F 1103

ACADÉMIE DE LA RÉPUBLIQUE SOCIALISTE DE ROUMANIE

REVUE ROUMAINE DE CHIMIE

Hommage à l'académicien ELENA CEAUŞESCU

TOME 34

N° 1

Janvier 1989

Rev. Roumaine Chim.

RRCHAX, **34,** *1,* p. 1 — 434 (1989), **Bucarest**

EDITURA ACADEMIEI REPUBLICII SOCIALISTE ROMÂNIA

ACADÉMIE DE LA RÉPUBLIQUE SOCIALISTE DE ROUMANIE

COMITÉ DE RÉDACTION

Rédacteur en chef :

I. G. MURGULESCU, membre de l'Académie de la République Socialiste de Roumanie

Rédacteurs en chef adjoints :

A. T. BALABAN et V. EM. SAHINI, membres correspondants de l'Académie de la République Socialiste de Roumanie

Collège de rédaction :

EM. BRATU, ELENA CEAUȘESCU, ECATERINA CIORĂNESCU-NENITZESCU, CR. SIMIONESCU, membres de l'Académie de la République Socialiste de Roumanie ; P. SPACU, membre correspondant de l'Académie de la République Socialiste de Roumanie : M. BANCIU, M. D. GHEORGHIU, I. HAIDUC, D. I. MARCHIDAN, G. NIAC et D. SĂNDULESCU

La Revue Roumaine de Chimie paraît 10 fois par an. Toute commande de l'étranger sera adressée à ROMPRESFILATELIA — sectorul Export-Import Presă, P.O. Box 12—201, télex 10376 prsfi r 78104 Bucarest, Calea Griviței nr. 64—66, Roumanie

Les manuscrits, les livres et les revues proposés en échange, ainsi que toute correspondance seront envoyés à la rédaction :

REVUE ROUMAINE DE CHIMIE

125, Calea Victoriei, 79717 Bucarest, Roumanie, téléphone 50 76 80

EDITURA ACADEMIEI REPUBLICII SOCIALISTE ROMÂNIA
125, Calea Victoriei 79717, Bucarest, Roumanie, téléphone 50 76 80

HOMMAGE À L'ACADÉMICIEN

ELENA CEAUȘESCU

ORSZÁGOS MŰSZAKI INFORMÁCIÓS KÖZPONT ÉS KÖNYVTÁR
1983

ORSZÁGOS MŰSZAKI INFORMÁCIÓS KÖZPONT ÉS KÖNYVTÁR 1883

IN HONOUR OF
ELENA CEAUȘESCU, D. CHEM. ENG.,
MEMBER OF THE ACADEMY OF THE SOCIALIST REPUBLIC OF ROMANIA

On January 7, this year, we celebrate the birthday and 50 years of revolutionary activity of Academician Elena Ceaușescu. A Doctor of Chemical Engineering, Member of the Executive Political Committee of the Central Committee of the Romanian Communist Party, First Vice-Prime Minister of the Government of the Socialist Republic of Romania, President of the National Council for Science and Education, Dr. Elena Ceaușescu chairs a vast scientific, political and social enterprise meant to bring into effect the country's plans for economic and social development, the important programs geared to a better organization and modernization of production, to increasing work productivity and efficiency, to a comprehensive implementation of the overall policy of the Romanian Communist Party and State, for the benefit of Romanian science, education and culture. The organization and management of the scientific research in this country, most especially in the fields of chemistry, and chemical technology and engineering, largely rely upon the innovative scientific spirit of, and direct guidance by Dr. Elena Ceaușescu.

As a direct outcome, the entire research and development system in chemistry has been given an appropriate coordination and has been integrated, along with the higher education in the field, with the respective industry.

The research work undertaken by Dr. Elena Ceaușescu is focused mainly on the chemistry and technology of macromolecular compounds; she has contributed to elucidating a number of major problems in the area — a most dynamic one in chemistry today, while also providing valuable contributions in all stages of applied research and

engineering, thus fostering the implementation in industry of the results of fundamental research.

Her studies dwell, *inter alia*, upon procedures for monomer and solvent purification; procedures for obtaining polymers via stereospecific polymerization and emulsion polymerization; procedures for obtaining polycondensates; studies on the structural characteristics of polymers and the relationship between structure and properties, as well as methods for the characterization of polymers. A series of studies deal with the use of complex catalysts for polymer synthesis in solution, with special emphasis on catalysts based on transition metals. Other works are concerned with the obtaining of polymers modified by isomerization, degradation and substitution reactions.

The stereospecific polymerization of isoprene holds an important place in the research work developed by Dr. Elena Ceauşescu, owing to the paramount relevance of this problem in today's chemistry of synthetic rubber. Part of the results were gathered in Dr. Ceauşescu's doctoral thesis. A special emphasis was placed on the synthesis of *cis*-1,4-polyisoprenic rubber that displays properties and structures similar to those of natural rubber, and substitutes for the latter in the tyre and technical item industry. Theoretical aspects connected with the reaction mechanism and kinetics, and the properties of the polyisoprene were also dealt with. Research was focused on the optimization of basic parameters, the obtaining of catalytic systems and development of the main steps of the technological flow-chart. The results have led to an industrial process for manufacturing *cis*-1,4-polyisoprenic rubber in Romania.

Dr. Elena Ceauşescu's scientific activity is also reflected in numerous papers published in scientific journals and in six monographs, first put out by Editura Academiei R. S. România, Bucharest, namely, "Research Work on Synthesis and Characterization of Macromolecular Compounds" (1974), "Stereospecific Polymerization of Isoprene" (1979), "Recent Research in the Field of Macromolecular Compounds" (1981), "Research in the Chemistry and Technology of Polymers" (1983), "Advances in Polymer Chemistry and Technology" (1986), and "Hydrocarbon Resins" (1988). Many publishing houses worldwide were soon to offer their readers translations of these books.

Dr. Elena Ceauşescu chaired the National Congress of Chemistry in the years 1978, 1981, 1988, and the IUPAC's Macro '83 Symposium. Her opening address at the 1988 National Congress of Chemistry gives important guidelines to the chemical research in Romania, also providing for the strengthening of the international scientific co-operation. Dr. Elena Ceauşescu contributed valuable papers to many scientific congresses and symposia — an outcome of her comprehensive scientific activity in the field of elastomer chemistry.

Dr. Elena Ceauşescu's scientific merits won well-deserved national and worldwide recognition. She is a member of the Academy of the Socialist Republic of Romania. She was also elected member of numerous international chemical societies of high renown and was nominated honorary professor by important higher education institutions abroad. Dr. Ceauşescu is a honorary member of the International Society of Industrial Chemistry, France; active member of the Academy of Sciences, New York; honorary member of the College of Chemists and Chemical Engineers in Costa Rica; honorary member of the University Council and of the Management Council of the Central University in Ecuador; honorary member of the Ecuador Institute of Natural Sciences; honorary member of the School of Information Science of the Central University of Ecuador; honorary professor of the National Engineering University, Peru; honorary member of the American Institute of Chemists (A.I.C.); Doctor Honoris Causa of the University of Buenos Aires; Doctor Honoris Causa of the University of South-Bahia Blanca, Argentina; Doctor Honoris Causa of the Feminine University of Manila, the Philippines; honorary member of the Chemical Society of Mexico; Doctor Honoris Causa of the University of Yucatan, Mexico; Extraordinary Professor of the Autonomous National University of Mexico; Doctor Honoris Causa of Sciences, University of Teheran; honorary member of the Society of Polymer Science in Japan; corresponding member of the Academy of Athens; awardee of the Silver Medal of the Science University of Kuweit; honorary member of the Academy of Arts and Sciences in Ghana; honorary member of the Academy of Sciences of the State of Illinois, USA; Fellow of the Royal Institute of Chemistry, UK; Professor Honoris Causa of the Polytechnics of Central London; member of the European Academy of Sciences, Arts

and Humanities, and member of the Honorary Committee of the Academy; Doctor Honoris Causa of the Technical University of the Middle East, Ankara; Doctor Honoris Causa of the University of Malta; Doctor Honoris Causa for Sciences of the Islamabad University, Pakistan; Doctor Honoris Causa for Sciences of the University of Liberia; Doctor Honoris Causa in Chemical Sciences, D.P.R. of Korea.

The high praise enjoyed by Dr. Elena Ceaușescu is also reflected in her being awarded important titles and distinctions of merit. Among these are: the highest Romanian title of honour "Hero of the Socialist Republic of Romania"; the title "Hero of Socialist Labour"; the medal "Star of the Socialist Republic of Romania", as well as other orders and medals, Romanian and foreign. She was also awarded the Gold Medal of the Institute for the Problems of a New International Economic Order, the Gold Medal "Marie Curie" and the Jubilee Gold Medal of the Institute of International Relations in Rome, and the Gold Badge of the European Academy of Sciences, Arts and Humanities. By virtue of these, Academician Elena Ceaușescu is the most prestigious representative of the Romanian contemporary science, education and culture.

Active in the national scientific and political life as well as in the international arena, presiding over the Romanian National Committee "Scientists and Peace", Academician Elena Ceaușescu makes an outstanding contribution to the carrying into effect of Romania's policy of independent domestic development, many-sided international co-operation, and struggle for peace, a policy designed under the guidance of Comrade Nicolae Ceaușescu, Secretary General of the Romanian Communist Party, President of the Socialist Republic of Romania, Honorary President of the Academy of the Socialist Republic of Romania.

The National Council for Science and Education, the Ministry of the Chemical and Petrochemical Industry, the Academy of the Socialist Republic of Romania, and the Central Institute for Chemistry join whole-heartedly in the feelings of highest esteem and praise the Romanian people has for Academician Elena Ceaușescu, and express deepest appreciation for her exceptional contribution

to the building of modern Romania, to the development of scientific research and education in this country, particularly in the field of chemistry, chemical technology and engineering. We wish the most distinguished Romanian scholar many happy returns and a long and fruitful activity in order that science, education and culture in the Socialist Republic of Romania be raised onto ever higher levels of performance, for the benefit of our society, of world progress and peace.

THE NATIONAL COUNCIL
FOR SCIENCE AND EDUCATION

THE MINISTRY
OF THE CHEMICAL
AND PETROCHEMICAL
INDUSTRY

THE ACADEMY
OF THE SOCIALIST
REPUBLIC OF ROMANIA

THE CENTRAL INSTITUTE
FOR CHEMISTRY

REVUE ROUMAINE DE CHIMIE

Tome 34, N° 1 **Janvier, 1989**

IN HONOUR OF
ELENA CEAUȘESCU, D. CHEM. ENG.
MEMBER OF THE ACADEMY OF THE
SOCIALIST REPUBLIC OF ROMANIA

ELENA CEAUȘESCU, M. DIMONIE, VICTORIA FIEROIU, G. HUBCĂ, V. GRUBER, ELENA GABRIELA BADEA, M. VLĂDULESCU, A. VERESTOI, H. IOVU and IOANA VASILE, Aspects concerning the polymerization of isoprene with lanthanide-based catalysts 5–13

ELENA CEAUȘESCU, VICTORIA FIEROIU, V. DRĂGUȚAN, EUGENIA SIMIONESCU, ELENA GRUBER, CORNELIA PIROJOC, C. ION, and VIORICA APOSTOL, Mechanism and stereochemistry of 1,3-butadiene polymerization in the presence of modified $TiCl_4$-TIBA-I_2 catalyst . 15–23

EMILIAN ANGELESCU, GAVRIL MUSCĂ, GRIGORE POP, ECATERINA POP, DANIELA SMOLEANU and GEORGIANA POGONARU, Conversion of C_2-C_4 alkenes into gasolines by using ZSM–5 zeolites catalysts 25–34

RADU AVRAM and DUMITRU SAVU, Relationship between a structure and effect of some organic compounds containing sulphur on steel corrosion inhibition process in acid medium 35–40

ALEXANDRU T. BALABAN and TEODOR-SILVIU BALABAN, Pyrylium salts formed by diacylation of olefins. Part XXIV. Synthesis of *meta*-terphenyl derivatives and heterocyclic analogs *via* bis-pyrylium salts obtained by bis-diacetylation of *meta*-diisopropenylbenzene 41–50

CAMELIA BELDIE, GH. NEMȚOI, EM. DUMITRIU and V. BĂRBOIU, The behaviour of diethyl maleate – vinyl acetate copolymers in solution . . 51–58

ANIŞOARA BOLD, ANGELICA POPA, AURELIA VASILE, M. CRUCEANU, EVELINE POPOVICI and MARIA ALEXANDROAEI, Zeolite molecular sieves as stationary phase in thin layer chromatography. V. On migration mechanism 59–63

GH. C. BUJGOI, World-wide and national concerns and tendencies regarding the turning to account of non-ferrous metals from low grade raw materials 65–78

Rev. Roumaine Chim. **34**, *1*, 1–434 (1989), Bucarest

E. CHIFU, I. STAN, M. SĂLĂJAN and EUGENIA GAVRILĂ, Surface mobility of surfactant solutions. XIII. Influence of the magnetic field . . . 79 — 85
ECATERINA CIORĂNESCU, ANCA VOICU and M. ELIAN, Carbonium ion reactions. XIX. The solvolysis of 5-(1′,1′-dimethylethyl)-5-hydroxy-5*H*-dibenzo[*a*,*d*]-cycloheptene and some related compounds. An uncommon neopentyl rearrangement . . . . 87 — 102
FELICIA CORNEA, ADALGIZA CIOBANU, I. BACIU, O. MAIOR and A. A. EL BAHNASAWY, Synthesis of some new heterocyclic derivatives of di- and tetrahydroquinazoline . . . . 103 — 109
KEVEN A. CURRAN, JOHN O. PETERSON and EMANUEL MERDINGER, Progress in hemodialysis . . . . 111 — 114
RAYMOND DAUDEL, Electronic structure of molecules. Applications in physics, chemistry and biology (in French) . . . . 115 — 119
A. HAAS, Recent developments in perfluoroorgano chemistry of selenium in various oxidation states . . . . 121 — 128
MARIA IONESCU, Polymers of permanently antistatic ε-caprolactam (in French) . . . . 129 — 142
M. IVAȘCU, D. N. POENARU, I. IVAȘCU, E. HOURANI and W. GREINER. Vibration energy of new kinds of radioactivities . . . . 143 — 148
GHEORGHIȚA JINESCU and VASILE LAVRIC, Mass transfer in an air-lift biological reactor. Part I. An experimental study . . . . 149 — 160
VALERIU V. JINESCU, A fundamental property of matter. Part II . . . 161 — 167
VALENTIN AFANASIEVICH KOPTYUG, Dependence of substituent electronic effects in π-systems on the character of molecular orbitals . . . . . 169 — 189
DIAMANTA LAUDONIU, S. CIOBANU, A. MANEA, M. SCARLETE, C. BARTHA, V. VANCA, D. VASILIU, V. NINULESCU and G. CRISTIANI, Decreased thermodynamical activity of oxygen in silicon single crystals grown by Czochralski method . . . . 191 — 195
C. LUCA, A. ANDREI and G. SEMENESCU, Considerations concerning oxide/metal/electrolyte system in non-equilibrium regime . . . . 197 — 205
GH. MARCU, MARIANA RUSU and A. BOTAR, Unsaturated heteropolytungstates with Th(IV) central ion . . . . 207 — 213
BUJOR OLTEANU, Achievements and expectations in crude oil processing 215 — 233
A. M. PROKHOROV, V. I. KONOV, V. P. AGEEV, I. URSU and I. N. MIHĂILESCU, Surface structuring by UV-laser irradiation in a gaseous atmosphere . . . . 235 — 245
JOSEF ŘÍMAN, Contribution of the Czechoslovak Academy of Sciences to the development of the modern Czechoslovak biotechnologies . . . . . . 247 — 252
V. E. SAHINI and CRISTINA POP, A molecular orbital approach to some radiogenetic mechanisms . . . . 253 — 257
DUMITRU SĂNDULESCU and GABRIELA SAVA, Thermodynamics of irreversible processes on electroosmosis of aqueous electrolyte and nonelectrolyte solutions . . . . 259 — 270
WERNER SCHROTH, New aspects in the chemistry of pyrylium salts : changes due to dialkylamino substituents . . . . 271 — 285
E. SEGAL and T. COSEAC, Basic versatile program for nonisothermal kinetics 287 — 295
ȘERBAN SEVER, STELUȚA CHIPER and SILVIU-DUMITRU POPESCU, Determination of Cu^{2+}, Pd^{22} and Zn^{22} by differential-pulse polarography 297 — 303

LUMINIȚA SILAGHI-DUMITRESCU, IOAN SILAGHI-DUMITRESCU and IONEL HAIDUC, The sulfotropic molecular rearrangement of tetraorganodiarsine disulfides 305–315

CRISTOFOR I. SIMIONESCU, AURA ANGELICA POPA, EUGENIA COMĂNIȚĂ and VIRGIL BĂRBOIU, Azoamide derivatives obtained from ethyl phenylazocarboxylate 317–322

P. SPACU, SILVIA PLOȘTINARU, LUMINIȚA PATRON, ADRIANA CONȚESCU, D. CRIȘAN and N. STĂNICĂ, Rare earth mixed oxides with transition metals. II. Mixed oxides with Fe(III) having a perovskite and garnet structure 323–329

R. STEFANOVA, I. BANCHOV and L. PETROVA, On the structure of the disodium *p*-isononylphenylethoxysulphosuccinate 331–336

SOLOMON STERNBERG, MIHAELA UNGUREANU and SORIN ROȘCA. Electrochemical oxidation of carboxylic acids. I. Electrode processes in the electrochemical oxidation of 3-phenylpropionic acid 337–349

RODICA A. STURZA, V. E. NENNO and A. M. ROMANOV, About the electrochemical durability of dioxide manganese titanium anodes obtained by electric spark method (in Russian) 351–356

I. TEOREANU and ANNEMARIE PURI, Formation and stability of 3(CaO$\cdot$Al$_2$O$_3$)$\cdot$BaSO$_4$ (in German) 357–363

CLEOPATRA VASILIU OPREA and MARCEL POPA, Tensile creep of monofilaments based on acrylonitrile-vinyl acetate-α-methyl styrene ternary copolymer (in German) 365–375

RADU VÂLCEANU, ZENO SIMON and LUDOVIC KURUNCZI, Quantum chemical calculations for dipole moments of phosphorus compounds . . 377–385

RODICA VÎLCU and MINODORA LECA, Thermodynamic characterization of polymers by chromatography with gas mobile phase 387–395

LIAN-WAN YANG and XIU-YUAN WANG, Studies on the hydrocarbon production by immobilized *Botryococcus braunii* cells 397–401

K. B. YATSIMIRSKII, Application of macrocyclic compounds for biosynthesis modelling (in Russian) 403–408

N. M .ZHAVORONKOV, Chemical technology as science and subject (in Russian) 409–433

Revue Roumaine de Chimie, **34,** *1,* 5 – 13 (1989)

ASPECTS CONCERNING THE POLYMERIZATION OF ISOPRENE WITH LANTHANIDE-BASED CATALYSTS

ELENA CEAUŞESCU, M. DIMONIE[a], VICTORIA FIEROIU[b], G. HUBCĂ[a], V. GRUBER[b], ELENA GABRIELA BADEA[b], M. VLĂDULESCU[c], A. VERESTOI[c], H. IOVU[b] and IOANA VASILE[b]

[a] Polytechnic Institute, Bucharest, Romania
[b] ICECHIM, Bucharest, Romania
[c] IAMN, Bucharest, Romania

Received November 21, 1988

The polymerization of isoprene catalyzed by indigenous lanthanide trichloride has been studied. These investigations made it possible to put in evidence the influence of the catalyst aging time, the Al/Nd molar ratio and the nature of the complexing agent upon conversion, the molecular weight and the microstructure of the obtained polymer.

INTRODUCTION

The lanthanide-based catalysts are Ziegler-Natta systems made up of a compound of an "f" transition metal belonging to the lanthanide series, an organic aluminium compound and a cocatalyst which may be a complexing or halogenating agent, as a function of the nature of the compound in which the transition metal occurs. Hence, if lanthanide halides are employed as cocatalyst, a complexing agent is added : tributyl phosphate, alcohols, hydroxyaldehydes, hydroxyesters, phenyl ethers, etc. If the transition metal is introduced in the form of an organic compound (alcoholate, carboxylate, chelate compounds, etc.) a chlorinating agent is used as a third component : AlR_2Cl, $Al_2(C_2H_5)_3Cl_3$, etc.

These catalytic systems exhibit a high catalytic activity at low concentration in the system, high stereospecificity and they lead to linear structure polymers, free of gel and oligomers, of high molecular weight and a large distribution of their molecular weights.[1]

It is worth pointing out several peculiarities that sharply differentiate these catalytic systems from the classical Ziegler-Natta titanium-based catalysts. They firstly refer to the fact that the catalytic and stereospecific activities are much more affected by the Al/Ln ratio, reaching a maximum at a molar ratio of 30-40-1. If we start from the fact that "f" transition metals have the stable valence state of +3, it results that the role of the organic aluminium compound is only to alkylate the transition metal. This fact was demonstrated by Dolgoplosk who succeeded in polymerizing isoprene and butadiene with lanthanide organic compounds (of the $RNdCl_2$ type) in the absence of the organic aluminium compounds.[8] Under these conditions, the activity of the latter depends on its alkylation capacity and the stability of the active centre depends on the nature of the organic radical. A high activity is exhibited by the organic aluminium compounds which are not associated at room temperature, such as triisobutylaluminium. The way in which the nature of the organic aluminium compounds influences the activity of the catalytic complex has been much studied but the results are contradictory.[1,7]

The second important peculiarity of these catalysts is the fact that the polymerization proceeds according to the "living polymers" system. The investigations have shown that the ideal living polymerization occurs only at low temperature (−70°C).[9] The process is of importance in obtaining stereo-regular block-copolymers.[10]

Remarkable peculiarities of these catalysts refer also to the fact that the halides of the "f" transition metals do not possess a cationic catalytic activity and the alkenes do not interact with the growing chain, the latter being some of the best solvents for the polymerization process.[11]

RESULTS AND DISCUSSION

The purpose of this work has been the study of the polymerization of isoprene with $LnCl_3 \cdot 3L-AliBu_3$ catalytic systems, considering the high activity of the lanthanide halide-based catalysts. As trihalides of the transition metals, there have been used pure neodime trichlorideneodime trichloride of IAMN institute origin and didim (a mixture of neodim trichloride, praseodime trichloride and lanthane trichloride in a 72 : 8 : 20 molar ratio). Tributylphosphate (TBP) and ethyl alcohol have been used as complexing agents.

The investigations undertaken have made evident the fact that didime and neodime chloride of IAMN institute origin exhibit a satisfactory catalytic activity but the resulting polymers have a more reduced content of 1,4-*cis* (table 1) as compared with those obtained with pure neodime chloride. This fact is probably determined by a series of impurities that have not been removed from these halides yet.

Table 1

The polymerization of isoprene with lanthanide-based catalytic systems. The influence of the nature of the lanthanide

AL/Ln = 20/L ; TBP/Ln = 3/L ; Complexing time = = 1 h ; Aging time = 1 h ; Reaction time = 4 h ; t = 25°C ; $[NdCl_3] = 2.3 \cdot 10^{-3}$ moles/L

LnX_3	Conversion %	[η] inh (dl/h)	$\overline{M}_v \cdot 10^{-5}$	1,4-*cis* %
Pure $NdCl_3$	97.64	3.22	5.2	93.2
Didim IAMN	99.26	2.23	3.2	82.8
$NdCl_3$ IAMN	37.0	8.16	17.2	86.1

Factors which highly influence the polymerization process are the time of complexing neodime trichloride with tributylphosphate or ethyl alcohol and the aging time of the catalyst, the latter being prepared in situ by using neodime trichloride of IAMN institute origin.

In figure 1, curve 1, an increase of conversion is to be noted, function of the aging time, increase which reaches a limit at reaction time of over 5 hours. This result is inconsistent with the results obtained by Monakov and coworkers.[12] (Fig. 1, curve 2) who assert that in the case of triisobutylaluminum, the activity of the active centre decreases in time and, consequently, the conversion too. The above-mentioned authors support the idea that, on the basis of the results obtained with tridecylaluminium, along with the increase of the sizes of the organic radicals from the organoaluminium compounds, a stabilisation of the active site takes place (Fig. 1, curve 3). The differences between our results and those mentioned in the literature are probably due to different experimental conditions.

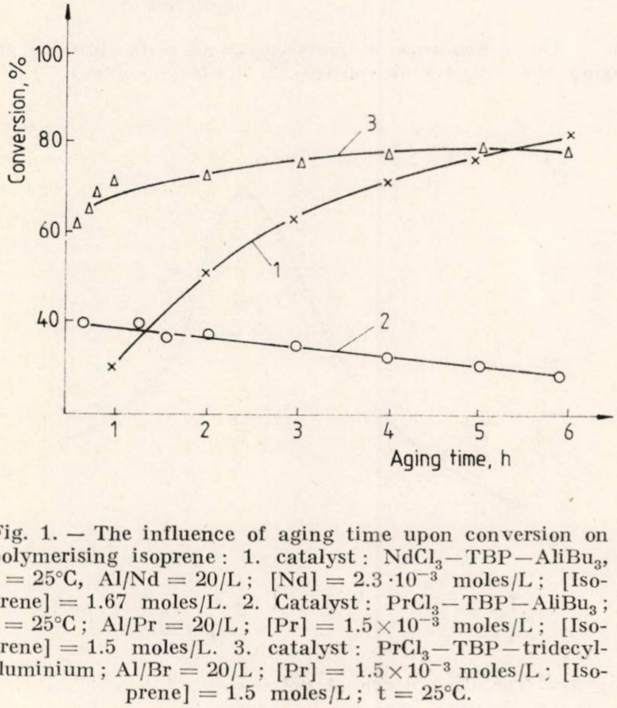

Fig. 1. — The influence of aging time upon conversion on polymerising isoprene : 1. catalyst : $NdCl_3$—TBP—$AliBu_3$, t = 25°C, Al/Nd = 20/L ; [Nd] = $2.3 \cdot 10^{-3}$ moles/L ; [Isoprene] = 1.67 moles/L. 2. Catalyst : $PrCl_3$—TBP—$AliBu_3$; t = 25°C ; Al/Pr = 20/L ; [Pr] = 1.5×10^{-3} moles/L ; [Isoprene] = 1.5 moles/L. 3. catalyst : $PrCl_3$—TBP—tridecylaluminium ; Al/Br = 20/L ; [Pr] = 1.5×10^{-3} moles/L ; [Isoprene] = 1.5 moles/L ; t = 25°C.

The aging time of the catalyst also influences the microstructure of the resulting polyisoprene and its inherent viscosity. As can be seen in Fig. 2, the 1,4 contents *cis* undergoes a slight decrease in favour of *trans*-1,4 contents. Higher viscosities are obtained at a 4 hours aging time of the catalyst (Fig. 3).

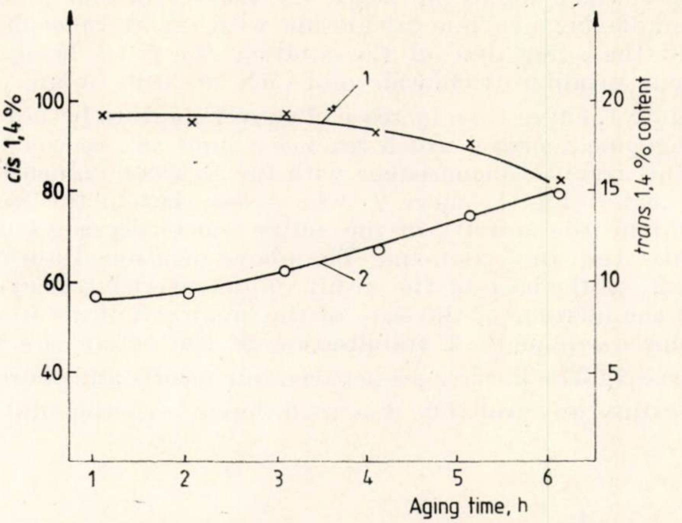

Fig. 2. — The dependence of polyisoprene microstructure on the aging time. 1. 1,4-*cis* content; 2. 1,4-*trans* content.

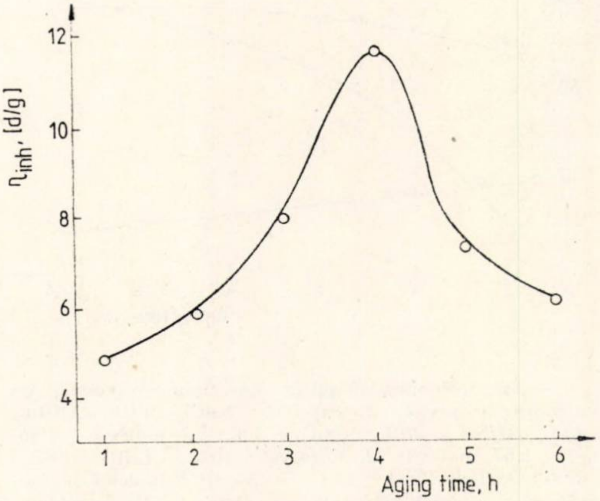

Fig. 3. — The dependence of polyisoprene inherent viscosity on the catalyst aging time.

It has been noticed that, for the investigated catalysts, the Al/Ln ratio influences the activity of the catalyst and the microstructure of the resulting polymer (table 2). The decrease of this ratio below 20/1 has a negative influence upon the microstructure and the molecular weight of the resulting polyisoprene.

By comparing the results obtained during the polymerization of isoprene with tributylphosphate and ethyl alcohol as complexing agents it is noticed that higher conversions are obtained in the first case while for ethyl alcohol higher molecular weights and *cis*-1,4 contents are obtained (table 3). It should also be noticed that the solubility of the metallic complex is higher for the TBP systems than for those based on ethyl alcohol which are pseudohomogeneous.

Table 2

The polymerization of isoprene with lanthanide-based catalytic systems. The influence of the Al/Ln molar ratio
TBP/Ln = 3/L : The reaction time = 4 h ; t = 25°C ; [Isoprene] = = 1.5 moles/L ; Aging time = 1 h ; [$NdCl_3$] = $2.3 \cdot 10^{-3}$ moles/L

Al/Ln	Conversion %	[η] inh (dl/lg)	$\vec{M}_v \cdot 10^{-5}$	1,4-*cis* %	1,4-*trans* %
10	36.0	9.27	10.17	90.0	5.8
20	37.0	8.16	17.12	86.1	9.6
30	69.2	5.03	9.21	88.0	7.4

Table 3

The polymerization of isoprene with lanthanide-based catalytic systems. The influence of the nature of complexing agents.
Al/Nd = 30/L : TBP/Nd = 3/L ; EtOH/Nd = 5/L
t = 25°C ; [Nd] = $2.3 \cdot 10^{-3}$ moles/L ;
[isoprene] = 1.5 moles/L

Complexing agent	Conversion %	[η] inh (dl/g)	$M_v \cdot 10^{-5}$	1,4-*cis* %	1,4-*trans* %
TBP	69.2	5.03	9.21	88.0	7.4
EtOH	30.6	7.19	14.53	91.0	4.7

EXPERIMENTAL PART

Polymerization was carried out in an n-hexane medium. The solvent was purified by fractionation in a column with 20 theoretical trays, whereupon it was stored on a sodium potassium alloy in a totally sealed vessel (Fig. 4) and freshly distilled prior to each polymerization.

The hexahydrated neodime and didime trihalides were subjected to an anhydrizing process. Their anhydrizing cannot be accomplished by simple heating as in the case of the crystal-hydrates of the elements in the main groups, because they react with the crystallization water or with oxygen and form oxi-halides which are completely inert during the polymerization process :

$$LnCl_3 + H_2O \rightarrow Ln\ OCl + 2\ HCl \qquad (1)$$

$$LnCl_3 + 1/2O_2 \rightarrow LnOCl + Cl_2 \qquad (2)$$

Because of these reasons the anhydrizing process must be carried out in a chlorinating atmosphere, which ensures the conversion of oxi-halides to trihalides according to the reaction :

$$LnOCl + 2\,HCl \rightarrow LnCl_3 + H_2O \quad (3)$$

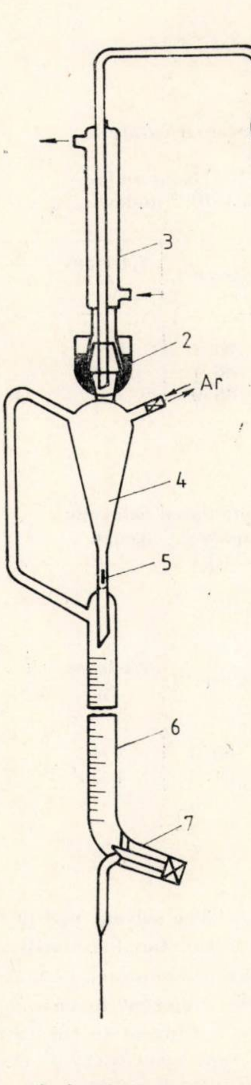

Fig. 4. — Installation for *n*-hexane purification. 1. reservoir; 2. hydraulic closing (with mercury); 3. condenser; 4. buffer reservoir; 5. magnetic tape; 6. graduated cylindrical tube; 7. teflon-type valve.

The chlorinating atmosphere is ensured either by passing a stream of dry gaseous hydrochloric acid, or by introducing ammonium chloride, which decomposes at the working temperature releasing HCl. In our case, the anhydrizing process was carried out in the presence of ammonium chloride, according to the method described by Taylor and Carter.[13] The anhydrized chlorides were run over under a cushion of argon into the proportioner represented in Fig. 5 and closed into glass balls or little tubes, as desired.

Triisobutylaluminium was diluted with n-hexane and dosed in phials under argon, by means of the proportioner presented in Fig. 6. Tributylphosphate was purified by vacuum distillation and its high drying was accomplished by an azeotropic distillation in a totally sealed vessel (Fig. 7). The anhydrizing process is carried out under vacuum. Pure n-hexane, stored on a Na—K alloy was passed from the buffer-vase 2 into the vase 1, containing TBP, by introducing liquid nitrogen in Dewar condenser 4′. After the homogenisation by introducing liquid nitrogen in Dewar pypa condenser 4, the n-hexane-water azeotrope was distilled in the buffer-vase 2. After the reaction of water with Na—K alloy, the operation was repeated and carried on till the samples drawn with the burette 6 had a content of humidity below 10 ppm. The tributylphosphate thus anhydrised was diluted with pure n-hexane at the desired concentration and was dosed in phials by means of a proportioner similar to that employed for the dosage of triisobutylaluminium (Fig. 6).

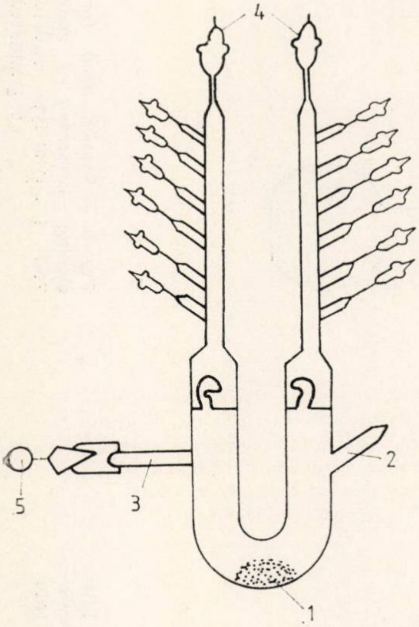

Fig. 5. -- Apparatus used for stocking and encapsulating known amounts of $LnCl_3$. 1. reservoir; 2. lateral arm; 3. loading system; 4. Argon admission. 5. Bubble containing $LnCl_3$.

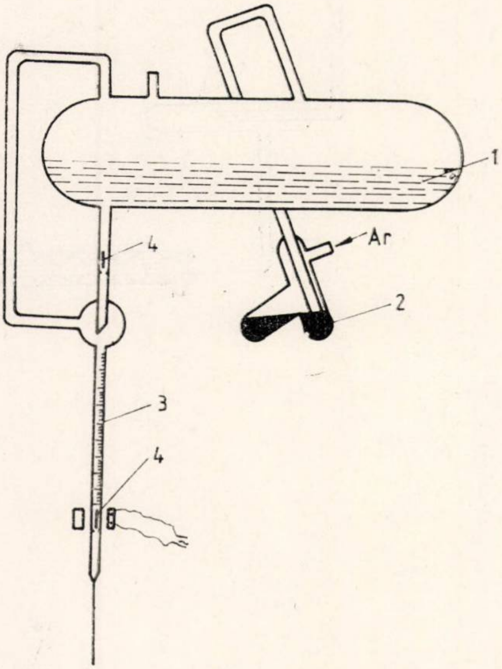

Fig. 6. — Measuring system used for the organo-aluminium compound. 1. reservoir; 2. hydraulic closing; 3. graduated tube; 4. magnetic tape.

The absolute ethyl alcohol was subjected to a further anhydrizing process with magnesium ethylate in a totally sealed of vessel (Fig. 8), whereupon it was diluted with n-hexane and dosed in phials as in the case of tributylphosphate.

Isoprene was purified by the fractionation of triisobutyl-aluminium and, prior to polymerization, by distillation out of the Na—K alloy.

The polymerizations were carried out in glass reactors with magnetic stirring, in a purified argon atmosphere, at a temperature of 25°C. The polyisoprene thus obtained was precipitated with methanol, stabilized with Santoflex — IP and analysed to determine the gel contend, the molecular weight and the microstructure.

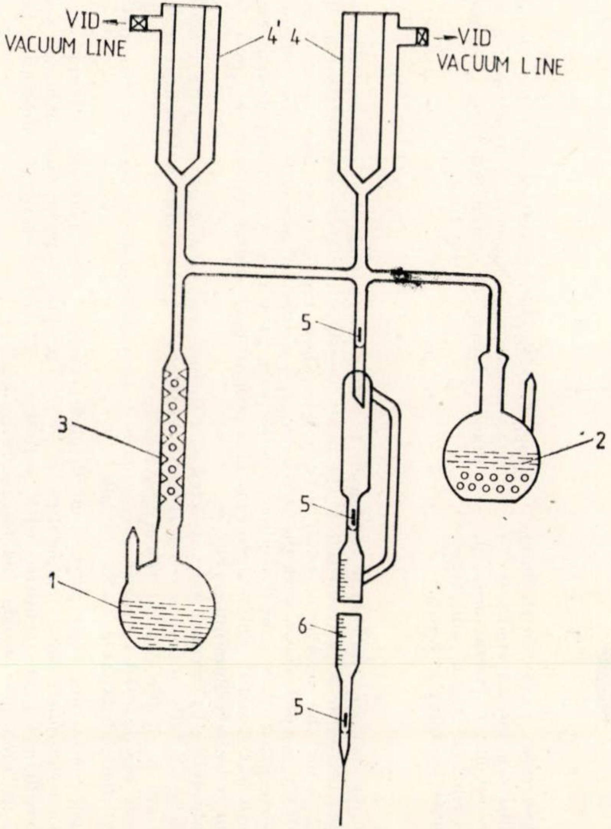
VID
VACUUM LINE
4'
4
VID
VACUUM LINE
5
3
5
2
1
6
5

Fig. 7. — System used in order to obtain anhydrous TBP. 1. reservoir; 2. reservoir; 3. Vigreoux column; 4. Dewar-type condensing device; 5. magnetic tap; 6. graduated tube.

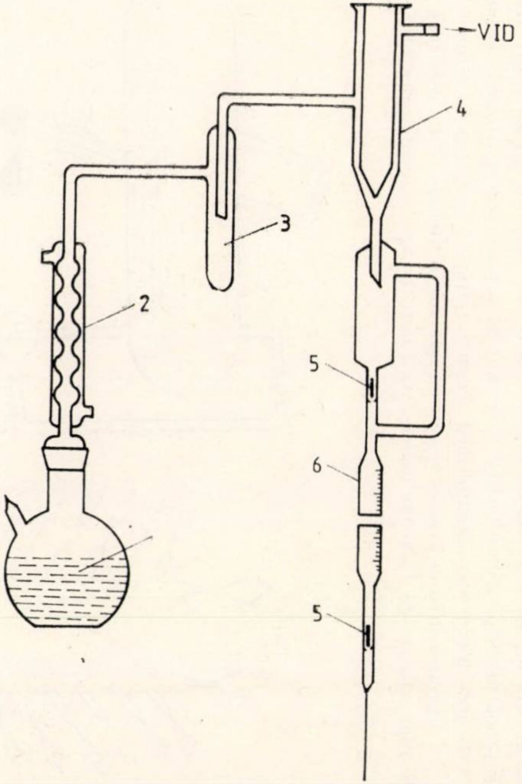

Fig. 8. — System used for anhydrising of ethyl alcohol: 1.reservoir; 2. condenser; 3. buffer reservoir; 4. Dewar-type condenser; 5. magnetic tap; 6. graduated tube.

REFERENCES

[1] Elena Ceaușescu, "Progrese în chimia și tehnologia polimerilor", Ed. Academiei, București, 1986.

[2] A. Mazzei, *Makromolec. Chem.*, **182**, Suppl. 4, 61 (1981).

[3] J. Yang, J. Hu, S. Feng., E. Pan, D. Xie, C. Zhong and J. Ouyang, *Sci. Sin.*, **23**, (6), 734 (1980).

[4] M. C. Throckmorton, *Kautschuk und Gumii Kunststoffe*, **22** (6), 293 (1969).

[5] S. K. Rafikov, Yu. B. Monakov, Ya. H. Bishshev, I. F. Valitova, Yu. I. Murinov, G. A. Tolstikov, and Yu. E. Nikitin, *Dokl. Akad. Nauk. S.S.S.R.*, **229** (5), 1174 (1976).

[6] Yu. B. Monakov, N. G. Marina, I. G. Savelieva, L. E. Kibor, V. G. Kozlov, and S. R. Rafikov *Dokl. Akad. Nauk S.S.S.R.*, **265** (6), 1431 (1982).

[7] N. G. Marina, Yu. B. Monakov, S. R. Rafikov, and H. K. Gadaleva, *Visokomol. Soedineniya*, **26** (6), 1123 (1984).

[8] E. L. Vollershtein, N. N. Glebova, S. B. Golishtein, E. N. Zavadovskaya, O. K. Saraev, V. A. Yakolev, E. I. Tinyakova, and B. A. Dolgoplosk, *Dokl. Akad. Nauk S.S.S.R.*,**284**, (1), 140 (185).

[9] Ji. Xianzhong, P. Shufen, Li Yuliang and G. Jun, *Sci. Sin.*, Series B, **29** (1), 8 (1986).

[10] V. S. Bodrova, *Dokl. Akad. Nauk S.S.S.R.*, **293** (3), 645 (1987).

[11] G. Ricci, *Makromol. Chem. Rapid Commun.*, **7**, 335 (1986).

[12] N. G. Marina, H. K. Gadeleva, Yu. B. Monakov, and C. R. Rafikov, *Dokl. Akad. Nauk S.S.S.R.* **274** (3) 641 (1984).

[13] M. D. Taylor and C. P. Carter, J. Imoy, Chem., **24**, 387 (1962).

Revue Roumaine de Chimie, **34**, *1*, 15 – 23 (1989)

MECHANISM AND STEREOCHEMISTRY OF 1,3-BUTADIENE POLYMERIZATION IN THE PRESENCE OF MODIFIED $TiCl_4$-TIBA-I_2 CATALYST

ELENA CEAUŞESCU, VICTORIA FIEROIU, V. DRĂGUŢAN, EUGENIA SIMIONESCU,
ELENA GRUBER, CORNELIA PIROJOC, C. ION and VIORICA APOSTOL
ICECHIM, Splaiul Independenţei 202, Bucharest, Romania

Received November 21, 1988

New catalytic systems based on TIBA-I_2-$TiCl_4$ have been studied in 1,3-butadiene polymerization using aromatic hydrocarbons as a solvent. It is found that when 1,3- and *cis, cis*-1,5-cyclooctadiene are employed as the catalyst modifier highly active and stereospecific systems can be obtained. Gel-free polymers were prepared and variable molecular weights resulted, as a function of the amount of modifier. The influence of some characteristic parameters of the catalytic systems such as the order of introduction of the catalytic components, the manner of formation of the catalytic complex, the molar ratio of the modifier, etc. on the polybutadiene properties has been studied. The mechanism and stereochemistry of 1,3-butadiene polymerization in the presence of the above catalysts are discussed.

Widespread industrial application of *cis*-1,4-polybutadiene, particularly in tyre production, has stimulated new research in obtaining highly stereospecific polymers and developing catalytic systems with improved activity and stability.[1]

Although at present a large number of studies on the mechanism and stereochemistry of 1,3-butadiene polymerization in the presence of various catalytic systems are known,[2-6] several important aspects of the reaction mechanism such as formation of initiating species and their nature, structure of the active centres of propagation, origin of the reaction stereochemistry or the mode of variation of polymer molecular weight are not completely elucidated.

The present work focuses on some aspects concerning the mechanism and stereochemistry of 1,3-butadiene polymerization in the presence of the quaternary catalytic system consisting of titanium tetrachloride, triisobutylaluminium, iodine and cyclooctadiene (1,3-and *cis*, *cis*-1,5-cyclooctadiene). This catalytic system displayed a high stereospecificity allowing obtention of 1,4-polybutadiene with the *cis* content between 92 and 95%.

The polymerization reaction was carried out discontinuously under inert gas (argon), at the atmospheric pressure, in homogeneous medium using toluene as the solvent. The reaction temperature was 30±2°C. The catalyst was prepared "in situ" or by precomplexing; the order of introduction of its components was varied to optimize the process.

RESULTS AND DISCUSSION

On polymerizing 1,3-butadiene under the above-mentioned conditions, using 1,3- and *cis,cis*-1,5-cyclooctadiene as the catalyst modifier, the results presented in Table 1 were obtained.

Table 1

Effect of reaction time on the conversion and microstructure of polymer

Run no.	Polymerization time, min.	Conv. %	Microstructure, %		
			cis-1,4	*trans*-1,4	1,2
TIBA + 1,3-COD + I_2 + $TiCl_4$					
1.	10	15.4	92.4	3.6	4.0
2.	15	65	93.0	3.0	4.0
3.	20	75	93.2	2.6	4.2
4.	30	85	91.8	3.5	4.7
5.	90	97	92.6	3.5	3.9
TIBA + 1,5-COD + I_2 + $TiCl_4$					
6.	10	28	92.3	2.2	5.5
7.	15	53	91.7	2.4	4.9
8.	20	68	91.3	3.2	5.5
9.	30	72	93.2	1.9	5.1
10.	90	78	92.1	2.6	5.3

Experimental conditions:
[C] = 4 mmol/100 g butadiene
Molar ratios of : Al/Ti = 8 ; Ti/Iodine = 0.5 ; COD/Al = 0.25
Temperature = 30 ± 2°C

From these data it can be observed that during the first 20 min. of reaction the conversion of 1,3-butadiene substantially increases to about 70% then slowly varies for the next 90 min. It can be seen that the catalyst modified with 1,3-cyclooctadiene exhibits a higher activity as compared to that with *cis*, *cis*-1,5-cyclooctadiene thus allowing to readily attain monomer conversions between 95 and 100%. In most experiments polymers with gel traces having molecular weights which increase as the conversion progresses were obtained.

The microstructure of polybutadiene as determined by IR spectroscopy indicated a high content of *cis*-units ranging between 92 and 95%. The content of both *trans*-1,4- and 1,2-polybutadiene was low (2—3,5% and 3—5,5%, respectively). It was found that the content of *cis*-1,4-, *trans*-1,4- and 1,2 units was constant during the polymerization reaction even under slight variation of the reaction parameters.

Similar results concerning the 1,3-butadiene conversion and polymer microstructure were obtained regardless of the manner of catalyst preparation (in situ or by precomplexing) (Table 2).

Table 2

Influence of the manner of catalyst preparation, TIBA $-$ COD $-$ I_2 $-$ $TiCl_4$

Run no.	Catalyst preparation	Conv. %	ηinh dl/g	Gel, %	Microstructure, %		
					cis-1,4	*trans*-1,4	1,2
1.	precomplexing	80.0	2.94	traces	94.0	2.1	3.9
2.	precomplexing	100.0	4.11	,,	92.8	3.7	3.5
3.	in situ	92.2	2.18	,,	93.4	2.7	3.9
4.	in situ	90.2	1.96	,,	92.5	3.6	3.9

Experimental conditions :

$[C] = 4$ mmol/100 g butadiene
Molar ratios of : $Al/Ti = 8$; $Ti/I = 0.5$; $COD/Al = 0.125$
Time of reaction : 2h
Temperature : $30 \pm 2°C$

It may be observed, however, that the induction period is prolonged when the catalytic system is obtained by precomplexing.

On addition of a supplementary amount of 1,3-butadiene toward the end of the reaction (after 90 min.) a substantial increase of the conversion of the monomer is recorded (Table 3).

Table 3

Butadiene polymerization using catalytic system TIBA$-$COD$-I_2-TiCl_4$. The monomer was introduced in two steps

Run no.	Time of reaction min.	Conv. %	η_{inh} dl/g	$i = \overline{M}_w/\overline{M}_n$
1.	10	15.4	1.42	2.59
2.	15	65	2.66	1.79
3.	20	75	2.64	1.86
4.	30	85	2.61	1.67
5.	90	97	2.60	1.91
6.	140	94	2.94	2.46

Experimental conditions :

$[C] = 4$ mmol/100 g butadiene
Molar ratios of : $Al/Ti = 8$; $Ti/I = 0.5$;
1.3 $COD/Al = 0.\ 25$
Temperature $= 30 \pm 2°C$

The rise in conversion is accompanied by the corresponding increase of the molecular weight. This particular behaviour suggests the occurrence of living catalytic centres at the end of the polymerization reaction. The same phenomenon has been reported by other authors using related catalytic systems.[7]

Preliminary studies by electron spectroscopic resonance concerning the nature of the active centres of catalysts prepared "in situ" pointed out the occurrence of paramagnetic Ti(III) species with g-factor of 1.950 at the very first moments of interaction. Similar paramagnetic species were also observed by Bressler and coworkers[8] on a related catalyst. It was found that the activity of our catalytic system depended on the concentration of this paramagnetic species. In case that this paramagnetic species disappears by a side reaction, the polymerization of 1,3-butadiene occurs slowly obeying characteristic kinetics. It is noteworthy that with the catalytic system prepared by precomplexing, the paramagnetic Ti(III) species were not observed.

The polybutadiene molecular weight changes slightly as the reaction progresses (Table 3). At short polymerization time (i.g. up to 20 min), an unimodal distribution of the polymer molecular weight was found (Figure 1). On the other hand, at polymerization time longer than 20 min., an increase of the dispersion degree could be observed.

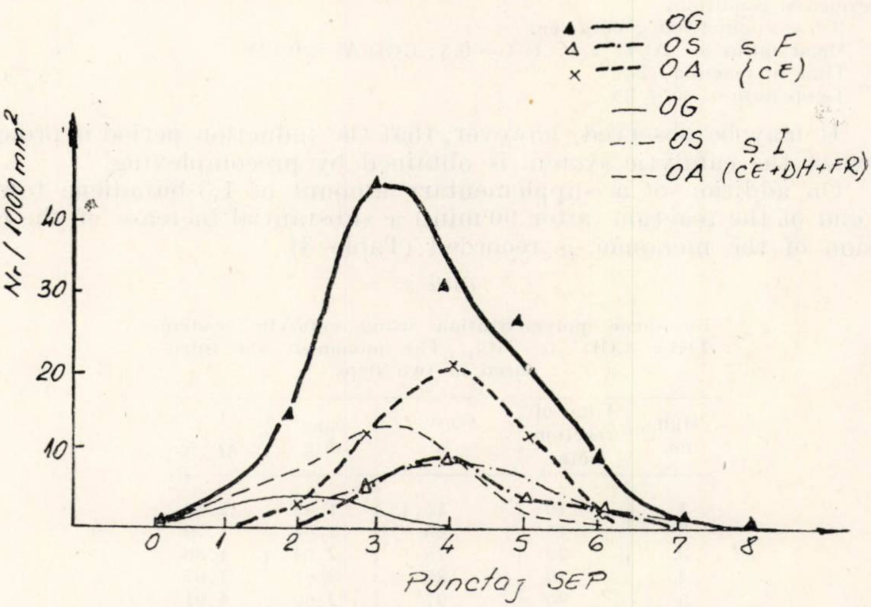

Fig. 1. — Dependence of molecular weight distribution on the time of polymerization. Experimental conditions: [C] = 4 mmol/100 g butadiene. Molar ratios of: Al/Ti = 8; Ti/I = 0.5; COD/Al = 0.25. Temperature: 30 ± 2°C. Time of reaction: 2h.

Formation of active species. Initiation reaction

Based on the above results, it can be inferred that the active species are formed by a reaction sequence involving alkylation and reduction of titanium tetrachloride by triisobutylaluminium (Eqs 1 and 2) and further substitution of chlorine ligand by iodine (Eqs 3–5).[9]

$$AlR_3 + TiCl_4 \rightarrow R_2AlCl + RTiCl_3 \rightarrow TiCl_3 + R^\cdot \quad (1)$$

$$\rightarrow \left| \begin{array}{l} \rightarrow R - R \\ \rightarrow R_{-H} + R_{+H} \end{array} \right.$$

$$AlR_3 + TiCl_3 \rightarrow RTiCl_2 + R_2AlCl \quad (2)$$

$$AlR_3 + I_2 \rightarrow R_2AlI + RI \quad (3)$$

$$R_2AlI + RTiCl_2 \rightarrow \underset{I}{RTiClI} + R_2AlCl \quad (4)$$

$$R_2AlI + RTiClI \rightarrow \underset{II}{RTiI_2} + R_2AlCl \quad (5)$$

By this way, trivalent Ti species, I and II, can arise having at least one iodine atom as the ligand. In the presence of 1,3- and *cis*,-*cis*-1,5-cyclooctadiene, the species I and II will lead to coordination complexes which stabilize the reaction centres. Due to the presence of the halogenated organometallic compound resulted from Eq. 1, the active species may be of a bridge type (Ia).

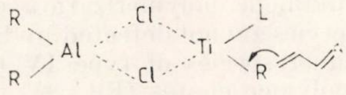

Ia

L = I, 1,3-COD, 1,5-COD

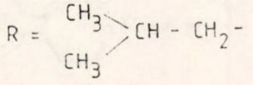

$$R = (CH_3)_2CH-CH_2-$$

After their formation, the active species I initiate the polymerization process through a bidentate coordination of 1,3-butadiene and subsequent insertion into the Ti-C bond ; allyl complexes will result as illustrated in eq. 6.

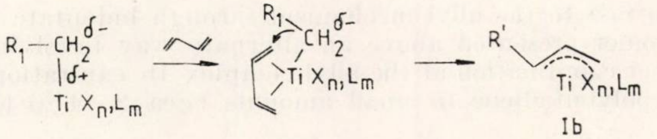

Ib (6)

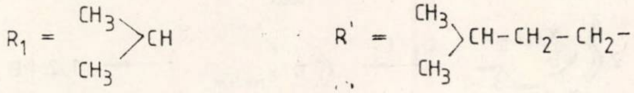

$$R_1 = (CH_3)_2CH \qquad R' = (CH_3)_2CH-CH_2-CH_2-$$

where R′ is the growing radical.

The bidentate coordination of 1,3-butadiene at the titanium complex is of cisoid type while the insertion reaction into the Ti—C bond occurs by a nucleophilic attack of the allyl carbon atom at the $C=C$ double bond of the complexed butadiene.

Mechanism of propagation reaction

Polymerization of 1,3-butadiene to *cis*-1,4 polybutadiene (92—95%) in the presence of the above modified $TiCl_4$ catalysts can be explained by a propagation mechanism involving π-allyl intermediates as represented in Eq.7.

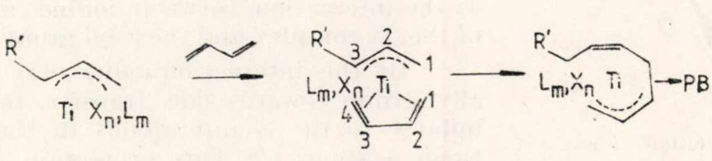

Ib III *cis*-η^4 (7)

The propagation mechanism supposes a bidentate coordination of 1,3-butadiene at the allyl complex Ib, formation of a coordination complex III, cis-η^4, and subsequent insertion of coordinated butadiene into the allyl ligand by C_1-C_1 addition. Through this insertion reaction anti allyl complexes arise having one more C_4 unit in the chain. On continuing these reaction steps polybutadiene of high *cis*-1,4 content resulting from the anti isomer can be obtained.

The fact that butadiene polymerization occurs slowly even when paramagnetic Ti(III) species are not detected by ESR spectroscopy suggests the possibility that dimer species of type IV to be present which lead to formation of two polymer chains (Eq. 8).

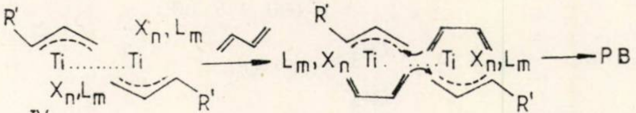

(8)

These dimer species favor both bimolecular chain transfer and termination reactions resulting in a wide molecular weight distribution at longer reaction time. Similar dimer species had been proposed earlier by Kormer[10] and Dolgoplosk[11] in butadiene polymerization induced by Ni catalysts.

In contrast to the allyl mechanism through bidentate coordination of the monomer presented above an alternate way involving monodentate monomer coordination at the allyl complex Ib can rationalize formation of 1,2-polybutadiene in small amounts (cca 2–4%) (Eq. 9).

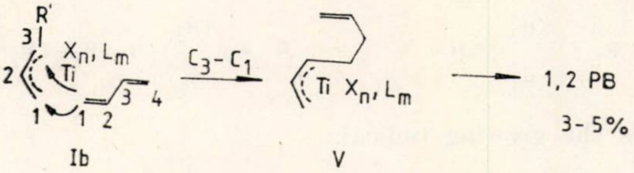

(9)

In this case the propagation reaction can occur by an $C_3 - C_3$ insertion leading to vinyl bonds in the allyl complex V. It is noteworthy that a similar mechanism is encountered at Dawans and Teyssié in butadiene polymerization with nickel complexes.[12]

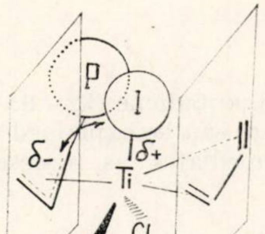

Fig. 2. — Multiple interaction in titanium allyl complexes bearing iodine ligand.

The occurrence of living centres demonstrated by both the rise of conversion when supplementary monomer is added at the end of the polymerization and concomitant increase of the molecular weight can be assigned to the interaction between iodine as a ligand of the Ti complex and the allyl group (Figure 2).

By this interaction iodine may protect the allyl group towards side transfer reactions similarly to the counteranions in the living cationic systems.[13] This protection imparts to the catalytic species the living propensity.

Stereochemistry of polymerization reaction

The polymerization reaction of 1,3-butadiene in the presence of the above employed modified $TiCl_4$ catalysts showed to be particularly stereoselective leading to 1,4-polybutadiene with 92–95% and 2–4% *cis* and *trans* content, respectively. The high stereoselectivity of the reaction suggests the formation of intermediate Ti species where significant steric interactions of iodine and/or cyclooctadiene with the reaction centre occur.

Formation of *cis*-1,4-polybutadiene can be explained by an allyl mechanism involving insertion of coordinated butadiene into the allyl ligand by C_1-C_1 addition. The anti-η^3 isomer resulted, A, gives rise to the *cis*-1,4-units of the polymer in the propagation process (Scheme 1).

Scheme 1

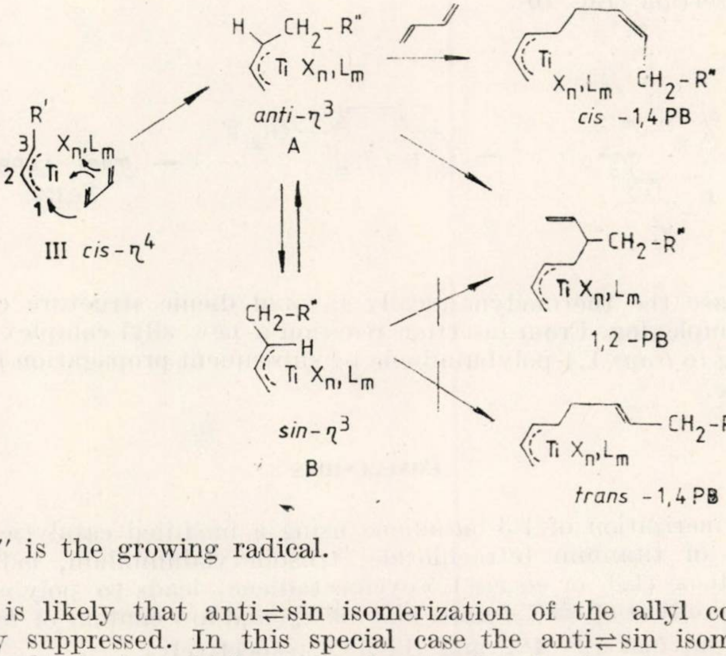

where R'' is the growing radical.

It is likely that anti⇌sin isomerization of the allyl complex is sterically suppressed. In this special case the anti⇌sin isomerization A⇌B would imply a high energy barrier due to the strong steric interaction of the polymer chain with the bulky ligands of the titanium atom in the intermediate σ-complex, C (Figure 3).

Although anti⇌sin isomerization known from Pd allyl complexes[14] is frequently encountered in 1,3-butadiene polymerization whith Ni catalysts[15] in the Ti allyl systems this process involves significant steric restrictions due to the small size of the titanium atom and the high steric hindrance.

On the other hand, formation of small amounts of *trans*-1,4-polybutadiene (cca 2–4%) suggests a different pathway, i.e. *via* a mono-

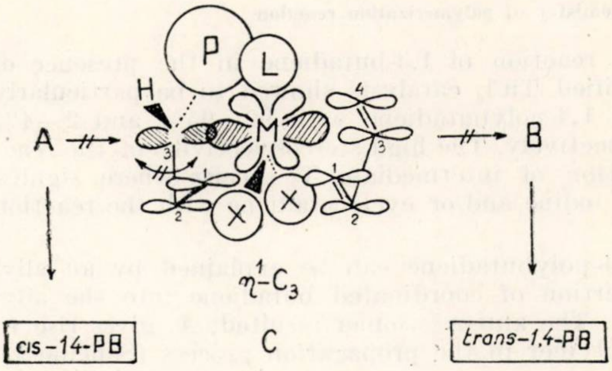

Fig. 3. — Steric interaction during anti ⇄ sin isomerization (A ⇄ B) in 1,3-butadiene polymerization with $TiCl_4$ catalyst.

dentate complex, VI, involving a free rotation of the C_2-C_3 bond during C_1-C_1 insertion (Eq. 10).

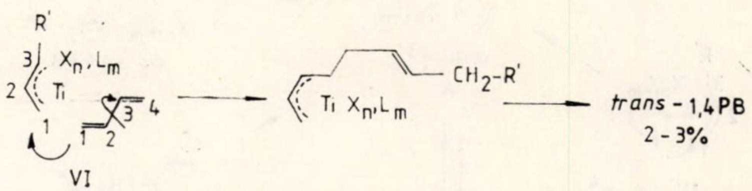

(10)

In this case the thermodynamically favored dienic structure can arise during complexing. From insertion reaction a new allyl complex of type VI leading to *trans*-1,4-polybutadiene by subsequent propagation reactions will arise.

CONCLUSIONS

Polymerization of 1,3-butadiene using a modified catalytic system consisting of titanium tetrachloride, triisobutylaluminium, iodine and cyclooctadiene (1,3- or *cis,cis*-1,5-cyclooctadiene) leads to polybutadiene with high content of *cis*-1,4-units (92–95%) and low content of *trans*-1,4- and 1,2- polymer (2–4% and 3–5%, respectively).

The reaction mechanism was interpreted in terms of an allyl complex of trivalent titanium as the active species formed in a process involving mainly bidentate coordination of 1,3-butadiene at the active centre and subsequent diene insertion into the allyl metal bond. The insertion reaction occurs via stereospecific C_1-C_1 addition leading to *cis*-1,4-polymer. Formation of small amounts of *trans*-1,4- and 1,2-polybutadiene was rationalized by a monodentate allylic pathway. The main active species appears to be the paramagnetic trivalent Ti complex identified by ESR spectroscopy.

The high stereoselectivity of the polymerization reaction was assigned to the strong steric interactions occurring during monomer insertion. These steric interactions direct butadiene insertion mainly to *cis*-1,4-polymer via "anti complex". The anti ⇄ sin isomerization was ruled out on sterical reasons. Formation of *trans*-1,4-polymer was explained by monodentate monomer coordination implying free rotation around the C_2-C_3 bond of 1,3-butadiene leading to the thermodynamically stable *trans* isomer.

EXPERIMENTAL

Starting materials. Butadiene of 99.8% purity with acetylenes content less than 100 ppm (Brazi Petrochemical Works) was distilled to remove the inhibitor and purified by passing over Cu and molecular sieves to less than 5 ppm oxygen and water and less than 50 ppm acetylenes. Toluene (Brazi Rafinery) was degassed and dried over molecular sieves to less than 5 ppm water. i-Bu_3Al (Merck) of 93% purity was used as a solution (toluene) without further purification. 1,3- and *cis, cis*-1,5-cyclooctadiene (Merck) of commercial grade were stored over molecular sieves. Iodine (Fluka) and $TiCl_4$ (BDH, England) of commercial grade were used without further purification.

Polymerization process. Both the contacting of the reactants and the polymerization reaction were carried out in glass apparatus under inert gas (argon). The catalyst was prepared "in situ" or by precomplexing from 5—10% solution (toluene). The polymerization reaction was carried out under vigorous stirring with cooling at temperatures about 30 ± 2°C. The reaction was quenched with methanol.

Analytical methods. The inherent viscosity was determined using an Ubbelohde viscosimeter with suspended level in toluene at 25°C. Molecular weight distribution was determined on a MOM 3170B ultracentrifuge in hexane/heptane (1/1 volume) at 45 000 rpm and 20°C. ESR spectra were recorded at room temperature on a JES-3B (JEOL) spectrometer using peroxylamine disulphonate as a standard. Polymer microstructure was determined by IR measurements on a Perkin-Elmer 255.

REFERENCES

[1] J. Witte, *Angew. Makromol. Chem.*, **94**, 119 (1981).
[2] L. Porri, G. Natta, M. C. Gallazzi, *J. Polym. Sci.*, C, **16**, 2525 (1967).
[3] M. Julemont, Ph. Teyssié, *Aspects of Homogeneous Catalysis*, **4**, 100 (1981).
[4] B. A. Dolgoplosk, S. I. Belin Yu. V. Korshak, K. L. Makovetski, E. I. Tinyakova, *J. Polym. Sci.*, A-1, **11**, 2569 (1973).
[5] J. Furukawa, *Pure Appl. Chem.*, **42**, 495 (1975).
[6] R. Taube, J. P. Gehrke, U. Schmidt, *Makromol. Chem. Macromol. Symp.*, **3**, 389 (1986).
[7] V. B. Murachev et al., *Vys. Soed. Krat. Soobsch.*, **25**, 706 (1983).
[8] L. S. Bressler et al., *Vys. Soed.*, **XI B**, 151 (1969).
[9] W. M. Saltman, T. H. Link, *IEC. Prod. Res. Develop*, **3**, 199 (1964).
[10] N. N. Drus, V. A. Zak, M. I. Lobach, V. A. Vasiliev, V. A. Kormer, *Eur. Polym. J.*, **14**, 21 (1978).
[11] B. A. Dolgoplosk, E. I. Tinyakova, "Metalorg. Cataliz. Prots. Polim"., Moscow, "Nauka", 1985.
[12] F. Dawans, Ph. Teyssié, *IEC, Prod. Res. Develop.*, **10**, 261 (1971).
[13] T. Higashimura, M. Sawamoto, *Adv. Polym. Sci.*, **62**, 49 (1984).
[14] C. A. Tolman, J. *Amer. Chem. Soc.*, **92**, 6777 (1970).
[15] R. Taube, J. P. Gehrke, P. Böhme, *Wiss.-Zeitschr. THLM*, **29**, 310 (1987).

Revue Roumaine de Chimie, 34, *1*, 25 – 34 (1989)

CONVERSION OF C_2—C_4 ALKENES INTO GASOLINES BY USING ZSM—5 ZEOLITES CATALYSTS

EMILIAN ANGELESCU[a], GAVRIL MUSCĂ[b], GRIGORE POP[b], ECATERINA POP[b],
DANIELA SMOLEANU[a] and GEORGIANA POGONARU[a]
[a] Polytechnic Institute, Bucharest, Faculty of Chemical Technology, Splaiul Independenţei N° 313, Bucharest 76206 Romania
[b] ICECHIM — The Institute of Chemical and Biochemical Energetics, Bucharest — Splaiul Independenţei N° 202, Bucharest, Romania

Received October 22, 1988

Investigations regarding the conversion of C_2—C_4 alkenes and of their binary or ternary mixtures into gasolines in the presence of some ZSM—5 zeolites catalysts in acid form or containing Ni, Cu, Fe transitional cations are presented. Considerations are made on the steps of the reaction mechanism by correlating the isomere composition of gasolines and the composition of the reaction gases with the structure and reactivity of the alkenic reagents.

INTRODUCTION

The catalytic conversion of methanol in the presence of ZSM—5 (H^+) zeolites into gaseous and liquid fractions of hydrocarbons provides an important nonconventional alternative, for obtaining fuels and petrochemical raw materials from non-oil sources.

The conversion selectivity depends on the catalytic composition given as SIO_2/Al_2O_3 module; the gasolines resulted mainly contain either aromatic hydrocarbons ($SIO_2/Al_2O_3 = 30$) or higher alkanes ($SIO_2/Al_2O_3 = 300$).

The process kinetics is complex, involving many reactions, parallel or subsequent ones, with rather close rates and thus with an advanced coupling degree.

The reaction mechanism is still discussed: the literature propose mechanism schemes by such intermediates like carbenes, absorbed radicals or carbocations.[1,2] The first stage is almost unanimously considered to be the methanol or dimethylether conversion into C_2—C_3 alkenes.

This process could be made competitive with the technologies of obtaining octanic and Diesel fuels and lubricants from oil by converting the gaseous hydrocarbons resulted from methanol conversion—mainly C_2—C_4—into higher hydrocarbons. Thus, supplementary amounts of oligomeric or aromatic gasolines can be obtained by increasing the overall conversion of methanol into liquid fractions of hydrocarbons.

In the last few years a large amount of research work was carried out in this field, on the catalytic conversion of alkenes into gasolines.[3–8]

These studies can also contribute to the theory of the process and especially of the reaction mechanism.

This paper presents the conversion of some alkenes, individually or in mixtures, into higher hydrocarbons within the composition range of gasolines.

The conversion of alkenes was studied as a function of the reaction temperature and the composition of the reactives flow. The catalysts used were ZSM—5 zeolites, in acid form or containing Ni, Cu, Fe transitional cations.

The catalytic activity specific to different specific reaction temperatures was correlated with the nature of the reactive hydrocarbon and with the isomere composition of the gasoline obtained.

The conclusions of these correlations were used to clear up the reaction mechanism and they can be extended, with certain restrictions, to the mechanism of methanol conversion into gasolines.

EXPERIMENTAL

The catalytic conversion was performed both on individual alkenes, ethene, propene, butene and 1-heptene and on binary mixtures of ethene—propene, ethene—butene and on a ternary mixture of ethene—propene—butene.

A specific catalyst was used for the conversion of methanol into aromatic gasoline: ZSM—5 (H^+) zeolite with 30% aluminium oxide having a module $SiO_2/Al_2O_3 = 70$ and 100% crystallinity.

The conversion reactions of the alkenes were carried out in a vertical quartz reactor with a fixed catalyst bed and in reactive flow at atmospheric pressure.

The analysis of the gaseous or liquid reaction products was performed by gas-liquid chromatography or by chromatography coupled with mass spectroscopy.

RESULTS AND DISCUSSION

At first, reactions of ethene conversion were performed in the temperature range of 260—400°C, the other operating conditions being identical. The results are given in Figure 1.

The total conversion of ethene increases linearly between 240—360°C and remains constant at higher reaction temperatures.

At 240°C, an unsignifiant amount of gasoline results; at 260°C, the gasoline yield is already of 42% and increases with the working temperature going through a maximum of 320°C and having lower values for reactions carried out between 320 and 400°C.

The gaseous products reaction yield is minimum at 240°C, almost equal to the gasoline yield at 320°C, having the maximum value at 400°C, when endothermal decomposition reactions take place with high frequency

The data presented in Figure 2 show that the gases resulted from the reaction contain small amounts of hydrogen and ethene of 2—5%, irrespective of the reaction temperature. But these gases contain large quantities of propane and butanes (40—50%) and the formation of these components is favoured by the increase of the working temperature.

The diagrams in Figure 3 illustrate the variation of the composition of gasoline resulted from reactions carried out at different temperatures.

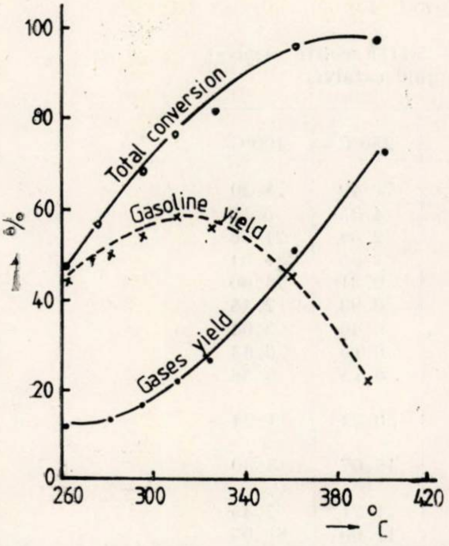

Fig. 1. — Conversion of ethene catalysed by ZSM—5 (H^+) zeolite at various reaction temperatures: $V_v = 500\ h^{-1}$; reaction time = 60 minutes.

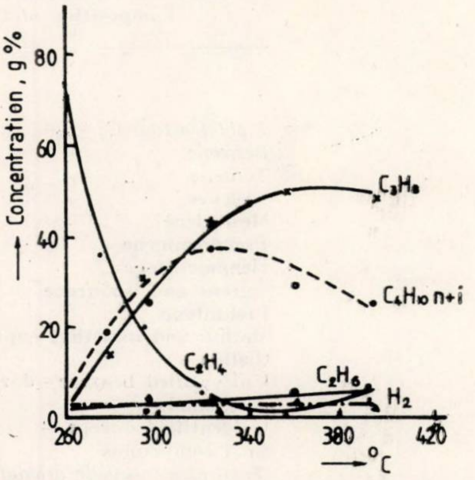

Fig. 2. — Composition in mass percentage of gases resulted from the conversion of ethene on ZSM—5 (H^+) zeolite catalyst: $V_v = 500\ h^{-1}$; reaction time = 60 minutes.

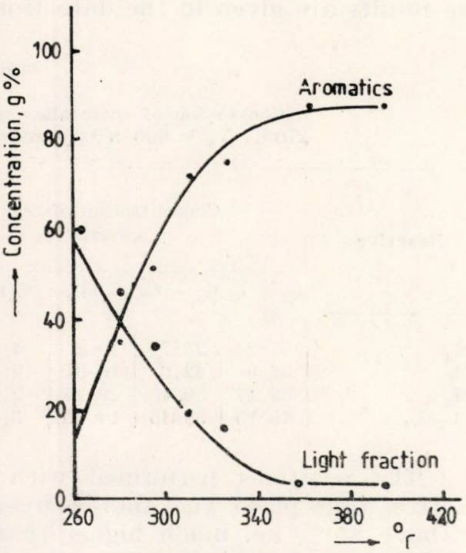

Fig. 3. — Variation of the composition of the liquid fraction resulted from the ethene conversion on ZSM—5 (H^+) zeolite catalyst function of the reaction temperature; $V_v =$ $= 500\ h^{-1}$; reaction time = 60 minutes.

The liquid fraction mainly contains aromatic hydrocarbons when the reaction takes place at a temperature higher than 320°C and a predominant light fraction (alkanes — alkenes C_2—C_7) when the ethene conversion is performed in the range 270—320°C.

The concentrations of the main components of the gasoline obtained at two reaction temperatures are given in Table 1.

The conversion of ethene on ZSM—5(H^+) zeolite catalyst, carried out at 320—400°C and small rate of volume flow, takes place with formation of gasolines whose composition is similar with the composition of the gasoline obtained by the catalytic conversion of methanol.

We considered important to investigate mainly the thermal reaction conditions range of 260–340°C in order to study the variation of light fraction/aromatics mass ratio from the gasolines obtained.

Table 1

Conversion of ethene on ZSM–5(H^+) zeolite catalyst. Composition of the liquid catalyst

	250°C	400°C
Light fraction C_2–C_6	71.49	8.20
Benzene	4.35	5.10
Toluene	2.66	21.56
Xylenes	1.95	31.04
Mesitylene	0.31	16.60
Pseudocumene	0.92	2.48
Hemimellitene	0.46	3.06
Durene and isodurene	0.19	0.63
Prehnitene	0.15	0.58
Methyl and dimethyl naphthaline	0.24	1.24
Unidentified benzene–durene compounds	16.07	3.30
Unidentified durene – final compounds	1.21	7.45
Total of monocyclic aromatics	11.00	81.05
BTX	8.96	57.70

A second series of reactions was carried out at 270°C using different alkenes as reactives. The other working conditions were kept constant. The results are given in the data from Table 2.

Table 2

Conversion of some alkenes on ZSM–5 (H^+) zeolite 270°C; $V_v = 600\ h^{-1}$; reaction time 60 min. $t_c = 5.9$ s

Reactive	Concentration of reaction gases, %					Concentration of liquid, %		Total conversion %	Conversion into liquid, %
	$C_2 + C_2'$	$C_3 + C_3'$	C_4H_{10}	C_4H_8	C_5H_{10}	$C_5 + C_5'$	$C_6 + C_6'$		
C_2H_4	57.2	23.7	19.2	4.12	2.08	5.22	7.52	71.2	49.5
C_3H_6	36.9	42.0	16.31	2.92	1.87	6.92	22.44	94.0	86.8
C_4H_8	33.47	39.40	22.25	3.95	0.90	14.23	24.00	91.5	88.8
$1-C_7H_{14}$	45.15	36.46	14.70	3.20	0.49	18.40	22.73	88.7	91.4

The reactions performed with propene, butene or 1-heptene as reactives take place with total conversion and conversions into gasolines of above 85%, i.e. much higher than in the case of ethene conversion at the same temperature.

The gasoline obtained in these cases contains 30–40% C_5–C_6 light fractions. The high conversions in liquid and its high content of light hydrocarbons can be correlated with the capacity of alkenes having more than two carbon atoms to form secondary or tertiary carbocations by protonic addition following the substrate interaction with the Brönsted acidity centre of the catalyst. The carbocationic intermediates can induce dimerization or oligomerization processes resulting in acyclic hydrocarbons, components of the light fraction from gasoline.

Taking into account the fact that the concentration of the C_5—C_6 fraction in gasolines is almost the same irrespective of the nature of the reactive alkenes and that in the case of operating with butene, the octenes content from gasoline is small, the conclusion can be drawn that such polymerization reactions degenerated by carbocationic mechanism have a relatively small share even in the case of some low reaction temperatures. They cannot explain satisfactorily the isomere composition of the gasolines obtained.

The gases resulted from the conversion reactions of various alkenes have almost equal concentrations of alkanes and C_2—C_4 alkenes.

By correlating these observations with the fact that, at 240°C, very small amounts of gasoline result, while at 260°C the alkenes conversion into liquid hydrocarbon fraction is of above 40%, one can reach the hypothesis that this is formed only above a certain thermal threshold, imposed by the endothermal reactions of carbon and hydrogen cracking and disproportionation.

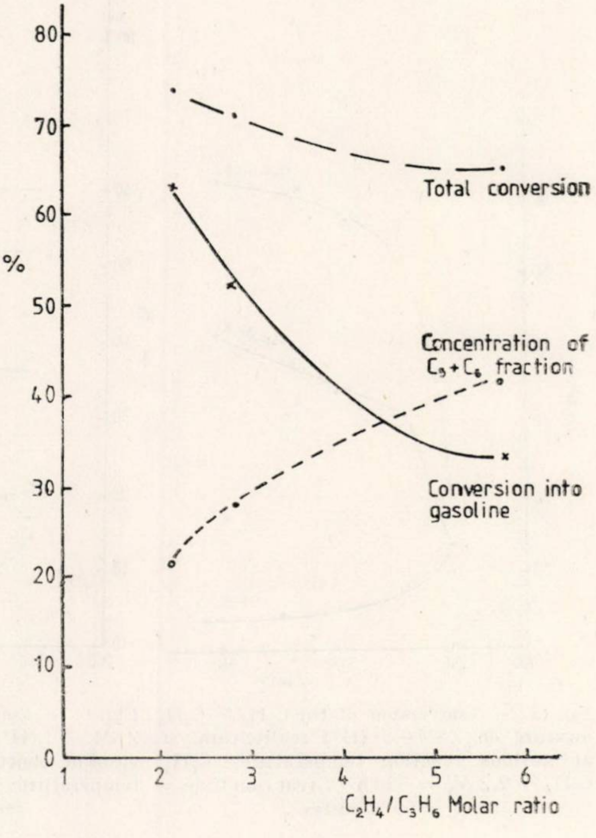

Fig. 4. — Variation of total conversion, of the conversion into gasoline and of the concentration of gasoline in C_5+C_6 function of the C_2H_4/C_3H_6 molar ratio of the reactives flow: 270°C; V_v = 330 h^{-1}; reaction time = 60 minutes.

If these reactions have the greatest share, they justify the comparable concentrations of C_2-C_4 terms from the reaction gases which result irrespective of the reactive alkene used.

A third series of reactions was performed with synthetic mixtures of ethene—propene with different molar compositions.

The results given in Figure 4 show that the increase of the ethene concentration in the reactive flow leads to the decrease of the total conversion and to a sharp decrease of the conversion into gasoline.

When operating with a mixture of ethene—propene with a molar composition of 2.2 at constant rate of volume flow, one can see that at temperatures in the range 240—300°C, the conversion into gasoline increases significantly. The hydrocarbon liquid resulted from the reaction contains higher amounts of aromatics when the thermal condition of the reaction is higher, and lower light fraction in gasoline when the thermal condition is lower. The results of these reactions are illustrated in figures 5 and 6.

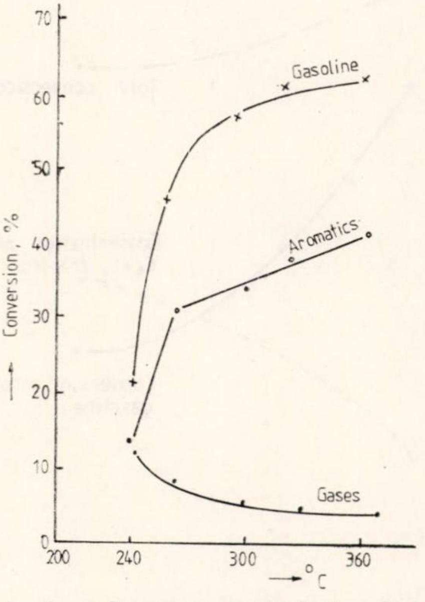

Fig. 5. — Conversion of the $C_2H_4 + C_3H_6$ mixture on ZSM—5 (H^+) zeolite catalyst at various reaction temperatures: $C_2H_4/C_3H_6 = 2.2$ $V_v = 330\ h^{-1}$; reaction time = =60 minutes.

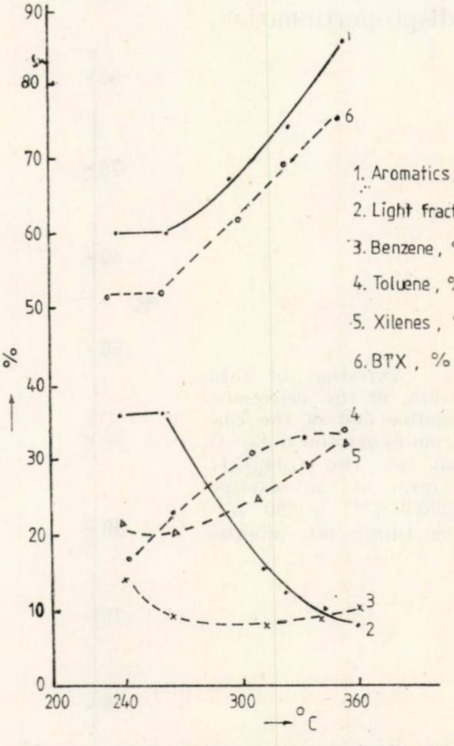

Fig. 6. — Conversion of $C_2H_4 + C_3H_6$ mixture on ZSM—5 (H^+) zeolite catalyst; variation of gasoline concentration function of the reaction temperature: $C_2H_4/C_3H_6 = 2.2$; $V_v = 330\ h^{-1}$; reaction time = 60 minutes.

The analysis by chromatography coupled with mass spectroscopy of the gasoline obtained at 320°C from ethene—propene evidenced th- presence of 107 components, belonging to the following hydrocare bon classes :

— alkanes and cycloalkanes	27.81 g %
— alkenes	10.06 g %
— arenes	56.65 g %
— unidentified compounds	5.48 g %

From the total of 37.87% alkanes and alkenes, 21.2% is C_5-C_6 fraction, while from the total of 56.65% arenic compounds, 31.92% is made up by the BTX fraction.

The fourth series of reactions was performed by using binary or ternary alkenes mixtures as reactive. The results are given in Table 3.

Table 3

Conversion of ethene—propene mixtures on ZSM—5 (H^+) zeolite catalyst; 270°C, $V_v = 600h^{-1}$, reaction time 60 min.

Reactive	Gas phase					Liquid phase		Total conversion %	Conversion into gasoline, %
	C_2+C_2'	C_3+C_3'	C_4H_{10}	C_4H_8	C_5H_{10}	C_5+C_5'	C_6+C_6'		
$C_2H_4 + C_3H_6$ 79.15% 20.85%	40.5	12.6	40.0	6.33	1.12	18.9	22.1	64.80	32.76
$C_2H_4 + C_4H_6$ 77.37% 22.63%	41.7	13.42	24.9	18.15	1.83	19.4	20.3	71.74	54.06
$C_2H_4 + C_3H_6 + C_4H_8$ 55.23% 18.52% 26.25%	44.0	13.56	28.6	12.40	1.44	17.5	24.4	79.88	71.80

At the temperature of 270°C and $V_v = 600\ h^{-1}$ the total conversion is higher than 42%, which is the value characteristic to the ethene conversion.

The presence of propene, butene or of both these alkenes in the reactive mixture, with a concentration mainly of ethene, leads tó high values of the conversion into gasoline.

These experiments indicated that the nature of the alkenes from the reaction flow does not modify the composition of the gases developed from the process or the concentration of the light fraction from the gasoline obtained.

Reactions were carried out by using a reactive made up of a mixture of 75% C_2H_4 and 25% C_3H_6 and a ZSM—5(H^+) zeolite catalyst on which Ni, Cu, Fe was impregnated at a concentration 1 and 5% Fe, respectively.

The data presented in Figure 7 indicate the fact that the presence of 1% transitional metal in the catalyst increases the concentration of light fraction of the gasoline resulted the from reaction and diminishes accordingly its concentration in BTX fraction.

The order of activity is Ni < Cu < Fe. The catalyst with 5% Fe has a higher activity than the one with 1% Fe.

The catalysts with 1% Ni, Cu, Fe provide higher conversion in light fractions as compared with the basic zeolite. From this point of view, the catalytic system with 5% Fe is three times more active.

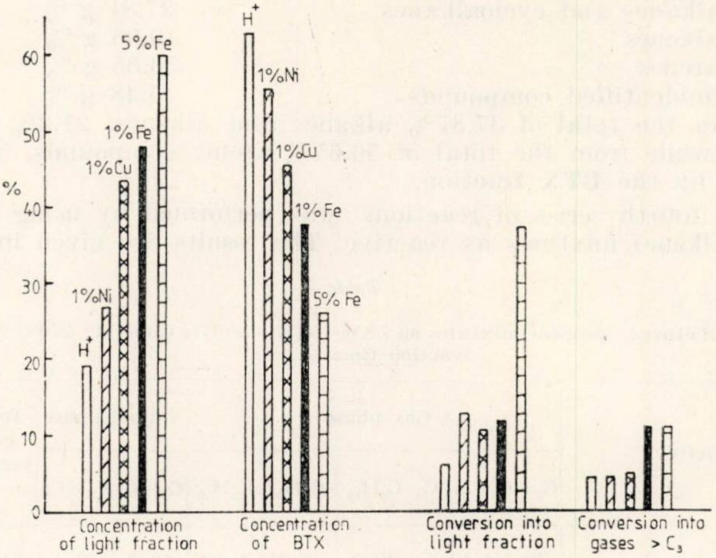

Fig. 7. — Conversion of $C_2H_4 + C_3H_6$ mixture on ZSM−5 (H^+) zeolite catalysts containing tranzitional cations: 320°C; $V_v = 500\ h^{-1}$ 75% C_2H_4 + 25% C_3H_6; reaction time = 60 minutes.

One should mention the fact that the presence of iron in the catalyst leads to higher conversions in gaseous fraction having a higher cracking activity than the other catalytic systems.

The results presented lead to the conclusion that the forming of the higher hydrocarbons, components of the gasoline obtained by the conversion of the C_2-C_4 alkenes on a ZSM−5(H^+) zeolite catalyst, does not occur mainly by a cationic mechanism of low polymerization. It is more likely that in the first step, there take place cracking processes and mainly disproportionation ones of the reactives, resulting in C_2-C_4 alkenes in different concentrations, depending on the working temperature, irrespective of the nature of the reactive alkene (Figure 8 a). The alkenes formed can be subjected to dimeric or oligomeric growing processes, responsible for the formation of the light fraction from the gasoline. The dimeric or oligomeric intermediates can also be cracked, a fact wich explains the relatively low concentrations of dimers, trimers, etc. in the gasoline, corresponding to the reactive alkenes.

The acid function of the catalyst would induce these reactions, which justify — at the same time — both the relatively equal concentrations of C_5-C_6 terms obtained by the conversion of various alkenes and the composition of the reaction gases (Figure 8 b).

But it is reasonable to consider that the formation of the aromatic hydrocarbons, the main constituents of the gasoline obtained by the alkenes conversion, takes place by complex processes of carbon and hydrogen disproportionation between molecules of identical or different alkenes (Figure 8 c).

It is difficult to explain the mechanism of these processes but it is certain that in carrying out these processes the main role is played by the shape function of the catalyst, specific to the ZSM—5 type zeolite structure.

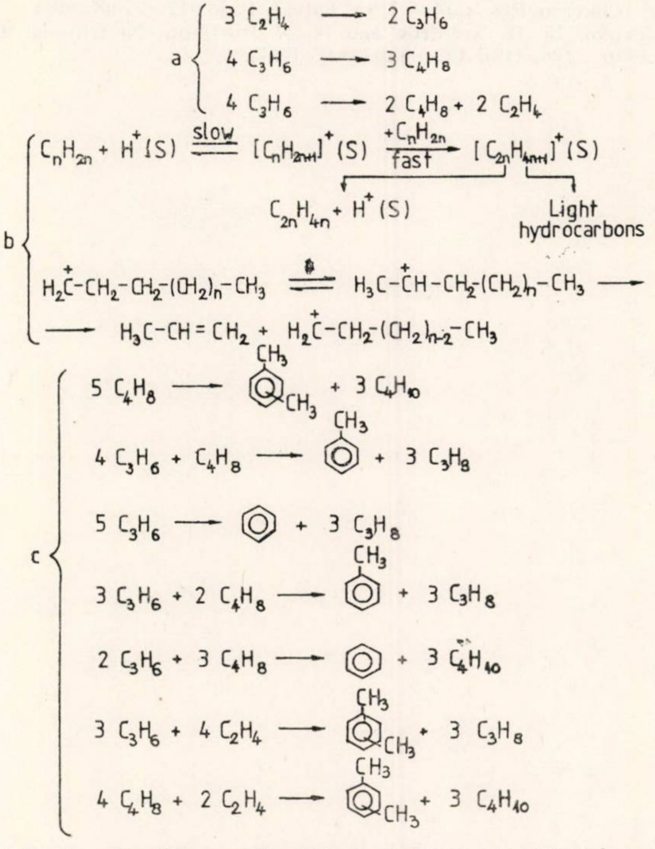
a
$3\,C_2H_4 \rightarrow 2\,C_3H_6$
$4\,C_3H_6 \rightarrow 3\,C_4H_8$
$4\,C_3H_6 \rightarrow 2\,C_4H_8 + 2\,C_2H_4$
b
$C_nH_{2n} + H^+(S) \xrightleftharpoons{slow} [C_nH_{2n+1}]^+(S) \xrightarrow[fast]{+C_nH_{2n}} [C_{2n}H_{4n+1}]^+(S)$
$C_{2n}H_{4n} + H^+(S)$
Light hydrocarbons
$H_2\overset{+}{C}-CH_2-CH_2-(CH_2)_n-CH_3 \rightleftharpoons H_3C-\overset{+}{C}H-CH_2-(CH_2)_n-CH_3 \rightarrow$
$\rightarrow H_3C-CH=CH_2 + H_2\overset{+}{C}-CH_2-(CH_2)_{n-2}-CH_3$
c
$5\,C_4H_8 \rightarrow$ + $3\,C_4H_{10}$
$4\,C_3H_6 + C_4H_8 \rightarrow$ + $3\,C_3H_8$
$5\,C_3H_6 \rightarrow$ + $3\,C_3H_8$
$3\,C_3H_6 + 2\,C_4H_8 \rightarrow$ + $3\,C_3H_8$
$2\,C_3H_6 + 3\,C_4H_8 \rightarrow$ + $3\,C_4H_{10}$
$3\,C_3H_6 + 4\,C_2H_4 \rightarrow$ + $3\,C_3H_8$
$4\,C_4H_8 + 2\,C_2H_4 \rightarrow$ + $3\,C_4H_{10}$
CH_3

Fig. 8. — Possible reactions in mechanisms of conversion of alkenes into gasolines.

The conclusion can be drawn that the gaseous fraction containing alkenic components which results from the methanol conversion into gasolines, catalysed by ZSM—5 zeolitic systems can be recycled in the process or can be used in a second reaction step, thus enhancing the total conversion of methanol into gasolines.

The mechanism of the process is complex, it involves many reactions, the great majority being carbon and hydrogen cracking and disproportionating reactions.

The modification of the catalysts with transitional metals cations induces selectivity effects which are reflected in the composition by hydrocarbon fractions of the gasoline resulted from the process.

REFERENCES

[1] C. D. Chang and A. J. Silvestri, *J. of Catalysis*, **47**, 249 (1977).

[2] P. Dejaifve, J. Védrine, V. Bolis and E. Derouane, *J. of Catalysis*, **63**, 331 (1981).

[3] C. D. Chang (Mobil Oil Co.), USA Patent 4 554 396 (19.11.1985).

[4] D. Seldon, U. K. Patent 2 156 380 (9.10.1985).

[5] C. D. Percival and D. Seldon, U. K. Patent 2.156.381 (9.10.1085).

[6] M. G. Long, (Union Carbide Co.) — Eur. Patent 142 154 (22.05.1986).

[7] S. J. Miller, (Chevron Res. Co.) — USA Patent 4 538 012 (27.08.1985).

[8] D. E. Radenenko, K. B. Nefedrov and N. N. Rostanin, Neftehimia, **2**, 3 (1987) from *Chem. Abstr.*, **106**, (18), 142, (140738d) (1987).

Revue Roumaine de Chimie, **34**, *1*, 35–40 (1989)

RELATIONSHIP BETWEEN STRUCTURE AND EFFECT OF SOME ORGANIC COMPOUNDS CONTAINING SULPHUR ON STEEL CORROSION INHIBITION PROCESS IN ACID MEDIUM

RADU AVRAM and DUMITRU SAVU
Faculty for Chemical Technology
Polytechnical Institute, Bucharest

Received February 8, 1988

The paper records the experimental results concerning the effect of corrosion inhibition upon acid pickling of some grades of steel, by sulphur-containing organic compounds belonging to the class of sulphur ethers and corresponding sulphoxides. The effects of molecule structure, of inhibitor concentration and of temperature upon the corrosion rate of steel grades and stability of inhibitor in the pickling bath are described. At the same time the effect of these parameters on steel brittlenes has also been studied.

INTRODUCTION

Pickling in inhibited acid solution results in undesired dissolution of basic metal and high acid consumption. By adding inhibitors in the pickling bath the acid attack is limited only to oxides thus reducing metal losses and acid consumption. The inhibitor also reduces steel brittleness by limiting the amount of hydrogen produced by acid attack on metal.

EXPERIMENTAL

Now everybody has accepted the idea that organic molecules inhibit corrosion by their adsorption at metal-solution interface.

There are a great many possibilities of inhibitor adsorption. Figure 1 (a + b) shows "funnel" and "umbrella"-types of adsorption. Corrosion may occur only in front of the pores between the inhibitor molecules adsorbed (Fig. 1 c).

A resitant film of inhibitor forms on the metal surface in dependence upon the chemical structure of inhibitor molecule, upon the chemical analysis of the solution, upon the nature of metal surface etc.[1,2]. Traube & Kuhn[3] have settled a direct dependence of adsorption capacity (J) of the inhibitor molecule on metal surface and gramme-molecular weight.

$$J = \frac{M^{1.83}}{15.3} \times n \qquad (1)$$

where :
M = gramme-molecular weight of inhibitor ; and
n = number of absorbed inhibitor moles.

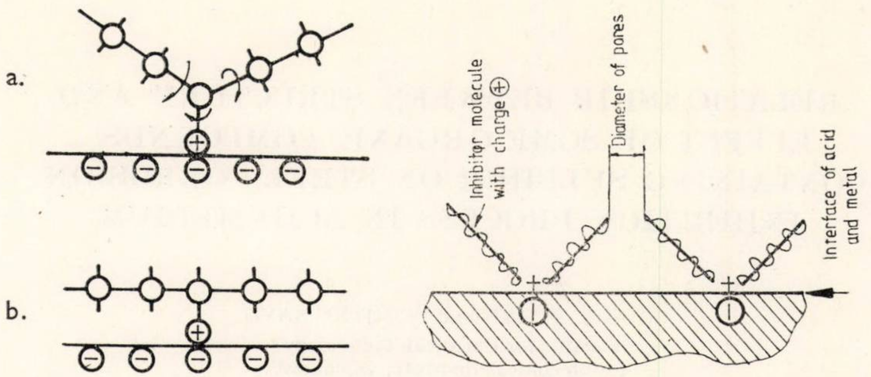

Fig. 1. — Schematic representation of adsorption of inhibitor molecules : a. funnel-type adsorption ; b. umbrella-type adsorption ; c. formation of pores between inhibitor molecules.

Numerous authors [4,8] mention the good inhibiting properties of organic compounds having sulphur atoms as active nuclei. Starting from these statements the effect has been studied of corrosion inhibition in sulphuric acid of some sulphur-containing organic compounds of various structures such as : di-n-butyl sulphur ether, di-s-butyl sulphur ether, dibenzyl sulphur ether, tribenzyl sulphonium chloride, di-n-butyl sulphoxide, di-s-butyl sulphoxide, di-n-pentyl sulphioxide, di-n-hexyl sulphoxide, diphenyl sulphoxide, benzyl phenyl sulphoxide and dibenzyl sulphoxide.

Tests have been run for pickling steel grades OL 37.2 and OL Cr Mo V in sulphuric acid of various concentrations with inhibitors present and absent.

The corrosion rates have been determined both gravimetrically (metal losses) and volumetrically (hydrogen emissions).

For a good study of inhibitor effect on direct acid attack of metal, three successive picklings have been run as follows :

— pickling A (half an hour) required to remove the layer of oxides off the metal surface according to the chemical reactions[9] :

$$FeO + H_2SO_4 = FeSO_4 + H_2O \tag{2}$$

$$Fe_3O_4 + 4H_2SO_4 = FeSO_4 + Fe_2(SO_4)_3 + 4H_2O \tag{3}$$

$$Fe_2O_3 + 3H_2SO_4 = Fe_2(SO_4)_3 + 3H_2O \tag{4}$$

— pickling B (a quarter of an hour) to determine the inhibition degree of the reaction :

$$Fe + H_2SO_4 = FeSO_4 + H_2 \tag{5}$$

by the organic compound tested.

— pickling C(a quarter of an hour) effected to the same end as pickling B.

The results got during picklings B and C have been averaged. By using the volumetric method, the volume of hydrogen released by acid attack of metal has been determined. The amount of hydrogen adsorbed on metal surface has been determined by the difference of total hydrogen released [corresponding to metal loss caused by reaction (5)] and hydrogen trapped by the volumetric method.

The efficiency of inhibitors tested has been expressed by the value of corrosion control coefficient (γ) which is the ratio between the corrosion rate with no inhibitor and the corrosion rate with inhibitor.

The deficiency of the inhibitor in the process of metal getting brittle as a result of adsorption of hydrogen on metal surface has been calculated by means of the relation :

$$E = \frac{N_{\text{inhibitor}} - N_0}{N_{\text{initial}} - N_0} \times 100 \tag{6}$$

where :

N = number of steel sheet bendings until its breaking;
$N_{\text{inhibitor}}$ = for steel sheet pickled with inhibitor;
N_0 = for steel sheet pickled with no inhibitor;
N_{initial} = for unpickled steel sheet.

RESULTS AND DISCUSSION

The corrosion inhibition effect of compounds tested is evident both in the curves of corrosion rate against inhibitor concentration (Fig. 2, 3) and in the polarization curve (Fig. 4).

It is explained, on the one hand, by surface film formation due to some reactions taking place at metal surface, and on the other hand, by the chemisorption process of organic molecule on metal surface. The dissolved inhibitors (sulphoxides and tribenzyl sulphonium chloride) or colloid ones (sulphur ethers) react — at the very moment of adding them — totally or partially with H^+ ions of acid and yield spontaneously a positive ion, which is stable in acid solution. The positive charge of sulphur ion is formed as per the following reactions :

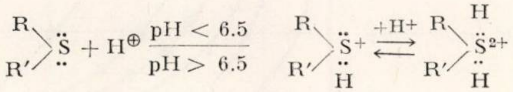

$$\begin{matrix}R\\R'\end{matrix}\!>\!\ddot{\underset{..}{S}} + H^{\oplus} \underset{\mathrm{pH} > 6.5}{\overset{\mathrm{pH} < 6.5}{\rightleftharpoons}} \begin{matrix}R\\R'\end{matrix}\!>\!\underset{\underset{H}{..}}{\ddot{S}^{+}} \overset{+H^{+}}{\rightleftharpoons} \begin{matrix}R\\R'\end{matrix}\!>\!\overset{H}{\underset{\underset{H}{..}}{S^{2+}}} \qquad (7)$$

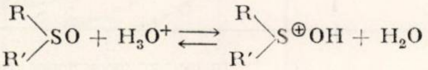

$$\begin{matrix}R\\R'\end{matrix}\!>\!SO + H_3O^{+} \rightleftharpoons \begin{matrix}R\\R'\end{matrix}\!>\!S^{\oplus}OH + H_2O \qquad (8)$$

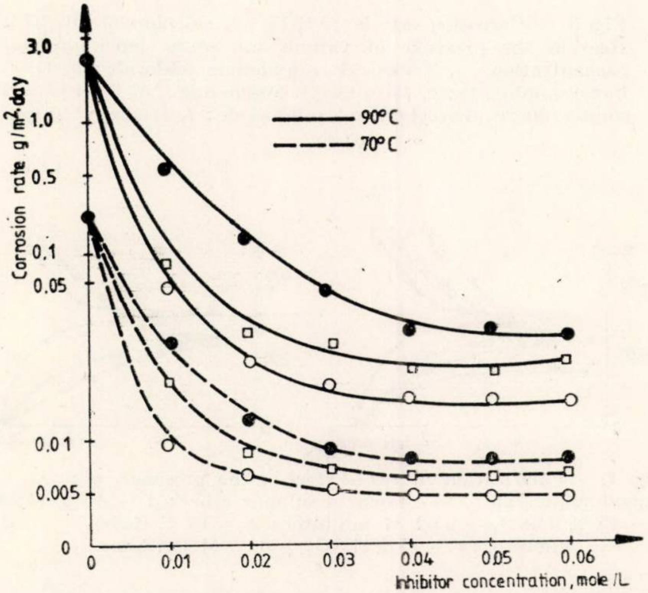

Fig. 2. — Effect of inhibitor concentration on steel (OL 37.2) corrosion rate in H_2SO_4 in the presence of dybenzyl sulphoxide

○ −5 % H_2SO_4 ; □ −10 % H_2SO_4 ; ● −15 % H_2SO_4.

Both sulphur ethers and sulphoxides tested show mobile adsorption mechanism which make further reactions of metal ions detachment to be much reduced (almost to zero) due to the filming process.

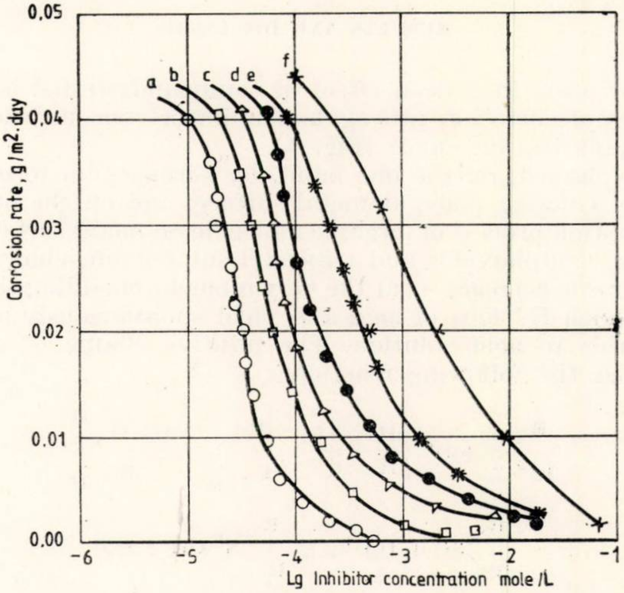

Fig. 3. — Corrosion rate in 15% H_2SO_4 solution of OL 37.2 steel in the presence of various inhibitors depending on concentration : a, Tribenzyl sulphonium chloride ; b, Di-s-butyl sulphixide ; c, Di-n-hexyl sulphoxide ; d, Di-n-pentyl sulphoxide ; e, Benzyl phenyl sulphoxide ; f, Diphenyl sulphoxide.

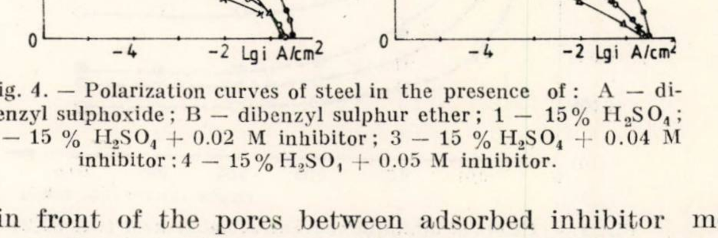

Fig. 4. — Polarization curves of steel in the presence of : A — dibenzyl sulphoxide ; B — dibenzyl sulphur ether ; 1 — 15% H_2SO_4 ; 2 — 15 % H_2SO_4 + 0.02 M inhibitor ; 3 — 15 % H_2SO_4 + 0.04 M inhibitor : 4 — 15% H_2SO_4 + 0.05 M inhibitor.

Only in front of the pores between adsorbed inhibitor molecules (space between adsorbed inhibitor molecules) (Fig. 1c), the reaction develops further, as if the solution were uninhibited, but much slower.

For the same inhibitor, efficiency gets poorer with temperature increase (Fig. 2). It is explained by the inhibitor film being diminished on the surface under temperature influence.

The corrosion rate decreases with inhibitor concentration down to a limit of 0.02 mole/L.

From data shown in Fig. 3 and Table 1 one can settle the efficiency of inhibitors.

Table 1

Corrosion control coefficients (γ) for OL. 37.2 and OL.CrMoV, in 15% sulphuric acid solution, at 70°C ($C_{\text{inhib.}} = 0.02$ mole/L).

Ref. no.	Inhibitor	γ	
		OL.37.2	OL.CrMoV
1.	Di-*n*-butyl sulphur ether	74.6	52.4
2.	Di-*s*-butyl sulphur ether	81.4	71.3
3.	Di-*n*-pentylsulphoxide	76.8	54.1
4.	Di-*n*-hexylsulphoxide	80.4	69.7
5.	Diphenyl sulphoxide	59.7	46.4
6.	Benzyl phenyl sulphoxide	64.2	50.5
7.	Dibenzyl sulphoxide	116.3	92.8
8.	Di-*n*-butyl sulphur ether	62.1	48.7
9.	Di-*s*-butyl sulphur ether	70.3	50.2
10.	Dibenzyl sulphur ether	89.4	73.6
11.	Tribenzyl sulphonium chloride	124.9	112.6

For the inhibitors tested a decrease in efficiency has been found out in the following sequence:

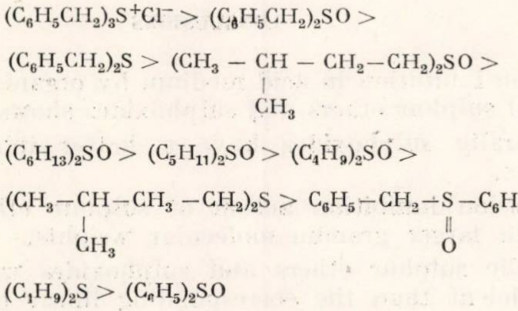

$$(C_6H_5CH_2)_3S^+Cl^- > (C_6H_5CH_2)_2SO >$$

$$(C_6H_5CH_2)_2S > (CH_3 - \underset{\substack{|\\ CH_3}}{CH} - CH_2-CH_2)_2SO >$$

$$(C_6H_{13})_2SO > (C_5H_{11})_2SO > (C_4H_9)_2SO >$$

$$(CH_3-\underset{\substack{|\\ CH_3}}{CH}-CH_3-CH_2)_2S > C_6H_5-CH_2-\underset{\substack{\|\\ O}}{S}-C_6H_5 >$$

$$(C_4H_9)_2S > (C_6H_5)_2SO$$

At the same time these data also show that:

— sulphoxides are better inhibitors than corresponding sulphur ethers;

— with sulphur ethers and sulphoxides the inhibiting action is stronger when the gramme-molecular weight is larger;

— aliphatic sulphur ethers and sulphoxides with branched chains have much stronger inhibiting action than the linear alkyl compounds.

The polarization curves for dibenzyl sulphoxide and dibenzyl sulphur ether show analogous shapes. As shown in Fig. 4 the protection action of sulphoxides and sulphur ethers is related to the control of both the cathodic reaction and the anodic one.

Yet, note that the anodic process is much slower. When adding the inhibitor to the solution a displacement of metal potential occurs toward the positive side.

Table 2 shows the results regarding the effect of inhibitor on steel brittleness. Note that both sulphur ethers and sulphoxides tested are efficient in preventing steel from getting brittle.

In this case too, sulphoxides are better than sulphur ethers.

Table 2

Effect of sulphur ethers and sulphoxides on OL 37.2 steel brittleness in 15% H_2SO_4 solution, inhibitor concentration : 10^{-5} mole/L

Inhibitor	No. of bendings until breaking	Efficiency, %
Tempered un-polarized specimens	104	—
Tempered polarized specimens, 15% H_2SO_4	79	—
Dibenzyl sulphur ether	105	100
Diphenyl sulphur ether	99	80
Benzylphenyl sulphur ether	104	100
Diethyl sulphur ether	104	100
Di-*s*-butyl sulphur ether	104	100
Di-*n*-butyl sulphur ether	99	80
Di-*n*-butyl sulphoxide	102	92
Diphenyl sulphoxide	100	84
Dibenzyl sulphoxide	104	100

CONCLUSIONS

Corrosion inhibition in acid medium by organic sulphur compounds of the type of sulphur ethers and sulphoxides shows that:

1. Generally sulphoxides have a better inhibiting action than sulphur ethers.
2. Corrosion inhibition action of sulphur ethers and sulphoxides is better with larger gramme-molecular weights.
3. Alkylic sulphur ethers and sulphoxides with branched chains are more efficient than the corresponding linear compounds.

REFERENCES

[1] G. Trabanelli, *Brit. Corros. J.*, **4** (5), 267(1969).
[2] M. R. Hudson, J. C. Warning, *Metal Finishing*, **64** (10), 58(1966).
[3] I. Putilova, S. Balerin, V. Barannik, "Metallic Corrosion Inhibitors", Pergamon Press, New York, 1960.
[4] H. Uhlig, "Corrosion et protection", Dunod, Paris, 1970, p. 242.
[5] D. N. Jones, D. P. Cottam, J. Davies, *Tetrahedron Lett.*, **51**, 4977 (1979).
[6] E. Rodzewich, *Corrosion/74*, *Int. Corros. Forum*, **74**, 1—74/9 (1974).
[7] J. S. Robinson, "Corrosion Inhibitors", Park Ridge, New Jersey, 1979.
[8] G. P. Panigrahi, R. Panda, *Bull. Chem. Soc. Japan*, **53** (8), 2366(1980).
[9] P. Driver, R. J. Makins, *Brit. Corros. J.*, **12** (1), 45—60 (1977).

Revue Roumaine de Chimie, 34, *1*, 41–50 (1989)

PYRYLIUM SALTS FORMED BY DIACYLATION OF OLEFINS. PART XXIV.[1]

SYNTHESIS OF *META*-TERPHENYL DERIVATIVES AND HETEROCYCLIC ANALOGS *VIA* BIS-PYRYLIUM SALTS OBTAINED BY BIS-DIACETYLATION OF *META*-DIISOPROPENYLBENZENE

ALEXANDRU T. BALABAN[a] and TEODOR-SILVIU BALABAN[b]
[a] Polytechnic Institute, Organic Chemistry Department,
Splaiul Independenţei 303, 77206 Bucharest, Romania
[b] Centre of Organic Chemistry — ICECHIM,
Splaiul Independenţei 202 B, 78100 Bucharest, Romania

Received October 9, 1988

meta-Diisopropenylbenzene was bis-diacetylated to the bis-pyrylium salts 1 (disulfoacetate, diperchlorate, bis-tetrafluoroborate and diiodide) which were converted in high yields into the corresponding bis-pyridine 3, bis-N-methyl- and bis-N-phenylpyridinium salts 4 and 5 respectively, bis-phenol 6, and bis-dihydropyran 7, all of which are new and interesting _meta_-terphenyl analogs and derivatives.

INTRODUCTION

In the course of our investigations on the reduction of pyrylium salts with sodium borohydride in acetic acid,[2] we needed the bis-pyrylium salt **1** in which both pyrylium rings have α- (2- and 6-) methyl groups and a γ- (4-) phenyl group. One α-alkyl group and a γ-phenyl group were proved to be structural requirements for reducing in high or quantitative yields pyrylium salts with the $NaBH_4$ + acetic acid system,[3] to Δ^3-dihydropyrans.[4] In order to explore further these requirements, bis-pyrylium salt **1** was required. A literature search revealed that it was unknown.

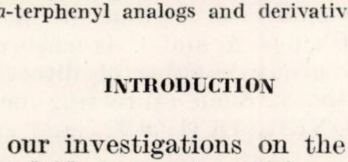

1

Dorofeenko and Krivun[5] have synthesized analogous bis-pyrylium salts **2a** and **2b** from terephthalaldehyde (**a**) or isophthalaldehyde (**b**) by condensation with aromatic methyl ketones, and bis-cyclisation of the resulted tetraketones in the presence of perchloric acid and acetic anhydride or of triphenylmethyl perchlorate in acetic acid :

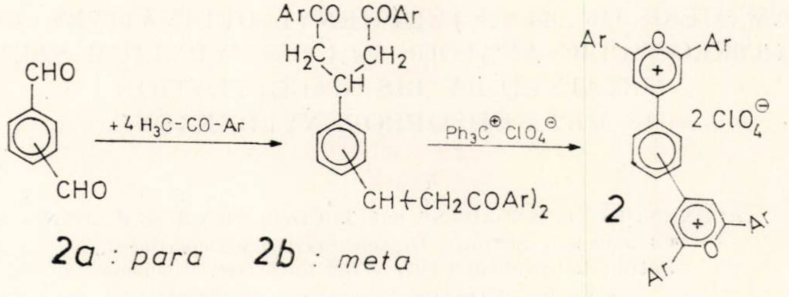

Although the global yields in pyrylium salts **2a**, **b** are above 75%, we were not attracted towards the above reaction sequence for synthesizing **1** because of the condensation step which is uncertain with non-aromatic methyl(ene) ketones (e.g. acetone).*

Bis-pyrylium salts **1** and **2b** are interesting precursors for hetero- or carbocyclic analogs of the *meta*-terphenyl system for which few general syntheses exist. One such synthesis of *meta*-terphenyls was published recently by Snieckus et al ;[6] similarly to the Dorofeenko synthesis of **2b**, it elaborates the outer aromatic rings A and C using a stepwise metallation—cross-coupling procedure of arylboronic acids with aryl halides. The *meta* orientation of rings A and C is ensured by the presence in the central ring B of a group capable of directing the metallation in the *ortho* positions exclusively. Such *o*-directing metallation groups (DMG) are e.g. $CON(iPr)_2$, $OCONEt_2$, OCH_2OCH_3 and others.

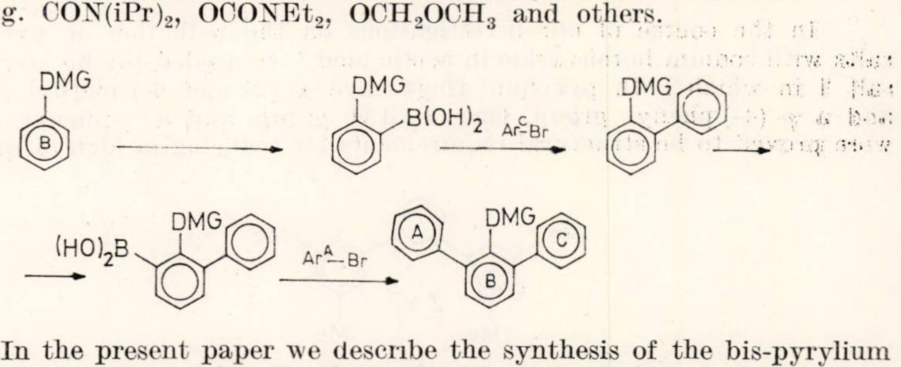

In the present paper we describe the synthesis of the bis-pyrylium salt **1** by means of a bis-diacylation reaction of a diolefin, namely *meta*-diisopropenylbenzene ; we elaborate also the outer heterocyclic rings which become *meta* oriented due to the starting material. Although in the almost thirty years from the beginning of the series of papers devoted to the diacylation of olefins,[7] this reaction has become widely used for the preparation of pyrylium salts with identical α-substituents[8,9], no preparation of a bis-pyrylium salt was reported by using this reaction. Moreover, previous attempts to isolate a bis-pyrylium salt from dienes or diene precursors failed.[5b,10]

---

* We use letters **a**—**d** for **1** to indicate various anions, and letters **a**, **b** for **2** to denote *m*/*p* structure.

We also report in this paper the conversion of **1** into hetero- and carbocyclic analogs of *meta*-terphenyl by making use of the versatility of pyrylium salt chemistry. About the reduction of **1** with acetoxyborohydrides only a brief account will be given here.

PREPARATION OF THE *META*-PHENYLENE-BRIDGED BIS-PYRYLIUM SALT *1* BY BIS-DIACETYLATION OF *META*-DIISOPROPENYLBENZENE (m-DIPEB)

The bis-pyrylium salt **1** was prepared by elaboration of the outer heterocyclic rings, in a single-step procedure, starting from *meta*-diisopropenylbenzene (*m*-DIPEB). It is the first example of a bis-pyrylium salt obtained by a bis-diacylation of a diolefin; *m*-DIPEB is a common reticulating agent and a by-product of α-methyl-styrene production, and is therefore commercially available at relatively low cost; *m*-DIPEB polymerizes readily in contact with acids. In order to isolate salts **1** from the strongly acidic acylating medium, suitable conditions had to be found, both for reducing the polymerization of *m*-DIPEB, and for the separation of the bis-diacylated product from the polymeric material.

Attempts for the diacetylation of *m*-DIPEB with acetic anhydride and 70%-perchloric acid led to tars from which the diperchlorate **1b** was inseparable owing to its poor solubility. Our experience with pyrylium sulfoacetates,[11] and their exceptionally high solubility in protic solvents, led us to bis-diacylating *m*-DIPEB with acetic anhydride and sulfoacetic acid :

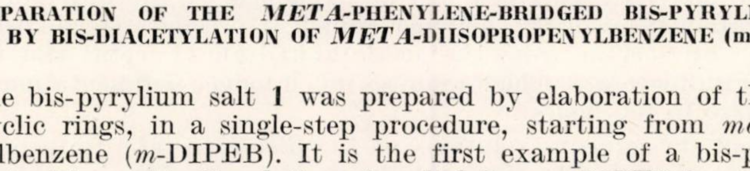

$SAC^{\ominus} = HOOC-CH_2-SO_3^{\ominus}$ **1a**

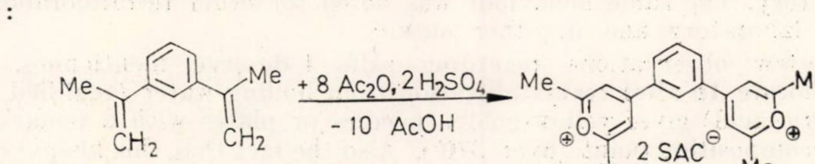

X	ClO_4	BF_4	I
1	*b*	*c*	*d*

In order to separate the bis-pyrylium disulfoacetate **1a** from the polymeric material, the reaction product was successively diluted with acetone by pouring the reaction mixture into acetone and decanting the supernatant from the sedimented material into a new portion of acetone. While linear oligomers are solubilized by acetone, reticulated polymers and the bis-pyrylium disulfoacetate **1a** are practically insoluble in acetone. From these insoluble, acetone-washed deposits, the disulfoacetate is easily extracted into water (to which it conveys a deep orange-red colour) and is thus readily separated from the water-insoluble polymeric material. Interestingly, the highest contents of **1a** are found in the third or fourth decantation batch, the first ones being rich in gummy polymeric material. This fact can be explained by the difference in the sedimentation rates of the polymer (which is precipitated almost instantaneously by acetone from the acetic anhydride — acetic acid medium) and the disulfoacetate (which requires much longer sedimentation periods, namely five to ten hours).

From the aqueous solutions of the disulfoacetate **1a**, after boiling with charcoal and filtration, the treatment with 70% perchloric acid, with 40% tetrafluoroboric acid, or with a saturated solution of sodium iodide, led to the diperchlorate **1b**, the bis-tetrafluoroborate **1c** and the diiodide **1d**, respectively, by the appropriate anion exchange reactions. From the salts **1a**—**1d** only the diperchlorate **1b** proved to be easily recrystallizable (from 1% $HClO_4$) and gave a satisfactory elemental analysis. From the other salts (the disulfoacetate **1a** and the diiodide **1d**), although the spectral data advocate their structure (see the experimental section), the fact that they did not crystallize readily prevented their correct analysis. The bis-tetrafluoroborate **1c** with correct spectra gave upon repeated combustion analyses a much lower carbon content than calculated, although the hydrogen microanalysis was reproductibly satisfactory. The same behaviour was noted for other tetrafluoroborates in our laboratory and in other ones.[12]

A few observations regarding salts **1** deserve mentioning. The diperchlorate **1b** after recrystallization from boiling water (acidified with perchloric acid) gives yellow-golden needles or plates with a remarkably high decomposition point (over 370°). Also the fact that this bis-pyrylium salt does not decompose upon heating to such a high temperature is an uncommon feature for pyrylium perchlorates; however, when **1b** is heated directly in the flame, it explodes without melting.

The temperature at which the bis-diacylation reaction is conducted influences the yield in the disulfoacetate **1a**. Optimum temperatures were between 70 and 80°; while at lower temperatures no bis-diacylated product is formed, at higher temperatures, the increased polymerization of *m*-DIPEB lowers the yield. The yield in recrystallized **1b** remains low, only 2%. Despite this low yield, salts **1** are accessible due to the cheap starting materials and the easy separation from the one-step bisdiacylation procedure. Compared to the 25% yield of the related diacetylation of α-methylstyrene,[11b] the much lower present yield can be explained by the greater polymerization tendency of *m*-DIPEB in the presence of acids.

In the ^{1}H-NMR spectra of the bis-pyrylium salts **1** in trifluoroacetic acid (TFA) as solvent, the four methyl groups give rise to a single peak at $\delta = 3.10$ ppm, comparable to the resonance at 3.04 ppm of the two methyl groups of 2,6-dimethyl-4-phenylpyrylium salts. The infrared absorption spectra of salts **1** confirm their structures: the pyrylium breathing band is at 1632 cm^{-1}, the *m*-phenylene ring has absorptions at about 800 and 680 cm^{-1} and additional intense bands appear due to the specific anions. The ultraviolet-visible spectra of salts **1** recorded in a slightly acidic aqueous medium exhibit two composite bands at 211 and 308 nm while in plain water the latter band is hypo- and hypsochromically shifted (λ_{max} 285 nm) probably due to a ring-opening of one of the two pyrylium rings.

PREPARATION OF HETEROCYCLIC ANALOGS OF *META*-TERPHENYL *3–5* FROM THE BIS-PYRYLIUM SALTS *1*

Conversion of salts **1** into heterocyclic analogs of *meta*-terphenyl was effected by known methods,[13] as depicted in formulas **3—5**.

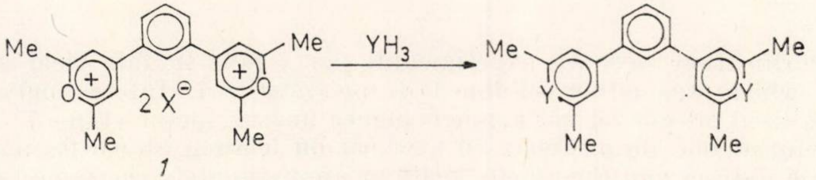

Y	N	$\overset{\oplus}{N}$Me	$\overset{\oplus}{N}$Ph
	3	*4*	*5*

High yields were obtained in all cases when the crystalline diperchlorate or bis-tetrafluoroborate (**1b** and **1c**, respectively) were used. The bis-pyridine **3** may also be conveniently obtained by using the aqueous solutions of the disulfoacetate **1a**. The ^{1}H-NMR spectrum of the bis-pyridine **3** exhibits one methyl resonance at 2.68 ppm in CDCl$_3$, comparable to the methyl resonance in 2,6-dimethyl-4-phenylpyridine which occurs at 2.58 ppm (also in CDCl$_3$). Also the relative molar induced shifts by Eu(fod)$_3$ in CDCl$_3$ for the latter compound [14] and **3** are similar.

Reactions of the diperchlorate **1b** with an ethanolic solution of methylamine or a boiling solution of aniline in methanol gave in good yields the corresponding N, N'-disubstituted bis-pyridinium salts **4** and **5**, respectively.

In the ^{1}H-NMR spectra of the N, N'-diphenyl-derivative **5** a high field shift was observed for the singlet of the four α-methyl groups when compared to the N,N'-dimethyl salt ($\Delta\delta = 0.35$ ppm in TFA). This value agrees well with similar diamagnetic shieldings of α-methyl signals in 2,4,6-trimethyl-N-aryl-pyridinium salts.[15] No change was observed in the UV spectra recorded in water compared to acidified water for the bis-pyridinium salts. A small bathocromic shift occurs when the N-methyl substituent in **4** which exhibits the λ_{max} at 284 nm, is replaced by an N-phenyl group (**5**, $\lambda_{max} = 290$ nm).

PREPARATION OF 3,3''-DIHYDROXY-5,5''-DIMETHYL-*META*-TERPHENYL **6**

Treatment of the aqueous solution of the disulfoacetate **1a**, or of an aqueous suspension of the diperchlorate or bis-tetrafluoroborate (**1b**, or **1c**, respectively), with 25% aqueous sodium hydroxide led to the dihydroxyterphenyl **6** by the known reaction.[13]

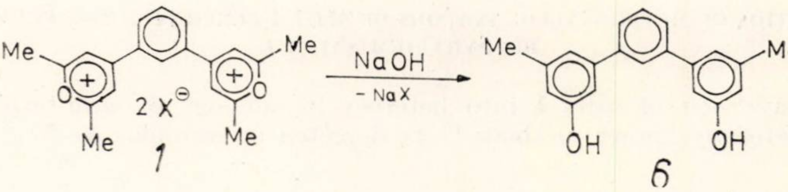

Purification (see the experimental part) gave in fair yield a bis-phenol which was either sublimed or recrystallized. Interestingly, the recrystallized bis-phenol has a much higher melting point (146–7°) than the sublimed one (m.p. about 70°), which on heating above its melting point, resolidifies and then melts again at approximately the same temperature (about 140°) as the recrystallized bis-phenol. It appears as if two crystalline forms of this bis-phenol exist : one which is obtained by sublimation and which by melting or dissolving in solvents is converted into the thermodynamically more stable form which melts at 146–7°. No notable differences could be seen between the infrared spectra of these two forms when recorded in KBr pellets.

REDUCTION OF BIS-PYRYLIUM SALTS *1* WITH SODIUM BOROHYDRIDE IN ACETIC ACID

We have recently shown that pyrylium salts with at least one of the α-substituents being an alkyl group, are easily reduced in good yields to Δ^3-dihydropyrans by sodium borohydride in acetic acid medium.[2] When a 4-phenyl group is present in the pyrylium salt (which, however, must not be 2,4,6-triphenyl-substituted), Δ^3-dihydropyrans result in quantitative yields in a convenient and rapid synthetic method.[4]

It seemed worthwhile to find out if the *meta*-phenylene group could act simultaneously as a 4-phenyl group for both pyrylium rings by blocking the γ-addition for hydride nucleophiles, in which case no by-products should be formed. This was indeed observed. The bis-Δ^3-dihydropyran **7** was formed in quantitative yield by reducing the diperchlorate **1b** with sodium borohydride in acetic acid.

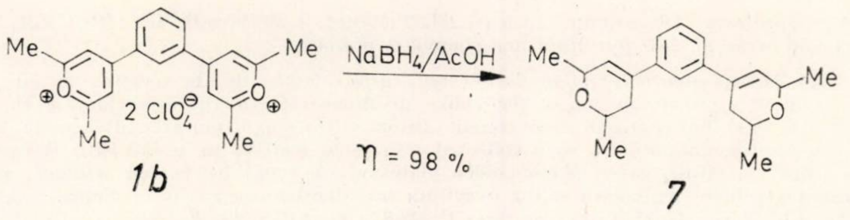

CONCLUSION

We have shown that the bis-diacylation of a diolefin (*meta*-diisopropenylbenzene) is possible and that it affords in a low yield the bis-pyrylium salts **1**. Subsequent conversions of salts **1** with high or quantitative yields into the new terphenyl bis-phenol **6**, or heterocyclic analogs (**3**, **4**, **5**, **7**) illustrate the synthetic potential of the "pyrylium route".

Application of these reactions to *para*-diisopropenylbenzene is in progress.

Acknowledgement. The help of the American Cynamid Co. is gratefully acknowledged for a generous sample of *m*-DIPEB.

EXPERIMENTAL PART

Melting points were measured on a hot-stage melting point apparatus and are uncorrected. Infrared spectra were obtained on a Zeiss UR 20 spectrometer from solid samples as KBr pellets or as specified otherwise. UV-Vis spectra were run also on a Zeiss intrument. ^{1}H—NMR spectra were recorded in $CDCl_3$ or CF_3COOH (TFA) solutions containing tetramethylsilane, on a Varian A—60A spectrometer operating at 60 MHz.

Bis-diacetylation of m-diisopropenylbenzene. 1,3-Bis-(2,6-dimethylpyryliumyl-4)-benzene disulfoacetate, **1a**. Sulfoacetic acid was prepared by adding dropwise 49 mL of concentrated sulfuric acid (90 g, 0.92 moles) into 550 mL acetic anhydride (486 g, 4.76 moles) over a period of ten minutes. The mixture was heated to 70 °C when it turned orange, and then 80 mL of commercial *m*-DIPEB (74 g, 0.47 moles) containing hydroquinone were added, very slowly at first, over a period of two hours. After the first drops of *m*-DIPEB, the mixture darkened completely. The exothermicity of the reaction had to be controlled with occasional external cooling, at the beginning of the addition. The temperature was maintained at 70 °C throughout the period of addition and during the subsequent 30 min, after which the mixture was left to stand overnight. The dark, viscous reaction mixture was poured into 350 mL of acetone; a polymeric material settled down immediately, thus allowing the liquid portion to be decanted into a second 500 mL portion of fresh acetone. After keeping in the refrigerator for two hours, the liquid was again decanted into a third 750 mL portion of fresh acetone which was left in the refrigerator overnight. Each crop of sedimented material was washed twice with acetone after which it was boiled with water (acidified with a few drops of conc. H_2SO_4) and charcoal. Filtration through celite afforded clear, deep red-brown solutions of the bis-pyrylium disulfoacetate **1a**. The concentrations of the various fractions could be measured spectrophotometrically and these were checked by precipitation with perchloric acid (see below). Our attempts to isolate a crystalline sample of the disulfoacetate **1a** failed. However, from the acetic acid solutions of the residue which remained upon drying the aqueous solutions of **1a**, diethyl ether precipitated a product with correct spectral data. The yield in **1a** (estimated from all the aqueous solutions of disulfoacetate) is 3%. From these solutions of known concentration, the crystalline salts **1b**—**1d** and derivatives **2** and **5** could be obtained directly.

IR spectrum (KBr; cm^{-1}): 522 m, 610 m, 710 mw, 820 m, 1045 s, 1200 s (broad), *1400* m, 1530 m, 1593 m, 1630 s, *1710* s, *1720* s, *2700—3400* m (broad). (italicised bands are due to the anion). UV spectrum in H_2SO_4 1%, λ_{max}, nm : 209, 213, 303 and 316 (shoulder).

^{1}H-NMR spectrum (TFA; δppm); 3.5 (s, 2H, 2′,6′-Me); 4.50 (broad s, 4H, HOOC-CH_2-SO_3^-); 8.33 (s and broad m, 8H, pyrylium and phenylene protons).

1,3-Bis-(2,6-dimethylpyryliumyl-4)-benzene diperchlorate, **1b**. On addition of 70% perchloric acid to a warm solution of the above disulfoacetate **1a**, the diperchlorate **1b** precipitated and was allowed to stand overnight before filtration. From all sulfoacetate solutions 5.0 g of diperchlorate **1b** were collected (2% yield relative to *m*-DIPEB). Recrystallization from 1% $HClO_4$ gave yellow-golden plates which could be heated without melting to surprisingly high temperatures for pyrylium perchlorates (over 370°C). Found: C, 49.04 H, 4.38; Cl, 14.57; $C_{20}H_{20}Cl_2O_{10}$ requires C, 48.87; H, 4.07; Cl, 14.89%.
IR spectrum (KBr; cm^{-1}): 565 w, *625*ms, 675 mw, 805 mw, *1100 vs*, 1215 mw, 1325 mw, 1530 ms, 1595 m, 1632 s, 3080 mw; italicised bands are due to the ClO_4^- anion. UV spectrum in $HClO_4$ 1% or in phosphate pH=2 buffered aqueous solution, λ_{max}, nm(lg ε_{max}): 211 (4.30); 215 (4.29); 308 (4.68); UV spectrum in water, λ_{max}, nm (lgε_{max}) 211 (4.14), 218 (4.20), 290 (4.45).
^{1}H-NMR spectrum (TFA, ppm): 3.10 (s,12H, 2,6-Me$_2$), 8.40 (s and broad m, 8H, pyrylium and *meta*-phenylene-H).

1,3-Bis-(2,6-dimethylpyryliumyl-4)-benzene bis-tetrafluoroborate, **1c**. Similar treatment of solutions of **1a** with 40% tetrafluoroboric acid, precipitated the salt **1c**. Recrystallization from 1% HBF_4 gave after prolonged standing an orange crystalline powder with m.p. higher than 370 °C, with identical ^{1}H-NMR and UV spectra as **1b**. Found: H, 4.11; $C_{20}H_{20}B_2F_8O_2$ requires H, 4.31%. The carbon analyses gave systematically with about 7% less than calculated.
IR spectrum (KBr; cm^{-1}): differs from the IR spectrum of **1b** with the bands due to the BF_4^- anion at 1060 s and 615 mw.

1,3-Bis-(2,6-dimethylpyryliumyl-4)-benzene diiodide, **1d**. A concentrated aqueous solution of sodium iodide was added to a solution of **1a** and gaseous sulfur dioxide was passed through the resulted suspension for reducing any triiodide anions (I_3^-) to iodides (I^-). Filtration and recrystallization from acetic acid and diethyl ether gave a sample with m.p higher than 350 °C and with identical ^{1}H—NMR spectrum as **1b**.
UV spectrum in phosphate pH = 2 buffered aqueous solution λ_{max}(nm): 227, 308; UV spectrum in water, λ_{max}(nm): 227, 287. No charge transfer bands could be detected by recording the UV-VIS spectrum in dichloromethane or tetrachloroethane. IR spectrum (KBr; cm^{-1}): as for **1b**, without the bands due to the anion.

1,3-Bis-(2,6-dimethylpyridyl-4)-benzene, **2**. Treatment of the aqueous solution of **1a** with NH_4OH followed by diethyl ether extraction, separation of suspended material and addition of 20% HCl yielded an aqueous solution of the dihydrochloride of **2**. This solution was extracted twice with ether and neutralized with an aqueous solution of sodium hydroxide. The dipyridine separated as an oil and was taken up in ether. The ethereal extract was dried over powdered NaOH and subsequently evaporated leaving a colourless solid m.p., 117—119 °C. From 0.5 g (1 mmol) of recrystallized **1b**, 0.233 g (99% yield) of crude bis-pyridine **3** were obtained after the first diethyl ether extraction and evaporation of the solvent. Found: N, 9.25%; $C_{20}H_{20}N_2$ requires N, 9.72%.
IR spectrum (KBr; cm^{-1}): 520 w, 545 mw, 671 w, 708 mw, 795 m, 865 m, 878 mw, 910 w, 995 w, 1030 w, 1095 w, 1190 w, 1215 w, 1238 w, 1338 w, 1402 m, 1447 m, 1551 ms, 1592 s 2850 w, 2920 mw, 3040 w.
UV spectrum in ethanol, λ_{max}, nm (lg ε_{max}): 216 (4.39), 252 (4.47).
^{1}H-NMR spectrum ($CDCl_3$, δppm): 2.68 (s, 12 H, 2′,6′-Me$_2$); 7.30 (s, 4H, 3′- and 5′-H); 7.70 (m, 3H, 4-, 6- and 5-H); 7.92 (m, 1H, 2-H). In CS_2 a high field shift of 0.15—0.17 ppm is experienced by all signals.

1,3-Bis-(1,2,6-trimethylpyridiniumyl-4)-benzene diperchlorate, **3**. The diperchlorate **1b** (1.45 g, 3 mmoles) was added to a 20% methanolic solution of methylamine (30 mL) and heated gently for 30 minutes. Filtration gave 1.50 g (98% yield) of **3** which after recrystallization from 1% $HClO_4$ gave a light tan crystalline powder with m.p. over 370 °C. On prolonged heating it becomes brown. Found: N, 5.07; $C_{22}H_{26}Cl_2N_2O_8$ requires N, 5.41%.
IR spectrum (KBr, cm^{-1}): 625 s, 695 mw, 762 mw, 807 mw, 880 mw, 1100 vs, 1260 mw 1320 mw, 1338 mw, 1375 mw, 1425 m, 1438 m, 1470 m, 1565 ms, 1625 s, 1990 w, 2920—3080 mw.
UV spectrum in $HClO_4$ 1%, λ_{max}, nm (lg ε_{max}): 211 (4.25), 215 (4.30), 284 (5.37); an identical spectrum is obtained in water.
^{1}H—NMR spectrum (TFA, δppm): 3.00 (s, 12H, 2′,6′-Me); 4.25 (s, 4H, $\overset{+}{N}$—Me); 8.15 (s, 4H, 3′- and 5′-H), 8.0—8.5 (m, 4H, phenylene protons).

1,3-Bis-(2,6-dimethyl-1-phenylpyridiniumyl-4)-benzene diperchlorate, **4.** Similarly, 1 g of the diperchlorate **1b** (2 mmoles) reacted with aniline (2 g, 21 mmoles) in 10 mL methanol affording 1.1 g (84% yield) of crystalline diperchlorate **4**, mp. over 360°. Found : N, 4.20; $C_{32}H_{30}Cl_2N_2O_8$ requires N, 4.37%.
IR spectrum (KBr, cm^{-1}) : 625 ms, 705 ms, 770 m, 800 mw, 1100 s, 1205 ms, 1340 mw, 1430 mw, 1460 mw, 1482 m, 1555 m, 1582 ms 1622 s, 2920—3070 w.
UV spectrum in $HClO_4$ 1% (or in H_2O), λ_{max}, nm : 216 and 290.
^1H—NMR (TFA, δppm) : 2.65 (s, 12H, 2′,6′-Me); 7.60 (s, 4H, 3′ and 5′-H); 7.88 (m, 10H $\overset{+}{N}$—Ph); 8.10—8.30 (m, 4H, phenylene protons).

3, 3″-Dihydroxy-5,5″-dimethyl-[1,1′: 3′,1″]-terphenyl, **5**. An aqueous solution of **1a** was admixed with excess of 20% aqueous sodium hydroxide, the precipitated bisphenol being dissolved at pH values higher than 12. The bisphenoxide solution was extracted twice with diethyl ether, warmed to remove any residual ether, neutralized while warm with an excess of hydrochloric acid and left overnight in the refrigerator. The crystalline bisphenol was easily removed by filtration and purified by sublimation in vacuum (1 Torr). The colourless, sublimed bisphenol melted at 70 °C, resolidified and then melted again between 128 and 135° C. Left to cool it crystallized again in needles with a sharp melting point of 140 °C. The sublimed bisphenol is initially dissolved by chloroform, trichloroethylene and other solvents but after a short period colourless fluffs were deposited from these solutions. The fluffy material melted at 145—147 °C. Recrystallization from benzene yielded colourless fine needles with m.p. 146—147 °C. Found : C, 82.62%; H, 6.48%; $C_{20}H_{18}O_2$ requires : C, 82.73% H, 6.24%.
No major difference between the IR spectra recorded as KBr pellets of the sublimed and recrystallized bis-phenol samples could be detected.
IR (KBr, cm^{-1}) : 3320 s (board), 1610 m, 1583 s, 1315 ms, 1155 ms, 810 ms, 700 m, 670 w, 545 w.
UV spectrum in ethanol, λ_{max}, nm (lg ε_{max}) : 222 (5.79); 2.53 (5.45), 291 shoulder (3.97).
^1H—NMR ($CDCl_3$, low solubility), δ(ppm) : 2.36 (6H, s, Me), 6.82 (broad s, 2H, 4- and 4″-H 7.06 (broad s, 2H, 6- and 6″-H), 7.15 (broad s, 2H, 2- and 2″-H), 7.48 (broad s, 3H, 4′, 6′- and 5′-H), 7.73 (m, 1H, 2′-H).

Bis-1,3-(2,6-dimethyl-5,6-dihydro-2H-pyranyl-4)benzene, **6**. The diperchlorate **1b** (1.5 g, 3.0 mmol) was suspended in anhydrous acetic acid (15 mL) and was reduced under dry argon with excess of sodium tetrahydroborate (2.75 g, 72 mmol) at 50 °C. The mixture was stirred for two hours and then it was decomposed with 50 mL water and extracted with diethyl ether. The ethereal extracts were neutralized with aqueous sodium carbonate, dried over anhydrous magnesium sulfate, and concentrated in vacuum yielding 0.85 g (93% yield) of pale yellow oil. Found : C, 80.87; H, 8.75. $C_{20}H_{26}O_2$ requires : C, 80.53; H, 8.72%.
IR spectrum (CS_2; cm^{-1}) : 700 w, 735 s, 845 mw, 851 mw, 910 ms, 974 w, 1055 m, 1070 m, 1100 ms, 1148 s, 1178 ms, 1225 w, 1320 m, 1370 ms, 1382 m, 1665 w, 2810 mw, 2850 m 2888 m, 2925 ms, 2972, s, 3030 w, 3055 vw. In CCl_4 : 1621 w, 1638 mw, 1680 vw, 1592 w, 1665 w.
UV spectrum in hexane, λ_{max}, nm : 244.
^1H—NMR spectrum in $CDCl_3$, δppm : 1.37 (d, 6H, 2-Me, 2″-Me, J = 6.5 Hz); 1.39 (d, 6H, 6-Me, 6″-Me, J = 6.0 Hz); 2.42. (m, 4H, 5-H_2, 5″-H_2); 3.89. (2H, sextet. 6-H, 6″-H, J = = 6.5 Hz) 4.50 (m, 2H, 2-H, 2″-H); 6.13 (q, 2H, 3-H, 3″-H, J = 1.5 Hz) 7.40 (m, 4H, 1′, 3′-phenylene-H).

REFERENCES

[1] Previous part in this series, XXIII, A. T. Balaban, A. Bota, F. Chiraleu, E. Sliam, A. Haneş and C. Drăghici, *Rev. Roumaine Chim.*, **22**, 1003 (1977).
[2] T.-S. Balaban and A. T. Balaban, *Tetrahedron Lett.*, **28**, 1341 (1987).
[3] G. W. Gribble and C. F. Nutaitis, *Org. Prep. Proc. Int.*, **17**, 317 (1985).
[4] T.-S. Balaban and A. T. Balaban, *Org. Prep. Proc. Int.*, **20**, 231 (1988).
[5] S. V. Krivun and G. N. Dorofeenko, a) *Zh. Obschei Khim.*, **34**, 2091 (1964); b) *Khim. Geterotsikl. Soedin.*, 656 (1966).
[6] M. J. Sharp, W. Cheng and V. Snieckus, *Tetrahedron Lett.*, **28**, 5093 (1987).
[7] Part I in this series, A. T. Balaban and C. D. Nenitzescu, *Justus Liebigs Ann. Chim.*, **625**, 66(1959).
[8] A. T. Balaban and C. D. Nenitzescu, *Org. Synth. Coll. Vol.* **5**, 1106(1973).

[9] A. T. Balaban and A. J. Boulton, *Org. Synth. Coll. Vol.* **5**, 1112 (1973).

[10] Previous attempts made by one of us (A.T.B.) for the diacylation of 2,3-dimethyl-1,3-butadiene.

[11] a) A. Dinculescu and A. T. Balaban, *Org. Prep. Proc. Int.*, **14**, 39 (1982); b) T.-S Balaban A. Dinculescu and A. T. Balaban, *Org. Prep. Proc. Int.*, **20**, 289 (1988).

[12] A. Dinculescu, private communication.

[13] A. T. Balaban, A. Dinculescu, G. N. Dorofeenko, G. W. Fischer, A. V. Koblik, V. V. Mezheritskii and W. Schroth, "Pyrylium Salts. Syntheses, Reactions and Physical Properties", *Adv. Heterocycl. Chem. Suppl. Vol.* 2, Editor, A. R. Katritzky, Academic Press, New York, 1982.

[14] T.-S. Balaban, C. Uncuţa, M. D. Gheorghiu and A. T. Balaban, *Tetrahedron Lett.*, **26**, 4669 (1985).

[15] A. T. Balaban, A. Dinculescu, H. N. Koutrakis and F. Chiraleu, *Tetrahedron Lett.*, 437 (1979).

Revue Roumaine de Chimie, 34, *1*, 51–58 (1989)

THE BEHAVIOUR OF DIETHYL MALEATE – VINYL ACETATE COPOLYMERS IN SOLUTION

CAMELIA BELDIE [a], GH. NEMŢOI [a], EM. DUMITRIU [b] and V. BĂRBOIU [c]
[a] Department of Physical-Chemistry, Faculty de Chemical Technology, Jassy 6600
[b] Department of Organic Technology, Faculty of Chemical Technology, Splai Bahlui 71, Jassy 6600
[c] Institute of Macromolecular Chemistry, Jassy 6600, Romania

Received September 12, 1988

Six copolymers of diethyl maleate with vinyl acetate having different molecular weights were synthesized. The behaviour of copolymers in solution, using as solvents : toluene, acetone and chloroform, was studied. The osmometry and viscosimetry were used as experimental methods of investigation. From the experimental data the Mark-Houwink constants (K and a), for the three solvents were determined. Also, the structural parameters were estimated using the Stockmayer-Fixman, Schaefgen-Flory and Kurata-Stockmayer-Roig equations and a comparison of the results was made.

The development of modern economy has imposed a new orientation of the industry of organic coatings from the classical polymers such as phenolic resins, nitrocellulose etc. to the coatings based on acrylic and vinyl polymers, polyurethane etc. The coatings obtained on the basis of the last type of polymers show a large range of properties : some are very flexible, others are very rigid or very resistant. In order to satisfy the demands of various industries : chemical, electrotechnical, buildings, foods etc., a large variety of organic coatings, with a large spectrum of properties, is necessary. The demands of these industries, in relation to certain properties, can be satisfied by the combination of different polymers, but a more advantageous method, leading to excellent results, consists in the preparation of these materials by copolymerization.

For this reason, our studies were oriented to the synthesis of some copolymers of maleic esters being known that these copolymers are recommended for the manufacture of fibers, adhesives, coatings etc.

As is known, the formation of a coating is determined by the chemical composition of polymer material, the degree of polymerization, the nature of the solvent used and other factors. From the point of view of structure, the coatings are formed from molecular aggregates of different forms and sizes. The formation of molecular aggregates is the consequence of the intermolecular forces which are manifested in the polymer solutions. Moreover, these forces determine many important properties for the technology of coatings such as : volatility, viscosity, surface tension, friction, solubility and compatibility. Some of these properties can be investigated by the thermodynamic study of polymer solutions.

Therefore, the aim of this paper is to investigate the thermodynamic behaviour of the copolymers of diethyl maleate with vinyl acetate solved in various solvents. There are no data about these polymer solutions in the literature.

MATERIALS AND METHODS

Vinyl acetate (VAc) was purified by distillation under nitrogen. Diethyl maleate (DEM) was synthesized by azeotropic esterification of maleic anhydride with ethanol using *p*-toluenesulfonic acid as catalyst. This monomer was also purified by distillation under vacuum and nitrogen. The purity of both monomers was checked by gaschromatography. 2,2'-Azo bis (isobutyronitrile), AIBN, was used as polymerization initiator after three recrystallizations from ethanol.

The solvents (benzene, toluene, acetone, chloroform and methanol) were purified by the common methods.

The copolymerization of diethyl maleate with vinyl acetate was carried out in benzene solution at 60°C. In order to vary the molecular weights of copolymers, the amount of AIBN was varied between 0.1 and 1% (by weight). The copolymers obtained at medium conversions were purified by reprecipitation from the benzene-light petroleum system (solvent and nonsolvent), then they were dried at 50°C under vacuum.

The copolymer compositions were determined by NMR analysis on a JEOL C-60 HL spectrometer using the integral of signals of CH (VAc) and CH_2 (DEM). The molar fraction of vinyl acetate units was calculated by the following relations :

$$f_{\mathrm{VAc}} = \frac{I_{\mathrm{CH}}}{I_{\mathrm{CH}} + 1/4\, I_{\mathrm{HC}_2}} \tag{1}$$

$$f_{\mathrm{VAc}} = \frac{1}{100}\, C_{\mathrm{VAc}}$$

where C_{VAc} is the molar concentration.

In Figure 1 a typical spectrum of this copolymer is shown. The copolymer compositions are presented in table 1.

Table 1

The composition of diethyl maleate-vinyl acetate copolymer

Sample	1	2	3	4	5	6
Initiator % by weight	0.15	0.30	0.39	0.45	0.60	0.80
Mole concentration C_{VA}	62.6	55.4	54.0	51.5	58.3	59.3
Mole fraction*VA	0.626	0.554	0.540	0.515	0.583	0.595

Number-average molecular weights were determined on the basis of osmometric measurements at 31 ± 0.5°C using a Knauer type osmometer. Viscosimetric measurements were carried out at 25 ± 0.2°C on a suspended level viscosimetry of the Ubbelohde type, with internal dilution. Toluene, acetone and chloroform (reagent grade) were used as solvents. The osmometric and viscosimetric measurements were performed using polymer solutions of concentrations ranging between 0.2 and 1.0 g/dL.

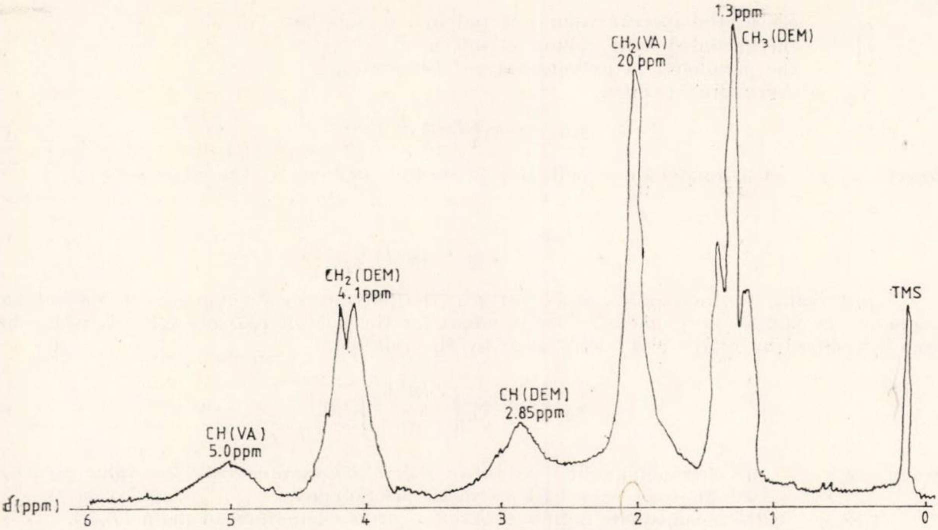

Fig. 1. — Spectrum of poly(DEM-co-VAc).

Number-average molecular weight ($\overline{M}_n$) was calculated on the basis of the following equation :

$$\frac{\pi}{C} = \frac{RT}{M_n} + RTA_2C \tag{2}$$

The limit viscosity index was determined on the basis of the Huggins and Fuoss-Mead equations[1] by double extrapolation. In order to interpret the dimension of macromolecules in solution three representative equations were used :

1) The Stockmayer-Fixman equation[2] :

$$\frac{[\eta]}{M^{1/2}} = K_\theta + 0.51\Phi_0\, BM^{1/2} \tag{3}$$

2) The Schaefgen-Flory equation :[3]

$$\frac{[\eta]^{2/3}}{M^{1/3}} = k_\theta^{3/2} + 4.085\, \Phi_0 B\, \frac{M}{[\eta]} \tag{4}$$

3) The Kurata-Stockmayer-Roig equation :[4]

$$\frac{[\eta]^{2/3}}{M^{1/3}} = k_\theta^{2/3} + 0.365\, \Phi_0\, Bg\, (\alpha_\eta)\, \frac{M^{2/3}}{[\eta]^{1/3}} \tag{5}$$

where :

$[\eta]$ — the limit viscosity index of the polymer in the considered solvent ;
M — the molecular weight of polymer sample ;
B — coefficient depending on the polymer-solvent interaction forces, which is correlated with the second virial coefficient A_2 by the following relationship :

$$B = \frac{2\nu_2^2}{N_m \nu_1}\,(1/2 - \chi) = \frac{2A_2}{N_m} \tag{6}$$

where :

ν_2 — the partial specific volume of polymer in solution ;
ν_1 — the partial specific volume of solvent ;
χ — the parameter of polymer-solvent interaction ;
N_m — Avogadro's number

$$g(\alpha_\eta) = 8\alpha_\eta^2/(3\alpha_\eta^2 + 1)^{3/2} \tag{7}$$

where : α_η is the thermodynamic coefficient of swelling defined by the relation :

$$\alpha_\eta^3 = \frac{[\eta]}{[\eta]_\theta} = \frac{[\eta]}{k_\theta M^{1/2}} \tag{8}$$

$[\eta]\theta$ being the limit index of viscosity of the polymer in θ conditions of solvent and temperature ; and k is a characteristic constant for the pair of polymer-solvent, which has been introduced by Flory[5] and Yamakawa[6] by the relation :

$$k_\theta = 6^{3/2}\Phi_0 \left(\frac{\langle R^2 \rangle \theta}{M} \right)^{3/2} \tag{9}$$

where : Φ_0 — is the thermodynamic constant of Flory, having obviously the value of 2.5×10^{21} dL·mol^{-1} cm^{-3} for unfractioned polymers.

$\langle R^2 \rangle_\theta$— is the mean square radius of gyration of the unperturbed chain ($R_{G\theta}$).

The mean square radius of gyration of the real chain (R), in a given solvent, can be directly determined using the Flory-Fox[7] equation :

$$[\eta] = 6^{3/2}\Phi_0 \frac{\langle R^2 \rangle}{M} \tag{10}$$

The study of behaviour of the DEM-VAc copolymer in solution of toluene, acetone and chloroform compares the results obtained with the aid of the above mentioned equations, in order to state the most adequate equation which allows to interpret the experimental data in relation to the limit index of viscosity and the molecular weight and also, in order to obtain certain thermodynamic parameters of the copolymer in the respective solvents.

In order to estimate the structural-thermodynamic parameters, the experimental data were processed by the method of the least squares which was applied for all three equations. In relation to the Kurata-Stockmayer-Roig equation, where the function $g(\alpha_\eta)$ is unknown, it must be specified that in order to find the k_θ coefficient the interaction method was applied. Thus, first the value $g(\alpha_\eta) = 1$ was adopted and, successively, k_θ, α_θ and $g(\alpha_\eta)$ were estimated and the calculus was resumed until two successive values of k_θ differ only by an imposed value. Here, the imposed value was :

$$\frac{K_{n+1} - K_{(n)}}{K_{(n)}} \leqslant 0.01 \tag{11}$$

RESULTS AND DISCUSSION

The results of $[\eta]$ and M determination are shown in Table 2. Also, the values of the second virial coefficient, determined by osmotic measurements in the toluene solutions, are given in the same table.

It can be observed that the second virial coefficient is a decreasing function vs. molecular weight and it can be expressed by the empirical relation :

$$A_2 = C \cdot M^{-\gamma}$$

which can be also found in the literature.

Molecular weights and the second virial coefficient were determined by the method of the least squares obtaining the following value for constants :

Table 2

The results of osmometric and viscometric measurem en ts

Solvent	Determined property	Sample					
		1	2	3	4	5	6
Toluene	$M_n(\mathrm{g \cdot mol^{-1}})$	130.0000	98.300	51.200	47.200	38.400	30.700
	$10^7 A_2(\mathrm{dm^3 \cdot mol \cdot g^{-2}})$	3.01	4.08	7.085	7.753	9.375	11.86
	$[\eta]$ $(\mathrm{dL \cdot g^{-1}})$	0.4015	0.3447	0.2351	0.2320	0.2011	0.1760
Acetone	$[\eta]$ $(\mathrm{dL \cdot g^{-1}})$	0.5005	0.4169	0.2693	0.2572	0.2281	0.1978
Chloroform	$[\eta]$ $(\mathrm{dL \cdot g^{-1}})$	0.7033	0.5769	0.3624	0.3427	0.2921	0.2503

$$\gamma = 0.9267 \pm 0.085$$

$$C = 0.01674 \pm 0.00785$$

the correlation coefficient being 0.9919 for the dependence ln $[\eta]$ vs. ln M_n. This proves that there are very small deviations from linearity.

Therefore, for the solution of DEM—VAc copolymer in toluene, the following relation can be obtained, which describes the dependence of the second virial coefficient vs. molecular weight.

$$A_2 = (0.016 \pm 0.00785)\,\bar{M}_n - (0.9267 \pm 0.0851)$$

The relatively high value of γ can be due to the fact that the study was carried out using polydisperse samples of polymer having relatively small molecular weights. For the dependence of A_2 vs. molecular weight for poly(vinyl acetate) the value $A_2 = 0.0176\ M_n^{-0.365}$ was found when the toluene was used as solvent.[8]

The dependence of ln $[\eta]$ vs. the corresponding logarithm of molecular weight indicates only a small deviation from linearity in the studied range. This is also confirmed by the value of correlation coefficient (Table 3).

Table 3

The coefficients of the Mark-Houwink equation

Solvent	$10^4(K \pm \Delta K)\mathrm{dl \cdot g^{-1}}$	$a \pm \Delta a$	The coefficient of linear correlation
Toluene	4.98 ± 0.83	0.5688 ± 0.0519	0.9992
Acetone	2.47 ± 0.18	0.6459 ± 0.0349	0.9997
Chloroform	1.52 ± 0.03	0.7169 ± 0.0172	0.9999

Using the method of the least squares the values of the Mark-Houwink coefficients (a and K) were determined. These values are presented in Table 3, too.

The value of a for toluene solutions indicates that this solvent is not so good, whereas in the other two solvents the macromolecular chains are more flexible. If we compare these results with those obtained for the poly(vinyl acetate)-toluene system,[8] a diminution of the properties of toluene as good solvent for the copolymer-toluene system can be observed.

Taking into account the thermodynamic properties of the studied solvents, which are underlined by the a coefficients, the following order can be obtained : chloroform $>$ acetone $>$ toluene. The values of viscosimetric constant (K_θ) obtained with the aid of the three equations (3—5) are shown in Table 4.

The K_θ values depend on the solvent nature. If the value of K_θ, calculated by the Schaefgen-Flory equation, is different from those obtained by the Stockmayer-Fixman and Kurata-Stockmayer-Roig equations for the copolymer-chloroform and copolymer-acetone systems, in the case of toluene, the K values are very close to one another, irrespective of the equation used.

Table 4

The values of k_θ for diethyl maleate-vinyl acetate copolymer versus nature of solvent

Solvent	Equation					
	Stockmayer-Fixman		Schaefgen-Flory		Kurata-Stockmayer-Roig	
	$10^4(k_\theta \pm \Delta k_\theta)$	Liniar correlation coefficient	$10^4(k_\theta \pm \Delta k_\theta)$	Liniar correlation coefficient	$10^4(k_\theta \pm \Delta k_\theta)$	Liniar correlation coefficient
Toluene	9.209 ± 1.166	0.9421	9.052 ± 0.3025	0.9285	9.167 ± 0.3912	0.9378
Acetone	8.790 ± 0.513	0.9981	7.6601 ± 0.2135	0.9944	8.542 ± 0.1381	0.9975
Chloroform	9.524 ± 1.185	0.9974	5.797 ± 0.3995	0.9974	8.822 ± 0.2901	0.9982

According to the adopted premises, the Schaefgen-Flory equation is not suitable for the systems consisting of polymer and a good solvent, but the results obtained applying the Schaefgen-Flory equation approach the real values where the system draws nearer to the theta point. These facts demonstrate that the K_θ values, which are in agreement irrespective of the equation used when the copolymer is solved in toluene, prove that this copolymer-solvent system draws nearer to the theta point ; this is also confirmed by the values of the a constant from the Mark-Houwink equation.

The gyration radii of the unperturbed chain $R_{G,\theta}$ and those of the real chains R_G, as well as the η values are shown in Tables 5—7.

These tables show that the gyration radii of the real chain in solution are of the same order of magnitude, in the case of acetone and chloroform, and they are smaller by about 8—14% for the toluene solutions. Therefore, these data indicate that acetone and chloroform are better solvents than toluene.

Table 5

The structural parameters of diethyl maleate-vinyl acetate copolymer in toluene solution

Equation	Parameter	Sample					
		1	2	3	4	5	6
	R_G, Å	107.36	92.96	65.84	63.79	56.78	50.41
Stockmayer-Fixman	$R_{G\theta}$, Å	100.77	87.63	63.24	60.72	54.77	48.97
	α_η	1.0654	1.0608	1.0410	1.0506	1.0368	1.0294
Schaefgen-Flory	$R_{G\theta}$, Å	100.20	87.13	62.88	60.37	54.46	48.69
	α_η	1.0715	1.0669	1.0470	1.0567	1.0427	1.0353
Kurata-Stockmayer-Roig	$R_{G\theta}$,Å	100.62	87.50	63.15	60.63	54.69	48.90
	α_η	1.0670	1.0624	1.0426	1.0522	1.0383	1.0309

Table 6

The structural parameters of diethyl maleate-vinyl acetate copolymer in chloroform solution

Equation	Parameter	Sample					
		1	2	3	4	5	6
	R_G, Å	115.54	99.05	68.89	66.03	59.22	52.41
Stockmayer-Fixman	$R_{G\theta}$, Å	99.22	86.28	62.27	59.79	53.93	48.22
	$\alpha\eta$	1.1645	1.1479	1.1063	1.1043	1.0981	1.0870
Schaefgen-Flory	$R_{G\theta}$, Å	94.77	82.41	59.48	57.11	51.51	46.06
	$\alpha\eta$	1.2192	1.2018	1.1582	1.1562	1.1497	1.1380
Kurata-Stockmayer-Roig	$R_{G\theta}$, Å	98.28	85.46	61.68	59.22	53.42	47.76
	$\alpha\eta$	1.1756	1.1589	1.1169	1.1149	1.1087	1.0974

Table 7

The structural parameters of diethyl maleate-vinyl acetate copolymer in chloroform solution

Equation	Parameter	Sample					
		1	2	3	4	5	6
	R_G, Å	129.42	110.37	76.75	72.65	64.31	56.69
Stockmayer-Fixman	$R_{G\theta}$,Å	102.49	89.12	64.32	61.76	55.70	49.81
	$\alpha\eta$	1.2627	1.2384	1.1932	1.1764	1.1544	1.1382
Schaefgen-Flory	$R_{G\theta}$, Å	86.37	75.10	54.20	52.04	46.94	41.97
	$\alpha\eta$	1.4985	1.4696	1.4031	1.3961	1.3699	1.3507
Kurata-Stockmayer-Roig	$R_{G\theta}$, Å	99.41	86.44	62.39	59.90	54.03	48.31
	$\alpha\eta$	1.3019	1.2678	1.2191	1.2129	1.1903	1.1735

The gyration radii of the unperturbed chain are of the same order of magnitude for the three solvents when the experimental data are interpreted by the Stockmayer-Fixman and Kurata-Stockmayer-Roig equations whereas if the Schaefgen-Flory equation is used the gyration radii of the unperturbed chain for the systems acetone and chloroform-copolymer differ from the values obtained by the other two methods. This indicates that acetone and chloroform are far from the theta conditions. We can also mention that the gyration radii both for the unperturbed and the real chain of copolymer in toluene solution are greater than those of the poly-(vinyl acetate) in the same solvent.

CONCLUSIONS

On the basis of the experimental measurements which allowed us to find *a* and *K* constants from the Mark-Houwink equation and the dimensions of macromolecular chain of the copolymer in the three solvents, the following aspects can be concluded. Both the values of the Mark-Houwink coefficients and the dimensions of copolymer macromolecules in these solvents indicate that acetone and chloroform are good solvents while toluene is a less good solvent. In the last case (the copolymer/toluene system) it was stated that the second virial coefficient depends on the molecular weight following a decreasing function. In relation to the unperturbed dimensions of macromolecules it was observed that the Stockmayer-Fixman and Kurata-Stockmayer-Roig equations lead to comparable results for the good solvents whereas the Schaefgen-Flory equation is adequate for the systems tending to the theta conditions.

REFERENCES

[1] L. J. Huggins, D. Mead and R. Fuoss, *J. Amer. Chem. Soc.*, **64**, 2716 (1942).
[2] W. H. Stockmayer and M. Fixman, *J. Polymer Sci.*, part. C., **1**, 137 (1963).
[3] J. R. Schaefgen and P. J. Flory, *J. Amer. Chem. Soc.*, **70**, 2709 (1948).
[4] M. Kurata, W. H. Stockmayer and A. Roig, *J. Chem. Phys.*, **33**, 151 (1960).
[5] P. J. Flory, *Makromol. Chem.*, **98**, 128 (1966).
[6] H. Yamakawa, "Modern Theory of Polymer Solutions", Harper and Row, New York 1971.
[7] P. J. Flory and T. G. Fox, *J. Amer. Chem. Soc.*, **73**, 1904 (1951).
[8] N. Aelenei, V. Nagacevschi, *Materiale plastice*, **21**, 204 (1984).

Revue Roumaine de Chimie, 34, 1, 59–63 (1989)

ZEOLITE MOLECULAR SIEVES AS STATIONARY PHASE IN THIN LAYER CHROMATOGRAPHY. V

ON MIGRATION MECHANISM

ANIȘOARA BOLD, ANGELICA POPA, AURELIA VASILE, M. CRUCEANU,
EVELINE POPOVICI and MARIA ALEXANDROAEI
Department of Chemical Technology, Polytechnic Institute, 71, Splai Bahlui,
Iași, Romania

Received October 4, 1988

This paper deals with a study on separation of the Fe(III), Co(II), Cu(II) and Ni(II) ions on NaX molecular sieves by TLC and ion exchange in solution. Correlation of the kinetical quantities of ion exchange and R_f values shows that the migration is based on ion exchange phenomenon.

INTRODUCTION

At present, the thin layer chromatography (TLC) uses as stationary phase a great number of organic or inorganic solid substances which by their adsorptive properties favour separations in different classes of compounds. Recently, side by side with well-known stationary phases are, with good results, the zeolite molecular sieves.[1-4] These products have besides the properties proper to powder state adsorbents, the selective adsorption and ion exchange, due to their porous crystalline structure and crystallochemistry. Due to these properties, by the TLC with zeolite molecular sieves, good separations have been performed for dye stuffs,[5] alkaloids[5] or inorganic cations.[7]

Taking into account the excellent results obtained in the inorganic cations separations, the present paper deals with a preliminary investigation on the separation mechanism of the Fe(III), Co(II), Cu(II) and Ni(II) by TLC compared with the ion exchange in solution.

EXPERIMENTAL

A zeolite molecular sieve NaX with uniform pore size of 13 Å, synthetized hydrothermally[8] in our laboratory has been employed. The maximum ion exchange capacity of zeolite powder was of 6.3 m equiv/gramme anhydrous zeolite. After calcination at 450°C and granulometric classification, the fraction with mean granule size of $2.16 \cdot 10^{-4}$ cm has been taken for experiments. The plates preparation has been carried out as previously described.[9]

The tested cations belong to 0.1 N aqueous solutions of nitrates, from which the spots of 20 μl have been applied.

Based on the experimental results obtained[7,10] the buffer solution (1 M acetic acid — 1 M sodium acetate) : ethanol (1 : 1 ; v/v) has been employed.

Localization and identification of the separated spots have been performed with specific reactifs such as solution 5 M of potassium ferrocyanide for Fe(III); alcoholic solution of 1% of rubeanic acid for Co(II) and Cu(II) and alcoholic solution of 1% of dimethylglyoxime for Ni(II).

The ion exchange in solution has been investigated in the same system, used as mobile phase in TLC, i.e. buffer 0.1 M acetate — ethanol (v/v). Concentration of the exchange cations was $4 \cdot 10^{-2}$M and the temperature of 20 and 40°C. The equilibrium concentrations have been determined complexometrically and flamphotometrically.

RESULTS AND DISCUSSION

The data as regards the TLC separation of the above-mentioned cations are set out in Figure 1.

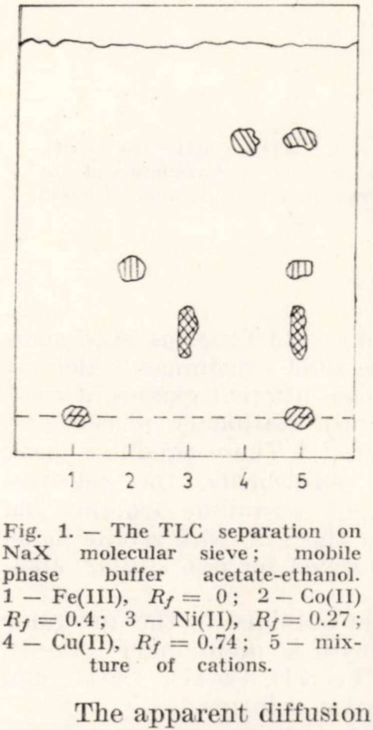

Fig. 1. — The TLC separation on NaX molecular sieve; mobile phase buffer acetate-ethanol. 1 — Fe(III), $R_f = 0$; 2 — Co(II) $R_f = 0.4$; 3 — Ni(II), $R_f = 0.27$; 4 — Cu(II), $R_f = 0.74$; 5 — mixture of cations.

Referring to the separation mechanism by TLC we suggest that it is based on ion exchange phenomenon. We consider that this hypothesis can be confirmed only by some correlations between the quantities proper to chromatographic separation, namely R_f and the quantities proper to ion exchange phenomenon, i.e. distribution separation and diffusion coefficients and activation energy. For this reason the ion exchange kinetics in the systems written below has been investigated and the results obtained are illustrated in Figures 2 and 3.

$$\mathrm{NaX} + \mathrm{Fe}^{3+} \rightleftharpoons \mathrm{FeX} + 3\mathrm{Na}^{+} \quad (1)$$

$$\mathrm{NaX} + \mathrm{Co}^{+2} \rightleftharpoons \mathrm{CoX} + 2\mathrm{Na}^{+} \quad (2)$$

$$\mathrm{NaX} + \mathrm{Ni}^{2+} \rightleftharpoons \mathrm{NiX} + 2\mathrm{Na}^{+} \quad (3)$$

$$\mathrm{NaX} + \mathrm{Cu}^{2+} \rightleftharpoons \mathrm{CuX} + 2\mathrm{Na}^{+} \quad (4)$$

For the Fe(III) ion we could not draw kinetical curves because in this case the supplementary influences occur, such as the clusters formation.[11]

The apparent diffusion coefficients and activation energy have been calculated using Boyd — Adamson [12] and Arrhenius equations, respectively. The obtained results are summarized in Table 1.

The distribution coefficients, $K_d = \dfrac{\text{m equiv. Me}^{2+}\text{/g zeolite}}{\text{m equiv. Me}^{2+}\text{/ml solution at equilibrium}}$

and selectivity coefficients,

$$K_{d_{\mathrm{Na}^+}}^{\mathrm{Me}^{2+}} = K_d^{\mathrm{Me}^{2+}} / K_d^{\mathrm{Na}^+},$$

are set out in Table 2.

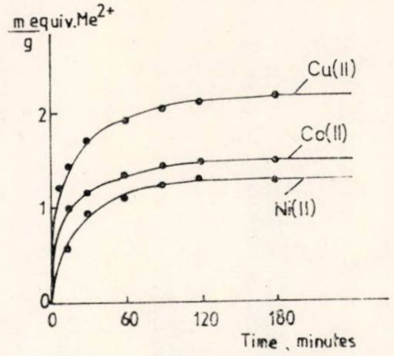

Fig. 2.—Kinetics of the ion exchange $Me^{2+} \rightleftharpoons 2Na^{+}$ in ethanol — buffer acetate solution at 20°C.

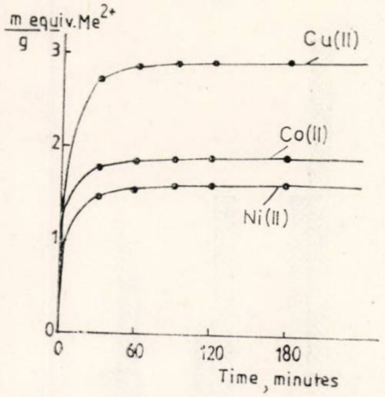

Fig. 3.—Kinetics of the ion exchange $Me^{+} \rightleftharpoons 2Na^{+}$ in ethanol — buffer acetate solution at 40°C.

Table 1

Diffusion coefficients and activation energy

Exchange ion	Apparent diffusion coefficients, $cm^2 \cdot s^{-1}$		Activation energy, $cal \cdot ion\ g^{-1}$
	$t = 20°C$	$t = 40°C$	
Cu(II)	$4.26 \cdot 10^{-13}$	$5.85 \cdot 10^{-13}$	2892
Co(II)	$4.73 \cdot 10^{-13}$	$8.04 \cdot 10^{-13}$	4818
Ni(II)	$4.87 \cdot 10^{-13}$	$9.19 \cdot 10^{-13}$	5767

Table 2

Distribution and selectivity coefficients

Exchange ion	Distribution coefficient		Selectivity coefficient	
	$t = 20°C$	$t = 40°C$	$t = 20°C$	$t = 40°C$
Cu(II)	11.56	16.80	0.316	0.737
Co(II)	7.42	9.75	0.118	0.202
Ni(II)	6.18	7.60	0.083	0.144

Comparing the R_f values, which show the chromatographic relation with zeolite stationary phase of the three cations, with the values of their distribution and selectivity coefficients ilustrated in Figures 4 and 5, which point out the behaviour of cations in the ion exchange reaction in solution, a good enough agreement can be seen.

As good as above-mentioned agreement can be seen in the case of correlation between diffusion coefficients and activation energy, respectively with R_f, Figures 6 and 7.

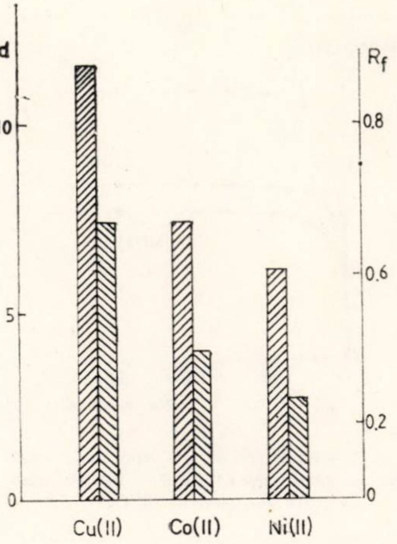

Fig. 4. — Distribution coefficients and R_f for the tested cations.

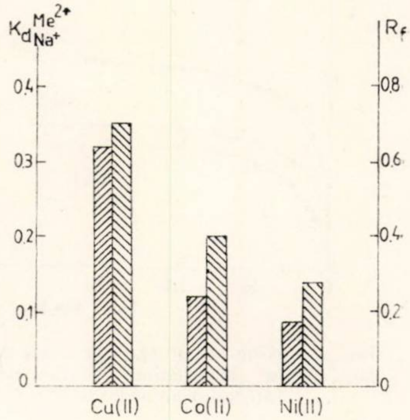

Fig. 5. — Selectivity coefficients and R_f for the tested cations.

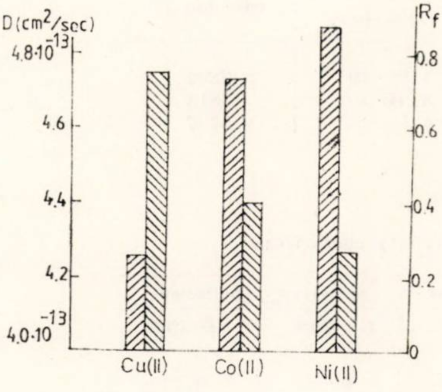

Fig. 6. — Diffusion coefficients and R_f for the tested cations.

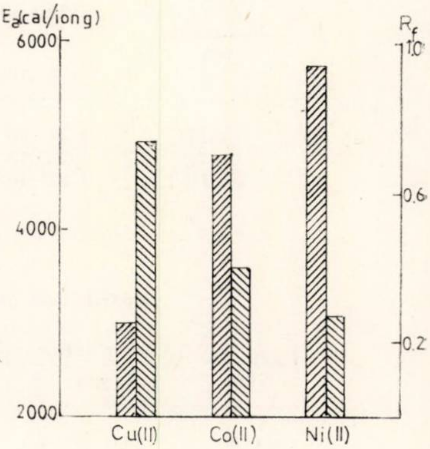

Fig. 7.—Activation energy and R_f for the tested cations.

The cation which requires a greater activation energy, i.e. Ni^{2+}, covers a lesser distance in comparison with the cations for which diffusion necessitates a lesser activation energy, i.e. Cu^{2+} and Co^{2+}.

Correlation between R_f values and kinetical quantities of the ion exchange testifies to the previously suggested hypothesis on separation mechanism of the inorganic ions by TLC on zeolite molecular sieves.

In the case of investigated cations the property of molecular sieve of the products employed in layer preparation does not work, because the

NaX zeolite has pore diameter of 13 Å, while the hydrated ion diameter does not exceed 5 Å (the ionic radius of hydrated ions are : 4.04 Å for Ni(II) and 4.2 Å for Cu (II)).

CONCLUSIONS

In the TLC separation of the Cu(II), Co(II) and Ni(II), on NaX molecular sieve as stationary phase, the separation mechanism is based on ion exchange phenomenon. Correlation of the R_f values and kinetical quantities of the ion exchange supports suggested hypothesis. Due to the difference between zeolite pore diameter and hydrated ions radius, in this case the "molecular sieve effect" does not take place.

REFERENCES

[1] A. Bold, A. Popa, M. Cruceanu, Ev. Popovici and M. Găburici, "European Conference on Analytical Chemistry", Euroanalysis, Cracovia, 1984.

[2] M. Cruceanu, Ev. Popovici, N. Bîlbă, R. Rusu, A. Vasile, N. Naum and L. Vlădescu, "Site moleculare zeolitice", Ed. Ştiinţifică şi Enciclopedică, Bucureşti, (1986).

[3] E. Sawicki, *Chemist. Analyst.*, **53**, 56 (1964).

[4] L. R. Snyder and D. L. Saunders, J. Chromat., **44**, 4238 (1969).

[5] A. Bold, A. Popa, M. Găburici, Ev. Popovici and M. Cruceanu, *Bul. Inst. Polytechnic Iaşi* (in print).

[6] A. Bold, M. Cruceanu, I. Bâra, Ev. Popovici, A. Vasile and A. Popa, *Rev. Chim. (Bucureşti)*, (in print).

[7] A. Bold, A. Popa, M. Cruceanu, Ev. Popovici and M. Găburici, *Rev. Chim. (Bucureşti)*, **36**, 928 (1985).

[8] E. Popovici and M. Cruceanu, *Rev. Chim. (Bucureşti)*, **33**, 732 (1982).

[9] A. Bold, A. Popa, M. Cruceanu, and Ev. Popovici, *Rev. Chim. (Bucureşti)*, **35**, 1123 (1984).

[10] A. Popa, A. Bold, M. Cruceanu, E. Popovici and C. Luca, 1st Symposium "Zeoliţii în tehnologia modernă", Iaşi, 136, 1983.

[11] F. Iacomi, E. Trif, E. Popovici, A. Vasile, M. Alexandroaei, M. Cruceanu and G. Singurel, *Rev. Roum. Chim*, **33**, 149 (1988).

[12] A. Vasile, Ph. D. Diss., Inst. Politechnic Iaşi, 1986.

Revue Roumaine de Chimie, **34**, *1*, 65–78 (1989)

WORLD-WIDE AND NATIONAL CONCERNS AND TENDENCIES REGARDING THE TURNING TO ACCOUNT OF NON-FERROUS METALS FROM LOW GRADE RAW MATERIALS

GH. C. BUJGOI
Research, Engineering and Design Institute for Inorganic and Non-Ferrous Metals Industry,
Bucharest, Romania

The paper presents the main tendencies regarding the production and turning into account of non-ferrous metals from low grade raw materials. Due to their physical and chemical characteristics, non-ferrous metals, their alloys and compounds have been playing a decisive part in the progress and development of human society.

INTRODUCTION

The increase and diversification of the non-ferrous metals production during the last 50 years, stimulating the development of the other economic branches, led to the increase, approx 10 times, of the Pb, Cu, Zn, Ni production and over 25 times of the Al production. This intimate correlation between the non-ferrous metals production and the assembly of the industrial activities implies a direct dependence of the first in comparison with the fluctuations and tendencies of the world economy.

The diversified and extensive use of non-ferrous metals during the sixties, which was a period of economic development, led though to an important decrease of the ore deposits with high content of non-ferrous metals. Thus, during 1960–1980 the content of Cu, Zn, Pb, Ni, Mo, W in the ores decreased 4–20 times. In this way the evaluations made on basis of the lowering of the useful content indicated a possible exhaustion of the resources for basic non-ferrous metals (copper zinc, lead).

The decrease of the content of the useful elements in ores leads to the exponential increase of the energy consumed in mining and metallurgical departments, as well as to the increase of investments.

These negative factors were also aggravated by the energetic crisis at the beginning of the seventies. Besides, the rapid and impetuous development of the non-ferrous metallurgy created also a quite critical situation concerning environment pollution.

All these aspects created a complex situation for the production and applications of non-ferrous metals.

THE MAIN DATA REGARDING THE NON-FERROUS METALS PROBLEM

To solve this situation a first solution would be the elaboration of new non-metallic materials as substitutes, especially organic polymers, ceramic materials on basis of oxides and inorganic compounds and composite materials. Still, we have to show that in spite of the successes obtained within the fabrication of these new materials, these substituted only partially the non-ferrous metal consumption due to the fact that no massive substitutions are to be expected for the next 10—20 years.

A second way would be the rational use and the recycling of nonferrous metals. Thus, the replacement of anticorrosive allows on basis of Ni and Cr with allows of larger spreading on the earth, like for example : of important quantities of Ni, Cr, W, Ni, Ta and other expensive alloying metals. Ti has exceptional anticorrosive characteristics especially for organic media and for mineral acid media, under conditions in which its density is almost half of that of alloyed steels.

Aluminium, due to its special physico-chemical characteristics, offers a maximum efficiency in manufacturing of vehicles, railway carriages, aircrafts, in electric power transportation ; 50 kg of aluminium included in a vehicle as pieces and sub-assemblies results in an economy of 600 l gasoline/year vehicle.

The recovery of non-ferrous metals out of wastes is part of the process of rational use of these and of resources conservation. Even the rich countries pay a greater deal of attention to waste recovery. Thus, in the U.S.A., during the last 10 years, the quantity of Al recovered from different types of packages has increased 20 times, the recycling percentage of the other common metals, Cu, Pb, Zn, exceeding 50%.

Another way of rational use of non-ferrous metals is represented by the elaboration of high purity alloys and of alloys with superior characteristics.

The manufacturing of very pure metals and of certain metals with special characteristics, like Al, Li, Al alloys with elements of the rare earths group, Sm, Nd, It, Ti and Zr alloys, etc., led to the decrease of metal consumption by the increase of useful life and by the decrease of the quantities included in pieces and sub-assemblies.

On the same line we can mention the elaboration of thermal processing technology without the modification of chemical composition for the generation of the continuous metals casting directly from the elaboration process, development of some new rolling technologies introduction on large scale of energy concentrated sources; electromagnetic fields, lasers, plasma.

All these directions solve but partially the problem of the need for non-ferrous metals, while the non-ferrous metal deposits known cannot provide the world economy consumption.

Taking into consideration this goal, the main problem is the enlargement of the raw material basis by prospecting new deposits and by the introduction within productive circuit of ores with low content of metals and with complex chemical-mineralogic composition.

The earth deposits, including the poor ones and with complex composition, can still provide the necessities of mankind for dozens of years, in what concerns metals like : Al, Cu, Ni, Ti, Zr, rare earths, W, Cr, etc. If we also take into consideration the working of sea knots and of dissoluted elements like salt in sea water, the mankind requirement of alkaline metals, magnesium, manganese, nickel, gold, uranium are provided for even a longer period of time.

The experts state that in the area of the Pacific Ocean there are sea deposits of metallic knots containing approx. 2000 billion tons of useful ores, out of which 16 billion tons are nickel, 270 times more than the volume of the known earth deposits.

The essential problem under these conditions is the development of new technologies, non-conventional technologies, by means of which this large range of new raw materials could be worked-out under economical, non-polluted conditions. These non-conventional technologies must be the result of a more rapid penetration of the technical-scientific revolution in non-ferrous metal industry.

Which should be the characteristics of these technologies ?

— At first they must allow the turning to account of some complex ore with low content, must be flexible and adjust themselves to the composition variations.

— Must allow the whole and selective turning to account of all the elements in the raw material.

— Must not generate wear waters, polluting gases or wastes.

Of course, it is not always possible to reach entirely these goals but the tendency is to get nearer to them.

From the fundamental point of view, the non-conventional technologies aim at carrying out a succession of chemical processes within energy auditing as near to the energy decomposition theory of the respective chemical product as possible. These hydro- and pyro-metallurgical processes can be achieved by :

— the use of chemical compounds with special characteristics (solubilization, extraction agents, ion exchangers),

— use of chemical compounds with high reactivity (acids, halogens, salts),

— use of biotechnologies,

— use of energy concentrated sources (high pressures and temperatures, electrical fields, ultrasounds, plasma, radiations, laser, etc.).

These processes can be applied individually or in couples, for example solubilization under pressure or electrolysis in fluidized bed or chlorination and extraction with solvents.

The examples of these non-conventional technologies will be presented further for different poor and complex raw materials, including the achievements of the IAMN Institute in this respect.

Turning to account of basic non-ferrous metals : Cu, Zn, Pb

Beside useful metal content (lead, copper, zinc and accompanying metals) Romanian low grade native ores also show modification of chemical and mineralogic composition in respect of sulphide content decrease and increase of silicates and oxides content. At the same time, ores with only one basic useful component are found very seldom, their complex character being thus increased.

These last factors, together with the low useful content, make the technological processes become more complicated, the energy consumptions increase and the extraction output decrease.

In view of solving this situation the first direction was towards the improvement of the performances of mining processes, in deposit, of the flotation processes, as well as those of obtaining and elaboration of the metal.

The improvement of the performances of the mining equipment for drilling, transportation, breaking-grinding, led, on world level, to an important decrease of the costs on ton of ore sent to flotation.

Within the concentration department, important progresses were achieved by the development of new flotation methods. These are based on the use of new reagents of high selectivity and by the introduction of vertical flotation columns. These improve with 5—10% the content in concentrates, increasing thus the extraction output, too.

The use of flotation columns allows the increase of the output of M at over 55%.

A first solution for polymetallic ores was also the selective flotation in several stages. Using this method the Centromin company processes concentrate like : Pb—Zn, Cu—Zn and Cu—Pb obtaining in the end, besides the basic metals : Pb, Zn, Cu, also a number of 21 accompanying metals.

Within the metallurgical field efforts have been also made in view of updating old processes and of performing new technologies.

Thus, in copper metallurgy, the melting in suspension and the improvement of this technology by carrying out only one aggregate for roasting and costing operations, represents an important progress in comparison with the traditional methods. In this way, almost the entire, thermal power of sulphur is turned to account, the tendency being an autogenous operation and at the same time a turning to account of the useful accompanying metals (Au, Ag, Cd, Zn, Pb, So, Te) and a superior turning to account of sulphur, respectively the reduction of pollution with SO_2.

Within Zn and Pb metallurgy an important progress was the introduction of continuous melt in great capacity furnaces of the type I.S.P., method used at Copşa Mică too, which brings an economy of 1—2.5 t.c.f./t, in comparison with the classical processes and which displays a high productivity and allows the turning to account of accompanying metals Au, Ag, Cu, Sb, Si, Cd, In.

By these intensive technologies the complex poor ores cannot be processed and any improvement brought would not provide the compensation of the ever greater energy consumption necessary for the vehiculation of huge quantities of mining concentrates.

Beside this, the pyrometallurgical processes, like melting in suspension and in furnace type I.S.P., are important sources of pollution with SO_2.

Under these circumstances, in view of turning to account in acceptable rentability conditions the poor raw materials in useful elements, the unique technological possibility is the introduction of hydrometallurgical processes on large scale. The essential advantages of these processes are :

— allow the turning to account of certain poor raw materials and can be used directly in the deposit or in the dump,

— can be used in the same way to the oxidic and sulphurous ores allowing the turning to account of all the components,

— have the flexibility necessary for the adjustment of some composition variations of useful components as well as some mineralogic complex structures,

— eliminate the advanced grinding operation necessary to flotation operations which, for 1 t of Cu requires an energy consumption of approx. 10,000 kwh ;

— allow the regeneration and recirculation of a great part of reagents.

These new hydrometallurgical processes are :

a) leaching in deposit with turning to account of pressure and eventually of geothermal energy, leaching in dump, leaching under pressure, leaching with very active chemical agents like $FeCl_3$, $CuCl_2$, mineral acids, bacteriological leaching,

b) extraction by means of solvents, ionic exchange, electrolysis in fluidized bed.

Turning to account of basic non-ferrous metals

Cu turning to account out of poor ores

For Cu extraction and turning to account out of poor ores the most modern hydrometallurgical processes were applied on large scale.

By the research works presented, new classes of most selective extraction agents were presented, LIX (liquid ion exchanger) and Kellex, of a new range of equipment which were further enlarged to the fabrication of other metals.

For the first time, for copper, the leachings in deposit at big depths, using conventional and nuclear explosives, were applied in view of creating excavations in U.S.A., Soviet Union, Chile, and so on.

Bacteriological leaching processes were also used and improved. These processes are based on the use of autotrophic bacteria like thiobacillus ferrooxidantus and thiobacillus thioxidantus.

These bacteria oxidized the sulphides at pH = 1.5—3.5 at temperatures of 25—40°C obtaining diluted solutions which are then treated by extraction with solvent followed by electrolysis.

The process is interesting owing to reduced reactives consumption and practically complete investment elimination.

Cu, Zn, Pb turning to account of complex ores

Complex and poor ores are practically pyrite ores which contain also some minerals of Pb, Cu, Zn finely concrescent. This character, even in the case of an advanced grinding and of a selective flotation in several stages leads to obtaining of low quality and very high costs (low outputs, electric energy consumptions and big flotation reagents).

On world level this type of ores was not introduced in the economic circuit because up to now there has not been yet finished off an economic technology comparable with the processing of the other types of ores. As these ores have a large spreading and taking into consideration the working out of rich deposits, several countries in the world are researching the processing of ore types (complex and poor).

In Czechoslovakia, which possesses exclusively complex ores, there exists since 1982 a pilot hydrometallurgical plant. The researches were performed in collaboration with Lurgi and Outokumpu companies.

The technology includes the following phases :

- oxidant roasting
- solubilization with H_2SO_4 in three stages ;
- Fe precipitation as hydronium jaruzite and thermal jaruzite ;
- concentration of solution and crystallization of $CuSO_4$ and $ZnSO_4$;
- Cu extraction with solvents followed by electrolysis ;
- chemical purification of the $ZnSO_4$ solution and electrolysis.

An industrial plant with a processing capacity of 60 thousand t/year collective concentrates is going to be carried out.

In general as solubilization processes of complex ores the following can be used : solubilization with chlorides, mainly $FeCl_3$, solubilization under pressure in presence of H_2SO_4 and an oxidant : sodium bichromate, nitric acid, most often oxygen.

The leaching with $FeCl_3$ is used in several variants (Fig. 1).

The St. Joe Minerals Corps company performs a selective solubilization of Pb by potentiometric control of the process. From the fundamental point of view operates the different kinetics of galena (PbS), blende (ZnS), and chalcopyrite, $PbCl_2$ is crystallized and the next phase is selective leaching of Zn and then of Cu. In the case of Zn they use the extraction with di(-2 ethylhexil)phosphoric acid. In the Cymet process Cu is removed from the solution by the reduction of H_2 under pressure, but a scheme of the type extraction with solvents-electrolysis can be also used.

The CANMET (Canada) uses a leaching process with $FeCl_3$, which also, from the fundamental point of view, was known a long time ago, could not be applied but in the moment of developing some materials resistant in chlorides, in essence titanium and its alloys.

The leaching process with sulphate at 150° and 7.8 atm is used by the Sherritt Gordon Mines (Canada), based on the Cu separation from Fe and Zn by extraction with a liquid cethyonite Acorga P5000, fabricated by the Imperial Chemical Industries company. Zn is separated further by extraction with di-(2 ethylhexyl)phosphoric acid. Both Cu and Zn are re-extracted with H_2SO_4 and settled down by electrolysis.

Worn out electrolyte is recirculated at re-extraction with H_2SO_4 and settled down by electrolysis. The worn out electrolyte is recirculated at re-extraction.

The problem of complex concentrates presents a special interest for the conditions characteristic for our country.

In Romania the working out of such complex ores was started 25 years ago at Leşul Ursului and Baia Borşa. The working out of these ores and the processing in even more economical conditions will

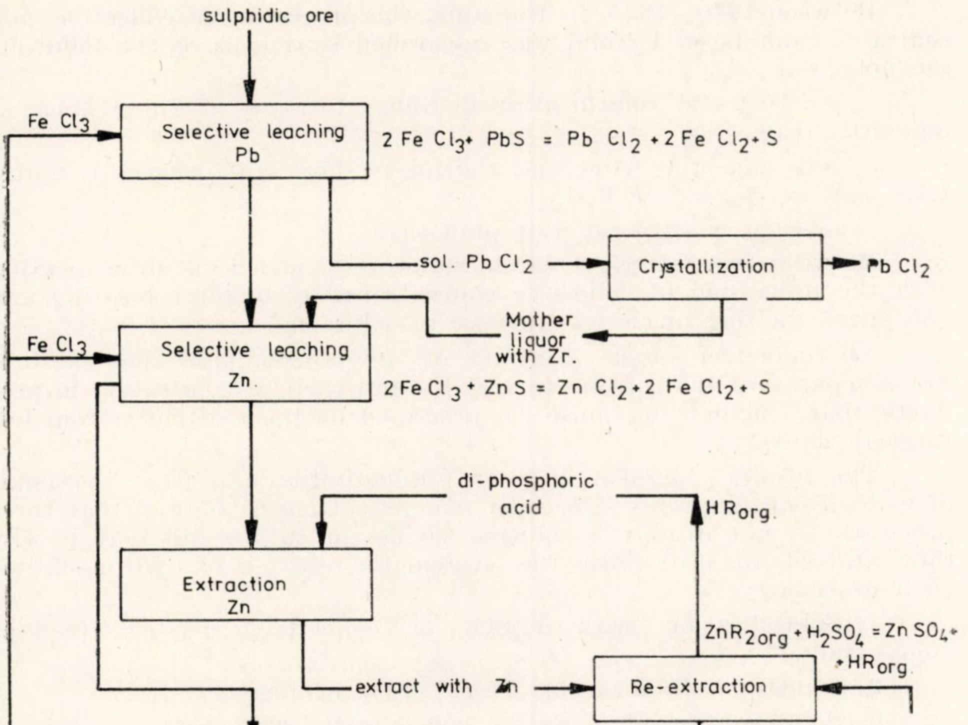
sulphidic ore
$FeCl_3$
Selective leaching Pb
$2FeCl_3 + PbS = PbCl_2 + 2FeCl_2 + S$
sol. $PbCl_2$
Crystallization
$PbCl_2$
Mother liquor with Zr.
$FeCl_3$
Selective leaching Zn
$2FeCl_3 + ZnS = ZnCl_2 + 2FeCl_2 + S$
di-phosphoric acid
$HR_{org.}$
Extraction Zn
$ZnR_{2org} + H_2SO_4 = ZnSO_4 + + HR_{org}$
extract with Zn
Re-extraction
worn electrolyte
$FeCl_3$
Cu leaching
H_2
$ZnSO_4$
waste with sulphur
Under pressure reduction
Electrolysis
$ZnSO_4 + H_2O = Zn + H_2SO_4 + + 1/2\ O_2$
Copper powder
Cathode Zn
waste
Extraction S
Sulphur
Regeneration $FeCl_3$

Fig. 1. — $FeCl_3$ selective leaching methods followed by solvent extraction under pressure reduction.

be dealt with even more seriously as the metal content, Pb, Zn, Cu, which at present is approx 3% will decrease in future at 1.5%.

Between 1970–1975, in Romania, the processing of collective concentrates from Leşul Ursului was researched by means of the following technologies :

— roasting and volatilization in rotary furnaces at Copşa Mică, at industrial scale,

— roasting, briquetting and melting in short pot furnaces at industrial scale at Ocker – F.R.G.

— melting in suspension at pilot scale.

Between 1982–1987, research works were carried out in connection with the processing of collective concentrates by oxidant roasting and volatilized melting in electric furnace at pilot scale.

All these technologies continue ore preparation, but they perform but a separation of Cu from Zn and Pb and their concentration in products that, further on, must be processed on the existent pyrometallurgical plants.

The results obtained, both as productivities and from the point of view of consumptions (especially energetical ones), showed that these processes do not display a solution viable for future and that is why they started to deal with the systematic research of hydrometallurgical processes :

1) Solubilization with H_2SO_4 of collective, roasted, oxidant concentrate.

2) Oxidant solubilization with H_2SO_4 in digester.

3) Solubilization of collective concentrates with $FeCl_3$.

The technological flows are presented in Figs 2–4.

The researched processes were elaborated following :

a) the solubilization agent should ascertain outputs of minimum 90%, should be regenerated within the process as much as possible, should be cheap, should be produced in Romania, should be as stable chemically as possible and non-polluted,

b) should achieve the separation of metals in the solutions of solubilization, with the turning to account of all the components, without wastes on dump and economically,

c) should allow the carrying out of equipment and apparatus with high resistance at corrosion under conditions of high temperatures and pressures.

These hydrometallurgical non-conventional technologies can be applied successfully and in view of turning to account of disperse elements out of volatile dusts from the Zn, Pb and Cu metallurgy. Thus, we can mention the process elaborated by IAMN of indium recovery out of the wastes from the electrolytic manufacturing of Pb of the more complex process of Cd and Zn out of volatile dusts and washing waters at the I.S.P. plant at Copşa Mică (Fig. 5).

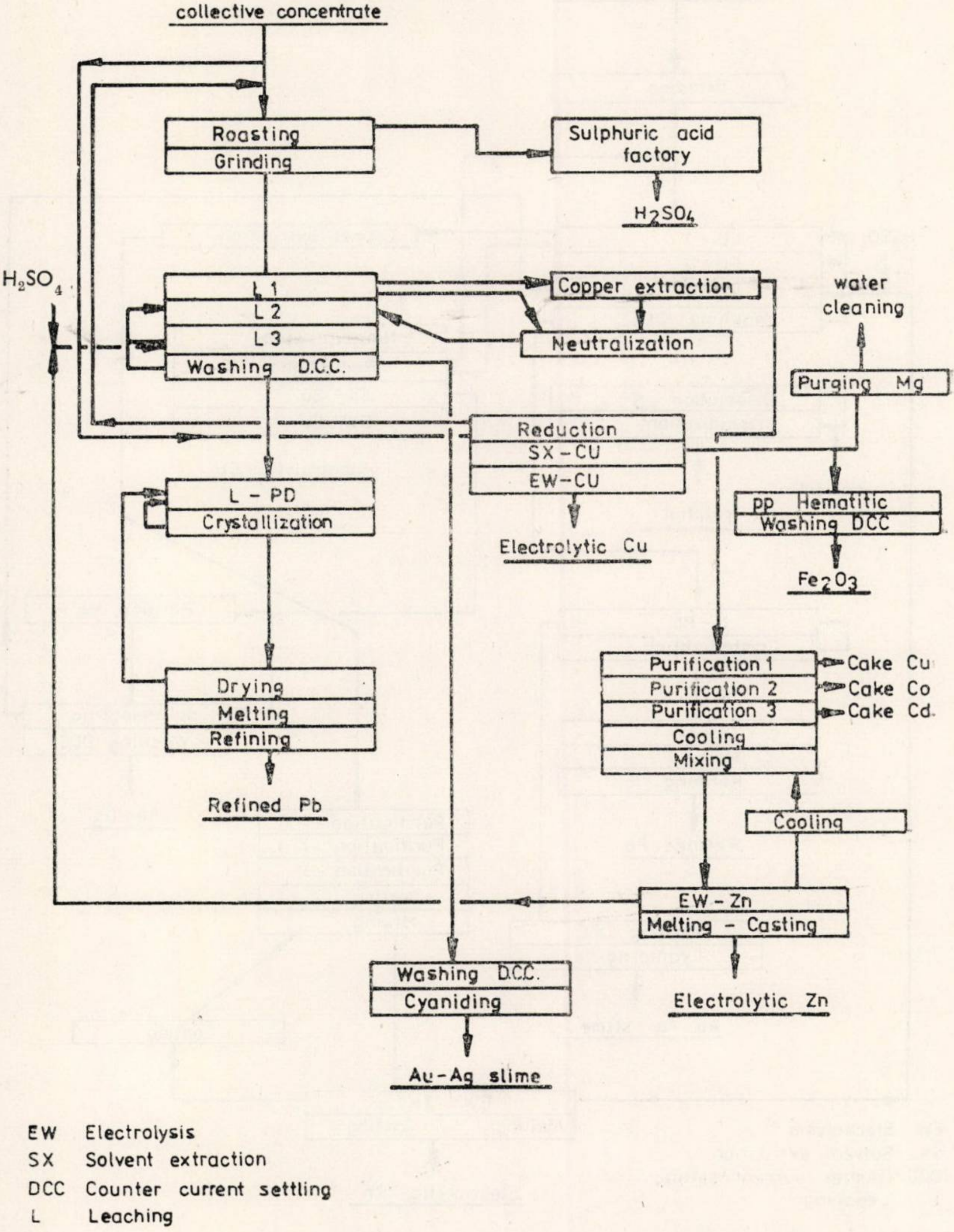
collective concentrate
Roasting
Grinding
Sulphuric acid factory
H_2SO_4
H_2SO_4
L 1
L 2
L 3
Washing D.C.C.
Copper extraction
Neutralization
water cleaning
Purging Mg
Reduction
SX-CU
EW-CU
Electrolytic Cu
pp Hematitic
Washing DCC
Fe_2O_3
L - PD
Crystallization
Drying
Melting
Refining
Refined Pb
Purification 1
Purification 2
Purification 3
Cooling
Mixing
Cake Cu
Cake Co
Cake Cd
Cooling
EW - Zn
Melting - Casting
Electrolytic Zn
Washing D.C.C.
Cyaniding
Au-Ag slime
EW Electrolysis
SX Solvent extraction
DCC Counter current settling
L Leaching

Fig. 2. — Collective concentrate processing. Flowsheet of roasting and solubilization with sulphuric acid.

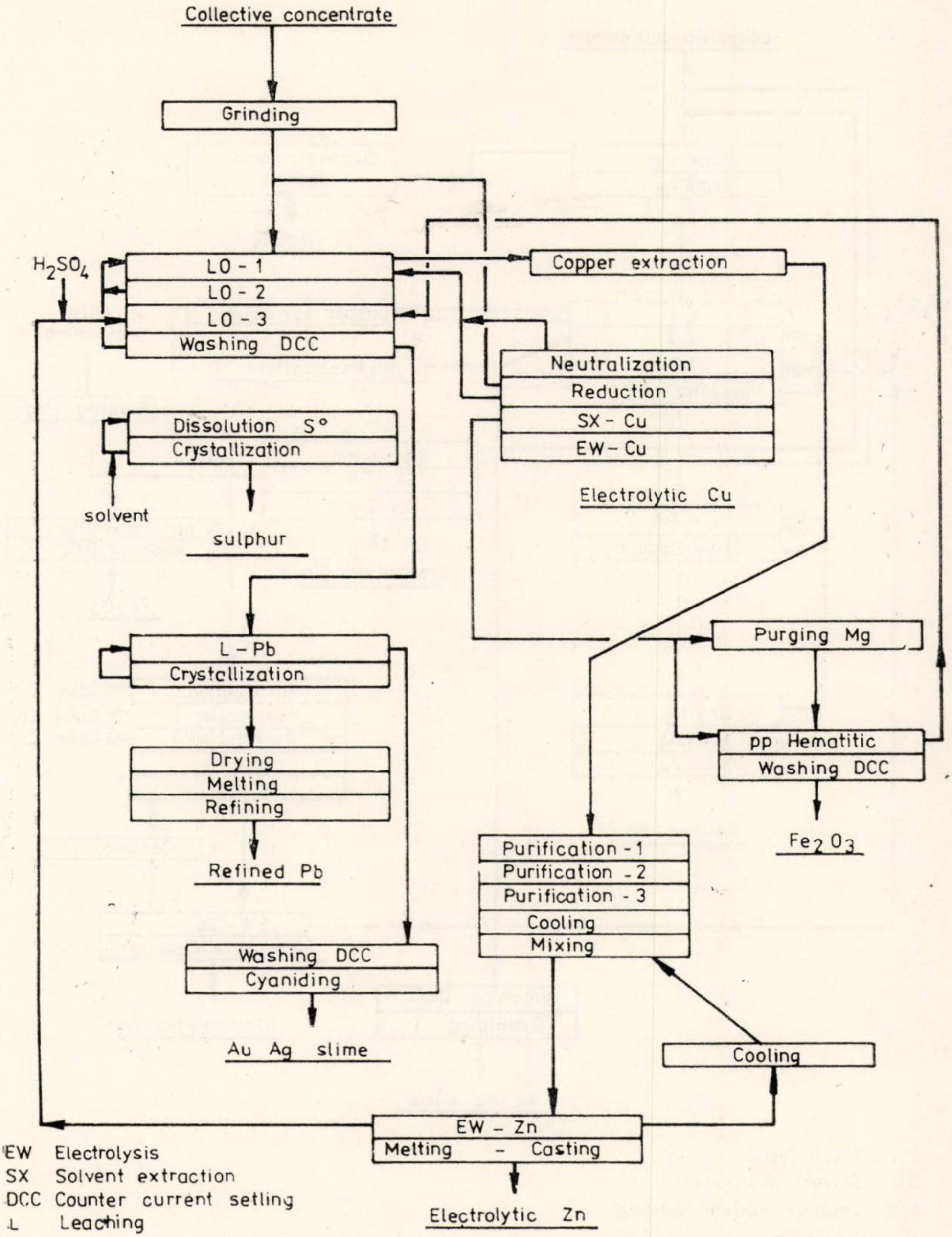
Collective concentrate
Grinding
H_2SO_4
LO - 1
LO - 2
LO - 3
Washing DCC
Copper extraction
Neutralization
Reduction
SX - Cu
EW - Cu
Electrolytic Cu
Dissolution S°
Crystallization
solvent
sulphur
L - Pb
Crystallization
Drying
Melting
Refining
Refined Pb
Washing DCC
Cyaniding
Au Ag slime
Purging Mg
pp Hematitic
Washing DCC
Fe_2O_3
Purification - 1
Purification - 2
Purification - 3
Cooling
Mixing
Cooling
EW - Zn
Melting - Casting
Electrolytic Zn
EW Electrolysis
SX Solvent extraction
DCC Counter current setling
L Leaching

Fig. 3. — Collective concentrate processing. Flowsheet of oxidant solubilization with sulphuric acid in autoclave.

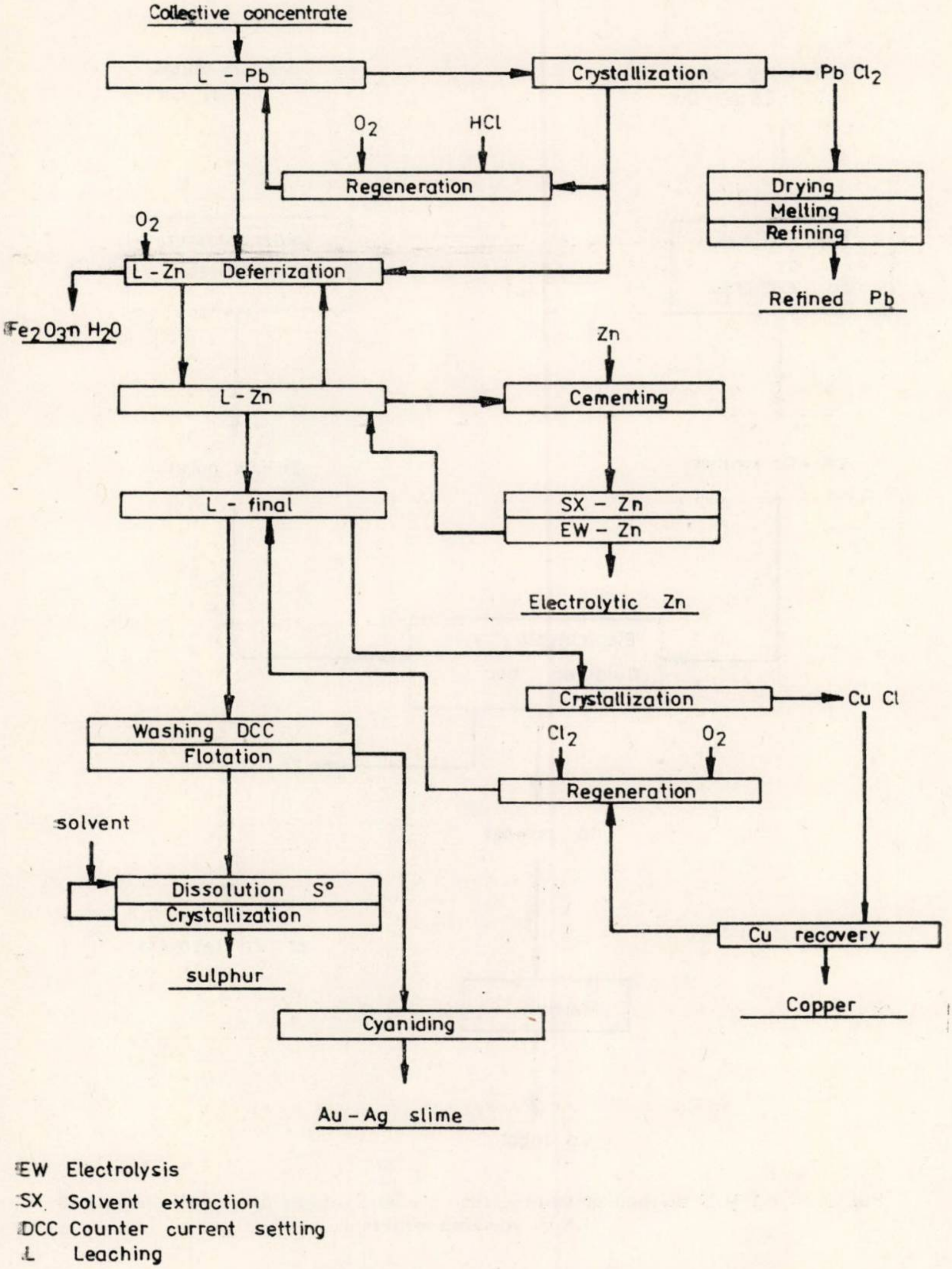
Collective concentrate
L - Pb
Crystallization
Pb Cl2
O2
HCl
Regeneration
Drying
Melting
Refining
O2
L - Zn
Deferrization
Refined Pb
Fe2O3n H2O
Zn
L - Zn
Cementing
L - final
SX - Zn
EW - Zn
Electrolytic Zn
Crystallization
Cu Cl
Washing DCC
Flotation
Cl2
O2
Regeneration
solvent
Dissolution S°
Crystallization
Cu recovery
sulphur
Copper
Cyaniding
Au - Ag slime
EW Electrolysis
SX Solvent extraction
DCC Counter current settling
L Leaching

Fig. 4. – Collective concentrate processing. Chloride solubilization flowsheet.

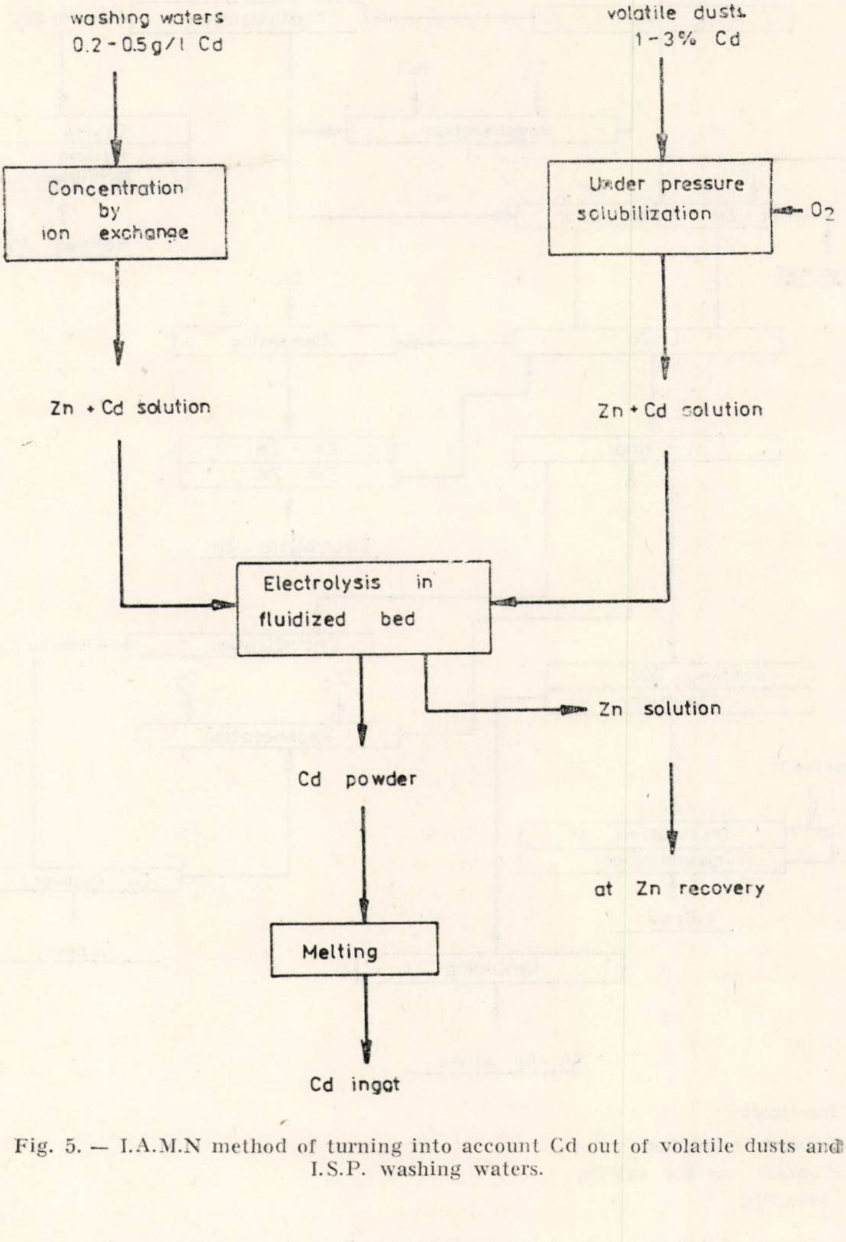
washing waters
0.2 - 0.5 g/l Cd
volatile dusts
1 - 3% Cd
Concentration by ion exchange
Under pressure solubilization
O2
Zn + Cd solution
Zn + Cd solution
Electrolysis in fluidized bed
Zn solution
Cd powder
at Zn recovery
Melting
Cd ingot

Fig. 5. — I.A.M.N method of turning into account Cd out of volatile dusts and I.S.P. washing waters.

CONCLUSIONS

The main non-conventional processes presented extraction with solvents, ionic exchange, electrolysis in fluidized bed, volatilized chloride, decomposition under pressure, represent but a part of the existent or long-term technologies for non-ferrous metallurgy. Even these technologies are continuously subject to improvements and adjustments. All the time there appear new classes of extraction agents, ion exchangers with large capacities and high selectivity. The work techniques are directed towards the more intensive equipment with smaller volumes. Thus in the field of extraction with solvents appeared new apparatus with selective membrane, impregnated with extractants. Thus the quantity of circulated materials decreases considerably while the solvent quantity decreases hundreds of times. More and more are used the organometallic volatile compounds in processes of separation and purification as well as of obtaining some metallic compounds with special characteristics.

The biotechnologies, by the creation of new types of micro-organisms through genetic engineering will probably play a more and more important role in direct leaching in deposit of very poor ores of Cu, Zn, Mo, U, etc., even in Romania, in geological levels with geo-thermal energy disponibilities.

Also, the expectations are of increasing importance for the leaching processes in deposit at high depths, processes which can turn to account in a superior way the geothermal pressure and energy.

The technologies using the concentrated sources of energy, mainly plasma, represent an important expectation, especially for mineral decomposition with complex chemical composition, intensive chlorination and decomposition reactions of chlorides, obtaining of metals and mainly of those high-melting ones.

The chemical processes stimulated by the use of lasers will become an important way of rapid and efficient separation in few stages of elements with very near chemical characteristics and even of the isotopes of the same element.

In future, the new non-conventional raw materials will generate technologies specifical to non-conventional raw materials. These technologies, based on a more and more rigorous application of the physics of the solid bodies of physical chemistry and of electrochemistry, will be more and more influenced by the last achievements of different industrial branches.

The complexity of these technologies, the special conditions the end-products have to fulfill, will require a more and more rigorous control of the processes, this fact determining a more and more advanced extension of cybernetics and information.

Generally in Romania important progresses have been carried out in view of the introduction of non-conventional technologies, in view of the elaboration of efficient technological processes of turning to account the poor and complex rare materials, but new approaches based on inter-discipline cooperation are necessary.

At present, this problem is firstly posed for the turning to account of complex ores : Pb, Zn, Cu, of accompanying and rare metals, of aluminium of non-bauxitic rare materials.

These non-conventional methods have a limited viability in time, like any other technical achievement, thus, even from the introduction of any new technology we have to think about other more improved variants and what forecasts will the technical-scientific revolution bring about in the near future.

Revue Roumaine de Chimie, **34**, *1*, 79–85 (1989)

SURFACE MOBILITY OF SURFACTANT SOLUTIONS. XIII *

INFLUENCE OF THE MAGNETIC FIELD

E. CHIFU [a], *, I. STAN [b], M. SĂLĂJAN [a] and EUGENIA GAVRILĂ [a]

[a] Department of Physical Chemistry, str. Arany J., N° 11, 3400 Cluj-Napoca, Romania

[b] Department of Differential Equations and Mechanics, University of Cluj-Napoca, Romania

Received October 1, 1988

Calculated data are reported about the influence of magnetic field upon the flow induced by interfacial tension gradients in thin liquid layers situated on an inclined solid plane. The velocity profiles and the rates of flow have been evaluated on the basis of the semi-infinite pellicle model, for magnetic field intensities characterized by Hartmann numbers found between 0 and 15. The magnetic field exhibits a damping effect on the Marangoni flow.

INTRODUCTION

The effect of surface tension gradients upon the liquid/gas interface has been studied in earlier works, under the circumstances created either by the presence of surfactants [1,2] or by temperature differences.[3] The flow processes, induced by interfacial tension gradients into thin liquid layers, have been interpreted on the basis of the semi-infinite pellicle model.[4] The flow rates have also been determined for this model as well as for canals with triangular section.[5]

In the present work the influence of the magnetic field upon the surface mobility is analysed. The liquid pellicle, of thickness δ, is supported by an inclined solid plane (Fig. 1).

The Ox axis is oriented with the maximum slope of the plane, Oy is perpendicular to this plane and Oz links the points situated at the same level. The surface tension σ at the liquid/gas interface varies along the Ox axis, having the values σ_0 (for $x = 0$) and σ(for $x = L$), chosen so that $\sigma < \sigma_0$.

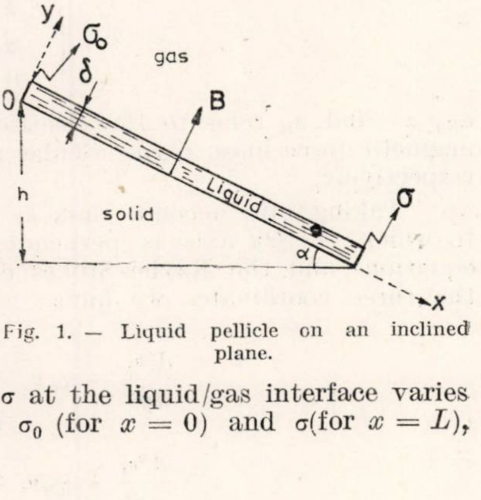

Fig. 1. — Liquid pellicle on an inclined plane.

---

* Part XII; see reference [5]

THE EQUATIONS OF THE MODEL

Two types of forces act simultaneously upon a similar pellicle, in the absence of the magnetic field : surface and gravity forces. Supposing that the liquid is viscous and uncompressible and the flow in the thin layer is laminar and steady, the semi-infinite pellicle model allows to calculate the Marangoni flow velocity — in competition with the gravity flow — on the inclined plane. The expression [4,Eq (16)] :

$$v_x = \frac{1}{\mu L}\left[\Gamma g h - (\sigma_0 - \sigma) + \rho g h \delta\right] y - \frac{\rho\, g h}{2\,\mu L} y^2 \tag{1}$$

has been obtained, in which L is the length of the pellicle, μ the liquid viscosity, ρ the liquid bulk density, h the level difference, Γ the surface density, g the gravity acceleration and y the position coordinate oriented with the Oy axis.

If the liquid in the pellicle is electrically conductive, a magnetic field B, perpendicular to the liquid surface ($Oy \parallel B$ — Fig. 1), will perturb its flow. The effect derives from the fact that the bulk force will have — besides the component due to the gravity field — also the component of the magnetic field,[6,7] as can be seen from the equation :

$$\vec{\mathrm{F}} = \rho \vec{\mathrm{g}} + \frac{1}{c} \vec{\mathrm{j}} \times \vec{\mathrm{B}} \tag{2}$$

where c is the light velocity. The current density vector $\vec{\mathrm{j}}$ is expressed by the Ohm law :

$$\vec{\mathrm{j}} = \hat{\alpha} \cdot \vec{\mathrm{E}} \tag{3}$$

in which $\vec{\mathrm{E}}$ represents the intensity of the induced electric field and $\hat{\alpha}$ is the electrical conductivity tensor :

$$\hat{\alpha} = \begin{pmatrix} \alpha_\perp & \alpha_\mathrm{H} & 0 \\ -\alpha_\mathrm{H} & \alpha_\perp & 0 \\ 0 & 0 & \alpha_\parallel \end{pmatrix} \tag{4}$$

$\alpha_\parallel$, $\alpha_\perp$ and α_H refer to the electrical conductivities : oriented with the magnetic force lines, perpendicular to them and due to the Hall current, respectively.

Taking into account that xz is considered as the inclined plane, to which the Oy axis is perpendicular (Fig. 1), from the continuity equations and the Navier-Stokes equation written in projection [4] onto the three coordinates we have :

$$\frac{\mathrm{d}^2 v_x}{\mathrm{d}y^2} - \gamma_\perp v_x - \gamma_\mathrm{H} v_z = -\,\Omega \tag{5}$$

$$\frac{\mathrm{d}^2 v_z}{\mathrm{d}y^2} + \gamma_\mathrm{H} v_x - \gamma_\perp v = 0 \tag{6}$$

in which

$$\hat{\gamma} = \frac{B^2}{\mu c^2}\hat{\alpha}, \qquad \Omega = \frac{g\rho h}{\mu L}. \tag{7}$$

In conditions in which the Hall effect can be neglected ($v_z = 0$), the undiagonal components of the tensor (4) vanish and the diagonal ones equal each other (so that $\gamma_H = 0$, $\gamma_\perp = \gamma_\parallel$). In this case, the solution of the system (5), (6), with the boundary conditions:

$$\Gamma g \frac{h}{L} - \mu\left(\frac{\partial v_x}{\partial y}\right)_{y=\delta} - \frac{\sigma_0 - \sigma}{L} = 0 \tag{8}$$

and

$$\frac{\partial v_z}{\partial y} = 0 \tag{9}$$

is reduced to

$$v_x = \frac{\delta}{\mu L}\left\{\left[\left[\Gamma g h - (\sigma_0 - \sigma)\frac{\operatorname{sh} H \frac{y}{\delta}}{H \operatorname{ch} H}\right] + \frac{\delta\rho g h}{H^2}\left[1 - \frac{\operatorname{ch} H\left(1 - \frac{y}{\delta}\right)}{\operatorname{ch} H}\right]\right]\right\} \tag{10}$$

in which the Hartmann number, expressing the ratio of the magnetic forces to the viscosity ones, is given by the relationship:

$$H = \frac{B\delta}{c}\sqrt{\frac{\alpha_\perp}{\mu}}. \tag{11}$$

The analysis of Eq. (10) makes evident the existence of an "antiparallel" flow what happens also in the absence of the magnetic field. As a function of the value for the h level difference one may have the following cases:

a) $h > \frac{(\sigma_0 - \sigma)H}{g(\rho\delta + \Gamma)}\operatorname{ctgh}\frac{H}{2}$, the liquid mass exhibits a downward flow on the inclined plane;

b) $h < \frac{(\sigma_0 - \sigma)H}{g(\rho\delta + \Gamma)}\operatorname{sh}^{-1} H$, the liquid moves upwards;

c) in the interval
$\frac{(\sigma_0 - \sigma)H}{g(\rho\delta + \Gamma)}\operatorname{ctgh}\frac{H}{2} > h > \frac{(\sigma_0 - \sigma)H}{g(\rho\delta + \Gamma)}\operatorname{sh}^{-1} H$ the two "antiparallel" flows coexist.

Quantitatively, the influence of the magnetic field upon the velocity of the liquid layers and of the rates of flow was evaluated by the numerical calculus methods.

NUMERICAL RESULTS AND DISCUSSION

By making use of a computer programme on the basis of Eqs. (1) and (10), the flow velocities in the thin liquid layer as a function of the relative thickness of the pellicle $\bar{y}$ have been calculated, both in the absence and in the presence of the magnetic field. Also, there have been evaluated, for a section of the pellicle having the area equal to $(1 \times \delta)$ cm^2, the rates of the upward flow — due especially to surface forces —, those of the downward flow — due to the gravity — and the global rates of flow. For simplicity, we shall denote these rates of flow as Q_-, Q_+, and Q respectively.

The examined parameters have the following value:
$\Gamma = 10^{-7}$ g/cm^2, $\delta = 2.39 \times 10^{-2}$ cm, $\Delta\sigma = 1 \div 10$ mN/m, $g = 981$ cm.s^{-1} $\mu = 10^{-2}$P, $L = 10$ cm, $h = 0 \div 0.5$ cm, $\bar{y} = y/\delta$ (0, 1].

The influence of the magnetic field intensity has been studied by adopting for the Hartmann numbers (H) the range between 0 and 15, where they can be considered as moderate [8] and corresponding to electrolyte solutions.

In Figs. 2 and 3 we present the variation of the flow velocities inside the pellicle. A first conclusion resulting from the analysis of the diagrams is that the magnetic field effect on the flow velocity is one of damping. At zero level difference (Fig. 2) the only possible type of flow is the Marangoni flow. In the absence of the magnetic field ($H = 0$)

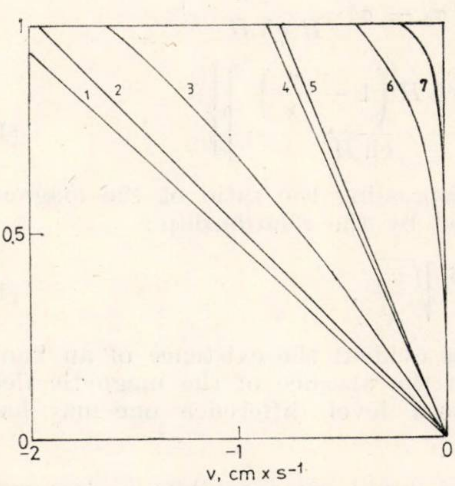

Fig. 2. — The profile for flow velocities in the thin liquid pellicle, at non-zero level difference. Curve (1) $H = 0$, $\Delta\sigma = 8.82$ mN/m; (2) $H = 0.5$, $\Delta\sigma = 8.82$ mN/m; (3) $H = 1$, $\Delta\sigma = 8.82$ mN/m; (4) $H = 0$, $\Delta\sigma = 3.53$ mN/m; (5) $H = 0.5$, $\Delta\sigma = 3.53$ mN/m; (6) $H = 5$, $\Delta\sigma = 8.82$ mN/m; (7) $H = 10$, $\Delta\sigma = 8.82$ mN/m.

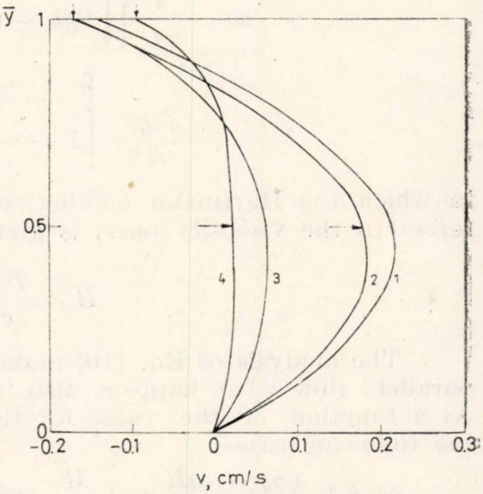

Fig. 3. — The profile for the flow velocities as function of the relative depth of the thin liquid pellicle, at level difference $h = 0.4$ cm and surface tension gradient $\Delta\sigma = 5.29$ mN/m. Curve (1) $H = 0$; (2) $H = 1$; (3) $H = 5$; (4) $H = 10$.

the dependence of the velocity on the relative thickness of the pellicle is linear. With increasing the intensity of the magnetic field this dependence is no more valid (see curves 1—3, 6, 7). The decrease of the surface tension gradient leads to the decrease of the flow velocity (see, for comparison, curves 1, 2 and 4, 5) and the dependence of the velocity on the gradient is a linear one (Eqs. (1) and (10)).

From the analysis of Figs. 2 and 3 it results that there is a preponderant influence of the magnetic field on the bulk forces acting upon the liquid pellicle and that the damping forces manifest themselves more pregnantly in the profoundness of the pellicle. In the strata immediately subjacent to the liquid/gas interface this effect is weaker. So, in Fig. 3 it can be seen that, when the Hartmann number is increased by an order of magnitude, the flow velocity inside the pellicle ($\bar{y} = 0.5$) is decreased by approximately one order of magnitude while for the liquid/gas interface ($\bar{y} = 1$) the velocity decrease is of only 30 percent for the same increase of H (see the arrows in Fig. 3).

Using the numerical integration method the values of the rates of flow were obtained, for the aforementioned conditions.

In Fig. 4 is given the variation of the upward (curves 1 and 1′) and of the downward (curves 2 and 2′) rates of flow, both in the absence ($H = 0$) and in the presence ($H = 1$) of the magnetic field, as functions of the level difference h. The interfacial tension gradient was maintained constant. The diagrams make evident the existence of the three flow domains: upward, ‘antiparallel" and downward. As the two types of flow rates are of opposite signs, in the diagrams they were given positive and negative values. As a matter of fact, the same was done in denoting the velocities (Fig. 3). The existence limits of these ranges (the h intervals) are different and they are better evidenced in Table 1. In the presence of the magnetic field, for the given case, the level difference h in which the antiparallel flow occurs is more extended than in its absence. The extension of the domain is explained by the damping effect of the magnetic

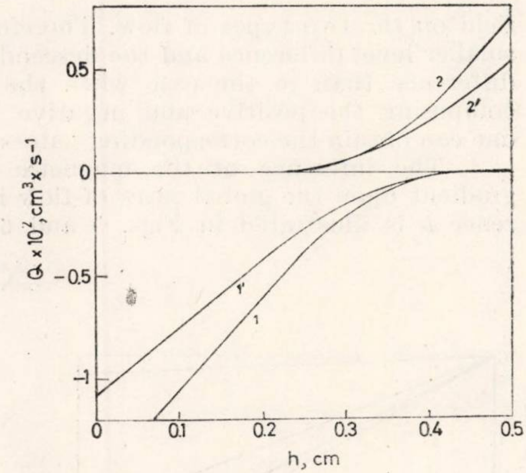

Fig. 4. — Dependence of the rates of flow, Q, on the level difference h, for a surface tension gradient $\Delta\sigma = 5.29$ mN/m. Curve (1) Q^0_-, $H=0$; (2) Q^0_+, $H = 0$; (1′) Q_-, $H = 1$; (2′) Q_+, $H = 1$.

Table 1

Evolution of negative and positive flow rates in the liquid pellicle as a function of the level difference, h, of the inclined plane in the absence ($Q^0_\pm$) and in the presence ($Q_\pm$) of the magnetic field, at the surface tension difference $\Delta\sigma = 5.29$ mN/m

h cm	$H = 0$			$H = 1$		
	Q^0_- cm$^3 \times$ s^{-1}	Q^0_+ cm$^3 \times$ s^{-1}	Type of flow	Q_- cm$^3 \times$ s^{-1}	Q_+ cm$^3 \times$ s^{-1}	Type of flow
0.190	-6.63×10^{-3}	—	(−)	-4.57×10^{-3}	—	(−)
0.195	-6.40×10^{-3}	—	(−)	-4.41×10^{-3}	2.21×10^{-8}	(− +)
0.200	-6.18×10^{-3}	—	(−)	-4.25×10^{-3}	4.93×10^{-7}	(− +)
0.220	-5.29×10^{-3}	—	(−)	-3.63×10^{-3}	1.79×10^{-5}	(− +)
0.230	-4.84×10^{-3}	1.30×10^{-7}	(− +)	-3.33×10^{-3}	4.13×10^{-5}	(− +)
0.445	-2.69×10^{-6}	4.76×10^{-3}	(− +)	-7.22×10^{-5}	3.65×10^{-3}	(−, +)
0.450	—	4.98×10^{-3}	(+)	-5.60×10^{-7}	3.79×10^{-3}	(− +)
0.485	—	6.54×10^{-3}	(+)	-3.25×10^{-8}	4.85×10^{-3}	(− +)
0.490	—	6.77×10^{-3}	(+)	—	5.01×10^{-3}	(+)
0.500	—	7.21×10^{-3}	(+)	—	5.33×10^{-3}	(+)

field on the two types of flow. Therefore, the ascendant flow arises at a smaller level difference and the descendant one vanishes at a greater level difference than in the case when the magnetic field does not act. By composing the positive and negative branches of the curves in Fig. 4 one can obtain the corresponding values of the global rates of flow.

The influence of the magnetic field and of the surface tension gradient upon the global rates of flow in the case of constant level difference h is illustrated in Figs. 5 and 6.

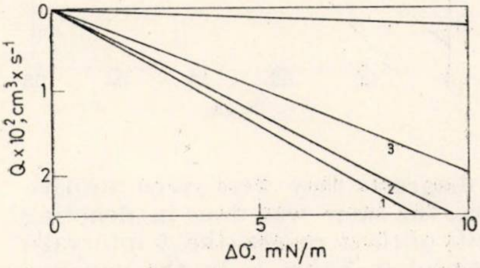

Fig. 5. — Dependence of the rates of flow, Q, on the surface tension gradient, $\Delta\sigma$, at zero level difference. Curve (1) $H = 0$; (2) $H = 0.5$; (3) $H = 1$; (4) $H = 5$

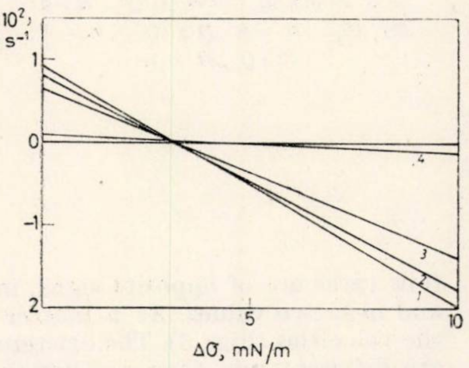

Fig. 6. — Dependence of the rates of flow, Q, on the surface tension gradient $\Delta\sigma$, for the level difference $h = 0.2$ cm. Curve (1) $H = 0$; (2) $H = 0.5$; (3) $H = 1$; (4) $H = 5$

In Fig. 5 is presented the situation corresponding to zero level difference. In this case the flow is only of the Marangoni type and the rates of flow will increase in the absolute value as the gradient $\Delta\sigma$ increases. In the case when the level differences are different from zero — Fig. 6 — , at low gradients the global rates of flow present positive values (the descendant flow has a greater weight) which decrease with increasing the value of the tension gradient. At large values of the surface tension gradient the rates of flow become negative (the ascendant flow predominates) and their absolute values increase. The dependence of the global rates of flow on the tension gradient is linear. The damping effect produced by increasing the magnetic field intensity upon the magnitude of the rates of flow is evidenced. An increase by circa one order of magnitude of the Hartmann number may lead to the decrease by about two orders of magnitude for the global rate of flow. Fig. 6, referring to a certain level difference, shows that there is always a value of the interfacial tension gradient ($\Delta\sigma$) at which the rate of flow is not influenced by the presence of the magnetic field (see intersection of the straight lines). It is to mention that the situation is quite different from the case of the zero level difference (Marangoni flow on a horizontal — Fig. 5) when the magnetic field influence is present on the whole domain of surface tension gradients.

Due to the fact that, in zero gravity conditions, the natural convection disappears, it is the Marangoni convection that presents interest. This one intervenes in processes such as : mass transfer through interfaces or interfacial turbulence involved in extraction, tertiary recovery of oil, reactions at the liquid/liquid interface etc. On the other hand, in modelling the phenomena of motion and deformation at the biomembrane level, one also resorts to the Marangoni effect. Taking into account this consideration, the results of such studies concerning the influence of magnetic fields upon the surface flow have got an increasing interest.

REFERENCES

[1] E. Chifu and I. Albu, *Stud. Univ. Babeş-Bolyai Chem.*, **13** (1), 99 (1968).

[2] E. Chifu, C. I. Gheorghiu and I. Stan, *Rev. Roumaine Chim.*, **29**, 31 (1984).

[3] E. Chifu, I. Albu, C. I. Gheorghiu, E. Gavrilă, M. Sălăjan and M. Tomoaia-Cotişel, *Rev. Roumaine Chim.*, **31** (1), 105 (1986).

[4] E. Chifu and I. Stan, *Rev. Roumaine Chim.*, **27** (6), 703 (1982).

[5] E. Chifu and C. I. Gheorghiu, *Rev. Roumaine Chim.*, **32** (9—10), 945 (1987).

[6] R. V. Deutsch, "Teoria magnetohidrodinamică în fizica plasmei", Ed. Academiei, Bucureşti, 1966, p. 301.

[7] R. V. Deutsch, *Rev. Roumaine Phys.*, **4**, 309 (1966).

[8] J. P. Roach and T. Z. Fahidy, *Canad. J. Chem. Eng.*, **50**, 414 (1972).

Revue Roumaine de Chimie, **34**, *1*, 87–102 (1989)

CARBONIUM ION REACTIONS. XIX[1]

THE SOLVOLYSIS OF 5-(1′,1′-DIMETHYLETHYL)-5-HYDROXY-5*H*-DIBENZO*[a,d]*CYCLOHEPTENE AND SOME RELATED COMPOUNDS. AN UNCOMMON NEOPENTYL REARRANGEMENT

ECATERINA CIORĂNESCU, ANCA VOICU and M. ELIAN
Centre of Organic Chemistry — ICECHIM
202 B, Spl. Independenţei, 78100, Bucharest

Received October 12, 1988

The unbuffered trifluoroacetolysis of the alcohol **6** gave the spirane **15** in variable amounts (6-30%) depending on the ratio **6** : trifluoracetic acid, along with the alcohols **14**. The spirane **15** was the major product (> 70%) of the buffered solvolysis of alcohol **6**, with hydrocarbon **20** as by-product. The behavior of the alcohol **6** contrasts that of the structurally related alcohols **8**, **9** and **10**. None of these last compounds gave spiranic hydrocarbons ; **9** and **10** yielded in the buffered solvolysis analogs of the hydrocarbon **20** exclusively. The neopentyl rearrangement of the alcohol **6** leads to an "abnormal" product in a stereoselective reaction (only the sterically crowded conformer **15a** is produced), together with smaller quantities of the "normal" product of this rearrangement, namely the hydrocarbon **20**. A reaction mechanism is advanced implying, as the key step, an intramolecular proton shift from the reaction centre to the double bond acting as an internal nucleophile. The substitution of the carbon atom bearing the leaving-group (**5** compared to **1**, R=H) suppresses the phenonium route, leading under thermodynamic control to π-route products exclusively.

INTRODUCTION

In the previous works[1] we described the solvolytic behavior of compounds with general formula **1** where X is a leaving-group. It was shown that system **1** can react by two different routes. In one of them, the phenonium route, the breakage of the C—X bond is assisted by the aromatic ring in β-position and consequently, ring enlargement (**1** → **2**, kinetic control) or ring contraction (**2** → **1**, thermodynamic control) took place. The second reaction path, the π-route gave, by double bond assisted ionization the bicyclic compounds **3** and **4**. The parent system (**1**, R=H) reacts mainly by phenonium route, the π-route having only a small weight (cca 8%).[2] An alkyl substituent at the double bond modifies its nucleophilicity bringing an important change in the behavior of the system which in this case reacted exclusively by π-route.[1]

It seemed interesting to study the solvolytic behaviour of compounds with alkyl substituents at the carbon atom bearing the leaving-group, which would generate carbonium ions of type **5** stabilized by the substituents. A convenient starting point appeared to be the known and

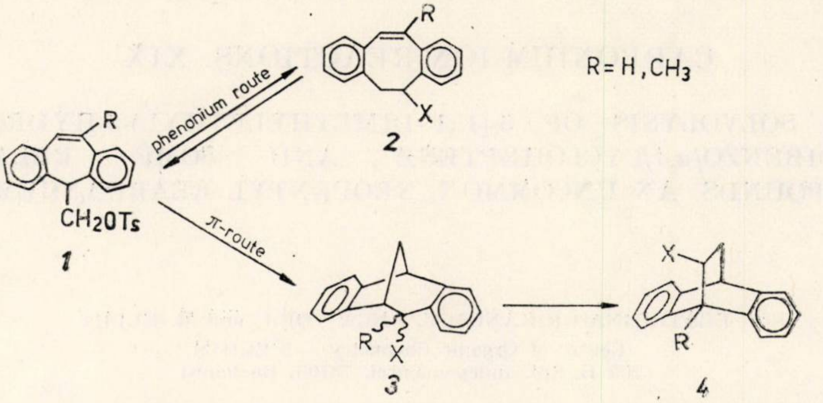
R
R = H, CH3
X
2
phenonium route
R
CH2OTs
1
π-route
R
X
3
X
R
4

relatively easily accessible 5-(1′,1′-dimethylethyl)-5-hydroxy-5*H*-dibenzo[*a*, *d*]cycloheptene **6**, which would generate by a neopentyl rearrangement the ion **7** substituted with two methyl groups at the ionic center. For comparison, the solvolytic behaviour of alcohols **8**, **9** and **10** was also studied.

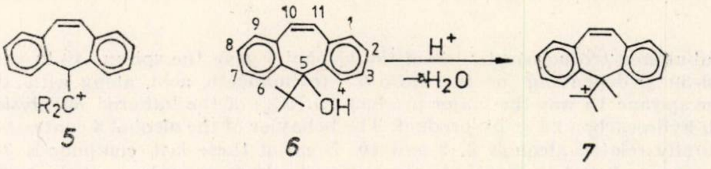
R2C+
5
10 11
9
1
8
2
7
6
5
4
3
OH
6
H+
−H2O
+
7

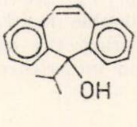

8

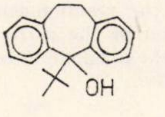

9

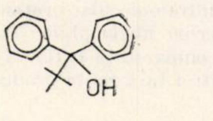

10

RESULTS

Starting materials

The alcohol **6** was synthesized, according to literature data[3] from dibenzotropone (**11**) and *t*-butyl magnesium chloride. Besides **6**, another

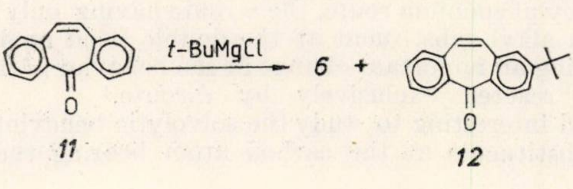
O
11
t-BuMgCl
6
+
O
12

product formed in this reaction which, after separation by column chromatography was shown to be the ring alkylated ketone **12**. The alkylation of the double bond is well known for α, β-unsaturated ketones [4] and was demonstrated also for aromatic ketones under these conditions.[5]

The alcohols **8** and **9** were obtained from the corresponding ketones and organomagnesium compounds ; the alcohol **10** was prepared according to the literature data.[5] In all cases, ring alkylated ketones were also obtained. The alcohols **8** and **9** were separated by column chromatography on silica. However, it was not possible to separate the alcohol **10** by chromatography, so a mixture of 44% **10** and 56% of the corresponding aromatic ring alkylated ketone was used for the subsequent reactions.

The conformation of the alcohols **6**, **8** and **9** is important for understanding their solvolytic behaviour. There are two possible conformations in which the substituent R is either axial (**13a**) or equatorial (**13b**). By

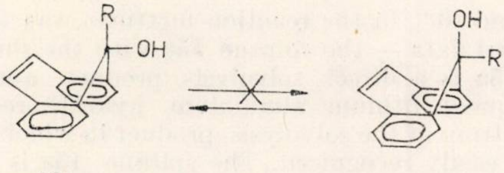

13a *13b* R= *t*-Bu, *i*-Pr.

NMR-spectroscopy with lanthanide shift reagents it was shown that in the alcohols **6**, **8** and **9** the larger alkyl substituent is predominantly or exclusively in the axial position.[6]

The reactions of alcohol 6

The alcohol **6** was treated with excess trifluoroacetic acid (1 : 10 moles) at 25°C for 24 h. The acid was neutralized and after the usual work-up an oily product was obtained (90% yield) which was reduced with $LiAlH_4$ in ether. The g.l.c. analysis showed three main components (72, 18 and 6%) which were separated by preparative g.l.c. From elemental analysis, NMR- and IR-spectra, two of them were shown to be the alcohols with dibenzobicyclo[3.2.1]octane skeleton **14a** (*endo* configuration 72%) and **14b** (*exo* configuration 18%).[8] The main arguments for configuration assignment rely on NMR-spectra ($J_{10,11} = 5.5$ Hz in **14a** and 1.5 Hz

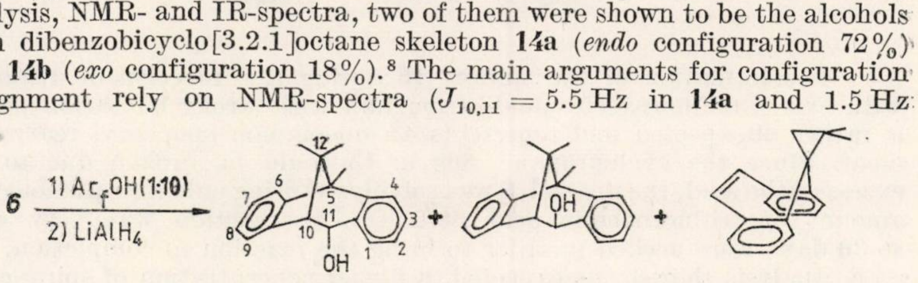

14a *14b* *15a*

$Ac_f = CF_3\text{-}CO\text{-}$

in **14b** in good agreement with literature data [7]), and IR-spectra ($\nu_{OH} = 3585$ cm^{-1} indicating intramolecular hydrogen bridge with an aromatic ring in **14a** and 3623 cm^{-1} in **14b**). The structure of the two alcohols was confirmed by oxidation with Jones reagent to the ketone **16** and subsequent reduction with hydrazine to the hydrocarbon **17**, both with corresponding analytical and spectral data. The reduction of the ketone **16** with lithium aluminium hydride gave a mixture of alcohols **14** in which the *endo* : *exo* ratio, 1 : 4 was reversed as compared to solvolysis.

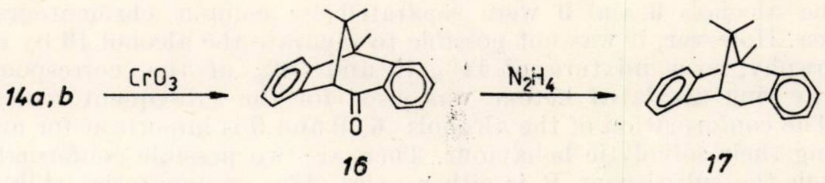

The third compound (6% in the reaction mixture) was — according to analytical and spectral data — the spirane **15a** with the shown conformation. The spirane **15a** is a direct solvolysis product and does not result from the subsequent lithium aluminium hydride reduction, as shown by the NMR-spectrum of the solvolysis product in which the methyl signals of **15a** could be easily recognized. The spirane **15a** is known and was obtained by Looker and coworkers [3] from alcohol **6** and thionyl chloride in dimethylformamide. The cited authors have shown that the cycle inversion in **15** requires a large activation energy, the two conformers **15a** and **15b** being stable at room temperature. From the two conformers, **15a** is the less stable one since it converts entirely into **15b** at cca 200°C.

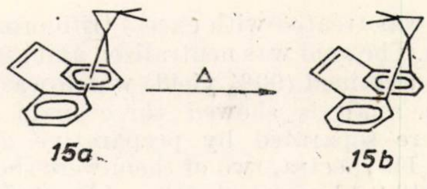

The formation of the spirane **15** during the reaction of alcohol **6** with excess trifluoroacetic acid, a medium with strong ionisation power, is rather unexpected and represents an uncommon neopentyl rearrangement. Since the cyclopropane ring in **15** could be broken due to the excess of the acid, the alcohol **6** was solvolysed using only an equimolecular amount of trifluoroacetic acid at 25°C. The reaction was very slow, so 36 days were needed in order to bring the reaction to completion. The g.l.c. analysis showed, as expected, a higher concentration of spirane **15a** (30%).

To gain new information about the solvolysis of the alcohol **6**, a reaction with excess trifluoroacetic acid (1 : 10 moles) at longer reaction time (120 h) was performed. After lithium aluminium hydride reduction, only one reaction product was isolated, namely the alcohol **18** with a dibenzobicyclo[2.2.2]octane skeleton, whose structure resulted from its spectral data as well as from those of the corresponding ketone **19**. The same product (**18**) resulted from a mixture of alcohols **14** and excess trifluoroacetic acid.

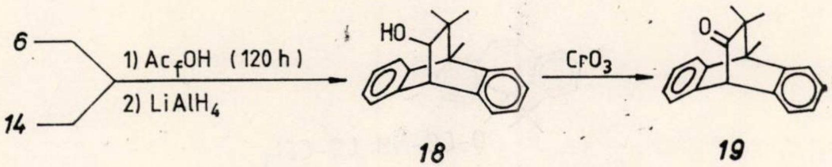

The spirane **15a** was transformed into the same reaction products with excess trifluoroacetic acid. After 24 h the trifluoroacetates of the alcohols **14** were formed; the prolongation of the reaction time to 120 h gave the trifluoroacetate of the alcohol **18**.[9]

In the previous works [2] the reactions of the compounds **1** ($X=OTs$) were performed under thermodynamic control conditions (acetic acid and *p*-toluenesulfonic acid resulting from the reaction) as well as under kinetic control conditions (sodium acetate buffered medium). All reactions of the alcohol **6** presented above were performed under thermodynamic control. For comparison with system **1**, as well as for better understanding the formation of spirane **15** we have tried to find kinetic control conditions for the reactions of the alcohol **6**. For this purpose the alcohol **6** was treated with trifluoroacetic anhydride and pyridine (molar ratio 1 : 1 : 2) in tetrachloroethene. The reaction was monitored at room temperature by NMR spectroscopy. During the reaction the spectrum changed progressively; the signals corresponding to the protons of the *t*-butyl group (0.7 ppm) and double bond (6.8 ppm) in the alcohol **6** diminished, and two other signals, corresponding to the same groups at 0.8 and 6.6 ppm respectively, appeared and increased. This transformation, which was complete at room temperature after 5 days, retains the original skeleton of the molecule and is due to the conversion of the alcohol **6** into the corresponding trifluoroacetate **6—OAc$_f$**. After heating the reaction mixture for 2 h at 90°C the trifluoroacetate **6—OAc$_f$** transformed completely. The NMR-spectrum exhibited the signals of the spirane **15a** along with signals of another compound containing an isopropenyl group. Further heating did not produce any change. The spirane **15a** and the hydrocarbon **20** were isolated by column chromatography from the reaction mixture. The crude product of this reaction showed the following compo-

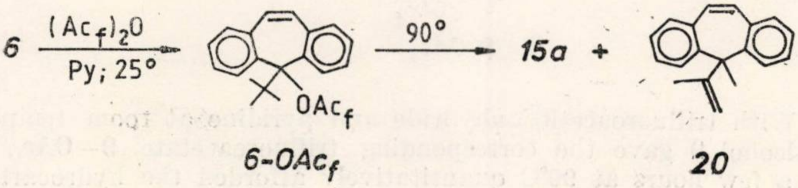

sition : 72.6% **15a**, 22.9% **20** and 0.8% **6**, the remaining of 3.7% consisting of several components, each under 1%. No product of π-route (the alcohols **14**, **18** or the corresponding trifluoroacetates) was formed; instead the neopentyl rearrangement took place, but only one of its products, the minor one, **20**, was the normal product of this rearrangement.

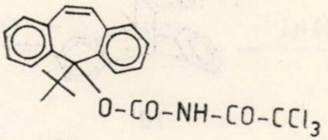

21

Under similar conditions (95°C in tetrachloroethene) the trichloroacetylurethane **21** reacted to give a mixture of spirane **15a** (50.4%) and hydrocarbon **20** (31.0%) together with other unidentified products.

The reactions of alcohol 9

Alcohol **9** with excess trifluoroacetic acid (1 : 10 moles) gave, after 24 h at 25°C, the hydrocarbon **23** with a double bond in the cycloheptane ring in 90% yield. With catalytic amounts of trifluoroacetic acid an intermediate product could be detected monitoring the reaction by NMR. This product was separated and proved to be the hydrocarbon **22** which preserves the saturated median ring. With excess trifluoroacetic acid **22** was transformed rapidly into **23**.

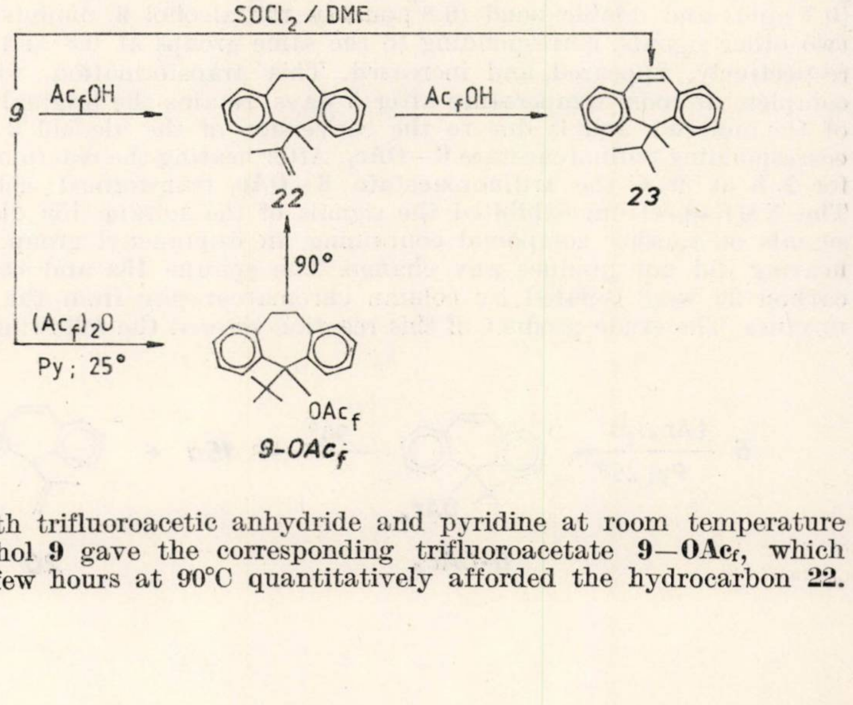

With trifluoroacetic anhydride and pyridine at room temperature the alcohol **9** gave the corresponding trifluoroacetate **9—OAc**$_f$, which after a few hours at 90°C quantitatively afforded the hydrocarbon **22**.

In none of these reactions spiranic hydrocarbons analogous to **15** were obtained. The alcohol **9** behaved also differently from its unsaturated congener **6** in reaction with thionyl chloride in dimethylformamide; under these conditions **9** gave only the hydrocarbon **23**.

The reactions of alcohol 8

With trifluoroacetic acid, the alcohol **8** gave the trifluoroacetates **25** and **26** through the hydrocarbon **24**. After 2 h at 25°C the hydrocarbon **24** was isolated in 90% yield, while after 10 h at reflux in chloroform a mixture of trifluoroacetates **25** and **26** resulted. With thionyl chloride in dimethylformamide only the elimination product, hydrocarbon **24**, was obtained.

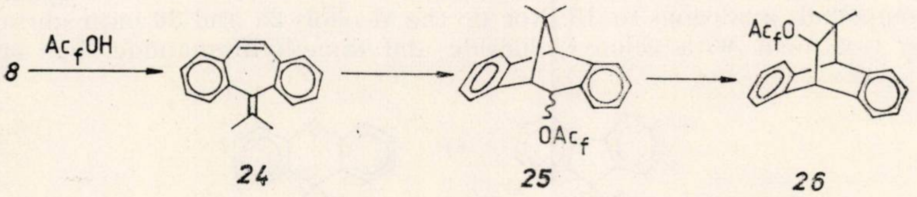

The reactions of alcohol 10

With trifluoroacetic acid the alcohol **10** gave the hydrocarbon **27** by dehydration accompanied by rearrangement. All attempts to evidence intermediates in this reaction failed, even with catalytic amounts of trifluoroacetic acid. The reaction of alcohol **10** with trifluoroacetic anhydride and pyridine at room temperature gave the corresponding trifluoroacetate **10−OAc$_f$** which at 90°C transformed entirely into the hydrocarbon **28**.

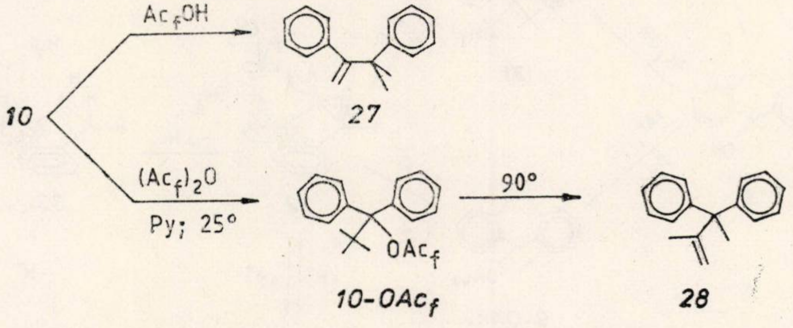

DISCUSSION

The alcohol **6** gave with trifluoroacetic acid π-route products (the trifluoroacetates **14—OAc$_f$**) and the spirane **15**. At longer reaction time trifluoroacetate **18—OAc$_f$** was the sole product. The ratio spirane vs. π-route products changed with the acidity of the reaction medium. With excess acid (1 : 10 moles) after 24 h the spirane was only 6%, while with equimolecular amounts of acid and alcohol, the spirane was as high as 30%. Under kinetic control conditions (trifluoroacetic anhydride and pyridine) the π-route vanished; over 70% spirane **15** was obtained along with the hydrocarbon **20**.

None of the alcohols **8**, **9** or **10**, closely related to **6**, gave spiranic compounds analogous to **15**. Nor do the alcohols **29** and **30** form spiranes by treatment with thionyl chloride and dimethylformamide, but only

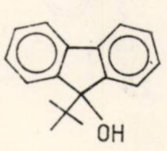

29

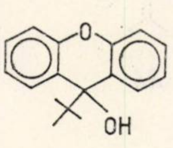

30

the "normal" reaction products.[3] The spirane did appear exclusively in the reactions of the alcohol **6**. It is worth mentioning also that only the unstable conformer **15a** of the spirane **15** was obtained in the reactions presented here as well as elsewhere.[3] Therefore the reaction is stereoselective.

The solvolytic behaviour of the alcohol **6** raises two questions: *i*) the predominance of π-route over phenonium route as compared to the parent system (**1**, R = H), and *ii*) the formation of the spirane and the stereo-

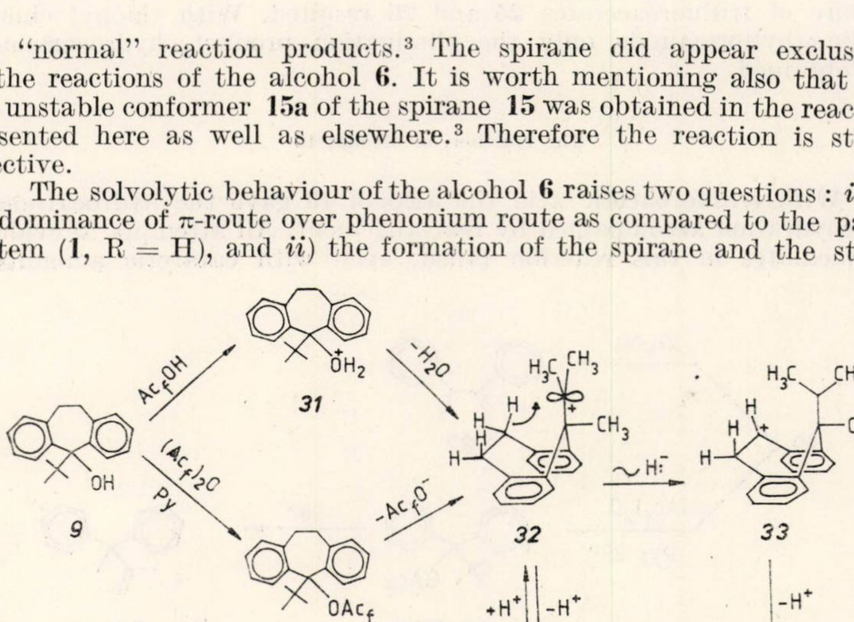

chemical implications. We want to discuss first the alcohols **8**, **9** and **10**, with "normal" solvolytic behavior and to return later to the uncommon behaviour of the alcohol **6**.

The alcohol **9** leads through the protonated intermediate **31** or the trifluoroacetate **9-OAc**$_f$ to the ion **32** by a neopentyl rearrangement. This ion can follow two routes : proton elimination to the hydrocarbon **22** or transannular hydride migration to the ion **33**, which stabilizes to **23**. Most probably, the elimination **32**→**22** takes place much more rapidly than the hydride shift **32**→**33**. When a base is present the protonation reaction **22**→**32** is suppressed and only the formation of hydrocarbon **22** — stable in the reaction medium and representing a kinetic control product — takes place. In the presence of an acid the reaction **32**⇄**22** becomes reversible, so the hydrocarbon **22** and the corresponding ion equilibrate. In these conditions the thermodynamic control takes over, and the hydrocarbon **22** evolves by the route **22**⇄**32**⇄**33**⇄**23** into the product which is most stable in the reaction medium. Transannular hydride migrations (**34**→**35**) are known in the dibenzocycloheptene system[10]. However, the transannular hydride shift taking place in the reaction of the alcohol **9** with trifluoroacetic acid is different from those described in the literature, because it starts from the two carbon atoms bridge to end at an atom placed outside the ring. The reason for this easy rearrangement is very probably the shown conformation of **32**, with the larger alkyl group in the axial position, conformation which brings the two reaction centers in close proximity. For hydrocarbon **23** with the same skeleton the conformation could be easily assigned : in the NMR-spectrum the protons of isopropyl group ($\delta = 0.38$ ppm) are strongly shielded by the double bond, this shielding being possible only for the axial substituent.

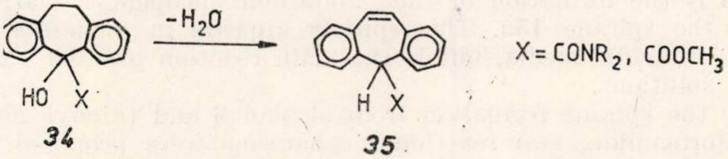

The alcohol **10** leads by a neopentyl rearrangement to the ion **36** from which, by phenyl migration, the benzylic ion **37** results. The two final products of the reaction, the hydrocarbons **28** and **27**, are formed under kinetic and thermodynamic control conditions respectively.

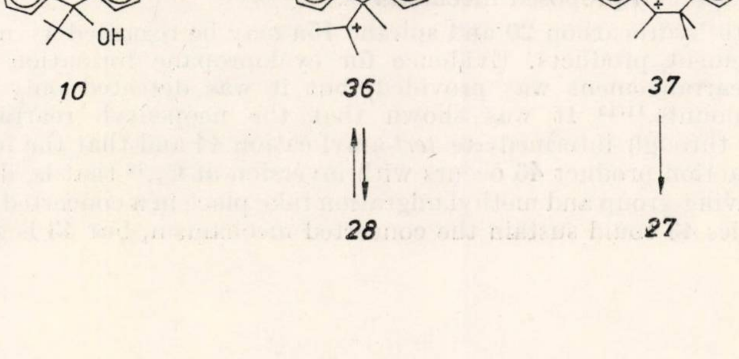

The alcohol **8** gives only π-route products, namely the trifluoroacetates **25** and **26**. Very likely, the initially formed alkene **24** is in equilibrium with the ions **38** and **39** and the latter generates the π-route products.

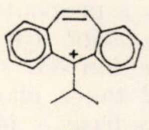

38

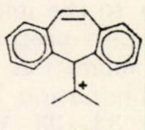

39

With trifluoroacetic acid the alcohol **6** undergoes at short reaction time a neopentyl rearrangement like the alcohols **9** and **10**. At longer reaction time the system evolves by π-route like the alcohol **8**. The main difference between the behaviour of the alcohols **8**, **9**, **10** and that of the alcohol **6** is the formation of the "abnormal" neopentyl rearrangement product, the spirane **15a**. This spirane appears in moderate amounts (6–30%) in acidic media, but is the main reaction product (>70%) in buffered solutions.

For the spirane formation from alcohol **6** and thionyl chloride in dimethylformamide, two reaction mechanisms were proposed.[3] One of these postulates the intermediacy of dibenzotropylium ion **40** in which one C–H bond attacks the positively charged carbon atom, with release of the steric strain as driving force. According to the second mechanism,[3] the carbene **41** and isobutene result as intermediates and react further to give a three membered ring. However, it should be pointed out that neither of these two mechanism explains the reaction stereoselectivity, namely that only the less stable and more crowded spirane **15a** results. One should rather expect the more stable conformer **15b** to be formed by either of the two proposed mechanisms.

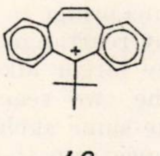

40

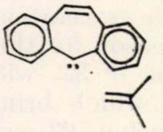

41

Both hydrocarbon **20** and spirane **15a** may be regarded as neopentyl rearrangement products. Evidence for cyclopropane formation in neopentyl rearrangement was provided, but it was detected only in very small amounts.[11,12] It was shown that the neopentyl rearrangement proceeds through intermediate *tert*-amyl cation **44** and that the formation of the reaction product **45** occurs with inversion at C_α,[12] that is, departure of the leaving-group and methyl migration take place in a concerted manner. The species **43** could sustain the concerted mechanism, but **43** is generally

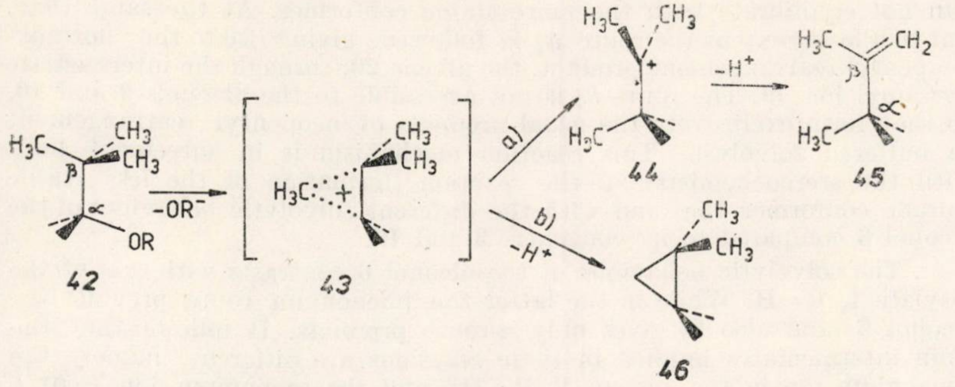
H$_3$C
CH$_3$
CH$_3$
β
α
OR
42
-OR$^-$
H$_3$C
+
CH$_3$
CH$_3$
43
a)
b)
-H$^+$
H$_3$C
CH$_3$
H$_3$C
+
44
-H$^+$
H$_3$C
CH$_2$
β
α
H$_3$C
45
CH$_3$
CH$_3$
46

believed to be rather a transition state than an intermediate.[12,13] To our knowledge only in the adamantane system, a species similar to **43** was proved to be an intermediate.[14]

The ratio between the two routes *a)* and *b)* leading to the reaction products could be affected by electronic factors and by the nature of the proton acceptor in the final step of the reaction. Since the alcohols **6**, **9** and **10** are structurally very similar it could be supposed that the electronic difference is too small to afflict a different solvolytic behaviour. However, the uncommon behaviour of the alcohol **6** could be explained admitting that the double bond in the cycloheptene ring may act as a very efficient intramolecular proton acceptor.

As was shown, the alcohols **6** and **9** have the same conformation [6] with an axial *t*-butyl group. By migration of the methyl group in **6-OR**,

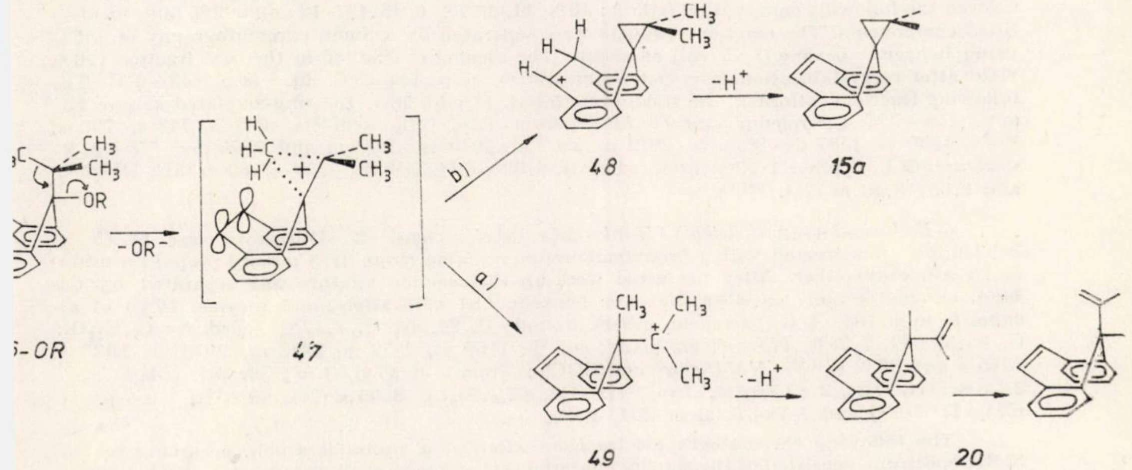
CH$_3$
CH$_3$
OR
-OR$^-$
-OR
H
H-C
H
+
CH$_3$
CH$_3$
47
b)
a)
H
H
H
+
CH$_3$
CH$_3$
48
-H$^+$
15a
CH$_3$
CH$_3$
+
C
CH$_3$
49
-H$^+$
20

concerted with the departure of the leaving-group the species **47** occurs. In this species the double bond can efficiently accept a proton from the closely placed protonated cyclopropane forming the benzylic ion **48** by route b).[15] This latter ion leads by proton elimination, to the spirane **15a** with the shown conformation, which at the reaction temperature ($<100°C$) can not equilibrate with the more stable conformer. At the same time, but to a lesser extent the route *a*) is followed, giving rise to the "normal" neopentyl rearrangement product, the alkene **20**, through the intermediate *tert*-amyl ion **49**. The route *b*) is not accessible to the alcohols **9** and **10**, so they form exclusively the usual products of neopentyl rearrangement in buffered solvolysis. This reaction mechanism is in agreement both with the stereochemistry of the reaction (formation of the less stable spirane conformer **15a**) and with the different solvolytic behaviour of the alcohol **6** compared to its congeners **9** and **10**.

The solvolytic behaviour of the alcohol **6** contrasts with that of the tosylate **1**, R=H. While in the latter the phenonium route prevails the alcohol **6** (and also **8**) gives only π-route products. It follows that the main intermediates implied in these reactions are different, namely the phenonium ion in the system **1**, R=H[16] and the carbonium ion **7** or a double bond assisted species for the alcohol **6**.

The behaviour of the tosylate **1** is singular; the insertion of a donor substituent at the double bond of the cycloheptene ring as well as substitution at the reaction centre entirely changes the reactivity of the system.

EXPERIMENTAL

Melting points are uncorrected. The IR spectra were recorded with an UR–20 Carl Zeiss-Jena double beam spectrophotometer and the ^{1}H–NMR spectra with a VARIAN A60–A spectrometer using TMS as internal standard.

5-(1′,1′-Dimethylethyl)-5-hydroxy-5H-dibenzo[a, d]*cycloheptene*, **6** and *2-(1′,1′-dimethylethyl)-5H-dibenzo*[a,d] *cycloheptene-5-one*, **12**. The alcohol **6** was obtained according to literature [3] from dibenzotropone **11** and *t*-butyl-magnesium chloride. After the usual work-up, the crude product showed the following composition (g.l.c.): 48% **11**, 36.7% **6**, 13.1% **12** and 2.2% four unidentified components. The reaction products were separated by column chromatography on silica using benzene : hexane (1 : 5 vol) as eluent. The alcohol **6** resulted in the first fraction (20% yield after recrystallization from petroleum ether), m.p. 144–5°C. lit. [3] m.p. 145–6°C. The following fractions afforded the starting material, **11** and then the ring-alkylated ketone **12**: m.p. 115–7°C (petroleum ether): *IR-spectrum* (CS_2, CCl_4 : cm^{-1}): 698 s, 742 s, 793 s, 808 s, 1300 vs, 1597 vs, 1633 vs, 2872 m, 2907 m, 2970 vs, 3033 m and 3070 m: *^{1}H-NMR-spectrum* (CCl_4, δppm): 1.37 s (9H, *t*-butyl), 6.92 s (2H, $H^{10,11}$), 7.35–7.60 m (5H, $H^{1,3,7-9}$) and 8.05–8.40 m (2H, $H^{4,6}$).

5-Hydroxy-5-(1′-methylethyl)-5H-dibenzo[a,d]*cycloheptene*, **8**. Dibenzotropone **11** (5 g, 24.2 mmol) was treated with *i*-propylmagnesium bromide (from 81.3 mmol *i*-propyl bromide) in 25 mL ethyl ether. After the usual work-up the reaction mixture was separated by column chromatography on silica (hexane : benzene 4 : 1 vol) affording 1 g (yield 16%) of alcohol **8**, m.p. 103–4°C (petroleum ether). Found: C, 86.55; H, 7.47%. Calcd. for $C_{18}H_{18}O$: C, 86.36 : H, 7.25% *IR-spectrum* (CCl_4; cm^{-1}): 1167 vs, 2872 m, 2932 m, 2970 vs, 3023 s, 3065 s and 3622 s. *^{1}H–NMR-spectrum* ($CDCl_3$; δppm): 0.46 d, J = 7 Hz (6H, $CH(CH_3)_2$), 2.28 s (1H, OH), 2.87 septet, J = 7 Hz (1H, $CH(CH_3)_2$), 6.90 s (2H, $H^{10,11}$), 7.0–7.5 m (6H, $H^{1-3,7-9}$) and 7.75–8.00 m (2H, $H^{4,6}$).

The following chromatographic fractions afforded a material which, according to the NMR-spectrum, consisted of the starting material (**11**) and a ring-alkylated ketone ($\delta = 1.20$ d, J = 7 Hz. $CH(CH_3)_2$; $\delta = 2.85$ septet, J = 7 Hz. $CH(CH_3)_2$).

5-(1′, 1′-Dimethylethyl)-10, 11-dihydro-5-hydroxy-5H-dibenzo[a, d]*cycloheptene*, **9**, was synthetized from 10,11-dihydro-5*H*-dibenzo[a, d] cyclohepten-5-one (10 g, 48.1 mmol) and *t*-butylmagnesium chloride (from 150 mmol *t*-butyl chloride) in 240 mL diethylether. Column chromatogaphy on silica (petroleum ether : benzene 4 : 1 vol) afforded 1 g (yield 8%) **9**, m.p. 99–101 °C (petroleum ether). Found: C, 85.34; H, 8.46%. Calcd. for $C_{19}H_{22}O$: C, 85.67; H, 8.32%. *IR.-spectrum* (CCl_4, cm^{-1}): 992 s, 1203 m, 1485 s, 2872 m, 2932 s, 2962 s, 2986 s, 3020 m, 3060 m and 3595 s. *^{1}H-NMR-spectrum* (CCl_4, δppm); 0.95 s (9H, *t*-butyl), 1.95 s (1H, OH), 2.5—3.8 m (4H, $H^{10,11}$), 7.05—7.35 m (6H, $H^{1-3,7-9}$) and 7.95—8.20 m (2H, $H^{4,6}$). The g.l.c. analysis of the reaction mixture indicated the following composition: 15% unreacted starting material, 45% alcohol **9**, 21% ring-alkylated ketone and 19% thirteen unidentified components. The presence of the ring-alkylated ketone was inferred from the ^{1}H—NMR-spectrum of the reaction mixture as well as that of the fractions separated bv column chromatography (*t*-butyl signal at 1.33 ppm).

The solvolysis of alcohol **6** *with trifluoroacetic acid (1 : 10 mol), 24 h.* 1 g (3.8 mmol) alcohol **6** in 50 mL chloroform was treated with 3 mL (4.6 g, 40.4 mmol) trifluoroacetic acid for 24 h at room temperature. After neutralization of the excess acid with 10 mL sodium carbonate 30%, the reaction mixture was washed with 2×20 mL water and dried over natrium sulfate. Evaporation of the solvent left 1.2 g oily product, which was reduced with 0.8 g (21.1 mmol) lithium aluminum hydride in 25 mL ethyl ether by heating at reflux for 6 h. The reaction mixture was decomposed with cold 10% sulfuric acid, washed and the solvent was removed. The composition of the crude product resulted from g.l.c analysis as 72% **14a,** 18% **14b,** and 6% **15a**. The three compounds were separated by preparative g.l.c.

*10, 11-Dihydro-11-*endo-*hydroxy-5, 12, 12-trimethyl-5, 10-methano-5H-dibenzo* [a, d]*cycloheptene,* **14a,** m.p. 86—8 °C. Found: C, 85.73; H. 7.72%. Calcd. for $C_{19}H_{20}O$: C, 86.32; H, 7.63%. *IR-spectrum* (CCl_4, cm^{-1}): 1054 m, 1393 s, 1471 m, 2873 m, 2923 m, 2973 m, 3023 m, 3070 m and 3585 m. *^{1}H-NMR-spectrum* (CCl_4, δppm): 0.99 s (6H, CH_3^{12}). 1.50 s (1H, OH), 1.55 s (3H, CH_3^5), 3.03 d, J = 5.5 Hz (1H, H^{10}), 4.80 d, J = 5.5 Hz (1H, H^{11}) and 6.9—7.4 m ($8H^{1-4,6-9}$).

*10,11-Dihydro-11-*exo-*hydroxy-5,12,12-trimethyl-5,10-methano-5H-dibenzo*[a,d]-*cycloheptene,* **14b,** m.p. 134—6 °C. Found: C, 85.91; H, 7.67%. Calcd. for $C_{19}H_{20}O$: C, 86.32; 7.63%. *IR-spectrum* (CCl_4, cm^{-1}): 1041 m, 1043 m, 1388 m 1470 m, 2873 m, 2926 m, 2972 m, 3020 m, 3071 m and 3623 m. *^{1}H-NMR-spectrum* (CCl_4, δppm): 0.97 s (3H, CH_3), 1.12 s (3H, CH_3), 1.57 s (3H, CH_3^5), 3.00 d. J=1.5 Hz(1H,H^{10}), 4.61 d, J = 1.5 Hz (1H, H^{11}) and 6.9—7.4 m (8H, $H^{1-4,6-9}$).

Spyro[*2,2-dimethylcyclopropane-1,5′-dibenzo*[a, d]*cycloheptene*], **15**, m.p. 104—6 °C, lit.[3] m.p. 104—5 °C: ^{1}H—NMR-spectrum identical with the reported one [3] for the conformer **15a**.

10, 11-Dihydro-5,12,12-trimethyl-5,10-methano-5H-dibenzo[a,d]*cyclohepten-11-one,* **16**. A mixture of alcohols **14a** and **14b** (1.2 g, 4.5 mmol, ratio **14a**: **14b** = 4 : 1) in 20 mL acetone was oxidized with Jones reagent until a stable, brown colour developed. The excess reagent was destroyed with *i*-propyl alcohol the reaction mixture was diluted with 120 mL water and extracted with 2×25 mL ethyl ether. After the evaporation of the solvent 1 g (yield 85%) ketone **16** resulted, mp. 104—5 °C (ethanol). Found: C, 87.12; H, 6.96%. Calcd. for $C_{18}H_{18}O$: C, 86.99; H, 6.92%. *IR-spectrum* (CCl_4, cm^{-1}): 1290 s, 1461 s, 1695 vs, 2873 m, 2943 s, 2978 vs, 3023 m and 3071 m. *^{1}H-NMR-spectrum* (CCl_4, δppm): 1.04 s (6H, CH_3^{12}), 1.62 s (3H, CH_3^5), 3.58 s (1H, H^{10}), 6.9—7.4 m (7H, $H^{2-4,6-9}$) and 7.80—7.95 m (1H, H^1).

10, 11-Dihydro-5,12,12-trimethyl-5,10-methano-5H-dibenzo[a,d]*cycloheptene,* **17.** 0.3 g (1.15 mmol) **16,** 1.15 g potassium hydroxide and 1.65 mL hydrazine hydrate in 10 mL diethyleneglicol were heated 2 h at 150 °C. The reaction mixture was maintained for 3 h at 220 °C and 24 h at room temperature, then 7 mL hydrochloric acid was added and extracted with 2×20 mL ethyl ether. After chromatography on silica with petroleum ether, 0.2 g (70% yield) hydrocarbon **17** resulted, m.p. 49—51 °C. Found: C, 91.49; H, 8.14%. Calcd. for $C_{19}H_{20}$: C, 91.88; H, 8.12%. *IR-spectrum* (CCl_4, cm^{-1}): 1039 m, 1376 s, 1387 s, 1474 s, 2839 m, 2879 s, 2918 vs, 2971 vs, 3018 s and 3061 s. *^{1}H-NMR-spectrum* (CCl_4, δppm): 0.95 s (6H, CH_3^{12}), 1.55 s (3H, CH_3^5), 2.50—3.45 ABC-type multiplet, 13 lines (3H, $2H^{11}$, H^{10}) and 6.8—7.3 (8H, $H^{1-4,6-9}$). The ABC-type subspectrum was computer-resolved, the following values resulting: 2.69 (H^{11endo}), 2.80 (H^{10}), 3.21 (H^{11exo}), $J_{11endo,\,11exo} = 16.9$ Hz, $J_{11endo,\,10} = 2.2$ Hz, $J_{11exo,\,10} = 4.8$ Hz.

The reaction of alcohol **6** *with trifluoroacetic acid (1 :1 mol).* 0.2 g (1.14 mmol) **6** was treated with 0.1 mL (1.35 mmol) trifluoroacetic acid in 30 mL chloroform at room temperature. The reaction was monitored by NMR-spectroscopy until the starting material was consumed (36 days). After reduction with lithium aluminium hydride the crude product showed the following composition (g.l.c.) : 35.1% **14a** + **14b**, 30.9% **15a**, 3% **6** and 31% eighteen unidentified components. The reaction mixture was separated into two fractions by chromatography on neutral alumina. The first of these (eluent petroleum ether) contained the spirane **15a** (91% g.l.c., identical IR- and NMR-spectra with an authentic sample). The second fraction (eluent petroleum ether : benzene 4 : 1 vol) gave the following g.l.c. composition : 1% **15a**, 45.2% **14a**, 37.6% **14b** and 1.6% **6**.

The reaction of alcohol **6** *with trifluoroacetic acid (1 : 10 mol), 120 h.* Alcohol **6** (1 g, 3.8 mmol) in 50 mL chloroform was treated with 3 mL (40.4 mmol) trifluoroacetic acid for 120 h at room temperature. After the usual work-up, 1 g (2.8 mmol) *9,10-dihydro-9,12,12-trimethyl-9, 10-ethanoanthracen-11-yl trifluoracetate*, **18—OAc$_f$** resulted as colourless oil. ^{1}*H—NMR-spectrum* (CCl_4, δppm) ; 0.58 s (3H, CH_3), 0.80 s (3H, CH_3), 1.82 s (3H, CH_3^9), 4.37 d, J = 3.5 Hz (1H, H^{10}), 4.98 d, J=3.5Hz (1H, H^{11}) and 7.0—7.5 m (8H, H^{1-8}).

The ester **18—OAc$_f$**, (1 g, 2.8 mmol) was reduced with lithium aluminum hydride (0.6 g, 15.8 mmol) in ethyl ether giving 0.7 g (yield 95%) *9,10 -dihydro-11-hydroxy-9, 12, 12-trimethyl-9, 10-ethanoanthracene* (**18**). *IR-spectum* (CCl_4 cm^{-1}) : 1053 m, 1392 s, 1470 m, 2870 m, 2920 m, 2970 m, 3020 m, 3070 m and 3578 m. ^{1}*H-NMR-spectrum* (CCl_4, δppm) : 0.52 s (3H, CH_3^9), 0.60 s (3H, CH_3), 1.70 s (3H, CH) 3.49 d, J = 3 Hz (1H, H^{10}), 4.09 d, J = 3 Hz, (1H, H^{11}) and 6.9—7.3 m (8 H, H^{1-8}).

9, 10-Dihydro-9, 12, 12-trimethyl -9, 10-ethanoanthracen-11-one, (**19**). 0.4 g (1.5 mmol) **18** in 30 mL dichloromethane was oxidized with 0.7 g chromium trioxide in 17 mL pyridine 3 h at 25 °C. After decomposition with 150 mL hydrochloric acid (10%), extraction with dichloromethane, neutralization with natrium hydrogen carbonate (5%) and solvent evaporation, an oil was obtained. The crude product was purified by column chromatography on silica resulting 0.3 g (yield 77%) **19**, m.p. 80—2 °C (methanol). Found : C, 86 .71 ; H, 7.02%. Calcd. for $C_{19}H_{18}O$: C, 86.99 ; H, 6.92%. *IR-spectrum* (CCl_4 cm^{-1}) : 1082 m, 1371 m, 1383 s, 1468 s, 1708 vs, 2872 m, 2974 s, 3022 m and 3072 m, ^{1}*H-NMR-spectrum* (CCl_4, δppm) : 0.71 s (6H, CH_3^{12}), 1.84 s (3H, CH_3^9), 4.69 s (1H, H^{10}) and 7.0—7.5 m (8H, H^{1-8}).

The reaction of alcohols **14** *with trifluoroacetic acid.* A mixture of alcohols **14a** and **14b** (0.5 g, 1.9 mmol) was treated with trifluoracetic acid (1.5 mL, 20.2 mmol) in chloroform (25 mL) for 100 h at room temperature. After the usual work-up, 0.4 g (1.1 mmol) ester **18—OAc$_f$**, resulted with NMR-spectrum identical with that of an authentic sample.

The reaction of spirane **15a** *with trifluoroacetic acid.* A solution of 0.5 g (2.0 mmol) spirane **15a** in 25 mL chloroform was treated with 1.5 mL (20.2 mmol) trifluoroacetic acid for 24 h at room temperature. After the work-up, 0.45 g of a mixture of trifluoroacetates of the alcohols **14a** and **14b** resulted, which were identified by the NMR-spectrum.

The reaction of alcohol **6** *with trifluoroacetic anhydride and pyridine.* To 1 g (3.78 mmol) alcohol **6** in 45 g tetrachloroethene, 3.83 g (18.24 mmol) trifluoroacetic anhydride and 2.43 g (30.76 mmol) pyridine were added. The reaction was monitored by NMR-spectroscopy. After 5 days at room temperature the transformation of the alcohol **6** into its trifluoroacetate was complete. The reaction mixture was heated afterwards at 90 °C for 4 h. The g.l.c analysis of the crude product gave 72.6% **15a**, 22.9% **20** and 0.8% **6**. The crude product was separated by column chromatography on neutral alumina (eluent petroleum ether). First, the spirane **15a** was eluted. In the last fractions *5-methyl-5-(1′-methylethenyl)-5H-dibenzo*[a, d]*cycloheptene*, **20** was obtained ^{1}*H—NMR-spectrum* (CCl_4, δδm) ; 1.27 m (3H, $CH_3—C=CH_2$), 2.06 s (3H, CH_3^5), 4.10 m (1H, $C=CH_2$), 4.60 m (1H, $C=CH_2$), 6.95 s (2H, $H^{10,11}$) and 7.1—7.7 m (8H, $H^{1-4,\ 6-9}$).

5-(1′, 1′-Dimethylethyl)-5H-dibenzo[a, d]*cyclohepten-5-yl-trichloroacetylcarbamate*, **21**. Alcohol **6** (0.5 g, 1.9 mmol) in carbon tetrachloride (5 mL) was treated with trichloroacetylisocyanate (3 mL 20% solution in carbon tetrachloride). After 30 min urethane **21** crystallized, m.p. 144—6 °C. *IR-spectrum* (KBr, cm^{-1}) : 1177 vs, 1527 vs, 1805 vs, 3320 s and 3355 m. ^{1}*H-NMR-spectrum* ($CDCl_3$, δppm) : 0.94 s (9H, *t*-butyl), 6.64 s (2H, $H^{10,11}$), 7.2—7.5 m, (8H, $H^{1-4,\ 6-9}$) and 8.53 broad s (1H, NH).

The thermolysis of urethane **21**. 0.5 g (1.10 mmol) **21** in 5 mL tetrachloroetene was heated at 95 °C for 10 h. The g.l.c. analysis showed the following composition : 50.4% **15a**, 30.9% **20** and 18.7% five unidentified components.

The reaction of alcohol **9** *with trifluoroacetic acid.* Alcohol **9** (1 g 3.8 mmol) in chloroform (50 mL) was treated with trifluoroacetic acid (2.3 mL, 31 mmol) for 24 h at room temperature. After the work-up, 0.75 g (yield 80%) *5-methyl-5-(1'-methylethyl)-5H-dibenzo*[a, d]*cycloheptene*, **23** was obtained m.p. 109—10° C (ethanol). Found: C, 91.64; H, 8.39%. Calcd. for $C_{19}H_{20}$: C, 91.88; H, 8.12%. *IR-spectrum* (CCl_4, cm^{-1}); 1036 m, 1364 m, 1370 m, 1388 m 1454 m, 1478 m, 2878 s, 2972 vs, 3028 s and 3068 s. *^1H-NMR-spectrum* (CCl_4 δppm); 0.38 d, J = 7 Hz (6H, $(CH_3)_2$ CH), 1.83 s (3H, CH_3^5), 3.12 heptet, J = 7 Hz (1H, $(CH_3)_2CH$), 6.93 s 2H, $H^{10,11}$) and 7.05—7.60 m (8H, $H^{1-4, 6-9}$).

When the alcohol **9** (0.1 g, 0.38 mmol) was treated with catalytic amounts of trifluoroacetic acid in chloroform (5 ml) for 24 h at room temperature *9,10-dihydro-5-methyl-5-(1'-methylethenyl)-5H-dibenzo*[a, d]*cycloheptene*, **22** was obtained (yield after chromatography on silica 55%), m.p. 77—9° C. Found: C, 91.63; H, 8.38%, Calcd. for $C_{19}H_{20}$: C, 91.88; H, 8.12%. *IR-spectrum* (CS_2 cm^{-1}); 746 s, 758 s, 896 m, 2932 m, 2964 m, 2984 m, 3016 m and 3059 m. *^1H-NMR-spectrum* (CCl_4, δppm); 1.55 m (3H, $CH_3-C=CH_2$), 1.90 s, (3H, CH_3^5), 2.60—3.70 m (4H, $H^{10,11}$), 4.71 m (1H, $C=CH_2$), 4.98 m (1H, $C=CH_2$) and 6.9—7.6 m (8H, $H^{1-4, 6-9}$).

The reaction of alcohol **9** *with trifluoroacetic anhydride and pyridine.* Alcohol **9** was treated with trifluoroacetic anhydride and pyridine (molar ratio 1 : 4 : 8) in tetrachloroethene. The reaction was monitored by NMR-spectroscopy. The transformation of alcohol **9** into its corresponding trifluoroacetate was complete after one day at room temperature. The reaction mixture was heated for 2 h at 110 °C. The *NMR*-spectrum indicated complete conversion to hydrocarbon **22**. No signals which could be assigned to a spiranic hydrocarbon were observed.

The reaction of alcohol **9** *with thionyl chloride in dimethylformamide.* 1.2 g (4.5 mmol) alcohol **9**, 0.6 mL dimethylformamide and 1.2 mL (16.7 mmol) thionyl chloride were heated at reflux for 30 min. After removal of excess thionyl chloride, extraction with diethylether and chromatography on silica (eluent petroleum ether) 1.0 g (yield 90%) **23** was obtained.

5-(2'-Methylethylidene)-dibenzo[a, d]*cycloheptene* **24**. To a solution of alcohol **8** (1 g, 4.0 mmol) in chloroform (20 mL), trifluoracetic acid (3 mL, 40.4 mmol) was added. After 2 h at 25 °C the excess acid was neutralized and the product extracted, resulting 0.85 g (yield 90%) **24**, m.p. 99—101 °C (after column chromatography on silica). *^1H-NMR-spectrum* ($CDCl_3$, δppm); 1.63 s (6H, CH_3), 6.83 s (2H, $H^{10, 11}$) and 7.20 s (8H, $H^{1-4, 6-9}$). The same hydrocarbon was obtained (yield 88%) from alcohol **8** (1 g, 4.0 mmol), thionyl chloride (1 mL, 10.1 mmol) and dimethylformamide (0.5 mL) after 30 min at reflux.

The reaction of alcohol **8** *with trifluoroacetic acid.* Alcohol **8** (1 g, 4.0 mmol) was treated with trifluoroacetic acid (3 mL, 40.4 mmol) in chloroform (20 mL) for 10 h at reflux. The crude product was separated by column chromatography on silica (eluent petroleum ether : benzene 9 : 1 vol). The first fraction afforded a small amount (0.2 g) of hydrocarbon **24**. In the following fractions the trifluoroacetates **25** and **26** were identified by NMR-spectroscopy. *^1H-NMR-spectrum of trifluoroacetate* **25** (CCl_4, δppm): 1.06 s (3H, CH_3), 1.13 s (3H, CH_3), 3.29 d, J = 5.5 Hz (1H, H^{10}), 3.40 s (1H, H^5) and 6.23 d, J = 5.5 Hz (1H, H^{11}). *^1H-NMR-spectrum of trifluoroacetate* **26** (CCl_4, δppm): 0.67 s (3H, CH_3), 0.91 s (3H, CH_3), 3.66 s (1H, H^9), 4.33 d, J = 3.5 Hz (1H, H^{10}) and 4.80 d, J = 3.5 Hz (1H, H^{11}).

The reaction of alcohol **10** *with trifluoroacetic acid.* Alcohol **10** could not be separated from the corresponding ring-alkylated ketone, so in the reactions described below a mixture of 44% **10** and 56% ring-alkylated ketone was used. 1 g mixture of alcohol **10** and ketone (1.83 mmol **10**) was treated with 3mL (40.4 mmol) trifluoroacetic acid for 24 h at room temperature. The NMR-spectrum showed that the ring-alkylated ketone did not change under these conditions, while alcohol **10** converted completely into *3-methyl-2,3-diphenyl-1-butene* **27**. *^1H-NMR-spectrum* (CCl_4, δppm): 1.43 s (6H, CH_3), 5.09 d, J= 1.5 Hz (1H, $C=CH_2$) and 5.34 d, J = 1.5 Hz (1H, $C=CH_2$).

The reaction of alcohol **10** *with trifluoroacetic anhydride and pyridine.* 0.05 g mixture of alcohol **10** and ring-alkylated ketone (0.09 mmol **10**) in 5 mL tetrachloroethene was treated with 0.55 mL (3.9 mmol) trifluoroacetic anhydride and 0.32 mL (4.0 mmol) pyridine. After 5 days at room temperature the NMR-spectrum showed the complete transformation of the alcohol **10** into its corresponding trifluoroacetate. The reaction was heated at 90 °C for 2 h. The NMR-spectrum showed that the ring-alkylated ketone did not change, whereas the trifluoroacetate of the alcohol **10** converted completely into *2-methyl-3,3-diphenyl-1-butene*, **28**.

^{1}*H-NMR-spectrum* ($Cl_2C{=}CCl_2$, δppm): 1.63 m (3H, $CH_3{-}C{=}CH_2$), 1.90 s (3H, CH_3^5), 4.55 m (1H, $C{=}CH_2$) and 4.98 m (1H, $C{=}CH_2$).

REFERENCES AND NOTES

[1] Note XVIII: M. Stănescu, M. Elian and E. Ciorănescu, *Rev. Roumaine Chim.*, **32**, 969 (1987).

[2] E. Ciorănescu, A. Bucur, M. Elian, M. Banciu, M. Voicu and C. D. Nenitzescu, *Tetrahedron Lett.*, **1964**, 3835; E. Ciorănescu, A. Bucur, M. Elian and C. D. Nenitzescu, *Rev. Roumaine Chim.*, **10**, 149 (1965); E. Ciorănescu, A. Bucur, M. Elian M. Banciu, M. Voicu and C. D. Nenitzescu, *ibid.*, **10**, 161 (1965); E. Ciorănescu, A. Bucur, F. Badea, M. Rentzea and C. D. Nenitzescu, *Tetrahedron Lett.*, **1969**, 1867; M. Stănescu, M. Elian and E. Ciorănescu, *Rev. Roumaine Chim.*, **31**, 1001 (1986).

[3] J. J. Looker, D. P. Maier and T. H. Regan, *J. Org. Chem.*, **37**, 3401 (1972).

[4] M. S. Karasch and O. Reinmuth, "Grignard Reactions of/Nonmetallic Substances", Constable and Co., London, 1954.

[5] C. Blomberg, *Bull. Soc. Chim. France*, **1972**, 2144.

[6] M. Elian, A. Voicu and E. Ciorănescu, to be published.

[7] A. R. Katritzky and B. Wallis, *Chem. & Ind.*, **1964**, 2025.

[8] The *endo*/*exo* ratio was 72 : 18 = 4 :1 at the end of the reaction. It was shown, following the reaction by NMR-spectroscopy, that the *exo*-epimer builds more rapidly and equilibrates then slowly with the *endo*-isomer.

[9] The trifluoroacetates were identified by NMR-spectroscopy and gas-liquid chromatography.

[10] D. E. Horning and J. M. Muchowski, *Canad. J. Chem.*, **46**, 3665 (1968).

[11] W. G. Dauben and J. L. Chitwood, *J. Amer. Chem. Soc.*, **90**, 6876 (1968); G. M. Fraser and H. M. R. Hoffmann, *Chem. Commun.*, **1967**, 561.

[12] H. S. Mosher, *Tetrahedron*, **30**, 1733 (1974).

[13] T. Ando, H. Yamataka, H. Morisaki, J. Yamawaki, J. Kuramochi and Y. Yukawa, *J. Amer. Chem. Soc.*, **103**, 430 (1981): V. J. Schiner jr., and J. J. Tai, *ibid.*, **103**, 436 (1981); H. Yamataka and T. Ando, *ibid.*, **104**, 1808 (1982).

[14] J. E. Nordlander, S. P. Jindal, P. v. R. Schleyer, R. C. Fort jr., J. J. Harper and R. D. Nicholas, *J. Amer. Chem. Soc.*, **88**, 4475 (1966).

[15] The proton migration **47**→**48** recalls the reverse hydride ion migration **32**→**33** observed for the alcohol **9**. The dibenzocycloheptene system seems to be very prone to transannular hydrogen migrations.

[16] The intervention of the phenonium ion is supported by the observation that in magic acid at low temperature the dibenzohomotropilium ion was evidenced. *See*: G. D. Mateescu, C. D. Nenitzescu and G. A. Olah, *J. Amer. Chem. Soc.*, **90**, 6235 (1968).

F 1/103
raktári szám

Revue Roumaine de Chimie
folyóirat címe

1988 év 1. szám (hó)

oldalszám (tól—ig)

Dékány
olvasható aláírás

1989 ápr 1.
dátum

omikk

Revue Roumaine de Chimie, **34**, *1*, 103—109 (1989)

SYNTHESIS OF SOME NEW HETEROCYCLIC DERIVATIVES OF DI- AND TETRAHYDROQUINAZOLINE

FELICIA CORNEA[a], ADALGIZA CIOBANU[a], I. BACIU[a], O. MAIOR[a] and
A. A. EL BAHNASAWY[b]
[a] Faculty of Chemical Technology, Polytechnic Institute, Bucharest, Romania
[b] Zagaziz University, Faculty of Science, Chemistry Department, Egypt

Received October 6, 1988

The investigations for obtaining new heterocyclic compounds with a potential biological activity have been carried on for synthesizing some derivatives of quinazoline. Alkylated derivatives of α-formyl-cyclohexenone and -cyclohexanone were condensed with ammonia and formamide, urea, thiourea and guanidine. Compounds having in their molecule a pyrimidinic cycle condensed with a cyclohexene or alkylated cyclohexanering, derivatives of di- and tetrahydroquinazoline (characterized by physico-chemical methods) have been thus obtained.

The importance of heterocyclic compounds having in their molecule a pyrimidinic nucleus, and especially their biological properties, made us study the synthesis of some heterocyclic compounds of this kind, i.e. quinazoline derivatives.

As a sequel to our previous investigations,[1] and taking into account the considerable reactivity of several cyclic ketones and of their σ-formylated derivatives, we focused our attention on some condensation reactions of these carbonylic compounds with convenient reagents.

1-Methyl—4-(2-propenyl) 1,6-ene-2-cyclohexanone—(+)carvone (obtained from ethereal oil of *Carum carvi*[2]) and 1-methyl-4(2-propyl)-3 cyclohexanone — (—)menthone — (obtained by oxidation of menthol[3]) were formylated, yielding compounds I and II.

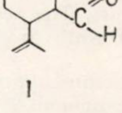

I

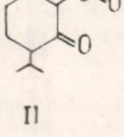

II

— Formyl derivatives I and II presented tautomerism and the equilibrium is shifted towards enolic form (enolization of the formyl group).

After condensation of compounds I and II with ammonia and formamide, urea, thiourea and guanidine, di- and tetrahydro derivatives of

3—H quinazoline were obtained. These heterocyclic systems are interesting for their steric structure, reactivity and biological properties.

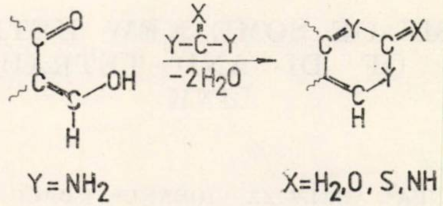

The reaction conditions were established, the compounds obtained were purified, the purity degree was checked by chromatography in thin layer and the structure formulas were attributed on the basis of analytical and spectral data.

The compounds synthesized were formulated as shown below, using *a* and *b* type formulas.

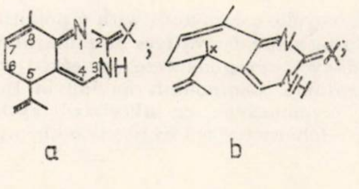

Derivatives of 5,6-dihydro-3-H-quinazoline ;

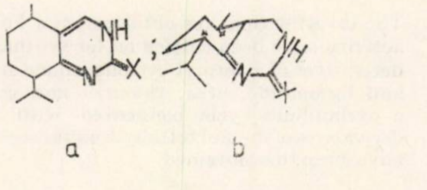

Derivatives of 5,6,7,8-tetrahydro-3-H-quinazoline

EXPERIMENTAL

1. *8-Methyl-5-(2-propenyl)-5,6-(3H)-dihydroquinazoline* was synthesized starting from 0.5 mol I dissolved in 100 chloroform. The solution was cooled to −10°C, and gaseous ammonia was bubbled for 5 hours. After removing chloroform by distillation at low pressure, the enamine formed by preparatory chromatography was separated. In the second stage of synthesis, 0.02 mol enamine, 0.1 mol formamide and 1 g piperidine acetate, freshly prepared, were refluxed at 160—190°C for 12—14 hours. To the reaction mixture cooled to room temperature, 100 mL chloroform were added. The solution was dried on anhydrous $MgSO_4$ and filtered. After removing chloroform, the viscous product obtained was further processed with ethylic ether. The final yellowish product was recrystallized from benzene. Yield 51% ; m.t. = 195—197°C.

2. *8-Methyl-(5-(2-propenyl)-5,6-dihydro-2(3H)quinazolinone* was synthesized in three variants starting from I and urea without solvent or in solvent, DMF or n-butanol, with which the best yield was obtained. 0.02 mol I, 0.02 mol urea, 30 mL n-butanol and several drops of anhydrous piperidine were refluxed for 4 hours. The reaction mixture was left at room temperature for three days and then the yellowish white product separated was recrystallized from benzene. Yield, 72%, m.t. = 177—179°C.

3. *8-Methyl-5-(2-propenyl)5,6-dihydro 2(3H)quinazolinthione* was synthesized using I and thiourea, the method being the same as for compound 2. Yield 59% ; m.t. = 201—203°C.

4. *8-Methyl-5-(2-propenyl)5,6-dihydro 2(3H)quinazolinimine* was synthesized by refluxing 0.02 mol I, 0.02 mol guanidine and 50 mL DMF for 4 hours. The brown compound obtained was recrystallized from benzene. Yield 78% ; m.t. = 163—165°C.

5. *5-Methyl-8-isopropyl-5,6,7,8-tetrahydro-2(3H)quinazolinone* was synthesized from II and urea in similar conditions to those used for obtaining compound **2**. Before cooling the

Table 1

New derivatives of di- and tetrahydroquinazoline

No.	Name and molecular formula	Structural formula	M.t. (°C)	Recrystallization solvent	Colour	Yield (%)	NMR ppm
1.	8-Methyl-5-(2-propenyl)5,6-dihydroquinazoline $C_{12}H_{14}N_2$	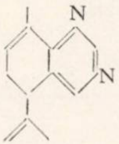	195−197	Ethanol	yellowish	80	$-CH_3$ 1.60−2.22 $>CH_2$ 2.20−2.80
2.	8-Methyl-5-(2-propenyl)5,6 dihydro2(3H)quinazolinone $C_{12}H_{14}N_2O$	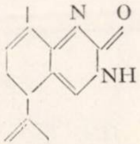	177−179	Benzene	yellowish white	38	$>CH$ 3.10−3.60 $\gg CH$ 6.40−7.30
3.	8-Methyl-5(2-propenyl)5,6-dihydro 2(3H)quinazolinthione $C_{12}H_{14}N_2S$	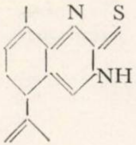	201−203	Benzene	reddish-brown	59	$=C\langle{}^{H}_{H}$ 4.74−5.50 $>N-H$

Table 1 (continued)

No.	Name and molecular formula	Structural formula	M.t. (°C)	Recrystallization solvent	Colour	Yield (%)	NMR ppm
4.	8-Methyl-5(2-propenyl)5,6-dihydro 2(3H)quinazolinimine $C_{12}H_{14}N_3$	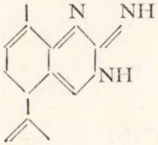	163–165	Ethylic ether Benzene (1V : 1V)	brown	70	$-OH$ 6.80–7.30
5.	8-Methyl-8-(2-propyl)5,6,7,8-tetrahydroquinazolinone $C_{12}H_{18}N_{20}$	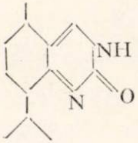	215–217	Benzene	white with a yellowish tint	68	$-CH_3$ 0.5–1.00 $>CH_2$ 1.20–1.80
6.	5-Methyl-8-(2-propyl)5,6,7,8-tetrahydro-2(3H)quinazolinthione $C_{12}H_{18}N_2S$	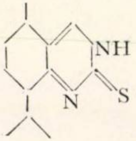	200–202	Benzene	yellow	42	$(H_3C)_2>C-H$ 1.70–2.50
7.	5-Methyl-8-(2-propyl)5,6,7,8-tetrahydro-2(3H)quinazolinimine $C_{12}H_{18}N_3$	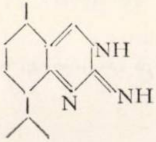	165–168	Ethylic ether Benzene (1V : 1V)	light brown	35	$>C-H$ 2.25–3.50

reaction mixture, several drops of alcoholic ferric chloride solution 1% were added. The product obtained (white with a slightly yellowish tint) was recrystallized from absolute ethanol. Yield 68%, m.t. = 215—217°C.

6. *5-Methyl-8-isopropyl-5,6,7,8-tetrahydro 2(3H) quinazolinthione* was synthesized similarly to compound **3,** starting from II. The yellow product obtained was recrystallized from benzene. Yield : 42%; m.t. = 200—202°C.

7. *5-Methyl-8-isopropyl1-5,6,7,8-tetrahydro-2(3H)quinazolinimine* was synthesized similarly to compound **4,** starting from II. The reaction mixture was poured, after cooling, into 300 mL water with ice. The light-brown product obtained was recrystallized from a mixture of ethylic ether : benzene (1V : 1V). Yield 35%; m.t. = 165—168°C.

Apparatus

IR spectra were recorded on a UR-20 Karl Zeiss Jena spectrometer in KBr disk. NMR spectra were recorded on a 60 MHz Varian A 60 spectrometer, using TMS as reference system and DMSO as solvent.

For chromatographic determinations (CSS) the following were used : Merck chromatographic plates with G silicagel as fixed phase and a mixture of solvents : ethylic ether : heptane (1V : 3V); ethyl acetate : chloroform (1V : 9V); petroleum ether : ethylicether(20V : 1V); ethylic ether : benzene (1V : 1V) as mobile phase and iodine for identification.

RESULTS AND DISCUSSION

The newly synthesized compounds are shown in table 1. Except, for compounds **1** all the others show the existence of a tautomeric equilibrium.

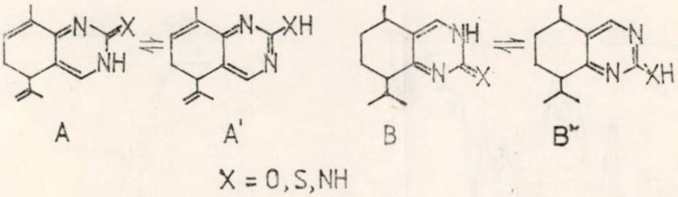

IR spectra

IR spectra of the compounds in table 1 give the characteristic frequencies that explain, together with the data obtained form the NMR, spectra, the structure assigned. Within the ranges 3100—2850 cm^{-1} ν_{sym} and ν_{asym} can be found for the C—H bonds : 1350—1380 cm^{-1} deformation vibrations for the —C—H bond; 920—980 cm^{-1} deformation vibrations for the =C—H bond. Within the range 1700—1600 cm^{-1} the vibration frequencies for the C=N, C=C, C=O bonds, including the amide band I, can be found.

The shape of the spectra within the 1700—900 cm^{-1} range shows interesting differences among compounds; splitting of some bands together with other frequencies explains the existence of the tautomeric forms. For the sulfur containing compounds, the complex thioamidic band appears at 1475, 1415 cm^{-1}.

The 3080—3500 cm^{-1} range shows the presence of the vibrations characteristic for the associated or nonassociated N—H, NH$_2$and —O—H bonds. One could appreciate that the tautomeric equilibrium is shifted towards the carbonylic, thiocarbonylic and imino forms. Intermolecular associations by the hydrogen bonds of the types: N—H— ... :O< N—H ... :N; O—H ... :N; O—H ... :O< and even N—H ... S= and S—H ... N are shown in the spectra. Figures 1, 2 and 3 give the IR spectrum of compound **2** and, comparatively, ranges from the spectra of compounds **2** and **3** (1700—900 $\mathrm{cm^{-1}}$) and of compounds **2**, **3** and **4** (3500—3000 $\mathrm{cm^{-1}}$).

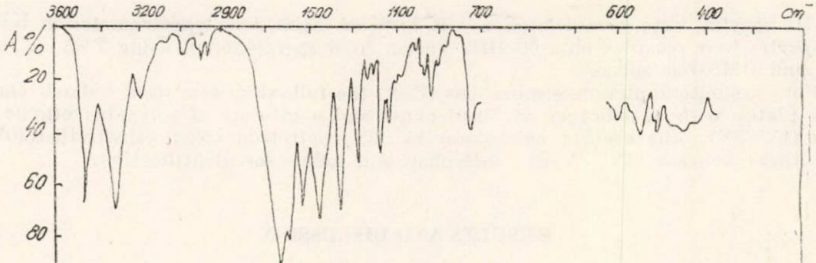

Fig. 1. — Infrared spectra of compound **2**.

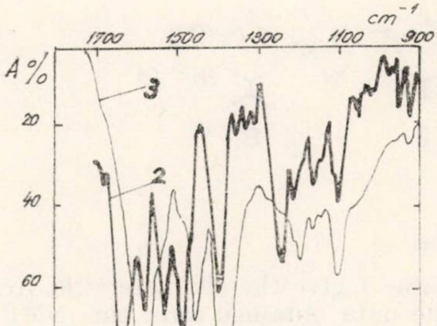

Fig. 2. — Infrared spectra of compounds **2** and **3** (1700—900 $\mathrm{cm^{-1}}$).

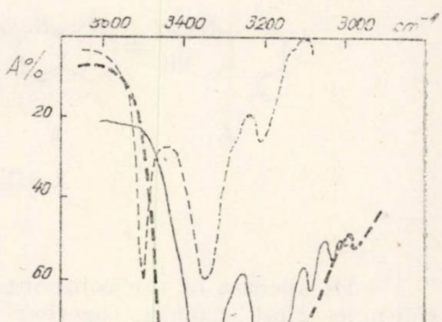

Fig. 3. — Infrared spectra of compounds **2**, **3** and **4** (3500—3000 $\mathrm{cm^{-1}}$).

They show clearly the effect generated by the replacement of oxygen by S and by the = NH group respectively.

The shape of the IR spectrum of compound **3** within the 600—400 $\mathrm{cm^{-1}}$ range, and the existence of a very broad band between 550 and 450 $\mathrm{cm^{-1}}$ should also be considered. It also suggests the existence of an intermolecular association in which the sulfur atom takes place.

CONCLUSIONS

Seven new derived heterocyclic compounds of di- and tetrahydroquinazoline were synthesized and characterized. Except for compound **1** all the others presented tautomerism. The compounds are interesting from the point of view of their sterical structure, reactivity and biological properties.

REFERENCES

[1] F. Cornea, O. Maior, I. Baciu and N. H. El Sayed, *Rev. Chim. (București)*, **38**, 570 (1987).

[2] D. I. A. Iglesias and J. A. Retamar, *Rev. Ital. E.P.P.O.A.S.C.A.*, **1957**, 210.

[3] H. C. Brown and C. P. Garg, *J. Amer. Chem. Soc.*, **83**, 2952 (1961).

Revue Roumaine de Chimie, 34, *1*, 111–114 (1989)

PROGRESS IN HEMODIALYSIS

KEVEN A. CURRAN, JOHN C. PETERSON and EMANUEL MERDINGER
Division of Nephrology, University of Florida

Received October 1, 1988

The present paper deals with some biochemical aspects involved in the clinical technique of hemodialysis. At the same time, this technique is presented in its actual state, its achievements and difficulties.

One of the pioneers of Nephrology, Homer Smith, once said : "Bones can break, muscles can atrophy, glands can loaf, even the brain can go to sleep, without immediately endangering our survival" ; when the kidneys fail and the biochemical perturbations associated with uremia ensue the therapeutic options are limited to renal transplantation or some form of dialysis, either hemo-, or peritoneal.

Dialysis involves the diffusion of small solute molecules across a semipermeable membrane from an area of high concentration to an area of lower concentration. When the kidney ceases to function effectively, ingested substances or metabolites accumulate. These are believed to exhibit concentration-dependent toxicity known as the "uremic syndrome." Although a specific "uremic toxin" has not been identified,this concept is supported by the fact that dialysis is an effective long-term therapy for patients with uremia.

William Kolff, working in the Netherlands, was the first physician to perform hemodialysis or as he termed it "blood washing." He passed blood through a cellophane tube wrapped around wooden slats on a steel drum which rotated in a bath containing the dialysate. Since that time dialysis has undergone drastic improvements. The currently disposable hollow-fiber kidneys are made of a reconstituted celluloid derivative called cuprophane with an average pore diameter of 10–12 microns. Efficiency of solute removal has been increased by modifications which allow for countercurrent flow of blood and dialysate. Currently over 80,000 patients are maintained on chronic hemodialysis in the U.S.

Although a large number of patients are maintained on dialysis with only a small mortality each year, it is not without continuing problems. Patients on dialysis for more than 10 years have a much higher incidence of cardiovascular mortality when compared to "normal controls", probably related to multiple on-going problems including hypertension and hyperlipidemia.

Recent advances have improved dialysis efficiency. Undialyzed middle molecular weight molecules (mol. wt 200–2000) have long been thought to cause many of the side effects associated with dialysis. Recently (polysulfone) membranes have been developed which allow improved filtration of middle molecules. With these membranes, a dialyzer has been developed which takes advantage of greatly increased blood flow and improved membrane permeability to shorten dialysis time from 4 to $2\frac{1}{2}$ hours. The use of these new techniques is limited by blood flow from the patients fistula, and by the hypotension caused by rapid fluid removal from the intravascular space. Currently, research into the plasma refill time required for such "high-flux" dialysis is underway. If these limitations can be overcome the high-flux dialysis technique will improve efficiency both in regard to filtration of middle molecules and time spent on a dialysis machine.

The combination of more permeable membranes and increased blood flow, from the previous maximum of 250 mc/min to 400—500 ml/min, is now called "high flux" dialysis.

One of the major complications of chronic renal insufficiency and dialysis is chronic anemia. Up to 25% of dialysis patients require regular blood transfusions. This places them at increased risk for infection with hepatitis and the acquired immunodeficiency syndrome virus, as well as iron overload. The cause of this anemia is not well defined but is believed to occur via three mechanisms (see Table 1). These mechanisms are decreased erythropoietin (a hormone produced in the kidney which stimulates the bone marrow's production of red blood cells) production relative to the severity of the anemia, plasma "uremic toxins" that inhibit the bone marrow's response to erythropoietin and mild hemolysis.

Table 1

Mechanisms of the anemia of chronic renal failure

(1) Decreased renal mass — decreased erythropoietin production relative to the severity of the anemia
(2) "Uremic toxins" — inhibit bone marrow response to erythropoietin
(3) Mild hemolysis

A study by Pavlovic-Kentera showed that patients with acquired polycystic kidney disease and mild anemia had much higher erythropoietin levels than chronic renal failure patients with severe anemia (see Table 2).

Table 2

Erythropoietin and hematocrit levels in patients

	Hematocrit	Erythropoietin level
Adult polycystic kidney disease	38±7	151.1±15.4
Chronic renal failure	19±3	20.7±4

Further, patients on hemodialysis have a slightly higher erythropoietin level than patients with chronic renal failure but these levels are much lower than patients without renal failure who have comparable hematocrits. Thus the diseased kidneys are unable to produce adequate erythropoietin to normalize red blood cell production.

A number of uremic toxins have been implicated in the pathogenesis of the anemia of chronic renal failure. Some of these are listed in Table 3 and include unfiltered middle molecules and high molecular weight substances, low molecular weight proteins and biopolar lipids. Also implicated is elevated parathyroid hormone from the secondary hyperparathyroidism of chronic renal insufficiency. These substances are thought to inhibit the end-organ response to erythropoietin thus inhibiting the ability of the bone marrow to respond to the erythropoietin present.

Table 3

Plasma "uremic toxins" associated with the anemia of chronic renal failure

---

- Unfiltered "Middle Molecules"
- Parathyroid hormone
- Low molecular weight proteins
- High molecular weight substances
- Bipolar lipids

A number of factors are associated with hemolysis in dialysis patients. These are listed in Table 4. The procedure of dialysis itself can induce hemolysis by mechanical injury and copper in the dialysis membrane. Elevated aluminum levels and changes in plasma osmolality resulting from dialysis can also induce hemolysis. Hypersplenism and a microangiopathic hemolytic anemia also can occur in patients with chronic renal failure. Finally, low phosphate levels resulting from the use of phosphate binders can produce hemolysis.

Table 4

Factors associated with hemolysis in dialysis patients

Dialysis associated
- Mechanical injury
- Osmolality changes
- Copper
- Aluminum

Microangiopathic hemolysis
Hypophosphotemia
Hypersplenism

For several decades it has been postulated that the administration of erythropoietin to chronic renal failure patients would improve this anemia; however, adequate amounts of this hormone were not available. In the last 10 years erythropoietin has been sequenced and the gene coding for its production has been cloned. Through recombinant DNA technology using bacteria, sufficient quantities of erythropoietin are now available for clinical studies.

Winearls et al administered erythropoietin to ten patients three times a week. All ten patients had a rise in hemoglobin after eleven weeks. Eschbach et al. studied 25 patients with varying doses of erythropoietin and demonstrated a dose related increase in hematocrit. Currently, a double blind placebo controlled study is underway to definitively evaluate erythropoietin. Side effects of this therapy have included : worsening hypertension, fistula clotting, iron deficiency anemia, and an increase in predialysis blood urea nitrogen and creatinine. Not only do these patients no longer require transfusions with its attendant risks and costs but they have a marked improvement in their sense of well-being and increase their activity level. The combination of erythropoietin and high-flux dialysis offer the hemodialysis patient a greatly improved quality of life, which is, after all, the reason for dialysis therapy.

Revue Roumaine de Chimie, 34, *1*, 115–119 (1989)

STRUCTURE ÉLECTRONIQUE DES MOLÉCULES. APPLICATIONS EN PHYSIQUE, CHIMIE ET BIOLOGIE

RAYMOND DAUDEL

Président d'honneur de l'Académie Internationale des Sciences Moléculaires Quantiques

Reçu le 25 novembre 1988

The paper reports the modification of radioactive period due to chemical effects, the concept of chemical bond, the relation of molecular electronic structure with chemical reactivity and carcinogenic capacity.

L'article présente la modification des périodes radioactives sous des effets chimiques, le concept de liaison chimique, les relations entre la structure électronique des molécules, leur réactivité chimique et leur pouvoir cancérogène.

INTRODUCTION

En 1981 j'avais eu l'honneur d'écrire la préface de l'édition française de l'ouvrage de l'Académicien Docteur Ingénieur Elena Ceaușescu dédié à de «Nouvelles recherches dans le domaine des composés macromoléculaires»[1].

J'avais pu ainsi mesurer l'importance des recherches réalisées par Madame Ceaușescu et ses collaborateurs dans un domaine qui comporte à la fois des recherches fondamentales et des applications pratiques très utiles à notre société.

C'est donc pour moi un grand privilège d'être invité à contribuer à la rédaction de ce livre jubilaire destiné à rendre hommage à un savant qui de plus préside au destin de la recherche scientifique et technologique de la République Socialiste de Roumanie qui joue un rôle éminent dans la production de la connaissance scientifique mondiale.

Je me propose d'évoquer brièvement quelques travaux que j'ai réalisés avec différents collaborateurs afin de mieux comprendre la structure électronique de molécules et d'en tirer quelques applications à la physique, à la chimie et à la biologie.

MODIFICATION DES PÉRIODES RADIOACTIVES SOUS DES EFFETS CHIMIQUES

On a longtemps pensé que les propriétés des noyaux des atomes et des molécules sont insensibles à leur environnement électronique. On avait en particulier remarqué que la période radioactive d'un noyau, autrement dit le rythme de sa désintégration, ne dépend pas de la molécule qui le renferme.

En 1947, réfléchissant à l'image que la mécanique ondulatoire donne des atomes et des molécules, je suis arrivé à la conclusion inverse. En effet, selon les idées de cette mécanique, les électrons qui peuplent les atomes et les molécules entrent de temps à autre en contact avec leurs noyaux.

J'étais ainsi arrivé à la conclusion que dans le fluorure de béryllium, où le fluor attire les électrons plus fortement vers lui que le béryllium, le noyau de béryllium devrait être moins souvent visité par les électrons que le même noyau de béryllium dans le métal. J'avais donc prévu que la vie moyenne de l'isotope 7 du béryllium qui se désintègre par capture électronique devait être plus grande dans le cas du fluorure que dans le cas du métal. [2] J'ai découvert le phénomène, peu de temps après, en réalisant l'expérience en collaboration avec R. Bouchez, P. Daudel et R. Muxart. [3] Dans le même article (2) je signalais que la vie moyenne des isomères nucléaires devait également dépendre de la structure électronique des molécules qui les contiennent. Ce nouveau phénomène a été découvert deux années plus tard. [4]

Actuellement, la relation qui existe entre la période radioactive d'un noyau et la structure chimique des molécules dont il fait partie est bien connue. Cette relation constitue un moyen d'élection pour la détermination de la nature chimique de traces radioactives. [5]

Dans le cas de la capture électronique, la période du noyau dépend directement de la valeur de la densité électronique en ce noyau. La mesure de la période permet de mesurer cette densité.

LE CONCEPT DE LIAISON CHIMIQUE

Le concept de liaison chimique joue un rôle central dans les études qui visent à préciser la structure électronique des molécules. Pendant longtemps, suivant les idées de Lewis, on a admis que des électrons particuliers servent à établir des liens, des liaisons entre les atomes d'une même molécule. Deux électrons servant, par exemple, à établir une liaison simple de covalence entre deux atomes.

Cette conception se heurte à une difficulté sérieuse car, en mécanique ondulatoire, tous les électrons sont indiscernables et doivent de ce fait jouer le même rôle dans la molécule. On ne peut distinguer des électrons particuliers.

Pour lever cette contradiction j'ai introduit le concept de loge. [6] Une loge est un domaine de l'espace où il existe une haute probabilité de rencontrer un certain nombre d'électrons (avec une certaine organisation de leurs spins). Pour trouver de telles loges dans les atomes et les molécules on peut minimiser l'information manquante.

Dans la molécule B H on peut, par exemple, délimiter une région située entre le noyau du bore et celui de l'hydrogène où il existe une haute probabilité de rencontrer deux électrons de spins contraires : c'est une loge de liaison. On notera la différence avec la conception initiale. La liaison n'est plus constituée par deux électrons. Elle est devenue une région de l'espace où l'on trouve souvent deux électrons et deux seulement, mais bien entendu n'importe lesquels ; ce ne sont plus deux électrons particuliers ; le principe d'indiscernabilité est respecté.

Par ailleurs, puisque les loges s'obtiennent en minimisant l'information manquante, elles donnent le maxium possible d'information sur la distribution des électrons dans l'espace de l'atome ou de la molécule étudiés.

Pour préciser encore le concept de liaison chimique, en collaboration avec Mesdames Besnaïnou et Roux[7] j'ai introduit la notion de densité électronique différentielle.

Cette fonction est la différence entre la densité électronique existant effectivement en un point d'une molécule et la densité électronique qui existerait en ce même point si les densités électroniques des atomes qui constituent la molécule s'étaient simplement superposées sans se perturber.

En chaque point d'une molécule la densité électronique différentielle mesure donc l'effet de la liaison sur la densité. En un point où la densité différentielle est positive, la liaison entre les atomes a apporté un enrichissement électronique. Un appauvrissement électronique a été causé par ce même phénomène de liaison en un point d'une molécule si cette densité différentielle est au contraire négative en ce point. Ce concept a été largement utilisé pour étudier les transferts électroniques provoqués par les phénomènes de liaison. A. Pullman [8] a, par exemple, montré en utilisant cette méthode qu'un net appauvrissement électronique se produit au voisinage du proton qui sert à établir «une liaison hydrogène» .

STRUCTURE ÉLECTRONIQUE ET RÉACTIVITÉ CHIMIQUE

La famille des hydrocarbures conjugués constitue un important ensemble de molécules organiques tant au plan théorique qu'au plan pratique. Rappelons que cette famille qui comprend le benzène, le naphtalène, l'anthracène comporta des molécules très cancérogènes come le 3,4 benzopyrène.

Les distances qui dans ces molécules séparent les atomes de carbone adjacents ne sont pas identiques. Les liaisons les plus courtes sont bien sûr les plus fortes et L. Pauling a défini, pour caractériser les différentes liaisons, un indice de liaison qui mesure la force de la liaison, son «énergie de liaison».

Certains réactifs qui se fixent volontiers sur une liaison carbone-carbone des hydrocarbures conjugués choisissent de préférence la liaison la plus forte. C'est le cas de l'ozone et du tétraoxyde d'osmium.

Les méthodes de la chimie quantique permettent le calcul des indices de liaison d'un hydrocarbure conjugué et, par conséquent, la détermination de la liaison la plus apte à réagir par addition avec un réactif comme l'ozone : c'est la liaison qui possède le plus grand indice de liaison.

Les hydrocarbures conjugués dits alternants possèdent une propriété intéressante : la charge électronique autour de chaque atome de carbone est sensiblement la même. Il en résulte que les ions positifs, les ions négatifs et les radicaux libres ne se fixent pas habituellement sur le même atome de carbone.

Afin de pouvoir prévoir sur quel atome ces réactifs se fixent de préférence, j'ai, en collaboration avec A. Pullman, introduit le concept d'indice de valence libre[9] à partir d'une idée de Swartholm. L'indice de valence libre d'un atome est la différence entre une constante (d'ailleurs arbitraire) et la somme des indices de liaison qui aboutissent à cet atome.

Dans la famille des hydrocarbures alternants les ions, les radicaux libres se fixent préférentiellement sur l'atome de carbone possédant le plus grand indice de valence libre.

Et sur ces bases s'est peu a peu développée une méthode qui établit un pont entre les structures électroniques et la réactivité chimique : la méthode des diagrammes moléculaires.

STRUCTURE ÉLECTRONIQUE ET POUVOIR CANCÉROGÈNE

Pour interpréter certains phénomènes d'antagonismes entre composés cancérogènes découverts par A. Lacassagne, N. P. Buu-Hoi et G. Rudali, j'avais été conduit à supposer que les hydrocarbures cancérogènes se fixent sur certaines molécules importantes des cellules vivantes. [10]

Un peu plus tard, A. Pullman [11] nota la présence d'une liaison possédant un fort indice de liaison (donc apte à donner des réactions d'addition) chez les hydrocarbures conjugués cancérogènes.

Ces observations, jointes a différentes données expérimentales conduisirent mon épouse P. Daudel à élucider en collaboration avec Duquesne, Vigny, Grover et Sims, le mécanisme de la fixation des hydrocarbures cancérogènes sur les acides nucléiques des tissus animaux. [12]

Ces auteurs traitèrent des souris par du benzopyrène et montrèrent clairement grâce à une méthode spectrophotométrique très performante que le benzopyrène ne se fixe pas directement sur les acides nucléiques cellulaires.

Il subit d'abord une oxydation sous l'influence d'un enzyme qui cherche à se débarasser de la molécule importune. Par malheur, cet enzyme transforme le benzopyrène en un diol-époxyde très agressif qui constitue lui le véritable canérogène et se fixe solidement aux acides nucléiques. [13]

BIBLIOGRAPHIE

[1] Elena Ceauşescu, « Nouvelles recherches dans le domaine des composés macromoléculaires », Pergamon Press (1981).

[2] R. Daudel, *La Revue Scientifique*, **85**, 162 (1947).

[3] R. Daudel, R. Bouchez, P. Daudel et R. Muxart, *J. de Physique*, II, 336 (1947).

[4] Bainbridge, Goldhaber et Wilson, *Physical Review*, **75**, 897 (1949).

[5] Vargas, *M.T.P. Int. Rev. Sci. Series*, 1, 8, 75 (1971).

[6] R. Daudel, *C. R. Académie des Sciences*, 237, 601 (1953).

[7] *J. Chim. Phys.*, **53**, 218 (1956).

[8] dans R. Daudel et A. Pullman ,« Aspects de la chimie quantique contemporaine », CNRS éditeur, p. 253 (1971).

[9] R. Daudel et A. Pullman, *C. R. Académie des Sciences*, **220**, 888 (1945).

[10] A. Lacassagne, N. P. Buu-Hoi, R. Daudel et G. Rudali, *Compt. Rend. Soc. Biol.*, **138**, 282 (1947).

[11] A. Pullman, *Ann. Chim., Paris*, **2**, 5 (1947).

[12] P. Daudel, M. Duquesne, P. Vigny, Ph. L. Grover et P. Sims, *FEBS Letters*, **57**, 250 (1975).

[13] L'ensemble des travaux évoqués dans ce bref article se trouve développé en détail dans les livres suivants : R. Daudel, « Théorie quantique de la liaison chimique », Gauthier Villars (1967) ; P. Daudel et R. Daudel, « Chemical Carcinogenesis and Molecular Biology », Wiley (1966) ; R. Daudel, G. Leroy, D. Peeters et M. Sana, « Chimie cuantică », Ed. Academiei Republicii Socialiste România (1988).

Revue Roumaine de Chimie, 34, 1, 121–128 (1989)

RECENT DEVELOPMENTS IN PERFLUOROORGANO CHEMISTRY OF SELENIUM IN VARIOUS OXIDATION STATES

A. HAAS
Lehrstuhl für Anorganische Chemie II, Ruhr-Universität Bochum,
Postfach 102 148, D–4630 Bochum

Received November 29, 1988

A review is presented for the following developments in the field of perfluoroorgano-chemistry of selenium in various oxidation states.

Following the last review on perfluorohalogenoorgano Selenium Chemistry [1] in 1985 it seems appropriate to report on new activities and accomplishments in this field. Progress has been achieved in the following areas :

1) Perfluoroorgano-selenocarbonyls and –1,3-Diselaetanes
2) Trifluoromethyl- and Pentafluorphenylselenonic Acid
3) Selenium-containing cationic Ring Compounds

Selenocarbonyls are still rare compounds in comparison with their sulfur analogues. This is mainly due to their great reactivity, toxicity and unpleasant smell. Two such compounds are known so far : F_2CSe[2] and $(CF_3Se)_2CSe$.[3] The key compound is without any doubt F_2CSe, which can be made by thermal decomposition of $B(SeCF_3)_3$ [2] or $(CH_3)_3SnSeCF_3$, [4] or by reacting $Hg(SeCF_3)_2$ with AlI_3^3 or $(CH_3)_2AlI$.[5] All these methods have in common the elimination of F_2CSe from a CF_3Se-group, with simultaneous formation of an E–F bond according to

$$E(SeCF_3)_n \rightarrow n\ F_2CSe + EF_n$$

For E = B, n = 3 ; E = Hg, n = 2 ; E = $(CH_3)_3Sn$ n = 1.

It seemed therefore most appropriate to use such methods for the preparation of other selenocarbonyls.

If $Hg(SeC_2F_5)_2$ is reacted with AlI_3 or $(C_2H_5)_2AlI$ in octamethylcyclotetrasiloxane at 40 to 50°C/$5 \cdot 10^{-3}$ Torr, a deep violet liquid of $CF_3C(Se)F$ condenses in a trap cooled to –196°C in 43% yield. Since the reaction is carried out in a dynamic vacuum, the product is contaminated mainly by some solvent and $(C_2H_5)_2AlI$. The product tends to polymerize even at – 100°C to a waxy colourless solid in a few minutes. Possibly this polymerisation process is catalyzed by impurities. The purified solid pyrolyses at 300 to 400°C to yield 13% $CF_3C(Se)F$. It has been characterized in a mixture with its two isomeric dimers by ^{77}Se— and ^{19}F—NMR-spectroscopy.

^{77}Se—NMR (−50°C, d_8-toluene): (Se) = 1560 (d), J(Se—F) = 315 Hz; external standard: CH_3SeCH_3. ^{19}F—NMR: (CF) = 60.2 (qu), J(F—F) = 16.9 Hz, $^2J(Se-F) = 314.7$ Hz; (CF_3) = −71.3 (d), $^3J(F-F) = 16.9$ Hz.

Thermal decomposition of the polymer gives as volatile products 13% $CF_3C(Se)F$, 35% *cis*- and 46% *trans*-2,4-difluoro-2,4-bis (trifluoromethyl)-1,3-diselanetane, estimated by ^{19}F—NMR spectroscopy at − 50°C. They are trapped in $CFCl_3$ and vigorous stirring is essential on warming up to 20°C to prevent polymerisation of the monomer. It dimerizes in $CFCl_3$ solution at 20°C within 30 minutes quantitatively to the *cis*-, *trans*-dimers according to the following scheme.

$$Hg(SeC_2F_5)_2 + (C_2H_5)_2AlI \xrightarrow[C_2H_5HgI_2]{} \langle CF_3C(Se)F\rangle$$

$$\rightarrow [CF_3C(Se)F]_n$$

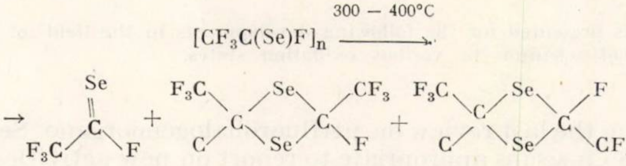

Pyrolysis of $[CF_3C(Se)F]_n$ takes place in complete agreement with that of $(F_2CSe)_x$. The product distribution for $[CF_3C(Se)F]_n$ is $CF_3C(Se)F$:*cis*-, *trans*-$[CF_3C(Se)F]_2$ = 14 : 86 and for $(F_2CSe)_x$ the ratio $F_2C = Se : (F_2CSe)_2$ is 40 : 60. These results show that $CF_3C(Se)F$ is more reactive (less stable) than F_2CSe.

The mixture of *cis*, *trans*-dimers can be separated by gas chromatography methods. They are separated on a 4.5 m (i.d. = 6 mm) column packed with 10% Marlophen 814 on Chromosorb P NAW, 60−80 mesh, 75°C, He-stream: 80 ml/min. *Trans*-$[CF_3C(Se)F]_2$ is a pale yellow coloured crystalline substance (m.p. 27.5°C) and *cis*-$[CF_3C(Se)F]_2$ is a yellow liquid.

The monomer undergoes as a dienophil (2+4) cyclo additions and forms with cyclopentadiene a mixture of exo-, endo-3-fluoro-3-trifluoromethyl-2-selenabicyclo [2.2.1] hept-5-ene in a 5 : 4 ratio according to

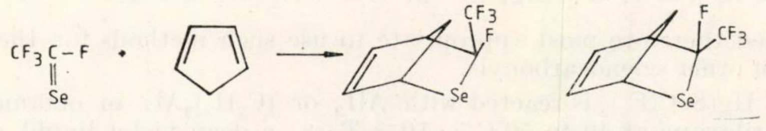

It is remarkable that in the ^{19}F—NMR-spectrum of the isometric mixture only one signal representing (CF) is splitted into a doublet by coupling with the proton of C−4. The other isomer shows only a quartet by coupling with the adjacent CF_3-group. These observations are in agreement with the results obtained from F_2CSe-cyclopentadiene addition products. Here again the endo-fluoratom only couples with the adjacent proton.[4]

Analogous to the preparation of $CF_3C(Se)F$ the homolog $CF_3CF_2C(Se)F$ is made from $Hg(SeCF_2CF_2CF_3)_2$ and $(C_2H_5)_2AlI$ in good yields. The liquid monomer is deep violet coloured and can be handled in a vacuum system without greater losses by polymerisation. When kept in daylight a solution of $C_2F_5C(Se)F$ in $CFCl_3$ or pentane dimerizes at 20°C in about 15 to 30 minutes to yield *cis-*, *trans-*$[C_2F_5C(Se)F]_2$, a yellow mobile liquid. It was not possible to separate these two isomers by gas chromatography. As far as polymerisation is concerned, $C_2F_5C(Se)F$ is more stable than $CF_3C(Se)F$ but less than F_2CSe. With cyclopentadiene $C_2F_5C(Se)F$ reacts in pentane immediately to form the corresponding $(4+2)$-cyclo adduct. In this reaction the formation of only one product is observed probably the endo-fluoro compound. Preparation and reactivity of $C_2F_5C(Se)F$ is summarized in the following scheme:

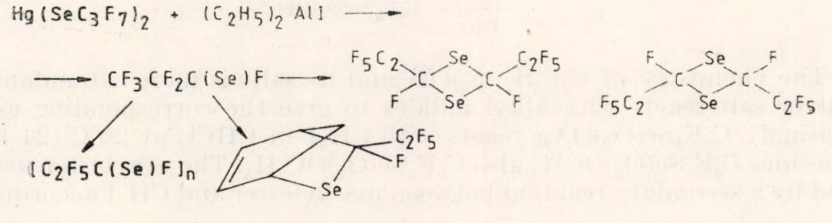

Since each of the starting materials C_2F_5COOH and C_3F_7COOH are contaminated with up to 5% of the latter, during the distillation of $(CF_3C(Se)F)_2$ and $[C_2F_5C(Se)F]_2$ small amounts of an additional product are isolated, which according to spectroscopic investigations is probably a mixed *cis-*, *trans-*dimer of $CF_3C(Se)F$ and $C_2F_5C(Se)F$. When the reaction between $Hg(SeCF_3)_2$ and AlI_3 is carried out in vacuo ($5 \cdot 10^{-3}$ Torr) under the conditions described above for the preparation of $CF_3C(Se)F$, then in addition to the already known products F_2CSe and $CF_3SeSeCF_3$ a new selenocarbonyl can be isolated. It is the linear dimer of selenocarbonyldifluoride. Spectroscopic investigations at -50°C, $^{19}F-$, $^{13}C-$ and $^{77}Se-$NMR-spectra prove unambigously the formula $CF_3SeC(Se)F$. The deep orange to red coloured liquid dimerizes in solution similar to F_2CSe. After keeping a sample in sunlight for 3 days *cis-* and *trans-*$[CF_3SeC(Se)F]_2$ is formed in a 3 : 1 ratio.

Since the preparation of the first perfluoroorganoselenonic acid only little progress has been achieved concerning the chemistry of this acid.[6] Reaction of CF_3SeO_3Ag and C_2H_5I in $CHCl_3$ at 20°C (24 h) yielded 60% $CF_3SeO_2OC_2H_5$. The colourless liquid (m.p. 5°C) has been fully characterized. Some advance has been achieved in pentafluorophenyl-selenium (VI) chemistry.

The oxidation of $C_6F_5Se(O)OH$ (made from $C_6F_5SeSeC_6F_5$ and HNO_3) with $KMnO_4$ in aqueous solution took place according to

$$3\ C_6F_5Se(O)OH + 2\ KMnO_4 \rightarrow 2\ C_6F_5Se(O_2)K$$

$$+ C_6F_5Se(O_2)OH + MnO_2 + H_2O$$

$$C_6F_5Se(O_2)OH + MOH \rightarrow C_6F_5Se(O_2)OM + H_2O$$

$$M = NH_4^+,\ Li^+,\ Na^+,\ 1/2\ Ba^{++}$$

Similarly Cs- and Ag-salts are made from $C_6F_5Se(O_2)OH$ and equimolar amounts of $CsNO_3$ or $AgNO_3$. Besides the silver salt, which is only slightly soluble, the others dissolve in water. On heating decomposition without melting takes place in the range of 245 to $> 350°C$.

When the potassium salt is treated with $HClO_4$ in aqueous solution the free acid is obtained. The solution was boiled down till colourless blades precipitated. Elemental anaylsis and spectroscopical data proved that the compound is the monohydrate $C_6F_5Se(O_2)OH \cdot H_2O$ (m.p. 120°C). On heating in vacuo water evaporates and the pure acid $C_6F_5Se(O_2)OH$ is obstained (m.p. 160°C).

$$C_6F_5Se(O_2)OK + HClO_4 \xrightarrow[-KClO_4]{H_2O} C_6F_5Se(O_2)OH \cdot H_2O$$

$$\xrightarrow[H_2O]{} C_6F_5Se(O_2)OH$$

The chemistry of $C_6F_5Se(O_2)OH$ and its salts is more abundant, as the silver salt reacts with alkyl iodides to give the corresponding esters. Surprisingly $C_6F_5Se(O_2)OAg$ reacts with CH_3I in $CHCl_3$ at 20°C (24 h) to give besides $C_6F_5Se(O_2)OCH_3$ also $C_6F_5Se(O_2)OC_2H_5$. The ethylester may be formed by a secondary reaction between methylester and CH_3I according to

$$C_6F_5Se(O_2)OAg + CH_3I \xrightarrow[-AgI]{} C_6F_5Se(O_2)OCH_3\ CH_3I \xrightarrow[-HI]{CH_3I}$$

$$\longrightarrow C_6F_5Se(O_2)OC_2H_5$$

As the reaction products could not be separated, this process provides only a mixture of these two esters. Therefore the methylester has been characterized spectroscopically only. In opposition to mentioned esterification $C_6F_5Se(O_2)OAg$ forms with C_2H_5I and $CH_3CH_2CH_2I$ the corresponding ester in a pure state.

$$C_6F_5Se(O_2)OAg + RI \longrightarrow C_6F_5Se(O_2)OR\,;$$

$$R = C_2H_5 \text{ (m.p. 15°C)},\ n-C_3H_7 \text{ (m.p. 18°C)}$$

Both substances are colourless liquids with almost no vapour pressure at 20°C and soluble in polar organic solvents.

Similarly $C_6F_5Se(O_2)OAg$ forms with $(CH_3)_3SiCl$ in $CHCl_3$ the corresponding silylester

$$C_6F_5Se(O_2)OAg + (CH_3)_3SiCl \xrightarrow[-AgCl]{} C_6F_5Se(O_2)OSi(CH_3)_3$$

At room temperature the silylester is a colourless liquid (m.p. about 10°C) and has almost no vapour pressure at 20°C.

The NMR-spectra were carried out in D_2O, CH_3OD or $CDCl_3$. As standards were used for $^{19}F-CFCl_3$ (internal) and for ^{77}Se-NMR-spectra CH_3SeCH_3 (external). ^{19}F-chemical shifts for the F-atoms in C_6F_5 are lowest for $C_6F_5Se(O_2)OC_2H_5$ in $CDCl_3$ at $\delta(2\text{-}, 6\text{-F}) = -132.9$, $\delta(4\text{-F}) = -139.7$ and $\delta(3\text{-}, 5\text{-F}) = -155.1$ ppm and highest for $C_6F_5Se(O_2)OH$ in

CH_3OD at $\delta(2\text{-},\ 6\text{-F}) = -136.9$, $\delta(4\text{-F}) = -148.8$ and $\delta(3\text{-},\ 5\text{-F}) = = -160.3$ ppm. The signals for the other compounds are placed between.

Because of Se—F coupling $\delta(^{77}Se)$ is observed as a complex multiplet for all compounds in the range of 982.4 for $C_6F_5Se(O_2)OSi(CH_3)_3$ and 1027.9 ppm for $CF_3Se(O_2)OC_2H_5$. The others absorb inbetween. ^{13}C- and ^1H—NMR-spectra were also measured and the results observed confirmed the structures. In $C_6F_5Se(O_2)OSi(CH_3)_3$ δ $(^{25}Si) = 38.9$ ppm. IR- and mass spectra were also recorded but no unexpected observations were made.

A considerable revival and extension has been achieved in the field of selenium-sulfur-nitrogen cationic ring compounds. Since $S(NSO)_2$ reacts with $SbCl_5$ or $TiCl_4$ to yield either S_4N_4 [7] or S_2N_2, [8] it was desirable to synthesize $Se(NSO)_2$ and to study its chemistry. It is made from Se_2Cl_2 and $(CH_3)_3SiNSO$ dissolved in CH_2Cl_2 or hexamethyldisiloxane in 80 to 85% yield. Lower yields are obtained from $SeOCl_2$ or $SeCl_4$ and $(CH_3)_3SiNSO$.[9] The yellow crystalline solid proved to be the expected, many-sided synthon for the preparation of thiodiselenazyl cations. Preparation of $[Se_4S_2N_4]^{++}[MF_6^-]_2$ from $Se(NSO)_2$ and MF_5 (M = As, Sb, Nb) in SO_2 at 22°C (2—3 d) is superior to the one carried out by Gillespie et al. [10] They prepared $[Se_4S_2N_4]^{++}[M'F_6^-]_2$ (M' = As, Sb) from S_4N_4 and $Se_4[AsF_6]_2$, $Sb_4[Sb_2F_{11}]_2$ or $Se_8[AsF_6]_2$ in SO_2 or CH_2Cl_2. As the starting materials $Se(NSO_2)_2$ and MF_5 are better available than S_4N_4 and $[Se_{4\langle 8\rangle}]^{++}[AsF_6{}^-]_2$ or $Se_4{}^{++}[S_2F_{11}{}^-]_2$ methods (1) is more favourable.

$$Se(NSO)_2 + MF_5 \xrightarrow[\text{in}SO_2]{22°C} [Se_4S_2N_4]^{++}\ [MF_6{}^-]_2 \qquad (1)$$

1

M = As, 2 h, dark blue to violet, 40%, **1a**; Sb, 2 h, dark green, 38%, **1b**; Nb, 3 h, dark blue, 59%, **1c**.

$$[Se_{4(8)}]^{++}[AsF_6{}^-]_2 + S_4N_4 \xrightarrow[\text{in } SO_2]{22°C} [Se_4S_2N_4]^{++}[AsF_6{}^-]_2 \qquad (2)$$

1a

$$[Se_4]^{++}[Sb_2F_{11}{}^-]_2 + S_4N_4 \xrightarrow[\text{in } SO_2]{22°C} [Se_4S_2N_4]^{++}[SbF_6{}^-]_2$$

1b

From reaction with $Se_8{}^{++}[AsF_6{}^-]_2$ in SO_2 37% [9] **1a** are obtained.

As the infrared spectra of the products prepared from $Se(NSO)_2$ according to (1) differed substantially from the one yielded by (2), additional characterizations were carried out. A complete microanalysis proved that the dark blue to violet coloured crystals have the composition $As_2F_{12}N_4S_2Se_4$. Magnetic measurements showed that the product is diamagnetic and it gave no ESR- spectrum as a solid.

A final proof for the identity of $[Se_4S_2N_4]^{++}[AsF_6^-]_2$ made by route (1) or (2) has been achieved by crystal structure investigation. The structure was elucidated and is identical with the one published.[10] $[Se_4S_2N_4]^{++}[NbF_6^-]_2$ has been synthesized for the first time. When $Se(NSO)_2$ was reacted with $SbCl_5$ (ratio 1 : 0.5 to 0.7) dissolved in CH_2Cl_2 at 22°C (20 h) a new thiodiselenazyl cation is formed in 53.6% according to

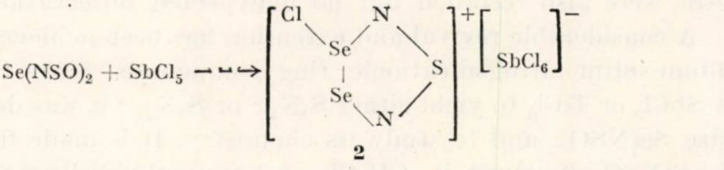

2 (3)

Besides a complete elemental analysis orange coloured **2** was characterized by its IR-, Raman-, ^{77}Se- and ^{14}N−NMR-Spectra. It shows no ESR-spectrum and is diamagnetic. The crystal structure investigation proved the five membered ionic ring structure with an exocyclic chlorine bound to one selenium atom and the $[SbCl_6]$ unit. Similarly $Se(NSO)_2$ forms with PCl_5 (ratio 1 : 1) in CH_2Cl_2 by an oxidative halogenation process 27% $[ClSe_2N_2S]^+Cl^-$(**3**) as an orange-red solid compound. It undergoes a complete halogen exchange reaction with $AgAsF_6$ in SO_2 and provides colourless $[Se_2N_2S]^{++}[AsF_6^-]_2$ in 90% yield. This substance can also be made from $Se(NSO)_2$ and AsF_5 (ratio 1 : 3) in SO_2 in 70% yield. The following scheme ilustrates the described reactions.

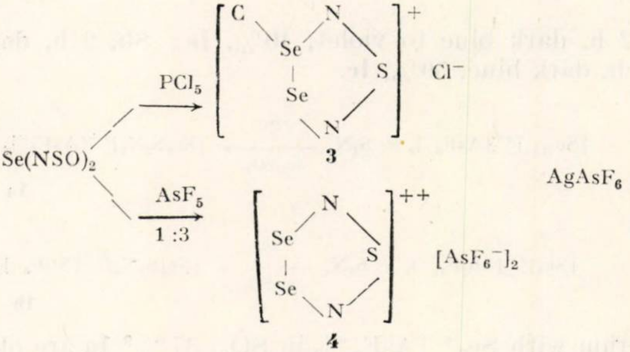

The fact that **3** is insoluble in CH_2Cl_2, SO_2 and $POCl_3$ supports an ionic structure but investigations carried out so far (eg. reaction with $AgAsF_6$ to **4**) can not rule out that both chlorine atoms form covalent bonds with one Se-atom. **2a** and **2c** proved to be good starting materials for the preparation of halogenated thiadiseladiazyl cations. They react with Cl_2 at

22°C in SO_2 almost quantitatively to yield $[ClSe_2SN_2]^+AsF_6^-$ (**5a**) and $[ClSe_2SN_2]^+NbF_6^-$ (**5b**). Similarly **2a** forms with bromine 99% $[BrSe_2SN_2]^+ AsF_6^-$ (**6**) according to

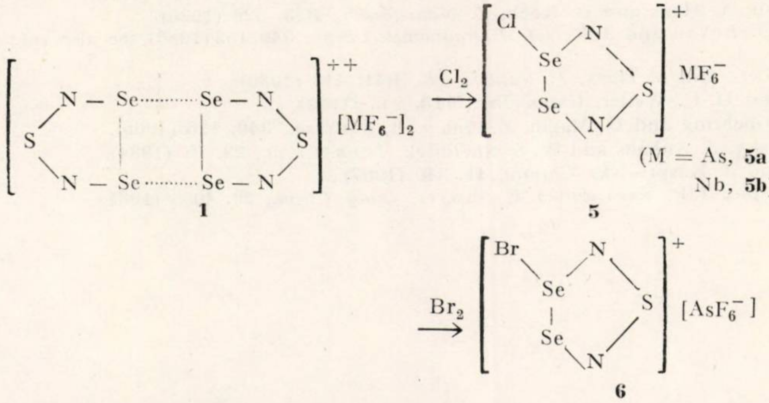
Cl₂
Br₂
[MF₆⁻]₂
MF₆⁻
[AsF₆⁻]
1
5
6
(M = As, 5a, Nb, 5b)

The structure of **5b** was determined by an X-ray analysis. It proved the five-membered ionic ring structure with an exocyclic chlorine bound to one selenium atom. This is in complete agreement with the structure of **2**.

Substances **5a, b** and **6** were characterized by elemental analysis, infrared- and ^{77}Se-NMR spectra. There is no doubt, that **5a** and **6** have the same structure as **5b**. No reaction takes place with **1a** and iodine in SO_2 at room temperature. The following scheme summarizes the results.

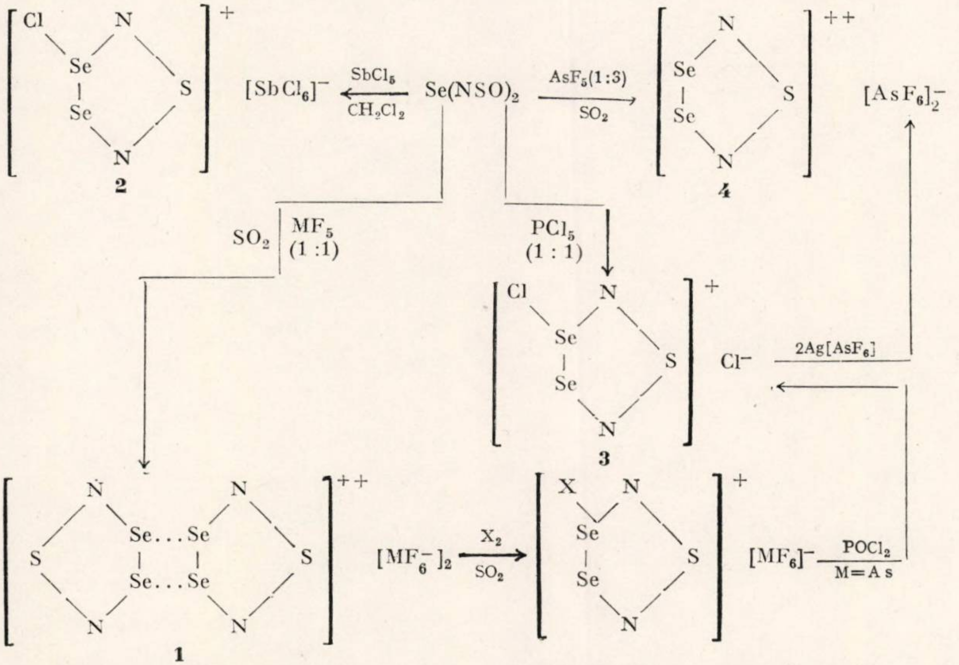
[SbCl₆]⁻
SbCl₅
CH₂Cl₂
Se(NSO)₂
AsF₅(1:3)
SO₂
[AsF₆]₂⁻
2
4
SO₂
MF₅ (1:1)
PCl₅ (1 : 1)
Cl⁻
2Ag[AsF₆]
3
[MF₆⁻]₂
X₂
SO₂
[MF₆]⁻
POCl₂
M=As
1

M = As (**1a**), Sb (**1b**), Nb (**1c**)

X = Cl (**5**), M = As (**5a**), Nb (**5b**);
X = Br, M = As (**6**)

REFERENCES

[1] A. Haas, J. *Fluorine Chem.*, **32,** 415 (1986).
[2] A. Haas, B. Koch and N. Welcman, *Z. Anorg. Allg. Chem.*, **427,** 114 (1976).
[3] A. Darmadi, A. Haas and B. Koch, *Z. Naturforsch.*, **B35,** 526 (1980).
[4] J. Grobe, D. LeVan and J.Welzel, *J. Organomet. Chem.*, **340,** 153 (1988), see also ref. [11] there.
[5] F. Fockenberg and A. Haas, *Z. Naturforsch.*, **B41,** 413 (1986).
[6] A. Haas and H.-U. Weiler, *Chem. Ber.*, **118,** 943 (1985).
[7] M. Becke-Goehring and G. Magin, *Z. Anorg. Allg. Chem.*, **340,** 126 (1965).
[8] H. W. Roesky, J. Anhaus and W. S. Sheldrick, *Inorg. Chem.*, **23,** 75 (1984).
[9] A. Haas and J. Kasprowski, *Chimia*, **41,** 340 (1987).
[10] R. J. Gillespie, J. P. Kent and J. F. Sawyer, *Inorg. Chem.*, **20,** 4053 (1981).

Revue Roumaine de Chimie, **34**, *1*, 129–142 (1989)

POLYMÈRES DE ε-CAPROLACTAME À PROPRIÉTÉS ANTISTATIQUES PERMANENTES

MARIA IONESCU
Institut Central de Chimie, 77208, 202, Splaiul Independenţei, Bucarest, Roumanie

Reçu le 21 décembre 1988

The paper presents a highly efficient process for obtaining permanently antistatic polyamide fibers, by the introduction in the polymerization stage of certain modifiers as for instance the polymethyleneglycols or the polyethyleneglycol esters with phosphoric or boric acid (mono- and di-esters). The modifiers are chemically added to the polyamide macromolecular chain, and act both as initiators or as regulating agents of the molecular mass. Polyamide fibers with an antistatic degree similar to that of the cotton (resistivity = $10^7-10^8\ \Omega$ cm), with physical-chemical properties comparable to those of the unmodified fibers, and with thermal and fatigue strengths higher than the standard ones have been obtained. The studied process may be applied to conventional polymerization-spinning plants, without any modification of the equipment or of the working conditions.

INTRODUCTION

Le polycaprolactame, $[NH(CH_2)_5-Co]_n$ (polyamide 6, ou Nylon 6), est le plus repandu polyamide obtenu par la polymérisation à ouverture du cycle des lactames, étant à présent l'un des plus importants polymères pour l'industrie des fibres synthètiques, à applications majeures dans l'industrie textile, la fabrication des pneus, des transporteurs à ruban, des articles techniques, etc. Au processus de traitement textile, des fils et des fibres, de même que pendant l'utilisation, à cause des frottements, le fil est chargé à électricité statique, phénomème qui conduit à de nombreux inconvénients et difficultés de traitement à cause de la répulsion électrostatique des fils, des étincelles électriques qui peuvent apparaître au déchargement, etc. La charge électrostatique des fibres dépend de la vitesse de travail, de l'effet des frottements, de l'humidité du milieu environnant, de la nature chimique du polymère, de même que de la nature des pièces qui déterminent le frottement. Ainsi, par frottement naturel par rapport à l'acier, les polyamides, la laine, la viscose, la soie naturelle, le coton sont chargés (+), à la différence des fibres polyacrylonitryliques, polyesthériques et polyoléfiniques qui sont chargées (—)[2-4,7]. A présent, pour éviter les inconvénients mentionnés ci-dessus, on fait des efforts considérables pour éliminer l'effet de charge électrostatique des fibres en général, donc une antistatisation de celles-ci.

L'expérience accumulée jusqu'à présent au traitement des fibres textiles a démontré que si la fibre est fortement hydrophile, si elle a une absorption plus grande d'eau, tels que les fibres cellulosiques (le coton, la viscose, la soie acétate) les fibres sont chargées statiquement beaucoup moins et sont traitées beaucoup plus facilement que les fibres synthétiques, fortement hydrophobes, qui présentent de grandes difficultés au traitement textile. Au tableau **1** on peut observer la croissance de la résistance spécifique R ou de la résistivité (une mesure du degré d'antistatisation qui est grande aux valeurs petites de R) en fonction de la nature chimique des fibres et de leur absorption spécifique d'eau.

Tableau 1

Résistance spécifique des fibres en fonction de la nature chimique et de l'absorption d'eau

Type de la fibre	Résistance spécifique cm	Absorption d'eau %
Viscose	$10^{7}-10^{8}$	12—13
Coton	$10^{7}-10^{8}$	8—8,5
Acétate	$10^{11}-10^{12}$	7—7,5
Polyamide 6	$10^{12}-10^{13}$	4—4,5
Polyacrylonitryle	$10^{13}-10^{14}$	1—2
Polyesther	$10^{14}-10^{15}$	0,4—0,5
Polyoléfines	$10^{15}-10^{16}$	0—0,2

On a constaté expérimentalement que par la croissance de la valeur de la conductibilité de surface de la fibre (mesurée par l'inverse de celle-ci — résistance spécifique en Ω cm, c'est-à-dire une mesure quantitative du degré d'antistatisation), par l'action de quelques substances nomées antistatisantes, on peut assúrer une décharge rapide de la charge électrostatique.

En comparant le système fibre—corps de frottement à un condensateur, la présence de l'eau dans la couche superficielle de la fibre ou même dans l'atmosphère environnante par la croissance de la constante diélectrique (eau à une constante diélectrique très grande $\varepsilon = 78,5$ à 25°C) réalise le déchargement rapide des charges électriques.

Il résulte clairement qu'une substance antistatisante doit actionner par la croissance de la conductibilité des surfaces de la fibre. Cela peut être réalisé soit par le traitement de la fibre à substances polarisées dont les molécules ont des charges (+) ou (—) partielles ou séparées, soit à substances tensioactives ayant des segments fortement hydrophiles et hydrophobes. Il est suffisant que l'on fixe à la surface de la fibre un nombre élevé de molécules d'eau, à structure fortement polarisée, pour permettre un transfert puissant de la charge accumulée.

Toutes les substances tensioactives présentent un effet antistatisant, parce qu'elles sont orientées avec la partie hydrophobe vers le polymère synthétique et avec la partie hydrophile vers l'extérieur, en permettant l'absorption d'une quantité élevée d'eau à la surface de la fibre.

Dans le contexte des principes généraux présentés ci-dessus, la majorité des procédés actuels pour l'antistatisation des fibres réside dans la croissance de leur hydrophilie par le traitement superficiel au processus d'usinage textile avec une série de substances hygroscopiques (glycérine, glycols, polyglycols), des ions amphotériques (de type betaïnique) ou substances tensioactives anioniques (carboxylates, sulfates, phosphates), cationiques (sels quanternaires d'ammonium) et non ioniques (produits polyéthoxylats) [2,4,7].

Les traitements superficiels avec ces substances conduisent à une antistatisation temporaire, importante pour la facilité des usinages textiles; ensuite après les premiers lavages du tissu fini, l'effet d'antistatisation disparaît peu à peu. C'est pourquoi on fait des efforts pour la réalisation d'une antistatisation permanente des fibres qui ne disparaisse pas à des lavages répétés. Notre ouvrage présente un procédé d'efficience élevée pour la réalisation de fils et fibres polyamidiques à antistatisation permanente, directement au processus de polymérisation par l'introduction dans la structure chimique de la chaîne macromoléculaire de quelques substances fortement hydrophiles telles que : polyéthylèneglycols à M = 400—4000 et de quelques esthers acides (mono et diesthers) des polyéthylèneglycols (phosphates et borates).

PARTIE EXPÉRIMENTALE

La polymérisation de ε-caprolactame à été réalisée, en présence des modificateurs, dans une installation semi-industrielle de polymérisation, à une pression atmosphérique du type VK (fig. 1), en appliquant tout justement les technologies courantes de fabrication de ε-caprolactame.

Les conditions de travail ont été les suivantes :

Eau déminéralisée, initiateur de polymérisation	: 0,3—0,4 %
Additif antistatisant (variable)	: 0,5—4 %
Température de travail	: 256—260°C
Temps de polymérisation	: 18 h

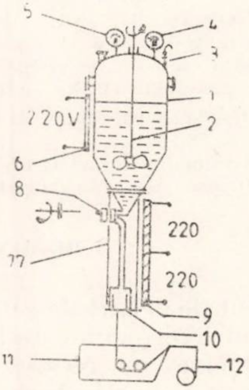

Fig. 1. — Schéma technologique de l'installation de polymérisation continue de ε-caprolactame à pression atmosphérique de type VK, à trois sections. 1. vaisseau d'alimentation à lactame ; 2. vaisseau d'alimentation à additifs ; 3. colonne d'alimentation ; 4. filtre de ε-caprolactame fondu ; 5. vaisseau de fusion ; 6. tuyau d'élimination de l'eau ; 7. réfrigérateurs de reflux pour débit ; 8. tête d'extrusion ; 9. frotteur de niveau ; 10. pompe à roues dentées.

On a fait extraire le polymère sous la forme d'un câble, ensuite on l'a granulé et on a extrait les granules (de monomère, d'oligomères et de traces de modificateur qui n'a pas reactionné) à 90°C, pendant 4 heures ; puis le polymère a été séché, pendant 44—48 heures, à 90°C et vidé de 30—40 mmHg, jusqu'à une teneur en eau de max. 0,07 % par rapport au polymère.

Ensuite le polymère séché a été filé de la coulée dans l'installation, dont le schéma technologique est présenté dans la figure 2.

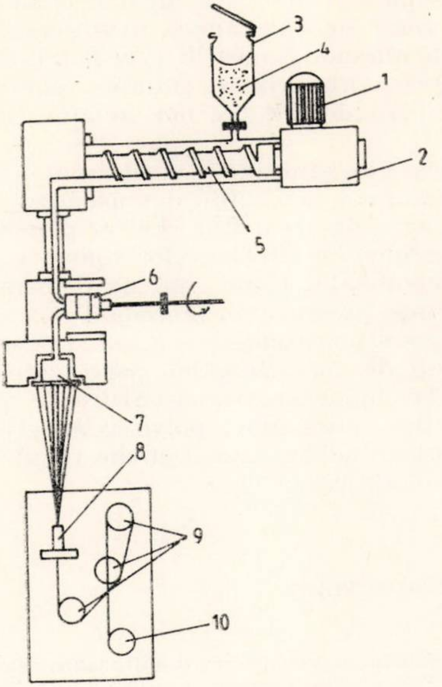

Fig. 2. — Schéma technologique de l'installation de filage : 1 — électromoteur ; 2 — réducteur ; 3 — trémie granules ; 4 — granules ; 5 — vis transporteuse ; 6 — pompette ; 7 — filière ; 8 — galet de préparation ; 9 — galets ; 10 — bobine à fil.

Matières premières

ε-caprolactame : (type A conf. STAS 7311—1969)
p.t. 68,8°C
chiffre de $KMnO_4 = 3000$ sec.
Acidité libre, 0,01 m val/kg
couleur APHA,
solution aqueuse 50% : 5

Polyéthylèneglycols: $HO-CH_2-CH_2(-O-CH_2-CH_2)_{n-2}-O-CH_2-CH_2-OH$, produits au C. P. Brazi (n ≈ 7—88) à M = 400 — 4000.

Phosphates et borates de polyéthylèneglycol : on les obtient usuellement par la réaction du pentaoxyde de phosphore (P_2O_5) ou de l'anhydride borique (B_2O_3) à polyéthylèneglycols à $\overline{M} = 1500$. La résistance spécifique ou la résistivité (Ω cm) a été mesurée à l'aide d'un ultramégohmètre UM. 18.

On a déterminé les caractéristiques physico-mécaniques des fibres (résistance à la traction, ténacité, finesse, allongement) conformément à STAS—8283/2—77 ; 11192—78.

RÉSULTATS ET DISCUSSIONS

Le point de départ de cette étude a été de trouver quelques substances fortement hydrophiles, telles que les chaînes de polyéthylène-oxyde, qui peuvent être insérées chimiquement dans la structure macromoléculaire du poly ε-caprolactame. Par la liaison chimique des structures de polyéthylène-oxyde, les chaînes ne sont plus extraites du polymère aux lavages répétés, en conférant, de la sorte à la fibre, une hydrophilie élevée et en même temps une antistatisation à caractère permanent.

Le mecanisme de la polymérisation hydrolytique de ε-caprolactame unanimement accepté jusqu'à présent consiste dans une succession de réactions, la polymérisation de ce monomère étant une polymérisation d'équilibre [1–4,7].

1. Réaction d'ouverture du cycle lactamique par l'eau à formation d'acide ε-aminocaproïque :

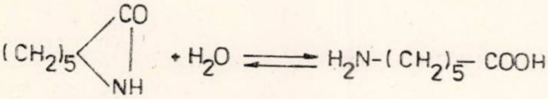

2. Réaction de polycondensation (réaction entre les groupes carboxyle et amino à élimination d'eau et formation de la liaison amidique) :

$$H_2N-(CH_2)_5-COOH + H_2N-(CH_2)_5-COOH \rightleftharpoons$$
$$H_2N-(CH_2)_5-CO\,NH-(CH_2)_5-COOH + H_2O$$

$$H_2N-(CH_2)_5-[CO-NH-(CH_2)_5]_n-COOH + H_2N-(CH_2)_5-[CO-NH-(CH_2)_5]_m COOH \rightleftharpoons$$
$$H_2N-(CH_2)_5-[CO-NH-(CH_2)_5]_{m+n}-COOH + H_2O$$

3. Réaction de polyaddition du cycle lactamique aux groupes terminaux des macromolécules en croissance (aux groupes COOH) :

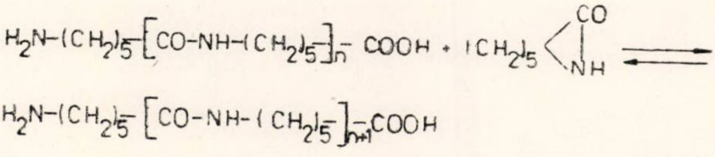

4. Réaction de «lyse» des chaînes polyamidiques (de transamidation, hydrolyse, acidolyse, aminolyse des liaisons amidiques 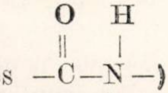 $-\overset{O}{\overset{\|}{C}}-\overset{H}{\overset{|}{N}}-$) à formation d'oligomères, de ε-caprolactame, d'acide ε-aminocapronique, parallèlement à un équilibre entre les chaînes. Ces réactions ont lieu dans un poids beaucoup plus petit que les réactions 1—3, la polyaddition réversible étant la réaction de base par l'ouverture du cycle de ε-caprolactame aux chaînes en croissance.

Les données de la littérature mettent en évidence le fait que l'initiation de la polymérisation de ε-caprolactame peut être réalisée non seulement avec de l'eau, mais aussi avec des alcools et des acides organiques ou inorganiques. On a essayé, à partir de ces données, d'utiliser dans le système d'initiation les polyéthylèneglycols qui contiennent des groupes hydroxyle terminaux (donc ce sont des alcools capables d'initier la polymérisation de ε-caprolactame) et des esthers partiels de l'acide phosphorique et borique à polyéthylèneglycols contenant des groupes acides

$>\overset{\overset{O}{\uparrow}}{P}-OH$, $>B-OH$), de même que des groupes hydroxyle, tous les deux capables d'initier la polymérisation du monomère :

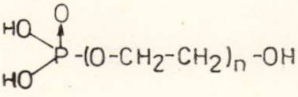

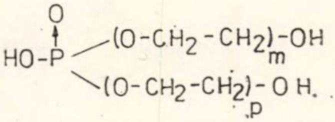

On a démontré, par les expérimentations effectuées, le fait que les polyéthylèneglycols, de même que les esthers partiels (phosphoriques ou boriques) des polyéthylèneglycols sont insérés par liaison chimique dans les chaînes polyamidiques sans être extraits du polymère ni même après les lavages répétés. En analysant les réactions 1—4, on propose quelques possibilités de liaison chimique des modificateurs utilisés dans les chaînes polyamidiques (réactions a—e).

Les polyéthylèneglycols [5,6] peuvent initier la polymérisation de ε-caprolactame (a) ou peuvent participer à des réactions d'esthérification aux groupes carboxyle terminaux (b) :

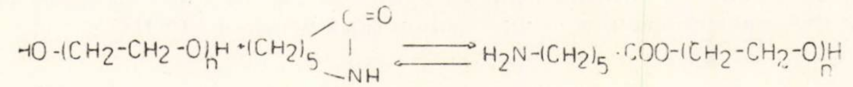

(a)

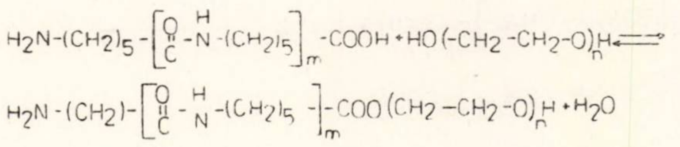

(b)

Les esthers partiels de l'acide phosphorique et borique [5,6] peuvent initier la polymérisation de ε-caprolactame, de même que les acides libres (c); ils peuvent aussi quaterniser les groupes aminiques terminaux (d) et peuvent produire la destruction des liaisons amidiques, avec la formation du phosphoramide (e)

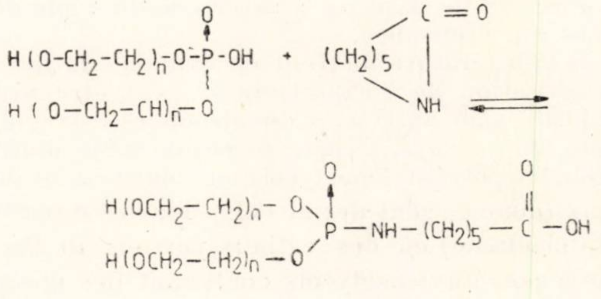

(C)

(d)

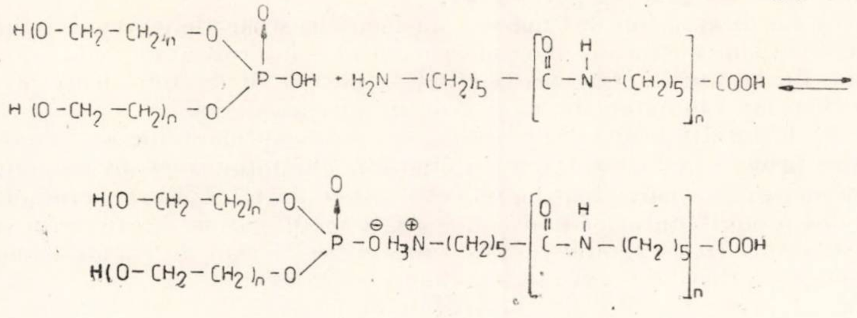

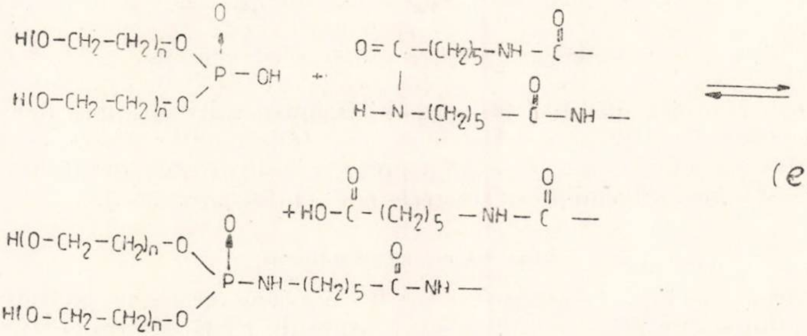

(e)

Analysant les réactions (a—e), proposées pour expliquer l'insertion chimique des modificateurs, on constate que, par n'importe quelle réaction, le modificateur est lié chimiquement, à grande probabilité comme groupe terminal. Par la participation de tous les groupes hydroxyle aux polyéthylèneglycols, de même que des groupes hydroxyle des esthers partiels, il existe la possibilité de l'insertion des modificateurs à l'intérieur des chaînes macromoléculaires.

Parce que l'on a constaté une diminution des masses moléculaires parallèlement à la croissance de la concentration de modificateurs, les polyéthylèneglycols, de même que les esthers phosphoriques ou boriques partiels des polyéthylèneglycols peuvent être considérés comme initiateurs, de même que des régulateurs de chaîne à la polymérisation de ε-caprolactame. A l'appui des réactions a—e, proposées pour la liaison chimique des PEG et des esthers PEG à l'acide phosphorique et borique il existe les suivants arguments expérimentaux :

a) Après des extractions répétées, les polyéthylèneglycols sont décalés en spectres, IR (les liaisons etheriques à 1100 cm^{-1} et les groupes OH alcooliques à 3400—3600 cm^{-1}). Au cas d'un mélange physique de polyamide 6 à PEG, le modificateur est extrait quantitativement. Ce fait démontre clairement la liaison chimique du polyéthylèneglycol par la chaîne polyamidique.

b) La réduction des concentrations de groupes — COOH, aux polymères traités à PEG et la diminution de la concentration de groupes $-NH_2$, à ceux modifiés à esthers partiels, phosphariques ou boriques, prouvent l'interaction chimique des groupes hydroxyle et acides des modificateurs avec les groupes terminaux.

c) La diminution des masses moléculaires parallèlement à la croissance de la concentration de modificateur et à la croissance de la concentration de groupes — OH actifs (PEG à petites M de 400—600) prouve l'intervention chimique du modificateur au processus.

d) L'initiation de la polymérisation de ε-caprolactame à ces modificateurs prouve nettement une intéraction chimique avec le monomère, de même qu'une participation à la croissance de la chaîne macromoléculaire des produits intermédiaires formés, le modificateur étant inséré dans leur structure (par exemple les réactions entre l'esther de l'acide ε-aminocapronique à PEG et les groupes amino terminaux) :

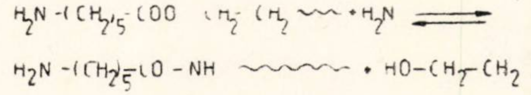
H2N-(CH2)5-COO CH2-CH2 ~~~ + H2N
H2N-(CH2)5-CO-NH ~~~~~ + HO-CH2-CH2

On présente, ensuite, les caractéristiques antistatiques des polyamides obtenus en présence des deux classes de modificateurs, de même que l'effet de celles-ci sur les autres propriétés des fibres obtenues (physico-mécaniques, thermiques, résistance à la fatigue, etc.).

Effet des polyéthylèneglycols

Parce que l'on a constaté, dans les expérimentations préliminaires « micropilot », que plus de 4% concentration de PEG par rapport à ε-caprolactame conduit à de grandes réductions des masses moléculaires, effet d'autant plus prégnant que la masse moléculaire du PEG est plus petite (donc à une concentration plus grande de groupes hydroxyle réactifs), l'étude a été effectuée avec PEG à M = 1500, masse moléculaire où le phénomène est beaucoup diminué.

Vu qu'au-dessus de 4% concentration de modificateur les valeurs de résistivité électrique restent pratiquement invariables, on a étudié le domaine de concentrations 0,5—4%, PEG—1500 par rapport au monomère.

Tableau 2

L'effet antistatisant du PEG—1500 — Résistivité Ω/cm

Contenu en PEG %	Initial	Après un lavage	Après 10 lavages
0 (Témoin)	$2,3\cdot10^{11}$	$3,4\cdot10^{11}$	$3,2\cdot10^{12}$
0,5	$1,2\cdot10^{11}$	$1,2\cdot10^{11}$	$1,7\cdot10^{9}$
1,0	$5,8\cdot10^{8}$	$2,2\cdot10^{10}$	$0,9\cdot10^{8}$
2,0	$3,7\cdot10^{9}$	$1,6\cdot10^{9}$	$0,2\cdot10^{7}$
4,0	$0,9\cdot10^{9}$	$2,1\cdot10^{8}$	$2,7\cdot10^{9}$

Au tableau 2 on peut observer l'effet antistatisant marquant du PEG—1500, dans le domaine de concentration 0,5—4% et la conservation de cet effet après 10 lavages successifs, par comparaison à l'essai témoin (polyamide synthétisé selon la technologie courante, sans addition de modificateur).

En analysant la concentration de groupes terminaux (aminiques et carboxyliques), on a constaté une réduction de la concentration de groupes carboxyliques et une croissance des groupes aminiques, parallèlement à la concentration du modificateur.

Tableau 3

Effet de la concentration du PEG—1500 sur la concentration de groupes terminaux des polyamides synthétisés

Contenu en modificateur PEG—1500 %	Groupes aminiques n° équiv/g	Groupes carboxyliques n° équiv/g
0,0	$54,5 \cdot 10^{-6}$	$74,4 \cdot 10^{-6}$
0,5	$65,4 \cdot 10^{-6}$	$66,7 \cdot 10^{-6}$
2,0	$60,0 \cdot 10^{-6}$	$67,1 \cdot 10^{-6}$
2,0	$60,0 \cdot 10^{-6}$	$67,3 \cdot 10^{-6}$
4,0	$65,0 \cdot 10^{-6}$	$65,0 \cdot 10^{-6}$
6,0	$76,3 \cdot 10^{-6}$	$65,0 \cdot 10^{-6}$

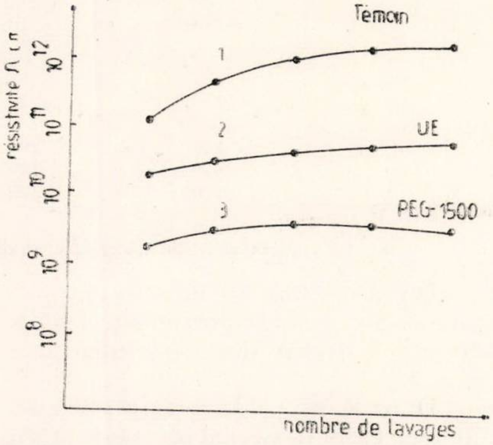

Fig. 3. — Effet d'antistatisation réalisé à polyéthylèneglycol PEG—1500 (3) comparativement au polyamide étalon (1) et à un polyamide antistatisé par un mélange physique dans la coulée (2).

Cet effet de réduction de la concentration des groupes carboxyliques parallèlement à la disponibilité de ceux aminiques représente une preuve indiscutable de la réaction d'esthérification des groupes OH du modificateur avec les groupes carboxyle (réaction b).

La fig. 3 présente la réduction de la charge électrostatique des fibres antistatisées en permanence (courbe 3), comparativement à l'essai témoin, sans modificateur (courbe 1), et avec un polyamide antistatisé par le mélange physique d'un antistatisant et le polymère fondu au processus de filage (antistatisant UE).

La stabilité thermique des polymères n'a pas été affectée par l'introduction de quelques pourcentages réduits de PEG—1500, ce qui est mis en évidence par le fait que la température initiale de la dégradation thermique, à tous les essais, est comprise au domaine 285—320°C, les pertes thermogravimétriques avant la dégradation thermique (élimination des traces d'eau, de monomère nonextrait, etc.) étant petites, de 1,3—2%, tel qu'on peut remarquer au tableau 4.

De plus, la température de fusion du produit modifié n'est pas modifiée compartivement au témoin : ($T_m = 223°$) variant entre $T_m = 220,5 - 224°C$.

Tableau 4

La résistance thermique du polyamide antistatisé avec PEG—1500

Pourcentage de PEG—1500 %	Température initiale de dégradation °C	Perte thermogravimétrique avant la dégradation
0	320	1,3
0,5	287	1,30
1,0	296	1,33
2,0	320	1,86
4,0	322	1,46

Effet des esthers partiels des acides phosphorique et borique à PEG—1500

On a réalisé l'étude de la polymérisation de ε-caprolactame en présence des esthers partiels de l'acide phosphorique et borique à PEG—1500, en utilisant des concentrations de modificateur qui varient de 1% à 5%.

Dans la fig. 4 on peut remarquer l'efficacité antistatique exceptionnelle des esthers de l'acide phosphorique (mono et diesther) à polyéthylèneglycol PEG—1500 et la diminution marquante de la résistivité parallèlement à la croissance de la concentration d'additif.

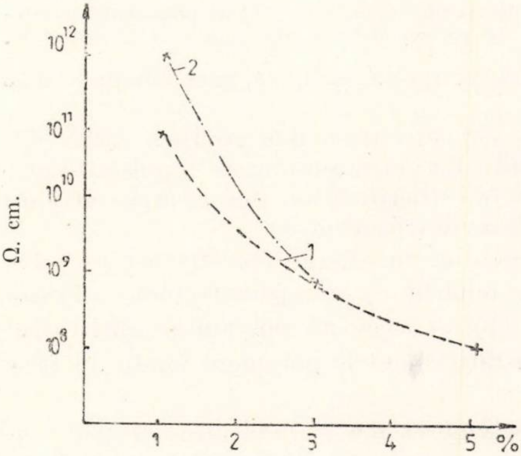

Fig. 4. — Efficacité antistatique en fonction de la concentration du modificateur : 1. monophosphate de PEG—1500 ; 2. diphosphate de PEG—1500.

Il reste à présenter l'effet des modificateurs sur d'autres caractéristiques des fibres polyamidiques finies. Au tableau 5, on peut observer l'effet du borate de PEG—1500, au domaine de concentrations 0,5—2,5%, sur la résistivité, de même que sur quelques propriétés physico-mécaniques des polyamides modifiés.

Au tableau 6 est donnée la réduction des viscosités dynamiques des polyamides modifiés à borate de PEG—1500, en fonction de la température et de la concentration du modificateur. L'explication de cette réduction consiste soit dans la diminution des masses moléculaires, soit dans un possible effet de plastification des chaînes polyéthylène-oxydiques.

Il est surprenant de remarquer que dans la présence des modificateurs, outre l'effet marquant d'antistatisation et de conservation des principales caractéristiques physico-mécaniques des fibres obtenues, celles-ci ont une résistance à la fatigue 2—4 fois plus grande qu'aux essais témoins (Tableau 7).

Les figures 5 et 6 représentent la modification de la résistance et de la ténacité par l'exposition pendant 16 heures, à 125°C, en milieu d'oxygène ; on constate que la vitesse de dégradation est plus lente pour tous les polymères modifiés par comparaison au témoin (fig. 6 c).

CONCLUSIONS

1. On a obtenu des fibres polyamidiques à antistatisation permanente par l'addition des polyéthylèneglycols (M—1500) et des esthers phosphoriques et boriques des polyéthylèneglycols, directement dans la phase de polymérisation hydrophile à ε-caprolactame, obtenant des valeurs de la résistivité de 10^8—10^9 Ω cm proches des valeurs pour le coton, l'étalon pour une fibre à antistatisation efficiente.

2. Les modificateurs testés agissent comme initiateurs de polymérisation et comme des régulateurs de la masse moléculaire, étant insérés chimiquement dans la structure de la chaîne polymère. Les modificateurs ne peuvent pas être extraits des polyamides, ni même après 10 lavages répétés, conférant à l'antistatisation un caractére permanent.

3. La majorité des propriétés physico-mécaniques des polyamides modifiés, synthétisés (résistance à la traction, finesse, allongement, ténacité) se trouvent aux domaines admis, étant comparables à l'étalon non modifié. Les viscosités dans la coulée des polymères modifiés sont plus petites que celles de l'étalon, prouvant un meilleur traitement au processus de filage ou à l'obtention des repères techniques (des lampes de mine). Par le maintien dans des conditions de température élevée (16 heures à 125°C), de dégradation forcée (100 heures), à radiations UV (Xenotest), les polymères modifiés conservent mieux que le polymère étalon toute une série de propriétés, telles la résistance à la traction, la ténacité, le degré de blanc. Au polymère étalon ces propriétés se trouvent au-dessous des valeurs admises.

4. Les polymères modifiés ont une résistance à la fatigue à des flexions répétées 2—4 fois plus grande que celle de l'étalon, propriété particulièrement importante pour les fibres cord (pour les pneus d'autos).

5. Le procédé d'obtention des fibres polyamidiques à antistatisation permanente, présenté ci-dessus, peut être appliqué aux installations

Tableau 5

L'effet antistatisant et les propriétés physico-mécaniques des fils polyamidiques modifiés à borate de PEG-1500

Caractéristiques Résistivité (cm)	Concentration en borate de PEG-1500				
	0,5%	1%	1,5%	2%	2,5%
	$2,3 \cdot 10^{12}$	$4,3 \cdot 10^{12}$	$1,7 \cdot 10^{11}$	$3,1 \cdot 10^{12}$	$2,4 \cdot 10^{9}$
Allongement, %	20	19	22	20	19
Contraction, %	17	18,3	17,8	17,9	17,8
Résistance, gf	539	222	530	225	527
Ténacité	5,72	5,3	5,47	5,6	5,6

Tableau 6

Les viscosités dynamiques des polyamides modifiés à borate de PEG-1500

T°C	esther 0,5%	1%	1,5%	2%	2,5%	3%	3,5%
250	12.510	11.614	11.718	11.230	10.830	11.115	9.720
260	9.314	9.450	8.916	8.452	8.142	8.210	7.822
270	3.210	2.924	2.865	2.784	2.540	2.614	2.416
280	1.131	1.210	980	973	847	883	812

Tableau 7

Comportement à la fatigue, à des flexions répétées des polyamides modifiés, comparativement au polyamide témoin (n° de cycles)

Additif	Nombre cycles $\cdot 10^3$
(Témoin)	$245 \cdot 10^3$
Monophosphate de PEG	$674 \cdot 10^3$
Diphosphate de PEG	$901 \cdot 10^3$
Borate de PEG	$826 \cdot 10^3$
PEG—1500 (4%)	$982 \cdot 10^3$

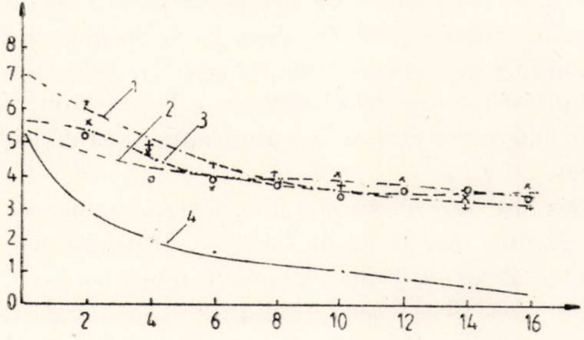

Fig. 5. — Modification de la résistance à la rupture des polyamides antistatisés en permanence par traitement thermique (16 heures à 125°C) : 1 — Monophosphate de PEG-1500 (2,5%); 2 — Diphosphate de PEG-1500 (2,5%); 3 — PEG-1500 (2,5%); 4 — Etalon (polyamide monoadditionné).

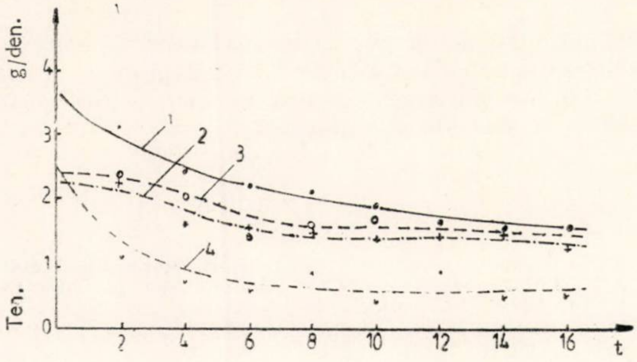

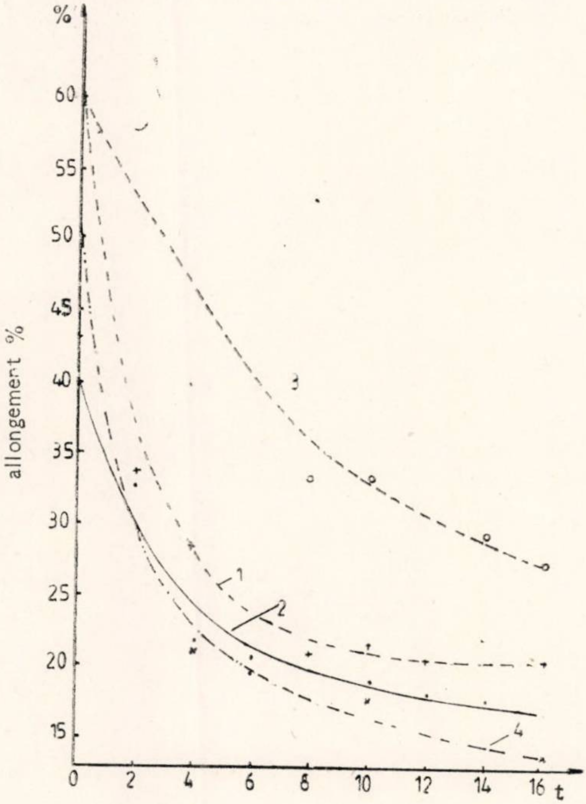

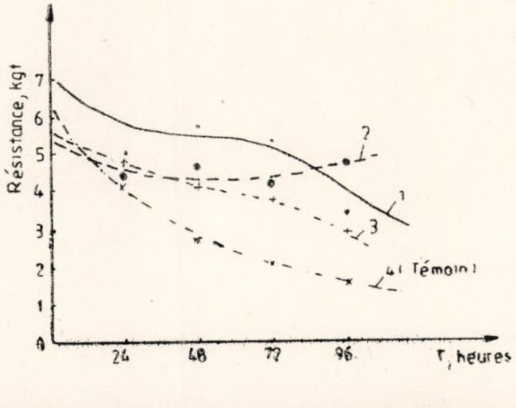

Fig. 6. — Modification de la ténacité des polyamides antistatisés sans cesse par traitement thermique (16 heures à 125°C) : 1— Monophosphate de PEG-1500 (2,5%) ; 2 — Diphosphate de PEG-1500 (2,5%) ; 3 —PEG-1500 (2,5%) ; 4 — Etalon (polyamide nonadditionné).

de polymérisation et filage existantes, sans aucune modification de celles-ci ou des conditions technologiques de travail.

6. Le polymère peut être utilisé aux pièces qui fonctionnent en milieu à danger d'explosion.

BIBLIOGRAPHIE

[1] V. V. Korshak, « Progrese în chimia polimerilor », Ed. Tehnică, 1968, București, pp. 13—48.

[2] * * *, « Fibre Sintetice », Ed. Tehnică, 1960, pp. 23—115.

[3] L. Alexandru et S. Borică « Fibre Sintetice », Ed. Tehnică, 1966, pp. 168—284.

[4] Maria Ionescu, « Cartea operatorului în fibre chimice », Ed. Tehnică, 1983, IIIe éd.

[5] Brevet RSR, 78746, 1979.

[6] Brevet RSR, 74324, 1978.

[7] Maria Ionescu, « Contribuții la obținerea unor polimeri ai ε-caprolactamei cu proprietăți speciale », Thèse de doctorat, Institut Polytechnique, București, 1988.

Revue Roumaine de Chimie, **34**, *1*, 143–148 (1989)

VIBRATION ENERGY OF NEW KINDS OF RADIOACTIVITIES

M. IVAŞCU [a], D. N. POENARU [a,b], I. IVAŞCU [a], E. HOURANI [c] and W. GREINER [b]

[a] Central Institute of Physics, Bucharest, Romania
[b] Institut für Theoretische Physik, Frankfurt am Main, F. R. Germany
[c] Institut de Physique Nucléaire, Orsay, France

Received October 15, 1988

The main results obtained in the framework of the analytical superasymmetric fission model unifying the description of heavy ion radioactivities, alpha decay and cold fission are briefly resumed. Predicted half lives for ^{14}C, ^{24}Ne and ^{28}Mg spontaneous emission in the range $10^{11} - 10^{25.5}$ s have been experimentally confirmed with 1.5 orders of magnitude. The most probable asymmetric and symmetric measured cold fission fragments are reproduced. Zero point vibration energy is calculated from the stiffness of the barrier, by using Yukawa-plus-exponential potential showing pronounced shell effects.

Les principaux résultats obtenus dans le cadre du modèle analytique de la fission superasymmétrique unifiant la description des radioactivités par émission d'ions lourds, la désintégration alpha et la fission froide sont résumées. Les durées de vie prévues, dans l'interval $10^{11} - 10^{25.5}$ s ont été confirmées expérimentalement à 1.5 ordres de grandeur près. Les plus probables fragments de fission froide asymmétrique et symmétrique sont réproduits par nos calculs. L'énergie de vibration du niveau fondamental, déterminé à partir de la rigidité de la barrière, en utilisant le potentiel Yukawa-plus-exponentielle montre des effets de couches prononcés.

1. INTRODUCTION

Besides the well known α, β and γ radiations discovered by H. Becquerel in 1896, many other kinds of nuclear decay modes are known at present. Theory and experiments on proton radioactivity, α-decay, heavy ion radioactivities, spontaneous fission from the ground state and from shape isomeric states, cold fission, particle accompanied fission, beta-delayed emission of: protons, two-protons, α-particles, neutrons, two-neutrons, three-neutrons and tritons are reviewed [1] by many scientists with outstanding contributions to these fields.

Heavy ion radioactivities possess a mass asymmetry parameter intermediate between fission and α-decay. The theory of these new phenomena had been developed correspondingly by extending either the fission models toward higher asymmetry, or the traditional image of a preformed α-particle, to heavier clusters. Both directions were presented in two review papers in 1980 (see also Refs. 2–5) where, among other theoretical predictions we have shown that ^{14}C should be the most probable emitted ion from ^{222,224}Ra.

In 1984, Rose and Jones from Oxford University [6] discovered experimentally ^{14}C radioactivity of the intermediate nucleus, ^{223}Ra.

The analytical superasymmetric fission model [3] (ASAFM) developed by us in 1980, has been improved and exploited intensively since 1983. It allows to consider more than 10^5 combinations parent-emitted ion requested in a systematic search for new decay modes. After fitting one parameter of the model to the α-decay data of about 385 emitters and to the first measurement of ^{14}C emission, reliable values of the half-lives have been predicted, which have been used to guide the experiments. It was shown that the largest branching ratio (less than 10^{-9}) relative to the α-decay was measured from the beginning. Highest emission rates are obtained for combinations leading to a doubly magic daughter ^{208}Pb, or to its neighbours, but all nuclei with $Z \geqslant 40$ are metastable with respect to several heavy ion radioactivities.

Up to now three of more than 140 new decay modes theoretically predicted, have been experimentally confirmed [6–10] by various groups from Oxford, Moscow, Orsay, Berkeley, Geneva, Dubna—Bucharest—Moscow, Argonne and Livermore. The measured life-times of ^{14}C spontaneous emission from $^{222-224,226}Ra$, of ^{24}Ne emission from ^{230}Th, ^{231}Pa, $^{232-234}U$ and of ^{28}Mg emission from ^{234}U are in good agreement with predicted half-lives [11–15] within 1.5 orders of magnitude. After including an even-odd effect,[14] the agreement became much better.

The model was also extended [13,16,17] to the cold fission mechanism, observed in two regions of nuclei : U, Np, Pu[18–20] and Fm, Md, No[21], where the estimated properties are dominated by the closed shell number of neutrons $N = 82$ and protons $Z = 50$ in one or both of the two fragments. The highest symmetry of the mass distribution is expected for ^{264}Fm, where cold fission should be the strongest mechanism. The unified treatment of α-decay, heavy ion emission and cold fission is best illustrated [17] on ^{234}U parent for which all mentioned groups of nuclear disintegrations have been measured.

An improved description of the fission dynamics is obtained by replacing the reduced mass with the hydrodynamical inertia tensor calculated [22,23] in the framework of the Werner-Wheeler approximation and by taking into consideration the neck degree of freedom.[24]

In the following we would like to present another development, namely a self-consistent calculation of zero-point vibration energy parameter in a wide range of mass asymmetry including alpha decay and the cold fission. In order to understand better this contribution we shall review briefly some related elements of theory.

2. NUCLEAR STABILITY AGAINST NEW DECAY MODES

One possibility to study the stability of a parent nucleus AZ relative to the spontaneous division in two nuclei A_dZ_d (the daughter or the heavy fragment) and A_eZ_e (emitted ion or the light fragment) is to use the deformation energy of the system with constrained mass and charge asymmetry versus separation distance, R, between fragment centers.[3] By taking for the origin of the potential the sum of individual energies of two final nuclei at infinite separation distance, for spherical shapes, we get initially at $R = R_i = R_0 - R_2$, the energy released in the process (Q — value):

$$E(R_i) = Q = M(A, Z) - [M(A_1, Z_1) + M(A_2, Z_2)] \tag{1}$$

where $R_0 = r_0 A^{1/3}$, $R_j = r_0 A_j^{1/3}$ $(j = 1, 2)$ and $M(A, Z)$ is the nuclear mass expressed in MeV.

By denoting with E_{SP} the saddle point energy, the fission barrier height is given by

$$E_b = E_{SP} - Q \tag{2}$$

A nucleus is metastable (or in other words it is radioactive) with respect to a given split, if both the Q-value and the barrier height are positive quantities ($Q > 0$, $E_b > 0$). In this case only temporarily the fragments are held together by the potential barrier. There is a finite probability, P, per time unit for the penetration through the barrier by quantum mechanical tunneling effect. The classical theory of the decay assumes a disintegration probability independent of the past history of the decaying nucleus, leading to the exponential decay law. The half-life, T, is the time after which the number of nuclei is reduced to 50%.

By introducing a complex energy, $E = E_0 - i\Gamma/2$, with $\Gamma \ll E_0$, in the stationary state Schrödinger equation, the exponential law is $\exp(-\Gamma t/\hbar)$, hence the disintegration width

$$\Gamma = \hbar \ln 2/T = \hbar\lambda \tag{3}$$

is directly related to the half-life and the disintegration constant λ.

3. SPONTANEOUS FISSION HALF LIVES

In general the nuclear deformation energy is a function of several independent generalized coordinates $q = \{q_1, q_2, \ldots, q_n\}$ determining the shape of the system. Deformation energy hypersurface in this n-dimensional space gives the generalized forces acting on the nucleus. The information concerning how the system reacts to these forces is contained in a tensor of inertia (or the effective masses) $\{B_{ij}\}$. One can define a path (or trajectory) followed by the nuclear system during the fission process. If we denote by R a new (curviliniar) coordinate along this trajectory, defined by $q_1 = q_1(R)$, $q_2 = q_2(R)$, $\ldots$, $q_n = q_n(R)$, the multidimensional problem can be reduced to one dimension for which

$$E(R) = E[q_1(R), q_2(R), \ldots, q_n(R)] \tag{4}$$

$$B(R) = \sum_{i=1}^{n} \sum_{j=1}^{n} B_{ij}\,[q_1(R), q_2(R), \ldots, q_n(R)]\,\frac{\partial q_i}{\partial R}\,\frac{\partial q_j}{\partial R} \tag{5}$$

From the classical point of view a nuclear system which has a potential energy barrier of the shape mentioned above (with $Q > 0$ and $E_b > 0$) is perfectly stable. Only quantum-mechanics is able to explain the disintegration of such a nucleus, by tunneling through the barrier, leading to a half-life

$$T = \frac{h \ln 2}{\Gamma} = \frac{\ln 2}{\nu} \cdot \frac{1}{P} = \frac{h \ln 2}{2E_v} \cdot \frac{1}{P} \tag{6}$$

where $\nu = \omega/(2\pi)$ is the number of assaults on the fission barrier in a time unit (the characteristic frequency of the collective mode leading to fission), h is the Planck constant, $E_v = h\omega/2$ is the zero point vibration energy and P is probability of the penetration through the barrier.

In the framework of semi-classical Wentzel-Kramers-Brillouin (WKB) approximation, for a one dimensional case

$$P = [1 + \exp(K)]^{-1} = \exp(-K) \tag{7}$$

where

$$K = \frac{2}{\hbar} \int_{R_i}^{R_b} \{2B(R)\,[E(R) - Q]\}^{1/2}\, \mathrm{d}R \tag{8}$$

is the action integral usually computed along the trajectory for which it takes a minimum value (least action path). R_i and R_b are the classical turning points given by $E(R_i) = E(R_b) = Q$.

In this way both the overlapping and separated fragments (coulombian forces) stages of the process are contributing to the integral.

4. ZERO POINT VIBRATION ENERGY

In the previous variants of the superasymmetric fission model, the zero point vibration energy had been obtained by fit to some experimental data on α-decay and ^{14}C radioactivity. A semiempirical law had been used to interpolate and extrapolate the behaviour of this parameter in the regions of not measured decay modes in order to make predictions.

Now the zero point vibration energy can be estimated from the stiffness of the potential barrier, C, and the value of the effective mass parameter, B, taken at the constrained saddle point, where the asymmetrical split is decided

$$E_v = \frac{h\omega}{2} = \frac{h}{2}(C/B)^{1/2}; \qquad C = \frac{\partial^2 E}{\partial R^2} \tag{9}$$

in which

$B = \mu$ — the reduced mass (at the touching point).

For a parabolic variation of the initial part $E(R)$ from $R = R_i$ to $R = R_t = R_1 + R_2$, we get

$$E_v = \frac{1}{R_t - R_i}\left[\frac{\hbar^2}{2\mu}(E_t - Q)\right]^{1/2} \tag{10}$$

with

$$E_t = E(R_t).$$

In order to perform calculations one takes into account that $\mu = m A_d A_e / A$ and $\hbar^2/m = 41.47$ MeV·fm². The energy at the touching point, E_t, as well as the radius constant, r_0, depend on the adopted variant of the liquid drop model. We are using the Yukawa-plus-exponential model [25] extended for binary systems with different charge densities [26] with the recently prescribed parameter values.[27]

The results obtained for α-decay and ^{14}C radioactivity are plotted in Fig. 1 a and 1 b, respectively, versus the neutron number of the daughter nucleus, N_d.

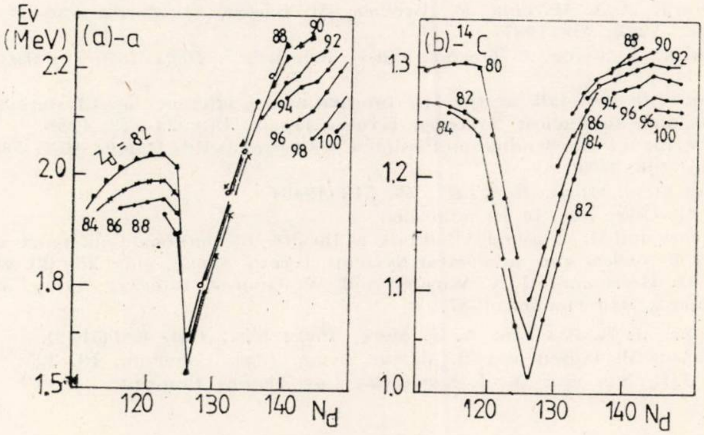

Fig. 1. — Zero-point vibration energy vs. neutron number of the daughter nucleus for α-decay (a) and ^{14}C radioactivity (b).

One can see very pronounced shell effects leading to lower values of E_v at the magic number of neutrons $N_d = 126$ and protons $Z_d = 82$, and a trend toward smaller E_v for heavier emitted ion, approaching 0.5 MeV around $A_e = 48$.

Fig. 1a is very similar with a plot of reduced width for alpha decay, but the range of E_v values is much smaller than 2—3 orders of magnitude.

REFERENCES

[1] "Particle Emission From Nuclei". Vol. I : "Nuclear Deformation Energy". Vol. II : "Alpha-, Proton- and Heavy Ion Radioactivities". Vol. III : "Fission and Beta-Delayed Decay Modes", D. N. Poenaru and M. Ivașcu, Eds., CRC Press, Boca Raton, Florida, USA, 1988.

[2] D. N. Poenaru, M. Ivașcu and W. Greiner, Chapter 7, Vol. III. Ref. 1

[3] D. N. Poenaru and M. Ivașcu, Chapters 3—5, vol. II, Ref. 1.

[4] W. Greiner, M. Ivașcu, D. N. Poenaru and A. Sandulescu, in "Treatise on Heavy Ion Physics", D. A. Bromley Ed., Vol. VIII, Plenum Press, New York, in print.

[5] F. Barranco, R. A. Broglia and G. F. Bertsch, *Phys. Rev. Lett.*, **60**, 507(1988).

[6] H. J. Rose and G. A. Jones, *Nature*, **307**, 245 (1984).

[7] E. Hourani and M. Hussonnois, Chapter 6, Vol. II, Ref. 1.

[8] W. Henning and W. Kutschera, Chapter 7, Vol. II, Ref. 1.

[9] P. B. Price and S. W. Barwick, Chapter 8, Vol. II, Ref. 1.

[10] D. Haşegan and S. P. Tretyakova, Chapter 9, Vol. II, Ref. 1.

[11] D. N. Poenaru, M. Ivaşcu, A. Sandulescu and W. Greiner, *J. Phys.* G, **10** L-183 (1984); *Phys. Rev.*, C**32** 527 and 2198 (1985).

[12] D. N. Poenaru, W. Greiner, K. Depta, M. Ivaşcu, D. Mazilu and A. Sandulescu, *Atomic Data and Nucl. Data Tables*, **34**, 423 (1986).

[13] D. N. Poenaru, M. Ivaşcu, D. Mazilu, R. Gherghescu, K. Depta and W. Greiner, Central Institute of Physics, Bucharest, Preprint NP-54-1986.

[14] D. N. Poenaru, W. Greiner, M. Ivaşcu, D. Mazilu and I. H. Plonski, *Z. Phys.*, A**325** 435 (1986).

[15] D. N. Poenaru, M. Ivaşcu, D. Mazilu, I. Ivaşcu, E. Hourani and W. Greiner, invited talk at the International Symposium on Developments in Nuclear Cluster Dynamics, Sapporo, Japan, August 1—3, 1988.

[16] D. N. Poenaru, M. Ivaşcu and W. Greiner, *Nucl. Tracks*, **12**, 313 (1986).

[17] D. N. Poenaru, J. A. Maruhn, W. Greiner, M. Ivaşcu, D. Mazilu and R. Ghergescu, *Z. Phys.*, A**328**, 309 (1987).

[18] C. Signarbieux, G. Simon, J. Trochon and F. Brissard, *J. Phys. Lettres* (Paris), **46**, L-1095 (1985).

[19] P. Armbruster, invited talk at the 5th International Conference on Clustering Aspects in Nuclear and Subnuclear Systems, Kyoto, Japan, July 25—29, 1988.

[20] F. Gönnenwein, in Proc. Seminar on Fission, C. Wagemans Ed., Report BLG 586 SCK/CEN Mol, pp. 106, 1986.

[21] E. K. Hulet et al., *Phys. Rev. Lett.*, **56**, 313 (1986).

[22] I. Ivaşcu, St. Cerc. Fiz., to be published.

[23] D. N. Poenaru and M. Ivaşcu, invited talk at the 5th International Conference on Clustering Aspects in Nuclear and Subnuclear Systems, Kyoto, Japan, July 25—29, 1988.

[24] K. Depta, R. Herrmann, J. A. Maruhn and W. Greiner, Internat. Symp. on Collective Phenomena, Bad Honnef, 1987.

[25] H. J. Krappe, J. R. Nix and A. J. Sierk, *Phys. Rev.*, **C20**, 992 (1979).

[26] D. N. Poenaru, M. Ivaşcu and D. Mazilu, *Comp. Phys. Commun.*, **19**, 205.

[27] P. Möller, J. R. Nix and W. J. Swiatecki, Los Alamos Preprint.

Revue Roumaine de Chimie, 34, 1, 149–160 (1989)

MASS TRANSFER IN AN AIR-LIFT BIOLOGICAL REACTOR. Part I

AN EXPERIMENTAL STUDY

GHEORGHIŢA JINESCU and VASILE LAVRIC

Department of Chemical Engineering,
77128, Polizu, 1, Bucharest, Romania

Received April 2, 1988

The paper presents an experimental setup for air-lift studies, that was conceived, realized and tested, both for gas-liquid hydrodynamics and for oxygen transfer. The chosen method permitted the experimental determination of the local specific mass transfer coefficient, k_La, in some points of interest of the air-lift reactor. Since the sensor constant, k_s is much less than k_La, the experimental data were processed accordingly. Some interesting conclusions about the relation between k_La and volumetric gas flow rate were drawn.

INTRODUCTION

First discovered by Lefrançois,[1] the air-lift biological reactor has known, since then, an increasing interest, many industrial applications being reported beginning with the eighties. While simple in design, the air-water circulation is very complex, thus difficult to be transposed in mathematical models. The increasing demand of robust and economic reactors focused the specialists' attention on this apparatus, many articles being published [2–12] after the pioneering works of Hatch [2,3] regarding the mass transfer capabilities of the air-lift biological reactors. The liquid-phase circulation and mixing are ensured without mechanical drivers or pumps. The driving force is the difference between the densities of the gas-liquid suspension formed near the nozzle and that of the liquid from the recirculation zone,[10] which may be a tube concentric to the draft one or an external one, intended to the recirculation of the free-gas liquid-phase (Fig. 1, a and b).

In larger configurations, the aeration capacity of an air-lift reactor is higher than that of a mechanically agitated gas-liquid reactor, the former being more economical.[13]

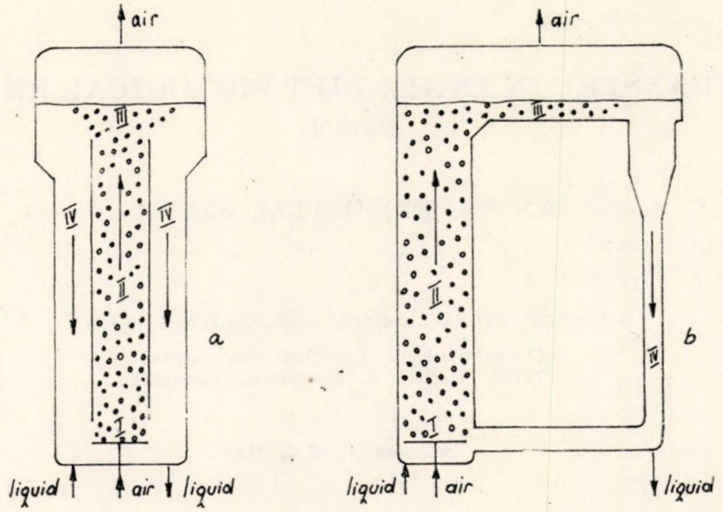

Fig. 1. — Air-lift reactor. a) with draft tube ; b) with external loop (I — mixing region ; II — draft tube region ; III — head region ; IV — loop region).

THEORETICAL CONSIDERATIONS

In aerobic fermentation, the transport of the oxygen from the gas-phase to the interior of the cells is of great importance, especially when cells density into the biological process volume is great, when their growth is limited by their possibility of getting enough oxygen from the liquid-phase. When a large need for dissolved oxygen (DO) exists — hydrocarbon substrate fermentations — the design of a fermentor that provides optimal oxygen transfer values requires the intimate understanding of this process and its determining mechanism. The implied stages of a typical mass transfer process from a gas-bubble to a cell are shown in Fig. 2., considering that Whitmann's two-film theory is applicable.[14] As can be seen, there are six consecutive elementary stages, which determine the global oxygen transfer coefficient value. It must be pointed out that only two of them are rate controlling : 2 and 5.

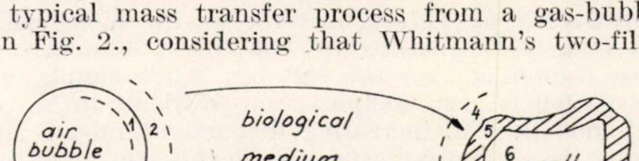

Fig. 2. — Oxygen transfer steps from air-bubble to cell : 1. Diffusion through gas-film ; 2. Diffusion through liquid-film surrounding the bubble ; 3. Oxygen transport through bulk liquid to cell ; 4. Diffusion through liquid-film surrounding the cell ; 5. Oxygen transport through cell membrane ; 6. Oxygen consumption into the cell.

If one designs well a fermentor (the liquid and gas velocities are big enough), the liquid-side film surrounding the gas-bubble can be narrowed, which determines an improvement of the global mass transfer. The rate controlling step is, almost always, the oxygen transport through cell membrane, that cannot be increased with the usually operating methods.

Although the oxygen transfer mathematical modelling was achieved for the steady state behaviour,[15] there is still need for experimentally determined values for the specific mass transfer coefficient, k_La, suitable to each reactor, as there are no theoretical correlations that can predict it, taking account of the appropriate two-phase hydrodynamics of this type of fermentor.

THE EXPERIMENTAL APPROACH

The experimental setup, presented in Fig. 3, is composed of the air-lift reactor, with its draft-tube, the air and water circuits and the measurement apparatus. The volumetric air flow rate can be modified, with three rotameters, from 100 to 3600 l/h, while volumetric water flow rate can take values from 5 to 200 l/h. Supplementary, by a three-way tap, the nitrogen circuit was connected to the air-lift nozzle; this supplementary circuit is used for the complete water deaeration.

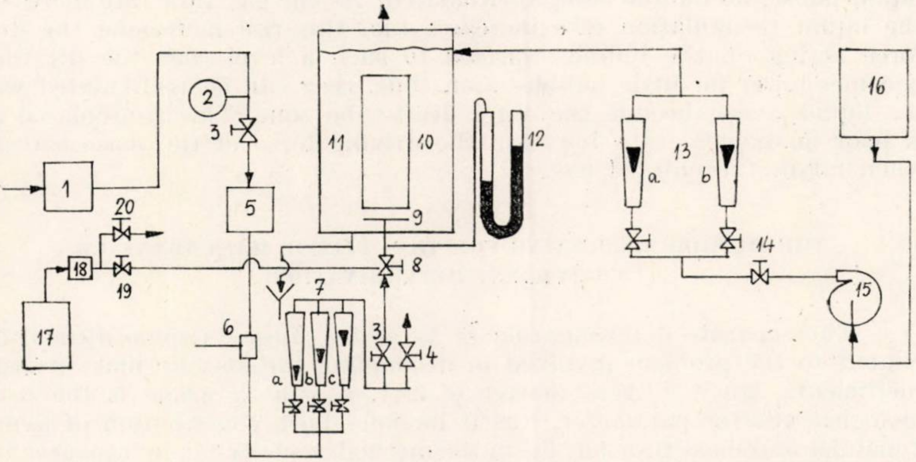

Fig. 3. — The experimental setup : 1. compressor ; 2. manometer ; 3. air tap ; 4. air by-pass tap ; 5. filter ; 6. thermometer ; 7. rotameters (a : 10—100 l/h ; b : 200—1200 l/h ; c : 100—1000 l/h) ; 8. three way tap ; 9. gas sparger ; 10. draft tube ; 11. outer tube ; 12. Hg manometer ; 13. flowmeter (a : 5—50 l/h ; b : 10—150 l/h) ; 14. water tap ; 15. pump ; 16. water tank ; 17. nitrogen source ; 18. pressure reducing gear ; 19. nitrogen tap ; 20. nitrogen by-pass.

The draft-tube diameter was chosen so that its cross section equals the annular one. The air-water separator, at the top of the air-lift reactor, is large enough to prevent foam exit from the fermentor.

A special attention has been paid to the gas-sparger, which must provide a good bubble dispersion in the liquid-phase at the bottom of the air-lift reactor and, at the same time, does not disturb the liquid-phase recirculation in the draft-tube, obturating its entrance. After some tests, the chosen gas sparger was of the perforated plate type, having a total area equal to three quarters of the draft-tube one.

The gas-liquid circulation inside the air-lift reactor is complex, depending mainly on : the reactor and draft-tube diameters ratio, the height of the draft-tube, the liquid height above the draft-tube, the gas sparger type, the gas and liquid flow rates and the rheological properties of the liquid-phase.

For low gas flow rates, the bubbles which are generated from the sparger are of the same diameter. The air-water suspension aroused on the top of the gas sparger has a lower density than that of the surrounding liquid and, thus, arisis a driving force which generates the suspension rise to the top of the draft-tube. The living liquid is replaced by one coming from the outside draft-tube zone. The impact between this supplied liquid and the gas evolved from the gas sparger contributes to the mixing of the liquid-phase. Because of the low flow rate of the recirculated liquid, the lifting force that is acting on the gas bubbles is large enough, compared with the drag force, and, thus, the gas-phase can leave the liquid-phase, no bubble being recirculated. As the gas flow rate increases, the liquid recirculation rate increases too, this rise increasing the drag force acting on the bubbles surface to such a level that the lift force becomes lower for little bubbles and, thus, they can be recirculated with the liquid-phase through the outer draft-tube zone. This recirculated air is poor in oxygen, thus lowering the driving force of the mass transfer when mixes the entered gas.[11,15]

THE METHOD ACCOUNTING FOR THE SPECIFIC MASS TRANSFER COEFFICIENT DETERMINATION

The separate determination of k_L and a presents some difficulties, related to the problem involved in decoupling the specific mass transfer coefficient, k_La.[16,17] As a matter of fact, $k_L\ a$ as a whole is the usual biological reactor parameter,[13] as it includes both contribution of hydrodynamics and mass transfer. From the methods usually taken into account, some gained a larger popularity : the sodium sulfite method, [16] the dynamic method [17,18,19] and the direct method,[17] respectively.

The sodium sulfite procedure,[16] which takes place in the absence of the biological process, has all the drawbacks of any chemical method, i.e. it is laborious and the obtained k_La is a global one. If one is interested in comparing the different zones of an air-lift reactor from the point of view of mass transfer capability, this sodium sulfite method is not adequated because of its averaging property.

The dynamic method, a physical one based on DO probes, applies mainly in the presence of the biological process [18,19]; the important drawback of this method consists in stopping the aeration for a sufficiently long period of time, so that the biological process is perturbed and so, the information obtained corresponds to the unsteady state of the system instead of the stationary one.

A dynamic method variant, which permits the determination of the specific mass transfer coefficient in the absence of the biological process is based on the measurements, with a DO probe, of the DO concentration in the liquid-phase.[17,19] The two major types of steam sterilizable DO electrodes are [17,18]: polarographic (Beckman electrode, Ag anode and Au cathode) and voltametric (Mackereth electrode, Pb anode and Ag cathode) electrodes, which are covered by a polymeric membrane and contain an electrolyte between the membrane and the cathode (Fig. 4).

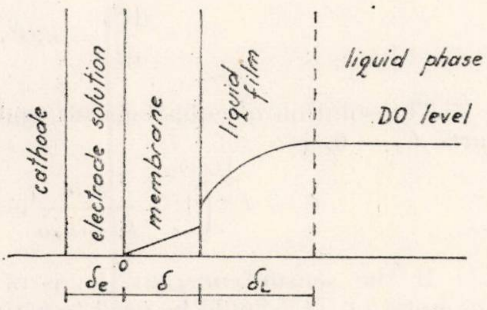

Fig. 4. — Oxygen profiles inside and outside DO probe immersed in liquid phase.

The DO in the liquid-phase difuses through the membrane and the electrolyte layer and is reduced at the cathode surface according to the reaction [18]:

$$O_2 + 2\,H_2O + 4e^- \longrightarrow 4\,OH^- \tag{1}$$

The hydroxyl ions formation on the surface of the cathode produces a current between the electrodes, the intensity of which is proportional to the flux of oxygen through the electrode-membrane, n_{02}.

$$n_{02} = k(p_L - p_e) \tag{2}$$

Considering that the steady state is reached in a short period, the intensity of current is:

$$i = nFAn_{02} \tag{3}$$

In the case of reaction (1), the transferred electrons number, n, is four. Substituting (3) for (2), one obtains the equation relating the partial pressure of the liquid-phase DO to the partial pressure of the oxygen on the membrane-electrolyte interface:

$$p_L = p_e + \frac{i}{n\,F\,A\,K} \tag{4}$$

In general, the dynamic response characteristics of the DO probe must be considered in the determination of k_La by the dynamic method.

In the absence of the microbial cells, and, thus, of the cells respiration, the dynamic balance on DO is [17] :

$$\frac{\mathrm{d}C_L}{\mathrm{d}t} = k_La(C^* - C_L) \tag{5}$$

If, when the aeration process starts, the DO concentration is zero, the solution of equation (5) is :

$$C_L = C^*(1 - \mathrm{e}^{-k_Lat}) \tag{6}$$

If the response of the DO probe is of the first order, the rate of change in the probe readings is :

$$\frac{\mathrm{d}C_s}{\mathrm{d}t} = k_s(C_L - C_s) \tag{7}$$

The solution of equations (6) and (7), knowing that before aeration starts $C_s = 0$, is :

$$C_s = C^*\left(1 + \frac{k_La}{k_s - k_La}\,\mathrm{e}^{-k_st} - \frac{k_s}{k_s - k_La}\,\mathrm{e}^{-k_Lat}\right) \tag{8}$$

If the sensor constant, k_s, is of the same order of magnitude as k_La, equation (8) should be used to estimate the value of k_La by measuring the values of C_s as a function of time and using a trial and error procedure, if the k_s value is known *a priori*. In some cases, the probe response is much more rapid than the rate of oxygen transfer ($k_s \gg k_La_v$), which implies $C_s \simeq C_L$ and the response of the probe is given by equation (6). Linearising equation (6), one obtains :

$$\mathrm{Ln}\,\frac{C^*}{C^* - C_L} = k_Lat \tag{9}$$

Using linear regression with equation (9), one obtains the specific mass transfer coefficient, k_La from experimental data of C^* and C_L vs time.

However, for imperfectly mixed fermentation broth (such as mycelial or polysaccharide fermentation), the probe constant is smaller than the specific oxygen transfer coefficient ($k_s \ll k_La$) and the response of the sensor is very slow compared to the actual changes in DO concentration. In such cases, equation (8) should be used to estimate the value k_La.

RESULTS AND DISCUSSION

The experimental determinations of DO concentrations were done for three volumetric gas-phase flow rates (1.2 ; 2.4 ; 3.6 m^3/h), the liquid-phase being operated batch-wise. Fig. 5 illustrates the probe locations inside the experimental air-lift reactor, for each one being determined the local specific mass transfer coefficient, $k_L a$. The liquid height was kept the same in each experiment.

The DO probe utilized for the experimental determination of the DO concentrations was made by Denki Kogaku Keiki Co., with $k_s \ll k_L a$. Consequently, the experimental data processing was carried out with equation (6) in the linearized form (9).

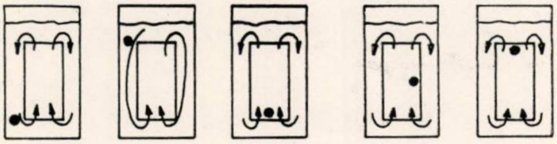

Fig. 5. — DO probe locations inside air-lift reactor.

To be sure of the reproducibility of the experimental data and the correct measurement of the DO concentrations, it must be ensured a correct calibration of the DO probe, for each temperature and pressure and, at the same time, a complete deaeration of the liquid-phase, for that the DO concentration be zero everywhere inside the liquid-phase. For each experiment, the time varying DO concentrations were recorded until the oxygen saturation level was reached.

The experimental data are presented in Figs. 6—10, both the deaeration period and the aeration one. Analysis of these results shows that

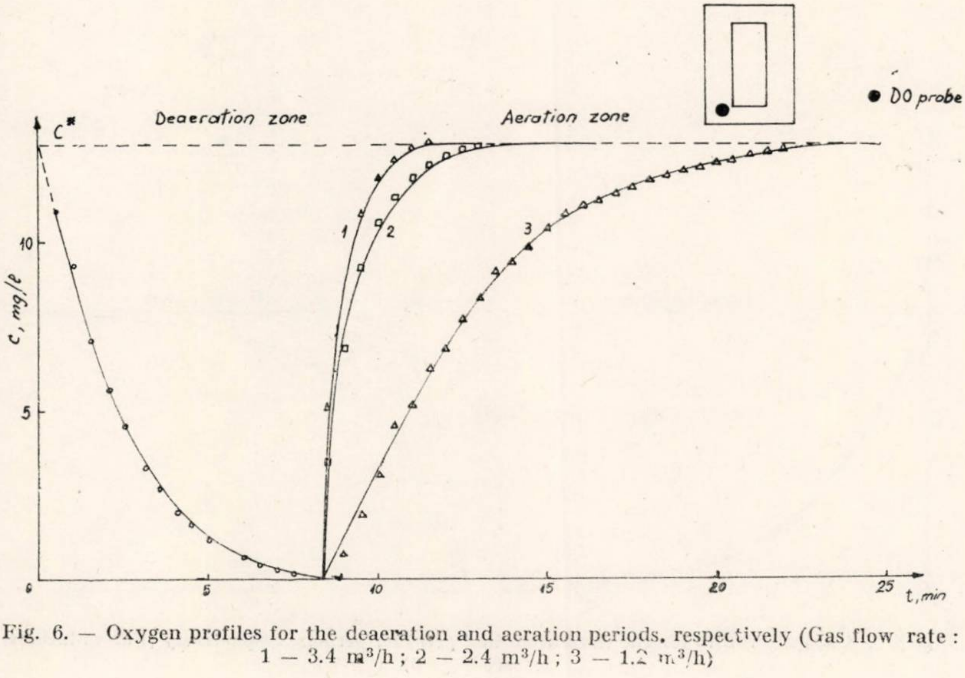

Fig. 6. — Oxygen profiles for the deaeration and aeration periods, respectively (Gas flow rate : 1 — 3.4 m^3/h ; 2 — 2.4 m^3/h ; 3 — 1.2 m^3/h)

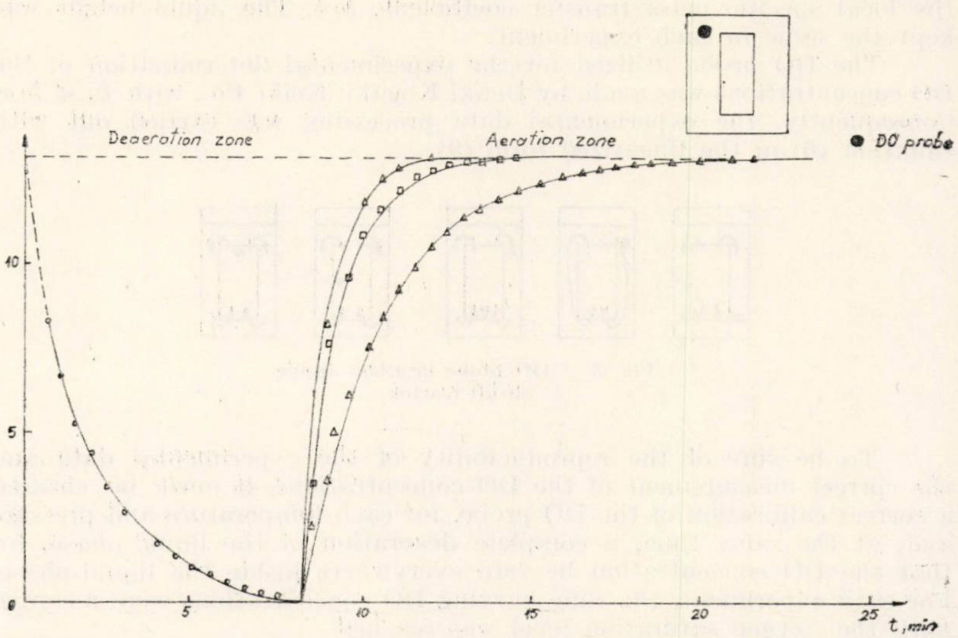

Fig. 7. — Oxygen profiles for the deaeration and aeration periods, respectively (For notations, see Fig. 6).

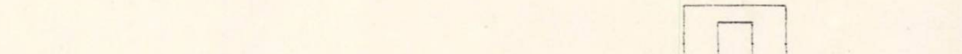

Fig. 8. — Oxygen profiles for the deaeration and aeration periods, respectively (For notations, see Fig. 6).

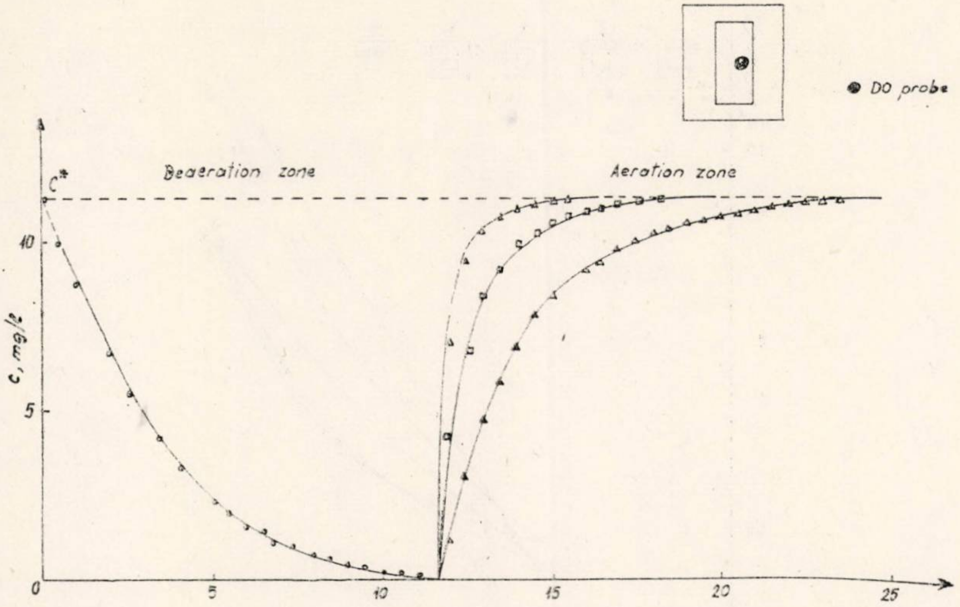

Fig. 9. — Oxygen profiles for the deaeration and aeration periods, respectively (For notations see Fig. 6).

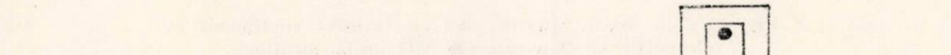

Fig. 10. — Oxygen profiles for the deaeration and aeration periods, respectively (For notations, see Fig. 6).

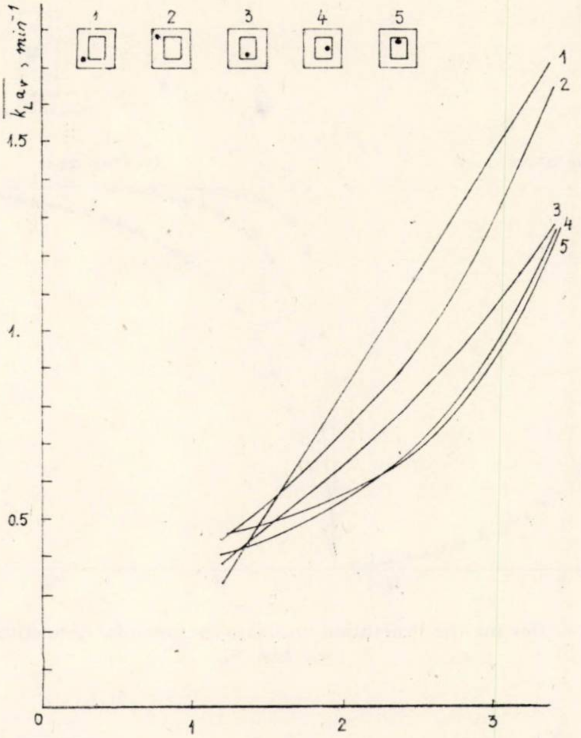

Fig. 11. The mean specific oxygen transfer coefficient *vs* volumetric air-flow-rate (● DO probe location).

irrespective of the DO probe location, the following general conclusions can be drawn :

a) the time ellapsed till the oxygen saturation level is reached, significantly reduces with the increasing gas flow rate. This can be explained by the proportionality between the volumetric gas flow rate and :

— the liquid recirculation rate inside the air-lift reactor, which has as a consequence the decrease of the stagnant liquid film surrounding the gas bubble ; so, the liquid mass transfer resistance decreases too, increasing the specific oxygen transfer coefficient.

— the void fraction in the whole air-lift reactor, which increases the interfacial area, and, thus, the $k_L a$.

b) the oxygen saturation level is not influenced by the volumetric gas flow rate, but is dependent on the liquid height inside the reactor, due to the hydrostatic pressure. The minimum value of the DO concentration (experimentally determined), of about 8.3 ppm, in the gas sparger region can be explained taking account of two effects :

— the injected gas stream induces a great local liquid turbulence which has as effect the partial deoxygenation of the liquid-phase coming from the outside of the draft-tube region with a saturation concentration of about 13 ppm, by the nitrogen from the air, which, although less soluble than oxygen, is in greater concentration.

— at the bottom of the draft-tube, the hydrostatic pressure is less than those corresponding to the same height, but in the outer draft-tube region, because of the different void fractions on both zones : greater value for the draft-tube.

With the upward movement of the gas-liquid suspension, the turbulence dissipates onto the whole liquid-phase and, adequately, the lower solubility of the nitrogen vs oxygen contributes to the rise of the concentration in liquid-phase, up to a maximum on the top of the draft-tube. In the outer draft-tube region, the DO saturation level is practically constant, taking account, on the one hand, of the low void fraction in this region and, on the other, of the relatively slow motion of the liquid-phase in this recirculation zone. Besides, the liquid-phase reaches this zone saturated in oxygen.

c) the specific oxygen transfer coefficient, k_La, is proportional to the volumetric gas flow rate. Surprising is the way in which this increase appears in different zones of the air-lift reactor. At the bottom of the draft-rube region, the increase is linearly with the volumetric gas flow rate, having the maximum variation rate, consequence of the linear dependence between the liquid-phase recirculation rate and the gas flow rate and the modification of the gas-liquid hydrodynamic structure. For the top of the outer draft-tube region, the k_La changes in the same manner, the main difference being the accelerated increase with the gas flow rate. This is plausible, taking account of the increase on both gas void fraction and liquid recirculation rate.

In the draft tube region, the increase of the specific mass transfer coefficient k_La is slower, with the same tendency to the accelerated increase for the height gas flow rates. For the draft-tube zone, the k_La values are smaller than the corresponding outer draft-tube zone ones. This can be explained taking account of the driving force acting on both zones, the difference $C^* - C_L$, which is lower for the draft-tube one.

CONCLUSIONS

An experimental setup for the air-lift reactor studies was conceived, realized and tested, both from the point of view of the gas-liquid hydrodynamics and the oxygen transfer. For the characterization of the mass transfer process the dynamic method was utilized, which permits the determination of the specific mass transfer coefficient, k_La, on the basis of the experimental data taken with a DO probe, consisting in oxygen concentration profiles in time for the liquid-phase. The experimental evidence indicates an increase of the k_La with the volumetric gas flow rate, more marked for the outer draft-tube region. The saturation DO levels are lower in the draft-tube region than those corresponding to the outer draft-tube one.

It must be pointed out that the experimentally determined values of k_La in the present work are well correlated with similar results presented in other papers, for the same range of volumetric gas flow rates. [6,11,13,15,18,20].

NOTATIONS

A — cathode surface area, m^2
C^* — saturation DO level, mg/l (ppm)
C_L — DO concentration, mg/l
F — Faraday's constant, (96500 C/kg equiv.)
i — intensity of the current at steady state, A
K — global mass transfer coefficient, $mol/m^2 \cdot at \cdot min$.
k_s — sensor constant, min^{-1}
n_{02} — flux of oxygen, $mol/m^2 \cdot min$
p_e — partial pressure in the electrolyte-membrane surface, at
p_L — partial pressure in the bulk-liquid, at
t — time, min.

REFERENCES

[1] L. Lefrançois, C. G. Mariller and J. V. Mejane, Brevet D'Invention France, No 1102200, Delivreé le 4 Mai, 1955.

[2] R. T. Hatch, Experimental and Theoretical Studies of Oxygen Transfer in the Airlift Fermentor, Ph. D. thesis, MIT, 1973.

[3] R. T. Hatch, Fermentor Design, in "Single-Cell Protein II", S. R. Tannenbaum and D. I. C. Wang, Eds., MIT Press, Cambridge, Mass, 1975, p. 46.

[4] M. Chakravarty et al., Biotechnol. Bioengngn. Symp, **4**, 363, 1973.

[5] P. G. Cooper et al., Semi-Commercial Studies of a Petroprotein Process Based on n-Paraffines, in "Single-Cell Protein II", S. R. Tannenbaum and D. I. C. Wang, Eds., MIT Press, Cambridge, Mass., 1975, p. 454.

[6] H. Blenke, *Adv. Biochem. Engng.*, **13**, 1 (1979).

[7] N. Blakebrough and K. Sambarurthy, *Biotechnol. Bioengng.*, **8**, 25 (1966).

[8] C. Kleinstreuer and T. Poweigha, *Adv. Biochem. Engng.*, **30**, 91 (1984).

[9] K. Schügerl, Nonmechanically Agitated Bioreactor Systems, in "The Principles of Biotechnology: Engineering Considerations", M. Moo-Young, Ed., 1985, p. 99.

[10] J. C. Merchuk and Y. Stein, *A.I.Ch.E.J.*, **27**, 377 (1981).

[11] N. Blenke, "Biochemical Loop Reactors", in "Biotechnology II", H.-J. Rehm and G. Reed, Eds., VCH Verlagsgesellschaft, Weinhein, 1985.

[12] Y. C. Hsu and M. P. Duduković, *Chem. Engng. Sci.*, **35**, 135 (1980).

[13] G. A. Legrys, *Chem. Engng. Sci.*, **33**, 83 (1978).

[14] G. W. Whitmann, *Chem. Met. Engng.*, **29**, 147 (1923).

[15] C. S. Ho et al., *Biotechnol. Bioengng.*, **19**, 1503 (1977).

[16] V. Linek and V. Vacek, *Chem. Engng. Sci.*, **36**, 1747 (1981).

[17] F. Kargi and M. Moo-Young, Transport Phenomena in Bioprocesses, in "The Principles of Biotechnology. Engineering Considerations", M. Moo-Young, Ed., 1985, p. 5.

[18] V. Linek and V. Vacek, *Biotechnol. Bioengng.*, **18**, 1537 (1976).

[19] B. Bandyopadhyay et al., *Biotechnol. Bioengng.*, **9**, 533 (1967).

[20] C. H. Liu et al., *Biotechnol. Bioengngn.*, **18**, 1557 (1976).

Revue Roumaine de Chimie, **34**, *1*, 161–167 (1989)

A FUNDAMENTAL PROPERTY OF MATTER. Part II

VALERIU V. JINESCU
Polytechnic Institute of Bucharest, Department of Mechanics, Romania

Received April 15, 1988

The principle of reluctance, stated in the first part of the paper, gives the possibility of a new interpretation of the first principle of thermodynamics. It can be accepted as a unitary principle, including the transfer, change and conservation of energy. At the same time the reluctance property is correlated with the concept of material degradation as well with that of reluctance force.

This paper has the sections and relationships numbered sequentially in continuation of those presented in Part I.[9]

4. SEVERAL OBSERVATIONS SUPPORTING THE IDEA OF A FUNDAMENTAL, UNIQUE, PROPERTY OF MATTER

At present, the reluctance for a given action upon a material body is estimated through different physical characteristics, depending on the nature (electrical, magnetical, mechanical etc...) and the type of the external load (accumulation, transport or propagation energy).

Sometimes, although the *external actions are different*, the characteristics conveying their behaviour are alike. E.g.:

— the iron magnetizing curve and the stretching-compression stress curve are alike; if mechanically speaking an iron body is remanently deformed, magnetically speaking it is remanently magnetized;

— at not very low temperatures, the metals thermal conductivity, λ, is proportional to the electric conductivity, λ_e, (Wiedman and Franz's law)

$$\lambda = K \cdot T \cdot \lambda_e,$$

where K is a proportionality factor; T — temperature in K;

— equations describing material behaviour in the electric and the magnetic fields have similar structures,

$$\vec{D} = \varepsilon \cdot \vec{E} \text{ — in the electric field;}$$

$$\overline{B} = \mu \cdot - \overline{H} \text{ in the magnetic field,}$$

where $\vec{D}$ is the electric induction; $\vec{E}$ — electric field vector; $\overline{B}$ — magnetic induction; $\overline{H}$ — magnetic field vector; ε — dielectric constant and μ — magnetic permeability.

The fact that *external actions of a certain nature* may determine effects of a nature differing from that of the action, backs up the idea of a unique fundamental property (reluctance).

Such are for instance the piezoelectric effect (electric polarization of some crystalline substances following their mechanical deformation), the pyroelectric effect (electric polarization determined by body temperature variation), magnetostrictive effect (body deformation when an electric field is applied to it) as well as the thermoelectric, thermomagnetic, galvanometric effects, etc.

5. A GENERALIZED EXPRESSION FOR THE RELUCTANCE PROPERTY

On the basis of the above analysis we suggest the following general relationship for reluctance,[10]

$$\mathbf{R} = -k \cdot \frac{\mathrm{d}E_a}{\mathrm{d}e}, \tag{11}$$

where k is a constant dependent on the nature of obtained effect, e, and $\mathbf{R}$ — the reluctance property or generalised inertia (property of opposition).

The minus sign shows that the action energy and the reluctance are contrary.

Hence, reluctance $\mathbf{R}$ is proportional to the action energy variation, E_a (which acts upon the body) with respect to the obtained effect, e. Constant k includes, for every type of external load, the physical characteristics corresponding to the nature and type of the obtained effect. For example :

— in the case of gravity, $e = h$ and $k = -1/g$;

— in the case of thermal energy accumulation $e = T$, whereas $k = -1/c_p$.

If the energy load E yields n different effects, then relation (11) may be written as

$$\mathbf{R} = -\sum_{i=1}^{n} k_i \cdot \frac{\mathrm{d}E_a}{\mathrm{d}e_i}, \tag{12}$$

where

$$E_a = \sum_{i=1}^{n} E_{a,i} \text{ and } \frac{\mathrm{d}E_a}{\mathrm{d}e_i} = \frac{\mathrm{d}E_{a,i}}{\mathrm{d}e_i}$$

Writting

$$\mathbf{R}_i = -k_i \cdot \frac{\mathrm{d}E_{a,i}}{\mathrm{d}e_i} \tag{13}$$

yields

$$\mathbf{R} = \sum_{i=1}^{n} \mathbf{R}_i,$$

or

$$\sum_{i=1}^{n} \frac{\mathbf{R}_i}{\mathbf{R}} = 1. \tag{14}$$

Then in the case of several effects, the sum of reluctance participation ratios corresponding to each obtained effect is equal to 1.

6. CONSEQUENCES OF THE RELUCTANCE PRINCIPLE

6.1. A new interpretation of the first principle of thermodynamics on the basis of the reluctance principle

If the effect obtained is measured in energy units, E_e, relationship (11) becomes

$$\mathbf{R} = -k \cdot \frac{\mathrm{d}E_a}{\mathrm{d}E_e}, \tag{15}$$

so that $k = -1$. Since the energy effect, irrespective of the energy forms involved, is equal to the action energy (according to the postulate stated in the introduction) all the above give

$$\mathbf{R} = +1. \tag{16}$$

From relationships (15) and (16) one has, generally,

$$E_a = \frac{-1}{k} \cdot E_e. \tag{17}$$

Through k we highlight the sign of energy; one writes

$$-\frac{1}{k} = \mathrm{sign}(E_{e,j}/E_{a,j}),$$

where energy effect $E_{e,j}$ of the type j, may have the same sign as $E_{a,j}$ or it may be contrary to it, so that

$$\mathrm{sign}\left(\frac{E_{e,j}}{E_{a,j}}\right) = \begin{cases} +1, & \text{if } E_{e,j} \text{ has the same sense as } E_{a,j}; \\ -1, & \text{if } E_{e,j} \text{ has a sense contrary to } E_{a,j}. \end{cases}$$

Now, relationship (17) becomes

$$E_a = E_e \cdot \mathrm{sign}\left(\frac{E_a}{E_e}\right) \tag{18}$$

For example, if a deforming work L is exerted upon a material body and the heat amount Q is transferred at the same time (Fig. 5, a) and the effect obtained lies only in the variation of the internal energy $\Delta U = U(T_2) - U(T_1)$ (Fig. 5.b), then relationship (18) becomes,

$$L + Q = \Delta U. \tag{19}$$

On the other hand, if a certain amount of heat Q by acting upon a material body causes both the variation of the internal energy ΔU and work, then

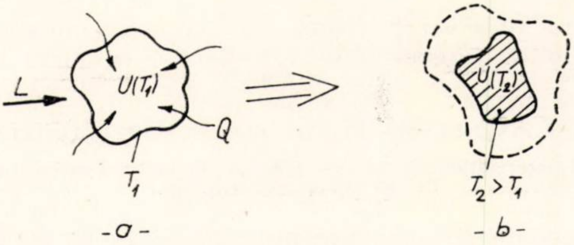

Fig. 5. — Variation in the internal energy of a material body undergoing deformations under the work L and heated with the amount Q.

$$Q = \Delta U + L. \tag{20}$$

Relationships (19 and 20) are two different forms of the first principle of thermodynamics. Starting from relationship (18) the first principle of thermodynamics can be written under the general form of

$$Q = \Delta U + L \cdot \operatorname{sign}\left(\frac{L}{\Delta U}\right), \tag{21}$$

where

$$\operatorname{sign}\left(\frac{L}{\Delta U}\right) = \begin{cases} +1, & \text{if work } L \text{ is ``energy'' effect like } \Delta U\,; \\ -1, & \text{if work } L \text{ is action ``energy''.} \end{cases}$$

6.2. Reluctance and material degradation

A sequence of actions $E_{a,j}$ determines by means of reluctance a sequence of oppositions on the part of the material. Each action leaves, on account of reluctance, "a trace" in the material; this represents a micro- or a macro-degradation of the material. We write D_j the degradation caused by action j. The sum of *successive degradations* equals the total degradation D of the material

$$D = \sum_j D_j. \tag{22}$$

Relationship (22) may be also written as

$$\sum_j \mathbf{d}_j = 1, \tag{23}$$

where $\mathbf{d}_j = \dfrac{D_j}{D}$ is the relative degradation caused by action $E_{a,j}$. In the case of *simultaneity action* of $E_{a,j}$ the same relationship (22) is used for the calculation of the total degradation.

If the total degradation D corresponds to the point when the material reaches the critical state (i.e. : failure, melting etc.) then $D = D_{cr}$. In this case

$$\sum_j \mathbf{d}_j^* = 1, \tag{24}$$

where $\mathbf{d}_j^* = \frac{D_j}{D_{cr}}$ may be calculated on the basis of the critical energy principle.[10]

All the above prove that the relative reluctance (14) and the relative degradation of the materials (23) are formally similar variables, degradation being an outcome of reluctance.

6.3. **Reluctance and force equilibrium**

Reluctance is, as we have shown, an intrinsic property of matter; it manifests itself, for instance, when the material body undergoes the action of external forces, $\vec{P}_j$. In this case reluctance is also a force, *the reluctance force* $\vec{F}_r$. Because the reluctance force is at work only when the material body undergoes the action of some forces, this means that it behaves as a *latent force.*

Therefore the reluctant force is a real force, specific to the body in motion.

The sense of the reluctant force $\vec{F}_r$ is, obviously, opposite to the sense of external motion. Hence, the reluctant acceleration, $\vec{a}_r$, has a direction contrary to the motion acceleration, $\vec{a}$. When only inertia is present, for instance,

$$\vec{F}_r = \vec{F}_i = m \cdot \vec{a}_r \tag{25}$$

where $\vec{a}_r = -\vec{a}$.

Consequently, when there is no friction, the forces acting upon a body, including the reluctance force, form together a system of forces in equilibrium, respectively

$$\sum_j \vec{P}_j + \vec{F}_r = 0 \tag{26}$$

or

$$\sum_j \vec{P}_j - m \cdot \vec{a} = 0. \tag{27}$$

Relationship (27) represents the well-known *d'Alembert principle* from Analytical Mechanics.[11] In the d'Alembert principle the inertia forces are considered as fiction forces for the body undergoing the action of forces $\vec{P}_j$. Consequently, the equilibrium from d'Alembert principle is considered as a fiction equilibrium.

The reluctant *force is real*, intrinsic to the material body and consequently the equilibrium of action forces $\vec{P}_j$ and reluctant force $\vec{F}_r$ (26) is real.

If a system subjected to connections becomes free of connections, and if we introduce instead the connection forces, $\vec{R}_l$, then the action forces $\vec{P}_j$, the connection forces, $\vec{R}_l$, and the reluctant force, $\vec{F}_r$, form a system of forces in equilibrium, respectively

$$\sum_j \vec{P}_j + \sum_l \vec{R}_l + \vec{F}_r = 0, \tag{28}$$

which represents a reformulation of the d'Alembert principle,[11] with reluctance consideration.

Hence, the reluctant force is a real force; it appears in the interactions and must be taken into account when we write the forces equilibrium equation.

Consequently, the virtual work of the resultant forces, forces which are in equilibrium, is zero, respectively

$$(\sum_j \vec{P}_j + \vec{F}_r) \cdot \Delta\vec{r}_j = 0, \tag{29}$$

where $\Delta\vec{r}_j$ is the virtual motion along the direction of force $\vec{P}_j$.

If $\vec{F}_r = \vec{F}_i = - m \cdot \vec{a}$, relationship (29) represents the analytical transposition of the d'Alembert-Lagrange principle from Analytical Mechanics.[11]

In the case of a system with friction, the reluctant force is made up of the inertia force and the friction force, $\vec{F}_f$, respectively,

$$\vec{F}_r = \vec{F}_i + \vec{F}_f = m \cdot a_r \tag{30}$$

The positive sign of the reluctant force corresponds to the positive sense of the friction force which is contrary to the positive sense of speed.

In this case, relationships (26), (28) and (29) remain valid.

7. CONCLUSIONS

The investigation of some physical, chemical, biological phenomena as well as of some wellknown principles and laws, together with the induction method application, proved the existence of a fundamental property, **reluctance**, or generalised inertia; the **principle of reluctance** was stated, a generalizing principle covering the validity fields of some wellknown laws and principles which are specific only to some particular departments of science.

From the general expression (11) proposed for reluctance, it follows that it is proportional to the energy variation with respect to the effect obtained. One may conclude that **the analysis of interactions should be made by using the energy concept.**

Mention should be made that the nature of external action determines the kind of behaviour of the material bodies (mechanical, electrical, chemical, thermal, magnetical...) and the composition and structure of the material body determines its kind of response to external action; the agregation state of the material body determines the level of its reluctance.

Owing to the reluctance property, the effect opposes the cause, matter opposes the change in the equilibrium of the local forms of energy ; **the overall amount of the energy involved in the interaction is preserved, but the form of implied energy and its amount are generally not preserved.**

REFERENCES

[9] V. V. Jinescu, *Rev. Roumaine Chim.*, **33**, 763 (1988).

[10] V. V. Jinescu, *Revista de Chimie* (București), **35**, 858 (1984).

[11] R. Voinea, D. Voiculescu and V. Ceaușu, "Mecanica", Ed. Didactică și Pedagogică, Bucharest, 1983.

Revue Roumaine de Chimie, **34**, *1*, 169–189 (1989)

DEPENDENCE OF SUBSTITUENT ELECTRONIC EFFECTS IN π-SYSTEMS ON THE CHARACTER OF MOLECULAR ORBITALS

VALENTIN AFANASIEVICH KOPTYUG
Inst. of Organic Chemistry, Siberian Branch of the USSR Academy of Sciences,
Novosibirsk 90, USSR

Received October 10, 1988

A comprehensive review is presented for a new approach to the problem of calculating electronic effects in π-systems on the basis of ionization potentials. This approach is more general than the well-known method of Hammett, and can be applied to polycyclic benzenoids as well.

One of the important problems of theoretic organic chemistry is elucidation of quantitative relationship between the structure and reactivity of organic compounds. Traditionally there are two approaches to this problem. The first one uses the $\rho\sigma$ type correlations where the effect of structure modification, such as introduction of substituent X, is defined using the σ(X) parameter. This approach is theoretically non-substantiated and should be regarded as empirical or semi-empirical. Despite the apparent simplicity and certain convenience, it has some serious demerits. The main demerit is in the fact that substituent electronic effect "constants" σ(X) are not constants in reality. Depending on the character of the compound frame, we have to use either the induction or resonance "constants", which in addition depend on the substituent position relative to the reaction centre. Thus in the benzene series one has to use three position σ constants – σ_{ortho}, σ_{meta}, and σ_{para}, and in the naphthalene series – already 14 such constants (Scheme 1). Depending on the character of reaction centre in the benzene series, the Hammett, σ^+, and σ^- constants are used. Such a multitude of constants brings this formerly attractive approach to a deadlock.

Another approach uses quantum-chemical calculations of different complexity. It is theoretically well-substantiated and will doubtless be the principal approach in the future. But it also has some demerits. One of them is temporary, being a consequence of insufficient reliability of the existing calculation methods. Only one example will be given relating to the problem of the structure of a complex formed by the proton addition to benzene. For some reasons this question was once a subject of widespread interest. Some chemists considered (Scheme 2) that the complex has π-structure (hybridization of carbon atoms remains undisturbed), whereas others maintained the σ structure (one of the carbon sp^2 hybrid atoms of the benzene ring changes to the sp^3 hybrid state).

During the recent two decades, complexes of aromatic compounds with protons and other strong electrophiles have been thoroughly investigated by various physical methods, and found to have the σ structure.

Scheme 1

$$\lg \frac{K_{i-x}}{K_H} = \rho\sigma_{i-x}$$

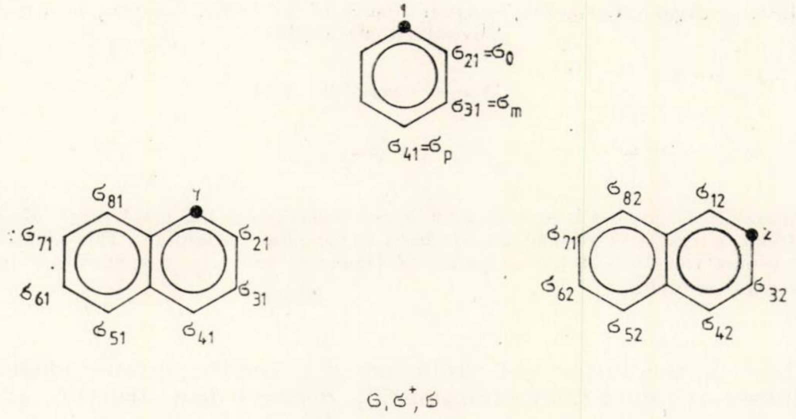

As to the calculations, they give different results depending on the calculation procedure. Some calculations predict the greater stability of the

Scheme 2

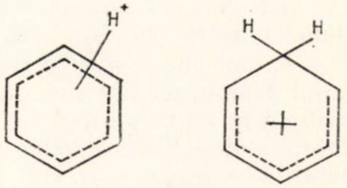

π structure, whereas others, of the σ structure. Similar results have been obtained in the calculations of a simpler proton-ethylene system (Scheme 3).

The reliability of quantum-chemical calculations will obviously increase with improvement of calculation methods. But this will enhance another demerit of this approach — the lack of perceptivity, and, as a consequence, difficulties in understanding the reasons for the effects predicted. The calculation program will become a kind of a "black box", on one side of which the data are input and on another the results are output, while the relationship between the starting data and the results remains obscure.

It seems important to span these two approaches into one which would combine the simplicity of the first approach and at least the simplified theoretic substantiation of the second.

This proved to be quite a simple affair in the case of defining substituent effect on the reactivity of aromatic and unsaturated systems.

Scheme 3

Calculation method	More stable structure		$\Delta E_{(E_B-E_A)}$ kcal/mol
	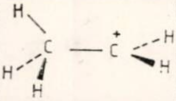	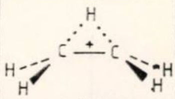	
Extended Hückel Theory (1964)	⊕		+ 2
Extended Hückel Theory (1968)	⊕		+24
Intermediate Neglect of Differential Overlap (1968)		⊕	−12
Neglect of Diatomic Differential Overlap (1969)		⊕	−33
Complete Neglect of Differential Overlap — FK (1971)		⊕	−10
Partial Retention of Diatomic Differential Overlap (1974)	⊕		+20
Modified Intermediate Neglect of Dif. Overlap — 3(1975		⊕	− 8
ab initio LGGO (1968)	⊕	⊕	0
STO — 3G (1970)	⊕		+11
4 — 31 G (1972)	⊕		+ 7
6 — 31 G (1972)	⊕	⊕	0
MSTO (1973)	⊕		+12
C — PeGTO (1973)		⊕	− 9

I shall give two examples where the expected correlations between the reactivity and σ constants of substituents are not in effect. As a "chemical process" to simplify the deductions we chose the electron elimination from the π system.

Example **1**. (Scheme 4). The substituent effect on the reactions of electrophilic substitution in the benzene ring proceeding via formation of σ complexes is known to be well defined in terms of $\rho\sigma$ correlations using substituent σ^+ constants. Then why the oxidation potentials characterizing one of the reactivity types of such σ complexes have no clear-cut relation to position (*orho*, *meta*, *para*) σ^+ constants?

Example **2** (Scheme 5). It is common to think that the *ortho* and *para* isomers in the series of disubstituted benzene derivatives are analogus in their reactivity, and *me a* isomers are dramatically different. Then why the first ionisation potentials are similar for *ortho* and *meta* isomers, whereas the *para* isomer has a different ionisation potential?

This is a nice example as it prompts an answer to such questions.

Benzene has two highest occupied orbitals — a_2 and b_1: they are degenerate. The introduction of substituents removes the degeneracy. In the radical cation formed upon the electron elimination, the highest occupied orbital is the one which suffers the greatest stabilizing effect of substituents. This effect should depend on the properties of substituent and on the efficiency of its interaction with the molecular π-orbital, which depends on the character of this orbital.

Thus the stabilizing effect of an electron-donating substituent on the highest occupied orbital of radical cation is stronger the greater the c_i^2 value at a substituent position. In the case of disubstituted benzenes, this requirement is satisfied by the a_2, orbital for *ortho* and *meta* isomers,

Scheme 4

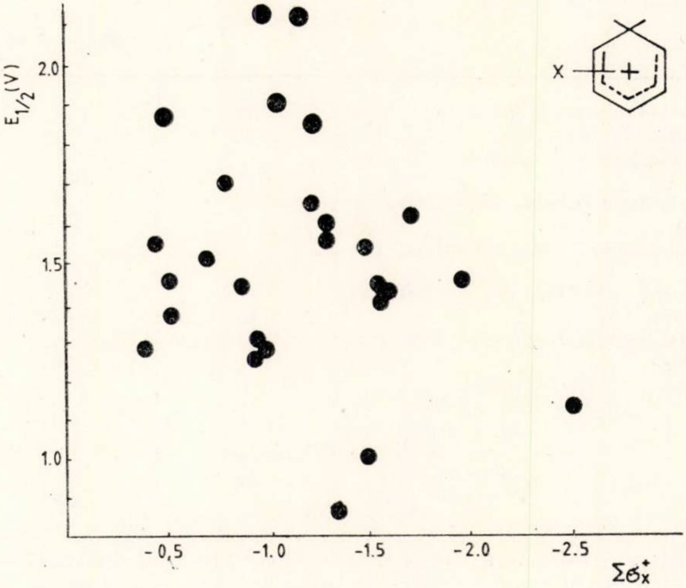

Scheme 5

π-HOMO : FI method, +M Substituent

Substituted benzene	First I. P. (eV)
H	9.25
1,2 - $(CH_3)_2$	8.56
1,3 - $(CH_3)_2$	8.56
1,4 - $(CH_3)_2$	8.44
1,2 - F, CH_3	8.92
1,3 - F, CH_3	8.92
1,4 - F, CH_3	8.78

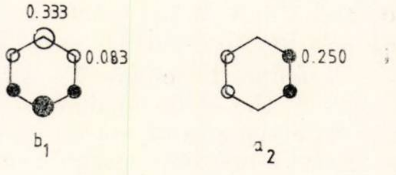
0.333
0.083
0.250
b_1
a_2

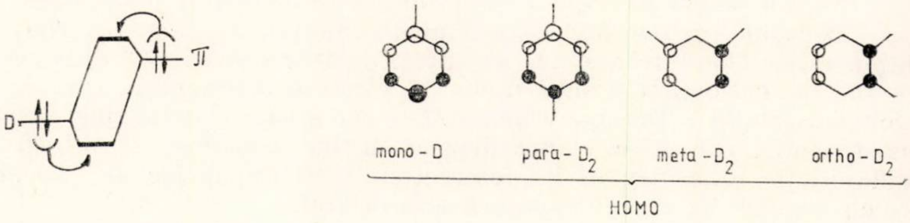
D
π
mono - D
para - D_2
meta - D_2
ortho - D_2
HOMO

and the b_1 orbital for the *para* isomer. Just this accounts for the similarity of first ionisation potentials of *ortho* and *meta* isomers and the difference of ionisation potential of the *para* isomer.

This example reveals an important circumstance — the substituent electronic effect in π-systems depends on the character of molecular orbital involved in the reaction. Let us try to deal with this problem more closely, considering that the total substituent electronic effect involves the resonance and induction contributions. The reaction series in question — electron elimination from benzene derivatives — is very suitable for such consideration if we take into account not only the first ionisation potential but also the second one, that is if we compare variation of ionisation potentials of orbitals b_1 and a_2.

Evidently, the resonance term of substituent electronic effect depends above all on the c_i^2 value of the orbital at substituent position (Scheme 5: $c_i^2 = 0$ for a_2), whereas the induction (electrostatic) term, on the character of positive charge distribution all over the orbital. Dependence of the induction term (Φ_X) on charge distribution in the orbital may be defined by a usual correlation given in Scheme 6, taking into account that $q_i = c_i^2$. In this correlation D_X is a constant defining substituent, which may be easily determined numerically making use of the fact that variation of ionisation potential (Δ_X^I) of the a_2 orbital of monosubstituted benzene is defined only by the induction effect of substituent, as $c_i^2 = 0$.

Using this correlation it is easy to estimate the variation of the induction term from benzene to other π-systems. We shall need this later and now it should only be noted that the substituent induction effect on electron elimination from the b_1 and a_2 orbitals of benezene has close values and we shall regard it to be the same in both cases.

Scheme 6

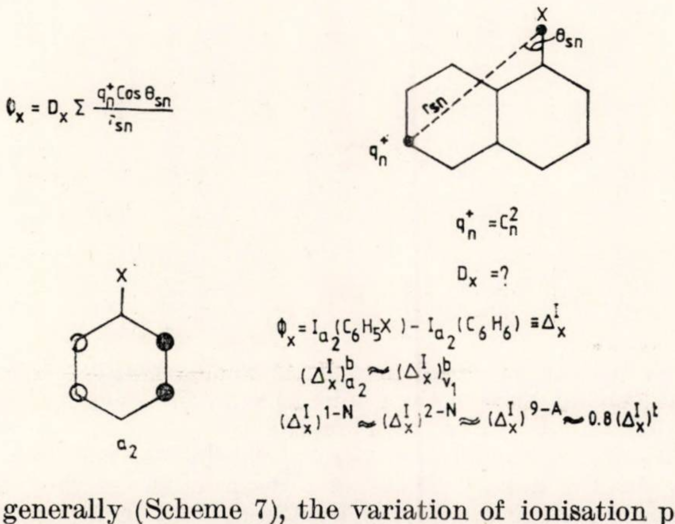

$$\Phi_X = D_X \Sigma \frac{q_n^+ \cos\theta_{sn}}{r_{sn}}$$

$$q_n^+ = c_n^2$$

$$D_X = ?$$

$$\Phi_X = I_{a_2}(C_6H_5X) - I_{a_2}(C_6H_6) \equiv \Delta_X^I$$

$$(\Delta_X^I)^b_{a_2} \sim (\Delta_X^I)^b_{v_1}$$

$$(\Delta_X^I)^{1-N} \sim (\Delta_X^I)^{2-N} \approx (\Delta_X^I)^{9-A} \sim 0.8(\Delta_X^I)^t$$

Thus, generally (Scheme 7), the variation of ionisation potential of substituted benzene involves the induction term irrespective of the orbital character, and the resonance term Δ_X^I which depends on the c_i^2 value. As for the benzene b_1 orbital $c_i^2 = 0.333$, on passing to other orbitals we should introduce the standardizing factor $c_i^2/0.333$.

Scheme 7

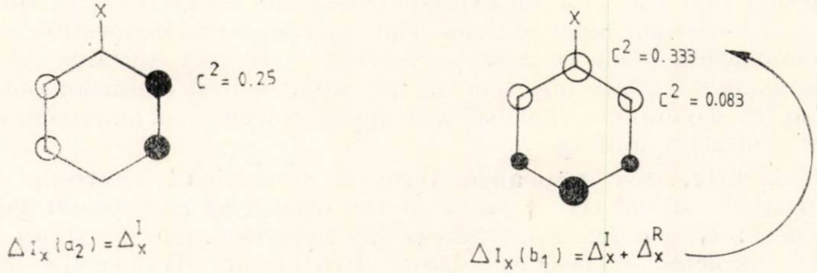

$$\Delta I_{i-x}(\pi) = \frac{c_i^2}{0.333}\,\Delta_x^R + b\Delta_x^I$$

Table 1 shows the Δ_X^I and Δ_X^R values for a number of substituents and, for the sake of comparison, the σ_m^+ and $(\sigma_p^+ - \sigma_m^+)$ values, generally used to estimate the induction and resonance effects of substituents in the benzene series for the reactions giving rise to a positive charge in the π-system. The σ^+ values are usually determined in the solvolysis reaction of substituted cumyl chlorides.

Table 1

Values of ΔI_X^I and Δ_X^R units (Photoelectron spectroscopy)

X	Δ_X^I	Δ_X^R	σ_{m-X}^+	$\sigma_{p-X}^+ - \sigma_{m-X}^+$
$N(CH_3)_2$	−0.27	−1.55	−0.27	−1.43
NH_2	−0.15	−1.10	−0.16	−1.14
OCH_3	−0.03	−0.82	+0.03	−0.83
OH	+0.05	*−0.59*	+0.12	*−1.04*
CH_3	−0.05	−0.28	−0.07	−0.24
F	+0.36	−0.43	+0.35	−0.42
CHO	+0.32		+0.35	
CN	+0.43		+0.56	
NO_2	+0.63		+0.67	

It was reasonable to expect a linear correlation between the Δ_X and σ^+ values, but they were found to coincide even in their absolute values, which is, of course, accidental.

The Δ_X values seem to be more preferable for use as a measure of induction and resonance effects of substituents, as they have a clear physical sense and are unaffected by the solvent (compare the data for the OH group).

Using the Δ_X^I and Δ_X^R values found for monosubstituted benzenes, it is possible to calculate ionisation potentials of polysubstituted compounds in the context of an additive scheme of substituent effects, considering the dependence of the resonance term on the σ_I^2 values. As an example Table 2 shows comparison between the calculated and experimental values for polyfluorinated benzenes. It is easy to see that the agreement is quite good.

Table 2

Fluorine-substituted benzenes
(Photoelectron-spectroscopic method)

Position of fluorines	Ionisation potentials	
	Expt.	Calc.
1	9.19, 9.63	9.19 (b_1), 9.59 (a_2)
1,2	9.30, 9.68	9.29 (a_2), 9.67 (b_1)
1,3	9.32, 9.68	9.29((a_2), 9.67 (b_1)
1,4	9.15, 9.98	9.13 (b_1), 9.91 (a_2)
1,3,5	9.62	9.62 (b_1, a_2)
1,2,3,4	9.56, 9.88	9.55 (b_1), 9.95 (a_2)
1,2,3,5	9.56, 9.93	9.55(b_1), 9.95 (a_2)
1,2,4,5	9.36, 10.34	9.33 (a_2), 10.09 (b_1)
1,2,3,4,5	9.64, ?	9.66 (a_2), 10.03 (b_1)
1,2,3,4,5,6	9.90	9.98 (b_1, a_2)

The use of this calculation scheme encounters some difficulties which will be mentioned below on. But the main thing which should be stressed here is that consideration of the substituent resonance effect dependence on the character of molecular orbital involved in the reaction essentially expands the applications of the correlation schemes describing the reactivity and physical characteristics of substituted π-systems. In this connection let us return to the question asked at the beginning of the lecture — how can we define substituent effect on the electrochemical oxidation of benzenonium ions (Scheme 8)?

Scheme 8

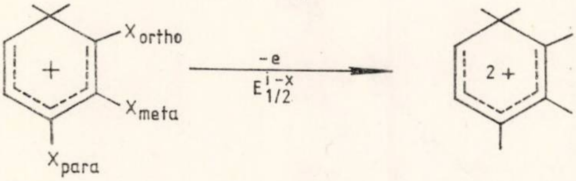

$X = H, CH_3, OH, OCH_3, Cl, Br, NO_2$

The character of the highest occupied molecular orbital of benzenonium ion, which releases an electron, is shown in Scheme 9. Taking into account the character of the orbital, it is clear that the resonance effects of *ortho* and *para* substituents should strongly differ ($c_2^2 = 0.25$, $c_4^2 = 0$).

This difference may be considered in the same way as with ionisation potentials and recalculated using a known correlation between the ionisation potentials and electrochemical oxidation potentials of benzene derivatives.

Scheme 9

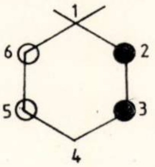

$$C_4^2 = 0$$

$$C_2^2 = C_3^2 = C_5^2 = C_6^2 = 0.25$$

For substituted benzenes :

$$E_{1/2}^{x} = 0.62\, I_X^{HOMO} - 3.70$$

For substituted benzene ions :

$$E_{1/2}^{x} = E_{1/2}^{0} + \Sigma\Delta E_{1/2}^{x} = E_{1/2}^{0} + 0.62\, \Sigma\Delta I_X^{calc}$$

with Δ_X^R and Δ_X^I

Scheme 10 compares the calculated values of oxidation potentials of substituted benzenonium ions and the experimental values. If one compares the oxidation potentials correlated (Scheme 4) with the σ^+ values of *ortho*, *meta*, and *para* substituents, no other comments are necessary.

Scheme 10

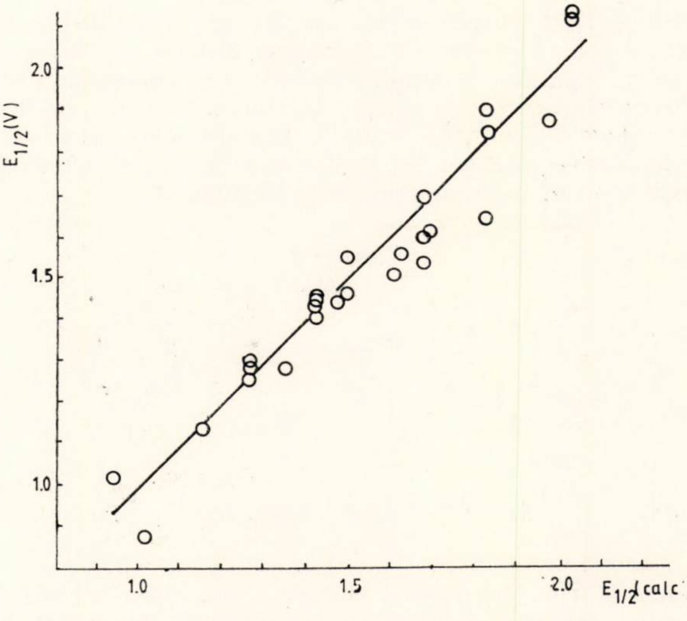

There is another example demonstrating the necessity to consider the dependence of the resonance term of substituent electronic effect on the character of molecular orbitals. This example concerns the problem of substituent effect on the electronic absorption spectra of benzenonium ions (Scheme 11).

Scheme 11

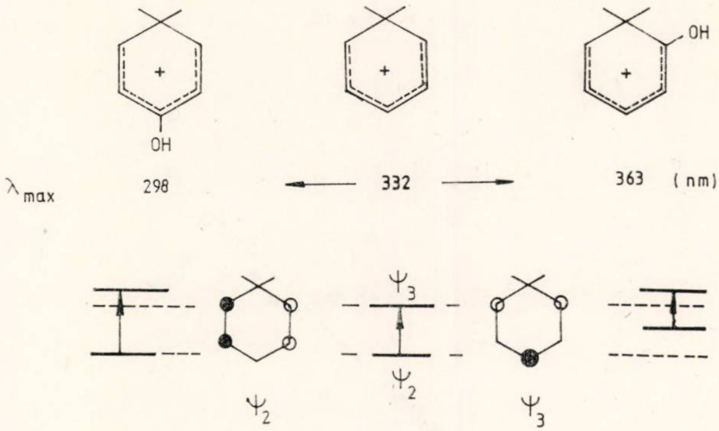

$$\Delta E_X^* = \alpha_2 \frac{c_i^2(\Psi_2)}{0.333} \Delta_X^R - \alpha_3 \frac{c_i^2(\Psi_3)}{0.333} \Delta_X^R$$

For many years it was not clear why the introduction of the hydroxy group in *ortho* positions leads to a shift of absorption band towards higher wavenumbers, whereas in *para* positions to a shift towards lower wavenumbers. However, if we take into consideration the character of the highest occupied and lowest unoccupied orbitals involved in the electron transitions upon its absorption of a light quantum, things straighten out.

Table 3 compares the experimental λ_{max} values for substituted benzenonium ions with the values calculated using the Δ_X^I and Δ_X^R para-

Table 3

Electron absorption maxima of substituted benzenonium ions ($\alpha_2 = 1$ $\alpha_3 = 0.45$)

Substituent	Acid	λ_{max}^{exp}	λ_{max}^{calc}
H	HBr—$AlBr_3$	332	
4-CH_3	HBr—ABr_3	326	323
2,3,4,6-$(CH_3)_4$	HF—BF_3	365	352
2,3,4,5,6-$(CH_3)_5$	HF	377	371
2-CH_3-4-OH	$HClO_4$	298	300
2,6-$(CH_3)_2$-4-OH	HF—BF_3	308	305
2,4-$(OH)_2$	$HClO_4$	311	319
6-CH_3-2,4-$(OH)_2$	HF—BF_3	324	325
4,5,6-$(CH_3)_3$-2-OH	HSO_3F	380	378
2,4,6-$(OH)_3$	HF—BF_3	324	325
2,4,6-$(OCH_3)_3$	$HClO_4$	347	344
2,4,6-$(NH_2)_3$	H_2SO_4	360	350

meters. Scheme 12 shows a more complete comparison (the number of ions is doubled). The agreement is quite good.

Thus, in describing the substituent effect in π-systems, the character of molecular orbital involved, defined by the c_i^2 values, is taken into account. However there is another, equally important characteristic of molecular orbitals, which is also not to be ignored — the orbital energy. The extent of substituent-induced perturbation in the π-system depends on the energy ratio between the interacting π-orbital of the system and the orbital of substituent (Scheme 13). The closer the energies of interact-

Scheme 12

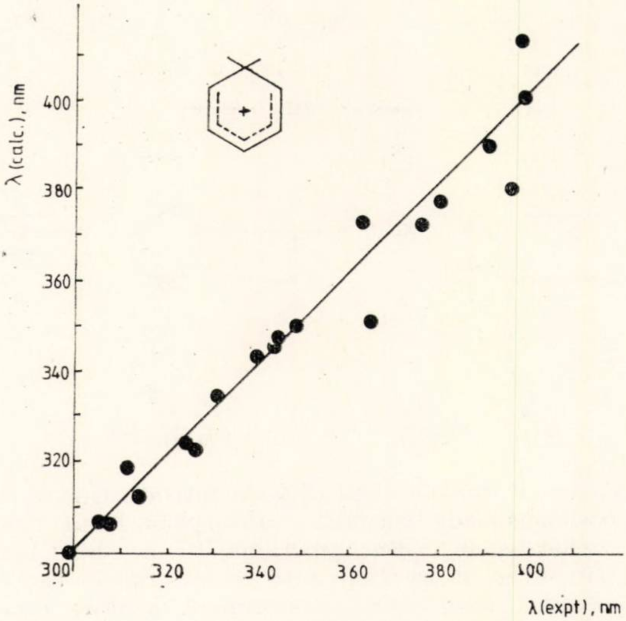

Scheme 13

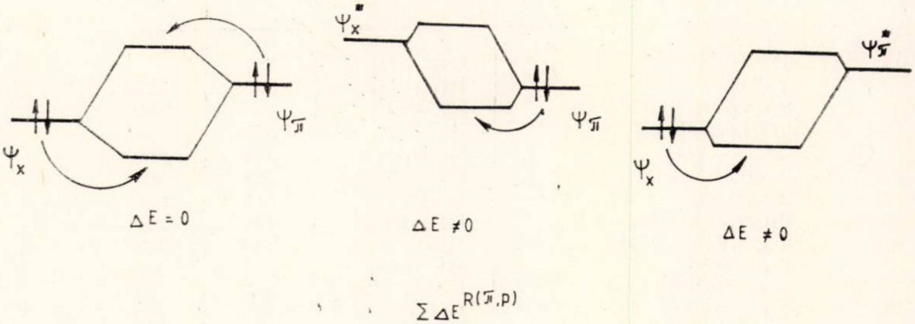

ing orbitals, the stronger the perturbation. This leads to the conclusion that the substituent effect in polysubstituted π-systems may not be strictly additive. Thus if, for example, we introduce the amino group into the benzene ring, this will decrease the energy of the b_1 orbital by 1.25 eV. Evidently, upon introduction of another amino group into the 4-position, the energy variation of this orbital will have different values. This accounts for the non-additivity of the effect of substituents having a strong resonance effect.

The non-additivity of substituent effect in correlations is usually defined by the so-called "cross-terms". Introduction of a cross-term is also necessary when substituent effect is specified using the Δ_X values instead of the σ ones. For example, ionisation potentials of the b_1 and a_2 orbitals of disubstituted benzenes with different combinations of substituents are well defined by the correlation presented in Scheme 14. As might be expected, the cross-term should only be considered when both substituents are strong electron donors.

Scheme 14

$$\mathrm{i - X - C_6H_4 - Y - j}$$

$$\Delta \mathrm{I}_{x,y} = \frac{\mathrm{C}_i^2}{0.333}\,\Delta_x^R + \Delta_x^I + \frac{\mathrm{C}_j^2}{0.333}\,\Delta_y^R + \Delta_y^I + \underbrace{0.5\,\frac{\mathrm{C}_i^2}{0.333}\,\Delta_x^R\,\frac{\mathrm{C}_j^2}{0.333}\,\Delta_y^R}_{\mathrm{x,y\,=\,NR_2,\ OR}}$$

Verified upon I_1 and I_2 for 54 compounds

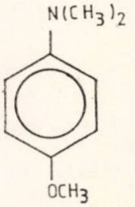

$\mathrm{I}_{\mathrm{C_6H_6}} = 9.27$ (b_1, a_2)

$\mathrm{I}^{\mathrm{exp}} = 7.22$, 8.90 to 8.98

$\mathrm{I}^{\mathrm{calc}} = 7.23$ (b_1), 8.97 (a_2)

This approach gave good results in the case of naphthalene and anthracene derivatives. An ordinary comparison of ionisation potentials of substituted aromatic system with the σ constants of substituents does not provide the general description of substituent effects — every group of compounds has its own correlation (Scheme 15). The approach suggested, which takes into consideration the character of molecular orbitals, covers the whole set of data (Scheme 16).

Good results have also been obtained in defining the electrochemical oxidation potentials of benzene, naphthalene, and anthracene derivatives. As an example Scheme 17 compares the experimental and calculated values of oxidation potentials of mono- and polysubstituted benzenes.

Despide good results in all these cases, the approach is still methodologically unacceptable, as introduction of a cross-term is non-substantiated. Moreover, the energy of π-orbitals may substantially vary not only upon introduction of substituents but also from one π-system to another — for example, from benzene ($\mathrm{I}_1 = 9.27$ eV) to ethylene ($\mathrm{I}_1 = 10.51$ eV). Therefore it would be reasonable to take advantage of the molecular orbital theory and try to consider the dependence of substituent resonance

Scheme 15

Data of L. Klasinc et al., *Pure Appl. Chem.*, **55**, 289 (1983).

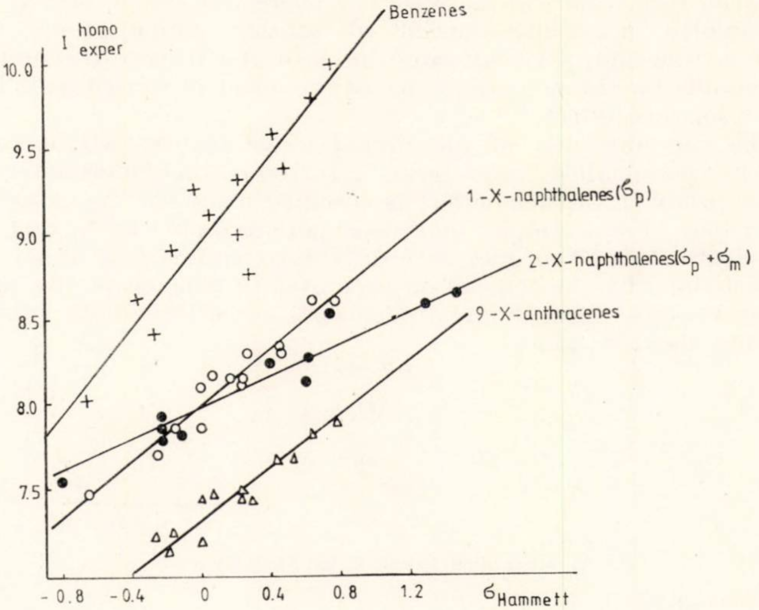

Scheme 16

Correlation between experimental and calculated values of the lst (1) and 2nd (2) ionization potentials (in eV) of monosubstituted naphthalenes, and also of the first (3) and second (4) ionization potential of 9-substituted anthracenes.

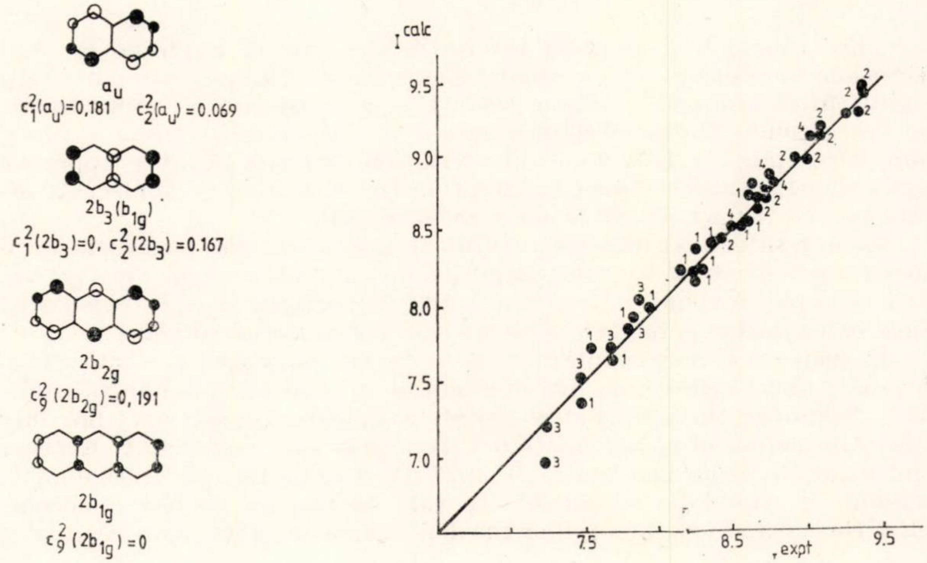

effect on the energy of disturbed orbital in terms of a very simple method — the method of linear combination of fragment orbitals (LCFO). This method designs the molecular orbitals of substituted π-systems from the π-orbitals of a parent system AH_n and the p (or π)-orbitals of substituents X.

Scheme 17

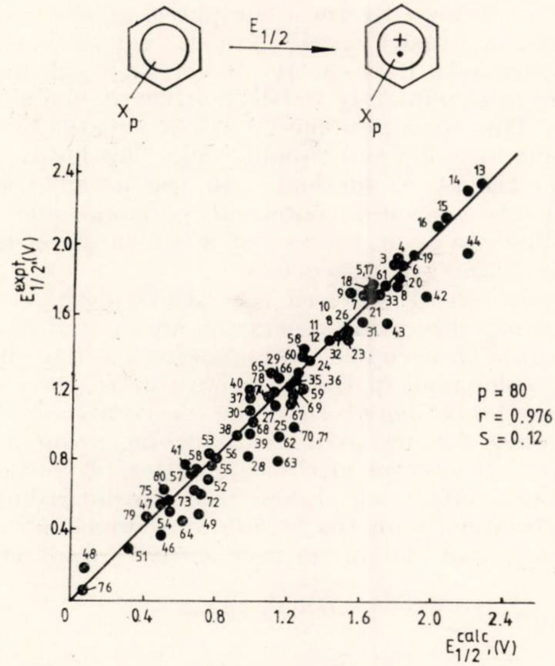

Scheme 18 shows the principal equations for calculating the energies of π-molecular orbitals in the case of monosubstituted benzenes. It should be noted that the energy of π-orbital calculated in this way

Scheme 18

$$\psi_{AX_1X_2X_3\ldots X_n} = C_{AH_n}\psi_{AH_n} + C_{X_1}\psi_{X_1} + \ldots + C_{\ n}\psi_{X_n}$$

$$\psi_{C_6H_5X} = C_{C_6H_6}\psi_{C_6H_6} + C_X\psi_X$$

$$\begin{vmatrix} [E_{C_6H_6}(b_1,a_2) - E^0_{C_6H_5X}(b_1)] & [H_{C-X} - S_{C-X}E^0_{C_6H_5X}(b_1)] \\ [H_{C-X} - S_{C-X}E^0_{C_6H_5X}(b_1)] & [E_X - E^0_{C_6H_5X}(b_1)] \end{vmatrix} = 0$$

$$f_{C-X} = H_{C-X} - S_{C-X}E^0_{C_6H_5X}(b_1) \approx \text{const}(X)$$

$$c_i^2 = 0.333$$

$$f^2_{C-X} = \overbrace{[-I_{C_6H_6} + (I_{C_6H_5X}(b_1) - \Delta x)]}^{\Delta^P_X}\,[-I_{HX} + (I_{C_6H_5X}(b_1) - \Delta x)]$$

$$f_{C-X}(\pi) = f_{C-X}(C_6H_5X)\sqrt{\frac{c^2_{1-X}(\pi)}{0.333}}$$

$$I_{m-XC_6H_4Y} = -E^0_{m-XC_6H_4Y} + \Delta^I_X + \Delta^I_Y$$

(E°) differs from the full energy of π-orbital (E), which shows itself in molecular ionisation, by the induction term value of the substituent (Δ^i_X). Correction of the induction term upon a change of π-system is carried out as described above.

If we know parameters I_{AH_n}, c_i^2, f^2_{c-x}, I_{HX}, and Δ^i_x, we can calculate, by the LCFO method the ionisation potential for any substituted π-system. There is no need to use a computer, as the order of the equations to be solved is usually small ($N + I$, where N is the number of substituents). Scheme 19 lists the results of such calculations of ionisation potentials for approximately 100 derivatives of benzene, naphthalene and anthracene. The ionisation potentials of substituted pyridines, and especially ethylenes, are defined equally well. This indicates a reasonably high similarity of the LCFO method with the parametrization obtained from consideration of ionisation potentials of monosubstituted benzenes. This approach allows to avoid the use of a multitude of substituent position constants in defining π-systems.

We have also effectively used the LCFO method for the description of the electronic absorption spectra of mono- and disubstituted benzenes. The energies of occupied and unoccupied π-orbitals in benzene derivatives were calculated in the same way as in the case of ionisation potentials. It should be noted that the electron-accepting groups like NO_2 do not produce any pronounced disturbing resonance effect in the occupied π-orbitals. Therefore in the calculation of ionisation potentials only their induction effect was taken into consideration. However the effect of such substituents on the lowest unoccupied π^* orbitals of benzene is significant and should be necessarily considered in the LCFO

Scheme 19

$$I_{AH_p}, c_i^2, f^2_{c-x}, I_{HX}; \Delta^I_X$$

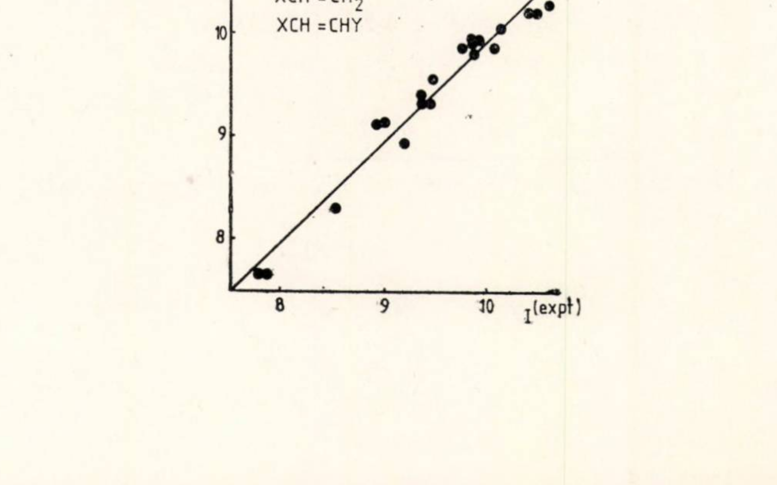

calculations. The E^*_{c-x} and f^*_{c-x} values were found by the spectral data for pairs of compounds C_6H_5A and 4-$(CH_3)_2$ NC_6H_4A. Tables 4 and 5 show comparison of the calculated and experimental positions of absorption bands $^1B_{14}$ (the p-band) and $^1B_{24}$ (the α-band) (for C_6H_6, 203 and 255 nm respectively).

Table 4

Correlation between experimental (in hydrocarbon solvents) and calculated absorption maxima of *para*- band α-ands of mono- and disubstituted benzenes with electron-donor substituents

Substituent	λ^{exp}_{max}(nm)	λ^{calc}_{max}(nm)
H	203.5, 254	
F	204, 259	210.5, 266
CH_3	207, 260	208, 262
OH	210, 269	214,6 270.5
OCH_3	220, 275	222, 277.5
NH_2	233.5, 286	228, 286.5
$N(CH_3)_2$	250, 297	250, 302
1,4-$(NH_2)_2$	246, 315	239, 310
1,3-$(NH_2)_2$	240, 293	234, 290.5
1,2-$(NH_2)_2$	235.5, 289	234, 290.5
1,4-$(OCH_3)_2$	226, 290	232, 295
1,3-$(OCH_3)_2$	220, 277.5	227, 281
1,2-$(OCH_3)_2$	225, 275	227, 281
1,4-$(OH_2)_2$	223, 292	222, 285
1,3-$(OH)_2$	217, 273.5	218.5, 273.5
1,2-(OH_2)	214, 274	218.5, 273.5
1-NH_2, 4-OH	235, 304	232, 298.5
1-NH_2, 3-OH	234, 283.5	227.5, 283
1-NH_5, 2-OH	235, 288	227.5, 283
1-NH_2, 4-OCH_3	236, 303	235.5, 303
1-NH_2, 3-OCH_3	233.5, 283	231, 286
1-NH_2, 2-OCH_3	237, 286	231, 286
1-OCH_3, 4-OH	223.5, 288	227, 290
1-OCH_3, 3-OH	220, 271.5	223, 277.5
1-OCH_3, 2-OH	216, 273.5	223, 277.5
1-NH_2, 4-CH_3	237, 293	229, 292.5
1-NH_2, 3-CH_3	237, 289	228, 284
1-NH_2, 2-CH_3	234, 283	228, 284
1-OCH_3, 4-CH_3	222,5, 276.5	224, 284
1-OCH_3, 3-CH_3	217, 277	222.5, 275
1-OCH_3, 2-CH_3	215.5, 270	222.5, 275
1-OH, 4-CH_3	220, 277	218, 277.5
1-OH, 3-CH_3	214, 271	215, 268.5
1-OH, 2-CH_3	213, 270	215, 268.5
1-NH_2, 4-F	230, 296	229, 296
1-NH_2, 3-F	234, 283	225, 281
1-NH_2, 2-F	230, 281	225, 281
1-OCH_3, 4-F	218.5, 281.5	224, 287.5
1-OCH_3, 3-F	220, 269.5	220, 275
1-OCH_3, 2-F	219.5, 271	220, 275
1-OH, 4-F	212.5, 278.5	218.5, 281.5
1-OH, 3-F	213.5, 279.5	215, 270.5
1-OH, 2-F	214, 269	215, 270.5

The knowledge of the E^*_{c-x} and f^*_{c-x} values allowed to pass to the description of substituent effect on the reactions involving electron addition to the aromatic system. Schemes 20 and 21 compare the electrochemical reduction potentials of X-substituted nitrobenzenes and benzonitriles with the calculated energies of lowest unoccupied orbitals of the respective compounds.

Table 5

Correlation between experimental (in hydrocarbon solvents except when otherwise stated) and calculated absorption maxima of *para*- and α-bands of mono- and disubstituted benzenes with one electron-withdrawing substituent

Substituent	λ_{max}^{exp}(um)	λ_{max}^{exp}(nm)
H	203.5, 254	
CN	225	225^B, 27
	$224, 271^A$	
COOH	239, 275	230^B, 274
$COCH_3$	237.5, 277	237.5^B, 279
CHO	242	242^B, 282
NO_2	252, 280	252, 289
1-NO_2, 4-CH_3	264	264.5
1-NO_2, 4-OH	285	280.5
1-NO_2, 3-OH	262, 319	258.5, 303
1-NO_2, 4-OCH_3	292	294.5
1-NO_2, 3-OCH_3	260, 313	261.5, 310
1-NO_2, 4-NH_2	319	312.5
1-NO_2, 4-$NCH_3)_2$	353	353^B
1-CHO, 4-OH	265.5	264.5
1-CHO, 3-OH	244, 302	247.5, 296
1-CHO, 4-OCH_3	265	277
1-CHO, 3-OCH_3	246, 304	250, 302
1-CHO, 4-NH_2	291.5	291.5
1-CHO, 3-NH_2	243, 327.5	253, 308.5
1-CHO, 4($NCH_3)_2$	325	325
1-$COOCH_3$, 4-CH_3	247, 273	247.5
1-$COCH_3$, 3-CH_3	241.5, 283	241, 286.5
1-$COCH_3$, 4-OH	267	259
1-$COCH_3$, 3-OH	246, 306	243.5, 292
1-$COCH_3$, 4-OCH_3	266	270
1-$COCH_3$, 3-OCH_3	246, 304	246, 298
1-$COCH_3$, 4-NH_2	285	283
1-$COCH_3$, 3-NH_2	246, 320	248, 305
1-$COCH_3$, 4-$N(CH_3)_2$	315	315^B
1-COOH, 4-CH_3	238, 279	289.5
1-COOH, 4-OH	251	252
1-COOH, 3-OH	235.5, 296	235.5, 287
1-COOH, 4-OCH_3	255	263
1-COOH, 3-OCH_3	238, 295	237.5, 292
1-COOH, 4-NH_2	277	277^B
1-COOH, 3-NH_2	244, 320	240, 299
1-CN, 4-NH_2	261	261
1-CN, 3-NH_2	238, 310	233, 293

^{A}In water; ^{B}These bands were used for obtaining parameters F^*_{c-x} and E^*_x

The above example of description of substituent effect on the reactivity of π-systems concern the simplest reactions – those of electron elimination or addition. Will these approaches be effective in the case of reactions involving bond cleavage? In order to demonstrate such a possi-

Scheme 20

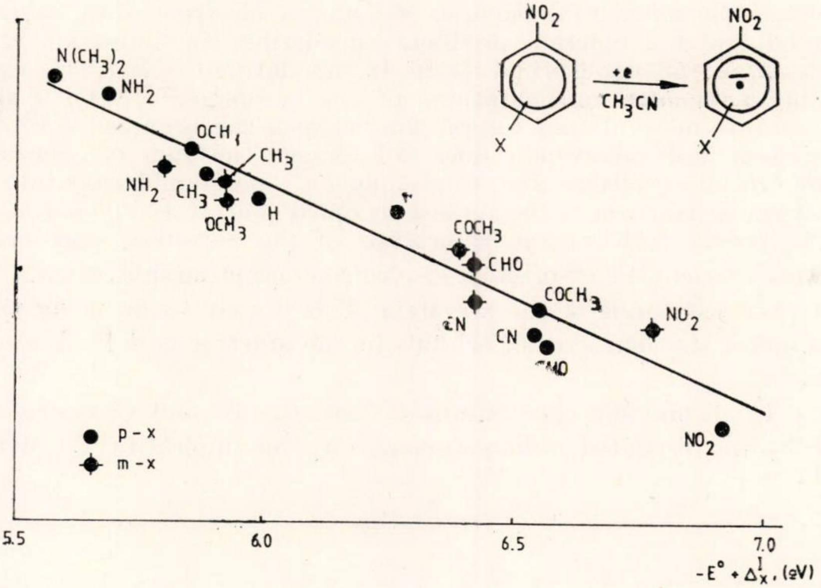

Scheme 21

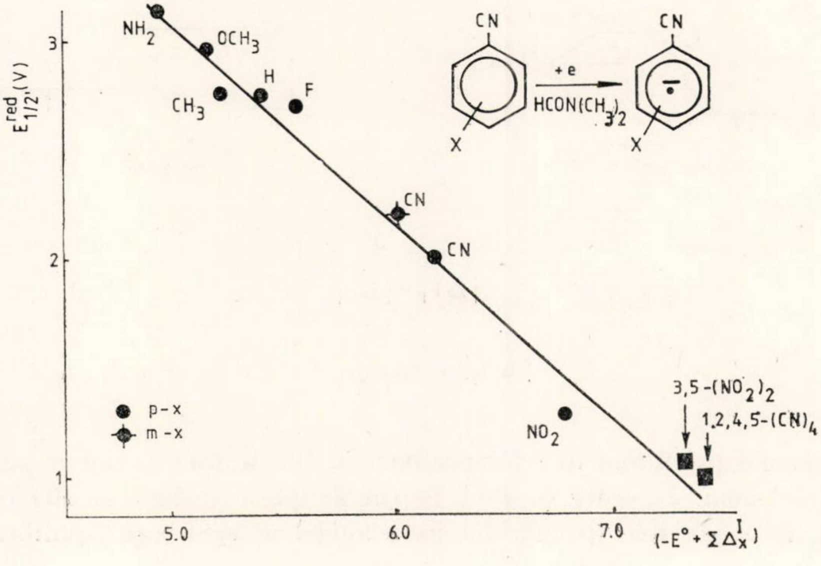

bility, we shall discuss the substituent effect on acid-base equilibria o substituted anilines — a typical reaction where for the $\rho\sigma$ description on should use two constant scales (the σ Hammet and σ^- ones).

To evaluate the substituent effect on the equilibrium transformation of a substituted π system, it is necessary to calculate the variatio in the full energy of π- and ρ-electrons of the π system and substituen upon the addition of substituent to the π system ($\Sigma_\Delta E^{R(\pi,p)}$). Differenc betwen the changed full energies of π- and ρ^- electrons of the starting compound and the reaction product, considering the induction effect, wil determine the equilibrium state. In calculating the $\Sigma_\Delta E^{R(\pi,p)}$ values (th R index denotes considerations of the resonance effect), it should b taken into account that interaction between the occupied orbitals of th π-system and substituent does not change the sum of energies of th two orbitals (Scheme 22). Consequently, one should take into accoun only the interaction of the highest occupied p-orbitals of electron-donatin substituents with vacant π^*-orbitals of the π-system, and that of th lowest unoccupied π^*-orbitals of electron-accepting substituents with th occupied π-orbitals of the π-system. This is easy to do using the LCFO method if the character of orbitals in the starting and final π-systems is known.

In all previous calculations we used the E^J and C_i^2 values obtained for the unsubstituted carbon π-systems by the simplest LCAO MO method

Scheme 22

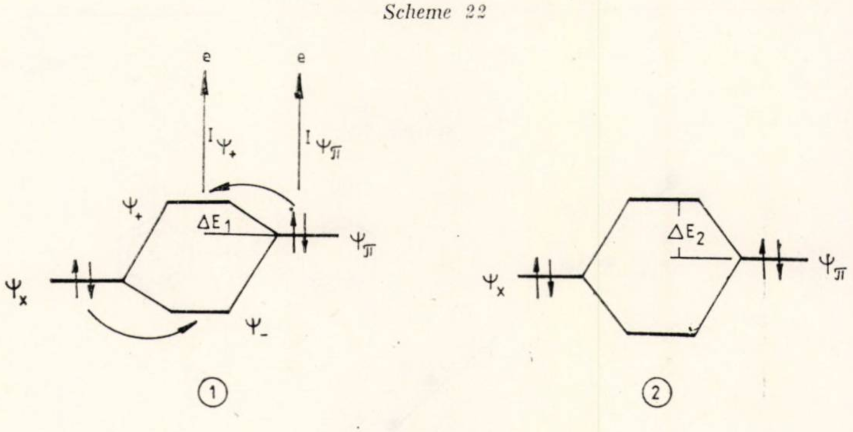

$$|\Delta I| = |\Delta E|$$

$$|\Delta I_1| < |\Delta I_2|$$

(the values are found in reference-books). But aniline is not a pure carbon π-system. In order to stick to the simplest variant of MO calculations, it is possible to consider as a model of acid-base equilibrium o substituted anilines the protonation reaction of substituted benzyl anions (Scheme 23). A measure for the changed free energy of the reaction is the A_X parameter.

Scheme 23

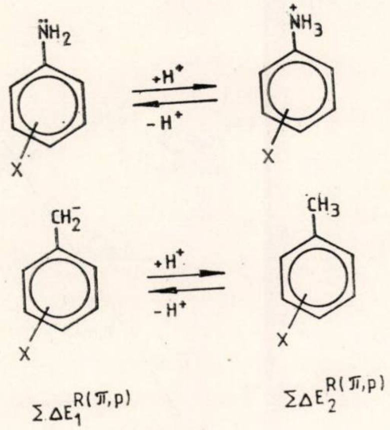

$\ddot{N}H_2$
$+H^+$
$-H^+$
$\overset{+}{N}H_3$
X
X
CH_2^-
$+H^+$
$-H^+$
CH_3
X
X
$\Sigma\Delta E_1^{R(\pi,p)}$
$\Sigma\Delta E_2^{R(\pi,p)}$

$$(\Delta_X^I)^{BA} = (\Delta_X^I)^B \cdot 0.7$$

$$A = \delta\Sigma\Delta E^{R(\pi,p)} + 0.7(\Delta_X^I)^B$$

Scheme 24 compares the free energy variation in formation of the anilinium ion under substituent effect in gas phase with the A_X parameter.

Scheme 24

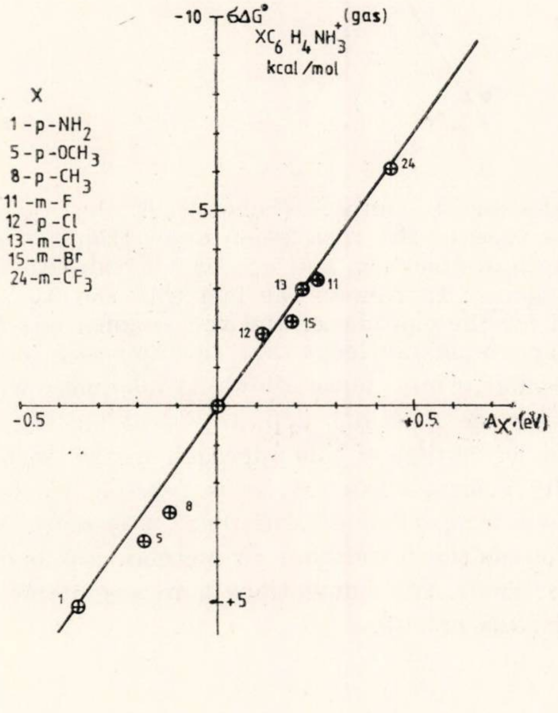

Unfortunately, the literature contains little data on this reaction for gas phase. But for the data available the correlation is quite satisfactory.

Scheme 25 represents the same comparison for the reaction in water, for which there are enough data. The correlation here is also satisfactory ($n = 20$, $r = 0.96$, $s = 0.48$), though one could expect complications caused by solvention effects.

Scheme 25

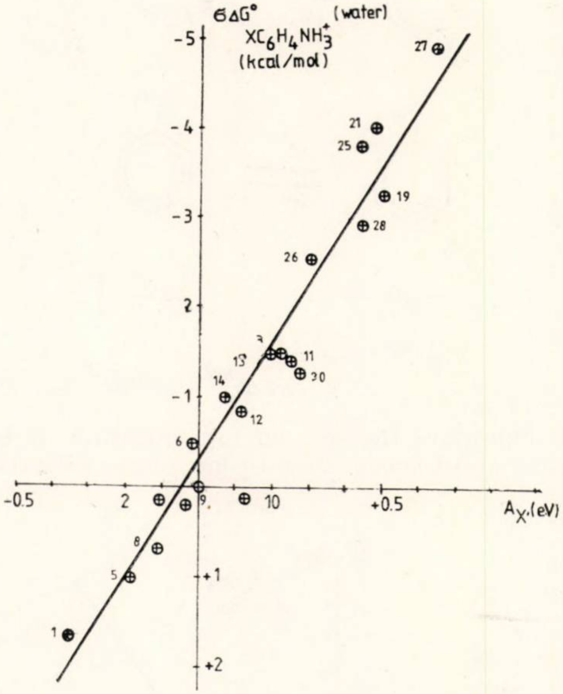

It is interesting to compare (Scheme 26) the A_X parameters with the σ constants used in the correlation descriptions of acid-base equilibria of substituted anilines (σ_m and σ_p for ^+M substituents, σ_m and σ_p^- for $-M$ substituents). In view of the fact that the A_X parameters have been calculated for the gas phase, and the σ constants for the reactions in solution, we are to acknowledge that this approach based on the physically clear molecular orbital ideas allows an adequate description of substituent effect for the reactions typically used for the $\rho\sigma$ correlations.

We see the advantage of this approach in the fact that, using one set of physically clear parameters, it is possible to define substituent effect on various properties of different π-systems. Methodologically it essentially exceeds the correlation $\rho\sigma$ method, and as opposed to quantum-chemical methods, the calculations here are simple and perceptive though certainly less precise.

Scheme 26

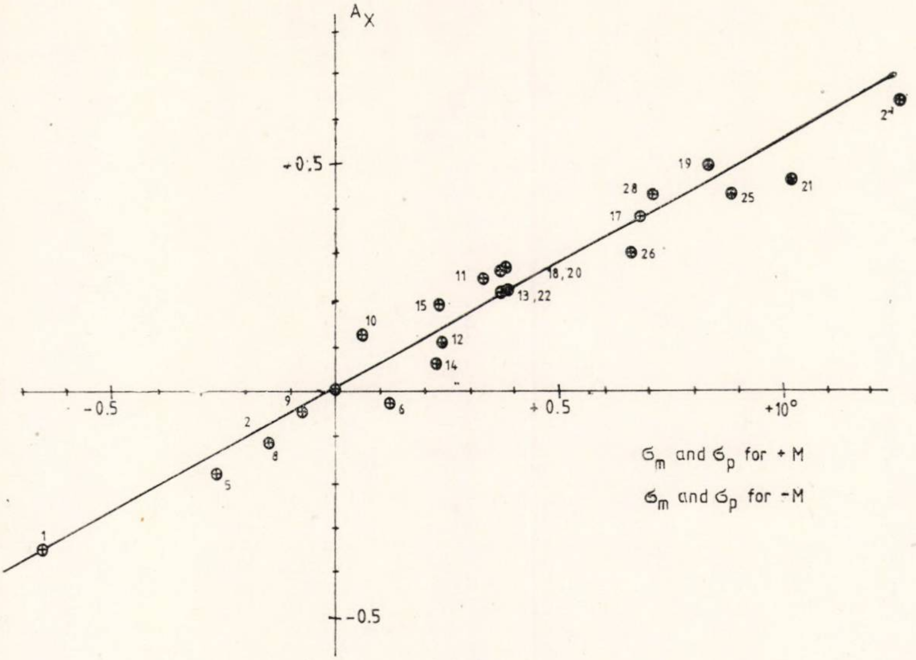
A_X
+0.5
-0.5
-0.5
+0.5
+1.0
1
2
5
8
9
6
10
12
14
15
11
13, 22
18, 20
17
26
28
19
25
21
24
σm and σp for + M
σm and σp for − M

Revue Roumaine de Chimie, **34**, *1*, 191–195 (1989)

DECREASED THERMODYNAMICAL ACTIVITY OF OXYGEN IN SILICON SINGLE CRYSTALS GROWN BY CZOCHRALSKI METHOD

IAMANTA LAUDONIU, SILVIA CIOBANU, ADRIAN MANEA, MIHAI SCARLETE,
CONSTANTIN BARTHA, VASILE VANCA, DUMITRU VASILIU, VALERICĂ
NINULESCU and GEORG CRISTIANI

Research and Production of High Purity and Semiconductor Materials Institute,
Bucharest, Romania

Received October 22, 1988

Factors governing the concentration of oxygen thermal donors — OTD — related to the incorporation of oxygen and carbon into extralightly boron-doped (111) Czochralski silicon single crystals, during a nonconventional Cz process involving an "active atmosphere" containing added carbon monoxide into argon flow, are studied. Carbon contamination occurs mainly via dissolution from the gaseous atmosphere, obeying Henry's law. An impurification model of the crystal including the incorporation of carbon and oxygen in the form of the molecular CO is presented and related to the OTD level. This CO "doping" process is proper to decrease the thermodynamical activity of oxygen in OTD formation in as grown and heat treated silicon single crystals.

I. INTRODUCTION

The most abundant impurities in the silicon single crystals grown by Czochralski (Cz) method are oxygen and carbon, whose concentrations are $10^{17}-10^{18}$ and $10^{16}-10^{17}$ at/cm^3, respectively. Among the most important properties of the single crystal which are related to the concentrations and distributions of these elements in the body of the single crystal, the development and destruction of the oxygen related thermal donors — OTD — in as grown and heat treated (HT) Cz-silicon play an important role. For example, the maximum concentration of OTD species producible during a special HT is proportional to the 4,4-th power of interstitial oxygen content.[1] Such an expression is valuable also for OTD in as grown silicon. It is accepted today that crystal impurification with the two above mentioned impurities occurs mainly from two independent sources: so, the oxygen supply is the reaction between SiO_2 crucible and the liquid silicon during the crystallization process, and the carbon source is the polysilicon raw material. After this impurification, the obtained resistivity of the bulk single crystal is quite different from the expected values corresponding to the IRVIN dependence related to the dopant concentration. So, in a specific way of each as grown sample (dependent on its thermal history and microstructure) it is possible that OTD in concentration of about 10^{15} cm^{-3} appear. So a material whose "true" resistivity can be reached only after elimination of OTD a HT being obtained the residual amount of the thermal fluctuant species still remaining is however $1-3 \times 10^{14}$ cm^{-3}. This fact imposes a large enough dopant concentration to make the OTD added influence on the silicon bulk resistivity negligible. Today, the Cz method is used to produce silicon single crystals up to 80 ohmcm, by a fine control of oxygen impurification and a proper HT of the as grown crystals.

This paper presents a modality to decrease the thermodynamical activity of oxygen related to as grown silicon crystals used in electronic devices, permitting a subsequent decrease in the residual level of OTD of $1-3 \times 10^{13}$ cm^{-3}. In such a way it is possible to obtain with a good reproductibility silicon with a stable resistivity up to 110 ohmcm.

II. EXPERIMENTAL

To influence the incorporation of oxygen and carbon in the crystal, an "active atmosphere" formed by the injection of a known quantity of purified carbon dioxide in the stream of the spectral pure argon flow is used. The obtained dependence of the substitutional carbon concentration in the crystal at a solidified fraction of 0.1 — 0.7 was studied. The concentration measurements of the extralightly boron doped crystals were made by room temperature infrared (IR) absorption at 605 cm^{-1}. The results are presented in Fig. 1. The longitudinal

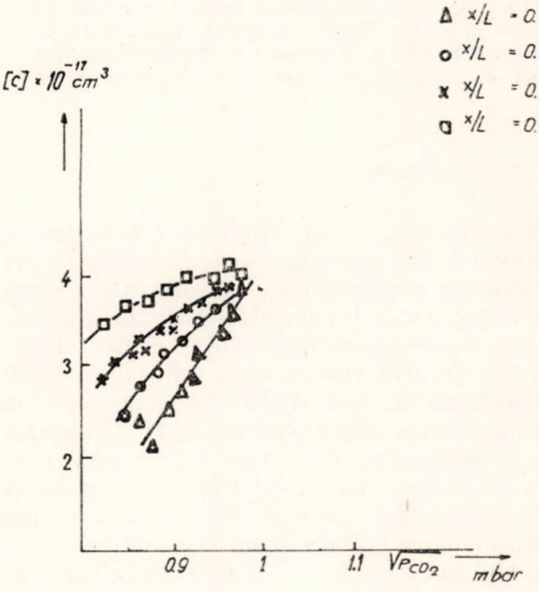

Fig. 1 — Substitutional carbon concentration at various solidified fractions versus ln $P[CO_2]$. The linearity relation is visible at small fractions, but altered to fractions greater than 0.6.

variation of substitutional carbon concentration in crystals grown in an atmosphere containing 3.5% (by volumes) CO_2 in Ar is represented in Fig. 2, which reveals also the difference between the experimental values and a perfect segregation curve with a repartition coefficient of 0.1 (the estimated k for carbon repartition). Fig. 3 shows the as grown OTD concentration related to the solidified fraction in two crystals of 45 and 80 ohmcm grown in active atmosphere. These results were obtained by resistivity measurements with a four pins resistivimeter. Another set of determinations was dedicated to a statistical determination of the solidified fraction for which the dependence of as grown OTD concentration obeys the law of the 4,4-th power of oxygen concentration. The fraction obtained is 0.1 for crystals grown in an inert Ar atmosphere.

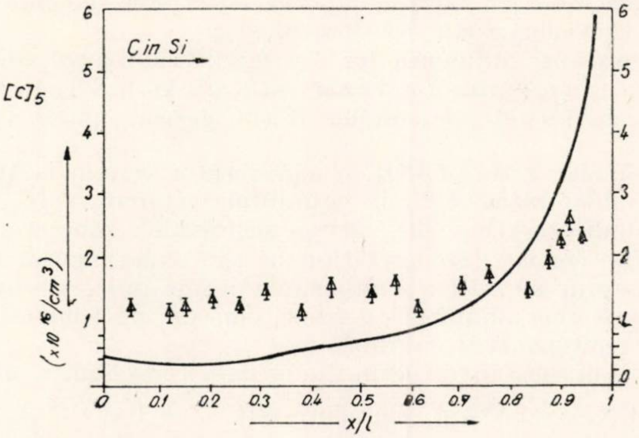

Fig. 2. — The axial variation of substitutional carbon versus solidified fraction (measurement points) and a perfect segregation curve for a repartition coefficient of 0.1.

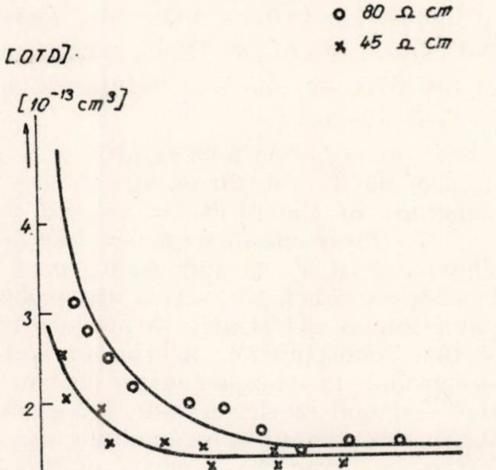

Fig. 3. — As grown thermal donor species versus solidified fraction in extralightly boron-doped silicon single crystals.

III. DISCUSSION

1. Theoretical model of impurification with C, O and CO of silicon single crystal

The chemical reactions equilibrium involved in the carried species containing carbon and oxygen between the phases of the heterogeneous system associated to the Cz environment, built from 14 atomic and molecular species distributed in 5 phases was the searching target for the FORTRAN program MINIMG, presented in[2]. The results were the following :

i) vitreous SiO_2 is not a stable component of this system (this means that the reaction between the crucible and the liquid silicon is not, in fact, thermodynamically controlled);

ii) the pressure influence on the equilibrium composition of the gaseous phase is negligible for molar ratio of Ar less than 0.1 ;

iii) the significant compounds of the gaseous phase are SiO, CO and Si ;

iv) the molar ratio of CO_2 in equilibrium system is 10^{-6};

v) the molar ratio of O_2 in equilibrium system is 10^{-19}.

Fig. 2 indicates that the carbon segregation process is not satisfactory for the correct interpretation of the experimental results. The alternative we propose is that a major role in this process is due to the CO incorporation at the solidification front, considering conclusions iii) and iv) from thermodynamical equilibrium.

So, the equilibria involved in the proposed mechanism are :

a) $CO_2(g) + C(gr) \rightleftharpoons 2\,CO(g)$, therefore $P[CO] = Ka\sqrt{P[CO_2]}$

b) $CO(g) \rightleftharpoons Co(diss)$, therefore $x[CO] = Kb \times P[CO]$

c) $SiO_2(vitr) + Si(liq) \rightleftharpoons 2\,SiO(diss)$

d) $SiO(diss) \rightleftharpoons SiO(cr)$

e) $CO(diss) \rightleftharpoons CO(cr)$, congruent segregation of CO

f) $CO(diss) \rightleftharpoons C(cr) + O(cr)$, incongruent segregation of CO

g) $SiO(diss) + C(diss) \rightleftharpoons Si(liq) + CO(diss)$

h) $C(diss) \rightleftharpoons C(cr)$

where the abbreviations signify : g — gas, gr — graphite, diss — dissolute form in the liquid silicon, vitr — vitreous, Ka and Kb are the equilibrium constants of the reactions a) and b), and x reprсsents the molar ratio.

In this reactions sequence, four new appearing equilibria are included. These are b), e), f) and g). b) must be included in the carried carbon mechanism when the active atmosphere is used and the kinetics of CO_2 reduction to CO is able to produce considerable amount of CO, so that carbon incorporation in the crystal via molecular CO is appreciable as considered to the elementary carbon segregation ; this fact is proper to the seed end of the crystal, for example at a solidified fraction of 0.1. When the amount of elementary segregated carbon becomes appreciable, differences from the linearity of the substitutional carbon related to the logarithm of the partial pressure of CO_2 are visible, like at solidified fractions greater than 0.6 (Fig. 1). For the equilibrium e) and f) there is no experimental evidence until today, the determination of CO molecule in solid silicon being an actual problem.[3-6] The influence of the equilibrium g) on the incorporation of carbon and oxygen in silicon single crystals was presented elsewhere.[7]

At the solidified fraction 0.1 the dependence of the OTD concentration in crystals grown in the active atmosphere is presumed to obey the law of the 4,4-th power of oxygen activity. By comparing the as grown OTD concentration in a typical Cz-silicon single crystal, and the experimental results obtained after using the active atmosphere, the resulting statistical value is

$$[\mathrm{OTD}]/[\mathrm{COTD}] = 7.5 \times 10^{-2}$$

where [OTD] is the concentration of as grown thermal donors and [COTD] is the concentration of the donor species at the same solidified fraction of 0.1 and the same concentration of interstitial oxygen, but in a crystal grown with CO_2 doped Ar flow. In this case, considering that the activity coefficient of the oxygen is 1, the resulting oxygen activity for the CO doped crystal is

$$\mathrm{f} = \mathrm{f}_0\sqrt{[\mathrm{COTD}]/[\mathrm{OTD}]}$$

and $\mathrm{f} = 0.55$.

IV. CONCLUSIONS

1. The possibility to form an "active atmosphere" by creating a significant partial pressure of CO in the gaseous phase of the thermodynamical system associated to the Cz environment controlling the incorporation of carbon in silicon single crystals is evidenced.
2. The incorporation of CO in the liquid phase obeys Henry's law.
3. The CO doping procedure reduces the thermal donor species level to $1-3 \times 10^{13}$ cm^{-3}, and this phenomenon is associated to a decreased phenomenological activity of oxygen in silicon single crystals.

REFERENCES

[1] P. Gaworzewski, *Phys. stat. sol.*, (a), **94**, 233 (1986).
[2] D. Geana and F. Danes, "The National Chemical Conference", Bucharest, 1976, vol. I, p. 138.
[3] B. Svensson, *Phys. stat. sol.*, (a), **95**, 587 (1986).
[4] N. Magnea, *Appl. Phys. Lett.*, **45** (1), 322 (1984).
[5] F. Shimura, *Appl. Phys. Lett.*, **47** (8), 421 (1985).
[6] L. Wien, *J. Appl. Phys.*, **54** (2), 123 (1985).
[7] S. Sternberg and M. Scarlete, "The Semiconductors Conference", vol. I, Bucharest, p. 266, 1987.

Revue Roumaine de Chimie, **34**, *1*, 197–205 (1989)

CONSIDERATIONS CONCERNING OXIDE/METAL/ ELECTROLYTE SYSTEM IN NON-EQUILIBRIUM REGIME

C. LUCA[a], A. ANDREI[b] and G. SEMENESCU[b]
[a]Central Institute of Chemistry, Department of Physical Chemistry
Bucharest, 202, Splaiul Independenţei
[b]Institute for Nuclear Power Reactors, Piteşti

Received October 9, 1988

The behaviour of the oxide electrolyte system in dynamic regime is presented by means of the "transition layer" model. The transition layer is considered as a well-defined thermodynamic system. The role of the surface states is also emphasized. The existence of the threshold values of the electrode/electrolyte potential difference, which correspond to the irreversible transformations at the transition layer level, is also explained.

INTRODUCTION

Many technologically important processes are controlled, to a considerable extent, by the properties of the surfaces. Of particular practical interest are the metallic oxides properties and especially their interaction with the adsorbed molecules.[1]

To understand the mechanisms which are supposed to underlie practical importance electrochemical processes, one has to know the phenomena which are carried out at the electrolyte/oxide contact, these being the object of many theoretical and experimental investigations. The understanding of the electrolyte/oxide interface behaviour presents a great interest in the thermodynamic equilibrium conditions, as well as in the dynamic regime by using the "transition layer" model.[2]

Thermodynamical considerations concerning the solid / electrolyte interface

The surface composition is generally different from the bulk one (fact confirmed by the modern analytic techniques which deal with the solid surfaces study).[3,4]

A realistic view of a solid surface is not an ideal plane. On an atomic scale, the surface includes crystal faces for which composition, orientation, and perfection are determined by prior treatment of the solid.[4]

The understanding of the oxide surface behaviour is difficult because of the large limits in which the surface composition can vary[3]. Many structures and compositions that cannot exist in the bulk are allowed in the region of reduced symmetry at a surface. The surface stoichiometry can be altered by certain treatments which are commonly used in the preparation of a controlled surface (chemical cleaning, ionic bombardment, annealing).

To understand the behaviour of interfaces are required experimental efforts to characterize them from the point of view of their electronic, geometric and compositional properties. [4]

Theoretical efforts are also required — trying to elucidate the phenomenologic understanding at a microscopical level for the phenomena at the interface.

In terms of the thermodynamic theory, developed by Gibbs for the treatment of the interfacial region, it is considered that all the transition layer properties are determined by the area and also by the curvatures of an idealized geometrical surface.

Let us consider an extensive property, expressed by a quantity X associated with the thermodynamic system composed of two phases α and β and of the interfacial zone. In the bulk of the two phases, the density of the quantity X will be X_α and X_β, respectively.

Gibbs takes into account a geometrical surface called surface of tension, placed in the interface zone.

If one imagines homogeneous bulk phases α, β supposedly extending right up to the dividing surface with volumes V_α, V_β they would have total amounts of extensive property X_α and X_β, respectively.

$$X_\alpha = x_\alpha V_\alpha \tag{1}$$

$$X_\beta = x_\beta V_\beta \tag{2}$$

Obviously, we have :

$$X \neq X_\alpha + X_\beta \tag{3}$$

because the densities in the interfacial zone will be different from those of the bulk phases α and β.

Gibbs associates defined quantities to the dividing surface, as follows :

$$X^S = X - (X_\alpha + X_\beta) \tag{4}$$

None of the three quantities X^S, Y_α, X_β is the actual value of the extensive property of any part of the real system, but the scheme is a convenient and correct one to define the surface amounts (which can be positive or negative) of all extensive properties.

The Gibbs method has the advantage to supply results with general applicability, without referring to the concrete structure of a particular transition layer. But such treatment does not allow a detailed understanding for the mechanisms of the phenomena at the interface.[5] That is why it is necessary to specify, in detail, the structure of the transition layer.

In the model advanced,[2] it is thought that the transition layer at the solid/ electrolyte interface has a finite thickness and consists of Helmholtz Inner Plane (PHI) and adjacent solid phase plane which contains donor and acceptor active sites.

We mention that, in the following, the quantities with the superscript "S" refer to the transition layer unlike other papers[6,7] where there is a reference to the surface of tension.

In the transition layer both the geometric arrangement of the atoms and the relative proportions of the different atomic species present will not be the same as in the interior of either phase.

Consequently, the transition layer atoms will have different energies, as compared to the bulk ones and thus a certain energy can be associated to this transition layer.[1,6,7]

In order to minimize the total energy of the system, the atoms existing in the interface region will occupy the lowest energy positions consistent with the constraints imposed by the atoms in the interior. As a result of these constraints, the interface region (the transition layer)[2] is left in a state of stress, even at equilibrium.[1,6,7]

It is shown [1] that one of the reasons which make the thermodynamic description of interfaces a little confused is the use of the term "surface tension" for the surface stress description, as well as for the surface energy description.

In the following, we will consider the quantity "effective surface stress" g, which generally has an elastic component f and a plastic component γ. The significance of the quantities g, γ and f will be defined as follows.

The quantities g and f have a tensor character, but for simplicity we must consider the case :

$$g_{11} = g_{22} = g \qquad g_{33} = g_{12} = g_{23} = g_{13} = 0 \tag{5}$$

$$f_{11} = f_{22} = f \qquad f_{33} = f_{12} = f_{23} = f_{13} = 0$$

We consider that a uniform flat sample of a chemically homogeneous isotropic material, liquid or solid, amorphous or single crystalline, is stretched uniformly through an infinitesimally small length change at constant temperature and constant pressure, increasing its surface area from A to A + dA and the number of its surface atoms from N^S to $N^S + dN^S$.

The work increment δW^S which is expended to overcome the effective surface stress g[6] is given by

$$\delta W^S = g\mathrm{d}A \tag{6}$$

In principle, the increment δW^S can be obtained by subtracting from the total work term corresponding to the deformation, that portion which corresponds to stretching the bulk.

In ideally elastic straining, the number of surface atoms remains constant and the area per surface atom ($a = A/N^S$) changes while in ideally plastic straining the area per surface atom remains unchanged but the number of surface atom changes.

The quantity γ, defined as a necessary reversible mechanical work used to modify the surface with a unity, by a transformation that implies the transfer of the bulk atoms at the surface, in pressure, temperature and elastical deformation (ε_e^S) constant conditions, represents the surface specific free energy.

The variable quantity g has the significance of a specific superficial mechanical work and depends on the transformation by means of which the area is modified with dA, while the quantity γ is determined by the surface physical state and not by the concrete transformation through which the surface is modified.

The superficial mechanical work to create a new area $\mathrm{d}A_P$, where $\mathrm{d}A_P$ is the surface increasing under plastic deformation condition is [7]

$$\mathrm{d}W_P^S = \gamma \mathrm{d}A_P \tag{7}$$

If the surface is isothermically extended maintaining constant the superficial atoms N^S number, then the area modification will be produced by a purely elastical transformation and the corresponding elementary mechanical work is [7]:

$$\mathrm{d}W_e^S = f\mathrm{d}A_e \tag{8}$$

In the case of a real transformation, the deformation is not an ideally elastic one, neither an ideally plastic one. If p is the plastic fraction of the total deformation ε' and $(1 - p)$ — its elastic fraction, we have

$$g = (\varepsilon_p/\varepsilon')\gamma + (\varepsilon_e/\varepsilon')f \tag{9}$$

where $\varepsilon_p = p\varepsilon'$ and $\varepsilon_e = (1 - p)\varepsilon'$.

Obviously, for simplicity, the deformation tensorial character was neglected.[7]

If the tensorial properties are not neglected we obtain :

$$g_{ij} = \delta_{ij}\gamma + \frac{\partial \gamma}{\partial e'_{ij}} \tag{10}$$

where e'_{ij} is the linear component of the total strain.[7]

In the case of the purely elastic deformations, the following relation is available :

$$f_{ij} = \gamma\delta_{ij} + \frac{\partial \gamma}{\partial e_{ij}} \tag{11}$$

(which is known as Shuttlerworth relation for the isotrope case) where e_{ij} is the elastic strain tensor, and δ_{ij} — the Kronecker symbol.

In the electrolyte/semiconductor interfaces case, some surface states are present in the transition layer, and they appear as a consequence of a solid lattice termination through a surface (intrinsic states) or as a consequence of the superficial impurities existence (extrinsic states).[8,9]

The surface states are energetical levels, located at the surface, able to receive electron excess (acceptor states) or to release electrons (donor states).

The surface states studies is very important for the electrolyte/semiconductor interface understanding.[10]

The surface states generate an interfacial charge (the occupied acceptor states are negatively charged, while the empty donor states are positively charged).[9] They contribute to the free energy of the double layer.

The effective surface stress tensor and implicitly the surface free energy are functions of the charge density of the electric double layer.[1]

By applying a potential at the interface, the sign and the value of the charge on the surface of the electrode can be established.

Depending on the applied field direction, the electrons move towards the solid or towards the electrolyte so that the polarity of the charge system can be modified by polarization around the potential of zero charge (pzc).

The existence of a negative or positive charge excess on the surface determines that the necessary force to maintain the lattice parameter in the transition layer zone to the bulk value vary because of the electrostatic repulsion between the charges.

In the simplified case, when all the tensor g_{ij} components are null, excluding $g_{11} = g_{22}$, it can be shown that for a polarized solid electrode to the superficial net change density q, the following relation is available:

$$\left(\frac{\partial g_{11}}{\partial \varphi}\right)_{T,P,\mu_i} = -q \tag{12}$$

In the case of a mercury electrode in relation (9) we have $p = 1$, $g = \gamma$ and thus we obtain Lippmann's relation

$$\left(\frac{\partial \gamma}{\partial \varphi}\right)_{T,P,\mu_i} = -q \tag{13}$$

Thus, generally, in the case of solid/electrolyte interfaces, the effective surface stress tensor is the quantity directly affected by the charge density on the solid surface.

The dependence of the inner potential difference φ between the transition layer and the electrolyte on the charge density q, can be established by adopting one of the double layer models (Guy Chapman, Helmholtz-Perrin or other models [11]).

Thus, considering relations (9) and (12), g_{ij} and implicitly γ and f are depending on φ.

The transition layer model in dynamic regime

We consider the oxide/electrolyte interface in the non-equilibrium regime. At interface, many charge exchange reactions are simultaneously possible.

For simplicity, we consider a homogeneous solid surface and only an electronation and a deelectronation reaction which imply only monovalent species at interface.[2]

$$\begin{array}{l} A^+ + e \rightleftarrows A_t^* \\ A_t^* + \mathscr{D} \rightleftarrows (\mathscr{D}A)_t^* \\ \hline A^+ + \mathscr{D} + e \underset{K_{a_2}}{\overset{K_{C_2}}{\rightleftarrows}} (\mathscr{D}A)_t^* \end{array} \tag{14}$$

$$\begin{array}{l} D^- \rightleftarrows D_t^* + e \\ \mathscr{A} + D_t^* \rightleftarrows (\mathscr{A}D)_t^* \\ \hline D^- + \mathscr{A} \underset{K_{C_1}}{\overset{K_{a_1}}{\rightleftarrows}} (\mathscr{A}D)_t^* + e \end{array} \tag{15}$$

The equation which describes the behaviour of an interface in closed circuit (in potentiostatic and intensiostatic, as well as potentiodynamic regime) is :

$$c\frac{\mathrm{d}\varphi}{\mathrm{d}t} = i_d + i_a - i \tag{16}$$

Donor (D_t^*) and acceptor (A_t^*) species can participate to chemical reactions with active acceptor and respective donor sites, after charge exchange chemisorption ; also, is possible the chemical reaction of species D_t^* and A_t^*, respectively with release or deposition of substance. According to general thermodynamic criteria for equilibrium and evolution, the chemical reactions with the participation of the transition layer species can occur, only when the adequate free energy variation is negative.

Because, according to relation (12) both the free energy γ of the transition layer and the quantity f depend on the inner potential difference φ, as being the components of the effective surface stress g, the chemical reactions of the transition layer species can occur after the outrunning of some threshold values for the inner potential difference.

Because there is the possibility of the chemical reactions when the threshold conditions are satisfied, in the relations of the currents i_d and i_a considered,[2] for the dynamic regime case some terms must be added, representing the contribution of the species which, after charge exchange chemisorption, do not yield variation of surface species concentration in active state but participate in the reactions in the transition layer, in accordance with Faraday's law.

Regarding the sign of the current we adopt the following convention : when there is net flow of electrons from the solution to the solid, the current is taken as positive ;

We have :

$$\begin{aligned} i_d &= FS\left(\frac{\mathrm{d}\Gamma(D_t^*)}{\mathrm{d}t} + \lambda_1\frac{\mathrm{d}\Gamma_f(D_t^*)}{\mathrm{d}t}\right) = \\ &= FS\{K_{a_1}\mathrm{e}^{-\beta_1\frac{\Gamma_{Sd}}{\Gamma_{SD}-\Gamma(D_t^*)}}\mathrm{e}^{-\alpha\varphi}a_{D^-}[\Gamma_{Sd} - \Gamma(D_t^*)] - K_{C_1}\mathrm{e}^{-\alpha\varphi}\Gamma(D_t^*)\} \end{aligned} \tag{17}$$

$$\begin{aligned} i_a &= -FS\left(\frac{\mathrm{d}\Gamma(A_t^*)}{\mathrm{d}t} + \lambda_2\frac{\mathrm{d}\Gamma_f(A_t^*)}{\mathrm{d}t}\right) = \\ &= -FS\{-K_{a_2}\Gamma(A_t^*)\mathrm{e}^{\alpha\varphi} + K_{C_2}\mathrm{e}^{-\beta_2\frac{\Gamma_{Sa}}{\Gamma_{SA}-\Gamma(A_t^*)}}a_{A^+}\mathrm{e}^{\alpha\varphi}[\Gamma_{Sa} - \Gamma(A_t^*)]\} \end{aligned} \tag{18}$$

Where

$$\lambda_1(\varphi) = \begin{cases} 1 & \text{for} \quad \varphi \in \Delta(D) \cup \Delta(AD) \\ 0 & \text{for} \quad \varphi \notin \Delta(D) \cup \Delta(AD) \end{cases}$$

$$\lambda_2(\varphi) = \begin{cases} 1 & \text{for} \quad \varphi \in \Delta(A) \cup \Delta(AD) \\ 0 & \text{for} \quad \varphi \notin \Delta(A) \cup \Delta(AD) \end{cases}$$

Equations (17) and (18) should be completed with the equations regarding the kinetic description of the chemical reactions which can occur with participation of transition layer species, when the threshold conditions are satisfied.

For example, in the case of the following reactions :

$$2D_t^* \xrightarrow{K_D} D_2 \uparrow \tag{19}$$

$$2A_t^* \xrightarrow{K_A} A_2 \uparrow \tag{20}$$

$$\mathscr{A}\mathscr{D} + A_t^* + D_t^* \xrightarrow{K_{AD}} (\mathscr{A}D)_t + (\mathscr{D}A)_t \tag{21}$$

we have :

$$\frac{\mathrm{d}\Gamma_f(D_t^*)}{\mathrm{d}t} = \begin{cases} K_D\Gamma^2(D_t^*) & \text{for } \varphi \in \Delta_I(D) \\ K_{AD}\Gamma(A_t^*)\Gamma(D_t^*) & \text{for } \varphi \in \Delta_I(AD) \\ K_D\Gamma^2(D_t^*) + K_{AD}\Gamma(A_t^*)\Gamma(D_t^*) & \text{for } \varphi \in \Delta(D) \cup \Delta(AD) \end{cases} \tag{22}$$

$$\frac{\mathrm{d}\Gamma_f(A_t^*)}{\mathrm{d}t} = \begin{cases} K_A\Gamma^2(A_t^*) & \text{for } \varphi \in \Delta_I(A) \\ K_{AD}\Gamma(A_t^*)\Gamma(D_t^*) & \text{for } \varphi \in \Delta_I(AD) \\ K_A\Gamma^2(A_t^*) + K_{AD}\Gamma(A_t^*)\Gamma(D_t^*) & \text{for } \varphi \in \Delta(A) \cup \Delta(AD). \end{cases} \tag{23}$$

In the previous equations the case of the concentrated electrolytes has been considered, when the diffusion is not rate determining step and the diffuse Guy Chapman layer can be considered negligible. Also, the surface states density was considered so high that the potential drop in the Garrett Brettain space charge region can be considered negligible.

The free energy in the transition layer represents the sum of contributions of all interface atoms, including their interaction with the neighbouring region.

The specific free energy of the active acceptor sites including sites with occupied acceptor level $\bar{G}^S(\mathscr{A})$ and of the active donor sites, including sites with free donor level $\bar{G}^S(\mathscr{D})$ and also of the donor species $G^S(D^*)$ and acceptor species $G^S(A_t^*)$ in adsorbed state, are functions of the inner potential difference φ, because they are additive parts of the specific transition layer free energy :

Thus, we have :

$$\bar{G}^S(\mathscr{A}) = \Gamma_{Sa}\mu(\mathscr{A}) + \Gamma(D_t^*)\bar{\mu}(e) \tag{24}$$

$$\bar{G}^S(\mathscr{D}) = \Gamma_{Sd}\mu(\mathscr{D}) - \Gamma(A_t^*)\bar{\mu}(e) \tag{25}$$

$$G^S(A_t^*) = \Gamma(A_t^*)\mu(A_t^*) \tag{26}$$

$$G^S(D_t^*) = \Gamma(D_t^*)\mu(D_t^*) \tag{27}$$

Because the quantities $\bar{G}^S(\mathscr{A})$, $\bar{G}^S(\mathscr{D})$, $G^S(A_t^*)$, $G^S(D_t^*)$, $\Gamma(D_t^*)$, $\Gamma(A_t^*)$, $\bar{\mu}(e)$ are functions of φ, according to relations (24)—(27) there results that $\mu(\mathscr{A})$, $\mu(\mathscr{D})$, $\mu(A_t^*)$, $\mu(D_t^*)$ are also functions of φ.

The following reaction:

$$\mathscr{A}\mathscr{D} + A_t^* + D_t^* \rightarrow (\mathscr{A}D)_t + (\mathscr{D}A)_t \tag{28}$$

is possible when potential difference belongs to the range of potentials $\Delta(AD)$ for which is satisfied the condition:

$$\mu(\mathscr{A}\mathscr{D}) + \mu(A_t^*) + \mu(D_t^*) > \mu(\mathscr{A}D)_t + \mu(\mathscr{D}A)_t \tag{29}$$

The appearance of some potentials difference is also possible, which corresponds to the elastical strain and then mechanical destruction of transition layer structure, according to the second term in the right side of relation (9).

We note the fact that the chemical reaction of deposition or oxide dissolution as well as the mechanical oxide destruction implies the changes of the interface nature, which involves some quantitative and qualitative active sites modifications.

The "transition layer" model can explain the shape of the current-potential diagram used in materials corrosion behaviour evaluation.

The mechanism explanation of the steels passivation with the "transition layer" model will make the object of a future study.

CONCLUSIONS

The "transition layer" model allows the approach of the solid/electrolyte interface in the thermodynamic equilibrium conditions as well as in the non-equilibrium conditions.

This model approaches the interface from a phenomenological point of view and considers the transition layer as a thermodynamic system with well-defined structure, which is characterized by the functions of the state.

The role of the surface states is emphasized.

The existence of the threshold values of the electrode-electrolyte potential difference, which corresponds to the irreversible transformations at the transition layer level, is also explained.

The detailed understanding of phenomena which occur at the solid-electrolyte interface requires a theoretical treatment at microscopic level.

GLOSSARY OF SYMBOLS

D^- — the donor ionic species
$\mathscr{A}$ — the acceptor active centre
A^+ — the acceptor ionic species
$\mathscr{D}$ — the donor active centre
t — the species existing in the transition layer
K_{a_1}, K_{a_2} — the rate constants for the anodic components of the reactions 1 and 2.
K_{C_1}, K_{C_2} — the rate constants for the catodic components of the reactions 1 and 2
$\Gamma(D_t^*)$ — the superficial concentration of the species D in adsorbed state
Γ_{Sd} — the superficial concentration of the active centres, for the donor species.
$\Gamma(A_t^*)$ — the superficial concentration of the species A in adsorbed state
Γ_{Sa} — the superficial concentration of the active centres for the acceptor state

Γ_{SD} — the saturation superficial concentration for the species D in adsorbed state
Γ_{SA} — the saturation superficial concentration for the species A in adsorbed state
$\alpha = \frac{1}{2}\frac{F}{RT}$
$\varphi = \varphi_t - \varphi_e$, the inner potential difference between the transition layer and the electrolyte
a_{D^-} — the activity of the donor species in the electrolyte
a_{A^+} — the activity of the acceptor species in the electrolyte
i_d — the net current of the charge transfer reaction of the species D.
i_a — the net current of the charge transfer reaction of the species A.
i — the current through the external circuit
S — the surface of the electrode.
$\frac{\mathrm{d}\Gamma_f(D_t^*)}{\mathrm{d}t}$ = the Faraday variation of the superficial concentration of the species D as a consequence of one chemical reaction which implies the species D.
$\frac{\mathrm{d}\Gamma_f(A_t^*)}{\mathrm{d}t}$ = the Faraday variation of the superficial concentration of the species A as a consequence of one chemical reaction which implies the species A.
$\Delta(AD)$ — the range of potentials for which the following reaction is possible:

$$\mathscr{A}\mathscr{D} + A_t^* + D_t^* \rightarrow (\mathscr{A}D)_t + (\mathscr{D}A)_t$$

$\Delta(D)$, $\Delta(A)$ — the range of potentials in which a chemical reaction implying the species D and respectively A is possible.
$\Delta_1(D)$ — the range of potentials for which $\varphi \in \Delta(D)$ but $\varphi \notin \Delta(AD)$
$\Delta_1(A)$ — the range of potentials for which $\varphi \in \Delta(A)$ but $\varphi \notin \Delta(AD)$
$\Delta_1(AD)$ — the range of potentials for which only the following dissolution reaction is possible:

$$\mathscr{A}\mathscr{D} + A_t^* + D_t^* \rightarrow (\mathscr{A}D)_t + (D\mathscr{A})_t$$

REFERENCES

[1] M. R. Latanision N. H., Macmillan and R. G. Lye, *Corrosion Science*, **P3**, 387 (1973)
[2] V. E. Henrich, *Progress in Surface Science*, **9**, 143 (1979).
[3] "Electron Spectroscopy, Theory, Techniques and Applications", vol. 4, Academic Press, 1981.
[4] Richard C. Tolman. Chem. J. Phys., **16**, p. 8 (1948).
[5] P. R. Couchman, W. A. Jesser and D. Kuhlman-Wilsdorf, *Surface Science*, **33**, 429 (1972).
[6] C. Luca, G. Semenescu and A. Andrei, *Rev. Roumaine Chim.*, **29**, 67 (1984).
[7] P. R. Couchman and W. A. Jesser, *Surface Science*, **34**, 212 (1973).
[8] Peter Mark and W. R. Botoms, "Progress in Solid State Chemistry", vol. 6, edited by H. Reiss J. O. Mc Caldin, Pergamon Press, Oxford, New York, 1971.
[9] *Surface Science* **1**, 213 (1964).
[10] J. O. M. Bockris and A. K. N. Reddy, "Modern Electrochemistry", vol. 11, Plenum Press, New York, 1970, p. 822.

Revue Roumaine de Chimie, **34**, *1*, 207–213 (1989)

UNSATURATED HETEROPOLYTUNGSTATES WITH Th(IV) CENTRAL ION

GH. MARCU[a], MARIANA RUSU[a] and A. BOTAR[b]
[a] Faculty of Chemical Technology, Cluj-Napoca, 3400 Romania
[b] Institute of Chemistry, Cluj-Napoca, 3400 Romania

Received October 8, 1988

Th(IV) ion reacts relatively easily with the unsaturated heteropolyanions of type $PMo_2W_9O_{39}^{7-}$ and $P_2MoW_{16}O_{61}^{10-}$ forming stable heteropolymolybdotungstates. The potassium salts of these heteropolyanions were isolated and then characterized by UV and IR spectra. According to the results of the studies undertaken the new heteropolycompounds are situated in the category of heteropolymolybdotungstates with modified Keggin and Dawson structures.

1. INTRODUCTION

The category of heteropolycombinations has been enriched in the last two decades with new classes of heteropolytungstates, characterized by the presence of two heteroatoms in the polytungstic anion. We are taking into account the unsaturated heteropolycombinations of type 1 : 1 : 11 and 1 : 2 : 17.

The first investigations in this direction were initiated by L. C. W. Baker and co-workers [1–4] who isolated and studied representatives of these classes. The theoretical and practical importance of the new classes of heteropolycombinations explains the interest aroused and also the rapid rate of development of a great number of synthesized representatives as well as the extension of the studies undertaken on them.[5–14]

Marcu and co-workers [15–27] made attempts to extend and develop this class of heteropolycombinations by obtaining new representatives as a result of studying their formation mechanisms, respectively, by elucidating the problems referring to their structure. The isolation of some heteropolycombinations of ML_2 type was achieved, where $L = PW_{11}O_{39}^{7-}$, $SiW_{11}O_{39}^{8-}$, $BW_{kk}O_{39}^{9-}$, $P_2W_{17}O_{61}^{10-}$ and $As_2W_{17}O_{61}^{10-}$ and $M = Th^{4+}$, U^{4+}, Se^{4+}, Ru^{3+}, Rh^{3+} and In^{3+}.

We are proceeding now on reporting the most important results of our researches on heteropolytungstates.

2. EXPERIMENTAL

If a solution that contains Th^{4+} ion is rapidly added to the solutions of potassium salts of $PMo_2W_9O_{39}^{7-}$ and $P_2MoW_{16}O_{61}^{10-}$ heteropolyanions, the following reactions take place, the heteropolytungstate molar ratio being 2 : 1 :

$$2K_7[PMo_2W_9O_{39}] + Th(NO_3)_4 = K_{10}[Th(PMo_2W_9O_{39})_2] + 4KNO_3 \tag{1}$$

$$2K_{10}[P_2MoW_{16}O_{61}] + Th(NO_3)_4 = K_{16}[Th(P_2MoW_{16}O_6)_2] + 4KNO_3 \tag{2}$$

Table 1

Results of the chemical analysis

Compound	K%		Th%		P%		Mo%		W%		H_2O%	
	calculated	found	calculated	found	calculated	found	calculated	found	calculated	found	calculated	found
$K_{10}[Th(PMo_2W_9O_{40}H_2)_2] \cdot 22H_2O$	7.05	6.98	4.29	4.32	1.11	1.07	6.92	6.95	59.71	59.95	7.14	7.25
$K_{16}[Th(P_2MoW_{16}O_{62}H_2)_2] \cdot 28H_2O$	6.51	6.42	2.41	2.48	1.91	1.87	1.99	2.05	61.24	61.39	5.24	4.30

In order to establish the optimum conditions of synthesis of heteropolycombinations of ThL_2 type, a study has been accomplished on their formation by chemical reaction (1) and (2) in solutions of 10^{-2}M concentration, using the method of electrophoresis at high tension. The pH range was 2.0—6.5, the Th(IV) cation was deposited on chromatographic paper with the help of a micropipette. By reducing W(IV) with UV rays to blue tungsten, the shift/displacement of the heteropolyanions formed has been watched. The Kunkel and Tiselius [28] method has been applied to estimate the sum of the electrophoretic mobilities of the ions formed, subsequently represented graphically depending on pH to obtain the stability range and the optimum pH of formation of heteropolycombinations.

$K_{10}[Th(PMo_2W_9O_{40}H_2)_2] \cdot 22H_2O$ *Synthesis* : 6.018 g (0.002 mol) $K_7[PMo_2W_9O_{39}] \cdot 13H_2O$ are dissolved in 75 mL distilled water and the solution is heated to 60—70°C. Another solution containing 0.552 g (0.001 mol) $Th(NO_3)_4 \cdot 4H_2O$ is added to the one already mentioned by continuous stirring in 25 mL distilled water. The pH of the mixture is maintained about 4.00 value while adding the Th(IV) solution. The reaction mixture is cooled to the room temperature, the possible impurities deposited under the form of precipitate are filtered and kept at a 5°C temperature. Small well-formed colourless crystals are separated from the solution after a few days. The product is recrystallized with warm water at a pH adjusted to the value.

$K_{16}[Th(P_2MoW_{16}H_2)_2] \cdot 28H_2O$ *Synthesis.* A solution containing 0.552 g (0.001 mol) $Th(NO_3)_4 \cdot 4H_2O$ in 25 mL water is added slowly and by continuous stirring to a solution containing 9.608 g (0.002 ml) $K_{10}[P_2MoW_{16}W_{61}] \cdot 18H_2O$ in 74 mL distilled water heated to 70°C. While adding the Th(IV) solution, the pH is maintained at the value of 5. The solution is cooled to room temperatures, filtered from the possible traces of precipitate and is kept at 5°C. In a few days, small well-formed colourless crystals are separated from the solution and recrystallized/from warm water with a pH adjusted to 5.0 value.

Chemical Analysis was performed according to the well-known method.[29] Thorium was dosed/proportioned under the form of thorium oxalate that was calcinated to ThO_3[30] molibdenum [31] and tungsten [32] were determined gravimetrically, potassium was determined by precipitation as potassium tetraphenylborate, phosphorus was determined as $Mg_2P_2O_7$[34] and the water content was determined by calcinating the samples at 600°C. The results of the analysis are rendered in Table 1. The electronic spectra in UV were recorded on the aqueous solutions of the synthesized compounds having a $5 \cdot 10^{-5}$M concentration in complex. The records were performed on a "Specord UV-VIS" spectrophotometer with self recording, the electronic absorption spectra in UV are shown in figure 2.

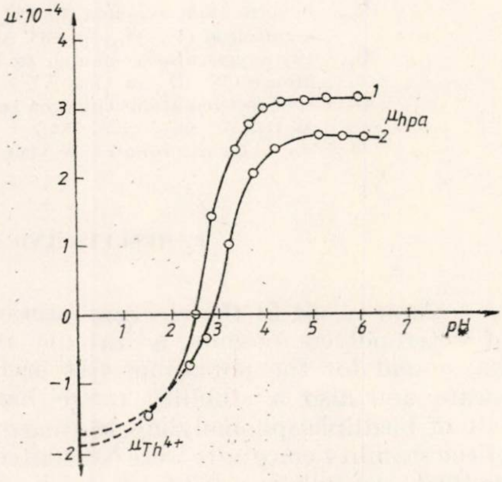

Fig. 1 — The graphic representation of the sum of the electrophoretic mobilities u depending on pH : (1) for the Th(IV) $PMo_2W_9O_{39}^{7-}$ system ; (2) for the Th(IV) $P_2MoW_{16}O_{61}^{10-}$ system.

The IR spectra were recorded on tablets containing the potassium salts of the heteropolyanions synthesized in KBr. The records were performed on a UR-10 Zeiss Jena spectrophotometer ; the values attributed to frequencies are rendered in Table 2. The existence of a constitutional water molecule in the edifice of the complex heteropolyanions studied was confirmed by the substitution reaction of Py in aqueous solution when the pyridonium salts of the complex heteropolyanions substituted were obtained under the form : $(C_5H_5N)_{10}[Th(PMo_2W_9O_{39})_2(C_5H_5N)_2]$ and $(C_5H_5N)_{16}[Th(P_2MoW_{16}O_{61})_2(C_5H_5N)_2]$ respectively.

Table 2

Results of the spectral analysis in IR

Compound	νcm^{-1}	Assignment
$K_{10}[Th(PMo_2W_9O_{40}H_2)_2] \cdot 22H_2O$	1080 1045	$P-O_{(1)}(\nu_{asym})$
	950	$W_0-O_{(4)}(\nu_{asym})$
	800 760 725	$W-O_{(3)}-W(\nu_{asym})$
	605	$O_{(1)}-P-O_{(1)}(\delta)$
$K_{16}[Th(P_2MoW_{16}O_{62}H_2)_2] \cdot 28H_2O$	1084 1059(u) 1015	$P-O_{(1}(\nu_{asym})$
	952 922	$W_{(0)}-O_{(4)}(\nu_{asym})$
	894	$W-O_{(2)}-W(\nu_{asym})$
	596 550	$O_{(1)}-P-O_{(1)}(\delta)$

$O_{(1)}$ oxygen atom common to PO_4 tetrahedron to the three belonging octahedron $(W-O_{(1)} = 1.84$ Å)

$O_{(2)}$ two oxygen atoms common to two octahedrons of different W_3O_{13} groups $(W-O_{(2)}= 1.93$ Å).

$O_{(3)}$ two oxygen atoms common to two octahedrons of the same group $W_3O_{13}(W-O_{(3)}=1.97$ Å).

$O_{(4)}$ an exterior, isolated oxygen atom $(W-O_{(4)} = 2.01$ Å).

3. RESULTS AND DISCUSSION

As a result of the electrophoretic study on the formation reactions of heteropolycompounds, a stability range with a pH between 2.5 and was found for the potassium salt of bis-(phospho-dimolybdo-9-tungsto)-tarate and also a stability range between 3 and 7 for the potassium salt of bis(diphosphomolybdo-16-tungsto)tarate. Subsequently, the values of the stability constants were calculated according to the above-mentioned method, as follows : $2.42 \cdot 10^6$ for $K_{10}[Th(PMo_2W_9O_{40}H_2)_2] \cdot 22\ H_2O$ and $2.16 \cdot 10^6$ for $K_{16}[Th(P_2MoW_{16}O_{62}H_2)_2] \cdot 28\ H_2O$

The electrophoretic study on the synthesized heteropolycompounds informs us of the optimum pH of formation, 4 and 5 respectively for the two compounds, of the relatively high stabilities of these combinations as well as of their purity. These compounds are unitary and not mixtures of heteropolycompounds.

The results of the chemical analysis are given in Table 1. The values represent the arithmetical mean of four determinations and are in agreement with the formulations already assigned to the analyzed compounds. At the same time the chemical analysis confirms the substitutions of the constitutional water molecule in the polytungstic edifice with pyridine. This water molecule is part of the polytungstic edifice, occupying the site corresponding to the terminal oxygen atom of the octahedron in which centre half of the secondary Th(IV) ion is coordinated.

The electronic absorption spectra in UV (rendered in figure 2), exhibit a characteristic band that lies between 42.500–39.000 cm^{-1} for the 1 : 1 : 11 series (curve 1) and a wide band superposed against the background, that lies between 41.000–36.000 cm^{-1} for the 1 : 2 : 17 series. These bands may be attributed to the electron transitions in the tricentral bond W–O–W and are specific to polytungstic edifices of type ($PMo_2W_9O_{39}^{7-}$) and ($P_2MoW_{16}O_{61}^{10-}$)[35], respectively.

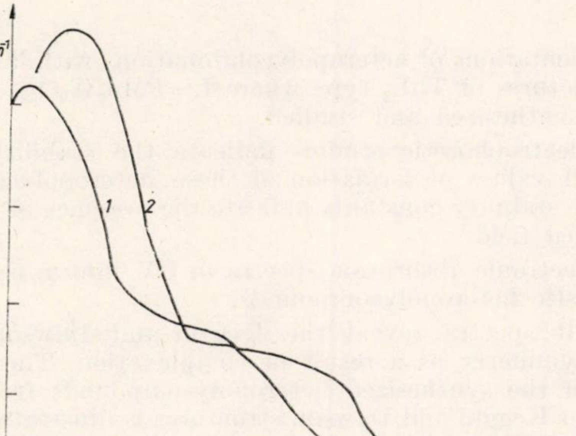

Fig. 2 — The electronic absorption spectra in UV recorded on aqueous solutions of $5 \cdot 10^{-5}$M concentration in complex.
(1) $K_{10}[Th(PMo_2W_9O_{40}H_2)_2] \cdot 22H_2O$;
(2) $K_{16}[Th(P_2MoW_{16}O_{62}H_2)_2] \cdot 29H_2O$.

The blurring and shift of the studied heteropolycompounds towards higher energies of maxima, as compared to ligands, are due to a stronger transition in ThL_2 than in the ligands and to formation of Th–O bonds with the oxygen of some terminal W=O bonds of the ligands, as well as to the strengthening of the other W=O bonds that do not take part in the formation of Th–O bond. These electronic absorption bands follow the tail ends of more intense absorption bands due to $p_\pi-d_\pi$ transition of electrons from terminal oxygen atoms to ligands in W—O terminal bonds, with an absorption maximum situated at 49.000 cm^{-1} in the compound of the 1 : 1 : 11 series and at 48.800 cm^{-1} in the compound of the 1 : 2 : 17 series.

Table 2 presents the spectral analysis and the assignments of the existing bands in the IR absorption spectra recorded on synthesized compounds.

The IR spectra exhibit three absorption bands, four respectively-due to the valence vibrations of the W—O and W—O—W bonds, characteristic to all polytungstic edifices and specific to the structure of Keggin type combinations of 1 : 1 : 11 series and to the structure of Dawson type combinations of 1 : 2 : 17 series.[37]

About 1080 cm^{-1} value there occur bands specific to P—O bond that appears singular in $H_3[PW_{12}O_{40}]$ and splits into distinct bands with the heteropolycompounds 1 : 1 : 11 and 1 : 2 : 17 respectively.

4. CONCLUSIONS

Representations of heteropolycombinations with lacunar Keggin and Dawson structures of ThL_2 type where $L=PMo_2W_9O_{39}^{7-}$ and $P_2MoW_{16}O_{61}^{10-}$ have been synthesized and studied.

The electrophoretic studies indicate the stability range and the optimum pH values of formation of these heteropolycombinations. The values of the stability constants indicate the presence of stable compound n the studied field.

The electronic absorption spectra in UV inform us of the formation of polytungstic heteropolycompounds.

The IR spectra reveal the Keggin and Dawson structures and growth of symmetry as a result of complexation. The deviation of the symmetry of the synthesized heteropolycompounds from the symmetry of the perfect Keggin and Dawson structures is illustrated by the splitting of the absorption band $P-O_{(1)}$ into two components and three respectively, the latter emphasizing a weaker complexation.

The modified Keggin structure of the heteropolyligand $PMo_2W_9O_{39}^{7-}$ arises from that one of the complete Keggin anion α-$PW_{12}O_{40}^{3-}$ by substituting three W(VI) ligand atoms from the centre of 3 there adjacent octahedra, belonging to the same group, with two Mo(VI) atoms as addends inserting half of Th(IV) atom as secondary heteroatom together the terminal oxygen from the centre of the octahedron that coordinated it beside a constitutional water molecule.

The modified Dawson structure of the complex heteropolyanion $P_2MoW_{16}O_{61}^{10-}$ proceeds from that one of the complete Dawson anion α-$P_2W_{18}O_{62}^{6-}$, by substituting two addend W(VI) atoms, the first one, equatorial with a Mo(VI) atom as addend and the latter one, polar with half of the Th(IV) atom as secondary heteroatom, that is of the terminal oxygen atom from the centre of the octahedron where the secondary Th(IV) heteroatom was coordinated beside a constitutional water molecule.

REFERENCES

[1] L. C. W. Baker and M. T. McCutcheon, *J. Amer. Chem. Soc.*, **78**, 4503 (1965).

[2] L. C. W. Baker and J. S. Figgis, *J. Amer. Chem. Soc.*, **92**, 3794 (1970).

[3] L. C. W., V. Simmons Baker, K. Eriks, M. T. Pope, M. Shibata, O. W. Rollins, J. H. Fang and L. L. Koh, *J. Amer. Chem. Soc.*, **88**, 2329 (1966).

[4] L. C. W. Baker, V. Simmons Baker, K. Eriks, M. T. Pope, M. Shibata, O. W. Rollins, J. H. Fang and L. L. Koh, Proceedings pth ICCC St. Moritz – Switzerland, Sept. 1966, 1 Fri., p. 421.

[5] T. J. R. Weakley and S. A. Malik, *J. Inorg. Nuclear Chem.* **29**, 2935 (1967).

[6] S. A. Malik and T. J. R. Weakley, *Chem. Commun*, **1094** (1967).

[7] C. M. Tourne, G. Tourne, *Bull. Soc. Chim. France*, **4**, 1124 (1969).

[8] C. M. Tourne, G. F. Tourne, S. A. Malik and T. J. R. Weakley, *J. Inorg. Nuclear Chem.*, **32**, 3875 (1970).

[9] R. D. Peacook and T. J. R. Weakley, *J. Chem. Soc.* (A), **1971**, 1836.

[10] A. Botar and T. J. R. Weakley, *Rev. Roumaine Chim.*, **18**, 1155 (1973).

[11] H. T. Evans Jr., *Perspectives Struct. Chem.*, **4**, 1 (1971).

[12] S. A. Malik and T. J. R. Weakley, *J. Chem. Soc.* (A), **1968**, 2647.

[13] M. Bauchet, C. M. Tourne and G. F. Tourne, *Compt. rend.* (C), **275**, 407 (1972).

[14] O. W. Rollins, *J. Inorg. Nuclear Chem.*, **33**, 75 (1971).

[15] Gh. Marcu, Mariana Rusu and A. Botar, *Rev. Roumaine Chim.*, **19**, 827 (1974).

[16] Gh· Marcu and Mariana Rusu, *Rev. Roumaine Chim.*, **21**, 385 (1976).

[17] Gh. Marcu and I. Ciogolaş, *Rev. Roumaine Chim.*, **24**, 1048 (1979).

[18] Gh. Marcu and I. Duca, *Rev. Roumaine Chim*, Teză de Doctorat, Inst. de Chimie Cluj-Napoca, 1981.

[19] A. Botar and T. J. R. Weakley, *Rev. Roumaine Chim.*, **18**, 1155 (1973).

[20] Gh. Marcu, A. Botar and Mariana Rusu, *Rev. Roumaine Chim.*, **24**, 1465 (1979).

[21] Mariana Rusu, A. Botar and Cornelia Trocan, *Studia Univ. Babeş-Bolyai, Chemia*, **XXVI**, 56 (1981).

[22] Mariana Rusu, A. Botar and Siegbriche Richi, *Studia Univ. Babeş-Bolyai, Chemia*, **XXIX**, 45 (1984).

[23] Gh. Marcu and Mariana Rusu, *Rev. Roumaine Chim.*, **22**, 227 (1971).

[24] Gh. Marcu, Mariana Rusu and Livia Ocheşel, *Rev. Roumaine Chim.*, **22**, 849 (1977).

[25] Gh. Marcu, Mariana Rusu and Mariana Oneaga, *Stud. Univ. Babeş-Bolyai, Chem.*, **XXIV**, 2 (1979)

[26] Mariana Rusu and A. Botar, *Stud. Univ. Babeş-Bolyai, Chem.* **XXXI**, 84 (1986).

[27] Gh. Marcu, Mariana Rusu and A. Botar, *Stud. Univ. Babeş-Bolyai, Chem.*, **XXXI**, 76 (1986).

[28] H. G. Kunkel and A. Tiselius, *J. Gen. Physiol.*, **35**, 89 (1951).

[29] V. E. Simmons, Ph. Dissertation, Boston University, 1963.

[30] I. M. Kolthoff, P. J. Elving, "Treatise on Analytical Chemistry of Inorganic and Organic Compounds", Part II, vol. 5, John Wiley & Sons, New York, London, Sidney, 1961, p. 154.

[31] A. I. Vogel, "A Text Book of Quantitative Inorganic Analysis", 2nd ed, London, 1951, p. 418.

[32] H. P. Knowles, *J. Res. Nat. Bur. Stand*, **9**, 1 (1932).

[33] G. H. Glass, *Chemist Analyst*, **42**, 50 (1953).

[34] A. I. Vogel, "Quantitative Inorganic Analysis", 3rd. ed. London, 1961, 1575.

[35] G. M. Varga Jr., E. Papaconstantinou, M. T. Pope, *Inorg. Chem.*, **9**, 662 (1970).

[36] Hynsoo So, M. T. Pope, *Inorg. Chem.*, **11**, 1441 (1972).

[37] O. Glemser, W. Holznagel, W. Hopte, E. Schwarzmann, *Naturforsch.*, **20b**, 7258 (1965).

Revue Roumaine de Chimie, **34**, *1*, 215–233 (1989)

ACHIEVEMENTS AND EXPECTATIONS IN CRUDE OIL PROCESSING

BUJOR OLTEANU
The Romanian Institute of Research, Development and Design for Oil Refineries (ICITPR)
Ploieşti, Romania

Received October 6, 1988

The reduction of world crude oil resources determined all scientists to concentrate their efforts in finding new energy resources, so that hydrocarbons should be used in a more rational way. Romania, a country with old traditions in crude oil processing, recorded significant progress in the field of modern crude oil processing and in the increase of feedstocks required for petrochemical industry. Scientific research, development and design had an outstanding contribution to the development of new technologies, to the design and revamping of refineries in Romania as well as to the performance of important projects abroad. The new trends in crude oil processing foreseen for the next decade constitute the main directions for the research, development and engineering design of the specialists from the Romanian Institute of Research, Development and Design for Oil Refineries (ICITPR), Ploieşti.

1. Changes in the Production and Offer of Crude Oil and Energy

The reduction of world crude oil resources, estimated now at about 300 billion tons, and the production control within the OPEC countries after the year 1980 determined a decrease of world crude oil production and consumption. Figures 1 and 2 show the modifications occurred in the world production and consumption of crude oil beginning with the year 1965 and the prognosis till 1995.

The cease of war between Iran and Iraq as well as the increase of crude oil production within the OPEC countries which have the largest crude oil resources (Fig. 3) shall stimulate the increase of the world crude oil consumption.[1]

The more rational use of crude oil will lead to changes in world energy offer. Table 1 shows the changes expected to appear in the energy offer till the year 2000.[2]

The increased use of heavy crude oils having a high sulphur content and the low prices offered for fuel oils call for the development of new processes and the revamping of existing ones, so that to ensure an increased efficiency of high quality products and the reduction of energy consumptions in order to upgrade the crude oil processing.

2. Achievements of Crude Oil Processing in Romania

Crude oil processing in Romania has old traditions and in the year 1990 it celebrates 150 years from the date of building the first unit for crude oil processing at Lucăceşti.

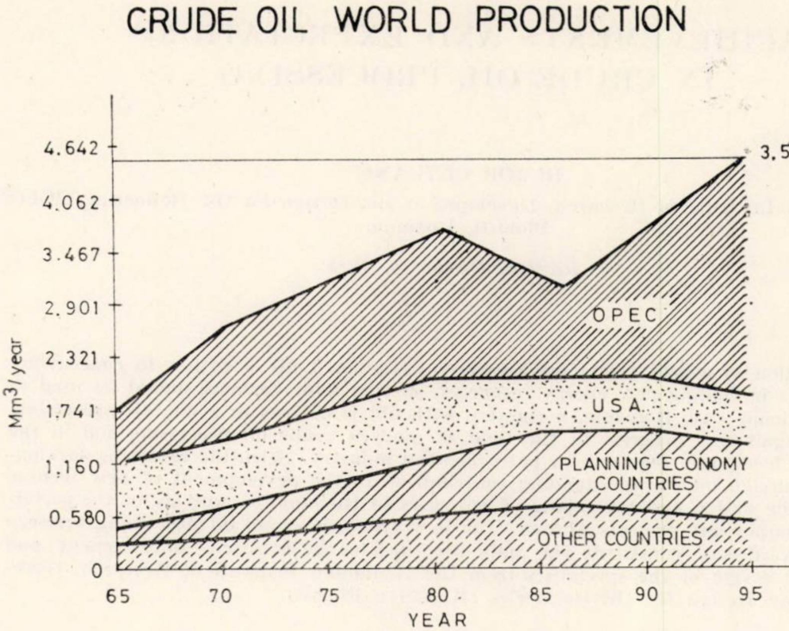
CRUDE OIL WORLD PRODUCTION
4.642
4.062
3.467
2.901
2.321
1.741
1.160
0.580
0
Mm3/year
3,5 G.m3/year
OPEC
USA
PLANNING ECONOMY COUNTRIES
OTHER COUNTRIES
65
70
75
80
85
90
95
YEAR

FIG. 1

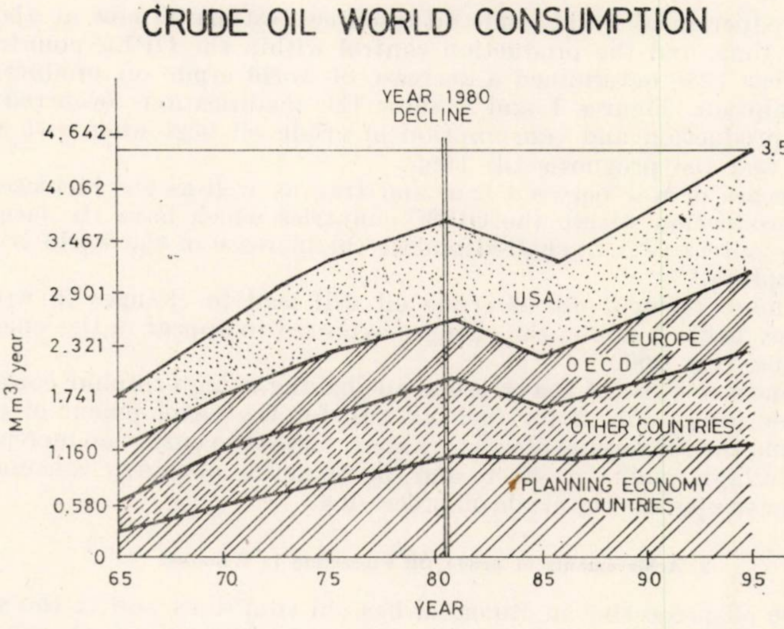
CRUDE OIL WORLD CONSUMPTION
YEAR 1980 DECLINE
4.642
4.062
3.467
2.901
2.321
1.741
1.160
0,580
0
Mm3/year
3,5 Gm3/year
USA
EUROPE
OECD
OTHER COUNTRIES
PLANNING ECONOMY COUNTRIES
65
70
75
80
85
90
95
YEAR

FIG. 2

During the 40 years that passed since the nationalization of the petroleum industry, crude oil processing passed through 3 development stages which are shown in a simplified form in figure 4.

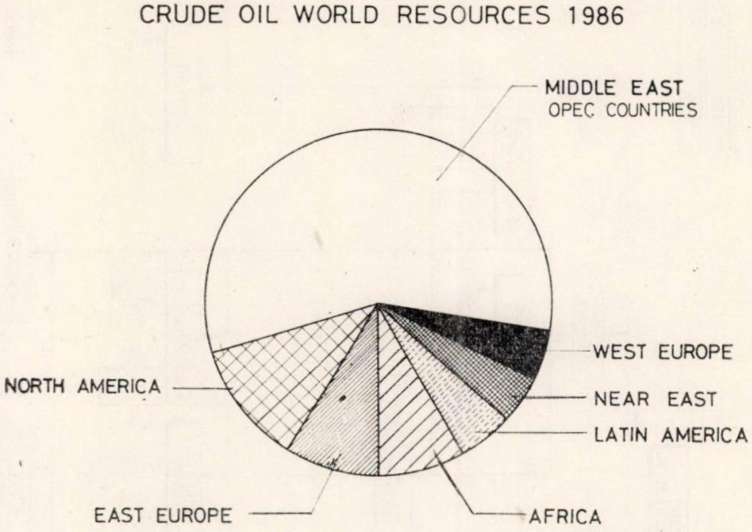

FIG. 3

An impetuous development of the crude oil processing industry took place after the 9th Congress of the Romanian Communist Party, when new refineries and petrochemical complexes were built, based upon the latest world technical progress and, mainly, on the scientific research activity directed with high competence by Academician dr. eng. Elena Ceaușescu, president of the National Council for Science and Education, prime vice-prime minister of the Romanian Government.

Table 1

Estimative offer of world energy [2]

No.	Type of energy	1980		2000	
		Exajouls	%	Exajouls	%
1.	Crude oil	133	38	113	26
2.	Coal	82	24	105	24
3.	Natural gases	61	18	79	18
4.	Nuclear energy	8	2	23	5
5.	Non-conventional sources	63	18	113	26

[1] exajoule = 10^{15} joule
1 joule = 0.238846 cal

The Romanian Institute of Research, Development and Design for Oil Refineries (ICITPR), belonging to the Central Institute of Chemistry, has designed and engineered the new refineries from Borzești, Pitești, Midia and developed new technologies and designs for revamping the

STAGES FOR FURTHER PROCESSING OF CRUDE OIL

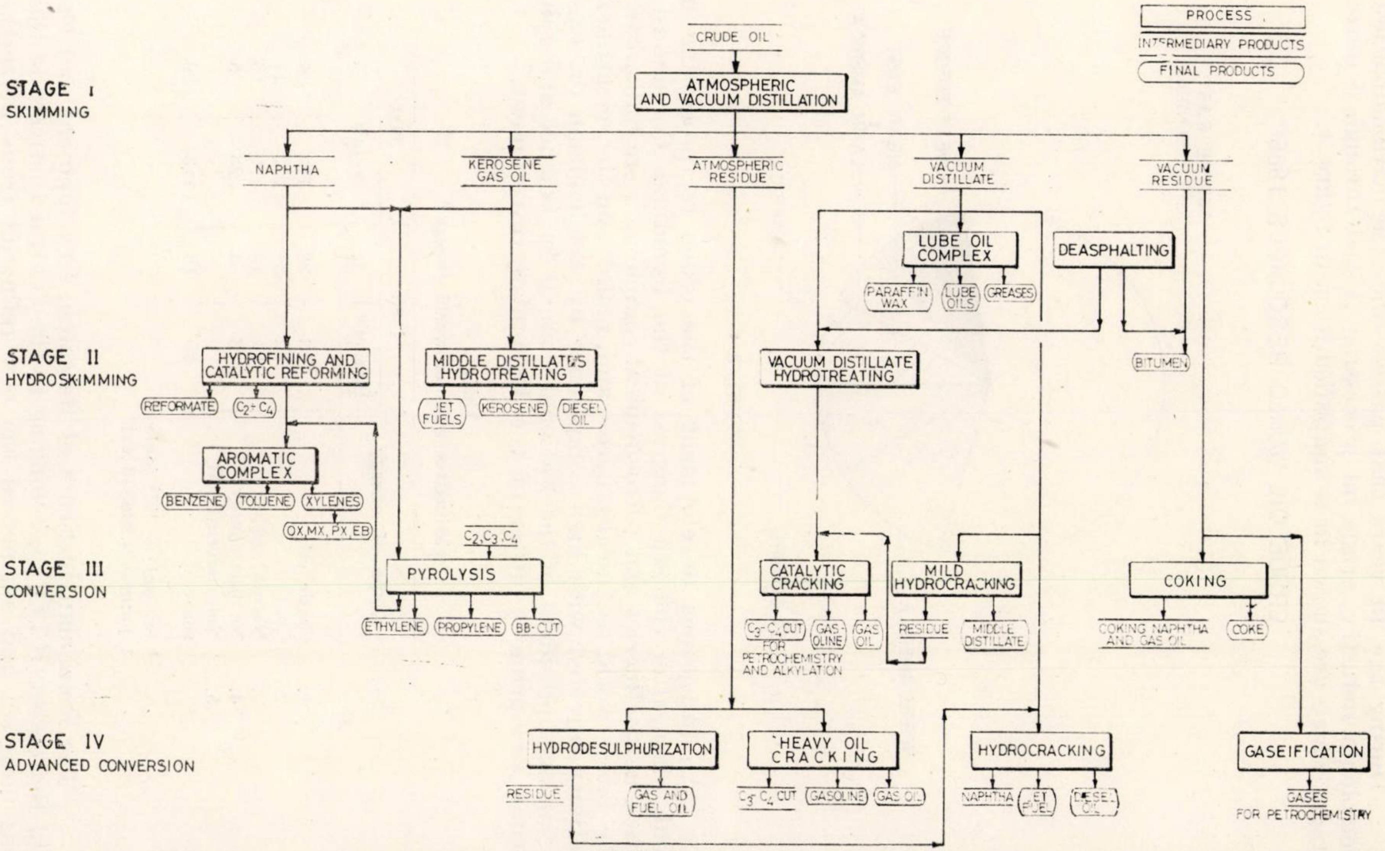
PROCESS
INTERMEDIARY PRODUCTS
FINAL PRODUCTS
CRUDE OIL
STAGE I
SKIMMING
ATMOSPHERIC AND VACUUM DISTILLATION
NAPHTHA
KEROSENE GAS OIL
ATMOSPHERIC RESIDUE
VACUUM DISTILLATE
VACUUM RESIDUE
LUBE OIL COMPLEX
DEASPHALTING
PARAFFIN WAX
LUBE OILS
GREASES
STAGE II
HYDROSKIMMING
HYDROFINING AND CATALYTIC REFORMING
MIDDLE DISTILLATES HYDROTREATING
VACUUM DISTILLATE HYDROTREATING
BITUMEN
REFORMATE
C2÷C4
JET FUELS
KEROSENE
DIESEL OIL
AROMATIC COMPLEX
BENZENE
TOLUENE
XYLENES
OX, MX, PX, EB
C2, C3, C4
STAGE III
CONVERSION
PYROLYSIS
ETHYLENE
PROPYLENE
BB-CUT
CATALYTIC CRACKING
MILD HYDROCRACKING
COKING
C3-C4 CUT FOR PETROCHEMISTRY AND ALKYLATION
GASOLINE
GAS OIL
RESIDUE
MIDDLE DISTILLATE
COKING NAPHTHA AND GAS OIL
COKE
STAGE IV
ADVANCED CONVERSION
HYDRODESULPHURIZATION
HEAVY OIL CRACKING
HYDROCRACKING
GASEIFICATION
RESIDUE
GAS AND FUEL OIL
C3-C4 CUT
GASOLINE
GAS OIL
NAPHTHA
JET FUEL
DIESEL OIL
GASES FOR PETROCHEMISTRY

FIG. 4

refineries from Brazi, Teleajen, Ploiești, Cîmpina, Brașov, Vega, Dărmănești, Crișana.

The policy of large international economic cooperation, supported by Romania, offered the possibility to intensify the economic, technical and scientific exchanges. Thus, ICITPR prepares the technical documentation for many refineries, lube oil complexes, products and crude oil depots, complex equipment for world-wide owners among which :

- India, the Gauhati refinery, the lube oil complex at Haldia and SO_2 extraction units at Baraouni ;
- Pakistan, the expansion of the refinery and the lube oil complex at NRL Karachi ;
- Syria, the Banias refinery ;
- Jordan, the Zarqa Refinery ;
- Turkey, the Central Anatolia Refinery ;
- Iraq, the depots at Zubair and Fao ;
- Egypt, tanks for Assyut and Suez refineries.

Figure 5 shows the main projects designed and other activities achieved by ICITPR for foreign partners.[3]

For the time being the up-to-date refineries in Romania ensure a complex processing of crude oil and integrate well within the petrochemical complexes recently built.

The thermocatalytic processes are of major importance in crude oil processing schemes. In hydrofining, hydrotreating and hydrodesulphurization units there are processed the gasolines, kerosenes, gas oils, vacuum distillates and lube oils, which represent over 80% from the total sulphur crude oil subjected to processing.

Straight run naphtha is processed in catalytic reforming units ; heavy distillates are processed in catalytic cracking units ; n-pentanes and n-hexanes are processed in isomerization units.

M-xylene extraction, separation and isomerization units were built to obtain aromatic hydrocarbons and gas fractionation units were built to obtain light hydrocarbons.

The processing schemes made possible the increased use of products for chemistry, about 15%, as compared to the crude oil subject to processing.

3. THE MAIN DEVELOPMENT DIRECTIONS OF CRUDE OIL PROCESSING

The development of crude oil processing industry in the next years will be intensively oriented to the processing ot heavier and high metal content crude oils.

The increased development of processed crude oil will be ensured mainly by revamping the existing units, improving the processes, the catalysts, the equipment and the processing schemes, in order to reduce the energy consumption.

The next step will be the erection of new units, specific to the conversion of heavy distillates and residual products into gas used in chemical industry as well as into medium and light distillates.

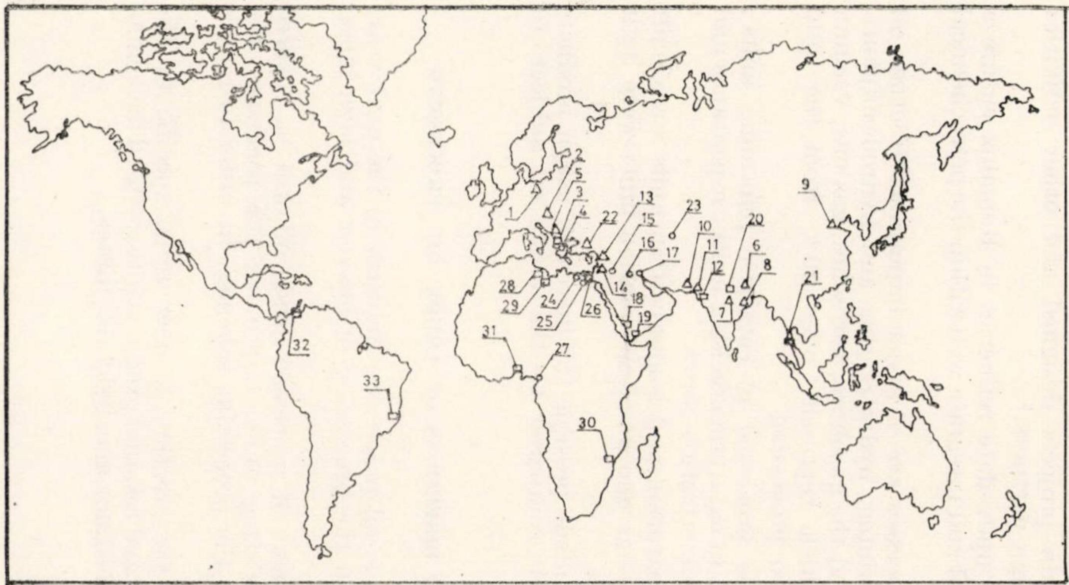

EUROPE

G.D.R.	△ 1. BOHLEN REFINERY
YUGOSLAVIA	△ 2. PANCEVO REFINERY
GREECE	□ 3. ASPROPIRGOS REFINERY
	○ 4. ASPROPIRGOS REFINERY
ALBANIA	△ 5. BALLSH LUBE OIL COMPLEX

ASIA

INDIA	△ 6. GAUHATI REFINERY
	△ 7. BARAUNI REFINERY
	△ 8. HALDIA REFINERY
P.R. OF CHINA	△ 9. LUBE OIL COMPLEX
PAKISTAN	△ 10. N.R.L. KARACHI REFINERY
	△ 11. KARACHI LUBE OIL COMPLEX
	□ 12. HYDROCRACKER UNIT KARACHI REFINERY
SYRIA	△ 13. BANIAS REFINERY
YORDAN	△ 14. ZARQA REFINERY
	○ 15. PRODUCT STORAGE
IRAQ	○ 16. ZUBAIR CRUDE STORAGE
	○ 17. FAO CRUDE STORAGE
P.D.R. OF YEMEN	□ 18. ADEN REFINERY
A.R. OF YEMEN	□ 19. BAJIL REFINERY
NEPAL	□ 20. AMLEKHGUNJ REFINERY
MALAYSIA	□ 21. PETRONAS CORPORATION
TURKEY	△ 22. CENTRAL ANATOLIAN REFINERY
USSR	○ 23. GASES PROCESSING COMPLEX SOVETABAD

AFRICA

EGYPT	○ 24. CRUDE OIL AND PRODUCTS STORAGE ASSYUT REFINERY
	○ 25. CRUDE OIL AND PRODUCTS STORAGE SUEZ REFINERY
	□ 26. PETROCHEMICAL COMPLEX
NIGERIA	○ 27. HARCOURT HARBOUR REFINERY
LIBYA	□ 28. NATIONAL OIL CORPORATION
	□ 29. MISURATA REFINERY
MOZAMBIQUE	□ 30. MATOLA REFINERY
BENIN	□ 31. COTONOU REFINERY

SOUTH AMERICA

COLUMBIA	□ 32. TUMACO REFINERY
BRAZIL	□ 33. PETROQUISA CORPORATION

LEGEND

△ COMPLEX PROJECTS FOR REFINERIES AND LUBE OIL COMPLEX

○ PROJECTS FOR DELIVERY OF EQUIPMENT FOR REFINERIES, PETROCHEMICAL COMPLEXES, DEPOTS

□ STUDIES, TECHNICAL ASSISTANCE, OTHER ENGINEERING SERVICES

THE MAIN PROJECTS DESIGNED AND OTHER ACTIVITIES ACHIEVED BY ICITPR FOR FOREIGN PARTNERS

FIG. 5

To obtain high quality products at world market level and a wide range of products in refineries and petrochemical complexes, new processes will be developed for the separation of high purity paraffin, aromatic and olefin hydrocarbons.

At the same time, the oxygen compounds obtained by etherification will be largely used for the preparation of superior gasolines.

The refinery gases used as fuels represent a potential source for the increase of the production of C_{2+} hydrocarbons aimed for chemical industry as well as a source of hydrogen required for new hydroconversion processes.

The membrane and molecular sieve separation processes represent more attractive alternatives as compared to cryogenic processes and they will develop rapidly in the next years.

The main modification directions with respect to petroleum products are outlined below:

— a reduced production of heavy fuels;

— an increased production of chemical industry gases, aromatic hydrocarbons, diesel gas oils, jet fuels, sulphur, n-paraffins;

— an improved quality of petroleum products: motor gasoline, jet fuels, acicular coke, lube oils mainly, for longer utilization periods.

3.1. Processes for further processing of crude oil

The reduction of crude oil quantity for obtaining petroleum products required for national economy, i.e. the reduction of crude oil consumption necessary to obtain one ton of gas for chemical industry, gasolines and medium distillates is performed by further processing of crude oil. Table 2 shows the crude oil consumption necessary to obtain one ton of processed products depending on the refineries profile.[4]

Table 2

Required amount of crude oil subject to processing in order to obtain one ton of gasoline, gas for chemical industry and oil products

Prccessing scheme	Specific consumption Crude oil (tons)
AD, CF, GF	1.87
AD, CR, VD, CC, GF	1.3
AD, CR, VD, CC, GF, C_x	1.12
AD, CR, VD, CC, GF, C_x, HDR	1.02

Note:

AD — Atmospheric Distillation
CR — Catalytic Reforming
GF — Gas Fractionation
VD — Vacuum Distillation
CC — Catalytic Cracking
C_x — Delayed Coking
HDR — Atmospheric Residue Hydrodesulphurization

The conversion processes of residual products will be of major importance in the modification of products distribution, in the increase of distillate products yield and in the reduction of heavy fuels production.

Figures 6 and 7 show the main catalytic and thermal processes to be used for future development of crude oil processing.

New visbreaking and delayed coking units will be commissioned in Romania.

In the world oil industry, besides visbreaking and delayed coking, flexicoking and fluid coking processes also developed.[5]

In the case of residual feedstocks having a high sulphur content, the coking process leads to a high sulphur content coke, for which the prices are considered to be lower than the prices for the coke used for normal and special electrodes.

Coke having sulphur content over 3% is used mainly as fuel.

The following alternatives may be taken into account in order to reduce the production of coke having a high sulphur content :

— long residue hydrodesulphurization followed by vacuum distillation, that is vacuum residue coking ;

— combination of coking with gaseification and obtaining of synthesis gas.

Table 3 shows the yields achieved by flexicoking processes.[6]

Residual products and conversion thermocatalytic processes of heavy distillates may be divided into :

Table 3

Flexicoking yields [6]

Feed	Athabasca tar sands bitumen	Arab heavy vacuum residue
Sulphur, wt. %	4.9	6.0
Con carbon, wt. %	12.7	27.7
Ni + V, WPPM	325	269
Yields on feed		
C_4, wt. %	8.7	13.8
C_5/510°CVR, LV %	83.4	58.9
Coke gas, std. m^3/m^3	900	2100
Coke gas LHV, MJ/Nm^3	3.5	4.0
Net coke, wt. %	0.8	0.7

— catalytic processes without hydrogen addition (with removal and redistribution of carbon);

— catalytic processes with hydrogen addition.

Catalytic cracking continues to be the first among the thermocatalytic processes for conversion of residual products and heavy distillates without hydrogen addition.

As metals (Ni and V) and asphaltenes from processed feedstocks deactivate the zeolitic catalysts used now, the catalytic cracking units developed processes which lead to the improvement of performances and to the increase of feedstock sources.

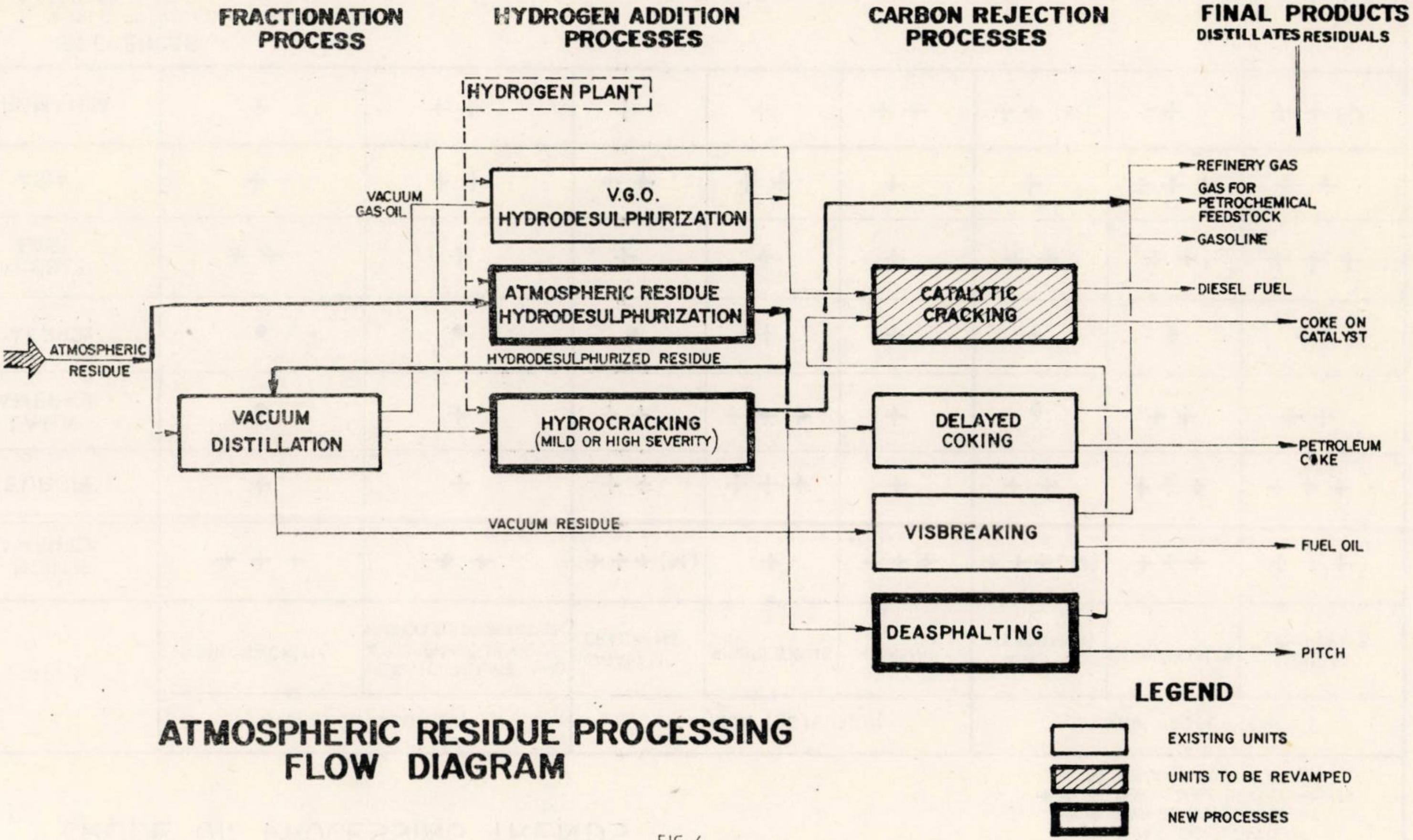
FRACTIONATION PROCESS
HYDROGEN ADDITION PROCESSES
CARBON REJECTION PROCESSES
FINAL PRODUCTS
DISTILLATES
RESIDUALS
HYDROGEN PLANT
VACUUM GAS-OIL
V.G.O. HYDRODESULPHURIZATION
ATMOSPHERIC RESIDUE HYDRODESULPHURIZATION
ATMOSPHERIC RESIDUE
HYDRODESULPHURIZED RESIDUE
VACUUM DISTILLATION
HYDROCRACKING (MILD OR HIGH SEVERITY)
VACUUM RESIDUE
CATALYTIC CRACKING
DELAYED COKING
VISBREAKING
DEASPHALTING
REFINERY GAS
GAS FOR PETROCHEMICAL FEEDSTOCK
GASOLINE
DIESEL FUEL
COKE ON CATALYST
PETROLEUM COKE
FUEL OIL
PITCH
LEGEND
EXISTING UNITS
UNITS TO BE REVAMPED
NEW PROCESSES

ATMOSPHERIC RESIDUE PROCESSING FLOW DIAGRAM

FIG. 6

CRUDE OIL PROCESSING TRENDS

LEGEND
● NO DEVELOPMENT
+ MINOR DEVELOPMENT
++ LARGE DEVELOPMENT
+++ VERY LARGE DEVELOPMENT
M REVAMPING

AREA	HYDROGEN ADDITION		CARBON REJECTION			OTHER PROCESSES		
	HYDROCRACKING	HEAVY DISTILLATE AND ATMOSPHERIC RESIDUE HYDRODESULPHURIZATION	CATALYTIC CRACKING	VISBREAKING	COKING	CATALYTIC REFORMING	ETHERIFICATION	LUBE OIL COMPLEXES
NORTH AMERICA	+++	++	+++(M)	+	+++	+++(M)	+++	+++
EUROPE	+	+	++	+++	+	++	+++	+++
LATIN AMERICA	●	+	++	+++	+	●	++	++
AFRICA	●	●	●	+	+	+	●	+
MIDDLE EAST	++	+	+	+	+	++	++	+++
ASIA	+	++	++	++	+	+	+++	++
ROMANIA	+	++	+	+	++	++ (M)	+	++ (M)

REFERENCES
1. WORLD PETROLEUM CONGRESSES
2. I.F.P. STUDIES

FIG. 7

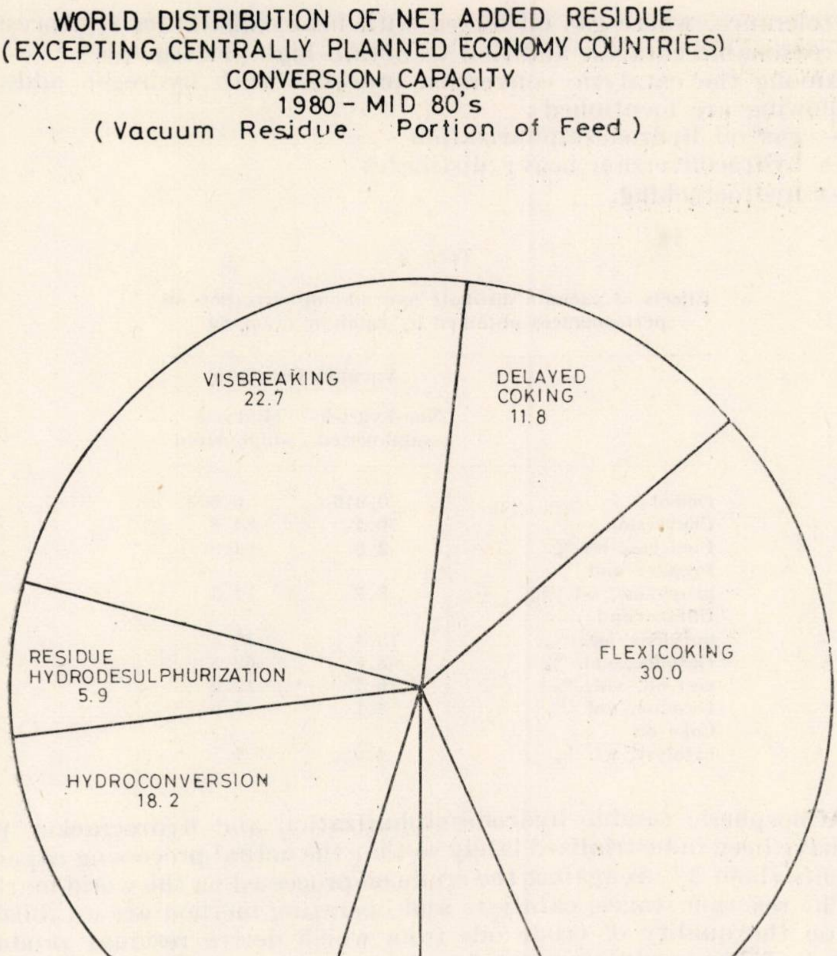

FIG. 8

Hydrodesulphurization processes were achieved for preparation of eedstocks.

Table 4 shows the performances obtained by catalytic cracking f desulphurized vacuum distillate as compared to non-desulphurized vacuum istillate processing.[7]

Demetallization and deasphalting with isobutane or C_3-C_7 hydroarbons mixtures of residual feedstocks aimed at the catalytic cracking.

The most attractive way of catalytic conversion of residual products vithout hydrogen addition is represented by the up-to-date catalytic racking processes that use ultrastable catalysts (type L.Z.200) having metal tolerance, where gas oil mixed with heavy distillates is processed, under reasonable catalyst addition to obtain high performances.[8]

Among the catalytic conversion processes with hydrogen addition the following are mentioned :

— gas oil hydrodesulphurization
— hydroconversion heavy distillates
— hydrocracking.

Table 4

Effects of vacuum distillate hydrodesulphurization on performances obtained by catalytic cracking

	Vacuum Distillate	
	Non-hydrodesulphurized	Hydrodesulphurized
Density	0.916	0.903
Conversion	79.1	84.8
Fuel gas, wt.%	2.8	1.9
Propane and propylene, wt. %	8.7	11.3
Butane and butylene, wt. %	15.4	19.6
Gasoline, vol. %	68.1	69.5
Gas oil, vol. %	16.7	12.2
Residue, vol. %	4.1	3.0
Coke on catalyst, wt. %	4.9	4.7

Atmospheric residue hydrodesulphurization and hydrocracker processes have been industrialized lately so that the actual processing capacity represents about 3% as against the crude oil processed on the world market.

The reaction stages, catalysts and operating method are established based on the quality of crude oils from which derive residual products subject to hydrodesulphurization.[9]

Due to severe working conditions (pressures up to 200 bars, temperatures at 370—440°C, volume velocity 0.3—1 h^{-1}) to hydrogen consumption of about 1.3%, to special equipment and steel, the specific investment is high and this leads to a limited application of the process, depending on the efficiency of an atmospheric residue complex processing.

Table 5

Yields obtained by atmospheric residue hydrodesulphurization

Gases	1.5%
H_2S+NH_3	2.5%
Gasoline	2.0%
Gas oil	12.0%
Vacuum distillate	55.0%
Vacuum residue	27.0%

Table 5 shows the yields obtained by hydrodesulphurization of a long residue having 4% sulphur.

The valorification methods of desulphurized atmospheric residue which may lead to an increased efficiency of atmospheric residue processing are the following : vacuum distillation, catalytic cracking, hydrocracking, that is coking for production of coke having a sulphur content below 1.5% destined for the fabrication of electrodes.

3.2. Evolution of Petroleum Products Quality and Ways of Meeting the Market Demands

The evolution of petroleum products quality is determined by the new conditions imposed by an increased efficiency equipment, by the new regulations regarding environment protection as well as by the rational use of hydrocarbons.[10]

The quality of Premium and Regular gasolines should comply with the new governmental decisions of each country with respect to lead content. Starting with year 1990 it is foreseen to remove the lead from the gasolines available in the USA, Japan and the OPEC countries from Europe.

Premium and Regular gasolines should have the octane numbers $\frac{R+M}{2}$ 91 and $\frac{R+M}{2}$ 87 respectively; final boiling point max. 205°C; 50% vol. to distillate up to 120°C; vapors pressure max. 450 mm Hg for summer time and 550 mm Hg for winter time.

Regarding the utilization of oxygen compounds the oxygen content in gasoline is limited to 3.5 wt. %, corresponding to about 9.5% MTBE (and a higher rate of TAME).[11,12]

To provide a good quality gasoline the following steps should be taken:

— to increase the octane number of catalytic reforming and catalytic cracking gasolines (which represent about 75% from the components of gasolines preparation) by revamping the units and by the use of new, more selective catalysts for dehydrocycling reactions to the detriment of hydrocracking reactions;

— to increase the production of isopentane, isohexane, alkylate, MTBE, TAME and other ethers up to 8 carbon atoms.

Table 6 shows the octane numbers of pentanes and hexanes having normal and isoparaffin structure and the excess of octane numbers to be obtained by C_6-C_5 cuts isomerization.

Table 6

C_5-C_6 Hydrocarbons octane numbers and the excess of octane numbers that can be achieved by isomerization

	Structure		Octane No. excess
	Normal	Iso	
Pentane	61.7	92.3	30.6
Hexane	24.8	91.8	77

By recirculation of normal hydrocarbons (nC_5-nC_6) the octane number $\left(\frac{R+M}{2}\right)$ can be higher than 88.

Table 7 shows the maximum allowable concentrations [12,13] of oxygen compounds in gasolines from the USA and CEE countries.

In countries where LPG stocks are available (C_3—C_4), catalytic cyclisation processes based on zeolites could be used at temperatures of about 540°C and pressures of about 1—20 bar.

Table 7

Maximum allowable concentrations of oxygen compounds in gasolines

	In USA		In CEE countries	
	O_2 conc., wt. %	Oxygen compound conc., vol. %	Allowable concentration, vol. %	
Methanol without cosolvent	excluded	—	Methanol incl. 40% stabilization agent	5
TBA	3.5	16		7
Oxinol (50% methanol+50% TBA)	3.5	9.6		
Ethanol	3.5	10.0	incl. 30% stabilization agent	7—10
MTBE	2.0	12.0		10—15
Isopropanol				5—10
Mixtures				10

Table 8 shows the yields to be obtained by LPG aromatization.[14] C_2—C_{10} olefins and C_3—C_{10} paraffins can be aromatized on HZSM-5 type catalysts.

Kerosenes of TH and T1 type should correspond to the conditions for reactors, regardless of the feedstocks nature.

Table 8

Yields obtained by propane-butane cyclisation

Feedstock:		Propane	Butane
Yields, % wt.			
	Benzene	20	18
	Toluene	27	29
	Xylene	11.6	14
Aromatics C		5	14
Total		63.6	67.5

A hydrocracker can ensure the flexibility required for obtaining increased amounts of jet fuels, regardless of the feedstocks nature and this represents one of the major ways of meeting the jet fuel demands.

Diesel fuels for high speed engines should have a final boiling point (FBP) of max. 370°C, a sulphur content below 0.3% (to avoid pollution) and a cetane number of 45 up to 50.

Table 9 shows the main characteristics of Diesel fuel components.

The increase of lube oils quality and the large use of Super 1, 2, 3 oils using additives comply with the requirements of a larger utilization period having favourable effects on both the increase of the engine operating time and the reduction of the specific consumption at 1000 km.

Table 9

Components for Diesel fuels

Properties	Quality commercial Diesel oil (Average values)	Atmospheric distillation gas oil		Catalytic cracking gas oil	Visbreaking gas oil	Delayed coking gas oil	Hydro-cracking gas oil
		Paraffin crude oils	Non-paraffin crude oils				
1. Density 15°C	0.810−0.890	0.835−0.843	0.846−0.870	0.930−0.963	~0.845	~0.900	~0.835
2. Initial−Final °C		170−400	140−400	160−370	170−570	170−370	200−360
% to 300°C	50−75						
% to 350°C	88−97						
3. Cloud point °C	0÷−15	0÷−12	13÷−30	−5÷−18	−4÷−18	−5÷−20	−14÷−25
4 Cetane number	45−50	50−54	43−54	24−25	40	25−28	50

Calcined petroleum coke used for the fabrication of anodes in aluminium industry should have a low metal content besides the sulphur content (below 3%). This requirement can be followed by selecting the feedstocks used for coke fabrication as well as by desulphurization and demetallization of feedstocks for coking.

With regard to greases, the multi-functional lithium greases, calcium complex greases and special greases will be largely used.

Improvement of quality, within the economically justified limits, can also be achieved with the remaining petroleum products.

3.3. The main ways to reduce energy consumptions in refineries

Refineries consume huge amounts of energy; refineries having a medium degree of complexity consume about 7% of the crude oil processed (about 2.6% in electrical desalting units, atmospheric and vacuum distillation units; 2.8% in naphtha hydrofining units, catalytic reforming and gases fractionation units; 1% in catalytic cracking units, etc.).

The conversion processes of residual products and the petrochemical processing require an additional energy consumption which may reach 12% of the crude oil processed.

To reduce the energy consumptions in refineries, complex steps were taken, i.e.:

—the development of new processes that may ensure crude oil processing at reduced energy consumption;

— the revamping of units, including combination of units in order to eliminate the cooling-reheating phases;

— a larger utilization of steam boilers with turbogenerators, steam turbines and low pressure steam as well as waste heat from medium temperature streams;

— heat recovery from secondary energy resources (waste gases, hot water, hot air from air coolers, etc.);

— use of medium temperature streams (below 100°C) for domestic water heating;

— use of multi-functional additives in order to avoid deposits in heat exchangers;

— crude oil desalting in two stages;

— increased yields at heaters and other equipment.

4. UPDATING OIL PROCESSING

Completion of refineries block flow diagrams with new units will increase the complexity and, as a result higher value products obtained by reducing fuel oil production, thus ensuring an increased value of the products obtained from one ton of crude oil.

Figure 9 shows the block flow diagram of crude oil processing in Romania.

Future development of crude oil processing based on new processes and the revamping of existing units will be performed so that to meet the demands of national economy.

Fig. 10 shows the increased value of the products obtained from one ton of crude oil with further processing.

CRUDE OIL PROCESSING IN ROMANIA

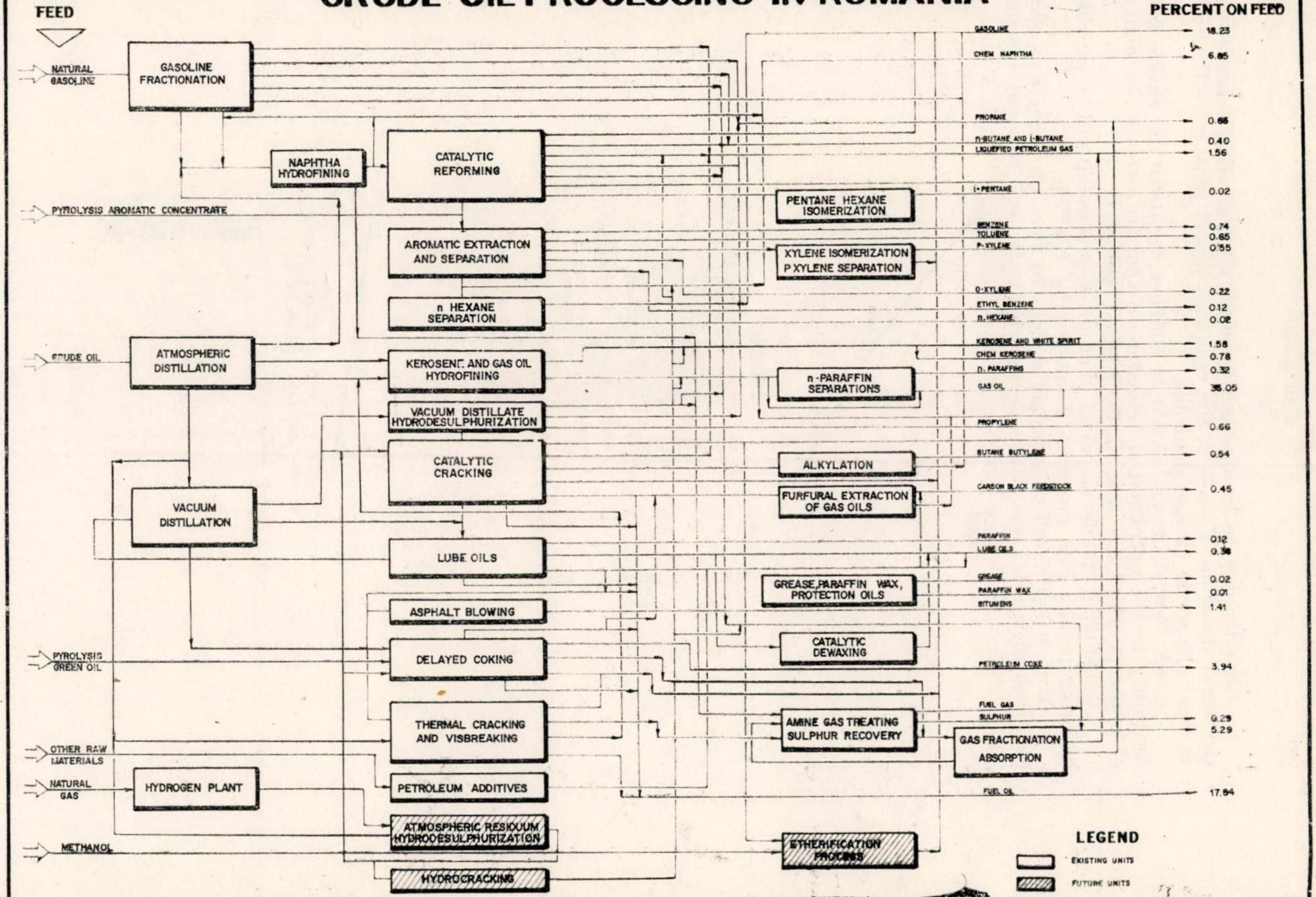
FEED
PERCENT ON FEED
NATURAL GASOLINE
GASOLINE FRACTIONATION
NAPHTHA HYDROFINING
CATALYTIC REFORMING
PYROLYSIS AROMATIC CONCENTRATE
AROMATIC EXTRACTION AND SEPARATION
n HEXANE SEPARATION
CRUDE OIL
ATMOSPHERIC DISTILLATION
KEROSENE AND GAS OIL HYDROFINING
VACUUM DISTILLATE HYDRODESULPHURIZATION
CATALYTIC CRACKING
VACUUM DISTILLATION
LUBE OILS
ASPHALT BLOWING
PYROLYSIS GREEN OIL
DELAYED COKING
THERMAL CRACKING AND VISBREAKING
OTHER RAW MATERIALS
NATURAL GAS
HYDROGEN PLANT
PETROLEUM ADDITIVES
ATMOSPHERIC RESIDUUM HYDRODESULPHURIZATION
METHANOL
HYDROCRACKING
PENTANE HEXANE ISOMERIZATION
XYLENE ISOMERIZATION P XYLENE SEPARATION
n-PARAFFIN SEPARATIONS
ALKYLATION
FURFURAL EXTRACTION OF GAS OILS
GREASE, PARAFFIN WAX, PROTECTION OILS
CATALYTIC DEWAXING
AMINE GAS TREATING SULPHUR RECOVERY
GAS FRACTIONATION ABSORPTION
ETHERIFICATION PROCESS
GASOLINE 18.23
CHEM NAPHTHA 6.85
PROPANE 0.66
n-BUTANE AND i-BUTANE 0.40
LIQUEFIED PETROLEUM GAS 1.56
i-PENTANE 0.02
BENZENE 0.74
TOLUENE 0.65
P-XYLENE 0.55
O-XYLENE 0.22
ETHYL BENZENE 0.12
n. HEXANE 0.02
KEROSENE AND WHITE SPIRIT 1.58
CHEM KEROSENE 0.78
n. PARAFFINS 0.32
GAS OIL 35.05
PROPYLENE 0.66
BUTANE BUTYLENE 0.54
CARBON BLACK FEEDSTOCK 0.45
PARAFFIN 0.12
LUBE OILS 0.38
GREASE 0.02
PARAFFIN WAX 0.01
BITUMENS 1.41
PETROLEUM COKE 3.94
FUEL GAS
SULPHUR 0.29
5.29
FUEL OIL 17.84
LEGEND
EXISTING UNITS
FUTURE UNITS

FIG. 9

The efficiency to be obtained by crude oil processing depends upon the world situation. Therefore, the refineries should have more flexibility to meet the world market demands.

Block flow diagrams should be further improved to ensure more flexibility in the operation of refineries so that to increase the number of products which are sold at the highest prices.

Revamping and development of crude oil processing will be provided by using mainly new processes developed by ICITPR.

Also, ICITPR will take proper actions to meet the directions given by Academician dr. eng. Elena Ceaușescu at the 3rd National Congress

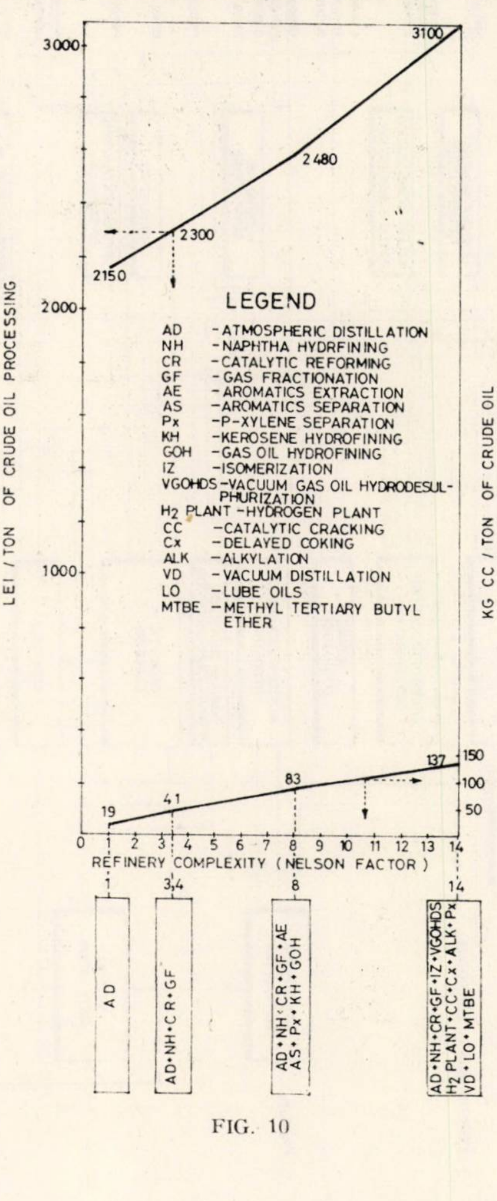

FIG. 10

of Chemistry, including also the extension of the international collaboration with world partners.

5. CONCLUSIONS

Crude oil processing in Romania will continue to be at the level of modern refineries in the world as a result of the steps taken for revamping the processes and of the new processes developed for crude oil processing, residue conversion and improvement of products quality.

The processing schemes of refineries will be optimized and adapted to the requirements of national economy and to the tendencies existing on world market for high value products, reduction of fuel oil production and mainly to obtain increased amounts of hydrocarbons destined for petrochemistry.

Units for obtaining high octane number compounds will be developed in order to produce TEL-free superior gasoline.

Special attention should be paid to the research and production of new additives for oils and petroleum products and catalysts for the existing processes as well as to the new processes which will be industrialized.

The improvement of products quality imposed by the better technical condition of the equipment and machines as well as by the regulations on the environment protection keep on being in the attention of researchers and designers.

Considering that oil refineries are big energy consumers, studies should be continued to reduce the utility consumptions by revamping the units, recovery of secondary energy resources, etc.

New actions will be taken for the rational utilization of the petroleum products and for an increased efficiency of crude oil processing.

The Romanian Institute of Research, Development and Design for Oil Refineries (ICITPR) will take the necessary steps to meet the objectives included in the development programs of the national economy as well as to extend the international collaboration.

REFERENCES

[1] T. Acosta, Hydrocarbon Processing, **67**, 2, 90A (1988).

[2] V. Barauşan, I. Corobea and G. Muscă, "Economia hidrocarburilor", Ed. Ştiinţifică şi Enciclopedică, vol. I, 1980, vol. II, 1987.

[3] B. Olteanu and P. Valter, *Revista Economică*, **41**, 9 (1987).

[4] B. Olteanu and I. Zirnă, *Revista de Chimie*, **32**, 760.

[5] E. S. Ellis, J. Sosnowski, R. L. Hood, M. G. Luzarraga and K. L. Riley, 46th Midyear Refining Meeting Session on Heavy Oils Processing, Chicago, Illinois, May 13, 1981.

[6] * * * The 10th Petroleum Congress P.D. 18, Developments in Thermal and Catalytic Cracking Process for Heavy Feeds, Bucharest, Sept. 1979.

[7] * * * *Hydrocarbon Processing*, **66**, Sept., 94 (1986).

[8] C. Ionescu, The 3rd National Congress of Chemistry, Inferences of the New Types of Catalysts upon Certain Industrial Oil Treating Processes, Bucharest, Sept. 1988.

[9] R. E. Boening, N. K. McDaniel, R. D. Petersen and R. P. Van Driesen, *Hydrocarbon Processing*, Sept., 59 (1987).

[10] * * * *Oil and Gas Journal*, **83**, 50 (1985).

[11] G. H. Unzelman, *Oil and Gas Journal*, **82**, No. 27, 59 (1984).

[12] G. H. Unzelman, *Oil and Gas Journal*, **84** No. 14, April, 88 (1986).

[13] * * * *Hydrocarbon Processing*, **65**, Oct., 19 (1986).

[14] R. F. Andreson, J. A. Johnson and J. R. Mowry, The American Institute of Chemical Engineers Spring National Meeting, Houston, Texas, March 1985.

Revue Roumaine de Chimie, **34**, *1*, 235–245 (1989)

SURFACE STRUCTURING BY UV-LASER IRRADIATION IN A GASEOUS ATMOSPHERE

A. M. PROKHOROV[a], V. I. KONOV[a], V. P. AGEEV[a], I. URSU[b] and I. N. MIHĂILESCU[a]
[a]Institute of General Physics of the USSR Academy of Sciences, Moscow, USSR
[b]Central Institute of Physics, Bucharest, Romania

Received November 21, 1988

New results on excimer laser application for fine surface structuring are presented. One discusses the peculiarities of the UV-photon-induced processes of : (i) chemical deposition on dielectric substrates of carbon and silicon carbide films from CCl_4 and CH_3SiCl_3 vapour precursors, and (ii) chemical etching of c-Si in a CCl_4 vapour environment. The fundamental role of the concurrence of thermal and photo-stimulated processes is also discussed.

1. INTRODUCTION

Fine processing of surfaces is one of the most important and successfully developing fields of laser applications.[1] Our investigations started by experiments on laser-induced etching of W and Mo [2,3] using metal combustion.[4] Another interesting possibility for surface processing is associated with the growth of oxide (nitride) films in a laser beam [5,6] when the radiation not only serves as an efficient and localized heat source but also enables a control of chemical reactions to be performed by measuring the reflectivity and absorptivity of a material.[7] And, finally, it is to some extent feasible to perform a fine surface processing using the surface plasma that occurs as a result of the breakdown of active gases by the laser radiation.[8]

All these experiments were performed using the CO_2-laser radiation with $\lambda = 10 \cdot 6$ μm The option for the excimer lasers generating a powerful pulse UV radiation is first determined by its offering a sharper focusing, which in turn provides for obtaining on a processed surface thin film structure with a spatial resolution which is the best obtainable with the existing technological lasers.

Excimer lasers provide also quite a number of other advantages for surface microprocessing. Firstly, within the spectral generation range of these lasers the majority of the materials of practical interest have an exceptionally high absorption coefficient. Secondly, the quantum energy of their light (3.5–7.9 eV) is quite sufficient for breaking the bonds in the irradiated materials. These factors make excimer lasers highly efficient devices for the photo- and thermo-induced modification of materials

Our studies on the microconditioning of surfaces using excimer laser included the following processes [9-13]:

1. Oxidation of silicon plates;
2. Laser sputtering of materials to obtain thin films on variou types of substrates;
3. Recrystallization of thin films of amorphous silicon on orientated sapphire substrates;
4. Photo- and thermal decomposition of metallo-organic films ont volatile destruction products and non-organic film phase (metallic an oxide);
5. Chemical etching of semiconductor surfaces;
6. Local deposition of films from gas phase; and others.

This paper reports our results on points 5 and 6.

2. DEPOSITION FROM A GAS PHASE

In the laser deposition from a gas phase, we discriminate betwee a parallel- and perpendicular-to-the-surface-of-material exposure of reagent. In the case of the parallel geometry, the UV quanta produce onl a photolytic activation of the reagent in the bulk, which leads to non-local growth of films on the substrate surface. In the case of th perpendicular illumination of the surface, powerful UV pulses activat the gas phase medium and also produce a photo-induced decompositio of the adlayer molecules. Sometimes they cause a local heating of substrates as well. Thereby the perpendicular illumination localizes the growt of films mainly within the laser spot. We now consider some aspect of deposition under a normal UV exposure of a substrate. We will us as an example a deposition of films of hydrogenated silicon carbide fro three-chlormethylsilane vapours.

We have studied experimentally the dependence of deposition rates o the pulsed energy density of XeCl-laser radiation E ($\lambda = 308$ nm), th number of laser pulses N, vapour pressure P, and the substrate back ground temperature T_0. Using a projection scheme we performed a unifor illumination of the surface within the 500 μm spot. Substrates wer monocrystalline silica plates with the surface orientation $\langle 111 \rangle$ and sample from fused silica and magnesium fluorite transparent to the UV radiation To control the deposition dynamics during the laser exposure we recorde the amplitude of the UV pulse passing through the substrate and throug the growing film. Optical measurements and actual thicknesses of film were correlated using a profilometer-profilograph to an accuracy no lower than 200 Å.

Our experiments have shown that as the irradiation dose increase $D = EN$ (N is the number of laser pulses) the deposition process goe through three typical stages: activation, extended growth, and self limiting (Fig. 1). The deposition dynamics and properties of films ar largely determined by the background substrate temperature T_0. Whe T_0 varies within the range 20–130°C the UV absorption coefficients i the film matter increase by two orders of magnitude (see Table 1), whic is an indication of different structures of deposited films.

Investigations of the element composition of the films by the X-ray microanalysis and laser mass spectrometry show that in the deposited material Cl atoms are practically absent. Together with adsorbent lines the mass-spectra contain the C^+, Si^+, SiC^+, SiC_2^+ lines, as well as the lines of the hydrogen-containing compounds $SiCH_2^+$ and SiC_2H^+. This allows to conclude that during deposition hydrogenated silicon carbide films are growing. This conclusion is indirectly confirmed by the fact that the measured values of the UV absorption coefficient for the films deposited on a heated substrate are close to those typical for the silicon carbide phases $K = 5 \cdot 10^3 - 5 \cdot 10^4$ cm^{-1} [14]. At low substrate temperatures some silicon-organic polymer appear to be deposited, which is also of interest.

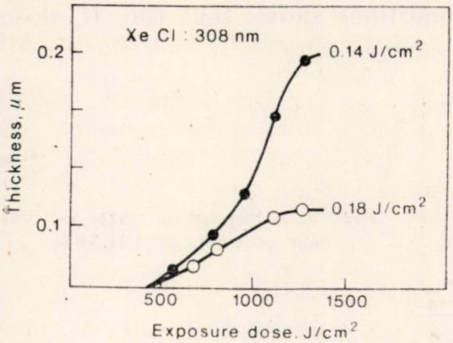

Fig. 1. — Typical deposition curves.

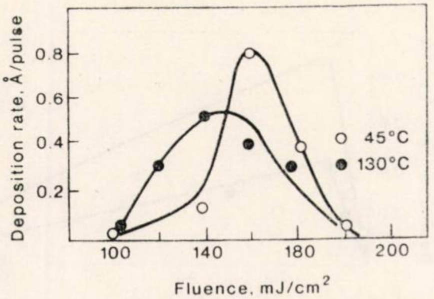

Fig. 2. — Deposition rates vs. fluence at different substrate temperatures.

Table 1

Values of coefficients of absorption (k) and reflection (R) of UV radiation by films of various substrate temperature T_0

T_0, °C	20	45	130
k, cm^{-1}	$7 \cdot 10^3$	$5 \cdot 10^3$	$4 \cdot 10^4$
R	0.1	0.15	0.2

The most efficient film deposition occurs within a sufficiently narrow range of fluence $E = 0.1-0.2$ J/cm². For $E < 0.2$ J/cm², a uniform growth of films over the entire irradiated substrate surface takes place. For large E the deposition occurs chiefly on the periphery of the laser action zone producing a typical volcano profile (Fig. 3).

Another distinctive feature of the process is a non-trivial dependence of deposition rates at the developed growth stage v on the energy fluence E (see Fig. 3) and vapour pressure P (Fig. 4). As seen from the curves, the deposition rates have their maxima at definite values of these parameters. The values of the optimal rates also depend on T_0, i.e. with the increase in T_0 they decrease to a certain extent.

From our point of view, the observed mechanisms of deposition indicate a close relationship and mutual influence of the photo- and thermal activation of the non-equilibrium processes on the substrate surfaces at various stages of the deposition. Thus the analysis of dependences $H(D)$ obtained under various experimental conditions shows that the D_a dose of the activation stage is practically independent of the pulse energy and weakly increases with the rise in the substrate temperature. Therefore it is possible to infer that at least in the early stage of the deposition (in the activation stage) the process is purely photolytic. Evaluations using measurements of the photolytic process cross-sections ($\sigma = 10^{-21}$ cm^2) yield the values of the deposition rates for this case. They are $v \simeq 3 \cdot 10^{-4}$ and 10^{-2} Å per pulse due to decomposition of CH_3SiCl_3 molecules, respectively, in the vapour phase (with $p = 10$ Torr) and in the equilibrium adlayer.

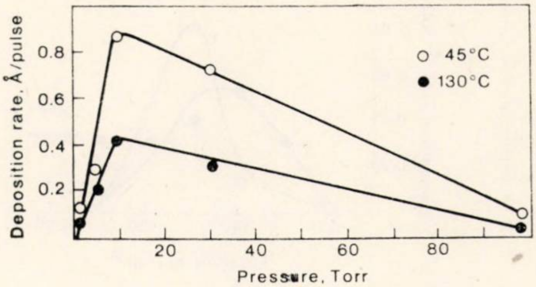

Fig. 3. — Deposition rate vs. vapour pressure of CH_3SiCl_3.

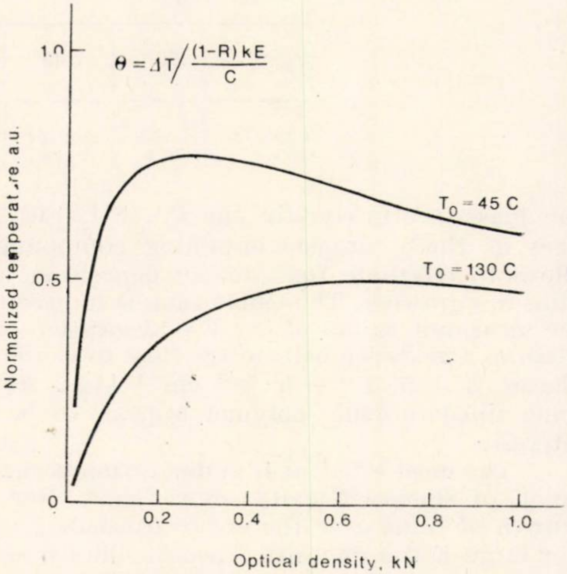

Fig. 4. — Normalized increase in temperature of silicon carbide films on quartz substrate, $\Delta Tc/(1-R)kE$, vs. their optical densities, kH.

The evaluations of the growth rates of films via the decomposition of the adlayer molecules are of the same order of magnitude as those in the experiments at $D < D_a$, i.e. at the initial stage the gas phase decomposition of molecules plays a minor role. Note as well that the growth of the activation doses with the increase in the substrate temperature also indirectly confirms the assumption that the decomposition of the adlayer molecules mainly contributes to the process, since the equilibrium thickness of the adlayer decreases with the increase in temperature (see, e.g.[15]).

Nevertheless, consistent with the assumption of a photolytic nature of the deposition, neither the self-acceleration, nor the subsequent limiting of the film thickness growth at the increase in the exposure dose can be explained. We should seek the origins of this and other phenomena in the activation of the processes due to the laser heating of the initial nuclei and then of the films themselves. To evaluate a pulse increment in temperature T we use a simple equation of energy balance which takes into account a homogeneous release of laser energy in the growing film as well as a heat removal into the transparent-to-UV substrate:

$$(1 - R)E(1 - \exp(-kH)) = (cH + c_0(\chi_0\tau_{1/2})^{1/2}\Delta T \tag{1}$$

Here one of the required conditions for the homogeneous heating of the film is considered to be satisfied

$$kH \langle\langle 1\,;\; H \langle\langle (\chi\tau_{1/2})^{1/2} \tag{2}$$

In (1), (2) c, c_0 and χ, χ_0 are the specific heat and thermal diffusivity of the film and substrate material, respectively; R — reflectance of the UV radiation from the outer boundary of the film; $\tau_{1/2}$ — FWHM (for the XeCl-laser employed in the experiment $\tau_{1/2} = 20$ ns).

Solving (1) for T after the corresponding rearranging of the terms, it is easy to obtain

$$\theta = \frac{\Delta T}{(1 - R)Ek/c} = \frac{1 - \exp(-kH)}{kH + a} \tag{3}$$

where $a = k\dfrac{c_0}{c}(\chi_0\tau_{1/2})^{1/2}$.

Fig. 4 presents a dimensionless temperature parameter versus optical thickness kH of the deposited film at the operating wavelength. Note that as H increases pulse increments in temperature at constant fluence levels also increase initially and reach the maximum

$$\theta = (I - a/2)/(I + a/2) \tag{4}$$

at certain values of thicknesses $\widetilde{H}$ which, according to (3), are defined from

$$\widetilde{H} = H = (2c_0\chi_0\tau_{1/2}/kc)^{1/2} \tag{5}$$

Having passed through the maximum the heating temperature begins to decrease as the film continues to grow under the laser exposure.

The essential slow-down in the deposition process observed at large doses takes place just at the existing film thicknesses $\widetilde{H} = H$ which are functions of the radiation absorption coefficient, and hence of the background substrate temperature (see the Table). It is also important to note that for the typical experimental conditions ($E = 0.15\ \mathrm{J/cm^2}$, $T_0 = 130°\mathrm{C}$, $k = 4 \cdot 10^4\ \mathrm{cm^{-1}}$) silicon carbide films on quartz substrates at $H = \widetilde{H} = 0.2\ \mu\mathrm{m}$ will be heated to the temperatures $T \simeq 10^3$ K which are sufficient for the activation of the thermal decomposition of the initial molecules on the surface, yet much lower than the sublimation temperatures of the deposited material.

On the one hand, these evaluations confirm the primary role of film heating at the stage of self-limiting of the film growth. On the other hand, the decrease in the growth rate noted in the experiment is much sharper than it should be due to a weaker action of the thermal factor at $H > \widetilde{H}$. In this connection we would like to note the following. Firstly, one is warranted to assume that at a thermally-induced deposition the film growth is due to the molecules of the adlayer. Then, with a rise in the film temperature the deposition process will be increasingly counteracted by a thermally-induced desorption of molecules from the growing surface. In our opinion, this is indirectly indicated by the existence of maxima on the curves $v(E)$, as well as by a decrease in the maximal deposition rates at the increase in the background substrate temperature T_0 (i.e., in fact, at the decrease in the equilibrium adlayer thickness). Secondly, at both the photo- and thermal decomposition of the initial gas molecules, active radicals (Cl, H) capable to produce etching of growing films form together with the fragments participating in the deposition. The essential decrease in the deposition rate at the increase in the vapour pressure (i.e., in fact, at the increase in the concentration of etching decomposition products) is an evidence for the existence of such a thickness limiting mechanism.

Thus, we have seen that the film deposition from the gas phase occurs under a powerful action of the laser radiation on surfaces via decomposition of molecules of the adlayer whose thicknesses at operating pressures are several monolayers. Now we discuss the situation when "thick" (about 1 μm) organo-metallic films preliminarily deposited on substrates by some technological procedure decompose due to laser irradiation.

3. THE UV-INDUCED ETCHING OF SILICON IN CCl_4 VAPOURS

The action of the UV laser radiation on the surface of a silicon wafer in CCl_4 vapours is another interesting example of the competition of the photo-induced film deposition and substrate etching.

For our experiments we applied ArF and KrF excimer lasers ($\lambda = 193$ and 248 nm, $\tau = 20$ ns). Silicon samples were irradiated in a chemical reactor under the pressure of CCl_4 vapours up to 100 Torr. Using a projection scheme, the radiation was focused through a quartz window. Preliminarily, by placing the silicon substrates (n-type, 0.01 Ω cm) into a HF solution, the natural oxide was removed.

The experiment revealed the following features of the laser-induced interaction of the radiation with gas and Si surface. Firstly, when exceeding a certain typical fluence level $E \simeq 1$ mJ/cm^2 at the input window of the reactor (from the inside) a transparent-in-the-visible carbon film was deposited. With the increase in its thickness, the film considerably blocked the penetration of the UV radiation inside the reactor. Fig. 5 shows the curves for the dependences of transmittance of films as they grow at the reactor window under the action of the radiation with $\lambda = 248$ nm of various intensity. The transmittance was measured at the operating wavelength.

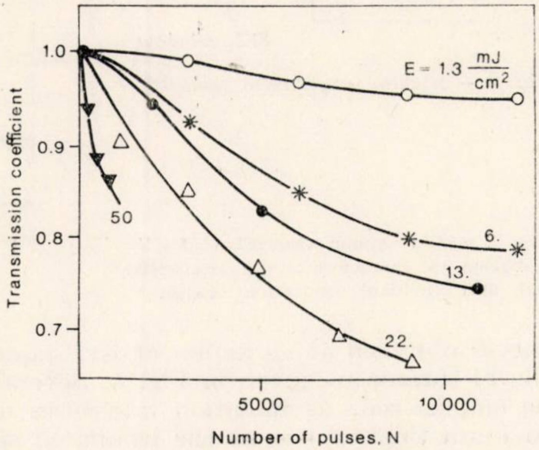

Fig. 5. — Transmission of growing amorphous carbon films vs. number of pulses.

When a certain threshold fluence $E_{max} \simeq 30$ mJ/cm^2 was reached opaque films were formed. At a further increase in the number of pulses they partially cracked. Probably, at such intensities the amorphous metastable phase of carbon transformed into a stable modification — graphite, with a large UV absorption coefficient. Thus, the films broke due to an increase in the pulse temperature (curves with $E = 50$ mJ/cm^2).

To prevent the surface of the Si samples from shielding we used a focusing scheme (Fig. 6) which provided fluences at the quartz window of the reactor lower than the threshold E. Since the fluence varies with the beam narrowing, nonhomogeneous interaction of laser radiation with gas may occur. Fig. 7 demonstrates the absorption of the KrF-laser irradiation by gas in the sample-free reactor as a function of the fluence corresponding to sample surface plane.

One can see that the absorption behaviour is essentially non-linear, indicating a successive photofragmentation of the CCl_4 molecule. The first plateau corresponds to the initial step of reaction : $CCl_4 + h\nu \rightarrow CCl_3 + Cl$ with the cross-section $\sigma = 2 \cdot 10^{-21}$ cm^2 ($8 \cdot 10^{-19}$ cm^2 at $\lambda = 193$ mm), which correlates to cross-section values measured using cylindrical beam geometry in the low intensity limit. It must be noted that the photo-induced absorption resulting from the step-wise fragmentation is mainly concentrated near the lens focus. This is also confirmed by the luminescence in this area. Consequently, an additional shielding of the sample surface occurs which is difficult to take into account (particularly for the ArF laser light).

The etching of silicon was observed only at an excess of fluence $E = 0.15\ \mathrm{J/cm^2}$ for both ArF and KrF lasers, and only after a certain number of activating pulses, i.e. a certain dose D. Some typical etching curves obtained at an action of KrF laser pulses of various fluences on the Si surface are given in Fig. 8. Several details of the process should be emphasized. As radiation intensities increase a graphite deposit (up to 1 μm thick) forms at the irradiated spot. Then the thickness of the deposit quickly decreases and an etched groove appears in its place. Due to this effect the effective etching activation dose D_a increases, although the slope of the straight lines remains the same at low intensities. It is only after reaching the melting threshold $E = 0.7\ \mathrm{J/cm^2}$ of Si [18] that the slope of the straight line changes.

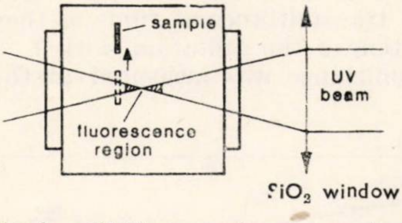

Fig. 6. — Etching experiment geometry

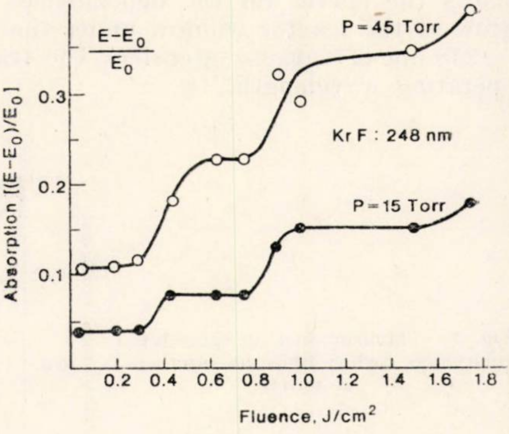

Fig. 7. — CCl_4 vapour absorption of UV radiation vs. fluence (E and E_0 transmitted and incident radiation energies).

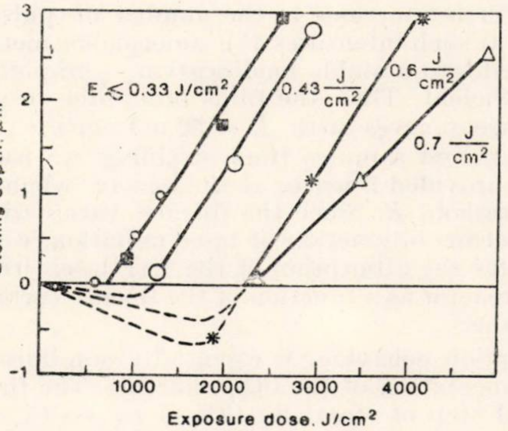

Fig. 8. — Etching curves (c—Si) vs. KrF laser $P = 40$ Torr.

Nevertheless, the question of the etching threshold and activation dose D_a is not clear. From our point of view, their existence is due to the fact that the surface with ⟨111⟩ orientation is closely packed with Si atoms. Because of this, it is difficult for Cl atoms to penetrate into the surface; therefore it is necessary to loosen the lattice beforehand. Due to this, reacting surface enlarges and thus the reaction rate increases.

Fig. 9 shows the etching depth as a function of vapour pressure for ArF and KrF lasers. Particularly notable is this dependence for the radiation with $\lambda = 193$ nm. Such behaviour of the etching may be explained by, first, the shielding of the radiation through a disregarded non-linear absorption near the sample surface; and second, by the elimination of the reaction velocity not due to the gas phase, but due to conditions on the surface.

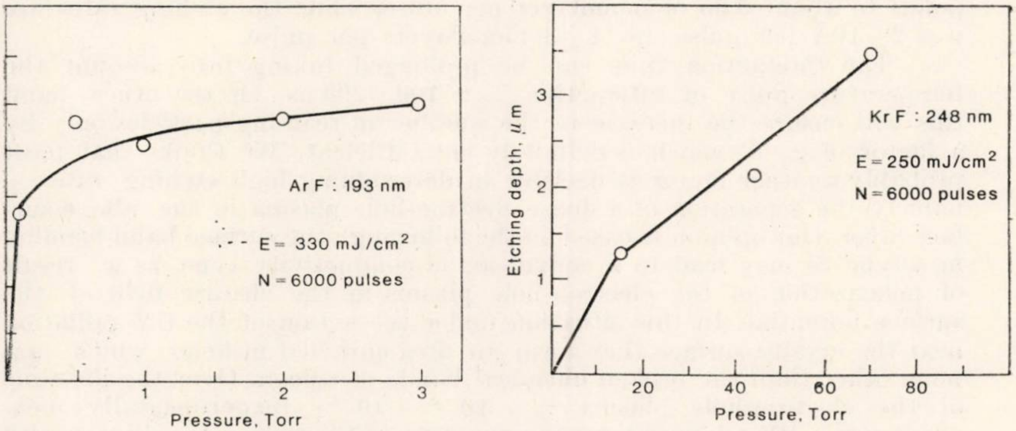

Fig. 9. — Etching depth vs. CCl_4 vapour pressure under fixed irradiation conditions.

Figure 10 presents etching rates $v = \Delta H/\Delta N$ (Å/pulse) defined by the experimental curves Fig. 8 in the $D > D_a$ area. At rather low laser intensities etching rates are about linearly dependent on them. At $E = 0.5$ J/cm^2 (for KrF-laser) the rates reach their maximum and then near the melting threshold fluence they fall. Fig. 10 also gives the etching rates for polycrystalline silicon by ArF-laser in pure Cl_2 [19]. The

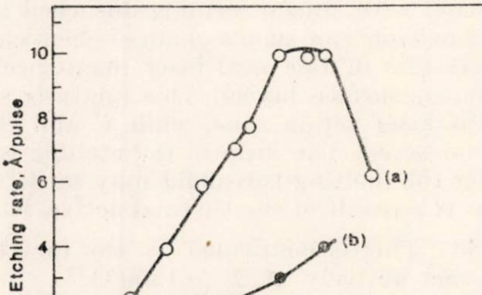

Fig. 10. — Etching rate vs. fluence for silicon : a. KrF : $\lambda = 248$ nm $p(CCl_4) = 15$ Torr; b. ArF : $\lambda = 193$ nm $p(CCl_4) = 2$ Torr; c. ArF : $\lambda = 193$ nm $p(Cl_2) = 400$ Torr (for polysilicon [19])

radiation was weakly absorbed by the gas, so the conditions were similar to those experienced in the etching by KrF laser in CCl_4. However, the etching rates in CCl_4 exceeded those in Cl_2 by almost an order of magnitude. The difference may be accounted for by a less effective excitation of the Cl_2 gas and poly-Si surface by the ArF laser light.

The observed etching rates necessarily require the gas-surface interaction time to be much longer than a laser pulse duration. Evaluations show that if during the pulse duration $\tau = 20$ ns all particles which collide with the surface react, then at a pressure of 15 Torr a number of removed Si atoms per unit square will be $N_0 = 10^{14}$ cm^2, which corresponds to about 0.05 of monolayer per pulse, while the etching rates are $v = 2-10$Å per pulse, i.e. 1—3 monolayers per pulse.

The interaction time can be prolonged taking into account the temperature pulse of interaction $\tau_a \simeq 100-200$ ns. On the other hand this will ensure the increase in the number of reacting particles only by a factor of 2—5, which is definitely not sufficient. We think that most probably another factor is decisive in determining high etching rates — namely the generation of a dense electron-hole plasma in the above-surface layer. Our opinion is based on the following : the surface band bending in *n*-type Si may lead to a conversion of conductivity type, as a result of polarization of the electron-hole plasma in the electric field of the surface potential. In this situation under the action of the UV radiation near the crystal surface they form an area enriched in holes which are none other than the broken chemical bonds of silicon. Over the life-time of the electron-hole plasma $\tau_p = 10^{-6} - 10^{-5}$ s (experimentally measured using RF relaxometers) the number of CCl_4 molecules colliding with the surface due to natural wall flux reaches $N = 2 \cdot 10^{16} - 2 \cdot 10^{17}$ mol/cm^2 (for $p = 15$ Torr).

From our viewpoint, these free chemical bonds may react not only with photodecomposition products, but directly with CCl_4 molecules as well. The released carbon, in turn, may also adsorb on the surface or react with silicon forming adsorbed layers of silicon carbide. A possible existence of such a chain of chemical transformations is evidenced by the results of the local laser mass-spectrometric analysis of the composition of surface layers. This analysis showed that Cl is, in fact, absent in the laser action zone, while C and SiC lines of various stoichiometry are observed. The drop in the etching rate under high intensities approaching the melting threshold may be attributed to the SiC film formation, now as a result of the thermal activation of the competing reaction $\mathrm{Si} + \mathrm{C} \xrightarrow{T} \mathrm{SiC}$. This is confirmed by the fact that silicon and carbon begin to interact actively at $T > 1200$°C.[20]

REFERENCES

[1] "Laser Processing and Diagnostics", Ed. D. Bauerle, Springer-Verlag, Berlin, Heidelberg, New York, Tokyo, 1984.

[2] M. I. Arzuov, A. I. Barchukov, F. V. Bunkin, V. I. Konov and A. A. Ljubin, *Kvantovaya Elektronika*, **2**, 1717 (1975), (in Russian).

[3] M. I. Arzuov, J, I. Djumambekov, V. I. Konov, V. G. Ral'chenko and N. I. Chapliev, *Kratkije Soobschenija Fiz.*, N⁰ **9**,22 (1987) (in Russian).

[4] M. I. Arzuov, A. I. Barchukov, F. V. Kunkin, V. I. Konov and B. S. Lukjanchuk, *Kvantovaya Elektronika*, **6**, 1339 (1979) (in Russian).

[5] V. I. Konov in Proc. Int. Conf. "Lasers and Application", Bucharest 665, 1982.

[6] I. Ursu et al., *Appl. Phys. Lett.*, **46**, 110 (1985).

[7] V. I. Konov, V. G. Ral'chenko and V. N Tokarev, *Izv. Akad. Nauk SSSR, Ser. Fiz.*, **46**, 1065 (1982), (in Russian).

[8] I. N. Mihăilescu, V. I. Konov and S. A. Uglov, in "Proc. Conf. on Laser Advanced Material Processing Science and Application", Osaka, Japan (1987), 465.

[9] "Laser and Particle-Beam Chemical Processing for Microelectronics", Ed. D. J. Ehrlich, G. S. Higashi and M. M. Oprysko in MRS Symposium Proc., **101**, 33 (1987), Boston, USA.

[10] V. P. Agev, A. F. Chernyschev, A. A. Gorbunov, V. I. Konov, A. V. Kuzmichev and A. A. Orlikovsky in Proc. of 2nd Conf. "Trends in Quantum Electronics", Bucharest, 1985.

[11] V. P. Ageev, V. I. Konov, A. V. Kuzmichev et al., *Pis'ma Zh. Tekh. Fiz.*, **14**, 313 (1988), (in Russian).

[12] V. P. Ageev, A. B. Barysh, I. V. Baranenkov, V. I. Konov et al., Preprint IOFAN, N^0 278 (1987), (in Russian).

[13] V. P. Ageev, I. N. Belokon', V. I. Konov, A. V. Kuzminchev, *Kratkije Soobschenija Fiz.*, N^0 **12**, 16 (1987).

[14] Landolt-Bornstein, "Numerical Data and Functional Relationships in Science and Technology", new series, 17a, 22a, 1984.

[15] A. W. Adamson, "Physical Chemistry of Surfaces", Los Angeles, California, 1976.

[16] "Energies of Chemical Bonds", Ed. V. N. Kondratjev, Moscow, Nauka, 1984 (in Russian).

[17] V. P. Ageev, A. L. Builov, V. I. Konov, A. V. Kuzmichev et al., *Dokl. Akad. Nauk SSSR* (to be published) (in Russian).

[18] C. K. Ong, E. H. Sin and H. S. Tan, *J. Opt. Soc. Am.*, B/ **3**, 812 (1986).

[19] S. V. Naguyen, S. Fridmann, *J. Rembetsky*, **33** in ref. [9].

[20] K. A. Andrianov, "Silicon-organic compounds", Goskhimizdat, Moscow, 1955 (in Russian).

Revue Roumaine de Chimie, **34**, *1*, 247–252 (1989)

CONTRIBUTION OF THE CZECHOSLOVAK ACADEMY OF SCIENCES TO THE DEVELOPMENT OF THE MODERN CZECHOSLOVAK BIOTECHNOLOGIES

JOSEF ŘÍMAN
President of the Czechoslovak Academy of Sciences

Received November 28, 1988

The paper reports on some results obtained in the research institutes of the Czechoslovak Academy of Sciences in the field of biotechnology.

The level of our academic research achieved at the beginning of the seventies in general and special biology (particularly in microbiology, immunology and retrovirology), chemistry and biochemistry of nucleic acids and proteins, bioorganic chemistry (including the synthesis of nucleic acid compounds and physiologically active peptides), physical chemistry, and chemical engineering enabled us to monitor all new important trends in the world research of living systems and gradually develop them with our own original contributions.

For these reasons our Academy has become since the early eighties an ideological initiator and direct methodical mediator in the development of modern biotechnologies in our country. This development is now being realized as one of the Czechoslovak governmental programmes of scientific and technological development linking up to the 5th direction of the Complex Programme of Scientific and Technological Progress of member countries of the Council for Mutual Economic Aid.

Although the Czechoslovak programme of the development of biotechnologies follows the long traditions of some Czechoslovak fermentation industries, as the production of beer, but also the production of wine, citric acid, and antibiotics, its goal in our conditions is the optimal utilization of the wide prospective possibilities of modern biotechnologies developed on the basis of application of the newest basic knowledge of the science and possibilities of the present techniques which transform the conventional fermentation and biological technologies, processes, and services into new "high" technologies of the end of this century.

The main innovation charge of the biotechnologies being developed in the world in the present time is a wide application of the methods and techniques of gene manipulation of all types, the productive and processing application of immobilized biological systems, approaches involving large-scale cultivation of plant and animal cells, as well as economization and optimization of technological biological processes on the principles of system and process engineering.

It is in the direct participation of our basic academic research in the mediation of the practical transfer and development of these main innovation components of modern biotechnologies that we saw the primary task of the Czechoslovak Academy of Sciences at the beginning of the eighties.

The six years of our concrete experience and the results achieved in the Czechoslovak Academy of Sciences during our participation in the development of biotechnologies in our country have shown us that the most effective aid of science in speeding up the scientific and technological progress of society and the development of society in general can be expected particularly in those branches where science concentrates on the formation and spreading of foci of basic innovations in the strategically important fields of economic and social development.

This approach of our science to the needs of society posed from the very beginning a great many new tasks associated not only with the establishment of adequate links between the basic research, applied research, and industry, but also many tasks associated with further orientation and development of different branches of our science, the close cooperation of which is a prerequisite for the stimulation of the development of modern biotechnologies. One of these tasks is the formation of research teams capable of interdisciplinary work, provided with specialized services, apparatuses, and preparations of specialized research materials, considering also the material and moral stimulation of high-quality and fast work.

As it follows from the very character of the scientific work, we have not found a uniform prescription for its organization in all individual tasks which our Academy fulfilled and continues to fulfil in the framework of this programme. The access must be in this case always differentiated according to the character of the topic under study. A definitely positive experience with increasing the effectiveness of the research work has been obtained if the work was organized and performed by means of special projects of basic research, the closest goal of which was, besides the medium-term and long-term studies of concrete topics, a rapid establishment of complete methodical sets necessary for a rapid introduction of main innovations into the development of our biotechnologies.

And now some concrete examples of the results obtained in the Czechoslovak Academy of Sciences in this field in the period of less than the six last years.

In the area of genetic engineering, the work with recombinant DNA molecules including the introduction of structural and functional sequence regions for cloning and expression of heterogenous genetic information has been mastered completely. For ensuring the production of synthetic fragments, a Czechoslovak prototype of fully automated and programmed gene-synthesizer, so-called SYNGEN-1, has been constructed from entirely Czechoslovak components including the electronic ones. It is able to synthesize chains of up to 50 nucleotides from protected deoxyribonucleosides in solid phase on a carrier (Fraktosil-1000) using either a modified methylphosphochloridite method or 2-cyanoethyl-N,N-diisopropylphosphoamidite method for the formation of internucleotide bonds.

With this methodical and technical background four genes have been constructed:

Synthetic oligogene of pro-met-enkephalin containing 11-neurohormone-coding units separated always by two codons for the amino acid arginine. A product, which can be cleaved by trypsin to give an active hormone, was obtained by expression in *E. coli*.

Similarly a gene for the cow's colostrum trypsin inhibitor has been synthesized. Its protein product contains 67 amino acids. An original method of composing the gene from 22 oligonucleotide fragments in solid phase on a Sephacryl S-50 carrier was used. This method enables a consecutive binding to the first covalently bound oligonucleotide groups of three or four oligonucleotides and at the last stage also a non-linearized vector. It also enables to obtain by a one-stage ligase reaction, a complete recombinant molecule, which can be released by restriction endonuclease at the site of purposefully inserted polylinker.After circularization of the released molecule, a high yield of the recombinant vector utilizable for the transformation of host cells can be obtained.

A gene for calf chymosin, the enzyme used in cheese production, has been constructed using enzymatic and chemical synthesis. In an expression system with a tac-promoter, the production of more that 1 mg of enzyme per 1 g of *E. coli* biomass has been obtained. This amount of enzyme provides not only sufficient material for experimental production of cheese, but is also used for the preparation of a sufficient amount (ca 30 mg) of a mutant product for protein engineering, for which purposeful mutagenesis of the inserted gene is employed (Val is replaced by Phe in the P_3 enzyme region responsible for enzyme-substrate interaction).

Recently we have obtained expression of the cDNA gene of prochymosin in the expression vector pJDB in *Sacharomyces cerevisiae*, which ensures the continual secretion of an active enzyme product into the medium in the amount of several tens of milligrams per 1 litre of culture. This result opens a way to real application of genetic engineering in food production and in an innovated production of special proteins in the pharmaceutical industry in our country.

In the Czechoslovak Academy of Sciences, methods of genetic engineering have also been introduced and developed in the area of manipulation with plant material. After it had been found that a portion of the Ti plasmid of *Agrobacterium tumefaciens*, designated as T-DNA, is stable following insertion into plant material and can serve as a vector for the transfer of heterogenous genes, methods modifying the structure and function of T-DNA (removal of the genes controlling the formation of phytohormones and insertion of new genes) have been developed. After the introduction of recombined T-DNA (a linear vector with a vir-region) into plant cell nucleus, pollen sterility was induced in tomatoes and a gene for the formation of legumin (a leguminous storage protein) and sets of genes leading to the overproduction of plant growth hormones, auxins and cytokinins, were introduced into the genome of tobacco as a model plant. The goal of our further work in this field is the introduction of pertinent viral genetic information enabling the induction of resistance of plants to some viral infections.

Genetic engineering has been also relatively widely developed in the microbiological area of activities of the Czechoslovak Academy of Sciences, specifically in industrial microbiology. The greatest progress has been made with streptomycetes, where promotor regions of streptomycete DNA were found, which are identified by RNA-polymerase of *E. coli*. By cloning these promotors into a streptomycete promotor probe and junction of the newly formed plasmid with the replicon of *E. coli* plasmid pBR 322, shuttle vectors were obtained expressing the cloned genetic information in the cells of both streptomycetes and *E. coli*. Many other new vectors have also been constructed and used for cloning and expression of genes coding the synthesis of alpha-amylase, thermostable amylase, and agarase. The multiple presence of these genes in the plasmid vectors led to a marked increase in the output of the corresponding enzymes in both the streptomycete host (5,000—10,000 U/L), and the *E. coli* host (4,000—5,000 U/L). In methylotrophic and coryneform bacteria, vectors have been constructed and genes for the synthesis of amino acids have cloned in order to improve the properties of these strains (particularly from the viewpoint of methionine synthesis).

Also cellular engineering has been pursued in the Cezechoslovac Academy of Sciences. Its constitution led to the establishment of a basic production of defined monoclonal antibodies and 43 hybridomas have been constructed. The first Czechoslovak monoclonal antibodies are being industrially produced and have been made available to medical practice for diagnostic purposes. Important sets of monoclonal antibodies have been prepared for the needs of the scientific work proper and have found application not only in our country, but also in the world. This concerns particularly monoclonal antibodies against the cytoskeletal components (tubulin, vimentin, desmin), but also for the determination of hormones (progesterone, insulin, and beta-subunits of human choriogonadotropin), and sets of monoclonal antibodies for the detection of the surface and core antigens of hepatitis B. Moreover, a set of antibodies for phytosanitary diagnostics has been prepared.

Another significant contribution of the Czechoslovak Academy of Sciences in this field is the systematic study of the applicability of synthetic media for mass cultivation of animal cells. It has been found that the transferrin component of medium can be replaced by a defined complex of iron compounds, which results in a simplication and lower price of media for the production of monoclonal antibodies.

Marked progress has also been achieved at the level of genetic engineering in whole animal organisms. Teratocarcinoma cells have been used as totipotent carriers of heterogenous genetic information into the mammalian organism; early embryos have been used for cloning model animals and animals of economic importance and for creation of animal chimeras. Several laboratories of our Academy have introduced important methods for the transfer of genes into animal cells, ranging from the precipitates of calcium-phosphate salts of nucleic acids up to utilization of the most prospective retroviral vectors.

Results applicable in practice have been achieved in the laboratories dealing with the biogenesis of natural substances, the traditions of which have enabled the preparation of highly productive strains of *Streptomyces cinnamonensis* synthesizing the very valuable anticoccidial drug monensin A without admixture of monensin B. The industrial production of monensin A for practical use has already been started.

A great attention is paid to the studies of biopesticides, which are performed mainly at the Institute of Entomology of the Czechoslovak Academy of Sciences. The investigations concern three principal topics : microbial insecticides, biorational pesticides, and breeding of predators and parasites and mass production of arthropods for the control of pests. Results obtained in all of these three subjects are already used in practice. Methods of mass breeding of codling moth caterpillars used for the production of granulosis virus have been developed, as well as methods for the detection of this virus in the host. A series of *Bacillus thuringiensis*-based agents have been prepared, which will be produced for practical application in the forestry and agriculture. Other agents have been based on the fungus *Bauveria bassiana*. A strain of a fungus belonging to the genus Tolipocladium has been isolated and prepared for the production of cyclosporin A, which is an effective insecticide and at the same time an emportant imunosupressant.

Great attention has been paid to the research of technology without liquid wastes. Significant results have been obtained in the paper and cellulose industries. An original Czechoslovak fermentation technology has been worked out utilizing the sulphite waste liquors of cellulose production as substrates for continual cultivation of fodder yeast in 800-m^3 fermentors. For this purpose, a strain in *Candida utilis*, resistant to a high SO_2 concentration and utilizing all available saccharides in the liquors, has been selected. The separated washed biomass has excellent nutritive properties as single-cell protein. The fermentation fluid after separation and thickening is burned under an advantageous energetical balance and the remaining inorganic component (sulphite) is returned to cellulose production. This biotechnology without liquid wastes, thanks to which our most modern cellulose factory in Paskov can produce 22,000 tons of fodder yeast in a year, is extremely important also from the ecological point of view.

Of no lesser importance for ecology are the results achieved in thickening of sludge from sewage plant and in obtaining biocatalysts with denitrifying activity. The denitrifying activity of sludges thickened by bioflotation has also been used for the preparation of immobilized microbial cells capable of denitrifying different sorts of water.

In addition to many other activities, the participation of Czechoslovak Academy of Sciences in the Czechoslovak biotechnological programme also involves process engineering and automation of microbial technologies, which are pursued along four main lines :

Information engineering concentrated on the formation of data banks collecting the information particularly from the pharmaceutical, chemical, and food industries, from the viewpoint of their patent, publication, and marketing activities.

System engineering deals with the analysis and synthesis of complex biotechnological processes and formation of programme sets for the simulation and optimalization of individual operations and operation complexes.

The development of facilities for monitoring and automation is concerned with the development of hardware, as well as of software control of adaptive methods for optimum management of dynamic systems.

Exploration of physiological bases of process engineering is directed at the elaboration of methods for quantitative evaluation of changes in the physiological activity of microorganisms in relation to the technological optimum, the goal being to respect the biological character of the process in relation to the rentability of computer-controlled technological processes. Many results obtained also in this field have already been applied in the innovations of the Czechoslovak biotechnological practice.

Revue Roumaine de Chimie, **34**, *1*, 253–257 (1989)

A MOLECULAR ORBITAL APPROACH TO SOME RADIOGENETIC MECHANISMS

V. E. SAHINI and CRISTINA POP
Bucharest Polytechnic Institute, Department of Physical Chemistry, Bucharest, Romania

Received October 12, 1988

An HMO-based mechanism of DNA andRNA damage on γ-irradiation at the level of chemical bonds between deoxyribose and the pyrimidinic and purinic bases is proposed. The relative stability of some intermediate radicals and their capacity to react with water molecules are examined in the framework of this model.

1. INTRODUCTION

The interest in the field of radogenetics is continuously increasing because of its fundamental aspects as well as of some biomedical implications in the study of mutaion processes, of radiation professional diseases, in cancer therapeutics, in the research of the radiation effects on the population after nuclear accidents, etc. The physico-chemical aspects of radiogenetical phenomena, especially those connected with their molecular interpretations, present a particular significance in the quantitative explanation of a large amount of biological experimental data. The present paper deals with an elementary MO approach to some radiogenetic mechanisms in the framework of the oldest and mostly used model of these processes, based on chromosome DNA breaks subsequently followed by the binding of different fragments.[1,2]

2. BASIC SUPPOSITIONS AND EXPERIMENTAL DATA

The single strand break of DNA macromolecule's covalent bonds was considered as the main initial elementary process of the mutation produced by γ-radiation, breaks of single DNA strands being supposed to result mostly from the destruction of the phosphate-ester bonds.[3] The study of the experimental conditions dependance of the efficiency of the chromosomial transformations on γ-irradiation led to the conclusion that the mechanism seems to be a much more complex one. The present paper deals with the examination of a mechanism of DNA damage at the level of the chemical bonds between deoxyribose and the purinic or pyrimidinic bases.

In the normal state of the cell nucleus, the DNA macromolecular structure protects these bonds to a great extent. In order to simplify the approach, we shall suppose that, due to the much higher energy of γ-quanta in comparison with those of the chemical bonds of DNA, an equal probability of each bond cleavage is to be supposed in the interaction of DNA with γ-radiation.

A second supposition to be considered in the present paper is that, due to the very high specificity of DNA molecular structure involved in the genetic expression of biochemical codification,[4] only the forms of irradiated DNA in which the sequence of pyrimidinic (1) and purinic (2) bases may differ in respect of the initial DNA molecular structure can be considered as being able to continue, in some modified forms, the protein synthesis leading to a possibly different sequence of resulting aminoacids.

The homolytic cleavage of $N-C^d$, as well as of C^d-C^d and C^d-H bonds (the carbon atoms belonging, in all cases, to the deoxyribose molecule) is responsible for the formation of some radicals (Fig. 1), which, in recombination processes with different positions of the macroradicals, can form such modified DNA molecular structure capable of continuing the synthesis of some new proteins. The relative stability of these radicals and their reactivity towards water molecules might be important properties to be taken into account as arguments which could support a mechanism of radio-mutation, as well as such remarkable experimental results: the mutation efficiency is significantly higher when the γ-radiation acts in the mitotic and meiotic phases of cell division, when the chromosomic DNA macromolecules are to be found by the γ-quanta in their less coiled and more mobile forms as before irradiation, centrifugation determines a decrease in the percentage of chromosomial aberrations, but when acting during and after irradiation, it determines an increase of this. Ultra-sound has similar effects. Older approximations concerning the existence of some fragile points of chromosomial DNA in respect of the radiation [4] are well represented in this mechanism by the N—C deoxyribose bonds.

A third supposition is that the radicals issued from γ-irradiation of DNA can be classified according to the interaction of their unpaired electrons with the rest of the radicals' electrons as:

σ-radicals, with the single electron localised in a σ-orbital, generally having short-distance interaction, low stability and short life;

π-radicals, caracterised by a significant intramolecular interaction of the unpaired electron with those belonging to the radicals' π-systems, relatively stable and with longer life.[5]

3. RESULTS AND DISCUSSION

In order to compare the relative stability of π-radicals formed by the homolytic cleavage of $N-C^d$ bonds (labelled I) with that of the radicals obtained by the C^d-C and C^d-H bonds cleavage (labelled II), their delocalization energy per π-electron (DE) were computed using the Hückel and ω-technique methods for all DNA pyrimidinic and purinic I and II radicals. To account for radiation effects on RNA, uracil has also been included and, for some abnormal pairing, tautomeric forms of pyrimidinic and purinic bases were also considered.

The influence of the Coulomb integral on the π-energetic results was studied in relation with a frequently used set [6] by systematically changing, as presented in table 1. The resonance integral was constantly used as listed in table 2.

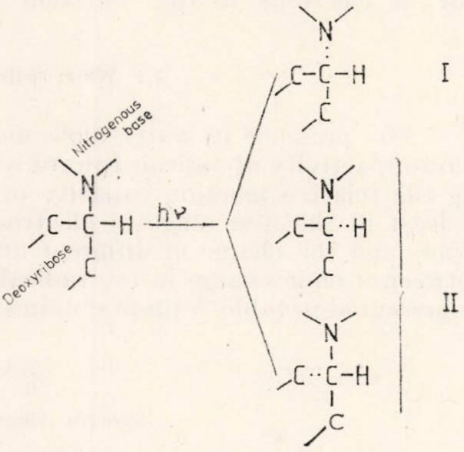

Fig. 1. — Radicals formed by γ-irradiation at the level of deoxyribose-nitrogenous base bond.

Table 1

Coulomb Integrals on Atoms

Atom	Coulomb integral
$\dot{N}$	$\alpha + (0.4 \pm 0.2)\beta$
$\ddot{N}$	$\alpha + (1 \pm 0.2)\ \beta$
$\dot{O}$	$\alpha + (1.2 \pm 0.2\ \beta$
$\ddot{O}$	$\alpha + (2 \pm 0.2)\ \beta$

Table 2

Resonance Integrals on Bonds

Bond	Resonance integral
C=N	β
C–N	$0.9\ \beta$
C=O	$2\ \beta$
C–O	$0.9\ \beta$

Table 3

D. E. (β units) in Radicals

Radical	I	II
Base		
U	0.26–0.27	0.21–0.24
T	0.22–0.25	0.16–0.19
C	0.29–0.31	0.21–0.27
G	0.31–0.35	0.24–0.29
A	0.38–0.40	0.32–0.35

For all the five bases studied (T, C, U, A, G), values of DE for I are higher in respect of the corresponding II radicals in the range of listed parameters, pointing out a higher stability.

Using the ω-technique and starting from the initial set of parameter,[6] the values of DE found at the convergence are presented in table 4, with DE(I) > DE(II).

Table 4

D.E. (β units), ω-technique

	U	T	C	A	G
I	0.24	0.25	0.29	0.38	0.32
II	0.18	0.18	0.21	0.23	0.25

All these results, proving that I radicals are significantly more stable than II radicals, are not a matter of parameter choice or of computing method (meaning those used in the present paper), and these radicals are to be considered as molecular fragments able to take part in some mutagenic processes. To a certain extent, this stability appears to be due to the modification Coulomb integral of nitrogen atom, according to the hypothesis that this involves its participation with a single or a pair of electrons to the π-system of radical.[5]

3.2. Water-radicals interaction

The presence of water molecules in all living matter and the well-known reactivity of radicals toward water suggest some comments concerning the relative reaction capacity of I radicals in relation with II ones, at least in the first stage of electrostatic interaction between the water dipole and the charge of different atoms. The most significant difference between atomic charge in the radicals is located at the radicalic nitrogen as presented in table 5 (data obtained using HMO and usual parameters[6]), and suggesting a significantly stronger interaction capacity with water molecules of radicals II and consequently a lower stability.

Table 5

Nitrogen charge in radicals

	U	T	C	A	G
I	−0.06	−0.10	−0.09	−0.13	−0.20
II	+0.36	+0.35	+0.40	+0.41	+0.41

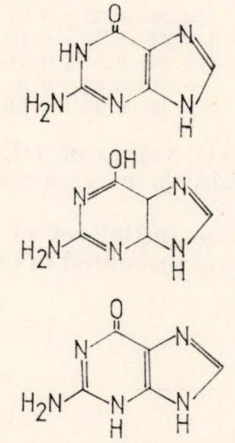

Fig. 2. — Tautomeric forms of guanine.

Table 6

D.E. (β units) and nitrogen charge in tautomeric forms of guanine

Tautomeric forms		1	2	3
	Radicals			
D.E.	I	0.32	0.35	0.30
	II	0.25	0.28	0.24
atomic charge	I	−0.20	−0.14	−0.21
	II	+0.41	+0.40	+0.41

These results are independent of the tautomeric forms of the bases. For instance, in the three tautomeric forms (Fig. 2) of guanine, the DE and charge values of the nitrogen ($N-C^d$) atom are listed in table 6, proving the same significant differences between the I and II radicals.

REFERENCES

[1] I. J. Stadler, "Genetics Effects of X-Rays in Plants, Columbia Univ. Press, New York, 1950.

[2] R. Rieger, "Die Genommutationen", Fischer, Jena, 1936.

[3] J. E. Coggle, "Biological Effects of Radiation", Wykelem, London, 1971.

[4] I. Nicolae and A. Nasta, "Radiogenetica", Edit. Științifică și Enciclopedică, București, 1975.

[5] V. E. Sahini, "Water and Ions in Biological Systems" (A. Pullman, V. Vasilescu, L. Packer Eds.), Union of Societies for Medical Sciences, Bucharest, 1985, p. 417.

[6] B. Pullmann and A. Pullman, "Quantum Biochemistry", Interscience Publ., New York, 1963.

[7] V. E. Sahini and Mihaela Hillebrand, "Chimie Cuantică", Edit. Academiei, București, 1985.

Revue Roumaine de Chimie, **34**, *1*, 259–270 (1989)

THERMODYNAMICS OF IRREVERSIBLE PROCESSES IN ELECTROOSMOSIS OF AQUEOUS ELECTROLYTE AND NONELECTROLYTE SOLUTIONS

DUMITRU SĂNDULESCU and GABRIELA SAVA
Institute of Petroleum and Gas, 39, București Blvd, Ploiești, Romania

Received September 30, 1988

This paper studies the electroosmosis of aqueous electrolyte and nonelectrolyte solutions and the results are interpreted by using thermodynamics of irreversible processes and phenomenological coefficients L_{11} and L_{12}.

1. INTRODUCTION

The study of electrokinetic phenomena by using the classical Helmholtz-Smoluchowski formula and determining the electrokinetic potential (potential zeta) turned out to be difficult because of the necessity of experimentally determining many experimental values with several errors which may appear as a result of the changes of the values in the double electric layer.[1] Therefore, in the last twenty years, the studies in this field have used for interpreting the experimental data obtained from electrokinetic measurements, the method of thermodynamics of irreversible processes.[2,3]

The use of this method is relatively simple and allows the correlation and interpretation of experimental data by means of thermodynamic values, that is the phenomenological coefficients which are more important than some conventional properties of transport (diffusion coefficients, equivalent conductibilities, numbers of transport) inasmuch as they offer information regarding the interactions existing in the studied systems.

The electrokinetic method allowed the determination of the values of the phenomenological coefficients L_{11} and L_{12} in simple systems such as water-electrolyte (NaCl, KCl) and also water-electrolyte-nonelectrolyte (urea, glycerol, HMT *, PAA), systems for which the number of data is small or missing.

---

* HMT hexamethylentetramine; PAA polyacrylamide; L_{11} phenomenological coefficient ($cm^5dyne^{-1}s^{-1}$); L_{12} phenomenological coefficient ($cm^3s^{-1}V^{-1}$); $(J)_{\Delta P=0}$ volumetric flow at zero difference of pressure (cm^3s^{-1}); $(J)_{\Delta \varnothing=0}$ volumetric flow at zero difference of electric potential (cm^3s^{-1}); $\Delta \varnothing$ difference of electric potential (V); ΔP difference of pressure (N/m^2, $dyne/cm^2$); D dielectric constant; r capillary radius; l capillary length; ξ electrokinetic potential; η viscosity coefficient.

In all the studied cases the validity has been established of the linear phenomenological equations and the dependence of the values on the phenomenological coefficients from the composition of solutions.

2. EXPERIMENTAL

a. Substances

For the experimental determinations the following substances have been used : NaCl, KCl, urea, glycerol, HMT, PAA $\overline{M} = 4.9.10^6$ (p.a).

The electrolytes – urea, HMT, PAA – before being used were dried at 110–115° C for 24 h.

The dried substances, kept in a desiccator over $CaCl_2$, have been used to obtain solutions of different concentrations.

To obtain solutions of PAA, the samples of 1 g at 1 L water bidistilled have been melted, blending continuously and leaving it for complete solubilization. The solution thus obtained has been filtered on a filtering crucible G_1. After the determination of the concentration by the method of residues, the solution thus obtained was used as a basic solution for the obtaining of solutions of different concentrations.

b. Apparatus and experimental procedure

For experimental determinations on original electroosmotic cell was used endowed with a glass frit (Pyrex G_4). Because the experimental results can be easily influenced by the impurities especially in the dilute solutions, before each determination the frit was treated with hot HNO_3 (1 : 1), washed repeatedly with bidistilled water and dried.

To avoid permeability changes of the glass frit its equilibration was used for 24 h with the studied solution.

The electroosmotic volumetric flow $(J)_{\Delta P=0}$ was determined by measuring the advancing velocity of the liquid menisk in the lateral graded tubes with which the cell is endowed and the time of movement with a chronometer with precision of ± 0.1 s. The electrical potential difference was applied with a continuous source of current SIT RV 5040.

By connecting to one of the lateral tubes of some electroosmotic cells of a system with dried nitrogen and by using a differential mercur manometer in the thus realised installation the volumetric flow at zero potential difference $(J)_{\Delta \emptyset=0}$ was experimentally determined.

3. RESULTS AND DISCUSSIONS

For the substance transport in an electroosmotic cell the linear relation (6) can be written

$$J = L_{11}\Delta P + L_{12}\Delta \emptyset \qquad (1)$$

which in the case of ordinary permeability becomes

$$(J)_{\Delta \emptyset=0} = L_{11}\Delta P \qquad (2)$$

and for electroosmotic flowing velocity

$$(J)_{\Delta P=0} = L_{12}\Delta \emptyset . \qquad (3)$$

The experimental results are presented in tables 1 and 2.

It is known that a great number of transport phenomena through membranes, as ions migrations, hydraulic permeability, membrane potential, are connected with the phenomenological coefficients. The deter-

Table 1

The phenomenological coefficients values L_{12} in the aqueous electrolyte and nonelectrolyte solutions

Nonelectrolyte concentration	Electrolyte concentration	$\Delta\O(\mathrm{v})$	$(J)_{\Delta P=0} \cdot 10^3$ ($cm^3\ s^{-1}$)	$L_{12} \cdot 10^4$ ($cm^3 s^{-1} V^{-1}$)
0	10^{-3} M NaCl	5.88	3.052	5.091
		7.84	4.361	
		9.80	4.579	
		13.72	6.990	
		19.60	9.543	
		25.48	12.647	
	10^{-3} M KCl	5.80	4.579	8.750
		6.63	5.887	
		8.28	8.222	
		11.60	10.030	
		14.91	13.301	
		16.57	14.609	
2.5 HMT	10^{-3} M NaCl	3.64	6.213	18.188
		4.85	8.500	
		6.07	11.222	
		8.50	13.956	
		10.92	19.843	
		12.13	24.858	
	10^{-3} M KCl	3.14	9.594	28.571
		3.92	11.666	
		4.70	14.392	
		5.49	15.482	
		7.05	19.990	
		7.84	22.630	
5 HMT	10^{-3} M NaCl	3.40	4.444	15.550
		4.53	6.722	
		5.66	9.158	
		7.93	11.555	
		10.20	16.136	
		11.32	17.663	
	10^{-3} M KCl	2.99	8.643	31.818
		3.75	11.990	
		4.49	15.730	
		5.24	16.800	
		6.74	21.200	
		7.49	22.822	
10 HMT	10^{-3} M NaCl	4.08	5.887	16.666
		5.09	8.222	
		7.13	11.000	
		9.17	13.519	
		10.19	15.918	
	10^{-3} M KCl	2.96	4.444	15.094
		3.71	5.620	
		4.45	7.196	
		5.19	8.504	
		6.67	10.030	
		7.41	9.813	

Table 1 (continued)

Nonelectrolyte concentration	Electrolyte concentration	$\Delta Ø(v)$	$(J)_{\Delta P=0} \cdot 10^3$ $(cm^3\ s^{-1})$	$L_{12} \cdot 10^4$ $(cm^3\ s^{-1}\ V^{-1})$
5 glycerol	10^{-3} M NaCl	8.15	5.180	6.486
		14.27	10.466	
		18.34	12.647	
		20.38	12.865	
		26.49	17.321	
	10^{-3} M KCl	10.45	8.333	6.452
		13.06	10.990	
		15.68	13.301	
		18.29	13.737	
		23.52	17.550	
		26.12	20.000	
10 glycerol	10^{-3} M NaCl	6.79	6.977	8.571
		9.06	7.820	
		11.32	10.210	
		15.85	15.264	
		20.38	16.572	
		22.65	19.788	
	10^{-3} M KCl	5.32	7.632	10.909
		7.09	8.213	
		8.86	10.500	
		10.63	11.775	
		12.41	14.174	
		17.22	17.663	
15 glycerol	10^{-3} M NaCl	8.15	3.110	3.750
		10.87	4.000	
		13.59	5.233	
		19.02	7.500	
		24.46	8.940	
		27.18	10.467	
		35.33	12.865	
	10^{-3} M KCl	7.99	5.555	6.666
		9.99	6.663	
		11.98	7.850	
		13.99	9.158	
		17.98	10.903	
		19.98	11.993	
5 urea	10^{-3} M NaCl	5.09	7.120	13.793
		6.79	9.183	
		8.49	12.083	
		10.19	13.828	
		11.89	16.200	
		15.28	21.666	
		16.98	23.999	
	10^{-3} M KCl	6.39	6.105	8.695
		7.96	7.850	
		9.55	8.286	
		11.15	10.685	
		14.33	11.121	
		15.92	13.519	

Table 1 (continued)

Nonelectrolyte concentration	Electrolyte concentration	$\Delta\varnothing$(v)	$(J)_{\Delta P=0} \cdot 10^3$ ($cm^3\ s^{-1}$)	$L_{12} \cdot 10^4$ ($cm^3\ s^{-1}\ V^{-1}$)
10 urea	10^{-3} M NaCl	4.53	10.466	16.666
		6.04	12.647	
		7.55	15.045	
		10.57	18.220	
		13.58	23.423	
		15.09	26.300	
	10^{-3} M KCl	4.43	6.300	14.084
		5.91	10.466	
		7.38	11.338	
		8.86	12.211	
		10.34	13.301	
		14.77	20.715	
15 urea	10^{-3} M NaCl	4.37	5.455	12.121
		5.82	7.222	
		7.28	8.833	
		8.73	11.000	
		10.19	12.810	
		13.10	16.810	
		14.56	17.880	
	10^{-3} M KCl	4.31	7.450	13.333
		5.74	8.995	
		7.18	12.600	
		8.61	13.859	
		10.05	15.220	
		12.92	18.753	
		14.35	23.210	
0.01 PAA	0	2.07	19.888	7.547
		2.76	20.600	
		3.45	21.550	
		4.15	21.777	
		4.84	22.677	
		6.90	24.750	
	10^{-3} M NaCl	5.09	2.616	9.090
		6.79	5.669	
		8.49	7.850	
		11.89	10.466	
		13.58	13.083	
		16.98	21.805	
	10^{-3} M KCl	4.22	5.233	10.000
		5.62	6.977	
		7.03	7.414	
		8.43	8.722	
		9.84	9.594	
		12.65	10.902	
		14.05	12.647	
0.05 PAA	0	6.04	7.500	11.666
		9.06	12.220	
		12.08	14.287	
		15.09	19.625	
		18.18	22.677	
		21.14	26.766	

Table 1 (continued)

Nonelectrolyte concentration	Electrolyte concentration	ΔØ(V	$(J)_{\Delta P=0} \cdot 10^3$ ($cm^3\ s^{-1}$)	$L_{12} \cdot 10^4$ ($cm^3 s^{-1} V^{-1}$)
0.05 PAA	10^{-3} M NaCl	4.89	4.797	9.231
		6.52	5.669	
		8.15	9.158	
		9.78	9.588	
		11.41	12.211	
		16.31	13.519	
	10^{-3} M KCl	4.10	5.233	12.500
		5.47	7.850	
		6.84	8.722	
		8.21	9.158	
		9.57	13.519	
		12.31	14.392	
		13.68	14.827	
0.1 PAA	0	3.62	6.105	16.949
		7.24	13.519	
		10.85	17.008	
		13.26	22.677	
		13.68	23.550	
		18.09	30.964	
	10^{-3} M NaCl	4.22	5.669	11.428
		5.62	8.786	
		7.03	8.286	
		8.24	10.466	
		9.84	10.903	
		12.65	14.080	
		14.05	14.550	
	10^{-3} M KCl	3.73	4.220	12.800
		4.97	6.111	
		6.21	7.599	
		7.45	9.599	
		8.70	11.350	
		11.18	14.012	
		12.43	15.443	
0.2 PAA	0	5.14	5.200	10.526
		6.85	7.500	
		10.27	11.338	
		11.98	11.513	
		15.41	14.653	
		18.84	14.827	
		25.69	28.260	
	10^{-3} M NaCl	4.70	2.398	6.456
		6.27	3.925	
		9.41	6.542	
		10.97	7.850	
		12.54	9.158	
		15. (8	10.903	
	10^{-3} M KCl	4.55	5.669	6.951
		5.69	6.105	
		6.83	6.977	
		9.11	7.850	
		12.52	9.594	
		14.80	12.444	

Table 2

The phenomenological coefficient values L_{11} in the aqueous electrolyte and nonelectrolyte solutions

Nonelectrolyte concentration	Electrolyte concentration	$\Delta P \cdot 10^{-4}$ (dyne cm^{-2})	$(J)_{\Delta \varnothing = 0} \cdot 10^{2}$ (cm^{3} s^{-1})	$L_{11} \cdot 10^{7}$ (cm^{5} dyne^{-1} s^{-1})
0	10^{-3} M NaCl	2.63	1.121	4.820
		3.95	2.041	
		11.05	5.547	
		18.82	9.289	
		23.42	11.775	
	10^{-3} M KCl	6.71	2.915	
		8.29	3.588	
		10.79	4.859	
		11.05	5.233	
		16.97	7.646	
		18.42	8.495	
2.5 HMT	10^{-3} M NaCl	6.18	2.691	4.166
		7.35	2.776	
		8.16	3.738	
		9.21	3.887	
		10.53	4.336	
		13.16	5.496	
	10^{-3} M KCl	5.26	2.317	4.387
		7.37	3.140	
		8.42	3.887	
		11.84	5.457	
		12.89	5.831	
		16.44	7.700	
5 HMT	10^{-3} M NaCl	6.71	2.616	3.871
		10.00	3.813	
		14.07	5.607	
		15.79	6.729	
		18.55	7.476	
		16.45	7.626	
	10^{-3} M KCl	6.58	2.542	4.285
		6.97	3.088	
		8.03	3.887	
		13.68	5.831	
		14.60	6.355	
		18.16	7.159	
10 HMT	10^{-3} M NaCl	6.84	2.317	3.018
		9.21	2.915	
		10.00	2.990	
		11.84	3.663	
		20.39	6.666	
		22.63	7.213	
	10^{-3} M KCl	5.92	2.093	4.00
		9.34	3.215	
		10.53	3.864	
		8.42	3.588	
		13.16	4.785	
		22.37	7.925	

Table 2 (continued)

Nonelectrolyte concentration	Electrolyte concentration	$\Delta P \cdot 10^{-4}$ (dyne cm^{-2})	$(J)_{\Delta\varnothing=0} \cdot 10^{2}$ (cm^{3} ; $^{-1}$)	$L_{11} \cdot 10^{2}$ (cm^{2} $dyne^{-1}$ s^{-1})
5 glycerol	10^{-3} M NaCl	6.79	2.732	4.402
		10.53	4.336	
		10.79	4.560	
		16.32	7.252	
		27.05	8.917	
		22.23	9.994	
	10^{-3} M KCl	2.76	1.546	4.244
		6.97	2.841	
		7.11	3.065	
		10.26	4.929	
		14.34	6.728	
		16.84	7.476	
10 glycerol	10^{-3} M NaCl	10.13	3.588	3.523
		11.18	4.111	
		11.71	4.485	
		13.16	5.009	
		17.24	5.756	
		22.03	9.121	
	10^{-3} M KCl	4.21	1.046	4.000
		7.37	2.467	
		10.13	3.962	
		11.58	4.410	
		14.47	5.607	
		21.18	8.184	
15 glycerol	10^{-3} M NaCl	6.32	2.168	3.333
		6.78	2.019	
		9.21	2.691	
		9.86	3.439	
		11.71	3.887	
		23.68	7.883	
	10^{-3} M KCl	7.50	2.668	3.333
		6.97	2.243	
		14.21	4.710	
		13.82	5.084	
		18.68	6.481	
5 urea	10^{-3} M NaCl	4.21	2.168	4.571
		8.82	3.738	
		12.62	5.682	
		13.42	6.056	
		15.26	7.177	
		20.39	9.794	
	10^{-3} M KCl	5.20	2.306	4.322
		7.34	3.120	
		8.40	3.867	
		12.59	5.267	
		11.62	5.437	
		16.22	7.561	

Table 2 (continued)

Nonelectrolyte concentration	Electrolyte concentration	$\Delta P \cdot 10^{-4}$ (dyne cm^{-2})	$(J)_{\Delta\varnothing=0} \cdot 10^{2}$ (cm^3 s^{-1})	$L_{11} \cdot 10^{7}$ (cm dyne^{-1} s^{-1})
10 urea	10^{-3} M NaCl	7.37	2.916	4.117
		8.82	3.364	
		10.92	4.560	
		13.82	5.682	
		15.13	6.280	
		15.79	6.803	
	10^{-3} M KCl	5.72	2.060	3.973
		8.41	2.867	
		9.21	3.192	
		10.50	3.593	
		12.98	4.762	
		22.17	7.903	
15 urea	10^{-3} M NaCl	5.79	2.093	3.636
		9.74	3.663	
		11.05	4.119	
		14.87	5.009	
		22.37	10.466	
	10^{-3} M KCl	5.76	2.112	3.529
		9.53	3.412	
		11.02	4.002	
		12.40	4.510	
		14.40	4.998	
		20.34	10.266	
		$(J)\Delta\varnothing=0 \cdot 10^{3}$ (cm^3 s^{-1})		
0·01 PAA	0	12.24	10.466	0.769
		19.21	15.700	
		24.47	18.840	
		30.65	26.166	
		31.84	25.073	
		57.24	45.250	
	10^{-3} M NaCl	8.68	5.114	0.581
		19.74	11.338	
		24.61	13.933	
		27.63	15.700	
		61.84	34.666	
	10^{-3} M KCl	8.03	7.420	1.375
		19.34	17.793	
		26.32	22.344	
		31.84	31.400	
		32.23	28.260	
		41.84	37.680	
0·05 PAA	0	34.61	4.556	0.130
		54.61	7.326	
		63.42	8.266	
		68.42	9.160	
		86.45	11.680	

Table 2 (continued)

Nonelectrolyte concentration	Electrolyte concentration	$\Delta P \cdot 10^{-4}$ (dyne cm^{-2})	$(J)_{\Delta \varnothing = 0} \cdot 10^{3}$ (cm^{3} s^{-1})	$L_{11} \cdot 10^{7}$ (cm^{5} dyne^{-1} s^{-1})
0.05 PAA	10^{-3} M NaCl	14.08	4.533	0.313
		14.87	5.687	
		23.68	7.550	
		31.84	10.466	
		39.08	13.519	
		37.11	12.283	
	10^{-3} M KCl	17.50	11.420	0.666
		17.76	11.467	
		27.76	16.746	
		33.82	21.980	
		35.53	23.027	
		39.47	26.167	
0.1 PAA	0	25.00	2.626	0.125
		47.37	6.433	
		52.63	6.794	
		85.53	10.883	
	10^{-3} M NaCl	27.89	1.638	0.060
		28.68	1.962	
		37.11	2.244	
		45.00	2.616	
		51.32	3.270	
	10^{-3} M KCl	18.55	2.616	0.166
		34.21	5.233	
		51.32	8.250	
		55.26	8.747	
		59.21	10.466	
		73.68	12.500	
0.2PAA	0	18.42	1.986	0.107
		31.97	3.256	
		47.63	5.083	
		54.60	5.950	
		60.13	6.643	
	10^{-3} M NaCl	20.13	0.981	0.044
		38.82	1.526	
		33.68	1.425	
		49.08	2.181	
	10^{-3} M KCl	38.16	5.416	0.145
		55.92	7.633	
		57.89	8.542	
		66.45	9.466	
		74.34	10.547	

mining of these values is also considered as an important stage in the kinetic study of ionic transport through membrane.

The phenomenological theory of irreversible processes can then be applied to the transport phenomena in electrolyte and nonelectrolyte solutions and the modern macroscopic form of the theory[4] has been primarily suggested by the first papers on statistics mechanics by Onsager. He achieved a general description of the ionic transport in solutions in the phenomenological coefficients terms.

The phenomenological coefficients values L_{11} and L_{12} have been determined by the slope of the linear representations indicated by equations 2 and 3. The obtained values as the order of value are in good agreement with the existing data from the speciality literature in the case of NaCl, KCl.

The experimental results prove the validity of linear phenomenological equations for all the studied systems and for all the compositions of solutions.

The linear dependence of thermodynamic flows on the thermodynamic forces justifies the studied transport phenomenon, showing the application of the general hypothesis of the theory of the thermodynamics of irreversible processes justified in the case of some small forces.

From the data in tables 1 and 2 the dependence of L_{11} and L_{12} coefficients on the composition of the solutions can be observed. Greater values of L_{12} are observed in nonelectrolyte solution than in the electrolyte solution, high values of this coefficient in solution with HMT and urea, the rise of L_{12} value while passing from the NaCl solutions to the KCl solutions.

Using as basis the double electric diffuse layer, L_{12} coefficient is correlated with medium characteristics and the sizes of capillaries by the relation :

$$L_{12} = Dr^2 \xi / 4 \eta\, l \tag{4}$$

Equation 4 also correlates the experimental data which verify relation 3 with the electric potential appeared between the fixed and moving part of the double electric layer, zeta potential, which is a concept based on microscopic model thus explaining the higher values of L_{12} in systems with great zeta potentials.

Examining the data from table 2 one notes a drop of the L_{11} phenomenological coefficient value, when adding the nonelectrolyte to electrolyte solution, drop which becomes important with the rising of the nonelectrolyte concentration.

Equation 5 established the double electric diffuse layer model :

$$L_{11} = \pi r^4 / 8 \eta\, l \tag{5}$$

which allows a justification of this experimental observation. The observed dependence of this phenomenological coefficient on concentration agrees with the existing data in the speciality literature[5,6] concerning the variation of this thermodynamic value with the composition of the solutions.

4. CONCLUSIONS

a. The electroosmotic method has been applied to the study of aqueous electrolyte and nonelectrolyte solutions.

This method has allowed the obtaining of some experimental data which are necessary to estimate the phenomenological coefficients values, L_{11} and L_{12}.

b. The validity of the phenomenological linear equations has been established by applying the thermodynamics of irreversible processes in cases of electrolyte and nonelectrolyte solutions for all studied compositions and for all applied entrance forces.

c. The phenomenological coefficients values L_{11} and L_{12} have been estimated by the linear representations $(J)_{\Delta P=0} - \Delta\varnothing$ and $(J)_{\Delta\varnothing=0} - \Delta P$.

d. The dependence of these coefficients on the nonelectrolyte added concentration has been observed from the obtained data. A rise of L_{12} coefficient of the electrolyte solution while adding nonelectrolyte has been generally observed. The presence in electrolyte solutions causes in all the studied cases a drop of the value of L_{11} coefficient.

REFERENCES

[1] G. Sava, Thesis, Institute of Petroleum and Gas, Ploiești.
[2] I. Prigogine, "Etude Thermodynamique des phenomènes irreversibles", Paris, Liège, 1947.
[3] R. Haase, "Thermodynamique of irreversible processes", Addison Wesley Publ. Comp., Massach., 1969.
[4] D. Miller, *Chem. Rev.*, **60**, 15 (1960).
[5] R. P. Rastogi, R. C. Srivastava, S. M. Singh, *J. Phys. Chem.*, **74** (15) 2960 (1970).
[6] R. C. Srivastava, M. G. Abraham, *Trans. Faraday Soc.*, **72**, 2631 (1976).
[7] H. Schönert, *J. Phys Chem.*, **73**, 62 (1962).

Revue Roumaine de Chimie, **34**, *1*, 271–285 (1989)

NEW ASPECTS IN THE CHEMISTRY OF PYRYLIUM SALTS: CHANGES DUE TO DIALKYLAMINO SUBSTITUENTS

WERNER SCHROTH

Martin-Luther University, Halle-Wittenberg
Sektion Chemie, W. B. Organische Chemie, Postfach, 4010 Halle, DDR

Received October 12, 1988

The classical pyrylium chemistry, based on the high acceptor reactivity of organyl-substituted pyrylium salts, comprises a large variety of synthetically valuable ring-opening and ring-transformation reactions. The pyrylium cation stands for the extreme situation of a singly-perturbed heterobenzenoid ring with a strong electron deficit in positions $2 \equiv 6$ and 4. A very different behaviour could be observed for the newly synthesized dialkylamino-substituted pyrylium salts **1**–**3** as well as for the related γ-pyrones **4**. The ground state of the salts in polymethine-like and the ring-heteroatom acts more as a π-inert bridging fragment. The salts **1**–**3** are more or less resistant to nucleophilic agents and give electrophilic substitutions, a novelty in pyrylium chemistry. The pyrones **4** are extremely reactive as donors. Several pyrylium precursors are also of interest; the reactivity of 2-acyl-1-chloroenamines [$R-CO-CH=C(NR_2)Cl$], readily available from acylketenedichlorides, is mainly determined by the presence of dialkylamino group. Chemical and physical peculiarities of dimethylamine–carbon dioxide complex (DIMCARB), advantageously used as aminolysis agent, are commented.

INTRODUCTION

As was well known for a long time, the pyrylium cation contains an aromatic π-system which is strongly perturbed by the positively charged oxygen. Consequently, pyrylium salts show both a high formation tendency and a high acceptor reactivity. Accordingly, pyrylium salts act as a turntable in various synthetic routes and represent, on the whole, an ideal example for the general significance of heterocycles in organic synthesis.

The main feature of pyrylium chemistry is the large variety of ring-opening and ring-transformation reactions following nucleophilic additions to active sites of the pyrylium cation. As illustrated in Scheme 1, the transfer of the five-carbon ring segment offers an easy access to a host of other hetero- and carbocycles.

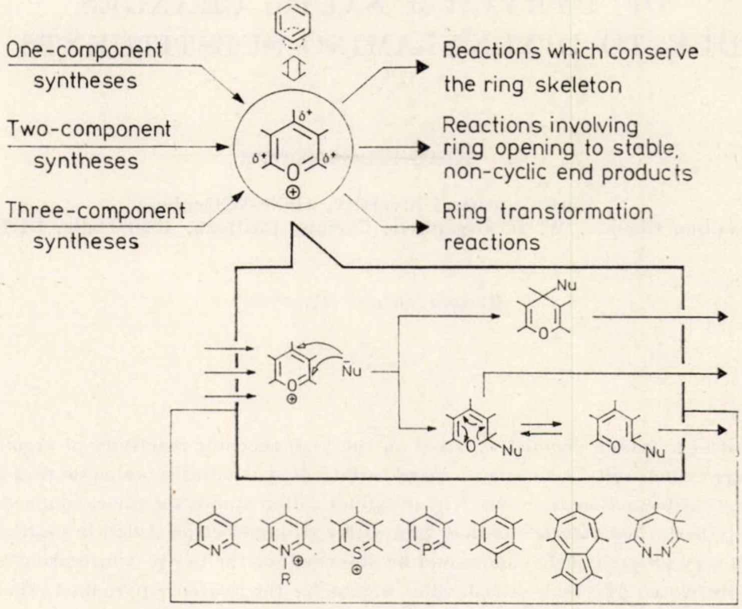
One-component syntheses
Two-component syntheses
Three-component syntheses
δ+
δ+
δ+
O
⊕
Reactions which conserve the ring skeleton
Reactions involving ring opening to stable, non-cyclic end products
Ring transformation reactions
Nu
Nu
Nu
Nu
N
N
R
⊕
S
⊕
P
N–N

Nevertheless, it should be emphasized that the synthetically useful pyrylium salts inevitably contain organyl substituents in the reactive positions 2, 4 and 6. In contrast, the knowledge about pyrylium salts with heterofunctional substituents has remained still very poor.

The traditional pyrylium chemistry reveals another serious limitation. As late as 1982, we had reason enough to make the following statement in our four-country (S. R. Romania, Deutsche DR, USSR, USA) book on pyrylium salts : [1] "Thus pyrylium salts give *no electrophilic substitution*, but only addition of nucleophiles (as primary reaction step)". Now, the time has come to put a question mark to this statement in view of the changes in pyrylium salt chemistry brought about by heterofunctional substituents. A comparison with benzenoid-aromatic series is appropriate. Effenberg's basic studies demonstrated the activation by donor substituents in 1,3,5-tris(dialkylamino)benzenes. The question arose whether the same substituents in cationic heterocycles would be able to produce comparable effects and to compensate the notorious π-electron-deficiency of these heterocycles. Such structures are pyrylium and thiopyrylium salts with dialkylamino groups in the 2-, 4-, and 6-positions, as represented by formulas **1**, **2** and **3**; γ-pyrones and γ-thiopyrones of type **4** are to be mentioned as well. A final remark concerns the 2- and 4-dialkylamino-pyrylium salts **5** and **6**, respectively, which display, as already known, pyrylium-like properties.

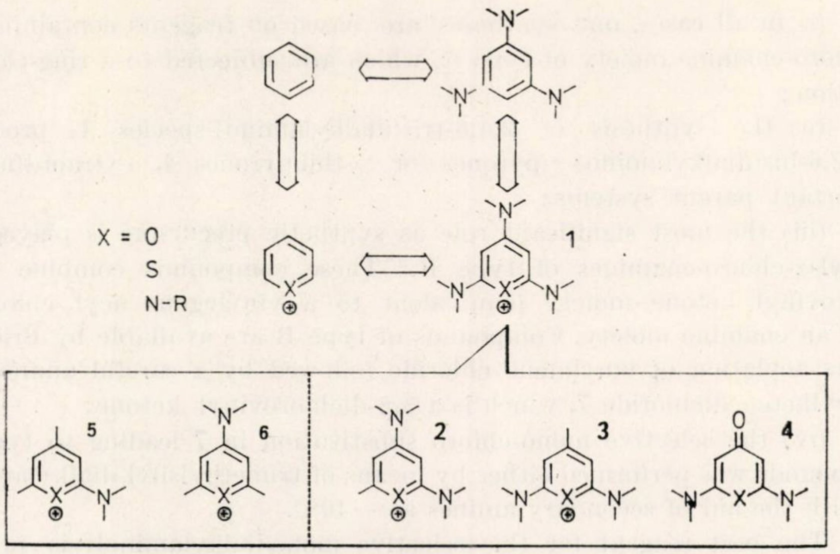
X = O
S
N-R
1
2
3
4
5
6

SYNTHESIS AND ELECTROPHILIC SUBSTITUTIONS IN POLY(DIALKYLAMINO) PYRYLIUM SALTS

Several synthetic principles and tools used in the preparation of poly-dialkylamino-substituted pyrylium salts [2] are outlined in Scheme 2:

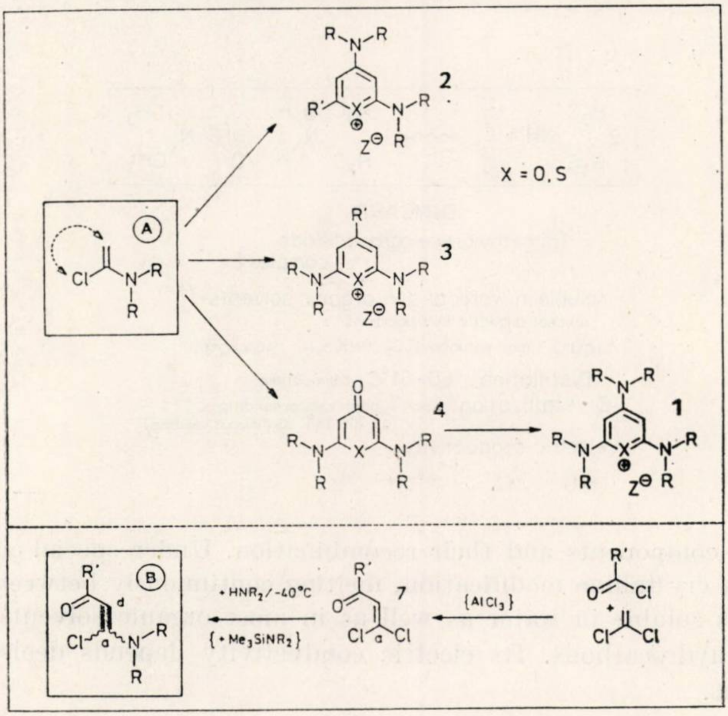
2
X = O, S
A
3
4
1
B
d
a
7
+ HNR₂ / -40°C
{+ Me₃SiNR₂}
{AlCl₃}

(i) in all cases, our syntheses are based on reagents containing an α-chloro-enamine moiety of type A, which are subjected to a ring-closure reaction ;

(ii) the synthesis of 2,4,6-tris(dialkylamino)-species **1** proceeds *via* 2,6-bis(dialkylamino)-γ-pyrones or γ-thiopyrones **4,** extraordinarily important parent systems ;

(iii) the most significant role as synthetic precursors is played by β-acyl-α-chloro-enamines of type B.[3] These compounds combine a β-chlorovinyl ketone moiety (equivalent to a vinylogous acyl chloride) with an enamine moiety. Compounds of type B are available by Friedel-Crafts acylation of vinylidene chloride followed by a careful aminolysis of acylketenedichloride **7,** which is a β,β-dichlorovinyl ketone;

(iv) the selective mono-chloro substitution in **7** leading to type B compounds was performed either by means of trimethylsilyl-dialkylamines or with the aid of secondary amines at −40°C.

The best reagent for this selective monodialkylaminolysis proved to be the dimethylamine—carbon dioxide complex, DIMCARB for short, easily prepared from gaseous dimethylamine and carbon dioxide in a simple one-pot operation. Formally a salt (dimethylammonium-dimethylcarbamate), DIMCARB presents unusual properties. At ambient temperature it exists as a liquid. It is distillable at 60°, with intermediate thermolysis into components and their recombination. Under special condition one gets a crystalline modification, melting continuously between 20 and 35°C. It is soluble in water as well as in most organic solvents, except aliphatic hydrocarbons. Its electric conductivity depends decisively on the solvent.

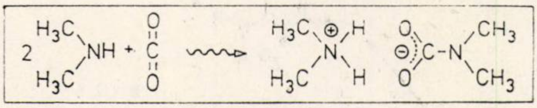

DIMCARB
{dimethylamine carbondioxide complex}

soluble in water and in organic solvents
(except aliphatic hydrocarbons)
Liquid (bond enthalpy [$CO_2/HN(CH_3)_2$]: 40 kJ/mol)
Distillation: 60-61°C, combustible
Crystallization, in part (under special conditions, at 20-35°C continuous melting)
electric conductivity

All these facts suggest a dynamic equilibrium between different tructures,[4] as displayed in Scheme 3 :

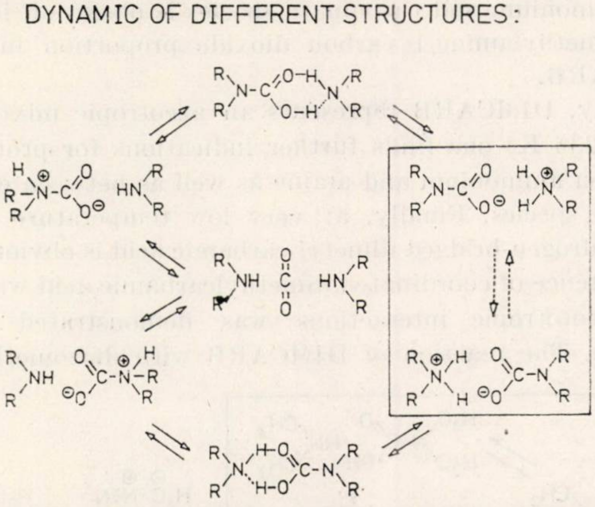

The ^1H-, ^{13}C- and ^{15}N-NMR spectra of DIMCARB are also proofs or the existence of such equilibria. The ^1H-NMR spectra of DIMCARB t several temperatures are presented in Fig. 1. The ambient temperature

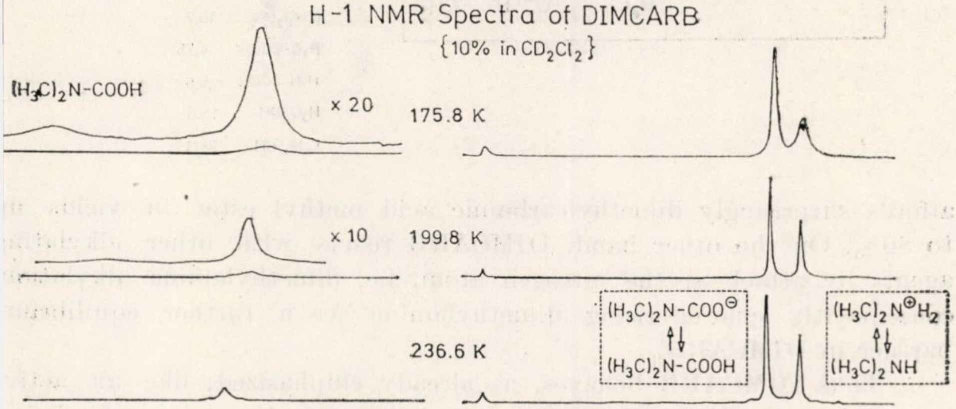

Fig. 1. — Variable-temperature ^1H—NMR spectra of DIMCARB.

spectrum (at the bottom) displays one signal for both ammonium and carbamate species. At lower temperature (262 K), a splitting into separat signals for ammonium and carbamate species is observed, in a ratio indicating 1.8 dimethylamine/1 carbon dioxide proportion in the distille liquid DIMCARB.

Obviously, DIMCARB represents an azeotropic mixture. At lowe temperature (236 K) one finds further indications for prototropic interactions between ammonium and amine as well as between carbamate an carbamic acid species. Finally, at very low temperature (175.8 K) th presence of hydrogen-bridged dimetyl-carbamic acid is obviously indicated

The existence of coordinated dimethylcarbamic acid within and equilibrium of prototropic interactions was demonstrated by chemica means as well. The reaction of DIMCARB with diazomethane in ethe

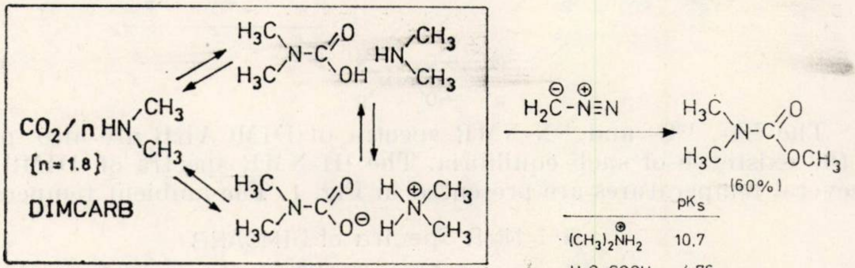

	pK$_s$
$(CH_3)_2\overset{\oplus}{N}H_2$	10.7
$H_3C-COOH$	4.76
$H_2N-COOH$	~5.6
H_3C-OH	15.5
C_6H_5-OH	9-11

affords surprisingly dimethylcarbamic acid methyl ester in yields u to 80%. On the other hand, DIMCARB reacts with other alkylatin agents by attack at the nitrogen atom, i.e. dimethylamine alkylation consequently characterising dimethylamine as a further equilibriun partner in DIMCARB.

Thus DIMCARB behaves, as already emphasized, like an activ dimethylamine. It is indeed the dimethylaminolysis reagent of choice because it can be kept and handled like all other liquid secondary amine such as diethylamine, pyrrolidine, morpholine, and so on. Moreover, i can be used as a refluxing solvent, too. Scheme 4 presents selected examples of preparations using DIMCARB as dimethylaminolysis reagent We call attention to the smooth selective aminolysis of phosgene leadin to dimethylcarbamoyl chloride (pathway 6), to the Willgerodt-Kindle reaction[5] (pathway 9 ; to note that this reaction normally requires highe boiling secondary amines, such as morpholine) and finally to the alread mentioned monoaminolysis of acylketene-dichlorides leading to β-acyl-

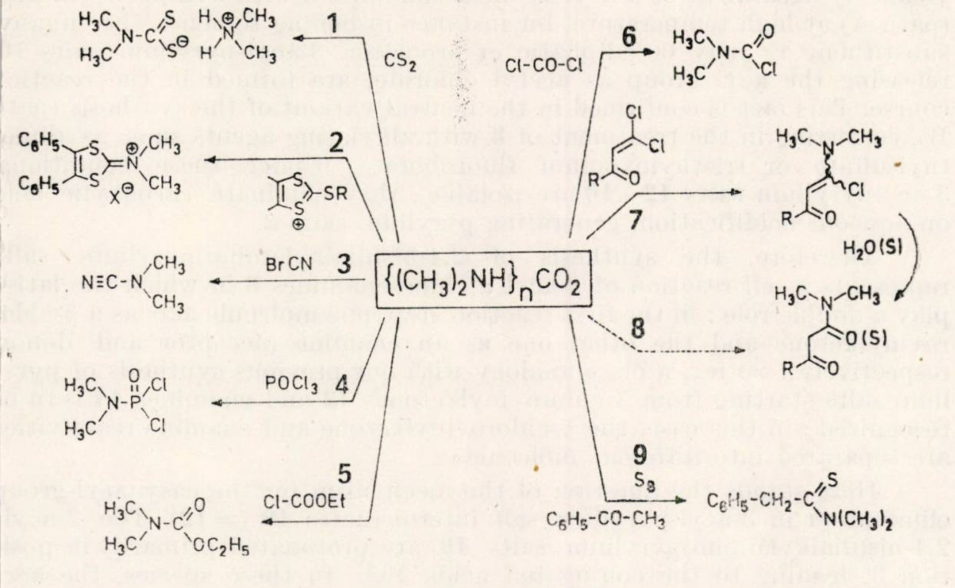
1
CS_2
2
3
BrCN
4
$POCl_3$
5
Cl-COOEt
$\{(CH_3)_2NH\}_n CO_2$
6
Cl-CO-Cl
7
$H_2O(S)$
8
9
S_8
C_6H_5-CO-CH_3

β-chloroenamines (pathway 7). The latter may be easily transformed by reaction with water or hydrogen sulfide into β-keto- or β-thioketo-dimethylamides; aminolysis and hydrolysis may be effected as one-pot operations (pathway 8).

Synthesis of 2,4-bis(dialkylamino)pyrylium salts **2** (Scheme 5). This synthesis was performed amazingly smoothly and usually in good

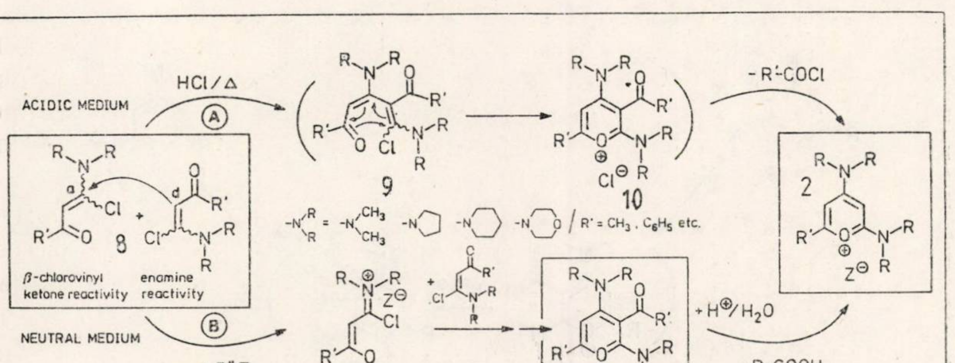
ACIDIC MEDIUM
HCl / Δ
A
9
10
- R'-COCl
2
a
d
8
β-chlorovinyl ketone reactivity
enamine reactivity
R' = CH_3, C_6H_5 etc.
NEUTRAL MEDIUM
B
+ R"-Z
$\{(CH_3)_2SO_4, (C_2H_5)_3OBF_4\}$
11
12
+ $H^{\oplus}$/ H_2O
-R-COOH
13
14
15
16
17
$H^{\oplus}Z^{\ominus}$
- HN
β-chlorovinyl ketone / enamine

yields by treatment of β-acyl-α-chloroenamines **8** with hydrogen chlorid (path A) at high temperature, for instance in boiling toluene. The organy substituent R′ may be aliphatic or aromatic. 3-acyl-pyrylium salts **1** releasing the acyl group as acetyl chloride, are formed in the reactio course. This fact is confirmed in the neutral variant of the synthesis (pat B), consisting in the treatment of **8** with alkylating agents such as dimethylsulfate or triethyloxonium fluoroborate. Under these conditions 3-acylpyrylium salts **12**—**10** are isolable ; they eliminate carboxylic aci on aqueous acidification, generating pyrylium salts **2**.

Therefore, the synthesis of 2,4-bis(dialkylamino)pyrylium salt represents a self-reaction of β-acyl-α-chloroenamines **8** in which the latte play a double role : in the first reaction step, one molecule acts as a β-chlorovinylketone and the other one as an enamine (acceptor and donor respectively). So far, a close analogy with our previous synthesis of pyrylium salts starting from β-chlorovinylketones **13** and enamines **14** is to b recognized ; in this case, the β-chlorovinylketone and enamine reactivitie are separated into different molecules.

Here stands the question of the mechanism for the easy acyl-grou elimination in 3-acyl-pyrylium salt intermediates **10** (=**12**). The 3-acyl-2,4-bis(dialkylamino)pyrylium salts **10** are protonated primarily in position 3, leading to the conjugated acids **10A**. In these species, the ary group is released in coherence with an attack of the nucleophile Y, the driving force being the generation of the 2,4-bis(dialkylamino)pyrylium salt **2**. On the whole, this reaction path represents a protolytic displacement, in other words, an electrophilic substitution of the acyl group, a statement to be returned to, later.

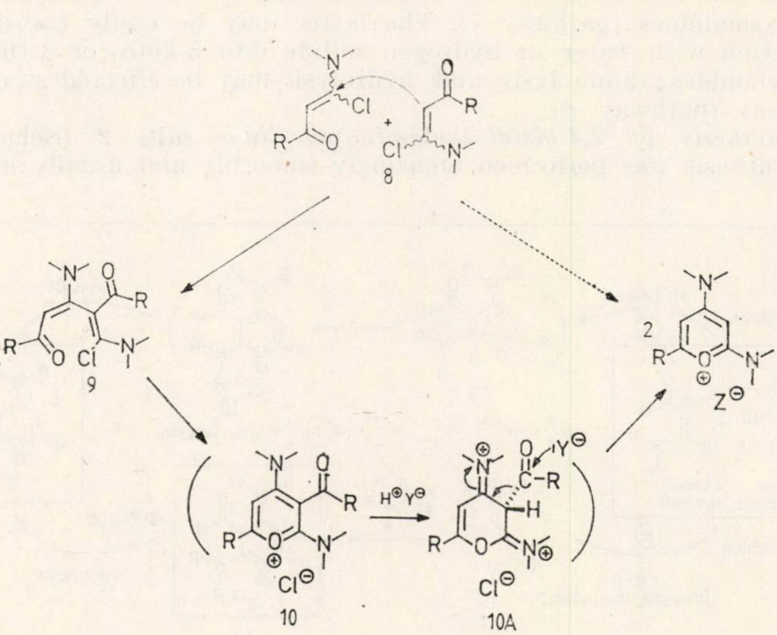

The donor-reactivity, consequently the ability of proton-addition in position 3, is revealed by UV as well as NMR spectroscopical findings (see Fig. 2). In concentrated perchloric acid, the character of the UV-absorption is dramatically changed. The ^{13}C-NMR analysis also proved the preference of the ring-position 3 for proton-addition. The signal at 79.4 ppm for carbon 3 in cation **A** disappeared on protonation and a new signal was obtained at 30.4 ppm, corresponding to carbon 3 in dication **B**; the signal for carbon 5 remained more or less unchanged. Furthermore the chemical shift of carbon 3 in cation **A** compared with that of carbon 5 indicated position 3 as a relatively electron-rich site.

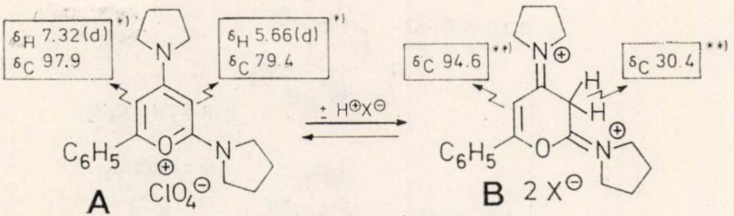

*) in DMSO-d_6

**) in 75% H_2SO_4

λ_{max} (log ε)	
H_2O	$HClO_4$ [70%]
298 (4.26)	350 (4.38) nm
261 (4.66)	269 (3.91) nm

Fig. 2. — ^{1}H— and ^{13}C—NMR chemical shifts and UV data of **A** and dication **B**.

The proton-addition in position 3 points, in principle, to the possibility of electrophilic substitution in this position. Indeed, this fundamental deviation from the traditional pyrylium chemistry has been confirmed experimentally.

Electrophilic substitution in 2,4-bis(dialkylamino)pyrylium salts 2

Several examples of electrophilic substitutions in position 3 of 2,4-bis(dialkylamino)pyrylium salts **2** are presented in Scheme 6. The deuterium exchange (**2** → **18**) is straightforward. The nitration proceeded under very mild conditions leading to the 3-nitro compound **19**. The reaction with Vilsmeier reagent afforded iminium salt **20**; the attempted hydrolysis of **20** regenerated the starting pyrylium salt **2** by a protolytic displacement of the whole formiminium group. With cyanogen bromide under Friedel-Crafts conditions and at low temperatures, the 3-cyano salt **21** was obtained. The structure of the 3-cyanoderivative **21** was unequivocally confirmed by an independent synthesis starting from cyanoacetic acid pyrrolidide **24**, with a final ring-closure step (**25** → **21**) performed under acidic conditions.

The cyanopyrylium salt **21** could be converted into 3-cyanopyridine **22** with ammonia at 20°C. This ring-transformation reaction, in accordance with the notorious behaviour of "normal" pyrylium salts, is to be kept in mind. We have good reason to admit that this is due to the presence of the cyano group, compensating for the donor-active influence of the amino groups. Otherwise, all attempts to transform the 2,4-bis(dialkylamino) pyrylium salts **2** into the corresponding pyridines **27** failed, even

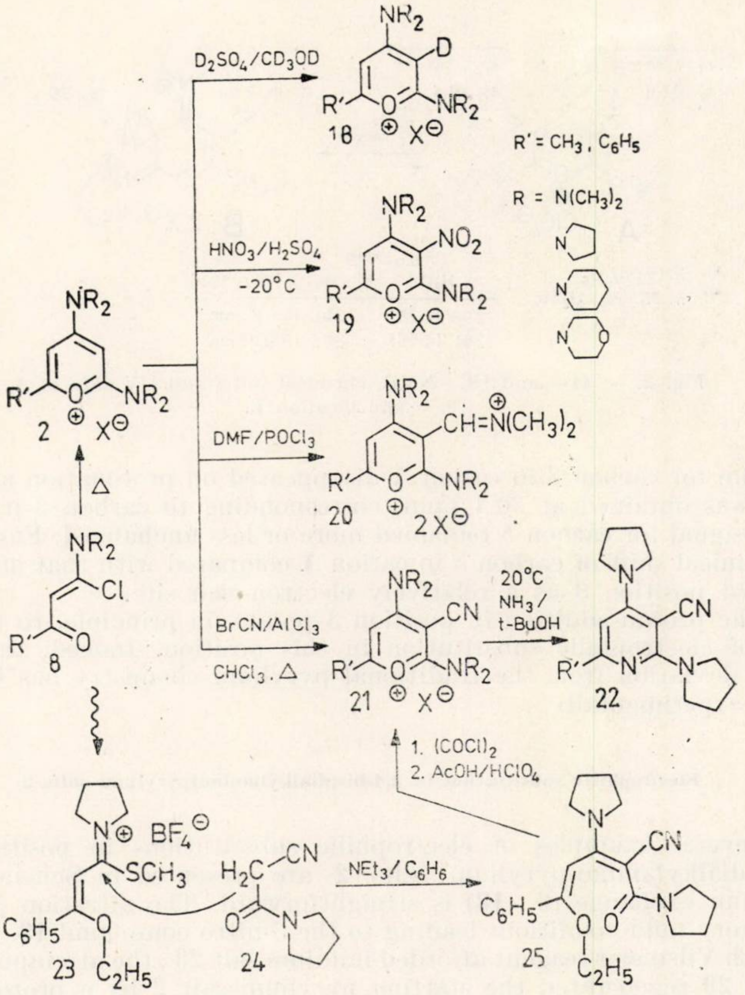

D_2SO_4/CD_3OD
18
HNO_3/H_2SO_4
-20°C
19
DMF/POCl$_3$
20
2 X$^\ominus$
BrCN/AlCl$_3$
CHCl$_3$. Δ
21
20°C
NH$_3$/
t-BuOH
22
R' = CH$_3$, C$_6$H$_5$
R = N(CH$_3$)$_2$
2
Δ
8
1. (COCl)$_2$
2. AcOH/HClO$_4$
BF$_4^\ominus$
SCH$_3$
NEt$_3$/C$_6$H$_6$
23
24
25

with molten urea (see Scheme 7). Only in concentrated aqueous sodium hydroxide solution did the ring-opening succeed, giving the enolate sodium salt **26**. This, however, regenerated the pyrylium salt **2** on dilution in the presence of sodium perchlorate (Scheme 7).

To sum up, these findings allow the statement that nucleophilic attack has no, or at most very limited chances, at 2,4-bis(dialkylamino) pyrylium salts, and this is the second fundamental anomaly compared with the conventional pyrylium chemistry.

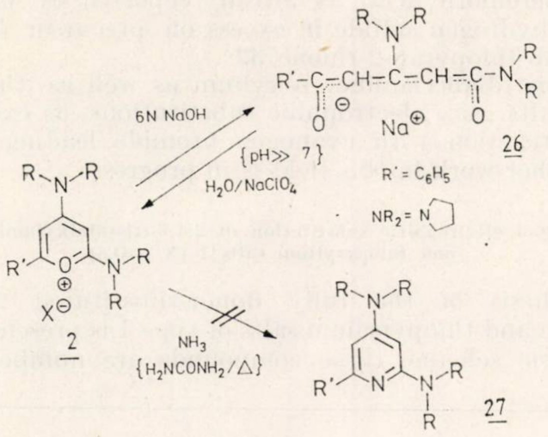
6N NaOH
{pH>> 7}
H₂O/NaClO₄
26
R' = C₆H₅
NR₂ = N
2
NH₃
{H₂NCONH₂/Δ}
27

Synthesis and electrophilic substitution of 2,6-bis(dialkylamino)pyrylium and thiopyrylium salts 3 X(O,S) (Scheme 8)

The synthesis of 2,6-bis (dialkylamino) pyrylium and thiopyrylium salts is based on H. G. Viehe's previous work. The key-precursor of the synthesis is 1,5-dichloro-tetramethylpentamethinium chloride **30** obtained

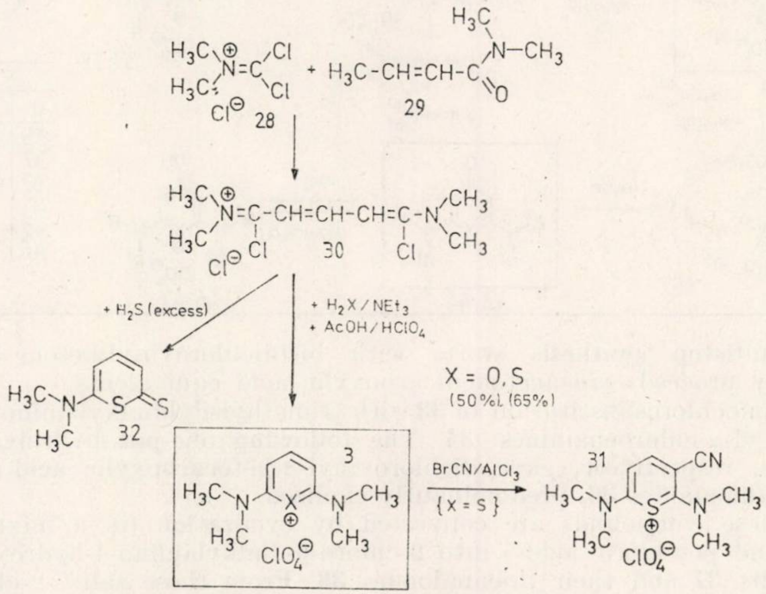
28
29
30
+ H₂S (excess)
+ H₂X / NEt₃
+ AcOH / HClO₄
X = O, S
(50%), (65%)
32
3
BrCN/AlCl₃
{X = S}
31

from the reaction of Viehe's salt **28** with N,N-dimethylcrotonamide **29.** This precursor **30** offers the access to both 2,6-bis(dimethylamino)pyrylium and thiopyrylium salts (**3,** X = O and S, respectively). The preparation was performed by careful mono-hydrolysis or mono-thiolysis, respectively, in the presence of a base, followed by treatment with a mixture of acetic and perchloric acid. As already reported by Viehe and others the action of hydrogen sulfide in excess on precursor **30** gives rise t 6-dimethylamino-thiopyran-2-thione **32**.

The 2,6-bis (dialkylamino) pyrylium as well as the correspondin thiopyrylium salts gave electrophilic substitutions, as exemplified by th Friedel-Crafts reaction with cyanogen bromide leading to 3-cyanoderivative **31**. Further work in this field is in progress.

Synthesis and electrophilic substitution of 2,4,6-tris(dialkylamino)pyrylium and thiopyrylium salts 1 (X = O,S)

The synthesis of the fully donor-substituted 2,4,6-tris(dialkylamino)pyrylium and thiopyrylium salts of type **1** is presented in Scheme (in the synthetic scheme, these compounds are numbered **41** and **42**)

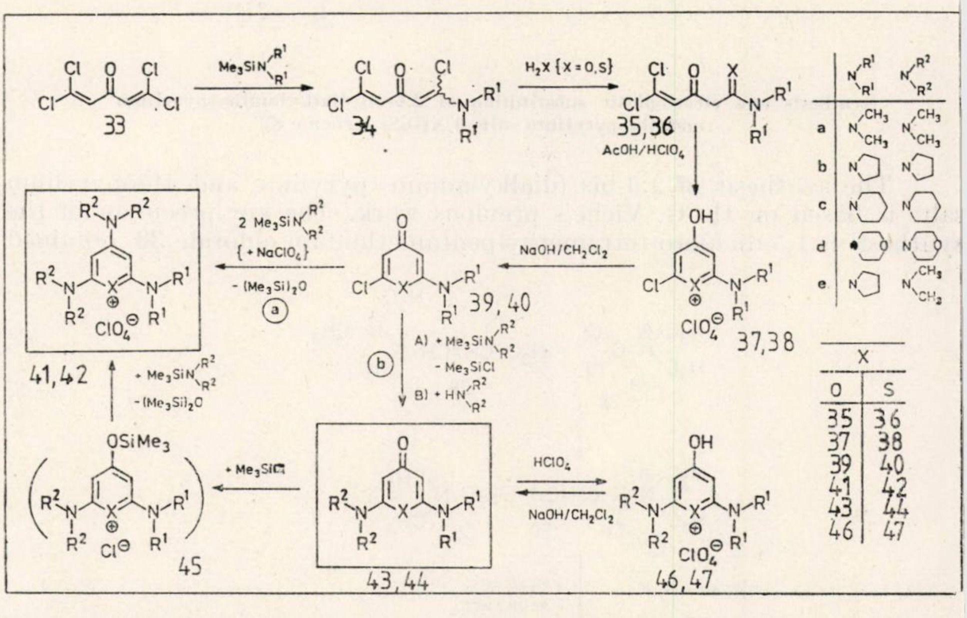
33
Me₃SiN(R¹)₂
34
H₂X {X = O,S}
35,36
AcOH/HClO₄
NaOH/CH₂Cl₂
37,38
39, 40
2 Me₃SiN(R²)₂
{+ NaClO₄}
- (Me₃Si)₂O
ⓐ
ⓑ
A) + Me₃SiN(R²)₂
- Me₃SiCl
B) + HN(R²)₂
41,42
+ Me₃SiN(R²)₂
- (Me₃Si)₂O
+ Me₃SiCl
HClO₄
NaOH/CH₂Cl₂
45
43,44
46,47
a
b
c
d
e
X
O S
35 36
37 38
39 40
41 42
43 44
46 47

This multistep synthesis starts with bis(dichlorovinyl)ketone **33** and generally proceeds *via* acetonedicarboxylic acid equivalents.

Monochlorosubstitution of **33** with trimethylsilyldialkylamines yielded β-acyl-α-chloroenamines **34**. The following one-pot hydrolysis and thiolysis, respectively, gave dichlorovinyl-β-ketocarboxylic acid amides **35** and thioamides **36**, predominantly enolized.

These compounds are converted by cyclization (in a mixture of acetic and perchloric acids) into 2-chloro-6-dialkylamino-4-hydroxypyrylium salts **37** and their thioanalogues **38**. From these salts, 2-chloro-6-dialkylamino-γ-pyrones **39** and γ-thiopyrones **40** were liberated under basic conditions.

Reaction on compounds **39** and **40** with an excess of trimethylsilyldialkylamines afforded immediately 2,4,6-tris(dialkylamino)pyrylium salts **41** and thiopyrylium salts **42**, readily precipitated with sodium perchlorate in basic medium (pH about 12 till 13). Here again, the preparation of a (thio) pyrylium salt in alkaline medium contrasts with the experience in the field of normal pyrylium salts.

The two-fold amino group transfer, leading directly from γ-pyrones **39** and **40** to salts **41** and **42**, obviously involves 2,6-bis(dialkylamino)-γ-pyrones **43** and γ-thiopyrones **44** in the primary step. The ***in-situ*** generated trimethylsilyl chloride produces O-silylation to 4-trimethylsilyloxy-salts **45**, this formation of final products **41** and **42** releasing hexamethylsiloxane. The release of hexamethylsiloxane seems to be the driving force of the whole reaction sequence. Actually, γ-pyrones **43**, obtained from **39** and one molar equivalent of trimethylsilyl-dialkylamine, reacted successively with trimethylsilyl chloride and trimethylsilyl-dialkylamine to form the same pyrylium salts **41**. Moreover, γ-pyrones **43** and γ-thiopyrones **44** may be obtained by aminolysis of **39** and **40** with secondary amines and isolated *via* alkaline decomposition of their hydroperchlorates **46** and **47**, previously precipitated in acidic medium.

As already mentioned in the introduction, special attention should be paid to 2,6-bis(dialkylamino)-γ-pyrones and γ-thiopyrones of type **4** (X = O,S). These structures are not only γ-(thio)pyrones, but also two-sided vinylogous ureas bonded by a heteroatom. Thus, they should display a highly donor-activated reactivity of their carbonyl-oxygen. Several significant data in this respect are presented in Fig. 3.

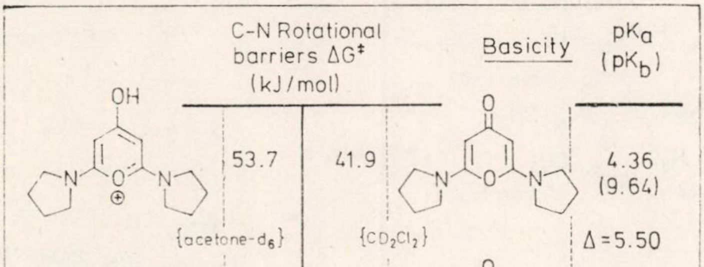

Fig. 3. — $\mathrm{pK_a}$ or $\mathrm{pK_b}$ Values and rotational barriers of 4- thio) pyrones and corresponding rotation barriers of the respective conjugate acids i.e. thio) pyrylium salts.

The pK_a-values in **4** are significantly enhanced in comparison with unsubstituted γ-pyrones, indicating a dramatically increased basicity. The difference in the case of 2,6-dipyrrolidino-γ-pyrone and its thioanalogue is as high as 6 pH units, meaning that the protonation to the corresponding 4-hydroxypyrylium salt and its thioanalogue should be favoured by about 35 kJ/mole.

Rotational barriers of dialkylamino groups in **4** are expected to be in the range of those for vinylogous dialkylamides. The rotational barriers are, of course, distinctly increased after protonation to the 4-hydroxypyrylium salts and their thioanalogues.[6]

Last but not least, the enhanced reactivity of 2,6-bis(dialkylamino)-γ-pyrones and thioanalogues is expressed in their ready acylation to isolable 4-acyloxy-pyrylium salts and corresponding thiopyrylium salts. These compounds are useful acyl-transfer reagents. This part of our work is still in progress.

The 2,4,6-tris(dialkylamino)pyrylium salts and their thioanalogues are very sensitive towards electrophilic agents. For instance, the tris(dimethylamino) pyrylium salt **48**(X=O) is smoothly nitrated already at — 40°C, forming the fully heterofunctionalized pyrylium salt **49** (see Scheme 10). This compound can explode under rapid mechanical shock.

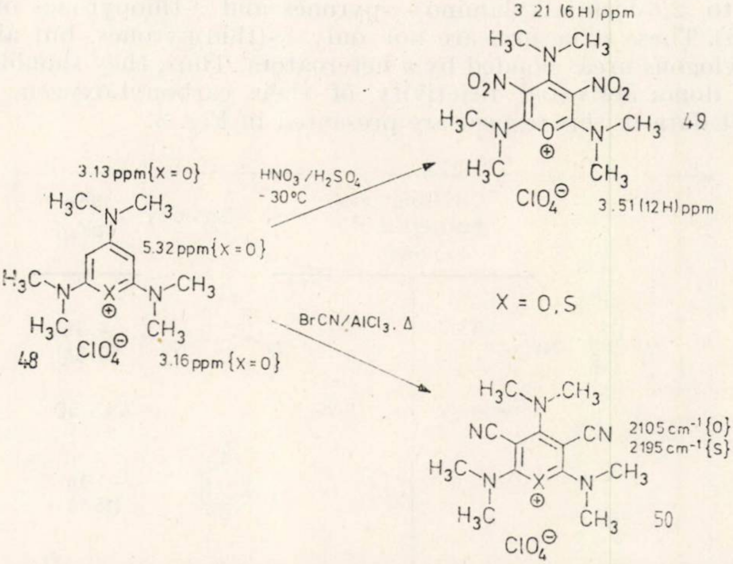

Pyrylium salt **48** (X=O) and its thioanalogue **48** (X=S) reacted with cyanogen bromide under Friedel-Crafts conditions, leading to 3,5-dicyano-pyrylium sal **50** (X=O) and its thioanalogue **50** (X=S).

Conversely, tris(dialkylamino)pyrylium salts of type **1** are relatively stable towards nucleophilic attack. As already mentioned, their perchlorates are formed in alkaline medium, a fact which would be an absolute impossibility in the series of normal pyrylium salts.

The main question is how far these poly-donor-substituted pyrylium salts represent true pyrylium salts.

On one hand, these structures may be considered over-compensated π-deficient systems. On the other hand, an electronic cooperativity between dialkylamino groups has to be taken into account. This means that these cyclic systems may be better described as bridged polymethinium salts, namely tri- and pentamethinium salts, as depicted in Scheme 11. The main physico-chemical arguments for this statement are the following :

(i) the NMR-chemical shifts and the rotational barriers of the hindered amino-group rotation, as stated in our very extended NMR studies ;

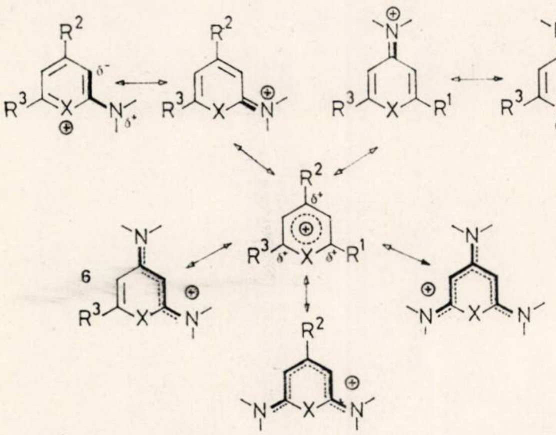

(ii) the different bond-lengths, as elucidated by X-ray analysis of 2,4-dipyrrolidino-6-phenylpyrylium tetraphenylborate ;

(iii) the chemical behaviour : electrophilic substitutions are already well-known in the polymethinium series.

The reply to this question is reminiscent of the situation where we are asked about the meaning of an expressionistic painting : beauty is in the eye of the beholder.

ACKNOWLEDGEMENTS. Thanks are expressed to Dr. R. Spitzner, Mrs. K. Ziemann, Mr. U. Andersch for skilful synthetic contributions, to Doz. H.D. Schädler for theoretical discussions, to Professors E. Kleinpeter and R. Radeglia for NMR investigations, and to Dr. John C. Barnes from the Dundee University in Scotland for X-ray investigations.

REFERENCES

[1] A. T. Balaban, A. Dinculescu, G. N. Dorofeenko, G. W. Fischer, A. V. Koblik, V. V. Mezheritskii and W.Schroth, "Pyrylium Salts. Syntheses, Reactions and Physical Properties", Adv. Heterocyclic Chem., Suppl. Vol. 2, A. R. Katritzky Editor, Academic Press, New York, 1982.

[2] W. Schroth and R. Spitzner, *Tetrahedron Letters*, **26**, 3963 (1985) ; R. Spitzner, R. Radeglia and W. Schroth, *Tetrahedron Letters*, **26**, 3967 (1985) ; W. Schroth, R. Spitzner and E. Kleinpeter, *Tetrahedron Letters*, in press.

[3] W. Schroth, R. Spitzner and S. Hugo, *Synthesis*, **1982**, 199 ; W. Schroth, *Khim. Geterotsikl. Soedin.*, **1985**, 1587 ; W. Schroth and R. Spitzner, *Monatsh. Chem.*, **118**, 1263 (1987) ; R. Spitzner, S. Freitag and W. Schroth, *Monatsh Chem.*, **118**, 1383 (1987) ; W. Schroth, M. Richter, B. Dobner, R. Spitzner and S. Freitag, *Monatsh. Chem.*, **119**, 463 (1988).

[4] R. Radeglia, J. Andersch and W. Schroth, *Z. Naturforsch. B*, in press ; W. Schroth, H.D. Schädler and J. Andersch, *Z. Chem.*, in press.

[5] W. Schroth and J. Andersch, *Synthesis*, in press.

[6] E. Kleinpeter, R. Spitzner and W. Schroth, *Magn. Reson. Chem.*, **25**, 688 (1987) ; E. Kleinpeter, R. Spitzner, W. Schroth, K. Philaja and J. Mattinen, *Magn. Reson. Chem.*, **26**, 707 (1988) ; E. Kleinpeter and R. Spitzner, *Z. Chem.*, **28**, 306 (1988).

Revue Roumaine de Chimie, **34**, *1*, 287–295 (1989)

BASIC VERSATILE PROGRAM FOR NONISOTHERMAL KINETICS

E. SEGAL and T. COSEAC
Polytechnic Institute of Bucharest, Faculty of Chemical Technology,
Department of Physical Chemistry and Electrochemical Technology,
Blvd Republicii 13, Bucharest, Romania

Received July 24, 1988

The authors present a BASIC program for automatic data processing in nonisothermal kinetics according to six methods.

This paper deals with a versatile program to process experimental data for nonisothermal kinetics. The program uses the following methods based on equations which can be brought to linear forms :

1. Kissinger's method, based on the equation[1] :

$$\frac{\mathrm{d}\ln\dfrac{a}{T_{\max}^2}}{\mathrm{d}\left(\dfrac{1}{T_{\max}}\right)} = -\frac{E}{R} \tag{1}$$

where a stands for the heating rate, $T_{\max}$ — for the temperature corresponding to the maximum reaction rate, E — for the activation energy, and R — for the universal gas-constant ($R = 1.986$ cal/mol. K). From the slope of the linear plot $\ln a/T_{\max}^2$, $1/T_{\max}$ the value of the activation energy can be obtained.

2. Freeman-Carroll's method, based on the equation[2] :

$$\frac{\ln\dfrac{\mathrm{d}\alpha}{\mathrm{d}t}}{\ln(1-\alpha)} = n - \frac{E\,\Delta\left(\dfrac{1}{\mathrm{T}}\right)}{R\,\Delta\ln(1-\alpha)} \tag{2}$$

where α is the degree of conversion, $\dfrac{\mathrm{d}\alpha}{\mathrm{d}t}$ express the reaction rate, n is the reaction order, E — the activation energy, T — the temperature K) and Δ a difference between two-values operator. From the intercept and slope of the linear plot $\dfrac{\Delta\ln\dfrac{\mathrm{d}\alpha}{\mathrm{d}t}}{\Delta\ln(1-\alpha)}$, $\dfrac{\Delta\left(\dfrac{1}{T}\right)}{\Delta\ln(1-\alpha)}$ the values of the reaction order and activation energy can be obtained. As far as the preexponential factor is concerned, its value is calculated accordin to the formula [3]:

$$A(\mathrm{s}^{-1}) = \frac{\dfrac{\Delta\alpha}{\Delta t}}{(1-\alpha_i)}\,\mathrm{e}^{\frac{E}{1.986\,T_i}} \qquad (3$$

where

$$\frac{\Delta\alpha}{\Delta t} = \frac{\alpha_{i+1}-\alpha_i}{t_{i+1}-t_i}$$

is obtained from two points of the *TG* curve $P_i(\alpha_i,\ T_i,\ t_i)$ and $P_{i+1}(\alpha_{i+1}$ $T_{i+1},\ t_{i+1})$ obtained at temperatures T_i and T_{i+1}(K) which are reache at the moments t and t_{i+1}.

3. Coats-Redfern's method based on the equation [4]:

$$\ln\frac{F(\alpha)}{T^2} = \ln\frac{AR}{aE}\left(1-\frac{2RT}{E}\right)-\frac{E}{RT} \qquad (4$$

where $F(\alpha)$ is the integral conversion function given by:

$$F(\alpha) = \frac{1-(1-\alpha)^{1-n}}{1-n} \text{ for } n \neq 1 \qquad (5$$

$$F(\alpha) = -\ln(1-\alpha) \text{ for } n = 1$$

the other notations having known meanings. The program chooses th optimum value of n corresponding to the maximum absolute value o the correlation coefficient r for the linear plot $\ln\dfrac{F(\alpha)}{T^2},\ \dfrac{1}{T}$.

The other three methods are based on Flyn-Wall's equation [5]

$$\log F(\alpha) = \lg\frac{AE}{T^2} - \log a - 2.315 - 0.457\,\frac{E}{RT} \qquad (6)$$

with the following variants.

4. For $\alpha = \text{const}$ the slope of the linear plot $\log a,\ \dfrac{1}{T}$, allows to obtain the value of the activation energy.

5. For $a = \text{const}$, from the slope and intercept of the linear plot $\log F(\alpha),\ \dfrac{1}{T}$ the values of the activation energy and preexponential factor, can be obtained. The optimization of the linear plot is performed as previously shown for the Coats-Redfern method.

6. For $T = \text{const}$, the compatibility of the function $F(\alpha)$ can be checked by the linear plot $\log F(\alpha), \log a$ whose slope should be equal to -1.

The flow (logical) diagram of the program given in figure 1 is followed by the program listing.

FLOW DIAGRAM

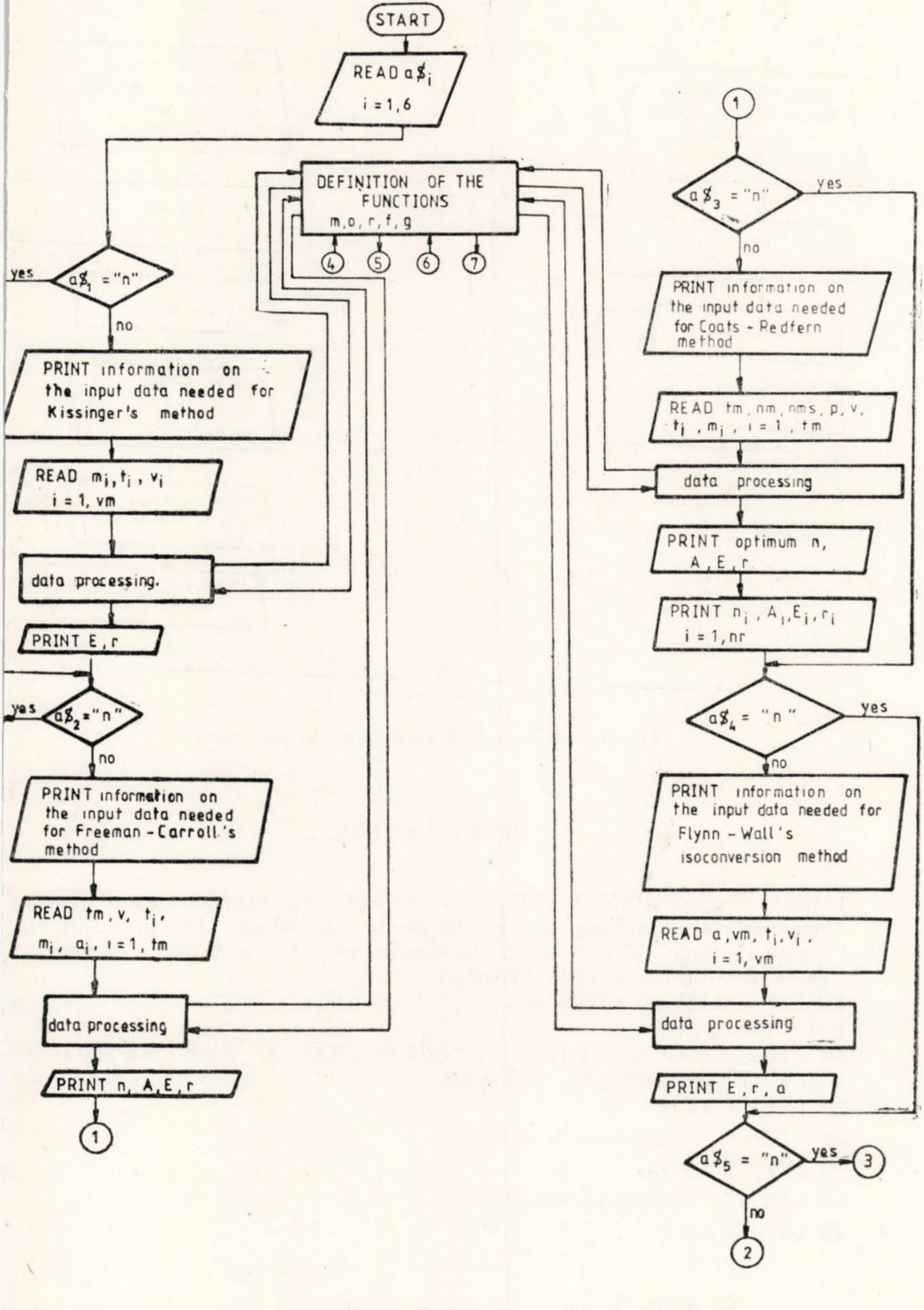
START
READ a$$_i$ i = 1,6
DEFINITION OF THE FUNCTIONS m,o,r,f,g
4
5
6
7
yes
a$$_1$ = "n"
no
PRINT information on the input data needed for Kissinger's method
READ m_i, t_i, v_i i = 1, vm
data processing.
PRINT E, r
yes
a$$_2$ = "n"
no
PRINT information on the input data needed for Freeman - Carroll's method
READ tm, v, t_i, m_i, a_i, i = 1, tm
data processing
PRINT n, A, E, r
1
1
a$$_3$ = "n"
yes
no
PRINT information on the input data needed for Coats - Redfern method
READ tm, nm, nms, p, v, t_i, m_i, i = 1, tm
data processing
PRINT optimum n, A, E, r.
PRINT n_i, A_i, E_i, r_i i = 1, nr
a$$_4$ = "n"
yes
no
PRINT information on the input data needed for Flynn - Wall's isoconversion method
READ a, vm, t_i, v_i, i = 1, vm
data processing
PRINT E, r, a
a$$_5$ = "n"
yes
3
no
2

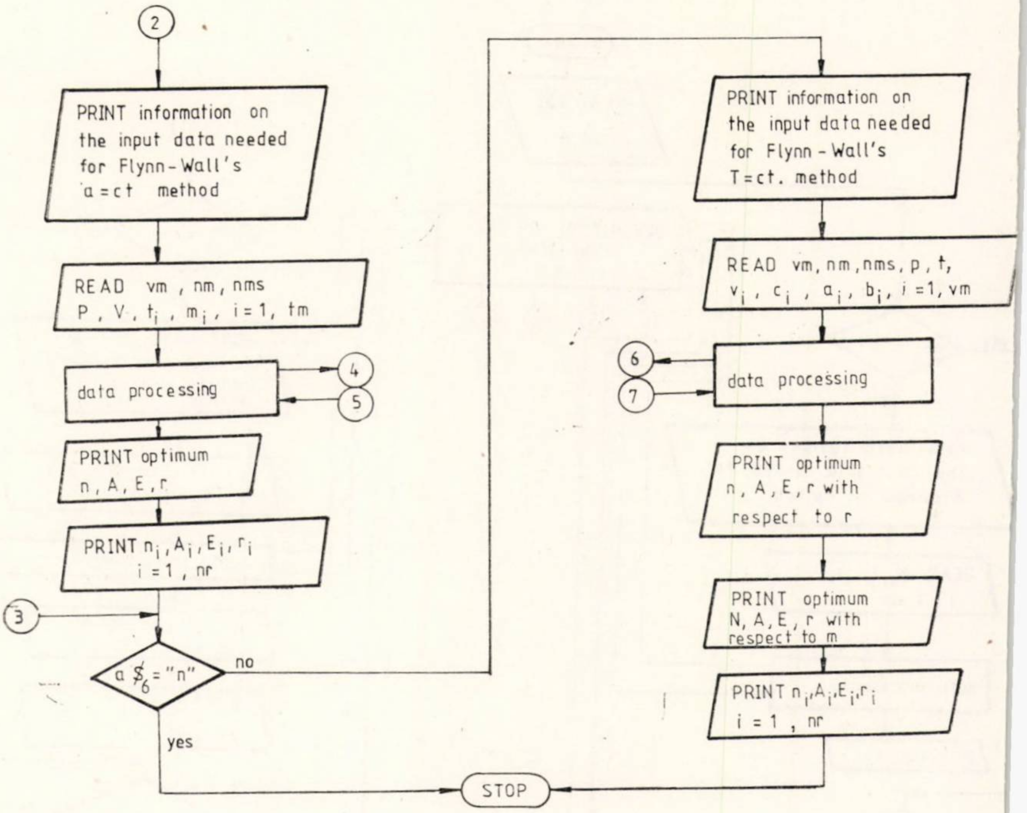
2
PRINT information on the input data needed for Flynn-Wall's a=ct method
READ vm, nm, nms P, V, t_i, m_i, i=1, tm
data processing
4
5
PRINT optimum n, A, E, r
PRINT n_i, A_i, E_i, r_i i=1, nr
3
a $6 = "n"
no
yes
STOP
PRINT information on the input data needed for Flynn-Wall's T=ct. method
READ vm, nm, nms, p, t, v_i, c_i, a_i, b_i, i=1, vm
6
7
data processing
PRINT optimum n, A, E, r with respect to r
PRINT optimum N, A, E, r with respect to m
PRINT n_i, A_i, E_i, r_i i=1, nr

Fig. 1. — Flow (logical) diagram of the program.

PROGRAM LISTING

```
1 REM Program VERSATILE to evaluate the nonisothermal kinetic
  parameters according to the methods: Kissinger, Freeman-Carroll,
  Coats-Redfern, Flynn-Wall, isoconversion, Flynn-Wall, a = const
  (a = heating rate), Flynn-Wall, T = const.
5 CLS : PAPER 7 : INK 0
10 DIM A $ (6)
20 PRINT PAPER 1; INK 7; "SELECTION OF THE METHODS"
  '''PAPER 7; INK 0; "Kissinger?"
30 INPUT a$ (1)
40 PRINT '"Freeman-Carroll?"
50 INPUT a$ (2)
60 PRINT '"Coats-Redfern?"
70 INPUT a$ (3)
```

```
 80 PRINT ' "Flynn-Wall, isoconversion?"
 90 INPUT a$ (4)
100 PRINT ' "Flynn-Wall, a = const?"
110 INPUT a$ (5)
120 PRINT ' "Plynn-Wall, T = const?"
130 INPUT a$ (6)
140 DEF FN m (a, b, c, e, n) = (e—a * c/n)/(b—ABSa ↑ 2/n)
150 DEF FN 0 (a, b, c, e, n) = (b *c — a *e)/(n *b—ABSa ↑ 2)
160 DEF FN r (a, b, c, d, e, n) = (e—a *c/n)/SQR(b—ABSa ↑ 2/n)/
    SQR(d—ABS c ↑ 2/n)
170 DEF FN f (a, n) = (1—(1—a) ↑ (1—n))/(1—n)
190 DEF FN g (a)= — LN(1—a)
200 IF a$ (1) = "n" THEN GO TO 320
210 CLS ; PRINT PAPER 1 ; INK 6 ; "Kissinger" ''' PAPER 7 ; INK 0 ;
    "INPUT DATA :" ' " — number of points" ' "— pairs of values
    (temperature corresponding to maximum reaction rate (°C), heating
    rate)"
220 INPUT vm
230 DIM t (vm) : DIM v (vm)
240 FOR i = 1 TO vm ; PRINT i : INPUT t (i), v (i) : LET t (i) =
    = t (i) + 273 : NEXT i
245 CLS : PRINT AT 10, 5 ; "COMPUTER IS WORKING!"
250 LET S 1 = 0 : LET S2 = 0 : LET S3 = 0 : LET S4 = 0 : LET
    S5 = 0
260 FOR i = 1 TO vm
270 LET x = 1/t (i) : LET y = LN (v(i)/t(i) ↑ 2)
280 LET S1 = S1 + x : LET S2 = S2+x ↑ 2 : LET S3 = S3 + y :
    LET S4 = S4 + ABSy ↑ 2 : LET S5=S5+x *y
290 NEXT i
300 LET e=—1.986 *FNm (S1, S2, S3, S5, vm) :
    LET r=FN r(S1, S2, S3, S4, S5, m) BEEP 1,4 : BEEP 1.5, 0
310 PRINT ''' "E = "; e '' "r = "; r : STOP
320 IF a$ (2) = "n" THEN GO TO 580
330 CLS : PRINT PAPER 1 ; INK 6 ; "Freeman-Carroll" ''' PAPER 7 ;
    INK 0 ; "INPUT DATA :" ' "-number of points" ' "-heating rate"
    ' "values (T, TG, DTG)" ' "Observation :" ' "-first group of values
    should correspond to conversion 0" ' "-last group of values should
    correspond to conversion 1"
340 INPUT tm, v
350 DIM t(tm) : DIM a(tm) : DIM m(tm)
360 FOR i = 1 TO tm : PRINT i : INPUT t(i), m(i), a(i) : LET t(i) =
    = t(i) + 273 : NEXT i
365 CLS : PRINT AT 10, 5 ; "COMPUTER IS WORKING!"
370 LET S1 = 0 : LET S2 = 0 : LET S3 = 0 LET S4=0 : LET S5=0 :
    LET S6 = 0
380 FOR i = 2 TO tm —1
390 LET a1 = (m(i) — m(1))/(m(tm)—m(1))
400 FOR j = i + 1 TO tm—1
430 LET a2 = (m(j) — m(l))/(m(tm) — m(1))
460 LET x = (1/t (j) — 1/t(i))/LN((1—a2)/(1—a1))
```

```
470 LET  y = LN (a(j)/a(i))/LN ((1−a2)/(1−a1))
480 LET  S1 = S1 + x :  LET  S2 = S2+ABSx ↑ 2 :  LET  S3=S3+y :
    LET  S4 = S4+ABS  y ↑ 2 :  LET  S5=S5+x ∗ y :  LET  S6=S6+1
490 NEXT  j
500 NEXT  i
510 LET  n = FN 0 (S1, S2, S3, S5, S6) LET  e = −1.986 ∗ FN  m(S1,
    S2, S3, S5 ; S6) : LET r=FN r (S1, S2, S3, S4, S5, S6) : LET zm=0.
515 BEEP 1,4 : BEEP 1.5, 0
560 PRINT "E="; e, "n="; n, "r="; r
561 FOR  i=1 TO tm−1
562 LET z = v ∗ (m(i + 1) − m(i))/(t(i + 1)−t(i))/(m(tm) −m (1)) ∗ EXP
    (e/1.986/t(i)−40 ∗ LN 10)/((m(tm)−m(i))/(m(tm)−m (1))) ↑ n/60
563 LET zm = zm+z :  NEXT  i
564 LET zm = zm /(tm−1) : PRINT "AE−40="; zm
570 STOP
580 IF a$ (3) = "n" THEN GO TO 860
590 CLS : PRINT PAPER 1;  INK  6;  "Coats-Redfern" ''' PAPER  7;
    INK  0;  "INPUT  DATA :" ' "-number  of  points" '  "- initial  value
    of  n " ' "-final  value  of  n" ' "-step  n" '' "-heating  rate"  / "-pairs
    of values (T, TG)" ' "Observation :" ' "-first  pair  should  correspond
    to  conversion  0" ' "-last  pair  should  correspond  to  conversion  1"
600 INPUT  tm,  nm,  nms,  p,  v
610 LET nr = INT  ((nms−nm)/p+1)
620 DIM t(tm) : DIM m(tm) : DIM e(nr) : DIM z(nr) : DIM r (nr)
630 FOR i = 1 TO tm : PRINT i :  INPUT t(i), m(i) : LET  t(i) = t(i) +
    +273 :  NEXT  i
635 CLS :  PRINT AT 10, 5 ; "COMPUTER IS WORKING!"
640 LET  S6 = tm−2 :  LET  r = 0
650 LET n = nm : LET  j = 0
635 LET  S1=0 :  LET  S2=0 :  LET  S3=0 :  LET  S4=0 :  LET  S5=0
660 FOR i = 2 TO tm−1
670 LET x = 1/t (i) : LET a = (m(i)−m(1))/(m(tm)−m(1))
680 IF ABS (n−1) < 10 ↑ −4  THEN  GO TO 710
700 LET  x = LN (FNf(a, n)/t(i) ↑ 2) : GO TO 730
710 LET  y=LN  (FNg(a)/t(i) ↑ 2)
730 LET   S1=S1+x :   LET   S2=S2+ABSx ↑ 2 :    LET   S3=S3+y :
    LET S4=S4+ABS y ↑ 2 :  LET S5=S5+x ∗ y
740 NEXT  i
750 LET  j=j+1 : LET  e(j)=−1.986 ∗ FN  m(S1,  S2,  S3,  S5,  S6) : LET
    z(j)=e(j) ∗ v ∗ EXP (FN (S1, S2, S3, S5, S6)−40 ∗ LN  10)/1.986/60 :
    LET r(j)=FN r (S1, S2, S3, S4, S5, S6)
760 IF r(j) >r  THEN   GO TO 780
770 LET  e=e(j) : LET  z=z(j) : LET  r=r(j) : LET  no=n
780 LET  n=n+p
790 IF n<=nms+10 ↑ −4 THEN GO TO 655
795 BEEP 1,4 :  BEEP  1.5,0
800 PRINT PAPER  1;  INK 6;  ' "OPTIMUM VALUES :" '  PAPER 7;
    INK  0;  "E ="; e ' "n=", no;  ' "AE−40="; z ' "r="; r
810 STOP
820 CLS :  LET  n = nm−p
```

```
830 FOR i = 1 TO nr : LET n=n+p
840 PRINT PAPER 1 : INK 6; "n=" n ' PAPER 7; INK 0; "E =";
    e(i) ' "AE−20 = "; z(i) ' "r="; r(i); NEXT i
850 STOP
860 IF a$ (4) = "n" THEN GO TO 990
870 CLS : PRINT PAPER 1; INK 6; "Flynn-Wall" ' "isoconversion"
    ''' PAPER 7; INK 0; "INPUT DATA :" ' "-conversion" ' "-number
    of points" ' "-pairs of values (temperature (°C), heating rate)"
880 INPUT a, vm
890 DIM t (vm) : DIM v (vm)
900 FOR i=1 TO vm : PRINT i : INPUT t(i), v(i) : LET t(i) = t(i)+
    +273 : NEXT i
905 CLS : PRINT AT 10, 5; "COMPUTER IS WORKING!"
910 LET S1=0 : LET S2=0 LET S3 = 0 : LET S4 = 0; LET S5 = 0
920 FOR i = 1 TO vm
930 LET x = 1/t(i); LET y = LN v(i)
940 LET S1 = S1 + x : LET S2=S2+ABS x ↑ 2 : LET S3=S3+y :
    LET S4=S4+ABS y ↑ 2 : LET S5=S5+x * y
950 NEXT i
960 LET e = −1.986/1.052 * FN m(S1, S2, S3, S5, vm) : LET r=FN
    r(S1, S2, S3, S4, S5, vm)
965 BEEP 1,6 : BEEP 1.5, 0
970 PRINT ' "E="; e ' "r="; r' "conversion ="; a : STOP
990 IF a$ (5) = "n" THEN GO TO 1290
1000 CLS : PRINT PAPER 1; INK 6; "Flyn-Wall" ' "a = ct." '''
     PAPER 7; INK 0; "INPUT DATA :" ' "-number of points" '
     "- initial valuent n" ' "- final value of n" ' "-step n" ' ,,heating
     rate" ' "- pairs of values (T, TG) " ' "Observation :" ' "- first
     pair should correspond to conversion 0" ' "- last pair should cor-
     respond to conversion 1"
1010 INPUT tm, nm, nms, p, v
1020 LET nr = INT ((nms − nm)/p + 1 )
1030 DIMt (tm) : DIM m(tm) : DIM (e(nr) : DIM z(nr) : DIM r(nr)
1040 FOR i = 1 TO tm : PRINT i : INPUT t(i), m(i) : LET t(i) =
     t(i) + 273 : NEXT i
1045 CLS : PRINT AT 10,5 ; "COMPUTER IS WORKING"
1050 LET S6 = tm − 2 : LET r = 0
1060 LET n = nm : LET j = 0
1065 LET S1 = 0 : LET S2 = 0 : LET S3 = 0 : LET S4 = 0 : LET
     S5 = 0
1070 FOR i = 2 TO tm − 1
1080 LET x = 1/t(i) : LET a = m(i) − m (1))/(m(tm)−m(1))
1090 IF ABS (n−1) < 10 ↑ −4 THEN GO TO 112 0
1110 LET y = LN (FN f (a, n)) : GO TO 114 0
1120 LET y = LN (FN g (a))
1140 LET S1 = S1 + x : LET S2 = S2 + ABSx ↑ 2 : LET S3 =
     = S3 + y : LET S3 = S4 + ABS y ↑ 2 : LET S5 = S5 + x * y
1150 NEXT i
```

```
1160 LET j = j + 1 : LET e(j) = −1.986/1.052 * FN (m (S1, S2, S3,
     S5, S6) : LET z(j) = 1.986/60*v*EXP (FN 0 (S1, S2, S3, S5,
     S6) + 5.33−40*LN 10)/e(j) : LET r(j) = FN r (S1, S2, S3, S4,
     S5, S6)
1180 IF r(j) > r THEN GO TO 1200
1190 LET e = e (j) : LET z = z(j) : LET r = r (j) : LET no = n
1200 LET n = n + p
1210 IF n < nms + 10 ↑ −4 THEN GO TO 1065
1215 BEEP 1,4 : BEEP 1.5, 0
1220 PRINT PAPER 1 ; INK 0 ; ' “OPTIMUM VALUES :” ' PAPER 7 ;
     INK 0 ; “n =”; no ' “E =”; e ' “AE−40 =”; z ' “r =”; r
1230 STOP
1240 CLS : LET n = nm − p
1250 FOR i TO nr : LET n = n+p
1260 PRINT PAPER 1 ; INK 6 ; “n=”; n ' PAPER 7 ; INK 0 ; “E”;
     e(i) ' “AE−20 =”; z(i) ' “r =”; r(i) : NEXT i : STOP
1290 IF a$ (6) = “n” THEN GO TO 1550
1300 CLS : PRINT PAPER 1 ; INK 6 ; “Flynn-Wall” ' “T = ct.” '''
     PAPER 7 ; INK 0 ; “INPUT DATA :” ' “—number of points”
     ' “-initial value of n” ' “-final value of n” ' “-stop n” '“-temperature
     (°C)” ' “-group of values (heating rate, weight of the evolved gas,
     initial weight of the evolved gas which equals zero, final weight
     of the evolved gas corresponding to conversion 1)”
1310 INPUT vm, nm, nms, p, t ; LET nr = INT (nms−nm)/p+1)
1330 DIM v(vm) : DIM c(vm) : DIM a(vm) : DIM b(ym) : DIM m(nr) :
     DIM n(nr) : DIM : r(nr)
1340 FOR i = 1 TO vm : PRINT i : INPUT v(i), c(i), a(i), b(i) : NEXT i
1345 CLS : PRINT AT 10,5 ; “COMPUTER IS WORKING”
1350 LET r = 0 : LET m2 = 10 ↑ 10 : LET n = nm : LET j = 0
1355 LET S1 = 0 : LET S2 = 0 : LET S3 = 0 : LET S4 = 0 : LET S5 = 0
1360 FOR i = 1 TO vm
1370 LET x = Ln v(i) : LET a = (c(i)−a(i))/(b(i)−a(i))
1380 IF ABS (n−1) < =10 ↑ −4 THEN GO TO 1410
1400 LET y = LN (FN f(a, n)) : GO TO 1430
1410 LET y = LN (FN g(a))
1430 LET S1 = S1 + x : LET S2 = S2 + ABSx ↑ 2 : LET S3 = S3+y :
     LET S4 = S4 + ABS y ↑ 2 : LET S5 = S5+x*y
1440 NEXT i
1445 LET j = j + 1 : LET n(j) = n : LET m(j) = FN m (S1, S2, S3,
     S5, vm) : LET r(j) = FN r (S1, S2, S3, S4, S5, vm)
1450 IF r(j) > r THEN GO TO 1470
1460 LET r=r (j) : LET no = n (j) : LET m1 = m(j)
1470 IF ABS (m(j)+1)>ABS (m2+1) THEN GO TO 1490
1480 LET m=m(j) : LET nov = n (j) : LET r1 = r(j) : LET m2 = m(j)
1490 LET n = n + p : IF n<=nms+10 ↑ −4 THEN GO TO 1355
1495 BEEP 1,4 : BEEP 1.5, 0
1510 PRINT PAPER 1 ; INK 6 ; '' “Optimum values with respect to
     r :” ' PAPER 7 ; INK 0 ; “n =”; no ' “m =”; m1 ' “r = ”; r.
1520 PRINT PAPER 1 ; INK 6 ; '' “Optimum values with respect to
     m” : ' PAPER 7 ; INK 0 ; “n =”; nov ' “m =”; m2 ' “r =”; r1
```

```
1530 STOP
1540 FOR i = 1 TO nr. : PRINT PAPER 1 ; INK 6 ; "n="; n(i) ' PA-
     PER 7 ; INK 0 ; "m ="; m(i) ' "r ="; r(i) : NEXT i
1550 STOP
```

The selection of the methods is performed conversationally, the computer asking the user if he wants to apply them in the order given in instruction 1. The answers are "y" (or any other letter) for the methods that the user is going to apply and "n" for the others.

In instructions 140—160 m, o and r are the notations used for the slope, intercept and correlation coefficient of the linear plot, a, b, c, d, e are the notations for the sums which enter their expressions according to the least squares method and n stands for the number of experimental points; in the following instructions for the same sums the notation S1, S2, S3, S4, S5 are used. The notation S6 is used for the number of points, which is used as a sum in the Freeman-Carroll method.

The meanings of other notations can be established through comparison of the instructions.

210 with 220 and 240 for Kissinger's method
330 with 340 and 360 for Freeman-Carroll's method
590 with 600 and 620 for Coats-Redfern's method
870 with 880 and 900 for Flynn-Wall's method (α = const)
1000 with 1010 and 1040 for Flynn-Wall's method (a = const)
1300 with 1310 and 1340 for Flynn-Wall's method (T = const)

In the input data, instead of α or $\frac{d\alpha}{dT}$ (in Freeman-Carrol's method) arbitrary units as the ordinates of TG and DTH curves can be used.

In instructions 330, 590, 1000, T means temperature in °C, *TG* — the conversion degree or any quantity directly proportional to it, and DTG the ordinate of the DTG curve corresponding to the temperature T.

The program was run using a TIM S personal computer to evaluate the kinetic parameters of some coordination compounds of Ni^{II} and Co^{II}[6].

REFERENCES

[1] H. E. Kissinger, *Analyt. Chem.*, **29**, 1702 (1957).
[2] E. S. Freeman and B. Carroll, *Z. Phys. Chem.*, **62**, 394 (1958).
[3] I. G. Murgulescu and E. Segal, *Rev. Roumaine Chim.*, **11**, 13 (1966).
[4] A. W. Coats and J. P. Redfern, *Nature*, **20**, 68 (1964).
[5] J. H. Flynn and L. M. Wall, *Polym. Lett.*, **4**, 323 (1966).
[6] Mihaela Badea, Dana Marinescu and E. Segal, *Thermochim. Acta.*, (in print).

Revue Roumaine de Chimie, **34**, *1*, 297–303 (1989)

DETERMINATION OF Cu^{2+}, Pd^{2+} AND Zn^{2+} BY DIFFERENTIAL-PULSE POLAROGRAPHY

ŞERBAN SEVER, STELUŢA CHIPER and SILVIU-DUMITRU POPESCU
Institute of Chemical Research
202, Spl. Independenţei, 77208-Bucharest, Romania

Received November 20, 1988

The polarographic conditions used for the reduction of Cu^{2+}, Pd^{2+} and Zn^{2+} at the dropping mercury electrode are described. The polarographic peaks were obtained in aqueous media, using hydrochloric acid as solvent, Congo red paper for pH determination, ammonia solution for transforming the sample into a base and as main electrolyte, and gelatin as maximum suppressor. By this method concentrations as low as 0.1–0.5 mg/mL could be determined for each cation. A differential-pulse polarographic method was used to increase the sensitivity and accuracy over classical polarography. The concentration limits given above are valid for both methods. The proposed method is selective, reproducible and very suitable for determining (simultaneously, if necessary) the cations investigated.

INTRODUCTION

Copper, palladium and zinc are elements which have a great importance for the chemical and electrotechnical industries, and also for research laboratories, since they are used as catalysts in some organic technological processes. They are also constituents of some alloys such as Au-Pd or Ag-Pd, particularly used in stomatological and dental techniques.

For these reasons, a method was needed for determining quantitatively these elements in various samples and alloys as exactly, selectively and efficiently as possible. At the same time, a method which would be able to establish the degree of impurification with Zn and Cu of some noble metals was desirable as well.

The many methods already published in the literature would not entirely satisfy the stringent conditions imposed by modern technologies, since these require analytical results which are as accurate as possible and also quickly delivered. For this reason, the best method seems to be that of differential-pulse polarography, which offers a broad spectrum of possibilities corresponding to the present requirements.

The method described below is selective and very convenient due to its simplicity, and it also can become apt to being applied in various domains. Compared to classical polarography,[1-12] the differential-pulse polarography has a higher sensitivity.

THE POLAROGRAPHIC METHOD

The reduction of Cu^{2+}, Pd^{2+} and Zn^{2+} ions on the dropping mercury electrode can be represented schematically by the following equilibrium :

$$Me^{2+} + 2e^- \rightarrow Me_{(Hg)} \ (Me = Cu^{2+}, Pd^{2+} \text{ or } Zn^{2+})$$

The overall formula of the above reaction includes all the steps of reduction of the investigated ions up to the corresponding metals. In this way, the peaks and steps easily measurable correspond to the reduction of two electrons, a fact which permits to determine polarographically the mentioned ions.

The mechanism of the above reactions is straightforward and well understood : it depends on the reduction process at the dropping mercury electrode, a fact which proves from a practical point of view the viability of the polarographic theory.

The proposed method has proved to be reproducible and characteristic for the Cu^{2+}, Pd^{2+} and Zn^{2+} ions ; the impurities present in the samples did not modify the peaks or the step heights, therefore they did not affect adversely the analysis results.

EXPERIMENTAL

Reagents :

HCl conc., p.a.
HNO_3 conc., p.a.
Congo red indicator paper
NH_4OH, 1 : 1 solution in water
NH_4OH conc., p.a.
Gelatin, 0.5% solution in water
Copper, fine powder GR (Merck)
Palladium, powder (LAB — Merck)
Zinc, granular GR (Merck).

Standard solution of Cu :

0.1 g of Cu were accurately weighted and dissolved in aqua regia (3 parts HCl and one part HNO_3). After dissolution, the solution was evaporated to remove the nitrous vapours ; the residue was re-taken 3—4 times with conc. HCl in order to create an adequate medium. The residue was then dissolved in 10 mL of conc. HCl and introduced in a 100—mL volumetric flask ; this was brought to the mark with distilled water. The solution was stirred vigorously for homogeneization. 1 mL of the standard solution contains 1 mg of Cu.

Standard solutions of Pd and Zn :

The standard solutions of Pd or Zn were prepared as follows. 0.1 g of Pd or Zn were accurately weighted and dissolved in 10 mL of conc. HCl, then introduced in a 100—mL volumetric flask and brought to the mark with distilled water. The solution was stirred vigorously for homogeneization. 1 mL of the standard solution contains 1 mg of Pd or Zn.

Apparatus :

An OH-107 Radelkis (Budapest) multifunction routine polarograph was used, set on the "Differential Pulse" position, 2 V potential range, and 1 mV/*n* potential rate. The fine current sensitivity was set at position 0.6 and the pulse amplification at 50 mV. The starting potential was 0.0 V. We worked with normal peak, therefore with the "Hammer" push-button off. The paper speed was 0.6 cm/min. and the damping was set at position 3. The height of the mercury column was of 70 cm. As dropping electrode we used a 0.07 mm capillary, adjusting the mercury dropping rate at one drop in 3 s. This was the measuring electrode, whereas the mercury introduced in advance in the Novak cell was the reference electrode.

In the case of classical polarography, the recording conditions were the usual and known ones.

Procedure

0.1 g of the sample were weighted and dissolved in 5—10 mL of conc. HCl. When copper or other hardly soluble elements were present, the sample or alloy was subjected to the same disaggregation process as in the case of the standard solution of copper, that is with aqua regia. The 100—mL volumetric flask was brought to the mark with distilled water, then stirred vigorously to homogenize the solution. An aliquot of this solution was transferred to a 50—mL calibrated flask. The solution was then neutralized with a 1 : 1 solution of NH_4OH in the presence of Congo red paper until the blue paper (in acid media) turns to its initial red color (in basic media). An excess of 10 mL of concentrated solution of NH_4OH (for forming the medium or the pH suitable for the reduction at the dropping mercury electrode and as main electrolyte) and 1 mL of a 0.5% solution of gelatin were added as maxima suppressor. After addition of each reagent, the flask was carefully stirred and cooled. The flask was brought to the mark with distilled water and thoroughly homogeneized. After cooling, the solution was allowed to stand for 5 minutes, was bubbled in a Novak cell with an inert gas (methane or argon) for 3 minutes, then polarographed. (Bubbling is necessary to remove oxygen from samples.)

In the case of differential-pulse polarography, the relation which allows to estimate the results of the determination is

$$C(\%) = (A_s \cdot C_{std}/A_{std} \cdot G) \cdot 100$$

whereas in classical polarography it is

$$C(\%) = (H_s \cdot C_{std}/H_{std} \cdot G) \cdot 100$$

where C is the concentration in the sample, A_s and A_{std} are the areas of the sample's and of the standard's curves, H_s and H_{std} are the step heights of the sample and standard solutions (in mm), respectively, C_{std} is the concentration in the standard solution (in mg/mL), and G is the sample's weight (in g).

DISCUSSION

1. It is worth mentioning that when determining the elements in an alloy, attention must be paid to the fact that these should not exceed 30% in each component of the investigated material, since otherwise the errors would be too large.

2. The polarographic calibration curves of the investigated Cu^{2+}, Pd^{2+} and Zn^{2+} ions, representing the variation of the polarographic peaks and step heights, are given in Figures 1 and 2, respectively, where the concentration of the depolarizer is also specified. The results obtained were affected by errors which did not fall outside the ± 2% range.

The sensitivity of the method was estimated at 10^{-4} mg Cu^{2+}, Pd^{2+} and Zn^{2+} for differential-pulse polarography, and at 10^{-3} mg Cu^{2+}, Pd^{2+} and Zn^{2+} for classical polarography.

By comparing Fig. 1 to Fig. 2, we could remark nothing special, since the linear curves are characteristic to the studied cations.

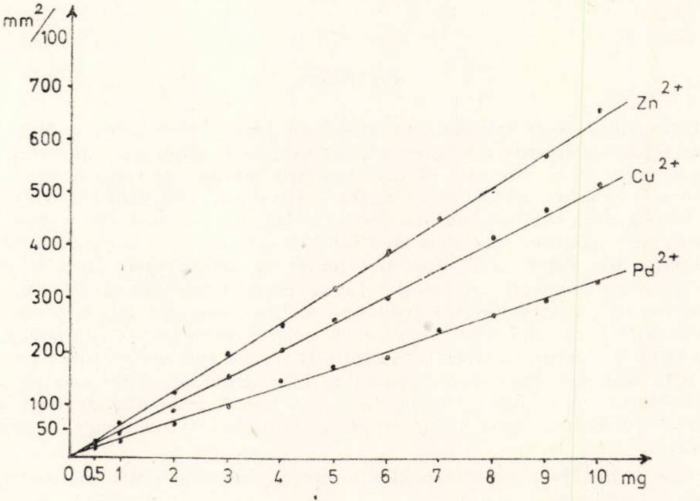

Fig. 1. — The linear calibration curves obtained by differential pulse polarography for Cu^{2+}, Pd^{2+} and Zn^{2+}.

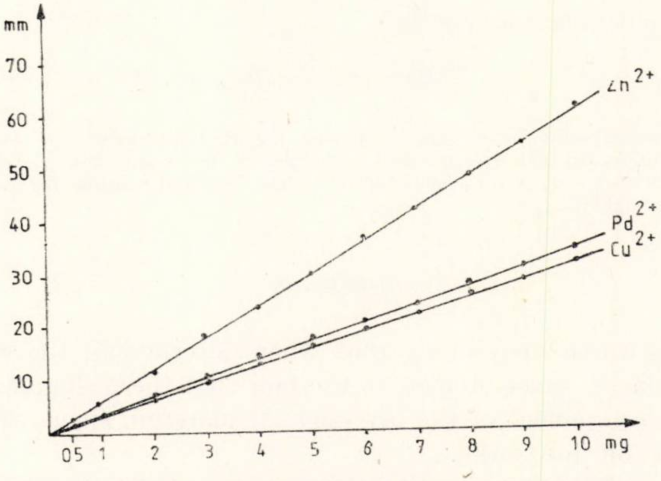

Fig. 2. — The linear calibration curves obtained by classic polarography for Cu^{2+}, Pd^{2+} and Zn^{2+}.

3. Although very well-shaped steps can be obtained by classical polarography, the peaks obtained by differential-pulse polarography are easier measurable and the resulting errors are smaller, whereas the sensitivity of the method is greatly improved.

4. After recording the polarograms at various time intervals, similar peaks or curves were obtained, and after 48 hours no modification was

noticed in the step heights or the peaks, which remained constant over all this interval.

5. The results obtained for Cu, Pd and Zn prove that the differential-pulse polarographic method and the classical polarographic method are very reproducible and suitable for determining the compounds investigated.

6. In the case in which Au^{3+} ions are present, the shape of the polarographic peaks and steps is modified. This makes it necessary to use the method of additions, in order to decrease the possible errors. At the same time, it turned out to be useful for the sample to be filtered before bubbling it with inert gas in the Novak cell, in order to remove the $Au(OH)_3$ precipitate.

In what concerns the presence of Ag^{2+} ions, these do not affect the analysis results, i.e. they do not modify the polarographic peaks and steps, whereas the formed Ag_2O precipitate dissolves in the added excess of NH_4OH.

7. The Co^{2+} ions impede only the determination of Zn^{2+} ions, since their reduction potentials are identical. Unlike Co^{2+}, the Ni^{2+} ions show a peak or some steps which are well formed, selective and with interposing potentials, and they do not interfere with the other investigated elements (Figs. 3 and 4). The Cd^{2+} ions also impede to some extent the Pd^{2+} determination by limiting the selectivity, despite the fact that the configuration of the curves is satisfactory.

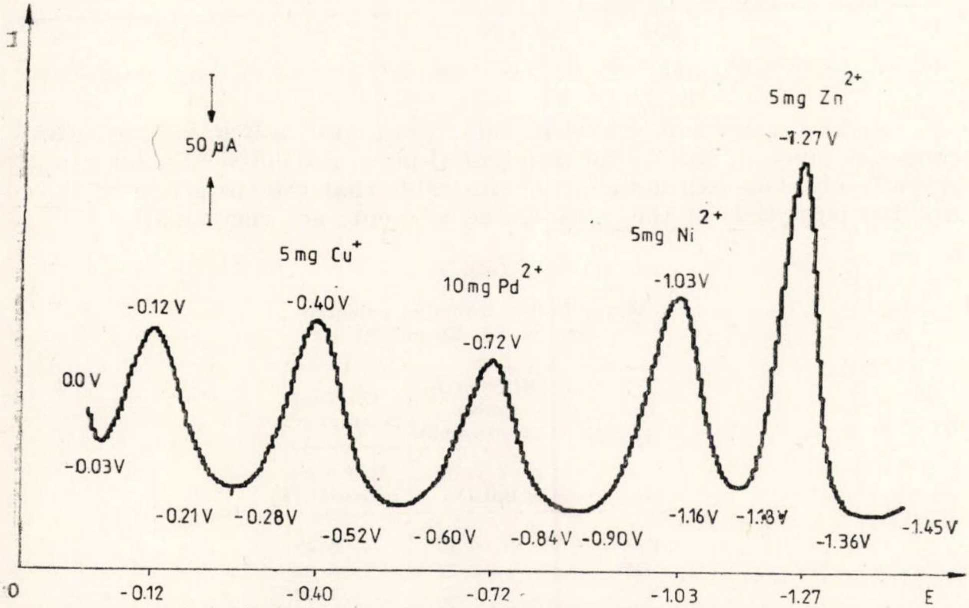

Fig. 3. — Cu^{2+}, Pd^{2+}, Ni^{2+} and Zn^{2+} peaks obtained by differential pulse polarography.

In order to obtain well-shaped polarograms, the 5*M* ammonium chloride (which had been introduced as main electrolyte) was eliminated from the method, this being replaced by the added excess of ammonia and by the acidic medium used for the dissolution of the samples. It was noticed that the presence of the $5M$ NH_4Cl solution prevents the clear appearance of the polarographic peaks and steps, especially when nickel is also present.

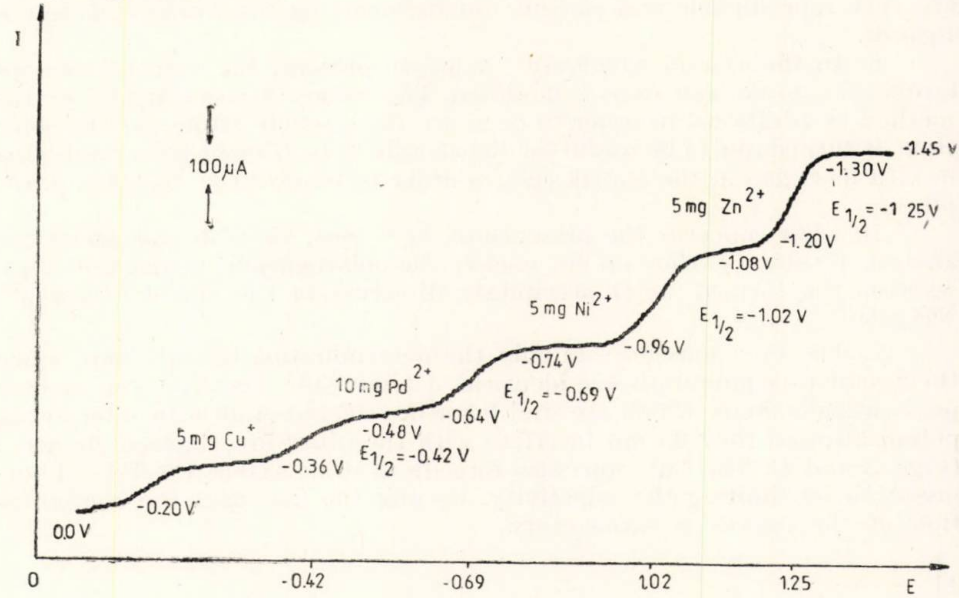

Fig. 4. — Step heights for Cu^{2+}, Pd^{+2}, Ni^{+2} and Zn^{+2} obtained by classic polarography.

8. The values of the reduction (peak and half-wave) potentials range are given in Table 1 for differential-pulse and classical polarography, respectively. One can notice from this table that the variations of the reduction potentials of the investigated elements are very small.

Table 1

Values of the reduction potential for Cu, Pd, Ni and Zn

Symbol	Differential-pulse polarography	Classical polarography
	peak potential (V)	half-wave potential (V)
Cu^{2+}	-0.40	-0.42
Pd^{2+}	-0.72	-0.69
Ni^{2+}	-1.03	-1.02
Zn^{2+}	-1.27	-1.25

9. The recordings for various samples or for mixtures containing the elements in various concentrations gave polarograms fully suitable to such mixtures.

CONCLUSIONS

This work describes a rapid, selective and economical polarographic method for determining Cu^{2+}, Pd^{2+}, Ni^{2+} and Zn^{2+}.

The method may be applied both to samples which contain the mentioned elements and to the impurities in noble metals. In the case of alloys, the method is applicable only if each constitutive element does not exceed 30%; otherwise, the absolute error may increase over the acceptable analytical limits.

Comparatively with classical polarography, the differential-pulse polarography offers good recordings, easily measurable peaks, a much increased sensitivity — that is, in other words, it is a much more efficient method.

REFERENCES

[1] Kalousek, M., *Coll. Czech. Chem. Comm.*, **11**, 592 (1939).
[2] Menzel, R. G. and Jackson, M. L., *Anal. Chem.*, **23**, 1861 (1951).
[3] Willis, J. B., *J. Am. Chem. Soc.*, **67**, 547 (1945).
[4] Pleticha, R., *Coll. Czech. Chem. Comm.*, **15**, 807 (1950).
[5] Pribil, R., Roubal, Z. and Svatek, E., *Coll. Czech. Chem. Comm.*, **18**, 43 (1953).
[6] Allsopp, W. E. and Arthur, T. E., *Anal. Chem.*, **23**, 1883 (1951).
[7] Lingane, J. J., *Ind. Eng. Chem., Anal. Ed.*, **15**, 583 (1943).
[8] Ligane, J. J., *J. Am. Chem. Soc.*, **67**, 919 (1945).
[9] Ligane, J. J., Electroanal. Chem. Interscience Publishers, New York, 330 (1953).
[10] Voriskova, M., *Coll. Czech. Chem. Comm.*, **11**, 580 (1939).
[11] Loveridge, B. A., Thesis, Ph. D., Harvard University, 1947.
[12] Meites, L., "Polarographic Techniques", Interscience Publishers, New York, 1955, p. 261, 274, 278 and 294.

Revue Roumaine de Chimie, **34**, *1*, 305–315 (1989)

THE SULFOTROPIC MOLECULAR REARRANGEMENT OF TETRAORGANODIARSINE DISULFIDES

LUMINIŢA SILAGHI-DUMITRESCU, IOAN SILAGHI-DUMITRESCU
and IONEL HAIDUC

Chemistry Department, University of Cluj-Napoca Str. Kogălniceanu
No. 1, R-3400 Cluj-Napoca, Romania

Receeived October 1, 1988

The reaction of sodium diorganodithioarsinates with diphenylarsenic chloride provides a mixture of isomeric compounds identified by IR and ^{1}H-NMR spectroscopy as Ph_2As-S-(S)AsR_2, Ph_2As(S)-S-AsR_2 and Ph_2As-S-S-AsR_2 ($R = CH_3$, C_6H_5). The intensities of the observed resonance peaks in the ^{1}H-NMR spectra are highly temperature dependent; equilibrium constants and free energy changes were calculated at different temperatures. Enthalpy and entropy changes were also estimated. Extended Hückel MO calculations on simplified models suggest a tetrahedral As_2S_2 intermediate.

INTRODUCTION

Organometallic derivatives of dithioarsinic acids, $R_mM(S_2AsR'_2)_n$, with M = tin,[1,2] silicon, germanium, lead,[3] phosphorus,[4] arsenic[5,6] have been described, most of them in the recent literature. When $R_mM = Ph_2P(n = 1)$ it was found that a sulfotropic molecular rearrangement occurs, with migration of the sulfur atom from arsenic to phosphorus, and formation of diorganoarsenic(III) diphenyldithiophosphinates, $R_2As{-}S{-}(S)PPh_2(R{=}CH_3,\ C_6H_5)$:[4]

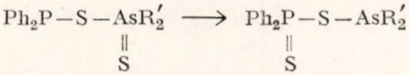

$$\mathrm{Ph_2P{-}S{-}\underset{\underset{\displaystyle S}{\|}}{As}R'_2 \longrightarrow Ph_2\underset{\underset{\displaystyle S}{\|}}{P}{-}S{-}AsR'_2}$$

In extension of these studies we found of interest to investigate the behavior of unsymmetrical diorganoarsenic(III) dithioarsinates (tetraorganodiarsine disulfides), $R_2AsS_2AsR'_2$.

The already known tetraorganodiarsine disulfides are symmetrical compounds, $R_4As_2S_2$ ($R{=}CH_3$, C_3H_7) which have been obtained in a somewhat unexpected manner. Thus, $Me_4As_2S_2$ is formed on treating dimethylarsinic acid, $HO(O)AsMe_2$, with hydrogen sulfide,[7,8] while $Pr^n_4As_2S_2$ is formed by heating dipropyl(ethylthio)arsine, Pr^n_2AsSEt, with elemental sulfur.[6] In the case of methyl derivative an X-ray diffraction established structure I, with the arsenic atoms in different oxidation states, (III) and (V) : [5]

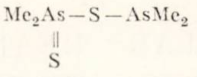

$\mathrm{Me_2}\underset{\underset{\mathrm{S}}{\|}}{\mathrm{As}}\mathrm{-S-AsMe_2}$

I

$\mathrm{Me_2As-S-S-AsMe_2}$

II

In solutions ^{1}H-NMR spectra demonstrate the presence of a second form, II, containing only arsenic (III). [8]

It can be expected that a larger class of tetraorganodiarsine disulfides, including unsymmetrical compounds, $R_2AsS_2AsR'_2$, could be prepared by reacting diorganoarsenic halides, R_2AsCl, with sodium diorganodithioarsinates, $NaS_2AsR'_2$.

Here we report the synthesis of the first unsymmetrical tetraorganodiarsine disulfide, $Ph_2Me_2As_2S_2$, obtained in the reaction of Ph_2AsCl with NaS_2AsMe_2. A tetraphenyl derivative $Ph_4As_2S_2$ was also prepared from Ph_2AsCl and NaS_2AsPh_2. The resulting compounds undergo an interesting molecular rearrangement which has been investigated in some detail.

RESULTS AND DISCUSSION

The equilibrium of molecular rearrangement

In our hands the reaction of chlorodiphenylarsine, Ph_2AsCl, with sodium diorganodithioarsinates, $NaS_2AsR'_2 (R'=CH_3,\ C_6H_5)$ in CCl_4 gave, after the removal of sodium chloride, a viscous oil which does not crystallize on standing, cooling or treating with petroleum ether. The infrared and ^{1}H-NMR spectra could not be interpreted in terms of a unique compound.

For a tetraorganodiarsine disulfide with different organic groups at the two arsenic atoms, three isomeric structures (A), (B) and (C) are possible :

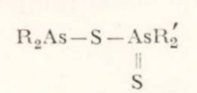

$\mathrm{R_2As-S-}\underset{\underset{\mathrm{S}}{\|}}{\mathrm{As}}\mathrm{R'_2}$

(A)

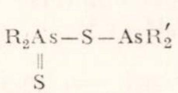

$\mathrm{R_2}\underset{\underset{\mathrm{S}}{\|}}{\mathrm{As}}\mathrm{-S-AsR'_2}$

(B)

$\mathrm{R_2As-S-S-AsR'_2}$

(C)

The relationship between the three forms, (A), (B) and (C), together with thermodynamic parameters of their interconversion has been investigated with the aid of the ^{1}H-NMR and infrared spectroscopy. The study was also extended to the tetraphenyl derivative.

The infrared spectra exhibit a large number of bands in the arsenic-sulfur stretching region. The temperature dependence of the relative intensities corroborated with the spectra of the starting materials and the related dithioarsinic compounds with known molecular structure lead to the assignments presented in Table 1.

The ^{1}H-NMR spectra of $Ph_2AsS_2AsMe_2$ recorded on the reaction mixture, at room temperature contain three peaks, at 2.06, 1.56, and

Table 1

Arsenic-sulfur stretchings in the IR spectra of thioarsenorganic compounds

Compound	$\nu_{As^1 = S}$	$\nu_{As^2 = S}$	$\nu_{As^1 - S}$	$\nu_{As^2 - S}$	Ref.
$Ph_2As^1-S-As^2(S)Me_2$	—	480	418	410	this work
$Ph_2As^1(S)-S-As^2Me_2$	484	—	423	400	,,
$Ph_2As^1-S-S-As^2Me_2$	—	—	418	400	,,
$Ph_2As^1-S-As^2(S)Ph_2$	—	484	416	423	,,
$Ph_2As^1-S-S-As^2Ph_2$	—	—	416	416	,,
$Me_2Sn[S-As^2(S)Me_2]_2$	—	480	—	410	[2]
$Me_2Sn[S-As^2(S)Ph_2]_2$	—	484	—	416	[2]
$Me_2As^1-S-As^2(S)Me_2$	—	488	400	400	[8]

1.37 ppm (δ) for methyl protons. The three peaks were assigned as follows :

(a) $\delta = 2.06$ ppm to the methyl groups attached to arsenic(V) in $(CH_3)_2As(S)-S-AsPh_2$ as for $NaS_2As(CH_3)_2$,[8] $(CH_3)_2As(S)-S-AsMe_2$,[8] $Me_2Sn[S_2As(CH_3)_2]_2$.[2] These methyl groups are present only in the (A) form.

(b) $\delta = 1.56$ ppm to $(CH_3)_2As-S-(S)AsPh_2$ in structure (B) : the same signal is present in the ^1H-NMR spectrum of tetramethyldiarsine disulfide, structure II.[8]

(c) $\delta = 1.37$ ppm corresponds to methyl protons attached to arsenic(III) in a $(CH_3)_2As-S-$ unit.[8]

The ^1H-NMR spectra were recorded in solutions of different concentrations (0.04 M, 0.1 M, 0.5 M, 1 M) and were found concentration nondependent. The relative intensities of the signals are highly temperature dependent, as shown in Table 2. The thermodynamic parameters characterising the system were estimated from the ^1H-NMR quantitative measurements.

Table 2

Equilibrium constants related to ^1H-NMR data

T(K)	%			k_1	k_2	k_3
	A	B	C	B :A	C :A	C :B
293	46.5	20.3	25.2	0.608	0.542	0.840
301	42.3	26.3	31.5	0.610	0.745	1.206
309	37.7	23.3	39.0	0.619	1.035	1.671
350	28.2	16.8	55.0	0.597	1.955	3.275

$\Delta H_{fAB} = 0.10$ kcal·mol^{-1} $\Delta S = -1.31$ cal·mol^{-1}·deg^{-1}

$\Delta H_{fCA} = 4.30$ kcal·mol^{-1} $\Delta S = +13.70$ cal·mol^{-1}·deg^{-1}

$\Delta H_{fCB} = 4.41$ kcal·mol^{-1} $\Delta S = +15.03$ cal·mol^{-1}·deg^{-1}

A = $Ph_2As-S-As(S)Me_2$ ($\delta = 2.06$ ppm)

B = $Ph_2As(S)-S-AsMe_2$ ($\delta = 1.56$ ppm)

C = $Ph_2As-S-S-AsMe_2$ ($\delta = 1.37$ ppm)

The following equilibria must be taken into account:

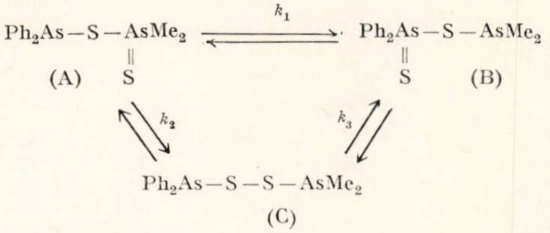
Ph₂As—S—AsMe₂
(A)
S
k_1
Ph₂As—S—AsMe₂
S
(B)
k_2
k_3
Ph₂As—S—S—AsMe₂
(C)

characterized by three equilibrium constants, k_1, k_2 and k_3:

$$k_1 = \frac{[A]}{[B]}; \quad k_2 = \frac{[C]}{[A]}; \quad k_3 = \frac{[C]}{[B]}.$$

The values of the equilibrium constants and the related free energy changes were calculated for each temperature (Fig. 1, Table 2). The enthalpy and entropy changes were estimated from these data by the graphic method (Table 2).

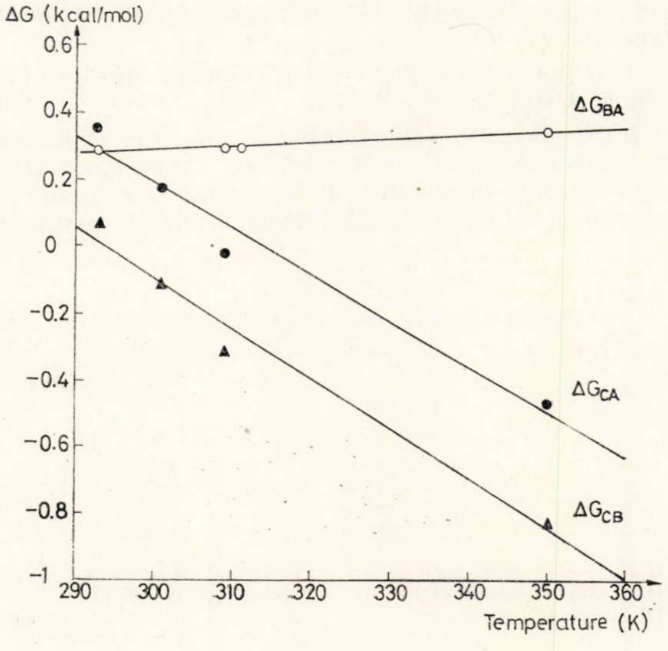

Fig. 1. — Temperature dependence of the free energy changes.

The following thermodynamic features of the system should be pointed out:

(a) The free energy changes for $A \rightleftharpoons B$ equilibrium is almost negligible and temperature independent (Fig. 1), consequently the value of ΔH_{AB} is very small (Table 2).

(b) The free energy changes in the $A \rightleftharpoons C$ and $B \rightleftharpoons C$ systems are strongly temperature dependent (Fig. 1), implying higher values for ΔH. Accordingly, values of $13.7 - 15.03$ cal·mol^{-1}·deg.$^{-1}$ were found for entropy changes in the last two equilibria, while a very small value was found for $A \rightleftharpoons B$ equilibrium.

The highest value for entropy changes was related to form (C), the most flexible structure (highest number of degrees of freedom).

The B form is the most stable, perhaps because of the possibility of conjugation in the Ph−As=S system.

The values of ΔH and ΔS obtained for $Ph_2AsS_2AsMe_2$ are close to those reported before for tetramethyldiarsine disulfide, $\Delta H = 6.77$ kcal·mol^{-1}, $\Delta S = 15.2$ cal·mol^{-1}·deg^{-1} when the $I \rightleftharpoons II$ equilibrium was considered.

An inspection of the molecular orbitals of the system

In order to get a deeper insight into these transformations, we investigated the electronic structure of some model compounds related to the chemical species involved. These include the arsinyl cation H_2As^+ (III), the dithioarsinic anion $H_2AsS_2^-$ (IV), as well as various conformers of arsinyldithioarsinate (V) and diarsine disulfide (VI).

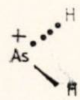

III

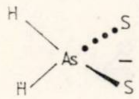

IV

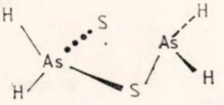

V

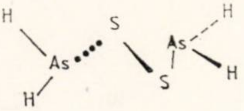

VI

The method employed is of Extended Hückel type[10] with parameters given in ref. 11, 12. Calculations were carried out by using a computer program developed in our laboratory.[13]

The shape of the arsinyl cation molecular orbitals resemble those of the AH_2 triatomics.[14] However, for the sake of completeness, we calculated and give here the interaction diagram for this system (see Fig. 2). With six valence electrons, only $1a_1$, $1b_2$ and $2a_1$ are occupied. The next nonbonding $1b_1$, is empty, and has a quite low energy so it is suitable for interaction with the proper mo's of dithioarsinic anion (IV).

The dithioarsinic anion has been little investigated and to the best of our knowledge, no molecular orbital calculations have been reported so far. Consequently a short description of the most important mo's of this fragment is worthwhile at this point. Figure 3 shows the sequence of the occupied molecular orbitals, resulted from our EH calculation.

Contrasting AsH_2, we can notice a large gap between HOMO and LUMO, and the involvement of the latter in bonding with other fragments is very little probable. In fact this anion should act only as a good donor and to a less extent as acceptor. Taking into account the valence orbitals of H_2As^+, we may select four of the $H_2AsS_2^-$ mo's allowed to interact with $2a_1$ and $1b_1$ of Fig. 2. These are $3b_2$ (π_1), $4a_1$ (n_+), $2b_1$ (π_2) and

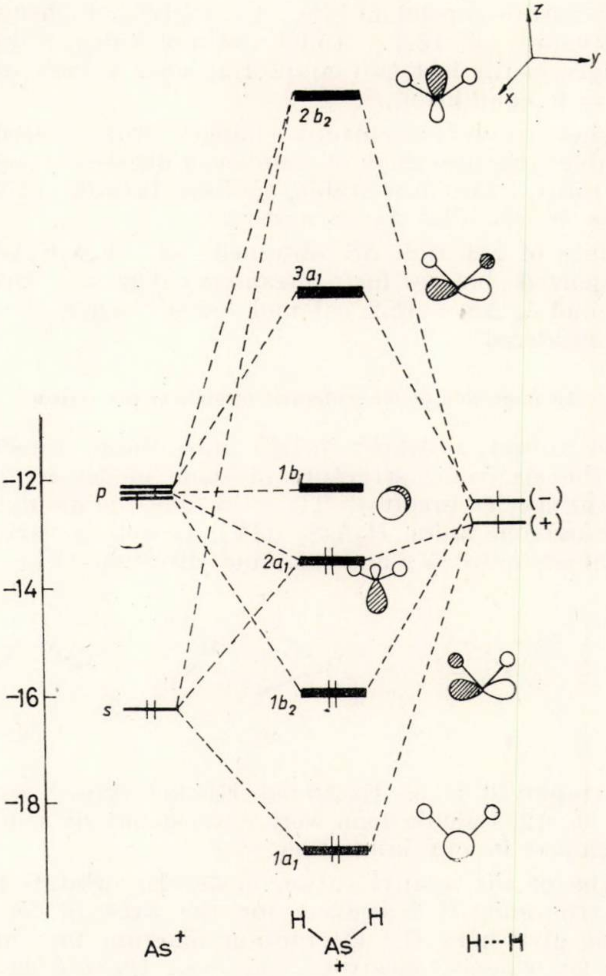

Fig. 2. — The orbital interaction diagram in $AsH_2^{\pm}$. As the higher two mo's ($3a_1$, $2b_2$) are at 1.88 and 23.17 eV, their position is not scaled in the diagram.

$4b_2$ (n_-) and are shown in the rectangle of the top part of figure. Two of them are of π type ($3b_2$, $2b_1$), the other two of sigma type ($4a_1$, $4b_2$) are well localized at the sulfur atoms (excepting $2b_1$-with contribution from As p_z orbital) so they describe nonbonding electron pairs of this atom.

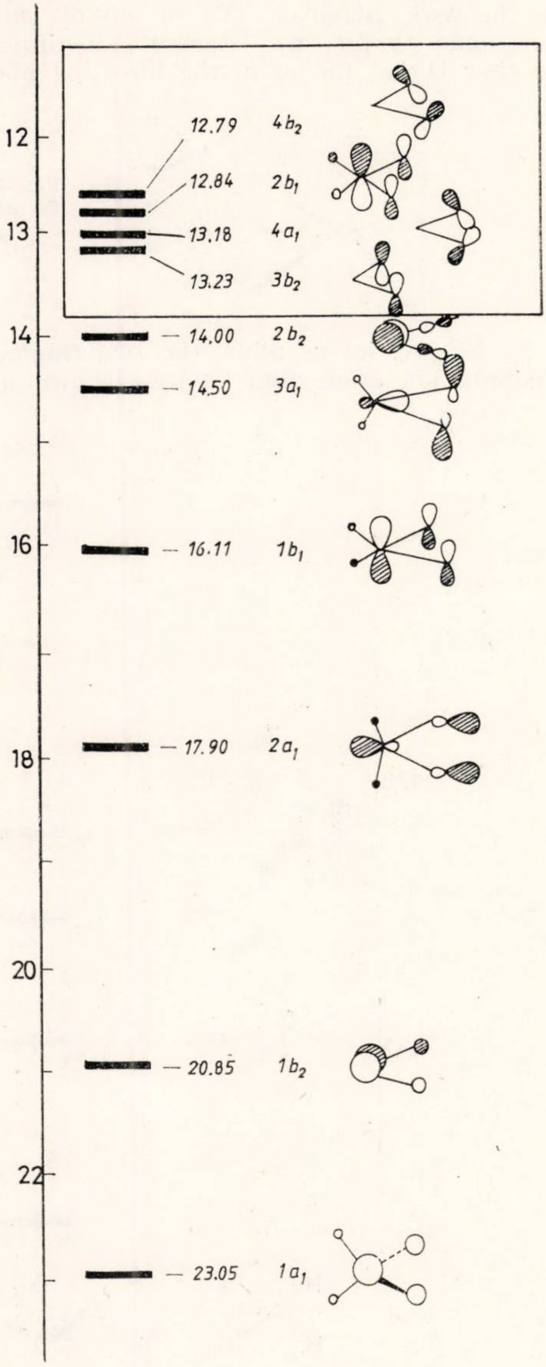
12
13
14
16
18
20
22
12.79 4b₂
12.84 2b₁
13.18 4a₁
13.23 3b₂
14.00 2b₂
14.50 3a₁
16.11 1b₁
17.90 2a₁
20.85 1b₂
23.05 1a₁

Fig. 3. — The occupied molecular orbitals of dithioarsinate anion ($H_2AsS_2^-$).

The attack of H_2As^+ cation could proceed basically in two ways: in the AsS_2 plane of (IV) or out of this plane. As both sulfur have the same charge, we "started" the interaction in a symmetrical way, so that H_2As^+ moves in the bisecting plane of the SAsS angle (Fig. 4).

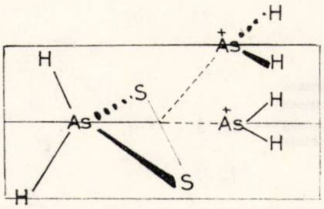
H
As
S
S
H
As
H
H
As
H
H

Fig. 4. — Two possible ways for the attack of H_2As^+ at the sulfur atoms of dithioarsinate.

Firstly, let us allow the two fragments to interact in plane. The arsinate ion offers four orbitals shown in the left part of Fig. 5. The

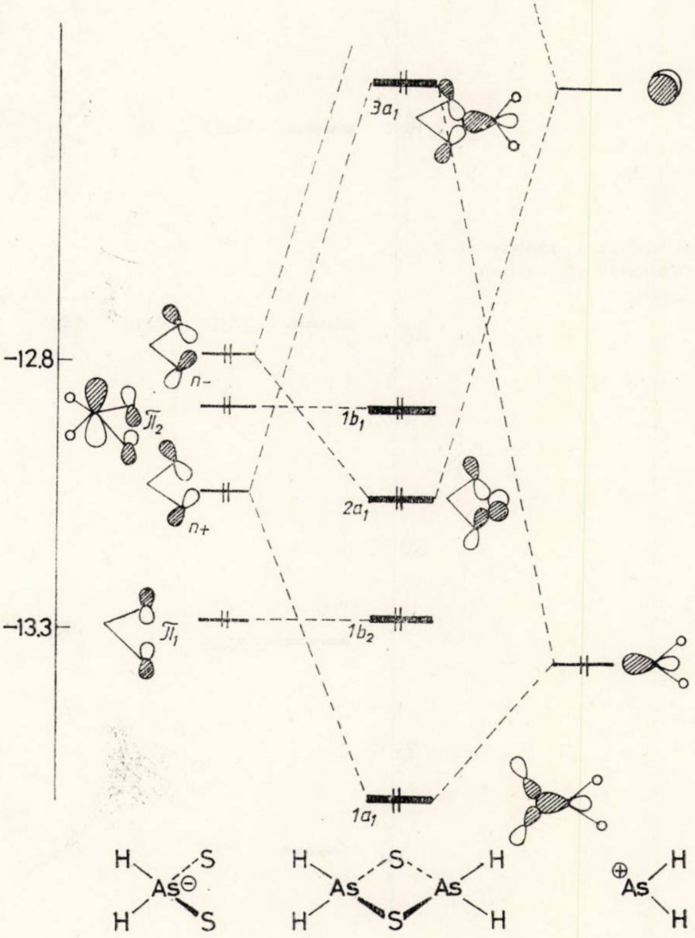
−12.8
−13.3
n−
π2
n+
π1
3a1
1b1
2a1
1b2
1a1
H
As⊖
S
S
H
H
As
S
S
As
H
H
H
⊕As
H
H

Fig. 5. — The "in plane" interaction of $H_2AsS_2^-$ and H_2As^+.

arsinyl cation (right hand part of Fig. 5) is rotated around the y axis, otherwise, the "reaction product" would contain an As atom in a planar environment. This particular geometry reduces to zero all the overlaps of π_1 and π_2 with $2a_1$ and $1b_1$ and leaves π_1 and π_2 as nonbonding orbitals. It is n_+ and n_- which are stabilized by interaction with $2a_1$ and $1b_1$ of H_2As^+. Four of the five electron pairs are accommodated in the four lower energy mo's of the system but the last pair should take the highly unfavorable fifth mo shown in the top of Fig. 5.

What happens if the attack of H_2As^+ occurs out of SAsS plane? This situation is sketched in Figs. 6 and 7. At variance with the previous case, $2a_1$ and $1b_1$ may interact not only with n_+ but also with π_2 and no destabilizing effect occurs. Consequently, all five electron pairs occupy energetically more favorable mo's than those resulted from the in plane interaction.

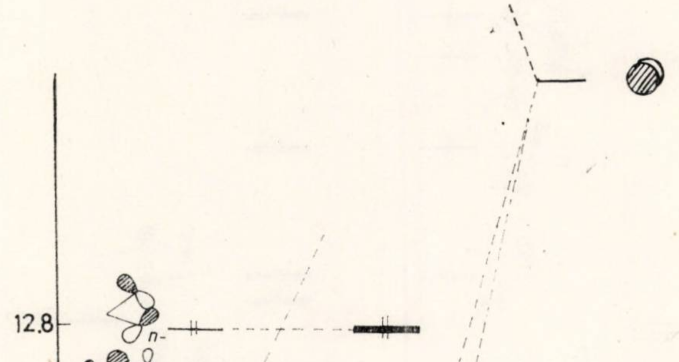

Fig. 6. — "Out of plane", symmetric attack of arsinyl cation.

These results suggest that during the reaction of dithioarsinates with halogenoarsines, cyclic tetraatomic AsS_2As intermediates (folded along the SS axis to give a pseudotetrahedral geometry) occur, which

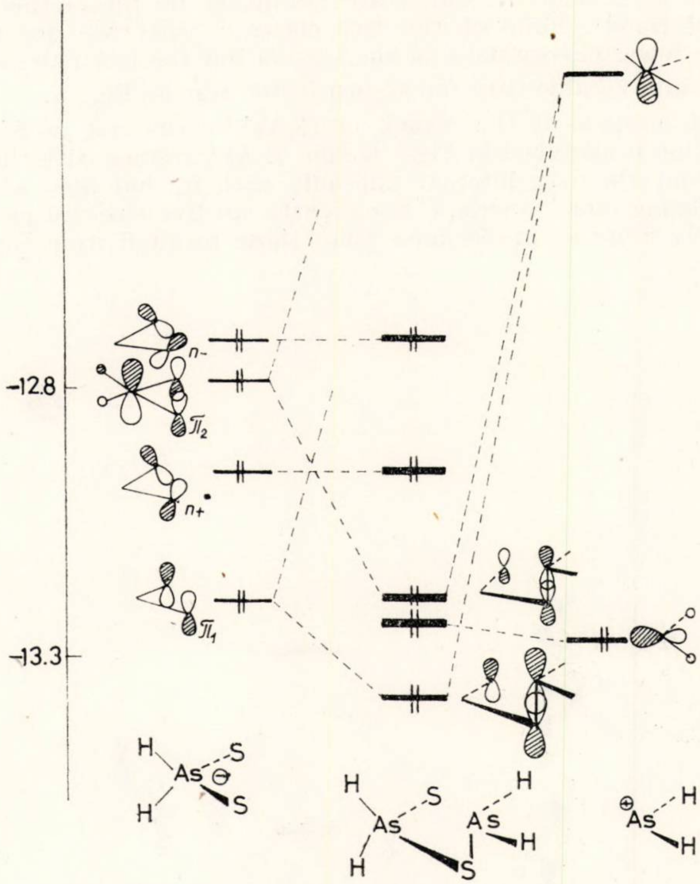

Fig. 7. — "Out of plane" asymmetric reaction product.

eventually lead to the primary product (V). The conformation of arsinyldithioarsinate (Fig. 7) is in accordance with that of $(CH_3)_2As(S)SAs(CH_3)_2$ found by X-ray diffraction analysis.[5]

It is beyond the scope of this paper the swiping of the entire potential surface of the rearrangements described in the previous section. Though, qualitative arguments derived from the present calculations may shed some light on the possible way of VI ⇌ V isomerization.

The propensity of the S—S bonds toward rotations make probable various conformers of VI. Their relative energies, for example at 180°, 90° and 0° AsSSAs dihedral angles, are 1.00, 0.00 and 290 kcal/mole, respectively. These figures clearly show the preference of diarsine disulfide for trans or gauche conformers over the eclipsed one.

Turning back to Fig. 6 we note that the arsinate diarsinedisulfide rearrangement would require a concerted As—S bond breaking and the formation of a new S—S bond. The S—S bond could stem from n_+ which have the proper symmetry for a σ interaction. π_2 also play an important role here since, moving down As_1, the out of phase overlap of $p_z(As_1)$ with $p_z(S_2)$ gradually decreases and reaches a position with positive (bonding) overlap (VII), at the same time, the overlap with $p_z(S_1)$ is greatly diminished and the disulfide form takes some advantage over the arsinate. This way, the trans conformer of diarsinedisulfide is attainable (VII), which in turn, is in equilibrium with the gauche form.

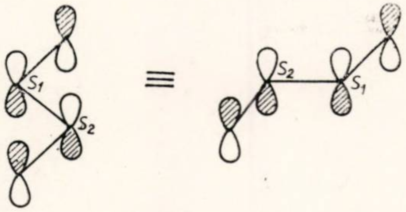

VII

REFERENCES

[1] I. Haiduc and L. Silaghi-Dumitrescu, *J. Organometal. Chem.*, **225**, 225 (1982).
[2] L. Silaghi-Dumitrescu, I. Haiduc and J. Weiss, *J. Organometal. Chem.*, **263**, 159 (1983).
[3] L. Silaghi-Dumitrescu and I. Haiduc, *J. Organometal. Chem.*, **259**, 65 (1983).
[4] L. Silaghi-Dumitrescu and I. Haiduc, *J. Organometal. Chem.*, **252**, 295 (1983).
[5] N. Camerman and J. Trotter, *Canad. J. Chem.*, **42**, 219 (1964).
[6] L. S. Sagan, R. A. Zingaro and K. J. Irgolic, *J. Organometal. Chem.*, **39**, 301 (1972).
[7] R. Bunsen, *Liebigs Ann. Chem.*, **46**, 1 (1843).
[8] R. A. Zingaro, K. J. Irgolic, D.H.O'Brien and L. J. Edmonson Jr., *J. Amer. Chem. Soc.*, **93**, 5677 (1971).
[9] I. Silaghi-Dumitrescu, L. Silaghi-Dumitrescu and I. Haiduc, *Rev. Roumaine Chim.*, **27**, 911 (1982).
[10] R. Hoffmann, *J. Chem. Phys.*, **39**, 1397 (1963).
[11] J. Hinze and H. H. Jaffé, *J. Chem. Phys.*, **71**, 1240 (1974).
[12] A. G. Turner, "Methods in Molecular Orbital Theory", Prentice Hall Inc., New Jersey, 1974.
[13] Program EHOK is written in SuperBasic for a SINCLAIR QL computer.
[14] R. G. Pearson, "Symmetry Rules for Chemical Reactions. Orbital Topology and Elementary Processes", Wiley, New York, 1976.

Revue Roumaine de Chimie, **34**, *1*, 317–322 (1989)

AZOAMIDE DERIVATIVES OBTAINED FROM ETHYL PHENYLAZOCARBOXYLATE

CRISTOFOR I. SIMIONESCU[a], AURA ANGELICA POPA[b],
EUGENIA COMĂNIŢĂ[a] and VIRGIL BĂRBOIU[b]

[a] Department of Organic and Macromolecular Chemistry, "Gheorghe Asachi" Polytechnic Institute, 23 August Street, No. 11, 6600 Jassy, Romania
[b] "Petru Poni" Institute of Macromolecular Chemistry, Grigore Ghica Vodă Alley, No. 41/A, 6600 Jassy, Romania

Received October 6, 1988

Azoamides containing the alkylazocarbonyl group were prepared by the reaction of ethyl phenylazocarboxylate with ammonia, aliphatic diamines and amino acids. Some characteristics of ^1H-NMR spectra which are in agreement with the structures of the synthesized compounds are described. Some data on the thermal behaviour are presented.

INTRODUCTION

Like ethyl azodicarboxylate, [1] the ethyl phenylazocarboxylate can easily react with nucleophilic reagents, such as ammonia and amines, giving azoamides. Their structure would indicate a stability at the azo group due to the extended conjugation which limits their use as initiators in radical polymerization. However, the azo group (in azoesters, azoamides) may be activated by decomposition by a Lewis acid or by other procedures.[2,3] Since some compounds contain reactive groups permitting the "coupling" with other monoazo derivatives they may be used as intermediates in the synthesis of bifunctional initiators.

RESULTS AND DISCUSSION

In the present paper some reactions of the ethyl phenylazocarboxylate (I) with ammonia and other basic reagents are reported.

In the first part the behaviour of (I) toward ammonia, ethylene diamine (EDA), hexamethylenediamine (HMDA) and ethanolamine (EA) is presented :

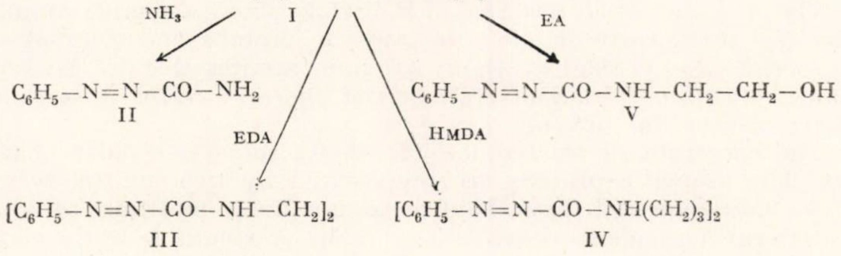
$C_6H_5-N=N-COOC_2H_5$
I
NH_3
EA
$C_6H_5-N=N-CO-NH_2$
II
$C_6H_5-N=N-CO-NH-CH_2-CH_2-OH$
V
EDA
HMDA
$[C_6H_5-N=N-CO-NH-CH_2]_2$
III
$[C_6H_5-N=N-CO-NH(CH_2)_3]_2$
IV

The phenylazocarboxamide (II) results simply by bubbling gaseous ammonia into a suspension of I in water. The N, N′-ethylene-bis(phenylazoformamide) (III) and N, N′-hexamethylene-bis(phenylazoformamide) (IV) are obtained from I and the corresponding amines in ethanol medium.

The N-(β-hydroxyethyl)-phenylazoformamide (V) was synthesized as described in a previous paper and used for the synthesis of a bifunctional initiator.[4]

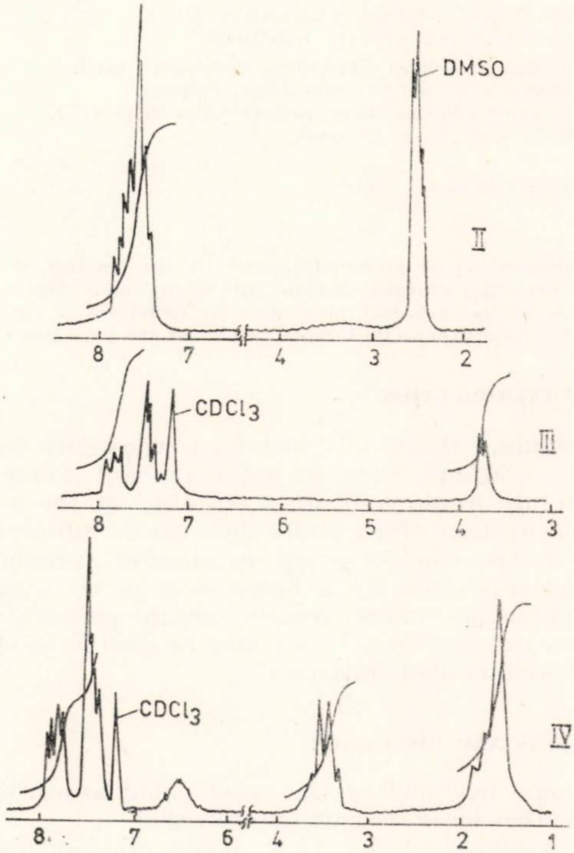

Fig. 1. — ^{1}H-NMR spectra of phenylazocarboxamide (II), N, N′-Ethylene-bis(phenylazoformamide) (III) and N, N′-Hexamethylene-bis(phenylazoformamide)(IV).

The structures of amides II, III and IV were confirmed by elemental analysis data as well as by IR and ^{1}H-NMR spectroscopy. In Fig. 1 the ^{1}H-NMR spectra of the three compounds are given.

The spectrum of II, recorded in DMSO-d_6, shows a complex multiplet at 7.5—7.9 ppm, corresponding to aromatic protons and a broad signal with a peak (less visible) at about 3.5 ppm attributable to the isotopic exchange between the amide protons and those of water present as an impurity within the solvent.

The spectrum of azodiamide III shows some particular characteristics. The aromatic protons are represented by two multiplets within the 7.3—8.0 region and the methylene groups by a multiplet at 3.9 ppm whose lateral components constitute a doublet attributable to the coupling with the NH—CO proton and the central component to a coupling cancelled by the isotopic exchange between the NH—CO proton and those in water traces. The amide protons give a wide signal within the 6—8 ppm range due to the dipolar relaxation of the ^{14}N nucleus.

The ^1H—NMR spectrum of the compound IV shows the same signals as III for the aromatic protons, an unresolved multiplet at 6.5 ppm corresponding to the NH—CO protons and two multiplets at 3.5 ppm (CH_2 group near the amide group) and at 1.5—1.9 ppm (the other CH_2 group). It is worth mentioning that the multiplet at 3.5 ppm is a quartet due to the J_{CH_2, CH_2} and $J_{CH_2, NHCO}$ couplings.

The second part of the paper deals with the reaction of I with two amino acids, glycine and β-alanine, according to the following equations :

$$C_6H_5-N=N-COOC_2H_5 + H_2N-(CH_2)_n-COO^-Na^+ \dashrightarrow$$

$$C_6H_5-N=N-CO-NH-(CH_2)_n-COO^-Na^+ \xrightarrow{H^+}$$

$$C_6H_5-N=N-CO-NH-(CH_2)_n-COOH$$

$$n = 1{,}2 \qquad \text{VI and VII}$$

The amino acid has been previously converted into its sodium salt to assure its solubility in water and the basicity of the amino group. The synthesis was carried out in a homogeneous medium, by adding the azo ester dissolved in ethanol to the aqueous solution of the aminoacid salt. Similar acids containing azoamide group have been previously prepared from ethyl azodicarboxylate.[5]

The ^1H—NMR spectrum of the compound VI, recorded in DMSO-d_6 (Fig. 2) shows two multiplets at 7.4—8 ppm (aromatic protons) and 3.95 ppm (protons CH_2), a triplet at 8.9 ppm (NHCO proton) and a very wide signal within the 5—7 ppm region for the protons in —COOH, H_2O and NHCO, involved in rapid reactions of isotopic exchange. As in the case of the compound III, the signal of the CH_2 group is a superimposing of a doublet and a singlet (curve a). The former is due to the $J_{CH_2, NHCO}$ coupling and its intensity is correlated with that of the NHCO signal at 8.9 ppm. The relative intensity of the latter signal corresponds to less than a proton, as noticed also with the compound III, because the signal is generated only by the molecules in which the NH—CO proton exchanges slowly with other labile protons within the system.

Figure 3 presents the ^1H—NMR spectrum of compound VII.

Among the azoamides synthesized the compounds III and V have been investigated for their behaviour under heating. The thermodifferential analysis (Fig. 4) made on a PAULIK-PAULIK MOM Budapest apparatus at a heating rate of 1.56° and 2.5°C/min shows rather high melting points (185°C for compound III and 140°C for compound V, respectively) followed by a sudden decomposition (maximum at 192° and 162°, respectively). It deserves mentioning that the weight losses during this stage coincide with the nitrogen content of the compound III (17%) and with nitrogen and carbon dioxide contents of the compound V (34%).

A differential scanning calorimetry (DSC) study (Fig. 5) on the compound V performed within the 100—250°C temperature range also indicates the melting point which coincides with the beginning of the

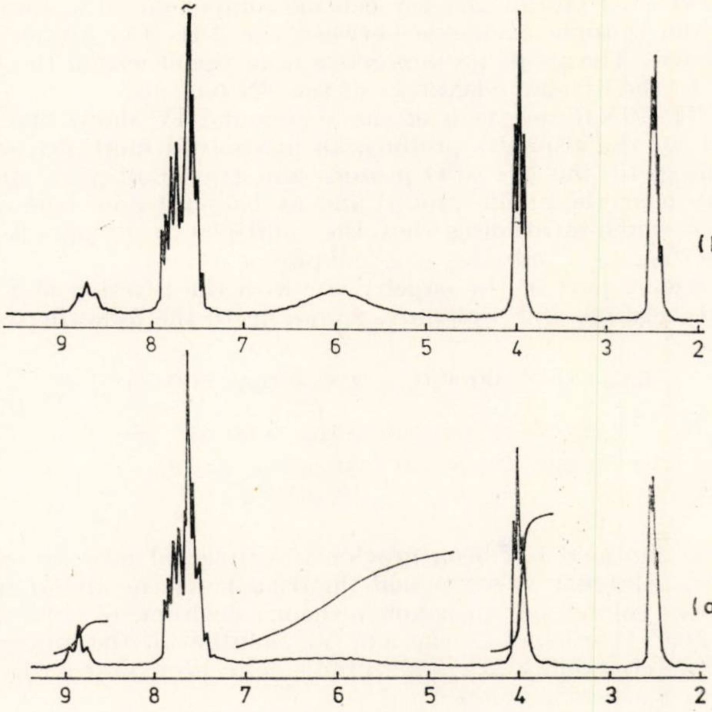

Fig. 2. — ^{1}H—NMR spectrum of phenylazoformamidoacetic acid (VI) at 20 °C (a) and 55 °C (b), in DMSO-d_6.

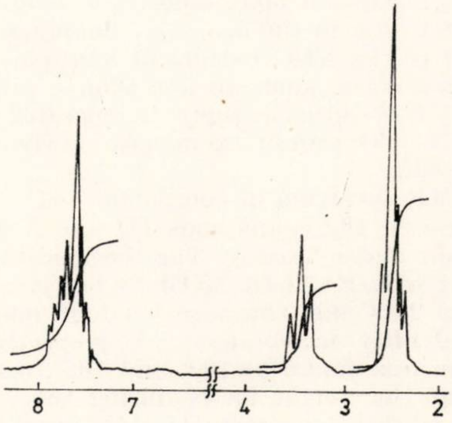

Fig. 3. — ^{1}H—NMR spectrum of phenylazoformamidopropionic acid (VII), in DMSO-d_6.

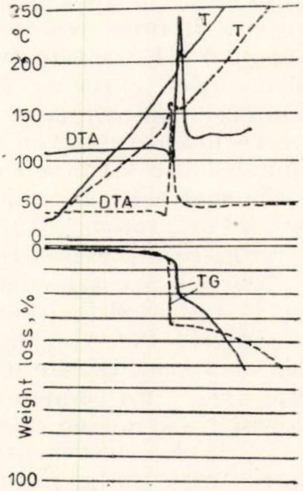

Fig. 4. — The thermograms of N,N′-Ethylene-bis(phenylazoformamide) (——) and phenylazoformamidoacetic acid (— — —).

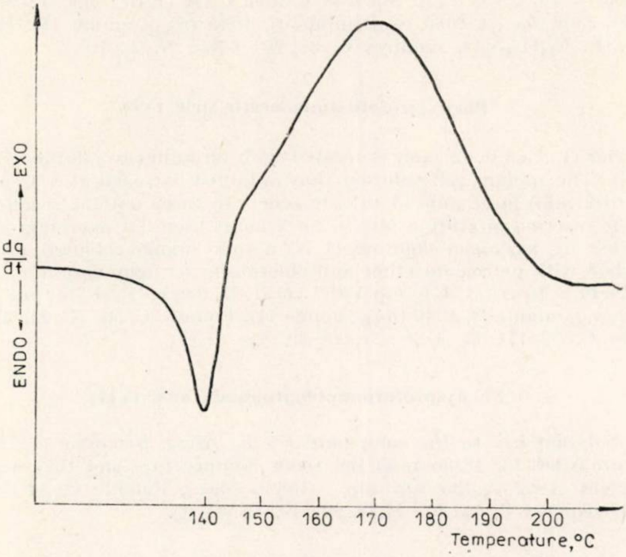

Fig. 5. — The DSC curve of phenylazoformamidoacetic acid (VI).

decomposition process. The thermogram was recorded on a Perkin-Elmer DSC-1B calorimeter at a heating rate of 10°C/min.

EXPERIMENTAL

Ethyl phenylazocarboxylate (I)

It was prepared by the oxidation of ethyl phenylhydrazocarboxylate by $KMnO_4$.[6]

Phenylazocarboxiamide (II)

Gaseous ammonia is bubbled into a suspension of I in water. The precipitate appearing after 5 minutes was washed with petroleum ether to remove the unconverted I, then dried under vacuum at 40 °C. Yield 1.5 g (75 %); mp 110 °C (dec.). IR (KBr; cm^{-1}) : 3380, 3220 (ν_{NH}), 1690 (ν_{CO}, amide I), 1545 (δ_{NH}, amide II). Found : C, 56.53 ; H, 5.30 ; N, 28.41 ; $C_7H_7N_3O$ requires C, 56.37 ; H,4.69 ; N, 28.18 %.

N, N′-Ethylene-bis(phenylazoformamide) (III)

1.78 g (0.01 moles) of I dissolved in 5 mL ethanol are cooled at 5 °C then treated dropwise with EDA (0.3 g ; 0.005 moles). A precipitate is noticed to form toward the addition end. The product is yellow-orange when recrystallized from benzene and red from ethanol. Yield 1.18 g (73 %) ; mp 192—194 °C (dec.). IR (KBr ; cm^{-1}) : 3295 (ν_{NH}), 3060 (ν_{CH}), 1695 (ν_{CO}, amide I), 1545 (δ_{NH}, amide II). Found : C, 59.36 ; H, 5.05 ; N, 26.14 ; $C_{16}H_{16}N_6O_2$ requires C, 59.26 ; H, 4.94 ; N, 25.92 %.

N, N′-Hexamethylene-bis(phenylazoformamide) (IV)

0.56 g (0.005 moles) HMDA solvent in ethanol (4 mL) are added to solution of I (1.78 g ; 0.01 mol) in 6 mL ethanol, cooled on ice bath. The product is noticed to separate immediately. It is washed with petroleum ether, then with water to remove the unreacted I

and diamine. Yield 1.10 g (58 %); mp 148 °C (dec.). IR (KBr; cm^{-1}): 3300 (ν_{NH}), 3060 ($\nu_{=CH}$), 2960, 2920, 2865 (ν_{C-H}), 1680 (ν_{CO}, amide I), 1545 (δ_{NH}, amide II). Found: C, 62.26; H, 6.09; N, 22.31; $C_{20}H_{24}N_6O_2$ requires C, 63.16; 6.32; N, 22.10 %.

Phenylazoformamidoacetic acid (VI)

The glycocoll (1.5 g; 0.02 mol) is treated with an aqueous solution (5 mL) of NaOH (0.8 g; 0.02 mol). The sodium salt solution thus obtained is cooled at 5 °C and then treated with I (3.56 g; 0.02 mol) in ethanol (5 mL) in order to carry out the reaction in a homogeneous medium. The reaction mixture is stirred for 2 hours then left overnight (24 h) in a cold place. By acidifying by hydrogen chloride (1 N) a solid orange-coloured product separates. It is filtered, washed with petroleum ether and chloroform for removing the unreacted I and the amino acid. Yield 2.19 g (53 %); mp 140 °C (171 °C dec.). IR (KBr; cm^{-1}): 3300 (ν_{NH}), 3050 ($\nu_{=CH}$), 1700 (ν_{CO}, amide I), 1540 (δ_{NH}, amide II). Found: C, 50.77; H, 4.28; N, 20.52; $C_9H_9N_3O_3$ requires C, 52.17; H, 4.35; N, 20.29 %.

Phenylazoformamidopropionic acid (VII)

It is prepared similarly to the compound VI by using β-alanine (1.78 g; 0.01 mol). The reaction mixture is left for 48 hours at the room temperature and then separated as described above. Yield 1.62 g (35 %); mp 156 °C (dec.). Found: C, 54.38; H, 4.84; N, 19.28; $C_{10}H_{11}N_3O_3$ requires C, 54.30; H, 4.98; N, 19.00 %.

REFERENCES

[1] C. I. Simionescu, A. A. Popa, E. Comăniță and V. Bărboiu, The III-rd National Congress of Chemistry, București, 21–24 Sept. 1988.

[2] C. S. Sheppard and R. E. MacLeay, *B.R.D. Pat.*, 1940473 (February 10, 1970); cf. *Chem. Abstr.*, **72**, 90983 m (1970).

[3] R. E. MacLeay and C. S. Sheppard, *U. S. Pat.*, 3987024 (October 10, 1976); cf. *Ref. Zh.*, **13** (II), 13.H. 297 P (1977).

[4] C. I. Simionescu, E. Comăniță, M. Păstrăvanu and A. A. Popa, *Polym. Bull.*, **18**, 13 (1987).

[5] C. I. Simionescu, E. Comăniță, M. Păstrăvanu and B. Comăniță, *Acta Chim. Acad. Sci. Hungaricae*, in press.

[6] O. Widman, Ber. dtsch. chem. Ges., **28**, 1927 (1895).

Revue Roumaine de Chimie, **34**, *1*, 323–329 (1989)

RARE EARTH MIXED OXIDES WITH TRANSITION METALS. II[1]

MIXED OXIDES WITH Fe(III) HAVING A PEROVSKITE AND GARNET STRUCTURE

P. SPACU, SILVIA PLOŞTINARU, LUMINIŢA PATRON, ADRIANA CONŢESCU, D. CRIŞAN and N. STĂNICĂ

Center of Physical Chemistry, Bucharest, Romania

Received October 3, 1988

The present paper deals with the study of the mixed oxides $LnFeO_3$ and $Ln_3Fe_5O_{12}$ obtained using polynuclear coordination compounds, as precursors. All oxides were analysed by X-ray diffraction and were characterized by physico-chemical methods (electronic and IR spectra, magnetic measurements).

A previous contribution [1] dealt with the preparation and the study of ABO_3 perovskite type mixed oxides of lanthanides with Co(III) and Ni(III).

In recent years, special attention has been devoted to the basic and applied investigations on mixed oxides of this type. The use of mixed oxides containing lanthanides and transition metals as catalysts in oxidation-reduction,[2] hydrogenation [3] and depollution reactions [4,5] is mentioned in literature. The catalytic activity is strongly dependent on the atomic number, electrical and magnetic properties as well as on the large coordination tendency of lanthanide ion. Therefore, the recent studies have dealt with developing rapid and efficient methods of obtaining pure oxidic phases. This involved the diversification of the type of mixed oxides and of preparation methods, often resorting to non-conventional methods. The mixed oxides resulted are more reactive and obtained at lower temperature.

This contribution is a study of Ln(III) and Fe(III) mixed oxides of perovskite structure, $LnFeO_3$, and garnet structure $Ln_3Fe_5O_{12}$ obtained by the decomposition of polynuclear coordination compounds.

RESULTS AND DISCUSSION

The crystalline orthoferrites ($LnFeO_3$) and the garnets ($Ln_3Fe_5O_{12}$) are usually obtained by sintering oxide mixtures Ln_2O_3 and Fe_2O_3, at very high temperatures ($\simeq 1300°$).

Recently, the orthoferrites and garnets were obtained by decomposition of hydroxide coprecipitates [6,7] or of stoichiometric mixtures of hydroxidic components. [8]

A newer and more efficient method, only seldomly employed is the thermal decomposition of coordination compounds. Thus, orthoferrites were obtained through decomposition of complex cyanides of the $LnFe(CN)_6$ type.[9]

In M(III) — Fe(III) system, depending on the ratio of metallic ions and on temperature, various types of oxidic combinations are obtained. When M(III) = Ln(III), due to the phenomenon called "contraction of lanthanides", only orthoferrites ($LnFeO_3$) are obtained, both for ceritic and yttric series, at 1 : 1 component ratio (regardless of temperature and the method of synthesis employed). For a component ratio Ln(III) : Fe(III) = 3 : 5, the garnet is formed only for the yttric series, while for ceritic series only orthoferrites and mixtures of simple oxides are obtained.

The studied oxidic compounds were prepared from polynuclear coordination compounds of Fe(III) and Ln(III), in 1 : 1[10] and 3 : 5 ratio, with gluconic acid as precursors.

The coordination compounds used as precursors have the following general formula :

$LnFe(Gluc)_4 \cdot 4\,H_2O$ where Ln(III) = La . . . Tb

and

$Ln_3Fe_5(Gluc)_{12} \cdot 5\,H_2O$ where Ln(III) = Gd . . . Yb

The oxidic products resulted from the decomposition of polynuclear coordination compounds were analysed by X-ray diffraction.

The diffractogrames have shown that after decomposition of coordination compounds, whose Ln : Fe ratio is 1 : 1, the perovskite phase coexists with the traces of component oxides. Therefore, these products were subject to a suitable thermal treatment, until the X-ray spectra indicated the formation of pure perovskite phase.

Thus the orthoferrites form between 500 and 600°. The temperature of crystalline phase formation is at least 100° lower than in the systems previously studied.[1] The diffractogram of the oxidic residuum obtained at 600° indicates the formation of a less crystallized pure oxidic phase. After the thermal treatment of 5h at 700°, the lines of very well crystallized $LnFeO_3$ appear (Fig. 1, 2).

The formation of garnet phase from Ln—Fe—Gluconic acid begins at 650°. The X-ray diffraction spectra show that between 300 and 500°, the oxidic residuum is amorphous. After a 5h thermal treatment at 800° the sample resulted from Gd—Fe—Gluconic acid system, a very well crystalized $Gd_3Fe_5O_{12}$ garnet phase is obvious (Fig. 3).

Because the literature data show that an increase of calcination temperature to 1000—1300° influences the formation and increases the crystalinity of garnet phase, the samples were further subjected to a thermal treatment of 5h/1000°.

The oxidic phases obtained :

$LnFeO_3$ where Ln(III) = La . . . Tb

and

$Ln_3Fe_5O_{12}$ where Ln(III) = Gd . . . Tb

are black powders slightly soluble in warm mineral acids. They are characterized by IR, electron spectroscopy and magnetic measurements.

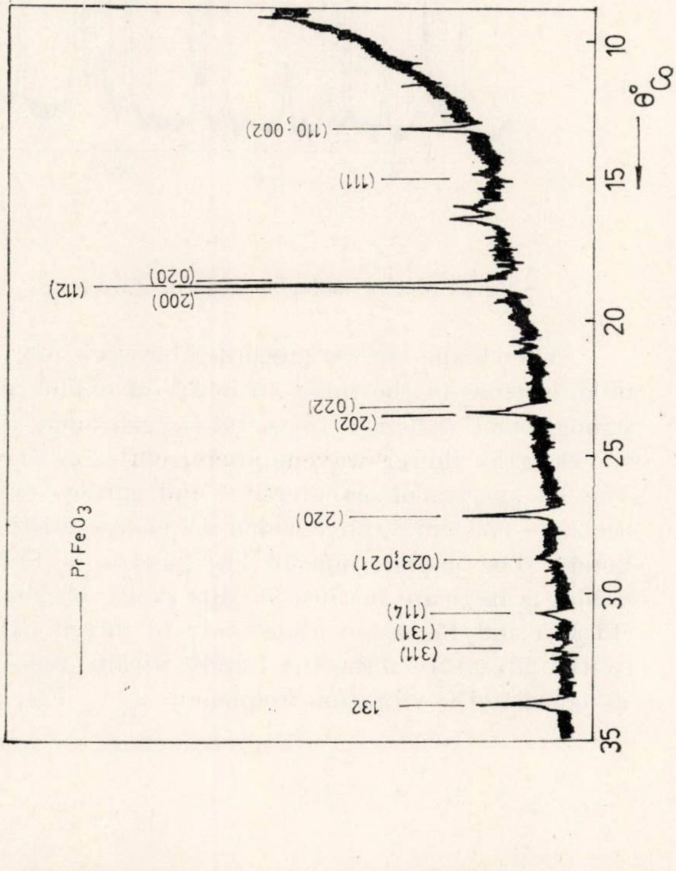

Fig. 1. — X-ray diffraction pattern of PrFeO$_3$.

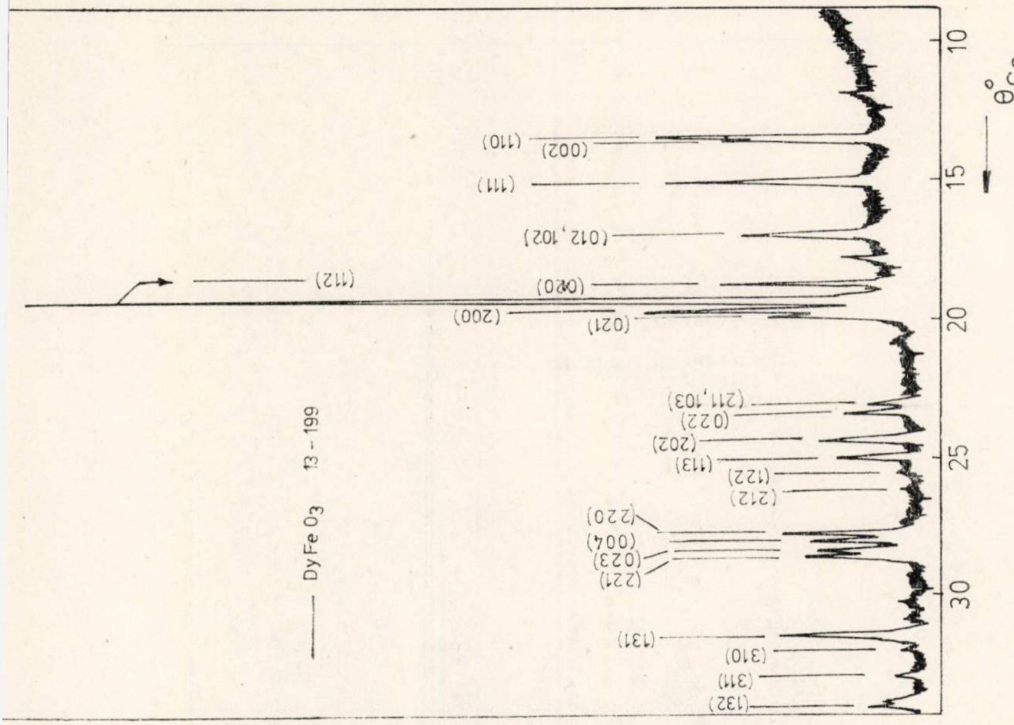

Fig. 2. — X-ray diffraction pattern of DyFeO$_3$.

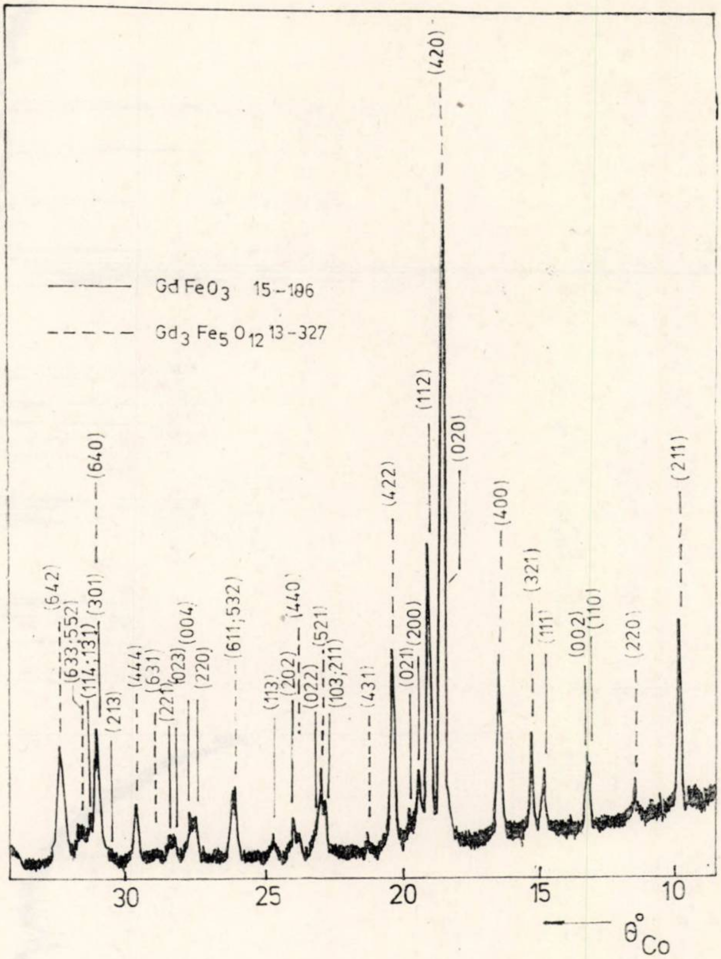

Fig. 3. — X-ray diffraction pattern of Gd FeO_3 (—) and $Gd_3Fe_5O_{12}$.(---)

The IR spectra were recorded between 400—800 cm^{-1}; they evidence modifications in the inner structure of oxidic phases. Thus the relatively strong band assigned to metal-oxygen bond vibration shifts to larger wavelengths (lower wavenumbers, cm^{-1}) as the oxide weight increases. The IR spectra of orthoferrites and garnets exhibit absorption bands in the 250—660 cm^{-1} range which are characteristic of Fe—O and O—Fe—O bonds. The explanation of IR spectra of Fe(III) and Ln(III) mixed oxides is intricate because in this range, the bands of lanthanides oxides (Ln_2O_3) and Fe_2O_3, overlap those of mixed oxides. However, according to the literature data the bands within 400—600 cm^{-1} range may be assigned to the vibration frequency ν_{Fe-O}. Fig. 4 shows the IR spectrum of $LaFeO_3$ whose absorption maximum lies at 570 cm^{-1} and is assigned to the vibration mode of ν_{Fe-O}.

The electronic spectra recorded for the orthoferrites of rare earths evidence several maxima assigned to the transitions of Fe(III) (d^5) ion in an octahedral configuration of minimum spin. Fig. 5 shows the electronic spectra of $LaFeO_3$ and $NdFeO_3$.

The Fe(III) mixed oxides which contain lanthanides exhibit very interesting magnetic properties. The orthoferrites are antiferromagnetic with some superimposed magnetism. Gileo [11] elucidated the magnetic behaviour of this class of oxides.

The strong dependence of La(III) orthoferrite susceptibility on the conditions of oxide preparation points to the existence in this oxide of some impurities or lattice defects. Because La(III) is a nonmagnetic ion the magnetism is assigned to Fe(III) ion.

The value of the magnetic moment of $LaFeO_3$, at room temperature, is 1.93 MB corresponding to Fe(III)(d^5) of octahedral coordination with minimum spin.

Soviet literature [12] mentions weak ferromagnetic properties for $DyFeO_3$; the maximum value of saturation magnetization (σ_{sat}) at 750° is 3.64 gauss · cm^3/g.

The experimental values of magnetization for various strengths of the field in $HoFeO_3$ (obtained by decomposition of gluconate mixtures) at room temperature correspond to a weak ferromagnetism (Table 1).

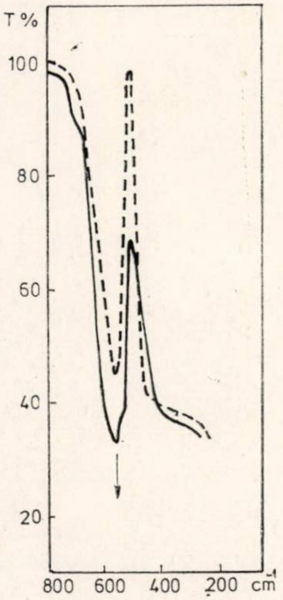

Fig. 4. — The IR spectrum of $LaFeO_3$.

Elucidation of the magnetic properties of the garnet has occurred together with the establishment of their crystalline structure. All lanthanide garnets are magnetic at room temperature except $GdFeO_3$ which is ferromagnetic at lower temperatures.

Chealyi [12] has studied the variation of magnetic properties of Yb and Gd garnets from their crystallization temperature (750°) to 1300°. Although at 750° the formation reaction is practically finished after 10 minutes, the value of saturation magnetization (σ_{sat}) points to the formation of a 95% garnet phase. The rising of temperature to 1300° entails an increase of saturation magnetization from 11.9 to 12.8 gauss·cm^3/g which indicates the improvement of sample crystalinity.

The data yielded by samples initially subjected to treatments at 800°/5 h and then at 1000°/5 h confirm Chealyi's findings. Table 1 lists the values of saturation magnetization of $Dy_3Fe_5O_{12}$ sample subjected to the two treatments.

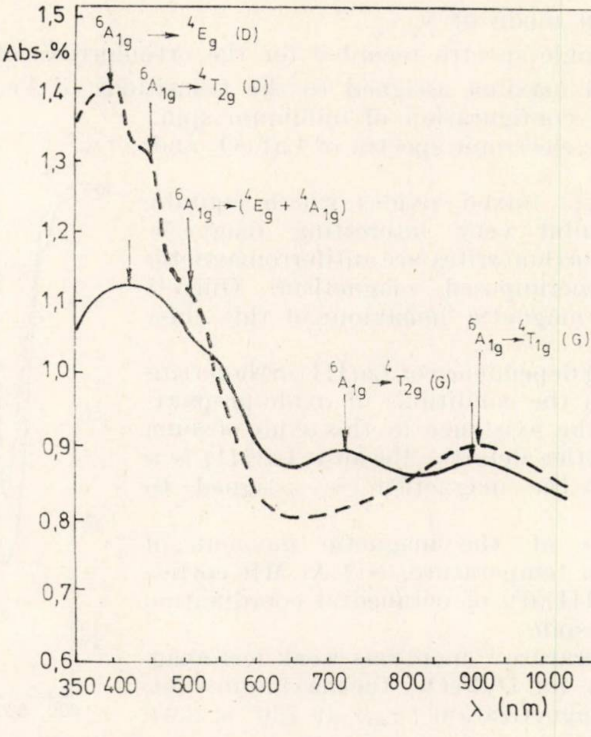

Fig. 5. — The electronic spectra of $LaFeO_3$ (———) and $NdFeO_3$ (— — —).

Table 1

The values of magnetization on for various strengths of the field in $HoFeO_3$ and $Dy_3Fe_5O_{12}$

	$H(Oe) \times 10^3$	$\chi S^{(u.e.m./g)}$
$HoFeO_3$	2.2 4.2 6.2 8.1	1.465 1.623 1.86 2.046
$Dy_3Fe_5O_{12}$ (5h/800°)	2.2 4.2 6.2 8.1	1.82 2.42 2.50 2.99
$Dy_3Fe_5O_{12}$ (5h/1000°)	2.2 4.2 6.2 8.1	2.59 2.99 3.59 4.59

REFERENCES

[1] P. Spacu, S. Ploştinaru, L. Patron, A. Conţescu, D. Crişan and N. Stănică, *Rev. Roumaine Chim.*, **32**, 877 (1987).

[2] Yung-Fang Yu, *J. Catal.*, **36**, 266 (1975).

[3] R. H. Voorhaeve, *Science*, **177**, 353 (1972).

[4] L. Ray and V. Sunivasan, *J. Catal.*, **65**, 121 (1980).

[5] J. O. Petuneli, *J. Catal.*, **70**, 356 (1981).

[6] M. Robbins, *Mat. Res. Bull.*, **7**, 233 (1972).

[7] V. P. Chealyi, *Izv. Akad. Nauk SSSR, Neorg. Mat.*, **9**, 1208 (1973).

[8] Ya. Macarova, L. C. Gavrilova, *Ukr. Khim. Zh.*, **12**, 1330 (1977).

[9] P. K. Gallagher, *Mat. Res. Bull.*, **3**, 225 (1968).

[10] P. Spacu, S. Ploştinaru, L. Patron, A. Conţescu, N. Stănică and D. Crişan, *Rev. Roumaine Chim.*, in press.

[11] N. A. Gilleo, *J. Chem. Phys.*, **24**, 1239 (1956).

[12] V. P. Chealyi, *Izv. Akad. Nauk SSSR, Neorg. Mat.*, **10**, 2028 (1974).

Revue Roumaine de Chimie, 34, *1*, 331–336 (1989)

ON THE STRUCTURE OF THE DISODIUM *p*-ISONONYLPHENYLETHOXYSULPHOSUCCINATE

R. STEFANOVA[a], I. BANCHOV[a] and L. PETROVA[b]

[a] Organic Chemistry Institute, Bulgarian Academy of Sciences, Sofia, Bulgaria
[b] Scientific Polymer Centre, Sofia, Bulgaria

Received February 16, 1988

The structure of *p*-isononylphenylethoxysulphosuccinate has been investigated by means of model compounds and using ^1H-NMR spectroscopy and quantum-chemical calculations. On the basis of the chemical shifts and theoretical calculations it has been found that SO_3Na and COONa hydrophilic functional groups are in α-position with respect to each other. The conformation of the compound investigated in d_6-DMSO and $CDCl_3$ has been determined from the measured vicinal constants. A strong tendency to the conformation with SO_3Na and p-iso-$C_9H_{19}C_6H_4O(CH_2CH_2O)_nOC$ groups anti-oriented to each other has been also found.

INTRODUCTION

The investigation of disodium monoalkylsulphosuccinates arouses interest, in connection with their wide use as surfactants as well as in order to find the mechanism of their formation.

The data known from literature show that the formation of disodium monoalkylsulphosuccinates is accompanied by the obtaining of undesirable diesters and other by-products,[1,2,3,4] depending on the temperature, the reaction time, the reaction medium pH, and on the ratio of the starting components of the reactions. The mechanism of sodium bisulphite addition to the carbon-carbon double bond of the maleic monoester as well as the SO_3Na group position in the disodium monoalkylsulphosuccinate is not well understood. The investigations of Panaeva[5] show that at reaction medium pH above 7 a product having SO_3Na and COONa groups in α-position is formed, whereas at pH less than 7 a product with β-oriented SO_3Na groups is additionally present in the reaction mixture.

By using physical methods and on the basis of theoretical considerations the authors[6] have found out that [in *p*-isononylphenylethoxysulphosuccinic acid converted into its disodium salt at pH = 6 and pH = = 6.3, the SO_3Na group is in α position in respect to the COONa group. In the present work, the structure of disodium *p*-isononylphenylethoxysulphosuccinate obtained at pH = 6.3 is studied by using ^1H-NMR and quantum-chemical calculations.

THEORETICAL

In order to define the intimate stages of the mechanism of this reaction, quantum-chemical calculations have been performed.

It is well-known that the reactions can be classified into two main groups : charge-controlled and orbital-controlled. [7] Usually, the reactions of the first type take place when one or the other reagent is of ionic or approximately ionic nature, i.e. when individual atoms or groups of atoms are so strongly charged that the electrostatic interactions between them are prevailing. With orbital-controlled reactions the contribution of the transfer of a charge from the highest occupied orbital (HOMO) to the lowest unoccupied molecular orbital (LUMO) plays the main role. In order to determine which of both mechanisms applies in our case, the following scheme of the process has been assumed.

The reaction proceeds in alkaline medium (NaOH solution). Therefore, the first stage of the process will be the reaction of the base with the carboxylic group of the intermediate product :

$$\mathrm{ROOC{-}CH = CH{-}COOH} \qquad \text{(I)}$$

with the formation of a sodium salt. $NaHSO_3$ dissociates to Na^+ and HSO_3^-. We suppose a dissociation of the HSO_3^- anion according to the scheme [9] :

$$\mathrm{HSO_3^- \rightleftarrows H^+ + SO_3^{--}}$$

and subsequent recombination with the Na^+ ion :

$$\mathrm{Na^+ + SO_3^{--} \rightleftarrows NaSO_3^-}$$

Therefore, the main reagents attacking the intermediate product are the H^+ cation and the $NaSO_3^-$ anion, i.e. reagents having a marked ionic nature. In order to estimate the possible paths of the attack, on condition that the charge-controlled mechanism of the reaction is assumed on the basis of the above-mentioned considerations, the values of electron charge densities of all atoms of the product I must be obtained.

Our investigations have been performed using the CNDO/2 method. Since the molecule being studied is too large and is out of the limits of our program, the following structure has been used as a model for this molecule :

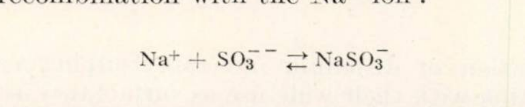

$$\mathrm{CH_3{-}O{-}CH_2{-}CH_2{-}O{-}\overset{\overset{O}{\|}}{C}{-}CH{=}CH{-}C\genfrac{}{}{0pt}{}{\diagup ONa}{\diagdown\!\!\!= O}} \qquad \text{(I″)}$$

As assumed $n = 1$ for the $(CH_2CH_2)_n$ fragment and further it is considered that the influence of the p-iso-$C_9H_{19}{-}C_6H_4O$ group on the central double bond (carbon atoms 1 and 2) is negligible so that this group can be modelled with a single methoxy group without significant effects on the results.

The calculated charge densities are presented in Table 1 (densities of non-carbon atoms are given only).

From the results in Table 1 it can be seen that except for the high electron density at oxygen atom due to the presence of a free electron pair, the highest electron density (the highest negative value) is observed for carbon atom 1. We will expect the most probable proton attack with the subsequent breaking of the double bond. The intermediate product obtained will react with the $NaSO_3^-$ anion which will take α-position in respect to the COONa group. Of course, due to the slight difference between the electron densities of the carbon atoms 1 and 2, under other conditions (different pH, etc.), the shifting of the mechanism towards the formation of β-derivative or most probably of both isomer mixtures is also possible (α-isomer content is always expected to be higher).

Table 1

Charge densities of individual atoms without the hydrogen atoms of compound I″

Atom N°	Kind of atom	Charge density	Atom N°	Kind of atom	Charge density
1	C	−0.0607	8	O	−0.2089
2	C	−0.0162	9	C	0.1649
3	C	0.3867	10	C	0.3715
4	O	−0.2449	11	O	−0.4364
5	O	−0.3203	12	O	−0.5506
6	C	0.1651	13	Na	0.7230
7	C	0.1599			

EXPERIMENTAL

The disodium p-isononylphenylethoxysulphosuccinate, respectively ethoxysulpho- succinate, has been obtained according to the following reaction scheme using the procedure described in work[7]:

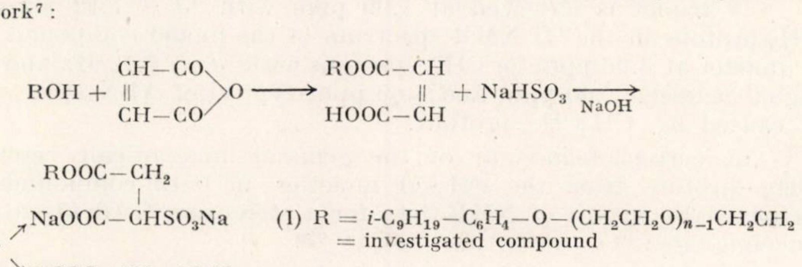

$$ROH + \begin{matrix}CH-CO\\ \| \\ CH-CO\end{matrix}\!\!>O \longrightarrow \begin{matrix}ROOC-CH\\ \| \\ HOOC-CH\end{matrix} + NaHSO_3 \xrightarrow[NaOH]{}$$

$$\longrightarrow \begin{cases} \begin{matrix}ROOC-CH_2\\ | \\ NaOOC-CHSO_3Na\end{matrix} & (I)\ R = i\text{-}C_9H_{19}-C_6H_4-O-(CH_2CH_2O)_{n-1}CH_2CH_2 = \text{investigated compound} \\ \begin{matrix}ROOC-CH-SO_3Na\\ | \\ CH_2COONa\end{matrix} & (II)\ R = CH_3CH_2 = \text{model compound}\end{cases}$$

From this scheme it can be seen that two possibilities for isomeric end products (I and II) exist. So far the exact structure has not been determined. The process of maleic anhydride esterification with the corresponding alcohol resulting in the formation of the corresponding ester has been carried out under the following experimental conditions: molar ratio of starting reagents = 1.05 : 1; reaction temperature = 95–100°C; reaction time = 180 min.

The process has been followed by means of the acid number and the saponification number of the reacting mixture. The addition of the sodium bisulfite to the monoesters obtained has been carried out under the following conditions: molar ratio 1 : 1.30; temperature = = 68–70°C; reaction medium pH = 6.3; reaction time = 60 min.

^{1}H-NMR Spectra

The ^{1}H–NMR spectra of the disodium *p*-isononylphenylethoxysulphosuccinate (I) and of the disodium alkylethoxysulphosuccinate (II) used as a model compound have been registered on WM–250 NMR Brucker spectrometer operating at 250.13 MH for ^{1}H in FT mode, at room temperature. d_6-DMSO and $CDCl_3$ have been used as solvents and TMS as an internal standard. The normal conditions for spectral analysis were as follows: pulse width about 40°; spectral width of 4000 Hz, 16 K data point for the Fourier transformation.

RESULTS AND DISCUSSION

A broad multiplet signal for the (OCH_2CH_2) polyethyleneglycol unit is observed at about 3.59 ppm, (3.55 ppm respectively in $CDCl_3$), in the ^{1}H–NMR spectrum of the investigated compound in d_6-DMSO. The widened downfield triplet signals at 3.70 ppm and at 4.02 ppm, (respectively 4.12 ppm in $CDCl_3$) and are caused by the CH_2-protons and $COOCH_2$-protons bonded like ethers to the aromatic substituent. The protons of the isononyl substituent are classified as follows: overlapping triplets at 0.72 ppm and 0.74 ppm related to the CH_3–protons; broad multiplet at 1.21 ppm and 1.42 ppm for three CH_2–groups and two CH_2–groups; for the aromatic ring protons, a doublet is observed at 6.82 ppm (and 6.84 ppm respectively in $CDCl_3$), for H_m with respect to the isononyl group and a multiplet centered at 7.16 ppm (7.17 respectively $CDCl_3$) for H_0 with respect to the isononyl group, with a coupling constant which is typical for *ortho*-interacting protons, $J = = 8.42\ Hz$, 8.52 Hz respectively ($CDCl_3$). In the region between 2.5 ppm and 3.9 ppm three groups of signals are observed corresponding to both diastereotopic methylene and methine protons of the CH_2CH ethane fragment.

A triplet is observed at 1.09 ppm with $^3J = 7.12$ Hz due to the CH_3-protons in the ^{1}H-NMR spectrum of the model compound, as well as a quartet at 3.96 ppm for CH_2–protons with $^3J = 7.12$ Hz and a multiplet signal between 2.60 ppm and 3.60 ppm typical of ABX spin systems and is caused by CH_2CH–protons.

A correct behaviour of the geminal magnetically non-equivalent CH_2–protons from the CH_2CH moieties in both compounds has been achieved by means of NMR-data for a stereospecific deuterated methylsuccinic acid.[10]

Based on the ABX analysis, the spectral characteristics, the chemical shifts and the spin interaction constants have been obtained (Table 2). The determination of the structure of the investigated compound has been achieved on the basis of the measured chemical shifts of the CH_2CH-protons. As can be seen from Table 2, the values of the chemical shifts for these protons in the investigated compound and in the model compound are almost equal. From the experimentally observed chemical shifts it follows that the positions of the SO_3Na and COONa substituents in the investigated compound are similar to those from model compound. The downfield shift of the CH-proton can be explained by a deshielding effect caused by the hydrophilic SO_3Na and COONa functional groups α-oriented to each other. Such a position is implemented as shown on the reaction scheme of the investigated compound and is in accordance with the theoretical calculations presented in the preceding section. The greater value of the shifts for the CH-proton of the investigated compound can be explained by the presence of a conformation in which this proton falls in the deshielding zone of the aromatic ring. The hindered conformations are shown in Fig. 1 for both compounds : compound I (investigated) and compound II (model). It is obvious that the *c* conformation with two gauche-group interactions has a slight contribution to the conformational equilibrium (the three substituents are in gauche-position with respect to each other). When considering the Newman projection formulas, it can be seen that in *b* conformation an *anti*-orientation of both vicinal H_A and H_X protons is implemented. In agreement with the measured vicinal proton coupling constants ($J_{AX} > J_{BX}$, see Table 2) one can conclude that *b* conformation is prevailing. The shift of the conformational equilibrium towards the conformation with the ROCO and SO_3Na groups in *anti*-positions and minimum number of gauche-group interactions is obviously determined by steric considerations. The steric volume of the ROCO substituent defines the following order of stability of the conformations : $q > a > c$.

Table 2

Chemical shifts and proton-proton coupling interaction constants of the CH_2CH-fragment in both compounds investigated

Compound	Solvent	Chemical shifts δ, (ppm)			Spin interaction constant J(Hz)		
		H_A	H_B	H_X	$^3J_{AB}$	$^3J_{AX}$	$^3J_{BX}$
Investigated	$CDCl_3$	2.80	2.69	3.93	−16.21	10.76	4.11
	d_6-DMSO	2.84	2.64	3.97	−16.58	9.98	4.20
Model	d_6-DMSO	2.80	2.61	3.58	−16.64	10.29	4.21

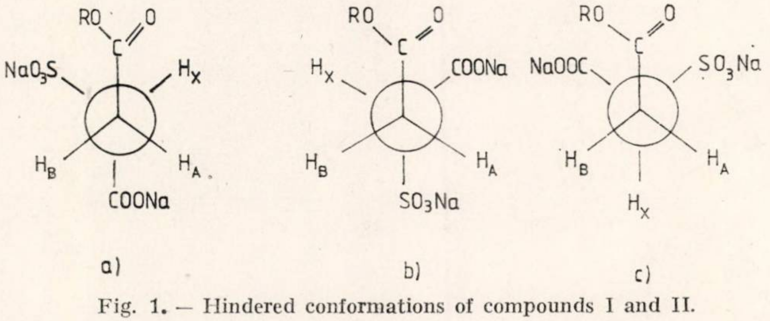

a) b) c)

Fig. 1. — Hindered conformations of compounds I and II.

The study of the effect of the reaction medium on the position of the conformational equilibrium of the investigated compound shows that the vicinal coupling constant values are not influenced by this factor (see Table 2). The latter fact is an indication for the conformational stability of the investigated compound. From the integral intensity of the signal for the polyglycolic unit of the investigated compound in $CDCl_3$ it has been calculated that *n* is equal to six.

REFERENCES

[1] J. Valee, *Parfum. Cosm. Savon*, **4**, 285 (1961).

[2] H. Hoffmann, *J. Soc. Cosm. Chem.*, **14**, 591 (1963).

[3] A. M. Schwartz, J. W. Perry and J. Berch, "Surface Active Agents and Detergents ", Vol. 2, Interscience, New York, 1958.

[4] E. E. Gilbert, "Sulfirovanie organicheskikh soedinenii", Izd. "Chimia", Moskwa, 1969.

[5] Sv. Panaeva, I. V. Ivanov and P. D. Stognusko, *Jurnal Prikladnoy Khimii*, **61**, 1300 (1986).

[6] L. Petrova, Cr. Simionescu and M. Ivanova, *Die Angewandte Makromolekulare Chemie*, in press.

[7] G. Klopman, *J. Amer. Chem. Soc.*, **90**, 223 (1968) ; G. Klopman, *ibid.*, **86**, 1463 (1964) ; G. Klopman, *J. Chem. Phys.*, **43**, 124 (1965) ; G. Klopman and B. O'Leary, *Fortschr. Chem. Forsch.*, **15**, 4 (1970) ; G. Klopman and R. F. Hudson, *Theoret. Chim. Acta* (Berlin), **8**, 165 (1967).

[8] K. Fukui, in "Chemical Reactivity and Reaction Paths", G. Klopman Ed., Moscow, MIR (1977), p. 30 (in Russian) ; K. Fukui, *Chem. Forsch.*, **15**, 1 (1970).

[9] L. Petrova, *Bul. Sert.*, **35**, 389 (1983).

[10] I. Retey, E. H. Smith and B. Zagalav, *Eur. J. Biochem.*, **83**, 437 (1987).

Revue Roumaine de Chimie, **34**, *1*, 337–349 (1989)

ELECTROCHEMICAL OXIDATION OF CARBOXYLIC ACIDS. I

ELECTRODE PROCESSES IN THE ELECTROCHEMICAL OXIDATION OF 3-PHENYLPROPIONIC ACID

SOLOMON STERNBERG[a], MIHAELA UNGUREANU[a] and SORIN ROȘCA[b]
[a] Laboratory for Applied Physical Chemistry, Faculty of Chemical Technology, Polytechnic Institute, 76206 Bucharest, Splaiul Independenței 313
[b] Department of Organic Chemistry, Polytechnic Institute, Bucharest

Received November 20, 1987

The present paper reports an application of the cyclic voltammetric method to the study of the processes of electrochemical oxidation of 3-phenylpropionic acid (PH) on platinum and graphite electrodes. It was shown that the two-electron oxidation on graphite occurs at about 1 V more electronegative potential than one-electron oxidation on platinum. Oxidation of PH and monomethyladipic acid (MH) on platinum was comparatively studied.

INTRODUCTION

The following general scheme :

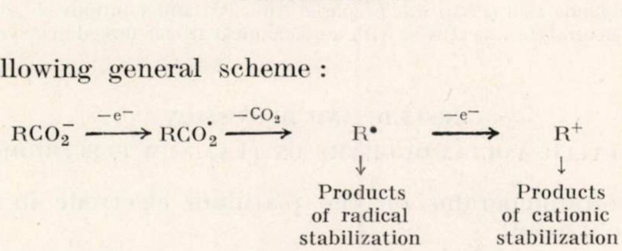

$$\begin{array}{ccccc} RCO_2^- \xrightarrow{-e^-} RCO_2^{\bullet} & \xrightarrow{-CO_2} & R^{\bullet} & \xrightarrow{-e^-} & R^+ \\ & & \downarrow & & \downarrow \\ & & \text{Products of radical stabilization} & & \text{Products of cationic stabilization} \end{array}$$

is known to illustrate oxidation processes in the case of carboxylic acids (in the form of their salts).

The fact is also known that large current densities favour one-electron oxidation on platinum electrodes and two-electron oxidation on graphite electrodes.[1]

The present paper makes a comparative study of the electrochemical oxidation of 3-phenylpropionic acid (PH) on platinum and graphite respectively, employing the method of cyclic voltammetry. It is an attempt at explaining the differences noticed in the preparatory electrolyses whose aim was to identify PH oxidation products. They showed that in case of PH oxidation on platinum, 84% products of radical stabilization and 16% products of cationic stabilization were obtained, whereas on graphite those percentages stood at 7 and 93 respectively.[2]

PH behaviour when oxidized on platinum was compared with the behaviour of the methylic monoester of the adipic acid $CH_3OOC(CH_2)_4COOH$(MH), when oxidized in similar conditions.

EXPERIMENTAL

Potentiostatic determinations were performed in non-steady-state conditions in an installation consisting of a Princeton Applied Research Model 179 potentiostat, an ORION EMG—1117/2 pulse generator and an X—Y recorder, all linked to an electrochemical cell with separate compartments.

The working electrode was either a platinum plate (area = 0.84 cm^2) or a graphite disk (area = 0.84 cm^2), and a platinum gauze served as counterelectrode. The reference electrode was an aqueous saturated calomel electrode. Prior to each determination, the platinum electrode was prepared as follows : oxidation with *aqua regia*, wash-up with distilled water, polarization at −0.01 V in a H_2SO_4 1 N solution for about ten minutes and slow return to +0.30 V. Further on, employing the same solution, the electrode was cycled with a 1.8 V triangular signal until a characteristic cyclovoltammogram was obtained. [3] Finally, the electrode was rinsed in distilled water and dried up. Before each determination, fine emerization provided for the renewal of the graphite electrode. All potentials were referred to the normal hydrogen electrode potential.

The working electrolyte employed was a methanolic solution containing a small amount of water (1% in volumes), the sodium salt of the 3-phenylpropionic acid (PNa) of various concentrations and free 3-phenylpropionic acid (PH) in a concentration of 0.5 M. In the case of MH oxidation, the electrolyte was a methanolic solution containing a small amount of water (1% in volumes), the sodium salt of the methylic monoester of the adipic acid (MNa) of various concentrations and the methylic monoester of the free adipic acid (MH) in a concentration of 0.5 M.

All substances used in the determinations were analytically pure. The 3-phenylpropionic acid (PH) was synthesized through an electrochemical reduction of the cinnamic acid, purified through distillation and then assessed from a physico-chemical point of view. The sodium salt of the 3-phenylpropionic acid (PNa) was prepared from PH and solutions of sodium methoxide in methanol. The electrolyte was stirred with a mechanical stirrer linked to a synchronous motor of 1,500 rpm.

RESULTS AND DISCUSSION

A. CYCLIC VOLTAMMOGRAMS ON PLATINUM ELECTRODE

Cyclic voltammograms on the platinum electrode in the range of 0—6 V were obtained.

Figure 1 shows the first five cyclic voltammograms obtained when PNa concentration was of 0.3 M ($C_{PNa} = 0.3M$). The curves in figure 1 show the first cycle to differ from the others (in which similar current values are yielded for the same potential value). Furthermore one may note that after cycle 3 the electrode processes become reproducible as the subsequent cyclic voltammograms were recorded.

Cyclic voltammogram 5 in figure 1 shows three strongly irreversible oxidation processes. The first process starts at 1 V and features a peak, P_1, of roughly 0.55 mA at 1.9 V. After P_1 the current drops to 0.15 mA.

The second oxidation process starts at roughly 2.4 V and features a shoulder, L_2, of 0.7 mA at 3 V or so. Superposed over the second process is a third oxidation process, whose salient feature is a limiting current, L_3, of some 1 mA, reached at roughly 3.4 V and maintained up to a potential of about 6 V. The three oxidation processes are clearly differentiated on the first cyclic voltammogram.

The return curve differs from the forward curve within the ranges of processes 1 and 2 and virtually runs over it within the range of the third oxidation process (the hysteresis characteristic of a diffusive process, however, is not obtained).

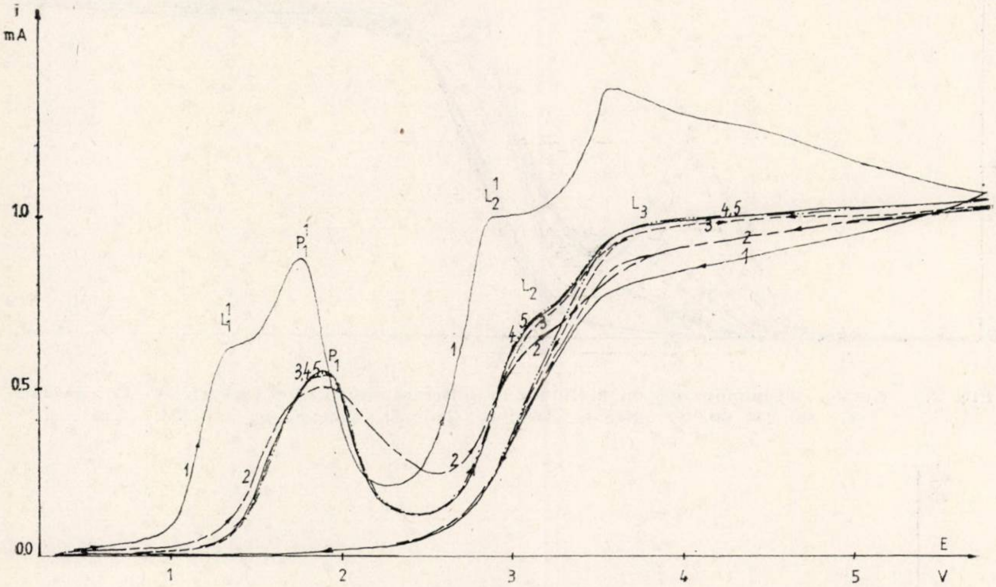

Fig. 1. — Successive cyclovoltammograms (cycles 1—7) on platinum ($C_{PNa} = 0.3$ M ; $v = 12$ mV/s).

Figure 2 shows the height of peak P_1 to decrease with the rise in sweep rate, while shoulder L_2 turns into peak P_2 whose height increases along with the sweep rate (from 0.8 mA at 12 mV/s to 1.33 mA at 360 mV/s). The limiting current L_3 is in no way affected by the sweep rate growth.

Figure 2 shows the cyclic voltammograms obtained on platinum at $v = 12$ mV/s for varied PNa concentrations. The fact is noteworthy that within the range of relatively high anion concentrations (0.1—0.3 M), oxidation processes are not practically influenced by anion concentration. The same dependence at the sweep rate of 180 mV/s is shown in figure 4.

Representations in figure 5 point to the linear dependence of the peak P_2 current on the square root of the sweep rate for anion concentrations of 0.1, 0.2 and 0.3 M, respectively.

Figures 3 and 4 show that when anion concentrations are smaller than 0.1 M, the aspect of the cyclic voltammograms changes, the limiting current L_3, recorded in case of high anion concentrations, disappears and the rise in the current knows no limits.

For an anion concentration of 0.02 M (figure 3) the first and second oxidation processes are marked by two high limiting currents—L_1 and L_2—whose values increase along with the sweep rate.

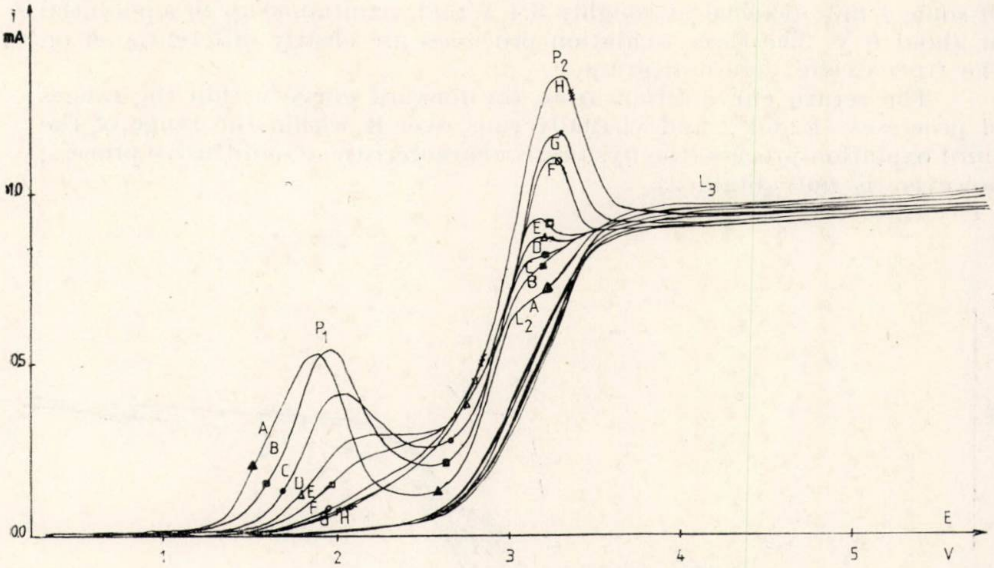

Fig. 2. — Cyclic voltammograms on platinum at different sweep rates (mV/s) ; A : 12 ; B : 24 ; C : 36 ; D : 60 ; E : 84 ; F : 180 ; G ; 240 ; H : 360 ; $C_{\mathrm{PNa}} = 0.3\mathrm{M}$.

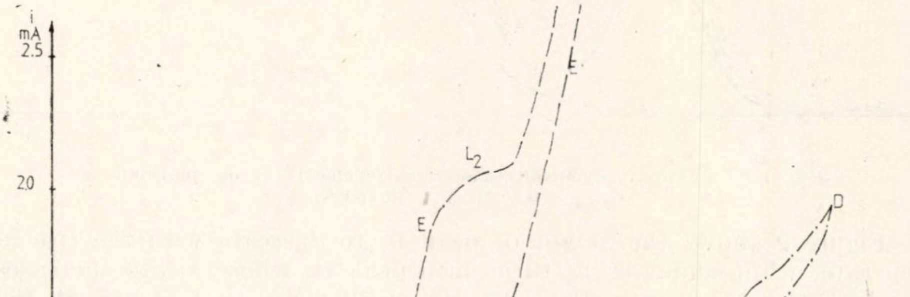

Fig. 3. — Cyclic voltammograms on platinum at various PNa concentrations (M) ; A : 0.3 ; B : 0.2 ; C : 0.1 ; D : 0.05 ; E : 0.02 ; $v = 12$ mV/s.

The behaviour of the 3-phenylpropionate anion (P^-) when oxidized was compared with that of the anion of monomethyladipate $CH_3OOC(CH_2)COO^-(M^-)$, which was analysed in the same conditions.[4]

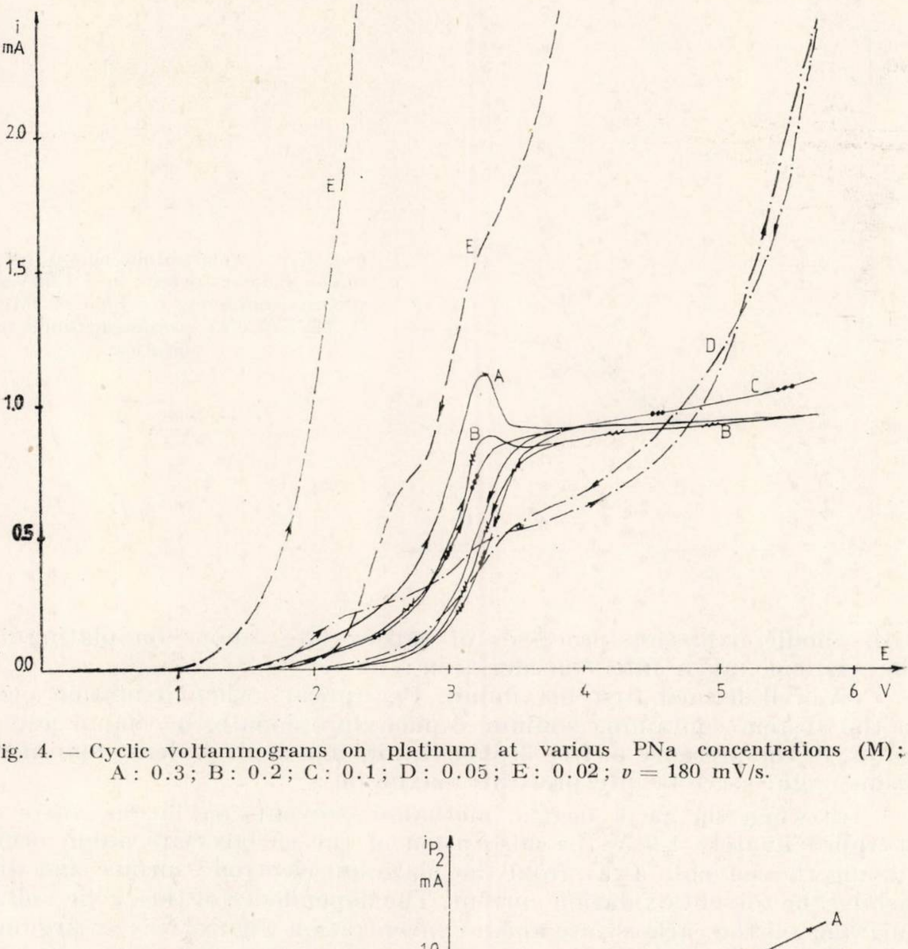

Fig. 4. — Cyclic voltammograms on platinum at various PNa concentrations (M); A : 0.3 ; B : 0.2 ; C : 0.1 ; D : 0.05 ; E : 0.02 ; $v = 180$ mV/s.

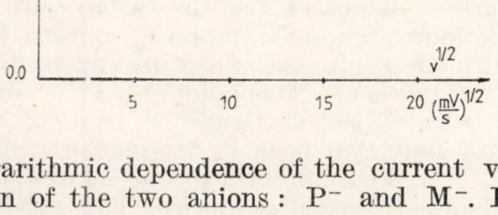

Fig. 5. — The dependence of the peak P_2 current on the sweep rate at various PNa concentrations (M) ; A : 0.3 ; B : 0.2 ; C : 0.1.

Figure 6 shows the semi-logarithmic dependence of the current values on potential for the oxidation of the two anions : P^- and M^-. I- also outlines the major differences between the oxidation processes ot the two anions on platinum and, primarily, the current values which are far higher in the case of M$^-$ than in the case of F$^-$ oxidation.

The cyclic voltammograms and their processing yielded, which are given in figures 1—6, lead to the following conclusion in connection

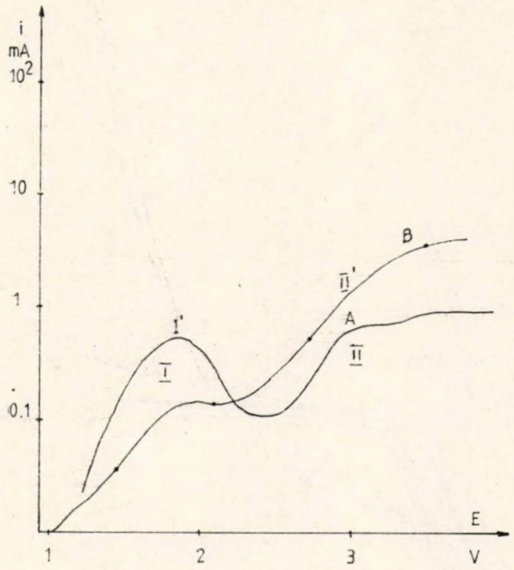

Fig. 6. — Polarization curves on platinum (anodic sweep; $v = 12$mV/s) in systems containing A : PNa (0.3M) and B : MNa (0.3M); semilogarithmic representation.

with anodic oxidation processes of carboxylate anions on platinum in the systems taken into consideration :

A well-defined first maximum, P_1, appears when oxidation occurs in the system containing sodium 3-phenylpropionate, methanol and 1% water, in the presence of free 3-phenylpropionic acid. At least four mechanisms might serve to interpret this maximum :

a) when the peak begins, methanol (solvent) oxidation starts and at approximately 1.9 V the adsorption of the carboxylate anion occurs, moving the solvent away from the platinum electrode surface and diminishing the solvent oxidation current. The dependence of the cyclic voltammograms on the carboxylate anion concentration (figure 3) is an argument in favour of this hypothesis. So, for instance, when anion concentration stands at 0.02 M (the lowest concentration under study) the prevailing process is that of methanol oxidation, with the salt serving primarily as an ion-bearing electrolyte. When salt concentration goes up, the overall current decreases and the carboxylate anion is adsorbed more than the methanol whose oxidation it inhibits. Figure 2 shows peak P_1 to decrease with the rise in the sweep rate and to disappear when sweep rates are higher than 180 mV/s. This points to the occurrence of slow adsorptive processes. When comparing figures 3 ($v = 12$ mV/s) and 4 ($v = 180$ mV/s) one may note that peak P_1 disappears when sweep rates are high.

b) Peak P_2 may be accounted for by HO$^-$ ion discharge, when adsorbed oxygen is formed. This process should have a cathodic correspondence : the reduction of the adsorbed oxygen in cathodic sweep.

This cathodic process was not observed on the cyclic voltammograms obtained within a 1 or 2 V restricted potential range.

c) Platinum oxidation might occur within the peak P_1 range, leading to the formation of platinum oxides. According to numerous authors this oxidation process precedes any other molecular oxidation process on both platinum [5] and other metals.[6] The first cycle is characterized by the limiting current L_1^1 and the maximum P_1^1. Total carboxylate oxidation [5] was shown to occur on free platinum, which might correspond to the limiting current L_1^1 (obtained in the first cycle). Peak P_1 would correspond to the oxidation of the platinum electrode. The second cycle occurs on an electrode covered with platinum oxide formed in the first anodic sweep and L_1^1 disappears. Further on, the processes are virtually reproducible.

d) As will be shown in what follows, within the range of the potential characteristic of peak P_1 two-electron oxidation of the 3-phenylpropionate anion occurs on graphite electrodes. The same process might occur within the P_1 range on platinum, though, as yet, there is no evidence to support this hypothesis.

Of the four above-mentioned mechanisms, our working hypothesis will rely on the first interpretation of peak P_1(a).

The faradaic process of 3-phenylpropionate anion oxidation, according to scheme $C_6H_5CH_2CH_2COO^- \xrightarrow{Pt} C_6H_5CH_2\dot{C}H_2 + CO_2 + e^-$ (2) followed by reactions of stabilization of the formed radical, for instance, by dimerization (3)

$$2\,C_6H_5CH_2\dot{C}H_2 \rightarrow C_6H_5CH_2CH_2CH_2CH_2C_6H_5 \tag{3}$$

starts at about 2.1 V. The polarization curve is characterized by peak P_2, which, at low sweep rates, is a shoulder, and by the limiting current L_3. The limiting current L_3 is probably caused by a relatively thick porous layer of reaction products (resins). A forced rather than a semiinfinite linear diffusion occurs through the porous layer of thickness δ. This is probably responsible for the same "return", respectively, for the lack of hysteresis within the limiting current L_3 range.

Furthermore, the fact should be underscored that the system under study contains no "indifferent" electrolyte, the only anion being the electrochemically active one. Under similar circumstances, diffusion is combined with electromigration. Frumkin [7] showed that in the case of a combined mass transport : diffusion-electromigration, the limiting current doubles if the ion passes through the two mechanisms in the same sense. And this is our case, too. The transformation of the limiting current L_2 into peak P_2, along with a sweep rate growth, attests the existence of a mass transport limit (figures 2 and 5).

The diffuse limitation of the process of electrooxidation of the 3-phenylpropionate anion is proved also by the study of the system in conditions in which the electrolyte is stirred (figure 7). In this case, the limiting current L_2 increases threefold or so as compared with the voltammograms obtained without stirring. Owing to stirring, the passivating anodic layer "grows thinner" and the anodic current increases ; peak P_1 is not disturbed by stirring.

The absence of a clear law concerning the role of the concentration may be due to the complexity of the process in question. Probably, the anodic current has two competitive components, respectively: $i = i_1$ (anion oxidation) $+ i_2$ (solvent oxidation).

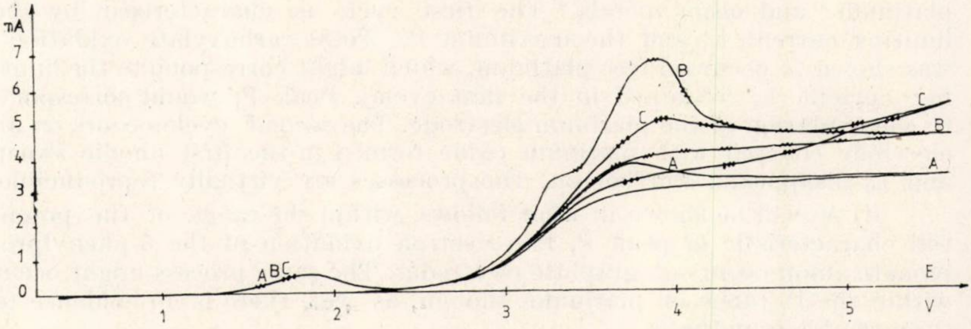

Fig. 7. — Cyclic voltammograms on platinum in conditions of electrolyte stirring, at various PNa(M) concentrations; $A : 0.3$; $B : 0.2$; $C : 0.1$; $v = 12$ mV/s.

A higher anion concentration is favourable to current i_1 and detrimental to current i_2. In the case of the cyclic voltammograms obtained without stirring, the respective competitivity masks the $i = i(C_{\mathrm{PNa}})$ dependence. In the case of the experiments involving stirring, total current is high and i $(C_{\mathrm{PNa}} = 0.3)$ is higher than $i(C_{\mathrm{PNa}} = 0.1)$. This might indicate a weight of i_2 in i larger than that of i_1. A current maximum is obtained for i $(C_{\mathrm{PNa}} = 0.2)$, as an outcome of the competition between the two anodic processes.

As concerns the comparison of the cyclic voltammograms obtained for the two carboxylates under study (figure 6) a marked difference may be noted in the behaviour of the two anions. For the system containing M^- two oxidation ranges are also obtained.[4] The first range (I′) — between 0 and 2.2 V — probably corresponds to solvent oxidation, while the second (II′), which starts from 2.2 V, stands for anion oxidation. There is no clear separation between the two ranges in the case of M^- oxidation. The currents obtained in the case of M^- oxidation are higher than those yielded in the case of P^- oxidation — by about three times within the first range and, respectively, 25 times or so within the second range. So, for instance, in the case of an anion concentration of 0.3 M the currents registered at 3.3 V amount to 20 mA (M^-) and 1 mA(F^-). These differences seem to prove that M^- adsorption of platinum is stronger than P^- adsorption. Supporting the same point is the absence of a minimum region between the two oxidating processes in case of M^- oxidation. Another work [4] showed that the current increases with anion concentration growth in the domain of M^- anion oxidation (II′) which differs from the behaviour of the P^- anion when oxidized, as shown above.

Here are the possible explanations of the very marked differences in the behaviour of the two carboxylate anions:

(i) The real concentration of P^- ions is far lower than the nominal one; probably, ion pairs form in this metabolic medium with a high PNa association constant. This explains the very low currents obtained for this salt in comparison with MNa. In the case of MNa, the real anion concentration is very high, virtually equaling nominal concentration. Then i_2 in equation (4) is negligible and $i = i_1$, which explains the current rise along with MNa concentration growth. In the preparatory electrolyses, for the same value of current intensity, terminal voltage is some threefold smaller in the case of MNa oxidation than in the case of PNa oxidation.

(ii) Within the system that contains MH, the passivating layer does not form, the limiting current L_3 does not emerge and M^- oxidation proceeds freely up to a very high potential (range II'; figure 6). The Tafel apparent slopes within range II' are substantial (roughly 500 mV per decade), which cannot be explained by a charge transfer control combined with adsorption, but rather by an ohmic control of the electrode process. Even more substantial slopes are obtained in the case of PNa and their explanation is also an ohmic control within a system whose conductivity is lower than that of MNa.

B. Cyclic Voltammograms on Graphite Electrode

A study was conducted onto the behaviour of the system consisting of sodium 3-phenylpropionate of various concentrations, 3-phenylpropionic acid (0.5 M), methanol and water (1% in volumes) on graphite electrode. Figure 8 shows a cyclic voltammogram obtained when $C_{\mathrm{PNa}} =$

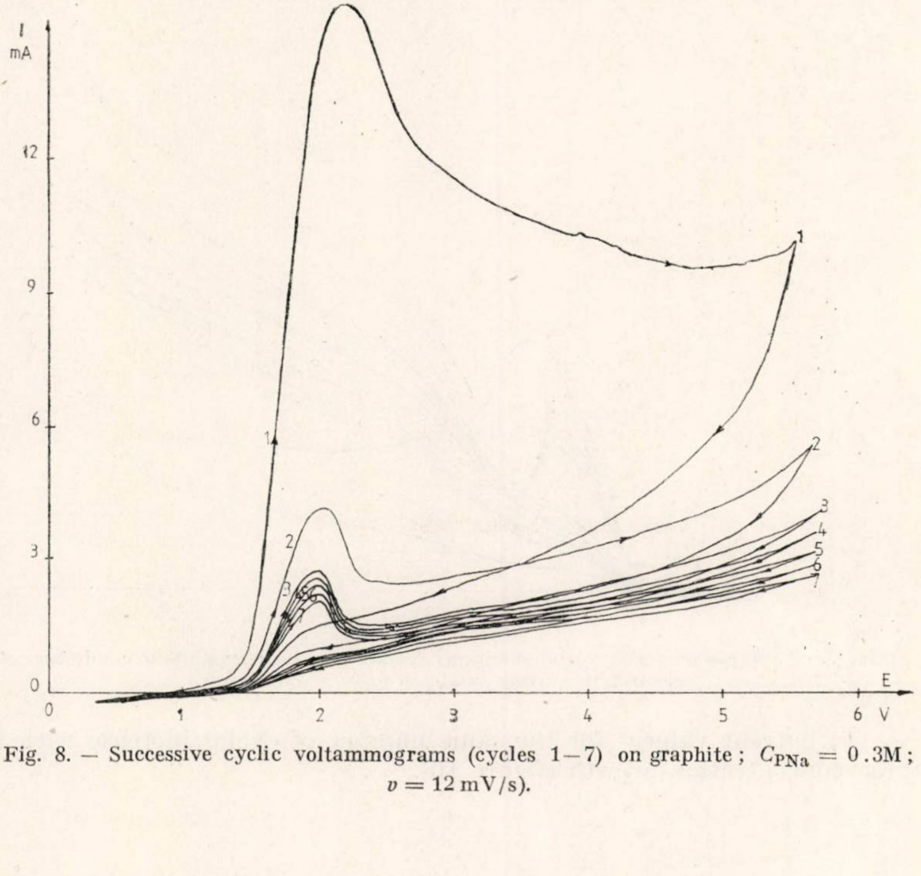

Fig. 8. — Successive cyclic voltammograms (cycles 1—7) on graphite ; $C_{\mathrm{PNa}} = 0.3\mathrm{M}$; $v = 12\ \mathrm{mV/s}$).

$= 0.3$ M. A behaviour different from that registered on the platinum electrode (figure 1) can be noted as follows :

a) a rapid oxidation process, with currents far higher than those registered on platinum, starts at about 1.4 V. The current reaches a maximum at roughly 2 V, then drops and again increases, this time slowly. A value of some 2.4 mA is attained at 5.3V (cycle 7). Given the same potential, the current stands at about 1 mA on platinum ;

b) the voltammograms obtained on graphite feature a marked hysteresis ;

c) to a great extent, registered current values depend on the number of cyclings to which the electrode was subjected. So, for instance, the value of the peak current at 1.9 V drops 3.7 times from the first to the second cycle and 1.5 times from the second to the third cycle. Further on, current values decline about seven per cent for every cycle. Such a behaviour may be accounted for by the formation of a layer of reaction products oxidized on the electrode surface.

d) just like in the case of the platinum electrode, oxidation processes are intensified by electrolyte stirring (figure 9) ;

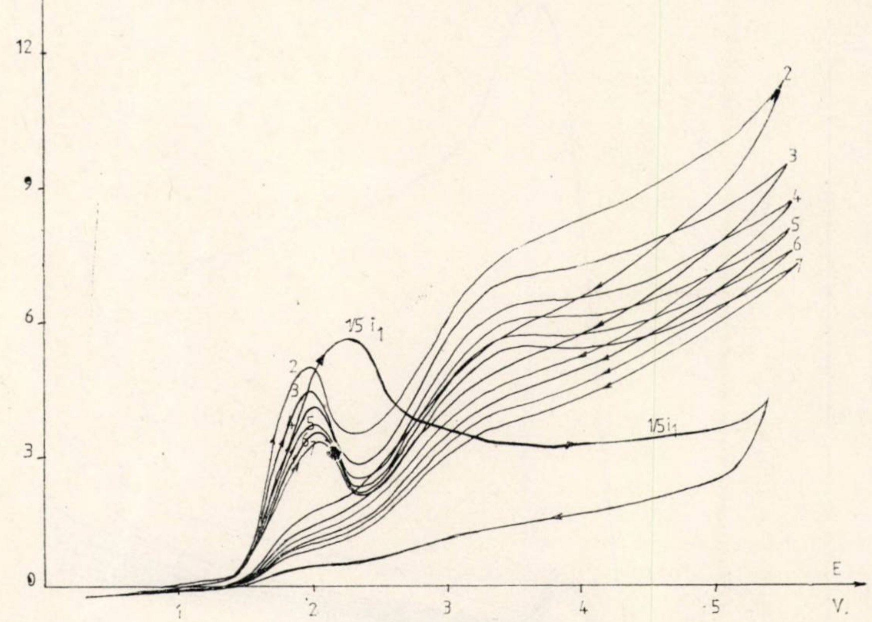

Fig. 9. — Successive cyclic voltammograms (cycles 1—7) on graphite in conditions of electrolyte stirring ; $C_{\mathrm{PNa}} = 0.3$; $v = 12$ mV/s.

e) current values for the same number of cycles increase with the anion concentration growth (figure 10).

The results of the previously performed preparatory electrolyses [2] on graphite electrodes show that the oxidation reaction of the sodium

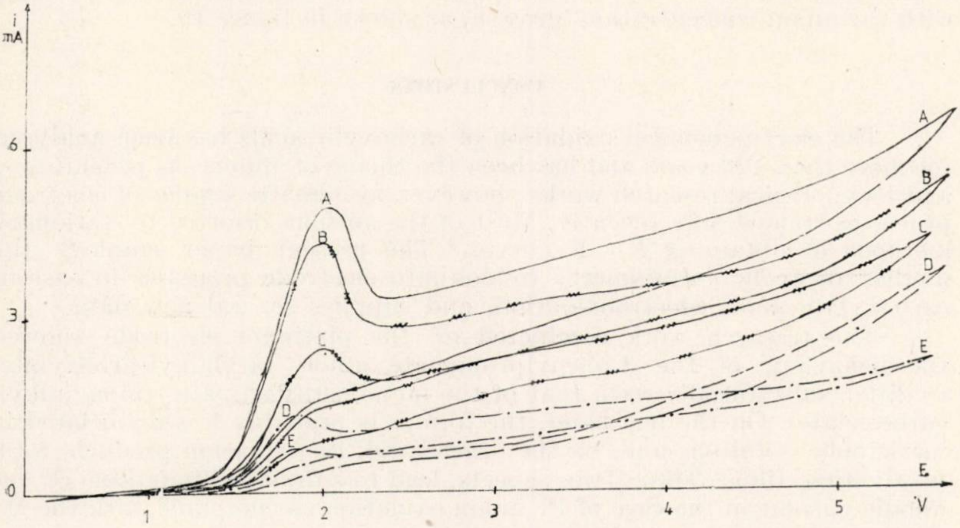

Fig. 10. — Cyclic voltammograms on graphite at various PNa (M) concentrations; A : 0.3; B : 0.2; C : 0.1; D : 0.05; E : 0.02; $v = 12$ mV/s.

3-phenylpropionate proceeds according to a two-electron mechanism, that is :

$$C_6H_5CH_2CH_2COO^- \rightarrow C_6H_5CH_2CH_2^+ + CO_2 + 2\ e^- \qquad (5)$$

Reaction (5) is followed by stabilization reactions, yielding mainly alcohols and ethers :

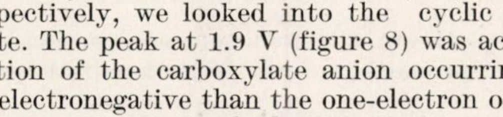

$$\begin{tikzcd} C_6H_5CH_2CH_2^+ \arrow[r, "CH_3OH"] \arrow[d, "\sim H^{-\cdot\cdot}"] & C_6H_5CH_2CH_2OCH_3 \quad (6) \\ C_6H_5CH^+CH_3 \arrow[r, "CH_3OH"] & C_6H_5\underset{\displaystyle OCH_3}{\underset{|}{C}}HCH_3 \quad (7) \end{tikzcd}$$

Confining our analysis to the electrochemical aspect of the process, to reaction (5) respectively, we looked into the cyclic voltammograms obtained on graphite. The peak at 1.9 V (figure 8) was accounted for the two-electron oxidation of the carboxylate anion occurring at potentials of about 1 V more electronegative than the one-electron oxidation process on platinum, where currents are far higher. Oxidation currents are much higher in the first cycle in particular (that is, some 16 times). Even in the case of cycle 7 (figure 8) the currents are approximately two times higher on a platinum. One may also note a passivation of the electrode after repeated cyclings, which may be accounted for by the formation of a passive film of hardly soluble reaction products (possibly resins).

In the case of the graphite electrode, solvent oxidation and carboxylate anion oxidation are probably superposed. Current i_2 in equation (4) is probably far lower than current i_1. That is why, the current increases with the anion concentration growth, as shown in figure 10.

CONCLUSIONS

The electrochemical oxidation of carboxylic acids has been analysed for more than 120 years and has been the theme of numerous preparatory and technological research works; however, systematic studies of electrode processes started only recently. Most of the authors resorted to stationary methods of obtaining $I - E$ curves.[8] The present paper employs the method of cyclic voltammetry to look into electrode processes in case of carboxylate anion electrooxidation, and supplies several new data.

The research work conducted on the platinum electrode showed the behaviour of the 3-phenylpropionate anion (arylalkylcarboxylate) to differ substantially from that of the monomethyladipate anion (alkylcarboxylate). On the one hand, the former is probably less dissociated in methanolic solutions and, on the other hand, its oxidation products form passivating films. These two aspects lead to a drastic diminution of the anodic current in the case of P^- anion oxidation as compared with the M^- anion oxidation.

Further items of information were obtained as concerns the nature of the electrode. Previous preparatory studies[2] showed that the use of a graphite electrode is favourable to a two-electron oxidation of the carboxylate anions. The present paper gives an "electrochemical answer" to this question. Two-electron electrooxidation on graphite proceeds at potentials about 1 V more electronegative than the one-electron electrooxidation on platinum. Therefore, platinum is an "anticatalyst" of the two-electron oxidation; in exchange, it is favourable to a selective run of the one-electron oxidation and, implicitly, of Kolbe dimerization, which, in most cases, is the most interesting from a technological point of view. The first oxidation stage (8) occurs both on platinum and on graphite.

$$\mathrm{RCOO^-} \rightarrow [\mathrm{RCOO}\cdot]_{\mathrm{ads}} + e^- \qquad (8)$$

According to Wendt[9] on platinum the electrode surface is blocked with the adsorbed intermediary and, further on, the charge transfer reaction occurs no longer on the inner plane of the Helmholtz electrical double layer but on its outer plane, that is:

$$\mathrm{R{-}COO^-} \rightarrow \mathrm{RCOO^\bullet} + e^- \qquad (8a)$$

Further on, on platinum, the homogeneous reactions of decarboxylation and dimerization, primarily, of the formed radical occur:

$$\mathrm{RCOO^\bullet} \rightarrow \mathrm{R^\bullet} + \mathrm{CO_2} \qquad (8b)$$

$$2\,\mathrm{R} \rightarrow \mathrm{R{-}R} \qquad (8c)$$

On graphite, the decarboxylation reaction proceeds according to scheme (9a)

$$[\mathrm{RCOO^\circ}]_{\mathrm{ads}} \rightarrow [\mathrm{R^\circ}]_{\mathrm{ads}} + \mathrm{CO_2} \qquad (9a)$$

The adsorbed radical may be further oxidized to carbocation (9b) :

$$[R^\bullet]_{ads} \rightarrow \overset{+}{R}_{ads} + e^- \qquad (9b)$$

As is known, charge transfer from the outer Helmholtz plane (according to equation (8a)) needs a far higher energy consumption than in the case the anion is adsorbed on the electrode surface (located in the inner Helmholtz plane). This probably explains the energy difference of about 1 eV between graphite and platinum, mentioned in this paper.

Other authors [10] relate the two-electron process on graphite to the existence of a number of paramagnetic centers on the graphite surface and on a larger real surface. This hypothesis seems more plausible, as it implies carboxylate-ion adsorption on both platinum and graphite, with different adsorption energies, however.

REFERENCES

[1] N. L. Weinberg, "Technique of Electroorganic Syntheses", John Wiley & Sons, New York, 801, 1974.

[2] S. Roşca, Mihaela Ungureanu and S. Sternberg, *Rev. Roumaine de Chimie*, in press.

[3] D. Pletcher and V. Solis, *Electrochim. Acta*, **27**, 779 (1982).

[4] S. Sternberg, Mihaela Ungureanu and S. Roşca, *Rev. Roumaine de Chimie*, in press.

[5] D. F. A. Koch and R. Woods, *Electrochim. Acta*, **13**, 2101 (1968).

[6] O. Radovici and I. Gh. Murgulescu, "Introducere în chimia fizică. 4. Electrochimia", 303, Ed. Academiei, 1986.

[7] V. V. Damaskin and D. A. Petri, "Vedenie v elektrokhimicheskuyu kinetiku", 169, Vyshaya shkola, Moskva, 1975.

[8] Yu. V. Vassiliev, E. P. Kovsman and G. N. Freidlin, *Electrochim. Acta*, **27**, 937 (1982); *Electrochim. Acta*, **27**, 953 (1982).

[9] H. Wendt, *Electrochim. Acta*, **29**, 1513 (1984).

[10] S. Torii, "Electroorganic Syntheses", Kondansha VCH, Tokyo, 12 (1985).

Revue Roumaine de Chimie, **34**, *1*, 351–356 (1989)

ОБ ЭЛЕКТРОХИМИЧЕСКОЙ СТОЙКОСТИ ТИТАНДВУОКИСНОМАРГАНЦЕВЫХ АНОДОВ, ПОЛУЧЕННЫХ ЭЛЕКТРОИСКРОВЫМ СПОСОБОМ

РОДИКА А. СТУРЗА, В. Э. НЕННО и А. М. РОМАНОВ
Лаборатория электрофлотации веществ, Институт прикладной физики АН МССР, Кишинев, СССР

Получена 2 октября 1988 г.

Изучена электрохимическая стойкость титандвуокисномарганцевых анодов (ТДМА), активное покрытие которых наносилось импульсными электрическими разрядами при одновременной подаче в межэлектродное пространство дисперсного материала. Установлено, что двуокисномарганцевое покрытие с добавкой небольшого количества палладия обладает удовлетворительными электрохимическими характеристиками. При плотности тока до 100 мА/см^2) срок службы анодов достигает 50—64 тысяч часов до износа 70% покрытия. Методами рентгенофазового анализа и авторадиографии исследованы глубина проникновения, фазовый состав и получены кривые распределения материала покрытия в титане.

The electrochemical durability of dioxide manganese titanium anodes actively coated by impulse electric discharges with the simultaneous feeding of the disperse material to the interelectrode gap has been studied. It has been stated that the dioxide manganese coating with the addition of a small quantity of palladium possesses satisfactory electrochemical characteristics. When the current density is up to 1000 A/m^2 the anodes are used for 50000—64000 hours and the wear equals 70 % of the active coating. The penetration depth of the coating material in titanium and its phase composition have been investigated by the X-ray phase and radioactive isotopes methods. The distribution curves have been obtained.

ВВЕДЕНИЕ

В последнее время титандвуокисномарганцевые аноды (ТДМА) находят все более широкое применение в различных областях электрохимического производства.[1] Как правило, они изготовливаются путем термического разложения $Mn(NO_3)_2$ или осаждением из растворов в условиях электролиза $MnSO_4$. С целью улучшения электрического контакта между основой и покрытием наносят промежуточный слой из металлов платиновой группы или их оксидов.[2] Кроме того, небольшие добавки благородных металлов оказывают также влияние на каталитическую активность анода.

Однако при получении и эксплуатации анодов существуют сложности, связанные со склонностью покрытия к потере механической прочности (растрескивание). Более того, создание многокомпонентных металлооксидных анодных материалов включает в себя, как правило, ряд энергоемких технологических операций.

В данной работе при нанесении оксида марганца (IV) и электрокаталитической добавки — палладия на титановую подложку использовали метод электроискрового легирования (ЭИЛ) с одновременной подачей в межэлектродное пространство дисперсного материала. Способ разработан в ИПФ АН МССР[3] и в определенной мере совмещает преимущества традиционного ЭИЛ компактными материалами с широкими технологическими возможностями порошковых методов нанесения покрытий.

Порошковый материал подается в межэлектродное пространство (в зону действия разрядов) в момент движения легирующего электрода вниз к катоду. При воздействии плазмы искрового разряда порошковый материал расплавляется и происходит его взаимодействие с поверхностью детали. Метод удобен, не требует специального оборудования и позволяет использовать различные шихты, концентрации компонентов которых легко регулируются. Многокомпонентные покрытия формируются за одну технологическую операцию, не требуют предварительной подготовки поверхности основы и последующего диффузионного отжига.

Покрытия, полученные импульсными электрическими разрядами, отличаются высокой степенью сцепления с основой, что снижает вероятность их отслоения в процессе анодной поляризации.

ЭКСПЕРИМЕНТАЛЬНАЯ ЧАСТЬ

Смесь порошков оксида марганца (IV) марки (ХЧ) и палладия наносилась на основу из титана ВТ1-0 импульсными электрическими разрядами длительностью 200 мкс и рабочей частотой 100 Гц на установке типа ,,ЦИЛИНДР'' с источниками технологического тока серии ,,ЭФИ'' и ,,ЭЛИТРОН''. Для нанесения покрытия использовали электродный инструмент вибрирующего типа с одновременной подачей в межэлектродное пространство порошкового материала. Легирующим материалом анода служил титан.

Образцы имели цилиндрическую форму, рабочей поверхностью служила торцевая часть (S_{pad} = 1,1 см^2). С целью снижения шероховатости до необходимого класса чистоты рабочая поверхность подвергалась поверхностно-пластической деформации стальным закаленным шариком диаметром 5 мм.

Электрохимические исследования проводились на потенциостате П-5827М с автоматической записью на потенциометре ПДП4-002 в 0,01 N растворе $CaCl_2$. Контроль за содержанием марганца в растворе после окисления его периодатом[4] осуществлялся фотоколориметрически на приборе ФЭК-56П. Электрохимические потенциалы в статье даны относительно нормального водородного электрода.

Рентгенофазовый анализ проводился на установке ДРОН-3 в кобальтовом K_α-излучении. Распределение элементов в поверхностных слоях титана изучалось методом авторадиографии на установке БЕТА-1. Шероховатость поверхности измерялась на профилографе-профилометре (модель 252) с автоматической цифровой записью.

РЕЗУЛЬТАТЫ И ОБСУЖДЕНИЕ

Электрохимическая стойкость ТДМА определяется стойкостью титана и оксида марганца (IV). Стойкость титана обуславливается защитной пленкой TiO_2, потенциал пробоя которой обычно в несколько раз выше рабочего потенциала ТДМА. В условиях, когда химическое растворение

MnO_2 ничтожно мало, его стойкость определяется скоростью электрохимического окисления. Так как покрытия, нанесенные известными методами (кроме плакирования) обладают достаточной пористостью в условиях анодной поляризации происходит рост оксидной пленки на титане. В результате этого увеличивается переходное сопротивление и нарушается электрический контакт между основой и покрытием. Эти два фактора определяют срок службы ТДМА.

При электрохимической поляризации ТДМА (покрытие — 100% MnO_2) в области потенциалов 0,2—0,5 В наблюдается линейная зависимость φ—lgi с константами $a = 300$ мВ и $b = 67$ мВ (рис. 1, кривая 1). Это связано с растворением низковалентных, хорошо растворимых оксидов марганца, которые всегда присутствуют в его диоксиде. Данный процесс подтверждается изменением массы электрода в процессе гальваностатической поляризаци ($i = 40$ мА/см²). Вначале наблюдается потеря массы (18 мг/см² в час), а затем масса электрода увеличивается, что связано с образованием фазы TiO_2. Потенциал анода вначале неустойчив и устанавливается в области выделения кислорода лишь по истечению одного часа, через три часа работы потенциал электрода возрастает.

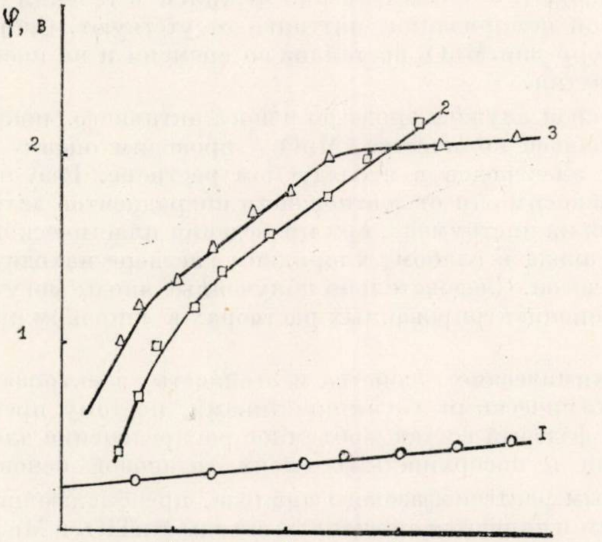

Рис. 1. — Потенциодинамические анодные поляризационные кривые в 0,01 N растворе $CaCl_2$. Материал анода: 1 — MnO_2/Ti, 2 — $MnO_2/TiC/Ti$, 3 — $(MnO_2 + Pd)/Ti$.

Согласно [5], в качестве токопроводящего подслоя в ТДМА можно использовать карбид титана, который обладает хорошей электропроводностью. Исследование ТДМА с предварительно нанесенным слоем TiC показало, что перенапряжение по кислороду невысокое (рис. 1, кривая 2), однако поляризуемость анода значительна ($tg\beta = 0{,}46$). Через 4—5 часов работы электрический контакт между титаном и покрытием нарушается. По данным рентгенофазового анализа TiC в условиях анодной поляризации разрушается. Так как покрытия нанесенные методом ЭИЛ, отличаются высокой пористостью, условия работы в подслое оказались жесткими и его окисление происходит с той же скоростью, что и окисление покрытия.

На потенциодинамической поляризационной кривой образцов с покрытием можно выделить два участка газовыделения: от 1,5 до 2,0 В и выше 2,0 В (рис. 1, кривая 3). Первый характеризуется углом наклона $tg\beta=0,46$, второй носит явно тафелевский характер с константами $a = 1291$ и $b = 77$ при $i = 100$ мА/см^2. Гальваностатическая поляризация образца в течении 25 часов показала, что потенциал анода устанавливается практически сразу на уровне 2,2 В и не меняется во времени, хотя через 17—18 часов на поверхности электрода были обнаружены питтинги.

Шероховатость поверхности после ЭИЛ находится в пределах 3—6 мкм. Питтинговая коррозия образца происходит, по-видимому, в наивысших точках шероховатой поверхности, где возникает максимальный градиент потенциала, приводящий к точесному пробою защитной пленки TiO_2. После проведения поверхностно-пластической деформации шероховатость рабочего покрытия образца снижается до 0,6—1,25 мкм. Потенциал такого анода ($i = 100$ мА/см^2) не меняется в течении 60 часов гальваностатической поляризации, питтинги отсутствуют. Скорость электрохимической коррозии MnO_2 постоянна во времени и не превышает 0,15—0,16 г/м^2 в сутки.

Приняв срок службы анода до износа активного покрытия на 70% и определив общее количество MnO_2, проводим оценку длительности эксплуатации электродов в исследуемом растворе. Результаты показывают, что в зависимости от соотношения инградиентов активного покрытия и давления на инструмент, при проведении пластической деформации, срок службы анода в слабом хлоридном растворе находится на уровне 50—64 тысяч часов. Следовательно полученные аноды могут быть использованы в слабоконцентрированных растворах в широком интервале плотностей тока.

Электрохимические свойства и стойкость электрода определяется его физико-химическими характеристиками, поэтому представляло интерес изучить фазовый состав и объемное распределение элементов активного покрытия в поверхностных слоях титановой основы электрода.

По данным рентгенофазового анализа, преобладающими фазами в составе покрытия являются смешанные оксиды $MnTiO_3$ и Mn_2TiO_4. Обнаружены также Ti, TiO и следы интерметаллида Ti Pd. Чистые фазы MnO_2 и Pd отсутствуют. Очевидно, отсутствие MnO_2 положительно влияет на механическую прочность активного покрытия. Ответственными за высокую каталитическую активность и стабильность работы анода являются, вероятно, фазы $MnTiO_3$ и Mn_2TiO_4. Сплав вентильного и благородного металлов создает эффективный барьер протеканию ионного тока, что предотвращает окисление подложки в процессе анодной поляризации.

Распределение легирующего материала в поверхностных слоях изучалось методом авторадиографии. С увеличением энергии разряда интенсифицируется глубина диффузионной зоны и повышается концентрация легирующих элементов в объеме легируемого материала (рис. 2). При этом, однако, ухудшается качество покрытий так как образуется

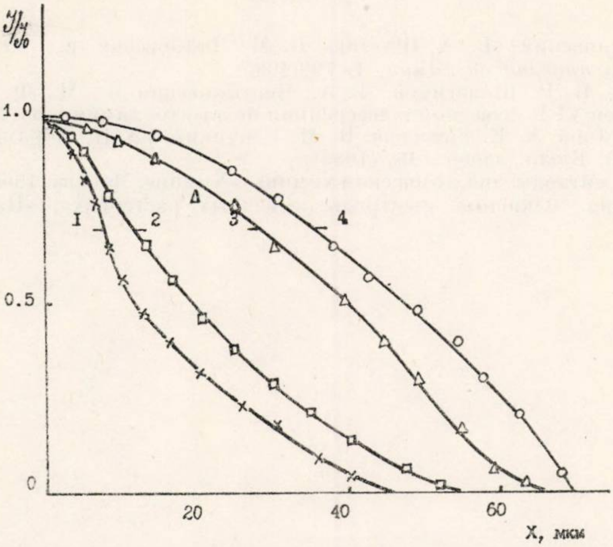

Рис. 2. — Распределение легирующего материала ($MnO_2 + Pd$) в поверхностных слоях титана при энергии электроискрового легирования: 1 — $W_{\text{и}} = 0{,}27$; 2 — $W_{\text{и}} = 0{,}84$; 3 — $W_{\text{и}} = 2{,}7$: 4 — $W_{\text{и}} = 6{,}4$ Дж.

множество микротрещин и увеличивется шероховатость покрытий. Поэтому рабочий режим нанесения покрытия по энергии разряда был оптимизирован, как по однородности слоя активного покрытия, так и по концентрации легирующих компонентов в его объеме.

ЗАКЛЮЧЕНИЕ

Методом электроискрового легирования с одновременной подачей в межэлектродное пространство материала в дисперсном виде получены двуокисномарганцевые покрытия на титане. Отсутствие компонентов благородных металлов в покрытии приводит к возрастанию переходного сопротивления и нарушению электрического контакта между основой и активным слоем. Электроискровое легирование составом, содержащим палладий сопровождается образованием новой фазы — сплава TiPd, являющейся эффективным барьером протеканию ионного тока и предотвращающей окисление подложки. Высокая активность и механическая прочность покрытия связана с присутствием электрокаталитически активных смешанных оксидов $MnTiO_3$ и Mn_2TiO_4

Условия электроискрового легирования существенно влияют на структуру и распределение материалов в поверхностных слоях титановой основы электрода.

ЛИТЕРАТУРА

[1] Е. А. Калиновский, В. А. Шустов, В. М. Чайковская и Ю. К. Россинский, *Журнал прикладной химии*, **4**, 799(1985).

[2] Д. М. Шуб, В. В. Шалагинов, Т. А. Чертыковская и М. Ф Резник, «Тезисы докладов VI Всесоюзной конференции по электрохимии», т. 2, Москва, 1982.

[3] В. В. Михайлов, А. Е. Гитлевич, В. М. Ревуцкий и А. П. Абрамчук, *А. С. СССР*, 1151403, Бюлл. изобр., **15**, (1985).

[4] Г. Шарло, «Методы аналитической химии», «Химия», Москва, 1966.

[5] Н Ф. Разина, «Окисные электроды в водных растворах», «Наука», Алма-Ата, 1978.

Revue Roumaine de Chimie, **34**, *1*, 357–363 (1989)

BILDUNG UND STABILITÄT VON $3(CaO \cdot Al_2O_3) \cdot BaSO_4$

I. TEOREANU und ANNEMARIE PURI
Polytechnische Hochschule Bukarest, Polizustr. 1, Bukarest, Rumänien

Eingegangen am 12. Oktober 1988

Es werden die Reaktionsvorgänge und die Natur der Mineralphasen welche sich beim Brennen von Massen aus dem System $CaO-Al_2O_3-BaSO_4$ bilden, untersucht. Die Zusammensetzung der untersuchten Massen entspricht den Molverhältnissen $CaO : Al_2O_3 : BaSO_4$ von 3 : 3 : 1, bzw. 9 : 3 : 1 ; als Ausgangssubstanzen wurden neben $BaSO_4$, sowohl $CaCO_3$ und Al_2O_3, als auch $CaO.A_2O_3$ verwendet. In den über 1000°C gebrannten Massen bildet sich ein Sulfataluminat dessen Zusammensetzung, Gitterkonstanten und thermische Beständigkeit von der Natur der Ausgangssubstanzen beeinflusst werden.

The interaction processus and the nature of mineralogical phases which result by burning the masses from the $CaO-Al_2O_3-BaSO_4$ system are examined. The compositions of the examined masses were in accordance with the mol ratios $CaO : Al_2O_3 : BaSO_4 =$ $= 3 : 3 : 1$, respectively 9 : 3 : 1. As starting materials were used, except $BaSO_4$, both $CaCO_3$ and Al_2O_3 and also $CaO \cdot Al_2O_3$. In the masses burned over 1000°C sulfataluminate was present ; its composition, lattice constant and thermal stability depend on the nature of the starting materials.

1. EINLEITUNG

Die ersten Informationen über die Bildung und thermische Beständigkeit von $3(CaO \cdot Al_2O_3) \cdot CaSO_4$ sind in der Fachliteratur vor ungefähr drei Jahrzehnten erschienen,[1–10] sie wurden nachträglich durch weitere Forschungen über die Struktur des $3(CaO \cdot Al_2O_3) \cdot CaSO_4$[11] und sein Hydratationsverhalten, allein oder zusammen mit verschiedenen Mengen CaO, $CaSO_4 \cdot 2\,H_2O$, $2\,CaO \cdot SiO_2$, $3\,CaO \cdot SiO_2$, Zementklinker, Puzzolane oder Gemischen von diesen Stoffen,[5,6,8–10,12–15] ergänzt. In der Arbeit [16] wird die Möglichkeit der Bildung von Sulfataluminaten der Art $3(CaO \cdot Al_2O_3) \cdot Me_x(SO_4)_y$ gezeigt, wobei $Me_x(SO_4)_y$ Sulfate mit grosser thermischer Beständigkeit sind.

Scholze und Hildebrandt [11] haben die Ähnlichkeit der Struktur des Calciumsulfataluminates mit derjenigen des natürlichen Minerals Hauyn $Na_6[Al_6Si_6O_{24}](CaSO_4)_2$ gezeigt ; durch Ersetzen der Na^+-Ionen mit Ca^{2+} und der Si^{4+}-Ionen mit Al^{3+} entsteht $Ca_6[Al_{12}O_{24}](CaSO_4)_2$. Die Elemente aus der eckigen Klammer bilden ein dreidimensionales Netzwerk aus über Ecken verknüpften $[AlO_4]$-Tetraedern, in dessen Hohlräumen sich die Ca^{2+}-und SO_4^{2-}-Ionen befinden (Bild 1). In einer solchen Struktur ist das SO_4^{2-}-Ion sehr stabil gebunden ; nach Halstead und Moore[17] ist bei 1400°C der SO_3-Verlust von $CaSO_4$ 30-mal schneller als der von $3(CaO \cdot Al_2O_3) \cdot CaSO_4$.

Es ist zu erwarten dass der Radius des Kations, welches zusammen mit dem SO_4^{2-}-Ion in die Hohlräume eingebaut wird, die Dimensionen der kubischen Elementarzelle der entsprechenden Sulfataluminate beeinflusst; Teoreanu und Mitarbeiter[16] haben, für die Sulfataluminate der Reihe $3(CaO \cdot Al_2O_3) \cdot MeSO_4$, eine Verschiebung der entsprechenden Roentgeninterferenzen, parallel mit dem Anwachsen des Ionenradius von Mg^{2+} zu Ba^{2+} festgestellt.

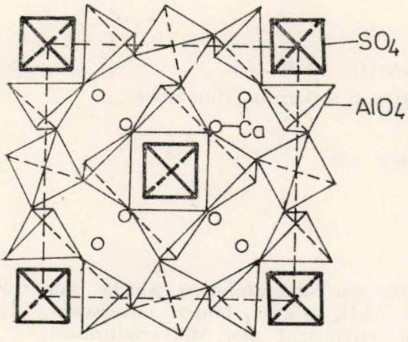

Bild 1. — Struktur des $3(CaO \cdot Al_2O_3) \cdot CaSO_4$

In dieser Arbeit werden die Reaktionsvorgänge und die Mineralphasen, welche beim Brennen von Massen aus dem System $CaO-Al_2O_3-BaSO_4$ entstehen, untersucht.

2. VERSUCHSBEDINGUNGEN

Es wurden Massen welche stoichiometrisch dem $3(CaO \cdot Al_2O_3) \cdot BaSO_4$ entsprechen und auch solche mit einem Überschuss an CaO(deren basischere Natur den silikatischen Sulfataluminatzementen vergleichbar ist), untersucht. Den untersuchten Massen entsprechen folgende Molverhältnisse:

— für die Masse SAB I — $CaO : Al_2O_3 : BaSO_4 = 3 : 3 : 1$;

— für die Masse SAB II — $CaO : Al_2O_3 : BaSO_4 = 9 : 3 : 1$.

Es wurden folgende Ausgangssubstanzen verwendet:

— $CaCO_3$, Al_2O_3 und $BaSO_4$, die entsprechenden Massen wurden SAB Ia und SAB II a notiert;

— $CaO \cdot Al_2O_3$ und $BaSO_4$ für die Masse SAB I, welche SAB Ib notiert wurde.

Die homogenisierten Ausgangsmischungen wurden zu Formlingen (Zylinder mit $\varnothing = 10$ mm) gepresst, 3 Stunden lang bei 800—1500°C gebrannt und langsam im Ofen abgekühlt. Die Reaktionsvorgänge und die Natur der sich bildenden Mineralphasen wurden durch analytische Bestimmung des ungebundenen CaO und durch Roentgendiffractometrie untersucht.

3. DARSTELUNG UND DISKUSSION DER ERGEBNISSE

Die aus den Diffractogrammen ermittelten Informationen über die Natur der sich bildenden Mineralphasen wurden graphisch bearbeitet und als Variation der Intensität der entsprechenden Roentgeninterferenzen mit der Brenntemperatur, dargestellt. In die gleichen Diagramme wurde auch der analytisch bestimmte Gehalt an ungebundenem CaO eingetragen.

Die Masse SAB Ia

Das Verschwinden der dem $CaCO_3$ entsprechenden Interferenzen in der bei 1000°C gebrannten Probe, korreliert mit dem kleinen Wert des analytisch bestimmten freien CaO (Bild 2) und der progressiven

Abschwächung der Intensität der Interferenzen des Al_2O_3 zeigen, dass schon unter 1000°C Reaktionsvorgänge zwischen CaO und Al_2O_3 stattfinden. Roentgenographisch werden die, dem $CaO \cdot Al_2O_3$ und $12\ CaO \cdot 7\ Al_2O_3$ entsprechenden Interferenzen nachgewiesen, deren Intensität bis zu ungefähr 1150°C anwächst; bei höheren Temperaturen wird die

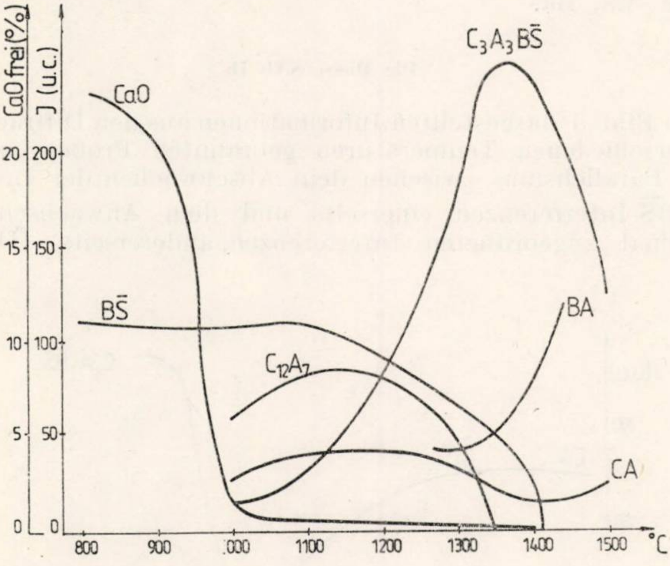

Bild 2. — Temperaturäbhängigkeit der Mineralphasen beim Brennen der Masse SAB Ia

Intensität der Calciumaluminatinterferenzen wieder schwächer, so dass in der bei 1350°C gebrannten Probe kein $C_{12}A_7$* mehr nachgewiesen werden kann.

Bei über 1000°C wird die Intensität der $BaSO_4$-Interferenzen langsam schwächer, nach 1100°C beschleunigt sich diese Abschwächung, parallel mit dem raschen Anwachsen der Intensität von, dem $3(CaO \cdot Al_2O_3) \cdot BaSO_4$ zugeordneten Interferenzen. Bei ungefähr 1350°C erreicht die Intensität der Sulfataluminatinterferenzen maximale Werte um dann, besonders über 1400°C, rasch abzufallen. In den bei über 1200°C gebrannten Massen bildet sich $BaO \cdot Al_2O_3$.

Die Tatsache dass die Abschwächung der Intensität der Sulfataluminatinterferenzen beim Überschreiten von 1350—1400°C, nicht von einem Anwachsen der $BaSO_4$-Interferenzen begleitet wird, sowie auch das Anwachsen der BA-Interferenzen, weisen darauf hin, dass bei diesen Temperaturen sowohl das $3\,CA \cdot B\bar{S}$ als auch das $BaSO_4$ in dem untersuchten System unbeständig werden.

---

* Es werden folgende, in der Silikatchemie übliche Symbole verwendet: $C = CaO$; $A = Al_2O_3$; $B = BaO$; $B\bar{S} = BaSO_4$.

Das bei der thermischen Zersetzung des Sulfataluminates bedeutendere Anwachsen der BA-Interferenzen, im Vergleich mit denjenigen des CA, könnte eine Folge der Bindung als Aluminat nicht nur des Calciums, sondern auch des Bariums sein, mit entsprechenden Folgen für die Gitterkonstante des Sulfataluminates. Demnach würde das so gebildete Sulfataluminat eher der Formel $3\,(MeO \cdot Al_2O_3)BaSO_4$ entsprechen, in welcher Me=Ca, Ba.

Die Masse SAB Ib

Die in Bild 3 dargestellten Informationen aus den Diffractogrammen der bei verschiedenen Temperaturen gebrannten Proben, zeigen einen deutlichen Parallelismus zwischen dem Abschwächen der Intensität der CA- und $B\overline{S}$-Interferenzen einerseits und dem Anwachsen der, dem Sulfataluminat zugeordneten Interferenzen, andererseits. Überraschend erscheint die Feststellung dass das, aus CA und $B\overline{S}$ gebildete $3\,CA \cdot B\overline{S}$ auch bei Temperaturen über 1350°C beständig bleibt, die Untersuchungen wurden bis einschliesslich 1430°C geführt.

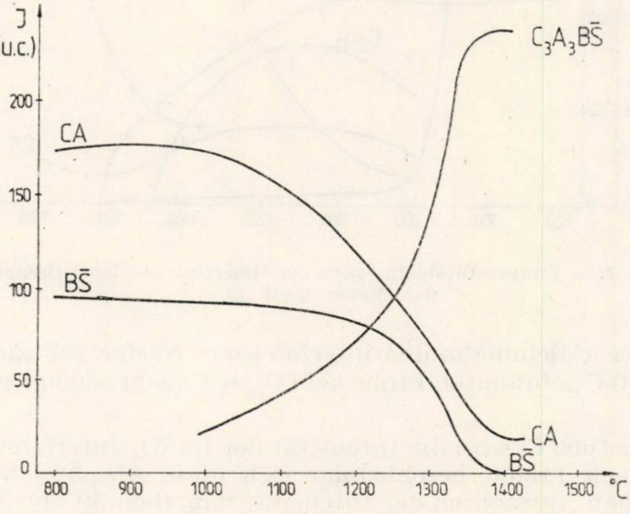

Bild 3. — Temperaturabhängigkeit der Mineralphasen beim Brennen der Masse SAB Ia

Um diese unterschiedliche Temperaturbeständigkeit des aus verschiedenen Ausgangssubstanzen synthetisierten Sulfataluminates zu überprüfen, wurden die Massen SAB Ia und SAB Ib bei 1350° und 1400°C, eine bzw. fünf Stunden lang, gebrannt; Bild 4 zeigt die Werte der Intensität der Hauptinterferenz des Sulfataluminates. Die grössere Temperaturbeständigkeit des aus CA und $B\overline{S}$ synthetisierten Sulfataluminates ist deutlich sichtbar.

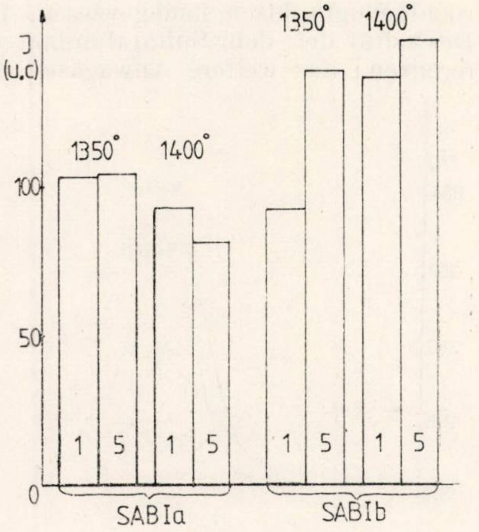

Bild 4. — (Temperatur-Zeit)-Abhängigkeit der Intensität der Hauptinterferenz (422) des Sulfataluminates für SAB Ia und SAB Ib

Die Masse SAB IIa

Die Intensitäten der, den verschiedenen Mineralphasen charakteristischen Interferenzen (Bild 5), zeigen schon von 900°C an, Reaktionsvorgänge (durch das Abschwächen der Al_2O_3 Werte und des Anteils an ungebundenem CaO). Als neugebildete Phasen werden in der, bei 1000°C gebrannten Probe, mit Sicherheit $C_{12}A_7$, C_3A und Erdalkalisulfataluminat

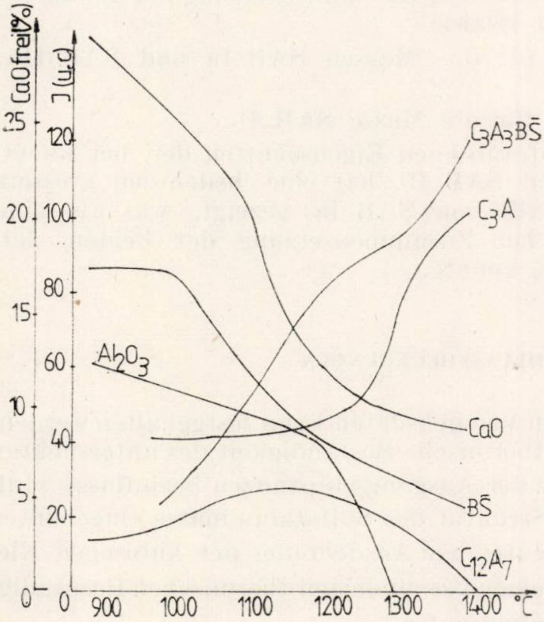

Bild 5. — Temperaturabhängigkeit der Mineralphasen beim Brennen der Masse SAB IIa

roentgenographisch nachgewiesen. Bis 1200°C wächst hauptsächlich die Intensität der, dem Sulfataluminat und dem $C_{12}A_7$ entsprechenden Interferenzen; das weitere Anwachsen der Brenntemperatur führt zu einem raschen Verbrauch des gebildeten $C_{12}A_7$, sowie auch des Al_2O_3, CaO und $BaSO_4$, während der Anteil an C_3A und $3\,CA \cdot B\overline{S}$ wächst. In der, 3 Stunden bei 1400°C gebrannten Probe coexistieren $3\,CA \cdot B\overline{S}$, C_3A, $B\overline{S}$ und ungebundenes CaO (8,6%). Es wird keine Bildung von BA festgestellt.

Bild 6 zeigt die Verschiebung der Hauptinterferenz des Sulfataluminates bei Anwachsen der Brenntemperatur. Für alle untersuchten Massen wird eine Ausdehnung des kubischen Gitters des Sulfataluminates bis 1400°C festgestellt, gefolgt von einer Schrumpfung im, der Sulfataluminatzersetzung entsprechenden Temperaturbereich.

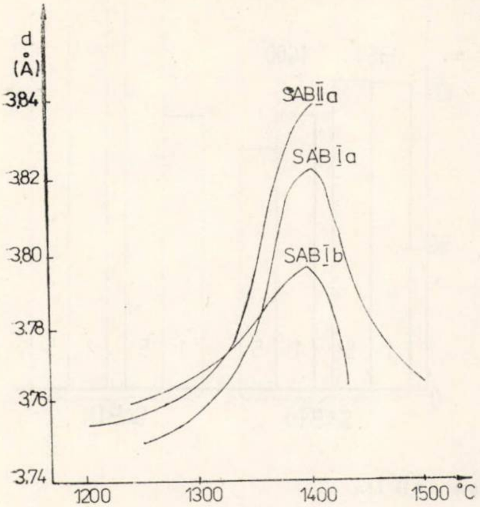

Bild 6. — Temperaturabhängigkeit der Hauptinterferenz (422) des Sulfataluminates

Für die Massen SAB a, welche aus $CaCO_3$, Al_2O_3 und $BaSO_4$ synthetisiert wurden, ist die Ausdehnung des Gitters entschieden bedeutender als für die Masse SAB Ib aus $CaO \cdot Al_2O_3$ und $BaSO_4$. Diese Feststellung könnte auf eine unterschiedliche Zusammensetzung der gebildeten Sulfataluminate hinweisen, und zwar:

— $3(MeO \cdot Al_2O_3)BaSO_4$ — für die Massen SAB Ia und SAB IIa, wobei MeO=CaO, BaO und

— $3(CaO \cdot Al_2O_3) \cdot BaSO_4$ — für die Masse SAB Ib.

Die Untersuchung der hydraulischen Eigenschaften der, bei 1350°C gebrannten Massen SAB Ia und SAB Ib, hat eine bedeutend grössere Reaktivität mit Wasser im Falle von SAB Ia gezeigt, was als eine Bestättigung der unterschiedlichen Zusammensetzung der beiden Sulfataluminate angesehen werden könnte.

4. SCHLUSSFOLGERUNGEN

Auf Grund der angeführten Versuchsdaten kann festgehalten werden, dass die Zusammensetzung und thermische Beständigkeit des untersuchten Sulfataluminates von der Natur der Ausgangssubstanzen beeinflusst wird. Ein grösserer Anteil an, in die Struktur des Sulfataluminates eingebauten Ba^{2+}-Ionen führt zu einer bedeutenden Ausdehnung der kubischen Elementarzelle und gleichzeitig zu einer verminderten thermischen Beständigkeit des entsprechenden Sulfataluminates.

LITERATURVERZEICHNIS

[1] J. A. Rogozina, *Zhur. priklad. Khim.*, **30**, 1742 (1957).

[2] J. A. Rogozina und M. A. Ahmedov, *Epitöanyag*, **22**, 259 (1968).

[3] N. Fukada, *Semento Gjiutso Nengo*, **15**, 26 (1961) ; *Bull. Chem. Soc. Japan*, **34**, 138 (1961).

[4] S. D. Okorokov, S. L. Golynko-Volfson, T. N. Yarkina und R. A. Chepik, *Zhur. priklad. Khim.*, **35**, 256 (1962) ; **35**, 2554 (1962).

[5] P. P. Budnikov, *Cement-Wapno-Gips*, **17/29**, 39 (1962) ; **22/34**, 281 (1967).

[6] P. P. Budnikov, T. V. Kuznetsova und V. G. Saveliev, *Silikattechnik*, **16**, 414 (1965) ; *Cement-Wapno-Gips*, **20/32**, 153 (1965) ; *Zhur. priklad. Khim.*, **41**, 953 (1968).

[7] W. Gutt und M. A. Smith, *Trans. Brit. Ceram. Soc.*, **67**, 487 (1968).

[8] P. K. Mehta, *J. Amer. Ceram. Soc.*, **56**, 305 (1973).

[9] I. Teoreanu und M. Muntean, *Rev. Roum. Chim.*, **19**, 1483 (1974).

[10] I. Teoreanu und M. Muntean, *Rev. Roum. Chim.*, **30**, 575 (1985).

[11] H. Scholze und U. Hildebrandt, *Zement-Kalk-Gips*, **23**, 573 (1970).

[12] I. Teoreanu und M. Muntean, *Cem. Concr. Res.*, **13**, 711 (1983).

[13] I. Teoreanu und M. Georgescu, "Processes in the systems $3(CaO \cdot Al_2O_3) \cdot CaSO_4 - CaO - CaSO_4 \cdot 2H_2O - H_2O$", unter Druck bei *Il Cemento*.

[14] I. Teoreanu, M. Georgescu und A. Puri, *Bul. Inst. Polit. București*, **48**, 29 (1986).

[15] I. Teoreanu, M. Georgescu und C. Chirica, "Hydratations und Erhärtungsvorgänge in $C_2S - C_4A_3\bar{S} - H_2O$ Systemen", vol. 1, IBAUSIL **10**, Weimar–DDR, 1988, S. 202.

[16] I. Teoreanu, M. Muntean und I. Dragnea, *Il Cemento*, **83**, 39 (1986).

[17] P. E. Halstead und E. Moore, *J. Appl. Chem.*, **12**, 413 (1962).

Revue Roumaine de Chimie, 34, 1, 365—375 (1989)

DAS KRIECHVERHALTEN BEI ZUGBEANSPRUCHUNG DER MONOFILAMENTEN AUS DEM TERNÄREN KOPOLYMERISAT AUF DER GRUNDLAGE VON AKRYLNITRIL-VINYLACETAT-α-METHYLSTYROL

CLEOPATRA VASILIU OPREA und MARCEL POPA
Polytechnisches Institut Jassy
Lehrstuhl für organische und makromolekulare Chemie 23 August, 11 A, 6600
Jassy, Rumänien

Eingegangen am 18. Januar 1988

Die Arbeit behandelt das Studium des Zugkraftverhalten der Monofilamenten aus dem Kopolymerisat (Akrylnitril — Vinylacetat-α-Methylstyrol) nach verschiedenen Etappen der technologischen Herstellungsprozesses. Es wurden die Koeffizienten der Kriechgleichungen ermittelt, und auf deren Basis wurden eine Reihe von physikalisch-mechanischen und rheologischen Kennziffern des Polymers berechnet. Man stellte fest, dass diese nach den einzelnen Etappen des technologischen Spinoprozesses aus einer Lösung sich ändern und somit auf die Verfestigung des Materials hinweisen. Die beobachteten strukturellen und morphologischen Veränderungen bestätigen die Strukturversteifung und erklären die Veränderung der rheologischen Eigenschaften.

The creep of monofilaments based on poly(acrylonitrile-co-vinyl acetate-co-α-methyl styrene) selected after different phases of the technological process is studied, under tensile stress conditions. The coefficients of the creep equations were established, and thus, some physico-mechanical and rheological characteristics were evaluated. Their modification after different phases of the wet-spinning technology was observed, indicating the polymer rigidization. The structural and morphological modifications confirm the rigidization and explain the changes of the rheological properties.

EINLEITUNG

Während der Herstellungs- und Verarbeitungsprozesse sowie deren Nützung sind die Monofilamenten, aus denen man kunst- und synthetische Fasern, erhält, einem Komplex von mechanischen Beanspruchungen unterworfen, die das Auftreten von reversiblen oder plastischen Verformungen verursachen können. Die Beschreibung eines solchen Deformierungsprozesses setzt die Kenntnis der rheologischen Gleichung voraus, die der mathematische Ausdruck der Verbindung zwischen der Kraft, der Deformierung und der Belastungsdauer oder zwischen der Kraft der Geschwindigkeit der Belastung ist.

Das rheologische Verhalten von Fasern wurde in zahlreichen Arbeiten behandelt, sowohl hinsichlich der einer mechanischen Beanspruchung unterworfenen Natur, als auch der Chemiefasern, wobei die Korrelationen zwischen den rheologischen Elementen [1] festgelegt wurden, die dann in Modelform verallgemeinert wurden. [2-4] Durch die Untersuchung des Einflusses der strukturellen Elemente und der technologischen Bearbeitungsparameter wurden Informationen mit augenscheinlichem praktischen Nutzen erhalten.[6, 5]

Das ternäre Kopolymerisat auf der Basis von Akrylnitril, Vinylazetat und α-Methylstyrol wird seit langem industriell hergestellt und verarbeitet und nimmt einen wichtigen Platz im Ensemble der Chemiefasern ein. Trotzdem findet man in der Fachliteratur sehr wenige Informationen hinsichtlich seines rheologischen Verhaltens bei verschiedenen Beanspruchungen. Obwohl im allgemeinen die durch die einzelnen Etappen des Verarbeitungsprozesses auftretenden Einflüsse auf die Struktur und die Eigenschaften der spinnbaren Polymere und im einzelnen derer, aus denen man Monofasern vom Typ ,,Melana" erhält, bekannt sind, existieren jedoch nur wenige Arbeiten, in denen eine Korrelation der rheologischen Eigenschaften und der Strukturveränderungen versucht wird, und man findet nicht eine Arbeit bzgl. des vorher erwähnten ternären Kopolymerisats.

Somit wird in dieser Arbeit die Festlegung des rheologischen Verhaltens der Monofasern aus dem ternären Kopolymerisat ,,Melana" nach verschiedenen Herstellungsetappen, die bestimmung der Koeffizienten der entsprechenden Kriechgleichungen und der rheologischen Parameter, sowie eine Korrelierung ihrer Veränderungen und der durch mechanische Behandlung (Reckung, Kräuselung) und physikalisch-chemische (Avivage) erhaltenen Transformationen in der molekulären und übermolekulären Struktur verfolgt. Gleichfalls wurden einige Informationen hinsichtlich Molekularmechanismus der Deformierung des Polymers gewonnen.

EXPERIMENTELLER TEIL

Die untersuchten Monofilamenten wurden durch Spinnen aus einer Lösung, bestehend aus dem Kopolymerisat Akrylnitril-Vinyl-azetat-α-Methylstyrol mit einer Zusammensetzung von 92,2% Akrylnitril, 4,5% Vinylazetat und 3,3% α-Methylstyrol gewonnen. Es wurden Monofilamenten mit einer Feinheit von 6 den nach verschiedenen Etappen des Verarbeitungsprozesses (spinnen, Avivage, Trockenrechung).

Das Kraft-Dehnungs-Diagramm wurde durch Bildung des mittleren Wertes aus 15 Versuchen (aktiver Sektor 20 mm) mit dem Dynamometer "Fafegraf" erhalten. Das Kriechen bei Zugbeanspruchung wurde mit Hilfe einer Waage zur Bestimmung der Stabilität der Fasern beim Kräuseln untersucht.

Die Kristallinitätszahlen und der Orientierungsfaktor wurden durch Diffraktion von X-Strahlen mit dem Röntgenapparat Typ 24 M (DDR) mit Kobaltanode bei einer Spannung von 25 kV und einer Stärke von 30 mA bestimmt. Aus dem Diffraktionsspektrum, das ein Maximum bei $\theta = 10°$ aufweist, wurde die amorphe Zone auf graphischem Wege separiert.

$$I.C. = \frac{A_c}{A_t}\,(\%)$$

mit $I.C.$ — Kristallinitätszahl

A_c — dem kristallinen Bereich entsprechende Fläche

A_t — totale Fläche unter der Kurve bei $\theta = 10°$.

Der Orientierungsfaktor wurde aus den aufgezeichneten Diffraktionsspektren in Äquatorebene bestimmt :

$$F_0\,(\%) = \frac{90 - \alpha}{90} \times 100$$

wobei α die grösse ist, die aus dem Diffraktionsspektrum der X — Strahlen bestimmt wird.

Der kalorische Lösungseffekt wurde mit einem Leitungsmikrokalorimeter Typ Calvet, gemessen, das mit einem Aufzeichnungsgerät, Typ Zonen ausgestattet ist und mit einer Messgenanigkeit von 0,5 mV/200 mm und einer Aufzeichnungsgeschwindigkeit von 2 mm/min, arbeitet (die Konstante β des Systems beträgt $2{,}68 \times 10^{-4}$ cal/min²)

$$Q = \frac{\beta \times S}{m}$$

mit

β — Systemkonstante,

S — Fläche die von der Kurve eingeschlossen wird, die die Änderung des Flusses in der Zeit darstellt,

m — Masse des gelösten Stoffes,

Q — gesamte Lösungswärme.

Die elektronenmikroskopischen Untersuchungen wurden mit dem Apparat "TESLA BM" (CSSR) ausgeführt, wobei die Technik der 2-Stufen-Schichten angewendet wurde (Film von Polystyrol + Kohle).

ERGEBNISSE UND DISKUSSION

Eine erste rheologische Charakterisierung der untersuchten Monofilamenten bestand in der Aufzeichnung der Kraft-Deformierungs-Kurven, wobei der Wert der Zerreisskraft (T_r) und der der Bruchdehnung erhalten wurde. Man stellte selbstverständlich ein Anwachsen der Bruchkraft nach dem Reckprozess fest, wobei die trocken gereckten Monofilamenten den grössten Wert hatten (16,5 gf). Ihr rheologisches Verhalten zeigt gleichfalls das Auftreten der viskoelastischen Komponente, die bei den anderen Proben fehlt.

Für eine vollständigere rheologische Charakterisierung des Polymers wurden die Kriechkurven bei Zugbeanspruchung festgelegt. In allen Fällen wurde mit einer Belastungskraft von 9 gf gearbeitet, was sich in der Zone des elastischen Verhaltens der trocken gereckten Monofilamenten bewegt.

Abb. 1 veranschaulicht diese Kurven, die durch Mittelwertbildung von 3 Versuchen für jede Probe erhalten wurden.

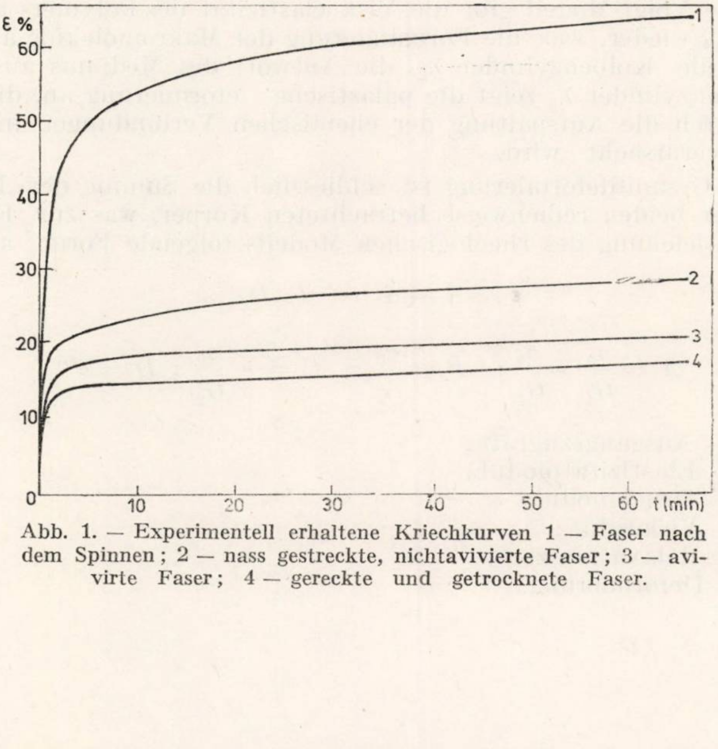

Abb. 1. — Experimentell erhaltene Kriechkurven 1 — Faser nach dem Spinnen; 2 — nass gestreckte, nichtavivierte Faser; 3 — avivirte Faser; 4 — gereckte und getrocknete Faser.

Man beobachtet, dass sowohl die momentane Deformierung als auch die gesamte Deformierung (nach einer Beanspruchung von 60 min) sich bei Anwendung mechanischer Behandlungen (Reckung) vermindern, weniger aber bei Anwendung der physikalisch-chemischen Verfahren (Avivage), die spezifisch sind für die Herstellungstechnologie der Faser ,,MELANA". Dieses Verhalten stimmt klar überein mit den Daten aus den vorher diskutierten Kraft-Dehnungs-Diagrammen.

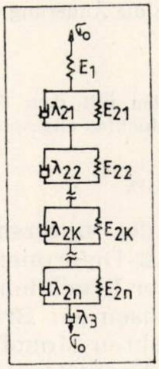

Abb. 2. — Das verallgemeinerte Bürgers-Modell, anwendbar auf das Fliessen der Monofilamenten von ,,Melana" Typ.

Das rheologische Verhalten der untersuchten Monofilamenten kann durch das mechanische Modell nach Bürger beschrieben werden, das man durch aufeinanderfolgendes Zusammenstellen des Modells ,,Kelvin-Voigt" mit dem Modell ,,Maxwell" (Abb. 2) erhält, da der Körper eine Momentelastizität, eine verspätete Elastizität und ein viskoses Fliessen besikt. Somit drückt die Feder E die Materialelastizität, eine Folge der Veränderung der interatomaren Abstände und Valenzwinkel, aus. Das verallgemeinerte Voigt-Modell gibt die Viskoelastizität des Polymers durch die Federn E_{2k} wieder, was die Formänderung der Makromoleküle ausdrückt, während die Kolbenzylinder λ_{2k} die Antwort des Mediums ausdrücken. Des Kolbenzylinder λ_3 zeigt die palastische eformierung an, die im einzelnen durch die Aufspaltung der chemischen Verbindungen in der Basiskette verursacht wird.

Die Gesamtdeformierung ist schliesslich die Summe der Deformierungen der beiden reihenweise betrachteten Körper, was zur Folge hat, dass die Gleichung des rheologischen Modells folgende Form [7] annimmt :

$$\varepsilon = A + B \cdot t - C . D^{-t}$$

$$A = \frac{\sigma_0}{G_1} + \frac{\sigma_0}{G_2} \; ; \quad B = \frac{\sigma_0}{\eta} \; ; \quad C = - \frac{\sigma_0}{G_2} \; ; \; D = e^{1/\theta_r}$$

mit : σ_0 — Ausgangszugraft ;
G_1 — Elastizitätmodul ;
G_2 — Druchmodul ;
η — Viskosität ;
θ_r — Relaxationszeit ;
ε — Deformierung.

Die Koeffizienten $A \ldots D$ und die obengenannten, experimentell schwer, bestimmbaren Grössen, deren Werte in Tab. 1 wiedergegeben sind, wurden aus den experimentell erhaltenen Kriechkurven berechnet.[7] Man stellt fest, dass alle rheologischen Parameter bei mechanischer Behandlung (Recken) wertmässig anwachsen, aber keine wesentliche Veränderung durch die Avivage zu verzeichnen ist. Die Richtung, in der besonders die Relaxationszeit und die Viskosität sich änderen, deutet auf eine leichte Strukturversteifung hin. Als Folge wächst der Elastizitäts- und Druckmodul, wodurch die Anwendung einer mechanischen Behandlung (Reckung) zur Verbesserung der physikalisch-mechanischen Eigenschaften des untersuchten Kopolymers gerechtfertigt wird.

Tabelle 1

Rheologische Parameter, berechnet aus den experimentellen Kriechkurven für die 6 den Faser

Bearbeitungsetappe	Koeffizienten der rheologischen Gleichen				Rheologische Kennzifern			
	A	$B \times 10^4$	C	D	θ_r (s)	G_1 (gf/mm)	G_2 (gf/mm)	$\eta \times 10^4$ (gf. s/mm)
Spinnen	17,25	3,409	12	1,004	242	1,714	0,75	2,64
Nassreckung	7,68	2,272	3,18	1,003	273	2,00	2,83	3,96
Reckung und Trocknung	4,50	1,515	1,20	1,002	460	2,727	7,50	5,94

Die Nassreckung (an der Spinndüse) hat einen kleineren Versteifungseffekt, einerseits durch die Tatsache, dass sie bei kleineren Werten des Dehnungsverhältnisses durchgeführt wird, und andererseits durch die Tatsache, dass unter diesen Bedingungen die Makromoleküle vor allem die Tendenz des Gleitens im Verhältnis zu den anderen aufweisen und weniger die einer Formänderung. Aus diesem Grunde gibt es kaum in dieser Bearbeitungsphase mechanochemische Reaktionen einer homolytischen Aufspaltung der kovalenten chemischen Bindungen in der Basiskette.

Die Nachreckung wird bei erhöhten Werten des Dehnungsverhältnisses durchgeführt, wenn die Makromoleküle sich unter der Krafteinwirkung formmässig verändern, indem sie sich aufwinden und ausrichten. Folglich nähern sie sich an, wodurch die Wechselwirkung vom Typ ,,Van der Waals'' oder die Wasserstoffverbindungen sich verstärken und somit auch die physikalisch-mechanischen Eigenschaften der Monofilamenten sich verbessern. Die im Polymer existierenden Strukturdefekte, unter ihnen sogar Trennungszonen der kristallinen und amorphen Bereiche, die Faktoren einer Kraftkonzentration darstellen, führen zur Überspannung einiger chemischer Verbindungen in der Basiskette des Polymers, die sich dann homolytisch aufspalten, so dass in dieser Bearbeitungsetappe die Häufigkeit mechano-chemischer Vorgänge viel grösser ist im Vergleich zur Nassreckung. Das industriell bearbeitet Polymer verkleinert durch die die Reckung seine Molekularmasse von 64850 auf 61230, was scheinbar unbedeutend ist, aber auf die Existenzvon Reaktionen eines mechanischen Abbaus hindeutet. Die mechano-distruktiven Effekte sind jedoch gering im Vergleich zu den vorteilhaften Folgen der Reckung, sowohl durch die kurze Dauer der Krafteinwirkung als auch durch die Absicherung der thermo-dynamischen Bedingungen für das Auftreten von Formveränderungen, so dass im grossen und ganzen die Monofilamenten qualitativ höhere Eigenschaften haben als die Nichtgereckten.

Das untersuchte ternäre Kopolymer weist eine 2-Phasen-Struktur auf, in der die Makromoleküle nacheinander mehrere Bereiche mit maximaler (kristallisierte Bereiche) und minimaler (amorphe Bereiche) Anordnung durchlaufen. Unter der Wirkung der Dehnungskraft bei der Reckung erleiden die Kristallite eine Orientierung entsprechend der Kraftwirkung, wobei auch die Fragmente der Makromoleküle angesprochen werden, die die amorphen Bereiche durchlaufen. Durch das Anwachsen ihres Verpackungs-und Ordnungsgrades wird die Kristallisierung erleichtert. So steilt man fest, dass das dem Polyakrylnitril mit 10° charakteristische Beugungsmaximum nach der mechanischen Beanspruchung (Abb. 3) schmaler und intensiver wird, was das Anwachsen der Kristallitätszahl begründet.

Eine Verstärkung der mechanischen Beanspruchung, z. B. während der Kräuselungsoperation, wenn die Monofilamenten starken unterliegen, führt zum Abfall der Kristallitätszahl von ca. 20 % auf 45 % (Abb. 3, Kurve 4).

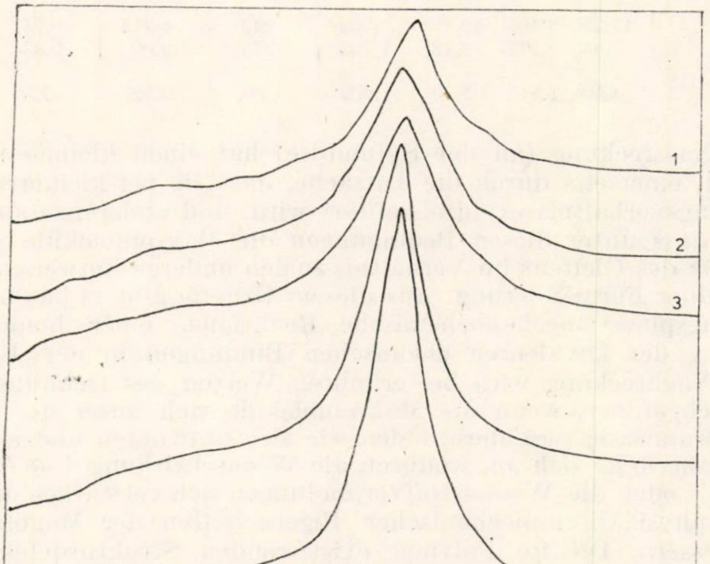

Abb. 3. — Beugungsdiagramme der X-Strahlen 1 — Faser nach dem Spinnen ; 2 — nassgereckte, nicht avivierte Faser ; 3 — gekräuselte Faser ; 4 — gereckte und getrocknete Faser.

Der Effekt ist sicher auf die unter diesen Bedingungen teilweise Zerstörung der kristallinen Struktur zurückzuführen, was sogar zum Auftreten von Mikronissen in der Oberfläche der Monofilamenten führt (Abb. 6,d).

Die Korellation zwischen der Veränderung einiger rheologischer Eigenschaften der Monofilamenten und der Veränderung der Kristallinität scheint einleuchtend zu sein (Abb. 4).

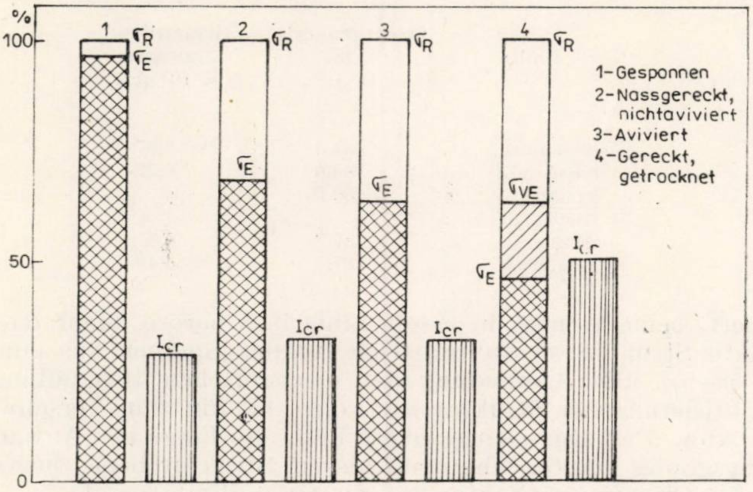

Abb. 4. — Histogramm der mit den Kristallinitätszahlen korrelierten rheologischen Eigenschaften für die 6 den- Faser.

Somit ist die Zugkraft σ_E (elastisch) nach dem Spinnen fast gleich der Zugkraft σ_R, wobei die Kristallinitätszahl den Wert 20% hat. Durch Nassreckung wächst die Kristallinität, wodurch der elastische Grenzwert sich verkleinert im Vergleich mit dem Bruchs. Die Avivage beeinflusst praktisch nicht die Kristallinität und nicht das elastische Verhalten der Probe. Die Entreckung hat jedoch ein starkes Anwachsen der Kristallinität (*I.C.* = 50%) und einem Abfall von σ_E gegenübber σ_R zur Folge, aber besonders das Auftreten und die Verstärkung des viskoelastischen Verhaltens des Polymers.

Man kann also einschätzen, dass die Veränderung der rheologischen Eigenschaften während des Herstellungsprozesses der Monofilamenten Typ ,,Melana'', bedeutende Veränderungen der molekulären und übermolekulären Struktur zu Grunde liegen. Ein zusätzliches Argument in diesem Sinne ist durch die Veränderung des Orientierungsfaktors (F_0) bei der angewendeten mechanischen Behandlung (Tab. 2).

Man stellt fest, dass die sofort nach dem Spinnen gewonnene Probe einen ziemlich hohen Orientierungsgrad durch das Fliessen durch die Spinndüsenöffnung hat. Die Nassreckung bewirkt das Anwachsen des F_0 — Wertes, der durch die Avivage praktisch unverändert bleibt.

Ein stark ausgeprägtens Anwachsen verzeichnet man bei der Nachreckung (F_0 = 87,7%), eine Folge der Orientierung sowohl der Kristalliten als auch der amorphen Bereiche im Sinne der Kraftwirkung.

Die beobachteten Veränderungen in der übermolekulären Struktur ziehen auch bedeutende Veränderungen in der Fasermorphologie nach sich. Wenn man die Mikrofotografien der Monofilamentenausschnitte nach verschiedenen Etappen des technologischen Herstellungsprozesses

Tabelle 2

Wert des Orientierungsfaktors (F_0) und der Gesamten Lösungswärme

Probe	Orientierungsfaktor (F_0), %	Gesamtlösungswärme $Q \times 10^4$ (cal/g)
— gesponnen	83,3	3,87
— nassgerekt	85,0	6,32
— aviviert	85,2	—
— trockengereckt	87,7	6,95
— gekräuselt	87,5	6,49

analysiert, bemerkt man in erster Linie ihre poröse, mehr oder weniger kompakte Struktur, charakteristisch für das Spinnen aus einer Lösung (Abb. 5a—c). Die Anwendung der mechanischen Behandlung hat die Kompaktisierung der Struktur zur Folge, bis hin zum Verschwinden der Poren (Abb. 5 c). Das ist ein erster Linie die Folge des Anwachsens des Packungsgrades in der übermolekulären Strukturebene, hervorgehoben durch den Orientierungsfaktor und die Kristallinitätszahl.

Eine klare Orientierung der strukturellen Einheiten im Sinne des Krafteinwirkung erscheint auch bei der Analyse der Faseroberfläche mit dem Elektronenmikroskop (Abb. 6). Die gekräuselte, einer schnellen und intensiven Zugkraft unterworfene, Faser zeigt im Querschnitt eine kompakte Struktur, verzeichnet jedoch auf der Oberfläche einen mechanischen Zerfall in Form von Rissen (Abb. 6 d).

Auch die physikalisch-chemischen und mechanischen Eigenschaften variieren bei der mechanischen Behandlung, eine Folge der bedeutenden, schon aufgezeigten, strukturellen Veränderungen. Eine von diesen ist die totale Lösungswärme, deren Werte für verschiedene Etappen des technologischen Prozesses in Tab. 2 dargestellt sind. Man stellt fest, dass durch die mechanische Behandlung die Gesamtlösungswärme anwächst, was eine Folge des Anwachsens des Ordnungsgrades ist, der das Lösungsmittel hindert, leicht in die Faser einzudringen. Der leicht verkleinerte Wert dieser Eigenschaft für die gehräuselte Faser steht in gutem Einklang mit der Kristallinitätszahl, die, wie vorher erwähnt wurde, auf eine teilweise Zerstörung der kristallinen Struktur hinweist.

Die thermokinetischen Lösungskurven (Abb. 7) lassen bedeutende Unterschiede zwischen den Proben erkennen, ebenfalls im Sinne eines Anwachsens der Schwierigkeit des Lösungsmittels in die orienterten Proben einzudringen. Die Kräuselung zieht eine leichte Verkleinerung der von der Kurve eingeschlossenen Fläche bzw. der Gesamtlösungswärme nach sich.

Man kann also einschätzen, dass der Änderung des rheologischen Verhaltens der untersuchten Monofilamenten wichtige, in ihrer Morphologie und übermolekulären Struktur eingetretene Veränderungen durch die Anwendung einer mechanischen Behandlung zugrunde liegen.

Die Reckung hat jedoch zur Folge nicht nur Veränderungen im Aufbau der Makromoleküle, was zur Orientierung und dem Anwachsens

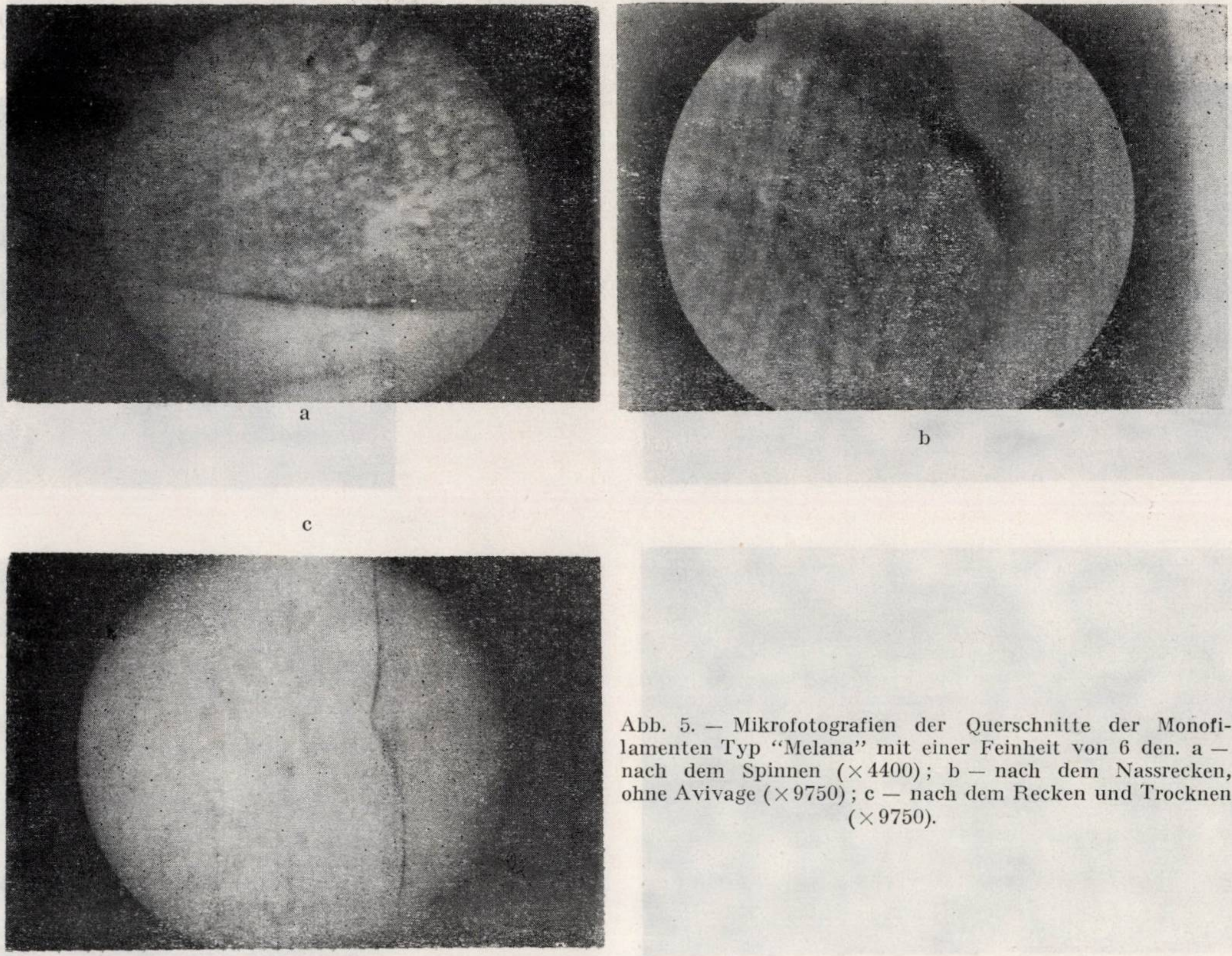

Abb. 5. — Mikrofotografien der Querschnitte der Monofilamenten Typ "Melana" mit einer Feinheit von 6 den. a — nach dem Spinnen (×4400); b — nach dem Nassrecken, ohne Avivage (×9750); c — nach dem Recken und Trocknen (×9750).

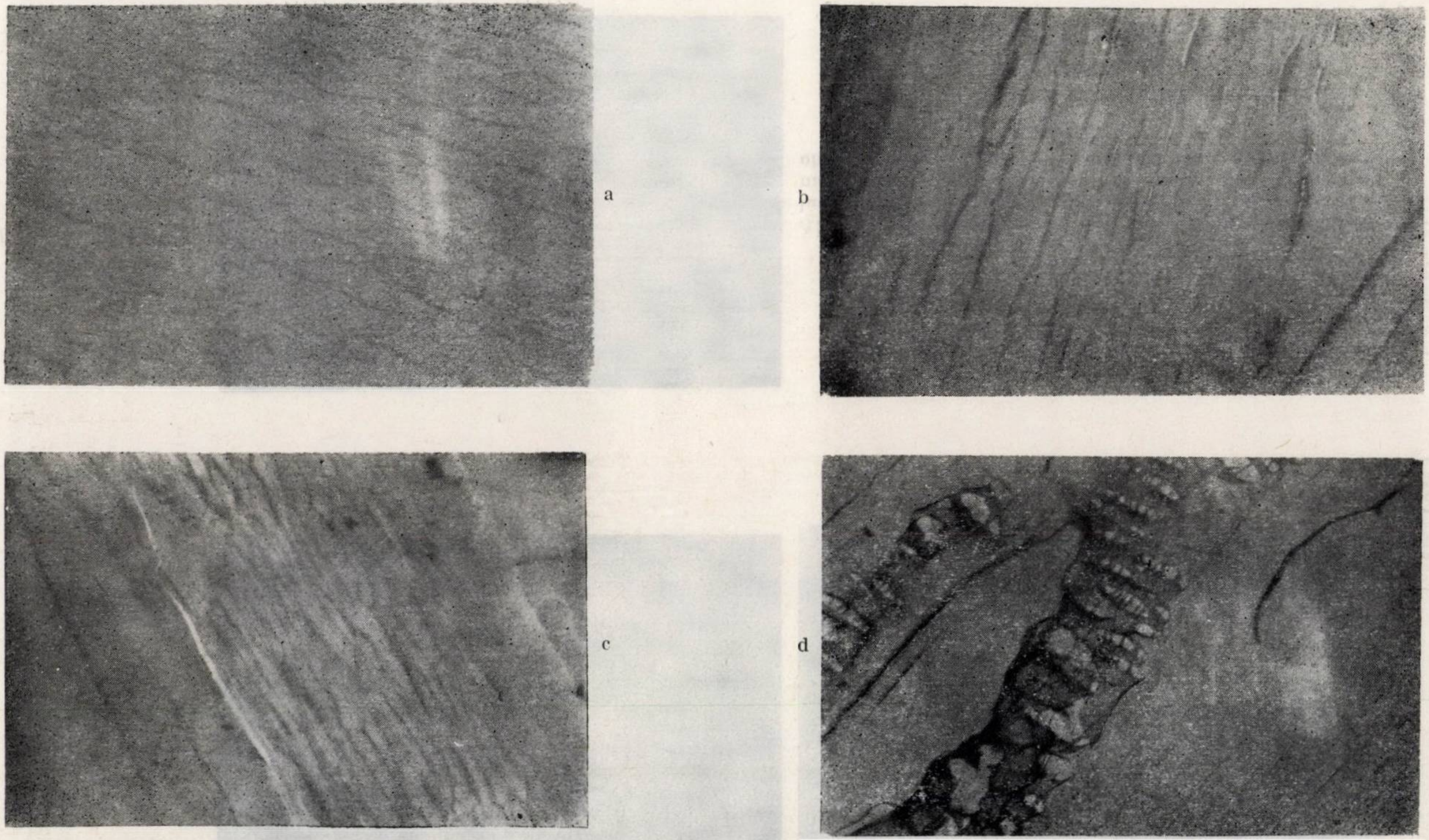

Abb. 6. — Mikrofotografien der Oberfläche von Monofilamenten Typ "Melana", mit einer Feinheit von 6 den. a — nach dem Spinnen (× 4400); b — nach der Nassreckung, ohne Avivage (× 4400); c — nach dem Recken und Trocknen d — nach dem Kräuseln (× 4400).

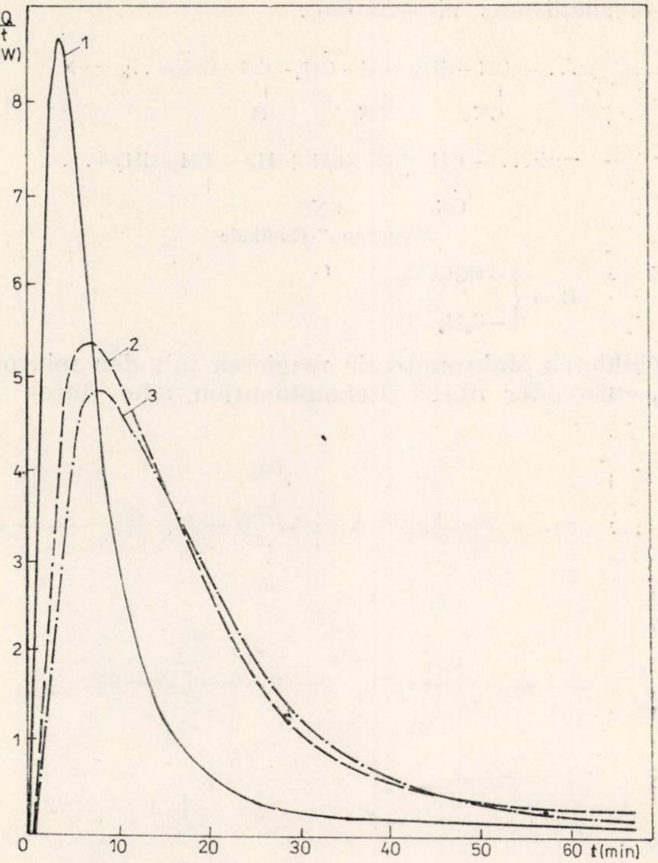

Abb. 7. — Thermokinetische Lösungs kurven der Monofilamenten Typ "Melana" mit der Feinheit 6 den. 1 — nach dem Spinnen ; 2 — nach dem Recken und Trocknen ; 3 — nach der Kräuselung.

des Packungsgrades führt, sondern auch chemorheologische Effekte. Die mechanische Energie konzentriert sich in den chemischen Verbindungen der Grundkette, was ihre homolytische Aufspaltung verursacht und in der Bildung von „Mechano"-Radikalen endet. Sie wurden durch die Spannung einiger gereckter und nichtgereckter Monofilamenten in Methanollösungen von Radikalakzeptoren des Typs DPPH oder aromatischer Diaminen herausgestellt. Somit wurden gefärbte Monofilamenten erhalten, stabil bei der Extraction in organischen Lösungsmitteln, was die chemische Bindung der mikromolekularen Verbindung an das Polymer beweist. Diese Fasern wurden nachträglich einer Diazotierung und einer Kopplung mit Phenolderivaten unterworfen, wodurch eine variierte Skala von spezifischen Farben erhalten wurde. Es folgt dass während der mechanischen Beanspruchung im Bearbeitungsprozess der Monofilamenten, auch mechano-chemische Krackungsreaktionen nach folgendem Mechanismus stattfinden:

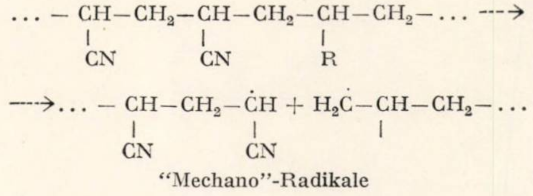

$$\ldots -\underset{\substack{|\\ \mathrm{CN}}}{\mathrm{CH}}-\mathrm{CH_2}-\underset{\substack{|\\ \mathrm{CN}}}{\mathrm{CH}}-\mathrm{CH_2}-\underset{\substack{|\\ \mathrm{R}}}{\mathrm{CH}}-\mathrm{CH_2}-\ldots \dashrightarrow$$

$$\dashrightarrow \ldots -\underset{\substack{|\\ \mathrm{CN}}}{\mathrm{CH}}-\mathrm{CH_2}-\underset{\substack{|\\ \mathrm{CN}}}{\dot{\mathrm{C}}\mathrm{H}} + \mathrm{H_2\dot{C}}-\underset{|}{\mathrm{CH}}-\mathrm{CH_2}-\ldots$$

"Mechano"-Radikale

$$R = \begin{cases} -\mathrm{OCOCH_3} \\ -\mathrm{C_6H_5} \end{cases}$$

Die gebildeten Makroradikale reagieren mit den mikromolekulären Substanzen, entwender durch Rekombination oder durch Kettenübertragung:

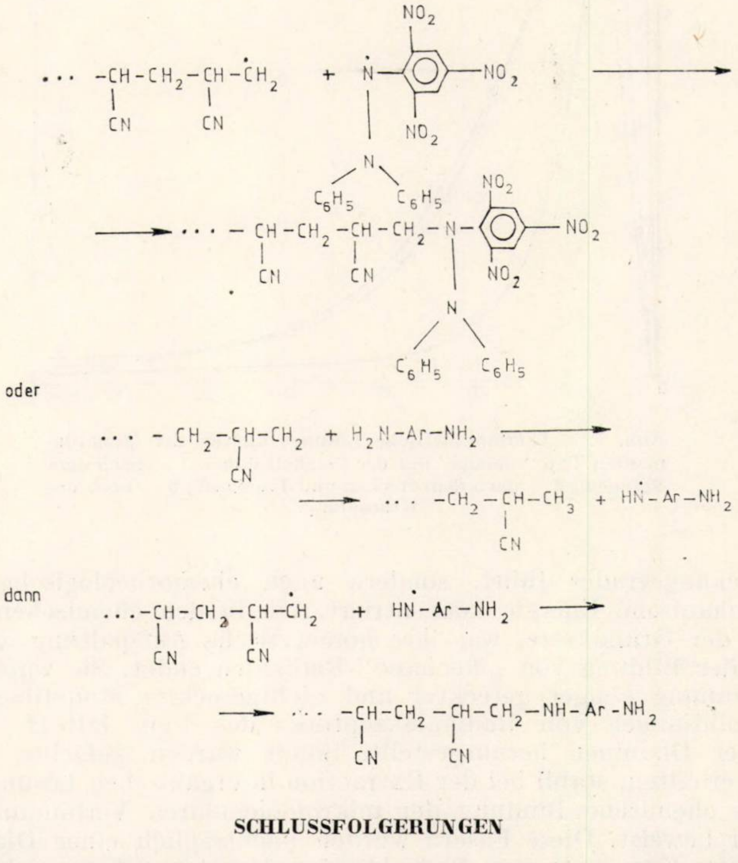

SCHLUSSFOLGERUNGEN

1. Während der Herstellung und Bearbeitung der Monofilamenten aus dem Kopolymerisat Akrylnitril-Vinylazetat-α-Methylstyrol finden bedeutende morphologische und strukturelle Veränderunge statt, die ihr rheologisches Verhalten beeinflussen.

2. Die mechanische Beanspruchung der Monofilamenten bewirkt eine „Verstärkung" der Struktur (bzw. ihre leichte Versteifung), eine Tatsache, die durch die aus den Kriechkurven festgelegten rheologischen Kennziffern widergespiegelt wird.

3. Während der mechanischen Beanspruchung der Monofilamenten aus „Melana" unter statischen oder dynamischen Bedingungen werden Reaktionen hervorgerufen die mit dem mechanochemischen Zerfall des Polymers, der als Grundlage einen Radikalmechanismus hat, endet.

LITERATURVERZEICHNIS

[1] H. Morton, "Physical Properties of Textile Fibers", London, 1962.

[2] R. S. Lenk, "Plastics Rheology", London, 1968.

[3] P. Winkler, A. Baner und K. Nitsche, *Faserforsch. Textiltechn.*, **25**, 10, 445 (1974).

[4] R. Z. Tudose, "Procese şi utilaje in industria de prelucrare a compuşilor macromoleculari", Ed. Tehnică, Bucharest, 1976.

[5] B. M. I. Chapman, *J. Appl. Polym. Sci.*, **18**, 21, 3523 (1974).

[6] R. Z. Tudose, S. Ciovica und M. Condeanu, Bull. I.P.I., **XXV** (XXIX), (1–4), **21** (1979).

[7] I. Volintiru und Gh. Ivan, "Introducere în fizico-chimia polimerilor", Ed. Tehnică, Bucharest, 1980.

Revue Roumaine de Chimie, 34, 1, 377–385 (1989)

QUANTUM CHEMICAL CALCULATIONS FOR DIPOLE MOMENTS OF PHOSPHORUS COMPOUNDS

RADU VÂLCEANU[a], ZENO SIMON[b] and LUDOVIC KURUNCZI[a]
[a] Chemical Research Center, B-dul Mihai Viteazul 24
1900 — Timişoara, Romania
[b] Department of Biophysics, Institute of Medicine, P-ţa 23 August 2, 1900 — Timişoara, Romania

Received October 5, 1988

In a search for a quantum chemical method able to give reliable charge distributions for trivalent phosphorus compounds, we developed a parametrization within the Del Re method, based upon experiamental dipole moments of fifteen phosphorus compounds with an essentially *sigma* bond character. The results obtained by this method are compared with experimental dipole moments and with results of advanced methods. Within a series of similar compounds, there is a general parallelism between the dipole moments calculated by our Del Re method, and by advanced methods. The results of the last ones are rather far from the experimental values, and depend strongly on the used method and on the basis set of functions. For a test series of seven trivalent phosphorus derivatives with a defined conformation, the correlation coefficient between experimental dipole moments and those calculated by our Del Re method is r = 0.937.

INTRODUCTION

The importance of phosphorus compounds, and especially the organic ones, in various fields — such as chemical reagents, pesticides and other biological active compounds etc.[1] — justifies the search of methods of theoretical chemistry able to give reliable predictions for such molecules.

Structural calculations by advanced quantum-chemical methods were performed for a relatively large number of such compounds, but generally for small molecules.[2–14] The results of different methods and even of different parametrizations within one method, as concerns the dipole moment of one molecule fall within a rather wide range. Also, for larger molecules, the time required even with modern fast computers would be prohibitively large. The relative success of a simple empirical method [15–17] encouraged us to develop a parametrization within the Del Re method[18] for charge distributions in molecules of inorganic and organic phosphorus compounds even for large molecules. Here we discuss our results obtained for dipole moment calculations, and compare them with experimental values, and with the values obtained by more advanced methods. We shall demonstrate hereby that our results have a sufficient reliability, which is not inferior to the one of the advanced methods.

SHORT SURVEY OF ADVANCED METHODS

The largest number of dipole moment calulations were peformed for the phosphine molecule (**1**), for which the experimental value of 0.57 D (Debye) is accepted (see Table 1). Hillier and Saunders [2] obtain 0.34 D with an *ab initio* SCF-MO using a minimal set of Slater type orbitals, with the best atom exponents augmented by phsphorus 3*d* orbitals. Unfortunately, in *ab initio* calculations the result depends strongly on the basisset functions. For example Roberts *et al.*[3] obtain 0.38 D for the dipole moment when they use 7 *s*, 3 *p* (phosphorus) and 2 *s* (hydrogen) uncontracted Gaussian type orbitals and 0.95 D for 9, 5 and respectively 3 such orbitals; introduction of one *d* orbital at the P atom reduces the dipole moment vaule to −0.10 D and repectively 0.44 D. Lehn and Munsch [4] obtain valus between 0.62 D and 1.22 D for different sets; the most elaborated computation — with 12 *s*, 9 *p*, 2 *d* orbitals for the P atom, 5 *s* and 1 *p* for the H atom yields 0.66 D. The CI and SCF results of Scott and Sutcliff [8] range between 0.219 and 1.565 D for different basis sets and parametrizations of the atomic orbitals. The semiempiric methods yield also divergent results. The CNDO/2D of Kuznesof *et al.*[6] yields 0.01 D (with *d* orbital at the P atom) the MNDO calculations of Frenking et al.[11] — 1.35 D, the CNDO/2-FPP of Rhee et al.[12] — 0.916 D. Other theoretical results, see Table 1.

For the trihalogenides of phosphorus Ewig, Coffey and Van Wazer [7] with an *ab initio* valence only SCF (NOCOR) obtain for PF_3, (**2**), PCl_3 (**3**), PBr_3 (**13**) and PJ_3 (**14**) 0.52; 0.63; 0.32 and respectively 0.06 D, while the experimental values are (as quoted by these authors 7)) 1.03; 0.78; 0.61 and 0.00 D.

For the methyl derivatives with CNDO/2D and *d* orbital at the P atom Kuznesof *et a.*[6] obtain: $H_2P(CH_3)$ (**5**), $HP(CH_3)_2$ (**6**), $P(CH_3)_3$ (**7**) — 1.52; 1.81; 1.81 D. The experimental values are 1.10; 1.23 and 1.19 D (Table 1). For the same molecules the MNDO results [11] are: 1.61; 181 and 1.94 D, while the results of Bowen and Allinger [14] with a molecular mechanical technique (quoted MM2) are 0.99; 1.11 and 1.19 D.

Results for other molecules are listed in Table 1. While in series of derivatives there is a general parallelism between calculated and experimental values, the agreement between the individual experimental and calculated values is not very good and depends strongly upon parametrization, even within one given type of method. This suggests the search for a less elaborated semiempiric method able to give satisfactory results due to a successful parametrization. With that end in view we shall use the Del Re method. The method used by Smith *et al.*[15,16] has a lower degree of generality and it is more difficult to use the parameters obtained in one class of molecules for another class of molecules.

Table 1

Calculated and experimental dipole moments[a]

Compound	Del Re moment	Other methods	Experimental values	Structural data
1	*2*	*3*	*4*	*5*
1 PH_3^*	0.65	0.34 *ab initio* SCF[2] 0.44 *ab initio* SCF[3] 0.66 *ab initio* SCF[4] 1.247 CI[20] 1.276 SCF[20] 0.01 CNDO/2D[6] 0.767 CI[8] 0.759 SCF[8] 0.776 *ab initio* SCF[9] 1.35 MNDO[11] 2.70 MINDO[3 11] 0.916 CNDO/2-FPP[12]	0.55±0.01 M[21] 0.579±0.012 M[22] 0.578±0.01 M[23] 0.57395±0.0003 Re[24]	M[25]
2 PF_3^*	1.062	1.44 *ab initio* SCF[2] 1.78 *ab initio* SCF[5] 0.52 NOCOR[7] 0.51 SCF[7] 2.641 *ab initio* SCF[9] 2.06 MINDO[3,10,11] 2.44 MNDO[11]	1.025±0.009 M[26] 1.03±0.01 M[27] 1.00±0 03 G[28]	M[29]
3 PCl_3^*	0.801	0.63 NOCOR[7] 1.59 MINDO[3,10,11] 1.39 MNDO[11]	0.91 B[30] 0.78±0.01 G[31] 0.89 B[32] 0.56±0.02 M[33] 0.57 On[34] 0.94 B Hg[35]	M – IR[36]
4 PF_2H^*	1.184	1.99 *ab initio* SCF[9]	1.35±0.02 G[37] 1.32±0.01 M[38]	M[38]
5 $H_2PCH_3^*$	1.02 *i*	1.52 CNDO/2D[6] 1.61 MNDO[11] 2.30 MINDO[3,11] 1.00[17] 0.99 MM2[14]	1.10±0.01 M[39]	M *i*[39]
6 $HP(CH_3)_2^*$	1.174 *i*	1.81 CNDO/2D[6] 1.81 MNDO[11] 1.75 MINDO[3,11] 1.16[17] 1.11 MM2[14]	1.23±0.01 M[40]	M *i*[41]
7 $P(CH_3)_3^*$	1.274 *i*	1.08 *ab initio* SCF[2] 1.81 CNDO/2D[6] 1.94 MNDO[11] 1.13 MINDO[3,11] 1.19 MM2[14]	1.192±0.005 M[42]	M – E *i*[43]

Table 1 (continued)

1	*2*	*3*	*4*	*5*
8 FPH_2	1.145	1.81 *ab initio* SCF[9]	1.30[b 37]	*c*
9 $P(OH)_3$	—	2.54 MINDO[3,10]	—	—
10 P_4O_6	—	0.0 MINDO[3,10]	—	—
11 F_2PPF_2	0.175 ∼ *t*	0.01 MINDO[3,10]	—	E ∼ *t*[44] (IR + R: G,L,S ∼ ∼ *t*[45])
12 Cl_2PPCl_2	—	0.19 MINDO[3,10]	—	—
13 PBr_3	—	0.32 NOCOR[7]	0.52 B[46] 0.62 C[47]	—
14 PJ_3	—	0.06 NOCOR[7]	0.0[48] 0.34 Sc[49] 0.34 B[50]	—
15 Cl_2PCH_2Cl	1.228 *g* 1.874 *t*	2.29 MINDO[3,10] 1.86[17]	2.97 Ch[51]	E*g*[52d]
16 Cl_2PCH_2Br	—	1.73[17]	—	—
17 Cl_2PCH_3	2.253 *i*	3.08 MINDO[3,10] 1.88[17]	—	E*i*[53]
18 Cl_2PCCl_3	—	0.26 MINDO[3,10]	—	—
19 $ClP(CH_2Cl)_2$	—	0.61 MINDO[3,10]	—	—
20 $F_2PC_2H_5$	2.192 *g* 1.896 *t*	—	2.1678 ± 0.0002 M *g*[54] 2.081 ± 0.01 M *t*[54]	M*g*[54] M*t*[54]
21 $ClP(CH_3)_2$	—	2.71 MINDO[3,10] 2.37[17]	—	—
22 $H_2PC_2H_5$	1.12 *g*, 1.429 *t*, *i*	1.09[17]	1.17 ± 0.02 G[55] 1.11 ± 0.05 B[55] 1.15 ± 0.05 B[55] 1.22 ± 0.07 M *g*[56] 1.226 ± 0.005 M *t*[56]	M*g*,*i*[56] M*t*,*i*[56] (IR + R: eq.of t ⇌ g[57])
23 $P(OCH_3)_3$	—	0.73 MINDO[3,10,11] 1.60 MNDO[11]	1.83 C[58] 1.81 B[59] 1.90 B[60] 1.85 B[61] 1.60 B[62] 1.55 On[62]	—

Table 1 (continued)

1	2	3	4	5
24 $H_2P\,C(CH_3)_3$	1.391 *i*	0.98 MM2[14]	1.17±0.02 M[63]	M *i*[63]
25 $HP(C_2H_5)_2$	1.101 *g-g* 0.981 *g-g′* 1.603 *t-g* 1.621 *t-g′*	1.36[17]	1.39±0.06 B[55] 1.36±0.05 B[55]	*i*[c]
26 $P(C_2H_5)_3$	1.043 *g-g-g* 1.262 *g-g-g′* 1.589 *t-g-g* 1.628 *t-g-g′* 2.214 *t-t-g* 2.674 *t-t-t*	1.77 MNDO[11] 1.41 MINDO[3,11] 1.39[17]	1.84 Ch[64] 1.48 B[65] 1.45 B[55] 1.35±0.05 B[55] 2.9±0.1 D[66] 1.42 B Hg[35]	*i*[e] (IR:eq. of 3 conf.[67])
27 $P(OC_2H_5)_3$	—	0.59 MINDO[3,10,11] 1.61 MNDO[11]	1.96 C[58] 1.82 D[68] 1.71 Ch[68] 1.80 B[59] 1.84±0.03[66] 1.64 On[34] 1.61 On[62] 1.69 B[62]	—
28 $P(C_3H_7)_3$	1.145 *g-g-g* 1.332 *g-g-g′* 1.760 *t-g-g* 1.699 *t-g-g′* 2.22 *t-t-g*	1.45[17]	1.48 B[65] 2.6±0.1 D[66] 126±0.03 B[69] 1.16±0.08 B[69] 1.74 On[34]	*i*[c]
29 $P(OCH(CH_3)_2)_3$	—	0.46 MINDO[3,11]	1.98 C[58] 1.82 B[59]	—
30 $P(C_4H_9)_3$	1.101 *g-g-g* 1.315 *g-g-g′* 1.604 *t-g-g* 1.867 *t-g-g′* 2.24 *t-t-g*	1.46[17]	2.22 Ch[64] 1.49 B[65] 2.4±0.1 D[66] 1.56 D[70] 1.60 B[70] 1.55 Ch[70] 1.76 On[34]	*i*[c]
31 $P(C(CH_3)_3)_3$	2.152 *i*	0.78 MM2[14]	1.59 B Hg[35]	E*i*[71]
32 $P(C_6H_{11})_3$	—	1.46[17]	1.48 B[65]	—

[a] Literature quotations in superscripts. Compounds used in calibration of the Del Re method are marked by an asterisk *. Molecular conformations: *g* — *gauche*; *g′* — *antigauche*; *t* — *trans*; *i* — *staggered*. Methods for dipole moment and structural determination: M — microwave spectroscopy; E — electron diffraction; IR — *infrared* spectroscopy; R — Raman spectroscopy; Re — electronic resonance method. G, L, S — gaseous, liquid and solid state; solvents: B — benzene; Ch — cyclohexane; C — carbon tetrachloride; Sc — carbon disulphide; D — dioxane with Debye theory. Hg and On — Higasi and respectively Onsager formulae Dipole moments in Debye (1 Debye — $3.336.10^{-30}$ C·m) units.

[b] Estimated value.

[c] Bond lengths and bond angles estimated by us.

[d] For the *t* conformer we used the *g* geometrical parameters.

CALCULATION OF DIPOLE MOMENT BY THE DEL RE METHOD

The Del Re method [18] was devised for calculations of not atomic charges in molecules with *sigma* bonds using a parametrization of atomic electronegativities and inductive effects based upon experimental values for molecular dipole moments. Obviously the knowledge of the molecular geometry is required within this method. The parametrization used here is based on the geometry and dipole moments of 15 simple phosphorus compounds : number 1—**7** of Table 1 and also $ClPF_2$, H_2PPH_2, $HPPF_2$, $H_2P(CF_3)$, $F_2P(CH_3)$, $Cl_2P(C_2H_5)$, $ClP(C_2H_5)_2$ and $P(CH_2O)_3CCH_3$. Molecules containing only the bonds PH, PC, PF, PP and PCl were considered, as these bonds can be assumed to have an almost pure *sigma* character (for trivalent phosphorus). The optimized value hereby obtained for the electronegativity parameter of the P atom $\delta^\circ = 0.066$, while for the inductive and exchange parameters the vlues $(\gamma_{AB}/\gamma_{BA}\,;\ \varepsilon_{AB})$ — 0.362/0.744 ; 0.747 — 0.306/0.787 ; 0.426—0.207/0.151 ; 0.92—0.279/0.279 ; 0.837 and 0.265/0.265 ; 0.251 were obtained for the PH, PC, PF, PP and respectively PCl bonds. Details concerning the parameter optimization method and the stereochemical considerations for dipole moment calculations will be given in a further note.[19]

RESULTS

Table 1 lists all phosphorus derivatives for which dipole moments were calculated with advanced methods (and also the method of Smith *et al* [15–17]). Experimental values and dipole moments calculated by our Del Re method are also given. Comparisons are difficult also because larger molecules present several conformers. Therefore in the last column (**5**) of Table 1 the method for structural determination is listed, and also, where known, the predominant conformer.

In order to assess the predictive value of our Del Re method, Table 2 lists the molecules for which the calculated moments can be compared

Table 2

Experimental and Del Re dipole moments [a]

	Compound	Experimental value	Calculated value
	$FPCl_2$	0.86 [b]	0.77
20	$F_2PC_2H_5$ — *g*	2.168	2.192
20	$F_2PC_2H_5$ — *t*	2.081	1.896
22	$H_2PC_2H_5$ — *g*	1.22	1.12
22	$H_2PC_2H_5$ — *t*	1.226	1.429
	$H_2PCH(CH_3)_2$ — *g*	1.23 [c]	1.453
24	$H_2PC(CH_3)_3$	1.17	1.391
31	$P(C(CH_3)_3)_3$	1.59	2.152

[a] Only compounds not used for calibration included. Notation of conformation is the same as in Table 1. References for experimental dipole moments and for structural data, where not quoted, see also Table 1. Dipole moments in Debye units.

[b] From ref. 28.

[c] From ref. 72.

[d] Structural data from ref. 73.

[e] Structural data from ref. 72.

with experimental ones. Only eight molecules are listed because for larger molecules the existing equilibrium mixture of conformers makes calculations practically impossible. The correlation coefficient between the eight calculated and experimental values is r = 0.874. The highest disagreement is obtained for the tri-*butyl*-butyl-derivative (**31**); the discrepancy may be explained by the steric crowding of the three t-*butyl*-butyl groups and the hereby produced deformation of charge distributions. With this compound eliminated r = 0.937 is obtained.

Concerning comparison between calculated dipole moments by the Del Re method and by advanced methods, for the methylated phosphine derivatives PH_3 (**1**), $H_2P(CH_3)$ (**5**), $HP(CH_3)_2$ (**6**) and $P(CH_3)_3$ (**7**) the CNDO/2D calculations of Kuznesof *et al* [6] yield 0.01; 1.52; 1.81 and 1.81, the calculated Del Re values are 0.65; 1.02; 1.174 and 1.274 D. The parallelism is acceptable.

For the same series of compounds the MNDO and the MINDO/3 values calculated by Frenking *et al* [11] are 1.35 1.61; 1.81; 1.94 and respectively 2.70; 2.30; 1.75; 1.13 D. Only the MNDO values present a parallelism with the Del Re values, but the agreement with the experimental values is less satisfactory. The MM2 results of Bowen and Allinger [14] are in good agreement with both experimental and Del Re values.

For the fluorinated series PH_3 (**1**), H_2PF (**8**), HPF_2 (**4**) and PF_3 (**2**) the *ab initio* results of Schmiedekamp *et al.*[9] are with *sp* basis for the P atom 1.207; 2.305; 2.588; 2.641 D, while with *spd* basis 0.776; 1.810; 1.990. The corresponding Del Re and experimental values are 0.65; 1.145; 1.184; 1.062 and 0.57; 1.30 (estimated); 1.32; 1.025 D respectively. The parallelism with the Del Re results is satisfactory but the calculated *ab initio* values are much higher than the experimental ones.

There is generally a good agreement between the calculated Del Re dipole moments and the experimental ones. Even for larger molecules where a comparison with experimental results is difficult because of the conformational equilibrium, the experimental value is within the range of the values calculated for the different possible conformers.

CONCLUSIONS

Dipole moments calculated by our calibrated Del Re method are in satisfactory agreement with the experimental results. The dipole moments evaluated by more sophisticated methods generally agree less with experimental data, even if there is a parallelism with the Del Re results within a series of compounds.

Our method can thus be recommended for an evaluation of atomic charge distribution within phosphorus compounds without appreciable *pi* bonding character. The time cost advantages of our method would be appreciable for calculation of charge distributions in large molecules; with an about 50 kbytes home computer dipole moments can be calculated overnight for molecules with up to 40—50 atoms.

REFERENCES

[1] D. Purdela and R. Vâlceanu, "Khimiya organicheskikh soedinenii fosfora", Izd. Khimiya, Moskva, 1972.

[2] I. H. Hillier and V. R. Saunders, *J.C.S., Chem. Commun.*, **1970**, 316.

[3] J. B. Robert, H. Marsmann, L. J. Schaad and J. R. Van Wazer, *Phosphorus*, **2**, 11 (1972).

[4] J. M. Lehn and B. Munsch, *Mol. Phys.*, **23**, 91 (1972).

[5] M. F. Guest, I. H. Hillier and V. R. Saunders, *J. C. S. Faraday Trans.* 2, **1972**, 114.

[6] P. M. Kuznesof, F. B. T. Pessine, R. E. Bruns and D. F. Shriver, *Inorg. Chim. Acta.*, **14**, 271 (1975).

[7] C. S. Ewing, P. Coffey and J. R. Van Wazer, *Inorg. Chem.*, **14**, 1848 (1975).

[8] J. M. Scott and B. T. Sutcliff, *Theor. Chim. Acta*, **41**, 141 (1976).

[9] A. Schmiedekamp, S. Skaarup, P. Pulay and J. E. Boggs, *J. Chem. Phys.*, **66**, 5769 (1977).

[10] G. Frenking, F. Marschner and H. Goetz, *Phosphorus and Sulfur*, **8**, 337 (1980).

[11] G. Frenking, F. Marschner and H. Goetz, *Phosphorus and Sulfur*, **8**, 343 (1980).

[12] C. H. Rhee, R. M. Metzger and F. M. Wiygul, *J. Chem. Phys.*, **77**, 899 (1982).

[13] M. Corosine, F. Crasnier, M. C. Labarre, J. F. Labarre and C. Leibovici, *Chem. Phys. Letters*, **20**, 111 (1973).

[14] J. P. Bowen and N. L. Allinger, *J. Org. Chem.*, **52**, 2937 (1987).

[15] R. P. Smith, T. Ree, J. L. Magee and H. Eyring, *J. Am. Chem. Soc.*, **73**, 2263 (1951).

[16] R. P. Smith and E. M. Mortensen, J. Amer. Chem. Soc., **78**, 3932 (1956).

[17] N. Saraswathi and S. Soundararajan, *J. Organometal. Chem.*, **46**, 289 (1972).

[18] G. Del Re, *J. Chem. Soc.*, **1958**, 4031.

[19] L. Kurunczi, R. Vâlceanu and Z. Simon, to be published.

[20] J. D. Pethke and J. L. Whitten, *J. Chem. Phys.*, **59**, 4855 (1973).

[21] C. C. Loomis and M. W. P. Strandberg, *Phys. Rev.*, **81**, 798 (1951).

[22] M. E. Sirvetz and R. E. Weston, *J. Chem. Phys.*, **21**, 898 (1953).

[23] C. A. Burrus, *J. Chem. Phys.*, **28**, 427 (1958).

[24] P. B. Davies, R. M. Neumann, S. C. Wofsey and W. Klemperer, *J. Chem. Phys.*, **55**, 3564 (1971).

[25] F. Y. Chu and T. Oka, *J. Chem. Phys.*, **60**, 4612 (1974).

[26] R. G. Shulman, B. P. Dailey and C. H. Townes, *Phys. Rev.*, **78**, 145 (1950).

[27] S. N. Ghosh, R. Trambarulo and W. Gordy, *J. Chem. Phys.*, **21**, 308 (1953).

[28] J. G. Morse and R. W. Parry, *J. Chem. Phys.*, **57**, 5372 (1972).

[29] E. Hirota and Y. Morino, *J. Mol. Spectroscopij*, **33**, 460 (1970).

[30] J. W. Smith, *Proc. Roy. Soc.*, **A**, **136**, 256 (1932).

[31] U. Grassi, *Nuovo Cime to*, **10**, 3 (1933).

[32] N. Hacket and R. J. W. Le Fèvre, *J. Chem. Soc.*, **1961**, 2612.

[33] C. R. Nave, L. T. Weatherly and Q. Williams, *J. Chem. Phys.*, **40**, 1413 (1968).

[34] Yu. P. Egorov, V. I. Katolichenko, Yu. Ya. Borovikov, N. G. Katolichenko and V. Ya. Semenii, *Teor. Eksp. Khim.*, **8**, 761 (1972).

[35] J. P. Van Lindthoudt, E. V. Van den Berghe, G. P. Van der Kelen, *J. Mol. Struct.*, **67**, 269 (1980).

[36] G. Cazzoli, *J. Mol. Spectroscopy*, **53**, 37 (1974).

[37] J. G. Morse and R. W. Parry, *J. Chem. Phys.*, **46**, 4159 (1967).

[38] R. L. Kuczkowski, *J. Amer. Chem. Soc.*, **90**, 1705 (1968).

[39] T. Kojima, E. L. Breig and C. C. Lin, *J. Chem. Phys.*, **35**, 2139 (1961).

[40] R. Nelson, *J. Chem. Phys.*, **39**, 2382 (1963).

[41] J. R. Durig, S. D. Hudson, M. R. Jalilian and Y. S. Li, *J. Chem. Phys.*, **74**, 772 (1981).

[42] D. R. Lide and D. E. Mann, *J. Chem. Phys.*, **29**, 914 (1958).

[43] B. Beagley and A. R. Medwid, *J. Mol. Struct.*, **38**, 229 (1977).

[44] H. L. Hodges, L. S. Su and L. S. Bartell, *Inorg. Chem.*, **14**, 599 (1975).

[45] K. H. Rhee, A. M. Snider, Jr. and F. A. Miller, *Spectrochim. Acta*, **A**, **20**, 1029 (1973).

[46] K. Suenga and A. Krotera, *J. Chem. Soc. Japan, Pure Chem. Soc.*, **70**, 116 (1949); *Chem. Abstr.*, **45**, 4107 *c* (1951).

[47] E. A. Ishmaeva, I. I. Patsanovskii, M. Mikolajczik, B. Zemnitskaya, Ya. Kzhivanskii and A. N. Pudovik, *Doklady Akad. Nauk S.S.S.R.*, **242**, 620 (1978).

[48] M. G. Malone and A. L. Ferguson, *J. Chem. Phys.*, **2**, 99 (1934).

[49] M. Baudler and G. Fricke, *Z. anorg. allg. Chem.*, **320**, 11 (1963).

[50] R. P. Arshinova, T. D. Sorokina, A. B. Remizov, G. E. Koroleva and B. A. Arbuzov, *Izvest Akad. Nauk S.S.S.R., Ser. Khim.*, **1979**, 2242.

[51] R. P. Arshinova and S. G. Vul'fson, *Zhur. strukt. Khim.*, **20**, 862 (1979).

[52] L. L. Tuzova and V. A. Naumov, *Zhur. strukt. Khim.*, **20**, 923 (1979).

[53] V. A. Naumov and O. N. Kataeva, *Zhur. strukt. Khim.*, **24**, No. 2, 160 (1983).

[54] P. Groner, J. S. Church, Y. S. Li and J. R. Durig, *J. Chem. Phys.*, **82**, 3894 (1985).

[55] G. Kodama, J. R. Weawer, J. La Rochelle and R. W. Parry, *Inorg. Chem.*, **5**, 710 (1966).

[56] J. R. Durig and A. W. Cox, Jr., *J. Chem. Phys.*, **64**, 1930 (1976).

[57] J. R. Durig and A. W. Cox, Jr., *J. Chem. Phys.*, **63**, 2303 (1975).

[58] A. E. Arbuzov and I. P. Rakov, *Izvest Akad. Nauk S.S.S.R., Otdel. khim. Nauk*, **1950**, 237.

[59] M. J. Aroney, L. H. L. Chia, R. J. W. Le Fèvre and J. D Saxby, *J. Chem. Soc.*, **1964**, 2948.

[60] J. G. Verkade, *Coord. Chem. Reviews*, **9**, 1 (1972/73).

[61] D. Bessere and M. Troquet, *Bull. Soc. Chim. France*, **1974**, 845.

[62] H. Waeschke and R. Mitzner, *Z. Chem.*, **17**, 228 (1977).

[63] Y. S. Li, A. W. Cox, Jr. and J. R. Durig, *J. Mol. Spectroscopy*, **70**, 34 (1978).

[64] G. Klages and R. Langpape, *Z. Elektrochem.*, **63**, 533 (1959).

[65] C. W. N. Cumper, A. A. Foxton, J. Read and A. J. Vogel, *J. Chem. Soc.*, **1964**, 430.

[66] P. Mauret, J. P. Fayet, M. C. Labarre and J. F. Labarre, *J. Chim. Phys.*, **65**, 549 (1968).

[67] J. H. S. Green, *Spectrochim. Acta*, **A**, **24**, 137 (1968).

[68] T. L. Brown, J. G. Verkade and T. S. Piper, *J. Phys. Chem.*, **65**, 2051 (1961).

[69] J. G. Morse and R. W. Parry, *J. Chem. Phys.*, **57**, 5367 (1972).

[70] J. P. Fayet, M. Pradayrol and P. Mauret, *C. R. Ăcad. Sci.*, **C**, **271**, 1033 (1970).

[71] H. Oberhammer, R. Schmutzler and O. Stelzer, *Inorg. Chem.*, **17**, 1254 (1978).

[72] J. R. Durig and Y. S. Li, *J. Mol. Spectroscopy*, **70**, 27 (1978).

[73] L. O. Brockway and J. V. Beach, *J. Amer. Chem. Soc.*, **60**, 1836 (1938).

Revue Roumaine de Chimie, **34**, *1*, 387–395 (1989)

THERMODYNAMIC CHARACTERIZATION OF POLYMERS BY CHROMATOGRAPHY WITH GAS MOBILE PHASE

RODICA VÎLCU and MINODORA LECA

Polytechnic Institute of Bucharest, Faculty of Chemical Technology, Department of Physical Chemistry, Blvd Republicii 13, R 70346, Bucharest, Romania

Received October 9, 1988

Thermodynamic quantities and properties of polymers which can be obtained by gas mobile phase chromatography, or by the so-called inverse gas chromatography are reviewd. In gas-liquid chromatography, from the equilibrium partition of the injected substances between the stationary and mobile phase, the activity coefficients of the injected substances, the polymer-solvent and polymer-polymer interaction parameters, the enthalpy of dilution, and the solubility parameters of polymers may be obtained at infinite dilution of the injected sample in polymer. In gas-solid chromatography the adsorption isotherms and surface specific areas are available from the equilibrium adsorption of the injected substances on polymers. The melting transitions of polymers, their crystallinity, kinetics of crystallization, glass transitions, multiple transitions in crystalline-amorphous polymers, segregation of block copolymers, diffusion coefficients, etc. are also obtainable owing to the different retention mechanisms both below and above the glass transition. Inverse gas chromatography allowed the check up of some theories of solution such as : regular solutions theory, contact points and segments theory, perturbation theory, Flory-Huggins' theory, Flory's equation of state theory.

Polymers, on account of their negligible vapour pressure below the decomposition temperature, cannot be analysed by gas chromatography. However, this very feature makes them very convenient as stationary phases. Chromatographic analysis successfully uses a wide variety of polymeric stationary phases in the separation of complex mixtures of substances.

Because chromatographic separation is determined by the equilibrium partition (distribution) of the injected components between stationary and mobile phases, the gas chromatographic technique may be used to measure some thermodynamic quantities such as :[1] partition coefficients of the injected substance between stationary and mobile phases, activity coefficient of the injected substance at infinite dilution, the second virial coefficient of the vapour mixture injected substance-carrier gas, excess thermodynamic functions, partition and adsorption isotherms, vaporization enthalpies, mixture and adsorption enthalpies, specific surfaces, boiling temperature, etc.

The above quantities are determined from the interaction of an "unknown" injected sample with a well known stationary phase in the technique of direct gas chromatography. Inversing the unknowns, i.e. the injected substances have known properties and stationary phase unknown ones, the properties of polymeric phases may be obtained from their interaction. Guillet [2] gave the name of inverse gas chromatography to this second technique. This last technique will be the object of the present work.

The chromatography is gas-liquid (GLC), partition or distribution if the stationary phase is liquid at the operating temperature and gas-solid (GSC) or adsorption if this is solid.

In GLC the injected micromolecular substances dissolve practically at infinite dilution in the polymeric stationary phase. Therefore, the thermodynamic quantities of dissolution at polymer volume fraction, φ_2, close to unity are directly available. The solute-solute interactions both before and after mixing are thus eliminated.

The activity coefficient at infinite dilution of the injected sample defined on the basis of mole fraction x_1, ${}^x\gamma_1^\infty$, is given by the equation :

$$\ln {}^x\gamma_1^\infty = \ln\left(\frac{a_1}{x_1}\right)^\infty = \ln\frac{RTm_2}{p_1^0 V_N M_2} - (B_{11} - V_1)\frac{p_1^0}{RT} + (2B_{13} - V_1)\frac{p_0 J_3^4}{RT} \quad (1)$$

where a_1 is the activity of the injected substance, R the gas constant, t the operating temperature, m_2 the mass of the stationary phase, p_1^0 the vapour pressure of the injected substance, V_N the net retention volume, M_2 the molecular weight of the stationary phase, B_{11} the second virial coefficient of the solute vapours, V_1 the molar volume of the solute, B_{13} the second virial coefficient of the solute vapour-carrier gas mixture, p_0 the pressure at the column outlet, J_3^4 the correction factor for the pressure drop along the column.

In terms of the specific retention volume V_g, equation (1) is written :

$$\ln {}^x\gamma_1^\infty = \ln\frac{273\cdot 16 R}{p_1^0 V_g M_2} - (B_{11} - V_1)\frac{p_1^0}{RT} + (2B_{13} - V_1)\frac{p_0 J_3^4}{RT} \quad (2)$$

and in terms of the specific retention volume extrapolated to zero column pressure, V_g^0 simplifies to :

$$\ln {}^x\gamma_1^\infty = \ln\frac{273\cdot 16\, R}{p_1^0 V_g^0 M_2} - (B_{11} - V_1)\frac{p_1^0}{RT} \quad (3)$$

In order to calculate ${}^x\gamma_1^\infty$ from equations (1)—(3), the molecular weight of the stationary phase must be known. The synthetic polydisperse polymers are characterized by average molecular weights. Equations (1)—(3) lead to $\ln {}^x\gamma_1^\infty \to -\infty$ when $\bar{M}_2 \to \infty$. This suggests [3] that ${}^x\gamma_1^\infty$ is not the most meaningful quantity for comparing the thermodynamic quantities calculated from GLC data with theories of solutions when polymers are used as stationary phases. Mole fractions are not used in the thermodynamic theories of polymer solutions ; they are replaced by volume fractions φ_i in the Flory-Huggins theory and by segment fractions Φ_i in Flory's equation of state theory. An appropriate reference function for the activity can be any concentration variable of solute which does not nvolve the number of moles of polymer, such as the weight fraction w_1, he volume fraction φ_1, the molarity, etc. Patterson et al.[3] selected the veight fraction as a reference function for defining the activity coefficient t infinite dilution of the solute. Replacing x_1 by w_1 in equation (3), he activity coefficient defined in terms of the weight fraction, ${}^{w}\gamma_1^{\infty}$, is :

$$\ln {}^{w}\gamma_1^{\infty} = \ln \left(\frac{a_1}{w_1}\right)^{\infty} = \ln \frac{273.16R}{p_1^0 V_g^0 M_1} - (B_{11} - V_1)\frac{p_1^0}{RT} \tag{4}$$

where M_1 is the molecular weight of the injected sample. The following correlations exist between activity coefficients defined in terms of mole, weight, and volume fractions :[4]

$${}^{w}\gamma_1^{\infty} = {}^{x}\gamma_1^{\infty} M_2/M_1 \tag{5}$$

$${}^{\varphi}\gamma_1^{\infty} = {}^{w}\gamma_1^{\infty} \rho_1/\rho_2 \tag{6}$$

${}^{w}\gamma_1^{\infty}$ and ${}^{\varphi}\gamma_1^{\infty}$ do not require knowledge of the polymer molecular weight and polydispersion. The new activity coefficients still depend on the above mentioned factors, but through the values of V_g or V_g^0. Their values tend to a limit with increasing molecular weight of the stationary phase.[3]

According to the Flory-Huggins theory the solute activity is given by the equation :

$$\ln a_1 = \ln \varphi_1 + (1 - 1/m)\varphi_2 + \chi_{12}\varphi_2 \tag{7}$$

where m is the number of segments for a polymer molecule considered monodisperse and χ_{12} the injected substance-polymer interaction parameter. For polydisperse polymers, m is given by the ratio :

$$m = (\bar{V}_2)_n/V_1 = (\bar{M}_2)v_2/V_1 \tag{8}$$

$(\bar{V}_2)_n$ being the number average of molecular volumes in polydisperse polymer sample.

For the infinite dilution condition in GLC equation (7) becomes :

$$\ln {}^{w}\gamma_1^{\infty} = \ln (v_1/v_2) + \left(1 - \frac{V_1}{\bar{M}_2 v_2}\right) + \chi_{12} \tag{9}$$

Taking account of the relation (4) the interaction parameter becomes, using the Flory-Huggins theory :

$$\chi_{12} = \ln \frac{273.16\,Rv_2}{p_1^0 V_g^0 V_1} - \left(1 - \frac{V_1}{\bar{M}_2 v_2}\right) - (B_{11} - V_1)\frac{p_1^0}{RT} \tag{10}$$

and :

$$\chi_{12}^{*} = \ln \frac{273.16\, R v_2^{*}}{p_1^0 V_g^0 V_1^{*}} - \left(1 - \frac{V_1^{*}}{\bar{M}_2 v_2^{*}}\right) - (B_{11} - V_1)\frac{p_1^0}{RT} \qquad (11$$

using Flory's equation of state theory. The new volumes v^{*} correspond to the specific volumes of the close-packed hypothetical liquid at 0 K and are independent of temperature.

Equations (10) and (11) are both approximations assuming that virial coefficients arising from carrier gas-solvent interactions may be neglected and, similarly, that solute-carrier gas interactions in the gas phase have a negligible effect on the measured V_g^0 value.

According to Flory et al.,[5-7] the interaction parameter χ_{13}^{*} can be written :

$$\chi_{12}^{*} = \frac{p_1^{*} V_1^{*}}{RT\Phi_2^2}\left[\left((3\,\tilde{T}_1 \ln \frac{\tilde{v}_1^{1/3} - 1}{\tilde{v}_2^{1/3} - 1} + \tilde{v}_1^{-1} - \tilde{v}_2^{-1}\right) + \frac{X_{12}}{\tilde{v}_2 p_1^{*}\theta_2^2}\right] \qquad (12)$$

where $\tilde{z}$ are the reduced quantities and X_{12} the contact interaction parameter. The relationship between χ_{12} and χ_{12}^{*} is :[8]

$$\chi_{12}^{*} - \chi_{12} = \ln (v_1/v_2) \qquad (13)$$

The values of χ_{12}^{*} are in very good agreement with those obtained by equilibrium absorption [9] for hydrocarbons-polydimethylsiloxane systems.

The total interaction parameter between the volatile substance and the binary mixture of the polymeric stationary phases, $\chi_{1(23)}$ is given by the relation : [10]

$$\chi_{1(23)} = \chi_{12}\varphi_2 + \chi_{13}\varphi_3 + \chi_{23}\frac{V_1}{V_2}\varphi_2\varphi_3 =$$

$$= \ln \frac{273.16(w_2 v_2 + w_3 v_3)}{p_1^0 V_g^0 V_1} - \left(1 - \frac{V_1}{V_2}\right)\varphi_2 - \left(1 - \frac{V_1}{V_3}\right)\varphi_3 - (B_{11} - V_1)\frac{p_1^0}{RT} \qquad (14)$$

where χ_{12} and χ_{13} are the interaction parameters between the injected substance and the individual polymers and χ_{23} the polymer-polymer interaction parameter. Hence, using the binary systems 1—2 and 1—3, the polymer-polymer interaction parameter can be obtained from gas chromatographic data.

The enthalpy of dilution of a solute at infinite dilution in polymer $\Delta\bar{H}_1^{\infty}$ is obtained by the equation : [3]

$$\Delta\bar{H}_1^{\infty} = \bar{H}_1^{\infty} - H_1^0 = R\frac{\partial \ln a_1}{\partial(1/T)} = R\frac{\partial}{\partial(1/T)}\left[-\ln V_g^0 p_1^0 - \frac{p_1^0}{RT}(B_{11} - V_1)\right] \qquad (15)$$

vhere $\bar{H}_1^\infty$ is the partial molar enthalpy of the solute at infinite dilution ind H_1^0 its molar enthalpy in the pure liquid state. Equation (15) may be vritten : [3]

$$\Delta \bar{H}_1^\infty = RT^2(\alpha_2 - \alpha_1) + R\,\frac{\partial \chi_{12}}{\partial(1/T)} \tag{16}$$

α_1 and α_2 being the thermal expansion coefficients of components in he liquid state.

At constant pressure, the Gibbs free energy of dilution is given lirectly by the solubility parameters of components δ_1 and δ_2 : [11]

$$\bar{G}_1^\infty = V_1(\delta_1 - \delta_2)^2 = RT \ln {}^w\gamma_1^\infty \tag{17}$$

The Flory-Huggins treatment combined with the Hildebrand-Scatchard heory gives the following relationship for the polymer-solute interaction arameter : [11]

$$\chi_{12} = V_1(\delta_1 - \delta_2)^2/RT \tag{18}$$

vhich can be written :

$$\frac{\delta_1^2}{RT} - \frac{\chi_{12}}{V_1} = \frac{2\delta_2}{RT}\,\delta_1 - \frac{\delta_2^2}{RT} \tag{19}$$

Therefore a plot of the left side of this equation versus δ_1 yields a straight ine with a slope of $2\delta_2/RT$ and the intercept of $-\ \delta_2^2/RT$.

The solubility parameter defined by equation (17) is different from hat conventionally measured by solubility, swelling, or surface tension ata, since in the first case the solute is at infinite dilution in polymer, vhile in the last one its concentration is high. Since δ_1 has a unique hermodynamic definition, a solubility parameter at infinite dilution for olymer, δ_2^∞, may be defined in terms of measurable thermodynamic uantities : [12]

$$\chi_{12}^\infty = V_1(\delta_1 - \delta_2^\infty)^2/RT \tag{20}$$

The quantity related to the solubility parameters of the two componets which can be determined by GLC is $\Delta\bar{H}_1^\infty$. If non-polar substances re injected into polar polymers, only interactions through dispersion orces are basically involved. If δ_1 of the injected substance is known, hen from $\Delta\bar{H}_1^\infty$ thus determined the polymer solubility parameter due to ispersion forces for the polymer, δ_{2d}, is obtained.[13,14] By injecting polar ubstances whose structure is similar to that of the polymer, the total olubility parameter of the polymer, δ_2, is determined and using the elation :

$$\delta^2 = \delta_{2d}^2 + \delta_{2p}^2 \tag{21}$$

ne solubility parameter due to polar forces, δ_{2p}, is obtained.

GSC is the only method of studying adsorption characteristics o surfaces at very low coverage. At the same time the method applies a higher concentrations. Thus a range of concentrations of the adsorbe substance may be covered and hence the adsorption isotherms can b determined. The specific surface area of the adsorbed substance may b determined, as a rule, from adsorption isotherms.[1]

The inverse gas chromatography allows the determination of polymer-injected substance interactions as well as of some properties of th polymers themselves.

The determination of polymers phase transitions by gas chromatography is founded on the different interactions of injected substance with ordered and isotropic phases : the injected substance vapours ma penetrate only in the amorphous regions of the polymer below the meltin temperature, the crystalline ones being impenetrable.[15] At the meltin point, T_m, the amorphous content rises sharply, which causes an increas of the retention volumes and an obvious discontinuity on the $\ln V_g = f(1/T)$ diagram, which is called the retention diagram. Above th melting temperature the polymer is completely amorphous and the retention diagram is perfectly linear. Below T_m the retention volumes ar lower than those calculated by extrapolation of the linear section of th diagram to higher temperatures. The retention diagrams for some substances injected on poly(ethylene oxide) are shown in Fig. 1.[16]

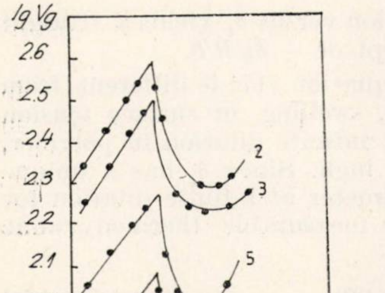

Fig. 1. — Retention diagrams of : 1 — benzene ; 2 — toluene ; 3 — chloroform ; 4 — carbon tetrachloride ; 5 — n-octane on poly(ethylene oxide).

Because the melting of polymer involves no change in the retention mechanism of the injected substance, the crystalline fraction X_c of the polymeric stationary phase may be determined at a temperatures by the equation : [15]

$$V_g = (1 - X_c)V_g' \qquad (22$$

where V_g' is the retention volume corresponding to a completely amorphous polymer. V_g' is obtained by linear extrapolation of the straight section of th retention diagram from higher temperatures where the polymer is amorphous t temperatures below T_m.

The adsorption phenomenon at th polymer-carrier gas interface also take place for crystalline-amorphous polymer and the adsorption contribution must b subtracted from the measured V_g bot above and below T_m.

A comparison of the degrees of crystallinity obtained by gas chromatography for poly(ethylene oxide) of molecular weight 40000 with thos determined by IR spectroscopy and X-ray diffraction yields the following results :[17] 74% for the first method when the film thickness wa 6.5×10^{-5} cm, 75.9% for the second (film thickness 5.1×10^{-3} cm) an

79.1% for the last method. The differences were ascribed to the incomplete development of the crystallinity in the films used in gas chromatography and IR spectroscopy, these films being thinner than the diameter of spherulites.

The gas chromatographic method is the only one which does not require a knowledge of the properties of the 100% crystalline polymer and is based on the assumption that the properties in question vary linearly with the degree of crystallinity. In copolymers the additivity may no longer operate and inverse gas chromatography, which does not need information regarding polymer, becomes particularly convenient. Moreover, to avoid sample dissolution, the copolymer may be introduced in the column as a powder mixed with the support. In such a system the diameter of the particles should be taken into account, because if it exceeds 200 μm the equilibrium is not reached even at temperatures close to T_m.

Monitoring the time variation of the retention volume at constant temperature, gas chromatography may be used to study the kinetics of crystallization. As a polymeric stationary phase cools from the melt to a temperature below T_m, the retention volume decreases at the rate of formation of crystalline regions. Maximum possible crystallinity at a given temperature expressed in percent, $X_{c\,\max}$, is given by the relation : [18,19]

$$X_{c\,\max} = 100(1 - V_g^c/V_g^d) \tag{23}$$

where V_g^c is the specific retention volume at the time that equilibrium between crystalline and amorphous phases has been reached and V_g^d the specific retention volume due to dissolution. The percentage of crystalline phase at any time t is then :

$$X_c = 100(V_g^d - V_g^t)/(V_g^d - V_g^c) \tag{24}$$

V_g^t being the specific retention volume measured at time t.

The retention diagrams are linear whenever, in the temperature range where retention data were determined for a chromatographic system, there is no transition of phase or physical state of the stationary phase. Near the glass transition, T_g, the polymeric stationary phases exhibit a Z-shaped retention diagram [20,21] which, within a certain temperature range, shows an increase of retention volume with temperature (Fig. 2). Retention originates in surface adsorption on the polymer surface in the glassy state at temperature below T_g (region I) ; owing to an increasing molecular mobility at and above T_g the solute molecules penetrate the polymer bulk, causing an increase of retention volume with rising temperature (non-equilibrium region II) ; at even higher temperatures (region III) the equilibrium distribution of solute between gas phase and polymer bulk (dissolution in the stationary phase) occurs along with adsorption contribution. This method becomes particularly important and useful in highly crystalline polymers which have multiple transitions, in block copolymers with incompatible blocks, and in fibers, making possible the study of the effect of thermal treatment on transitions.

Comparison of retention diagrams with those from differential calorimetry data has shown that[21,22] T_g is derived from the first deviation from linearity in the adsorption region (I), T_1, which corresponds to the first measurable contribution of dissolution (of the penetration of sample vapours into the polymer bulk) to the overall retention volume. The non-equilibrium region II, characterized by the strong dependence of retention volume on carrier gas flow rate, are due to the slow solute diffusion into the bulk of the polymer stationary phase. Because of the sharp decrease of diffusion coefficient as T_g is approached, the equilibrium repartition cannot be attained during the passage of the solute through the column and therefore the measured retention volumes differ from equilibrium values denoted by dotted lines in Fig. 2.

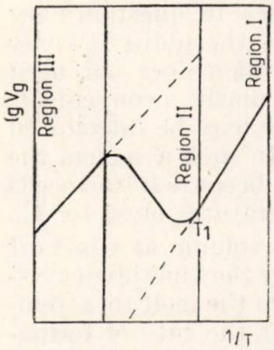

Fig. 2. — Generalized retention diagram for an amorphous polymer.

Many polymers undergo second order transitions at temperatures below T_g[23]; the transitions are caused by rotation of side groups about an axis which is perpendicular to the chain, by the motion of sequences of 3–5 methylenic groups from the backbone or by motion of chain portions in polymers containing heteroatoms in the main chain.[24,25] The second kind of motion, noted by Schatzki[26,27] in ethene copolymers and in many homopolymers, is referred to as the crankshaft effect and it occurs immediately below T_g. Because it is almost insensitive to the crystalline phase percentage compared to T_g, it is the dominant transition in crystalline polymers and is often confused with T_g; it is frequently encountered as glass transition temperature II.

Some polymers may undergo transitions above the glass transition temperature, which Boyer[23] called intermediate transition: at $T > T_g$ for amorphous polymers and $T_g < T < T_m$ for crystalline amorphous polymers.

Segregation of block copolymers with incompatible blocks which form an interface at a molecular scale,[1] diffusion coefficients of the injected substance vapours in polymers,[1] the polymer capacity to incorporate plasticizers, the compatibility of polymers with oligomers, the rate of setting of paints and film-forming polymers may also be determined.

Some other applications can be forseen,[28,29] such as the study of polymer chemical modifications, the quality control of polymer powders or fibres.

In order to obtain correct thermodynamic data it is necessary to modify the standard chromatographs so that the column temperature, pressure and flow rate of carrier gas can be controlled with higher precision.

REFERENCES

[1] R. Vîlcu and M. Leca, "Termodinamica polimerilor prin cromatografie de gaze", Ed. Academiei, Bucharest, 1987.
[2] J. E. Guillet in "New Development in Gas Chromatography" vol. 11, J. H. Purnell Ed., Wiley, New York, 1973.

[3] D. Patterson, Y. B. Tewari, H. P. Schreiber and J. E. Guillet, *Macromol.*, **4**, 356 (1971).

[4] A. J. Ashworth, C. F. Chien, D. L. Furio, D. M. Hooker, M. M. Kopečni, R. J. Laub and G. J. Price, *Macromol.*, **17**, 1090 (1984).

[5] B. E. Eichinger and P. J. Flory, *Trans. Faraday Soc.*, **64**, 2035 (1968).

[6] R. A. Orwoll and P. J. Flory, *J. Amer. Chem. Soc.*, **89**, 6814 (1967).

[7] R. A. Orwoll and P. J. Flory, *J. Amer. Chem. Soc.*, **89**, 6822 (1967).

[8] Yu. K. Leung and B. E. Eichinger, *J. Phys. Chem.*, **78**, 60 (1974).

[9] W. R. Summers, Y. B. Tewari and H. P. Schreiber, *Macromol.*, **5**, 12 (1972).

[10] D. Desphande, D. Patterson, H. P. Schreiber and C. S. Su, *Macromol.*, **7**, 530 (1974).

[11] D. Patterson, *Rubb. Chem. Technol.*, **40**, 1 (1967).

[12] G. DiPaola-Baranyi and J. E. Guillet, *Macromol.*, **11**, 228 (1978).

[13] M. Leca, L. Groswald-Cremer and M. Surmeian, *Mat. plastice*, **16**, 114 (1979).

[14] M. Leca and M. Enache, *Rev. Roumaine Chim.*, **28**, 287 (1983).

[15] J. E. Guillet and A. N. Stein, *Macromol.*, **3**, 102 (1970).

[16] M. Leca and M. Surmeian, *Mat. plastice*, **17**, 175 (1980).

[17] M. Leca, M. Surmeian and C. Mandravel, *Bul. Inst. Pol. București*, **XLII**, 33 (1980).

[18] D. G. Gray and J. E. Guillet, *Macromol.*, **4**, 129 (1971).

[19] A. N. Stein, D. G. Gray and J. E. Guillet, *Br. Polymer J.*, **3**, 175 (1971).

[20] O. Smidsrød and J. E. Guillet, *Macromol.*, **2**, 272 (1969).

[21] A. Lavoie and J. E. Guillet, *Macromol.*, **2**, 443 (1969).

[22] J. M. Braun, A. Lavoie and J. E. Guillet, *Macromol.*, **8**, 311 (1975).

[23] R. F. Boyer, *Rubb. Chem. Technol. Rev.*, **36**, 1303 (1963).

[24] M. Leca, "Chimia macromoleculelor și coloizilor", Ed. Didactică, Bucharest, 1977.

[25] A. D. Jenkins, "Polymer Science", North Holland Publ. Comp., Amsterdam, 1972.

[26] T. F. Schatzki, *Polymer Preprints*, **6**, 646 (1965).

[27] R. F. Boyer, *J. Polymer Sci., Symp.*, **50**, 189 (1975).

[28] D. G. Gray, "Gas-Chromatographic Measurement on Polymer Structure and Interactions" in "Progress in Polymer Science" vol. 5, no. 1, Pergamon Press, Oxford, 1979.

[29] J. M. Braun and J. E. Guillet, "Study of Polymers by Inverse Gas Chromatography", in "Advances in Polymer Science" vol. 21, Springer-Verlag, Berlin, 1976.

Revue Roumaine de Chimie, **34**, *1*, 397–401 (1989)

STUDIES ON THE HYDROCARBON PRODUCTION BY IMMOBILIZED *BOTRYOCOCCUS BRAUNII* CELLS

LIAN-WAN YANG and XIU-YUAN WANG *
* Institute of Microbiology, Academia Sinica, 100080 Beijing

Received September 29, 1988

The morphology, growth, photosynthetic activity and hydrocarbon production of free cells of the hydrocarbon-rich *Botryococcus braunii* and of its immobilized cells on two carriers (cotton gauze or polyurethane foam 5000) were tested under batch culture. During 14 days on a shaker culture in light, the biomass, O_2 evolution and hydrocarbon production of the *B. braunii* immobilized on cotton gauze were $0.88\ g \cdot L^{-1}$, $1.66\ \mu$ moles $\cdot\ min^{-1} \cdot L^{-1}$ and $0.817\ g \cdot L^{-1}$, respectively, which were comparable with that of its free cells, but higher than that of its cells immobilized on the polyurethane foam. These results indicated that the cotton gauze may be a new suitable carrier for the immobilized cells to produce hydrocarbon by the continuous cultivation.

INTRODUCTION

Studies on the hydrocarbon biosynthesis began in nineteen thirties and forties with investigations on the role of microorganisms in the hydrocarbon accumulation and in the petroleum genesis. With the development of gas chromatography, the qualitative and quantitative analyses of trace hydrocarbon became easier, hence studies on the hydrocarbon components of microbial cells as a classification characteristic were adopted. Many species of algae, photosynthetic and non-photosynthetic bacteria, fungi, as well as yeasts have been reported to be able to synthesis trace hydrocarbons,[1] of which the freshwater *Botryococcus braunii* [2–5] and the seawater *Dunaliella salina* [6] gave the high production of liquid hydrocarbon.

The green colonial alga *Botryococcus braunii* is a widespread photoplankton in freshwater lakes. Its fossil has been found in organic sediments of different countries.[7–9] This alga is characterized by its unusually high hydrocarbon contents ranging from 15 to 75% (dry weight),[4,5] and named "oil alga". Thus carboniferous deposits, various paleozoic oil-bearing rocks, as well as some tertiary sediments are assumed to derive their hydrocarbon contents from this alga. Interest in this alga has been aroused in some countries because of its ability to provide a renewable source of hydrocarbon usable as fuel or feedstock directly.

This report describes the morphology, growth, photosynthetic activity and hydrocarbon production of *B. braunii* cells immobilized on cotton gauze or polyurethane foam, comparing with its free cells.

RESULTS

1. Morphology

The scanning electron micrographs of the three kinds of *B. braunii* cultures (Fig. 1) on a shaker at 25°C for 21 days showed that their colonies were constituted from two, four or more cells. The morphology of cells immobilized on cotton gauze (C) or in holes of polyurethane foam 5000 (B) were comparable with that of its free cells (A). It means that the two kinds of carrier have no obvious effect on the cell morphology.

2. Growth and Photosynthetic Activity

A comparative studies on cotton gauze and polyurethane foam 5000 as an immobilization carrier of *B. braunii* cells indicated that the former was better than the latter based on both O_2 evolution and biomass as index of growth and photosynthetic activity. On the 14th day of incubation on a shaker, both O_2 evolution and biomass reached to their maxima, 1.66 μmoles $\cdot$min.$^{-1}\cdot$L^{-1} (Table 1) and 0.88 g$\cdot$L^{-1} (Table 2), espectively, which almost draws near those of its free cells.

Table 1

Variations in O_2 evolution, against culture duration, of *B. braunii* cells immobilized on two carriers and of free cell controls *

Culture duration (days)		O_2 evolution (μmole $\cdot$ min$^{-1}\cdot$ L^{-1} culture)		
		7	14	21
Free cell controls		1.44	1.76	1.46
Carriers of cells immobilized	Cotton gauze	1.32	1.66	1.58
	Polyurethane foam 5000	0.78	1.00	0.82

* Free cells used to initial the cultures. The initial O_2 evolution was 0.38 μmole $\cdot$ min$^{-1}\cdot$ L^{-1} culture.

Table 2

Variations in biomass, against culture duration, of *B. braunii* cells imobilized on two carriers and of free cell controls *

Culture duration (days)		Dry biomass (g$\cdot$L^{-1} culture)		
		7	14	21
Free cell controls		0.64	0.96	0.92
Cariers of cells immobilized	Cotton gauze	0.60	0.08	0.82
	Poliyurethane foam 5000	0.46	0.76	0.68

* Free cells used to initial the cultures. The initial dry cells were 0,25 g$\cdot$L^{-1} culture.

Table 3

Comparison of two carriers of *B. braunii* cells immobilized for hydrocarbon production *

Carrier	Total biomass (dry weight $g \cdot L^{-1}$ culture)	Hydrocarbon yield of the culture ($g \cdot L^{-1}$ culture)	Total hydrocarbon level (as % of biomass)
Free cell controls	4.05	0.835	20.6
Cotton gauze	3.84	0.817	21.3
Polyurethane foam 5000	2.85	0.574	20.1

* Free cells used to initial the cultures. The initial dry cells were 0.32 $g \cdot L^{-1}$ culture. The sample were incubated at 25 °C for 21 days under air-lift culture conditions.

3. **Hydrocarbon Yield and Components**

Data in table 3 indicated that 0.817 $g \cdot L^{-1}$ of liquid hydrocarbon was produced by *B. braunii* cells immobilized on cotton gauze after 21 days cultivated under air-lift condition. The total hydrocarbon yield and level were over 20% of its biomass. This result is near those of its free cells, while the hydrocarbon yield obtained by its cells immobilized on polyurethane foam 5000 was only attainable to 0.574 $g \cdot L^{-1}$ (Table 3).

Gas chromatography analyses of hydrocarbons produced by three kinds of *B. braunii* culture mentioned above showed that the nature and distribution of major external hydrocarbons produced by them were the same, while the relative abundances were slightly different (Fig. 2, Table 4). They produced an homologous series of dienic unbranched compounds with odd carbon number from C_{25} to C_{31} and trienic C_{29} and C_{31} derivatives. It means that the nature and distribution of the major external hydrocarbons were not affected by immobilization compared with its free cells under air-lift cultivation.

Table 4

Nature and distribution of the major external hydrocarbons produced by immobilized *B. braunii* cells *

Carrier	Relative abundance (%) *					
	$2\Delta C_{25}$	$2\Delta C_{27}$	$2\Delta C_{29}$	$3\Delta C_{29}$	$2\Delta C_{31}$	$3\Delta C_{31}$
Free cell controls	1.5	10.9	44.5	15.8	24.6	2.7
Cotton gauze	1.3	10.8	41.3	15.9	28.2	2.5
Polyurethane foam 5 000	1.2	14.5	41.4	19.2	21.4	2.3

* The samples were incubated at 25°C for 21 days under air-lift culture conditions. General formula of the major dienic hydrocarbons of *B.braunii* $CH-(CH_2)_7-CH=CH-(CH_2)_x-CH=CH_2$ (x = 13, 15, 17 and 19). The above derivatives, added to the triene hydrocarbons account for more than 95% derivatives of total hydrocarbons,

DISCUSSION

The previous studies on the hydrocarbon synthesis by *Botryococcus braunii* were mainly concerned with its morphology, nutrients, hydrocarbon components, etc.[2,3,10,12-16] According to the studies on the oil-rich *B. braunii* in the Darwin River Reservoir, Hillen and Wake(5,7) indicated that its hydrocarbon yield was about 35 t·ha^{-1}·year^{-1}. They considered that it is worthwhile to breed this alga in reservoirs. In recent years, Bailliez et al[11,17,18]. reported the results of hydrocarbon production by the *B. braunii* cells immobilized on alginate or polyurethane foam, but the yields were much lower than that of its free cells, which were demonstrated by our present experiments using polyurethane foam as carrier. It seemed to be due to their slight toxicity and worse transparency.

B. braunii cells immobilized on the cotton gauze exhibited a rapid growth, high photosynthetic activity and higher hydrocarbon yield, which were comparable to that of its free cells. These promising results may be attributed to its toxicity-free and good transparency, and demonstrated that the cotton gauze is a novel suitable carrier for *B. braunii*. It is obvious that this immobilized method is simple, easy and cheaper. The mechanical strength of cotton gauze is better than that of alginate. Therefore, the cotton gauze may be applied to hydrocarbon production by continuous cultivation. Its operation stability remains to be investigated in the future.

EXPERIMENTAL

Alga strain: *Botryococcus braunii* Kützig was obtained from the Wuhan Institute of Aquatic Biology, Academia Sinica.

Carrier materials: Cotton gauze was Beijing Health Material Factory, China, cut into small pieces (ca. 1 cm^2) and washed three times with distilled water. Polyurethane foam 5000 was from Rexilin Chemicals AB, Helsingborg, Sweden, cut into small cubes (ca. 0.5 mm^3), washed five times in distilled water and dried at 80 °C for 1 day.

Medium and cultivation: The modified CHU 13 medium [10] was used for present study. Three different cultivation conditions were employed as follows.

1. Inoculation and cultivation of free cells: The free cells were grown in modified CHU 13 medium in 250 mL conical flasks. 30 mL of its suspension were inoculated into 70 ml medium. Growth was performed on a shaker (100 rpm, 25°C) at light flux density 24 w/m^2 for 14 days.

All cultures were harvested by centrifugation (2000 rpm, 10 min.). The collected cells were used as inocula and some fresh medium was added so as to obtain a high density algal suspension.

A part of the suspension was directly inoculated into fresh medium (5 mL of the algal suspension into 95 ml of medium in 250 mL conical flasks). Cultures were incubated on a shaker.

2. Inoculation and cultivation of immobilized cells: A part of the suspension was inoculated in 250 mL conical flasks containing 95 mL of medium and 1.5 g of carriers for 5 mL of algal suspension. Growth was performed in the same manner as above conditions.

The pieces of carriers were then picked up. A few pieces were dried to determine the weight of cells adsorbed/g of carrier on the 14 th day cultivation.

The others were inoculated (1.5 g of carrier containing about 25 mg of cells in 100 mL of fresh medium) in 250 mL conical flasks. Growth was performed as above conditions.

Cell concentration was also determined from the free cell cultures and a calculated amount of algal suspension was inoculated in 100 mL of fresh medium in 250 mL conical flasks so as to offer the same amount of alga as in the immobilized cultures. Some of the resulting immobilized cultures and of the free controls were immediately used for determining O_2 evolution at time zero. The others were grown on a shaker as mentioned above. Algal dry weight and O_2 evolution were regularly determined for two types of cultures.

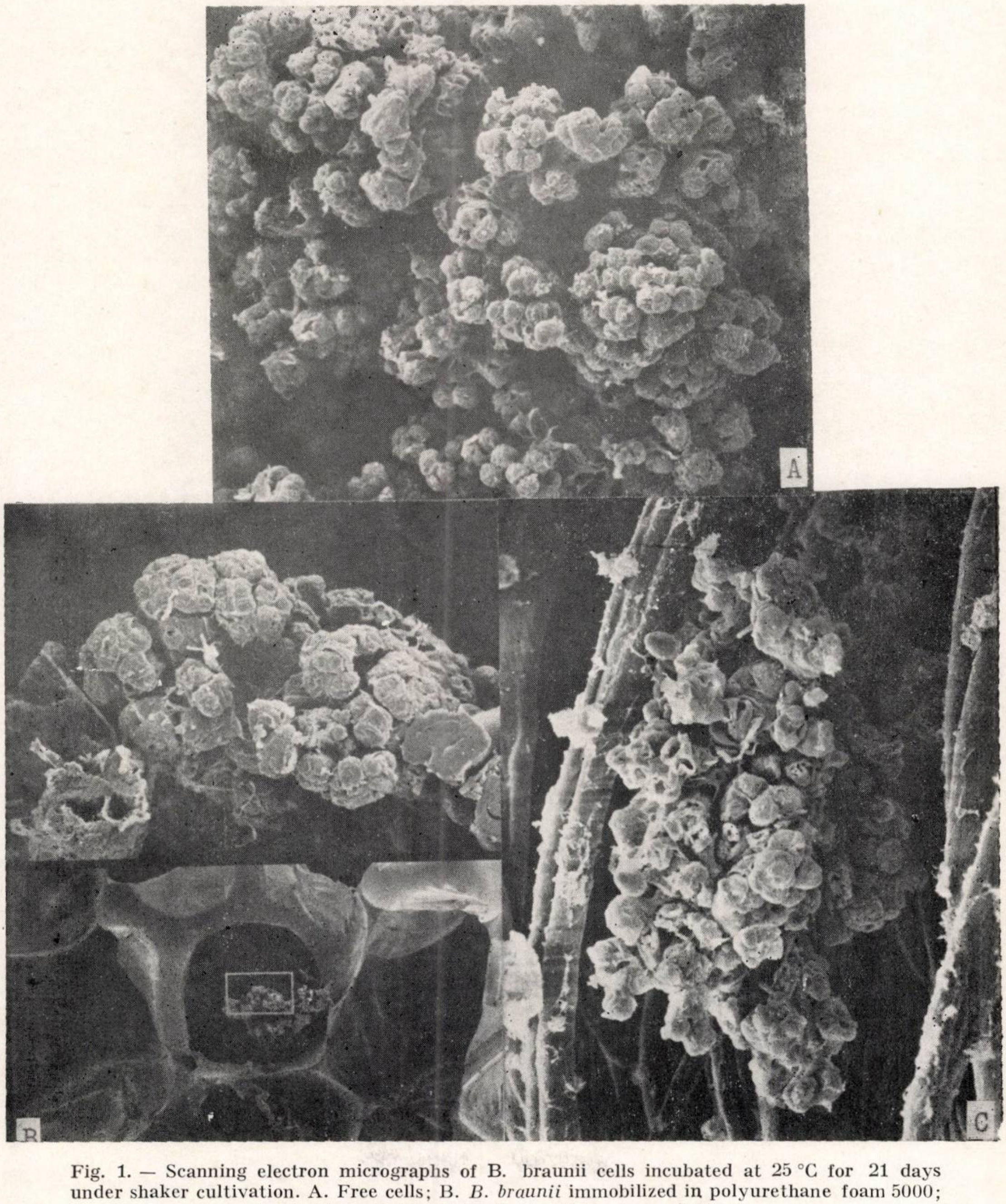

Fig. 1. — Scanning electron micrographs of B. braunii cells incubated at 25 °C for 21 days under shaker cultivation. A. Free cells; B. *B. braunii* immobilized in polyurethane foam 5000; C. *B. braunii immobilized on cotton gauze.* (600 ×).

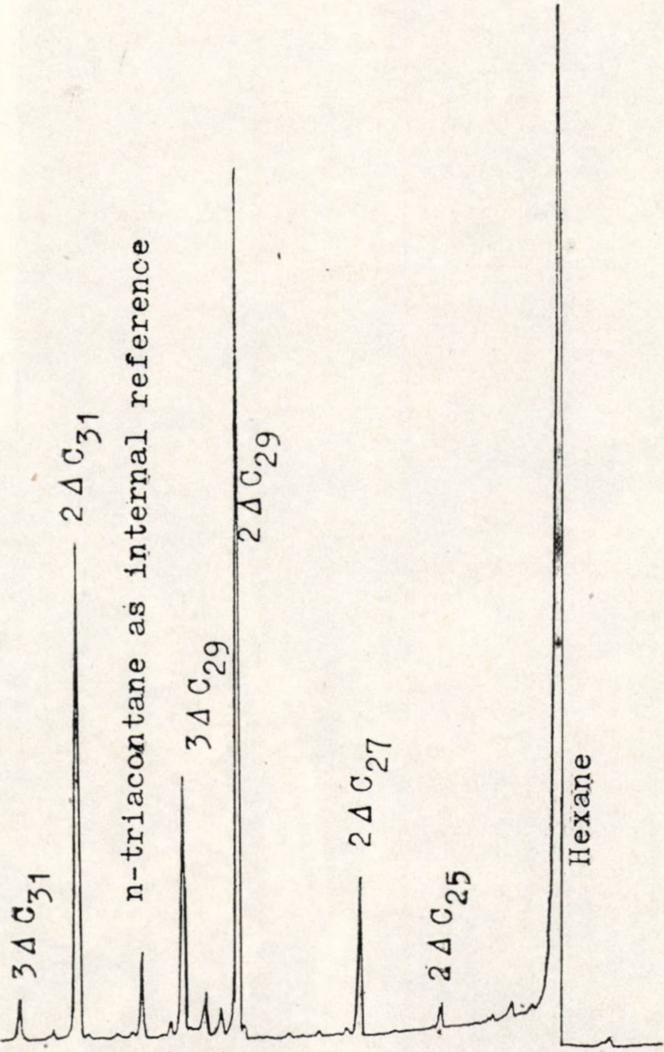

Fig. 2. — Gas chromatogram of the hydrocarbon constituents produced by *B. brauni* under air-lift batch condition at 25°C for 21 days.

3. Air-lift cultivation : The immobilized algae and free controls were grown in 250 mL cylindrical tubes, 35 mm in internal diameter (approximatly 100 mL of culture per tube) at 25 °C. The cultures were continuously illuminated. Sterile air enriched with 1% CO_2 was admitted at the bottom of the tubes (about 5L · h^{-1} per tube) providing both stirring and aeration. The air outlets were protected by Microflow line filters.

Assays

Measurement of O_2 was carried out by a Biological Oxygen Monitor Model 53. For free control cultures, 5 mL of the algal suspension was sampled for each measurement. For immobilized cultures 1/5 of the pieces (i.e. 0.1 g of gauzes or polyurethane foams) were taken for each measurement in 5 mL fresh medium.

Dry weight determination : Aliquots of free cell controls and immobilized cells were filtrated on filters, then the filters were thoroughly rinsed (5 ml of free cell control or immobilized culture containing 0.1 g of carrier were washed using 30 ml of distilled water and dried at 80 °C for one day.

Hydrocarbon analyses : External hydrocarbons were extracted as previously described [10] from the dried free cultures and immobilized cells. Hydrocarbon purification was performed on column chromatography; the qualitative and quantitative analyses of hydrocarbon fraction thus obtained were carried out by the gas chromatograph with *n*-triacontane as an internal reference. [10]

Morphology observation

The immobilized cells and the free cells were fixed with 1% glutaraldehyde in 0.1 M caccodylate buffer (pH 7.4) for one day and washed in the same buffer for one day. Osmic acid (1% in coccodylate buffer, pH 7.4, for 3 h in 4 °C refrigerator) added into the samples. After dehydration with an ethanol series the samples were dried using the CO_2 critical point technique, coated with gold and observed with a CAMECA MEB 07 Microscope.

REFERENCES

[1] E. G. Dediukhina and V. K. Eroshin, *Uspekhi Sovrem. Biol.*. **76**, 351 (1973).

[2] J. R. Maxwell, A. G. Douglas, G. Eglinton and A. McCormick, *Phytochemistry*, **7**, 2157 (1968).

[3] A. C. Brown, B. A. Knights and E. Conway, *Phytochemistry*, **8**, 543 (1969).

[4] J. D. Weete, in "Chemistry and Biochemistry of Natural Waxes" (ed. by P. E. Kolattukudy), Elsevier, Amsterdam, 1976, p. 350.

[5] L. W. Hillen and L. V. Wake, in "1st National Conference, Energy Sources-Australia's Needs" (Australian Energy Institute, Newcastle, 1979), pp. 18—25.

[6] T. C. Tornabene, G. Holzer and S. L. Peterson, *Biochem. Biophys. Res. Commun.*, **96**, 1349 (1980).

[7] L. V. Wake and L. W. Hillen, *Biotechnol. Bioeng.*, **22**, 1637 (1980).

[8] Chengquan He, *Acta Paleontologica Sinica*, **20**, 116 (1981).

[9] Guangjia Zhou, Dunxiang Zhang, Jingrong Li and Zhilin Chen, in "Proceedings of the 2th Conference on Organic Chemistry", The Petroleum Industry Press, Beijing, 1984, pp. 177—190.

[10] C. Largeau, E. Casadevall, C. Berkaloff and P. Dhamelincourt, *Phytochemistry*, **19**, 1043 (1980).

[11] C. Bailliez, C. Largeau, C. Berkaloff and E. Casadevall, *Appl. Microbiol. Biotechnol.*, **23**, 361 (1986).

[12] C. Largeau, E. Casadevall and C. Berkaloff, *Phytochemistry*, **19**, 1081 (1980).

[13] E. Schnepf and W. Koch, *Bot. Jahrb.*, **99**, 370 (1978).

[14] E. Gelpi, J. Oro, H. J. Schneider and E. O. Bennett, *Science*, **161**, 700 (1968).

[15] E. Gelpi, H. J. Schneider, J. Mann and J. Oro, *Phytochemistry*, **9**, 603 (1970).

[16] B.A. Knights, A. C. Brown, E. Conway and B. S. Middleditch, *Phytochemistry*, **9**, 1371 (1970).

[17] C. Bailliez, C. Largeau and E. Casadevall, *Appl. Microbiol. Biotechnol.*, **23**, 99 (1985).

[18] C. Bailliez, C. Largeau, C. Casadevall, L. W. Yang and C. Berkaloff, *Appl. Microbiol. Biotechnol.*, **29**, 141 (1988).

Revue Roumaine de Chimie, 34. 1, 403–408 (1989)

ПРИМЕНЕНИЕ МАКРОЦИКЛИЧЕСКИХ СОЕДИНЕНИЙ ДЛЯ МОДЕЛИРОВАНИЯ БИОСИНТЕЗА

К. Б. ЯЦИМИРСКИЙ
Институт физической химии им. Л. В. Писаржевского Академии наук УССР,
Киев-28, Проспект науки 31, С С С Р

Получена 3 октября 1988 г.

Macrocyclic compounds are widely used for the modelling of biological systems ("biomimetics"). As new examples of such modelling the different types of analogues of ionophores, electron transfer agents (blue proteins and cytochromes), enzymes ("synzymes"), oxygen and free radical transfer agents are considered.
For research activity in the field of ionophores, bulk liquid membranes were used, which were solutions of macrocyclic compounds in 1,2-dichloroethane. The relationship between extraction coefficient values and ionophore ability of macrocycles in solutions was established. New types of siderophores were found. For modelling the active centres of blue proteins sulfur-containing macrocyclic compounds were chosen. The peculiarity of copper(II) interaction with such kind of ligands consists in significant electron transfer from sulfur donor atoms to copper(II) ions. Some iron(II) polyazamacrocyclic compounds possess pronounced peroxidase activity. Cobalt (II) polyazamacrocyclic compounds are considered from united position both as dioxygen and as free radicals transfer agents (vitamin B_{12} analogues). A new type of dioxygen transfer agents, namely cobalt tetraazamacrocyclic complexes, are suggested.

Макроциклические соединения широко применяются для моделирования биологических систем: переноса ионов через мембраны, активных центров (сайтов) электронотранспортных белков (редокспротеинов), энзимов („синзимов"), белков обратимо связывающих радикалы и молекулы O_2 (бирадикалы). Это связано с тем, что как в биомолекулах, так и в металлокомплексах с макроциклическими лигандами ионы металлов окружены определенным числом, расположенных в определенном порядке донорных атомов кислорода, азота или серы. Задача моделирования металлобиомолекул входит в качество составной части интенсивно развивающейся в последнее время науки — биомиметики.

Краун-эфиры и криптанды могут моделировать такие ионофоры как валиномицин, энниатин, актины и другие.

Для исследования ионсфорной активности мы использовали жидкостные мембраны, представляющие собой два слоя водных растворов изучаемых солей, разделенных слоем, не смешивающегося с водой раствора макроциклического соединения (10^{-3}M) в дихлорэтане ($C_2H_4Cl_2$). При этом установлено, что скорость транспорта солей через жидкостную мембрану зависит от величины константы экстракции, достигая максимума при величине константы экстракции порядка 10^5—10^6. Если значения константы экстракции меньше этой величины то замедляется экстрагирование соли на границе источник-мембрана, при бо́льших значениях константы экстракции замедляется перенос ионов из жидкостной мембраны в приемник.

Скорость переноса солей металлов через жидкостные мембраны зависит также от природы анионов: чем они менее гидратированы, тем легче осуществляется трансмембранный транспорт. В некоторых случаях нами установлено увеличение скорости переноса солей через жидкостные мембраны в результате образования стэкинг-аддуктов между макроциклическими лигандами и анионами переносимых через мембраны солей. Так, например, пикраты щелочных металлов переносятся через жидкостные мембраны с дибезно-18-краун-6 быстрее, чем другие соли щелочных металлов. В случае жидкостных мембран с 18-краун-6 этот эффект не наблюдается (невозможность образования стэкинг-аддуктов с ароматическим кольцом пикратов).[1]

Изученные нами системы с жидкостными мембранами могут быть использованы для изучения транспорта соединений железа (III). В качестве ионофоров (сидерофоров) использованы макроциклические соединения с донорными атомами кислорода и азота. Наибольшую ионофорную активность проявляет 18-краун-6 (скорость переноса в 25 раз больше скорости переноса с дибензо-18-краун-6) и тетраметилдибензо [14] гексаен N$_4$. При этом совершенно необходимо присутствие хлорид ионов в растворе. При помощи различных методов (включая ЭПР-спектроскопию) установлено, что в жидкостной мембране образуется соединение $[FeLCl_2][FeCl_4]$.[2]

Во многих биосистемах большую роль играют так называемые ,,синие протеины'', переносящие электроны, они участвуют, в частности, в фотосинтетических системах (пластоцианины). ,,Синие белки'' содержат атомы меди, окруженные двумя донорными атомами серы (цистеина и метионина) и двумя донорными атомами азота (гистидина) с изменяющейся степенью окисления меди (I, II). Характеризуются такие белки довольно высоким редокспотенциалом пары медь (II) / медь (I) (в области 0,7—0,8 В), наличием в спектре поглощения интенсивной полосы в области 600 нм (молярный коэффициент погашения около 2000) и низкими значениями параметра сверхтонкого расщепления в спектре ЭПР.

В наших экспериментах было показано, что активные центры синих белков можно моделировать при включении во внутреннюю сферу комплексов не только атомов азота и серы, [3] но и просто атомов серы, то-есть путем использования в качестве лигандов различных тетратиамакроциклов, содержащих в макроцикле от 12 до 14 атомов. В качестве примера можно привести комплекс меди с $[14]_{\text{ан}}S_4$. В этом случае редокспотенциал пары $Cu^{II}L/Cu^{I}L$ равен 0,98 В, весьма интенсивная полоса с $\varepsilon = 1200$ наблюдается в области 630 нм.

В спектрах ЭПР комплексов меди (II) с различными тетратиамакроциклическими лигандами, наряду с полосами, вызванными наличием парамагнитных ионов меди (II), наблюдаются острые пики, свидетельствующие о наличии в растворе свободных радикалов.

Эти данные в совокупности с другими наблюденными, позволяют предположить образование катион-радикалов тетратиамакроциклических комплексов по такой схеме:

$$Cu^{2+} + [12]_{\text{ан}}S_4 \rightleftharpoons Cu^{2+}[12]_{\text{ан}}S_4 \rightleftharpoons$$
$$\rightleftharpoons Cu^{+}[12]_{\text{ан}}S_4^{\dot{+}} \rightleftharpoons Cu^{+} + [12]_{\text{ан}}S_4^{\dot{+}} \qquad (1)$$

Можно полагать, что многие особенности ,,синих белков'' и их моделей объясняются протеканием указанных процессов, в частности, легкость переноса электрона, интенсивная окраска и др.

Для моделирования цитохромов (гемсодержащих переносчиков электронов) выбраны пентаазамакроциклические комплексы железа (II), железа (III) и в частности $Me_2Pyo[13]$ триен N_5. Комплекс железа (III) с этим лигандом характеризуется довольно высоким редокспотенциалом.

Установлено протекание приведенных ниже трех реакций, кинетика которых изучается.

$$2FeL^{3+} + 2CysSH = 2FeL^{2+} + CysS - SCys + 2H^{+} \qquad (2)$$

$$2FeL^{3+} + QH_2 = 2FeL^{2+} + Q + 2H^{+} \qquad (3)$$

$$2FeL^{3+} + H_2Asc = 2FeL^{2+} + DAsc + 2H^{+} \qquad (4)$$

В этих уравнениях L — $Me_2Pyo[13]$ триен N_5, CysSH — цистеин, QH_2 и Q парагидрохинон и хинон, соответственно, H_2Asc и DAsc аскорбиновая и дегидроаскорбиновая кислоты, соответственно.

Во многих биометаллических комплексах важную роль играют комплексы металлов с порфирином и его аналогами. Для моделирования порфирина и его комплексов использованы сравнительно простые тетраазамакроциклические соединения и, в частности, весьма доступный лиганд — $Bzo_4[16]$ октаен N_4 (обозначаемый в дальнейшем через TAAB). Этот лиганд напоминает порфирин по жесткой плоской структуре, числу донорных атомов азота, по величине макроцикла (16 атомов) и по большому числу двойных связей (16).

О том, что данный лиганд является подходящей моделью порфирина, можно судить по результатам квантово-химических расчетов. С целью сопоставления электронных характеристик этих двух соединений был произведен квантовохимический расчет комплексов $Ni^{II}Porph$ и $NiTAAB^{2+}$, в результате которого определены эффективные заряды на атомах металла, донорных атомах азота и атомах углерода. Эффективные заряды на указанных атомах для NiPorph и $NiTAAB^{2+}$, соответственно, равны: Ni 0,241 и 0,322; N — 0,186 и — 0,179; C_1 — 0,048 и — 0,053; C_2 0,116 и 0,172; C_3 — 0,003 и 0,253.

Обращает на себя внимание близость эффективных зарядов на донорных атомах азота в обоих комплексах, близость зарядов на углеродных атомах C_1 и сопоставимые величины для эффективных зарядов на атомах никеля и атомах углерода C_2. Большие различия зарядов на атомах углерода C_3 в рассматриваемых комплексах объясняется тем, что несмотря на одинаковые обозначения, эти атомы занимают различные положения в макроциклах: C_3 в порфирине входят в состав удаленных от центрального атома пиррольных участков пиррольных колец, а атомы C_3 в ТААВ непосредственно связаны с донорными атомами азота.

Конечно, необходимо отдавать себе отчет и в существенном различии MPorph и модельного соединения $MTAAB^{2+}$: первое — электронейтральная молекула, второе — катион.

И тем не менее комплексы ТААВ с железом (II) и медью (II)обладают пероксидазной и аскорбатоксидазной активностью соответственно, то-есть эти макроциклические соединения можно с известным приближением рассматривать как ,,синтетические энзимы'' (,,синзиин'').

Комплекс $Fe(TAAB)^{2+}$ имеет выраженную пероксидазную активность, но для него нехарактерна каталазная активность. В присутствии этого комплекса ускоряются реакции окисления пероксидом водорода различных субстратов: эриохромчерного Т, фенолов, ароматических аминов.

Кинетика реакции окисления эриохромчерного Т пероксидом водорода в присутствии $FeTAAB^{2+}$ в качестве катализатора, моделирующего пероксидазу, изучалась спектрофотометрическим методом. При этом получено такое кинетическое уравнение:

$$-\frac{d[ЭХТ]}{dt} = k[H_2O_2]\,[ЭХТ]\,[FeTAAB^{2+}] \qquad (5)$$

с $k = 2{,}9.10^4 M^{-2}C^{-1}$ при 20°C.

Действие аскорбатоксидазы может быть промоделировано применением $CuTAAB^{2+}$. При этом наблюдается каталитическое окисление аскорбиновой кислоты до дегидроаскорбиновой кислоты растворенным кислородом по схеме

$$O_2 + HAsc^- = HO_2^- + DAsc \qquad (6)$$

Механизм этой реакции, установленный нами, [5] описывается четырьмя стадиями:

$$CuTAAB^{2+} + HAsc^- \overset{k}{\rightleftharpoons} CuTAAB(HAsc^-)^+ \qquad (7)$$

$$CuTAAB(HAsc^-)^+ \xrightarrow{k} CuTAAB^+ + HAsc^{\cdot} \qquad (8)$$

$$HAsc^{\cdot} + O_2 \rightarrow DAsc + HO_2^{\cdot} \qquad (9)$$

$$HO_2^{\cdot} + CuTAAB^+ \rightarrow HO_2^- + CuTAAB^{2+} \qquad (10)$$

Стадия (8) является скорость-определяющей и общее кинетическое уравнение имеет такой вид:

$$k_{набл} = (kKC_A/1 + KC_A) \cdot \frac{1}{[H^+]} \qquad (11)$$

где C_A — концентрация аскорбиновой кислоты, $k = 3{,}4.10^{-6} M^{-1}C^{-1}$ и $K = 180$ M.

Как видно, медь в каталитическом процессе изменяет степень окисления от $+2$ до $+1$ и обратно — от $+1$ до $+2$.

Многочисленные макроциклические соединения, особенно кобальта (II), могут моделировать действие витамина B_{12} (генерация свободных радикалов) и действие переносчиков молекулярного кислорода (бирадикала). Обобщенные схемы этих процессов приводятся ниже:

$$LM^{II} + R^{\cdot} \rightleftharpoons LM^{III}R^{-} \qquad (12)$$

$$LM^{II} + O_2 \rightleftharpoons LM^{III}O_2^{-} \qquad (13)$$

$$LM^{II} + LM^{III}O_2^{-} \rightleftharpoons LM^{III}O_2^{2-}M^{III}L \qquad (14)$$

В этих уравнениях L — тетраазамакроциклический лиганд, M — железо, кобальт или никель.

В качестве примера реакции (12), моделирующей действие витамина B_{12}, приведем изученную нами термическую диссоциацию $LCoCH_3$ в толуоле при 50°C — с L — $Me_2(CH_2C(O))_2$ [14] тетраен N_4^{2-}, описываемую уравнением:

$$LCo^{III}CH_3 - LCo^{II} + CH_3^{\cdot} \qquad (15)$$

Указанная здесь реакция подчиняется кинетическому уравнению первого порядка по макроциклическому комплексу $CoCH_3$ с $k = 2{,}1 \cdot 10^{-4} c^{-1}$. Энергия активации этой реакции составляет 82,3 к Дж/моль, а $\lg A = 9{,}6$. Энергия активации реакции (15) близка к энергии разрыва связи Co^{II} — C, определенной другими методами. Молекулы переносчиков кислорода в организмах реагируют с O_2 по схеме (13) — (миоглобин, гемоглобин) и по схеме (13) и (14) (гемэритрин, гемоцианин). Реакции модельных соединений (макроциклические соединения кобальта (II)) протекают по обеим схемам, в зависимости от природы макроцикла, выбранной среды и некоторых других условий.

В качестве примера можно привести тетраазамакроциклические соединения кобальта, обратимо присоединяющие молекулярный кислород по схеме: [6]

$$2\,Co^{II}L + O_2 \rightleftharpoons L\,CoO_2CoL \qquad (16)$$

Здесь L — Me_6[14] диен N_4.

Итак, макроциклические комплексы металлов могут использоваться как в качестве структурных, так и в качестве функциональных моделей тех биосистем, в состав которых входят ионы металлов в определенном окружении донорных атомов. Такие модели в некоторых случаях могут оказаться весьма эффективными заменителями природных соединений (например, металлоэнзимов). Так как в макроциклических лигандах можно варьировать размеры макроцикла, число и природу донорных атомов, а также вводить различные заместители в боковые цепи, то для моделирования металлобиомолекул здесь открываются весьма широкие перспективы.

ЛИТЕРАТУРА

[1] К. Б. Яцимирский, Г. Г. Таланова, А. А. Чайковская, *Теорет. экспер. химия*, **21**, *5*, 600–604 (1985).

[2] К. Б. Яцимирский, Г. Г. Таланова, Е. В. Рыбак-Акимова, Доклады Акад. наук СССР, **288**, *3*, 646–649, 1986.

[3] V. V. Pavlishchuk, P. E. Strizhak, K. B Yatsimirskii, J. Labuda, *Inorg. Chim. acta*, **151**, *1*, 133–137 (1988).

[4] И. П. Белецкий, *Теорет. экспер. химия*, **23**, *4*, 421–424 (1987).

[5] К. Б. Яцимирский, Я. Лабуда, Докл. Акад. наук СССР, **276**, *4*, 880–883 (1984).

[6] К. Б. Яцимирский, Ю. И. Братушко, Я. Д. Лампека, *Теорет. экспер. химия*, **15**, *5*, 598–601 (1979).

Revue Roumaine de Chimie, 34, *1*, 409–453 (1989)

ХИМИЧЕСКАЯ ТЕХНОЛОГИЯ КАК НАУКА И УЧЕБНАЯ ДИСЦИПЛИНА

НИКОЛАЙ МИХАЙЛОВИЧ ЖАВОРОНКОВ
Институт общей и неорганической химии, Москва, СССР

Получена 3 октября 1988 г.

Химическая технология как наука и учебная дисциплина представлена в ее сущности и в развитии во времени. Изложены ее основные разделы, где соответствующие процессы дивизированы по гидромеханике, технике, рассеиванию или изменению массы, механическому или химическому, с разнообразными аппликациями в инженерии химических процессо

Chemical Technology, as science and education subject, is presented both in its content and its development. Its main chapters also are described, while the respective processes are divided into hydromechanical, thermal, mechanical and chemical ones, diffusion or mass exchange; their various applications in chemical processes engineering is also shown.

Во все времена вопрос о том, какие вещества и материалы создавать, какие свойства им придавать, был и всегда будет неотделим от проблемы, как их производить. Ответы на такой первостепенной важности вопрос дает технология — наука о промышленном производстве. Но прежде всего необходимо напомнить, что означает термин ,,технология''. Он появился в конце XVIII в., когда начался переход от основанных на ручном труде ремесел и мануфактур к крупной машинной индустрии. Термин ,,технология'' составлен из греческих слов techne (искусство, мастерство, ремесло) и logos (слово, учение, наука) и означает ,,наука о ремеслах'', или в современном смысле — ,,наука о промышленном производстве''. Впервые эта наука была названа технологией в 1777 г. профессором Геттингенского университета И. Бекманом в его работе ,,Введение в технологию''. Позже он издал и первые учебные пособия (1779—1788 гг.)[1]. В 1795 г. в Германии был опубликован двухтомный курс И. Ф. Гмелина ,,Руководство по технической химии'', переведенный на русский язык В. М. Севергиным под названием ,,Химические основания ремесел и заводов''. Химическая технология с конца XVIII — начала XIX вв. стала обязательной учебной дисциплиной в университетах и высших технических училищах всех наиболее развитых стран Европы.

---

[1] В. Фрацшер, Технология и ее задачи в связи с материально-техническим обеспечением производственных процессов в промышленности, 1982 г. (перевод с немецкого).

В России, которая во второй половине XVIII в. не уступала в промышленном развитии западно-европейским странам, химической технологии уделялось не меньшее внимание, чем в Германии. В училищах коммерческого и технического профиля в России общая технология, как учебная дисциплина была введена уже в конце XVIII в. С 1807 по 1817 г. Главное управление училищ четырежды издавало курс под названием ,,Технология''. Курс химической технологии был впервые введен в Московском университете в 1806 г. Читал этот курс профессор И. А. Двигубский, который вначале пользовался учебными пособиями И. Бекмана и И. Ф. Гмелина, а затем в 1807—1808 гг. издал свой учебник ,,Начальные основания технологии, или краткое показание работ, на заводах и фабриках производимых''. С тех пор в России в течение всего XIX столетия учебники по химической технологии выходили в свет один за другим. Среди них особенно выделяются труды Ф. А. Денисова, П. А. Ильенкова, М. Я. Киттары, Ф. Лесгафта, М. В. Скобликова, Н. Н. Любавина. Примечательно, что за первое полустолетие XIX в. как в России, так и за рубежом было издано учебников по химической технологии значительно больше, чем по общей химии.

В 1804 г. в соответствии с Уставом 1803 г. Академия наук приступила к изданию ,,Технологического журнала, или собрания сочинений и известий, относящихся до технологии, и приложения учиненных в науках открытий к практическому употреблению''. В предисловии к первому номеру журнала, написанном его главным редактором академиком В. М. Севергиным, излагаются соображения о необходимости тесной связи науки и практики. В этом предисловии говорится, что успехи ремесел и заводов находятся в необходимой связи с успехами наук. Та же мысль красной нитью проходит в статье В. М. Севергина ,,Краткое обозрение начала успехов и пользы технологии'', также опубликованной в первом номере. В ней технология рассматривается как прикладная наука о промышленном производстве, основывающаяся на приложении механических, физических и химических знаний к ремеслам и искусствам.

Таким образом, более 200 лет тому назад термин ,,технология'' вошел в европейские языки как наименование одной из важнейших прикладных инженерных наук — науки о промышленном производстве.

Д. И. Менделеев дает следующее определение этого термина в Энциклопедическом словаре Брокгауза и Ефрона: ,,. . . . технология или учение о выгодных (т.е. поглощающих наименее труда людского и энергии природы) приемах переработки природных продуктов в продукты, потребные (необходимые или полезные, или удобные) для применения к жизни людей. Хотя технология по своему предмету глубоко отличается от социально-экономических учений, но у ней с ними много прямых и косвенных связей, так как экономия (сбережение) труда и материала (сырья), а через них времени и сил, составляет первую задачу всякого производства, и существо учения о фабрично-заводских производствах совершенно теряет почву, если утрачивается из вида выгодность (экономичность) производства. Дело, например, химии изучать получение железа из его руд или из иных веществ природы, где оно содержится, а дело технологии изучить выгоднейшие для того способы, выбрать из возможностей наиболее применимую — по выгодности — к данным условиям времени и места, чтобы придать продукту наибольшую дешевизну при желаемых свойствах и формах''.

,,Технология, — отмечал Д. И. Менделеев, — принадлежит к числу наук очень молодых, возникших всего лишь в XIX столетии. Систематическое изложение, сопровождаемое не только описанием существующего (применяемого или предлагаемого), но и оценкою его достоинства, т.е. сопоставлением достигаемого с возможным (теоретическим по расходу работы и материала), стало появляться в отношении к отдельным производствам только в XIX в., особенно же во второй половине, когда явилось уже много специально-технических журналов''.

Подчеркивая существо технологии как науки, Д. И. Менделеев писал: ,,Учение о способах, применяемых заводами и фабриками, освещает научными началами то, что вырабатывается практикою и через это не только усовершенствуется производство, но и расширяется область научного понимания вещей и явлений ...

И хотя многие приемы, применяемые на заводах и фабриках, ведут свое начало от опытом оправданных начал естествознания, тем не менее в практическом сочетании частностей должно ждать своих обобщений, с которыми в будущем может выступить технология как самостоятельная, прикладная наука''.[2]

Это определение Д. И. Менделеева полностью соответствует современному пониманию технологии как науки о промышленном производстве, которая, образно говоря, ногами стоит на фундаменте естественных наук, а головой упирается в экономику.

Прежде всего технология — наука о производстве средств производства. Ее задача — изучение, разработка и непрерывное совершенствование основных процессов и их совокупности в производстве машин, аппаратов, приборов и других современных орудий труда. Технология служит научной основой машиностроительной станкостроительной, приборостроительной отраслей промышленности. Важнейшее значение для машиностроения имеет технология металлов — получение и обработка черных и цветных металлов и их сплавов; горячая их обработка (литье, ковка, прессование, штамповка, прокатка, сварка, закалка, отжиг); холодная обработка (холодная прокатка, волочение, калибровка); обработка металлов резанием (обточка, сверление, фрезерование, шлифование и т.д.). Технология черных металлов иллюстрируется табл. 1, цветных — табл. 2, 3.

Большим и наиболее разнообразным разделом технологии является химическая технология — наука о наиболее экономичных методах и средствах массовой химической переработки сырых природных материалов и первичных продуктов сельскохозяйственного производства в продукты потребления и промежуточные продукты, применяемые в других отраслях материального производства.

Химическая технология — научная база химической, нефтехимической, коксохимической, целлюлозно-бумажной, пищевой промышленности, промышленности стройматериалов, электронной и многих других отраслей промышленности (табл. 4). В табл. 4 включена и черная метал-

---

[2] Энциклопедия Брокгауза – Ефрона, 1901, т. 33, с. 132.

Таблица 1

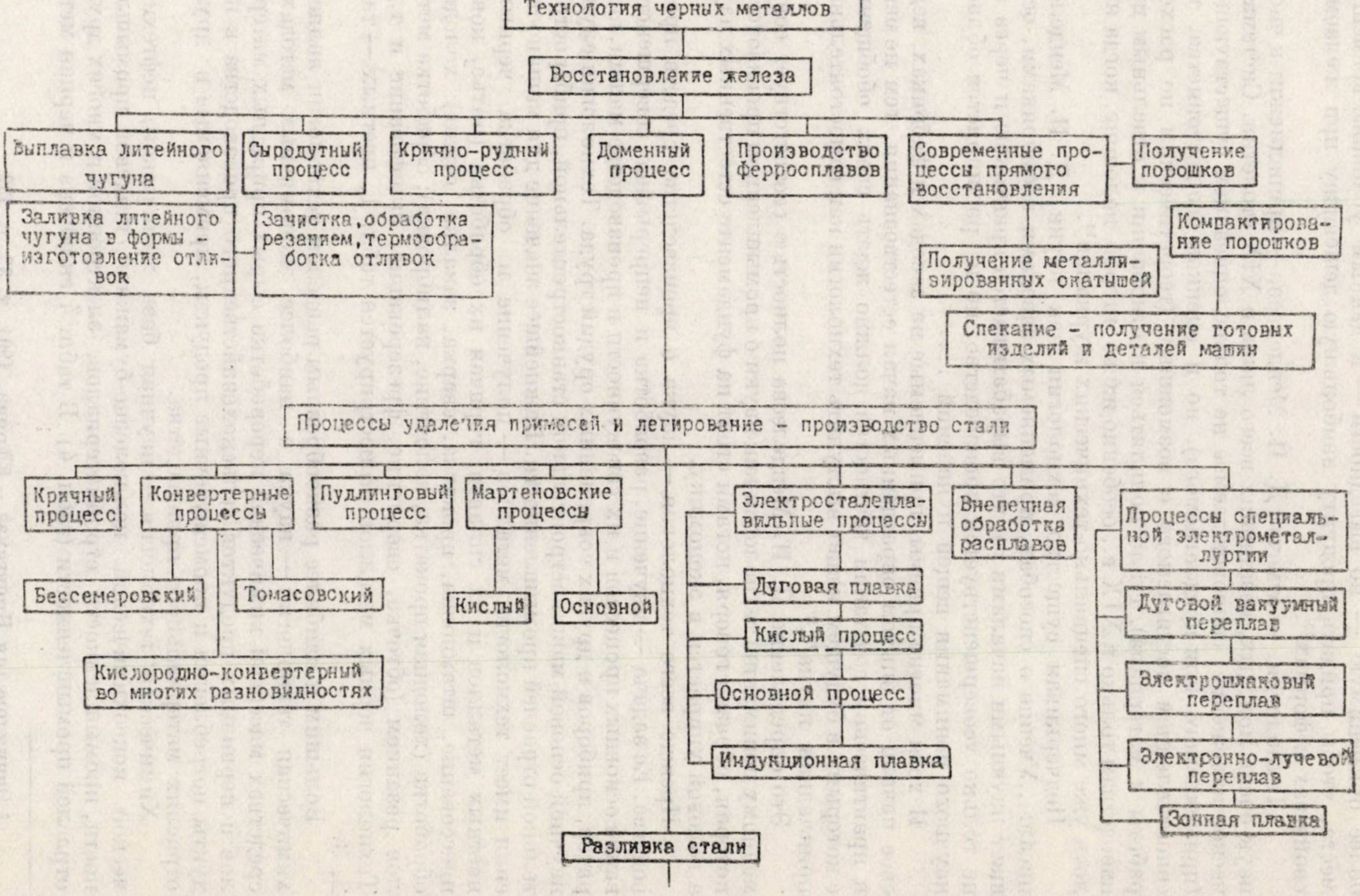
Технология черных металлов
Восстановление железа
Выплавка литейного чугуна
Сыродутный процесс
Кричнo-рудный процесс
Доменный процесс
Производство ферросплавов
Современные процессы прямого восстановления
Получение порошков
Заливка литейного чугуна в формы - изготовление отливок
Зачистка, обработка резанием, термообработка отливок
Компактирование порошков
Получение металлизированных окатышей
Спекание - получение готовых изделий и деталей машин
Процессы удаления примесей и легирование - производство стали
Кричный процесс
Конвертерные процессы
Пудлинговый процесс
Мартеновские процессы
Электросталеплавильные процессы
Внепечная обработка расплавов
Процессы специальной электрометаллургии
Бессемеровский
Томасовский
Кислый
Основной
Дуговая плавка
Кислый процесс
Основной процесс
Индукционная плавка
Дуговой вакуумный переплав
Электрошлаковый переплав
Электронно-лучевой переплав
Зонная плавка
Кислородно-конвертерный во многих разновидностях
Разливка стали

Таблица 2

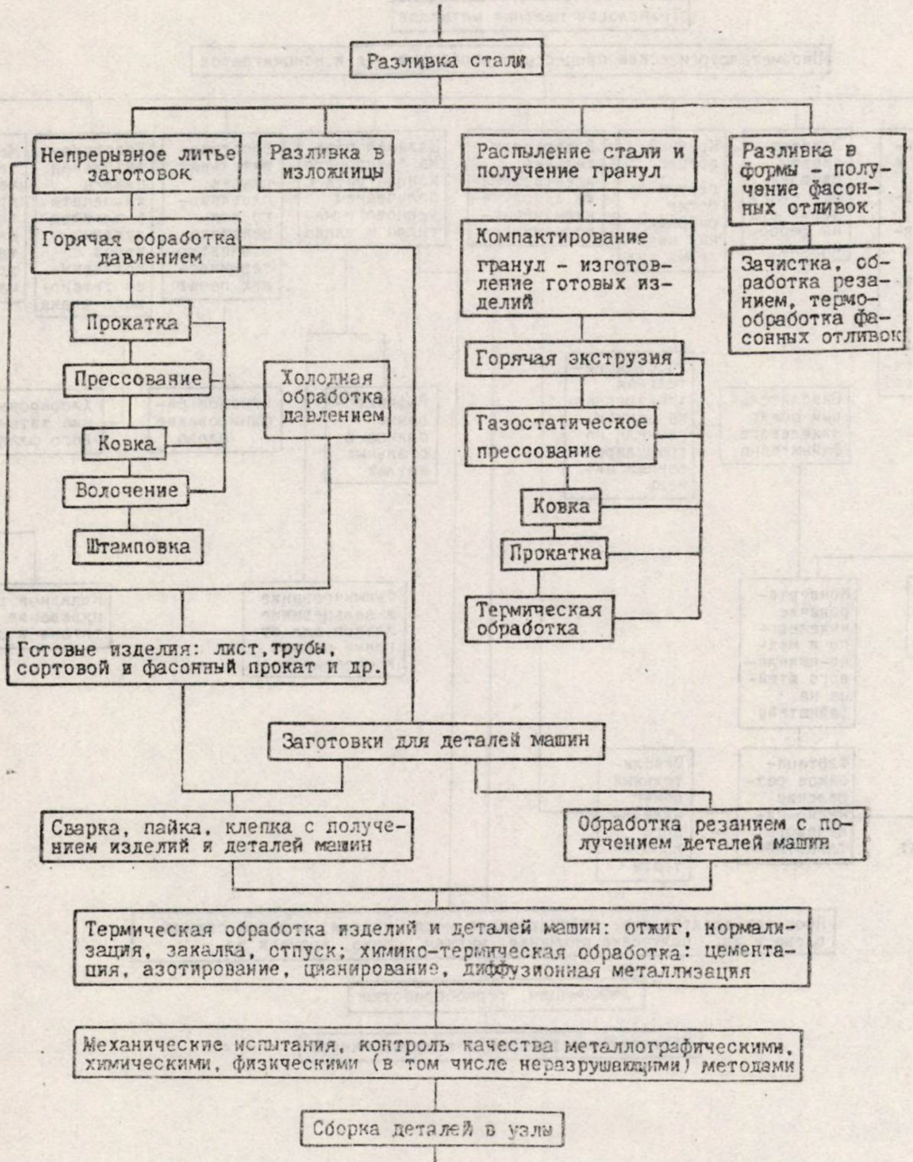
Разливка стали
Непрерывное литье заготовок
Разливка в изложницы
Распыление стали и получение гранул
Разливка в формы - получение фасонных отливок
Горячая обработка давлением
Компактирование гранул - изготовление готовых изделий
Зачистка, обработка резанием, термообработка фасонных отливок
Прокатка
Прессование
Холодная обработка давлением
Ковка
Волочение
Штамповка
Горячая экструзия
Газостатическое прессование
Ковка
Прокатка
Термическая обработка
Готовые изделия: лист, трубы, сортовой и фасонный прокат и др.
Заготовки для деталей машин
Сварка, пайка, клепка с получением изделий и деталей машин
Обработка резанием с получением деталей машин
Термическая обработка изделий и деталей машин: отжиг, нормализация, закалка, отпуск; химико-термическая обработка: цементация, азотирование, цианирование, диффузионная металлизация
Механические испытания, контроль качества металлографическими, химическими, физическими (в том числе неразрушающими) методами
Сборка деталей в узлы
Сборка узлов в механизмы и машины

Таблица 3

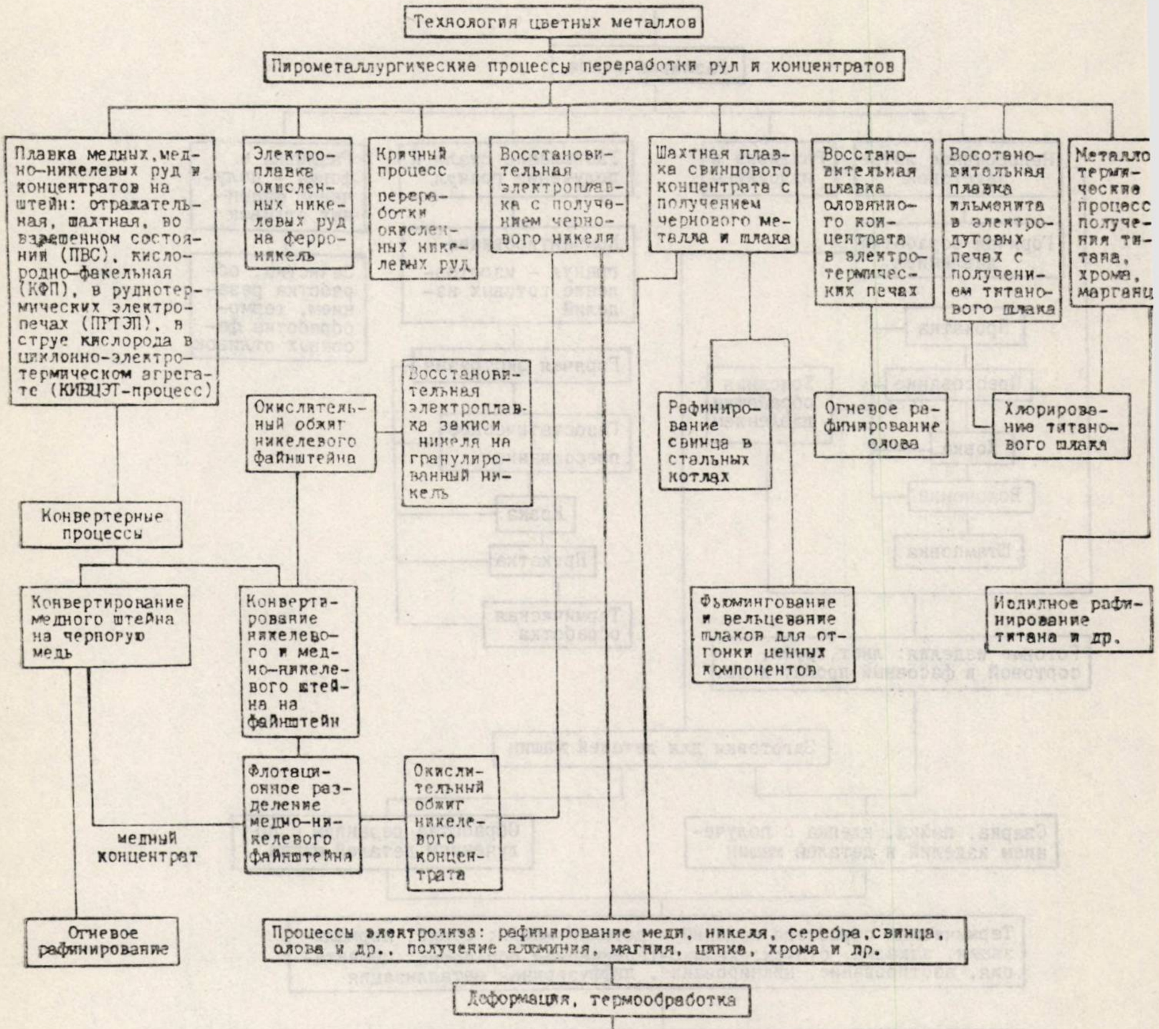
Технология цветных металлов
Пирометаллургические процессы переработки рул и концентратов
Плавка медных, медно-никелевых руд и концентратов на штейн: отражательная, шахтная, во взвешенном состоянии (ПВС), кислородно-факельная (КФП), в руднотермических электропечах (ПРТЭП), в струе кислорода в циклонно-электротермическом агрегате (КИВЦЭТ-процесс)
Электроплавка окисленных никелевых руд на ферроникель
Кричный процесс переработки окисленных никелевых руд
Восстановительная электроплавка с получением чернового никеля
Шахтная плавка свинцового концентрата с получением чернового металла и шлака
Восстановительная плавка оловянного концентрата в электротермических печах
Восотановительная плавка ильменита в электродутовых печах с получением титанового шлака
Металло термические процесс получения титана, хрома, марганц
Окислительный обжиг никелевого файнштейна
Восстановительная электроплавка закиси никеля на гранулированный никель
Рафинирование свинца в стальных котлах
Огневое рафинирование олова
Хлорирование титанового шлака
Конвертерные процессы
Конвертирование медного штейна на черновую медь
Конвертарование никелевого и медно-никелевого штейна на файнштейн
Фъюмингование и вельцевание шлаков для отгонки ценных компонентов
Иолидное рафинирование титана и др.
Флотационное разделение медно-никелевого файнштейна
Окислительный обжиг никелевого концентрата
медный концентрат
Огневое рафинирование
Процессы электролиза: рафинирование меди, никеля, серебра, свинца, олова и др., получение алюминия, магния, цинка, хрома и др.
Деформация, термообработка
Изготовление изделий и полуфабрикатов

Продолжение таблицы 8

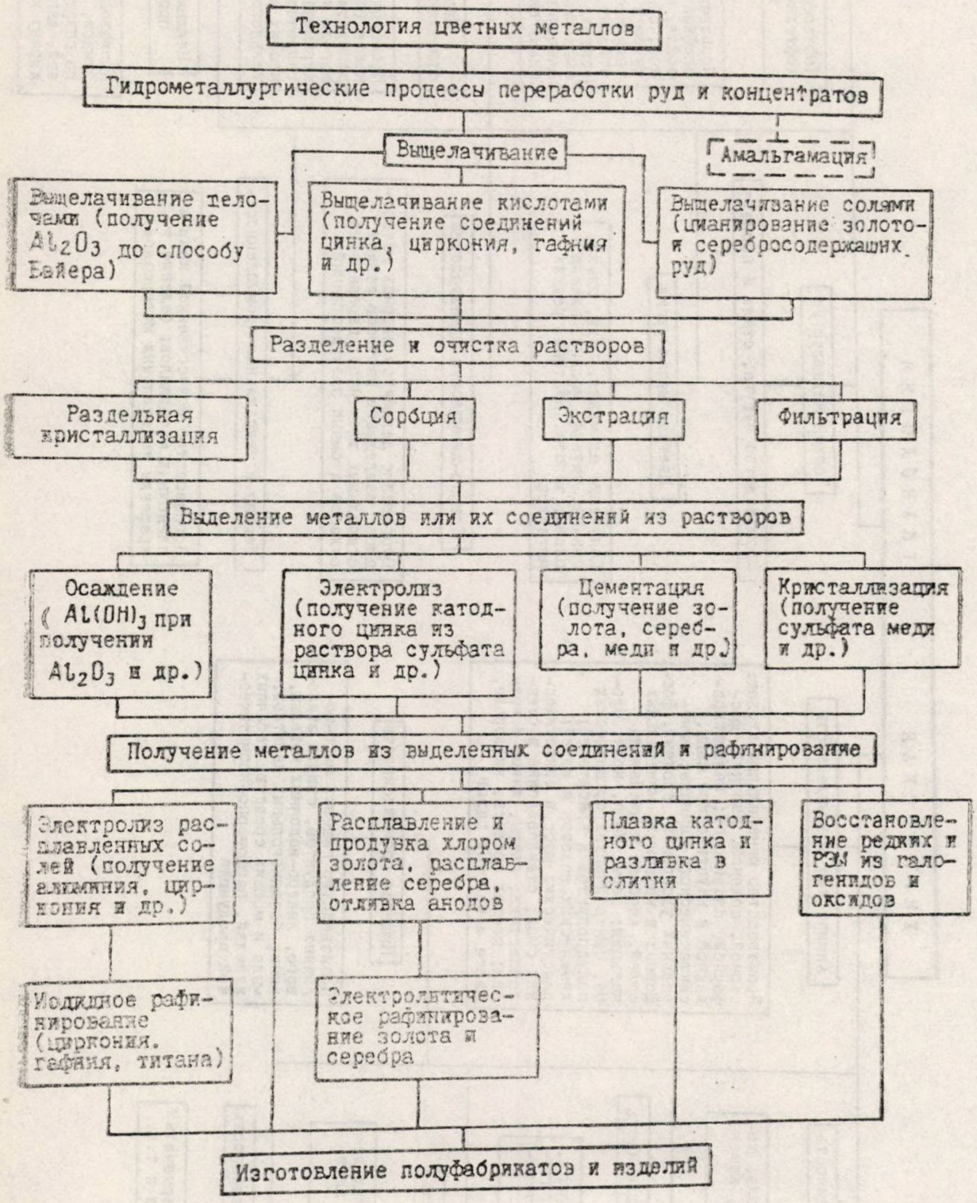
Технология цветных металлов
Гидрометаллургические процессы переработки руд и концентратов
Выщелачивание
Амальгамация
Выщелачивание щелочами (получение Al_2O_3 по способу Байера)
Выщелачивание кислотами (получение соединений цинка, циркония, гафния и др.)
Выщелачивание солями (цианирование золото- и серебросодержащих руд)
Разделение и очистка растворов
Раздельная кристаллизация
Сорбция
Экстрация
Фильтрация
Выделение металлов или их соединений из растворов
Осаждение ($Al(OH)_3$ при получении Al_2O_3 и др.)
Электролиз (получение катодного цинка из раствора сульфата цинка и др.)
Цементация (получение золота, серебра, меди и др.)
Кристаллизация (получение сульфата меди и др.)
Получение металлов из выделенных соединений и рафинирование
Электролиз расплавленных солей (получение алюминия, циркония и др.)
Расплавление и продувка хлором золота, расплавление серебра, отливка анодов
Плавка катодного цинка и разливка в слитки
Восстановление редких и РЗМ из галогенидов и оксидов
Иодидное рафинирование (циркония, гафния, титана)
Электролитическое рафинирование золота и серебра
Изготовление полуфабрикатов и изделий

Таблица 4

ХИМИЧЕСКАЯ ТЕХНОЛОГИЯ

- Коксо-химическая промышленность
  - Производство кокса, бензола, толуола, фенолов, пиридина, каменноугольной смолы и др.
- Микробиологическая промышленность
  - Производство кормовых белков, аминокислот, витаминов, антибиотиков, ферментов, бактерицидных препаратов
- Медицинская промышленность
  - Производство синтетических лекарственных препаратов, антибиотиков
- Военно-химическая промышленность
  - Производство порохов, взрывчатых веществ, ракетных топлив и т.д.
- Химическая промышленность
  - Производство минеральных кислот: серной, соляной, азотной, фосфорной, плавиковой; кальцинированной и каустической соды, синтетического аммиака; минеральных удобрений: азотных, фосфорных и калийных; минеральных солей, карбида и цианамида кальция; серы, бора, иода, брома; синтетических органических полупродуктов и красителей; химических волокон и нитей; пластических масс и синтетических смол; стекловолокна и стеклопластика; олифы, лаков и красок; моющих средств; кислорода, азота и инертных газов
- Пищевая промышленность
  - Производство пищевых мясо-молочных продуктов, спирта этилового, ликеро-водочных изделий, вина, безалкогольных напитков, мыла и моющих средств, табачных изделий, парфюмерно-косметической продукции
- Черная металлургия
  - Производство чугуна, стали и проката
- Цветная металлургия
  - Получение алюминия, меди, цинка, свинца, титана, магния, никеля, олова, золота, платины, редких металлов
- Ядерно-химические производства
  - Обогащение делящихся ядерных материалов; разделение изотопов легких стабильных элементов; переработка отходов атомных электростанций
- Легкая и текстильная промышленность
  - Производство искусственной кожи и пленочных материалов; беление и крашение текстильных материалов
- Нефтеперерабатывающая и нефтехимическая промышленность
  - Производство бензинов, олефинов, керосина, газойля, мазута и гудронов; синтетических каучуков и резины, шин; технического углерода; этилена, окиси этилена, винилхлорида, стирола; смазочных, электроизоляционных и консервационных масел
- Промышленность строительных материалов
  - Производство портландцемента (быстротвердеющего, декоративного, расширяющегося и т.п.), стекла, керамического материала, теплозащитных и акустических материалов, строительного гипса
- Целлюлозно-бумажная промышленность
  - Производство целлюлозы, бумаги, картона, этилового спирта, кормовых дрожжей, канифоли, скипидара, жирных кислот

лургия, в основе которой лежат химические процессы восстановления железа, а также цветная металлургия, практически целиком основанная на использовании химико-технологических процессов, в чем нетрудно убедиться, анализируя данные табл. 2 и особенно табл. 3.

В последние десятилетия химико-технологические процессы широко используются практически во всех областях промышленного производства. Развитие машиностроения, энергетики, строительства, транспорта, связи, сельского хозяйства, здравоохранения, обеспечение человека питанием связаны с использованием разнообразных материалов, веществ, продуктов и препаратов с определенным комплексом механических, физических, химических и биологических свойств. Разработка и производство этих веществ и материалов было и всегда будет главной задачей химии и химической технологии.

Цель любого производства, в том числе химического, — получение конечного продукта при минимальных удельных капитальных вложениях и эксплуатационных затратах — достигается выбором соответствующих технологических процессов, необходимого оборудования и построением рациональной системы производства, а также путем автоматизации контроля и управления технологическими процессами и производством в целом.

Все многообразие процессов химической технологии разделяют по их природе на пять основных классов: 1) гидромеханические, 2) тепловые, 3) диффузионные, или массообменные, 4) механические, 5) химические. Перечень процессов, входящих в первые 4 класса, приведен в табл. 5. Заметим, что за последние годы массообменные процессы пополнились новой и весьма важной группой мембранных процессов.

Класс химических процессов — наиболее многочисленный, что вызвано исключительно широкой номенклатурой производимых в современных условиях веществ и материалов на основе химических превращений например: *процессы горения и окисления* — сжигание твердого, жидкого и газообразного топлива, серы, серного колчедана для производства серной кислоты, производство стали из чугуна в мартеновских печах, электропечах и конвертерах; *процессы восстановления* — получение железа и других металлов из руд; *электрохимические процессы* — электролиз воды и водных растворов солей, электроосаждение металлов, электролиз в расплавленных средах — производство алюминия, магния и других металлов; *электротермические* — получение карбида кальция, электровозгонка фосфора, электросварка металлов; *металлотермия* — процессы восстановления металлов из их соединений (оксидов, галогенидов и др.) более активными металлами (алюминием, магнием), а также кремнием, протекающие с выделением тепла, — производство титановой губки, безуглеродистых легирующих сплавов; *плазмохимические процессы* — химические реакции в низкотемпературной плазме — получение порошков тугоплавких металлов и неметаллических материалов; *синтез простых неорганических соединений* — кислот, щелочей, солей, металлических сплавов и других неорганических веществ и материалов; *комплексообразование* — разделение и рафинирование платиновых и других благородных металлов, очистка газов от оксида углерода, получение особо чистых металлов синтезом и разложением комплексных соединений; *обжиг и спекание* — высокотемпературный синтез силикатов, получение цементного клинкера, глинозема из нефелинов, керамических материалов и изделий; *термическая диссоциация* — получение извести, кальцинация двууглекислого натрия, гидроксида алюминия; *химическое обогащение руд ценных металлов*, в которых последние входят изоморфно в кристаллическую решетку сопутствующих минералов, например, путем хлорирующего или сульфатизирующего обжига с целью перевода металла в летучие или способные к выщелачиванию водой соединения; *окислительно-восстановительные процессы* — газификация твердых и жидких топлив, конверсия углеводородов с водяным паром, парциальное окисление углеводородов; *гидрирование* — синтез аммиака, метанола и высших спиртов, гидрокрекинг и гидроочистка нефти и продуктов ее переработки от сернистых соединений, гидрогенизация жиров; *пирогенные процессы* — коксование и полукоксование углей и сланцев, пиролиз и крекинг жидких и газообразных нефтепродуктов, сухая перегонка древесины; *синтез органических вещест* на основе оксида углерода, олефинов, парафинов, ароматических углеводородов, ацетилена и других органических соединений; *химическое разложение сложных органических веществ* — варка древесной щепы с растворами химических веществ (каустическая сода, бисульфит кальция и др.) с целью делигнификации древесины в производстве целлюлозы; *полимеризация и поликонденсация* — получение высокомолекулярных соединений и на их основе синтетических смол, пластмасс, синтетических каучуков, резины и других эластомеров, полимерных пленок, лакокрасочных покрытий, клеев, искусственных и синтетических волокон; *синтез сложных органических* соединений — красителей, промежуточных продуктов, лекарственных препаратов, пестицидов, детергентов и других; *аммонолиз* — окисление углеводородов совместно с аммиаком с целью получения синильной кислоты, акрилонитрила и других веществ; *аминирование* — получение карбамида и органических аминосоединений жирного и ароматического рядов; *нитрование* — получение нитропроизводных органических соединений, порохов, взрывчатых веществ; *хлорирование* — получение хлорорганических веществ, химических средств борьбы с вредителями сельскохозяйственных растений, четыреххлористого титана; *сульфирование* — получение сульфоорганических веществ, синтетических моющих средств; *циклизация* — превращение органических соединений с открытой цепью в циклические или ароматические соединения с целью улучшения качества моторного топлива; *биохимические процессы* — брожение в производстве вина, пива, хлеба, микробиологический синтез белка, биологическая очистка промышленных и бытовых сточных вод и т.п.; *гидролиз* — реакция обменного разложения между различными веществами и водой, гидролиз солей — получение гидроксидов металлов, разложение целлюлозы и других полисахаридов, содержащихся в отходах деревообрабатывающей промышленности и сельскохозяйственного производства, обработкой слабыми растворами минеральных кислот для получения глюкозы и других моносахаридов; *ядерно-химические процессы* — получение ядерного горючего из природных руд, выделение чистых трансурановых элементов и непрореагировавшего урана из продуктов деления радиоактивных элементов, использование радиации в химическом синтезе и т.п.

В настоящее время в стадии становления находится новый большой и очень перспективный раздел технологии — биотехнология. Здесь особенно важна технология продуктов, получаемых в результате совокупности сложных процессов тонкого синтеза биохимическими методами (аминокислоты, простогландины, интерфероны и т..п.).

Для ускорения химических реакций, лежащих в основе многих из перечисленных выше процессов, в промышленности широко используется катализ.

Количественное описание процессов химической технологии основано на законах химической термодинамики и химической кинетики в совокупности с законами переноса количества движения, теплоты, массы. Круг задач, связанный с описанием явлений на микроуровне, когда рассматриваются физико-химические эффекты, определяющие скорость протекания процессов на молекулярном уровне и в локальном объеме аппарата, и на макроуровне, когда на эффекты микроуровня накладываются гидродинамические, тепловые, диффузионные явления крупномасштабного характера, структура которых определяется конструктивными особенностями промышленного аппарата, характером подвода к нему внешней энергии и т.п., составляет ядро теоретических основ химической технологии.

Многообразие химических и физико-химических процессов, используемых на практике, обусловливает разнообразие конструкций аппаратов, в которых осуществляются химико-технологические процессы. Создание высокоэффективных аппаратов с оптимальным энерго-ресурсо-потреблением—важнейшая задача химического машиностроения, которая должна решаться на основе новейших достижений теоретических основ химической технологии. Конструкции таких аппаратов должны обеспечивать возможность создания и поддержания оптимальных (с позиции химической технологии) режимов работы и одновременно соответствовать требованиям современного машиностроения. Очевидно, что для оптимального проведения большого числа химических процессов требуется исключительно широкий спектр вариантов химического оборудования. В то же время для ускорения проектирования и изготовления этого оборудования машиностроителям необходимо иметь ограниченный выбор типовых решений. Это противоречие может быть разрешено путем создания химической аппаратуры как гибкой совокупности унифицированных узлов или модулей. Унифицировать следует машиностроительные узлы, изготавливаемые по единой технологии обеспечивая максимально возможное количество сочетаний этих узлов для создания того или иного варианта аппарата или машины. К оборудованию для крупнотоннажных производств должны предъявляться требования повышенной надежности в сочетании с максимальной эффективностью. При создании оборудования для производства малотоннажных химических продуктов главным является легкость переналаживания и резервирование мощностей для обеспечения широкого диапазона областей применения.

Химический реактор является тем элементом технологической схемы, от совершенства которого зависит возможность осуществления в промышленных условиях всего производства. Общая теория химических реакторов стала развиваться сравнительно недавно. Весьма плодотворным при этом оказалось применение метода математического моделирования для решения задачи масштабного перехода от результатов лабораторных экспериментов к промышленным условиям. Успехи в области изучения химической кинетики, переноса теплоты и массы, сопровождающих химическую реакцию, и применение математического моделирования позволяют теперь более строго подходить к проектированию промышленных реакторов. На этой основе уже создан ряд новых эффективных конструкций реакторов большой единичной мощности и определены оптимальные условия проведения некоторых важных для практики процессов.

Современные химико-технологические процессы должны осуществляться непрерывно и с большими скоростями, с применением средств самонастройки на оптимальный режим, отвечать условиям комплексного использования сырья и энергии, комбинирования и кооперирования различных производств, исключающих возможность загрязнения воздушного и водного бассейнов вредными выбросами. Химизация является одним из важнейших факторов, способствующих интенсификации развития всей экономики в целом. Поэтому химическая промышленность развивается и будет развиваться опережающими темпами. Требуются серьёзные шаги в направлении разумного использования сырья, топлива и энергии. Необходимы радикальные качественные изменения технологических процессов, в том числе разработка катализаторов нового поколения, внедрение в промышленную практику таких перспективных процессов и аппаратов, как мембранные процессы, экстракция сжатыми газами при сверхкритических давлениях, а также новые методы воздействия на технологические процессы с целью их интенсификации. В качестве примеров можно привести, в частности, влияние градиентов поверхностного натяжения, способствующих возникновению поверхностной конвекции и резкой интенсификации массообмена при абсорбции с химическими превращениями, ректификации, экстракции; создание нестационарных условий путём циклического проведения процессов в химических реакторах, экстракторах, абсорберах; использование электрических и магнитных полей, пульсаций, вибраций и др.

Перспективы развития химической технологии определяются необходимостью создания новых экономичных интенсивных технологических процессов, высокопроизводительной аппаратуры и разработки системы автоматизации, контроля, управления и оптимизации не только отдельных процессов, но и их взаимосвязанных комплексов, т.е. целых производств с широким использованием электронно-вычислительной техники.

Это — задачи инженера-химика-технолога. Многие инженерные вопросы имеют фундаментальный научный характер. Химик-исследователь постоянно добывает новые знания, синтезирует новые вещества, изучает их свойства, кинетику реакций. Инженер-химик творчески ,,овеществляет'' эти знания, соединяет их с элементами обширных знаний других областей науки — физики, математики, механики, биологии, экономики, кибернетики. Такое объединение различных знаний служит инженеру-химику для разработки новых методов производства, новых технологических процессов, аппаратов, пригодных для практического использования. Образно говоря, химик-иследователь познает новое, инженер-химик-технолог создаёт новое. Наибольший успех достигается лишь тогда, когда объединяются усилия исследователей и инженеров, и они могут по праву разделить этот успех.

Для развития химической индустрии подготовка инженерных и научных кадров имеет первостепенное значение. Первый технологический институт в России был основан в Санкт-Петербурге в 1828 г. Как гласил первый пункт положения об организации института, ,, ... цель Практического Тенологического института есть та, чтобы приготовить людей, имеющих достаточные Теоретические и Практические познания, для управления фабриками и частями оных''. По учебному плану, составленному академиком Г. И. Гессом, предписывалось наиболее подробно излагать химию, механику, а также общий курс технологии. Изучение учебного материала подразделялось на два важнейших раздела: механический и химический. Первый раздел в свою очередь делился на отделения обработки твердых материалов и мягких (волокнистых) с получением нитей и тканей. Второй раздел включал химические процессы, необходимые для обработки нитей и тканей, и в первую очередь беление, крашение и печатание узорами. В 60-х годах прошлого века исходя из потребностей развивающейся промышленности институт был преобразован в высшее учебное заведение для подготовки инженеров-технологов по двум специальностям — механической и химической.

В 1830 г. в Москве для подготовки инженеров-технологов по тем же специальностям было основано Высшее техническое училище. Позже, уже в XX в. в России были основаны технологические и политехнические институты для подготовки инженеров химиков в других крупных городах.

В XIX веке химическая технология была в основном описательной наукой. Начало нового этапа развития химической технологии относится к первой четверти нашего века, когда стало формироваться учение об основных процессах и аппаратах (юнит оперейшенс). Однако любопытно отметить, что ёще в начале прошлого века в одном из первых учебных пособий по химической технологии (1828 г.) его автор, профессор Московского университета Ф. А. Денисов подчеркнул общность многих процессов и аппаратов для различных химических производств, или, как он писал: ,,... средств, орудий и машин, употребляемых в разных химических искусствах''. В развитии современной химической технологии как самостоятельной научной дисциплины основополагающая роль принадлежит Д. И. Менделееву. Он предвосхитил создание курса основных процессов и аппаратов как теоретической основы химической технологии.

Идеи Д. И. Менделеева в этом направлении были развиты в дореволюционной России известными учёными—инженерами А. К. Крупским в Петербургском технологическом институте и И. А. Тищенко в Москве. Профессор А. К. Крупский, специалист в области технологии стекла а также промышленных печей и топок, одним из первых опубликовал (1909 г.) курс процессов и аппаратов химической технологии, в котором дал описание производственных химических процессов на основе принципов физической химии.

Почти одновременно и независимо И. А. Тищенко — специалист в области технологии сахара, а также термодинамики и теплопередачи — прочитал курс ,,Основные процессы и аппараты химической технологии'' студентам химического факультета Московского высшего технического училища (1911 г.). Этот курс был опубликован в 1913—1914 гг. И. А. Тищенко считал, что главное отличие высшего химико-технологического образования от университетского должно заключаться в том, что его основой и спецификой должны быть инженерно-химические дисциплины и в первую очередь курс основных процессов и аппаратов химической технологии и курс общей химической технологии. При этом курс ,,Основные процессы и аппараты химической технологии'' по своему содержанию охватывал первые четыре группы процессов — гидромеханические, тепловые, диффузионные и механические, т.е. физические и физико-химические, а курс ,,Общей химической технологии'' — химические процессы. Базируясь на фундаменте общехимических дисциплин, главным образом физической химии, — с одной стороны, и общеинженерных — технической термодинамики, теоретической механики, сопротивления материалов, деталей машин, теплотехники и электротехники — с другой, инженерно-химические дисциплины в свою очередь должны служить основой для дисциплин специальных, отражающих потребность конкретных отраслей промышленности. И. А. Тищенко прекрасно понимал значение новой дисциплины для формирования инженера-химика-технолога. В курсе процессов и аппаратов химической технологии он увидел то недостающее звено, которое завершало подготовку инженеров-технологов нового типа и связывало в единое целое общенаучную и общеинженерную подготовку со специально-технологической. Эти идеи И. А. Тищенко претворил в жизнь будучи назначен в 1923 г. ректором Московского химико-технологического института им. Д. И. Менделеева. В то же время в Петроградском технологическом институте в развитие идей Д. И. Менделеева большой вклад внес его ученик и соратник академик Д. П. Коновалов. Он опубликовал в 1924 г. фундаментальную монографию ,,Материалы и процессы химической технологии''.

Важным этапом в развитии химической технологии как науки явилась книга профессора Петроградского технологического института Л. Ф. Фокина ,,Методы и орудия химической техники'', которая вышла в свет в 1923 г. одновременно с известной монографией американских ученых В. Уокера, В. Льюиса и В. Мак-Адамса ,,Принципы инженерной химии''. Обе эти книги в течение нескольких лет были основными пособиями при подготовке инженеров-химиков. В 1935—1937 гг. вышел в свет учебник профессора МХТИ им. Д. И. Менделеева А. Г. Касаткина ,,Основные процессы и аппараты химической технологии'', выдержавший 9 изданий. Последние два издания, выпущенные уже после смерти А. Г. Касаткина, существенно дополнены его сотрудниками (1970 и 1973 г.).

Из многочисленных учебников и учебных пособий по общей химической технологии следует упомянуть книги П. М. Лукьянова, двухтомный курс авторского коллектива под руководством С. И. Вольфковича, учебник под редакцией И. П. Мухленова и другие, сыгравшие большую положительную роль в подготовке инженеров-химиков-технологов. В послевоенные годы было опубликовано много учебных пособий и монографий советских и иностранных авторов как по общим проблемам химической технологии, так и по важнейшим её разделам.

Начиная с 30-х годов по настоящее время опубликовано много учебников, учебных пособий и монографий по процессам и аппаратам химической технологии и общей химической технологии, которые свидетельствуют об успехах международного сотрудничества ученых этой области знания. Подтверждением этого является прилагаемый к докладу большой, но далеко не полный список литературы.

В становлении и пропаганде химической технологии огромную роль сыграли возникшие на грани XIX—XXвв. национальные химические общества и общества инженеров-химиков, которые в послевоенные годы послужили основой инженерно-технических международных сообществ: Европейской федерации инженерной химии, Межамериканской конфедерации инженерной химии и Азиатско-тихоокеанской конфедерации инженерной химии.

Научно-технический прогресс предполагает взаимосвязанное и взаимообусловленное развитие науки, производства и образования. При этом образование как наиболее дальнодействующий фактор, закладывающий фундамент успехов в будущем, требует научно обоснованной перспективной программы развития. Подготовка кадров, бесспорно, неотъемлемая часть научно-технического прогресса и один из самых существенных факторов его ускорения. Высшее образование и подготовка кадров при этом являются производительной отраслью народного хозяйства. Недаром академик В. И. Вернадский говорил: ,,Высшая школа есть орудие в мировой борьбе за существование более сильное, чем дредноуты''. Поэтому инженерно-химическое образование требует сегодня рациональной системы разнообразных мер по его укреплению. К этим мерам относится в первую очередь дальнейшее повышение оснащенности вузов новейшим научным оборудованием и электронно-высчислительной техникой. Целесообразно также в ряде научных и технических химических журналов ввести систематические рубрики, посвященные различным конкретным аспектам совершенствования инженерно-химического образования.

Мы заслуженно гордимся развитием высшего, и особенно инженерного образования, обусловившего успехи нашей науки и промышленности. В современных условиях необходимо дальнейшее совершенствование высшего химико-технологического образования с учетом новейших достижений науки и техники, реальной оценки тех огромных возможностей, которые открываются в изучении и использовании в промышленности процессов химической технологии при широком применении методов кибернетики и ЭВМ.

В настоящее время уже достигнуты определенные успехи в преподавании общеинженерных и инженерно-химических дисциплин, принята и реализуется новая программа курса процессов и аппаратов. В учебные планы введен ряд новых дисциплин, отвечающих современным требованиям. К их числу относятся такие курсы, как ,,Химические процессы и реакторы''. ,,Теплотехника химических производств'', ,,Применение ЭВМ в химической технологии''. Однако в целом уровень инженерно-химической подготовки специалистов всё ещё существенно отстаёт от требований, предъявляемых к ним современной промышленностью и особенно промышленностью завтрашнего дня. Будущим инженерам необходимы новые знания. А это требует использования таких методов обученя, которые развивали бы научно-инженерный интеллект, инженерное мышление, основанное на системном анализе. Системный подход к образованию, требует, в частности, неразрывности в преподавании курсов процессов и аппаратов химической технологии и химических процессов и реакторов. В то же время в курсе общей химической технологии следует шире знакомить студентов с вопросами комплексной переработки сырья, оптимальной с экономической точки зрения организации химико-технологических систем, с конкретными производствами, тесно увязывая эти знания с энергетическими и экологическими проблемами.

Инженеру-химику необходимы обширные знания многих смежных дисциплин. Здесь уместно напомнить афоризм древних греков, перефразированный Бернардом Шоу: ,,Узкий специалист узнает всё больше о все меньшем и так до тех пор, пока не будет знать все ни о чём и ничего обо всем''.

Химическая технология как инженерная наука ответственна за ликвидацию выбросов вредных продуктов производства в первую очередь потому, что методы переработки и утилизации отходов в большинстве своем — химические и физико-химические. Одним из важнейших путей исправления ,,экологического спазма'', вызванного человеческой деятельностью, является повышение качества высшего химико-технологического образования. Оно призвано перестроить мировоззрение инженеров-химиков и указать основные направления разработки экологически чистых производственных систем.

Стержневую роль в комплексе общеинженерных и инженерно-химических дисциплин играет курс процессов и аппаратов химической технологии. Программа этого курса должна нацеливать на углубленное изучение фундаментальных закономерностей, лежащих в основе методов расчета, исследования и моделирования основных процессов и их аппаратурного оформления. Программа должна предусматривать преподавание отдельных разделов курса в глубокой системной взаимосвязи друг с другом. В ней акцентировано внимание на том, чтобы приобретаемые студентами знания могли быть использованы как для практической деятельности на предприятиях, так и для проектной и иследовательской работы.

Очень важный вопрос — подготовка инженеров широкого профиля. В настоящее время создаются большие комбинаты, производящие разнообразные продукты с применением различных методов и технологических процессов. Поэтому ведущие специалисты этих предприятий должны быть вооружены глубокими фундаментальными знаниями основных процессов и аппаратов химической технологии. В этой связи необходимо подумать об укрупнении узких профилирующих специальностей, по которым готовят инженеров-химиков. Комплекс инженерно-химических дисциплин не только является одной из основ образования инженера-химика-технолога, но играет большую роль в формировании инженерно-химического мышления и общего мировоззрения выпускников химико-технологических вузов и факультетов.

При всей важности конкретных знаний, получаемых студентами, например, в курсе ,,Процессы и аппараты химической технологии'', главной задачей является развитие творческого характера инженерно-химического мышления. Это возможно лишь при проблемном характере преподавания: наука о процессах и аппаратах должна преподноситься студентам в развитии — с ее достижениями и нерешенными вопросами, с анализом вероятных путей их решения.

Изложение ряда конкретных проблем совершенствования процессов и аппаратов должно быть подчинено решению важнейших вопросов развития экономики, связанных с необходимостью повышения эффективности производства и качества продукции. В химической технологии проблемы повышения эффективности и качества могут решаться лишь в глубокой диалектической взаимосвязи. Так, переход от сравнительно небольших производств к агрегатам большой единичной мощности приводит не только к количественному росту производительности установок, но и к резкому повышению качественных показателей. Снижение капитальных и эксплуатационных затрат, улучшение условий контроля технологических процессов дает в итоге улучшение качества продукции, как это имеет место, например, в производстве аммиака. Эволюция азотной промышленности, начиная с первой промышленной установки фиксации азота дуговым методом (1905 г.) и до наших дней, представляет собой яркий пример борьбы за резкое снижение энергоемкости производства и себестоимости продукта.

Инженерно-химическое образование может дать человеку очень многое. В книге Д. Росса ,,Энергия волн''[3] говорится о Г. Гудвине — научном руководителе Министерства энергетики Великобритании'': ,,Он инженер-химик и утверждает, что такое образование является идеальной основой, ибо охватывает любую инженерную область и позволяет разговаривать с механиками, конструкторами и электриками на их языке''.

В заключение остановимся на вопросах классификации и упорядочения научной терминологии в области химической технологии.

Классификация основных процессов и аппаратов сыграла свою положительную роль в формировании химической технологии как науки и учебной дисциплины. Строгая классификация какой-либо отрасли науки требует установления четкой терминологии, характерной для данной области знания.

Из всех языков науки (логического, физического, математического и др.) химический язык является наиболее пригодным вспомогательным средством для международного научного общения (особенно в письменной форме) вследствие таких своих отличительных особенностей, как широко разветвленная химическая номенклатура и общепринятая символика. Однако для упорядочения научной терминологии в области химической технологии нельзя ограничиться простым сложением физических, математических и других терминов в отрыве от сущности описываемых процессов и аппаратов, в которых они осуществляются. Важнейшие проблемы современной научной терминологии заключаются, во-первых, в упорядочении самой терминологии, во-вторых, — ее стандартизации. Эти проблемы тесно связаны с потребностью автоматизации, машинного хранения и поиска научно-технической информации, а также с необходимостью международного общения и плодотворного сотрудничества специалистов смежных отраслей промышленности.

Большая работа в этом направлении была проведена отделом химии Института СЭВ по стандартизации в связи с разработкой темы ,,Классификация и терминология основных процессов химической технологии''. Проведенное исследование представляет собой первую попытку заложить твердую основу для сотрудничества стран СЭВ в области химической технологии и машиностроения при оформлении поставок оборудования и проектировании путем унификации основных понятий. Классифиация основных процессов химической технологии составлена с учетом общности закономерностей, характеризующих процессы, а также их целенаправленность и способ осуществления. Разработанная классификация может быть положена в основу классификации химического оборудования, так как классификационные схемы отдельных процессов иерархически доведены до непосредственного выхода на типовые аппараты или их группы.

---

[3] Д. Росс, Энергия волн, Гидрометеоиздат, 1981.

Основные результаты исследования опубликованы П. Г. Романковым и М. И. Курочкиной [4] и отражены в табл. 5, в которой нами добавлен только подкласс 3. 5 ,,Мембранные прцессы''. В основу классификации положены общепринятые пять основных классов процессов химической технологии (см. выше). Классы делятся на подклассы, различающиеся по физико-химической сущности процессов. Подклассы в свою очередь делятся на группы процессов, отличающиеся способом осуществления или целенаправленностью. Классификация предусматривает более детальную разработку, не показанную в табл. Так, группы процессов делятся на подгруппы по способу осуществления или отличию агрегатного состояния вещества, например, группа ,,Диспергирование'' состоит из подгрупп ,,Диспергирование газов в жидкости'', ,,Диспергирование жидкостей'', ,,Диспергирование твердых тел в газах и жидкостях''.

Подгруппы процессов делятся на виды по условиях проведения процесса или различию его аппаратурного оформления. На последней классификационной ступени виду процесса соответствует название типа аппарата, в котором данный процесс осуществляется.

Такая классификационная система основных процессов химической технологии удобна еще и тем, что дает возможность установить единую номенклатуру типовой химической аппаратуры, используемой для проведения этих процессов, и может служить основой для составления классификации машин и аппаратов химической технологии. Четкая классификация необходима для планирования научных исследований, при оценке полноты информации и для решения ряда экономических задач (планирование закупок, поставок и др.).

Рациональная классификация химических процессов исключительно сложна и работа здесь еще не закончена. Большое внимание следует также уделить вопросам дальнейшего упорядочения терминологии, обеспечивающей взаимопонимание и неразрывно связанной с классификацией. Следует подчеркнуть, что тщательно разработанная классификация и устоявшаяся терминология являются признаком зрелости любого раздела науки.

После проведения заключительного этапа работы — классификации химических процессов — ее результатами сможет воспользоваться многочисленный отряд химиков, которым до сих пор более половины времени, отведенного для исследования, приходится тратить на поиск научной информации.

Разработка стандартов на отдельные процессы, а затем и на аппараты является необходимым условием технического прогресса.

---

[4] П. Г. Романков. М. И. Курочкина, *Журн, прикл. химии*, 1972, 14, *11*, *Теор. основы хим. технол.*, 1974. 8, *3*.

Таблица 5

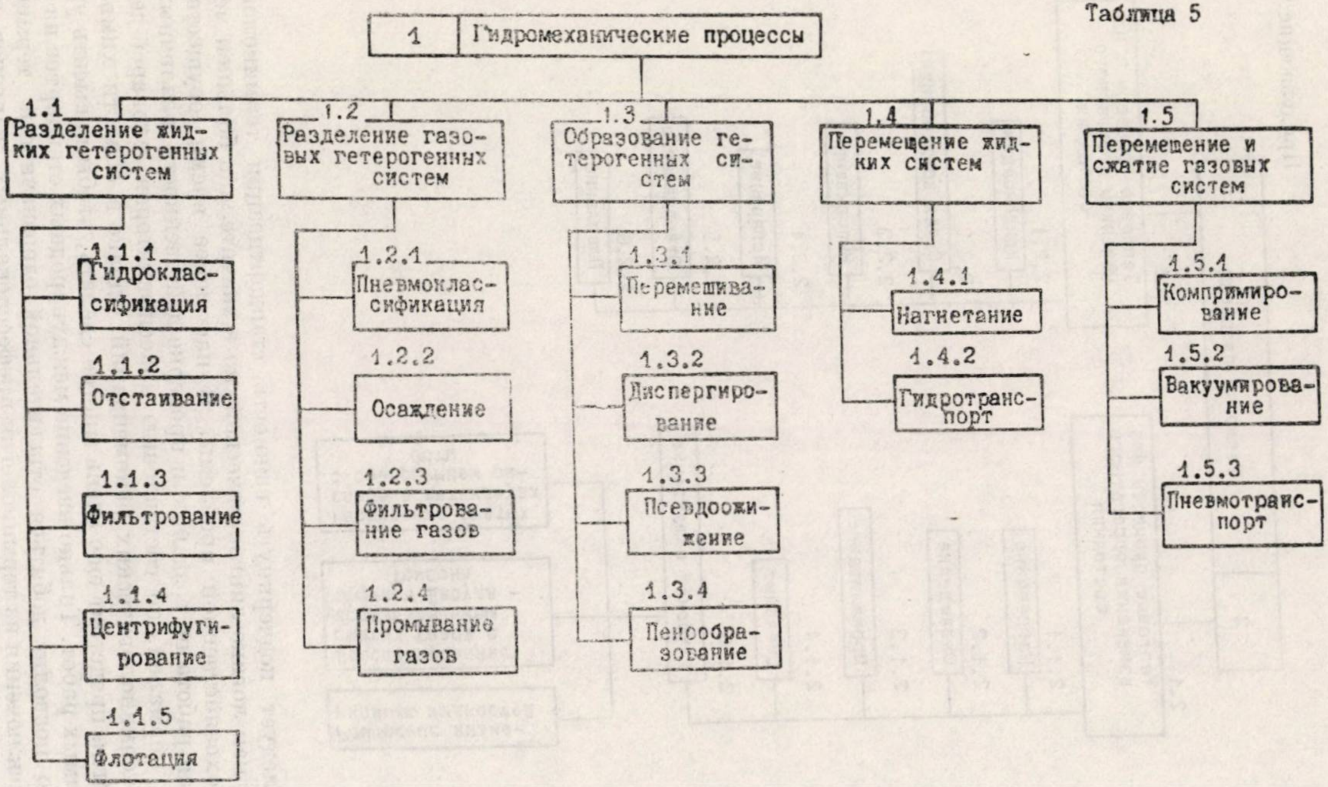
1 Гидромеханические процессы
1.1 Разделение жидких гетерогенных систем
1.1.1 Гидроклассификация
1.1.2 Отстаивание
1.1.3 Фильтрование
1.1.4 Центрифугирование
1.1.5 Флотация
1.2 Разделение газовых гетерогенных систем
1.2.1 Пневмоклассификация
1.2.2 Осаждение
1.2.3 Фильтрование газов
1.2.4 Промывание газов
1.3 Образование гетерогенных систем
1.3.1 Перемешивание
1.3.2 Диспергирование
1.3.3 Псевдоожижение
1.3.4 Пенообразование
1.4 Перемещение жидких систем
1.4.1 Нагнетание
1.4.2 Гидротранспорт
1.5 Перемещение и сжатие газовых систем
1.5.1 Компримирование
1.5.2 Вакуумирование
1.5.3 Пневмотранспорт

Продолжение таблицы 5

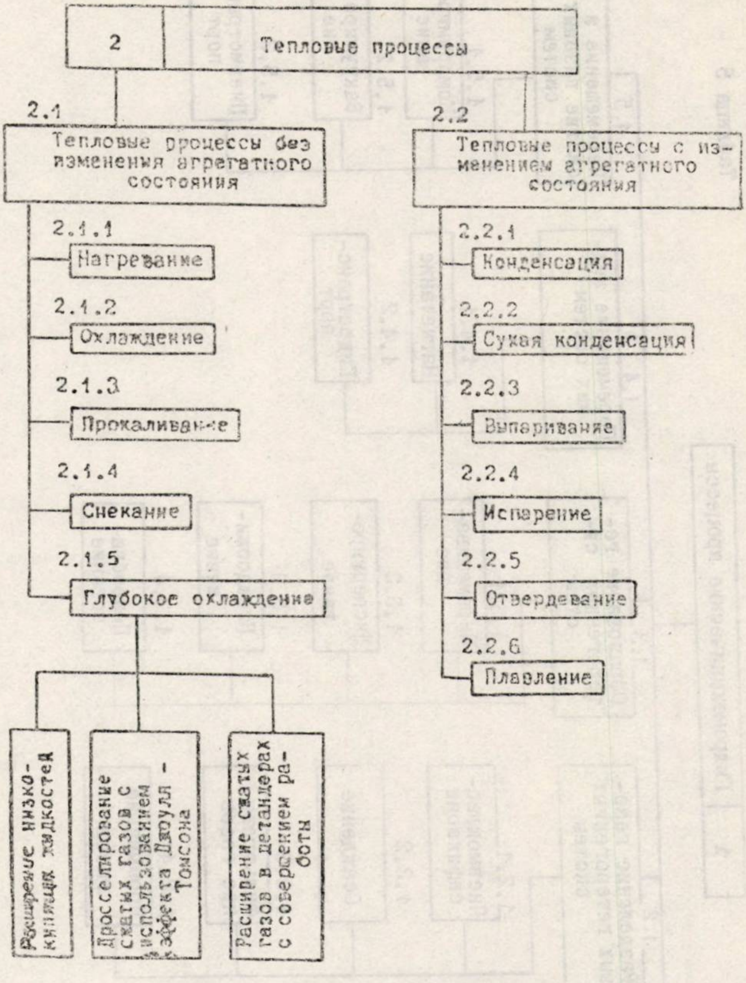
2
Тепловые процессы
2.1
Тепловые процессы без изменения агрегатного состояния
2.1.1
Нагревание
2.1.2
Охлаждение
2.1.3
Прокаливание
2.1.4
Снекание
2.1.5
Глубокое охлаждение
Расширение низкокипящих жидкостей
Дросселирование сжатых газов с использованием эффекта Джоуля - Томсона
Расширение сжатых газов в детандерах с совершением работы
2.2
Тепловые процессы с изменением агрегатного состояния
2.2.1
Конденсация
2.2.2
Сухая конденсация
2.2.3
Выпаривание
2.2.4
Испарение
2.2.5
Отвердевание
2.2.6
Плавление

Следует подчеркнуть важность стандартизации терминологии не только как логико-лингвистической, но в значительно большей мере как народнохозяйственной проблемы. В настоящее время осуществляется огромная работа по созданию и проверке действенности различных стандартов, нормалей, по составлению классификаторов, словарей-дескрипторов, терминологических рекомендаций. Однако в области химической технологии предстоит еще очень многое сделать, чтобы повысить уровень проводимых работ. Только введение международных стандартов на терминологию позволит добиться относительной однозначности терминовя а также исключения из терминологии профессиональных жаргонов, засоряющих язык. Еще Декарт говорил: ,,Определяйте значения слов, и вы избавите человечество от многих заблуждений''. Эта мысль особенно верна для областей науки в период их бурного развития, в который вступает сейчас химическая технология.

Продолжение таблицы 5

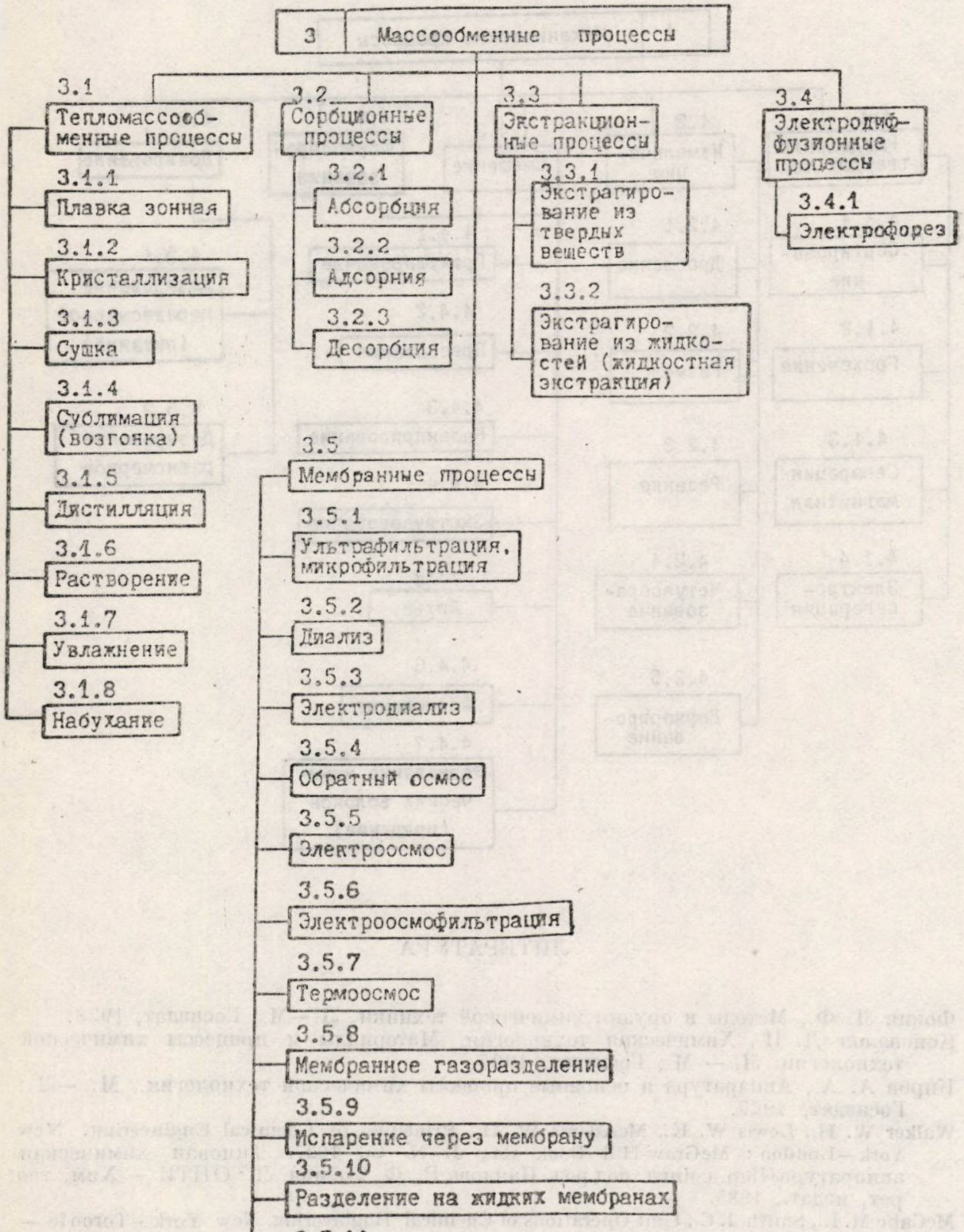
3 Массообменные процессы
3.1 Тепломассообменные процессы
3.1.1 Плавка зонная
3.1.2 Кристаллизация
3.1.3 Сушка
3.1.4 Сублимация (возгонка)
3.1.5 Дистилляция
3.1.6 Растворение
3.1.7 Увлажнение
3.1.8 Набухание
3.2 Сорбционные процессы
3.2.1 Абсорбция
3.2.2 Адсорбция
3.2.3 Десорбция
3.3 Экстракционные процессы
3.3.1 Экстрагирование из твердых веществ
3.3.2 Экстрагирование из жидкостей (жидкостная экстракция)
3.4 Электродиффузионные процессы
3.4.1 Электрофорез
3.5 Мембранные процессы
3.5.1 Ультрафильтрация, микрофильтрация
3.5.2 Диализ
3.5.3 Электродиализ
3.5.4 Обратный осмос
3.5.5 Электроосмос
3.5.6 Электроосмофильтрация
3.5.7 Термоосмос
3.5.8 Мембранное газоразделение
3.5.9 Испарение через мембрану
3.5.10 Разделение на жидких мембранах
3.5.11 Экстракция через мембрану

Продолжение таблицы 5

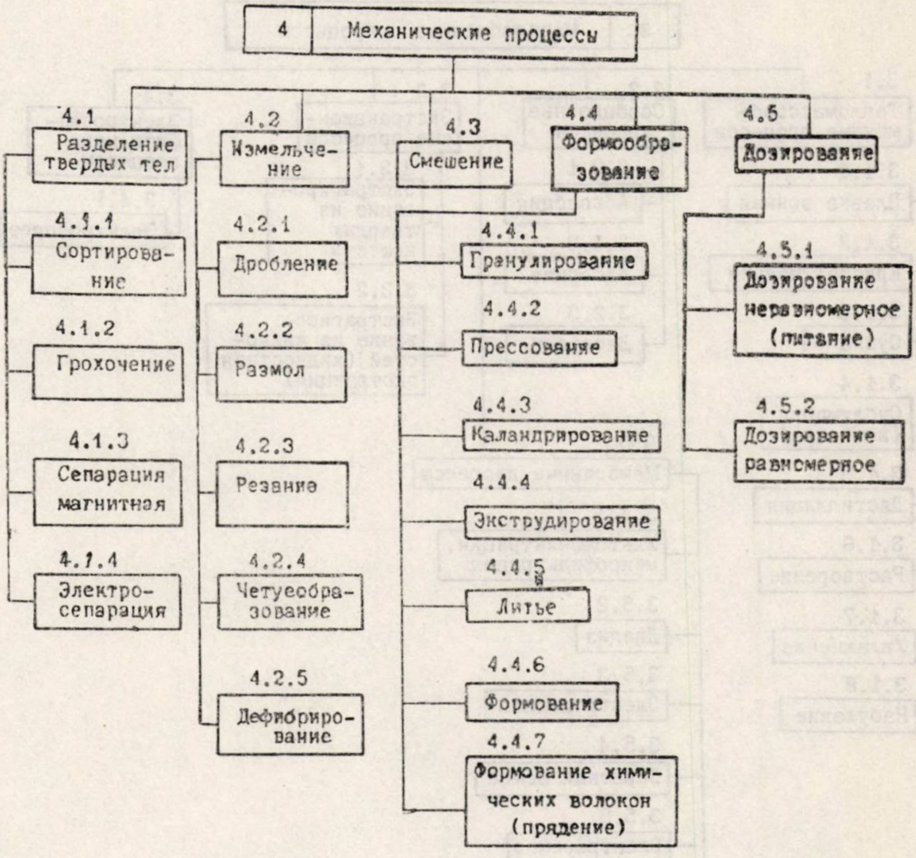
4
Механические процессы
4.1
Разделение твердых тел
4.1.1
Сортирование
4.1.2
Грохочение
4.1.3
Сепарация магнитная
4.1.4
Электросепарация
4.2
Измельчение
4.2.1
Дробление
4.2.2
Размол
4.2.3
Резание
4.2.4
Четуеобразование
4.2.5
Дефибрирование
4.3
Смешение
4.4
Формообразование
4.4.1
Гранулирование
4.4.2
Прессование
4.4.3
Каландрирование
4.4.4
Экструдирование
4.4.5
Литье
4.4.6
Формование
4.4.7
Формование химических волокон (прядение)
4.5
Дозирование
4.5.1
Дозирование неравномерное (питание)
4.5.2
Дозирование равномерное

ЛИТЕРАТУРА

[1] Фокин Л. Ф., Методы и орудия химической техники. Л.—М.: Госиздат, 1923.

[2] Коновалов Д. П., Химическая технология, Материалы и процессы химической технологии. Л. — М.: Госиздат, 1925.

[3] Киров А. А., Аппаратура и основные процессы химической технологии. М. —Л.: Госиздат, 1927.

[4] Walker W. H., Lewis W. K., McAdams W. H., Principles of Chemical Engineering. New York—London: McGraw-Hill Book Co., J. N. C., 1927. Типовая химическая аппаратура/Пер. с англ. под ред. Павлова Е. Ф. 2-е изд. Л.: ОНТИ — Хим. теорет, издат., 1935.

[5] McCabe M. L., Smith J. C., Unit Operations of Chemical Engineering, New York—Toronto — London: McGraw-Hill Book Co., J. N. C., 1956.

[6] Badger W. L., Banchero J. T., Introduction to Chemical Engineering. Ibid., 1955.

[7] Касаткин А. Г., Основные процессы и аппараты химической технологии. М.: Химия, 1973.

[8] Циборовский Я., Процессы химической технологии/Пер. с польск. под ред. Романкова П. Г. Л.: Гос. научно-технич. изд-во хим. лит., 1958.

[9] Франк-Каменецкий Д. А., Диффузия и теплопередача в химической кинетике. М.: Наука, 1967.

[10] Коган В. Б., Теоретические основы типовых процессов химической технологии. Л.: Химия, 1977.

[11] Плановский А. Н., Николаев П. И., Процессы и аппараты химической и нефтехимической технологии. М.: Гос. научн.-техн. изд. нефт. и горно-топливной пром-сти , 1960.

[12] Перри Дж., Справочник инженера-химика/Пер. с англ. под ред. Жаворонкова Н. М., Романкова, П. Г. Л.: Химия , 1969.

[13] Бретшнайдер С., Свойства газов и жидкостей. Инженерные методы расчета/ Пер. с польск. под ред. Романкова П. Г. М. — Л.: Химия, 1966.

[14] Рид Р., Праусниц Дж., Шервуд Г., Свойства газов и жидкостей. Л.: Химия, 1982. 591 с.

[15] Бенедек П., Ласло А., Научные основы химической технологии/Пер, с нем. под ред. Романкова П.Г.Л.: Химия, 1970.

[16] Жаворонков Н. М., Гидравлические основы скрубберного процесса и теплопередача в скубберах. М.: Советская наука. 1944. 224 с.

[17] Lewa M., Tower Packings and packed tower desigh. U. S. Stoneware C., 1953, 214 p.

[18] Morris G. A., Jackson J., Absorption towers, Butterworths Sci. Publ., 1953, 150 p.

[19] Danckwerts P. V., Insights into Chemical Engineering. Oxford : Pergamon Press, 1981, 307 p.

[20] Process Heat Exchanger/Ed. Cavaseno Y. New York : McGraw-Hill Publication, 1979, 607 p.

[21] Handbook of Separation Techniques for Chemical Engineering/Ed. Schweitzer P. A. New York : McGraw-Hill Book Co., 1979, 1120 p.

[22] Plant Design and Economics for Chemical Engineering/Ed. Peters M. S., Timmerhaus K. D. Tokyo : McGraw-Hill Kogakusha Ltd., 1980, 973 p.

[23] Павлов К. Ф., Романков П. Г., Носков А. А., Примеры и задачи по курсу процессов и аппаратов химической технологии. Л.: Химия, 1976, 552 с.

[24] Романков П. Г., Курочкина М. Н., Гидромеханические процессы химической технологии. Л.: Химия, 1982, 287 с.

[25] Авербух Я. Л., Заостровский Ф. Н., Матусевич Л. Н., Процессы и аппараты химической технологии. Гидравлические и механические процессы,/Под ред. Шабалина К. Н. Свердловск: Урал. политехн. ин-т, 1969.

[26] Малиновская Т. А. Кобринский Н. А., Кирсанов О. С., Рейнфарт В. В., Разделение суспензий в химической промышленности. М.: Химия, 1983, 263 с.

[27] Пажи Д. Г., Галустов В. С., Основы техники распыливания жидкостей. М.: Химия, 1984, 254 с.

[28] Брагинский Л. Н., Бегачев В. Н., Барабаш В. М., Перемешивание в жидких средах. Л.: Химия, 1984.

[29] Жужиков В. А., Фильтрование. Теория и практика разделения суспензий. М.: Химия, 1980, 398 с.

[30] Михеев М. А., Основы теплопередачи. М. — Л.: Госэнергоиздат, 1947.

[31] Кутателадзе С. С., Основы теории теплообмена, М.: Атомиздат, 1979, 415 с.

[32] Хоблер Т., Теплопередача и теплообменники/ Пер. с польск. под ред. Романкова П. Г. Л.: Госхимиздат, 1961.

[33] Романков И. Г., Фролов В. Ф., Теплообменные процессы химической технологии. Л.: Химия, 1982.

[34] Теплопередача в двухфазном потоке/ Нод ред. Баттерворса Д., Хьюитта Г. М.: Энергия, 1980, 326 с.

[35] Гаусбрант Э., Гирш М., Выпаривание, конденсация и охлаждение/Пер. с нем. под ред. Накшвера А. Б. М.: ОНТИ, 1936.

[36] Таубман Е. И., Выпаривание, М.: Химия, 1982, 327 с.

[37] Боттерилл Дж., Теплообмен в всевдоожиженном слое. М.: Энергия. 1980, 345 с.

[38] Толубинский В. И., Теплообмен при кипении. Киев: Наук. думка. 1980, 315 с.

[39] Кутепов А. М., Стерман Л. С., Стюшин Н. Г., Гидродинамика и теплообмен при парообразовании. М.: Высш. школа, 1983.

[40] Лыков А. В., Тепломассообмен. М.: Энергия, 1972.

[41] Гидромеханика и тепломассообмен в невесомости. М.: Наука, 1982, 263 с.

[42] Делайе Дж., Гио М., Ритмюллер М., Теплообмен и гидродинамика в атомной и тепловой энергетике. М.: Энергоатомиздат, 1984, 422 с.

[43] Берд Р., Стьюарт В., Лайтфут Е., Явление переноса/Пер. с анг. под. ред. Жаворонкова Н. М., Малюсова В. А. М.: Химия, 1974.

[44] Данквертс И. В., Газожидкостные реакции. М.: Химия, 1973,

[45] Шервуд Т., Пигфорд Р., Уилки Ч., Массопередача/Пер. с англ. под ред. Малюсова В. А. М.: Химия, 1982.

[46] Кафаров В. В., Основы массопередачи. М.: Высш, школа, 1972.

[47] Ворошнин Л. Г., Хусид Б. М., Диффузионный массонеренос в многокомпонентных системах. Минск: Наука и техника, 1979, 225 с.

[48] Тепло- и массобмен. Теплотехнический эксперимент: Справочник Под. ред. Григорьева В. А., Зорина В. М. М.: Энергоиздат, 1982, 510 с.

[49] Bergles A. E., Collier T. G., Delhaye J. M., Hewitt G. F., Majinger F., Two-phase flow and heat transfer in the power and process industries. Washington—New York—London : Hemisphere Publ. Corp. 1981, 707 p.

[50] Матусевич, Л. Н., Кристаллизация из растворов в химической промышленности. М.: Химия. 1968.

[51] Бэмфорт А. В., Промышленная кристаллизация/Пер. с англ. под ред. Матусевича Л. Н. М.: Химия, 1969.

[52] Хамский Е. В., Кристаллизация в химической промышленности. М.: Химия, 1979.

[53] Тодес О. М., Себалло В. А., Гольцикер А. Д., Массовая кристаллизация из растворов Л.: Химия, 1984, 232 с.

[54] Сажин Б. С., Основы техники сушки. М.: Химия, 1984, 319 с.

[55] Трегубов А. М., Теория перегонки и ректификации. Баку: Гос. научн.-тех. изд. нефт. и горно-топливной лит., 1946.

[56] Гельперин Н. И., Дистилляция и ректификация. М. — Л.: Госхимиздат. 1947.

[57] Хоблер Т., Массопередача и абсорбция/Пер. с польск. под ред. Романкова П. Г. Л.: Госхимиздат. 1964.

[58] Рамм В. М., Абсорбция газов. М.: Химия, 1976 655 с.

[59] Astatita G., Savage D. W., Bisio A., Gas treating with chemical Solvents. N. Y. : J. Wiley and Sons, 1983.

[60] Протодьяконов И. О., Сипаров С. В., Механика процесса адсорбции в системах газ — твердое тело. Л. Наука. 1985.

[61] Кельцев Н. В., Основы адсорбционной техники. М.: Химия, 1976.

[62] Ягодин Г. А. и др., Основы жидкостной экстракции. М.: Химия, 1981.

[63] Хансон К., Последние достижения в области жидкостной экстракции. М.: Химия, 1974.

[64] Ритчи Г. М., Эшбрук А. В., Экстракция. Принципы и применение в металлургии. М.: Металлургия, 1983, 407 с.

[65] Романков П. Г., Курочкина М. И., Экстрагирование из твердых материалов. Л.: Химия, 1983. 256 с.

[66] Дытнерский Ю. И., Обратный осмос и ультрафильтрация. М.: Химия, 1978.

[67] Дытнерский Ю. И., Баромембранные процессы. М.: Химия, 1986. 271 с.

[68] Хванг С.-Т., Каммермейер К., Мембранные процессы разделения М.: Химия, 1981, 464 с.

[69] Розен А. М. и др., Масштабный переход в химической технологии. Разработка промышленных аппаратов методом гидродинамического моделирования. М. Химия, 1980.

[70] Кафаров В. В., Дорохов, И. И., Системный анализ процессов химической технологии. М.: Наука, 1976.

[71] Вильямс Т. Дж., Проектирование химико-технологических процессов методами системотехники. М. — Л.: Химия, 1967.

[72] Ротертс С., Динамическое программирование в процессах химической технологии. и методы управления/Пер. с англ. под ред. Кафарова В. В. М.: Мир., 1965.

[73] Протодьяконов И. О., Муратов О. В., Евлампиев И. И., Динамика процессов химической технологии. Л.: Химия, 1984.

[74] Peters M. S., Plans Design and Economics for Chemical Engineers. New York—Toronto—London : McGraw-Hill Book Co., 1958.

[75] Усюкин И. П., Установки, машины и аппараты криоге техники. М.: Пищ. пром-сть, 1976.

[76] Тодес О. М., Цитович О. Б., Аппараты с кипящим слоем. Л.: Химия, 1981.

[77] Карпачева С. М., Рябчиков Б. Е., Пульсационная аппаратура в химической технологии. М.: Химия, 1983. 223 с.
[78] Крапивина С. А., Плазмохимические технологические процессы. Л.: Химия, 1981. 246 с.
[79] Вольфкович С. И. и др., Общая химическая технология, В 2 т. М. — Л.: Гос. научн. техн. изд. хим., лит. 1959.
[80] Михленов И. П. и др., Общая химическая технология. М.: Высш. школа. 1977.
[81] Амелин А. Г., Манахов А. И., Зубова И. Е., Зайцев В. Н., Общая химическая технология. М.: Химия, 1977.
[82] Bretsznajder S., Kawecki W., Leyko J., Marcinkowski R., Podstawy Ogolne Technologii Chemicznej. Warszawa, 1973. Общие основы химической технологии/Пер. с польск. под Романова П. Г., Курочкиной М. И. Л.: Хилия, 1977
[83] Кутепов А. М., Бондарева Т. Н., Беренгартен М. Т., Общая химическая технология. М.: Высш. школа, 1985.
[84] Бесков С. Д., Технологические расчеты. М. — Л.: Госхимиздат, 1950.
[85] Денбиг К., Теория химических реакторов/Пер. с англ. под ред. Жаворонкова Н. М. М.: Наука, 1968.
[86] Арис Р., Анализ процессов в химических реакторах/Пер. с англ. под ред. Иоффе И. И. Л.: Химия, 1967.
[87] Корсаков-Богатков С. М., Химические реакторы как объект математического моделирования. М.: Химия, 1967.
[88] Крамерс Н., Вестертерп К., Химические реакторы. Расчет и управление ими. М.: Химия, 1967.
[89] Леонов А. Л., Ревдин Ф. Я., Автоматизация химических производств и пути ее развития. М.: Химия, 1967.
[90] Левеншпиль О., Инженерное оформление химических процессов/Пер. с англ. под ред. Слинько М. Г. М.: Химия, 1969.
[91] Вейлас С., Химическая кинетика и расчеты промышленных реакторов. М.: Химия, 1967.
[92] Островский Г. М., Волин Ю. М., Методы оптимизации химических реакторов. М.: Химия, 1967.
[93] Леонов А. Л., Ревзин Ф. Я., Автоматизация химических производств и пути ее развития. М.: Химия, 1967.
[94] Слинько М. Г., Моделирование химических реакторов. Новосибирск: Наука, 1968.
[95] Закгейм А. Ю., Введение в моделирование химико-технологических процессов. М.: Химия, 1982.
[96] Кузнецов В. И., Зайцева З. А., Химия и химическая технология. Эволюция взаимосвязей. М.: Наука, 1984.
[97] Математическое моделирование химических реакторов/Под ред. Марчука Г. И. Новосибирск: Наука, 1984.
[98] Industrial Gas separations. (ACS Symp. Ser. N. 223)/Ed. Jhaddeus E. Washington, Amer. Chem. Soc., 1983, 292 p.
[99] Chemical Reaction Engineering. The 8th Intern. Symp. on Chemical Reaction Engineering Pergamon Press. 1984, 826 p.
[100] Condensers : Theory and Practice, Pergamon Press, 1983. 510 p.
[101] Chemical and Catalytic Reactor Modeling (ACS Symp. Ser. No. 237), Ed.Milorad P. Washington : Amer. Chem. Soc., 1983, 426 p.

PRINTED IN ROMANIA

ORSZÁGOS MŰSZAKI INFORMÁCIÓS KÖZPONT ÉS KÖNYVTÁR
1883

NOTE POUR LES AUTEURS

La **Revue Roumaine de Chimie** publie des articles en anglais, français, russe, allemand ou espagnol. Les auteurs sont priés d'envoyer des articles et des comptes rendus inédits.

Les manuscrits seront dactylographiés à double interligne. La bibliographie, les tableaux et la légende des figures seront placés après le texte.

Si l'article fait partie d'une série numérotée, la partie précédente sera donnée comme première référence.

Chaque article sera précédé d'un résumé comprenant quinze lignes au maximum.

Les références bibliographiques dans le texte seront faites par des exposants sans parenthèses et paraîtront à la fin de l'ouvrage.

Les publications périodiques mentionnées dans la bibliographie seront présentées suivant les prescriptions internationales : le nom de l'auteur précédé de l'initiale du prénom, le titre du périodique abrégé conformément à « Chemical Abstracts » et souligné par une ligne, le numéro du tome indiqué par des chiffres arabes et souligné par deux lignes, suivi de la première page de l'article : à la fin, l'année de la parution sera placée entre parenthèses. Le numéro de la revue ne sera pas indiqué si les pages du volume sont numérotées consécutivement.

Les textes des livres ou traités incluеront : le nom des auteurs, précédés de l'initiale du prénom, le titre du livre entre guillemets et sans être souligné, le numéro du tome précédé par l'abréviation « vol. » (ou « Bd. »), le numéro de l'édition, les éditions (the publisher), la localité de la parution du livre, l'année de la parution et la page de la référence précédée(s) par l'abréviation « p » (ou « S »).

Les brevets seront indiqués comme suit : l'auteur ou la firme, le pays et le numéro du brevet, la date de la revue *(Chem. Abstr.)*. Par ex. : M. Jones (to Union Carbide Co.), Brit. Pat. 610 238, 2 Sept. 1959 : cf. *Chem. Abstr.*, **54**, 12808 (1960).

Si la référence n'a pas été lue en original, on indiquera aussi la revue de références consultée.

Les diagrammes seront tracés à l'encre de Chine sur papier calque. Les tableaux et les figures (en nombre strictement nécessaire), ainsi que les courbes dans les figures seront numérotés par des chiffres arabes. Leur explication sera donnée dans la légende des figures. Prière de ne pas inscrire les mêmes données dans les tableaux et les figures. Chaque tableau aura un titre. On indiquera dans le texte la place approximative des tableaux et des figures. Les formules chimiques seront incluses dans le texte ; en outre, elles seront transcrites sur papier calque, à l'encre de Chine.

Les auteurs sont priés d'indiquer les caractères italiques (en soulignant les lettres au crayon), ainsi que tout autre caractère spécial : les préfixes *ortho*, *méta*, *para*, *cis*, *trans*, etc. seront soulignés pour indiquer leurs caractères italiques et ne seront jamais écrits avec des majuscules.

Aucune correction à la main ne sera admise sur le manuscrit. Les corrections seront frappées à la machine. Les lettres grecques ou d'autres symboles spéciaux seront insérés à la main à l'encre clairement.

Le manuscrit sera signé par l'auteur.

Le titre courant aura 50 lettres au maximum.

L'entière responsabilité du contenu des articles appartient aux auteurs.

Sur demande on peut obtenir une note plus complète.

PRINTED IN ROMANIA

TRAVAUX PARUS AUX ÉDITIONS DE L'ACADÉMIE DE LA RÉPUBLIQUE SOCIALISTE DE ROUMANIE

ELENA CEAUŞESCU, **Răşini de hidrocarburi, vol. 1**, 1988, 344 p.

ELENA CEAUŞESCU, **Progrese în chimia şi tehnologia polimerilor**, 1986, 446 p.

ELENA CEAUŞESCU, **Forschungen im Bereich der Chemie und Technologie der Polymere**, 1986, 444 p.

ELENA CEAUŞESCU, **Cercetări în chimia şi tehnologia polimerilor**, 1983, 520 p.

ELENA CEAUŞESCU, **Noi cercetări în domeniul compuşilor macromoleculari**, 1981, 536 p.

ELENA CEAUŞESCU, **Polimerizarea stereospecifică a izoprenului**, 1979, 307 p.

ELENA CEAUŞESCU, **Research work on synthesis and characterization of macromolecular compounds. Contributions**, 1974, 251 p.

I. G. MURGULESCU, **Introducere în chimia fizică, vol. I. 1. Atomi, molecule, legătură chimică**, 1976, 560 p.

I. G. MURGULESCU, V. EM. SAHINI, **Introducere în chimia fizică, Vol. I, 2. Structura şi proprietăţile moleculelor**, 1979, 604 p.

I. G. MURGULESCU, E. SEGAL, **Introducere în chimia fizică, Vol. II. 1. Teoria molecular-cinetică a materiei**, 1979, 1036 p.

I. G. MURGULESCU, TATIANA ONCESCU, E. SEGAL, **Introducere în chimia fizică, Vol. II. 2. Cinetică chimică şi cataliză**, 1981, 1024 p.

I. G. MURGULESCU, J. PĂUN, **Introducere în chimia fizică, Vol. I, 3. Nucleul atomic, reacţii nucleare, particule elementare**, 1982, 606 p.

I. G. MURGULESCU, RODICA VÎLCU, **Introducere în chimia fizică. Vol. III. Termodinamica chimică**, 1982, 624 p.

I. G. MURGULESCU, O. M. RADOVICI, **Introducere în chimia fizică, Vol. IV. Electrochimia**, 1986, 416 p.

CRISTOFOR I. SIMIONESCU, VALERIA GORDUZA, **Implicaţii bioenergetice ale coloranţilor**, 1988, 208 p.

R. VÎLCU, M. LECA, **Termodinamica polimerilor prin cromatografie de gaze**, 1987, 238 p.

I. ZUGRĂVESCU, M. PETROVANU, **Cicloadiţii 3+2 dipolare**, 1987, 446 p.

RAUL MIHAIL, ION GROZEANU, **Estimarea secvenţială aplicată sistemelor chimice**, 1986, 406 p.

M. BREZEANU, I. PATRON, M. ANDRUH, **Combinaţii complexe polinucleare şi aplicaţiile lor**, 1986, 244 p.

A. T. BALABAN et al., **Labelled Compounds and Radiopharmaceuticals Applied in Nuclear Medicine**, coédition avec John Wiley and Sons, 1986, 742 p.

D. PURDELA, **Nomenclatura chimiei organice — IUPAC**, 1986, 451 p.

PETRU BUDRUGEAC, **Probleme de chimie**, 1986, 280 p.

T. ONCESCU, S. G. IONESCU, **Conversie fotochimică şi stocare de energie**, 1985, 272 p.

V. DRĂGUŢAN, A. T. BALABAN, M. DIMONIE, **Olefin Metathesis and Ring-Opening Polymerization of Cyclo-Olefins**, coédition avec John Wiley and Sons, 1985, 544 p.

C. LITEANU, I. RÎCĂ, **Optimizarea proceselor analitice**, 1985, 360 p.

N. PERESCU, **Chimia extracţiei cu solvenţi şi aplicaţii**, 1985, 212 p.

V. EM. SAHINI, M. HILLEBRAND, **Chimie cuantică în exemple şi aplicaţii**, 1985, 382 p.

GH. MARCU, **Chimia compuşilor coordinativi**, 1984, 415 p.

E. CORDOŞ, C. MANOLIU, **Spectrometria de absorbţie şi fluorescenţa atomică**, 1984, 178 p.

C. BODEA, **Tratat de biochimie vegetală, p. II, t. V**, 1984, 438 p.

N. ASANDEI, A. GRIGORIU, **Chimia şi structura fibrelor**, 1984, 395 p.

N. IONESCU, M. CĂLDĂRARU, **Oxidarea catalitică a olefinelor inferioare**, 1983, 178 p.

C. I. SIMIONESCU, F. DANEŞ, **Originea vieţii**, 1984, 110 p.

C. BODEA, **Tratat de biochimie vegetală, p. II, t. IV**, 1982, 408 p.

CR. SIMIONESCU, VALERIA GORDUZA, **Polimeri biocompatibili şi biologic activi**, 1980, 479 p.

M. FLORESCU, **Metode ştiinţifice în dezvoltarea industriei chimice moderne**, 1979, 495 p.

C. GH. MACAROVICI, **Analiza chimică cantitativă anorganică**, 1979, 457 p.

ISSN 0035–3930

I. P. Informaţia c. 2673

43 426

Lei 40

F 1103

ACADÉMIE DE LA RÉPUBLIQUE SOCIALISTE DE ROUMANIE

REVUE ROUMAINE DE CHIMIE

Hommage à l'académicien
ELENA CEAUȘESCU

TOME 34

N° 2

Février 1989

Rev. Roumaine Chim. RRCHAX, **34**, *2*, p. 435 – 708 (1989), Bucarest

EDITURA ACADEMIEI REPUBLICII SOCIALISTE ROMÂNIA

ACADÉMIE DE LA RÉPUBLIQUE SOCIALISTE DE ROUMANIE

COMITÉ DE RÉDACTION

Rédacteur en chef :

I. G. MURGULESCU, membre de l'Académie de la République Socialiste de Roumanie

Rédacteurs en chef adjoints :

A. T. BALABAN et V. EM. SAHINI, membres correspondants de l'Académie de la République Socialiste de Roumanie

Collège de rédaction :

EM. BRATU, ELENA CEAUȘESCU, ECATERINA CIORĂNESCU-NENITZESCU, CR. SIMIONESCU, membres de l'Académie de la République Socialiste de Roumanie ; P. SPACU, membre correspondant de l'Académie de la République Socialiste de Roumanie ; M. BANCIU, M. D. GHEORGHIU, I. HAIDUC, D. I. MARCHIDAN, G. NIAC et D. SĂNDULESCU

La Revue Roumaine de Chimie paraît 10 fois par an. Toute commande de l'étranger sera adressée à ROMPRESFILATELIA – sectorul Export-Import Presă, P.O. Box 12–201, télex 10376 prsfi r 78104 Bucarest, Calea Griviței nr. 64–66, Roumanie

Les manuscrits, les livres et les revues proposés en échange, ainsi que toute correspondance seront envoyés à la rédaction :

REVUE ROUMAINE DE CHIMIE

125, Calea Victoriei, 79717 Bucarest, Roumanie, téléphone 50 76 80

EDITURA ACADEMIEI REPUBLICII SOCIALISTE ROMÂNIA
125, Calea Victoriei 79717, Bucarest, Roumanie, téléphone 50 76 80

HOMMAGE À L'ACADÉMICIEN
ELENA CEAUȘESCU

ORSZÁGOS MŰSZAKI INFORMÁCIÓS KÖZPONT ÉS KÖNYVTÁR 1983

IN HONOUR OF
ELENA CEAUȘESCU, D. CHEM. ENG.,
MEMBER OF THE ACADEMY OF THE SOCIALIST REPUBLIC OF ROMANIA

On January 7, this year, we celebrate the birthday and 50 years of revolutionary activity of Academician Elena Ceaușescu. A Doctor of Chemical Engineering, Member of the Executive Political Committee of the Central Committee of the Romanian Communist Party, First Vice-Prime Minister of the Government of the Socialist Republic of Romania, President of the National Council for Science and Education, Dr. Elena Ceaușescu chairs a vast scientific, political and social enterprise meant to bring into effect the country's plans for economic and social development, the important programs geared to a better organization and modernization of production, to increasing work productivity and efficiency, to a comprehensive implementation of the overall policy of the Romanian Communist Party and State, for the benefit of Romanian science, education and culture. The organization and management of the scientific research in this country, most especially in the fields of chemistry, and chemical technology and engineering, largely rely upon the innovative scientific spirit of, and direct guidance by Dr. Elena Ceaușescu.

As a direct outcome, the entire research and development system in chemistry has been given an appropriate coordination and has been integrated, along with the higher education in the field, with the respective industry.

The research work undertaken by Dr. Elena Ceaușescu is focused mainly on the chemistry and technology of macromolecular compounds; she has contributed to elucidating a number of major problems in the area — a most dynamic one in chemistry today, while also providing valuable contributions in all stages of applied research and

engineering, thus fostering the implementation in industry of the results of fundamental research.

Her studies dwell, *inter alia*, upon procedures for monomer and solvent purification; procedures for obtaining polymers via stereospecific polymerization and emulsion polymerization; procedures for obtaining polycondensates; studies on the structural characteristics of polymers and the relationship between structure and properties, as well as methods for the characterization of polymers. A series of studies deal with the use of complex catalysts for polymer synthesis in solution, with special emphasis on catalysts based on transition metals. Other works are concerned with the obtaining of polymers modified by isomerization, degradation and substitution reactions.

The stereospecific polymerization of isoprene holds an important place in the research work developed by Dr. Elena Ceaușescu, owing to the paramount relevance of this problem in today's chemistry of synthetic rubber. Part of the results were gathered in Dr. Ceaușescu's doctoral thesis. A special emphasis was placed on the synthesis of *cis*-1,4-polyisoprenic rubber that displays properties and structures similar to those of natural rubber, and substitutes for the latter in the tyre and technical item industry. Theoretical aspects connected with the reaction mechanism and kinetics, and the properties of the polyisoprene were also dealt with. Research was focused on the optimization of basic parameters, the obtaining of catalytic systems and development of the main steps of the technological flow-chart. The results have led to an industrial process for manufacturing *cis*-1,4-polyisoprenic rubber in Romania.

Dr. Elena Ceaușescu's scientific activity is also reflected in numerous papers published in scientific journals and in six monographs, first put out by Editura Academiei R. S. România, Bucharest, namely, "Research Work on Synthesis and Characterization of Macromolecular Compounds" (1974), "Stereospecific Polymerization of Isoprene" (1979), "Recent Research in the Field of Macromolecular Compounds" (1981), "Research in the Chemistry and Technology of Polymers" (1983), "Advances in Polymer Chemistry and Technology" (1986), and "Hydrocarbon Resins" (1988). Many publishing houses worldwide were soon to offer their readers translations of these books.

Dr. Elena Ceauşescu chaired the National Congress of Chemistry in the years 1978, 1981, 1988, and the IUPAC's Macro '83 Symposium. Her opening address at the 1988 National Congress of Chemistry gives important guidelines to the chemical research in Romania, also providing for the strengthening of the international scientific co-operation. Dr. Elena Ceauşescu contributed valuable papers to many scientific congresses and symposia — an outcome of her comprehensive scientific activity in the field of elastomer chemistry.

Dr. Elena Ceauşescu's scientific merits won well-deserved national and worldwide recognition. She is a member of the Academy of the Socialist Republic of Romania. She was also elected member of numerous international chemical societies of high renown and was nominated honorary professor by important higher education institutions abroad. Dr. Ceauşescu is a honorary member of the International Society of Industrial Chemistry, France; active member of the Academy of Sciences, New York; honorary member of the College of Chemists and Chemical Engineers in Costa Rica; honorary member of the University Council and of the Management Council of the Central University in Ecuador; honorary member of the Ecuador Institute of Natural Sciences; honorary member of the School of Information Science of the Central University of Ecuador; honorary professor of the National Engineering University, Peru; honorary member of the American Institute of Chemists (A.I.C.); Doctor Honoris Causa of the University of Buenos Aires; Doctor Honoris Causa of the University of South-Bahia Blanca, Argentina; Doctor Honoris Causa of the Feminine University of Manila, the Philippines; honorary member of the Chemical Society of Mexico; Doctor Honoris Causa of the University of Yucatan, Mexico; Extraordinary Professor of the Autonomous National University of Mexico; Doctor Honoris Causa of Sciences, University of Teheran; honorary member of the Society of Polymer Science in Japan; corresponding member of the Academy of Athens; awardee of the Silver Medal of the Science University of Kuweit; honorary member of the Academy of Arts and Sciences in Ghana; honorary member of the Academy of Sciences of the State of Illinois, USA; Fellow of the Royal Institute of Chemistry, UK; Professor Honoris Causa of the Polytechnics of Central London; member of the European Academy of Sciences, Arts

and Humanities, and member of the Honorary Committee of the Academy; Doctor Honoris Causa of the Technical University of the Middle East, Ankara; Doctor Honoris Causa of the University of Malta; Doctor Honoris Causa for Sciences of the Islamabad University, Pakistan; Doctor Honoris Causa for Sciences of the University of Liberia; Doctor Honoris Causa in Chemical Sciences, D.P.R. of Korea.

The high praise enjoyed by Dr. Elena Ceaușescu is also reflected in her being awarded important titles and distinctions of merit. Among these are: the highest Romanian title of honour "Hero of the Socialist Republic of Romania"; the title "Hero of Socialist Labour"; the medal "Star of the Socialist Republic of Romania", as well as other orders and medals, Romanian and foreign. She was also awarded the Gold Medal of the Institute for the Problems of a New International Economic Order, the Gold Medal "Marie Curie" and the Jubilee Gold Medal of the Institute of International Relations in Rome, and the Gold Badge of the European Academy of Sciences, Arts and Humanities. By virtue of these, Academician Elena Ceaușescu is the most prestigious representative of the Romanian contemporary science, education and culture.

Active in the national scientific and political life as well as in the international arena, presiding over the Romanian National Committee "Scientists and Peace", Academician Elena Ceaușescu makes an outstanding contribution to the carrying into effect of Romania's policy of independent domestic development, many-sided international co-operation, and struggle for peace, a policy designed under the guidance of Comrade Nicolae Ceaușescu, Secretary General of the Romanian Communist Party, President of the Socialist Republic of Romania, Honorary President of the Academy of the Socialist Republic of Romania.

The National Council for Science and Education, the Ministry of the Chemical and Petrochemical Industry, the Academy of the Socialist Republic of Romania, and the Central Institute for Chemistry join whole-heartedly in the feelings of highest esteem and praise the Romanian people has for Academician Elena Ceaușescu, and express deepest appreciation for her exceptional contribution

to the building of modern Romania, to the development of scientific research and education in this country, particularly in the field of chemistry, chemical technology and engineering. We wish the most distinguished Romanian scholar many happy returns and a long and fruitful activity in order that science, education and culture in the Socialist Republic of Romania be raised onto ever higher levels of performance, for the benefit of our society, of world progress and peace.

THE NATIONAL COUNCIL
FOR SCIENCE AND EDUCATION

THE MINISTRY
OF THE CHEMICAL
AND PETROCHEMICAL
INDUSTRY

THE ACADEMY
OF THE SOCIALIST
REPUBLIC OF ROMANIA

THE CENTRAL INSTITUTE
FOR CHEMISTRY

REVUE ROUMAINE DE CHIMIE

Tome 34, N° 2 **Février 1989**

IN HONOUR OF
ELENA CEAUȘESCU, D. CHEM. ENG.
MEMBER OF THE ACADEMY OF THE SOCIALIST REPUBLIC OF ROMANIA

ELENA CEAUȘESCU, CONSTANȚA SDRULA, M. PÎRLOG, LUCIA FIERĂSCU, ANA-MARIA HINTZ, LINA CORNEA, N. LUCACIU and MARIA PĂTRU, Polyesters for polyurethanes. Triethanolamine based polyesters 437–443
CAMELIA BELDIE, NICOLAE AELENEI, ANA ONU, GHEORGHE NEMȚOI and FELICIA SĂNDESCU, Thermochemical aspects of the reaction between aliphatic alcohols and $POCl_3$ 445–451
ALEXANDRINA DONESCU, JOSETTE WEINBERG and V. EM. SAHINI, Solute-solvent interactions in carbenicillin solubility processes. 453–457
MIHAIL FLORESCU, Biotechnologies in the chemical industry. 459–475
AURELIA GHENCIULESCU, LUCIAN ENESCU, FILIP CHIRALEU and ILIE G. DINULESCU, Reaction of *endo*- and *exo*-benzocyclobutenonorbornan-7-one with dimethyloxosulfonium methylide 477–480
MIRCEA D. GHEORGHIU, ANGELA POPESCU and GHEORGHE SURPĂȚEANU, ^{1}H—NMR spectra of 5,9-methano-5H-benzo[3,4]cyclobuta[1,2]-cycloheptene derivatives 481–489
VALERIU V. JINESCU, The high degree generality of the principle of critical energy 491–502
V. N. KALININ, S. K. MOISEEV, V. I. BAKHMUTOV and N. I. UDALOV, Synthesis of 6,7-benzomorphanes using arenetricarbonylchromium complexes (in Russian) 503–508
V. G. KHARCHENKO and S. N. CHALAYA, Nucleophilic and electrophilic reactions of 1,5-diketones (in Russian) 509–516
MARIANA KHRISTOVA, D. PANAYOTOV and D. MEKHANDJIEV, Neutralization of nitrogen oxides on CuO and Co_3O_4 catalysts and $Cu_xCo_{3-x}O_4$ spinels (in Russian) 517–526

Rev. Roumaine Chim. **34**, *2*, 435–708 (1989), Bucarest

KH. M. MINACHEV and V. V. KHARLAMOV, Oxidative acetoxylation of hydrocarbons over metal-containing catalysts (in Russian) 527–536

L. ONICIU, MARIA JITARU and I. A. SILBERG, Mediated electrocatalysis. I. General aspects 537–549

D. PAVLOV, B. MONAKHOV, M. MAJA and N. PENAZZI, Sn-free effect at the positive lead acid battery plates 551–559

LILIANA PETROVA, JULIETA STOYANOVA, TSVETANKA NEDYALKOVA and ELSA TORBOVA, Purification of the air from styrene in production of glass reinforced resin by chemical methods (in Russian) . . 561–566

C. POPESCU and E. SEGAL, On the temperature integral used in nonisothermal kinetics 567–575

GEORGETA POPESCU, GHEORGHE NECHIFOR, BUJOR ALBU and NICOLAE LUCA, Microporous polyethersnlphone membranes. 577–580

CARMEN POSTOLACHE and TATIANA ONCESCU, Kinetics of hemoglobin and casein hydrolysis catalyzed by alcalase 581–584

S. A. SILING, Synthesis and research of polymers based on nitriles of polycarboxylic acids and on diamines (in Russian) 585–595

CRISTOFOR I. SIMIONESCU, AURICA CHIRIAC, VIORICA RUSAN and IORDANA NEAMŢU, Adhesive emulsions. 4. Synthesis of the vinyl acetate/methyl methacrylate/acrylamide copolymer in the absence of emulgators 597–601

I. STAN, E. CHIFU, Z. FINTA and EUGENIA GAVRILĂ, Marangoni translational motion of a free drop initially at rest 603–615

MICHAELA STĂNESCU, MIRCEA BANCIU and ALEXANDRU T. BALABAN, 1-Oxonia and 1-aza analogues of triptycene 617–622

S. STERNBERG, I. V. COTÂRŢĂ and D. CONSTANTINESCU, Oscillating phenomena during anodic polarization of sulphur containing nickel electrodes 623–633

N. STRIBECK, S. POLIZZI, P. BÖSECKE and H. G. ZACHMANN, Investigations of strained S-B-S block copolymers with dilute elastic networks 635–648

I. TEOREANU and MARIA GEORGESCU, Hydratation processes in the $3CaO \cdot SiO_2 - 3(CaO \cdot AL_2O_3)CaSO_4 - H_2O$ system (in French) 649–659

VIORICA TRANDAFIR, MINODORA LECA and CRISTINA MANDRAVEL, Characterization of complexes formed by chromium basic salts with natural and synthetic tanning polyphenols 661–666

I. URSU, R. ALEXANDRESCU, I. MORJAN, I. N. MIHĂILESCU, C. GRIGORIU, A. M. PROKHOROV, V. I. KONOV and YU. N. PETROV, Prospects for IR laser applications in chemical technology 667–681

M. I. VASS, I. BALINT and V. POPA, Methane oxidation on supported palladium catalysts 683–688

I. I. VATAMAN, L. S. KOPANSKAYA, L. G. KIRIYAC, V. A. SMELOV and V. G. RUSSU. The polarography determination of lead and tin in alloys (in Russian) 689–696

RODICA VÎLCU, I. GĂINAR, ŞT. PERIŞANU and GH. ANIŢESCU, Vapour pressures of *cis*- and *trans*-2-butenes 697–701

MARIA ZAHARESCU, CONSTANŢA PÎRLOG, MARIA CRIŞAN and MARINA SAHINI, Structural characterization of vitreous SiO_2 made from gels 703–707

Revue Roumaine de Chimie, **34**, *2*, 437–443 (1989)

POLYESTERS FOR POLYURETHANES. TRIETHANOLAMINE BASED POLYESTERS

ELENA CEAUȘESCU, CONSTANȚA SDRULA, M. PÎRLOG, LUCIA FIERĂSCU,
ANA-MARIA HINTZ, LINA CORNEA, N. LUCACIU and MARIA PĂTRU
Chemical Research Institute
Spl. Independenței 202, Bucharest, Romania

Received November 21, 1988

Some aspects regarding triethanolamine (TEA) behaviour in the direct esterification reaction of adipic acid (AA) with different diols and/or triols were studied in a previous work.[2] The present paper continues by evaluating the possibility of using the TEA-based polyesters as polyolic component for polyurethane (PUR) rigid foams. The influence of TEA content on the physical and mechanical properties of the foam, as well as on the dynamics of the foaming process was studied. The results reveal the effect of TEA in the polyols-isocyanate reactions and also in the structural properties of the resulting foam. These are important factors, determining the amount to which TEA can be introduced in PUR rigid foams formulation, to obtain good thermal insulation applications.

Polyols with triethanolamine (TEA) content are of particular interests for polyurethane (PUR) rigid foams, due to the fact that they lead to more homogeneously structured foams, a higher fire-resistance and hydrolytic stability and a catalytic effect in the foaming process.[1]

Previous work [2] regarding the TEA behaviour in the direct esterification reaction of adipic acid (AA) outlined some important features :

1. Triethanolamine, as a polyol, is more reactive than the most common triols used in polyesters for PUR manufacturing (Fig. 1).

If we use, for monitoring the reaction-rates, the decrease of the acidity index (AI, mgKOH/g) in time (in the very first step of the esterification process, which is unaltered by the viscosity changes in the reaction medium), it follows that the reaction-rate varies with the nature of triol in the order :

$$\mathrm{TEA} > \mathrm{TMP} > \mathrm{HT} > \mathrm{G}$$

Comparing only glycerol (G), 1, 2, 6-hexanetriol (HT) and trimethylolpropane (TMP), this order is an experimental evidence of the fact that secondary hydroxyl groups are less reactive in esterification reaction than the primary ones. The higher reactivity of TEA is based merely on its higher stability against hydrolysis, the inverse esterification reaction.[3]

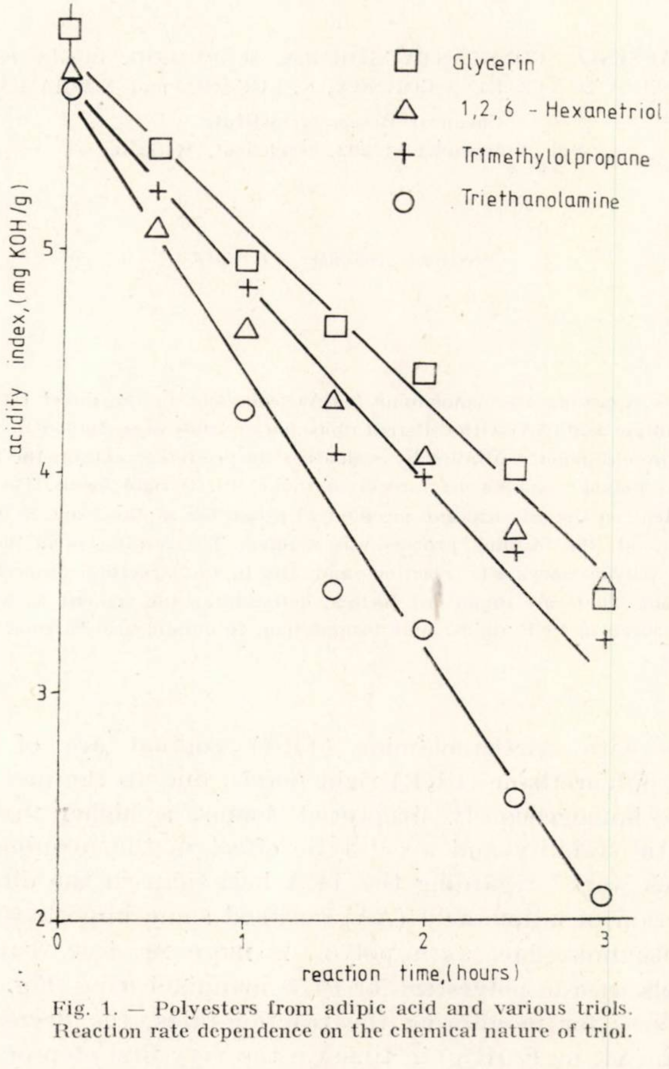

Fig. 1. — Polyesters from adipic acid and various triols. Reaction rate dependence on the chemical nature of triol.

2. Triethanolamine-based polysters have lower bulk viscosities than other corresponding oligoadipates (Fig. 2). One can see that, at similar molecular weights, the bulk viscosity of oligoadipates from different triols varies with the nature of triol as follows :

TMP > G > HT > TEA

First of all, this order points again to the effect of the secondary hydroxyl groups in G and HT, which leads to more linear structures of the chains. The lowest viscosity of the TEA containing adipates is probably explained by the higher mobility of the branching points of these chains.

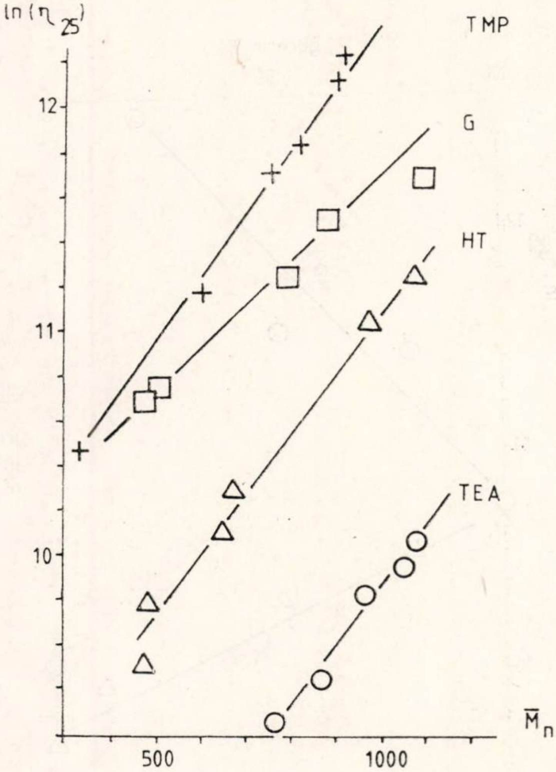

Fig. 2. — Polyesters from adipic acid and various triols. Correlation between no. av. mol. wt. ($\overline{M}_n$) and dynamic viscosity at 25°C, (η_{25}, mPa.s).

3. Triethanolamine has a low thermo-oxidative stability and during the reaction time is affected by partial decomposition.

In fact, TEA itself has a good thermal stability. But, in the esterification medium and at temperatures over 180°C, the reaction mixture is subjected to a strong colouring process, and the balance of the reactive groups in the formulation is drastically affected.

Consequently, by introducing TEA in the initial reaction mixture, the result is a growth in viscosity, instead of the expected lowering one. This phenomenon is illustrated on polyesters based on TEA and G, because the corresponding TMP based polyadipates, at the usual formulation, imply a higher risk of gelation (Fig. 3). It can be seen that, at a reaction temperature of 200°C, the viscosity increases with the increase of the TEA content, because of the lowering of the hydroxyl groups excess in the formulation by the TEA decomposition. On the other hand, at lower reaction temperatures (160°C), this phenomenon cannot be observed and the viscosity varies normally with TEA content in the starting formulation, between the values corresponding to the homopolymers.

Starting from this point, the possibility of using this kind of polyesters as polyolic component in PUR rigid foams manufacturing was further studied.

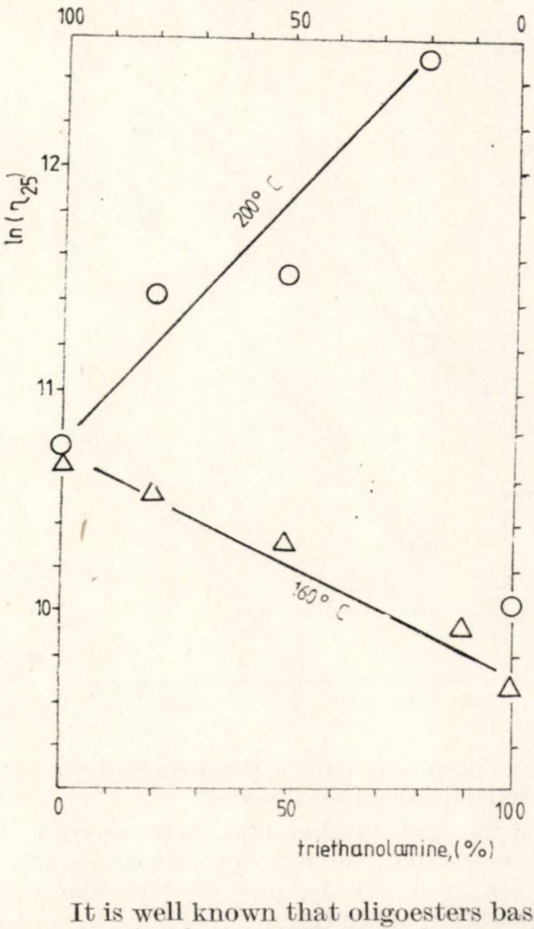

Fig. 3. — Polyesters from adipic acid, glycerin and triethanolamine. Influence of triethanolamine-content on dynamic viscosity (η_{25}, mPa.s) of polyester.

It is well known that oligoesters based only on AA and triols generally are not suitable for PUR rigid foams: they exhibit a very poor compatibility with the other components in the foaming formulation (due to their high viscosities) and lead to very friable foams.

Consequently, for the study it was necessary to obtain typical polyolic components, as the oligoadipates based on diethyleneglycol (DEG) and TMP are with various TEA contents.

All these polyols showed apparently a normal behaviour in the foaming process and lead to rigid PUR foams with acceptable physical and mechanical characteristics.

The effect of the TEA content reveals first of all from the dynamic of the foaming process and from the structures of the resulting foams.

1. From the beginning, it can be seen that the TEA containing polyesters have a considerable catalytic effect in the foaming process.

It is well known that, among the foaming process parameters, the cream-time is the most significant one for the activity of the catalytic system itself.

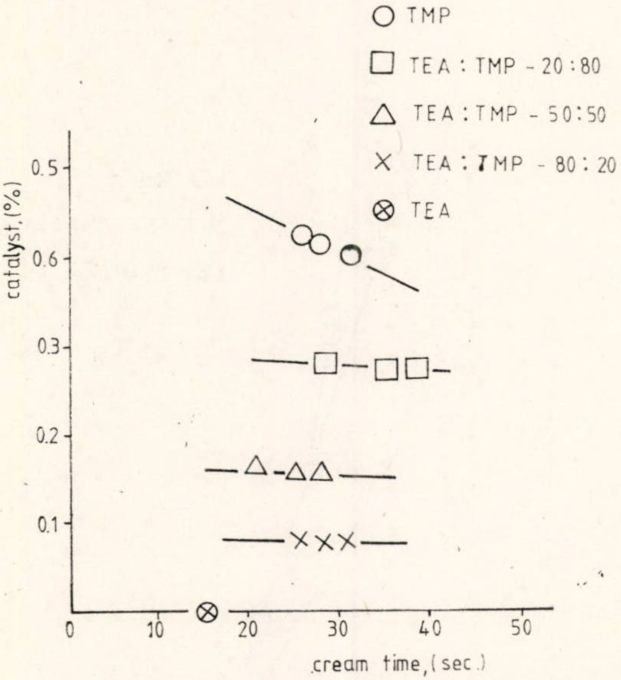

Fig. 4. — Polyesters from adipic acid, diethyleneglycol and triethanolamine. Influence of triethanolamine-content and catalyst (triethylamine) concentration on cream time.

In figura 4 are represented the cream-time values vs. the added aminic catalyst concentrations (triethylamine), calculated for 3 different amounts of expanding agent — Freon 11, for formulations with various TEA contents in polyol. It is obviously shown that TEA containing polyesters lead to lower values of the cream-time, even with smaller amounts of added catalyst.

Moreover, in spite of the fact that by dilution with freon the concentration of the added catalyst varies unsignificantly, the cream-time values support real changes. All these lead to the conclusion that the concentration of the effective catalytic system is greater than the added catalyst one, that is exactly the catalytic effect of TEA.

2. The overall foaming process is a most complex one, which consists at least in a competition between the expanding process, due to the expanding agent and the thermal effect of the reaction with isocyanate,

and the stiffness process, by rising the viscosity during the crosslinking reactions.

But, for the same catalytic system, the rise-time will depend mainly on the expander agent quantity and the polyol nature.

Figure 5 shows the variation of the rise-time with the freon content in formulation (illustrated by the recalculated added catalyst concentration), for different TEA containing polyols.

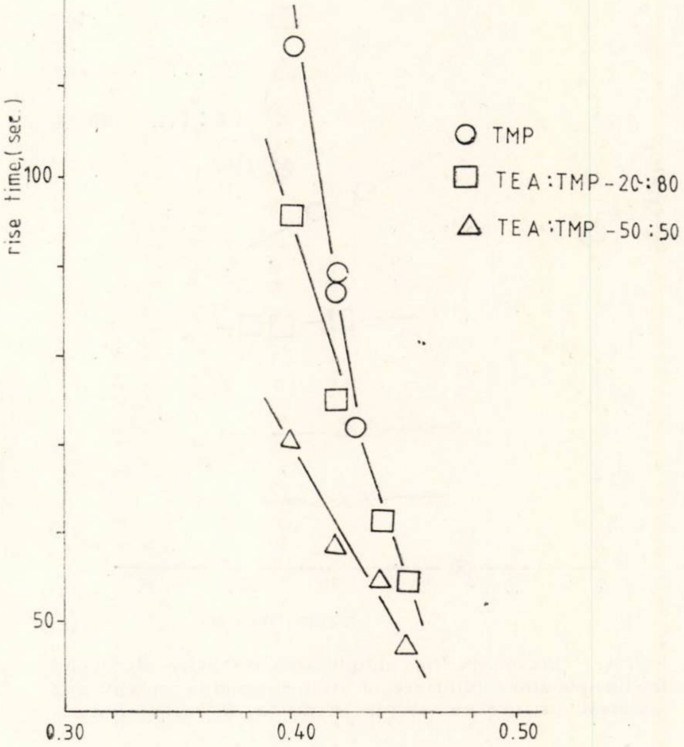

Fig. 5. — Polyesters from adipic acid, diethyleneglyco and triethanolamine. Influence of triethanolamine-content on rise time.

It can be seen that free polyols have the strongest variation of the rise-time with dilution. Lower values and smaller greadient of variation are obtained by introducing TEA in formulation. Because TEA-containing and TMP-containing polyesters present similar molecular structures, this behaviour difference cannot be assessed only to the crosslinking reaction, but also to the previously mentioned catalytic effect of TEA.

3. Finally, as regards the structure of the resulting foam (by commonly used siliconic emulsifiers as Polyurax SR 235), it can be seen that the rising of the TEA content in polyol leads to a drastic fall of the closed cell-content in the foam (Fig. 6).

Moreover, for more than 50% TEA in polyol (related to the TMP content), the foam will finally colapse. But, even with small amounts of TEA, the resulting foams will have an important open-cells content, which makes them improper for thermal insulation uses.

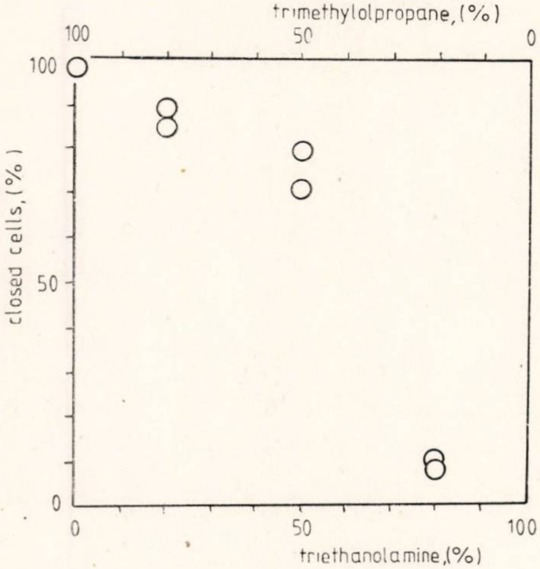

Fig. 6. — Polyesters from adipic acid, diethyleneglycol, trimethylolpropane and triethanolamine. Effect of triethanolamine-content on foam structure.

In conclusion, polyesters based on AA, DEG, TMP and TEA are easy-to-obtain, they have low viscosity, high compatibility and selfcatalytic polyolic components for PUR foams. They lead to rigid PUR foams with good physical and mechanical properties. For the further thermal insulation applications, additional research work is also necessary with the aim to minimize the open-cells content of the resulting foams (as an emulsifier study).

REFERENCES

1. Pat USA 3574167 (1971).
2. Elena Ceaușescu "Progrese în chimia și tehnologia polimerilor", Edit. Academiei, Bucharest, 1986, p. 353.
3. I. R. Metlyakova, M. V. Shoshtaeva. *Plast. Massy.* 112—4 (1977).

Revue Roumaine de Chimie, **34**, *2*, 445–451 (1989)

THERMOCHEMICAL ASPECTS OF THE REACTION BETWEEN ALIPHATIC ALCOHOLS AND $POCl_3$

CAMELIA BELDIE, NICOLAE AELENEI, ANA ONU,
GHEORGHE NEMŢOI and FELICIA SĂNDESCU*
Physical Chemistry Department, Faculty of Technological Chemistry, Polytechnic Institute "Gh. Asachi", Splai Bahlui no. 71, 6600, Iassy, Romania
* Synthetic Fibre Work of Săvineşti, Piatra-Neamţ, Romania

Received October 20, 1988

The thermal effect and its dependence on the temperature of the phosphating reaction of higher aliphatic alcohols with $POCl_3$, using an adiabatic calorimeter fitted with an isothermal mantle, was measured. The measurements performed on industrial alcohol samples (C_{12} – C_{18} fraction) emphasized the dependence of the thermal effect on the average chemical composition of the samples. An abnormal thermal effect dependence on temperature was recorded when the industrial alcohol samples were used for the measurements. That might be the result of the different behavior of the C_8–C_{12} alcohol fraction and of the C_{16}–C_{18} alcohol one within 15–60°C temperature range. The performed study might be used with a view to the mathematical modelling and the process optimalization in order to prepare indigenous antistatic compounds.

1. INTRODUCTION

The features of textile products made from synthetic fibres and threads (for instance; the antistatic properties, utilization comfort, maintenance behaviour) do not depend only on the chemical structure and the fibre production technology, but also, to a great extent, on the utilization of some higher finishing products during their processing. For this reason a few preparation products are used which play an important part in decreasing the fibre–fibre and fibre–metal frictions, increasing the fibre elasticity, decreasing the electrostatical charges, the modification of the tensioactive properties, etc., during processing.[1]

The adequate chemical compounds used ensure high output of the synthetic fibres and thread processing, and also remove the subsequent difficulties which occur during the next textile processing stages.

The requirements imposed by a suitable preparation cannot be accomplished only by a chemical compound. As a rule, the main functions of the various recipes are the same, but the industrial products differ by their chemical composition and the percent included in the industrial preparation products.

In processing the acrylic fibres spun from the solution, which present a rugged surface, some ethoxylated and high molecular weight compounds should be used in the industrial preparation products to assure a uniform deposition on the fibre surface, as an elastic and resistant film. That enables an adequate fibre processing, when it is subjected to very harsh mechanical stresses, for example, in the case of the cable break machine, or the carding operations. For this purpose, ethoxylated amides of the $RCONH-(CH_2-CH_2O)_nH$ type, where R is an aliphatic radical ($C_{16}-C_{18}$), were used in practice.

Recently, the preparation products of alkyl phosphites and alkyl phosphates which confer very good features to the fibres have been largely applied.[2-7]

One of the preparation methods of phosphites is based on phosphating the aliphatic alcohols with $POCl_3$; the reaction is followed by the partial elimination of hydrochloric acid and subsequent neutralization of mono- and di-phosphoric esters with ethanolamine or ethoxylated compounds. The neutralization reaction is performed in the presence of poly(glycol) esters, which have antifoam effect and ensure a better dispersion of the neutralization agent within the reaction medium. Good antistatic properties are obtained when the content of mono-ester into the phosphates is higher than 50.0 %. Such a high percent of mono-ester in the phosphating product is obtained by a correct dosing of the reactants and a severe temperature control. For this reason, the reaction thermal effect and its dependence on the temperature should be known.

This paper presents the experimental data obtained for the phosphating reaction of the aliphatic alcohols (C_8; C_{10}; C_{12}; C_{16}; C_{18}) with $POCl_3$. The literature suffers from lack of data concerning the reaction thermal effect values.

2. EXPERIMENTAL

The reaction thermal effects were measured using an adiabatic calorimeter fitted with an isothermal mantle. The calorimetric installation consists of a calorimetric vessel (Dewar type) fitted with an adjustable velocity stirrer (propeller type), thermometer, standard electric resistance, Beckmann termometer in order to measure the temperature variation (± 0.001 °C) and a reaction vessel.

In order to reduce the heat exchange with the exterior, the calorimetric vessel was placed in an air thermostate, whose temperature was kept with 1—2 °C higher than the calorimetric vessel temperature. The temperature was kept constant during the initial period adjusting the air thermostate temperature and stirrer velocity.

The caloric capacity of the calorimeter (the calorimeter constant) was determined by the electric calibration. For this reason, the discharged power by the electric resistance was measured with an EL-21 type Watt-meter (0.2 accuracy). The heating time was measured with a ± 0.1 s accuracy. The temperature variation of the calorimetric vessel, as a result of the electric heating was measured applying the graphic interpolation of the temperature-time data. The calorimeter constant was measured after the achievement of the chemical reaction in the reaction vessel. For each experiment 3—5 measurements were performed. A good reproduction of the measurements was recorded. The experimental errors were less than 1.0 %.

The reaction vessel (50 mL capacity) is made of glass, with thin walls in order to ensure the temperature transfer in the optimum conditions. $POCl_3$, heated at the working temperature, was measured with a pippete and poured over alcohol, previously weighted and thermostated, in the reaction vessel.

The temperature variation of the calorimetric vessel, as a result of the chemical reaction, was also estimated by means of the graphic interpolation technique.

The thermal effect was calculated applying the relationship :

$$\Delta H = - \frac{\overline{K} \cdot \Delta T}{n} \text{ (J/mol)} \qquad (1)$$

where : $\overline{K}$ — is the average value of the calorimetric constant (J/mol) ; ΔT — is the temperature variation of the calorimetric vessel (K) and n — is the $POCl_3$ (moles).

For each sample, 3 up to 4 measurements, at a determined temperature value, were carried out. In this case, the measurement errors ranged between 1.0 % and 2.0 %.

3. RESULTS AND DISCUSSION

The thermal effect measurements of the phosphating reaction upon the industrial samples of higher aliphatic alcohols ($C_{12}-C_{18}$ fraction), containing high percent of $C_{16}-C_{18}$ fraction, were performed.

Taking into account the heterogeneity of the industrial high alcohol samples, it was absolutely necessary to check if the sample collecting technique influenced the reaction thermal effect values. The measured values are given in table 1.

Table 1

The sample collecting technique influence on the reaction thermal effect

Sample	t,(°C)	m(R—OH) (g)	$\overline{K}$, (J/K)	ΔT, (K)	$\Delta_r H$(kJ/mol)
1	25.1	9.6906	971.69	0.760	−20.64
2	25.2	15.6401	987.27	1.640	−26.51
3	25.1	6.8390	991.15	0.639	−23.71

Sample 1 was collected after the centrifugation of the industrial alcohol sample, and liquid fraction removing. Therefore, it contains a small percent of the lower molecular weight alcohols. Sample 2 was collected from the liquid fraction, and it contains a higher percent of the C_{12} alcohol fraction, but it also contains higher molecular weight alcohols which are soluble in the lower alcohol fraction. Sample 3 was collected after the fusion and homogenization of the industrial alcohol sample.

One can notice that the termal effect values differ from a sample to another though all measurements were performed at 25.1°C.

The thermal effect data of the homogenized samples lie between the values obtained for the samples having smaller percent of lower molecular weight alcohols and larger contents of lower molecular weight alcohols, respectively. All subsequent measurements were carried-out on the homogeneous samples collected from the fusion of the industrial alcohol samples.

The experimental data of the two groups of the industrial alcohol samples are summarized in table 2.

A good reproduction of the measurements for the same sample group was noticed. But the average values obtained for the two sample groups vary with about 5.0%. The first sample group may possibly contain a larger percent of the higher alcohols.

The caloric effect dependence on temperature was investigated on a sample series collected from the first sample group. All samples were collected after the fusion and homogenization of the industrial alcohol sample. A stoichiometric quantity of $POCl_3$, for the hypothetic formation only of the mono-ester was taken into account. Table 3 shows the experimental results.

Table 2

The thermal effect of the phosphating reaction for the two groups of the industrial alcohol samples with $POCl_3$

Sample	t (°C)	m (g)	$\overline{K}$ (J/K)	ΔT_R (K)	Δ_rH (kJ/mol)	$\Delta_r H$(average) (kJ/mol)
I	24.3	11.0169	983.26	1.041	−23.79	−23.78
	25.1	6.8390	991.51	0.639	−23.71	
	25.0	10.2233	985.82	0.962	−23.75	
	24.8	12.4660	999.35	1.163	−23.87	
II	25.0	9.6906	982.24	0.956	−24.81	−25.01
	25.4	12.2321	981.97	1.220	−25.07	
	25.1	6.8400	991.15	0.678	−25.15	

Table 3

The thermal effect variation against the temperature of the posphating reaction of the industrial alcohol samples with $POCl_3$

No. of measurements	t (°C)	$m_{\text{calc.}}$ (g)	$\overline{K}$ (J/K)	ΔT_r (K)	$\Delta_r H$ (kJ/kg)	$\Delta_r H$ (kJ/mol)
1	16.6	5.7429	986.50	0.464	-79.70^{+}	-20.41^{+}
2	19.8	13.7352	1022.73	1.110	-82.65^{+}	-21.16^{+}
3	21.8	6.5916	977.75	0.588	−87.21	−22.33
4	23.3	6.0431	988.60	0.549	−89.81	−22.99
5	24.3	11.0169	983.26	1.041	−92.91	−23.79
6	24.6	12.4660	999.35	1.163	−93.29	−23.87
7	25.0	10.2233	985.82	0.962	−92.76	−23.75
8	25.1	6.8390	991.15	0.639	−92.61	−23.71
9	28.0	12.9394	1051.37	1.262	−102.51	−26.26
10	30.3	6.9081	1014.97	0.720	-105.86^{+}	-27.10^{+}
11	32.9	10.2569	1064.20	1.022	−109.10	−27.20
12	36.1	10.3244	1032.55	1.159	−115.91	−29.67

The study of these data points out a linear dependence of the thermal effect on the temperature. The experimental results marked with (+) were performed after the introduction into the reaction medium of an ester resulted from a fatty acid with poly(ethyleneglycol), used as antifoam and dispersion agent in the preparation product technology. The ester/alcohol ratio used in all the three determinations was 1 : 6. The thermal effects obtained for the three measurements lie very well between the results obtained when the experiments were carried out without poly(ethyleneglycol) ester. That proves that the addition of ester has no influence on the thermal effect of the phosphating reaction.

The processing of the experimental data (Table 3) applying the least squares method leads to an equation which gives the variation of the caloric effect as a function of temperature.

$$\Delta_r H = -23.94 - 0.49(T - 298.2) \text{ kJ/mol} \qquad (2)$$

Both the dependence of the thermal effect on the sample composition, expressed by the lower and higher alcohol ratio, and its large exaggerated dependence on temperature show a different behaviour of lower and higher aliphatic alcohols against the phosphating reaction with $POCl_3$. With a view to define more accurately these differences, the thermal effects of the pure alcohol phosphating reaction containing C_8; C_{10}, C_{12}, C_{16} and C_{18} were measured. $POCl_3/R-OR$ molar ratios of 1 : 1 and 2 : 1, respectively, were used for the measurements.

Table 4 shows the experimental results of C_8-C_{12} alcohol samples.

Table 4

The thermal effect of the reaction between $C_nH_{2n+1}OH$ and $POCl_3$ (n = 8; 10; 12); $\Delta_r H$ (kJ/mol)

	$t = 25°C$		$t = 60°C$
	$n(POCl_3) : n(R-OH)$		$n(POCl_3) : n(R-HO)$
	1 : 1	2 : 1	2 : 1
$C_8H_{17}OH$	−38.24	−38.92	−27.08
$C_{10}H_{21}OH$	−40.29	−41.79	−21.95
$C_{12}H_{25}OH$	−41.38	−43.02	−21.05

The thermal effects shown by table 4 represent the average of 3 to 5 measurements. The experimental values obtained when $POCl_3$ was taken in excess were higher with about 4% than when reactant stoichiometric quantities were used. That should be explained by the fact that during the phosphating reaction, small quantities of $POCl_3$ are removed due to the elimination of gaseous HCl.

It is surprising that the thermal effect values at 60°C are smaller (30% to 50%) than those measured at 25°C. We suppose that this is due to the fact that at 25°C prevails the formation of mono-ester, while at higher temperature values the yield of the di- and tri-esters is favoured. The last two stages develop with a much lower exothermic thermal effect.

The behaviour of the higher aliphatic alcohols ($C_{16}H_{30}OH$ and $C_{18}H_{37}OH$) is much more complex. For instance, cetyl alcohol (m.p. 49.5°C) behaves completely different during the phosphating reaction with $POCl_3$, at 25°C in comparison with that performed above its melting point temperature. From the thermal point of view, at 25°C there are two reaction stages: an endothermal stage followed by an exothermal one, which overlaps partially the endothermal stage. At 50°C and 60°C, respectively, the phosphating reaction of cetyl alcohol with $POCl_3$ develops exothermally.

The average thermal effect values of the cetyl alcohol phosphating reaction with $POCl_3$ are listed in table 5.

Table 5

The thermal effect of cetyl alcohol phosphating reaction with $POCl_3$

t(°C)	t = 25 °C				t = 50 °C	t = 60 °C
$\frac{n_{POCl_3}}{n_{R-OH}}$	1 : 1		2 : 1		2 : 1	2 : 1
Stage	I	II	I	II		
$\Delta_r H$ (kJ/mol)	+18.44	−3.34	+20.44	−4.67	−26.15	−27.15

It seems that the endothermal stage has to be assigned to the alcohol fusion, assumption supported also by the fact that the sum of the absolute values, corresponding to the thermal effects during the two stages (25.11 kJ/mol) has the same magnitude as the values recorded at 50° and 60 ° respectively.

Octadecyl alcohol ($C_{18}H_{37}OH$, m.p. 58.8°C) does not react practically at 25°C, while at 60°C it gives an exothermic thermal effect, comparable with the thermal effects recorded during the phosphating reaction of lower aliphatic alcohols and for cetyl alcohol at the same temperature

$$\Delta_r H = -20.37 \text{ kJ/mol}.$$

CONCLUSIONS

The thermal effects of the phosphating reaction of higher aliphatic alcohols with $POCl_3$ were determined. From the recorded experimental results the following conclusions can be withdrawn :

— The thermal effect of the phosphating reaction of the industrial alcohol samples depends on the industrial sample type and the collecting technique from the same sample; for a given sample the thermal effect increases strongly with the temperature.

— For the pure alcohol fractions ($C_8 \ldots C_{12}$) which at 25 °C are liquids, the recorded measurements show a high thermal effect dependence on temperature; at 60°C the thermal effect values are 30...50% smaller than at 25 °C. This abnormal behaviour was assigned to the fact that at high temperature di- and tri-esters yield, particularly, while at 25 ° prevails the formation of the mono-esters.

– The pure alcohols, higher than C_{12}, have the thermal effect dependence on temperature much more complex; that is determined by the melting point of the alcohol.

REFERENCES

[1] P. Ehrler and W. Sprenkmann, Chemiefasern Textilindustrie, Sept. 1981, p. 656.
[2] Patent R.S. Romania no. 85368, 1984.
[3] Patent R.S. Romania no. 67013, 1979.
[4] Patent R.S. Romania no. 65923, 1979.
[5] Patent R.S. Romania no. 67012, 1979.
[6] Patent R.S. Romania no. 85369, 1984.
[7] Patent R.S. Romania no. 83303, 1984.

Revue Roumaine de Chimie, **34**, *2*, 453–457 (1989)

SOLUTE-SOLVENT INTERACTIONS IN CARBENICILLIN SOLUBILITY PROCESSES

ALEXANDRINA DONESCU[a], JOSETTE WEINBERG[a] and V. EM. SAHINI[b]
[a] ICECHIM, Centre of Physical Chemistry, Spl. Independenţei 202, Bucharest
[b] Polytechnical Institute, Laboratory of Physical Chemistry, B-dul Republicii 13, Bucharest

The solute-solvent interaction of carbenicillin with various solvents in the temperature range 5–42° was studied. Solubility curves, solubility factor and thermodynamic functions were established. The experimental results could be rationalized taking into account the model of localized interactions between the carbenicillin molecule and the solvent molecules in the first solvation layer.

The present work presents solubility data of carbenicillin in the saturated C_1-C_8 alcohol series, acetone, chloroform, dichloromethane, benzene and glycerol, in the temperature range 5–42°. The solubility curves were obtained by plotting the logarithm of the dissolved molar fraction ($\log x_2$) *vs* the reversed absolute temperature ($1/T$). From the solubility data, the thermodynamic functions as well as the solubility factor of carbenicillin were determined. The experimental results were interpreted in terms of solute-solvent interaction, considering also departure from ideal behaviour.

EXPERIMENTAL PART

Carbenicillin, a β-lactam antibiotic, has the structure shown in Fig. 2.

The carbenicillin employed in this work was a pharmaceutical commercial product of the Antibiotic Enterprise Iași. All the solvents employed were p.a. grade reagents. For the determination of the dissolved carbenicillin, the UV extinction at $\chi = 264$ nm, characteristic for β-lactam cycle absorption,[1] measured with a UV-VIS Specord spectrophotometer, was used.

RESULTS AND DISCUSSIONS

Among the solvents used in solubility measurements, only methanol, ethanol and glycerol are of interest since the carbenicillin solubility in the remaining solvents was $< 10^{-3}$ g/100 mL in the temperature range investigated. The solubility data are presented in Table 1, and the solubility curves in Fig. 1.

Table 1

Solubility of carbenicillin in methanol, ethanol and glycerol

Solvent	t°C	$10^4/T$	x_2	log x_2
Methanol	5	35.97	4.170×10^{-3}	-2.379
	15	34.72	5.362×10^{-3}	-2.270
	22	33.89	7.845×10^{-3}	-2.105
	42	31.74	2.340×10^{-2}	-1.630
Ethanol	5	35.97	5.673×10^{-4}	-3.246
	15	34.72	6.114×10^{-4}	-3.213
	22	33.89	6.502×10^{-4}	-3.187
	42	31.74	1.826×10^{-3}	-2.738
Glycerol	5	35.97	6.491×10^{-4}	-3.187
	22.5	33.84	1.931×10^{-3}	-2.714
	31.5	32.84	3.316×10^{-3}	-2.479
	42.5	31.69	3.928×10^{-3}	-2.405

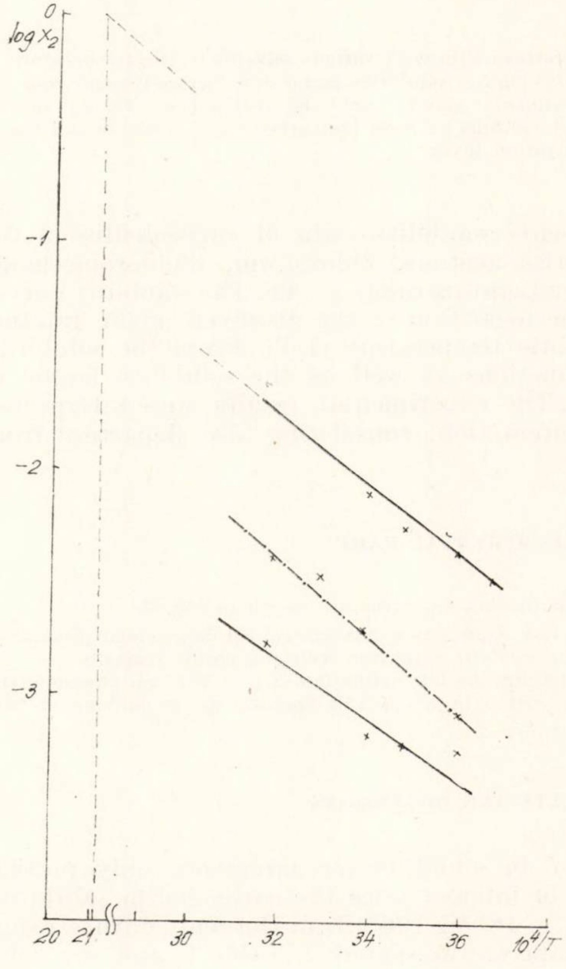

Fig. 1. — The solubility curves of carbenicillin in : ——— methanol; +.— ethanol; —..— glycerol.

The temperature dependence of carbenicillin solubility in methanol (Fig. 1) is a curve corresponding to an ideal solution,[2] whose intercept at $\log x_2 = 0$ is the melting point of carbenicillin (203°C). Using Raoult's rule, melting heat ΔH^F of carbenicillin was calculated. The enthropy variation on mixing and free energy variation on dissolution were calculated from solubility data :

$$\Delta H^F = 8097 \text{ cal/mol}$$

$$\Delta S_2 = 9.62 \text{ cal}$$

$$\Delta G_2 = -2840 \text{ cal/mol}$$

Departure from ideal behaviour was observed for the solubility, of carbenicillin in ethanol. Constant B values (table 2) were obtained using Hildebrand's relationship[2], indicating that solution of carbenicillin in ethanol is regular

$$RT \ln \frac{x_2^i}{x_2} = B\, x_1^2 \qquad (1)$$

x_2^i = ideal solubility = $7{,}845 \cdot 10^{-3}$
x_2 = molal fraction of carbenicillin in ethanol
x_1 = molal fraction of solvent (ethanol)
B = constant

The solubility parameter of ethanol, δ_1, calculated from vaporization heat,[3] is 12.29. This value and the previously determined ideal solubility x_2^i enabled the calculation of the solubility factor of carbenicillin δ_2 according to eq. (2); $\delta_2 = 10.22$ was obtained

$$\log \frac{x_2^i}{x_2} = \frac{\rho_1^2 V_2(\delta_1 - \delta_2)}{4{,}575\ T} \qquad (2)$$

Table 2

B constant at different temperatures

T°K	B
278	1451
288	1461
295	1461

ρ_1 = fraction volume of solvent (ethanol)
V_2 = molal volume of carbenicillin.

The thermodynamic parameters calculated for this regular solution were the following : partial molal energy of mixing $\Delta E^M = 1452$ cal/mol; free energy variation of solvation $\Delta G^M = -2890$ cal/mol.

The solubility of carbenicillin in glycol presents neither ideal nor regular behaviour.

According to literature,[4] the water solubility of carbenicillin is high (> 100 g/100 mL at 25°C). There seems to exist a correlation between the solubility of carbenicillin and the dielectric constant of the solvents. Data in Table 3 indicate that in solvents having $\varepsilon < 20$, the carbenicillin solubility is under 10^{-4} g/100 mL solvent.

Table 3

Dielectric constant and solubility of carbenicillin

Solvent		Solubility g/100 mL (25°C)
Water	78.54	> 100[4]
Glycerol	42.5	—
Methanol	32.63	8.25
Ethanol	24.30	0.47
Acetone	20.7	$<10^{-3}$
Propanol	20.0	$<10^{-4}$
n-Buthanol	17.8	$<10^{-4}$

Among the factors determining the solvation power of a certain solvent, its dipole moment, polarizability, molecular size and ability to form hydrogen bonds or donor-acceptor complexes are to be considered.[5] The simple electrostatic models for solvation emphasized the importance of the dielectric constant of the medium (representing a measure of its polarity). Carbenicillin is very soluble in water, soluble in methanol and moderately soluble in ethanol; one may ascribe this solubility difference to the dielectric constant of these solvents.

Formation of hydrogen bonds may also play an important role in the solubilization of carbenicillin in solvents possessing hydroxyl group. The polar molecules of the solvent are oriented towards the polar centers of the carbenicillin molecule in the ground state. In order to establish this specific solute-solvent interaction through hydrogen bonds, theoretical calculations were performed in MO—LCAO-Hückel formalism for carbenicillin molecule. The whole molecule of antibiotic was taken into account, with corrections for noncoplanarity. In Fig. 2 is presented the numbering of the centers and in table 4 are displayed the net charge and bond order. The charge density values and the low bond order indicate the N_9 atom and O_8, O_{14} carbonylic oxygen atoms as most probable sites for hydrogen bond formation.

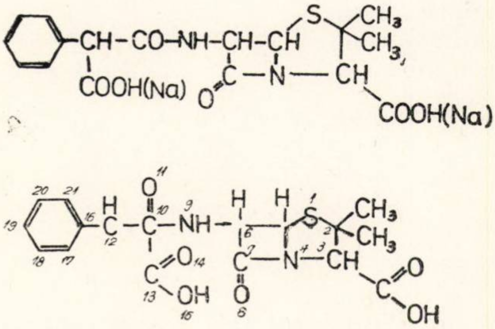

Fig. 2. — Numbering of the centers in carbenicillin.

Table 4

Net charges and mobile band orders in carbenicillin

Atom/Bond	Net charge q	Bond order p_{r-s}
O_8	−0.5637	
C_7-O_8	—	0.2768
N_9	−0.5269	—
O_{11}	−0.6497	—
$C_{10}-O_{11}$	—	0.6387
O_{14}	−0.6254	—
$C_{13}-O_{14}$	—	0.3204
O_{23}	−0.5636	—
$C_{22}-O_{23}$	—	0.7487

To sum up, carbenicillin dissolution in the afore-mentioned solvents consists in surrounding of carbenicillin molecule by solvent molecules with interaction by hydrogen bonds, as revealed by the free energy variation of solution values calculated from solubility data and by the theoretical charge distribution and bond order data.

REFERENCES

[1] T. Yamana, A. Tsuji, *J. Pharm. Sci.*, **65** (11), 1563 (1976).
[2] J. H. Hildebrand, R. L. Scott, "The Solubility of Nonelectrolytes" USA, 1950.
[3] C. D. Hodman, "Handbook of Chemistry and Physics", 1959.
[4] Pyopen, "Britisch Pharmacopeea", 1981.
[5] I. G. Murgulescu, E. Segal, Tațiana Oncescu, "Introduction to Physical Chemistry — Chemical Kinetics and Catalysis", vol. II, Ed. Acad., 1981 (in Romanian).

Revue Roumaine de Chimie, **34**, *2*, 459–475 (1989)

BIOTECHNOLOGIES IN THE CHEMICAL INDUSTRY

MIHAIL FLORESCU

National Council for Science and Technology, Bucharest, Romania

An interdisciplinary field largely opened towards industry, towards the solving of some grave problems of the world economy such as raw materials and energy, proteins and drugs shortage and environment pollution, biotechnology is one of the most fascinating elements for promoting the technical progress. The paper reflects the achievements in biotechnology, both world wide and in Romania, the joined efforts of Romanian specialists, who, within the framework of a wide international collaboration, have proved, by an original, concrete contribution, the idea that the role of biotechnology, its implication in the national economy are immense.

Nowadays, we are flooded by more and more news concerning a certain domain which, around 1960, seemed to become the future of a very promising, largely usable chapter of biology, namely biotechnology.

Like all the beginnings, this promise was not very clearly formulated. This was the consequence of a phenomenon typical of the appearance and development of new domains, which later proved to be of revolutionary importance for mankind, that is the very rapid, even explosive formation of a theoretical conception starting from a great amount of fresh knowledge and also the restructuring of quite a number of conceptions, which theoretically reflected this knowledge.[1] Much was said about the term "biotechnology" which essentially defined the trend emerging from the junction of the traditional chemical technology with the useful application of the biosystems, by the exploitation of an already known, insufficiently studied process – bioconversion – but, unfortunately, on certain occasions, accuracy was overlooked.[2]

Nowadays, we are talking about the practical origins of biotechnology associated to the area of immobilized enzymes, about the theoretical bases related to biology and to molecular genetics and, finally, we are dealing with artificial systems of gene synthesis and we continue to state, with the naïveté of the beginning, that this is one of the most fascinating domains of biology. It is as if we said that we are dealing with one of the most fascinating domains of chemistry, of computed techniques, of electronics, of immunochemistry, a.s.o.

Today's biotechnology, with its practical results in multiple bioindustries is a technological science characterized by the use of biosystems (enzymes, polyenzymatic systems, organelles, immobilized cells, associations of populations, etc.) as conversion agents for the obtaining of useful products.

From this viewpoint, biotechnology, with its amazing results, is not new. Practically speaking, it is impressively old and we may talk about a stage based on intuition and human practice as in the case of domestic animal and plant selection, for instance.

At present, biotechnology represents a revolution owing to a new theoretical, scientific and technological conception in this domain.

In this respect, of great importance is the stabilization of the tendencies characterized by the thorough theoretical study of the practical bases of the phenomenon consisting in the promotion of biotechnologies. In 1978, The European Federation of Biotechnology was created, a body whose goal is the unification of all research endeavours in this field and the promotion of a unitary theoretical conception based on the knowledge and application of the fundamental principles of biotechnology.[1] First of all, mention should be made that biotechnology belongs both to chemical technology (better said to that of organic synthesis) because of the industrial equipment it needs, and to biology, owing to the biosystems used as conversion agents. Anyway, some of the biosystems (the enzymes for instance) are indirectly related to biology and closely linked to biochemistry.

The application of the polyenzymatic systems, organelles or microbial populations, is, strictly speaking, the result of the intensive application of biochemistry and of molecular biology. Its position acquires a great importance in areas where it was not highly considered,[1,3] namely taxonomy and evolution. The identification of the exact position of a microbial conversion agent in a system for instance, and the determination (by biochemical means) of its metabolic evolution is of huge practical importance, representing a genuine biological item that belongs to biotechnology.

The obtainment of a monoclonal antigen is a preoccupation of immunochemistry; the creation, by the recombinant DNA technique of a synthesis biosystem for a protein fragment consists of a sequence of biochemical activities which deal only generally with the aspects of biology proper. It is a paradoxical characteristic of biotechnology : the handling of the most intimate properties of biosystems also means the thorough application of the most typical methods of biochemistry, and of molecular biology. This is the secret as well as the strength of biotechnology. The thorough application of chemical methods determined the appearance of the technology of biosystems and, on the basis of chemical equipment, the huge progress in the computer area could be associated to the above mentioned technology.[1-3] The computer was associated to biotechnology with the help of chemistry which imposed its accuracy. Biotechnology is based on molecular biology or on molecular genetics, that is the biochemistry of the genetic material and the static (compositional) or dynamic (metabolic) biochemistry of living structures. All these facts show the evolution of this domain, its future possibilities, its main course of development and make us understand the necessity for placing biotechnology within the framework of chemical research, whether it is organic chemistry, farmaceutical chemistry foodstuff chemistry, or agricultural chemistry.

Highly trained biologists and geneticians also make contributions of great importance. Nowadays, integrated units of research production-marketing dealing with biotechnology have been founded worldwide. Their importance is so great that certain UN specialized bodies, as for instance FAO, UNESCO and WHO, are engaged in the achievement of some programmes of research and application of biotechnologies.[1] Many of the most critical problems of mankind like famine, health, environmental protection etc. could be solved with the help of biotechnology. This up-to-date and efficient approach to these problems augments research activities in the respective domain, and stimulates achievement of the industrial capacities.

Thus, in the U.S.A. and in the west-European countries many private associations have been created, yet there is a certain drawback typical of the impact of these technologies with the existing social structures. Legal, economic, military, social, ecological complications have cropped up. The solving of these problems requires a great attention and implies a great responsibility, because of the consequences of handling such complex and uncertain systems as the biosystems are. That is why many programmes of international cooperation have been created to support and manage the industrial application of biotechnological processes.

The Bucharest Institute of Chemical and Biochemical Energetics (IECB), and implicitly Romania, is the beneficiary of a UNDP programme, called "Chemical Products from the Biomass". This programme has enhanced the scientific and technical contribution to approaching a prioritary field — the obtainment of chemicals from the biomass, thus ensuring a real basis for continuing the research activity, both by providing new fundamental research directions and by the implementation of biotechnologies developed in production plants. The results of such an activity are highly useful. We are willing to take part in such scientific cooperation activities in the future, too. Many research institutes of chemistry, biology, health protection, agriculture and alimentation participate in carrying out important researches in the socialist countries within the priority direction of "Speeding up biotechnological development in the framework of the CMEA-member countries' programme of techno-scientific cooperation up to the year 2000".

Unlike the initial image characterized by spontaneity and unpredictability, the concept of biotechnological achievement has emerged in our social system given that fundamental and applied research are coordinated by the state with the help of highly competent Romanian men of science, and especially with the help of Academician doctor engineer Elena Ceaușescu, President of the National Council for Science and Education.

In Romania, the state and party leadership attaches a great importance to biotechnology. As a state problem, it develops according to the unique plan of research and development and, in its turn, it is integrated into the general efforts of the CMEA member-countries. From this viewpoint, many institutions and institutes coordinated by the National Council for Science and Technology cooperate with similar bodies in other socialist countries. All these show the important part played by biotechnology and the necessity for its accelerated development in a highly organized framework subordinated to the highest concern of our society — man.

The President of the Socialist Republic of Romania, Nicolae Ceaușescu, has often insisted on the need for a better cooperation among research activities, on the interconnection between theoretical and practical training of students. This phenomenon was very clearly devined as proved by the technological development worldwide and which is valid for the biotechnological science and engineering as well.

EXPANSION OF THE RAW MATERIAL BASIS FOR THE CHEMICAL INDUSTRY

The main problem of any production process is, first of all, that of obtaining the necessary feedstock, because, many times, the production processes become highly economical, were faced with the exhaustion of the national feedstock. Such situations are unavoidable under the conditions of accelerated technical-scientific progress, which lay at the basis of the most dynamic economic and social development in the history of mankind. The discrepancy between the limited nature of resources and the unlimited capacity of industrial development has led to this deadlock, which has to be overcome by means of new solutions. Such solutions can be dialectically derived from an infinitely generous element, knowledge. Only thus can our efforts be oriented towards a continuous, sure and efficient economic development.

A critical analysis of the factors which give birth to all the new materials of industrial importance has shown that, of all the feedstock-generating factors, the most mobile, efficient and rapid are the biogenes. Even in the case of ores, as for instance the phosphates, the iron ores (paludous ones) etc., the formation is impressive as to purity, concentration, rapidity and efficiency, if the process is compared to a strictly geochemical one.

This fact shows that it is high time we undestood the formation mechanism of certain raw materials, we stopped being the passive beneficiaries of the natural processes, we began taking part in the great natural economy, we competently and wisely directed the major biochemical cycles; it is high time we changed our environment into a place where everything rational is possible, without any existentialist impossibilites.

It is true that the decrease of the traditional basis of raw materials was the characteristic feature of the last decades, especially 1950—1970, but, at the same time, an unconventional extension of this basis by processes of high economic efficiency represented by biotechnologies manifested itself.[4,5] Many processes of this kind have appeared which have emphasized the value of phenomena considered as uneconomical. Let us compare the classical energointensive metallurgy to the bacterial metallurgy, which, at present, recovers many of the deficient elements not only in the already exploited poor ores, but also in the depositions resulted from rich ores transformation. The geological prospecting itself benefits nowadays from the advantages of the application of the biotechnological concepts. As is well known, above certain ores, an absolutely specific flora grows, by which the ores are easily recognizable.

The biosystem represents a huge force which secures a rich raw material basis, starting even from modest natural conditions. Therefore, the notion of raw material has to be reconsidered from the viewpoint of the efficient exploitation imposed by the application of the biotechnological processes. Besides this quite passive criterion, the active aspect of the possible formation of certain raw materials by means of biotechnologies has to be considered. The accelerated formation of certain kinds of biomass, made of compounds of great importance for certain industrial branches, is one of those directions whose development has merely begun. An example would be the exploitation of certain vegetal species which produce organic substances (certain alkaloids) constituting the raw materials for highly valuable industries.[4] The increase of the content of these products is a typical biotechnological problem. There is also the problem of the bioformation of certain compounds which have never appeared in a biosystem[3] until now, and such compounds with very complicated structures, whose chemical synthesis would imply several costly stages, are formed with the consumption of the most common raw materials and energies, namely water, carbon dioxide and solar light and with the accumulation of "residues" which are not inconvenient but desirable : oxygen and non-toxic organic matter from which many useful products can be derived.

The bioenergetic crops represent a great promise for obtaining hydrocarbons as they ensure a renewable and practically inexhaustible raw materials basis.

The most important associate of biotechnology is the domain of raw materials, the material side of life (of the biosystems), namely the biomass. From the point of view of its fundamental features, the biomass has properties that make it the most important source of raw materials for the future. Here are some of these properties :

a. The biomass occurs in large quantities compatible with industrial exploitation.
b. It involves very low expenses.
c. It is selfregenerating.
d. It does not imply environmental protection and its genesis is not polluting.
e. The formation of the biomass proceeds from unconventional energetic forms, therefore without exhausting the already limited reserves of fossil fuel.
f. The biomass embodies very big energies which could not be stored otherwise.
g. The biomass may lead to highly valuable products (alcohols, proteins, sugars, fats, hydrocarbons a.s.o.) by the application of controlled conversion technologies without a special financial effort.
h. The biomass is an inexhaustible source of fuels whose intermediates are methanol and ethanol.
i. The processing of the biomass by certain technologies is not inconsistent with our industrial experience.[2]

According to its origin, the biomass falls into the following three main categories : microbial biomass, vegetal biomass and animal biomass. Each of these three categories has many applications. The vegetal biomass is very abundant, is formed by biosynthesis and incorporates the solar energy received by our planet, in the form of certain compounds (cellulose, for instance). The protein content is smaller than in the case of the animal biomass. At the same time, the circulation of the constituent matter is slower. The exploitation of the energetic vegetal biomass involves certain inconveniencies, as for instance : a) the reduction of the surfaces necessary to obtaining agricultural foodstuffs ; this may be recovered by the higher quality of the crops secured by highly efficient cross-breedings obtained by improvement and by genetic engineering ; b) in the beginning, the production has a random character and c) it needs fertilizers, watering and pedologic improvement.[5] But these disadvantages derived from the material quality of the biomass are unimportant as compared to the advantages it offers.

All the programmes elaborated for the period up to the year 2,000 and the next millennium, such as : the CMEA Programme, the U.S.A. and Japan Programme, the Eureika Programme of Western Europe pay great attention to the economic development on the basis of new biotechnologies of high productive capacity and efficiency.

This interest is well illustrated by the national programme and strategies concerning the biomass, existing in the developed countries as well as in the developing and underdeveloped ones where these programmes represent an economic alternative.[5] Therefore, in 1979, the USA invested $ 40 million, quite a modest sum, for the research, for production and controlled conversion of the biomass. If only 10% of the existing surface were assigned to the energetic agriculture, it would be possible to obtain electric power, ammonia, methanol, ethanol, gas fuels with average caloric value and other raw materials and energy forms.

Canada is considering the replacement of up to 42% of the existing transportation fuels with methanol, by 2,025. Australia has a long-term plan for the selection of plants with a high-energy yield and continuous harvesting (eucalyptus, manioc, hibiscus, elephant grass and sugar cane). New Zeeland is interested in the fuel alcohols (methanol and ethanol) from wood (pine) and in the organic fermentation gas (maize and savoy). Brasil is already known for its PNA (Pro-alcohol) programme which has started in 1975, and in 1977 had already determined the replacement of 20% of the fuel gasoline by the energy potential of the sugar cane, manioc and sweet sorghum.

In 1977, China already had 4,700,000 biogas units. This reflects the turning to good account of two very important elements : the tradition of biogas production and application and the intensive research activity. Better said, it is a question of the results with a very good theoretical and practical basis, in a country of great possibilities. Under these conditions, mention must be made that in Romania we are not only interested in this domain but we have also obtained remarkable results. In this country, a method and an equipment were developed for obtaining the biogas at the Institute of Research for the Treatment of Waste Waters (ICPEAR) resulting in the removal of very polluting waste waters, as for instance those from the live-stock farms or the turning to good account of waters with a high organic content, as for instance those from the food industry and the town waste waters. Conceived for the turning to good account of a great number of organic resources, the process may extend rapidly. The equipment is entirely original, being built from domestic materials and by our own means and represents an undisputed Romanian achievement requested for exportation.

India and the Philippines also announced their national programmes of making use of the rapid growing, nitrogen-fixing trees, *Casuarina* and *Leucaena acidophila*, respectively.

Europe is especially interested in fast-growing species of softwood (*Salix* and *Populus*). In this respect, an extensive research activity has been developed in Romania and remarkable results have been obtained with energetic cultures. At the Institute for Agrosylvicultural Research — Bucharest (ICAS) many studies were done for the selection of fast-growing species of trees, especially *Populus* and also *Paulownia tomentosa*), for which pulp forming rates 20 times bigger than those of the natural process have been obtained. This is not the only example of a research work that led to a biotechnology with high performances and indisputable economic effects. The increase of the pulp forming rate determines a decrease of the lignin content which represents a great advantage for this type of energetic biomass, because the pulp is more easily accesible to enzymatic hydrolysis. Even if this biomass from fast-growing wood species vere processed by gasifying, the economic advantage would be very great. Considering all the elements of the turning to good account of the fast-growing forest biomass illustrated by the results and research activity of the Institute for Forest Research and Improvements (ICAS) and the Institute for Chemical and Biochemical Energetics (IECB), the best strategy is the exploitation by gasifying. This fact is also proved by the results obtained in other countries with a much greater experience in this domain, and shows the high value of the studies done by our specialists, who, with by far more modest means, have obtained the same results like other specialists who work with the most up-to-date equipment.

Sometimes, in certain geographical areas, such as Sahel for instance, this seems to be the only economic alternative.

The photochemical bioconversion leads to the obtainment of a quantity of biomass 10 times bigger than the world energy needs. The exploitation of the biomass means therefore the exploitation of its power content. Considering that the volume of the existing fossil fuel reserves is equal to the volume of the existing wood biomass and that by intensive treatment, this biomass volume may increase 10 times, it is obvious that the directions of research established in accordance with the national programmes and strategies have a very realistic basis. At present, photosynthesis generates fuels (oil, petroleum, natural gas, wood), food, fibres and other chemical products. In the future, the photosynthetic process will probably be used stagwise and some biomimetic systems will be developed. Water photolysis may provide the best and cleanest fuel known hydrogen. The second stage, the reduction of carbon dioxide followed by the formation of sugars, already leads to a series of useful applications. For the time being it is hindered by the consecutive process of sugar polycondensation giving birth to macromolecular products among which glucides have a lower reactivity.

The water biomass has great prospects, too. The Institute of Biological Sciences from Bucharest harvested *Pistia*, rich in proteins, vitamins and mineral salts for fodder, for obtaining some valuable pigments — chlorophil and betacaroten, fighting environment pollution by the biological treatment of waste waters from towns and animal breeding.

The microbial biomass is also important, some types of such biomass being already produced in big tonnage. This is the case of the so-called single cell proteins (i.e. products with a very high proteic concentration resulted from the metabolic activity of microorganisms (bacteria and fodder yeasts) [1] that tend to become the most important raw material for obtaining some concentrates of aminoacids, monosaccharides, lipids, vitamins, etc., i.e. of some foodstuffs of great complexity, very easily assimilable and with a very high nutritive value.[7] An important aspect of using the microbial biomass (bacterial, levuric, fungic, etc.) is the possibility that this biomass for fodder or food use originates from integrated biotechnologies or even from some manufacturing processes as secondary products. This is the case of the micelia resulted from the manufacturing of antibiotics, of the residual yeasts from the alcoholic fermentation, of the bacterial mass which helped to the synthesis of some organic polymers, etc. Thus, in Romania they are operating a large plant for manufacturing fodder yeast from *n*-alkanes at Curtea de Argeş, as well as many smaller plan tspertaining to different cellulose manufacturing combines. Researches and achievements in this field have been obtained by the institutes of the Academy of Agricultural and Forestry Sciences viz, the Institute of Biology and Animal Nutrition, Baloteşti, where they are concerned mainly with increasing the nutritive value of some fodders (straws) by enriching them with microbial biomass and, implicitly, with fodder protein. At the same time, at the Institute for Chemical and Biochemical Energetics (IECB), the conversion of hemicelluloses from the sewage lye into fodder protein is studied in a pilot plant, which is going to operate within the Cellulose, Paper and Synthetic Fibers Plant — Brăila, in the Fibers Section, which coordinates this research work. Still at IECB, intense research work is carried on in the field of the enzymatic hydrolysis of the cellulosic, lignocellulosic and hemicellulosic materials, as well as in the technology of alcoholic fermentation with living cells of immobilized yeasts. In this way, the overall yield of the alcoholic fermentation reaches the theoretical figure, the retention time of the bioreactor (column type) is reduced very much and the productivity increases significantly compared with the classical processes. The Institute for Food Chemistry has similar preoccupations and results along with other remarkable technological achievements. Among these, the biotechnology of enzymatic conversion of glucose from glucosic syrups into fructose is of the greatest interest. This very modern technology uses glucosizomerase as a bioconversion agent, namely an enzyme for whose induction they use the sylosic concentrates obtained as microproduction within the IECB biotechnology laboratory. The melioration of the strains increases the yield of bioprocesses. In the same direction, they investigate some single cell algae and several other biomass categories. The algae biomass type has very interesting elements which make its exploitation very promising in the future. It is possible to obtain many useful products by biotechnological practice, as in Japan, where certain algae are used as foodstuff, in the manufacturing of drugs, the obtainment of ores concentrates, etc. The manufacturing of chemicals from algae is a field with most current applications, because it implies, among other things, the possibility of a profitable exploitation of oceans. In this respect, valuable results were achieved in the production of some microalgae like *Spirulina* at IECB, at the Institute of Biological Sciences and at the University of Cluj-Napoca, as well as at other institutes. This fact proves the good orientation of our specialists, their continuous preoccupation to meet the needs of the national economy and especially their ability to solve the complex aspects which are facing science in this revolutionary age of biotechnologies. The biomass is, indeed, the key to break the present deadlock of the narrowing of the raw materials basis of different industries, and mainly of the chemical one. That is why it is absolutely necessary to reconsider the possibility of exploring it. Many countries and especially the developed ones have undestood this requirement of the present world and have made enormous investments in their research programmes in this field.

In our national economy certain categories of biomass play a capital role and require nation-wide efforts for turning to good account the vegetal and animal biomass. The animal biomass produced by animal husbandry can take advantage of the progress made by biotechnology. In this respect, the specialized institute, IBNA—Baloteşti, has scored good results and has found efficient practical solutions. Still the demand for fodder protein is growing continuously due to the need to increase the production of meat, eggs, etc., namely animal biomass which has most important implications for the quality of human life. For this reason, the concentration and orientation of the efforts of specialists from other institutes, and especially from IECB, towards a national programme of speeding up the application of some biotechnologies for the conversion of the cellulosic vegetal biomass into fodder proteic biomass would be a decisive step in the direction of solving this very actual practical problem. Such an effort would also imply the finding of solutions in some other top biotechnology fields like the obtaining of protoplasts, which have an extraordinary importance for plant culture, animal breeding, the antibiotics industry, etc. In this direction, some institutes like the Institute of Biology and the Institute for Chemico-Pharmaceutical Research obtained a series of promising successes. The research on the monoclonal antibodies developed rapidly and in a short time they became the basis of a very profitable production of higher means of diagnosis and treatment in many diseases which imply an immune response, mainly of the human body. This type of biotechnologies is very widely spread and it continues to expand.

Very important as a raw material for biotechnologies is oil, a metamorphic fossil biomass. Lately, it has become a highly appreciated raw material for obtaining some single cell proteins, by using *n*-paraffins as a carbon resource by a *Candida* stem (named *Candida paraffinica* for this reason). The use of paraffins as raw material has a great importance for this country, and a plant of this type was built at Curtea de Argeş.

The synthesis of hydrocarbons starting from the biomass is just as interesting. There exists a very intense synthesis of alkenes in some algae (*Botryococcus braunii*, from 15 to 17% of the dry weight)[1] and in some superior plants (cabbage, *Equisetum arvense*—horse tail). This category also includes the production of oleaginous plants, the oil of some of them having 50% higher fat acids (alkenes with one hydrogen atom — one from 36 for $C_{16}H_{33}$—COOH— substituted for a COOH group) as is the case of rape-oil, and represent a very appreciated Diesel fuel. If we add the conversion of alcohols into the corresponding alkenes, the way from the biomass to the petrochemical industry is paved.[2]

MICROORGANISMS – THE BASIS OF SOME HIGH PERFORMANCE BIOTECHNOLOGIES

Microorganisms have played and will play a special role in the development of biotechnologies. They are some of the most efficient bioconversion agents known and their use brings about the following big advantages : a) a very rapid sequence of the generations, providing a very rapid growth and big productions per time unit (reduced retention time); b) very modest living conditions, namely, relatively simple installations and unpretentious culture media, so that no special investments are needed; c) the transformation of a great number of substrates, which means the turning into account of many substrates, i.e. of all the usable compounds; d) very big possibilities of controlling the metabolic processes, that is a good control of bioproducts; e) stability and relatively easy to operate variability, namely the possibility of obtaining the best bioconversion agents looked for ;f) very diverse genetic structures (both pro- and eu-kariots) namely the possibility to operate both with inferior and superior bioconversion agents.

There are, of course, certain disadvantages but they are mastered by quite a vast experience which tends to neutralize them. From a chronological point of view, the oldest application of using microorganisms consists in the different types of fermentation. Some of them induced real revolutions in human nutrition — as in the case of bakery which marked a huge step forward along with the yeasting of dough.

The most important fields which took advantage of the use of microorganisms as instruments of some biotechnologies were usually associated with the food industry, which has developed a series of fermentations with a great nutritive value, such as : a) alcoholic fermentation resulting in very valuable primary products, eg, wine and beer; acetic fermentation yielding the acetic acid; c) citric fermentation; d) lactic fermentation leading to borsch, pickles, etc.; e) fermentation of cheese.

The experience showed that one can obtain high quality products in large amounts and at low costs only with microorganisms with high fermentative capacities. For a long time, microorganisms were obtained exclusively by natural selection so that this field advanced very slowly and the raw materials were somewhat limited. There are some fields of activity which traditionally were considered to have no connection with the use of microorganisms. They were recognized as important but things did not go further. Such a field was medicine which recognized the role of some microbial patogenes, but things remained in the same stage for a long time. The discovery of microbial antagonisms has sharply changed the situation. Nowadays, the production of antibiotics is absolutely indispensable to the medical practice. The incomes obtained in this way by many developed countries make up more that 60% of the incomes resulted from biotechnological practice. The application of some top techniques, like recombinant-DNA, brought medicine the new and very big advantages of using microorganisms. The microbial synthesis of insuline or of the human growth hormone are only two of the best known biotechnological industrial achievements. Finally, there are some domains such as pedology and, through it, agriculture, which have recognized the importance of microorganisms for soil formation and evolution, but for a long time they could not go beyond this stage. Nowadays, such a situation belongs to the past. The coming into use of microbial fertilizers is only one of the most modern and efficient aspects of applying microorganisms in agriculture. But this is not the only one. Like in the field of medicine, the practice of recombinant-DNA technique opens most attractive perspectives. The transfer of nitrogen-fixing genes (NIF genes) towards certain culture plants makes possible the tremendous increase of the production of most basic crops. Such preoccupations focus the interest of some prestigious institutes such as the Institute for Biological Sciences and the Institute for Cereals and Technical Plants-Fundulea, where this topic has been studied for a long time now.

The improvement of microorganism strains, the development of installations specific to bioprocesses, the development of the fermentative raw materials basis, the use of some new separation and purification processes of biosynthesis products, the carrying out of fermentation via new metabolic ways made this field — usually associated with the oldest domestic traditions — become one of the most up-to-date domains of biotechnology.

Highly developed nations which do not have a rich raw materials basis, like Japan, obtain a great part of their national gross product due to the fermentative industry and they solve a great part of a difficult food supply problem this way. Most difficult problems of mankind, such as the energy crisis and the increasing lack of nutritive proteins makes more and more actual the need for using biotechnologies of conversion of the fermentescible sugars into proteic fodder or edible biomass. The same sugars can become the substrate for an alcoholic fermentation which results in a substitute for gasoline used as fuel in the engines with internal combustion. A substitution of gasoline of up to 20% does not require constructive modifications of the engines so that the solution can be applied (and many countries do so already). There is a perspective of converting these fermentation alcohols into hydrocarbons and, generally speaking, into petrochemical type products.[3]

This trend, although at the beginning, is not only promising but also in an advanced stage of implementation. Within IECB, the catalytic conversion of some alcohols (for the moment, of methanol and ethanol) into olefins is not only a research direction but also a material achievement. There are already some industrial pilots in which the conversion into olefins is carried out with good yields and as soon as the corresponding microorganisms for obtaining new alcohols are found, new qualities of alcohols can be produced. This is a route that can be discussed. Even the negative elements of microorganisms — the patogene microorganisms — ended up by being attenuated and used. They were dealt with by a very prodigious branch of the pharmaceutical industry — the industry of sera and vaccins (brilliantly representated in Romania by the "I. Cantacuzino" and "L. Pasteur" institutes) and the industry of antibiotics (with large capacity units like the Enterprise of Antibiotics, Iași, "Terapia", Cluj-Napoca, etc.). The Romanian-made products are of good quality they are competitive and are well exported. The fact should be mentioned that it is possible to increase the production capacities under the quality requirements of the most severe international standards due to the activity of the specialised institute — the Institute for Chemico-Pharmaceutical Research, which is endowed with a rich material basis and has a very rich collection of microorganisms useful for medical purposes. These achievements make us consider that Romania can have even more important developments in the biotechnological, biomedical research and production, such as the obtainment of monoclonal antibodies.

Another direction in which the microbiological industry could have good results is in the preparation of pigments (for instance, carotenoids) and of edible dyestuffs. Such an example is provided by the various red shade dyestuffs produced by the fungus *Monascus purpureus*.[1] But less known is the role played by all these dyestuffs. Many of them act as antibiotics, too. Thus, biotechnologies become possible which produce nontoxic edible dyestuffs and have the capacity to provide the sterility of foodstuff without any treatment that would diminish the nutritive properties (some treatments can even lead to undesired compounds).[2]

This list of useful products synthesized by microorganisms is very long. Still, from among the possible and applicable biotechnologies, some come into evidence due to their great importance, being actually fields of activity. The synthesis of some organic polymers, of the biopolymers is such a field. Out of these, the synthesis of microbial polysaccharides (of the *Xantan* type, produced by the *Xantomonas bacteria*) has a great importance for many domains. The synthesis of polyhydroxybutirate, a bacterial product too, is also very important (this is a reserve product) as it has many industrial applications (in biotechnology, in the organic industry, in medicine, etc.).[2]

Widely discussed lately, the process of biogas production is one of the most important biotechnologies whose development is based on the activity of some microorganisms.

The bacteria used to enhance the secondary recovery of oil from some deposits should be considered as implication in the energetics of fuels, as well. These bacterial populations, together with a corresponding amount of medium are injected into the deposits where they contribute to the formation of some gaseous products that exercise a certain pressure on the deposit, making thus possible to obtain new oil quantities.

Such processes are experimented in four oil fields in Romania, with promising results. The Institute for Biological Sciences and the Institute for Oil and Gas from Cîmpina have scored important results in this field by cooperating with the USSR, the USA and the United Kingdom. Important results in bacterial extraction processes e.g. the extraction of copper from poor, ores, were achieved by the Institute for Biological Sciences and the Institute of Research for Nonferrous Ores from Baia-Mare in collaboration with universities from West Germany.

But the most spectacular application of the microbial metabolism is in the preparation of hormones (especially of the peptidic ones) and of enzymes. Some hormones, like the human growth hormone and insuline, can be prepared by using the recombinant-DNA.[3] The biotechnologies of obtaining enzymatic preparations of microbial origin are very important. At this moment, the beer industry, the milk industry and the industry of meat products cannot be conceived without the use of enzymatic concentrates. The specialized unit, the Institute for Food Chemistry, has many wellknown achievements. Of particular interest is the substitution of indigenous products for imported ones. Thus, the initiative taken by IECB to produce catalase for the milk industry should be extended to other products of this type. This case is not unique, as many other institutes are making efforts to put microorganisms to work.

These preparations are impressively varied. Moreover, due to the possibility of obtaining large amounts of enzymes by using microorganisms as producers, the use of enzymatic preparations is in full swing and we are faced now with the use of immobilized enzymes, which is considered to be the most important moment of industrial enzymology.[3,6] The immobilization of enzymes is a trend that has been manifest a long time ago. But the enzymes could not be produced in big quantities, but once this problem solved, every thing could be reconsidered. A great surprise was the fact that even the enzymatic immobilization existing in the microbial cells could be used. Thus, the dead cells of some *actinomicetes* have acted for a long time as immobilized enzymes, in the case of a certain enzyme (glucosoisomerase).[7] A similar situation can occur in the case of certain organelles which continue to work in some yeast cells practically killed by the destruction of the cell membrane, by adding some solvents that extract the lipids from the semipermeable cell membrane, with a lipoproteic structure.[2]

The immobilized preparations obtained in this country represent theoretical and practical successes of our specialized institutes (ICCF, ISBB, IECB and ICA), a strong direction for the development of biotechnology. In this respect, the capacity of adjusting the chemical industry production to the requirements for adequate carriers is of the greatest importance. Going along this rather uneasy way, the Institute of Macromolecular Chemistry "Petru Poni", Iași, succeeded to go beyond the stage of lab investigations in the immobilization of some biopreparations and score many achievements.

Just as spectacular is the immobilization of some cells or special types of cells, too, as their industrial use tends to develop high performance biotechnologies.

GENETIC ENGINEERING – A DETERMINANT FACTOR OF BIOTECHNOLOGICAL DEVELOPMENT

Genetic engineering appeared as a consequence of the development of the knowledge of the structure of the genetic material; nucleic acids and associated proteins (such as hystones).

At the same time, with the progress of knowledge acquired by specialized biochemical investigations, new data have emerged on the structure and physiology of the nucleic acids as well as on the current techniques for their manipulations. Thus, separations of some morphophysiological units, like the genes, has become possible.

Simultaneously, the enzymes characteristic of gene physiology are isolated and the way they act is characterized. So *in vitro* models appear in which gene physiology is reproduced and very important phenomena like the restriction and the modification are modelled.[3] Taking such physiological processes out of the cell space and their development under controlled conditions made possible their orientation in other directions than the ones in which they had evolved in nature. Thus, starting from the observation that a chromosome can divide into fragments in a natural way, at the level of the link between two neighbouring genes, one can see that, still in a natural way, the mending of such a break-up is possible, on condition that the two ends that must be linked be correspondingly complementary. From this observation to the substitution of another gene for the broken one, which should encode the synthesis of a compound of great interest for us, there was only one more step to be taken. The technology of recombinant-DNA was immediately applied in practice, with most important economic consequences.[4] By this route, it was possible to achieve the biosynthesis of the human growth hormone in large quantities and at low prices, using the traditional equipment of the fermentation industry, that is without any extra investments. The only important investment was the research activity. Such a situation is characteristic for the way in which the biotechnology becomes a means, of material progress due to the force of the ideas created by research work. This first success has allowed us to believe that more ample genetic reprogramming solutions will be reached in future. [3]

These techniques of genetic reprogramming belong to the future but, at the same time, they are already proved possibilities. In this direction, certain genetic manipulations were carried out, which are not strictly genetic engineering acts, resulting in most encouraging results, promptly applied in practice, such as the technique of protoplasts fusion.[3] This originates in the observation that the removing of the cell wall, by digestion with cellulase and pectinase, releases the cell content in the form of a whole named protoplast. This tends to remake its cell wall, but till the building of a new wall, such protoplasts exhibit the phenomenon of fusion, consisting in the uniting of two or more such formations, resulting in one alone. This unique formation will have a double, triple, etc. genome, thus being polyploid, tetra-, hexa-, etc. respectively, or generally speaking, polyploid. It is well known that the polyploid bodies have much higher characteristics compared with the diploid ones, which makes up a very solid basis for increasing the production of culture crops. For this reason the process is largely used and, consequently, it is considered a solid means of increasing the biomass production in future. Its association with a judicious selection has already led to very useful results. Of course, there are still many aspects to be studied, but they are of the greatest utility. It is very important to emphasize the fact that this lab scale achievement and then its implementation on a large industrial level corresponds to some proven natural principles. Thus, it is well known that polyploidy is one of the natural means of adjusting plants, the inferior ones — gymnosperms — and the higher ones — the angiosperms — making use of it in proportion of 46% and 47%, respectively. So, we follow the natural route of mobilization of plant energies and we get associated with the whole evolution potential of the vegetal world in this attempt at increasing our material means.

Many of the qualities of the vegetal products are limited by the characteristics of the species, so that the product with the desired qualities is not always achieved by the simple mixture of products coming from the species which individually produce one of the qualities we expect from a unique product. A producer having all the desired characteristics of a product would be the real solution. This means a hybrid product obtained from a hybrid species coming from individual producers, carriers of the desired characteristics. The answer is positive, again. In nature there is the phenomenon of alopolyploidy, consisting in a natural synthesis of a hybrid genom starting from two or three different genoms. Such an example is wheat (*Triticum aestivum*), the result of the successive addition of the genoms *Aegilops speltoides* and *Aegilops squarrosa* to the *Triticum monococcum* genom. This means that the approach to the fusion of protoplasts belonging to different species has good prospects and will yield good results. From an economical point of view, such a technology leads to the achievement, from the many possible species, of those of a great practical interest, which would probably never occur naturally or perhaps they would, but only after an enormous lapse of time. The fusion of protoplasts proves to be a valuable method of synthesis of higher genoms from which economically efficient phenotypes are derived. In future, this route will be followed by many valuable biotechnological processes such as the one referring to the production of proteic, polysaccharidic, oil-producing, hydrocarbonic, etc. biomass. The practice of techniques based on the achievement of plants starting from protoplasts shortens by about 20 years the time required by the traditional experiments, in the difficult cases. One of the theoretical consequences, out of many, is the fact that this route makes possible the achievement of a fundamental taxonomy founded on the genetic complexity. The study of these laws of genetic compatibility that are valid at the forming of mixed protoplasts will have very important practical consequences for the future biotechnologies.

Finally, another technique of synthesising highly valuable genoms for practice is haploidy by androgenesis, consisting in the germination of pollen grains on adequate media. This way, a special type of embryons — embryoids — are formed which give birth to plants having a genetic material equal with half a genom. In these plants, a phenotype — genotype identity will exist, which means that the selection operations are performed in a single generation. The hybridization taking place in the second generation will lead to homozygot species, also known as isogenic lines. With these species, the characters become practically definitive. Such a procedure has a high economic value and makes up one of the richest reservoirs of the biotechnology of the future. Of no less interest is the practice of selection based on the mutagenesis technique. Although this technique is not a real genetic engineering process, the fact that it is a process that modifies the genom, makes it to be dealt with within the framework of genetic engineering. The method consists in applying some physical mutagenic factors (irradiation, X-rays, ultraviolet radiations, caloric radiations, etc.) or chemical ones (alkylating agents, insertion agents, disaminating agents, agents of homologue substitution, etc.) to a certain genom. The genom will be more or less modified, as a function of the mutagene agent, time and power. Generally speaking, the mutant genoms appear at a lethality of over 50%, their selection leading to the disadvantage that revertants can appear, but there is also the advantage that through its mechanism of a random statistical distribution, the phenomenon is very close to the natural mutagenesis, being superior to it as it proceeds at a higher rate. Moreover, the association of two mutagenous factors applied simultaneously or sequentially leads to a great number of schemes capable of yielding very good results. One should bear in mind that this technique can be much improved and that the very good results obtained so far represent but a small part of its possibilities.

But what makes up the most spectacular process of genetic engineering at the moment seems to be the machines for gene synthesis. They are automated devices for the synthesis of a polynucleotidic chain. Such a device has two very useful elements : it uses the synthesis in an immobilized regime and the synthesis process proceeds under computer control. Otherwise said, the operation requires a knowledge of the amino-acid sequence of the protein and its conversion by means of the genetic code into a polynucleotidic sequence. Started in 1980 (Itakura) this direction is continued today, making a big progress, that opens up practical prospects.

It is evident that biotechnology has become an extremely dynamic field of the technico-scientific activity and that it represents one of the factors promoting the new. For scientists worldwide, biotechnology means, at the same time, a field of active cooperation in the spirit of the lofty and noble ideals of economic and social development, of solving the grave problems facing mankind today — alimentation and famine control, satisfying the energy demand, preventing and controlling some grave diseases, environmental protection.

All researchers and scientists from Romania are willing to actively contribute to this cooperation, to validate by original, concrete contributions the idea that the role of biotechnology in our country is far-reaching. The orientations and directives of our party and state leadership, the important financial effort directed towards biotechnology make up the basis of some promising achievements and developments. For this purpose, we benefit from the guidelenes given by the Secretary General of the Romanian Communist Party, the President of the Socialist Republic of Romania, Nicolae Ceaușescu, who, on the occasion of the Meeting with the workers from agriculture said that : "...we should think of a revolution in genetics in Romania, in order to obtain new species. These problems are facing the whole world and they can and should be solved. Nature has solved them along hundreds of thousands of years, while man, using his knowledge, must solve them in a few years only."

This stimulating and noble appeal is reverberating in the minds of our biotechnologists and they are decided to spare no efforts in attaining the targets set by the National biotechnological research programme.

REFERENCES

A. S ason, "Biotechnology, Challenge and Promises" (Romanian translation), Ed. tehnică, Bucharest, 1988.

[2] M. Zamfir, *Rev. Chim. (București)*, **39**, nos. 1–8 (1988).

[3] * * * "Genetic and Biotechnological Engineering under the Conditions of the New Contemporary Scientifico-Technical Revolution", Mihail Florescu (coord.), Ed. politică, Bucharest, 1988.

[4] * * * "General Report. Events and Achievements in the Chemical Industries". Report I, part 3. The 9th Session of the Comission for Chemical Industries, Geneve, 1988.

[5] * * * "EERG (Energy, Saving, Recycling, Management)", 5, Ed. tehnică, Bucharest, 1988.

[6] * * * "Biology, Biophysics, Biochemistry", Technico-scientific Bulletin, **26**, VI (1988).

[7] * * * "Biological Reactors", Technico-scientific Bulletin, **25**/17, VI (1988).

Revue Roumaine de Chimie, **34**, 2, 477–480 (1989)

REACTION OF *endo*- AND *exo*-BENZOCYCLOBUTENONORBORNAN-7-ONE WITH DIMETHYLOXOSULFONIUM METHYLIDE [1]

AURELIA GHENCIULESCU, LUCIAN ENESCU, FILIP CHIRALEU and ILIE G. DINULESCU
Organic Chemistry Department, Polytechnic Institute TCH, 313, Splaiul Independenţei, 76206 Bucharest, Romania

Received June 8, 1987

The reaction of *endo*- (**1**) and *exo*-benzocyclobutenonorbornan-7-one (**2**) with dimethyloxosulfonium methylide (**5**) yields exclusively the products of *exo* attack, namely the *endo* oxides **9** and **10**, respectively. Ketones **1** and **2** react with ylide **5** in a highly stereoselective manner in comparison with norcamphor (**6**). Furthermore, the reaction opens a convenient route to a number of other polycyclic systems.

As part of our studies concerning the chemistry of polycyclic systems with cyclobutene ring,[2] we reported previously on the behaviour of *endo*- (**1**) and *exo*-benzocyclobutenonorbornan-7-one (**2**) in the course of reactions with nucleophiles.

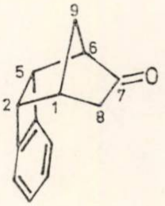

1

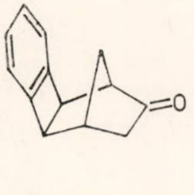

2

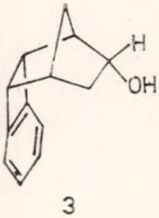

3

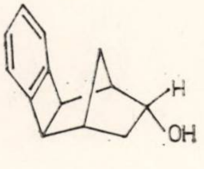

4

It was shown in earlier papers that the reaction of the ketones **1** and **2** with mixed-metal hydrides yields exclusively the *endo*-hydroxy derivatives **3** and **4** respectively.[3] To see if the orientation of the benzocyclobutene ring influences the composition of the product in the reaction with nucleophiles, we studied the reaction of the ketones **1** and **2** with dimethyloxosulfonium methylide (**5**). As known the sulfur ylides react with ketones to yield epoxides.[4]

As reported previously, norcamphor (**6**) reacts with dimethyloxosulfonium methylide (**5**) to give a mixture of 88% *endo* oxide **7**, 10%

exo oxide **8** and 2% unreacted ketone **6**.[5]

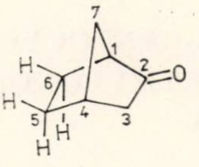

6

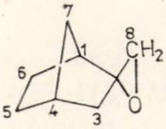

7

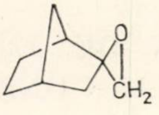

8

Dimethyloxosulfonium methylide (**5**) was prepared using the usual procedure,[4,6] by addition of trimethyloxosulfonium iodide [7] to a stirred suspension of sodium hydride in dimethyl sulfoxide. All experiments were carried out under nitrogen.

The reaction of *endo*-benzocyclobutenonorbornan-7-one (**1**)[3] at 50° with an excess of dimethyloxosulfonium methylide (**5**) in dimethyl sulfoxide afforded a mixture containing the epoxide **9** and unreacted ketone **1**, in a ratio 1 : 2.35, established on the basis of its ^1H-NMR spectrum. The crude mixture was separated by chromatography on alumina column.

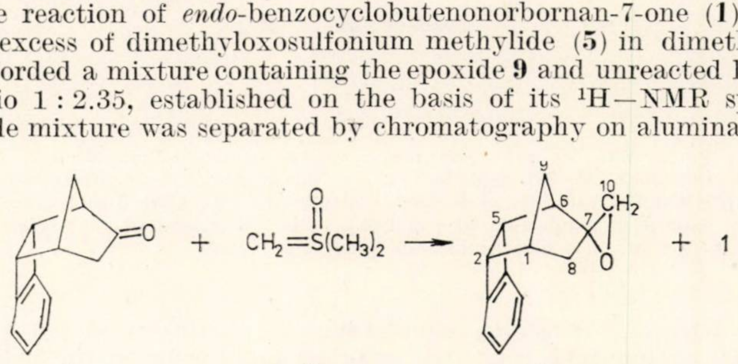

1 5 9

In the reaction of *exo*-benzocyclobutenonorbornan-7-one (**2**)[3] with dimethyloxosulfonium methylide, only the *endo* oxide **10** was obtained.

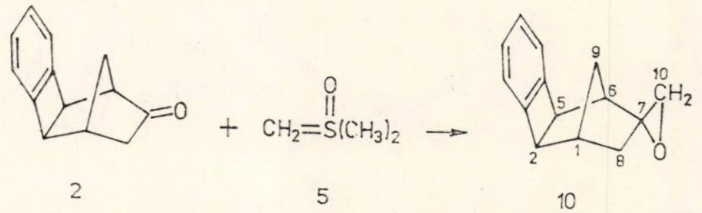

2 5 10

The structures of the epoxides **9** and **10** were ascribed on the basis of analytical and spectral data. Thus, the *endo* orientation of the benzocyclobutene ring in the epoxide **9** was confirmed on the basis of the ^1H-NMR spectral pattern of the benzylic protons H—2 and H—5, which are coupled with the bridgehead protons H—1 and H—6, leading to a complex multiplet.[8] The ^1H-NMR spectrum of the epoxide **9** had complex patterns in the region δ 1.00—2.60 ppm. The structure and stereochemistry for the epoxidic ring are provided by lanthanide induced shift experiment using $Eu(fod)_3 \cdot d_{27}$. The ^1H-NMR spectra of the epoxide **9** displayed significant diamagnetic shifts for protons H—6 and H—8-*endo*, in accordance with the *exo* orientation of the H—10 methylenic protons.

The structure of the epoxide **10** was ascribed on the basis of spectral data and by comparison with the previously described 7-*endo*-substituted *exo*-benzocyclobutenonorbornanes. Thus, the *endo* orientation of the epoxidic oxygen is supported by the ^{1}H—NMR spectrum, namely by the signals of H—2 and H—5 protons which appear as an AB system, at δ 3.40 and 3.80 ppm with $J = 3.50$ Hz.[8] At it is known, in 9-substituted and 7-*exo*-substituted *exo*-benzocyclobutenonorbornanes, the H—2 and H—5 protons exhibit as a sharp singlet, in accordance with the lack of coupling between the benzylic protons of this system and the bridgehead protons.[8]

Furthermore, the ^{1}H—NMR spectrum of the epoxides **9** and **10** showed and AB system due to the slightly nonequivalent epoxidic protons (called H—10 in this paper), in contrast to epoxides of norcamphor (**7** and **8**), which exhibit a singlet for H—8 protons.[5]

According to our expectation, the reaction of dimethyloxosulfonium methylide (**5**) with the ketones **1** and **2**, yielded compounds of *exo* attack, namely the epoxides **9** and **10**, respectively. The remarkable regio-, and stereospecificity of this reaction in comparison with the similar reaction of norcamphor (**6**) may be explained by intervention of steric factors. Thus, in polycyclic ketones such as **1**, **2** or **6**, *exo* attack is favoured,[59'] but more in ketones **1** and **2** than in **6**. On the other hand, the intermediates resulted by *endo* attack, namely **11** and **12**, are disfavoured geometrically, because of the impossibility to perform the geometry necessary for C—S bond assistance at the displacement of the leaving group, *viz* dimethyl sulfoxide, in comparison with intermediates of *exo* attack (for example **13**).

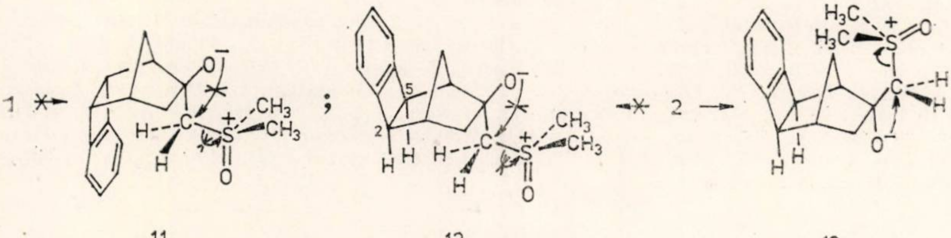

11 12 13

The steric hindrance due to H—5 and H—6 atoms in the intermediate derived from norcamphor is less severe than that due to H—2 and H—5 atoms in the intermediate **12**, which explains the small differences of stereospecificity between the reactions of **1** or **2** and **6**.

EXPERIMENTAL

IR spectra were recorded on a double beam Jena UR—20 spectrophotometer. ^{1}H-NMR spectra were recorded on a Varian EM—3 601 spectrometer using TMS as internal standard. Gas-chromatographic analyses were carried out on a Chromatron gas-chromatograph, using a 1.0 m × 4 mm diameter column filled with 20% methylsilicone SE 30 on Chromosorb W 30—60 mesh, at 220°, and with 30 mL/min hydrogen as carrier gas. *Starting materials.* The ketones 1 and 2 were obtained after the procedures previously described.[3] Dimethyl sulfoxide was distilled from calcium hydride at reduced pressure. Sodium hydride was available as a 80%

dispersion in mineral oil from Fluka AG Chem. Fab. The reactions were carried out under nitrogen in oven-dried apparatus.

The reaction of endo-benzocyclobutenonorbornan-7-one (**1**) *with dimethyloxosulfonium methylide* (**5**). A 80% suspension of sodium hydride in mineral oil (0.4 g, 13 mmoles) was washed with petroleum ether (bp 35°) by decantation. Dry dimethyl sulfoxide (11 mL) was added and the mixture was stirred for 15 min at room temperature, under nitrogen.[4] Trimethyloxosulfonium iodide (2.1 g, 9.54 mmoles) was introduced during 15 min and suspension was stirred and heated for 20 min at 40—50°. When the evolution of hydrogen had ceased, a solution of 1.5 g (8.15 mmoles) ketone **1** in 10 mL dimethyl sulfoxide was added dropwise during 15 min, under nitrogen. The reaction mixture was stirred and heated for 7 hrs at 50°, cooled, poured in 20 mL water and extracted with ether. The ether solution was washed with water, then with saturated aqueous salt solution, dried and the solvent was removed in vacuo, yielding 1.23 g oily product. ^{1}H-NMR spectrometry analysis shows a content of epoxide **9** and ketone **1** in a 1 : 2.35 ratio.

The crude product was separated by column chromatography on neutral alumina (activity II). The first fraction (eluent : petroleum ether-diethyl ether in ratio 5 : 1) afforded 0.39 g (54.2% raported to reacted ketone) pure **9**.

Spiro[endo-benzo[c]tricyclo[4.2.1.0^{2,5}]*nonan-3-en-7,2′-endo-oxacyclopropane*] (**9**), oily.- Anal. $C_{14}H_{14}O$ (198.24) Calcd. : C, 84.81 ; H, 7.11. Found : C, 84.53 ; H, 7.01.-IR (CCl_4, cm^{-1}) : 950, 1190, 1280. — ^{1}H-NMR ($CDCl_3$, δ, ppm) : 1.07 (dd, 1H, H-8-*endo*, $J_{8,8}$ = 14 Hz, $J_{1,8-exo}$ = = 3.6 Hz), 1.76 (dd, 1H, H-8-*exo*, $J_{8,8}$ = 14 Hz, $J_{1,8-exo}$ = 5 Hz), 1.93 (AB system, 2H, H-9-*syn*, H-9-*anti*), 2.01 (m, 1H, H-6), 2.31 (AB system, 1H, H-10, J_{AB} = 5 Hz), 2.58 (m, 1H, H-1), 2.61 (AB system, 1H, H-10, J_{AB} = 5 Hz), 3.72 (m, 2H, H-2, H-5), 6.90—7.30 (m, 4 aromatic H).

Further elution with a mixture of petroleum ether — diethyl ether in ratio 5 : 2 afforded 0.83 g unreacted ketone **1** (44.6% conversion of ketone).

The reaction of exo-benzocyclobutenonorbornan-7-one (**2**) *with dimethyloxosulfonium methylide* (**5**). Working as above, from 1.5 g (8.15 mmoles) ketone **2**, 1.45 g crude product were obtained. The gas-chromatographic analysis of crude product indicated only one compound, which was identified to be the epoxide **10**. The crude epoxide was purified by chromatography on neutral alumina using a mixture of petroleum ether — diethyl ether (1 : 1) as eluent. Removal of the solvent afforded 1.4 g (87.5%) epoxide **10**.

Spiro[exo-benzo[c]tricyclo[4.2.1.0^{2,5}]*nonan-3-en-7,2′-endo-oxacyclopropane*] (**10**), colourless oil. — Anal. $C_{14}H_{14}O$ (198.24) Calcd. : C, 84.81 ; H, 7.11. Found : C, 84.58 ; H, 6.98. -IR (CCl_4, cm^{-1}): 970, 1200, 1290. —^{1}H-NMR ($CDCl_3$, δ, ppm) : 1.01 (AB system, 1H, H-9-*syn*, J = 10 Hz), 1.21 (d, 1H, H-8-*endo*, $J_{8,8}$ = 13 Hz), 1.35 (AB system, 1H, H-9- *anti*, J_{AB} = = 10 Hz), 1.91 (m, 1H, H-6), 1.93 (dd, 1H, H-8-*exo*, $J_{1,8-exo}$ = 5 Hz), 2.38 (m. 1H, H-1), 2.60 (AB system, 1H, H-10, J_{AB} = 5.5 Hz), 2.80 (AB system, 1H, H-10, J_{AB} = 5.5 Hz), 3.40 (AB system, 1H, H-2, J_{AB} = 3.5 Hz), 3.80 (AB system, 1H, H-5, J_{AB} = 3.5 Hz), 6.90—7.03 (m, 4 aromatic H).

REFERENCES

[1] Part LXII in the series "Investigations in the Cyclobutane series". For part LXI see : N. Ştefan, I. G. Dinulescu and M. Avram, *Rev. Roumaine Chim.*, in press.

[2] A. Ghenciulescu, M. D. Gheorghiu, L. Enescu, I. G. Dinulescu and M. Avram, *Rev. Roumaine Chim.*, **29**, 49 (1984) ; L. Enescu, M. D. Gheorghiu, A. Ghenciulescu, I. G. Dinulescu and M. Avram, *Rev. Roumaine Chim.*, **28**, 1001 (1983) and references therein cited.

[3] R. Baker and J. Hudec, *Chem. Comm.*, **1967**, 929 ; R. Baker and T. J. Mason, *J. Chem. Soc. C.*, **1970**, 596.

[4] E. J. Corey and M. Chaykovsky, *J. Amer. Chem. Soc.*, **87**, 1353 (1965).

[5] R. S. Bly, C. M. DuBose, Jr., and G. B. Konizei, *J. Org. Chem.*, **33**, 2188 (1968).

[6] E. J. Corey and M. Chaykovsky, *Org. Synth., Coll. vol. V*, 755 (1973).

[7] R. Kuhn and H. Trischmann, *Liebigs Ann. Chim.*, **611**, 117 (1958).

[8] M. Avram, F. Chiraleu and I. Pogany, *Rev. Roumaine Chim.*, **15**, 1219 (1970).

[9] H. C. Brown and J. Muzzio, *J. Amer. Chem. Soc.*, **88**, 2811 (1966) ; S. Beckmann and R. Mazger, *Chem. Ber.*, **89**, 2738 (1956) ; C. H. DePuy and P. R. Story, *J. Amer. Chem. Soc.*, **82**, 627 (1960) ; N. J. Toivonen, E. Siltanen and K. Ojala, *Ann. Acad. Sci. Fennicae*, *AII*, No. 64 (1955) ; D. C. Kleinfelter and P. Schleyer, *J. Org. Chem.*, **26**, 3740 (1961) ; H. C. Brown, F. S. Chloupek and M-H. Rei, *J. Amer. Chem. Soc.*, **86**, 1246 (1964).

Revue Roumaine de Chimie, **34**, *2*, 481–489 (1989)

^{1}H–NMR SPECTRA OF 5,9-METHANO-5H-BENZO[3,4]CYCLOBUTA[1,2]CYCLOHEPTENE DERIVATIVES[1]

MIRCEA D. GHEORGHIU[a], ANGELA POPESCU[a] and GHEORGHE SURPĂŢEANU[b]

[a] Department of Organic Chemistry, Polytechnic Institute-TCH, 76206 Bucharest-16, Romania

[b] Department of Organic Chemistry, Polytechnic Institute, 71, Splai Bahlui, Iassy, Romania

Received November 29, 1988

The spectral parameters (chemical shifts and coupling constants) of seventeen bicyclo [3.2.1] octene derivatives are reported. The chemical shifts are dependent on the configuration of benzocyclobutane fragment and on substitution at C_7 and C_8. Bridgehead protons couple only with H_{10}^{anti}, while there is no interaction with the methano-bridge proton H_{10}^{syn}. This result was rationalized, with the aid of NMR calculations and Karplus relationship. All vicinal coupling constants and two types of long-range interactions are also reported.

INTRODUCTION

The ^{1}H–NMR spectra analysis of 5,9-methano-5H-benzo[3, 4] cyclobuta[1, 2]cycloheptenes (hereafter called bicyclo[3.2.1]octene derivatives) was initiated independently in 1963 by Moore *et al* [2a] and De Selms *et al* [2b], and extended in 1976 by Winstein et al[3]. One year later, Jefford and Ramey [4] published a thorough analysis of the ^{1}H–NMR of substituted bycyclo[3.2.1]oct-2-enes. All their findings regarding chemical shifts and especially coupling constants were recognized in many related systems. Such is the case of nonannelated[5], benzo-[6] or dibenzoannelated derivatives [7] of bicyclo[3.2.1]oct-2-ene. As expected, coupling constants magnitude is especially very powerful in assigning unequivocally the stereochemistry of substituted bicyclo[3.2.1]-octenes. In addition to vicinal coupling constants, long-range interactions were recognized as conspicuous for the bicyclo[3.2.1]octene skeleton.

In the present paper we intend to provide new examples from the up to now unexplored class of *endo*- and *exo*-benzocyclobuta annelated to bicyclo[3.2.1]octene skeleton [8]. Our results are in close agreement with Jefford's findings[4], pointing out that indeed, the spectral parameters of the parent system are preserved in the annelated bicyclo[3.2.1]octenes. We shall also provide experimental evidence for some of the earlier assignments resulted from analogies with related structures [2–4]. Finally, from the dihedral angles resulted from MM-2 calculations, with the aid of the

Karplus type equations, the pattern of the methano-protons ^1H-NMR signals (H_{10}^{syn} and H_{10}^{anti}) is now uncovered. All spectra were recorded at 60 MHz and only occasionally at 400 MHz.

RESULTS AND DISCUSSION

A. Chemical shifts

We have summarized our results in Table 1, where the chemical shifts of the *exo*- and *endo*-benzocyclobutabicyclooctenes 1 and 2, respectively, are displayed.

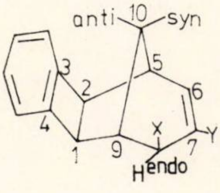

1

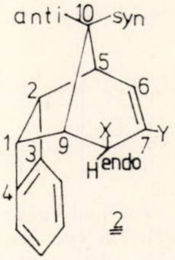

2

	X	Y
a	H	H
b	OH	H
c	OH	Cl
d	$OCOCH_3$	H
e	$OCOCH_3$	Cl
f	Cl	Cl
g	=O	Cl
h	=O	H
i	C_6H_5	Cl

The bridgehead proton signals of H_5 and H_9 are (at 60 MHz) depending on the configuration of the benzocyclobuta fragment, more or less overlapping and only in few cases distinguishable.

However, as for other overlapping signals discussed below, the assignment was very much assisted by europium shift reagents, double resonance experiments and for compounds by the well differentiated spectra obtained at 400 MHz. As a rule, the chemical shifts of bridgehead protons H_5 and H_9 are downfield shifted in the *endo*- isomer relatively to the *exo*-isomer. In the case of the *exo*-benzocyclobuta[3.2.1]octenes, **1** H_5 is more deshielded with approximately0.1 — 0.3 ppm than H_9. However, only in the case of the chloroketone **1g**, as result of the proximity of the shielding region of the ketone group, H_5 is more shielded than H_9 (see fig. 1b)

A spectacular difference in the chemical shifts of the bridgehead protons was achieved when C_8 was *exo*-substituted, **1i**, with a phenylgroup (see fig. 1a). For obvious steric reasons, due to the lack of free rotation, H_9 faces the shielding region of the aromatic ring, therefore occurring at lower field. Bicyclo[3.2.1]octenes substituted at C_8 with good Lewis bases centre as -OH, -OAc or keto group, were all subjected to complexation with Eu $(fod)_3$. d_{27}. The closer H_5 proton to the complexation centre does present a higher gradient for the induced shift than the most remote H_9 proton. Also when the signals of H_5 became distinguished from H_9, as result of the added shift reagent, we have carried out decoupling experiments, irradianting successively the bridgehead protons and observing the signals of vinylic protons H_6 and H_7 respectively. For compounds with $Y = H$, H_6 is easily distinguishable from H_7 both as pattern and chemical shift (see below), while for Y = Cl, H_6 is obviously assigned, although slightly overlapping with the aromatic protons. In the latter case, irradiating the vinylic proton, as for example the chloroketone **1g**, the lower field H_5 signal became a doublet, as a result of the remaining coupling with H_{10}^{anti} proton.

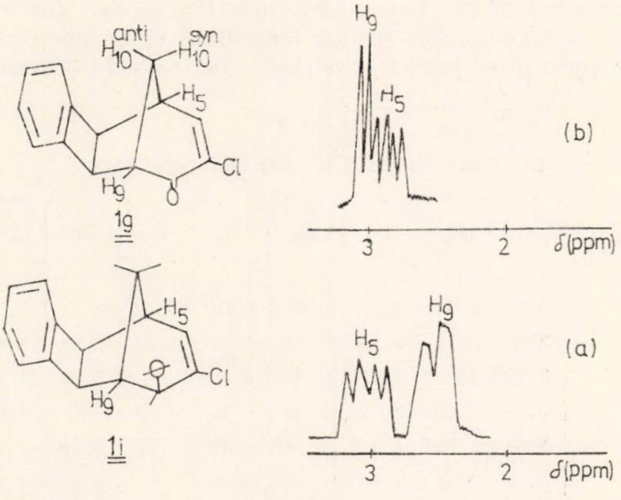

Fig. 1. — Patterns of well resolved H_5 and H_9 protons.

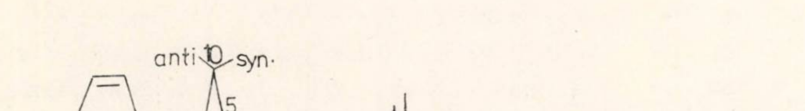

Fig. 2. — The ^{1}H — NMR spectrum (at 60 MHz) of the chloroketone **1g**. In the upper part is presented the resulted spectrum after irradiating the vinylic H_6 proton.

As a result of these extensive experimental observations, we propose for H_5 and H_9 the chemical shifts in Table 1.

Next, our concerns are the chemical shifts assignments of the methano-bridge protons, H_{10}^{anti} and H_{10}^{syn}, respectively. From the outset, we shall emphasize that the chemical shift of these protons is strongly dependent on the configuration of the benzocyclobuta fragment. The *exo*-configuration produces a relative upfield shift of both methylene protons with approximatively 0.4 ppm in respect to the *endo*- benzocyclobutabicyclo [3.2.1] octene derivatives. However the patterns of H_{10}^{anti} and H_{10}^{syn} are strikingly different. The H_{10}^{syn} is a doublet, while H_{10}^{anti} is a doublet of triplets (see the comments below).

Table 1

Chemical shifts (in ppm, internal standard TMS)

Compound	H_1	H_2	H_5	H_9	H_6	H_7	H_8	H_{10}^{syn}	H_{10}^{anti}
1a	3.62	3.87	2.42	2.08	6.01	5.43	2.1	2.0	
1b	3.30–3.71		2.46	2.34	6.83	5.50	3.89	1.65	1.16
1c	3.72*	3.52*	2.6[c]	2.53[c]	6.25	—	3.92	1.70	1.23
1d	3.47–3.80		2.55	2.45	6.25	5.42	5.0	1.65	1.16
1e	3.8*	3.72*	2.77[b]	2.58[b]	6.48	—	5.18	1.74	1.25
1f	3.74	3.54	2.62[a]	2.68[a]	6.20	—	4.25	1.95	1.28
1g	3.86*	3.7*	2.91	3.09	7.33	—	—	2.15	1.53
1h	3.83	3.7	2.9	2.93	7.31	5.83	—	2.04	1.56
1i	3.82	3.63	2.45	2.21	6.2	—	3.35	1.47	1.09
2a	3.82	3.97	2.60	2.43	5.37	5.01	2.10	2.0	
2b	3.81		2.65	2.42	5.51	5.08	3.67	2.05	1.61
2c	3.93		2.4–3.1		5.66	—	3.76	2.11	1.78
2d	3.88[d]	3.86[d]	2.7[a]	2.5[a]	5.66	5.10	4.78	2.05	1.69
2e	3.90		2.8[a]	2.5[a]	5.65	—	4.87	2.08	1.71
2f	3.9–4.0		2.66–3.16		5.60	—	4.13	2.43	1.68–2.02
2g	4.23		3.25		6.96	—	—	2.44	2.14
2h	4.28		2.70–3.20		6.55	5.40	—	2.38	2.06

* ambiguous assignment

[a] from typic coupling constants of bicyclo[3.2.1]oct-2-ene derivatives

[b] from double resonance

[c] from $Eu(fod)_3 \cdot d_{27}$ dopped spectrum at 60 MHz

[d] from simulation (noniterative)

Although, our assignments coincide with those proposed more than twenty years ago [2-4], we would like to emphasize here, that our results are based on experimental support. When to compounds with X=OH, -OAc or >C=O, was added incrementally $Eu(fod)_3 \cdot d_{27}$, the greater induced shift was experienced by H_{10}^{syn}. Moreover, as will be presented while discussing the coupling constants, MM—2 calculations carried out for the isomeric ketones **1h** and **2h**, combined with the Karplus relationship[10], are in fully agreement with the pattern of H_{10} signals.

The vinylic proton H_6 is always more deshielded than H_7 with 0.3—1.5 ppm (see Table 1). The actual chemical shift is dependent upon configuration of the benzocyclobuta fragment. When *endo-* oriented, both vinylic protons are relatively shielded with approximatively 0.3—0.4 ppm. Our assignments, presented in Table 1, are based on (i) the pattern of the signals defined by the constituent coupling constants, (ii) when Y=Cl, H_6 both as signal pattern and relative chemical shift was unequivocally defined, (iii) decoupling experiments carried out for bridgehead protons H_5 and H_9, and with H_{10}^{anti} (when these protons display a long-range coupling), unvailed the proximity of the H_5 — H_6 protons.

The allylic protons, H_8^{exo} and H_8^{endo} are not resolved at 60 MHz, for both **1a** and **2a** hydrocarbons. Since compounds **b** — **f**, **1i** are all *exo*-substituted at C_8, as a result of the magnitude of the coupling constant with the vicinal bridgehead proton H_9, the assignment of H_8^{endo} is straightforward. As is seen in Table 1, the actual chemical shift of H_8^{endo} is dependent on the configuration of the benzocyclobuta-fragment and on the nature of the substituent at C_7 and C_8. An *endo-* orriented benzocyclobuta fragment will shield with approximately 0.1—0.3 ppm in respect with the *exo*-oriented phenylidene fragment.

The assignments of benzylic H_1 and H_2 protons is rather ambiguous. Our proposals are only occasional. Thus the ABCD pattern of the *endo-*

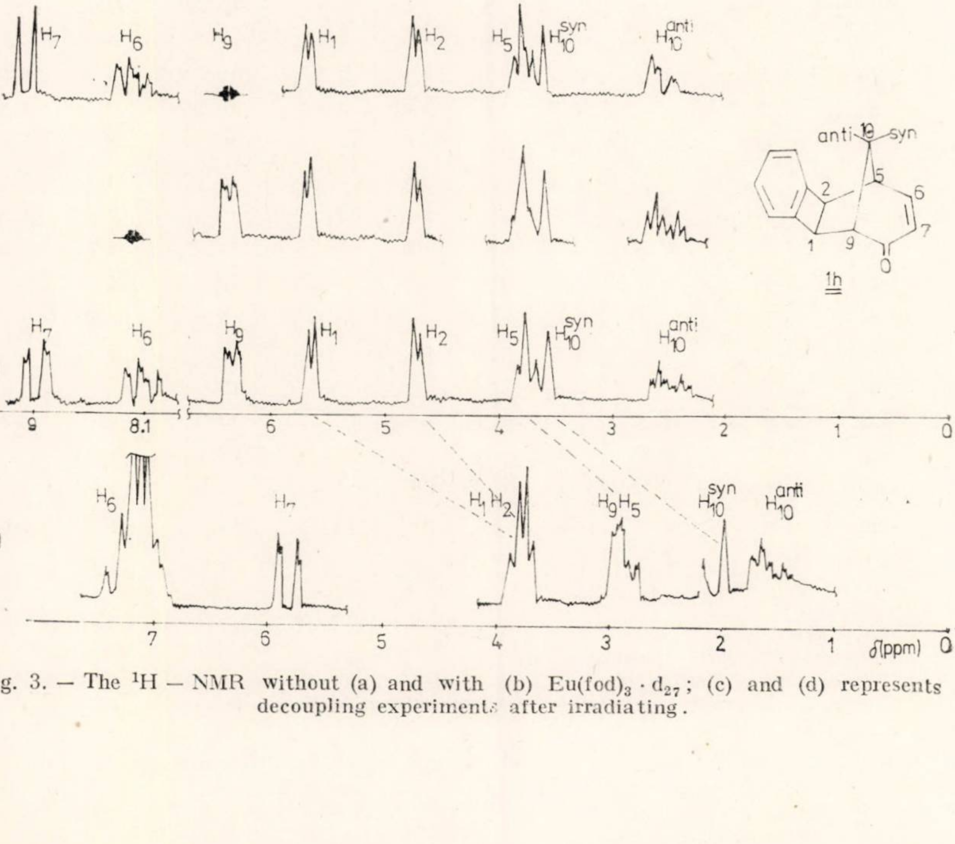

Fig. 3. — The ¹H — NMR without (a) and with (b) Eu(fod)$_3$ · d$_{27}$; (c) and (d) represents decoupling experiments after irradiating.

benzocyclobutabicyclo[3.2.1]octene **2d** was simulated non-iteratively with the SIMEQ program from the FT—80A software of Varian Company. The higher field signal ($\delta = 3.86$ ppm) was assigned to H_2, while the lower field signal ($\delta = 3.88$ ppm) was assigned to H_1. When the *exo*-ketone **1h** was subjected to complexation with Eu $(fod)_3 \cdot d_{27}$ (fig. 3), H_1 signal was more rapidly shifted than H_2. Therefore we estimate that H_1 has a relative downfield shift in respect to H_2. A more convincing evidence, we believe to produce with quantitative evaluation of the induced shift correlated with the geometry was obtained with MM—2 calculation for **1h**.

B. Coupling constants

Geminal, vicinal and long-range coupling constants are collected in Table 2. They were estimated either as first order parameters from the 60 MHz spectra, without or with Eu $(fod)_3 \cdot d_{27}$, from 400 MHz spectra carried out for **1g** and compounds or from noniterative simulation. The coupling constant magnitudes are decisive for defining the configuration of the bicyclo[3.2.1] octene substituents.

Table 2

Coupling constants of compounds **1** and **2** (J : Hz)

Compound	$J_{5,6}$	$J_{5,10^a}$	$J_{8,9}$	$J_{1,2}$	$J_{6,7}$	$J_{7,8}$	$J_{10^s,10^a}$	$J_{9,10^a}$	$J_{9,7}$
1b	7.5	4	2.5	3	9.5	3.5	12	3.5	1.5
2b	7.1^b	4	1.5	—	9.4^b	3.68^b	10.95^b	4	1.5^b
1c	6^c	4	2	3	—	—	12	4	—
2c	7.5	4	2.5	—	—	—	11	4	—
1d	7	4	3	3	9	4	12	4	1.5
2d	7^d	4.5^d	2.7^d	6^d	9.5	4	11	4.5	1.5
1e	7	4	2.5	4	—	—	12	4	—
2e	7	4.25	2.5	—	—	—	11.5	4.25	—
1f	7	4	2.5	3.5	—	—	12	4	—
2f	7		2.5		—	—	12	—	—
1g	8^b	4^b	—	3.47^b	—	—	12.1^c	4^c	1.5
2g	7^c	4.25	—		—	—	12.5	4.25	—
1h	7	4	—	3.5	10	—	12	4	2
2h		4	—		10	—	11	4	1.5
1i	7	4	2	3	—	—	12	4.5	—

a — anti
s — syn
[a] from 400 MHz spectrum
[b] from using $Eu(fod)_3 \cdot d_{27}$
[c] from noniterative simulation of the spectrum of acetoxiderivative, **2d**

a) Vicinal coupling constants

Bridgehead protons H_5 and H_9 present in all cases studied here three-bonds interactions as well as four-bonds interactions, the latter but only in a few examples.

In *exo*-benzocyclobuta derivatives **1**, bridgehead H_5 couples with the vinylic H_6 and H_{10}^{anti} protons, while H_9 interacts with H_8^{endo} and H_{10}^{anti}. Neither H_5, nor H_9 couple with the *endo* orriented H_1 and H_2 proton, respectively. The coupling J_{H_5, H_9} is in the range of 6—8 Hz, while J_{H_9, H_8} is

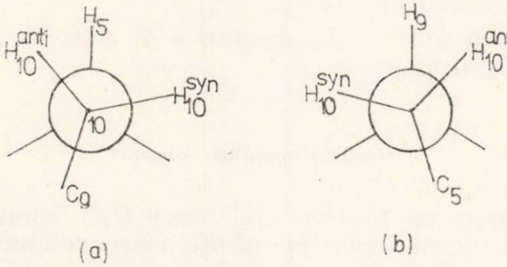

Fig. 4. — Newman projections along (a) $C_{10} - C_5$ bond and (b) $C_5 - C_{10}$ bond.

of 2—3 Hz magnitude. The latter value is typical for an *endo*-oriented H_8 proton, and therefore this coupling constant is significant for the configuration of a substituent at C_8^5. A larger value, for J_{H_9, H_8} is typical for an *exo*-oriented H_8^5. Both H_5 and H_9 couple with only one of methano-bridge, protons, namely H_{10}^{anti} and do not interact with H_{10}^{syn}.

MM—2 calculation carried out for compounds **1h** and **2h** respectively, revealed that the dihedral angles $H_5 - C_5 - C_{10} - H_{10}^{syn}$ are 69.69° for **1h** and 67.74° for **2h**, respectively. The dihedral angles $H_9 - C_9 - C_{10} - H_{10}^{syn}$ are 71.76° for **1h** and 69.67° for **2h** respectively. The calculated values, using the quoted dihedral angles, are in the range of 0.5—0.9 Hz.

We have not observed a coupling constant between the bridgehead protons with H_{10}^{syn}. However because the dihedral angles $H_5—C_5—C_{10}—H_{10}^{anti}$ are 52.11° in *exo*-ketone **1h** and 52.73° for *endo*-ketone **2h**, and $H_9—C_9—C_{10}—H_{10}^{anti}$ is 49.99° for *exo*-ketone **1h** and 54.69° for *endo*-ketone **2h** H_{10}^{anti} gives coupling constants of 2.5—3.2 Hz with bridgehead protons. The experimental value is approximatively 4 Hz.

In the case of *endo*-benzocyclobutabicyclo[3.2.1]octene derivatives, the bridgehead protons are also coupling with the benzylic protons H_1 and H_2 respectively. Our estimation resulted from spectra simulation in the case of acetate **2d**. The magnitude of coupling is of 6 Hz. An extrapolation of this finding to the related *endo* derivatives **2**, is not risky, since the patterns for all *endo*-benzocyclobutabicyclo[3.2.1]octenes are quite similar.

The allylic proton H_8^{endo} couples additionally to the vicinal vinylic proton, with H_7. A magnitude of 4Hz was obtained in the case of acetoxy-derivatives **1d** and **2d**, respectively, while at 400 MHz, the same coupling constant is 3.68 Hz for the hydroxyderivative **2b**.

b) Long range interactions

Jefford *et al.*[4] have noticed five distinct long-range interactions in the case of the nonannulated bicyclo[3.2.1]octene derivatives. By annulation, as is the case of our **1** and **2** type compounds, the bicyclo[3.2.1] octene system still retains two types of four-bonds couplings, all belonging to the well-known W type geometry.

Thus H_{10}^{anti} interracts with the vinylic proton H_6. The magnitude of the coupling was estimated to be 1.09 Hz from the 400 MHz spectrum of ketone **1g**. At 60 MHz by irradiating H_6, the pattern of H_{10}^{anti} becomes a very nice doublet of triplets (see fig. 2).

The bridgehead proton H_9, display a W pattern interaction with H_7 of 1—2 Hz magnitude.

c) Geminal coupling constant

The methano-group protons H_{10}^{anti} and H_{10}^{syn} interact with 11—12 Hz, irrespective of the configuration of the benzocyclobuta fragment or of substitutions at C_7 and C_8. The geminal coupling constant for the parent hydrocarbons **1a** and **2a** are unknown at present stage of investigations.

CONCLUSIONS

The spectral parameters of 17 bicyclo[3.2.1] derivatives, most of them presented here for the first line, have resulted by analyzing the ^1H—NMR spectra at 60 MHz and 400 MHz. These parameters are typical for the bicyclo[3.2.1]octene system and are useful in difining the stereochemisty of the system. Some vicinal coupling constants, as for example $J_{H_5H_{10}^{anti}}$ and $J_{H_9H_{10}^{anti}}$, were rationalized with the aid of MM—2 calculations combined with Karplus equation.

EXPERIMENTAL PART

The syntheses of compounds **1a**, **2a**, **1f**, **2f** were reported by us previously. The synthesis of the other examples discussed here will be reported in a forthcoming paper. The 60 MHz ^1H-NMR were recorded with a Varian EM 360 L spectrometer, using solutions of **1** or **2** in $CDCl_3$ or CCl_4, with internal TMS.

The dopped spectra were obtained by incrementally adding $Eu(fod)_3 \cdot d_{27}$ to the respective solution.

The 400 MHz ^1H-NMR spectra were recorded on an AM Bruker instrument as solution in dimethyl-sulfoxide-d_6. MM-2 calculations were performed on an IBM — XT PC.

The Karplus relationship[10] used here was

$$J = 8.5 \times \cos^2 \varnothing - 0.3$$

where $\varnothing$ is the dihedral angle between protons H_i and H_j.

REFERENCES

[1] Taken in part from the Ph. D. Thesis of A.P.

[2] (a) W. R. Moore, W. R. Moser, J. E. La Prade, *J. Org. Chem.*, **28**, 2200 (1963); (b) R. C. De Selms and C. M. Combs, *J. Org. Chem.*, **28**, 2206 (1963).

[3] S. Winstein, M. Ogliarusso, M. Sakai and J. M. Nicholson, J. *Amer. Chem. Soc.*, **89**, 3656 (1967).

[4] C. W. Jefford and K. C. Ramey, *Tetrahedron*, **24**, 2927 (1968).

[5] M. A. Battiste, J. M. Coxon and R. Edelman, *Tetrahedron Lett.*, **1972**, 4577.

[6] J. M. Brown, E. Cain and M. C. McIvor, *J. Chem. Soc.* (B), **1971**, 730; H. Tanida, K. Tori and K. Kitahonoki, *J. Amer. Chem. Soc.*, **89**, 3212 (1967).

[7] S. J. Cristol, J. R. Mohring and D. E. Phorde, *J. Org. Chem.*, **30**, 1956 (1965); S. J. Cristol R. Caple, R. M. Sequeira and L. O. Smith, Jr., *J. Amer. Chem. Soc.*, **87**, 5679 (1965)

[8] Our previous contributions are devoted to a specific and do not represent a general discussion of the system :
a) L. Pârvulescu and M. D. Gheorghiu, *Rev. Roumaine Chim.*, **22**, 1089 (1977).
b) A. Popescu, L. Pârvulescu, L. Stănescu and M. D. Gheorghiu, *Rev. Roumaine Chim.*, **31**, 1025 (1986).

[9] L. M. Jackman and S. Sternhell, "Applications of Nuclear Magnetic Resonance Spectroscopy in Organic Chemistry", 2nd Edition, Pergamon Press, New York, 1969, p. 281.

Revue Roumaine de Chimie, 34, 2, 491–502 (1989)

THE HIGH DEGREE GENERALITY OF THE PRINCIPLE OF CRITICAL ENERGY

VALERIU V. JINESCU
Polytechnical Institute of Bucharest,
Faculty of Mechanics, Romania

Received September 30, 1988

The present paper underlines the importance of the energy concept in the analysis of interactions. On this basis a new principle is formulated: the principle of critical energy. It has a great degree of generality and includes some well-known principles, such as Boltzmann' principle, the principle of force action independence and so on. With this principle we can obtain some well known laws, such as Dalton's law, Amagat's law and so on, as well as some new relations, especially the interdependence between groups of external actions upon material bodies. The principle of critical energy allows the determination of the critical groups of loads, for loads of different nature and of different types.

1. CRITICAL ENERGY

A certain amount of energy, E_k, of nature k, in certain conditions is capable of generating a force F, of the same nature k, or of a different one. The electrical energy, for example, may generate forces of electrical, mechanical, thermal etc. ... nature. The energy action E_k on a certain body M (Fig. 1) is carried out by the force F whose nature depends on the type of the process (physical, chemical or biological) determining the transfer and/or conversion of energy. In other words, a generalized force F in action carries with it a certain amount of energy E_k (Fig. 2, a).

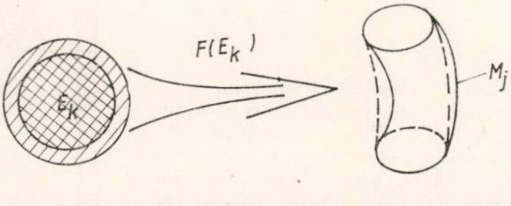

Fig. 1. — The energy action E_k on the body M, carried out by the force F.

During its action on a material body M_j (containing the energy E), the force F will transfer to it the amount of energy $E_k^* \leqslant E_k$ (Fig. 2, b). Hence, an interaction, irrespective of its material support, is based on a certain amount of energy. Consequently, one may say that the energy is the *golden standard* for changes or processes of any kind. The use of the energy concept both for the cause and the effect of an interaction allows a unitary approach of phenomena or processes of various types.

In nature a certain exchange of energy takes place between particles, material bodies and so on. After a certain amount of energy accumulation, the bodies, or the substances out of which they are made, undergo slow or sudden changes.

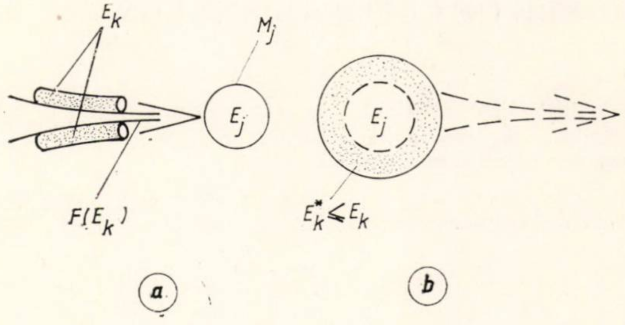

Fig. 2. — The force F : a — before action, carries with it a certain amount of energy E_k ; b — after its action upon a body M_j, has transferred to it an amount of energy $E_k^* \leqslant E_k$; the body M_j contains now the total energy $E_j + E_k^*$.

The accumulated amount of energy, which makes the material body to pass from a state of equilibrium to a new state of equilibrium which is *qualitatively different* from the first one, has been termed ***critical energy*** E_{cr} (Fig. 3). In Fig. 3, *a* since $E < E_{cr}$, the shape of the body is unchanged, while the volume is not. In Fig. 3, *b* since $E > E_{cr}$, both the shape and the volume of the deformed body differ from the shape and the volume of the non-deformed body.

1.1. Several well-known examples

Several well-known examples are given to prove that a certain phenomenon (a physical or physical-chemical process) is initiated only when the stored energy attains a certain value, to be called here the *critical energy* of the considered phenomenon or process.

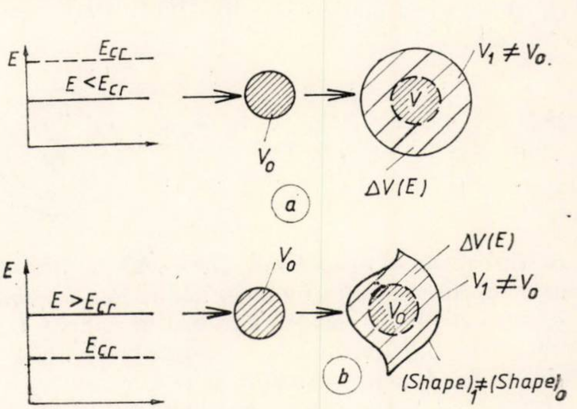

Fig. 3. — The effect of amount of energy, E, accumulated by a body : a—when $E < E_{cr}$; b — when $E \geqslant E_{cr}$ the body passes to a new state of equilibrium, qualitatively different from the first one (for example the final shape is different from the initial shape of the body).

a. In the decomposition of a molecule into its constituents, $AB \rightarrow \rightarrow A + B$, it should accumulate an amount of energy equal to the energy of molecular formation (E_b — binding energy), (Fig. 4).

b. In extracting an *electron from a metal*, the electron should be given a certain amount of energy; the minimum energy required is called the *extraction energy*, E_e.

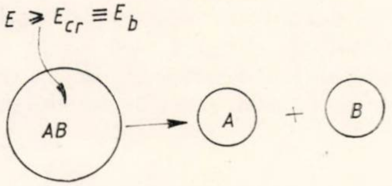

Fig. 4. — The decomposition of a molecule into its constituents after the accumulation of an amount of energy $E \geqslant E_{cr}$, where $E_{cr} = E_b$ is the binding energy.

c. In the case of an isolated atom, a photon of an incident wave can snatch an electron from the atom only if a certain amount of energy, greater than the *extraction energy*, E_{ex}, is transferred to the latter.

d. The existence of a certain ordering of the energy levels which characterized the atom structure is consonant with the idea of *some critical energy values*.

1.2. Some new examples

a. At a macroscopical scale, some changes of substances occur at a characteristic fixed temperature; they correspond to the accumulation of certain amounts of thermal energy. For example, one could mention the specific thermal energy for the melting of a crystalline body, E_m, at a certain pressure, as well as the specific thermal energy required to *vaporize* a crystalline solid substance, E_v, at a certain pressure.

The two changes of state, at a given pressure, are characterized by some fixed values of accumulated thermal energy; they represent *the two levels of the specific stored energy* for a crystalline solid material (Fig. 5 a).

With the increase of pressure p, the melting and vaporization temperatures will rise, and E_m and E_v as well.

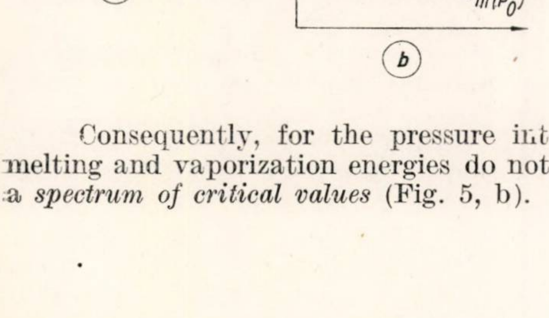

Fig. 5. — The levels of critical energy (corresponding to the change of physical state by melting and vaporization) for a crystalline substance: a — at a given pressure p_0; b — at different pressures $p \in [p_0\,;\, p_n]$.

Consequently, for the pressure interval $p \in [p_0\,;\, p_n]$, the specific melting and vaporization energies do not have just one single value but a *spectrum of critical values* (Fig. 5, b).

b. A body may be lifted in the gravitational filed only when the applied mechanical energy (in the required direction) exceeds the energy corresponding to the inertia (reluctance) of the body.

The energy accumulated by a material body may be determined by the action of one or several external factors. If the critical state is attained through the action of several external factors carrying the amounts of energy E_1, E_2, . . .E_n, then that group of factors is called the *critical group* for the considered phenomenon or process (Fig. 6).

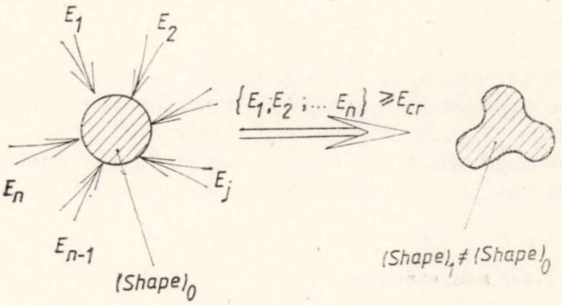
E_1
E_2
$\{E_1;E_2;\dots E_n\} \geq E_{cr}$
E_n
E_j
E_{n-1}
$(Shape)_0$
$(Shape)_1 \neq (Shape)_0$

Fig. 6. — A body undergoing several energy actions.

It follows therefore that if n external factors differing in their nature (mechanical, electrical, chemical, magnetic etc. . . .) or of the same nature but of various types, act on a material body then arises the question : *when is the critical state attained*?! Which should be the ratio of the external factors of action, each of them the carrier of a certain amount of energy, likely to induce a critical state in the material undergoing the interaction?!

The answer to this question is to be given by the *principle of critical energy* as stated below.

2. PRINCIPLE OF CRITICAL ENERGY

In the development of a phenomenon or process one reaches the critical state when the sum of the energy transferred upon the body and acting in the sense to achieve it, becomes equal to the value of critical energy characteristic of the phenomenon or process under consideration.

The mathematical expression of this principle is the following[1]

$$\sum_j \left(\frac{E_j}{E_{\mathrm{cr}}}\right) \cdot \operatorname{sign}\left(\frac{F_j}{F}\right) = 1 \tag{1}$$

where E_j is the energy accumulated by the matter involved in the process ; energy E_j is "carried" by the generalized force F_j or is determined by such a "force".

The critical energy, E_{cr}, in a given case is a *constant*, independent of the types of energy involved. To emphasize this fact, E_{cr} is to be replaced by $E_{\mathrm{cr}.j}$ so that relation (1) becomes

$$\sum_j \left(\frac{E}{E_{\mathrm{cr}}}\right)_j \cdot \operatorname{sign}\left(\frac{F_j}{F}\right) = 1 \tag{2}$$

In the previous relations, "force" F acts in the sense which determines the critical state ; it is a reference force for the considered phenomenon, so that

$$\operatorname{sign}\left(\frac{F_j}{F}\right)=\begin{cases} +1, \text{ if the effect of "force" } F_j \text{ has the same sense as the effect of force } F \text{ ;} \\ -1, \text{ if the effect of "force" } F_j \text{ is opposite to the effect of the action of force } F. \end{cases}$$

Energies E_j and E_{cr} are *specific energies* expressed in J/kg. With the aid of the critical energy principle, *depending on the meaning given to critical energy*, by particular restrictions, one obtains some well-known principles and laws as well as some new relations, particularly in the case of simultaneous actions of several external factors.

2.1. Well-known principles and laws resulting from particular applications of the principle of critical energy

a. Boltzmann's superposition principle ("the total response of a body is the sum of the individual responses the body would give to each of the applied actions, or forces") may be applied only to those cases where material behaviour is linear (the cause-effect dependence is linear). The principle of critical energy refers to the summation of effect energies ; this sum may be worked out irrespective of the type of material behaviour (linear or nonlinear).

Consequently, the principle of critical energy is more general than Boltzmann's superposition principle.

b. The principle of force independence action states that the effect of the action of a force is independent of the effects of other force actions. In other words the effect of several forces action is equal to the sum of the effect generated independently by each force in its turn, respectively

$$\bar{a} = \sum_{i=1}^{n} a_i, \tag{3}$$

where $\bar{a}_i$ is the acceleration produced by force $\bar{F}_i$ and $\bar{a}$ — the resulting acceleration produced by the resultant force $\bar{F} = \sum_{i=1}^{n} \bar{F}_i$.

By replacing energy E_j transferred to the body by work W_j in rel. (1), one obtains

$$\sum_{j=1}^{n} \frac{W_j}{W} = 1,$$

where $W_j = \bar{F}_j \cdot l$ is the work of force $\bar{F}_j$ for the motion of a body with mass m over distance l, while $W = \bar{F} \cdot l$ — the overall work for the motion of a body with mass m over distance l under the action of $\bar{F}$ (Fig. 7).

Out of the previous relations we obtain

$$\bar{F} = \sum_{j=1}^{n} \bar{F}_j,$$

that is the resultant force.

Out of (4), by dividing it by mass m one obtains relation (3) which expresses the principle of force independence action,

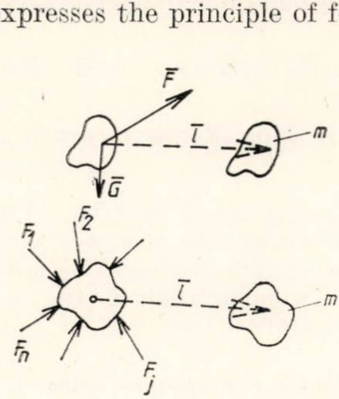

Fig. 7. — The same motion, $\bar{l}$, of a body of mass m, undergoing: a — a force $\bar{F}$; b — several forces $F_1, F_2 \ldots F_n$.

c. *Dalton's law and Amagat's law.* The capable (or potential) energy of a mixture of perfect gases occupying volume V at a pressure p is $E = p\,.V$. The capable energy of a component of this mixture under partial pressure [*] p_j is $E_j = p_j\,.V$.

$$\sum_j \frac{p_j \cdot V}{p \cdot V} = 1,$$

or

$$\sum_j p_j = p, \tag{5}$$

which represents the expression of Dalton's law or the law of partial pressures in mixtures of perfect gases ("total pressure, p, of a mixture of gases equal to the sum of partial pressures, p_j, of the mixture components").

By analogy, the capable energy of a component from a mixture of perfect gases under pressure p, which occupies the partial volume V_j is $E_j = p_j\,V$. From relation (1) one obtains (with $E_{cr} = p\,.V$)

$$\sum_j \frac{p \cdot V_j}{p \cdot V} = 1,$$

or

$$\sum_j V_j = V, \tag{6}$$

which represents *Amagat's law* or the law of partial volumes in perfect gases ("the volume, V, of a perfect gas mixture is equal to the sum of partial volumes V of the mixture components"). Hence, Dalton's and Amagat's laws come out as particular cases from the expression of the principle of critical energy.

2.2. New relations obtained from the principle of critical energy

More examples of new relations for the calculation of critical state are to be supplied further, particularly for the case of simultaneous action of several external factors, e.g. in the case of combined static or cyclic loading.

a. *Structure stability.* A structure made from a linearly elastic material will lose its stability under compression loads when the applied load P becomes equal to its critical value P_{cr} (Fig. 8, a); the critical load indicates the point of behaviour branching (Fig. 8, b).

---

[*] the *partial pressure* of a component in a mixture represents the pressure the component might have if it were the only one to occupy volume V.

If several loads act simultaneously upon the same structure — some of them being compression loads — the attaining of the critical state, or the critical loads group may be obtained by applying the principle of critical energy.

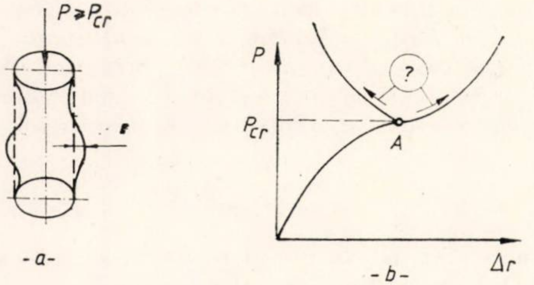

Fig. 8. — A cylindrical shell subjected to compression load $P\,(a)$, and the dependence of the load P on the deformation Δr before buckling ($P < P_{\text{cr}}$). At $P == P_{\text{cr}}$ the structure buckles (A = point of branching).

For the material with nonlinear elastic behaviour ($\sigma = M_e \cdot \varepsilon^a$) we got :[2]

$$\sum_j \left(\frac{P_j}{P_{\text{cr},j}}\right)^{\frac{1}{a}+1} \cdot \text{sign}\left(\frac{P_j}{P}\right) = 1, \tag{7}$$

where P_j is any load whose critical value is $P_{\text{cr},j}$ and P the reference load, so as

$$\text{sign}\left(\frac{P_j}{P}\right) = \begin{cases} +1, \text{ if } P_j \text{ causes compression;} \\ -1, \text{ if } P_j \text{ causes extension.} \end{cases}$$

For a material with a linear elastic behaviour, $a = 1$.

For example, a shell from a linear-elastic material under compression (F), torsion (M_t), bending (M_b) and under internal pressure (p_i) will collapse if the load group fulfils condition

$$\left(\frac{F}{F_{\text{cr}}}\right)^2 + \left(\frac{M_t}{M_{t,\text{cr}}}\right)^2 + \left(\frac{M_b}{M_{b,\text{cr}}}\right)^2 - \left(\frac{p_i}{p_{i,\text{cr}}}\right)^2 = 1 \tag{7, a}$$

which results from relation (7).

b. *Isothermal fatigue.* In the case of fatigue loading by an asymmetrical cycle (Fig. 9) of a material with an elastic nonlinear behaviour, the problem of determining the moment of its failure raises, owing to its cyclic loading. By applying the principle of critical energy we get[5]

$$\left(\frac{\sigma_m}{\sigma_y}\right)^{\frac{1}{a}+1} + \left(\frac{\sigma_v}{\sigma_R}\right)^{\frac{1}{a}+1} = 1, \tag{8}$$

where σ_m is the mean-stress applied ; σ_v — the stress amplitude ; $\sigma_{m,\text{cr}} = \sigma_y$ — is the material yield stress ; $\sigma_{v\text{-cr}} = \sigma_R$ — the fatigue limit for a stress ratio $R = \sigma_{\text{min}}/\sigma_{\text{max}}$.

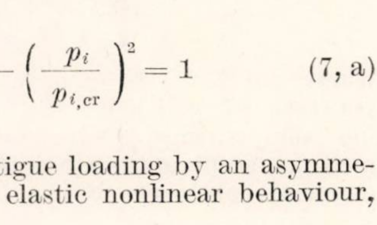

Fig. 9. — An asymmetrical cycle of stresses.

For a material with a linear elastic behaviour ($a = 1$) for symmetrical loading ($R = -1$), rel. (8) becomes

$$\left(\frac{\sigma_m}{\sigma_y}\right)^2 + \left(\frac{\sigma_v}{\sigma_{-1}}\right)^2 = 1 \tag{9}$$

The relation has been obtained in a different way by Buzdugan.[3]

c. *Fatigue loading with continuous temperature increase.* Similarly, for the case of fatigue loading with continuous temperature increase, the expression of the critical energy principle applied to a material of nonlinear elastic behaviour resulted into rel. (10)

$$\left[\frac{\sigma_m}{\sigma_c(t)}\right]^{\frac{1}{a}+1} + \left[\frac{\sigma_v}{\sigma_f(N)}\right]^{\frac{1}{a}+1} = 1, \tag{10}$$

where $\sigma_c(t)$ is the creep rupture strength at a time t equivalent to $N = t/f$ cycles of loading with frequency f;
$\sigma_f(N)$ — strength at N cycles of loading.

For $a = 1$, one obtains

$$\left[\frac{\sigma_m}{\sigma_c(t)}\right]^2 + \left[\frac{\sigma_v}{\sigma_f(N)}\right]^2 = 1, \tag{11}$$

which is a good approximation for Crawford and Benham experimental results, obtained for an acetal copolymer.[4]

Quite a few relations useful to the mechanical design deduced from the principle of critical energy have been already published[5] so I will not insist upon them.

d. *The melting temperature*, T_t, of a material, depends — as everybody knows — on the tension (pressure) applied to it. The following general correlation has been obtained on the basis of the critical energy principle,

$$\left[\frac{T_t(\sigma) - T_0}{T_t(0) - T_0}\right]^\alpha + \left[\frac{\sigma}{\sigma_{\mathrm{cr}}(T_0)}\right]^\beta = 1, \tag{12}$$

where $\sigma_{\mathrm{cr}}(T_0)$ is the compressive stress which alone, applied at the temperature T_0, will bring the body to the melting state; $T_t(0)$ — the melting temperature when mechanical stress is not present, $T_t(\sigma)$ — the melting temperature when mechanical stress, σ, is present; α and β are material constants. For a linear behaviour of the material $\alpha = 1$ and $\beta = 2$.

e. For *the vitrification temperature*, T_v, it has been experimentally found that for an amorphous polymer or a semicrystalline polymer T_v decreases with the stress increase. Measurements carried out on thermally and mechanically loaded samples have shown that the vitrification temperature decreases linearly with the increase of tension (Fig. 10).

Starting from the principle of critical energy (1), we obtain:
— for a mechanical nonlinear behaviour of the material ($\sigma = M_e \cdot \varepsilon^a$)

$$\frac{T_v(\sigma) - T_0}{T_v(0) - T_0} + \left(\frac{\sigma}{\sigma_{\mathrm{cr}}}\right)^{\frac{}{a}+1} = 1; \tag{13}$$

— for a mechanical linear behaviour of the material ($\sigma = M_e \cdot \varepsilon$)

$$\frac{T_v(\sigma) - T_0}{T_v(0) - T_0} + \left(\frac{\sigma}{\sigma_{\rm cr}}\right)^2 = 1, \tag{14}$$

where $T_v(\sigma)$ is the vitification temperature under the stress σ; $T(0)$ — the vitrification temperature when the stress is not present; $\sigma_{\rm cr}$ — the mechanical stress which acting alone leads to the vitrification temperature.

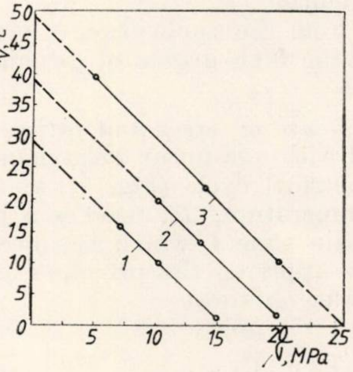

Fig. 10. — Vitrification temperature decrease with the increase of tension for[4]: 1 — Polyvinyl acetal; 2 — Polystyrene; 3 — Polyvinylbutyral.

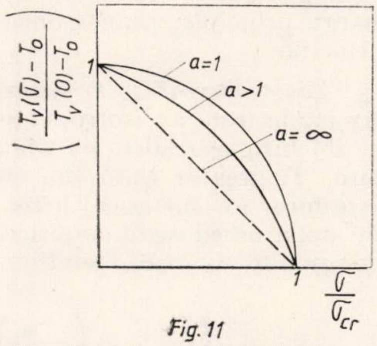
$\left(\frac{T_v(\sigma) - T_0}{T_v(0) - T_0}\right)$
1
a=1
a>1
a=∞
1
$\frac{\sigma}{\sigma_{cr}}$

Fig. 11

Fig. 11. — A nondimensional representation of the $T_v(\sigma) - \sigma$ dependence, function of the material mechanical behaviour given by the value of a.

The graphical representation of the dependence $T_v(\sigma) - \sigma$ is, generally speaking, a curve whose concavity faces the origin of the coordinate axes (Fig. 11);

— in the case of a rigid body, ($a \to \infty$), relation (14) is a straight line (Fig. 11) so as

$$\frac{T_v(\sigma) - T_0}{T_v(0 - T_0} + \frac{\sigma}{\sigma_{\rm cr}} = 1 \tag{15}$$

Relation (15) is proved by some experimental results, as shown in Fig. 10.

f. *Strength theories*. In the case of a tridimensional loading with normal main stresses σ_1, σ_2, σ_3, of a body made from a matérial with a linear-elastic behaviour, the energy which determines the shape variation of the body is expressed as:[6,7]

$$E_s = \frac{1+\mu}{6M_e} \cdot \left[(\sigma_1 - o_2)^2 + (\sigma_2 - \sigma_3)^2 + (\sigma_3 - \sigma_1)^2\right], \tag{16}$$

where μ is Poisson's coefficient; M_e — the elasticity modulus ($\sigma = M_e \cdot \varepsilon$).

By only j-direction loading until the normal critical stress is reached, $\sigma_{{\rm cr},j}$, the critical value of the shape variation energy is expressed as

$$(E_{s,j})_{\rm cr} = \frac{1+\mu}{6M_e} \cdot (2 \cdot \sigma_{j,{\rm cr}}^2). \tag{17}$$

Out of relations (1), (16) and (17) one obtains

$$\left(\frac{\sigma_1 - \sigma_2}{\sqrt{2} \cdot \sigma_{1,\mathrm{cr}}}\right)^2 + \left(\frac{\sigma_2 - \sigma_3}{\sqrt{2} \cdot \sigma_{2,\mathrm{cr}}}\right)^2 + \left(\frac{\sigma_3 - \sigma_1}{\sqrt{2} \cdot \sigma_{3,\mathrm{cr}}}\right)^2 = 1, \tag{18}$$

where the normal critical stresses are considered to differ along the three directions of loading.

Relation (18) represents the general expression of the failure of an anisotropic material with a linear-elastic behaviour.

For an isotropic material, $\sigma_{1,\mathrm{cr}} = \sigma_{2,\mathrm{cr}} = \sigma_{3,\mathrm{cr}} = \sigma_y$, so that relation (18) becomes the Huber-Hencky-Mises relation.

The general relation (18), resulted from the application of the critical energy principle, proves once again the high degree of generality of this principle.

g. *Time interval up to failure in the case of creep and fatigue loads.* A body made from an isotropic material with non-linear behaviour ($\sigma = M_e \cdot \varepsilon^a$) fatigue loaded by an asymmetrical cycle (Fig. 9), at a temperature, T, greater than the creep temperature, T_c, reaches a critical state (failure, for instance) after a certain time t, which has been previously determined semi-empirically. By applying the principle of critical energy for $\sigma_m > \sigma_y$, relation (19) was obtained

$$\left(\frac{t}{t_{\mathrm{cr}}}\right)^{\varkappa} + \left(\frac{\sigma_m}{\sigma_{m,\mathrm{cr}}}\right)^{\frac{1}{a}+1} + \left(\frac{N}{N_{\mathrm{cr}}}\right)^{\beta} = 1, \tag{19}$$

where $\varkappa > 1$ is the exponent in the law of material creep behaviour; β — the exponent in the law of material fatigue behaviour; N — stress cycles ($\Delta\varepsilon = C \cdot N^{\beta}$); t_{cr} -- the time interval up to failure under stress σ at $T > T_c$; N_{cr} — the number of stress cycles until failure (at temperature T, with amplitude σ_v); $\sigma_{m,\mathrm{cr}}$ — the critical mean stress corresponding to static loading at temperature $T > T_c$.

If the fatigue load is exerted with constant frequency, f, then the relation $N = t \cdot f$ will be between t, N and f so that relation (19) becomes

$$\left(\frac{t}{t_{\mathrm{cr}}}\right)^{\varkappa} + \left(\frac{t \cdot f}{N_{\mathrm{cr}}}\right)^{\beta} + \left[\frac{\sigma_m}{\sigma_{m,\mathrm{cr}}^{(T)}}\right]^{\frac{1}{a}+1} = 1. \tag{20}$$

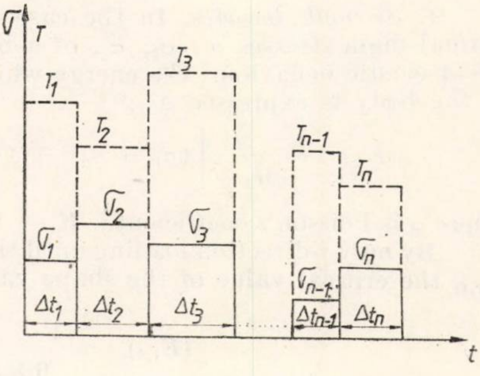

Fig. 12. — A body differently loaded — mechanical (σ_i) and thermal (T_i) — ove different time intervals (Δt_i).

For a material with a linear elastic behaviour ($a = 1$), whose behaviour under creep is characterized by a time linear increase of the strain ($\varkappa = 1$) and by a linear strain increase with the increase of load cycles, out of relations (19) and (20) one obtains, respectively,

$$\frac{t}{t_{\text{cr}}} + \left[\frac{\sigma_m}{\sigma_{m,\text{cr}}^{(T)}}\right]^2 + \left(\frac{N}{N_{\text{cr}}}\right)^2 = 1\,; \tag{21}$$

$$\frac{t}{t_{\text{cr}}} + \left(\frac{t \cdot f}{N_{\text{cr}}}\right)^2 + \left[\frac{\sigma_m}{\sigma_{m,\text{cr}}^{(T)}}\right]^2 = 1. \tag{22}$$

Relations like (21) have been *empirically* established for steel used in airplane engines, for gas turbine in aeronautics, for steam turbines in the field of energetics, etc. Such relations are to be used for example in the calculation of reactors for catalytic reformation, for catalytic cracking, etc.

When a body is loaded over time intervals Δt_i at different stresses σ_i and different temperatures, T_i (Fig. 12), it is impossible to determine empirically the time to failure.

Using the principle of critical energy, starting from relation (20), we obtain the following general relation, in the case $\sigma_m > \sigma_y$,

$$\sum_{i=1}^{n} \left(\frac{\Delta t_i}{t_{\text{cr},i}}\right)^{\varkappa} + \sum_{i=1}^{n} \left[\frac{\sigma_m}{\sigma_{m,\text{cr}}^{(T)}}\right]^{\frac{1}{\varkappa+1}} + \sum_{i=1}^{n} \left(\frac{N_i}{N_{\text{cr},i}}\right)^{\beta} = 1. \tag{23}$$

3. THE FIRST PRINCIPLE OF TERMODYNAMICS

Taking into account the considerations leading to the principle of critical energy, the first principle of thermodynamics may be written as

$$\frac{\mathrm{d}U}{\mathrm{d}Q} + \frac{\mathrm{d}L}{\mathrm{d}Q} \cdot \operatorname{sign}\left(\frac{L}{Q}\right) = 1 \tag{24}$$

which allows the highlighting of *inversion points* in the development of some phenomena. In relation (24), in the case of compression or expansion processes,

$$\operatorname{sign}\left(\frac{L}{Q}\right) = \begin{cases} +1, \text{ if } T > T_{\text{inv}}\,; \\ 0, \text{ if } T = T_{\text{inv}}\,; \\ -1, \text{ if } T < T_{\text{inv}}, \end{cases}$$

where T_{inv} is the inversion temperature. For example, for water, $T_{\text{inv}} = 4°\text{C}$; for hydrogen $T_{\text{inv}} = -80°\text{C}$.

Similar relations can be written for other phenomena as well, if they feature inversion points such as magnetostriction, stretching of rubber samples, etc.

4. CONCLUSIONS

Some relations used in the calculation of machine parts under combinations of different types of loads have been obtained starting from the principle of critical energy.^{5} One can point out that further applications of this principle are likely to be developed.

The high degree of generality of this principle lies in the use of the energy concept in its statement.

Thus stated, it has become a fruitful principle, which not only covers the fields of validity of some well-known classical laws, in science, but it also leads to new results, which could not have been established in other ways up to now.

I suppose this principle is likely to be applied to changes occurring at the molecular level of living matter. We could ask ourselves whether, for example, all disequilibria occurring in diseases are the outcome of a deflection from a certain critical value of the specific energy accumulated at a certain time. And the list of questions might continue.

It seems that the principle of critical energy is going to have a wide range of applications in science and technology and I certainly hope so.

REFERENCES

[1] V. V. Jinescu, *Rev. Chim.* (București), **35**, 858 (1984).

[2] V. V. Jinescu, *Rev. Chim.* (București), **33**, 70 (1982).

[3] Gh. Buzdugan, *Studii și Cercetări de Mecanică Aplicată*, **XIV**, 827 (1962).

[4] R. J. Crawford, and P. P. Benham, *Journal Mech. Eng. Science*, **16**, 178 (1974).

[5] V. V. Jinescu, *Contrucția de mașini* (București), **37**, 183 (1985).

[6] J. F. Harvey, "Theory and Design of Modern Pressure Vessels", second edition, V Nostrand, Reinhold Comp., New Yok, 1974.

[7] Gh. Buzdugan, "Rezistența materialelor", Editura tehnică, București, 1980.

Revue Roumaine de Chimie, **34**, *2*, 503—508 (1989)

СИНТЕЗ 6,7-БЕНЗОМОРФАНОВ С ИСПОЛЬЗОВАНИЕМ АРЕНХРОМТРИКАРБОНИЛЬНЫХ КОМПЛЕКСОВ

В. Н. КАЛИНИН, С. К. МОИСЕЕВ, В. И. БАХМУТОВ и Н. И. УДАЛОВ
Институт элементоорганических соединений, ул. Вавилова, 28,
Москва 117813, СССР

Получена 3 октября 1988 г.

Действием амида натрия на трикарбонил-η^6-[1′,2′,3′,4′-тетрагидро-спиро(1,3-диоксолан-2,1-нафталин)]хром (**4**) с последующей обработкой бромацетатом натрия приводит к образованию кетокислоты **5**. Кислота **5** использована для синтеза 1-(N-бензил-2-аминоэтил)-1,2-дигидронафталина (**11**), циклизацией которого получен 3-бензил-1,2,3,4,5,6-гексагидро-1-гидрокси-2,6-метано-3-бензазоцин(**12**).

The action of sodium amide on tricarbonyl-η^{12}-[1′, 2′, 3′, 4′-tetrahydro-spiro(1,3-dioxolane-2,1′-naphthalene)]chromium (**4**) followed by the reaction with sodium bromoacetate produces ketoacid **5**. This compound was used for the preparation of 1-(*N*-benzyl-2-aminoethyl)-1,2-dihydronaphthalene (**11**), which was cyclised into 3-benzyl-1,2,3,4 5, 6-hexahydro-1-hydroxy-2,6-methano-3-benzazocine (**12**).

Ранее нами был разработан способ получения β-арилпропионовых кислот через α-металлирование аренхромтрикарбонилов действием $NaNH_2$ в жидком аммиаке с последующей обработкой $BrCH_2COONa$.[1] В развитие этого метода в настоящей работе предлагается способ получения хромтрикарбонильного комплекса 11-(,2,3,4-тетрагидро-4-оксонафталин) уксусной кислоты (**5**), исходя из диоксоланового производного тетралона-1 (**3**). Эта кислота может быть превращена в β-аминоэтильное производное 1,2-дигидронафталина, используемое в синтезе 6,7-бензоморфанов (**1**) методом внутримолекулярной циклизации.[2]

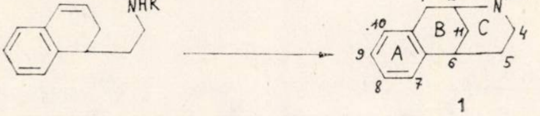

1

Схема 1

Ключевая стадия данного метода — синтез 1-(1, 2, 3, 4-тетрагидро-4-оксонафталин) уксусной кислоты, осуществляемый прямым введением карбоксиметильного заместителя в положение *4* тетралона-1. Возможность такого замещения обеспечивается комплексообразованием аренового лиганда с хромтрикарбонильной группой. Координация группы

$Cr(CO)_3$ вызывает необходимое для стадии металлирования увеличение CH-кислотности в положении *4* тетралонового лиганда. С этой целью действием $Cr(CO)_6$ на диоксолан **3** (получен из тетралона-1 (**2**) для защиты карбонильной группы) в смеси дибутиловый эфир (ТГФ синтезирован хромтрикарбонильный комплекс **4**, который легко металлируется в бензильное положение по разработанной нами методике [1] действием $NaNH_2$ в жидком аммиаке. Последующее взаимодействие полученного натриевого производсного с $BrCH_2COONa$ в среде NH_3 (жидк.)). ТГФ приводит после обработки реакционной смеси 10%-ной HCl (при этом одновременно снимается диоксолановая защита) к хромтрикабонильному

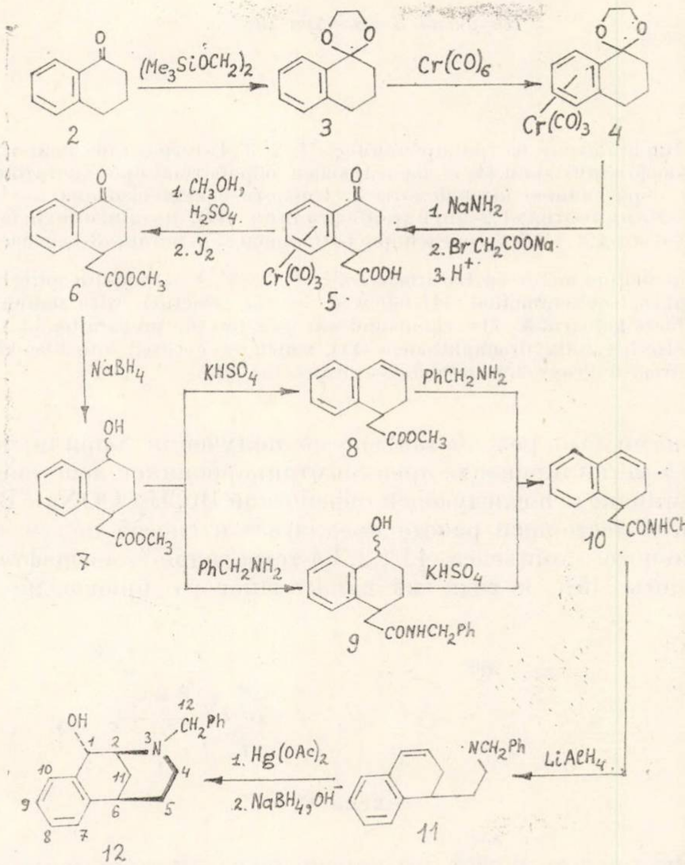
2
(Me3SiOCH2)2
3
Cr(CO)6
Cr(CO)3
4
1. NaNH2
2. BrCH2COONa
3. H+
Cr(CO)3
COOH
5
1. CH3OH, H2SO4
2. J2
COOCH3
6
NaBH4
OH
COOCH3
7
KHSO4
PhCH2NH2
COOCH3
8
CONHCH2Ph
10
PhCH2NH2
OH
KHSO4
CONHCH2Ph
9
LiAlH4
NCH2Ph
11
1. Hg(OAc)2
2. NaBH4, OH−
OH
CH2Ph
12
12

Схема 2

комплексу кетокислоты **5.** Последний легко этерифицируется метанолом в присутствии H_2SO_4. После декомплексования (I_2, 20°C) выделен соответствующий метиловый эфир **6.** Кетонная карбонильная группа сложного эфира **6** селективно восстановлена действием $NaBH_4$ в изопропиловом спирте, давая смесь изомерных *цис-* и *транс-*оксиэфиров **7.** Эта смесь может быть двумя путями превращена в *N*-бензиламид 1-(1,2 дитидронафталин) уксусной кислоты **10.** Первый путь включает дегидратацию **7** кипячением в бензоле в присутствии $KHSO_4$ с образованием сложного эфира **8**, который затем переводится в *N*-бензиламид **10** действием бензиламина в присутствии NH_4Cl. Второй путь представляет собой обратную последовательность двух указанных стадий с промежуточным образованием оксиамида **9.**

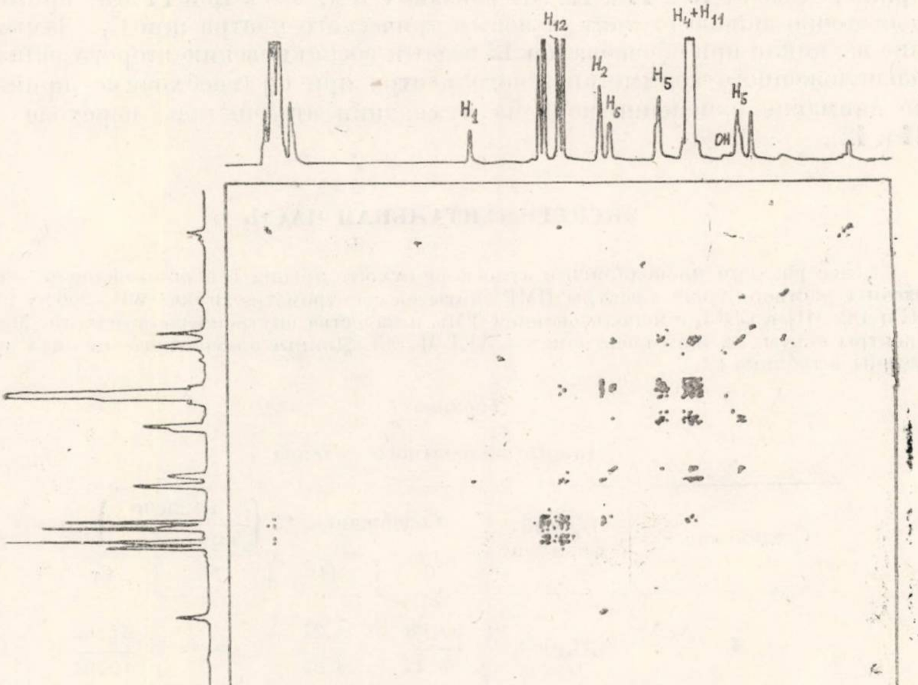

Рис. 1. — Корреляционный $^1H-^1H$ 2D COSY спектр соединения 12.

Восстановление амида **10** $LiAlH_4$ в ТГФ приводит к целевому синтону **11**, из которого действием сначала $Hg(OAc)_2$ в смеси ТГФ/ вода, а затем $NaBH_4$ в щелочной среде [2] получен 6,7-бензоморфан **12.**

Строение **12** подтверждено ПМР- и масс-спектрами. Отнесение сигналов протонов произведено на основании данных корреляционного

^{1}H–^{1}H 2D COSY спектра **12**(рис.1). Взаимное расположение гидроксильной группы и кольца C бензоморфановой структуры (*цис*- или *транс*- по отношению к кольцу *B*) определено с помощью двойного гомоядерного протонного резонанса. Величина $^3J_{H_1H_2}$ равна 1,1 Гц, что соответствует *транс*-расположению протонов H_1 и H_2. Следовательно, гидроксильная группа и аминогруппа расположены также в транс-положении по отношению друг к другу. Следует также отметить резкое увеличение разности химических сдвигов диастереотопных протонов в бензильном положении при переходе от **10** и **11** к **12**. Это связано с тем, что в **10** и **11** эти протоны достаточно далеко отстоят от асимметрического центра при C_1. Замыкание же цикла при образовании **12** ведет к возникновению второго близко расположенного асимметрического центра при C_1 (необходимо принять во внимание изменение порядка нумерации атомов при переходе от **11** к **12**).

ЭКСПЕРИМЕНТАЛЬНАЯ ЧАСТЬ

Все реакции проводились в атмосфере сухого аргона с использованием абсолютных растворителей. Спектры ПМР сняты на спектрометре Bruker WP–200 SV (200 МГц для ^{1}H) в $CDCl_3$ с использованием ТМС в качестве внутреннего стандарта. Масс-спектры сняты на масс-спектрометре AEI-M -30. Данные элементного анализа приведены в таблице 1.

Таблица 1

Данные элементного анализа

Соединение	Брутто-формула	Содержание, % $\left(\frac{\text{найдено}}{\text{вычислено}}\right)$			
		C	H	N	Cr
4	$C_{15}H_{14}CrO_5$	$\frac{55,08}{55,22}$	$\frac{4,27}{4,33}$	—	$\frac{15,62}{15,94}$
5	$C_{15}H_{12}CrO_6$	$\frac{52,83}{52,94}$	$\frac{3,39}{3,53}$	—	$\frac{15,50}{15,29}$
2,4-Динитрофенилгидразон **6**	$C_{19}H_{18}N_4O_6$	$\frac{57,50}{57,29}$	$\frac{4,60}{4,55}$	$\frac{14,02}{14,06}$	—
4-Нитробензоат **7**	$C_{20}H_{19}NO_6$	$\frac{65,00}{65,03}$	$\frac{5,15}{5,18}$	$\frac{3,71}{3,79}$	—
10	$C_{19}H_{19}NO$	$\frac{82,02}{82,28}$	$\frac{6,98}{6,90}$	$\frac{4,90}{5,05}$	—
12	$C_{19}H_{21}NO$	$\frac{81,60}{81,68}$	$\frac{7,85}{7,58}$	$\frac{4,96}{5,01}$	—

1′,2′,3′,4′-Тетрагидро-спиро(1,3-диоксолан-2,1′-нафталин) (**3**). К охлажденнмуо до −78°C раствору 91,0 г (0,44 моля) 1,2-бис (триметилсилилокси) этана и 63,6 г (0,44 моля) **2** в 100 мл CH_2Cl_2 добавили 0,84 мл $CF_3SO_3SiMe_3$. Смесь перемешивали при этой температуре в течение 35—40 ч (контроль за ходом реакции осуществляли методом ГЖХ ;

в случае необходимости добавляли 1—2 мл $CF_3SO_3SiMe_3$ или, при выпадении большого количества осадка, 50 мл CH_2Cl_2). К реакционной смеси при —78°С медленно добавляли 25 мл пиридина, затем воду, насыщенный раствор $NaHCO_3$ и эфир. Водный раствор отделяли, экстрагировали эфиром. Экстракт и органический слой объединяли, растворитель отгоняли, остаток перегоняли в вакууме. Получили 87,0 г (58%) **3**, т. кип. 118—124°С/3 мм рт. ст.

Трикарбонил-η^6- [1′,2′,3′,4′-тетрагидро-спиро (1, 3-диоксолан-2, 1′-нафталин)] хром (**4**). Смесь 3,39 г (17,84 ммоля) **3** и 23,55 г(107,05 ммоля) $Cr(CO)_6$ кипятили в смеси 100 мл дибутилового эфира и 20 мл ТГФ в течение 28 ч. После охлаждения раствор профильтровали через слой Al_2O_3 (5 см). Растворитель отгоняли, остаток перекристаллизовали из смеси бензол/гептан. Получили 4,30 г (74%) **4**, т. пл. 122,5—124°С. Масс-спектр: M^+ 326.

Трикарбонил-η^6- [1-(1,2,3,4-тетрагидро-4-оксонафталин) уксусная кислота] хром (**5**). К суспензии $NaNH_2$ (получали из 0,70 г натрия) в 120 мл жидкого NH_3 добавляли при —70°С 25 мл ТГФ и 8,40 г (25,8 ммоля) **4**. Смесь перемешивали 1 ч при этой температуре, а затем нагревали до —50°С и перемешивали еще 30 мин. К реакционной смеси добавляли 4,90 г (30,4 ммоля) $BrCH_2COONa$, большую часть NH_3 испаряли, после чего реакционную смесь обрабатывали 1 г NH_4Cl, водой, 10%-ным раствором NaOH. Щелочной раствор экстрагировали эфиром и подкисляли при охлаждении 10%-ной HCl. Продукт экстрагировали эфиром, эфир отгоняли. Получили 5,65 г (64%) **5**, т. пл. 202—205°С. Масс-спектр: M^+ 340.

Метиловый эфир 1-(1,2,3,4-тетрагидро-4-оксонафталин) уксусной кислоты (**6**). Раствор 4,00 г (11,8 ммоля) **5** и 20 мл MeOH в 200 мл CCl_4 кипятили в присутствии 0,5 мл H_2SO_4 (конц.) в течение 4 ч. Смесь охлаждали, промывали 1 *М* раствором NaOH водой. Органический слой отделяли, растворитель отгоняли. Остаток растворяли в 50 мл 50%-ного водного ацетонитрила и перемешивали 45 мин. при комнатной температуре в присутствии избытка иода. Непрореагировавший иод удаляли обработкой реакционной смеси раствором $Na_2S_2O_3$. Продукты реакции экстрагировали эфиром, эфир отгоняли. Получили 1,97 г (82%) **6** в виде масла. Масс-спектр: M^+ 218. ПМР-спектр (δ, м.д.): 3,78 (3Н, OCH_3). 2,4-Динитрофенилгидразон **6**: т. пл. 136—137°С, масс-спектр: M^+ 398.

Метиловый эфир 1-(1,2,3,4-тетрагидро-4-гидроксинафталин)-уксусной кислоты (**7**). К раствору 1,31 г (34,4 ммоля) $NaBH_4$ в 100 мл изопропилового спирта добавляли раствор 1,50 г (6,88 ммоля) **6** в 25 мл изопропилового спирта. Смесь оставляли на ночь, затемобрабатывали водой и 3%-ной HCl. Продукты экстрагировали эфиром, экстракт промывали водой, сушили над Na_2SO_4, растворитель отгоняли. Получили 1,01 г (67%) **7** (смесь *цис-* и *транс-*изомеров) в виде масла. 4-Нитробензоат **7**: масс-спектр: M^+ 369.

Метиловый эфир 1-(1,2-дигидронафталин) уксусной кислоты (**8**). Раствор 0,05 г 7 кипятили в 5 мл бензола в присутствии избытка $KHSO_4$ в течение 2ч. После охлаждения раствор профильтровали, растворитель отгоняли. Получили 0,04 гл (86%) **8** в виде масла. Масс-спектр: M^+ 202. ПМР-спектр (δ, м.д): 3,65 (3Н, OCH_3), 5,91 (IH, H_3), 6,48 (IH, H_4), $^3J_{3,4}$ 9,5 = Гц.

N-Бензиламид 1-(1,2-дигидронафталин) уксусной кислоты (**10**). 0,24 г (1,18 ммоля) **8** нагревали в 1,5 мл бензиламина в присутствии 0,025 г (0,47 ммоля)NH_4Cl в течение 17 ч при 130°С. Реакционную смесь разбавляли водой, обрабатывали 10%-ной HCl. Продукты экстрагировали хлороформом. Растворитель отгоняли, остаток хроматографировали на колонке SiO_2 в хлороформе. Получили 0,25 г (76%) **10**, т. пл. 123,5—124,5°С (бензол/гексан). ПМР-спектр (δ, м.д.): 4,32 и 4,35 (IH и IH, $PhCH_2$, AB-система), 5,70 (IH, NH), 5,88 (IH, H_3), 6,42 (IH, H_4), $^3J_{3,4}$ = 9,55 Гц.

1-(N-Бензил-2-аминоэтил)-1,2-дигидронафталин (**11**). Раствор 0,33 г (1,19 ммоля) **10** в 25 мл ТГФ добавляли по каплям к суспензии избытка $LiAlH_4$ в 20 мл ТГФ. Смесь кипятили 18 ч, затем разлагали водой и обрабатывали 10%-ной HCl. Кислотный слой отделяли, органический промывали водой. Кислый раствор и водные вытяжки объединяли, обрабатывали NaOH (тв.), продукты реакции экстрагировали эфиром. Экстракт сушили над NaOH, растворитель отгоняли. Получили 0,21 г (67%) **11**. Масс-спектр: M^+263. ПМР-спектр (δ, м.д.); 3,72 (2Н,$PhCH_2$)$_2$ 5,88 (IH,H_3), 641(IH, H_4).

3-Бензил-1,2,3,4,5,6-гексагидро-1-гидрокси-2,6-метано-3-бензазоцин(**12**). К раствору (0,21 г (0,80 ммоля) **11** в 35 мл ТГФ добавлялм 0,26 г 0,80 ммоля $(HgOAc)_2$. Смесь перемешивали 10 мин, при 20°С, после чего к ней добавляли 15 мл воды и перемешивали еще 75 ч. К смеси добавляли 15 мл 10%-ного раствора КОН и 0,30 г $NaBH_4$. Смесь перемешивали 1 ч. Раствор профильтровали, продукты экстрагировали эфиром и промывали 10%-ной HCl (3×30 мл). Кислотные вытяжки обрабатывали 1 *М* раствором NaOH до щелочной реакции, продукты экстрагировали эфиром. Эфирный раствор сушили над NaOH, растворитель отгоняли. Остаток хроматографировали на колонке $Si_2O-CHCl_3/MeOH$(20: 1)). Получили 0,09 г (45%) **12**, т. пл. 139—141°С (из гексана). Масс-спектр: M^+ 279.

ЛИТЕРАТУРА

[1] В. Н. Калинин, Н. И. Удалов и А. В. Усатов. *Изв. АН СССР, серия хим.*, **1987,** 1672.

[2] H. Inoue and E. L. May, *J. Med. Chem.*, **19,** 259 (1976).

Revue Roumaine de Chimie, **34**, *2*, 509–516 (1989

НУКЛЕОФИЛЬНЫЕ И ЭЛЕКТРОФИЛЬНЫЕ РЕАКЦИИ 1,5-ДИКЕТОНОВ

В. Г. ХАРЧЕНКО и С. Н. ЧАЛАЯ
Саратовский государственный университет, Саратов, СССР

Получена 18 ноября 1988 г.

Описываются реакции 1,5-дикетонов с нуклеофильными (аммиак, амины, гидроксиламины, сернистый водород) и электрофильными реагентами (кислоты, хлор, бром и т.д.). Приводится также реакция каталитического гидрирования.

The paper describes the reactions of 1,5-diketones with nucleophiles such as ammonia, amines, hydroxylamines, hydrogen sulphide, and with electrophiles: acids, chlorine, bromine, etc. Also the catalytic hydrogenation is described.

1,5-Дикетоны относятся к весьма доступным и исключительно перспективным карбонильным соединениям, широко используемым в органическом синтезе. Характерным свойством 1,5-директонов является их способность подвергаться циклизации с образованием шести- либо пятичленных карбо- и гетероциклических систем. При наличии в α-положении к CO-группам метильных или метиленовых групп возможна циклизация, в результате которой уже в условиях синтеза дикетонов наблюдается образование продуктов внутримолекулярной альдольной или кротоновой конденсации.[1]

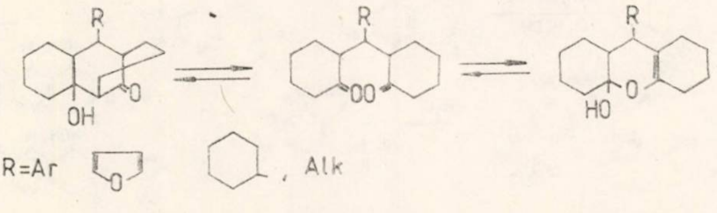

Следует отметить, что арилиденсбисциклогексаноны существуют преимущественно в полуацетальной форме, стабилизация которой осуществляется, видимо, за счет арильной группы в метиленовом мостике. Указанные процессы карбо- и гетероциклизации являются примерами внутримолекулярных нуклеофильных процессов 1,5-дикетонов.

Действие кислот способствует гетероциклизации 1,5-дикетонов и сопровождается образованием кислородных гетероциклических систем — пиранов и солей пирилия. В реакциях с $HClO_4$, CF_3COOH или эфиратом трехфтористого бора в уксусной кислоте нам удалось выделить наряду с солями пирилия соответствующие тетрагидропираны, являющиеся продуктами диспропорционирования пиранов:[2]

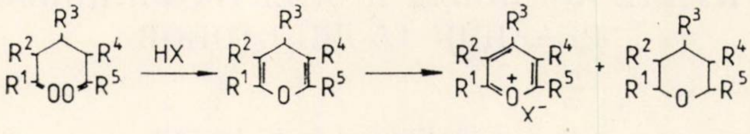

Реакции 1,5-дикетонов с аммиаком и первичными аминами приводят к образованию 1,4-дигидропиридинов, которые в ряде случаев могут быть выделены, но чаще претерпевают дальнейшие превращения: подвергаются пиридинизации с образованием пиридиновых оснований или их солей, присоединяют второй нуклеофил (например, CN, H_2O_2 и другие), если такой имеется в реакционной смеси, либо диспропорционируют с образованием смеси пиридиновых, тетра- либо гексагидропиридиновых производных:[1]

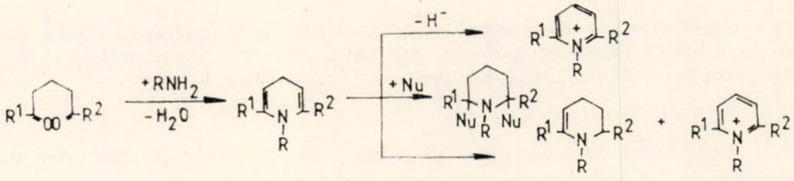

При действии солянокислого гидроксиламина на оксо-1,5-дикетоны наряду с обычным процессом пиридинизации наблюдается процесс изомеризации возникающего пиридинового производного и образование двух изомерных оксогидрохинолинов:[3]

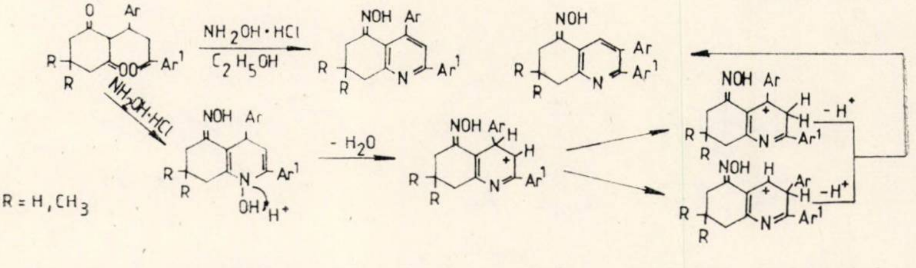

Каталитическое гидроаминирование 1,5-дикетонов включает нуклеофильный процесс аминирования и каталитическое гидрирование. Гидрометиламинирование протекает с высокой селективностью и образованием N-метилпиперидинов, N-метилгидрохинолинов, N-метилпергидроакридинов и родственных соединений. В анологичных условиях бициклические 1,5-дикетоны с этаноламином дают N-(β-оксиэтил)-дициклипиперидины; нециклические и семициклические 1,5-дикетоны реагируют как бинуклеофилы, образуя производные оксазологидропиридинов. При гидроаминировании посредством H_2/NH_3 на никеле, модифицированном рутением, 1,5-дикетоны образуют смеси пиридинов и пиперидинов либо соответствующие диолы :[4]

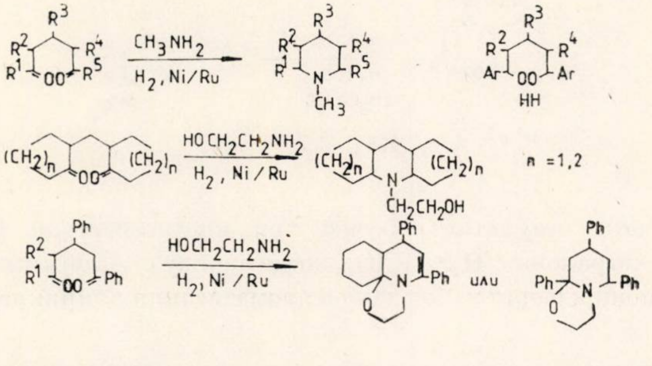

Циклизация 1,5-дикетонов с сернистыми реагентами (H_2S или P_xS_y) осуществляется с образованием тиопиранов либо продуктов их диспропорционирования — тиациклогексанов или дигидротиопиранов и соответствующих солей тиопирилия. Характер возникающих продуктов определяется структурой дикетонов и условиями реакций :[5]

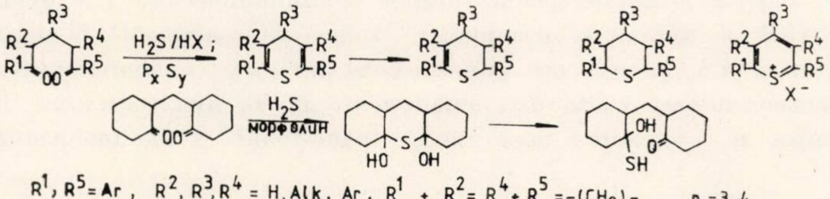

$R^1, R^5 = Ar$, $R^2, R^3, R^4 = H, Alk, Ar$, $R^1 + R^2 = R^4 + R^5 = -(CH_2)_n-$, n = 3,4

В случае реакции метиленбисциклогексанона с H_2S в морфолине выделен интермедиат — тиобисполуацеталь, который при действии кислоты превращается в соль тиопирилия и тиациклогексан.

При действии на 1,5-дикетоны H_2S/HCl в метаноле чаще образуются тиопираны, а в среде уксусной кислоты с теми же реагентами — продукты их диспропорционирования. Влияние характера заместителей в 1,5-дикетонах проявляется на глубине диспропорционирования. Так, 2,4-диметил-1,5-дифенилпентандион с H_2S/HCl в уксусной кислоте образует смесь хлорида тиопирилия и дигидротиопирана, тогда как метиленбисциклогексанон и в метаноле дает продукты полного диспропорционирования. Для 1,Б-диарил-3-(5R-фурил) пентандиона реакции с H_2S/HCl протекают легко только в метаноле, а в уксусной кислоте фурановый цикл разрушается, проявляя ацидофобные свойства.

Электронодонорные заместители в 1,5-дикетонах, как оказалось, способствуют диспропорционированию. Этот факт оказался особенно ценным в случае оксо-1,5-дикетонов, когда при введении метоксифенильных заместителей удалось получить соли тиопирилия.

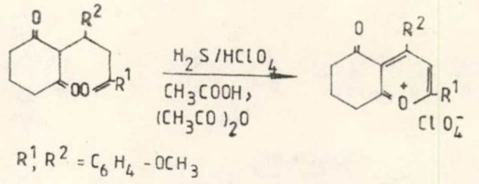
O
R²
R¹
H₂S/HClO₄
CH₃COOH,
(CH₃CO)₂O
ClO₄⁻
R¹, R² = C₆H₄-OCH₃

Необычный результат получен при взаимодействии 1,3-дифенилпропанонил-тетралона с $H_2S/HClO_4$, когда наряду с обычными продуктами диспропорционирования наблюдается ароматизация алицикла:

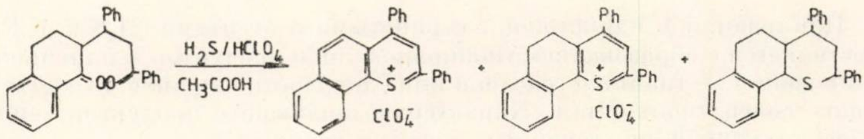
Ph
H₂S/HClO₄
CH₃COOH
S
ClO₄⁻
+

В случае реакций трео-изометров семициклических 1,5-дикетонов с H_2S/HCl в метаноле возникают транс-транс-метокси-3,5-диарил-2-тиабицикло-[4,4,0]-дец-3-ены, образование которых является результатом взаимодействия указанных дикетонов с двумя нуклеофилами. Незамещенный в C^3-дикетон дает смесь транс-транс- и цис-цис-изомеров:

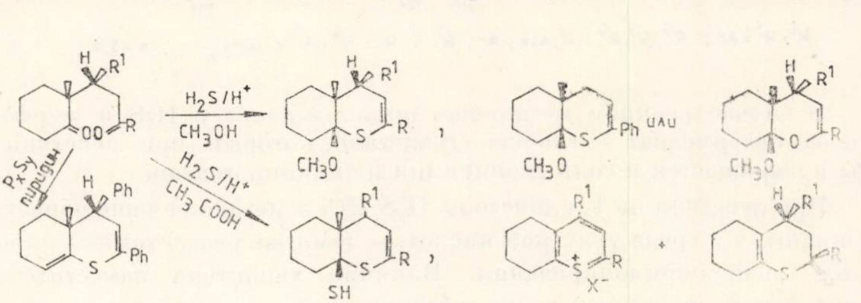
H
R¹
R
H₂S/H⁺
CH₃OH
CH₃O
S
Ph
или
O
PₓSᵧ
пиридин
H₂S/H⁺
CH₃COOH
SH
X⁻
+

Уменьшение размера алицикла в молекуле семициклических 1,5-дикетонов меняет характер процесса и приводит к образованию только 4Н-тиопирана. В реакциях семициклических 1,5-дикетонов с P_xS_y в пиридине образуется сульфид, который содержит двойную связь в алицикле.

3(4-Пиразонил)-пропанолы в реакцию с H_2S и P_xS_y в описанных условиях не вступают, а в ,,жестких'' условиях образуют пираны. Видимо, причина состоит в образовании соли пиранопиразолия. Соответствующие соли пирилия удалось получить только выше 140 °C:

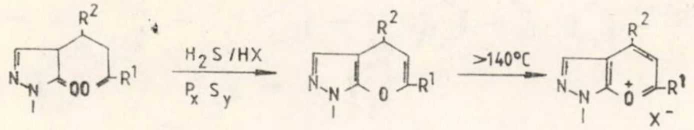
R²
R¹
H₂S /HX
PₓSᵧ
>140°C
X⁻

Нуклеофильные реакции 1,5-дикетонов с селеноводородом возможны лишь в инертной атмосфере в отсутствии кислорода воздуха. Характер превращения 1,5-дикетонов с H_2Se/HX аналогичен их реакциям с сероводородом. Важной особенностью реакций дикетонов с H_2Se является образование моно- или диселенолов селеноциклогексанов наряду с солями селенопирилия и селеноциклогексанами:[6]

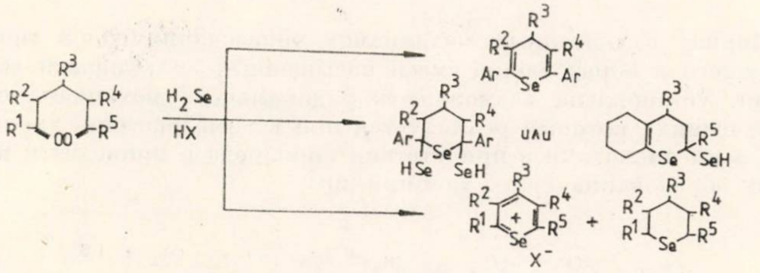
H₂Se
HX
R¹ R² R³ R⁴ R⁵
Ar
Se
HSe
SeH
или
X⁻
+

В результате кинетических исследований реакции гетероциклизации 1,5-дикетонов с сероводородом установлено, что присоединение сероводорода идет по одной карбонильной группе, лимитирующей стадией является взаимодействие нуклеофила с протонированной карбонильной группой, дальнейшее превращение гем-ол-тиола протекает быстро с образованием тиопирана:[5]

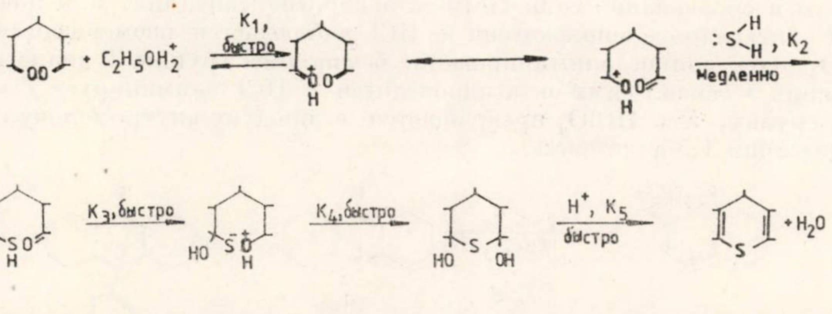
+ C₂H₅OH₂⁺
K₁, быстро
:S H H , K₂
медленно
K₃, быстро
K₄, быстро
H⁺, K₅
быстро
+ H₂O
HO
OH
H

Тиопираны в ряде случаев уже в условиях реакции подвергаются диспропорционированию до циклических сульфидов и солей тиопирилия.

Процесс диспропорционирования протекает по катионному механизму ступенчато, включая протонирование тиопирана, стабилизацию возникающего карбкатиона за счет межмолекулярного переноса гидрид-иона из положения C^4:

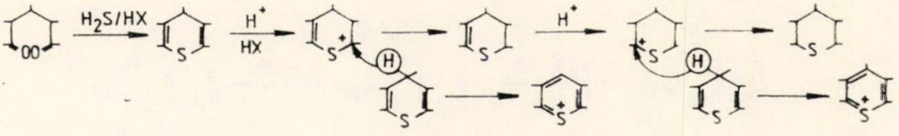

Межмолекулярный гидридный перенос и образование при протонировании карбкатионов по C^2 и C^6 подтверждается экспериментально в реакции дейтерированного тиопирана с CF_3СООД :[5]

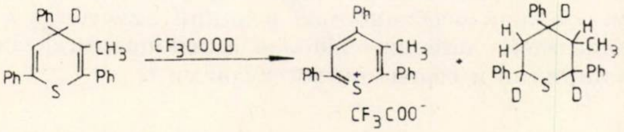

Наряду с указанным механизмом образования солей тиопирилия приводящего к образованию смеси насыщенных сульфидов и солей тиопирилия, установлена возможность радикального механизма образования последних, который реализуется при взаимодействии тиопиранов с протонными кислотами в присутствии кислорода и приводит к количественному образованию солей тиопирилия:

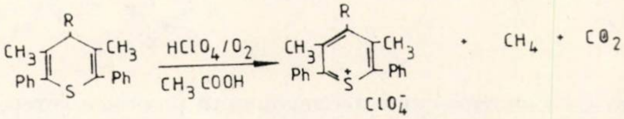

Следует отметить своеобразное действие кислот HCl и $HClO_4$ на 9-бензил-симм-октагидротио(селено)ксантены. В этом случае возникающий в результате протонирования тиопиранового цикла карбкатион стабилизируется за счет электрофильного взаимодействия с ароматическим циклом. Наряду с этим наблюдается элиминирование бензильной группы и образование соли симм-октагидротиоксантилия. Для 9-бензил-симм—октагидроселеноксантена с HCl наблюдается изомеризация, а с $HClO_4$ почти полное элиминирование бензильной группы. В аналогичных условиях 9-бензил-симм-октагидроксантен с HCl элиминирует бензильную группу, а с $HClO_4$ превращается в продукт внутримолекулярной конденсации 1,5-дикетона:

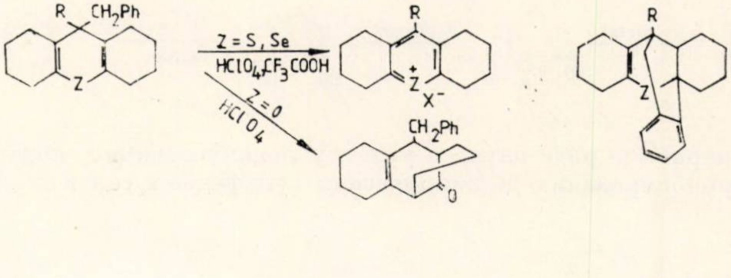

Исходя из структурных особенностей 1,5-дикетонов (наличие карбонильных групп и подвижных атомов водорода в α-положении), свидетельствующих о том, что для соединении подобного типа должны легко протекать не только реакции с нуклеофильными реагентами, но и с электрофильным, мы изучили реакции 1,5-дикетонов с галогенами. В результате были найдены условия электрофильного замещения атомов водорода. Так, при действии хлора в CCl_4 при 60°C наблюдается преимущественное образование 2,4-дихлорпентандионов. В ряде случаев удается выделить моно- и трихлорзамещенные продукты:[7]

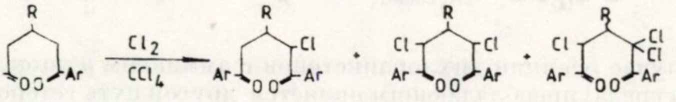

Реакции 1,5-дикетонов с бромом в зависимости от условий осуществляются по двум направлениям: при действии брома в CCl_4 при 60°C образуются продукты электрофильного замещения — соответствующие бромзамещенные дикетоны, при нагревании в уксусной кислоте наблюдается солеобразование:

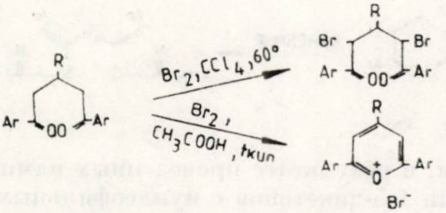

Изучены структурные особенности дихлорзамещенных пентандионов, выявлено определяющее влияние заместителей в положении C^3 на структуру дихлорпроизводных. На основании спектральных исследований и рентгеноструктурного анализа установлено, что для 1,5-диарил-2,4-дихлорпентандионов реализуется симметричная структура с заслоенным положением атомов кислорода и хлора, в молекуле 1,3,5-тризамещенных 2,4-дихлорпентандионов существует различное пространственное расположение бензоильных групп — с заслоненным и незаслоненным расположением атомов кислорода и хлора:

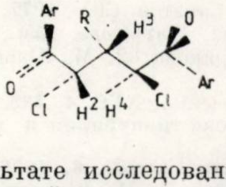

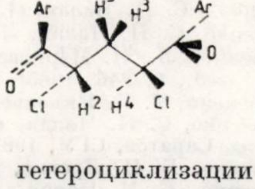

В результате исследований реакций гетероциклизации дихлордикетонов с нуклеофильными реагентами выявлены новые аспекты превращений дикарбонильных соединений, обусловленные наличием в их структуре подвижных атомов хлора.[8] Установлено, что реакции дихлордикетонов с ацетатом аммония в уксусной кислоте осуществляются обычным путем, включающим легко протекающие в кислой среде присоединение нуклеофила по карбонильной группе и гетероциклизацию с участием второго карбонила, приводящую к образованию пиридиновых производных. Следует отметить селективную направленность процесса гетероциклизации дихлордикетонов в указанных условиях, протекающую с количественным образованием 3-хлорпиридинов:

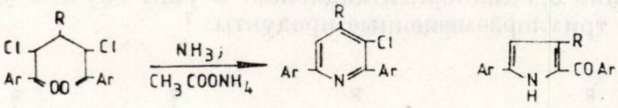

В случае реакции дихлордикетонов с аммиаком в диоксане при 60°С (основная среда) преобладающим является другой путь гетероциклизации, включающий участие атомов хлора и СО-групп, в результате чего основными продуктами являются ароилпирролы. Характер превращения дихлордикетонов зависит также и от заместителя в положении C^3.

Реакции дихлордикетонов с динуклеофиоами-тио-и фенилтиомочевинами приводят к бисаминотиазолам, образование которых является также результатом взаимодействия реагента по атомам хлора и СО-группам:

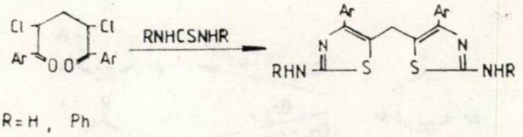

Таким образом, в результате проведенных нами исследований установлено, что реакции 1,5-дикетонов с нуклеофильными реагентами (серо- и селеноводородом, а также реакции каталитического гидроаминирования) осуществляются с образованием соответствующих шестичленных серо-, селен- и азотсодержащих систем. При действии хлора и брома наблюдается электрофильное замещение атомов водорода с образованием соответствующих галогенпроизводных. Введение хлора в структуру 1,5-дикетонов проявляется в новых аспектах их гетероциклизации с нуклеофильными реагентами, в частности, реакции с аммиаком осуществляются по двум конкурирующим направлениям с образованием хлорпиридинов и бензоил-пирролов.

ЛИТЕРАТУРА

[1] В. Г. Харченко, С. Н. Чалая, «1,5-Дикетоны», Саратов, СГУ, 1977, 58 с.

[2] В. Г. Харченко, С. Н. Чалая, Л. Г. Чиченкова, *Журн. орг. хим.*, **7**, 444(1975).

[3] В. Г. Харченко, Л. И. Маркова, Т. Д. Казаринова, Л. М. Юдович, *Хим. гетероцикл. соед.*, **6**, 846 (1985).

[4] А. П. Кривенько, Т. Г. Николаева, В. Г. Харченко, ХГС, **4**, 435 (1987).

[5] В. Г. Харченко, С. Н. Чалая, «Тиопираны, соли тиопурилия и родственные соединения», Саратов, СГУ, 1987, 160 с.

[6] В. Г. Харченко, Б. И. Древко, *Хим. гетероцикл. соед.*, **6**, 1636 (1984).

[7] В. Г. Харченко, С. Н. Чалая, О. В. Литвинов, Л. М. Юдович, В. К. Промоненков, *Журн. орг. хим.*, **20**, *6*, 1208 (1984).

[8] В. Г. Харченко, С. Н. Чалая, О. В. Литвинов, *Хим. гетероцикл. соед.*, **3**, 352 **(1985)**.

Revue Roumaine de Chimie, **34**, *2*, 517–526 (1989)

КАТАЛИТИЧЕСКАЯ НЕЙТРАЛИЗАЦИЯ ОКСИДОВ АЗОТА НА ПОВЕРХНОСТИ КАТАЛИЗАТОРОВ CuO, Co_3O_4 И $Cu_xCo_{3-x}O_4$ ШПИНЕЛЯХ

МАРИЯНА ХРИСТОВА, Д. ПАНАЙОТОВ и Д. МЕХАНДЖИЕВ
Институт общей и неорганической химии БАН, София 1040, ул. Акад. Г. Бончев, бл. 11, Болгария.

Получена 3 октября 1988 г.

Исследовано взаимодействие NO с CO на поверхности CuO, Co_3O_4 и на $Cu_xCo_{3-}O_4$ шпинелях ($0 \leqslant x \leqslant 1$) в интервале температур 60–240°C. Установлено, что скорость обеих реакций восстановления NO до N_2O и N_2 соответственно повышается с увеличением содержания Cu(x). Увеличение скорости второй реакции наблюдется лишь при $x \geqslant 0.5$. Это связано с присутствием различных активных центров, на которых формируются N_2O и N_2.
Состояние поверхности катализатора в ходе каталитического процесса было исследовано методом переходного отклика при последовательном использовании катализаторов со смесями NO + CO + Ar (стехиометрическая смесь реагентов) NO+Ar. Было установлено, что в присутствие стехиометрической смеси (NO+CO) протекает вторичное взаимодействие CO с кислородом поверхности катализатора. Количество взаимодействующего CO с поверхностью увеличивается значительно для катализаторов, при которых $x \geqslant 0,5$. При $Cu_xCo_{3-x}O_4$ катализаторах восстановление на поверхности приводит преимущественно к ускорению восстановления NO до N_2. Предполагается, что механизм восстановления NO до N_2O при температурах ниже 170°C один и тот же для всех катализаторов, лишь скорость лимитирующий этап реакции меняется с изменением содержания меди в катализаторах.

The interaction of NO with CO on CuO and Co_3O_4 catalysts and $Cu_xCo_{3-x}O_4$ spinels ($0 \leqslant x \leqslant 1$) at temperatures of 60–240°C was investigated. It was found that the two reactions of NO reduction, to N_2O and N_2, respectively, are accelerated with increasing Cu(x) content. An increase in the rate of the second reaction was only observed at $x \geqslant 0.5$. This is attributed to the presence of different active sites on which N_2O and N_2 are formed. The state of the catalyst surface during the catalytic process was investigated by the transient response method, the catalysts being successively used with NO + + CO + Ar (a stoichiometric mixture of the reagents) and NO + Ar. It was found that a secondary interaction of CO with the oxygen from the catalyst surface proceeds in the presence of the stoichiometric mixture NO + CO. The amount of CO interacting with the surface considerably increases with catalysts in which $x \geqslant 0.5$. In the case of $Cu_xCo_{3-x}O_4$ catalysts, the reduction of the surface accelerates mainly the reduction of NO to N_2. The mechanism of NO reduction to N_2O at temperatures below 170°C is supposed to be the same for all catalysts, the rate-determining step changing with the copper content in the catalysts.

ВВЕДЕНИЕ

Оксиды азота являются одними из наиболее токсических соединений, выбрасываемых в атмосферу отходящими газами промышленных предприятий и выхлопными газами двигателей внутреннего сгорания.

Перспективным методом удаления оксидов азота от выхлопных газов является их каталитическое восстановление. В качестве восстановителей могут быть использованы углеводороды, аммиак, водород, оксид углерода.

В настоящее время среди катализаторов, применяемых в практике для очистки выхлопных газов существенную роль имеют катализаторы на основе благородных металлов, в первую очередь платины. К идеям замены платиновых катализаторов с оксидными, оксидами переходных металлов или другими придерживаются все меньшее число сторонников. Кроме высокой активности этих катализаторов, оптимизм поддерживается еще фактом, что среди них существуют такие оксидные катализаторы со шпинельной структурой, которые сохраняют своя активность в присутствии каталитических ядов.

Каталитическое восстановление оксида азота с CO протекает следующим образом:

$$2NO + CO = N_2O + CO_2 \tag{1}$$

$$2NO + 2CO = N_2 + 2CO_2 \tag{2}$$

В общих чертах, получение N_2 можно представить схемой двух маршрутов:

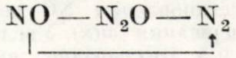

$$NO - N_2O - N_2$$

По первому маршруту NO восстанавливается до N_2 после получения N_2O. По второму маршруту осуществляется прямое восстановление NO до N_2. Среди оксидных катализаторов самую большую активность в отношении восстановления NO с CO проявляют оксиды переходных металлов. Алхазов и сотр.[1] получили следующий порядок активности оксидных катализаторов:

$$CuO > Co_3O_4 > Mn_3O_4 > Fe_2O_3 > NiO > Cr_2O_3 > ZnO$$

Однако, надо отметить, что при окислах наблюдаются фазовые изменения даже в стехиометрической смеси NO + CO, которое приводит к изменению их активности.

Нами был получен[2] порядок каталитической активности шпинельных катализаторов, имеющий общую формулу $MCo_2O_4/M=Cu$, Ni, Mn/ в отношении восстановления NO с CO:

$$CuCo_2O_4 > CuO > Co_3O_4 > NiCo_2O_4 > MnCo_2O_4$$

Установлено, что для оксидных систем образование на поверхности каталитического активного слоя является важным этапом гетерогенно каталитических процессов.[3]

Для исследования процессов, при которых на поверхности катализаторов наблюдаются изменения вследствие ее взаимодействия с газовой фазой, особо подходящим оказывается метод переходного отклика. В основе этого метода лежит запись отклика данного параметра реакционной системы при определенном скачкообразном нарушении стационарного состояния.

Из вышесказанного стало видно почему представляет интерес изучение каталитического восстановления NO с CO на $Cu_xCo_{3-x}O_4$ (где $0 \leqslant x \leqslant 1$) шпинелях. Для сравнсния были изучены также катализаторы CuO и Co_3O_4.

ЭКСПЕРИМЕНТАЛЬНАЯ ЧАСТЬ

Методика получения образцов подробно описана в. [4] Рентгенофазовый анализ показывает, что $Cu_xCo_{3-x}O_4$ образцы монофазовые и обладают .шпинельной структурой. Удельная поверхность (по методу БЭТ) CuO равна 8 м²/г, Co_3O_4—9м²/г, $Cu_{0,3}Co_{2,7}O_4$ — — 14 м²/г, $Cu_{0,54}Co_{2,46}O_4$ — 12 м²/г, $Cu_{0,94}Co_{2,06}O_4$ — 4 м²/г и $CuCo_2O_4$ — 5 м²/г.

Каталитические измерения проводили в проточной аппаратуре с модельной газовой смесью CO — 0,12 об.%, NO — 0,12 об. % и остальное — аргон. Содержание CO и NO в выходящем из реактора газовом потоке непрерывно контролировали NDIR газанализаторами ,,Maihak'' (производство ФРГ), а содержание N_2O путем газовой кювети (Z = 1м) ,,Specac'' (Англия) на спектрофотометре ,,Specord'' 75—IR (ГДР), при объемной скорости газового потока $26000h^{-1}$. Соотношения между длиной каталитического слоя (30 мм) и размером зерен (0,3—0,6) с одной стороны, и между диаметром реактора (8 мм) и размером зерен, с другой стороны, соответственно выше 30 и 4.

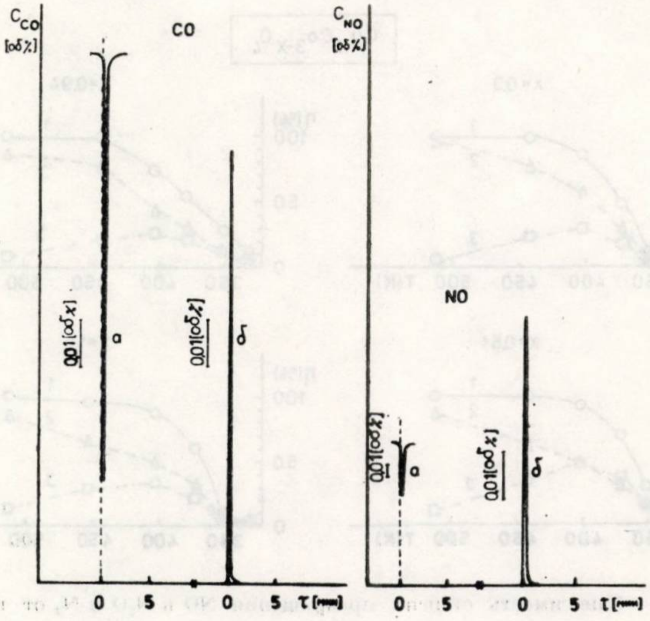

Рис. 1. — Старт- и стоп кривые отклика CO и NO для реактора, заполненного кварцем.

Согласно Doraiswamy [5] эти соотношения обеспечивают минимальные градиенты концентрации и температуры в случае проточного реактора.

На рис. 1 даны записи кривых отклика для CO и NO когда в реакторе на месте катализатора находился слой кварца того же роста и размера частиц.

ОПЫТНЫЕ РЕЗУЛЬТАТЫ И ИХ ОБСУЖДЕНИЕ

На рис. 2 предствлена зависимость степени превращения NO и CO от температуры катализаторов Co_3O_4, CuO, и $Cu_xCo_{3-x}O_4$(x = 0,3 ;0,54 ; 0,94 и 1).

Сравнивая активность ηNO и селективность (γN_2 и ηN_2O) катализаторов устанавливается, что содержание Cu(x) в катализаторах $Cu_xCo_{3-x}O_4$ в

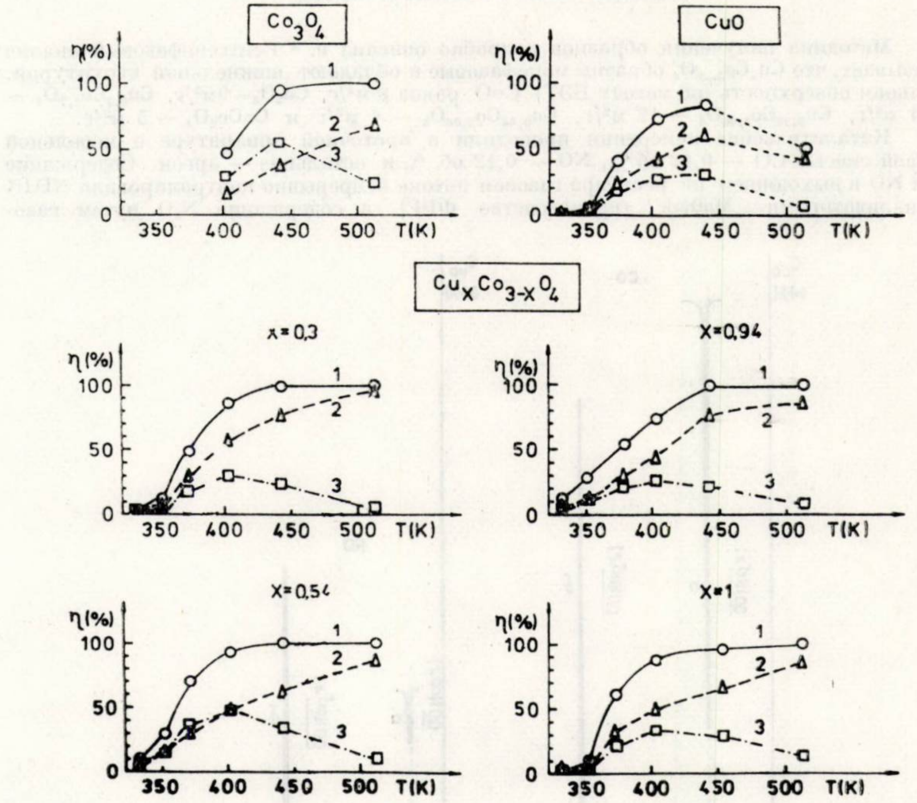

Рис. 2. — Зависимость степени превращения NO в N_2O и N_2 от температуры.

значительной степени оказывает влияние на их каталитические свойства. Как видно от рисунка, с увеличением содержания Cu в решетке шпинеля повышается эффективность восстановления NO.

Максимумы образования N_2O находятся при ~ 400 K для всех $Cu_xCo_{3-x}O_4$, а для CuO и Co_3O_4 они при 440 K. Образование N_2 для всех катализаторов начинается одновременно с образованием N_2O. С повышением температуры образование N_2 монотонно нарастает.

Чтобы показать роль содержания Cu(x) в образцах, нами была подсчитана средняя скорость восстановления $NO-I_S^{NO}$ до N_2O и до N_2 при определенной температуре, выраженная в граммах NO конвентированный до N_2O и N_2 на 1 м² поверхности катализатора за 1 час. Для этой цели выбрали температуру максимального образования N_2O для Cu-содержащих катализаторов, которая равняется 400 K. Данные представлены на рис. 3.

От рисунка стало ясно, что в зависимости от содержания Cu(x) интенсивность превращения $NO(I_S^{NO})$ до N_2O и N_2 меняется разным образом. Этот факт дает основание допустить, что реакции, ведущие к образованию N_2O и N_2 протекают на различных активных центрах.

С другой стороны факт, что еще в начале исследуемого интервала температур наблюдается одновременное формирование N_2O и N_2, как и сам ход кривых $\eta \sim (T)$, говорит о наличии независимых маршрутов обеих реакций $NO \genfrac{}{}{0pt}{}{\nearrow N_2O}{\searrow N_2}$.

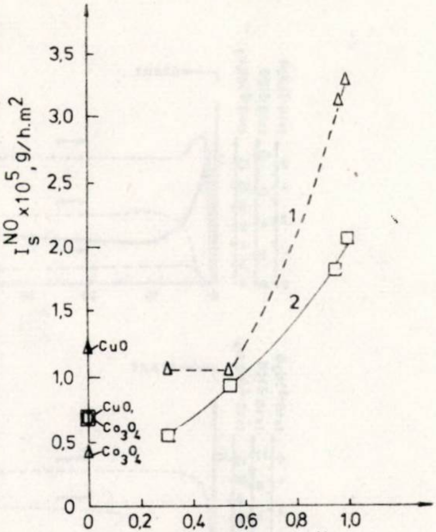

Рис. 3. — Средняя скорость восстановления I_S^{NO} до N_2O и N_2 в зависимости от содержания Cu(x).

Интересный способ анализа кривых отклика, полученных в переходном периоде, предлагает Кобаяши.[6] Он классифицирует кривые отклика, отражающие изменение со временем концентрации продуктов от реакции согласно их виду. Вид этих кривых со своей стороны несет информацию о скорость-лимитирующем этапе в реакции образования продуктов.

Были проведены 3 серии экспериментов:

$A = Ar \rightarrow$ (старт) $NO + CO + Ar \rightarrow$ (стоп) Ar

$B = A \rightarrow$ (старт) $NO + Ar \rightarrow$ (стоп) Ar

$C = A \rightarrow B \rightarrow$ (страт) $NO + CO + Ar \rightarrow$ (стоп) Ar

На рис. 4 представлены кривые отклика экспериментов серии А при 400 К.

Кривые отклика N_2O для Co_3O_4 при 400 К указывают на индукционный период в стартовом этапе и постепенное медленное уменьшение концентрации N_2O в стоп-этапе в течение ~30 мин. (появляющееся в виде хвоста десорбционного пика). Это кривая S — образного типа. При Cu-содержащих катализаторах не наблюдается индукционный период в старт-этапе, а в стоп-этапе выделение N_2O заканчивается более быстро с нарастанием содержания Cu(x). Кривые отклика N_2O для образцов, имеющих x = 0,3 и x = 0,54 можно определить как монотонно нарастающие, а другие, с x = 0,94 — как кривые моментального типа. При температуре 400 К, одновреемнно с образованием N_2O протекает также образование N_2 в соизмеримых количествах в начальном периоде.

Кривые отклика для СО показывают, что с увеличением содержания Cu(x) нарастает количество СО, которое участвует во вторичном релаксационном процессе — по всей вероятности отбирает кислород от поверхности катализаторов.

На рис. 5 показаны кривые отклика экспериментов той самой серии А, но при температуре 510 К. Изменения вида кривых отклика по сравнению с наблюдаемыми при 400 К очевидны. Кривые отклика N_2O для Co_3O_4 моментального типа, а для Cu — содержащих катализаторов — т.н. надрастающего типа. Кривые отклика N_2 монотонно нарастающего типа

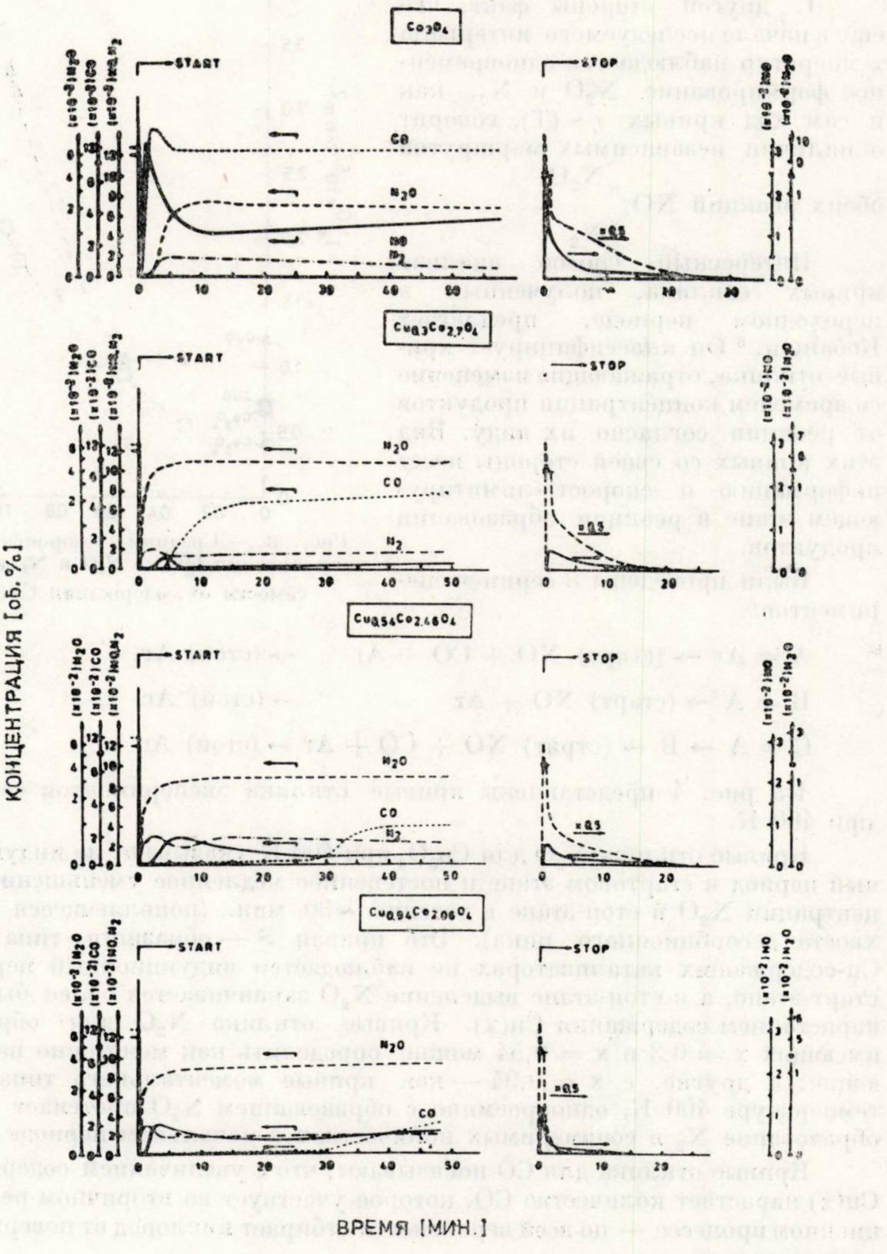

Рис. 4. — Кривые отклика экспериментов серии A при 403 K.

указывают на постепенное нарастание скорости образования N_2 со временем. Кривые отклика для CO отсутствуют — CO полностью адсорбируется в ходе каталитического и вторичного процесса. Можно предполо-

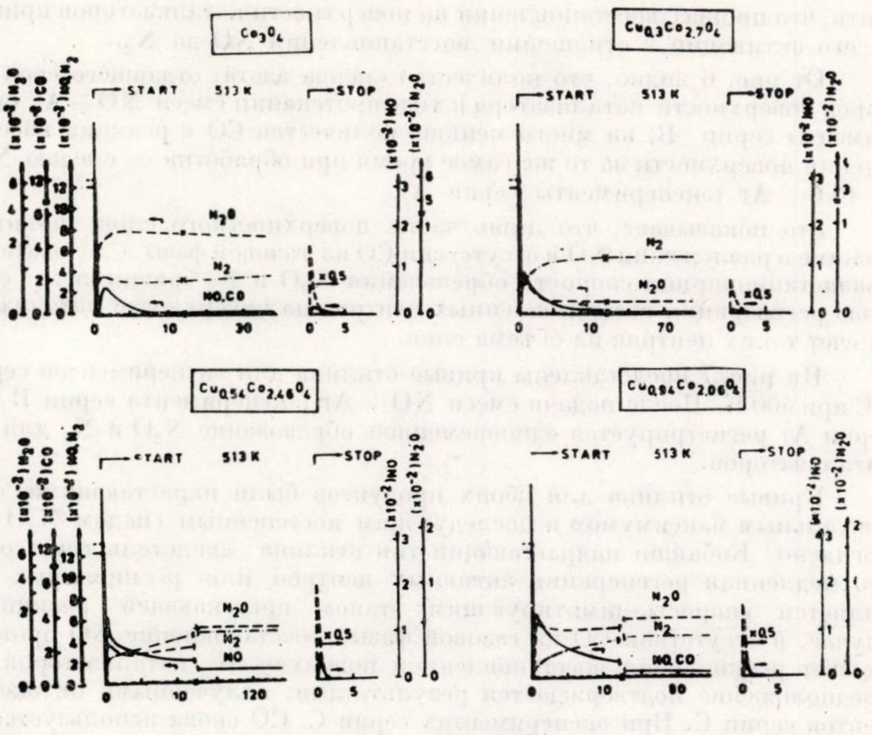

Рис. 5. — Кривые отклика экспериментов серии А при 513 К.

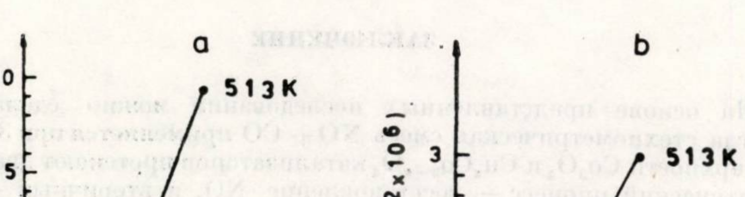

Рис. 6. — а) эксперименты серии А: Количество CO, используемое при восстановлении поверхности в зависимости от содержания Cu(x). б) эксперименты серии В: Количество NO, отдавшее свой кислород поверхности в зависимости от содержания Cu(x).

жить, что процесс восстановления на поверхности катализаторов приводит к его активации в отношении восстановления NO до N_2.

От рис. 6 видно, что количество оксида азота, отдавшего свой кислород поверхности катализатора в ходе протекания смеси NO+ Ar (эксперименты серии В) на много меньше количества CO в реакции восстановления поверхности за то же самое время при обработки со смесью NO + + CO + Ar (эксперименты серии А).

Это показывает, что лишь часть поверхностного слоя принимает участие в разложении NO в отсутствии CO из газовой фазы. Следовательно, квазистационарная скорость образования N_2O и N_2 сравнима со скоростью регенерации восстановленных центров на поверхности катализатора за счет таких центров из объема слоя.

На рис. 7 представлены кривые отклика для экспериментов серии В и С при 400 К. После подачи смеси NO+ Ar (эксперимента серии В после серии А) регистрируется одновременное образование N_2O и N_2 для всех катализаторов.

Кривые отклика для обоих продуктов были нарастающими с моментальным максимумом и последующим постепенным спадом N_2O и N_2. Согласно Кобаяши надрастающий тип отклика свидетельствует о том, что медленная регенерация активных центров или реакционных форм является скорость-лимитирующим этапом протекающей реакции. В случае, в отсутствии CO из газовой фазы, восстановление NO протекает за счет реокисления восстановленной поверхности катализаторов. Это предположение подтверждается результатами, полученными от экспериментов серии С. При экспериментах серии С, CO снова используется для восстановления поверхности катализаторов, что соответствует стационарному состоянию стехиометрической смеси NO + CO.

ЗАКЛЮЧЕНИЕ

На основе представленных исследований можно сделать вывод что когда стехиометрическая смесь NO+ CO применяется при 333—513 К, на поверхности Co_3O_4 и $Cu_xCo_{3-x}O_4$ катализаторов протекают два процесса: каталитический процесс — восстановление NO, и вторичный процесс — взаимодействие CO с O_2 поверхности катализатора. Вторичный процесс приводит к активации поверхности катализаторов в отношении восстановления NO. При низких температурах, в случае Co_3O_4, восстановление NO до N_2O ускоряется, в то время как восстановление NO до N_2 ускоряется в случае $Cu_xCo_{3-x}O_4$ катализаторов.

Механизм восстановления NO до N_2O при температурах ниже 400 К по всей вероятности не различается для различных катализаторов. Лишь скорость лимитирующий этап реакции меняется с увеличением содержания Cu. По нашему мнению механизм ассоциативен и включает образование промежуточных соединений на поверхности, устойчивость которых уменьшается с увеличением содержания Cu в катализаторах. Эти соединения являются самыми устойчивыми на поверхности Co_3O_4 (кривые отклика S — типа N_2O в старт-этапе и хвост десорбционного пика для N_2O в стоп-этапе) (рис. 4).

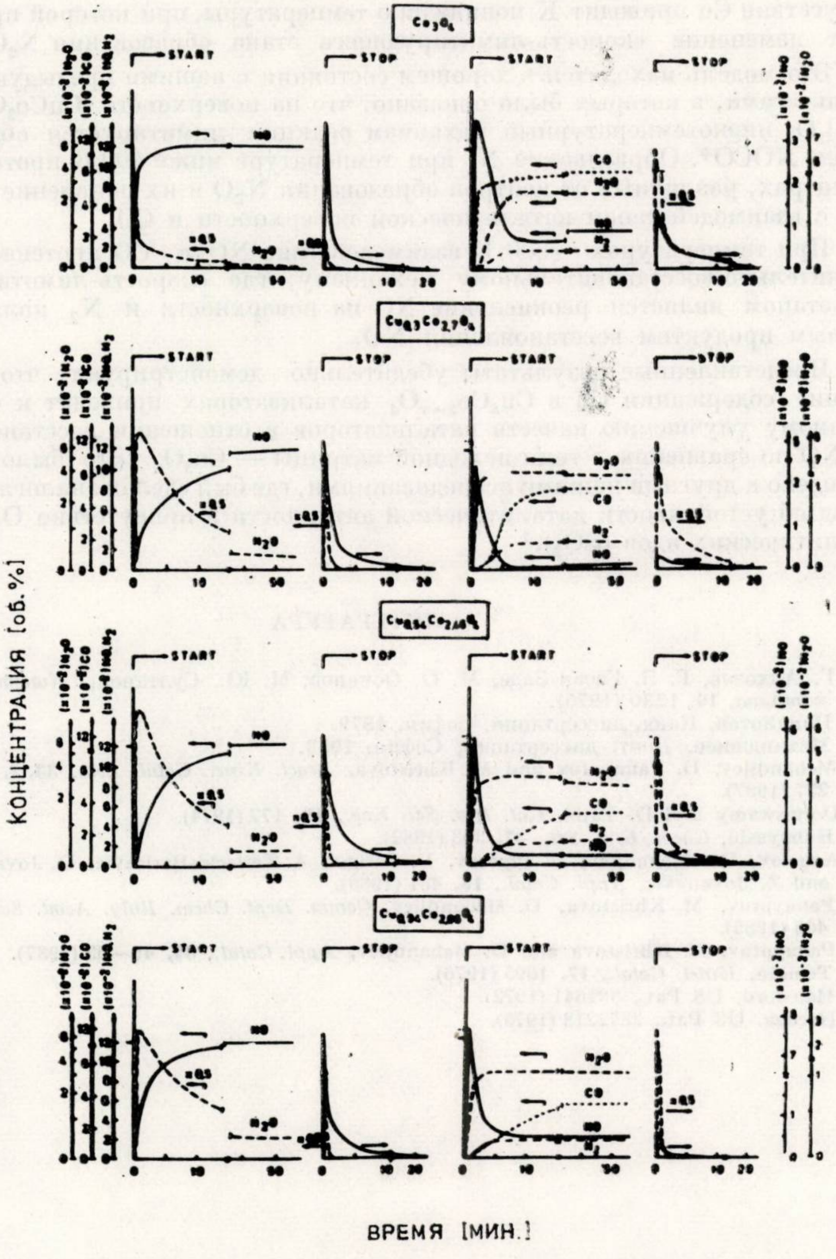

Рис. 7. — Кривые отклика экспериментов серии В и С при 403 К.

Для Cu-содержащих катализаторов устойчивость более низка при x = 0,3 где скорости реакции на поверхности и десорбции N_2O сравнимы. При катализаторах с максимальным содержанием Cu (x = 0,94) реакция на поверхности является скорость-лимитирующим этапом. Следовательно, притугствие Cu приводит К понижению температуры, при которой происходит изменение скорость-лимитирующего этапа образования N_2O.

Эта модель находится в хорошем состоянии с нашими предыдущими результатами, в которых было показано, что на поверхности $CuCo_2O_4$ на $\gamma-Al_2O_3$ низкотемпературный механизм реакции лимитируется образованием NOCO*. Образование N_2 при температуре ниже 400 К протекает на центрах, различных от центров образования N_2O и их появление связано с взаимодействием каталитической поверхности и CO.

При температурах ~500 К взаимодействие NO с CO протекает по окислительно-восстановительному механизму, где скорость-лимитирующим этапом является реокисление NO на поверхности и N_2 является главным продуктом восстановления NO.

Представленные результаты убедительно демонстрируют, что увеличение содержания Cu в $Cu_xCo_{3-x}O_4$ катализаторах приводит к определенному улучшению качеств катализаторов в отношении восстановления NO по сравнению с теми исходной матрицы — Co_3O_4. Это было подтверждено и другими нашими исследованиями, где был сделан аналогичный вывод об устойчивости каталитической активности в присутствии O_2 и ли каталитических ядов (SO_2).[7]

ЛИТЕРАТУРА

[1] Т. Г. Алхазов, Г. З. Гасан-Заде, М. О. Османов, М. Ю. Султанов, *Кинетикап катализ*, **16**, 1230 (1975).

[2] Д. Панайотов, Канд, диссертация, София, 1979.

[3] Д. Механджиев, Докт. диссертация, София, 1983.

[4] D. Mehandjiev, D. Panayotov and M. Khristova, *React. Kinet. Catal. Lett.*, **33, 2**, 273—277 (1987).

[5] L. Doraiswamy and D. Tajbl, *Cat. Rev. Sci. Eng.*, **10**, 177 (1974).

[6] M. Kobayashi, *Chem. Eng. Sci.*, **37**, 393 (1982).

[7] S. Angelov, D. Mehandjiev, B. Piperov, V. Zarkov, A. Terlecki-Baricevic, D. Jovanovic, and Z. Jovanovic, *Appl. Catal.*, **16**, 431 (1985).

[8] D. Panayotov, M. Khristova, D. Mehandjiev, *Comm. Dept. Chem. Bulg. Acad. Sci.*, **18**, 405 (1985).

[9] D. Panayotov, M. Khristova and D. Mehandjiev, *Appl. Catal.*, **34**, 49—63 (1987).

[10] M. Temkin, *Kinet. Catal.*, **17**, 1095 (1976).

[11] R. Hansford, US Pat., 381641 (1972).

[12] C. Heceba, US Pat., 3872213 (1975).

Revue Roumaine de Chimie, **34**, *2*, 527–536 (1989)

ОКИСЛИТЕЛЬНОЕ АЦЕТОКСИЛИРОВАНИЕ УГЛЕВОДОРОДОВ НА МЕТАЛЛОСОДЕРЖАЩИХ КАТАЛИЗАТОРАХ

Х. М. МИНАЧЁВ и В. В. ХАРЛАМОВ
Институт органической химии имени Н. Д. Зелинского АН СССР,
Москва

Получена 16 ноября 1988 г.

Каталитическое окислительное ацетоксилирование углеводородов является удобным, одностадийным методом синтеза ненасыщенных сложных эфиров карбоновых кислот — винилацетата, аллилацетата, бензилацетата и др., имеющих важное значение в производстве полимеров, синтетических душистых веществ и др. Исследование окислительного ацетоксилирования пропилена на Pd-содержащих катализаторах на основе кристаллических (цеолиты) и аморфных алюмосиликатов показало, что активность катализатора существенно зависит от способа его приготовления, а также определяется составом и пористой структурой носителя. Так, например, в случае цеолитов найдено, что активность катализатора растёт с увеличением величины соотношения окислов кремния и алюминия и необходимой стадией приготовления катализатора является нейтрализация кислотных центров, т.к. в их присутствии цеолитные катализаторы не проводят данную реакцию. Исследование кинетики и механизма реакции с использованием меченой ^{18}O-уксусной кислоты позволило предположить схему процесса с промежуточным образованием аллилового спирта в хемосорбированном состоянии. В случае катализаторов на основе аморфных алюмосиликатов их активность зависит от способа распределения палладия по грануле носителя — равномерное или ,,корочковое'' распределение. При этом для обоих типов катализаторов получена единая зависимость активности от поверхностной концентрации металла, что свидетельствует о существовании оптимальной дисперсности кристаллитов палладия. Сопоставление активности Pd-цеолитных катализаторов в ацетоксилировании различных углеводородов указывает на зависимость скорости реакции от величины энергии рвущейся C—H связи с строения углеводорода.

The catalytic oxidative acetoxylation of hydrocarbons is a convenient method for the synthesis of unsaturated esters vinyl acetate, allyl acetate, benzyl acetate and others, which are important in the production of polymers, drugs and so on. The propylene oxidative acetoxylation over Pd-containing catalysts on the basis of crystalline (zeolites) and amorphous aluminosilicates has been investigated. The catalyst activity was shown to depend on the method of its preparation. The chemical composition and porous structure of the carrier play an important role too. For instance in the case of zeolites the catalyst activity increases with silica-alumina ratio and besides the neutralization of acidic centres is the needed stage in the catalyst preparation, because zeolites with acidic centres are inactive in this reaction. The kinetics and the mechanism of the reaction have been studied. Experiments with acetic acid labelled by ^{18}O indicated that allyl alcohol is probably the intermediate species which undergoes the esterification with acetic acid into allyl acetate. The activity of the catalyst on the basis of amorphous aluminosilicates was shown to depend on the method of palladium distribution on the carrier pellet — uniform or "crust"-type distribution. Both types of the catalyst give a common dependence of the activity on the surface

concentration of the metal. This dependence indicates the existence of an optimal dispersity of palladium crystallites. Comparison of the activity of Pd-zeolite catalyst in the acetoxylation of various hydrocarbons indicates the dependence of the reaction rate on the value of C—H bond energy and on the hydrocarbon structure.

Реакцией окислительного ацетоксилирования углеводородов, как известно, называют каталитический процесс взаимодействия ненасыщенного углеводорода с кислородом и уксусной кислотой, в реультате которого образуется ненасыщенный сложный эфир и вода.

$$RH + AcOH + 1/2\,O_2 \longrightarrow AcOR + H_2O$$

где $R: C_2H_3$, C_3H_5, C_6H_5, $C_6H_5CH_2$ и др. Реакция обычно в большей или меньшей степени сопровождается процессом глубокого окисления исходного углеводорода

$$RH + O_2 \longrightarrow CO_2 + H_2O$$

В качестве исходного углеводорода используют этилен, пропилен бензол, толуол и др.[1]

Эта реакция была открыта в СССР в 1960 г. при исследовании механизма окисления этилена, когда в среде уксусной кислоты в присутствии хлористого палладия вместо ацетальдегида в качестве основного продукта реакции был получен винилацетат.[2] Помимо винилацетата по этой реакции можно получать и ряд других ценных продуктов: аллилацетат, бензилацетат и т.д. В результате интенсивных исследований, осуществлённых в различных странах, было показано, что данную реакцию можно проводить не только в жидкой, но и в газовой фазах с использованием в качестве катализатора палладия или его соединений с добавками различных промотеров на таких носителях, как окись алюминия, силикагель, активированный уголь и др.[3,9] Помимо палладия обязательным компонентом катализатора в данном случае является ацетат щелочного металла, который добавляют к катализатору в количестве 10—15% (вес.).

Цеолиты в качестве основы для приготовления катализаторов окислительного ацетоксилирования углеводородов до начала наших работ не применялись,[10] поэтому задачей нашего исследования было выяснить возможность приготовления активных и селективных катализаторов для данного процесса на основе кристаллических и аморфных алюмосиликатов, а также изучить закономерности реакции.

РЕЗУЛЬТАТЫ И ОБСУЖДЕНИЕ

В табл. 1 представлены данные по влиянию типа цеолита на активность и селективность Pd-катализаторов синтеза аллилацетата. Как видно, свойства катализатора существенно зависят от соотношения окислов кремния и алюминия в составе цеолита. Наиболее подходящим для приготовления катализатора является цеолит типа ЦВМ с соотношением $SiO_2/Al_2O_3 = 30 \div 47$.

Pd-цеолитные катализаторы окислительного ацетоксилирования припилена имеют одну особенность, которая не встречается в других реакциях окислительного типпа. Оказалось, что активностью в синтезе аллилацетата обладают катализаторы на основе Na-форм цеолитов, в

Таблица 1

Влияние типа цеолита на свойства Pd-катализатора (1,5% Pd, 15% AcOK) при 180°C, 1 атм, $C_3H_6 : AcOH : O_2 = 2 : 1 : 0,5$, $V_{AcOH} = 2$ $час^{-1}$, $g_{кат} = 1,5$ г.

Цеолит	$\frac{SiO_2}{Al_2O_3}$	Активность, $\frac{г\text{-}моль}{г.\ кат.\ час} \times 10^3$	Селективность, %
NaA	2,0	0	0
NaX	2,9	0	0
NaУ	4,8	0,35	35
K, Na-шабазит	5,0	0,44	34
K, Na-эрионит	6,5	0,15	100
Na-морденит	11,9	0,19	26
ЦВМ-408	29,6	7,33	96
ЦВМ-364	47	7,43	94
ЦВК-XI	68	5,52	87
ЦВК-III	78	3,04	89

то время как в случае Н-форм, имеющих кислотные центры, вместо окислительного ацетоксилирования протекает лишь простое присоединение уксусной ккислоты к пропилену с образованием изопропилацетата. Присоединение уксусной кислоты к пропилену, как известно, осуществляется

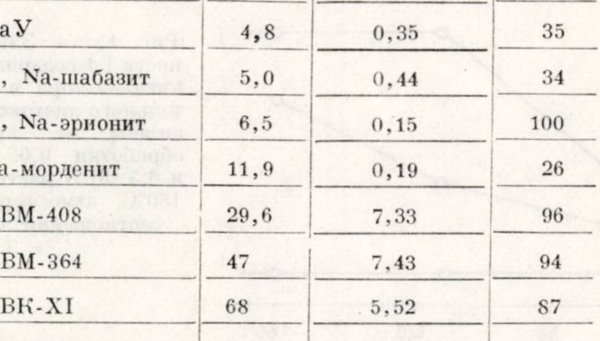

$$C_3H_6 + AcOH + 1/2\ O_2 \begin{cases} \xrightarrow{Pd/HM} AcO-CH(CH_3)_2 \\ \xrightarrow{Pd/NaM} AcOC_3H_5 + H_2O \end{cases}$$

на кислотных центрах катализатора, а на металлическом компоненте при этом происходит глубокое окисление пропилена до CO_2 и H_2O. Важно отметить, что для такого изменения направления реакции достаточно присутствия в катализаторе небольшого числа кислотных центров, которое возникает после введения палладия в цеолит методом ионного обмена с последующим восстановлением его водородом.

Причина указанного явления могла заключаться либо в том, что в присутствии кислотных центров цеолита изменяются свойства металлического компонента катализатора и в таком случае это должно проявляться и в других реакциях, которые могут протекать на металле, например в гидрировании пропилена, либо в присутствии кислотных центров происходит изменение селективности окисления пропилена, например, в результате того, что окислению будет подвергаться не молекула пропилена, а пропильный карбокатион. Для ответа на поставленный вопрос был приготовлен ряд образцов Pd-цеолитных катализаторов, обработанных в различных условиях раствором щёлочи с целью нейтрализации кислотных центров. Варьировались концентрация раствора щёлочи и продолжительность обработки катализаторов. Затем была определена активность этих образцов в трёх реакциях: в окислительном ацетоксилировании, гидрировании и окислении пропилена.

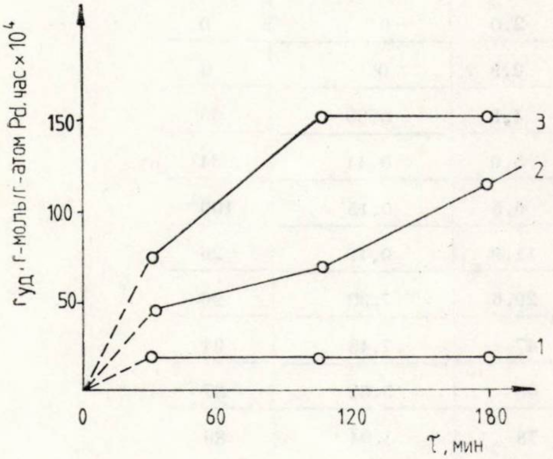

Рис. 1. — Зависимость активности Pd-содержащего цеолитного катализатора в реакции окислительного ацетоксилирования пропилена от продолжительности обработки 0,05 (1), 0,275 (2) и 0,5 (3) N растворами NaOH при 180°C, атмосферном давлении и соотношении $C_3H_6:AcOH:O_2 = 2:1:0,5$.

Как видно из рис. 1, активность катализатора в реакции окислительного ацетоксилирования пропилена увеличивается с ростом концентрации раствора щёлочи и продолжительности обработки. Необработанный щёлочью катализатор, как уже отмечалось выше, не проводит реакцию окислительного ацетоксилирования пропилена.

Аналогичная картина наблюдается и в реакции гидрирования пропилена (рис. 2). Отличие заключается только в том, что исходный,

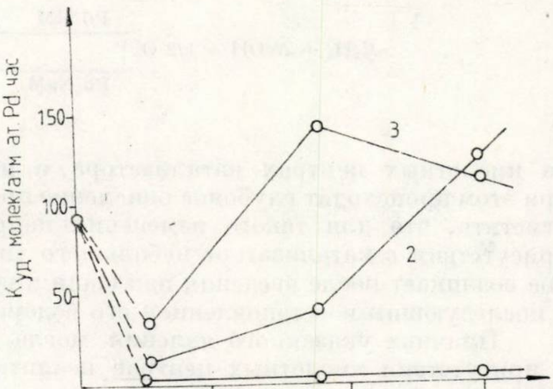

Рис. 2. — Зависимость активности Pd-содержащего цеолитного катализатора в реакции гидрирования пропилена от продолжительности обработки 0,05 (1), 0,275 (2) и 0,5 (3) N растворами NaOH при комнатной температуре в импульсном микрореакторе.

необработанный щёлочью катализатор проявляет такую же активность в гидрировании пропилена, как и обработанный в оптимальных для реакции ацетоксилирования условиях. Это указывает на то, что свойства металлического компонента катализатора не изменяются в присутствии кислотных центров цеолита.

Другая картина наблюдается в реакции окисления пропилена (рис. 3). Одним из основных продуктов неполного окисления пропилена был акролеин и скорость его образования увеличивалась с продолжительностью обработки катализатора раствором щёлочи, как увеличивалась и общая скорость окисления пропилена. Однако на необработанном щёлочью катализаторе акролеин не образовывался, т.е. подтвердилось второе предположение, что в присутствии кислотных центров цеолита происходит изменение селективности окисления пропилена на металлическом компоненте катализатора.

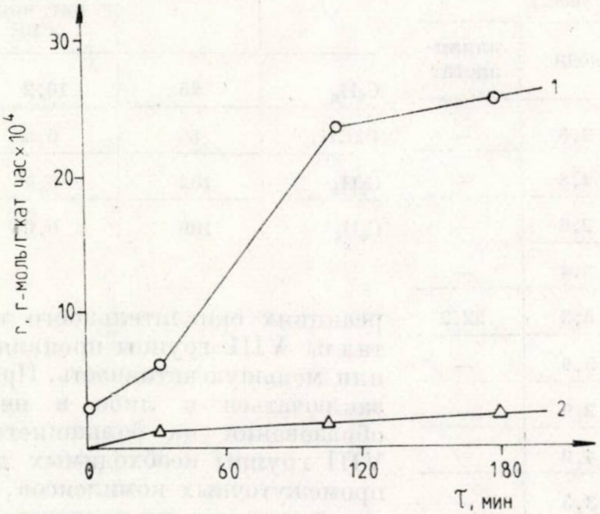

Рис. 3. — Зависимость общей скорости окисления пропилена (1) и скорости образования акролеина (2) от продолжительности обработки катализатора 0,5 N раствором NaOH при 200°С, атмосферном давлении, $V_{C_3H_6} = 0,5$ л/час, $V_{возд.} = 2,5$ л/час, $g_{кат.} = 1$ г.

Согласно литературным данным в качестве катализаторов реакции окислительного ацетоксилирования пропилена обычно используют палладий с различными добавками на носителях. В тоже время отсутствуют сведения о каталитических свойствах других металлов VIII группы. Полученные нами данные по каталитическим свойствам металлов VIII группы в синтезе аллилацетата представлены в табл. 2. Из неё следует, что из всех металлов VIII группы лишь Pd проявляет каталитическую активность в данной реакции. На других металлах, в том числе и на таком типичном катализаторе окисления как Ag, протекает лишь реакция глубокого окисления пропилена, о чём можно судить по образованию воды в продуктах реакции. Необычность этого результата в том, что в других

Таблица 2

Активность монометаллических катализаторов на основе цеолита типа ЦВМ-408 (содержание металла 1,5%, АсОК — 15%) при 180°C, 1 атм, $C_3H_6 : AcOH : O_2 = 2 : 1 : 0,5$, $V_{AcOH} = 2$ час$^{-1}$, $g_{кат} = 1,5$ г.

Металл	Состав катализатора, % (вес.)		
	уксусная кислота	вода	аллилацетат
Co	96,2	3,8	—
Ni	95,2	4,8	—
Ru	97,4	2,6	—
Rh	96,6	3,4	—
Pd	71,5	6,3	22,2
Os	94,1	5,9	—
Ir	97,1	2,9	—
Pt	95,1	4,9	—
Ag	96,5	3,5	—

Таблица 3

Окислительное ацетоксилирование различных углеводородов на катализаторе 1,5% Pd/ЦВМ + + 15% АсОК при 180°C, 1 атм, $RH : AcOH : O_2 = (6 \div 0,2) : 1 : (0,2 \div 0,5)$

RH	Q_{C-H}, ккал/моль	Скорость реакции $\frac{\text{г-моль}}{\text{г. кат. час}} \times 10^3$	Селективность образования продукта, %
C_3H_6	86	10,2	86
$PhCH_3$	85	0,3	85
C_2H_4	102	0,5	9
C_6H_6	109	0,02	88

реакциях окислительного типа все металлы VIII группы проявляют большую или меньшую активность. Причина может заключаться в либо в невозможности образования на большинстве металлов VIII группы необходимых для реакции промежуточных комплексов, либо в высокой скорости их расходования в реакции глубокого окисления. Этот вопрос требует дальнейшего исследования.

Изучение Pd-содержащих катализаторов на основе аморфных алюмосиликатов показало, что их активность зависит как от характеристик пористой структуры носителя, так и от способа распределения металла,

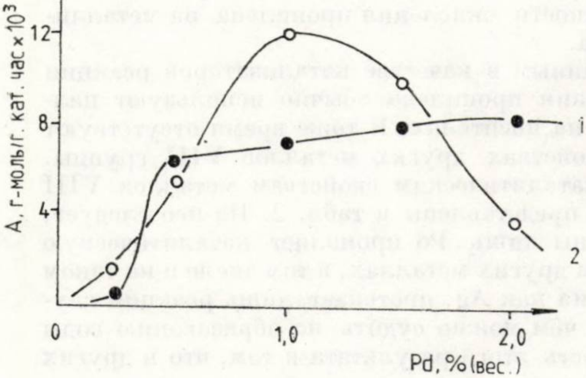

Рис. 4. — Зависимость активности катализатора от содержания палладия при равномерном (1) и „корочковом" (2) распределении металла по грануле носителя ($S = 67$ м^2/г, $\gamma = 205$ Å) при 180°C, атмосферном давлении, $C_3H_6 : AcOH : O_2 = 2 : 1 : 0,5$, $V_{AcOH} = 2$час$^{-1}$, $g_{кат.} = 1,5$ г.

по грануле носителя: равномерное или ,,корочковое'' распределение. Из следующего рисунка видно (рис. 4), что в случае алюмосиликата с удельной поверхностью 67 м²/г и средним радиусом пор 205Å при равномерном распределении металла по грануле носителя активность катализатора с ростом содержания палладия сначала увеличивается резко, затем более плавно. Иная зависимость получилась для ,,корочкового'' распределения палладия, когда активность проходит через максимум при содержании металла 1%.

Однако на другом носителе ($S = 300$ м²/г, $\gamma = 40$ Å) характер зависимости для ,,корочкового'' катализатора остался таким же (кривая с максимумом), а при равномерном распределении металла ход кривой изменился: активность медленно нарастала до содержания Pd до 1—1,5%, затем наблюдался резкий подъём (рис. 5).

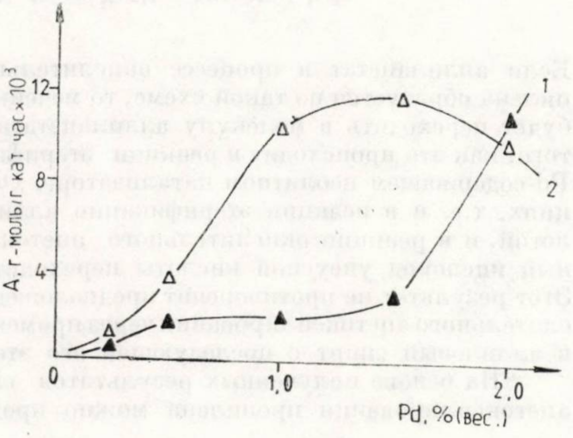

Рис. 5. — Зависимость активности катализатора от содержания палладия при равномерном (1) и ,,корочковом'' (2) распределении металла по грануле носителя ($S = 300$ м²/г, $\gamma = 40$ Å) при 180°С, атмосферном давлении, $C_3H_6 : AcOH : O_2 = 2 : 1 : 0{,}5$, $V_{AcOH} = 2$ час$^{-1}$, $g_{ка} = 1{,}5$ г.

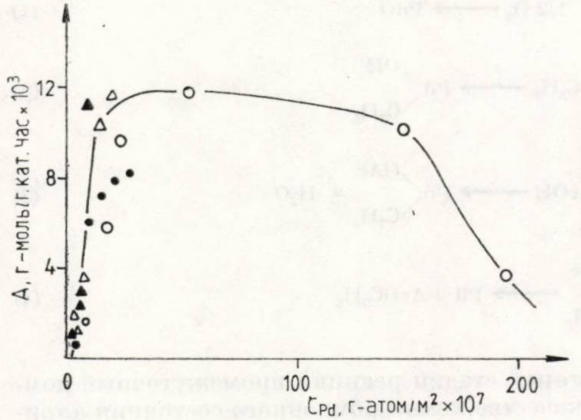

Рис. 6. — Зависимость активности катализатора от концентрации Pd на поверхности носителя при равномерном (●, ▲) и ,,корочковом'' (○, △) распределении металла на гранулах алюмосиликата с $S_{уд} = 67$ м²/г и $\gamma = 205$ Å (●, ○) и с $S_{уд} = 300$ м²/г, $\gamma = 40$ Å (▲, △) при 180°С, атмосферном давлении, $C_3H_6 : AcOH : O_2 = 2 : 1 : 0{,}5$ $V_{AcOH} = 2$час$^{-1}$, $g_{кат.} = 1{,}5$ г.

Интересно отметить, что если построить зависимость активности катализатора от концентрации палладия на поверхности носителя (рис. 6), то экспериментальные данные для 4-х исследованных серий катализаторов укладываются на одну обобщённую кривую с пологим максимумом. При этом в случае ,,корочкового'' распределения палладия при расчёте его поверхностной концентрации учитывалась только та часть поверхности носителя, на которой располагался металл. Максимум на этой кривой свидетельствует, по-видимому, о существовании оптимальной дисперсности Pd на поверхности носителя.

Механизм реакции исследован с использованием ^{18}O-меченой уксусной кислоты. Была проверена возможность протекания реакции окислительного ацетоксилирования пропилена через промежуточное образование аллилового спирта с последующей его этерификацией.

$$
\begin{array}{l}
C_3H_6 + 1/2\ O_2 \longrightarrow C_3H_5OH \\
C_3H_5OH + !\ Ac^{18}OH \longrightarrow Ac^{18}OC_3H_5 + H_2O \\
\hline
C_3H_6 + Ac^{18}OH + 1/2\ O_2 \longrightarrow Ac^{18}OC_3H_5 + H_2O
\end{array}
$$

Если аллилацетат в процессе окислительного ацетоксилирования пропилена образуется по такой схеме, то меченый кислород уксусной кислоты будет переходить в молекулу аллилацетата или воды в зависимости от того, как это происходит в реакции этерификации аллилового спирта на Pd-содержащем цеолитном катализаторе. Оказалось, [11] что в обеих реакциях, т.е. и в реакции этерификации аллилового спирта уксусной кислотой, и в реакции окислительного ацетоксилирования пропилена меченый кислород уксусной кислоты переходит в молекулу аллилацетата. Этот результат не противоречит предположению о протекании реакции окислительного ацетоксилирования через промежуточное окисление пропилена в аллиловый спирт с последующей его этерификацией.

На основе полученных результатов схему реакции окислительного ацетоксилирования пропилена можно представить следующим образом

$$Pd + 1/2\ O_2 \longrightarrow PdO \qquad (1)$$

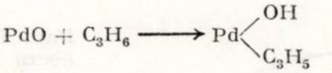

$$PdO + C_3H_6 \longrightarrow Pd\begin{cases} OH \\ C_3H_5 \end{cases} \qquad (2)$$

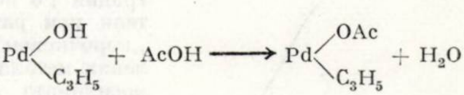

$$Pd\begin{cases} OH \\ C_3H_5 \end{cases} + AcOH \longrightarrow Pd\begin{cases} OAc \\ C_3H_5 \end{cases} + H_2O \qquad (3)$$

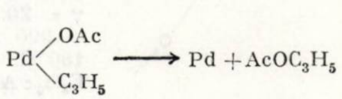

$$Pd\begin{cases} OAc \\ C_3H_5 \end{cases} \longrightarrow Pd + AcOC_3H_5 \qquad (4)$$

При этом образующийся на второй стадии реакции промежуточный комплекс можно рассматривать в качестве хемосорбционного состояния аллилового спирта.

Исследование различных углеводородов в реакции окислительного ацетоксилирования важно с точки зрения установления зависимости активности катализатора от строения исходного углеводорода и от величины энергии C—H связи, участвующей в реакции. В табл. 3 представлены результаты исследования активности и селективности Pd-цеолитного катализатора в окислительном ацетоксилировании различных углеводородов: пропилена, толуола, этилена и бензола. Как видно, скорость реакции уменьшается на порядок и более при переходе от аллильного типа С—Н связи (пропилен, толуол) к С—Н связи винильного типа (этилен, бензол), т.е. при увеличении энергии рвущейся связи от 85—86 до 102—109 ккал/моль. При этом необходимо сравнивать углеводороды с близкими размерами молекул: пропилен-этилен, толуол-бензол. С другой стороны, если сравнить углеводороды с близкими величинами энергии С—Н связи (пропилен — толуол, этилен — бензол), но отличающихся своим строением и размерами, то можно заключить, что при переходе от олефиновых углеводородов к ароматическим, т.е. с увеличением размеров молекул исходных углеводородов, скорость реакции уменьшается также не менее, чем на порядок. Следовательно, в реакции окислительного ацетоксилирования углеводородов играют роль как энергетические, так и стерические факторы.

Таким образом, проведённое исследование показало, что на основе кристаллических и аморфных алюмосиликатов можно приготовить высокоактивные Pd-содержащие катализаторы окислительного ацетоксилирования пропилена. Активность таких катализаторов существенно зависит от способа их приготовления: равномерное или ,,корочковое'' распределение палладия в случае аморфного алюмосиликата, наличие или отсутствие кислотных центров в цеолитах.

Скорости реакции окислительного ацетоксилирования различных углеводородов в значительной мере различаются между собой, что связано с энергетическими и стерическими факторами. Возможно, что при этом происходит также изменение лимитирующей стадии процесса. Этот вопрос требует дополнительных исследований.

На примере реакции с пропиленом исследован механизм процесса. Показано, что возможным путём образования аллилацетата является промежуточное окисление пропилена до аллилового спирта с последующей его этерификацией уксусной кислотой.

ЭКСПЕРИМЕНТАЛЬНАЯ ЧАСТЬ

Катализаторы готовили на основе цеолитов и аморфных алюмосиликатов Использовали Na-формы цеолитов А, X, У, шабазит, эрионит, морденит, ЦВМ и ЦВК, в которых соотношение SiO_2/Al_2O_3 изменялось в пределах от 2,0 до 78. Палладий вводили в цеолиты ионным обменом или пропиткой. Порошкообразный цеолитных катализатор формовали без связующих веществ придавлении 100 атм, дробили и отбирали фракцию частиц 0,5—1,0 мм.

Аморфные алюмосиликаты, использованные для приготовления катализатора, имели форму шариков с диаметром 2—3 мм. Пропитку раствором палладия проводили двумя способами. По первому способу при нагревании с перемешиванием производилось выпаривание растворителя с последующим прокаливанием в токе воздуха или азота и восстановлением водородом при 500°С. Получался катализатор с равномерным распределением палладия по грануле носителя. Второй способ пропитывания заключался в добавлении к носителю такого объёма раствора соли палладия, который поглощался взятой навеской носителя без остатка. Затем проводилась обработка слабым раствором щёлочи, промывка дистиллированной водой, прокаливание и восстановление водородом, как в предыдущем случае. При этом получали катализатор с ,,корочковым'' распределением палладия по грануле носителя.

Каталитические опыты проводили в стеклянном проточном реакторе, обогреваемом силиконовым маслом из термостата. Условия реакции: атмосферное давление, температура 160—190°С, молярное соотношение углеводород: уксусная кислота: кислород = (6÷0,2): 1: (0,2÷0,5). Количество загружаемого в реактор катализатора составляло 1—6 см^3. Жидкие продукты реакции собирали в охлаждаемый при 0°С сборник и анализировали хроматографически.

Меченую ^{18}O уксусную кислоту готовили взаимодействием CH_3COCl с $H_2{}^{18}O$. Продукты реакций с использованием меченой ^{18}O уксусной кислоты анализировали с помощью хроматомасс-спектрометрии на приборах „Varian MAT — 111" и „Kratos MS—70".

ЛИТЕРАТУРА

[1] Б. В. Суворов и Н. Р. Букейханов, Окислительные реакции в органическом синтезе, Изд. „Химия", М. 1978.
[2] И. И. Моисеев, М. Н. Варгафтик и Я. К. Сыркин, *Докл. Ан. СССР*, **133**, 377 (1960).
[3] В. Крёниг и Г. Шарфе, Пат. ФРГ, 1901289 (1969).
[4] Г. Рошер и Г. Шмитц, Пат. ФРГ, 2038120 (1970).
[5] П. Гейден и Дж. В. Ирвинг, Англ. пат. 1310225 (1970).
[6] Х. Кисаки, Ю. Цуцуми и К. Такешиго, Пат. ФРГ, 2165738 (1971).
[7] В. К. Бояджан, С. С. Хачатрян, Г. Г. Степанян и др., Пат. ФРГ, 2603550 (1976).
[8] T. Kunugi, H. Arai and K. Fujimoto, Bull. Jap. Petr. Inst.. **12**, 97 (1970).
[9] С. Ф. Политанский, А. М. Шкитов, В. В. Харламов, Х. М. Миначёв, И. И. Моисеев и О. М. Нефёдов, Изв. АН СССР, сер. хим., **7** 1479(1981).
[10] Х. М. Миначёв, О. М. Нефёдов, В. В. Харламов, С. Ю. Панов и С. Ф. Политанский, *Изв. АН СССР, сер. хим.*, **7**, 1490 (1981).
[11] Х. М. Миначёв, О. М. Нефёдов, В. В. Харламов, О. С. Чижов, А. П. Родин и В. И. Каденцев, *Изв. АН СССР, сер. хим.*, **6**, 1253 (1985).

Revue Roumaine de Chimie, 34, 2, 537–549 (1989)

MEDIATED ELECTROCATALYSIS. I

GENERAL ASPECTS

L. ONICIU[a], MARIA JITARU[b] and I. A. SILBERG[b]

[a] University of Cluj-Napoca, Dept. of Chemical Technology, 11, Arany Ianos str., R–3400 Cluj-Napoca, Romania
[b] ICECHIM, Institute of Chemical and Biochemical Energetics, Cluj-Napoca Research Group, 11, Arany Ianos str., R–3400 Cluj-Napoca, Romania

Received October 15, 1988

The paper presents a brief critical review of literature data concerning the notion of mediated electrocatalysis, formulating proposals for the simplification and uniformity of the terminology in this field. Starting from the probable mechanism of action of a mediator redox system, the advantages of using mediated electrocatalysis are discussed, with reference to the mediated oxidation or reduction of organic, inorganic and biologic systems. The practical criteria of choosing a mediator redox system able to ensure maximum selectivity and minimum energy consumption are underlined.

1. THE CONCEPT OF MEDIATED ELECTROCATALYSIS

Defining mediated electrocatalysis is a deceptively simple task. This concept is, obviously, subordinated to the notion of electrocatalysis: consequently, the way the latter is defined and outlined will directly affect the definition of mediated electrocatalysis.

In its most general acception, *electrocatalysis encompasses the totality of factors modifying the kinetic parameters of the charge-transfer processes in systems involving electrodic interfaces*. In a way entirely similar to that followed when defining catalysis, it is tacitly assumed here that the usual thermodynamic parameters (temperature, pressure and concentration of the main reactants) are kept at constant values while comparing catalyzed and uncatalyzed processes. However, the variation of such factors as the pH or the concentration of some ionic species is not excluded, in order to allow the extension of the area of general electrocatalysis so as to include the specific contribution of acid-base catalysis, of ion-pairing, etc. Thus, *electrocatalysis practically amounts to selective modifications of the reaction rates in processes involving at least one heterogeneous charge-transfer step.*

The explicit mentioning of the electrode interface is necessary for at least two reasons:

— there are a score of catalyzed homogeneous charge-transfer processes (e.g. $V^{3+} + Fe^{3+} \rightarrow V^{4+} + Fe^{2+}$ catalyzed by Cu^{2+} ions) without direct bearing on the function of an electrochemical reactor;

— the presence of the electrode couple is ensuring, in all cases, the fulfilling of the classical condition of catalysis, namely, the cyclic sequence character, with the catalyst being recovered unmodified at the end of a full cycle : this is done by regenerating at the electrode at least one catalytic species.

Both in the cases when the act of catalysis occurs in the electron-transfer (ET) step, or the catalytic effect is exerted at another stage of the investigated reaction sequence, the directly observable result consists of the modification, usually the increase of the current density under constant potential. Thus, for instance the electric parameters characterising the function of a fuel-cell or of an electrochemical reactor can be substantially influenced by the modification of pH, which exerts acid-base catalysis upon a reaction step, not directly involved in the electrode process.

The ET reaction at the electrode takes place with the direct participation of the substrate S in the case of the usual, non-mediated electrocatalysis. However, if this electrode reaction involves the electronation or deelectronation of another chemical species (the mediator) the substrate will react with the reduced or oxidized form of the mediator and we are already in the realm of mediated electrochemical processes. Thus, *mediated electrocatalysis represents the catalytic effect exerted in the homogeneous phase by a redox system, regenerated by a heterogeneous process at the electrode*.

The terminology adopted by various authors for defining the basic notions encountered in this field is rather different, each of the suggested terms emphasizing a single aspect of the process complexity. Thus, the name "*redox catalysis*" [1–7] does not point out the "electrode side" of the process, while the term "*indirect electrochemical reaction*" [2] was used for stressing also the fact that the electrochemical regeneration of the mediator takes place in another reactor.[3] Both the definition used by Antropov,[4] "*electrochemical reaction with external electron transfer agents*", and that of Mayranovski [5] "*electrochemical reactions against the standard potential fall*" are lacking in concision, and insights into the process mechanism are required in order to understand them. It is often observed that the authors themselves do not use consistent terminology, several different terms being used in parallel within the same paper. For instance, Weinberg [6] employs the term "*reaction with an electrochemically regenerated oxidizing agent*" as well as the notion of "*oxygen carriers*" for ceric salts involved in mediated anodic oxidation processes. Among the more recent papers dealing with mediated electrochemical processes [2,4,5,8] in the review of Wendt,[8] which is of outstandingly ample scope, a distinction is made between the homogeneous and the heterogeneous mediated ET, also called mediated electrochemical conversion. In the conception of Wendt, the homogeneous mediators are redox systems soluble in the electrolysis medium, whereas the heterogeneous mediators are fixed on the electrode surface by chemical bonds. The chemically modified electrodes, obtained by attaching the mediating redox system to the electrode, are also functioning on the basis of ET between the electrode and the substrate by the intermediacy of the mediator.

For Shano[9] there is a clear-cut distinction between the homogeneous mediator systems, directly oxidizing or reducing the substrate S, and the heterogeneous mediatoı systems, which are also electrochemically regenerated, but react chemically in the bulk phase, with S, by oxidizing or reducing it. It is quite obvious that in the last two quoted cases, the notions of "heterogeneous" and "homogeneous" refer to principially different classifications criteria. Using the same terms for different phenomena is bound to create confusion, especially in a complex field, like the one under scrutiny here, that makes precise delineations quite difficult to come by.

We suggest that *the catalytic effect exerted in the homogeneous phase should be called "mediated electrocatalysis" and that the redox system involved in the ET and regenerated by a heterogeneous process at the electrode be named "mediator redox system" (MRS), or, simply, "mediator"*.

The above considerations lead to the outlining of several definitory features of the mediated electrocatalysis, which represent as many differences with respect to the direct electrocatalysis:

— the mediated electrocatalytic process *involves at least two ET steps* occurring in the electrochemical cell, at least one of these steps being of heterogeneous nature and taking place at the electrode. One can already anticipate the existence of two classes of mediated electrocatalytic processes, with the ET step involving the electrode preceding or following the reaction between the mediator and the substrate S;

— the proceeding of mediated electrocatalytic processes assumes an interaction between the mediator and the electrode, that is, between those orbitals of the mediator which are susceptible of occupation or depopulation, and the Fermi level of the electrons within the electronically conducting phase of the electrode *;

— the homogeneous ET-step, that is, the one occurring in the bulk phase of the solution involves the interaction between S and the electrodically generated active species of the mediator, interaction yielding oxidized or reduced forms of S which collapse to reaction products, while the mediator is regenerated and reenters the catalytic cycle.

Thus, the mediated electrocatalysis encompasses the electrocatalytic processes in which the electrode reaction (the regeneration of the active species of the mediator) is distinct from the ET step leading to the reaction products.

GENERAL MECHANISM OF ACTION OF A MEDIATOR REDOX SYSTEM

In discussing the mediated electrocatalytic processes the localization of the electrochemical reaction at the electrode surface has to be considered, emphasizing the heterogeneous character of the phenomenon. Fig. 1 (a, b, c) is intuitively substantiating the possible cases occurring in electrocatalysis, in comparison with a process (Fig. 1 d) which cannot be considered as electrocatalytic. Under certain conditions (Fig. 1 c), a monolayer of the mediator redox system (MRS)A/A$^+$ is somewhat modifying the electrode surface, and the respective system can serve as ET mediator.

---

* The electrode interface consists of one electronically conducting phase (metal, semiconductor, graphite) and one ionic conducting phase (electrolyte solution, ionic conducting ceramic, molten salt).

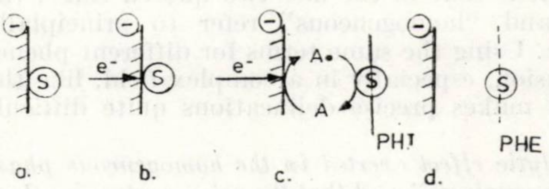

Fig. 1. — Possible cases occurring in electrocatalyses.

By extrapolating the case in Fig. 1, if the MRS A/A$^-$ is chemically bonded to the electrode surface, a chemically modified electrode is obtained which, also operates according to a mediated electrocatalysis mechanism.

When a substrate S is subjected, for instance, to a reduction reaction, the action of a MRS regardless of its organic or inorganic nature, can be imagined as depicted in Fig. 2.

Under certain conditions, an electron from the Fermi level of the cathodic metal can be accepted, at a given potential, either in a *d* vacant orbital (if the mediator A is an inorganic redox system) or in the LUMO of A, if the latter is an organic mediator. In its turn, S, which is to be reduced should have an antibonding orbital similar in energy with that orbital of the mediator which is accommodating the electron received from the cathode.

At a given moment, the electron will be equally shared by the S and A orbitals of common energy, and eventually it will be entirely appropriated by the molecular orbitals of the substrate.

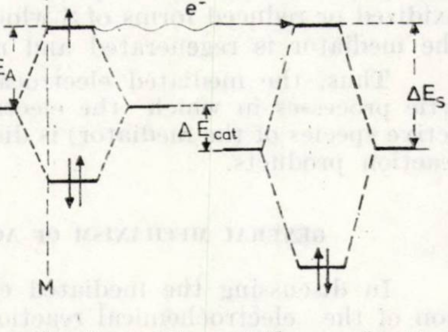

Fig. 2. — Action of MRS on a reduction reaction.

The reaction sequence leading to the formation of the reduction product of substrate S

$$\mathrm{A} + e^- \rightleftharpoons \mathrm{A}^{\dot{-}} \tag{1}$$

$$\mathrm{A}^{\dot{-}} + \mathrm{S} \rightleftharpoons \mathrm{S}^{\dot{-}} + \mathrm{A} \tag{2}$$

$$\mathrm{S}^{\dot{-}} \rightarrow \text{reaction products} \tag{3}$$

should be very fast, significantly surpassing in rate the competing transformation of $A^{\overline{\cdot}}$ into products.

$$A^{\overline{\cdot}} \rightarrow \text{secondary reaction products} \qquad (4)$$

The mediator A is heterogeneously oxidized [9] or reduced at positive or negative potentials, respectively, which are of lower values than the standard reduction or oxidation potentials of S. If, for instance, the oxidation potential of S is much more positive than A^+/A, the equilibrium described by equation (2′) is strongly displaced to the left and the overall reaction rate depends to a very large extent upon the transformation rate of the active species of S into products, according to eq. (3′).

$$A - e^- \rightleftharpoons A^+ \qquad (1')$$

$$A^+ + S \rightleftharpoons S^+ + A \qquad (2')$$

$$S^+ \rightarrow \text{reaction products} \qquad (3')$$

If the oxidation or reduction potential is very large, the proceeding of the reaction sequence (1—4) is impossible even if the rate of conversion of $S^{\overline{\cdot}}$ into products is very large.

As far as the concrete way of effecting the "mediation" of the homogeneous ET is concerned, the life-time of MRS is a decisive factor. By extrapolating, if the life MRS is very long it can be taken that the regeneration of its active species occurs in another reactor. Sometimes, the use of multiple redox systems [40] allows the achieving of optimal thermodynamic and kinetic conditions for the mediated oxidation or reduction of S. From a practical point of view, the combined action of two or more mediators reduces the transformation potential of S into the electrochemically active species, able to generate the desired products with maximal yields. For instance, the secondary alcohols are oxidized to the respective ketones in the presence of two MRS,

Br^-/Br^+ and $R_2'S^+Br/R_2'S$ according to the scheme (9)—(Fig. 3)

At this moment, a kinetic criterion is looming out which will compete along with the thermodynamic one to the selection of the pathway the mediated electrocatalytic reaction will follow.

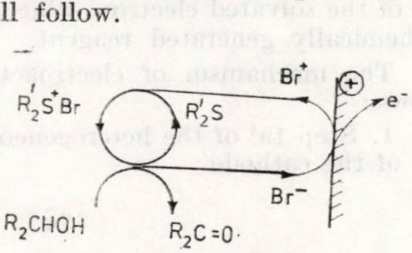

Fig. 3. — Oxidation of alcohols in the presence of a double MRS.

The energy gain of the process occurring by mediated electrocatalysis is ΔE_{cat}, the energy difference between ΔE_s and ΔE_A ($\Delta E_{cat} = \Delta E_S - \Delta E_A$). There are reasons to consider in this respect the occurrence of a redox resonance between the mediator and the substrate, a similitude of the redox potential of the mediator A and of the substrate S which is to be oxidized or reduced.

According to our views, the inorganic redox systems in Table 1 could be used for the reductive cleavage of the C—X bond, the selective hydrogenation of double and triple bonds, the reduction of epoxides to olefines and many others, on account of the compatibility of the corresponding redox potentials. As yet, only the $S_n^{4+/2+}$ has been used.[11,12] Research carried out in our laboratory proved that in the mediated electroreduction of aromatic nitroderivatives to the corresponding amines the redox system involved is $S_n^{2+/0}$ and not $S_n^{4+/2+}$.[13]

For mediated electrocatalytic oxidation reactions the most frequently used mediator redox systems are listed in Table 2.

Table 1

Inorganic MRS

Reduction		Oxidation	
MRS	E_e(V)	MRS	E_e(V)
$Ti^{3+/2+}$	−0.37	MnO^-/MnO_4^{-2}	0.54
$Sn^{2+/2+}$	+0.15	$Cl_2O_4^{-2}/Cl^{3+}$	1.36
$Cu^{2+/+}$	+0.15	$Cl^{4+/2+}$	0.48
$Cr^{3+/2+}$	−0.41	$Co^{3+/2+}$	1.84
$V^{3+/2+}$	−0.25	MnO_4^-/Mn^{2+}	1.62

The scheme herewith advanced for explaining the action of the mediator, in general, does not contradict the literature data, namely, Antropov's conception of solvated electron[4] and the mechanism of external activation with the transfer of electron through the medium, put forward by Mayranovski.[5]

2.1. The formation of solvated electron

Antropov[4] assumes that the oxidation or reduction of the substrate S in the presence of the promoter A does not occur at the electrode surface, but at a certain distance, in the electrolyte bulk phase. In other words[5] the reaction sequence involved in the mediated electrocatalytic process includes :

— a "heterogeneous" ET reaction at the electrode interface, at the level of the electric double layer, and

— a homogeneous ET reaction in the bulk phase.

According to Antropov[4] these two ET steps involve the participation of the solvated electron, which can be regarded as the simplest electrochemically generated reagent.

The mechanism of electroactive species formation is described as follows :

1. Step $1a^I$ of the heterogeneous reduction takes place in the vicinity of the cathode :

$$e_M^- + L \rightarrow e_L^- \tag{5}$$

when the electron supplied by the metal — e_M^- — is converted into a solvated electron — e_L^- — by the solvent molecules L.

2. Step $1b^I$ of homogeneous oxidation in which the electron leaves the particle subjected to oxidation and is solvated in its turn :

$$R + L \rightarrow R^{\dot{+}} + e_L^- \tag{6}$$

3. Step 2 a^{II} of homogeneous reduction, in the bulk phase, corresponds to the accepting of the solvated electron by the particle subjected to reduction :

$$e_L^- + Ox \rightarrow Ox^{\overline{\cdot}} + L \qquad (7)$$

4. Step 2 b^{II} of heterogeneous oxidation, consisting of the transfer of solvated electron to the anode :

$$e_L^- \rightarrow e_M^- \qquad (8)$$

Several electroactive species ($R^{\dot{+}}$, $Ox^{\overline{\cdot}}$) appeared in the process, and their subsequent evolution will be governed by thermodynamic and kinetic factors, essentially, by their nature and by the reaction conditions.

2.2. The mechanism of external activation with through-medium ET

The theory of Mayranovski[5] applied to the mediated electrocatalysis involving organic mediators represents the first attempt to explain this type of reactions. Up to the publication of Mayranovski's paper there existed only reports referring to the reduction of organic substrates, favoured by the presence of, for instance, small amounts of naphthalene and anthracene.[6]

Mayranovski's theory is supported by the experimental observation that nitrohaloalkanes and nitrohalobenzenes eliminate the X group at the reduction potential of the NO_2 group, that is much easier than the respective unsubstituted compounds.

It follows that the NO_2 group exerts an internal activation action upon the molecule, by increasing its affinity for the electron, thus facilitating the electron injection into the $ArXNO_2$ or the $AlkXNO_2$ molecules.

The acceptor fragment A — the NO_2 group in this case — lowers the energy of the substrate LUMO (4b) as compared to the energy of the same orbital, in the absence of the activating group.

If instead of the acceptor fragment — the NO_2 group — a mediator ion or molecule A is introduced in the system (4c) we can induce, by analogy, an external activation, the electron will be accepted into the LUMO of the mediator A and then transferred to the substrate. The case depicted in Fig. 4c corresponds to a mediated electrocatalytic reaction.

An intermediate case suggests itself at this stage, namely, the one corresponding to an internal activation, but with the ET occurring through space. An insu-

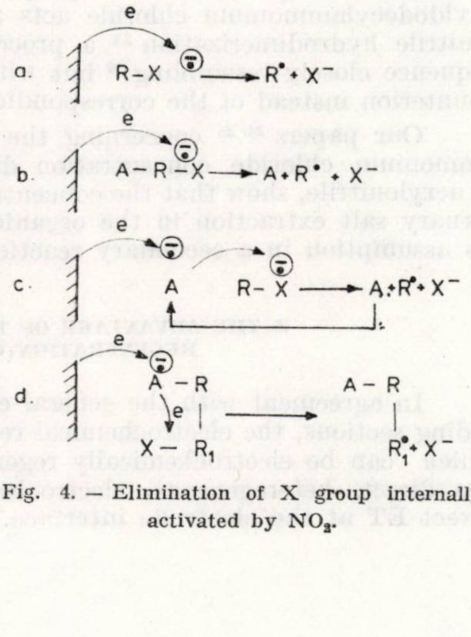

Fig. 4. — Elimination of X group internally activated by NO_2.

lating fragment R, present in the molecule, keeps A apart from S, so that their orbitals cannot interact and the ET form A to S will occur through the surrounding medium, that is, in the bulk of the solution.

The a, b, c cases, taken from the paper of Mayranovski, allow a similar interpretation for the formation of the anion radical of acrylonitrile CH_2CHCN^- facilitated by the presence of organic MRS, such as naphthalene and anthracene.[14]

Taking into account these general views on the probable action mechanisms of a MRS, it is assumed [15] that, in the particular case of CrO_4^{2-}/Cr^{3+} and $Cr_2O_7^{2-}/Cr^{3+}$ type systems, the oxidation reaction proceeds by oxygen transfer from the chromate or dichromate anion. Other authors [16,17] maintain that the anodically generated radicals obtained from various anions are able to bind oxygen from the substrate to be oxidized. Of course, the increase in concentration of the active species electrochemically generated in the vicinity of the electrode leads to the formation of dimer products.[18] Whatever the real mechanism of the electrochemical reaction proceeding, it involves in agreement with the general considerations already presented, heterogeneous processes at the electrode as well as ulterior homogeneous processes, occurring in the bulk phase. These homogeneous processes, in their turn, can be catalyzed or not. The tetraalkylammonium salts catalyze the acetophenone reduction reaction[19] and their favourable effect on the electrohydrodimerization process might ba due to the formation of a complex between the acrylonitrile anion — radical and the quaternary ammonium salts :

$$H_2C{=}C{-}C{=}{-}N + e^- + [AlK_4N]^+ \rightleftharpoons [H_2C{-}CH{-}CN]^{\dot{-}} \ldots {}^+[NAlK_4]$$

$$2\,[CH_2{-}CH{-}CN]^{\dot{-}} \ldots {}^+[NAlK]_4 + 2\,H^+ + e^- \rightleftharpoons NC{-}(CH_2)_4{-}CN + 2[NAlK_4]^+$$

similar to the acetophenone pinacolization process.[8]

Kinetic studies on the competitive acrylonitrile electroreduction reactions to adiponitrile [20] and propionitrile [21, 22] underlined that trimethyldodecylammonium chloride acts as phase-transfer catalyst in acrylonitrile hydrodimerization [23] a process which ammounts to a reaction sequence closely resembling [8] but with the $/{:}CH_2CH_2CN/^-$ anion as the counterion instead of the corresponding anion-radical.

Our papers [24, 25] concerning the determination of trimethyldodecylammonium chloride concentration during the electrohydrodimerization of acrylonitrile, show that the concentration variations are due to the quaternary salt extraction in the organic phase, and to a lesser extent, to its assumption in a secondary reaction of anodic oxidation.

3. THE ADVANTAGE OF THE ELECTROCHEMICAL REGENERATION OF THE MRS

In agreement with the general considerations presented in the preceding sections, the electrochemical reaction mediated by a redox system which can be electrochemically regenerated has many advantages over the direct, heterogeneous, electrochemical reaction, which involves a direct ET at the electrode interface.

The effecting of the mediated ET is possible and advantageous when the following criteria are observed :

(a) the thermodynamic criterion, referring to the irreversibility of the oxidation or reduction process;

(b) the kinetic criterion, requiring high values for the rates of the reactions 1—3, leading to the reaction products, so that the anionic radical $A^{\overline{\cdot}}$, appeared in the first monoelectronic transfer, would not be consumed in competing deactivation reactions ;

(c) optimal diffusion conditions, that is, an efficient mass transfer favouring the through-space ET against the standard potential fall.

When this set of conditions is fulfilled, an endoergic ET against the standard potential fall becomes not only possible but even advantageous from a certain point of view.

It is known [26] that, when the electrode material displays a good electrocatalytic activity, a variation of only 0.15 V of the electrode potential results in an 80% modification of the selectivity. If, in addition to the indisputable advantages of the electrochemical reactions, one benefits from the presence of a MRS the selectivity is further increased, *via* the possibility of controlling the formation rate of $A^{\overline{\cdot}}$.[27]

From the economic point of view, by the use of a MRS the reaction can proceed at lower potentials. As an example can serve the electrochemical reduction of vitamin D_2 in the presence of p-tolunitrile.[28] In the absence of the organic MRS, vitamin D_2 presents a certain reduction wave at the half-wave potential E_{12} (S) (Fig. 5).

The p-tolunitrile is reduced at lower potentials E_{12}(A). In the presence of this organic mediator, the shift of the redox potential of the triene system towards lower values $\varepsilon_{1/2}(A + S)$ is observed, along with an increase of the current up to the value i_3.

A spectacular example illustrating the advantages of the mediated electrocatalytical reactions is represented by the reduction of carbobenzoxy — N — butylamine in the presence of biphenyl.[28] It can be observed (Fig. 6) that within the electrochemical range of the supporting electroyte (curve 1) the substrate alone shows no reduction wave (curve 2)

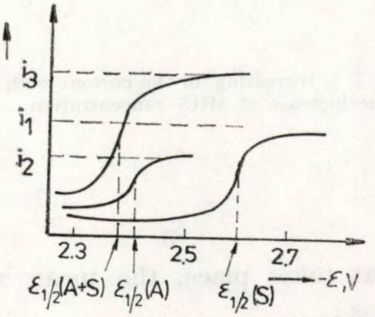

Fig. 5. — Electrochemical reduction of vitamin D_2 in the presence of p-tolunitrile.[28]

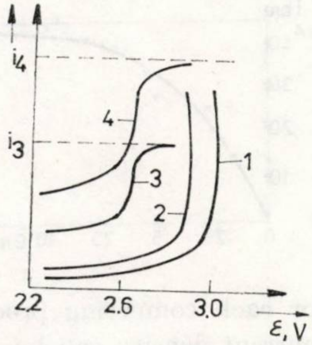

Fig. 6. — Electrochemical reduction carbobenzoxy-N-butylamine in the presence of biphenyl.

whereas the biphenyl is reduced (curve 3). When the carbobenzoxy derivative and biphenyl are simultaneously present, there is a dramatic increase of the current (curve 4) at the half-wave potential corresponding to biphenyl $E_{1/2}=2.6$ V/SCE. In this case, the possibility of carrying out electrochemical reactions which would not occur in the absence of the MRS is demonstrated.

On account of the appearance of a supplementary catalytic component, the reaction proceeds at lower potentials with larger faradaic yields and in the desired direction.

From the viewpoint of the direct electrochemical processes, it is impossible to extract homolytically an H atom from an organic substrate. This homolytic cleavage can be, however, carried out by the intermediacy of the MRS $NO_3^-/NO_3^{\cdot}$; the $NO_2^{\cdot}$ radical, anodically generated $NO_3^- - e^- \rightarrow$ $\rightarrow NO_3^{\cdot}$ is able to extract $H^{\cdot}$ as a neutral particle, bringing about, by a mediated route, a chemical transformation no electrode can perform directly.[29]

From the theoretical point of view, the maximum specificity of a mediated electrocatalytic reaction[30] depends, among other things, upon the following factors :

— the nature of the electrode surface ;

— the nature of the MRS ;

— the energetics of the electrosorption of reactants, intermediates, and reaction products ;

— the values of the rate contants for the occurring competing reactions.

In the presence of 4—4′ bipyridine, in an aqueous phosphate medium, the proteinic substrate — cytochrome — leads to the appearance of a reduction peak. In the presence of this MRS, an increase of the current with the increase of 4—4′ bipyridine concentrations is observed. (Fig. 7).[31]

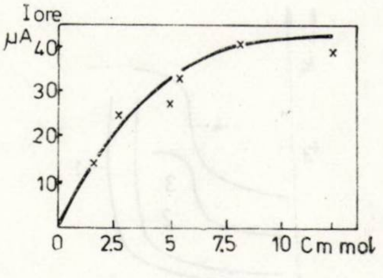

Fig. 7. — Increasing of the current with the increase of MRS concentration.

For each competing process j that takes place, the mean value of the current density can be written as :

$$i = n\mathscr{F}\{k_f^0 \cdot f(c_j)\exp.^{-\frac{\alpha_c \mathscr{F} E}{RT}} - k_b^0 \cdot f'(c_j)\exp.^{-\frac{\alpha_a \mathscr{F} E}{RT}}\} \tag{9}$$

where $f(c_j)$ and $f'(c_j)$ are function of reactants and reaction products, and can be written in the form:

$$f(c_j) = \frac{\prod_j k_j c_j^{a_j}}{[1 + \sum_{j=1} k_j c_j]^m} \tag{10}$$

If the electrocatalytical reaction can follow x different pathways, the total current can be expressed as a sum of the currents corresponding to each route:

$$\bar{i}_t = \sum_x \bar{i}_x = \sum_x n_x \mathscr{F} k_x \tag{11}$$

where K_x stand for the corresponding rate constants.

We have dealt with mean values of the current densities because in an electrochemical reaction *i* is a variable depending upon temperature and concentration. The selectivity of the formation of product P can be defined as the ratio:

$$\Phi_P = \frac{\bar{k}_P}{\sum k_x} \tag{12}$$

$$\Phi_P = \Phi_P(c_j, a_j, E, \alpha_x, \Delta E_x^{\neq}, T)$$

and is a function of concentration, c_j, a_j, potential ε, transfer coefficients α_x, action energy $\Delta E_x^{\neq}$ for route x and temperature.

Among the above listed factors, the value of the electrochemical potential at which the electrochemical reaction occurs, the transfer coefficients [32] and particularly the activation energies necessary for the proceeding of the reaction are decisively influenced by the presence of the MRS. These values, which differ in the case of a reaction occurring by a mediated route with respect to the corresponding values recorded in a direct electrochemical reaction, influence the process selectivity according to eq. (12).

By widening the scope of the mediated electrochemical reactions, the association of electrochemistry with enzymology is coupling the enzyme specificity with the versatility of the electrochemical detection and with the advantages of steering the electrochemical regeneration of the enzyme.

The enzymes are the catalysts of biochemical reactions, and are regenerated, as of now, by enzymatic routes, but such methods involve the presence, within the enzymatic reactor, of at least two enzymes and two substrates, as well as of their corresponding oxidation and reduction products. (Fig. 8).

Electrochemistry replaces the enzymatic regeneration system with an electrochemical regeneration of the coenzyme (Fig. 8) so that the S′/P′ system is substituted by an electrocatalytically active anode, thus avoiding the presence of any secondary species in the system.[33]

We shall return to the concrete examples of successful application of mediated organic and inorganic electrosynthesis in the section devoted to a review of the state-of-the-art in the mediated electrocatalysis. A last argument shows how the choosing of optimal MRS could lead to the mediated reduction of NO_2 groups simultaneously with the oxidation of the side-chains of aromatic nitroderivatives, yielding aminoacids of outstanding practical importance (Fig. 9).

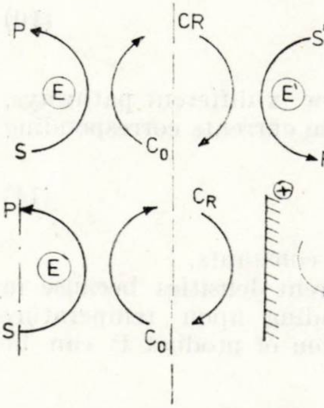

Fig. 8. — Electrochemical regeneration of the coenzyme.

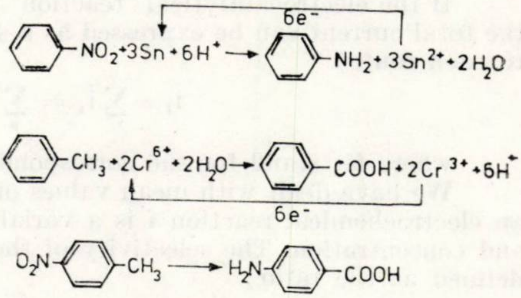

Fig. 9. — Mediated reduction of NO_2 groups simultaneously with the oxidation of the side-chains of aromatic compounds.

The above presented considerations put forward several practical criteria which might be of assistance in choosing the optimal MRS :

(a) *The structural criterion*, referring to the necessity of a similitude between the structure of the substrate S (which is to be oxidized or reduced) and of the MRS ; such similitudes should ensure the compatibility of the electron levels involved in the ET.

(b) *The equivalent electron exchange criterion*, requiring a rapid exchange of an equivalent number of electrons between A and S.

(c) *The electrochemical criterion*, underlining the decisive part played by the potential in the proceeding of the electrochemical reactions.

(d) *The thermodynamic criterion*, which states the necessity of a negative overall variation of G during the transformation of the system.

(e) *The kinetic criterion*, pointing out that when electrolyzing a mixture of compounds, there is preferential transformation of those substances which form, under the given conditions the ET product of lowest kinetic stability, that is, which are transformed the fastest.

After this presentation of general aspects, regarding the concept of mediated electrocatalysis the probable mechanism of mediated electrocatalytical reactions and the advantages of conducting an electrochemical reaction by a mediated route, it is necessary to review the actual stage of research in field of practical use of MRS.

REFERENCES

[1] G. P. Sachelaroupoulos, *Adv. Catalysis*, **30**, 217 (1981).
[2] "Comprehensive Treatise of Electrochemistry", Ed. J. O'Bockris, B. E. Conway, R. White and E. Yeager, Plenum Press, New York, 1981, tome 2, p. 291.
[3] M. Ya. Fyoshin, *Electrokhimiya*, **13**, (1), 3, (1977).

[4] L. Antropov, "Theoretical Electrochemistry", Mir, Moscova, 1979, p. 468.
[5] "Electrosintez monomerov", Nayka, Moskva, 1980, p. 245.
[6] "Techniques J. Electroorganic Synthesis", Ed. N. L. Weinberg, John Wiley and Sons, New York, 1975, part 1, p. 235.
[7] F. Beck, *Ber. Bunsenges Phys. Chem.*, **77**, 353 (1973).
[8] H. Wendt, *Electrochim. Acta*, **29**, (11), 1513 (1984).
[9] T. Shono, "Electroorganic Chemistry as a New Tool in Organic Synthesis", Springer-Verlag, 1984, vol. 20, p. 116.
[10] T. Shono, Y. Matsumura, Y. Hayashi and M. Mizoguchi, *Tetrahedron Letters*, **21**, 1867 (1980).
[11] H. V. K. Udupa and M. V. Rao, *Electrochim. Acta*, **12**, 353, 1967.
[12] H. V. K. Udupa, K. S. Udupa and K. Jayaraman, (CSIR India), Indian Patent, 142 241; C.A., 92, 84928 u (1980).
[13] L. Oniciu, I. A. Silberg, Virginia Danciu, Maria Olea and Simona Bran, Extended Abstracts of the 36th Meeting of ISE, Salamanca, Spain, September 25—28, 1985, p. 289.
[14] H. Lundt, *J. Electroanalyt. Chem.*, **65**, 205 (1975).
[15] K. B. Wiberg, "Oxidation in Organic Chemistry", Academic Press, New York, 1965, p. 218.
[16] L. Eberson, *Acta Chem. Scand.*, **B 34**, 481 (1980).
[17] F. M. Halla, J. Pinson and J. M. Seaveant, *J. Amer. Chem. Soc.*, **102**, 4120 (1980).
[18] R. Wienkamp and E. Steckham, *Angew. Chem.*, **21**, 783 (1982).
[19] W. J. M. van Pilborg, C. S. Smit, *Tetrahedron Letters*, **41**, 3651 (1977).
[20] L. Onciu, I. A. Silberg, I. Baldea, Florentina Ciomos, Maria Jitaru, D. A. Löwy,. O.H. Oprea and Liliana Radu, Extended Abstract of the 36th Meeting of ISE, Salamanca, Spain, September 25—28, 1985, p. 13010—12.
[21] L. Onciu, D. A. Löwy, Maria Jitaru, I. A. Silberg, B. C. Toma, *Rev. Roumaine Chim.*, **32** (7), 701—706 (1987).
[22] L. Onciu, Maria Jitaru, D. A. Löwy, I. A. Silberg, B. C. Toma, Extended Abstracts of the 38th Meeting of OSE, Maastricht, The Netherlands, September 13—18, 1987, p. 285—287.
[23] L. Oniciu, I. A. Silberg, Florentina Ciomos, Maria Jitaru, P. Popescu, D. A. Löwy, O. H. Oprea, Romanian Patent, 88417/1985 (C.A.107; p. 25114f).
[24] L. Oniciu, D. A. Löwy, I. A. Silberg, D. F. Anghel, Florentina Ciomos and Maria Jitaru, Proceedings of the Second Symposium of Applied Electrochemistry, Timişoara, 4—5 October 1985, p. 207—15.
[25] L. Oniciu, D. A. Löwy, I. A. Silberg and D. F. Anghel, *Analysis*, **14**, 456 (1986).
[26] G. P. Sachelaroupoulos, S. H. Langer, *J. Catal.*, **44**, 25 (1976).
[27] V. G. Levich, *Adv. Electrochem. Electrochem.* **4**, 249 (1966).
[28] V. G. Mayranovskii, I. A. Timova, *Doklady Akad. Nauk S.S.S.R.*, **239**, 1167 (1976); **223**, 643 (1975).
[29] R. Tomat, A. Rigo, *J. Appl. Electrochem.*, **16**, 8 (1986).
[30] A. Bennett, "Electrocatalyses", Ed. Brewster, New York, 1974, p. 49.
[31] C. Jourdainne, Thèse, Université Paul Sabatier, Toulouse, p. 39, 1985.
[32] Sak, G. A. Francis, *J. Electrochem. Soc.*, **126**, 1928 (1979).
[33] A. Bergel, Thèse du grade de docteur-ingénieur, Université Paul Sabatier, Toulouse, 27 nov. 1984.

Revue Roumaine de Chimie, 34, 2, 551 – 559 (1989)

Sn-FREE EFFECT AT THE POSITIVE LEAD ACID BATTERY PLATES

D. PAVLOV[a], B. MONAKHOV[a], M. MAJA[b] and N. PENAZZI[b]

[a]Central Laboratory of Electrochemical Power Sources, Bulgarian Academy of Sciences, Sofia 1040, Bulgaria

[b]Polytechnic of Turin, Department of Material Science and Chemical Engineering, 10129 Turin, Italy

Received November 25, 1988

When the lead-acid battery positive plate is made of pure Pb or of low-antimony non-Sn lead alloys, the positive plates are often passivated due to the formation of an uninterrupted layer of tet-PbO with high resistance. It was established that Sn keeps down these passivation phenomena in the plate. Through SLV and photoelectrochemical investigations it was found that Sn facilitates the process of oxidation of PbO to PbO_n $(1 < n < 2)$, and lowers the potential at which this reaction starts. This phenomenon is explained using a semiconductive model of oxidation of PbO to PbO_n.

INTRODUCTION

During operation of the lead-acid battery, the PbO_2 plate has high positive potential at which the lead grid is thermodynamically unstable and is oxidized to PbO_2. Thus an oxide corrosion layer is formed between the grid and the active mass. The thickness of this layer depends on the corrosion rate. The properties of the oxide layer exert a strong effect on battery performance. This effect is realized in three directions posing three types of problems to lead-acid battery experts.

1. Grid corrosion. Very often it determines the battery life.

2. Problems related to the chemical and electrochemical properties of the corrosion layer. During battery charge and discharge, a competition between the rates of the electrochemical processes in the active mass and in the corrosion layer appears. If the PbO_2 reduction rate is higher in the corrosion layer than in the active mass,a $PbSO_4$ sublayer is formed in the corrosion layer and the electric contact between grid and active mass is hampered. This decreases the battery capacity. Practice showed that not always the whole amount of $PbSO_4$ in the corrosion layer undergoes re-oxidation to PbO_2. A barrier $PbSO_4$ layer is formed. It cannot only bring about a decrease in battery capacity but also cause battery failure.

3. The electrical properties of the corrosion layer are of critical importance, when a tet-PbO sublayer is formed on the positive grid.

What is the essence of the last problem?

Grid oxidation proceeds in three stages: [1,2] The rate of these processes is denoted by V.

$$1.\ \mathrm{Pb} \xrightarrow{V_1} \text{tet-PbO}$$

$$2.\ \text{tet-PbO} \xrightarrow{V_2} \text{tet-PbO}_n \qquad (1 < n < 1.5)$$

$$3.\ \text{tet-PbO}_n \xrightarrow{V_3} \alpha\text{-PbO}_{(2-x)}$$

$$V_1 \neq V_2 \neq V_3$$

During the first stage Pb is oxidized to tet-PbO, during the second one, through solid state reactions, PbO is oxidized to a non-stoichiometric oxide, $\mathrm{PbO_n}$. The stoichiometric coefficient n of this oxide increases from 1.1 to 1.5. The third stage includes oxidation of this oxide to alpha-$\mathrm{PbO_2}$. The above three reactions proceed at different rates. Depending on the ratio between these rates corrosion sublayers with different stoichiometric coefficients can be formed.

The oxide conductivity depends on the stoichiometric coefficient. Figure 1 presents this dependence based on the data established by Lappe.[3]

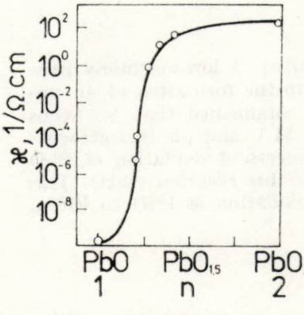

Fig. 1. — Dependence of the conductivity, χ, on the stoichiometric coefficient of $\mathrm{PbO_n}$. The graph was built using Lappe's data.

PbO has a specific conductivity of about 10^{-10} reciprocal Ohm · cm. When the stoichiometric coefficient becomes greater than 1.2, the conductivity increases sharply and when n reaches the value of 1.5, the conductivity becomes equal to that of lead dioxide. Consequently, the formation of a tet-PbO layer will lower the electrical characteristics of the plate.

Bullock and coworkers [4,5] established that when battery positive plates made of Sb-free alloys are kept at potentials around 1.2 V (vs. $\mathrm{Hg/Hg_2SO_4}$ electrode), a Pb/tet-PbO/$\mathrm{PbO_2}$ electrode system is formed. As a result, a notable deterioration of battery performance is observed.

Which battery parameters can be affected by the tet-PbO corrosion sublayer?

First, the charge acceptance of the battery is strongly reduced. Second, during discharge, batteries have reduced power and energy. Third, after formation of the positive plates, tet-PbO is formed when plates are dried at temperatures higher than 80°C. This causes thermopassivation. Fourth, after a long stay at open circuit, due to reactions between the metal and the corrosion layer, a continuous tet-PbO layer is formed leading to passivation of the electrode.

The formation of the tet-PbO layer depends strongly on the type and quantity of the alloying additives.

It was established that Sn suppresses strongly this process. Giess [6] found that, when the positive plate grids are made of low-Sb alloys containing tin, no tet-PbO layer is formed and the batteries have higher charge acceptance. Wiesener *et al.*[7] reported that tin strongly suppresses the thermo- and storage passivation of the positive plates.

The mechanism of action of tin preventing tet-PbO formation remains still unexplained. The aim of this lecture is to present a model of the mechanism of action of tin on the processes of tet-PbO sublayer formation.

RESULTS

The effect of Sn of the rate of PbO to PbO oxidation was studied in the electrode system Pb/PbO layer/$PbSO_4$ membrane. This electrode system was formed by potentiostatic polarization of lead and lead-tin electrodes at +0.6 V for 16 hrs. in 1 N H_2SO_4 solution.

The formation of a PbO sublayer depends on the ratio between the rates of oxidation of Pb and of PbO.

$$\mathrm{Pb} \xrightarrow{V_1} \text{tet-PbO}$$

$$\text{tet-PbO} \xrightarrow{V_2} \text{tet-PbO}_\mathrm{n}$$

$$\text{for}: \; V_1 > V_2 - \mathrm{Pb/PbO/PbO_n/PbO_2}$$

$$V_2 > V_1 - \mathrm{Pb/PbO_n/PbO_2}$$

If the oxidation rate of PbO is higher than that of Pb oxidation, no PbO corrosion sublayer will be formed. Thus, the purpose of our investigation was reduced to revealing the mechanism of action of Sn on the rate of PbO oxidation.

This reaction can be carried out in two ways : i) in the dark, by increasing the electrode potential far deep into the PbO_2 potential region, $\varphi > 0.95$ V (vs. Hg/Hg_2SO_4 electrode), and ii) by illuminating the electrode at potentials more positive than 0 V. The irradiation of the system with white light decreases by 1 V the starting potential of PbO oxidation.[9]

Oxidation of the $Pb/PbO/PbSO_4$ system in the dark was carried out using linear potential sweeps to an upper potential value situated deep into the PbO_2 potential range. After oxidation, a cathodic potential sweep followed indicating the formation of PbO and PbO_2 phases. The electrode stayed for 10 min. at 0.60 V before the next sweep was started.

Figure 2 presents a series of potentiodynamic sweeps in the dark of Pb and Pb − 0.5% Sn electrodes. The serial sweep number is encircled. An arrow is used for marking the start of the oxidation reaction. The sweeps for the pure Pb electrode are presented by a dashed line, while a continuous line marks those for the Pb-Sn electrodes.

This figure shows that Sn decreases the starting potential of the oxidation reaction.

Figure 3 represents the dependence of the potential at which the oxidation reaction starts on the number of successive sweeps.

Sn decreases this potential by approximately 0.2 V. It may be expected that this effect is due to the action of tin ions incorporated in the oxide.

Does this effect appear from the beginning of PbO formation? To answer this question, we oxidized Pb and Pb-Sn electrodes for one hour at a constant potential in the high positive potential range. Then the circuit was open and the potential transients were registered. Next figure presents these transients.

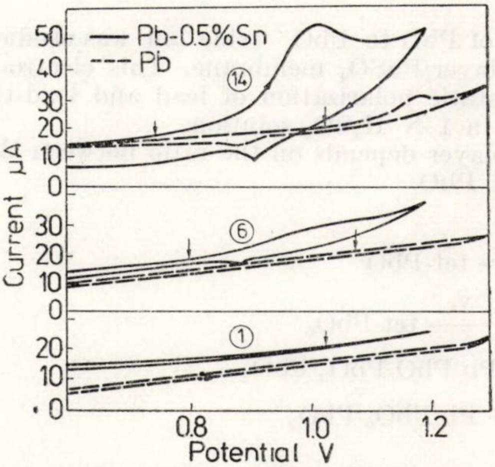

Fig, 2. — First, sixth and fourteenth voltammograms (or Pb — 0.5 % Sn/PbO/PbSO electrode at up to 1.3 V sweeps. The arrow marks the start of PbO oxidation. Sweep rate 10 mV/s.

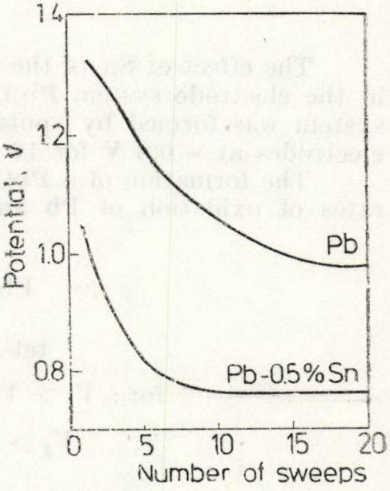

Fig. 3. — Dependence of the potential at which PbO oxidation starts on the number of sweeps for different Pb—Sn alloy electrodes.

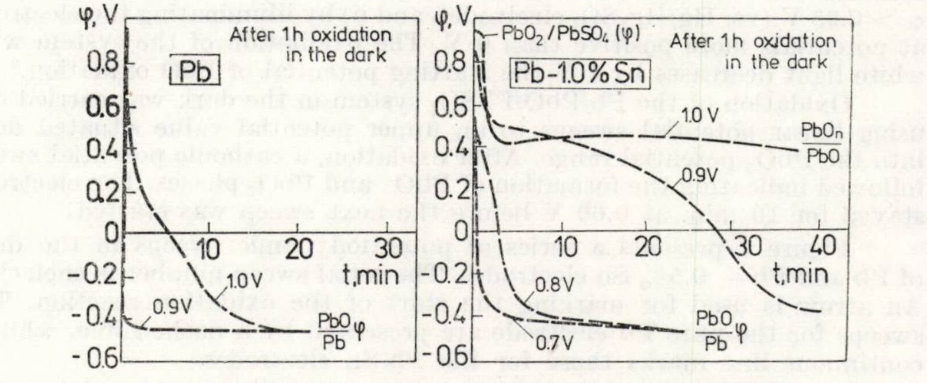

Fig. 4. — Potential decay of Pb and Pb — 1% Sn electrodes after one hour oxidation at constant potentials in the dark.

When the oxidation of the Pb electrode was carried out at up to +0.9 V, at open circuit the potential dropped to a plateau coinciding with the equilibrium potential of the Pb/PbO electrode. This means that up to the above potential PbO does not undergo oxidation.

When the Pb — 1% Sn electrode was oxidized at +0.8 V, at open circuit a potential arrest appeared on the transient. After oxidation at higher potentials, a plateau is formed at about +0.5 V at open circuit. This plateau is due to the formation of a non-stoichiometric oxide. It has to be distinguished from the PbO_2 plateau which appears at 0.9 V after oxidation at 1.0 V.

What is this electrocatalytic effect of Sn due to?

The answer to this question was looked for in studying the semiconductive behaviour of the electrode by photoelectrochemical methods. Pb and Pb-Sn electrodes were anodically polarized and periodically illuminated with white light for 3 min. Figure 5 presents the photocurrent during the 1st, 2nd, 3rd and 6th light pulses.

When light energy falls on the electrode, a photocurrent flows which grows with increasing the quantity of light energy. As was established earlier,[9] the photocurrent increase is due to an increase of the oxide stoichiometric coefficient. After a certain amount of light energy has fallen on the electrode, the photocurrent passes through a maximum and then decreases reaching a stationary value. It was found that the photocurrent decrease is caused by the formation of an oxygen layer at the oxide/solution interface which hampers the current flow. When the light is switched off, this oxygen layer is reduced, whereby a cathodic current flows.

A comparison between the photocurrent curves for pure Pb and Pb — 0.5% Sn electrodes shows that Sn facilitates significantly the photooxidation of PbO.

We studied the processes of photoactivation of electrodes with different tin content. Figure 6 presents the respective relative photocurrent/light energy curves. The photocurrent is referred to its maximum value.

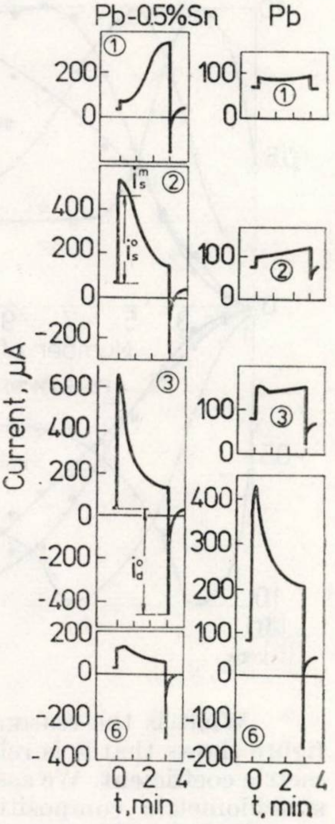

Fig. 5. — Photocurrent determined during the first, second, third and sixth light pulses of the photoactivation of Pb and Pb — 0.5% Sn electrodes. Oxidation potential 0.6 V. Intervals between two light pulses 15 min.

For pure Pb electrodes the maximum photocurrent is reached after 13 light pulses, while for Pb-Sn electrodes the higher the amount of Sn the smaller the light energy necessary for reaching the maximum. Obviously, the electrocatalytic effect of Sn becomes stronger with increasing its content in the alloy.

The last figure illustrates another phenomenon, too. After passing through the maximum, the photocurrent decreases, and for Pb — 0.5% Sn alloy it reaches a stationary value which is 30% of the maximum photocurrent.

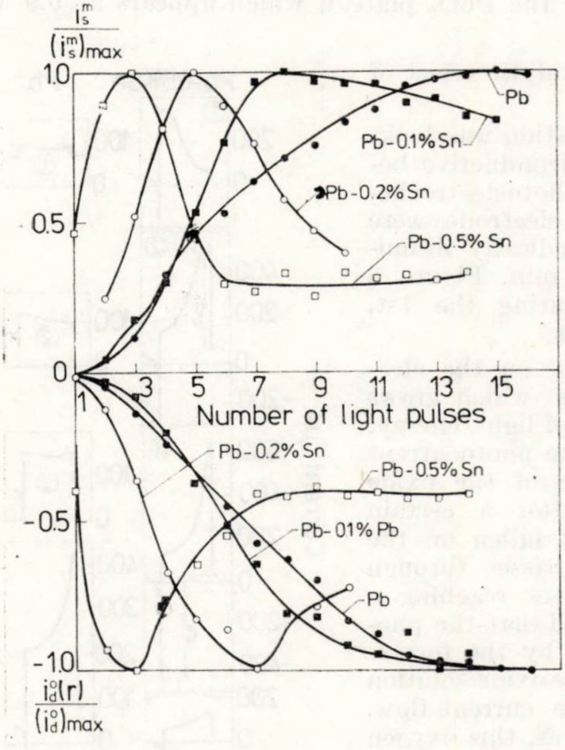

Fig. 6. — Dependence of initial photocurrent (in relative units) and the initial cathodic current in the dark (in relative units) on the number of light pulses during photoactivation of $Pb/PbO/PbSO_4$ and $Pb-Sn/PbO/PbSO_4$ electrodes.

What is the reason for this photopassivation of the electrode? The figure shows that it is related to the amount of Sn and the oxide stoichiometric coefficient. We assumed that a lead-tin oxide is formed with a fixed stoichiometric composition and weaker photoproperties.

Looking through the literature we found two lead-tin oxides with a fixed composition : lead orthostannate, Pb_2SnO_4, and lead metastannate, $PbSnO_3$.[10] There may be other ones, too. Probably the formation of some of them causes electrode photopassivation.

The oxidation of PbO is associated with transfer of electrons from the Pb^{2+} ions over the band gap of the oxide. Tin decreases the potential at which PbO formation starts. Is this not due to narrowing of the band gap? The optical band gap was determined from the spectral curve. Figure 7 represents these curves for Pb and Pb-Sn electrodes.

The band gap is determined by that segment on the abscissa at which the photocurrent begins to increase. The figure shows that the photocurrent starts growing at one and the same wave length for both electrodes. That means that Sn does not affect the band gap width. The lower starting potential of PbO oxidation is obviously due to some other reason.

The Sn effect on the photocurrent/potential dependence was studied, too. Figure 8 represents these curves for photoactivated electrodes.

It is seen that the higher the potential the stronger the photocurrent. For the Pb electrode the photocurrent passes through a maximum at about +0.9 V after which it decreases due to the formation of PbO_2 which has a high conductivity. The photocurrent growth as well as the potential maximum depend on the tin content in the alloy. The higher the tin content the more negative the potential maximum.

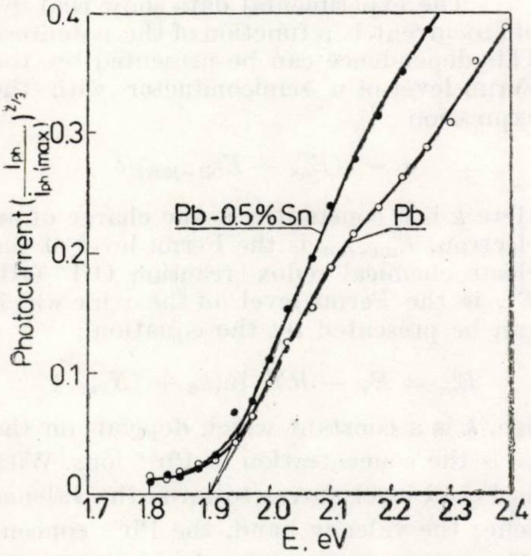

Fig. 7. — Spectral curves of photoactivated Pb/PbOn/$PbSO_4$ and Pb — 0.5% Sn/PbO_n/$PbSO_4$ electrodes formed at +400 mV.

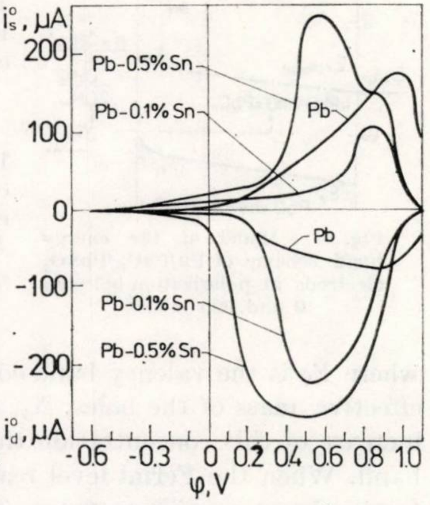

Fig. 8. — Dependence of i_s^0 and i_d^0 on, the potential for Pb, Pb — 0.1% Sn Pb — 0.5% Sn/lead oxide/lead sulfate electrodes.

The bottom part of the figure presents the initial current in the dark which passes through the electrode, when the light is switched off (Fig. 5). It is much stronger for Pb-Sn electrodes than for pure Pb ones. Evidently, Sn facilitates the adsorption of oxygen atoms on the oxide surface.[9]

DISCUSSION

On the basis of the photoelectrochemical behaviour of the Pb/PbO/$PbSO_4$ electrode, a semiconductive model of oxidation of PbO to a non-stoichiometric oxide was suggested.[11] The scheme on Fig. 9 illustrates this model.

When a Pb^{2+} ion of the PbO crystal lattice absorbs a quantum with energy greater than that of the band gap, an electron-hole pair is formed. Under the action of the electric field this pair is divided. The electron passes into the metal and the hole reaches the oxide/solution interface. There it reacts with the OH- ions of the solution forming an OH radical.

This is the only elementary electrochemical reaction in the whole process of PbO oxidation. The OH radicals recombine between themselves forming oxygen atoms. The latter diffuse into the PbO crystal lattice oxidizing it to a non-stoichiometric oxide. This oxide contains 3-valency lead ions which create p-type conductivity. The latter is a function of the stoichiometric coefficient. This is in agreement with Lappe's curve.

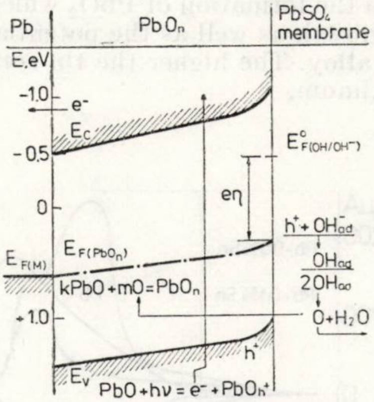

Fig. 9. — Model of the energy band scheme of $Pb/PbO_n/PbSO_4$ electrode at polarization between 0 and 900 mV.[11]

The experimental data show that the photocurrent is a function of the potential. This dependence can be presented by the Fermi level of a semiconductor with the expression :

$$i \sim k(E^{\mathrm{F}}_{\mathrm{ox}} - E^{\mathrm{F}}_{\mathrm{OH-/OH}})/e$$

Here k is a constant, e is the charge of an electron, $E^{\mathrm{F}}_{\mathrm{OH-/OH}}$ is the Fermi level of the electrochemical redox reaction OH^-/OH, $E^{\mathrm{F}}_{\mathrm{ox}}$ is the Fermi level of the oxide which can be presented by the equation :

$$E^{\mathrm{F}}_{\mathrm{ox}} = E_{\mathrm{V}} - RT \ \ln(k_{\mathrm{h}} + /N_{\mathrm{Pb3^+}})$$

where E_{V} is the valency band edge, k is a constant which depends on the effective mass of the holes, $N_{\mathrm{Pb3^+}}$ is the concentration of Pb^{3+} ions. With increase of this concentration the Fermi level moves towards the valence band. When the Fermi level reaches the valency band, the Pb^{3+} concentration has a maximum value. The semiconductor turns into a degenerated one, and attains a conductivity equal to that of metals. Such high concentration of Pb^{3+} ions causes transformation of the tet-PbO_n crystal lattice into an alpha-Pb_2 one. This behaviour of the Pb electrode is observed, when the potential exceeds 0.9 V.

How does Sn influence this process ?

The equilibrium potentials of Sn/SnO and Sn/SnO_2 are as follows :[12]

$E_{\mathrm{Sn/Sn0}} = -0.784$ V (vs. Hg/Hg_2SO_4)

$E_{\mathrm{Sn/Sno_2}} = -\ 0.786$ V

The difference between these two electrodes is only 2 mV and appears at highly negative potentials. That is why when the Sn electrode is polarized, two-, three- and four-valent Sn ions are formed simultaneously. We can suppose that the same process takes place, when Pb-Sn electrodes are oxidized. Sn ions are incorporated into the PbO crystal lattice and being three-valent they create p-type conductivity in the valency band of the mixed $PbSnO_m$. This conductivity is represented schematically in Fig. 10.

The holes created by the Sn^{3+} ions react with OH^- ions resulting in the formation of oxygen atoms. They diffuse into the oxide increasing its stoichiometric coefficient and conductivity. Thus, Sn^{3+} ions play the role of a dopant and the Fermi level depends on their concentration according to the equation :

$$E^{\mathrm{F}}_{\mathrm{ox}} = E_{\mathrm{V}} + RT\ln\left(k_{\mathrm{h}}/N_{\mathrm{Pb3+}} + N_{\mathrm{Sn3+}}\right)$$

The Sn^{3+} ion concentration is included in the denominator of the logarithmic member. That is why the potential at which the oxidation of PbO starts will be reached at a more negative value. This was confirmed by the LV sweeps as well as by the dependencies of the photocurrent on the fallen light energy.

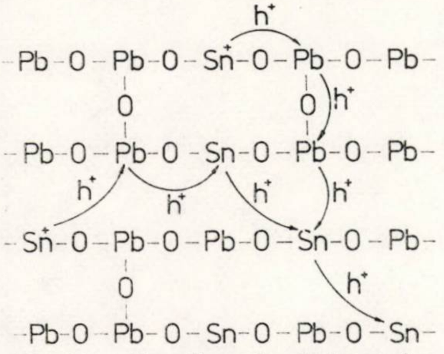

Fig. 10. — Two-dimensional scheme of a PbO crystal lattice containing Sn^{2+} and Sn^{3+} dopant ions.

Let us again turn to the problem of the passivation phenomena caused by the formation of a PbO layer. The latter is formed when the rate of Pb oxidation is greater than that of PbO oxidation. When the alloy contains Sn, the Sn^{3+} ions in the corrosion layer act in two directions : first, they shift the Fermi level closer to the valency band thus reducing the potential drop at the corrosion layer/active mass interface, and second, they increase the rate of PbO oxidation to a value greater than that of lead oxidation. In this way no separate tet-PbO layer is formed. The corrosion layer has high conductivity and no plate passivation occurs.

REFERENCES

[1] D. Pavlov and T. Rogachev, *Electrochim. Acta*, **3**, 1237 (1978).
[2] D. Pavlov and Z. Dinev, *J. Electrochem. Soc.*, **127**, 855 (1980).
[3] F. Lappe, *J. Phys. Chem. Solids*, **23**, 1563 (1962).
[4] K. R. Bullock and E. C. Laird, *J. Electrochem. Soc.*, **129**, 1393 (1982).
[5] K. R. Bullock and M. A. Butler, *J. Electrochem. Soc.*, **133**, 1085 (1986).
[6] H. K. Giess, "Advances in Lead-Acid Batteries", K. R. Bullock and D. Pavlov (eds.), Vol. 84–14, The Electrochemical Soc. Inc., USA, 1984, p. 241.
[7] K. Wiesener, J. Garche and N. Anastasijevic, *Power Sources*, **9**, 17 (1983).
[8] D. Pavlov, B. Monakhov, M. Maja and N. Penazzi, *J. Electrochem. Soc.*, (under press).
[9] D. Pavlov, S. Zanova and G. Papazov, *J. Electrochem. Soc.*, **124**, 1522 (1977).
[10] D. Greniger, V. Kollonitsch and Ch. H. Klein, "Lead Chemicals", ILZRO, N. Y. USA, p. 111.
[11] D. Pavlov, *J. Electroanal. Chem.*, **118**, 167 (1981).
[12] C. I. House and G. H. Kelsall, *Electrochim. Acta*, **29**, 1459 (1984).

Revue Roumaine de Chimie, **34**, *2*, 561—566 (1989)

ОЧИСТКА ВОЗДУХА ОТ СТИРОЛА ПРИ ПРОИЗВОДСТВЕ СТЕКЛОПЛАСТОВ ПОСРЕДСТВОМ ХИМИЧЕСКИХ МЕТОДОВ

ЛИЛЯНА ПЕТРОВА, ЖУЛИЕТА СТОЯНОВА, ЦВЕТАНКА НЕДЯЛКОВА
и ЕЛЗА ТОРБОВА
Центр для конструкционных полимеров
1528 София, гара Искър , ул. ,,5003'', Болгария

Получена 3 октября 1988 г.

Проведены исследования в лабораторных условиях для хемосорбции стирольных паров в воздухе при производстве стеклопластов. В качестве гемоабсорбентов использованы минерализованные воды, содержащие Br, I, бисульфит натрия, полимерные системы. Установлена степень хемосорбции стирола 80—98%, которой достигается предельно допустимая концентрация стирола в воздухе рабочей среды 5 мг/м^3 и 0,003 мг/м^3 в населенных местах.

The paper presents some methods for the elimination of styrene from polluted air in production of glass reinforced resins materials using different chemical methods. For styrene absorption are used : polymer systems, $NaHSO_3$, mineral waters containing Br, I and others. The absorptions degree of the syterene vapour from air by the investigated methods is determined (in limits) 80—98%.

I. ВВЕДЕНЕ

Проблема очистки воздуха от стирола при производстве стеклопластов не разрешена в мировом масштабе. В промышленных условиях используются физические, химические и комбинированные методы в различных вариантах.[1–5] Широко применяются химические методы, более важными из которых являются: окисление в жидкой фазе (водяной раствор гипохлорида натрия),[6] фосфорная и серная кислоты,[7] в газовой фазе посредством сгорания,[8] каталитическая очистка воздуха от стирола.[9]

Применение этих методов связано с употреблением дорогих реактивов, расходом энергии, экономической невыгодностью, что ограничивает их массовое применение.

Цель настоящей работы исследовать возможность очистки воздуха от стирола при производстве стеклопластовых изделий посредством некоторых доступных химических веществ и в результате получить безвредные продукты. Критерием эффективности очистки считается достижение предельно допустимой концентрации стирола в воздухе: 5 мг/м^3 в рабочей среде и 0,003 мг/м^3 для воздуха в населенных местах.

II. ЭКСПЕРИМЕНТАЛЬНАЯ ЧАСТЬ

Исследование хемосорбционной способности при применении химических веществ проведено на лабораторной установке (рис. 1), при которой вводятся искусственные газовые смеси, содержащие стирольные пары различной концентрации от 30 до 1926 мг/м^3. Принципиально установка работает таким способом: воздух, который подается из газодувки 1 посредством маностата 2, используемый для поддержки постоянного давления в системе, разделяется на два потока. Первый поток воздуха через тройник 5 и кран 7 проходит через ротаметр 2 для измерения дебита и подается в основу абсорбера 10 для барботирования. Второй поток воздуха через тройник 6 и кран 7 проходит через ротаметр 4 для измерения дебита и направляется в основу барботера 9 для насыщения стирольными парами и смешивается с первым потоком воздуха в смесителе 15. Посредством изменения дебита в двух потоках воздуха и температуры в барботере 9 получается газовая смесь с желанной концентрацией стирольных пар.

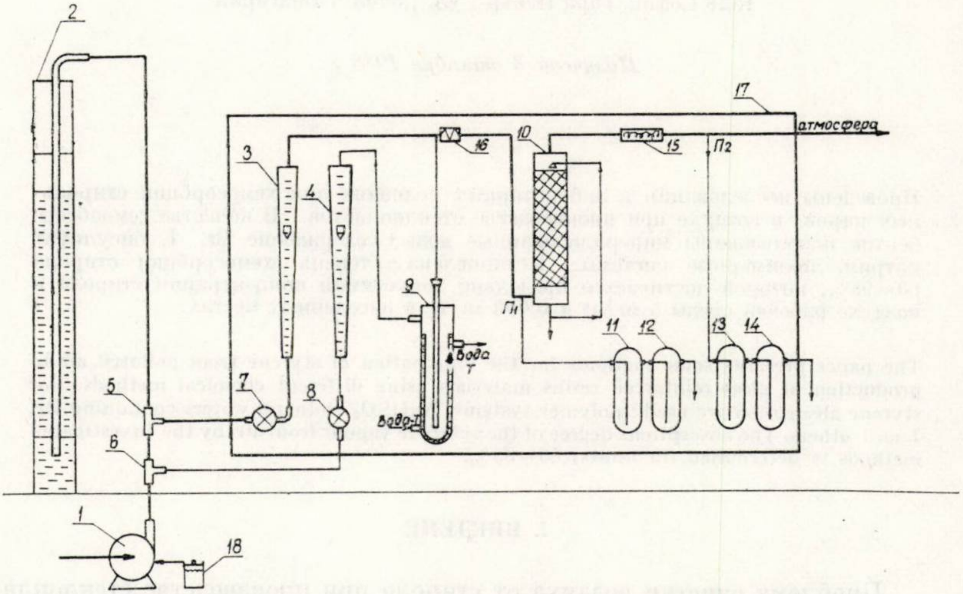

Рис. 1. — Лабораторная установка для хемосорбции стирольных пар из воздуха Обозначения: 1 — газодувка, 2 — маностат, 3,4 — ротаметры, 5, 6 — тройники, 7,8 — краны, 9 — барботер, 10 — абсорбер, 11, 12 — поглотители — вход, 13, 14 — поглотители — выход, 15 — каплеуловитель, 16 — смеситель, 17 — табло, 18 — Латр.

Для правильного протекания процесса и равномерного распределения потока воздуха по всему сечению система является термостатированной. Полученная газовсмесь с желанной концентрацией стирола барботирует в колонне абсорбции, где протекает хемосорбция.

Для полного протекания химического процесса воздушная смесь аспирируется в системе со скоростью 3 л/ч, при этом количество абсорбированной этанолом пробы 1 л для 20 мин.

На основе данных анализов вычисляется степень поглощения по формуле:

$$\eta = \frac{C_{\text{вх.}} - C_{\text{вых.}}}{C_{\text{вх.}}} \cdot 100\%,$$

где $C_{\text{вход}}$, $C_{\text{выход}}$ являются концентрациями стирола в воздушной смеси, соответственно входа и выхода абсорбционной колонны.

Анализ газовой смеси до и после абсорбции проводится путем газохроматогравского определения абсорбированных стирольных паров от этанола помещенного в пробоотборные пробирки 11, 12, 13, 14. В этом случае используется газхроматограф типа Сигма — 300 фирмы Перкин-Елмер, оборудованный пламенно-ионизационным детектором. Используется метод абсолютной калибровки. Условия анализа следующие: стеклянная колонна длиной 1,8 м и внутренним диаметром 2 мм наполнена 20% динонилфталатом и нанесена на инертный носитель — Газ — Хром Q,

$T_{\text{колонна}} = 120°C$;
$T_{\text{инжектор}} = 200°C$;
$T_{\text{деткетор}} = 250°C$;
Газ носитель — азот.
Скорость газа — носителя = 25 мл/мин
Время протекания анализа — 3,5 мин.

Средняя статистическая погрешность анализа выражена как вариационный коэффициент — 6,2%.

Объем одного определения — 1 мл.

Исследованы следующие хемосорбционные системы:

1. Минерализированпая вода, содержащая 289 мг Br/л, 100 мг Br/л.
2. Минерализованная вода, содержащая 293 мг I/л 33,96 мг I/л; модельный раствор, содержащий 50 г/л KI.
3. Бисульфит натрия — 34% водяной раствор.
4. Полимерная система в водяной эмульсии.

Полимеризация стирольных пар в полистироле одна из возможностей очистки воздуха от стирола. С этой целью использована полимерная система следующего состава:

Декалин	— 84.7%
Малеиновый ангидрид	— 8.5%,
Ронгалит	— 0.3%,
Диэтиленгликоль	— 3.6%,
Co-октоат	— 0,4%,
Метил-этил-кетон	— 2.5%.

Хемосорбционная способность используемых по отношению стирольных пар из воздуха показана графически, как зависимость от степени абсорбции к начальной концентрации стирольных пар в приложенных рис. 2, 3, 4, 5.

III. Обсуждение результатов

Как известно, поглощение пар в жидкой фазе начинается от поверхности и распространяется на глубину жидкости. Этот эбсорбционный процесс протекает в результате физических (вандерваальсовых) сил и с появлением химических валентных сил (хемосорбция). В рассмотренном случае физическая абсорбция способствует протеканию химического взаимодействия.

Анализ опытных данных, отраженные в рис. 2, 3, 4, 5 водят до следующие толкования процессов: присоединения галогенов к двойной связи углерод — углерод протекает легко. Реакция начинается с предварительной поляризации молекулы галогена, которая действует на двойную связь этиленового радикала у стирола. Теоретически, в поляризованной молекуле калогена X: $X — X^{\delta+} \ldots X^{\delta-}$ более сильное поляризованное действие должно иметь положительно зареженный атом галогена, под влиянием которого наступает поляризация двойной связи этиленового радикала стирола:

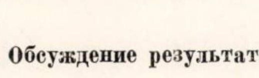

Электрофильное присоединение молекулы галогена к двойной связи протекает по двуэтапному механизму

1. Присоединение галогеного катиона X^+ к паре электронов двойной связи углерод — углерод (π) с образованием катиона I и катиона II:

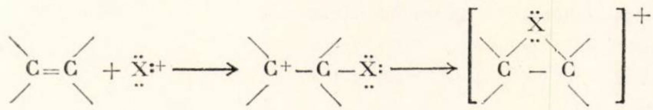

2. Присоединение анионного галогена X^- к катиону II через бимолекулярную заместительную реакцию и образование дигалогенного производного.

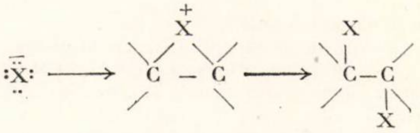

Анализ графики от рис. 2,3, отражающие зависимость между степенью хемосорбции начальной концентрации стирола показывают, что более богатые бромом и йодом минерализованные воды связывают стироль в более высокую степень.

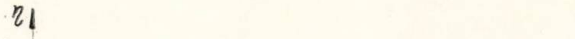

Рис. 2. — Зависимость степени хемосорбции с начальной концентрации стирола. 1. Минерализированная вода, содержащая 288 Br/л.2. Минерализированная вода, содержащая 100 мг Br/л. W — скорость продувания газовой смеси через абсорбер $W_1 = 3$ см/сек;$W_2 = 6,0$ см/сек; $W_3 = 7,3$ см/сек; t=23°C).

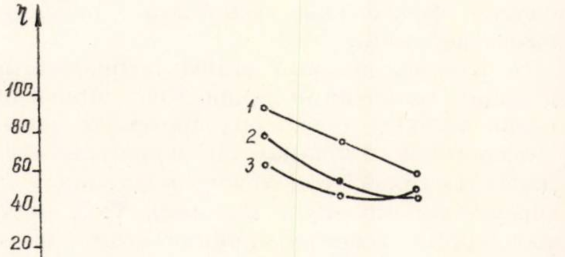

Рис. 3. — Зависимость от степени-хемосорбции с начальной концентрации стирола. 1. Минерализированная вода, содержащая 293 мг I/л. 2. Минерализированная вода, содержащая 33.96 мг I/л. 3. Модельный раствор, содержащий 50 г/л KI. W — скорость продувания газовой смеси через барботер ($W_1 = 4,3$ см/сек; $W_2 = 6,0$ см/сек; $W_3 = 7,3$ см/сек; t = 25°C).

На рис. 4 показана зависимость степени хемосорбции стирола от водного раствора бисульфита натрия. В этом случае использована харак-

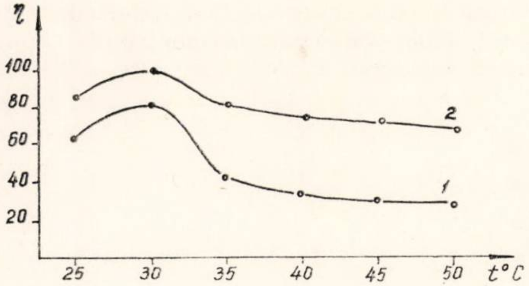

Рис. 4. — Зависимость степени хемосорбции бисульфита натрия от температуры. Водный раствор бисульфита натрия (34%): 1. без инициатора; 2. с инициатором. W — скорость, продувания газовой смеси через систему ($W_1 = 4{,}3$ см/сек).

терная реакция двойной углерод — углерод связь для нуклеофильного присоединения бисульфита натрия. В водяном растворе бисульфит натрия дисоциирует по следующей схеме:

$$NaHSO_3 \rightarrow Na^+ + HSO_3^-$$

$$3HSO_3^- \rightleftarrows 3SO_3^{2-} + 3H^+$$

Так как стирол представляет систему сопряженных двойных связей, механизм присоединения является йонным. Химическая реакция между стиролом и бисульфитом натрия протекает вероятно по следующей схеме

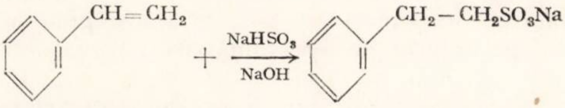

В результате хемосорбции α-2-фенилэтансульфоната натрия получается безвредное поверхностно активное вещество. В присутствии пероксидов как инициаторы, степень гемосорбции стирола более большая, как видно из графика на рис. 4.

Использованная полимерная система для уловления стирольных пар в воздухе и их полимеризирование в полистирол имеет следующий вероятный механизм: Co-октоат переносит электрон к перекису (R-OO-R), при котором Co переходит из более низкой в более высокую валентность. Ронгалит как сильный редуктор повышает валентность Co. Таким образом освобождается радикал, который инициирует полимеризацию стирола. Малеиновый ангидрид инициирует процесс полимеризации, но из-за своей симметричности он не влияет на дальнейший ход реакции.

Процесс проходит по следующей схеме:

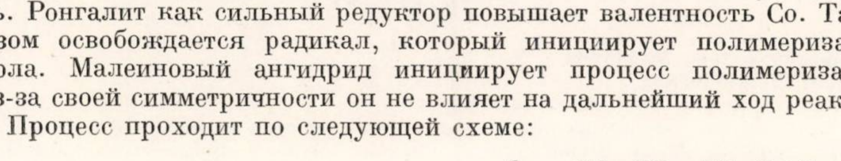

Сделанные ИК- спектры полученной смолы доказывают полимеризацию стирола в полистирол посредством отсуствия двойной связи стирола при 1620 см$^{-1}$ и в интервале 900—1000 см$^{-1}$, как и в присуствии характерных для полистирола каркасных колебаний в интервале 538—560 см$^{-1}$. Зависимость полимеризации стирола в полимерной системе от времени отражено в рис. 5.

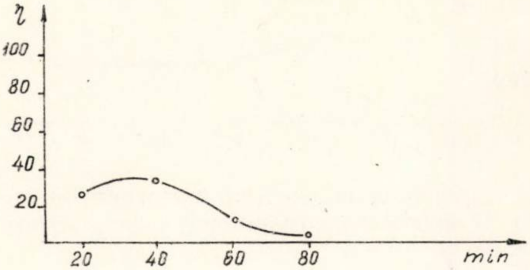

Рис. 5. — Зависимость степени хемосорбции полимерной системы от. времени ($W_1 = 4,3$ см/сек; t = 25°C)

IV. РЕЗУЛЬТАТЫ

От результатов опытных х данных можно сделать следующие выводы:

1. Исследованные химические вещества и системы являются подходящими хемоабсорбентами для стирольных пар в воздухе. Степень абсорбции находится в переделах 80—98% абсорбционный капацитет хемоабсорбентов при многократном продувании газовой смесью уменьшается до 30%.

2. Данные показывают, что при более богатом содержании стирольных паров в рабочей газовой смеси абсорбция является более высокой.

3. С увеличением скорости через абсорбционную установку степень абсорбции уменьшается.

4. Сравнительные результаты показывают, что самая высокая абсорбционная способность имеет бисульфит натрия и очень близкие показатели имеет полимерная система для полимеризации стирола.

ЛИТЕРАТУРА

[1] Японский патент 52-111469.
[2] Патент США 5907524.
[3] H. Arsovio, *Gesunh. Ing.*, **97**, 253 (1976).
[4] О. Ю. Семенов, ,,Промышленная и санитарная очистка газов'', 1978.
[5] Н. С. Злобина, В. В. Яржевский, ,,Гигиена труда и профессиональные заболевания'', 1983.
[6] O. Geichi, *J. Jap. Air Pollut.*, **15**, 21 (1980).
[7] Г. Д. Харламович, ,,Безотходные технологические процессы в химической промышленности'', Химия, Москва, 1978.
[8] H. J. Mathys, *Silikat J.*, **18**, 63 (1979).
[9] К. Сычевска, Ю. Войтех, ,,Защита атмосферы'', 1983.

Revue Roumaine de Chimie, 34, 2, 567–575 (1989)

ON THE TEMPERATURE INTEGRAL USED IN NONISOTHERMAL KINETICS

C. POPESCU[a] and E. SEGAL[b]

[a] Research Centre for Raw Material, Auxiliaries and Environment Protection, Str. Siret 95, Bucharest, Romania

[b] Department of Physical Chemistry and Electrochemical Technology, Faculty of Chemical Technology, Polytechnic Institute of Bucharest, Blvd Republicii 13, Bucharest, Romania

Received January 18, 1988

The paper presents a comparative analysis of some approximations of the temperature integral for linear and nonlinear heating programmes.

The rate of heterogeneous reactions, r, is usually expressed as:

$$r = \mathrm{d}\alpha/\mathrm{d}t \tag{1}$$

where α is the conversion degree and t the time.[1]

Generally the reaction rate is considered as depending on the separable variables temperature, T, and conversion degree, α, thus:

$$\mathrm{d}\alpha/\mathrm{d}t = k(T)\cdot f(\alpha) \tag{1'}$$

In nonisothermal kinetics one assumes that: [2]

— equation (1′) describes adequately the reaction rate although other equations to express it are available; [3]

— the investigated systems are heated with the rate, a, given by:

$$a = \mathrm{d}T/\mathrm{d}t \tag{2}$$

which is kept constant in most of the thermoanalytical equipments; nevertheless in special investigation nonlinear heating programmes (hyperbolic, parabolic, exponential) are used; [2]

— the rate constant $k(T)$ in eqn. (1′) is given by the Arrhenius equation:

$$k(T) = A\exp(-E/RT) \tag{3}$$

where the preexponential factor, A, and the activation energy, E, are considered independent of temperature,[4] statement which has been criticized in the last time.[5]

Taking into account these assumptions, the nonisothermal rate equation can be written as :

$$\frac{\mathrm{d}\alpha}{\mathrm{d}T} = \frac{1}{a} A\, f(\alpha) \exp(-\, E/RT) \tag{4}$$

Equation (4) and its integrated form :

$$\int_0^{\alpha} \frac{\mathrm{d}z}{f(z)} = A \int_0^{T} \frac{1}{a(y)} \exp(-\, E/Ry)\, \mathrm{d}y \tag{5}$$

are used to evaluate the kinetic parameters of a given reaction or physical change as well as to find the right form of the function $f(\alpha)$, called conversion function. The integral from the left member of equation (5) is known as the conversion integral. Correspondingly, the integral from the right member of equation (5) :

$$I(T) = \int_0^{T} \frac{1}{a(y)} \exp(-\, E/Ry)\mathrm{d}y \tag{6}$$

is known as the temperature integral. Introducing the notation $F(\alpha)$ for the conversion integral equation (5) can be shortly rewritten as :

$$F(\alpha) = A \cdot I(T) \tag{5'}$$

or, in the logarithmic form :

$$\ln F(\alpha) = \ln A + \ln I(T) \tag{5''}$$

In the following considerations the temperature integral will be considered for two main cases, namely :

i) linear heating programme, for which $\mathrm{d}T/\mathrm{d}t = a = \text{const.}$

i) nonlinear heating programme, for which the heating rate depends on temperature, $\mathrm{d}T/\mathrm{d}t = a(T)$.

CASE 1 : LINEAR HEATING PROGRAMMES

For this case the heating rate being constant, the temperature integral (6) takes the form :

$$I(T) = \int_0^{T} \exp(-\, E/Ry)\, \mathrm{d}y \tag{6'}$$

Obviously in this case the right member of equation (5'') should contain the supplementary term independent of temperature, $-\ln a$. The usual treatment of equation (6') consists in the change of variable :

$$x = -\, E/Ry$$

which gives:

$$I(T) = \frac{E}{R}\left(-\frac{e^x}{x} + \int_{-\infty}^{x} \frac{e^x}{x}\,\mathrm{d}x\right) \tag{7}$$

or

$$I(T) = E/R\, p(x) \tag{7'}$$

where $p(x)$ is the expression between the brackets, followed by the approximation of $p(x)$ through series developments or semiempirically.[2] Among these approximations we mention:

– Doyle's approximation: [6]

$$\ln p(x) \simeq -5.324 - 1.063\, x \tag{8}$$

– Coats and Redfern's approximation: [7]

$$p(x) \simeq \frac{e^x}{x^2}(1 + 2/x) \tag{9}$$

– Gorbachev-Doyle's approximation: [8]

$$p(x) \simeq \frac{e^x}{x^2}\frac{1}{1 - 2/x} \tag{10}$$

These three approximations generated the following three integral methods to evaluate the nonisothermal kinetic parameters:

– Flynn and Wall's method based on the equation [9]

$$\ln F(\alpha) = \ln AE/R - \ln a - 1.063\, E/RT - 5.324 \tag{11}$$

– Coats and Redfern method [7] which uses the equation:

$$\ln F(\sigma) - 2 \ln T = \ln AR/aE(1 - 2\, RT/E) - E/RT \tag{12}$$

– Gorbachev-Doyle's method according to which the nonisothermal kinetic parameters can be obtained by working the experimental data by means of the equation: [8]

$$\ln F(\alpha) - 2 \ln T = \ln \frac{AR}{aE}\frac{1}{1 + \dfrac{2RT}{E}} - \frac{E}{RT} \tag{13}$$

In all these three methods the preexponential factor A and the activation energy, E, are obtained from the intercept and respectively slope of the straight line $\ln F(\alpha)$, or $\ln F(\alpha)/T^2$, versus $1/T$. As far as the function $F(\alpha)$ is concerned, its form is obtained using other methods or it is supposed to be described by the reaction order model, i.e.,

$$f(z) = (1 - z)^n$$

and

$$F(\alpha) = \frac{1 - (1 - \alpha)^{1-n}}{1 - n} \tag{14}$$

where n is the reaction order.

A way to check the correctness of $F(\alpha)$ is to find the activation energy from the slope of the straight line $\ln a$ versus $1/T$, according to equation (11) and to compare it with the value obtained by the same equation using the slope of the straight line $\ln F(\alpha)$ versus $1/T$ for a given heating rate.

In an attempt to solve the temperature integral we considered :[10]

$$I(T) = q(T)\exp(-E/RT) \tag{15}$$

where $q(T)$ is an unknown function.

Considering the derivative of equation (15) with respect to temperature and taking (6′) we obtain :

$$\frac{\mathrm{d}q}{\mathrm{d}T} + \frac{E}{RT^2}q = 1 \tag{16}$$

a) For [11]

$$q(T) = hT^i \tag{17}$$

where i is a parameter, from equation (16) it turns out that :

$$ihT^{i-1} + \frac{E}{RT^2}hT^i = 1$$

and

$$hT^i = \frac{RT^2}{iRT + E}$$

Introducing these results in relationship (15) it turns out that :

$$I(T) = \frac{RT^2}{iRT + E}\exp(E/RT) \tag{18}$$

Using Gorbachev's idea [8] to compare the approximations of the temperature integral, taking the derivative of (18) with respect to temperature :

$$\frac{\mathrm{d}I(T)}{\mathrm{d}T} = \frac{iR^2T^2 + iERT + 2ERT + E^2}{(iRT + E)^2}\exp(-E/RT) =$$

$$= 1 - \frac{i^2R^2T^2 + i(ERT - R^2T^2) - 2ERT}{(iRT + E)^2}\exp(-E/RT)$$

and identifying with (4) the following result is obtained :

$$i^2 + i(E/RT - 1) - \frac{2E}{RT} = 0 \tag{19}$$

The solutions of equation (19) are :

$$i_{1,2} = \frac{1 - E/RT \pm \sqrt{(1 - E/RT)^2 + \frac{8E}{RT}}}{2} \tag{20}$$

It is easy to observe that one of the solutions lies in the range $(1 \ldots 2)$, the function from equation (19) being negative for $i = 1$ and positive for $i = 2$, and it can be shown that the best approximation of i in natural numbers is $i = 2$, value which leads to Gorbachev-Doyle's approximation.[11]

Writing $i_{1,2}$ as :[12]

$$i_{1,2} = \frac{1 - E/RT \pm \left(1 - \dfrac{E}{RT} + 2l\right)}{2} \tag{21}$$

where l is an adjusting parameter, the following two approximations of the temperature integral can be considered :

$$I^{i1} = \frac{RT^2}{E - lRT} \exp(-E/RT) \tag{22}$$

formally identical with the Gorbachev-Doyle's approximation, and :

$$I^{i2} = \frac{T}{1 + l} \exp(-E/RT) \tag{23}$$

b) **For**[12]

$$q(T) = c \cdot e^{jT} \tag{24}$$

where c is a constant and j a parameter, equation (16) turns into :

$$cj \exp(jT) + \frac{E}{RT^2} \cdot c \cdot \exp(jT) = 1$$

hence :

$$c \exp(jT) = \frac{RT^2}{jRT^2 + E}$$

Taking into account these results, the temperature integral takes the form :

$$I(T) = \frac{RT^2}{jRT^2 + E} \exp(-E/RT) \tag{25}$$

Taking the derivative with respect to temperature and identifying with equation (4) we get :

$$\frac{E^2 + jERT^2 + 2RTE}{(jRT^2 + E)^2} = 1$$

and

$$j^2 + \frac{E}{RT^2} j + \frac{2E}{RT^3} = 0 \tag{26}$$

whose solutions are :

$$j_{1,2} = \frac{-\frac{E}{RT^2} \pm \left(\frac{E}{RT^2} - 2m\right)}{2}$$

where m is an adjusting parameter. For these two solutions the following two approximations of the temperature integral have been obtained :

$$I^{j1} = \frac{RT^2}{E - mRT} \exp(-E/RT) \tag{27}$$

and

$$I^{j2} = -\frac{1}{m} \exp(-E/RT) \tag{28}$$

The four approximations of the temperature integral (22—23) and (27—28) introduced in (5″) with a = const., lead to the following integral equations :

$$\ln F(\alpha) = \ln A/a - E/RT - \ln m \tag{29}$$

$$\ln F(\alpha) - \ln T = \ln A/a - E/RT - \ln(1 + l) \tag{30}$$

$$\ln F(\alpha) - 2 \ln T = \ln A/a - E/RT + \begin{cases} \ln R/(E - lRT) \\ \ln R/(E - mRT^2) \end{cases} \tag{31}$$

Equations (29) and (31) are formally identical with those used in the methods Flynn-Wall-Ozawa and Coats-Redfern-Gorbachev-Doyle. Equation (30) is a new one, worked by us.

Equations (29—31) can be shortly written as :

$$\ln F(\alpha) - s \ln T = \ln A/a - E/RT + L(s) \tag{32}$$

where

$$s \in \{0, 1, 2\}$$

and $L(s)$ is a correction factor.

Equation (32) with $L(s) = 0$ and $f(z) = 1 - z$ was used to work up the data concerning the dehydratation of calcium oxalate monohydrate. The obtained results are listed in Table 1.

Table 1

Nonisothermal kinetic parameters for the dehydration of $CaC_2O_4 \cdot H_2O$ (solid)

a(K/min)	E(kcal/mole)			A(s^{-1})			correlation coefficient		
	$s = 0$	$s = 1$	$s = 2$	$s = 0$	$s = 1$	$s = 2$	$s = 0$	$s = 1$	$s = 2$
2.3	23.0	22.1	21.2	10^{11}	10^{10}	$9 \cdot 10^{10}$	0.997	0.997	0.996
7.4	22.3	21.4	20.5	$6 \cdot 10^{10}$	$5 \cdot 10^{10}$	$4 \cdot 10^{10}$	0.996	0.996	0.986
14.8	21.5	20.6	19.6	$4 \cdot 10^{10}$	$3 \cdot 10^{10}$	$2 \cdot 10^{10}$	0.995	0.994	0.994

By comparing the value of the activation energy values with that obtained by differential method,[13] the closest one is obtained for $a = 2.3$ K/min and $s = 0$. One has to emphasize that although $L(s)$ was neglected the values of the preexponential factor are quite close.

CASE 2: NONLINEAR HEATING PROGRAMMES

In this case the temperature integral keeps the form (6), i.e. :

$$I(T) = \int_0^T \frac{1}{a(y)} \exp(-E/Ry)\mathrm{d}y$$

On the other hand if :

$$I(T) = q(T)\exp(-E/RT)$$

and following the same procedure as in case 1 we get :

$$a(T) = \frac{1}{\dfrac{\mathrm{d}q}{\mathrm{d}T} + \dfrac{E}{RT^2}q} \tag{33}$$

As

$$a(T) = \mathrm{d}T/\mathrm{d}t$$

it turns out that :

$$t = q + E/R\int_0^T q/y^2\mathrm{d}y \tag{34}$$

a) If $q(T)$ is given by :[14]

$$q(T) = bT^i \tag{35}$$

equation (34) takes the form :

$$t = \begin{cases} bT^i + b'\dfrac{E}{R}T^{i-1}, & i \neq 1 \\ bT + b\dfrac{E}{R}\ln T, & i = 1 \end{cases} \tag{36}$$

where $b' = b/(i-1)$.

For $i = 0$ and $i = 2$ equation (36) leads to the hyperbolic and parabolic, respectively, heating programmes.

For this case equation (5″) takes the particular form :

$$\ln F(\alpha) - i\ln T = -E/RT + \ln Ab \tag{37}$$

b) If $q(T)$ is given by :[14]

$$q(T) = b\exp(j/T) \tag{38}$$

equation (34) takes the form :

$$t - b(1 - E/Rj)\exp(j/T) \qquad (39)$$

which actually describes an exponential heating programme.

Taking into account eqn. (39), eqn. (5″) takes the particular form :

$$\ln F(\alpha) = -\frac{E/R - j}{T} + \ln Ab \qquad (40)$$

To summarise, the following general equation is valid for most nonlinear heating programmes :

$$\ln F(\alpha) - i \ln T = \ln Ab - E/RT \qquad (41)$$

It is easy to observe that for $L(s) \to 0$, equations (32) and (41) have the same form but the coefficient of $\ln T$ has different meanings. In eqn. (32) s and $L(s)$ give the approximation of the temperature integral while in eqn. (41) i is a variable whose values give the heating programmes. Taking into account the condition of independence of i of the right member of eqn. (41), one concludes that the conversion integral seems to depend on i and thus on the heating programme.

Another way of treatment of the temperature integral consists in using some iterative methods together with a suitable computing programme. Such a method based on the Gauss approximation of the integral[15] has been recently suggested.[16] The iterative treatment is advantageous as it leads to kinetic parameters values with the desired precision. Its disadvantage consists in the need of a high amount of calculations as well as in its insensitivity to changes of the reaction kinetics.

CONCLUSIONS

1) Many of the integral methods used in nonisothermal kinetics with linear heating programme are based on a general equation of the form :

$$\ln F(\alpha) - s \ln T = -E/RT + \ln A/a + L(s), \quad s \quad \{0, 1, 2\}$$

The equation is applied in the linear coordinates $\ln F(\alpha)/T^s$, $1/T$ using the least square method.

2) For many of the integral methods with nonlinear heating programmes, the general integral equation is :

$$\ln F(\alpha) - i \ln T = -E/RT + \ln Ab, \quad i \in Z$$

3) The temperature integral can be treated with iterative methods too.

REFERENCES

[1] I. Murgulescu, E. Segal and T. Oncescu, "Introduction to Physical Chemistry" (in Romanian), vol. III, Ed. Academiei, Bucharest, 1979.

[2] E. Segal and SD. Fătu, "Introduction to Nonisothermal Kinetics" (in Romanian) Ed. Academiei, Bucharest, 1981.

[3] J. R. Mac Callum and J. Tanner, *Nature*, **225**, 1127 (1970).
[4] W. W. Wendlandt, J. Šestak and V. Šatava, *Thermochim. Acta*, **7**, 333 (1973).
[5] E. Urbanovici and E. Segal, *Thermochim. Acta*, **94**, 399 (1985).
[6] C. D. Doyle, *J. Appl. Polymer Sci.*, **6**, 639 (1962).
[7] A. W. Coats and J. R. Redfern, *Nature*, **201**, 68 (1964).
[8] V. M. Gorbachev, *J. Thermal Anal.*, **8**, 349 (1975).
[9] J. H. Flyn and L. A. Wall, *J. Res. Nat. Bur. Stand.*, **70A**, 487 (1966).
[10] V. Marcu and E. Segal, *Thermochim. Acta*, **24**, 178 (1978).
[11] C. Popescu and E. Segal, *Thermochim. Acta*, **75**, 253 (1984).
[12] C. Popescu and E. Segal, *Thermochim. Acta*, **107**, 365 (1986).
[13] J. Leyko, M. Maciejewski, R. Szuniewicz, *J. Thermal Anal.*, **17**, 263 (1979).
[14] C. Popescu, E. Segal, M. Tucsnak and C. Oprea, *Thermochim. Acta*, **121**, 487 (1987).
[15] A. Myshkis "Mathematics for Engineers", P. H. Myr, Moscow, 1971.
[16] M. Tucsnak, C. Popescu and E. Segal, Comunication to the 4-th ESTAC Jena, 1987.

Revue Roumaine de Chimie, 34, 2, 577–580 (1989)

MICROPOROUS POLYETHERSULPHONE MEMBRANES

GEORGETA POPESCU, GHEORGHE NECHIFOR, BUJOR ALBU
and NICOLAE LUCA*
Center of Physical Chemistry-ICECHIM, Spl. Independenţei 202, Bucharest
* Polytechnic Institute of Bucharest

Received October 26, 1988

Microporous polyethersulphone membranes with asymmetrical structure were prepared by phase inversion method. The influence of solvent, coagulation agent and additions of polyethylene glycols with various molecular weights was studied. The membrane morphology was characterized by scanning electron microscopy and their hydrodynamic properties by solvent permeation and standard system filtering. The results recommend these membranes for utilization in micro- and ultrafiltration.

INTRODUCTION

The non-conventional technologies generated by the science of membranes have determined the growing interest shown to this field of research. The processes occurring in membranes have been dealt with in many studies which underlined the development of several advantageous separation processes employed in chemistry, medicine, biology, food and textile industry, agriculture, microelectronics, polymer science, etc.

Mathematics, physical and colloidal chemistry, physiology, biology, thermodynamics of irreversible processes as well as other branches of science have contributed to transforming membranology into an independent study with adequate theoretical foundations and well defined applications.

Among the separation processes mentioned by Porter,[1] the membrane processes cover a wide range of molecular diameter or molecular weight; the molecular weights of the constituents retained are higher than the exclusion characteristics. From the standpoint of particle size the process of ultrafiltration (UF) ranges within 10^{-6}–10^{-2} mm i.e. from ionic range to macromolecular domain, the micron-particles having a wide applicability. The selective diffusion through semipermeable membranes occurs either spontaneously as osmotic and dialysis phenomena or driven by pressure or vacuum as in case of ultrafiltration. Unlike the regular filtration in which particles accumulate at filtering surface to form progressively a colmation layer, in UF and reverse osmosis (RO) the membrane behaves as a selective barrier.[2]

This contribution presents the results of a study on preparation and characterization of polyethersulphone membranes designed for ultrafiltration.

EXPERIMENTAL

The polymer employed was a Udel-type polyethersulphone whose structure is the following:

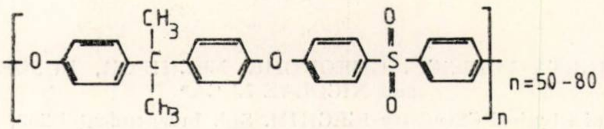

It was obtained starting up with 4-4′-dichlordiphenyl-sulphone and aromatic diphenols prepared at the Institute of Macromolecular Chemistry "P. Poni" Iassy.[3] The IR spectrum of the polymer has evidenced the adsorption bands characteristic of the C—S—C bond located at 780—1100 cm^{-1} and of the sulphoxide group at 1364—1380 cm^{-1}; the spectrum is identical to that of Udel polysulphone P_{1700}.

Polyethersulphone (PESF) is very resistant over the whole pH range to alcohols, organic and inorganic acids and bases. It is incompatible with polar aprotic solvents whose solubility parameter exceeds 10 (e.g. dimethylformamide (DMF), dimethylsulfoxide (DMSO), N-methylpyrolidone (NMP).[4] It is thermoplastic, amorphous, rigid, hard; it retains its mechanical properties over a wide range of temperatures from —101°C to 175°C. Its degradation in the air is fast at temperatures above 460°C. The temperature of continuous utilization (CU) is 149°C while that of deformation is high (174°C).

Polyethersulphone membranes were prepared by phase inversion,[5,6] particularly by immersion precipitation technique.[7] The solvents were DMF and NMP, the coagulation agents were water, isopropanol, mineral acid solution and mixtures of solvent and nonsolvent. The influence of polyethylene glycols (PEG) of various molecular weights (300—10.000) on the hydrodynamic parameters of sinthesized microporous membranes was studied. Use has been made of Loba Feinchemie Austranal ($M = 300$, 600, 1500, 4000) Merck ($M = 6000$) and Fluka AG ($M = 10.000$) samples.

The characterization of membranes has taken account of microstructure determinations and of the performance of the UF process. To determine the pore size distribution which ensures the efficiency of separation use has been made of flow rate (solvent permeation) method.[8] The results obtained for membranes width have to be supplemented by information supplied by other techniques as e.g. scanning electron microscopy[9,10]. Use has been made of a Leitz REM 1600 T microscope; the samples were immersed in liquid nitrogen to avoid structural deformations (that may cause fracture) and plated with platinum.

The exclusion characteristics, i.e. the ability of membrane to retain a certain molecular species whose size and shape is well defined was determined by the method of standard filtering.[11] The exclusion curves were determined with bovine serum albumin ($M = 67000$), ovine serum albumin ($M = 43000$), chymotripsinogen A ($M = 25000$), blue dextran ($M = 2000000$), all Pharmacia Fine Chemicals and γ-globulin ($M = 160000$) Serva. The determination of initial concentration (C_0) and ultrafiltrate (C) was carried out by UV absorption and the retention was calculated by the equation:

$$R(\%) = \frac{C_0 - C}{C_0} \cdot 100$$

In the field of microfiltration testing was performed on monodisperse polystyrene latex whose particle size was known.[12]

The hydrodynamic tests were performed in a cell of our own manufacturing whose useful volume was 100 cm^3 and inert gas pressure between 0.2 — 1 MPa.

RESULTS AND DISCUSSION

Figures 1 and 2 show the electron micrograms for PESF membranes obtained from DMF and NMP, respectively. They evidence an asymmetrical structure (image a cross section) whose active surface ranges between 0.5

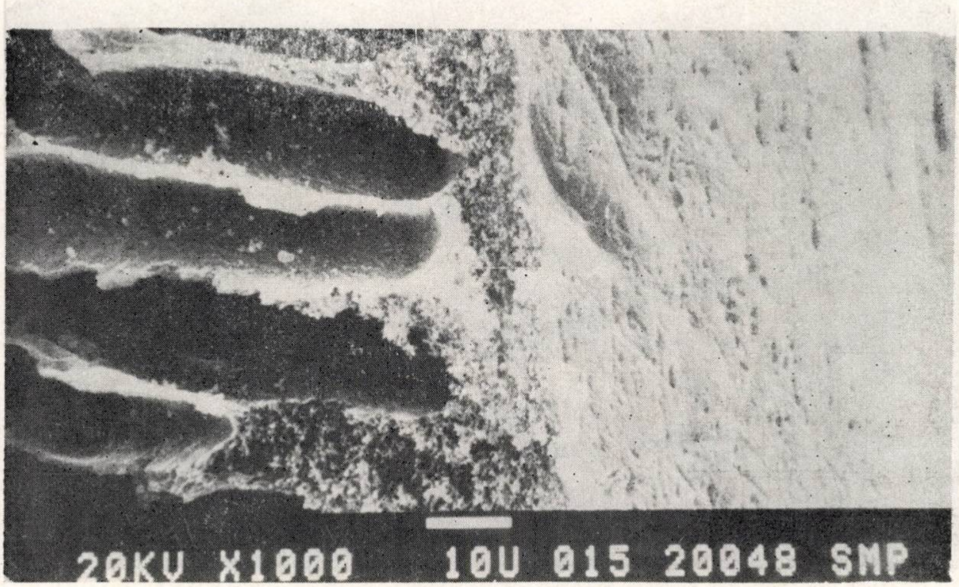
20KV X1000 10U 015 20048 SMP

Fig. 1. — a) Cross section of a PESF/DMF asymmetric membrane;

20KV X5070 10U 004 21048 SMP

b) Close-up.

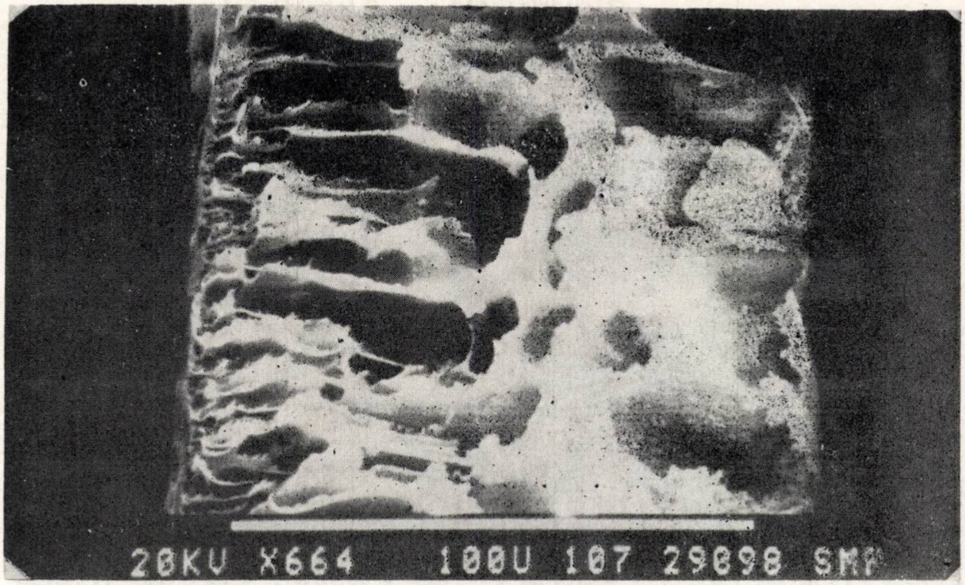
20KV X664 100U 107 29098 SMP

Fig. 2. — a) Cross section of a PESF/NMP asymmetric membrane ;

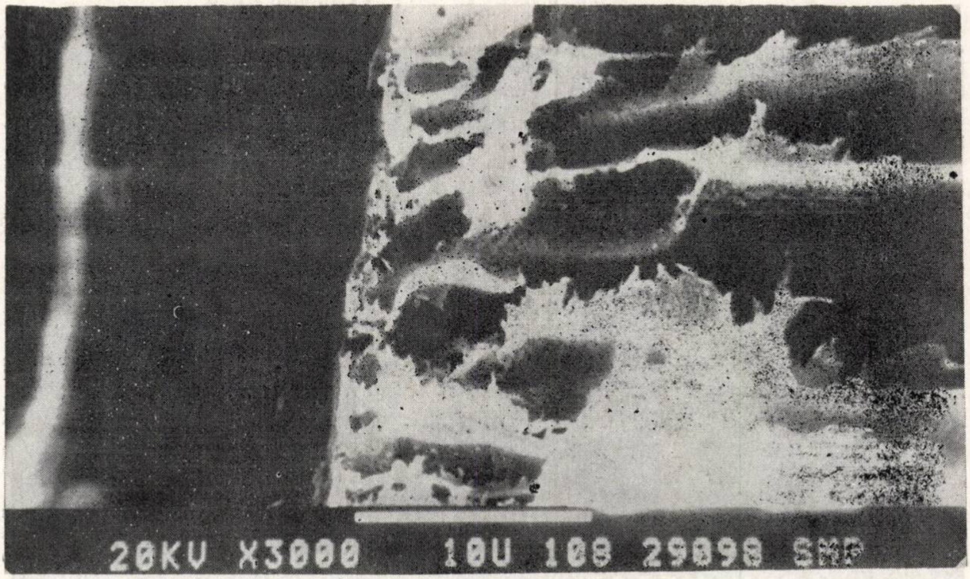
20KV X3000 10U 108 29098 SMP

b) Close-up

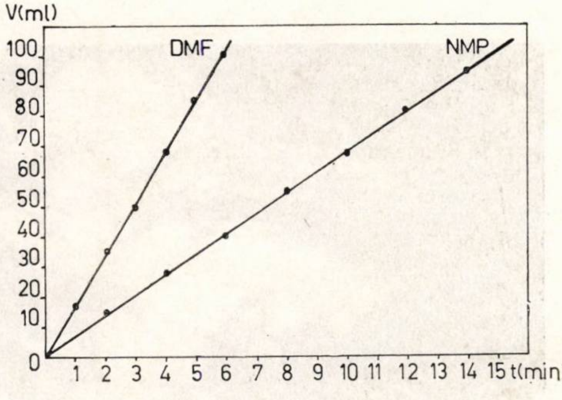

Fig. 3.—Permeation of water through a PESF/DMF and PESF/NMP membrane.

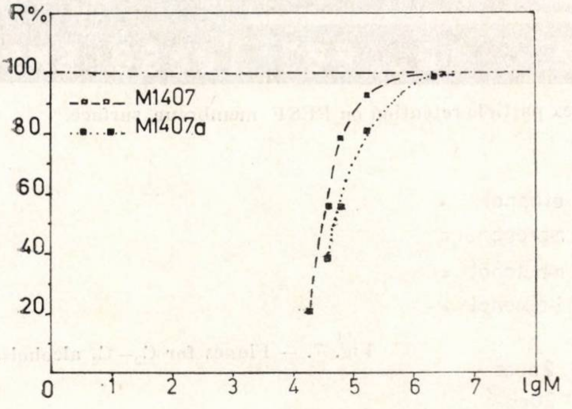

Fig. 4. — Exclusion curves for M 1407 and M 1407a membranes.

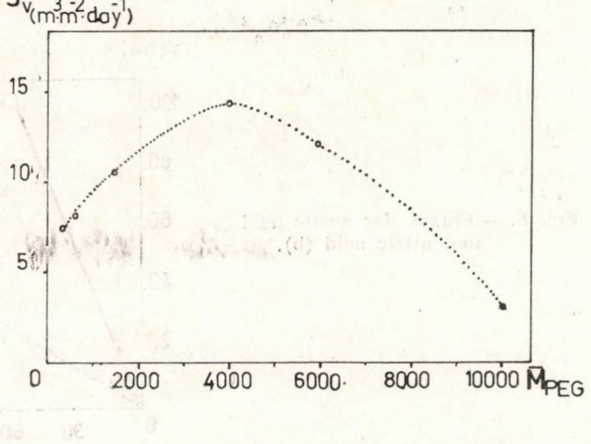

Fig. 5.—The dependence of PESF membrane permeability on the molecular weight of PEG employed as addition.

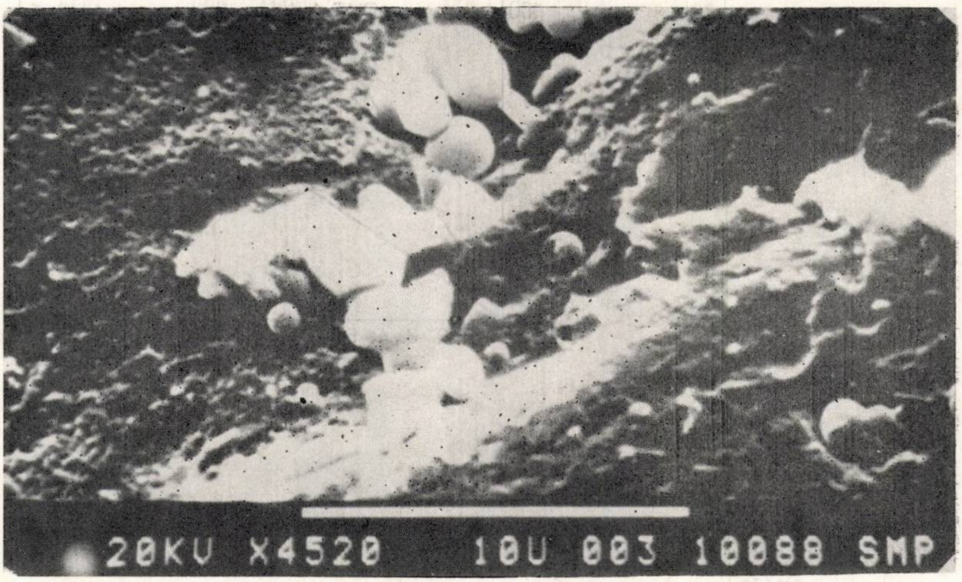
20KU X4520 10U 003 10088 SMP

Fig. 6. — Microgram of latex particle retention on PESF membrane surface.

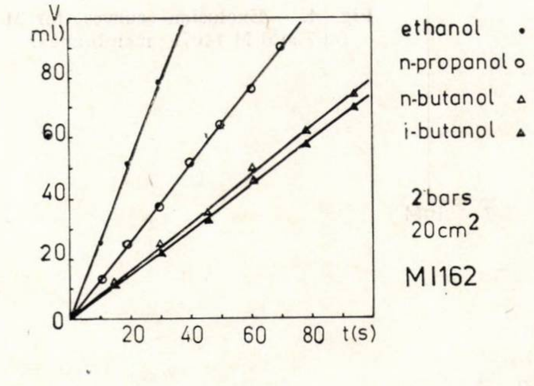

Fig. 7. — Fluxes for C_2-C_4 alcohols.

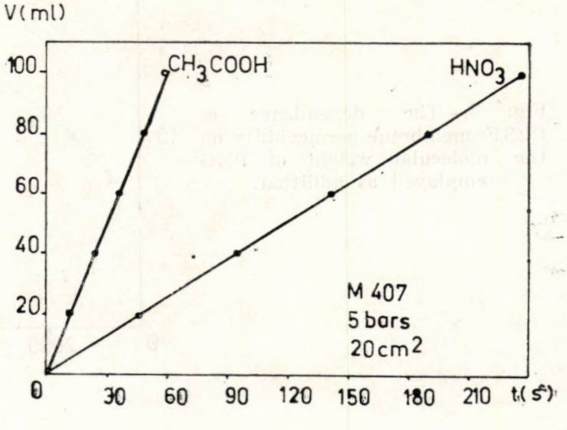

Fig. 8. — Fluxes for acetic acid (
and nitric acid (b).

and 10 μm and the porous support between 100 and 200 μm. Figures 1 and 2 also show the details of macroporous dimensions of pores beneath the active surface of the membrane which are smaller than 0.1 μm. At the same polymer concentration in DMF and NMP (15%), the NMP membrane is more compact exhibiting smaller macropores. These findings are according to the permeation data (fig. 3), the permeability of membranes prepared from DMF is higher than that of membranes prepared from NMP.

The membranes obtained from 15% PESF solution in NMP with various coagulants show specific exclusion characteristics (fig. 4). The membrane M 1407 was coagulated with 33% acetic acid aqueous solution while M 1407a was coagulated with water.

The cut-off molecular weight, i.e. that molecular weight value which corresponds to a minimum 90% retention decreases from 500.000 for M 1407a to 150000 for M 1407 evidencing the influence of the coagulation agent. Depending on the molecular weight of PEG added to the polymer solution [13] the membranes come out with different permeabilities (fig. 5) which increase with the molecular weight, reach a maximum at PEG 4000, then decrease.

Likewise the results of filtration tests carried out on latexes whose particle size were of 0.2—0.8 μm and 2 μm (fig. 6) show that membranes of PESF in DMF retain on their surface all particles. This confirms the possibility of utilizing these membranes in purification of the reagents of electronic use.

The permeation tests for a series of reagents as demineralized water, alcohols, organic and inorganic acids have come out with fluxes of 7—15 m^3/m^2 day which are very important for their application.

To exemplify, the curves in Figs. 7 and 8 show the fluxes for C_2-C_4 alcohols as well as for an organic and inorganic acid. As the alcohol hydrocarbon chain increases, the flux decreases according to the Hagen-Poseuille law. One may note the difference between isomer butanol fluxes. On the other hand the flux of nitric acid is lower than that of acetic acid.

In *conclusion*, the phase inversion method allows the obtaining of PESF Udel-type membranes with asymmetrical structure and the structural and hydrodynamic characteristics that make them suitable to ultrafiltration.

REFERENCES

[1] M. C. Porter and A. S. Michaels, *Chem. Tech.*, **1**, 56, 248, 440, 633 (1971); **2**, 56 (1972).

[2] S. T. Hwang and K. Kammermeyer, "Membranes in Separations", vol. VII, John Wiley, New York, 1975.

[3] E. Butuc and E. Melnic, The Ist National Symposium on Membranology, Săvinești Piatra Neamț, 24—27 May 1988.

[4] Filterprogramm, Sartorius Membranfilter GmbH, FRG.

[5] A. J. Reuvers, J. W. A. van den Berg and C. A. Smolders, *J. Membr. Sci.*, **34**, 45 (1987); A. J. Reuvers and C. A. Smolders, *J. Membr. Sci.*, **34**, 67 (1987).

[6] P. Meares, *J. Chem. Tech. Biotechnol.*, **37**, 189 (1987).

S. Loeb and S. Sourirajan, *Advan. Chem. Ser.*, **38**, 117 (1962).

[8] C. J. Van Oss, in "Progress in Separation and Purification" (E. S. Perry and C. J. Van Oss, Editors) Interscience, vol. III, New York, 1970, p. 97.

[9] R. Kesting, M. Engdahl and W. Stone, *J. Macromol. Sci.*, **A3**, 155 (1969).

[10] Pellicon Ultrafiltration (Application Report AR-21), Millipore Co., Bedford, Massachusetts, SUA.

[11] J. G. Wijmans, J. P. B. Baaij and C. A. Smolders, *J. Membr. Sci.*, **14**, 263 (1983).

[12] H. J. Van den Hul and J. W. Vanderhoff, in "Polymer Colloids" (R. M. Fitch Editor), Plenum Press, New York, 1971.

[13] N. Chlubek, 2nd. Intern. Sch. on Membrane Phenomena and Processes, Gdansk-Sobieszewo, 1988.

Revue Roumaine de Chimie, **34**, 2, 581–584 (1989)

KINETICS OF HEMOGLOBIN AND CASEIN HYDROLYSIS CATALYZED BY ALCALASE

CARMEN POSTOLACHE[a] and TATIANA ONCESCU[b]

[a]Polytechnic Institute, Department of Physical Chemistry, 13, Republicii Blvd, R–70346, Bucharest

[b]Institute of Chemical Pharmaceutical Research, 112, Şos. Vitan, Bucharest, R–74379

Received October 5, 1988

A comparative study was made between hemoglobin and casein hydrolysis catalysed by alcalase at pH 8.5 and various temperatures. One determined the kinetic parameters: the scission constant of the enzyme-substrate complex and the activation parameters ΔE^*, ΔH^*, ΔS^* and ΔG^* of this reaction, as well as the Michaelis constant K_M.

I. INTRODUCTION

The alkaline protease alcalase hydrolyzes the most common proteins, such as casein, hemoglobin, albumin, gelatin, gluten, etc. For this reason alcalase is used in the detergent industry for the cleansing of proteic stains (blood, cocoa, milk products) as well as in the food industry to remove proteins from fish meal and biscuits.

In this paper we studied the kinetics of the reaction between alcalase and hemoglobin, irrespective of casein, in the temperature range 25–55°C.

II. EXPERIMENTAL

A Spekol Colorimeter (Karl Zeiss Jena) was used to determine product concentration in mmoles tyrosine, by Anson [1] method, at different reaction times.

Alcalase was obtained from *Baccillus subtilis* I.C.C.F.–22. Hemoglobin and Casein Merck were used as such.

Trichloracetic acid (TCA) Fluka was used to stop the enzymatic reaction.

Folin-Ciocalteu's phenol reagent Merck, was utilized for colorimetric measurements.

All the experiments were carried out at pH = 8.5 using a phosphate buffer.

III. RESULTS AND DISCUSSION

We considered the reaction scheme :

$$E + S \underset{k_{-1}}{\overset{k_1}{\rightleftharpoons}} ES \underset{k_{-2}}{\overset{k_2}{\rightleftharpoons}} P + E \qquad (1)$$

which characterizes a large number of enzyme-catalyzed reactions. To this effect we plotted the concentration of the reaction products obtained in our experiments, versus times and determined the initial rate v_0 by using the mirror method, for six various initial substrate concentrations $[S_0]$ at constant enzyme concentration $[E_0]$. The kinetic of reaction (1) holds Briggs-Haldane [2] equation :

$$\left(\frac{d[P]}{dt}\right)_{t=0} = v_0 = \frac{k_2[E_0]}{\frac{k_{-1}+k_2}{k_1[S_0]}+1} = \frac{v_0}{\frac{K_M}{[S_0]}+1} . \tag{2}$$

A plot of v_0 versus $[S_0]$ gives a hyperbolic curve if $k_{-1} \gg k_2$ or k_{-1} of comparable magnitude with k_2.

Our experimental data give such a behaviour, as shown in fig. 1

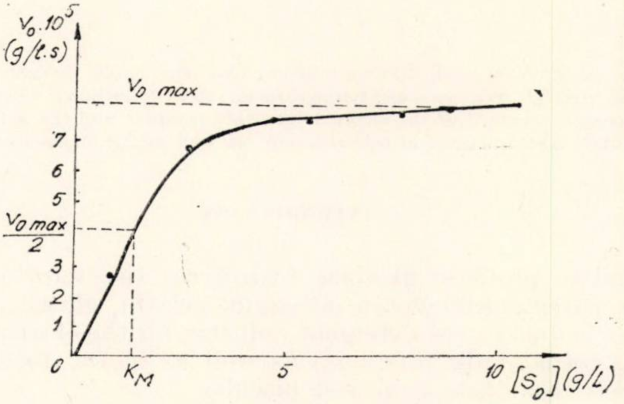

Fig. 1. — Plot of the initial rates versus hemoglobin concentration, at 35°C; $[E_0] = 0.45$ g/L.

For a more satisfactory approach of $v_{0\,max}$ and K_M we employed Hanes [3] equation :

$$\frac{[S_0]}{v_0} = \frac{K_M}{v_{0\,max}} + \frac{1}{v_{0\,max}}[S_0] \tag{3}$$

which predicts a linear variation of $\frac{[S_0]}{v_0}$ versus $[S_0]$. As figure 2 shows, both v_{0max} and K_M can be obtained from the slope and intercept of the straight line.

From the maximum value of the initial velocity $v_{0\,max}$, one immediately determines the rate constant k_2 :

$$k_2 = \frac{v_{0\,max}}{[E_0]} \tag{4}$$

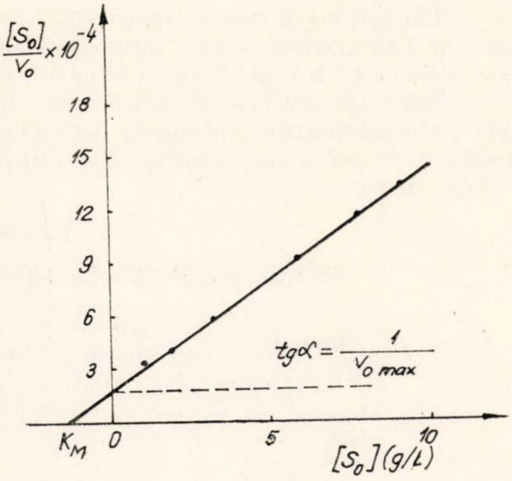

Fig. 2. — Hanes plot with data of Fig. 1

The same treatment was applied using casein as substrate. Our results are synthetized in table 1.

Table 1

Kinetic parameters of hemoglobin and casein hydrolysis, catalyzed by alcalase

Substrate	Temp. (K)	v_0 max (g/L.s)	k_2 (s^{-1})	K_M (g/L)
Hemoglobin	308	7.8×10^{-5}	1.7×10^{-4}	1.50
	318	1.4×10^{-4}	3.1×10^{-4}	2.10
	328	1.8×10^{-4}	4.0×10^{-4}	2.70
Casein	308	3.7×10^{-5}	8.3×10^{-5}	0.15
	318	6.6×10^{-5}	1.5×10^{-4}	0.20
	328	1.1×10^{-4}	2.3×10^{-4}	0.25

The concentrations used to determine the kinetic parameters from table 1 were expressed in g/L because the molecular weight of enzyme and casein utilized are unknown. In the case of hemoglobin with a molecular weight of ~65.000 we converted the K_M value in molarity ($\sim 2 \times 10^{-5}$M) which ranges between 10^{-1} and 10^{-6}M, reported for K_M of the most single-substrate reactions.[4] Table 1 shows that the catalytic constant k_2 for hemoglobin is two times higher than that of casein and the Michaelis constant K_M differs with one order of magnitude.

If $k_{-1} \gg k_2$, Michaelis constant K_M becomes the dissociation constant $\frac{k_{-1}}{k_1}$ of the enzyme-substrate complex ES. The higher value of K_M constant in the case of alcalase-hemoglobin complex therefore denotes a lower stability of this complex and also a lower substrate specificity $\left(\frac{k_2}{K_M}\right)$.

The values of rate constants k_2 at various work temperatures permitted the calculation of the activation energy ΔE^* and the preexponential coefficient A, by plotting Arrhenius equation for both substrates.

With the values obtained one computed the activation enthalpies ΔH^*, the activation entropies ΔS^* and the activation free energy ΔG^*. Table 2 presents our results (the temperature of 35°C was used to calculate ΔS^*).

Table 2

Activation parameters of hemoglobin and casein hydrolysis

Substrate	ΔH^* (kcal/mol)	ΔS^* (cal/mol.K)	ΔG^* (kcal/mol)
Hemoglobin	10.2	−31.4	19.8
Casein	12.2	−32.1	20.1

It is noticed that the activation parameters for both substrates are close. At the same time one remarks the negative value of ΔS^* which suggests the possibility of charge separation in the transition state, precursor of the hydrolysis imposing a more ordered structure.

From our presented data there results that there are no significant differences in the kinetics of hemoglobin and casein hydrolysis in the presence of alcalase.

REFERENCES

[1] M. L. Anson, *J. Gen. Physiol.*, **22**, 99 (1938).

[2] G. E. Briggs, J. B. S. Haldane, *Biochem. J.*, **19**, 338 (1925).

[3] S. C. Hanes, *Biochem. J.*, **128**, 425 (1940).

[4] R. Chang, "Physical Chemistry with Application to Biological Systems", Mac Millan Publishing Co. Inc., N. Y., 401, 1977.

Revue Roumaine de Chimie, **34**, *2*, 585–595 (1989)

СИНТЕЗ И ИССЛЕДОВАНИЕ ПОЛИМЕРОВ НА ОСНОВЕ НИТРИЛОВ ПОЛИКАРБОНОВЫХ КИСЛОТ И ДИАМИНОВ

С. А. СИЛИНГ

Институт Элементоорганических Соединений А. Н. СССР Москва, СССР

Получена 18 ноября 1988 г.

Конденсация полимеров на основе нитрилов поликарбоновых кислот и диаминов ведет к формированию полимеров или циклических структур.

The condensation of nitriles of aromatic polycarboxylic acids (di- and tetracarbonitriles) with aromatic diamines yields polymers or cyclic structures.

В настоящее время получение многих полимерных материалов, играющих ключевую роль в научно-техническом прогрессе, основано на использовании полимеров, среди которых особое место принадлежит полигетероариленам. К числу полимеров циклоцепного строения относятся и полимеры с изоиндольными циклами, которые получают поликонденсацией тетранитрилов тетракарбоновых кислот и диаминов.

Целью настоящей работы явилось исследование процесса поликонденсации, синтез этим методом новых полимеров и изучение их свойств. Основные закономерности данного типа реакций были исследованы нами на примере модельного взаимодействия фталодинитрила с моно- и диаминами.

Для определения условий, при которых взаимодействие фталодинитрила с диаминами в наибольшей степени направлено в сторону образования макрогетероцикла, было предпринято исследование зависимости состава продуктов реакции от природы реакционной среды. В качестве среды были выбраны бутиловый спирт, циклогексанол, фенол, фенолы с электронодонорными и электроноакцепторными заместителями, а в качестве реагентов—фталодинитрил и *п*-фенилендиамин.

Исследование продуктов реакции показало, что природа реакционной среды является одним из решающих факторов, который определяет состав продултов реакций (схема 1).

Установлено, что реакция фталодинитрила с диаминами в фенолах с электроноакцепторными заместителями не приводит к образованию макрогетероцикла.[1] Фенол в этом случае входит в состав продуктов реакции и является не только реакционной средой, но и одним из реагентов. Продукты конденсации фталодинитрила с диаминами в алифатических и циклоалифатических спиртах содержат широкий спектр соединений.

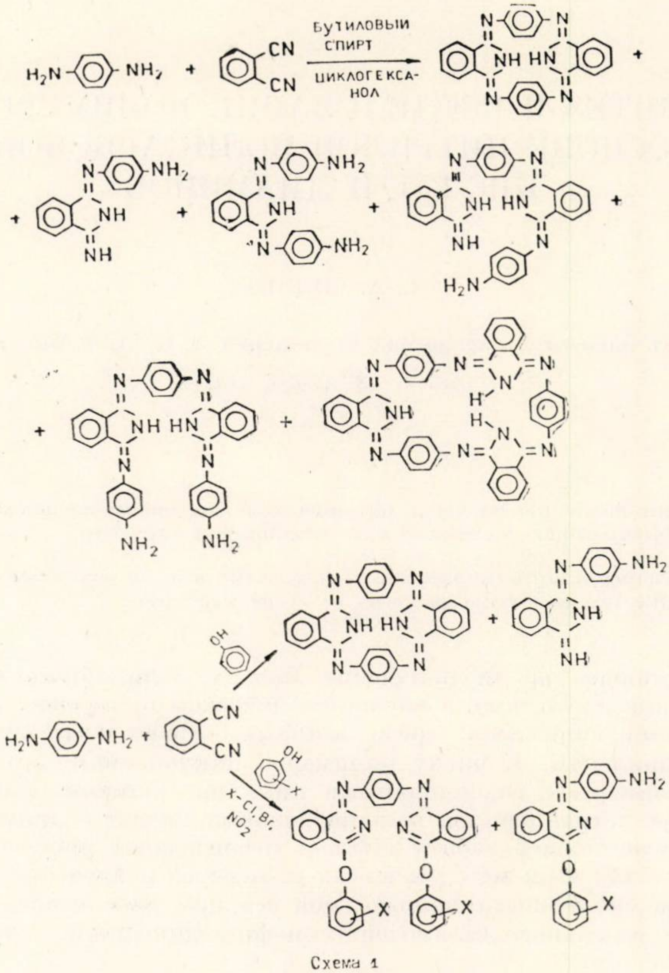

Схема 1

Выход макрогетероцикла, который мы предложили называть гексазоцикланом, не превышает 50%. При реакции этих же исходных в феноле и фенолах с электронодонорными заместителями гексазоциклан является основным продуктом реакции и получается с количественным выходом.[2] Общая схема образования гексазоциклана предложена на основании полученных результатов (схема 2).

Термодинамика процесса была изучена на примере конденсации фталодинитрила с м-фенилендиамином.[3] Были рассчитаны энтальпия, энтропия,энергия Гиббса и константы равновесия образования гексазоциклана при 60—530°К. Рассчеты показали, что в этом интервале температур константа равновесия изменяется от $9,3.10^5$ до $5,3.10^3$, т.е. конденсацию фталодинитрила с диаминами можно отнести к необратимым процессам. Энтропия реакции отрицательна, так что термодинамичская разрешенность процесса образования гексазоциклана и то, что равновесие

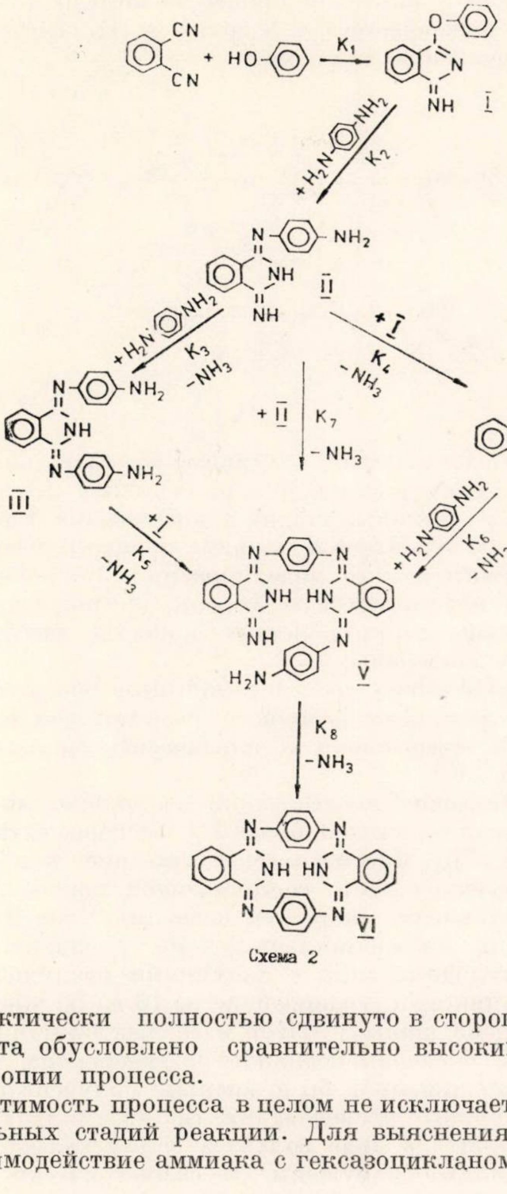
CN
CN
+ HO-
K₁
I
NH
+H₂N- -NH₂
K₂
II
N- -NH₂
NH
+H₂N- NH₂
K₃
-NH₃
+ II
K₇
-NH₃
+ I
K₄
-NH₃
III
IV
+ I
K₅
-NH₃
K₆
-NH₃
V
H₂N
K₈
-NH₃
VI

Схема 2

системы практически полностью сдвинуто в сторону образования конечного продукта обусловлено сравнительно высоким отрицательным значением энтропии процесса.

Необратимость процесса в целом не исключает возможности обратимости отдельных стадий реакции. Для выяснения этого вопроса было изучено взаимодействие аммиака с гексазоцикланом в условиях его получения.

Полученные результаты позволили заключить, что те стадии процесса образования гексазоциклана, которые протекают с выделением аммиака, являются необратимыми. Следовательно, необратимость реакции фталодинитрила с диамином следует отнести на счет ее начальных стадий.

Кинетика и механизм образования гексазоциклана были исследованы нами на примере взаимодействия фталодинитрила с *п*-фенилендиамином в феноле при 140°.[4] За ходом процесса следили по уменьшению интенсивности полосы поглощения $C \equiv N$-групп в ИК-спектре реакционного раствора и по выделению аммиака.

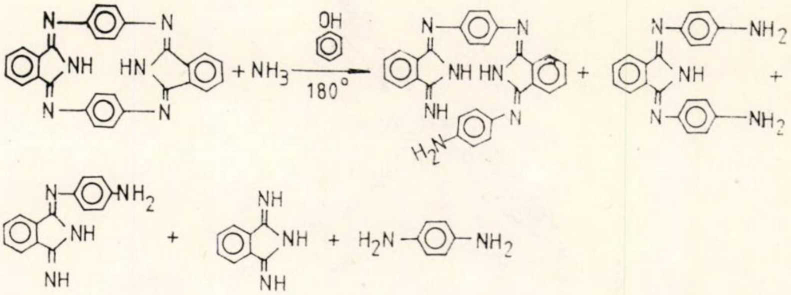

Конденсация фталодинитрила с диаминами-многостадийный процесс, состоящий из восьми последовательно-параллельных стадий. Поэтому для определения вклада отдельных стадий в образование гексазоциклана и установления наиболее вероятого механизма процесса решено было использовать метод математического моделирования. Большое количество констант, входящих в математическую модель, предопределило необходимость предварительной оценки констант скоростей тех реакций, для которых это оказалось возможным.

В результате кинетических исследований была обнаружена каталитическая активность третичных аминов в реакции фталодинитрила с фенолом и предложена эффективная каталитическая система, состоящая из третичного амина и LiCl.

На основе кинетических исследований составлена математическая модель процесса, которая описывает более 100 экспериментальных точек со средним отклонением 5%. Математическое описание дало возможность рассчитать скорости всех реакций, составляющих процесс образования гексазоциклана. Сопоставление скоростей позволило определить основную схему образования гексазоциклана (схема 2, двойные стрелки).

Конденсацией фталодинитрила с диаминами различного строения синтезированы гексазоцикланы, содержащие от 16 до 56 членов в цикле. Их строение подтверждено данными ИК- и масс-спектрометрии и элементного анализа. Прямое экспериментальное подтверждение макроциклического строения гексазоцикланов было впервые получено нами с помощью рентгеноструктурного исследования гексазоциклана, кристаллы которого удалось получить в виде сольвата с диметилформамидом.[5] В исследованных кристаллах обнаружены две симметрически независимые молекулы. Геометрия основных групп атомов близка к обычной, т.е. образование макрогетероцикла практически не требует искажения валентных углов и длин связей (рис. 1).

Наличие в гексазоцикланах большого внутрициклического пространства позволило предположить вероятность образования соединений включения. В частности впервые показано, что соединения включения с гексазоцикланами образует воды.[6] Кулонометрическим титрованием в среде реактива Фишера, а также методом элементарного анализа установлено,

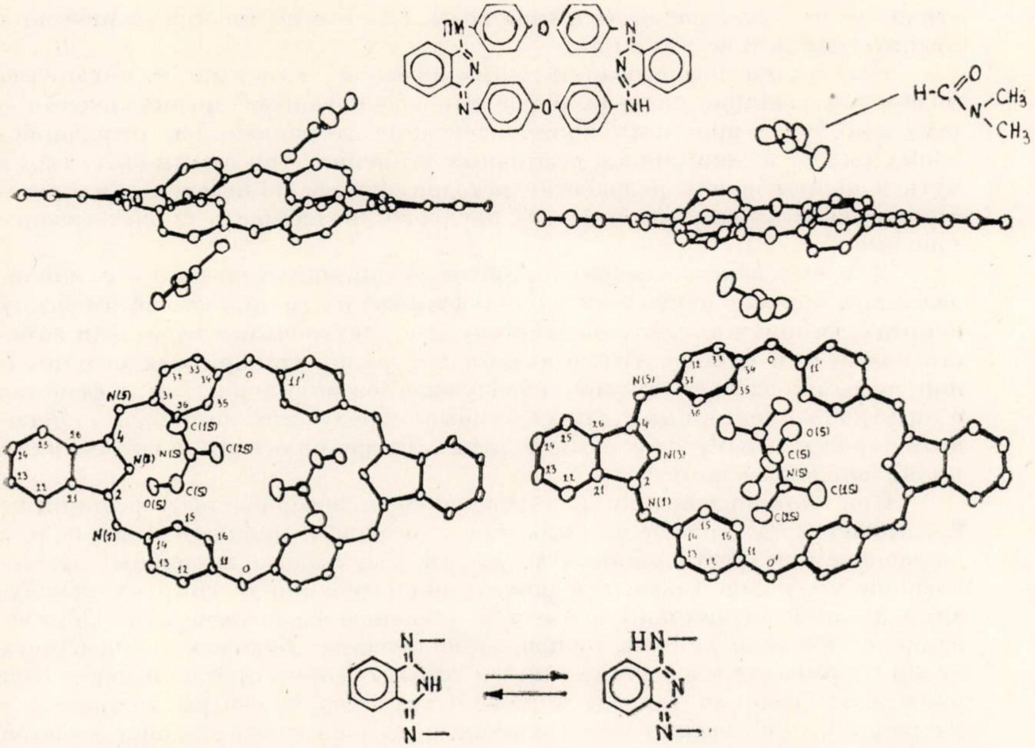

Рис. 1. — Проекции молекул гексазоциклана с ближайшими к макрогетероциклу сольватными молекулами диметилформамида. Верхние — на плоскость, перпендикулярную средней полскости гексазоциклана, нижние — на его среднюю плоскость.

Таблица 1

Данные элементного анализа

Соединение	Брутто-формула	Найдено/вычислено		
		C	H	N
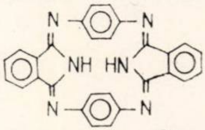	$C_{28}H_{16}N_6$	73,54/76,71	4,73/4,12	18,06/19,17
	$C_{28}H_{16}N_6 \cdot H_2O$	73,54/73,66	4,73/4,39	18,06/18,42
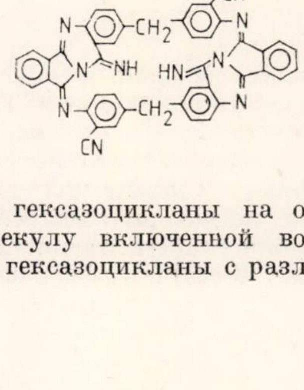	$C_{46}H_{26}N_{10}$	76,42/76,87	3,99/3,65	19,09/19,49
	$C_{46}H_{26}N_{10} \cdot 2H_2O$	76,42/73,20	3,99/3,44	19,09/18,56

что гексазоцикланы на основе одноядерных диаминов содержат одну молекулу включенной воды, остальные — две молекулы. Показано, что гексазоцикланы с различными группами во внутрициклическом пространстве не содержат включенной воды, т.к. там не имеется стерических препятствий для ее удаления.

Результаты исследования термодинамики, кинетики и механизма модельной реакции позволили сделать обоснованные предположения о том, как будет протекать поликонденсация тетранитрилов тетракарбоновых кислот и диаминов в различных условиях. Тем самым был открыт путь к направленной разработке методов синтеза полимеров с иакрогетероциклами в цепи, которые мы предложили называть полигексазоцикланами.

Для выяснения влияния природы реакционной среды на поликонденсацию процесс проводили в алифатических и циклоалифатических спиртах, фенолах с электронодонорными и электроноакцепторными заместителями и в феноле. Исследования показали, что природа реакционной среды определяет строение образующегося полимера. Так, в фенолах с электроноакцепторными заместителями образуются полимеры с боковыми ароксильными группами в цепи. Такие полимеры названы нами полиизоиндоксазенами.[1]

При поликонденсации в спиртах степень завершенности реакции не превышает 25%, полимеры выпадают в осадок в процессе синтеза и в дальнейшем не растворяются. С учетом результатов модельных исследований можно полагать, что при поликонденсации в спиртах образуются полигексазоцикланы с высокой степенью разнозвенности. Образование в процессе синтеза большого количества боковых полимерных цепей и приводит в конечном итоге к структурированию полимера. При проведении реакции в среде фенола и крезолов полимеры находятся в растворе на протяжении всего синтеза, и их растворимость определяется только строением полимера.

Совокупность полученных результатов позволила сделать важный вывод о том, что полигексазоцикланы с максимальным содержанием макрогетероциклов могут быть получены в среде фенола и крезолов.

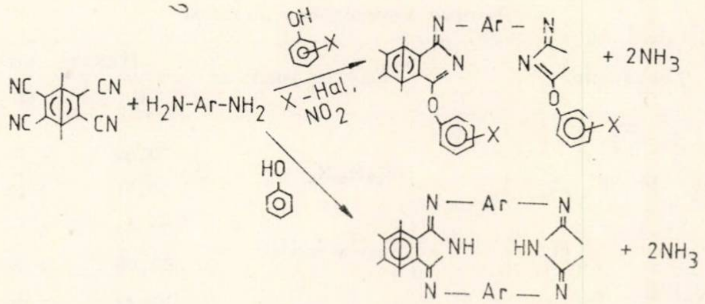

Полигексазоцикланы получаются с высоким выходом и высокой степенью завершенности реакции. Данные, полученные методом ТГА, свидетельствуют о сравнительно высокой термостойкости полимеров.[7] Более полная информация о термических превращения полигексазоцикланов была получена при исследовании механизма термической термогидролитической деструкции полимеров и их модельных соединений. Исследования показали, что процессы разложения полигексазоцикланов различного строения носят одинаковый характер. В состав газообразных продуктов реакции входят двуокись углерода и аммиак, образование которых в виде следов наблюдается при 350°. При более высоких температурах появляются водород, метан и окись углерода, незначительные количества цианистого водорода, анилина и бензола. Твердые продукты деструкции представляют собой диамины и олигомерные соединения.

Тот факт, что до 400° двуокись углерода является практически единственным, а до 450° — основным продуктом деструкции, позволяет заключить, что до 450° решающую роль в термической деструкции полигексазоцикланов играют гидролитические процессы распада. Установлено, что основным гидролизующим агентом является вода, включенная в макрогетероцикл. При температуре выше 450° преобладают гомолитические процессы распада.

Большинство полигексазоцикланов хорошо растворимо в апротонных растворителях, серной и муравьиной кислотах. При исследовании вязкости разбавленных растворов полигексазоцикланов в апротонных растворителях было установлено, что вне зависимости от степени завершенности реакции приведенная вязкость 0,5% растворов очень низка. Другой аномалией является то, что приведенная вязкость 0,3—1% растворов полимеров в апротонных растворителях не зависит от концентрации. При центрифугировании ; этих растворов происходит полное осаждение полимеров. Совокупность приведенных данных дала нам основание полагать, что полигексазоцикланы находятся в растворе в виде метастабильных агрегатов, т.е. эти растворы являются не истинными, а переходными к коллоидным или коллоидными.[8] В пользу этого предположения свидетельствует тот факт, что по данным электронной микроскопии проекции полимерных частиц представляют собой пирамидки размером до 1000 Å или неправильные образования размером до 3000 Å. (рис. 2).

При исследовании растворов полимеров в муравьиной кислоте было обнаружено, что абсолютные значения приведенной вязкости полимеров в муравьиной кислоте значительно выше, чем в N-метилпирролидоне. Обращает на себя внимание повышение вязкости раствора полимера в муравьиной кислоте с уменьшением его концентрации. Наиболее вероятной причиной увеличения вязкости является то, что полигексазоцикланы, представляющие собой слабые основания, в растворе муравьиной кислоты присоединяют протон и становятся полиэлектролитами. Поэтому повышение приведенной вязкости может быть проявлением полиэлектролитного эффекта. Это предположение подтверждается тем, что приведенная вязкость растворов полимеров в 85% муравьиной кислоте понижается с уменьшением концентрации раствора.

Исследование концентрированных растворов полимеров в муравьиной кислоте показало, что, начиная с определенной концентрации у ряда полимеров происходит гелеобразование, являющееся очевидно, следствием взаимной укладки вытянутых молекул. При центрифугировании растворов полигексазоцикланов в муравьиной кислоте выпадения полимеров в осадок не наблюдается. По данным электронной микроскопии размер полимерных частиц в растворе не превышает 80—100 Å. Приведенные факты свидетельствуют о том, что растворы полигексазоцикланов в муравьиной кислоте являются молекулярно-дисперсными.

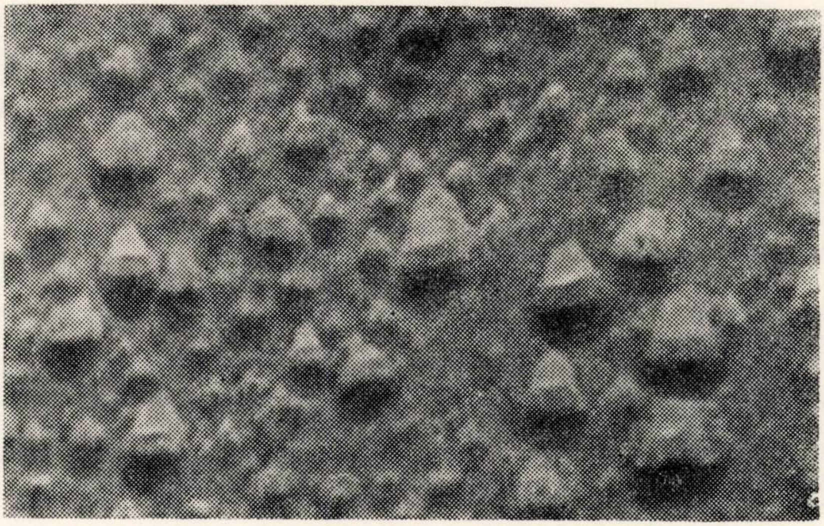

Рис. 2. — Микрофотография полигексазоциклана.

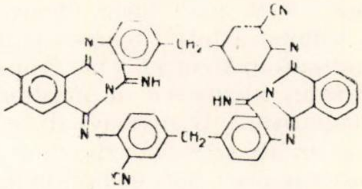

(0,002% раствор в N-метилпирролидоне). Увеличение × 50000

Термостойкость, заложенная в структуре полигексазоцикланов, в полной мере не реализуется, поскольку включенная в макрогетероцикл вода обуславливает протекание гидролитических процессов при относительно низких температурах. Это сделало необходимым разработку методов синтеза таких полигексазоцикланов, строение которых предопределило бы отсутствие включенной воды, т.е. полимеров, у которых часть внутрициклического пространства занята какими-либо группами. Наиболее целесообразным в этом аспекте представлялся синтез полимеров, в макрогетероцикле которых содержатся гетероциклы, конденсированные с изоиндольным. Мы полагали, что такие полимеры могли быть получены при использовании в качестве мономеров диаминов, содержащих в ортоположении заместители, способные к взаимодействию со вторичными аминогруппами изоиндольного цикла, например C ≡ N-группу.

При использовании для синтеза полимеров бис (о-цианаминов) получены полигексазоцикланы с конденсированным изоиндольным и хиназолиновым циклами.[9]

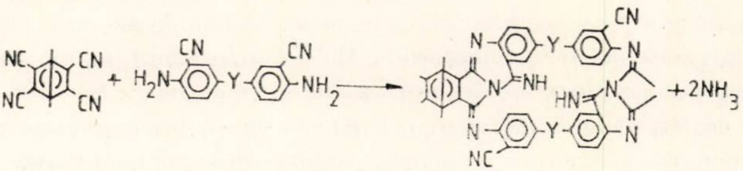

Данная реакция интересна тем, что позволяет получать систему конденсированных гетероциклов путем изомеризационной циклизации без выделения летучих продуктов. Полимеры образуются с количественным выходом и высокой степенью завершенности реакции. Они хорошо растворимы в огранических растворителях, устойчивы к действию кислот и щелочей.

Как и ожидалось, полумеры такого строения по данным элементного анализа не содержат включенной воды, что не могло не отразиться на термической устойчивости полимеров.[7] Гидролитические процессы распада рассмотренных ранее полигексазоцикланов уже при 250—300° сопровождаются появлением в ИК-спектре полосы поглощения 1730 см$^{-1}$, относящеся к экзоциклической C = O-группе, образовавшейся в процессе гидролиза. В ИК-спектрах полимеров с конденсированными циклами, входящими в макрогетероцикл, слабое поглощение в этой области наблюдается лишь после прогрева при 450°. Количество CO_2, выделившегося в результате термической деструкции полигексазоциклана на основе п-фенилендиамина при 450° в 4—6, а при 500—550° в 2—4 раза больше чем у полимера на основе о-цианамина. Количество выделившейся окиси-углерода у полимеров с конденсированными гетероциклами также существенно ниже.[7]

Таким образом, полимеры с системой конденсированных гетероциклов, входящих в макроцикл, обладают значительно более высокой термической устойчивостью, чем полигексазоцикланы на основе незамещенных диаминов.

Нами разработан принципиально новый метод синтеза полигексазоцикланов, отличительной особенностью которого является использование в качестве одного из реагентов гексазоциклана.[10] При этом бифункциональные соединения могут реагировать со вторичными иминогруппами изоиндольного цикла. Такой метод интересен тем, что позволяет получать полимеры, не обладающие разнозвенностью в отношении макрогетероциклов.

Так, при поликонденсации гексазоцикланов с дихлорангидридами дикарбоновых кислот впервые синтезированы полимеры, названные нами полиамидогексазоцикланы.

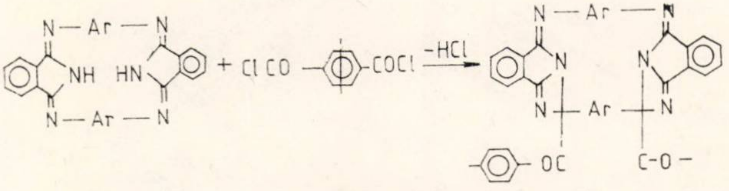

По данным элементного анализа эти полимеры не содержат включенной воды, что нашло свое отражение в термических характеристиках полигексазоцикланов. По термостойкости полиамидогексазоцикланы значительно превосходят полигексазоцикланы: гидролитические процессы в них не наблюдаются до 450°, о чем свидетельствует отсутствие CO_2 в продуктах деструкции.[7] По результатам изотермического анализа на воздухе потеря массы у полиамидогексазоцикланов в 4 раза ниже, чем у полигексазоцикланов.

Поликонденсацией тетранитрилов тетракарбоновых кислот и бисантраниловых кислот в полифосфорной ккислоте получены полимеры немакроциклического строения, названные нами полиизоиндолхиназолоны.[11] Термостойкость этих полимеров достаточно высока. Однако, нельзя не отметить, что как гидролитические, так и гомолитические процессы распада в полиизоиндолхиназолонах протекают в значительно большей степени, чем в полигексазоцикланах, что свидетельствует о вкладе макроциклической структуры в термическую устойчивость полимеров.

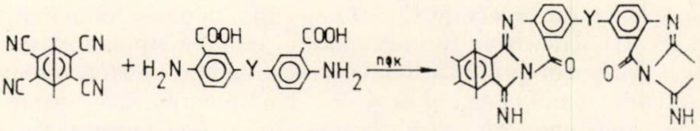
NC
CN
NC
CN
COOH
COOH
$+H_2N$
Y
NH_2
пфк
N
Y
N
N
O
O
N
NH
NH

Таким образом, изучение химии и установление физико-химических закономерностей поликонденсации бисфталодинитрилов с диаминами и соответствующих модельных реакций позволило сформулировать общие представления о механизме этих реакций и создало основу для целенаправленного синтеза серии новых классов полимеров, что свидетельствует о широких синтетических возможностях реакции о-динитрилов с ароматическими диаминами (см. схему 3).

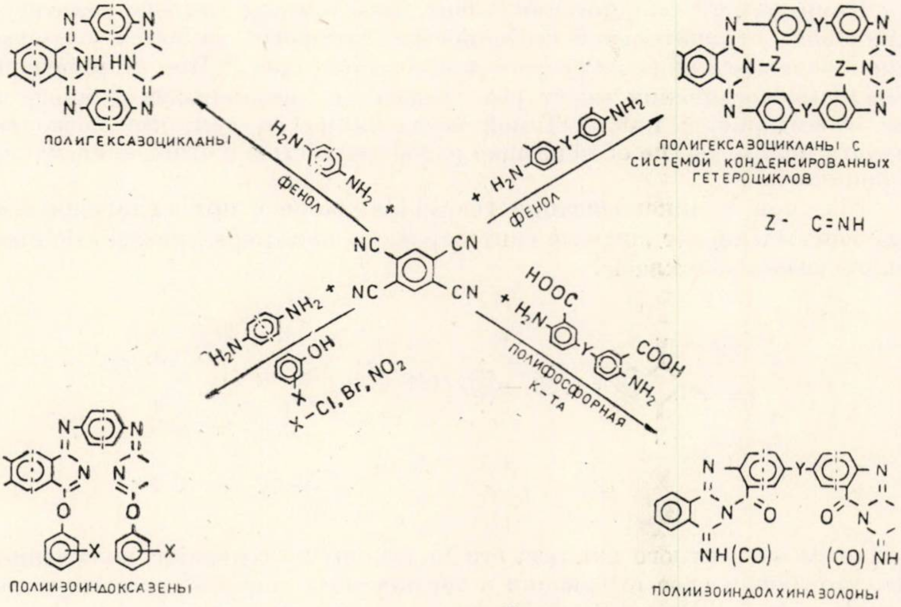
ПОЛИГЕКСАЗОЦИКЛАНЫ
ПОЛИГЕКСАЗОЦИКЛАНЫ С СИСТЕМОЙ КОНДЕНСИРОВАННЫХ ГЕТЕРОЦИКЛОВ
Z - C=NH
ФЕНОЛ
ФЕНОЛ
NC
CN
NC
CN
HOOC
COOH
ПОЛИФОСФОРНАЯ К-ТА
OH
X-Cl, Br, NO2
ПОЛИИЗОИНДОКСАЗЕНЫ
ПОЛИИЗОИНДОЛХИНАЗОЛОНЫ
NH(CO)
(CO) NH

Схема 3

Найденные закономерности поликонденсации тетранитрилов тетракарбоновых кислот и диаминов, установленные связи между строением и свойствами образующихся полимеров могут служить фундаментом для развития новых направлений в области полимерной химии.

ЛИТЕРАТУРА

[1] В. В. Коршак, С. В. Виноградова, С. А. Силинг, В. Н. Соловьев, *ДАН СССР* **222**, *1*, 114 (1975).

[2] S. A. Siling, S. V. Vinogradova, V. N. Solovjov, *Macromol. Chem.*, **177**, 1905 (1976),

[3] Н. Б. Рабинович, Н. В. Карякин, Э. С. Джаримова, С. А. Силинг и др., *Изв. АН СССР, сер. хим.*, **4**, 779 (1984).

[4] С. А. Силинг, И. И. Пономарев, В. В. Кузнецов и др., *Изв. АН СССР, сер. хим.*, **4**, 771(1984).

[5] С. В. Линдеман, В. Е. Шкловер, Ю. Т. Стручков и др., *Изв. АН ССР, сер. хим.*, **9**, 2015 (1984).

[6] С. А. Силинг, Н. Н. Годовиков, И. И. Пономарев и др., *Изв. АН СССР, сер. хим.*, **6**, 1471 (1984).

[7] S. A. Siling, P. N. Ciacova, I. I. Ponomarev, *J. Pol. Sci.*, **21**, *9*, 2675 (1983).

[8] С. А. Силинг, И. И. Пономарев, В. Г. Васильев и др., *Высокомол соед.*, **1**, **162** (1987).

[9] В. В. Коршак, С. В. Виноградова, С. А. Силинг и др,. *Высокомол. соед.*, **5**, 1120 (1981).

[10] С. В. Виноградова, С. А. Силинг, В. Н. Соловьев, В. В. Коршак, *Высокомол. соед.* **1**, 288 (1979).

[11] С. В. Виноградова, С. А. Силинг, И. И. Пономарев, В. В. Коршак, *Высокомол. соед.*, **1**, 138 (1979).

Revue Roumaine de Chimie, **34**, *2*, 597–601 (1989)

ADHESIVE EMULSIONS. PART 4*

SYNTHESIS OF THE VINYL ACETATE/METHYL METHACRYLATE/ACRYLAMIDE COPOLYMER IN THE ABSENCE OF EMULGATORS

CRISTOFOR I. SIMIONESCU, AURICA CHIRIAC,
VIORICA RUSAN and IORDANA NEAMŢU

Institute of Macromolecular Chemistry "P. Poni",
Aleea Gr. Ghica Vodă 41 A, Jassy, Romania

Received February 18, 1988

The present paper studies the acrylamide copolymerization — in aqueous emulsion — of the" vinyl acetate/methyl methacrylate/acrylamide" system, both by the classical method, in the absence of emulgators and the presence of performed homopolymers (polyvinyl acetate, methyl polymethacrylate, polyacrylamide), and in the absence of homopolymers and emulgators. The stability of the obtained emulsions has been reported to the classical system of synthesis.

Previous investigations dealt with the obtainment — in aqueous emulsion — of the "vinyl acetate/methyl methacrylate/acrylamide" copolymer, in the presence of the anionic-nonionic system of emulgators, natrium di-2-ethylhexylsulphosuccinate/nonylphenolpolyethoxylate.[1] Studies in this field attest that emulgator removal from the system improves optical and dielectrical properties, as well as the stability of the emulsions.[2]

The possibilities of aqueous emulsion formation without using tensioactive agents has been already proved in the radicalic polymerization of vinyl acetate, methyl and ethyl acrylate, styrene or in their copolymerization by using comonomers with ionizable groups (e.g.: $-COOH$, $-NH_2$, $-SO_4$).[3-9]

On the other hand, some attempts of synthesizing vinylic copolymers in aqueous emulsion, in the presence of polymers pre-existing in the system, are known.[10-11]

The present paper studies the copolymerization — in aqueous emulsion — of the "vinyl acetate/methyl methacrylate/acrylamide" system, both through the classical method (I), in the absence of emulgators and in the presence of homopolymers (polyvinyl acetate II, methyl polymethacrylate III, polyacrylamide IV) and in their and in the homopolymers absence.

---

* Part 3 : *Materiale plastice*, **2**, 70 (1988).

The stability of the obtained emulsions has been reported to the classical system of synthesis.

EXPERIMENTAL

The vinyl acetate/methyl methacrylate/acrylamide copolymer has been synthesized by radicalic mechanism, starting from the initial gravimetric composition of the comonomers : 60/27/13, in the presence of potassium persulphate (0.7%, as compared with the comonomer mixture), with a view to obtaining a stable aqueous emulsion. The reaction was conducted at 70 °C for 5 hours, followed by a post-thermal treatment at 85 °C, for 30 minutes.

The synthesis conditions applied were the following :

— emulsion of standard copolymer (I), obtained with an anionic/nonionic emulsion system (1/1)— natrium-di-2-ethylhexyl sulphosuccinate and nonylphenol polyethoxylate—(3%, as compared with the comonomer mixture) ;

— copolymer emulsion (II) obtained in the presence of polyvinyl acetate (synthesized in standard conditions for aqueous emulsion and introduced into the reaction mixture concomitantly with the comonomers, 3% as compared with them) ;

— copolymer emulsion (III) synthesized in the presence of methyl polymethacrylate (homopolymer produced and introduced into the reaction as above) ;

— copolymer emulsion (IV) produced in the presence of polyacrlylamide (synthesized and used as in cases II and III) ;

— copolymer emulsion (V) deriving from comonomer polymerization in the reaction system, in the absence of emulgators or preformed homopolymers.

The products have been characterized from the viewpoint of the emulsion stability in time and of their thermal degradation.

Optical microscopy (MC—1 IOR-type optical microscope ; magnifying power of films obtained from synthesized copolymers 600×) and electron microscopy (Tesla BS 513 A type transmission electron microscope ; 0.005% concentrated solutions have been magnified 4600× times), conductometry (PP-type conductomer, 1% concentrated emulsions) and thermogravimetry (Paulik-Paulik Erdely-type derivatograph ; heating rate of the films from the obtained emulsions, 12 °C/min, in air ; DTA drop calibration with $NaNO_3$), techniques have been applied.

RESULTS AND DISCUSSION

The system of vinyl acetate/methyl methacrylate/acrylamide comonomers, in an initial gravimetric ratio of 60/27/13, always leads to stable emulsions, showing adhesive properties.

The copolymerization reaction is seen to proceed much slowly in the absence of emulgators or homopolymers pre-existent in the system (Fig. 1 — curve 5).

By introducing a water-soluble prepolymer — polyacrylamide — the process rate — as compared with the variant lacking in emulgator — considerably increases (figure 1, curve 4). Mention must be made of the positive influence of emulgators upon the reaction rate (figure 1, curve 1 as compared with 2—5). The emulgator absence from the system doubles the reaction time.

As to the microscopical aspect of the films from the synthesized copolymers, Figure 2 evidences a strong homogeneity of emulsions in variant V (absence of emulgators and homopolymers) as compared with copolymers I—IV.

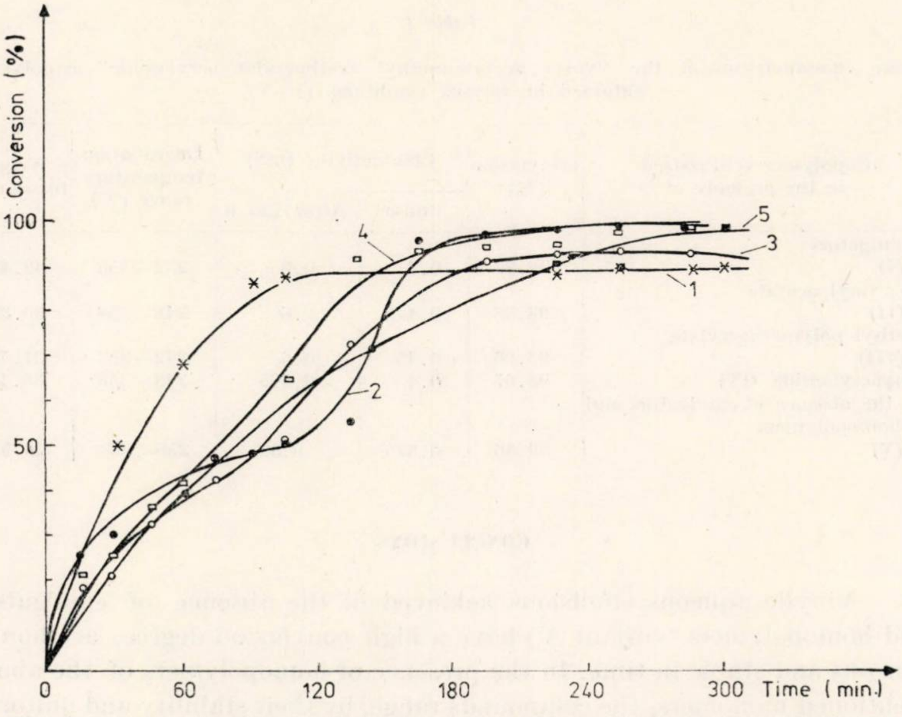

Fig. 1. — Conversion of synthetized latex : classical latex (1) ; in the presence of polyvinyl acetate (2), methyl polymethacrylate (3), polyacrylamide (4) ; in the absence of emulgators and preformed homopolymers (5).

The morphology of latex individual particles, investigated by electron microscopy, also shows the homogeneity of the emulsion prepared in the absence of emulgators or homopolymers. Figure 3 (a—e) evidences clearly individualized spheroidal particles of methacrylovinylic copolymers.

Conductimetric determination of the emulsion stability in time leads to optimal values for samples 5, which confirms the high stability of the system performed in the absence of emulgators and preformed homopolymers. The time variation of conductivity is presented in Figure 4.

The copolymer thermal behaviour (Table 1) evidences the stability of the emulsions obtained in the absence of emulgators and homopolymers (variant V), which is argumented by the initial and maximum decomposition temperature, as well as by weight losses. Thus, the initial decomposition temperature increases with 20°C, while weight losses decrease with up to 15% in the thermal decomposition interval ($T_i - T_{\max}$).

As regards the adhesive character of the emulsions, it is not influenced by the nature of the compounds playing the role of emulgators, the time of set remaining within the same limits for all variants of synthesized copolymer.

Table 1

Some characteristics of the "vinyl acetate/methyl methacrylate/acrylamide" copolymer, obtained in various conditions (I—V)

Copolymer synthesized in the presence of	Conversion (%)	Conductivity (mS)		Degradation temperature range (°C)	Weight losses (%)
		Initia	After 720 h		
Emulgators (I)	98.93	0.7	0.9	232—356	39.48
Polyvinyl acetate (II)	98.98	0.425	0.6	248—358	30.82
Methyl polymethacrylate (III)	98.96	0.45	0.6	242—358	31.70
Polyacrylamide (IV)	98.95	0.4	0.575	248—358	30.43
In the absence of emulgators and homopolymers (V)	99.86	0.375	0.55	256—360	26.53

CONCLUSIONS

Vinylic aqueous emulsions achieved in the absence of emulgators and homopolymers (variant V) have a high conversion degree, are homogeneous and stable in time. In the presence of homopolymers of the above mentioned monomers, the compounds range, by their stability and uniformity, between the emulsion obtained by classical procedures and the one without emulgator and homopolymers.

The present paper opens the way for subsequent investigations on the correlation between the chemical structure, method of synthesis and the characterization of the emulsions obtained in the absence of classical tensioactive substances, by applying nonconventional procedures which offer the advantages of higher conversions and improved properties.

REFERENCES

[1] A. Chiriac, A. Leonte, I. Neamţu, V. Rusan, to be submitted for publication.

[2] V. I. Eliseeva, "Emulsyonaya polimerizatsia", 1976.

[3] R. Patsiga, L. M. Stannet, *J. Phys. Chem.*, **64**, 801 (1960).

[4] V. I. Eliseeva, I. B. Nazarova, S. A. Petrova, *Kolloid. J.*, **30**, 37 (1968).

[5] V. I. Eliseeva, S. A. Petrova, *Vysokomol. Soedineniya*, A, **12**, 1621 (1970).

[6] V. I. Eliseeva, K. M. Zurabian, A. L. Zaides, *Doklady Akad. Nauk SSSR*, **162**, 1086 (1964).

[7] A. Kotera, K. Furusawa, J. Takada, *Koll. Z. i Z. Polymere*, **239**, 677 (1970).

[8] V. I. Eliseeva, I. V. Nazarova, A. B. Taubman, *Doklady Akad.. Nauk SSSR*, 1082 (1967).

[9] D. P. Sheetz, *J. Appl. Polymer Sci.*, **9**, 3759 (1954).

[10] C. Hagiopol, M. Georgescu, I. Deaconescu, *Acta Polymerica*, **36**, 540 (1985).

[11] W. D. Hergeth, K. Schmutzler, *Acta Polymerica*, **35**, 472 (1986).

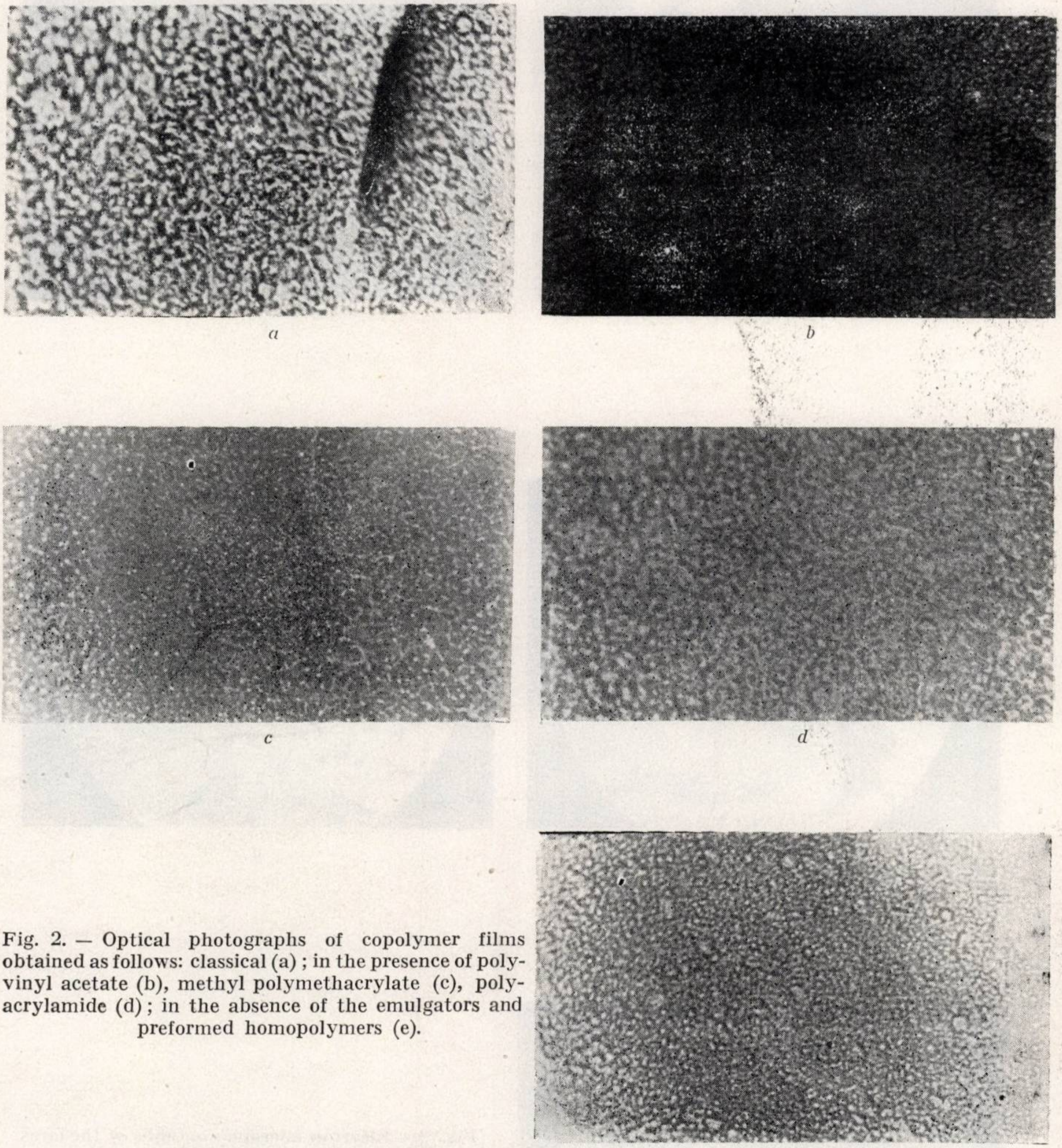

Fig. 2. — Optical photographs of copolymer films obtained as follows: classical (a) ; in the presence of polyvinyl acetate (b), methyl polymethacrylate (c), polyacrylamide (d) ; in the absence of the emulgators and preformed homopolymers (e).

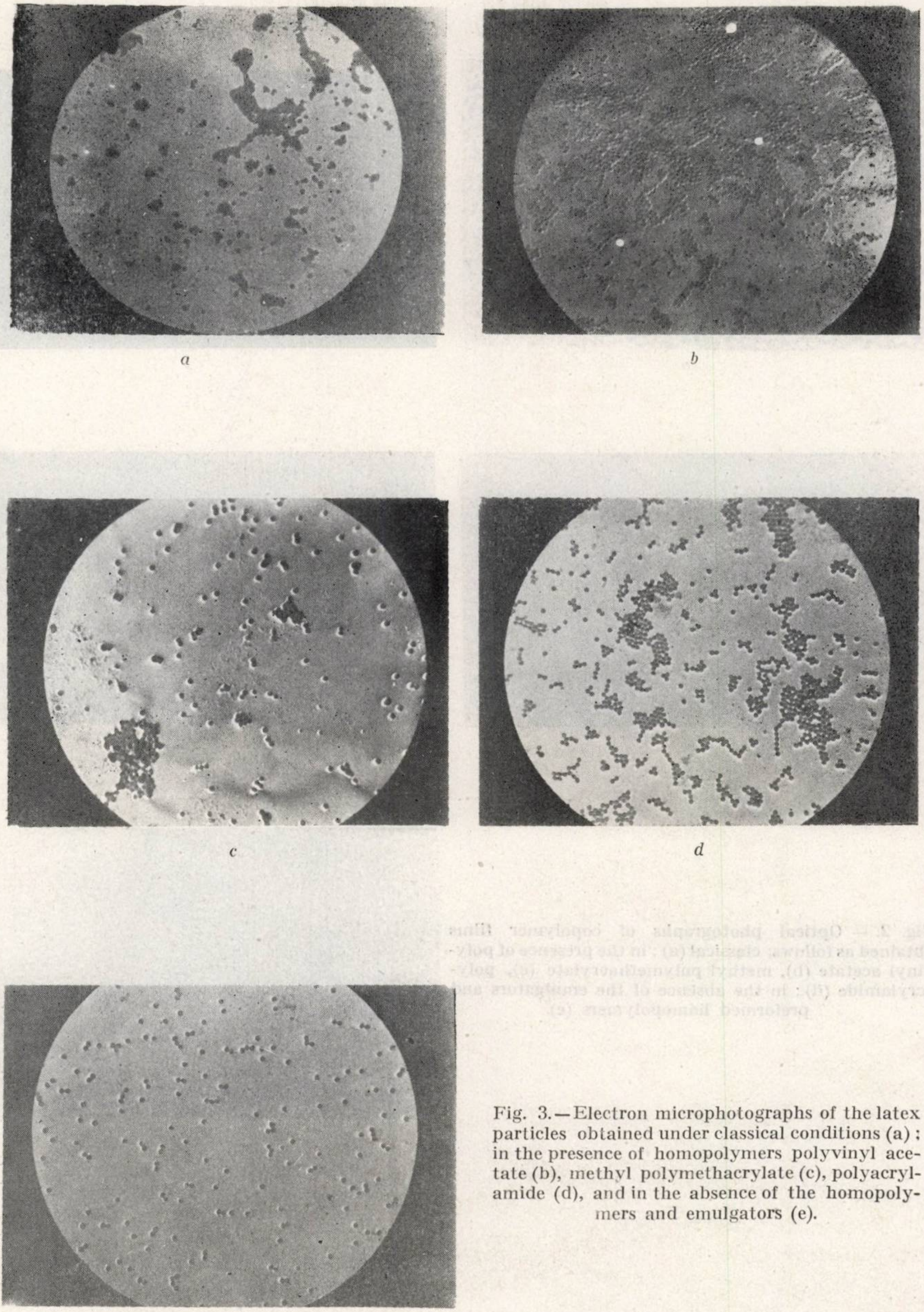

Fig. 3.—Electron microphotographs of the latex particles obtained under classical conditions (a); in the presence of homopolymers polyvinyl acetate (b), methyl polymethacrylate (c), polyacrylamide (d), and in the absence of the homopolymers and emulgators (e).

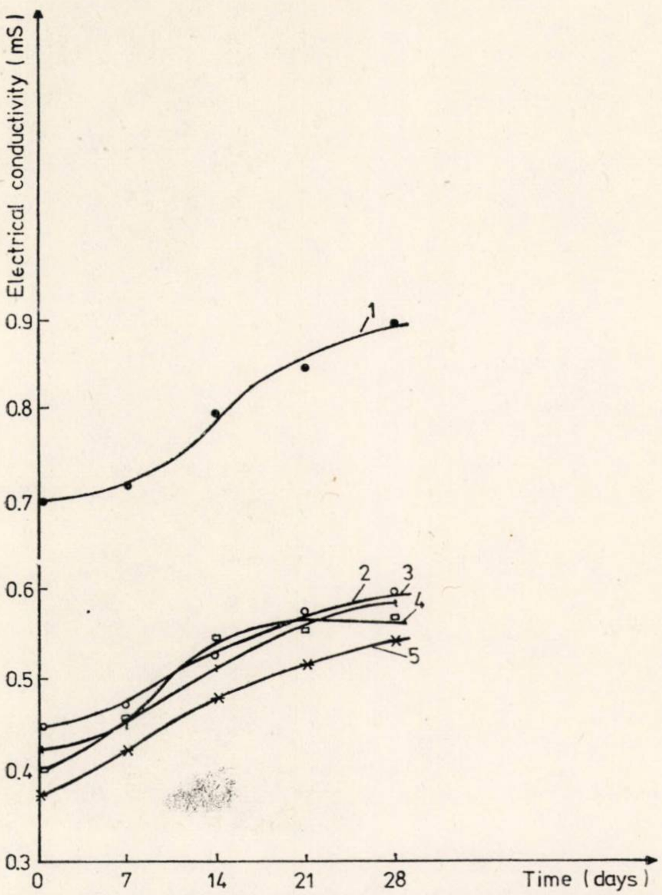

Fig. 4. — The influence of the synthesis conditions on the electrical conductivity of the polymers emulsions : classical (1), in the presence of polyvinyl acetate (2) methyl polymethacrylate (3), polyacrylamide (4), in the absence of emulgators and preformed homopolymers (5).

Revue Roumaine de Chimie, **34**, 2, 603–615 (1989)

MARANGONI TRANSLATIONAL MOTION OF A FREE DROP INITIALLY AT REST

I. STAN[b], E. CHIFU[a,1], Z. FINTA[a] and EUGENIA GAVRILĂ[a]

[a] Department of Physical Chemistry

[b] Department of Differential Equations and Mechanics, University of Cluj-Napoca, Romania

Received December 25, 1987

Experimental and theoretical results are presented concerning the translational motion of a drop, acted by interfacial tension gradients. The drop is initially motionless, being at neutral buoyancy (or at zero gravity). The interfacial tension gradients are induced by injecting the free drop with surfactant in a determined point of its surface. As a result a Marangoni flow is started, developing with a well-defined front of the surfactant, as we have previously reported. The theoretical model proposed in this paper stipulates that the translation of the drop "in toto" arises as a consequence of the Marangoni spreading. The translational velocity varies with the covering degree, namely with the position of the surfactant front. The experimental translational velocities of the drop, determined by filming, satisfactorily fit the theoretical values foreseen by our model, especially for relatively large Reynolds numbers.

INTRODUCTION

Under the action of interfacial tension gradients, a free drop immersed in an equidense liquid performs complicated movements [1] such as :

- translational motion ;
- possible rotation ;
- deformation and even fission ;
- oscillation, waves on its surface, etc.

The study of the phenomena generated by interfacial tension gradients is of present interest in the mass transfer processes, in conceiving models of movement at the biological membrane level, as well as in the space science and technology of liquids.[2–7]

In a previous work [7] we showed that the first consequence of the interfacial tension gradients is the Marangoni-type surface flow. We have succeeded in determining quantitatively the spreading velocity of a surfactant under the Marangoni effect, by using practically undeformable drops. Such undeformable drops are obtained when a liquid drop the viscosity of which is much higher than that of the continuous medium is used and the interfacial tension gradients are small. At the same time we elaborated, for the quasi-steady flow, a hydrodynamic theory which is in a satisfactory agreement with our experimental data.

---

[1] To whom correspondence should be sent : Department of Physical Chemistry, str. Arany J., 11, 3400 Cluj-Napoca, Romania

In the present paper it was possible for us to experimentally "isolate" the translational motion (the first of the above-listed processes) from the other effects (deformation, oscillation, etc.), also by making use of undeformable drops. Moreover, we have performed quantitative measurements of the displacement velocity of the entire drop.

The translation of the drop had been predicted in the well-known theory of the viscous drop oscillations [8] and, more recently,[3] this movement was found as a secondary effect in theoretical studies regarding the interfacial instability.

Other authors [9-11] theoretically examine the case of a drop which moves under the action of the gravity field in a continuous solution of surfactant; the velocity of the drop and that of the interface are both altered by the interfacial tension gradient due to the unequal distribution of the surfactant on the surface of the drop.

The theoretical and experimental model reported here is essentially different. The drop is initially at rest — at neutral buoyancy. Subsequently the drop is "injected" with a surfactant in a well-determined point on its surface. As a result, the Marangoni spreading of the surfactant takes place, with a distinct front which advances continuously.[7] This work aims at correlating the Marangoni spreading on the surface of the initially motionless drop with the translational motion induced by the spreading of the surfactant and undergone by the drop "in toto".

MODEL FOR THE TRANSLATION OF THE UNDEFORMABLE FREE DROP

It will be considered a drop L' of radius a, suspended in an immiscible liquid L. The force $\vec{F}$ acting on the unit volume of the drop will be cancelled :

$$\vec{F} = (\rho' - \rho)\vec{g} = 0, \tag{1}$$

either when the densities of the two liquids are equal ($\rho = \rho'$), or in the absence of gravity ($\vec{g} = 0$). Such a drop will be called "free" and it is motionless.

Let us take the system of spherical coordinates r, θ, φ (Fig. 1), with the origin placed at the centre of the drop. It will be admitted that the interfacial tension is σ_1 in the point where the positive Oz axis intersects the sphere and σ_0 at the opposite "pole", in such a manner that $\sigma_1 < \sigma_0$.

The fact can be performed by injecting the drop with a surfactant which lowers the interfacial tension from the value σ_0 to σ_1, in the point corresponding to the above-mentioned intersection with the Oz axis. Local variations of the temperature or of the electric charge on the surface would produce a similar effect. Then the interfacial tension difference ($\sigma_0 - \sigma_1$) arises along the meridians of the drop, determining the Marangoni flow of the L/L' interface ; this interfacial flow is accompanied by the drag of the adjacent liquids, due to the lack of slippage between the interface and the bulk liquid L and L', respectively.

In the following we shall only deal with the case in which the difference $(\sigma_0 - \sigma_1)$ is induced by injecting a surfactant in a point of the drop surface where the interfacial tension now becomes σ_1 (Fig. 1). As a consequence, the Marangoni spreading of the surfactant is initiated. As the spreading is symmetrical with respect to the Oz axis, the interfacial flow velocity, as well as the velocities of the outer and inner liquid flows, are not functions of the angle φ. The surfactant front position at a given moment is characterized only by the value θ_f of the angle θ (Fig. 2). The interfacial tension is constant (σ_0) in any point of the uncovered surface, while the interfacial tension difference $(\sigma_0 - \sigma_1)$ arises only in the invaded region, so that we have always σ_1 in the injection point and σ_0 at the limit of the surfactant front (Fig. 2).

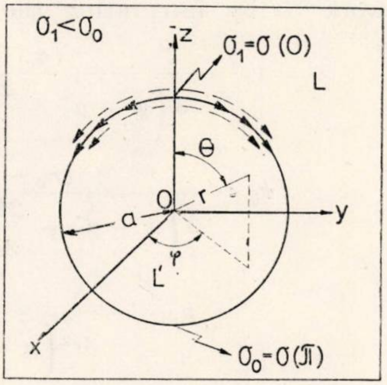

Fig. 1. — The system of spherical coordinates.

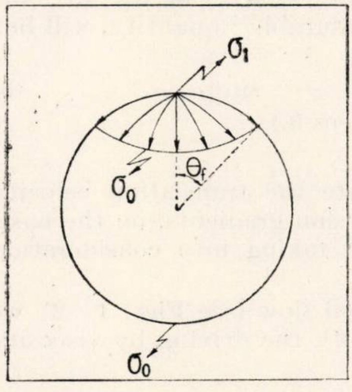

Fig. 2. — The spreading of the surfactant on the drop surface.

It is obvious that only σ_1 and σ_0, i.e. only the minimum and the maximum values of the interfacial tension, can be experimentally measured, as we had already reported in our previous work.[7] As a matter of fact, the very difference $\sigma_0 - \sigma_1$ is the driving force of the spreading as well as of the drop translation in our experiments. The local variation of the interfacial tension inside the invaded region is experimentally unapproachable for the moment.*

We assume, in a first approximation, that a steady flow process is established in the invaded region. The distribution of the flow velocities (v) respectively of the pressures (p) for the continuous medium L in the interval $0 \leqslant \theta \leqslant \theta_f$ is then obtained — as we had shown in a previous work [7] — by integrating the hydrodynamic equations and results in :

$$v_r = \frac{(\sigma_0 - \sigma_1)a^3}{3\left(\mu + \mu' + \frac{2K}{3a}\right)(1 - \cos\theta_f)}\left(\frac{1}{r^3} - \frac{1}{a^2 r}\right)\cos\theta, \tag{2}$$

$$v_\theta = \frac{(\sigma_0 - \sigma_1)a^3}{3\left(\mu + \mu' + \frac{2K}{3a}\right)(1 - \cos\theta_f)}\left(\frac{1}{2r^3} + \frac{1}{2a^2 r}\right)\sin\theta, \tag{3}$$

$$p = -\frac{\mu(\sigma_0 - \sigma_1)a}{3r^2\left(\mu + \mu' + \frac{2K}{3a}\right)(1 - \cos\theta_f)}\cos\theta, \tag{4}$$

where μ and μ' are the bulk viscosities of the liquids L and L' and K is the surface dilatational viscosity of the interfacial fluid.

Equations for the inner liquid L' can be obtained, correspondingly.[7]

The liquid flows tangentially at the surface of the drop, within the invaded region, with the velocity :

$$(v_\theta)_{r=a} = \frac{\sigma_0 - \sigma_1}{3\left(\mu + \mu' + \frac{2K}{3a}\right)(1 - \cos\theta_f)}\sin\theta. \tag{5}$$

By taking now $\theta = \theta_f$ as a variable $(0 < \theta_f \leqslant \pi)$ in Eq. (5), the velocity of the surfactant front, a directly measurable [7] quantity, will be :

$$v_f = \frac{\sigma_0 - \sigma_1}{3\left(\mu + \mu' + \frac{2K}{3a}\right)(1 - \cos\theta_f)}\sin\theta_f. \tag{6}$$

In the following we attempt to calculate the translation velocity of the entire free drop acted by interfacial tension gradients, on the basis of the Marangoni flow processes respectively taking into consideration the preceding equations.

If we analyse the model of the Marangoni flow (see Figs. 1—2) we immediately find that — as the flow occurs with the driving by viscosity of the outer liquid L — forces of hydrodynamic pressure will act on the drop L'. The resultant F, of the forces exerted by the fluid on the drop, projected on the Oz axis will be of the form [12]:

---

* Nevertheless, from the theoretical point of view, it can be seen in Eqs. (12) and (13) of our work[7], that the variation of the interfacial tension $\sigma(\theta)$ with the angle θ inside the invaded region is of the form $\sigma(\theta) = \sigma_m + a_1\cos\theta$, where $\sigma_m = (\sigma_0 - \sigma_1\cos\theta_f)/(1 - \cos\theta_f)$, and $a_1 = -(\sigma_0 - \sigma_1)/(1 - \cos\theta_f)$. For the particular case when the surface of the entire drop is covered with surfactant ($\theta_f = \pi$) the equation obtained is similar to that proposed by other authors — see Eq. (26) in Ref.[10] — with the value $\sigma_m = (\sigma_0 + \sigma_1)/2$, σ_m being now the average interfacial tension.

$$F = \iint_S (p_{rr} \cos \theta - p_{r\theta} \sin \theta) \, \mathrm{d}s, \tag{7}$$

where ds is the element of surface, while S is the covered (invaded) surface; p_{rr} and $p_{r\theta}$ are the normal and the tangential components of the viscous stress tensor:

$$p_{rr} = -p + 2\mu \frac{\partial v_r}{\partial r}, \tag{8}$$

$$p_{r\theta} = \mu \left(\frac{1}{r} \frac{\partial v_r}{\partial \theta} + \frac{\partial v_\theta}{\partial r} - \frac{v_\theta}{r} \right). \tag{9}$$

At the surface of the drop (for $r = a$), taking into account Eqs. (8), (2) and (4), one obtains for the normal component of the stress tensor:

$$p_{rr} = - \frac{\mu(\sigma_0 - \sigma_1)}{a\left(\mu + \mu' + \dfrac{2\mathrm{K}}{3a}\right)(1 - \cos \theta_f)} \cos \theta, \tag{10}$$

while the tangential component of this tensor is, in accordance with Eqs. (9), (2) and (3):

$$p_{r\theta} = - \frac{\mu(\sigma_0 - \sigma_1)}{a\left(\mu + \mu' + \dfrac{2\mathrm{K}}{3a}\right)(1 - \cos \theta_f)} \sin \theta. \tag{11}$$

The element of surface on the spherical drop being

$$\mathrm{d}s = 2\pi a^2 \sin \theta \, \mathrm{d}\theta,$$

equation (7) can be rewritten as:

$$F = \int_0^{\theta_f} (p_{rr} \cos \theta - p_{r\theta} \sin \theta) 2\pi a^2 \sin \theta \, \mathrm{d}\theta. \tag{12}$$

By introducing the values p_{rr} and $p_{r\theta}$ from Eqs. (10)—(11) into Eq. (12), one obtains after integration:

$$F = \frac{2\pi\mu a(\sigma_0 - \sigma_1)}{3\left(\mu + \mu' + \dfrac{2\mathrm{K}}{3a}\right)} (1 - 2 \cos \theta_f - 2 \cos^2 \theta_f). \tag{13}$$

It can be seen in Eq. (13) that the resultant force F is dependent on the angle θ_f, namely on the extent to which the drop surface is covered with surfactant (see also Fig. 2).

If we consider the part dependent on θ_f

$$f(\theta_f) = 1 - 2\cos\theta_f - 2\cos^2\theta_f, \tag{14}$$

we see that this function vanishes for $\cos\theta_0 = \dfrac{\sqrt{3}-1}{2}$, that is at $\theta_0 = 68.53°$. For θ_f values found in the interval $[0, \theta_0]$ it can be seen that $f(\theta_f) < 0$; further on, for θ_f values found in the interval $[\theta_0, \pi]$, the function $f(\theta_f)$ has only positive values and it exhibits a maximum at $\theta_f = 2\pi/3$.

This discussion results in the finding that, for $\theta_f < \theta_0$, the resultant F of the forces (in conformity with Eq. (13)) is negative, and for $\theta_f > \theta_0$, it is positive and presents a maximum at the above-mentioned θ_f value.

This fact can be interpreted by making explicit the normal and the tangential components of the resultant force F. Indeed, the normal component is:

$$F_n = \iint_S p_{rr}\cos\theta\, ds$$

or, by taking Eq. (10) into account,

$$F_n = \frac{2\pi\mu a(\sigma_0 - \sigma_1)}{3\left(\mu + \mu' + \dfrac{2K}{3a}\right)}(-1 - \cos\theta_f - \cos^2\theta_f). \tag{15}$$

The tangential component will be:

$$F_t = -\iint_S p_{r\theta}\sin\theta\, ds$$

and, with Eq. (II) taken into consideration:

$$F_t = \frac{2\pi\mu a(\sigma_0 - \sigma_1)}{3\left(\mu + \mu' + \dfrac{2K}{3a}\right)}(2 - \cos\theta_f - \cos^2\theta_f). \tag{16}$$

From expressions (15) and (16) it is found that the tangential component F_t is practically zero for small values of θ_f, while the normal component F_n is negative in the same circumstances. Consequently, the resultant F of the forces exerted by the external liquid upon the drop is oriented towards the negative direction of the Oz axis.

As the surface of the drop is covered with surfactant and θ_f increases, the tangential component F_t oriented towards the positive direction of the Oz axis, increases too, leading to the reduction of the resultant force F (oriented towards the negative direction of the Oz axis); when θ_0 becomes 68.53°, F vanishes.

At greater coverings of the surface, i.e. at $\theta_f > \theta_0$, the resultant of the forces, F, is oriented towards the positive direction of the Oz axis.

From the above discussion it results that the propulsive force F_p corresponding to a covering degree up to the angle $\theta_f (\theta_f > \theta_0)$, and representing the resultant of the forces exerted by the outer fluid L on the drop L' towards the positive direction of the Oz axis (see Fig. 3) is :

$$F_p = \int_{\theta_0}^{\theta_f} (p_{rr} \cos\theta - p_{r\theta} \sin\theta) 2\pi a^2 \sin\theta \, d\theta. \tag{17}$$

By integrating, with Eqs. (10) and (11) taken into account, we find

$$F_p = \frac{2\pi a \mu (\sigma_0 - \sigma_1)[3(\cos\theta_0 - \cos\theta_f) - 2(\cos^3\theta_0 - \cos^3\theta_f)]}{3\left(\mu + \mu' + \dfrac{2K}{3a}\right)(1 - \cos\theta_f)} \tag{18}$$

To the propulsive force F_p responsible for the movement of the drop, another force is opposed, deriving from the viscous resistance of the continuous phase in which the motion takes place. The expression of this latter force depends upon the flow conditions, given by the Reynolds number. Consequently, in selecting the proper equation, we shall take into account the manner the velocity varies during the displacement of the drop. As initially it is at neutral bouyancy and situated in an uncontaminated continuous phase, the drop is at rest. From the moment when the surfactant is injected at one of its poles, a certain "induction time" is necessary for the drop to be set in motion with the positive direction of the Oz axis. In other words, a certain time is necessary for the surfactant to cover the drop surface such as $\theta_f = \theta_0$. Further on, the velocity of the drop increases until a given moment, then it decreases, as a function of the surfactant front position, i.e. of the surface covering degree. Finally the translational velocity is vanished. It follows that the displacement occurs under small Reynolds numbers at the beginning of the motion, then under greater ones as the drop velocity increases. Unlike this situation, the surfactant flow on the drop surface takes place only under small Reynolds numbers,[7] on account of the high viscosity of the drop. Consequently, it is only for a short while at the beginning of the translation (Re $<$ $<$ 1), that the two phenomena develop in identical conditions. Therefore,in the following, two situations will be discussed.

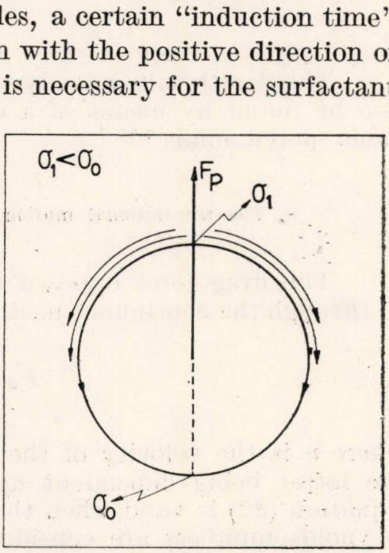

Fig. 3. — The propulsive force.

a. The translational motion at Reynolds numbers less than unity

The translational velocity is determined by the forces acting on the drop, i.e. by equating the propulsive force F_p (18), corresponding to a certain covering degree of the drop surface, with the drag force acting on the interface. Denoting by u the velocity of the drop displacement corresponding to the θ_f angle of the invaded region, we assume, in a first approach, that the drag force acting on the drop for Reynolds numbers less than unity is[11]:

$$F_d = \frac{2\pi\mu a u\left(2\mu + 3\mu' + \dfrac{2\mathrm{K}}{3a}\right)}{\mu + \mu' + \dfrac{2\mathrm{K}}{3a}}\,. \tag{19}$$

By equating the forces (18) and (19), the translation velocity is

$$u = \frac{(\sigma_0 - \sigma_1)}{3\left(2\mu + 3\mu' + \dfrac{2\mathrm{K}}{3a}\right)} \cdot \frac{3(\cos\theta_0 - \cos\theta_f) - 2(\cos^3\theta_0 - \cos^3\theta_f)}{(1 - \cos\theta_f)}\,. \tag{20}$$

For the particular case of total covering $\theta_f = \pi$ we find the final velocity

$$u_f = \frac{(\sigma_0 - \sigma_1)}{3\left(2\mu + 3\mu' + \dfrac{2\mathrm{K}}{3a}\right)} \tag{21}$$

This last result, namely the drop final velocity and only itself, can also be found by means of a more general calculation using the Gegenbauer polynomials.[9,10]

b. The translational motion at Reynolds numbers greater than unity

The drag force opposed to the displacement of the spherical drop L' through the continuous medium L will have the well-known form[1,11,13]:

$$F_d = \frac{1}{2}\pi a^2 \rho u^2 C_d \tag{22}$$

where u is the velocity of the displacement and C_d the drag coefficient, the latter being dependent upon the Reynolds number (Ref.[13] p. 15). Equation (22) is valid when the drops are sufficiently large and when the Reynolds numbers are considerably greater than unity, (Ref.[11] p. 429), namely in the case studied by us (Table 3). At Reynolds numbers inferior to 300, the C_d coefficient for the liquid drop is the same as for a solid sphere of identical radius [1] and can be obtained by interpolation from the $R = R(C_d)$ type curves (Ref. 13 p. 16).

By equalling the forces in the equations (18) and (22), the translational velocity is obtained, along the positive Oz axis, at a certain covering degree (θ_f) of the surface:

$$u = \sqrt{\frac{2F_p}{\pi a^2 \rho C_d}} \,. \tag{23}$$

It can be seen from Eqs. (18) and (23), that u increases rapidly in the interval $\theta_f = 68.53° - 90°$, then a slow variation follows, between $90° - 180°$, with a flat maximum at 120°. This fact is well reflected in table 1, where the dependence of the dimensionless function

$$A = \sqrt{\frac{3(\cos\theta_0 - \cos\theta_f) - 2(\cos^3\theta_0 - \cos^3\theta_f)}{1 - \cos\theta_f}}$$

on the angle θ_f is presented.

Table 1

The values of the parameter A for various angles θ_f (see the text)

θ_f	A
68.53°	0.000
70°	0.309
80°	0.770
90°	1.000
100°	1.134
110°	1.204
120°	1.225
130°	1.208
140°	1.166
150°	1.110
160°	1.055
170°	1.015
180°	1.000

Eq. (23) represents a generalization of an earlier equation proposed by us[14] for the translation of the free drop under the action of interfacial tension gradients. In that equation ((22) in the work[14]) the surface viscosity was neglected and, what is more important, the angle θ_f, characterizing the position of the surfactant front, was not taken into account, because the complete covering of the drop ($\theta_f = \pi$) was admitted; as a consequence, the translation velocity of the drop did not appear as a function of θ_f, which represented a first approximation.

In conclusion, in our hydrodynamic model, the practically underformable free drop found at neutral buoyancy (or at zero gravity), and initially motionless, undergoes a translational displacement. This displacement occurs when interfacial tension gradients are engendered by injecting the drop with a surfactant, in a well-determined point of its surface. We explain the translation of the drop by the occurrence of a propulsive force determined by a Marangoni spreading which develops with a well-defined front of the surfactant. After the covering of the drop with surfactant has reached a certain degree ($\theta_0 = 68.53°$), this translation takes place in a direction joining the points of maximum and minimum interfacial tension on the drop (see Fig. 3). The translational velocity varies with the position of the surfactant front (θ_f) and exhibits a maximum at $\theta_f = 2\pi/3$.

EXPERIMENTAL

The measurement of the translational motion of the undeformable free drop was performed on the liquid/liquid systems of equal densities given in Table 2.

The parameters characterizing the systems (the density $\rho = \rho'$, the bulk viscosities μ and μ' of the liquids, the interfacial tensions σ_0 and σ_1) were determined by the methods previously described.[7]

Table 2

Composition and parameters of the liquid/liquid systems of equal densities ($\rho = \rho' = 0.863$ g/cm^3) with the phase L' (drop) made of paraffin oil ($\mu' = 0.80$ poise)

System	Phase L (continuous)			Surfactant		Interfacial tension difference ($\sigma_0 - \sigma_1$), dyn/cm
	Composition (% vol.)	Viscosity (μ, poise)	Interfacial tension (σ_0, dyn/cm)	Composition % vol.)	Interfacial tension (σ_1, dyn/cm)	
1.	Ethanol 78.6 Water 21.4	0.0226	7.9	Propanol 77.3 Water 22.7	3.5	4.4±0.4
2.	Methanol 78.0 Water 22.0	0.0133	10.2	Isopropanol 76.0 Water 24.0	4.7	5.5±0.4
3.	Methanol 78.0 Water 22.0	0.0133	10.2	Propanol 77.3 Water 22.7	3.5	6.7±0.4

The experiments upon the translation of the drop were carried out in the following manner :

— the free drop is positioned inside the continuous phase which is kept in a parallelepipedic vessel having transparent walls ; the system is thermostatted at 20±0.1° C ;

— the drop, initially motionless, is injected — in the intersection point of the positive Oz axis with the surface of the drop (see Fig. 1.) — with a small quantity ($10^{-3} - 10^{-2}$ cm^3) of the surfactant solution, by using a micrometric syringe ;

— as a result of the interfacial tension difference $\sigma_0 - \sigma_1$ produced like this, the Marangoni spreading occurs (Fig. 2) ; the latter can be visualized by colouring the surfactant solution (see also Fig. 6 in our previous work[7]).

— after an "induction period", takes place the translation of the drop which is watched by filming (24 images/s) ;

— in order to make sure that the movement of the drop is not affected either by the manner in which the drop is injected, or by the removal of the syringe from the "front side" of the advancing drop, blank experiments were made, by injecting the drop with surface-inert liquids ; no movement of the drop occurs in these circumstances ;

— the distance z travelled through by the drop in the time t is read on the cinematographic negatives, against a fixed reference point, at a determined aggrandizement (approximately 1/10 linear ratio) ; as the numbering of the cinematographic sequence is directly correlated with the time, the translation velocity can be immediately evaluated as $u = \mathrm{d}z/\mathrm{d}t$.

A number of sequences illustrating the translation of the drop is given in Fig. 4.

The motion can be followed against the vertical line in the centre of the picture.

RESULTS AND DISCUSSION

Our experiments show that if the surface of the drop is injected with surfactant in the point having the interfacial tension σ_1 (Figs. 1 and 3) the translation of the drop "in toto" takes place always towards the positive direction of the Oz axis.

The reproducibility of the results is the best when the injection is performed sidewise, because the accidental occurrence of a small density gradient along the vertical could affect the translation of the drop.

In Fig. 5 the results concerning the dependence $z = z(t)$ are plotted for some of the studied systems.

It can be seen in Fig. 5 that the translation movement of the drop begins only a certain time after the injection with surfactant. By correlating the time t with the covering degree θ_f of the drop surface, as can be

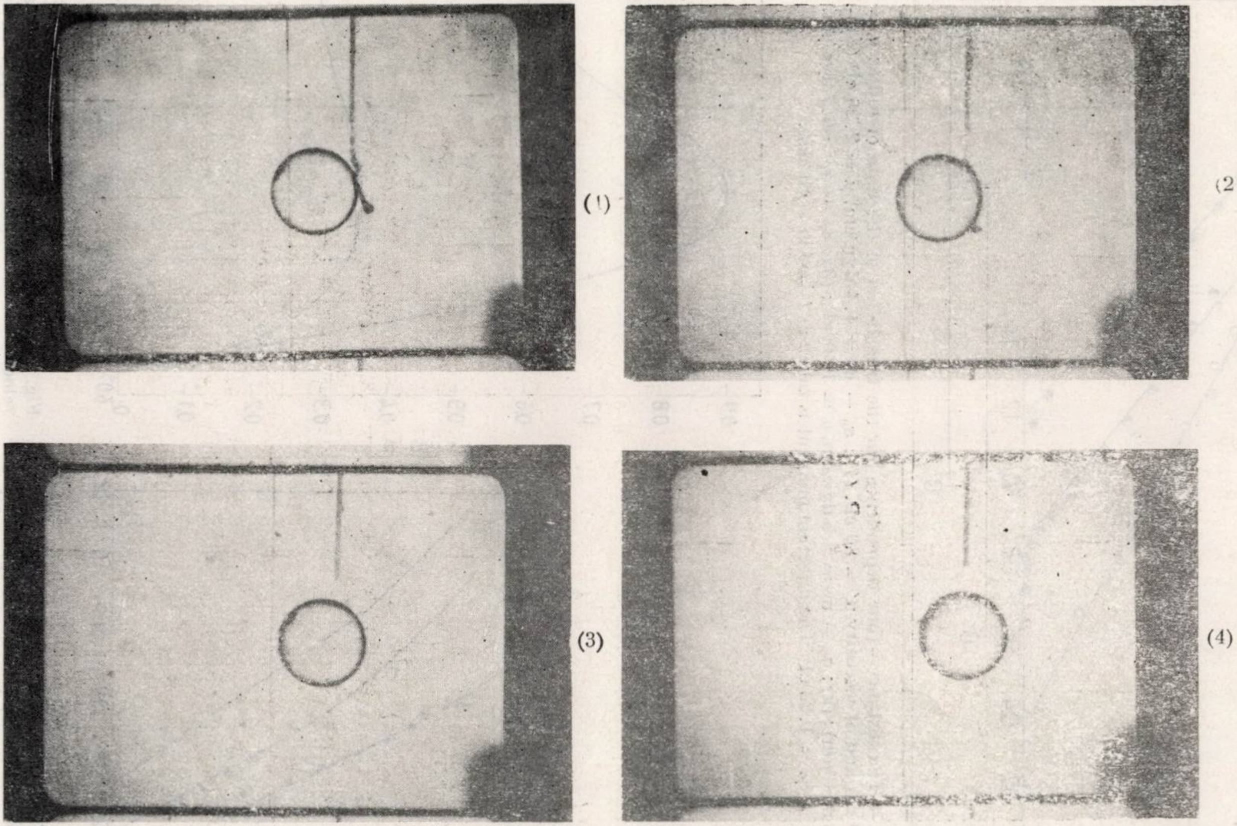

Fig. 4. — Filmed pictures representing the translation of the drop against a fixed reference (vertical line). Drop radius : $a = 0.62$ cm ; interfacial tension difference : $\sigma_0 - \sigma_1 = 5.5$ dyn/cm ; viscosities : $\mu = 1.33$ cP (the continuous medium L), and $\mu' = 80$ cP (the drop L'). (1) : $t = 0$ s ; (2) : $t = 0.7$ s ; (3) : $t = 1.4$ s ; (4) : $t = 2.6$ s.

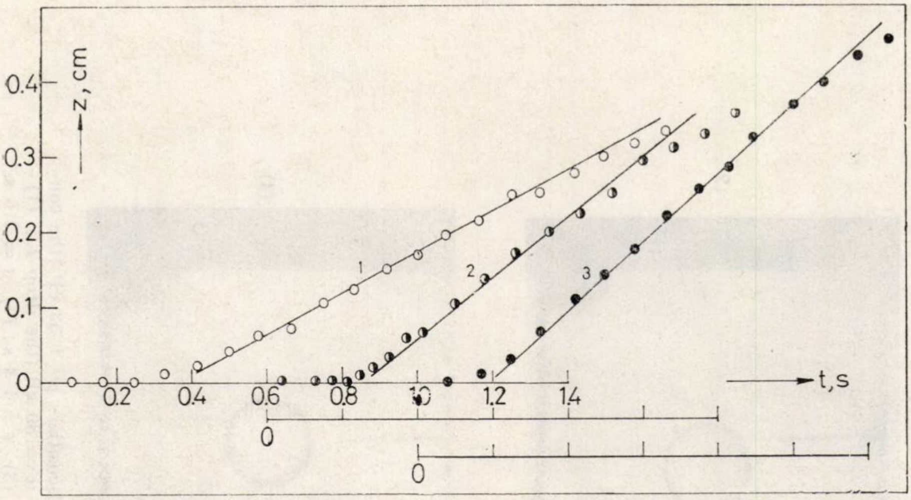

Fig. 5. — The distance—time dependence for the translation of the drop of radius $a = 0.49$ cm and of viscosity $\mu' = 80$ cP. (1) : $\sigma_0 - \sigma_1 = 4.4$ dyn/cm, $\mu = 2.26$ cP (continuous medium) ; (2) ; $\sigma_0 - \sigma_1 = 5.5$ dyn/cm, $\mu = 1.33$ cP ; (3) : $\sigma_0 - \sigma_1 = 6.7$ dyn/cm, $\mu = 1.33$ cP. The injection moment is taken as $t = 0$ in each case.

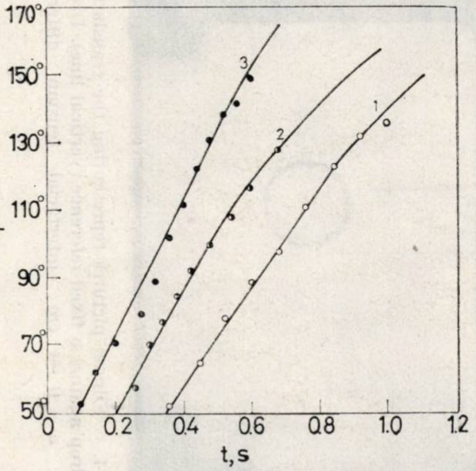

Fig. 6. — The $\theta_f = f(t)$ dependence for the drop of radius $a = 0.49$ cm. The other parameters are identical to those in Fig. 5.

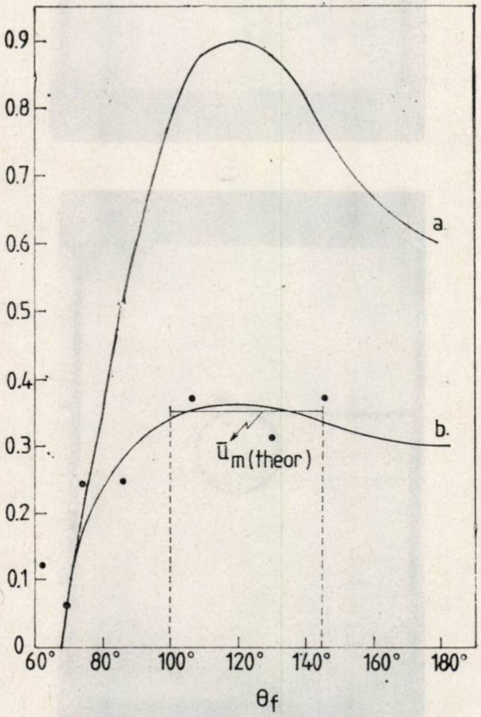

Fig. 7. — Theoretical curves : momentary velocity vs. the angle characterizing the surfactant front position (θ_f). Curve a) $u = f(\theta_f)$ from Eq. (20) for Re < 1 ; curve b) $u = f(\theta_f)$ from Eq. (23) for Re > 1 ; ● experimental values ; both curves correspond to system 1 in table 2 ; drop radius $a = 0.49$ cm.

seen in Fig. 6, one finds that the translation begins at values of the θ_f angle within approximately $50° \div 75°$, that is – if we have in mind the experimental difficulties – in a satisfactory agreement with the value indicated by the theory : $\theta_0 = 68.53°$.

At smaller values of the time – corresponding to $\theta_f < \theta_0$ – no translation of the drop can be experimentally noticed. However we suggest that the energy corresponding to the negative force F might be dissipated under other forms of activity of the drop [1] unobservable in the described experimental conditions.

The S-shape of the curves $z = f(t)$ presented in Fig. 5 reveals that after an initial period in which the velocity increases, a roughly linear dependence follows, corresponding to a maximum average of the translation velocity of the drop $\bar{u}_{m(\mathrm{exp})} = \mathrm{d}z/\mathrm{d}t$ (see the full lines). Further on, for relatively large t or θ_f values, the translation velocity is reduced.

The shape of the curves generally agrees from the qualitative point of view with our theoretical predictions, because the $u = f(t)$ or $u = f(\theta_f)$ curve must present a maximum (see also Fig. 7). Of course, the theory makes sense only until θ_f reaches π. The following decrease of the translational velocity is due to the transient character of the phenomenon.

In order to quantitatively verify the theoretical predictions, it is necessary to evaluate the momentary velocities at various covering degrees.

The experimental values have been evaluated by the relation $u_{\mathrm{exp}} = \Delta z/\Delta t$.

The theoretical curves $u = f(\theta_f)$, calculated by the relationships (20) and (23) for the two situations determined by the hydrodynamical regimes of the translational motion, are given – as an example – on the case of the system in Fig. 7. It can be seen that the experimental values of the momentary velocities are close – within the experimental errors – to the calculated ones for all covering degrees in the model of drop translation under Reynolds numbers greater than unity (Fig. 7, curve b). The experimental velocities agree with the theoretically derived values also for small Reynolds numbers, but only in the case of small covering degrees (Fig. 7, curve a), indicating that the applicability of this model in the conditions of our experiment is restricted to the outset of the translational motion.

Taking into account the difficulties in accurately measuring the momentary velocities, we considered it convenient to verify the theoretical model of translation under Reynolds numbers greater than unity, by means of the maximum translational velocity, which can be determined with a satisfactory accuracy from the experimental data.

The value of the maximum instantaneous velocity is calculated, according to the theory, with Eqs. (18) and (23) in which one takes $\theta_0 = 68.53°$ and $\theta_f = 120°$. The following expression is obtained :

$$u_{m(\mathrm{theor})} = 1.41 \sqrt{\frac{\mu(\sigma_0 - \sigma_1)}{a\rho C_a\left(\mu + \mu' + \dfrac{2K}{3a}\right)}} . \qquad (24)$$

Because from the shape of experimental curves, like those in Fig. 5, only one maximum average velocity can be evaluated, $\bar{u}_{m(\mathrm{exp})} = \mathrm{d}z/\mathrm{d}t$

it is resonable to compare this value also with a maximum average theoretical velocity.

In order to value the averaging interval, in Fig. 7 b the theoretical curve $u = u(\theta_f)$ is presented for one of the studied systems. Taking into account the shape of this curve, it seems reasonable to do the averaging along the $\theta_f = 100° \div 145°$ interval. Besides, the time (t)-covering degree (θ_j) correlation suggests that the roughly linear dependence $z = z(t)$ corresponding to the maximum average value of the velocity is situated approximately in this interval. Therefore the theoretical maximum average value has been calculated by averaging 10 instantaneous values proper to the above-indicated interval. The following expression is obtained :

$$\bar{u}_{m(\text{theor})} = 1.19 \sqrt{\frac{\mu(\sigma_0 - \sigma_1)}{a\rho C_d\left(\mu + \mu' + \dfrac{2K}{3a}\right)}}\,. \tag{25}$$

In table 3 are listed the maximum average experimental values of the translational velocity $\bar{u}_{m(\text{exp})}$ obtained for the systems in Table 2, with drops having different radii. The theoretical values $u_{m(\text{theor})}$ and $\bar{u}_{m(\text{theor})}$ are

Table 3

Experimental ($\bar{u}_{m(\text{exp})}$) and calculated ($u_{m(\text{theor})}$ and $\bar{u}_{m(\text{theor})}$) translation velocities of free drops acted by interfacial tension gradients

Interfacial tension difference $\sigma_0 - \sigma_1$ (dyn/cm)	Drop radius a (cm)	$\bar{u}_{m(\text{exp})}$ (cm/s)	Reynolds number R	Drag coefficient C_d	$u_{m(\text{theor})}$ (cm/s)	$\frac{\bar{u}_{m(\text{exp})}}{u_{m(\text{theor})}}$ %	$\bar{u}_{m(\text{theor})}$ (cm/s)	$\frac{\bar{u}_{m(\text{exp})}}{\bar{u}_{m(\text{theor})}}$, %
4.4	0.49	0.29	10.9	4.4	0.36	81	0.35	83
	0.62	0.31	14.7	3.6	0.35	89	0.34	91
	0.84	0.24	15.4	3.5	0.31	77	0.30	80
	1.19	0.21	19.1	3.2	0.27	78	0.26	81
5.5	0.49	0.42	26.7	2.7	0.40	105	0.39	108
	0.62	0.34	27.4	2.6	0.36	94	0.35	97
	0.84	0.31	33.8	2.2	0.33	94	0.33	94
	1.19	0.31	47.9	1.7	0.32	97	0.31	100
6.7	0.49	0.45	28.6	2.4	0.46	98	0.45	100
	0.62	0.47	37.8	1.9	0.46	102	0.45	104
	0.84	0.37	40.3	1.8	0.41	90	0.40	92
	1.19	0.36	55.6	1.6	0.36	100	0.35	103

also given, as they have resulted from Eqs (24) and (25) by using the experimental parameters $(\sigma_0 - \sigma_1)$, μ, μ', ρ and a. The term $2K/3a$, corresponding to the surface dilatational viscosity, is considered as negligible, what is plausible in our experimental conditions, where the drops are large enough, and K has probably low values for the weak surfactants employed.

As the calculus of the u_{theor} values compels the knowledge of the drag coefficients, the Reynolds numbers have been evaluated first:

$$R = \frac{2a\rho u_{\text{exp}}}{\mu}$$

and then, on the basis of the $R = R\ (C_d)$ type diagrams,[13] the C_d values have been obtained by interpolation.

By examining the data in Table 3 a good agreement can be noticed between the experimental and the theoretical velocities. The theoretical values $u_{m(\text{theor})}$and $\bar{u}_{m(\text{theor})}$ are close; the agreement is still better if the averaged $\bar{u}_{m(\text{theor})}$ values are compared with the $\bar{u}_{m(\text{exp})}$, what is to be expected.

In the case of drops acted by large interfacial tension differences (5.5 and 6.7 dyn/cm) the agreement is very good ($\approx 100\%$).

A certain systematic deviation arises only at relatively small Reynolds numbers, namely in the case of drops acted by small interfacial tension differences (4.4 dyn/cm); that is also to be expected, because equation (22) is valid especially when the Reynolds numbers are large enough.[1,11]

As a rule, the influence of various parameters such as the interfacial tension difference, the drop radius, and the viscosities of the liquids, is well reflected in the data presented in tables 2 and 3.

It has not been possible to evaluate with sufficient accuracy the instantaneous values of the experimental translation velocities of the free drop for each covering degree θ_f. In spite of that, the maximum average values are in good agreement with those stipulated by our theory, especially for relatively large Reynolds numbers.

REFERENCES

[1] R. S. Valentine, N. F. Sather and W. J. Heideger, *Chem. Eng. Sci.*, **20**, 719 (1965).

[2] F. Deyhimi and A. Sanfeld, *Compt. rend. Acad. Sci., Ser. D*, **279**, 437 (1974).

[3] T. S. Sorensen, M. Hennenberg, A. Steinchen and A. Sanfeld, J. Colloid Interface Sci., **56**, 191 (1976).

[4] T. S. Sorensen and J. L. Castillo, *J. Colloid Interface Sci.*, **76**, 399 (1980).

[5] J. F. Patzer II and G. M. Homsy, *Phys. Fluids*, **24**, 567 (1981).

[6] C.-H. Chun and W. Wuest, *Acta Astronautica*, **5**, 681 (1978).

[7] E. Chifu, I. Stan, Z. Finta and E. Gavrilă, *J. Colloid Interface Sci.*, **93**, 140 (1983).

[8] L. Landau and E. Lifschitz, "Mecanique des fluides", Chap. VII, Mir, Moscow, 1971, p. 301.

[9] M. D. Levan and J. Newman, *Amer. Inst. Chem. Engineers J.*, **22**, 695 (1976).

[10] M. D. Levan, *J. Colloid Interface Sci.*, **83**, 11 (1981).

[11] V. G. Levich, "Physicochemical Hydrodynamics", Chap. VIII, Prentice-Hall, Englewood Cliffs, New Jersey, 1962.

[12] Ref. 8, Chap. II, p. 84.

[13] H. Schlichting, "Boundary Layer Theory", Chap. I, McGraw-Hill, New York, 1960.

[14] E. Chifu and I. Stan, *Rev. Roumaine Chim.*, **25**, 1449 (1980).

Revue Roumaine de Chimie, **34**, *2*, 617–622 (1989)

1-OXONIA AND 1-AZA ANALOGUES OF TRIPTYCENE

MICHAELA STĂNESCU, MIRCEA BANCIU and ALEXANDRU T. BALABAN
Organic Chemistry Laboratory – Polytechnic Institute Bucharest, Splaiul Independenţei 313, 76206 Bucharest 16, Romania

Received October 21, 1988

9,10-Dihydro-9,10-ethanoanthracen-11-one (**4**) afforded, on treatment with ethyl formate, the β-ketoaldehyde **5**, existing in two tautomeric forms **5a** and **5b**. Compound **5** was converted successively into pyrylium salt **6** and pyridine **9**, two new heterocycles with a triptycene skeleton.

INTRODUCTION

Previous papers of this laboratory described the syntheses of heterocyclic compounds **1a**, **1b**[1] with homotriptycene, and **2**[2] with tribenzobullvalene structures, respectively (oxonia, azonia and aza-analogues of homotriptycene and bullvalene).

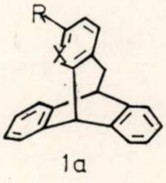

1a

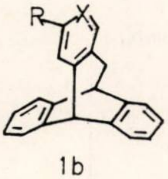

1b

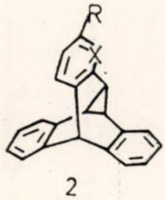

2

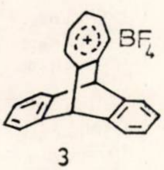

3

$X = \overset{+}{O}\ ClO_4^-$; N.
$R = C_6H_5$

It seemed interesting to investigate related compounds which include a triptycene skeleton. A compound **3** in which a benzenic ring of triptycene is replaced by a tropylium one was obtained in 1977 by Murata and coworkers.[3] In this paper we describe the synthesis of two new heterocycles having triptycene skeleton.

RESULTS AND DISCUSSION

Reaction of the known ketone **4**[4] with ethyl formate in the presence of sodium methoxide led to the formyl-derivative **5**, m.p. 144–147°. Three tautomeric structures can exist for compound **5**, namely **5a**, **5b** and **5c**, but only the ketoaldehyde **5a** and the ketoenol **5b** were proved to coexist in equilibrium.

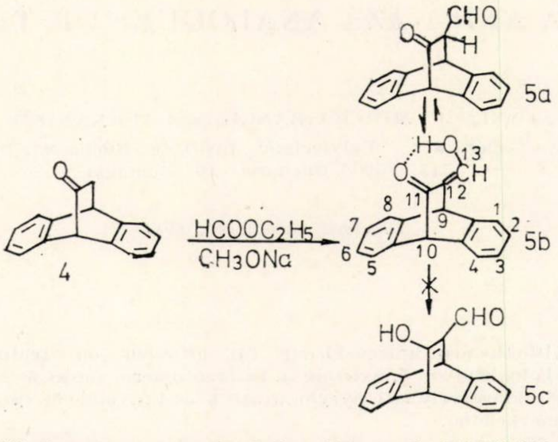

This equilibrium was studied by IR and ^{1}H-NMR spectrometries. Table 1 illustrates the spectral data for both tautomers.

Table 1

IR and ^{1}H-NMR spectral data of equilibrating ketoaldehyde **5a** and ketoenol **5b**

Compound	IR ($CHCl_3$, cm^{-1})	^{1}H-NMR ($CDCl_3$; δ_{ppm})					
		H^9	H^{10}	H^{12}	H^{13}	H_{arom}	HO
5a	$1700_{C=O ket}$; $1725_{C=O ald}$; $2835_{C-H ald.}$	4.95(d) J=2.5 Hz	4.90(s)	3.20(d) J = 2.5 Hz	9.40(s)	7.0–7.6(m)	—
5b	$1600_{C=C conj}$; $1672_{C=O conj}$; 3000–3300 large	5.00(s)[a]		—	7.0–7.6(m)		9.7–10.3

[a] Accidental isochronism

As could be seen, in the IR spectrum (in $CHCl_3$) the characteristic absorptions for ketoaldehyde **5a** – at 1700 (νC=O ket.), 1725 (νC=O ald.) and 2835 cm^{-1} (νCH ald.) – as well as those for ketoenol **5b** – at 1600 (νC=C conj.), 1672 (νC=O conj.) and 3000 – 3300 cm^{-1} (νOH ; large) – are observable. The ^{1}H-NMR spectrum (in $CDCl_3$) reveals also the presence of both tautomers (Table 1). Characteristic signals for **5a** appear at $\delta = 4.90$ and 4.95 ppm (bridgehead protons) and 9.40 ppm (CHO proton) whereas those for **5b** occur at $\delta = 5.00$ ppm (bridgehead protons appearing accidentally isochronous) and $\delta = 9.7 - 10.3$ ppm (OH proton).

Analysis of the ^{1}H-NMR spectrum of **5** indicated a keto/enol (**5a**/**5b**) ratio of 1/3 in $CDCl_3$. Interestingly, in DMSO only the enolic form **5b** was present.

Intramolecular hydrogen bonding occurring in the enolic form **5b** explains its higher stability with respect to the ketoaldehyde **5a**. No trace of **5c** was noticed, probably due to the greater steric strain which would be present in such a structure with a shorter —C=C— bond than **5a** and **5b**.

Treatment of compound **5** with acetophenone in acetic acid in the presence of perchloric acid afforded, as in numerous other similar cases,[5] a pyrylium salt **6**, isolated in 15% yield as a brown-green solid with m.p. 204—6°.

The IR, UV and ^{1}H-NMR spectral data (see Experimental) are in agreement with the structure **6** and not with the other possible isomeric structure **7**. A proof in this respect comes out from the occurrence of a low-field signal at $\delta = 8.20$ ppm (doublet, $J = 9$ Hz) in the ^{1}H-NMR spectrum of **6**. This signal is due to a deshielded aromatic proton $H^{5'}$ in **6** from the pyrylium ring and its *ortho*-relationship with the neighbouring proton ($H^{4'}$) results from the above mentioned coupling characteristic for ^3J *ortho*.[6]

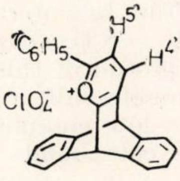

6

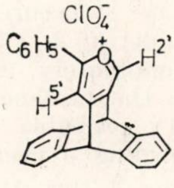

7

In the presumable pyrylium salt **7** the two pyrylium protons $H^{5'}$ and $H^{2'}$ would be in *para*-relationship and, consequently, they should have a much smaller coupling constant ^5J of about 1—1.5 Hz.[6]

One may notice that, similarly to compound **2** ($X=O^+$)[2], only one of the two possible isomeric pyrylium salts was obtained in the present case while for compound **1** both heterocycles **1a** and **1b** ($X=O^+$) were isolated. Formation of **6** from **5** is in agreement with the enhanced reactivity of the aldehydic (hydroxymethylenic) group as compared to the ketonic one in the condensation with the methyl group of acetophenone.

In the pyrylium salt **6**, possessing a triptycene skeleton, interactions between the π-electrons of benzene rings and the positive charge of pyrylium ring are possible. The electronic spectrum of this compound **6** presents an absorption maximum at 412 nm (in CH_2Cl_2) and 396.5 nm (in CH_3CN). These absorptions may be considered as due to charge transfer interactions and the blue shift (negative solvatochromy) noticed on increasing the polarity of the solvent is in agreement with literature data for similar compounds e.g. **3**.[3] In this connection it could be interesting to mention that recently [7] intramolecular interactions between a positive oxygen atom and aromatic π-electrons were proved by ESR spectroscopy in a radical-cation **8** with triptycene skeleton (the oxygen atom in **8** is exocyclic whereas in pyrylium salt **6** is endocyclic).

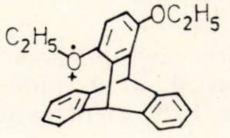

8

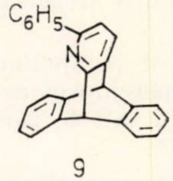

9

The conversion of pyrylium salt **6** into pyridine **9** was performed by reaction with gaseous ammonia in *t*-butanol at 60°. From the resulting reaction mixture, the pyridine **9** was separated by thin layer chromatography on silica as a yellow crystalline product with m.p. 169–170°. Attempts to obtain the pyridine **9** from pyrylium salt **6** by treatment with aqueous ammonia were unsuccessful.

The ^{1}H-NMR spectrum of pyridine **9** (see Experimental) is in agreement with its structure. One of the two pyridinic ring protons appears as a doublet at $\delta = 7.90$ ppm ($J = 8$ Hz) confirming their *ortho*-relationship. Unfortunately, the second proton of this ring could not be observed even in the presence of lanthanide shift reagent [Eu(DPM)$_3$] (molar ratio 1 : 1), probably due to the low complexing ability owing to steric overcrowding expected in this compound.

A correlation of the ^{1}H-NMR signals for the bridgehead protons (H^9 and H^{10}) for the newly synthesized compounds **5**, **6**, **9**, the known compounds **4**[4] and **10**[8] (with a dibenzobicyclo[2.2.2]octane skeleton) and the related compounds **1a** ($X{=}O^+$, N)[1], **11**,[9] **12**[10] as well as **13**[11] (with a dibenzobicyclo[3.2.2]nonane skeleton) is presented in Figure 1.

From the data in Fig. 1 a good correlation of similar protons in both series of compounds may be seen. The strong deshieldings of bridgehead protons in pyrylium salts **6** and **1a** ($X{=}O^+$) and the smaller ones in pyridines **9** and **1a** ($X{=}N$) are due to the strong electron withdrawing effect of the positive oxygen atom and the weaker effect of the nitrogen atom (in comparison with a carbon atom). The lower-field position of bridgehead protons signals in bicyclo[2.2.2]octane derivatives resides in different skeletal characteristics of these systems.

In conclusion, two new heterocyclic compounds with triptycene skeleton, namely the pyrylium salt **6** and the pyridine **9** were synthesized and characterized.

EXPERIMENTAL

Melting points are uncorrected. ^{1}H-NMR spectra were recorded on a Varian EM-360L instrument, with TMS as internal standard; IR spectra were performed on an UR-20 Zeiss-Jena spectrometer and UV spectra on a Specord UV–VIS Zeiss Jena double beam spectrometer.

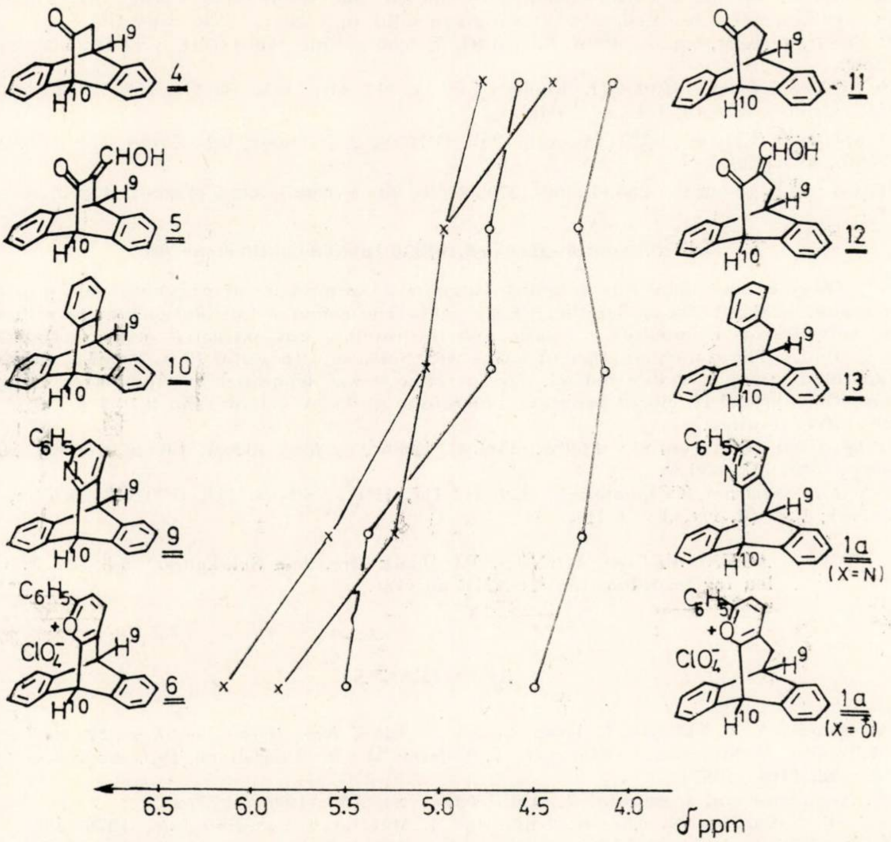

Fig. 1. — Correlation of ^{1}H-NMR signals for bridgehead protons in bicyclo[2.2.2] octane (x) and bicyclo[3.2.2]nonane (o) derivatives. The right-band peak is due to H^9, the left-band signal to H^{10}.

9,10-Dihydro-9,10-ethanol-12-hydroxymethyleneanthracen-11-one (5a + b)

To a cold benzenic (50 mL) suspension of dry sodium methoxide, freshly prepared from 1.15 g (0.05 gram-atoms) sodium and methanol, a solution of 4.4 g (20 mmoles) ketone **4** and 7.4 g (100 mmoles) freshly distilled anhydrous ethyl formate, in 50 mL benzene, was added with stirring. After additional 5 hrs of stirring at room temperature the mixture was left overnight. The resulted suspension was filtered in vacuum and the obtained solid was added with cooling to a mixture of 50 mL water and 10 mL 33% hydrochloric acid. The compound **5** was isolated by filtration as a yellowish-white solid (3 g, 60%), m.p. 144—147°C (washed with diethyl ether). Found: C, 82.59; H, 5.10%. $C_{17}H_{12}O_2$ requires: C, 82.24%; H, 4.86%.

IR Spectrum ($CHCl_3$, cm^{-1}): 950w, 1075m, 1145s, 1345w, 1390w, 1458m, 1600m, 1672vs, 1700s, 1725m, 2835w and 3000—3300w.
^{1}*H-NMR Spectrum* (see Table 1).

9,10-Dihydro-6′-phenyl-1′-oxonia-9,10[2′,3′]benzenoanthracene perchlorate (6)

A solution of formyl derivative **5** (2.8 g; 11.3 mmoles) in 20 mL anhydrous acetic acid was treated with 2.5 g (20.8 mmoles) freshly distilled acetophenone and 3 mL 70% perchloric acid. The mixture was heated on an oil bath at 105—110°C for 2 hrs with stirring.

The reaction was poured after cooling into 600 mL anhydrous diethyl ether. After filtration the pyrylium salt **6** resulted as a brown-green solid, m.p. 204 – 206°C (dec.).
IR Spectrum (KBr, cm^{-1}); 490w, 625s (ClO_4^-), 685m, 765m, 1100s (ClO_4^-), 1450s, 1510s, 1620s, 1720w.
^1H-NMR Spectrum (CF_3COOH, δppm) : 5.95 (s, 1H, H^9); 6.15 (s, 1H, H^{10}); 7.2 – 8.4 (m, 15H, Harom.), 8.20 (d, 1H, J = 9Hz).
UV Spectrum (CH_2Cl_2 ; $\lambda_{max}^{nm}(\varepsilon\ max)$) : 257 (12400), 287 (8000), 301 (7700), 353 (7300), 411 (12500), 495 (1200).
(CH_3CN ; λ_{max}^{nm} (ε max)) : 250 (12000), 279 (8700), 339.5 (6800), 396.5 (12400), 478 (1200).

9,10-Dihydro-6′-phenyl-9,10[2′,3′]pyridinoanthracene (9)

Gaseous ammonia was bubbled through a suspension of pyrylium salt **6** (0.86 g, 2 mmoles) in 20 mL *t*-butanol during 3 hrs at 50°C. The colour of the solution became yellow-red. The solvent was evaporated *in vacuo* and the residue was extracted with diethyl ether (4 × 50 mL). The combined ethereal layers were washed with water (2 × 20 mL), dried and evaporated giving a yellow-red oil. The pyridine **9** was separated by thin layer chromatography on silicagel H, eluent benzene : chloroform (9 :1). A yellow solid **9**, 0.2 g (30%) m.p. 169–170°C resulted.
IR Spectrum (CCl_4, cm^{-1}): 1130w, 1160w, 1290w, 1320w, 1385w, 1460m, 1600w, 1670m, 2860m, 2960 m, 3080 w.
^1H-NMR Spectrum (CCl_4, δppm) : 5.25 (s, 1H, H^9); 5.60 (s, 1H, H^{10}) ;6.9–8.2 (m, 15H, Harom) ; 7.90 (d, 1H, J = 8 Hz).

ACKNOWLEDGEMENTS. We thank Mrs. Ana Schiketanz and Dr. F. Chiraleu for recording the ^1H-NMR spectra.

REFERENCES

[1] M. Banciu, A. T. Balaban, C. Drăghici and R. Vlad, *Rev. Roumaine Chim.*, **27**, 1037 (1982).

[2] M. Banciu, M. Stănescu, C. Florea, A. T. Balaban and E. Ciorănescu, *Rev. Roumaine Chim.*, **32**, 1161 (1987).

[3] T. Nakazawa and I. Murata, *J. Amer. Chem. Soc.*, **99**, 1996 (1977) : T. Nakazawa, N. Abe, K. Kubo and I. Murata, *Tetrahedron Lett.*, **1979**, 4995.

[4] P. F. Huldrik, A. M. Huldrik and Chung Non Wan, *J. Org. Chem.*, **40**, 1116 (1975).

[5] A. T. Balaban, A. Dinculescu, G. N. Dorofeenko, G. W. Fischer, A. V. Koblik, V. V. Mezheritskii and W. Schroth, "Pyrylium Salts, Syntheses, Reactions and Physical Properties", *Adv. Heterocyclic Chem.*, Suppl. 2, 1982, Academic Press, New York, 1982.

[6] P. Sandor and L. Radics, *Org. Mag. Reson*, **14**, 98 (1980).

[7] H. Quast and H. L. Fuchsbauer, *Chem. Ber.*, **119**, 1016 (1986).

[8] W. Theilacker, K. Albrecht and H. Uffmann, *Chem. Ber.*, **98**, 428 (1965).

[9] E. Ciorănescu, M. Banciu, R. Jelescu, M. Rentzea, M. Elian and C. D. Nenitzescu, *Rev. Roumaine Chim.*, **14**, 911 (1969).

[10] M. Banciu, *Rev. Roumaine Chim.*, **27**, 769 (1982).

[11] S. J. Cristol and D. K. Pennelle, *J. Org. Chem.*, **35**, 2357 (1970).

Revue Roumaine de Chimie, **34**, 2, 623–633 (1989)

OSCILLATING PHENOMENA DURING ANODIC POLARIZATION OF SULPHUR CONTAINING NICKEL ELECTRODES

S. STERNBERG, I. V. COTÂRȚĂ and D. CONSTANTINESCU
Chair of Physical Chemistry and Electrochemical Technology,
The Polytechnic Institute, Bucharest, Romania

Received January 20, 1988

In this paper is shown that considerably high current values occur at anodic polarization of the sulphur doped nickel electrodes in sulphuric acid solutions, both in the active and passive ranges. It is also shown that there is a potential range of about 70 mV, where oscillating phenomena occur. These aspects have been interpreted on the basis of two steady states with different stability.

INTRODUCTION

It is known that the anodic dissolution of sulphur doped nickel electrodes is much more intense than that of pure nickel electrodes. [1-12]

Nevertheless to date, there are not many studies concerning the kinetics of the electrode processes on a Ni–S anode and this is what justifies our research in this field. In the present work we report some experimental data obtained.

EXPERIMENTAL

The experiments have been carried out with sulphur doped nickel electrodes having 0.0743 ; 0.12 and 0.23% sulphur concentrations as mass percentages. They have been electrochemically obtained by a method described in another paper.[3] The disk shaped electrode has been sealed in a glass tube using an epoxy resin. A saturated calomel electrode was used as reference and the counter electrode was a large area Pt sheet.

The anodic behaviour of the sulphur doped nickel electrodes in 1M H_2SO_4 solutions was studied by the method of cyclic voltametry using a PRINCETON POTENTIOSTAT Model 173. The equipment has also included a PHILLIPS PM 5168 functions generator and a XY COMPENSOGRAPH SIEMENS RECORDER.

The sulphur doped nickel electrodes were obtained electrochemically from Watts-type nickel plating solutions with sodium sulphite addition reagent. The anodes of the cell tube have been made from pure nickel and the cathode was a chemically passivated brass electrode. The cathodic deposit thus obtained has been stripped off from the support. Its sulphur content was analysed.[3]

RESULTS AND DISCUSSIONS

All electrode potentials discussed in the present work were reported as overpotential versus stationary potential. We found the values $E_{st} = -0.716$ V (n.h.e) for nickel electrode with $S = 0.12\%$ and -0.635 V(n.h.e) for the electrode with $S = 0.0743\%$.

A representative cyclovoltammogram using a Ni—S alloy is given in Fig. 1. In Fig. 2 is given for comparison another cyclovoltammogram obtained on pure nickel, in the same conditions as those for Ni—S electrodes.

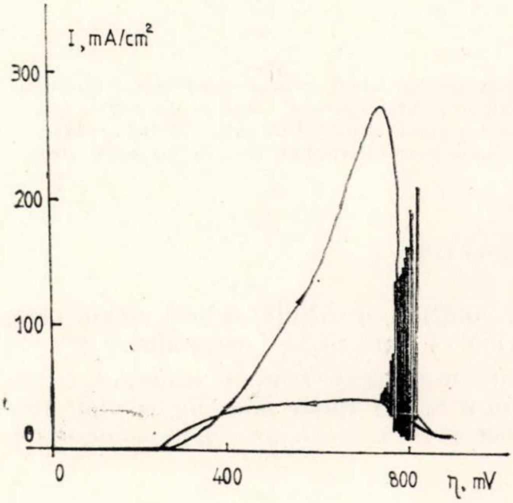

Fig. 1. — Voltammogram obtained on a Ni—S electrode with 0.0743% S in H_2SO_4 1 M solution; $v = 0.7$ mV/s.

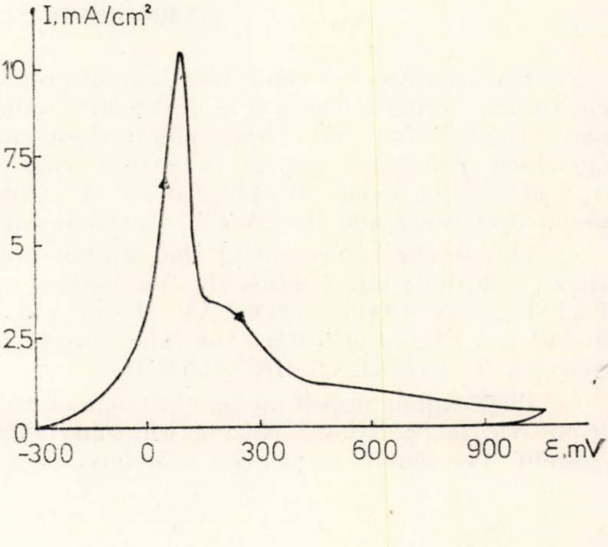

Fig. 2. — Voltammogram obtained on a pure nickel electrode in H_2SO_4 1 M solution; $v = 0.7$ mV/s.

It can be noticed that the two voltammograms are significantly different. Thus at anodic polarization curve of the sulphur doped nickel, there appear the currents which are one order higher than those occurring when a pure nickel electrode is used. These currents rise with the concentration of doped sulphur. Moreover reactivation curves with reverse scan can be noticed, which do not exist in the case of pure nickel. Also, it is characteristic for the Ni—S alloys, the existence of the reversal curve on a potential range $\Delta\eta_{osc}$ where current oscillations with high amplitude occur, which, for high sulphur concentrations (0.12% and 0.32% S) of electrodes, exceed the peak current recorded in active dissolution.

In Fig. 3 some representative current/time oscillations for constant potential are shown. According to our working conditions, at 25°C, the oscillating potential range $\Delta\eta_{osc}$ of about 70 mV was found far more electropositive than the Flade potential. The oscillogrammes can be obtained either by stopping the potential scan rate on the reverse curve, or directly by maintaining the desired potential in the $\Delta\eta_{osc}$ range itself. In the latter case, after some seconds of a continuous decrease of current, the electrode enters in the oscillating regime with sustained oscillations which are practically lasting until the total dissolution of nickel. As can be easily seen from Table 1 both the frequency and the amplitude of these oscillations vary highly with the potential. Though such oscillating phenomena have been previously noticed in the anodic dissolution of some metals (Fe, Zn, Co, Au), they are not known yet, for nickel electrodes. [13-22]

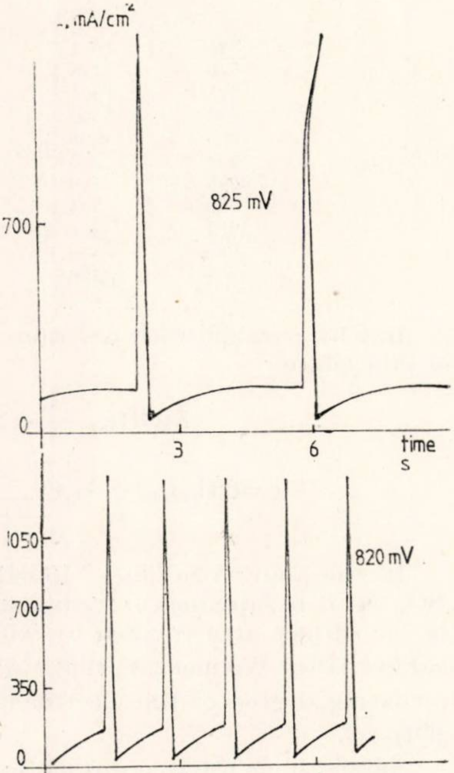

Fig. 3. —Current oscillations obtained in potentiostatic conditions on Ni—S electrode with 0.12% S.

A. Anodic dissolution of nickel-sulphur alloys

Various mechanisms have been previously proposed for anodic dissolution of pure nickel as well as for that of iron.[23-25] According to these mechanisms, the nickel active dissolution reaction follows the pattern mechanism shown below:

$$\mathrm{Ni}+\mathrm{H_2O}\underset{k_{-1}}{\overset{k_1}{\rightleftharpoons}}(\mathrm{NiOH})_{ads}+\mathrm{H}^{+}+e^{-} \qquad (1)$$

$$(\mathrm{NiOH})_{\mathrm{ads}} \rightarrow (\mathrm{NiOH}^+)_{\mathrm{sol}} + e^- \tag{2}$$

$$(\mathrm{NiOH}^+)_{\mathrm{sol}} + \mathrm{H}^+ \rightleftharpoons \mathrm{Ni}^{2+}_{\mathrm{aq}} + \mathrm{H_2O} \tag{3}$$

Table 1

Values of the potentials, frequency, maximum and minimum current obtained in the oscillating range on a Ni–S (0.12% S) electrode in H_2SO_4 1 M solution

η, mV	$I_{\max}$, mA/cm²	f, Hz	$I_{\min}$ mA/cm²
825	1514.7	0.066	31
820	1438.2	0.11	31
815	1361.7	0.14	31
810	1300.5	0.2	38.75
805	1208.7	0.5	38.75
800	596.7	2.5	77.55
995	520.2	2.85	77.5
990	504.9	2.5	85.25
985	581.4	1.33	85.25
980	550.8	1	85.5
975	596.7	0.29	85.5

But in parallel with reactions (2) and (3), reactions (4) and (5) can also take place :

$$(\mathrm{NiOH})_{\mathrm{ads}} \xrightarrow{k_4} (\mathrm{NiOH}^+)_{\mathrm{ads}} + e^- \tag{4}$$

$$(\mathrm{NiOH}^+)_{\mathrm{ads}} + \mathrm{H_2O} \underset{k_{-5}}{\overset{k_5}{\rightleftharpoons}} [\mathrm{Ni(OH)_2}]_{\mathrm{ads}} + \mathrm{H}^+ \tag{5}$$

In the above reactions $Ni(OH)_2$ is a hydroxide partially soluble in H_2SO_4 but it is supposed to form a smooth layer of $(1-A)$ porosity, where A is the surface area covered by $Ni(OH)_2$ and assumed to act as an electrical insulator. We mention that "A" is different from θ_i, which stands for the coating degree of the electrochemically active oxides $(NiOH)_{ads}$ and $(NiOH_2)_{ads}$.

Taking θ_0 as the free surface area with $\theta_{[Ni(OH)_2]_{ads}} = A$ and neglecting the coating with $Ni(OH)_{ads}$ we shall have $\theta_0 + \theta_{[NiOH^+)_{ads}} + A = 1$ and $1 -$ $- A = \theta_0 + \theta_{NiOH^+)_{ads}}$ will be the dielectrically uncoated area where the electrochemical and diffusion processes herein discussed take place.

By structural studies, Oudar and Marcus [1-2] have shown that the formation of nickel oxides NiO and Ni_2O_3 is unlikely to happen on a NiS electrode : therefore, we have also assumed that the final product of the oxidation process is $Ni(OH)_2$, which can dissolve itself in sulphuric acid as : [25]

$$[\mathrm{Ni(OH)_2}]_{\mathrm{ads}} + 2\mathrm{H}^+ \underset{k_{-6}}{\overset{k_6}{\rightleftharpoons}} \mathrm{Ni}^{2+}_{\mathrm{aq}} + 2\mathrm{H_2O} \tag{6}$$

We have admitted the symplifying hypothesis that sulphur induces only an activation of nickel surfaces, by modifying the growing lattice of the polycrystal, generating a very active plane, from the energetical point of view, hence the sulphur is not directly involved in the process of anodic dissolution of nickel.

Following a very simplified scheme, let us consider that in the steady state, the active dissolution process of nickel is controlled by the reaction (2) and the current is given by the relation :

$$i = 2Fk_2\theta_{(\mathrm{NiOH}^+)_{\mathrm{ads}}}\exp\left[\frac{(1-\alpha)\cdot F\eta}{RT}\right]$$

where η is the overpotential measured versus the stationary potential. In Fig 4, a characteristic $I - \eta$ polarisation curve is given plotted on the basis of experimental data obtained on an electrode with S content of 0.12%.

The dielectric A fraction is equal to zero, in the Tafel range, up to $i \cong 0.3\ I_{\max}$, the "ab" section in Fig. 4 respectively.

The A surface area grows along the "bc" section and reaches a maximum value in the "cd'e" section. In this case, the overall reaction rate is assumed to be controlled by the current of the dissolution reaction (6). For the "cd'e" section, the following equation can be approximately given for the current density :

$$i_{\mathrm{diff}} = \frac{FD(c_0 - c_s)}{\delta}(1 - A) \qquad (9)$$

where : i_{diff} is the diffusion current ;
δ = the thickness of the porous layer ;
A = the surfaces area covered with $\mathrm{Ni(OH)_2}$:
c_0 = concentration of the H^+ in the bulk solution (at the film-solution interface) where the chemical dissolution takes place ;
c_s = concentration of the H^+ at the interface between the free metal surface and the solution (see Fig. 6).

The "cd" section includes a dotted range which indicates an unstable stationary state showing the minimum oscillation values.

It is possible that this "cd'e" section corresponds to a growing process of the $\mathrm{Ni(OH)_2}$ porous layer, where the thickness δ is increased.

As a simplification, we have neglected the growing current of the $\mathrm{Ni(OH)_2}$ layer, and chemical dissolution (equation (6)).

On the other hand, Oudar$^{1-2}$ has shown, by structural studies, that the formation of NiO and $\mathrm{Ni_2O_3}$ oxides (the latter being stable in suphuric acid and responsible for the metal passivation) is unlikely to occur on the NiS electrode. On the other hand, the current values in the "cdd'" section are much higher than the $I_{\max}$ in Fig. 2. Therefore, it can be assumed that a proper passivation is unlikely to occur on a Ni—S electrode, but rather a "prepassivation" takes place in such a case (over the whole "cdd'" section), characterized by the presence of some nickel hydroxides or oxides soluble in H_2SO_4 The "prepassivation" has been also illustrated on pure Fe electrodes.[23]

In this simplified scheme, the current given by reaction (7) stands for the current of the electrochemical dissolution of nickel, according to equations (1), (2), and (3), while the reaction rate is given by the diffusion rate of hydrogen consumed in reaction (3).

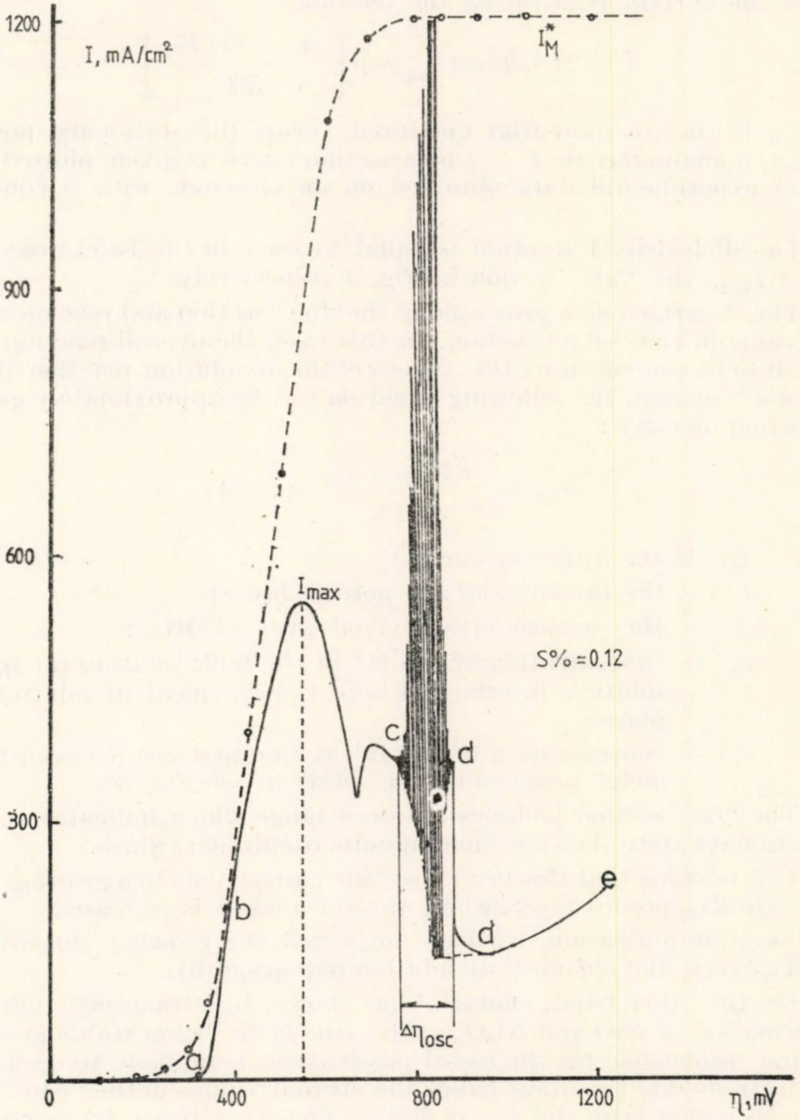

Fig. 4. — Anodic polarization curve drawn up on a Ni–S electrode (0.12% S) in H_2SO_4 1 M solution; $v = 0.7$ mV/s. ——— Theoretical curve of the upper stationary state calculated by equation (9) for $i_0 =$ $= 0.1 \text{mA/cm}^2$ (—·—).

B. Current oscillations in anodic dissolution of sulphur doped nickel

In the $\Delta\eta_{osc}$ potential range conditions for the occurrence of some dissipative structures (as described in the irreversible processes thermodynamics or in the bifurcation theory [26-28]) are created.

The existence of some sustained oscillations can be explained by the simultaneous occurrence of the reaction of formation of the $Ni(OH)_2$ insulating film (the reactions (4) and (5)) and the dissolution reaction (6).

The periodical variation of the H_2SO_4 concentration over the electrode surface, in the $\Delta\eta_{osc}$ potential range, brings about the current oscillations observed in this paper.

In Figure 5 is shown a typical oscillation of the current-time variation, and table 1 gives the values of overvoltage, frequency and minimum and maximum current for the whole oscillating range investigated.

The main process which is taking place during the oscillation time is, probably, the nickel dissolution, either directly by electrochemical reaction (2), or indirectly, by chemical dissolution (reaction (6)). Probably, a rather small quantity of current is used in order to form and grow $Ni(OH)_2$. The reactions (2) and (3) have a consumption of H^+ ions, while the film-forming reaction (5) induces a pH growing. But, the film-formation current is much less than that of the active dissolution (equation (2)), and therefore the consumption of H^+ ions is predominant. Thus, it can be assumed that in the "s" (or "m") point, when the film-forming is over, there exists a concentration gradient between the electrolyte-film and the electrolyte/metal interfaces (see Fig. 6).

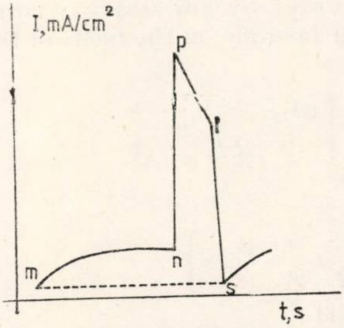

Fig. 5. — Oscillation profile of current on a Ni—S electrode (0.12 %S) for explaining the mechanism proposed.

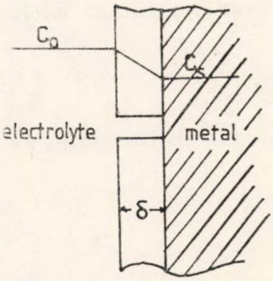

Fig. 6. — The H^+ ions diffusion pattern through pure nickel.

Since in the "cd'e" section of the potential-current curves the dissolution current is relatively high, it results that A will not be equal to 1 and that there is a $(1-A)$ remanent porosity of an order of magnitude $\cong 0.1$.

The "mn" section corresponds also to the nickel electrochemical dissolution (reactions : (1), (2), (3)), but in the conditions of a deficit of H^+ ions which are necessary for reaction (3). The H^+ ions come to the metal-electrolyte interface by diffusion through the $Ni(OH)_2$ film, a process which controls the anodic dissolution rate along the "mn" section. This is an unsteady diffusion, $\partial C_{H^+}/\partial t$, but the process is complicated by the simultaneous dissolution of the $Ni(OH)_2$ films, hence, by a complex variation of δ thickness and of the $(1 - A)$ free surface area. The point "n" corresponds to the dissolution of the last layer of the film. At the "*n*" point, the dielectrical A surface passes abruptly from high values to very small ones, and the active dissolution reaction is controlled by reactions (2) and (3). At the "*n*" point, the H_2SO_4 concentration at the metal electrolyte interface becomes equal to that in the bulk.

The role of sulphuric acid on the occurrence of oscillations is also supported by the fact that these oscillations do not occur in dilute sulphuric acid solutions or solutions of $H_2SO_4 + MgSO_4$.[4]

The current value grows suddenly due to the charging of the electrical double-layer and when I^*_{max} is reached, an intense dissolution of nickel takes place.

We have marked by (*) the steady state parameters in the upper stability state.

At the same time with the electrochemical dissolution of nickel (reactions (2) and (3)), the film forming $Ni(OH)_2$ reactions (4) take place too. In the "rs" section (see Fig. 5), these reactions lead to the passivation of the electrode, after which the process repeats itself in a cyclic way.

In fact, in the range of the (I^*_{max}) maximum oscillating currents, an extension of the "ab" domain takes place, but in the conditions when the η_a anodic overpotential is much higher than in the common anodic dissolution the electrode is passivated in this potential range.

On the basis of these considerations, we shall try to make a calculation of the upper stationary states marked by low stability corresponding to I^*_{max} currents. The evaluation can be done on the basis of the transfer equation combined with diffusion :

$$i = i_{cor}\left(i - \frac{i}{i^*_L}\right)\exp\left[\frac{(1-\alpha)F\cdot\eta}{RT}\right] \tag{8}$$

which can be also written as :

$$i = \frac{i_{cor}\exp\left[\frac{(1-\alpha)}{R\cdot T}F\cdot\eta\right]}{1+\frac{i_{cor}}{i^*_L}\exp\left[\frac{(1-\alpha)}{R\cdot T}F\cdot\eta\right]} \tag{9}$$

where the limiting current refers to the H^+ ions diffusion from the solution bulk at the metal surface. In this case, the H^+ ions involved are those consumed in reaction (3), and the diffusion is not made through pores, but over the $(1 - A^*)$ free surface area.

For the "ab" section (the classically active domain), the slowest step is the charge transfer reaction (2). Nevertheless the situation changes for very high overpotentials, when reaction (2) becomes very fast, and the rate of supplying the H^+ ions by diffusion (reaction (3)) is comparable with that of reaction (2), so correction made by means of the limiting current (equation (9)) is required.

The dotted curve in Fig. 4 has been calculated according to equation (9), using for $i_{cor} = 0.1$ mA/cm^2 according with other work.[4] It has also been considered that $i^*_{max} = i_L \cdot \rho^*$, where ρ^* is a factor depending on the potential, structure and thickness of the $Ni(OH)_2$ layer, which is involved in the dissolution-precipitation oscillating processes.

It should be also written down $i^*_L \cong \beta\ (i_L)$, where β is a "structural roughness coefficient", deriving from the substantial modification of the metallic network of the Ni—S alloy.

One can see that, for each composition of Ni—S electrodes, different i^*_L current values were obtained. Taking $\rho^* = 1$ for $i^*_{max,1}$, then the dotted curve in Fig. 4 stands for an example often upper stationary state for the Ni—S electrode, with $S = 0.12\%$. In the $\Delta\eta_{osc}$ oscillating range, the current varies between two stationary states: the lower state (with a higher stability) shown by "cd'" dotted line and the upper state (with a low stability) which depends on the i^*_L limiting current (obtained by extrapolating the "ab" active dissolution range to very high overpotentials).

From a coulometric calculation $q = \int_{t_1}^{t_2} I dt$ made for the "ne" section (Fig. 5), for the first oscillation with a frequency $= 0.066$Hz, a thickness of $\cong 1000$ Å is obtained, that means about 300 hydroxide molecular layers. For the last oscillation having a higher frequency, the calculation is very approximate, but a smaller δ is obtained, namely films of several molecular layers.

Therefore, it can be assumed that the whole "cd'e" section stands for the growing range of the hydroxide film, and that along the "cd" dotted section, the structure of the $Ni(OH)_2$ film facilitates the occurrence of oscillating phenomena.

In Figure 7, there are shown some oscillogrammes obtained on a Ni—S electrode with a 0.0743% sulphur content.

It has been noticed that a decrease in the sulphur content is followed by a diminution of the oscillating current amplitude. An increase of the oscillation frequency corresponding to the potential shift in cathodic direction can be noticed in this case too. The existence of more complex oscillations characterized by the occurrence of an additional peak

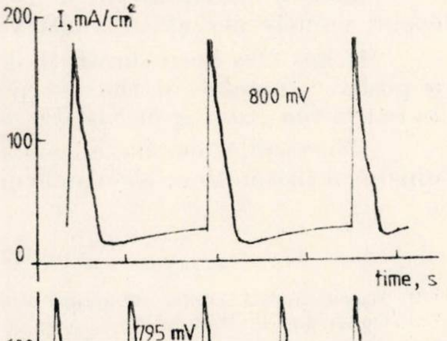

Fig. 7. — The current oscillations for anodic dissolution of a Ni—S electrode (0.0793%) in H_2SO_4 1 M solution.

current can also be de noted by "m" (Fig. 7). This may be attributed to a growing current of the $Ni(OH)_2$ layer thickness.

It is interesting to note that "m" peak current occurs periodically every fourth cycle. For very small frequencies, this "m" peak current has not appeared.

The current decrease due to the decrease of sulphur concentration can be explained by the decrease of the structural roughness coefficient β. Due to this decrease, I^*_{max} and i_{cor} also decrease at a lower sulphur percentage in the Ni—S electrodes. [4]

CONCLUSIONS

It has been shown that the anodic polarization of the sulphur doped nickel has certain remarkable peculiarities in comparison with that of pure nickel.

Thus, the anodic currents are much higher than for pure nickel along the whole scanned potential range.

There has been made the assumption that a proper passivation of the anode cannot be done. A "prepassivation" is done instead. This is characterized by the formation of a $Ni(OH)_2$ porous film, which is soluble in sulphuric acid solution.

With the reverse scan of potential the chemical dissolution of the $Ni(OH)_2$ film takes place, inducing a reactivation of the surface.

Also, a potential range is obtained where oscillating phenomena occur, namely periodical variations of current at a constant potential.

It has also been shown that the oscillation frequency decreases with a positive increase of the overpotential. This behaviour has been attributed to the growing of $Ni(OH)_2$ thickness.

The oscillations have been explained by the periodical phenomena o chemical dissolution, electrochemical reformation of $Ni(OH)_2$ porous film

REFERENCES

[1] P. Marcus and J. Oudar, *Materials Science and Engineering*, **42**, 191 (1980).

[2] J. Oudar and P. Marcus, *Appl. Surf. Sci.*, **3**, 48 (1979).

[3] D. Constantinescu, I. V. Cotârţă, V. Diaconescu and S. Sternberg, *Rev. Roum. Chim.*, to be published.

[4] S. Sternberg and I. V. Cotârţă, to be published.

[5] G. A. DiBari and J. V. Petrocelli, *J. Electochem. Soc.*, **112**, 99 (1965).

[6] A. C. Hart, *Metalloberflache*, **31**, 334 (1977).

[7] A. C. Hart, *Metal Finishing Journal*, **19**, 332 (1973).

[8] R. Parkinson, *Galvanotehnica*, **10**, 181 (1979).

[9] E. Raub and A. Disam, *Metalloberflache*, **13**, 308 (1959).

[10] T. S. De Gromoboy and L. L. Shreir, *Electrochim. Acta*, **11**, 895 (1966).

[11] S. A. Watson, *Metal Finishing Journal*, **18**, 18 (1972).

[12] T. P. Hoar, *Corrosion Sci.*, **7**, 341 (1967).

[13] J. J. Podesta, R. C. V. Piatti and A. J. Arvia, *J. Electrochem. Soc.*, **126**, 1363 (1979).

[14] J. J. Podesta, R. C. V. Piatti and A. J. Arvia, *Electrochim. Acta*, **24**, 633 (1979).

[15] B. Mazza and P. Podeferi, *Electrochim. Acta*, **23**, 78 (1979).

[16] I. Epelboin, M. Ksouri and R. Wiart, *J. Less Common Metals*, **43**, 235 (1975).

[17] K. J. Vetter, "Elektrochemische Kinetik", Springer, 1961, p. 641.

[18] U. F. Franck, *Z. Elektrochem.*, **62**, 649 (1958).

[19] M. N. Hull, J. E. Ellison and J. E. Toni, *J. Electrochem. Soc.*, **117**, 192 (1970).

[20] D. Constantinescu, C. Ghica and I. V. Cotârţă, *Bul. Inst. Politehnic Bucureşti*, 4, **XLII**, 73 (1980).

[21] M. C. H. McHubre and D. D. Mcdonald, *J. Electrochem. Soc.*, **128**, 524 (1981).

[22] C. B. Diem, *A. I. Ch. Journal*, **33**, 218 (1987).

[23] A. A. El Miligy, D. Geana and W. J. Lorentz, *Electrochim. Acta*, **20**, 273 (1975).

[24] D. Geană, A. A. El Miligy and W. J. Lorentz, *Corrosion Sci.*, **13**, 505 (1973).

[25] J. R. Vilche and A. J. Arvia, *Corrosion Sci.*, **18**, 441 (1978).

[26] Y. Kuramoto, "Chemical Oscillations Waves and Turbulence", Springer-Verlag, 1984.

[27] P. Ortoleva and J. Ross, *J. Chem. Phys.*, **58**, 5673 (1973), **56**, 5090 (1974); **63**, 3389 (1975).

[28] P. Glausdorff and I. Prigogine, "Thermodynamic Theory of Structure Stability and Fluctuations", J. Wiley, London, 1971.

Revue Roumaine de Chimie, **34**, *2*, 635–648 (1989)

INVESTIGATIONS OF STRAINED S-B-S BLOCK COPOLYMERS WITH DILUTE ELASTIC NETWORKS*

N. STRIBECK, S. POLIZZI [a], P. BÖSECKE and H. G. ZACHMANN
Institut für Technische und Makromolekulare Chemie, Universität Hamburg
[a] Dipartimento di Chimica Fisica, Università degli Studi di Venezia

Received October 26, 1988

Spin cast films of one pure SBS and two oil extended SBS samples are observed under first cycle straining in the synchrotron radiation beam at HASYLAB. A scattering curve is extracted by intersecting the scattering pattern in drawing direction. This scattering curve is analyzed by fitting a one dimensional fibrillar two phase model. Essential to a fit with parameters of physical sense is the assumption of a least two components. One of the two main components is identified by fibrils containing PS cylinders orientated parallel to strain, the other by such containing cylinders orientated in cross direction. Splitting of cylinder orientation in the drawn state seems to be essential to the mechanical properties of the thermoplastic rubber, since only those cylinders orientated with their axis in the direction of strain are rigid while those orientated cross to drawing direction are yielding. The amount of cylinders alotted to each of the two components is varying as a function of the diluting agent and appears mainly to be influenced by topological parameters : the cylindrical particle dimensions within a two dimensional pseudo lattice cell of slightly varying dimenions in longitudinal and cross cylinder direction respectively. While paraffinic mineral oil dilution causes the cylinders length to decrease and thus improves cylinder orientability within the pseudo lattice cell, aromatic oil dilution increases the particles diameter. The results are compared with those of a preceding study, which allowed determination of the degree of phase separation by absolute SAXS and with first TEM micrographs.

1. INTRODUCTION

The main objective of this article is the presentation of our actual state of research in studying the morphology of a SBS three block copolymer and its oil diluted descendants under strain. Our main experimental method is small angle X-ray scattering (SAXS), and the study comprises absolute measurements of the samples SAXS in the undrawn state,[1] development of an adapted theory for the evaluation of the scattering patterns of the drawn samples,[2] a report on experimental method and on first results for samples under strain [3] and a comprehensive presentation and discussion of the fully evaluated scattering patterns.[4]

*** Lecture presented at the 3rd National Congress of Chemistry, Bucharest, Romania, Sept. 22nd, 1988**

Early in 1967 Hendus et al.[5] observed an originally isotropical scattering pattern from an SBS sample, that under strain deforms towards "a very narrow ellipse with an intensity accumulation of layer line character". Papers recently published on this subject [6,7,8] use sample films prepared by solvent casting. This procedure is known to yield a very perfect microstructure, as was shown by many authors using transmission electron microscopy (TEM). Thus the SAXS patterns of these samples are very detailed, showing many distinct reflections which are difficult to interpret. In the present paper we are dealing with sample films that are produced by our Romanian collaboration partners.[9,10] Their rapid spin casting process, far from equilibrium, is closer to technical processes like injection moulding and the general scattering pattern of these samples looks like the rather simple one described by Hendus et al. in 1967. For this type of pattern we were able to develop a new evaluation tool and to analyze the scattering patterns. Beyond that D. Hong made first electron micrographs of two of the samples that we additionally present here.

Blending of SBS block copolymers with typically 50 pph (parts per hundred parts of polymer) of a mineral oil fraction is of technological interest, since it is known to improve tensile strength of the product and processing capabilities.[6] This improvements cannot be obtained by the use of highly aromatic mineral oil fractions, so normally a light, mainly paraffinic/naphthenic mineral oil fraction is used. Although there is a lot of patent literature on this topic, we did not find papers on the morphology of oil extended grades of SBS copolymers except the ones of Ceauşescu et al.[7,8] Our collaboration partners by the use of rubber network theories, indirectly conclude that the PS particles in the sample diluted with 50 pph of paraffinic mineral oil should be closer to spherical shape than the ones in the undiluted sample.

2. EXPERIMENTAL

The base sample investigated is a poly(styrene)—poly(butadiene)—poly(styrene) three block copolymer with molecular weights $M_n = 80{,}800$ g/mole for the middle and $M_n = 21{,}200$ g/mole for each of the end blocks. A polymer film was spin cast from toluene solution. This base sample shall be referred to as "SBS". It was modified by blending 50 pph (parts per 100 parts of the polymer) of each a highly paraffinic/naphthenic and highly aromatic mineral oil fraction to the solution before spin casting (samples "P50" and "A50"). Synthesis [11] and sample preparation [10] were described elsewhere. The SAXS of the samples under first straining was measured at the Hamburg Synchrotron Radiation Laboratory (HASYLAB) and recorded with a two-dimensional detector (VIDICON). The experiment in detail was described in a previous publication on the undiluted sample.[3] For each positive and integer stretching ratio $\lambda = \varepsilon + 1$ a scattering pattern was accumulated for 60 s. In a second experiment the accumulation time after applying strain was chosen to be 5 s. This was the minimal time to get a sufficient signal/noise ratio with the VIDICON detector. By comparison between both experiments we took a first glance at creep of orientation and order.

Absolute SAXS measurements of the undrawn samples were performed with a Kratky camera using the moving slit method. TEM micrographs were obtained from cuts of ca. 100 nm thickness, stained with OsO_4. TEM measurements were carried out using a Japanese H-800 electron microscope at Yanshan research institute, Beijing, P. R. China, operated at 200 kV.

3. RESULTS AND DISCUSSION

3.1. Influence of Diluents on Phase Separation

Fig. 1 shows the electron density difference (contrast) $\Delta \rho_{OB}$ between the two phases of our base SBS sample diluted with various diluent oils as a function of the volume fraction of oil in the poly(butadiene) phase, v_{OB}. The value of 24 el/nm^3, obtained for the undiluted SBS, is far below the theoretical value for optimal phase separation (38 el/nm^3) (cf.[1]). It could be shown that the electron density of the paraffinic/naphthenic oil is close to that of pure PB and the electron density of the aromatic oil is close to that of pure PS. All kinds of oil mainly invade the PB phase. The curve for paraffinic mineral oil clearly shows that oil dilution improves phase separation and can be extrapolated towards the theoretical value of contrast for infinite dilution of the PB phase. Concerning aromatic oil dilution, interpretation is more difficult. The three samples that were investigated while straining are indicated in the figure.

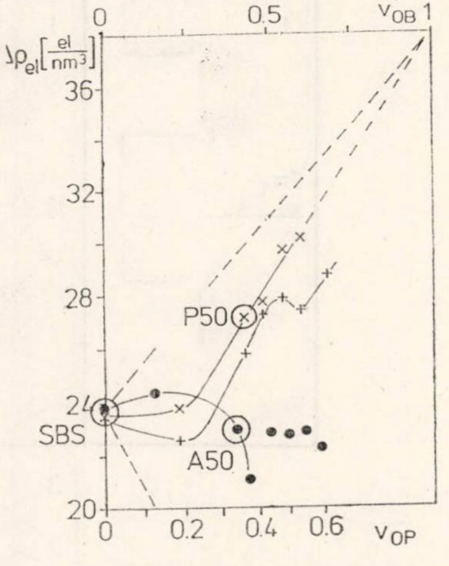

Fig. 1.— Contrast $\Delta\rho_{el}$ between the two phases of oil extended SBS three block copolymers as a function of v_{OB}, the volume fraction of oil in the PB phase for different kinds of diluents. (+): Low molecular weight PB (Lithene PM). (×): Paraffinic mineral oil fraction. (o): Aromatic mineral oil fraction

3.2. SAXS Results of Sample Straining

As an example the variation of the scattering pattern of SBS with elongation $\varepsilon = (l - l_0)/l_0$ and accumulation time after applying the additional strain is shown in Fig. 2. Here l_0 is the initial and l the actual length of the sample. Creep effect of the scattering pattern is visible, but too fast that it could be studied with the VIDICON detector and the experimental method chosen. Only for $\varepsilon = 1$ and 2 an effect of layer line straightening could be observed. Thus the study of creep phenomena would require an adapted experimental method and possibly a faster detector. For the further evaluation we decided to use the "relaxed" scattering patterns that were accumulated for 60 s.

The general type of the scattering pattern, in the simplest case, suggests a one dimensional model of fibrils containing cylindrical particles within. Due to the closed layer lines a correlation among cylinders belonging

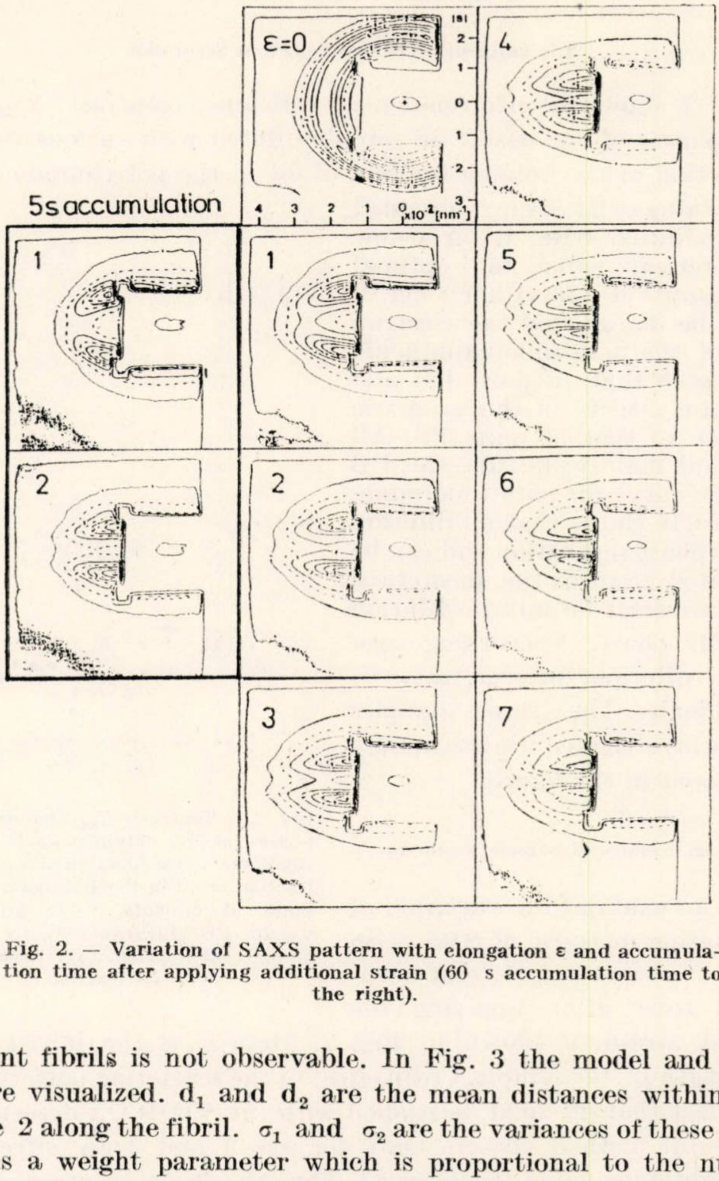

Fig. 2. — Variation of SAXS pattern with elongation ε and accumulation time after applying additional strain (60 s accumulation time to the right).

to different fibrils is not observable. In Fig. 3 the model and its parameters are visualized. d_1 and d_2 are the mean distances within phase 1 and phase 2 along the fibril. σ_1 and σ_2 are the variances of these distances and A_P is a weight parameter which is proportional to the number of cylinders contributing to the fibrillar model component and some other quantities. These five parameters in general are sufficient to describe the one dimensional fibrillar scattering curve $I_1(s)$, if the statistics how to build up the fibril is known. So we have two problems, namely to extract the one dimensional fibrillar scattering curve from the scattering pattern and to find out about the fibrillar statistics. It[1] was shown that one can extract the one dimensional scattering curve from the pattern by taking the intersection of the pattern in the direction of draw. So we can take the curve along the s_3-component of the scattering vector in cylindrical coordinates, as is illustrated in Fig. 4. If one does not want

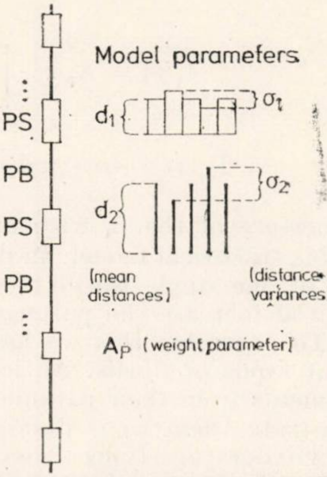
Model parameters
PS
PB
PS
PB
d_1
σ_1
d_2
σ_2
(mean distances)
(distance variances)
A_P (weight parameter)

Fig. 3. — Illustration of a one dimensional fibrillar model and its parameters.

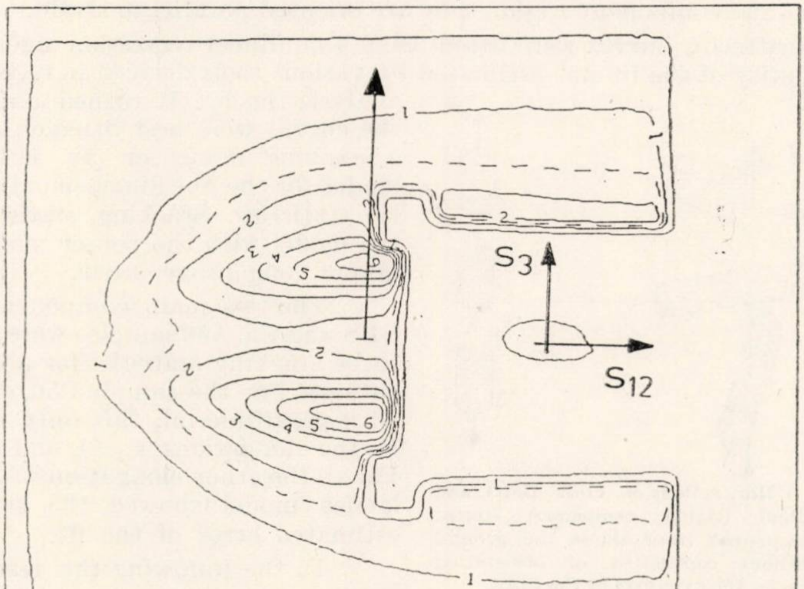

Fig. 4. — Illustration of intersecting the two dimensional SAXS pattern with cylindrical symmetry to get the one dimensional scattering curve I_1 (s^3). s_{12} and s_3 are the components of the scattering vector $\vec{s}$ in cylindrical coordinates.

to make assumptions on the fibrillar statistics, one can use a formula based on Rulands theory of interface distributions [12] and express the one dimensional scattering curve by an infinite sum over attenuated cosine terms :

$$I_1(s) = A_p/s^2 \cdot \left[1 - \sum_{i=1}^{\infty} w_i H_i(s)\right]$$

$$H_i(s) = \cos(2\pi\, d_i s) \cdot \exp(-\, 2\pi^2 \sigma_i^2 s^2) \tag{1}$$

Thus the increase of the σ_i with increasing i should give hints on the most probable statistical model. In doing the latter we found out that the assumption of one single fibrillar component was of no physical sense. After an initial increase the parameters σ_i^2 dropped and again increased thereafter. To overcome this we had to assume the presence of a least two different kinds of fibrils. Anticipating the identification of the two main components from their parameters values and response to straining, we can illustrate them as is done in Fig. 5. In the cross component (left), the cylinders are lying cross to straining direction, while in the longitudinal component (right) they are oriented parallel to strain.

Scattering curves were fitted using a nonlinear regression algorithm. The quality of the fit was estimated by various tools derived in regression analysis theory. It turned out that the curves were best fitted either by a stacking model or by a lattice model for the one dimensional fibrillar statistics. Stacking statistics is the model with the poorer model inherent long range order.

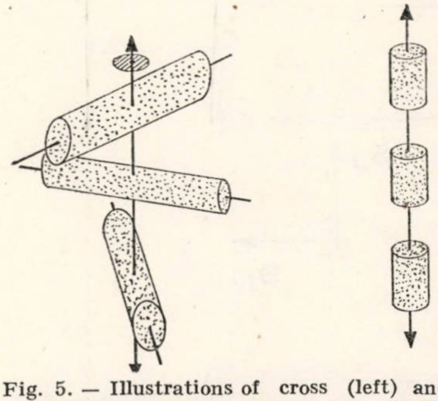

Fig. 5. — Illustrations of cross (left) and longitudinal (right) component fibrils. Cross component fibril shows the general case without correlation of orientation among the cylinders in the fibril.

The two main components for SBS and the A50 samples were found to be stacking statistics for all elongations. For the sample P50, diluted with paraffinic oil, this only is true for the elongations $\varepsilon = 1$ and $\varepsilon = 3$. For all the other elongations a double lattice model showed the smallest estimated error of the fit.

In the following the results of the three samples shall be presented by plotting the various model parameters versus the elongation ε. The individual parameter values and intervals of confidence will be shown by symbols with error bars. The height of the bar is chosen to mark a "$2\,\sigma$"-interval of confidence, assuming the error is normally distributed. I.e. the probability to find the true value of the parameter within the interval of confidence is 0.95. Considering the height of the error bars, smooth graphs are drawn through the points evaluated. Points without error bars have an error smaller than symbol height.

Because of the fact that the layer lines for all samples and $\varepsilon = 1$ are still somewhat bent, indicating imperfect orientation, it is not strictly allowed to apply our one dimensional model to these data. Therefore especially the weight parameters of this elongation should be interpreted cautiously. In the plots they are put in parenthesis. Furthermore bad model adaptation at $\varepsilon = 1$ in any case causes stacking statistics to fit better than the one dimensional lattice model, even if morphology really presents a lattice.

3.2.1. **Pure SBS**

Fig. 3 shows the distance parameters d_i from the double unidimensional model. The closed line graphs can be identified as the dimensions of hard particles, the PS-cylinders. The broken lines describe a weaker phase and shall be identified by the linear dimensions of the PB-matrix in the direction of strain. The first model is marked by triangles, the second by circles. Let us identify the triangle marked component by fibrils containing cylinders with their axis in the direction of strain (longitudinal component) and the circle marked component by fibrils with cylinders cross to drawing direction (cross component) and verify this identification by the response of its parameters to elongation and variation of oil dilution.

Looking at the closed line graphs, describing the PS-domains, it is obvious that the cylinders are rigid if orientated in longitudinal direction, while in cross direction they are weak and extend up to an elongation of $\varepsilon = 3$, where their dimension has increased from 22 nm to 60 nm. After this elongation the cross system fails, as can be seen from the following decrease of the mean radial dimension of the cross cylinders and the relaxation of the corresponding gap height. The strong increase of the gap in the longitudinal component denotes a takeover by this system. An extrapolation to $\varepsilon = 0$ is possible and leads to a cylinder height $h_c = 38$ nm and a diameter $d_g = 23$ nm. The initial heights of the gaps can be coarsely estimated, from an extrapolation in a plot $d_2(\varepsilon)/(\varepsilon + 1)$ vs. ε for the first three data points. The estimates result in a gap length of $d_g = 19$ nm for the longitudinal and $d_g = 42$ nm for the the cross component.

The weights A_P of both the longitudinal and cross component of the scattering under extension are given in Fig. 5. As one can see, the sum of the two main model weights is nearly constant from $\varepsilon = 3$. At low elongations an orientation effect can be observed : cylinders orientated indifferently at $\varepsilon = 2$ are comprised in the cross model. At $\varepsilon = 3$ they are oriented in longitudinal direction. In a middle range of ε a plateau for both weights is observable. The weight A_P is always proportional to the number of cylinders allotted to the component, but in such a plateau region even certain approximations should hold, allowing to assume the proportionality constants for both components to be the same. We recognize that the height of the plateau is identical for both main components and thus can state that about 50% of the cylinders can be oriented parallel to the direction of strain.

Double stacking statistics was found to be the model best fitted to data. From this we deduce, that the order of the superstructure is a poor one.

3.2.2. SBS Diluted with Paraffinic Oil

For the sample P50, Fig. 6 shows the dimensions d_g of the two phase system in drawing direction. As one can see, up to $\varepsilon = 3$ the PS particles of both the longitudinal and the cross component can be considered to be rigid. The extrapolation to $\varepsilon = 0$ yields cylinders of $d_g = 22$ nm and $h_c = 28$ nm. The initial heights of the gaps can be estimated, if one plots $d_2(\varepsilon)/(\varepsilon + 1)$ vs. ε for the first three data points and extrapolates towards zero. The estimates result in a gap length of $d_g = 35$ nm for both the longitudinal and the cross component.

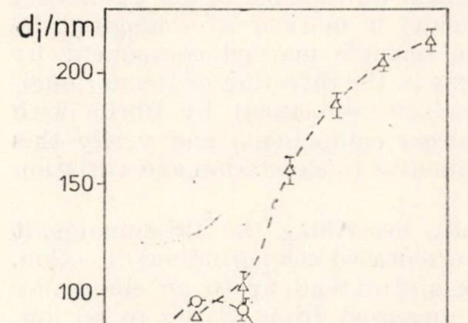

Fig. 6. — Dimension parameters d_i vs. elongation ε of pure SBS sample fitted with double fibrillar stacking statistics. (0) : Fibrils with cylinders lying cross drawing direction. (Δ) : Fibrils with cylinders orientated in drawing direction. Closed graphs : Cylinder dimensions (PS). Broken graphs : Gap dimensions (PB).

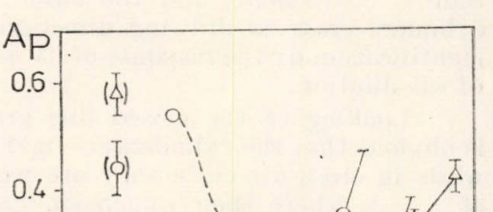

Fig. 7. — Weights A_p vs. elongation ε of pure SBS sample fitted with double fibrillar stacking statistics. (⊙) : Component of fibrils with cylinders lying cross drawing direction. (Δ) : Fibrils with cylinders orientated in drawing direction. Parenthesis for $\varepsilon = 1$ denotes poor model adaptation due to bent layer lines.

Near $\varepsilon = 4$ the cross cylinders begin to yield, with the cylinder diameter increasing up to 80 nm. Both matrix dimensions respond by relaxation to a constant value, further elongation advances by disruption of the cylinders lying cross to the direction of deformation, until again matrix material is elongated after $\varepsilon = 7$. At an elongation of $\varepsilon = 3$ the scattering curve is best fitted with a stacking model, which points to the fact that the instable state is inducing disorder to the morphology.

The following scattering curves again are lattice model fitted, but now in the cross component an inversion of the phase decorating the lattice has taken place. While at $\varepsilon = 2$ the curve was fitted best with a cross component in which the PS phase was decorating the lattice, from now on the PB matrix is forming the decoration. For the longitudinal component no such inversion of lattice decoration was observed.

Fig. 8 shows the development of the weights A_P as a function of elongation. The initial orientation effect can be observed until $\varepsilon = 3$, where the plateau is reached. In the plateau the amount of cylinders oriented parallel to strain is approximately 87%.

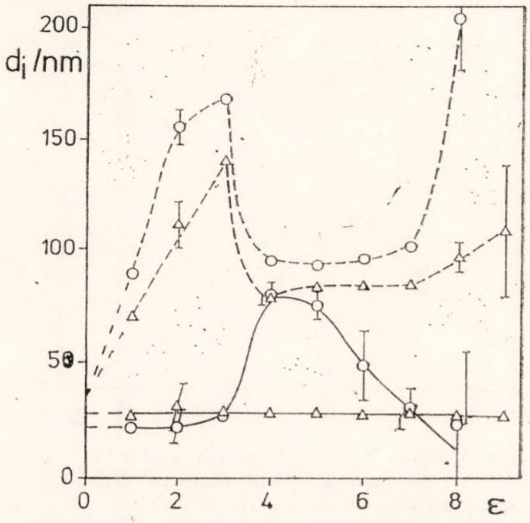

Fig. 8. — Dimension parameters d_i vs. elongation ε of P50 sample containing 50 pph of paraffinic oil. (⊖): Fibrils with cylinders lying cross drawing direction. (Δ): Fibrils with cylinders orientated in drawing direction. Closed graphs: Cylinder dimensions (PS). Broken graphs: Gap dimensions (PB).

Thus, paraffinic oil dilution decreases the cylinders anisotropy, helps the cylinders optimal orientation parallel to stress and in cross direction improves the relative hardness of the cylinders with respect to the matrix. Due to lattice model fit the morphology can be said to show a goad degree of order.

3.2.3. **SBS Diluted with Aromatic Oil**

For the sample A50 the response of the distances d_c to straining is plotted in Fig. 9. The cylinders orientated in the direction of strain are rigid again. Extrapolation of the cylinders height will be discussed in the next passage. The cylinders cross drawing direction, on the other hand, are flexible even at $\in = 1$, so that no extrapolation to their initial thickness is possible. A very coarse estimate for the initial cylinder diameter and the gaps can be done the same way as for the preceding samples. The values are indicated in the plot. The cylinder diameter thus can be estimated by $d_c = 29$ nm and for the gap lengths we get values of $d_g = 19$ nm for the longitudinal and $d_g = 30$ nm for the cross component.

At $\in = 5$ the cross system has failed and one finds a takeover by the longitudinal system, indicated by a sudden increase of as well PB anb PS mean distance. A similar behaviour was found in the undiluted SBS sample at an elongation of $\in = 4$.

In Fig. 11 the weights A_P of the sample A50 are plotted. As one can see, the plateau is reached lately at $\varepsilon = 5$. Here the amount of the longitudinal component is very low while most of the cylinders contribute

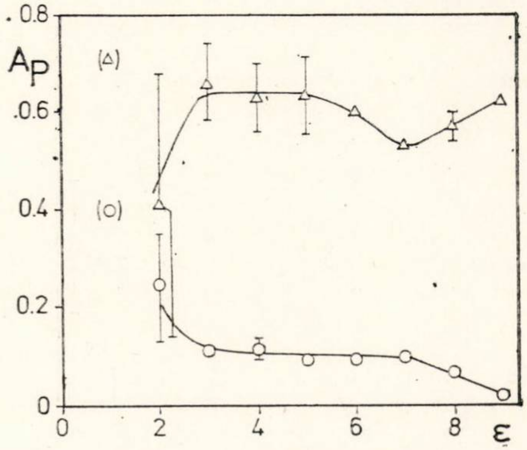

Fig. 9. — Weights A_P vs. elongation ε of P50 sample. (○) : Component of fibrils with cylinders lying cross drawing direction. (Δ) : Fibrils with cylinders orientated in drawing direction. Parenthesis for $\varepsilon = 1$ denotes poor model adaptation due to bent layer lines.

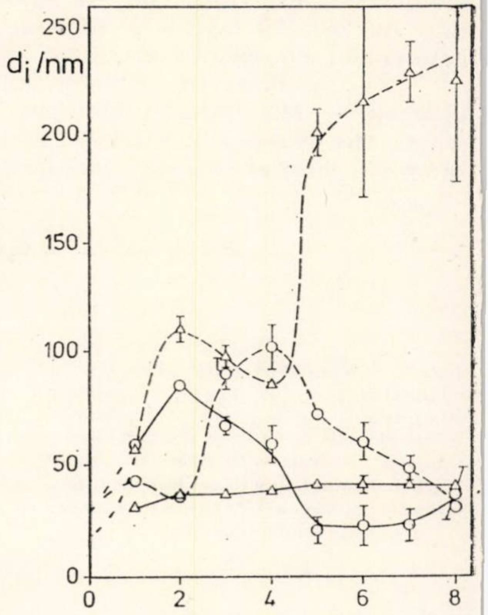

Fig. 10. — Dimension parameters d_i vs. elongation ε of A50 sample fitted with fibrillar stacking statistics. (○) : Fibrils with cylinders lying cross drawing direction. (Δ) : Fibrils with cylinders orientated in drawing direction. Closed graphs : Cylinder dimensions (PS). Broken graphs : Gap dimensions (PB).

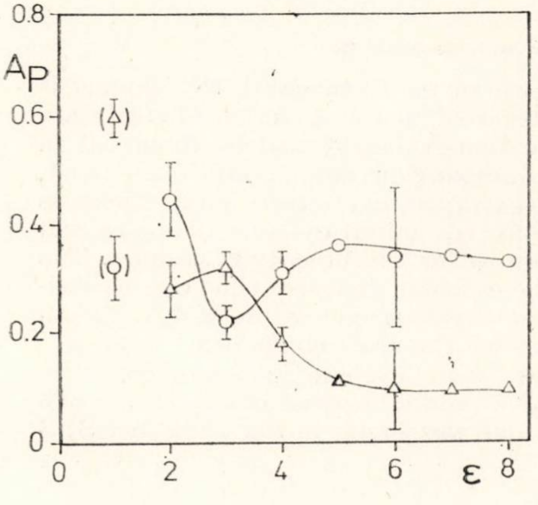

Fig. 11. — Weights A_P vs. elongation ε of A50 sample. (○) : Component of fibrils with cylinders lying cross drawing direction. (Δ) : Fibrils with cylinders orientated in drawing direction. Parenthesis for $\varepsilon = 1$ denotes poor model adaptation due to bent layer lines.

to the cross component. At $\varepsilon = 3$ there is a significant valley in the cross component that is accompanied by a peak in the longitudinal component. The peak coincides with the range of longitudinal fibril relaxation and the valley does so with the range of cross cylinder disruption. The explanation by an orientation phenomenon is supported by results of the variance (σ) plots, that are not presented in this paper. We assume that the increase of the longitudinal components amount is caused by a latent (and only fair) longitudinal orientation of a certain amount of cylinders at low elongations, so that the longitudinal component is increased. While cross cylinders under tension are disrupting, an orientation relaxation from longitudinal to cross orientation occurs, which can be observed in the decrease of the longitudinal component and the corresponding increase of the cross component between $\varepsilon = 3$ and 5. Thus we take the true cylinder height from high elongations and find $h_c = 14$ nm.

In the plateau, found at high elongations, approximately only 21% of the cylinders are oriented parallel to strain.

Thus aromatic oil dilution slightly increases the cylinders height, hinders the optimal cylinder orientation parallel to stress and reduces the relative hardness of the cylinders lying cross to drawing direction. The morphology shows a low degree of order, as is true for the undiluted SBS.

3.3. Discussion of Extrapolated or Estimated Dimensions

In the preceding paragraphs we could extrapolate or estimate values for the mean dimensions of the particles and the mean distances between them in the undrawn state, which are compiled in Table 1.

As one can see, pure SBS shows a rather wide gap d_{gc} in cross direction between neighbouring cylinders. Anticipating a look at the corresponding electron micrograph, we interpret this as an effect of bad phase separation (see [1]): Imperfect PS "particles" between the more stable cylinders that are even vanishing at a very low elongation. So in d_{gc} we just estimate the mean PB distance between two more stable cylinders, "blended" with some additional imperfect PS material.

Paraffinic oil dilution only affects the cylinder height, while aromatic oil dilution mainly seems to influence the cylinder diameter. Both diluents cause a reduction of the h_c/h_c-ratio of the cylinders, but parafinic oil dilution decreases the cylinder height, while aromatic oil dilution seems to increase the cylinder diameter.

If we trust in the estimated values for the mean initial distances between the cylinders, the result on the particle dimensions can even be generalized. From the values in Table 1 we construct nearly the same "pseudo lattice cell" for P50 and A50 (see Fig. 14). The lattice cell of pure SBS appears only somewhat wider in cross

Table 1

Extrapolated or estimated (*) values for the cylinder dimensions and the distances in between for the undrawn state h_c, d_c: cylinder height and diameter. d_{gl} d_{gc}: gaps in longitudinal and cross direction (with respect to the cylinder axis)

	SBS	P50	A50
h_c/nm	38	28	41
d_c/nm	23	22	*23
d_{gl}/nm	*19	*35	*19
d_{gc}/nm	*42	*35	*30

cylinder direction. A result compatible with this was found in a preceding work on the unstretched samples : a long period nearly constant for three kinds of diluents and oil dilutions up to 140 pph.[1].

Thus a reasom for the different a mount of cylinders allotted to each of the two components with different cylinder orientation is obviously given by topology : the cylindrical particles dimensions within a pseudo lattice cell of nearly constant extent, determining the particles possibility to rotate and follow an external torque.

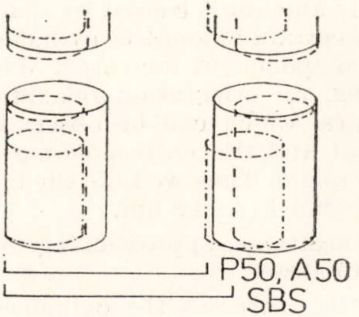

Fig. 12. — Pseudo lattice cells containing cylindrical particles constructed from extrapolated or estimated dimensions for the undrawn state. Broken line : Pure SBS. Dashed and dotted line : Sample P50, 50 pph paraffinic oil dilution. Full line : Sample A50, 50 pph aromatic oil dilution. Decrease of lattice constants cross component on oil dilution is indicated.

3.4. TEM Micrographs

In fig. 13 the first two electron micrographs obtained from SBS and a sample diluted with 60 pph of paraffinic oil (P60) are presented. The PS particles appear light, while the PB phase, due to staining, is the darker one. As one can see, the results of our SAXS study are excellently verified by the TEM pictures.

Bad phase separation of SBS is visible by the comparatively bad staining of the interstices, meaning a pollution of the PB phase by poly (styrene). The microstructure is rather a chaotic one, which is in agreement to the stacking model fit of the sample.

Measurements of the cylinder dimeusions and the distances between them in well developed regions resulted in the same values that were found by the SAXA pattern analysis for the samples SBS and P50, which is very close to P60 sample.

Looking at the topology of P60, one finds clusters of ordered cylinders, built up from few cells of lattice character. The cells contain one cylinder in the middle that is surrounded by 5 to 8 other cylinders, the most frequent number being 6. Thus we recognize a disturbed hexagonal lattice structure.

4. OUTLOOK

The results of this work show that using an adapted theoretical approach and model for the evaluation of the small angle X-ray scattering can give profound information on the two phase topology of an (oil diluted) SBS block copolymer not only in the drawn state.

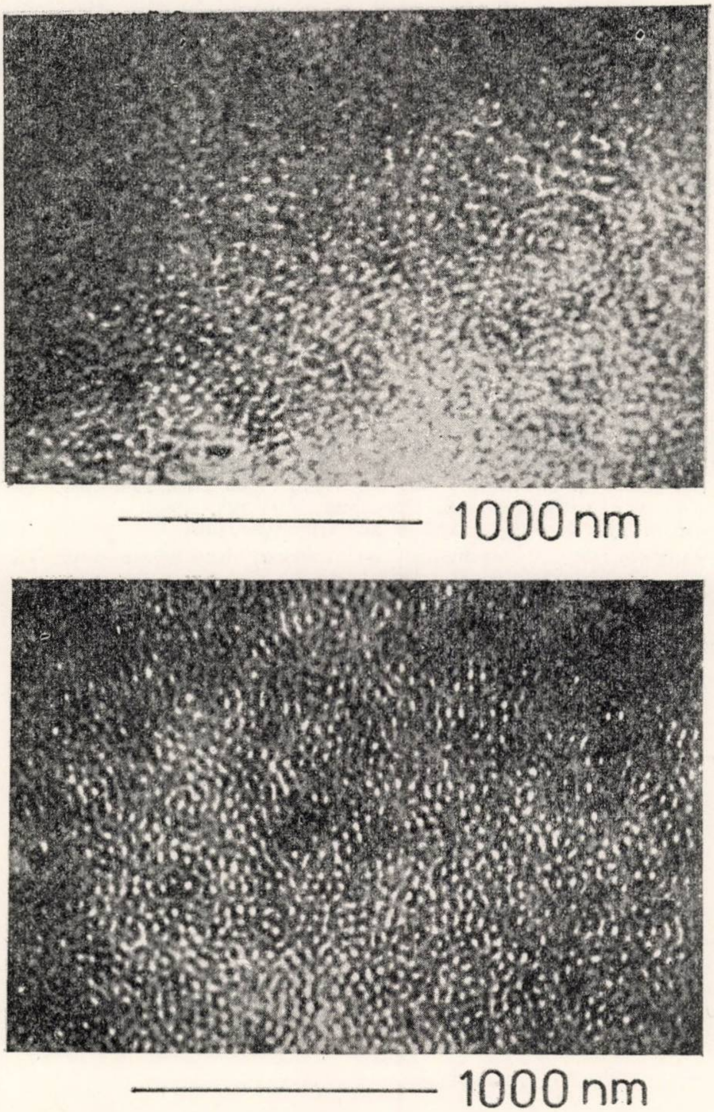

Fig. 13. — TEM micrographs of pure SBS (above) and P60 (SBS + 60 pph of paraffinic mineral oil, below). Length of the bars : 1000 nm.

After having studied linear three block copolymers, it will be interesting to investigate diluted SBS star block copolymers. These types are more frequently used than the linear ones. Also resin diluted SBS block copolymers are of interest for the production of adhesives and thus could be studied.

Creep could be studied in an adapted experiment : samples could rapidly be strained from their initial length to a medium elongation (ε ≅ 2) and variation of the scattering curve in the direction of strain could be recorded rapidly, if a fast diode array detector were used.

The effect of oil dilution to the relaxed morphology could be studied by further TEM investigations.

As noted in the discussion to the lecture, changes of the PS domain dimensions could have occurred between preparation and measurements (more than 1 year, samples kept at room temperature) due to thermal aging.

REFERENCES

[1] S. Polizzi, et al., (1988) submitted to *Colloid Polym. Sci.*
[2] N. Stribeck (1988) submitted to *Colloid Polym. Sci.*
[3] S. Polizzi, et. al., (1988) submitted to *Polymer.*
[4] N. Stribeck, et. al., (1988) submitted to *Colloid Polym. Sci.*
[5] H. Hendus, et. al., *Colloid Polym Sci.*, **216**, 110—119, (1967).
[6] R. Séguéla and J. Prud'homme, *Macromolecules*, **21**, 635—643 (1988).
[7] T. Pakula, et. al., *Macromolecules*, **18**, 1294—1302, (1985).
[8] R. W. Richards and J. T. Mullin, *Mat. Soc. Symp. Proc.*, **79**, 299—308, (1988).
[9] E. Ceaușescu, et. al., *Rev. Roumaine Chim.*, **28**, 299—323, (1983).
[10] E. Ceaușescu, et. al., *Pure Appl. Chem.*, **56**, 319—328 (1984).
[11] In : E. Ceaușescu (ed) "Forschungen im Bereich der Chemie und Technologie der Polymere. Birkhäuser, Basel, 1986", pp. 65—77.
[12] W. Ruland, *Colloid Polym. Sci.*, **255**, 417—427 (1977).

Revue Roumaine de Chimie, **34**, 2, 649—659 (1989)

PROCESSUS D'HYDRATATION ET DE DURCISSEMENT DANS LE SYSTÈME $3CaO\cdot SiO_2-3(CaO\cdot Al_2O_3)CaSO_4-H_2O$

I. TEOREANU et MARIA GEORGESCU
Institut Polytechnique Bucarest

Reçu le 28 septembre 1988

On a étudié l'évolution des processus d'interaction et de formation de la structure de durcissement, dans le système $C_3S-C_4A_3\bar{S}-H_2O$, pour des compositions avec rapport $C_3S/C_4A_3\bar{S} = 1...10$, sans et avec addition de gypse. Les expériences ont mis en évidence l'existence des interinfluences parmi les processus d'interaction $C_3S + H_2O$ et $C_4A_3\bar{S} + H_2O$. La présence de C_3S, par $Ca(OH)_2$ qui résulte par hydrolyse, détermine des modifications dans la vitesse d'interaction de sulfataluminate avec l'eau, ainsi que dans la nature des produits d'hydratation formés et leur degré de cristallisation. Les masses des systèmes examiné, avec des compositions différentes, présentent des propriétés différentes — tant parmi elles, ainsi que par rapport avec les systèmes $C_3S - H_2O$ et $C_4A_3\bar{S}-H_2O$.

This paper studies the evolution of the interactions and hardening structure formation, in the $C_3S-C_4A_3\bar{S}-H_2O$ system, for compositions characterised by $C_3S/C_4A_3\bar{S} = 1...$ $...10$ ratios, with and without gypsum addition. The investigations evidenced the existence of some reciprocal influences between $C_3S + H_2O$ and $C_4A_3\bar{S} + H_2O$ interaction processes. The presence of the tricalcic silicate in this system, through $Ca(OH)_2$ released by hydrolysis, determines some changes of the velocity in the interaction between water and calcium sulfataluminate, in the nature of hydrocompounds which are forming, as well as in their crystallinity degree. The examined systems, having different compositional features, present different binding properties, among themselves, as well as in relation with $C_3S - H_2O$ and $C_4A_3\bar{S} - H_2O$ systems.

1. INTRODUCTION

Les renseignements fournis par des recherches antérieures [1-8] attestent l'influence que le sulfataluminate de calcium exerce sur le comportement liant de certains systèmes dont il est le constituant, par suite des transformations qu'il détermine dans la cinétique des interaction chimiques, dans la nature et la proportion des hydrocomposés qui se forment.

Pour l'obtention des renseignements supplémentaires concernant cette classe de systèmes liants, dans le présent travail on a étudié les processus d'hydratation et de durcissement pour des mélanges ($C_3S +$ $+ C_4A_3\bar{S} + H_2O$) * sans et avec addition de gypse.

---

* On va utiliser les notations suivantes : $C = CaO$, $A = Al_2O_3$, $S=SiO_2$, $\bar{S} = SO_3$ $H = H_2O$.

Tableau 1

Indicatif du système	Rapport $C_3S/C_4A_3\bar{S}$	Addition $CaSO_4 \cdot 2H_2O$(%)
I_1	1	—
II_1	2	—
III_1	3	—
IV_1	10	—
I_2	1	5
II_2	2	5
III_2	3	5
IV_2	10	5

2. INVESTIGATIONS EXPÉRIMENTALES

En utilisant du silicate tricalcique et du sulfataluminate de calcium synthétisés au laboratoire à partir des réactifs chimiquement purs, on a préparé des mélanges caractérisés par des rapports $C_3S/C_4A_3\bar{S}$ = 1 ... 10 (voir aussi[7]), sans et avec addition de 5% gypse (voir tableau 1).

Ces mélanges ont été broyés conformément à des surfaces spécifiques (Blaine) de 3 400—3 600 cm^2/g.

L'évolution des processus d'interaction avec l'eau des phases anhydres ainsi que la nature des hydrocomposés qui en résultent, ont été étudiées par des déterminations d'eau chimiquement liée et par des analyses diffractométriques sur des pâtes ayant le rapport eau/liant = 0,5, conservées en milieu humide pendant 3 heures — 28 jours.

Des renseignements, concernant les propriétés liantes des masses étudiées, ont été obtenus par des déterminations de la résistance mécanique sur des échantillons en mortier dont le rapport liant/sable = 1/3 et 13% eau, conservés en milieu humide 1,3, 7 et 28 jours.

3. RÉSULTATS

Les données d'eau chimiquement liée et les analyses diffractométriques à partir desquelles on a estimé le degré de transformation du sulfataluminate de calcium (en tant que indice concernant la vitesse des processus chimiques des systèmes liants) mettent en évidence un comportement différencié des masses sulfataluminate-silicate en fonction de la teneur en C_3S et $C_4A_3\bar{S}$ (fig. 1—4).

Les courbes de la figure 1, ainsi que celles de la figure 2, où on a représenté l'évolution du degré de liaison de l'eau (en rapportant la valeur déterminée pour 1, 3 et 7 jours à la valeur de l'eau chimiquement liée après 28 jours), en fonction de la teneur en C_3S, mettent en evidence le caractère de la dépendance du degré de liaison de l'eau des caractéristiques compositionnelles du système anhydre et par conséquent du système liant durci : les processus d'hydratation se développent plus intensément avec la liaison des quantités plus élevées d'eau dans les compositions plus riches en sulfataluminate (I) et moins intensément dans les masses ayant une teneur plus élevée en C_3S (III, IV).

Pour toutes les masses, l'allure des courbes de la figure 1 suggère l'existence, peut-être, après une période négligeable d'induction, de deux étapes de développement des processus d'hydratation :

— une étape d'accroissement poussé de la quantité d'eau chimiquement liée (jusqu'à 3 jours), par suite du développement intense des interactions chimiques et

— une deuxième étape, d'accroissement lent de la quantité d'eau chimiquement liée, déterminé par le développement à une vitesse plus petite des processus d'hydratation (3—28 jours).

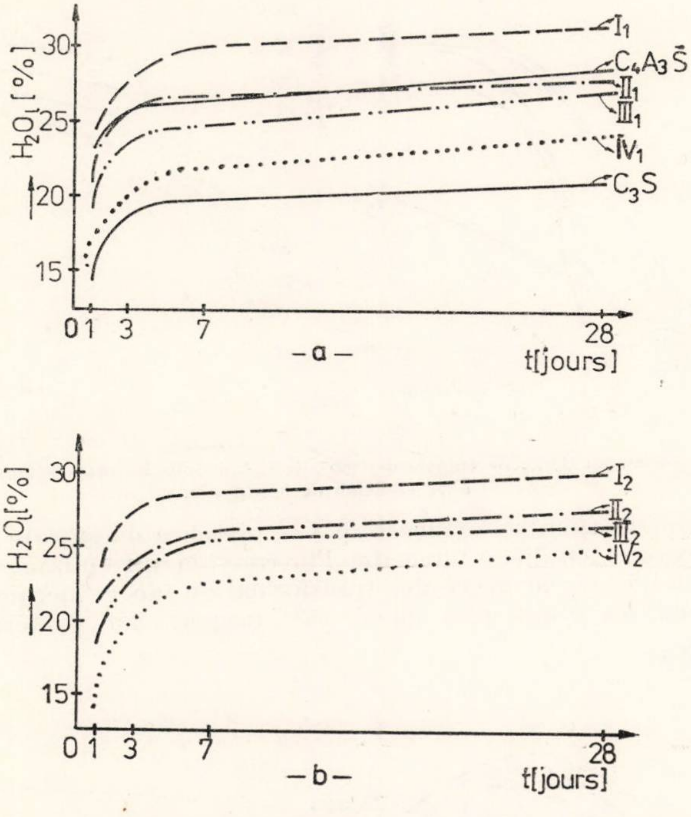

Fig. 1. — Evolution de l'eau chimiquement liée pour les masses sans gypse (a) et avec addition de 5% gypse (b).

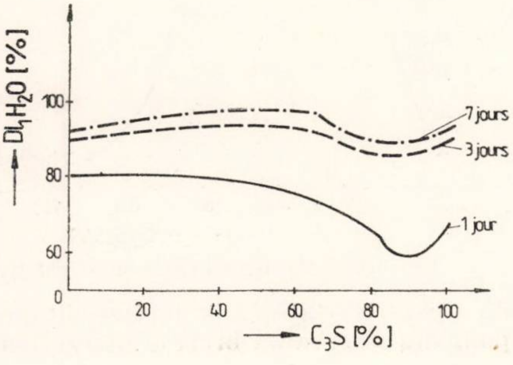

Fig. 2. — Evolution du degré de liaison de l'eau, en fonction de la teneur en C_3S.

Tout en considérant que l'interaction $C_4A_3\bar{S} + H_2O$ ait un rôle important pour l'évolution des processus de durcissement des systèmes sulfataluminate-silicate, on a réalisé les représentations des figures 3–4.

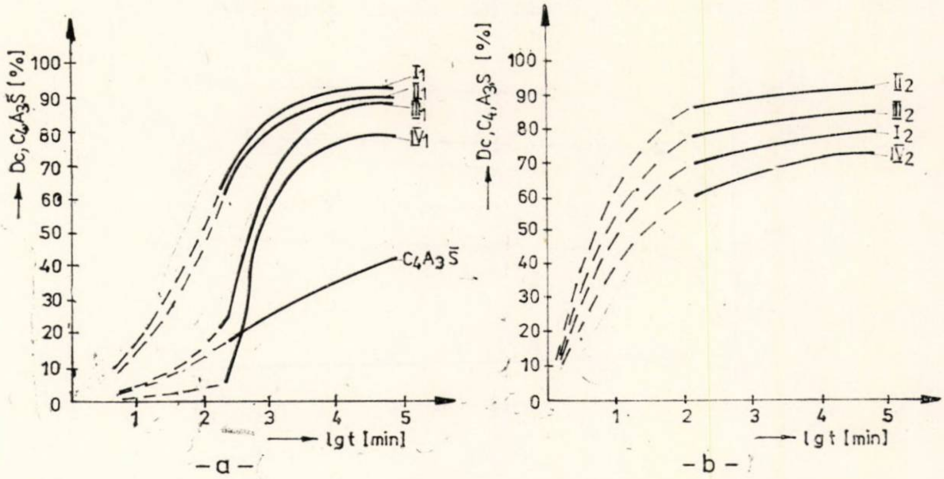

Fig. 3. — Evolution du degré de transformation de $C_4A_3\bar{S}$ pour les masses sans gypse (a) et avec addition de 5% gypse.

Ces dernières mettent en évidence que la présence du silicate tricalcique dans les masses étudiées intensifie l'interaction du sulfataluminate de calcium avec l'eau, le degré de transformation de ce dernier dans les systèmes mixtes étant plus élevé par rapport au système binaire $C_4A_3\bar{S} + H_2O$.

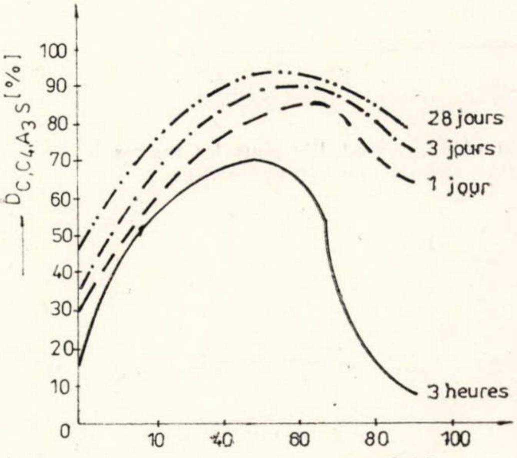

Fig. 4. — Evolution du degré de transformation de $C_4A_3\bar{S}$, en fonction de la teneur en C_3S du système.

On constate que l'influence du gypse sur le degré de transformation de $C_4A_3\bar{S}$ des systèmes mixtes étudiés est plus significative seulement pour des intervalles brefs d'interaction et surtout pour des systèmes plus riches en silicates (III et IV), où l'addition de 5% gypse favorise l'interaction avec l'eau de $C_4A_3\bar{S}$ (voir fig. 3b par rapport à 3a). Une influence semblable a été signalée antérieurement pour des masses du système $C_2S-C_4A_3\bar{S}-H_2O$.[7]

L'interaction avec l'eau du silicate tricalcique contenu dans les systèmes mixtes sulfataluminate-silicate est influencée, à son tour, par la présence du sulfataluminate de calcium qui imprime une cinétique plus lente aux réactions $C_3S + H_2O$, surtout quand il est contenu en proportions plus élevées dans le système liant (voir fig. 5).

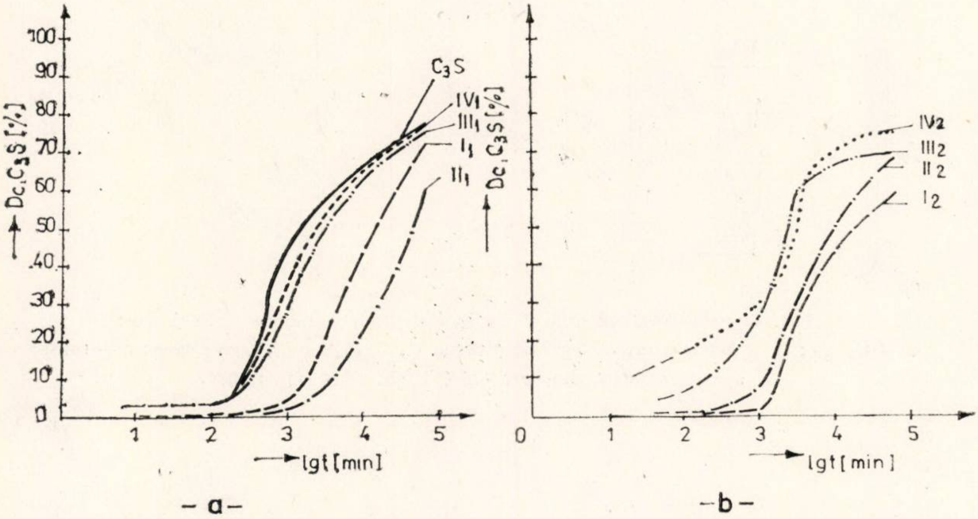

Fig. 5. — Evolution du degré de transformation de C_3S pour les masses sans gypse (a) et avec addition de 5% gypse (b).

Les analyses diffractométriques des masses I—IV, sans et avec addition de 5% gypse, durcies à des intervalles de temps différents (fig. 6—9) fournissent des renseignements concernant la nature des hydrocomposés formés et leur évolution, compte tenu aussi de la basicité du système. Elles mettent en évidence que la présence du silicate tricalcique favorise la formation de l'ettringite cristalline même à partir des stades initiaux des processus d'interaction (3 heures). Les interférences 9,5—9,6 Å, 5,5—5,6 Å, 3,8 Å visibles sur les diffractogrammes des systèmes mixtes après 3 heures d'hydratation et, qui pour le sulfataluminate de calcium hydraté durant une même période n'apparaissent que partiellement et à très faible intensité (fig. 6a) peut constituer un argnment dans ce sens.

Pour des intervalles plus grands d'hydratation, la teneur en ettringite cristalline des systèmes liants mixtes, estimée en fonction de l'interférence 9,5—9,7 Å, se réduit à cause de la transformation partielle en hydroalu-

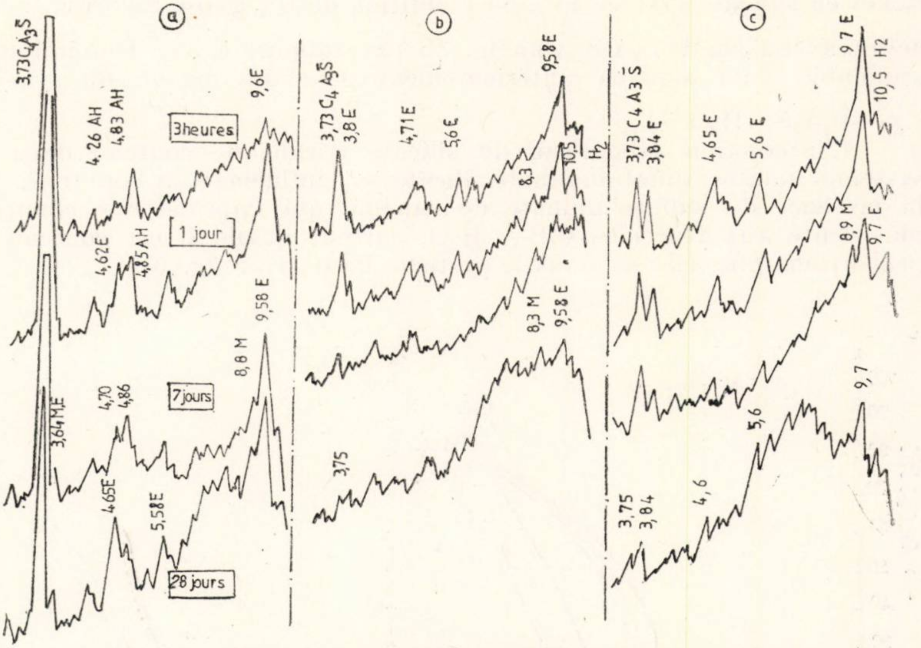

Fig. 6. — Diffractogrammes des liants durcis 3 heures — 28 jours : a — $C_4A_3\overline{S}$; b — masse à rapport gravimétrique $C_3S/C_4A_3\overline{S} = 1$, sans gypse ; c — masse ayant le même rapport $CaO/C_4A_3\overline{S}$, avec 5% gypse.

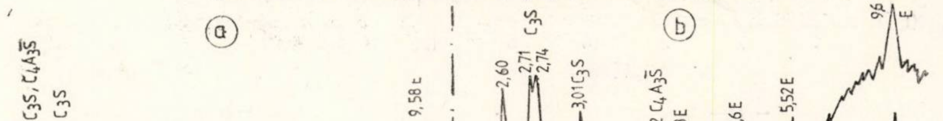

Fig. 7. — Diffractogrammes des liants à rapport gravimétrique $C_3S/C_4A_3\overline{S}=2$, durcis 3 heures — 28 jours : a — sans gypse ; b — avec 5% gypse.

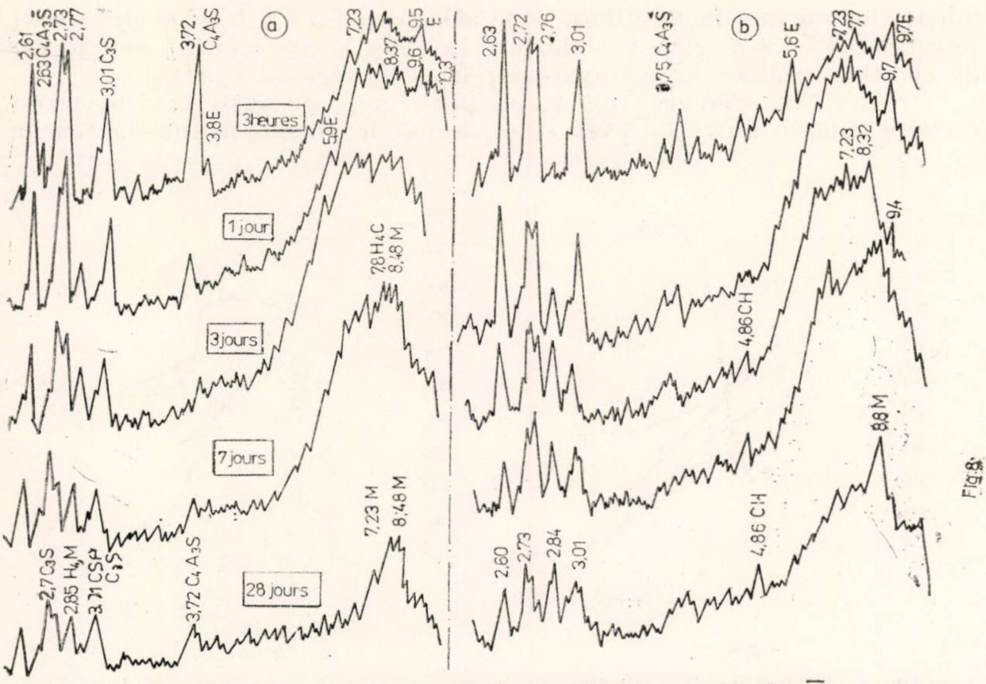

Fig. 8. — Diffractogrammes des liants à rapport gravimétrique $C_3S/C_4A_3\overline{S} = 3$, durcis 3 heures — 28 jours : a — sans gypse ; b — avec 5% gypse.

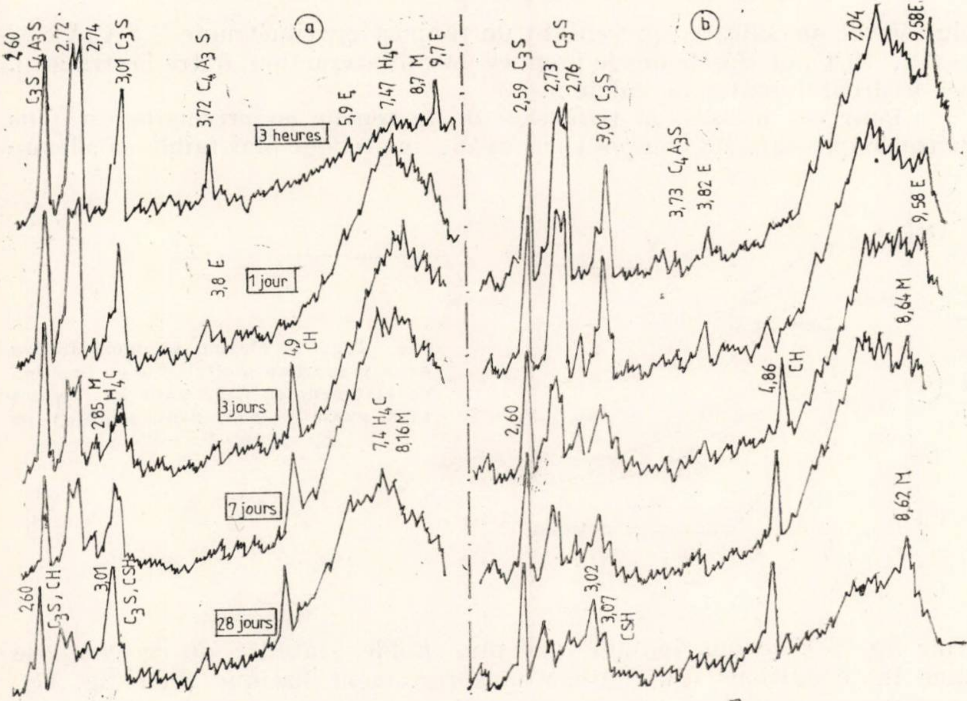

Fig. 9. — Diffractogrammes des liants à rapport gravimétrique $C_3S/C_4A_3\overline{S} = 10$, durcis 3 heures — 28 jours : a — sans gypse ; b — avec 5% gypse.

minate de calcium monosulfaté — 3 CaO . Al_2O_3 . $CaSO_4$. 12 H_2O (les interférences 8,3—8,8 Å, 2,85 Å — fig. 6b, 7a—9a), le cas échéant sous forme de solutions solides avec l'hydroaluminate hexagonal C_4AH_{13}.

Selon l'interférence 10,5 Å, on peut supposer aussi l'existence de certaines phases du type C_2AH_8. Dans le cas des masses ayant une teneur plus élevée en silicate (présentant un rapport gravimétrique $C_3S/C_4A_3\bar{S} = 3/1, 10/1$), on décèle dès le premier jour d'interaction, outre l'ettringite, des hydroaluminates de calcium.

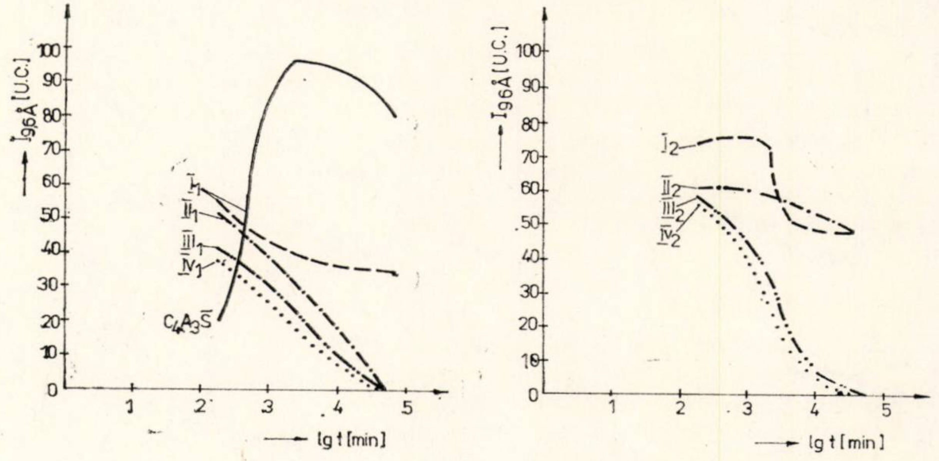

-a-

-b-

Fig. 10. — Evolution semiquantitative de la teneur en ettringite pour : a — masses sans gypse ; b — masses avec 5% gypse.

Pour ces masses, la réduction de la teneur en ettringite est plus marquée que dans les compositions ayant une teneur plus faible en silicate (voir fig. 10), ce qui indique une plus faible stabilité de ce composé dans les conditions d'un milieu plus fortement basique (voir fig. 11).

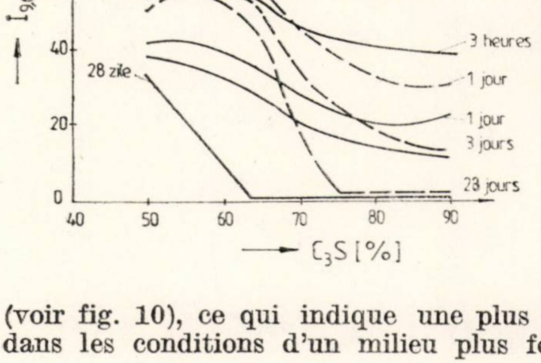

Fig. 11. — Evolution semiquantitative de la proportion d'ettringite en fonction de la teneur en C_3S, pour les masses sans gypse (—) et avec addition de 5% gypse (— — —).

Ce même phénomène est à retenir aussi pour des systèmes du type $C_4A_3\bar{S}-CaO-H_2O$.[6, 8]

L'addition de 5% gypse détermine, bien sûr, l'accroissement de la teneur en ettringite, surtout pour des intervalles d'hydratation plus brefs, tandis que cet accroissement est plus élevé pour les compositions plus riches en sulfataluminate (I et II) (voir fig. 6c, 7b, 9b et 10).

Dans le cas des masses très riches en silicate, on constate le même caractère instable de l'ettringite, qui se transforme intégralement après 28 jours en hydroaluminate monosulfaté (voir fig. 8, 9 et 10).

La présence des phases hydrosilicate qui résultent à la suite de la réaction du silicate tricalcique avec l'eau est difficile à mettre en évidence par des rayons Röntgen, pas tant à cause de leur faible cristallinité, surtout pour des intervalles brefs d'hydratation, qu'à cause de superposition des interférences spécifiques de ces phases (3,01—3,07 Å, 2,8 Å) avec des interférences des composés mieux cristallisés (C_3S, $CaCO_3$, hydrosulfataluminates).

En ce qui concerne les masses à haute teneur en silicate (IV_1 et IV_2) on décèle certe, après des périodes dépassant une journée, la présence de $Ca(OH)_2$, composé résultant du processus d'hydrolyse du silicate tricalcique (voir fig. 9 — les interférences 4,9 Å et 2,60 Å); dans les masses à une teneur plus faible en silicate, le calcium hydroxide résulte en plus faibles proportions et il est consommé dans le processus de formation des hydrosulfataluminates de calcium.

La nature et la proportion des produits d'hydratation, ainsi que la cinétique des processus d'interaction des systèmes sulfataluminate-silicate étudiés, constituent des facteurs décisifs dans leur comportement différencié au point de vue de leurs résistances mécaniques. Les courbes des figures 12—13 mettent en évidence l'influence sur les propriétés

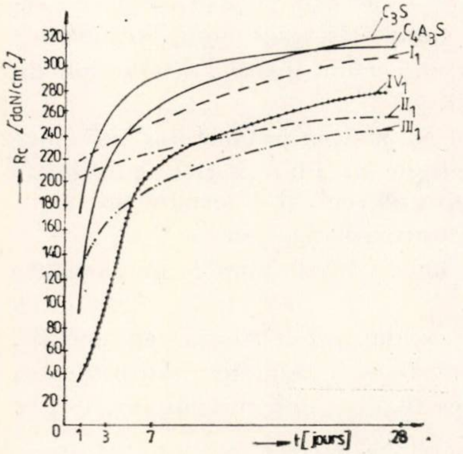

Fig. 12. — Evolution des résistances mécaniques des masses sulfataluminate — silicatiques.

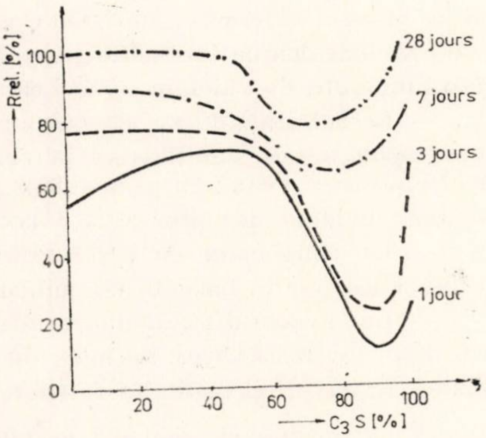

Fig. 13. — Evolution des résistances mécaniques relatives, en fonction de la teneur en silicate tricalcique.

mécaniques des masses liantes durcies, des caractéristiques structurales du système en corrélation avec la durée du durcissement. La figure 13 où sont représentées les résistances mécaniques des masses étudiées rapportées à la résistance du sulfataluminate de calcium durci pendant 28 jours, met en évidence l'existence d'un rapport gravimétrique optimum $C_3S/C_4A_3\bar{S}_1$ (égal à 1) pour les résistances mécaniques initiales (1 jour).

Pour des périodes de durcissement plus grandes, les résistances mécaniques diminuent un peu avec l'accroissement de la teneur en C_3S jusqu'à des valeurs du rapport gravimétrique $C_3S/C_4A_3\bar{S}$ égal à 1 ; pour des valeurs plus élevées du rapport mentionné, la diminution est sensible, avec la mise en évidence d'un minimum déplacé vers des rapports $C_3S/C_4A_3\bar{S}$ d'autant plus petites que la période de durcissement est plus grande.

L'évolution des résistances mécaniques par rapport aux caractéristiques compositionnelles du système liant est bien en corrélation avec la dépendance du degré de transformation de $C_4A_3\bar{S}$ et du degré de liaison de l'eau, en fonction de la basicité du système (fig. 2 et fig. 4) ce qui démontre le rôle essentiel de la vitesse de formation et la proportion d'hydrosulfataluminates de calcium, en particulier l'ettringite, pour les propriétés mécaniques de ces systèmes surtout pour des périodes brèves de durcissement.

4. CONCLUSIONS

Les renseignements obtenus dans le présent travail conduisent aux conclusions suivantes :

— Les processus d'interaction du système $C_3S-C_4A_3\bar{S}-H_2O$ decoulent à vitesse différente, fonction des caractéristiques compositionales ; le silicate tricalcique intensifie jusqu'à un certain degré l'interaction du sulfataluminate de calcium avec l'eau.

— Le sulfataluminate de calcium, en petites proportions influence d'une façon moins significative la cinétique de l'interaction du silicate tricalcique avec l'eau ; en proportions plus élevées, il détermine un ralentissement évident des processus d'hydratation-hydrolyse de C_3S.

— La conversion de l'ettringite en hydroaluminate monosulfaté est favorisée par la basicité du milieu.

— Les hydrosulfataluminates de calcium, l'ettringite en spécial, favorisent les résistances initiales du système durci ; les hydrosilicates influencent favorablement les résistances finales. Par conséquant, il y a des valeurs optimes du rapport gravimétrique entre $C_4A_3\bar{S}$ et C_3S, dans le système envisagé, au point de vue des résistances mécaniques après durcissement.

BIBLIOGRAPHIE

[1] P. P. Budnikov, .I. V. Kuznetsova et V. G. Saveliev, *Silikattechnik*, **16**, 414 (1965).

[2] P. K. Mehta, *Zhur. Amer. Ceram. Soc.*, **56**, 315 (1973).

[3] I. V. Kravcenko, I. V. Kuznetsova et B. V. Kliusov, *Tsement*, **8**, 7 (1978).

[4] K. Ykeda et V. Yamaguchi, « Ciments aux $C_4A_3\bar{S}$ et C_2S », 7e Congrès de la Chimie des Ciments, vol. 2, Paris, p. III/31, 1980.

[5] I. Teoreanu et M. Muntean, *Cement and Concrete Research*, **13**, 711 (1983).

[6] I. Teoreanu et M. Georgescu, « Processes in the Systems $C_4A_3\bar{S}$ — CaO—$C\bar{S}H_2$—H_2O », à paraitre dans la revue *Il Cemento*.

[7] I. Teoreanu, M. Georgescu et C. Chiricâ, « Hydratation und Erhärtungsvorgänge in C_2S—$C_4A_3\bar{S}$—H_2O Systemen », vol. 1, IBAUSIL 10 — Weimar RDG, p. 202 (1988).

[8] I. Teoreanu et M. Georgescu, « Procese de hidratare și întărire în sisteme $C_4A_3\bar{S}$ —CaO— —$C\bar{S}H_2$—H_2O, în corelare cu mediul de conservare », CONSILOX 5, Timișoara, Roumanie, 1988.

Revue Roumaine de Chimie, 34, *2*, 661–666 (1989)

CHARACTERIZATION OF COMPLEXES FORMED BY CHROMIUM BASIC SALTS WITH NATURAL AND SYNTHETIC TANNING POLYPHENOLS

VIORICA TRANDAFIR[a], MINODORA LECA[b] and CRISTINA MANDRAVEL[b]
[a]Leather and Footwear Research Institute, Bucharest
[b]Polytechnic Institute, Faculty of Chemical Technology, Department of Physical Chemistry, Bucharest

Received October 5, 1988

A new type of tanning material, named cromtan, was obtained by complexing the polyphenols from oak tanning extract and synthetic tanning materials (sintans) with chromium basic salts. It is used for retanning rarely structured skin, which represents a superior revaluation of the native oak extract. The new complex was characterized by quantitative chemical analysis, gel permeation chromatography on Sephadex G 25 and IR spectroscopy.

INTRODUCTION

The vegetable tanning materials are a class of compounds that have the property of tanning animal skin to which they impart stability in time to micro-organisms and to some physico-chemical agents and mechanical forces.

They are polyphenol derivatives with two or three adjacent hydroxyl groups (similar to pyrocatechin or to pyrogallol) at least in regard to one of the aromatic nuclei. The phenolic hydroxyl groups stand for 15–30% of the molecular weight of the tanning material.[1]

The tanning materials from plants (oak, quebracho, chestnut, mimosa-bark and wood) have a polydisperse nature, due especially to the size of the tanning particles and of the non-tanning compounds (organic acids, simple phenols, etc.).

The native tanning extract from oak wood and bark is a composite pyrogallolic and pyrocatechinic tanning material or, following another classification, able to undergo hydrolysis and therefore a condensate. In the pyrogallolic tanning materials the esteric or glycosidic type of bonds prevail and in the catechinic ones, the covalent C–C type of bonds, which are more resistant.

The native oak tanning material has technologic properties (tanning properties) of lesser value than those offered by quebracho or mimosa extracts (exotic wooden species). This is due to their high proportion of high molecular weight particles and of insoluble substances specific to the oak wood. Therefore the oak extracted tanning particles have a reduced power to penetrate the skin resulting in a prolonged tanning time.

The synthetic tanning materials (sintans) were thought of as a substitute for the vegetable tanning materials or as auxiliary tanning materials due to their ability to disperse the particles of the vegetable materials. They are mono- or polynuclear sulphonic polyphenolic compounds.

The best tanning material can be obtained using phenol and naphthol (especially β-naphthol).[2] Their action as tanning agents and their tanning effect are determined by: their polyaromatic nature, the number and position of their hydroxyl groups, the presence and number of sulphonic groups, their colloidal nature, etc.

The benzenic nucleus in the tanning materials is polarized and therefore it is given affinity to collagenous protein in the skin. Due to their position the hydroxyl phenolic groups enhance the tanning characteristics of the tanning materials, bringing about inductive effect to the aromatic nucleus. For example, the tanning materials based on β-naphthol, *ortho*- and *para*-cresol are more active than those based on α-naphthol. Besides tanning materials with hydroxyl phenolic groups, tanning materials with sulphon-amidic groups are also used.

Unlike the vegetable tanning materials the synthetic ones contain aromatic monomers linked by many and different bonds : methylene, sulphone, sulphonamide, etc.

The molecular weight of the synthetic tanning materials is much lower than that of the vegetable ones, a fact that determines a much lower astringency, a higher dispersing power, a rapid and deep diffusion in the skin. That is why synthetic tanning materials are convenient to be used for dispersing the vegetable tanning ones.

The size and solubility of native oak tanning particles were modified using sintans of the naphthalenesulphonic type and better tanning properties were obtained.[3]

Small molecule polyphenols resulted from the reaction between the two tanning materials were used in this work as masking agent for chromium basic salts, currently used as mineral tanning material. A chelating complex, which is a new type of tanning material, was finally obtained. This new type of tanning material, named cromtan, is used for retanning rarely structured skin since it combines vegetable and mineral tanning characteristics.

EXPERIMENTAL

Cromtan was prepared using oak extract modified with a mixture of β-naphthalenesulphonic and phenol-sulphonic sintans as atomized powder (pulvis) having the following characteristics:

— dry substance	94.58 %
from which:	
— tanning substances	53.9 %
— ash	6.3 %
— non-tanning substances	37.0 %
— insoluble substances	2.9 %

The modified oak extract was characterized according to the size of the particles by means of fractioned precipitation with sodium chloride of different concentrations (STAS 6829/76). The results show the following: the percent of very large particles was reduced to a half as compared to the non-modified oak extract, whereas the percent of small particles was doubled, the latter representing ligands from chromium basic salts complex.

The chromium basic salt used contains 150 g/L of Cr_2O_3 and has a basicity of 30%. The cromtan complex is a viscous solution with the following characteristics:

— dry substance	33.0%
— Cr_2O_3	4.96%
— tanning substance	6.76%
— non-tanning substances (solubles)	20.73%
— pH = 3	

The cromtan complex can be atomized to a brownish-greenish powder. Both the components and the complex were characterised by chromatography on Sephadex G 25 gel, using 0.1 M potassium chloride as eluent, UV adsorption at 230 nm and IR spectroscopy within 4600—400 cm^{-1} range using IR 71 and IR 75 spectrophotometers.

RESULTS AND DISCUSSION

It was concluded that the best dispersing agents for the oak tanning extract are the synthetic tanning materials of the acid type with sulphoaromatic structure. Their dispersing action is probably due to the lyophilic exchange of tanning particles determined by factors as : the capacity of the tanning particles to adsorb sulphonic acid, the change of the acidity in the system, the peptizing of the particles and the effect of the electrolytes.[4]

The native oak tanning extract has a high percentage of high molecular weight particles. The sintan based on β-naphthalin-sulphonic acid has the best dispersing effect, due to the capacity the vegetable tanning particles have to adsorb the sintan, thus conferring them a more pronounced lyophilic character and to the chemical combinations between the two tanning materials that gives lyophilic particles less sensible to the coagulation action of the electrolytes (Figure 1). Gel chromatography on Sephadex G 25 shows that all three materials taking part in the formation of the cromtan complex are much more polydisperse as regards molecular weight distribution than cromtan (Figures 1 and 2).

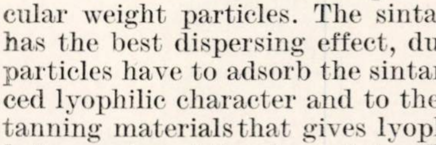

Fig. 1. — Gel permeation chromatograms on Sephadex G 25 using a 0.1 M solution as eluent: 1 — sintan; 2 — oak tanning extract; 3 — chromium basic salt.

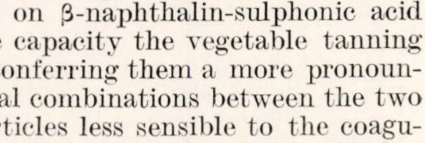

Fig. 2. — Gel permeation chromatograms on Sephadex G 25 using the same eluent as in Figure 1 for: 1 — liquid cromtan; 2 — atomized cromtan.

The components that pass through the gel chromatographic column after an elution volume of 340 mL are considered non-tanning substances (very small molecules). In Figure 2 the data for cromtan show a narrower distribution of the molecular weight of the particles in the system, having a molecular weight range of about 800—3000, with tanning characteristics. Therefore part of the non-tanning materials as well as small molecule polyphenols are trapped in the newly formed complex and act as binding agents (ligands). Atomized cromtan gives different chromatograms (Fig. 2), the percentage of high molecular weight particles (fraction 1—136 ml) is reduced, a common feature in materials that underwent atomization.

Then cromtan and the basic components were studied by IR spectrophotometry. IR spectra of the oak tanning extract, sintan, cromtan and chromium basic salts were run in the range 4600 400 cm^{-1} using IR 71 and IR 75 spectrophotometers.

For the first substance the spectrum was considered using only pellets in KBr ; for cromtan the IR spectra were obtained using two techniques : pellets of atomized product in KBr and using the aqueous solution, in the capillary layer between KRS-5 windows ; for sintan and the chromium basic salt the spectrum was determined only in the aqueous solution using the technique mentioned in Table 1.

Table 1

KBr oak extract pellets	Sintan aqueous solution	Atomized cromtan KBr	Cromtan aqueous solution	Chromium basic salt aqueous solution	Comments	Notes
3410blm	3970 fs	3400 blm		3300 bli	ν OH associated in dimer, trimer phenols	
2980 m	2980 u, s	2980 m	2960 bl, m	3400 u, m	ν OH associated in basic salt	
2370 u, s	2950 bl, m	2370 s	2370 u, s			
	1875 u, s					
1750 m	1700 s	1730 m	1725 s	1645 as, i		bl—wide band
1625 m		1680 m				
1525 m	1550 u, s	1580 u, m	1580 s			u—shoulder
		1550 u, m				
1450 m	1430 b	1525 m				as-asymmetric
		1475 m				
1375 m		1425 m	1425 s	1450 m		ν—valential type of vibrations
1325 m		1350 m	1325 s	1400 m		
		1200 i				i—intense
1190 m, u	1190 m	1150 i	1100 i	1100 i	νC—OH in phenols ν_3 SO_4^{2-} ion	m — medium s — weak
1050 i	1075 m	1050 i	1025 u, m	975 m	ν_1 SO_4^{2-} ion T_d	(i < 30 % T; 70 > m > > 30 % T; s > 70 % T)
	1030 m		975 u, s			
	925 s					
875 m		875 m				
825 m		825 m				
775 m		775 m				
750		750 m				
		690 u, m		620 i	ν_4 SO_4^{2-} ion	
		620 m				
		590 m			νCr—O	Specific for Cr—O in chromium complexes
		545 u, m				
		475 u, m				

The comparison between the oak tanning extract spectrum and that of the sintan shows great similitude in the regions 2900–3400 cm^{-1} and 1800–700 cm^{-1}. There appear bands characteristic of: hydroxyl groups intermolecularly associated in phenols at 3410 cm^{-1}, ν C=O frequency at 1190 cm^{-1} (the most intense band in sintan), the vibration ν C–C in the benzenic ring in the range 1450–1600 cm^{-1}, ν C=O frequency at 1700 cm^{-1}, very weak in sintan and at 1750 cm^{-1} respectively, of medium intensity in the oak extract, the ν C–O vibration at 1050 cm^{-1}, prevailing in the oak extract, and of medium intensity and shifted position in sintan, due to benzenic rings condensed by means of C=O bonds in the large molecules of natural extracts. Considering the literature data[5 6] these characteristics show that the oak tanning extract as well as the sintan contain phenols, dimers, trimers, etc., and polyphenols, carbonil groups grafted on the aromatic ring in the oak extract and bound to the methylene chain in the sintan. Characteristic frequencies for sulphate ion appear on chrome basic salt spectrum, in T_d sorrounding: 1100 cm^{-1} (ν_3) intensive, 975 cm^{-1} (ν_1) medium, 620 cm^{-1} (ν_4) intensive, 3300 and 1645 cm^{-1} corresponding to the complex hydroxyl groups,[7] respectively.

One of the common tests to determine the centre of coordination when interpreting the IR spectra of complexes, is the shift of valence vibrations that are specific to the ligands molecules, molecules which have more donor atoms or groups, phenolic and cetonic groups, in which case the maximum of specific absorption bands shifts in opposite directions.

Changes in intensity of valence vibration and deformation in the ligands are also of importance for coordination.

Another test on coordination reveals the presence of other new absorption bands that are characteristic of M-ligand or M–M bonds.[7]

With the IR spectrum of aqueous solution of cromtan, the band of sulphate ion in tetrahedral symmetry at 110 cm^{-1}, prevailing in intensity, has a complex shape with shoulders at 1025 and 975 cm^{-1}. The first has the maximum shifted to lower frequencies than that of sintan and oak tanning extract. The spectrum shows another band of lower intensity at 1580 cm^{-1} that certifies conjugation of the aromatic rings in phenols with substituents.

In the IR spectrum of the atomized cromtan, the most intense band is positioned at 1150 cm^{-1} followed by the intense one at 1050 cm^{-1}, a fact demonstrating that, as in the case of the chromatogram on Sephadex gel, some changes in the complex conformation due to the removal of water by atomizing take place; the more compact structure leads to a lower molecular weight. Figure 3 shows a comparison

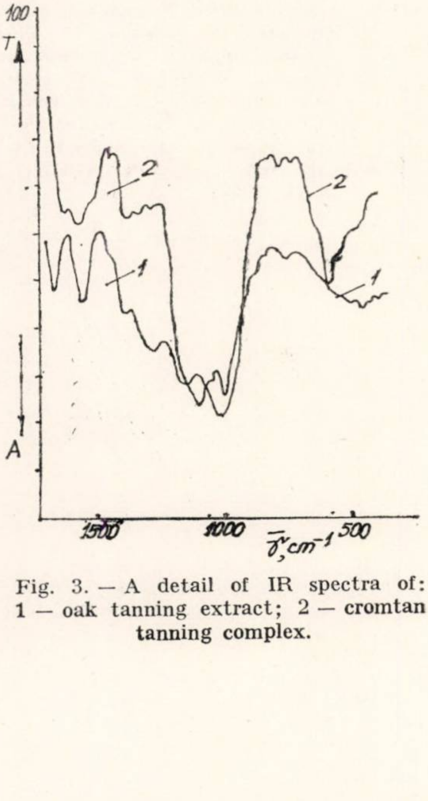

Fig. 3. — A detail of IR spectra of: 1 — oak tanning extract; 2 — cromtan tanning complex.

between a detail of this spectrum (2) and that for the oak extract (1). It can be asserted that in cromtan the basic components of the oak extract are coordinated around chromium ion. This statement is supported by the shift of the characteristic frequency ν C—OH in phenols, to frequencies higher by 40 cm^{-1}, this shift being correlated to the change in intensity ratio of the spectrum as compared to the band situated at 1050 cm^{-1}, and considering the 10 cm^{-1} shift towards lower frequencies of the position of the maximum in the absorption band ν OH valential 3400 cm^{-1}. The band corresponding to the aromatic carboxyl group from the oak extract at ν C=O 1750 cm^{-1} also shifts to lower frequencies in cromtan with $\Delta\nu = 20$ cm^{-1} that indicates the coordination of the above group. There also appear some shoulders on the specific band of the sulphate ion from the small wave length region at 620 cm^{-1}, namely 545 and 475 cm^{-1}. Having in view the literature on vibration ν M—O in the trioxalatochromic complex positioned at 543 cm^{-1} and the oak extract spectrum in this region, the shoulder at 545 cm^{-1} is possibly said to correspond to this vibration Cr—O in cromtan.

The chromatographic study, the data on chemical analysis (that show a ratio Cr : tanning material of 2 : 1 . . .2), and the IR spectra have demonstrated the formation of a chelatic complex between chromium and natural and synthetic polyphenols, time resistant for pH up to 5.5, a functional region for this complex used as retanning agent.

REFERENCES

[1] K. Venkataboopathy and K. K. Redly, *Leather Sci.*, **5**, 171 (1982).

[2] S. I. Trahtenberg, *Technologya legkoy promishlennosti*, **2**, 65 (1986).

[3] V. Trandafir, S. Simache, D. Vidu and G. Zăinescu, *Industria Ușoară*, **35**, 487 (1985).

[4] K. Venkataboopathy, V. S. Sundara and T. Viyayarama, *Leather Sci.*, **4**, 21 (1981).

[5] S. Bădilescu, M. Toader, M. Giurgiuca and V. Tălpuș, "Spectroscopia în IR a polimerilor și auxiliarilor", Editura Tehnică, București, 1982.

[6] N. B. Colthup, L. H. Daly and S. E. Wiberley, "Introduction to Infrared and Raman Spectroscopy", Academic Press, New York, 1975.

[7] K. Nakamoto, "Infrared Spectra of Inorganic and Coordination Compounds", Wiley, New York, 1964.

Revue Roumaine de Chimie, 34, 2, 667–681 (1989)

PROSPECTS FOR I.R. LASER APPLICATIONS IN CHEMICAL TECHNOLOGY

I. URSU, R. ALEXANDRESCU, I. MORJAN, I. N. MIHĂILESCU, C. GRIGORIU
Central Institute of Physics, Bucharest, Romania

A. M. PROKHOROV, V. I. KONOV and YU. N. PETROV
Institute of General Physics of the Academy of Sciences of the USSR, Moscow

Recived November 14, 1988

New results concerning laser induced chemical processes in different media and their potential technological applications are presented. Examples are given on laser homogeneous chemical synthesis of high purity compounds such as reagents, ceramic powders, polymers, etc. In laser purification and substance separation methods heterogeneous interface processes are playing a dominant role. An overlook on the mechanism of some laser induced chemical reactions and process kinetics is also given.

INTRODUCTION

Laser applications in chemical technology were initiated and developed together with the improvement and dissemination of laser sources. A new and dynamic interdisciplinary research field has thus evolved, aiming to : (i) the synthesis of materials by laser chemical processing ; (ii) the study of fundamental problems connected with physical phenomena (as e.g. laser energy absorption, excitation and multiphoton dissociation, surface induced polarization, etc.) [1–4].

The potential applications of lasers in chemical technology requires the knowledge of many complex chemical and physical processes involved in the effect of laser radiation on substances.

Chemists are well acquainted with the fact that light may affect the course of some chemical reactions.

Since Einstein's stimulated emission principle materialized, lasers with emission in varied spectral ranges, from UV and visible down to the IR regions were made available for applications. Characteristic of the laser radiation sources are the emission of a controlled quantity of energy, which allows for the control of the induced photochemical processes ; the emission in a well-defined spectral range, so that the radiation is absorbed by molecules with resonant spectral response to laser radiation ; and finally, the coherence and high intensity, which allows for nonclassical heating of substances, and feed-back reactions.

A special position in the field of laser applications is held by the lasers with medium infrared emission (at 10.6 μm), i.e. the CO_2 lasers (photon energy – 0.11 eV). CO_2 lasers are currently the most advanced technologically and show an even larger area of applications. Among their characteristics are a high quantum efficiency and versatility in both continuous wave and pulsed operation, with powers and energies in the order of kW and J, respectively. From the standpoint of photochemistry, CO_2 lasers have originated a new chemistry branch — the vibrational chemistry, based on molecular vibrational excitation by the absorbed light quanta.

Physical-chemical processes stimulated by laser radiation can be divided in : A — homogeneous processes, which take place in gaseous media, surrounded by surfaces, B — processes at the surface of solid substances and C — heterogeneous processes, at the gas-solid and liquid-solid interfaces.

A. HOMOGENEOUS PROCESSES IN GASEOUS MEDIA

Laser activation of chemical reactions in gaseous media is based on : photolytic mechanisms (photochemical), and/or pyrolytic mechanisms (photothermal), which may either concur, or follow each other in contributing to the reaction.

In photolysis, the constituents are in nonequilibrium states. Dissociative states may be reached, ensuing with species selectivity and radical formation. In pyrolysis fast thermalisation of laser excitation occurs, resulting in homogeneous gas heating [12].

Laser pyrolysis has a tremendous potential for applications in chemical technology. Some features of laser pyrolysis are : (1) fast local heating, without unwanted heated wall effects (contaminated) ; (2) the achievement of states with vibrational temperatures higher than the surrounding gas, providing for chemical processes with high activation barrier, followed by chemical kinetic selectivity among the products ; (3) the molecules which accept laser energy are vibrationally excited and transfer the received energy to the gaseous media by collisions ; the acceptor may be a sensitizer which is inert against the chemical reaction.

This paper will follow the classification above. As examples of laser homogeneous reactions in gases, we shall present laser pyrolysis of the mixture $SiH_4 + NH_3$ with silicon nitride formation [1], and also, laser multiphoton dissociation of SiH_4 in the presence of methyl methacrylate [2, 3].

Laser thermochemical reactions induced in solids in powder form will be illustrated by the laser decomposition and dehydration of $MnCO_3$ and H_3BO_3 respectively [5, 7].

In the last category, of laser processes induced at the interface of heterogeneous media, we shall include liquid-solid interface processes, like concentration modifications induced in uranyl aqueous solutions at the contact with a solid surface [4]. Finally, we shall emphasize the gas-solid interface processes, focusing on the substance separation through induced polarization in metal capillaries [6, 8].

A.1. Laser pyrolysis : ultrafine silicon nitride powder obtained by laser irradiation of gaseous silane and ammonia mixture

It is known that ceramic powders (like silicon nitride) are the precursors of ceramic materials. In a Si_3N_4 ceramic sintering process, the densification qualities are favoured if the initial powders are of high purity, also showing fine grains and a homogeneous distribution of diameters.

The mechanism of the laser reaction with silicon nitride formation, which may be expressed as

$$3\ SiH_4(g) + 4\ NH_3(g) \xrightarrow{h\nu} Si_3N_4(s) + 12\ H_2(g)$$

is most probably based on some successive steps [5].

Initially there is radiation absorption by reactant gases. It is known that NH_3 as well as SiH_4 absorb laser radiation. The greatest absorption occurs in the ν_4 mode of SiH_4 for the P(20) laser line (10.59 μm) (see Fig. 1).

By radiation absorption and thermalisation of the initial excitation, high local temperatures are reached, which bring the silane in highly excited and/or dissociative states. Radicals are formed, followed by dimolecular reactions among decomposition products.

The nucleation and particle growth from gaseous phase is the final step in the process of silicon nitride laser — synthesis.

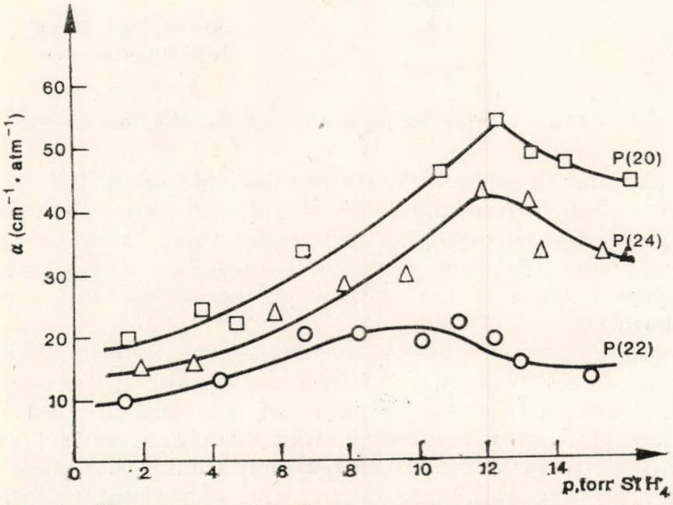

Fig. 1. The pressure dependence of the absorption coefficient α ($cm^{-1} \cdot atm^{-1}$) of silane for different laser emission lines in the 10.4 μm band of the CO_2 laser. The greatest absorption occurs for the P(20) line.

The main parts of the experimental installation for Si_3N_4 production in a continuous-flow system are : a vacuum and flowing gas system, with gas feeding device ; the reaction chamber (Fig. 2) ; and a 25 W cw CO_2 laser as radiation source.

The vacuum system also ensures a permanent gas flow during irradiation.

In the reaction chamber [6], the reactant gases (premixed silane and ammonia gases at known concentrations) enter through a nozzle (approx. 2 mm in diameter) and intersect at a right angle the laser beam. The spatial confinement of reactant gases and of the formed powders during the reaction is achieved by injecting an inert gas (Ar), through a coaxial tube and through two lateral inlets placed in the vicinity of KCl cell windows which close the ends of the cell arm. Long-life operation of the windows was ensured by protecting them from unwanted nitride powder deposition. The laser effect was amplified by backward reflection and focalization via a curved mirror placed at one end and outside the reaction chamber.

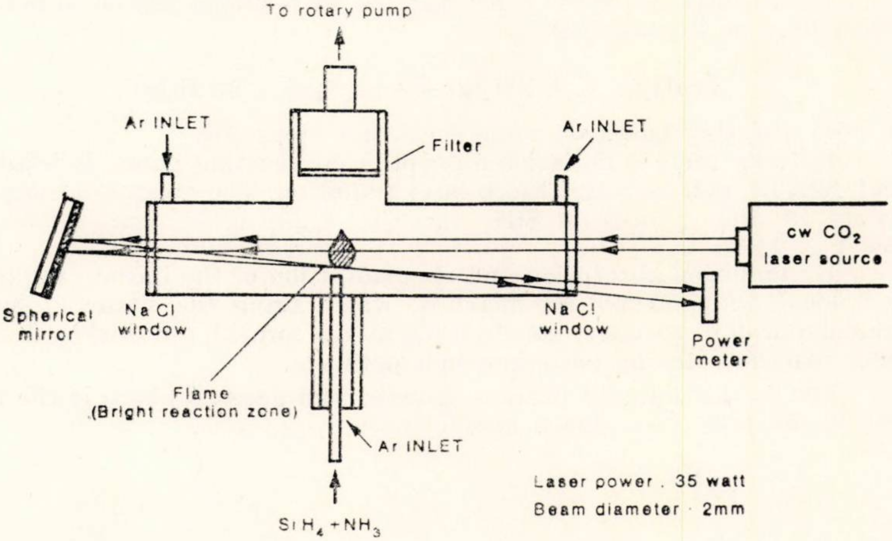
To rotary pump
Ar INLET
Filter
Ar INLET
cw CO_2 laser source
Spherical mirror
Na Cl window
Na Cl window
Power meter
Flame (Bright reaction zone)
Ar INLET
Laser power . 35 watt
Beam diameter 2mm
$SiH_4 + NH_3$

Fig. 2. — Reaction chamber for laser synthesis of silicon nitride powder.

The silicon nitride powder formed in the reaction bright flame in the center of the cell was collected in a microporous filter, perpendicularly to the laser beam, in the sense of pump suction and gas flow.

The installation allows for: concentration control (in time and space); temperature control of the reaction zone — by space confinement of reactant gas flow and laser beam; and also composition, dimensions and morphology control of the formed powders.

The parameters which affect the reaction and reaction products were found to be the relative concentration of the components, the total pressure in the reaction chamber and, most of all, the flow values of silane and ammonia (Fig. 3).

The significant increase in the absorbed laser energy with the active gas flow will allow for scaling up the process by circulating more important flows, and also by using a laser of higher average power.

Transmission electron microscopy of the silicon nitride powder obtained by laser processing showed a spherical shape of particles, with narrow range of diameters ($\Phi = 150-250$ Å). It is probable that the chain-agglomerates have not an internal microstructure.

It is worth mentioning some of the advantages of the laser technique of silicon nitride powder production, like the positive energy balance (the reaction temperature is sustained by the reaction exothermicity and by the minimized losses obtained by argon confinement) and also the good productivity (expressed by the quantity of reacted silane, which exceeds 90%).

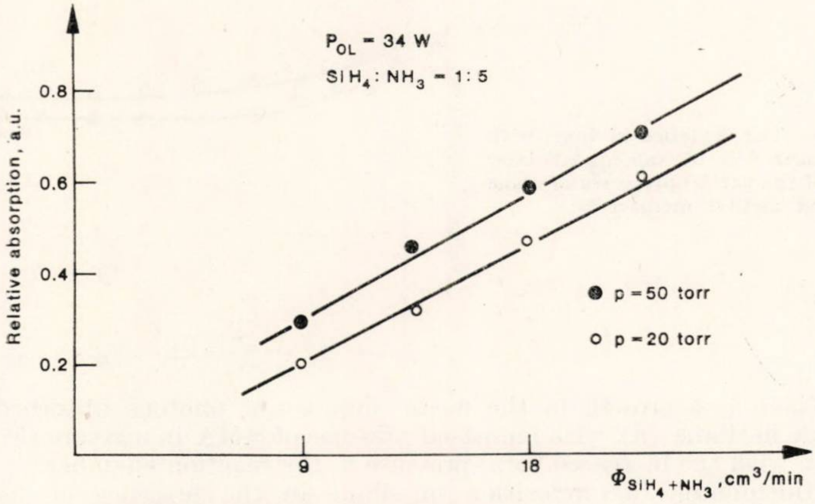

Fig. 3. — The dependence of the absorbed laser energy on the mixture SiH_4 + + NH_3 flow (for two values of total pressure in the reaction chamber).

Characterization studies of silicon nitride powders obtained by laser synthesis (morphology, composition stoichiometry, etc.) will be developed in connection with the basic parameters which govern the processes.

A.2. Laser multiphoton dissociation: silane decomposition in the presence of methyl methacrylate (MMA) with siloxane polymer deposition

The goal of this research was to get films of silicon-containing polymers (with application in encapsulation, membrane preparation, dielectric coatings, etc.) [7] and also to study the mechanism of infrared decomposition of silane, which is not yet well understood [8, 9].

The experimental device mainly consists of a pulsed CO_2 laser (frequency repetition rate of $f \sim 2$ Hz, energy per pulse — 5 J, pulse duration — 100 ns) and a reaction chamber filled with SiH : MMA (1 : 1 concentration, total pressure 20—35 torr).

The analysis and control methods of laser-induced reaction were IR spectrophotometry and mass spectrometry. Using these methods, the time evolution of reactant and reaction products relative concentration was monitored.

The mixtures were irradiated with 5,50 and 100 pulses, and changes in their composition were monitored.

The depletion in time, with the number (N) of laser pulses, of the partial pressures of silane and methyl methacrylate (Fig. 4) shows that the laser induced reaction proceeds much faster during the first pulses with a yellow luminescence [8].

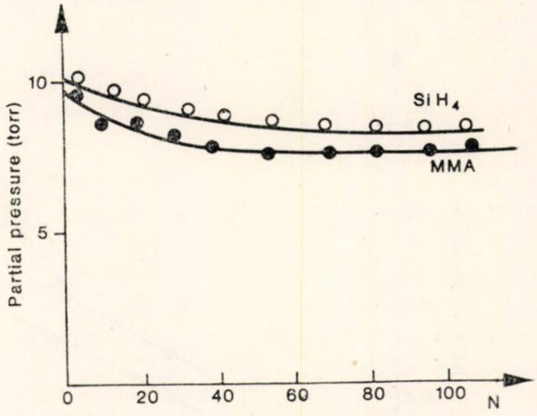

Fig. 4. — The depletion in time, with the number (N) of subsequent laser pulses, of the partial pressures of silane and methyl methacrylate.

There is a growth in the mean number of photons absorbed per molecule in silane ($\vec{n}$), with increased pressure of MMA in mixture (Fig. 5), but also with the increased total pressure in the reaction chamber.

Multiphoton decomposition of silane in the presence of methyl methacrylate leads almost exclusively to an organosiloxane polymer formation (brown coloured), which is deposited on the whole inner surface of the cell. The deposit is growing with the number of pulses (up to 5—8 μm thickness).

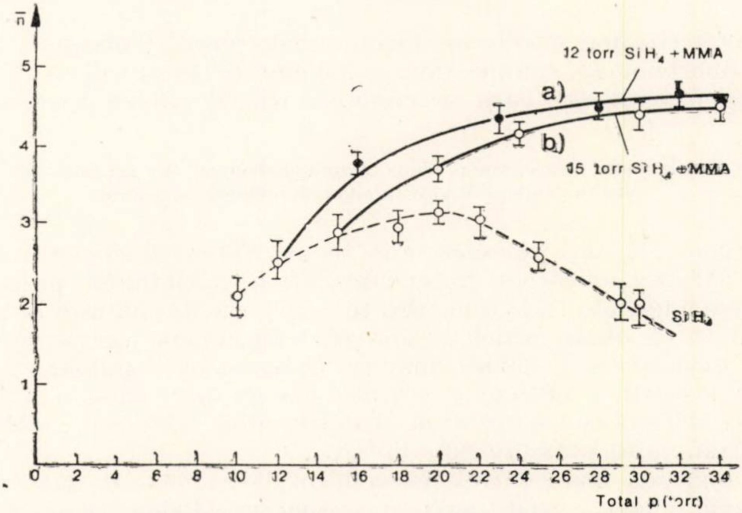

Fig. 5. — The dependence of the mean number $\bar{n}$ of photons absorbed per SiH_4 molecule with increased MMA pressure in the mixture. For comparison, the dotted curve shows the pressure dependence of $\bar{n}$ in pure silane.

Small amounts of volatile compounds resulted from reaction (methane, butenes, carbon monoxide) were also monitored by mass spectrometry technique.

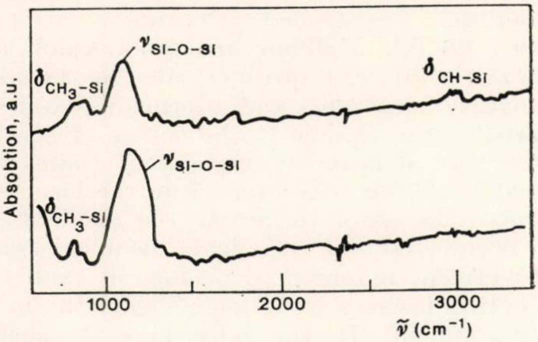

Fig. 6. — The IR spectrum of the deposited siloxane polymer.

From IR spectral analysis (Fig. 6) and XPS (X-ray photoelectron spectroscopy) analysis, the formed polymer structure has most probably as basic unit :

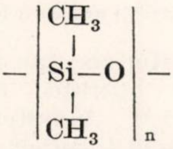

$$-\left|\begin{matrix} CH_3 \\ | \\ Si-O \\ | \\ CH_3 \end{matrix}\right|_n-$$

The mechanism of the laser-induced and driven reaction in the mixture $SiH_4 + MMA$ can be explained through an initial silane decomposition by a multiphoton process with silylene releasing :

$$SiH_4 \xrightarrow{nh\nu} SiH_2 + H_2,$$

followed by the addition of SiH_2 radical to the double bond of MMA and the adduct decomposition with siloxane polymer formation. To mention also the possible development — at high SiH_4 partial pressures of the process of Si formation and deposition :

$$SiH_4 \rightarrow SiH_2 \rightarrow Si$$

The research concerning silicon-blended polymer deposition by laser-induced chemical reactions are in line with up-to-date silane processing techniques aiming to obtain thin films (of silicon, amorphous hydrogenated silicon, silicon dioxide, silicone carbide and nitride, etc.) with outstanding applications in the field of surface processing for microelectronic devices.

B. CHEMICAL PROCESSES STIMULATED AND DRIVEN BY LASERS AT SOLID SURFACES : DECOMPOSITION AND DEHYDRATION THROUGH LASER-INDUCED THERMOCHEMICAL REACTIONS IN SOLID INORGANIC POWDERS

The dynamics of laser thermochemistry is affected by many interrelated factors among which the rather fast variation in temperature, which strongly influences the reaction kinetics and also the reciprocal influence of chemical and thermal freedom degrees of the process [15], [19]. Consequently, the main features of the laser thermochemical processes are the local thermal action, high thermal gradients, the control of the process dynamics by laser power variation (focusing and collimating conditions, controlled atmosphere, etc.), reaction kinetics peculiarities and, finally, feedback reactions which establish themselves and evolve in the absorbant medium, due to the absorptivity (at the laser wavelength) of reactants and intermediate and final products. This last characteristic may change in the course of the induced chemical reaction [10]. The goal of laser decomposition studies was to obtain high purity compounds taking advantage from the laser light which is a "clean" heating source. In order to clarify the similarities and differences between the laser-assisted and "classical" chemical reactions a comparative study was performed, in order to decide, in each case, the advisability of implementing laser-assisted technologies in the laboratory or in the industrial environment. In the followings we shall briefly outline some results [10, 15].

B.1. Manganese oxide (Mn_3O_4) and boron oxide (B_2O_3) obtained by laser decomposition of manganase carbonate ($MnCO_3$) and boric acid (H_3BO_3), respectively

The irradiation of raw materials was performed with the aid of a cw CO_2 laser source, which was operated on the P(20) (944 cm^{-1}) line, at an output power of $P = 25$ W. A system for material recirculation and homogeneous heating was used together with a system for deflection, focusing and measurement of the laser beam (Fig. 7).

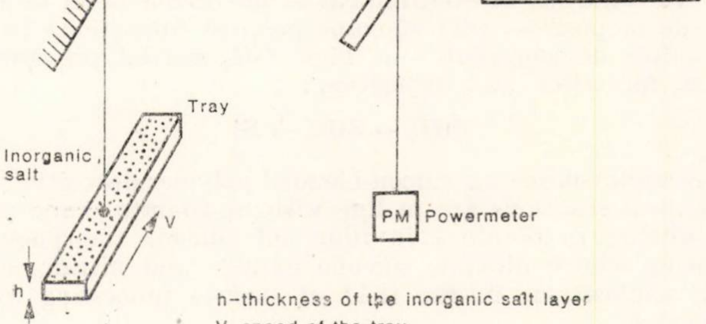

Fig. 7. — The experimental arrangement for laser decomposition of inorganic salts.

The determination of the conversion factor C and of the dependence $\log(\mathrm{d}C/\mathrm{d}t)$ on $\log C$ for $MnCO_3$ conversion to Mn_3O_4 (Fig. 8) shows that for a laser-driven reaction the process implies two elemental steps (I and III on the curve in Fig. 8) coupled by a complex intermediary region.

Table 1 summarizes some features derived from the performed study comparing laser kinetics with controlled heating kinetics [11]. Thus, at $MnCO_3$ decomposition, there are significant differences between reaction orders in the first and the second reaction steps. Also, at H_3BO_3 decomposition, one notices that laser dehydration is a unique stage process

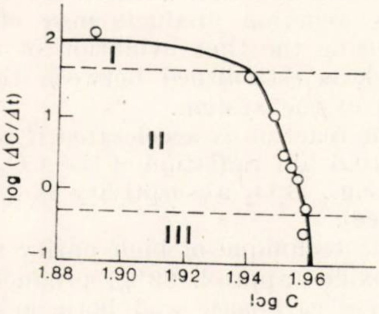

Fig. 8. — The plot of $\log(dC/dt)$ against $\log C$ as derived from the time dependence of the conversion factor C of $MnCO_3$ to Mn_3O_4.

Table 1

Stages and reaction orders

	Laser reaction	Reaction order	Step-by-step (controlled) heating reaction	Reaction order *
$MnCO_3$ decomposition	I. $MnCO_3 \rightarrow MnO_2 + CO$	0	I. $MnCO_3 \rightarrow MnO_2 + CO$	1
	II. $MnO_2 + CO \rightarrow MnO + CO_2$ $3MnO_2 \xrightarrow[-\frac{3}{2} O_2]{} 3MnO \xrightarrow{+\frac{1}{2} O_2} Mn_3O_4$ $2MnO_2 \rightarrow Mn_2O_3 + \frac{1}{2} O_2$	undetermined (continuously changing)	II. $2MnO_2 \rightarrow$ $\rightarrow Mn_2O_3 + 1/2O_2$	2/3
	$3Mn_2O_3 \rightarrow 2Mn_3O_4 + \frac{1}{2} O_2$	0	III. $3Mn_2O_3 \rightarrow$ $\rightarrow 2Mn_3O_4 + \frac{1}{2} O_2$	0
H_3BO_3 dehydration	I. $2H_3BO_3 \rightarrow B_2O_3 + 3H_2O$	$\frac{3}{2}$	I. $4H_3BO_3 \rightarrow$ $\rightarrow H_2B_4O_7 + 5H_2O$ II. $H_2B_4O_7 \rightarrow$ $\rightarrow 2B_2O_3 + H_2O$	1

* The kinetical data of controlled heating (reaction order n, activation energy E, preexponential factor A) were obtained by the derivatographic method, using the relation

$$\frac{d\alpha}{dt} = \frac{A}{b} (1 - \alpha)^n \exp(-E/RT)$$

where b — heating rate, $d\alpha/dt$ — reaction rate [5, 11].

with a reaction order differing from unity $\neq 1$ (which is in this case a characteristic of the controlled heating).

These characteristics point out to diffusion processes which dominate the chemical reaction induced by laser. The diffusion of reactants and (gaseous) reaction products may change in the course of irradiation.

During the time evolution of the laser thermochemical reaction, a feed-back is established between the chemical and thermal degrees of freedom of the system.

The reaction is accelerated if reaction products exhibit absorptivity (at the 10.6 μm radiation of the CO_2 laser), due to the fast rise in temperature (e.g., B_2O_3 absorptivity is 25% larger than that of the starting substance).

The technique of high purity manganese oxide (approx. 95%) and boron oxide (approx. 99%) production by CO_2 laser decomposition of manganese carbonate and boric acid allows also for a high conversion coefficient (more than 90%), low raw material losses and high efficiency (in the energy and mass balance).

C. PURIFICATION AND SUBSTANCE SEPARATION BY LASER-INDUCED POLARISATION IN HETEROGENEOUS INTERFACE PROCESSES (LIQUID-SOLID, GAS-SOLID INTERFACES)

The principle of these new methods is the selective action of laser radiation on molecules in a mixture presenting an absorption band at the radiation wavelength. By the excitation of molecules near a solid surface or in the vicinity of the phase-separation border, a variation in the adsorption potential occurs, with diffusion and/or concentration modifications on the surface [16], [17].

C1. Laser-induced photoadsorption of uranyl ions in solution

In a quite simple experimental device (Fig. 9) a nitrate uranyl aqueous solution was placed in a thin metallic cell, closed at one end by a ZnSe window.

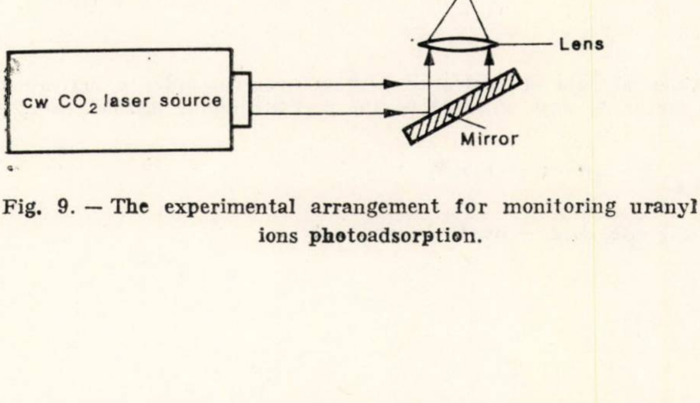

Fig. 9. — The experimental arrangement for monitoring uranyl ions photoadsorption.

Half of the window aperture was irradiated by a cw CO_2 laser (P(20) emission line – 945 cm^{-1}) – line intensity 40 W/cm^2. The other half of the ZnSe window was screened.

The radiation was defocalized, so as to cover the entire surface of the window.

After three minutes of irradiation, the uranyl solution was evacuated and the adsorbed uranyl amount on the surface was determined by IR spectrophotometrical methods.

It may be observed that the radiation acts directly at the separation border interface between the solution and the solid surface (to minimize the influence of the solvent layer in which the excitation energy received is rapidly transferred ($\sim 10^{-11}$ s)) [9].

It is known that the uranyl group is linear in coordination compounds. On the other hand, CO_2 laser radiation is in resonance with the asymmetrical valence vibration ν_3 of the UO_2^{++} complex (945 cm^{-1}). By monitoring the IR absorption in this intense band it was found that the uranyl amount deposited on the irradiated surface (curve 2) is larger than that cumulated on the screened surface (curve 3), the difference in concentration reaching $\sim 20\%$.

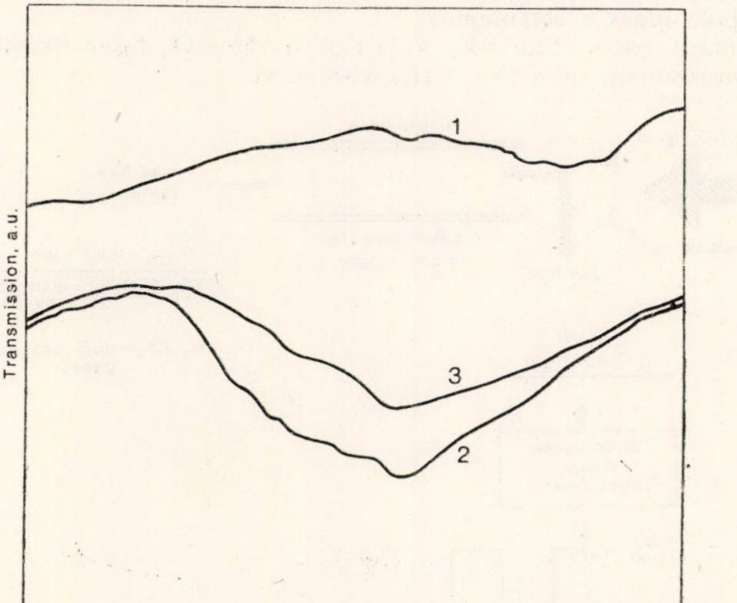

Fig. 10. — The IR transmission spetrum of the two halves of ZnSe plate, which was containing uranyl nitrate solution: 1 — initial ZnSe plate, 2 — screened half of the plate (after irradiation), 3 — irradiated half of the plate.

It was also found that the thermal action of the laser radiation accounts for a thermal desorption process, which is stronger in the irradiation zone.

Laser stimulation of surface adsorption for ions in solutions is a complex process in which more investigations are needed in order to elucidate complicate structures like adsorbed layers, ligands in solution, etc. Nevertheless, it offers a promising field, in which the increased density of the substance (as compared to similar processes in gaseous media) may increase the efficiency of photoadsorption processes.

C.2 Substance separation in capillaries by laser-induced polarization at the gas-solid interface

Experimental and theoretical evidence pointed out the possibility of a laser selective control of the permeability of capillaries to gas flows [6, 8]. It was found that the electromagnetic field modifies the resonant (to radiation) diffusion of the molecule through a variation in the adsorption potential. The macroscopical effect is a sudden decrease in the resonant molecular flow at the switch-on of the laser radiation into the capillary, while the non-resonant flow in the mixture remains constant.

The experimental installation mainly consists of a Ni capillary (0.5 mm in diameter, 10 cm in length) connected at one end with a gas feeding system, and at the other end with the high vacuum chamber of a quadrupole mass spectrometer.

Resonant gases (like SF_6, $C_2H_4F_2$) to the CO_2 laser radiation as well as non-resonant ones (N_2, CH_4) were used.

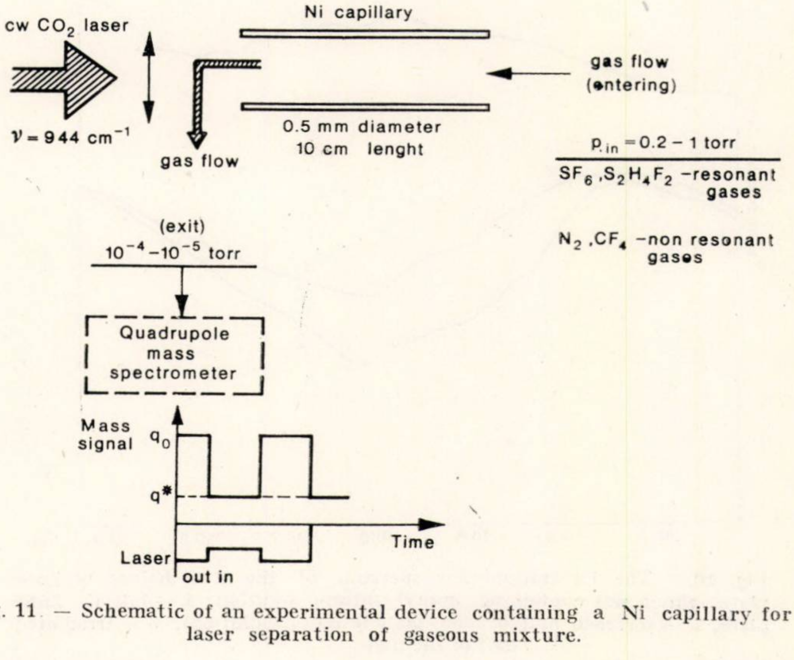
cw CO_2 laser
Ni capillary
gas flow
(entering)
$\nu = 944$ cm^{-1}
gas flow
0.5 mm diameter
10 cm lenght
$p_{in} = 0.2 - 1$ torr
SF_6, $S_2H_4F_2$ -resonant gases
N_2, CF_4 -non resonant gases
(exit)
$10^{-4} - 10^{-5}$ torr
Quadrupole mass spectrometer
Mass signal
q_0
q^*
Time
Laser
out in

Fig. 11 — Schematic of an experimental device containing a Ni capillary for laser separation of gaseous mixture.

The cw CO_2 laser, rated at 10 W power, $\tilde{\nu} = 944$ cm^{-1} was propagating in a sense opposite to the gas flow, and was focalized at the capillary entrance by a ZnSe lens.

The effect of laser blocking of the flow was analyzed by recording the mass signal of the molecules in transit (lower part in Fig. 11), where q_0 and q^* are the flow values in the absence of laser radiation and in the presence of laser radiation, respectively.

One important result obtained in the experiments was that the laser separation action is strongly enhanced by increasing the laser radiation intensity into the capillary (Fig. 12).

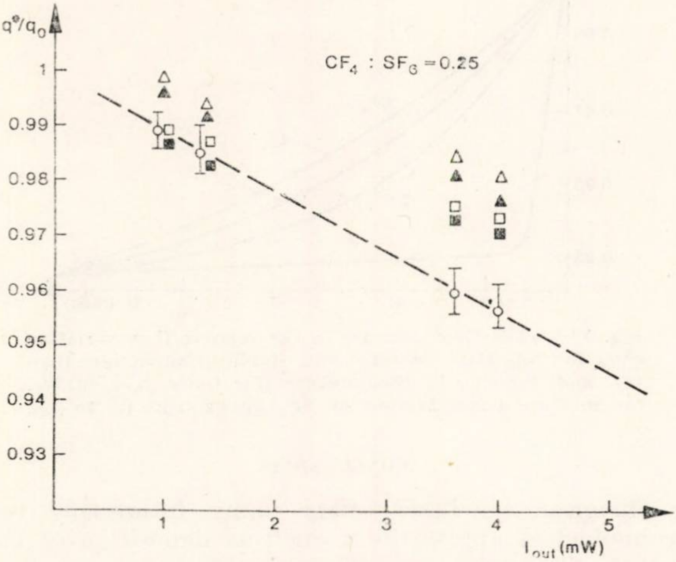

Fig. 12. — The dependence of the relative flow variation q^*/q_0 for CF_4:SF_6 = 1:4 mixture on laser intensity (measured at the capillary output) for different total pressures: $\overset{\top}{\underset{\perp}{\circ}}$ — SF_6; ■ 0.2 torr CF_4; □ 0.3 torr CF_4; ▲ 0.6 torr CF_4; △ 0.9 torr CF_4.

By analyzing the flow regions along the capillary (which could markedly depart from a free molecular character as the gaseous mixture pressure grows), optimum separation regimes were evidenced (as against the temporal and pressure characteristic parameters).

During the first 2—3 seconds of irradiation, it was found that the separation coefficient η reaches high values ($n \geqslant 1.06$) (Fig. 13).

The limitation with time of the separation coefficient is due to the heating effect (the heat is released to the capillary walls by excitation thermalisation through collision of the resonant SF_6 molecules.

As the resonant gas concentration and the pressure decrease, this thermal transfer diminishes and the separation coefficient improves.

Despite some controversial heat effects which are still under study, a selective action of laser radiation on gas flows transiting through capillaries was found and the separation of components in gaseous mixtures was obtained.

The process is favoured by an increased laser intensity and a decreased pressure at the capillary input (which could maintain a free molecular flow of gases).

The technique of laser substance separation by using metal capillaries could present advantages over other heterogeneous systems by allowing for more important gas flows, greater laser intensities, relative transparency in a wide range of laser wavelengths and simple thermal evacuation.

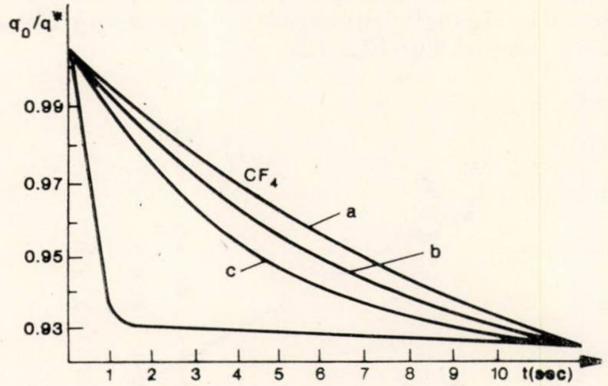

Fig. 13. — The time decrease in the relative flow variation q^*/q_0 for SF_6 (fast decrease and stabilization in less than 1s) and for CF_4 in the mixture (for the a, b, c curves, the mixture concentration in SF_6 grows from (a) to (c)).

CONCLUSIONS

Laser chemical synthesis offers many interesting results, with potential technological applications, such as deposition of thin films of polymers, metals, dielectrics, semiconductors (for components and circuits, for integrated sensors, etc.); the synthesis of high purity compounds (reagents, ceramic powders, polymers); the possibility of obtaining catalytic-active media, chain-reaction initiation and chemical reaction acceleration (by orders of magnitude). These new methods and chemical techniques may constitute a technological alternative, which will prove its viability together with the lowering of laser photon costs and the improved reliability of optical laser components.

As a research tool in basic chemistry, lasers are now difficult to replace, because they offer the possibility of detailed investigation of the mechanism of chemical reactions, also providing new information on process kinetics in gases, liquids and solids.

REFERENCES

[1] E. Grunwald, D. F. Dever, P. M. Keehn, "Megawatt Infrared Laser Chemistry", Wiley, N. Y., 1987.

[2] Yu. Molin, V. N. Panfilov, A. K. Petrov, "Infrakrasnaya fotochimya", Nauka, Novosibirsk, 1985.

[3] K. Kleinermanns, J. Wolfrum, *Angew. Chem. Int. Ed. Engl.*, **26**, 38 (1987).

[4] D. Bauerle, "Laser Processing and Diagnostics", Springer Verlag, Berlin, 1985.

[5] J. S. Haggerty, W. R. Cannon, in "Laser-Induced Chemical Processes", J. I. Steinfeld Ed., Plenum Press, N. Y., London, 1981.

[6] I. Ursu, R. Alexandrescu, I. Morjan, C. Grigoriu, I. N. Mihăilescu, J. Tlaskal, "Laser Driven Ultrafine Silicon Nitride Production in a Flowing System", Proceedings of TQE International Conference, Bucharest, 29 Aug.—3 Sept. 1988.

[7] R. Alexandrescu, I. Morjan, C. Grigoriu, I. N. Mihăilescu, Z. Bastl, J. Tlaskal, R. Mayer, J. Pola, *Appl. Phys.*, A, **46**, 275 (1988).

[8] I. Ursu, I. Morjan, R. Alexandrescu, I. N. Mihăilescu, D. Sorescu, J. Pola, J. Tlaskal, "Laser assisted decomposition of silane", Proceedings of the TQE International Conference, Bucharest, 29 Aug.—3 Sept. 1988.

[9] I. Ursu, R. Alexandrescu, C. Grigoriu, D. Dragulinescu, I. Morjan, I. N. Mihăilescu, A. M. Prokhorov, Yu. N. Petrov, A. N. Orlov, V. A. Pustavoi, "Laser Action on Aqueous Solutions through Porous Membranes", Proceedings of the TQE International Conference, Bucharest, 29 Aug.—3 Sept. 1988.

[10] C. Popescu, V. Jianu, R. Alexandrescu, I. N. Mihăilescu, I. Morjan, M. L. Pascu, *Thermochimica Acta*, **129**, 269 (1988).

[11] I. Ursu, R. Alexandrescu, V. Drăgănescu, C. Grigoriu, I. N. Mihăilescu, I. Morjan, A. M. Prokhorov, A. N. Orlov, A. S. Lagutchev, Yu. N. Petrov, *Appl. Phys.* B, **47**, 61 (1988).

[12] I. Ursu, R. Alexandrescu, V. Crăciun, I. Morjan, I. N. Mihăilescu, *Appl. Lasers*, **6**, 157 (1986).

[13] I. Ursu, I. Morjan, R. Alexandrescu, I. N. Mihăilescu, C. Grigoriu, A. M. Prokhorov, A. N. Orlov, Yu. N. Petrov, A. S. Lagutchev, *Infrared Physics*, **27**, 339 (1987).

[14] P. A. Longway, F. N. Lampe, *J. Am. Chem. Soc.*, **103**, 6813 (1981).

[15] R. Alexandrescu, I. N. Mihăilescu, I. Morjan, M. L. Pascu, V. Jianu, M. Popescu, F. V. Bunkin, B. S. Lukianchuk, *Phys. stat. sol.* (a), **104**, 687 (1987).

[16] V. A. Kravchenko, A. N. Orlov, Yu. N. Petrov, A. M. Prokhorov, "Resonance Heterogeneous Processes in a Laser Field" (in Russian), Trudy IOFAN, Vol. II (1988).

[17] N. V. Karlov, A. S. Lagutchev, A. N. Orlov, Yu. N. Petrov, A. M. Prokhorov, *JEPT Lett.*, **10**, 598 (1983).

[18] I. Ursu, R. Alexandrescu, I. N. Mihăilescu, I. Morjan, V. Jianu, C. Popescu, *J. Phys.* B : *At. Mol. Phys.*, L825 (1986).

[19] I. Ursu, R. Alexandrescu, I. N. Mihăilescu, I. Morjan, A. M. Prokhorov, F. V. Bunkin, B. S. Lukyanchuk, E. A. Morozova, G. A. Shafeev, *J. Phys.* D, *Appl. Phys.*, **20**, 407 (1987).

Revue Roumaine de Chimie, **34**, 2, 683–688 (1989)

METHANE OXIDATION ON SUPPORTED PALLADIUM CATALYSTS

M. I. VASS, I. BALINT and V. POPA

ICECHIM-Center of Physical Chemistry, Spl. Independenţei 202, Bucharest 79611, Romania

Received March 26, 1988

The complete oxidation of methane over palladium supported catalysts has been studied using a microcalorimeter technique. Kinetic parameters of reaction have been measured. The results indicate that methane and oxygen react on the catalyst surface following a Langmuir-Hinshelwood kinetics. Some correlations between experimental results and thermogravimetric measurements have been found which explain reaction rate variation with temperature.

The complete oxidation of methane on supported or unsupported platinic metals has been extensively studied by many authors.

Eyraud and coworkers [1–5] investigated the catalytic combustion of methane on Pt and Pt alloys. Measurable oxidation rate was found on pure Pt filaments only at temperatures higher than 600°C with a maximum value for 1300°C. They observed that the reaction takes place heterogeneously on the metal surface at low temperatures and homogeneously at higher temperatures.

The complete oxidation of methane over supported platinic metals (Pd, Pt, Rh, Ir) was investigated by Firth [6] and Cullis.[7,8] They found that the reaction occurs between adsorbed methane and oxygen on catalyst surface following a Langmuir-Hinshelwood route. Two types of active sites were identified by Firth on the catalyst surface : one type for the competitive adsorption of methane and oxygen at low temperature and one type only for methane adsorption at high temperatures. The same heterogeneous mechanism was found by Cullis [7,8] which demonstrated that both methane and oxygen molecules are adsorbed on the catalyst surface. Akuja,[9] Schwartz [10] and Pitchai [11] also found that methane and oxygen react on the supported catalyst surface. Brennan [12] and Bell [13] have identified both the strongly bound oxygen and the oxide type structures on catalyst surface .Methane adsorption on different metals surfaces (Pd, Re, Ni, Mo, W, Ta) was identified at pressures higher than 10^{-2} torr by Liénard and Frennet.[14–19]

The aim of this paper is to report the results of an extensive kinetic study of the methane oxidation over Pd supported catalyst and to elucidate the reaction rate variation with temperature.

EXPERIMENTAL

The kinetic mesurements were performed with a microcalorimeter similar to that used by Firth.[20] The rate of methane oxidation was evaluated by measuring the heat effects of the reaction.

The microcalorimeter forms one arm of a simple Wheatstone bridge. A variable resistor set on the arm parallel to the calorimeter allowed the bridge to be balanced. Out of balance voltages were measured using digital voltmeter with a sensitivity of 0.1 mV. The measurements were carried out at normal pressure (101 kN m^{-2}). The microcalorimeter was imersed in flowing methane/air mixture. The partial pressure of methane in air did not exceed 2.5 kN $\cdot m^{-2}$.

The microcalorimeter consists of Pt thermoresistance embedded in an alumina pellet on which the Pd catalyst was deposited. The temperature of the pellet was measured in its center using an inserted chromel-alumel thermocuple. A stabilisation process was applied to catalyst prior to utilisation in order to obtain reproductible results.

The catalytic oxidation of methane on the pellet was conducted at constant temperatures. The heat dissipated by the catalytic pellet is directly proportional to its temperature. The variation of electrical power *vs.* pellet temperature plotted on Fig. 1 was used for the microcalorimeter calibration. Taking into account the associated Joule effects, the heat dissipated by the catalytic pellet in time unit at temperature T_i is :

$$\frac{dQ}{dt} = U \cdot I = P \tag{1}$$

where U is the applied voltage, I the current through the Pt coil and P the dissipated power.

Plotting P vs. the measured T_i, a straight line is obtained (Fig. 1), the slope of which represents the variation of the dissipated heat in time unit with temperature, $S = (dQ/dT)/dT$. When the catalytic pellet is introduced in a methane-air mixture, an increase of temperature takes place from T_1 to T_2 as a consequence of the oxidation reaction : the pellet will dissipate a new flux of heat $(dQ/dT)_{T_2}$.

The heat effect of oxidation is therefore :

$$\left(\frac{dQ}{dt}\right)_{OX} = \left(\frac{dQ}{dt}\right)_{T_2} - \left(\frac{dQ}{dt}\right)_{T_1} \tag{2}$$

Taking into account the slope of linear presentation in Fig. 1 one gets :

$$\left(\frac{dQ}{dt}\right)_{OX} = S \cdot (T_2 - T_1) \tag{3}$$

Using relation (3) the heat associated with methane oxidation dissipated in time unit an be evaluated from the experimental data.

On the other hand the rate of the catalytic oxidation at temperature T_i of CH_4 can be written :

$$v = \frac{d[CH_4]}{dt} = \left(\frac{dQ}{dt}\right)_{OX} \cdot \frac{1}{\alpha \cdot \Delta H} \tag{4}$$

where ΔH is the enthalpy of methane oxidation and α the fraction of the heat absorbed by calorimeter.

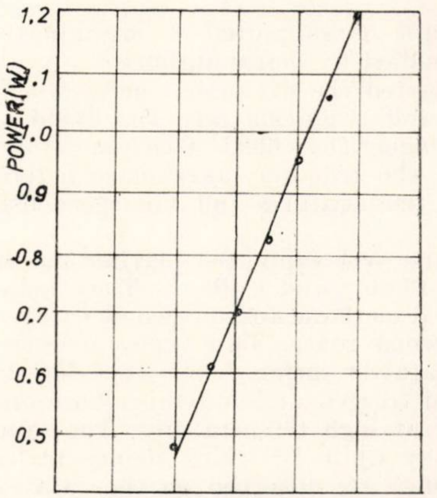

Fig. 1. — The heat dissipated by the catalytic pellet in air in the temperature range 300—700 °C.

From eqs (3) and (4) an expression of the rate of methane total oxidation is obtained :

$$v = S(T_2 - T_1) \cdot \frac{1}{\alpha \cdot \Delta H} \tag{5}$$

RESULTS AND DISCUSSION

Relation (5) was used to evaluate the rate of methane complete oxidation on the supported Pd catalysts over the temperature range 350–800°C. In this temperature range the reaction rate increases with temperature up to a plateau (approximatively between 600 and 700°C), then decreases with the increasing temperature (Fig. 2).

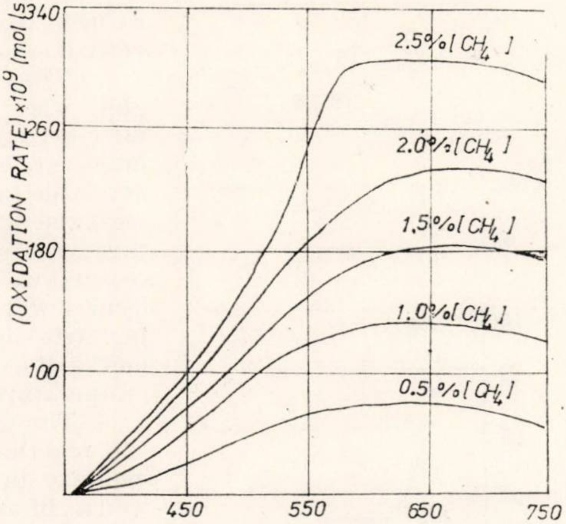

Fig. 2. — The variation of the methane oxidation rate vs. catalytic pellet temperature.

The reaction rate dependence on methane pressure over the same temperature range is also shown in Fig. 3.

The apparent activation energies for the reaction over Pd catalyst can be determined from plots of ln K_{ap} against reciprocal of the absolute temperature. Such representations are shown in Fig. 4. The Arrhenius

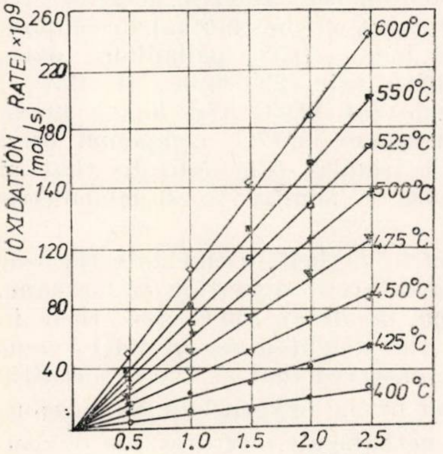

Fig. 3. — The variation of the methane oxidation rate vs. methane concentration at different pellet temperatures.

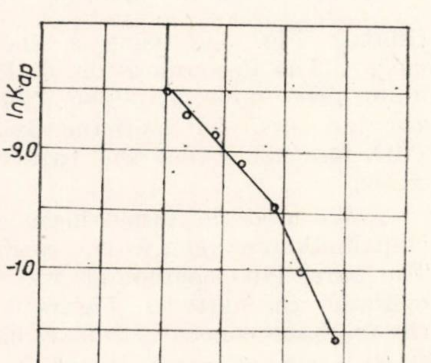

Fig. 4. — Arrhenius plots for methane oxidation over palladium catalyst.

plots exhibit a change in apparent activation energy E_{app} at about 450°C giving a value of about 96 kJ/mol (11 kcal/mol) at higher temperatures, in good agreement whith the reported values over Pd catalysts ranging between 17 and 24 kcal/mol in flow methods respectively 10—14 kcal/mol in static methods.[7,8,13,21,22,23] At temperatures higher than 600°C the apparent activation energy E_{app} tends to be zero.

These results (two activation energies) were explained by Firth [6] taking into account the palladium property to have, at low temperatures, empty sites available for the competitive adsorption of methane and oxygen. At higher temperatures, the palladium surface is completely covered with oxygen and the methane molecules will be adsorbed without competing with oxygen. It is supposed that the methane oxidation occurs by two distincts temperature dependent mechanisms.

The good agreements concern also the reaction order in methane found to be unity in our measurements (Fig. 3) as well as in other reported studies.[20,24]

To explain the decrease of the oxidation rate over 700°C, the kinetic data have been further correlated with thermogravimetric determinations. The measurements were carried out on a Dupont 1090 System. Some authors [6,7,8,11,13] have supposed that the surface palladium oxide is responsible for the catalytic activity. We have investigated the thermal decomposition of high purity palladium oxide (Fluka), Fig. 5 a, using a linear heating rate (20°C/min., air flow, 1 cm^3/s). The decomposition of PdO begins at 811°C and has a maximum rate value at 820°C. The thermogram of Pd compound on α alumina used for methane oxidation is similar (Fig. 5 b) to that of PdO, indicating that the catalytic phase is similar to stoichiometric oxide.

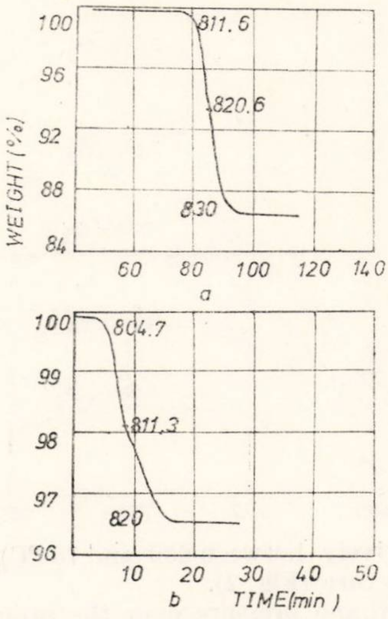

Fig. 5. — The thermal decomposition of high purity palladium oxide in air (flow rate 1 cm^3/s, heating rate 20 °C/min), (a), and the thermogram of palladium compound on α alumina which catalyses the oxidation reaction in air (heating rate 5 °C/min), (b).

We used the same thermogravimetric method to elucidate the role of palladium-oxygen atoms ratio during catalytic oxidation of methane. The pure PdO compound was exposed in air at 750°C and then in methane air mixtures. Figure 6 shows the weight losses of PdO versus the methane concentration. It has been observed that at 750°C the ratio Pd/O atoms increases in air as a result of the oxygen loss, to an equilibrium value. In the presence of the methane-air mixtures the oxygen loss increases as methane concentration increases. The removal of the reducing gase (methane) brings about an increase of the oxygen uptake reaching an equilibrium value at 750°C.

Consequently it may be concluded that the decrease of the methane oxidation rate on supported Pd catalyst can be attributed to the oxygen loss of surface species of the PdO type.

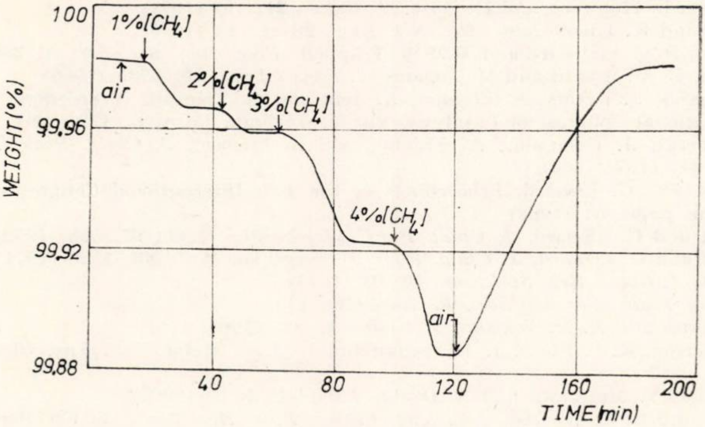

Fig. 6. — The change of Pd/O ratio for palladium oxide in relation to the methane concentration at an initial temperature 750°C.

CONCLUSIONS

In the temperature range of 350—750°C the methane oxidation is a kinetically controlled surface reaction; the reaction rate is not significantly dependent on the flow rate. On the Pd catalyst surface the reaction occurs between the adsorbed methane and adsorbed oxygen, following a Langmuir-Hinshelwood route.

It has been found out that the reaction is first order in methane over the temperature range studied and methane pressure used, indicating weak and nondissociative adsorption for methane, respectively strong oxygen adsorption.

The reaction rate decreases at temperatures higher than 700°C, as a consequence of the ratio Pd/O increasing. The temperature increase brings about a weakening of Pd—O bonds inducing the formation of a non stoichiometric Pd—O surface compound.

The Pd—O ratio is influenced by the methane concentration; the increase of the methane concentration results in oxygen loss from the catalyst surface, while the methane removal leads to oxygen gain reaching the initial equilibrium value.

REFERENCES

[1] Ch. Eyraud, B. Domanski and L. de Mourgues, *Bull. Soc. chim. France*, **1956**, 808.
[2] Ch. Eyraud, B. Domanski and P. Bussière, *Compt. rend.*, **243**, 905 (1956).
[3] M. M. P. Devore, Ch. Eyraud and M. Prettre, *Compt. rend.*, **246**, 1200 (1958).
[4] M. F. Cabannes and Y. Thibaut, *Compt. rend.*, **249**, 502 (1959).
[5] Ch. Eyraud, P. Bussière and B. Domanski, *Bull. Soc. chim. France*, **1956** (1604).

[6] J. G. Firth and H. B. Holand, *Trans. Faraday Soc.*, **65**, 1121 (1969).

[7] C. F. Cullis and D. E. Keane, *Trans. Faraday Soc.*, **67**, 864 (1971).

[8] C. F. Cullis, T. G. Newell and D. L. Trimm, *J. Chem. Soc. Faraday Trans.*, 1, **68** (pt 3). 1406 (1972).

[9] O. P. Akuja and G. P. Mathur, *Canad. J. Chem. Eng.*, **45**, 367 (1967).

[10] A. Schwartz, L. Holbrook and H. Wise, *J. Catal.*, **21**, 199 (1971).

[11] R. Pitchai and K. Klier, *Catal. Rev. Sci. Eng.*, **28** (1), 13 (1966).

[12] D. Brennan, D. O. Hayward and B.M.W. Trapnell, *Proc. Roy. Soc. Ser. A*, **256**, 81 (1960).

[13] W. E. Bell, R. E. Inyard and M. Tagami, *J. Phys. Chem.*, **70**, 3735 (1960).

[14] R. Coekelbergs, J. Derots, A. Frennet, A. Jelli and G. Liénard, Proceedings of the 2-nd International Congress of Catalysis, Vol. 1, Technip. Paris, p. 427 (1961).

[15] R. Coekelbergs, J. Delannois, A. Frennet and G. Liènard, *J. Chim. Phys. Physicochim. Biol.*, **61**, 1167 (1964).

[16] A. Frennet and G. Liénard, Proceedings of the 4-th International Congress on Catalysis, Moscow, paper 51 (1968).

[17] A. Frennet and G. Liénard, *J. Chim. Phys. Physicochim. Biol.*, **67**, 598 (1970).

[18] A. Frennet and G. Liénard, *J. Chim. Phys. Physicochim. Biol.*, **68**, 1526 (1971).

[19] A. Frennet, *J. Catal. Rev. Sci. Eng.*, **10**, 37 (1974).

[20] J. G. Firth, *Trans. Faraday Soc.*, **62**, 2566 (1966).

[21] G. M. Schwab and A. M. Watson, *J. Catal.*, **4**, 570 (1965).

[22] R. B. Anderson, K. C. Stein, J. J. Feenan and L. J. E. Hofer, *Ind. Eng. Chem.*, **53**, 809 (1961).

[23] Y. Moro-aka, Y. Morikawa and A. Ozaki, *J. Catal.*, **7**, 23 (1967).

[24] R. Mezaki and C. C. Watson, *Ind. Eng. Chem. (Proc. Res. Dev.)*, **5**, 62 (1966).

Revue Roumaine de Chimie, **34**, *2*, 689—696(1989)

ПОЛЯРОГРАФИЧЕСКОЕ ОПРЕДЕЛЕНИЕ СВИНЦА И ОЛОВА В СПЛАВАХ

И. И. ВАТАМАН, Л. С. КОПАНСКАЯ, Л. Г. КИРИЯК, В. А. СМЕЛОВ и В. Г. РУССУ

Институт химии Академии наук Молдавской ССР, 277028, г. Кишинев, Ул. Гросула, 3; СССР

Получена 3 октября 1988 г.

Разработаны полярографические методы определения свинца и олова в оксалатном растворе азура 1 и свинца в экстракте после селективной экстракции при pH 10—11 хлороформенным раствором диэтилдитиокарбамината в сплавах Pb—Sn—Te из навесок малой массы. Методами переменно-токовой полярографии, хроноамперометрии с линейной разверткой потенциала и снятием электрокапиллярных кривых показано, что электродный процесс осложнен адсорбцией всех компонентов раствора и особенно продуктов электродной реакции.

The analytical procedure for determining lead and tin from oxalate solution of azure 1 and lead from extract after the selective extraction by pH 10 — 11 of chloroform solution of NaDDC in alloys Pb — Sn — Te was proposed. AC-polarography, chronoamperometry with linear potential and electrocapillary curves have shown that the electrode process is complicated by adsorption of initial substances as well as by electrode reaction products.

ВВЕДЕНИЕ

Изучение влияния ПАВ на электровосстановление комплексов ионов металлов с различными лигандами имеет принципиальное значение для аналитической химии. Ингибирование разряда поверхностно-активными веществами может быть использовано как способ повышения селективности определения, а способность ПАВ ускорять процесс электровосстановления — для повышения чувствительности в водных и водно-органических средах.[1]

Экстракционное разделение и концентрирование, органично сочетаясь с полярографией экстракта, исключает неизбежные потери при реэкстракции. Экстрагирование металлов предпочтительно осуществлять в виде хелатов, т.к. электрохимические процессы хелатов меньше осложнены предшествующими химическими реакциями, влияющими на форму волн и их положение по оси потенциалов; они в меньшей степени подвержены сольватации, что улучшает условия увеличения аналитического сигнала.[2]

На примере свинца и олова можно проиллюстрировать, что целенаправленный поиск условий реализации механизма электровосстановления, осложненного адсорбцией на электроде ряда органических реагентов как в водных, так и в водно-органических средах приводит к повышению аналитического сигнала, что позволяет подобрать условия раздельного их определения.

Тиазиновые красители, используемые в экстракционнофотометрическом методе определения ряда элементов,[3] в полярографии используются мало. Исключение составляет метиленовый голубой.[4-7] Изучено влияние адсорбции тионина [8] и азура I на восстановление олова из оксалатных растворов с целью разработки методики одновременного определения свинца и олова в системе свинец-олово-теллур из навесок малой массы. Наряду с этим разработаны методики определения свинца и олова, изолированных от сопутствующих элементов, что позволило оценить правильность методики без разделения.

ЭКСПЕРИМЕНТАЛЬНАЯ ЧАСТЬ

Переменно-токовые полярограммы регистрировали на полярографе ПУ-I с прямоугольным напряжением, хроноамперограммы на осциллографическом полярографе ЦЛА-03. Индикаторный электрод — ртутный капающий, электрод сравнения— насыщенный каломельный, вспомогательный — платиновая пластинка. Характеристики капилляра: $m = 2{,}6$ мг/с; $t = 5{,}3$ с (ПУ-1) и 7,5 с (ЦЛА-03). В работе использовали термостатированную ячейку ($25 \pm 0{,}2^2$С). Кислотность раствора проверяли pH-метром pH-262 со стеклянным электродом. Кислород из раствора удаляли продуванием электролитического водорода. Растворы готовили на дважды перегнанной воде из х.ч. и перекристаллизованных реактивов.

РЕЗУЛЬТАТЫ И ИХ ОБСУЖДЕНИЕ

Электровосстановление Sn(IV) и Sn(II) в оксалатных растворах в присутствии тионина (азура I) сопровождается резким увеличением тока. Наблюдается один хорошо выраженный пик при потенциале — 0,550 В, отвечающий двухэлектронному переходу Sn(II) — Sn(0). Высота пика зависит от концентраций $H_2C_2O_4$, красителя, олова, pH, ионной силы раствора. Максимальный пик олова наблюдается при pH I. При этом pH восстановление красителя происходит в положительной области потенциалов и к началу съемок полярограмм олова поверхность электрода покрыта восстановленными частицами тиазинового красителя. Именно в этих условиях наблюдается максимальный пик олова. На рис. 1 приведены зависимости высоты пика восстановления (переменно-токовая полярограмма) олова от концентраций красителя, щавелевой кислоты, и самого деполяризатора. Наблюдаемая область насыщения на кривой зависимости $H_{п}$—$C_{крас}$. характерна для процессов, осложненных адсорбцией. Хроновольтамперограмма олова на фоне 0,5M раствора $H_2C_2O_4$ в присутствии тионина (рис. 2) имеют предволну и характерны для случая сильной адсорбции продукта реакции.[9] Резкое увеличение тока восстановления олова можно объяснить накоплением на поверхности электрода восстановленных частиц тионина и образованием энергетически более выгодной частицы олово — щавелевая кислота — протонированная молекула лейкооснования тионина.

Электрокапиллярные кривые (ЭКК), снятые методом счета капель в трехэлектродной ячейке с медленно капающим электродом по отношению к 0,2 М раствору серной кислоты также указывают на адсорбцию всех компонентов раствора. В растворах щавелевой кислоты максимум ЭКК смещается в отрицательную область потенциалов и происходит заметное снижение положительной ветви ЭКК, что характерно для адсорбции анионов. При pH I степень диссоциации щавелевой кислоты незначительна. Однако адсорбироваться на поверхности электрода может не только преобладающая в растворе форма, но и присутствующая в незначительном

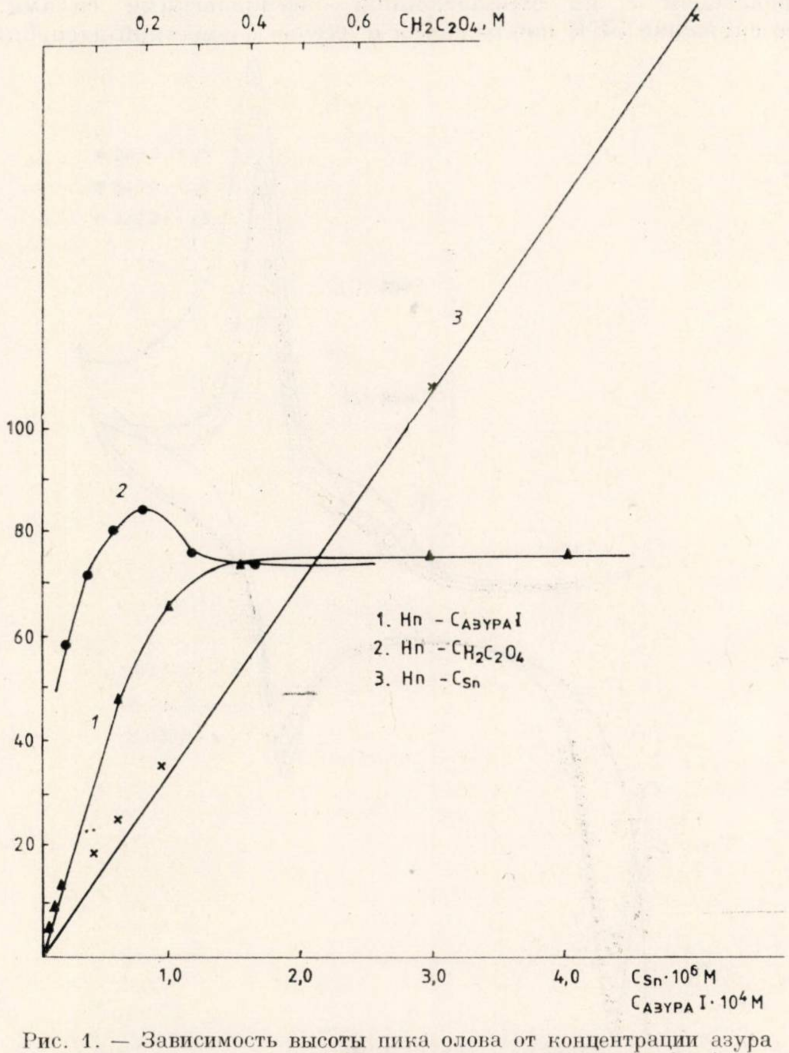

Рис. 1. — Зависимость высоты пика олова от концентрации азура (1), $H_2C_2O_4$ (2) и олова (3). Состав раствора (М): Sn—210^{-6} (1, 2), $H_2C_2O_4$—0,5 (1, 3), азур 1 — 10^{-4}(2,3). E = 12мВ, v = 2мВ/с,t = 25°C.

количестве.[10] В данном случае адсорбироваться могут частицы $HC_2O_4^-$. По отношению к фону ЭКК раствора красителя снижается заметно, причем ее максимум расположен при том же потенциале, что и максимум ЭКК фона. Можно предположить, что как и для ароматических аминов, адсорбция на положительной ветви ЭКК определяется π — электронным взаимодействием а на отрицательной — кулоновскими силами. Еще большее снижение ЭКК наблюдается в случае совместной адсорбции ща-

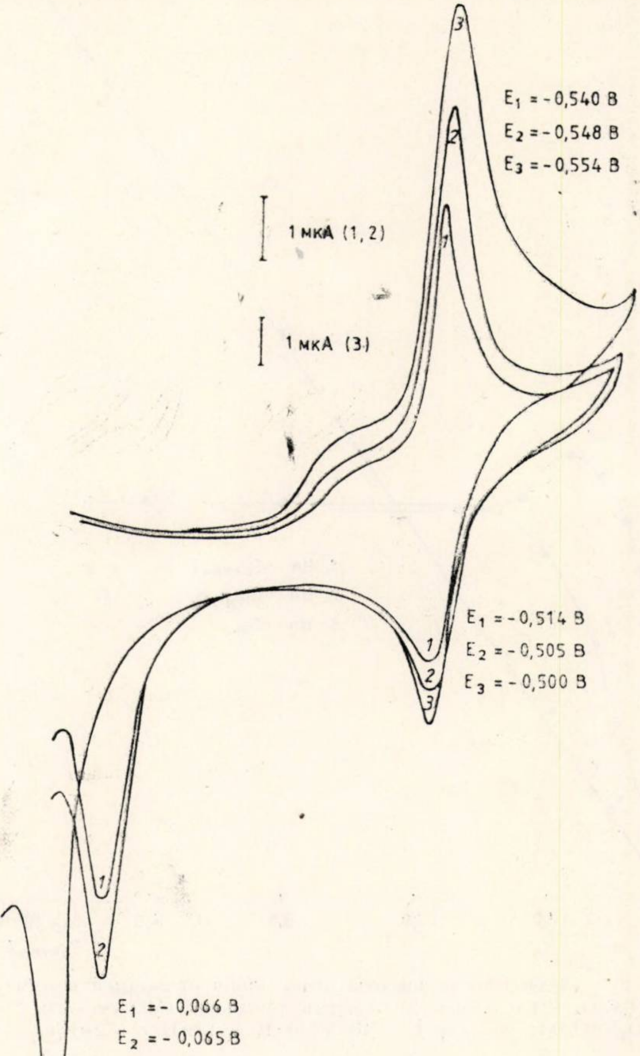

Рис. 2. — Хроноамперограммы олова. Состав раствора (М): Sn — 5 10^{-6}, $H_2C_2O_4$ — 0,5, тионин — 1, 5, 10^{-4} v(В/с): 0,5 (№) 5 ; 1,0 (2) ; 2,0 (3).

велевой кислоты и красителя. Это указывает на то, что в присутствии адсорбированных восстановленных частиц красителя происходит усиление адсорбции анионов щавелевой кислоты, а излом на ЭКК указывает на образование соединения типа ассоциата между восстановленными частицами красителя и аниона щавелевой кислоты. Введение олова в смесь красителя и щавелевой кислоты почти не изменяет характер кривых на ЭКК (рис. 3). Повидимому адсорбированные частицы аниона щавелевой кислоты вступают в дополнительное комплексообразование с оловом на поверхности электрода, ведущее к облегчению разряда деполяризатора.

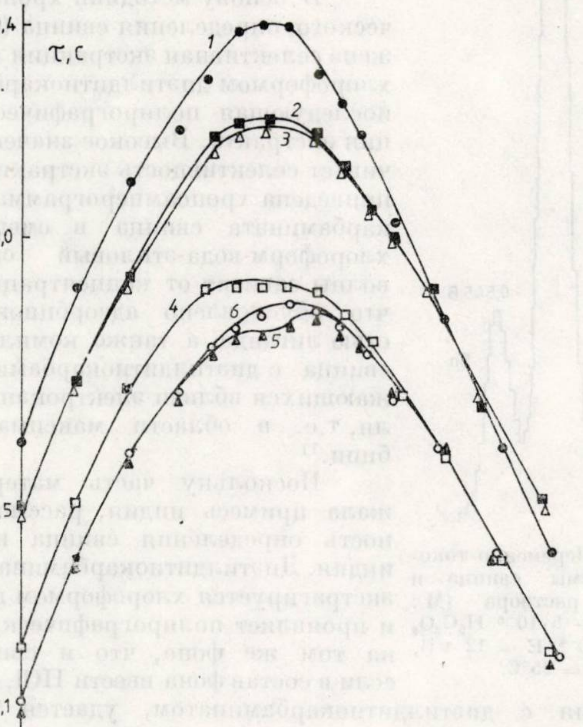

Рис. 3. — Электрокапиллярные кривые. 1—0,2М H_2SO_4 2—1+0,5М $H_2C_2O_4$; 3—2+5·10^{-6}М Sn(IV) 4—1 + 1,5.10^{-4}М тионина; 5—2+1,5·10^{-4}М тионина, 6—5+5·10^{-6}М олова.

Между высотой пика и концентрацией олова в растворе сохраняется пропорциональная зависимость в пределах 2.10^{-7}—5.10^{-5} М.

Определение олова на фоне 0,5 М щавелевой кислоты в присутствии 10^{-4}М азура 1 отличается высокой чувствительностью и селективностью. Определению олова не мешают 100-кратные избытки многих металлов, в том числе и свинца. Возможность определения олова в присутствии избытка свинца основана на том, что из-за дополнительного комплексообразования олова на поверхности электрода облегчается его разряд и увеличивается аналитический сигнал более, чем на порядок. В этих условиях азур 1 не влияет на электровосстановление свинца на оксалатном фоне. Высокая чувствительность определения олова и разность потенциалов вершин свинца и олова (рис. 4) позволяют проводить определение олова в присутствии свинца без их разделения.

На фоне 0,5 М щавелевой кислоты в присутствии азура 1 теллур восстанавливается и на переменно-токовой полярограмме наблюдаются два пика, однако они не мешают определению олова.

В основу методики хроноамперометрического определения свинца (метод Б) положена селективная экстракция при pH 10—11 хлороформом диэтилдитиокарбамината Pb и последующая полярографическая регистрация экстракта. Высокое значение pH обеспечивает селективность экстракции. На рис. 5 приведена хроноамперограмма диэтилдитиокарбамината свинца в смешанной среде: хлороформ-вода-этиловый спирт. Форма волны зависит от концентрации комплекса, что обусловлено адсорбционной активностью лиганда, а также комплексных частиц свинца с диэтилдитиокарбаминатом, разряжающихся вблизи электрокапиллярного нуля, т.е. в области максимальной адсорбции.[11]

Поскольку часть материалов содержала примесь индия, рассмотрена возможность определения свинца в присутствии индия. Диэтилдитиокарбаминат индия также экстрагируется хлороформом при pH 10—11 и проявляет полярографическую активность на том же фоне, что и свинец. Однако, если в состав фона ввести HCl, разрушающий комплекс индия с диэтилдитиокарбаминатом, удается устранить его влияние на волну свинца.

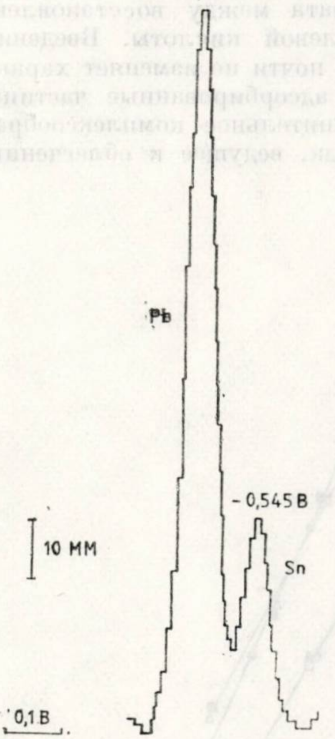

Рис. 4. — Переменно-токовые полярограммы свинца и олова. Состав раствора (М: Pb — $5\cdot10^{-5}$ Sn — $5\cdot10^{-6}$ $H_2C_2O_4$ — 0,5 азур 1—10^{-4}, E = 12 мВ, v=мВ/с, t = 25°C.

В основу определения олова с отделением положено отделение соосаждением с гидроксидом бериллия в присутствии ЭДТА.[12] При этом вместе с оловом частично отделяется и теллур. Дальнейшее определение осажденного олова проводится точно также, как было описано выше.

Растворение образцов. Тонко измельченную навеску сплава, массой 5—10 мг растворяют в царской водке.

Определение свинца и олова без разделения (метод А). Аликвотную часть раствора в мерной колбе на 50 мл смешивают с щавелевой кислотой, добавляют раствор азура 1, создают pH I. Полученный раствор переносят в полярографическую ячейку, удаляют кислород и снимают переменно-токовую полярограмму. Содержание свинца и олова находят методом добавок. В таблице 1 приведена метрологическая характеристика метода, а результаты определения свинца и олова в сплавах приведены в таблице 2. Полярограммы регистрировали на полярографе ПУ-1 с прямоугольным напряжением в трехэлектродной ячейке.

Таблица 1

Метрологические характеристики методик одновременного (А) и раздельного (Б) определения свинца и олова в искусственных смесях ($P = 0{,}95$)

Метод	Элемент	Введено $C \cdot 10^{-5}$ М				n	Найдено $\overline{X}$ 10^5, М	S_r	$(\overline{X} \mp \delta) \cdot 10^5$
		Te	In	Sn	Pb				
А	свинец	5,0	—	5,0	0,5	5	0,496	0,009	$0{,}496 \mp 0{,}07$
В	свинец	6,0	0,6	6,0	6,0	4	5,65	0,059	$5{,}65 \mp 0{,}53$
А	олово	5,0	—	0,84	4,0	6	0,837	0,013	$0{,}837 \mp 0{,}012$
В	олово	5,0	—	0,84	4,0	5	0,826	0,023	$0{,}826 \mp 0{,}024$

Таблица 2

Результаты определения свинца и олова в сплавах Pb—Sn—Te ($P = 0{,}95$)

Образец	Определ. элемент	Метод А (без разделения)				Метод Б (с разделением)			
		Найдено: $\overline{X}$, вес. %	n	S_r	$\overline{X} \mp$	Найдено: $\overline{X}$, вес. %	n	S_r	$\overline{X} \mp \delta$
1	свинец	53,3	5	0,019	$53{,}3 \mp 1{,}2$	53,9	5	0,020	$53{,}9 \mp 1{,}4$
2	—"—	—	—	—	—	47,1	8	0,025	$47{,}1 \mp 1{,}0$
3	—"—	53,2	6	0,013	$53{,}2 \mp 0{,}7$	55,4	5	0,028	$55{,}4 \mp 1{,}9$
1	олово	6,73	4	0,013	$6{,}73 \mp 0{,}14$	6,74	5	0,017	$6{,}74 \mp 0{,}08$
2	—"—	9,64	3	0,049	$9{,}64 \mp 1{,}17$	9,84	10	0,018	$9{,}84 \mp 0{,}13$
3	—"—	6,44	6	0,022	$6{,}44 \mp 0{,}15$	6,37	6	0,013	$6{,}37 \mp 0{,}06$

Определение олова с разделением (метод Б), К аликвотной части рствора прибавляют смесь кислот и раствор, содержащий 1 мг бериллия в 1 мл 3 М HCl. Добавляют 10% раствор ЭДТА. Образовавшийся осадок фильтруют и затем растворяют в горячей щавелевой кислоте. Дальнейшая работа проводится по вышеописанной методике.

Определение свинца с разделением (метод Б). Определение свинца осуществляют в аликвотной части раствора, которую нейтрализуют до pH 8—9. Вводят буферный раствор с pH 10, 4 мл 10% диэтилдитиокарбамината натрия и 2 мл хлороформа. Интенсивно встряхивают. После расслоения фаз водный слой сливают. Отбирают 1 мл органической фазы. Смещивают с фоном 1М $LiClO_4$ + 1 М HCl в этаноле. Раствор помещают в полярографическую ячейку и удаляют кислород. Хроноамперограмму свинца регистрируют на осциллографическом полярографе ОП - 5122. Содержание свинца находят по градуировочному графику. Результаты определения свинца представлены в таблице 2.

Как видно из таблицы, результаты, полученные двумя независимыми способами, хорошо между собой согласуются.

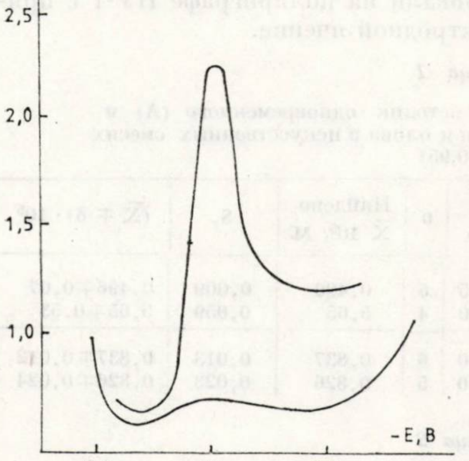

Рис. 5.—Хроноамперограмма свинца. Состав раствора(1 М): $LiClO_4 + HCl$ в C_2H_5OH, $Pb - 6{,}5 \cdot 10^{-5}$.

ЛИТЕРАТУРА

[1] И. И. Ватаман, В. Т. Мерян, Б. Ф. Пинтилий, О. А. Борищак, И. Д. Грама и И. Ф. Фиштик, «Кинетика и механизм гетерогенных и гомогенных химических процессов», изд. Штиинца, Кишинев, 1977.

[2] Г. К. Будников и Т. В. Троепольская, *Успехи химии*, **48**, 829 (1979).

[3] А. А. Арбутис, Р. М. Казлаускас, Л. Р. Нарушкявичус и Л. Г. Казлаускене, «Органические реагенты в аналитической химии», изд. Пермск. ун-та, Пермь, 1983.

[4] Л. Г. Петрова, В. И. Игнатов и Е. Я. Нейман, *Ж. аналит. химии*, **33**, 1949 (1978).

[5] Л. Н. Васильева, З. Л. Юстус и С. Г. Засадыч, *Ж. аналит. химии*, **32**, 273 (1977).

[6] Т. Д. Горностаева и С. В. Логунова, *Заводск. лаборатория*, **49**, 5 (1983)).

[7] J. Lexa, and K. Stulik, *Talanta*, **29**, 1089 (1982).

[8] И. И. Ватаман, Л. Г. Кирияк и А. В. Бодю, *Ж. аналит. химии*, **42**, 1999 (1987).

[9] M. N. Hubert and J. Shain, *Anal. Chem.*, **39**, 1514, 1927 (1967); **42**, 162 (1970).

[10] I. F. Fishtik, I. I. Vataman and F. A. Spatar, *J. Electroanal. Chem.*, **165**, 1 (1984).

[11] Г. К. Будников и Н. А. Улахович, *Успехи химии*, **49**, 147 (1980).

[12] T. Mikoyama, T. Jamane, N. Kida and M. Tanaka, *Anal. Chim. Acta*, **61**, 83 (1972).

Revue Roumaine de Chimie, 34, 2, 697—701 (1989)

VAPOUR PRESSURES OF *sı̣ɔ*- AND *trans*-2-BUTENES

RODICA VÎLCU, I. GĂINAR, ȘT. PERIȘANU and GH. ANIȚESCU
Laboratory of Physical Chemistry, Polytechnic Institute, Bd. Republicii 13, Bucharest, Romania

Received October 1, 1988

The vapour pressures of 2-butenes were measured by means of an original equipment in the range of −20° to + 90°C. The data fit very well in four-term equations, obtained by a regression procedure and agree satisfactorily with those from the literature.

1. INTRODUCTION

The data of vapour pressures for *cis* and *trans*-2-butenes in the over-atmospheric range are scarce. The main sources of data in this field are the gas data books of Matheson and Linde Co[1,2] and the paper of Carmichael et al.[3] The agreement between the data of different sources is good up to about 50°C, some discrepancies being observed above this temperature especially for the *cis* isomer.

The parameters for the Harlacher equation :

$$\ln p^{sat} = A + B/T + C \ln T + D \cdot p^{sat}/T^2$$

given in the book of Reid, Prausznitz and Sherwood[4] lead to reliable values of vapour pressures up to 50—60°C.

2. EXPERIMENTAL

The cell, a 300 ccm chromium plated brass autoclave is immersed in a RK4 Lauda Thermostate having an automatic control with Pt resistance thermometer. Cell's cover provided with a circular channel having inside a teflon gasket, assures by means of six screws the perfect tightness.

The thermostating bath contains a 1:1 ethyleneglycol-water mixture. The thermostating accuracy was ±0.02°C. The connexions between the working cell and the pressure measuring system were made of stainless steel capillaries with $Ø_{int} = 0.2$ mm in order to reduce the dead volume of the equipment.

The pressure measurement was made by means of two manometers M_1 and M_2 (see Fig. 1). The manometer M_1 made from glass, allows measurement within the range of 0—2400 mm Hg ; the M_2 one, an equipment with rotating piston and weights (precision class 0.05) is provided with a stainless steel U-shaped tube (Ø = 8 mm) filled with mercury, in order to equilibrate pistons weight and to prevent the contact between the gas and the oil. The insulation oil was put in the upper side of the U tube in order to diminish friction of the piston.

The U-shaped tube is provided with a thermostated shield which allows heating of the contact zone between mercury and vapours up to a few degrees above the temperature of the cell. Thus, the vapour condensation in the manometer is avoided.

The samples, delivered by Merck–Schuchardt, had a purity of 99.5%.

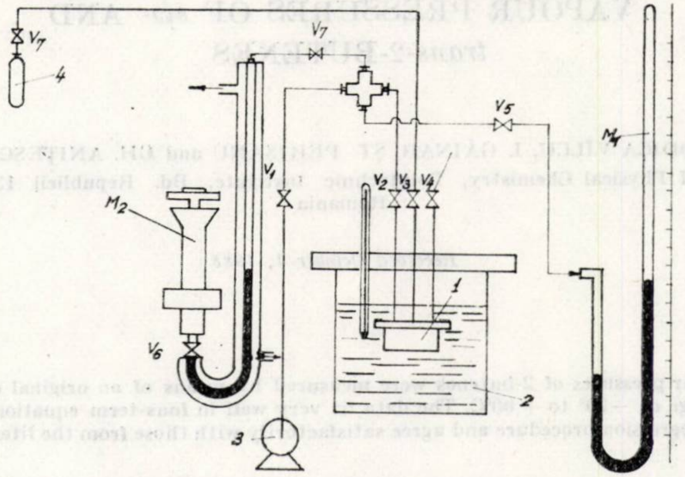

Fig. 1 — Experimental set up for the measurement of vapour pressures: 1 — cell, 2 — thermostating bath, 3 — vacuum pump, 4 — gas ampoule, V_1—V_7 — gas valves, M_1 — mercury manometer, M_2—rotating piston manometer.

An experiment consists of the following operations:

— vacuum is firstly made in the whole equipment up to about 10^{-2} mm Hg.

— the gas ampoule is weighted during the distillation of the desired amount of substance into the cell, immersed in the thermostate at about — 20°C.

— the vapour pressures are measured when equilibrium is attained, by means of the M_1 manometer up to 15—20°C and using M_2 manometer at higher temperature.

3. RESULTS AND DISCUSSION

The pressure measurements were accurate within ±3 mm Hg in the range of 300—2500 mm. At higher pressures, when the piston manometer was used, the error was of about ±0.05 bar. The accuracy of the temperature measurement was of ±0.05°C.

In tables 1 and 2 the experimental values of vapour pressures for *cis-* and *trans*-butenes together with the corresponding values from references[1-3] are listed.

A good agreement between literature data[1-3] and ours is observed for *trans*-2-butene. For *cis*-2-butene the agreement with the data of Matheson Gas Data Book [1] is good, but not with those of Linde [2] and Carmichael [3] at temperatures above 50°C. Our data of vapour pressures seem to be somewhat higher than those of Matheson [1] in the range of 70—90°C.

The experimental data of vapour pressures were fitted in equations of the form:

$$\ln P = A + B/T + C \ln T + DT \qquad (1)$$

by means of a regression computer program based on the least squares method.

Table 1

Experimental and literature data of vapour pressures of *cis*-2-butene

t°C	P_{exp}(mm Hg)	P_{lit}(mm Hg)[a]	P_{lit}(mm Hg)[b]	P_{lit}(mm Hg)[c]
−16	346	325	340	—
−10	444	442	430	—
0	670	659	650	—
3.7	764	760	760	—
10	965	960	960	—
15	1162	1147	1130	—
25	1585	1604	1610	—
30	1879	1880	1875	—
40	2526	2540	2525	2536
50	3387	3360	3325	3342
60	4377	4369	4225	4318
70	5623	5593	5330	5559
80	7108	7080	6675	6967
90	8850	8805	8250	8730

[a] Data from reference[1]
[b] Data from reference[2]
[c] Data from reference[3]

Table 2

Experimental and literature data of vapour pressures of *trans*-2-butene

t°C	P_{exp}(mm Hg)	P_{lit}(mm Hg)[a]	P_{lit}(mm Hg)[b]	P_{lit}(mm Hg)[c]
−16	386	381	375	—
−10	486	492	490	—
0	736	735	720	—
0.9	764	760	760	—
10	1064	1052	1050	—
20	1470	1495	1460	—
30	2033	2053	2000	—
40	2754	2759	2700	2721
50	3641	3642	3560	3596
60	4708	4720	4690	4634
70	6058	6046	6000	6002
80	7630	7629	7600	7380
90	9500	9480	9300	9130

[a] Data from reference[1]
[b] Data from reference[2]
[c] Data from reference[3]

The coefficients of equation (1) for *cis*- and *trans*-2-butenes are listed in table 3.

Table 3

Coefficients of equation (1) of vapour pressures for *cis*- and *trans*-2-butenes

Parameter	*Cis*-2-butene	*Trans*-2-butene
A	17.54250	18.48430
B	−2945.825	−3003.430
C	−0.0009858	−0.088660
D	−0.00092862	0.0014683
Standard deviation	0.0048	0.0040
Correlation coefficient	0.999999	0.999999

In tables 4 and 5 the experimental values of vapour pressures are compared with those calculated by means of equation (1). The agreement is very good, including the data outside the range of our experiments, taken from literature (two values below −20°C and the critical pressure). The possibility of extrapolation of the vapour pressure equations confirms the reliability of our experimental data which were used to obtain the above-mentioned equations.

Table 4

Experimental and calculated data of vapour pressures of *cis*-2-butene

T(K)	P_{exp}(mm Hg)	P_{calc}(mm Hg)
240	144*	154
250	240*	250
257.2	346	345
263.2	444	446
273.2	670	666
276.9	764	766
283.2	965	965
288.2	1162	1152
298.2	1585	1606
303.2	1878	1881
313.2	2526	2542
323.2	3387	3368
333.2	4377	4387
343.2	5623	5622
353.2	7108	7103
363.2	8850	8854
435.6	31575*	31867

* taken from reference[1]

Table 5

Experimental and calculated data of vapour pressures of *trans*-2-butene

T(K)	P_{exp}(mm Hg)	P_{calc}(mm Hg)
240	168*	169
250	275*	274
257.2	386	379
263.2	486	489
273.2	736	729
274.1	764	755
283.2	1064	1056
293.2	1470	1490
303.2	2033	2052
313.2	2754	2767
323.2	3641	3658
333.2	4708	4751
343.2	6058	6072
353.2	7630	7648
363.2	9490	9500
428.7	30750*	30443

* taken from reference[1]

REFERENCES

[1] "Matheson Gas Data Book", East Rutherford, N. J. 1971.

[2] "Linde Gase Katalog für Forschung, Entwicklung und Messtechnik", Höllrigelskreuth, 1973.

[3] L. T. Carmichael, K. C. Hwang, V. M. Berry and B. H. Sage, *J. Chem. Eng. Data,* **7,** 331 (1962).

Revue Roumaine de Chimie, 34, 2, 703–707 (1989)

STRUCTURAL CHARACTERIZATION OF VITREOUS SiO_2 MADE FROM GELS

MARIA ZAHARESCU, CONSTANȚA PÎRLOG, MARIA CRIȘAN and MARINA SAHINI
ICECHIM — Center of Physical Chemistry, Bucharest, 202, Splaiul Independenței, Romania

Received September 12, 1988

Vitreous SiO_2 has been prepared through thermal treatment of gels synthesized through the hydrolysis of organometallic compounds. The structural modifications induced by polymerization at room temperature and by thermal treatment at temperatures between 600 and 1000 °C have been detected using IR spectroscopy, DTA, DTG, XRD, TEM, and pore size and density measurements.

1. INTRODUCTION

The preparation of glasses by the sol-gel method, starting from organo-metallic compounds (metal alkoxides), which avoids melting of crystalline mixtures has raised much attention over the recent years. Four international scientific meetings have been held so far on this matter.[1-4]

As a rule, metal alkoxides hydrolyze in the presence of water and catalysts, and a spontaneous polymerization occurs subsequently.[6]

Many recent papers describe the low temperature polymerization of metal alkoxides, followed by adequate thermal treatment. The products obtained by this method are bulk [5] and porous [7,8,9] glasses, glass films,[10,11] glass fibers drawn directly from the solution [7,12] a.o. The main advantages of the method are the possibility to design the structure of the resulted glasses and the feasibility of the production of vitreous masses from substances which cannot be prepared in vitreous form by conventional techniques.

The present paper deals with the synthesis of silica glasses with a tridimensional network, through the hydrolysis-polycondensation of $Si(OC_2H_5)_4$ followed by adequate thermal treatment. The structura changes accompanying the sol-gel and gel-glass transformations have been also studied.

2. EXPERIMENTAL PART

Unicomponent silica glasses have been prepared from ethyl silicate.

In Table 1 the compositions of the starting alcoholate — water — ethanol — catalyst solutions are presented. Water is needed in the hydrolysis process, ethanol is used in diluting the alcoholate and HCl and NH_4OH act as catalysts of the hydrolysis reaction.

The hydrolysis reaction is allowed to proceed over rather long-time ranges, under refluxing, continuously stirring the solution heated at 80° C.

The sol-gel transition has been studied by viscosity measurements at room temperature, using the RVT Brookfield viscometer, at intervals of 72 hours each.

In order to study the gel-glass transition, gel samples dried at room temperature have been treated according to the following temperature schedule: heating between 20 and 1000°C at 3°C/min., with one-hour annealing at 600, 800, 900 and 1000°C. The dry gel and the glass resulted from the thermal treatment have been studied by the following methods:

— DTA, using a MOM-OD-103 Derivatograph, between 20 and 1300°C;

— IR spectroscopy performed on a Carl Zeiss Jena Specord 75 IR spectrophotometer;

— TEM, on a TESLA BM540, transmission electron microscope, using Pt—C replicas;

— X-ray diffraction on a HZG-3 diffractometer, working with $Cu_{K\alpha}$ radiation;

— BET adsorption of nitrogen gas at the temperature of liquid nitrogen. The pore volume and the surface area have been determined using the absorption-desorption isotherm;

— density measurements done in CCl_4 by the picnometer method.

3. RESULTS AND DISCUSSION

Preliminary measurements made on the mixtures listed in Table 1 showed that mixtures A—C lead to transparent gels, whose gelling periods were different from each other. In the other mixtures where NH_4OH has been used as catalyst, the gelling process has been achieved relatively fast, resulting in opaque bodies.

Mixture A, whose hydrolysis is slower and thus allows polymerization measurements to be made while still being a sol, has been therefore selected among the five mixtures investigated.

Table 1

Composition of initial solutions (mole ratios)

Solution	$\frac{H_2O}{SiEt_4}$	$\frac{EtOH}{SiEt_4}$	$\frac{HCl}{SiEt_4}$	$\frac{NH_4OH}{SiEt_4}$	Catalyst	pH of starting solution	Gelling period
A	15	4.3	0.25	—	HCl	3	16 days
B	11.9	3.5	0.65	—	HCl	2	1 hour
C	11.2	4.3	—	—	—	5	30 days
D	—	4.3	—	0.13	NH_4OH	7.5	2 hours
E	—	4.3	—	1.62	NH_4OH	8.5	1 hour

The sol-gel route of glass preparation involves three steps:

— alkoxide group hydrolysis accompanied by silanol group formation;

— condensation of silanol groups resulting in silicate polymers;

— bridging of polymers and formation of a gel.

The sol-gel transition depends on the respective amounts of catalyst and water, on the pH of the solution and on the hydrolysis temperature.

In the case of $Si(OC_2H_5)_4$, the solutions with a small water content were composed of a linear polymer when catalyzed by HCl. Fibers could be drawn from such solutions just before gelation. Solutions catalyzed by HCl and containing a large amount of water behaved analogously to solutions catalyzed by NH_4OH, suggesting that a high water content causes the formation of non-linear or network colloidal polymers in a hydrolysis-polycondensation process. Such solutions did not exhibit spinability, but gelled into elastic bulk masses which were easily converted to bulk glasses.[12]

In figure 1 is plotted the viscosity of the hydrolyzed solution A vs. time.

In the first stage the viscosity slowly increases, then, when the gel structure is achieved, a sharp increase is noted. This stepwise increase is noted after about 250 hours, which is a duration similar to that reported by other investigators working with similar compositions.[6,12] The result of this process is a transparent gel.

The DTA made on a gel sample dried at room temperature shows only a dehydration effect, whose maximum is at 130°C. The total weight loss amounts to about 18%. The DTA samples calcinated at 900°C show a small weight loss assigned to the loss of residual hydroxyl groups in the glass sample and an exothermal effect at 1340°C, assigned to crystallization.

X-ray diffraction shows that over the whole temperature range under investigation (20—1000°C), only an amorphous phase is present. Above 1000°C, the crystallization process is initiated, according to the X-ray patterns.

DTA and X-ray diffraction results are in agreement with IR spectroscopy data, given in Figure 2.

The starting gel and the calcinated samples show the same absorption bands whose assignment is established, well-documented,[13-15] except the band at 960 cm^{-1} which has been assigned to SiO(OH) [16,17], SiO^- vibrations,[18,19] and to vibrations associated with non-bridging oxygen bonding a proton.[20]

The Si—O—Si structural units found in gels are similar with those in molten quartz, as shown by the similarities in the IR spectra of both materials.[21]

The absorptions with maxima at 1080 cm^{-1} (in this case the maximum itself does not shift), 800 cm^{-1} and 460 cm^{-1} shift towards higher wave numbers in the case of annealed samples.

For the sample annealed at 600°C the band at 960 cm^{-1} is transformed into an inflexion at 980 cm^{-1}, which vanishes in the samples annealed at higher temperatures.

The increase in the relative intensities of the bands at 800 cm^{-1} and the disappearance of the one at 960 cm^{-1} supports the assumption that the SiO(OH) bonds pass into Si—O—Si bonds and the total pore volume decreases accordingly. The shift towards greater wavelengths of the bands assigned to Si—O—Si skeleton vibrations shows that the silicate network is strengthened.

The shape of the band at 460 cm^- leads to the hypothesis of a wider distribution of Si—O—Si bond angle than in molten quartz.

The spectrum of the sample calcinated at 1000°C shows that a mixture of crystalline phases is formed. A marked decrease in the intensity of the band at 1630 cm^{-1} is noted, which is assigned to the vibrations of bound or adsorbed water.

Over the range 3700—3100 cm^{-1} assigned to the vibrations of constitutional hydroxyl groups and adsorbed water, the increase in the temperature of thermal treatment is accompanied by a decrease in intensities and a narrowing of the absorption ranges.

In Figure 3 the microphotographs of the studied samples are compared to those of quartz glass. The shape of the calcinated samples is similar to that of the quartz glass. The room-temperature dried gel is similar to silicagel, and the sample annealed at 1000°C exhibits microcrystals.

In Table 2 the texture properties of samples calcinated up to 900°C and the density of the latter sample are given.

Table 2

Texture properties

Thermal treatment temperature, °C	Volume of pores (0–150 Å) cm³/g	Volume of micropores (0–15 Å) cm³/g	Diameter pores Å	BET surface area m²/g	Density g/cm³
20	$357.3 \cdot 10^{-3}$	$337.4 \cdot 10^{-3}$	14.4	481.5	
600	$352.0 \cdot 10^{-3}$	$340.8 \cdot 10^{-3}$	13.6	522.6	
800	$307.1 \cdot 10^{-3}$	$299.3 \cdot 10^{-3}$	13.7	451.7	
900	$268.1 \cdot 10^{-3}$	$257.8 \cdot 10^{-3}$	14.3	385.2	2.0688

The most remarkable feature is the occurrence of micropores of diameters situated within a restricted range (13.6—14.4 Å) at all temperatures. The pore diameter (around 14 Å) and the DTA weight loss support Klein and Garvey's[8] structural model of the starting gel. According to this model, the predominant structural units are cycles of 14 silicon atoms, linked by one bridging oxygen, which is situated at very sixth silicon atom. The diameter of such cycles is 15 Å, and the total weight loss for the formation of bridging oxygen at every OH group amounts to 25%.

The thermal treatment exerts no influence on the pore diameter, but a decrease in the pore number (and a subsequent decrease in surface area) is noted.

The picnometer density in CCl_4 is close (around 90%) to the previously reported data for similar glasses[8,12,22] and for the molten quartz glass. The differences in density are in connection with the amount of pores in the glass.

4. CONCLUSIONS

The above described procedure has been successfully used in the synthesis of porous glass whose density was approximately 90% of the density of molten quartz. These glasses may have some special uses. An adequate thermal schedule may lead to dense glasses, with properties similar to those of the conventionally prepared glasses.

The corroboration of data obtained by the methods used by the authors leads to the conclusion that glass-like structural units are preformed in solution during the hydrolysis-polymerization process and their form and assemblage are predetermined by changes in the conditions of reaction.

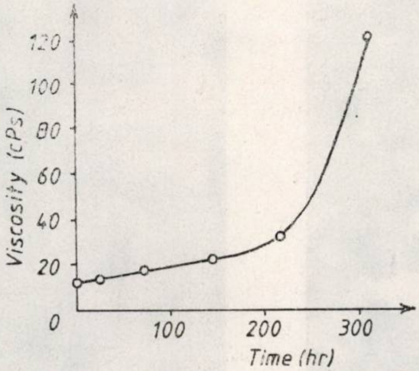

Fig. 1. — Viscosity vs. time plot for the hydrolysed solution A.

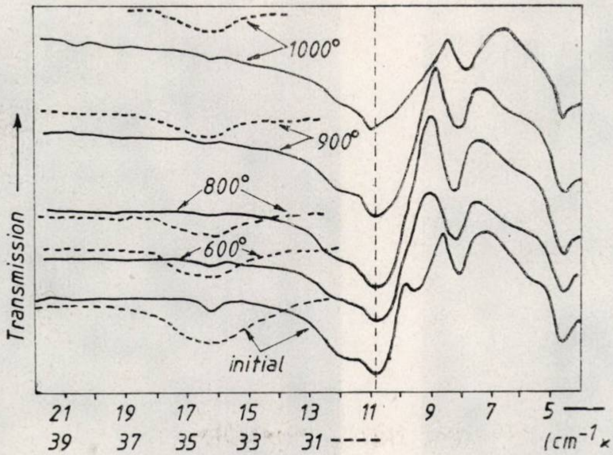

Fig. 2. — IR spectra of the starting gel and of samples calcinated at different temperatures.

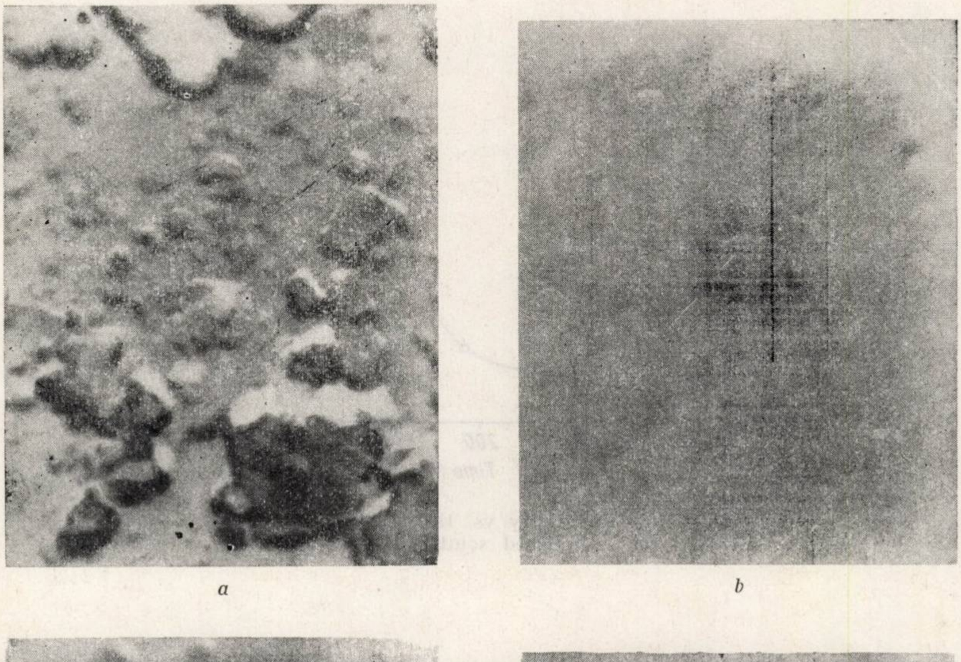

a *b* *c* *d*

Fig. 3. — The microphotographs of the studied samples (× 30.000); a — starting gel; b — sample calcinated at 900°C; c — sample calcinated at 1000°C; d — quartz glass.

REFERENCES

[1] V. Gottardi (editor), "Glasses and glass ceramics from gels". Proc. Int. Workshop on Glasses and Glass Ceramics from Gels. Padova, Italy, October 8–9, 1981; *J. Non-Cryst. Solids*, **48**, 1 (1982).

[2] H. Scholze (editor), "Glasses and glass ceramics from gels". Proc. 2nd Int. Workshop on Glasses and Glass Ceramics from Gels. Würzburg, Federal Republic of Germany, July 1–2, 1983; *J. Non-Cryst. Solids*, **63**, 1–2 (1984).

[3] J. Zarzycki (editor), "Glasses and glass ceramics from gels". Proc. 3rd Int. Workshop on Glasses and Glass Ceramics from Gels. Montpellier, France, September 12–14, 1985; *J. Non-Cryst. Solids*, **82**, 1–3 (1986).

[4] S. Sakka (editor), "Glasses and glass ceramics from gels. Proc. 4th Int. Workshop on Glasses and Glass Ceramics from Gels. Kyoto, Japan, July 13–15, 1987; *J. Non-Cryst. Solids*, **100**, 1–3 (1988).

[5] J. D. Mackenzie, *J. Non-Cryst. Solids*, **48**, 1 (1982).

[6] M. Nogami and Y. Morya, *J. Non-Cryst. Solids*, **37**, 191 (1980).

[7] G. Wilkinson, *Chemistry in Britain*, **18**, 850 (1982).

[8] L. C. Klein and J. Garvey, *J. Non-Cryst. Solids*, **48**, 97 (1982).

[9] G. Carturan and colab., *J. Non-Cryst. Solids*, **48**, 219 (1982).

[10] H. Dislich and P. Hinz, *J. Non-Cryst. Solids*, **48**, 11 (1982).

[11] S. P. Mukherjee and W. H. Lowdermilk, *J. Non-Cryst. Solids*, **48**, 177 (1982).

[12] S. Sakka and K. Kamiya, *J. Non-Cryst. Solids*, **48**, 31 (1982).

[13] P. H. Gaskel, "The Vitreous State" in *Disc. Faraday Soc.*, 55, 1970.

[14] M. Miller, *Czech. J. Phys.*, *B*, 18 (1968).

[15] J. Bock and G. J. Su, *J. Amer. Ceram. Soc.*, **53**, 69 (1970).

[16] A. W. Pliskin and H. S. Lehman, *J. Electrochem. Soc.*, **112**, 1013 (1965).

[17] J. Zarzycki and F. Naudin, *J. Chim. Phys.*, 830 (1961).

[18] D. M. Sanders and W. B. Person, *Appl. Spectroscop.*, **28**, 247 (1974).

[19] M. Sahini, M. Zaharescu, L. Constantinescu, E. Bărbulescu and G. Jitianu, *Epitoanyag*, **34**, 170 (1982).

[20] M. Yamans, T. Kojima, *J. Non-Cryst. Solids.*, **44**, 181 (1981).

[21] A. Bertoluzza, C. Fagnano, M. Morelli, V. Gottardi and M. Guglielmi, *J. Non-Cryst. Solids.*, **48**, 117 (1982).

[22] M. Yamane, S. Aso, S. Okano and T. Sakaino, *J. Mat. Sci.*, **47**, 607 (1974).

PRINTED IN ROMANIA

ORSZÁGOS MŰSZAKI INFORMÁCIÓS KÖZPONT ÉS KÖNYVTÁR 1883

16

NOTE POUR LES AUTEURS

La **Revue Roumaine de Chimie** publie des articles en anglais, français, russe, allemand ou espagnol. Les auteurs sont priés d'envoyer des articles et des comptes rendus inédits.

Les manuscrits seront dactylographiés à double interligne. La bibliographie, les tableaux et la légende des figures seront placés après le texte.

Si l'article fait partie d'une série numérotée, la partie précédente sera donnée comme première référence.

Chaque article sera précédé d'un résumé comprenant quinze lignes au maximum.

Les références bibliographiques dans le texte seront faites par des exposants sans parenthèses et paraîtront à la fin de l'ouvrage.

Les publications périodiques mentionnées dans la bibliographie seront présentées suivant les prescriptions internationales : le nom de l'auteur précédé de l'initiale du prénom, le titre du périodique abrégé conformément à « Chemical Abstracts » et souligné par une ligne, le numéro du tome indiqué par des chiffres arabes et souligné par deux lignes, suivi de la première page de l'article : à la fin, l'année de la parution sera placée entre parenthèses. Le numéro de la revue ne sera pas indiqué si les pages du volume sont numérotées consécutivement.

Les textes des livres ou traités inclueront : le nom des auteurs, précédés de l'initiale du prénom, le titre du livre entre guillemets et sans être souligné, le numéro du tome précédé par l'abréviation « vol. » (ou « Bd. »), le numéro de l'édition, les éditions (the publisher), la localité de la parution du livre, l'année de la parution et la page de la référence précédée(s) par l'abréviation « p » (ou « S »).

Les brevets seront indiqués comme suit : l'auteur ou la firme, le pays et le numéro du brevet, la date de la revue *(Chem. Abstr.)*. Par ex. : M. Jones (to Union Carbide Co.), Brit. Pat. 610 238, 2 Sept. 1959 : cf. *Chem. Abstr.*, **54**, 12808 (1960).

Si la référence n'a pas été lue en original, on indiquera aussi la revue de références consultée.

Les diagrammes seront tracés à l'encre de Chine sur papier calque. Les tableaux et les figures (en nombre strictement nécessaire), ainsi que les courbes dans les figures seront numérotés par des chiffres arabes. Leur explication sera donnée dans la légende des figures. Prière de ne pas inscrire les mêmes données dans les tableaux et les figures. Chaque tableau aura un titre. On indiquera dans le texte la place approximative des tableaux et des figures. Les formules chimiques seront incluses dans le texte ; en outre, elles seront transcrites sur papier calque, à l'encre de Chine.

Les auteurs sont priés d'indiquer les caractères italiques (en soulignant les lettres au crayon), ainsi que tout autre caractère spécial : les préfixes *ortho*, *méta*, *para*, *cis*, *trans*, etc. seront soulignés pour indiquer leurs caractères italiques et ne seront jamais écrits avec des majuscules.

Aucune correction à la main ne sera admise sur le manuscrit. Les corrections seront frappées à la machine. Les lettres grecques ou d'autres symboles spéciaux seront insérés à la main à l'encre clairement.

Le manuscrit sera signé par l'auteur.

Le titre courant aura 50 lettres au maximum.

L'entière responsabilité du contenu des articles appartient aux auteurs.

Sur demande on peut obtenir une note plus complète.

PRINTED IN ROMANIA

TRAVAUX PARUS AUX ÉDITIONS DE L'ACADÉMIE DE LA RÉPUBLIQUE SOCIALISTE DE ROUMANIE

ELENA CEAUŞESCU, **Răşini de hidrocarburi, vol. 1, 1988, 344 p.**

ELENA CEAUŞESCU, **Progrese în chimia şi tehnologia polimerilor, 1986, 446 p.**

ELENA CEAUŞESCU, **Forschungen im Bereich der Chemie und Technologie der Polymere, 1986, 444 p.**

ELENA CEAUŞESCU, **Cercetări în chimia şi tehnologia polimerilor, 1983, 520 p.**

ELENA CEAUŞESCU, **Noi cercetări în domeniul compuşilor macromoleculari, 1981, 536 p.**

ELENA CEAUŞESCU, **Polimerizarea stereospecifică a izoprenului, 1979, 307 p.**

ELENA CEAUŞESCU, **Research work on synthesis and characterization of macromolecular compounds. Contributions, 1974, 251 p.**

I. G. MURGULESCU, **Introducere în chimia fizică, vol. I. 1. Atomi, molecule, legătură chimică, 1976, 560 p.**

I. G. MURGULESCU, V. EM. SAHINI, **Introducere în chimia fizică, Vol. I, 2. Structura şi proprietăţile moleculelor, 1979, 604 p.**

I. G. MURGULESCU, E. SEGAL, **Introducere în chimia fizică, Vol. II. 1. Teoria molecular-cinetică a materiei, 1979, 1036 p.**

I. G. MURGULESCU, TATIANA ONCESCU, E. SEGAL, **Introducere în chimia fizică, Vol. II. 2. Cinetică chimică şi cataliză, 1981, 1024 p.**

I. G. MURGULESCU, J. PĂUN, **Introducere în chimia fizică, Vol. I, 3. Nucleul atomic, reacţii nucleare, particule elementare, 1982, 606 p.**

I. G. MURGULESCU, RODICA VÎLCU, **Introducere în chimia fizică. Vol. III. Termodinamica chimică, 1982, 624 p.**

I. G. MURGULESCU, O. M. RADOVICI, **Introducere în chimia fizică, Vol. IV. Electrochimia, 1986, 416 p.**

CRISTOFOR I. SIMIONESCU, VALERIA GORDUZA, **Implicaţii bioenergetice ale coloranţilor, 1988, 208 p.**

R. VÎLCU, M. LECA, **Termodinamica polimerilor prin cromatografie de gaze, 1987, 238 p.**

I. ZUGRĂVESCU, M. PETROVANU, **Cicloadiţii 3+2 dipolare, 1987, 446 p.**

RAUL MIHAIL, ION GROZEANU, **Estimarea secvenţială aplicată sistemelor chimice, 1986, 406 p.**

M. BREZEANU, I. PATRON, M. ANDRUH, **Combinaţii complexe polinucleare şi aplicaţiile lor, 1986, 244 p.**

A. T. BALABAN et al., **Labelled Compounds and Radiopharmaceuticals Applied in Nuclear Medicine,** coédition avec John Wiley and Sons, **1986, 742 p.**

D. PURDELA, **Nomenclatura chimiei organice — IUPAC, 1986, 451 p.**

PETRU BUDRUGEAC, **Probleme de chimie, 1986, 280 p.**

T. ONCESCU, S. G. IONESCU, **Conversie fotochimică şi stocare de energie, 1985, 272 p.**

V. DRĂGUŢAN, A. T. BALABAN, M. DIMONIE, **Olefin Metathesis and Ring-Opening Polymerization of Cyclo-Olefins,** coédition avec John Wiley and Sons, **1985, 544 p.**

C. LITEANU, I. RÎCĂ, **Optimizarea proceselor analitice, 1985, 360 p.**

N. PERESCU, **Chimia extracţiei cu solvenţi şi aplicaţii, 1985, 212 p.**

V. EM. SAHINI, M. HILLEBRAND, **Chimie cuantică în exemple şi aplicaţii, 1985, 382 p.**

GH. MARCU, **Chimia compuşilor coordinativi, 1984, 415 p.**

E. CORDOŞ, C. MANOLIU, **Spectrometria de absorbţie şi fluorescenţa atomică, 1984, 178 p.**

C. BODEA, **Tratat de biochimie vegetală, p. II, t. V, 1984, 438 p.**

N. ASANDEI, A. GRIGORIU, **Chimia şi structura fibrelor, 1984, 395 p.**

N. IONESCU, M. CĂLDĂRARU, **Oxidarea catalitică a olefinelor inferioare, 1983, 178 p.**

C. I. SIMIONESCU, F. DANEŞ, **Originea vieţii, 1984, 110 p.**

C. BODEA, **Tratat de biochimie vegetală, p. II, t. IV, 1982, 408 p.**

CR. SIMIONESCU, VALERIA GORDUZA, **Polimeri biocompatibili şi biologic activi, 1980, 479 p.**

M. FLORESCU, **Metode ştiinţifice în dezvoltarea industriei chimice moderne, 1979, 495 p.**

C. GH. MACAROVICI, **Analiza chimică cantitativă anorganică, 1979, 457 p.**

ISSN 0035—3930

1989 APR 0 [illegible]

I. P. Informaţia c. 2673

43 426

Lei 40

F1103

ACADÉMIE DE LA RÉPUBLIQUE SOCIALISTE DE ROUMANIE

REVUE ROUMAINE DE CHIMIE

Hommage à l'académicien
ELENA CEAUȘESCU

TOME 34

N° 3

Mars 1989

Rev. Roumaine Chim.

RRCHAX, 34, *3*, p. 709 – 904 (1989), Bucarest

EDITURA ACADEMIEI REPUBLICII SOCIALISTE ROMÂNIA

ACADÉMIE DE LA RÉPUBLIQUE SOCIALISTE DE ROUMANIE

COMITÉ DE RÉDACTION

Rédacteur en chef :

I. G. MURGULESCU, membre de l'Académie de la République Socialiste de Roumanie

Rédacteurs en chef adjoints :

A. T. BALABAN et V. EM. SAHINI, membres correspondants de l'Académie de la République Socialiste de Roumanie

Collège de rédaction :

EM. BRATU, ELENA CEAUŞESCU, ECATERINA CIORĂNESCU-NENITZESCU, CR. SIMIONESCU, membres de l'Académie de la République Socialiste de Roumanie ; P. SPACU, membre correspondant de l'Académie de la République Socialiste de Roumanie ; M. BANCIU, M. D. GHEORGHIU, I. HAIDUC, D. I. MARCHIDAN, G. NIAC et D. SĂNDULESCU

La Revue Roumaine de Chimie paraît 10 fois par an. Toute commande de l'étranger sera adressée à ROMPRESFILATELIA – sectorul Export-Import Presă, P.O. Box 12–201, télex 10376 prsfi r 78104 Bucarest, Calea Griviţei nr. 64–66, Roumanie

Les manuscrits, les livres et les revues proposés en échange, ainsi que toute correspondance seront envoyés à la rédaction :

REVUE ROUMAINE DE CHIMIE

125, Calea Victoriei, 79717 Bucarest, Roumanie, téléphone 50 76 80

EDITURA ACADEMIEI REPUBLICII SOCIALISTE ROMÂNIA
125, Calea Victoriei 79717, Bucarest, Roumanie, téléphone 50 76 80

HOMMAGE À L'ACADÉMICIEN

ELENA CEAUȘESCU

ORSZÁGOS MŰSZAKI INFORMÁCIÓS KÖZPONT ÉS KÖNYVTÁR
1883

IN HONOUR OF
ELENA CEAUŞESCU, D. CHEM. ENG., MEMBER OF THE ACADEMY OF THE SOCIALIST REPUBLIC OF ROMANIA

On January 7, this year, we celebrate the birthday and 50 years of revolutionary activity of Academician Elena Ceauşescu. A Doctor of Chemical Engineering, Member of the Executive Political Committee of the Central Committee of the Romanian Communist Party, First Vice-Prime Minister of the Government of the Socialist Republic of Romania, President of the National Council for Science and Education, Dr. Elena Ceauşescu chairs a vast scientific, political and social enterprise meant to bring into effect the country's plans for economic and social development, the important programs geared to a better organization and modernization of production, to increasing work productivity and efficiency, to a comprehensive implementation of the overall policy of the Romanian Communist Party and State, for the benefit of Romanian science, education and culture. The organization and management of the scientific research in this country, most especially in the fields of chemistry, and chemical technology and engineering, largely rely upon the innovative scientific spirit of, and direct guidance by Dr. Elena Ceauşescu.

As a direct outcome, the entire research and development system in chemistry has been given an appropriate coordination and has been integrated, along with the higher education in the field, with the respective industry.

The research work undertaken by Dr. Elena Ceauşescu is focused mainly on the chemistry and technology of macromolecular compounds; she has contributed to elucidating a number of major problems in the area — a most dynamic one in chemistry today, while also providing valuable contributions in all stages of applied research and

engineering, thus fostering the implementation in industry of the results of fundamental research.

Her studies dwell, *inter alia*, upon procedures for monomer and solvent purification; procedures for obtaining polymers via stereospecific polymerization and emulsion polymerization; procedures for obtaining polycondensates; studies on the structural characteristics of polymers and the relationship between structure and properties, as well as methods for the characterization of polymers. A series of studies deal with the use of complex catalysts for polymer synthesis in solution, with special emphasis on catalysts based on transition metals. Other works are concerned with the obtaining of polymers modified by isomerization, degradation and substitution reactions.

The stereospecific polymerization of isoprene holds an important place in the research work developed by Dr. Elena Ceauşescu, owing to the paramount relevance of this problem in today's chemistry of synthetic rubber. Part of the results were gathered in Dr. Ceauşescu's doctoral thesis. A special emphasis was placed on the synthesis of *cis*-1,4-polyisoprenic rubber that displays properties and structures similar to those of natural rubber, and substitutes for the latter in the tyre and technical item industry. Theoretical aspects connected with the reaction mechanism and kinetics, and the properties of the polyisoprene were also dealt with. Research was focused on the optimization of basic parameters, the obtaining of catalytic systems and development of the main steps of the technological flow-chart. The results have led to an industrial process for manufacturing *cis*-1,4-polyisoprenic rubber in Romania.

Dr. Elena Ceauşescu's scientific activity is also reflected in numerous papers published in scientific journals and in six monographs, first put out by Editura Academiei R. S. România, Bucharest, namely, "Research Work on Synthesis and Characterization of Macromolecular Compounds" (1974), "Stereospecific Polymerization of Isoprene" (1979), "Recent Research in the Field of Macromolecular Compounds" (1981), "Research in the Chemistry and Technology of Polymers" (1983), "Advances in Polymer Chemistry and Technology" (1986), and "Hydrocarbon Resins" (1988). Many publishing houses worldwide were soon to offer their readers translations of these books.

REVUE ROUMAINE DE CHIMIE

Tome 34, N° 3 Mars, 1989

IN HONOUR OF
ELENA CEAUŞESCU, D. CHEM. ENG., MEMBER OF THE ACADEMY OF THE SOCIALIST REPUBLIC OF ROMANIA

ELENA CEAUŞESCU, P. GHIOCA, H. PAVEN, GABRIELA BĂNICĂ, E. BUZDUGAN, IRINA CERCHEZ, RODICA STANCU, ANCA ION and DANIELA MARDARE, Thermoplastic plastomer/elastomer systems. Mechanical properties of the compounds of polyolefins and thermoplastic elastomer block-copolymers (in French) 711–724

CAMELIA BELDIE, I. GROSU, M. BOURCEANU and G. BOURCEANU, Periodically driven Briggs-Rauscher reaction 725–731

MARIA BRIE and IOAN A. SILBERG, Derivatives of 1,2-pyrazoles. I. Synthesis and IR-spectra of some new 3-methyl-5-aryl-1,2-pyrazoles 733–737

MARIANA CIUREANU, JEAN HERDAN and ALEXANDRU T. BALABAN, Electrochemical oxidation of N-(nitro-substituted phenyl)-4-amino-2,6-di-tert-butyl-phenols studied by cyclic voltammetry 739–748

V. COCHECI, E. GERASIMOU, C. CSUNDERLIK, L. COTARCĂ and A. NOVAC, Ozone oxidation of alkylamines in aqueous solution. I. Rate constants of ozone reactions with primary, secondary and tertiary amines 749–757

V. DRĂGUŢAN, I. DRĂGUŢAN, F. CHIRALEU and A. M. GLATZ, Friedel-Crafts chemistry of unsaturated alicyclic systems. III. Friedel-Crafts reaction of unsaturated alicyclic acids in the presence of various Lewis acids 759–763

LUCIAN ENESCU, AURELIA GHENCIULESCU, FILIP CHIRALEU and ILIE G. DINULESCU, Facile synthesis of 9-substituted *exo*-benzocyclobutenonorbornenes 765–769

I. GĂNESCU, J. ZSAKÓ, CS. VÁRHELYI and EDITH PÁLL, Study on the tetranitro-platinites(II) and hexanitro-platinates(IV) 771–777

N. I. IONESCU, MELANIA BOZEŞANU and ILEANA IOSIF, The influence of propylene on the mechanism of homogeneous pyrolysis of n-heptane . . 779–784

Rev. Roumaine Chim. 34, 3, 709–904, (1989), Bucarest

OCTAVIAN IORDACHE, GHEORGHIŢA JINESCU, DANIELA LAVRIC and VASILE LAVRIC, Kinetic theory of gas-liquid dispersions . . . . . . 785—795

ABETA IVAN and D. BECHERESCU, Ceramic pigments in the TiO_2—BaO—M_xO_y system . . . . 797—805

D. I. KRAVTSOV, V. M. PACHEVSKAYA, L. S. GOLOVCHENKO, B. A. KVASOV and E. I. FEDIN, Substituent effect on ^{19}F chemical shifts in 2-halo- and 2,6-dihalo-4-fluorophenols and anisoles (in Russian). . . . . 807—810

MINODORA LECA, MIHAELA OLTEANU and INGRID IONESCU-BUJOR, Interpolymer complexes formed by carboxylic polyacids with quaternary ammonium polysalts . . . . 811—819

A. MANTASHYAN, L. A. KHACHATRYAN and A. A. SUKIASYAN, he study of chain gas phase reactions of hydrocarbon — oxygen mixtures conversion in laser irradiation conditions (in Russian) . . . . 821—829

VERA A. MATVEEVICH, A. M. ROMANOV, RITA V. DRONDINA, V. N. SHAFRANSKI and VALENTINA P. MOTSPAN, Investigation of aluminum hydroxyfluoride complexes composition as a result of natural waters defluorination (in Russian) . . . . 831—837

M. R. MOSTAFA, H. M. ABU EL-NADER and G. M. ABU EL-REASH, Effect of acetophenone benzoyl hydrazone derivatives as corrosion inhibitors for the dissolution of aluminum in HCl solution . . . . 839—844

S. NEAGOE, LUCIA ANTONESCU, MARIA NEGOIU, VIORICA NEAGOE, D. NEGOIU and CORNELIA CERCASOV, Transition metal complexes with thioamides . . . . 845—854

V. V. POPOVSKII, Main problems in the field of ecologic catalysis (in Russian) 855—858

SOLOMON STERNBERG and MIHAELA DRĂGĂNOIU, The mean activity coefficient of $CuSO_4$ and excess functions in the aqueous e elctrolyte systems : $CuSO_4+Na_2SO_4+H_2O$; $CuSO_4+K_2SO_4+H_2O$ and $CuSO_4+ZnSO_4+H_2O$ 859—867

I. TEOREANU, ECATERINA ANDRONESCU and SIMONA CONSTANTINESCU, Compatibility relations in the $Li_2O-BaO-SiO_2$ system 869—876

D. N. TODOR, A. TĂNASE, V. DAVID and G. E. BAIULESCU, Thermoanalytical study of the complexes of palladium with α, α′-dipyridyl, *p*-nitrosodimethylaniline and *p*-nitrosodiphenylamine . . . . 877—881

CLEOPATRA VASILIU-OPREA, ALEXANDRU C. CONSTANTINESCU and SEVERIAN DUMITRIU, Study of thermal complexing of microcrystalline celluloses with transition metals. . . . . 883—894

LUMINIŢA VLĂDESCU and IRINEL BADEA, Analytical applications of a few azopyrazolonic derivatives. I. Spectrometric determination of iron(III) with an azopyrazolonic derivative of anthranilic acid . . . . 895—899

YA. V. ZACHINYAEV, A. I. BOBROV and A. I. GHINAC, 1,3-Dipolar cycloaddition reactions of nitril-imines with potassium salts of ethinylthio (seleno) lates (in Russian) . . . . 901—903

Revue Roumaine de Chimie, 34, 3, 711–724 (1989)

SYSTÈMES PLASTOMÈRE/ÉLASTOMÈRE THERMOPLASTIQUE. PROPRIÉTÉS MÉCANIQUES DES COMPOUNDS DE POLYOLÉFINES ET DE BLOC-COPOLYMÈRES ÉLASTOMÈRES THERMOPLASTIQUES

ELENA CEAUŞESCU, P. GHIOCA, H. PAVEN, GABRIELA BĂNICĂ, E. BUZDUGAN, IRINA CERCHEZ, RODICA STANCU, ANCA ION et DANIELA MARDARE
Institut de Recherches Chimiques, Spl. Independenţei 202, Bucarest, Roumanie

Reçu le 21 novembre 1988

This study shows the influence of linear butadiene-styrene block-copolymers on the physical and mechanical properties of high density polyethylene and polypropylene. There is a remarkable effect with a special emphasis on a higher shock resistance of the studied polyolefines.

La présente étude met en évidence l'influence des bloc-copolymères butadiène-styrène linéaires sur les propriétés physiques et mécaniques du polypropylène et du polyéthylène de haute densité. Cette influence est bien remarquable particulièrement sur la croissance de la résistance au choc des polyoléfines étudiées.

Les polyoléfines font partie dès plastomères les plus utilisés à la suite de leurs bonnes propriétés mécaniques et diélectriques, de la résistance chimique satisfaisante et de leur prix relativement bas. Leur résistance aux chocs (particulièrement aux températures basses) et leur flexibilité limitée diminuent pourtant leur domaine d'utilisation. L'amélioration des propriétés mécaniques des polyoléfines peut néanmoins être réalisée soit par copolymérisation aux différentes oléfines, comme par exemple le propylène à l'éthylène, ou l'éthylène à l'acétate de vinyl ou à 1-butène [1,2], soit par compoundage aux élastomères tels le polybutadiène [3], le butil-caoutchouc [4] ou le polyisobutène [5], les copolymères éthylène-propylène [6,7], etc. L'effet favorable des caoutchoucs s'étend aussi sur les compounds de polyoléfines, comme par exemple celui de polyéthylène de haute densité mélangée au polypropylène isotactique [8,9].

L'apparition des caoutchoucs thermoplastiques à base de bloc-copolymères butadiène-styrène offre une nouvelle manière pour renforcer les polyoléfines par compoundage [10,13], ce qui permet d'obtenir de nouveaux matériaux dont les propriétés sont supérieures à celles des élastomères conventionnels.

La présente étude se propose de réaliser une investigation systématique des effets d'un bloc-copolymère butadiène-styrène linéaire SBS) sur le polyéthylène à haute densité (HDPE) et à basse densité

(LDPE) et sur le polypropylène (PP). On a utilisé aussi comme modificateur un tribloc-copolymère hydrogéné dont le bloc central est un copolymère élastique d'ethylène et de 1-butène. Parmi les variétés de HDPE utilisées il y a eu aussi un copolymère de 1-butène, afin d'évaluer l'effet combiné de la copolymérisation et de la modification par un bloc-copolymère butadiène-styrène.

Les propriétés des polyoléfines utilisées sont preséntées dans le ableau 1. L'on a choisi comme polymères de base les polyoléfines de a production indigène courante.

Tableau 1

Propriétés des polyoléfines

Propriétés	Polyéthylène haute densité		Polypropylène
Type	A52BB	6131 M1)	F 401
Code	HDPE-1	HDPE-2	PP
Masse moléculaire (Mv)	77000	95100	95100
Densité, g·cm^{-3}	0.9370	0.9394	0.8955
Indice d'écoulement, g/10 min	0.702)	0.232)	1.423)
Résistance maxima, σcs, MPa	26.4	23.5	35.7
Résistance à la traction, σb MPa	24.9	—	30.6
Allongement à la rupture, %	980	—	680
Dureté, °ShD	65	63	74
Résistance au choc Izod, +22°C, 7/min	4.84	1.06	0.28
Resistance au choc Izod, −20°C, 7/min	3.34	0.49	0.16
Module complexe de courbement, E, MPa	559±29	604±30	995
Module dynamique d'élasticité, E′, MPa	1570	1365	1915
Module de pertes mécaniques, E″, MPa	158	235	195
Facteur de pertes dynamiques, $\beta = E''/E_0$	0.112	0.175	0.102
Vitesse de propagation du son à 1 MHz, m/s	2433	2350	

Note : 1) Copolymère à 4% 1-buthène
2) à 190°C
3) à 230°C

Les propriétés des élastomères thermoplastiques utilisés comme modificateurs des polyoléfines sont présentées dans le tableau 2.

La concentration de l'élastomère dans le système a été variée entre des limites larges (la fraction de volume d'élastomère $\varnothing_R$, fut entre 0 et 0,5), ce qui est une suite d'une étude antérieure, où l'on a étudié les propriétés des systèmes où la phase prédominante était l'élastomère thermoplastique /14/. Les compounds ont été réalisés par un calandre de laboratoire à coefficient réduit de friction (le rapport de rotation des rouleaux étant de 20 : 22).

L'ordre de dosage des compounds fut toujours le même : d'abord la polyoléfine et, après l'avoir fait adhérer aux rouleaux, l'on a ajouté le bloc-copolymère. La température des rouleaux fut de 190°C dans le cas des compounds de polypropylène, de 180—185°C dans le cas du polyéthylène à haute densité et de 155—160°C dans le cas du polyéthylène à basse densité. L'aspect final du mélange, après l'avoir soumis au calandrage, fut une feuille d'une épaisseur de 2—4 mm.

Tableau 2

Propriétés des bloc-copolymères élastomères thermoplastiques

Type	Bloc-copolymères butadiène-styrène C. P. Brazi	Bloc-copolymères butadiène-styrène hydrogéné
Code	Eltar-L L-2	Elexar 8421Z Shell HL
Structure [1]	S–B–S	S–EB–S
Contenu en styrène, %	35	—
Module réel d'élasticité à la traction, E', (MPa)	3.4[2]	121
Module de pertes à traction, E'' (MPa)	—	17
Module de rigidité, Es (MPa)	1[3]	33
Rapport de Poisson	0.5	0.5

[1] S = bloc styrène, B = bloc butadiène, EB = bloc copolymère, statistiquement éthylène-1-butène

[2] selon /15/

[3] estimé

Le calandrage a été prolongé suffisamment pour que la morphologie du compound soit la plus rapprochée de l'état morphologique stationnaire /16/, qui est relativement indépendante par rapport à l'histoire thermique et mécanique de l'échantilllon.

Ces compounds ont été transformés en plaques nécessaires aux test-physico-mécaniques, par pressage à 190°C (pour PP et HDPE) respectivement 170°C (pour LDPE) pendant 15 min., suivi d'un brusque refroidissement sous pression.

Les propriétés mécaniques ont été déterminées selon les méthodes normalisées.

Les indicateurs physico-mécaniques ont été déterminés sur des éprouvettes matricées (selon STAS 6642/73) à une vitesse de traction de 100 cm/s).

Les propriétés à la traction ont été déterminées selon STAS 6642/73, la dureté Shore D selon STAS 8643/73, le module de rigidité selon ASTM D 747/70 et, la résistance au choc Izod sur des éprouvettes matricées en une plaque de 4 mm d'épaisseur selon STAS 7310/87. Les déterminations dynamiques ont été réalisées selon ISO 6721/83.

LES PROPRIÉTÉS DES COMPOUNDS PRESSÉS

Les compounds pressés contenaient en tant que polymères de base du polyéthylène à haute densité (HDPE-1), du copolymère d'éthylène avec du 1-butène (HDPE-2) et, respectivement, du polypropylène (PP), modifiés avec du tribloc-copolymère butadiène-styrène linéaire L-2; dans le cas du polypropylène l'on a aussi étudié le mélange au bloc-copolymère hydrogéné HL.

La dureté de ces compounds (mieux dit le rapport entre la dureté du compound et la dureté de la polyoléfine (H/H_c) se situe, selon la fraction de volume du caoutchouc ($Ø_R$) sur deux curvilignes distinctes le compound avec HL présentant, pour n'importe laquelle des concentrations d'élastomère, des valeurs plus élevées (fig. 1). Ceci est une conséquence naturelle du fait que le bloc-copolymère hydrogéné a une dureté

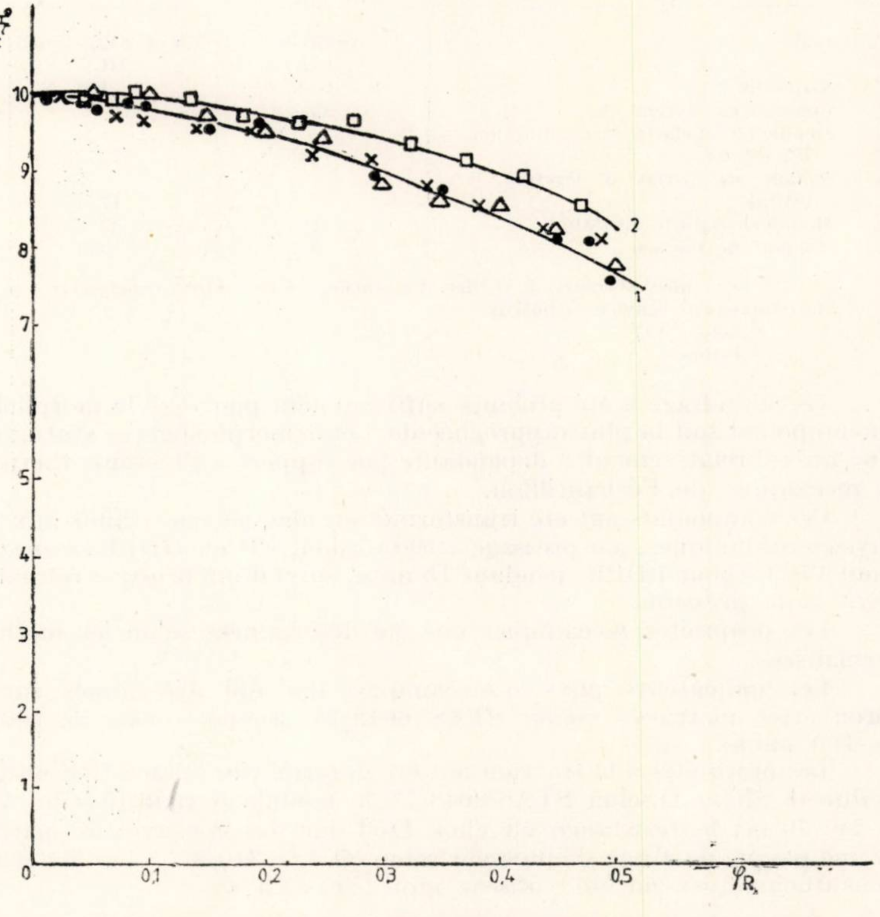

Fig. 1. — Variation de la dureté des compounds de polyoléfines selon la fraction de volume de caoutchouc thermoplastique. △ HDPE-1/L-2 ; ● HDPE-2/L-2 ; × PP/L-2 ; □ PP/HL 1: Compounds à bloc-copolymère butadiène-styrène; 2: Compounds de PP à bloc-copolymère hydrogéné.

plus élevée par rapport au bloc-copolymère butadiène-styrène. Par conséquent l'on remarque que la nature de l'élastomère a une influence déterminante sur le rapport H/H_0. L'effort unitaire maximal (à la limite du fluage) enregistre, à son tour, une baisse avec la concentration du ccaoutchouc de compound, touchant un minimum aux valeurs du $Ø_R$ de

0,5, respectivement à l'inversion des phases. Ce comportement concorde à la diminution du caractère plastique (caractérisé par des valeurs élevées de l'effort unitaire de fluage) et la croissance de celui élastique (chez lequel l'effort de fluage, si fluage il y a, est moindre que la résistance à la traction) (fig. 2). Le phénomène est déterminé morphologiquement, la phase continuelle étant, pour $Ø_R < 0,5$-polyoléfine, et pour $Ø_R > 0,5$-élastomère. Pour $Ø_R \approx 0,5$ le matériel contient un réseau interpénétré de polyoléfine et de l'élastomère [10-17].

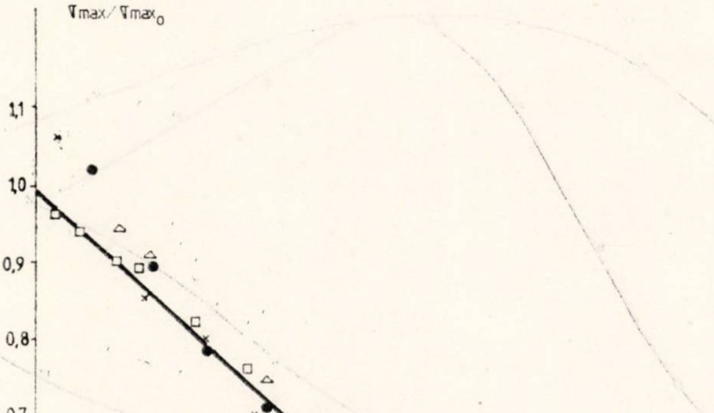

Fig. 2. — Variation de l'effort unitaire max. selon la fraction de volume de caoutchuc thermopalastique du compound. △ HDPE-1/L-2 ; ● HDPE-2/L-2 ; × PP/L-2 ; □ PP/HL.

Du point de vue de la résistance au choc à T = 20°C les compound à base de HDPE ont un comportement différent par rapport à ceux à base de PP (fig. 3), les deux séries de compounds contenant du HDPE; elles présentent déjà de petites concentrations de caoutchouc à croissances considérables de la résistance au choc, qui passent par un maximum à $\varnothing_R$ 0,2. A ce contenu de caoutchouc l'on obtient pratiquement la même résistance au choc pour HDPE-1 et HDPE-2. Au contraire, dans le cas des mélanges à base de polypropylène, les modifications de la résistance au choc sont, jusqu'à un $\varnothing_R$ 0,2, relativement mineures, mais pour des concentrations plus élevées de caoutchouc on peut constater une croissance monotone de la résistance. La variation relative de la résistance au choc (en tant que rapport entre la résistance du compound et celle du polymère de base, I/I_0) est présentée dans la figure 4. A ce que l'on peut constater, une telle expression de la résistance au choc des compounds à base de PP dépasse, pour des concentrations élevées d'élastomère, celle des compounds de HDPE.

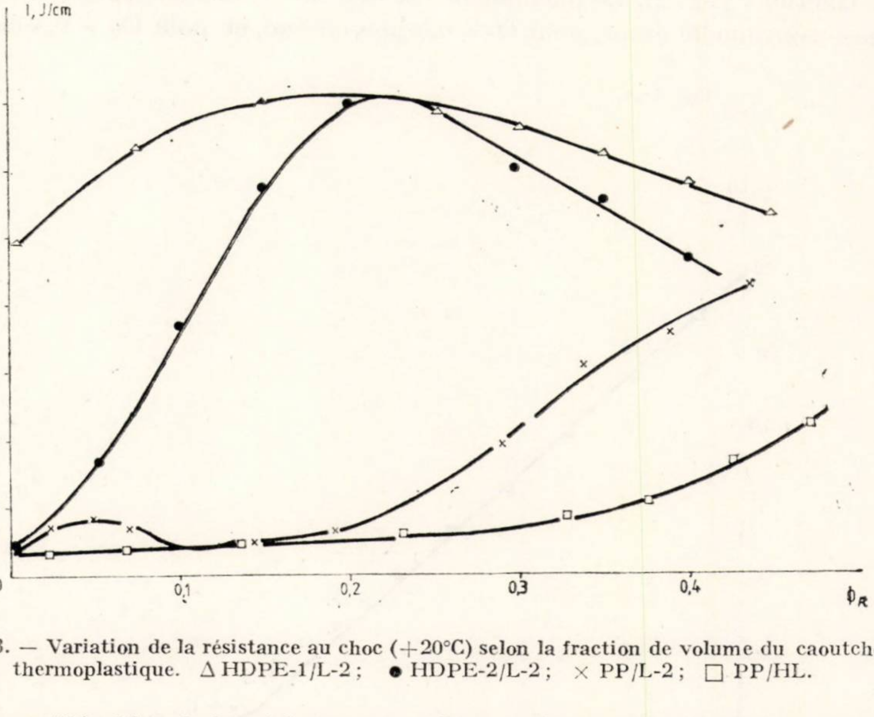

Fig. 3. — Variation de la résistance au choc (+20°C) selon la fraction de volume du caoutchouc thermoplastique. △ HDPE-1/L-2 ; ● HDPE-2/L-2 ; × PP/L-2 ; □ PP/HL.

Généralement, on peut remarquer un effet d'autant plus puissant du modificateur que la résistance initiale au choc du plastomère est plus réduite. Dans la figure 4 l'on remarque un maximum local de la résistance au choc du système polypropylène/L-2 qui se manifeste pour $\varnothing_R$0,05. A —20°C le tableau de la résistance au choc se modifie, car les compounds à base de copolymère éthylène-1-butène (HDPE-2) présente un maximum accentué pour $\varnothing_R$ 0,7. Quoique l'effet du bloc-copolymère

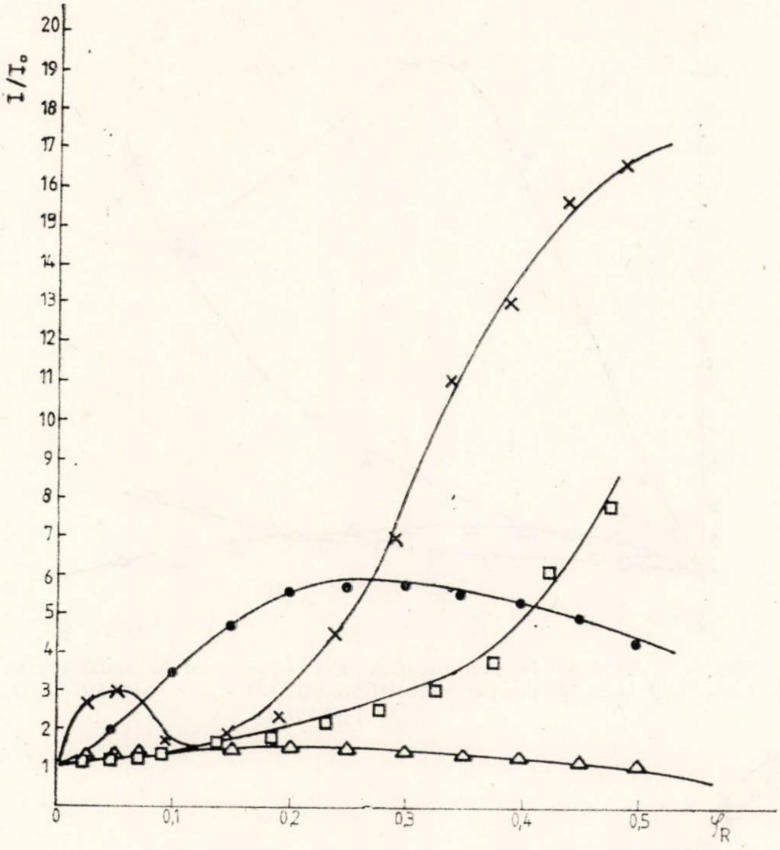

Fig. 4. — Effet de la concentration d'élastomère sur la résistance relative au choc (+20°C) des compounds à polyoléfines. △ HDPE-1/L-2 ; ● HDPE-2/L-2 ; × PP/L-2 ; □ PP/HL.

butadiène-styrène L-2 sur le polypropylène soit en quelque sorte plus réduit à T= −20°C, ce système présente une croissance sensible de la résistance au choc, même aux températures basses. Pour essayer de tirer au clair le mécanisme par lequel les élastomères influent la résistance au choc des polyoléfines étudiées, l'on a déterminé les propriétés mécaniques dynamiques des compounds. Dans la figure 6, l'on présente la variation du module dynamique d'élasticité selon la fraction de volume d'élastomère dans les compounds. On peut aisément constater que E′ diminue au fur et à mesure que le contenu en caoutchouc augmente comme prévu, compte tenu de la très grande différence entre les valeurs E′ des constituants (tableaux 1 et 2). La manière dont on peut modeler mathématiquement cette variation a été examinée en détail par une autre étude.[18] Du point de vue de la qualité, l'effet sur le module complexe semble, dans le cas des polyoléfines, plus compliqué par rapport à celui des systèmes purement amorphes, par exemple PCV/SBS.[19] Ceci est une conséquence de la complexité des systèmes fondés sur des polyoléfines contenant, par

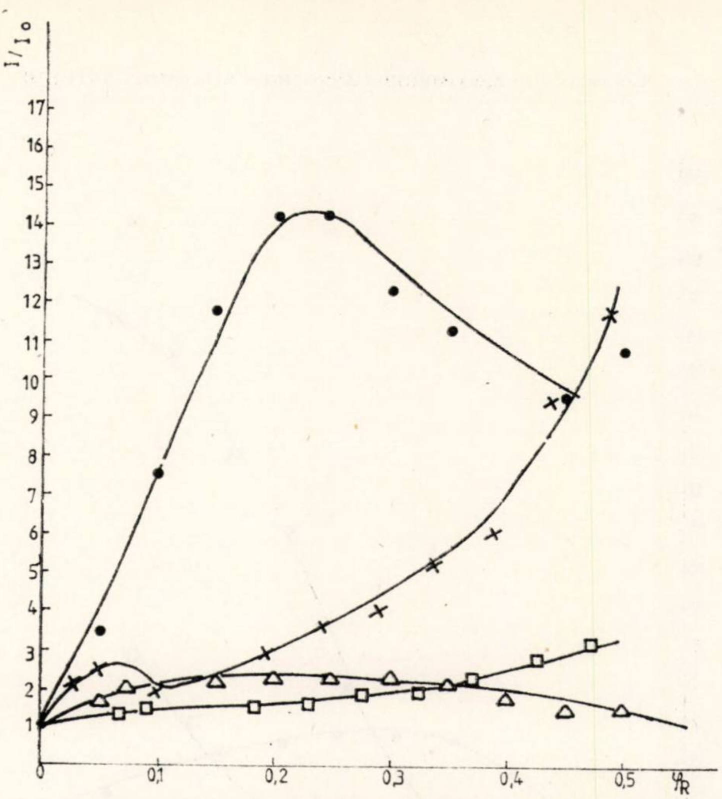

Fig. 5. — Effet de la concentration d'élastomère sur la résistance au choc (−20°C) des compounds à polyoléfines. ΔHDPE-1/L-2 ; ●HDPE-2/L-2 ; × PP/L-2 ; □ PP/HL.

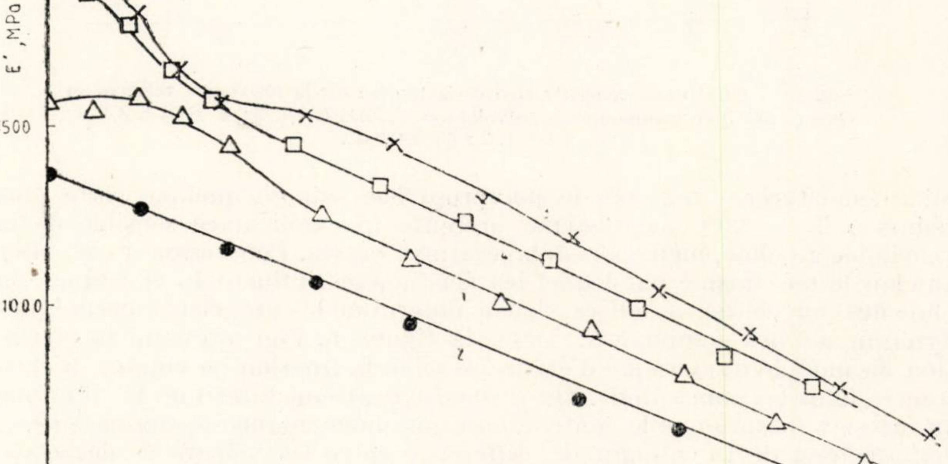

Fig. 6. — Variation du module dynamique d'élasticité E' selon la fraction de volume de l'élastomère dans les compounds. 1. HDPE-1/L-2; 2. HDPE-2/L-2; 3. PP/L-2; 4. PP/HL

exemple dans le cas de la modification avec des copolymères butadiène-styrène, les phases suivantes :

- phase cristallin de polyoléfine
- phase amorphe de polyoléfine
- phase élastomère formé de :
    - matrice polybutadiène
    - domaines polystyrène.

L'alure des curvilignes de la figure 6 nous fait constater une différence entre l'aspect relativement uniforme de la variation du module des compounds à base de copolymère éthylène-1-butène (HDPE-2) et les variations de pente enregistrées dans le cas des autres polyoléfines. Selon nous, ces manques d'uniformité sont liés aux modifications de la phase cristalline induites par la présence de l'élastomère. On sait que la cristallisation des polyoléfines est influencée non seulement par le degré de tacticité[20] mais aussi par la nature et la proportion des élastomères présents en tant qu'additifs [5,7,8-21]. La structure de ces systèmes dépend fortement de la température de cristallisation [7]. Le manque de l'uniformité susmentionée dans le cas du polymère HDPE-2 pourrait s'expliquer par son degré plus réduit de cristallisation comme une conséquence de la présence dans la chaîne des unités distribuées de manière statistique de 1-butène.

Le module complexe de pertes E'' présente une variation différente dans le cas des compounds contenant du HDPE-2 par rapport aux autres polyoléfines, puisqu'il enregistre une croissance plafonnée à un large maximum dans l'intervalle $\O_R = 0{,}1 - 0.3$.

La variation relative du facteur de pertes B défini comme le rapport entre E'' et E (fig. 8) est tout aussi différente, car elle présente une croissance à un maximum pour $\O_{\hat{R}} = 0{,}3$ pour tous les autres compounds ayant une relative constance du rapport β/β_0.

Ayant pour base les propriétés mécaniques déjà mentionnées, l'on peut essayer d'établir des corrélations capables de mettre en lumière le mécanisme de la modification. Ainsi, la variation de la résistance au choc (à +20°C) en fonction de E'' (fig. 9) nous fait constater que dI/dE'' a des valeurs positives (dans le sens de la croissance de la concentration d'élastomère), mais selon la première branche de la curviligne figurant les compounds à base de HDPE-2, l'on peut conclure que, pour ces mélanges, le mécanisme prédominant d'action de l'additif élastomère est la croissance de l'énergie dissipée au moment du choc.

La théorie classique du renforcement des plastomères en ajoutant des caoutchoucs considère cet effet comme celui des domaines d'élastomère qui empêcheraient la propagation des microfissures à travers la matrice plastomère. [22,23]

La nouvelle théorie, due à Hsiao et Buckwall [24,26] explique le renforcement par cela que les particules de caoutchouc déterminent la formation de microfissures, dont la moitié à peu près du volume nouvellement formé est occupée par les fibres de plastomère, puissamment étirées. L'existence de ces fibrilles de plastomère a pu être mise en évidence par microscopie électronique [27,28]. Au niveau macroscopique ceci équivaut à une modification du mécanisme de destruction, depuis le cassant au ductile. Des études de microscopie électronique à balayage (SEM) ont

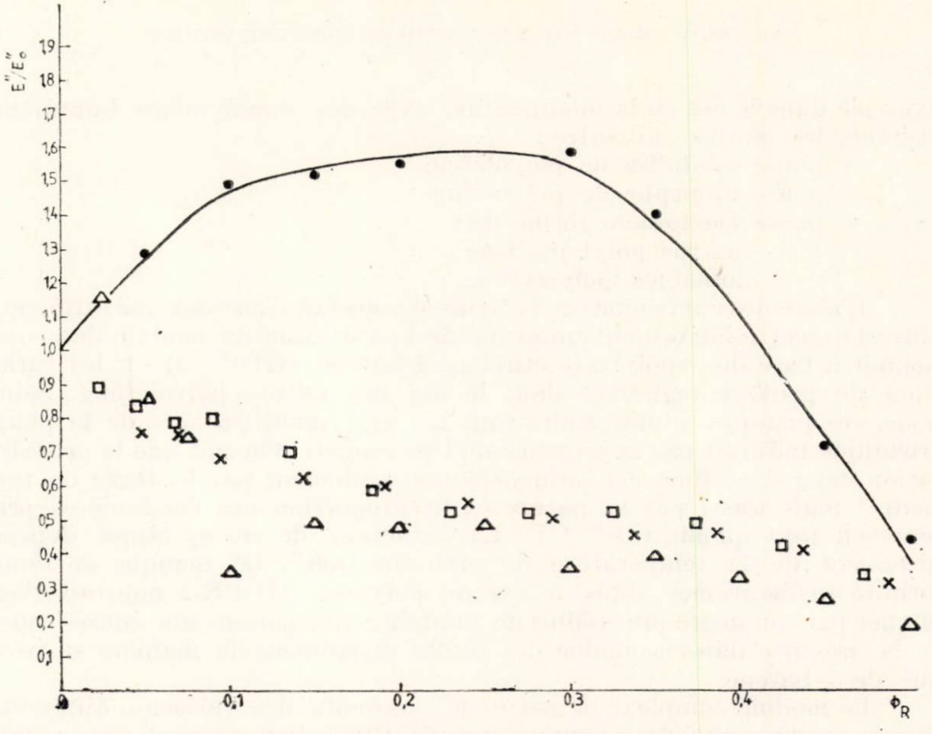

Fig. 7. — Variation relative du module de pertes dynamiques E'' selon la fraction de volume de l'élastomère dans les compounds. △ HDPE-1/L-2 ; ● HDPE-2/L-2 ; × PP/L-2 ; □ PP/HL.

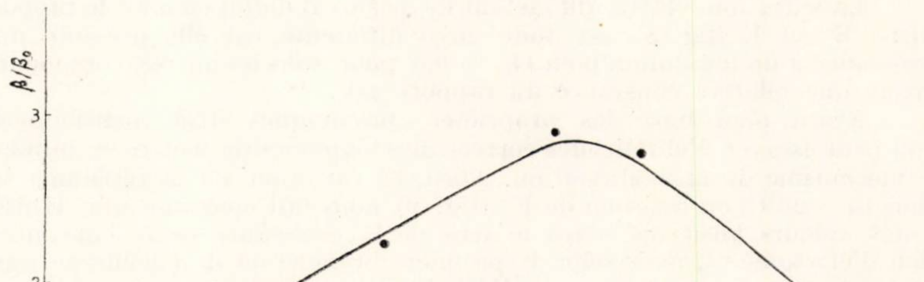

Fig. 8. — Variation relative du facteur de pertes β selon la fraction de volume de l'élastomère dans le compound. △ HDPE-1/L-2 ; ● HDPE-2/L-2 ; × PP/L-2 ; □ PP/HL

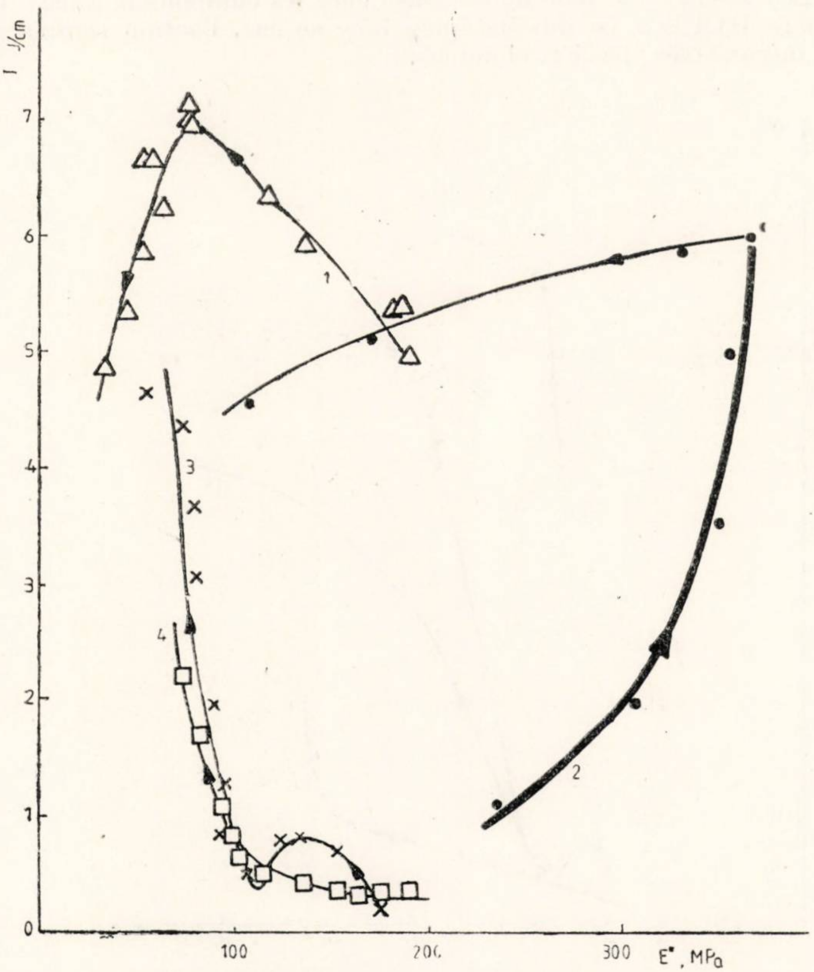

Fig. 9. — Dépendance de la résistance au choc (+20°C) du module de pertes dynamiques. Le sens de croissance de la concentration d'élastomère dans les compounds est indiqué par des flèches : 1. HDPE-1/L-2 ; 2. HDPE-2/L-2 ; 3. PP/L-2 ; PP/HL.

prouvé que dans le polypropylène pur la destruction est cassante et que dans l'HDPE, quoique le comportement soit principalement cassant, il y a une quelconque déformation plastique accompagnée de l'apparition des fibrilles.

La figure 10, représentant la dépendance de la résistance au choc de l'inverse du module dynamique d'élasticité, est un argument en faveur du fait que ce passage depuis la destruction cassante à celle ductile est celui qui intervient chez les autres compounds. L'on constate que cette dépendance présente dans tous les cas des tronçons linéaires relativement étendus, ce qui démontre la corrélation entre la résistance au choc et la plasticité du compound.

Il y a aussi une telle dépendance chez les compounds à base de copolymère HDPE-2, ce qui indique, dans ce cas, l'action semblable des deux mécanismes décrits ci-dessus.

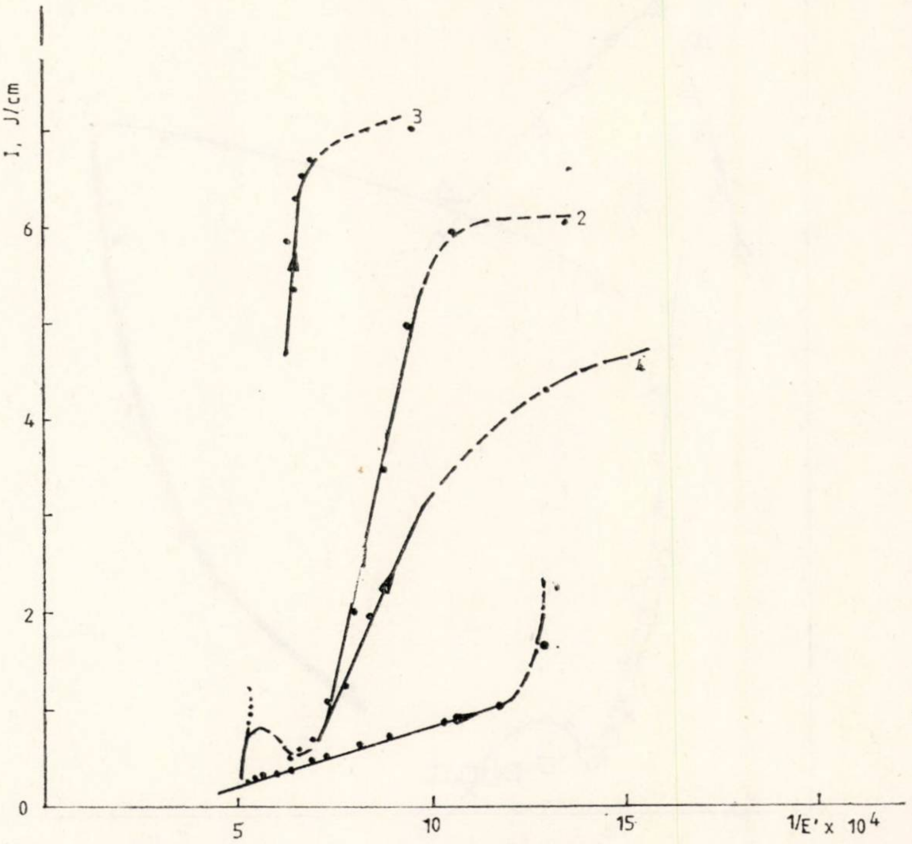

Fig. 10. — Dépendance de la résistance au choc (+20°C) selon l'inverse du module dynamique d'élasticité. Le sens de croissance de la concentration d'élastomère dans le compound est indiqué par des flèches. 1. HDPE-1/L-2 ; 2. HDPE-2/L-2 ; 3. PP/L-2 ; 4. PP/HL.

Le diagramme Petrich représenté dans la figure 11 qui indique la corrélation entre la résistance au choc et la résistance maxima à la traction (σ_{max}) soutient à son tour ces affirmations. Il est difficile de préciser la manière exacte dont agit l'élastomère pour modifier le caractère du comportement mécanique de la matrice.

Selon toute probabilité, le caoutchouc détermine une plastification de la phase amorphe de la polyoléfine. Les données dont nous disposons n'indiquent non plus la raison pour laquelle, dans les compounds contenant du HDPE, la résistance au choc présente un maximum à $Ø_R = 0.2$ (fig. 3). Ceci pourrait être corrélé à une modification de la cristallinité de la matrice produite de la résistance de la matrice à la suite de l'inclusion d'élastomère dans la phase cristalline.

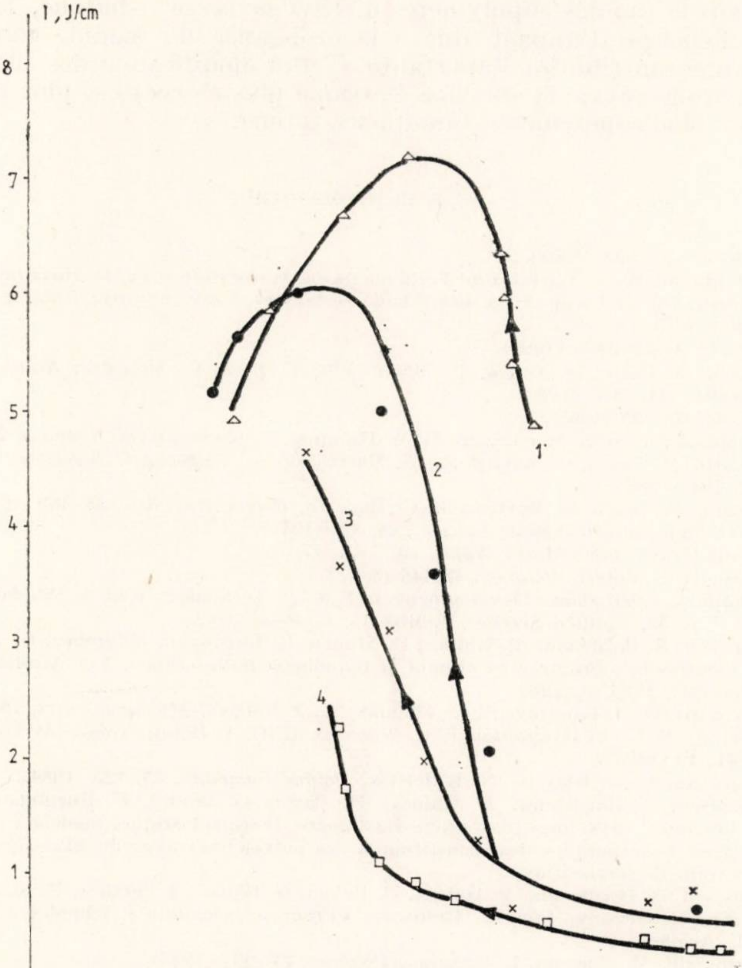

Fig. 11. — Corrélation entre la résistance au choc et la résistance maxima à la traction des compounds de polyoléfines et d'élastomères thermoplastiques. Le sens de croissance de la concentration d'élastomère est indiqué par des flèches.

En conclusion, l'on peut affirmer que la modification des polyoléfines (HDPE et PP) avec des bloc-copolymères élastomères thermoplastiques représente une manière convenable pour améliorer certaines propriétés mécaniques, particulièrement la résistance au choc. Cette amélioration est d'autant plus importante que la résistance initiale au choc de la polyoléfine est plus réduite. Dans le cas du polyéthylène à haute densité et du polypropylène, le mécanisme principal est celui de modification de la destruction depuis le cassant au ductile par l'initiation de la formation de microfissures contenant des microfibrilles étirées.

Dans le cas des copolymères d'éthylène avec 1-butène, la dissipation de l'énergie d'impact due à la croissance du module complexe de pertes a une contribution importante. L'effet modificateur des bloc-copolymères hydrogénés (à T_g du bloc élastique plus élevée) est plus réduit que celui des bloc-copolymères butadiène-styrène.

BIBLIOGRAPHIE

[1] Brev. R. U. 915622 (1963).

[2] A. J. Wildschut, dans « Chemie und Technologie der Kunststoffe », éd. R. Houwink., A. J. Staverman, vol. II/1, cap. II, p. 125, Akad. Verlagsges. Geest & Portig, Leipzig, 1963.

[3] Brev. Belg. 617870 (1962).

[4] Brev. E. U. A. 2939860 (1960).

[5] L. Bianchi, A. Forte, R. Greco, E. Martuscelli, F. Riva, C. Silvestre, *Kautschuk Gummi Kunstst.*, **34**, 281 (1984).

[6] Brev. Belg. 623729 (1963).

[7] F. Coppola, R. Greco, E. Martuscelli, H. W. Kammer, C. Kummerlöwe, *Polymer*, **28**, 47 (1987).

[8] L. D'Orazio, R. Greco, C. Mancarella, E. Martuscelli, G. Ragosta, C. Silvestre, *Polym. Eng. Sci.*, **22**, 536 (1982)

[9] L. D'Orazio, R. Greco, E. Martuscelli, G. Ragosta, *Polym. Eng. Sci.*, **23**, 489 (1983).

[10] K. von Henten, *Gummi Asbest. Kunstst.*, **26**, 387 (1973).

[11] A. L. Bull, *Plast. Rubb. Mater. Appl.*, 1977 (2), 27.

[12] S. Danesi, R. S. Porter, *Polymer*, **19**,448 (1978)

[13] F. Mistralli, A. Proni, dans « Developments in Rubber Technology » ed. A. Whelan, K. S. Lee, vol. 3, p. 59, Applied Science Publishers, London, 1982.

[14] E. Ceauşescu, R. Bordeianu, P. Ghioca, R. Stancu, E. Buzdugan, I. Cerchez, G. Bănică, dans E. Ceauşescu, « Progrese în chimia şi tehnologia polimerilor », Ed. Academiei R.S.R., Bucureşti, 1986, p. 226.

[15] D. B. Alward, D. J. Kinning, E. L. Thomas, L. J. Fetters, *Macromolecules*, **19**, 215 (1986).

[16] C. J. Nelson, G. N. Avgeropoulos, F. C. Werssert, G. G. A. Böhm, *Angew. Makromol. Chem.*, **60/61**, 49 (1977).

[17] J. Karger-Kocsis, L. Kiss, V. N. Kuleznev, *Polym. Commun.*, **25**, 122 (1984).

[18] E. Ceauşescu, R. Bordeianu, P. Ghioca, H. Paven, G. Bănică, E. Buzdugan, R. Stancu I. Cerchez : « Systèmes plastomère-élastomère thermoplastique, modelage de certaines propriétés mécaniques des constituants des polyoléfines avec du bloc-copolymère » v.o (en train de publication).

[19] E. Ceauşescu, R. Bordeianu, P. Ghioca, H. Paven, G. Bănică, I. Cerchez, R. Stancu, E. Buzdugan, M. Olteanu, dans E. Ceauşescu « Progrese în chimia şi tehnologia polimerilor » Ed. Academiei.

[20] E. Martuscelli, M. Pracella, L. Crispino, *Polymer*, **24**, 693 (1983).

[21] L. Bianchi, S. Cimmino, A. Forte, R. Greco, E. Martuscelli, F. Riva, C. Silvestre, *J. Mater Sci.*, **20**, 895 (1985).

[22] E. H. Merz, G. V. Claver, M. Bear, *J. Polym. Sci.*, **22**, 325 (1956).

[23] L. E. Nielsen, « Mechanical Properties of Polymers », Reinhold, New York, 1962, chap. 6.

[24] C. B. Buckwall, R. R. Smith, *Polymer*, **6**, 437 (1965).

[25] C. C. Hsiao, J. A. Sauer, J. Appl. Phys., **21**, 1071 (1950).

[26] C. B. Buckwall, « Toughened Plastics », Applied Science Publ., London, 1977.

[27] M. Matsuo, C. Nozaki, Y. Jyo, *Polym. Eng. Sci.*, **9**, 197, 206 (1969).

[28] R. P. Kambour, R. R. Russel, *Polymer*, **12**, 237 (1971).

[29] R. P. Petrich, *Polym. Eng. Sci.*, **13**, 248 (1973).

Revue Roumaine de Chimie, **34**, *3*, 725–731 (1989)

PERIODICALLY DRIVEN BRIGGS-RAUSCHER REACTION

CAMELIA BELDIE, I. GROSU, M. BOURCEANU and G. BOURCEANU
Department of Physical Chemistry, Polytechnic Institute "Gh. Asachi", Jassy, Romania

Received October 22, 1988

The influence of the external periodical perturbations on the stability of the self organization chemical reactions was studied using a reactor fed in continous flux (C.S.T.R.), in which the oscillatory reaction took place. In the reactor, sinusoidal periodical perturbations with different frequencies of the one of the reactants were introduced.

The first oscillatory chemical reaction was accidentally discovered by Bray [1] (1921) within closed homogeneous systems. The reaction consists of the catalytic decomposition of H_2O_2 by the iodic acid – iodine mixture in the presence of Mn^{2+}. The reaction was overlooked for a long time. The second oscillatory chemical reaction was discovered, also accidentally, by Belousov[2] (1958) using closed homogeneous systems during the oxidation of citric acid by $KBrO_3$ catalyzed by the $Ce^{4+} - Ce^{3+}$ mixture.

The existence of the oscillatory reactions until 25 years ago was regarded with scepticism and it was the topic of some hard controversy in the chemical world [3]. The great part of chemists were convinced that the appearance of the temporal or spatial order in the chemical systems was only an artificial arrangement of the investigation, going into contradiction with the 2nd principle of thermodyamics.

The belief in the existence of these true oscillatory chemical reactions and therefore the interest in their study increased with the development of the nonlinear thermodynamics at the Bruxelles school[4–8]. Indeed, far from the thermodynamical equilibrium, within the nonlinear systems, the appearance of the order is compatible with the second principle of thermodynamics. [9].

Likewise, the interest of the chemists in the oscillatory chemical reactions was aroused by Zhabotinski who reinvestigated Belousov's reaction in 1964 and studied it in several ways. [10,11] Today, the reaction is well known as the Belousov-Zhabotinski reaction.

In 1973, Bray's reaction was restudied and slightly modified by Briggs and Rauscher, and it is known under the name Briggs-Rauscher's reaction. [12]

The oscillatory reactions were carried out within closed systems up to 1975, without substance exchange with the exterior. Such systems present periodical oscillations for short periods of time because the reactant concentrations decrease fast below the critical value, and the system tends towards an equilibrium state.

Taking into consideration the theoretical results of the nonlinear thermodynamics — which proved that the temporal or spatial order may arise and can be unlimitedly preserved only in the open systems subject to some constant constraints — in 1975 the Bordeaux school led by Professor Pacault performed periodical chemical oscillations in an open system. The system consists of a reactor fitted with a perfect stirrer continuously supplied with reagents. The system is well-known under the name "continuous flow stirred tank reactor" (C.S.T.R).

By means of the phase diagram called "Cross-shaped phase diagram" given by Boissonade and De Kepper,[13] in 1980—1986 it was possible to discover over 100 chemical oscillatory systems.

Today, the discovery of new oscillatory chemical systems does no longer arouse scientific curiosity. The investigator may serendipitously discover, in a certain field of constraint parameters, that a special reactant presents periodical oscillations of the type "limit cycle".[14]

At present, the researches effort is aimed, besides other topics, to the discovery of a thermodynamical size able to characterize the self organization systems [15] and to the study on the self organization system behaviour under the periodical perturbations.

Theoretical studies, concerning the "Brusselator" trimolecular model behaviour under the periodical perturbations, were performed by Tomita.[16] The experimental studies carried out on the real chemical systems (the cool flame oxidation of acetaldehyde) were performed by Ross and coworkers. [17,18]

This paper deals with the study of the Briggs-Rauscher oscillatory system behaviour (BR) under dynamical conditions at periodical perturbations introduced after a sinusoidal component.

EXPERIMENTAL

The reactant mixture for the Briggs-Rauscher reaction has the following initial composition:

$$Co_{KIO_3} = 4.4\times 10^{-2}\ M;\ Co_{H_2O_2} = 1.2\ M;\ Co_{HClO_4} = 5.3 \times 10^{-2}\ M$$

$$Co_{CH_2(COOH)_2} = 5 \times 10^{-2}\ M;\ Co_{MnSO_4} = 5.5\times 10^{-3}\ M.$$

The total feed output of the reactor was 11.3 mL/min. The KIO_3 concentration was periodically introduced according to a sinusoidal component.
Hence:

$$C_{KIO_3(t)} = Co_{KIO_3} + C'_{KIO_3} \sin \frac{2\pi}{T} t\ (\mathrm{mol/L}) \qquad (1)$$

where: T is the perturbation period and t is the time.

The device which supplies periodically the KIO_3 concentration according to equation (1) is presented in Fig. 1. It consists of a flywheel (1) driven by an electromotor and an arm (2) having several equidistant bores is welded on the flywheel (1). A screw (3) which screws up in these bores has on the other end a bearing (4). A frame (5) leans upon the bearing (4). A vessel (6) with $2 \times C_0KIO_3$ concentration is attached to the frame (5). The 2nd vessel (7) is connected to the vessel (6) by two pulleys (8), (9).

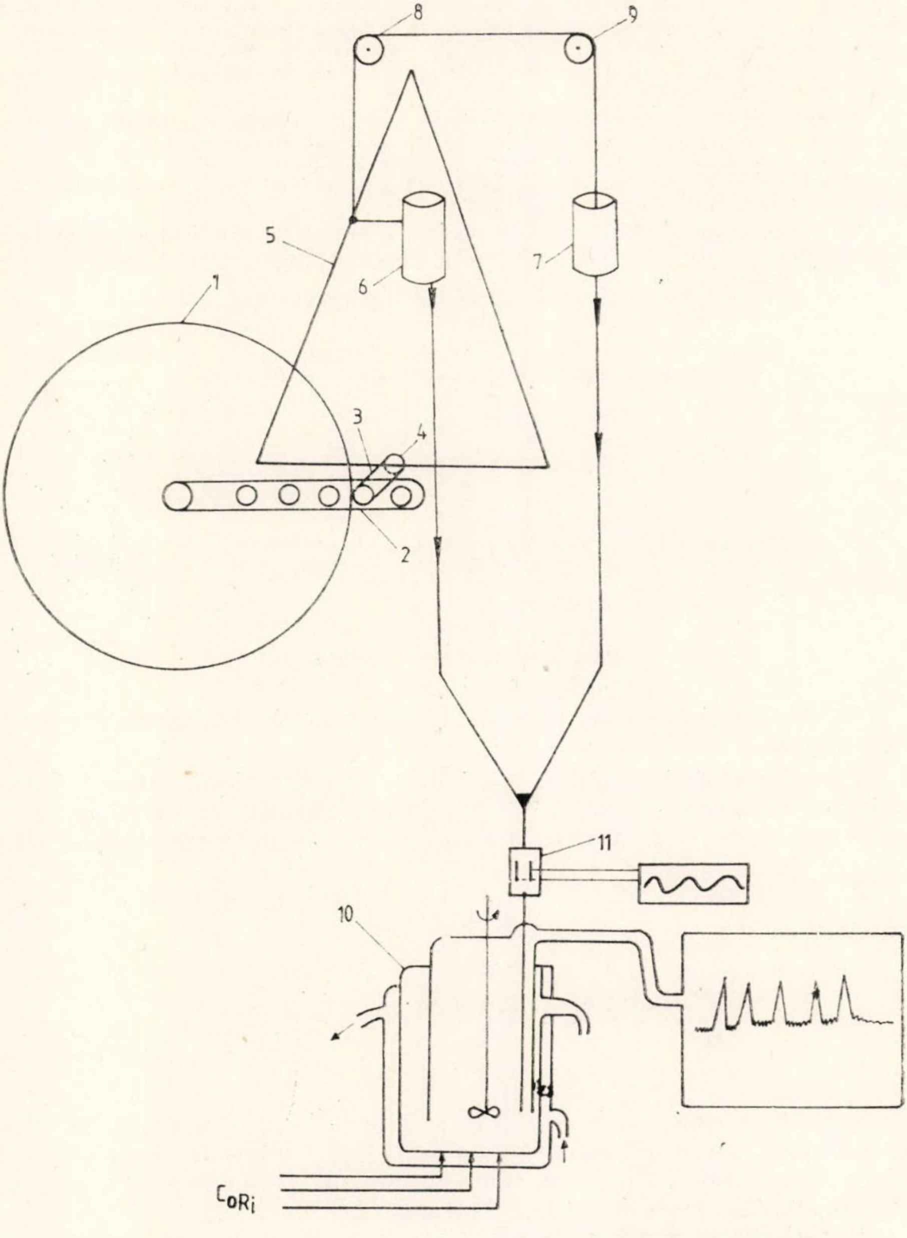

Fig. 1. – The device which supplies periodically the KIO_3 concentration.

Water and KIO_3 solution contained by the two vessels, flow into the reactor (10) through capillary pipes (Ø=0.1 mm), after mixing. The reactor volume is 36.0 mL and is thermostated. The response parameter was the redox potential $Mn^{2+}/MnOH^{2+}$. It is evident that if both vessels have the same level (the arm (2) is perfectly horizontal) then the feed flows in reactor, and the two vessels, are equal. When the flywheel (1) runs 360°, the frame (5) drives two moves, one on the vertical direction and another on the horizontal direction (sliding on the bearing (4)). When the arm is on the vertical position, the vessel (6) which contains KIO_3 solution gets the maximum height and the other having water gets the minimum level. The KIO_3 solution feed flow will be maximum and minimum for water, respectively. It should be noticed that the feed flow sum (KIO_3 solution and water) after mixing is always constant at the reactor entrance.

In order to prove that the KIO_3 concentration is sinusoidally supplied, an electroconductive microcell (11) was attached just at the reactor solution entrance. The cell was connected to a conductometer fitted with a recorder of the Y-t type.

Indeed, when the flywheel (1) runs 360° and the frame (5) has a vertical move, a sinusoidal graph is recorded on the recorder.

The perturbation amplitude modifies by the means of the arm bores. The frequency of the periodical perturbation modifies from the rotation velocity of the flywheel (1) driven by the electromotor.

Two amplitudes and four frequencies for each amplitude were used, i.e.:

$$C_{KIO_3} = 0.044 + 0.125 \times 0.044 \sin \frac{2\pi}{T} t \text{ (mol/L)}$$

$$C_{KIO_3} = 0.044 + 0.2 \times 0.044 \sin \frac{2\pi}{T} t \text{ (mol/L)}$$

The ratios $T/T_0 = 1/1$; $T/T_0 = 2/1$; $T = T_0 = 3/1$ and $T/T_0 =$ decimal number for each amplitude were performed (T_0 is the autonomous period and T is the period of perturbation).

RESULTS AND DISCUSSION

As mentioned above, the reactant system is fed with a variable concentration.

The theoretical study of periodical perturbation systems led to a series of interesting results.[16,19] So, Tomita studied periodically driven Brusselator model. This system is described by the differential equation.[16]

$$\frac{dX}{dt} = X^2Y - BX + A - X + a \cos \frac{2\pi}{T} t \qquad (2)$$

$$\frac{dY}{dt} = BX - X^2Y$$

where A, B, a and T are constants; X an Y are functions of time. For different values of parameters a and T the solution $(X(t), Y(t))$ gets various behaviours. If T_0 is the autonomous period (when $a = 0$) and T for $a \neq 0$, then solution $(X_{(t)}, Y_{(t)})$ may be[16]:

i) periodical, when $\overline{T} = nT$

ii) quasiperiodical, when $\overline{T} = \alpha T$ (α — non-integer number)

iii) double periodical, when $\bar{T} = 2^k T$ (k — integer number)

iv) chaotic behavior, when $\bar{T} = \infty$.

The experimental results which we measured and computed will be given in agreement with this classification. A convenient way to study the response of the system is by means of Poincaré's next phase plots. [17,18 20]

This graphical technique consists in representing the studied points $X(t + (n + 1)T)$ vs $X(t + nT)$, where $X(t)$ is a response parameter. If the plot contains one point, it results that $X(t)$ is periodical, having the period T and if the plot contains k points the period is $\bar{T} = kT$. If the points are dispersed at random then the solution $X(t)$ is chaotic.

For

$$C_{\mathrm{KIO_3}} = 0.044 + 0.125 \times 0.044 \sin \frac{2\pi}{T} t \ (\mathrm{mol/L})$$

$C_{\mathrm{Mn^{2}}_+}(t + (n+1)T$ vs $C_{\mathrm{Mn^{2+}}}(t + nT)$ (Fig. 2) were plotted.
For $T/T_0 = 1$ we have obtained oscillations of the type *i* (Fig. 2 a). If $T/T_0 = 2/1$ then the oscillations are of the type *ii* (Fig. 2 b). For $T/T_0 = 3/1$ and $T/T_0 = 35/9$ the oscillations are chaotic (Fig. 2 c and 2 d).

For another amplitude of the concentration

$$C_{\mathrm{KIO_3}} = 0.044 + 0.2 \times 0.044 \sin \frac{2\pi}{T} t \ (\mathrm{mol/L})$$

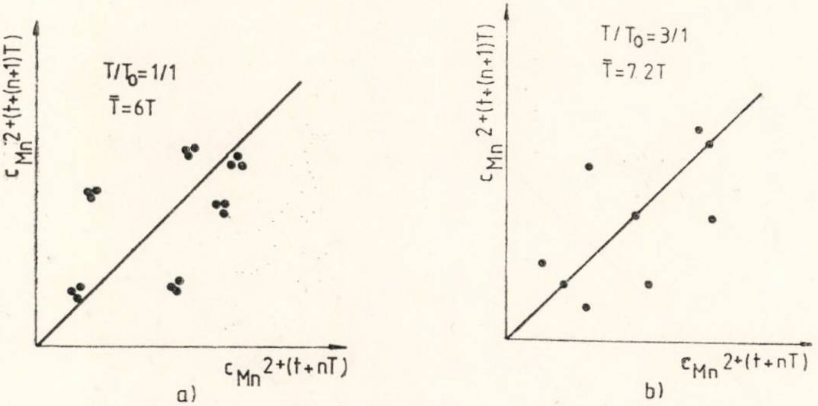

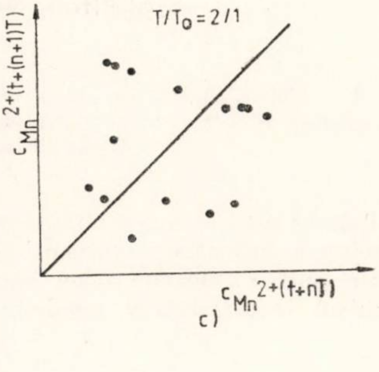

Fig. 2. — Plot $c_{\mathrm{Mn^{2+}}}$ $(t + (n + 1)T)$vs$\cdot$ $\cdot c_{\mathrm{Mn^{2+}}}(t+nT)$ for c'=0.125$\cdot$0.044(mol/L.)
a) oscillations of type i ; b) oscillation of type ii ; c) chaotic oscillations.

but for the same values T/T_0, the results are quite different.

Comparison of the system behaviour for the two amplitudes (Fig. 2 and Fig. 3) shows that at a larger amplitude the system is more easily entrained, in agreement with theoretical results. [16]

Today it is accepted that the number and variety of the dynamical structures are complex and that there is a need for a mathematical theory classification.[21]

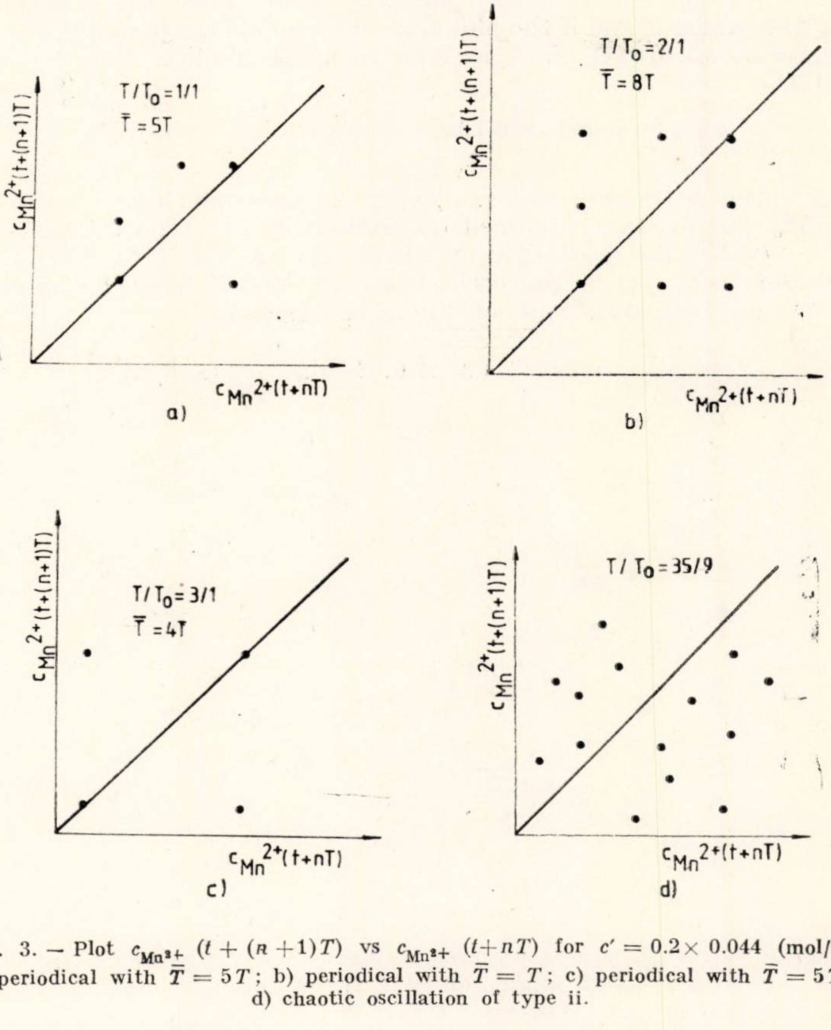

Fig. 3. — Plot $c_{Mn^{2+}}$ $(t + (n + 1)T)$ vs $c_{Mn^{2+}}$ $(t + nT)$ for $c' = 0.2 \times 0.044$ (mol/L). a) periodical with $\bar{T} = 5T$; b) periodical with $\bar{T} = T$; c) periodical with $\bar{T} = 5T$; d) chaotic oscillation of type ii.

Taking into account these preliminary results, it is quite necessary to develop a full study of reaction dynamic for various values of parameters c' and T. On the other hand, a theoretical study on the reaction mechanism is absolutely needed.

REFERENCES

[1] W. C. Bray, *J. Amer. Chem. Soc.*, 43, 1262 (1921).

[2] B. P. Belousov, Sb. Ref. Radiats. Med. 1958. Medgiz. Moscow., pp, 145.

[3] I. R. Epstein, "Chemical Instabilities", eds, G. Nicolis and F. Baras, D. Reidel Publishing Company, 1983, p. 3.

[4] I. Prigogine and G. Nicolis, *J. Chem. Phys.*, 46, 3542 (1967).

[5] I. Prigogine and R. Lefever, *J. Chem. Phys.*, 48, 1695 (1968).

[6] I. Prigogine et P. Glansdorff, *Bull. Acad. Roy. Belg. (Cl. Sc)*, **7**, 672 (1973),

[7] P. Glansdorff and I. Prigogine, "Thermodynamic Theory of Structure, Stability and Fluctuation", Wiley-Interscience, New York N. Y. 1978.

[8] G. Nicolis and I. Prigogine, "Self-Organization in Nonequilibrium System", Wiley-Interscience, New York, N. Y. 1977.

[9] G. Bourceanu and G. Moroşanu, *J. Chem. Phys.*, **82**, 3685 (1985).

[10] A. M. Zhabotinskii, *Biofizika*, **9**, 3, 306 (1964).

[11] A. M. Zhabotinskii, Doklady Akad. Nauk. SSSR, **157**, 2, 392 (1964).

[12] T. S. Briggs and W. C. Rauscher, *J. Chem. Educ.*, **50**, 496 (1973),

[13] J. Boissonade and P. De Kepper, *J. Phys. Chem.*, **84**, 5, 501 (1980).

[14] N. Ionescu, M. Chirica, T. Danciu and D. Marchidan, "Oxidarea catalitică a metanolului în regim oscilant" paper presented at the 3rd National Congress of Chemistry, Bucharest, 1988.

[15] C. Beldie, G. Bourceanu and I. Grosu, in "Proceedings of Chemical Reactivity in Liquids", Paris, 1987, Ed. Plenum Publishing Corp. N.Y., 1988.

[16] K. Tomita, *Physics Reports*, **86**, 3, 115 (1982).

[17] S. A. Pugh, M. Schell and. J. Ross, *J. Chem. Phys.*, **85**, 868 (1986).

[18] S. A. Pugh, B. Dekock and J. Ross, *J. Chem. Phys.*, **85**, 879 (1986).

[19] D. Cartianu, "Synchronization Phenomena in Reaction-Diffusion Systems" Tubner— Texte zur Physik, Leipzig, 1986.

[20] Ph. Rachetti, Thèse d'Etat, Université de Bordeaux I, 1987.

[21] J. Ross, Pugh and M. Schell in : "Proceedings of Chemical Reactivity in Liquids", Paris, 1987, Ed. Plenum Publishings Corp. N.Y. 1988.

Revue Roumaine de Chimie, **34**, *3*, 733–737 (1989)

DERIVATIVES OF 1,2-PYRAZOLES. I

SYNTHESIS AND IR-SPECTRA OF SOME NEW 3-METHYL-5-ARYL-1,2-PYRAZOLES

MARIA BRIE[a] and IOAN A. SILBERG[b]

[a] Institute of Chemistry, 30, Fîntînele Str., 3400 Cluj-Napoca, Romania
[b] ICECHIM-Institute of Chemical and Biochemical Energetics, Cluj-Napoca, Research Group, 11, Arany Janos 11 Str.

Received April 30, 1988

The condensation of ethyl, *o*-nitrobenzoyl-acetoacetate and of *o*-nitrobenzoyl acetone with hydrazine and phenylhydrazine yielded new 5-*o*-nitrophenyl-3-methyl-pyrazoles, which were characterized by IR-spectroscopy.

1. INTRODUCTION

The importance of pyrazoles in medicine, agriculture and technology, as well as their usefulness as intermediates in organic syntheses is well known.[1–4] Recent investigations continually enlarge the scope of practical applications of pyrazole derivatives pointing out, at the same time, new interesting theoretical aspects concerning their chemical and spectral behaviour. A distinct position is held by 3,5-disubstituted-1,2-pyrazoles owing to their availability *via* well-investigated syntheses,[1,2] and to the complex interactions which may occur between the substituents in these positions and the nitrogen atoms of the heterocycle.

Bearing in mind these facts and taking into account a series of earlier reports, both of our group,[5] and of other authors [6,7] regarding the substituent-heteroatom interaction phenomena in the case of five-membered heterocycles, we decided to carry out a chemical and physico-chemical study on a new series of 3-methyl-5-aryl-1,2-pyrazoles, characterized by the presence on the aryl substituent of some groups able to exert enhanced interactions with the heteroatoms of the main ring. The present paper reports the preparation and characterization by IR-spectroscopy of some 3-methyl-5-*o*-nitrophenyl-1,2-pyrazoles; subsequent communications will be devoted to further investigations of their behaviour, in the wider context of our work in the field of organic compounds with two adjacent nitrogen atoms.

2. SYNTHESIS

The compounds resulted from the condensation of ethyl acetoacetate with *o*-nitrobenzoyl chloride served as starting materials for obtaining 5-*o*-nitrophenyl-1,2-pyrazoles. The synthetic procedure used to obtain these starting materials is essentially that reported by Gevekoht,[8] consisting in the transformation of ethyl acetoacetate I into its organomagnesium compound II, followed by condensation with the acyl chloride III; both ethy *o*-nitrobenzoyl-acetoacetate IV and *o*-nitrobenzoyl-acetone V (yellow, well-formed crystals, m.p. 55°), prepared from IV by hydrolysis and decarboxylation (in 30% H_2SO_4) were successfully used as β-diketone components in the reaction with hydrazine (VI R=H) and phenyl-hydrazine (VI, $R=C_6H_5$) δ an often employed route to 1,2-pyrazoles. %[1-3]

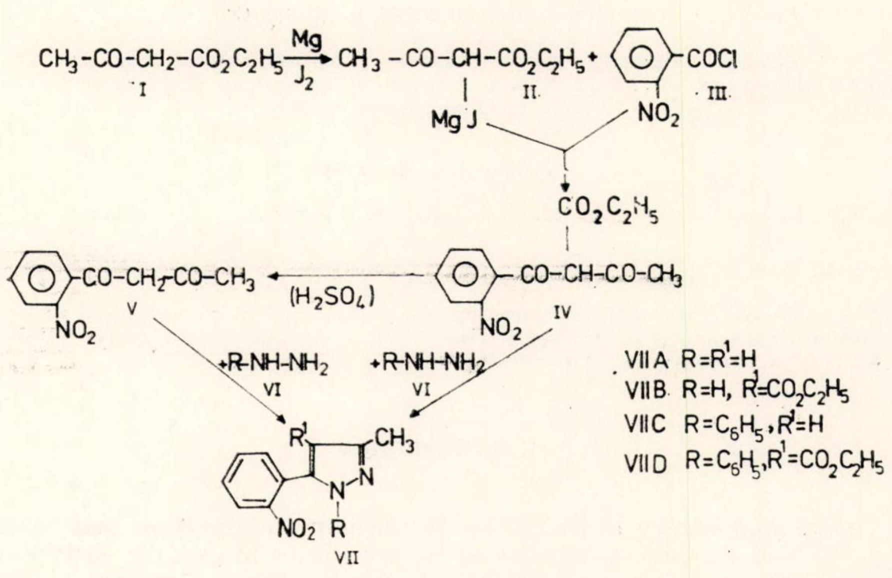
CH₃-CO-CH₂-CO₂C₂H₅
I
Mg
J₂
CH₃-CO-CH-CO₂C₂H₅
II
MgJ
+
COCl
III
NO₂
CO₂C₂H₅
CO-CH-CO-CH₃
IV
NO₂
(H₂SO₄)
CO-CH₂-CO-CH₃
V
NO₂
+R-NH-NH₂
VI
+R-NH-NH₂
VI
R¹
CH₃
N
N
NO₂
R
VII
VII A R=R¹=H
VII B R=H, R¹=CO₂C₂H₅
VII C R=C₆H₅, R¹=H
VII D R=C₆H₅, R¹=CO₂C₂H₅

The condensation reactions were carried out by refluxing for 2 hrs. a mixture obtained by adding an ethanolic solution of IV or V to an ethanolic solution containing an excess of VI. After diluting with cold water, the pyrazole derivatives were obtained; recrystallizations from ethanol, aqueous ethanol or benzene yielded the pure compounds.

5-*o*-Nitrophenyl-3-methyl-1,2-pyrazoles (VII, A–D) thus obtained are solid substances, soluble in ethanol, benzene, chloroform, toluene and ether. The melting points and elemental analyses are presented in Table 1.

3. IR-SPECTRA

The main characteristics of the IR-spectra (700–3500 cm^{-1} range) of the newly synthesized pyrazoles are displayed in Table 2; the spectra were recorded on a UR-10 Carl Zeiss Jena spectrometer in chloroform solution. Along with literature data,[9,10] we also used in the interpretation of IR spectra the direct comparison with the spectrum of 3,5-dimethyl-1,2-pyrazole; the most important bands arising from the vibration of this molecule are given in the last column of Table 2.

Table 1

Elemental analyses of compounds VII A–D

Compound	Structural formula	Molecular formula Mol.wt.	Calculated C%	Calculated H%	Calculated N%	Found C%	Found H%	Found N%
VII A	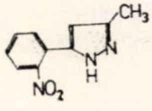	$C_{10}H_9N_3O_2$ 203.201	59.11	4.46	20.68	58.93	4.50	20.01
VII B	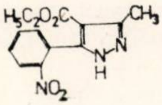	$C_{13}H_{13}N_3O_4$ 275.265	56.72	4.76	15.27	57.00	4.80	15.15
VII C	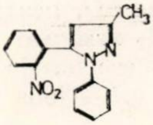	$C_{16}H_{13}N_3O_2$ 279.299	68.80	4.69	15.04	68.20	4.30	15.06
VII D	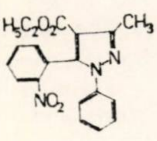	$C_{19}H_{17}N_3O_4$ 351.363	64.95	4.88	11.96	64.90	4.79	11.90

Table 2

Assignments of the main bands in the IR-spectra

Assignment		Experimental wave number (cm^{-1})				
		VII A	VII B	VII C	VII D	3,5-dimethyl-1,2-pyrazole
N–H	unassocd.	3425	3405	—	—	3450
	assocd.	3200	3200			3210
C–H	aromatic	2940	2940	—	—	3115 2900
C–H	methyl	2870	2870	—	—	2810
C=N		1710	1698	1705	1695	1595
C=O		—	1705	—	1705	—
C=C		1545 1460	1490 1450	1545 1485	1540 1480	1440
$-NO_2$	symm.	1370	1360	1365	1360	—

3.1. Vibrations assigned to the heterocyclic nucleus

In the 900—1000 and 1100—1300 cm^{-1} ranges, where the sets of bands characteristic of the molecular skeleton usually appear, the spectra of the herewith investigated compound present specific absorption profiles ("fingerprints") of potential analytical interest in identification problems.

Some of the vibrations originating in the structure elements belonging to the heterocycle are overlapping with those stemming from the substituents. Here can be listed the C—H valence vibrations in compounds VII A and C with a free 4-position, as well as some C=C vibrations.

3.2. Vibrations assigned to the substituents

Continuing to dwell upon the high wave-numbers region, it is to be noted that the methyl group might be responsible for the occurrence of absorption bands between 2800—2900 cm^{-1} due to the stretching vibrations of C—H bonds. The disubstituted benzene ring, in its turn, gives rise to weak absorption bands between 2920 and 2980 cm^{-1}; around 760 cm^{-1} the C—H out-of-plane vibrations can be noted.

On the other hand, in compounds VII C and D, bearing a carbethoxy substituent in position 4, the intense bands assigned to the C=O group appear, as expected, around 1700 cm^{-1}. These bands are of comparable intensity with those attributed to C=N vibrations which occur at slightly lower wave numbers.

A very striking feature revealed by the comparison between the spectra of 3,5-dimethyl-pyrazole and those of the newly synthesized pyrazoles consists of the presence of nitro groups in the molecule of the latter. It is to be emphasized that while the symmetric ν_{NO_2} vibrations at 1360—1370 cm^{-1} are present in the spectra of all 5-*o*-nitrophenyl derivatives as some of the most intense bands, the asymmetric vibrations of the same group around 1540 cm^{-1} is much less individualized, being even hardly discernable in the case of compounds containing the carbethoxy substituent in the molecule.

The series of bands between 1450 and 1600 cm^{-1} is certainly due to the C=C valence vibrations, originating mainly in the mono- and disubstituted phenyl groups, but also, to some extent, to the corresponding structural element of the heterocycle.

3.3. Vibrations revealing substituent-heterocycle interactions

The absorption bands around 1700 cm^{-1} in the spectra of compounds VII A—D were assigned, as already mentioned, to the stretching vibrations of C=N bonds. A comparison with the spectrum of 3,5-dimethyl-pyrazole points out to the fact that the presence of the nitro groups in the *ortho* position of the phenyl substituent entails a hypsochromic shift of about 100 cm^{-1}, very probably as a result of the electronic inductive and mesomeric effects exerted by these groups. The intensities of these bands are also affected by the $—NO_2$ substituents.

The interactions between the $—CO_2C_2H_5$ substituent in position 4 and the C=N and C=C bands manifest themselves also as intensity changes. Thus, whereas the intensity of the C=N bands raises, the C=C vibrations are less intense when the ester groups are present in the molecule.

A comparative study of spectra emphasizes the strong perturbations of the state of N—H bonds in compounds VII A and B, (with a free 1-position) *via* formation of hydrogen bonds. This phenomenon is indicated by a strong absorption band, unusually shifted — by about 300 cm^{-1} — with respect to the band at 3400—3450 corresponding to the unassociated forms. In the case of our compounds besides the association in dimers VIII, which obviously affects the spectrum of 3,5-dimethyl-pyrazole, one has to take into account the possibility of hydrogen bonds involving the nitro groups, as depicted in IX. The seven-membered rings required by such associations could be provided by non-planar dispositions of the participating structural elements. This hypothesis accounts well for the large shifts of the N—H bands, being at the same time compatible with the existence of a certain amount of molecules having conformations which allow the existence of unassociated NH groups.

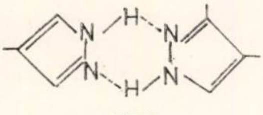

VIII

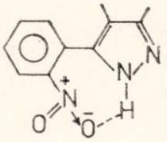

IX

4. CONCLUSIONS

The analytical data and the IR-spectral characterization support the structures assigned to compounds VII A—D which represent a new group of 1,2-pyrazoles. This is of importance both in the context of studies concerning the substituent-heterocycle interactions (which will be developed in subsequent papers) and in connection with the fact that, in the synthesis of compounds VII, the structural peculiarities of the starting materials and intermediates determine, along with the classical cyclization route to the expected pyrazoles, the formation of reaction products which denote deviations from this pattern, as will be shown in following reports.

ACKNOWLEDGEMENTS. Thanks are due to the Microanalyses Laboratory of the Institute of Chemistry, Cluj-Napoca, for carrying out the elemental analyses, and to physicist Rodica Grecu for recording the IR-spectra.

REFERENCES

[1] T. L. Jacobs, "Pyrazoles and Related Compounds" in "Heterocyclic Compounds" (R. C. Elderfield, ed.), vol. 5 p. 46; J. Wiley, New York, 1957.

[2] A. N. Kost and I. I. Grandberg, *Adv. Heterocycl. Chem.*, **6**, 347 (1965).

[3] R. A. Firestone, *Tetrahedron*, **33**, 3009 (1977).

[4] Yu. A. Naumov and I. I. Grandberg, *Usp. Khim.*, **35**, 21 (1966).

[5] I. A. Silberg, R. Macarovici and N. Palibroda, *Tetrahedron Letters*, **1976**, 1321.

[6] S. T. Reid, *Adv. Heterocycl. Chem.*, **11**, 1 (1970) and references cited therein.

[7] M. F. Marshalkin and L. N. Yakhontov, *Usp. Hhim.*, **42**, 1593 (1973); *ibid*, **55**, 1785 (1986).

[8] H. Gevekoht, *Liebigs Annal. Chem.*, **221**, 323 (1883).

[9] G. Zerbi and C. Alberti, *Spectrochim. Acta*, **18**, 407 (1962); *ibid.* **19**, 1273 (1963).

[10] W. Ried and F. J. Königstein, *Liebigs Annal. Chem.*, **625**, 53 (1959).

Revue Roumaine de Chimie, **34**, *3*, 739–748 (1989)

ELECTROCHEMICAL OXIDATION OF N-(NITRO-SUBSTITUTED PHENYL)-4-AMINO-2,6-DI-*tert*-BUTYL-PHENOLS STUDIED BY CYCLIC VOLTAMMETRY

MARIANA CIUREANU[a], JEAN HERDAN[b] and ALEXANDRU T. BALABAN[a]
[a]Polytechnic Institute of Bucharest, Faculty of Chemical Technology,
313, Splaiul Independenţei, 76206 Bucharest, Romania
[b]Institute of Technological Engineering, Research and Refinery Design (ICITPR)
Ploieşti, Romania

Received September 29, 1988

Cyclic voltammograms in acetonitrile are presented and discussed for: (**1**) 4′-nitro-, (**2**) 2′,4′-dinitro- and (**3**) 2′,4′,6′-trinitro-N-phenyl-4-amino-2,6-di-*tert*-butyl-phenol. Three oxidation waves were evidenced on the anodic scan for **1**, whereas only one was observed for **2** and **3**. In order to explain the electrode behaviour of the investigated compounds, a mechanism is proposed, in which a superposition of an ECEC sequence with a disproportionation pathway is considered. Arguments are presented to prove that the oxidation products are the corresponding nitro-substituted N-phenyl-4-imino-(2,6-di-*tert*-butyl)-benzoquinones, which may in turn hydrolyse with the traces of water present in the solvent. The differences in the electrochemical behaviour of the investigated compounds (particularly those between **1** and **2**, **3**) are discussed in terms of the steric inhibition of conjugation, produced by the presence of the *ortho*-nitro substituents.

INTRODUCTION

Because of the practical importance of phenols, the electrochemical behaviour of these compounds has received considerable attention. Despite the important number of studies concerning the anodic reactions of phenols performed by classical polarography, voltammetry and coulometry, there are still conflicting theories concerning the primary electrode reactions. Thus, opinions on the number of electrons transferred in the primary step were divided between 1*e* and 2*e*; the first theory was advanced by Hedenberg *et al.*[1] and Ginzberg,[2] whereas the second was favoured by Gaylor *et al.*[3] Vermillon and Pearl showed that for simple phenols in acetonitrile solution the initial reaction corresponded to a bielectronic process, but shifted to a monoelectronic charge transfer in the presence of a strong base.[4] Defined proof in favour of an initial 1*e* oxidation was found from ESR experiments for sterically hindered phenols by Vozdinsky *et al.*[5] Our previous studies have demonstrated that relatively stable aroxyls are obtained also by chemical oxidation of sterically hindered phenols.[6,7]

The electrode behaviour of aminophenols is still more complicated, since the presence of two oxidizable groups in the same molecule increases the complexity of the chemical reaction following the initial charge transfer Thus, Marcus *et al.*[8] have shown that for *p*-dimethylaminophenol in aqueous media the mechanism of electrooxidation is highly dependent on the acidity of the medium: in acidic media, the compound undergoes a two-electron transfer, whereas in the 6–9 pH range the global oxidation is a four-electron process; in basic media the first charge transfer is 1*e*, leading to an aroxyl. For substituted N-phenyl-*p*-aminophenols in acetone–$HClO_4$ media, the electrochemical oxidation is bielectronic, leading to the corresponding *p*-quinoneimine.[9] However, relatively stable aminyls were shown to appear by the chemical oxidation of related compounds, such as diphenylamine having nitro- and alkoxy substituents.[10] Taking into account the enhanced stability of such capto-dative aminyls, we decided to investigate their possible intermediacy in the electrooxidation of diarylamines possessing a polynitrophenyl group as electron acceptor and a 3,5-di-*tert*-butyl-4-hydroxyphenyl group as electron donor.

The following series of compounds was investigated by syclic voltammetry: (**1**) 4′-nitro-, (**2**) 2′,4′-dinitro-, and (**3**) 2′,4′,6′-trinitro-N-phenyl-4-amino-2,6-di-*tert*-butyl-phenol, as well as the quinoneimine (**4**) obtained on oxidation of **2**.

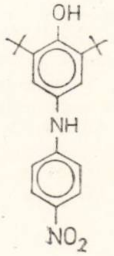

1

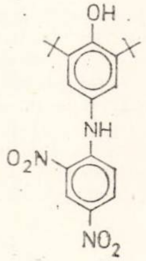

2

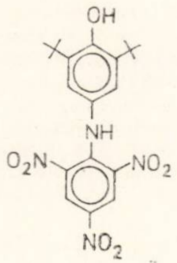

3

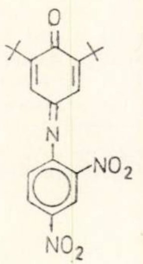

4

EXPERIMENTAL

The electrochemical measurements were performed with a Princeton M173 potentiostat equipped with a Radelkis VLF function generator and an ENDIM 620.02 x–y recorder. The working and counterelectrode were made of bright platinum. The apparent area of the working electrode was 0.5 mm^2. The reference electrode was of the Ag/Ag^+ (0.01 M) type, with acetonitrile as a solvent and a bridge compartment filling of 0.1 M $LiClO_4$ in acetonitrile. The concentration of the substrate was in the range $5 \times 10^{-4}-10^{-2}$ M. Spectrograde purity acetonitrile was used as a solvent and $LiClO_4$ as supporting electrolyte at a concentration of 10^{-1} M. The solutions were de-aerated and then held under an atmosphere of dry nitrogen.

The compounds were synthetized and purified as described in a separate paper.[10]

RESULTS

The cyclic voltammograms of the compounds under investigation are presented in figures 1–3. It may be seen that compound **1** shows three oxidation waves (*A*, *B*, *C*), whereas only one is observed for **2** and **3**. The values of the peak potentials are presented in Table 1.

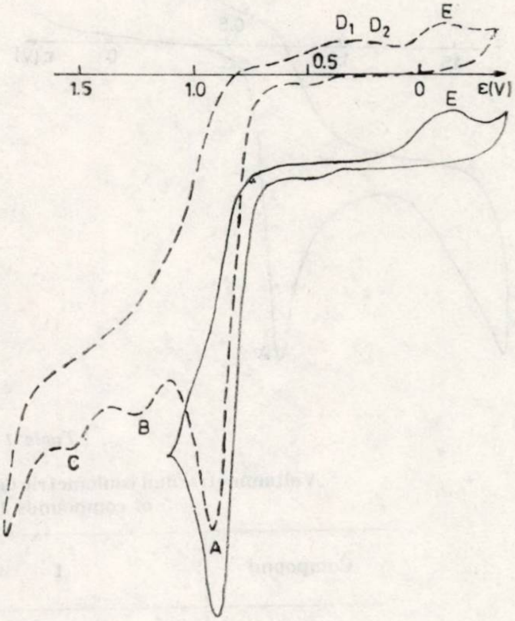

Fig. 1. — Steady state cyclic voltammograms of compound **1** recorded at a scan rate of 0.040 Vs^{-1}: — — —sweep range (−0.2) to 1.8 V; — sweep range (−0.2) to 1.1 V.

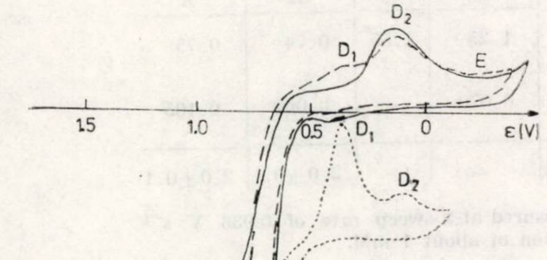

Fig. 2. — Steady state cyclic voltammogram of compound **2**, recorded at a scan rate of 0.040 Vs^{-1}: a) — — — sweep range (−0.2) to 1.8 V; b) ——— sweep range (−0.3) to 1.5 V; c) . . . same as b, with $HClO_4$ added.

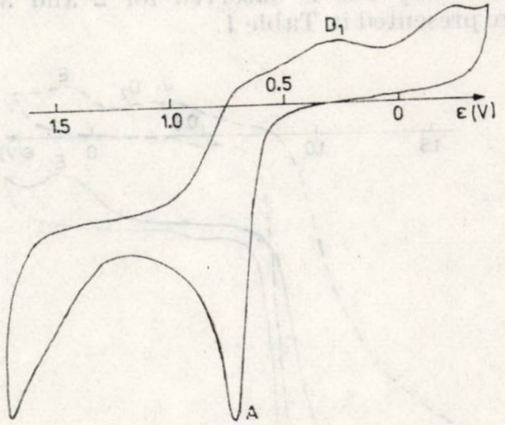

Fig. 3. — Steady state cyclic voltammogram of compound **3** recorded at a scan rate of 0.040 Vs^{-1}.

Table 1

Voltammetric and coulometric data for the anodic waves of compounds **1**, **2**, **3**

Compound	1			2	3
Wave	*A*	*B*	*C*	*A*	*A*
ε (V)	0.93	1.25	1.55	0.74	0.75
$\frac{d\varepsilon}{d(\log v)}$ (V/decade)	0.082	0.070	—	0.065	0.105
n_s	1.6±0.1	—	—	2.0±0.1	2.0±0.1

The peak potentials are measured at a sweep rate of 0.036 V · s^{-1} and a substrate concentration of about 1 mM.

The oxidation waves were subjected to the usual electrochemical tests,[11,12] the results of which are presented in figures 4 and 5. It may be seen that the current function

$$i_A/cv^{1/2}$$

evaluated for wave *A* decreases markedly with increasing sweep rate *v*; the dependence is similar for the three compounds under investigation although the current function measured in identical conditions is smaller for **1** than for **2** and **3** by a factor of 1.5 (figure 4).

For the three investigated compounds the anodic waves A show a definite shift toward positive potentials as the sweep rate (v) is increased. From figure 5 it may be seen that the $\varepsilon_A - f(\log v)$ dependences are straight lines with slopes between 70 and 105 mV per decade. These values show that the corresponding oxidation process is irreversible in all cases. For wave B of compound **1**, the $\varepsilon - f(\log v)$ dependence was found to be also linear.

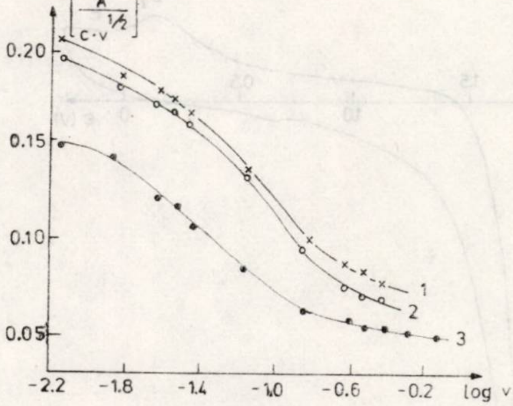

Fig. 4. — Plot of the intensity function $i_A/cv^{1/2}$(in A $s^{1/2}V^{-1/2}$ mole^{-1}) *vs.* log *v*: x, compound **1**; ○, compound **2**; ●, compound **3**.

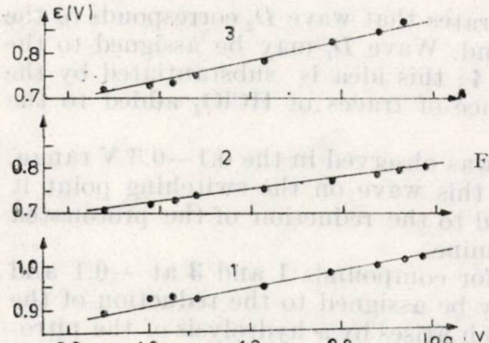

Fig. 5. — Dependence of the peak potential ε_A on the scan rate.

The number of electrons transferred in the oxidation process corresponding to wave *A* was determined by controlled potential microcoulometry. For **2** and **3** the results are consistent with a bielectronic process; for **1**, the apparent number of electrons (n_e) was found to have a non-integral value of 1.6 ± 0.1.

On the cathodic scan two waves, hereafter denoted by *D* and *E*, were observable. These waves are clearly due to the reduction of the products resulting by chemical reactions following the primary oxidation; no cathodic wave could be detected if the anodic scan was switched off before wave *A* and there were no waves in the background in this range. For **1** and **3**, waves *D* and *E* are of comparable heights, whereas for **2**, wave *E* is very small.

For compound **1**, wave *D* is very broad and arises obviously from a superposition of two waves: the first one (D_1), located at more positive potentials (0.30—0.35 V) was found to be highly dependent on the switching potential on the anodic scan; asseen from figure 1, this wave could not be observed if the switching potential was smaller than 1.6 V. Wave D_2, located at about 0.1 V, is broad and small.

For compound **2**, wave D_2 is considerably more intense than D_1. A comparison of the cyclic voltammograms of **2** with that obtained for an authentic sample of N-(2,4-dinitrophenyl)-4-imino-(2,6-di-*tert*-butyl-*p*-benzoquinone) (**4**) (figure 6) demonstrates that wave D_2 corresponds to the reduction peak of the latter compound. Wave D_1 may be assigned to the reduction of the protonated form of **4**; this idea is substantiated by the observed increase of D_1 in the presence of traces of $HClO_4$ added to the solvent (Figure 2).

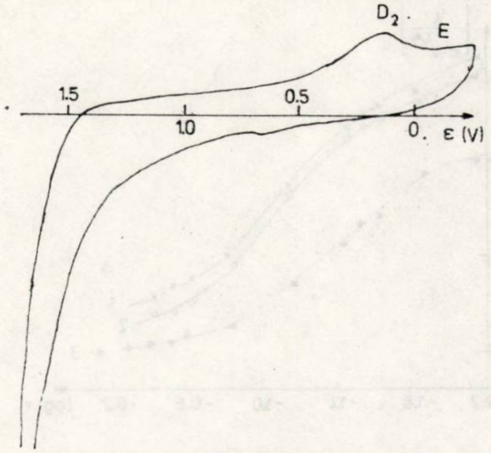

Fig. 6. — Steady state cyclic voltammogram of compound **4** recorded at a scan rate of 0.040 Vs^{-1}.

For compound **3** a single wave was observed in the 0.1—0.3 V range, at 0.26 V. From the dependence of this wave on the switching point it was inferred that it may be assigned to the reduction of the protonated form of the corresponding quinoneimine.

Wave *E* was clearly observed for compounds **1** and **3** at —0.1 and —0.3 V, respectively. This wave may be assigned to the reduction of the 2,6-di-*tert*-butyl-*p*-benzoquinone, which arises by a hydrolysis of the nitro-substituted N-phenyl-(2,6-di-*tert*-butyl)-quinoneimine with the residual water present in the solvent.*

DISCUSSION

Mechanism of oxidation

The experimental voltammetric data presented so far are consistent with the following overall mechanism of oxidation for the electrochemical oxidation of the investigated compounds:

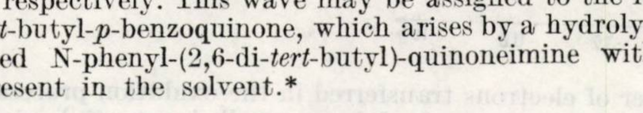

(1)

---

* It is known that even in very carefully dehydrated solvents, the concentration of residual water amounts to several mM, which is the usual range of substrate concentration in voltammetric studies.

The main problem to be solved is to ascertain the pathway by which the first step of this overall mechanism proceeds. Actually, the first step in (1) involves four elementary processes, because four particles (two electrons and two protons) are lost from each molecule of starting material. Since no ESR signals could be detected by the *in situ* electrooxidation of the investigated compounds, it may be inferred that either the initial oxidation is bielectronic, or the first step in (1) proceeds via an ECEC sequence (where E denotes an electron transfer and C a chemical reaction); in the latter case, the initial $1e$ transfer is followed by a sequence of rapid chemical and electrochemical reactions, so that the radical cannot accumulate to give a detectable ESR signal. The possibility of a mechanism involving a bielectronic charge transfer may be ruled out on the basis of the observed decrease of the peak intensity function with increasing sweep rate. Therefore, only the ECEC sequence will be discussed below :

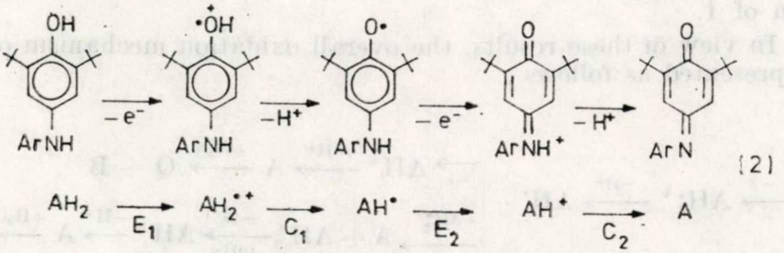

(2)

For compound **1**, the presence of the anodic waves A and B demonstrates that oxidation proceeds, at last in part, *via* the pathway (2), which involves two successive heterogeneous charge transfers, separated by a deprotonation step. However, the other experimental data require also the consideration of the pathways involving the disproportionation of the resulting radicals :

$$2\,\mathrm{AH}^{\bullet} \rightleftharpoons \mathrm{AH}_2 + \mathrm{A} \qquad (3)$$

$$\mathrm{AH}_2^{\bullet +} + \mathrm{AH}^{\bullet} \rightleftharpoons \mathrm{AH}_2 + \mathrm{AH}^{+} \qquad (4)$$

$$\mathrm{AH}_2^{\bullet +} + \mathrm{AH}^{\bullet} \rightleftharpoons \mathrm{AH}_3^{+} + \mathrm{A} \qquad (5)$$

where the notation is that of (1) and (2) and AH_3^+ denotes the protonated substrate. Several arguments plead in favour of a considerable interference of these disproportionation reactions :

(a) The apparent number of electrons determined coulometrically at the peak potential of wave A lies, for compound **1**, between $1e$ (the value correspondindg to the first charge transfer in (1)) and $2e$ (the value expected if all the radicals formed after a first electron transfer would disproportionate).

(b) As it may be observed from figure 1, the reduction wave E appears even if the anodic scan is switched off before reaching the peak potential of wave B; it is inferred that reaction (1) may be completed even if the heterogeneous abstraction of a second electron is not possible.

(c) The appearance of a third anodic wave (*C*) may be assigned to the oxidation of the protonated form of the substrate, according to the overall equation :

$$AH_3^+ \xrightarrow[-2H^+]{-2e} AH^+ \tag{6}$$

This assignment of wave *C* implies that for compound **1** the preferred disproportionation pathway is that described by eq. (5). A direct support for the process represented by (6) is provided by the cathodic wave D_1 ; this wave, which was assigned to the reduction of the protonated form of the quinoneimine, could be observed only if the anodic scan had reached the peak potential of wave *C*.

(d) The observed decrease of the peak intensity function with increasing sweep rate may be explained only in terms of an interference of the ECEC and disproportionation mechanisms in the electrochemical oxidation of **1**.

In view of these results, the overall oxidation mechanism of **1** may be represented as follows :

(7)

$$\begin{tikzcd}
AH_2 \arrow[r, "-e"] & AH_2^{\bullet +} \arrow[r, "-H^+"] & AH^{\bullet} \arrow[r, "-e"] \arrow[dr, "+AH_2^{\bullet +}"'] & AH^+ \arrow[r, "-H^+"] & A \arrow[r, "+H_2O"] & Q + B & \\
 & & & A + AH_3^+ \arrow[r, "-2e", "-2H^+"'] \arrow[d, "+H_2O"] & AH^+ \arrow[r, "-H^+"] & A \arrow[r, "+H_2O"] & Q + B \\
 & & & Q + B & & &
\end{tikzcd}$$

An important point to be solved is to establish whether the rate-determining step in this mechanism is the deprotonation (C_1),or the disproportionation. The observed decrease of the peak intensity function with increasing sweep rate night be assigned either a fast deprotonation followed by a slow disproportionation, or to a slow deprotonation followed by a rapid disproportionation. In the former case, the oxidation kinetics is second order, whereas in the second, the formal kinetics is first order, as in an uncomplicated ECEC mechanism. The distinction criterion between these cases is provided by the effect of initial concentration (*c*) on the peak intensity (i_A) ; since our experiments demonstrated the proportionality of i_A with *c*, which is characteristic of first-order processes, it may be inferred that the rate-determining step is the deprotonation of the cation-radical $AH_2^{\bullet +}$. This conclusion is also supported by the observed decrease of the peak intensity function for wave *B* ($i_B/cv^{1/2}$) with increasing sweep rate *v* : if the disproportionation step were rate-determining, this function would be expected to increase with *v*.

The mechanism described by eq. (7) explains why no ESR signal could be detected by the *in situ* electrolysis of compound **1** ; the cation radicals $AH_2^{\bullet +}$ can not accumulate, since the first charge transfer is intrinsically slow, as demonstrated by the totally irreversible nature of wave *A* ; the radicals $AH^{\bullet}$ cannot accumulate either, owing to the fast disproportionation following the deprotonation step.

For compounds **2** and **3**, the overall mechanism of oxidation should be similar to that for **1**, with two important differences :

(a) since no anodic wave similar to *B* was observed, it may be inferred that the oxidation potential of the phenoxy radicals $AH^{\bullet}$ is equal or even lower than that of the parent molecule AH_2 ;

(b) if condition (a) is fulfilled, the extent of participation of the disproportionation process described by eq. (4) is expected to become important ; the predominance of this disproportionation path over that described by eq. (5) offers an explanation for the observation that no anodic wave similar to *C* could be detected for compounds **2** and **3**.

Comparison within the investigated series

The experimental data presented so far evidenced some differences in the electrochemical behaviour of compound **1**, as compared with **2** and **3**. These differences may be discussed in terms of the effects produced by the successive introduction of the nitro substituents in the *ortho* position of the N-phenyl ring :

(*a*) the introduction of an electron-withdrawing group is expected to lower the electron density on the oxidizable groups (OH and NH) and thus to lower their capacity to lose electrons. Therefore, on the basis of this electronic effect, the oxidation potential would be expected to increase in the series $\mathbf{1} < \mathbf{2} < \mathbf{3}$;

(*b*) The introduction of an *ortho* substituent produces a steric hindrance to coplanarity of the two cycles, which decreases the conjugation of the electrons in the π-electronic system ; this effect is expected to produce an increase of the electron density on both oxidizable groups, thus lowering the oxidation potential.

A comparison of the oxidation potentials within the investigated series demonstrates the predominance of the second effect : the peak potential of wave *A* is higher by about 0.2 V for **1** as for **2** ; the difference between **2** and **3** is very small, since the introduction of the third nitro group does not produce a substantial change of the equilibrium geometry of the molecule. The steric effect should also be made responsible for the fact that for **2** and **3** the ionization potentials of $AH^{\bullet}$ and AH_2 are very close, so that a single anodic wave is observed, similarly as for unsubstituted *p*-aminophenol.[13]

The steric effect should be also made responsible for the observed decrease of hydrolysis rate of the 2,4-dinitro-substituted quinoneimine as compared with the 4-nitro-substituted compound. This trend, which was qualitatively observed from the intensity of wave *E*, is different from that predicted if only electronic effects are taken into consideration.[9]

CONCLUSIONS

The anodic oxidation of nitro-substituted N-phenyl-4-amino-2,6-di-*tert*-butyl-phenol was explained in terms of a superposition of an ECEC sequence with a disproportionation reaction. For the mono-nitro-derivative, the oxidation potentials corresponding to the electron transfers are different, so that two anodic waves are observed ; for the remaining derivatives, these potentials practically coincide, so that a single anodic wave is apparent. The oxidation products are the corresponding nitro-substituted quinoneimines, which hydrolyse in the presence of traces of water extant in the solvent.

REFERENCES

[1] J. F. Hedenberg and H. Freiser, *Anal. Chem.*, **25**, 1355 (1953).
[2] V. I. Ginzberg, *Zh. Fiz. Khim.*, **33**, 1504 (1959).
[3] V. F. Gaylor, A. L. Conrad and J. H. Lendere, *Anal. Chem.*, **29**, 224 (1957).
[4] F. J. Vermillon and J. A. Pearl, *J. Electrochem. Soc.*, **111**, 1392 (1964).
[5] I. V. Vozdinsky, A. A. Vasilieva, I. A. Korshinov and G. A. Abakumov, *Elektrokhimia*, **7**, 24 (1971).
[6] J. Herdan, G. Iordache, N. Negoiţă, N. Grecu and A. T. Balaban, *Rev. Roumaine Chim.*, **27**, 69 (1982).
[7] J. Herdan, A. T. Balaban, N. Negoiţă and N. Grecu, *Rev. Roumaine Chim.*, **28**, 129 (1983).
[8] M. F. Marcus and M. D. Hawley, *J. Electroanal. Chem.*, **18**, 175 (1968).
[9] D. W. Leedy and R. N. Adams, *J. Amer. Chem. Soc.*, **92**, 1647 (1970).
[10] A. T. Balaban, P. T. Frangopol, M. Frangopol and N. Negoiţă, *Tetrahedron*, **23**, 4661 (1967).
[11] R. S. Nicholson and I. Shain, *Anal. Chem.*, **37**, 178 (1965).
[12] R. S. Nicholson and I. Shain, *Anal. Chem.*, **36**, 707 (1964).
[13] D. Hawley and R. N. Adams, *J. Electroanal. Chem.*, **10**, 376 (1965).

Revue Roumaine de Chimie, 34, 3, 749–757 (1989)

OZONE OXIDATION OF ALKYLAMINES IN AQUEOUS SOLUTION. I

RATE CONSTANTS OF OZONE REACTIONS WITH PRIMARY, SECONDARY AND TERTIARY AMINES

V. COCHECI, E. GERASIMOU, C. CSUNDERLIK, L. COTARCĂ and A. NOVAC

Polytechnic Institute "Traian Vuia", Timişoara, Chemical Technology Faculty,
Blvd 30 Decembrie no. 2, 1900 Timişoara, Romania

Received November 1, 1988

In aqueous solutions the reaction of zone with aliphatic amines proceeds in the first step by an electrophilic attack of ozone on the nitrogen atom of the free amine. The adduct ozone-amine then rapidly decomposes to products that can be nitroderivatives, amides, carboxylic acids, aminoxides or substituted hydroxylamines. The reaction products can be further oxidized to total degradation by an excess of ozone.

In many countries ozone is largely used for the treatment of drinking water in order to improve its quality and for the oxidation of certain organic pollutants that may exist in industrial waste-water. It is known from such applications that zone is an oxidizing agent of increased selectivity.[1] Many of the ozonation products of some organic compounds existing in aqueous solutions have been observed or postulated of which some have been subsequently oxidized only by prolonged ozonation.[2]

Consequently, kinetic data are extremely necessary for estimating the advantages and risks of the ozonation procedures and to predict the nature of chemical compounds remaining in water after a certain duration of the ozonation process. Kinetic data are also important for understanding the effects of the ozone absorbed in natural aquatic systems on the environment.

Ozone initiates rather complex oxidation reactions in water; only a part of it reacts directly with the dissolved organic compounds[3–5] — another part may selfdecompose before the reaction. Such decompositions are catalysed by the hydroxide ions or other dissolved compounds. Hence OH· radicals are formed which exhibit a behaviour of extremely reactive secondary oxidants, considerably accelerating the ozone decomposition.[4–6] Radicalic chain reactions take place which consume ozone competing with the direct reaction with the organic dissolved compound. These reactions are schematically presented in Figure 1 and Figure 2.

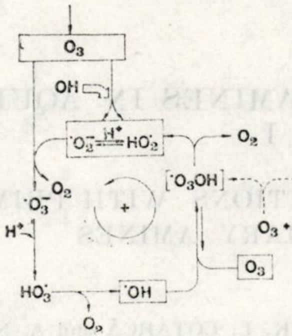

Fig. 1

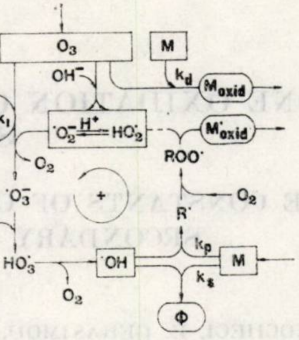

Fig. 2

For the surface and underground waters used as sources of drinking water (pH = 7 – 8) the two reaction paths are of comparable importance. Nevertheless, very different parameters are determining for the pathway of these reactions and the oxidation products are also different enough.

Despite the numerous practical applications of the ozonation process, papers dealing with the rate constants of the ozone reactions with organic compounds dissolved in water are scarce.[4,5,7,8] The rate constants determined for ozonation reactions in organic solvent cannot be directly applied to aqueous systems.

The studies concerning ozone reactions with amines have exclusively been carried out in organic solvents (hydrocarbons, chlorinated solvents – especially chloroform) at relatively low temperatures (0 to –60°C).[9–11] They provide the basis for establishing the mechanism of amine oxidation by ozone, which depends on the amine nature. The first step is in all the cases an electrophilic attack of ozone on the amine nitrogen atom with the formation of an amphionic adduct.[9] Its further decomposition depends on the amine structure and reaction conditions :

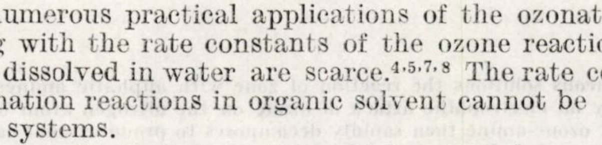

Scheme 1

– the primary and particularly tertiary amines are subsequently oxidized to aminoxies, hydroxylamines, nitroso and finally nitroderivatives[12–15];

– the amines with CH or CH_2 groups in the α-position are oxidized through unstable α-hydroxylamines to amides, formamides, carboxylic acids, aminoxides.[16–18]

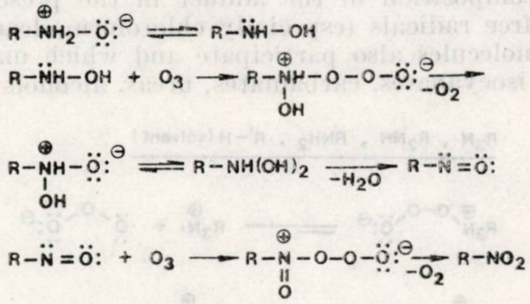

Scheme 2

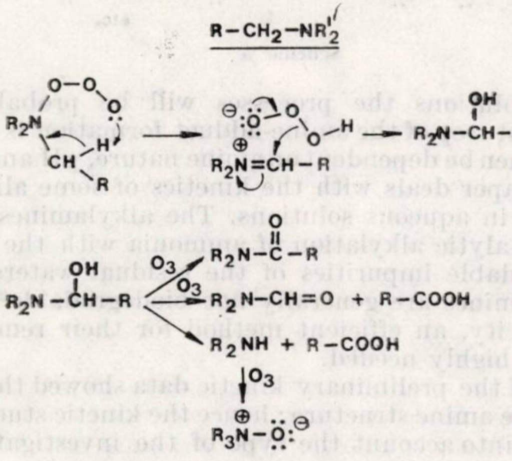

Scheme 3

— with the secondary amines the adduct decomposes through aminoxide radicals to nitroderivatives and trisubstituted hydroxylamines[19–21];

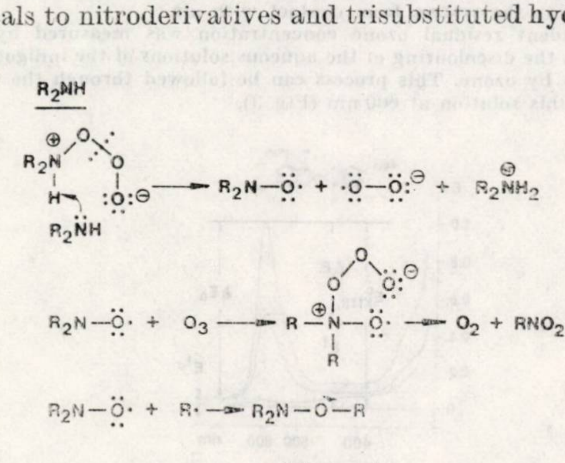

Scheme 4

— the decomposition of the adduct in the presence of a solvent easily forming free radicals (especially chloroform) leads to products in which solvent molecules also participate and which may be very different (phosgene, isocyanates, carbamates, ureas, alcohols etc.).[9]

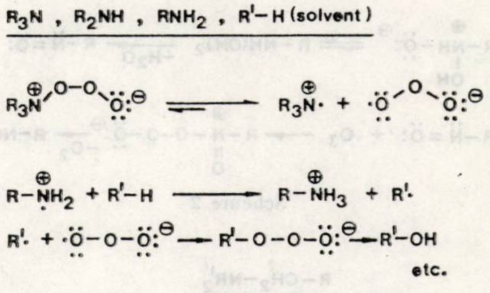

Scheme 5

In aqueous solutions the processes will be probably similar, at least as far as the first step of the amine-adduct formation is concerned. Its decomposition will then be dependent on amine nature, pH and temperature.

The present paper deals with the kinetics of some aliphatic amines oxidation by ozone in aqueous solutions. The alkylamines commercially produced by the catalytic alkylation of ammonia with the corresponding alcohols are unavoidable impurities of the residual waters. Taking into account that alkylamines are generally not biodegradable[22] and are of a relatively high toxicity, an efficient method for their removal from the aqueous medium is highly needed.

The analysis of the preliminary kinetic data showed that the reaction rate depended on the amine structure ; hence the kinetic studies (condition, method) had to take into account the type of the investigated compound.

EXPERIMENTAL

The reaction was initiated by adding the ozone solutions under the level of the amine solutions, thus protecting the system from contact with air.

The time-dependent residual ozone concentration was measured by the INDIGO method [23,25] which uses the discolouring of the aqueous solutions of the indigotrisulphonic acid tripotassic salt (KITS) by ozone. This process can be followed through the evolution of the characteristic band of this solution at 600 nm (Fig. 3).

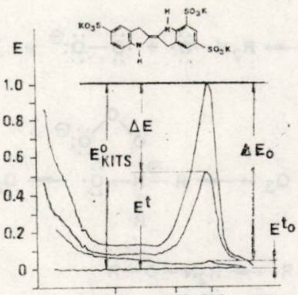

Fig. 3

The method is sensitive to ozone concentrations as low as 0.5 micromoles with an accuracy better than 10%. For each series of determinations the values measured for the ozone concentration decrease in time to zero. Thus no interference occurs with intermediate or by-products like peroxides.

For the more rapid reactions ($t_{1/2}$ less than 100 seconds) the reaction was stopped at different moments using as "freezing" reagent just the indigotrisulphonate solution.

The water used in the kinetic experiments was deionised and bidistilled in glassware in the presence of potassium permanganate. Its purity was spectroscopically (UV) and chromatographically (HPLC) verified. Before the ozonation water was refluxed for half an hour and then cooled to 5°C under nitrogen.

The aqueous ozone solutions were prepared by bubbling a stream of oxygen with 5—8% ozone produced by an analytical Fisher 500 M microozonizer through a column with water purified as above described in a glass contact apparatus provided with sintherised frit.

The duration of the water saturation with ozone varied depending on temperature. The water volume used was of 250 mL for which at ozone outputs of 25 mg/min, at 4°C and $pH = 2$, absorption yields of 0.2% were obtained. In all the cases buffered solutions were submitted to ozonation. The pH adjustment was carried out with $NaOH/H_3PO_4$ buffer such as the total phosphate ions concentration of the final solution did not exceed 0.05 M.

The alkylamine solutions were prepared using as above described deionised and bidistilled water and were submitted to "preliminary ozonation" to remove any reactive impurities that could affect the kinetic measurements.

The initial alkylamine concentrations of the aqueous solutions were simultaneously determined by three methods volumetry, gas-liquid chromatography and near infrared spectroscopy.[24]

INTERPRETATION OF THE KINETIC RESULTS

The rate constants were calculated by introducing the measured values of the extinction at 600 nm (in fact the difference between the extinctions of the standard KITS solutions and that of the samples taken from time to time) in the rate equation integrated for a reaction of pseudofirst order :

$$\ln \frac{\Delta E_0}{\Delta E} = \ln \frac{E^{\circ}_{\mathrm{KITS}} - E^{t_0}}{E^{\circ}_{\mathrm{KITS}} - E^{t}} = k_0 t$$

where $E^{\circ}_{\mathrm{KITS}}$ is the extinction of the standard KITS solution and E^{t_0} and E^{t} are the extinctions of the sample respectively for 0 and t seconds.

A calculation example for the reaction of n-butylamine with ozone is presented in table 1.

The rate constants of pseudofirst order were determined at various amine concentrations; the amine concentrations were always 10—200 times greater than the ozone concentration. The pseudofirst order rate constants determined for the reaction of n-butylamine with ozone are presented in table 2.

The second order rate constants, k_2, were obtained by plotting the pseudofirst order constants versus the amine concentration according to the equation :

$$k_0 = {}_{2}{}_{0}k + k_2\ [\mathrm{Amine}]$$

where k_0, is the rate constant for the ozone selfdecomposition.

Table 1

The calculation of the pseudofirst order rate constant for the reaction of n-butylamine ($2.56 \cdot 10^{-4}$ M) with ozone (initial concentration $3.59 \cdot 10^{-6}$ M) at pH = 2 and 20°C

t	ΔE	$\frac{\Delta E_0}{\Delta E}$	$\ln \frac{\Delta E_0}{\Delta E}$
0	0.206		
300	0.179	1.1508	0.1407
540	0.164	1.2561	0.2280
1140	0.140	1.4714	0.3860
1800	0.122	1.6885	0.5237
2340	0.108	1.9074	0.6456
2940	0.089	2.3146	0.8394
3540	0.076	2.7105	0.9972
4200	0.063	3.2698	1.1849
4740	0.056	3.6786	1.3028
5340	0.049	4.2041	1.4362

Table 2

The pseudofirst order rate constants (k_0) determined for the reaction of n-butylamine with ozone at 20°C and pH = 2

No.	$[\text{n-BuNH}_2] \times 10^4$ M	$[O_3] \times 10^6$ M	$\frac{[\text{n-BuNH}_2]}{[O_3]}$	$k_0 \times 10^4\ s^{-1}$
1	2.56	3.59	71.3	2.816
2	4.39	2.43	180.6	4.550
3	5.13	4.47	114.7	5.251
4	5.77	3.54	162.9	5.878

$k_0 = 0.374 \cdot 10^{-4} + 0.952\ [\text{nBu}-\text{NH}_2] \quad (r = 0.99)$
$k_2 = 0.952\ \text{M}^{-1} \cdot \text{L} \cdot \text{S}^{-1}$

RESULTS AND DISCUSSION

The second order rate constant for the reaction of various primary secondary and tertiary aliphatic amines with ozone are presented in table 3.

One observes that generally the values fall within the range $1-7\ \text{M}^{-1} \cdot \text{L} \cdot \text{s}^{-1}$. The most significant exception is benzylamine, the rate constant of which is much greater than those of the other amines. One may conclude that in this case the reaction mechanism is a different one. Low values of the rate constant were obtained for tert-butylamine, cyclohexylamine and tri-n-butylamine.

A preliminary study of the reaction products indicates for n-butylamine and tert-butylamine almost the same type of compounds as described in literature for the reaction in organic solvents. This seems to be in agreement with a quite similar reaction mechanism, namely the

Table 3

Second order rate constants for the reaction of alkylamines $R^1R^2R^3N$ with ozone at 20°C and pH = 2

No.	R^1	R^2	R^3	k_2 $M^{-1} \cdot L \cdot s^{-1}$	σ^*	E_s
1	Me	H	H	6.180	0	0
2	n-Bu	H	H	0.952	−0.130	−0.39
3	i-Bu	H	H	1.547	−0.125	−0.93
4	sec-Bu	H	H	1.730	−0.210	−1.13
5	tert-Bu	H	H	0.436	−0.300	−1.54
6	cyclo-C_6H_{11}	H	H	0.581	−0.150	−0.79
7	n-Bu	n-Bu	H	4.505	−0.260	−2.11 [a]
8	i-Bu	i-Bu	H	1.974	−0.250	−2.47
9	n-Bu	Et	H	2.530	−2.230	−2.11 [a]
10	i-Bu	Et	H	2.830	−0.225	−2.47 [a]
11	i-Pr	i-Pr	H	3.647	−0.250	−2.40 [a]
12	cyclo-C_6H_{11}	Et	H	7.520	−0.250	−1.50 [a]
13	Et	Et	Et	1.640	−0.300	−3.80 [a]
14	n-Bu	n-Bu	n-Bu	0.085	−0.390	−4.00 [a]
15	$C_6H_5CH_2$	H	H	39·420	0.215	−0.38

[a] Values estimated from literature data [26] according to the usual procedure

electrophilic attack of ozone on the amine nitrogen atom and degrading of the formed adduct by a chain of fast subsequent reactions. To prove this assumption the second order rate constants were correlated with the Taft-type electronic and steric parameters σ* (Fig. 4) and E_s (Fig. 5).

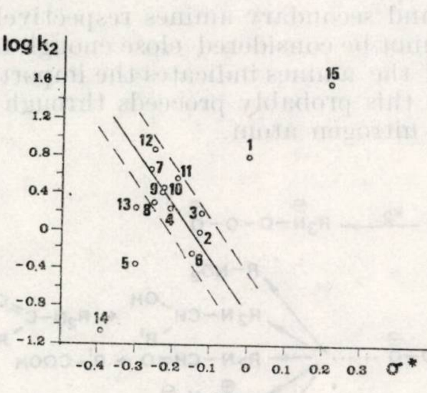

Fig. 4

As one can observe from Figure 4 the correlation between log k_2 and σ* is not very conclusive; the existence of a significant correlation for a part of the studied amines being not doubtless. However, the plot was drawn to account for a general variation tendency of the k_2 values with respect to the electronic (inductive) effect of the alkyl radicals. Thus one notes that for the amines with normal steric effects (n-butyl, cyclohexyl, isobutyl) the reaction rate increases with the increasing electron-donating effect of the alkyl. For the amines that significantly deviate from this tendency (tert-butylamine, tri-n-butylamine, triethylamine, methylamine and of course benzylamine) one may assume either an important steric hindrance or a different reaction mechanism.

Nevertheless one may consider as significant the increase of the reaction rate with the increasing nucleophilic character of the amine, thus supporting the assumption of the slow electrophilic attack of the ozone on the amine molecule.

The correlation of the rate constants with the steric parameters E_s is not fairly better than that with σ^* (Fig. 5). One observes that the amines are grouped along the two straight lines of the figure, which correspond to primary and secondary amines respectively. Tertiary amines and benzylamine cannot be considered close enough to any of the two lines. Such a grouping of the amines indicates the importance of the steric effect on the reaction as this probably proceeds through the electrophilic attack of ozone on the nitrogen atom.

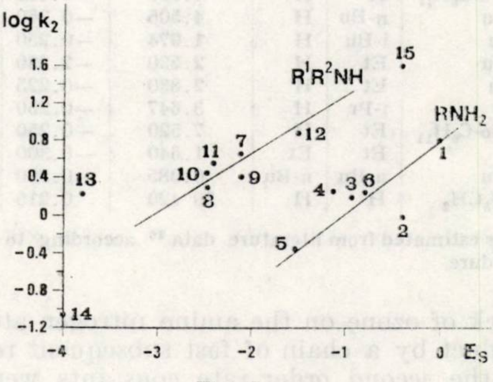

Fig. 5

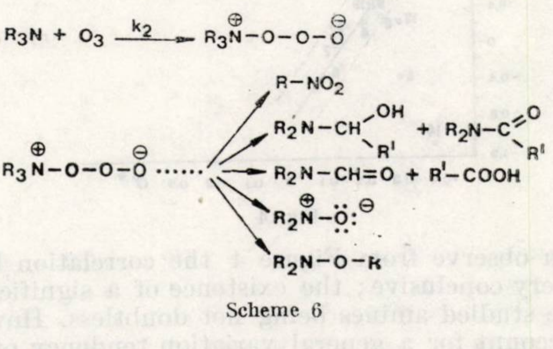

Scheme 6

As far as benzylamine is concerned, the reaction pathway is probably different; one may assume that the significantly higher reaction rate is due to ozone attacking the aromatic ring and not the nitrogen atom.

CONCLUSION

The kinetic data and the correlations with the amine structure produce evidence that in aqueous solutions the reaction of ozone with aliphatic amines proceeds in the first step by an electrophilic attack of ozone on the nitrogen atom of the free amine. The adduct ozone-amine then rapidly decomposes to products that can be nitroderivatives, amides carboxylic acids, aminoxides or substituted hydroxylamines. The reaction products can be further oxidized to total degradation by an excess of ozone.

REFERENCES

[1] M. Horvath, L. Bilitzky and J. Hüttner, "Topics in Inorganic and General Chemistry", vol. 20, Ozone, Elsevier, Amsterdam, 1985, p. 257.

[2] H. W. Prengle Jr., C. E. Mank, R. W. Legau and C. G. Hewes, *Hydroc. Process.*, **82** (10), 82 (1975).

[3] J. Staehelin and J. Hoigné, *Environ. Sci. Technol.*, **19**, 1206 (1985).

[4] J. Hoigné and H. Bader, *Water Res.*, **17**, 173 (1983).

[5] J. Hoigné and H. Bader, *Water Res.*., **17**, 185 (1983).

[6] V. Cocheci, E. Gerasimou, C. Csunderlik, L. Cotarca and A. Novac, *Rev. Chim. (București)*, in press (no. 9 — 1988).

[7] J. Hoigné, "Mechanisms, Rates and Selectivities of Oxidations of Organic Compounds Initiated by Ozonation of Water", in "Handbook of Ozone Technology and Applications", R. C. Rice and A. Netzer (eds.) Ann Arbor Science, 1982, p. 341.

[8] J. Hoigné and H. Bader, *Prog. Wat. Techn.*, **10**, 657 (1978).

[9] P. S. Bailey, "Ozonation in Organic Chemistry", vol. II "Nonolefinic Compounds", Academic Press, New York, 1982, pp. 155—200.

[10] P. S. Bailey, *Chem. Rev.*, **58**, 925 (1958).

[11] P. S. Bailey, J. E. Keller, D. A. Mitchard and H. M. White, *Adv. Chem.Ser.*, **77**, 58 (1968).

[12] P. S. Bailey and J. E. Keller, *J. Org. Chem.*, **33**, 2680 (1968).

[13] P. S. Bailey and T. P. Carter Jr., L. M. Southwick, *J. Org. Chem.*, **37**, 2997 (1972).

[14] E. Keinan and Y. Mazur, *J. Org. Chem.*, **42**, 844 (1977).

[15] P. S. Bailey, D. A. Lerdal and T. P. Carter Jr., *J. Org. Chem.*, **43**, 2662 (1978).

[16] P. S. Bailey, D. A. Mitchard and A. J. Khashab, *J. Org. Chem.*, **33**, 2675 (1968).

[17] H. B. Henbest and M. J. Stradford, *J. Chem. Soc.*, **1964**, 711.

[18] G. P. Shulman, *Can. J. Chem.*, **43**, 3069 (1965).

[19] P. S. BAILY, L. M. SOUTWICK, and T. P. CARTER Jr., *J. Org. Chem.*,**43**, 2657 (1978)

[20]. P. S. Bailey, J. F. Keller, and T. P. Carter Jr., *J. Org. Chem.*,**35**, 2777 (1970).

[21] P. S. Bailey, J. E. Keller, *J. Org. Chem.*, **35**, 2782 (1970).

[22] L. M. Vaicum, "Epurarea apelor uzate cu nămol activ", Ed. Academiei, București, 1981, p. 99.

[23] H. Bader and J. Hoigné, "Ozone : Science and Engineering", vol. 4, 1982, p. 169.

[24] V. Cocheci, E. Gerasimou, L. Cotarca and C. Cotarca, The 3rd National Congress of Chemistry, Abstracts vol. III, Bucharest, 1988, p. 949.

[25] V. Cocheci, E. Gerasimou, C. Csunderlik, L. Cotarca and A. Novac, The 3rd National Congress of Chemistry, Abstracts vol. III, Bucharest, 1988, p. 922.

[26] J. E. Leffler and E. Grunwald, "Rates and Equilibria of Organic Reactions", J. Wiley and Sons, New York, 1963, p. 222—228.

Revue Roumaine de Chimie, 34, 3, 759–763 (1989)

FRIEDEL-CRAFTS CHEMISTRY OF UNSATURATED ALICYCLIC SYSTEMS. III[1,2]

FRIEDEL-CRAFTS REACTION OF UNSATURATED ALICYCLIC ACIDS IN THE PRESENCE OF VARIOUS LEWIS ACIDS

V. DRĂGUȚAN *, I. DRĂGUȚAN, F. CHIRALEU and A. M. GLATZ
Center of Organic Chemistry, 202B Spl. Independenței, R-78100 Bucharest, Romania

Received November 8, 1988

The reaction of cyclohexylideneacetic acid and 1-cyclohexenylacetic acid with benzene catalyzed by $AlCl_3$, $AlCl_3 \cdot CH_3NO_2$, $BF_3 \cdot (C_2H_5)_2O$, $FeCl_3$, $TiCl_4$, $SnCl_4$ and $ZnCl_2$ is presented. Mixtures of phenylated acids were obtained in which the phenyl group entered the 2, 3 and 4 position of the cyclohexane ring (*trans*, *cis* and *trans*, respectively) depending on the catalyst employed. The mechanism of the phenylation reaction is discussed in terms of a carbocationic scheme involving ion-pairs.

INTRODUCTION

The phenylation reaction of cyclohexylideneacetic and 1-cyclohexenylacetic acids in the presence of $AlCl_3$ was reported by Nenitzescu and Gavăt[3] and simultaneously by Cook and Goulden[4] in 1937. The main reaction product they found was 4-phenylcyclohexaneacetic acid.

Later, thorough analysis[1] of the phenylation of these unsaturated alicyclic acids carried out at 40–45°C with $AlCl_3$ indicated that equilibrium mixtures of phenylated acids are formed in which the phenyl group enters the 2, 3 and 4 position of the cyclohexane ring. The reaction was stereoselective leading mainly to *trans*-1,2-, *cis*-1,3- and *trans*-1,4-phenylcyclohexaneacetic acids. The results were interpreted by a carbocationic mechanism involving 1,2- and 1,3-hydride ion shifts and formation of intermediate lactoid species accompanied by subsequent isomerization of the phenylated products.

The present study focuses on the reaction of cyclohexylideneacetic acid (**1**) and 1-cyclohexenylacetic acid (**2**) with benzene in the presence of a wider range of Lewis acids as the catalysts. Under these conditions *trans*-1,2- (**3**), *cis*-1,3- (**4**) and *trans*-1,4-phenylcyclohexylacetic (**5**) acids in proportions depending on the catalyst were recorded. In some cases, the product distribution allowed the isolation of pure phenylcyclohexylacetic acids useful for synthetic purposes, e.g. preparation of benzobicyclic compounds of interest for their potential biological activity.

RESULTS AND DISCUSSION

The reactions of cyclohexylideneacetic (**1**) and 1-cyclohexenylacetic (**2**) acids with benzene in the presence of different Lewis acid catalysts were carried out at 20–45°C using molar ratios acid : catalyst : benzene in the range 1 : 1.2–2.2 : 20–40 (Eqs. 1 and 2); *trans*-1,2- (**3**), *cis*-1,3- (**4**) and *trans*-1,4-phenylcyclohexylacetic (**5**) acids were obtained in various amounts as a function of the catalytic system and reaction time (see Table 1).

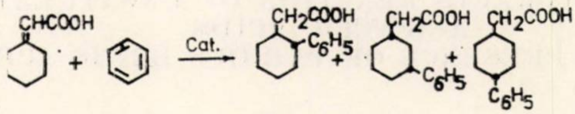

1 3 4 5

(1)

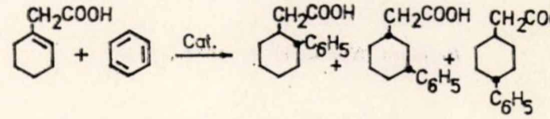

2 3 4 5

(2)

Table 1

Reaction of cyclohexylideneacetic acid (**1**) with benzene in the presence of various Lewis acids [a]

Catalytic system	Reaction time, hr	Reaction temp., °C	Conv. %	Product composition, % [b]		
				3	**4**	**5**
$AlCl_3$	1/4	40–45	99	1.6	59.0	38.0
$AlCl_3 \cdot CH_3NO_2$		40–42	35	22.0	5.5	6.8
$BF_3 \cdot (C_2H_5)_2O$		30–35	48	43.0	1.8	2.1
$FeCl_3$		40–42	20	8.4	4.9	2.1
$TiCl_4$		40–42	21	18.0	1.0	1.5
$SnCl_4$		40–42	12	10.7	0.7	0.4
$AlCl_3$	1	40–45	99	2.6	60.0	35.0
$AlCl_3 \cdot CH_3NO_2$		40–42	40	18.5	7.0	10.5
$BF_3 \cdot (C_2H_5)_2O$		30–35	62	56.0	2.2	2.3
$FeCl_3$		40–42	42	32.8	6.0	2.5
$TiCl_4$		40–42	39	35.0	1.2	2.0
$SnCl_4$		40–42	24	21.3	0.6	0.5
$ZnCl_2$		40–42	3.5	1.0	1.0	0.5
$AlCl_3$	4	40–45	99	2.7	60.0	35.0
$AlCl_3 \cdot CH_3NO_2$		40–42	55	16.8	14.0	23.8
$BF_3 \cdot (C_2H_5)_2O$		30–35	66	61.0	2.4	2.5
$FeCl_3$		40–42	77	53.7	9.9	12.5
$TiCl_4$		40–42	45	40.0	1.2	2.0
$SnCl_4$		40–42	40.5	38.0	0.8	0.7
$ZnCl_2$		40–42	5	1.4	1.1	0.8

[a] Molar ratio cyclohexylideneacetic acid : catalyst : benzene = 1 : 1.6–1.8 : 20;
[b] The remainder are several small unidentified components.

Table 1 clearly indicates that from acid **1** conversions and product compositions vary with the catalyst. A sharp difference between $AlCl_3$ and the other catalysts can be readily noticed even at shorter reaction times. Thus, whereas with $AlCl_3$ high conversions of acid **1** (over 90%) along with equilibration of products **3**, **4** and **5** occur even after 15 min, with $AlCl_3 \cdot CH_3NO_2$ and $BF_3 \cdot (C_2H_5)_2O$ only conversions of 35.0% and 48.0%, respectively are reached and the reaction mixtures contain product **3** as the major component. On the other hand, $FeCl_3$, $TiCl_4$ and $SnCl_4$ afford appreciable conversions (77.0%, 45.0% and 40.5%, respectively) after 4 hr when the product composition is still far from equilibrium. Formation in turn of *trans*-1,2-, *cis*-1,3- and *trans*-1,4-phenylcyclohexylacetic acids as the main products under different reaction conditions allowed these compounds to be easily separated from the reaction mixture and used in further synthetic work.

When starting from acid **2** with the above catalytic systems, conversions and product compositions (see Table 2) parallel generally those derived from acid **1**. It is noteworthy however that in the presence of majority of these catalysts the amount of product **3** is slightly greater in this case than that with acid **1**. At longer reaction times, *trans*-1,2-, *cis*-1,3- or *trans*-1,4-phenylcyclohexylacetic acids became major products and they could also be isolated from the respective reaction mixtures.

These two sets of results (Table 1 and 2) can be rationalized assuming a carbocationic mechanism in accordance with earlier proposals [1] (Scheme 1).

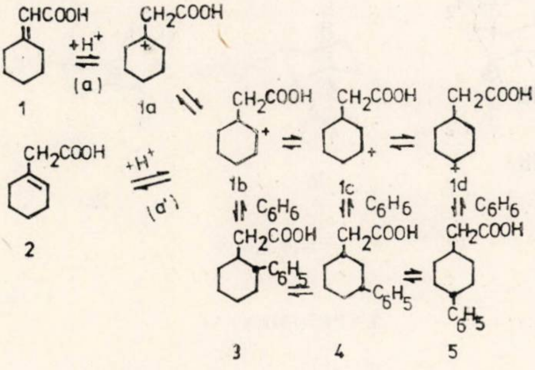

Scheme 1

This mechanism essentially involves generation of carbocations **1a** and **1b** from either the acid **1** and **2** under the action of the catalytic complex, rearrangements of these ions by 1,2- and 1,3-hydride shifts to ions **1c** and **1d**, alkylation of benzene by all intervening carbocations and subsequent isomerization of the phenylated products.

As also stated for Friedel-Crafts reaction of unsaturated esters,[2] the rate of each reaction step is greatly dependent on the Brönsted and Lewis acidity of the catalytic systems. The difference in the Brönsted and

Lewis acidities of the catalysts employed can readily account for their different catalytic behaviour during phenylation reaction of acids **1** and **2**. Thus, the increased conversion of the two alicyclic acids **1** and **2** in the presence of $AlCl_3$ reveals the high rate of formation of the intermediate carbocations **1a**—**1d** *via* pathways (a) and (a′) due to the significant Brönsted acidity connected with the catalytic complex. Furthermore, the great selectivity in products **4** and **5** shows rapid rearrangements (1,2- and 1,3-hydride shifts) in ions **1a** and **1b** in the presence of the same catalytic system. By contrast, the lower conversions with the systems $AlCl_3 \cdot CH_3NO_2$, $BF_3 \cdot (C_2H_5)_2O$, $FeCl_3$, $TiCl_4$ and $SnCl_4$ indicate a more moderate rate of formation of the carbocations **1a** and **1b**. In addition, the reduced amount of products **4** and **5** obtained with the last catalysts suggests that 1,2- and 1,3-hydride shifts in ions **1a**—**1d** and their alkylation on benzene are greatly hindered in the ion pairs arising from these systems.

The high stereoselectivity observed in the phenylation reaction of acids **1** and **2** implies a stereospecific attack of benzene ring on the ions **1b**—**1d** in accordance with earlier proposals.[1] Thus, for formation of *trans*-1,2-phenylcyclohexylacetic acid stereospecific attack on the lactoid species derived from ion **1b** must occur while generation of *cis*-1,3- and *trans*-1,4-phenylcyclohexylacetic acids results from the attack on ions **1c** and **1d** also undergoing simultaneous equilibration *via* hydride ion migration (Scheme 2).

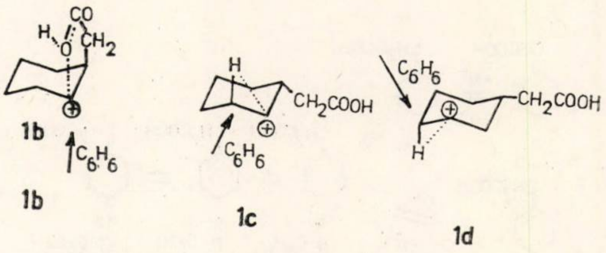

Scheme 2

EXPERIMENTAL

The purity and structure of the starting materials and authentic samples were checked by elemental analyses, v.p.c., NMR and IR spectra. All melting points are uncorrected. V.p.c. analyses were carried out on a Willy Giede model 18.3 gas chromatograph using a 3 m × 4 mm column packed with 10% ethyleneglycol-succinate on Chromosorb W (60—80 mesh), column temperature 190°C. NMR spectra were recorded on a Varian A 60-A spectrometer using TMS as internal standard. IR spectra were recorded on UR-20 Carl Zeiss-Jena spectrophotometer.

Starting materials and authentic samples

Cyclohexylideneacetic acid (**1**) was prepared *via* Wittig reaction starting from cyclohexanone and triethylphosphonoacetate after Wiberg and Hiatt.[6] 1-Cyclohexenylacetic acid (**2**) was obtained by alkaline hydrolysis of its ethyl ester prepared *via* Reformatsky reaction and subsequent dehydration.[7] For *trans*-1,2-, (**3**), *cis*-1,3- (**4**) and *trans*-1,4-phenylcyclohexaneacetic (**5**) acids the procedure mentioned elsewhere [1] was followed. Benzene (Reactivul) was purified by distillation and dried over sodium wire. $AlCl_3$ (Merck-Schuchardt), $BF_3 \cdot (C_2H_5)_2O$ (Merck-

Schuchardt), $FeCl_3$ (Merck-Schuchardt), $TiCl_4$ (Merk-Schuchardt), $SnCl_4$ (BDH, England), $ZnCl_2$ (Merck-Schuchardt) and nitromethane (Merck-Schuchardt) of commercial grade were used without further purification.

Reaction of cyclohexylideneacetic acid (1) and 1-cyclohexenylacetic acid (2) with benzene

The reactions of acids **1** and **2** with benzene in the presence of $AlCl_3$, $AlCl_3 \cdot CH_3NO_2$, $BF_3 \cdot (C_2H_5)_2O$, $FeCl_3$, $TiCl_4$, $SnCl_4$ and $ZnCl_2$ were performed at temperatures between 20° and 45°C using molar ratios acid : catalyst : benzene 1 : 1.2–2.2 : 20–40 according to the method described earlier.[1] The results inferred from v.p.c. analyses are given in Tables 1 and 2.

Table 2

Reaction of 1-cyclohexenylacetic acid (**2**) with benzene in the presence of various Lewis acids[a]

Catalytic system	Reaction time, hr	Reaction temp., °C	Conv. %	Product composition, %[b]		
				3	**4**	**5**
$AlCl_3$	1/4	40–45	98.0	1.8	58.0	38.0
$AlCl_3 \cdot CH_3NO_2$		40–42	36.0	24.0	5.4	6.6
$BF_3 \cdot (C_2H_5)_2O$		30–35	47.0	41.0	1.7	2.0
$FeCl_3$		40–42	20.0	8.6	5.0	2.2
$TiCl_4$		40–42	22.0	18.5	1.0	1.2
$SnCl_4$		40–42	12.0	10.5	0.6	0.4
$AlCl_3$	1	40–45	98.0	2.7	59.0	35.4
$AlCl_3 \cdot CH_3NO_2$		40–42	39.0	18.8	7.2	10.0
$BF_3 \cdot (C_2H_5)_2O$		30–35	59.0	52.0	2.6	2.0
$FeCl_3$		40–42	41.5	33.2	5.8	2.4
$TiCl_4$		40–42	38.8	35.5	1.2	2.5
$SnCl_4$		40–42	23.5	22.0	0.6	0.5
$ZnCl_2$		40–42	3.0	1.2	1.0	0.4
$AlCl_3$	4	40–45	99.0	2.8	60.0	35.0
$AlCl_3 \cdot CH_3NO_2$		40–42	53.0	17.5	12.4	21.2
$BF_3 \cdot (C_2H_5)_2O$		30–35	67.0	61.5	2.4	2.4
$FeCl_3$		40–42	76.0	53.8	9.8	12.3
$TiCl_4$		40–42	47.0	42.0	1.2	2.0
$SnCl_4$		40–42	38.0	35.0	0.6	0.6
$ZnCl_2$		40–42	4.0	1.5	1.0	0.8

[a] Molar ratio 1-cyclohexenylacetic acid : catalyst : benzene = 1 : 1.6–1.8 : 20;
[b] The remainder are several small unidentified components.

REFERENCES

[1] Part I, V. Drăguţan, L. Stănescu and A. M. Glatz, *Rev. Roumaine Chim.*, **22**, 1045 (1977).
[2] Part II, V. Drăguţan, Zs. Arvay and A. M. Glatz, *Rev. Roumaine Chim.*, **23**, 1283 (1978).
[3] C. D. Nenitzescu and I. Gavăt, *Ber. dtsch. chem. Ges.*, **70**, 1883 (1937).
[4] J. W. Cook and F. Goulden, *J. Chem. Soc.*, **1937**, 1559.
[5] V. Drăguţan, I. Drăguţan, C. Condeiu and A. M. Glatz, *Rev. Roumaine Chim.*, **34**, 000 (1989).
[6] K. B. Wiberg and H. Hiatt, *J. Amer. Chem. Soc.*, **90**, 6495 (1968).
[7] R. L. Shriner, "Organic Reactions", Vol. 1, J. Wiley, New York, 1942, p. 1.

Revue Roumaine de Chimie, **34**, *3*, 765–769 (1989)

FACILE SYNTHESIS OF 9-SUBSTITUTED *exo*-BENZOCYCLOBUTENONORBORNENES [1]

LUCIAN ENESCU, AURELIA GHENCIULESCU, FILIP CHIRALEU and
ILIE G. DINULESCU
Organic Chemistry Department, Polytechnic Institute TCH, 313, Splaiul Independenței,
76206 Bucharest, Romania

Received December 7, 1987

The reaction of benzyne with 7-*t*-butoxynorbornadiene (**5**) gave 9-substituted *exo*-benzocyclobutenonorbornenes (the *anti*/*syn* ethers **7** and **9**), together with tetracyclic compound **8**, in 1.1:1.0 ratio. The reaction on the more hindered side of the diene **5**, leading to an *anti*-9-substituted adduct, was explained by the participation of the *t*-butoxy group in the stabilisation of the diradicalic intermediate.

As already shown,[2–4] 9-substituted derivatives of *exo*-benzocyclobutenonorbornene (**1**) can be obtained by the electrophilic additions to *endo*-benzocyclobutenonorbornene (**2**).

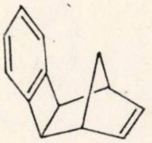

1

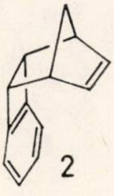

2

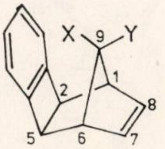

3a X=OH, Y=H
3b X=H, Y=OH

A similar rearrangement occurs during the cycloaddition reactions with *t*-butylcyanoketene [5] as well as with methyl propiolate.[6]

The alcohol **3b** was prepared from the alkene **2** by catalytic addition of palladium acetate-chloride and elimination of hydrochloric acid,[3] or by epoxidation of the alkene **2** and the opening of the epoxide ring with hydrobromic acid, followed by dehydrobromination.[4]

In connection with our studies on the behaviour of benzocyclobutenonorbornenes (**1** and **2**), we were interested in preparing the alcohols **3a** and **3b**. We wish to report herein another pathway in the synthesis of these alcohols based on the reaction of benzyne (**4**) with *t*-butoxynorbornadiene (**5**). Benzyne was generated *in situ*, by the procedure described previously.[7]

Thus, a suspension of diazo-anthranilic acid hydrochloride (**6**) in dichloroethane was refluxed with the diene **5** in the presence of propylene oxide, until the gas evolution ceased. The gas-chromatographic analysis of the crude product revealed the presence of three compounds, i.e. the ethers **7**, **8** and **9**, in 2.3 : 3 : 1 ratio. The compounds were isolated by column chromatography on silica gel.

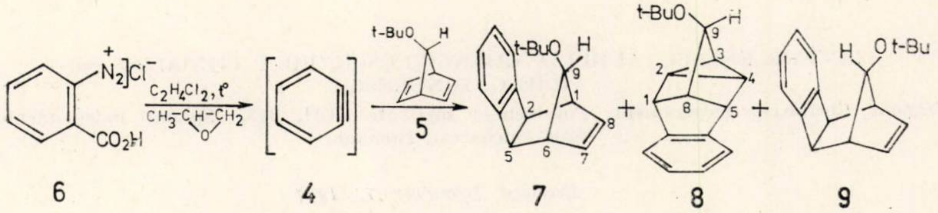

Afterwards, the ethers **7** and **9** were converted into the acetates **10** and **11**, respectively, by reaction with the acetic acid in presence of perchloric acid. The treatment of the acetates **10** and **11** with lithium aluminium hydride yielded the corresponding alcohols, **3a** and **3b** respectively.

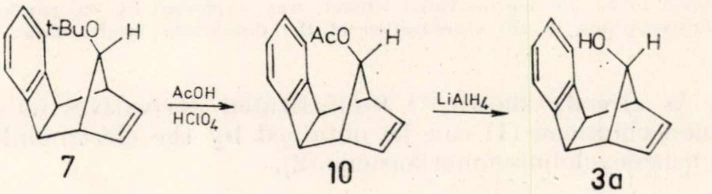

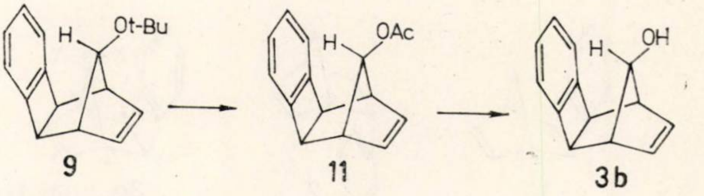

The physical and spectral characteristics of the alcohol **3b** are in agreement with those of an authentic sample obtained from the alkene **2** by Baker's procedure.[4]

The IR and ^{1}H-NMR spectral data of the new compounds support the ascribed structures. Thus, the *exo* configuration of the benzocyclobutene ring is supported by the signal of H—2 and H—5 protons which appear as a sharp singlet uncoupled with the bridgehead protons.[2,8] The features agree with the ascribed *anti*-orientation for the bulky substituents in **7**, **10** and **3a** and consequently the *syn*-orientation for H-9 proton. We observed a significant deshielding of the H-*syn* proton in compounds **7**, **10** and **3a** as compared with the H-9-*anti* in **9**, **11** and **3b**.[3,4] At the same time, the signals of the bulky group in **7** and **10** appear more shielded because of the aromatic ring. The ^{1}H-NMR spectrum of the ether **8** was compared with those of the similar nonsubstituted compound.[7] Thus, the *t*-butoxy group induces a downfield shift for the H-9 proton and an upfield shift for the H-5 and H-8 protons.

Concerning the reaction of benzyne with 7-*t*-butoxynorbornadiene our results reveal that the thermally unconcerted and the favoured concerted cycloaddition occur in somewhat equal ratio; for comparison, in the corresponding reaction of benzyne with norbornadiene, this ratio has been 3 : 1.[7] We suggest that an electron-rich group such as *t*-butoxy enhances the homo-Diels-Alder reactivity of norbornadiene in the thermally allowed process under the Woodward-Hoffmann orbital symmetry rules.[9] Furthermore, the unconcerted cycloaddition occurred at the more hindered side of 7-*t*-butoxynorbornadiene, when the major product was 9-*anti*-adduct, **7**. In view of the assumption that the thermally forbidden cycloadditions may be approximated by a two-step reaction with a diradical intermediate,[10] we suggest that in the course of the reaction of benzyne with 7-*t*-butoxynorbornadiene, the electron-donating group stabilizes the diradicalic intermediate (**12**).

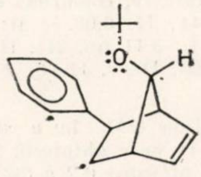

12a

or

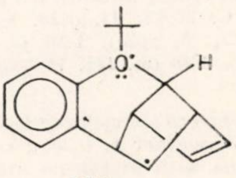

12b

EXPERIMENTAL

Gas-chromatographic analyses were carried out on a Chromatron gas-chromatograph, using a 1.0 m × 4 mm diameter column filled with 20% methylsilicone SE 30 on Chromosorb W 30—60 mesh, at 220°, and with 30 mL/min hydrogen as carrier gas. IR spectra were recorded on a Jena UR-20 spectrophotometer. ^{1}H—NMR spectra were recorded on a Varian A60-A spectrometer using TMS as internal standard, by Dr. F. Chiraleu.

The reaction of benzyne with 7-t-butoxynorbornadiene (**5**). In a two-necked flask fitted with a condenser were placed 11.4 g (69.5 mmoles) diene **5**,[11] 1.5 mL propylene oxide dissolved in 500 mL dichloroethane and 5.8 g (31.4 mmoles) diazo-anthranilic acid hydrochloride.[12] The suspension was gently boiled for 5 hrs. After this time the evolution of carbon dioxide and nitrogen ceased. The solvent was evaporated *in vacuo* and the residue was extracted with petroleum ether (b.p. 35°, 500 mL). After filtration from the polymeric material, the solution was washed with water (3 × 50 mL), with saturated sodium hydrogene carbonate solution (four runs of 50 mL) and then dried. The solvent and unreacted diene **5** (4.9 g, b.p. 85—87°/2.0 mm) were removed *in vacuo* using a Vigreux column (200 mm × 15 mm diameter) yielding 3.5 g oily product. The gas-chromatography analysis of the crude product indicated a content of three components in a 2.3:3.0:1.0 ratio. The crude mixture was separated by chromatography on silica gel column. The first fraction (eluent: petroleum ether, b.p. 35°) afforded 1.08 g (14.3%) ether **7**.

anti-9-t-Butoxy-exo-benzo[c]tricyclo[4.2.1.0$^{2.5}$]*non-3-ene* (**7**), colourless oil. — Anal. $C_{17}H_{20}O$ (240.33) Calcd.: C, 84.95; H, 8.39. Found: C, 84.73; H, 8.30. — IR (CCl_4, cm^{-1}): 900, 1195, 1030, 1360. — ^{1}H—NMR (CCl_4, δ, ppm): 0.75 (s, 9H, 9-*t*-butoxy), 2.78 (m, 2H, H—1, H—6), 3.30 (s, 2H, H—2, H—5), 3.46 (m, 1H, H-9-*syn*), 6.18 (t, 2H, H—7, H—8, $J = 2$ Hz), 6.80 — 7.30 (m, 4 H aromatic).
Further elution with a mixture of petroleum ether: diethyl ether in 2:1 ratio yielded 1.4 g (18.57%) ether **8**.

9-t-Butoxy-benzo[f]tetracyclo[3.2.1.1$^{3.8}$.0$^{2.4}$] *non-6-ene* (**8**), colourless crystals, m.p. 47—48° — Anal. $C_{17}H_{20}O$ (240.33) Calcd.: C, 84.95; H, 8.39. Found: C, 84.87 H, 8.22. — IR (CCl_4, cm^{-1}): 915, 1220, 1345. — ^{1}H—NMR ($CDCl_3$, δ, ppm): 1.10—1.90 (m, 12H, 9-*t*-butoxy, H—2, H—3, H—4), 2.28 (m, 1H, H—8), 3.11 (m, 1H, H—5), 3.61 (m, 1H, H—1), 4.08 (m, 1H, H—9), 7.00—7.50 (m, 4 H aromatic).

The last fraction, obtained by elution with diethyl ether as solvent, afforded 0.47 g (6.24 %) ether **9**.

syn-9-t-Butoxy-exo-benzo[c]tricyclo[4.2.1.0^{2,5}]*non-3-ene* (**9**), colourless crystals, m.p. 69—70°. — Anal. $C_{17}H_{20}O$ (240.33) Calcd.: C, 84.95; H, 8.39. Found: C, 84.70; H, 8.27. — IR (CCl_4, cm^{-1}): 907, 1070, 1250, 1380. — ^{1}H—NMR ($CDCl_3$, δ, ppm): 0.93 (s, 9H, 9-*t*-butoxy), 2.73 (m, 2H, H—1, H—6), 3.15 (s, 2H, H—2, H—5), 3.41 (m, 1H, H—9-*anti*), 6.21 (s, 2H, H—7, H—8), 6.90—7.50 (m, 4 H aromatic).

anti-9-Acetoxy-exo-benzo[c]tricyclo[4.2.1.0^{2,5}]*non-3-ene* (**10**). A solution of 0.6 g (2.5 mmoles) ether **7** into a mixture of 4.1 mL (4.3 g, 70 mmoles) anhydrous acetic acid and 0.86 mL acetic anhydride was allowed to stay at room temperature for 30 min. The solution was cooled in an ice bath, added to 0.55 g (3.8 mmoles) of 70 % perchloric acid previously cooled to 0° and mixture was kept at this temperature for 1 min. After this time, the mixture was poured into a separatory funnel containing 50 mL water and ice and extracted with dichloromethane (2 × 50 mL). The dichloromethane solution was washed with saturated sodium hydrogene carbonate solution (3 × 50 mL), water (2 × 50 mL), saturated sodium chloride solution (2 × 50 mL) and dried over magnesium sulfate. The solvent was removed *in vacuo*, yielding 0.53 g crude oil product. The chromatography on neutral alumina with petroleum ether as eluent afforded 0.5 g (88.5 %) acetate **10**, colourless oil. — Anal. $C_{15}H_{14}O_2$ (226.26) Calcd.: C, 76.62; H, 6.23. Found: C, 76.44; H, 6.08. — IR (CCl_4, cm^{-1}): 1720. — ^{1}H—NMR (CCl_4, δ, ppm): 1.16 (s, 3 acetoxy H), 3.11 (m, 2H, H—1, H—6), 3.35 (s, 2H, H—2, H—5), 4.28 (m, 1H, H-9-*syn*), 6.20 (t, 2H, H—7, H—8, $J = 2$ Hz), 6.83—7.30 (m, 4 H aromatic).

syn-9-Acetoxy-exo-benzo[c]tricyclo[4.2.1.0^{2,5}]*non-3-ene* (**11**). In a similar manner, from 0.4 g (1.66 mmoles) ether **9**, 0.25 g crude acetate **11** were obtained. The chromatography on neutral alumina with petroleum ether as eluent afforded 0.2 g (53.3 %) acetate (**11**) colourless crystals, m.p. 91—92°. — Anal. $C_{15}H_{14}O_2$ (226.26) Calcd.: C, 76.62; H, 6.23. Found: C, 76.54; H, 6.19. — IR (CCl_4, cm^{-1}): 1728. — ^{1}H—NMR (CCl_4, δ, ppm): 1.61 (s, 3 acetoxy H), 3.00 (m, 2H, H—1, H—6), 3.16 (s, 2H, H—2, H—5), 4.13 (m, 1H, H-9-*anti*), 6.10 (m, 2H, H—7, H—8), 7.11 (m, 4 H aromatic).

anti-9-Hydroxy-exo-benzo[c]tricyclo[4.2.1.0^{2,5}]*non-3-ene* (**3a**). In a two-necked flask fitted with a magnetical stirrer, dropping funnel and condenser were placed 0.06 g (1.31 mmoles lithium aluminium hydride and 5 mL anhydrous diethyl ether. A solution of 0.4 g (1.76 mmoles) acetate **10** in 10 mL anhydrous diethyl ether was added to the well stirred suspension over a period of 20 min. After addition the reaction mixture was allowed to stir at room temperature for 60 min. After this time, 1 mL water and 0.5 g sodium sulfate were added and the product was extracted with diethyl ether (3 × 15 mL). The ethereal extract was washed with water (2 × 10 mL) and dried over anhydrous sodium sulfate. Removal of the solvent afforded 0.3 g (92.5 %) alcohol **3a**, colourless crystals, m.p. 63—64°. — Anal. $C_{13}H_{12}O$ (184.22) Calcd.: C, 84.74; H, 6.56. Found: C, 84.45; H, 6.49. — IR (CCl_4, cm^{-1}): 1600, 3600. — ^{1}H—NMR (CCl_4, δ, ppm): 0.63 (bs, 1H, OH), 2.90 (m, 2H, H—1, H—6), 3.41 (s, 2H, H—2, H—5), 3.50 (m, 1H, H—9-*syn*), 6.20 (t, 2H, H—7, H—8, $J = 2$ Hz), 7.20 (m, 4 H aromatic).

syn-9-Hydroxy-exo-benzo[c]tricyclo[4.2.1.0^{2,5}]*non-3-ene* (**3b**). Working as above, from 0.15 g (0.66 mmoles) acetate **11**, 0.12 g crude alcohol **3b** were obtained, which was purified by chromatography on neutral alumina (activity II) using a mixture of petroleum ether: diethyl ether (10:1) as eluent. Removal of the solvent yielded 0.10 g (82.6 %) alcohol **3b**, m.p. 91—92°. The IR and ^{1}H—NMR spectra of the alcohol **3b** thus obtained were identical with those of an authentic sample prepared by Baker's procedure. [4]

REFERENCES

[1] Part LXIII in the series "Investigations in the Cyclobutane series". For part LXII see: A. Ghenciulescu, L. Enescu, F. Chiraleu and I. G. Dinulescu, *Rev. Roumaine Chim.*, (1989).

[2] a) M. Avram, I. Pogany, F. Badea, I. G. Dinulescu and C. D. Nenitzescu, *Tetrahedron Letters*, **1969**, 3851.

b) M. Avram, I. Pogany, I. G. Dinulescu, F. Chiraleu and C. D. Nenitzescu, *Rev. Roumaine Chim.*, **15**, 1207 (1970).

[3] M. A. Battiste and W. Nebzydosky, *J. Amer. Chem. Soc.*, **91**, 6887 (1969).

[4] R. Baker and J. C. Salter, *J. Chem. Soc.*, **1973**, 150.

[5] M. D. Gheorghiu, C. Drăghici and L. Pârvulescu, *Tetrahedron*, **33**, 3295 (1977).

[6] L. Enescu, M. D. Gheorghiu, A. Ghenciulescu, I. G. Dinulescu and M. Avram, *Rev. Roumaine Chim.*, **28**, 1001 (1983).

[7] a) L. Friedmann and R. L. Rise, quoted by F. M. Logullo, Ph. D. Thesis, Case Institute of Technology, Cleveland, 1965.
b) L. Enescu and M. Avram, *Rev. Roumaine Chim.*, **22**, 1061 (1977).

[8] H. E. Simmons, *J. Amer. Chem. Soc.*, **83**, 1657 (1961).

[9] R. B. Woodward and R. Hoffmann, *Angew. Chem., Int. Ed. Engl.*, **8**, 827 (1969).

[10] M. Taagepera and E. R. Thornton, *J. Amer. Chem. Soc.*, **94**, 1168 (1972).

[11] P. R. Story, *J. Org. Chem.*, **26**, 287 (1961); P. R. Story and S. R. Fahrenholtz, *Org. Synth., Coll.* **5**, 151 (1973).

[12] G. R. Ziegler, *J. Amer. Chem. Soc.*, **91**, 446 (1969).

Revue Roumaine de Chimie, **34**, *3*, 771–777(1989)

STUDY ON THE TETRANITRO-PLATINITES(II) AND HEXANITRO-PLATINATES(IV)

I. GĂNESCU, J. ZSAKÓ, CS. VÁRHELYI and EDITH PÁLL
Chemical Faculty, University of Craiova, 1100–Craiova,
Str. Al. I. Cuza, No. 13, Romania
University of Cluj-Napoca, Faculty of Chemical Technology
3400 – Cluj-Napoca, str. Arany János 11, Romania

Received September 21, 1987
Revised March 21, 1988

IR spectra of some simple salts of the $H_2[Pt(NO_2)_4]$ and $H_2[Pt(NO_2)_6]$ acids were discussed and the force constants of the co-ordinated nitro-groups calculated. A number of 23 new cobalt (III) amine salts of these complex acids were obtained by double decomposition reaction with monoacido-pentamine- and diacido-tetramine type complex salts and characterized.

INTRODUCTION

The nitro-complexes of the metals in the VIIIth group of the periodic system are mainly of analytical importance (e.g. $[Co(NO_2)_6]^{3-}$, $[Rh(NO_2)_6]^{3-}$ etc.). Some derivatives of this type can be used also for preparative purposes. The substitution reactions of $Na_3[Co(NO_2)_6]$ and $Na_3[Rh(NO_2)_6]$ with amines, phosphines, α-dioximes, β-diketones, Schiff's bases, etc. lead to the formation of a large number of mixed classical complexes and chelates. [1–5]

The hydrolysis kinetics of some nitro-complexes of Co(III) and Rh(III) was also studied.

Nitro-complexes of platinum were obtained by various substitution reactions. It was observed that during the reaction of $H_2[PtCl_6]$ with $NaNO_2$ the Pt(IV) → Pt(II) redox process occurs and $Na_2[Pt(NO_2)_4]$, is formed. [6] The tetranitro-platinite can be transformed easily in platinum (IV) nitro-derivatives by oxidation with free halogens: $K_2[PtX_2(NO_2)_4$, $K_2[PtX_3(NO_2)_3]$ and $K_2[PtX_4(NO_2)_2]$ (X = Cl, Br, I). [7–9] Conc. HNO_3 transforms them into $Na_2[Pt(NO_2)_6]$.[10]

Some substitution reactions of $Na_2[Pt(NO_2)_4$ with neutral and acidic ligands were also mentioned in the literature. The interaction with ammonia leads to the formation of *cis*-$[Pt(NH_3)_2(NO_2)_2]$. [11] With pyridine *cis*-$[Pt(py)_2(NO_2)_2]$ [12] and with some phosphines (e.g. R_3P), nitro-phosphino-complexes : $[Pt(R_3P)_2(NO_2)_2]$ can be obtained. [13] The reaction product with oxalic acid is *cis*-$[Pt(C_2O_4)(NO_2)_2]^{2-}$.[14]

In the present paper IR spectra of some simple salts of $H_2[Pt(NO_2)_4]$ and $H_2[Pt(NO_2)_6]$ have been recorded. An attempt was made to calculate force constants for the co-ordinated nitro group.

A series of new cobalt (III)-amine salts of these complex acids have been obtained by double decomposition reactions and characterized by chemical methods and by means of derivatographic measurements.

EXPERIMENTAL

The *IR spectra* were recorded in KBr pellets with a UR-20 Carl Zeiss Jena spectrophotometer.

$K_2[Pt(NO_2)_4]$ was obtained from $H_2[PtCl_6]$ and KNO_2, as described in the literature, in form of bright yellow rhombohedral prisms.

$K_2[Pt(NO_2)_6]$ was obtained according to the reaction scheme :

$$K_2[Pt(NO_2)_4] + HNO_3 + NO + NO_2 \rightarrow K_2[Pt(NO_2)_4(NO)(NO_3)] \rightarrow K_2[Pt(NO_2)_6]$$

3 g $K_2[Pt(NO_2)_4]$ were treated with 5–6 mL conc. HNO_3 and warmed on a water bath. A mixture of $NO + NO_2$ gas (from the reaction of Cu + 40–45% HNO_3) was bubbled through the warm solution for 35 – 50 minutes. A green-blue mass precipitated from the solution. After 1–2 hours the solid substance became yellow. It was filtered off and recrystallized from warm water (Yield : 40–45 %).

$[Co(DH)_2(amine)_2]$acetate — salts were obtained by the oxidation of a mixture of $Co(CH_3COO)_2 \cdot 4\,H_2O$, dimethylglyoxime and the corresponding amine (molar ratio : 1 : 2 : 3) in diluted methanol (60–70 %), by air bubbling (3–4 hours). The filtered 0.02 molar brown solutions were used for double decomposition reactions.

cis-$[Co(en)_2Cl(amine)]\,Cl_2$. 25 mmoles of *trans*-$[Co(en)_2Cl_2]Cl$ were moistened with 1–2 mL water and treated with the corresponding amine (30 – 35 mmoles) by rubbing in a mortar for 3–4 hours. The dark red mass was recrystallized from warm 2% HCl. The complex salt was dissolved in 40–50 mL water, filtered and used for double decomposition reactions.[15]

Tetranitro-platinites and hexanitro-platinates of the cobalt(III)-amines. 10 mmoles of the corresponding cobalt(III) amine in 50–75 mL water or in dil. methanol (1 : 1) were treated with 5 mmoles $K_2[Pt(NO_2)_4]$, or $K_2[Pt(NO_2)_6]$ in 20–25 mL aqueous solution. After 30 – 60 minutes the separated crystalline products were filtered off, washed with water and dried on air.

Analysis. The Co content was determined complexometrically after destruction of the samples with conc. H_2SO_4 and some crystals of KNO_3. Platinum was determined microgravimetrically as metallic platinum in the disaggregated and diluted samples. Nitrogen was determined by means of the usual gasvolumetrical method.

Recovery of the platinum rests. The solutions of the platinum complexes and the solid residues were evaporated to dryness and calcinated at 800–900°C. The black porous residue was heated with conc. H_2SO_4 and cryst. KNO_3, and after dilution with water the metallic platinum was filtered off from the violet solution of the $CoSO_4$.

Termogravimetric measurements were carried out by means of a derivatograph MOM (Budapest). Heating rate 20°/min.

RESULTS AND DISCUSSION

The IR spectra of $K_2[Pt(NO_2)_4]$, $K_2[Pt(NO_2)_6]$ and $Tl_2[Pt(NO_2)_6]$ have been recorded in the spectral region 400 – 3500 cm^{-1}.

From the six normal vibrations of the NO_2 group linked to a metal atom, five appear in this region.[16] They were identified by comparing the spectra of the compounds studied with the IR spectra of the analogous complexes containing Cl and Br instead of NO_2. The wave numbers of the vibration bands are given in table 1.

Table 1

Wave numbers (cm^{-1}) of the vibration bands of the $Pt-NO_2$ group

Compound	$\nu_3(Pt-N)$	$\delta_{w(NO)_2}$	$\delta_{s(NO_2)}$	$\nu_{s(NO_2)}$	$\nu_{as(NO_2)}$
$K_2[Pt(NO_2)_4]$	410	635	830	1345	1420
$K_2[Pt(NO_2)_6]$	420	605	840	1338	1410
$Tl_2[Pt(NO_2)_6]$	425	605	840	1335	1410

By using the Urey-Bradley Force Field approximation,[17] i.e. by neglecting the force constants of the modifications of bond angles and retaining only the force constant f_{11} of the attraction between N and O atoms, the force constant f_{12} of the repulsion between both O atoms and the force constant f_{33} of the attraction between Pt and N atoms, the force constants can be calculated from the wave numbers of the valence vibrations $\nu_s(Pt-N)$, $\nu_s(NO_2)$ and $\nu_{as}(NO_2)$. Details of these calculations are given in our earlier paper.[18]

The force constants obtained are given in table 2.

Table 2

Force constants derived from the IR spectra of the nitro-complexes

Compound	f_{11} (N/m)	f_{12} (N/m)	f_{33} (N/m)
$K_2[Pt(NO_2)_4]$	857.4	164.4	217.1
$K_2[Pt(NO_2)_6]$	854.2	151.3	232.2
$Tl_2[Pt(NO_2)_6]$	845.8	152.7	238.4
mean of (2) and (3)	850.0	152.0	235.3
mean for Co complexes of the type $[Co(DH)_2(NO_2)X]^n$	850.3	134.1	232.9

The same table contains also the mean value of the force constants obtained from the IR spectra of a number of nine nitro-bis-dimethylglyoximato-cobalt (III) complexes $[Co(DH)_2(NO_2)X]^n$; X = Cl, Br, NO_2, various amines, DH = deprotonated dimethylglyoxime; (n = 0, −1), containing a ligand able to give retrodative type $M \rightarrow L$ π-bonds.[17] By comparing this mean value with the arithmetical mean of the force constants obtained for the platinum complexes studied, one can see that f_{11} and f_{33} do not differ essentially but f_{12} is much higher with Pt complexes, as compared to the cobalt complexes. The high repulsion between the O atoms indicates a large negative charge, which might result from the formation of retrodative π-bonds implying an electron transfer from the Pt atom towards the empty antibonding π-orbital of the NO_2 ligand. This π bond formation may be expected to occur easier in the case of Pt, as compared to Co, since the 5 d energy level of Pt must be closer to the energy of the antibonding NO_2 π-orbital than the 3 d energy of Co.

Concerning the differences between the f_{12} values obtained for the three platinum complexes studied, they seem to be reasonable. The formation of retrodative π-bond with 4 ligands in the case of a d^8 system ($K_2[Pt(NO_2)_4]$ must lead to a higher electron density on the O atoms, than the formation of retrodative π-bonds with 6 ligands in the case of a d^6 system ($K_2[Pt(NO_2)_6]$.

By taking into account the polarizing effect of the Tl^+ ion, one might expect the increase of the electron density on the O atoms. The higher f_{12} value of $Tl_2[Pt(NO_2)_6]$ as compared to $K_2[Pt(NO_2)_6]$, seems to be in agreement with this expectation.

The retrodative π-bond formation leads to the increase of the M—N bond strength and consequently to increase of f_{33}, but it diminishes the N—O bond strength and entails the diminution of f_{11}. These effects appear if one compares compounds $K_2[Pt(NO_2)_6]$ and $Tl_2[Pt(NO_2)_6]$ with each other.

The comparison of $K_2[Pt(NO_2)_4]$ with $K_2[Pt(NO_2)_6]$ is rather difficult due to their different geometry and the effect of π-bond formations upon f_{11} and f_{33} is not obvious. By comparing the Pt(IV) complexes with the Co(III) ones, one must take into account that the strengths of the M—N σ-bonds are different. Due to the larger dimensions of the Pt atom as compared to the Co one, the Pt—N σ-bond is expected to be weaker than the Co—N one, but the f_{33} values are even a little higher. This means that the retrodative π-bonds become stronger in the platinum complexes, as compared to the cobalt ones, and this effect compensates the diminution of the M—N σ-bond strength. The effect upon f_{11} is not so clear. On the basis of the above discussion one might expect f_{11} to be less in the case of platinum complexes than with cobalt ones, but the difference of only 0.3 N/m is not very convincing.

New cobalt(III)-amine salts of $H_2[Pt(NO_2)_4]$ and $H_2[Pt(NO_2)_6]$

Our preliminary study shows that these dibasic complex acids form easily characteristic crystalline salts with various metal(III)-amine salts. The formation of ammonium and phosphonium salts of the type : $(amine\cdot H)_2[Pt(NO_2)_4]$ $(amine\cdot H)_2[Pt(NO_2)_6]$, $(phosphine\cdot H)_2[Pt(NO_2)_4]$, etc. with the hydrochlorides of some aliphatic and heterocyclic amines and tertiary phosphines is not characteristic. The hexamine type Co(III) and Cr(III) complexes are also unsuitable for this purpose. We noticed that the mono-acido-pentamines and diacido-tetramines precipitate the $[Pt(NO_2)_4]^{2-}$ and $[Pt(NO_2)_6]^{2-}$ anions as well defined, slightly soluble crystalline salts.

From the monoacido-pentamines some *cis*-$[Co(en)_2Cl(amine)]X_2$ derivatives were used for the above mentioned purpose. Generally, the $[Co(NH_3)_5X]Y_2$ type derivatives are not suitable for these reactions, since they are sparingly soluble in water (X and Y halides or pseudohalides).

From the diacido-tetramine type complexes, mainly the $[Co(en)_2X_2]Y$ ("en"-ethylenediamine) and $[Co(DH)_2\ (amine)_2]X$ (DH = deprotonated dimethylglyoxime) salts were used for double decomposition reactions aqueous or dil. alcoholic solutions. These complex salts form usually well

Table 3

New cobalt(III)-amine salts of the $H_2[Pt(NO_2)_4]$ acid

Formula	Mol. wt. calcd.	Yield (%)	Appearance	Analysis		
					calcd.	found
trans-$[Co(pn)_2Cl_2]_2 \cdot A \cdot H_2O$	953.5	50	green needles	Co	12.36	12.00
				Pt	20.47	20.22
				N	17.61	17.44
				H_2O	1.89	1.30
trans-$[Co(pyridine)_4]_2 \cdot A \cdot 2\ H_2O$	1307.4	80	square green plates	Co	9.01	8.98
				Pt	14.93	14.44
				N	12.85	12.62
				H_2O	2.75	2.30
$[Co(ec)(\alpha\text{-naphthylamine})_2]_2 \cdot A \cdot 3\ H_2O$	1568.0	75	brown spears	Co	7.51	7.29
				Pt	12.45	12.24
				N	10.71	10.46
				H_2O	2.82	3.04
$[Co(DH)_2(m\text{-toluidine})_2]_2 \cdot A$	1389.7	80	short, yellow-brown prisms	Co	8.48	8.23
				Pt	14.04	13.92
				N	16.11	16.02
$[Co(DH)_2(m\text{-xylidine})_2]_2 \cdot A$	1446.1		brown cryst. crops	Co	8.15	8.10
				Pt	13.50	13.30
				N	15.48	15.29
$[Co(DH)_2(NH_3)_2]_2 \cdot A\ H_2O$	1043.5	40	dark yellow spears	Co	11.25	10.99
				Pt	18.63	18.26
				N	21.38	21.14
				H_2O	1.72	1.68
$[Co(DH)_2(pyridine)_2]_2 \cdot A \cdot H_2O$	1295.8	70	bright brown irregular prisms	Co	9.09	8.80
				Pt	15.06	14.87
				N	17.28	17.09
				H_2O	1.39	1.09
cis-$[Co(en)_2Cl(benzylamine)] \cdot A$	700.7	40	pink, thick irregular prisms	Co	8.41	8.37
				Pt	27.86	27.80
				N	17.98	17.56
cis-$[Co(en)_2Cl(p\text{-toluidine})] \cdot A$	700.7	50	short, red-brown prisms	Co	8.41	8.13
				Pt	27.86	27.33
				N	17.98	17.49

"pn" = 1,2-propylenediamine ; "DH" = deprotonated dimethylglyoxime ; "ec. H_2" = ethylenediimino-bis-acetylacetone ; A = $[Pt(NO_2)_4]^{2-}$

Table 4

New cobalt(III)-amine salts of the $H_2[Pt(NO_2)_6]$ acid

Formula	Mol. wt. calcd.	Yield (%)	Appearance	Analysis		
				calcd.		found
trans-$[Co(en)_2Br_2]_2\cdot B$	1148.8	40	sparkling, green, thin, hexagonal plates	Co	10.26	10.07
				Pt	16.99	16.50
				N	17.06	16.87
trans-$[Co(pn)_2Cl_2]_2\cdot B$	1027.4	40	green-yellow dendrites	Co	11.47	11.19
				Pt	18.92	18.74
				N	19.07	18.88
trans-$[Co(pn)_2(NCS)_2]_2\cdot B$	1117.9	60	brown needles	Co	10.50	10.33
				Pt	17.40	17.16
				N	22.46	22.26
$[Co(DH)_2($*p*-toluidine$)_2]_2\cdot B$	1481.7	85	brown hexagonal plates	Co	7.95	7.73
				Pt	13.17	12.99
				N	17.00	16.92
$[Co(DH)_2($*m*-xylidine$)_2]_2\cdot B$	1538.1	90	dark brown square prisms	Co	7.66	7.41
				Pt	12.69	12.44
				N	16.38	16.14
$[Co(DH)_2($*m*-chloraniline$)_2]_2\cdot B$	1567.5	80	thick, dark brown rhomb. prisms	Co	7.52	7.38
				Pt	12.45	12.19
				N	16.07	15.88
$[Co(DH)_2(NH_3)_2]_2\cdot B\cdot H_2O$	1135.6	60	gold yellow rhomb. plates	Co	10.34	10.18
				Pt	17.13	17.01
				N	22.11	21.92
				H_2O	1.58	1.90
$[Co(DH)_2(\text{thiourea})_2]_2\cdot B$	1357.9	60	brown rhomb. plates	Co	8.68	8.53
				Pt	14.37	14.13
				N	22.68	22.19
$[Co(DH)_2($*o*-anisidine$)_2]_2\cdot B$	1545.7	70	thick, brown irreg. cryst.	Co	7.62	7.43
				Pt	12.63	12.50
				N	16.30	16.11
$[Co(DH)_2(\text{pyridine})_2]_2\cdot B$	1369.8	85	yellow-brown needles	Co	8.60	8.49
				Pt	14.25	14.02
				N	18.39	18.20
cis-$[Co(en)_2Cl(\text{pyridine})]\cdot B$	764.7	50	pink crops	Co	7.70	7.67
				Pt	25.53	25.16
				N	20.13	20.00
cis-$[Co(en)_2Cl(\text{p-toluidine})]\cdot B$	792.7	50	pink needles	Co	7.43	7.13
				Pt	24.62	24.33
				N	19.42	19.14
cis-$[Co(en)_2Cl(\text{benzylamine})]\cdot B$	792.7	55	pink crops	Co	7.43	7.40
				Pt	24.62	24.29
				N	19.42	19.22

$B = [Pt(NO_2)_6]^{2-}$

defined, characteristic crystalline products with other mono- and dibasic complex acids (e.g. $H[Co(DH)_2X_2]$, $H[Co(NH_3)_2(NO_2)_4]$, $H[Cr(NCS)_4(amine)_2)]$ too.

23 new tetranitro-platinites (II) and hexanitro-platinates (IV) are characterized in tables 3 and 4.

These complex salts are, generally, sparingly soluble in water and soluble in some organic polar solvents, e.g. dimethylformamide, tetrahydrofurane, dimethylsulphoxide, acetonitrile. They decompose by heating with conc. sulfuric acid and nitric acid.

The thermogravimetric study of some derivatives of these types shows that the crystallization water is lost up to 120 – 140°C (heating rate 20°/min) and the further decomposition occurs over 160–200°C, generally suddenly, with explosion, and a part of the sample is thrown out from the crucible. Thus, the final sample weight at 800–900°C may become much less than the weight of the stoechiometric amount of Co_3O_4 + Pt.

In some cases, if the decomposition is slower, the residue corresponds to this stoichiometric mixture and some relatively stable intermediates appear on the thermogravimetric curves, but they correspond to no clear stoichiometric ratio.

REFERENCES

[1] A. Tsugaeff, *Ber. dtsch. chem. Ges.*, **41**, 2226 (1908).
[2] K. A. Pilkington and P. J. Staples, *J. Inorg. Nucl. Chem.*, **29**, 1029 (1967).
[3] J. Szakó, Z. Finta and Cs. Várhelyi, *J. Inorg. Nucl. Chem.*, **34**, 2887 (1972).
[4] B. P. Cotsoradis and R. D. Archer, *Inorg. Chem.*, **6**, 800 (1967).
[5] A. Tsugaeff and L. L. Lebedinskii, *Z. anorg. Chem.*, **83**, 1 (1913).
[6] M. Vèzes, *Ann. chim. phys.*, (6), **29**, 211 (1893).
[7] S. W. Blomstrand, *Ann. chim. phys.*, (2), **3**, 215 (1871).
[8] J. J. Cernjaev and F. M. Kijackina, *Akad. Nauk SSSR, Izv. Sekt. Platiny*, **7**, 83 (1929).
[9] M. Vèzes, *Compt. rend. Acad. Sciences*, **115**, 45 (1892).
[10] J. J. Cernjaev, L. A. Nazarova and A. C. Mironova, *Zhur. neorg. Khim.*, **6**, 2444 (1961).
[11] A. Tsugaeff and S. S. Kiltinovic, *J. Chem. Soc.*, **109**, 1288 (1916).
[12] J. Lang, *J. prakt. Chem.*, **83**, 420 (1861).
[13] K. A. Jensen, *Z. anorg. Chem.*, **229**, 252 (1936).
[14] M. Vèzes, *Bull. Soc. chim. France* (3), **21**, **144** (1899).
[15] H. Meisenheimer and E. Kiderlen, *Liebigs Ann. Chem.*, **438**, 217 (1924).
[16] K. Nakamoto "Infrared Spectra of Inorganic and Coordination Compounds", J. Wiley Ed., New York, 1963.
[17] H. Urey and C. A. Bradley, *Phys. Rev.*, **38**, 1969 (1931).
[18] J. Zsakó, J. Máthé, E. Kästner-Marian and Cs. Várhelyi, *Acta Chim. Acad. Sci. Hung.*, **117**, 323 (1984).

Revue Roumaine de Chimie, 34, 3, 779–784 (1989)

THE INFLUENCE OF PROPYLENE ON THE MECHANISM OF HOMOGENEOUS PYROLYSIS OF n-HEPTANE

N. I. IONESCU, MELANIA BOZEȘANU and ILEANA IOSIF
ICECHIM – Center of Physical Chemistry, 202, Spl. Independenței, Bucharest, Romania

Received October 8, 1988

The homogeneous pyrolysis of n-alkanes is characterised by a selfinhibition due to the reaction products. Assuming that the reaction order is one, the rate constants decrease with conversion increase.

The selfinhibition of the homogeneous pyrolysis of n-alkanes by reaction products is as pronounced as the temperature is higher and was pointed out in the homogeneous pyrolysis of n-heptane.[1-3] Many experimental data suggest that propylene could be one of the reaction products which can influence the kinetics and mechanism of homogeneous pyrolysis of n-heptane.[4-7]

In this paper we aim at studying the influence of some of the reaction products, especially propylene in the homogeneous pyrolysis of n-heptane.

EXPERIMENTAL

The experiments were performed in a flow-reactor[2] at atmospheric pressure, within the temperature range 550–680°C.

The mole fraction of n-heptane in argon or propylene was within the range 0.2–0.8. In all experiments, the contact time was 21 seconds. The analysis of reaction products was performed by gas chromatography.[2]

RESULTS AND DISCUSSION

Experiments were carried out in order to obtain data concerning:

– the influence of propylene on the conversion, global reaction order and reaction rate of n-heptane pyrolysis.

– the influence of propylene on the products distribution of this reaction.

In order to determine the reaction order by Kerschenbaum and Martin's method,[8] two types of runs have been performed, the first one in the presence of argon, the second one in the presence of propylene.

In the first case, experiments were carried out at temperatures of 559, 605, 628 and 680°C, at mole fractions of n-heptane in argon which ranged from 0.2 to 0.8. The results of first type of runs are presented in Fig. 1.

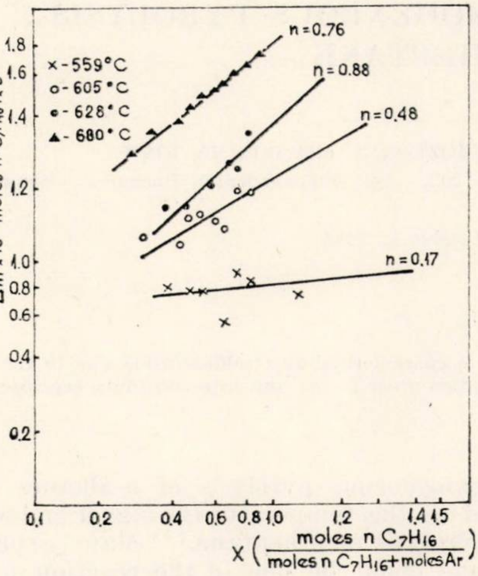

Fig. 1. — Variation with temperature of the reaction order in the homogeneous pyrolysis of n-heptane.

From the examination of Fig. 1 it results that the reaction order changed from the values of 0.2 to 0.8, when the temperature increases from 559 to 680°C. By repeating these experiments at the same temperatures, reaction time and mole fraction with propylene instead of argon it was concluded that at lower temperatures, 559°C and 605°C, the reaction rate decreases with the increase of the mole fraction of n-heptane in propylene. This result could be explained by the fact that in our experiments propylene is not an inert diluent like argon. In these conditions the premises required by Kerschenbaum and Martin's method are not fulfilled.

At higer temperatures, 628 and 680°C, the reaction rate increases by increasing the mole fraction and the reaction order is 0.2 at 628°C and 0.8 at 680°C.

The influence of propylene on the reaction rate and conversion of n-heptane is presented in Figs 2 and 3. In both cases, conversion decreases with the increase of the mole fraction of n-heptane in propylene or argon. At the same time, the conversion is lower in experiments carried out in the presence of propylene in the entire range of temperatures. The differences between the values of conversion of n-heptane in presence and absence of propylene increase with the temperature increases.

From Fig. 3 which presents the variation of the reaction rate with the mole fraction of n-heptane it can be seen that excepting the temperatures 559°C and 605°C, the reaction rate increases with the increases of the considered mole fraction. This behaviour is less pronounced in the experi-

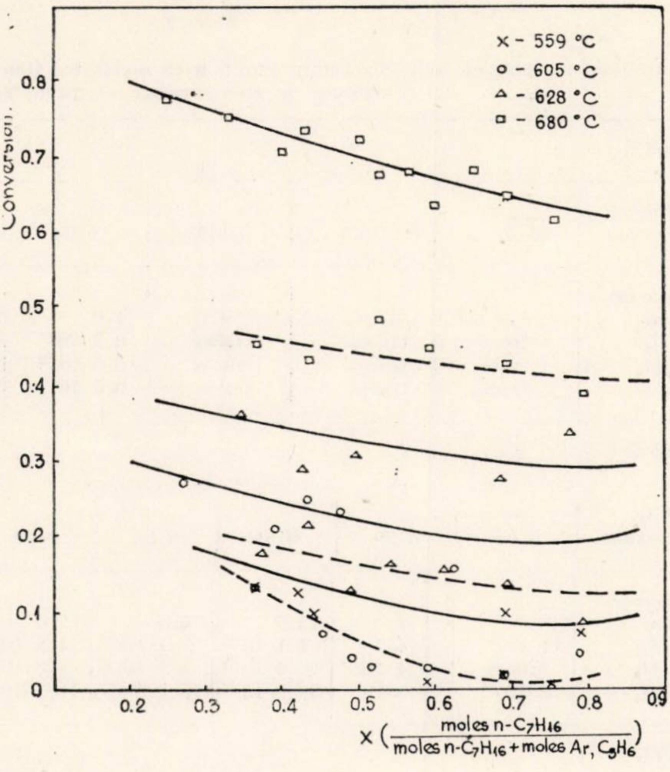

Fig. 2. — Variation of the n-heptane conversion with its mole fraction at different temperatures (dotted line presents the system n-heptane-propylene).

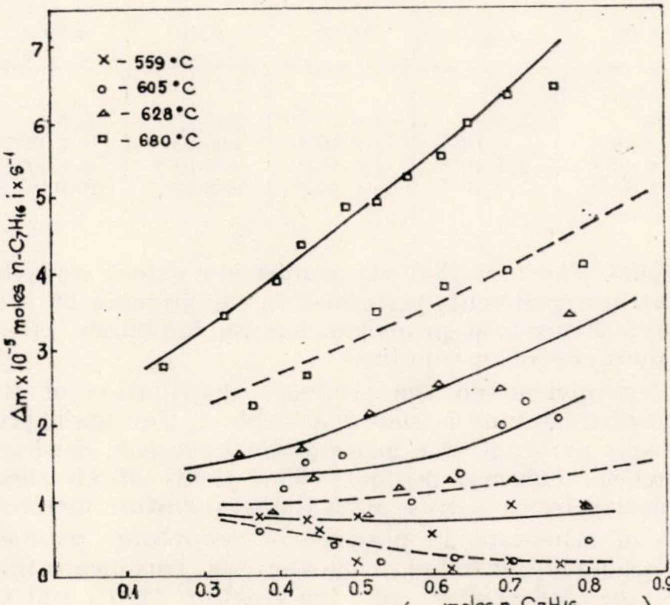

Fig. 3. — Variation of the n-heptane reaction rate with its mole fraction at different temperatures (dotted line represents the system n-heptane-propylene).

Table 1

Variation of yields of main reaction products with molar fraction in homogeneous pyrolysis of n-heptane in the presence of propylene

559°C

Mole fraction	0.37	0.45	0.49	0.62	0.70	0.76
Conversion	13.0	10.0	4.0	1.0	2.0	1.0
CH_4	traces	traces	traces	$0.2\cdot10^{-2}$	$0.5\cdot10^{-2}$	$0.5\cdot10^{-2}$
C_2H_6	traces	traces	traces	$0.3\cdot10^{-2}$	$0.4\cdot10^{-2}$	$0.5\cdot10^{-2}$
C_2H_4	traces	traces	traces	$0.6\cdot10^{-2}$	$0.8\cdot10^{-2}$	$0.8\cdot10^{-2}$

605°C

Mole fraction	0.38	0.35	0.51	0.54	0.66	0.77	0.69
Conversion	18.0	5.2	13.0	15.8	17.0	16.0	9.5
CH_4	$14\cdot10^{-2}$	$5.6\cdot10^{-2}$	$4.1\cdot10^{-2}$	$3.1\cdot10^{-2}$	$4.8\ 10^{-2}$	$4.7\cdot10^{-2}$	$5.0\cdot10^{-2}$
C_2H_6	traces	$3.4\cdot10^{-2}$	$10.6\cdot10^{-2}$	$3.6\cdot10^{-2}$	$4.8\cdot10^{-2}$	$4.4\cdot10^{-2}$	$6.3\cdot10^{-2}$
C_2H_4	$9\cdot10^{-2}$	$10.5\cdot10^{-2}$	$29.0\cdot10^{-2}$	$10.0\cdot10^{-2}$	$11.2\cdot10^{-2}$	$18.3\cdot10^{-2}$	$30.0\cdot10^{-2}$

28°C

Mole fraction	0.37	0.46	0.53	0.62	0.70	0.79
Conversion	13.0	7.0	3.0	3.0	2.0	5.0
CH_4	traces	$1.2\cdot10^{-2}$	$1.6\cdot10^{-2}$	$1.6.10^{-2}$	$1.8\cdot10^{-2}$	$1.2\cdot10^{-2}$
C_2H_6	traces	$2.0\cdot10^{-2}$	$2.7\cdot10^{-2}$	$2.4\cdot10^{-2}$	$2.8\cdot10^{-2}$	$4.1\cdot10^{-2}$
C_2H_4	traces	$4.8\cdot10^{-2}$	$5.7\cdot10^{-2}$	$5.6\cdot10^{-2}$	$6.2\cdot10^{-2}$	$10.0\cdot10^{-2}$

ments made in propylene. The fact that the conversion values and the reaction rates are lower in experiments performed in the presence of propylene supports the hypothesis that propylene has an inhibitory effect in the homogeneous pyrolysis of n-heptane.

The influence of propylene on the products distribution of the homogeneous pyrolysis of n-heptane is shown in table 1. The main products of the homogeneous pyrolysis of n-heptane are hydrogen, methane ethane, etylene, propylene, butenes, pentenes. The yields of all these reaction products, excepting butenes, raise with the temperature increase.

In the pyrolysis of n-heptane in presence of propylene, butenes, pentenes and hexenes are no longer found in the analysis. This means that propylene increases the selectivity of the reaction for C_1 and C_2 hydrocarbons.

The change of the products distribution in homogeneous pyrolysis of n-heptane in the presence of propylene could be explained according to Voevodskii and Kondratiev's hypothesis[9] concerning the influence of bimolecular chain initiation especially when the involved molecule is an unsaturated one.

The variation of 1-butene yield has a maximum which is better defined, the higher the temperature. Voevodskii and Kondratiev[9] have shown that this unsaturated molecule can be one of the reaction products, 1-butene for instance. The reactivity of olefines increases with the number of carbon atoms. At the same time the probability is not excluded that a disproportion reaction between two molecules of olefines should occur.[10]

In the absence of an initial addition of propylene, 1-butene formed by the decomposition of radicals with a great number of carbon atoms after the maximum of its concentration is attained, begins to be consumed in the reaction with another chain carrier radical, $CH_3^{\cdot}$, $C_2H_3^{\cdot}$, $C_2H_5^{\cdot}$ or $C_3H_7^{\cdot}$.

$$C_4H_8 + CH_3^{\bullet} \rightarrow CH_4 + C_4H_7^{\bullet}. \tag{1}$$

In experiments in which propylene was initially added, this can react with n-heptane or 1-butene according to the reactions.

$$C_3H_6 + 1{-}C_4H_8 \rightleftarrows C_3H_7^{\bullet} + C_4H_7^{\bullet} \tag{2}$$

$$C_3H_6 + C_7H_{16} \rightleftarrows C_3H_7^{\bullet} + C_7H_{15}^{\bullet} \tag{3}$$

It seems that the initial presence of propylene provides a supplementary quantity of alkyl radicals as shown in reactions 2 and 3. This can be another way for the consumption of 1-butene. These hypotheses can explain the disappearrance of 1-butene from the reaction products of the homogeneous pyrolysis of n-heptane in the presence of propylene.

The inhibitory effect of propylene wich leads to the decrease of the conversion and reaction rate could be explained by a mechanism proposed by Semenov.[10]

$$C_3H_6 \rightarrow H^{\bullet} + C_3H_5^{\bullet} \tag{4}$$

$$R^{\cdot}(CH_3^{\bullet},\ C_2H_5^{\bullet}) + C_3H_6 \rightarrow RH + C_3H_5^{\bullet} \tag{5}$$

In our experiments there was no evidence for an inversion in the nature of propylene influence, in other terms its transformation from inhibitor into promotor, at a given concentration. The above experiments have been carried out at atmospheric pressure. Gorohovskii and Stepuhovich[4] have shown that the possibility to observe this inversion is limited when the experiments are performed at pressures higher that 0.2—0.4 Pa.

In conclusion our results have shown that propylene has an inhibitory effect in the homogeneous pyrolysis of n-heptane. At the same time, propylene increases the selectivity for C_1 and C_2 hydrocarbons by the disappearance of butenes, pentenes and hexenes from the reaction products.

REFERENCES

[1] I. Iosif, M. Bozeşanu, N. I. Ionescu and G. Pop, *Rev. Chim. (Bucureşti)*, **31**, 231 (1980).

[2] I. Iosif, N. I. Ionescu, M. Bozeşanu and G. Pop, in "Aktuelle wissenschaftliche Probleme der Pyrolyse von Kohlenwasserstoffen", Leipzig, 1979, p. 130.

[3] M. Bozeşanu and N. I. Ionescu, *Rev. Roumaine Chim.*, **30**, 963 (1985).

[4] A. V. Gorohovskii and A. D. Stepuhovich, *Kinet. i Katal.*, **22**, 839 (1970).

[5] G. I. Zjkova and A. D. Stepuhovich, *Kinet. i Katal.*, **11**, 1371 (1970).

[6] L. I. Karmauhova and A. D. Stepuhovich, *J. Fiz. Khimii*, **53**, 2617 (1979).

[7] M. Bozeşanu, I. Iosif and N. I. Ionescu, *Rev. Chim. (Bucureşti)*, **34**, 1152 (1983).

[8] L. S. Kershenbaum and J. J. Martin, *AICHEI*, **13**, 1948 (1968).

[9] V. V. Voevodskii and V. N. Kondratiev, *Usp. Khim.*, **19**, 673 (1950).

[10] N. N. Semenov, "O nekotorykh problemakh khimicheskoy kinetiki i reactsionoy sposobnosti", Izd. A. N. SSSR, 1958, p. 150.

Revue Roumaine de Chimie, 34, 3, 785—795 (1989)

KINETIC THEORY OF GAS-LIQUID DISPERSIONS

OCTAVIAN IORDACHE, GHEORGHIŢA JINESCU, DANIELA LAVRIC
and VASILE LAVRIC
Department of Chemical Engineering, Faculty of Chemical Technology, 79590,
Splaiul Independenţei 313, Bucharest,
Romania

Received April 2, 1988

By means of a Boltzmann-like model, the stability of the flow in gas-liquid dispersions is studied. The regimes of flow and the domains of stability are examined. Homogeneous and heterogeneous types of flow, separated by transition zones, are outlined. A critical condition for transition from a homogeneous movement of individual bubbles at different velocities to a heterogeneous flow of gas bubbles as a group is determined using the velocity distribution function obtained from bubble size distribution and terminal velocities. The void fraction-superficial gas velocity dependence is calculated. A good agreement with experimental data is obtained.

1. INTRODUCTION

Though easy to use, bubble columns are difficult to design due to the complexity of flow characteristics. In bubble column reactors mixing and interphase mass and heat transfer depend strongly on the flow regime.

Various criteria for differentiating flow regimes have been proposed. Usually, three separate flow regimes occurring in the order of increasing flow rate are discussed.[1] They are : bubbly flow or quiescent bubbling, the churn turbulent or heterogeneous flow regime, and the slug flow. Notice that boundaries between the different flow regimes are only approximate.[2]

A kinetic model was proposed to describe the flow in gas-liquid dispersions.[3] This model is an attempt to apply Boltzmann-like equations to a variety of phenomena occurring in two-phase flow.[4] The cited model takes into account the bubble-bubble interactions as well as the bubble-fluid ones. Here, the alignment of bubbles to the global flow is incorporated into the previous existent stochastic approach. Various regimes of flow and limiting behaviour are obtained using the model presented here. For instance, a homogeneous flow of individual bubbles at different velocities and a collective flow of gas-bubbles as a group are outlined.

The theory allows to calculate the gas hold-up vs superficial velocity dependence for every domain of stability. The agreement with our experimental data as well as with those of Bucholz et al.[5] is emphasized.

Finally, different limiting cases of the general model are also presented.

2. RESULTS AND DISCUSSION

2.1. The model

In a previous work,[3] it was considered that bubble-bubble interactions are subjected to the rule :

$$v_1 + v_k \rightarrow \max(v_1,\ v_k) \tag{1}$$

that is : when two bubbles of velocities v_1 and v_k interact, they reach the same velocity v_1 if $v_1 > v_k$ or v_k if $v_k > v_1$. The rule (1) seems to be confirmed by some experiments due to Hills [6] and Hills and Darton .[7] In the experiments cited above, the rising velocity of a single faster bubble injected into a swarm is either a little different from that in still liquid or greater ; velocities below the range of the still water values were not observed. This signifies that the faster bubbles are essentially unaffected by the presence of the slower ones. Of course, there are domains of flow in which the effect of a faster bubble overtaking a slower one is to increase both their velocities. Notice that, in such cases, the average effect is an accelerated bubbling, which is in agreement with the rule (1). The rule (1) proposed here does not exclude the possibility that every interacting bubble keeps its velocity. Especially at low void fraction, it is hard to see how interactions will necessarily prevent different sized bubbles to continue to rise at different velocities on average (unless interaction of bubbles results in a coalescence). It should be pointed out that interaction occurs at large distance by means of the velocity distribution generated in the liquid surrounding each moving bubble.

The model proposed by Iordache and Muntean [3] as an approach to the hydrodynamics of gas-liquid dispersion was :

$$\frac{\partial u}{\partial t} + v\,\frac{\partial u}{\partial x} = -\,a^{\theta}(u - u^0) + anu(v - \bar{v}) \tag{2}$$

Here we denote by u^0 the velocity distribution in the individual flow of bubbles, i.e. in the absence of interactions. The velocity distribution u^0 is achieved for very low gas-holdups. In fact, u^0 is the distribution of terminal velocities. It is defined by reference to the same spatial distribution of bubbles as those that actually exists, but assuming that each bubble rises at its zero void fraction velocity, rather than at the velocity that it actually has at the instant.

The first term of the rhs of equation (2) describes a relaxation of the velocities distribution u to the individual flow distribution u^0 while the second term corresponds to the bubbles interactions. According to the interaction term in (2), the more a bubble velocity differs from the mean, the greater is the number of interactions with other bubbles.

Some experiments in tall bubble columns suggest that it is necessary to introduce in the model (2) a new term corresponding to bubble alignment and having the following meaning : each bubble is subjected to a kind of collective effect exerted by the total ensemble on each bubble which tends to increase the velocity of slow bubbles and to decrease the velocity of rapid bubbles.

The effect of the alignment term on the slow bubbles is similar to that of the interaction term while the effect on the rapid bubbles is opposite to the interaction term. Notice that the relaxation term in equation (2) is proportional to $(u^0 - u)$. The alignment term has similar form as it is proportional to $[n\delta(v - \bar{v}) - u]$. Here, $\delta(v)$ is the Dirac delta function

We may combine all mechanisms for velocity changement (i.e. relaxation, interaction and alignment) and write a more general model:

$$\frac{\partial u}{\partial t} = -a^0(u - u^0) + anu(v - \bar{v}) + a^1[n\delta(v - \bar{v}) - u] \tag{3}$$

The mean velocity $\bar{v}$ is given by:

$$\bar{v} = \frac{1}{n}\int vu(v)\mathrm{d}v \tag{4}$$

Observe that the alignment term does not change the number of bubbles. Indeed:

$$\int [n\delta(v - \bar{v}) - u]\,\mathrm{d}v = n\int \delta(v - \bar{v})\,\mathrm{d}v - \int u\mathrm{d}v = n - n = 0 \tag{5}$$

Therefore, the time evolution of the linear concentration n is not affected by the alignment effects. Similarly, the mean velocity $\bar{v}$ is not altered by such effects. Really:

$$\int v[n\delta(v - \bar{v}) - u]\mathrm{d}v = n\bar{v} - n\bar{v} = 0 \tag{6}$$

The main physical effect of the alignment term is to reduce the dispersion in the velocity distribution. Indeed, we have:

$$-\int (v - \bar{v})^2[u - n\delta(v - \bar{v})]\,\mathrm{d}v = -n\sigma^2 \leqslant 0 \tag{7}$$

Notice that σ^2 denotes the velocity disperson defined by:

$$\sigma^2 = \frac{1}{n}\int (v - \bar{v})^2 u(v)\,\mathrm{d}v \tag{8}$$

The model (3) is a nonlinear integro-differential equation. Due to mathematical difficulties, we will consider first some particular cases.[8,9]

2.2. Relaxations and interactions

The space homogeneous $\left(\text{i.e. } \frac{\partial u}{\partial x} = 0\right)$ and time stationary $\left(\text{i.e. } \frac{\partial u}{\partial t} = 0\right)$ solution of the model (3) in which the alignment is neglected (i.e. $a^1 = 0$) is :

$$u(v)\left[1 + \frac{a}{a^0}(\bar{v} - v)n\right] = u^0(v) \tag{9}$$

The solution of (9) is :

$$u(v) = \frac{u^0(v)}{1 + \frac{a}{a^0}(\bar{v} - v)n} \tag{10}$$

when :

$$1 + \frac{a}{a^0}(\bar{v} - v)n > 0 \tag{11}$$

The solution (10) describes the quiescent bubbling. This corresponds to the homogeneous flow regime valid for reduced values of n which satisfies equation (11). In such a flow regime, bubbles rise without remarkable interactions. The bubbles move independently with different velocities. This regime characterizes dispersions with almost uniformly sized bubbles.

Due to the fact that when $(1 + a/a^0(\bar{v} - v)n < 0$ the distribution function becomes negative, the solution (10) cannot be valid in general for arbitrary high concentrations n. If $(1 + a/a^0(\bar{v} - v)\, n = 0$, that is :

$$v = v + a^0/an \tag{12}$$

then the solution (10) must be replaced by :

$$u(v) = \frac{u^0(v)}{1 + \frac{a}{a^0}(\bar{v} - v)n} + bn\ \delta\left[1 + \frac{a}{a^0}(\bar{v} - v)n\right] \tag{13}$$

Here b is an arbitrary constant. The general solution (13) outlines a new flow regime.

Equation (10) or the first term in (13) corresponds to the quiescent bubbling. The last term in (13) corresponds to a collective flow. The bubbles characterized by this term of (13) have same velocity v and move together in a group.

Obviously the group rises with much higher velocity than that of individual bubbles and the main motion of gas-liquid dispersion is determined by the associated bubbles.

It should be noted that if the bubbles have a wide distribution of velocities, they cannot be distinguished from the coalesced bubbles. The general solution (13) describes a heterogeneous regime flow in which the homogeneous and the collective flow coexist. The fraction of bubbles being in collective flow is denoted by b.

According to the model, as the buble concentration n increases, the homogeneous gas-liquid dispersion cannot be maintained and an unsteady flow pattern with collective flow occurs. The heterogeneous flow regime is characterized by swarms of bubbles moving with high rise velocities in the presence of bubbles with independent behaviour.

To obtain b the normalization condition :

$$n = \int_0^\infty u(v)\mathrm{d}v = \int_0^\infty u^0(v)\mathrm{d}v \tag{14}$$

is useful. From (13) we obtain :

$$n = \int_0^\infty \frac{u^0(v)\,\mathrm{d}v}{1 + \frac{a}{a^0}(\bar{v} - v)n} + bn \tag{15}$$

In fact $b = 0$ in the homogeneous flow, $0 < b < 1$ in the transition zone and $b = 1$ in the totally collective flow. These regimes occur in the order of increasing gas flow rate.

2.3. The critical conditions

For practical purposes it is useful to establish the critical conditions for the bubbles velocities and concentration corresponding to the transition from homogeneous to heterogeneous flow. The condition is given by (12). The homogeneous flow is described by relation[3] :

$$\bar{v} = \frac{\bar{v}^0}{1 - \varepsilon^{1/3}} \tag{16}$$

where $\bar{v}$ is the mean velocity defined by (4) and $\bar{v}^0$ is the mean velocity in the individual flow (obtained using $u^0(v)$ in (4)). Observe that $\bar{v}^0$ is the mean bubbles terminal velocity. The relation $v_F = \varepsilon\bar{v}$, where $\bar{v}$ is given by (16), offers a good estimate for the homogeneous regime.

Multiplying (10) by v and integrating for all possible velocities, we obtain :

$$\frac{1}{n}\int_0^\infty vu(v)\left[1 + \frac{a}{a^0}(\bar{v} - v)n\right]\mathrm{d}v = \frac{1}{n}\int_0^\infty vu^0(v)\,\mathrm{d}v \tag{17}$$

Therefore :

$$\bar{v} - \frac{an}{a^0}\sigma^2 = \bar{v}^0 \tag{18}$$

To obtain the critical value (minimum in this case) of the gas void fraction ε_c, we start from equation (12). The critical value of the linear concentration n_c is reached when $v = v_m$, where v_m is the maximum value of the velocity of bubbles. Using (12), with $v = v_m$, and (18) with $\bar{v}$ and σ^2 obtained from theory or experiment, a relation between the critical mean velocity $\bar{v}_c$ and $\bar{v}^0$ results.
Considering, for instance, that : $v_m = r\bar{v}$ and $\sigma^2 = k^2\bar{v}^2$, where r and k are supposed constant during the process, we obtain following the above

described procedure that:

$$\frac{a^0}{an_c} = (r-1)\bar{v}_c\,; \quad \bar{v}_c = \frac{\bar{v}^\circ}{1-k^2/(r-1)} \tag{19}$$

Therefore:

$$\varepsilon_c = \left(\frac{k^2}{r-1}\right)^3 \tag{20}$$

Consider for instance that the velocity distribution is of parabolic type, i.e.:

$$u(v) = \begin{cases} 3nv^2/v_m^3\,; & 0 \leqslant v \leqslant v_m \\ 0\,; & v > v_m \end{cases} \tag{21}$$

Observe that $u(v)$ satisfies the normalization condition. Using (21) we obtain

$$\bar{v} = \frac{3v_m}{4} \quad \text{and} \quad \sigma^2 = \frac{3v_m^2}{80}\,.$$

Hence $r = 4/3$, $k^2 = 1/15$. Consequently, using (20) we obtain $\varepsilon_c = 1/125$. It the velocity distribution is uniform we obtain $\varepsilon_c = 1/27$ in the same manner.

Such calculations are based upon the hypothesis that r and k do not depend on ε. Obviously, this is an approximation to what happens. It is preferable to obtain ε_c directly using (12) and (18) with v_m, $\bar{v}$, σ^2 experimentally determined. In the homogeneous flow, the superficial velocity-gas hold-up dependence is, according to (16):

$$v_F = \frac{\bar{v}^0\varepsilon}{1-\varepsilon^{1/3}} \tag{22}$$

The heterogeneous flow will be described by the equation: $v_F = \varepsilon\bar{v}$ where, according to (13), $\bar{v}$ is given by:

$$\bar{v} = \frac{1}{n}\int_0^\infty \frac{vu^0(v)}{1+\dfrac{a}{a^0}(\bar{v}-v)n}\,\mathrm{d}v + b\left(\bar{v}_c + \frac{a^0}{an_c}\right) \tag{23}$$

Here the subscript c corresponds to the critical conditions. Accordiug to (23) for $\varepsilon > \varepsilon_c$ the particles velocity distribution splits into two parts, corresponding, respectively, to the quiescent bubbling and to the collective behaviour of the bubbles. The critical conditions and the values of b corresponding to different linear concentration n could be obtained nsing (15).

To avoid difficulties, we shall limit ourselves here to consider that in the transition zone, when $0 < b < 1$, the void fraction practically rests unchanged, $\varepsilon = \varepsilon_c$. In the collective regime $b = 1$. In this case the first term in the right hand side of (13) or (23) vanishes. Using also equations (19) in (23) we obtain $\bar{v} = r\bar{v}_c$. Consequently, in the collective flow regime, $v_F = \varepsilon r\bar{v}_c$. But the critical condition corresponds to a certain state belonging to the $\varepsilon - v_F$ dependence given by (22). Therefore, in the collective regime we have :

$$\bar{v}_F = \frac{\varepsilon r \bar{v}^0}{1 - \varepsilon^{1/3}} \tag{24}$$

In conclusion, the $\varepsilon - v_F$ dependence is given by equation (22) for $0 < \varepsilon < \varepsilon_c$. Then for v_F from $\varepsilon_c \bar{v}_c$ to $r\varepsilon_c\bar{v}_c$ we will consider that $\varepsilon = \varepsilon_c$. At higher gas velocities for $\varepsilon > \varepsilon_c$ the equation (24) is of use.

2.4. Analysis of experimental data

Many experiments about the gas hold-up in bubble columns are reported in literature.[2,5,10] Unfortunately, few simultaneous information about $\varepsilon - v_F$ dependence and the velocity distributions was available. The distribution $u(v)$ could be obtained either directly by velocity measurements, or indirectly, using the bubble size distributions as well as the terminal velocity vs bubble diameter dependente.

Bucholz et al [5] determined the gas hold-up superficial velocity dependence for aqueous solution of carboxy-methyl-cellulose (CMC) 1% as liquid phase and air as gas phase. To test our theory, we start from the bubble size distribution given for this system by Bucholz et al.[5]

In the next step we use the velocity-diameter dependence given by Acharya et al.[11] Thus, the velocity distribution could be obtained. It results : $\bar{v} = 0.33$ m/s, $\sigma^2 = 0.747$ m^2/s^2 ; $v_{\max} = 1$ m/s ; $k = 0.85$; $r = 3$, $\varepsilon_c = 0.048$.

The estimated average velocity in the individual flow is $\bar{v}^0 = 0.11$ m/s. A good estimation is obtained using (22) to correlate experiments for low values of ε.

Due to the fact that the liquid phase is mobile with velocity v_L, we will use :

$$v_F = \frac{\bar{v}^0 \varepsilon}{1 - \varepsilon^{1/3}} + \frac{v_L \varepsilon}{1 - \varepsilon} \tag{25}$$

instead of (22), as well as :

$$v_F = \frac{r\bar{v}^0 \varepsilon}{1 - \varepsilon^{1/3}} + \frac{v_L \varepsilon}{1 - \varepsilon} \tag{26}$$

instead of (24).

Fig. 1 contains a comparison between our theory and the experimental results of Bucholz et al.[5] In this case $v_L = 1.5$ cm/s ; for $0 < \varepsilon < \varepsilon_c$, we use equation (25). Then follows a domain with $\varepsilon = \varepsilon_c$ from the superficial velocity given by (25) with $\varepsilon = \varepsilon_c$ up to the superficial velocity given by (26) with $\varepsilon = \varepsilon_c$. For $\varepsilon > \varepsilon_c$ equation (26) is used. As mentioned above, in order to obtain diagrams as shown in Fig. 1, we start from bubble size distribution. Then terminal rise velocity vs bubble diameter dependence is used to obtain a velocity distribution. The terminal rise velocity of single bubble could be obtained on the basis of empirical correlations [12] or experimentally. The obtained velocity distribution is $u^0(v)$. It is assumed that the parameters k and r, obtained for $u^0(v)$, rest unchanged in the homogeneous domain of flow.

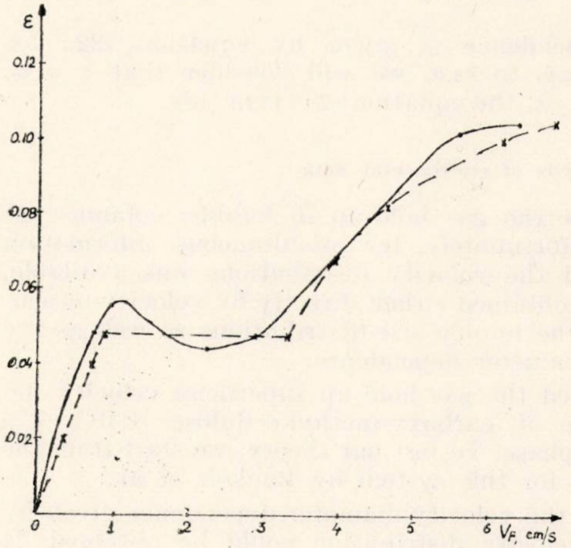

Fig. 1.— Comparison between theory (— — —) and the experimental results (———) of Bucholz et al.[5]

In a recent work due to Merchuk[13] Fig. 5 shows similar dependences of ε vs v_F like those observed by Bucholz et al,[5] for various gases. It must be pointed out that curves with critical points were reported only for bubble columns and not for air-lift reactors.

Our experimental work was carried out in a glass-made bubble column with a ratio H/D equal to 10, for different values of liquid heights and superficial gas velocities, with equipment for measurements of temperatures, pressures and flow rates. Terminal velocities of individual bubbles and their diameters were measured optically and photographically, respectively. Liquid-phase was tap water and the gas-phase was air. The air passed an oil separator, a pressure control device and entered the column from the bottom either through a porous plate, a rigid perforated plate or an elastic perforated one (rubber made). The superficial gas velocity was varied from 1.7 to 10.15 cm/s. The gas hold-up was determined by measuring the height of the aerated liquid H and that of the liquid without aeration, $H_0 : \varepsilon = (H - H_0)/H$. Three typical correlations between our ε vs v_F experimental points (▲) and the theory are presented in Fig. 2 (a, b, c), one for each plate. It must be pointed out that for the rigid perforated plate case, there was no critical point observed. Also, tap water favorises channeling and, thus, the collective flow regime was masked. Further experiments must be carried out confirming or not this observation.

2.5. Solution of the general model and some limiting situations

The stationary and homogeneous solution of the model (3) satisfies the equation.

$$u\left[1+\frac{an}{a^0}(\bar{v}-v)+\frac{a^1}{a^0}\right]=u^0+\frac{a^1 n}{a^0}\,\delta(v-\bar{v}) \qquad (27)$$

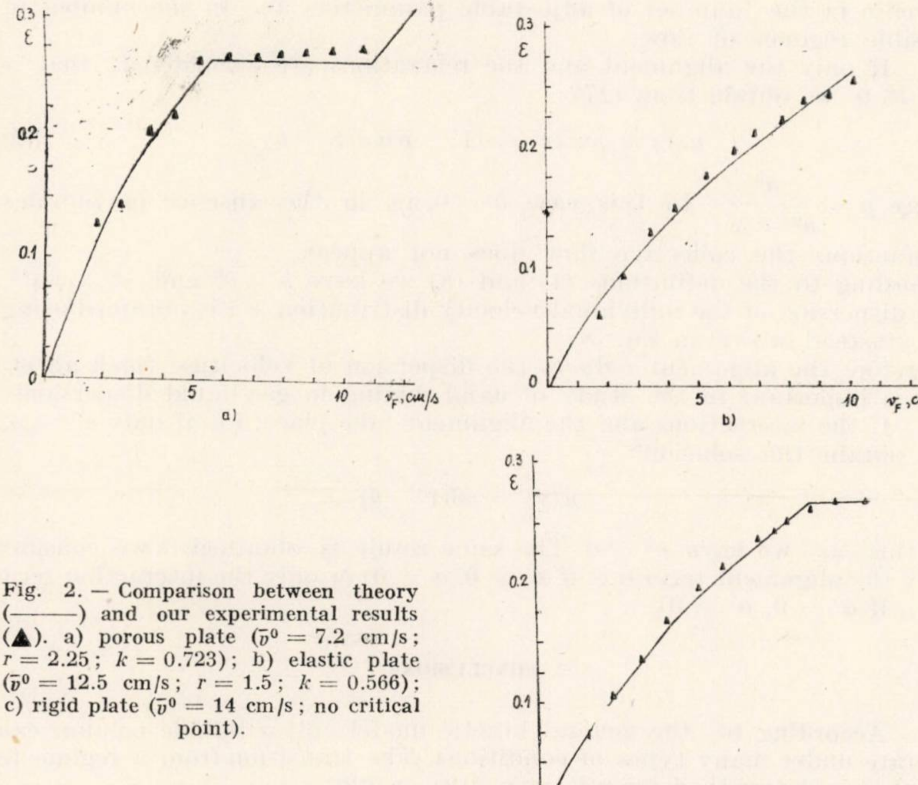

Fig. 2. — Comparison between theory (———) and our experimental results (▲). a) porous plate ($\bar{v}^0 = 7.2$ cm/s; $r = 2.25$; $k = 0.723$); b) elastic plate ($\bar{v}^0 = 12.5$ cm/s; $r = 1.5$; $k = 0.566$); c) rigid plate ($\bar{v}^0 = 14$ cm/s; no critical point).

The general solution of (27) is:

$$u=\frac{u^0+\dfrac{a^1}{a^0}n\,\delta(v-\bar{v})}{1+\dfrac{an}{a^0}(\bar{v}-v)+\dfrac{a^1}{a^0}}+bn\,\delta\left[1+\frac{an}{a^0}(\bar{v}-v)+\frac{a^1}{a^0}\right] \qquad (28)$$

Here, b is the constant giving the fraction of bubbles that moves into a swarm with velocity:

$$v=\bar{v}+\frac{a^0+a^1}{an} \qquad (29)$$

Observe that even if $b = 0$ there exists a singularity at the average velocity $\bar{v}$. This signifies that in the domain of validity of the general model (3), we are faced with a homogeneous flow and with two types of singular flow, corresponding to the collective flow with velocity given by (29) and to the aligned flow of velocity $\bar{v}$. The general feature of the results obtained in the absence of alignment is maintained. Obviously the introduction of additional terms in the kinetic model is accompanied by an increase in the number of adjustable parameters and in the number of possible regimes of flow.

If only the alignment and the relaxations are considered, that is if $a = 0$, we obtain from (27):

$$u(v) = pu^0(v) + (1 - p)n\delta(v - \bar{v}) \tag{30}$$

where $p = \dfrac{a^0}{a^0 + a^1}$. In this case $b = 0$, i.e in the absence of bubbles interactions the collective flow does not appear.

According to the definitions (4) and (8) we have $\bar{v} = \bar{v}^0$ and $\sigma^0 = p\sigma^{\circ 2}$. The dispersion of the individual velocity distribution $\sigma^{\circ 2}$ is obtained using $u^0(v)$ instead of $u(v)$ in Eq. (8).

Therefore the alignment reduces the dispersion of velocities. Such an effect is important in the study of axial mixing in gas-liquid dispersions.

If the interactions and the alignment take place, i.e. if only $a^\circ = 0$, we obtain the solution:

$$u(v) = n\delta(v - \bar{v})$$

In this case we have $\sigma^2 = 0$. The same result is obtained if we consider only the alignment term (i.e. if $a^\circ = 0$, $a = 0$) or only the interaction term (i.e., if $a^0 = 0$, $a^1 = 0$).

3. CONCLUSIONS

According to the general kinetic model (3) a bubble column can operate under many types of conditions. The transition from a regime to another is determined by relations (12) or (29).

Knowledge of the transitions from a regime to another is important because the axial mixing, heat and mass transfer as well as the achievable conversion depend strongly on the flow regime.

The critical conditions and the domains of flow calculated from the models proposed here show a good agreement with experimental data.

Obviously, individual parameters in the general model (3) such as a, a^0, a^1, are difficult to be determined from experimental data. However, these parameters could be determined from measured velocity distributions $u^\circ(v)$ and $u(v)$ or from observed transitions between regimes of flow.

It should be emphasized that the flow regime is highly sensitive to the conditions as for instance column diameter, the type of sparger used, the physico-chemical properties of both phases, the liquid velocity etc. The stability of flow under different conditions is not yet completely understood and it should be evaluated in more detail.

NOTATION

a, a^0, a^1 — constants, s^{-1}
b — fraction of associated bubbles
k $= \frac{\sigma}{\bar{v}}$
n — linear bubble concentration, no. of bubbles. m^{-1}
p $= \frac{a^0}{a^0 + a^1}$
r $= \frac{v_m}{\bar{v}}$
t = time, s
u — velocity distribution function, no. of bubbles, $s.m^{-1}$
v — rising bubble velocity, $m.s^{-1}$
v_L — liquid velocity, $m.s.^{-1}$
v_F — superficial gas velocity, $m.s.^{-1}$
x — space, m

Greek symbols

δ — Dirac delta function
ε gas void fraction (gas hold-up)
σ velocities dispersion

Superscripts

— mean
° values referring to the individual flow

Subscripts

m — maximum value
c — critical value

REFERENCES

[1] G. B. Wallis, "One-dimensional Two Phase Flow", McGraw Hill, New York, 1969.
[2] Y. T. Shah, B. G. Kelkar, S. R. Godbole and W. D. Deckwer, *A.I.Ch.E. Journal*, **28** 353(1982).
[3] O. Iordache and O. I. Muntean, *Ind. Eng. Chem. Fundam.*, **20**, 204(1981).
[4] O. Iordache, "Polystochastic Models in Chemical Engineering", VNU Science Press, Utrecht, The Netherlands, 1986.
[5] M. Bucholz, R. Bucholz and K. Schügerl, *Chem. Eng. Sci.*, **33**, 1061(1978).
[6] J. H. Hills, *Trans. Inst. Chem. Eng.*, **53**, 224 (1975).
[7] J. H. Hills and R. C. Darton, *Trans. Inst. Chem. Eng.*, **54**, 258 (1976).
[8] I. Prigogine, P. Resibois, R. Herman and R. L. Anderson, *Bull. de la Classe de Sciences*, **48**, 805 (1962).
[9] I. Prigogine and R. Herman, "Kinetic Theory of Vehicular Traffic", New York, 1971.
[10] K. Schugerl, J. Lucke and U. Oels, *Adv. Biochem. Eng.*, **7**, 1(1977).
[11] A. Acharya, R. A. Mashelkar and J. Ulbrecht, *Chem. Eng. Sci.*, **32**, 863 (1976).
[12] R. J. Klift, R. Grace and M. E. Weber "Bubbles, Drops and Particles" Chapter 7, Academic Press, New York, 1978.
[1] J. C. Merchuk, *Chem. Eng. Sci.*, **41**, 11 (1986).

NOTATION

[illegible]

REFERENCES

[illegible]

Revue Roumaine de Chimie, **34**, *3*, 797–805 (1989)

CERAMIC PIGMENTS IN THE $TiO_2-BaO-M_xO_y$ SYSTEM

ELISABETA IVAN and D. BECHERESCU
Polytechnic Institute "Traian Vuia", Faculty of Chemical Technology, Timişoara, Romania

Received October 22, 1988

The present paper investigates different possibilities of varying the range of ceramic pigments by evidencing the part played by mineralizers, in the synthesis of Ba-priderite and in the properties acquired by the reaction product with chromium, copper and nickel oxides.

1. INTRODUCTION

The literature records the existence of priderite, having the $(K, Ba)_{1.33}(Ti, F_e^{3+})O_{11}$ formula, which exhibits a lattice identical with that of "Criptomelan" and some properties identical with those of rutile. This mineral in its natural state can be found in leucite rocks from West Australia (Kimberley-Plateau).[1]

It is also known that the TiO_2-alkaline earth oxides binary systems are of interest in the fabrication of some special ceramic products of very high dielectrical properties. Among these systems, a very important one is the $BaO-TiO_2$ system, which constitutes the basis for obtaining some dielectrical materials from which high capacity condensers are made. In this system the following definite crystalline phases were identified: $BaOHTiO_2$; $BaO \cdot 3TiO_2$; $BaO \cdot 2TiO_2$; $BaO \cdot TiO_2$ and $2\ BaO \cdot TiO_2$. The last, $2\ BaO \cdot TiO_2$, is a compound which has a congruent melting, at the highest temperature of the system, of about 1860°C.

The Ba-priderite synthesis was carried out by Norrish (1951), by melting a TiO_2-BaCO_3 mixture in oxyacetylene flame, the compound structure being established roentgenographically by using $Cu_{K\alpha}$ radiation.[2]

Evans,[3] obtained Ba-priderite with Ni oxide, in order to use it as a pigment, for obtaining yellow colours in the ceramic industry.

The aim of our work was to obtain Ba-priderite at low temperatures and to use it in order to obtain some ceramic pigments.

It is known from the literature that the mechanisms of ceramic pigments formation, their dye absorptions and their behaviour in the presence of aggressive fluxes at the high temperature necessary, for ceramic products firing, are insufficiently studied and greatly disputed. Because of such severe conditions, relatively few materials can be used as ceramic pigments. The most resisting ones are the pigments which reproduce the crystalline structure of resistant substances at high temperatures. The main types of crystalline lattices that can ensure the characteristics of dyes imposed by their use in ceramics are shown in table 1. By the isomorphous replacement of one or of all the oxides in the formulae shown in the table by colour moulder oxides or by including in the lattice a chromophore element, ceramic dyes can be obtained.[4–6,8]

Table 1

Types of crystalline lattices reproduced in inorganic ceramic colour dyes

Crystalline lattices	The formulae	Melting temperature °C
Spinel I	$MgO \cdot Al_2O_3$	1850
Spinel II	$2\ ZnO \cdot TiO_2$	
Zircon	$ZrO_2 \cdot SiO_2$	1750
Granat	$3\ CaO \cdot Al_2O_3 \cdot 3\ SiO_2$	1200
Corindon	$\alpha\text{-}Al_2O_3$	2050
willemit	$2\ ZnO \cdot SiO_2$	1200–1250
Sfen	$CaO \cdot TiO_2$	1300
Mulit	$3\ Al_2O_3 \cdot 2SiO_2$	1800

2. EXPERIMENTAL PART

The raw materials used in the laboratory syntheses were : titanium dioxide as anatase, barium carbonate, nickel oxide, cupric oxide and chromic oxide of 98.7%, 98.2%, 98.4%, 98%, 98,7% purity, respectively and different mineralizers : alkaline chlorides and fluorides, of chemical purity. The mixtures investigated are shown in table 2.

Table 2

Investigated compositions

Specimens	Components (moles)					Alkali salts (mineralizers) %
	TiO_2	BaO	NiO	CuO	Cr_2O_3	
1	17	3	0.5	—	—	7–14
2	17	3	1.0	—	—	
3	17	3	1.5	—	—	
4	17	3	2	—	—	
5	17	3	—	0.5	—	7–14
6	17	3	—	1.0	—	
7	17	3	—	1.5	—	
8	17	3	—	2	—	
9	17	3	—	—	0.5	7–14
10	17	3	—	—	1.0	
11	17	3	—	—	1.5	
12	17	3	—	—	2	
13	17	3	—	—	—	7–14
14	17	3	—	—	—	

All the compositions studied were prepared by weighing on an analytical balance. The mixtures were homogenized either on a dry line in a mechanical agate mortar and then for 6—12 hours in a laboratory micronill, or on a wet line using ethyl alcohol. The homogenized specimens were moulded as tablets of Ø = 30 mm and h = 30 mm by semidry pressing and were dried at approx. 105°C in a drying chamber. The firing was made in an electric furnace with carbon silicide bars and in a superkanthal furnace at 1000°C, 1100°, 1200° 1300° and 1400°C.

In order to establish the optimal synthesis conditions the firing was made with and without mineralizers (such as: NaCl, CaF_2, KF, NaF, NH_4Cl in an amount of 7—14%, or with NaCl to which other two fluorides were added).

Specimens of 17 TiO_2, 3 BaO were melted in oxyacetylene flame and in plasma, too.

The sintered or melted specimens with or without mineralizers were ground in porcelain pot mills up to a complete sifting on the 0063 sizer, the ratio substance : procelain marbles : water being kept constant at 1: 1.5 : 0.6. Then the samples were washed in order to remove the soluble salts and dried at 105°C in a drying chamber.

The reaction products study was made roentgenographically, using a TUR-M 60 diffractometer with $Cu_{K\alpha}$ radiation. The IR absorption spectra were obtained with a Carl-Zeiss Jena Spectrograph U—R 10. The IR spectra have arbitrary units, representing relative scales in al cases. The thermal behaviour was studied with a MOM Paulik Erdely derivatograph. The granulometric composition of the powders was determined with a Coulter-Counter, and the colour of the samples with a MOM-COLOR colourimeter.

3. SOME OF THE OBTAINED RESULTS

The thermal analyses of the raw materials and of the mixtures are shown in fig. 1.

By comparing the diffraction spectra of the single compounds, and binary and ternary mixtures it was found that the effects are due to the $BaCO_3$ transformations. At temperatures between 850° and 1010°C the transformations $\alpha BaCO_3 \rightarrow \beta\ BaCO_3$ (the hexagonal form, for which the literature indicates 811°C) take place. From the abrupt altering of the DTA curve above —850°C a deep modification of the properties of the main product can be deduced.

On the cooling curve no effect can be noticed, confirming that all BaO was linked. The correlation between weight losses and thermal effects indicates the $BaCO_3$ decomposition process at a lower temperature than that in the single system. As a result of solid state reactions the weight losses are significant at 680°C and become approximately negligible at about 1180°C. The thermal behaviour of the mixtures containing $17\ TiO_2 \cdot 3BaO$ and $TiO_2 \cdot 3BaO \cdot 2NiO$ is identical. The compound containing NiO is yellow-greenish, a fact that indicates that the NiO is completely assimilated in the formed Ba-priderite structure.

The phasal composition of the studied specimens is shown in the diffraction spectra (Figs 2, and 4). The characteristic lines of the Ba-priderite as mentioned in the literature are shown in table 3.

The analysis of the diffraction spectra and the data given in table 3 show that by heat treatment in Ar-plasma and oxyacetylene flame, Ba-priderite (a compound of high heat-resistance) was obtained. Also, after the heat treatment at 1100° and 1200 °C for two hours at the highest temperature of the $17TiO_2 \cdot 3BaO$ mixture with 7—14% mineralizer (NaCl, and NaCl + NaF mixture) only Ba priderite was obtained. All the compositions studied in the presence of these mineralizers have led to the formation of Ba and Ni-priderite, Ba and Cu-priderite and Ba and Cr-prdiderite, the spectra showing only these compounds, differently coloured.

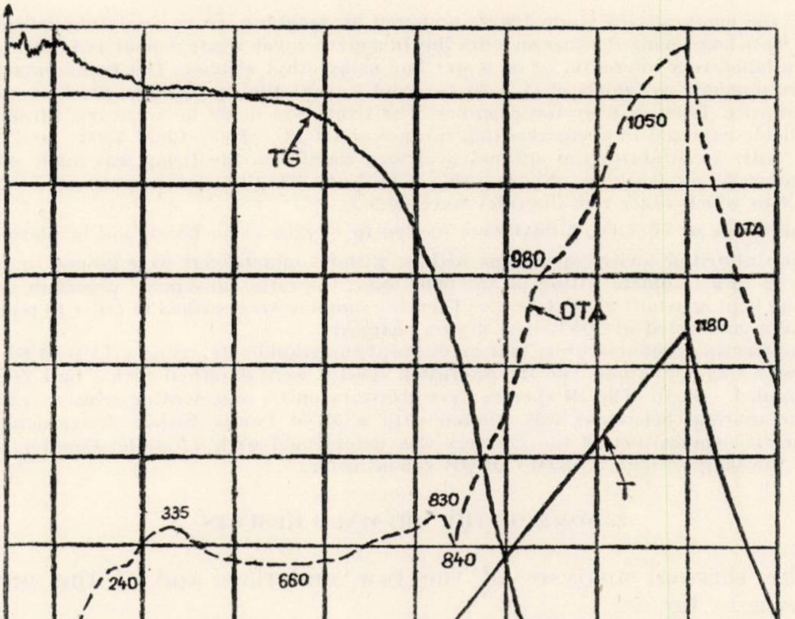

Fig. 1. — Differential thermal analysis curves for the mixture.

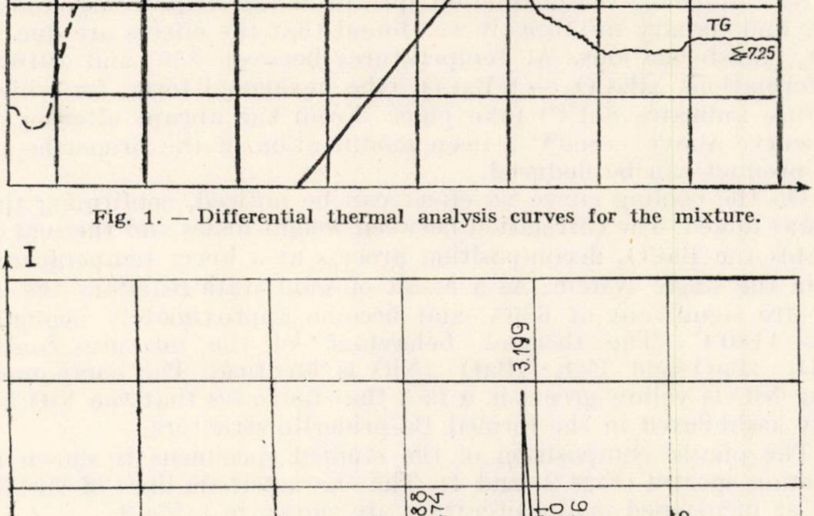

Fig. 2.—Diffraction spectra for the mixture 14 thermally treated.

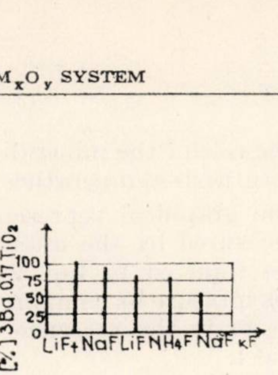

Fig. 3. — The influence of the mineralizers used measured by the intensity of the Ba-priderite fundamental diffraction line.

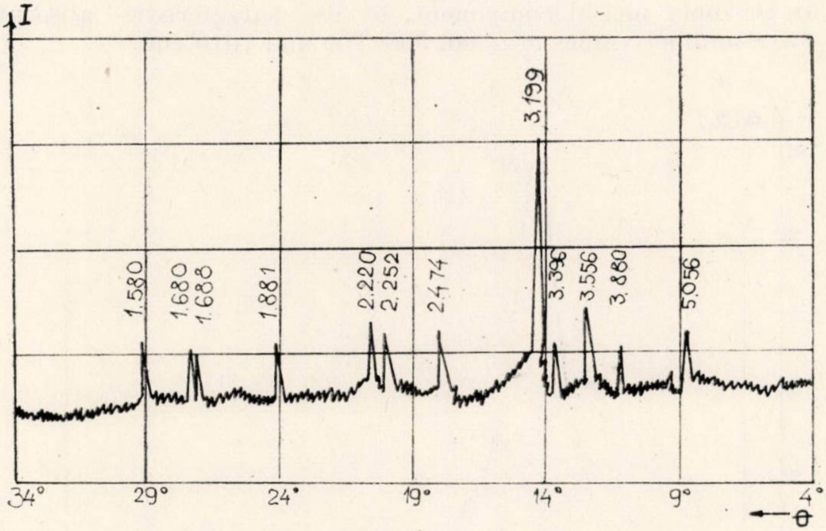

Fig. 4. — Diffraction spectra for the mixture 4 thermally treated.

Table 3

The principal diffraction lines of Ba-priderite for CuKα radiation [2]

Number line	Intensity	d, Å	θ degree
1	2	7.12	6.2154
2	4	5.06	8.7600
3	4	3.55	12.5200
4	10	3.19	13.9600
5	2	2.67	15.8559
6	8	2.47	18.1500
7	2	2.25	20.0027
8	6	2.223	20.2500
9	2	2.032	22.2600
10	2	1.977	22.9100
11	5	1.884	24.1100
12	6	1.683	27.21
13	5	1.583	29.09

The role of the mineralizers was very important as far as the decrease in the synthesis temperature of the Ba-priderite is concerned.[7]

The graphical representation of the efficiency of the mineralizers used, measured by the intensity of the Ba priderite fundamental diffraction line (plotted in Fig. 3) shows the increased efficiency of the two fluorides mixture as compared to the syntheses in the presence of only one fluoride, or in the presence of one fluoride with NaCl, in two fluorides with NaCl.

The IR absorption spectra (Fig. 5) confirmed the presence of Ba-priderite as the only phasal component, by its characteristic absorptions at the wave number values of : 500, 590, 700 and 1010 cm.

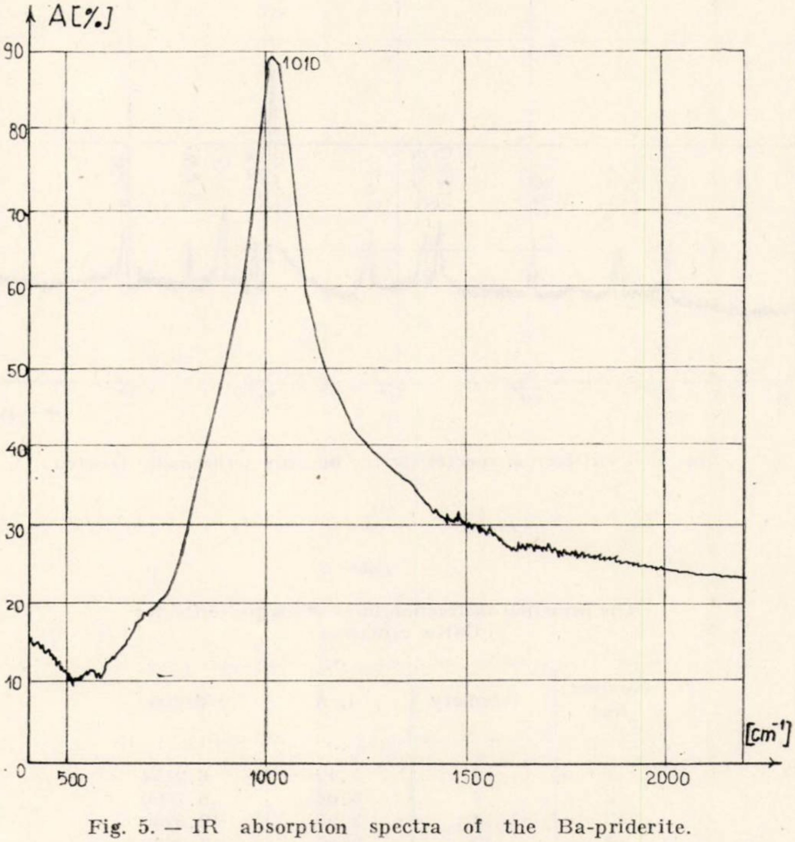

Fig. 5. — IR absorption spectra of the Ba-priderite.

4. THE UTILISATION POSSIBILITIES OF Ba-PRIDERITE WITH Ni, Cu AND Cr

As all the compositions obtained after the heat treatment were coloured, the possibility of using them as ceramic pigments was studied. The pigments were supposed to be used in glazes for tiles as well as for glazes having a 1200°—1300°C burning temperature, in industrial kilns at 50—70°C temperature gradient.

The granulometric composition of the powders, as obtained after the grinding is plotted in Fig. 6. It is obvious that most of the particles have a diameter ranging between 3 and 10 μm.

The finer particles have a tendency to be solubilized in glazes, while the coarser ones have a decreased colouring power.

Thus, the main characteristic of the pigments, their colour, was determined by a MOM COLOR colourimeter, both on the powders as such and on specimens obtained by simulating the utilization conditions for the pigments in ordinary glazes in fine building ceramic ware. After the calculation of the chromaticity indices, the results were graphically plotted in the chromaticity diagram (Fig. 7), the compositions being plotted in the region characteristic of yellow-greenish-brown mustard colours,

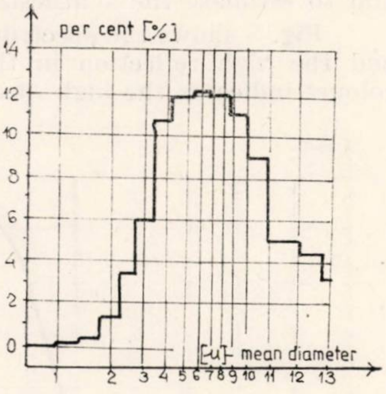

Fig. . — The granulometric composition of the powders.

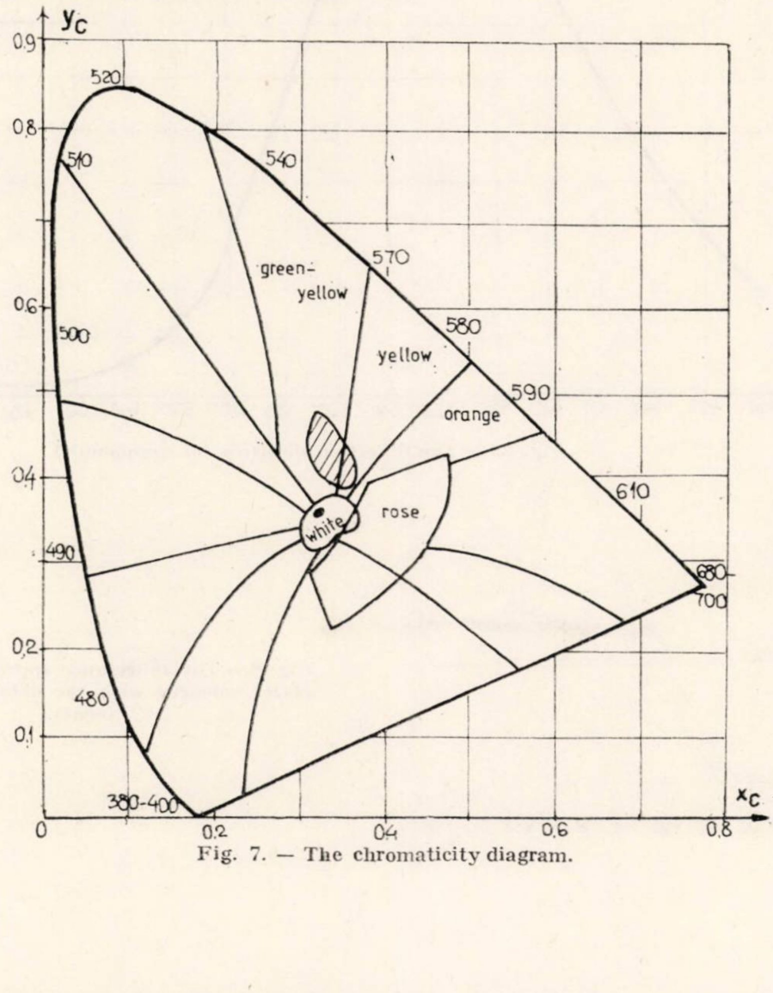

Fig. 7. — The chromaticity diagram.

with the wavelengths ranging between 565 and 590 nm. The best compositions were 4, 8 and 12.

The reflectance spectra determinations were made in order to control and to estimate the synthesized compounds.

Fig. 8 shows the spectrum for compound 4. The abrupt curve slope and the high reflection in the region characteristic of yellow-greenish colours indicates the high quality of the synthesized dyes.

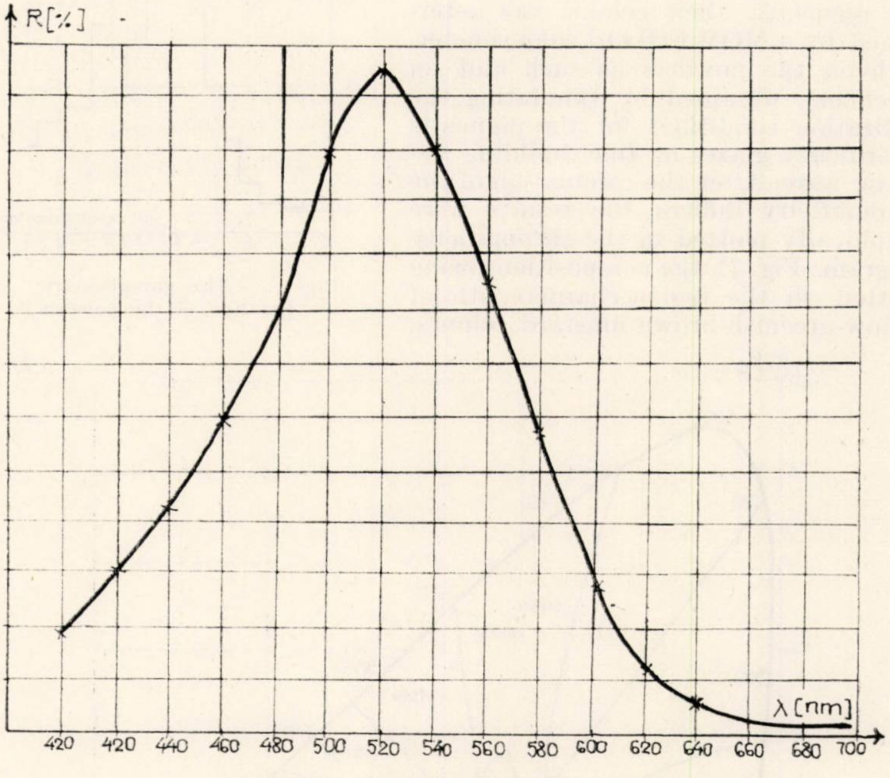

Fig. 8. — The reflection spectrum for compound 4.

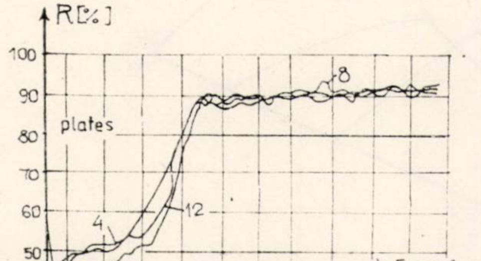

Fig. 9. — The reflectance spectra for the glazes coloured with the obtained pigments.

After the decoration of both the tiles and the sanitary objects, using only 5% synthesized dye and 95% ordinary white glaze, and firing at 1050°C and 1180°C respectively a various colour pallete was obtained. The colour was intense and uniformly distributed, while the glaze fluxes attack was insignificant. The reflectance spectra for the glazes coloured with the obtained pigments are shown in Fig. 9.

5. CONCLUSIONS

The possible interactions in the $TiO_2 \cdot BaO \cdot Me_xO_y$ systems were studied, especially the possibility of synthesizing the Ba-priderite ($17\ TiO_2 \cdot 3\ BaO$) at a lower temperature than that of approx. 1600°C.

The experimental determinations have proved the synthesis of Ba-priderite at 1150°C—1200°C in the presence of a 7—14% amount of mineralizers such as: NaCl; NaF + NaCl; NaF + LiF + NaCl or other mixtures of alkaline fluorides and chlorides. The Ba-priderite is a stable compound, having a lattice identical with that of the "criptomelan" and some identical properties with those of the rutile. The synthesized compound is black, with well-formed crystals visible with the naked eye.[7]

In the Ba-priderite host lattice, chromophores were added up to a proportion of 2 moles of NiO, CuO and Cr_2O_3, thus obtaining coloured inorganic compounds corresponding to the compositions $2\ NiO \cdot 17\ TiO_2 \cdot$ mustard, clean and stable, for the fluxes used in ceramic glazes, at burning temperatures up to 1250°—1300°C, in a neutral or in an oxidizing atmosphere.

Also, the paper highlights for the first time, the possibility of obtaining Ba-priderite ($17\ TiO_2 \cdot 3\ BaO$) at low temperatures of approx. 1200°C in the presence of some alkaline fluorides and chlorides, and contributes to widening the range of dyes used in the industry of construction of ceramic ware.

REFERENCES

[1] Gh. Mastacan and I. Mastacan, "Mineralogie" vol. I, Bucharest, Ed. Tehnică, 1975, p. 385.
[2] V. J. Miheev and D. P. Solidai, "Roentgenometricheskii opredelitelii mineralov", vol. II, Leningrad, Izd. "Medra", 1965, pp. 142—143.
[3] W. Ewans, *Trans. Brit. Ceram. Soc.*, **9**, 338 (1968).
[4] T. P. Tăvală, Dissertation, Polytechnical Institute "Traian Vuia" (1984).
[5] Maria Zaharescu and C. Gh. Macarovici, *Rev. Roumaine Chim.*, **16**, 1223 (1971).
[6] S. Y. Tumanov, *Steklo i Keram*, **1**, 33 (1967).
[7] D. Becherescu, Elisabeta Ivan and Lucia Gagea, Patent no., 92.250 September (1987).
[8] M. Marcinsca, *Szklo Keram.*, **11**, 340 (1974).

After the decoration of both the tiles and the sanitary objects using only 5% synthesized dye and 95% ordinary white glaze, and firing at 1050°C and 1180°C respectively a various colour palette was obtained. The colour was intense and uniformly distributed, while the glaze fluxes attack was insignificant. The reflectance spectra for the glazes coloured with the obtained pigments are shown in Fig. 9.

5. CONCLUSIONS

The possible interactions in the TiO_2–BaO–Me_2O systems were studied, especially the possibility of synthesizing the Ba-priderite (17 TiO_2 · 3 BaO) at a lower temperature than that of approx. 1600°C.

The experimental determinations have proved the synthesis of Ba-priderite at 1150°C–1200°C in the presence of a 7–14% amount of mineralizers such as: NaCl; NaF + NaCl; NaF + LiF + NaCl or other mixtures of alkaline fluorides and chlorides. The Ba-priderite is a stable compound, having a lattice identical with that of the "criptomelan" and some identical properties with those of the rutile. The synthesized compound is black, with well-formed crystals visible with the naked eye.

In the Ba-priderite host lattice, chromophores were added up to a proportion of 2 moles of NiO, CoO and Cr_2O_3, thus obtaining coloured inorganic compounds corresponding to the compositions 2 NiO · 17 TiO_2 · [illegible], chemically stable, for the fluxes used in ceramic glazes, at firing temperatures up to 1250–1300°C, in a neutral or in an oxidizing atmosphere.

Also, the paper highlights for the first time, the possibility of obtaining Ba-priderite (17 TiO_2 · 3 BaO) at low temperatures of approx. 1200°C in the presence of some alkaline fluorides and chlorides, and contributes to widening the range of dyes, used in the industry of construction of ceramic wares.

REFERENCES

1. Gh. Mantescu and I. Mantescu, "Mineralogie", vol. I, Bucharest, Ed. Tehnica, 1972, p. 365.
2. V. I. Mihees and D. P. [illegible], "Rentgenometriceskii opredelitel mineralov", vol. [illegible], Leningrad, Izd. "Nedra", 1965, pp. 142–145.
3. W. [illegible], Amer. J. of Ceram. Soc. 9, 353 (1955).
4. T. P. [illegible], Dissertation, Polytechnical Institute "Traian Vuia" (1983).
5. [illegible] Zaharescu and Gh. Mantescu, Rev. Roumaine Chim. 16, 1223 (1971).
6. [illegible], Steklo i Keram. 4, 12 (1977).
7. D. [illegible], Romanian Patent No. 92 286 September (1983).
8. M. [illegible], Steklo Keram. 11, 20 (1974).

Revue Roumaine de Chimie, 34, 3, 807—810 (1989)

ВЛИЯНИЕ ЗАМЕСТИТЕЛЕЙ НА ХИМИЧЕСКИЕ СДВИГИ ФТОРА В 2-ГАЛОИД- И 2,6-ДИГАЛОИД-4-ФТОРФЕНОЛАХ И -АНИЗОЛАХ

Д. Н. КРАВЦОВ, В. М. ПАЧЕВСКАЯ *, Л. С. ГОЛОВЧЕНКО,
Б. А. КВАСОВ и Э. И. ФЕДИН
Институт элементоорганических соединений им. А. Н. Несмеянова АН СССР,
г. Москва, СССР

Получена 3 октября 1988 г.

Методом ЯМР ^{19}F изучено влияние о-галоидных заместителей на химические сдвиги фтора, вызываемые CH_3O—и НО-группами.

The effects of ortho-halogen substituents on CH_3O- and HO-induced ^{19}F chemical shifts have been studied by ^{19}F NMR spectroscopy.

В ходе сравнительного исследования характера взаимодействия CH_3O- и НО-групп и металлоорганических группировок типа R_nMO с о-атомами галоида[1–3] возникла необходимость выяснить, каким образом различные о-галоидные заместители влияют на электронный эффект вышеуказанных групп в основном состоянии. В связи с этим в настоящей работе был изучен ряд 2-галоид- и 2,6-дигалоид-4-фторфенолов и соответствующих анизолов типа:

$$QC_6H_3X\text{-}2\text{—}F\text{-}4 \qquad QC_6H_2X_2\text{-}2,6\text{—}F\text{-}4$$
$$Q{=}HO,\ \ CH_3O; \qquad X{=}Cl,\ Br,\ I$$

Для указанных соединений были определены химические сдвиги фтора (ХСФ) в хлороформе по отношению к фторбензолу в том же растворителе и вычислены химические сдвиги фтора, вызываемые заместителем в соответствующей системе (ХСФВЗ) для CH_3O- и НО-групп. Величины ХСФ для изученных соединений и ряда 3-галоид- 3,5-дигалоидфторбензолов и ХСФВЗ для CH_3O- и НО-групп приведены в табл. 1.

Рассмотрим вначале характер влияния о-галоидных заместителей на ХСФВЗ для CH_3O-группы. Из табл. 1 следует, что введение о-атома хлора практически не влияет на ХСФВЗ для CH_3O-группы, тогда как о-бромный и в особенности о-иодный заместители заметно увеличивают ХСФВЗ и электронодонорный эффект указанной группы. Принимая во внимание, что 2-галоиданизолы существуют в S-транс-конформации, [4] можно полагать, что рост электронодонорной способности CH_3O-группы под влиянием о-галоидного заместителя вызван стереоэлектронным эффектом,[5] связанным с отталкиванием между неподеленными электронными парами атомов кислорода и галоида, а также пространственным усилением сопряжения CH_3O-группы с ароматическим кольцом.[6] Значительные различия во влиянии разноименных атомов галоидов на ХСФВЗ CH_3O-группы позволяет считать, что основное влияние оказывает первый фактор. Увели-

Таблица 1

Химические сдвиги фтора (ХСФ) относительно фторбензола для растворов в хлороформе и значения химических сдвигов фтора, вызываемых заместителем (ХСФВЗ) для CH_3O- и НО-групп (м.д.)

Соединение	ХСФ	ХСФВЗ	ХСФВЗ[а]	Соединение	ХСФ	ХСФВЗ	ХСФВЗ[а]
$CH_3OC_6H_4F$-4	11,3	11,3	—	HOC_6H_4F-4	11,1	11,1	—
$CH_3OC_6H_3Cl$-2-F-4	9,0	11,2	−0,1	HOC_6H_3Cl-2-F-4	8,8	11,0	−0,1
$CH_3OC_6H_3Br$-2-F-4	9,0	11,6	0,3	HOC_6H_3Br-2-F-4	8,8	11,4	0,3
$CH_3OC_6H_3I$-2-F-4	9,4	12,1	0,8	HOC_6H_3I-2-F-4	9,2	11,9	0,8
$CH_3OC_6H_2Cl_2$-2,6-F-4	2,3	6,2	−5,1	$HOC_6H_2Cl_2$-2,6-F-4	7,6	11,5	0,4
$CH_3OC_6H_2Br_2$-2,6-F-4	2,2	6,6	−4,7	$HOC_6H_2Br_2$-2,6-F-4	7,4	11,8	0,7
$CH_3OC_6H_2I_2$-2,6-F-4	2,9	7,3	−4,0	$HOC_6H_2I_2$-2,6-F-4	7,7	12,1	1,0
$NaOC_6H_4F$-4	19,7[б]	19,7[б]	—	$NaOC_6H_3Br$-2-F-4	19,2[б]	21,9[б]	2,1[б]
FC_6H_4Cl-3	−2,2	—	—	FC_6H_4Br-3	−2,6	—	—
FC_6H_4Br-3	−2,7[б]	—	—	FC_6H_4I-3	−2,7	—	—
$FC_6H_3Cl_2$-3,5	−3,9	—	—	$FC_6H_3Br_2$-3,5	−4,4	—	—
$FC_6H_3I_2$-3,5	−4,4	—	—				

а) — изменение ХСФВЗ для заметителя Q при переходе от QC_6H_4F-4 к QC_6H_3X-2-F-4 или $QC_6H_2X_2$-2,6-F-4

б) — в метаноле

чение изменения ХСФВЗ для CH_3O-группы при переходе от хлора к брому и иоду вероятно вызвано ростом степени перекрывания между орбиталями неподеленных электронных пар атомов кислорода и галоида при увеличении размеров последнего. Следует заметить, что увеличение электронодонорного эффекта CH_3O-группы из п-положения под влиянием о-галоидных заместителей наблюдалось также при изучении реакционной способности индикаторной карбэтоксильной группы.[6]

Можно было предположить, что интенсивность стереоэлектронного взаимодействия между группировками типа RO и о-атомом галоида будет зависеть от величины отрицательного заряда на атоме кислорода и полярности связи R—O. В связи с этим была исследована степень влияния о-атома брома на ХСФВЗ для группировки NaO. Как видно из табл. 1, в соответствии с данными для растворов соответствующих замещенных фенолятов натрия в метаноле ХСФВЗ для группировки NaO возрастает при введении о-атома брома в значительно большей степени, чем ХСФВЗ для CH_3O-группы. Этот результат свидетельствует о том, что стереоэлектронное взаимодействие между неподеленными электронными парами кислорода и галоида действительно возрастает при увеличении отрицательного заряда на атоме кислорода.

В соответствии с данными табл. 1 введение двух атомов галоида в положения 2 и 6 к CH_3O-группе вызывает не увеличение, а существенное уменьшение ее ХСФВЗ и электронодонорного эффекта. Это явление аналогично тому, которое наблюдается при введении двух CH_3-групп в положения 2 и 6 по отношению к CH_3O-группе,[7] и обусловлено тем, что введение двух о-заместителей существенно уменьшает степень копланарности CH_3O-группы с ароматическим кольцом. Это в свою очередь приводит к уменьшению или исчезновению электронодонорного эффекта р,π-сопряжения CH_3O-группы с ароматическим кольцом. Таким образом, пространственное влияние двух о-галоидных заместителей на электронный эффект CH_3O-группы превалирует над стереоэлектронным эффектом.

В то же время последний может играть определенную роль и в этом случае. Так, уменьшение ХСФВЗ CH_3O-группы под влиянием двух о-метильных групп составляет 6,3 м.д.,[7] что заметно больше величин, наблюдаемых при введении двух о-атомов галоида. Это имеет место также и для иода, ван-дер-ваальсов радиус которого практически равен ван-дер-ваальсову радиусу CH_3-группы. Кроме того, степень уменьшения ХСФВЗ CH_3O-группы под влиянием двух о-атомов галоида падает в ряду хлор > бром > иод. С другой стороны, рассмотрение молекулярных моделей Стюарта-Бриглеба показывает, что степень вывода CH_3O-группы из плоскости ароматического кольца под влиянием о-атомов галоида должна несколько возрастать при переходе от хлора к брому и иоду,что вызвано увеличением ван-дер-ваальсова радиуса в указанной последовательности. Антибатность вышеуказанных рядов может быть частично вызвана вкладом стереоэлектронного эффекта в общее влияние двух о-атомов галоида на электронный эффект CH_3O-группы.

Введение одного атома галоида в о-положение к HO-группе практически не изменяет ее ХСФВЗ в случае хлора и несколько увеличивает его в случае брома и иода. Поскольку 2-галоидфенолы существуют в инертных растворителях в основном в S-цис-конформации, [8] то указанный эффект не может быть вызван стереоэлектронным взаимодействием между неподеленными электронными парами кислорода и галоида. Возможно, что он является следствием образования внутримолекулярной водородной связи с о-атомом галоида,[8] которая несколько увеличивает электронодонорный эффект HO-группы из п-положения. Последнее обусловлено частичным переносом электронной плотности неподеленной электронной пары галоида на разрыхляющую σ^*-орбиталь H-O связи.[9]

Такой перенос электронной плотности должен увеличивать электронодонорный эффект HO-группы аналогично тому, как это имеет место при образовании ею водородной связи с координирующими растворителями.[10] Следует заметить, что частичный перенос электронной плотности с атома галоида должен в эквивалентной степени увеличивать его электроноакцепторный эффект. Однако изменение электронного эффекта атома галоида передается на индикаторный м-атом фтора в основном по индуктивному механизму,[11] тогда как изменение электронного эффекта HO-группы передается на индикаторный п-атом фтора как по индуктивному механизму, так и по механизму сопряжения. [11] Вследствие действия вышеуказанных факторов частичный перенос электронной плотности с о-атома галоида на HO-группу приводит к увеличению экранирования фтора. Интересно отметить, что изменение ХСФВЗ HO-группы возрастает в том же ряду, что и $\Delta\nu_{OH}$ при образовании HO-группой внутримолекулярной водородной связи с о-атомами галоида.[1]

Введение двух атомов галоида в положения 2 и 6 к HO-группе вызывает увеличение ее ХСФВЗ, что обусловлено отсутствием пространственных препятствий и совместным влиянием стереоэлектронного эффекта и внутримолекулярной водородной связи,[12] причем Δ ХСФВЗ возрастает в ряду: хлор < бром < иод. В то же время переход от 2-галоид-4-фторфенолов к 2,6-диагалоид-4-фторфенола увеличивает ХСФВЗ HO-группы в последовательности: иод < бром < хлор, что может быть связано с влиянием стереоэлектронного эффекта на внутримолекулярную водородную связь и ростом ее прочности в 2,6-дигалоидфенолах в ряду: иод < < бром < хлор.[12]

Таким образом, полученные в работе данные свидетельствуют о том, что введение о-атома галоида может увеличивать электронодонорный эффект CH_3O- и HO-групп. В противоположность этому введение двух о-атомов галоида увеличивет электронодонорный эффект HO-группы, но уменьшает электронодонорный эффект CH_3O-группы.

ЭКСПЕРИМЕНТАЛЬНАЯ ЧАСТЬ

Исследованные соединения получены по описанным в литературе методикам[13–15] и идентифицированы по температурам кипения и плавления. Контроль частоты проводился методом ЯМР ^{19}F. Спектры ЯМР ^{19}F регистрировались на спектрометре ,,Хитачи H-60'' и ,,Хитачи-Перкин-Элмер R-20'' на частоте 56,4 Мгц при температуре 34°C. Все измерения проводились для разбавленных растворов с концентрацией 0,1—0,2м. Химические сдвиги фтора определялись методом замещения относительно растворов фторбензола в том же растворителе и при той же концентрации, что и для исследуемых соединений. Положительный знак соответствует сдвигу сигнала в сильное поле по отношению к стандарту. Точность определения ХСФ не менее 0,1 м.д. Растворы замещенных фенолятов натрия получали растворением соответствующих фенолов в 1М растворе метилата натрия в метаноле.

ВЫВОДЫ

1. Изучено влияние о-галоидных заместителей на химические сдвиги фтора, вызываемые CH_3O- и HO-группами в 2-галоид- и 2,6-дигалоид-4-фторфенолах и -анизолах.

2. Найдено, что введение о-галоидного заместителя может вызыватьрост электронодонорного эффекта CH_3O- и HO-групп.

3. Установлено, что введение двух о-атомов галоида увеличивает электронодонорное влияние HO-группы, но уменьшает электронодонорный эффект CH_3O-группы.

ЛИТЕРАТУРА

[1] А. Н. Несмеянов, Д. Н. Кравцов, Э. И. Федин и др., *Докл. АН СССР*, **183**, 1098 (1968).
[2] Л. М. Эпштейн, Дау Зыонг, В. М. Пачевская и др., *Изв. АН СССР, Серия хим.*, 2447 (1975).
[3] Г. К. Семин, Е. В. Брюхова, Д. Н. Кравцов и др., *Изв. АН СССР, Серия хим.*, 1048 (1982).
[4] H. Lumbroso, J. Cure and C. G. Andrieu, *J. Molecul. Struct.*, **43**, 87 (1978).
[5] L. A. Cohen and W. M. Jones, *J. Amer. Chem. Soc.*, **84**, 1625 (1962).
[6] V. Baliah and V. M. Kavagasabapathy, *Tetrahedron*, **34**, 3611 (1978).
[7] L. Goodman and R. W. Taft, *J. Amer. Chem. Soc.*, **87**, 4385 (1965).
[8] A. W. Baker, *J. Amer. Chem. Soc.*, **80**, 3598 (1958).
[9] P. A. Kollman and L. C. Allen, *Chem. Rev.*, **72**, 283 (1972).
[10] D. Gurka and R. W. Taft, *J. Amer. Chem. Soc.*, **91**, 4794 (1969).
[11] W. J. Hehre, R. W. Taft and R. D. Topson, *Progr. Phys. Org. Chem.*, **12**, 159 (1976).
[12] A. W. Baker and W. W. Kaeding, *J. Amer. Chem. Soc.*, **81**, 5904 (1959).
[13] H. H. Hodgson and J. Nixon, *J. Chem. Soc.*, 1085 (1930).
[14] H. H. Hodgson and J. Nixon, *J. Chem. Soc.*, 1868 (1930).
[15] G. C. Finger, M. J. Gortowski, R. H. Shiley et al., *J. Amer. Chem. Soc.*, **81**, 94 (1959)

Revue Roumaine de Chimie, 34, 3, 811–819 (1989)

INTERPOLYMER COMPLEXES FORMED BY CARBOXYLIC POLYACIDS WITH QUATERNARY AMMONIUM POLYSALTS

MINODORA LECA, MIHAELA OLTEANU and INGRID IONESCU-BUJOR
Polytechnic Institute of Bucharest, Faculty of Chemical Technology,
Department of Physical Chemistry, Blvd Republicii 13, Bucharest, Romania

Received September 30, 1988

The formation of interpolymeric complexes was studied in three carboxylic polyacids i.e. poly(acrylic acid) (PAA), poly(acrylic acid-co-polyacrylamide) (PAA–AAm) and poly (maleic acid-co-polyacrylamide) (PAM–AAm) with a quaternary ammonium polysalt – poly(N,N-dimethyldialyl ammonium chloride). At a dissociation degree of zero the composition of complexes formed is 2 : 1 for the former two polyacids and 1 : 1 for the latter. The minimum values of the degree of conversion of carboxylic groups is located approximately at equimolecular compositions. The degree of conversion for all compositions of the mixture rises in the sequence PAA > PAM–AAm > PAA–AAm which is the inverse of the order of increasing acid strength expressed as intrinsic dissociation constant. This effect is accounted for in terms of the cooperative character of the interaction between complementary polyelectrolytes.

The products resulted from the interaction between two water-soluble polymers exhibit specific properties determined by the nature of the two polymers, the nature of bonds involved in interpolymer complex formation and the reaction conditions. The interpolymer complexes have been the object of numerous basic and applied studies. The basic interest is focused on the interactions between complementary polymers which represent models for interactions between biopolymers ; the interpolymeric complexes are used in formulation of semipermeable membranes, as floculants and stabilizers of dispersions, etc. Although the interpolymeric complexes have been studied over 20 years, very few rules regarding their formation have been established. Formation of interpolymeric complexes is strongly dependent on the nature of complementary polymers i.e. on the ratio of the two degrees of polymerization, the charge distribution on polymeric chains, the possibilities of hydrogen bond formation, etc.

The interactions between complementary polymers bear a cooperative character and may be electrostatic when both complementary polymers are ionogen, through hydrogen bonds whenever the polymers possess groups which are able to form such bonds and through charge transfer complex formation. According to Michaelis, [1,2] in the case of the reaction between strongly dissociated polyelectrolytes as e.g. polystyrene sodium sulphonate (PSNaS) and poly(vinyl chloride)-benzyl-trimethylammonium chloride a hardly soluble precipitate is formed even if one reactant is in excess. The polysalt formation at contact between two ionogen groups is followed by formation of salt-type bond according to a "zipper" mechanism. The screening of hydrophylic groups owing to the complex resulted is strongly hydrophobic assuming a compact configuration of lyophobic colloid type. The phenomenon is accompanied by the formation of a small molecule salt, of protons or hydroxides and by substantial modification of viscosity.

The formation of a small molecule compound allows the monitoring of complexing reaction through conductometry and potentiometry and after the formation of the complex one may also resort to turbidimetry, calorimetry, sedimentation, light scattering, spectroscopic methods (high resolution NMR included), gel permeation chromatography, etc. [3]

The formation of complexes from polyelectrolytes is directly dependent on the following major factors :

— the position of ionic groups in the polymer chain. One may distinguish the "pendant" type having side groups and the "integral" type having charges on the main chain ;

— the charge density on the polymeric chain which depends on the polymeric ionizable groups distance and the degree of dissociation of these groups ;

— the chemical structure of the main chain which is mirrored by the flexibility of polymeric chain.

Given the absence of some systematic information regarding the influence of the factors mentioned upon the capacity of formation of interpolymeric complexes, this contribution deals with the interactions between three carboxylic polyacids :

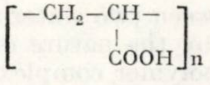

$$\left[-CH_2-\underset{\displaystyle COOH}{CH}-\right]_n$$

poly(acrylic acid) PAA

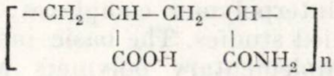

$$\left[-CH_2-\underset{\displaystyle COOH}{CH}-CH_2-\underset{\displaystyle CONH_2}{CH}-\right]_n$$

poly(acrylic acid-co-polyacrylamide) PAA−AAm

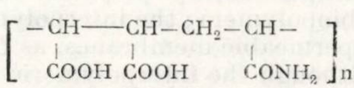

$$\left[-\underset{\displaystyle COOH}{CH}-\underset{\displaystyle COOH}{CH}-CH_2-\underset{\displaystyle CONH_2}{CH}-\right]_n$$

poly(maleic acid-co-polyacrylamide) PAM−AAm

and a quaternary amonium polysalt i. e. poly(N, N-dimethyl-dyalyl ammonium chloride) (Q).

EXPERIMENTAL

The synthesis of poly(acrylic acid) was carried out through radical polymerization in butanone medium ; AIBN was employed as initiator. The molecular weight was determined viscometrically in NaOH 2 N ; it was calculated by the Takahasi equation[4] : $[\eta] = 42 \times 10^{-5} M^{0.64}$ ·A value of 8.5×10^4 (PD = 1180) resulted.

The copolymer of acrylic acid with acrylamide was obtained by the hydrolysis of polyacrylamide in a basic medium whose degree of hydrolysis was 35% and the intrinsic viscosity in $NaNO_3$ 1N of 13 dL/g. The molecular weight of the initial polyacrylamide was of the order of 10^6. The solution of hydrolysed polymer was passed through a cationite column to transform the polysalt into polyacid.

The poly(N,N-dimethyl-dialyl ammonium chloride) has a molecular weight of 4×10^5 (PD = 2480) and in an aqueous solution behaves typically as a polyelectrolyte.[5]

The interactions between complementary polymers were studied by pH-metric titration (by adition of cationic polyelectrolyte to the polyanions) and by conductometric titration. The degree of conversion of ionogen groups was determined on the basis of pH change of some blends whose polyanion molar fraction varied between 0.1 and 1 against standard solutions whose H^+ ion concentration equaled that freed by the reaction, provided that it was stoichiometric. The degree of conversion θ was calculated by the equation :

$$\theta = \frac{C_{H^+}}{C_{H_0^+}} \qquad (1)$$

where $C_{H_0^+}$ stands for the concentration of H^+ in standard solution or the concentration of H^+ ions resulted from the total reaction of the minor component in the mixture and C_{H^+} for the concentration of H^+ ions resulted after mixing the two complementary polymers and the completion of reaction (I).

The degree of conversion θ may be expressed in terms of the ratio of concentration of the QP salt type groups formed over the overall concentration of QP groups that may be formed. The carboxylic polyacids employed are weak polyelectrolytes. For their characterization use was made of pH-metric titration ; the results were processed by the extended Henderson-Hasselbach equation :

$$pK_{ap} = pH + \lg\frac{1-\alpha}{\alpha} \qquad (2)$$

where α is the degree of dissociation of carboxylic groups and pK_{ap} the apparent dissociation constant. Extrapolation to $\alpha = 0$ supplies the intrinsic dissociation constant ($pK_{intr.}$) of the polyacid. Titration of polyacids whose concentration was 1×10^{-3} equiv$\cdot L^{-1}$ was performed with NaOH 0.1N solution.

Conductometric measurements were carried out with a Radelkis conductometer provided with platinated platinum cell.

RESULTS AND DISCUSSION

The carboxylic polyacids employed may be distinguished according to the intrinsic dissociation constants (Fig. 1) and to the dependence of pK_{ap} on the degree of dissociation. The poly(acrylic acid) yields the largest values of intrinsic dissociation constant and pK_{ap} which suggest it is the weakest on the whole dissociation degree range. PAA is followed in sequence by PAM—AAm and PAA—AAm. The strength of polyacid rises in a sequence which is determined by the distance between ionogen carboxylic groups.

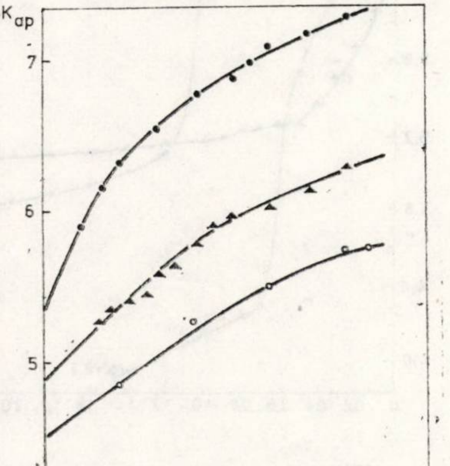

Fig. 1. — pK_{ap} versus the degree of dissociation for : ● —PAA ; Δ —PAA-AAm ; ○ — PAM—AAm.

When a polysalt [poly(N,N-dimethyl-dialyl ammonium chloride)] is added to a partially neutralized carboxylic polyacid the formation o interpolymeric complex may be represented as follows :

$$P^{-}H^{+} + Q^{+}Cl^{-} \rightleftarrows PQ + H^{+} + Cl^{-} \qquad (I)$$

$$P^{-}Na^{+} + Q^{+}Cl^{-} \rightleftarrows PQ + Na^{+} + Cl^{-} \qquad (II)$$

where P^{-} represents a dissociated carboxylic group, Q^{+} — the quaternary ammonium ion and PQ the electrostatic bond formed.

Reaction I shows that on mixing the two complementary polymers the pH changes of the system take place following the freeing of protons. The potentiometric titration curves for carboxylic polyacids of different degrees of dissociation with polysalt Q are shown in Figures 2–4.

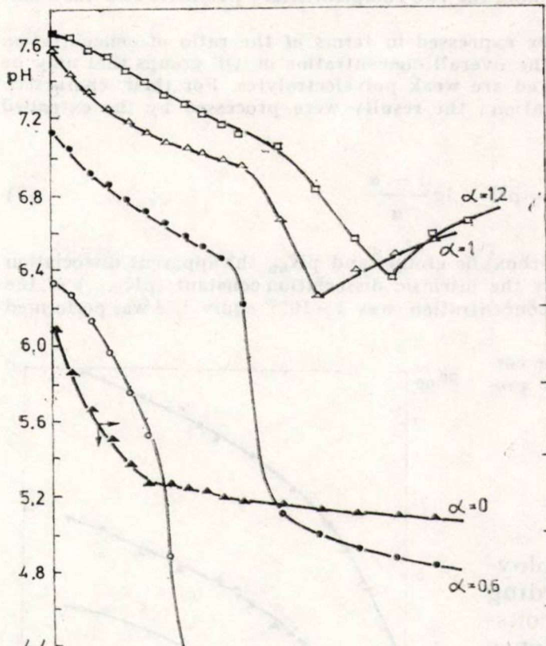

Fig. 2. — The titration curves of PAA with Q for the degrees of dissociation specified.

The titration curves were drawn by adding a Q solution of 0.2 equiv.L^{-1} to 40 mL 1×10^{-3} equiv $\cdot$ L^{-1} of polyacid solution ; they are presented as pH versus ρ ratio of ammonium quaternary group over a dissociable carboxylic group concentration :

$$\rho = [Q^{+}]/[P^{-}] \qquad (3)$$

In all carboxylic acids studied one may note the existence of a composition of the mixture for which the pH versus ρ plot undergoes a slope chan-

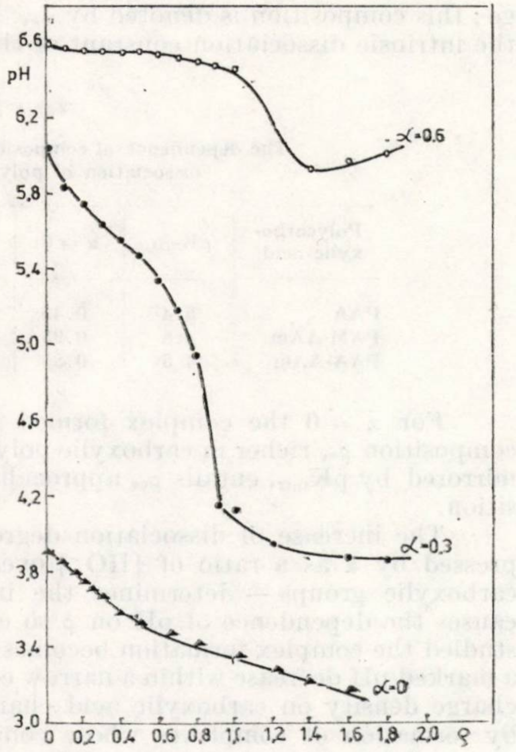

Fig. 3. — The titration curves of PAA-AAm with Q for various degrees of dissociation.

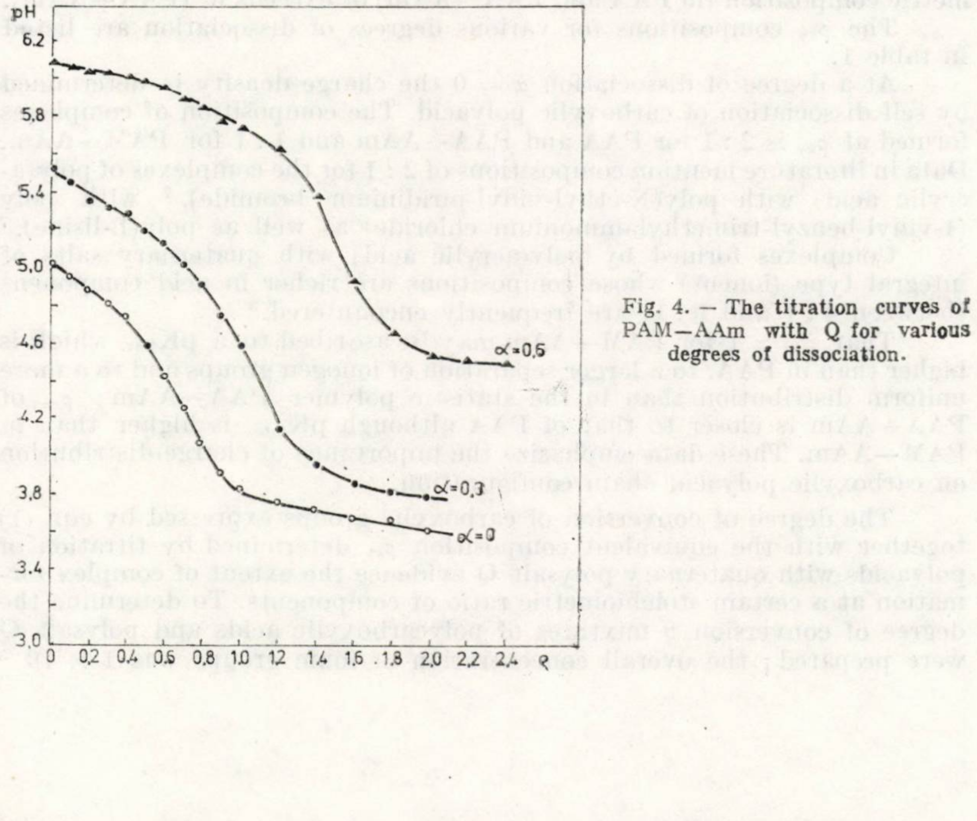

Fig. 4. — The titration curves of PAM—AAm with Q for various degrees of dissociation.

ge ; this composition is denoted by ρ_{ev}. The composition at ρ_{ev} depends on the intrinsic dissociation constant of the polyacid (Table 1).

Table 1

The dependence of composition ρ_{ev} on the degree of dissociation of polycarboxylic acids

Polycarboxylic acid	pK_{intr}	$\alpha = 0$	$\alpha = 0.3$	$\alpha = 0.6$	$\alpha = 1$
PAA	5.4	0.45	0.7	1.1	1.4
PAM-AAm	4.8	0.95	1.3	1.8	—
PAA-AAm	4.5	0.55	0.9	1.4	—

For $\alpha = 0$ the complex formed features $\rho_{ev} < 1$, which denotes a composition ρ_{ev} richer in carboxylic polyacid. The increase of acid strength, mirrored by pK_{intr}, entails ρ_{ev} approaching the 1 : 1 stoichiometric composition.

The increase of dissociation degree of poly(carboxylic acids) — expressed by α as a ratio of $[HO^-]$ over the concentration of dissociable carboxylic groups — determines the increase of ρ_{ev} composition which causes the dependence of pH on ρ to change. In all carboxylic polyacids studied the complex formation becomes strongly cooperative which entails a marked pH decrease within a narrow concentration range. The increase of charge density on carboxylic acid chains is expected to be accompanied by formation of complexes whose composition approaches the stoichiometric composition (in PAA and PAA—AAm) or exceeds it (PAA—AAm).

The ρ_{ev} compositions for various degrees of dissociation are listed in table 1.

At a degree of dissociation $\alpha = 0$ the charge density is determined by self dissociation of carboxylic polyacid. The composition of complexes formed at ρ_{ev} is 2 : 1 for PAA and PAA—AAm and 1 : 1 for PAM—AAm. Data in literature mention compositions of 2 : 1 for the complexes of poly(acrylic acid) with poly(N-ethyl-vinyl-piridinium bromide),[7] with poly (4-vinyl-benzyl-trimethylammonium chloride) as well as poly(L-lisine).[7]

Complexes formed by poly(acrylic acid) with quaternary salts of integral type (ionens) whose compositions are richer in acid component (between 4 : 1 and 9 : 1) are frequently encountered.[3]

That $\rho_{ev} \simeq 1$ for PAM—AAm may be ascribed to a pK_{intr} which is higher than in PAA, to a larger separation of ionogen groups and to a more uniform distribution than in the statistic polymer PAA—AAm ; ρ_{ev} of PAA—AAm is closer to that of PAA although pK_{intr} is higher than in PAM—AAm. These data emphasize the importance of charge distribution on carboxylic polyacid chain configuration.

The degree of conversion of carboxylic groups expressed by eqn (1) together with the equivalent composition ρ_{ev} determined by titration of polyacids with quaternary polysalt Q evidence the extent of complex formation at a certain stoichiometric ratio of components. To determine the degree of conversion θ mixtures of polycarboxylic acids and polysalt Q were prepared ; the overall concentration of ionic groups was 1×10^{-3}

equiv · L^{-1} while the mole fractions of polycarboxylic acid ranged within 0.1—0.9. Standard solutions were also prepared; they contained excess of polyelectrolyte and adequate amount of HCl to ensure the complete reaction of complementary polyelectrolytes.

The results of these determinations are shown in Figures 5—7.

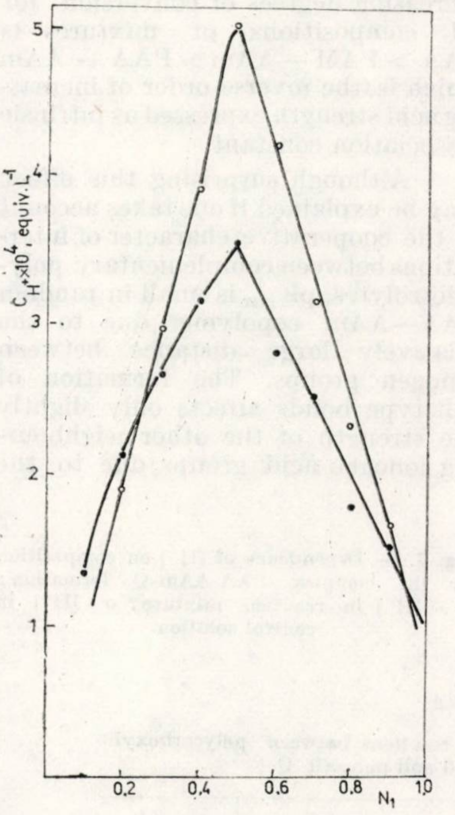

Fig. 5. — The composition dependence of $[H^+]$ at formation of PAA—Q complex: ● — $[H^+]$ in reaction mixture; ○ — $[H^+]$ in standard solution.

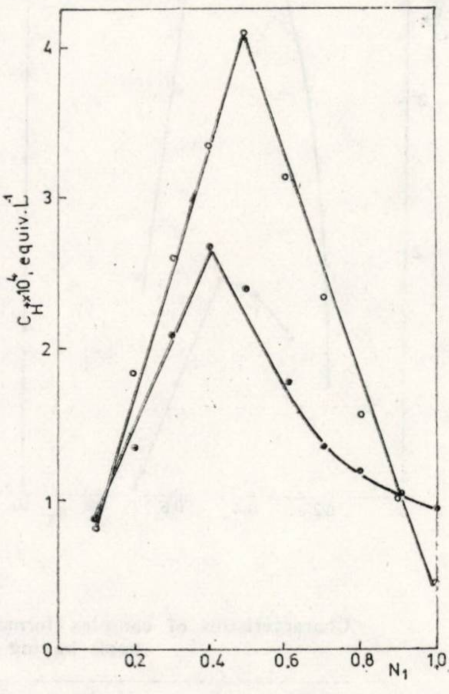

Fig. 6. — Dependence of $[H^+]$ on composition for the complex PAA—Q formation: ● — $[H^+]$ in reaction mixture; ○ — $[H^+]$ in control solution.

The composition of reaction mixture which ensures the maximum concentration of H^+ ions after reaction depends on the nature of polycarboxylic acid (Table 2).

Likewise, the specific conductivity of reaction mixture (Fig. 8) reaches a maximum (Table 2) whose location also depends on the acid nature. The compositions at maximum values of $[H^+]$ and the conductivities coincide satisfactorily.

The dependence of conversion θ, calculated by eqn (1), on the data in Figures 5 — 7 is shown in Figure 9; there are minima of the degree of conversion corresponding approximately to equimolecular mixtures, $N_1 =$

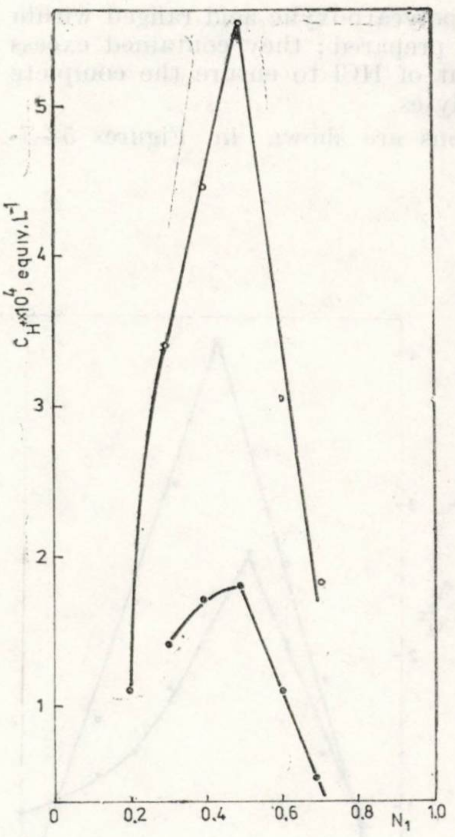

Fig. 7. — Dependence of [H$^+$] on composition for the complex PAA-AAm-Q formation: ● — [H$^+$] in reaction mixture; ○ — [H$^+$] in control solution.

= 0.5 (Table 2). The three carboxylic polyacids exhibit substantial difference between the degrees of conversion obtained at formation of complexes with Q salt.

One can note that the order of increasing degrees of conversion for all compositions of mixtures is PAA > PAM − AAm > PAA − AAm which is the inverse order of increasing acid strength expressed as intrinsic dissociation constant.

Although surprising this effect may be explained if one takes account of the cooperative character of interactions between complementary polyelectrolytes. pK$_{intr}$ is small in random PAA−AAm copolymer due to the relatively large distance between ionogen groups. The formation of salt type bonds affects only slightly the strength of the other neighbouring ionogen acid groups due to the

Table 2

Characteristics of complex formation reactions between polycarboxylic acids having $\alpha = 0$ and polysalt Q

Acid Properties	Composition	PAA	PAM-AAm	PAA-AAm
pH discontinuity	ρ_{ev} N_{1ev}	0.45	0.95	0.55
Composition at which $\overset{\circ}{C}_{H_+}$ is maximum	ρ_{max} N_{1max}	1.0 0.5	1.5 0.4	1.0 0.5
Composition at maximum on $\lambda = f(N_1)$ curve	ρ_M N_{1M}	0.66 0.60	1.5 0.4	1.0 0.5
Composition at minimum on $\theta = f(N_1)$ curve	c_m N_{1m}	0.66 0.60	0.66 0.60	0.43 0.70
Minimum value of θ	—	0.68	0.55	0.30

relatively low cooperative character. PAA behaves oppositely : its ionogen groups are close to each other, pK_{intr} is high and pK_{ap} depends strongly on the degree of dissociation. Formation of the complex through electrovalent bonds i.e. through screening of ionized groups rises the degree of dissociation of the other neighbouring groups (strongly cooperative character) leading to a higher degree of conversion at a certain composition like in the case of PAA—AAm. The PAM—AAm polyacid lies between the two polyacids mentioned because its density of ionizable groups takes intermediate values.

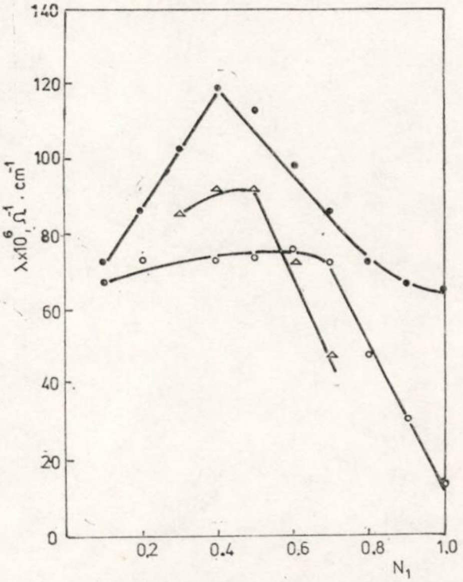

Fig. 8. — Specific conductivity in terms of reaction mixture composition : ○—PAA-Q ; Δ — PAA-AAm-Q ; ● — PAM-AAm-Q.

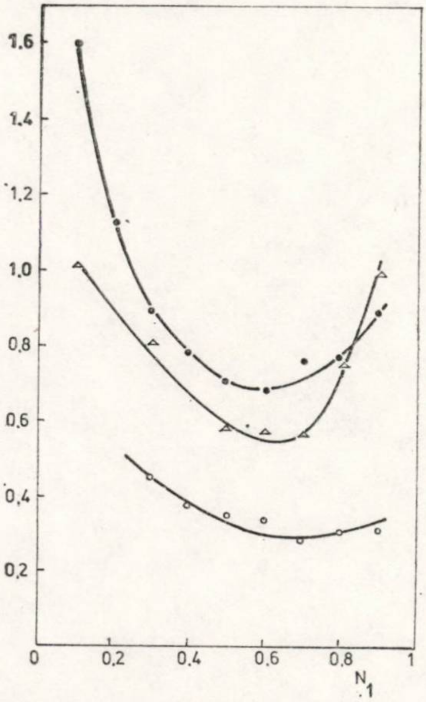

Fig. 9. — The variation of the degree of conversion on formation of complexes between polycarboxylic acids and salt Q for an overall concentration of 1×10^{-3} equiv $\cdot L^{-1}$ ● — PAA-Q ; Δ — PAM-AAm-Q ; ○ — PAAM-AAm-Q.

REFERENCES

[1] A. S. Michaelis and R. Miekka, *J. Phys. Chem.*, **65**, 1765 (1961).
[2] A. S. Michaelis, I. Mir and N. S. Schneider, *J. Phys. Chem.*, **69**, 1447 (1965).
[3] E. Tsuchida and K. Abe, "Advances in Polymer Science", vol. 45, Springer Verlag, Berlin, 1982, p. 1.
[4] A. Takahasi, *J. Chem. Soc. Japan*, **60**, 1059 (1957).
[5] M. Leca, *Rev. Chim. (Bucureşti)*, **8**, 764 (1982).
[6] E. Tsuchida, J. Osada and K. Abe, *Makromol. Chem.*, **175**, 583 (1974).
[7] E. A. Bekturov and L. A. Bimendina, "Advances in Polymer Science", vol. 41, Springer Verlag, Berlin, 1981, p. 99.

Revue Roumaine de Chimie, **34**, *3*, 821—829 (1989)

ИССЛЕДОВАНИЕ ЦЕПНЫХ ГАЗОФАЗНЫХ РЕАКЦИЙ ПРЕВРАЩЕНИЯ УГЛЕВОДОРОД—КИСЛОРОДНЫХ СМЕСЕЙ В УСЛОВИЯХ ЛАЗЕРНОГО ПОДОГРЕВА

А. А. МАНТАШЯН *, Л. А. ХАЧАТРЯН и А. А. СУКИАСЯН
ИХФ АН АрмССР, г. Ереван 375044, ул. Паруйра Севака 5/2

Получена 3 октября 1988 г.

Изучен процесс превращения простейших углеводородородов этана и пропана в условиях воздействия лазерного излучения инфракрасного диапазона ($\lambda = 944$ см$^{-1}$). Установлено, что в отсутствие гетерогенных факторов первичное образование радикалов (стадия инициирования) протекает гомогенно с необходимыми скоростями при температурах 800 К и выше. Возникающие в процессе алкильные радикалы R при этих температурах превращаются в олефины по реакциям

$$C_3H_7 \rightarrow C_2H_4 + CH_3,$$

$$C_3H_7 \rightarrow C_3H_6 + H$$

$$C_2H_5 \rightarrow C_2H_4 + H \text{ и т.д.}$$

Равновесие в реакции $R + O_2 \rightleftarrows RO_2$ образования алкилперекисных радикалов сдвинуто влево и соотношение концентраций $[RO_2]/[R] \ll 1$. По этой причине окислительный процесс, связанный с реакциями алкилперекисных радикалов RO_2 практически не протекает. Кислород в процессе не расходуется, т.к. он участвует в основном в первичной стадии зарождения радикалов

$$RH + O_2 \rightarrow R + HO_2.$$

Без кислорода процесс практически не протекает.

The conversion of simplest hydrocarbons — ethane and propane in the conditions of infrared laser irradiation ($\lambda = 944$ sm^{-1}) was studied. It was established that the primary formation of radicals (initiated step) proceeds homogeneously with necessary rates at temperatures of 800K and even higher. The alkyl radicals R which appear at these temperatures are converted into olefins by the reactions :

$$C_3H_7 \rightarrow C_2H_4 + CH_3,$$

$$C_3H_7 \rightarrow C_3H_6 + H$$

$$C_2H_5 \rightarrow C_2H_4 + H \text{ etc.}$$

The equilibrium in the formation of peroxy radicals is shifted to the left and the ratio of concentrations $[RO_2]/[R]$ is much less than 1. Therefore the oxidation process including the reactions of alkylperoxy radicals RO_2 practically does not proceed. Oxygen is not consumed because it takes part in the primary stage of chain initiation.

$$RH + O_2 \rightarrow R + HO_2$$

ВВЕДЕНИЕ

В настоящее время лазерное излучение получает широкое применение для осуществления различных химических превращений. Для изучения газофазных реакций эффективными оказываются лазеры, работающие в инфракрасном диапазоне. С их помощью изучен ряд газофазных процессов мономолекулярного распада различных веществ.[1,2] Показано, что энергию лазерного излучения в присутствии сенсибилизаторов удается трансформировать в тепловую энергию и осуществлять химическую реакцию в тепловом режиме. Важная информация о гомогенном механизме сложных цепных реакций, о путях ее целенаправленного осуществления может быть получена при осуществлении процесса непосредственно под пучком лазерного излучения в условиях его теплового воздействия, в отсутствие гетерогенных факторов, влияние которых неизбежно при осуществлении химических процессов в обычных реакторах.

В данной работе приводятся и обсуждаются результаты, полученные при изучении процессов превращения углеводород-кислородных смесей при воздействии излучением инфракрасного диапазона $\lambda = 944$ см$^{-1}$ от лазера на CO_2 в присутствии сенсибилизатора SF_6, трансформирующего энергию излучения в тепловую энергию. В этих условиях под пучком лазерного излучения удается реализовать различные температуры при ,,холодных'' стенках реактора. Превращение при этом протекает как бы в ,,бесстеночных'' условиях.

ЭКСПЕРИМЕНТ

Изучалось превращение пропан-кислородных и этан-кислородных смесей. Облучение реагирующей смеси проводилось в стеклянных цилиндрических кюветах по оси кюветы с торца, через оптически прозрачные окна из NaCl. Диаметр кюветы-реактора составлял $d = 40$ мм и существенно превышал диаметр лазерного пучка ($d = 7-8$ мм). В этих условиях под пучком удается осуществлять нагрев смеси до различных температур путем вариации мощности излучения, оставляя стенки реактора при комнатной температуре. Схема экспериментальной установки приводится на рис. 1. Методика эксперимента более подробно описана в работе.[3,4] Реагирующая смесь напускалась в откаченный реактор-кювету из стеклянных баллонов. Изучались превращения смесей следующих составов $C_3H_8 : O_2 = 1:5; 2:1; 5:1$ и $C_2H_6 : O_2 = 2:1$ разбавленные инерт-

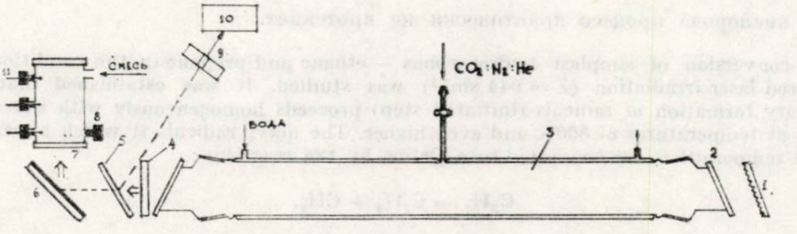

Рис. 1. — Схема экспериментальной установки: 1 — дифракционная решетка; 2 — окна из NaCl; 3 — разрядная трубка лазера; 4 — выводящее германиевое зеркало; 7 — реактор; 8 — штуцер для отбора пробы; 9 — ослабитель; 10 — измеритель мощности 2IMO—2H; 11 — термопары.

ным газом аргоном в 5—10 кратных соотношениях. Облучение кюветы производилось при давлении исходной смеси Р = 305 тор. Опыты проводились при различных мощностях лазерного луча и различных временах экспозиции. С целью построения кинетических кривых проводилась серия экспериментов с различными временами облучения исходной смеси при постоянной данной мощности излучения. Исходные углеводород и кислород, а также продукты реакции анализировались хроматографически. Формальдегид анализировался фотоколориметрически, а перекиси иодометрически. Для измерения температуры в непосредственной близости от пучка в реактор вводились тонкие хромель-алюмелевые термопары ($d = 60$ мкм). Наряду с термопарными измерениями проводилась также оценка средней температуры под пучком излучения с помощью так называемого метода ,,химического термометра'' на основе данных по осуществлению реакции распада азометана, для которой заведомо известна константа скорости реакции.[5]

Как показывают измерения по оси реактора, непосредственно под лучем устанавливается неизотермический режим и фиксируется резкий экспоненциальный спад температуры по мере удаления от пучка лазерного излучения (см. рис. 2). Этот режим устанавливается за время меньшее, чем время полного превращения. Таким образом, химическая реакция протекает в условиях исключающих вторичные гетерогенные реакции на поверхности реактора.

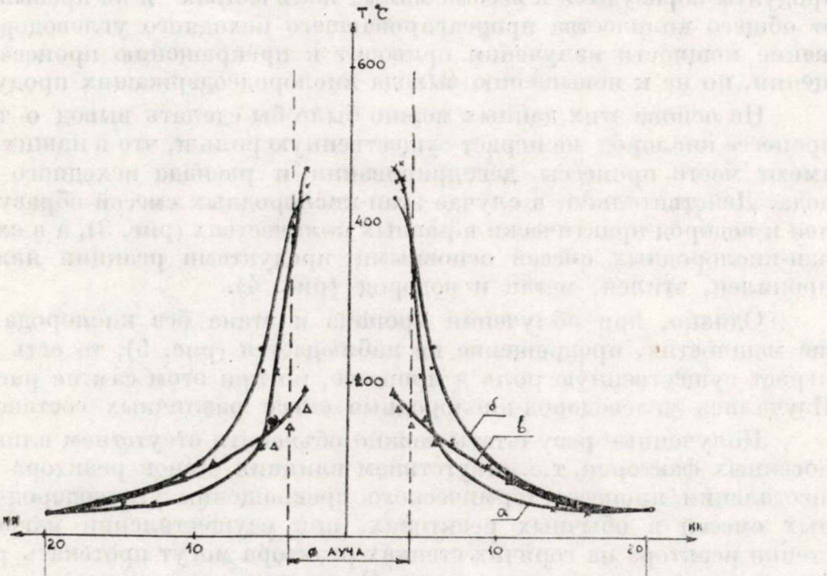

Рис. 2. — Профиль температуры, полученный в реакторе d=38 мм в трех горизонтальных плоскостях на различных высотах реактора.

РЕЗУЛЬТАТЫ И ОБСУЖДЕНИЕ

Облучение этан-кислородных и пропан-кислородных смесей привели к неожиданному, на первый взгляд, результату. Превращение наблюдается только при мощности лазерного излучения выше определенного значения, то есть существует пороговое значение по мощности излучения, способного вызвать химическое превращение. Этот факт можно объяснить тем, что при более низких мощностях не обеспечивается необходимая для протекания реакции температура. Известно, что превращение пропан-кислородных смесей в обычных условиях начинается уже при температурах 600÷650 К и основными продуктами реакции являются кислородсодержащие соединения: кислоты, перекиси, CO, CO_2, альдегиды, спирты, окиси и — вода. В наших условиях превращение начинается при мощности излучения 9 вт и выше. Измерения и оценки показывают, что температура при этом достигает 800 К.

Проведенные кинетические исследования как по превращению пропан-кислородных так и этан-кислородных смесей в условиях лазерного подогрева высветило тот факт, что основными продуктами реакции являются не кислородсодержащие продукты, а олефины. Кислородсодержащие продукты образуются в весьма малых количествах и не превышают 1,5% от общего количества прореагировавшего исходного углеводорода. Снижение мощности излучения приводит к прекращению процесса превращения, но не к повышению выхода кислородсодержащих продуктов.

На основе этих данных можно было бы сделать вывод о том, что в процессе кислород не играет существенную роль и, что в наших условиях имеют место процессы дегидрирования и распада исходного углеводорода. Действительно, в случае этан-кислородных смесей образуются этилен и водород практически в равных количествах (рис. 3), а в случае пропан-кислородных смесей основными продуктами реакции являются — пропилен, этилен, метан и водород (рис. 4).

Однако, при облучении пропана и этана без кислорода, при тех же мощностях, превращение не наблюдается (рис. 5), то есть кислород играет существенную роль в процессе, но при этом сам не расходуется. Изучались углеводород-кислородные смеси различных составов.

Полученные результаты можно объяснить отсутствием влияния гетерогенных факторов, т.е. отсутствием влияния стенок реактора. При осуществлении процесса термического превращения углеводород-кислородных смесей в обычных реакторах, при осуществлении нагрева через стенки реактора на горячих стенках реактора могут протекать различные первичные и вторичные процессы. В частности, гетерогенные реакции зарождения радикалов на поверхности реактора могут стать источником зарождения цепей уже при существенно низких температурах,[6] чем температуры, при которых наблюдается превращение в наших условиях. Из-за отсутствия горячих стенок реактора, зарождение радикалов, а следовательно, и цепей в наших условиях может протекать лишь гомогенно. Как показывает анализ, наиболее выгодным путем зарождения радикалов может быть взаимодействие углеводорода с кислородом:[7]

$$1.\ RH + O_2 \rightarrow R + H_2O + \Delta H.$$

Тепловой эффект этой реакции ΔH составляет в случае этана 49 ккал/моль, а пропана 47 ккал/моль [6] и реакции эти протекают с такими же энергиями активации соответственно. Следовательно, протекание их с необходимыми скоростями, обеспечивающими достаточную скорость зарождения для развития цепного превращения, может иметь место лишь при более высоких температурах.

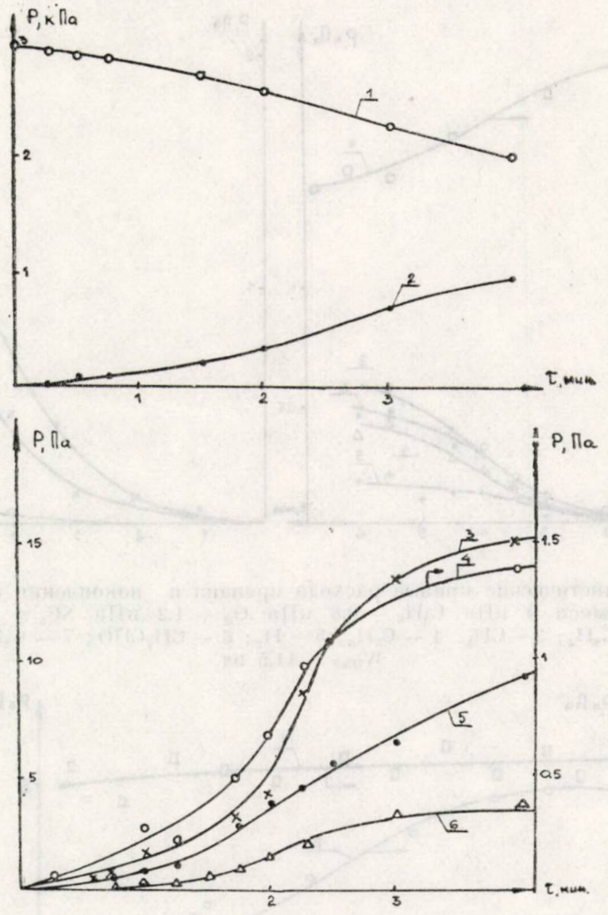

Рис. 3. — Кинетические кривые расходования исходного этана (1) и накопления продуктов реакции окисления этан-кислородной смеси 2 : 1 в присутствии сенсибилизатора SF_6(1,2 кПа). 2 — C_2H_4; 3 — C_2H_5OH; 4 — CH_3CHO; 5 — CH_2OH; 6 — C_2H_4O.

Известно, что алкильные радикалы R (этильные в случае этана и пропильные в случае пропана) могут взаимодействовать с кислородом и переходить в соответствующие перекисные радикалы

2. $R + O_2 \rightarrow RO_2$.

С повышением температуры эта реакция все заметнее протекает и в обратном направлении

2′. $RO_2 \rightarrow R + O_2$.

Образование кислородсодержащих соединений связано с превращениями этих радикалов. Они могут переходить в алкоксильные радикалы

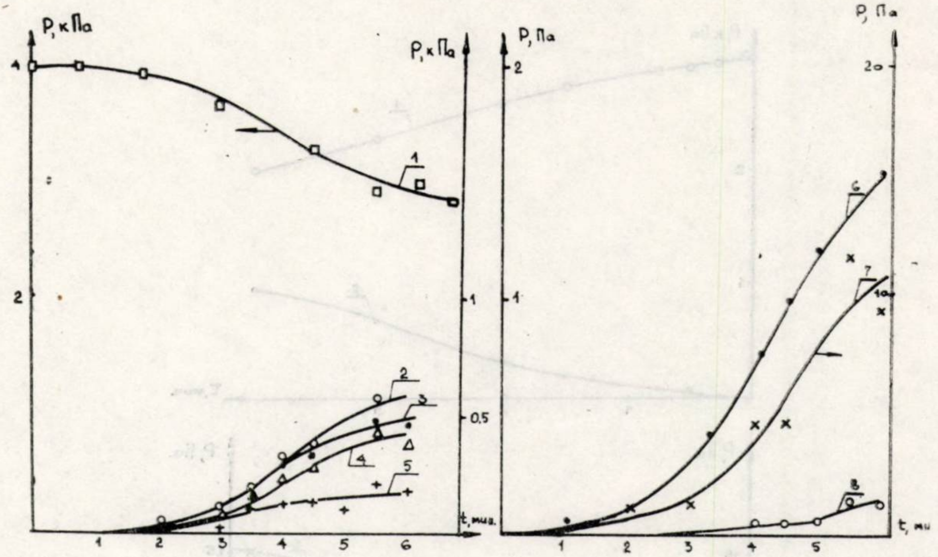

Рис. 4. — Кинетические кривые расхоца пропана и накопления продуктов при облучении смеси 4 кПа C_3H_8 + 0,8 кПа O_2 + 1,2 кПа SF_6 + 34,6 кПа Ar; 1 — C_3H_8; 2 — C_2H_4; 3 — CH_4; 4 — C_3H_6; 5 — H_2; 6 — CH_2CHO; 7 — C_2H_4O; 8 — C_3H_6O Wлаз = 11,5 вт.

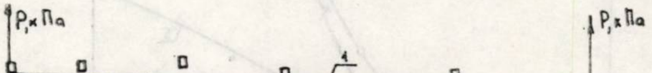

Рис. 5. — Кинетические кривые расходования пропана кривая 1 — смесь 4 кПа C_3H_8 + 1,2 кПа SF_6 + 35,5 кПа Ar; кривая 2 — смесь 4 кПа C_3H_8 + 1,2 кПа SF_6 + 0,8 кПа O_2 + 34,6 кПа Ar; кривая 3 — смесь 2,66 кПа C_3H_8 + 1,2 кПа SF_6 + 0,8 кПа O_2 + 36 кПа Ar и накопления продуктов: 4 — C_2H_4; 5 — C_3H_6; 6 — H_2 при пиролизе смеси соответствующей кривой 1 Wлаз = 11,5вт.

по реакциям

3. $RO_2 + RO_2 \rightarrow 2RO + O_2$

например $C_2H_5O_2 + C_2H_5O_2 \rightarrow C_2H_5O + O_2$

или $C_3H_7O_2 + C_2H_7O_2 \rightarrow C_3H_7O + O_2$

Последние будучи более активными обеспечивают дальнейшее развитие цепей и образование всей гаммы кислородсодержащих продуктов.[8,9]

4. $RO \rightarrow$ продукт $+ R'$

Например в случае пропана

$$C_3H_7O \rightarrow C_2H_5CHO + H$$
$$C_3H_7O + O_2 \rightarrow CH_3CH_2CHO + HO_2$$
$$C_3H_7O \rightarrow CH_3CHO + CH_3$$
$$C_3H_7O \rightarrow CH_2O + C_2H_5$$
$$C_2H_5O \rightarrow CH_3CHO + H$$
$$C_2H_5O + O_2 \rightarrow CH_3CHO + HO_2$$
$$C_2H_5O \rightarrow CH_2O + CH_3$$
$$CH_3O \rightarrow CH_2O + H$$
$$CH_3O + RH \rightarrow CH_3OH + R$$
$$C_2H_5O + RH \rightarrow C_2H_5OH + R$$
$$C_3H_7O + RH \rightarrow C_3H_7OH + R$$

Реакцией (2), усиливающейся с повышением температуры определяется соотношение радикалов R и RO_2 в реагирующей системе. Данные по константе равновесия для обратимого процесса (2), рассчитанные Бенсоном, на основе термодинамических данных, для различных алкильных радикалов приводятся в работах, [10] а для метильных радикалов также в работе, [11] полученное на основе прямых экспериментальных данных.

При температурах обычного окисления, согласно этим данным, алкильные радикалы быстро переходят в алкилперекисные радикалы и соотношение концентраций перекисных и алкильных радикалов сильно сдвинуто в пользу перекисных радикалов $[RO_2]/[R] \gg 1$. В результате окисление можно представить как цикл следующих элементарных стадий: исходный углеводород переходит в алкильные радикалы (1), которые образуют перекисные (2), а последние — алкоксильные (3). Далее происходит образование продуктов в результате реакции (4) и развитие цепи с восстановлением исходного радикала (R)

5. $R' + RH \rightarrow R'H + R$

С повышением температуры соотношение концентраций перекисных и алкильных радикалов будет меняться в пользу алкильных радикалов из-за усиления реакции обратного распада перекисных радикалов. Оценка показывает, что при температурах, возникающих под пучком лазерного излучения (800 K) и выше это соотношение $[RO_2]/[R] \ll 1$. Например, при T = 800 K оно в случае пропана $[C_3H_7O_2]/[C_3H_7]$ составляет 0,025, то есть при этих температурах концентрации алкильных радикалов в десятки и сотни раз превышают концентрации алкилперекисных радикалов. Это обстоятельство немедленно сказывается на усилении превращений радикалов R по другим каналам

6. $R \rightarrow$ олефин $+ R''$

Относительно высокая температура способствует усилению реакций типа (6) также непосредственно, через константу скорости этой стадии. Реакции типа (6) протекают с различной энергией активации в зависимости от радикала и конкретного пути превращения. Например, пропильные радикалы должны превращаться по следующим реакциям:

$$C_3H_7 \rightarrow C_3H_6 + H$$

$$C_3H_7 \rightarrow C_2H_4 + CH_3$$

с энергиями активации E = 37 и E = 31 ккал/моль соответственно.[12] По этой причине изменение температуры приводит к изменению соотношения пропилена и этилена в продуктах реакции.

Исходя из вышеизложенного механизм превращения пропан-кислородных смесей можно представить в виде следующей радикально-цепной схемы:

1. $C_3H_8 + O_2 \rightarrow C_3H_7 + HO_2$

2. $C_3H_7 + O_2 \rightarrow C_3H_7O_2$

2′ $C_3H_7O_2 \rightarrow C_3H_7 + O_2$

3. $2C_3H_7O_2 \rightarrow 2C_3H_7O + O_2$

4. $C_3H_7O \rightarrow CH_3CHO + CH_3$

(и другие реакции алкоксильных радикалов, рассмотренные выше)

5. $CH_3 + C_3H_8 \rightarrow C_3H_7 + CH_4$

6. $C_3H_7 \rightarrow C_3H_6 + H$

7. $C_3H_7 \rightarrow C_2H_4 + CH_3$

8. $H + C_3H_8 \rightarrow C_3H_7 + H$

9. $HO_2 + C_3H_8 \rightarrow C_3H_7 + H_2O_2$

Превращение этан-кислородных смесей можно представить по аналогичной схеме:

1. $C_2H_6 + O_2 \rightarrow C_2H_5 + HO_2$

2. $C_2H_5 + O_2 \rightarrow C_2H_5O_2$

2′. $C_2H_5O_2 \rightarrow C_2H_5 + O_2$

3. $2C_2H_5O_2 \rightarrow 2C_2H_5O + O_2$

4. $C_2H_5O \rightarrow CH_3CHO + H$

(и другие реакции алкильных радикалов)

4. $C_2H_5O \rightarrow CH_2O + CH_3$

5. $CH_3 + C_2H_6 \rightarrow C_2H_5 + CH_4$

6. $C_2H_5 \rightarrow C_2H_4 + H$

7. $H + C_2H_6 \rightarrow C_2H_5 + H_2$

Эти схемы отражают образование продуктов. Кислородсодержащие продукты образуются в малых количествах потому, что концентрации перекисных радикалов существенно уменьшаются с повышением температуры, а скорость их превращения по реакции (3), ведущей к образованию кислородсодержащих продуктов уменьшается пропорционально квадрату концентрации перекисных радикалов:

$$V_3 = K_3[RO_2]^2.$$

Окисление может усилиться, если понизить температуру, т.е. уменьшить мощность лазерного луча, но при этом понизится также скорость инициирования (реакция (1)) и процесс заглохнет. С целью проведения процесса при пониженных температурах были сделаны добавки инициатора азометана к углеводород-кислородной смеси. Облучение пропан-кислородной смеси состава $C_3H_8 : O_2 = 5 : 1$ с добавкой до 0,5% азометана, который распадается с образованием метильных радикалов CH_3, при более низких мощностях излучения приводит к превращению. Образование продуктов превращения наблюдается уже при мощности излучения 4 ват. Отношение кислородсодержащих продуктов к олефинам возрастает.

Таким образом превращение углеводород-кислородных смесей под воздействием лазерного излучения в ,,бесстеночных'' условиях, исключающих влияние каких-либо гетерогенных факторов не приводит к заметному образованию кислородсодержащих продуктов и превращение в основном протекает с образованием олефинов.

ЛИТЕРАТУРА

[1] Ю. Н. Самсонов. Дис. на соискание ученой степени канд. хим. наук. Новосибирск, ИХК и ГСО АН СССР (1977).

[2] Ю. И. Молин, В. И. Панфилов и А. К. Петров, ,,Инфракрасная фотохимия'', Новосибирск, ,,Наука'', (1985).

[3] А. А. Манташян, Л. А. Хачатрян и А. А. Сукиасян, ,,Кинетика и катализ'' (в печати).

[4] А. А. Сукиасян, Л. А. Хачатрян и А. А. Манташян, *Арм. хим. журн.*, **41**, 58(1988).

[5] А. А. Сукиасян, Л. А. Хачатрян и С. Д. Ильин, *Арм. хим. журн.*, **41**, 104 (1988).

[6] А. Б. Налбандян и А. А. Манташян, ,,Элементарные процессы в медленных газофазных реакциях'', Изд. АН АрмССР, Ереван (1975).

[7] Н. Н. Семенов, ,,О некоторых проблемах химической кинетики и реакционной способности'', АН СССР (1954).

[8] Б. А. Поладян, Г. Л. Григорян, Л. А. Хачатрян и А. А. Манташян, *Кинетика и катализ*, **17**, 304 (1976).

[9] A. A.Mantashyan, L. A. Khachatryan, O. M. Niazyan and S. D. Arsentyev, *Combustion and Flame*, **43**, 221 (1981).

[10] S. W.Benson, *J. Am. Chem. Soc.*, **87**, 972 (1965).

[11] L. A. Khachatryan, O. M. Niazyan, A. A. Mantashyan, V. I. Vedeneev and M. A. Teitelboim. *Internation. Journ. of Chem. Kinetics*. **14**, 1231 (1982).

[12] В. Н. Кондратьев, ,,Константы скоростей газофазных реакций. Справочник'', ,,Наука'' (1971).

Revue Roumaine de Chimie, 34, 3, 831–837 (1989)

ИССЛЕДОВАНИЕ СОСТАВА АЛЮМОГИДРОКСОФТОРИДНЫХ КОМПЛЕКСОВ, ОБРАЗУЮЩИХСЯ В ПРОЦЕССЕ ОБЕСФТОРИВАНИЯ ПРИРОДНЫХ ВОД

ВЕРА А. МАТВЕЕВИЧ, А. М. РОМАНОВ, РИТА В. ДРОНДИНА,
В. Н. ШАФРАНСКИЙ и ВАЛЕНТИНА П. МОЦПАН
Лаборатория электрофлотации веществ, Институт прикладной физики АН МССР, Кишинев, СССР

Получена 2 октября 1988 г.

Методами ИК спектроскопии и термогравиметрии исследован процесс образования гидроксофторидных комплексов алюминия при очистке природных вод от фтора. Изучение процесса комплексообразования ионов алюминия и фтора в водной среде в присутствии ионов Cl^-, SO_4^{2-}, HCO_3^- показало, что наиболее нагруженные по фтору гидроксофторидные комплексы алюминия типа $Al(OH)_2F \cdot nH_2O$, $Al(OH)F_2 \cdot nH_2O$ образуются при pH 6,5–6,7. При увеличении pH среды и начальной концентрации ионов алюминия в процессе обесфторивания природных вод происходит образование внешнесферных гидроксофторидных комплексов алюминия. Это обстоятельство обосновывает необходимость проведения процесса электрокоагуляционной очистки подземных вод от ионов фтора именно при вышеуказанном значении pH среды. При этом максимальный расход металлического алюминия составляет 10–15 кг на 1 кг извлекаемого фтора.

The process of aluminium hydroxyfluoride complexes formation during purification of natural waters from fluorine was investigated by IR-spectroscopy and thermogravimetry. The investigation of the process of aluminium and fluorine ions complex formation in water medium in the presence of Cl^-, SO_4^{2-}, HCO_3^- ions showed that more loaded by fluorine aluminium hydroxyfluoride complexes of the type $Al(OH)_2F \cdot nH_2O$, $Al(OH)F_2 \cdot nH_2O$ are formed at pH 6.5–6.7. With the increase of pH of the medium and of the initial concentration of aluminium ions in the process of defluorination of natural waters, outerspherical aluminium hydroxyfluoride complexes are formed. This requires electrocoagulational purification of underground waters from fluorine ions at the above-indicated value of the medium pH exactly. Thus the maximum consumption of metallic aluminium is 10–15 kg per 1 kg extracted fluorine.

ВВЕДЕНИЕ

Из литературы[1,2] известно, что в системе $AlCl_3-NaF-H_2O$ образуются ряд комплексных соединений алюминия с фтором от $[Al(H_2O)_5F]^{2+}$ до $[AlF_6]^{3-}$. Состав образующихся соединений определяется концентрационными условиями.[2] В присутствии ионов SO_4^{2-} и сопоставимых мольных отношениях конкурирующих лигандов $Al^{3+}:F^-$ и $Al^{3+}:SO_4^{2-}$ в растворе одновременно могут существовать комплексы состава $[Al(H_2O)_5F]^{2+}$, $[Al(H_2O)_4F_2]^+$, $[Al(H_2O)_3F_3]$, $[Al(H_2O)_4FSO_4]$, $[Al(H_2O)_3F_2SO_4]^-$.[3]

В присутствии OH^--ионов происходит образование гидроксофторидных комплексов алюминия, на что указано и в работах.[4,5]

В процессе обесфторивания природных вод гидроксидом алюминия происходит образование гидроксофторидных комплексов алюминия и их сорбция на гидроксиде алюминия. В задачу настоящего исследования входило изучение процесса комплексообразования в данной системе при различном pH среды, анионном составе и соотношении начальных концентраций ионов $C_{Al^{3+}}:C_{F^-}$, что позволяет оптимизировать процесс извлечения ионов фтора из природных вод.

ЭКСПЕРИМЕНТАЛЬНАЯ ЧАСТЬ

Нами изучен процесс образования гидроксофторидных комплексов алюминия в водных системах $AlCl_3-NaF-NH_4OH-H_2O$, $Al_2(SO_4)_3-NaF-NH_4OH-H_2O$, $Al_2(SO_4)_3-NaF-NaHCO_3-NH_4OH-H_2O$ при соотношении начальных концентраций ионов $C_{Al^{3+}}:C_{F^-}=1:3$; $1:2$; $1:1$; $1:0{,}5$; $1:0{,}25$; $1:0{,}05$ в зависимости от значения pH среды (от 5,0 до 8,5).

Концентрацию несвязанного фтора в маточяом растворе определяли потенциометрическим методом с использованием лантан-фторидного электрода ЭF/VI и хлорсеребряного электрода сравнения. Количество связанных ионов фтора определяли по разности между исходной концентрацией и концентрацией несвязанных ионов фтора. Содержание алюминия определяли методом атомно-абсорбционной спектрофотометрии на приборе ASS–1N (ГДР). Функцию образования ($\tilde{n}$) т.е. среднее число ионов фтора, координированных с каждым ионом алюминия рассчитывали по формуле: $\tilde{n}=\dfrac{\Sigma\,[C_{F^-}]_{CB}}{\Sigma\,[Al^{3+}]}$. $\Sigma[C_{F^-}]_{CB}$ — количество связанных ионов фтора с алюминием; $\Sigma[Al^{3+}]$ — количество связанных ионов алюминия с фтором. Результаты определения $\tilde{n}$ представлены в таблицах 1 и 2.

Свойства полученных твердых продуктов изучены методами ИК спектроскопии и термогравиметрии. ИК спектры высушенных на воздухе продуктов (соотношение ионов Al^{3+} и F^- в твердых продуктах и в растворе даны в таблице 3) получены на спектрофотометре UR – 20 в интервале 400 —3600 $см^{-1}$. Значения основных частот, найденных в ИК спектрах гидроксофторидных комплексов алюминия представлены в таблице 4.

Термогравиметрические (ТГ) исследования были выполнены на установке OD — 102 (фирма МОМ (ВНР)) для комплексного термического анализа системы Паулик-Паулик-Эрдей в атмосфере воздуха со скоростью нагрева 5 град./мин, и навесках 0,1 г. В таблице 5 приведены значения основных термических эффектов и соответствующая им убыль массы.

РЕЗУЛЬТАТЫ И ИХ ОБСУЖДЕНИЕ

Из данных таблицы 1 видно, что число координированных ионов фтора с алюминием $\tilde{n}$ зависит от pH среды. Для каждого определенного соотношения $C_{Al^{3+}}:C_{F^-}$ значение $\tilde{n}$ сначала растет с увеличением pH раствора, достигая свое максимальное значение ($\tilde{n}_{max}$) для данного соотношения $C_{Al^{3+}}:C_{F^-}$, а затем начинает падать. Также, можно отметить, что значение pH_{max}, соответствующее $\tilde{n}_{max}$, меняется вместе с изменением $C_{Al^{3+}}:C_{F^-}$. А именно, с ростом последнего от 1: 3 до 1: 0,05 pH_{max} сдвигается в более кислую область.

В связи с тем, что коллоидные частицы гидроксида алюминия увеличивают свой заряд положительного знака в интервале pH 6,5—5,0, то следует ожидать уменьшение сорбции на них положительно заряжен-

Таблица 1

Среднее число координированных ионов фтора при различных соотношениях ионов $C_{Al^{3+}} : C_{F^-}$ и значении pH

$C_{Al^{3+}} : C_{F^-}$	pH							
	5,0	5,5	6,0	6,5	7,0	7,5	8,0	8,5
1 : 0,05	0,046	0,048	0,048	0,049	0,048	0,048	0,048	0,047
1 : 0,25	0,198	0,243	0,245	0,250	0,246	0,242	0,238	0,223
1 : 0,50	0,455	0,491	0,500	0,514	0,507	0,504	0,497	0,478
1 : 1,00	0,327	0,537	0,718	0,823	0,834	0,822	0,764	0,673
1 : 2,00	0,836	0,966	1,035	1,368	1,745	1,871	1,805	1,652
1 : 3,00	0,881	0,987	1,681	1,820	2,307	2,610	2,768	2,758

ных гидроксофторидных комплексов алюминия, что и наблюдается на практике. Максимальная сорбция гидроксофторидных комплексов на гидроксиде алюминия происходит в изоэлектрической области сорбента. При дальнейшем увеличении pH поверхность начинает приобретать отрицательный заряд, вследствии перезарядки. При этом должна расти сорбция положительных алюмогидроксофторидных комплексов, однако, уменьшение степени связывания в комплекс ионов фтора с алюминием при увеличении $pH > 7$,[6] приводит к уменьшению общей сорбции ионов фтора на гидроксиде алюминия.

Смещение значения pH_{max} в более щелочную область с ростом начальной концентрации фторид-ионов, обусловлено увеличением количества положительно заряженных алюмогидроксофторидных комплексов в исследуемом растворе. Так как они являются потенциал-определяющими ионами для мицелл гидроксида алюминия, их сорбция повышает положительный заряд мицеллы. Как было указано выше, OH^--ионы конкурируют с F^--ионами за места в координационной сфере алюминия. Таким образом, с ростом pH среды, эта конкуренция обостряется. Но так как концентрация алюмогидроксофторидных комплексов возросла, следовательно, потребуется большее количество OH^--ионов для замещения F^--ионов в них и нейтрализации созданного ими положительного заряда, то есть должно наблюдаться увеличение значения pH_{max} для соотношения $C_{Al^{3+}} : C_{F^-}$ с большим содержанием фтора.

Размытость максимумов при высоких значениях $C_{Al^{3+}} : C_{F^-} = 1 : 0{,}25$; $1 : 0{,}05$ объясняется повышением количества Al^{3+}, который приходится на 1 г-экв F^-, что улучшает сорбцию фторид-ионов при любых значениях pH среды.

В табл. 2 приведены зависимости среднего числа $\bar{n}$ координированных ионов фтора от pH среды и анионного состава раствора при $C_{Al^{3+}} : C_{F^-} = 1 : 1$. Экспериментальные данные показывают, что лучше всего фторид-ионы связываются в присутствии хлорид-ионов. Наиболее существенно на процесс комплексообразования влияют сульфат- и бикарбонат-ионы. Полученные результаты хорошо согласуются с литературными данными,[2,7] авторы которых, сравнивая лигандные свойства некоторых анионов по отношению к алюминию, указывают на существование следующего ряда: $Cl^- < SO_4^{2-} \approx H_2O \ll F^- < OH$.

Таблица 2

Количество связанных ионов фтора с алюминием $\bar{n}$ при различном анионном составе и pH среды

Анионы	pH							
	5,0	5,5	6,0	6,5	7,0	7,5	8,0	8,5
Cl^-	0,351	0,563	0,723	0,830	0,846	0,831	0,770	0,681
SO_4^{2-}	0,327	0,537	0,718	0,823	0,834	0,822	0,764	0,673
$SO_4^{2-} + HCO_3^-$	0,316	0,530	0,697	0,803	0,823	0,805	0,733	0,638

На количество связанных в комплексов ионов фтора влияют и бикарбонат-ионы. Они смещают равновесие реакции гидролиза солей алюминия. В результате происходит снижение концентрации свободных ионов алюминия, принимающих участие в образовании комплексов с ионами фтора, что в свою очередь приводит к снижению степени закомплексованности фтора [8] (см. табл. 2).

Из анализа приведенных данных следует, что образование наиболее нагруженных по фтору алюмогидроксофторидных комплексов происходит в интервале pH 6,5—6,7. При сопоставлении ИК спектров полученных продуктов (см. табл. 3) (pH$=5{,}6$, $C_{Al^{3+}} : C_{F^-} = 1:1$) видно, что при повышении концентрации ионов F^- в составе продуктов происходят изменения, характеризующиеся соответствующими значениями частот валентных и деформационных колебаний Al—F, Al—O, Al—OH и др. Наблюдается повышение интенсивности полос поглощения ν(Al—F) и уменьшение интенсивности валентных и деформационных полос поглощения исходного гидроксида алюминия (продукт а) (см. табл. 4).

Таблица 3

Соотношение ионов Al^{3+} и F^- в твердых продуктах и в растворе

Продукт*	*б*	*в*	*г*	*д*	*е*	*ж*
$C_{Al^{3+}} : C_{F^-} = 1 : \bar{n}$	0,50	1,00	1,50	2,00	3,00	3,00
$Al^{3+} : F^- = 1 : \bar{n}$	0,48	0,81	0,96	1,10	2,18	3,00

* $\bar{n} = 0{,}5$ 1,0, 1,5 и т.д.

В области 410—420 см$^{-1}$ в спектрах продуктов наблюдается полоса поглощения относящаяся к связи Al—O. По интенсивности данной полосы можно судить о количестве образовавщихся однофтористых и двухфтористых гидроксокомплексов алюминия в исследуемых смесях. Изменении ширины и смещение интенсивности широкой полосы поглощения в областъ 450—670 см$^{-1}$, которая соответствует ν(Al—F), также подтверждает образование гидроксофторидных комплексов алюминия.[9] Постепенно широкая полоса поглощения октаэдров AlX_6 и тетраэдров AlX_4 комплексной струк-

Таблица 4

Основные частоты ($см^{-1}$), найденные и ИК спектрах гидроксофторидных комплексах алюминия

Продукт	$\delta(OH)$, $\delta(HOH)$	$\delta(Al-OH)$	$\delta(Al-OH)$	$\delta as(Al-OH)$	$\nu(Al-O)$, $\nu(Al-F)$	$\nu(Al-F)$	$\nu(Al-F)$, $[AlF_4]^-$
а	1650 сл	1160 пл	1030 ср	980 ср	665—530 ш		420 пл
б	1650 сл	1155 пл	1030 ср	970 ср	675—550 ш		420 сл
в	1650 ср	1155 пл	1030 ср	970 ср	675—550 ш		420 сл
г	1650 ср	1155 ср	1025 ср	970 ср	675—550 ш		420 сл
д	1650 сл	1155 сл	1025 ср	970 ср	650—550 ш		420 о.с.
е	1650 сл	1155 сл	1025 сл	970 сл	620—580 с		420 ср
ж	1650 пл	1155 пл	—	—	655 с	545ср	420 с

Примечание: о.с. — очень сильная, с. — сильная, ср. — средняя, сл. — слабая, пл. — плечо, ш. — широкая.

туры $\nu(Al-O)$ переходит в более узкую полосу поглощения с максимумом при 600 $см^{-1}$, которая по виду и положению в спектре, по всей вероятности, относится к поглощению тетраэдров AlX_4 и $\nu(Al-F)$. Полосы поглощения с максимумами при 970 и 1030 $см^{-1}$ относятся к поглощению $\delta(Al-OH)$.[10] При повышении содержания фтора в реакционной смеси максимумы этих полос понижаются и в чистом AlF_3 они полностью отсутствуют. Следовательно, поглощение в области 900—1100 $см^{-1}$, полосы которой могут быть обусловлены координированными молекулами воды или гидроксильными группами,[11] также свидетельствует об их замене в исходном гидроксиде алюминия на ионы фтора.

При сопоставлении максимумов этих полос (1030 и 970 $см^{-1}$) видно, что относительное уменьшение максимума полосы 1030—1025 $см^{-1}$ происходит постепенно при переходе от чистого $Al(OH)_3$ к продукту *е*, что связано, по-видимому, с замещением координированной воды ионами фтора. По мере увеличения содержания фтора (продукт *е*) происходит также изменение максимума полосы поглощения и при 970 $см^{-1}$, которая обусловлена $\delta(Al-OH)$.

Таким образом, при сопоставлении исследуемых продуктов видно, что при увеличении содержания ионов фтора вначале происходят изменения, связанные с замещением координированной воды, затем происходят изменения и в количестве координированных OH^--групп. По-видимому, в осадке образуется новое вещество $Al(OH)_2F\,.nH_2O$.

При переходе к продукту *е* наблюдается резкое уменьшение полос поглощения с максимумами при 1030 и 970 $см^{-1}$, что связано, по-видимому, с превращением $Al(OH)_2F\,.nH_2O$ в $Al(OH)F_2\,.\,nH_2O$. Этому переходу, действительно, должны соответствовать уменьшение поглощения в области OH^--групп и увеличение поглощения в области $\nu(Al-F)$. Результаты ИК спектроскопии свидетельствуют, что при переходе от продукта *а* к продукту *е* происходит постепенный переход:

$$Al(OH)_3\,.nH_2O \rightarrow Al(OH)_3\cdot HF\cdot nH_2O \rightarrow Al(OH)_2F\,.nH_2O \rightarrow Al(OH)F_2\,.nH_2O.$$

Термогравиметрические исследования полученных продуктов также указывают на изменение их состава и свойств в зависимости от соотношения $C_{Al^{3+}}:C_{F^-}$. Как видно из таблицы 5, при нагревании продуктов *а*—*е* до 510—540°С проявляются несколько сложных эндотермических эффектов, в результате которых происходит отщепление кристаллизационной воды до 200—210°С и конституционной воды в интервале температур 210—360°С, что связано с дегидратацией байерита и гидраргилита в осадке.[12] При дальнейшем увеличении температуры до 510—540°С происходит отщепление оставшейся конституционной воды. При этой же температуре происходит выделение и фтористого водорода.[13]

Таблица 5

Убыль массы продуктов в зависимости от температуры

Продукт	Номер эффекта*	t, °С	Δm, %	$\Sigma\Delta m$, %
а	I	130	17,0	34,0
	II	290	11,0	
	III	430	6,0	
б	I	190	23,0	39,0
	II	280	9,5	
	III	440	4,5	
в	I	190	19,0	35,5
	II	270	12,0	
	III	420	4,5	
г	I	150	12,0	33,5
	II	290	17,0	
	III	420	4,5	
д	I	140	11,5	33,5
	II	310	18,0	
	III	380	4,0	
е	I	130	6,0	15,5
	II	270	8,0	
	III	360	1,5	

* Эндотермический эффект. t — температура, Δm — убыль массы для соответствующего эффекта,
$\Sigma\Delta m$ — общая убыль массы.

По мере увеличения содержания ионов фтора в продуктах (*б—е*) происходит изменение убыли массы, рассчитанное из кривых ТГ для каждого эндотермического эффекта. Убыль массы, связанная с первым эффектом, уменьшается постепенно от 23 до 6%. Значение убыли массы для второго эффекта продуктов б—д увеличивается постепенно, а для продукта *е* резко сокращается и доходит до 8%. Суммарная убыль массы для указанных эффектов тоже уменьшается закономерно с увеличением содержания ионов фтора в твердых продуктах.

На основании полученных данных можно сделать вывод, что с увеличением содержания ионов фтора (до продукта *д*) происходит постепенное замещение кристаллизационной воды, связанное с убылью массы для соответствующего эффекта. В результате их нагревания одновременно с выделением кристаллизационной воды, по-видимому, происходит превращение и в составе продуктов, связанное с замещением OH^--групп из $Al(OH)_3$ (растет убыль массы, связанная с отщеплением конституционной воды).

При сопоставлении полученных величин убыли массы, найденных из ТГ-кривых, с вычисленными данными, можно предположить, что при соотношении $C_{Al^{3+}} : C_{F^-} = 1:1$ и более образуются внешнесферные гидроксофторидные комплексы алюминия типа $Al(OH)_3 \cdot HF \cdot nH_2O$, которые в результате нагревания превращаются в $Al(OH)_2F \cdot nH_2O$. При дальнейшем увеличении соотношения $C_{Al^{3+}} : C_{F^-}$ до 2: 1 (продукт *е*) происходит образование другого вещества, по всей вероятности $Al(OH)F_2 \cdot nH_2O$, т.е. увеличивается вероятность образования внутрисферных гидроксофторидных комплексов алюминия, что согласуется и с данными ИК спектроскопии.

Таким образом, нами показано, что при начальных соотношениях концентраций $C_{Al^{3+}} : C_{F^-} = 1:0{,}5$ и более, которые обычно наблюдаются при извлечении ионов фтора гидроксидом алюминия в процессе обесфторивания подземных вод, происходит образование внешнесферных гидроксофторидных комплексов алюминия. В более концентрированных фторсодержащих растворах, как видно из полученных данных, образуются внутрисферные гидроксофторидные комплексы алюминия.

ЛИТЕРАТУРА

[1] К. Е. Клейнер, *Ж. общ. химии*, **20**, 1747 (1950).

[2] Ю. А. Буслаев и С. П. Петросянц, *Ж. коорд. химии*, **5**, 163(1979).

[3] С. П. Петросянц и Е. Р. Буслаева, *Ж. коорд. химии*, **12**, 907(1986).

[4] А. С. Коробицын, Г. Н. Шапарова, О. Н. Каторина и др., *Ж. прикл. химии*, **53**, 2350 (1980).

[5] A. N. Crarke and D. J. Wilson, *Separ. Sci.*, **10**, 417 (1975).

[6] В. А. Матвеевич, Р. В. Дрондина, А. М. Романов и др., *Химия и технол. воды*, **6**, 312(1984).

[7] С. П. Петросянц и Е. Р. Буслаева. *Ж. неорган. химии*, **33**, 328(1988).

[8] А. Т. Пилипенко, Н. Ф. Фалендыш и Е. П. Пархоменко, *Химия и технол. воды*, **4**, 136(1982).

[9] A. K. Sengupta and K. Sew. *Ind. J. Chem.*, **17A**, 107 (1979).

[10] A. V. Nicolescu, Hurich Yasser and A. Nicolescu. *Rev. chem.*, **31**, 976 (1980).

[11] Б. Н. Иванов-Эмин, Мельядо Кампос, Б. Е. Зайцев и др. *Ж. неорган. химии*, **18**, 2942(1973).

[12] О. П. Криворучко, Р. А. Буянов, М. А. Федотов и др. *Ж. неорган. химии*, **23**, 1798 (1978).

[13] В. И. Москвитин, Д. И. Ушаков. *Изв. высш. учеб. завед. СССР. Цветная металлургия* (1977).

Revue Roumaine de Chimie, 34, 3, 839–844 (1989)

EFFECT OF ACETOPHENONE BENZOYL HYDRAZONE DERIVATIVES AS CORROSION INHIBITORS FOR THE DISSOLUTION OF ALUMINUM IN HCl SOLUTION

M. R. MOSTAFA[a], H. M. ABU EL-NADER[b] and G. M. ABU EL-REASH[b]
[a] Chemistry Department, Dumiatta Faculty of Science, Mansoura University, Egypt
[b] Chemistry Department, Faculty of Science, Mansoura University, Mansoura, Egypt

Received September 30, 1988

The inhibitive action of some acetophenone benzoylhydrazone derivatives on the dissolution of aluminum in 2M HCl has been investigated by hydrogen evolution and weight loss techniques. It is found that the dissolution reaction of aluminum in hydrochloric acid solution is of zero order and remains so when the additives are present. The rate constant decreases as the inhibition efficiency increases. The activation energy of the dissolution reaction increases with increasing inhibition efficiency of the additives used. The results indicated that the adsorption of acetophenone hydrazone derivatives occurs over the aluminum surface through the oxygen of the carbonyl group and nitrogen sites.

INTRODUCTION

A number of workers [1–4] have shown that carbonyl compounds have an effective corrosion inhibition on the dissolution of aluminum in hydrochloric acid. The inhibition was attributed [2,3] to the adsorption of these compounds on the aluminum metal surface *via* bonding through the carbonyl group, and the charge density on these groups was found to affect the inhibition efficiency. As acetophenone benzoylhydrazone derivatives are expected to exhibit higher corrosion inhibition efficiency, it was thought desirable to investigate the effect of some of these compounds on the retardation of aluminum dissolution in hydrochloric acid using weight loss and hydrogen evolution techniques. Kinetic studies were also carried out to compare the results with a previous [5] work which reported that the dissolution of aluminum in concentrated acetic acid solution is a zero order reaction.

EXPERIMENTAL

The acetophenone benzoylhydrazone derivatives used as corrosion inhibitors in this investigation are:

(I) *p*-Chloroacetophenone benzoylhydrazone

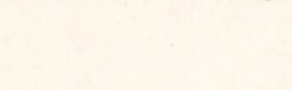

(II) Acetophenone benzoylhydrazone

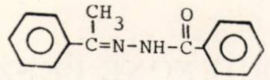

(III) *p*-Hydroxyacetophenone benzoylhydrazone

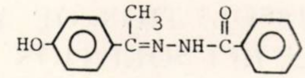

(IV) *p*-Methylacetophenone benzoylhydrazone

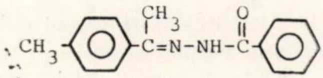

(V) *p*-Aminoacetophenone benzoylhydrazone

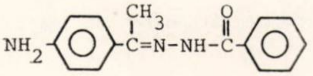

2M HCl solution was prepared by dilution from AR grade quality and its concentration was checked by standard carbonate free solution. The chemical composition of the aluminum sheet used was Al : 99.535, Si : 0.15, Fe : 0.19, Mn : 0.005, Mg : 0.1 and Cu : 0.02%. The dimensions of the test pieces used were 20×20×1.5 mm. These were cleaned and degreased as usual.[6]

In the hydrogen evolution method the vessel was the same as that employed before.[1] A weighed aluminum sample was dropped into 100 mL of 2M HCl and the volume of hydrogen evolved was recorded as a function of time (± 0.05 mL). The efficiency of a given inhibitor was evaluated as the percentage reduction in reaction rate (RR) viz.

% Reduction in $RR = (R_{\text{free}} - R_{\text{inh.}})\,100/R_{\text{free}}$ where R_{free} and $R_{\text{inh.}}$ are the rates of aluminum dissolution in the absence and in the presence of the given inhibitor, respectively (in mL $\text{cm}^{-2}\text{s}^{-1}$). The rate in all cases, given by the slope of the linear part of the volume of hydrogen evolved-time curve, must be measured at the same time.

The weight loss technique was used as previously reported.[6]

RESULTS AND DISCUSSION

The loss in the weight of aluminum strips in 2M HCl in the absence and in the presence of the additives was determined. The obtained weight loss-time curves are characterized by an initial slow rise in weight loss due to the formed surface oxide film[7] followed by a sharp rise. Curves for additive containing system fall below that of the free acid as indicated in Fig. 1. The curves indicate that weight loss of aluminum depends on both the type and the concentration of additives. The inhibition efficiencies of the additives after 60 min from the start and at a concentration of 10^{-4}M are included in Table 1. In this table the inhibitors examined are arranged in the order of decreasing inhibition efficiency. The order of increasing inhibition efficiency of the examined inhibitors is I > II > III > IV > V.

The effect of inhibitor concentration C on the retardation of aluminum dissolution was also studied. In all cases the increase in the concentration of the additives is accompanied by an increase in their inhibition efficiency as shown in Fig. 2. The increase of percentage inhibition with the increase of inhibitor concentration suggests[1] that inhibition is due

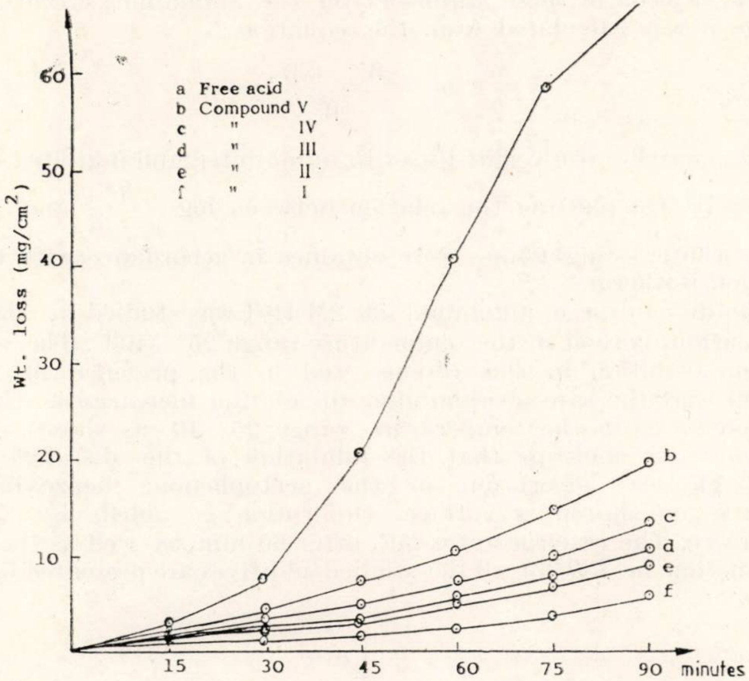

Fig. 1. — Weight loss-time curves for all additives used at concentration 10^{-4}M.

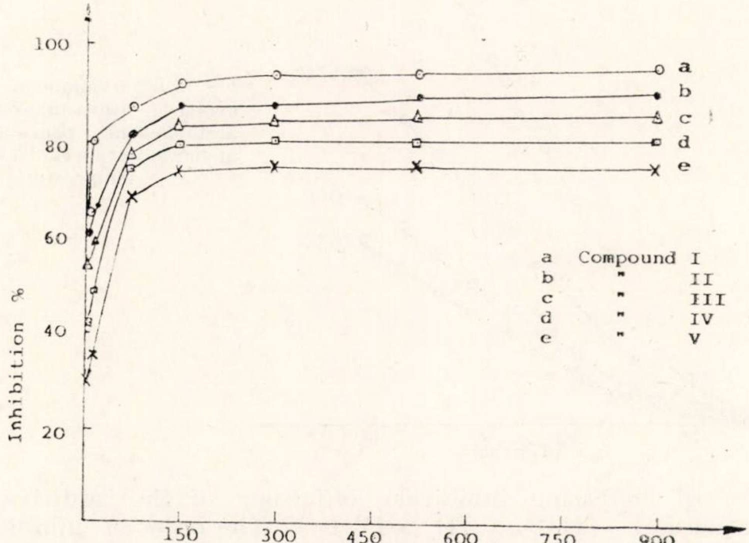

Fig. 2. — Percentage inhibition-concentration curves.

to the adsorption of these inhibitors on the aluminum surface. Surface coverage θ was calculated from the equation:

$$\theta = \frac{W_0 - W_i}{W_0}$$

where W_0 and W_i are weight-losses in uninhibited and inhibited solutions, respectively. On plotting the relation between $\log \frac{\theta}{1-\theta}$ and $\log C$ of the adsorbate, straight lines were obtained in accordance with Langmuir adsorption isotherm.[8]

The dissolution of aluminum in 2M HCl was studied by the hydrogen evolution method in the temperature range 25°—40°C. The volume of hydrogen evolution in the absence and in the presence of additives indicated that the rate of aluminum dissolution increases as the temperature increases in the temperature range 25—40° as shown in Fig. 3. This behaviour confirms that the inhibition of the dissolution occurs through physical adsorption of the acetophenone benzoylhydrazone derivatives on aluminum surface. Desorption is aided by increasing temperature. The reaction rate, *RR*, after 60 min, as well as the percentage reduction in *RR* for all the studied additives are presented in Table 1.

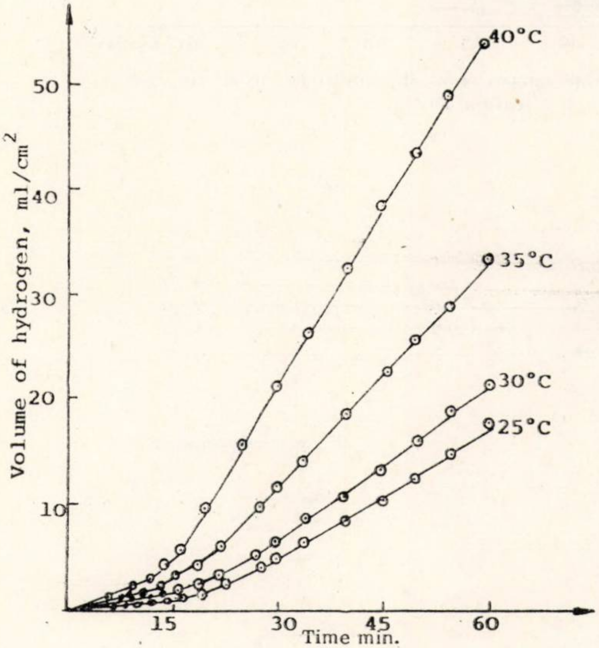

Fig. 3. — Volume of hydrogen evolved — time curves for *p*-chloracetophenone benzoylhydrazone at concentration 10^{-4}M at different temperatures.

The order of increasing inhibition efficiency of the additives under consideration is I > II > > III > IV > V. The order of inhibition efficiency of the additive compounds given by two different techniques is the same, indicating the validity of our studies.

Table 1

Comparison between the inhibitor efficiencies of all additives at 25 °C

Substance	*RR* (mg. cm^{-2}. min^{-1})	% Reduction in *RR*	% Inhibition
Free acid	2.07	—	—
I	0.30	85.5	92
II	0.33	84.06	87.8
III	0.36	82.60	85.36
IV	0.38	81.64	81.70
V	0.44	78.74	74.40

The curves obtained by the hydrogen evolution method indicated that after a certain interval the hydrogen evolution increases linearly with time. This initial slow rate may be attributed to both an induction period representing the breakdown of the oxide film on the metal surface and the start of attack.[7] The dissolution of aluminum oxide in acid solutions is not accompained by hydrogen evolution, so that the rate of hydrogen evolution increases slowly till the oxide film is completely dissolved. Consequently, it can be surmised that the dissolution of aluminum itself is linearly related to the reaction time. This behaviour is characteristic of zero order reactions. The zero order equation is generally given by

$$x = kt$$

where x is the fraction of aluminum converted into reaction products at time t, this being directly proportional to the volume of hydrogen evolved at time t, and k is the rate constant of the reaction. The value of k can be calculated from the slope of the $x-t$ curve at the given temperature. In this manner the rate constants of aluminum dissolution in 2M HCl in the absence and in the presence of 10^{-4}M acetophenone benzoylhydrazone derivatives were determined and collected in Table 2. It is evident that the value of k increases with the increase in temperature. Also, the value of k decreases with the increase in the inhibition efficiency of the acetophenone benzoylhydrazone derivatives.

Table 2

The rate constants and the activation energy of aluminum dissolution in 2M HCl

Substance	Rate constant at temp. °C				*E* kJ mol^{-1}
	25	30	35	40	
Free acid	1.585	1.778	2.188	2.818	33.60
I	0.399	0.499	0.72	1.14	65.10
II	0.383	0.517	0.732	1.086	54.42
III	0.433	0.523	0.75	1.142	57.54
IV	0.447	0.524	0.762	1.15	55.52
V	0.521	0.580	0.822	1.284	50.95

Arrhenius activation energy values, E, obtained from the slopes of $\log k$ vs $\frac{1}{T}$, are given in Table 2. These values increase with increasing inhibition efficiency of the acetophenone benzoylhydrazone derivatives and suggest that the process is activation controlled. Thus, the increase in activation energy of aluminum dissolution with the increase inhibition efficiency of acetophenone benzoylhydrazone derivatives could be attributed to an increased adsorption between the inhibitor and the metal surface.[9]

It is evident from Table 1 that the order of increasing inhibition efficiency of acetophenone benzoylhydrazone derivatives in 2M HCl is I > II > III > IV > V. The inhibition efficiency of the compounds would depend on the number of adsorption sites and their basicity.It is clear that the carbonyl groupoxygen and the substituent nitrogen atoms are the sites involved in adsorption of acetophenone benzoylhydrozone derivatives over the aluminum surface. All the additives have the same number of adsorption sites (one oxygen and two nitrogens). Thus, the power of the adsorption tendency of these sites would depend on the *p*-substituent which increases the charge density on these sites. The higher adsorption tendency of *p*-chloro-acetophenone benzoylhydrazone over that of the other additives may be due to a comparable increase in the basicity of the $C=O$ and $C=N$ groups resulting from the electron attracting character of the chloro-group in the *p*-position which decreases the enolization effect of the hydrogen in the NH adjacent to the carbonyl group. In the case of compounds III, IV and V, due to the presence of electron repelling groups in the *p*-position, the enolization effect leads to a decrease in the availability of electrons on the oxygen adsorption sites. NH_2 is more basic than $OH > CH_3 >$ unsubstituted compound. Accordingly the adsorption tendency increases in the order V < IV < < III < I. Bearing in mind that the adsorbability of the acetophenone-benzoylhydrazone derivatives would be comparable in the first place to the basicity of the oxygen and nitrogen sites involved, the order of inhibition efficiency is expected to follow the same order as the adsorbability of the organic inhibitors on the aluminum surface. This explanation supports the order obtained for the inhibition efficiency of the additives.

REFERENCES

[1] S. M. Hassan, Y. A. Elawady, A. I. Ahmed and A. O. Baghlaf, *Corrosion Sci.*, **19**, 691 (1979).
[2] M.N.H. Moussa, F.I.M. Taha, M.M.A. Gouda and G. M. Singab, *Corrosion Sci.*, **16**, 379 (1976).
[3] I. M. Issa, M. N. H. Moussa and M. A. A. Ghandour, *Corrosion Sci.*, **13**, 791 (1973).
[4] I.M. Issa, A.A. El-Samahy and Y.M. Temerek, *J.Chem. U.A.R.*, **13**, 121 (1970).
[5] I.V. Gimbitskaya, S.M. Beloglazov and M.E. Volkova, *Korros. Zaschch Met.*, (no. 1–2), 13 (1974).
[6] Aziz K. Shams and A. M. El-Din, *Corrosion Sci.*, **5**, 489 (1965).
[7] G. C. Wood et al., "Localised Corrosion", Ed. STAEHLE, p. 526 NACE, Houston, 1974.
[8] T. P. Hoar and R. D. Haliday, *J. Appl. Chem.*, **3**, 502 (1955).
[9] S. M. Hassan, M. N. H. Mousa, F. I. M. Taha and A. S. Fouda, *Corrosion Sci.*, **21**, 439 (1981).

Revue Roumaine de Chimie, **34**, *3*, 845–854 (1989)

TRANSITION METAL COMPLEXES WITH THIOAMIDES

S. NEAGOE[a], LUCIA ANTONESCU[a], MARIA NEGOIU[b], VIORICA NEAGOE[c],
D. NEGOIU[b] and CORNELIA CERCASOV[b]

[a] Institute of Petroleum and Gas, Ploiești, Blvd Bucharest no. 1–3, Ploiești, Romania
[b] Polytechnic Institute Bucharest, Str. Polizu no. 1, Bucharest, Romania
[c] School no. 50, Str. Ion Maiorescu no. 32, Bucharest, Romania

Received October 17, 1988

Complex compounds of several transition metals with thioamides in the series of thiobenzopiperidides and thiobenzomorpholides were synthesized and analyzed. The compounds obtained were formulated on the basis of elemental chemical analysis, determinations of molecular mass, thermal analysis, determinations of electrical conductibility, and also IR, UV-VIS and NMR spectra. The metal used was Pd(II).

Thioamides form complex compounds with the metallic ions due to the presence of the sulphur and nitrogen atoms in the functional group. These atoms can function as electron donors in the presence of some acceptors.[1,2]

The specialty literature offers certain data on the complex compounds formed by thioamides with the transition metal ions.[3–8]

Likewise, some complex compounds of Hg(II) with thioamides in the series of thiobenzopiperidides and thiobenzomorpholides were prepared and studied.[9]

The present paper reports the results of the study on the complex compounds of Pd(II) with thioamides in the thiobenzopiperidides (a) and thiobenzomorpholides (b) series :

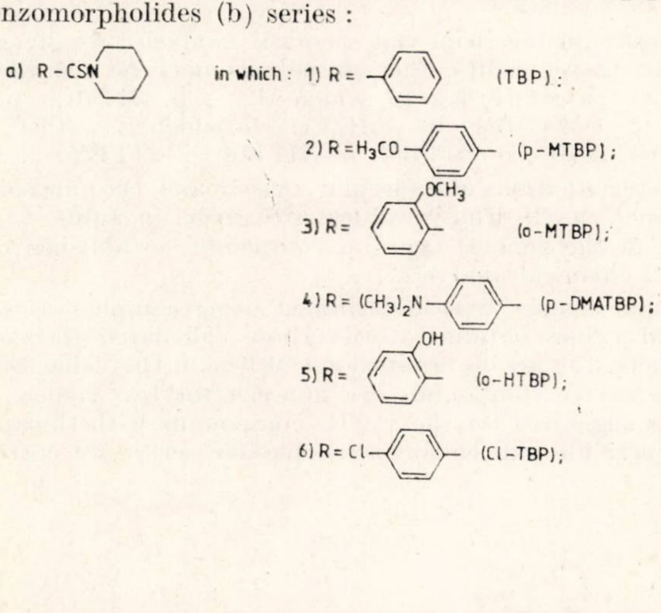

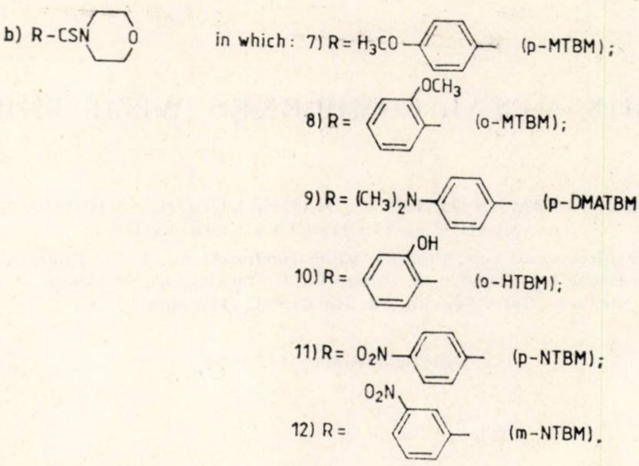
b) R-CSN O
in which: 7) R = H$_3$CO– (p-MTBM);
8) R = OCH$_3$ (o-MTBM);
9) R = (CH$_3$)$_2$N– (p-DMATBM);
10) R = OH (o-HTBM);
11) R = O$_2$N– (p-NTBM);
12) R = O$_2$N (m-NTBM).

RESULTS AND DISCUSSION

The complex compounds of Pd(II) with thioamides in the thiobenzopiperidides and thiobenzomorpholides classes are microcrystalline powders having various colours : orange-yellow, brick-red, red, dark-brown and higher melting points than the corresponding ligands. They are easily soluble in dimethylsulphoxide (DMSO), dimethylformamide (DMF), dichloromethane (CH_2Cl_2), camphor, sparsely soluble in nitromethane and insoluble in ethanol and acetone.

All compounds were obtained by similar methods. A solution of 0.1 M thioamide in ethanol or acetone was added gradually, while stirring, to an aqueous solution of $PdCl_2$, 0.1 M. According to the nature of the thioamide used, the compound appears instantaneously, after about 1/2 hour or after several hours. After at least one hour, the precipitate formed can be filtered off, washed in water and acetone or alcohol and then dried in vacuum.

The results of the elemental chemical analysis are given in table 1. According to these results, the compounds may be classified into two general types : a) $[PdLCl_2]$, in which L = p–MTBP, p–DMATBP p–MTBM, p–DMATBM ; b) $[PdL_2Cl_2]$, in which L = TBP, o–MTBP, o–HTBP, Cl–TBP ; o–MTBM, o–HTBM, p–NTBM, m–NTBM.

The determinations of molecular mass[10] and the measurements of molar conductivity,[11] whose values are given in table 2, confirm the formulation of the general types of compounds established on the basis of elemental chemical analysis.

Molecular masses were determined using camphor as solvent. The experimental values obtained verify those calculated theoretically. The molar conductivities are determined in DMSO and the values obtained show that the respective compounds are non-electrolytes. Hence, the general formulations suggested for the Pd(II) compounds with thioamides of the thiobenzopiperidide and thiobenzomorpholide series are correct.

Table 1

Elemental chemical analysis of the Pd(II) complex compounds with thiobenzopiperidides and thiobenzomorpholides

System	Element analysed Theores./Exp.					M.p.	Colour
	Pd%	C%	H%	S%	Cl%		
Pd(II)–TBP	18.11	49.03	5.10	10.89	12.07	177	dark-red
	18.30	49.26	5.29	10.96	12.66		
Pd(II)–(p-MTBP)	25.80	37.79	4.11	7.76	17.20	184	brick-red
	26.00	36.80	3.58	8.24	17.62		
Pd(II)–(o-MTBP)	16.43	48.20	5.25	9.88	10.95	164	brown
	16.55	48.34	5.60	9.80	10.76		
Pd(II)–(p-DMATBP)	25.02	39.50	4.70	7.52	16.67	186	brown
	25.34	40.00	4.92	8.00	16.84		
Pd(II)–(o-HTBP)	17.18	46.50	4.84	10.33	11.45	148	brick-red
	17.35	46.28	5.00	10.88	11.38		
Pd(II)–(Cl-TBP)	16.21	43.88	4.26	9.75	10.80	134	orange
	16.40	44.20	4.60	10.00	10.52		
Pd(II)–(p-MTBM)	25.68	34.75	2.65	7.72	17.11	169	dark-red
	25.50	34.30	2.42	7.68	17.55		
Pd(II)–(o-MTBM)	16.33	44.22	4.60	9.82	10.88	188	brown
	16.54	44.36	4.65	9.76	11.00		
Pd(II)–(o-HTBM)	17.07	42.35	4.17	10.26	11.37	218	brown
	17.30	42.50	4.18	10.62	11.07		
Pd(II)–(p-NTBM)	15.61	38.75	3.52	9.39	10.40	225	orange
	15.50	38.96	3.58	9.68	10.59		
Pd(II)–(m-NTBM)	15.62	38.75	3.52	9.39	10.40	203	orange-yellow
	15.50	38.20	3.48	9.02	10.66		

Table 2

Molecular mass and molar conductibility of the Pd(II) complex compounds with thioamides

Compound	Molecular mass		Concentration ($X.10^{-4}M$)	Molar conductibility ($\Omega^{-1}\ cm^2 \cdot mol^{-1}$)
	Theoret.	Experim.		
$[Pd(TBP)_2Cl_2]$	587.30	552.56	2.89	2.12
$[Pd(p\text{-}MTBP)Cl_2]$	412.30	402.65	5.09	1.44
$[Pd(o\text{-}MTBP)_2Cl_2]$	647.30	652.00	3.79	1.86
$[Pd(p\text{-}DMATBP)Cl_2]$	425.30	386.00	1.41	10.58
$[Pd(o\text{-}HTBP)_2Cl_2]$	619.30	628.44	2.64	3.66
$[Pd(Cl-TBP)_2Cl_2]$	656.20	664.00	2.55	2.36
$[Pd(p\text{-}MTBM)Cl_2]$	414.30	446.24	2.05	1.53
$[Pd(o\text{-}MTBM)_2Cl_2]$	651.30	683.00	2.24	3.05
$[Pd(o\text{-}HTBM)_2Cl_2]$	623.30	596.25	2.08	4.71
$[Pd(p\text{-}NTBM)_2Cl_2]$	681.30	648.45	2.27	5.76
$[Pd(m\text{-}NTBM)_2Cl_2]$	681.30	653.40	2.86	0.78

Thermal analysis

The compounds studied were thermally analyzed with the view of calculating their thermal stability and for confirmation of the general formulation suggested after the elemental chemical analysis and the determinations of molecular mass and molar conductivity. The ligand : metal 1/1 or 2/1 was thus established.

The thermal behaviour of the compound obtained with o—HTBM, $[Pd(o-HTBM)_2Cl_2]$ is highly interesting. Examination of the TG curve shows a good thermal stability of the compound up to a temperature of 220°C. Above this temperature, the compound decomposes in two stages : the former within the 220—350°C range and the latter within the 350—580°C. At 580°C the decomposition and oxidation of the organic substances is complete.

Within the 870—880°C temperature range, the decomposition effect appears : $PdO \rightarrow Pd + 1/2O_2$.

The experimental residue obtained, made ot metallic palladium, is 16.67% of the theoretical one, of 17.07%. This fact also confirms the combination ratio metal : ligand 2/1.

IR spectra

IR spectra of thioamides and of the corresponding complex compounds obtained with Pd(II) are given in table 3.

The interpretation of the IR spectra of tertiary thioamides is difficult, as a series of factors generating difficulties appear in the correct assignment of the characteristic bands :

a) internal conjugation p-π in the functional group;

b) the bands characteristic of thioamides appear within the 600—1700 cm^{-1} range, also very rich in other bands.

For the thioamides studied, the characteristic bands were assigned on the basis of Jensen and Nielsen's works.[12] Comparative analysis of the spectra of the ligands and of the corresponding complex compounds gives information on the atoms through which the ligand is bound to the central metallic ion.

The arguments for the achievement of the chemical bond in compounds of the type $[PdL_2Cl_2]$, through the sulphur atom of the thioamidic group under the "thioceto" form are :

a) changes in the band from 1050—850 cm^{-1} assigned to the $>C=S$ bond in thioamides. This band is shifted in the compounds studied with aboud 10 cm^{-1} towards higher or lower frequencies, but in both cases with decreased or sometimes much enlarged intensities;

b) changes in the bands from 1200—1000 cm^{-1}, assigned to the coupled vibrations $\nu_{NCS} + \gamma_{NH_2}$ of the thioamide spectra, which in the spectra of the compounds appear shifted either towards lower or towards higher frequencies but with changed intensity.

Non participation of the nitrogen atom in coordination, in the case of this type of compounds, is confirmed by the lack of important changes within the spectral range in which the bands corresponding to the coupled vibration $\nu_{CN} + \delta_{NH_2}$ and $\nu_{CC} + \nu_{CN}$ appear.

Table 3

Characteristic frequencies in the IR spectra of thioamides and their complex compounds with Pd(II), (cm^{-1})

Compound	Spectral range			
	1530–1490	1400–1200	1200–1000	1050–850
	$\nu_{CN}+\delta_{NH_2}$	$\nu_{CC}+\nu_{CN}$	$\nu_{NCS}+\gamma_{NH_2}$	$\nu_{C=S}$
1	2	3	4	5
TBP	1498w	1298w 1250s 1210m	1142m	1020m
p-MTBP	1495m	1260sh 1245w 1210s	1183m 1140s 1115s	1020m
o-MTBP	1490s	1250s 1280s 1300w	1010s 1100w 1175w	1010m
p-DMATBP	1492s	1275w 1240m 1215w	1195w 1175w 1140m	1020s
o-HTBP	1500s	1290m 1250m 1210m	1190w 1130m	1010m
Cl-TBP	1492m	1300m 1245s 1210w	1200s 1165w 1140m	1010m
p-MTBM	1490m	1250w 1235w	1185m	1040m
o-MTBM	1485m	1282m 1230s 1210w	1184w 1110s	1020m
o-HTBM	1515s	1290s 1265s 1210w	1165w	1035s
p-NTBM	1510w	1296m 1265m 1210m	1180m	1037s
m-NTBM	1500w	1295m 1270w 1215m	1180w	1040s
$[Pd(TBP)_2Cl_2]$	1488w	1290w 1245s 1205w	1138m	1010b
$[Pd(p\text{-}MTBP)Cl_2]$	1510w	1265w 1250w 1225w	1180s 1140m 1120w	1030b
$[Pd(o\text{-}MTBP)_2Cl_2]$	1485s	1242s 1284w 1300sh	1020s 1157s 1190s	1020s
$[Pd(p\text{-}DMATBP)Cl_2]$	1485sh	1290m 1260sh 1214sh	1175b	1030sh
$[Pd(o\text{-}HTBP)_2Cl_2]$	1510b	1295m 1242s 1210sh	1180w 1120m	1000w

Table 3 (continued)

1	2	3	4	5
[Pd(Cl-TBP)$_2$Cl$_2$]	1500m	1305m 1240s 1215sh	1210m 1155w	1000s
[Pd(p-MTBM)Cl$_2$]	1505w	1270m 1240w	1180s	1030m
[Pd(o-MTBM)$_2$Cl$_2$]	1480m	1295m 1225w 1205w	1180m 1120w	1010b
[Pd(o-HTBM)$_2$Cl$_2$]	1520w	1290w 1270m	1165sh	1030m
[Pd(p-NTBM)$_2$Cl$_2$]	1520sh	1300m 1265m 1205w	1180sh	1030m
[Pd(m-NTBM)$_2$Cl$_2$]	1535b	1305m 1270m 1215w	1175w	1030m

s = strong ; m = medium ; w = weak ; b = broad ; sh = shoulder

In the compounds of the type [PdLCl$_2$], the ligand is bound to the central metallic ion both through the sulphur atom and through the nitrogen atom in the functional group.

Proofs for participation of the nitrogen atom in achieving the chemical bond in these compounds, are given by the following :

a) change in the band within the 1530–1490 cm^{-1} spectral range, assigned to the coupled frequencies $\nu_{CN} + \delta_{NH_2}$, in thioamides, which in the complex compounds is shifted towards higher or lower frequencies as a function of the thioamide nature. Likewise, the intensity of these bands, within the spectra of complex compounds, is changed versus that within the spectra of noncomplexed thioamides ;

b) change and shift of bands from 1400–1200 cm^{-1}, assigned to the coupled vibrations $\nu_{CC} + \nu_{CN}$ in thioamides.

Comparative analysis of IR spectra, of ligands and of the corresponding compounds with Pd(II) shows that the thioamides used may be either monodentate or bidentate ligands, in which the sulphur and nitrogen atoms are donor atoms.

UV–VIS spectra

The ultraviolet-visible spectra of the complex compounds of Pd(II) with thioamides in the class of thiobenzopiperidides and thiobenzomorpholides were made in solid state after pelletizing in MgO.

The electronic reflection spectra show for ligands both transitions of the $n \rightarrow \pi^*$ type, appearing within the 360–405 nm range, and of the $\pi \rightarrow \pi^*$ type, within the 270–300 nm range.[13]

Comparison of the electronic spectra obtained, with those described by Gray and Ballhausen[14] for $[PdCl_4]^{2-}$ and $[PdBr_4]^{2-}$ led to the following assignments :

a) the rather intense band at 420 nm (23840 cm^{-1}), in the complex compounds was assigned to the $e_g(\pi^*) \rightarrow b_{1g}(\sigma^*)$, $(^1A_{1g} \rightarrow {}^1E_{1g})$ transition ;

b) the shoulder at 480 nm (20920 cm^{-1}) in the spectra of the complex compounds was assigned to the transition $a_{1g}(\sigma^*) \rightarrow b_{1g}(\sigma^*)$, $({}^1A_{1g} \rightarrow {}^1B_{1g})$;

c) the shoulder at 530 nm (18750 cm^{-1}) in the spectra of the complex compounds is assigned to the $b_{2g}(\pi^*) \rightarrow b_{1g}(\sigma^*)$, $({}^1A_{1g} \rightarrow {}^1A_{2g})$ transition.

These d–d type transitions are allowed by spin and forbidded by parity.

The assignments of the bands above allow the inclusion of the complex compounds studied within the square planar compounds belonging to the D_{4h} symmetry group.

NMR spectra

The coordination way of the ligands with the central metallic ion is also confirmed by the NMR spectra. The NMR spectra of the compounds, obtained with thiobenzopiperidide (TBP), p-methoxythiobenzopiperidide p(-MTBP), p-nitrothiobenzomorpholide (p-NTBM) and o-hydroxythiobenzomorpholide (o–HTBM) were recorded. The values of the chemical shifts of the aromatic protons in the complex compounds of Pd(II) with these ligands are given in table 4 versus those corresponding to the noncomplexed thioamides.

Table 4

Values of the chemical shifts of the aromatic protons in the complex compounds of Pd(II) with thioamides, versus those in the noncomplexed thioamides

Compound	δ(ppm)							
	Ligand				Complex compound			
	Ar	syn	anti	Δδ	Ar	syn	anti	Δδ
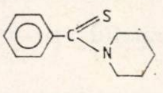	7.33	4.27	3.43	0.84	7.55 broad	4.27 broad	3.48 broad	0.48
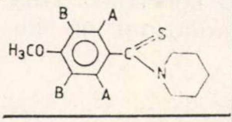	6.85B 7.20A	4.20	3.50	0.70	7.67 multi-plet 7.17	4.27 broad	3.602 4.10 broad	0.67
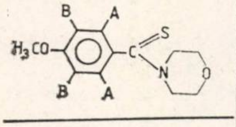	6.90B 7.26A	4.27	3.60	0.67	7.20B 7.64 broad	4.20 broad		
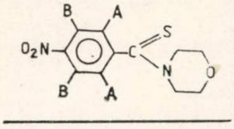	7.50A 8.20B	4.29	3.74	0.55	7.72 broad 8.30	4.35	3.80 slightly	0.55
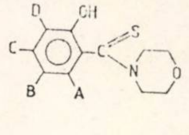	6.82CB 7.30AD	4.30	3.70	0.60	6.88CD 7.40 broad	4.33 broad	3.80 broad	0.53

The signals assigned to the aromatic protons appear within the 7–9 ppm zone and those due to the syn and antiprotons in the vicinity of the nitrogen atom in the piperidinic or morpholinic ring appear within the 4.5–3.5 ppm zone.

A higher deshielding of the protons neighbouring the thioamidic group is noticed in the aromatic zone of the complex compounds, in comparison with the other aromatic protons. The splitting in the spectrum of the ligand, due to the ortho coupling, appears in the spectrum of the complex compound as a slightly solved signal.

The signals assigned, in ligand, to the syn and anti protons neighbouring the nitrogen atom of the piperidinic or morpholinic ring, are subject to a slight perturbation in the complex compound. The spectrum of the compound shows a slight and constant shift towards lower fields and also a decrease of the distance between the two signals. All these findings show a decrease of the rotation barrier around the $>$C–N bond.

The changes in the spectra of the complex compounds, in comparison with the spectra of the ligands, show that in all the cases studied the $>$C=S group is involved in the formation of the complex compounds.

Worth noting is the case of the complex compound of Pd(II) with p–MTBP, [Pd(p-MTBP)Cl_2], for which the NMR spectrum shows a mixture of two compounds. This is indicated by the complexity of aromatic zone in the spectrum and also by the appearance of two unequal signals, at 3.68 and 3.87 ppm, for the methoxy group, CH_3O–. The assignment of three signals for the syn and antiprotons in the close vicinity of the nitrogen atom suggests the presence of two types of complex compounds, different from each other by the rotation barrier around the S$>$CN bond. For one of the compounds, one signal corresponds to the syn and antiprotons.

The conclusions drawn from the study of the NMR spectra of this compound, allow the assignment of the structural formulations of the I and II types :

I.

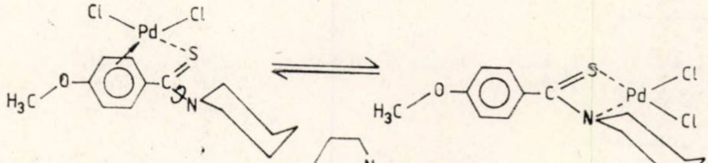

II.

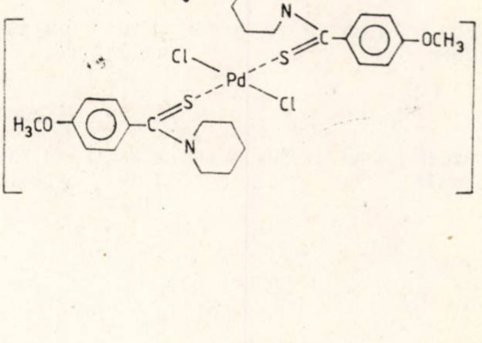

The ratio of the compounds in the mixture is $\frac{2:1}{1:1} = \frac{24}{29}$ but the share of the structure II is small. This thing explains the higher differences that appear in the elemental chemical analysis of the compound versus those calculated theoretically. The mixture of the two compounds was analyzed experimentally.

FORMULATION OF THE COMPLEX COMPOUNDS OF Pd(II) WITH THIOBENZOPIPERIDIDES AND THIOBENZOMORPHOLIDES. CONCLUSIONS

The study carried on the complex compounds of Pd(II) with tertiary thioamides, in the class of thiobenzopiperidides and thiobenzomorpholides, showed that they are of the form : $[PdLCl_2]$ or $[PdL_2Cl_2]$ in which L = the ligand.

The molar conductivity determinations indicated that the compound studied are nonelectrolytes, thus suggesting a donor-acceptor bond between the ligand and the central metallic ion.

Analysis of the infrared, ultraviolet-visible and NMR spectra allows the establishment of the structural formulas of the compounds studied. The ligands are either bidentate, the coordination being achieved both through the sulphur atom and the nitrogen atom (compounds of the $[PdLCl_2]$ type) or monodentate, the coordination being achieved through the sulphur atom in the "thioaceto" form (compounds of the type $[PdL_2Cl_2]$).

For the complex compounds of the $[PdLCl_2]$ type, the following tructures were assigned :

a)

1.

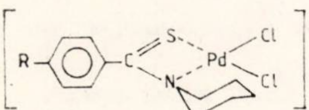

R : $(CH_3)_2N-$;

2.

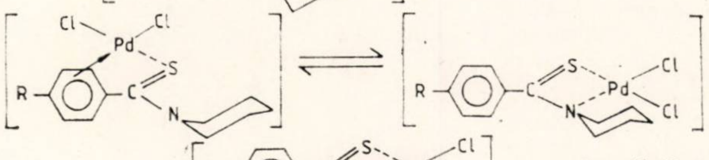

, R : H_3CO-;

3.

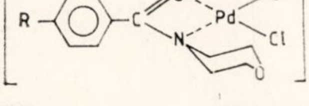

R : H_3CO-, $(CH_3)_2N-$;

b) for those of the $[PdL_2Cl_2]$ type

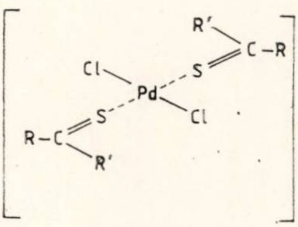

in which:

1. R = C_6H_5- and R' = 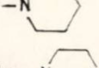

2. R = 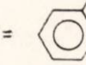

and R' = 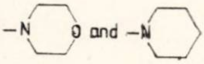

3. R = $H_3CO-C_6H_4-$ (o and p) and

R' = 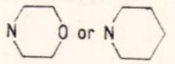

4. R = $O_2N-C_6H_4-$ (p and m) and R' = 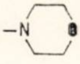

In these complex compounds, the coordination number of Pd(II) is four. This is in agreement with the oxidation state and with the results of the analysis of electronic spectra that shows a square-planar symmetry, belonging to the symmetry group D_{4h}.

The thermal analysis confirms the 1 : 1 or 1 : 2 metal : ligand ratio and the residue quantity left after pyrolysis corresponds to the theoretical one of the metallic palladium in the complex compounds.

EXPERIMENTAL

Reagents : $PdCl_2$, 0.1 M solution.

Thioamides, 0.1 M solutions in acetone or ethanol.

Apparatus : IR spectra of thioamides and of the corresponding complex compounds with Pd(II) were recorded with a Carl Zeiss Jena UR-20 spectrophotometer, using anhydrous KBr pellet.

Electronic spectra were recorded with a Carl Zeiss Jena VSU-1 spectrophotometer, using MgO pellet.

REFERENCES

[1] J. Chatt, *J. Inorg. Nucl. Chem.*, **8**, 515 (1958).

[2] R. G. Pearson, *J. Amer. Chem. Soc.*, **85**, 3533 (1963) : *Science*, **151**, 172 (1966).

[3] C. D. Flint and M. Goodgame, *J. Chem. Soc. A.*, **3**, 750 (1968).

[4] K. Kasparek and I. Mollin, *Colect. Czech. Chem. Commun.*, **25**, 2919 (1960).

[5] G. J. Sutton, *Aust. J. Chem.*, **19**, 2059 (1966).

[6] G. J. Sutton, *Aust. J. Chem.*, **22**, 2475 (1969).

[7] D. Negoiu, S. Neagoe and Maria Negoiu, *Rev. Roumaine Chim.*, **29**, 267 (1984).

[8] D. Negoiu, S. Neagoe and Ioana Saramet, *Rev. Roumaine Chim.*, **29**, 275 (1984).

[9] D. Negoiu, S. Neagoe, C. Cercasov, I. Saramet and C. Toma, *Rev. Roumaine Chim.*, **31**, 987 (1986).

[10] I. Tănăsescu and M. Ionescu, "Lucrări practice de chimie organică", vol. 2, Ed. Tehnică, Bucharest, p. 143 (1975).

[11] W. J. Geary, *Coord. Chem. Rev.*, **7**, 81 (1971).

[12] K. W. Jensen and P. H. Nielsen, *Acta Chem. Scand.*, **20**, 597 (1966).

[13] S. Neagoe, Doctoral Thesis, 1983.

[14] H. B. Gray and C. J. Ballhausen, *J. Amer. Chem. Soc.*, **85**, 260 (1963).

Revue Roumaine de Chimie, **34**, *3*, 855–858 (1989)

ОСНОВНЫЕ ЗАДАЧИ В ОБЛАСТИ ЭКОЛОГИЧЕСКОГО КАТАЛИЗА

В. В. ПОПОВСКИЙ
СССР, Новосибирск, Институт катализа СО АН СССР, Лаборатория экологического катализа

Получена 2 октября 1988 г.

В работе сформулированы основные задачи в области экологического катализа
- продвижение в области решения проблемы предвидения каталитического действия как основы предсказания катализаторов нейтрализации вредных газовых выбросов;
- разработка катализаторов с пониженным содержанием благородных металлов и без них;
- подбор носителей с оптимальной пористой структурой и создание катализаторов оптимальной формы;
- разработка методов приготовления прочных катализаторов;
- создание катализаторов малым сопротивлением слоя;
- разработка эффективных катализаторов очистки от окислов серы;
- разработка катализаторов восстановления окислов азота в присутствии кислорода;
- создание катализаторов очистки от соединений фосфора в производстве фосфора;
- разработка катализаторов комплексной очистки газов;
- создание энергосберегающих методов очистки выбросных и вентиляционных газов с максимальной утилизацией тепла (катализаторы, аппараты, технологические схемы).

Main problems in the field of ecologic catalysis have been formulated in this paper:
- progress in solving the problem of prediction of the catalytic action of catalysts applied in gas emissions detoxication;
- development of catalysts with low content in noble metals and without them;
- selection of supports with optimum porous structure and production of optimum catalysts;
- development of preparation procedures of strong catalysts;
- production of catalysts with low bed resistance;
- development of efficient catalysts for purification from sulphur oxides;
- development of catalysts for nitrogen oxides reduction in the presence of oxygen,
- development of catalysts for purification from phosphorus compounds in phosphorus production;
- development of energy-saving purification methods of vent and emission gases with maximum heat utilization (catalysts, apparatuses, technologic schemes).

Проблема защиты окружающей среды от вредных выбросов, производимых промышленными, сельскохозяйственными, горнодобывающими предприятиями, а также транспортом, является одной из глобальных проблем современности.

Основные виды производимых выбросов: отвалы твердых веществ, жидкие стоки, газовые выбросы в атмосферу.

Эффективными методами нейтрализации вредных веществ газовых выбросов являются каталитические, поскольку они достаточно надежны, простые и сравнительно недорогие.

Это определило рождение нового научно-технического направления — «Экологический катализ». Под этим термином понимается решение экологических задач средствами катализа в широком плане с включением разработки теоретических основ каталитических процессов газоочистки, развитие теории и научных основ приготовления катализаторов, внедрение каталитических методов очистки в практику.

Вредные газообразные вещества, выбрасываемые в атмосферу и оказывающие токсикологическое действие, можно объединить в несколько основных групп:

— органические соединения (условно CH_x) и CO;

— окислы азота (NO_x);

— соединения серы, прежде всего SO_2;

— прочие соединения, например, озон, соединения фосфора и т.д.

В настоящее время используются следующие каталитические методы очистки:

— каталитическое дожигание органических веществ и CO до практически безвредного углекислого газа и воды;

— каталитическое восстановление окислов азота до молекулярного азота такими газами-восстановителями, как NH_3, CO, CH_4, H_2;

— окисление сернистого ангидрида в SO_3 с последующим получением серной кислоты, либо восстановление SO_2 до элементарной серы;

— разложение озона и т.д.

Для основных групп процессов, лежащих в основе каталитических методов газоочистки, разработаны и используются катализаторы в основном платиновые, палладиевые (или их сочетания), окисные, смешанные металл-окисные и т.д.

Вместе с тем имеется ряд задач в области экологического катализа, требующих своего решения.

Эти задачи вытекают, прежде всего, из требований, предъявляемых к катализаторам газоочистки:

— высокая активность при умеренных температурах (иначе большие затраты энергии на подогрев очищаемого газа);

— достаточная механическая прочность;

— стойкость к действию отравляющих веществ (как правило, очищаемые газы содержат каталитические яды);

— необходимая термостойкость (следует иметь ввиду, что при эксплуатации возможны перегревы катализатора, например, вследствие нарушения технологического регламента;

— невысокое сопротивление слоя катализатора (иначе — большие затраты энергии на «проталкивание» газа через насадку катализатора);

— технологичность катализатора (доступность и стоимость сырья, простота операций приготовления, исключение вредных выбросов при приготовлении катализатора, возможность регенерации дорогостоящих катализаторов и.т.д.);

— длительный срок службы катализатора.

Задача 1. До сих пор все катализаторы подбираются эмпирическим путем, поскольку центральная проблема в катализе — проблема предвидения каталитического действия, являющаяся основой предсказания катализатора для данной реакции, остается нерешенной. Поэтому требуются усилия, направленные на её решение. Путь решения видится через вскрытие механизма реакций; установление природы активных центров; выявление приближенных корреляционных зависимостей и т.д.

Задача 2. Разработка катализаторов с пониженным содержанием благородных металлов (учитывая их дефицитность и дороговизну) или даже без них, но, естественно, сохраняющих все достоинства заменяемых катализаторов. Принципиально, это достижимо, например, платиновые низкопроцентные катализаторы, разработанные в НИФХИ им. Карпова, или низкопроцентные палладиевые катализаторы ИОКЭ АН Каз. ССР с очень малым содержанием палладия. В Институте катализа СО АН СССР созданы катализаторы дожигания на основе массивной окиси меди (ИК-12-4, ИК-12-9), не уступающие по активности платиновым или палладиевым катализаторам в модельных реакциях глубокого окисления СО и бутана.

Задача 3. Многие катализаторы имеют не оптимальную пористую структуру, не позволяющую полностью использовать всю внутреннюю поверхность катализатора, т.е. всю потенциальную возможность вещества активного компонента как катализатора. Можно существенно увеличить каталитическую активность единицы объема катализатора за счет регулирования пористой структуры, уменьшения размера зерен или изменения формы, например, перехода к кольцеобразным формам без перегородок или с перегородками. Весьма перспективными являются блочные носители сотовой структуры, на стенки каналов которых тонкой пленкой наносится активный компонент. Блочные катализаторы представляют интерес, в первую очередь, для разработки каталитических нейтрализаторов выхлопных газов автотранспорта.

Задача 4. Одно из основных требований к катализаторам газоочистки — иметь достаточную механическую прочность на раздавливание и истирание при одновременно высокой активности. Известны методы использования неорганических клеев для склеивания порошков при формировании или таблетировании. Эффективным оказался прием механохимической активации плохо формуемых порошков. Необходимо разрабатывать и другие методы упрочнения гранул катализатора.

Задача 5. Как правило, выбросные газы содержат каталитические яды: соединения серы, фосфора, мышьяка, ртути, свинца и т.д. Поэтому разработка неотравляемых или малоотравляемых катализаторов имеет огромное значение для практики. Например, существующие катализаторы для автотранспорта обеспечивают очистку выхлопных газов лишь в случае использования неэтилированных бензинов. Вместе с тем, значительная доля выпускаемых бензинов содержит тетраэтилсвинец, что приводит к появлению в выхлопных газах соединений свинца и отравлению катализатора. Задача состоит в разработке катализаторов, не отравляемых соединениями свинца в случае бензиновых карбюраторных двигателей или сернистыми соединениями — в случае дизельных двигателей.

Задача 6. Сопротивление слоя катализатора — один из факторов, определяющих экономику процесса очистки.

Особенно важно это в тех случаях, когда необходимо требуется пониженное газодинамическое сопротивление слоя катализатора (например, автовыхлоп; ТЭС, на которых расходы очищаемых газов составляют миллионы м^3 в час, и т.д.). Пути решения задачи видятся в создании определенных форм катализатора (блоки, кольца, пластины и т.д.) и в организации слоя катализатора.

Задача 7. Все ещё актуальными являются поиски катализаторов очистки от сернистых соединений. Исследования у нас в стране в этом направлении проводятся недостаточно интенсивно. Между тем, например, тепловые станции и электростанции, работающие на топливе, содержащем значительные количества сернистых соединений, выбрасывают в атмосферу много сернистого ангидрида.

Задача 8. Каталитическое восстановление окислов азота в смесях с малым содержанием кислорода является технически решенной задачей. Однако, положение резко осложняется, если концентрация кислорода велика. К настоящему времени известна лишь одна группа эффективных катализаторов — окисnúmeroванадиевых, способных избирательно восстанавливать окислы азота аммиаком в присутствии кислорода. Необходим поиск других каталитических систем восстановления окислов азота в присутствии кислорода и не только аммиаком, но и другими газами — восстановителями.

Задача 9. Эта задача возникла в связи с расширением класса процессов очистки. Так, стало необходимым очищать абгазы от соединений фосфора и фтористого водорода в производстве фосфора. При синтезе некоторых органических соединений необходима очистка выбросных газов от хлористого этила. Отсюда появилась задача по разработке катализаторов для очистки от этих и других соединений.

Задача 10. Задача поставлена из-за усложнения процессов. Например, часто требуется одновременная очистка газов от окислов азота и окислов серы; от окислов азота, окислов серы и продуктов неполного горения (ТЭС); от окислов азота, оксидов углерода, органических веществ и соединений серы (автовыхлоп). Все это требует разработки катализаторов комплексной очистки.

Задача 11. Необходимо продолжать разрабатывать энергосберегающие методы очистки выбросных и вентиляционных газов с максимальной утилизацией тепла. Для решения этой задачи следует разрабатывать нового типа аппараты, новые катализаторы, новые технологические схемы и т. д.

Х отя перечисленные задачи в области экологического катализа чат как прикладные и это действительно так, поскольку поставлены звуактикой, тем не менее для серьезного и глубокого решения каждой из прдач требуется участие и академической, и вузовской науки. Без фундазаентальной проработки вопросов, глубокого изучения и понимания сущемтва дела нельзя надеяться успешно развивать экологический катализ.

Revue Roumaine de Chimie, **34**, *3*, 859–867 (1989)

THE MEAN ACTIVITY COEFFICIENT OF $CuSO_4$ AND EXCESS FUNCTIONS IN THE AQUEOUS ELECTROLYTE SYSTEMS : $CuSO_4 + Na_2SO_4 + H_2O$; $CuSO_4 + K_2SO_4 + H_2O$ and $CuSO_4 + ZnSO_4 + H_2O$

SOLOMON STERNBERG and MIHAELA DRĂGĂNOIU
Department of Physical Chemistry, Polytechnic Institute of Bucharest,
Calea Griviței 132, Bucharest, Romania

Received February 21, 1988

Measurements of electromotive forces (emf) have been made in three ternary aqueous electrolyte systems and in the binary systems from which they derive. Thus it was possible to determine $\Delta\ln\gamma_1$, an extent chosen by us in order to characterize the deviation of the ternary system from the binary one. The results have been numerically analyzed and the coefficients of the polynomials of approximation have been given. A comparative discussion has been made.

Electrolyte systems of 2 : 2 sulphates are characterized by high values of the association constant ($K_{ass} \simeq 250$) comparatively to other aqueous electrolyte systems ($K_{ass} \simeq 0$ in halide solutions).[1,2,3]

In this context we have considered interesting to study the ternary aqueous mixtures of sulphates — systems with even greater deviations from the ideality than the binary ones from which they derive — a domain still poorly represented in the literature.

In some previous papers [4,5] the mean activity coefficients of $CuSO_4$ in the systems $CuSO_4 + MgSO_4 + H_2O$, $CuSO_4 + MnSO_4 + H_2O$ and respectively those of $ZnSO_4$ in systems of the types $ZnSO_4 + MeSO_4 + H_2O$ (where Me = Mg, Mn) and $ZnSO_4 + Me_2SO_4 + H_2O$ (where Me = = Na, K) were determined.

In the present paper results concerning the determination of $\gamma_\pm$ $CuSO_4$ in the systems : Cu–Na, Cu–K and Cu–Zn, as well as considerations about some excess properties of these solutions are presented.

EXPERIMENTAL PART

The determinations were made in cells with thermostatic mantle (at 25°C) using emf measurements. In each system measurements were made at four total ionic strengths and varying proportions of the two electrolytes.

The cells used were : Pt–Hg, $Hg_2SO_4/CuSO_4(m_1)$, $Me_nSO_4/(m_2)/Cu$–Pt.

The electrodes used were the following :

— the copper electrode — a plate made of copper, scaled, washed and dried before each determination.[6,7,8]

— the mercury — mercurous sulphate electrode chosen as reversible electrode to the sulphate ion because of the excellent reproducibility of the results (comparable to that of the hydrogen electrode).[8]

As far as the method of calculations is concerned, we consider having obtained an increase in accuracy compared to the classic method (that of calculating $a_\pm$, respectively $\gamma_\pm$ from Nernst's relation, using $\bar{E}^\circ$) by determining directly the difference $\Delta\ln\gamma_1$, which is :

$$\Delta\ln\gamma_1 = \ln\gamma^t_{1\pm} - \ln\gamma^b_{1\pm} \tag{1}$$

In (1), $\gamma^t_\pm$ is the mean activity coefficient of $CuSO_4$ in the studied ternary system and $\gamma^b_{1\pm}$ has the same significance in the binary system $CuSO_4 + H_2O$.

The emf in the binary system is :

$$E^b = E^0 - \frac{\nu RT}{nF}\ln a^b_{1\pm} = E^0 - \frac{RT}{F}\ln m^b_{1\pm} - \frac{RT}{F}\ln\gamma^b_{1\pm} \tag{2}$$

In the studied systems : $n = 2$ and $\nu = 2$, $m^b_{1\pm}$ is the medium molality of $CuSO_4$ in the binary system.

In the ternary system the emf is :

$$E^t = E^0 - \frac{\nu RT}{nF}\ln a^t_{1\pm} = E^0 - \frac{RT}{F}\ln m^t_{1\pm} - \frac{RT}{F}\ln\gamma^t_{1\pm} \tag{3}$$

with : $m^t_{1\pm} = [m_1(m_1 + m_2)]^{1/2}$ being the medium molality of $CuSO_4$ in the ternary system.

Substracting relation (2) from (3), we obtain directly :

$$\Delta\ln\gamma_1 = -\frac{E^t - E^b}{RT/F} - \ln\frac{m^t_{1\pm}}{m^b_{1\pm}} \tag{4}$$

We avoid thus the use in the calculation of $\bar{E}^\circ$ which is difficultly accessible. The main advantage is the direct obtention of $\Delta\ln\gamma_1$ which, in the form $(RT\Delta\ln\gamma_1)$, has the significance of a partial extent of excess and is proved to be the most valuable parameter for the characterization of the ternary system as compared to the binary one.

For the free enthalpy of mixing of a binary 1 : 1 electrolyte solution, Harned and Robinson[10] proposed the equation :

$$\Delta^m G^{ex} = RT[2m(\varphi^b_1 - \varphi^t) + 2m_2(\varphi^b_2 - \varphi^t) + 2m_1\ln(\gamma^t_{1\pm}/\gamma^b_{1\pm} + 2m_2\ln(\gamma^t_{2\pm}/\gamma^b_{2\pm}) \tag{5}$$

where the index m points out the fact that the mixing was made at constant molality $m = m_1 + m_2$, φ^t is the osmotic coefficient of the ternary solution at the molality m, φ^b_1 and φ^b_2 those of the binary solutions (electrolyte 1 + H_2O) and (electrolyte 2 + H_2O) respectively (both of molality m). For solutions of some electrolytes with superior ionic charges, replacing m_1, and m_2 by the partial ionic strengths I_1 and I_2, dividing by the total ionic strength I and introducing the coefficients ν_1 and ν_2 we obtain the equation :

$$\Delta^I G^{ex}/I = RT[\nu_1 y_1(\varphi^b_1 - \varphi^t) + \nu_2 y_2(\varphi^b_2 - \varphi^t) + \nu_1 y_1 \times$$

$$\times \ln(\gamma^t_{1\pm}/\gamma^b_{1\pm}) + \nu_2 y_2 \ln(\gamma^t_{2\pm}/\gamma^b_{2\pm}) = \Delta^I G^{ex}(I = 1). \qquad (6$$

We have introduced the notation $\Delta^I G^{ex}$ in order to point out the difference between it and G^E by which we usually indicate the free excess enthalpy of the ternary solution as compared to a ternary ideal solution.[11] In (6) the term $\ln(\gamma^t_{1\pm}/\gamma^b_{1\pm})$ is exactly $\Delta\ln\gamma_1$ determined experimentally by us and $RT\ln(\gamma^t_{1\pm}/\gamma^b_{1\pm})$ is μ^{ex}_1, the mean chemical excess potential of the electrolyte 1.

RESULTS

The results of the determinations are presented in tables 1, 2 and 3. In the last column the extent μ_1^{ex} is also given.

Table 1

The results of the determinations in the system

I	y_2	$\Delta E \cdot 10^3/V/$	$-\Delta \ln \gamma_1$	$\gamma_{1\pm}^t$	$a_{1\pm}^t$	$-\mu_1^{ex}$cal/kg H_2O echivg
3	0.09	3.8	0.1121	0.0438	0.0316	66.41
	0.19	5.9	0.1511	0.0421	0.0291	89.52
	0.30	10.4	0.2755	0.0371	0.0244	163.21
	0.39	14.4	0.3696	0.0338	0.0209	218.96
	0.49	19.9	0.5078	0.0294	0.0168	300.83
	0.60	22.5	0.5119	0.0293	0.0152	303.26
	0.69	27.1	0.5616	0.0279	0.0127	332.71
	0.79	33.4	0.6376	0.0258	0.0097	377.73
	0.90	33.1	0.2728	0.0372	0.0100	161.61
2.4	0.12	4.4	0.0864	0.0508	0.0290	51.19
	0.24	8.9	0.2438	0.0434	0.0234	144.43
	0.37	13.6	0.3551	0.0388	0.0195	210.37
	0.49	18.1	0.4254	0.0362	0.0165	252.02
	0.62	22.8	0.4948	0.0337	0.0136	293.13
	0.75	30.1	0.5942	0.0305	0.0102	352.02
	0.87	31.1	0.3030	0.0409	0.0098	179.50
1.8	0.16	5.8	0.1624	0.0561	0.0236	96.20
	0.33	12.8	0.3499	0.0465	0.0180	209.29
	0.49	20.2	0.5195	0.0392	0.0134	307.76
	0.66	28.0	0.6447	0.0346	0.0099	381.93
	0.83	26.7	0.2696	0.0504	0.0104	159.72
1.5	0.19	6.8	0.1863	0.0605	0.0209	110.37
	0.39	13.3	0.3267	0.0526	0.0162	193.54
	0.60	21.7	0.4806	0.0451	0.0117	284.72
	0.79	27.5	0.3911	0.0493	0.0093	231.70

In the ternary system for the determination of the mean activity coefficient $\gamma_{1\pm}^t$ we have used the relation :

$$\ln\gamma_{1\pm}^t = \ln\gamma_{1\pm}^b + \Delta\ln\gamma_1 \tag{7}$$

The values $\gamma_{1\pm}^b$ have been taken from the literature.[12]

The dependence of $\Delta\ln\gamma_1$ upon the ratio of the added sulphate has been expressed with the help of the ionic strength fractions y_2,[10] defined as :

$$y_2 = \frac{I_2}{I} \tag{8}$$

where I_2 is the partial ionic strength of electrolyte 2 and I is the total ionic strength. Thus, for the asymmetrical systems (alkaline sulphate added to $CuSO_4$), the expression of y_2 is :

$$y_2 = \frac{3m_2}{4m_1 + 3m_2} = \frac{3\ m_2^t}{4\ m_1^b} \tag{9}$$

Table 2

The results of the determinations in the system $CuSO_4 + K_2SO_4 + H_2O$

I	y_2	$\Delta E \cdot 10^3/V/$	$-\Delta \ln \gamma_1$	$\gamma^t_{1\pm}$	$a^t_{1\pm}$	$-\mu_1^{ex}$ cal/kg $H_2O \cdot$ echivg
3	0.09	9.6	0.3377	0.0349	0.0252	200.06
	0.19	11.0	0.3726	0.0337	0.0233	220.73
	0.30	13.1	0.3810	0.0334	0.0298	225.71
2.4	0.12	7.0	0.2270	0.0695	0.0398	131.66
	0.24	12.1	0.3688	0.0383	0.0207	197.88
	0.37	16.0	0.5274	0.0326	0.0164	302.44
1.8	0.16	5.6	0.1546	0.0565	0.0238	91.59
	0.33	16.0	0.3555	0.0462	0.0178	210.60
	0.49	20.0	0.5117	0.0395	0.0135	303.14
	0.66	31.6	0.7822	0.0278	0.0079	463.39
	0.83	36.6	0.6563	0.0342	0.0071	388.80
1.5	0.19	9.3	0.2839	0.0368	0.0127	168.19
	0.39	12.1	0.3504	0.0345	0.0106	207.58
	0.60	26.1	0.6525	0.0255	0.0066	386.55
	0.79	32.1	0.5673	0.0277	0.0052	336.08

Table 3

The results of the determinations in the system $CuSO_4 + ZnSO_4 + H_2O$

I	y_2	$\Delta E \cdot 10^3/V/$	$\Delta \ln \gamma_1$	$\gamma^t_{1\pm}$	$a^t_{1\pm}$	μ_1^{ex} cal/kg H_2O echivg
33	0.13	2.5	−0.0259	0.0477	0.0333	− 15.34
	0.26	3.7	0.0108	0.0495	0.0318	6.39
	0.40	7.4	−0.0329	0.0474	0.0275	− 19.49
	0.53	10.4	−0.0242	0.0478	0.0245	− 14.53
	0.66	15.4	−0.0506	0.0465	0.0201	− 29.97
	0.80	21.6	0.0368	0.0508	0.0170	21.80
	0.93	37.8	−0.1186	0.0435	0.0084	− 70.26
2.4	0.16	2.9	−0.0218	0.0449	0.0246	−124.40
	0.33	7.0	−0.0186	0.0543	0.0266	− 11.02
	0.50	8.80	−0.0452	0.0529	0.0224	− 26.77
	0.66	10.70	−0.0701	0.0516	0.0179	− 41.53
	0.83	24.3	−0.0509	0.0526	0.0129	− 30.15
1.8	0.22	2.7	0.0204	0.0669	0.0265	12.08
	0.44	7.6	−0.0023	0.0654	0.0219	− 1.36
	0.66	15.6	−0.0584	0.0618	0.0161	− 34.59
	0.88	29.3	−0.0429	0.0628	0.0094	− 25.41
1.5	0.26	4.0	−0.0010	0.0729	0.0234	− 0.59
	0.53	10.5	−0.028	0.0709	0.0181	− 16.58
	0.80	21.9	−0.0485	0.0695	0.0116	− 28.73

For the systems $CuSO_4(1) + ZnSO_4(2) + H_2O$:

$$y_2 = \frac{4m_2}{4m_1 + 4m_2} = \frac{m_2^t}{m_1^b} \tag{10}$$

For the activity coefficients determined at $I = \text{const}$, there are in the literature [10] equations of the form :

$$\ln \gamma^{t}_{1\pm} = \ln\gamma^{b}_{1\pm} + \alpha_1 I_2 + \beta_1 I_2^2 \tag{11}$$

For $\Delta\ln\gamma_1$ we have employed n order polynomial functions of the type :

$$\Delta \ln\gamma_1 = \sum_{i=1}^{n} Ci(y_2)^i = C_1 y_2 + C_2 y_2^2 + C_3 y_2^3 + \ldots \tag{12}$$

The substitution of the partial ionic strengths I_2 by the ionic strength ratio y_2 results from equation (11) by replacing $C_1 = \alpha_1 I$, $C_2 = \beta_1 I^2$, etc.

To determine this dependence of a polynomial type the least squares method has been used. The coefficients Ci for the approximation polynomials as far as the fifth order have been numerically computed in order to obtain a minimum mean standard deviation. No improvement can be obtained by polynomials of a higher order. For comparable standard deviations the polynomials with the least number of constants have been preferred.

The coefficients Ci of the selected polynomials are given in table 4.

Figures 1, 2 and 3 present the dependences $\Delta\ln\gamma_1 = f(y_2)$ for the three studied systems.

The curves have been drawn following the equations from table 4 and the experimental results are also mentioned. A very good agreement between the experimental and the calculated results can be observed.

Table 4

The coefficients of the computed polynomials

System	I	Degree of the poly-nomial	C_1	C_2	C_3	C_4	σi	μ_1^{extr} $\frac{cal}{H_2O}$ echivg
$CuSO_4$ +	3	IV	−1.4097	4.2346	−10.5147	7.9314	0.0578	143.88
Na_2SO_4 +	2.4	IV	−1.3525	3.7572	−9.2022	7.0855	0.0545	170.67
+H_2O	1.8	IV	−1.4673	4.5049	−12.9771	11.0614	0.0279	664.63
	1.5	III	−0.6412	−1.4159	2.0007		0.0381	−33.41
$CuSO_4$ +	3	II	−3.8134	8.6339			0.0647	−855.76
+ K_2SO_4	2.4	II	−2.2676	2.6820			0.0475	−245.50
+ H_2O	1.8	III	0.0182	−4.7086	4.4398		0.1067	−148.46
	1.5	II	−1.4657	0.8949			0.0984	−338.15
$CuSO_4$ +	3	I	0.0122	−0.0925			0.0482	−47.57
+ $ZnSO_4$ +	2.4	II	−0.1161	0.0535			0.0137	−37.08
+ H_2O	1.8	I	−0.0497				0.0259	29.44
	1.5	I	−0.0542				0.0102	32.11

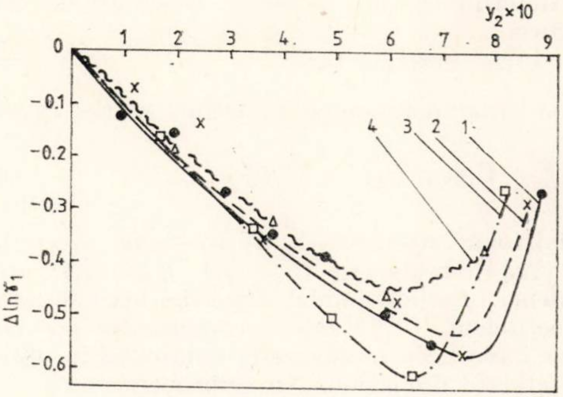

Fig. 1. — The dependences $\Delta \ln \gamma_1 = f(y_2)$ in the system $CuSO_4 + Na_2SO_4 + H_2O$: 1.I = 3; 2.I = 2.4 3.I = 1.8; 4.I = 1.5.

Fig. 2. — The dependences $\Delta \ln \gamma_1 = f(y_2)$ in the system $CuSO_4 + K_2SO_4 + H_2O$: 1.I = 3; 2.I = 2.4; 3.I = 1.8; 4.I = 1.5;

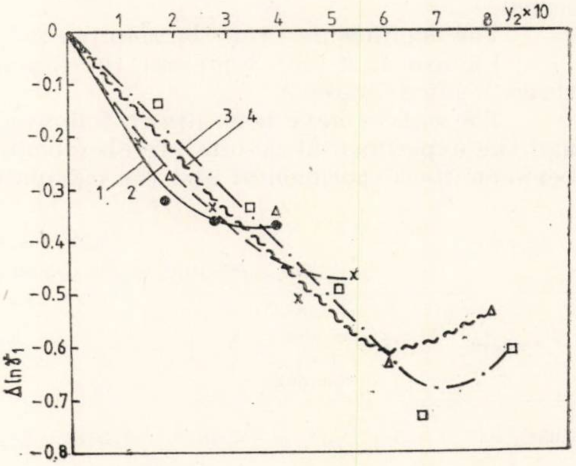

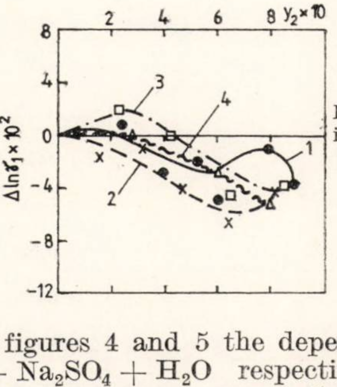

Fig. 3. — The dependences $\Delta \ln \gamma_1 = f(y_2)$: in the system $CuSO_4 + ZnSO_4 + H_2O$; 1.I = 3; 2.I = 2.4; 3.I = 1.8 4.I = 1.5.

In figures 4 and 5 the dependences $\ln \gamma^t_{1\pm} = f(m_1)$ for the systems $CuSO_4 + Na_2SO_4 + H_2O$ respectively $CuSO_4 + K_2SO_4 + H_2O$ as well as that for the binary system $CuSO_4 + H_2O$ are shown. Obviously the last one has not been drawn at constant ionic strength. At each ionic strength "the ideal behaviour" is given by the interrupted line parallel

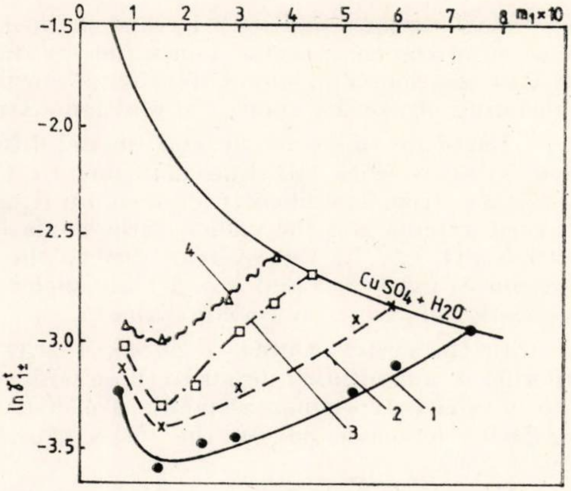

Fig. 4. — The dependences $\ln\gamma_{1\pm}^{t} = f(m_1)$ in the system $CuSO_4 + Na_2SO_4 + H_2O$: 1. I = 3; 2. I = 2.4; 3. I = 1.8; 4. I = 1.5.

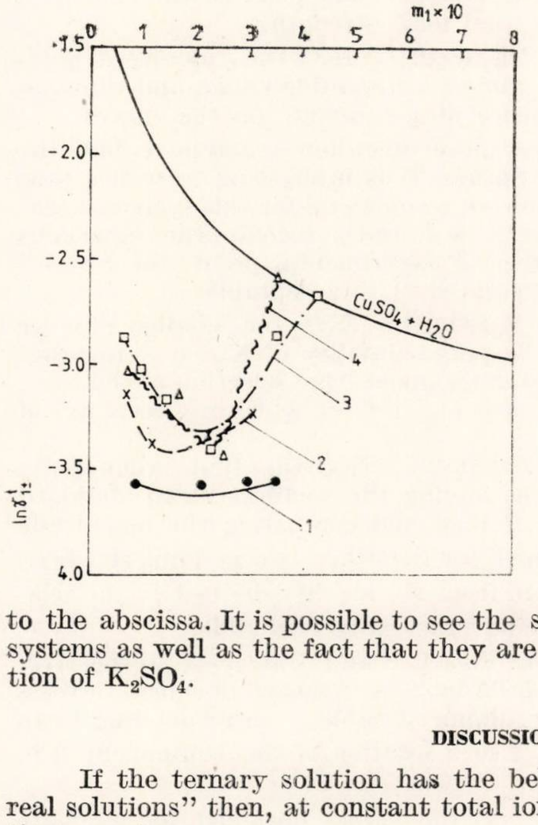

Fig. 5. — The dependences $\ln\gamma_{1\pm}^{t} = f(m_1)$ in the system $CuSO_4 + K_2SO_4 + H_2O$: 1. I = 3; 2. I = 2.4; 3. I = 1.8; 4. I = 1.5.

to the abscissa. It is possible to see the sense of the deviations in the two systems as well as the fact that they are greater in the system with addition of K_2SO_4.

DISCUSSION

If the ternary solution has the behaviour of "an ideal mixture of real solutions" then, at constant total ionic strength, the following equations are true:

$$\begin{cases} \Delta\ln\gamma_1 = 0 \\ \mu_1^{ex} = 0 \end{cases} \tag{13}$$

An "ideal ternary solution" is thus defined in relation to a real binary solution of the component 1 in water, at the same ionic strength as the ternary solution. The binary solution is considered as the "standard state" depending obviously upon the total ionic strength.

Based on this conventional model different behaviours for the studied systems with alkaline addition to $CuSO_4$ present great negative deviations from the ideality defined by equations (13). The curves have marked minima and the values of the deviations are greater in the system with K_2SO_4 (2). In this system, due to the poor solubility of K_2SO_4, the curves for $I = 3$ and $I = 2.4$ are incomplete because it was possible to work only up to a certain value y_2.

In the system $CuSO_4 + ZnSO_4 + H_2O$ the obtained values are by an order of magnitude inferior to those with addition of alkaline sulphates. The obtained experimental points are distributed without any apparent regularity on each side of the axis representing the ideal behaviour ($\Delta \ln \gamma_1 = 0$).

For none of the three studied systems was possible to evidence a convincing dependence upon the total ionic strength.

For the system $CuSO_4(1) + Na_2SO_4(2) + H_2O$ the calculated polynomials have for the coefficients C_1 and C_2 comparable values and of opposite sign explaining thus the existence of a minimum on the curves.

For the third order equations more precision is obtained but the prevalence of the constant C_1 disappears. It is interesting to notice that for the fourth order equations, which we recommend for this system, negative values for C_1 and neighbouring those from the second order equations reappear. Due to the reduced number of experimental points for $I = 1.5$ the third order curve has been represented (with acceptable σ_i).

For the system $CuSO_4(1) + K_2SO_4(2) + H_2O$ the smaller number of experimental points — due to the poor solubility of K_2SO_4 — together with the acceptable value for σ_i has determined the selection of the third order polynomials, excepting the case $I = 1.8$ for which we recommend the fourth order one.

For the system $CuSO_4(1) + ZnSO_4(2) + H_2O$ the first order polynomials have been recommended as having the smallest mean standard deviation. From a physical point of view and comparing the magnitude of the deviations with those obtained for the other two systems the deviation in the behaviour of this system from the ideality defined by the relations (13) can be considered as being practically negligible.

Extrapolating the curves from Figs 1, 2 and 3 at $y_2=1$ (respectively $y_1 = 0$), we obtain $\mu_1^{ex,tr} = RT\Delta \ln \gamma_1^{tr}$ a "mean chemical excess trace potential", given in the last column of table 4, corresponding to an infinite dilution of the component 1 in a solution of the component 2 in water of the same ionic strength.

For the system with Na_2SO_4 (2) the values obtained for $\mu_1^{ex,tr}$ are about 200 cal/kgH_2O · echiv ·g and for the system with $K_2SO_4(2)$ the values are slighty greater. The values for the system with $ZnSO_4(2)$ are with an order of magnitude smaller, that is about 30 cal/kg H_2O echiv·g.

REFERENCES

[1] E. M. Hanna, A. D. Pethybridge and J. E. Prue, *Electrochim. Acta*, **16**, 677, 1971.
[2] J.-C. Justice, *idem*, p. 701.
[3] M. C. Justice, R. Bury and J.-C. Justice, *idem*, p. 687.
[4] S. Sternberg and M. Drăgănoiu, *Rev. Roumaine de Chimie*, **30**, 209 (1985).
[5] S. Sternberg and M. Drăgănoiu, *Rev. Chim. București*, **38**, 3 (1987).
[6] A. Lewandowski, *Electrochim. Acta*, **29**, 547 (1984).
[7] B. G. Cox, A. J. Parker and W. E. Waghorne, *J. Phys. Chem.*, **78**, 1731 (1974).
[8] J. F. Coetzee and W. K. Istone, *Analyt. Chem.*, **52**, 53 (1980).
[9] D. J. D. Ives and G. J. Janz, "Reference Electrodes", Academic Press, New York, 1961.
[10] H. S. Harned and R. A. Robinson, "Multicomponent Electrolyte Solutions", Pergamon Press, London, 1971.
[11] M. Drăgănoiu, Ph. D. Thesis, Polytechnical Inst. of Bucharest, 1986.
[12] R. A. Robinson and R. H. Stokes, "Electrolyte Solutions", Butterworths Scientific Publications, London, 1955

Revue Roumaine de Chimie, **34**, 3, 869–876 (1989)

COMPATIBILITY RELATIONS IN THE Li_2O—BaO—SiO_2 SYSTEM

I. TEOREANU, ECATERINA ANDRONESCU and SIMONA CONSTANTINESCU
Polytechnical Institute Bucharest

Received October 6, 1988

It is necessary to know the subsolidus thermal phase equilibrium relations i.e. the compatibility established within a ternary system on the one hand, for the elaboration of the thermal phase equilibrium diagram and, on the other, for appreciating the usage of the ternary compositions considered in the system. The experimental results showed that the compatibility relations, established between the compounds in the $Li_2O-BaO-SiO_2$ system could be determined. Identification of the binary subsystems of the $Li_2O-BaO-SiO_2$ system, emphasized 13 ternary subsystems, made up of the considered oxidic system.

INTRODUCTION

The $Li_2O-BaO-SiO_2$ system is slightly known with respect to the thermal phase equilibrium. The data obtained by Dietzel, Wickert and Köppen [1] reveal that lithium and barium metasilicates establish compatibility relations which determine the binary subsystem $Li_2O \cdot SiO_2$—$BaO \cdot SiO_2$.

The ternary system $Li_2O-BaO-SiO_2$ does not include ternary compounds ; the respective binary compounds are the lithium and barium silicates : L_2S ; LS, LS_2, L_3S_2, LS_3, B_3S, B_2S, BS, B_2S_3, B_5S_8, B_3S_5, and BS_2.[2-8]

EXPERIMENTAL

A hypothetical model was considered necessary to evaluate the compatibility relations established in the $Li_2O-BaO-SiO_2$.

This was achieved starting from the existence of the above mentioned binary compounds and taking account of the only defined binary subsystem : $Li_2O \cdot SiO_2-BaO \cdot SiO_2$. The model proposed for the possible compatibility relations for the $Li_2O-BaO-SiO_2$ system is shown in fig. 1.

The analysis of the model presented in fig. 1, shows 28 possible binary subsystems, whose experimental checking proved to be a hard task.

We had in mind that two intersecting binary systems are excluding each other, and took this as a basis for selecting the ternary compositions to check the proposed model.

The selected ternary mixtures have been prepared either from previously synthesized, binary compounds supposed to establish binary subsystems, or from the Li_2CO_3, $BaCO_3$ and SiO_2 reactive (the raw materials employed had a high purity: 99.9%).

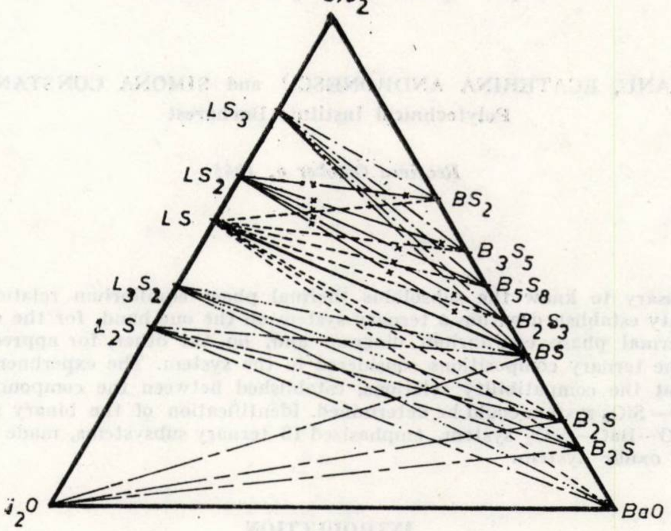

Fig. 1. — The model for the hypothetical compatibility lines for the $Li_2O-BaO-SiO_2$ system.

The experimental determinations made use of classical methods in order to determine certain phase relations (X-ray diffractometry, optic microscopy, differential thermal analysis).

By successive thermal treatments (followed by recurrent rehomogenizations) the considered compositions were brought to thermal equilibrium; the temperatures of these treatments were furnished by literature data and by laboratory practice.

A subsolidus equilibrium was considered reached when the recurrence of a thermal treatment for a certain period and temperature no longer determined modifications in quality and quantity, which could be experimentally evaluated, under phase composition.

Fig. 2 shows a less basic region of the system, where 14 binary subsystems may appear. Their checking started by selecting the composition marked 1, which appears in Table 1 and in fig. 2.

Mixture 1 results to be located in the possible binary subsystem LS_3-BS_2. Prepared both of reactive Li_2CO_3, $BaCO_3$ and SiO_2 and of lithium trisilicate and barium disilicate, the mixture was subject to thermal treatments mentioned in Table 1. The identified equilibrium phases are LS_3 and BS_2 which define the binary system LS_3-BS_2. Further a composition marked 2 was taken into consideration, oxidic and mineralogically rendered in Table 1. Mixture 2, as it results from fig. 2, is located at the crossing of the possible binary subsystems LS_2-BS_2 and LS_3-BS_2, respectively.

As two binary intersecting subsystems are excluding each other if the compatibility relation LS_2-BS_2 is real, the crossing subsystems $LS_3-B_3S_5$, $LS_3-B_5-S_8$, $LS_3-B_2S_3$ and LS_3-BS are cancelled, and if the compatibility line LS_3-BS is real then the subsystems : LS_2-BS_2, $LS_2-B_3S_5$, $LS_2-B_5S_8$, $LS_2-B_2S_3$, $LS-BS_2$, $LS-B_3S_5$, $LS-B_5S_8$ and $LS-B_2S_3$ are excluded.

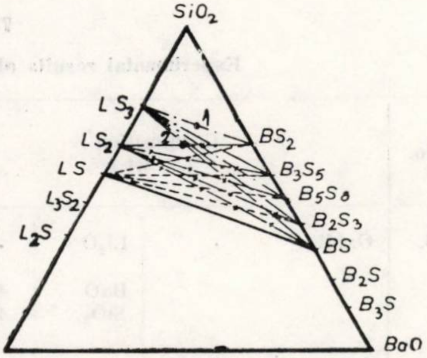

Fig. 2. — The model for the hypothetical compatibility lines for the subsystems.

Table 1

Experimental results obtained for composition 1 and 2

No.	Composition (% wt.)			Thermal treatments		Identified phases
				Temp. °C	Time h	
1.	Oxidic	Li_2O	7.14	900	3	LS_3 BS_2
		BaO	28.03	1000	3.5	LS_3 BS_2
		SiO_2	64.83	900	3	LS_3 BS_2
	Mineralogical	LS_3	50	900	3	LS_3 BS_2
		BS_2	50	900	2	LS_3 BS_2
2.	Oxidic	Li_2O	10	1000	2	LS_2, BS_2, LS
		BaO	28.02	700	5.25	LS_2, BS_2, LS
		SiO_2	61.98	700	4.5	LS_2, BS_2, LS
				700	7	LS_2, BS_2, LS
				700	7	LS_2, BS_2, LS
				800	5	LS_2, BS_2
	a) Mineralogical	LS_2	50	800	2.5	LS_2, BS_2
		BS_2	50	800	2.5	LS_2, BS_2
	b) Mineralogical	LS_3	51.53	900	1.5	LS_2, BS_2, LS_3,BS
		BS	48.46	900	2	LS_2, BS_2

Remarks: L = Li_2O; B = BaO; S = SiO_2

The experimental data proved that in composition 2 prepared of oxides we identified, as shown in Table 2, lithium disilicate, barium disilicate and lithium metasilicate. After successive thermal treatments (amounting to about 30 hrs.) the lithium metasilicate is no longer pulled out by

X rays. We further identified only LS_2 and BS_2 as equilibrium constituents of the considered composition. In the LS_2 and BS_2 mixture the components, thermally treated revealed no modifications in the phase composition able to illustrate the system development towards other phases; in the LS_3 and BS mixture there are emphasized transformations induced by the chemical interaction of the nonequilibrium phases LS_3 and BS turning into equilibrium phases LS_2 and BS_2, which determine the binary system and confirm the compatibility relations LS_2-BS_2.

Table 2

Experimental results obtained for composition 3

No.	Composition (% wt.)			Thermal treatments		Identified phases
				Temp. °C	Time h	
3.	Oxidic	Li_2O	8.24	1000	1.5	LS, BS_2, LS_2
				900	1	LS, BS_2 (LS_2) lin
		BaO	42.22	900	1	LS, BS_2
		SiO_2	49.52	800	1	LS, BS_2
				900	2.5	LS, BS_2
	a) Mineralogical	LS_2	41.21	900	5	LS, BS_2, LS_2, BS
		BS	58.79	900	3.5	LS, BS_2
	b) Mineralogical	LS	24.62	900	2	LS, BS_2
		BS_2	75.38	900	3.5	LS, BS_2

In the evaluation of the further compatibility relations we considered composition 3, oxidic and mineralogically shown in Table 2 and in fig. 3. Mixture 3 is located at the crossing of the possible binary subsystems LS_2-BS and $LS-BS_2$. By using, in the experimental approach, the same reasoning as for composition 2, we identified LS and BS_2 as subsolidus equilibrium phases in mixture 3. When establishing the $LS-BS_2$ compatibility relation the availability of the $LS_2-B_3S_5$, $LS_2-B_5S_8$, $LS_2-B_2S_3$ and LS_2-BS subsystems is cancelled. The subsystems $LS-B_3S_5$, $LS-B_5S_8$

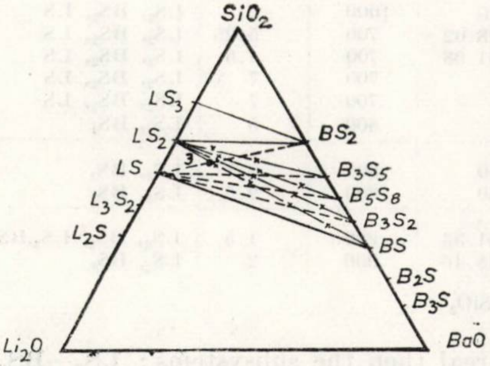

Fig. 3. — The probable compatibility lines of subsystems.

and LS—B_2S_3 are still very possible since the subsystem LS—BS is certain as shown by the data available in literature. To check the above mentioned subsystems the compositions marked 4—7 have been considered and shown in Table 3 and fig. 4. The experimental data obtained for compositions 4—7 evince that the lithium metasilicate establishes compatibility relations with B_3S_5, B_5S_8 and B_2S_3 determining the binary subsystems: LS—B_3S_5, LS—B_5S_8 and LS—B_2S_3.

Table 3

Experimental results obtained for composition 4—7

No.	Composition (% wt)			Thermal treatments		Identified phases
				Temp. °C	Time h	
4.	Mineralogical	LS	50	900	6.5	LS, B_3S_5
		B_3S_5	50	900	2	LS, B_3S_5
5.	Mineralogical	LS	50	900	6.5	LS, B_5S_8
		B_5S_8	50	900	2	LS, B_5S_8
6.	Mineralogical	LS	50	900	6.5	LS, B_2S_3
		B_2S_3	50	900	2	LS, B_2S_3
7.	Oxidic	Li_2O	16.66	1000	2	LS, BS
		BaO	35.91	900	1.5	LS, BS
		SiO_2	47.71	900	2	LS, BS
	Mineralogical	LS	50	900	3	LS, BS
		BS	50	900	3	LS, BS

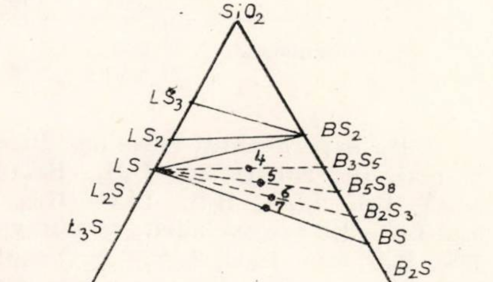

Fig. 4. — The compatibility lines for the LS—B_3S_5, LS—B_5S_8, LS—B_2S_3, LS—BS subsystems.

The subsolidus equilibrium relations in the more basic region of the system (under the LS—BS line) make it necessary to check some further 14 possible binary subsystems as results from fig. 5. Therefore we considered the ternary compositions marked 8—11 oxidic and mineralogically shown in table 4 and 5 and in fig. 5.

Composition marked 8 is located at the crossing of the LS—BaO and L_2S—BS subsystems.

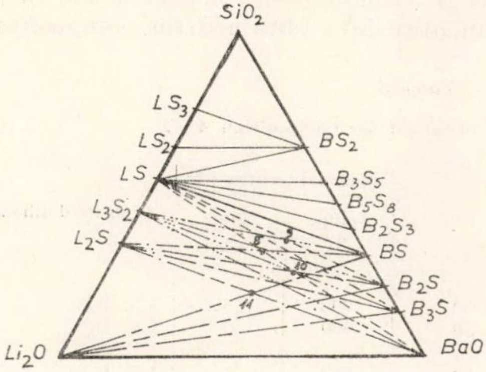

Fig. 5. — The probable compatibility lines for the subsystems.

Table 4

Experimental results obtained for composition 8

No.	Composition (% wt)			Thermal treatments		Identified phase
				Temp, °C	Time h	
8.	Oxidic	Li_2O	17.99	1000	1	LS, L_3S_2, BS
				900	1.5	LS, L_3S_2, BS
		BaO	46.02	900	4.5	LS, BS, L_3S_2
				900	3.5	LS, L_3S_2, BS
		SiO_2	35.98	900	8.5	LS, $BaCO_3$
				900	8.5	LS, $BaCO_3$
	a) Mineralogical	LS	53.98	900	5	LS, $BaCO_3$
		BaO	46.02	800	3.25	LS, $BaCO_3$
	b) Mineralogical	L_2S	35.43	900	5	LS, B_2S, BS
		BS	66.57	800	3.25	LS, $BaCO_3$

By experimental checking, in case the binary subsystem LS—BaO is real, the subsystems L_3S_2—BS, L_3S_2—B_2S, L_3S_2—B_3S, L_3S_2—BaO, Li_2O—BS, Li_2O—B_2S, Li_2O—B_3S, L_2S—BaO, L_2S—B_3S, L_2S—B_2S and L_2S—BS are excluded ; remain very possible the subsystems LS—B_2S, LS—B_3S, LS—BaO, L_3S_2—BaO and L_2S—BaO as shown in fig. 6. In case compatibility relations are established between L_2S and BS, then the subsystems LS—B_2S, LS—B_3S, LS—BaO, L_3S_2—B_2S, L_3S_2—B_3S and L_3S_2—BaO are cancelled and the binary subsystems L_3S_2—BS, L_2S—B_2S, L_2S—B_3S, L_2S—BaO remain as possibly substituting the last three subsystems Li_2O—BS, Li_2O—B_2S, Li_2O—B_3S, as shown in fig. 7.

The experimental results (Table 4) show that in composition 8, the lithium metasilicate and the barium oxide are identified as subsolidus equilibrium phase. Further on, the experimental data recorded for compositions 9—11 evidenced the binary subsystems LS—B_2S, LS—B_3S, LS—BaO, L_3S_2—BaO and L_2S—BaO.

Table 5

Experimental results obtained for composition 9—11

No.	Composition (% Wt)			Thermal treatments		Identified phase
				Temp. °C	Time h	
9	Mineralogical	LS	50	900	6.5	LS, B_2S
		B_2S	50	900	2	LS, B_2S
10	Oxidic:	Li_2O	16.04	1000	1	L_2S, LS, B_2S, BS
				900	1.5	LS, L_3S_2, $BaCO_3$
		BaO	60.04	700	5.25	LS, L_3S_2, $BaCO_3$
		SiO_2	23.89	700	7.5	LS, L_3S_2, $BaCO_3$
	Mineralogical:	LS	9.51	800	2	LS, L_3S_2, $BaCO_3$
		L_3S_2	30.53	800	3	LS, L_3S_2, $BaCO_3$
		BaO	59.94	900	3.5	LS, L_3S_2, $BaCO_3$
11	Oxidic:	Li_2O	22.33	1000	1	LS, L_2S, BS, B_2S, $BaCO_3$
				900	1.5	L_2S, LS, BS, B_2S, $BaCO_3$
		BaO	55.79	900	5.25	LS, L_2S, BS, B_2S, $BaCO_3$
				900	4.5	LS, L_2S, BS, B_2S, $BaCO_3$
				900	3.5	LS, L_2S, BS, B_2S, $BaCO_3$
		SiO_2	21.87	900	3	LS, L_2S, BS, B_2S, $BaCO_3$
				900	9.75	LS, L_2S, BS, B_2S, $BaCO_3$

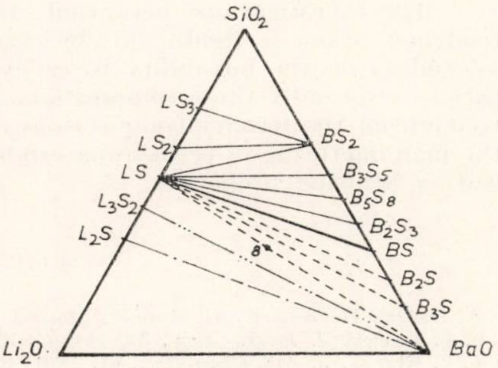
SiO_2
LS_3
BS_2
LS_2
LS
B_3S_5
B_5S_8
L_3S_2
B_2S_3
L_2S
BS
8
B_2S
B_3S
Li_2O
BaO

Fig. 6. — The compatibility lines for the LS—BaO subsystem.

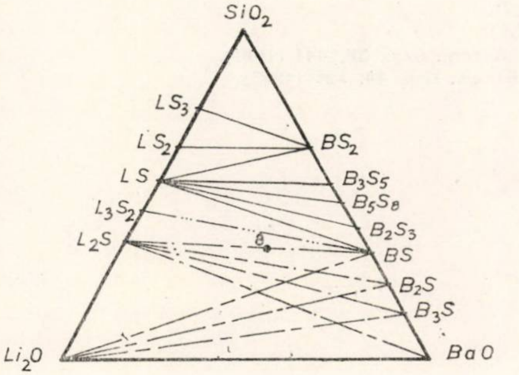
SiO_2
LS_3
LS_2
BS_2
LS
B_3S_5
B_5S_8
L_3S_2
B_2S_3
L_2S
8
BS
B_2S
B_3S
Li_2O
BaO

Fig. 7. — The compatibility lines for the L_2S—BS subsystem.

CONCLUSIONS

The experimental results lead to developing compatibility relationships between the respective compounds of the $Li_2O-BaO-SiO_2$ system.

By identifying the binary subsystems of the $Li_2O-BaO-SiO_2$ system, 13 ternary subsystems, which make up the considered oxidic system (fig. 8) were emphasized.

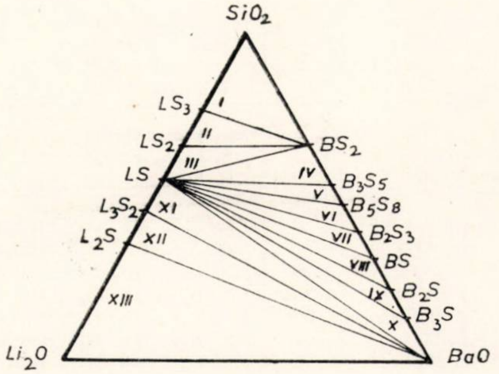

Fig. 8. — Compatibility relations in the $Li_2O-BaO-SiO_2$ system.

The investigations permitted considerations on the crystallization tendency which is significant for many of the investigated compounds as well as on the possibility to easily obtain certain controlled crystallizations (especially those compositions rich in LS and LS_2). Such remarks recommend the ternary compositions of the $Li_2O-BaO-SiO_2$ system for the manufacturing of certain materials of the vitroceram type with interesting utilising properties.

REFERENCES

[1] A. Dietzel, H. Wickert, H. Köppen, *Glasteck Ber.*, **27**, 5, 150 (1964).
[2] F. C. Kracek, *J. Phys. Chem.*, **34**, 2645 (1930).
[3] F. C. Kracek, *J. Am. Chem. Soc.*, **61**, 2870 (1939).
[4] P. Escala, *Am. I. Sci.*, **4**, 345 (1922).
[5] J. W. Grieg, *Am. I. Sci.*, **13**, 27 (1927).
[6] H. Müller, *Chem,. Fabrik*, **32**, 333 (1933).
[7] J. E. Planz, H., Müller, *Ber. Deutsch. Keram. Ges.*, **38**, 441 (1961).
[8] J. E. Planz, H. Müller, *Ber. Deutsch. Keram. Ges*, **40**. 191 (1963).

Revue Roumaine de Chimie, 34, 3, 877–881 (1989)

THERMO-ANALYTICAL STUDY OF THE COMPLEXES OF PALLADIUM WITH α,α'-DIPYRIDYL, *p*-NITROSODIMETHYLANILINE AND *p*-NITROSODIPHENYLAMINE

D. N. TODOR [a], A. TĂNASE [a], V. DAVID [b] and G. E. BAIULESCU [c]
[a] I.C.P.M.S., Str. Gării Cățelu 5, Sec. 3, Bucharest, Romania
[b] C.P.I.E.M., Str. Pop de Băsești 59, Sec. 2, Bucharest, Romania
[c] Department of Analytical Chemistry, National Institute of Chemistry, Spl. Independenței 202, 77207, Bucharest, Romania

Received November 21, 1987

A study was carried out upon the thermal behaviour of three compounds, i.e. α, α'-dipyridyl, *p*-nitrosodimethylaniline and *p*-nitrosodiphenylamine and their complexes with palladium divalent. The aim of the study was to find the temperature ranges within which the complexes can be used as stationary phases in gas chromatography.

INTRODUCTION

The divalent palladium complexes with *p*-nitrosodiphenylamine or *p*-nitrosodimethylaniline are chelate complexes having good application in visible spectrometric determinations of Pd(II) from different mixtures.[1-4] We have lately found that these three complexes of Pd(II) with *p*-nitrosodiphenylamine, *p*-nitrosodimethylaniline and α,α'-dipyridyl can be used in the determination of some atmospheric pollutants, e.g. :

- being used as reagents in UV/VIS spectrometric determination of carbon monoxide[5];
- being used as stationary phases in gas-chromatography.

For both purposes, the informations were needed with regard to the thermal behaviour of these complexes and their uncoordinated ligands.

EXPERIMENTAL

A Q 1500 (MOM) derivatograph was used to carry out the thermal behaviour of the investigated compounds. The determination were made for different heating rates of the furnace : 10, 5, 2.5 and 1.25°/min. The temperature and the differential temperature were measured with Pt/Pt-Rh thermocouples and the medium in the furnace was a static, environmental atmosphere. Samples weighing 100–200 mg were used.

We used reagents *p*-nitrosodiphenylamine and *p*-nitrosodimethylaniline obtained and verified by us, and α,α′-dipyridyl was of Merck quality. The complexes of ligands mentioned above with divalent palladium were synthesized using a solution of Pd(II) in 1 vol. % HCl and solutions of the ligands in 50 % C_2H_5OH, the reagent quantities used being in the following molar rations :

Pd(II) : *p*-Nitrosodiphenylamine = 1 : 2
Pd(II) : *p*-Nitrosodimethylaniline = 1 : 2
Pd(II) : α, α′-Dipyridyl = 1 : 1

RESULTS AND DISCUSSION

α,α′-Dipyridyl

From the thermal curves it results that α,α′-dipyridyl reagent shows on the DTA curve an endothermal effect assigned to the melting of the compound, whose peak is located at 350°. After this effect, a sublimation process of the reagent occurs, which is observable both on the DTA curve and the curves that show the mass variations (TG and DTG). This sublimation takes place entirely at 240°, with the heating rate specified in fig. 1a.

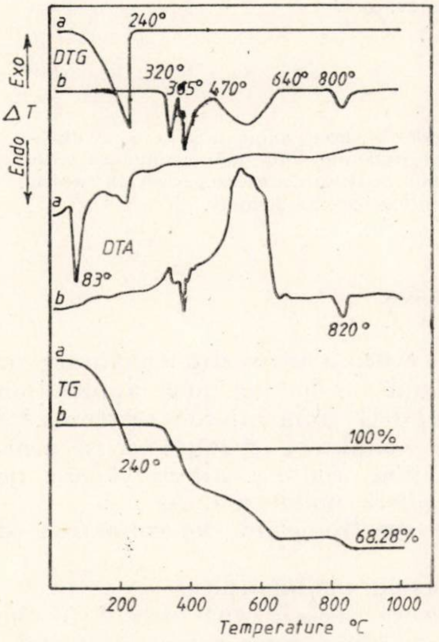

Fig. 1. — The thermal curves obtained at a heating rate of 5°/min up to 1000 °C for (a) α,α′-dipyridyl ; (b) α,α′-dipyridyl—Pd (II) complex.

α,α′-Dipyridyl — Pd(II) Complex

The complex obtained by us is thermally stable up to 320°. Further on, the decomposition occurs within a temperature domain rather wide, being finished up at 640° and measuring a total mass loss of 27 %. Within this temperature domain a series of thermal effects takes place, as such :

- in the range 320 — 365°, a mass loss of 8.25 % takes place, which is due to the release of N_2 (theoretical value is 8.40 %). For this process the DTA curve shows an exothermal effect.
- in the range 365—470° we suppose that chlorine and hydrogen found in the complex are released, while the partial oxidation of the Pd from complex to PdO occurs.
- in the range 470—640° the total degradation takes place, observable upon DTA curve by a very marked exothermal effect.

With the temperature increase the residue obtained after decomposition is thermally stable up to about 800°. At 820° an endothermal effect turned up and a mass loss was recorded according to the decomposition of PdO to Pd, the former being obtained during the thermal treatment, (Fig. 1b).

The total mass loss of the complex up to 1000° was of 68.28% and it was in a very good accordance with the theoretical value of 68.10%.

p-Nitrosodimethylaniline

By heating of the reagent it has a specific melting effect whose peak on the DTA curve is situated at 93°. At 110° the compound begins to decompose slighty, so that at the temperature of 180° the decomposition process gets an explosive character, recorded by pronounced effects upon all thermal curves (Fig. 2); the explosive decomposition process is closed at about 200°. Afterwards, the thermal curves show an oxidative degradation of the compound, which is finished up to about 680°. The total mass loss up to 1000° is 100%.

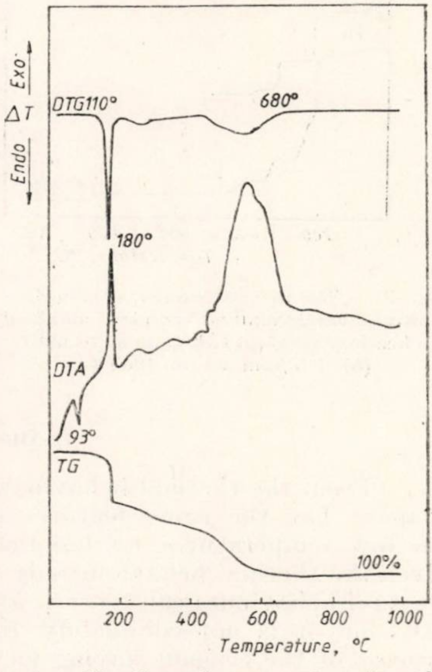

Fig. 2. — The thermal curves of *p*-nitrosodimethylaniline reagent at a heating rate of 5°/min.

p-Nitrosodimethylaniline — Pd(II) Complex

For this complex there were carried out two determinations with various heating rates: 1.25 and 2.5°/min. It was done for explaining the explosive effects that occur by heating of the complex. For both cases the complex is stable up to about 200° excepting a moisture loss. Within the range 200—250° the DTA curve shows an exothermal effect and TG and DTG curves show a pronounced mass loss, assigned to the explosive character of the compound decomposition. Within the range 250—300° we noticed a thermal stability of the compound partly decomposed, afterwards a new thermal phenomenon as the first one occurs, which at about 340° is completely finished up. Then, up to about 400° the thermal curves show an oxidative-like effect of the compound, observable mostly upon the curves obtained with the heating rate of 2.5°/min. Up to 800° the thermal purves show no thermal effect. After this temperature, the specific decomtosition effect of PdO to Pd takes place (Fig. 3).

The total mass loss up to 1000° is 77.25%, in a good agreement with the theoretical value, 77.42%.

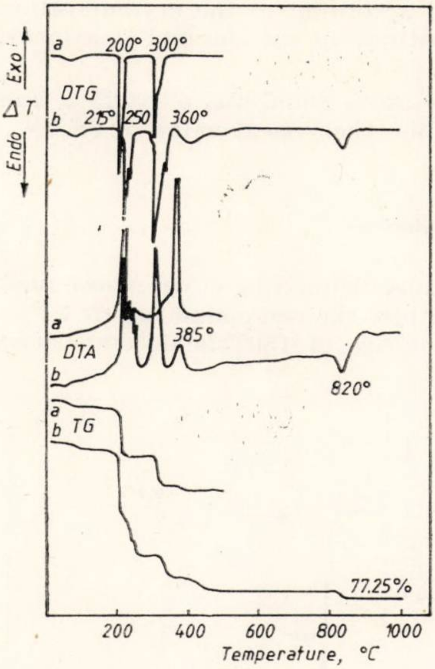

Fig. 3. — The thermal curves of Pd(II)—*p*-nitrosodimethylaniline complex obtained at a heating rate of (a) 1.25°/min up to 500 °C; (b) 2.5°/min up to 1000 °C.

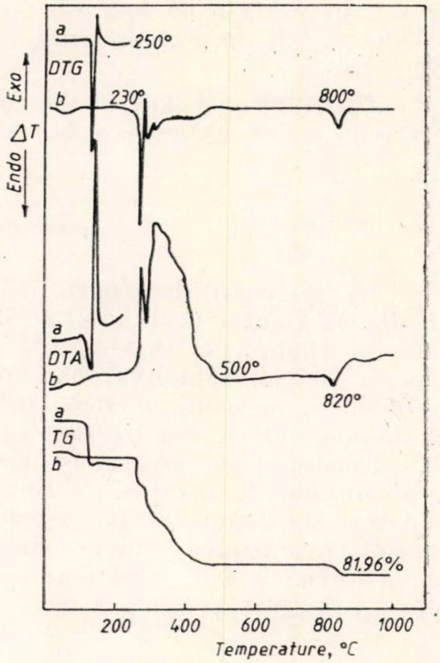

Fig. 4. — The thermal curves obtained at a heating rate of 5°/min up to 1000 °C for (a) *p*-nitrosodiphenylamine, (b) *p*-nitrosodiphenylamine—Pd(II) complex.

p-Nitrosodiphenylamine

From the thermal behaviour point of view, *p*-nitrosodiphenylamine reagent has the same features as *p*-nitrosodimethylaniline, excepting the low temperatures, i.e. less than 150°. For this reason in Fig. 4a it was given the thermal behaviour only up to 250°. The difference between their thermal behaviours can be seen at the melting process. It begins at about 110°, but it is not completely finished up because the decomposition process of the reagent having an explosive character occurs at the same time. The total mass loss up to 1000° is 100%.

p-Nitrosodiphenylamine—Pd(II) Complex

Up to 230° the complex is thermally stable excepting a slight moisture loss. At 230° the explosive decomposition of the complex occurs similarly to that of the uncoordinated reagent. The differences between them consist in the lack of the melting effect for the complex and the increase of the decomposition temperature. Soon after the explosive effect an oxidative effect can be seen, within a wide range, which at about 500° is completely finished up. With the temperature increase, over 800°, the thermal curves also show the specific effect of decomposition of

PdO to Pd, the former being oxidated during the thermal process. The total mass loss is 81.96%, being in a good accordance with the theoretical value, i.e. 81.45% (Fig. 4.b).

CONCLUSIONS

Since the aim of this study was merely to ascertain the thermal stabilities of the compounds, no attempts were made to interpret the thermal curves quantitatively. We found out that the complexes of Pd(II) with the two reagents containing the *p*-nitrosophenylamino functional group are stable up to 200°C, excepting a slight moisture loss ; α, α'-dipyridyl-Pd (II) complex is more stable than the previous ones and can be used as stationary phases in gas chromatography up to a working temperature of 320°C. The results of thermal behaviours of these compounds are very similar to those of other organic compounds containing phenylamino groups.[6]

REFERENCES

[1] L. G. Overholser and J. H. Yoe, *J. Amer. Chem. Soc.*, **61**, 2058 (1939).

[2] L. G. Overholser and J. H. Yoe, *J. Amer. Chem. Soc.*, **63**, 3224 (1941).

[3] J. H. Yoe and J. J. Kirkland, *Analyt. Chem.*, **26**, 1335 (1954).

[4] V. David, *Anal. Lett.*, **19**, 1199 (1986).

[5] V. David and G. E. Baiulescu, *Rev. Roumaine Chim.*, submitted for publication.

[6] M.E.M. Khalifa and D. H. Todor, *J. Therm. Anal.*, **24**, 165 (1982).

Revue Roumaine de Chimie, 34, 3, 883–894 (1989)

STUDY OF THERMAL COMPLEXING OF MICROCRYSTALLINE CELLULOSES WITH TRANSITION METALS

CLEOPATRA VASILIU-OPREA *, ALEXANDRU C. CONSTANTINESCU
and SEVERIAN DUMITRIU

Polytechnic Institute of Jassy, Department of Polymer Chemistry,
Calea 23 August 11, 6600 – Jassy, Romania

Received November 15, 1988

In this paper some data are presented, concerning microcrystalline celluloses utilization in thermal complexing reactions with different transition metals, in which cellulose macromolecules are used as ligand. As an application and a way of pointing out the complexes formation, they have been used in coupling reactions with enzymes (the invertase being used), which catalyse the common sugar hydrolysis reaction.

I. INTRODUCTION

The chemistry of complexes knows a rapid development, due to their involvement in many catalytic and biologic processes.[1-6]

The polychelate compounds are very numerous and varied owing – on the one hand – to the great number of cations able to generate complexes and – on the other – to the great number of inorganic and especially organic ligands. Generally, there are metal, molecular, inclusion and ionic change complexes.[1,7]

In biology, cyclic natural polychelates of transition metals are of a great importance (chlorophyll, haemoglobin). Synthetic complexes of the same type are employed either as models for investigating the mechanism of natural processes or as biologic-active-substances and supports as well, for immobilization of enzymes.

The metal-link method for immobilization of enzymes was initially developed by Novais.[8-10] He used, as support for titanium ions (III) complexing nitroaryl derivatives of cellulose.

The present paper reports the study of thermal complexing of microcrystalline cellulose (obtained according to an original procedure) with different transitional metals, being established at the same time the influence of the main parameters on the process. Synthesized cellulose complexes have been used for coupling reactions with invertase, an enzyme very important in food industry, for glucose and fructose obtention, by sugar hydrolysis.

II. EXPERIMENTAL

As complexing supports the microcrystalline cellulose was used, being obtained from beech chemical cellulose, according to an original hydrolytic procedure.[11]

Reaction conditions and the main microcrystalline cellulose properties are presented in Table 1. It can be noticed that the two celluloses used for complexing (C_{II} and C_{III}) are characterized by a high crystallinity, reduced particle sizes, high specific surface and low ash content. They are approved by the Romanian Health Ministry being non toxic for human beings.

Table 1

Microcrystalline cellulose properties and synthesis conditions

Cellulose type	Synthesis conditions			Characteristics				
	H_2SO_4 conc. (%)	Duration (Hrs)	Temp. (°C)	$\overline{DP}$	Cryst. (%)	Average particle size under 71 µ (%)	Specific surface (m^2/g)	Ash (%)
C_{II}	25	4	45	542	74.4	70.08	10.84	0.18
C_{III}	45	4	55	420	77.4	72.36	12.0	0.10

Transition metals used for complexing (in ionic form) belong to the IV-th period of Periodical System of the Elements: Ti^{3+}, VO_2^{2+}, Cr^{3+}, Mn^{2+}, Fe^{3+}, Co^{3+}, Ni^{2+}, Cu^{2+}, Zn^{2+}. For comparison two metals of the II-nd group were used: Mg^{2+} and Ca^{2+}.

Microcrystalline cellulose, dried at a constant weight, was mixed up (by stirring) with aqueous solutions of metal salts for four hours. After cellulose mixing and partial swelling, the obtained products were kept for 24 hours in a desiccator containing calcium chloride. Then, the cellulose was evacuated and separated by filtration (without washing) and dried in a vacuum-drying cupboard, at 50°C, for 24 hours. After the finishing of the thermal complexing reaction, the resulting samples were washed and extracted with distilled water, for 10 hours, to remove the metal salt excess which did not react. Then, the complexing products were dried at 105°C until constant weight.

For the microcrystalline cellulose characterization the following analysis techniques were used: average polymerization degree determination, as well as that of crystallinity, particle size distribution, specific surface, furnacing residue (ash). The average polymerization degree was viscometrically determined, using a Ubbelohde type viscometer, while as a solvent, a cupraammonium solution was used. It was calculated according to the following relation:

$$\overline{DP} = \frac{2000 \cdot \eta_{sp}}{C \cdot (1+0.29 \cdot \eta_{sp})} \qquad (1)$$

where: $\overline{DP}$ — average polymerization degree;

C — cellulose solution concentration (g/L);

η_{sp} — specific viscosity.

Crystallinity was determined by X-rays diffraction under small angles, using a TUR-M62 (East Germany) type apparatus. Particle-size distribution (expressed in %) was determined using a vibrating sieve, of the THYR-1 type (East Germany). The specific surface was measured using an apparatus built according to the BET modified method.[13] Furnacing residue (ash) was determined using a combustion furnace, at 800°C.

In the case of polychelates the following analysis techniques were used: furnacing residue (ash), bound metal content, crystallinity as well as thermal behaviour determinations. The bound metal content was obtained using an atomic absorption spectrophotometer, of the SP 90 Pye Unicam type. The thermal behaviour of the complexes was determined by differential thermal analysis, using a MOM Budapest (Hungary) thermobalance, at temperature range between 20° and 700°C, in an inert medium. The temperature was raised 12.4° per minute, the results being compared with those of the standard polymer.

The coupling reaction of complexed cellulose with invertase (Serva) was done in the following way : the complexed support was added to an acetate buffer solution (pH = 4.5) containing dissolved invertase, at 5°C, and mixed on, for 24 hours. The mixture was filtrate and washed with distilled water (2—3°C) to remove the uncoupled invertase. The filtrate was collected and preserved at 5°C, until the free enzyme activity determination. The solid product, left on filter, was washed with acetate buffer solution (pH = 4.5), being kept in wet state, in a closed bottle, at 5°C, until the coupled enzyme activity determination. The activity of the invertase was estimated by dosing the inverted sugar, respectively the glucose formed, by photocolorimetry, using a Spekol ZV (Carl Zeiss Jena) type apparatus.[14] The immobilized invertase was added to 50 mL solution of sucrose (0.25 M) in acetate buffer (pH = 4.5), at 37°C, and incubated for 15 min at this temperature. From this mixture, 0.5 mL were extracted and the enzymatic process stopped by adding 2 mL dinitrosalicylic reagent (prepared by dissolving 1 g of 3,5-dinitrosalicylic acid in 20 mL of 2M NaOH solution and diluting with 50 mL distilled water) and maintaining for 5 minutes on a boiling water bath. The sample was then cooled, diluted with distilled water until reaching 15 mL, and the absorbance at 540 nm was read in a cell of 1 cm against a standard sample in which the enzymatic reaction was stopped at zero time. The enzyme activity was calculated according to the relation :

$$A = (\text{nmoles inverted sugar for enzyme sample} - \text{nmoles inverted sugar for standard sample})/15 \qquad (2)$$

where : 15 — time of incubation, at 37°C (min).

III. RESULTS AND DISCUSSION

The synthesis conditions as well as the complexing capacity of studied metals expressed by the weight increase of both ash and quantity of bound metal are presented in Table 2. It is to be noticed that for the used metals an increase of residue value takes place, which differs according to the used ion nature. Lower values than 0.25% are explained by ion absorption on the cellulose support, without any coordination or covalent links formation. Higher values have been obtained by microcrystalline cellulose metal coordination. The greatest bound metal quantity has been recorded in the case of Ti^{3+} ion, fact which points out its capacity of form-

Table 2

Synthesis conditions and thermal complexation capacity of studied metals

Cellulosic support	Metal	Ion	Valence shell configuration	Initial anion	Reaction conditions			Bound metal (%)
					Ion conc. (moles/L)	Temp. (°C)	Duration (hrs)	
C_{III}	Ti	Ti^{3+}	$4s^23d^2$	Cl^-	0.4	50	24	3.81
C_{II}	V	VO^{2+}	$4s^23d^3$	Cl^-	0.2	50	24	0.62
C_{III}	Cr	Cr^{3+}	$4s^13d^5$	Ac^-	0.2	50	72	0.18
C_{II}	Mn	Mn^{2+}	$4s^23d^5$	Cl^-	0.2	60	72	0.54
C_{II}	Fe	Fe^{3+}	$4s^23d^6$	Cl^-	0.4	50	24	1.50
C_{III}	Co	Co^{3+}	$4s^23d^7$	Ac^-	0.4	50	96	1.76
C_{III}	Ni	Ni^{2+}	$4s^23d^8$	Cl^-	0.2	80	48	0.25
C_{III}	Cu	Cu^{2+}	$4s^13d^{10}$	Ac^-	0.4	50	96	1.19
C_{III}	Zn	Zn^{2+}	$4s^23d^{10}$	SO_4^{2-}	0.2	70	24	0.25
C_{III}	Mg	Mg^{2+}	$3s^2$	Ac^-	0.4	50	72	0.23
C_{III}	Ca	Ca^{2+}	$4s^2$	Ac^-	0.2	50	24	0.25

ing complexes with ligands, which have the oxygen as electrons donors atoms. Titanium (III) ion has only one unpaired electron on 3d orbital-electron, this explaining its high reactivity in complexing reactions. In aqueous solutions, Ti^{3+} ion is complexed with six water molecules. This complex stability is reduced, Ti^{3+} ion having the tendency to oxidize to Ti^{4+} ion, being obtained a hydrated oxide, which, by drying, converts to titanium oxide. The complex stability can be increased by acidulating the solution with hydrochloric acid 1% solution so that part of water molecules are replaced by Cl^- ions. The probable cellulose complexing mechanism with Ti^{3+} ion implies first the formation of complex ions, like: $[Ti(H_2O)_6]^{3+}$, $[Ti(H_2O)_5Cl]^{2+}$, $[Ti(H_2O)Cl_5]^{2-}$, $[TiCl_2]^{3-}$. Cellulose contains vicinal diol groups not involved in the glycosidic linkages between D-glucopyranose residues and therefore are amenable to chelation by transition metal ions, the polychelate being formed by replacement of two of the titanium ion ligands by polysaccharide hydroxy groups (Fig. 1).

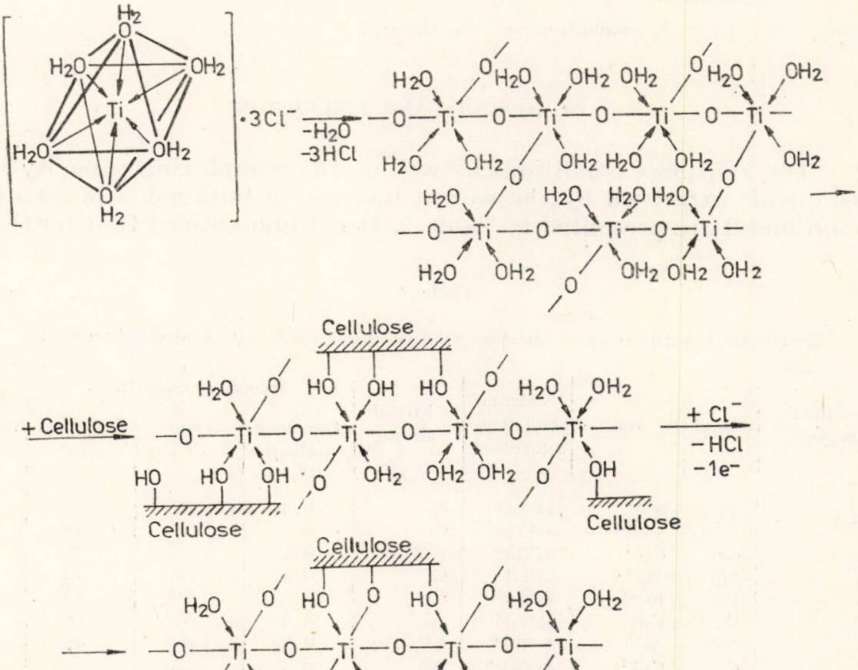

Fig. 1. — The probable mechanism of thermal complexing reaction in the case of titanium ion.

Thus, since cellulose is a polymer of β-1,4-linked D-glucopyranose units, the 2- and 3-hydroxy groups would be involved in chelate formation. The 6-hydroxy group of the D-glucopyranose residue can only be expected to participate in complexing of the cellulose chain by titanium, since sterically this hydroxy group is unable to become sufficiently close to any of the other hydroxy groups of the cellulose chain to be involved in chelate formation. The 6-hydroxy group of the D-glucopyranose residue can only be expected to participate in complexing of the cellulose chain by titanium, since sterically this hydroxy group is unable to become sufficiently close to any of the other hydroxy groups of the cellulose chain to be involved in chelate formation. Thus, titanium-treated cellulose material may be envisaged as being chelated and/or complexed along the length of its chain with various aquo, chloroaquo and chloro complex titanium species prevalent in solution. It should be noted that, for steric reasons, it is impossible for all the water or chloride ligands of titanium ion to become replaced by other hydroxy groups of the polysaccharide chain. Furthermore, these remaining ligands will not be extensively replaced by hydroxy groups of adjacent cellulose chains on account of the insolubility and lack of mobility of the cellulose molecules. Chelation may be achieved for any molecule containing groups appropriate to replace the ligands of the titanium bound to cellulose.

In the last stage, which takes place at reaction temperature there also appear covalent links between titanium and cellulose by means of the oxygen. During this stage the oxidation of Ti^{3+} ion to Ti^{4+} ion takes place, finally a high stability complex being obtained (Fig. 2).

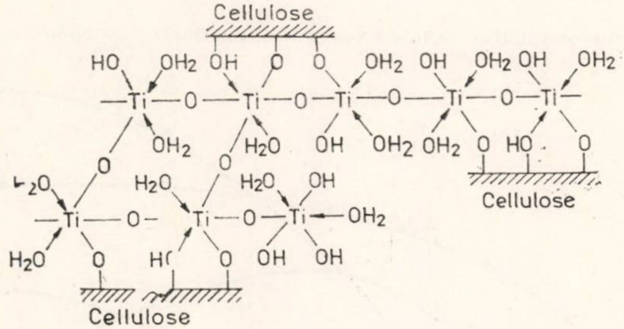

Fig. 2. — Final structure of complex formed by cellulose with titanium ion.

High values of bound metal percentage have been obtained in the case of the following ions : Co^{3+} (resulting from Co^{2+} ion oxidation in the presence of the ligand), Mn^{2+}, Fe^{3+} and Cu^{2+}. All these ions have been used further on for the study of the influence of thermal complexing conditions on the bound metal quantity.

The main parameters that influence the thermal complexing efficiency are the following : the metal ion nature, cellulose support nature (especially particles size), metal salt concentration, complexing duration and temperature.

The influence of the metal ion nature depends on the ratio between electrical charge and its ionic radius, i.e. on the polarization capacity.

The particles size of cellulose support influences the bound metal quantity in the manner presented in Fig. 3. It may be noticed that an

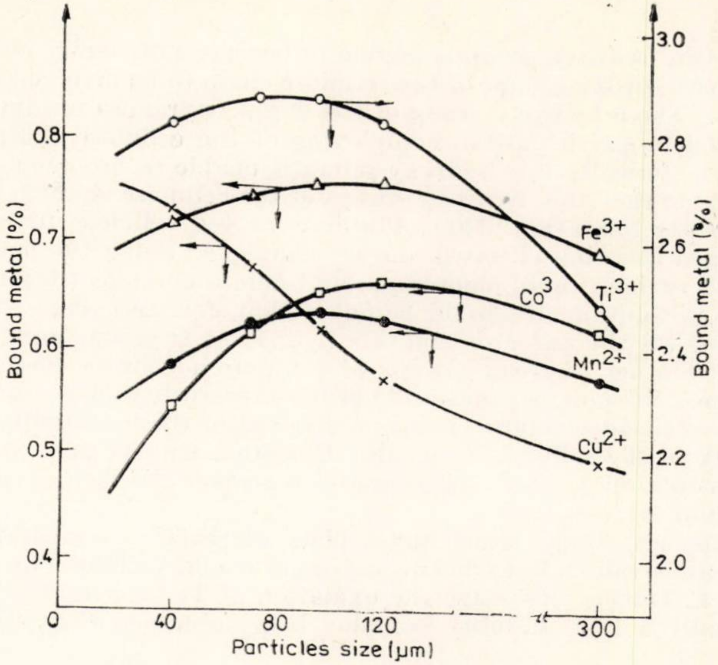

Fig. 3. — Microcrystalline cellulose particles size influence on bound metal quantity.

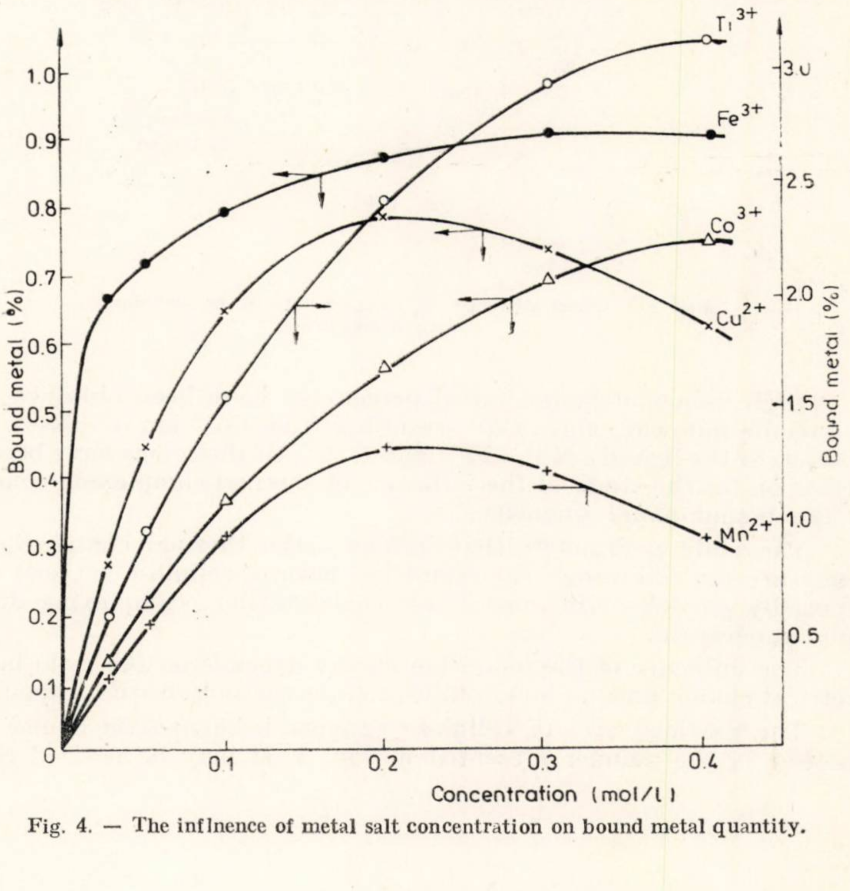

Fig. 4. — The inflnence of metal salt concentration on bound metal quantity.

increase of complexing process efficiency takes place, along with the diminution of cellulose particles size in the case of all metal ions studied.

The influence of metal salt concentration (Fig. 4) has been watched using as support C_{III} cellulose, a ratio cellulose/metal salt solution equal to 1 g/20 mL, 24 hours duration and 50°C. It is noticed that in the case of Mn^{2+} and Cu^{2+}, the curves present a maximum at a concentration equal to 0.2 M, while for the other ions the complexing capacity increases with the one of the concentrations up to the value of 0.4 M.

For curves representing temperature influence (Fig. 5), the maximum quantity of bound metal is recorded, at 50°C, for Mn^{2+}, Fe^{3+} and Cu^{2+} ions and at 60°C, for Co^{3+} ion. In the case of Ti^{3+} ion there does not exist a maximum in the studied temperature range, the curve shape suggesting a maximum at a higher temperature than 80°C. This could be explained by the fact that high temperatures favour the oxidation of Ti^{3+} ion to Ti^{4+} ion and as a consequence the increase of the complex stability.

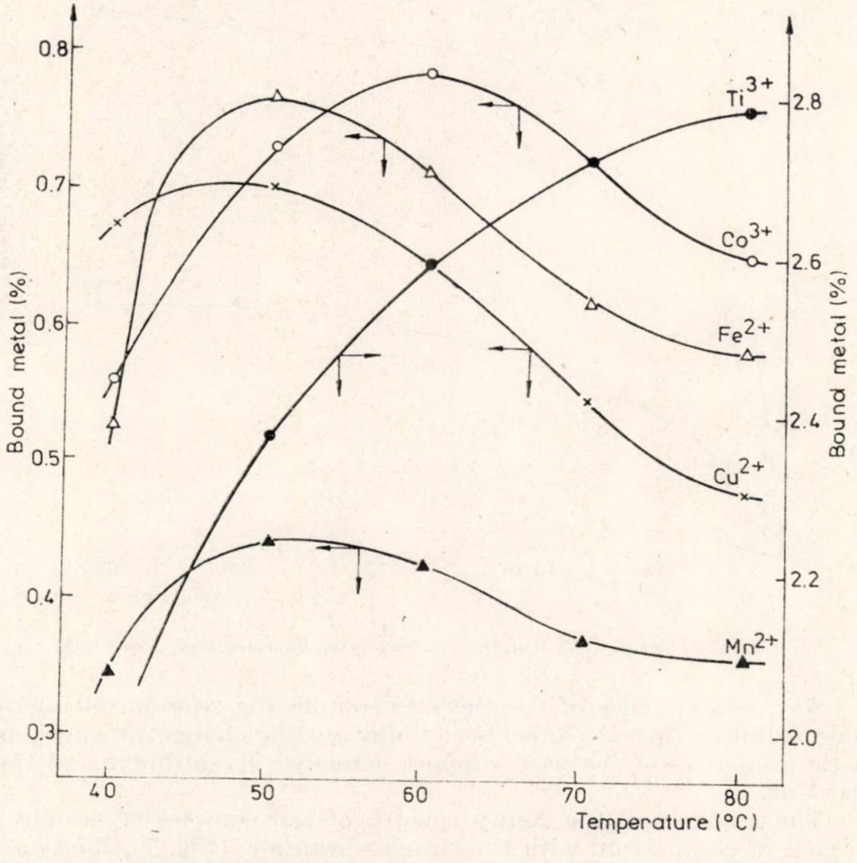

Fig. 5. — Complexing temperature influence on thermal complexing process efficiency.

As for complexing duration (Fig. 6) it is noticed an increase of bound metal quantity along with the time in the case of all metal ions. This increase is more pronounced (for the first 24 hrs) in the case of Cu^{2+} and Fe^{3+} ions and slower in the case of Co^{3+} and Ti^{3+} ones.

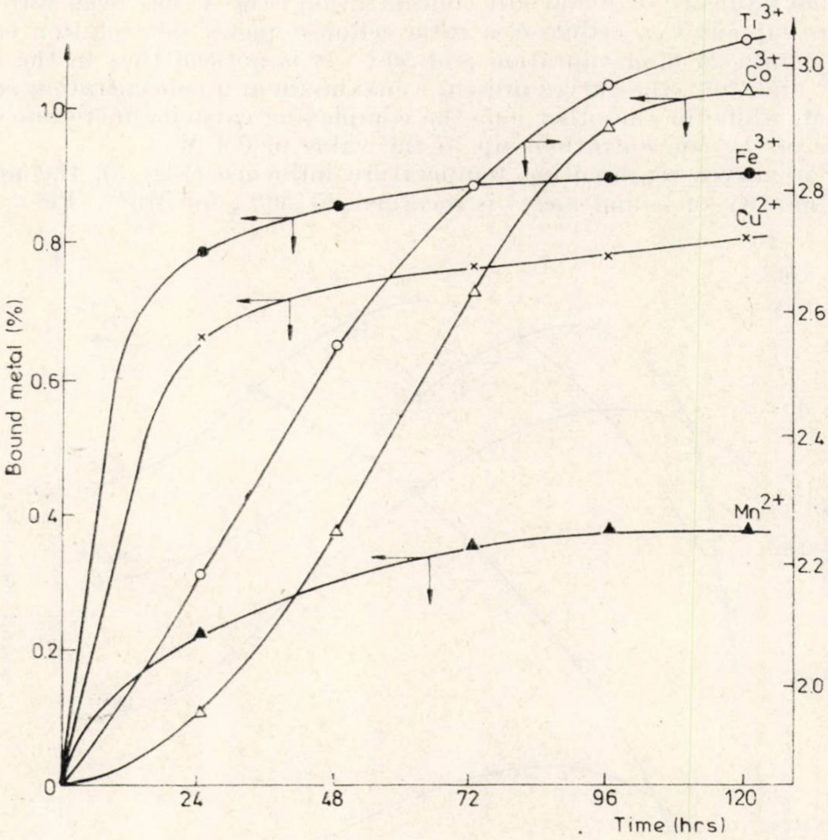

Fig. 6. — Complexing duration influence on bound metal percentage.

As a consequence of the thermal complexing reaction of microcrystalline cellulose there has also been found out the change of some characteristic properties of the used support, namely : crystallinity and thermal behaviour.

The analysis of the X-ray spectra of the complexed samples with Fe^{3+} ion, in comparison with the standard sample, (Fig. 7), shows a diminution of support crystallinity as a consequence of complexing (the reduction of the peak characteristic to the plane of glucopyranose cycles, noted [002]). At the same time there is noticed a diminution of the number of hydrogen bonds between the macromolecular chains (given by the peaks [101] and [$\overline{1}01$]). These data show on the one hand that oxygen occupied orbitals take part in complexing reaction, a fact proved by the reduction of the number of inter-chain hydrogen bonds and, on the other, that in the complexing process there are implied the OH groups from C_2 and C_3, which are to be found in the plane of glucopyranose cycles.

Table 3

The values of coupling yield and invertase activity in filtrate

Enzymatic filtrate	Extinction	Moles inverted sugar. 10^{-9}	A_i µmoles/g · min	Diminution of activity δ	Coupled enzyme $\frac{\delta}{A_i} 0.2$	Coupling yield %	Calculated activity $A_c = A_i \cdot M_E$
Enzyme	0.555	1425	4750	—	—	—	—
Cellulose	0.450	1160	3870	880	0.037	18.5	176
Cellulose + Ti^{3+}	0.230	600	2000	2750	0.115	57.5	546
Cellulose + Co^{3+}	0.400	1040	3470	1280	0.054	27.0	256
Cellulose + Mn^{2+}	0.360	930	3100	1650	0.069	34.5	328

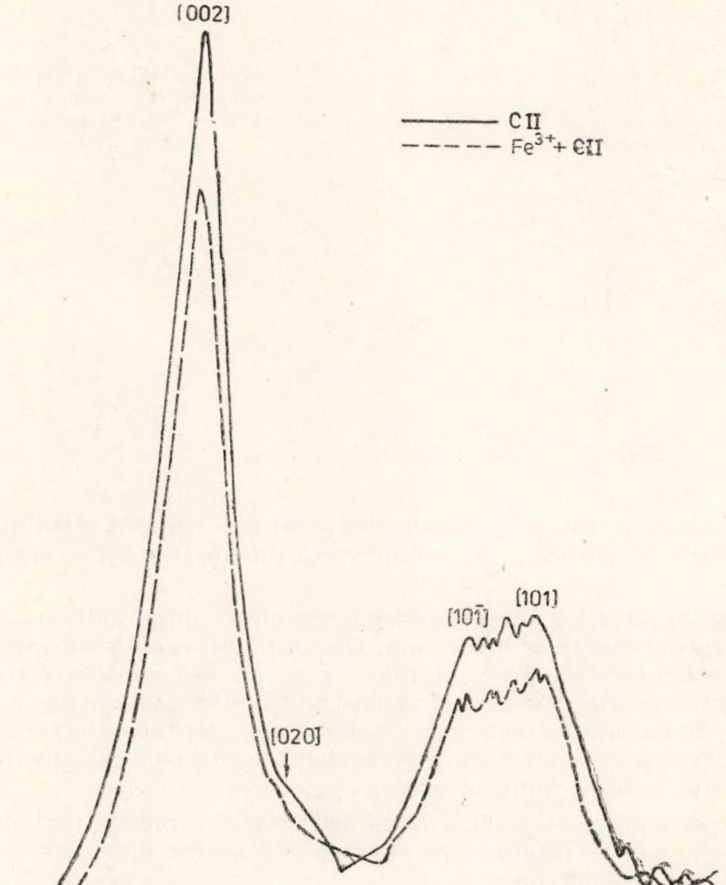

Fig. 7. — X-ray diffraction spectra for cellulose support (C_{II}) and complexed with Fe^{3+} ion.

Important changes appear in the thermal behaviour, pointed out by differential thermal analysis (DTA) (Fig. 8). Unlike the standard sample (C_{III} cellulose), the Cu^{2+} complexing one shows a less evident thermal decomposition process at 320°C. As in the case of C_{II} cellulose, instead of a strong endothermal process taking place at 320°C, an attenuation as well as a displacement toward higher temperatures appear, explained by a stronger thermal stability of complexes, due to the coordination links formation.

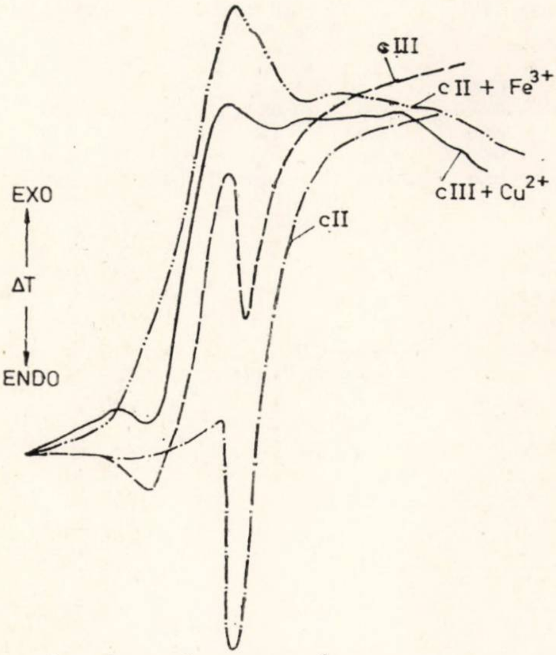

Fig. 8. — DTA curves for standard samples (C_{II} and C_{III} celluloses) and for their complexes with Fe^{3+} and Cu^{2+} respectively.

As an application of synthesized complex compounds, but also as a way of pointing out their formation, the titanium-cobalt- and manganese-treated cellulose have been coupled with an enzyme (invertase). Proteinaceous molecules such as enzymes, antibodies and antigens were the molecular types most frequently immobilized. Groups that can act as ligands in the case of enzymes will be the free carboxy groups from the C terminus of acidic amino acids.

The formation of such a bond between the metal-treated polymer and the enzyme, to produce an enzymically active derivative, would be expected to depend on:

a) the availability in the enzyme molecule of groups which can act as ligands;

b) steric factors which permit such groups to come in contact with the metal atom;

c) the non-involvement of such groups in the region of the active site(s) of the enzyme; and

d) the close proximity of enzyme molecules already bound in the polymer matrix.

The determination of coupling yield shows that unlike standard cellulose sample having a coupling yield of 18.5%, the complexed celluloses have higher yields (57.5% for Ti^{3+}, 34.5% for Mn^{2+} and 27.0% for Co^{3+}).

The values of the coupled enzyme activity have also been computed (Table 4). As the complexing enzyme quantities on each support were different, the enzyme activity (photocolorimetrically determined) has been related to the enzyme quantity existing on support, the K correction factor being calculated, according to the relation:

Table 4

The values of coupled enzyme activity

Enzyme support	Extinction	$M_{support}$ mg	A moles/ g · min	Total weight M_t $M_t = 0.2 + M_E$	$K = \frac{M_t}{M_E}$	$A_{cor} = K \cdot A$	$\Delta = A_{cor} - A_c$
Cellulose	0.20	20.11	1.724	0.237	6.4	11	−165
Cellulose + Ti^{3+}	0.65	0.54	208.0	0.316	2.7	571	+25
Cellulose + Co^{3+}	0.40	0.18	385.0	0.254	4.7	1810	+1554
Cellulose + Mn^{2+}	0.065	0.24	43.0	0.269	3.9	168	−160

$$K = \frac{M_{sup} + M_{enz}}{M_{enz}} \tag{4}$$

Applying this correction factor, an important increase of invertase activity has been found, which is coupled on cobalt complexed support (+1.554), which is justified by the role of co-activator of cobalt towards enzyme. This fact is important if it is taken into account that the literature does not mention the invertase co-activation by metal ions. In the case of the other ions, the activity increase is unimportant (+25 like in the case of Ti^{3+}) or there is a diminution of this activity (−160 in the case of Mn^{2+}).

IV. CONCLUSIONS

1. Microcrystalline celluloses obtained by an original hydrolytic process have thermal complexing capacity with transition metal salts, which is reflected by the values of bound metal quantities, which are higher in the case of titanium and cobalt.

2. There are favourable thermal complexing conditions for each metal ion, concerning: metal salt concentration, temperature and duration of the process.

3. The coupling capacity with enzymes of microcrystalline celluloses increases by their complexing with transition metals.

4. In the case of invertase, cobalt ion (III) determines a pronounced increase of enzyme activity, being a co-activator.

5. The immobilization of invertase on metal-treated microcrystalline cellulose can be used in food industry, for fructose and glucose production, by making columns for sugar hydrolysis able to work continuously.

REFERENCES

[1] M. Brezeanu and P. Spacu, "Chimia combinaţiilor complexe", 2nd ed., Ed. didactică şi pedagogică, Bucharest, 1974.

[2] C. Nuţă and C. Buşneag, "Investigaţii biochimice", Ed. didactică şi pedagogică, Bucharest, 1977.

[3] L. Roman and O. Bârzu, "Implicaţii biomedicale ale combinaţiilor complexe", Ed. Dacia, Cluj-Napoca, 1979.

[4] M. Străjescu and F. Teodor, "Elemente de chimie bioanorganică", Ed. Dacia, Cluj-Napoca, 1979.

[5] J. F. Kennedy and J. M. S. Cabral in "Solid-Phase Biochemistry" (W. H. Scouten, Editor), John Wiley, New York, 1983.

[6] J. F. Kennedy and J. M. S. Cabral in "Immobilized Cells and Enzymes—A Practical Approach" (J. Woodward, Editor), IRL Press, Oxford, 1985.

[7] C. Drăgulescu and E. Petrovici, "Chimie structurală modernă. Chimia coordinaţiei 8", Ed. Academiei RSR, Bucharest, 1977.

[8] S. A. Barker, A. N. Emery and J. M. Novias. *Process Biochem.*, **6**, 11 (1971).

[9] A. N. Emery, S. J. Hough, J. M. Novias and T. P. Lyons, *Chem. Eng.*, **259**, 71 (1972).

[10] J. M. Cabral, J. P. Cardoso and J. M. Novias, *Enzyme Microb. Technol.*, **3**, 41 (1981).

[11] C. Vasiliu-Oprea, G. Borhan, N. Merticaru, M. Popa, A. Constantinescu, J. Nicoleanu and C. Ailene, Rom. Pat., 87, 876 (June 27, 1985).

[12] M. Takai, K. Kohus and O. Hagashi, *Cell. Chem. Technol.*, **18**, 197 (1984).

[13] C. Vasiliu-Oprea, N. Bîlbă, F. Weiner, A. Constantinescu and J. Nicoleanu, *Cell. Chem. Technol.*, **19**, 231 (1985).

[14] C. Simionescu, M. I. Popa and S. Dumitriu, *Biotechnol. Bioengineering*, **29**, 361 (1987).

Revue Roumaine de Chimie, 34, 3, 895–899 (1989)

ANALYTICAL APPLICATIONS OF A FEW AZOPYRAZOLONIC DERIVATIVES. I

SPECTROMETRIC DETERMINATION OF IRON(III) WITH AN AZOPYRAZOLONIC DERIVATIVE OF ANTHRANILIC ACID

LUMINIŢA VLĂDESCU and IRINEL BADEA
National Institute of Chemistry, Laboratory of Analytical Chemistry, Splaiul Independenţei 202, 77207, Bucharest, Romania

Received October 10, 1988

The present paper reports the results of a spectrometric study on the iron(III) complexation with an organic reagent obtained by coupling 3-methyl-phenyl-5-pyrazolone with diazotized anthranilic acid. The data obtained were used in a spectrometric method for determining iron(III).

The presence of iron in varied proportions in the most part of the natural and synthetic compounds makes its quantitative determination very important for establishing the quality of the products.

The speciality literature describes a series of reagents which form, with the iron ions, stable compounds that lie at the basis of several methods for spectrometric determination.[1-4]

The present paper reports the results of a spectrometric study on the iron(III) complexation with a new organic reagent obtained by coupling 3-methyl-1-phenyl-5-pyrazolone with diazotized anthranilic acid. The reagent formula (further on noted R) is given in Fig. 1.

The data obtained were used in a spectrometric method for determining iron (III). After establishing the best working conditions, the method was checked on standard solutions and then it was applied for the determination of the iron content in alkaline hydroxides and carbonates.

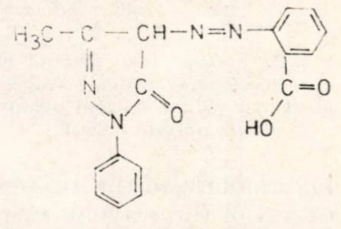

Fig. 1. — Chemical formula of the reagent.

EXPERIMENTAL

Chemicals and equipment

— Aqueous solutions of known titre of 10^{-3}M and $5 \cdot 10^{-4}$M of Fe^{3+} ions.
— Aqueous solutions 10^{-3}M—10^{-1}M of the ions : Ca^{2+}, Mg^{2+}, Sr^{2+}, Ni^{2+}, Co^{2+}, Cu^{2+}, Zn^{2+}, Ce^{3+}, Ce^{4+}, ZrO^{2+}, TiO^{2+}, Ag^{+}, Hg^{2+}.

- 10^{-3}M solution of azopyrazolonic reagent (R) in mixed solvent 50% water – 50% acetone, or 50% water – 50% ethanol.
- acetone, ethanol.
- SPECORD UV-VIS and SPEKOL Karl Zeiss Jena spectrometers.

The quantitative determination of iron(III) was performed by spectrometry in the presence of $KSCN$[5] or of feron.[6]

The solutions to be studied were prepared in 25 mL calibrated flasks where exactly measured volumes of the Fe(III) stock solutions and reagent were introduced ; the flasks were filled up to the mark with the mixed solvent in which the reagent was dissolved. Absorbance of each solution was measured against a corresponding reagent blank prepared analogously but which did not contain Fe(III).

RESULTS AND DISCUSSION

The establishment of the working conditions for spectrometric determination of iron (III)

The influence of the wavelength, of the reagent amount, of the organic solvent and of iron (III) concentration on the absorbance of the Fe(III) – organic reagent solutions was studied for establishing the best working conditions for the spectrometric determination of iron(III).

The azopyrazolonic derivative of anthranilic acid (noted R) forms a coloured complex with Fe(III) instantaneously at room temperature in the presence of mixed solvents water – acetone or water – ethanol (50% V/V).

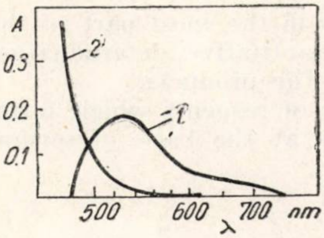

Fig. 2. – Absorption spectra (1 of the complex against reagent blank ; (2) of the reagent against mixed solvent blank.

The complex is stable more than 48 hours.

The absorption spectra of the Fe (III)-R complex and of the reagent solutions are shown in Fig. 2. The maximum absorbance of the complex is at λ = 525 nm where the absorbance of the reagent is very little.

All absorbance measurements were performed at λ = 525 nm against a corresponding reagent blank.

The effect of reagent concentration was examined by measuring the absorbance at λ = 525 nm of the solutions containing a known concentration of Fe (III) and varying amounts of the reagent. A curve in Fig. 3 shows that a 4-fold molar excess of the reagent over Fe(III) is required in order to obtain maximum constant absorbance.

The experimental results showed that the organic solvent does not influence the formation and spectral characteristics of the complex. As the reagent dissolves more rapidly in ethanolic than in acetonic medium, use of the mixed solvents 50% water – 50% ethanol is recommended.

The absorbance readings were constant in the temperature range 10–95°C.

The Fe(III)-R complex solutions obeys Beer's law over the concentration range 0.2–5 ppm (Fig. 4).

The molar absorptivity is $5 \cdot 10^3$ L $mole^{-1}$ cm^{-1}.

The relative error is ±2%.

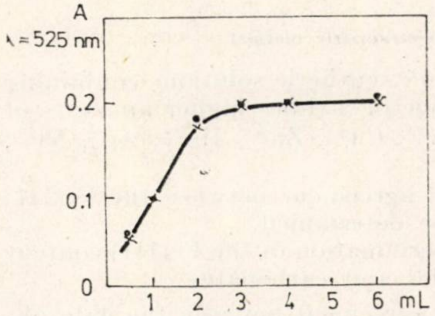

Fig. 3. — Influence of the reagent quantity on the absorbance of the complex (each sample contains 1 mL of 10^{-3}M Fe^{3+} solution): ●-mixed solvents 50 % water — 50 % acetone; ×-mixed solvents 50 % water — 50 % ethanol.

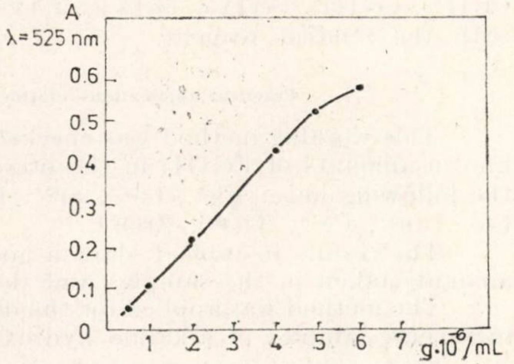

Fig. 4. — Variation of the absorbance with the Fe(III) concentration of solution (each sample contains 8 mL of 10^{-3}M R solution, mixed solvents 50 % water — 50 % ethanol).

Composition and nature of the complex

Job's method of continuous variation (Fig. 5) and spectrometric titration method were employed to establish the composition of the complex. The results indicated the formation of a 1 : 2 complex between Fe(III) and reagent.

Fig. 5. — Variation of the absorbance with the molar ratio of the reagent ($[Fe^{3+}] = [R] = 10^{-3}$M; mixed solvents 50 % water — 50 % ethanol).

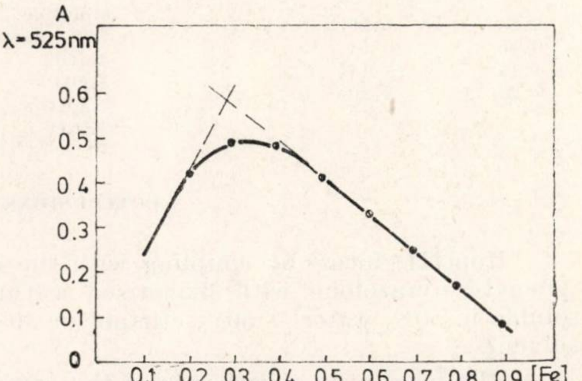

The apparent stability constant of the complex was calculated from the absorbance data by the mole ratio method. The value of log K obtained for the complex at 20 ± 1° was 6.0 ± 0.2.

The cationic nature of the complex was found by ion-exchange experiments.

Study of the interferences showed that the ions of alkaline, alkaline-earth metals and Ag(I), Cu(II), Zn(II), Co(II), Ni(II), Hg(II), Al(III), Cr(III), Ce(III), Ce(IV), Ti(IV), Zr(IV) do not form coloured compounds with the studied reagent.

Practical applications of the spectrometric method

This working method was checked on synthetic solutions containing known amounts of Fe(III) in the presence of 5-times higher amounts of the following ions : Mg^{2+}, Ca^{2+}, Sr^{2+}, Ba^{2+}, Cu^{2+}, Zn^{2+}, Hg^{2+}, Ag^{+}, Ni^{2+}, Co^{2+}, Ce^{3+}, Ce^{4+}, TiO^{2+}, ZrO^{2+}.

The results in table 1 show a good agreement between the Fe(III) amounts taken in the samples and those determined.

The method was applied for the determination of the Fe(III) content in several samples of alkaline hydroxides and carbonates.

The results in table 2 show a good agreement between the data obtained by the method proposed and those found starting from the known method in the literature.

Table 1

Results of the spectrometric determination of Fe(III) in synthetic samples

Quantity of Fe(III)	
In sample (mg)	Determined (mg)
0.56	0.59
0.56	0.54
1.12	1.14
2.24	2.20

Table 2

Results of the Fe(III) content determination in alkaline hydroxides and carbonates

Compound analysed	Fe(III) content %		
	Spectrometric determination with		
	KSCN	Feron	R
Solution 50% NaOH		0.0010	0.0010
NaOH	0.0034	0.0040	0.0036
KOH		0.0006	0.0007
Na_2CO_3	0.4560	0.4655	0.4700
K_2CO_3	0.0025	0.0030	0.0030

CONCLUSIONS

Iron(III) forms by coupling with the reagent obtained 3-methyl-1--phenyl-5-pyrazolone with diazotized anthranilic acid, a 1 : 2 complex soluble in 50% water – 50% ethanol or 50 water – 50% acetone mixed solvents.

The maximum absorbance of the complex is at $\lambda = 525$ nm where the absorbance of the reagent is very little. The molar absorptivity is $5 \cdot 10^3$ L mole^{-1} cm^{-1} at this λ, and log K at $20 \pm 1°$ was found 6.0 ± 0.2.

Data obtained were used in a spectrometric method for determining Fe(III). The range of the Beer – Lambert law validity is 0.2 – 5 ppm· The method was applied for the iron content determination in alkaline hydroxide and carbonates.

REFERENCES

[1] E. B. Sandell, "Colorimetric Determination of Traces of Metals", New York, Interscience, 1959.

[2] G. Charlot, "Colorimetric Determination of Elements", Elsevier Publishing Company, Amsterdam, 1964, p. 271.

[3] G. Popa and S. Moldoveanu, "Analiza chimică cantitativă cu reactivi organici", Ed. Tehnică, Bucharest, 1969, p. 290.

[4] J. Fries and H. Getrost, "Organic Reagent for Trace Analysis", E. Merck Darmstadt, 1977, p. 186.

[5] M. Zimmermann, "Photometric Metal and Water Analysis", W.V.C., M. B.H., Stuttgart, 1962, Section B—b 6/1 (61) and 6/2 (61).

[6] L. Vlădescu and C. D. M. Pop, *Rev. Roumaine Chim.*, **26**, 1019 (1981).

Revue Roumaine de Chimie, **34**, *3*, 901–903 (1989)

РЕАКЦИИ 1,3-ДИПОЛЯРНОГО ЦИКЛОПРИСОЕДИНЕНИЯ НИТРИЛИМИНОВ С КАЛИЕВЫМИ СОЛЯМИ ЭТИНИЛТИО(СЕЛЕНО(ЛОВ

ЯРОСЛАВ ВАСИЛЬЕВИЧ ЗАЧИНЯЕВ *, АЛЕКСАНДР ИВАНОВИЧ БОБРОВ
и АНАТОЛИЙ ИОСИФОВИЧ ГИНАК
Ленинградский технологический институт им. Ленсовета, г. Ленинград, СССР

Получена 3 октября 1988 г.

Взаимодействием N-арил-C-хлоргидразонов с калиевыми солями этинилтио(селено)лов в присутствии органического основания получены 4H—1,3,4-тиа(селена) диазины. Приведены выходы, физические константы и спектральные данные полученных соединений.

Interaction of N-aryl-C-chlorohydrazones with potassium ethinylthio(seleno)lates in bezene in the presence of organic base results in 4H-1,3,4-thia(selena)diazines. Yields, physical constants and spectral data of prepared compounds are described.

В данной работе приводятся результаты изучения взаимодействия этинилтиолятов и селенолятов калия [1,2] с N-арил-C-хлоргидразонами.[3] Установлено, что в присутствии органического основания в бензоле N-арил-C-хлоргидразоны превращаются в нитрилимины, которые реагируют с этинилтиолятами и селенолятами калия по схеме [3 + 3]-циклоприсоединения с образованием 2, 4, 5-тризамещённых 4H-1,3, 4-тиа-(селена) диазинов (I—X).

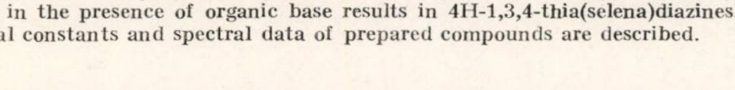

$$\mathrm{Ar{-}NH{-}N{=}\underset{\displaystyle Cl}{\underset{|}{C}}{-}R + Et_3N \xrightleftharpoons{C_6H_6} Et_3N\cdot HCl + Ar{-}\overset{-}{N}{-}N = \overset{+}{C}{-}R}$$

$$[\mathrm{R'} - \mathrm{C} \equiv \mathrm{C}-\mathrm{Z}^-]\mathrm{K}^+ + \mathrm{Ar} - \overset{-}{\mathrm{N}} - \mathrm{N} = \overset{+}{\mathrm{C}} - \mathrm{R} \rightleftarrows$$

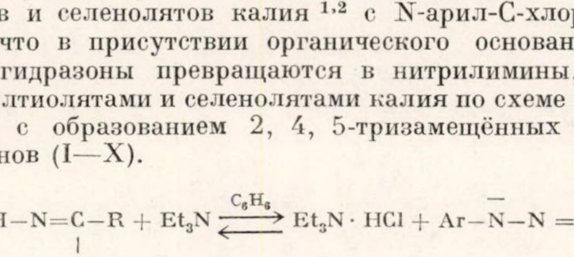

---

* Адрес для переписки: 191028, г. Ленинград, Д-28, ул. Пестеля, д. 13/15, кв. 106, Зачиняеву Ярославу Васильевичу.

Таблица

Выходы, константы и спектральные данные полученных тиа(селена) диазинов

№	Название	Выход, %	Т.пл., °C	ИК-спектр, ν (см$^{-1}$)			ПМР-спектр. δ (м.д.)			
				$>C=C<$	$>C=N-$	$>C=O$	H	R′	R	Ar
I	2-ацетил-4, 5-дифенил-4H-1,3,4-тиадиазин	58	145	1565	1590	1685	5.80 с	7.43 м	2.40 с	7.02 м
II	2-ацетил-4-фенил-5-п-толил-4H-1,3,4-тиадиазин	50	147	1600	1680	1710	5.84 с	2.26 с 7.24 д	2.42 с	7.24 м
III	2-ацетил-4-фенил-5-п-хлорфенил-4H-1,3,4-тиадиазин	62	133	1600	1690	1710	5.65 с	7.80 д	2.63 с	7.80 м
IV	2-ацетил-5-п-анизил-4-фенил-4H-1,3,4-тиадиазин	56	165	1610	1680	1710	5.58 с	3.75 с 7.33 д	2.48 с	7.33 м
V	2-ацетил-5-трет.-бутил-4-фенил-4H-1,3,4-тиадиазин	61	134	1590	1680	1660	5.60 с	0.80 с	2.38 с	7.06 м
VI	2-ацетил-4-п-толил-4-фенил-4H-1,3,4-тиадиазин	62	126	1570	1595	1680	5.79 с	7.24 м	2.41 с	7.08 д
VII	2-карбоэтокси-4-п-бромфенил-5-фенил-4H-1,3,4-тиадиазин	85	112	1580	1595	1715	5.91 с	7.50 м	CH_2 4.37 кв CH_3 1.40 т	7.45 кв
VIII	2-ацетил-4,5-дифенил-4H-1,3,4-селенадиазин	100	153	1580	1630	1665	6.09 с	6.88 м	2.45 с	7.14 м
IX	2-ацетил-4-п-толил-5-фенил-4H-1,3,4-селенадиазин	89	146	1575	1650	1665	5.95 с	6.88 м	2.40 с	7.11 д 2.40 с
X	2-карбоэтокси-4-п-бромфенил-5-фенил-4H-1,3,4-селенадиазин	90	175	1590	1670	1710	6,21 з	7.36 м	1.29 т 3.89 кв	6.98 д

I, Ar = Ph, R = Ac, R′ = Ph, Z = S ;

II, Ar = Ph, R = Ac, R′ = n-Me—C_6H_4, Z = S ;

III, Ar = Ph, R = Ac R′ = n-Cl—C_6H_4, Z = S ;

IV, Ar = Ph, R = Ac, R′ = n-CH_3O — C_6H_4, Z = S ;

V, Ar = Ph, R = Ac, R′ = t-Bu, Z = S ;

VI, Ar = n-CH_3—C_6H_4, R = Ac, R′ = Ph, Z = S ;

VII, Ar = n-Br — C_6H_4, R = CO_2Et, R′ = Ph, Z = S ;

VIII, Ar = Ph, R = Ac, R′ = Ph, Z = Se ;

IX, Ar = n-CH_3—C_6H_4, R = Ac, R′ = Ph, Z = Se ;

X, Ar = n-Br — C_6H_4, R = CO_2 Et, R′ = Ph, Z = Se.

ЭКСПЕРИМЕНТАЛЬНАЯ ЧАСТЬ

ИК-спектры снимали на спектрофотометре ,,ИКС-29'' в 5% растворе в $CHCl_3$. Спектры ПМР снимали на приборе ,,Tesla BS—487 С'' (80 МГц) в 10% растворе в CCl_4 с применением в качестве внутреннего стандарта ГМДС. Температуры плавления приводятся без поправки.

Соединения I—X получены по общей методике.

Выходы, температуры плавления и спектральные данные приведены в таблице.

Взаимодействие N-арил-С-хлоргидразонов с этинилтио(селено)лятом калия (синтез тиа(селена)диазинов I—X).

К раствору 0,01 моля соответствующего α-хлоргидразона [3] в 100 мл абсолютного бензола и 0,02 молях безводного триэтиламина при перемешивании добавляли 0,01 моля свежеприготовленного 2-арилэтинилтио(селено)лята калия .[1,2] Смесь окрашивается в тёмно-красный цвет. Её перемешивали 1 час, затем выдерживали 12 часов. Образовавшийся осадок KCl↓ отфильтровывали и промывали горячим бензолом. После отгонки в вакууме бензола и триэтиламина получаются тиа(селена)диазины I—X. Перекристаллизация из метанола.

ЛИТЕРАТУРА

[1] R. Huisgen, M. Seidel, G. Wallbillich und H. Knupfer, *Tetrahedron*, **17**, 3 (1962).

[2] Я. В. Зачиняев и Д. С. Орлов, *Реактивы и особо чистые вещества*, **6**, 51(1980).

[3] Я. В. Зачиняев, А. И. Бобров, Д. С. Орлов и С. А. Онохин, *Реактивы и особо чистые вещества*, **1**, 27(1982).

ORSZÁGOS MŰSZAKI INFORMÁCIÓS KÖZPONT ÉS KÖNYVTÁR 1883

NOTE POUR LES AUTEURS

La **Revue Roumaine de Chimie** publie des articles en anglais, français, russe, allemand ou espagnol. Les auteurs sont priés d'envoyer des articles et des comptes rendus inédits.

Les manuscrits seront dactylographiés à double interligne. La bibliographie, les tableaux et la légende des figures seront placés après le texte.

Si l'article fait partie d'une série numérotée, la partie précédente sera donnée comme première référence.

Chaque article sera précédé d'un résumé comprenant quinze lignes au maximum.

Les références bibliographiques dans le texte seront faites par des exposants sans parenthèses et paraîtront à la fin de l'ouvrage.

Les publications périodiques mentionnées dans la bibliographie seront présentées suivant les prescriptions internationales : le nom de l'auteur précédé de l'initiale du prénom, le titre du périodique abrégé conformément à « Chemical Abstracts » et souligné par une ligne, le numéro du tome indiqué par des chiffres arabes et souligné par deux lignes, suivi de la première page de l'article : à la fin, l'année de la parution sera placée entre parenthèses. Le numéro de la revue ne sera pas indiqué si les pages du volume sont numérotées consécutivement.

Les textes des livres ou traités inclueront : le nom des auteurs, précédés de l'initiale du prénom, le titre du livre entre guillemets et sans être souligné, le numéro du tome précédé par l'abréviation « vol. » (ou « Bd. »), le numéro de l'édition, les éditions (the publisher), la localité de la parution du livre, l'année de la parution et la page de la référence précédée(s) par l'abréviation « p » (ou « S »).

Les brevets seront indiqués comme suit : l'auteur ou la firme, le pays et le numéro du brevet, la date de la revue *(Chem. Abstr.)*. Par ex. : M. Jones (to Union Carbide Co.), Brit. Pat. 610 238, 2 Sept. 1959 : cf. *Chem. Abstr.*, **54**, 12808 (1960).

Si la référence n'a pas été lue en original, on indiquera aussi la revue de références consultée.

Les diagrammes seront tracés à l'encre de Chine sur papier calque. Les tableaux et les figures (en nombre strictement nécessaire), ainsi que les courbes dans les figures seront numérotés par des chiffres arabes. Leur explication sera donnée dans la légende des figures. Prière de ne pas inscrire les mêmes données dans les tableaux et les figures. Chaque tableau aura un titre. On indiquera dans le texte la place approximative des tableaux et des figures. Les formules chimiques seront incluses dans le texte ; en outre, elles seront transcrites sur papier calque, à l'encre de Chine.

Les auteurs sont priés d'indiquer les caractères italiques (en soulignant les lettres au crayon), ainsi que tout autre caractère spécial : les préfixes *ortho*, *méta*, *para*, *cis*, *trans*, etc. seront soulignés pour indiquer leurs caractères italiques et ne seront jamais écrits avec des majuscules.

Aucune correction à la main ne sera admise sur le manuscrit. Les corrections seront frappées à la machine. Les lettres grecques ou d'autres symboles spéciaux seront insérés à la main à l'encre clairement.

Le manuscrit sera signé par l'auteur.

Le titre courant aura 50 lettres au maximum.

L'entière responsabilité du contenu des articles appartient aux auteurs.

Sur demande on peut obtenir une note plus complète.

PRINTED IN ROMANIA

TRAVAUX PARUS AUX ÉDITIONS DE L'ACADÉMIE DE LA RÉPUBLIQUE SOCIALISTE DE ROUMANIE

ELENA CEAUŞESCU, **Răşini de hidrocarburi, vol. 1**, 1988, 344 p.
ELENA CEAUŞESCU, **Progrese în chimia şi tehnologia polimerilor**, 1986, 446 p.
ELENA CEAUŞESCU, **Forschungen im Bereich der Chemie und Technologie der Polymere**, 1986, 444 p.
ELENA CEAUŞESCU, **Cercetări în chimia şi tehnologia polimerilor**, 1983, 520 p.
ELENA CEAUŞESCU, **Noi cercetări în domeniul compuşilor macromoleculari**, 1981, 536 p.
ELENA CEAUŞESCU, **Polimerizarea stereospecifică a izoprenului**, 1979, 307 p.
ELENA CEAUŞESCU, **Research work on synthesis and characterization of macromolecular compounds. Contributions**, 1974, 251 p.
I. G. MURGULESCU, **Introducere în chimia fizică, vol. I. 1. Atomi, molecule, legătură chimică**, 1976, 560 p.
I. G. MURGULESCU, V. EM. SAHINI, **Introducere în chimia fizică, Vol. I, 2. Structura şi proprietăţile moleculelor**, 1979, 604 p.
I. G. MURGULESCU, E. SEGAL, **Introducere în chimia fizică, Vol. II. 1. Teoria molecular-cinetică a materiei**, 1979, 1036 p.
I. G. MURGULESCU, TATIANA ONCESCU, E. SEGAL, **Introducere în chimia fizică, Vol. II. 2. Cinetică chimică şi cataliză**, 1981, 1024 p.
I. G. MURGULESCU, J. PĂUN, **Introducere în chimia fizică, Vol. I, 3. Nucleul atomic, reacţii nucleare, particule elementare**, 1982, 606 p.
I. G. MURGULESCU, RODICA VÎLCU, **Introducere în chimia fizică. Vol. III. Termodinamica chimică**, 1982, 624 p.
I. G. MURGULESCU, O. M. RADOVICI, **Introducere în chimia fizică, Vol. IV. Electrochimia**, 1986, 416 p.
CRISTOFOR I. SIMIONESCU, VALERIA GORDUZA, **Implicaţii bioenergetice ale coloranţilor**, 1988, 208 p.
R. VÎLCU, M. LECA, **Termodinamica polimerilor prin cromatografie de gaze**, 1987, 238 p.
I. ZUGRĂVESCU, M. PETROVANU, **Cicloadiţii 3+2 dipolare**, 1987, 446 p.
RAUL MIHAIL, ION GROZEANU, **Estimarea secvenţială aplicată sistemelor chimice**, 1986, 406 p.
M. BREZEANU, I. PATRON, M. ANDRUH, **Combinaţii complexe polinucleare şi aplicaţiile lor**, 1986, 244 p.
A. T. BALABAN et al., **Labelled Compounds and Radiopharmaceuticals Applied in Nuclear Medicine**, coédition avec John Wiley and Sons, 1986, 742 p.
D. PURDELA, **Nomenclatura chimiei organice — IUPAC**, 1986, 451 p.
PETRU BUDRUGEAC, **Probleme de chimie**, 1986, 280 p.
T. ONCESCU, S. G. IONESCU, **Conversie fotochimică şi stocare de energie**, 1985, 272 p.
V. DRĂGUŢAN, A. T. BALABAN, M. DIMONIE, **Olefin Metathesis and Ring-Opening Polymerization of Cyclo-Olefins**, coédition avec John Wiley and Sons, 1985, 544 p.
C. LITEANU, I. RÎCĂ, **Optimizarea proceselor analitice**, 1985, 360 p.
N. PERESCU, **Chimia extracţiei cu solvenţi şi aplicaţii**, 1985, 212 p.
V. EM. SAHINI, M. HILLEBRAND, **Chimie cuantică în exemple şi aplicaţii**, 1985, 382 p.
GH. MARCU, **Chimia compuşilor coordinativi**, 1984, 415 p.
E. CORDOŞ, C. MANOLIU, **Spectrometria de absorbţie şi fluorescenţa atomică**, 1984, 178 p.
C. BODEA, **Tratat de biochimie vegetală, p. II, t. V**, 1984, 438 p.
N. ASANDEI, A. GRIGORIU, **Chimia şi structura fibrelor**, 1984, 395 p.
N. IONESCU, M. CĂLDĂRARU, **Oxidarea catalitică a olefinelor inferioare**, 1983, 178 p.
C. I. SIMIONESCU, F. DANEŞ, **Originea vieţii**, 1984, 110 p.
C. BODEA, **Tratat de biochimie vegetală, p. II, t. IV**, 1982, 408 p.
CR. SIMIONESCU, VALERIA GORDUZA, **Polimeri biocompatibili şi biologic activi**, 1980, 479 p.
M. FLORESCU, **Metode ştiinţifice în dezvoltarea industriei chimice moderne**, 1979, 495 p.
C. GH. MACAROVICI, **Analiza chimică cantitativă anorganică**, 1979, 457 p.

ISSN 0035—3930

I. P. Informaţia c. 2673

43 426

Lei 40

1989 APR

F 1103 ~~05~~

ACADÉMIE DE LA RÉPUBLIQUE SOCIALISTE DE ROUMANIE

REVUE ROUMAINE DE CHIMIE

Hommage à l'académicien ELENA CEAUȘESCU

TOME 34

N° 4

Avril 1989

Rev. Roumaine Chim.

RRCHAX, 34, 4, p. 905 – 1114 (1989), Bucarest

EDITURA ACADEMIEI REPUBLICII SOCIALISTE ROMÂNIA

ACADÉMIE DE LA RÉPUBLIQUE SOCIALISTE DE ROUMANIE

COMITÉ DE RÉDACTION

Rédacteur en chef :

I. G. MURGULESCU, membre de l'Académie de la République Socialiste de Roumanie

Rédacteurs en chef adjoints :

A. T. BALABAN et V. EM. SAHINI, membres correspondants de l'Académie de la République Socialiste de Roumanie

Collège de rédaction :

EM. BRATU, ELENA CEAUŞESCU, ECATERINA CIORĂNESCU-NENITZESCU, CR. SIMIONESCU, membres de l'Académie de la République Socialiste de Roumanie ; P. SPACU, membre correspondant de l'Académie de la République Socialiste de Roumanie ; M. BANCIU, M. D. GHEORGHIU, I. HAIDUC, D. I. MARCHIDAN, G. NIAC et D. SĂNDULESCU

La Revue Roumaine de Chimie paraît 10 fois par an. Toute commande de l'étranger sera adressée à ROMPRESFILATELIA — sectorul Export-Import Presă, P.O. Box 12—201, télex 10376 prsfi r 78104 Bucarest, Calea Griviţei nr. 64—66, Roumanie

Les manuscrits, les livres et les revues proposés en échange, ainsi que toute correspondance seront envoyés à la rédaction :

REVUE ROUMAINE DE CHIMIE

125, Calea Victoriei, 79717 Bucarest, Roumanie, téléphone 50 76 80

EDITURA ACADEMIEI REPUBLICII SOCIALISTE ROMÂNIA
125, Calea Victoriei 79717, Bucarest, Roumanie, téléphone 50 76 80

HOMMAGE À L'ACADÉMICIEN
ELENA CEAUȘESCU

ORSZÁGOS MŰSZAKI INFORMÁCIÓS KÖZPONT ÉS KÖNYVTÁR 1883

IN HONOUR OF
ELENA CEAUȘESCU, D. CHEM. ENG.,
MEMBER OF THE ACADEMY OF THE SOCIALIST REPUBLIC OF ROMANIA

On January 7, this year, we celebrate the birthday and 50 years of revolutionary activity of Academician Elena Ceauşescu. A Doctor of Chemical Engineering, Member of the Executive Political Committee of the Central Committee of the Romanian Communist Party, First Vice-Prime Minister of the Government of the Socialist Republic of Romania, President of the National Council for Science and Education, Dr. Elena Ceauşescu chairs a vast scientific, political and social enterprise meant to bring into effect the country's plans for economic and social development, the important programs geared to a better organization and modernization of production, to increasing work productivity and efficiency, to a comprehensive implementation of the overall policy of the Romanian Communist Party and State, for the benefit of Romanian science, education and culture. The organization and management of the scientific research in this country, most especially in the fields of chemistry, and chemical technology and engineering, largely rely upon the innovative scientific spirit of, and direct guidance by Dr. Elena Ceauşescu.

As a direct outcome, the entire research and development system in chemistry has been given an appropriate coordination and has been integrated, along with the higher education in the field, with the respective industry.

The research work undertaken by Dr. Elena Ceauşescu is focused mainly on the chemistry and technology of macromolecular compounds; she has contributed to elucidating a number of major problems in the area — a most dynamic one in chemistry today, while also providing valuable contributions in all stages of applied research and

engineering, thus fostering the implementation in industry of the results of fundamental research.

Her studies dwell, *inter alia*, upon procedures for monomer and solvent purification; procedures for obtaining polymers via stereospecific polymerization and emulsion polymerization; procedures for obtaining polycondensates; studies on the structural characteristics of polymers and the relationship between structure and properties, as well as methods for the characterization of polymers. A series of studies deal with the use of complex catalysts for polymer synthesis in solution, with special emphasis on catalysts based on transition metals. Other works are concerned with the obtaining of polymers modified by isomerization, degradation and substitution reactions.

The stereospecific polymerization of isoprene holds an important place in the research work developed by Dr. Elena Ceaușescu, owing to the paramount relevance of this problem in today's chemistry of synthetic rubber. Part of the results were gathered in Dr. Ceaușescu's doctoral thesis. A special emphasis was placed on the synthesis of *cis*-1,4-polyisoprenic rubber that displays properties and structures similar to those of natural rubber, and substitutes for the latter in the tyre and technical item industry. Theoretical aspects connected with the reaction mechanism and kinetics, and the properties of the polyisoprene were also dealt with. Research was focused on the optimization of basic parameters, the obtaining of catalytic systems and development of the main steps of the technological flow-chart. The results have led to an industrial process for manufacturing *cis*-1,4-polyisoprenic rubber in Romania.

Dr. Elena Ceaușescu's scientific activity is also reflected in numerous papers published in scientific journals and in six monographs, first put out by Editura Academiei R. S. România, Bucharest, namely, "Research Work on Synthesis and Characterization of Macromolecular Compounds" (1974), "Stereospecific Polymerization of Isoprene" (1979), "Recent Research in the Field of Macromolecular Compounds" (1981), "Research in the Chemistry and Technology of Polymers" (1983), "Advances in Polymer Chemistry and Technology" (1986), and "Hydrocarbon Resins" (1988). Many publishing houses worldwide were soon to offer their readers translations of these books.

Dr. Elena Ceauşescu chaired the National Congress of Chemistry in the years 1978, 1981, 1988, and the IUPAC's Macro '83 Symposium. Her opening address at the 1988 National Congress of Chemistry gives important guidelines to the chemical research in Romania, also providing for the strengthening of the international scientific co-operation. Dr. Elena Ceauşescu contributed valuable papers to many scientific congresses and symposia — an outcome of her comprehensive scientific activity in the field of elastomer chemistry.

Dr. Elena Ceauşescu's scientific merits won well-deserved national and worldwide recognition. She is a member of the Academy of the Socialist Republic of Romania. She was also elected member of numerous international chemical societies of high renown and was nominated honorary professor by important higher education institutions abroad. Dr. Ceauşescu is a honorary member of the International Society of Industrial Chemistry, France; active member of the Academy of Sciences, New York; honorary member of the College of Chemists and Chemical Engineers in Costa Rica; honorary member of the University Council and of the Management Council of the Central University in Ecuador; honorary member of the Ecuador Institute of Natural Sciences; honorary member of the School of Information Science of the Central University of Ecuador; honorary professor of the National Engineering University, Peru; honorary member of the American Institute of Chemists (A.I.C.); Doctor Honoris Causa of the University of Buenos Aires; Doctor Honoris Causa of the University of South-Bahia Blanca, Argentina; Doctor Honoris Causa of the Feminine University of Manila, the Philippines; honorary member of the Chemical Society of Mexico; Doctor Honoris Causa of the University of Yucatan, Mexico; Extraordinary Professor of the Autonomous National University of Mexico; Doctor Honoris Causa of Sciences, University of Teheran; honorary member of the Society of Polymer Science in Japan; corresponding member of the Academy of Athens; awardee of the Silver Medal of the Science University of Kuweit; honorary member of the Academy of Arts and Sciences in Ghana; honorary member of the Academy of Sciences of the State of Illinois, USA; Fellow of the Royal Institute of Chemistry, UK; Professor Honoris Causa of the Polytechnics of Central London; member of the European Academy of Sciences, Arts

and Humanities, and member of the Honorary Committee of the Academy; Doctor Honoris Causa of the Technical University of the Middle East, Ankara; Doctor Honoris Causa of the University of Malta; Doctor Honoris Causa for Sciences of the Islamabad University, Pakistan; Doctor Honoris Causa for Sciences of the University of Liberia; Doctor Honoris Causa in Chemical Sciences, D.P.R. of Korea.

The high praise enjoyed by Dr. Elena Ceaușescu is also reflected in her being awarded important titles and distinctions of merit. Among these are: the highest Romanian title of honour "Hero of the Socialist Republic of Romania"; the title "Hero of Socialist Labour"; the medal "Star of the Socialist Republic of Romania", as well as other orders and medals, Romanian and foreign. She was also awarded the Gold Medal of the Institute for the Problems of a New International Economic Order, the Gold Medal "Marie Curie" and the Jubilee Gold Medal of the Institute of International Relations in Rome, and the Gold Badge of the European Academy of Sciences, Arts and Humanities. By virtue of these, Academician Elena Ceaușescu is the most prestigious representative of the Romanian contemporary science, education and culture.

Active in the national scientific and political life as well as in the international arena, presiding over the Romanian National Committee "Scientists and Peace", Academician Elena Ceaușescu makes an outstanding contribution to the carrying into effect of Romania's policy of independent domestic development, many-sided international co-operation, and struggle for peace, a policy designed under the guidance of Comrade Nicolae Ceaușescu, Secretary General of the Romanian Communist Party, President of the Socialist Republic of Romania, Honorary President of the Academy of the Socialist Republic of Romania.

The National Council for Science and Education, the Ministry of the Chemical and Petrochemical Industry, the Academy of the Socialist Republic of Romania, and the Central Institute for Chemistry join whole-heartedly in the feelings of highest esteem and praise the Romanian people has for Academician Elena Ceaușescu, and express deepest appreciation for her exceptional contribution

to the building of modern Romania, to the development of scientific research and education in this country, particularly in the field of chemistry, chemical technology and engineering. We wish the most distinguished Romanian scholar many happy returns and a long and fruitful activity in order that science, education and culture in the Socialist Republic of Romania be raised onto ever higher levels of performance, for the benefit of our society, of world progress and peace.

THE NATIONAL COUNCIL
FOR SCIENCE AND EDUCATION

THE MINISTRY
OF THE CHEMICAL
AND PETROCHEMICAL
INDUSTRY

THE ACADEMY
OF THE SOCIALIST
REPUBLIC OF ROMANIA

THE CENTRAL INSTITUTE
FOR CHEMISTRY

REVUE ROUMAINE DE CHIMIE

Tome 34, N° 4 **Avril, 1989**

IN HONOUR OF
ELENA CEAUŞESCU, D. CHEM. ENG.
MEMBER OF THE ACADEMY OF THE SOCIALIST REPUBLIC OF ROMANIA

ELENA CEAUŞESCU, M. DIMONIE, ANNELIESE CORNILESCU, V. DRĂGUŢAN, ELENA NICOLESCU, S. COCA, LUCIA POPESCU, MIHAELA CUZMICI, C. OPRESCU, M. TEODORESCU, GH. HUBCA, R. GROSESCU, ALICE VASILESCU and M. CHIPARĂ, Aspects on the stereochemistry and mechanism of ring-opening polymerization of cycloolefins 907–916

MARIUS ANDRUH, O.D. CHIRICĂ and MARIA BREZEANU, Angular overlap model (AOM) calculations for the coordination compounds with macrocyclic ligands. II. AOM parameters for nickel(II) coordination compounds with saturated macrocyclic ligands 917–919

A. C. BANCIU, Bis(3-carbethoxy-1,5-di-*o*-anisyl-formasyl) Ni(II). A new unusual pentacoordinate formazane complex 921–932

C. M. BOGHINĂ, C. I. CINCU, N. N. MARINESCU, M. M. MARINESCU, M. V. DIMONIE and D. S. VASILESCU, Radical polymerization of acrylamide in homogeneous and heterogeneous systems. I. Solution properties of acrylamide in water 933–935

V. BRÂNZOI, S. STERNBERG and LILIANA APĂTEANU, Polarization behaviour of lead in sulphuric acid solution containing ammonium dichromate additions 937–944

MARIA BRIE, IOAN A. SILBERG and NICOLAE PALIBRODA, Derivatives of 1,2-pyrazoles. II. The influence of alkaline media on the reaction of 1,3-dicarbonyl compounds with hydrazine 945–952

ALEXANDRU CECAL and GRETY-IRINA CIUCHI, Radiochemical method for determination of solubility of some hard soluble compounds (in German) 953–960

Rev. Roumaine Chim. **34**, *4*, 905–1114 (1989), Bucarest.

E. DARVASI, H. MIOŞCU, A. MORARU, C. OANCEA and E. CORDOŞ, Microprocessor operated scanning UV-VIS monochromator 961–965

MIHAELA DRĂGĂNOIU and SOLOMON STERNBERG, The mean activity coefficient of $ZnSO_4$ and $CuSO_4$ in the electrolyte solutions: $ZnSO_4 + Li_2SO_4 + H_2O$ and $CuSO_4 + Li_2SO_4 + H_2O$ 967–975

V. DRĂGUŢAN, I. DRĂGUŢAN, C. CONDEIU and A. M. GLATZ, Friedel-Crafts chemistry of unsaturated alicyclic systems. IV. Effect of the catalytic system in Friedel-Crafts reaction of unsaturated esters 977–982

EMIL DUMITRIU, NICOLAE BÎLBĂ, VASILE HULEA and SPIRIDON OPREA, Selective alkylation of toluene on ZSM-5 zeolites 983–988

L. ENESCU, AURELIA GHENCIULESCU, F. CHIRALEU and I. G. DINULESCU, Reaction of ketones with benzocyclobuteno-norbornenic skeleton in the presence of dimethyloxosulfonium methylide 989–993

I. GERGEN, M. BOHL, H. SIMON and Z. SIMON, Structure-activity relations for steroids by the MTD method. Superposition procedure for molecules with different condensed cycles 995–1004

MIRCEA D. GHEORGHIU, ANA SCHIKETANZ, ATENA NECULA and ALEXANDRU T. BALABAN, Carbon-13 nuclear magnetic resonance assignments of the saturated segment from 1, 2, 3, 4-tetrahydrophenanthrene by means of ^{13}C and ^{2}H labelling 1005–1008

GH. IONESCU, ANA ONU and VALER NAGACEVSCHI, Determination of some liquid–vapour equilibrium data for acetone (1)–chloroform (2)–nonideal solution 1009–1015

G. IVAN, ERIKA TAVARU, MARIA GIURGINCA and D. N. NICOLESCU, Crosslinking of brominated butyl rubber by means of aromatic diamines 1017–1028

GH. MARCU, CS. VÁRHELYI, J. FÜLÖP and DANA ITUL, New cobalt chelates with ethylenediimino-bis-benzoylacetone 1029–1035

L. NEGULESCU, Considerations on the chemical regime maintenance in a water cooling system (in German) 1037–1046

I. V. NICOLESCU, GH. NEDELCU, RODICA MĂNĂILĂ, M. IVAŞCU, FLORENTINA AVRAMESCU, VIORICA SPÂNU and G. FILOTI, Phase composition and structure in Fe–Mg–O catalysts for oxydehydrogenation of n-butenes to butadiene 1047–1054

E. PINCOVSCHI, M. MERCHEŞ and KIM CHOL SIK, Synthesis and characterization of ZSM-5 zeolites 1055–1060

IG. C. POINESCU and A. CARPOV, Relationships between crosslinked copolymer synthesis and their features 1061–1073

IRINA SEROVA, GALINA OLEINIKOVA and A. I. GHINAC, Investigation of the processes of the oleandomycin phosphate inactivation (in Russian) 1075–1079

R. Z. TUDOSE, M. FOURAR, O. PETRUŞ and B. CONSTANTIN, Study of the performance of a new type of vibration extraction apparatus. I. Hydrodynamic characteristics of the apparatus (in French) 1081–1093

M. O. VLAD and E. SEGAL, Chemical systems with uncertain parameters. The method of integral equations 1095–1100

T. VOLINTIRU, G. IVAN, ELENA BUGARU and PAULA BUJENIŢĂ, Vulcanization of acrylonitrile-butadiene rubber with alkylphenol formaldehyde resin 1101–1106

FLORICA ZĂLARU, FELICIA CORNEA, AURELIA MEGHEA and D. IONESCU, Coordination compounds of $CuBr_2$ with some triazenoimidazole derivatives 1107–1114

Revue Roumaine de Chimie, **34**, *4*, 907–916 (1989)

ASPECTS ON THE STEREOCHEMISTRY AND MECHANISM OF RING-OPENING POLYMERIZATION OF CYCLOOLEFINS

ELENA CEAUȘESCU[a], M. DIMONIE[b], ANNELIESE CORNILESCU[a], V. DRĂGUȚAN[c],
ELENA NICOLESCU[a], S. COCA[a], LUCIA POPESCU[a], MIHAELA CUZMICI[a], C. OPRESCU[a],
M. TEODORESCU[b], GH. HUBCA[b], R. GROSESCU[d], ALICE VASILESCU[d]
and M. CHIPARĂ[d]

[a] Chemical Research Institute, Spl. Independenței 202, Bucharest, Romania
[b] National Institute for Chemistry, Bucharest, Romania
[c] Centre of Organic Chemistry, Bucharest, Romania
[d] Institute of Physics and Nuclear Engineering, Bucharest, Romania

Received November 21, 1988

Ring-opening polymerization of cycloolefins in the presence of WCl_6-based catalysts leads to polyalkenamers. The *cis-trans* content of these polymers depends on the reaction parameters (temperature, monomer concentration, etc.), initiation mode as well as on the nature of the organometallic compound, used as cocatalyst. Our studies indicated that at least two active species appear during this process : a very active species, unstable at high temperature which forms prevalently *cis*-polymer and a less active one, but more stable, leading to *trans*-polymer. Based on these data the reaction stereochemistry and the mechanism of initiation and propagation are discussed.

Although the ring-opening polymerization of cycloolefins has been known for more than 30 years, this process offers today still various research directions towards elucidating the reaction mechanism and stereochemistry or the nature of the active centres as well as in elaborating new highly stereoselective catalytic systems and polymerization procedures.[1–5] Under mild conditions, the olefin ring opens at the double bond to afford high molecular weight polyalkenamers containing in their chain the whole monomer unsaturation.

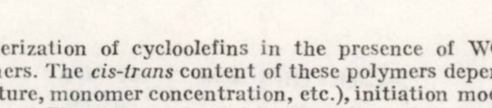

$$n\,\underset{(CH_2)_x}{CH=CH} \xrightarrow{-W-} \left[CH=CH-(CH_2)_x\right]_n$$

The reaction is of a general character and it is a new and direct way to the synthesis of polymers.

It has been undoubtedly demonstrated that during polymerization the olefin ring opens at the C=C double bond.[6]

Nowadays, it is almost unanimously accepted that this reaction takes place *via* carbenic species, namely metallacarbene complexes. The propagation reaction occurs by inserting the cycloolefin on the metal-carbene bond by intermediacy of a metallacyclobutane derivative. During this process the former double bond is cleaved to afford a new one and a new metallacarbene complex.[7,8]

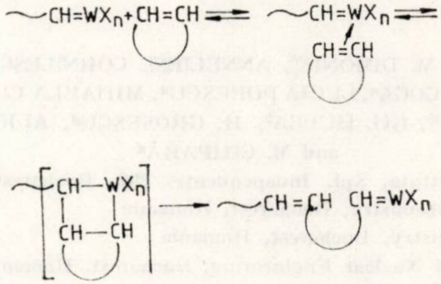
~CH=WXn+CH=CH
~CH=WXn
CH=CH
~CH—WXn
CH—CH
~CH=CH CH=WXn

In addition ,the reaction of the C=C double bond of the polymer chain on the active centres results in the formation of cyclic oligomers in a process occurring at equilibrium.

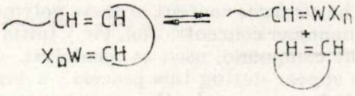
~CH=CH
XnW=CH
~CH=WXn
CH=CH

The most important factors which determine the microstructure of the polyalkenamers obtained by ring-opening polymerization of cycloolefins have proved to be the nature of the catalytic system and the temperature of the reaction. For instance cyclopentene can polymerize to *cis*- or *trans*-polypentenamer as a function of the catalyst employed.

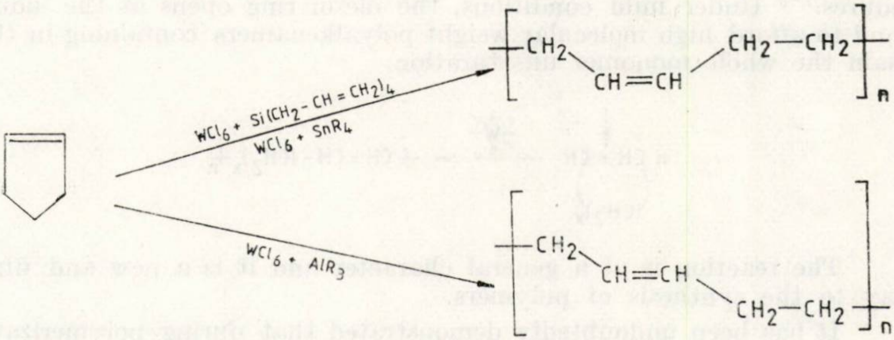
WCl6 + Si(CH2-CH=CH2)4
WCl6 + SnR4
WCl6 + AlR3
CH2
CH=CH
CH2—CH2
n
CH2
CH=CH
CH2—CH2
n

The influence of the temperature on the polymer microstructure differs with the nature of the catalyst. The polypentenamer obtained in the presence of WCl_6 and alumino-organic compounds catalysts has a prevailing "trans"-microstructure and it is practically not dependent on the temperature. In contrast, in the case of the polymerization of cyclopentene with the WCl_6-SnPh_4 or $WCl_6-SiMe_2Allyl_2$ systems, the temperature of the reaction has a decisive role on the microstructure of the obtained polymer. At low temperatures, polymers with a high content of *cis*-units are obtained. As the temperature rises beyond a certain value, the content of "cis" units drastically decreases and polymers with more and more abundant "trans" units are obtained. (Fig. 1).

Fig. 1. — Dependence of *cis*-content on temperature in ring-opening polymerization of cyclopentene with WCl_6-based catalysts : (O) catalytic system $WCl_6-SiAllyl_4$ [11] ; (□) catalytic system $WCl_6-SiMe_2Allyl_2$; (×) catalytic system WCl_6-AlR_3.

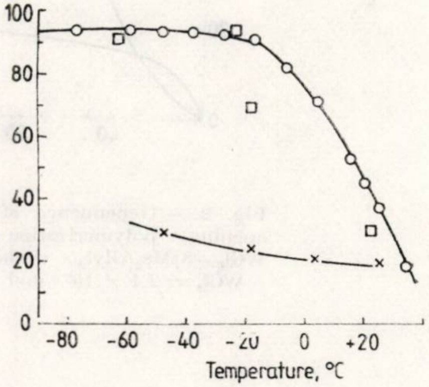

Kinetic measurements put into evidence the fact that the polymerisation of cyclopentene in the presence of $SnPh_4-WCl_6$ and $SiMe_2Allyl_2-WCl_6$ occurs at much higher rates at low temperatures (−20°C) when "cis" polypentenamer is obtained, than at a high temperature (+25°C) when polymers, with a high content of "trans" units are obtained. (Figs 2 and 3)

The polymerisation of cyclopentene induced by WCl_6-SnPh_4 or $WCl_6-SiMe_2Allyl_2$ occurs at low temperatures only when the initiation of the reaction takes place at a low temperature. If the reaction starts at high temperatures (+25°C), polymerisation stops completely on decreasing the temperature (−25°C).

Therefore, it is obvious that at least two types of active centres may appear during the polymerisation process : a very active one, but unstable at a high temperature and responsible for the formations of "cis" structures and the other one which is less active but stable at high temperature and leads to the formation of "trans" structures.

Studies of the polymerisation reaction by E.S.R. spectroscopy,[10] correlated to the results concerning the determination by ceriometric titration, of the valency of the transition metal from the catalytic system showed that, depending on the nature of the catalytic system employed and the temperature of the ring-opening polymerisation of cyclopentene, a multitude of active centres appears and they differ by the valence state of the transition metal. Furthermore, there is a direct relationship bet-

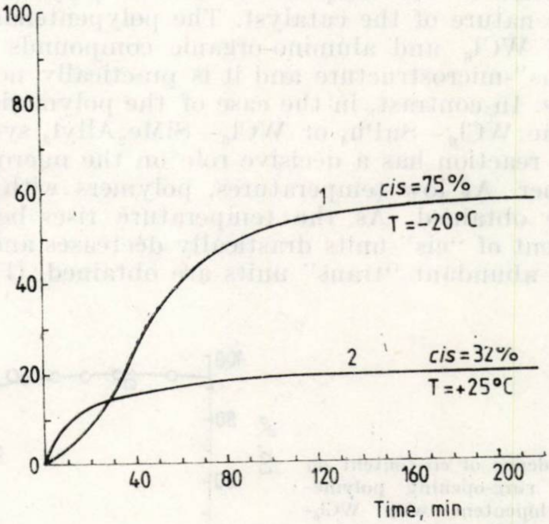

Fig. 2. — Dependence of conversion on time in ring-opening polymerization of cyclopentene initiated by $WCl_6-SiMe_2Allyl_2$. cyclopentene = 3.5 mol dm^{-3}; $WCl_6 = 2.1 \times 10^{-3}$ mol dm^{-3} $SiMe_2Allyl_2/WCl_6 = 2$

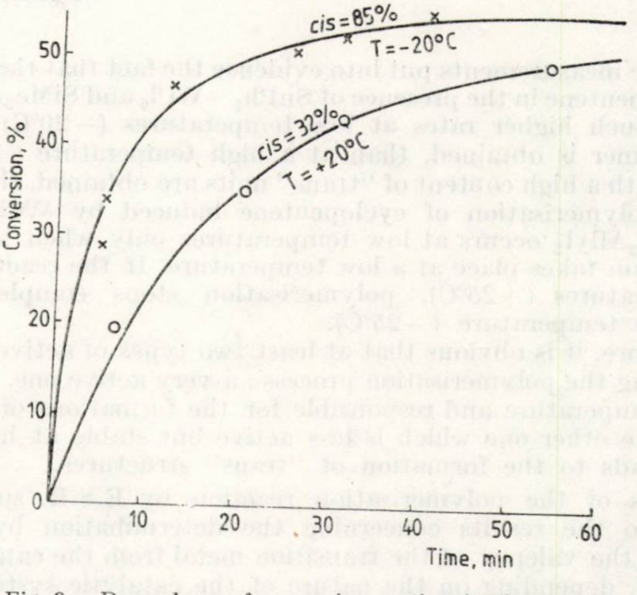

Fig. 3. — Dependence of conversion on time in ring-opening polymerization of cyclopentene with WCl_6-SnPh_4. cyclopentene = 3.5 mol dm^{-3}; $WCl_6 = 2.1 \times 10^{-3}$ mol dm^{-3} $Ph_4Sn/WCl_6 = 2$

ween the valence state of the transition metal of the catalytic system and the microstructure of the polymer which can be determined by IR spectroscopy and C^{13} NMR. (Fig. 4)

The active centres where the transition metal is in a low-valence state (W^{III}) lead to the formation of "trans" structures, those with high valency (W^{V}, W^{VI}) are responsible for producing "cis" structures.

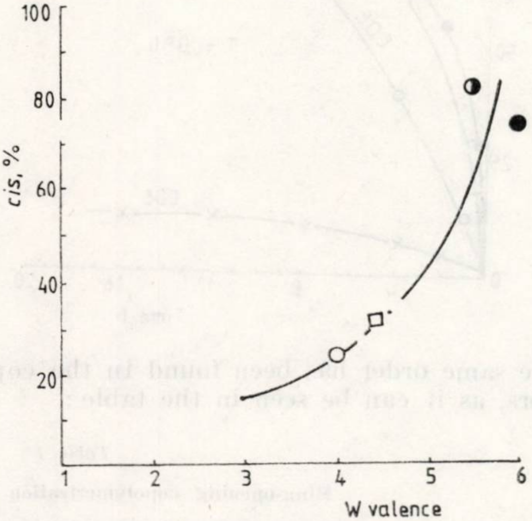

Fig. 4. — Variation of cis-content of polypentenamer with tungsten valence in the catalytic complex: (×) catalytic system WCl_6-AlR_3; temperature 0°C; (○) catalytic system WCl_6-SnPh_4; temperature 25° C; (□) catalytic system $WCl_6-SiMe_2Allyl_2$; temperature 20° C; (●) catalytic system $WCl_6-SiMe_2Allyl_2$; temperature −20°C; (◑) catalytic system WCl_6-SnPh_4; temperature −25°C.

Hence, it is obvious that by determining the degree of reduction of the transition metal, the temperature is a factor which acts only indirectly.

In the case of some organometallic compounds acting as weak reducing agents, the structure of the polymer depends sharply on the temperature, since the latter ultimately determines the valency of the transition metal in the active centre. In contrast, in the case of powerful reducing agents such as organoaluminium compounds, the structure of the polypentenamer is predominantly "trans" and not dependent on temperature.

We have obtained further information by a comparative study of the reactivity of several higher cycloolefins in the ring-opering polymerisations with the above-mentioned catalytic systems.

The results obtained can be summarized as follows: Catalysts of very low valence state which induce cyclopentene polymerization to *trans*-polypentenamer are also active in the polymerization of certain higher cycloolefins as cyclooctene (CO), cyclododecene (CDD) and cyclooctadiene (COD). (Fig. 5) Their reactivity varies in the series:

$$\mathrm{CP} \simeq \mathrm{COD} < \mathrm{CDD} < \mathrm{CO}$$

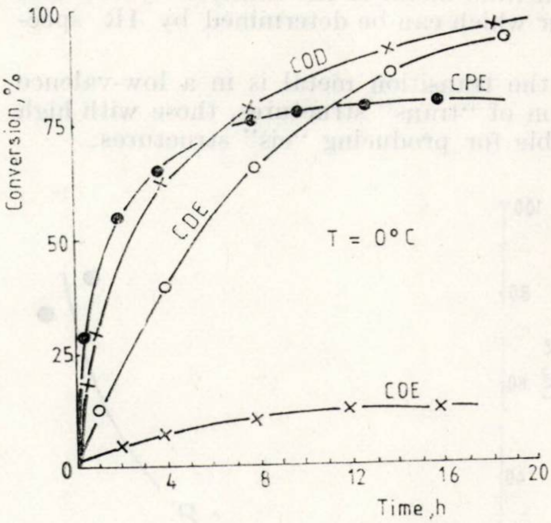

Fig. 5. — Time evolution of cycloolefin polymerisation with WCl_6. epichlorohydrin. Et_2Al catalyst : monomer = 3.5 mol dm^{-3} ; monomer/WCl_6 = 1500 ; Et_2AlCl/WCl_6 = 2 ; epichlorohydrin/WCl_6 = 2 ; temperature = 0°C, cyclopentene (CPE), cyclooctene (COE), 1,5-cyclooctadiene (COD), cyclododecene (CDE).

The same order has been found in the copolymerization of these monomers, as it can be seen in the table :

Table 1

Ring-opening copolymerization of cycloolefins

Copolymerization system $M_1 - M_2$	r_1	r_2
Cyclopentene-cyclooctene	1.07	0.45
Cyclopentene-cyclooctadiene	0.89	0.67
Cyclopentene-cyclododecene	3.94	0.33
Cyclooctene-cyclooctadiene	0.18	2.42
Cyclooctene-cyclododecene	1.24	4.19
Cyclooctadiene-cyclododecene	3.58	0.39

In contrast, the high-valency catalysts, responsible for the formation of *cis*-polypentenamer, are inactive in the polymerization of higher cycloolefins, cyclooctene and cyclododecene.

The $WCL_6 - SnPh_4$ or $WCl_6 - SiMe_2Allyl_2$ catalytic systems become active in the homopolymerization of cyclooctene or cyclododecene when small quantities of cyclohexene or cyclooctadiene are added. (Fig. 6) The same catalysts polymerize cyclooctadiene with high yields.

All the above obtained results indicate that : both the reactivity of higher cycloolefins in ring-opening polymerization and the stereochemistry of cyclopentene polymerization are highly governed by a common feature i.e. the steric hindrance around the reaction centre. Notwithstanding, the electronic factors constitute an important element as well.

In the case of catalysts of low valence state the steric hindrance will be less important : they will also be able to polymerize bulky cycloolefins and the insertion of the cyclopentene takes place by the most satisfactory pathway. A trigonal bipyramidal or octahedral symmetry may be admitted for the structure of the active centres. In the transition state, the polymer chain and the cycloolefin will have opposite positions to fulfil minimum steric interactions, fact which will afford the formation of "trans" structures. (Fig. 7)

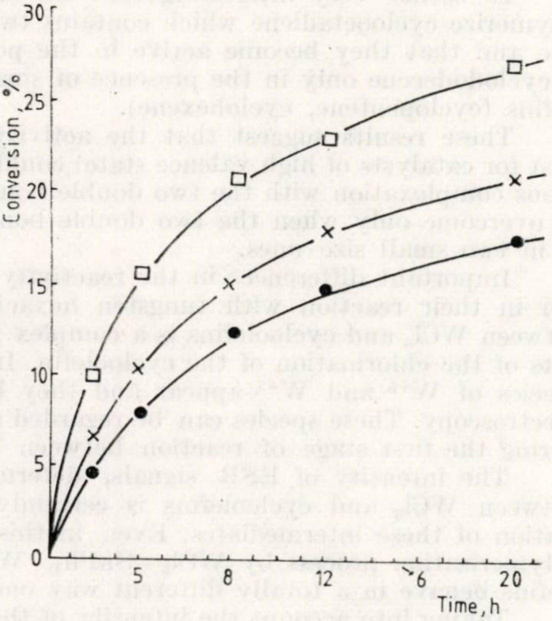

Fig. 6. — Time evolution of cyclooctene polymerisation with $WCl_6 \cdot Ph_4Sn$ catalyst in the presence of small amounts of cyclopentene □, cyclohexene × and 1,5 cyclooctadiene ●; cyclooctene = 3.5 mol dm^{-3} WCl_6 = 2.1×10^{-3} mol dm^{-3}; Ph_4Sn/WCl_6=2; temperature = 20°C.

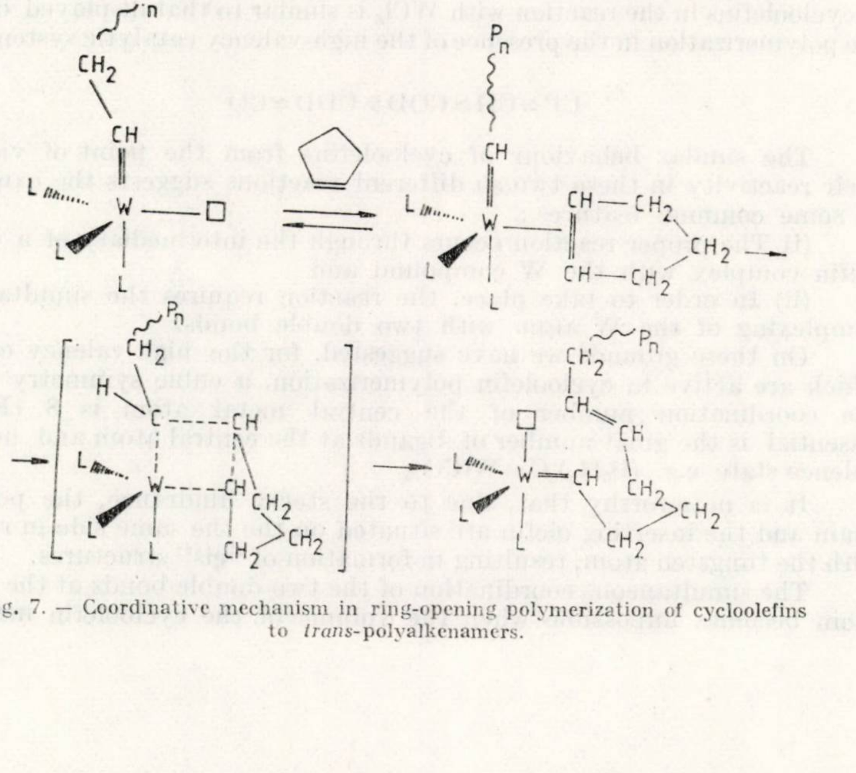
P_n
CH_2
CH
L
W
L
L
P_n
CH
CH — CH_2
CH_2
CH_2
P_n
CH_2
H
CH
CH
CH_2
CH_2
CH_2
L
W
L
L
P_n
CH_2
CH
CH
W
CH
CH_2
CH_2
CH_2
L
L
L

Fig. 7. — Coordinative mechanism in ring-opening polymerization of cycloolefins to *trans*-polyalkenamers.

On the other hand, in the case of catalysts of high valence state, the steric hindrance around the reaction centre become more important because of the great number of substituents. This is probably the main reason why these systems, so active in the case of cyclopentene polymerization, are totally inert toward higher cycloolefins.

It seems very interesting that the same systems are capable to polymerize cyclooctadiene which contains two double bonds in its molecule and that they become active in the polymerization of cyclooctene or cyclododecene only in the presence of small quantities of lower cycloolefins (cyclopentene, cyclohexene).

These results suggest that the activity during polymerization (at least for catalysts of high valence state) could be correlated with simultaneous complexation with the two double bonds. The steric hindrance can be overcome only when the two double bonds lie in the same molecule or in two small size ones.

Important differences in the reactivity of cycloolefins can be noticed in their reaction with tungsten hexachloride too. The interaction between WCl_6 and cycloolefins is a complex process whose first step consists of the chlorination of the cycloolefin. In this reaction paramagnetic species of W^{+5} and W^{+3} appear and they have been detected by ESR spectroscopy. These species can be regarded as intermediates which occur during the first stage of reaction between WCl_6 and the cycloolefin [4].

The intensity of ESR signals, determined during the interaction between WCl_6 and cycloolefins is certainly a measure of the concentration of these intermediates. Even in this interaction similarly to the polymerization process by WCl_6-SnPh_4, $WCl_6-SiMe_2Allyl_2$, the cycloolefins behave in a totally different way one from the other.

Taking into account the intensity of the W(V) signal, the reactivity of cycloolefins in the reaction with WCl_6 is similar to that displayed during the polymerization in the presence of the high-valency catalytic systems, i.e.

$$\mathrm{CP} \simeq \mathrm{CH} \simeq \mathrm{COD} \gg \mathrm{CDD} \simeq \mathrm{CO}$$

The similar behaviour of cycloolefins from the point of view of their reactivity in these two so different reactions suggests the existence of some common features :

(i) The proper reaction occurs through the intermediary of a cycloolefin complex with the W compound and

(ii) In order to take place, the reaction requires the simultaneous complexing of the W atom with two double bonds.

On these grounds we have suggested, for the high-valency centres which are active in cycloolefin polymerization, a cubic symmetry where the coordination number of the central metal atom is 8. (Fig. 8) Essential is the great number of ligands at the central atom and not the valence state e.g. $(C_6H_5)_2C{=}W(CO)_5$.

It is noteworthy that, due to the steric hindrance, the polymer chain and the inserting olefin are situated on the the same side in respect with the tungsten atom, resulting in formation of "cis" structures.

The simultaneous coordination of the two double bonds at the metal atom becomes impossible when the volume of the cycloolefin increases beyond a certain limit. Thereby it becomes explainable why these systems cannot polymerize higher cycloolefins, but are active in their copolymerization with cyclopentene or become activated in the presence of a small quantity of this monomer.

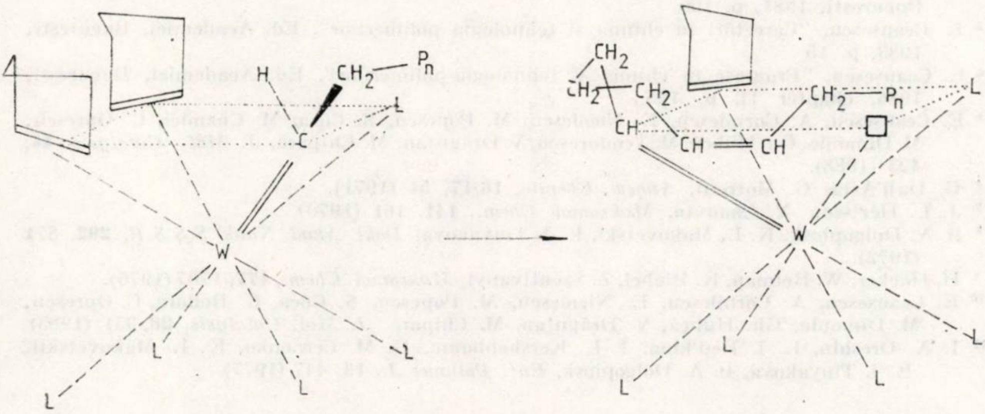

Fig. 8. — Coordinative mechanism in ring-opening polymerization of cycloolefins to *cis*-polyalkenamers.

The existence of certain complexes where the coordination number of tungsten should be superior to 6 originates from UV—VIS studies of WCl_6 complexes with arenes or cycloolefins.

The microstructures of polyalkenamer obtained by ring-opening polymerization of cycloolefins greatly depends on the nature of the catalyst employed and reaction temperature. Polyalkenamers with a high content of *cis-* or *trans*-units are obtained by using various WCl_6-based catalysts derived from organoaluminium, organotin or organosilicon compounds and working at low or high temperatures. The effect of temperature is dependent on the organometallic cocatalyst.

ESR spectroscopic measurements and ceriometric determinations revealed that at least two types of active centres appear in these catalytic system : high valency centres — stable at low temperatures and responsible for the formation of "cis" structures and low valency centres — stable at high temperatures leading preferentially to "trans" polymers. Catalysts of low valence state are active in the polymerization or copolymerization reaction of cyclopentene and higher cycloolefins e.g. cyclooctene, cyclododecene 1,5-cyclooctadiene, while catalysts of high valence state — active in cyclopentene or 1,5-cyclooctadiene polymerization — react with cyclooctene and cyclododecene only in the presence of traces of cyclohexene or 1,5-cyclooctadiene.

The differences in cycloolefin reactivity and polyalkenamer microstructure were rationalized by a metallacarbene mechanism involving a distinct steric hindrance around the reaction centre for the two types of catalytic systems. In the case of catalysts of high valence state, the simultaneous complexation of two double bonds from one or two cycloolefins was inferred. Furthermore, the different reactivity of cycloolefine displayed during polymerization and in the interaction with WCl_6 could be correlated with the appearance of paramagnetic W^{+5} and W^{+3} species.

REFERENCES

[1] K. J. Ivin, "Olefin Metathesis", Academic Press, London, 1983 ; V. Drăguţan, A. T. Balaban, M. Dimonie, "Olefin Metathesis and Ring-Opening Polymerization of Cyclo-Olefins" Ed. Academiei-J. Wiley, Bucharest-Chichester, 1985.

[2] E. Ceauşescu, "Noi cercetări in domeniul compuşilor macromoleculari", Ed. Academiei, Bucureşti, 1981, p. 100.

[3] E. Ceauşescu, "Cercetări în chimia şi tehnologia polimerilor", Ed. Academiei, Bucureşti, 1983, p. 15.

[4] E. Ceauşescu, "Progrese în chimia şi tehnologia polimerilor", Ed. Academiei, Bucureşti, 1986, chapter II, p. 105.

[5] E. Ceauşescu, A. Cornilescu, E. Nicolescu, M. Popescu, S. Coca, M. Cuzmici, C. Oprescu, M. Dimonie, Gh. Hubcă, M. Teodorescu, V. Drăguţan, M. Chipară, *J. Mol. Catalysis*, **46**, 423 (1988).

[6] G. Dall'Asta, G. Motroni, *Angew. Chemie*, **16/17**, 51 (1971).

[7] J. L. Hérisson Y. Chauvin, *Makromol. Chem.*, **141**, 161 (1970).

[8] B. A. Dolgoplosk, K. L. Makovetski, E. I. Tinyakova, *Dokl. Akad. Nauk. S.S.S.R*, **202**, 871 (1972).

[9] H. Höcker, W. Reiman, K. Riebel, Z. Szentivanyi, *Makromol. Chem.*, **177**, 1707 (1976).

[10] E. Ceauşescu, A. Cornilescu, E. Nicolescu, M. Popescu, S. Coca, C. Belloiu, C. Oprescu, M. Dimonie, Gh. Hubcă, V. Drăguţan, M. Chipară, *J. Mol. Catalysis*, **28**, 351 (1985).

[11] I. A. Oreshin, L. I. Red'kina, I. L. Kershenbaum, G. M. Cernenko, K. L. Makovetskii, E. I. Tinyakova, B. A. Dolgoplosk, *Eur. Polymer J.*, **13**, 447 (1977).

Revue Roumaine de Chimie, **34**, *4*, 917–919 (1989)

ANGULAR OVERLAP MODEL (AOM) CALCULATIONS FOR THE COORDINATION COMPOUNDS WITH MACROCYCLIC LIGANDS. II[1]

AOM PARAMETERS FOR NICKEL (II) COORDINATION COMPOUNDS WITH SATURATED MACROCYCLIC LIGANDS

MARIUS ANDRUH[a], O. D. CHIRICĂ[b] and MARIA BREZEANU[a]

[a]Laboratory of Inorganic Chemistry, Faculty of Chemical Technology, Polytechnic Institute, str. Dumbrava Roșie no. 23, Bucharest, Romania
[b]Enterprise for Semiconductor Devices-Băneasa, str. Erou Iancu Nicolae no. 32, Bucharest, Romania

Received November 19, 1988

The Angular Overlap Model parameters, taking into account all the configuration interactions, for nickel(II) coordination compounds with saturated macrocyclic ligands are calculated. The input data were derived from the electronic spectra and from the calculated electronic transition energies reported for these compounds (Busch, 1977). The corresponding parameters give information on the relative σ and π magnitude interactions of the nickel(II) ion with the macrocyclic and the axial ligands (Cl^-, Br^-, N_3^-, NCS^-).

In the preceding paper [1] we reported on the AOM calculations carried out for nickel (II) coordination compounds with a classical unsaturated macrocyclic ligand : tetrakis-anhydro-aminobenzaldehyde (TAAB). According to our results, TAAB seems to be a π-acceptor towards the nickel (II) ion. The π-acceptor ability of the TAAB macrocyclic ligand increases the Dq^{xy} parameter, favouring a diamagnetic behaviour (in a square-planar geometry) or a high spin$\rightleftharpoons$low spin equilibrium. This π-acceptor capability of the tetrakis-anhydro-aminobenzaldehyde may be understood by means of the conjugative effects which lower the energy of the ligands π^* orbitals, favouring metal-ligand back-bonding.

The complexes investigated in this paper are of the type **1**, containing saturated tetraaza macrocyclic ligands : [14] anN_4 (**2**), [15] anN_4(**3**), [16] anN_4 (**4**) and $TAABH_8$ (**5**) ; the latter derives from TAAB by reduction of the $\overset{|}{-C} = N-$ bonds.

All the coordination compounds are characterized by a high spin electronic configuration, *i.e.* a $^3B_{1g}$ ground state in D_{4h} symmetry[2] (*trans*-NiA_4B_2 type). Our calculation procedure was described in part I of this series. The set of AOM and Racah parameters were estimated by fitting the spectral data, [2] using a computer program. The energies of the six transitions are given by a linear equation, a two by two secular determinant and a three by three secular determinant. The matrix elements are expressed in terms of five parameters : e_σ^A, e_π^A, e_σ^B, e_π^B and B. In our calculations it was possible to made a simplification : the saturated macrocyclic ligands 2–5 do not have any π propensity (the assumption that the e_π^N parameters for the macrocycles are different from zero gives unreasonable solutions). Thus, for the complexes [Ni(MAC)X_2] e_π^N was written as zero, reducing the number of parameters to four. Tables 1 shows the AOM parameters calculated by us.

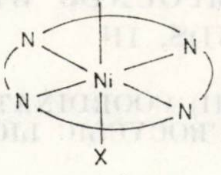

1.

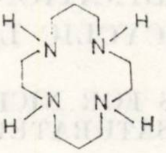

2

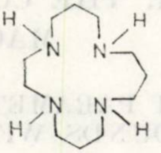

3.

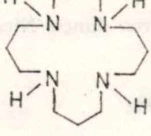

4.

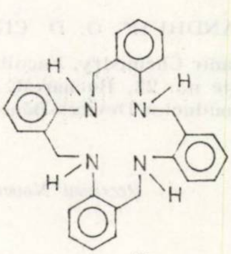

5.

Table 1

Angular Overlap Model Parameters (kK)

Compounds	e_σ^N (MAC)	e_π^N (MAC)	e_σ^X	e_π^X	B
[Ni([14]anN$_4$)Br$_2$]	4.950	0	0.465	−0.395	0.841
[Ni([14]anN$_4$)Cl$_2$]	4.917	0	1.372	−0.049	0.842
[Ni([14]anN$_4$)(N$_3$)$_2$]	4.827	0	2.040	−0.139	0.815
[Ni([14]anN$_4$)(NCS)$_2$]	4.717	0	2.668	−0.132	0.903
[Ni([15]anN$_4$)Br$_2$]	4.273	0	1.225	−0.208	0.820
[Ni([15]anN$_4$)Cl$_2$]	4.130	0	1.520	−0.325	0.834
[Ni([15]anN$_4$)(N$_3$)$_2$]	4.091	0	2.229	−0.237	0.797
[Ni([15]anN$_4$)(NCS)$_2$]	4.010	0	2.200	−0.622	0.839
[Ni([16]anN$_4$)Br$_2$]	3.752	0	1.309	−0.063	0.857
[Ni([16]anN$_4$)Cl$_2$]	3.719	0	1.525	−0.128	0.836
[Ni([16]anN$_4$)(N$_3$)$_2$]	3.624	0	2.048	−0.356	0.869
[Ni([16]anN$_4$)(NCS)$_2$]	3.575	0	2.430	−0.355	0.866
[Ni(TAABH$_8$)(NCS)$_2$]	3.750	0	2.440	−0.471	0.859
[Ni(TAAB)(N$_3$)$_2$]*	4.513	−0.290	1.880	−0.135	0.880
[Ni(TAAB)(NCS)$_2$]*	4.670	−0.162	2.060	−0.450	0.850

*— from ref[1]

The data collected in Table 1 allow to derive the following conclusions:

– e_σ^N(MAC) parameters are dependent on ring size (as well as the Dq^{xy} parameters [2]);

– the type and degree of unsaturation present in the macrocyclic ligands strongly determines the e_σ^N (MAC) parameters: the imines are, as a rule, stronger donors towards nickel ions than the secondary amines are ($e^{Nsp^2} > e^{Nsp^3}$);

– all the axial ligands (Cl^-, Br^-, N_3^-, NCS^-) have a π-acceptor behaviour;

– the calculated e_σ^X parameters suggest the following sequence of the spectrochemical series for nickel (II) coordination compounds, $Br^- < Cl^- < N_3^- < NCS^-$ in agreement with earlier observations.[3]

REFERENCES

[1] M. Andruh, C. I. Lepădatu and M. Brezeanu, *Rev. Roumaine Chim.*, **32**, 1033 (1987).
[2] L. Y. Martin, C. R. Sperati and D. H. Busch, *J. Amer. Chem. Soc.*, **99**, 2968 (1977).
[3] M. A. Hitchman, *Inorg. Chem.*, **11**, 2387 (1972).

Revue Roumaine de Chimie, **34**, *4*, 921–932 (1989)

BIS(3-CARBETHOXY-1,5-DI-*o*-ANISYL-FORMAZYL)Ni(II). A NEW UNUSUAL PENTACOORDINATE FORMAZANE COMPLEX

A. C. BANCIU
ICECHIM – Centre of Physical Chemistry,
77208-Bucharest, Spl. Independenţei 202, Sector 6, Romania

Received July 9, 1988

A new chelate Ni(II) complex has been synthesized using the 3-carbethoxy-1,5-di-*o*-anisyl-formazane as ligand. The complex has a pentacoordinate structure, unusual in the class of formazane complexes. In the complex the formazane anion acts both as di- and tridentate chelate ligand. The investigated chemical and physical properties (elemental chemical analysis, electrolytic and magnetic behaviour, IR and electronic spectra) show that the new complex is monomeric, nonionic, of high-spin type ($\mu_{\text{eff}} = 3.06 \pm \pm 0.15$ B.M.), containing the Ni(II)N_4O chromophore where the involved oxygen atom is anisolic and not esteric. The chromophore possesses, most likely, an intermediate geometrical structure, between square-pyramidal and trigonal-bipyramidal.

I. INTRODUCTION

The formazanes are well known as didentate chelate ligands.[1] Until now especially formazanes of type I have been used as ligands : [2]

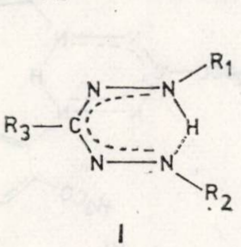

I

where R_1, R_2 = aryl or substituted aryl groups ; R_3=H, CH_3, CH_3CO ; H_5C_2OOC ; C^2H_5, etc.

Because the hydrogen atom of the imino group in I is chelate bounded it does not show acidic properties. However, in presence of bases (as triethylamine) it may dissociate. The corresponding anion, resulting from the proton dissociation from I, is the true chelate complexation agent. With divalent transition metal ions (M^{II}) it forms tetracoordinate complexes of type II, where R_1, R_2 and R_3 have the above-mentioned specifications.

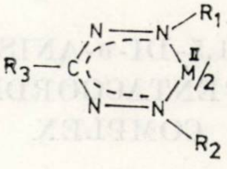

II

Until now, especially the formazane complexes of Co(II), Ni(II) and Cu(II) were synthesized and investigated.[2]

In the attempt to synthesize such a tetracoordinate Ni(II) complex, with the 3-carbethoxy-1,5-*o*-anisyl-formazane, a new pentacoordinate Ni(II) complex has been surprisingly obtained. The present paper describes the synthesis and the physical and chemical properties of this new and unusual pentacoordinate Ni(II) complex, obtained with a formazane ligand which acts both as di- and tridentate chelate ligand.

II. EXPERIMENTAL PART

All reagents used were of p.a. grade.

The synthesis of the organic ligand was performed using a method reported in the literature,[1] by the azoic coupling reaction (in alcoholic-aqueous solution and in strongly alkaline medium) of the acetylacetic ester with the diazonium salt of the *o*-anisidine (molar ratio ester : diazonium salt = 1 :2). By 1 :1 azoic coupling reaction an unstable intermediate results, which isomerizes immediately to the mono(*o*-methoxy)phenylhydrazone of the dicetobutyric ester. In strongly alkaline medium this compound undergoes desacylation and from the such formed intermediate carboanion, by 1 :1 azoic coupling reaction with the diazonium salt of the *o*-anisidine, the organic ligand III (the 3-carbethoxy-1,5-di-*o*-anisyl-formazane) is obtained.

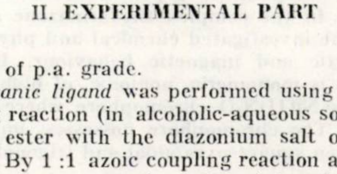

III

The crude product was purified by recrystallization from absolute methanol in presence of active charcoal. M.p. 84—87°. *Chemical analysis* : Calculated for $C_{18}H_{20}N_4O_4$: C 60.66%, H 5.67%. Found : C 61.82%; H 5.61%.

The synthesis of the Ni(II) complex. 0.90 g (2.5 mmoles) organic ligand (formazane III) was dissolved into about 150 mL hot methanol. 0.45 g $NiCl_2 \cdot 6\ H_2O$ (1.9 mmoles = = 150% from the theoretical amount for a complex of 1:2 metal : ligand type) was dissolved into 7—8 mL water and to the obtained solution 4—5 mL of concentrated aqueous NH_3 solution (containing at least 40—50 mmoles NH_3) were added. The ammonia-aqueous solution of the Ni(II) salt was added to the methanolic solution of formazane III and the obtained mixture was refluxed on a water bath for 45 min. The microcrystalline complex began to precipitate at cooling. It was filtrated on a Büchner funnel after the complete cooling of the reaction mass. The crude product was washed with 10—15 mL cool methanol and then purified from the unreacted inorganic salt. To this purpose the complex was impregnated into 50—60 mL 3% acetic acid, then warmed at 40°, under stirring, on a water bath and then filtrated on a Büchner funnel. This procedure was repeated for three times. Each washing with dilute acetic acid was followed by a washing with 8—10 mL cool methanol. The complex was finally purified by recrystallization from absolute methanol in presence of active charcoal. *Yield*: 0.55 g (= 57% of the theoretical one) complex, purified and dried (first in atmosphere then three days in a vacuum desiccator over P_4O_{10}). *Properties*: dark red-brown, almost black microcrystals. M.p. 210° (decomposition). The complex is insoluble in water, less soluble in methanol, soluble in ethanol, acetone, benzene, pyridine, dimethylformamide (DMF). All solutions are ruby-red. *Chemical analysis*: Calculated for $Ni(II)L_2$ (L = the anion of the 3-carbethoxy-1,5-di-*o*-anisyl-formazane): Ni 7.63%; C 56.18%; H 4.98%. Found: Ni 7.50% C 56.18%; H 5.19%.

The elemental chemical analyses (C, H) of the ligand and complex were performed by usual micromethods. The Ni content of the complex was determined by atomic spectroscopy. The Schöniger combustion, followed by mercurimetric titration, established that the complex does not contain chlorine.

The specific electric conductivities were determined with an OK 102/1 Radelkis conductometer. As solvents were used acetone "Merck", for spectroscopy, "Uvasol" (H_2O max. 0.1%) and DMF "Fluka" p.a. ($H_2O < 0.15\%$).

The IR spectra were recorded within the 200—4000 cm^{-1} range on a Perkin-Elmer type 225 spectophotometer and *the electronic diffuse reflectance spectra* were recorded within the 360—1150 nm range on a VSU-1 Carl Zeiss (Jena) spectophotometer, using MgO as standard.

The paramagnetic susceptibility of the solid complex was determined at room temperature, by Faraday method, using $Hg[Co(SCN)_4]$ as standard.

III. RESULTS AND DISCUSSION

The experimental conditions for the synthesis of the complex were those usual to obtain a tetracoordinate chelate complex of $Ni(II)L_2$ type (L = the anion of the formazane III). Much more, the elemental chemical analysis of the complex agrees with that for a tetracoordinate $Ni(II)L_2$ complex. Nevertheless, the obtained complex differs obviously (its colour is dark red-brown, almost black) from the usual $Ni(II)L_2$ complexes synthesized with ligands from the class of formazanes (whose colour is dark blue or dark blue-green). The band-rich electronic diffuse reflectance spectrum *excludes* undoubtedly *any tetra-* or *hexa*coordinate structure being *characteristic* for a *penta* coordinate Ni(II) complex (see below).

There are many possibilities to formulate the complex, which agree with : *i.* the pentacoordinate structure of the Ni(II) ions ; *ii.* the elemental chemical analysis data, and *iii.* the molecular and ionic species existing in the reaction medium of the complex synthesis. They are :

1. The monomeric structure $Ni(II)L_2L'$, where L = the formazane III anion and $L' = H_2O$ or NH_3 ;

2. The dimeric structure $[Ni(II)L_2]_2$ with a Ni(II)—Ni(II) chemical bond ;

3. The dimeric, trimeric or polymeric structure $[Ni(II)L_2]_n$, where $n = 2, 3, \ldots n$, with Ni(II)—O bonds formed with the oxygen atom of many esteric C=O groups. (In the dimeric structure both Ni(II) ions would be pentacoordinate, in the trimeric one the median Ni(II) ion would be hexacoordinate and the peripheric Ni(II) ions are pentacoordinate, etc.).

4. The monomeric structure Ni(II)L_2, built with the oxygen atom of an alkyl-aryl-etheric group, *i.e.* $CH_3-O-C_6H_4-$.

From the physical and chemical data of the complex (IR spectrum, the solubility in organic solvents, the specific magnetic susceptibility and the specific electric conductivities) and from many more recent experimental data, regarding the properties of some new formazane complexes (see below) one may conclude that the first three types of structure are excluded for the new Ni(II) complex herein discussed.

The monomeric structure *1*, anyhow less probable, is incompatible with the IR spectrum (see Table 1), which does not contain bands which may be ascribed to coordinated water or ammonia.

The dimeric structure *2* is excluded by sterical reasons (the bulky aryl substituents, existent at all donor nitrogen atoms, prevent from forming the Ni(II)—Ni(II) chemical bonds) and by magnetic arguments (the experimental data do not indicate a metal-metal interaction in the complex; see below).

All the polymeric structures *3* are excluded by the IR spectral data which show undoubtedly that the esteric C=O group does not participate to the coordination of the metal ions (see Table 1).

It results, therefore, that the structure of the new Ni(II) complex is monomeric, as above mentioned at point *4*. In this structure the pentacoordination of each Ni(II) ion is fulfilled by four Ni(II)—N bonds (existent in all formazane Ni(II) complexes) and an *intra*molecular Ni(II)—O bond, according to the formula IV of the complex.

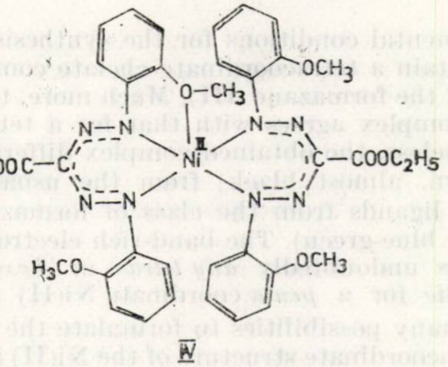

IV

This structure, unusual for the formazane complexes, needs some comments. Different organic ligands, having structures similar to those of the formazanes (i.e. didentate, able to form chelate rings of six atoms and having bulky aryl substituents linked to both donor nitrogen atoms) form *often* with the Ni(II) ions and *almost always* with the Co(II) ions *tetrahedral* complexes.[2] In contrast with these ligands, the formazanes, I, have the surprising and still unexplained property to form both with the Co(II) and Ni(II) ions practically only square-planar complexes.[2] To explain this property, it has been supposed that the chelate ring from the formazane complexes is formed only from five atoms.[2] In this case the azo group from the formazylic chain, $-N-N=\overset{|}{C}-N=N-$, remains outside the chelate ring and the bulky aryl substituent bounded to this group should be far from the central metal ion. In this way the steric hindrances should be avoided if the complex takes the square-planar structure. This explanation is perhaps valid, for some complexes. However, for other formazane complexes, as the bis(3-methyl-1-phenyl-5-*p*-tolylformazyl)Ni(II), it has been proved [3] by X-ray determinations, that the structure of the metal-ligand chemical bonds is square-planar, eventhough the formazane chelate rings are built from six atoms. The formazane Ni(II) complexes are almost always diamagnetic, with a "stepped" planar structure.[2] In this structure the central Ni(II) ion has a true square-planar surrounding, but the most part of the every formazane chelate ring forms a plane different from that of the Ni(II)—N chemical bonds. The planes formed by both formazylic groups are *parallel* between them and *interrupted* by the plane of the Ni(II)—N chemical bonds.[3] In this structure of the complex all the donor nitrogen atoms have a structure close to that of a sp^3 hybridized nitrogen atom (see [3]). From this reason, the valences between the donor nitrogen atoms and the arylic rings are obviously out of the plane of the $Ni(II)-N_4$ chemical bonds.

In contrast with these formazane complexes (*tetra*coordinate and *dia*magnetic) the new Ni(II) complex IV contains four methoxy-, CH_3O-, substituents, linked in the *ortho*-position (the closest to the central metal ion) to the benzene rings attached to the nitrogen donor atoms. Due to the *nature* of these substituents (having an *oxygen* atom which may act as a donor atom) and to their *position* (*ortho*), to the complex under discussion it is possible the occurrence of *new* supplementary metal-ligand bonds (of Ni(II)—O type), inexistent in the common (tetracoordinate) formazane complexes. Formally, assuming that the Ni(II)—N chemical bonds in the new complex have a square-planar structure (exactly as to the tetracoordinate formazane complexes) it follows that two from the four methoxy substituents form a Ni(II)—N bond (easily proved on steric models), the sixcoordination of the Ni(II) ion being in this way attained. Actually, surely only a Ni(II)—O bond is formed, since the complex IV is only pentacoordinated (see the electronic spectrum).

The electrolytic behaviour of the complex. A solution of 0.0193 g of complex IV in 50 mL acetone has, at 20°, the specific electric conductivity ($\varkappa$) of 0.6×10^{-6} ohm^{-1} cm^{-1} and a solution of 0.0192 g of complex IV in 25 mL DMF has, at 20°, $\varkappa = 6.4 \times 10^{-6}$ ohm^{-1} cm^{-1}. If the value M.W. = 769.53, corresponding to the monomeric structure IV is taken into account, one finds for the molar electric conductivities the following values : $\Lambda_M = 1.2$ ohm^{-1} cm^{2}mol^{-1} (acetone) and $\Lambda_M = 6.4$ ohm^{-1}cm^{2}mol^{-1} (DMF). Both values are characteristic for a nonelectrolyte,[4] in full agreement with the monomeric formula IV attributed to the complex.

The IR spectra. Table 1 summarizes the IR spectra of the free ligand (formazane III) and of the new Ni(II) complex IV, as well the most plausible assignments of the bands. The spectra are very similar in the whole 200—4000 cm^{-1} range, being mainly due to the numerous and intense bands of the esteric group and of the aromatic rings.

The IR spectrum of the formazane agrees with its attributed structure III. For example, the spectrum shows two important properties of the formazane : 1. its chelate structure (most probably of type III, with a pseudoaromatic ring formed from six atoms, where the conjugation of the C=N and N=N double bonds is extended over five atoms) and *2.* the conjugation of the esteric group with the formazane chelate ring. (The conjugation occurs as possible eventhough the chelate-ring is formed from five atoms). In the favour of the chelate structure is the fact that the band due to the $-\overset{\diagdown}{N}-N$ stretching vibration is absent in spectrum. This band should occur between 3300–3500 cm^{-1} (as in the secondary aromatic amines) if the formazane would have the free, nonchelate structure with the $\text{aryl}-\overset{\diagup}{N}-H$ group, (aryl = o-$CH_3O-C_6H_4$). Actually, in the formazane molecule the iminic hydrogen atom is bounded not only to one $\text{aryl}-\overset{\diagup}{N}-$ group, but, as a chelate, between the nitrogen atoms of two $\text{aryl}-\overset{\diagup}{N}-$ groups. For this reason the $-\overset{\diagdown}{N}-H$ stretching vibration is absent in the mentioned domain. For the conjugation of the esteric group, with the formazane chelate ring plead the wavenumbers at which they appear : *1.* the C=O stretching vibration (1712 cm^{-1}) ; *2.* the esteric C–O stretching vibration (1280 cm^{-1}) and *3.* the "second" band of the esters of primary alcohols (1120 cm^{-1}). If the conjugation is not present the mentioned vibrations must occur at approx. 1740 ; 1200 and 1035–1060 cm^{-1}, respectively.[5,6]

Between the complex and formazane there are some differences in their IR spectra, especially at 350 cm^{-1} and 560 cm^{-1} (where the complex has supplementary bands due, most likely, to the Ni(II)–ligand stretching vibrations) as well as in the domains : A : 1000–1045 cm^{-1} ; B : 1110–1140 cm^{-1} ; C : 1260–1350 cm^{-1} and D : 1490–1520 cm^{-1}. In the first three domains occur (see Table 1) different vibrations of the alkyl-aryl-etheric group (domains A and C) and of the ester group (domains A, B and C). Due to the conjugation of the esteric group with the formazane chelate ring its vibrations are obviously affected by the complexation with the metal ions. However, one may *surely* assert that the *esteric* group *does not participate* to the coordination of the Ni(II) ions, because the C=O stretching vibration occurs practically unchanged in the complex (1710 cm^{-1}), compared with 1712 cm^{-1} in the free formazane. If the esteric C=O group would participate to coordination, the formazane band at 1712 cm^{-1} would occur strongly shifed [5,6] in the complex, below 1665 cm^{1}, which is obviously not the case.

The strongest differences occurring in the IR spectra, between the free ligand (formazane III) and the complex IV may be seen within 1300–1350 cm^{-1} (Table 1). The free formazane III has in this domain bands due to the C–N stretching vibrations of the $\text{aryl}-\overset{\diagup}{N}-H$ group whereas the complex IV shows the same stretching vibration but from the $\text{aryl}-\overset{\diagup}{N}-Ni(II)$ group. These changes show the formation of the Ni(II)–N chemical bonds in the complex.

The existence of an intramolecular Ni(II)–O bond (formed with the oxygen atom of an alkyl-aryl-etheric-group) at the pentacoordination

Table 1

The IR spectra of the free organic ligand (formazane III) and of the new Ni(II) complex compound IV [cm^{-1}]

Free organic ligand III	New complex compound IV	Assignments
	350 w	metal-ligand stretching
375 w		
475 w		
478 w	480 w	
542 m	545 w	
	560 m	metal-ligand stretching
588 w	580 m	
602 w-m	600 w	
	617 w-m	
655 w		
	668 m	
740 vs	755 vs	out-of-plane C—H bending vibration for 1,2-disubst. benzene
768 vs	770 m-s	
790 w	795 w	
810 w	805 w	
860 w	850 w	
880 vw	878—892 w	
920 w		ring vibrations for 1,2-disubst. benzene
940 w	932 w	
960 vw		
1008 m-s	1005 sh	asym. $O-CH_2-C$ stretching vibration from ethylester group and aliphatic C—O stretching from aralkylether group
	1017 s	
	1022 s	
1028 vs	1032 s	
1042 s	1045 w	
1098 vs	1097 m	second C—O band for esters of primary alcohols
1110 s	1110 s	
1125 vs	1122 vs	
	1138 vs	
1160 s-vs	1158 m—s	disubstituted benzene ring vibrations
1170 s		C—N stretching from aryl-N-H or aryl-N$\overset{\diagup}{—}$ group, respectively, and aromatic C—O stretching from aralkylether group
1180 s	1178 s	
1200 s	1200 vs	
	1215 sh	
1242 sh	1238 m	
	1252 m	
1265 sh		C—O stretching vibration from ester group (conjugated with the pseudoaromatic formazane ring) and aromatic C—O stretching from aralkylether group
1278 vs	1275 vs	
1285 sh	1295 vs	
	1305 vs	C—N stretching from aryl-N-H or aryl-N$\overset{\diagup}{—}$ group, respectively
1310 sh	1315 vs	
1325 s	1327 vs	
1350 s	1345 vs	
1370 s-vs	1368 m	sym. CH_3 deformation vibration of the CH_3-C group
1390 m	1390 m	OCH_2 wag vibration from ethylester group

Free organic ligand III	New complex compound IV	Assignments
1415 sh	1410 sh	
1440 m	1440 m	asym. CH_3 deformation vibration from ethylester group; 1,2-disubst. benzene ring vibrations and sym. CH_3 umbrella deformation vibration from aralkylether group
1450 sh	1455 sh	
1468 s	1465 s	OCH_2 deformation vibration from ethylester group 1,2-disubst. benzene ring vibrations
1487 vs	1488 vs	
	1495 sh	
1502–1515 vs	1512 sh	
1590 m-s	1590 s	1,2-disubst. benzene ring vibrations and asym. stretching of the N⋯C⋯N "bond-and-a-half" bonds from pseudoaromatic formazane ring
1712 vs	1710 vs	C=O stretching vibration from ethylester group (conjugated with the pseudoaromatic formazane ring)
2840 m-s	2840 m	vibration of the OCH_3 group from the methylether group
2900 m-s	2910 m	CH_3 stretching vibration
2940 m-s	2940 m	asym. CH_2 stretching vibration
2980 m-s	2980 m	asym. CH_3 stretching vibration
3020 m	3020 sh	C–H stretching vibration of aromatic ring
3070 m	3070 m	C–H stretching vibration of aromatic rings

w = weak; vw = very weak; w-m = weak-medium; m = medium; m-s = medium-strong; s = strong; s-vs = strong-very strong; vs = very strong; sh = shoulder

of each Ni(II) ion is directly materialized in the IR spectrum. These are the obvious changes of the bands attributed to the vibrations of the alkyl-aryl-etheric-group,[7] occurring in the domains A (1000–1045 cm^{-1}) and *C* (1260–1350 cm^{-1}), as a consequence of the metal ions complexation.

In the favour of the mentioned pentacoordination are my recent experimental data,[8] regarding the synthesis and the properties of some new formazane complexes. Thus, from the six new Ni(II) complexes prepared with type I (formazanes where $R_1=R_2=$*o*-, *m*-, *p*$-CH_3-C_6H_4-$ and *o*-, *m*-, *p*-$CH_3O-C_6H_4-$, respectively, and $R_3=H_5C_2OOC$ the *only* pentacoordinate complex is the new Ni(II) complex IV, under discussion. This is the *only* complex where, due to the *nature* (OCH_3) and to the *position* (*ortho*) of the substituents one may form a $Ni(II)-O_{(etheric)}$ chemical bond. *All* the other mentioned complexes are *diamagnetic* and *tetra*-coordinate.

The special (pentacoordinate) structure of the new complex IV is therefore caused only by the special structure of the formazane III, which makes one from the two formazane anions, L, act in the complex molecule as a tridentate ligand (property which is inexistent for other formazane ligands). The fact that the special structure of the complex IV is achieved only by the special structure of the formazane ligand III excludes convincingly the other pentacoordinate structures formally possible for the complex and above excluded based on other physico-chemical properties.

The magnetic susceptibility measurements. The paramagnetic susceptibility per gram of complex is $\chi_g = (4.7 \pm 0.5) \times 10^{-6}$ c.g.s.u. The diamagnetic correction (χ_{dia}) calculated from the Pascal constants, for the monomeric pentacoordinate structure IV is of -311×10^{-6} c.g.s.u./mole.

Using the formula

$$\mu_{eff} = 2.828\sqrt{(\chi_g \text{M.W.} - \chi_{dia})T} \quad \text{B.M.}$$

valid for the mononuclear complexes and the values M.W. = 768.53 and $T = 298$ K one finds the value of 3.06 ± 0.15 B.M. This value is higher than the "spin only" value for two uncoupled electrons (2.83 B.M.) being practically comprised between the limits indicated in the literature for *high spin* pentacoordinate Ni(II) complexes, *i.e.* 3.2... 3.4 B.M.[9-12] Such Ni(II) complexes contain ligands having strong electronegative donor atoms (N and/or O), as the complex under discussion. (The pentacoordinate low spin Ni(II) complexes are formed with ligands having weak electronegative donor atoms, such as C, S, P or As and they do not have any uncoupled electron).

Assuming a dimeric structure for the complex, $[\text{Ni(II)L}_2]_2$, the values M.W. = 1539.06 and $\chi_{dia} = -622 \times 10^{-6}$ c.s.g.u./mole and using the formula

$$\chi_{eff} = 2.828\sqrt{\left(\frac{\chi_g \cdot \text{M.W.}}{2} - \frac{\chi_{dia}}{2}\right)T} \quad \text{B.M.}$$

valid for dinuclear complexes, for $T = 298$ K one finds an effective magnetic moment of 3.06 ± 0.15 B.M. per Ni(II) ion. This value is practically too high to show a real metal-metal interaction, which is to be expected if the dimeric structure is achieved through a Ni(II)—Ni(II) chemical bond. The experimental magnetic data are therefore in agreement with the monomeric structure IV for the complex, the dimeric structure with metal-metal bond being excluded by spatial arguments too. (The other dimeric structure formally possible for the complex, achieved by the esteric C=O group is undoubtedly excluded by IR spectral data, as has been above discussed).

The electronic spectra. Figure 1 gives the electronic diffuse reflectance spectra of the formazane III and of the complex IV. One observes directly that the spectrum of the complex, containing numerous absorption bands is *characteristic* for a *pentacoordinate* Ni(II) complex. It excludes any other tetracoordinate or hexacoordinate structures for the complex IV. If the spectra are compared, one observes that the two bands of the complex situated at lower wavelengths (480 nm = 20830 cm^{-1} and 530 nm = = 18870 cm^{-1}) are proper to the organic ligand (formazane III), being shifted with only 10 nm against the corresponding absorption bands of the free formazane. The band placed at 480 nm represents surely an allowed $\pi \rightarrow \pi^*$ transition. These bands, situated at 480 and 530 nm, are the most intense in the whole complex spectrum. The strong absorption corresponding to these bands determines practically the unusual color (for a formazane complex) of the complex IV (dark red-brown almost black in the solid state and red-ruby in solutions). The other four absorption bands of the complex (situated at 675, 710, 875 and 1090 nm, *i.e.* 14810, 14100, 11470 and 9170 cm^{-1}) are due to the ligand field and CT (charge transfer).

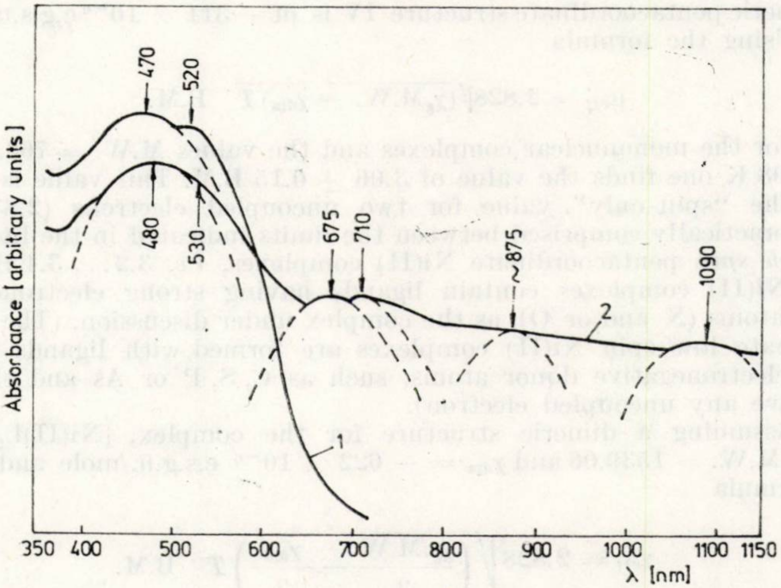

Fig. 1. — Electronic diffuse reflectance spectra of the free organic ligand (formazane III) and of the new pentacoordinate complex compound IV: 1 — the free organic ligand III; 2 — the new complex IV.

Table 2 summarizes the electronic spectra of some pentacoordinate high-spin Ni(II) complexes (all with magnetic moments between 3.2... ... 3.4 B.M.), compared with that of the new complex IV.

The structure of the complexes **1**—**4** is exactly known[9] by means of X-ray studies, and the square-pyramidal structure of the complex **5** is most probable, the complex being isomorphous with a similar Co(II) complex which has undoubtedly that structure.[11]

One directly observes that the spectra of *all* complexes from Table 2 are *similar*. These are similarities (the bands at 23000, 14500, 11500, and approx. 7100 cm^{-1}) between the spectra of the complexes **1** and **5**, eventhough their structures are very different (trigonal-bipyramidal and square-pyramidal, respectively). There are also differences between their spectra. The spectra of the complexes **4** and **5** (square-pyramidal) contain a band at about 16000 cm^{-1}, which is absent in the spectrum of the complex **1** (trigonal-bipyramidal). If the spectrum of the new complex IV (no. **6** in Table 2) is compared with those of the other complexes in Table 2, one observes numerous similarities. It is similar with that of the complex **1** (trigonal-bipyramidal) and to that of the complex **5** (square-pyramidal). The spectrum of the complex IV shows dissimilarities if it is compared with the spectra of the complexes **4** and **5** (square-pyramidal), having none band at about 16000 cm^{-1}, and is different from the spectrum of the complex **1** (trigonal-bipyramidal), because it does not contain a band

Table 2

The electronic diffuse reflectance spectra of some high-spin pentacoordinate Ni(II) complexes and of the new complex IV

No.	Ni(II) complex compounds	Electronic diffuse reflectance spectra Maxima of the corresponding absorption bands [cm^{-1}]								Structure	References
1	[$Ni(Me_6tren)Br$]Br [a,f]	7100	10500	sh 11400	14500			sh 20000	23000	irreg. TBP x	9
2	[$Ni(H$-Sal-en-$N(Et)_2$) (catec)]$_2$ [b,g]	6300	9700	11300	14200					INTERM. x	9
3	Ni[5Cl-Sal-en-$N(Et)_2$]$_2$ [c,g]	7600	9800	12700		16200				dist. SP x	9
4	[Ni(H-Sal-MeDPT)] [d,g]	8000	sh 9300	sh 12800		15800				INTERM. x	9
5	[$Ni(MePh_2AsO)_4(ClO_4)$] (ClO_4) [e,f]	sh 7100	sh 9100	11800	13700	16200	18400		23000	SP y	10
6	The new complex compound IV		9170	sh 11400	14100	14800	sh 18900	20800		INTERM.	this paper

[a] Me_6tren = tris(2-dimethylaminoethyl)amine;
[b] H-Sal-en-$N(Et)_2$ = N,N-diethylsalicylalethylenediamine; catec = cathecolate;
[c] 5Cl-Sal-en-$N(Et)_2$ = 5-chloro-N,N-diethylsalicylalethylenediamine;
[d] H-Sal-MeDPT = bis(salicylaldiminotrimethylene)methylamine;
[e] $MePh_2AsO$ = diphenyl-methyl-arsineoxide;
[f] Spectrum recorded in the 5000–25000 cm^{-1} range;
[g] Spectrum recorded only in the 5000–20000 cm^{-1} range;
[h] Spectrum recorded in the 8700–27000 cm^{-1} range;
sh = shoulder; TBP = trigonal-bipyramidal; SP = square-pyramidal;
INTERM = intermediate (between TBP and SP); x = Structure determined by X-ray diffraction technique; y = Determination of isomorphism with analogous compound with known SP structure

at about 10500 cm^{-1}. These similarities and dissimilarities show for the Ni(II)-ligand chemical bonds in the complex IV as most probable an *intermediate* geometrical structure, between square-pyramidal and trigonal-bipyramidal. In the favour of such a geometrical intermediate structure for the complex IV is the marked similarity between its spectrum and that of the complex **2** (which has most likely an intermediate structure). One thus observes (Table 2) that in the domain 9000–15000 cm^{-1} these spectra present three absorption bands which practically coincide (at 9200, 11300 and 14200 cm^{-1}).

CONCLUSIONS

From the analysis of all investigated physical and chemical properties (elemental chemical analysis, electrolytic and magnetic behaviour, IR and electronic spectra) of the new complex IV, *i.e.* the bis-(3-carbethoxy-1,5-di-*o*-anisyl-formazyl)Ni(II), one concludes that it is pentacoordinate, monomeric, nonionic, of high-spin type, containing the chromophore $Ni(II)N_4O$, where the involved oxygen atom is anisolic and not esteric. The pentacoordinate structure of the complex is due to the special property of the used ligand (the anion of III, *i.e.* of the 3-carbethoxy-1,5-di-*o*-anisyl-formazane) to act both as a chelate di- and tridentate ligand.

ACKNOWLEDGEMENT. The author is grateful to lecturer Dr. V. Mincu from the Polytechnic Institute of Bucharest for the magnetic susceptibility measurements.

REFERENCES

[1] C. D. Nenițescu, "Chimie organică", vol. 2, Ed. VIII, Ed. Didactică și Pedagogică, Bucharest. 1980, p. 77.
[2] R. H. Holm and M. J. O'Connor, "Progress in Inorganic Chemistry", vol. 14, Wiley, New York, 1971, p. 241.
[3] D. Dale, *J. Chem. Soc .*, **A, 1967**, 278.
[4] W. J. Geary, *Coord. Chem. Rev.*, **7**, 81 (1971).
[5] L. J. Bellamy, "The Infrared Spectra of Complex Molecules", Methuen, London, 1962, p. 178.
[6] N. B. Colthup, L. H. Daly and St. E. Wiberley, "Introduction to Infrared and Raman Spectroscopy", Academic Press, New York, 1975, p. 278.
[7] N. B. Colthup, L. H. Daly and St. E. Wiberley, Op. cit., p. 311.
[8] A. C. Banciu, unpublished results.
[9] L. Sacconi, "Transition Metal Chemistry", vol. 4, Marcel Dekker, New York, 1968, p. 199.
[10] P. L. Orioli, *Coord. Chem. Rev.*, **6**, 285 (1971).
[11] M. Ciampolini, *Structure and Bonding*, **6**, 52 (1970).
[12] A.B.P. Lever, "Inorganic Electronic Spectroscopy", Elsevier, 1968, p. 345.

Revue Roumaine de Chimie, **34, 4.** 933–935 (1989)

RADICAL POLYMERIZATION OF ACRYLAMIDE IN HOMOGENEOUS AND HETEROGENEOUS SYSTEMS. I

SOLUTION PROPERTIES OF ACRYLAMIDE IN WATER

C. M. BOGHINĂ, C. I. CINCU, N. N. MARINESCU, M. M. MARINESCU,
M. V. DIMONIE and D. S. VASILESCU
Laboratory of Macromolecular Chemistry, Polytechnical Institute,
Calea Victoriei 149, Bucharest, Romania

Received February 21, 1988

The apparent molecular weight of acrylamide in water increases with concentration; this fact indicates the formation of acrylamide associates, which, in turn, might be resposible for the high molecular weights of poly(acrylamide) obtained by radical polymerization in solution. Unlike acrylamide, acetamide does not exhibit the same behaviour.

INTRODUCTION

As is well known, the radical polymerization of acrylamide in aqueous solution is characterized by a high propagation constant (k_p), fact that explains to a great extent the unusually high molecular weights, which may be obtained by radical polymerization in homogeneous solution.[1]

In many cases, radical polymerizations are diffusion controlled;[2] as the addition of macroradical to monomer molecule represents the rapid step, the previous one, namely diffusion, is responsible for the global value k_p. Therefore, if the role of diffusive factor is somewhat diminished, this fact should manifest by an increase in the apparent value of k_p. Provided the monomer molecules are prearranged in a favourable position (associates, "matrices" etc.), then the phenomenon should express through a high value for k_p.

In order to verify this hypothesis, for the acrylamide-water system we have carried out numerical average molecular weight measurements, on acrylamide solutions, over a large concentration domain.

EXPERIMENTAL

Acrylamide — provenience American Cyanamid Co. — was recrystallized and dried in vacuum at room temperature. Acetamide — provenience BDH — and sodium acetate — provenience Reactivul — were also dried in vacuum. Pentadistilled water has been used as solvent. Solutions were prepared in the usual manner and their concentration has been calculated gravimetrically. Numerical average molecular weights were established by means of a Knauer-type microcryoscope; supercooling has been achieved with a Peltier element and temperature differences electronically measured. The calibration of the method has used aqueous solutions of water-soluble, nonionic, organic substances.

However, it must be said that cryoscopy is designed to work best with solutions in the range of 0.05–0.30 molal; a good reproducibility requires the use of the same supercooling in all tests. In the present case we have also used high concentrations (over 10 molal), and this fact has requested more advanced supercooling as well as reduced amplification for the output signal.

RESULTS AND DISCUSSION

The apparent molecular weights for acrylamide solutions are presented in Table 1. Up to 10–15%, the increase of apparent molecular weight is not spectacular. On the contrary, in the range of high concentrations an accentuated tendency towards association may be noticed. As several polymerization tests for acrylamide were carried out at high concentrations,[3] around 50%, it is plausible that aggregates formed prior to polymerization have an important role in obtaining high molecular weights of the resulting polymer.

In order to establish whether this behaviour of acrylamide in aqueous solution is peculiar, we have repeated the tests, using this time a similar compound, namely acetamide. As can be seen from Table 2 the apparent molecular weights are practically constant in this case ; this fact suggests the lack of association, or a nonsignificant importance in the range of high concentrations.

Table 1

Apparent molecular weights of acrylamide in aqueous solutions

No.	Acrylamide conc. g/100 g solution	Molal conc.*	Apparent $\overline{M}_{AA}$
1	0.77	0.1082	71.2
2	2.58	0.3654	70.6
3	3.99	0.5850	71.1
4	5.96	0.8686	73.3
5	9.90	1.4190	77.4
6	16.05	2.0085	79.9
7	24.84	4.0170	82.3
8	29.53	4.5908	91.3
9	33.87	5.1074	100.3
10	39.51	4.7520	133.4
11	42.34	4.5500	161.0

* cryoscopic measurements

Table 2

Apparent molecular weights of acetamide in aqueous solution

No.	Acetamide conc. g/100 g solution	Molal conc.*	Apparent $\overline{M}_{AcA}$
1	1.08	0.1905	57.5
2	1.99	0.3422	59.5
3	3.99	0.6846	60.7
4	6.30	1.1810	57.0
5	8.19	1.5223	58.6
6	11.05	2.1033	59.1
7	14.87	2.9246	59.7
8	19.78	4.1383	59.6
9	24.41	5.5792	57.8
10	29.26	7.0882	58.3
11	34.09	8.5984	60.1
12	39.48	9.4687	68.9

* cryoscopic measurements

Previous works[4] have reported the importance of salt co-presence, specifically natrium acetate, in the polymerization of acrylamide in aqueous solution. In the presence of sodium acetate, both the polymerization rate and the molecular weight of the polymer are affected. Consequently, we have measured the apparent molecular weights in the acrylamide-natrium acetate–water system ; the obtained data are presented in Table 3. Unlike the previous measurements, in this case we have prepared a solution of sodium acetate (0.2%) in water, and acrylamide has been dissolved in this "solvent". In the calculation of the apparent molality we have taken into account the dissociation-hydrolysis phenomena related to sodium acetate; thus, sodium acetate exhibits a molal concentration 1.6 times higher than the calculated one. As can be seen from Table 3 there are two rows of results regarding the apparent molecular weight, the first referring to the whole mixture, the second only to acrylamide (after subtracting the molality given by natrium acetate). It is remarkable that these data are similar to those obtained in the absence of sodium acetate (see Table 1). Thus it may be said that sodium acetate does not influence the degree of acrylamide association, and its influence on the kinetics of polymerization has to be connected to other phenomena (i.e. initiation).

Table 3

Apparent molecular weights of acrylamide in aqueous sodium acetate (0.2 %) solutions

No.	Acrylamide conc. g/100 g solution	Molal conc.*	Theoretical $\overline{M}_{AA}$**	Apparent $\overline{M}_{AA}$
1	1.99	0.3244	68.7	71.3
2	4.90	0.7954	67.3	68.1
3	9.91	1.5016	74.6	75.2
4	15.91	2.3847	79.6	80.1
5	23.33	3.5420	86.5	86.9
6	29.47	4.2848	98.0	99.0

* experimental data by cryoscopic measurements
** as resulted from Table 1

REFERENCES

[1] J. Brandrup and H. Immergut (editors), "Polymer Handbook", Second edition, Wiley, New York, 1975.

[2] See for instance: A. M. North and G. A. Reed, *J. Polymer Sci.*, A **1**, 1311 (1963).

[3] M. V. Dimonie, C. M. Boghină, N. N. Marinescu, M. M. Marinescu, C. I. Cincu and C. G. Oprescu, *Eur. Polymer J.*, **18**, 639 (1982).

[4] C. M. Boghină, C. I. Cincu, N. N. Marinescu, M. M. Marinescu, M. V. Dimonie, M. Lecca, G. Popescu, C. G. Oprescu, A. Roşanu and M. Lungu, *J. Macromol. Sci. Chem.*, A **22**, 591 (1985).

Revue Roumaine de Chimie, 34, 4, 937–944(1989)

POLARIZATION BEHAVIOUR OF LEAD IN SULPHURIC ACID SOLUTION CONTAINING AMMONIUM DICHROMATE ADDITIONS

V. BRÂNZOI[a], S. STERNBERG[a] and LILIANA APĂTEANU[b]
[a] Polytechnic Institute of Bucharest, Dept. of Physical Chemistry, Bucharest, Romania
[b] Biochemical and Chemical Energetics Institute, Bucharest, Romania

Received January 18, 1988

The polarization behaviour of the lead electrode in sulphuric acid solutions, with and without $(NH_4)_2Cr_2O_7$ additions, was studied, using the potentiodynamic method. The potential sweep of the working electrode was carried out within the (+800 to +1700) mV range. The values of the kinetic parameters, determined from the polarization curves, point out the intensification of the anodic and cathodic processes, on ammonium dichromate addition. Taking into account the shape of the potentiograms, the values of the kinetic parameters from these potentiograms and the coulometric ratios α, β, γ and δ, a succession of reactions was proposed, illustrating the processes occurring at the electrode, during the anodic and cathodic polarizations.

INTRODUCTION

The peculiar importance of lead acid batteries has determined the considerable development of the studies concerning the improvement of their performances. As everyone knows the life time of the lead acid battery is usually determined by the service time of the electrodes, the positive one especially. It was pointed out that, from the active mass of the positve electrode, only about 40–45% is utilized, the rest of 60–55% remaining unutilized. Any reduction of the unutilized mass of the positive electrode leads to the increase of the service time of the battery, that is to the improvement of its performances.

One of the methods usually employed for the improvement of the utilization index of the positive electrode active mass is the inclusion in the paste or in the electrolyte of different additives. In the present paper, the effect of $(NH_4)_2Cr_2O_7$ additions in the electrolyte, on the polarization behaviour of the lead electrode in sulphuric acid solutions (of $\rho = 1.24$ g/cm^3 density), was studied within a potential range changing from + 800 mV to + 1700 mV and back to + 800 mV. This potential range was chosen because the potential sweep (back and forth) within this range very well simulates the processes taking place on the positive plate of the lead acid battery during the charge-discharge cycles.

EXPERIMENTAL

The cyclic voltammetry of low potential sweep (300 mV/min in our case) was used, in order to obtain the polarization curves within the potential range specified above.

The working electrodes were made from pure lead with a surface of 50 mm^2. As counterelectrode a net of platinum was used and the $Hg/Hg_2SO_4/H_2SO_4$ 1 M electrode was used as a reference electrode.

The potential sweep within the $(+800 \div +1700)$ mV range was carried out using a Model 173 Potentiostat — Galvanostat (Princeton Applied Research) provided with a coulometric module, and coupled with an Orion Type pulses generator.

The potentiograms were registered by means of an X—Y register, and the potential of the working electrode was measured each moment using an electronic voltmeter against the reference electrode mentioned above.

Determinations were carried out in H_2SO_4 solutions (of $\rho = 1.24$ g/cm^3 with and without ammonium dichromate additions. For each determination a number of 20 cycles was realized in order to obtain an active and reproducible surface of the working electrode.

The electricity amount involved during the anodic and cathodic processes, as well as on the hole cycle were automatically registered by means of the coulometric module of the potentiostat. For each solution, that is for each $(NH_4)_2Cr_2O_7$ concentration, many determinations were carried out, until a good reproducibility of the results was obtained.

The scheme of the electric device, as well as the working way were described in a previous paper.[1] It is worthy of note that, before each run, the working lead electrode was mechanically polished with glass paper of different granulation, and then electropolished in a mixture of acetic and perchloric acids, rinsed in distilled water and in the studied solution, and finally introduced in the working cell and submitted to the electrochemical polarization.

Temperature in the working cell was maintained constant, at 20°C, by means of an UM-210 thermostat.

RESULTS AND DISCUSSION

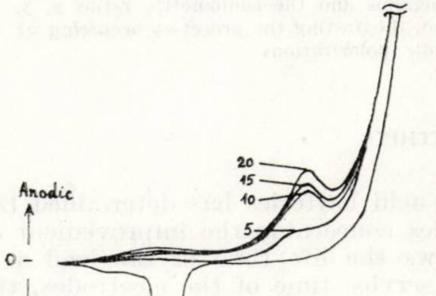

Fig. 1. — Potentiograms of the lead electrode in sulphuric acid solution of $\rho = 1.24$ g/cm^3 density.

Figure 1 shows the potentiograms of the lead electrode in a H_2SO_4 solution of $\rho = 1.24$ g/cm^3, obtained at the potential sweep within the mentioned range, with a sweep rate of 300 mV/min.

Analysis of the figure shows that at the increasing anodic sweep of the potential an anodic current maximum (A) obtains, within the $(+1200 \div +1500)$ mV potential range, corresponding to the reaction of PbO_2 formation from $PbSO_4$. At the going on of the potential sweep, the anodic maximum is followed by a high increase of the current, corresponding to the oxygen discharge. At the reverse potential sweep, from +1700 mV to +800 mV, a cathodic current maximum (B) registers, corresponding to the PbO_2 reduction to $PbSO_4$. One can consider that the cathodic maximum (B) entirely results from the reduction of PbO_2 formed during the anodic polarization. Further analysis of the figure shows the very different shape of the (A) and (B) maxima. While the (A) maximum is not too high and extends within a relatively wide potential range, the (B) maximum is much longer, very sharp and extends within a narrower potential range. The explanation is that the anodic process of transformation :

$$Pb^{2+} \rightarrow Pb^{4+} + 2\,e^-$$

is probably hindered by the diffusion of the Pb^{2+} ions (which exist in solution in a rather small concentration) through the pores of the $PbSO_4$ unconductible layer from the layer-metal interface. The diffusive control of the process is pointed out by the linear dependence ${}^{i}p_A = f\ (v^{1/2})$, too. The cathodic (B) maxima, very sharp, are free of diffusive hindering and probably kinetically controlled by the reduction of PbO_2 which is a semiconductor and allows a cathodic process :

$$Pb^{4+} + 2\,e \rightarrow Pb^{2+}$$

directly on the electrode surface. The Tafel slope on the ascendant side of the cathodic maximum is of ~ 30 mV, in agreement with the relation $b = RT/nF$, which applies to the transfer charge mechanism in the Debye layer at semiconductor electrodes. In this case the transfer coefficient is $\alpha = 1$ and not $\alpha = 0.5$, which corresponds to the Helmholtz double layer. The cathodic process represents a "stripping" process, a PbO_2 reduction process unhindered by diffusion, respectively.

Further analysis of the Fig. 1 shows an increase of the anodic and cathodic maxima height with the increasing number of cycles, and a very small modification of the potentials corresponding to the current maxima with the increase of the number of cycles. This fact demonstrates, as we had shown in previous papers,[2-7] that simultaneously with the increase of the number of cycles, the increase of the active layer thickness occurs at the electrode surface ; this layer participates in the oxidation and reduction reactions. In fact, as a result of the successive cyclings, the $PbO_2/PbSO_4$ electrode capacity (measured by Q_c) progressively increases and, after about 20 cycles a porous microelectrode obtains, with a sufficiently high capacity and with reproducible properties.

The ammonium dichromate addition in the sulphuric acid solution does not change the shape of the polarization curve (see figure 2). The

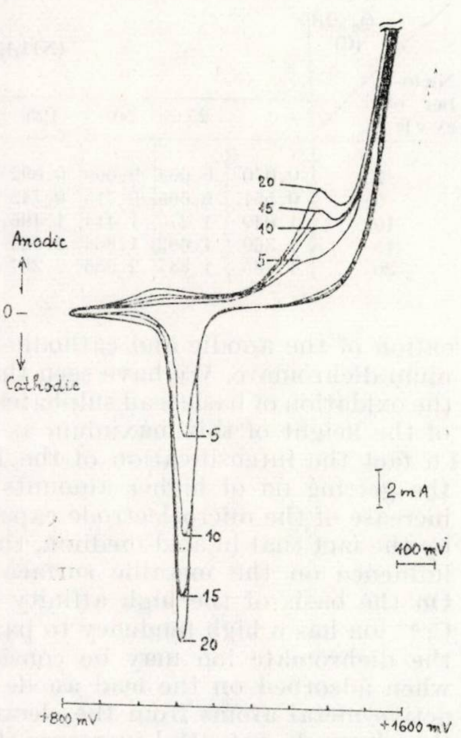

Fig. 2. — Potentiograms of the lead electrode in sulphuric acid solution of $\rho = 1.24$ g/cm³ density, containing ammonium dichromate addition (2 g/L).

two maxima (A) and (B) appear within the same potential ranges, but one can observe a considerable increase of the height of both maxima, as well as of the electricity amounts involved in the anodic (Q_a) and cathodic (Q_c) processes — see Tables 1 and 2. All these point out the intensification of the anodic and cathodic processes at the addition of the ammonium dichromate. We have seen that the (A) maximum actually represents the oxidation of basic lead sulphates and oxides to lead dioxide. The increase of the height of this maximum as a result of $(NH_4)_2Cr_2O_7$ addition means in fact the intensification of the Pb^{2+} oxidation process to Pb^{4+}, that is the getting on of higher amounts of lead dioxide and consequently the increase of the microelectrode capacity. This behaviour could be explained by the fact that in acid medium, the dichromate ion $Cr_2O_7^{2-}$ exerts a direct influence on the metallic surface characteristics of the lead electrode. On the basis of the high affinity of Cr^{6+} ion for reduction to Cr^{3+} (the Cr^{6+} ion has a high tendency to pass into the Cr^{3+} form, in acid medium), the dichromate ion may be considered as an electrophilic group which when adsorbed on the lead anode surface, leads to the oxidation of the active metal atoms from the electrode surface, to lead oxide and then as the electrode potential increases, to the lead dioxide.

Table 1

$Q_a \cdot 10$ (C) / Number of cycle	$(NH_4)_2Cr_2O_7$ concentration (ppm)									
	0	25	50	125	250	500	1000	2000	4000	6000
2	0.422	0.446	0.462	0.470	0.498	0.502	0.508	0.515	0.527	0.542
5	2.741	2.939	3.088	3.159	3.308	3.366	3.374	3.406	3.503	3.604
10	4.124	4.524	4.756	4.934	5.080	5.182	5.246	5.295	5.445	5.691
15	5.023	5.669	6.060	6.283	6.344	6.464	6.553	6.778	6.989	7.321
20	5.360	6.102	6.512	6.927	7.051	7.374	7.560	7.785	8.028	8.302

Table 2

$Q_c \cdot 10$ (C) / Number of cycle	$(NH_4)_2Cr_2O_7$ concentration (ppm)									
	0	25	50	125	250	500	1000	2000	4000	6000
2	0.070	0.084	0.090	0.092	0.098	0.100	0.102	0.105	0.111	0.115
5	0.551	0.666	0.715	0.743	0.793	0.812	0.819	0.850	0.899	0.937
10	1.049	1.270	1.414	1.496	1.545	1.588	1.646	1.689	1.771	1.869
15	1.369	1.692	1.866	2.029	2.081	2.167	2.236	2.325	2.412	2.557
20	1.485	1.847	2.055	2.287	2.376	2.513	2.599	2.688	2.796	2.964

On the other hand, some researchers [8-10] had shown that, at the cathodic polarization of the lead electrode in chromic acid solutions the dichromate ion reduction in preference to dissolved oxygen occurs, meaning that at the anodic polarization a higher amount of lead oxide and of PbO_2 respectively will form, at the same time with the increase of the dichromate concentration — as confirmed by our experimental results. The increase of the height of the (B) maxium, and of the electricity amount (Q) involved in the cathodic process respectively, at the same time with the increase of the $(NH_4)_2Cr_2O_7$ concentration is explicable, taking into account that this maximum represents in fact the reduction of PbO_2 formed during the increasing anodic sweep of the electrode potential; as the PbO_2 amount increased it is normally the reduction maximum to increase, too, confirming once again the increase of the lead microelectrode capacity (the increase of the PbO_2 amount, respectively) on the addition of the ammonium dichromate.

We consider that the electrode processes occurring in the presence of the dichromate ion, at the increasing anodic scan of the potential, from +800 mV to +1700 mV are the following:

$2\ Cr^{6+} + 3\ Pb \rightarrow 3Pb^{2+} + 2\ Cr^{3+}$ (at potentials between +800 mV ÷ +1200 mV)

$2\ Cr^{6+} + 3\ Pb^{2+} \rightarrow 3\ Pb^{4+} + 2\ Cr^{3+}$ (at potentials higher than +1200 mV)

$Pb^{2+} \rightarrow Pb^{4+} + 2\ e$

$Cr^{3+} - 3\ e \rightarrow Cr^{6+}$

At the reverse potential scan from +1700 mV to +800 mV the reduction of the formed PbO_2 occurs, that is:

$$Pb^{4+} \rightarrow Pb^{2+}$$

By means of the coulometric module of the potentiostat the electricity amounts involved in the anodic (Q_a) and cathodic (Q_c) process were measured — see tables 1 and 2.

Analysis of these tables shows a considerable increase of Q_a and Q_c respectively, at the same time with the increase of the $(NH_4)_2Cr_2O_7$ concentration. Considering that the main electrode processes within the studied potential range are the oxidoreduction $Pb^{2+} \rightleftarrows Pb^{4+}$ and the gaseous oxygen evolution, one can write:

$$Q_a = Q_{PbO_2} + Q_{O_2} = Q_C + Q_{O_2}$$

where:

Q_{PbO_2} (anodically formed) = Q_{PbO_2} (cathodically reduced) hence:

$$Q_{O_2} = Q_a - Q_c$$

We can write the following relations:

$$\alpha = \frac{Q_{O_2}}{Q^0_{O_2}} \cdot 100 = \frac{(Q_a - Q_c)}{(Q^0_a - Q^0_c)} \cdot 100$$

$$\beta = \frac{Q_{PbO_2}}{Q^0_{PbO_2}} \cdot 100 = \frac{Q_c}{Q^0_c} \cdot 100$$

$$\gamma = \frac{Q_{PbO_2}}{Q_{O_2}} \cdot 100 = \frac{Q_c}{(Q_a - Q_c)} \cdot 100$$

$$\delta = \frac{Q_{PbO_2}}{Q_{total}} \cdot 100 = \frac{Q_c}{Q_a} \cdot 100$$

where the "0" superscript refers to the H_2SO_4 solutions free of $(NH_4)Cr_2O_7$ addition.

The coulometric ratios, defined by the above equations, can provide some interesting informations concerning the influence of different factors on the electrode processes.

In the tables 3, 4, 5, 6 are given the values of the coulometric ratios α, β, γ, δ, calculated using the above equations.

Table 3

α / Number of cycle	$(NH_4)_2Cr_2O_7$ concentration (ppm)									
	0	25	50	125	250	500	1000	2000	4000	6000
2	100	102.84	105.68	107.39	113.64	114.20	115.34	116.48	118.18	121.31
5	100	103.79	105.82	110.32	114.84	116.62	116.67	116.71	118.90	121.78
10	100	105.82	108.68	111.80	114.96	116.88	117.07	117.27	119.48	124.29
15	100	108.84	114.78	116.42	116.67	117.60	118.14	121.87	125.26	130.38
20	100	109.80	115.02	119.74	120.65	125.45	128.03	131.54	135.02	138.53

Table 4

β / Number of cycle	$(NH_4)_2Cr_2O_7$ concentration (ppm)									
	0	25	50	125	250	500	1000	2000	4000	6000
2	100	120.00	128.57	131.20	139.70	143.00	145.34	150.00	157.70	163.70
5	100	120.90	129.82	134.80	144.00	147.35	148.62	154.20	163.24	170.00
10	100	121.10	134.79	142.60	147.30	151.40	156.90	161.00	168.75	178.20
15	100	123.57	136.28	148.20	152.00	158.32	163.27	169.84	176.20	186.80
20	100	124.37	138.37	154.00	160.00	169.16	175.00	181.00	188.34	197.60

Table 5

γ Number of cycle	$(NH_4)_2Cr_2O_7$ concentration (ppm)									
	0	25	50	125	250	500	1000	2000	4000	6000
2	19.88	23.20	24.19	24.34	24.50	24.88	25.12	25.61	26.68	26.93
5	25.16	29.30	30.13	30.75	31.53	31.79	32.05	33.26	34.52	35.13
10	34.11	39.03	42.31	43.51	43.71	44.18	45.72	47.76	48.20	48.90
15	37.47	42.54	44.49	47.70	48.82	50.43	58.80	52.21	52.70	53.67
20	38.32	43.41	45.45	49.29	50.82	51.70	52.39	52.76	53.44	54.66

Table 6

δ Number of cycle	$(NH_4)_2Cr_2O_7$ concentration (ppm)									
	0	25	50	125	250	500	1000	2000	4000	6000
2	16.588	18.834	19.481	19.574	19.679	19.920	20.079	20.388	21.062	21.218
5	20.10	22.661	23.154	23.520	23.972	24.123	24.274	24.956	25.664	25.999
10	25.44	28.072	29.730	30.320	30.410	30.640	31.380	32.325	32.531	32.840
15	27.25	29.847	30.79	32.29	32.80	33.52	34.121	34.302	34.511	34.927
20	27.71	30.267	31.557	33.017	33.697	34.079	34.378	34.528	34.830	35.341

One can observe the fact that the α ratio increases with the increase of the ammonium dichromate concentration, as well as with the number of cycles. As α represents the ratio between the oxygen amount evolved in the presence of the $(NH_4)_2Cr_2O_7$ and the oxygen amount evolved in the absence of the $(NH_4)_2Cr_2O_7$, one can conclude that the amount of the evolved oxygen increases with the increase of the $(NH_4)_2Cr_2O_7$ concentration, meaning that the anodic process is favoured by the ammonium dichromate presence.

Analysis of the γ and δ values shows in this case, too, their increase with the increase of the ammonium dichromate concentration. The increase of the δ ratio actually represents the increase of the PbO_2 amount formed during the anodic process, in respect to the total amount of electricity involved in the anodic process, while the increase of the γ ratio actually represents the increase of PbO_2 amount in respect to the electricity amount involved in the process of oxygen evolution. In both cases, the increase of γ and δ with the increase of the $(NH_4)_2Cr_2O_7$ concentration indicates the increase of the $PbO_2/PbSO_4$ electrode capacity, measured by the electricity amount involved in the process of Pb^{2+} oxidation to Pb^{4+} (that is the PbO_2 formation), or by the electricity amount involved in the process of PbO_2 reduction to $PbSO_4$, denoted by us by Q_c. On the other hand, β represents the ratio between the electricity amount involved in the PbO_2 obtention in the presence of the ammonium dichromate additions and that involved in the obtention of PbO_2 in the absence of ammonium dichromate; β actually represents the ratio between the lead microelectrode capacity in the presence of the $(NH_4)_2Cr_2O_7$ additions and the microelectrode capacity in the absence of the $(NH_4)_2Cr_2O_7$ and shows the most faithfully the influence of these additions.

Analysis of table 4 shows a pronounced increase of β, hence of the microelectrode capacity with the increase of the number of cycles, as well as of the ammonium dichromate concentration.

CONCLUSIONS

— At the potential sweep of the working (lead) electrode in H_2SO_4 solutions with and without ammonium dichromate additions, within the $(+800 \div +1700)$ mV potential range, on the polarization curves there are two current maxima which appear, one of them at the increasing anodic sweep, representing the Pb^{2+} oxidation to Pb^{4+} (hence the oxidation of $PbSO_4$ and of sulphates and basic lead oxides to lead dioxide) and the latter at the decreasing anodic sweep, representing, the reduction of the Pb^{4+} to Pb^{2+} (hence the reduction of the PbO_2, formed during the anodic process, to $PbSO_4$).

— The ammonium dichromate addition led in all cases to the increase of the lead electrode capacity, to the increase of the amount of the formed PbO_2, respectively.

— The increase of the number of cycles always results in the increase of the thickness of the active layer from the electrode surface, hence in the increase of the capacity, the increase of the formed PbO_2 amount respectively.

— Independently of the concentration and the number of cycles, the two curent maxima always appear within the same potential ranges.

— The increase of the $(NH_4)_2Cr_2O_7$ concentration and of the number of cycles always led to the increase of the electricity amounts Q_a and Q_c, hence to an intensification of the anodic and cathodic processes.

REFERENCES

[1] S. Sternberg, V. Brânzoi and Liliana Apăteanu, *Rev. Roumaine Chim.*, **29**, 833 (1984).
[2] S. Sternberg, V. Brânzoi, L. Apăteanu and A. Mateescu, *Rev. Roumaine Chim.*, **28**, 583 (1983).
[3] S. Sternberg, V. Brânzoi, L. Apăteanu, C. Doboş and E. Comănescu, *Rev. Chim.* (Bucureşti), **35**, 427 (1984).
[4] V. Brânzoi, S. Sternberg and Liliana Apăteanu, *Rev. Roumaine Chim.*, **30**, 199 (1985).
[5] S. Sternberg, V. Brânzoi, A. Mateescu and L. Apăteanu, *Rev. Roumaine Chim.*, **30**, 955 (1985).
[6] S. Sternberg, A. Mateescu, V. Brânzoi and Liliana Apăteanu, *Rev. Roumaine Chim.*, **32**, 457 (1987).
[7] S. Sternberg, V. Brânzoi and Liliana Apăteanu, *Rev. Roumaine Chim.*, **32**, 121 (1987).
[8] S. A. Awad, K. H. M. Kamel and Z. A. Elhady, *Electroanal. Chem. Interfacial Electrochemical*, **34**, 431 (1972).
[9] C. F. Yarnell, M. C. Weeks, *J. Electrochem. Soc.*, **126**, 1 (1976).
[10] K. R. Bullok and D. H. Mc. Clelland, *J. Electrochem. Soc.*, **123**, 327 (1976).

Revue Roumaine de Chimie, **34**, *4*, 945—952 (1989)

DERIVATIVES OF 1,2-PYRAZOLES. II[1]

THE INFLUENCE OF ALKALINE MEDIA ON THE REACTION OF 1,3-DICARBONYL COMPOUNDS WITH HYDRAZINE

MARIA BRIE[a], IOAN A. SILBERG[b] and NICOLAE PALIBRODA[c]

[a] Institute of Chemistry, 30, Fintinele Str., R—3400 Cluj-Napoca, Romania
[b] ICECHIM — Institute of Chemical and Biochemical Energetics, Cluj-Napoca Research Group, 11, Arany Janos Str., R—3400 Cluj-Napoca, Romania
[c] Institute for Isotopic and Molecular Technologies, 65—103, Donath Str., R—3400 Cluj-Napoca, Romania

Received September 12, 1988

In contrast to the normal cyclization reaction — carried out in neutral solutions — of the *o*-nitrophenyl-1,3-dicarbonylic compounds I and IX with hydrazine and phenylhydrazine, yielding the expected 3-methyl-5-*o*-nitrophenylpyrazoles, the use of alkaline media leads to reduction products modified at the level of substituents (VIII) and of the pyrazole ring (VI) as well as to the formation of the 3-hydroxy-pyrazole XI.

1. INTRODUCTION

Previous reports in the literature,[2-4] including our preceding communication,[1] demonstrated that the condensation of 1,3-dicarbonylic compounds with hydrazine and its derivatives is a very convenient route to pyrazoles, the reaction taking place, usually, in acidic or neutral media. It appeared of interest to investigate the course of the reaction of β-dicarbonyls with hydrazines under the influence of alkaline catalysts. Our experiments revealed that essential changes occur in the cyclization process, the interactions between the substituents and the reaction centers leading to the formation of different products.

2. EXPERIMENTAL

All melting points are uncorrected. The IR spectra were recorded in KBr pellets with an UR-10 Carl Zeiss Jena double-beam spectrophotometer, the ^1H-NMR spectra were taken in $CDCl_3$ solutions at 60 MHz with a Brucker-60 spectrometer (TMS served as internal reference) and the mass spectra were obtained with a Varian-MAT 311 spectrometer.

1H-3-Methyl-5-o-nitrophenyl-4,5-dihydropyrazole (VI)

A solution of I and 80% hydrazine hydrate (molar ratio I to N_2H_4 1:3) in ethanol was treated with 3% aqueous NaOH solution (1 ml for 100 ml ethanolic solution). The reaction mixture was refluxed under stirring for 2 hrs., cooled, and treated with a small amount of cold water. The precipitate was filtered, and cream-coloured crystals, easily soluble in benzene, ether or chloroform were thus obtained. After recrystallization from chloroform, the substance (short sticks) melted at 118–120°C. Reaction yield: about 50 %.

1H-3-Methyl-5-o-anilino-pyrazole (VIII)

A mixture of I and of 80 % hydrazine hydrate (molar ratio I to N_2H_4 1:1.5) in ethanol was treated with 3 % aqueous NaOH solution (5 ml for 100 ml ethanolic solution) then refluxed for 4 hrs. A pale-yellow precipitate separated on cooling; by recrystallization from ethanol, it gave VIII, m.p. 122°C (25 % yield).

1H-3-Hydroxy-5-o-nitrophenyl-pyrazole (XI)

A mixture of IX and of 80 % hydrazine hydrate (molar ratio IX to N_2H_4 1:1) was refluxed for 1.5 hrs in a 30 % ethanolic NaOH solution. On cooling and admixture of benzene a yellow precipitate separated; after filtration and recrystallization from ethanol, XI, m.p. 185°C, was obtained in a 55 % yield.

The elemental analyses of the compounds VI, VIII and XI are given in Table 1.

Table 1

Elemental analyses of compounds VI, VIII and XI

Compound	Molecular formula	M.p. °C	Calculated			Found		
			C %	H %	N %	C %	H %	N %
VI 1H-3-methyl-5-*o*-nitrophenyl-4.5-dihydropyrazole	$C_{10}H_{11}N_3O_2$	118	58.5	5.36	20.48	58.5	5.45	20.48
VIII 1H-3-methyl-5-*o*-aminophenyl-pyrazole	$C_{10}H_{11}N_3$	125	69.36	6.36	24.27	69	6.05	23.95
XI 1H-3-hydroxy-5-*o*-nitrophenyl-pyrazole	$C_9H_7N_3O_3$	185	52.68	3.41	20.48	50.93	3.24	20.05

2. RESULTS AND DISCUSSION

2.1. The formation of 1H-3-methyl-5-o-nitrophenyl-4,5-dihydropyrazole

As indicated above, when treating *o*-nitrobenzoyl acetone, I, prepared, as already reported,[1] by the method of Gevekoht,[5] with hydrazine in the presence of catalytic amounts of 3 % aqueous NaOH solution, the 1H-3-methyl-5-*o*-nitrophenyl-pyrazoline-2 (1H-3-methyl-5-*o*-nitrophenyl-4,5-dihydro-pyrazole) VI was isolated from the reaction mixture. Its structure is supported by elemental analysis data, as well as by the interpretation of IR, ^{1}H-NMR and mass spectra.

Literature data are very definite in pointing out δ the reluctance of pyrazoles — and especially of 1-unsubstituted pyrazoles — to undergo ring reduction reactions. Catalytic hydrogenation [6,7] and sodium/ethanol reduction of pyrazoles at 130° and 20 atm [8] are claimed to give, in some cases, pyrazolines; N-phenyl-pyrazoles, however, are more amenable to reduction with Na/ethanol systems [9]. On the other hand, pyrazolines can be prepared by the addition of hydrazine to ethylene-carbonyl compounds,[10] a reaction which, in a few instances, is reported to take place under base-catalysis conditions.[11]

Thus, faced with two principial possibilities of accounting for the occurrence of a pyrazoline derivative in our case, namely the reduction by the hydrazine/NaOH system of the already formed pyrazole ring, or the reduction of the *o*-nitrobenzoylacetone before the cyclization step, we are prone to favour the second alternative.

Indeed, the concommitant presence of a carbonyl compound, of hydrazine and of sodium hydroxide set up the necessary conditions for a Kijner-Wolff reduction to proceed. It appeared rather logical to put forward the following mechanism (which is a close parallel to the classical Kijner-Wolff reaction sequence) for the formation of VI. (Scheme 1)

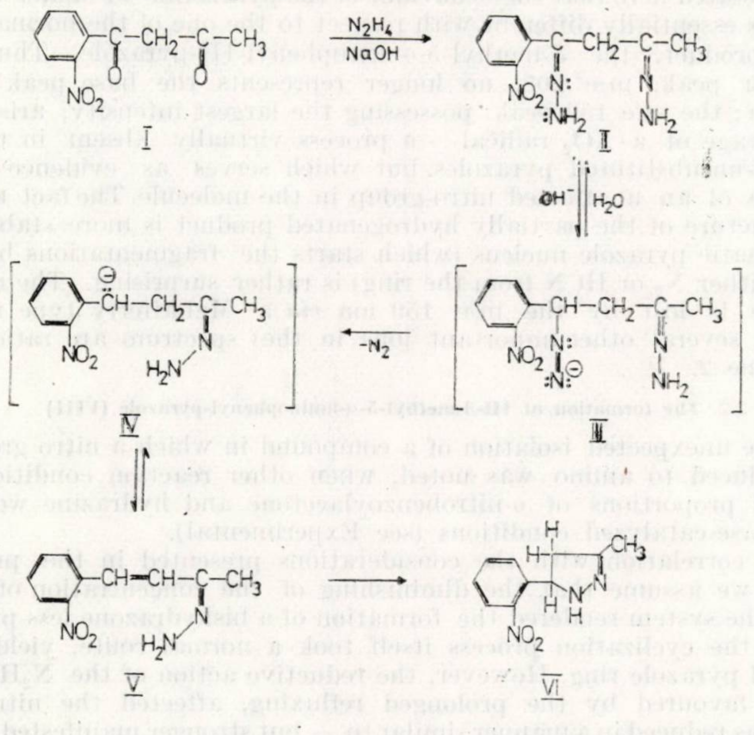

Scheme 1

The proposed mechanism includes the formation of a bishydrazone II; this is requested by the fact that a rather long-lived monohydrazone would prefer the route of cyclization to the normal, non-hydrogenated, pyrazole. The presence of an excess of hydrazine in this synthesis is also promoting the course towards the formation of a bishydrazone. However, a Kijner-Wolff reduction affecting both carbonyl groups is to be ruled out, since in this case no five-membered cyclic compound could be formed. We expect the electronic effects exerted by the nitro-group to differentiate enough the reactivities of the two carbonyls for an easier reduction of the CO group neighbouring the *o*-nitrophenyl moiety to take place, especially if one considers the acidifying influence of this group, which facilitates the protolytic steps involved by the assumed mechanism (steps II → III → IV).

In the ^{1}H-NMR spectrum of the pyrazoline VI, the characteristic signal of the CH_3 protons in position 3 at 1.30 ppm and especially the quadruplet at 4.34 ppm assigned to the adjacent CH_2 group (position 4), and the signal of the C_5-proton (7.60 ppm) are clearly supporting the proposed structure.

The IR-spectrum reveals the expected $C{=}N$ ($1690-1705\ cm^{-1}$) and $N-H$ ($3310-3480\ cm^{-1}$) vibrations.

The mass-spectra of the new series of pyrazoles synthesized during our research [1] will make the object of another report; however let it be stated here that the behaviour of the pyrazoline VI under electron impact is essentially different with respect to the one of the normal cyclization product, the 3-methyl-5-*o*-nitrophenyl-1H-pyrazole. Thus, the molecular peak, m/e 205, no longer represents the base peak of the spectrum; the m/e 159 peak, possessing the largest intensity, arises from the cleavage of a $\cdot NO_2$ radical — a process virtually absent in the case of our 4-unsubstituted pyrazoles, but which serves as evidence for the existence of an unaffected nitro-group in the molecule. The fact that the ring structure of the partially hydrogenated product is more stable than the aromatic pyrazole nucleus (which starts the fragmentations by eliminating either N_2 or HCN from the ring) is rather surprising. The nitrogen molecule is lost by the m/e 159 ion *via* a McLafferty type rearrangement; several other important ions in the spectrum are rationalized in Scheme 2.

2.2. The formation of 1H-3-methyl-5-o-aminophenyl-pyrazole (VIII)

The unexpected isolation of a compound in which a nitro group has been reduced to amino was noted, when other reaction conditions and modified proportions of *o*-nitrobenzoylacetone and hydrazine were used under base-catalyzed conditions (see Experimental).

In correlation with the considerations presented in the preceding section, we assume that the diminishing of the concentration of hydrazine in the system rendered the formation of a bishydrazone less probable, so that the cyclization process itself took a normal route, yielding the expected pyrazole ring. However, the reductive action of the $N_2H_4/NaOH$ system, favoured by the prolonged refluxing, affected the nitro-group which was reduced in a manner similar to — but stronger manifested than — other cases mentioned in the literature, even in the absence of nickel catalysts.[12] (See Scheme 3).

Elemental analysis as well as the most salient features of the IR — and ^{1}H-NMR spectra support the structure assigned to VIII; a detailed discussion of the fragmentation scheme rationalizing its mass-spectrum will be given in the paper devoted to the analysis of ring-substituent interaction in reactive states generated from our pyrazoles under electron impact.

2.3. The formation of 3-hydroxy-5-o-nitrophenyl-pyrazole (XI)

When using ethyl *o*-nitrobenzoylacetoacetate IX as starting material and employing more concentrated sodium hydroxide solution, the reaction takes a different course especially if the hydrazine hydrate is

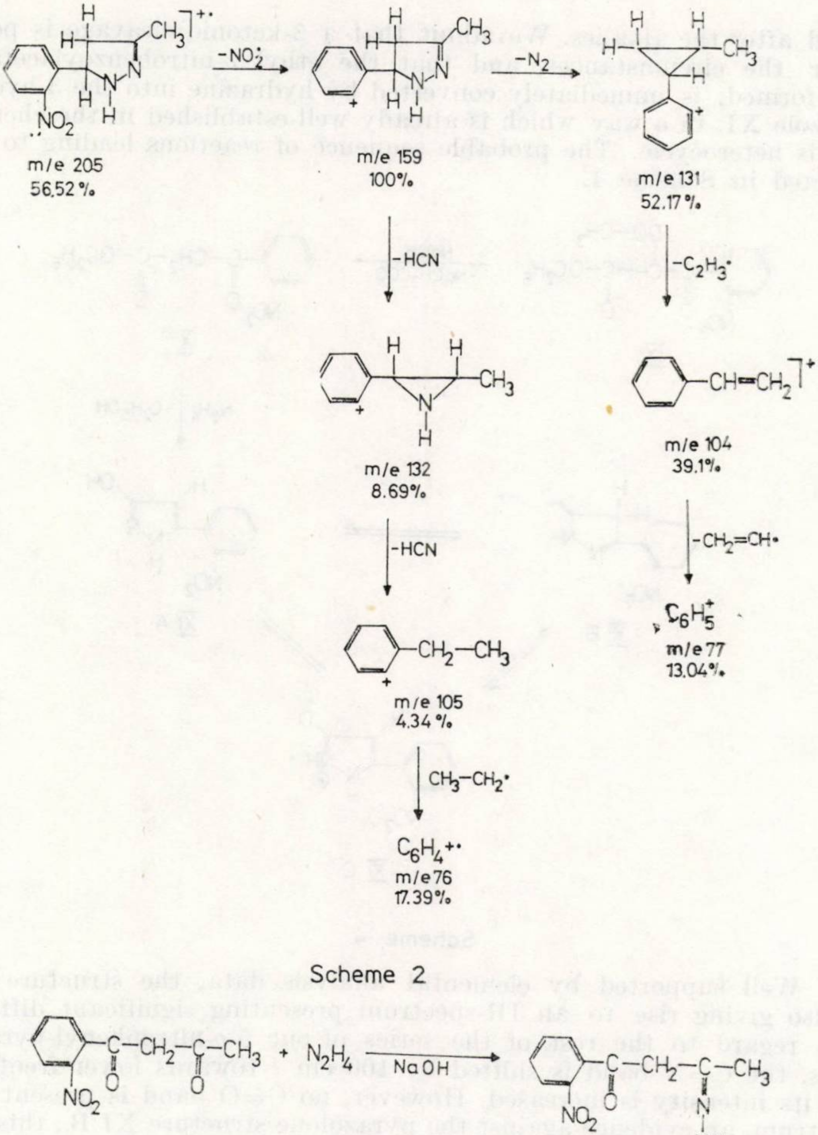
m/e 205
56.52 %
$-NO_2^{\cdot}$
m/e 159
100%
$-N_2$
m/e 131
52.17 %
-HCN
$-C_2H_3^{\cdot}$
m/e 132
8.69%
m/e 104
39.1%
-HCN
$-CH_2{=}CH^{\cdot}$
$C_6H_5^+$
m/e 77
13.04%
m/e 105
4.34 %
$CH_3-CH_2^{\cdot}$
$C_6H_4^{+\cdot}$
m/e 76
17.39%

Scheme 2

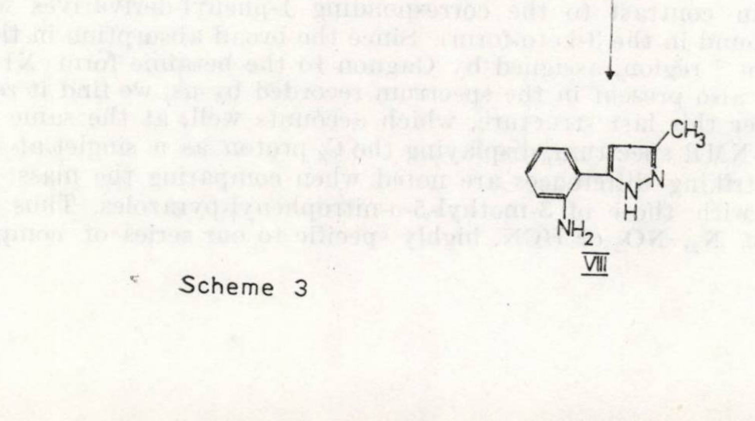
N_2H_4
NaOH
VII
VIII

Scheme 3

added after the alkalies. We admit that a β-ketonic cleavage is possible under the circumstances, and that the ethyl *o*-nitrobenzoylacetate X thus formed, is immediately converted by hydrazine into the 3-hydroxypyrazole XI, in a way which is already well-established in the chemistry of this heterocycle. The probable sequence of reactions leading to XI is depicted in Scheme 4.

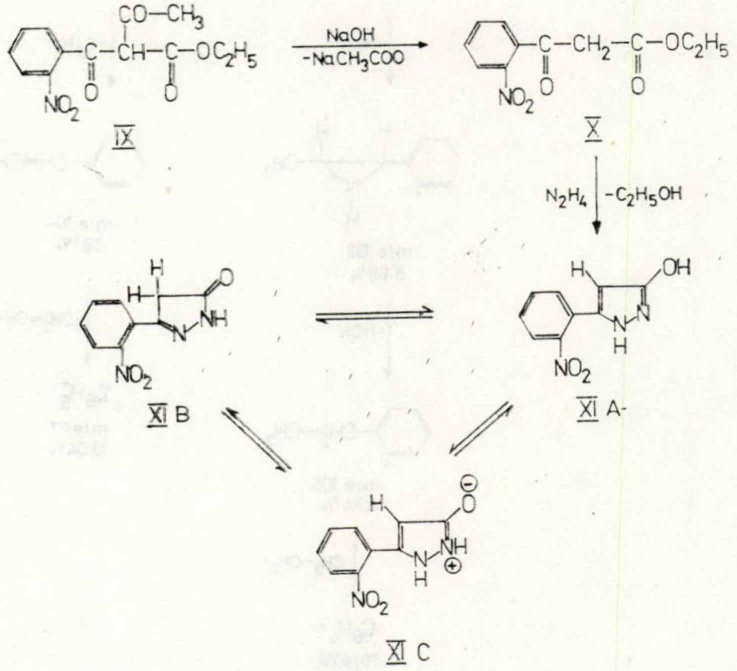

Scheme 4

Well supported by elemental analysis data, the structure of XI is also giving rise to an IR-spectrum presenting significant differences with regard to the rest of the series of our 5-*o*-nitrophenyl-pyrazoles.[1] Thus, the C=N band is shifted by 100 cm^{-1} towards lower frequencies, and its intensity is increased. However, no C=O band is present in the spectrum, an evidence against the pyrazolone structure XI B; this observation is in agreement with the reports by Gagnon *et al.*[13] concerning the preference of other N_1-unsubstituted-3-hydroxy-pyrazoles for the –OH form (in contrast to the corresponding 1-phenyl-derivatives which are to be found in the 3-keto-form). Since the broad absorption in the 2400–2700 cm^{-1} region, assigned by Gagnon to the betainic form (XI C in our case) is also present in the spectrum recorded by us, we find it reasonable to prefer this last structure, which accounts well, at the same time, for the ^{1}H-NMR spectrum, displaying the C_4 proton as a singlet at 5.62 ppm.

Striking differences are noted when comparing the mass spectrum of XI with those of 3-methyl-5-*o*-nitrophenyl-pyrazoles. Thus the cleavage of N_2, $\cdot NO_2$ or HCN, highly specific to our series of compounds, is insignificant in this case. The prevailing fragmentation routes are, in the case under scrutiny, the elimination of CHN_2O, $C_2H_2N_2O$ and C_2H_2O fragments from the ions m/e 205, m/e 204 and m/e 176 with the formation of the ions m/e 148 and m/e 134, which are among the most intense in

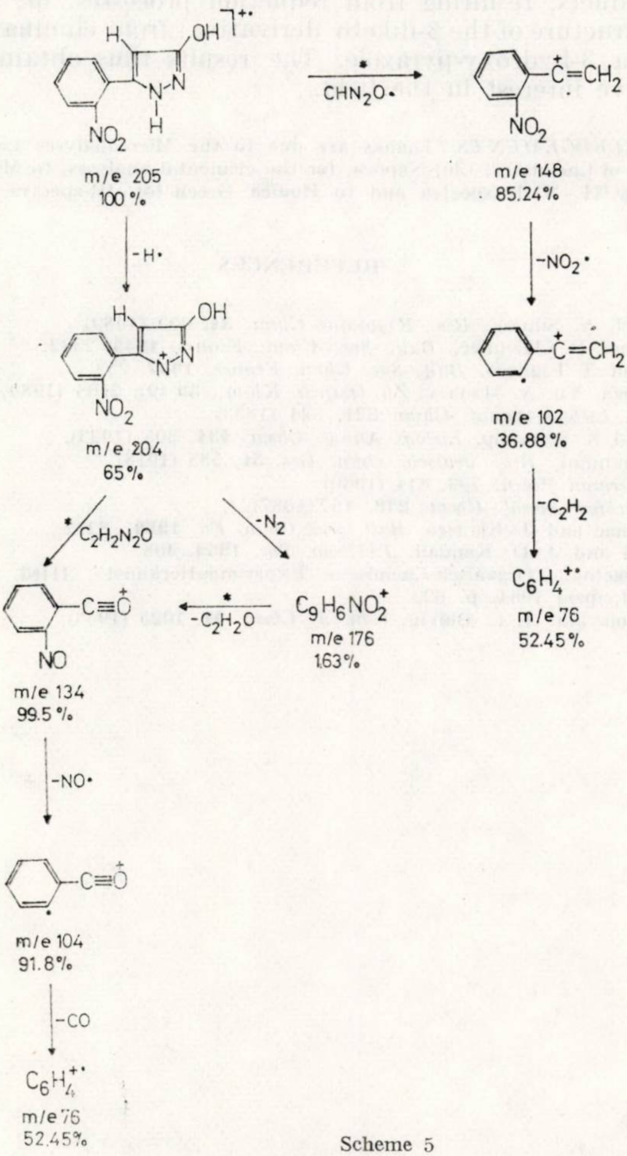
m/e 205
100 %
$-CHN_2O\cdot$
m/e 148
85.24%
-H·
$-NO_2\cdot$
m/e 204
65%
m/e 102
36.88 %
$-C_2H_2N_2O$
$-N_2$
$-C_2H_2$
$-C_2H_2O$
$C_9H_6NO_2^+$
m/e 176
1.63%
$C_6H_4^{+\cdot}$
m/e 76
52.45%
m/e 134
99.5 %
-NO·
m/e 104
91.8%
-CO
$C_6H_4^{+\cdot}$
m/e 76
52.45%

Scheme 5

the spectrum. These particular fragmentation processes were checked by determining the presence of the corresponding metastable peaks, as shown in Scheme 5; they originate, undoubtedly, from the specific properties of the betainic form XI C, which render less probable the usual elimination of N_2 or HCN.

3. CONCLUSIONS

The use of alkaline media in the condensation of *o*-nitrophenyl-β-diketonic compounds with hydrazine directs the reaction towards rather unusual products, resulting from reduction processes, or, (by affecting *in situ* the structure of the β-diketo derivative) from elimination reactions leading to a 3-hydroxy-pyrazole. The results thus obtained might be of preparative interest in the field.

AKNOWLEDGEMENTS. Thanks are due to the Microanalyses Laboratory of the Institute of Chemistry, Cluj-Napoca, for the elemental analyses, to Mircea Bogdan for recording ^1H-NMR spectra and to Rodica Grecu for IR-spectra.

REFERENCES

[1] M. Brie and I. A. Silberg, *Rev. Roumaine Chim,* **34,** 000 (1989).
[2] J. Elguero and R. Jacquier, *Bull. Soc. Chim. France,* **1966**, 2832.
[3] J. Bordou and J. Elguero, *Bull. Soc. Chim. France,* **1967**, 289.
[4] M. A. Andreeva, Yu. A. Manaev, *Zh. Obshch. Khim.,* **50** (9), 2106 (1980).
[5] H. Gevekoht, *Liebigs Annal. Chem.* **221**, 323 (1883).
[6] H. Thoms and S. Schnupp, *Liebigs Annal. Chem.* **434**, 305 (1923).
[7] K. W. Rosenmund, *Ber. deutsch. chem. Ges.* **51**, 585 (1918).
[8] H. Bohme, *German Patent* 703, 844 (1930).
[9] L. Knorr, *Liebigs Annal. Chem.* **238**, 137 (1887).
[10] J. L. Aubagnac and J. Elguero, *Bull. Soc. Chim. Fr.* **1969**, 3292.
[11] G. F. Duffin and J. D. Kendall, *J. Chem. Soc.* **1954**, 408.
[12] Weygand-Hilgetag, "Organisch-Chemische Experimentierkunst" IIIrd ed., J. A. Barth Verlag, Leipzig 1964, p. 622.
[13] P. E. Gagnon and J. L. Boivin, *Can. J. Chem.* **31**, 1025 (1953).

Revue Roumaine de Chimie, **34**, *4*, 953–960 (1989)

RADIOCHEMISCHE METHODE ZUR BESTIMMUNG DER LÖSLICHKEIT VON SCHWERLÖSLICHEN VERBINDUNGEN

ALEXANDRU CECAL und GRETY-IRINA CIUCHI
Fakultät für Chemische Technologie des Polytechnischen Instituts.
Splaiul Bahlui – 71, 6600 – Iaşi, Rumänien

Eingegangen am 18. Januar 1988

In dieser Arbeit wird eine radiochemische Methode zur Bestimmung der Löslichkeit einiger in Wasser und verschiedenen Gemischen von Wasser – Methanol, Wasser – Äthanol und Wasser – Isopropanol schwer lösbaren Verbindungen : $Zn(OH)_2$; $Cd(OH)_2$; $Hg(OH)_2$; $ZnCO_3$ und $CdCO_3$, vorgestellt, die auf der inneren isotopischen Verdünnung beruht. Für jede einzelne Probe wurden die Aktivitätskoeffizienten des Lösungsmediums berechnet, sowie die der freien Standardenergieschwankung entsprechenden Werte. Auf Grund dieser thermodynamischen Daten wurden anschliessend Schlussfolgerungen über den unterschiedlichen Solvatations- und Hydratationsgrad der Ionen schwerlöslicher Verbindungen während des Lösungsprocesses gezogen.

This paper presents a radiochemical method, based on the internal isotopic dilution, for the determination of solubility, in water or in several water-organic solvent mixtures, of some difficultly soluble compounds : $Zn(OH)_2$, $Cd(OH)_2$, $Hg(OH)_2$, $ZnCO_3$ and $CdCO_3$. From the experimental data, several parameters : solubility, solubility product, medium effect and the variation of standard free energy for these investigated systems, were determined.

EINFÜHRUNG

Es sind eine Reihe von Studien bekannt, die sich mit der Bestimmung der Löslichkeit von einigen schwerlöslichen Verbindungen in verschiedenen Gemischen von Wasser – organisches Lösungsmittel beschäftigen, wobei die thermodynamischen Parameter, die den Lösungsprozess beschreiben, berechnet werden.[1-9] In diesem Sinne wurde die Löslichkeit von Silber – und Lithiumhalogeniden in verschiedenen nichtwässrigen Lösungen oder in Gemischen von Wasser und organischen Lösungsmittel untersucht.

In der vorliegenden Arbeit wird eine radiochemische Methode zur Bestimmung der Löslichkeit einiger schwerlöslicher Verbindungen unter verschiedenen experimentellen Bedingungen vorgestellt, wobei die innere isotopische Verdünnung angewendet wurde.[10-11]

EXPERIMENTELLER TEIL

Zuerst wurden die Verbindungen $Zn(OH)_2$; $Cd(OH)_2$; $Hg(OH)_2$; $ZnCO_3$ und $CdCO_3$ in festem Zustand synthetisiert, wobei die Anweisungen aus der Fachliteratur berücksichtig wurden.[12–13] Danach wurden diese in festem Zustand sich befindlichen Substanzen 3 Stunden lang in einem Trockenschrank bei einer Temperatur von 110–115°C aufbewahrt, um die Wasserspuren zu beseitigen und dann in einem Exsikkator mit $CaCl_2$ gelagert.

In Erlenmayerkolben wurde das Lösungsmittel gefüllt: 90 ml Wasser oder 90 ml eines Gemisches aus Wasser und organischem Lösungsmittel (Methanol, Äthanol oder Isopropanol) in den folgenden Verhältnissen: 10, 20, 30, 40, 50, 60, 70, 80 und 90 %. In jeden dieser Kolben wurden noch je 10 ml radioaktive $^{65}ZnCl_2$ — Lösung für die Proben mit Zinkhydroxyd und Zinkkarbonat, $^{115}CdCl_2$ für Kadmiumhydroxyd und Kadmiumkarbonat sowie $^{203}HgCl_2$ für Quecksilberhydroxyd gefüllt. Die radioaktiven Lösungen wurden von IFIN Bukarest geliefert und hatten die in Tabelle 1 aufgeführten Konzentrationen und Aktivitäten.

Tabelle 1

Kennwerte der verwendeten radioaktiven Lösungen von $^{65}ZnCl_2$, $^{115}CdCl_2$ und $^{203}HgCl_2$

Verbindung	Konzentration (mg/mL)	Spezifische Aktivität (Bq/mL)
$^{65}ZnCl_2$	0,10	$1{,}48 . 10^4$
$^{115}CdCl_2$	0,15	$3{,}60 . 10^4$
$^{203}HgCl_2$	0,03	$1{,}05 . 10^4$

Dann wurden in jeden Erlenmayerkolben je 1 g von der entsprechenden schwerlöslichen Verbindung: $Zn(OH)_2$; $ZnCO_3$; $Cd(OH)_2$; $CdCO_3$ und $Hg(OH)_2$ gegeben. Die Proben wurden intermittierend geschüttelt und nach einer Pause von 30 min wurden aus jedem Kolben je 0,5 mL Lösung entnommen, deren Aktivität mit einem Szintillationsdetektor vom Typ NaI(Tl), angeschlossen an einen Ein-Kanal Analysator NK-150, gemessen wurde. Die gemessenen Aktivitäten, von denen der kosmische Grundwert abgezogen wurde, bezogen auf 1 ml Lösung, stellten die spezifischen Aktivitätswerte R_2 (Bq/mL) dar.

In weiteren 3 Kolben wurden folgende Proben vorbereitet:

— 90 ml Wasser + 10 mL $^{65}ZnCl_2$ — Lösung;

— 90 ml Wasser + 10 mL $^{115}CdCl_2$ — Lösung;

— 90 ml Wasser + 10 mL $^{203}HgCl_2$ — Lösung.

Aus diesen, wurden ebenfalls je 0,5 mL Lösung entnommen und ihre Aktivität, wie oben beschrieben, bestimmt. Nach Abzug des kosmischen Grundwertes wurden die erhaltenen Aktivitäten auf 1 mL Lösung bezogen, und somit wurde die spezifische Aktivität R_1 (Bq/mL) für jede dieser 3 Vergleichlösungen erhalten.

ERGEBNISSE UND DISKUSSION

Als Folge des Kontaktes der schwerlöslichen Verbindung mit dem Lösungsmittel, das die radioaktive Lösung enthält, findet eine intensive isotopische Verdünnung der radioaktiven Kationen ($^{65}Zn^{2+}$, $^{115}Cd^{2+}$ und $^{203}Hg^{2+}$) durch die entsprechenden nichtradioaktiven Kationen statt. Wenn C_1 die Konzentration der radioaktiven Kationen in der Ausgangslösung (mit der spezifischen Aktivität R_1) ist und C_2 die Konzentration der nichtradioaktiven Kationen, die von der festen Substanz (mit einer spezifischen Endaktivität R_2) in Lösung gegangen ist, dann kann man zwischen diesen Grössen die Beziehung:

$$C_2 = \frac{R_1 - R_2}{R_2} C_1$$

aufstellen, da als Folge der isotopischen Verdünnung die totale Aktivität der Lösung sich nicht ändert.

Für eine weniger lösliche Verbindung erhält man eine reduzierte innere isotopische Verdünnung, denn weniger nichtradioaktive Kationen gehen in die entsprechende radioaktive Lösung über. Infolgedessen ist die spezifische Aktivität der nach der eingeschränkten Auflösung der festen Probe erhaltenen Lösung nahe jener der Ausgangslösung.

Wenn jedoch die Löslichkeit der untersuchten Verbindung grösser ist, dann findet eine prägnantere isotopische Verdünnung statt, und somit ist die speczifische Aktivität der gegebenen Lösung viel kleiner als die der Ausgangslösung.

Während des Auflösungsprozesses kann man für eine Verbindung der Form AB folgendes Gleichgewicht aufstellen:

$$AB_n \rightleftharpoons A^{n+} + nB^-$$

Dann ist das Löslichkeitsprodukt:

$$K_s = [A^{n+}][B^-]^n = S(n\,S)^n = n^n S^{n+1};$$

Ist die Konzentration C_2 der Lösung nach der Auflösung der festen Probe (g/ml) bekannt, dann kann man danach die Löslichkeit S der entsprechenden schwerlöslichen Verbindung (mol/l) berechnen.

Es ist ein Unterschied zwischen den Werten der freien Solvatationsenergie (${}_sG_i^0$) und der der Hydratation (${}_wG_i^0$), was durch die folgende Beziehung wiedergegeben wird: [14–15]

$$\Delta G_{i,}^0 = {}_sG_i^0 - {}_wG_i^0 = RT \log {}_m\gamma_i = RT(\log {}_sK_s - \log {}_wK_s);$$

In diesem Ausdruck ist ${}_m\gamma_i$ das Mediumeffekt des gegebenen Reaktionsmediums auf den Lösungsprozess bzw. der Aktivitätskoeffizient des Lösungsmittels oder der Aktivitätskoeffizient des Lösungsmediums. Dieser Aktivitätskoeffizient weist auf die Tatsache hin, dass jedes Molekül des Lösungsmittels für sich und auf unterschiedliche Weise mit den Ionen jenes Systems reagiert. Gleichzeitig ist das Mediumeffekt ein Mass für die freie Standardübertragungsenergie des zu lösenden Stoffes vom Wasser zum nichtwässrigen Lösungsmittel. Zwischen der freien Standardübertragungsenergie und der Löslichkeit einer Verbindung in diesem Medium existiert ein umgekehrt proportionales Verhältnis.

Die erhaltenen praktischen Resultate zur Löslichkeit schwerlöslichen Verbindungen sowie jene bzgl. der entsprechenden thermodynamischen Grössen sind in den Tabellen 2–6 wiedergegeben.

Aus diesen Daten schliesst man, dass die Löslichkeit in Wasser der untersuchten Verbindungen grösser ist als die in den Gemischen Wasser–organisches Lösungsmittel.

In der Masse, in der Anteil an organischen Lösungsmittel wächst (bis 50%) stellt man einen Abfall der Löslichkeit fest und somit auch der anderen gefundenen Werte. Vergrössert sich weiter der Anteil von organischen Lösungsmittel, stellt man jedoch ein leichtes Anwachsen der Löslichkeit der untersuchten Verbindungen fest. Diese Resultate entsprechen den von anderen Autoren gefundenen Werte [16–18] für solche Systeme und

Tabellen 2—6

Abhängigkeit der Werte der untersuchten physikalisch-chemischen Parameter (Löslichkeit, Löslichkeitsprodukt, Mediumeffekt und Differenz der freien Solvatations -- und Hydratationsenergien) vom Lösungsmedium für die Verbindungen : $Zn(OH)_2$ (Tab. 2) ; $Cd(OH)_2$ (Tab. 3) ; $Hg(OH)_2$ (Tab. 4) ; $ZnCO_3$ (Tab. 5) und $CdCO_3$ (Tab. 6), bei 20,5°C.

Tabelle 2 : $Zn(OH)_2$

Auflösungsmedium	Wasser-organisches Lösungsmittel Verhältnis (%)	S (mol/1)	K_s	$\log_m \gamma_i$	ΔG_i^0 (J/mol)
Wasser	—	$3,26.10^{-9}$	$1,38.10^{-25}$	—	—
Wasser-Methanol	90 : 10	$3,08.10^{-9}$	$1,17.10^{-25}$	0,071	173,8
	80 : 20	$2,75.10^{-9}$	$8,31.10^{-26}$	0,220	534,6
	70 : 30	$2,39.10^{-9}$	$5,46.10^{-26}$	0,402	977,6
	60 : 40	$2,11.10^{-9}$	$3,75.10^{-26}$	0,565	1373,9
	50 : 50	$1,82.10^{-9}$	$2,41.10^{-26}$	0,757	1880,9
	40 : 60	$1,95.10^{-9}$	$2,96.10^{-26}$	0,670	1626,8
	30 : 70	$2,16.10^{-9}$	$4,03.10^{-26}$	0,534	1296,6
	20 : 80	$2,37.10^{-9}$	$5,32.10^{-26}$	0,413	1015,1
	10 : 90	$2,61.10^{-9}$	$7,11.10^{-26}$	0,288	699,3
Wasser-Äthanol	90 : 10	$3,13.10^{9}$	$1,22.10^{-25}$	0,056	136,6
	80 : 20	$2,92.10^{-9}$	$9,95.10^{-26}$	0,142	344,9
	70 : 30	$2,65.10^{-9}$	$7,44.10^{-26}$	0,268	651,4
	60 : 40	$2,38.10^{-9}$	$5,39.10^{-26}$	0,408	991,3
	50 : 50	$2,21.10^{-9}$	$4,32.10^{-26}$	0,504	1224,7
	40 : 60	$2,45.10^{-9}$	$5,88.10^{-26}$	0,370	899,6
	30 : 70	$2,77.10^{-9}$	$8,50.10^{-26}$	0,210	512,0
	20 : 80	$2,99.10^{-9}$	$1,05.10^{-25}$	0,118	288,2
	10 : 90	$3,03.10^{-9}$	$1,11.10^{-25}$	0,094	229,4
Wasser-Isopropanol	90 : 10	$3,17.10^{-9}$	$1,27.10^{-25}$	0,036	87,6
	80 : 20	$3,02.10^{-9}$	$1,10.10^{-25}$	0,099	239,1
	70 : 30	$2,89.10^{-9}$	$9,65.10^{-26}$	0,155	377,2
	60 : 40	$2,64.10^{-9}$	$7,36.10^{-26}$	0,273	662,8
	50 : 50	$2,42.10^{-9}$	$5,66.10^{-26}$	0,387	939,8
	40 : 60	$2,55.10^{-9}$	$6,63.10^{-26}$	0,318	773,0
	30 : 70	$2,74.10^{-9}$	$8,23.10^{-26}$	0,224	545,1
	20 : 80	$2,91.10^{-9}$	$9,85.10^{-26}$	0,146	355,5
	10 : 90	$3,01.10^{-9}$	$1,08.10^{-25}$	0,102	248,7

Tabelle 3: $Cd(OH)_2$

Auflösungsmedium	Wasser-organisches Lösungsmittel Verhältnis (%)	S (mol/L)	K_s	$\log_m \gamma_i$	ΔG_i^0 (J/mol)
Wasser	—	$3{,}91.10^{-5}$	$2{,}39.10^{-13}$	—	—
Wasser-Methanol	90 : 10	$3{,}72.10^{-5}$	$2{,}06.10^{-13}$	0,064	156,6
	80 : 20	$3{,}47.10^{-5}$	$1{,}67.10^{-13}$	0,155	380,1
	70 : 30	$3{,}25.10^{-5}$	$1{,}37.10^{-13}$	0,242	586,8
	60 : 40	$3{,}10.10^{-5}$	$1{,}19.10^{-13}$	0,303	735,3
	50 : 50	$2{,}94.10^{-5}$	$1{,}02.10^{-13}$	0,369	897,9
	40 : 60	$2{,}99.10^{-5}$	$1{,}07.10^{-13}$	0,348	850,2
	30 : 70	$3{,}19.10^{-5}$	$1{,}29.10^{-13}$	0,267	649,7
	20 : 80	$3{,}35.10^{-5}$	$1{,}50.10^{-13}$	0,203	491,2
	10 : 90	$3{,}39.10^{-5}$	$1{,}56.10^{-13}$	0,186	449,3
Wasser-Äthanol	90 : 10	$3{,}77.10^{-5}$	$2{,}14.10^{-13}$	0,047	116,5
	80 : 20	$3{,}61.10^{-5}$	$1{,}88.10^{-13}$	0,104	253,1
	70 : 30	$3{,}40.10^{-5}$	$1{,}57.10^{-13}$	0,182	443,1
	60 : 40	$3{,}22.10^{-5}$	$1{,}33.10^{-13}$	0,254	618,0
	50 : 50	$3{,}09.10^{-5}$	$1{,}18.10^{-13}$	0,306	744,2
	40 : 60	$3{,}14.10^{-5}$	$1{,}23.10^{-13}$	0,288	700,4
	30 : 70	$3{,}29.10^{-5}$	$1{,}42.10^{-13}$	0,226	549,0
	20 : 80	$3{,}38.10^{-5}$	$1{,}54.10^{-13}$	0,191	464,4
	10 : 90	$3{,}41.10^{-5}$	$1{,}64.10^{-13}$	0,148	363,7
Wasser-Isopropanol	90 : 10	$3{,}85.10^{-5}$	$2{,}28.10^{-13}$	0,024	48,8
	80 : 20	$3{,}69.10^{-5}$	$2{,}01.10^{-13}$	0,075	182,5
	70 : 30	$3{,}51.10^{-5}$	$1{,}73.10^{-13}$	0,140	340,7
	60 : 40	$3{,}37.10^{-5}$	$1{,}53.10^{-13}$	0,193	470,3
	50 : 50	$3{,}22.10^{-5}$	$1{,}33.10^{-13}$	0,256	618,1
	40 : 60	$3{,}29.10^{-5}$	$1{,}43.10^{-13}$	0,223	541,6
	30 : 70	$3{,}39.10^{-5}$	$1{,}56.10^{-13}$	0,185	449,8
	20 : 80	$3{,}46.10^{-5}$	$1{,}62.10^{-13}$	0,171	392,5
	10 : 90	$3{,}54.10^{-5}$	$1{,}77.10^{-5}$	0,130	326,6

Tabelle 4: $Hg(OH)_2$

Auflösungsmedium	Wasser-organisches Lösungsmittel Verhältnis (%)	S (mol/L)	K_s	$\log_m \gamma_i$	ΔG_i^0 (J/mol)
Wasser	—	$1{,}35.10^{-9}$	$9{,}84.10^{-27}$	—	—
Wasser-Methanol	90 : 10	$1{,}28.10^{-9}$	$8{,}38.10^{-27}$	0,069	169,3
	80 : 20	$1{,}17.10^{-9}$	$6{,}40.10^{-27}$	0,186	435,6
	70 : 30	$1{,}05.10^{-9}$	$4{,}63.10^{-27}$	0,327	795,0
	60 : 40	$9{,}98.10^{-10}$	$3{,}97.10^{-27}$	0,384	957,2
	50 : 50	$9{,}81.10^{-10}$	$3{,}77.10^{-27}$	0,416	1014,6
	40 : 60	$9{,}87.10^{-10}$	$3{,}84.10^{-27}$	0,408	992,3
	30 : 70	$9{,}92.10^{-10}$	$3{,}90.10^{-27}$	0,401	975,9
	20 : 80	$1{,}06.10^{-9}$	$4{,}76.10^{-27}$	0,325	785,7
	10 : 90	$1{,}11.10^{-9}$	$5{,}47.10^{-27}$	0,255	619,1

Tabelle 4 (continued)

Auflösungsmedium	Wasser-organisches Lösungsmittei Verhältnis %	(S mol/L)	K_s	$\log_m \gamma_i$	ΔG_i^0 (J/mol)
Wasser-Äthanol	90 : 10	$1,31.10^{-9}$	$8,98.10^{-27}$	0,039	95,3
	80 : 20	$1,26.10^{-9}$	$8,01.10^{-27}$	0,089	216,9
	70 : 30	$1,19.10^{-9}$	$6,74.10^{-27}$	0,164	397,8
	60 : 40	$1,11.10^{-9}$	$5,47.10^{-27}$	0,255	619,1
	50 : 50	$1,02.10^{-9}$	$4,42.10^{-27}$	0,365	887,7
	40 : 60	$1,07.10^{-9}$	$4,90.10^{-27}$	0,302	735,1
	30 : 70	$1,10.10^{-9}$	$5,32.10^{-27}$	0,267	648,4
	20 : 80	1ö15.10^{-9}	$6,08.10^{-27}$	0,209	507,7
	10 : 90	$1,21.10^{-9}$	$7,09.10^{-27}$	0,143	346,9
Wasser-Isopropanol	90 : 10	$1,32.10^{-9}$	$7,26.10^{-27}$	0,026	64,0
	80 : 20	$1,29.10^{-9}$	$8,58.10^{-27}$	0,058	144,1
	70 : 30	$1,24.10^{-9}$	$7,62.10^{-27}$	0,111	269,6
	60 : 40	$1,18.10^{-9}$	$6,57.10^{-27}$	0,175	425,9
	50 : 50	$1,12.10^{-9}$	$5,61.10^{-27}$	0,245	592,5
	40 : 60	$1,13.10^{-9}$	$5,77.10^{-27}$	0,231	562,8
	30 : 70	$1,17.10^{-9}$	$6,40.10^{-27}$	0,182	453,0
	20 : 80	$1,21.10^{-9}$	$7,08.10^{-27}$	0,143	347,1
	10 : 90	$1,24.10^{-9}$	$7,62.10^{-27}$	0,111	269,6

Tabelle 5: $ZnCO_3$

Auflösungsmedium	Wasser-organisches Lösungsmittel Verhältnis (%)	S (mol/L)	K_s	$\log_m \gamma_i$	ΔG_i^0 (J/mol)
Wasser	—	$1,72.10^{-4}$	$2,96.10^{-8}$	—	—
Wasser-Methanol	90 : 10	$1,41.10^{-4}$	$1,98.10^{-8}$	0,174	0,423,9
	80 : 20	$1,09.10^{-4}$	$1,18.10^{-8}$	0,398	969,2
	70 : 30	$9,75.10^{-5}$	$9,51.10^{-9}$	0,493	1197,3
	60 : 40	$9,32.10^{-5}$	$8,79.10^{-9}$	0,527	1280,3
	50 : 50	$9,01.10^{-5}$	$8,12.10^{-9}$	0,561	1363,8
	40 : 60	$9,12.10^{-5}$	$8,32.10^{-9}$	0,550	1330,1
	30 : 70	$9,33.10^{-5}$	$8,70.10^{-9}$	0,531	1290,6
	20 : 80	$9,69.10^{-5}$	$9,39.10^{-9}$	0,498	1211,0
	10 : 90	$9,92.10^{-5}$	$9,84.10^{-9}$	0,478	1161,3
Wasser-Äthanol	90 : 10	$1,59.10^{-4}$	$2,52.10^{-8}$	0,068	165,5
	80 : 20	$1,21.10^{-4}$	$1,46.10^{-8}$	0,306	745,2
	70 : 30	$1,02.10^{-4}$	$1,04.10^{-8}$	0,454	1102,9
	60 : 40	$9,81.10^{-5}$	$9,62.10^{-9}$	0,488	1185,1
	50 : 50	$9,58.10^{-5}$	$9,37.10^{-9}$	0,499	1217,2
	40 : 60	$9,70.10^{-5}$	$9,31.10^{-9}$	0,493	1196,1
	30 : 70	$9,82.10^{-5}$	$9,69.10^{-9}$	0,490	1198,7
	20 : 80	$9,97.10^{-5}$	$9,94.10^{-9}$	0,472	1150,6
	10 : 90	$1,12.10^{-4}$	$1,25.10^{-8}$	0,374	909,1
Wasser-Isopropanol	90 : 10	$1,66.10^{-4}$	$2,75.10^{-8}$	0,031	77,6
	80 : 20	$1,42.10^{-4}$	$2,02.10^{-8}$	0,165	402,9
	70 : 30	$1,22.10^{-4}$	$1,48.10^{-8}$	0,301	730,9
	60 : 40	$1,09.10^{-4}$	$1,18.10^{-8}$	0,399	968,8
	50 : 50	$9,92.10^{-5}$	$9,84.10^{-9}$	0,478	1161,3
	40 : 60	$1,03.10^{-4}$	$1,06.10^{-8}$	0,445	1082,2
	30 : 70	$1,17.10^{-4}$	$1,36.10^{-8}$	0,337	820,1
	20 : 80	$1,29.10^{-4}$	$1,67.10^{-8}$	0,248	603,5
	10 : 90	$1,45.10^{-4}$	$2,10.10^{-8}$	0,149	361,9

Tabelle 6: $CdCO_3$

Auflösungsmedium	Wasser-organisches Lösungsmittel Verhältnis (%)	S (mol/L)	K_s	$\log_m \gamma_i$	ΔG_i^0 (J/mol)
Wasser	—	$1,59.10^{-5}$	$2,53.10^{-10}$	—	—
Wasser-Methanol	90 : 10	$1,28.10^{-5}$	$1,64.10^{-10}$	0,188	457,0
	80 : 20	$1,09.10^{-5}$	$1,18.10^{-10}$	0,331	804,2
	70 : 30	$9,82.10^{-6}$	$9,64.10^{-11}$	0,419	1017,4
	60 : 40	$9,66.10^{-6}$	$9,34.10^{-11}$	0,433	1051,9
	50 : 50	$9,38.10^{-6}$	$8,79.10^{-11}$	0,459	1114,8
	40 : 60	$9,75.10^{-6}$	$9,51.10^{-11}$	0,424	1029,5
	30 : 70	$9,97.10^{-6}$	$9,94.10^{-11}$	0,405	985,1
	20 : 80	$1,07.10^{-5}$	$1,14.10^{-10}$	0,346	840,6
	10 : 90	$1,13.10^{-5}$	$1,27.10^{-10}$	0,284	633,1
Wasser-Äthanol	90 : 10	$1,39.10^{-5}$	$1,93.10^{-10}$	0,117	284,4
	80 : 20	$1,20.10^{-5}$	$1,44.10^{-10}$	0,244	594,3
	70 : 30	$1,03.10^{-5}$	$1,06.10^{-10}$	0,377	917,3
	60 : 40	$9,91.10^{-6}$	$9,82.10^{-11}$	0,439	1066,1
	50 : 50	$9,72.10^{-6}$	$9,44.10^{-11}$	0,428	1039,5
	40 : 60	$9,87.10^{-6}$	$9,73.10^{-11}$	0,414	1006,4
	30 : 70	$1,01.10^{-5}$	$1,02.10^{-10}$	0,394	957,9
	20 : 80	$1,09.10^{-5}$	$1,18.10^{-10}$	0,331	804,2
	10 : 90	$1,25.10^{-5}$	$1,56.10^{-10}$	0,210	509,9
Wasser-Isopropanol	90 : 10	$1,47.10^{-5}$	$2,16.10^{-10}$	0,068	166,7
	80 : 20	$1,29.10^{-5}$	$1,66.10^{-10}$	0,183	444,3
	70 : 30	$1,17.10^{-5}$	$1,37.10^{-10}$	0,266	646,8
	60 : 40	$1,04.10^{-5}$	$1,08.10^{-10}$	0,369	897,6
	50 : 50	$9,95.10^{-6}$	$9,90.10^{-11}$	0,407	989,4
	40 : 60	$1,05.10^{-5}$	$1,10.10^{-10}$	0,361	878,3
	30 : 70	$1,11.10^{-5}$	$1,23.10^{-10}$	0,313	760,5
	20 : 80	$1,22.10^{-5}$	$1,49.10^{-10}$	0,229	558,2
	10 : 90	$1,33.10^{-5}$	$1,76.10^{-10}$	0,157	382,6

können durch die unterschiedliche Basizität des Lösungsmediums erklärt werden.

In reinem Wasser sind die Wasserstoffverbindungen stärker als in den Gemischen Wasser — organisches Lösungsmittel. Aus diesem Grunde ist die Basizität des reinen Wassers kleiner als der verwendeten Lösungsmittelgemische. Wenn das reine Wasser Assoziationen vom Typ : $H^+(H_2O)_n$ enthält, nach dem Zusatz von organischem Lösungsmittel erhält man in erster Linie Hydroniumionen H_3O^+ und Assoziationen vom Typ : $(H_2O)_m$, wobei $m < n$. Aber es ist bekannt, dass die einzelnen Wassermoleküle oder die Assotiationen $(H_2O)_m$ mit einer kleineren Anzahl von Molekülen eine höhere Basizität haben als die des reinen Wassers. In diesem Zustand ist der Hydratationsgrad der Metallionen im Gemisch Wasser-organisches Lösungsmittel etwas niedriger, wodurch die Löslichkeit der festen Probe etwas kleiner ist. Also ist in diesem Fall die Bindung von Hydroniumionen wahrscheinlicher als die der hydratisierten Formen des Typs : $[M(H_2O)]^{n+}$.

Jedoch in dem Masse, in dem der Anteil des organischen Lösungsmittels im Lösungsmittelgemisch anwächst, werden die Ionen des Hydroniumions durch die des Oxoniums, ROH_2^+, ersetzt :

$$H_3O^+ + ROH \rightleftharpoons ROH_2^+ + H_2O$$

wodurch man ein weniger basisches Medium erhält als das des reinen Wassers. Wegen des Überschusses an organischem Lösungsmittel mit einem saueren Charakter als der des reinen Wassers können in diesem System solvatierte Formen des Typs : $[M(ROH)]^{n+}$ auftauchen und infolgedessen ist die Löslichkeit der festen Substanz grösser als im vorhergehenden Fall.

LITERATURVERZEICHNIS

[1] R. Shaw und J. A. V. Butler, *Proc. Roy. Soc.*, **129**, 517(1930).
[2] J. A. V. Butler und D. W. Thomson, *Proc. Roy. Soc.*, **141**, 86(1933).
[3] A. J. Parker, *Chem. Rev.*, **69**, 1(1969).
[4] J. Padova, *J. Phys. Chem.*, **72**, 796(1968).
[5] O. Popovich, *Crit. Rev. Anal. Chem.*, **1**, 79(1970).
[6] J. I. Kim, H. Duschner und T. Hashimoto, *Z. phys. Chem., Neuer Folge*, **103**, 15(1976).
[7] J. I. Kim und H. Duschner, *Z. phys. Chem., Neue Folge*, **106**, 1(1977).
[8] J. I. Kim, Al. Cecal, H.-J. Born und E. A. Gomaa, *Z. phys. Chem., Neue Folge*, **110**, 209(1978).
[9] Al. Cecal und I. Tepes, *Rev. Chim. (București)*, **37**, 1005(1986).
[10] Al. Cecal, *Isotopenpraxis*, **20**, 9(1984).
[11] Al. Cecal, *Isotopenpraxis*, **20**, 259(1984).
[12] G. Brauer, "Handbook of Preparative Inorganic Chemistry", Vol. 2, Second Edition, Acad. Press, New York, 1965.
[13] C. Gh. Macarovici, "Chimie analitică cantitativă", Ed. Tehnică, Bucharest, 1959.
[14] J. F. Coetzee und C. D. Ritchie, "Solute-Solvent Interactions", M. Dekker, New York, 1969.
[15] M. Kolthoff und M. K. Chantooni-Jr., *Anal. Chem.*, **44**, 915 (1972).
[16] E. A. Braude und F. S. Stern, *J. Chem. Soc.*, **1948**, 1976.
[17] M. Alfenaar, C. L. DeLigny, *Rev. Trav. Chim.*, **86**, 929(1967).
[18] I. T. Oiwa, *Sci. Rep. Tohoku Univ.*, **42**, 129 (1967).

Revue Roumaine de Chimie, **34**, *4*, 961–965 (1989)

MICROPROCESSOR OPERATED SCANNING UV-VIS MONOCHROMATOR

E. DARVASI, H. MIOŞCU, A. MORARU, C. OANCEA and E. CORDOŞ
Department of Chemistry, University of Cluj, Cluj-Napoca, Str. Arany Janos 11, Romania

Received October 3, 1988

A sequential monochromator for spectrophotometry computer operated has been designed and built. The monochromator covers the 200 to 700 nm spectral range with a spectral band halfwidth of 0.18 nm. The wavelength and order filter selection and the slit opening are automated and performed by computer.

Computing technique, respectively the microprocessors, has much improved the performances in spectroscopy and the efficiency of the instruments for spectral analysis, in the present the majority of the high performance spectrophotometers being computer driven.[1,2] Monochromators are among the spectral instruments components most subjected to profound constructive transformations in order to be computer operated. This fact has a high significance since in most cases the monochromators decide the performances of the whole spectrometer.

Attempts of modifying and adjusting the monochromators to the operation by computer date from the beginning of '70s, in most cases concern the modification of some existing systems. For this reason the computer control has been limited to the grating position without achieving all the advantages provided by the computer driving regarding the accuracy of the wavelength or signal intensity.[3-7]

The situation has not changed much, most of the spectral instruments designers employing traditional mechanical structures. Therefore the authors have designed and built a programmable sequential monochromator operated by the computer that can be used in the absorption spectrometry and molecular fluorescence as well as in the atomic absorption or emission. The novelty consists both in the arrangement of the optical and mechanical components and in the way they are controlled by computer. At present, the monochromator is included in the SPECTROM 01 UV–VIS spectrophotometer. All the following measurements have been accomplished in this system using the radiation source and the photodetector of the spectrophotometer.

From the optical point of view, the monochromator (Fig. 1) is of the Czerny-Turner type having a plane grating (G) with 651 lines/mm as the dispersion device. The focusing and collimating mirrors (M_1, M_2)

have 250 mm focal length. To reduce the stray light and eliminate the higher interference orders, five absorption filters (F) are mounted on a revolving disk (FD). The opening of the slits (S_1, S_2) is variable between

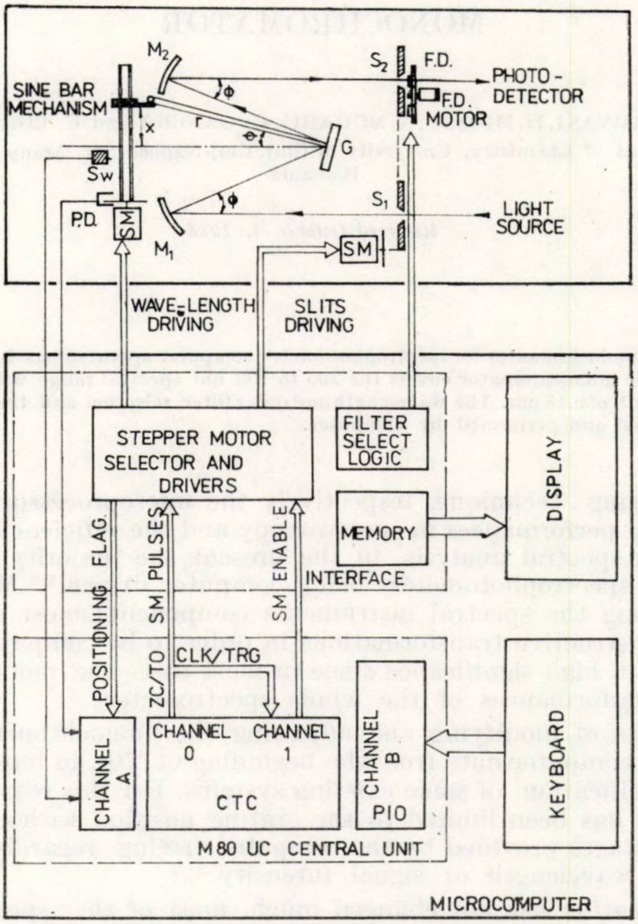
M2
SINE BAR MECHANISM
X
r
ϕ
ϕ
ϕ
G
Sw
P.D.
SM
M1
S2
F.D.
F.D. MOTOR
PHOTO-DETECTOR
S1
LIGHT SOURCE
SM
WAVE-LENGTH DRIVING
SLITS DRIVING
STEPPER MOTOR SELECTOR AND DRIVERS
FILTER SELECT LOGIC
MEMORY
DISPLAY
POSITIONING FLAG
ZC/TO SM PULSES
SM ENABLE
INTERFACE
CLK/TRG
CHANNEL A
CHANNEL 0
CHANNEL 1
CTC
CHANNEL B
PIO
KEYBOARD
M 80 UC CENTRAL UNIT
MICROCOMPUTER

Fig. 1. — Schematic diagram of the UV-VIS monochromator and the adjacent computer electronics. SM — stepper motor ; S_1, S_2 — slits ; FD — filter disk ; G — diffraction grating ; M_1, M_2 — spherical mirrors ; Sw — mechanical switch ; PD — position decoder.

20 and 2000 μm. It is actuated by a lever-type mechanical system driven by a stepper motor computer controlled, the system providing a simultaneous and identical opening. Taking into account the established relation between the slit opening and the number of the motor steps, one can obtain any opening in the above mentioned interval with an increment of 0.2μm. At the start of the working cycle the slits are closed until a microswitch is detected, then driven in the opposite direction to an optoelectronic switch, which serves as a position reference. To eliminate mechanical

backlashes, the change of the slit width is always made in the opening sense. In selecting a narrower width, it comes back to the position reference and then the slits are opened again to the desired value.

The wavelength selection is achieved by rotating the grating around its vertical axis. The equation of the grating for a symmetrical mounting is[8]:

$$m\lambda = 2d \cos \Phi \sin \theta \tag{1}$$

where m — the spectrum order
d — the distance between two successive lines of the grating
Φ — the angle between the incident ray on the grating and the symmetry axis of the monochromator
θ — the rotation angle of the grating

Since Φ is constant, the wavelength varies linearly with $\sin\theta$:

$$\lambda = \left(\frac{2a}{m} \cos \Phi\right) \sin \theta \tag{2}$$

The use of the computer allows the wavelength selection to be made based on equation (2) by driving the grating with a simple mechanical reduction. The simplicity of the mechanical reduction is not advantageous since there are no mechanical adjusting elements necessary for series production in order to bring all the instruments at the same parameters. Therefore, a driving mechanical system with a sinusoidal bar has been used,[9,10] which has no more backlashes than the simple mechanical transmission and, in addition, provides a linear relation between the wavelength and the movement of the bar.

Since

$$\sin \theta = \frac{x}{r} \tag{3}$$

where x — the distance of the sinusoidal bar travel
r — the sine-bar length

the wavelength can be expressed by the relation:

$$\lambda = 2 \frac{a \cos \Phi}{mr} \cdot x \tag{4}$$

Noting with P the step of the leading screw and with N the number of turns, the wavelength is expressed by a polynomial of the first order:

$$\lambda = \frac{2a\, P \cos \Phi}{mr} N \tag{5}$$

This linearity is not always rigorously respected owing to adjusting and mechanical errors. Computer enables a compensation of the eventual deviations by using equations where correction factors are introduced. Thus, in our system, a polynomial function between the wavelength and the number of steps N has been experimentally determined:

$$N(\lambda) = 4.7 \cdot 10^{-5}\lambda^2 + 19.8815\,\lambda + 0.5 \tag{6}$$

In selecting a certain wavelength the computer introduces its value into equation (6) and, on the basis of the resulted number of steps, a corresponding number of pulses is fed to the stepper motor. To drive the stepper motor, the computer has to provide the pulses at a frequency accepted by the motor and register the number of the performed steps by counting the transmitted pulses. The real position accuracy is checked through a feedback from an optical transducer mounted on the stepper motor axle yielding a constant number of pulses for each full rotation of the axle. At a given time, the wavelength is measured through the number of steps performed by the motor from the origin.

Since a mechanical reference for the origin of the wavelength scale cannot ensure the required accuracy, it has been resorted to a spectral reference which is the zero order spectrum of the grating. It is detected by turning the motor towards shorter wavelengths until a mechanical switch (Sw) placed beyond the zero order spectrum position is reached. At this point, the motor rotation is reversed and, while it continues its movement, the photodetector current is measured. The detection of the zero order consists in finding the maximum photodetector signal value by mathematical processing. This maximum represents the origin of the wavelength scale.

The advantage of this system is that it provides a reference with a very accurate position, its localization being facilitated by the intensity of the zero order spectrum that cannot be confused with other spectral lines.

The control system of the stepper motors has been accomplished by use of a programmable timer circuit of a Z80—CTC type. Each current position of the motors is memorized and related to the previous one adding or substracting the performed step number, depending on the moving sense. The positioning command is given by the central unit loading the number of the pulses into the CTC counter. From this moment the central unit is free to do other operations, the positioning being accomplished only under CTC control. The end of operation is signaled by CTC through an interruption. The stepper motor driving from the slit actuation is made on the basis of a similar algorithm.

The computer programme allows the spectrum scanning in 0.1 nm increments, working with a number of measured points between 10 and 250. The programmed spectral range is 200 to 700 nm. The accuracy and reproducibility of the wavelength, established by use of mercury spectral lines, is given in table 1.

Table 1

The accuracy and reproducibility of wavelength selection

Mercury line wavelength nm	Measured wavelength (10 points average) nm	Accuracy nm	Repro-ducibility mn
253.65	253.58	−0.07	0.19
334.15	334.01	−0.14	0.13
407.78	407.79	+0.01	0.10
435.83	435 86	+0.03	0.13
546.07	546.26	+0.19	0.28

The spectral qualities of the monochromators are expressed by the spectral band halfwidth, which is 0.18 nm at a 20 μm slit.

REFERENCES

[1] M. A. Floyd and V. A. Fassel, *Analyt. Chem.*, **52**, 431 (1980).
[2] A. Menna, *Internat. Lab.*, **15**, 65(1985).
[3] J. D. Norris and T. S. West, *Analyt. Chem.*, **45**, 226 (1973).
[4] I. F. Skene, D. C. Stuart et al., *Spectrochim. Acta*, Part. B, **29**, 339 (1974).
[5] J. B. Dawson, D. J. Ellis et al., *Spectrochim. Acta*, Part B, **23**, 695 (1968).
[6] E. Cordoş and H. V. Malmstadt, *Analyt. Chem.*, **45**, 425 (1973).
[7] R. W. Spillman and H. V. Malmstadt, *Analyt. Chem.*, **48**, 303 (1976).
[8] J. F. James and R. S. Sternberg, "The Design of Optical Spectrometers", London, 1969.
[9] E. F. Palermo and Akbar Montaser, *Analyt. Chem.*, **46**, 2154 (1974).
[10] E. Cordoş, "Analiza instrumentală", University of Cluj-Napoca, 1980.

The spectral qualities of the monochromators are expressed by the spectral band halfwidth, which is 0.15 nm at a 25 μm slit.

REFERENCES

1 R. A. Floyd and V. A. Fassel, Analyt. Chem., 52, 431 (1980).
2 [illegible] Meinel, [illegible] Opt., 13, 631 (1980).
3 J. D. Norris and T. S. West, Analyt. Chem., 45, 226 (1973).
4 J. P. Slene, D. G. Stuart et al., Spectrochim. Acta, Part B, 28, 227 (1973).
5 D. Dawson, R. J. Ellis et al., Spectrochim. Acta, Part B, 23, 463 (1968).
6 S. Fardos and H. V. Malmstadt, Analyt. Chem., 45, 425 (1973).
7 K. W. Spillman and H. V. Malmstadt, Analyt. Chem., 48, 303 (1976).
8 J. F. James and R. S. Sternberg, "The Design of Optical Spectrometers", London, 1969.
9 P. Paterno and Albert Montaser, Analyt. Chem., 46, 2164 (1974).
10 G. Cardos, "Modern Instrumentation", University of [illegible], 1978.

Revue Roumaine de Chimie, **34**, *4*, 967–975 (1989)

THE MEAN ACTIVITY COEFFICIENT OF $ZnSO_4$ AND $CuSO_4$ IN THE ELECTROLYTE SOLUTIONS: $ZnSO_4 + Li_2SO_4 + H_2O$ AND $CuSO_4 + Li_2SO_4 + H_2O$

MIHAELA DRĂGĂNOIU and SOLOMON STERNBERG
Department of Physical Chemistry, Polytechnic Institute of Bucharest,
Calea Griviței no. 132, Bucharest, Romania

Received February 21, 1988

As a sequel to the study of the ternary aqueous systems of sulphates we have determined the deviation of these systems from the respective binary ones. The obtained results have been numerically computed and the coefficients of the approximation polynomials are also given. An extended comparison among several ternary systems of sulphates is made and the deviations from the ideality are discussed in terms of excess functions.

After the thermodynamic study of the ternary aqueous systems of sulphates, the present paper synthesizes the results of the determinations made in the systems: $ZnSO_4$ (1) + Li_2SO_4 (2) + H_2O and respectively $CuSO_4$ (1) + Li_2SO_4 (2) + H_2O.

The purpose has been the determination of the mean activity coefficients of the two divalent sulphates, $\gamma_{\pm ZnSO_4}$, respectively $\gamma_{\pm CuSO_4}$. Concerning the obtained values, considerations have been made about the very nonideal behaviour of these solutions in terms of thermodynamic excess functions.

Based on the results presented in this paper as well as on those obtained by us and published previously[1,2,3] a comparison has been made between the behaviour of the ternary systems of sulphates having $ZnSO_4$ as component 1 and that of the systems with $CuSO_4$ component 1.

EXPERIMENTAL PART

For the determination of the mean activity coefficient of the electrolyte 1 from the ternary aqueous solutions of sulphates the emf method was used.

Working in cells with thermostatic mantle (at 25 °C) measurements were made in each system at four total ionic strengths and variable proportions of the two electrolytes.

For the determination of $\gamma_{\pm ZnSO_4}$ the following cell was used: Pt—Hg $Hg_2SO_4/ZnSO_4(m_1)$, $Li_2SO_4(m_2)/Zn_xHg$ — Pt.

For the determination of $\gamma_{\pm CuSO_4}$ the cell: Pt—Hg, $Hg_2SO_4/CuSO_4(m_1)$, $Li_2SO_4(m_2)$/Cu—Pt was employed.

The choice of the copper electrode and of the mercury — mercurous sulphate electrode was discussed in a previous paper.[3]

As zinc electrode, a two-phase amalgam with 25% weight mercury was used. It was obtained by dissolving zinc powder (99.9% purity) in mercury.[4]

From the emf measurements, the extent $\Delta\ln\gamma_1$ was directly computed as:

$$\Delta\ln\gamma_1 = \ln\gamma_{1\pm} - \ln\gamma^b_{1\pm} \quad (1)$$

The method of calculation and the significance of the employed symbols are discussed in the same previous paper.[3]

$\Delta\ln\gamma_1$ was chosen for the characterization of the presented systems with nonideal behaviour because in the form $RT\Delta\ln\gamma_1$, it has the significance of a mean chemical excess potential (μ^{ex}_1) of the electrolyte 1 ($CuSO_4$ respectively $ZnSO_4$) in the studied ternary systems.

RESULTS

Tables 1 and 2 present the results of the determinations as well a the values obtained for μ^{ex}_1.

Table 1

The results of the determinations in the system $ZnSO_4 + Li_2SO_4 + H_2O$

I	y_2	$E \cdot 10^3$(V)	$\gamma^t_{1\pm}$	$a^t_{1\pm}$	$\mu^{ex}_1 = RT\Delta\ln\gamma_1 \frac{cal}{kg\ H_2O \cdot echivg}$
3	0.09	−0.6	0.0593	0.0429	35.25
	0.19	1.1	0.0579	0.0401	21.56
	0.30	1.0	0.0612	0.0403	54.26
	0.39	1.5	0.0678	0.0419	114.46
	0.49	0.5	0.0717	0.0411	147.81
	0.60	0.6	0.0788	0.0409	203.50
	0.69	1.1	0.0877	0.0400	267.18
	0.79	3.6	0.0965	0.0364	323.58
	0.90	4.6	0.1295	0.0350	498.05
2.4	0.12	0.7	0.0595	0.0341	27.01
	0.24	−4.0	0.0661	0.0350	88.51
	0.37	1.1	0.065	0.0327	78.91
	0.49	−6.1	0.0774	0.0355	182.41
	0.62	−2.1	0.0832	0.0336	225.18
	0.75	2.1	0.0999	0.0335	337.77
	0.87	−1.7	0.1372	0.0331	521.63
1.8	0.16	0.1	0.0714	0.0301	35.66
	0.33	0.3	0.0771	0.0298	81.93
	0.49	−1.1	0.0918	0.0315	184.95
	0.66	0.8	0.1020	0.0293	247.46
	0.83	0.8	0.1411	0.0293	439.64
1.5	0.19	1.1	0.0905	0.0314	21.56
	0.39	−0.4	0.1073	0.0332	122.39
	0.60	−0.9	0.1305	0.0339	238.10
	0.79	4.7	0.1444	0.0272	298.17

The values of the mean activity coefficient of the electrolyte[1] in the ternary system ($\ln\gamma^t_{1\pm}$) have been computed on the basis of the experimental determinations and of the data existing in the literature[5] for the

Table 2

The results of the determinations in the system $CuSO_4 + Li_2SO_4 + H_2O$

I	y_2	$\Delta E \cdot 10^3$(V)	$\gamma^{t}_{1\pm}$	$a^{t}_{1\pm}$	$\mu_1^{ex} = RT\Delta \ln \gamma_1 \frac{\text{cal}}{\text{kg } H_2O \cdot \text{echiv.}}$
3	0.09	2.2	0.0464	0.0335	−29.32
	0.19	5.3	0.0429	0.0298	−75.30
	0.30	7.3	0.0418	0.0275	−91.11
	0.39	10.4	0.0383	0.0236	−144.26
	0.49	14.2	0.0367	0.0210	−168.13
	0.60	16.5	0.0370	0.0196	−163.45
	0.69	20.9	0.0355	0.0162	−187.86
	0.79	26.6	0.0352	0.0133	−193.66
	0.90	35.0	0.0346	0.0094	−203.50
2.4	0.12	4.1	0.0503	0.0288	−67.18
	0.24	6.6	0.0484	0.0256	−90.82
	0.37	11.0	0.0462	0.0232	−98.88
	0.49	13.1	0.0443	0.0203	−142.71
	0.62	19.8	0.0421	0.0169	−174.05
	0.75	23.6	0.0402	0.0135	−200.18
	0.87	35.3	0.0355	0.0086	−274.59
1.8	0.16	8.2	0.0565	0.0238	−102.79
	0.33	8.8	0.0493	0.0191	−183.47
	0.49	14.7	0.0459	0.0175	−225.83
	0.66	23.1	0.0381	0.0109	−336.44
	0.83	37.3	0.0341	0.0071	−402.79
1.5	0.19	0.5	0.0659	0.0226	−58.47
	0.39	10.0	0.0597	0.0185	−116.59
	0.60	10.4	0.0548	0.0143	−167.54
	0.79	28.3	0.0480	0.0091	−246.45

respective binary systems ($CuSO_4 + H_2O$ and $ZnSO_4 + H_2O$).

$$\ln \gamma^{t}_{1\pm} = \ln \gamma^{b}_{1\pm} + \Delta \ln \gamma_1 \tag{2}$$

The behaviour of the mean chemical excess potential μ_1^{ex} was characterized by the variation of $\Delta \ln \gamma_1$ with the ionic strength ratio y_2 — computed according to [3], for this type of ternary asymmetrical systems. Using the same program as in[3] the coefficients C_i for the approximation polynomials as far as the fifth order have been numerically computed. They are given in table 3. The calculated dependences are represented in figs. 1 and 2.

For the systems with $CuSO_4$ (1), the polynomials of the second order have been selected for all the ionic strengths except $I = 2.4$. For the solutions with $ZnSO_4$ (1) the second order polynomials are recommended, the curves being practically overlapped for all the ionic strengths.

On the same figures the experimental results are also mentioned. A good agreement between them and the calculated curves can be noticed.

The same agreement can be noticed in figure 3 where several system studied by us in the present paper and in other ones are sythesized[1,2,3]

Table 3

The coefficients of the computed polynomials

System	I	Degree of the polynomial	C_1	C_2	C_3	C_4	σ_i	$\mu_1^{ex,tr}$ cal/ kgH_2O echivg
$ZnSO_4$ + + Li_2SO_4 + + H_2O	3	III	0.4028	−0.3933	1.0496		0.0370	407.41
	2.4	III	0.6676	−1.1893	1.7858		0.0399	648.87
	1.8	II	0.1257	0.8810			0.0415	596.38
	1.5	III	−0.3427	3.1000	−2.3571		0.0008	337.08
$CuSO_4$ + + Li_2SO_4 + + H_2O	3	II	−0.7023	0.3589			0.0174	−203.86
	2.4	III	−0.9980	1.7166	−1.3451		0.0124	−371.15
	1.8	II	−0.9127	0.1209			0.0321	−469.08
	1.5	II	−0.4447	−0.0851			0.0130	−313.86
*$CuSO_4$ + + $MgSO_4$ + + H_2O	3	II	−0.0517	0.1584			0.0097	63.21
	2.4	II	0.0583	0.0361			0.0165	55.92
	1.8	III	−0.3749	0.9808	−0.5629		0.0107	25.47
	1.5	II	−0.1095	0.0953			0.0032	− 8.41
*$CuSO_4$ + + $MnSO_4$ + + H_2O	3	IV	−0.2952	1.7088	−2.5188	0.8812	0.0057	−654.74
	2.4	III	−0.5257	1.7035	−1.2202		0.0079	− 25.12
	1.8	II	−0.0921	0.1531			0.0116	36.14
	1.5	II	−0.0356	0.0607			0.0058	14.87

* The results are synthetizing the determinations from [3].

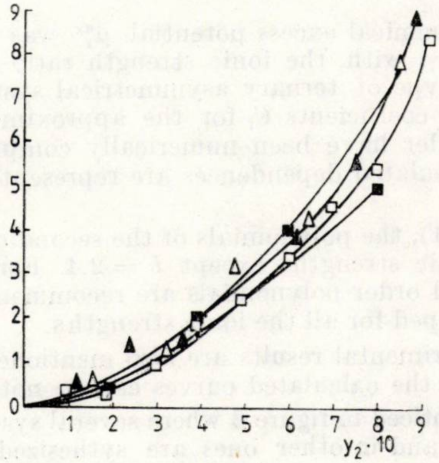

Fig. 1. — The dependences $\Delta \ln \gamma_1 = f(y_2)$ in the system $ZnSO_4 + Li_2SO_4 + H_2O$: —□—□— $I = 3$; —▲—▲— $I = 2.4$; —△—△— $I = 1.8$. —■—■— $I = 1.5$;

The comparison is made for a single total ionic strenght ($I = 1.8$) but a similar behaviour is obtained for the other ionic strengths too.

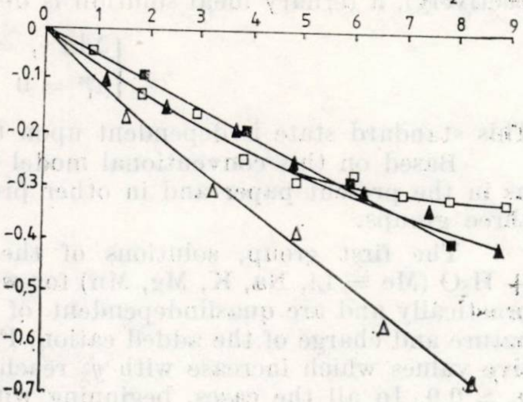

Fig. 2. — The dependences $\Delta\ln\gamma_1 = f(y_2)$ in the system $CuSO_4 + Li_2SO_4 + H_2O$: —□—□— $I = 3$; —▲—▲— $I = 2.4$; —△—△— $I = 1.8$; —■—■— $I = 1.5$.

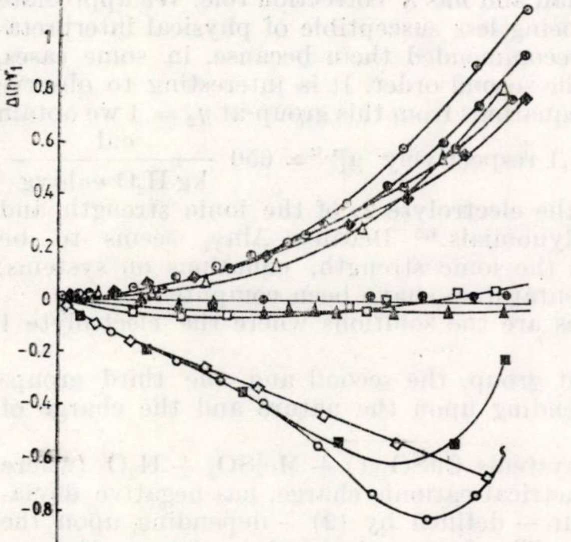

Fig. 3. — The dependence $\Delta\ln\gamma_1 = f(y_2)$, at $I = 1.8$, in all the studied systems: —◓—◓—Zn—Li; —△—△—Zn—Na; —⊙—⊙—Zn—K; ◐—◐—Zn—Mg; —◆—◆—Zn—Mn; —◇—◇—Cu—Li; —■—■—Cu—Na; —○—○—Cu—K; —□—□—Cu—Mg; —■—■—Cu—Mn; —▲—▲—Cu—Zn.

In all the cases studied by us, for a given system, a weak and unconvincing dependence of $\Delta\ln\gamma_1$ upon the total ionic strength was found.

Extrapolating the equations from table 3 at $y_2 = 1$ (respectively $y_1 = 0$), we obtain $\mu_1^{ex,tr} = RT\,\Delta\ln\gamma_1^{tr}$, a "mean chemical excess trace potential" corresponding to an infinite dilution of electrolyte 1 in a solution of electrolyte 2 of the same ionic strength.

DISCUSSION

Considering as "standard state" a real binary solution of component 1 in water (that is the solutions $CuSO_4 + H_2O$ and $ZnSO_4 + H_2O$ respectively), a ternary ideal solution is defined by:

$$\begin{cases}\Delta \ln \gamma_1 = 0 \\ \mu_1^{ex} = 0\end{cases} \tag{3}$$

This standard state is dependent upon the ionic strength.

Based on this conventional model the ternary solutions studied by us in the present paper and in other previous ones may be divided into three groups.

The first group, solutions of the type $ZnSO_4(1) + Me_nSO_4(2) + H_2O$ ($Me = Li, Na, K, Mg, Mn$) for which $\Delta\ln\gamma_1$ depends only upon y_2 practically and are quasiindependent of the ionic strength as well as the nature and charge of the added cation. For these systems $\Delta\ln\gamma_1$ has positive values which increase with y_2 reaching important values ($\simeq 1.0$) for $y_2 \simeq 0.9$. In all the cases, beginning with the second order polynomials, an acceptable mean standard deviation is obtained. For further theoretical considerations the most appropriate equations seem to be those of the second order which are formally similar to the equation of the regular solutions; the main term is small and has a correction role. We appreciate the third order equations as being less susceptible of physical interpretations but have nevertheless recommended them because, in some cases, they fit better than those of the second order. It is interesting to observe that by extrapolating all the equations from this group at $y_2 = 1$ we obtain the same value for $\Delta\ln\gamma_1^{tr} \simeq 1.1$ respectively $\mu_1^{ex,tr} \simeq 650 \dfrac{\text{cal}}{\text{kg } H_2O \text{ echivg}}$, irrespective of the nature of the electrolyte 2, of the ionic strength and the order of the chosen polynomials.[4,5] Because $\Delta\ln\gamma_1$ seems to be approximately independent of the ionic strength, equations on systems, from all the available experimental data, have been computed.[5]

The following two groups are the solutions where the electrolyte 1 is $CuSO_4$.

Differently from the first group, the second and the third groups have distinct behaviours depending upon the nature and the charge of the added cation.

The second group, the systems $CuSO_4(1) + Me_2^ISO_4 + H_2O$ (where $Me_2^I = Li, Na, K$) with asymmetrical cationic charge, has negative deviations from the ideal behaviour — defined by (2) — depending upon the nature of the alkaline cation. The forms of the dependences $\Delta\ln\gamma_1 = f(y_2)$ are also different from those of the first group. As far as $y_2 = 0.5$ all the systems are linear, the negative deviations increasing in the sequence Li, Na, K.

For the solutions $CuSO_4 + Li_2SO_4 + H_2O$, $\Delta\ln\gamma_1$ is decreasing over the whole domain of y_2 values. The equations recommended by us are those of the second order (Table 3). For the systems having Na_2SO_4 or K_2SO_4 as the addition sulphate, equations of the third and fourth orders are recommended.[6]

The third group, the systems $CuSO_4(1) + Me^{II}SO_4(2) + H_2O$ where $Me^{II} =$ Mg, Mn, Zn with symmetrical cationic charge, have very small deviations from the ideality defined by the equations (2). However t is necessary to remark that this quasiideality is relative, $\mu_1^{ex,tr}$ being of the same order of magnitude with the values obtained for the system $BaCl_2(1) + NaCl(2) + H_2O$, one of the mixed halides systems having the greatest deviations from the ideality. The orders of the polynomials recommeded by us for the systems from the third group (II, III and IV) are also greater than those given in the literature for the mixed chloride systems.

Figure 3 shows that although the deviations for these systems are small, the form of the curves is more complex than that for the systems belonging to the first two groups; here there are negative as well as positive deviations from the ideality.

In figures 4 and 5 are represented the dependences $\ln\gamma_{1\pm}^t = f(m_1)$ for the studied systems as well as those for the binary systems ($ZnSO_4 + H_2O$ respectively $CuSO_4 + H_2O$). The curves for the binary systems are not at total constant ionic strength.

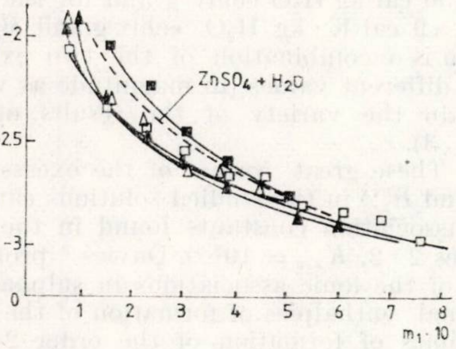

Fig. 4. — The dependences $\Delta\ln\gamma_{1\pm}^t = f(m_1)$ in the system $ZnSO_4 + Li_2SO_4 + H_2O$: $-\square-\square-I = 3$; $-▲-▲-I = 2.4$; $-\triangle-\triangle-I = 1.8$; $-■-■-I = 1.5$.

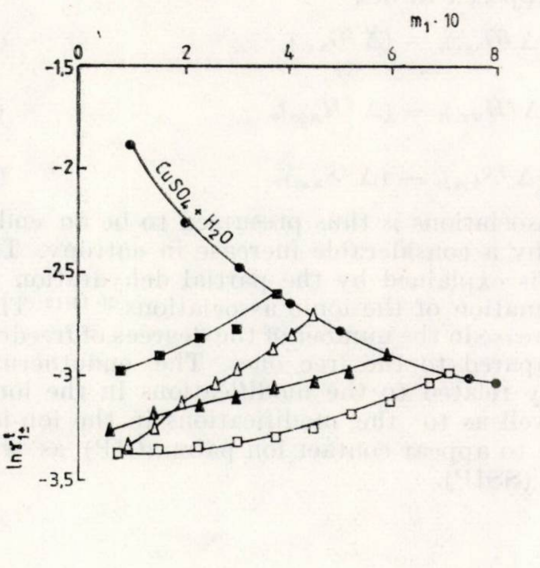

Fig. 5. — The dependen ce $\ln\gamma_{1\pm}^t = f(m_1)$ in the syst em $CuSO_4 + Li_2SO_4 + H_2O$: $-\square-\square I = 3$; $-▲-▲-I = 2.4$; $-\triangle-\triangle-I = 1.8$; $-■-■-I = 1.5$.

For the system $ZnSO_4(1) + Li_2SO_4(2) + H_2O$, with positive deviations, the dependences for all the ionic strengths are practically identical among them and with that for the binary system. A similar behaviour has been obtained for the other systems with $ZnSO_4(1)$ too.[5]

For the systems from the second group the experimental dependences $\ln\gamma^t_{1\pm}=f(m_1)$ are set under the ideal line [6] and those from the third group are near the ideal line.

The results obtained for all the mixtures studied by us are unexpected from several points of view.

First, the values $\Delta\ln\gamma_1$ obtained for the solutions from the first two groups are approximately with an order of magnitude superior to those given in the literature for the mixture of halides. From preliminary determinations for the dependence of $\Delta\ln\gamma_1$, upon the temperature, $\bar{S}_1^{ex}$ as well as $\bar{H}_1^{ex}$ for some of the ternary studied mixtures have been computed. Unexpectedly high values have been obtained for $\bar{S}_1^{ex}$ and $\bar{H}_1^{ex}$. These values differ very much with the nature of the system: for the system $CuSO_4 + Li_2SO_4 + H_2O$, $\bar{S}_1^{ex} \simeq 3$ cal/K · kg · H_2O echivg and $H^{ex}_{1(0.5)} \simeq$ $\simeq 500$ cal/kg H_2O · echiv g, both of them at $I = 2.4$. For the system $ZnSO_4 + Na_2SO_4 + H_2O$, $\bar{S}^{ex}_{1(0,5)} \simeq 3.5$ cal/K · kg H_2O · echivg and $\bar{H}^{ex}_{1(0.5)} \simeq$ $\simeq 1250$ cal/kg H_2O echiv g and for the system $CuSO_4 + Na_2SO_4 + H_2O$, $\bar{S}^{ex}_{1(0.5)} \simeq 9$ cal/K · kg H_2O · echiv g and $\bar{H}^{ex}_{1(0.5)} \simeq 2000$ cal/kg H_2O · echivg· μ_1^{ex} which is a combination of the two extents, $\mu_1^{ex} = \bar{H}_1^{ex} - T\bar{S}_1^{ex}$, can thus take different values (in magnitude as well as sign) a fact which could explain the variety of the results obtained for the different systems (Fig. 3).

These great values of the excess potentials (for μ_1^{ex} as well as for $\bar{S}_1^{ex}$ and $\bar{H}_1^{ex}$) in the studied solutions can be related to the great values of the association constants found in the respective binary systems (sulphates 2 : 2, $K_{ass} \simeq 10^{2.3}$). Davies [9] promoted the ideea that the formation of the ionic associations in sulphates 2 : 2 is accompanied by endothermal enthalpies of formation of the order 4000 cal/mole and positive entropies of formation of the order 24 cal/mole · K.

The μ_1^{ex} found by us is supposed to be:

$$\mu_1^{ex} = (\Delta\, {}^fG_{ass})_t - (\Delta\, {}^fG_{ass})_b \tag{4}$$

Similarly:

$$\bar{H}_1^{ex} = (\Delta\, {}^fH_{ass})_t - (\Delta\, {}^fH_{ass})_b \tag{5}$$

and:

$$\bar{S}_1^{ex} = (\Delta\, {}^fS_{ass})_t - (\Delta\, {}^fS_{ass})_b \tag{6}$$

The formation of ionic associations is thus presumed to be an endothermal process accompanied by a considerable increase in entropy. The positive entropy of formation is explained by the partial dehydration of the ions in the process of formation of the ionic associations.[10,11,12] This implies the hypothesis of an increase in the number of the degrees of freedom of the associated ions as compared to the free ones. The endothermal thermal effect can be probably related to the modifications in the ionic atmospheres of hydration as well as to the modifications in the ion-ion interactions. It is thus possible to appear contact ion pairs (CIP) as well as solvent separated ion pairs (SSIP).

The presence of water molecules in the hydrated ion association has been also proved by X-ray diffraction in liquid state.[13]

In solutions of sulphates 2 : 2 the role of the hydration structure has to be especially important taking into account the high values of the hydration numbers of the ions ($n_{Cu^{2+}} = 17.5$ and $n_{SO_4^{2-}} = 15.3$) confirmed recently by ultrasonic measurements [14] as well as by measurements of transport numbers in ion exchanging membranes.[15]

The results presented in this paper, show that both the hydration structures and the ionic interractions at the formation of the ternary solution from the binary ones, due to the presence of two different cations in the composition of the hydrated ion association, are modified. These modifications are probably greater in systems of the type $CuSO_4 + Na_2SO_4 + H_2O$ than in systems of the type $ZnSO_4 + Me_nSO_4 + H_2O$ explaining the difference in the $\Delta\ln\gamma_1$ values obtained by us.

For a more accurate interpretation of the presented results the completion of the studies of the temperature coefficient, calorimetric measurements for the integral thermal effects of mixing and determinations of osmotic coefficients are required.

REFERENCES

[1] S. Sternberg, M. Drăgănoiu and A. Mateescu, *Rev. Roumaine Chim.*, **25**, 793 (1980).
[2] S. Sternberg and M. Drăgănoiu, *idem*, **29**, 105 (1984).
[3] S. Sternberg and M. Drăgănoiu, *idem*, **30**, 209 (1985).
[4] M. Drăgănoiu, Ph. D. Thesis, Polytechnical Inst. of Bucharest, 1986.
[5] S. Sternberg, M. Drăgănoiu and L. Grigore, *Rev. Chim. (București)*, **38**, 3 (1987).
[6] S. Sternbeg and M. Drăgănoiu, *Rev. Roumaine Chim.*, **34**, 000 (1989).
[7] H. S. Harned and R. A. Robinson, "Multicomponent Electrolyte Solutions", Pergamon Press, London, 1971.
[8] S. Sternberg and M. Drăgănoiu, Conference of Chemistry and Chemical Engineering, Section VIII B, I.P.B. 1987.
[9] C. W. Davies, "Ion Association", Butterworths, London, 1962.
[10] J.-C. Justice, *Electrochim. Acta*, **16**, 701 (1971).
[11] P. Chang, R. V. Slates and C. M. Swar, *J. Phys. Chem.*, **70**, 3180 (1966).
[12] T. E. Hagen-Esch and J. J. Smid, *Amer. Chem. Soc.*, **88**, 307 (1966); **88**, 318(1966); **89**, 2764(1967); **91**, 4580(1969); **94**, 9240 (1972).
[13] Iizhak Marcus, "Ion Solvation", Wiley, 1985, p. 206.
[14] V. Ilgunas and A. Rutkunene, *Sov. Phys. Acoust.*, **31**, 58 (1985).
[15] S. Sternberg, L. Shirshina and S. Daneş, *Rev. Roumaine Chim.*, **25**, 467 (1980).

Revue Roumaine de Chimie, **34**, *4*, 977–982 (1989)

FRIEDEL-CRAFTS CHEMISTRY OF UNSATURATED ALICYCLIC SYSTEMS. IV[1]

EFFECT OF THE CATALYTIC SYSTEM IN FRIEDEL-CRAFTS REACTION OF UNSATURATED ESTERS

V. DRĂGUŢAN,* I. DRĂGUŢAN, C. CONDEIU and A. M. GLATZ
Center of Organic Chemistry, 202B Spl. Independenţei, R-78100 Bucharest, Romania

Received November 8, 1988

The Friedel-Crafts reaction of methyl esters of cyclohexylideneacetic acid and 1-cyclohexenylacetic acid was examined in the presence of a wide range of catalytic systems ($AlCl_3$, $AlCl_3 \cdot CH_3NO_2$, $BF_3 \cdot Et_2O$, $FeCl_3$, $TiCl_4$ and $SnCl_4$). It was shown that reaction kinetics and product distributions are dependent on the catalyst employed. The optimum conditions allowing to obtain specific phenylated products are revealed. The reaction mechanism and stereochemistry are discussed pointing out the effect of the catalytic system.

INTRODUCTION

Previous work [2] showed that when methyl esters of cyclohexylideneacetic acid and 1-cyclohexenylacetic acid are reacted with benzene under Friedel-Crafts conditions ($AlCl_3$, 40–45°C) mixtures of 1,2-, 1,3- and 1,4-phenylcyclohexaneacetic esters are obtained. Both stereoisomers *cis* and *trans* were formed for the product substituted in position 2 of the cyclohexane ring while reaction in positions 3 and 4 yielded either the isomer *cis* or *trans*. At lower reaction temperature (0–5°C) kinetic and thermodynamic control of the phenylation could be more readily evidenced.

In the present paper we proposed to investigate the same reaction using an array of the Lewis type acids in order to prove the role the catalyst plays on the reaction rate and product distribution and to enable the best choice when preparation of a specific product is required.

RESULTS AND DISCUSSION

The phenylation reaction of esters **1** and **2** independently was carried out with benzene in the presence of the following catalysts : $AlCl_3$, $AlCl_3 \cdot CH_3NO_2$, $BF_3 \cdot (C_2H_5)_2O$, $FeCl_3$, $TiCl_4$ and $SnCl_4$ working at temperatures between 20° and 50°C (Eqs. 1 and 2).

The molar ratios ester : catalyst : benzene were varied in the range 1 : 1 – 1.5 : 20 – 40. For each catalytic system similar conversions of esters **1** and **2** were obtained (Figures 1 and 2).

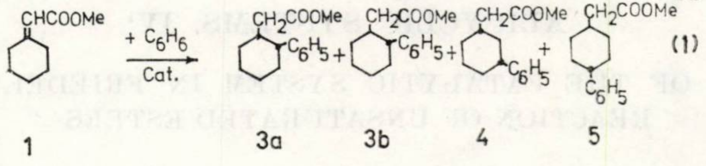

(1)

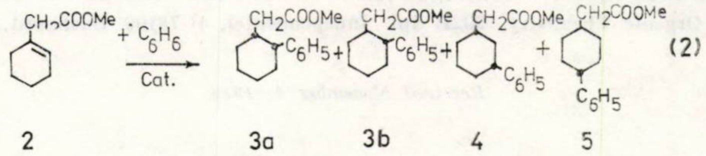

(2)

As can be observed from Figures 1 and 2, $AlCl_3$ proved to be the most active catalyst leading to high conversions even at short reaction times in accordance with our previous results.[2] By contrast, moderate conversions are obtained using $AlCl_3 \cdot CH_3NO_2$, $BF_3 \cdot (C_2H_5)_2O$, $FeCl_3$, $TiCl_4$ and $SnCl_4$ despite prolonged reaction time.

For the above catalytic systems significant differences were also recorded concerning the distribution of the phenylated esters (Tables 1 and 2).

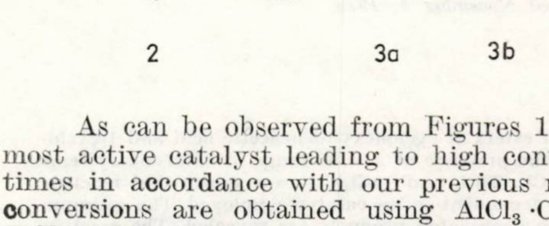

Fig. 1. Conversion of ester **1** with benzene in the presence of Friedel-Crafts catalysts (△ – $AlCl_3$, ○ – $AlCl_3 \cdot CH_3NO_2$, ▲ – $BF_3 \cdot (C_2H_5)_2O$, × – $FeCl_3$, ● – $TiCl_4$, □ – $SnCl_4$).

Thus, while $AlCl_3$ affords *cis*-1,3- (*4*) and *trans*-1,4-phenylated (*5*) esters as the main reaction products, large quantities of *cis*-1,2- (*3a*) and *trans*-1,2-phenylated (*3b*) esters are obtained using the other catalysts.

It is noteworthy that both *cis* and *trans* 1,2-stereoisomers are found in amounts varying with the catalyst activity but their ratio is roughly the same ; however, the percentage of *cis*-1,3 and *trans*-1,4 products depended essentially on the catalytic system. Furthermore, as previously stated,[2] the product distribution varied substantially during the progress of the reaction with $AlCl_3$ while on using other catalytic systems the product composition changed within narrow limits. This fact pointed out that isomerization of the phenylated esters under these reaction conditions is slowed down.

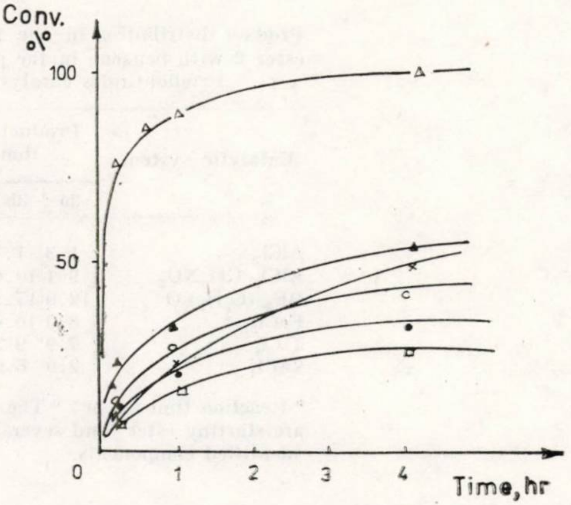

Fig. 2. — Conversion of ester **2** with benzene in the presence of Friedel-Crafts catalysts (Δ — $AlCl_3$, ○ — $AlCl_3 \cdot CH_3NO_2$, ▲ — $BF_3 \cdot (C_2H_5)_2O$, x — $FeCl_3$, ● — $TiCl_4$, □ — $SnCl_4$).

Table 1

Product distribution in the reaction of ester **1** with benzene in the presence of Friedel-Crafts catalysts[b]

Catalytic system	Product composition, % [b]			
	3a	3b	4	5
$AlCl_3$	1.4	1.1	44.5	46.8
$AlCl_3 \cdot CH_3NO_2$	9.2	10.0	4.5	6.0
$BF_3 \cdot (C_2H_5)_2O$	14.0	19.2	4.8	7.8
$FeCl_3$	8.1	11.2	3.0	2.5
$TiCl_4$	8.4	9.5	0.7	1.2
$SnCl_4$	3.0	7.1	0.4	0.3

[a] Reaction time : 1 hr ; [b] The remainder are starting ester and several small unidentified components.

The above results can be rationalized if a carbocationic mechanism similar to that proposed earlier for the phenylation reaction of esters **1** and **2** in the presence of $AlCl_3$ is considered.[2] The reaction pathway probably consists first of carbocation generation from the unsaturated ester under the action of the catalyst, further alkylation of benzene accompanied by concurrent hydride shift migration (1,2- and 1,3-hydride shift) in the intermediate carbocation and subsequent isomerization of the phenylated esters (Scheme 1).

Table 2

Product distribution in the reaction of ester **2** with benzene in the presence of Friedel-Crafts catalysts [a]

Catalytic system	Product composition, % [b]			
	3a	**3b**	**4**	**5**
$AlCl_3$	1.3	1.1	42.4	45.1
$AlCl_3 \cdot CH_3NO_2$	9.1	10.6	4.1	5.2
$BF_3 \cdot (C_2H_5)_2O$	12.0	17.1	2.2	3.8
$FeCl_3$	8.0	10.4	2.9	2.7
$TiCl_4$	7.9	9.2	0.5	0.8
$SnCl_4$	2.9	6.8	0.5	0.4

[a] Reaction time : 1 hr ; [b] The remainder are starting ester and several small unidentified components.

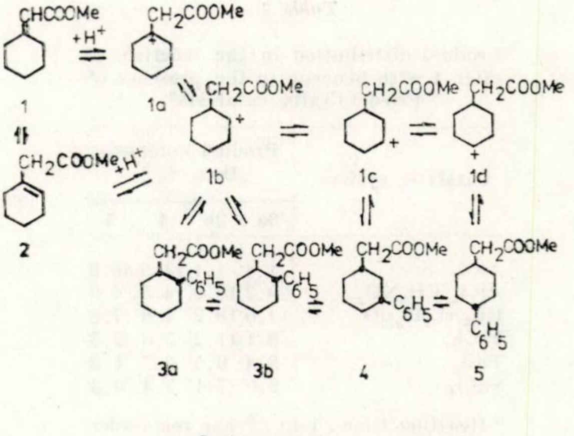

CHCOOMe
+H+
CH2COOMe
1
1a
CH2COOMe
CH2COOMe
CH2COOMe
CH2COOMe,H+
1b
1c
1d
2
CH2COOMe
C6H5
CH2COOMe
C6H5
CH2COOMe
C6H5
CH2COOMe
C6H5
3a
3b
4
5

Scheme 1

In addition, isomerization of esters **1** and **2** in the presence of Lewis acids is also occurring.

The difference between the catalytic systems appears in the mode they influence on each of these reaction steps. It may be inferred that the above catalysts act distinctly during the reaction course of esters **1** and **2** as a function of their actual Brönsted and Lewis acidity and their ability to form more or less tight ion pairs. The smaller their Brönsted acidity the lower the rate of carbocation generation and product isomerization. At the same time, with higher Lewis acidity of the catalyst more intimate (or tight) ion pairs are formed protecting thus the intermediate carbocation from 1,2- and 1,3-hydride shift migration and outer attack by benzene. Obviously, the nature of the corresponding counteranions plays a significant part in the transition states of 1,2- and 1,3-hydride shifts as well as of benzene alkylation by the respective carbocations. These effects of the catalytic systems in the phenylation reaction of esters **1** and **2** will result in higher overall reaction rates for $AlCl_3$ and lower with $AlCl_3 \cdot CH_3NO_2$, $BF_3 \cdot (C_2H_5)_2O$, $TiCl_4$ and $SnCl_4$. The rate of formation of carbocations **1a** and **1b** undergoing further 1,2- and 1,3-hydride shifts to carbocations **1c** and **1d** will be considerable in the presence of $AlCl_3$, a strong Brönsted and Lewis acid, while the rate will be lower in the presence of the other weaker Brönsted acids. On the other hand, the Lewis acidity of the weaker Brönsted acids will influence distinctly the hydride shifts in carbocations **1a**—**1d** as well as the attack of benzene ring on these carbocations by their power to form tight ion pairs; consequently, the structure of these ion pairs will determine correspondingly the product distribution of the phenylated esters.

Obtention of both stereoisomers *cis*-1,2- and *trans*-1,2-phenylcyclohexylacetic esters suggests that the nucleophilic attack by benzene ring on the carbocation **1b** occurs readily from both the axial and equatorial directions (Scheme 2), the generation of a lactoid species from the ester carbocations **1a** and **1b** being precluded.

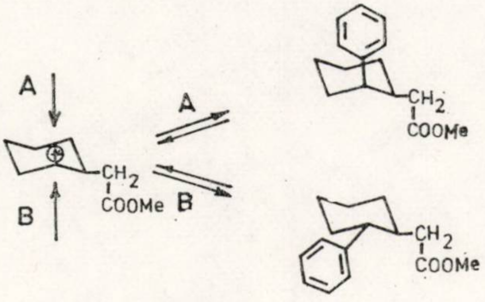

Scheme 2

Additionally, the lower reaction rate encountered in the phenylation of esters **1** and **2** as compared to the reaction of the corresponding acids [1] may be assigned to the deactivating effect of the ester group. This effect is also operative during the isomerization of the phenylated esters in the presence of the above catalytic systems.

EXPERIMENTAL

IR spectra were recorded on UR-20 Carl Zeiss-Jena spectrophotometer. NMR spectra were recorded on a Varian A 60-A spectrometer using TMS as internal standard. The v.p.c. analyses were carried out on a Willy Giede model 18.3 gas chromatograph using a 3 m × 4 mm column packed with 10% ethyleneglycol-succinate on Chromosorb W (60—80 mesh); column temperature 190°C.

Starting materials

The methyl esters of cyclohexylideneacetic acid (**1**) and 1-cyclohexenylacetic acid (**2**) were prepared from the corresponding acids by esterification with ethereal diazomethane solution as described previously.[2] The methyl esters of the phenylated cyclohexylacetic acids **3**, **4** and **5** were independently obtained by esterification of the corresponding acids with diazomethane as described elsewhere.[3] Benzene (Reactivul) was purified by distillation and further dried and stored over sodium wire. $AlCl_3$ (Merck-Schuchardt), $BF_3 \cdot (C_2H_5)_2O$ (Merck Schuchardt), $FeCl_3$ (Merck-Schuchardt), $TiCl_4$ (Merck-Schuchardt), $SnCl_4$ (BDH, England) and nitromethane (Merck-Schuchardt) were used without further purification. The structure and purity of the starting materials and authentic samples were checked by v.p.c., NMR and elemental analyses.

Reaction of methyl cyclohexylideneacetate (1) and 1-cyclohexenylacetate (2) with benzene

The reactions of the esters **1** and **2** with benzene in the presence of $AlCl_3$, $AlCl_3 \cdot CH_3NO_2$, $BF_3 \cdot (C_2H_5)_2O$, $FeCl_3$, $TiCl_4$, $SnCl_4$ were carried out at temperatures between 20° and 50°C using the method described elsewhere.[2] The v.p.c. retention times of the reaction products were compared to that of the authentic samples. The results obtained are given in Figures 1 and 2 and Tables 1 and 2.

REFERENCES

[1] Part III, V. Drăguțan, I. Drăguțan, F. Chiraleu and A. M. Glatz, *Rev. Roumaine Chim.*, **34**, 000 (1989).

[2] V. Drăguțan, Zs. Arvay and A. M. Glatz, *Rev. Roumaine Chim.*, **23**, 1283 (1978).

[3] V. Drăguțan, L. Stănescu and A. M. Glatz, *Rev. Roumaine Chim.*, **22**, 1045 (1977).

Revue Roumaine de Chimie, **34**, *4*, 983–988 (1989)

SELECTIVE ALKYLATION OF TOLUENE ON ZSM-5 ZEOLITES

EMIL DUMITRIU, NICOLAE BÎLBĂ, VASILE HULEA and SPIRIDON OPREA
Department of Organic Chemical Technology, Faculty of Chemical Technology,
Splai Bahlui 71, P.O. Box 483, Jassy 6600 Romania

Received September 5, 1988

The alkylation reaction of toluene with methanol was carried out on a pulse reactor using a ZSM-5 zeolite which was synthesized in presence of cyclohexanol. The influence of reaction conditions on the catalytic activity and selectivity has been studied. Also, the influence of nature of the substance used as template has been investigated. The results prove a very good selectivity and activity of these catalysts. The catalytic properties are improved by impregnation with phosphoric acid.

Obviously the ZSM-5 type zeolites are obtained by the crystallization of aluminosilicate gel using an organic substance as template. There are many reports on such templates as: quaternary ammonium salts,[1,2] amines,[3,4] alcohols [5,6] etc.[7] The mentioned zeolites can be also prepared without templates.[8,9] The X-ray diffraction studies on the crystals prepared using various substances as templates have demonstrated the crystallographic identity of these zeolites but not all properties, e.g. sorptive properties, the distribution of active centers, were always the same. Therefore, some peculiarities of the behaviour of such zeolites may appear just due to the affectation of these properties as a result of the condition of zeolite synthesis.

Taking into account this idea, our paper aims to present the results obtained in the alkylation reaction of toluene using a ZSM-5 zeolite prepared in presence of a cyclic alcohol (this alcohol having a volume of about the same magnitude as the molecule of toluene) and to compare this result with those obtained using a ZSM-5 catalyst synthesized in presence of quaternary ammonium salts.

EXPERIMENTAL

The ZSM-5 zeolite (Na^+form) was obtained by hydrothermal crystallization at 180°C for 24 hours of a mixture having the following molar composition : $SiO_2/Al_2O_3 = 64.2$, Na_2O (active)$/Al_2O_3 = 6.26$, $HO^-/SiO_2 = 0.134$ and $H_2O/Al_2O_3 = 1833$ respectively; the cyclohexanol was used as template. X-ray analysis indicated only a single crystalline phase and the crystallinity in relation to a standard sample was 100%. The crystals were uniform as size, well defined and without intergrowths. The H^+ form of catalyst (Z_{CH}) was obtained from the natrium form by ionic exchange, in two stages, using a 6.0 N hydrochloric acid solution, at 60°C for 2 hours.

The modified catalyst $Z_{CH}-P$ was obtained by the impregnation of H-ZSM-5 zeolite with an aqueous solution of H_3PO_4. The sample was maintained under stirring at 150°C for 3 hours, then it was calcined at 200°C for 4 hours and at 500°C for another 4 hours. The elementary analysis indicated a content of phosphorus about 10.2% by weight.

First, the catalysts were pelletized without binder, then they were ground, sieved and the fraction of 0.25–0.40 mm was retained. The alkylation reactions were carried out on a pulse microreactor (i.d. = 3 mm) containing 10 mg of catalyst.The microreactor was coupled at a gas chromatograph equipped with a flame ionization detector. The sample of reaction mixture was of 0.1 μL. The column was filled with dinonyl phthalate and Bentone 34 on Chromosorb W.

RESULTS AND DISCUSSION

It is known that the alkylation of toluene implies in the first stage the formation of *ortho* and *para* isomers of xylene.[10] This behaviour is determined by the electronic effects taking place at the level of aromatic ring and which influence this electrophylic substitution. But, from the point of view of the thermodynamic stability, the *meta* isomer is more stable than the other isomers and, as a consequence, the isomerization of *p*- and *o*-xylene to *m*-xylene is favoured, especially under the conditions of the acidic catalysis of zeolites. Therefore, the process of alkylation has two distinct stages : the alkylation reaction and the isomerization respectively, as can be observed from the following scheme :

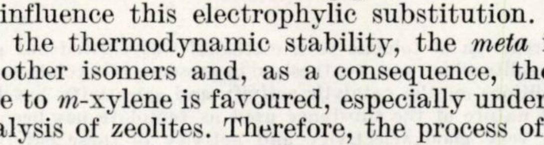

From the practical point of view it is interesting to state the reaction condition for which the first stage (*p*-xylene formation) will be prevalent.

An important realization has been the synthesis of zeolite catalysts of the pentasil type which, by their structure and size of micropores, limit drastically the diffusion of *ortho* and *meta* substituted alkylbenzenes comparatively with those *para*-substituted.[11] The selectivity in relation to *para* isomers was enhanced by the modification of these catalysts, especially by the following two methods :

i) – the impregnation of these zeolites with various oxides (on the basis of P, Mg[12] etc) having a certain implication on the size of pores;

ii) – the isomorphous substitution of aluminium in the pentasil structure with elements such as Fe, Cr, B[13], having influence on the porosity of catalyst, the strength and the distribution of active centers.

Further we shall analyse the behaviour of the ZSM-5 zeolites synthesized using cyclohexanol as template, in the alkylation reaction of toluene with methanol taking into account the above mentioned observations.

In the first stage of our study, the catalytic performances of Z_{CH} zeolite were followed in relation with various operation variables : temperature, contact time and number of pulses. Relative to the influence of temperature, both the toluene conversion and the selectivity in relation to *p*-xylene are dependent on temperature (Fig. 1). The conversion of aoluene rises with the increase of temperature and reaches a maximum bt about 375°C, then a decrease is observed. This behaviour can be explained by an important change of the concentration of electrophilic carrier as the conversion of methanol at paraffin and olefine hydrocarbons is favoured by the temperature increase. The decrease of *p*-xylene concentration in the favour of *m*-xylene at 400°C is determined by the intensification of *p*-xylene isomerization, this process being accelerated by the temperature increase.

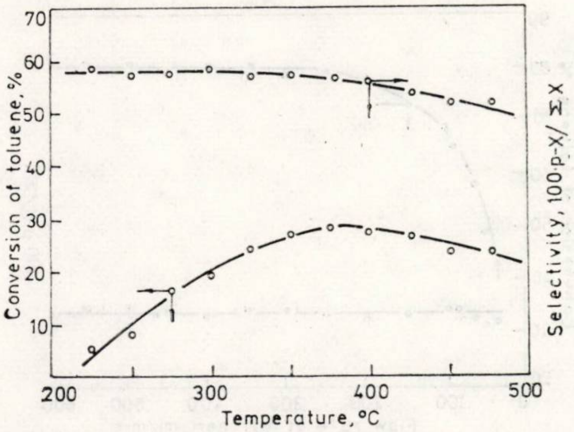

Fig. 1. — The effect of reaction temperature on the toluene conversion and selectivity to *p*-xylene; flow rate of nitrogen 60 mL/min; T/MeOH = 1/2 (mole).

It is also known that the zeolites of the ZSM-5 type have a very good thermal stability and an important resistance to the coke formation. Following the behaviour of Z_{CH} catalyst vs. the number of pulses it can be noticed that after about 25 pulses the activity of catalyst (expressed as toluene conversion) is practically unchanged, but the selectivity shows a certain increase (Fig. 2).

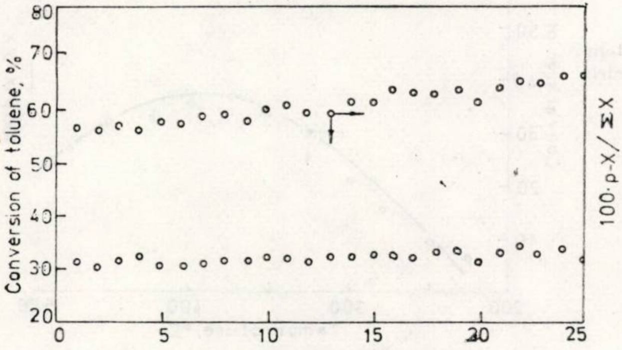

Fig. 2. — The influence of pulse number on the activity and selectivity; T = 375°C; carrier gas flow rate 60 mL/min; T/MeOH = 1/2 (mole); catalyst Z_{CH}.

This phenomenon can be explained by blocking the strongest acid centres by cocking, these centres being also responsible for the isomerization of *p*-xylene. It is remarkable that the catalyst entirely comes back at the initial properties after regeneration by the coke burning.

As is above mentioned the catalysts of pentasil type determine a certain diffusional limitation for *ortho* and *meta* isomers due to their shape and size of pores. The diffusion of reagents and products is also influenced by the flow conditions of gases, in other words, by the contact time.

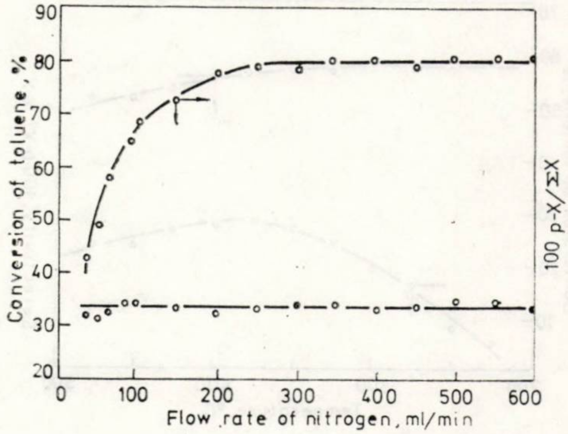

Fig. 3. — The influence of contact time on the activity and selectivity; T = 375°C; T/MeOH = 1/2 (mole); catalyst Z_{CH}.

By the modification of the flow rate of carrier gas various values of the contact time have been obtained and the results are shown in Figure 3.

The conversion of toluene remains practically unchanged but the selectivity is strongly affected. The selectivity increases in the range of flow rate of about 40—200 mL/min, after which it becomes independent of the contact time, this being a proof that the reaction occurs in the kinetic range.

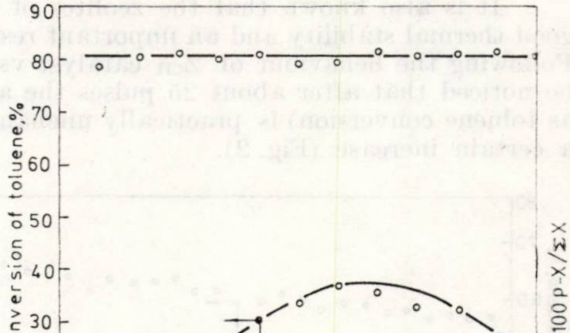

Fig. 4. — The effect of reaction temperature on the activity and selectivity; catalyst $Z_{CH}-P$.

The $Z_{CH}-P$ catalyst, obtained by the impregnation of the former catalyst (Z_{CH}), was investigated in the same conditions. At the beginning we must underline that this catalyst possess remarkable catalytic properties. Thus, it can be observed from Figure 4, where the influence of temperature on the toluene conversion is shown, that the conversion of toluene is greater than in the previous case and the selectivity too.

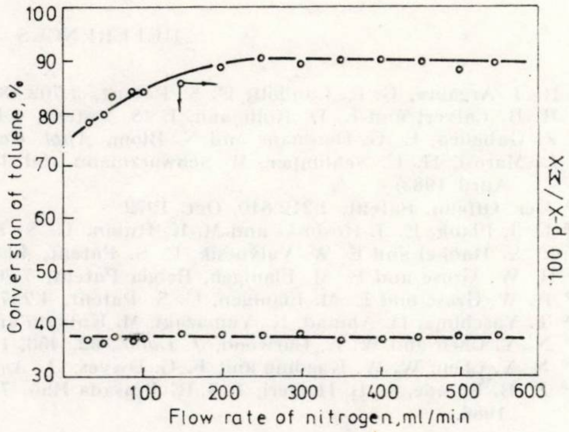

Fig. 5. — The influence of contact time on the activity and selectivity; catalyst Z_{CH}–P.

Like in the first case, the contact time determines the selectivity in relation to *p*-xylene only for the range of carrier gas flow rate of 40—200 mL/min, after which the selectivity remains constant at a value of about 90% (Fig. 5).

Finally, in order to compare the two zeolites of the ZSM-5 type which were synthesized using different templates, we studied the alkylation reaction of toluene, in the same reaction conditions using a sample of ZSM-5 catalyst which was obtained in the presence of a quaternary ammonium salt.

Table 1 shows a similar behavior of both catalysts, perhaps a greater selectivity of Z_{CH} than Z_B but at a smaller conversion of toluene.

Table 1

The influence of nature of catalyst on the activity and selectivity; flow rate nitrogen 60 mL/min; T/MeOH = 1/2 (mole)

Catalyst	Toluene conversion, %		*p*-Xylene selectivity, %	
	375°C	400°C	375°C	400°C
Z_{CH}	29.1	27.8	56.5	56.1
Z_{CH}–P	37.9	36.6	79.2	80.8
Z_B^x	33.2	32.8	53.6	52.9

We can conclude, on the basis of the above presented results, that the ZSM-5 zeolite synthesized in the presence of cyclohexanol possesses a very good activity and especially, selectivity for the alkylation of toluene with methanol. Of course, these performances are influenced by the reaction conditions, the maximum selectivity being obtained at small contact time. The modification of pore size and the acidic strength of active centers by impregnation with phosphoric acid enhances both the activity and selectivity.

REFERENCES

[1] R. J. Argauer, G. R. Landolt, U. S. Patent, 3.702.886, Oct. 1972.
[2] R. B. Calvert and L. D. Rollmann, U. S. Patent, 4.495.166, Dec. 1985.
[3] Z. Gabelica, E. G. Derouane and N. Blom, *Appl. Catal.*, **5**, 109, 1983.
[4] L. Marosi, H. U. Schlimper, M. Schwarzmann and J. Stabenow, U. S. Patent, 4.404.175, April 1983.
[5] Ger. Offenn. Patent, 2.212.810, Oct. 1972.
[6] C. J. Plank, E. J. Rosinski and M. K. Rubin, U. S. Patent, 4.199.556, Feb. 1980.
[7] L. A. Rankel and E. W. Valyocsik, U. S. Patent, 4.388.285, July 1983.
[8] R. W. Grose and E. M. Flanigen, Belgia Patent, 7.701.115, Dec. 1977.
[9] R. W. Grose and E. M. Flanigen, U. S. Patent, 4.257.885, Oct. 1981.
[10] T. Yaschima, H. Ahmad, K. Yamazaki, M. Katsuta and N. Hara, *J. Catal.*, **16**, 273, 1970.
[11] N. Y. Chen and W. E. Garwood, *J. Catal.*, **52**, 453, 1978.
[12] N. Y. Chen, W. W. Kaeding and F. G. Dwyes, *J. Am. Chem. Soc.*, **101**, 6783, 1979.
[13] R. B. Borade, A. B. Halgeri, T. S. R. Prasada Rao, 7-th Int. Zeolites Conf. Tokyo, Japan, 1986.

Revue Roumaine de Chimie, **34**, *4*, 989–993 (1989)

REACTION OF KETONES WITH BENZOCYCLOBUTENO-NORBORNENIC SKELETON IN THE PRESENCE OF DIMETHYLOXOSULFONIUM METHYLIDE[1]

L. ENESCU, AURELIA GHENCIULESCU, F. CHIRALEU
and I. G. DINULESCU
Organic Chemistry Department, Polytechnic Institute TCH, 313, Splaiul Independenţei, 76206 Bucharest, Romania

Received October 1, 1988

The reaction of *exo*- (6) and *endo*-benzocyclobuteno-norbornene-9-one (7) and *exo*- (8) and *endo*-benzocyclobuteno-norbornane-9-one (9) with dimethyloxosulfonium methylide (3) is described. The ketones 6, 7 and 8 yield exclusively the products of *syn* attack, namely the *anti* oxides 10,11 and 12 respectively. In particular, the ketone 9 afforded the mixture of the *anti*- (13) and *syn*-oxide (14) in a ratio 1 :1.65.

In a recent paper we reported on the reaction of benzocyclobuteno-norbornane-7-ones **1** and **2** with dimethyloxosulfonium methylide (**3**), yielding exclusively the products of *exo* attack, namely the *endo* oxides **4** and **5** respectively.[2]

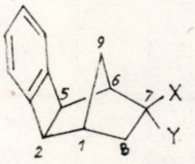

1 X=Y=O
4 -X-Y-=CH₂O-

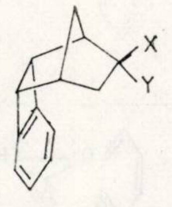

2 X=Y=O
5 -X-Y-=CH₂O-

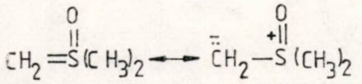

$$CH_2=\overset{O}{\overset{\|}{S}}(CH_3)_2 \longleftrightarrow \bar{C}H_2-\overset{O}{\overset{+\|}{S}}(CH_3)_2$$

3a 3b

In order to extend the investigation of the behaviour of polycyclic compounds with benzocyclobutene ring, we wish to present our results on the treatment of benzocyclobuteno-norbornene-9-ones, **6** and **7**, and benzocyclobuteno-norbornane-9-ones, **8** and **9**, with methylide **3**.

The reaction of ketones **6**, **7** and **8** with methylide **3** afforded the epoxides **10**, **11** and **12** respectively, with the *anti* orientation of the epoxidic oxygen, together with variable amounts of unreacted ketones. The similar treatment of the ketone **9** yielded a mixture of the isomeric epoxides **13** and **14**, in a 1 : 1.65 ratio, established on the basis of the ^{1}H-NMR spectrum. The general experiment consisted in addition of the ketone to a stirred suspension of methylide **3**, in dimethyl sulfoxide, at 25–60°, under nitrogen.

Dimethyloxosulfonium methylide (**3**) was prepared according to published syntheses,[3,4] by addition of trimethyloxosulfonium iodide [5] to a stirred suspension of sodium hydride in dimethyl sulfoxide under nitrogen.

Results are presented in table 1.

Table 1

Reaction of the ketones 6 – 9 with dimethyloxosulfonium methylide

Compound	Temp. [°C]	Time [min]	Products and ratio	Overall yield [%]
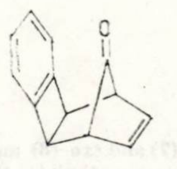 6	25	90	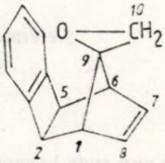 + 6 10 7.3 : 1	97.8
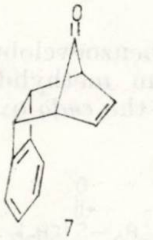 7	25	60	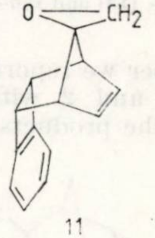 + 7 11 4.0 : 1	88.6
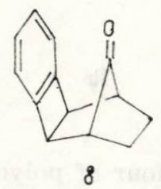 8	40–60	180	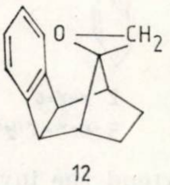 + 8 12 2.0 : 1	87.8
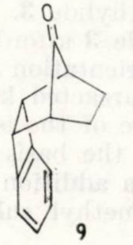 9	25	60	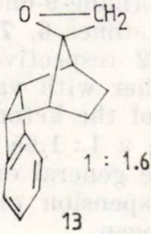 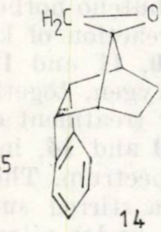 1 : 1.65 13 14	31.0

The analytical and spectral data were in accordance with the proposed structures. Thus, in the ^{1}H-NMR spectrum of the epoxide **11**, the signals of H—2 and H—5 benzylic protons appeared as a multiplet, because of the coupling with the bridgehead protons.[6] The *anti* orientation of the epoxidic oxygen is supported by the ^{1}H-NMR spectrum, i.e. by the signals of H—2 and H—5 protons, which appear more deshielded (δ 4.00 ppm) because of the neighborhood of the oxygen. A similar remark can be made concerning the same protons in the alcohol **15** (δ 3.95 ppm), previously described.[7] In the epoxides **10** and **12** the signals of the benzylic protons, as well as those of the H—10 protons appear as singlets. In this case, the assignment of these signals and the configuration of the oxiranic ring are provided by lanthanide induced shift experiments, using Eu(fod)$_3$ $\cdot$d$_{27}$.

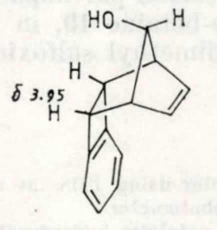

15

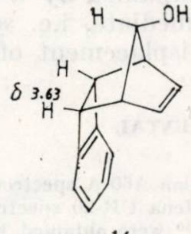

16

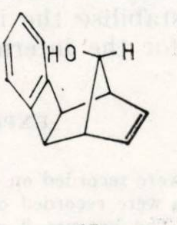

17

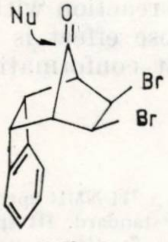

18

The ^{1}H-NMR spectra of these epoxides displayed significant diamagnetic shifts for H—10 protons (δ 3.55 ppm) and aromatic protons, in accordance with an *anti* orientation of the epoxide oxygen. It is interesting that the ^{1}H-NMR spectrum of the mixture of epoxides **13** and **14** could be interpreted because of chemical shift differences between their protons. Thus, the protons H—10 induce an upfield shifts for the benzylic protons in the epoxide **14** (δ 3.78 ppm). Finally, the epoxidic oxygen induces a downfield shift for the protons H—2 and H—5 in the epoxide **13** (δ 4.03 ppm).

It is known that 9-substituted ketones such as the ketones **6**—**9** are reactive toward nucleophiles, and that *syn* attack is favoured sterically as well as electronically.[8] Thus, as previously reported, in the reaction of *exo*- (**6**) and *endo*-benzocyclobuteno-norbornene-9-one (**7**) with mixed-metal hydrides, the alcohols formed by the *syn* attack, namely the alcohols **15** and **17**, were obtained.[7,9] The steric factor is more important in the case of bulky nucleophiles such as methylide **3**. The reaction of the ketones **6**, **7** and **8** with dimethyloxosulfonium methylide (**3**) is rapid and highly stereospecific yielding the products of the *syn* attack exclusively. However, in the case of the saturated ketone **9**, with *endo* oriented benzocyclobutene ring, the *syn* attack of the nucleophile can be relatively hindered because of *cis* oriented substituents from C—7 and C—8. Thus, as it is known, the dibromo derivative **18** reacts with mixed-metal hydrides on the *anti* side.[7] Thus it is not surprising that in the reaction of the ketone **9** we obtained also the product of the *anti* attack, i.e. the epoxide **14**, along with the expected epoxide **13**. We assume that the H—7-*cis* and H—8-*cis* protons hinder the bulky nucleophile (namely methylide **3**) to attack on the *syn* side.

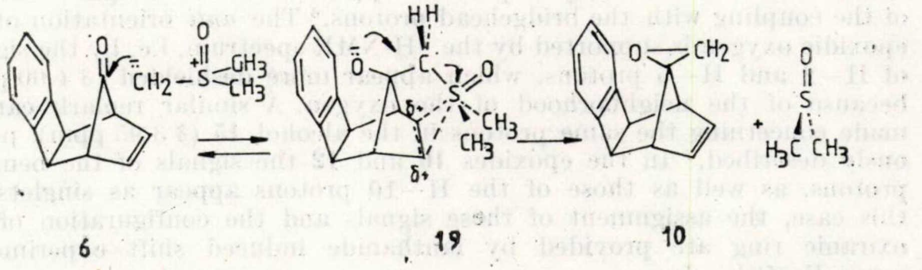

6 **19** **10**

Furthermore, it was suggested that in the case of ketones **6** and **7**, the reaction with methylide **3** is accompanied by π-electron participation whose effect is to stabilise the intermediate, i.e. *syn*-betaine **19**, in the best conformation for the internal displacement of dimethyl sulfoxide.[8]

EXPERIMENTAL

^{1}H-NMR spectra were recorded on a Varian A60-A spectrometer using TMS as internal standard. IR spectra were recorded on a Jena UR-20 spectrophotometer.

Starting materials. The ketones **8** and **9**[10] were obtained by catalytic hydrogenation of the corresponding unsaturated ketones **6**[9] and **7**[7], respectively, on palladium as catalyst. Dimethyl sulfoxide was distilled from calcium hydride at reduced preassure. Sodium hydride was available as a 80% dispersion in mineral oil from Fluka AG Chem. Fab. The reactions were carried out under nitrogen in an oven-dried apparatus.

The reaction of exo-benzocyclobuteno-norbornene-9-one (**6**) *with dimethyloxosulfonium methylide* (**3**). A 80% suspension of sodium hydride in mineral oil (0.13 g, 4.33 mmoles) was treated with 2 mL petroleum ether (b.p. 35°) and the solvent was removed by decantation. Dry dimethyl sulfoxide (4 mL) was added and the mixture was stirred for 15 min at room temperature, under nitrogen.[4] Trimethyloxosulfonium iodide[5] (0.65 g, 2.95 mmoles) was introduced portionwise during 15 min and suspension was stirred and heated for 20 min at 40—50°. When the evolution of hydrogen has ceased, a solution of 0.5 g (2.74 mmoles) ketone **6** in 3.5 mL dimethyl sulfoxide was added dropwise during 15 min, under nitrogen. The reaction mixture was stirred for 90 min at room temperature, poured in 20 mL water and extracted with diethyl ether (3 × 25 mL). The ether solution was washed with water (3 × 25 mL), then with saturated salt solution (2 × 10 mL), dried and the solvent was removed *in vacuo*, yielding 0.52 g product. ^{1}H-NMR spectrometry analysis showed a content of the epoxide **10** and of the ketone **6** in a 7.2 : 1 ratio. The residue was treated with petroleum ether and after 2 hrs, 0.46 g, white crystalline compound, epoxide **10**, m.p. 102—103° was isolated (97.8%).

Spiro[exo-benzo[c]tricyclo [4.2.1.0$^{2.5}$] nona-3,7-diene-9,2'-anti-oxacyclopropane] (**10**), colourless crystals, m.p. 102—103°. — Anal. $C_{14}H_{12}O$ (196.23) Calcd.: C, 85.68; H, 6.16. Found: C, 85.81; H, 6.06. — IR(CCl$_4$, cm^{-1}): 950, 1110, 1280. — ^{1}H-NMR (CDCl$_3$, δ, ppm): 2.36 (s, 2H, H—2, H-5), 2.55 (m, 2H, H-1, H-6), 3.45 (s, 2H, H-10), 6.36 (t, 2H, H-7, H-8, $J = 2$ Hz), 6.90 — 7.40 (m, 4 aromatic H).

The reaction of endo-benzocyclobuteno-norbornene-9-one (**7**) *with dimethyloxosulfonium methylide* (**3**). Working as above, from 0.13 g (4.33 mmoles) sodium hydride 80%, dimethyl sulfoxide (4 mL), 0.65 g (2.95 mmoles) trimethyloxosulfonium iodide and a solution of 0.5 g (2.74 mmoles) ketone **7** in 3.5 mL dimethyl sulfoxide, 0.48 g crude product was obtained ^{1}H-NMR spectroscopy analysis showed a content of the epoxide **11** and the ketone **7**, in a. 4.0 :1 ratio. The crude epoxide was purified by column chromatography on alumina yielding 0.39 g (88.6%). The purified oxirane **11** was an oil, which appeared to be quite pure as judged by its spectral properties, elemental analysis and behaviour on thin-layer chromatography.

Spiro[endo-benzo[c]tricyclo[4.2.1.0.$^{2.5}$]nona-3,7-diene-9,2'-anti-oxacyclopropane] (**11**) [2] colourless oil. — Anal. $C_{14}H_{12}O$ (196.23) Calcd. : C, 85.68 ; H, 6.16. Found : C, 85.86 ; H' 6.19. — IR(CCl_4, cm^{-1}) : 960, 1070, 1270. — ^{1}H-NMR ($CDCl_3$, δ, ppm) : 2.51 (m, 2H, H-1' H-6), 2.75 (s, 2H, H-10), 4.00 (m, 2H, H-2, H-5), 5.75 (m, 2H, H-7, H-8), 6.80 — 7.40 (m 4 aromatic H).

The reaction of exo-benzocyclobuteno-norbornane-9-one (**8**) *with dimethyloxosulfonium methylide* (**3**). The procedure used for compound **6** was followed except a solution of 0.1 g (0.5 mmoles) ketone **8** in 0.7 mL dimethyl sulfoxide was added over a suspension of the methylide **3**, prepared previously from 0.026 g (0.86 mmoles) sodium hydride 80% and 0.12 g (0.54 mmoles) trimethyloxosulfonium iodide in 1 mL dimethyl sulfoxide under nitrogen. The mixture was stirred for 3 hrs. at 40—60°. The crude product (0.1 g) contains a mixture of the epoxide **12** and the ketone **8** in a 2 :1 ratio, established on the basis of its ^{1}H-NMR spectrum. The product was purified by column chromatography on neutral alumina, yielding 0.065 g (87.8%) epoxide **12**.

Spiro[exo-benzo[c]tricyclo [4.2.1.0.$^{2.5}$]nona-3-ene-9,2'-anti-oxacyclopropane] (**12**), colourless crystals, m.p. 118—119°. — Anal. $C_{14}H_{14}O$ (198.25) Calcd. : C, 84.81 ; H, 7.11. Found :C 85.01 ; H, 6.92. — IR (CCl_4, cm^{-1}) : 925, 1100, 1280. — ^{1}H-NMR ($CDCl_3$, δ, ppm) : 1.38 (AB system, H-7-*exo* and H-8-*exo*, $J_{7\cdot8}$=11.5 Hz), 1.73 (AB system, H-7-*endo* and H-8-*endo*, $J_{7\cdot8}$ = 11.5 Hz), 1.95 (m, 2H, H-1, H-6), 2.43 (s, 2H, H-2, H-5), 3.55 (s, 2H, H-10), 6.93—7,46 (m, 4 aromatic H).

The reaction of endo-benzocyclobuteno-norbornane-9-one (**9**) *with dimethyloxosulfonium methylide* (**3**). A suspension of methylide **3** was prepared from 0.4 (13.33 mmoles) sodium hydride 80% and 2.1 g (9.54 mmoles) trimethyloxosulfonium iodide, at 40 — 50°, under nitrogen. A solution of 1.5 g (8.15 mmoles) ketone **9** in 10 mL dimethyl sulfoxide was added to above suspension, during 25 min. The mixture was stirred at room temperature for 60 min, under nitrogen. Then, the procedure followed for compound **6** was followed and 1.75 g crude product were obtained. From this resinous material, 0.5 g (31%) of a mixture of epoxide **13** and **14** was separated by preparative tlc on silica gel with petroleum ether — diethyl ether in a 7 : 3 ratio, as eluent. The attempt to separate the mixture of epoxides **13** and **14** was unsuccesful but their ^{1}H-NMR spectrum could be interpreted. Thus the ^{1}H-NMR spectral analysis showed a content of the epoxides **13** and **14** in a 1 :1.65 ratio.

Spiro [endo-benzo[c]tricyclo[4.2.1.0$^{2.5}$] nona-3-ene-9,2'-anti-oxacyclopropane] (**13**) and *spiro [endo-benzo[c] tricyclo [4.2.1.0.$^{2.5}$] nona-3-ene-9,2'-syn-oxacyclopropane]* (**14**), colourless oil. — Anal. $C_{14}H_{14}O$ (198.25) Calcd. : C, 84.81 ; H, 7.11. Found : C, 84.98 ; H. 7.00.— IR (CCl_4, cm^{-1}) : 930, 1065, 1090, 1220, 1235. *Epoxide* **13** : ^{1}H-NMR ($CDCl_3$, δ, ppm) : 0.80 — 1.40 (m, 4H, H-7, H-8), 1.78 (m, 2H, H-1, H-6), 2.90 (s, 2H, H-10), 4.03 (m, 2H, H-2, H-5), 6.90 — 7.50 (m, 4 aromatic H). *Epoxide* **14** : ^{1}H-NMR ($CDCl_3$, δ, ppm) : 0.80—1.40 (m, 4H, H-7 H-8), 1.95 (m, 2H, H-1, H-6), 3.03 (s, 2H, H-10), 3.78 (m, 2H, H-2, H-5), 6.90 — 7.50 (m, 4 aromatic H).

REFERENCES

[1] Part LXIV in the series "Investigations in the Cyclobutane series". For part LXIII see : L. Enescu, A. Ghenciulescu, F. Chiraleu and I. G. Dinulescu, *Rev. Roumaine Chim.*, in press.

[2] A. Ghenciulescu, L. Enescu, F. Chiraleu and I. G. Dinulescu, *Rev. Roumaine Chim.*, in press.

[3] E. J. Corey and M. Chaykovsky, *J. Amer. Chem. Soc.*, **87**, 1353 (1965).

[4] E. J. Corey and M. Chaykovsky, *Org. Synth. Coll. vol. 5*, 755 (1973).

[5] R. Kuhn and H. Trischman, *Liebigs Ann. Chim.*, **611**, 117 (1958).

[6] M. Avram, F. Chiraleu and I. Pogany, *Rev. Roumaine Chim.*, **15**, 1219 (1970).

[7] M. A. Battiste and J. W. Nebzydoski, *J. Amer. Chem. Soc.*, **92**, 4450 (1970).

[8] R. S. Bly, C. M. DuBose, Jr. and G. B. Konizer, *J. Org. Chem.*, **33**, 2188 (1968).

[9] M. A. Battiste and J. W. Nebzydoski, *J. Amer. Chem. Soc.*, **91**, 6887 (1969).

[10] Ch. J. R. Adderley, J. W. Nebzydoski, M. A. Battiste, R. Baker and D. E. Halliday *Tetrahedron Letters*, **1971**, 3545.

Revue Roumaine de Chimie, 34, 4, 995–1004 (1989)

STRUCTURE-ACTIVITY RELATIONS FOR STEROIDS BY THE MTD METHOD. SUPERPOSITION PROCEDURE FOR MOLECULES WITH DIFFERENT CONDENSED CYCLES

I. GERGEN[a], M. BOHL[b], H. SIMON[c] and Z. SIMON[c]
[a] Office for Studies in Pedology and Agrochemistry, Timişoara, Romania
[b] Zentralinstitut für Mikrobiologie und Experimentelle Therapie, 69 Jena, DDR
[c] Institute of Medicine, Timişoara-1900, P-ţa 23 August 2, Romania

Received October 20, 1988

A method for a least square deviation, atom per atom superposition of steroids with different skeletons was developed, using crystallographic atomic coordinates and a computerised technique. This method is used to construct the hypermolecule for the MTD method. A maximal interdistance of 0.5 Å is recommended for attribution of atoms from different molecules to the same hypermolecule-vertex based upon an analysis of van der Waals potential curves. For a series of 39 gestagenic testosterone derivatives with three types of skeletons, using MTD and a corrected hydrophobicity, the correlational equations yield a regression coefficient, $r = 0.932$. The use of the Hückel-resonance energy in such correlations is also discussed.

INTRODUCTION

One of the difficulties in establishing a QSAR by the Minimal Topological Difference (MTD) method for series of molecules with different condensed cycles, as steroids, is the construction of the hypermolecule.[1,2] The hypermolecule is constructed by an approximative atom per atom superposition. If differently condensed cycles are to be super-imposed, one must use atomic coordinates in order to ascertain that atoms of different molecules, superimposed upon the same vertex, are really near enough to the vertex. Here we describe a computerised superposition procedure which uses crystallographic atomic coordinates and also its application to three series of biologically active steroids with different steroid cycles.

METHOD

The superposition procedure for the hypermolecule construction requires the orientation of the molecules such that pharmacophoric groups or common molecular parts occupy the same positions in all molecules. Atoms, from different molecules, which by superposition fall less than about 0.5 Å apart, are considered to occupy the same vertex of the hypermolecule.[1,2]

The 0.5 Å-limit for the distance between atoms, which can be considered to occupy the same vertex, is justified in Appendix 1, by an analysis of van der Waals potentials and of flexibilities in torsional deformations. The existence of X-ray crystallography data for a great number of steroids[3-5] allows to perform complex structural calculations, such as molecular superposition with minimisation of the sum of quadratic differences between pairs of equivalent atoms (least squares fitting procedure). Graphical facilities of the computer techniques allow also visualization of molecules and of their rotations for the superposition. The following programs were used for the superposition :

MOLFIT — program for fitting the molecules according to the least square condition for distances between equivalent atoms,[6] written in FORTRAN-77 language and adapted for the Romanian Junior-computer.

SUPRAMOL — program for molecular superposition and graphical visualization, written in BASIC-language for the Romanian TIM-S computer.[7]

The following examples refer to gestagenic steroids which bind to the progesteronic receptor by hydrogen bonds with two oxygen atoms in position 3 and 17β (testosterone-derivatives) or 20 (progesterone derivatives) and by hydrophobic forces.[8,9] These two oxygen atoms are thus "key'-atoms and, together with the C_2 atom of the steranic cycle, are used for the orientation of molecules and for fitting by the least squares procedure.

MOLECULAR SUPERPOSITION OF GESTAGENIC STEROIDS

By a survey of published data, dissociation constants for binding to the uterine progesterone receptor were found for 128 steroids.[9-12] The available X-ray crystallography data[3-5] allowed us to consider for superposition upon progesterone and respectively testosterone, the steroids listed in Table 1 and Table 2. The least squares fitting procedure was applied for atoms C_2, O_3 and O_{20} or $OH_{17\beta}$, but in some cases all atoms for which interdistances are listed in Tables 1 and 2 were used for the least squares fit (cases marked by asterisk). The interdistances between pairs of equivalent atoms are also listed. Different cases of superpositions are visualized in Fig. 1. The 17β-acetyl side chain of progesterone and derivatives was considered with a torsional $C_{16}-C_{17}-C_{20}-C_{20}$ angle of $-46°$, according to Duax et al[4].

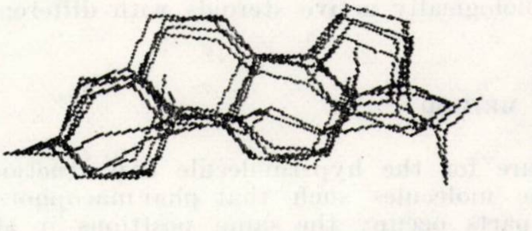

Fig. 1. — Common superposition figure of 1,4-P, 5-AHT, 17-CMT, testosterone and NORT upon progesterone. Viewed from above. Angles : Frontal 90°, Rolling 0°. See legend of Table 1 for abbreviations

If the key atoms O_3, O_{20} or 17β—CH and C_2 are used for the least squares fitting procedure in the superposition of testoterone upon progesterone (Table 1), there are several pairs of equivalent atoms with interdistances larger than 0.5Å, namely C_{12}, C_{13}, C_{15}, C_{16}, C_{17}, O_{20}. If steroids with both types of skeletons, 4-pregnene-3,20-dione and 17β-OH-4--androstene-3-one, would be used for a unique series for QSAR, new vertices are to be introduced for all these atoms and for the substituents at these atoms, increasing chance correlation. Therefore separate series for QSAR were considered for the steroids with each skeleton.[9,10]

An inspection of Tables 1 and 2 demonstrates that the 5αH-androstene-3-one (5AHT) skeleton can be superimposed upon the 4-androstene-3-one skeleton (and the same for the pregnene skeleton—see columns 5AHT*), if all skeleton atoms (C_3—C_{19}) are used for the least squares fitting procedure. Atoms C_1 and C_2 of 5AHT occupy different positions than the equivalent atoms in testosterone or progesterone, because of different lowest energy conformations of the *A*-ring[3-5]; the equivalent C_4-atoms also fall apart at distances larger than 0.5Å. Three new vertices must be thus introduced in the hypermolecule. The 4,9-an-

Table 1

Distances between equivalent atoms for superpostions of steroids upon the progesterone molecule

No Atom C	Distances (*A*) between equivalent atoms in the pairs progesterone and :						
	NORT	17-CMT	5-AHT	5 AHT*	4,9—T*	1,4P	T
C_1	0.399	1.052	0.328	—	—	0.652	0.419
C_2	0.394	0.540	0.357	—	—	0.338	0.414
C_3	0.341	0.498	0.411	0.193	0.282	0.180	0.339
C_4	0.437	1.335	1.078	0.551	0.140	0.334	0.297
C_5	0.426	1.707	0.369	0.323	0.041	0.465	0.311
C_6	0.712	2.894	0.827	0.204	0.081	0.575	0.269
C_7	0.894	2.781	1.049	0.059	0.096	0.646	0.335
C_8	0.574	1.701	0.681	1.074	0.143	0.410	0.383
C_9	0.407	0.587	0.382	0.127	0.402	0.433	0.417
C_{10}	0.345	1.122	0.309	0.098	0.364	0.454	0.376
C_{11}	0.523	1.161	0.442	0.185	0.237	0.627	0.475
C_{12}	0.631	0.987	0.591	0.146	0.120	0.831	0.587
C_{13}	0.478	1.505	0.526	0.041	0.105	0.490	0.559
C_{14}	0.805	1.457	0.879	0.029	0.060	0.545	0.495
C_{15}	1.265	2.587	1.309	0.128	0.055	0.650	0.514
C_{16}	1.372	1.775	1.440	0.325	0.048	0.630	0.658
C_{17}	0.844	0.632	0.886	0.052	0.226	0.664	0.651
C_{18}	0.389	1.841	0.476	0.111	0.151	0.347	0.500
C_{19}	—	—	0.438	0.231	—	0.529	0.328
C_{20}	3.217	1.733	—	—	—	0.689	—
C_{21}	—	—	—	—	—	1.552	—
O_3	0.358	0.275	0.432	0.279	0.159	0.165	0.320
O_{20}	0.751	0.765	0.779	—	—	0.425	0.728

* Superposition upon progesterone with least square deviation including all atoms ; 4,9-T stands for 17βOH-17αCCH-4,9 androstadiene-3-one ; NORT norethisterone ; 17 CMT : 17α-cyanomethyl-17βhydroxy-androsta-4,9-diene-3one ; 5AHT ; 5αH-androstane-3,20-dione, 1,4-P : 1,4-pregnadiene-3,2O-dione ; T-testosterone.

Table 2

Distances between equivalent atoms for superposition of steroids upon the testosterone molecule

No Atom C	Distances (A) between equivalent atoms in the pairs testosterone and :				
	NORT	17-CMT	5 AHT	ANOGA *	1,4-P
C_1	0.064	0.9244	0.103	—	0.733
C_2	0.045	0.148	0.142	—	0.141
C_3	0.097	0.379	0.317	0.117	0.234
C_4	0.327	1.353	1.095	0.584	0.442
C_5	0.347	1.711	0.284	0.241	0.542
C_6	0.683	2.948	0.804	0.081	0.597
C_7	0.774	2.931	0.953	0.244	0.588
C_8	0.443	1.803	0.577	0.036	0.299
C_9	0.063	0.426	0.143	0.056	0.512
C_{10}	0.090	1.017	0.209	0.037	0.508
C_{11}	0.428	0.897	0.329	0.062	0.815
C_{12}	0.411	0.689	0.307	0.059	1.002
C_{13}	0.109	0.633	0.184	0.040	0.697
C_{14}	0.464	1.776	0.586	0.015	0.466
C_{15}	0.979	2.968	1.035	0.086	0.431
C_{16}	0.882	2.311	0.964	0.033	0.391
C_{17}	0.235	1.016	0.341	0.039	0.770
C_{18}	0.648	1.741	0.641	0.092	0.791
C_{19}	—	—	0.425	—	0.415
O_3	0.050	0.102	0.146	0.256	0.210
O_{17}	0.025	0.047	0.060	0.065	0.305

Legend: See Table 1; * Superposition of ANOGA (17β-OH-5Hα-androstan-3-one) upon norethisterone with least square deviations including all atoms.

drostadiene-3-one skeleton can also be superimposed upon the 4-pregnene-3,20-dione skeleton (see column 4,9-T*, Table 1) and the same should be true also for superposition upon the 4-androstene-3-one skeleton which differs only by the lack of the 17β-acetyl group.

The *A*-ring conformation of the 4,9 diene-3-one-skeleton is also different from that of the 4-one-3-one-skeleton[13] and atoms C_1 and C_2 are not superposable.

Generally, superposition with least squares fitting for all C-atoms of the steranic skeleton (except C_1 and C_2 — for inverted *A*-ring conformations) allow better atom per atom superposition.

QUANTITATIVE STRUCTURE ACTIVITY RELATIONS

As an example we give here the QSAR by the MTD-method for a series of testosterone type derivatives. Out of the above mentioned 128 steroids with gestagenic activity, we could select 39 molecules superposable, without the introduction of several new vertices, upon testosterone: 27 derivatives with the 4-androsten-3-one skeleton, 4-with the 5αH-androstan-3-one skeleton and 8 with the 4,9 androstadiene-3-one skeleton, listed in Table 3.

Table 3

Testosterone derivatives with gestagenic activity

Na	Substituents	Occupied vertices	A	f	MTD	$\hat{A}$
a) Derivatives with 17β-OH-4-androsten-3-one (j :23—25) skeleton						
1	18-Me-NE	1,8,9,13,18,19	2.55	0.31	3	2.27
2	11=CH_2—18-Me-NE	1,7—9,13,18,19	2.54	0.47	3	2.35
3	7α17α-diMe-NT	1,4,8,13,19	2.33	0.52	3	2.38
4	11β-Cl-NE	1,6,8,13,18,19	2.32	−0.33	3	1.92
5	NE	1,8,13,18,19	2.19	−0.21	3	1.99
6	17α-Me-NT	1,8,13,19	2.00	0.00	3	2.10
7	17α-CH_2Cl-NT	1,8,13,14,19	1.93	0.16	3	2.19
8	17α-Et-NT	1,8,13,14,19	1.89	0.52	3	2.38
9	18-Et-NE	1,8—10,13,18,19	1.86	0.83	4	1.58
10	17α-Pr-18-norT	1,5,13—15,19	1.83	1.04	4	1.69
11	17α-CH=CH_2—NT	1,8,13,14,19	1.81	0.16	3	2.19
12	17α-CH_2CMe=CH_2—NT	1,8,13—16,19	1.68	1.19	4	1.78
13	18-Me—NT	1,8,9,19	1.53	0.00	4	1.13
14	7α-Me—NT	1,4,8,19	1.34	0.00	4	1.13
15	3-deoxy-17αMe—NT	8,13,19	1.30	0.00	4	1.13
16	E	1,5,8,13,18,19	1.28	0.31	4	1.30
17	3-deoxy-11=CH_2— —18Me—NE	7—9,13,18,19	1.20	0.47	4	1.39
18	3-deoxy-7-Me—NE	4,8,13,18,19	0.95	0.31	4	1.30
19	3-deoxy-NE	8,13,18,19	0.85	−0.21	4	1.02
20	NT	1,8,19	0.78	−0.52	4	0.86
21	18-Et—NT	1,8—10,19	0.65	0.52	5	0.45
22	4-Cl-17αMe—T	1,2,5,8,13,19	0.11	0.68	5	0.53
23	Testosteron	1,5,8,19	−0.22	0.00	5	0.17
24	17α-CH_2CN=T	1,5,8,13,14,17,19	−0.52	−0.42	5	−0.06
25	4-Cl-11β-OH-17αMe—T	1,2,5,6,8,13,19	−1.00	−0.97	5	−0.35
26	11=CH_2, 17αCCH—NT	1,7,8,13,18,19	2.48	−0.05	3	2.07
27	11β-Me, 17αCCH, 18Me—NT	1,6,8,9,13,18,19	2.18	0.83	3	2.55
b) Derivatives with 17β-OH-5-androstan-3-one (j :26—28) skeleton						
28	11=CH_2, 17αCCH, 18—Me, 19-nor	1,7—9,13,18,19	1.99	0.83	4	1.58
29	17α—CCH, 19-nor	1,8,13,18,19	1.23	0.15	4	1.22
30	17α-CCH	1,5,8,13,18,19	0.70	0.67	5	0.53
31	5Hα-Testosteron	1,5,8,19	−0.30	0.36	6	−0.60
c) Derivatives with 17β-OH-4,9-androstadiene-3-one (j :25—27) skeleton						
32	7α, 17α-diMe	1,4,8,13,19	2.30	0.16	3	2.19
33	17α-Me	1,8,13,19	1.85	−0.36	3	1.91
34	17α-CCH, 18-Me	1,8,9,13,18,19	1.83	−0.05	3	2.07
35	17α-CCH	1,8,13,18,19	1.62	−0.57	3	1.79
36	18-Me	1,8,9,19	1.42	−0.36	4	0.94
37	9Δ-Testosteron	1,8,19	1.23	−0.88	4	0.66
38	17α-CCH, 18-Et	1,8—10, 13, 18, 19	1.04	0.47	4	1.39
39	18-Et	1,8—10, 19	0.66	0.16	5	0.66

Legend: NT-19nortestosterone, E-ethisterone, NE-19-norethisterone, Me-methyl, Et-ethyl, Pr-propyl. For each molecule are indicted only the vertices occupied by the substituents to the steroidic skeleton. $A \rightarrow \log K_D$ is the binding affinity to the progesterone receptor; f — corrected hydrophobicity ($f = 0$ for progesterone); MTD — minimal topologic difference calculated with the optimised map $S_T^*(1)$; $\hat{A}$ — calculated activities with eq. (2).

The biological activity, A, represents the logarithm of the relative affinity to the progesteron receptor of rabbit uterus (progesterone 100%, $A = 2$) as defined in[9]. As structural parameters we consider the minimal topologic difference, MTD, and a corrected hydrophobicity, f (contribution of 3 and 17β substituents-neglected).[9,14]

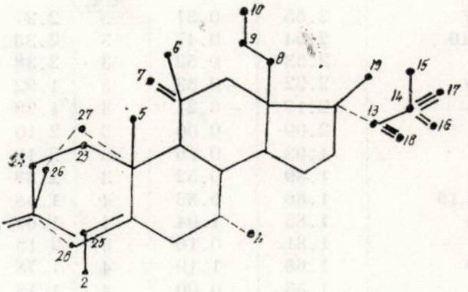

Fig. 2. — Hypermolecule and numerotation of the j-vertices, for the series of gestagenic steroids of Table 3.

The hypermolecule constructed for this series presents 22 vertices with different occupations in these 39 molecules. The vertex numerotation, j :1,2,4,—10,13—19, 23—28, corresponds to the one in papers[9,10].

$$S_T^*\begin{cases} j(\varepsilon=-1): 1,\ 13,\ 19,\ 23-27 \\ j(\varepsilon=0): 4,\ 6,\ 7,\ 9,\ 14,\ 16,\ 18,\ 28 \\ j(\varepsilon=+1): 2,\ 5,\ 8,\ 10,\ 15,\ 17 \end{cases} \tag{1}$$

$$\hat{A} = 5.000 - 0.966\ \mathrm{MTD} + 0.538\mathrm{f};\ N = 39,\ r = 0.932,\ s = 0.326,\ \mathrm{F} = 119 \tag{2}$$

The 4,9-diene-3-one-skeleton is stated to have a high conformational flexibility with respect to the A-ring conformation.[13] The corresponding derivatives (Nos. 32—39, Table 7) could adopt thus also the 4-en-3one-skeleton-type A-ring conformation and occupy vertices j :23—25 (instead of j :25—27); in this case the vertex j :26 or 27 could be declared as irrelevant ($\varepsilon = 0$) in S_T^*, the other (j : 23—25, 28 and 27 or 26) as cavity vertices ($\varepsilon = -1$). Anyway, the receptor map S_T^* satisfies the condition[2] that all cavity vertices ($\varepsilon = -1$) form a unique connected network if the common vertices, occupied by all molecules, are also considered cavity vertices.

Eq. (2) is to be compared with eq. (3) obtained in a previous paper[9] for a reduced series of compounds (Nos. 1—25, Table 3):

$$\hat{A} = 5.396 - 1.092\ \mathrm{MTD} + 0.639\ \mathrm{f};\ N = 25,\ r = 0.955 \tag{3}$$

The optimised receptor map for this reduced series is identical to S_T^*, except that it does not contain vertices j : 23—28.

The superpositional results here described were used also to obtain a QSAR for a series of $N = 55$ gestagenic progesterone derivatives (49 with a 4-one-3,20-dione skeleton, 2 with a 5Hα-3,20-dione skeleton and 4 with a 4,9-diene-3,20-dione skeleton)[10] and for a series of $N = 46$ steroid inhibitors of the enzyme aromatase (30 with the 4-androstene-3-one skeleton, 16 with a 5Hα-3-one skeleton).[15] For the series of 55 progesterone derivatives, the following correlational equation was obtained :

$$\hat{A} = 5.493 - 0.760\ \mathrm{MTD} + 0.698\mathrm{f}\ ;\ N = 55,\ r = 0.934 \qquad (4)$$

The correlational equations (2), (3) and (4), obtained for the same progesteronic receptor, for different series of molecules have similar regressional coefficients.

For the 46 aromatase inhibitors, the correlational equation is

$$\hat{A} = 1.621 - 0.566\ \mathrm{TD} + 0.535\mathrm{f} + 3.120\ \mathrm{R}\ ;\ N = 46,\ r = 0.914 \qquad (5)$$

with R — the resonance energy,[16] in β-units, for the systems of conjugated pi-electronic systems in the region of the *A* and *B*-rings. Details about the resonance energy calculations are given in Appendix 2. Attempts to consider resonance energy as a third parameter were done also for eqs. (2) and (4), but no sensible improvement was obtained.

CONCLUSIONS

Computational techniques and X-ray crystallography data for molecular structure were used to construct the hypermolecule by superposition of molecules with different condensed cycles. An upper threshold of about 0.5Å can be recommended for distances between atoms from different molecules which can be superimposed upon the same vertex of the hypermolecule.

Superpositions upon progesterone and respectively testosterone of skeletons of different steroids with gestagenic action were performed and used to construct the hypermolecule for a series of 39 gestagenic testosterone derivatives with 4ene-3-one, 5Hα-one and 4,9-diene-3-one-skeletons. The correlational equation and optimised receptor map hereby obtained are similar with those obtained for other two series of gestagenic steroids and this fact is a positive test for the reliability of the correlational results.

The superposition technique here described can be recommended for QSAR studies by the MTD method for series of molecules with different condensed cycles where the simple, by hand superposition of molecules does not yield a clear attribution of the atoms to the vertices of the hypermolecule.

Appendix 1

How exact must be the steric fit?

How far can an atom, of a certain molecule, be from the vertex of the hypermolecule to which it is attributed? The answer can be found if one knows how sensible is the van der Waals interaction energy to variations in interatomic distances. Also, how much depends the torsional potential upon the displacement of an atom (X in Fig. 3), displacement produced by a steric repulsion with the partner-molecule.

Consider the well known 6 – 12 van der Waals potential

$$U(r) = -Ar^{-6} + Br^{-12} \qquad (6)$$

The energy minimum, $U_{\min} = -A^2/4B$ is obtained for $r_0 = (2B/A)^{1/6}$. One can ask for which shift, Δr, from the equilibrium distance, r_0, one has :

$$U(r_0 + \Delta r) = \frac{1}{2} U_{\min} = -A^2/8B \qquad (7)$$

With $r = r_0 + \Delta r$, one has :

$$-A^2/8B = -Ar^{-6} + Br^{-12}$$

which can be brought in the quadratic form ($z = r^6$)

$$z^2 - \frac{8B}{A} z + \frac{8B^2}{A^2} = 0$$

with the solutions

$$z_{1,2} = \frac{2B}{A}(2 \pm \sqrt{2}) \text{ or : } r + \Delta r = \begin{cases} r_0 \cdot 3.41^{1/6} = 1.227\, r_0 \\ r_0 \cdot 0.59^{1/6} = 0.916 r_0 \end{cases}$$

With the usual van der Waals contact distance, $r_0 = 3.5$ Å, one has $\Delta r = +0.79$ Å and -0.33 Å

For the energy, ΔU, required in a torsional shift of the X atom (Fig. 3) one has, for a sinusoidal potential :

$$U(\alpha) = \frac{1}{2} U_0 (1 - \cos \alpha) \qquad (8)$$

$$\Delta U(\alpha) = U(\alpha) - U(0) = \frac{1}{2} U_0 (\cos \alpha - 1)$$

The shift of atom X produced for a torsion of α-radians is :

$$\Delta r \cong 1_{xy} \cdot \sin \widehat{XYZ} \cdot \alpha \qquad (9)$$

With $1_{xy} = 1.5$ Å, $\widehat{ZYX} = 108°30'$ (sp^3 hybridisation for Y) and $\Delta U =$

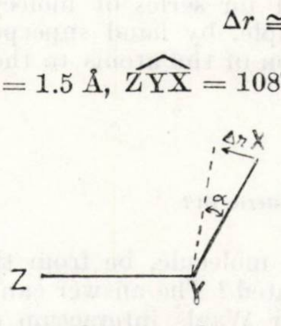

Fig. 3. — Shift Δr of atom X upon an α-rad torsion around the ZY-bond.

$= kT \cong 4 \cdot 10^{-21}\, j$, one obtains, for a potential barrier U_0 of 3 kcal/mol, 10 kcal/mol and respectively 40 kcal/mol ; Δr of 0.64 Å ; 0.34 Å and respectively 0.17 Å. These are the shifts which require an energy consumption equal to the mean thermal energy, kT.

Thus, while the shifts from equilibrium positions for van der Waals and torsional potentials (obtainable with energy consumptions near the thermal mean energy kT) depend rather strongly upon the particular situation, the guess of 0.5 Å for the precission of steric fit seems reasonable.

Appendix 2

Resonance energy calculations

Resonance energy, *R*, is defined as the difference between the pi-electron energy of the conjugated system and the one for the localised pi-bonds and atomic pi electron pairs.[16] Resonance energies were calculated by the simple HMO method with the parameters listed in Table 4. The parameters are generally those recommended by Streitwieser,[16] but as the conjugated pi-systems within the *A* and *B*-ring regions of steroid skeletons deviate from coplanarity, for the β-exchange integrals of simple bonds somewhat lower values were used than those generally adopted.

Table 4

Parameters used for HMO-calculations and resonance energies *R* (in β-units)

$$\alpha_C = \alpha\,;\ \alpha_{=O} = \alpha + \beta\,;\ \alpha_{-OH} = \alpha_{CH_3} = \alpha + 2\beta\,;$$

$$\alpha_{Cl} = \alpha + 1.8\beta$$

$$\beta_{C=C} = \beta_{C=O} = \beta\,;\quad \beta_{C-CH} = \beta_{C-C} = 0.8\beta\,;$$

$$\beta_{C-CH_3} = 0.6\beta\,;\quad \beta_{C-Cl} = 0.4\,\beta$$

No.	Conjugated model systems	R(β)
1.	$O=CH_2$	0.
2.	$O=CH-CH=CH_2$	0.341
3.	$O=CH-CH=CH-CH=O$	0.656
4.	$C=CH-CH=CH-CH=CH_2$	0.679
5.	$H_2C=CH-CO-CH=CH_2$	0.659
6.	$O=CH-C(CH_3)=CH_2$	0.451
7.	$O=CH-C(OH)=CH_2$	0.538
8.	$O=CH-C(Cl)=CH_2$	0.393
9.	$O=CH-CH=CH-CH=$ $=CH-CH=CH_2$	1.015
10.	$H_2C=CH-CO-CH=CH-$ $-CH=CH_2$	0.995
11.	$H_2C=CH-CO-CH=CH-$ $-CH=O$	0.998
12.	$H_2C=CH-CO-C(OH)=CH_2$	0.858

The *R*-values in β-units and the corresponding conjugated systems are listed in Table 4. As example, system No. 1 is the model for the 5Hα-3-one-steroid skeleton, No. 2 for the 4-ene-3-one-skeleton, No. 4 for the 4,9-diene-3one-skeleton, etc.

An increased resonance energy will reinforce the tendency towards coplanarity of the conjugated system; the rather high R-value for the 4,9-diene-3one skeleton may explain the flexibility of this skeleton concerning the transition between the noncoplanar sopha and half-chair conformations of the *A*-ring.[13] The polarisability of the pi-system also increases with the resonance energy, favouring van der Waals interactions with planar regions of the receptor.

REFERENCES

[1] A. T. Balaban, A. Chiriac, I. Moţoc and Z. Simon, "Steric Fit in Quantitative Structure-Activity Relations." Springer Verlag, Heidelberg (lecture Notes in Chemistry Series, **13** (1980), chap. 5.

[2] Z. Simon, A. Chiriac, S. Holban, D. Ciubotariu and G. I. Mihalaş, "Minimum Steric Difference. The MTD Method for QSAR Studies", Research Stud. Press, Letchworth, 1984, chap. 3.

[3] G. Reck, *Cryst. Struct. Com.*, **1**, 18 (1982).

[4] W. L. Duax, J. F. Griffin and D. C. Rohrer, *J. Amer. Chem. Soc.*, **103**, 6705 (1981).

[5] W. L. Duax, J. F. Griffin, D. C. Rohrer, D. C. Swenson and C. M. Weeks, *J. Steroid Biochem.*, **15**, 41 (1981).

[6] Details about the MOLFIT-program can be obtained from Dr. M. Bohl.

[7] Details about .the SUPRAMOL-program can be obtained from Dr. I. Gergen.

[8] W. L. Duax, J F. Griffin, D. C. Rohrer, C. M. Weeks and R. H. Ebright in : "Biochemical Actions of Hormones", Vol. XI, (G. Litwack, ed.), p. 187, Academic Press, New York 1984.

[9] M. Bohl, Z. Simon, A. Vlad, G. Kaufmann and K. Ponsold, *Z. Naturforsch*, **42c**, 935 (1987)

[10] M. Bohl, et al., in preparation.

[11] T. Kanoja, *J. Medic. Chem.*, **18**, 1143 (1975).

[12] J. Pitt, *J. Medic. Chem.*, **22**, 966 (1979).

[13] M. Bohl, G. Kaufmann, M. Hubner, G. Reck and R. Kretschmer, *J. Steroid Biochem.*, **23**, 895 (1985).

[14] R. F. Rekker and H. M. de Kort, *Eur. J. Med. Chem.*, **14**, 479 (1979).

[15] M. Bohl. Z. Simon, M. Lochmann, *Z. Naturforsch c*, submitted.

[16] A. Steitwieser Jr., "Molecular Orbital Theory for Organic Chemists," John Wiley, New York, 1961.

Revue Roumaine de Chimie, 34, 4, 1005–1008 (1989)

CARBON-13 NUCLEAR MAGNETIC RESONANCE ASSIGNMENTS OF THE SATURATED SEGMENT FROM 1,2,3,4-TETRAHYDROPHENANTHRENE BY MEANS OF ^{13}C AND ^{2}H LABELLING[1]

MIRCEA D. GHEORGHIU *, ANA SCHIKETANZ, ATENA NECULA and
ALEXANDRU T. BALABAN *

Department of Organic Chemistry, Polytechnic Institute-TCH, 77206 Bucharest 16, Romania

Received November 21, 1988

The ^{13}C-NMR assignments for the C_1-C_4 fragment of 1, 2, 3, 4-tetrahydrophenanthrene were arrived at on the basis of [1-^{13}C], [3-^{13}C], 2,2-d_2 and 3,3-d_2 labelled compounds. Unlike previous literature assignments for C_2 and C_3 (see refs. 6 and 7), the chemical shifts found by us for the C_1-C_4 carbon atoms are : C_1 : 30.40 ; C_2 : 22.93 ; C_3 : 23.21 ; C_4 : 25.59 ppm, respectively.

INTRODUCTION

The increasing interest in the last decade in liquid fuels obtained from coal liquefaction triggered many research projects for spectroscopical studies of hydroaromatics, including tetra- and octa-hydrophenanthrenes.[2-7] The Gulf Science & Technology scientists proposed the ^{13}C-NMR as analytical tool to investigate the structure of hydroaromatic molecules obtained in coal liquefaction processes; thus sixteen tetralins, hydrophenanthrenes and hydropyrenes were analyzed [6] by ^{13}C-NMR. For the compound which represents our interest in the present paper, 1,2,3,4-tetrahydrophenanthrene (THP), the aromatic signal assignments were obtained with the aid of model compounds such as 1- and 2-methylnaphthalene, 1,2-dimethylnaphthalene and phenanthrene. However, the assignment of the saturated carbon atoms of THP was not commented, but merely presented in a Table, probably considered as self-explanatory. Later, Grant, Pugmire et al.[7] have noticed that C_2 and C_3 assignments are ambiguous, as well as those for the quaternary carbons C_{4a} and C_{8a}, respectively.

The present paper contains a definite assignment of the saturated carbon atoms from THP, based on the experimental evidence resulted from the ^{13}C-NMR spectra of [1-^{13}C]-, [3-^{13}C]-, 2,2-d_2 and 3,3-d_2-tetrahydrophenanthrenes.

DISCUSSION OF THE RESULTS

The chemical shifts for the carbon atoms C_1-C_4 are collected in the Table.

Table

^{13}C-NMR chemical shifts (ppm, internal TMS, $CDCl_3$) for labelled and parent THP, including literature assignments

Compound		C_1	C_2	C_3	C_4	References
THP	1	30.3	23.2	22.9	25.5	lit. 6
		30.4	23.2*	23.0*	25.5	lit. 7
		30.40	22.93	23.21	25.59	present work
[1-^{13}C] THP	2	30.50	—	—	—	present work
[3-^{13}C] THP	3	—	—	23.21	—	present work
2,2-d_2-THP	4	30.20	—	23.00	25.54	present work
3,3-d_2-THP	5	30.36	22.71	—	25.40	present work

* ambiguous assignment according to ref. 7.

On the basis of reasoning by analogy, the benzylic carbon atoms C_1 and C_4 were correctly assigned previously.[6,7] The result obtained here from the experiment using [1-^{13}C] THP supports nicely the lower field chemical shifts assignment for the C_1 carbon atom, while the C_4 carbon atom resonates at higher field. The analogy used previously for assignment[6] of the two carbon atoms (C_1 and C_4) with the corresponding carbon atoms from 1-methyl- and 2-methylnaphthalene [8] is therefore supported by experimental facts. Additional support is provided by the isotopic upfield shift induced by deuterium atoms. Thus, in the case of 2,2-d_2-THP, the isotopic shift for C_1 is −0.2 ppm, while the higher resonating C_4, being three bonds remote, has a negligible isotopic shift. When the deuterium atoms are at C_3, then a −0.19 ppm isotopic shift is induced for C_4, and a negligible one for C_1.

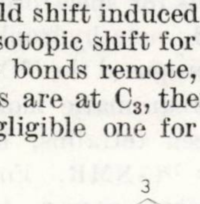

1

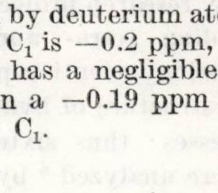

2

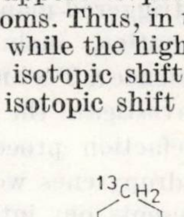

3

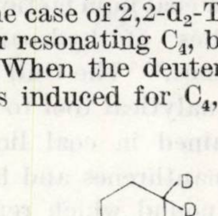

4

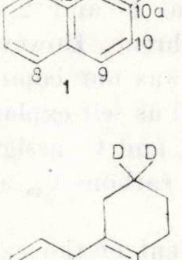

5

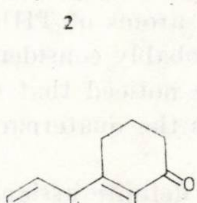

6

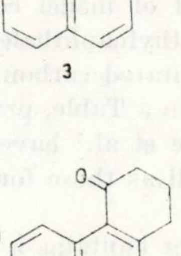

7

The remaining saturated carbon atoms were assigned incorrectly.[6,7] The ^{13}C-NMR spectrum of [3-^{13}C]THP (see Table) supports the assignment to C_3 of the signal occurring at relatively lower field. Thus the remaining signal at 22.93 ppm must be assigned to C_2. Additional support resulted from the ^{13}C-NMR spectra of 2,2-d_2- and 3,3-d_2-THP. On recording under standard conditions (see experimental part), in the case of 2,2-d_2-THP the signal of C_2 is missing, while the two vicinal carbon atoms C_1 and C_3 are shifted upfield with about -0.2 ppm. In the case of 3,3-d_2-THP, the "missing" signal is that corresponding to 23.21 ppm, while the isotopic 23.21 shift, as expected, is significant only for the vicinal carbon atom C_4. Therefore, we conclude that a definite assignment of the chemical shifts for the saturated fragment of THP is the following: C_1: 30.40; C_2: 22.93; C_3: 23.21 and C_4: 25.59 ppm, respectively, as shown in the Table.

We hope to bring in the future experimental evidence aiming to solve the remaining ambiguous assignment of C_{4a} and C_{8a}.[7]

EXPERIMENTAL

The ^{1}H—NMR spectra were obtained with a Varian EM-360 L instrument. The ^{13}C-NMR spectra were recorded with a Varian FT-80A instrument using the following parameters: spectral windows 4000 Hz and 5000 Hz, pulse width 10 μs, pulse delay 3 s, acquisition time 2.047 s or 1.638 s. The deuterated compounds **4** and **5** were obtained from the 1,2,3,4-tetrahydro-1-phenanthrenone (**6**) and 1,2,3,4-tetrahydro-4-phenanthrenone (**7**), respectively, by exchange with D_2O. The general procedure[9] was the following: a mixture of 2 g (10.2 mmoles) of ketone **6** or **7** carefully dried over P_2O_5, 20 ml D_2O (99.7%, Uvasol, Merck, West Germany) and 0.4 g (2.8 mmoles) anhydrous K_2CO_3 were refluxed for five hours. The crude reaction mixture was extracted with ethyl ether. After drying and removal of solvent, 1.8 g (89% yield) of deuterated ketone **4** (or **5** respectively) was obtained. By ^{1}H-NMR at least 80% of the recovered material was deuterated after a single exchange and was used further as such.

Deuterated 1,2,3,4-tetrahydrophenanthrenes **4** and **5** were obtained from the corresponding ketones **6** and **7**, respectively by reduction with $LiAlH_4+AlCl_3$.[10] A solution of $AlCl_3$ (0.85 g, 6 mmoles) in 7 mL absolute ethyl ether was added rapidly over a suspension of 0.3 g (7 mmoles) of $LiAlH_4$ and 7 mL absolute ethyl ether. After five minutes we added a mixture of 1 g (5 mmoles) of ketone **6** (or **7**), 0.7 g (5 mmoles) $AlCl_3$ and 13 mL ethyl ether. The mixture was gently refluxed for 30 minutes. After cooling, to the reaction mixture were added 10 mL of water and then 7 mL H_2SO_4 6N. The aqueous layer was extracted with 4 × 10 mL ethyl ether. The combined ethereal extracts were dried over anhydrous Na_2SO_4, and evaporated, giving 0.6 g (66% yield) of deuterated 1,2,3,4-tetrahydrophenanthrene **4**. The isomer **5** was obtained with a similar yield. Both **4** and **5** were of acceptable purity by ^{1}H—NMR and ^{13}C-NMR assessments.

1,2,3,4-Tetrahydro-1-phenanthrone (**6**) was obtained by cyclization of (1-naphthyl)-4-butanoic acid with polyphosphoric acid (PPA), by analogy with the synthesis of α-tetralone from *4*-phenylbutanoic acid.[11]

1,2,3,4-Tetrahydro-4-phenanthrone (**7**) was obtained from (2-naphthyl)-4-butanoic acid with PPA, in a kinetically controlled cyclization reaction.[12]

The m.p. and the spectral properties of the ketones **4** and **5** are identical with those reported in the literature.[12,13]

The synthesis of [1-^{13}C]- and [3-^{13}C]-1,2,3,4-tetrahydrophenanthrene was summarized in our note[14] and will be reported in detail in a full paper regarding the phenanthrene automerization.

REFERENCES

[1] Taken in part from the Ph. D. Thesis of A. S.
[2] T. J. Wozniak and R. A. Hites, *Anal. Chem.*, **57**, 1320 (1985).

[3] P. E. Hansen and B. Arne, *Spectr. Inter. J.*, **2**, 1 (1983) ; *Chem. Abstr.*, **100**, 5401z (1981).

[4] S. Huggenberg and M. Hesse, *Helv. Chim. Acta*, **63**, 2295 (1980).

[5] S. Berger and K. P. Zeller, *Org. Magn. Reson.*, **11**, 303 (1978).

[6] K. S. Seshadri, R. G. Ruberto, D. M. Jewell and H. P. Malone, *Fuel*, **57**, 111, 549 (1978).

[7] F. G. Morin, W. J. Horton, D. M. Grant, R. J. Pugmire and D.K. Dalling, *J. Org. Chem.*, **50**, 3380(1985).

[8] D. Doddrell and P. R. Wells, *J. Chem. Soc. Perkin II*, **1973**, 1333

[9] D. S. Noyce, G. L. Woo and M. J. Jorgenson, *J. Amer. Chem. Soc.*, **83**, 1160 (1963).

[10] R. F. Nystrom and C. R. A. Berger, *J. Amer. Chem. Soc.*, **80**, 2896(1958).

[11] D. G. Ott, "Synthesis with Stable Isotopes of Carbon, Nitrogen and Oxygen", Wiley, New York, 1981, page. 101 and references cited therein.

[12] I. Agranat and Yu.-S. Shih, *Synthesis*, 865 (1974).

[13] J. Haworth, *J. Chem. Soc.* **1932**, 1125 ; W. E. Bachmann and R. O. Edgerton, *J. Amer. Chem. Soc.*, **62**, 2219 (1940).

[14] A. T. Balaban, M. D. Gheorghiu, A. Schiketanz and A. Necula, *J. Amer. Chem. Soc.*, **111**, Jan (1989).

Revue Roumaine de Chimie, **34**, *4*, 1009–1015 (1989)

DETERMINATION OF SOME LIQUID—VAPOUR EQUILIBRIUM DATA FOR ACETONE (1)—CHLOROFORM (2)—NONIDEAL SOLUTION

GH. IONESCU, ANA ONU and VALER NAGACEVSCHI

Polytechnic Institute of Jassy, Faculty of Chemical Technology, Department of Physical Chemistry, Splai Bahlui 71, Jassy 6600, Romania

Received October 24, 1988

Using a device based on isoteniscope principle with some original changes, the overall pressure and compositions of the liquid and vapour phases at equilibrium, for the nonideal binary acetone (1) – chloroform (2) solution have been determined at 50°C. New data on liquid—vapour equilibrium for this significant nonideal system have been added to the literature ones. The partial vapour pressures and the coefficients of activity in the symmetrical convention have been calculated for the standard state. The thermodynamic consistency of the obtained experimental data on the activity coefficients have been proved using the Coulson – Herrington – Redlich – Kistes criterion. The computations implied by this criterion used for integration the Gauss method and for interpolation the Aitken – Newille method.

1. INTRODUCTION

The coefficients of activity are significant physical amounts used for the thermodynamic characterization of the nonideal liquid solutions.

Even under isothermal and isochoric conditions these amounts are complicated functions of the concentration which indicates the experimental method as a sure method for obtaining numerical values.

For most of nonideal nonelectrolyte solutions, the coefficients of activity can be calculated at low pressures, from the vapour pressures.

Thus, according to the symmetrical convention for the standard state :

$$\gamma_1 = \frac{p_1}{p_{01}} \cdot x_1 \quad \text{and} \quad \gamma_2 = \frac{p_2}{p_{02}} \cdot x_2 \tag{1}$$

With the asymmetric convention for the standard state :

$$\gamma_1 = \frac{p_1}{P_{01}} \cdot x_1 \quad \text{and} \quad \gamma_2 = \frac{p_2}{k_2} \cdot x_2 \tag{2}$$

if (1) stands for the solvent and (2) for the dissolved component ;

$$\gamma_1 = \frac{p_1}{k_1} \cdot x_1 \quad \text{and} \quad \gamma_2 = \frac{p_2}{p_{02}} \cdot x_2 \tag{3}$$

if (1) stands for the dissolved component and (2) for the solvent (γ_1, γ_2 are the coefficients of activity, p_1, p_2 — the partial vapour pressure, p_{01}, p_{02} — vapour pressure of the pure components, x_1, x_2 — mole fractions, k_1, k_2 — Henry's constants).

In Fig. 1 (a, b, c) the vapour pressure *vs.* concentration and the coefficients of activity *vs.* concentration curves are depicted for a solution with negative deviations from the ideality.

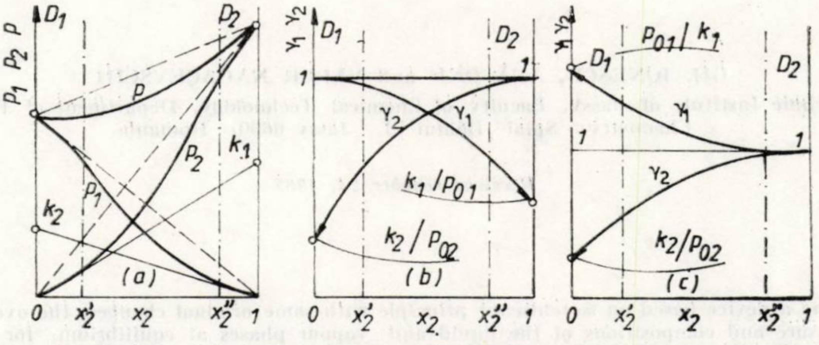

Fig. 1. — Variation of vapour pressure and coefficients of activity as a function of concentration : a) variation of the vapour pressure ; b) variation of the activity coefficients with the symmetrical convention ; c) variation of the activity coefficients with the asymmetrical convention.

The concentration ranges, D_1 and D_2, correspond to the nonideal diluted solutions, acetone in chloroform and chloroform in acetone, respectively, where the partial vapour pressures depend on the concentration according to Raoult's and Henry's laws. Within the concentration range $x'_1 \ldots x''$ the coefficients of activity are correlated with concentration by rather complicated relationships.

From the equation set . . . (1)—(3) it results that γ_1, and γ_2 can be calculated from the experimental data on vapour pressure and composition of liquid vapour at equilibrium.

The present paper determines experimentally the coefficients of activity for the components of the mentioned solution which has significant practical uses. The measurements were carried out at 50°C to bring additional information to the literature data.[1-4] The isothermal conditions have been preferred as, under these conditions, the correlation of experimental data is more accurate than under isobaric conditions.[5]

2. EXPERIMENTAL

2.1. Reagents

The substances used (chloroform and acetone of spectroscopical degree) have been supplied by E. Merck, Darmstadt.

2.2. Laboratory equipment

The experimental device is depicted in Fig. 2 and consists of the following :

1 — liquid vessel ;
2 — funnel with solution ;

3 — vessel for collecting the vapour sample;
4 — internal manometer for indicating the attaining of liquid—vapour equilibrium;
5 — external manometer for indicating the differences between the atmospheric pressure and the pressure inside the equipment;
6 — thermostat;
7 — phial for collecting the condensed sample after the condensation of vapours;
8 — three way cock.

Such an equipment works on the basis of the isoteniscope principle and is partially described in literature.[6] It can be used for studying the chemical equilibria during the decomposition of some solid substances to determine the dissociation pressure. For determining the overall vapour pressure and the phase composition at the vapour—liquid equilibrium the introduction of the devices 2 and 3 was required as well as the finding of an appropriate working manner.

2.3. Working procedure

The equipment is thermostated at the desired temperature. The equipment is vacuumed by means of R_1 (shut) and R_2 and R_3 (opened) cocks. Then the connection with the vacuum is cut off and the R_2 cock is shut. In this way the equipment is connected with the external manometer (5) only by means of internal manometer (4). Each change of the internal pressure is transmitted to the external manometer only by means of the internal one.

The required amount of solution is introduced in the vessel by means of the funnel (2). Immediately, a change of the Hg level in the internal manometer occurs, which has to be gradually counterbalanced by air admission.

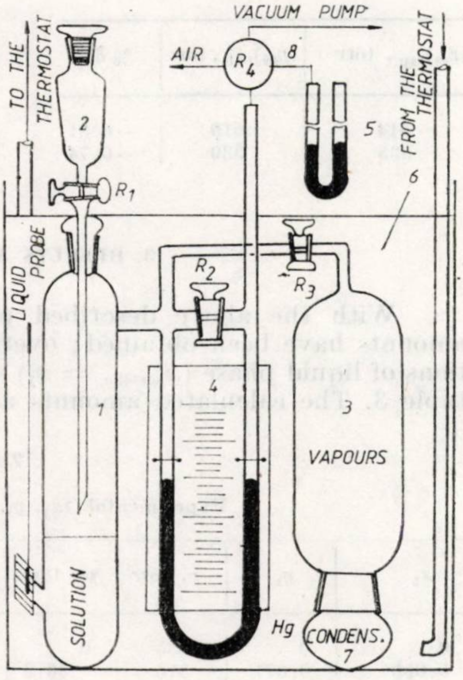

Fig. 2. — The experimental device.

The solution evaporation continues until the equilibrium is attained which is indicated by constant values on the manometers. The Hg height in both branches of the internal manometer is levelled by air admission. The barometric pressure and the residual uneveness indicated by the external manometer is read.

The difference between the barometric pressure and the residual uneveness, converted into torr by carrying out the temperature correction is the overall vapour pressure. The accuracy of reading the manometer scale was of ± 0.5 mm Hg.

The cock R_3 is shut and the vessel with the vapour phase is detached and introduced with its bottom (phial 7) in the acetone-carbonic ice cooling mixture (~ -80°C).

The vapours condense in the phial on the basis of cooled wall.

The obtained liquid and the residual solution were analysed refractometrically, based on a suitable standard curve, the phase composition at equilibrium being thus settled. The standard curve in $n_D^{20} - x_1$ coordinates was obtained with prisms thermostated at 20°C, at he natrium wavelength, D, the reading of the refractometer index having five digits.

2.4. Check of the equipment

To check the equipment and the working procedure, measurements were performed with pure components and their solutions and the obtained experimental pressure values compared with the literature ones.[2] The obtained data are listed in Tables 1 and 2, respectively.

T he obtained data indicated the equipment to offer vapour pressure with errors under 3 % which is within the limits generally accepted allowed for the liquid-vapour equilibrium.

Table 1

Experimental and tabulated data on the vapour pressure of pure components, at 50°C

$(p_{01})_{\text{exp.}}$, torr	$(p_{02})_{\text{tab.}}$, torr	% δ_r
614	619	−0.81
535	539	−0.74

Table 2

Experimental and tabulated data on the vapour pressure of some chloroform-acetone solution at 50°C.

x_1	$(p)_{\text{exp.}}$, torr	$(p)_{\text{tab.}}$, torr	% δ
0.300	470	485	−3.0
0.497	470	471	−0.1
0.820	553	547	+1.2

3. RESULTS AND DISCUSSION

With the above described procedure the following experimental amounts have been obtained ; overall vapour pressure (p), the compositions of liquid phase ($x_{\text{acetone}} = x_1$) and the vapour phase ($Y_{\text{acetone}} = Y_1$), table 3. The calculated amounts are also tabulated namely the experimental vapour pressure (p_1, p_2) the coefficients of activity in the symmetrical convention for the standard state (γ_1^I, γ_2^I) and the amount $\ln\left(\frac{\gamma_1}{\gamma_2}\right)^I$.

Table 3

Experimental (x_1, y_1, p) and calculated data

x_1	y_1	p, torr	p_1, torr	p_2, torr	γ_1^I	γ_2^I	$\ln\left(\frac{\gamma_1}{\gamma_2}\right)^I$
0	0	535	0	535	0.668*)	1	−0.4035
0.088	0.071	516	36.6	481	0.685	0.987	−0.3653
0.146	0.125	500	62	436	0.700	0.954	−0.3096
0.234	0.215	480	103	377	0.718	0.920	−0.2479
0.310	0.298	469	140	329	0.735	0.898	−0.2003
0.405	0.415	468	194	264	0.764	0.865	−0.1242
0.497	0.521	470	245	225	0.802	0.836	−0.0415
0.580	0.622	485	302	183	0.848	0.815	+0.0397
0.675	0.741	508	376	132	0.908	0.759	+0.1792
0.825	0.887	554	491	63	0.970	0.673	+0.3656
1	1	614	614	0	1	0.632*	+0.4589

*) $\gamma_1^I = k_1/p_{01}$; $\gamma_2^I = k_2/p_{02}$

Asymmetrical standard convention

Henry's constants, k_1 and k_2 have been determined graphically by plotting the tangents to the curves $p_1 = f(x_1)$ and $p_2 = f(x_1)$ at the points $x_1 \to 0$ and $x_1 \to 1$, respectively. The found values are :

$$k_1 = 410 \text{ Torr} \quad \text{and} \quad k_2 = 338 \text{ Torr}$$

The scale used : ordinate — 100 Torr = 50 mm ; abscissa : 0.1 mole fraction = 25 mm.

The data in Table 3, regarding the coefficients of activity have been checked thermodynamically by applying the Coulson-Herrington-Redlich-Kister general criterion of consistency [7] :

$$\int_0^1 \ln\left(\frac{\gamma_1}{\gamma_2}\right)^I \cdot \mathrm{d}x_1 = 0, \quad IaT = \text{const.} \tag{4}$$

To evaluate the integral, the amount $\ln(\gamma_1/\gamma_2)^I$ has been calculated (Table 3) as a function of x_1 variable. The numerical integration has been used, according to the Gauss method [8] which can be successfully applied in this case since the analysed data are not equally spaced on the x_1 abscissa. According to the Gauss method the integral is evaluated in five fixed points which are calculated by interpolation. For computer programming the interpolation based on the Aitken-Neville method [9] is recommended.

The integral is noted :

$$I = \int_a^b Y_i \cdot \mathrm{d}z_i \tag{5}$$

In equation (5) and the logical diagram, the following notations are used :

a, b — integral limits
p, q — integral limits after variable change
Y_i = values of the amount $\ln(\gamma_1/\gamma_2)$, Table 3
z_i = values of the amount x, Table 3
C_i — values of the coefficients of the five Gauss points
x_i — values of the Gauss points on the abscissa
T = values of the Gauss points on the abscissa after the variable change
F = values of the Gauss points on the ordinate obtained by interpolation.

For the integral "I" a value of $1.9\,56 \cdot 10^{-2}$ has been found. This is, in fact, the summation of two areas, one positive, the other one negative.

Consequently the two areas differ from each other by about 2%. Such an error lies within the allowed error range in determining the experimental amounts which allows the statement that eq (4) is satisfied and the obtained experimental data are thermodynamically consistent.

4. CONCLUSIONS

a) Using an apparatus based on the isoteniscope principle with an original modification which unlike the isoteniscope ensures the maintenance of the whole vapour phase at the equilibrium temperature and the collection of vapour phase, additional literature data regarding the nonideal acetone-chloroform solution at 50°C have been provided.

b) From the experimentally determined amounts, overall vapour pressure and composition of the liquid—vapour phases at equilibrium, the coefficients of activity in the symmetrical convention for the standard state have been calculated.

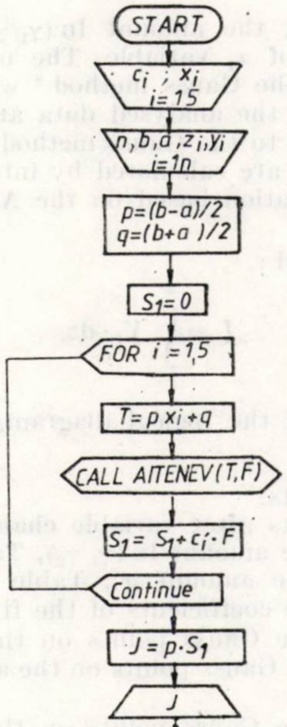
START
c_i ; x_i
$i=\overline{1,5}$
n, b, a, z_i, y_i
$i=\overline{1,n}$
$p=(b-a)/2$
$q=(b+a)/2$
$S_1=0$
FOR $i=\overline{1,5}$
$T=p x_i+q$
CALL AITENEV(T,F)
$S_1=S_1+c_i\cdot F$
Continue
$J=p\cdot S_1$
J
STOP

Logical diagram.

c) The thermodynamic consistency of the experimental data, regarding the coefficients of activity has been settled by means of the general Coulson-Herington-Redlich-Kister criterion, with an accuracy of 2%.

d) To prove the thermodynamic consistency of data, the Gauss integration method has been applied by using the Aitken-Newille method for which the suitable logical diagram and computer programme have been elaborated.

REFERENCES

[1] C. G. Schmidt, *Z. Phys. Chem.*, **121**,, 221 (1926).

[2] Landolt-Börnstein, "Eigenschaften der Materie in ihren Aggregatzuständen", 2 Teil, Bandteil a-Gleichgewichte Dampf — Kondensat und osmotische Phänomene. Berlin—Göttingen—Heidelberg, Springer-Verlag, 1960.

[3] H. Röch and W. Schröder, *Z. Phys. Chem.* (N.F.), **11**, 41 (1957).

[4] I. B. Rabinovici and P. N. Nikolaev, *Zhur. Fiz. Him.*, **34**, 2289(1960).

[5] * * * — International Council of Scientific Unions — Committee on Data for Science and Technology, Warsaw (PPR), April 14, 1986.

[6] * * * — Prakticheskje raboty po fizicheskoi khimii, Izd. Himia, Leningrad, 1967.

[7] D. Săndulescu, "Chimie fizică", vol. I, Ed. ştiinţifică şi enciclopedică, Bucharest, 1979, p. 576.

[8] V. Marinoiu, "Metode numerice aplicate în ingineria chimică", Ed. Tehnică, Bucharest, 1986.

[9] St. Dumitrescu, I. Dumitrescu and O. Paiu, "Aplicaţii inginereşti ale calculatoarelor cu exemple din industria petrolieră", Ed. Tehnică, Bucharest, 1974, p. 236.

REFERENCES

[1] G. Schmidt, Z. Phys. Chem., 121, 221 (1926).
[2] Landolt-Börnstein, "Eigenschaften der Materie in ihren Aggregatzuständen", 2 Teil, Band a "Gleichgewichte Dampf – Kondensat und osmotische Phänomene, Berlin – Göttingen – Heidelberg, Springer-Verlag, 1960.
[3] H. Bloch and W. Schröder, Z. Phys. Chem. (N.F.), 11, 41 (1957).
[4] B. Rabinovich and P. N. Nikolaev, Zhur. Fiz. Khim., 34, 2289 (1960).
[5] * * * International Council of Scientific Unions – Committee on Data for Science and Technology, Warsaw (CEE), April 14, 1980.
[6] * * * Prakticheskie raboty po fizicheskoi khimii, Izd. Khimia, Leningrad, 1967.
[7] D. Sandulescu, "Chimie fizică", vol. I, Ed. Ştiinţifică şi enciclopedică, Bucureşti, 1979, p. 570.
[8] V. Marinoiu, "Metode numerice aplicate în industria chimică", Ed. Tehnică, Bucureşti, 1986.
[9] St. Dumitrescu, I. Dumitrescu and O. Pală, "Aplicaţii [illegible] cu exemple din industria petrolieră", Ed. Tehnică, Bucureşti, 1974, p. 230.

Revue Roumaine de Chimie, 34, 4, 1017–1028 (1989)

CROSSLINKING OF BROMINATED BUTYL RUBBER BY MEANS OF AROMATIC DIAMINES*

G. IVAN, ERIKA TAVARU, MARIA GIURGINCA and D. N. NICOLESCU
Research Institute for Rubber and Plastics Processing, R-79628 Bucharest, Romania

Received March 26, 1988

The interaction of brominated butyl rubber with aromatic diamines in mechanochemical degradation conditions has been studied. The present work containing data regarding the process rate, the reactivity of tested amines, the diamine consumption and the crosslinking degree reached puts into evidence the significant factors and parameters which influence the complex crosslinking-destruction process taking place in a binary system consisting of brominated butyl rubber and certain aromatic diamines, submitted to a high shearing stress.

It has been known since long that butyl rubber exhibits outstanding properties regarding its resistance to thermal, oxidant and ozonant degradation, as well as low gas permeability. Such intrinsic qualities have been substantially improved by halogenation, thus obtaining an increased cure rate and better compatibility with diene elastomers. Moreover, the halogenation of butyl rubber has allowed the use of various cure systems; one may use classical systems (i.e. resins, sulphur and accelerators), as well as aminoacids,[1,2] polyfunctional acids,[3] quaternary ammonium salts,[3] or difunctional amines.[4]

It has been noticed[4] that by curing halogenated butyl rubber with amines, crosslinked products with good mechanical and thermal properties (including resistance to oxygen or ozone) have resulted.

The present work brings new experimental facts concerning the cure of brominated butyl rubber by using primary and secondary aromatic diamines.

EXPERIMENTAL

The starting point of this work is the experimental finding that the reaction between brominated butyl rubber and aromatic diamines may be carried out faster at moderate temperatures (60 to 100°C) if the elastomer-amine system is submitted to a high shearing stress.

Tests have been carried out on Bromobutyl X2 (Polysar Ltd.), containing 2.1% bromine. The primary and secondary aromatic amines used as curing agents are symbolised as can be seen from Table 1.

---

* Paper presented at the Seminar "Progress in Polymer Processing", Bucharest, 1987.

Table 1

Tested amines used as crosslinking agents

Symbol	Formula
R1	N-isopropyl-N′-phenyl-*p*-phenylenediamine
R2	N,N′-diphenyl-*p*-phenylenediamine
R3	*p*-phenylenediamine
R4	*o*-phenylenediamine
R5	*m*-phenylenediamine

The crosslinking process has been run into a Brabender Pl 3 S type plastograph: the mixing chamber has been provided with N-50 type rotors, usually having 60 r.p.m. The temperature has ranged from 50 to 100°C and the mixing time did not exceed 50 minutes. Such conditions have been selected to favour mechano-chemical destruction.

After crosslinking, samples have been subjected to thermo-oxidative degradation in the range 150—170°C; the evolution of carbonyl/carboxyl groups has been put into evidence by infrared spectrometry (Perkin Elmer 577 apparatus).

RESULTS AND DISCUSSION

The reaction between halogenated rubber and diamine may be considered as a typical amine alkylation *via* an ionic mechanism. However, this assessment raises the problem of the noticed synergism between this ionic process, on one hand, and the radicalic mechano-chemical destruction of the polymer, on the other. Bearing in mind this fact, the tests have been carried out to find the meaningful factors which influence the curing phenomenon of brominated butyl rubber submitted to the mechano-chemical process, in the presence of difunctional amines.

1. Crosslinking During Mechanical Processing

Figure 1 illustrates three types of torque diagrams obtained during experiments; obviously, the curves represent the average value of torque.

Crosslinking has been put into evidence by a supplementary peak, noticed in the diagram torque *vs.* time.

The first peak (I in Figure 1), present in all these diagrams, is due to the increase of shear forces in the moment of closing the mixing chamber after feeding (ram descending produces an overpressure). The second and the third peaks (II, respectively III in Figure 1) have been assigned to the interaction between the polymer and diamine, the noticed viscosity increase being explained by crosslinking processes taking place in the system. It is important to notice the fact that the third peak does not appear for all tested diamines; this feature will be discussed further.

The hypothesis according to which the second and third maxima may be assigned to crosslinking processes is furthermore supported by the amplification, in these parts of diagram, of the recorded band width

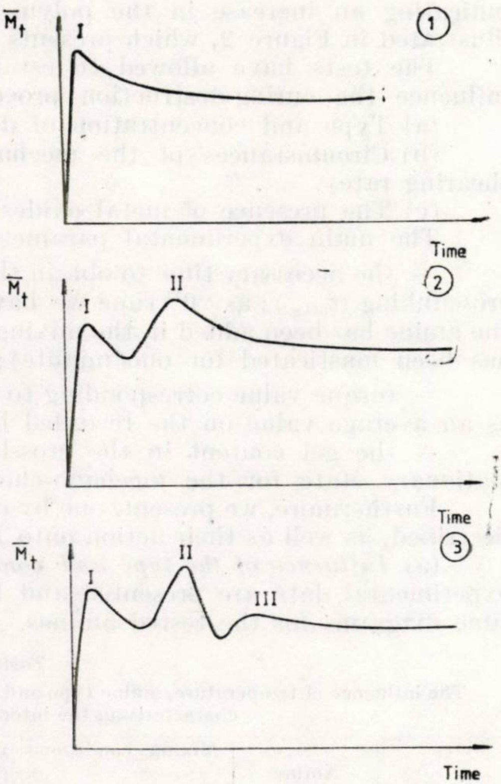

Fig. 1. — Typical experimental plottings for torque. 1 — mechano-chemical destruction ; 2, 3 — destruction-crosslinking.

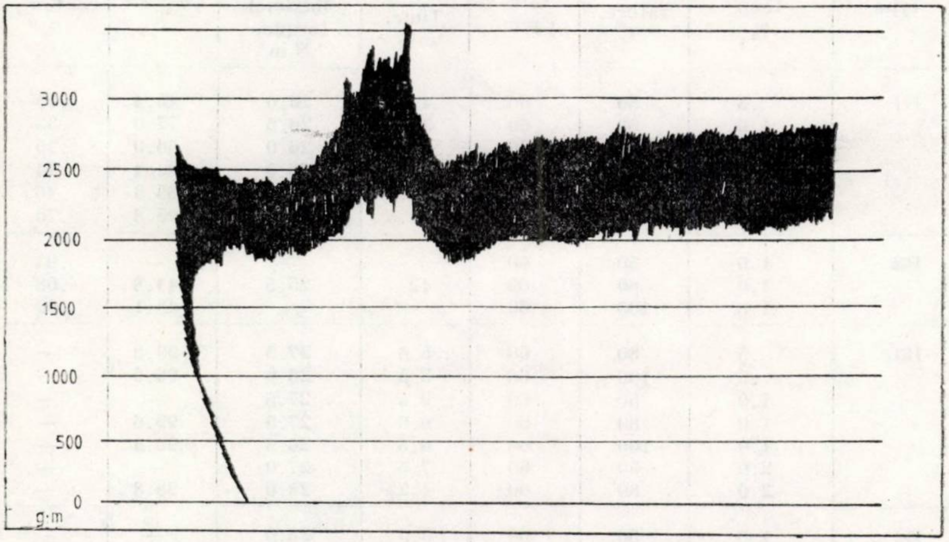

Fig. 2. — Diagram as recorded by plastograph for the sample of brominated butyl rubber containing 2% *p*-phenylenediamine, at 80°C and 60 r.p.m.

indicating an increase in the polymer elasticity; such a behaviour is illustrated in Figure 2, which presents a typical torque *vs.* time diagram.

The tests have allowed to establish the following factors which influence the curing-destruction process:

(a) Type and concentration of diamine

(b) Circumstances of the mechano-chemical process (temperature, shearing rate)

(c) The presence of metal oxides (i.e. ZnO, MgO)

The main experimental parameters are:

— the necessary time to obtain the peak corresponding to maximum crosslinking (t_{max}); as "0" time we have considered the moment in which the amine has been added in the mixing chamber (previously, the polymer has been masticated for one minute);

— torque value corresponding to the crosslinking maximum ($\overline{M}_{max}$), as an average value on the recorded band width;

— the gel content in the crosslinked product after reaching the stationary state for the mechano-chemical process.

Furthermore, we present, one by one, the specified factors previously described, as well as their action onto the process parameters.

(a) *Influence of the type and concentration of diamine.* In Table 2 experimental data are presented and Figure 3 illustrates the torque *vs.* time diagrams for the tested amines.

Table 2

The influence of temperature, amine type and concentration onto various parameters characterising the interaction with rubber

Amine type	Amine concentration, %	Mixing conditions		Main characteristics of Plastograph recordings		Gel content, %	Free amine content, %
		temperature, °C	rate, r.p.m.	Time, min	Maximal torque, N.m		
R1	.5	80	60	45	26.0	45.4	.15
	1.0	50	60	39	26.5	77.0	.33
	1.0	80	60	36	26.0	66.0	.35
	1.0	100	60	24	26.5	83.4	.24
	2.0	80	60	17.5	26.0	85.3	.46
	2.0	100	60	16.5	24.5	95.8	.70
R2	1.0	50	60	—	—	—	.63
	1.0	80	60	42	25.5	44.8	.58
	1.0	100	60	—	—	43.1	.60
R3	.5	80	60	5.0	27.5	99.0	—
	.5	100	60	5.5	26.0	96.6	—
	1.0	50	60	9.5	27.5	—	—
	1.0	80	60	6.0	27.5	99.6	—
	1.0	100	60	6.5	26.5	96.3	—
	2.0	50	60	7.5	27.0	—	—
	2.0	80	60	4.25	28.0	99.8	—
R4	1.0	50	60	5.0	28.0	—	—
	1.0	80	60	7.5	28.4	95.2	—
R5	1.0	80	60	10.5	25.5	99.0	—

Taking into account the necessary time to reach the maximal torque as an indication of amine reactivity, it results that, under the previously described conditions (80°C, 60 r.p.m., 1% of amine), the reactivity decreases in the order R3 > R4 > R5 > R1 > R2. This reactivity series indicates two effects, namely: the primary amines are more reactive than the secondary ones and the secondary amines with alkyl-aryl substituents present higher activity than the diaryl substituted ones.

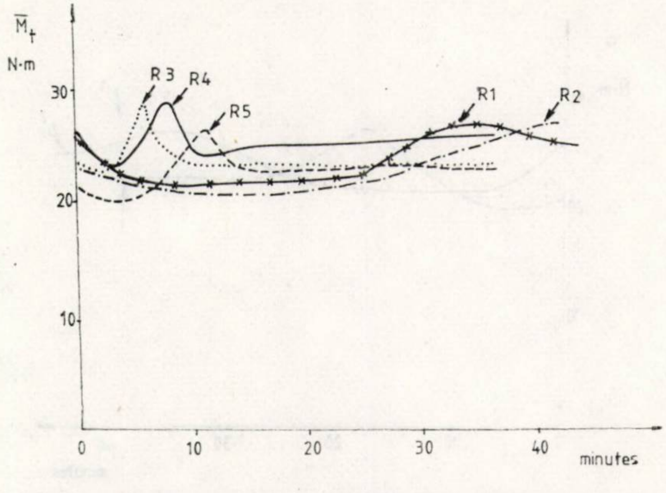

Fig. 3. — Torque values *vs.* time for the tested amines (80°C, 60 r.p.m.) (for the symbols see Table 1).

Among the primary diamines, at 80°C, the noticed order of reactivity has been para > ortho > meta, but, at the same time, at 50°C, the necessary time for reaching the maximal torque has been lower for *o*-phenylenediamine. This suggests that the observed crosslinking phenomenon is the result of two different crosslinking processes, one being thermal and the other mechano-chemical; obviously, the two processes take place simultaneously, but at different rates.

By considering the values for the maximal torque, it may be noticed that amines R3 and R4 lead to a similar crosslinking degree, but somewhat higher than that obtained for the other tested amines.

In order to express in a quantitative way the crosslinking degree, we have measured the gel content of samples at the end of the experiment (after reaching the stationary state in the crosslinking — mechano-chemical destruction process). Taking into account the values presented in Table 2, one may notice the high degree of crosslinking reached by using primary phenylenediamines; the network formation is more advanced by using alkyl-aryl — disubstituted diamines, than by using only a diaryl disubstituted *p*-phenylenediamine.

For samples crosslinked with R1 and R2, the free amine content has been measured as well. It has been found that R1 has reacted in a higher amount with the polymer, thus it may be considered more reactive than R2. However, this indication cannot be correlated with the crosslinking degree, taking into account the fact that diamines may be bound to polymer *via* only one functional group, leading to bound antioxidant.[5]

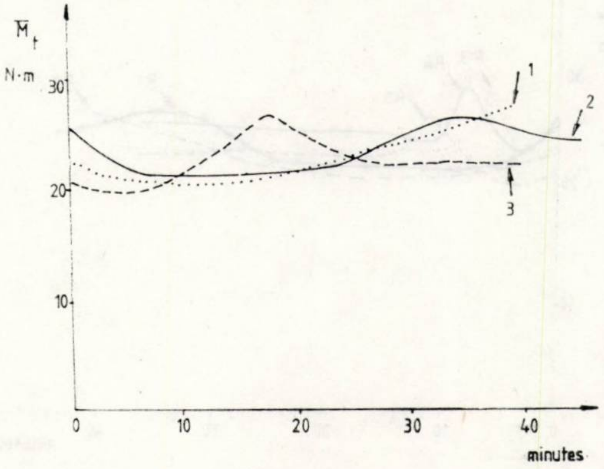

Fig. 4. — The influence of N-isopropyl-N'-phenyl-*p*-phenylenediamine concentration on the crosslinking process (80°C, 60 r.p.m.). 1 — 0.5%; 2 — 1%; 3 — 2%.

The experimental data show that the reactivity of amines towards rubber follows the same order as their corresponding basicity constants: for instance, the values pK_a for the first ionization step are: 2.1 (R1); 2.02 (R2); 6.10 (R3);[6] 4.58 (R4); 4.90 (R5).[7]

The influence of amine concentration upon the interaction with rubber has been put into evidence in the case of *p*-phenylenediamine (R3) and for its alkyl-aryl-substituted derivative. Figure 4 presents the curve corresponding to torque value as a function of time for crosslinking by means of R1 amine.

It may be noticed that, by increasing the amine content, the crosslinking becomes more rapid and, in turn, the final crosslinking degree (expressed by the content of the processed material — see Table 2) increases as well.

On the other hand, in the case of *p*-phenylenediamine, the concentration of crosslinking agent does not change neither the process rate, nor the crosslinking degree in any significant amount, as presented in Figure 5.

For the case of amine R3, in all experiments, higher crosslinking have been obtained; the measurements carried out at 80°C have exhibited a quite complete crosslinking (the gel content higher than 99%), but at 100°C a rather low value for the gel content (around 96%) has been obtained. Such a behaviour may be justified by a reduced efficiency of the mechano-chemical process, due to the change of rheological properties, as a result of temperature increase.

(b) *Influence of the circumstances of the mechano-chemical process.* It may be said that temperature represents a main factor affecting in different ways the process. From the point of view of chemical crosslinking, a higher temperature is, obviously, favourable; as it may be expected, this fact is put into evidence by the diminishing time to reach the structuration maximum for amines R1 and R2, possessing reduced chemical reactivity (see Table 2).

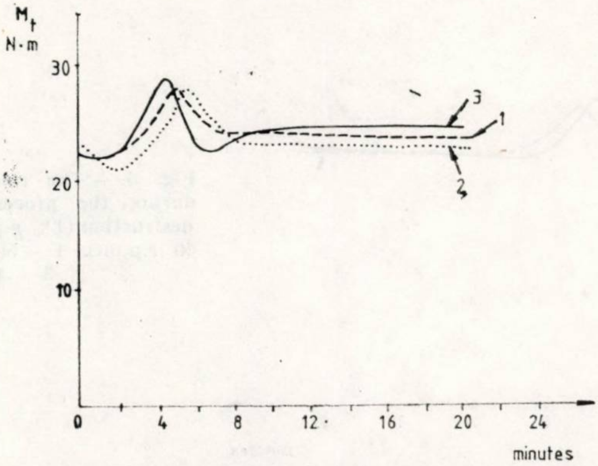

Fig. 5. — Torque *vs.* time, at different concentrations of *p*-phenylene-diamine (80°C, 60 r.p.m.). 1 — 0.5%; 2 — 1%; 3 — 2%.

When using amines with higher reactivity (R3 and R4), the chemical reaction between rubber and amine has a higher rate and, consequently, the influence of temperature upon reaction rate is buffered by the effect of reducing the efficiency of mechano-chemical process as a result of temperature increase; finally, the second effect becoming preponderant, a certain delay of crosslinking may be noticed as the temperature increases (see Figure 5, Table 2).

Table 3

The influence of shearing rate in the process of crosslinking, using 1% *p*-phenylenediamine

Mixing conditions		Main characteristics of Plastograph recordings	
Temperature °C	Rate r.p.m.	Time min	Maximal torque, N·m
50	40	12.5	27.5
50	60	9.5	27.5
50	80	6.0	28.4
50	100	2.75	28.0

This hypothesis regarding the role of temperature is sustained by the values obtained for the gel content.

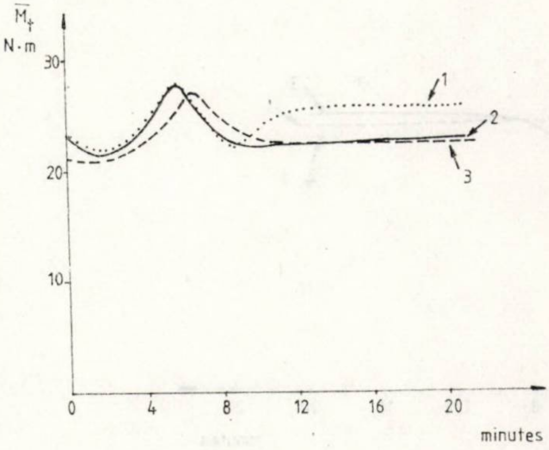

Fig. 6. — The role of temperature during the process crosslinking — destruction (1% *p*-phenylenediamine, 60 r.p.m.). 1 — 50°C; 2—80°C; 3 — 100°C

The data presented in Table 3 have put into evidence the effect of shearing rate for the crosslinking of brominated butyl rubber with 1% R3 in conditions favourable to mechano-chemical destruction.

Although no proportionality between shearing rate and reaction rate has been found, an increase in the crosslinking degree as the shearing rate increases has been noticed, likely based on a higher concentration of mechano-chemical generated free radicals.

(c) *The effect of metal oxides*. As it is known since long, some metal oxides may produce by themselves the crosslinking of halogenated rubbers. Accordingly, the interaction between aromatic diamines and brominated butyl rubber in the presence of zinc and magnesium oxides has been studied as well.

The data presented in Table 4 allow the remark that addition o selected metal oxides accelerates crosslinking and a clear synergistic effect between tested amine (R3) and zinc or magnesium oxides respectively, is present. Moreover, by adding magnesium oxide, besides the reducing of the necessary time for reaching the crosslinking maximum, a higher torque corresponding to the crosslinking maximum has been noticed as well, thus providing a higher crosslinking density. However, using the previously described conditions, ZnO and MgO did not induce the polymer crosslinking in the absence of amines.

The increase of the R3 content from 1 to 2%, keeping a constant amount of metal oxides, has produced a further time shortening for reaching the crosslinking maximum; this fact is more obvious in the case of zinc oxide.

Table 4

The influence of adding ZnO and MgO on the crosslinking process with *p*-phenylenediamine, at 50°C and 60 r.p.m.

Amine %	ZnO %	MgO %	Main characteristics of Plastograph recordings	
			Time, min	Maximal torque, N.m
—	3	—	—	—
—	—	3	—	—
1	—	—	9.5	27.5
1	3	—	5.5	27.5
1	—	3	4.8	28.4
2	—	—	7.5	27.0
2	3	—	4.0	26.5
2	—	3	4.5	28.4

2. Behaviour of Amine Modified Brominated Butyl Rubber During Thermo-oxidative Ageing

Starting from the presumption that in the crosslinked system there are units containing bound antioxidant, tests regarding the behaviour to thermo-oxidative ageing have been carried out, at temperatures in the range 150 — 170°C. Tests have been run on polymer films, pure or containing amine; the samples have been put on KBr windows. The films containing amine have been crosslinked in oven at 185°C during 15 minutes; the pure rubber films have been submitted to the same treatment. Subsequently, the films have been submitted to thermo-oxidative destruction at 150 and 165°C, respectively, examining the growth of oxygenated groups CO/COOH type, by means of infrared spectrometry, measuring the classical peak at 1720 cm^{-1} in time.

The plottings of extinction at 1720 cm^{-1} *vs.* time were used to obtain the data presented in Table 5, concerning the induction and propagation steps characteristic of the degradation process.

Table 5

Kinetical data regarding the thermo-oxidative degradation of crosslinked samples

Amine	Induction time, h		Propagation time, h		Reaction rate constant, min^{-1}		Activation energy, kJ/mole
	150°C	165°C	150°C	165°C	150°C	165°C	
None	5.8	2.3	6.0	2.7	.005	.023	160.3
R1	12.5	2.5	10.5	2.5	.0054	.023	152.0
R2	37.0	8.0	10.0	2.0	.0014	.0024	57.0
R3	8.8	7.2	2.6	2.4	.004	.017	150.0
6PPD*	20.0	5.2	11.0	1.8	.0029	.01	124.0

* N-1,3-dimethylbutyl-N′-phenyl-*p*-phenylenediamine

Taking into account the induction step, a high protecting efficiency may be noticed for the diamine R2, at both temperatures. During the propagation step at 150°C, diamines such as R1, R2 or N-dimethylbutyl-N′-phenyl-*p*-phenylenediamine exhibit high efficiency as well; such a superior protecting capability should be explained by the formation, during thermo-oxidative process, of the corresponding quinoneimine structures which possess antioxidant efficiency, as already observed [8,9] for ungrafted N,N′-disubstituted-*p*-phenylenediamines.

In all tests the same order of magnitude for reaction rate constants and, consequently, for the activation energy, has been found. For the brominated butyl rubber modified by amine R2, the activation energy is somewhat diminished with regard to the other amines; it is interesting to notice that this value (57 kJ/mole) is close to that obtained for the oxidation of the binary system isoprene rubber – R2 (83.7 kJ/mole) as found by us.[10,11]

The accumulated data suggest that in the process studied, there are several distinct phenomena: the polymer is modified by interaction with difunctional amines, as well as by mechano-chemical destruction. Taking as "zero time" the moment at which the amine is introduced over the previously plastified rubber, we presume the following stages:

a. In the first stage, the mechano-chemical destruction takes place mainly; accordingly, the molecular mass decreases and, in turn, this fact is reflected by the decrease in the torque value.

b. The second stage corresponds to an increase in the torque value due to the augmentation of the molecular mass, as a result of the reactions produced by free radicals generated *via* the mechano-chemical process, as well as from reactions involving diamines. This increase in the molecular mass may be, for instance, the result of rebonding of two macroradicals by a diamine molecule. In parallel, the macroradicals present in the system may be stabilized by extracting a bromine atom from the neighbouring chain. Such a supposition is justified taking into account, on one hand, the bond strengths (65 kcal/mole for C—Br and 98 kcal/mole for C—H respectively [12]) and, on the other, the fact that the bromine atom is placed in an allyl position.[14] The resulting macroradicals, containing radical centers alongside the chain, lead, by reacting with amine, to tridimensional structures:

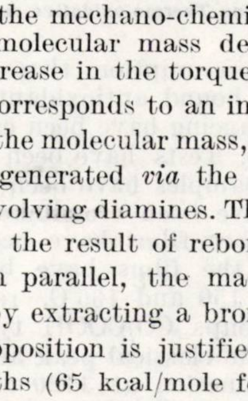

(1)

Amine alkylation may be considered as another process leading to crosslinked structures as well, accompanied by elimination of HBr. This fact has been confirmed by the presence of bromine in the alcoholic extract of crosslinked samples.

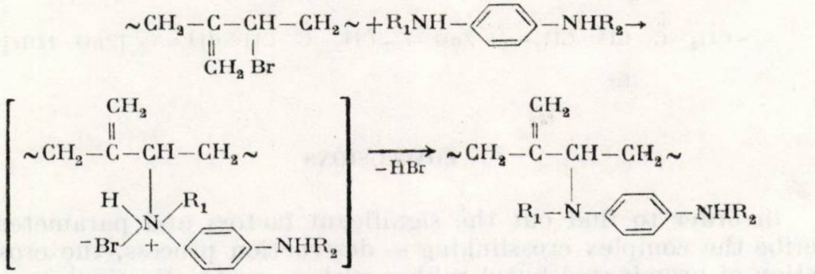

(2)

If a similar reaction takes place to the second amine group, this will lead to the above-mentioned structure (1).

c. The molecular weight increase on the basis of the previously discussed reactions is limited. During processing, the mechano-chemical destruction becomes preponderant as the viscosity increases and the amine is consumed. The equilibrium point between these contrary effects is the second maximum which may be noticed in the curves presented in Figure 1.

The mechano-chemical degradation takes place rapidly until reaching a stationary state that, in turn, appears in the diagrams for torque value as a plateau towards a minimal torque.

When using primary amines at rather high concentrations (1 or 2%), a third maximum may be noticed, however, not a clear-cut one.

Taking into account that the minimum torque value recorded between the second and the third maxima, respectively, is lower than the final value (characterising the process after reaching the stationary state), the third maximum should be assigned to a rapid mechano-chemical degradation of the network with a high crosslinking density accompanied by a decrease of the molecular mass under the critical value for destruction.

At the same time, another plausible explanation for the lower torque value between the second and the third maxima, with regard to that corresponding to the final stationary state may be given. Thus, the literature [13] points out that the critical molecular mass reached by mechano-chemical degradation decreases as the initial molecular mass increases. Accordingly, after reaching a second maximum, the molecular mass decreases by degradation, thus reaching a reduced critical value; subsequently, in the stationary state reached at a certain time, on the basis of the remnant free amine, as well as of single bound diamine molecules, the molecular mass would again increase, reproducing (this time with reduced magnitude) the previous crosslinking process until the mechano-chemical destruction would again limit the molecular weight to a value, this time higher than that reached after the second maximum. This last explanation is also supported by the experimental fact that we have obtained diagrams containing three maxima only when using primary diamines (the most reactive ones) at high concentrations.

The presence of metal oxides exhibits an accelerating effect on the reaction between rubber and amine, likely by forming a complex of conjugated double bonds[4]:

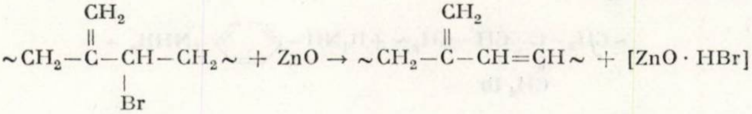

$$\sim CH_2-\overset{\overset{CH_2}{\|}}{C}-\underset{\underset{Br}{|}}{CH}-CH_2\sim + ZnO \rightarrow \sim CH_2-\overset{\overset{CH_2}{\|}}{C}-CH=CH\sim + [ZnO\cdot HBr] \qquad (3)$$

CONCLUSIONS

In order to find out the significant factors and parameters which describe the complex crosslinking – destruction process, the crosslinking reaction of brominated butyl rubber with aromatic diamines in mechanochemical degradation conditions has been studied.

The accumulated data regarding the process rate, the reactivity of tested amines, the diamine consumption and the crosslinking degree make us expect possible practical implications. For instance, the way we have led the experiments allows us to evaluate the scorch tendency for compounds based on brominated butyl rubber containing amines as protecting agents.

Taking into account that the bound amines keep their antioxidant effect after crosslinking, it results that the process of curing with diamines confers a long time protection, due to an obvious reducing of losses in antioxidant by extraction or by evaporation.

REFERENCES

[1] Masao Onizawa, *Patent F.R. Germany* 2, 548, 516, 1976.

[2] E. J. Buckler, G. Feniak, *Patent F. R. Germany* 2, 452, 915, 1975.

[3] R. E. Morris, *Patent F. R. Germany* 2, 506, 251, 1975.

[4] D. C. Edwards, *Elastomerics*, **118**, no. 4 (1986).

[5] M. E. Cain, K. F. Gazeley, I. R. Gelling, P. M. Lewis, *Rubber Chem. Technol.*, **45**, 204, (1972).

[6] F. M. Albert, M. Giurginca, A. Meghea, G. Ivan, *Revue Roumaine Chimie*, **25**, 1543 (1980).

[7] P. K. Gallagher, *J. Phys. Chem.*, **67**, 807 (1963).

[8] J. Tsurugi, S. Murakami, K. Goda, *Rubber Chem. Technol.*, **44**, 857 (1971).

[9] F. M. Albert, M. Giurginca, *Ind. Uşoară*, **27**, 347 (1980).

[0] M. Giurginca, *Ind. Uşoară*, **28**, 543 (1981).

[11] M. Giurginca, E. Tudor, G. Ivan, *Ind. Uşoară*, **29**, 67 (1982).

[12] C. D. Neniţescu, "Chimie Organică" vol. I, 7th edition, Editura Didactică şi Pedagogică Bucharest.

[13] C. Simionescu, C. Vasiliu Oprea, "Mecanochimia compuşilor macromoleculari", Editura Academiei, Bucharest, 1967.

[14] Chia Yeh Chu, K. N. Watson, R. Vukov, *Rubber Chem. Technol.*, **60**, 636 (1987).

Revue Roumaine de Chimie, **34**, *4*, 1029 – 1035 (1989)

NEW COBALT CHELATES WITH ETHYLENEDIIMINO-BIS-BENZOYLACETONE

GH. MARCU, CS. VÁRHELYI, J. FÜLÖP and DANA ITUL
Faculty of Chemical Technology, University of Cluj-Napoca, Romania

Received October 10, 1988

A number of 20 new complex salts of the type [Co(benzec) $(NH_3)_2$]X and [Co(benzec) $(\text{imidazole})_2$]X and the nonelectrolyte : Co(benzec) (benzec · H_2 — ethylenediimino-bis-benzoylacetone were obtained and characterized by IR and UV spectra. The thermal decomposition of some new compounds was followed by means of derivatographic measurements.

INTRODUCTION

The 1,2- and 1,3-aliphatic diamines (ethylenediamine (en), 1,2- and 1,3-propanediamine (pn) form easily bis Schiff's bases with α-substituted aromatic and heterocyclic hydrooxyaldehydes (e.g. salicylaldehyde, pyridin-2-aldehyde), ketones (e.g. *o*-amino-acetophenone, *o*-amino-benzophenone, β-diketones, mono- and dithio-β-diketones. These tetradentate chelating agents can be used for the synthesis of various types of complexes [1–3] and for the analytical determination of some transition metals.[4]

The first derivative with β-diketones : the ethylene-diimino-bis-acetylacetone (ec. H_2) was described by Combes.[5]

Mixed chelates of cobalt(III) with ammonia : $[Co(ec)(NH_3)_2]^+$ were obtained by Morgan and Smith.[6] In the previous papers [7–11] a series of new chelates of the type $[Co(ec)(amine)_2]^+$ (amine-aromatic and heterocyclic amines) and $[Co(ec)(H_2O)(Ar_3P)]^+$ were obtained and characterized.

RESULTS AND DISCUSSION

As a sequel to these investigations instead of acetylacetone, benzoylacetone was used for the synthesis of bis-Schiff's bases. It was noticed that ethylenediamine reacts easily with this aromatic β-diketone. The enolic form (I) of the obtained ethylenediimino-bis-benzoylacetone (benzec · H_2) is a tetradentate chelating agent. By complexing with M(II) and M(III) transition metal ions three heterocyclic rings are formed (II).

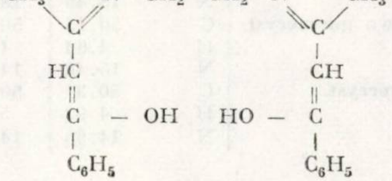

(I.)

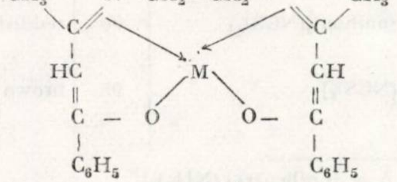

(II.)

We observed that by the interaction of some divalent transition metals (Co, Pd, Pt) with ethylenediimino-bis-benzoylacetone complexes of the M(benzec) type result, similarly as in the case of ethylenediimino-bis-acetylacetone (ec · H_2) : M(ec).

From these non electrolytic complexes the cobalt(II) derivative: Co(benzec) can be oxidized easily with perhydrol to mixed electrolytic chelates of cobalt(III) in the presence of amines, phosphines and arsines. *E.g.*

$$2Co^{2+} + 2\text{benzec} \cdot H_2 + 4\text{ amine} + 1/2O_2 = 2[Co(\text{benzec})(\text{amine})_2]^+ + HO_2 + 2H^+$$

In this paper 2 new chelate cations: $[Co(\text{benzec})(NH_3)_2]^+$ and $[Co(\text{benzec})(\text{imidazole})_2]^+$ were characterized by isolation of 20 salts, by means of double decomposition reactions from the alcoholic solutions of the acetates with alkaline salts of halides, pseudohalides, organic acids, complex acids of Co(III) and Cr(III).

The new complex salts obtained are characterized in tables 1 and 2.

Table 1

New complex salts of the $[Co(\text{benzec})(NH_3)_2]X$ type

Formula	Yield (%)	Appearance	Analysis		
				Calcd.	Found
A · Cl	65	short orange prisms	Co	12.41	12.30
			NH_3	7.17	7.35
A · Br	75	sparkling gold yellow needles	Co	11.35	11.10
			NH_3	6.56	6.77
A · I	85	yellow desks	Co	10.41	10.50
			NH_3	6.02	6.13
A · NO_3	60	gold-yellow thin long plates	Co	11.75	11.80
			NH_3	6.80	6.75
A · ClO_4	90	organe-yellow microcryst.	Co	10.94	11.05
			NH_3	6.32	6.43
A · NCS	60	orange prisms	Co	11.85	11.67
			S	6.45	6.60
$A_2 \cdot S_3O_6$	70	light yellow microcryst.	Co	11.01	10.81
			S	8.98	9.10
$A_2 \cdot S_2O_8$	75	light yellow microcryst.	Co	11.00	10.90
			S	5.99	5.77
$A_2 \cdot S_2O_6$	65	orange, long thin needles	Co	11.35	11.15
			S	6.18	6.02
A · picrate	95	lemon yellow irregular cryst.	Co	8.83	8.60
			N	14.69	14.90
A · $[Co(NH_3)_2(NO_2)_4]$	85	light-brown irregular cryst. aggregates	Co	16.45	16.58
			N	19.55	19.34
A · $[Cr(NH_3)_2(NCS)_4]$	95	reddish-brown microcryst.	C	41.20	40.80
			H	4.52	4.34
			N	18.49	18.80
A · $[Cr(\text{anilina})_2(NCS)_4]$	90	reddish-brown microcryst.	C	50.15	50.40
			H	4.64	4.33
			N	15.40	14.95
$A_3 \cdot Cr(NCS)_6]$	95	brown microcryst.	C	50.31	50.86
			H	4.93	5.10
			N	14.65	14.33

A = $[Co(\text{benzec})(NH_3)_2]^+$

Table 2

New complex salts of the [Co(benzec) (imidazole)$_2$]X type

Formula	Yield (%)	Appearance	Analysis		
				Calcd.	Found
B · I	30	reddish-brown microcryst.	Co	8.82	8.66
			N	12.57	12.35
B · ClO_4	30	light-brown microcryst.	Co	9.20	9.40
			N	13.11	12.86
B · picrate	75	yellow-brown microcryst.	Co	7.66	7.90
			N	16.38	16.14
B · $[Co(NH_3)_2(NO_2)_4]$	60	light-brown irreg. prisms	Co	14.40	14.30
			N	20.54	20.37
B · $[Cr(NH_3)_2(NCS)_4]$	75	reddish-brown microcryst.	C	44.69	44.10
			H	4.22	3.97
			N	19.55	19.93
B · [Cr(aniline)$_2$(NCS)$_4$]	80	reddish brown microcryst.	C	52.21	51.48
			H	4.38	4.29
			N	16.61	16.19

B = [Co(benzec) (imidazole)$_2$]$^+$

As compared to the analogous ethylenediimino-bis-acetylacetone derivatives ([Co(ec)(amine)$_2$]X), the [Co(benzec)(amine)$_2$]X salts are sparingly soluble in water and methanol, insoluble in benzene or ether. The solubility decreases in the order X : Cl > Br > I > ClO_4. The derivatives of the Reinecke-salt ($K[Cr(NCS_4)(NH_3)_2]$) and analogous compounds (amine · H[Cr(NCS)$_4$(amine)$_2$]) are insoluble in aqueous media and soluble in acetone, dimethylsulfoxide and dimethylformamide.

The geometric structure of these chelate cations corresponds to four asymmetric, optically active *cis* isomers and to one symmetric *trans* modification (Fig. 1).

The latter is probably the most stable geometric form from the thermodynamic point of view. The other isomers turn into the *trans* modification on standing. This geometric rearrangement was mentioned by Morgan and Smith[6] in connection with the analogous [Co(ec)(NH$_3$)$_2$]$^+$ derivatives.

The high stability of the *trans* isomer in the case of [Co(benzec) (amine)$_2$]$^+$ complexes is due to the very largely delocalized π-bond system, comprising 23 atoms in the equatorial plane of the complex. The same

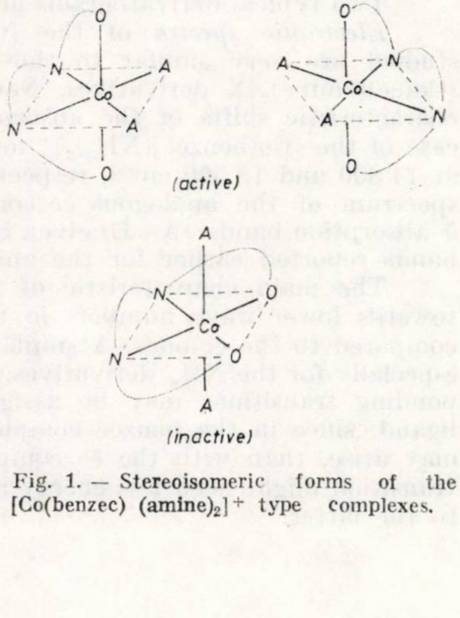

Fig. 1. — Stereoisomeric forms of the [Co(benzec) (amine)$_2$]$^+$ type complexes.

plane contains also 12 hydrogen atoms and 4 carbon atoms with sp^3 hybridization. Thus, from the 49 atoms indicated in formula below, only 10 hydrogen atoms are situated out of the plane. In the case of the optically active isomers, due to the lack of coplanarity, there are two delocalized π-bond systems, comprising only 12 atoms each.

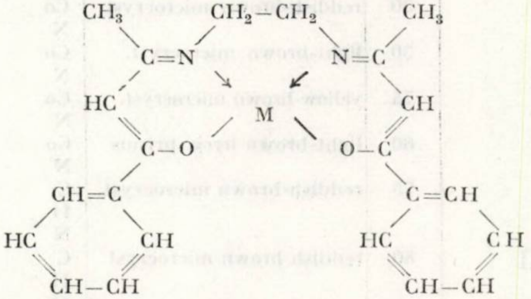

The thermal stability of some $[Co(benzec)(amine)_2]X$ type complexes and that of Co(benzec) was studied by means of derivatographic measurements. The complicated thermal degradation process begins at 140—60°C in the case of the $[Co(benzec)(amine)_2]X$ derivatives as a function of the nature of the amine component and of the external anion. The pyrolysis process in air atmosphere takes place with evolution of free amines, N_2, CO, CO_2 and other decomposition and oxidation products in non stoichiometrical ratios, the final product at 800—850° being Co_3O_4, or in some cases $Co_3O_4 + CoX_2$, $Co_3O_4 + Cr_2O_3$. This means an analogou behaviour, as in the case of [the $Co(ec)(amine)_2]X$ type complexes, the latter having a higher thermal stability. The exo- and endothermal peaks in a temperature range of 150—550° show these complicated decomposition and oxidation processes.

The Co(benzec) nonelectrolyte decomposes at higher temperature: 260—270°, the pyrolysis end product being Co_3O_4.

Two typical derivatograms are presented in Figs. 2 and 3.

Electronic spectra of the $[Co(benzec)(amine)_2]X$ type complexes studied are very similar to those reported earlier for the analogous $[Co(ec)(amine)_2]X$ derivatives. Nevertheless, some little differences and characteristic shifts of the absorption bands may be observed. In the case of the $[Co(benzec)(NH_3)_2]^+$ ion two weak crystal field bands appear at 14 800 and 18 500 cm^{-1}, respectively, which were not observed in the spectrum of the analogous *ec* complex. Both complexes studied have 5 absorption bands (A—E) given in table 3, together with the absorption bands reported earlier for the analogous *ec* complexes.

The main characteristic of these spectra is the shift of band A towards lower wave numbers in the case of the benzec derivatives. as compared to the ec-ones. A similar effect is observed also with band B, especially for the NH_3 derivatives. This suggests the idea that the corresponding transitions may be assigned to the co-ordinated tetradentate ligand, since in the benzec complex a larger delocalized π-bond system may arise, than with the ec complex and in such conditions a $\pi - \pi^*$ transition might need less energy in the case of the former, as compared to the latter.

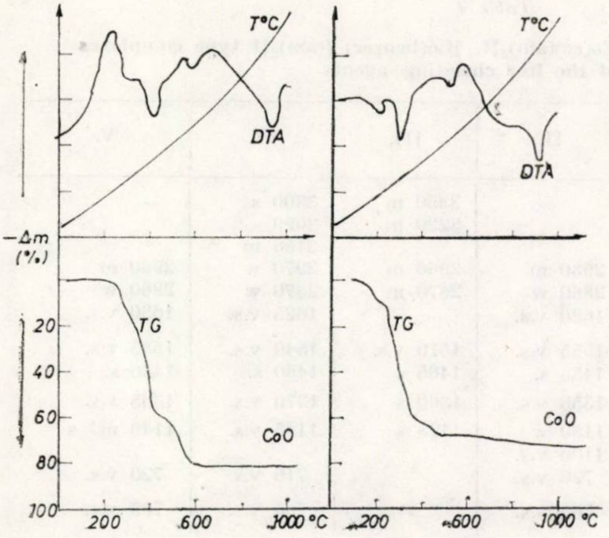

Fig. 2. — Derivatograms of — [Co benzec)] ; — [Co-(benzec) $(NH_3)_2$] I.

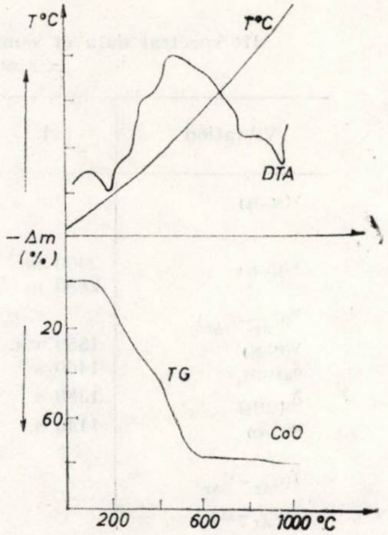

Fig. 3. — Derivatogram of — Co(benzec) $(imidazole)_2$]I.

The shifts of bond C are not relevant, since they were observed in opposite direction in the case of the two amine ligands. Both band D and E seem to be shifted towards higher wave numbers in the case of the benzec complexes as compared to the ec ones.

Table 3

Wave numbers (in cm^{-1}) of the absorption bands of some [Co X$(amine)_2$] Y type complexes

X	amine	Y	band				
			A	B	C	D	E
benzec	NH_3	I	21 800	27 300	34 000	43 500	49 300
	imidazole	acetate	19 700	29 500	36 200	40 200	47 800
ec	NH_3	ClO_4	24 600	29 900	37 400	42 500	45 800
	imidazole	I	23 700	29 600	34 500	38 600	45 200

The influence of the amine ligand appears in the clearest way with band D, having lower values in the case of imidazole, as compared to ammonia. This might be due to the possibility of imidazole to give π-bonds with the cobalt atom.

The infrared spectra of benzec·H_2, Co(benzec) and [Co(benzec)-$(amine)_2$]X have been recorded in kalium bromide pellets. Some IR spectral data are presented in table 4.

Table 4

IR spectral data of some $[Co(ec)(am)_2]I$, $[Co(benzec)\ ((am)_2]I$ type complexes and of the free chelating agents

Vibration	I.	II.	III.	IV.	V.
$\nu_{(N-H)}$	—	—	3350 m 3220 m	3300 s 3090– 3150 m	—
$\nu_{(C-H)}$	2960 m 2880 m	2980 m 2860 w	2960 m 2870 m	2970 w 2870 w	2980 m 2960 w
$\nu_{(C_{Ar}-C_{Ar})}$	—	1620 v.s.	—	1625 v.s.	1630 v.s.
$\nu_{(C-N)}$	1550 v.s.	1555 v.s.	1510 v.s.	1540 v.s.	1535 v.s.
$\delta_{as(CH_3)}$	1460 s	1455 s.	1465 s	1460 s.	1460 s.
$\delta_{s(CH_2)}$	1380 s	1355 v.s.	1360 s	1370 v.s.	1365 v.s.
$\nu_{(C-O)}$	1145 s	1180 w 1100 v.s.	1125 s	1145 v.s.	1140 m–s
$\gamma_{(C_{Ar}-C_{Ar})}$	—	720 v.s.	—	710 v.s.	720 v.s.
$\gamma_{(C_{Ar}-H)}$	—	765 v.s.	—	765 v.s.	765 v.s.

I. $ec.H_2$; II. $benzec \cdot H_2$; III. $[Co(ec)(NH_3)_2]I$; IV. $[Co(benzec)\ (NH_3)_2]\ I$ V. [Co (benzec) $(imidazole)_2]\ I$.

The most important frequencies of the free $benzec \cdot H_2$: $\nu_{C=N}$ and ν_{C-O} (of the enolic form) are shifted towards lower wave number values by chelation. The shifts observed indicate strong Co—N and Co—O covalent bonds. As compared to the spectra of the analogous acetylacetone derivatives, these shifts are slightly smaller (10—15 cm^{-1}) indicating an increase of the strength of the Co—N and Co—O covalent bonds in the order

$$Co(benzec) < Co(ec)$$

This might be due to the electron withdrawing effect of the phenyl groups, explaining also the lower thermal stability, mentioned above.

The ν_{N-H} stretching vibration bands of the ammonia derivative appear at 3300 and 3120 cm^{-1} shifted with 200—250 cm^{-1} towards lower frequencies against the free, noncoordinated ammonia, showing strong covalent $Co-NH_3$ bonds through the N-atom.

EXPERIMENTAL

Ethylenediimino-bis-benzoylacetone ($benzec \cdot H_2$) was obtained by refluxing benzoylacetone and ethylendiamine (molar ratio : 2 : 1) in methanol. Silky, irregular needles. M.p. 140 °C Co-(benzec). 0.1 mole cobalt acetate ($Co(CH_3-COO)_2 \cdot 4\,H_2O$) in 100 mL water and 0.1 mole $benzec \cdot H_2$ in 500 mL methanol were refluxed on a water bath for 30—40 minutes. The separated crystalline product is filtered off, washed with water and dried on air. Brilliant scarlet red needles.

Analysis :	calcd.	Co 14.41,	N 6.85,
$(Co(C_{22}H_{22}N_2O_2)$		(mol. wt. 408.9)	
	found	Co 14.42	, N 6.90

$[Co(benzec)\ (amine)_2]$ — acetate solution

The suspension of 50 mmoles of Co(benzec) with 5 g sodium acetate was treated in 400 mL methanol with 10 mL 20 NH_3, and with 120—140 mmoles of imidazole, respectively. The mixture was oxidized with 10—12 mL 30% H_2O_2 drop by drop under refluxing conditions. The scarlet red Co(benzec) dissolves slowly and dark brown Co(benzec) $(amine)_2$ acetate solutions are formed. After cooling the solutions were filtered off and used for double decomposition reactions.

[Co(benzec) (amine)2]X complex salts. 10 mmoles of [Co(benzec) $(amine)_2$]-acetate in 100 mL alcoholic solutions were treated with an excess of 2 — 10 % NaBr, KI, $NaNO_3$, $NaClO_4$, picric acid, $NH_4[Co(NH_3)_2(NO_2)_4]$, $H[Co(DH)_2X_2]$ (X = CN, NCS), $NH_4[Cr(NCS)_4(amine)_2]$, $K_3[Cr(NCS)_6]$, etc.

The obtained cryst. products were filtered off after 15—45 min standing, washed with dil. methanol and dried on air.

Analysis. The cobalt content of the samples was determined complexometrically after destruction of 80—100 mg substances with hot sulfuric acid and some crystals of KNO_3. After dilution with water the residue was neutralized with sodium acetate. The N content was determined by the usual microanalytical method.

The electronic spectra were recorded in methanol with a Specord recording spectrophotometer (Carl Zeiss Jena). Conc. $1-1.5\times10^{-3}$ mole/L (in visible) and $2\times10^{-5}-10^{-4}$mole/L in UV.

The IR spectra were recorded in kalium bromide pellets with a UR 20 spectrophotometer (Carl Zeiss Jena).

The thermal measurements were carried out with a Derivatograph (MOM — Budapest). Sample weight 100 mg, heating rate 10°/min.

REFERENCES

[1] R. H. Bailes and M. Calvin, *J. Amer. Chem. Soc.*, **69,** 1886 (1947).

[2] L. Sacconi, P. Nanneli and U. Campigli, *Inorg. Chem.*, **4,** 818, 984 (1965); **5,** 606, 1520 (1966).

[3] E. Uhlemann et al., *Z. anorg. Chem.*, **342,** 41 (1966); **353,** 26 (1967); **356,** 71 (1967); **364,** 153 (1969); **386,** 328 (1971); **393,** 215 (1972); **402,** 273 (1973); **470,** 177 (1980).

[4] E. Uhlemann et al., *Anal. chim. Acta*, **48,** 115 (1969); **63,** 236 (1973), **69,** 79 (1974); **116,** 153, 403 (1980).

[5] A. Combes, *Compt rend.*, **108,** 1252 (1889).

[6] G. T. Morgan and D. M. Smith, *J. Chem. Soc.*, **125,** 1996 (1924); **127,** 2030 (1925).

[7] G. Marcu, Cs. Várhelyi and I. Müller, *Rev. Roumaine Chim.*, **17,** 711 (1972).

[8] G. Marcu, Cs. Várhelyi and I. Müller, *Stud. Univ. Babeș Bolyai, Chem.*, **19,** (2), 13 (1974).

[9] M. Abdel Salam El Absy, G. Marcu, J. Zsakó and Cs. Várhelyi, *Rev. Roumaine Chim.*, **27,** 919 (1982).

[10] G. Marcu, Cs. Várhelyi, M. Abdel Salam El Absy and A. Hantz, Acad. RSR, Memoriile Secţiilor Ştiinţ. Ser. IV, **IV,** (2), 45 (1981).

[11] Cs. Várhelyi and I. Gănescu, *Monatsh.*, **109,** 83 (1978).

[12] K. Ueno and A. E. Martell, *J. physik. Chem.*, **59,** 998 (1955); **60,** 1270 (1956).

Revue Roumaine de Chimie, 34, 4, 1037—1046 (1989)

BEITRÄGE ZUM AUFBEWAHREN DER CHEMISCHEN FAHRWEISE IM KÜHLKREISLAUF

L. NEGULESCU

ICPEAR — Institut für Forschung und Projektierung der Abwasseraufbereitung,
Şos. Panduri 90—92, Bukarest, Rumänien

Eingegangen am 20. August 1988

In dieser Arbeit wird die Modalität zum Vorgreifen der chemischen Fahrweise in einem mit Rezirkulation vorgesehen Kühlungssystem gezeigt. Nachdem die für jeden Kühlturm gültigen Massengleichgewichtrelationen bestimmt werden, werden mehrere Entladungshypothesen vorausgesetzt. Da die Placierung der Messgeräte in einem gemischten Kreislauf grosse Schwierigkeiten verursacht und um das Fehlen solcher Geräte auszugleichen, wird das Massenverhalten eines Ions, das während des Vorgangs unverändert bleibt, berücksichtigt. Die Genauigkeit der Voraussetzungen wird durch eine praktische Anwendung bestätigt.

The paper presents the method of chemical regime prediction in a water cooling circuit with recirculation at a certain moment. After establishing the relations of mass balance on the cooling tower, different hypotheses in many discharge systems are adopted. In order to compensate the lack of measure equipment which is difficult to be placed in a mixed circuit, the mass evolution of a ion which is not submitted to transformation is used. The accuracy of the facts established by an application is confirmed.

In Ermangelung der geeigneten Messgeräte und wegen der technischen Placierungsschwierigkeiten, die beim Einsatz dieser Geräte im Kreislauf auftreten, kann die Massenbilanz der in einem gemischten Kühlkreislauf aufgelösten Stoffe nur schwer oder kaum bestimmt werden.

Nachstehend wird die Festlegung von Relationen, die zur Vorwegnahme der Zeit führen, erzielt.

In einem gemischten Kühlkreislauf erfolgt die Kühlung des Umlaufswassers in Türmen und zwar durch Verdunstung.

In diesem Kreislauf ergibt sich der im Bild 1 gezeigte Verluste.

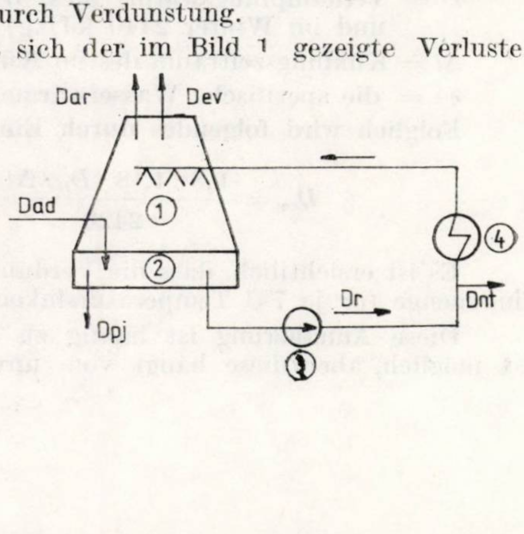

Bild 1 — Massenbilanz in einem gemischten Kühlsystem 1 — Kühlturm; 2 — Kühlwasserbecken; 3 — Kreislaufpumpe; 4 — Wärmeaustauscher.

Die Aufzeichnungen im Bild 1 bedeuten:

— D_{ev} = durch Verdunstung entstandener Verlust, m³/h,
— D_{ar} = durch Mitreissen der Tropfen entstandener Verlust, m³/h,
— D_{nt} = durch Undichtigkeit des hydrotechnischen Kreislaufs entstandener Verlust, m³/h,
— D_{pj} = durch Ablass entstandener Verlust, m³/h
— D_R = die Durchflussmenge des Wasserumlaufs, m³/h,
— D_{ad} = die Durchflussmenge des Zusatzwassers, m³/h.

Die Massenbilanz sieht wie folgt aus:

$$D_{ad} = D_{ev} + D_{ar} + D_{nt} + D_{pj} \tag{1}$$

Es ist bemerkenswert, dass die im Wasser aufgelösten Stoffe durch Verdunstung im Kreislauf verbleiben, während die im Wasser enthaltenen Stoffe durch den übrigen Verlust beseitigt werden. In dieser letzten Kategorie wird konventioneller Weise der während des Ablasses entstandene Verlust miteinbezogen, so dass:

$$D^*_{pj} = D_{pj} + D_{ar} + D_{nt} \tag{2}$$

Auf dieser Weise wird die Gleichung der Massenbilanz:

$$D_{ad} = D_{ev} + D^*_{pj} \tag{3}$$

Nachstehend werden die für die funktionellen Parameter gültigen Relationen bestimmt.

a. Durch Verdunstung entstandener Verlust

Die Wasserkühlung im Turm erfolgt auf grund der Verdunstung, so dass man schreiben darf:

$$D_{ev} = \frac{D_R \cdot e \cdot c \cdot \Delta t}{r} \tag{4}$$

wo:

e = durch Verdunstung evakuierter Wärmeanteil (z.B. im Sommer 0,8 ... 0,9 und im Winter 0,5 ... 0,6),
r = Verdampfungswärme des Wassers (im Sommer 2420 kJ/kg und im Winter 2440 kJ/kg),
Δt = Kühlungszeitraum des im Kühlturm vorhandenen Wasser, °C,
c = die spezifische Wasserwärme, kJ/kg.grd.

Folglich wird folgendes durch Einsetzen in Relation (4) erreicht:

$$D_{ev} = \frac{0{,}8 \cdot 4{,}18 \cdot D_R \cdot \Delta t}{2420} = 0{,}0014 \cdot D_R \Delta t \tag{5}$$

Es ist ersichtilich, dass die Verdunstung 1% von der Umlaufdurchflussmenge für je 7°C Temperatursinken im Kühlturm darstellt.

Diese Annäherung ist häufig zu gross, eine bessere Annäherung ist möglich, aber diese hängt vom unvorgesehenen Wetter ab.

b. Der Umfang des Kühlungsystems bezeichnet der gesamte im System enthaltene Wasserumfang, einschliesslich der Becken der Kühltürme, Leitungsröhre, Wärmeaustauscher, Schwingunsbecken u.s.w. Dieser Umfang ist mehr oder weniger gleichbleibend und wird als

1) V = $2V_T$ bewertet, wo V = der gesamte Systemumfang und V_T = Beckenumfang des Kühlturms,

2) V = 10 $D_R/60$, indem beide Bewertungen wirklichkeitsfremd sind.

Zur praktischen Bewertung des Gesamtumfangs wird eine ausreichende Quantität von *einem bestimmten Ion* (Chromat oder Chlorid) hinzugefügt, damit dieser analytischer Weise aufgefunden werden kann und keine Ablagerungen enstehen.

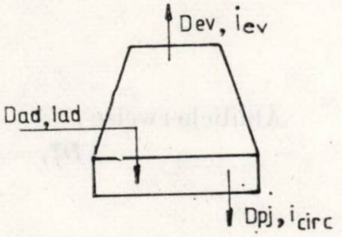

Bild 2 — Massenbilanz der aufgelösten Salze.

Die Ion-Konzentration wird analytisch bestimmt, in dem die Analyse nicht später als V/D_R Minuten nach der Hinzufügung des Ions anfangen soll.

Die Bewertungsberechnung des Systemumfangs wird wie folgt durchgeführt :

$$V = \frac{\text{kg, hinzugefügtes Ion}}{\text{ppm, Ion-Konzentration}} \cdot 10^3 \tag{6}$$

Bild 2 zeigt die im System vorhandene Salzenbilanz indem i_{ad}, i_R und i_{ev} die Ion-Konzentration im Zusatz- und Umlaufwasser und im Kühlturm vorhandener Wasserdampf darstellen.

Wenn man i_{ev} als Null betrachtet, wird die Salzenbilanz wie folgt bestimmt :

$$D_{ad} \cdot i_{ad} = D^*_{pj} \cdot i_R \tag{7}$$

und

$$D_{ad} = D^*_{pj} \cdot \frac{i_R}{i_{ad}} \tag{8}$$

aber

$$\frac{i_R}{i_{ad}} = C \tag{9}$$

wo C ist die Konzentrationsziffer (Eindickungsziffer), die auch als

$$C = \frac{D_{ad}}{D^*_{pj}} = \frac{i_R}{i_{ad}} \tag{10}$$

ausgedrückt werden darf.

Um die Relation $D_{ad} = f(D_{ev}, C)$ zu erreichen, darf die Relation (10) auch als :

$$D^*_{pj} = \frac{D_{ad}}{C}$$

geschrieben werden und durch Ersetzen wird die Relation (3): ,

$$D_{ad}\,D_{ev} + \frac{D_{ad}}{C} \text{ oder } D_{ad}\frac{C-1}{C} = D_{ev}$$

$$D_{ad} = D_{ev}\,\frac{C}{C-1} \tag{11}$$

Ähnlicherweise :

$D^*_{pj} = f(D_{ev}, C)$ man erreicht :

$$D^*_{pj} = \frac{D_{ev}}{C-1} \tag{12}$$

Tafel 1 stellt die Ergebnisse zusammenfassend dar.

Die für die chemische Fahrweise in einem gemischten Kühlungssystem spezifischen Grössen beziehen sich auf :

— Retentionszeit,
— Entladungszeit,
— Halbwertzeit,
— Zyklusdauer.

Tafel 1

Massenbilanzsrelationen des Kühlsystems

D_{ev}	D_{ad}	D^x_{pj}	C
$0{,}0014 \cdot \mathrm{D_R} \cdot t$	$D_{ev}\dfrac{C}{C-1}$	$D_{ev}\dfrac{C}{C-1}$	$\dfrac{i_\mathrm{R}}{i_{ad}}$
$D_{ad} - D_{pj}$	$D_{ev} + D^*_{pj}$	$D_{ad} - D_{ev}$	$\dfrac{D_{ad}}{D^*_{pj}}$

Retentionszeit *(t)*

Es wird vorausgesetzt, dass ein gewisses Ion (z.B. das hexavalente Chrom-Ion Cr^{+6}) zur Wasserkonditionierung verwendet wird. Zu diesem Zweck wird eine bestimmte Quantität von betreffenden Ionen, zusammen mit dem Zusatzwasser im Kreislauf hinzugefügt.

Wenn man das mit × kg notiert, dann wird x/V die Konzentration dieses Ions am Anfangsmoment t.

Der Ablass, der konventionellerweise laut Relation (2) definiert wird, verursacht die Konzentrationsverminderung des hinzugefügten Ions.

Es ergeben die folgenden 2 Fragen:

1) Wie lange bleibt das bevorzugte Ion im System, wenn dieses nicht mehr geimpft aber ununterbrochen beseitgt wird?

2) Wieviel Zeit wird dafür benötigt, damit ein bestimmtes Ion-Prozent beseitigt wird?

Der Ablass D^*_{pj} löst stündlich einen Wasserumfang aus dem System heraus, so dass es D^*_{pj} Chancen gibt, dass das bevorzugte Ion aus V herausgelöst wird. Die Probabilität dieses Ions innerhalb von 1 Stunde heraus gelöst zu werden ist D^*_{pj} oder wird dessen Elimination in V/D^*_{pj} Stunde erwartet.

Die Retentionszeit wird definiert, wie folgt:

$$t = \frac{V}{D^*_{pj}} \tag{12 a}$$

Die zweite Frage wird mathematisch beantwortet und zwar von der Gleichung ausgehend, die die Konzentrationsdifferenz dx definiert:

dx = hinzugefügte Quantität – herausgelöste Quantität und wenn keine neuen Ion-Quantitäten hinzugefügt werden, wird:

$$\mathrm{dx} = -D^*_{pj}\frac{\mathrm{x}}{\mathrm{V}}\cdot \mathrm{dt} \text{ oder } \frac{\mathrm{dx}}{\mathrm{x}} = -\frac{D^*_{pj}}{V}\cdot \mathrm{dt}$$

und durch Integrieren ergibt sich:

$$\ln \mathrm{x} = -\frac{D^*_{pj}}{V}\cdot t$$

und:

$$\mathrm{t} = -\frac{V}{D^*_{pj}}\cdot \ln \mathrm{x} \tag{13}$$

wo: dt = Retentionszeitänderung

Durch Anwendung von Relation (13) ergibt sich folgendes für einige Werte von x:

$$\mathrm{x} = 0{,}5 \ (50\,\% \text{ herausgelöst}) \rightarrow \mathrm{t} = 0{,}693\frac{V}{D^*_{pj}};$$

$$\mathrm{x} = 0{,}1 \ (90\,\% \text{ herausgelöst}) \rightarrow \mathrm{t} = 2{,}302\frac{V}{D^*_{pj}};$$

$$\mathrm{x} = 0{,}01 \ (99\,\% \text{ herausgelöst}) \rightarrow \mathrm{t} = 4{,}605\frac{V}{D^*_{pj}}.$$

Entladungszeit (t_d)

Die Entladungszeit wird als die vom Ablass um einem mit dem ganzen Systemumfang übereinstimmenden Wasserumfang zu eliminieren benötigte Zeit definiert; d.h.:

$$D^*_{pj}\cdot t_d = V \text{ oder } t_d = \frac{V}{D^*_{pj}} \tag{14}$$

Graphisch sieht das wie im Bild 3 aus.

Bemerkung: Praktisch weisen die Retentions- und Entladungszeit denselben mathematischen Ausdruck auf, indem die physikalischen Interpretationen identisch sind.

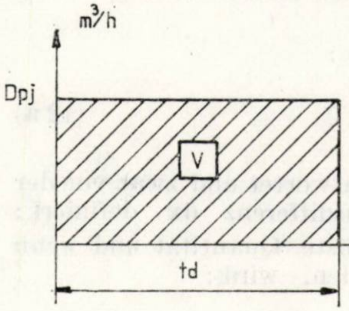

Bild 3 — Graphische Darstellung der Entladungszeit.

Weiter wird die Entladungszahl n, wie folgt, definiert:

$$n = \frac{t}{t_d} = \frac{t}{\dfrac{V}{D^*_{pj}}} = \frac{D^*_{pj}}{V} \cdot t \qquad (15)$$

Laut Relation (13) $\ln x = \dfrac{D^*_{pj}}{V} \cdot t$ und $x = e^{-\frac{D^*_{pj}}{V} \cdot t}$

Durch Ersetzen mit Relation (15) wird $x = e^{-n}$.

Durch Anwendung der Relation bei einer gewissen Zahl von Entladungen ergeben sich die nachstehenden Werte:

nach n Entladungen	gibt es noch im System x % aus der Anfangskonzentration des zugefügten Ions
1	36,80
2	13,50
3	5,00
4	1,84
5	0,68

Die Dauer eines Zyklus, t_c, stellt die Zeit dar in welcher der Wasserumlauf einmal erfolgt.

Mathematisch kann man es wie folgt umschreiben:

$$t_c = \frac{V}{D_R} \qquad (16)$$

Die Dauer eines Zyklus dient zur Bewertung der Systemsantwortzeit, so dass, durch die Dosierung eines Ions in Kühlturmbecken, nach t_c Minuten, das durch das Aufteilungssystem im Becken wiederkehrende Wasser das bevorzugte Ion enthält.

Halbwertzeit ($t_{1/2}$)

Die Halbwertzeit wird als jener Zeitraum definiert in dem die Ion-Quantität auf die Hälfte reduziert wird.

Aus der Relation (13) ergibt sich:

$$t_{1/2} = -\frac{V}{D^*_{pj}} \ln x = -\frac{V}{D^*_{pj}} \cdot \ln 0{,}5 = 0{,}693 \frac{V}{D^*_{pj}} \qquad (17)$$

oder $t_{1/2} = 0{,}693$. Retentionszeit

Durch nacheinanderfolgendes Ersetzen erlangt man:

$$t_{1/2} = 0{,}693 \frac{V}{\frac{D_{ev}}{C-1}} = 0{,}693 \frac{V}{\frac{0{,}0014 \cdot D_r \cdot t}{C-1}} = \frac{0{,}693}{0{,}0014} \cdot \frac{C-1}{t} \cdot \frac{V}{D_R}$$

oder $t_{1/2} = 495 \cdot \frac{C-1}{t}$. die Dauer eines Zyklus (18)

So kann man die Halbwertzeit nur aufgrund der bekannten Konzentrationsziffer und der Wasserkühlung im Kühlturm berechnen, indem die Dauer eines Zyklus schon bekannt ist. Eine ganze Reihe von Grössen, die für ein Kühlsystem spezifisch sind, sind definiert worden, wobei auch einige Berechnungsrelationen dafür bestimmt worden sind.

Nachstehend wird die Anwendung dieser Relationen zwecks ordungsmässiger Funktionierung eines solchen Systems (in bestimmten Fällen) gezeigt.

Die Ablasseinstellung

Die Ablasseinstellung sieht einer nicht funktionierenden Bremse ähnlich.

Man setzt ein mit Konzentrationsziffer = 2 (d.h. C=2) funktionierendes Kühlsystem voraus. Es wird gefragt wieviel Zeit zur Erhöhung der Konzentrationsziffer mit einer Einheit benötigt wird, wenn der Ablass eingestellt wird.

Sei es x_{ad} (kg/m^3) die im Zusatzwasser vorhandene Konzentration der aufgelösten Stoffe, so wird die Kreislaufwasserkonzentration $= 2\,x_{ad}$, die im Kreislauf enthaltene Stoffmenge $= 2x_{ad} \cdot V$, die hinzugefügten Stoffe $= x_{ad} \cdot D_{ad} \cdot t$ und die Endkonzentration $= 3x_{ad}$. In diesem Fall zeigt die Stoffenbilanz dass:

$$2x_{ad} \cdot V + x_{ad} \cdot D_{ad} \cdot t = 3x_{ad} \cdot V \text{ d.h.}$$

$$D_{ad} \cdot t = V \text{ wobei } t = \frac{V}{D_{ad}} \qquad (19)$$

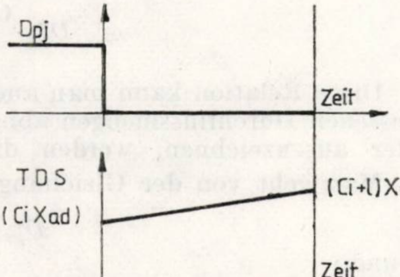

Bild 4 — Die Ablasseinstellung.

Graphisch sieht die Relation wie im Bild 4 aus.

Die auf dieser Weise berechnete Zeit hängt von der Anfangskonzentration der im System vorhandenen Stoffe nicht ab ; da der Systemumfang vorherbestimmt ist, wird die Zeitspanne, in der die Erhöhung mit einer Einheit erfolgt, nur aufgrund der der bekannten Zusatzdurchflussmenge (D_{ad}) berechnet.

Praktisch ist es vorteilhaft, dass es eine dauernde $t = \frac{V}{D_{ad}}$ erreicht wird ; dafür benötigt man einen je grösser desto passenden Systemumfang und einen geringeren Zusatz (d.h. eingeschränkter Verlust).

Die Ablassverdoppelung

Die Frage ist : welches ist die notwendige Zeitspanne, damit der Übergang von der Konzentrationsziffer C_i zu einer Konzentrationsziffer C_f erfolgt, wenn der Ablass verdoppelt wird ?

— die vor der Ablassverdoppelung vorhandene Stoffmenge $= C_i \cdot x_{ad}$,

— die nach der Ablassverdoppelung vorhandene Stoffmenge $= C_f \cdot x_{ad}$.

Die Verminderung der aufgelösten Stoffe :

$(C_i - C_f) \cdot x_{ad} \cdot V =$ beseitgte Stoffe — hinzugefügte Stoffe, kg.

Wenn man in dem betreffenden Zeitraum eine durchschnittliche Konzentration von $\frac{C_i - C_f}{2}$ annimmt, darf man wie folgt schreiben :

— beseitigte Stoffe $= D^*_{pj} \cdot \frac{C_i + C_f}{2} \cdot x_{ad} \cdot t$ (20)

(21)

— hinzugefügte Stoffe $= D_{ad} \cdot x_{ad} \cdot t$.

Durch einsetzen der Relationen (21) in (20) ergibt sich :

$$(C_i - C_f) \cdot x_{ad} \cdot V = D^*_{pj} \frac{C_i - C_f}{2} \cdot x_{ad} \cdot t$$

so dass :

$$t = \frac{(C_i - C_f) \cdot V}{D^*_{pj} \cdot \frac{C_i - C_f}{2} - D_{ad}} \tag{22}$$

Diese Relation kann man auch als von vor der Ablassverdoppelung gemessenen Durchflussmengen abhängige Relation. Um diese Gleichungsglieder auszuzeichnen, werden diese mit Index „o" gekennzeichnet.

Man geht von der Gleichung :

$$D^*_{pj} = 2\,D^0_{pj} \qquad (23$$

aus und :

$$D_{ad} = D_{ev} + D^*_{pj} = D_{ev} + 2D^0_{pj} \text{ oder } D^0_{pj} = D^0_{pj} + D^0_{ev} = D_{ev} + D^0_{pj}$$

Man bemerkt dieselbe Verdunstung, sowohl vor als auch nach der Ablassverdoppelung.

Durch die Differenz der obenangeführten Relationen ergibt sich :

$$D_{ad} = D^0_{ad} + D^0_{pj} \tag{24}$$

Wenn man (23) und (24) in (22) ersetzt, ergibt sich durch Reduzieren :

$$t = \frac{(C_i - C_f)\cdot V}{D^0_{pj}(C_i + C_f - 1) - D^0_{pj}} \tag{25}$$

Wenn man die Relationen (11) und (12) in Relation (25) und weiter D_{ev} durch Relation (5) ersetzt, ergibt es sich :

$$t = (C_i - C_f)\frac{C_i - 1}{C_f - 1}\cdot\frac{t_c}{0{,}0014\ \Delta t} \tag{26}$$

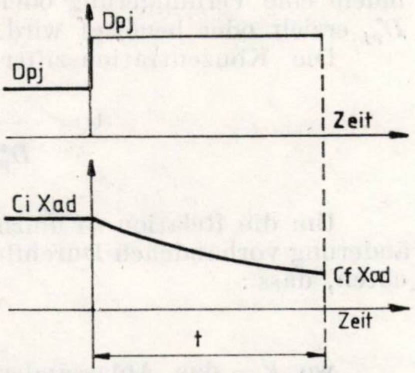

Bild 5 — Die Ablassverdoppelung.

Graphisch sieht die Ablassverdoppelung wie im Bild 5 aus.

Das Ablasshalbieren

Durch Ablassverminderung auf die Hälfte wird die Konzentrationsziffer nach einer Zeitspanne von C_i zu C_f steigen, was graphisch wie im Bild 6 aussieht.

In Analogie zu dem vorgenannten Fall der Ablassverdoppelung ergibt sich die Relation (27) :

$$t = \frac{(C_f - C_i)\cdot V}{D_{ad} - D^*_{pj}\dfrac{C_i + C_f}{2}} \tag{27}$$

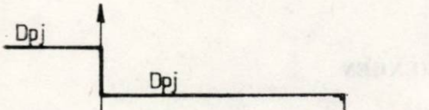

Bild 6 — Die Ablasshalbierung.

oder als von vor der Ablassverminderung gemessen Durchflussmengen abhängige Relation :

$$t = \frac{(C_f - C_i)\cdot V}{D^0_{pi} - 0{,}5D^0_{pj}\cdot\left(1 + \dfrac{C_i + C_f}{2}\right)} \tag{28}$$

Dem Ablasshalbieren zufolge kann, in einer aus den Relationen (27) und (28) resultierenden Zeit, der Übergang von der Konzentrationsziffer C_i zu C_f erreicht werden.

Praktisch sind die Relationen (22) und (27) identisch, d.h. dass die für die Erhöhung der Konzentrationsziffer (im Fall des Ablasshalbierens) notwendige Zeit mit der Zeit gleich ist, die für das entsprechende Sinken der Konzentrationsziffer (im Fall der Ablassverdoppelung) notwendig ist.

Verallgemeinerung

Sei es C_i die im Anfangsmoment vorhandene Konzentrationsziffer, indem eine Verminderung oder ein Zuwachs des Ablasses von D^0_{pj} zu D^*_{pj} erzielt oder benötigt wird.

Die Konzentrationsziffer C_f wird nach folgender Zeit erreicht:

$$t = \frac{(C_i - C_f) \cdot V}{D^*_{pj} \cdot \frac{C_i + C_f}{2} - D_{ad}} \tag{29}$$

Um die Relation so umzuformen, dass sie von den vor der Ablassänderung vorhandenen Durchflussmengen abhängig ist, sollte man beachten, dass:

$$D^*_{pj} = kD^0_{pj} \tag{30}$$

wo k = das Ablassänderungskoeffizient und $k \geqslant 0$ oder:

$$D_{ad} = D_{ev} + D^*_{pj} = D_{ev} + kD^0_{pj} \tag{31}$$

und:

$$D^0_{ad} = D^0_{ev} + D^0_{pj} = D_{ev} + D^0_{pj} \tag{32}$$

Aus den Relationen (31) und (32) ergibt sich:

$$D_{ad} = D^0_{pj} + (k - 1) \cdot D^0_{pj} \tag{33}$$

Durch Ersetzen von (30) und (33) in (29) ergibt sich:

$$t = \frac{(C_i - C_f) \cdot V}{kD^0_{pj} \cdot \frac{C_i + C_f}{2} - D^0_{pj} \cdot (k - 1) - D_{ad}} \tag{34}$$

SCHLUSSFOLGERUNGEN

Es wurden für ein gemischtes Kühlsystem gültige Berechnungsrelationen festgelegt, indem die für Gleichungen fähigen chemischen Indikatoren angewendet worden sind und zwar zwecks Determinierung der Umfänge und Durchflussmengen, die praktischerweise nicht bestimmt werden können.

Die demonstrierten Relationen gestatten die Berechnung der Verwirklichungszeit einiger erwünschten Situationen.

Die Schlussfolgerungen sind auf 200 MW-Gruppen angewendet worden, indem die Ergebnisse die praktizierten Werte bestätigen.

Die Entscheidungen, die getroffen wurden, können leichter festgelegt werden, wenn die zu deren Erfüllung benötigte Zeit bekannt ist.

Revue Roumaine de Chimie, **34**, *4*, 1047–1054 (1989)

PHASE COMPOSITION AND STRUCTURE IN Fe–Mg–O CATALYSTS FOR OXYDEHYDROGENATION OF n-BUTENES TO BUTADIENE

I. V. NICOLESCU[a], GH. NEDELCU[a], RODICA MĂNĂILĂ[b], M. IVAȘCU[b], FLORENTINA AVRAMESCU[a], VIORICA SPÂNU[b] and G. FILOTI[b]

[a] Technology and Catalysis Department, The Polytechnic, TCH, 313 Spl. Independentei, 76206 Bucharest, Romania

[b] Institute of Physics and Technology of Materials, Bucharest–Măgurele, P.O. Box, MG 07, Romania

Received October 10, 1988

The system Fe–Mg–O with various concentration ratios (Fe/Mg atomic ratio = 1–5) has been investigated by Mössbauer and X-ray diffraction data with respect to the phase structure in oxidated-reduced-tested state (post reaction). The experimental results show a dependence between catalytical properties (yield, selectivity) and active states of catalysts, non-stoichiometric spinellic solid solutions $MgFe_2O_4$–Fe_3O_4 in a highly disordered state.

1. INTRODUCTION

The dehydrogenation process of n-butenes to butadiene implying oxygen as acceptor of hydrogen, occurs by the reaction

$$C_4H_8 + 1/2O_2 \rightarrow C_4H_6 + H_2O \quad \Delta H = -130 \text{ KJ/mole}$$

This strong exothermal reaction is a thermodynamically nonequilibrium one. Yields of butadiene per step of 65–70% and selectivities more than 90% are obtained. In thermodynamically limited nonoxidative dehydrogenation of n-butene, yields of 16–34% and selectivities of 60–80% are obtained.[1]

These practical performances have intensified the investigation regarding different classes of catalysts, especially ferrite multiphase systems with structural defects.[2–4]

Phase composition and structure of $MgO \cdot nFe_2O_3$ system as a function of composition (Fe/Mg atomic ratio- "n"), calcination temperature and reaction atmosphere have been investigated in this paper. Also, we focused on the active catalytic structures appearing in the sample triplets: oxidated–reduced–tested (post reaction).

2. EXPERIMENTAL

2.1. Mössbauer spectrometry

Mössbauer data were collected using "home-made" spectrometer with symmetrical waveform. A ^{57}Co source in copper matrix, with an activity of 20 mCi, was used. The optimized thickness of the absorbers amounted to 35 mg/cm^2. The experimental spectra were processed by a computer program described elsewhere.[5]

2.2. X-ray diffraction

Diffraction patterns were recorded on a Siemens diffractometer, with CuK-α radiation monochromatized by a concave graphite crystal, placed before the scintillation counter. The profile of selected diffraction lines was recorded by step-scanning.

2.3. Preparation and testing of the catalysts

Catalysts in the system $MgO \cdot nFe_2O_3$ $(1 \leqslant n \leqslant 5)$ were prepared by mechanical homogeneization of a wet mixture of MgO and hydrated Fe_2O_3. The final mass was dried at 110°C and calcinated at a temperature between 500 and 1200°C.

Activity tests were performed in an isothermal fixed-bed dynamic reactor, in the following conditions: $T = 480°C$, $V_v = 600\ h^{-1}$ (calculated per butene), molar ratio n-butene: $O_2:H_2O = 1:0.9:15$; 5 cm^3 of catalyst with a granulation of 1–2 mm after reduction in butene or hydrogen was used.

Reaction products were analyzed by chromatography. The conversion, yield of butadiene and selectivity were calculated.

3. RESULTS AND DISCUSSION

3.1. Structure of catalysts in the oxidated state

X-ray diffraction and Mössbauer data agreed on a two-phase structure, comprising haematite ($\alpha-Fe_2O_3$) and a cubic spinellic Mg ferrite. Both phases contain Fe^{3+} only. Phase composition versus the "n" value (Fig. 1) shows for $n = 2$ roughly equal concentrations of both phases in the oxidated state catalyst calcinated at 1000°C.

Figure 2 shows the catalyst activity versus composition "n". The activity is characterized by yield (% mole), selectivity and conversion (% mole). A maximum of activity is noticed around $n = 2$.

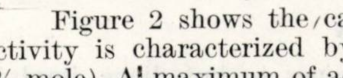

Fig. 1. — Concentrations of free haematite and Mg ferrite versus composition n. 1 — αFe_2O_3; 2 — $MgFe_2O_4$

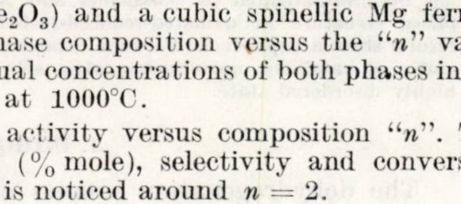

Fig. 2. — Catalytic activity versus composition n. 1 — yield of butadiene (% mole); 2 — conversion (% mole); 3 — selectivity

For this composition ($n = 2$) we investigated the effect of calcination temperature on the structure and on the Fe distribution between the two crystalline phases. Calcination was carried out at temperatures between 500 and 1200°C for 90 minutes. Figure 3 shows the phase composition of the catalysts with $n = 2$ versus calcination temperature, T_c. It can be seen that rising T leads to a more complete formation of the Mg ferrite. At $T_c = 1000$°C, Mössbauer data show equal concentrations of ferrite and haematite, as required by the chemical formula, pointing to a completed reaction of ferrite formation. For T_c above 1000°C, the spinellic lattice dissolves an amount of iron in excess Fe_2O_3 phase.

On the other hand, at low T_c 's the area of the haematite diffraction lines is lower (Fig. 3). This fact can be accounted for by a quasi-amorphous fraction, which escapes observation by diffraction methods. The explanation is supported by the strong variation of effective crystallite dimension with T_c, for both haematite and Mg ferrite (Fig. 4).

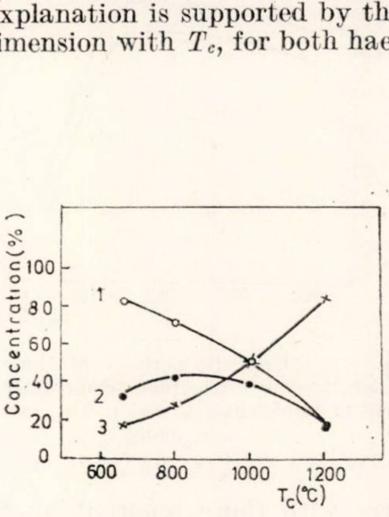

Fig. 3. — Concentrations of Mg ferrite and free haematite versus calcination temperature ($n = 2$). 1 — αFe_2O_3 from Mössbauer data; 2 — αFe_2O_3 from X-ray diffraction data; 3 — $MgFe_2O_4$.

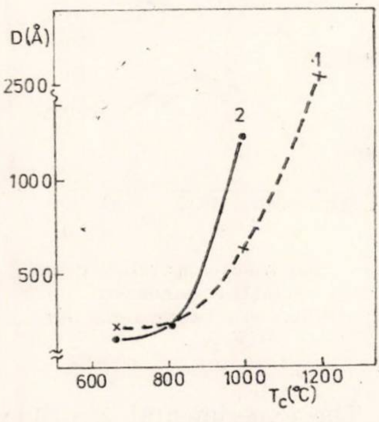

Fig. 4.—Effective crystallite dimension of spinellic ferrite $D_s(1)$ and haematite $D_H(2)$ versus calcination temperature, for $n = 2$ (reproducibility zone for 10 preparations).

Thus, low T_c's (660—800°C) result in incompletely formed and disordered Mg ferrite, while the unreacted Fe accounts for the free haematite. On the other hand, at $T_c = 1200$°C excess Fe is dissolved into the spinellic ferrite, as results both from X-ray diffraction (area of the haematite lines) and Mössbauer (energetical values of the spectrum) data. We conclude that the optimal T_c for composition $n = 2$, is 1000°C.

The lattice parameter a of $MgFe_2O_4$ varies with T_c as shown in figure 5. Increasing T_c from 660 to 1000°C results in an increased a value, which can be explained by the normalization of cation distribution, as reported. [6-8]

In order to check this hypothesis, we determined the parameter λ in the spinel formula:

$$Mg^{2+}_{\lambda}Fe^{3+}_{1-\lambda}[Mg^{2+}_{1-\lambda}Fe^{3+}_{1+\lambda}]O^{2-}_{4},$$

i.e. the Mg fraction on the tetrahedral spinellic sites. λ was evaluated from the intensity ratios of the X-ray diffraction spinellic lines (111)/(400) and (220)/(400) the former being particularly sensitive to cation distribution. Comparison of experimental ratios with those calculated from structure factors yielded the λ values shown in figure 5. The oxygen positional parameter was taken as its ideal value (0.250).

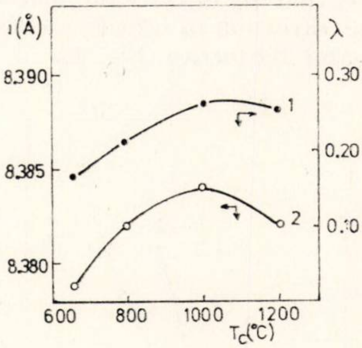

Fig. 5. — Variation of inversion degree λ (1) and of lattice parameter a (2) with calcination temperature, for $MgFe_2O_4$.

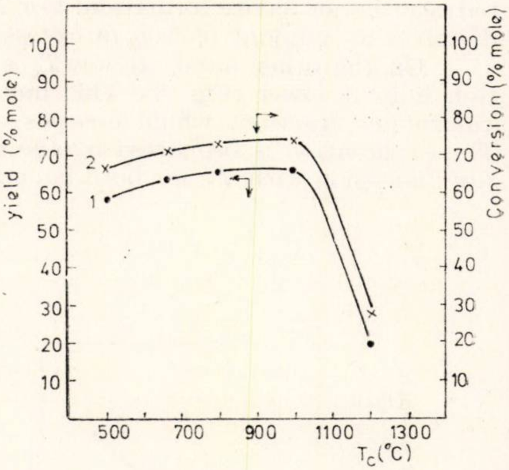

Fig. 6. — Catalytic activity of $MgO \cdot 2Fe_2O_3$ system versus calcination temperature. 1 — yield of butadiene (% mole); 2 — conversion (% mole).

The experimental λ values agree with those reported by Brabers and Klerk[6] for $MgFe_2O_4$ quenched from different T's and are in the range quoted by Mozzi and Paladino[7] and Faller and Birchenall[8] for the same compound.

Thus, increasing T_c causes a Fe distribution among cation sites closer to the statistical one ($\lambda = 1/3$). Mössbauer data support this redistribution, showing a strong increase of λ with T_c.

The experimental "a" values at different T_c's (Fig. 5) fall inside the relatively wide range of values reported in literature.[6-9] The decrease of the lattice parameter for $T_c = 1200$°C should be attributed to Fe dissolution in the spinel.[10]

As expected, the catalyst's activity is influenced by calcination temperature, as shown in figure 6. Catalysts with $n = 2$ calcinated between 800 and 1000°C present the best catalytical activity.

We noticed from Mössbauer data of $MgO \cdot 2Fe_2O_3$ catalysts, calcinated between 600 and 1200°C a similar variation of the yield in butadiene and of the ratio iron on tetrahedral positions (Fe_A) and iron occupying octahedral positions (Fe_B), Fe_A/Fe_B, for catalyst in the initial state, as results from table 1.

Table 1

Variation of Fe_A/Fe_B ratio versus calcination temperature and catalytic activity (R = yield in butadiene).

Calcination temperature, °C	% Fe composition in			Fe_A/Fe_B	R % mole
	α-Fe_2O_3	Fe_A	Fe_B		
660	47.00	4.00	6.00	0.66	63.70
800	71.00	15.00	14.00	1.07	65.00
1000	48.00	38.00	14.00	2.71	68.00
1200	14.00	18.00	66.00	0.27	18.90

3.2. Structure of reduced catalysts

Activation of the catalyst before the reaction was performed with a corresponding reducing agent. During activation, Fe^{3+} is transformed into Fe^{2+} or even into Fe function of the agent, the energetic and chemical equilibrium of the reduced lattice also requiring, in some cases, the creation of ion vacancies.

Activation of calcinated catalysts (1000°C for 90 minutes) was performed in butenes or hydrogen as reducing agent.

Reduction of samples with $n > 2$ in a butenes atmosphere (5 h at 540°C) induced a unique spinellic structure. It was assigned, on the basis of Mössbauer and X-ray diffraction data, to a solid solution of Mg ferrite and magnetite.

On the other hand, for $n \leqslant 2$ incomplete solubilization occurs, $MgFe_2O_4$ and Fe_3O_4 being noticed as separate phases. This was revealed by a profile analysis of the high-angle (731) + (553) spinellic line, as well as by the Mössbauer parameters.

The lattice parameter of Mg ferrite in samples with $n \leqslant 2$, reduced in butene, does not change significantly ($a = 8.384 \pm 0.002$ Å), as compared with $a = 8.385$ Å in the oxidated phase. This shows that reduction is supported mainly by $\alpha-Fe_2O_3$, while $MgFe_2O_4$ is practically not affected.

Figure 7 displays the concentration of Fe on spinellic tetrahedral sites (Fe_A), as derived from the area of the Mössbauer sextets, as a function of composition n, for samples reduced in butene. The curve shows a discontinuity at $n = 2$.

Figure 8 shows the isomer shift of the octahedral Fe(Fe_B) versus n, displaying a maximum around $n = 2$. This sugests an optimal homogeneity of the Fe_B distribution around this composition. This behaviour could be also related to interface effects between Fe_3O_4 and Mg ferrite, which are highest when the two-phase concentrations are equal ($n = 2$).

Mössbauer line width, Γ, which informs about the homogeneity of cation distribution, shows (Fig. 9) a minimum for octahedral Fe_B around the same composition, stressing again the improved homogeneity at $n = 2$. The general decreasing trend of Γ with increasing Fe/Mg ratio suggests that a Fe exces ($n > 1$) reduces the local distortion around Fe positions in Mg ferrite (or in the spinellic solid solution), induced by the reduction process.

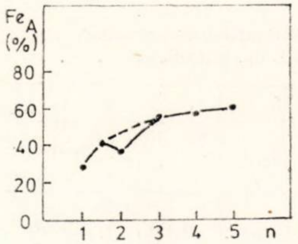

Fig. 7. — Concentration of tetrahedral Fe (Fe_A) versus composition, for samples reduced in butene (Mössbauer data).

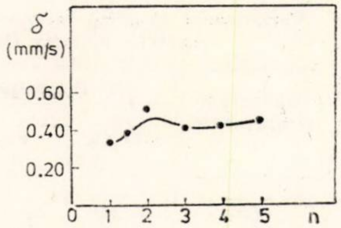

Fig. 8. — Isomer shift for octahedral Fe (Fe_B) versus composition, for samples reduced in butenes (Mössbauer data).

Thus, the study of oxidated state catalysts shows that the composition with $n = 2$ seems to offer an homogeneous and favourable distribution of ions, between the catalytic phases.

Reduction in hydrogen at the same temperature (540°C) but for 90 minutes only, causes a deeper reduction of Fe in catalysts. Metallic Fe and wüstite FeO appear, as well as the solid solution $MgFe_2O_4 - Fe_3O_4$. The degree of final reduction of Fe can be characterized by the amount of metallic $\alpha-Fe$.

Figure 10 shows the variation of Fe and FeO amounts versus composition, n, as derived by Mössbauer and confirmed by X-ray diffraction data. The concentration of FeO decreases with increasing Fe/Mg ratio in the catalysts. On the other hand, for $n > 2-3$, reduction in hydrogen leads to a considerable amount of metallic Fe (as well as to free MgO, originating in the partial decomposition of Mg ferrite).

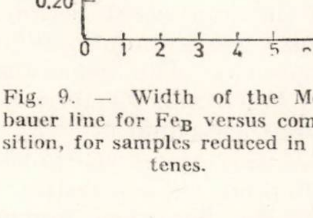

Fig. 9. — Width of the Mössbauer line for Fe_B versus composition, for samples reduced in butenes.

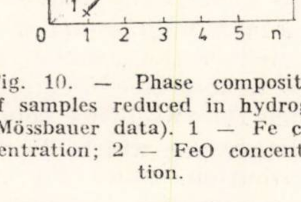

Fig. 10. — Phase composition of samples reduced in hydrogen (Mössbauer data). 1 — Fe concentration; 2 — FeO concentration.

Figure 11 shows Mössbauer line width for Fe_A and Fe_B versus composition in samples reduced with hydrogen. The line width for Fe_B from the spinellic solid solution, decreases for $n > 2$, as was also the case for the reduction in butene (Fig. 9). The line width of Fe_A shows no variation.

Large line widths of Fe_B point to defects introduced by reduction, especially at small n values as was also shown for samples reduced in butenes.

The solid solutions Mg ferrite-magnetite appearing for $n > 2$ as a result of reduction in butene show a reduced character. X-ray diffraction data showed that their lattice parameter is increased by $3-5 \cdot 10^{-3}$ Å, in comparison with the value calculated for a stoichiometric solid solution, pointing to an oxygen deficiency.

The reduced samples should be considered, from a structural point of view, as precursors of the active states formed in the catalyst, after testing in the most favorable conditions of reaction.

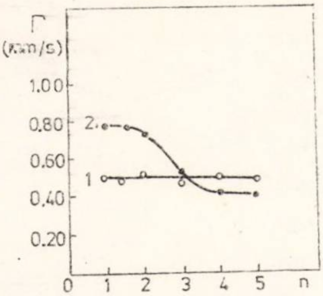

Fig. 11. — Mössbauer line width for $Fe_A(1)$ and $Fe_B(2)$ versus composition, in samples reduced with hydrogen.

3.3. Structure of tested catalysts

The catalysts reduced in butenes showed, after reaction, small amounts of $\alpha-Fe_2O_3$, appearing by partial reoxidation of the Fe_3O_4 in the reduced sample by the oxygen in the reaction medium. The magnetite present in the tested catalyst is strongly disordered.

In the catalysts reduced in hydrogen and tested, curves 1 and 2 in figure 12 show the variation of Fe_A and Fe_B concentrations versus compositional parameter n. A minimum and maximum inflexion can be noticed, respectively, for $n = 2$.

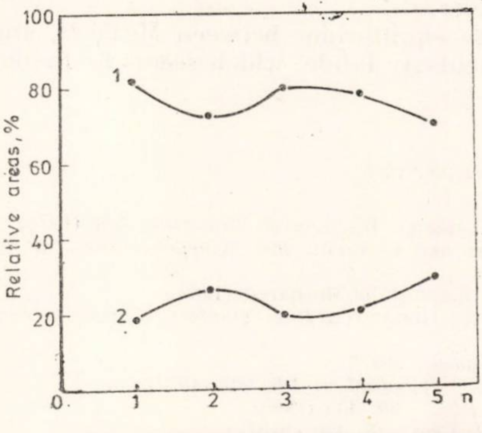

Fig. 12. — Variation of relative areas in the spinellic ferrite of catalysts reduced in hydrogen and tested, versus composition n. 1 — tetrahedral Fe, Fe_A; 2 — octahedral Fe, Fe_B.

The solid solution $Fe_3O_4-MgFe_2O_4$ formed during the activation, is also found in the tested catalysts, but with a smaller lattice constant, indicative of partial oxidation.

Figure 13 shows an inverse relation between the concentration Fe_A of tetrahedral iron in butenes or hydrogen reduced and tested catalysts (curves 1 and 2) and the butadiene yields (curve 3).

The optimum yield at $n = 2$ corresponds to a minimum concentration of Fe_A.

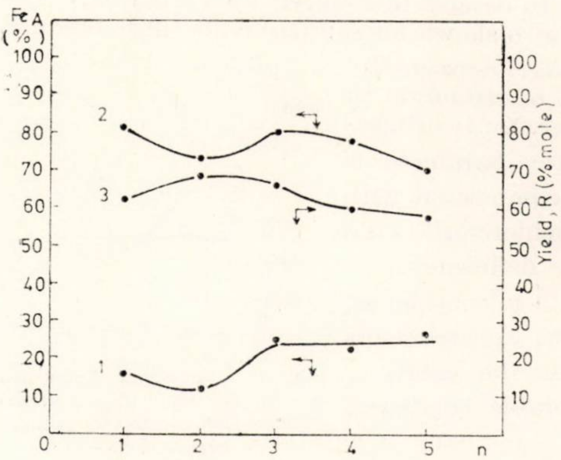

Fig. 13. — Fe_A concentration and yield of butadiene variation, versus composition *n*. 1 — Fe_A, catalysts reduced in butenes and tested; 2 — Fe_A, catalysts reduced in hydrogen and tested; 3 — yield of butadiene (R, % mole).

4. CONCLUSIONS

From experimental data resulted that, the specific activity of ferritic catalysts in the oxidehydrogenation of *n*-butenes to butadiene depends on the active structures formed by calcination—reduction—testing in specific media.

These active structures are related to the non-stoichiometric spinellic solid solutions $MgFe_2O_4—Fe_3O_4$ in a highly disordered state, due to the presence of cation and anion vacancies.

For the $n = 2$ composition, the equilibrium between $MgFe_2O_4$ and the $\alpha—Fe_2O_3$ (Fe_3O_4) phases is particularly labile, which seems to favour the formation of active states.

REFERENCES

[1] L. M. Welch, L. J. Croce and H. F. Christmann, *Hydrocarbon Processing*, 131 (1978).
[2] I. V. Nicolescu, R. Mănăilă, M. A. Chaar and G. Filoti, *Rev. Roumaine Chim.*, **31**, 99 (1986).
[3] Gh. Nedelcu, Chem. D. Thesis, Polytechnic Institute of Bucharest (1980).
[4] Chien-Ren Joe Yin, Tae-Jin Park and J. W. Hightower, *Proc. 9th Inter. Congr. in Catalysis*, Calgari, **4**, 1570 (1988).
[5] G. Filoti, Ph. D. Thesis, University of Bucharest (1971).
[6] V. A. M. Brabers and J. Klerk, *J. Phys. Coll. Cl, suppl.*, 4, **38**, 207 (1977).
[7] R. L. Mozzi and A. E. Paladino, *J. Chem. Phys.*, **39**, 435 (1963).
[8] J. G. Faller and C. E. Birchenall, *J. Appl. Cryst.*, **3**, 496 (1970).
[9] W. C. Allen, *J. Amer. Ceram. Soc.*, **49**, 257 (1966).
[10] B. I. Suharevski and B. G. Alapin, *J. Phys. Chem. Solids*, **29**, 1773 (1968).

Revue Roumaine de Chimie, 34, 4, 1055– 1060 (1989)

SYNTHESIS AND CHARACTERIZATION OF ZSM-5 ZEOLITES

E. PINCOVSCHI, M. MERCHEŞ and KIM CHOL SIK
Polytechnic Institute, Department of Inorganic Chemistry, Splaiul Independenţei 313,
76206 Bucharest, Romania

Received November 19, 1988

The hydrothermal synthesis requirements for ZSM-5 crystallization in the presence of isopropylamine (IPA) are examined. It is noted that IPA has a complex influence on the formation of zeolite framework by "templating" it and modifying its SiO_2/Al_2O_3 molar ratio. Temperature-programmed desorption (TPD) of NH_3 emphasizes the strength and the acid centers distribution during the ZSM-5 synthesis.

INTRODUCTION

In view of its catalytic properties (aromatization of n-paraffins, ethylbenzene synthesis, conversion of methanol to gasoline, etc.), ZSM-5 may be considered the most important member of the high silica (pentasil) zeolites.[1,2]

In order to obtain the ZSM-5 framework structure a great variety of organic additives may be used, as quaternary ammonium salts, hydroxides, or their precursors,[3,4] lower aliphatic amines and alcohols, alkyldiamines, cyclic amides, etc.[5-7] The changes effected by addition of organics to the reaction mixture have to be evaluated in connection with the other parameters controlling the process, among which, the nature and the purity of the reactants, the initial mixture composition, the order of mixing, the aging period, the temperature and the pressure of hydrothermal crystallization.

The reaction mixture composition plays an important role in the process of zeolite formation. SiO_2/Al_2O_3 and Na_2O/SiO_2 mole ratios, for example, control the number of SiO_4 and AlO_4 tetrahedra per unit cell, while OH^-/SiO_2 and H_2O/SiO_2 ratios influence the structural type and the crystal morphology, by rating the interconversion equilibrium between the polymeric and molecular species present, and this way the network formation. The role played by temperature is complex. Generally, as temperature is increased, the solution supersaturation and consequently the nucleation rate decrease. This way increases the chance of getting larger crystals. However, above 200° C there is the possibility to crystallize another phase, especially quartz, whereas below 160° C, the crystallization rate decreases sharply.

In the present paper we attempted first to analyse the influence of IPA on the structural characteristics of ZSM-5 zeolite, while keeping constant the other reaction parameters, and second, to determine the strength and the distribution of zeolite acid centers.

Selecting IPA as the organic additive is based both on steric (tetrahedral structure with 5.5 Å effective molecular size) and chemical grounds as well (basic, polar molecule, which may form, through its nitrogen lone pair, complexes with the atoms of the framework).[8]

The final product was characterized by X-ray powder patterns, optical and scanning electron microscopy, chemical analysis, thermal analysis, adsorption and subsequently TPD of NH_3.

EXPERIMENTAL

As starting materials for ZSM-5 synthesis were used commercial-grade waterglass type SE (26.6 SiO_2, 8.9 Na_2O, 64.5% wt/wt H_2O) and $Al_2(SO_4)_3 \cdot 18\,H_2O$. The pH has been adjusted with H_2SO_4.

We used the following steps in the synthesis : 7–38 hours digestion under autogenous pressure and 180° ± 3 C, of the alkaline reaction mixture (pH = 12–12.5), stirred by rotation ; filtering and water washing (pH = 8–9) of the RNaZSM-5 obtained (R – organic cation) ; removal of the organic template by 4 hours calcination at 550°C in order to obtain NaZSM-5 ; exchange of Na^+ with NH_4^+ by circulating a 2M NH_4NO_3 solution over a heated (80°C) zeolite column ; decomposition of NH_4ZSM-5 by 3 hours calcination at 600°C ; one obtains HZSM-5 as final product.

RESULTS AND DISCUSSION

Table 1 gives pertinent data for synthesis of zeolite ZSM-5. One notices that an increase in the crystallization time is accompanied by a slight increase in both the SiO_2/Al_2O_3 and the crystallinity of the final product, as for samples Nos 1 to 3. To a first approximation the extension of the crystallization time over 21 hours apparently brings no benefit.

Table 1

Synthesis of Zeolite ZSM-5

Exp. No.	Initial composition (mole ratio)				Cryst. time (h)	Product comp. (mole ratio)	Crystallinity (%)	Product zeolite
	$\frac{SiO_2}{Al_2O_3}$	$\frac{HO^-}{SiO_2}$	$\frac{H_2O}{SiO_2}$	$\frac{IPA}{SiO_2}$		$\frac{SiO_2}{Al_2O_3}$		
1	87.2	0.22	44.8	0.69	38	50.6	100	ZSM-5
2	87.2	0.22	44.8	0.69	28	48.8	98.8	ZSM-5
3	87.2	0.22	44.8	0.69	21	46.3	98.0	ZSM-5
4	110.0	0.25	44.8	0.69	21	56.3	98.2	ZSM-5
5	87.2	0.22	44.8	0.46	28	38.9	97.6	ZSM-5
6	87.2	0.22	44.8	0.46	21	36.2	86.2	ZSM-5 + amorphous
7	87.2	0.22	44.8	0.23	28	30.2	96.7	ZSM-5 + amorphous
8	87.2	0.22	44.8	0.23	21	28.1	75.2	ZSM-5 + amorphous
9	55.1	0.2	44.8	0.69	38	42.1	100	ZSM-5

The influence of the reaction mixture composition on the zeolite framework composition is evidenced by comparing samples Nos 3, 4 and 9. Indeed, the increase in the initial SiO_2/Al_2O_3 allows one to obtain a more siliceous zeolite.

It should be pointed out at the outset that the effect of the IPA content in the crystallization gel, specifically IPA/SiO_2, is of an intricate nature. As can be seen from Table 1 it is possible to improve the SiO_2/Al_2O_3 ratio of the zeolite and at the same time the crystallinity (samples Nos 3, 6 and 8, also 2, 5 and 7), keeping constant all the other parameters excepting IPA/SiO_2. One notices that the increase in IPA content shortens markedly the time required to obtain a certain crystallinity. This may be understood by admitting a combined action of IPA : templating the ZSM-5 structure and controlling the SiO_2/Al_2O_3 ratio in zeolite product. Both effects might be attributed to the above mentioned stereospecific and chemical factors. It seems that crystallization of ZSM-5 will continue until the aluminum in the reaction mixture is exhausted. One can argue that the process is accelerated by bringing into solution the aluminum containing species via complex formation with participation of IPA.

The importance of IPA addition for ZSM-5 synthesis resides not only in the possibility to achieve well crystallized samples with an advanced purity, but also in the high reproducible outcomes. Supporting this assertion were the results of the over 40 batches crystallized by the authors. The explanation for this finding might reside in the fact that the templating effect of IPA as well as of $(C_3H_7)_4N^+$ are little perturbed by the variation (in certain limits) of the other system parameters.

ACIDITY MEASUREMENTS

The catalytic activity and selectivity of zeolite HZSM-5 in many reactions involving carbonium ions intermediates are conditioned by the presence of acid centers associated with the negatively charged AlO_4^-.[9]

In order to establish the strength and the distribution of the acid sites NH_3—TPD has been used. NH_3 meets the requirements for a suitable probe molecule : basicity and a small critical diameter (2.6 Å).[10,11] Connecting the desorption reactor with a conductometric cell, equipped with a thermostatic control, it was possible to continuously record the integral titration curves of certain amounts of 0.01 N H_2SO_4 solution with the programmed evacuated ammonia,[12] as a function of temperature or time. Differentiation of the above curves gives the desorption profiles shown in Fig. 1, which represent the variation of the desorption rate (in arbitrary units) with time or temperature.

Only NaZSM-5 and HZSM-5 samples were saturated with NH_3 and then equilibrated in a sweep gas (nitrogen) at 293°K, until constant conductivity, prior to TPD, for the purpose of eliminating physically adsorbed ammonia.

The profile from NaZSM-5 (curve 1) indicates that some of the acid centers appear in the course of eliminating the organic template. One might be tempted, based on the position of the maximum (500—550° C) to consider the majority of these centers as fairly strong. Thermal decomposition of NH_4ZSM-5 (curve 2) shows a maximum localized approximately between the same limits as well. This would indicate, again, a departure of ammonia from strong acidic sites. However, the argument as to whether ammonia, initially located — as NH_4 — on weak sites, desorbs and readsorbs progressively on stronger ones with increasing temperature, or the site occupancy is maintained, until decomposition of NH_4 is a matter of speculation.

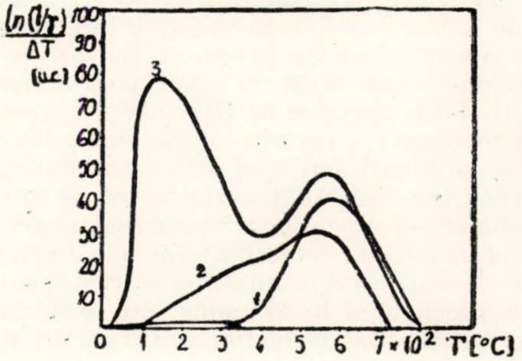

Fig. 1. — Differential TPD profiles for ammonia from NaZSM-5 (curve 1), NH_4ZSM-5 (curve 2), HZSM-5 (curve 3). Ammonia initially sorbed at 293°K, 1 atm. Heating rate 7°K min^{-1}. Sweep gas (nitrogen) flow rate 20 cm^3 min^{-1}.

In addition to the high temperature maximum, curve No 3, taken with a HZSM-5 sample of the same SiO_2/Al_2O_3 ratio as the other two, exhibits another maximum at much lower temperature (150—250°C), which might be attributed to weak acid sites.

The conductometric curves allow one to evaluate the number of acid centers on each temperature interval. It appears that the total number of acid sites increases, for the same SiO_2/Al_2O_3 ratio in the sequence : Na—, NH_4—, H—ZSM-5. This trend could be rationalized admitting that, for the first two cases, a certain amount of acid centers (both strong and weak) are neutralized by Na and NH_4, respectively. On the other hand, for the protonated samples of different compositions, this number decreases steadily as the SiO_2/Al_2O_3 ratio increases (e.g. as SiO_2/Al_2O_3 changes from 36.2 to 40.1 and 46.3 the number of acid centers decreases successively as 8.17, 7.48 and 5.56×10^{20}/g HZSM-5). It is assumed that in the competition between Si and Al the latter one prevails in creating acid sites.

The activation energy for desorption, E_d, may be estimated,[13-15] using NH_3—TPD curves as well. Assuming that NH_3 adsorbs on a monomolecular layer on HZSM-5 (idea supported by the Langmuir type of adsorption isotherms), the desorption rate is given by :

$$v_d = \frac{d\theta}{dt} = \theta^n A e^{-\frac{E_d}{RT}} \qquad (1)$$

where θ — coverage degree ; A — preexponential factor ; E_d — activation energy, n — kinetic order.

For a linear heating rate β, we obtain :

$$\frac{d\theta}{dT} = \theta^n \frac{A}{\beta} e^{-\frac{E_d}{RT}} \tag{2}$$

which gives :

$$\ln\left(\frac{1}{\theta^n}\frac{d\theta}{dT}\right) = \ln\frac{A}{\beta}\frac{E_d}{R}\frac{1}{T} \tag{3}$$

Plotted (Fig. 2) for a kinetic order, n, close to unity, relationship (3) allows direct evaluation of E_d and A only for high temperature peak. This fact is not a drawback because the majority of the acid catalyzed organic processes take place at relatively high temperatures (over 400°C).

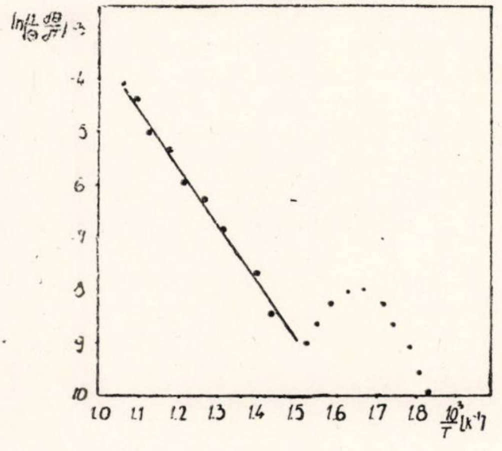

Fig. 2. — Log v_d (arbitrary units) versus 1000/T plot for sample No 1.

CONCLUSIONS

1. Use of IPA as structure directing agent makes it possible to obtain a well crystallized ZSM-5 zeolite with reproducible properties.

2. The main reaction parameters controlling the quality of the final product are the initial SiO_2/Al_2O_3, IPA/SiO_2 ratios, pH of the mixture, temperature and the time of hydrothermal crystallization.

3. Acid centers appear already in the stage of NaZSM-5 formation and increase in number and strength in the course of NH_4ZSM-5 decomposition.

REFERENCES

[1] H. Nakamoto and H. Takahashi, *Zeolites*, **2**, 67 (1982).
[2] P. A. Jacobs, H. K. Beyer and J. Valyon, *Zeolites*, **1**, 161 (1981).
[3] M. Cruceanu, E. Popovici, N. Bâlbă, N. Naum, L. Vlădescu, R. Russu and A. Vasile, "Site moleculare zeolitice", Ed. Ştiinţifică şi Enciclopedică, Bucharest, 1986.
[4] A. Vasile, "Zeoliţi de tip ZSM. Sinteză, caracterizare, utilizări". Doctoral Thesis, Iaşi, 1987.
[5] A. Vasile and M. Cruceanu, Romanian Patent 86 665 (1984).
[6] A. Vasile, M. Cruceanu and N. Bâlbă, Romanian Patent 80 122 (1985).
[7] A. Vasile, M. Cruceanu, N. Bâlbă and V. Ababi, Romanian Patent 86 668 (1984).
[8] E. Pincovschi, M. Merches and Kim Chol Sik, The 2nd Symposium on "Zeolites in modern technology" Iaşi, 1987, p. 124.
[9] I. Săndulescu, O. Şerban, S. Davidescu, R. Russu and L. Frunză, *Rev. Roumaine Chim.*, **23**, 1575 (1978).
[10] V. A. Sokolov, N. S. Torocheshnikov and N. V. Keltsev, Moleculearnye Sita i ih primenenie, Izd. Himia, Moscow, 1964.
[11] N. Y. Topsoe, K. Pedersen and E. G. Derouane, *J. Cat.*, **70**, 41 (1981).
[12] E. Pincovschi, M. Merches, I. Săndulescu and Kim Chol Sik, The 2nd Symposium "Zeolites in modern technology" Iaşi, 1987, p. 163.
[13] R. J. Cvetanovic and Y. Amenomiya, *Adv. Cat.*, **17**, 103 (1967).
[14] R. J. Gorte, *J. Cat.*, **75**, 164 (1982).
[15] M. Alnot and A. Cossuto, *Surf. Sci.*, **112**, 325 (1981).

Revue Roumaine de Chimie, **34**, *4*, 1061—1073(1989)

RELATIONSHIPS BETWEEN CROSSLINKED COPOLYMER SYNTHESIS AND THEIR FEATURES

IG. C. POINESCU and A. CARPOV
Institute of Macromolecular Chemistry "Petru Poni", Aleea Gr. Ghica-Vodă no. 41A, 6600
Iassy, Romania

Received October 23, 1988

The paper presents the influence of the δ-solubility parameter on the styrene—divinylbenzene copolymer features. It was also proved that porous copolymers prepared in the presence of "good solvent" have a better ordered texture that allows them to swell to a greater extent in methanol which is a "bad solvent". Using mixtures of diluents having various δ-values and taking into account the percent of divinylbenzene, it is possible to choose the synthesis parameters in order to predict a certain structure.

INTRODUCTION

The development of the bead internal macroreticular structure has a great importance in the ion-exchange industry adsorbents for technology of "Gel Permeation Chromatography" as precursors for carbon-beads and as networks for polymer-bound reagents (enzymes, drugs, etc.). It is necessary to establish the mechanism which governs the relationships between the conditions of the copolymerization process and the properties of the matrix. The structures of macroporous networks depend on the solvent-polymer solubility parameter and the crosslinking degree.[1-7] Due to the continuous changes that occur during the copolymerization process (the concentration of diluent and polymer, the variation of the crosslinking density as a function of the conversion reaction, the differences between the copolymerization constant values of the monomers within the monomer composition, etc.), the separation of the pure solvent phase outside the gel phase takes place gradually. That leads to a very heterogeneous network structure that influences strongly the features of the matrix which are used as adsorbents, supports for ion-exchanges or polymeric reagents.

It was also noticed that the pores in these networks can collapse during the synthesis process, particularly during the removal process of the inert diluent and the drying process.[6-9] The collapse phenomenon of the pores has to be considered as a result of the cohesional forces when the solvated polymer chains are approaching each other, by the loss of the diluent. It was also observed that the collapse effect is strongly related to the solubility parameter.[10] In the case of the porous matrix, the collapse effect is stronger in smaller pores than in larger ones, and in a few cases, it is a reversible process ; the collapsed networks can be reswollen in a proper solvent.

Lately, mixtures of two diluents; one "good solvent" and the other a "precipitant one" have been often used to perform a proper pore size and pore distribution.[8, 10, 12]

Generally, good solvents produce small pores, while, bad solvents (precipitants) give large pores. This is quite important, because the features of an adsorbant may be very well tailored in a wide range changing the diluent and the crosslinking degree, or the other synthesis parameters.

Alfrey and Lloyd,[13-14] found that the solubility parameter determines decisively the porous structure (pore internal distribution) of the networks and it can be computed using the equation

$$\delta^2 = (\Delta H - RT)/V = \text{CED} \qquad (\text{cal/ml}) \qquad (1)$$

where ΔH is the latent heat of vaporization, R is the gas constant, T is the absolute temperature, V is the molar volume, and CED means "cohesive energy density".[14]

The structure formation of the porous copolymers must be explained as the difference between the solvent-polymer solubility parameter values, because the heat of mixing for two or several substances depends on the square root of the solubility difference of the components. If δ_1 is the solubility parameter assigned to solvent, and δ_2 is the solubility parameter for the polymer, then when $\delta_1^2 \cong \delta_2^2$ the two sustances will be miscible.

Also, Alfrey and Lloyd[13,14] showed that $\delta_1 = \delta_2 \pm 0.8$ when a suitable solvent or mixture is used as a diluent medium to generate porous copolymers. In practice, the solvent or diluent mixture has a CED of about 65–85 (cal/ml).

This paper deals with the influence study of several diluents, or diluent mixtures on the network texture. The investigations try to emphasize the relationships between the solubility parameters and the macroporous copolymer features.

EXPERIMENTAL

1. Preparation of Porous Networks

Styrene (St) and divinylbenzene (DVB) were freed of inhibitor and vacuum-distilled before use. Practical-grade DVB had the following chemical composition (measured by gas chromatography); 59.75% DVB, 36.42% ethylstyrene, and 6.41% nonpolymerizable compounds. Because ethylstyrene, which accompanies always practical-grade DVB participes in the copolymerization process yielding a ternary copolymer which can be termed as styrene-ethylstyrene-divinylbenzene copolymer. The second comonomer (i.e. ethylstyrene) becomes dominant when high percents of crosslinking agent are used.

All inert diluents were practical-grade and were used as received. The suspension copolymerization technique of the monomers is used most frequently to obtain pearl-shaped networks for an organic/water phase ratio of 1 : 2.5, v/v.

The copolymerization process was run in a one liter capacity flask, cylindrical shape, fitted with a variable mechanical stirrer, thermometer, and reflux condenser. A solution of St, DVB and variable volumes of solvent was poured into the flask which contained an aqueous solution of styrene-maleic anhydride copolymer ammonium salt (0.25–0.50% vs. water), gelatine (0.10–0.25% vs. water) and 3.0% NaCl. The organic phase was dispersed as fine droplets and the copolymerization process was performed at 80°C for about 20 h in a thermostated bath. The copolymer beads were washed, sieved, extracted with methanolor steam.

2. Characterization of Copolymers

Porous networks were characterized from a physical point of view in order to obtain information on their inner structure. The beads vacuum-dried at 50°C for about 40 h, and the apparent density [15] (ρ_{ap}), solvent uptake coefficients,[16] pore volume,[15] porosity,[15] (P %) and the specific surface area [17] were measured.

The pore volume (P.V), or the whole macroporosity of the copolymers was calculated according to the equation

$$PV = 1/\rho_{ap} - 1/\rho_{sp} \tag{2}$$

where, ρ_{ap} is the apparent density (g/ml) and ρ_{sp} is the skeletal density (the mean value is 1.090 g/ml).

The porosity (P %) was calculated according to the relationship

$$P\,\% = 100(1 - \rho_{ap}/\rho_{sp}) \qquad (3$$

and reflects the pore percent contained by the porous network.

The mean-pore diameter size was computed applying the equation

$$\overline{D} = \frac{4 \cdot PV}{S_{BET}} \,.\, 10^4 \tag{4}$$

(the cylindrical model was assumed for the pore shape).

RESULTS AND DISCUSSION

During the network synthesis several diluents were used (cyclohexane, cyclohexanol, cyclohexanone, toluene, 2-ethyl hexyl alcohol or their mixtures) compounds whose δ-solubility parameter values lie within a large domain (Table 1).

Table 1

Solubility parameter values of several diluents [19]

No.	Diluent	(cal/ml)$^{1/2}$	Cohesive energy density (CED) (cal/ml)
1	Cyclohexane	7.81	60.99
2	Cyclohexanol	9.94	98.90
3	Cyclohexanone	9.90	98.01
4	Toluene	8.90	79.21
5	Chlorbenzene	9.50	90.25
6	Styrene	9.30	86.49
7	Polystyrene	9.10	82.81
8	Alyphatic hydrocarbons ($C_8 - C_{11}$)	7.50	56.25
9	2-Ethyl hexyl alcohol	9.96	99.20
10	di 2-Ethyl hexyl phosphoric acid	11.03 *)	121.66 *)
11	Tri-n-butyl phosphate	8.20	67.24

*) It was estimated from the structural formula the use of Small's "Molar-Attraction Constants" and it was applied the equation $\delta = \Sigma G/M$ where d is the density and M the molecular weight. ΣG is the sum for all atoms and grouping in the molecule of diluent.

It is observable that the study dealt with "good and bad solvents" of the polystyrenic chain. This led to a multitude of the network structures which might be performed. It has to be mentioned that during the copolymerization process performed in the presence of a bad solvent there is a mixture consisting of precipitating diluent and monomers that are solvating compounds of the polystyrenic chains and whose concentration decreases constantly. The ratio between them is changing function of the conversion degree of monomers. The system becomes richer in the precipitating diluent and the phase separation occurs. As the network chains form, they are no longer extended, as in the case where the diluent shows a high interaction with the copolymer, so there is an increasing tendency for growing chains to entangle inside the virtually unswollen nuclei. Therefore, the yielded network system is one in which large entangled nuclei are connected by a relatively small number of coiled and crumpled intermolecular chains and the polymer and dilute phase are segregated. The diluent-filled network can no longer be regarded as a swollen gel. This is the case when a *bad solvent* (*diluent*) is used.

When a copolymerization process is performed in the presence of a "good solvent", but otherwise an inert diluent, the chains are all the time fully solvated and thus during the copolymerization process, less shrinkage occurs than in corresponding systems, in the absence of a solvating compound. Therefore, the nuclei are less entangled and with the increasing dilution the growing chains attain greater length. Such networks swell even in methanol, though it is a "bad solvent". It must be pointed out that a porous texture results in using a minimum amount of crossliker and diluent. For instance, the porosity (%P), the volume swelling coefficient (β) and the specific surface area (S) depend strongly on δ-parameter for the three diluents (Figures 1–3). Cyclohexanol, used as diluent forms the highest porous matrix.

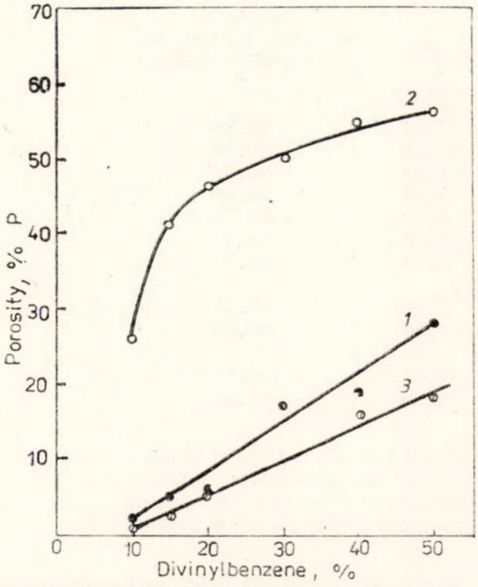

Fig. 1. — The porosity (%P) vs. DVB (%) for the macroporous networks prepared in the presence of 50% diluent; 1—cyclohexane; 2— cyclohexanol; 3 — cyclohexanone.

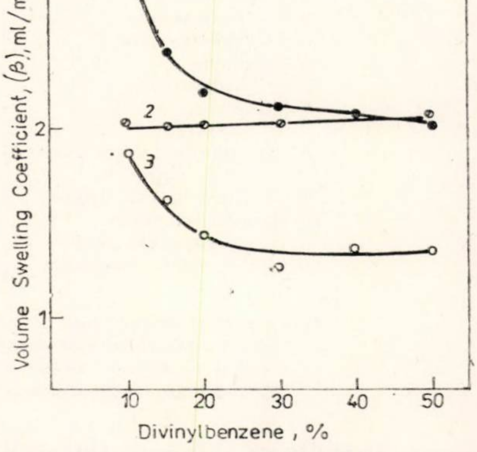

Fig. 2. — The volume swelling coefficient (β) vs. DVB (%) for the macroporous networks prepared in the presence of 50% diluent; 1 — cyclohexane; 2 — cyclohexanol; 3 — cyclohexanone.

It is well known that the St. DVB copolymers swell in solvating diluents and the degree of swelling depends on the crosslinking percent.

The macroporous matrix has, besides the permanent porosity (in dry state), a swelling porosity whose magnitude depends on the diluent kind used for monomer dilution. Therefore, the macroporous copolymers employed as packing cromatographic materials will swell in good solvents working with a higher porosity. The swelling porosity (β) measured using Dušek's equation[18]

$$\beta = \frac{\rho_{ap}}{\rho_{sp}} + (W-1)\times\frac{\rho_{ap}}{\rho_{solv}} \quad (\mathrm{ml/ml}) \qquad (5)$$

where, ρ_{solv} is the toluene density (0.8669) g/ml), W is the swollen copolymer weight/dried copolymer weight and $W-1$ has the same meaning and value as the solvent uptake coefficient, measured in toluene or other good solvent; it could be avoided (minimized) if a large percent of DVB (DVB 40.0%) had been used in the copolymerization process (Fig. 1). But the experimental results did not prove that assumption.

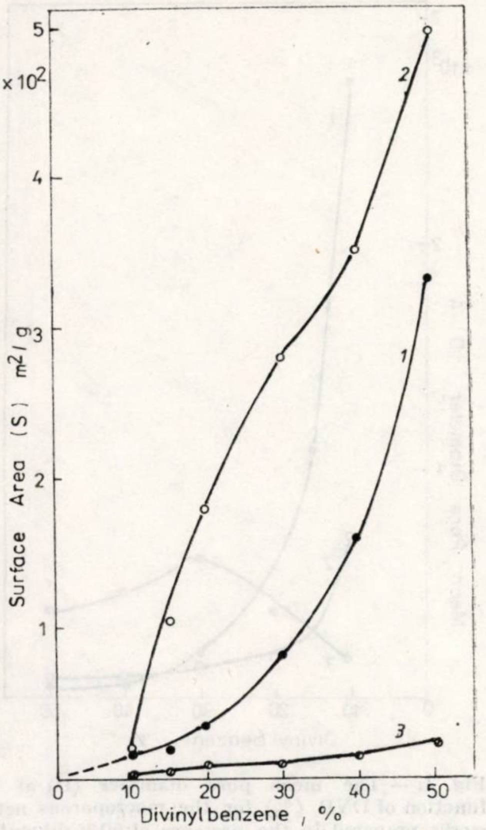

Fig. 3. — The specific surface area as a function of DVB (%) for the macroporous networks prepared in the presence of 50% diluent; 1 — cyclohexane; 2 — cyclohexanol; 3 — cyclohexanone.

The network with 50.0% DVB has a significant volume swelling coefficient (β), which depends on the kind and volume of diluent as well as the percent of DVB. The percent of DVB influences the volume swelling coefficient up to 20.0% DVB for cyclohexane and cyclohexanol, while it is almost constant for cyclohexanone (Fig. 2). The curves clearly show how δ-differences between the diluents influence the surface area magnitude and consequently, the pore size (Fig. 4).

Cyclohexane and cyclohexanol give networks with a higher specific surface area than cyclohexanone as a consequence of the CET values, i.e. δ-parameter, respectively (Fig. 3). For instance, the networks performed in the presence of toluene are characterized by high values of the surface area (small mean-pore diameter) while the networks prepared in the presence of cyclohexanone have low values of the surface area (large mean-pore diameter) (Figs. 3 and 4). We assume that this

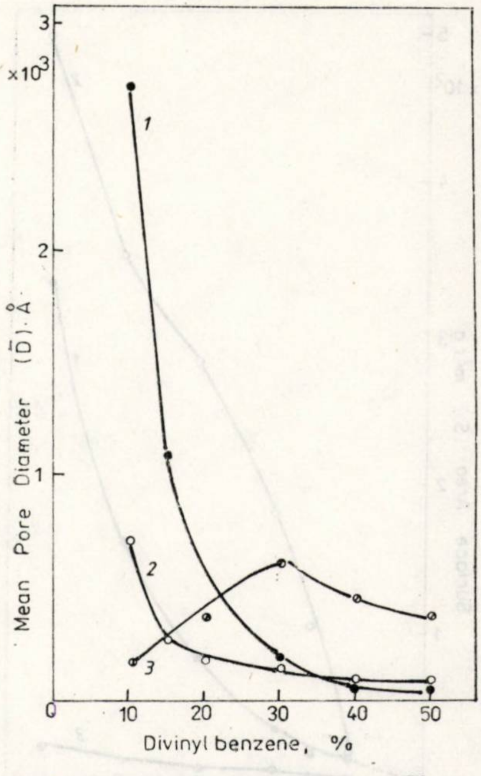

Fig. 4. — The mean pore diameter ($\overline{D}$) as a function of DVB (%) for the macroporous networks prepared in the presence of 50% diluent; 1 — cyclohexane; 2 — cyclohexanol; 3 — cyclohexanone.

peculiar behaviour of the two diluents results in the CED value differences (see Tab. 1). For instance, in the 50.0% DVB and 50.0% monomer mixture dilution, the measured surface area values of the performed networks are of 490.0 m²/g (cyclohexanol) and 280.0 m²/g (cyclohexanone), respectively (Fig. 3). Cyclohexane gets an intermediary place with its 332.0 m²/g.

The mean-pore diameters $\overline{D}$ show large differences for low percents of DVB, while the copolymers are more homogeneous when cyclohexane and cyclohexanol are used as diluents (Fig. 4). Also, the networks performed in the presence of cyclohexanone and whose percents of DVB vary from 10.0% to 50.0% DVB do not show significant modifications in the surface area values (Fig. 3). The mean-pore diameter presents a maximum at about 30.0% DVB (609.0 Å) and then it decreases to 387 Å for 50.0 % DVB. The largest mean-pore diameter measured for cyclohexane is about 2700 Å (10.0% DVB and 50.0% diluent; Fig. 4) and the highest porosity is obtained for cyclohexanol (Fig. 1).

The influence of phosphoric acid esters, used as diluents, on the St. DVB copolymers have an interesting behavior (Fig. 5,6).

The sample containing only 5.0% DVB prepared in the presence of tri-n-butyl phosphate (TBP) has a specific surface area of about 115 m²/g, while the sample containing 50.0% DVB (performed under the same conditions) has 550.0 m²/g (measured by means of BET method). It seems that the same volume of TBP for various percents of DVB has a little influence on the development of the specific surface area (Fig. 5). According to the values of the δ-solvent-polymer factor and the experimental results, one can notice that between the two inert media (TBP and Di-2-ethyl hexyl phosphoric acid, D2EHPA) there are large differences which are reflected in the porous structure of the networks (Table 2).

The high values of the surface area are similar to the networks prepared in the presence of the solvating diluents which swell the polymeric chains.

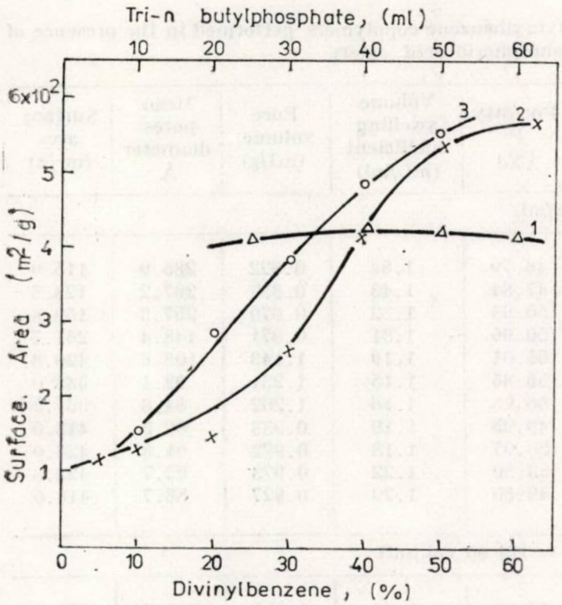

Fig. 5. — The specific surface area (S) vs. DVB (%), and TBP volume (1). 2 — 50 ml TBP; 3 — 50 ml D2EHPA/C_6H_5Cl.

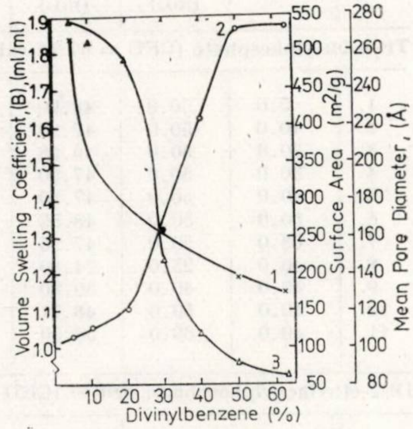

Fig. 6. — The volume swelling coefficient (β), (1), surface area (2) and the mean pore diameter (3) as a function of DVB (%). (Dilution : 50 ml TBP/50 ml monomer mixture).

It is well known that the principle of the synthesis of heterogeneous crosslinked copolymer consists in using a large quantity of DVB and diluting the monomer phase by a certain volume of diluent, which has to accomplish several conditions.[1] So, one can notice that the volume-swelling coefficient decreases with the increase of DVB percent. This is due to the increase of the stiffness of the porous networks. The polymeric chains become more rigid and solvation occurs only in the low crosslinked porous copolymers. Therefore, the higly crosslinked nuclei are only slightly swellable (Fig. 6).

The mean pore diameter decreases sharply with the increase of the upper limit of the DVB percent for which a further increase of the surface area does not occur ; the surface area values remain almost constant after addition of 50.0% DVB (Fig. 6).

Several samples of copolymers were characterized by the Hg-porosimetry measuring the pore diameter between 75.0 and 75000 Å (Table 3).

It can be noticed that the samples prepared in the presence of D2EHPA : C_6H_5Cl mixture have pores which range between 75 Å and 3000Å, while the ones obtained in the presence of TBP have larger pore diameters with a larger pore distributions. Also, it was measured a greater pore volume for TBP than the samples performed in the presence of D2EHPA : C_6H_5Cl mixture (Table 3).

Table 2

Main characteristics of porous styrene-divinylbenzene copolymers performed in the presence of organic phosphoric acid esters

Exp. no.	DVB (%)	Inert medium		Porosity P (%)	Volume swelling coefficient (mL/ml)	Pore volume (ml/g)	Mean pores diameter Å	Surface area (m^2/g)
		Added [a] (mL)	Found [b] (mL)					
Tri-n-butylphosphate (CED = 67.24 cal./ml)								
1.	5.0	50.0	48.90	46.79	1.84	0.822	285.9	115.0
2.	10.0	50.0	47.90	47.84	1.43	0.857	267.2	128.3
3.	20.0	50.0	46.98	50.93	1.32	0.970	257.3	150.8
4.	30.0	50.0	47.90	50.96	1.31	0.971	148.4	261.7
5.	40.0	50.0	47.80	55.01	1.19	1.143	108.6	420.8
6.	50.0	50.0	48.53	56.85	1.15	1.231	92.1	535.0
7.	63.0	50.0	47.95	56.25	1.16	1.202	84.8	567.0
8.	40.0	25.0	24.80	49.95	1.19	0.933	90.5	413.0
9.	40.0	40.0	39.80	50.97	1.18	0.972	91.3	426.0
10.	40.0	50.0	48.71	53.30	1.22	0.973	92.7	422.3
11.	40.0	60.0	58.50	49.80	1.20	0.927	88.7	418.0
Di-2-ethylhexylphosphoric acid [c] (CED = 121.66 cal./ml)								
12.	10.0	25.0	24.21	47.19	1.66	0.835	218.3	153.0
13.	20.0	25.0	24.72	48.77	1.56	0.889	124.8	285.0
14.	30.0	25.0	24.00	45.09	1.66	0.767	79.5	386.0
15.	40.0	25.0	24.17	45.61	1.66	0.784	64.7	485.0
16.	50.0	25.0	24.90	44.39	1.65	0.746	61.3	487.0

[a] Added to 50.0 g of the monomer mixture
[b] Included in 50.0 g of the copolymer
[c] 25 ml D2EHPA/25 ml C_6H_5Cl added to 50.0 g of the monomer mixture

In the introduction it was pointed out that using mixtures of two or several diluents it will be possible to predict the texture of the networks. So, there were carried-out experiments using mixtures of toluene-2-ethyl hexyl alcohol (TEHA), or toluene-gasoline (b.p. 115–150°C); (T.G.). The values of δ-solvent-polymer parameter was calculated applying Small's equation[20]

$$\delta = \frac{\delta_1 \cdot X_1 \cdot V_1 + X_2 \cdot V_2 \cdot \delta_2}{X_1 \cdot V_1 + X_2 \cdot V_2} \tag{6}$$

One can notice that the values of the pore volume for the three crosslinking degrees depend strongly on the δ-values. Samples having a high percent of DVB tend to have an almost linear dependence of the δ-parameter value (Fig. 7; curve 3). The CED values vary from 81.0 to 97.0 cal/ml that according to the theory[21] this domain lies towards the upper limit. Also, this domain of CED leads to spectacular variation both in the pore volume and pore diameter values (Figs. 7 and 8).

The mean pore diameter values are more influenced by the solubility parameter (δ) (Fig. 8). The curve shapes are almost similar, though

Table 3

Pore distribution measured by Hg-porosimetry

Exp. no.	DVB (%)	Pore volume (ml/g)	Pore distribution (%)						
			$0.75-1\times10^2$	Å $1-3\times10^2$ Å	$3-6\times10^2$ Å	$0.6-1\times10^3$ Å	$1-5\times10^3$ Å	$0.5-1\times10^4$ Å	$1-7.5\times10^4$ Å
Tri-n-butylphosphate (CED = 67.24 cal. ml)									
2.	10.0	0.7746	9.05	54.53	24.28	7.72	1.77	0.88	1.77
3.	20.0	0.8044	8.14	41.18	31.45	11.31	6.56	0.68	0.68
D-2-EHPA (CED = 121.66 cal./ml)									
12.	10.0	0.3008	30.62	53.13	4.38	1.24	3.76	0.62	6.25
13.	20.0	0.4532	15.63	65.62	6.64	3.52	5.47	1.17	1.95
14.	30.0	0.3162	26.74	59.28	5.67	3.61	2.58	2.06	2.06
15.	40.0	0.4368	16.03	68.58	8.02	1.60	3.53	0.96	1.28

Table 4

Influence of the toluene removal from the macroporous matrices on some physical features ($f_v = 0.35$)

Exp. no.	DVB (%)	Toluene was removed with								Uptake of dye-stuff	
		Steam				Methanol					
		Uptake coefficient (g/g)			Apparent density (g/ml)	Uptake coefficient (g/g)			Apparent density (g/ml)	Steam (g/l)	CH_3OH (g/l)
		CH_3OH	Toluene	Cycloh.		CH_3OH	Toluene	Cycloh.			
1	24.0	0.090	0.954	0.271	1.0341	0.219	1.682	0.820	1.0251	104.7	185.5
2	27.0	0.191	1.466	0.293	1.0160	0.601	1.850	1.091	0.9880	109.0	334.0
3	33.0	0.212	1.490	0.321	0.9982	1.240	2.120	1.770	0.9285	—	—
4	37.0	0.573	0.946	0.770	0.9562	1.365	1.735	1.200	0.8901	—	—
5	45.0	0.621	1.221	0.920	0.8832	1.960	2.230	1.720	0.5962	74.0	145.8
6	50.0	1.088	1.389	1.120	0.7752	1.630	1.902	1.890	0.5680	142.0	166.0
7	65.0	1.099	1.452	1.230	0.7328	1.830	2.080	1.970	0.5848	—	—

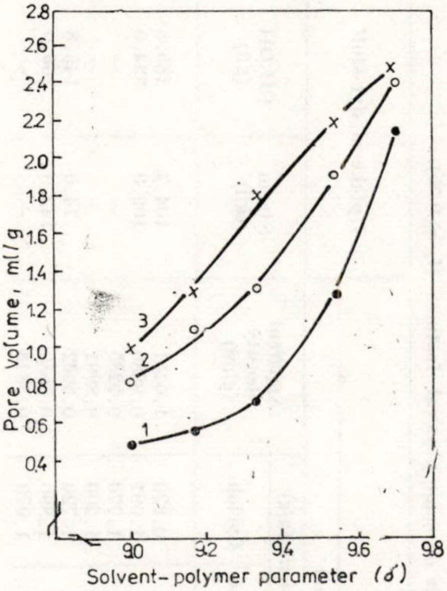

Fig. 7. — The pore volume (PV) vs. solvent-polymer solubility parameter (δ) for the diluent mixture "toluene-2-ethyl hexyl alcohol". 1 — 40% DVB; 2 — 50% DVB; 3 — 61% DVB.

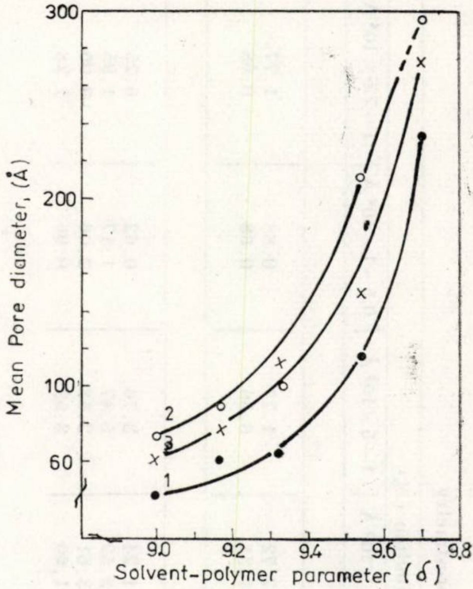

Fig. 8. — The mean pore diameter vs. solvent-polymer solubility parameter (δ) for the diluent mixture "toluene-2-ethyl hexyl alcohol"; 1 — 40% DVB; 2 — 50% DVB; 3 — 61% DVB.

the percent of DVB varies in wide range. If the TEHA ratio changes, the mean-pore diameter shifts from 53.46 Å to 236.85 Å (40.0 % DVB). The same remarks are also valid for the samples with 50.0% DVB and 61.0% DVB, respectively. The increase is due to the modification of the δ-value (Fig. 8).

Very interesting observations concerning the influence of diluent mixture composition variation on the specific surface area can be withdrawn (Fig. 9).

One can notice that a little bit queer behavior takes place. The variation of the surface area for the two copolymers (40.0% DVB and 50.0% DVB) shows a maximum for $\delta = 9.50$ $(\text{cal/ml})^{1/2}$ and $\delta = 9.33$ $(\text{cal/ml})^{1/2}$. This maximum moves towards the ordinate, so, for the samples which contain 61.0% DVB the curve starts from the highest value of the surface area and decrease when $\delta = 9.70$ $(\text{cal/ml})^{1/2}$, i.e., when the diluent mixture contains the largest amount of 2EtHA. The highest values of the specific surface area lie on a straight line whose slope gets the value $\text{tg}\alpha = -471.9$. This is a proof which demonstrates that between the δ-parameter, for a certain diluent mixture and the specific surface area there is a tight correlation which allows to choose an adequate composition of the organic phase in order to prepare a certain macroporous copolymer having determined features.

The porosity (%P) and the surface area (S) modifications of porous St. DVB copolymers, function of the DVB percent, for a constant TG ratio (1 : 1 by volume/volume) and 60.0% dilution of the monomer composition are plotted in Fig. 10.

The percent of DVB influences the specific surface area of the networks up to 50.0% DVB after that, it decreases for higher content of DVB. It is well known that the porous copolymers with large percent of DVB prepared in the presence of precipitating diluents still contain free vinyl groups, so that the true crosslinking degree is smaller than the quantity of DVB introduced in the mixture of monomers.[22]

The porous structure of St. DVB matrix varies with the diluent type in which the network was carried out due to the flexibility of macromolecular chains. It was observed that the copolymers prepared in the precipitating diluents and dried show a maximum porosity, which is close to the porosity in the swollen state.[23] If the drying process of the copolymers is performed in good solvent it may lead to a partial collapse of the pores. Recently Okay[24] and formerly Millar[25] have shown that during the drying process the pores collapse particularly in the rubbery

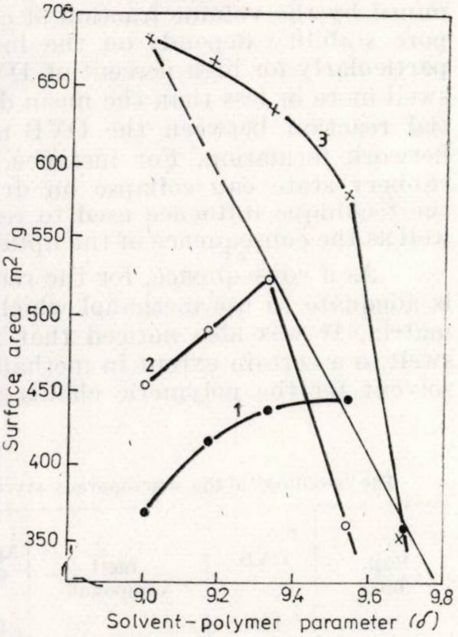

Fig. 9. — The specific surface area vs. solvent polymer solubility parameter (δ) for the diluent mixture "tolune-2-ethyl hexyl alcohol"; 1 — 40% DVB; 2 — 50% DVB; 3 — 61% DVB.

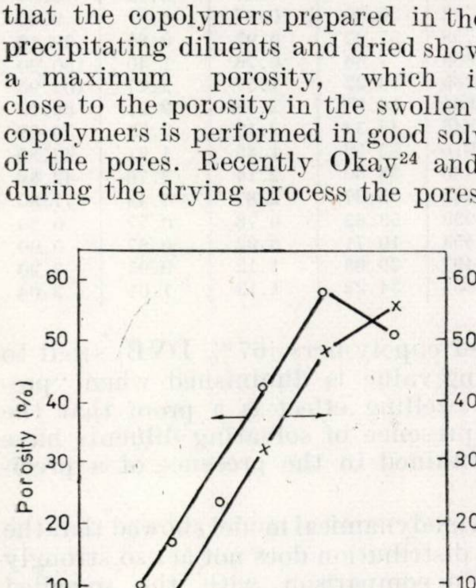

Fig. 10. — The porosity (%P) and the specific surface area as functions of DVB (%) for the diluent mixture "toluene-gasoline".

rather than in the glassy state and the pore structure stability is determined by the volume fraction of copolymer in the swollen gel. Also, the pore stability depends on the inhomogeneity in crosslink distribution, particularly for high percent of DVB. The samples contain regions which swell more or less than the mean degree of swelling, due to the preferential reaction between the DVB monomers and the mechanism of the network formation. For instance, the pores in network portion of the rubbery state can collapse on drying. The data of Table 4 emphasize the technique influence used to remove the inert medium from beads as well as the consequence of the uptake of dye-stuff by the anion-exchangers.

As a consequence, for the removal of the "good solvent" diluent it is adequate to use methanol which preserves the initial structure of the matrix. It was also noticed that the samples prepared in good solvent swell to a certain extent in methanol though this compound is the worst solvent for the polymeric chains (Table 5).

Table 5

The "swelling" of the macroporous styrene-divinylbenzene copolymers in methanol

Exp. no.	DVB (%)	Inert compound	Apparent density (g/ml)	Porosity (%)	Solvent uptake methanol (ml/g)	Coefficient cyclohexane (ml/g)	Swelling in methanol (%)
Amberlite	XAD-1	—	0.7316	31.62	0.49	0.72	6.55
Amberlite	XAD-2	—	0.6762	36.80	0.87	0.87	9.40
Amberlite	XAD-4	—	0.6738	37.02	0.97	0.85	29.10
28	27.00	Toluene	0.9880	7.66	0.76	1.40	130.00
29	33.00	Toluene	0.9285	13.22	1.57	2.27	102.90
30	45.00	Toluene	0.8901	16.81	2.48	2.21	96.70
31	67.00	Toluene	0.5848	45.34	2.13	2.53	79.09
32	35.00	Tol/Hep	0.5076	52.56	1.45	1.91	42.85
33	35.00	Tol/Hep	0.4430	58.60	2.14	3.76	42.86
34	40.00	Tol/Hep	0.6862	35.87	2.87	1.43	77.80
35	10.00	Hep/PS	0.4939	53.83	0.78	0.77	0.50
36	10.00	Gasoline	0.9554	10.71	0.92	0.87	0.00
37	10.00	2EH-alcohol	0.7497	29.93	1.12	0.93	2.20
38	10.00	2EH-alcohol	0.7234	34.22	1.13	1.01	2.04

Even samples of high crosslinked copolymers (67% DVB) swell to about 79.9% in methanol. The swelling value is diminished when "precipitants" are used as diluents. The swelling effect is a proof that the copolymer samples performed in the presence of solvating diluents have more ordered structures than those obtained in the presence of a precipitant one.

The studies carried out on the thermodynamical model showed that the heterogeneity of the crosslinked bond distribution does not act so strongly in the case of the solvating diluent in comparison with the so-called precipitants very often used as inert media.[1] This homogeneity (approximately) allows a light solvation and swelling of the polystyrenic chains.

Therefore, the use of methanol to measure the uptake coefficient of the networks is not recommended because it does not give a true value of the pore volume. The characterization of the networks by the uptake coefficient of cyclohexane seems to be quite a correct measurement.

CONCLUSIONS

It was demonstrated the influence of δ-parameter value on the copolymer bead features using several diluents and mixtures of diluents.

The study allows to predict certain features for each porous network type function of the δ-parameter value in good agreement with the percent of DVB.

Although the δ-parameter value has a high influence on the matrix, the degree of the crosslinking determines the mean characteristics of the macroporous copolymers, even for the mixtures of diluents.

REFERENCES

[1] J. Seidl, J. Malinsky, K. Dušek and W. Heitz, *Adv. Polym. Sci.*, **5**, 113 (1967).
[2] K. Dušek, *J. Polym. Sci., Part C 16*, 1289 (1967).
[3] K. Dušek and W. Prins, *Adv. Polym. Sci.*, **6**, 1 (1969).
[4] W. G. Lloyd and T. Alfrey jr., *J. Polym. Sci.*, **62**, 30 (1962).
[5] W. L. Sederel and G. J. De Jong, *J. Appl. Polym. Sci.*, **17**, 2835 (1973).
[6] K. A. Kun and R. Kunin, *J. Polym. Sci., A-1*, **6**, 2689 (1968).
[7] H. Jacobelli, M. Bartholin and A. Guyot, *J. Appl. Polym. Sci.*, **23**, 927 (1929).
[8] Ig. Poinescu, Cr. Vlad, A. Carpov and A. Ioanid, *Angew. Macromol. Chemie*, **156**, 105 (1988).
[9] O. Okay and T. I. Balkoş, *J. Appl. Polym. Sci.*, **31**, 1785 (1986).
[10] Piotr P. Wieczorek, Bozena N. Kolart and Henryk Galina, *Angew. Macromol. Chemie*, **126**, 39 (1984).
[11] Ig. Poinescu, Cristina Vlad, A. Carpov, *Reactive Polymers*, **2**, 261 (1984).
[12] Ogut Okay, *Angew. Macromol. Chem.*, **157**, 1—15 (1988).
[13] T. Alfrey jr. and W. G. Lloyd US Pat. 3, 322, 695 (Cl. 260—2.5), 1967.
[14] A. D. Jenkins, "Polymer Science", A. D. Jukins, Ed., North-Holland, Amsterdam and London, 1972, p. 550.
[15] J. Melinsky and J. Seidl, *Chem. Prum.*, **13**, 100 (1963).
[16] K. W. Pepper, *J. Appl. Chem.*, **1**, 126 (1951).
[17] S. Brunauer, "The Adsorption of Gases and Vapors", Princeton Univ. Press, Princeton, N.Y., 1954, p. 151.
[18] K. Dušek, *Coll. Czech. Chem. Comm.*, **30**, 3804 (1965).
[19] A. D. Jenkins, "Polymer Science", A. D. Jenkins Ed., North-Holland. Amsterdam and London, 1972, p. 552.
[20] P. A. Small, *J. Appl. Chem.*, **3**, 21 (1953).
[21] T. Alfrey, Jr. and W. G. Lloyd, *J. Polym. Sci.*, **62**, 159, 301 (1962).
[22] K. Dušek, *Collect. Czech. Chem. Commun*, **27**, 284 (1962).
[23] J. Baldrian, B. N. Kolart, H. Galina, *Coll. Czech. Chem. Commun*, **46**, 1575 (1981).
[24] O. Okay, T. I. Balkas, *J. Appl. Polym. Sci.*, **31**, 1785 (1986).
[25] J. R. Millar, D. S. Smith, W. E. Marr, T. R. Kresman, *J. Chem. Soc.*, p. 218, p. 2779 (1963).

Revue Roumaine de Chimie, **34**, *4*, 1075–1079 (1989)

ИССЛЕДОВАНИЕ ПРОЦЕССОВ, ПРИВОДЯЩИХ К ПОТЕРЕ БИОЛОГИЧЕСКОЙ АКТИВНОСТИ ПРЕПАРАТОВ ОЛЕАНДОМИЦИНА ФОСФАТА

ИРИНА СЕРОВА *, ГАЛИНА ОЛЕЙНИКОВА и
АНАТОЛИЙ ИОСИФОВИЧ ГИНАК

Ленинградский технологический институт имени Ленсовета, Ленинград, СССР

Получена 3 октября 1988 г.

Проведено комплексное исследование процесса инактивации препаратов олеандомицина фосфата. Выделены и изучены некоторые биологически неактивные компоненты, накапливающиеся в препарате при хранении. Предложена возможная схема инактивации антибиотика, включающая на ранних стадиях отщепление молекулы воды в положении C_{11} и присоединение H_2O по эпоксидному кольцу; на более поздних стадиях — гидролиз по гликозидным связям.

Complex study of the inactivation process of the oleandomycin phosphate has been performed. Some biologically inactive components accumulating in the preparation during the storage have been extracted and studied. A scheme accounting for the inactivating process of the antibiotic is suggested. This scheme involves the elimination of water in the C_{11} position at an earlier stage and the addition of water to the epoxy ring. At the later stages of this process a hydrolysis on the glycoside bonds occurs.

Сохранение качества препарата до его потребления пациентом является существенным требованием, предъявляемым к лекарственным веществам. В связи с лабильностью сложных органических молекул особенно актуальна проблема их стабильности в готовых лекарственных формах.

В настоящей работе изучен процесс инактивации макролидного антибиотика олеандомицина фосфата, препараты которого теряют биологическую активность уже через полгода хранения. Ранее было показано, что препараты данного антибиотика могут содержать ряд неактивных примесей.[1,2] Высказано предположение, что примеси являются катализаторами процессов, приводящих к инактивации олеандомицина.[3] Отмечено также существенное влияние влажности на стабильность препарата.[4]

Для установления возможных путей инактивации антибиотика использовали метод ,,ускоренного старения'' препаратов при повышенной температуре, инактивированные препараты исследовали методами гельпроникающей (ГПХ) и тонкослойной (ТСХ) хроматографии, ИК-, УФ-, масс-спектрометрии.

---

* Адрес для переписки: 199155, Ленинград, СССР, ул. Кораблестроителей, дом 38, корпус 1, кв. 201, Серовой И. П.

Как и ожидалось, старение препарата повлекло за собой изменение вида хроматограмм, что позволило наблюдать возникновение продуктов деструкции (рис. 1). До инактивации на хроматограмме ГПХ наблюдается два пика (I и II). I пик, по данным ТСХ, включает, кроме олеандомицина, незначительное количество ангидроолеандомицина. II пик представляет примесь, обозначаемую в литературе как ,,примесь-260''.[5]

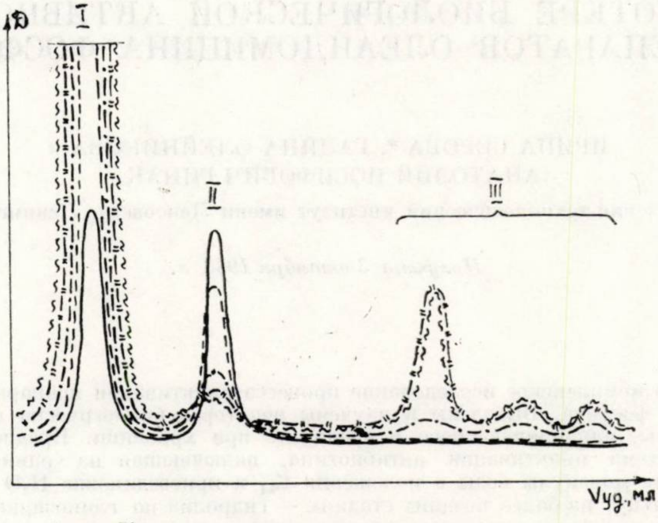

Рис. 1. — Кривые элюирования препаратов олеандомицина фосфата на разных стадиях ,,ускоренного старения'' при 37 °C: — перед началом старения; ······ — 2 недели старения; —·——4 недели; —,,——8 недель; ~~~—12 недель.

После двух недель ,,ускоренного старения'' наблюдалось сильное увеличение интенсивности I пика (рис. 1). Этот факт может быть связан с образованием ангидроолеандомицина, что подтверждается усилением поглощения в УФ-области при 235 нм, а также данным ТСХ со свидетелем — ангидроолеандомицином, полученным по известной методике.[6] Данные об образовании этого неактивного продукта имеются и в литературе.[4]

По мере старения препарата имело место уменьшение интенсивности II пика, что соответствовало, вероятно, деструкции ,,примеси-260'', а на более поздних стадиях (8, 12 недель хранения при 37°C) появилась группа пиков III, включающих низкомолекулярные продукты инактивации олеандомицина.

Наибольший интерес представляло изучение основных продуктов деструкции антибиотика, условно обозначенных А и Б , образующихся на ранних стадиях старения и не обладающих биологической активностью. Эти вещества были выделены из фракции, соответствующей пику I на хроматограмме ГПХ , методом препаративной ТСХ. Были изучены их физико-химические характеристики (табл. 1). Вещество Б по физико-химическим характеристикам было идентично ангидроолеандомицину.

Таблица 1

Физико-химические характеристики основных продуктов инактивации олеандомицина фосфата

Характеристика	Вещество А	Вещество Б
1. Элементный анализ		
вычислено С, %	53,50	62,78
Н, %	8,15	8,82
найдено С, %	53,34	62,57
Н, %	8,22	8,92
2. R_f в элюирующих системах:		
I ацетон-изобутанол-аммиак (25%)-вода (1: 8: 1: 6)	0,06±0,03	0,52±0,03
II бутанол-уксусная кислота-вода (3: 1: 1)	0,16±0,04	0,36±0,04
III. хлороформ-метанол-аммиак (17%) (2: 1: 1)	0,00±0,04	0,96±0,04
3. Температура плавления	207°С с разложением	201°С
4. Квазимолекулярный ион $(M+H)^+$	786	670

Для установления структуры продуктов инактивации были изучены ИК-, УФ- и масс-спектры этих соединений. Сравнивая ИК-спектры веществ А и Б со спектром олеандомицина, следует отметить их идентичность в области 3400—2700 см$^{-1}$ и 1000—1200 см$^{-1}$, что говорит о наличии в молекулах этих соединений N—H, O—H, C—C, C—H, C—O связей. [7]

Наибольший интерес представляет область полос поглощения, соответствующих валентным колебаниям C=O. В ИК-спектре олеандомицина полосу поглощения при 1730 см$^{-1}$ следует отнести к C=O лактона, а полосу при 1695 см$^{-1}$ — к C=O группе кетона.[8] Сопряжение с двойной углерод-углеродной связью при водит к понижению частоты поглощения C=O кетона в ИК-спектре вещества Б. Плечо при 1640 см$^{-1}$ можно отнести к валентным колебаниям C=C, полосу 1250 см$^{-1}$ — в спектрах олеандомицина и вещества Б — к симметричному валентному колебанию эпоксидного кольца. В ИК-спектре вещества А полоса при 1250 см$^{-1}$ отсутствует.

Для вещества А полоса поглощения, соответствующая валентным колебаниям C=O кетона, наблюдается при 1630 см$^{-1}$. Такое понижение частоты может быть вызвано дополнительным сопряжением C=O группы и двойной связи C=C, если происходит раскрытие эпоксидной группы с образованием гликоля ангидроолеандомицина, гидроксильная группа которого связывается прочной внутримолекулярной связью с C=O группой (рис. 2). Это предположение подтверждается также гипсохромным сдвигом R-полосы в УФ-спектре вещества А, по сравнению с олеандомицином, (λ_{max} = 280 нм), так как водородная связь понижает энергию n-орбитали.[8]

В масс-спектрах соединений А и Б наблюдается очень интенсивный пик протонированного квазимолекулярного иона $(M+H)^+$: м/z 786(100) — для вещества А, м/z 670(100) — для Б, а также пики фрагментных ионов,

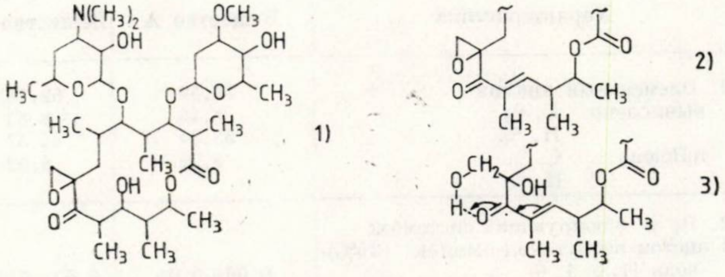

Рис. 2. — 1 — олеандомицин, 2 — ангидроолеандомицин, 3 — гликоль ангидроолеандомицина.

подтверждающие предложенную структуру анализируемых соединений Вещество А было идентифицировано как гликоль ангидроолеандомицина вещество Б-ангидроолеандомицин.

Кроме основных продуктов инактивации были выделены и проанализированы некоторые вещества, образующиеся на поздних стадиях старения (III, рис. 1). Исследование методом ТСХ показало, что вещества III$_1$ и III$_2$ не давали желтого окрашивания, характерного для антибиотиков-макролидов при проявлении хроматограмм в парах иода, не проявлялись анисальдегидным реактивом (специфическим реагентом на макролактон), однако давали характерное для сахаров окрашивание при проявлении анилиновым реактивом.

Полученные экспериментальные данные УФ- и ИК-спектров соединений III$_2$ и III$_3$ согласовались с характеристиками сахаров, входящих в молекулу олеандомицина, приведенными в литературе .$^{9-11}$ Анализ спектральных данных для другого соединения группы Ш$_1$ показал, что в молекуле этого вещества сохранен макролидный фрагмент и отсутствует углеводная часть. Вероятно, на поздних стадиях старения препаратов происходит деструкция антибиотика, связанная с гидролизом по гликозидным связям.

ЭКСПЕРИМЕНТАЛЬНАЯ ЧАСТЬ

Изучались экспериментальные образцы олеандомицина фосфата. Разделение компонентов проводили на жидкостном хроматографе ,,Farmacia'' (Швеция), используя сефадекс IH-20, элюент — 50% водный этанол. ИК-спектры снимали на приборе UR-10 (таблетки KBr), УФ-спектры — на СФ-26. Масс-спектры изучали на приборе ХЖ—МХ 3303 с электрогидродинамическим вводом раствора вещества в масс-спектрометр (метод ЭРИАД). Концентрация анализируемого соединения составляла 5.10^{-4}М в растворе CH_3OH-H_2O (9: 1).

Выделение и очистку продуктов инактивации проводили методом препаративной ТСХ в системе растворителей 1 (табл. 1). Чистоту веществ контролировали хроматографически в трех системах, применяемых в ТСХ для макролидных антибиотиков, значения R_f представлены в таблице 1. Использовали пластинки с закрепленным слоем силикагеля Силуфол УФ-254 (ЧССР). Хроматограммы проявляли в УФ-свете и анисальдегидным реагентом.[12] ,,Ускоренное старение'' препаратов проводили в предварительно вакуумированных и запаянных ампулах при 37°С.[13] Биологическую активность препаратов определяли методом диффузии в агар с помощью тест-культуры Bacillus mycoides.[14]

ЛИТЕРАТУРА

[1] Е. В. Комаров, Г. А. Олейникова, А. П. Селезнев и И. П. Серова, *Антибиотики и медицинская биотехнология*, **2**, 103(1982).

[2] Г. А. Олейникова, А. П. Селезнев и И. П. Серова, *Химико-фармацевтический журнал*, **8**, 1003(1984).

[3] Л. Д. Антоненко, Л. Р. Давиденков, Г. А. Олейникова и И. П. Серова, *Антибиотики и медицинская биотехнология*, **6**, 434(1986).

[4] А. А. Славин, И. З. Бруншетйн и Е. Д. Этингов, *Антибиотики*, **6**, 445 (1983).-

[5] С. П. Пышный, Т. И. Гайдукова и А. А. Славин, ,,Результаты научно-технического сотрудничества отраслевого НИИ(ВНИТИАФ) и ВУЗа (ЛТИ им. Ленсовета)'', Ленинград, 1980.

[6] F. A. Hochstein, H. Els and W. D. Celmer, *J. Amer. Chem. Soc.*, **82**, 3225 (1960).

[7] Л. Беллами, ,,Инфракрасные спектры сложных молекул'', Изд-во ,,Мир'', Москва, 1963.

[8] Р. Сильверстейн, Г. Басслер и Т. Моррил,,, Спектрометрическая идентификация органических соединений'', Изд-во ,,Мир'', Москва, 1977.

[9] F. Blindenbacher and T. Reichstein, *Helv. Chim. Acta*, **31**, 2061 (1948).

[10] R. K. Clark, *Antibiotics and Chemotherapy*, **3**, 663 (1953).

[11] H. Els, W. D. Celmer and K. Murai, *J. Amer. Chem. Soc.*, **80**, 3777 (1958).

[12] M. I. Weinstein, G. H. Wagman, *J. Chromat. library*, **15**, 273 (1978).

[13] ,,Временная инструкция по проведению работ с целью определения сроков годности лекарственных средств на основе метода ,,ускоренного старения'' при повышенной температуре'', Изд-во ЦБНТИ медпром., Москва, 1974.

[14] В. С. Димитриева и С. М. Семенов, ,Микробиологический контроль активности антибиотических препаратов'', Изд-во ЦБНТИ медпром. Москва, 1965,

Revue Roumaine de Chimie, 34, 4, 1081–1093 (1989)

ÉTUDE DES PERFORMANCES D'UN NOUVEAU TYPE D'EXTRACTEUR À PLATEAUX VIBRATOIRES. I.

CARACTÉRISTIQUES HYDRODYNAMIQUES DE L'EXTRACTEUR

R. Z. TUDOSE, M. FOURAR
Faculté de technologie chimique, Institut polytechnique de Jassy, 22, rue 23 August, Jassy Roumanie
O. PETRUȘ et B. CONSTANTIN
Université « Al. I. Cuza », Département de physique, 11, rue 23 August, Jassy, Roumanie

Reçu le 4 juillet 1988

Un nouveau type d'extracteur à étages multiples vibratoires est décrit. La colonne se compose d'une succession alternative de plateaux perforés fixes et vibratoires qui couvrent entièrement la section transversale. En l'absence de transfert de masse, les performances de l'extracteur ont été examinées à l'aide d'une technique cinématographique. Le diamètre moyen, la distribution en tailles et la vitesse terminale des gouttes ont été déterminés en fonction des conditions opératoires et des caractéristiques géométriques des plateaux.

A new type of multi-stage vibrating extraction apparatus is described. The column consists of an alternative sequence of perforated fixed and vibrating plates which close the whole cross section. The column performances have been investigated by means of a cinematographic technique in the absence of mass transfer. The mean diameter of drops, their distribution and the terminal drop velocity in the continuous phase as a function of operating conditions and the plate geometry have been followed.

A. INTRODUCTION

Dans les colonnes d'extraction liquide–liquide dépourvues de systèmes d'agitation, l'énergie nécessaire pour la pulvérisation de la phase dispersée se limite à l'énergie potentielle due à la différence de densité des phases de contact. Le degré de dispersion et, par conséquent, l'efficacité de l'extracteur, peuvent être améliorés par un rapport supplémentaire d'énergie mécanique. Cet apport d'énergie est habituellement réalisé par un système d'agitation mécanique (disques rotatifs, disques vibratoires) ou par un mécanisme de mouvement alternatif (pompes à piston sans soupapes).

A l'heure actuelle, les extracteurs agités mécaniquement sont les plus recherchés. Cependant, il est pratiquement impossible de dire lequel d'entre eux est le plus efficace. Il n'existe pas encore d'extracteur universel qui pourrait être utilisé pour tous les types de séparation. Il apparaît que les colonnes à dispositifs rotatifs sont les plus répandues. A côté de ces extracteurs, un intérêt de plus en plus croissant est porté aux colonnes à pulsations et à vibrations.

La première colonne à plateaux vibratoires fut construite par Van Dijck [1] qui proposa aussi une possibilité analogue de former une dispersion en faisant exécuter au liquide, le mouvement de va-et-vient des disques vibratoires. Sur la base de cette suggestion, un grand nombre de colonnes à pulsation est maintenant connu.

Parallèlement, quelques colonnes à vibration ont été proposées. Ces dernières peuvent être réparties en deux grandes catégories : extracteurs à mouvement réciproque des plateaux (reciprocating plate column) et extracteurs à étages multiples vibratoires (multi-stage vibrating disks column) qui est une modification du premier.

Ces deux types d'extracteurs, tels qu'ils sont décrits dans la littérature, présentent les inconvénients suivants :

— une partie du mouvement vibratoire des plateaux n'est pas pleinement utilisée pour la dispersion des phases et provoque un déplacement de la masse entière de liquide de la colonne vers les conduites d'alimentation et d'évacuation ;

— par les espaces libres qui existent entre les plateaux vibratoires et les parois de la colonne, une partie du liquide échappe à la dispersion réciproque des phases.

Dans la littérature très peu d'articles ont été publiés au sujet des colonnes à vibration. Karr,[2] Baird et Lane,[3] Prochazka et collab.[4] ont analysé les performances des colonnes à mouvement réciproque des plateaux et ont rapporté une grande efficacité de séparation.

L'extracteur à étages multiples vibratoires a été appliqué dans le domaine de l'absorption,[5] dans le cas des réactions chimiques gaz—liquide en présence de catalyseurs solides [6] et dans le traitement des eaux résiduelles.[7] Son utilité dans les processus d'extraction liquide—liquide a été récemment montrée par Tojo et Miyanami.[8] En dépit des nombreuses possibilités d'applications industrielles, beaucoup d'informations manquent sur cette colonne. C'est pourquoi de nouvelles recherches sont exigées pour élucider les caractéristiques de ce type d'extracteur.

Dans ces circonstances, nous suggérons une série d'études expérimentales sur l'effet des variables opératoires et des facteurs géométriques sur les performances d'une nouvelle colonne à étages multiples vibratoires. Le présent article décrit, conformément au brevet d'invention les caractéristiques géométriques de l'extracteur [9]. Il présente les diférentes conditions expérimentales auxquelles est soumise la colonne d'extraction et décrit les différentes techniques expérimentales nécessaires à cette recherche. De plus, il décrit en l'absence de transfert de masse, quelques principales caractéristiques hydrodynamiques de l'extracteur, à savoir la capacité de la colonne, le diamètre moyen, la distribution en tailles et les vitesses de chute des gouttes de la dispersion.

B. PARTIE EXPÉRIMENTALE

1. Description de la colonne d'extraction

La colonne d'extraction conforme au brevet d'invention (fig. 1) se compose d'un tube cylindrique (1) constitué de sept compartiments identiques. Chaque compartiment est formé d'un plateau perforé vibratoire (2) alterné à deux plateaux perforés fixes (3). L'ensemble des plateaux vibratoires est fixé à une tige (4) animée d'un mouvement vibratoire assuré par un mécanisme excentrique (5). L'amplitude et la fréquence des oscillations peuvent être réglées suivant les conditions imposées par l'expérimentation. Avec le système utilisé, l'amplitude peut être variée en modifiant le rayon de l'excentrique et peut atteindre une valeur maximale de 3,6 cm. La variation de la fréquence peut être obtenue en changeant le rapport de transmission avec un variateur de vitesse placé entre le moteur et l'excentrique. Une valeur maximale de 0,615 cycles par seconde peut être atteinte.

Les plateaux fixes au même titre que les plateaux vibratoires, occupent entièrement la section transversale de la colonne. Cette situation présente à la fois l'aspect original et la caractéristique principale de la colonne proposée par les auteurs. Elle introduit les avantages suivants que l'on ne rencontre pas dans les autres types d'extracteurs à plateaux vibratoires :

— sous l'action des plateaux vibratoires, la phase continue est forcée à passer à travers les perforations où les gouttes de la phase dispersée sont formées ;

— la présence des plateaux fixes a pour rôle d'éviter les pertes de liquide par les espaces libres qui existent entre les plateaux vibratoires et les parois de la colonne ;

— les plateaux fixes permettent également de réduire au minimum le déplacement de la masse entière de liquide à l'intérieur de la colonne dû à l'effet piston engendré par le mouvement des plateaux vibratoires ;

— l'énergie consommée est plus petite en raison de la réduction de la masse du dispositif actionné (le nombre de plateaux vibratoires étant plus petit) et elle est intégralement utilisée pour la dispersion réciproque des phases.

Les principales caractéristiques de construction de la colonne sont :

— hauteur 100 cm ;

— hauteur opératoire 70 cm ;

— nombre de plateaux : 15 dont 7 sont vibratoires et 8 fixes ;

— distance séparant deux plateaux fixes 10 cm ;

— nombre de perforations sur chaque plateau 116 ;

— diamètre des perforations variable de 0,15 à 0,3 cm, offrant ainsi une fraction de surface libre pouvant aller de 6,22 % à 24,9 % ;

— disposition hexagonale des perforations.

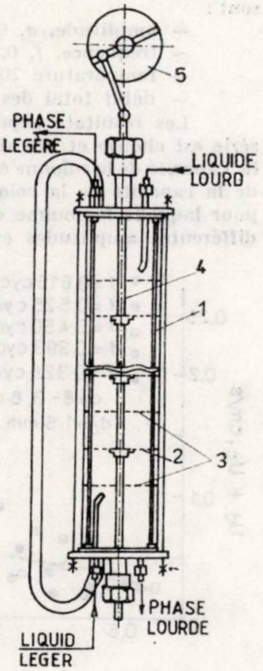

Fig. 1. — Colonne d'extraction.

2. Technique expérimentale

La technique cinématographique est utilisée pour étudier la dispersion du tétrachlorure de carbone dans l'eau. A cet effet, une caméra de fabrication soviétique type Quartz est employée. La dispersion est éclairée par l'arrière en lumière diffusée avec une lampe de 500 watts.

Pour chaque fraction de surface libre des plateaux, la phase dispersée est filmée pour une série d'intensités d'agitation, af, produit de l'amplitude par la fréquence. Les prises de vues sont réalisées à partir d'une distance de 48 cm de la colonne en utilisant une lentille supplémentaire de 1,75 dioptries.

Pour les conditions expérimentales qui viennent d'être évoquées, le diamètre volume—surface de Sauter est évalué à partir d'éléments situés près des parois. Un nombre suffisamment grand de photogrammes est dépouillé pour que le diamètre de Sauter calculé ne varie pas de manière significative. Ce nombre varie entre 100 aux faibles vitesses d'agitation et 400 pour les vitesses élevées, et seules les gouttes dont le contour est clairement défini sont analysées.

Pour un contrôle exact de l'agrandissement des images lors de la projection du film, un repère gradué en millimètres et fixé sur la colonne est enrégistré sur les péllicules.

3. Zones opératoires de la colonne

Les premières séries d'expériences hydrodynamiques sont consacrées à délimiter les régions opératoires de l'extracteur.

Avec le système binaire tétrachlorure de carbone—eau, la capacité de la colonne (somme des débats des phases à la sortie rapportée à la section de la colonne) est mesurée à différentes amplitudes et à différentes fréquences d'oscillations pour chaque fraction de surface libre des plateaux. Ces expériences sont réalisées sur une petite colonne constituée d'un seul étage composé d'un plateau vibratoire alterné à deux plateaux fixes. Les conditions expérimentales utilisées sont :

— amplitude, *a*, 0 ÷ 3,6 cm ;
— fréquence, *f*, 0,213 ÷ 0,615 cyles/s ;
— température 20°C ;
— débit total des phases 2.133 ÷ 33,53 l/h.

Les résultats expérimentaux sont groupés sous forme de séries expérimentales. Une série est choisie et une description qualitative est donnée sur la dépendance qui existe entre la capacité de la colonne et les variables opératoires. Dans la figure 2, est montrée la dépendance de la capacité de la colonne en fonction du produit af pour la première série d'expériences pour laquelle la somme des vitesses de passage des phases en fonction de la fréquence pour différentes amplitudes est représentée dans la figure 3.

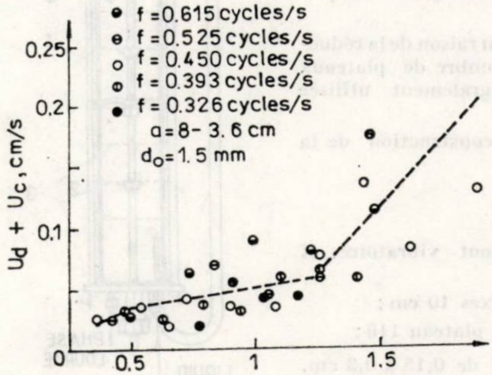

Fig. 2. — Effet de l'intensité d'agitation sur la capacité de la colonne pour différentes fréquences.

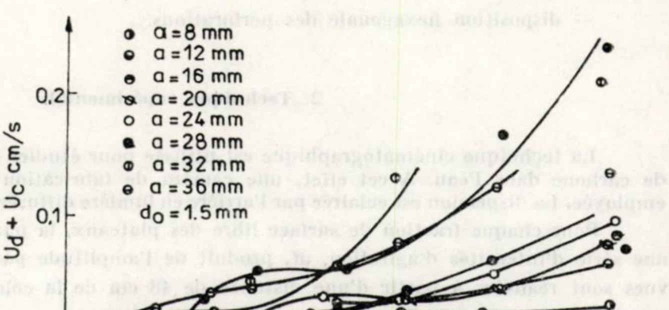

Fig. 3. — Effet de la fréquence et de l'amplitude de vibrations sur la capacité de la colonne.

Il est évident que les forces d'inertie jouent un rôle décisif sur la capacité de la colonne. Elles deviennent très importantes quand l'intensité d'agitation dépasse la valeur de 1,2 cm/s. Une dispersion assez fine est formée et la phase dispersée est déchargée à travers les perforations avec une grande vitesse. Des valeurs relativement élevées de la capacité de la colonne en résultent.

C. DIAMÈTRE MOYEN DES GOUTTES

A partir d'une certaine taille, de l'ordre de quelques millimètres dans les systèmes usuels, les gouttes s'écartent de la forme sphérique. Il convient alors de modéliser différemment la forme des gouttes pour calculer le diamètre de Sauter à partir du diamètre équivalent basé sur certaines grandeurs géométriques mesurées sur les profils observés. Cette modélisation n'est qu'approximative et il est impossible de connaître le degré de fiabilité des résultats obtenus.

Pour réaliser cette étude, nous avons considéré que la forme des gouttes résultait de la juxtaposition d'un hémisphère et d'un demi-ellipsoïde.[10] C'est un modèle commode car il permet de décrire des géométries trés différentes. Dans le cadre de ce modèle, le diamètre équivalent des gouttes est donné par :

$$de_i = (a_i^2 b_i)^{1/3} \tag{1}$$

et le diamètre de Sauter est calculé à partir de l'expression :

$$d_{32} = \frac{\sum_{i=1}^{n} n_i d_{ei}^3}{\sum_{i=1}^{n} n_i d_{ei}^2} \tag{2}$$

où n_i représente le nombre de gouttes de diamètre équivalent d_{ei}.

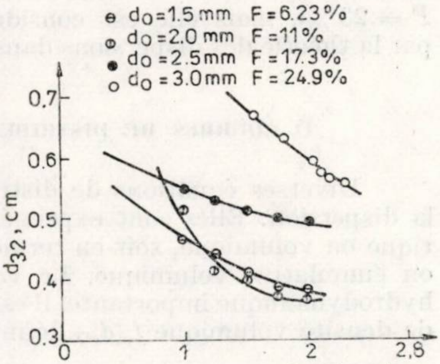

Fig. 4. — Effet de l'intensité d'agitation sur le diamètre de Sauter.

La phase dispersée est filmée à de différentes intensités d'agitation en lumière diffusée. Le film est projeté au moyen d'une visionneuse Fujicaéditor E_{55} sur un écran transparent où les images sont agrandies de 5 à 6 fois. La variation du diamètre de Sauter en fonction de l'intensité d'agitation est illustrée dans la figure 4 où le diamètre et la fraction de surface occupée par les perforations sont choisis comme paramètres.

Il est clair qu'avec l'augmentation de la vitesse d'agitation, le diamètre de Sauter décroît. La dépendance trouvée est du type puissance et elle est similaire à celle trouvée par d'autre auteurs.[3,11,13] Aux intensités élevées, les gouttes présentent une petite taille, ce qui correspond à un accroissement remarquable de l'aire interfaciale entre les phases dans l'extracteur. Le diamètre des perforations présente une forte influence sur la dimension des gouttes, essentiellement dans le domaine des intensités comprises entre 1 et 2 cm/s.

Les diamètres de Sauter mesurés sont utilisés pour vérifier l'équation (3) proposée par Hinze [14] et déduite de la théorie des dispersions dans un milieu turbulent isotropique :

$$d_{32} = K(af)^{-1,2} \tag{3}$$

où K est un coefficient qui dépend des propriétés physiques du système liquide—liquide. Il inclut aussi les effets de la fraction de surface libre et de la dimension des perforations. Pour le traitement des données expérimentales, la méthode des moindres carrés est utilisée et les corrélations obtenues sont groupées dans le tableau 1.

Tableau 1

Corrélation du diamètre de Sauter par l'équation Hinze

d_0, mm	F, %	Equations pour d_{32}, mm	Déviation moyenne absolue, %
1,5	6,23	$0,468\ (\text{a.f})^{-0,300}$	1,20
2,0	11,00	$0,487\ (\text{a.f})^{-0,460}$	3,54
2,5	17,30	$5,470\ (\text{a.f})^{-0,146}$	0,28
3,0	24,90	$8,170\ (\text{a.f})^{-0,480}$	0,82

La valeur de l'exposant (0,48) se rapproche de celle trouvée par Assenov et Penchev [13] dans l'étude d'une colonne à pulsations (0,5 pour $F = 23\,\%$), mais elle est considérablement plus faible que celle exigée par la théorie des dispersions dans un milieu turbulent isotropique.

D. COURBES DE DISTRIBUTION EN TAILLES DES GOUTTES

Diverses équations de distribution sont proposées pour représenter la dispersion. Elles sont exprimées soit en termes de distribution numérique ou volumique, soit en termes de distribution cumulative numérique ou cumulative volumique. Le volume de la goutte étant une quantité hydrodynamique importante, il est alors plus utile de considérer la fonction de densité volumique $f_v(d_{ei})$ définie par :

$$f_v(d_{ei})\,\Delta(d_{ei}) = \frac{n_i d_{ei}^3}{\sum\limits_{i=1}^{M} n_i d_{ei}^3} = V_i \tag{4}$$

où M est le nombre total d'intervalles.

Des fonctions exponentielles du type :

$$\frac{\mathrm{d}V}{\mathrm{d}r} = \frac{\delta}{\sqrt{\pi}} \exp(-\delta^2 r^2) \tag{5}$$

où r est une fonction du diamètre de la goutte, sont utilisées pour décrire la phase dispersée dans les extracteurs.

Selon la relation qui existe entre les variables r et d, on distingue :
— la simple loi log-normale avec deux paramètres :

$$\frac{\mathrm{d}V}{\mathrm{d}r} = \frac{\delta}{\sqrt{\pi}} \exp(-\delta^2 r^2) ; \; r = \ln \frac{d}{\bar{d}} \tag{6}$$

où δ et $\bar{d}$ représentent respectivement l'uniformité et le diamètre moyen volumique de la distribution.

L'expression du diamètre de Sauter pour cette loi de distribution est donnée par :

$$d_{32} = \bar{d} \exp(-1/4\delta^2) \tag{7}$$

la loi log-normale modifiée ou l'équation de Mugele et Evans [14] :

$$\frac{\mathrm{d}V}{\mathrm{d}r} = \frac{\delta}{\sqrt{\pi}} \exp(-\delta^2 r^2) ; \; r = \ln \frac{ad}{d_m - d} \tag{8}$$

où a et d_m représentent respectivement le paramètre de gonflement de la courbe de distribution (skewness parameter) et le diamètre maximum des gouttes.

L'expression du diamètre de Sauter est donnée par :

$$d_{32} = \frac{d_m}{1 + a \exp(1/4\delta^2)} \tag{9}$$

Une autre fonction de distribution exponentielle, basée sur un seul paramètre est proposée par Gal-Or et Hoelscher [15] :

$$\frac{\mathrm{d}V}{\mathrm{d}r} = 4\left(\frac{\delta^3}{\pi}\right) r^2 \exp(-\delta r^2) ; \; r = d \tag{10}$$

Les résultats expérimentaux obtenus dans la présente recherche sont utilisés pour tester ces fonctions de distribution. La fonction de densité volumique est calculée sur des intervalles de 0,25 mm pour cinq intensités d'agitation différentes. Les valeurs obtenues sont utilisées pour estimer les paramètres qui caractérisent chaque type de fonction de distribution.

Pour une meilleure précision, nous avons employé une méthode rigoureuse de calcul, basée sur les techniques d'analyse des régressions et d'optimisation non linéaire.

Les équations qui résultent et les résultats expérimentaux sont montrés dans les figures 5 à 7. Elles représentent la fonction de densité volumique en fonction du diamètre équivalent de la goutte pour différentes intensités d'agitation.

L'échec de la fonction de Gal-Or et Hoelscher pour représenter la distribution en tailles des gouttes sur tout le domaine considéré est clairement démontré. La fonction normale logarithme semble mieux approcher les données expérimentales que la fonction proposée par Mugele-Evans. Ceci est confirmé par la comparaison entre les diamètres de Sauter calculés par l'équation (2) et ceux estimés à partir des fonctions de distribution (tab. 2).

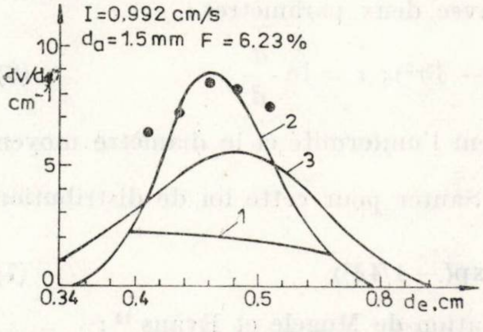

Fig. 5. — Courbes de distribution en tailles des gouttes ; modèles :
1 — Gal-Or et Hoelscher [15], 2 — log-normale, 3 — Mugele et Evans [14] et ● -points expérimentaux.

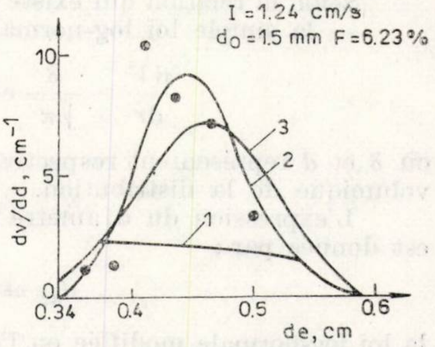

Fig. 6. — Courbes de distribution en tailles des gouttes ; modèles :
1 — Gal-Or et Hoelscher [15], 2 — log-normale, 3 — Mugele et Evans [14] et ● — points expérimentaux.

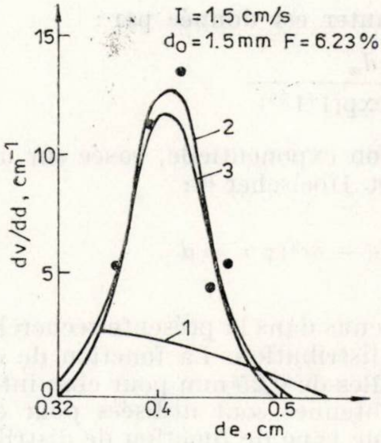

Fig. 7. — Courbes de distribution en tailles des gouttes ; modèles :
1 — Gal-Or et Hoelscher [15], 2 — log-normale, 3 — Mugele et Evans [14] et ● — points expérimentaux.

Tableau 2

Comparaison entre les diamètres de Sauter calculés et ceux estimés à partir des courbes de distribution

I = a.f cm	Diamètres d_{32}, cm			Déviation maximale absolue, %	
	exp.	Log. n.	$M - E$	Log. *n*.	$M - E$
0,992	0,4665	0,4666	0,4620	0,02	0,96
1,240	0,4443	0,4475	0,4520	0,72	1,73
1,500	0,4141	0,4084	0,4000	1,14	3,40
1,739	0,3851	0,3853	0,3813	0,05	0,98
1,987	0,3840	0,3890	0,3842	1,30	0,05

E. VITESSES TERMINALES

Le mouvement des gouttes de tétrachlorure de carbone dans l'eau, qui fait partie de l'étude du comportement hydrodynamique de la phase dispersée, est examiné dans cette investigation. Le déplacement des gouttes est déterminé par la technique cinématographique. Une vitesse de 48 photogrammes par seconde est utilisée pour filmer la phase dispersée. Les mesures des vitesses terminales obtenues sont montrées dans la figure 8 L'allure générale de la courbe est similaire à celles établies par différents chercheurs.[17-20] Le maximum de la courbe correspond à une transition entre deux mécanismes hydrodynamiques différents. Autour de ce sommet, la goutte commence à osciller et une augmentation dans la taille de la goutte au-delà de la valeur qui marque le début des oscillations conduit à une diminution de la vitesse terminale (partie B de la courbe).

Les résultats expérimentaux obtenus pour les gouttes oscillantes sont comparés à ceux calculés au moyen de l'équation proposée par Thorsen et collab.[18] pour des systèmes soigneusement purifiés (fig. 9).

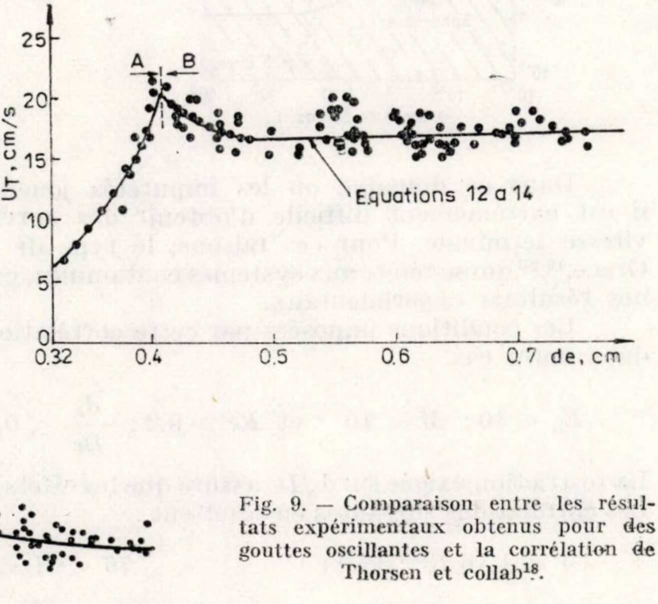

Fig. 8. — Vitesses terminales mesurées pour les gouttes de tétrachlorure de carbone dans l'eau.

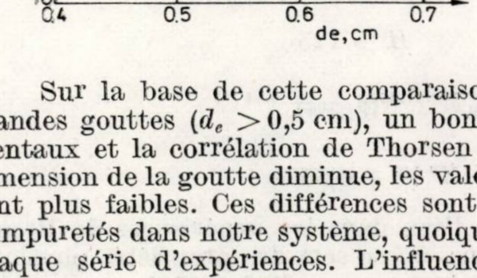

Fig. 9. — Comparaison entre les résultats expérimentaux obtenus pour des gouttes oscillantes et la corrélation de Thorsen et collab[18].

Sur la base de cette comparaison, on peut constater que pour de grandes gouttes ($d_e > 0{,}5$ cm), un bon accord entre les résultats expérimentaux et la corrélation de Thorsen est observé. Cependant, quand la dimension de la goutte diminue, les valeurs rapportées par notre recherche sont plus faibles. Ces différences sont probablement dues à la présence d'impuretés dans notre système, quoique les liquides soient distillés avant chaque série d'expériences. L'influence des impuretés sur les vitesses terminales a été signalée par un grand nombre de chercheurs.[18,21,22] Elle est particulièrement importante sur la zone de transition d'une goutte à circulation interne à une goutte oscillante.

L'utilisation du diagramme de Grace,[23] qui permet de prévoir la forme et la vitesse de chute d'une goutte dans un liquide pour tout régime d'écoulement, montre que sur le domaine examiné les gouttes présentent une forme elliptique (fig. 10).

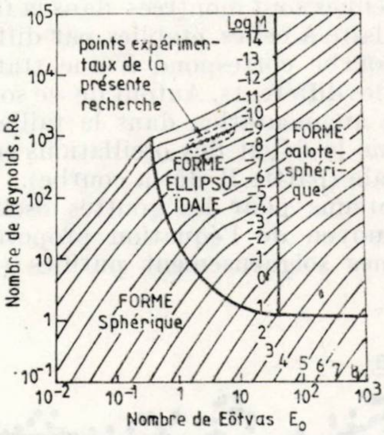

Fig. 10. — Différentes formes adoptées par les gouttes en mouvement dans un liquide.

Dans ce domaine où les impuretés jouent un rôle déterminant, il est extrêmement difficile d'obtenir des corrélations explicites de la vitesse terminale. Pour ces raisons, le type de corrélation proposé par Grace,[19,23] qui se réfère aux systèmes contaminés, est employé pour corréler nos résultats expérimentaux.

Les conditions imposées par cette corrélation sont dûment remplies dans notre cas.

$$E_0 < 40\,;\; M < 10^{-3} \text{ et } Re > 0{,}2\,;\; \frac{d_e}{Dc} < 0{,}12 \text{ pour } Re > 100 \qquad (11)$$

La restriction exigée sur d_e/Dc assure que les effets de parois soient négligés. Les corrélations suivantes en résultent :

$$J = 1{,}16\,10^{-4}\mathrm{H}^{2.71}\,; \qquad 76 < H < 94$$

$$J = 32{,}4\,\mathrm{H}^{-0.056}\,; \qquad 94 \leqslant H < 125 \qquad 12)$$

$$J = 2{,}03\,\mathrm{H}^{0.515}\,; \qquad H > 125$$

$$H = \frac{4}{3}\,E_0 M^{-0.149}(\mu_c/\mu_w)^{-0.14} \qquad 13)$$

$$J = Re\,M^{0.149} + 0{,}857$$

où $\mu_w = 0{,}9$ cp est la viscosité de l'eau dans les expériences de Braida. Pour l'utilisation de ces corrélations, on se sert des propriétés physiques du système et du diamètre équivalent pour calculer H.

J est ensuite calculé par l'une des équations citées plus haut suivant les différents cas qui se présentent. Enfin, la vitesse terminale par l'expression explicite suivante se trouve calculée :

$$U_T = \mu_c/\rho_c d_e)\ M^{-0.149}\ J - 0{,}857) \qquad (14)$$

Selon cette procédure, la corrélation est appliquée aux données expérimentales et la courbe résultante est montrée dans la figure 8. Un bon accord avec les résultats expérimentaux est obtenu.

Cette corrélation est recommandée pour estimer les vitesses de chute des gouttes quand les conditions signalées auparavant sont satisfaites et où la présence des impuretés est inévitable.

F. CONCLUSIONS

Quelques caractéristiques hydrodynamiques en l'absence de transfert de masse pour le nouveau type d'extracteur proposé sont décrites. La capacité maximale de la colonne est obtenue pour des valeurs de l'intensité d'agitation supérieures à 1,2 cm/s. Elle est significativement affectée par le diamètre des perforations ou par la fraction de surface libre.

Le diamètre moyen de la dispersion, exprimé par le diamètre de Sauter, diminue avec le produit de la fréquence par l'amplitude et augmente avec le diamètre des perforations. Les courbes obtenues sont du type puissance. Les valeurs[14] des exposants $I = af$ trouvées indiquent que, dans ces conditions expérimentales, le degré de turbulence exigé par la théorie des dispersions en milieu turbulent n'est pas atteint. Les travaux de Baird-Lane[3] révèlent que cette condition est satisfaite pour des valeurs de $I > 2$ cm/s.

Les mesures de la distribution en tailles des gouttes pour différentes intensités d'agitation sont utilisées pour tester les diverses fonctions de distribution proposées par la littérature. Les paramètres de ces fonctions sont estimés par une méthode de calcul basée sur les techniques d'analyse de régression et d'optimisation non linéaire. La comparaison entre les diamètres de Sauter mesurés et ceux estimés confirme que la distribution est mieux représentée par la loi log-normale.

Les vitesses terminales des gouttes de tétrachlorure de carbone (phase dispersée) dans l'eau sont mesurées par la technique cinématographique. Elles révèlent que la forme des gouttes est elliptique. Les gouttes qui présentent un diamètre équivalent inférieur à 0,4 cm sont le siège d'une circulation interne, les autres sont soumises à des oscillations. La comparaison entre les valeurs expérimentales obtenues et celles décrites par différents chercheurs montre des différences dans les mesures pour les gouttes dont le diamètre est compris entre 2 et 6 mm. Ces déviations sont attribuées au degré de pureté des systèmes utilisés.

NOTATION

Dc : diamètre intérieur de la colonne (cm)

Eo : nombre de Eötvas : $(\Delta\rho\, d^2 g)/\sigma$

F : fraction de surface libre des plateaux

H : hauteur utile de la colonne (cm) ; notation (eq. 13)
H_T : hauteur totale de la colonne (cm)
I(af) : intensité des vibrations ou intensité d'agitation (cm/s)
M : nombre de Morton : $(\Delta\rho g\mu_c^4)/(\rho_c^2\sigma^3)$
N : nombre de plateaux perforés
Re : nombre de Reynolds: $(U_T d_e \rho_c)/\mu_c$
Uc : vitesse de passage de la phase continue (débit rapporté à la section de la colonne), (cm/s)
Ud : vitesse de passage de la phase dispersée (cm/s)
U_T : vitesse terminale ou de chute des gouttes (cm/s)
V : volume de la goutte (cm^3)
a : amplitude des pulsations ou des vibrations (cm) ; axe vertical de l'ellipse (eq. 1, cm) ; paramètre de gonflement (skewness parameter, eq. 8)
b : axe horizontal de l'ellipse (cm)
d : diamètre de la goutte (cm)
$\bar{d}$: diamètre moyen volumique de la goutte (cm)
d_e : diamètre équivalent d'une goutte sphérique du même volume que la goutte (cm)
d_m : diamètre maximal de la goutte (cm)
d_0 : diamètre des perforations (cm)
d_{32} : diamètre volume-surface ou diamètre de Sauter (cm)
f : fréquence des vibrations (cycles/s)
f_v : fonction de densité volumique
g : accélération de la pesanteur (cm/s^2)
l : distance entre deux plateaux fixes (cm)
n : nombre de gouttes
r : fonction du diamètre de la goutte (cm)
ρ_d : densité de la phase dispersée (g/cm^3)
ρ_c : densité de la phase continue (g/cm^3)
$\Delta\rho$: différence de phases (g/cm^3)
σ : tension interfaciale (g/s^2)
μ_c : viscosité dynamique de la phase continue (g/cm·s)
δ : facteur d'uniformité de la distribution

BIBLIOGRAPHIE

[1] V. J. D. Van Dijck, Patent USA, nr. 2011186 (1935).
[2] A. E. Karr, *A.I.Ch.E.J.*, **5**, 446 (1959).
[3] M. H. I. Baird et S. J. Lane, *Chem. Eng. Sci.*, **28**, 947 (1973).
[4] J. Prochazka, J. Landau et F. Souhrada, *Brit. Chem. Eng.*, **16**, 42 (1971).
[5] J. Prochazka, J. Landau et F. Souhrada, *Brit. Chem. Eng.*, **14**, 1161 (1969).
[6] K. Takeba, T. Shirai et Y. Kimoto, Reprint of the 10th General Symposium of the Soc. Chem. Eng., Japan, 124 (1971).
[7] Y. Akai, Master thesis, University of Osaka, 1979.
[8] K. Tojo, K. Miyanami et T. Yano, *Chem. Eng. Japan*, **8**, 122 (1975).
[9] R. Z. Tudose, Romanian Patent No. 58918 (1974).
[10] H. Veteau, Thèse de doctorat ès sciences, Grenoble (France) (1981).
[11] H. Angelino, C. Alran, L. Boyadzhiev et S. P. Murkherjee, *Brit. Chem. Eng.*, **12**, 1893 (1967).

[12] S. Z. Kagan, N. E. Aerov, V. Lonik et T. S. Volkova, *Izv. Vysshikhl. Uchebn. Zavedeni Kim. i Khim. Tekh.*, **8**, 142 (1965).

[13] A. Assenov et I. Penchev, *Dokl. Bulg. Akad. Nauk.*, **24**, 1381 (1971).

[14] R. A. Mugele et H. D. Evans, *Ind. Eng. Chem.*, **43**, 1317 (1951).

[15] B. Gal-Or et H. E. Hoelscher, *A. I. Ch. E. J.*, **12**, 499 (1966).

[16] R. R. Scroeder et R. C. Kintner, *A. I. Ch. E. J.*, **11**, 5 (1965).

[17] S. Hu et R. C. Kintner, *A.I.Ch.E.J.*, **1**, 42 (1955).

[18] G. Thorsen, R. M. Stordalen et S. G. Terjessen, *Chem. Eng. Sci.*, **23**, 413 (1968).

[19] R. Clift, J. R. Grace et M. E. Weber, "Bubbles, Drops and Particles", Academic Press, New York, 1978.

[20] W. Licht, G. S.R. Narasimhamurty, *A.I.Ch.E. J.*, **1**, 366 (1955).

[21] R. M. Edge et C. D. Grant, *Chem. Eng. Sci.*, **27**, 1709 (1972).

[22] D. Raymond et S. A. Zieminski. *A.I.Ch. .J.*, **17**, 57 (1971).

[23] J. R. Grace, T. Wairegi et T.H. Nguyen, *Trans. Inst. Chem. Eng.*, **54**, 167 (1976).

Revue Roumaine de Chimie, 34, 4, 1095–1100 (1989)

CHEMICAL SYSTEMS WITH UNCERTAIN PARAMETERS. THE METHOD OF INTEGRAL EQUATIONS

M. O. VLAD [a] and E. SEGAL [b]

[a] Industrial Central for Medicinal Drugs and Cosmetics,
Blvd. Chimiştilor 50, CP 78014, Bucharest, Romania
[b] Polytechnic Institute, Department of Physical Chemistry and Electrochemical Technology,
Blvd. Republicii 13, Bucharest 70346, Romania

Received January 18, 1988

This paper reports some reacting chemical systems with uncertain parameters. A new method is developed to determine the probability density of rate constants $\psi(\mathbf{k})$ in terms of the probability density of composition vector $P(\mathbf{C}, t)$. The results are applied to the problem of confidence range for the experimental evaluation of kinetic constants.

1. INTRODUCTION

Systems of differential equations are important models of many processes in chemical kinetics. Homogeneous and isothermal chemical systems may be described by systems of coupled first order equations for the rates of change of concentrations $C_1, \ldots C_S$

$$d\mathbf{C}/dt = \mathbf{R}(\mathbf{k}, \mathbf{C}), \tag{1}$$

where $\mathbf{C}$ is the composition vector

$$\mathbf{C} = (C_1, \ldots, C_S), \tag{2}$$

and $\mathbf{k}$ is the vector of rate constants

$$\mathbf{k} = (k_1, \ldots, k_m). \tag{3}$$

Assuming that the rate constants $k_1, \ldots, k_m$ and the initial condition

$$\mathbf{C}(t = 0) = \mathbf{C}^0, \tag{4}$$

are known, the time evolution of the composition vector $\mathbf{C}(t)$ can be determined by means of analytical or numerical integration of (1). However, if the initial conditions and the reaction rates are not known accurately, it is important to assess the effect of the uncertainty of parameters $\mathbf{k}$ and $\mathbf{C}^0$ on the time evolution of composition vector. A solution of this problem may be given by applying the method of sensitivity analysis.[1] In literature systematic methods have been developed for studying the behaviour of solutions of differential equations to parameter variations.[1]

Within this note we shall use an alternative approach, based on a chemical Liouville equation (Costanza and Seinfeld[2]). The layout of the paper is as follows. First we shall give a new formulation of the Costanza-Seinfeld method. Further on, we shall derive an integral equation for the probability density of rate constants. Finally, our results will be applied to a chemical system comprising the formation of a reaction intermediate with a constant reaction rate.

2. THE CHEMICAL LIOUVILLE EQUATION

For simplicity, we consider chemical systems for which the solution

$$\mathbf{C} = \mathbf{\Pi}(\mathbf{C}^0, \mathbf{k}, t), \tag{5}$$

of Eq. (1) with the initial condition (4) fulfills the relationship

$$J(\mathbf{C}^0, \mathbf{k}, t) = \det |\partial \Pi_i(\mathbf{C}^0, \mathbf{k}, t)/\partial C_j^0| = \text{finite} \neq 0, \tag{6}$$

so that we can express the vector $\mathbf{C}^0$ explicitely as

$$\mathbf{C}^0 = \mathbf{\Xi}(\mathbf{C}, \mathbf{k}, t), \tag{7}$$

where

$$\mathbf{\Pi}(\mathbf{\Xi}(\mathbf{C}, \mathbf{k}, t), \mathbf{k}, t) = \mathbf{C}, \tag{7'}$$

and

$$\mathcal{J}(\mathbf{C}, \mathbf{k}, t) = \det |\partial \Xi_i(\mathbf{C}, \mathbf{k}, t)/\partial C_j| = J^{-1}(\mathbf{\Xi}(\mathbf{C}, \mathbf{k}, t), \mathbf{k}, t) = \\ = \text{finite} \neq 0. \tag{8}$$

Relationships (5) — (8) have been introduced by Vlad.[3] Although somewhat restrictive, these conditions are fulfilled by a broad class of physicochemical systems (see also Vlad[4]).

One of our purposes is to answer the following question : given the probability

$$\psi \, \mathrm{d}\mathbf{k} = \psi(\mathbf{k})\mathrm{d}\mathbf{k}, \quad \int_{\mathbf{k}} \psi(\mathbf{k})\mathrm{d}\mathbf{k} = 1. \tag{9}$$

that the values of rate constants are between k_i and $k_i + \mathrm{d}k_i$, $i = 1,2, \ldots m$, and the probability

$$P^0 \mathrm{d}\mathbf{C}^0 = P^{\circ}(\mathbf{C}^0)\mathrm{d}\mathbf{C}^0, \quad \int_{\mathbf{C}^0} P^0(\mathbf{C}^0)\mathrm{d}\mathbf{C}^0 = 1, \tag{10}$$

that the values of the initial concentrations lie between C_i and $C_i + \mathrm{d}C_i$, $i = 1, \ldots, S$, what is the probability

$$P \, \mathrm{d}\mathbf{C} = P(\mathbf{C}, t)\mathrm{d}\mathbf{C}, \quad \int_{\mathbf{C}} P(\mathbf{C}, t)\mathrm{d}\mathbf{C} = 1, \tag{11}$$

that at time t the values of the concentrations are between C_i and $C_i + dC_i$, $i = 1, \dots, S$?.

To answer this question we introduce the conditional probability

$$\Phi\, d\mathbf{C} = \Phi(\mathbf{C}|\mathbf{k};\, t)\; d\mathbf{C}, \quad \int_{\mathbf{C}} \Phi(\mathbf{C}|\mathbf{k};\, t) d\mathbf{C} = 1, \tag{12}$$

and observe that

$$P(\mathbf{C}, t) = \int_{\mathbf{k}} \Phi(\mathbf{C}|\mathbf{k};\, t)\psi(\mathbf{k}) d\mathbf{k}, \tag{13}$$

$$\Phi(\mathbf{C}|\mathbf{k}, t = 0) = P^0(\mathbf{C}). \tag{14}$$

On the other side, taking into account (1), we can write a continuity equation for Φ[2]:

$$\partial_t \Phi(\mathbf{C}|\mathbf{k};\, t) + \nabla_{\mathbf{C}} \cdot (\mathbf{R}(\mathbf{k}, \mathbf{C})\; \Phi(\mathbf{C}|\mathbf{k};\, t)) = 0. \tag{15}$$

The proof of (15) is straightforward: the initial probability density $P^0(\mathbf{C}^0)$ determines a distribution of points in the composition space. The time evolution of the points is described by the differential equation (1) with different initial conditions $\mathbf{C}^0_1, \mathbf{C}^0_2, \mathbf{C}^0_3, \dots\dots$ Eq. (15) expresses the conservation of the number of points. Obviously, (15) is similar with the Liouville equation of statistical mechanics.[5] However, in our case there is no reason why the flow in composition space should be incompressible, and then the operator $\nabla_{\mathbf{C}}$ should remain in front of **R**.

3. THE METHOD OF INTEGRAL EQUATIONS

Performing the transformation of coordinates

$$\mathbf{C}^0 = \Xi(\mathbf{C}, \mathbf{k}, t), \tag{16}$$

(15) becomes

$$\begin{gathered} d_t \Phi(\boldsymbol{\Pi}(\mathbf{C}^0, \mathbf{k}, t)|\mathbf{k}, t) + [\mathbf{R}(\mathbf{k}, \boldsymbol{\Pi}(\mathbf{C}^0, \mathbf{k}, t)) - d_t \boldsymbol{\Pi}(\mathbf{C}^0, \mathbf{k}, t)] \cdot \\ \cdot \operatorname{grad}_{\boldsymbol{\Pi}} \Phi(\boldsymbol{\Pi}(\mathbf{C}^0, \mathbf{k}, t)|\mathbf{k}, t) + \Phi(\boldsymbol{\Pi}(\mathbf{C}^0, \mathbf{k}, t)) \operatorname{div}_{\boldsymbol{\Pi}} \mathbf{R}(\mathbf{k}, \boldsymbol{\Pi}(\mathbf{C}^0, \mathbf{k}, t)) = 0. \end{gathered} \tag{17}$$

Taking into account (1), integrating (17) with the initial condition (14) and coming back to the initial state variable $\mathbf{C}_i$ we get

$$\begin{gathered} \Phi(\mathbf{C}|\, \mathbf{k};\, t) = \\ = P^0(\Xi(\mathbf{C}, \mathbf{k}, t)) \exp\left(- \int_0^t \operatorname{div}_{\boldsymbol{\Pi}} \mathbf{R}(\mathbf{k}, \boldsymbol{\Pi}(\Xi(\mathbf{C}, \mathbf{k}, t), \mathbf{k}, t')) dt' \right). \end{gathered} \tag{18}$$

The solution (18) can be expressed in terms of the Jacobian $\mathscr{J}(\mathbf{C}, \mathbf{k}, t)$.

Indeed, a theorem of linear algebra[6] states that if the matrix $\mathbf{M}(t)$ is the solution of the differential equation

$$\mathrm{d}\mathbf{M}(t)/\mathrm{d}t = \mathbf{A}(t)\,\mathbf{M}(t),\ \mathbf{M}(0) = \|\delta_{ij}\|, \tag{19}$$

then

$$\det|\mathbf{M}(t)| = \exp\left(\int_0^t T_r(\mathbf{A}(\tau))\mathrm{d}\tau\right). \tag{20}$$

The matrix elements $\Gamma_{ij} = \partial \Pi_i(\mathbf{C}^0, \mathbf{k}, t)/\partial C_j^0$ obey a system of linear differential equations similar with (19). Making use of (1) and (5) we come to

$$\mathrm{d}\,\Gamma_{ij}/\mathrm{d}t = \sum_{\alpha=1}^{S} [\partial R_i(\mathbf{k}, \mathbf{\Pi}(\mathbf{C}^0, \mathbf{k}, t))/\partial \Pi_\alpha]\Gamma_{\alpha j}, \tag{21}$$

and

$$\Gamma_{ij}(t=0) = \partial \Pi_i(\mathbf{C}^0, \mathbf{k}, 0)/\partial C_j^0 = \partial C_i^0/\partial C_j^0 = \delta_{ij}. \tag{22}$$

A straightforward application of (6), (8) and (20) yields

$$\mathscr{J}(\mathbf{C}, \mathbf{k}, t) = \exp\left(-\int_0^t \mathrm{div}_{\mathbf{\Pi}}\mathbf{R}(\mathbf{k}, \mathbf{\Pi}(\mathbf{\Xi}(\mathbf{C}, \mathbf{k}, t), \mathbf{k}, t'))\mathrm{d}t'\right), \tag{23}$$

and (18) may be rewritten as

$$\Phi(\mathbf{C}\,|\mathbf{k}\,; t) = \mathscr{J}(\mathbf{C}, \mathbf{k}, t)P^0(\mathbf{\Xi}(\mathbf{C}, \mathbf{k}, t)). \tag{24}$$

Combining now (13) and (24) we get the sought for expression of $P(\mathbf{C}, t)$:

$$P(\mathbf{C}, t) = \int_{\mathbf{k}} \mathscr{J}(\mathbf{C}, \mathbf{k}, t)P^0(\mathbf{\Xi}(\mathbf{C}, \mathbf{k}, t))\psi(\mathbf{k})\mathrm{d}\mathbf{k}. \tag{25}$$

Using (25) we can reduce the determination of the moments of random variables $C_i(t)$, $i = 1, \ldots, S$ to the evaluation of two different means

$$\langle \ldots \rangle^{(\mathbf{k})} = \int_{\mathbf{k}} \ldots \psi(\mathbf{k})\,\mathrm{d}\mathbf{k}, \tag{26}$$

and

$$\langle \ldots \rangle^{(\mathbf{C}^0)} = \int_{\mathbf{C}^0} \ldots P^0(\mathbf{C}^0)\mathrm{d}\mathbf{C}^0. \tag{27}$$

Indeed, combining (5) — (8) and (25) we obtain

$$\langle C_i(t)\rangle = \int_{\mathbf{C}} C_i P(\mathbf{C}, t)\mathrm{d}\mathbf{C} = \langle\langle \Pi_i(\mathbf{C}^0, \mathbf{k}, t)\rangle^{(\mathbf{k})}\rangle^{(\mathbf{C}^0)}, \tag{28}$$

$$\langle C_i(t)\Delta C_j(t)\rangle = \int_{\mathbf{C}} (C_i - \langle C_i(t)\rangle)(C_j - \langle C_j(t)\rangle)P(\mathbf{C}, t)\mathrm{d}\mathbf{C} =$$

$$= \langle\langle \Pi_i(\mathbf{C}^0, \mathbf{k}, t)\Pi_j(\mathbf{C}^0, \mathbf{k}, t)\rangle^{(\mathbf{k})}\rangle^{(\mathbf{C}^0)} - \langle C_i(t)\rangle\langle C_j(t)\rangle, \ldots, \text{etc.} \tag{29}$$

Now, we can formulate the inverse problem: given the probability densities $P^{\circ}(\mathbf{C}^0)$ and $P(\mathbf{C}, t)$, what are the statistical properties of the rate constants ?. At least in principle, the answer to this question may be given by solving the integral equation (25) for $\psi(\mathbf{k})$.

4. AN EXAMPLE

To illustrate our approach, we consider the formation of a reaction intermediate with a constant reaction rate

$$\mathrm{d}C/\mathrm{d}t = k = \text{constant}, \; k > 0. \tag{30}$$

We have

$$\Xi(C, k, t) = C - kt, \; t \leqslant C/k; \quad \mathscr{J}(C, k, t) = 1. \tag{31}$$

We assume that the results of concentration measurements may be fitted by gaussian functions

$$P^0(C^0) = \frac{1}{\sqrt{2\pi\langle\Delta C^{02}\rangle}} \exp\left(-\frac{(C^0 - \langle C^0\rangle)^2}{2\langle\Delta C^{02}\rangle}\right), \tag{32}$$

$$P(C, t) = \frac{1}{\sqrt{2\pi\langle\Delta C^2(t)\rangle}} \exp\left(-\frac{(C - \langle C(t)\rangle)^2}{2\langle\Delta C^2(t)\rangle}\right). \tag{32'}$$

Introducing the notation $\delta k = k - \langle k\rangle$ and supposing that the dispersion of the rate constant $\langle k^2\rangle - \langle k\rangle^2$ is sufficiently small we can neglect the boundary effects and integrate in (25) over δk from $-\infty$ to $+\infty$:

$$\frac{1}{\sqrt{2\pi\langle\Delta C^2(t)\rangle}} \exp\left(-\frac{(C - \langle C(t)\rangle)^2}{2\langle\Delta C^2(t)\rangle}\right) =$$

$$= \frac{1}{\sqrt{2\pi\langle\Delta C^{02}\rangle}} \int\limits_{\delta k = -\infty}^{+\infty} \exp\left(-\frac{(C - \langle k\rangle t - \langle C^0\rangle - \delta k t)^2}{2\langle\Delta C^{02}\rangle}\right)\psi(\langle k\rangle + \delta k)\mathrm{d}\delta k. \tag{33}$$

The integral equation (33) is amenable to solution through the method of the Fourier transform. After simple but lengthy manipulations we get:

$$\psi(k) = \sqrt{\frac{t}{2\pi(\langle\Delta C^2(t)\rangle - \langle\Delta C^{02}\rangle)}} \exp\left(-\frac{(kt - \langle C(t)\rangle + \langle C^0\rangle)^2}{2t(\langle\Delta C^2(t)\rangle - \langle\Delta C^{02}\rangle)}\right). \tag{34}$$

We see that the probability density function of the rate constant is a gaussian with mean $\langle k\rangle = (\langle C(t)\rangle - \langle C^0\rangle)/t$ and dispersion $\langle \Delta k^2\rangle = (\langle \Delta C^2(t)\rangle - \langle \Delta C^{02}\rangle)/t$. As expected, for $t = 0$ Eq. (34) leads to an indetermination. Indeed, the knowledge of a single probability density $P^0(C^0)$ is not sufficient for determination of $\psi(k)$.

ACKNOWLEDGEMENT. This work has been supported by CIMC Bucharest.

REFERENCES

[1] P. M. Frank, "Introduction to System Sensitivity Theory", Academic Press, New York, 1978.

[2] V. Costanza and J. H. Seinfeld, *J. Chem. Phys.*, **74**, 3852 (1981).

[3] M. O. Vlad, *J. Theoret. Biol.*, **126**, 239 (1987); *Math. Biosci.*, **87**, 173 (1987); *Ecological Modelling*, **41**, 229 (1988).

[4] M. O. Vlad, *J. Colloid Interface Sci.*, in press.

[5] D. ter Haar, "Elements of Statistical Mechanics", Constable, London, 1954., p. 101.

[6] R. Bellman, "Introduction to Matrix Analysis", McGraw-Hill, New York, 1960., ch. 10.

Revue Roumaine de Chimie, **34**, *4*, 1101–1106 (1989)

VULCANIZATION OF ACRYLONITRILE-BUTADIENE RUBBER WITH ALKYLPHENOL-FORMALDEHYDE RESIN

T. VOLINTU, G.RI IVAN, ELENA BUGARU and PAULA BUJENIȚĂ
Research Institute for Rubber and Plastics Processing R-79628 Bucharest, Romania

Received October 25, 1988

Curing of acrylonitrile-butadiene rubber with an alkylphenol-formaldehyde resin in presence of activation system, polychloroprene + zinc oxide have been studied. The influences of the curing system proportion as well as of the influence of acrylonitrile content on curing behaviour are discussed.

1. INTRODUCTION

Acrylonitrile-butadiene rubber was considered to be of unusual interest as a specialty rubber because of its properties. This rubber had, besides better oil and gasoline resistance, also better thermostability and lower gas permeability.

Vulcanization of acrylonitrile-butadiene rubber is possible with almost all known crosslinking agents, but, normaly, sulphur systems are used whenever they can produce the required balance of processing, curing and vulcanizate properties.[1]

Resin systems in rubber curing are known for a rather long time and a lot of studies have been made in attempt to explain the mechanism of resin cure [2–6] but the large majority are concerned with butyl rubber curing. In acrylonitrile-butadiene rubber, resin curing systems are used when high heat and steam resistance are required. Curing effect of resins is activated by the presence of the some metallic halogenides ($ZnCl_2$, $SnCl_2$) or by organic halogen donors (polychloroprene, halogenated butyl rubber, chlorosulfonated polyethylene, chlorinated parafin, etc.) associated with a metallic oxide, frequently zinc oxide.[7,8]

A great number of the published papers [9–12] are concerned mainly with final physical properties of vulcanizates and the vulcanization itself seems to be the object of the limited works.[13–15]

The present paper is meant to investigate the influence of the proportion of resin vulcanization system as well as the influence of acrylonitrile content on curing behaviour of acrylonitrile butadiene rubber.

2. EXPERIMENTAL

Materials used in the present study were as follows:

— acrylonitrile-butadiene rubber, types, Carom NBR 33.65 and Carom NBR 38.65 (Romania);

— polychloroprene, type Neoprene W (du Pont de Nemours Co., U.S.A.);

— zinc oxide (STAS 421-78);

— *p*-octylphenol-formaldehyde resin, type SP 1045 (Schenectady, France);

— styrene-butadiene rubber, type Carom 1500 (Romania);

— FEF carbon black (Romania).

Laboratory equipment. A WNR-2 laboratory mill (Troester KG, West Germany) was used for compounding. Curing curves have been recorded in a R100 Rheometer (Monsanto Co., U.S.A.).

Compounding. Studied recipes are presented in Table 1. They were selected as simple as possible in order to avoid an eventual influence of other components on the curing behaviour. All the components were added on the mill at 50°C, using a friction ratio 1.0 :1.4 ; a good incorporation was obtained in 25 minutes. Final compound was tested after a rest of minimum 24 hours but no more than 48 hours.

Table 1

Studied recipes, p.p.h.r.

Components	Recipes 1	2	3
Carom NBR 33.65	100.0	—	—
Carom NBR 38.65	—	100.0	—
Carom SBR 1500	—	—	100.0
Polychloroprene	10.0	10.0	10.0
Zinc oxide	5.0	5.0	5.0
Resin SP 1045	9.0	9.0	9.0

Rheograms were recorded with an oscillation of the rotor of ±3°, using a standard microdie. Cure curves have been obtained in isothermal conditions, selecting 170, 180 and 190°C as temperature steps, according to experiment design. (Fig. 1).

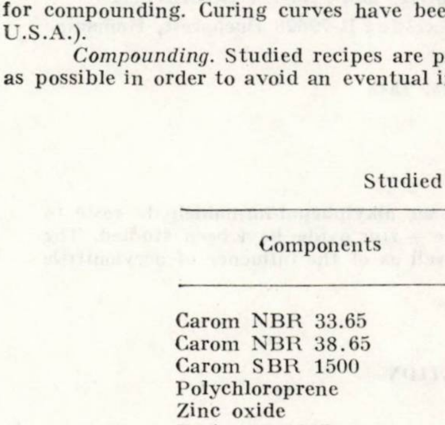

Fig. 1. — Experiment design.

3. RESULTS AND DISCUSSIONS

In attempt to elucidate the influence of the proportion of resin curing system, as well as the influence of acrylonitrile content on curing behaviour, two acrylonitrile butadiene rubber types with 33% and 38% acrylonitrile content have been cured with *p*-octylphenol-formaldehyde resin, using, polychloroprene + zinc oxide. Isothermal vulcanization was used to follow the crosslinking process from the curves recorded in the rheometer.

Curing rate, as usual in vulcanization studies,[16] is associated to time necessary to reach 50% (t_{50}) on vulcanization curve (torque).

The considerable amount of experimental data resulting from the realization of the experimental design for curing rate (t_{50}) and for maximum viscosity (recorded maximum torque) are presented in the most contracted form as contour graphs grouped for each temperature and resin proportion.

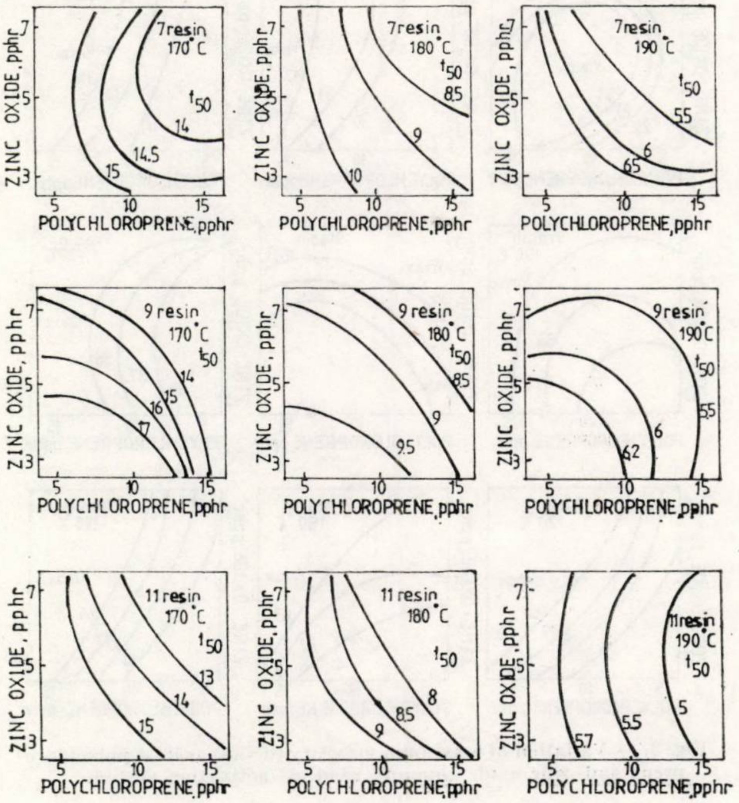

Fig. 2. — Variation of t_{50} (min) against polychloroprene and zinc oxide amounts used in the activation system.

The plottings for cure rate (t_{50}) and for maximum viscosity (maximum torque) are presented in figures 2 and 3. About these figures, there are some comments to be presented :

— cure rate (t_{50}) and maximum viscosity increase with the increase of the activator system proportion ;

— the increase of the curing temperature and of the resin proportion leads also to marked increase of the cure rate ;

— maximum viscosity is influenced by resin proportion which means that the increase of resin proportion increases maximum viscosity, while the temperature variation has little influence.

In order to explain the mechanism of resin cure it was investigated the influence of acrylonitrile content on curing behaviour of acrylonitrile butadiene rubber. Isothermal vulcanization (170°C) was used to follow the crosslinking process; the curves recorded in the rheometer, figure 4 exhibit the increase of the cure rate and of the maximum viscosity when the acrylonitrile content increases.

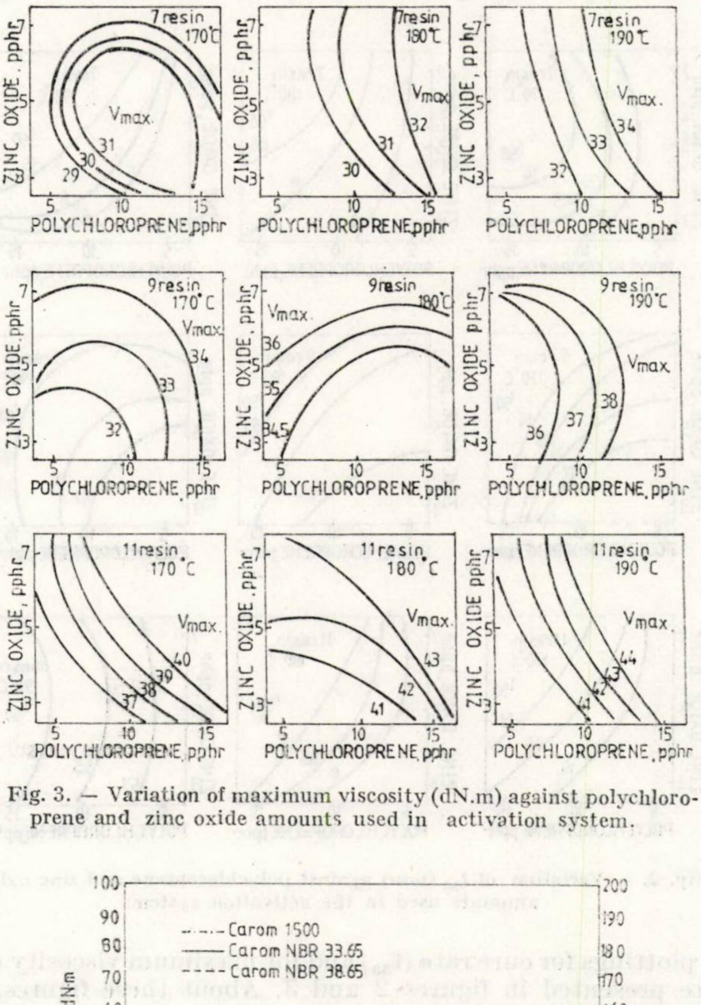

Fig. 3. — Variation of maximum viscosity (dN.m) against polychloroprene and zinc oxide amounts used in activation system.

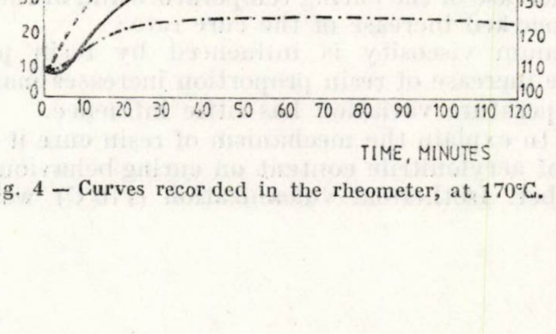

Fig. 4 — Curves recor ded in the rheometer, at 170°C.

According to literature data,[8,17] during curing process can be formed chromanique cycles by reactions of methylol groups of the resin with C=C double bonds (equation 1.a); a reaction of methylol groups with nitrile groups is possible also (equation 1b).

1 a.

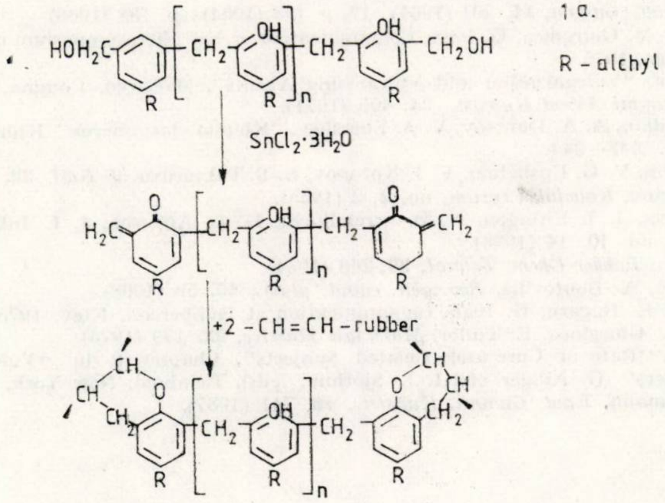

1 b.

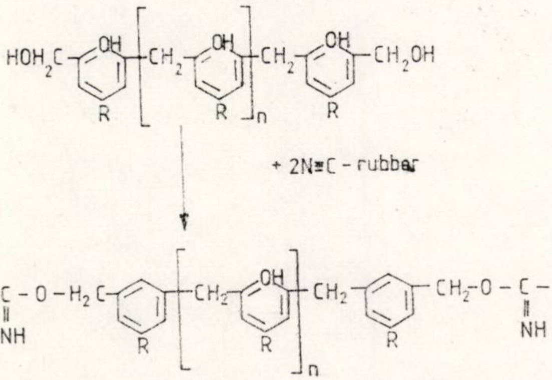

These reactions are activated by the presence of the some metallic halogenides added in compounds or formed *in situ* by reaction of zinc oxide with organic halogen donors.

4. CONCLUSIONS

The study of acrylonitrile-butadiene rubber curing by phenol-formaldehyde resins in the presence of an activation system, zinc oxide + + polychloroprene allows to ascertain the cure rate, and the maximum viscosity is influenced mainly by curing temperature. The increase of acrylonitrile content leads to a marked increase of the maximum viscosity the cure rate.

REFERENCES

[1] T. Volintiru, and G. Ivan, "Bazele tehnologice ale prelucrării elastomerilor" Ed. tehnică, Bucharest, 1974.
[2] J. Le Bras, *Rev. gén. caout.*, **20**, 63 (1974).
[3] P. O. Tawney, *Ind. Engng. Chem.*, **51**, 937 (1969).
[4] A. Giller, *Kaut. Gummi*, **14**, 201 (1961) ; **17**, p. 174 (1964) ; p. 188 (1966).
[5] T. Volintiru, M. Giurginca, G. Ivan, Communication of I-st Microsymposium on Macromolecules, Iași, 1975.
[6] W. Hofmann, "Vulcanization and Vulcanizing Agents", Maclaren, London, 1967.
[7] A. Giller, *Gummi Asbest Kunstst.*, **24**, 405 (1971).
[8] B. A. Dogadkin, A. A. Dontsov, V. A. Shershev, "Khimia elastomerov" Khimiya, Moscow, 1981, p. 343–344.
[9] Yu. N. Nikitin, V. G. Epshetein, V. I. Korobov, L. S. Tuktarova, *J. Koll.* **32**, p. 403 (1971).
[10] V. A. Sapronov, *Kauciuk i rezina*, no. 2, 2 (1965).
[11] A. G. Shvarts, I. I. Eitingon, N. P. Strelnikova, K. L. Aizinson, I. I. Jukova, *Kauciuk i rezina*, no. 10, 14 (1968).
[12] G. Thelamon, *Rubber Chem. Tehnol*, **36**, 268 (1964).
[13] M. Laurentie, A. Bouteville, *Rev. gén. caout. plast.*, **45**, 59 (1968).
[14] T. Volintiru, E. Bugaru, G. Ivan, Communication at Rubbercon, Kiev, 1978.
[15] G. Ivan, M. Giurginca, E. Tudor, *Materiale plastice*, **22**, 179 (1975).
[16] A. E. Juve, "Rate of Cure and Related Subjects", Chapter 2 in "Vulcanization of Elastomers" (G. Alliger end I. J. Sjothun, eds), Reinbold, New York, 1964, p. 30.
[17] Th. Kempermann, *Kaut. Gummi. Kunstst.*, **40**, 741 (1987).

Revue Roumaine de Chimie, **34**, *4*, 1107–1114 (1989)

COORDINATION COMPOUNDS OF $CuBr_2$ WITH SOME TRIAZENOIMIDAZOLE DERIVATIVES

FLORICA ZĂLARU, FELICIA CORNEA, AURELIA MEGHEA and D. IONESCU
Polytechnic Institute, Department of Chemical Technology,
Bucharest, Romania

Received September 21, 1987

The paper presents new complex compounds of $CuBr_2$ with triazenylimidazole derivatives of the type : $CuLBr_2$, CuL_2Br_2 and $CuLBrC_2H_5OH$, where L = 5–(3,3-dimethyl-1-triazenyl)imidazol-4-carbonamide and its corresponding ethyl ester. The compounds were characterized by elemental chemical analysis, electronic, IR and ESR spectra. The influence of bromide ion on the compound type was emphasized.

The coordination properties of imidazole and of some of its derivatives offer important data for understanding some of the reactions between the metallic ions and the natural or synthetical biologically active organic compounds. This explains the interest of the investigators in this ligand and especially in its triazenyl-imidazole derivative 5-(3,3-dimethyl-1-triazenyl)imidazole-4-carboxamide, an important antitumoral agent.[1–4] Antitumoral activity might be ascribed to its ability to act as a chelating agent,[1] although other mechanisms were considered.[2–3]

Interaction of $CuCl_2$ with the triazenylimidazole derivatives of type I

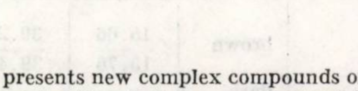

$R = -OCH_3, -NH_2, -NHCH_2COOC_2H_5$

I

shows the influence of the R substituent nature on the type compound CuL_4Cl_2, respectively $CuLCl \cdot C_2H_5OH$ and $CuLCl_2$, and also on the donor atoms.[4] On the basis of our previous experimental data,[4] this paper presents the influence of the bromide anion in the interaction of $CuBr_2$ with the same ligands.

RESULTS AND DISCUSSION

Synthesis was performed in ethanolic medium in a molar ratio Cu : L = 1 :1 and 1 : 2. Two different compounds were obtained for the 1 : 1 molar ratio as a function of the way of adding the reagents. When small amounts of the ligand solution were added on the copper bromide solution, a brown microcrystalline precipitate, soluble in hot dimethylformamide, formulated on the basis of the elemental chemical analysis, $CuLBr_2$, separated. When adding a $CuBr_2$ solution suddenly to the ligand solution, a pulverulent, green product was obtained. It is formulated $CuLBr.C_2H_5OH$ and is insoluble in cold or hot DMF (Table 1).

Table 1

The compound type and analytical data

Molar ratio Cu : L	No.	Compound for		colour	Cu %	Br %	N %
		R	R		F / C	F / C	F / C
1 : 1	1	$CuLBr_2$		brown	15.66 15.76	39.23 39.41	22.12 20.69
	2	$CuLBrS$		dark green	17.84 17.57	21.33 21.44	25.72 22.52
	3		$CuL'Br_2$	brown	14.17 13.01	33.55 32.52	18.54 17.07
1 : 2	4	CuL_2Br_2		green	9.89 0.81	28.30 27.18	27.44 28.57
	5		*cis*-CuL'_2Br_2	dark green	7.46 8.51	19.64 21.27	
	6		*trans*-CuL'_2Br_2	light green	6.79 8.51	20.81 21.27	

L = ligand for R = $-NH_2$; L′ = ligand for R = $-NHCH_2COOC_2H_5$; S = C_2H_5OH; F = Found; C = Calcd.

For the Cu : L = 1 : 2 molar ratio, two compounds having the same formula, CuL'_2Br_2 were obtained only from ligand L′ for which R = $-NHCH_2COOC_2H_5$. These compounds could be *cis-trans* isomers as suggested by the ESR and visible electronic spectra.

Electronic spectra

Figures 1 and 2 give the reflectance electronic spectra for the isolated compounds. The brown compounds (**1** and **2**) have an almost similar spectrum: a band whose $\lambda_{max} = 470$ nm might be assigned to a charge-transfer interaction Cu—Br and which gives them a brown colour and a $\lambda_{max} = 760$ nm band that might be assigned to a d—d transition expected for the Cu(II) compounds in a distorted tetragonal octahedron encirclement between 500 and 600 nm and which is shifted towards the near IR range as a function of the tetragonal distortion.[5–9] The spectrum of compound **1** has also a shoulder at 700 nm. The green compound, **2**, has in the

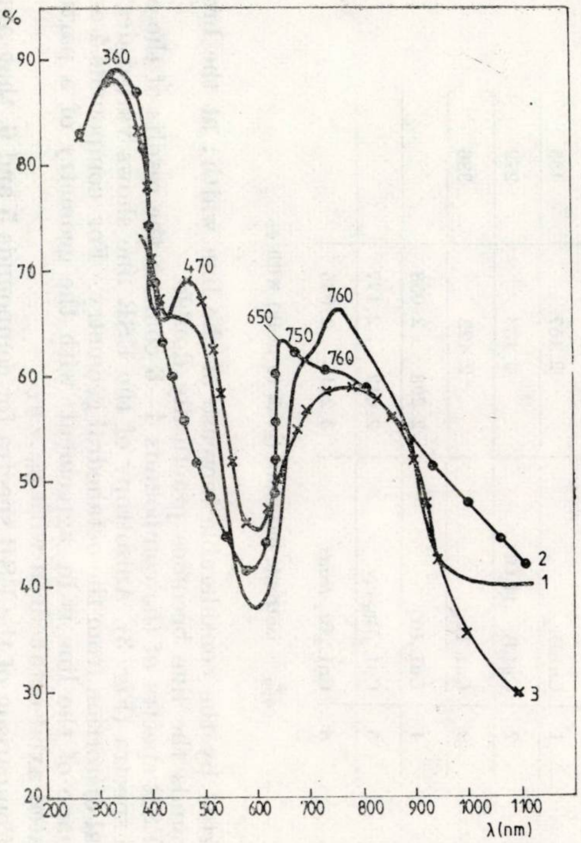

Fig. 1. — Electronic reflectance spectra: ——— compound (1); —·—·—·—·— (2): ×—×—×—×—× (3).

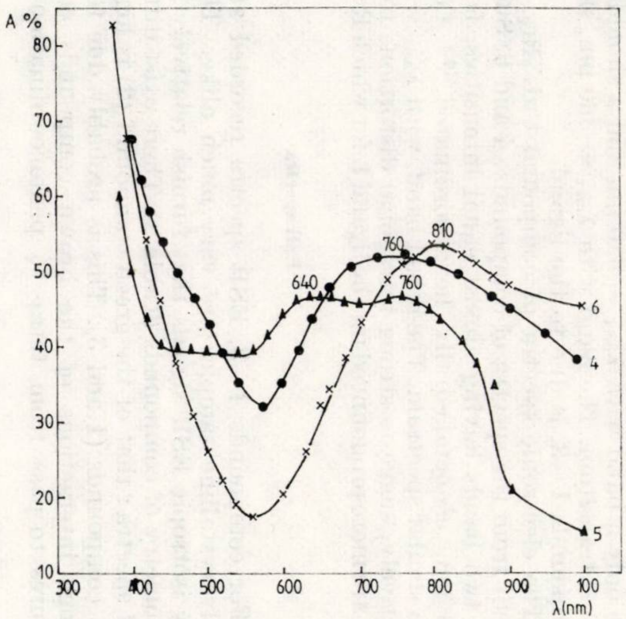

Fig. 2. — Electronic reflectance spectra: —·—·—·—·— compound (4); —▲—▲—▲ (5); —×—×—×— (6).

visible only a band with $\lambda_{max} = 650$ nm and a shoulder at 760 nm due to the d–d transition. The band with $\lambda_{max} = 360$ nm, shown by the spectra of compounds **1**–**3**, is due to the ligand.

The electronic spectra of compound CuL'_2Br_2, noted **5** (Fig. 2), are different from the spectra of compounds **4** and **6**. Such a spectrum, made up of two bands having almost equal intensities, is associated with the Cu(II) ion, *cis*-octahedrally hexacoordinated.[5,7,9] Compounds **4** and **6** show a similar spectrum. The broad band, with $\lambda_{max} = 760$ nm and 810 nm respectively, suggests strong tetragonal distortions towards square planar which are more pronounced for the ligand L for which $R = -NHCH_2CO_2C_2H_5$.

ESR spectra

For compounds **1**–**3**, ESR spectra recorded at room temperature on polycrystalline samples are very much alike. The compound shows largely isotropic ESR signals that furnish relatively little information on the geometry of compounds (Table 2). There exist differences in the intensity of spectra: that of the green compound (**2**) is higher than that of the brown compounds (**1** and **3**). This is probably due to the increase of the exchange interactions of the brown compounds enabling some dimer structures to pass from tetra- to pentacoordination. This hypothesis is supported by the considerable increase of the line width; at the brown compounds the line becomes practically double.

Table 2

ESR spectral parameters

No.	Compound	g_i		a^*_{pp} (Gauss)
		$g_{\parallel}$	$g_{\perp}$	
1	$CuLBr_2$	2.157		435
2	$CuLBrC_2H_5OH$	2.133		272
3	$CuL'Br_2$	2.122		336
4	CuL_2Br_2	2.298	2.058	
5	CuL'_2Br_2-*cis*	2.012	2.177	
6	CuL'_2Br_2-*trans*	2.244	2.045	

a^*_{pp} – isotropic linewidth (peak to peak) with g_i.

ESR spectra of the compounds **4**–**6** confirm the results of the electronic spectra (Fig. 3). Anisotropy of the ESR line shows varied degrees of axial distortion from the octahedral geometry. For compounds **4** and **6** the shape of the line is in agreement with the geometry of a partially elongated axial octahedron with $g_{\parallel} > g_{\perp}$.

Comparison of the ESR spectra for compounds **5** and **6**, that appear as geometrical isomers, shows an inversion of the axial distortion from the elongated octahedron, compound **6**, to a slightly flattened octahedron, compound **5** with $g_{||} < g_{\perp}$ in agrement with the assignment given on the basis of the electronic spectra.[5]

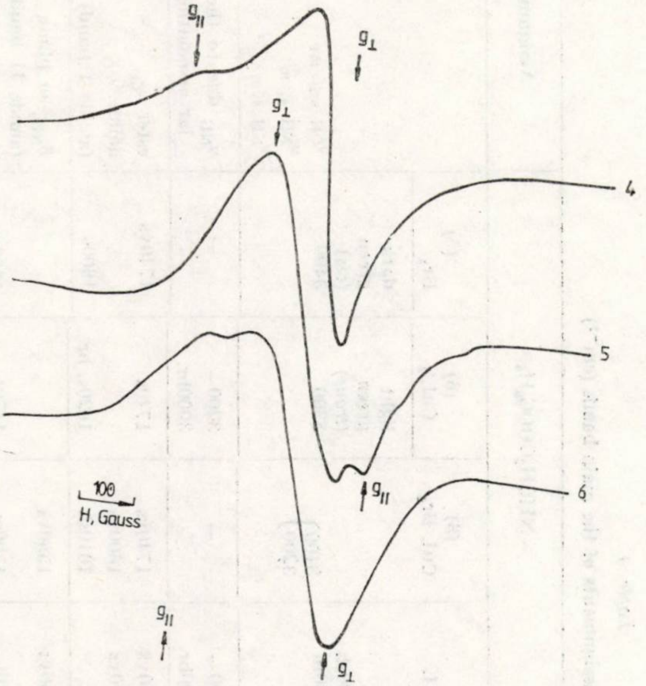

Fig. 3. — ESR spectra : **4** — CuL_2Br_2, 5 — CuL'_2Br_2-*cis*, 6 — CuL'_2Br_2—*trans*.

IR spectra

IR spectra for ligands and compounds have been recorded for obtaining information on the donor atoms. Comparison of the IR spectrum of compounds with that of ligands shows the following (Table 3).

1) In the green compounds, $CuLBrC_2H_5OH$, one notices the disappearance of the ν_{N-H} band, characteristic of the imidazole intermolecularly associated with hydrogen bonds (3100—2100 cm^{-1}) and also the existence of one single band in the asymmetrical and symmetrical ν_{N-H} range, showing the presence of a secondary amide. This change might suggest the participation of the amide group in the complex formation by replacing a hydrogen atom by the nitrogen atom. The second donor atom might be the imidazole nitrogen atom N(3), taking into account the changes within the 1500—1000 and 1000—700 cm^{-1} ranges, characteristic of the stretching vibrations and of the bending of the imidazole ring, respectively.[10] The other two coordinative points might be the bromine atom and oxygen atom of the solvent. If the structure formula of the compound is correlated with the data given by electronic and ESR spectra, Cu(II) atom would be tetracoordinated in a square planar geometry distorted to tetrahedron.[9]

Table 3

IR spectrum and assignments of the main bands (cm^{-1})

R	$-NH_2$			$-NHCH_2COOC_2H_5$				Assignments
L	(1) $CuLBr_2$	(2) CuLBrS	(4) CuL_2Br_2	L	(3) $CuL'Br_2$	(6) CuL'_2	(5) Br_2	
						light green (*trans*)	dark green (*cis*)	
 3390m 3180m	3400w 3350m 3180m	3400m	3600sh 3390w 3100w	3600sh 3360m	3400) 3200)	3300	3400	ν_{OH} associat ν_{NH} asym. ν_{NH} sym.
3200– 2100br.	—	—		3200– 2100br.	—	3200– 3000br.	—	ν_{NH} due to the molecular associations
 1665vs 1614vs	 1650)s 1580)	 1650) vs 1680)	 1650vs —	1740vs 1670vs	1740vs 1600vs 1610sh	1740s 1620s, br	1740vs 1600s	ester ν_{CO} amide ν_{CO} (amide I band)
1520) vs 1500) 1440) 1420) vs 1400) 1350) vs 1320)	1520m) 1490m) 1420w 1380s 1320m	1500vs 1420w 1380vs 1320w	1520w 1500s 1420s 1350vs 1320s	1550vs 1470s 1430) m 1390) 1350sh 1210) vs 1200)	1550vs 1500w 1430w 1390m 1320m 1210) s 1200)	1470s 1350v, br. 1210	1500w 1360w 1240vw	δ_{NH_2} in plane (amide II band) $\nu_{imidazole\ cycle}$
1080vs	1100w	1100vs	1090s	1080vs	1100s	1080s	1110vw	ν_{NNN}
965m 890m 870sh	965m 900m —	1050m 900	985m 910 870	960m 900m 870m	1000m 900vw 870vw	900vw		deformation of the imidazole cycle

s = C_2H_5OH ; vs = very strong, s = strong, w = weak, vw = very weak, m = medium sh = shoulder, br = broad.

2) For the brown compounds (**1** and **3**) the change due to the $\nu_{C=0}$ vibration (Band I amide) and those due to the stretching ($1500-1000$ cm^{-1}), and bending of the imidazole ring ($1000-700$ cm^{-1}), respectively, in shape, intensity and position, might suggest the involvement of the oxygen atoms of the carboxamide group and also the imidazole nitrogen atom N(3) in coordination. The other two coordinative points might be the bromine atoms.

3) The IR spectrum of compounds **4** and **6** shows changes within the $\nu_{C=0}$ range and within the ranges of stretching and bending vibrations of the imidazole ring, suggesting the involvement in coordination of the same donor atoms (oxygen atom of carboxamide group and nitrogen atom N(3) of imidazole). Spectrum of compounds **5**, although very changed in comparison with that of the free ligand, generally show changes that concern the same ranges.

The information given by the electronic, ESR and IR spectra, correlated with the structure formulae of the new compounds obtained, show that the copper atom is tetracoordinated between a square planar geometry, slightly distorted to tetrahedron by the O, N(3) imidazole nitrogen atoms and by bromine atoms (compounds **1** and **3**) and the nitrogen atom of carboxamide group by deprotonation, N(3) imidazole atom, oxygen atom of the solvent and the bromine atom (compound **2**). Likewise, we appreciate that the Cu(II) atom is hexacoordinated in a tetragonal *trans*-octahedron geometry, distorted to square planar for compounds **4** and **6** and *cis*-octahedron for compound **5**. The coordination is achieved by oxygen atoms of the carboxamide group, the imidazole N(3) nitrogen atom and the two bromine atoms.

CONCLUSIONS

The influence of bromide anion on the type of compound and on the number of compounds isolated was evidenced.

For the molar ratio Cu : L = 1 : 1, two compounds are obtained $CuLBr \cdot C_2H_5OH$ and $CuLBr_2$ as a function of the way of adding the reagents. For the molar ratio Cu : L=1 : 2 only the ligand L′ for which $R=-NHCH_2CO_2C_2H_5$ favours the separation of the two *cis-trans* geometrical isomers CuL'_2Br_2 while interaction of $CuCl_2$, in the same conditions determined the obtention of only two compounds : $CuLCl \cdot C_2H_5OH$ and $CuL'Cl_2$.

The arguments for the structure of the new compounds were supported by the spectral data in visible, IR and ESR.

EXPERIMENTAL

$CuBr_2$ and ligands prepared according to the data in the literature [11] were used. The compounds were prepared by the ethanolic solution of $CuBr_2$ and of the ligands. The compounds were separated by vacuum filtration, washed in small amounts of ethanol and then dried at room temperature.

$CuLBr_2$. Ethanolic solution of ligand (0.001 M) was added in small amounts under stirring to the $CuBr_2$ solution (0.001M). A brown solution was obtained, out of which a solid brown precipitate was separated in about 30 min. The compound is soluble in hot DMF.

$CuLBr \cdot C_2H_5OH$. The $CuBr_2$ (0.001M) ethanolic solution was added suddenly to the ethanolic ligand solution (0.001M). A green compound, insoluble in cold and hot DMF, was separated.

CuL'_2Br_2. The ethanol ligand solution (0.002M) was added to the ethanol solution of $CuBr_2$ (0.001M). From the green solution a dark green precipitate deposited and a light green precipitate, soluble in water, crystallized on the walls.

The analyses of copper were carried out by Spacu's method. Bromine analyses were performed by the gravimetric standard method. Diffuse-reflectance spectra were recorded with a Zeiss-Jena VSU−2 spectrophotometer in the 400−1000 nm range, using magnesium oxide as reference. Infrared spectra of the ligands and the complexes were recorded with a Specord 71 spectrophotometer in the range of 4000−700 cm^{-1}. Samples were prepared as KBr disk. The ESR spectra at room temperature were recorded on the polycrystalline powder using an ART-5-IFA spectrograph. The klystron frequency was 9060 MHz and the modulation of the magnetic field 100 kHz. The ESR spectral parameters were calculated versus a Mn(II) standard.

REFERENCES

[1] J. L. Skibba, D. D. Beal, G. Rairez and G. T. Bryan, *Cancer. Res.*, **30**, 147 (1970).
[2] Y. F. Shealy, J. A. Montgomery and W. R. Laster Jr., *Biochem. Pharmacol.*, **1**, 674 (1962).
[3] H. C. Freeman and N. D. Hutchinson, *Acta Cryst.*, **B35**, 2045, 2051 (1979).
[4] F. Zălaru, D. Ionescu, A. Meghea, F. Cornea and C. Gheorghiu, *Rev. Roumaine Chim.*, **28**, 811(1983).
[5] B. J. Hathaway and D. E. Billing, *Coord. Chem. Rev.*, **5**, 143 (1970).
[6] B. J. Hathaway, *J. Chem. Soc. A*, **1972**, 1196.
[7] B. J. Hathaway, I. M. Procter, R. C. Slade and A.A.G. Tomlinson, *J. Chem. Soc. A*, **1969**, 2219.
[8] E. D. McKenzie, *J. Chem. Soc. A.*, **1970**, 3095.
[9] B. J. Hathaway, "Structure and Bonding", 57, 56, Springer Verlag, Heidelberg, 1984.
[10] R. H. Carlson and T. L. Brown, *Inorg. Chem.*, **5**, 268 (1966).
[11] D. Ionescu, "Compuşi organici de sinteză cu acţiune biologică", Doctoral Thesis, Bucharest, 1981.

PRINTED IN ROMANIA

ORSZÁGOS MŰSZAKI INFORMÁCIÓS KÖZPONT ÉS KÖNYVTÁR 1883

NOTE POUR LES AUTEURS

La **Revue Roumaine de Chimie** publie des articles en anglais, français, russe, allemand ou espagnol. Les auteurs sont priés d'envoyer des articles et des comptes rendus inédits.

Les manuscrits seront dactylographiés à double interligne. La bibliographie, les tableaux et la légende des figures seront placés après le texte.

Si l'article fait partie d'une série numérotée, la partie précédente sera donnée comme première référence.

Chaque article sera précédé d'un résumé comprenant quinze lignes au maximum.

Les références bibliographiques dans le texte seront faites par des exposants sans parenthèses et paraîtront à la fin de l'ouvrage.

Les publications périodiques mentionnées dans la bibliographie seront présentées suivant les prescriptions internationales : le nom de l'auteur précédé de l'initiale du prénom, le titre du périodique abrégé conformément à « Chemical Abstracts » et souligné par une ligne, le numéro du tome indiqué par des chiffres arabes et souligné par deux lignes, suivi de la première page de l'article : à la fin, l'année de la parution sera placée entre parenthèses. Le numéro de la revue ne sera pas indiqué si les pages du volume sont numérotées consécutivement.

Les textes des livres ou traités incluеront : le nom des auteurs, précédés de l'initiale du prénom, le titre du livre entre guillemets et sans être souligné, le numéro du tome précédé par l'abréviation « vol. » (ou « Bd. »), le numéro de l'édition, les éditions (the publisher), la localité de la parution du livre, l'année de la parution et la page de la référence précédée(s) par l'abréviation « p » (ou « S »).

Les brevets seront indiqués comme suit : l'auteur ou la firme, le pays et le numéro du brevet, la date de la revue *(Chem. Abstr.)*. Par ex. : M. Jones (to Union Carbide Co.), Brit. Pat. 610 238, 2 Sept. 1959 : cf. *Chem. Abstr.*, **54**, 12808 (1960).

Si la référence n'a pas été lue en original, on indiquera aussi la revue de références consultée.

Les diagrammes seront tracés à l'encre de Chine sur papier calque. Les tableaux et les figures (en nombre strictement nécessaire), ainsi que les courbes dans les figures seront numérotés par des chiffres arabes. Leur explication sera donnée dans la légende des figures. Prière de ne pas inscrire les mêmes données dans les tableaux et les figures. Chaque tableau aura un titre. On indiquera dans le texte la place approximative des tableaux et des figures. Les formules chimiques seront incluses dans le texte ; en outre, elles seront transcrites sur papier calque, à l'encre de Chine.

Les auteurs sont priés d'indiquer les caractères italiques (en soulignant les lettres au crayon), ainsi que tout autre caractère spécial : les préfixes *ortho*, *méta*, *para*, *cis*, *trans*, etc. seront soulignés pour indiquer leurs caractères italiques et ne seront jamais écrits avec des majuscules.

Aucune correction à la main ne sera admise sur le manuscrit. Les corrections seront frappées à la machine. Les lettres grecques ou d'autres symboles spéciaux seront insérés à la main à l'encre clairement.

Le manuscrit sera signé par l'auteur.

Le titre courant aura 50 lettres au maximum.

L'entière responsabilité du contenu des articles appartient aux auteurs.

Sur demande on peut obtenir une note plus complète.

PRINTED IN ROMANIA

TRAVAUX PARUS AUX ÉDITIONS DE L'ACADÉMIE DE LA RÉPUBLIQUE SOCIALISTE DE ROUMANIE

MÁJ 1 2

ELENA CEAUŞESCU, **Răşini de hidrocarburi, vol. 1**, 1988, 344 p.
ELENA CEAUŞESCU, **Progrese în chimia şi tehnologia polimerilor**, 1986, 446 p.
ELENA CEAUŞESCU, **Forschungen im Bereich der Chemie und Technologie der Polymere**, 1986, 444 p.
ELENA CEAUŞESCU, **Cercetări în chimia şi tehnologia polimerilor**, 1983, 520 p.
ELENA CEAUŞESCU, **Noi cercetări în domeniul compuşilor macromoleculari**, 1981, 536 p.
ELENA CEAUŞESCU, **Polimerizarea stereospecifică a izoprenului**, 1979, 307 p.
ELENA CEAUŞESCU, **Research work on synthesis and characterization of macromolecular compounds. Contributions**, 1974, 251 p.
I. G. MURGULESCU, **Introducere în chimia fizică, vol. I. 1. Atomi, molecule, legătură chimică**, 1976, 560 p.
I. G. MURGULESCU, V. EM. SAHINI, **Introducere în chimia fizică, Vol. I, 2. Structura şi proprietăţile moleculelor**, 1979, 604 p.
I. G. MURGULESCU, E. SEGAL, **Introducere în chimia fizică, Vol. II. 1. Teoria molecular-cinetică a materiei**, 1979, 1036 p.
I. G. MURGULESCU, TATIANA ONCESCU, E. SEGAL, **Introducere în chimia fizică, Vol. II. 2. Cinetică chimică şi cataliză**, 1981, 1024 p.
I. G. MURGULESCU, J. PĂUN, **Introducere în chimia fizică, Vol. I, 3. Nucleul atomic, reacţii nucleare, particule elementare**, 1982, 606 p.
I. G. MURGULESCU, RODICA VÎLCU, **Introducere în chimia fizică. Vol. III. Termodinamica chimică**, 1982, 624 p.
I. G. MURGULESCU, O. M. RADOVICI, **Introducere în chimia fizică, Vol. IV. Electrochimia**, 1986, 416 p.
CRISTOFOR I. SIMIONESCU, VALERIA GORDUZA, **Implicaţii bioenergetice ale coloranţilor**, 1988, 208 p.
R. VÎLCU, M. LECA, **Termodinamica polimerilor prin cromatografie de gaze**, 1987, 238 p.
I. ZUGRĂVESCU, M. PETROVANU, **Cicloadiţii 3+2 dipolare**, 1987, 446 p.
RAUL MIHAIL, ION GROZEANU, **Estimarea secvenţială aplicată sistemelor chimice**, 1986, 406 p.
M. BREZEANU, I. PATRON, M. ANDRUH, **Combinaţii complexe polinucleare şi aplicaţiile lor**, 1986, 244 p.
A. T. BALABAN et al., **Labelled Compounds and Radiopharmaceuticals Applied in Nuclear Medicine**, coédition avec John Wiley and Sons, 1986, 742 p.
D. PURDELA, **Nomenclatura chimiei organice – IUPAC**, 1986, 451 p.
PETRU BUDRUGEAC, **Probleme de chimie**, 1986, 280 p.
T. ONCESCU, S. G. IONESCU, **Conversie fotochimică şi stocare de energie**, 1985, 272 p.
V. DRĂGUŢAN, A. T. BALABAN, M. DIMONIE, **Olefin Metathesis and Ring-Opening Polymerization of Cyclo-Olefins**, coédition avec John Wiley and Sons, 1985, 544 p.
C. LITEANU, I. RÎCĂ, **Optimizarea proceselor analitice**, 1985, 360 p.
N. PERESCU, **Chimia extracţiei cu solvenţi şi aplicaţii**, 1985, 212 p.
V. EM. SAHINI, M. HILLEBRAND, **Chimie cuantică în exemple şi aplicaţii**, 1985, 382 p.
GH. MARCU, **Chimia compuşilor coordinativi**, 1984, 415 p.
E. CORDOŞ, C. MANOLIU, **Spectrometria de absorbţie şi fluorescenţa atomică**, 1984, 178 p.
C. BODEA, **Tratat de biochimie vegetală, p. II, t. V**, 1984, 438 p.
N. ASANDEI, A. GRIGORIU, **Chimia şi structura fibrelor**, 1984, 395 p.
N. IONESCU, M. CĂLDĂRARU, **Oxidarea catalitică a olefinelor inferioare**, 1983, 178 p.
C. I. SIMIONESCU, F. DANEŞ, **Originea vieţii**, 1984, 110 p.
C. BODEA, **Tratat de biochimie vegetală, p. II, t. IV**, 1982, 408 p.
CR. SIMIONESCU, VALERIA GORDUZA, **Polimeri biocompatibili şi biologic activi**, 1980, 479 p.
M. FLORESCU, **Metode ştiinţifice în dezvoltarea industriei chimice moderne**, 1979, 495 p.
C. GH. MACAROVICI, **Analiza chimică cantitativă anorganică**, 1979, 457 p.

ISSN 0035–3930

I. P. Informaţia c. 2673

43 426

Lei 40

F 1103

ACADÉMIE DE LA RÉPUBLIQUE SOCIALISTE DE ROUMANIE

REVUE ROUMAINE DE CHIMIE

Hommage à l'académicien
ELENA CEAUȘESCU

TOME 34
N° 5
Mai 1989

Rev. Roumaine Chim.

RRCHAX, 34, 5, p. 1115 – 1290 (1989), Bucarest

EDITURA ACADEMIEI REPUBLICII SOCIALISTE ROMÂNIA

ACADÉMIE DE LA RÉPUBLIQUE SOCIALISTE DE ROUMANIE

COMITÉ DE RÉDACTION

Rédacteur en chef :

I. G. MURGULESCU, membre de l'Académie de la République Socialiste de Roumanie

Rédacteurs en chef adjoints :

A. T. BALABAN et V. EM. SAHINI, membres correspondants de l'Académie de la République Socialiste de Roumanie

Collège de rédaction :

EM. BRATU, ELENA CEAUȘESCU, ECATERINA CIORĂNESCU-NENITZESCU, CR. SIMIONESCU, membres de l'Académie de la République Socialiste de Roumanie ; P. SPACU, membre correspondant de l'Académie de la République Socialiste de Roumanie ; M. BANCIU, M. D. GHEORGHIU, I. HAIDUC, D. I. MARCHIDAN, G. NIAC et D. SĂNDULESCU

La Revue Roumaine de Chimie paraît 10 fois par an. Toute commande de l'étranger sera adressée à ROMPRESFILATELIA — sectorul Export-Import Presă, P.O. Box 12—201, télex 10376 prsfi r 78104 Bucarest, Calea Griviței nr. 64—66, Roumanie

Les manuscrits, les livres et les revues proposés en échange, ainsi que toute correspondance seront envoyés à la rédaction :

REVUE ROUMAINE DE CHIMIE

125, Calea Victoriei, 79717 Bucarest, Roumanie, téléphone 50 76 80

EDITURA ACADEMIEI REPUBLICII SOCIALISTE ROMÂNIA
125, Calea Victoriei **79717,** Bucarest, Roumanie, téléphone 50 76 80

ORSZÁGOS MŰSZAKI INFORMÁCIÓS KÖZPONT ÉS KÖNYVTÁR 1883

HOMMAGE À L'ACADÉMICIEN
ELENA CEAUȘESCU

IN HONOUR OF
ELENA CEAUŞESCU, D. CHEM. ENG.,
MEMBER OF THE ACADEMY OF THE SOCIALIST REPUBLIC OF ROMANIA

On January 7, this year, we celebrate the birthday and 50 years of revolutionary activity of Academician Elena Ceauşescu. A Doctor of Chemical Engineering, Member of the Executive Political Committee of the Central Committee of the Romanian Communist Party, First Vice-Prime Minister of the Government of the Socialist Republic of Romania, President of the National Council for Science and Education, Dr. Elena Ceauşescu chairs a vast scientific, political and social enterprise meant to bring into effect the country's plans for economic and social development, the important programs geared to a better organization and modernization of production, to increasing work productivity and efficiency, to a comprehensive implementation of the overall policy of the Romanian Communist Party and State, for the benefit of Romanian science, education and culture. The organization and management of the scientific research in this country, most especially in the fields of chemistry, and chemical technology and engineering, largely rely upon the innovative scientific spirit of, and direct guidance by Dr. Elena Ceauşescu.

As a direct outcome, the entire research and development system in chemistry has been given an appropriate coordination and has been integrated, along with the higher education in the field, with the respective industry.

The research work undertaken by Dr. Elena Ceauşescu is focused mainly on the chemistry and technology of macromolecular compounds; she has contributed to elucidating a number of major problems in the area — a most dynamic one in chemistry today, while also providing valuable contributions in all stages of applied research and

engineering, thus fostering the implementation in industry of the results of fundamental research.

Her studies dwell, *inter alia*, upon procedures for monomer and solvent purification; procedures for obtaining polymers via stereospecific polymerization and emulsion polymerization; procedures for obtaining polycondensates; studies on the structural characteristics of polymers and the relationship between structure and properties, as well as methods for the characterization of polymers. A series of studies deal with the use of complex catalysts for polymer synthesis in solution, with special emphasis on catalysts based on transition metals. Other works are concerned with the obtaining of polymers modified by isomerization, degradation and substitution reactions.

The stereospecific polymerization of isoprene holds an important place in the research work developed by Dr. Elena Ceauşescu, owing to the paramount relevance of this problem in today's chemistry of synthetic rubber. Part of the results were gathered in Dr. Ceauşescu's doctoral thesis. A special emphasis was placed on the synthesis of *cis*-1,4-polyisoprenic rubber that displays properties and structures similar to those of natural rubber, and substitutes for the latter in the tyre and technical item industry. Theoretical aspects connected with the reaction mechanism and kinetics, and the properties of the polyisoprene were also dealt with. Research was focused on the optimization of basic parameters, the obtaining of catalytic systems and development of the main steps of the technological flow-chart. The results have led to an industrial process for manufacturing *cis*-1,4-polyisoprenic rubber in Romania.

Dr. Elena Ceauşescu's scientific activity is also reflected in numerous papers published in scientific journals and in six monographs, first put out by Editura Academiei R. S. România, Bucharest, namely, "Research Work on Synthesis and Characterization of Macromolecular Compounds" (1974), "Stereospecific Polymerization of Isoprene" (1979), "Recent Research in the Field of Macromolecular Compounds" (1981), "Research in the Chemistry and Technology of Polymers" (1983), "Advances in Polymer Chemistry and Technology" (1986), and "Hydrocarbon Resins" (1988). Many publishing houses worldwide were soon to offer their readers translations of these books.

Dr. Elena Ceauşescu chaired the National Congress of Chemistry in the years 1978, 1981, 1988, and the IUPAC's Macro '83 Symposium. Her opening address at the 1988 National Congress of Chemistry gives important guidelines to the chemical research in Romania, also providing for the strengthening of the international scientific co-operation. Dr. Elena Ceauşescu contributed valuable papers to many scientific congresses and symposia — an outcome of her comprehensive scientific activity in the field of elastomer chemistry.

Dr. Elena Ceauşescu's scientific merits won well-deserved national and worldwide recognition. She is a member of the Academy of the Socialist Republic of Romania. She was also elected member of numerous international chemical societies of high renown and was nominated honorary professor by important higher education institutions abroad. Dr. Ceauşescu is a honorary member of the International Society of Industrial Chemistry, France; active member of the Academy of Sciences, New York; honorary member of the College of Chemists and Chemical Engineers in Costa Rica; honorary member of the University Council and of the Management Council of the Central University in Ecuador; honorary member of the Ecuador Institute of Natural Sciences; honorary member of the School of Information Science of the Central University of Ecuador; honorary professor of the National Engineering University, Peru; honorary member of the American Institute of Chemists (A.I.C.); Doctor Honoris Causa of the University of Buenos Aires; Doctor Honoris Causa of the University of South-Bahia Blanca, Argentina; Doctor Honoris Causa of the Feminine University of Manila, the Philippines; honorary member of the Chemical Society of Mexico; Doctor Honoris Causa of the University of Yucatan, Mexico; Extraordinary Professor of the Autonomous National University of Mexico; Doctor Honoris Causa of Sciences, University of Teheran; honorary member of the Society of Polymer Science in Japan; corresponding member of the Academy of Athens; awardee of the Silver Medal of the Science University of Kuweit; honorary member of the Academy of Arts and Sciences in Ghana; honorary member of the Academy of Sciences of the State of Illinois, USA; Fellow of the Royal Institute of Chemistry, UK; Professor Honoris Causa of the Polytechnics of Central London; member of the European Academy of Sciences, Arts

and Humanities, and member of the Honorary Committee of the Academy; Doctor Honoris Causa of the Technical University of the Middle East, Ankara; Doctor Honoris Causa of the University of Malta; Doctor Honoris Causa for Sciences of the Islamabad University, Pakistan; Doctor Honoris Causa for Sciences of the University of Liberia; Doctor Honoris Causa in Chemical Sciences, D.P.R. of Korea.

The high praise enjoyed by Dr. Elena Ceauşescu is also reflected in her being awarded important titles and distinctions of merit. Among these are: the highest Romanian title of honour "Hero of the Socialist Republic of Romania"; the title "Hero of Socialist Labour"; the medal "Star of the Socialist Republic of Romania", as well as other orders and medals, Romanian and foreign. She was also awarded the Gold Medal of the Institute for the Problems of a New International Economic Order, the Gold Medal "Marie Curie" and the Jubilee Gold Medal of the Institute of International Relations in Rome, and the Gold Badge of the European Academy of Sciences, Arts and Humanities. By virtue of these, Academician Elena Ceauşescu is the most prestigious representative of the Romanian contemporary science, education and culture.

Active in the national scientific and political life as well as in the international arena, presiding over the Romanian National Committee "Scientists and Peace", Academician Elena Ceauşescu makes an outstanding contribution to the carrying into effect of Romania's policy of independent domestic development, many-sided international co-operation, and struggle for peace, a policy designed under the guidance of Comrade Nicolae Ceauşescu, Secretary General of the Romanian Communist Party, President of the Socialist Republic of Romania, Honorary President of the Academy of the Socialist Republic of Romania.

The National Council for Science and Education, the Ministry of the Chemical and Petrochemical Industry, the Academy of the Socialist Republic of Romania, and the Central Institute for Chemistry join whole-heartedly in the feelings of highest esteem and praise the Romanian people has for Academician Elena Ceauşescu, and express deepest appreciation for her exceptional contribution

to the building of modern Romania, to the development of scientific research and education in this country, particularly in the field of chemistry, chemical technology and engineering. We wish the most distinguished Romanian scholar many happy returns and a long and fruitful activity in order that science, education and culture in the Socialist Republic of Romania be raised onto ever higher levels of performance, for the benefit of our society, of world progress and peace.

THE NATIONAL COUNCIL
FOR SCIENCE AND EDUCATION

THE MINISTRY
OF THE CHEMICAL
AND PETROCHEMICAL
INDUSTRY

THE ACADEMY
OF THE SOCIALIST
REPUBLIC OF ROMANIA

THE CENTRAL INSTITUTE
FOR CHEMISTRY

REVUE ROUMAINE DE CHIMIE

Tome 34, N° 5 **Mai, 1989**

IN HONOUR OF
ELENA CEAUŞESCU, D. CHEM. ENG.
MEMBER OF THE ACADEMY OF THE SOCIALIST REPUBLIC OF ROMANIA

ELENA CEAUŞESCU, M. CORCIOVEI, M. DIMONIE, D. BARB, M. CHIPARĂ and T. SÂRBU, ESR studies on $AlCl_3$ based catalytic systems 1117–1130

URSULA BOLOGA, ANA SCHIKETANZ, CORINA MUŞAT, DANIELA VÎLCICĂ, C. DRĂGHICI, M. D. GHEORGHIU and A. T. BALABAN, Synthesis and stereochemistry of 3,5-dialkyl-2-furyl *p*-substituted-styryl ketones (furanic analogues of chalcone) 1131–1137

GRIGORE BOZGA, CRISTIAN TSAKIRIS and ALEXANDRU ISOPESCU, Studies of the thermal regime influence on the ethylene yield in naphtha pyrolysis process 1139–1147

A. V. BULATOV, Hydrogenation of aromatic nitro compounds in the presence of dye-containing catalysts 1149–1154

V BUTUCEA, ADRIANA SÂRBU, CECILIA-SPERANŢA GEORGESCU, ADRIANA IONESCU and I. DEACONESCU, The evaluation and significance of kinetic parameters k_i and k_t in the emulsion polymerization of vinyl chloride 1155–1161

TATIANA Ya. DATSKO and V. I. ZELENTSOV, The role of electrolytic gases in the electrochemical stabilization of aluminium hydroxide (in Russian) . 1163–1167

A. DEAKY, T. ŞIMANDAN, N. MIRICĂ, S. DRAGOŞ and M. MEDELEANU, Hydroquinone electrosynthesis from phenol 1169–1173

MIRCEA V. DIUDEA and IOAN SILAGHI-DUMITRESCU, Molecular topology. I. Valence group electronegativity as a vertex discriminator 1175–1182

FLOREA DUMITRAŞCU and DAN RĂILEANU, Rearrangement of 4-alkyl-3-(*o*-carboxyphenyl)sydnones to 1-acyl-1,2-dihydro-3*H*-indazol-3-ones . . 1183–1193

EMIL DUMITRIU, VASILE HULEA, MILENA STOICA and SPIRIDON OPREA, Kinetic study of the maltodextrine hydrolysis catalyzed by immobilized glucoamylase 1195–1201

KRISTIANA GOŞA, DAN DONESCU, NICOLETA CARP and LIANA FUSULAN, Interactions between the emulsifiers utilized in polymerization of vinyl acetate 1203–1207

Rev. Roumaine Chim. 34, *5*, 1115–1290 (1989), Bucarest

OLGA IULIAN, ORTANSA LANDAUER, DAN GEANĂ and CORNELIA MATEESCU, The study of the vapor-liquid equilibrium in the dioxane-water system 1209–1216

GHEORGHIȚA JINESCU and ALEXANDRU ȘTEFAN, A study of the isothermal flow instability of polymeric fluids 1217–1223

N. K. KOCHETKOV, Synthesis ways of the o-antigenic polysacharides . . . 1225–1240

CANDIANO LEONTE and EUGENIA CARP, An extension of the Koch-Haaf reaction. N-acyl-glycines from N-hydroxymethyl-amides and -imides . . 1241–1243

D. NEGOIU, MARLENE HANDREA, MARIA NEGOIU and OVIDIU MAIOR, Complex compounds of divalent manganese 1245–1250

HORIA PETRIDE and DAN RĂILEANU, Mesoionic oxazolones. III. Planar and nonplanar acylated compounds 1251–1261

ALEXANDRU C. RĂZUȘ, MIRCEA D. GHEORGHIU and EMERIC BARTHA, Solvolyses in substituted cyclopropylcarbinylic systems. 5. Behaviour of spiro-cyclopropane-indanic alcohols 1263–1273

P. SPACU, LUMINIȚA PATRON, SILVIA PLOȘTINARU, ADRIANA CONȚESCU and N. STĂNICĂ, Coordination compounds as raw materials for mixed oxides. V. Mixed coordination compounds of lanthanides and Co(II), Ni(II) or Fe(III) with gluconic acid 1275–1280

S. STERNBERG, V. BRÂNZOI and LILIANA APĂTEANU, Contribution to the calculation of E–I curves, for electrode processes with insoluble films formation. I. The influence of the potential sweep rate on the Pb/Pb^{2+} electrode process, in sulphuric acid solutions 1281–1286

LUMINIȚA VLĂDESCU and STELUȚA CHIPER, Combined ion exchange-spectrometric study of the Ce(IV)–sulphanilic acid system. II. Spectrometric determination of sulphanilic acid 1287–1290

Revue Roumaine de Chimie, **34**, *5*, 1117–1130 (1989)

ESR STUDIES ON $AlCl_3$ BASED CATALYTIC SYSTEMS

ELENA CEAUȘESCU[a], M. CORCIOVEI[a], M. DIMONIE[b], D. BARB,[c]
M. CHIPARĂ[c] and T. SÂRBU[a]

[a] Chemical Research Institute, Spl. Independenței 202, Bucharest, Romania
[b] National Institute for Chemistry Bucharest, Romania
[c] Institute for Physics and Technology of Materials, Bucharest-Măgurele, Romania

Received November 21, 1988

Catalytic systems $AlCl_3$-aromatic hydrocarbon-cationogen, used in the initiation of unsaturated hydrocarbons polymerization, exhibit ESR signals with hyperfine structures that are dependent on the nature of the components. ESR spectra of many complexes prepared from anhydrous aluminum chloride in benzene, toluene, ethylbenzene and mesitylene with water, ethanol, HCl, ethyl chloride, benzyl alcohol, benzylchloride were studied. One can observe that the counterions (e.g. $AlCl_4^-$ or $AlCl_3OH^-$) have no influence on ESR spectra. These signals are strongly dependent on the nature of aromatic ring substituents. Hyperfine splitting constants derived from obtained spectra have been calculated. On the basis of experimental data, including other experiments (the change of Lewis acid, study of variation of signals with temperature) there are presented assumptions on the possible nature of paramagnetic species responsible for ESR spectra.

Carbocationic polymerization initiated with Lewis acids represents an important chapter of chemistry and technology of macromolecular compounds. Among Friedel-Crafts halides a major importance has $AlCl_3$ and – especially from technological point of view – catalytic systems based on aluminium chloride. Besides the advantages relating their dosing and handling, one can observe an increase of catalytic efficiency and also a decrease of crosslinkings in polymerizations, in respect to those initiated with powdered aluminium chloride, affording at the same time a possibility for the polymer properties modelling.[1–4] Though in literature there are references on the use of these catalytic systems based on $AlCl_3$ for the synthesis of hydrocarbon resins, the mechanism of initiation was little studied, especially owing to the system complexity.

Prepared in an aromatic solvent, in the presence of a complexing agent (Table 1) the catalysts based on $AlCl_3$ are homogeneous liquids, oily, deeply coloured from red to brown, similar to the so-called "red oils" well-known from alkylation reactions with $AlCl_3$.

The poor solubility in aromatic hydrocarbons, the intense colour and the sensitivity toward hydrolysis of these complexes indicate the presence of carbonium ions in their composition.[5] The ionic character of these systems has been emphasized from electrical conductivity studies.[1] The concentration of ionic species depends on the nature and concentra-

Table 1

Catalytic systems based on $AlCl_3$

Aromatic hydrocarbons (Ar)	Complexing agents (A)
toluene	water
	hydracids (HCl, HBr)
xylenes	mono- and poly-alcohols
	phenols
ethylbenzene	mono- or polyhalogenated aliphatic derivatives
trimethylbenzenes	halohydrines
	mercaptans
	aliphatic esters
iso-alkylbenzenes	aliphatic anhydrides
	aliphatic nitroderivatives
di-iso-alkylbenzenes	dimethylformamide
	lactames
	aliphatic cetones

Molar ratios :
$[AlCl_3] : [Ar] = 1 : 1.5 - 1 : 5$
$[AlCl_3] : [A] = 1 : 0.2 - 1 : 1$

tion of complexing agent and on the solvent nature. The electrophile is formed from the interaction of complexing agent with aluminium halide; this one will attack the aromatic ring, and it is obvious that electrophilic strength depends on the nature of complexing agent.

In the interaction of an electrophile with an aromatic substrate a weak complex (outer complex) [6] is formed first, reversibly, in which aromaticity is not lost. In the following stage by the overlapping of the aromatic π-orbital, containing an electron pair, with the empty orbital of the electrophile, a two-electron three center bond is formed, called by Olah [7] aronium ion or π-complex. Opening of the three-center bond of the aronium ion leads to the trivalent arenium ion — σ-complex — in which the bonding of the electrophilic reagent is accounted for a directing effect, the determining rôle having the nature of aromatic substrate, its localization energy.

The elimination of proton, energetically favoured, will be influenced by the nature of electrophilic part bounded to the ring.

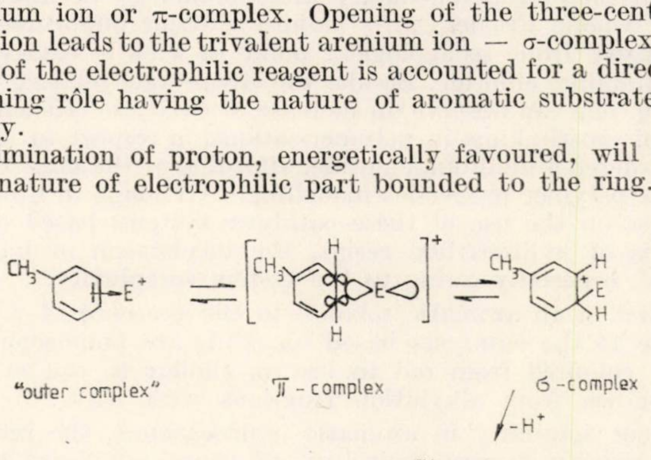

At prolonged contact with aluminium halide the process becomes reversible, the above systems being the result of equilibrium reactions between alkylarene species with different degrees of substitution, processes in which arenium ions intermediates or, in some cases, π-complexes appear. The molar ratios between the components used in the preparation of complexes based on $AlCl_3$ have an important rôle in this context.

Arenium ions have been evidenced by NMR spectroscopy at low temperatures in superacid systems like HSO_3F or $HF+SbF_5$.[8,9] Japanese authors [10] obtained ^{13}C-NMR spectra of arenium ions at 30°, important being the signals at $\delta > 190$ ppm, assigned to 0,0′ and p carbons, and also the signal at $\delta \simeq 50$ ppm assigned to sp^3 hybridized carbon atom. Ceaușescu and co-workers [11] have identified arenium ions with different degrees of substitution – and consequently stabilization – both at room temperature and low temperatures, for a series of catalytic systems based on $AlCl_3$.

Figure 1 presents the ^{13}C-NMR spectrum for the complex $AlCl_3$-ethylbenzene-HCl obtained on a Bruker SXP-90 spectrometer operating at 22.63 MHz.[11]

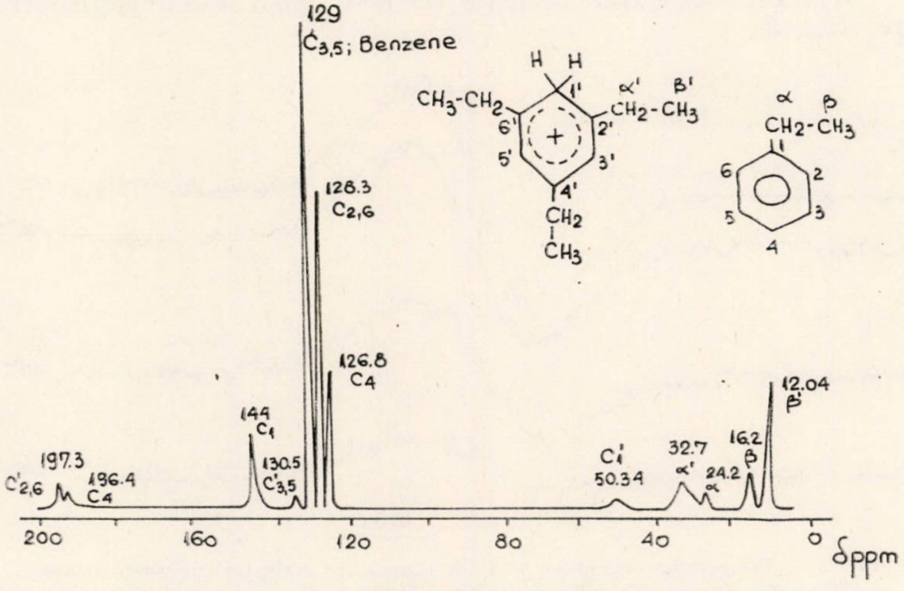

Fig. 1. – ^{13}C-NMR spectrum of $AlCl_3$-ethylbenzene-HCl complex, recorded at room temperature.

For the complexes prepared in mesitylene, with water and ethyl alcohol as complexing agents, ^{13}C-NMR signals of trisubstituted benzenonium ion have not been observed. This behaviour can be assigned to the much higher basicity of mesitylene, in this case, how Olah indicates,[12] the transition state being more of a π-complex in nature.

The complexes $AlCl_3$-aromatic hydrocarbons-electrophile agents show distinct ESR signals, with the hyperfine structure depending on the aromatic hydrocarbon nature and also complexing agent nature.

Thus $AlCl_3$-toluene-water complexes show a resonance signal at $g = 2$ (Fig. 2). The 10 lines can be ascribed to the delocalization of uncoupled electron over two CH_3 groups characterized by hyperfine splitting $a_1 = 4.8$ Gs and $a_2 = 2 \cdot 4$Gs.

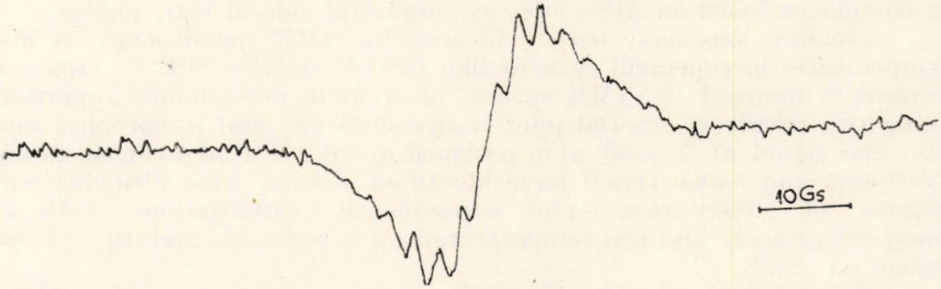

Fig. 2. — ESR spectrum of $AlCl_3$-toluene-water complex, at room temperature.

With the temperature decrease, the ESR signal loses hyperfine structure (Fig. 3)

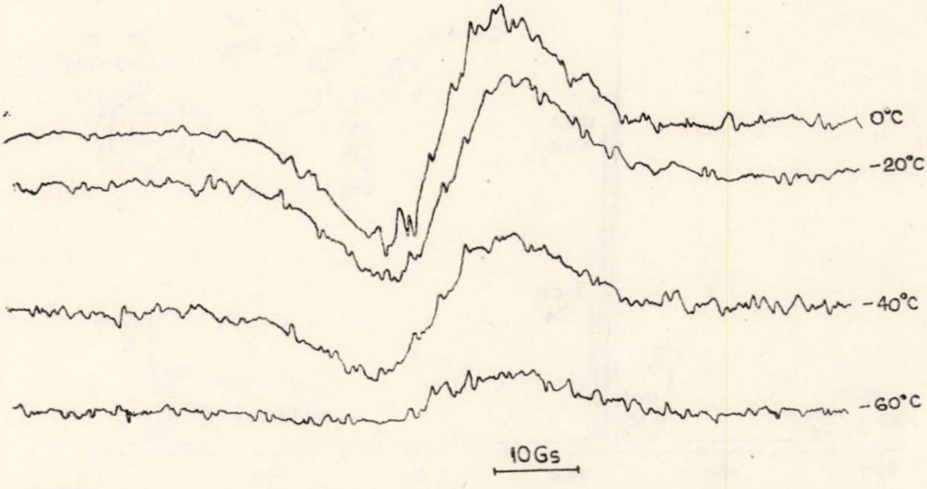

Fig. 3. — Temperature variation of ESR signals for $AlCl_3$-toluene-water complex.

The $AlCl_3$-mesitylene-water system shows 11 lines that can be assigned to 3 equivalent protons having $a_1 = 3$ Gs and 4 protons with $a_2 = 1.5$ Gs (Fig. 4).

By introduction of stabilizing ethyl groups in the complex $AlCl_3$-toluene-ethyl alcohol the ESR spectrum presents 19 lines assigned to delocalization of the electron over methyl and ethyl groups; hyperfine splittings are $a_1 = 7.2$ Gs, $a_2 = 4.8$ Gs and $a_3 = 2.4$ Gs (Fig. 5).

An increase of the electrophile agent amount in complex preparing leads to a moderate increase of the paramagnetic species concentration (Fig. 6).

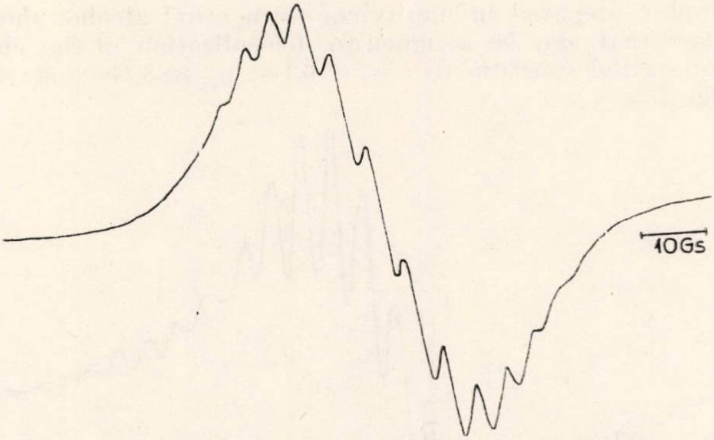

Fig. 4. — ESR spectrum of $AlCl_3$-mesitylene-water complex, at −5°.

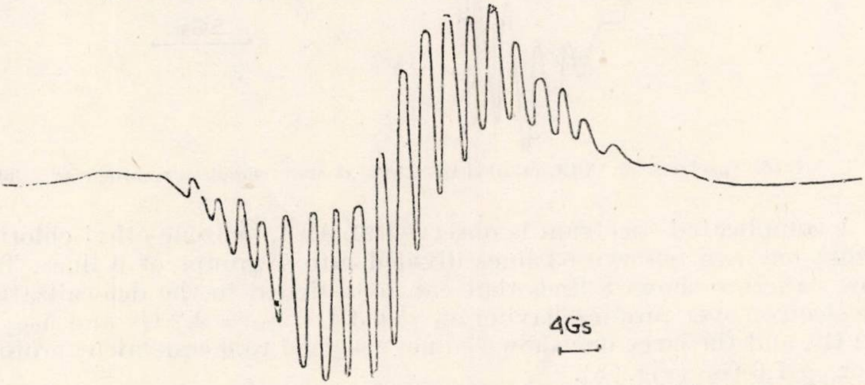

Fig. 5 — ESR spectrum of $AlCl_3$-toluene-ethyl alcohol=1: 2: 0.4(molar) at room temperature

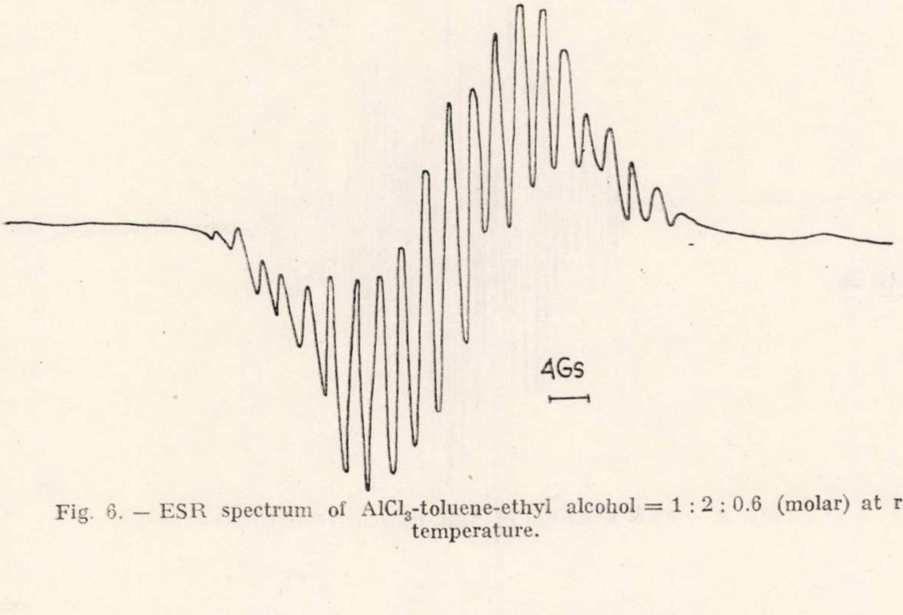

Fig. 6. — ESR spectrum of $AlCl_3$-toluene-ethyl alcohol = 1 : 2 : 0.6 (molar) at room temperature.

The complex prepared in mesitylene with ethyl alcohol shows 20 equidistant lines that can be assigned to delocalization of the electron over methyl and ethyl substituents: $a_1 = 6$ Gs, $a_H = 3$ Gs and $a_{C_2H_5} = 1.5$ Gs (Fig. 7).

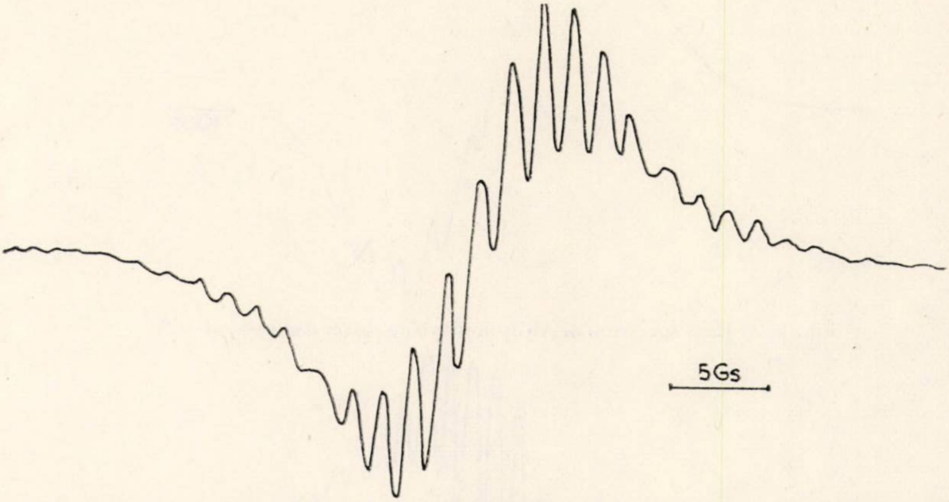

Fig. 7. — ESR spectrum of $AlCl_3$-mesitylene-ethyl alcohol complex recorded at −30°.

A complicated spectrum is observed at $AlCl_3$-benzene-ethyl chloride systems; one can observe 63 lines divided into 7 groups of 9 lines. The narrow structure shows 8 lines that can be assigned to the delocalization of the electron over protons having $a_H = 6.3$ Gs, $a_H = 4.2$ Gs and $a_{CH_3} = 1.2$ Gs, and the large one shows 7 lines assigned to 6 equivalent protons with $a = 7.6$ Gs (Fig. 8).

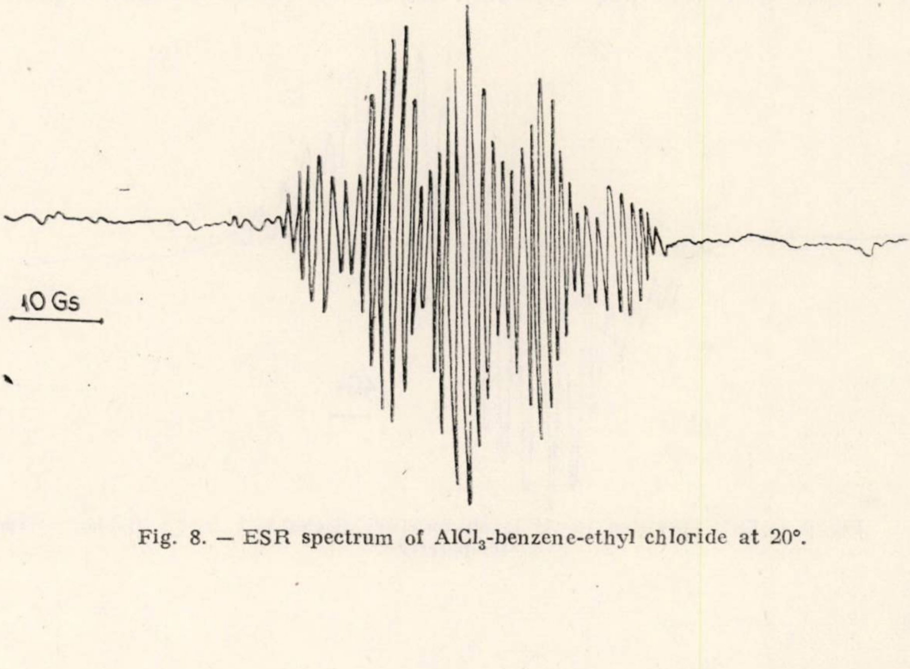

Fig. 8. — ESR spectrum of $AlCl_3$-benzene-ethyl chloride at 20°.

When ethyl chloride is replaced by ethyl alcohol as complexing agent, that means changes of counterion structure, ESR spectrum remains unchanged (Fig. 9).

The same type of spectrum is obtained also for $AlCl_3$-ethylbenzene-HCl system (Fig. 10).

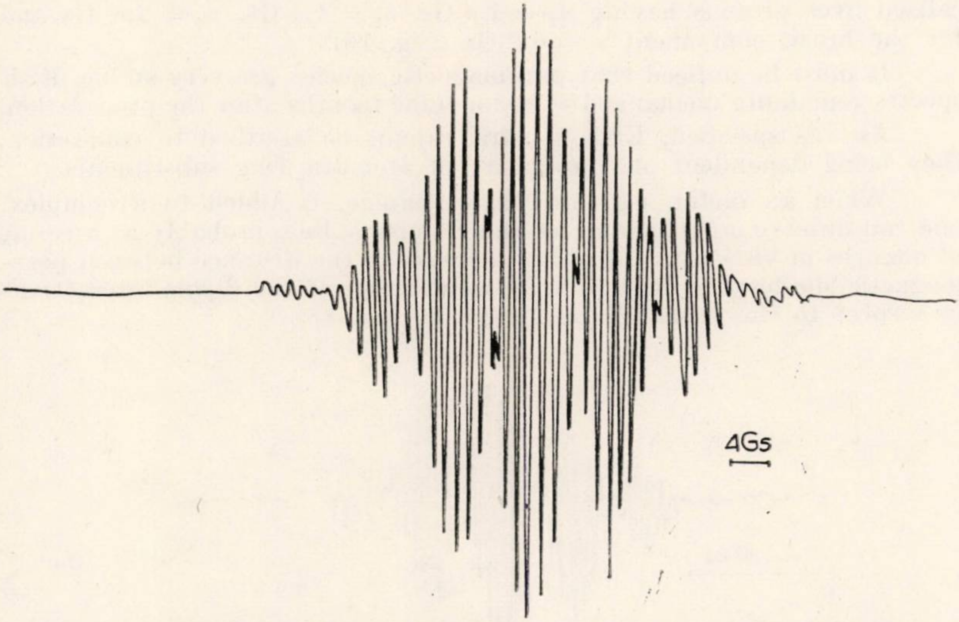

Fig. 9. — ESR spectrum of $AlCl_3$-benzene-ethyl alcohol complex at room temperature.

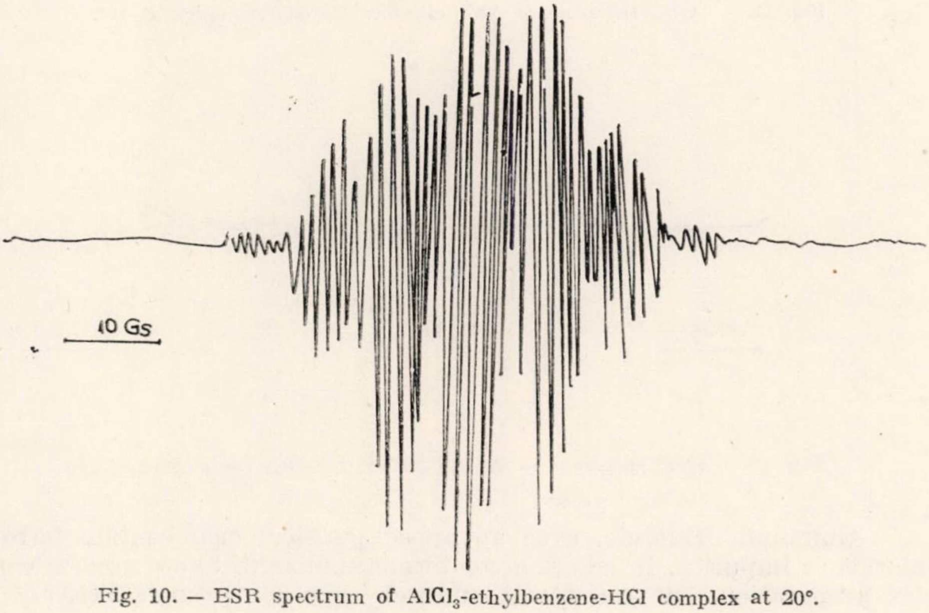

Fig. 10. — ESR spectrum of $AlCl_3$-ethylbenzene-HCl complex at 20°.

The variation with temperature exhibits a maximum at −20° followed by a decrease of the signal with temperature decrease, probably owing to ESR line broadening as a result of sample freezing (Figs. 11−15).

For the complexes prepared with benzyl alcohol or benzyl chloride ESR spectrum shows 33 lines that can be ascribed to the electron delocalized over protons having $a_1 = 1.4$ Gs, $a_2 = 1.4$ Gs, $a_3 = 2.8$ Gs and for the broad component $a = 6.2$ Gs (Fig. 16).

It must be noticed that paramagnetic species are very stable, ESR spectra remaining unchanged even for some months after the preparation.

As was specified, ESR spectra cannot be ascribed to counterion, they being dependent on the nature of aromatic ring substituents.

When an olefin, e.g. 2-methyl-1-butene, is added to a complex, one can observe a broadening of the resonance line, probably as a result of changes in viscosity and of the increase of the distance between paramagnetic species that lead to an intensification of the dipole interactions in respect to the exchange one (Figs. 17 and 18).

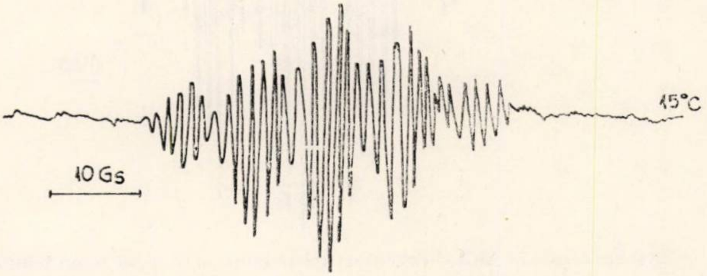

Fig. 11. — ESR spectrum of $AlCl_3$-ethylbenzene-HCl complex at 15°.

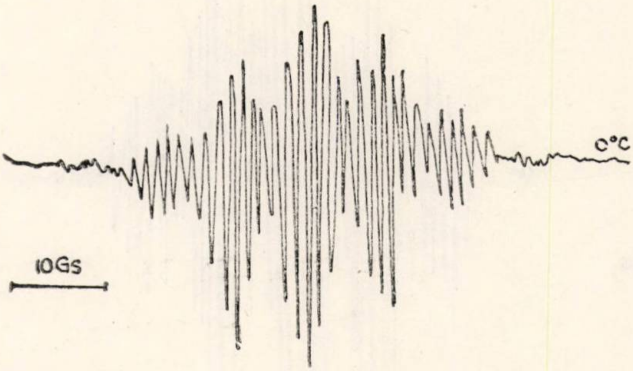

Fig. 12. — ESR spectrum of $AlCl_3$-ethylbenzene-HCl complex at 0°.

Aluminum chloride, even advanced purified, can contain ferrous chloride as impurity. In reaction conditions similar to those used in complex preparation, one can form sandwich type compounds $Fe(Ar)_2^{2+}$.[13]

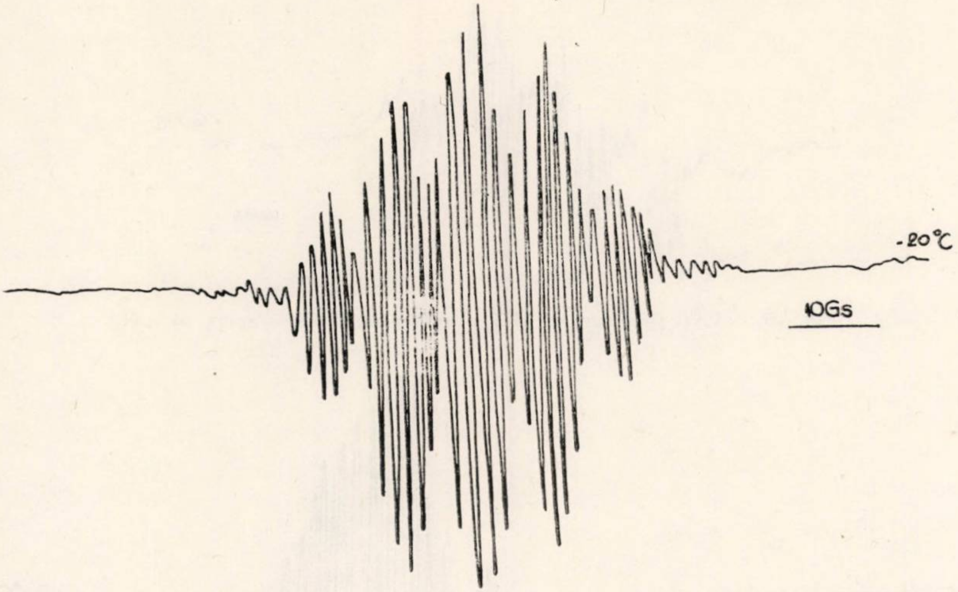

Fig. 13. — ESR spectrum of $AlCl_3$-ethylbenzene-HCl complex at −20°.

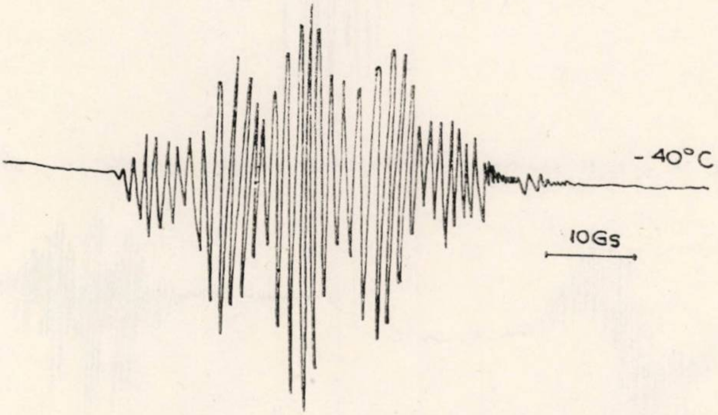

Fig. 14. — ESR spectrum of $AlCl_3$-ethylbenzene-HC complex at −40°.

The possibility that paramagnetic species mentioned above to be due to such sandwich compounds is not in agreement with spectroscopic investigations on the systems in which anhydrous ferrous chloride was added. One observes that ESR signal does not increase, how would be expected, but a central line would appear; this line has been assigned to Fe^{3+} (Fig. 19). Moreover the literature mentions the diamagnetic character of the sandwich complexes between aromatic hydrocarbons and iron.[14]

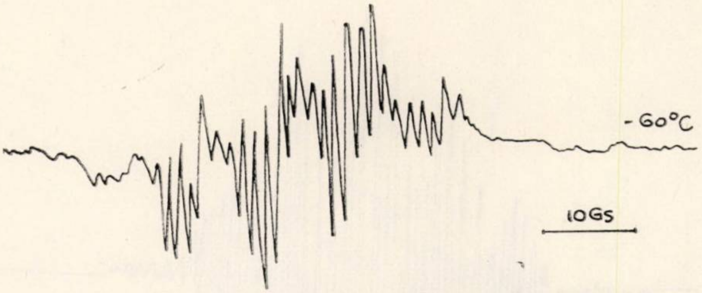

Fig. 15. — ESR spectrum of $AlCl_3$-ethylbenzene-HCl complex at —60°.

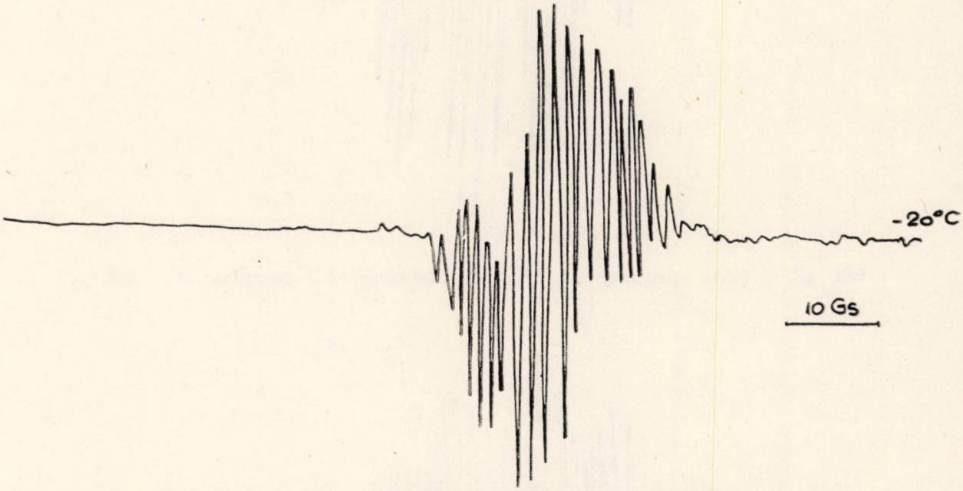

Fig. 16. — ESR spectrum of $AlCl_3$-benzene-benzyl chloride at —20°.

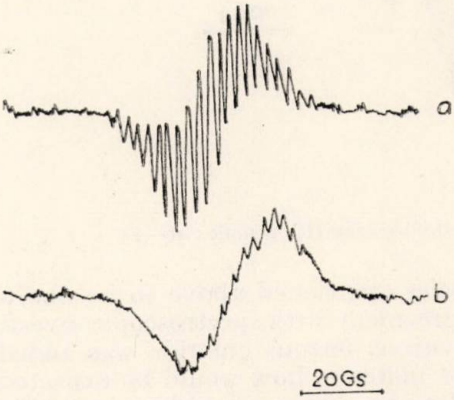

Fig. 17. — ESR spectra of $AlCl_3$-toluene-ethyl alcohol complex (a) and of the complex-2-methylbutene-1 mixture (b).

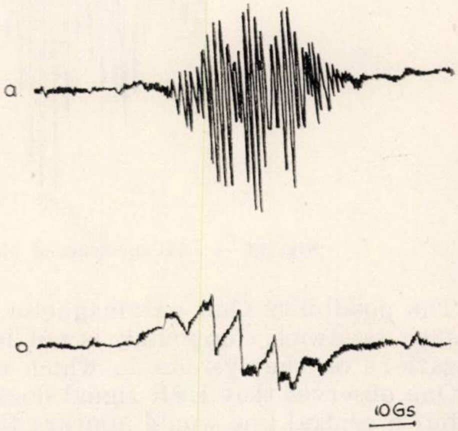

Fig. 18. — ESR spectra of $AlCl_3$-ethylbenzene-HCl complex (a) and of the complex -2-methylbutene-1 mixture (b).

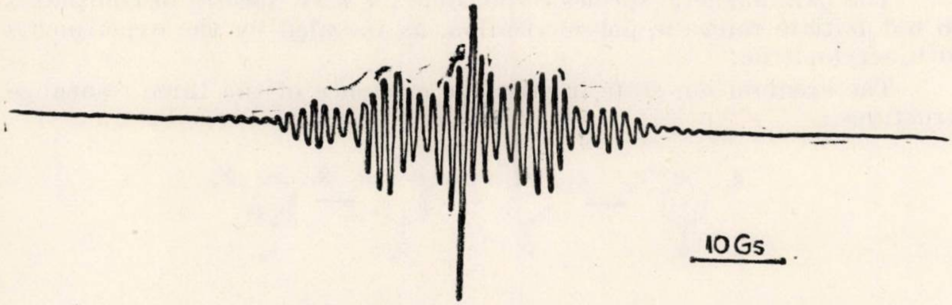

Fig. 19. — ESR spectrum of $AlCl_3$ + $FeCl_2$-benzene-ethyl alcohol complex.

Aluminum chloride is not the sole Lewis acid that forms complexes with aromatic hydrocarbon exhibiting ESR signals. Such signals have been observed also for complexes prepared with $SnCl_4$ (Fig. 20). No ESR spectra have been shown for boron chloride complexes.

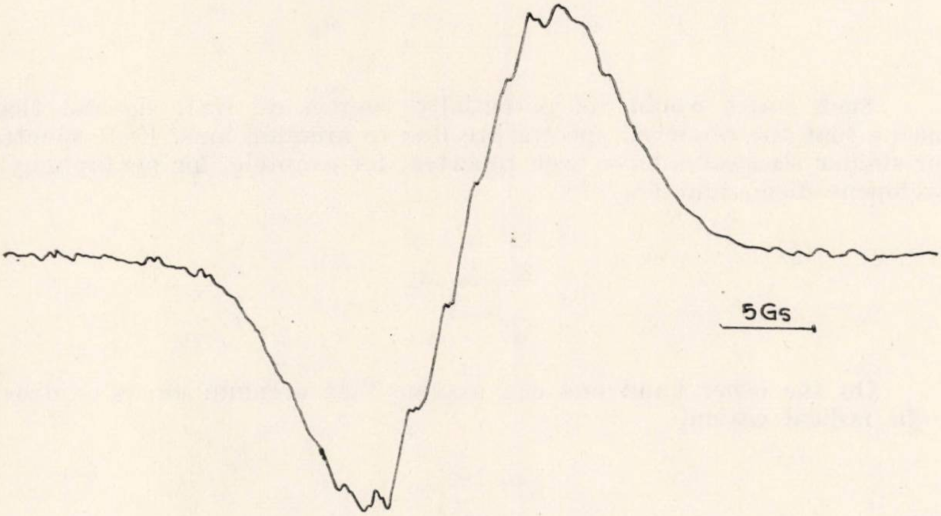

Fig. 20. — ESR spectrum of $SnCl_4$-benzene-benzyl chloride complex.

By gas-chromatography together with mass spectrometry analysis of hydrocarbon mixtures, arisen from alkaline hydrolysis of complexes, in some cases have been identified small concentrations of polynuclear aromatic hydrocarbons like biphenyl and alkylated derivatives of naphthalene and phenanthrene. Consequently, one can suppose that ESR spectra are due to radicalic species appeared from the well-known conjugations characteristic of some polynuclear aromatic hydrocarbons. This assumption cannot explain however the presence of ESR signals for the complexes prepared in mesitylene.

The paramagnetic species responsible for ESR spectra of complexes do not initiate radicalic polymerization, as revealed by the experiments with acrylonitrile.

The arenium ion state implies the existence of the three resonance structures :

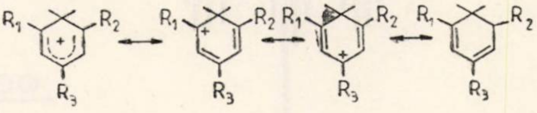

The shift from one to other resonance state lies in the jump of a π-electron pair from an orbital to another. If this is achieved by individual jumps of electrons then between the three resonance structures there will be intermediate states like :

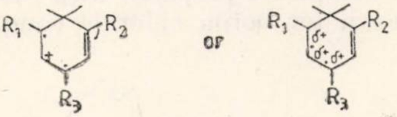

Such states would be potentially sources of ESR signals, that means that the observed spectra are due to arenium ions. ESR spectra for similar structures have been reported, for example, for pentaphenylcyclopentadienonium ion [15,16] :

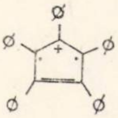

On the other hand one can assume that arenium ion is oxidized to a radical cation

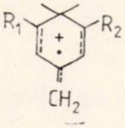

very similar to those supposed to appear from interaction of hexamethylbenzene with sulphuric acid [17] that offers another explanation to ESR spectra.

The initiation reaction of carbocationic polymerization with these catalytic systems occurs cationically, the first stage being the displacement toward the right of the equilibrium :

$$[ArH_2]^+Al_2X_7^- \rightleftharpoons ArH + H^+Al_2X_7^-$$

in the presence of the monomer that will be protonated to the first cation capable to propagate, in so-called cationation stage according to Kennedy's proposal[18]:

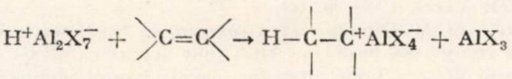

$$H^+Al_2X_7^- + \rangle C{=}C\langle \rightarrow H{-}\overset{|}{\underset{|}{C}}{-}\overset{|}{\underset{|}{C}}{}^+AlX_4^- + AlX_3$$

Aluminium halide will react with the monomer:

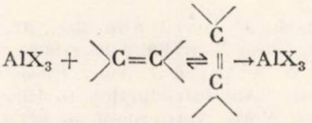

the reaction being favoured by the medium polarity.

According to the HSAB principle of Pearson[19] this interaction is a weak one, needing co-catalysis:

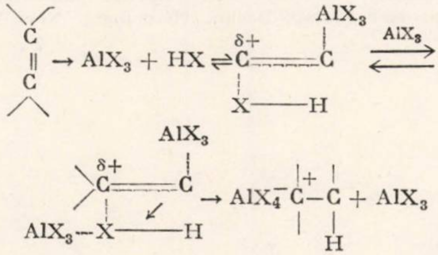

In this case HX will be represented by at least two species: HCl dissolved in catalytic complex and water traces from monomer.

The possibility for self-ionization of aluminium halide can be also neglected because of the complex polarity.

These reactions will take place simultaneously, the predominance of any one mechanism depending on the polymerization conditions, the monomers nature and the type of catalytic complex used.

REFERENCES

[1] E. Ceaușescu, M. Corciovei, T. Sârbu, G. Domneșteanu, F. Taran and S. Barac, *Acta Polymerica*, **34**, 690 (1983).

[2] E. Ceaușescu, M. Corciovei, C. Ioniță, T. Sârbu, M. Dițu, F. Taran, S. Barac, M. Mihăilescu, E. Marinescu and S. Ioniță, Rom. Pat. 86543 (1983).

[3] E. Ceaușescu, C. Ioniță, M. Corciovei, M. Dițu, T. Sârbu, M. Mihăilescu, E. Marinescu, F. Taran, S. Barac and S. Ioniță, Rom. Pat. 86623 (1983).

[4] E. Ceaușescu, M. Corciovei, T. Sârbu, F. Taran, S. Barac and R. Munteanu, *Mat. Plast.*, **22**, 77 (1985).

[5] C. D. Nenițescu, in "Carbonium Ions", vol. I, G. A. Olah and P. von R. Schleyer Eds., Intersci. Publs., New York, London, Sidney 1968.

[6] R. S. Mulliken, *J. Amer. Chem. Soc.*, **72**, 600 (1950); **74**, 811 (1952), refs. in G. A. Olah, „Friedel-Crafts Chemistry", Wiley Intersci., New York, London, Sidney, Toronto, 1972.

[7] G. A. Olah, *J. Amer. Chem. Soc.*, **94**, 808 (1972).

[8] T. Birchall and R. J. Gillespie, *Can. J. Chem.*, **42**, 502 (1964), refs. in "Carbonium Ions", G. A. Olah and P. von. R. Schleyer Eds. vol. II, Wiley Intersci., New York, London, Sidney, Toronto, 1970, p. 864.

[9] D. M. Brouwer, E. L. Mackor and C. MacLean, *Rec. Trav. Chim.*, **84**, 1564 (1965), refs. in "Carbonium Ions", G. A. Olah and P. von. R. Schleyer Eds., vol. II, Wiley Intersci., New York, London, Sidney, Toronto, 1970, p. 864.

[10] N. Nambu, K. Yamamoto, S. Hamanaka and M. Ogawa, Technology reports of Kansai University, no. 21, March 1980, p. 93.

[11] E. Ceaușescu, M. Corciovei, M. Dimonie, R. Grosescu, A. Vasilescu and T. Sârbu, C^{13}-NMR study on soluble complexes based on $AlCl_3$ that act as catalysts in cationic polymerization of dienes and olefines, Conference for Chemistry and Engineering, 5-th ed., Bucharest, 22th—23th October 1987.

[12] G. A. Olah, "Friedel-Crafts Chemistry", Wiley, Wiley Intersci. New York, London, Sidney, Toronto, 1972.

[13] J. F. Helling and D. M. Braitsch, *J. Amer. Chem. Soc.*, **92**, 7207 (1970).

[14] E. O. Fischer and B. Böttcher, *Chem. Ber.*, **89**, 2397 (1956).

[15] R. Breslow, H. W. Chang and W. A. Yager, *J. Amer. Chem. Soc.*, **85**, 2033 (1963).

[16] M. Bersohn and J. C. Baird, "An Introduction to Electron Paramagnetic Resonance", W. A. Benjamin Inc., New York, Amsterdam, p. 121 (1966).

[17] D. Bethell and V. Gold, "Carbonium Ions. An Introduction", Academic Press, London, New York (1967).

[18] J. P. Kennedy and E. Maréchal, *J. Polym. Sci.*, Part D, **10**, 123 (1981).

[19] R. G. Pearson, *Surv. Progr. Chem.*, **5**, 1(1969), refs. in A. Gandini, H. Cheradame, "Cationic Polymerization. Initiation Processes with Alkenyl Monomers, Advances in Polymer Science", 34/35, Springer Verlag, Berlin, Heidelberg, New York, p. 13 (1980).

Revue Roumaine de Chimie, **34**, *5*, 1131–1137 (1989)

SYNTHESIS AND STEREOCHEMISTRY OF 3,5-DIALKYL-2-FURYL *p*-SUBSTITUTED-STYRYL KETONES (FURANIC ANALOGUES OF CHALCONE)

URSULA BOLOGA, ANA SCHIKETANZ, CORINA MUŞAT, DANIELA VÎLCICĂ, C. DRĂGHICI, M. D. GHEORGHIU and A. T. BALABAN

Polytechnic Institute, Department of Organic Chemistry, Splaiul Independenţei 313, 76206 Bucharest, Romania

Received November 21, 1988

2-Acetyl-3-alkyl-5-methylfurans **2** obtained from pyrylium salts **1** and hydrogen peroxide (3–R = Me or Et) gave crystalline 3-alkyl-5-methyl-2-furyl *p*-substituted-styryl ketones **3a-f** by condensation with *p*-substituted benzaldehydes (*p*-R′ = H, Me, OMe, NMe_2, NEt_2). The structure was confirmed by IR, UV, ^1H–NMR and ^{13}C–NMR spectra. In the ^1H–NMR spectra, the vinylic and the 3-methyl protons gave the largest induced shift with $Eu(fod)_3$, and negative aromatic solvent induced shifts. The conformation is therefore **7**, *E-s-cis-s-cis* with respect to the mutual orientations of the carbonyl and the flanking double bonds.

INTRODUCTION

Starting from hydrogen peroxide and 2,4,6-trialkylpyrylium salts **1**, which are easily available by diacylation of alkenes,[1,2] it was shown[3] that 2-acyl-3,5-dialkylfurans **2** can be obtained in good yields by ring contraction. The present paper reports the synthesis and a conformational study of the condensation products obtained from such 2-acetyl-3,5-dialkylfurans and aromatic aldehydes. In all cases the 5-alkyl group is methyl; the 3-R alkyl was either methyl (**3a–e**) or ethyl (**3f**).

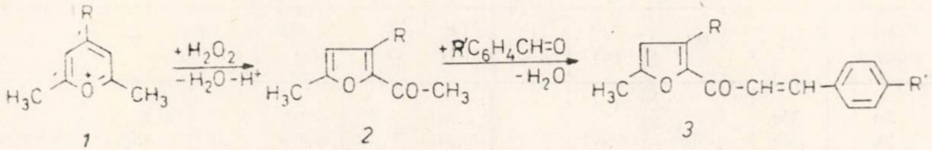

Synthesis, IR and ^{1}H-NMR spectra of dialkyl p-substituted-styryl ketones

Under reaction conditions similar to those used for obtaining chalcone from benzaldehyde and acetophenone, 2-acyl-3,5-dialkylfurans **2** undergo condensation with aromatic aldehydes *p*-R′-C_6H_4CHO affording title compounds **3a-f**. These α, β-unsaturated ketones are crystalline and may be purified by recrystallisation from ethanol (Table 1). Vibrational and ^{1}H−NMR spectra confirm the structure of **3**. The α, β-unsaturated carbonyl stretching vibration appears at 1640−1650 cm^{-1}.

Table 1

Data or 3,5-dialkyl-2-furyl *p*-substituted-styryl ketones **3a**−**f**

Compound	R	R′	M.p. °C	Yield %	$\nu_{C=O}$ KBr, cm^{-1}
3a	Me	H	75−6	49	1650
3b	Me	OMe	95−6	45	1650
3c	Me	Me	100−1	42	1645
3d	Me	NMe$_2$	141	30	1645
3e	Me	NEt$_2$	155−6	30	1645
3f	Et	Me	57−8	30	1645

^{1}H−NMR spectra were recorded in CDCl$_3$ when considerable overlap occurred, and in C$_6$D$_6$ when all peaks were resolved. This effect is illustrated in Tables 2 and 3. The large J^{CD} coupling constants (16 Hz) indicated that the vinylic protons are in *E*-configuration. Most ^{1}H-NMR assignments are straightforward. The single peak at 6.00 −6.10 ppm in CDCl$_3$ and 5.63−5.73 ppm in C$_6$D$_6$ is due to the furanic proton in agreement with literature data.[4] The two methyl groups in **3b**−**e** (three C-methyls in **3c**) made it necessary to synthetize **3f** for an unambiguous assignment; then

Table 2

^{1}H−NMR chemical shifts of 3,5-dialkyl-2-furyl *p*-substituted-styryl ketones **3a**−**f** in CDCl$_3$ (δ, ppm)

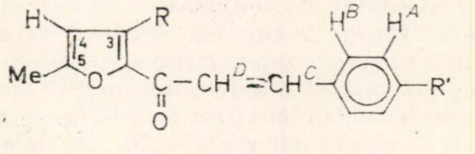

Compound	R	R′	H^A (d)	H^B (d)	H^C (d)	H^D (d)	4−H (s)	5−Me (s)	R	R′
3a	Me	H	[a]	[a]	7.80	7.40	6.08	2.33	2.42 (s)	—
3b	Me	OMe	6.83	7.56	7.70	7.33	6.05	2.38	2.43(s)	3.83(s)
3c	Me	Me	7.20	7.53	7.80	7.33	6.06	2.35	2.42(s)	2.35(s)
3d	Me	NMe$_2$	6.63	7.47	7.67	7.28	6.00	2.40	2.42(s)	3.00(s)
3e	Me	NEt$_2$	6.67	7.50	7.73	7.30	6.03	2.35	2.41(s)	3.38(q) 1.20(t)
3f	Et	Me	7.13	7.48	7.77	7.40	6.10	2.33	2.88(q) 1.20(t)	2.34(s)

[a] Phenyl multiplet at 7.50−7.63 ppm

Table 3

^{1}H—NMR chemical shifts of 3,5-dialkyl-2-furyl *p*-substituted-styryl ketones **3a—f** in C_6D_6 (δ, ppm)[a]

Compound	R	R′	H^A (d)	H^B (d)	H^C (d)	H^D (d)	4—H (s)	5—Me (s)	R	R′
3a	Me	H	*b*	*b*	7.98	7.63	5.61	1.95	2.45(s)	*b*
3b	Me	OMe	6.60	7.30	8.13	7.63	5.70	2.00	2.46(s)	3.20(s)
3c	Me	Me	6.83	7.26	8.06	7.63	5.61	1.91	2.48(s)	2.00(s)
3d	Me	NMe_2	6.40	7.43	8.30	7.70	5.67	1.96	2.53(s)	2.40(s)
3e	Me	NEt_2	6.36	7.40	8.26	7.67	5.67	1.92	2.50(s)	2.83(q) 0.76(t)
3f	Et	Me	6.83	7.25	8.10	7.63	5.73	1.93	3.05(q) 1.20(t)	2.00(s)

[a] $J_{AB} = 8$ Hz; $J_{CD} = 16$ Hz; $J_{Et} = 7$ Hz
[b] Multiplet at 6.90—7.40 ppm

it became evident that the peak at 1.90—2.00 ppm (in C_6D_6) is due to the 5-methyl present in all compounds **3a-e**, while the peak at 2.45—2.53 ppm (in C_6D_6) which is absent from **3f** is due to the 3-R group; in **3f** this peak becomes replaced by the ethyl signals. In $CDCl_3$ all methyl peaks are almost isochronous.

By subtracting the chemical shift values of C_6D_6 from those in $CDCl_3$ one obtains aromatic solvent induced shift (ASIS) Δ values which are negative for the hydrogens in close proximity of the carbonyl group (both vinylic protons, and the 3-R group protons); all remaining protons have positive Δ values (Table 4).

Table 4

Aromatic Solvent Induced Shift Δ values for compounds **3a—f** (ppm)

Compound	R	R′	H^A	H^B	H^C	H^D	4—H	5—Me	R	R′
3a	Me	H	—	—	−0.26	−0.27	0.47	0.38	−0.03	—
3b	Me	OMe	0.23	0.26	−0.43	−0.30	0.35	0.44	−0.03	0.57
3c	Me	Me	0.37	0.27	−0.06	−0.30	0.45	0.44	−0.06	0.35
3d	Me	NMe_2	0.23	0.04	−0.63	−0.42	0.33	0.44	−0.06	0.35
3e	Me	NEt_2	0.34	0.10	−0.53	−0.37	0.36	0.43	−0.09	0.55 0.44
3f	Et	Me	0.30	0.23	−0.33	−0.23	0.37	0.40	−0.17 0.00	0.33

In order to check the assignment of ^{1}H-NMR signals and to assist in determining the conformation of the molecules, we determined molar induced shifts (MIS) for compounds **3c** and **3f** in $CDCl_3$ using $Eu(fod)_3$ as lanthanide shift reagent (LSR). Results are indicated in Fig. 1 as MIS values relative to the induced shift due to the furanic 4-H signal; this signal had the smallest induced shift in an earlier study of conformations in 2-acyl-3,5-dialkylfurans **2**.[4]

It can be seen that the largest MIS values correspond to the protons in the close proximity of the carbonyl group (in the conformations shown in formulas **6** and **7**), i.e. exactly those protons which gave negative ASIS Δ values.

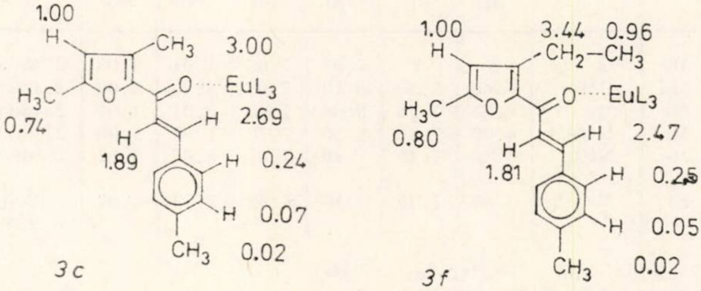
1.00
H
CH3
3.00
O···EuL3
H3C
O
0.74
H 2.69
H
1.89
H 0.24
H 0.07
CH3 0.02
3c
1.00
H
3.44 0.96
CH2–CH3
O···EuL3
H3C
O
0.80
H 2.47
H
1.81
H 0.25
H 0.05
CH3 0.02
3f

Fig. 1. — Relative induced shifts for compounds **3c** and **3f** in $CDCl_3$ with $Eu(fod)_3$.

From the four possible *E*-rotamers **4**—**7**, denoted by the conformation (*s-cis* / *s-trans*) at the α, β-enone group and then by the reciprocal position of the carbonyl and furanic double bonds, the first two (**4** and **5**) are ruled out. This leaves the conformations **6** and **7** which are the only ones having protons of the R group and the vinylic hydrogens (α and β, respectively) in the vicinity of the LSR coordination site close to the carbonyl oxygen. Conformation **7** has the β-vinylic proton (with the larger MIS value) closer to the coordination site, therefore this is the most plausible structure. By analogy with lanthanide induced shift studies with 2-acyl-3,5-dialkylfurans,[4] where an *s-cis* conformation **8** was favoured

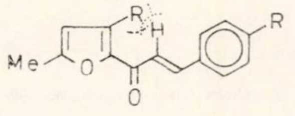

4, E-s-cis-s-trans

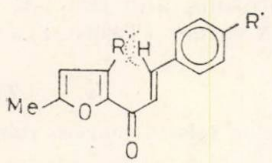

5. E-s-trans-s-trans

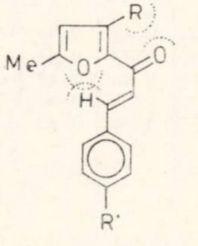

6, E-s-trans-s-cis

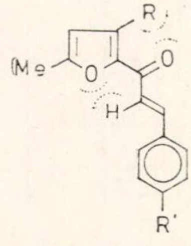

7, E-s-cis-s-cis

by the smaller steric strain in conformation **8** than in **9**, we consider that in the present case conformation **7**, which is also the least strained, is the most plausible.

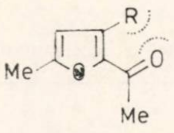

8, s-cis

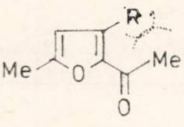

9, s-trans

^{13}C-NMR Spectra

The ^{13}C-NMR spectra were recorded for **3a-c** in $CDCl_3$. The three carbon peaks of the unsaturated carbonyl moiety, the furanic carbon atoms, and the benzenic carbon atoms were assigned taking into account chemical shifts, off-resonance multiplicities and peak intensities. The assignments presented in Table 5 agree with literature data of related compounds.[6]

Table 5

^{13}C-NMR chemical shifts in $CDCl_5$ (δ, ppm) for compounds **3a—c**

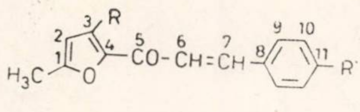

Compound	**3a**	**3b**	**3c**
C_1	148.20	148.23	148.24
C_2	113.32	113.22	113.25
C_3	133.53	132.93	132.52
C_4	155.31	155.03	155.06
C_5	178.99	179.03	178.96
C_6	122.35	120.01	121.29
C_7	142.30	142.01	142.22
C_8	135.29	127.94	133.10
C_9	128.43	130.07	128.40
C_{10}	128.80	114.28	129.55
C_{11}	130.10	161.39	140.13
Me	14.01	13.93	13.93
R	12.17	12.13	12.14
R′	—	55.24	21.41

Electronic absorption spectra

Table 6 contains the absorption maxima, determined in methanol. The longest wavelength absorption band, I, is also the strongest. A marked bathochromic shift is observed on increasing the donor ability of the *para*-substituent. A less pronounced bathochromic shift is also observed for the two other, weaker, absorption bands which are poorly resolved for the *p*-H, Me and OMe substituents.

Table 6

UV Absorption maxima of ketones **3a**—**e**, λ_{max}(nm) in methanol

Compound	I	II	III
3a	333	227	—
3c	343	227	238
3b	357	235	244
3d	424	263	247
3e	435	267	247

The bathochromic shift indicates gradually increased contributions of the dipolar limiting structure (e.g.**10b**) of the excited state on increasing the donor ability of the *para*-substituent.

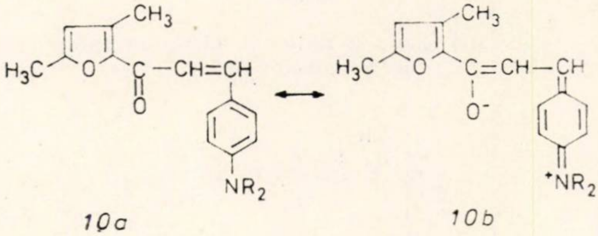

10a 10b

EXPERIMENTAL PART

IR Spectra were recorded in KBr pellets with a Jena UR-20 spectrometer. ^{1}H—NMR spectra were registered with a 60 MHz Varian EM-360L instrument. Melting points (uncorrected) were determined with a Boetius apparatus. Elemental analyses were satisfactory.

3,5-Dimethyl-2-furyl styryl ketones (**3a**). A homogenous solution of 3,5-dimethyl-2-acetylfuran[3] (1.38 g, 10 mmol) and freshly distilled benzaldehyde (1.30 g, 12 mmol) in cold aqueous methanol was treated with a solution of sodium hydroxide (0.40 g, 10 mmol) in the same solvent and left for 24 hrs at room temperature. The resulting crystals were filtered off and recrystallized from aqueous methanol, yellow leaflets m.p. 75—76°. From the filtrate a further crop was obtained by extraction with benzene, washing with aqueous $NaHCO_3$, drying, evaporation of the solvent, and recrystallization. Total yield 49%.

3,5-Dimethyl-2-furyl p-methoxystyryl ketone (**3b**), yellow crystals from methanol.

3,5-Dimeythyl-2-furyl p-methylstyryl ketone (**3c**) crystallized after several days, yellow crystals from methanol.

3,5-Dimethyl-2-furyl p-dimethylaminostyryl ketone (**3d**). Orange-coloured crystals.

3,5-Dimethyl-2-furyl p-diethylaminostyryl ketone (**3e**). No crystalline product was obtained from the aqueous methanolic solution on standing. After extraction with ether and evaporation of the solvent, the residue crystallized and the product was purified by recrystallization from methanol. Orange-coloured crystals.

3-Ethyl-5-methyl-2-furyl p-methylstyryl ketone (**3f**) was prepared similarly starting from 4-ethyl-2,6-dimethylpyrylium perchlorate (obtained from t-amyl chloride, acetyl chloride, and anhydrous aluminium chloride, and purified by recrystallization from water) which was converted by hydrogen peroxide into 2-acetyl-3-ethyl-5-methylfuran. This was condensed with *p*-tolualdehyde as described above. Yellow crystals.

REFERENCES

[1] A. T. Balaban and C. D. Nenitzescu, Org. Synth. Coll. Vol. 5, 1106 (1973); *Liebigs Ann. Chem.*, **625**, 74 (1969).

[2] A. T. Balaban, A. Dinculescu, D. N. Dorofeenko, G. W. Fischer, A. V. Koblik, V. V. Mezheritskii and W. Schroth, "Pyrylium Salts. Synthesis, Reactions, and Physical Properties", Adv. Heterocyclic Chemistry, Suppl. Vol. 2 (ed. A. R. Katritzky), Academic Press, New York, 1981.

[3] A. T. Balaban and C. D. Nenitzescu, *Chem. Ber.*, **93**, 599 (1960); A. T. Balaban, *Org. Prep. Proc.*, **1**, 63 (1969).

[4] A. T. Balaban, M. D. Gheorghiu and C. Drăghici, *Israel J. Chem.*, **20**, 168 (1980).

[5] P. Laszlo, *Progress in NMR Spectroscopy*, **3**, 231 (1967); M. Jauquet and P. Laszlo, in "Influence of Solvents on Spectroscopy" (ed. J. Dack), Wiley, New York, 1975, p. 243.

[6] A. Radeglia and W. Altenburg, *Z. Chem.*, **16**, 363 (1976).

Revue Roumaine de Chimie, **34**, *5*, 1139–1147 (1989)

STUDIES OF THE THERMAL REGIME INFLUENCE ON THE ETHYLENE YIELD IN NAPHTHA PYROLYSIS PROCESS

GRIGORE BOZGA[a], CRISTIAN TSAKIRIS[b] and ALEXANDRU ISOPESCU[c]
[a] Department of Chemical Engineering, Polytechnic Institute of Bucharest, Romania
[b] Brazi Petrochemical Works, Romania
[c] Computer Center of Chemical Industry, Bucharest, Romania

Received June 25, 1988

A theoretical study of thermal conditions for naphtha pyrolysis reactors is presented. The process kinetic is described by a global molecular model. The results confirm that the ethylene yield can be increased by operating at shorter residence times and higher temperatures than in industrial conventional reactors.

Liquid feedstocks from naphtha, kerosene and even gas oil classes, have an increasing importance in the fabrication of ethylene by pyrolysis. The big production capacities and the increasing part that raw materials have in the cost of pyrolysis products, accent the necessity of operating these installations, in conditions that ensure the highest transformation yields in olefines.

Optimization studies of the operating conditions for the pyrolysis reactors that are found in literature are predominantly directed to pure gas feedstocks (especially to ethane [1,2] and to a lesser degree to hydrocarbon mixtures). The explanation may probably be found in the quality of kinetic models, better for pure hydrocarbon feedstocks. An optimization study of operating conditions for a naphtha pyrolysis reactor is presented below. Among operating parameters, the most important is the reaction temperature and its profile along the reactor. Studies of the reaction temperature profile influence are correlated with those of raw material flow rate and steam to hydrocarbon ratio.

The performance index used represents the reactor ethylene yield penalized by a term proportional to global coking rate. The kinetics of the pyrolysis process is described by a molecular model, and the computational algorithm is derived from a first variational method.

MATHEMATICAL REACTOR MODEL

The flow of reaction mixture inside the pyrolysis reactor being in a strong turbulent state ($Re > 10^5$), the ideal plug flow model may be used, neglecting consequently temperature and composition variations across flowing direction, and taking into account the convective substance and heat transport only.

The mathematical reactor model consists of molar balance and pressure drop equations. The molar balance equations are used in the structure that represents the evolution of reaction molar extent along the reactor.[3]

$$\frac{d\xi_{mi}}{dz} = \frac{S}{D_m} v_{Ri}, \qquad i = 1, \dots r \tag{1}$$

The stoichiometry and the kinetics of the pyrolysis process is described by a global molecular model. In the kinetic model, the naphtha feedstock is assumed as a pseudo-pure compound and the pyrolysis is represented by a primary decomposition step, followed by a set of reactions between the primary products, as proposed by Hirato and Yoshioka.[4] Also, to take into account the coking phenomenon, an eighth reaction was added to the Hirato-Yoshioka model. The selectivities of primary reaction and the preexponential factors, were adaptaed to fit a set of industrial data. The complete reaction scheme is shown in Table 1.

Table 1

The kinetic model

i	Chemical equation	reaction rate	$k_i = k_{0i}\exp(-E_i/R)$	
			k_{0i}	$E_i/R(K)$
1.	$C_mH_n \rightarrow 0.231C_2H_6 + 0.016C_3H_8$ $+ 1.035C_2H_4 + 0.47C_3H_6 + 0.069C_4H_8$ $+ 0.534C_4H_6 + 0.941CH_4 + 0.523H_2$	$v_{R_1} = k_1 C_{C_mH_n}$	$8 \cdot 10^{13}$ s^{-1}	29527
2.	$C_2H_6 \rightarrow C_2H_4 + H_2$	$v_{R_2} = k_2 C_{C_2H_6} P_{C_4H_8}$	$0.189 \cdot 10^{15}$ $s^{-1}atm^{-1}$	30030
3.	$C_3H_8 \rightarrow C_2H_4 + CH_4$	$v_{R_3} = k_3 C_{C_3H_8}$	$0.139 \cdot 10^{17}$ s^{-1}	37987
4.	$C_2H_4 \rightarrow 0.15C_2H_6 + 0.1C_3H_6 +$ $+ 0.25C_4H_6 + 0.1H_2$	$v_{R_4} = k_4 C_{C_2H_4} P_{C_4H_8}$	$0.221 \cdot 10^{12}$ $s^{-1}atm^{-1}$	22577
5.	$C_3H_6 \rightarrow 0.028C_2H_6 + 0.444C_2H_4$ $+ 0.25C_6H_9 + 0.556\ CH_4$	$v_{R_5} = k_5 C_{C_3H_6} P_{C_4H_8}$	$0.36 \cdot 10^{15}$ $s^{-1}atm^{-1}$	29673
6.	$C_4H_8 \rightarrow 0.106C_2H_6 + 0.177C_2H_4$ $+ 0.301C_3H_6 + 0.35C_6H_9 + 0.425CH_4$	$v_{R_6} = k_6 C_{C_4H_8} P_{C_4H_8}$	$0.102 \cdot 10^{16}$ $s^{-1}atm^{-1}$	30725
7.	$C_4H_6 \rightarrow 0.667C_6H_9$	$v_{R_7} = k_7 C_{C_4H_6} P_{C_4H_6}$	$0.506 \cdot 10^{8}$ $s^{-1}atm^{-1}$	11364
8.	$C_6H_9 \rightarrow 6C + 4.5H_2$	$v_{R_8} = k_8 C_{C_6H_9}$	20.17 s^{-1}	15525

The pressure drop equation is deduced from Fanning's equation written for a reactor element:

$$\frac{dp}{dz} = -\left(\frac{\lambda_f}{2d_t} + \frac{\xi_f}{\pi r_c}\right)\rho_{am} w^2 ; \ \lambda_f = 0{,}184\ R_e^{-0{,}2} \tag{2}$$

The factor ξ_f used for the supplementary pressure drop in the bends, is computed from Necrasov's formula[5]:

$$\xi_f = \left(0.7 + \frac{\alpha}{90} \cdot 0.35\right)\left(0.051 + 0.19 \frac{d_t}{r_c}\right) \tag{3}$$

After substitutions, equation (2) results in the following form:

$$\frac{dp}{dz} = -1181.5 \frac{D_m^{1.8}}{d_t^{4.8}} \frac{\eta_{am}}{M_{am}} \frac{T}{p} \mathrm{Fe} \tag{4}$$

For straight portions of the reaction coil Fe = 1, and for the bends:

$$\mathrm{Fe} = 1 + 5.7038\, d_t^{0.8} D_m^{0.2} \eta_m^{-0.2} \frac{\xi_f}{\pi r_c} \tag{5}$$

Temperature being considered the control variable, the heat balance equation is not included in the reactor model, so this consists of equations (1) and (4) which may be written in the general form:

$$\frac{dx_i}{dz} = f_i(X(z), T(z)) \qquad i = 1, \dots r+1 \tag{6}$$

$$z = 0 \qquad x_i = 0, \qquad i = 1, \dots r$$

$$x_{i+1} = p_0$$

For a given reaction temperature profile, integrating the equation system (6) one obtains the evolution of reaction mixture composition and pressure along the reactor.

OPTIMIZATION PROBLEM AND THE COMPUTATIONAL ALGORITHM

For the reaction system described, it is desired to determine the reaction temperature evolution along the reactor, T(z) (the temperature profile), that maximizes the performance index:

$$I = \eta_{C_2H_4}(L)\left(1 - \beta \int_0^L v_{RC}(z)\,dz\right) \tag{7}$$

The second term represents a penalty of ethylene yield, dependent on global coking rate in industrial reactor, being related to the influence of coking on reactor economic efficiency.[6]

The problem so formulated is solved using an algorithm derived from Pontriaghin's Minimum Principle, consisting in the following steps[7]:

— an initial temperature profile T(z) is guessed;

— state equations (6) are integrated in forward direction (from z = 0 to z = L), and the performance index (7) is computed for the resulted trajectory;

— a set of "adjoint variables", $\lambda_i(z)$, is computed by the backward numerical integration (between $z = L$ and $z = 0$) of the adjoint system of differential equations (the costate equations):

$$\frac{d\lambda_i(z)}{dz} = -\sum_{j=1}^{r+1} \frac{\partial f_j}{\partial x_i} \lambda_j(z) \tag{8}$$

$$z = L \quad \lambda_i(L) = \frac{\partial I}{\partial x_i(L)}$$

— the temperature profile is improved by a correction proportional to the gradient of hamiltonian:

$$T^{(k+1)}(z) = T^{(k)}(z) - \varepsilon \frac{\partial H^{(k)}(z)}{\partial T}, \quad \text{with} \tag{9}$$

$$H = \sum_{i=1}^{i+1} \lambda_i(z)\, f_i(X, T) \tag{10}$$

The superscripts (k) and (k + 1) represent the improved iterations of the temperature profile. ε is the iteration step, obtained by a unidimensional searching method;

— the state equations system are integrated for the new temperature profile $T^{(k+1)}(z)$, computing the new value of performance index $I^{(k+1)}$;

— a convergence condition to the performance index is tested by the relation:

$$\left| \frac{I^{(k+1)} - I^{(k)}}{I^{(k)}} \right| \leqslant \gamma.$$

To integrate the differential equation system, the Runge-Kutta method is used. The numerical integration in the performance index expression is done by the trapezoids method (coking rate being much more slower than the other chemical reaction rates). To solve the problem using the presented algorithm, a computational program was elaborated in Fortran IV.

COMPUTATIONAL RESULTS

Constructional and operating data of the industrial reactor considered in this study are given in Table 2, and the naphtha feedstock characteristics

Table 2

The reactor operating data

The internal diameter of the tube	0.108 m
The coil length	72 m
Straight portion length of the coil	6.3 m
The radius of the bends	0.195 m
Naphtha feedrate	2345 kg/h
Steam to hydrocarbon ratio	0.7416 kg/kg
Inlet pressure	3.8 atm
Feed temperature	550 °C

in Table 3. The initial temperature profile necessary to start the computing procedure is obtained by simulation of the reactor, at a constant heat flux along the coil of 65000 kcal/m^{2}h, this being considered as the reference run.

Table 3

The characteristics of naphtha

P.O.N.A. (wt %):		Distillation cv. (°C)	
— parrafins 86.27		0	80
— olefins	0.88	20	103
— naphthenes	1.73	50	124
— aromates	11.12	80	151
C/H ratio (wt): 5.1		100	223
Mean molecular weight: 85.5			

The optimal temperature profile determined by the computational procedure described and from the operating data given in Table 2 is shown in Fig. 1, versus the industrial reference ones. The computed optimal evolution of temperature requires a sudden increase on the last portion

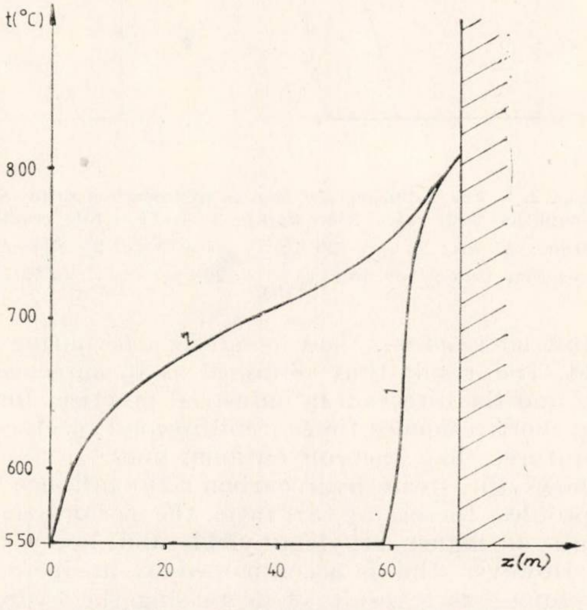

Fig. 1. — Optimal and reference run temperature profiles (naphtha feed rate: 2345 kg/h; 0.7416 kg steam/kg naphtha): 1 — optimal profile (reaction time; 116 ms; $\eta_{C_2H_4} = 25.6\%$; $\eta_{C_3H_6} = 14.3\%$; 2 — reference run profile (reaction time: 705 ms; $\eta_{C_2H_4} = 22.8\%$; $\eta_{C_3H_6} = 10.8\%$)

$$\frac{I_1 - I_2}{I_2} = \frac{12.3}{100}$$

of the reactor, from the inlet value, to values greater than 800°C. This result suggests that it would be more advantageous to operate at smaller reaction time (volume) and higher temperature than in the con-

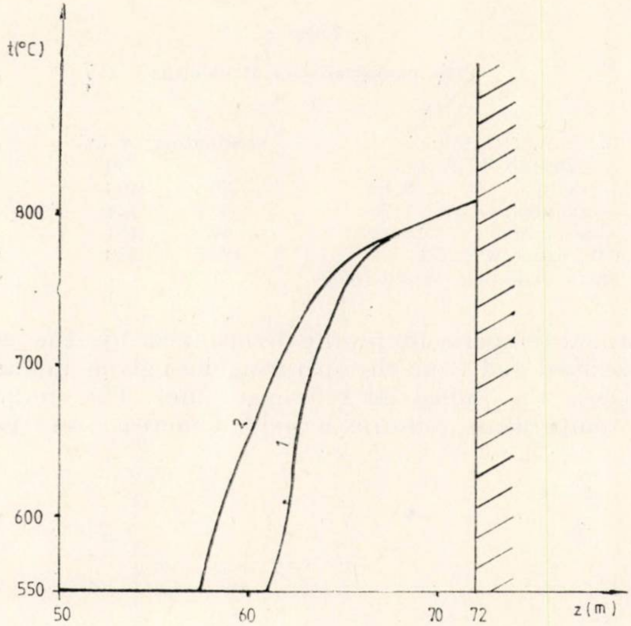

Fig. 2. — The influence of steam to hydrocarbon ratio (SH) (naphtha feed rate: 2345 kg/h): 1 — SH = 1.0; reaction time: 86 ms; $\eta_{C_2H_4} = 26\%$; $\eta_{C_3H_6} = 15\%$; 2 —SH=1.4; reaction time: 109 ms; $\eta_{C_2H_4} = 26.1\%$; $\eta_{C_3H_6} = 15.7\%$.

ventional industrial reactors, these conditions favouring the increase of ethylene yield. The result thus obtained is in agreement with experimental results and the direction in industrial practice, for pyrolysis reactors with very short residence times ("millisecond reactors"), operated at higher temperatures than the conventional ones.[8]

Fig. 2 shows the steam/hydrocarbon ratio influnce on the optimal temperature profiles. Increasing this ratio, the performance index increases, as a result of higher ethylene yields and lower values of global coking rates. However, this is accompanied by an increase in the reaction time (volume) as a result of decreasing the hydrocarbon partial pressure, and other economic disadvantages, not included in the model or in performance index.

The effect of naphtha flow rate, at constant inlet pressure and steam to hydrocarbon ratio is represented in Fig. 3. As the naphtha flow rate increases the reaction time increases, as a consequence of the pressure drop along the coil. Fig. 4 presents the inlet pressure effect on optimal temperature profile. Increasing the inlet pressure, the olefins yields decrease and the reaction time decreases. The relative increase of

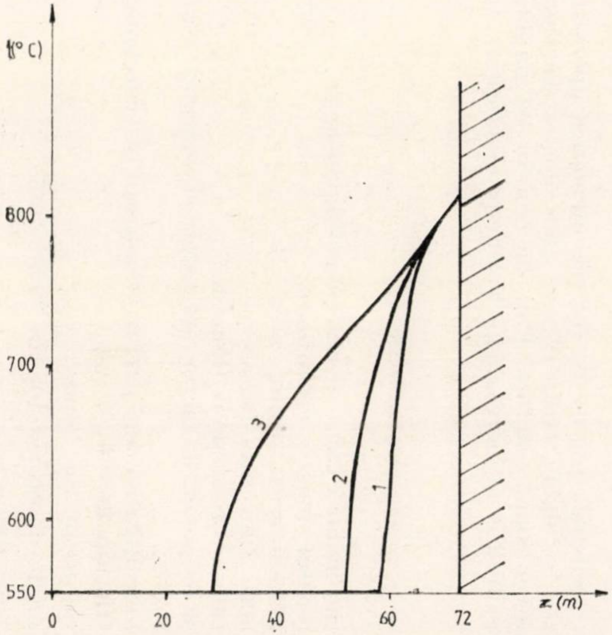

Fig. 3. — The influence of naphtha feed rate (D_m) (SH = = 0.7416 kg/kg) : 1 — D_m = 2500 kg/h ; reaction time : 124 ms ; $\eta_{C_2H_4}$ =25.7 % ; $\eta_{C_3H_6}$ = 14.5 % ; 2 — D_m = 3000 kg/h ; reaction time : 131 ms ; $\eta_{C_2H_4}$ = 25.7 % ; $\eta_{C_3H_6}$ = 14.7 % ; 3 — D_m = 3500 kg/h ; reaction time : 258 ms ; $\eta_{C_2H_4}$ = 25.7 % ; $\eta_{C_3H_6}$ = 15.3 %.

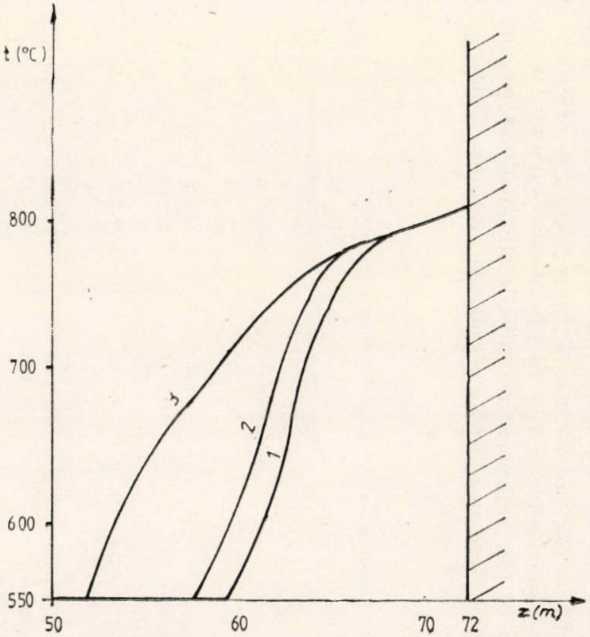

Fig. 4. — The influence of inlet pressure (p_0) : 1 — p_0 = = 3.8 atm ; reaction time : 116 ms ; $\eta_{C_2H_4}$ = 25.6 % ; $\eta_{C_3H_6}$ = = 14.3 % ; 2 — p_0 = 3.4 atm ; reaction time : 117 ms ; $\eta_{C_2H_4}$ = 25.9 % ; $\eta_{C_3H_6}$ = 14.7 % ; 3 — p_0 = 3.0 atm ; reaction time : 136 ms ; $\eta_{C_2H_4}$ = 26.0 % ; $\eta_{C_3H_6}$ = 15.5 %.

the performance index, versus the reference industrial case, is about 12%. The literature mentions the possibility of increasing the ethylene production from naphtha feedstocks, using millisecond reactors, up to 20%.[8] The positive effect of the temperature profile determined is noticed also in the increase of the yield in another pyrolysis products (butene, butadiene) as mentioned in Table 4.

Table 4

Main pyrolysis products concentrations

Product, j	Mass fraction (kg j/kg naphtha)	
	industrial profile	optimal profile
ethane	0.067	0.064
propane	0.047	0.005
ethylene	0.233	0.256
propylene	0.115	0.148
butene	0.032	0.033
butadiene	0.024	0.046
pyrolysis oil	0.347	0.259
methane	0.166	0.149
hydrogen	0.012	0.01
conversion	0.999	0.97

As a measure of the integrating method accuracy, the mass balance along the reactor was tested. The greatest computation error was 0.11%.

CONCLUSIONS

For naphtha feedstock pyrolysis, the recommended operating regimes are characterized by higher temperatures and shorter reaction times, versus those of conventional reactors. For the considered naphtha, the results show the possibilities of increasing ethylene production up to 12%.

NOTATIONS

ξ_{ni} — the molar extent of reaction i (kmol/kg);
z — reactor length coordinate;
S — reactor cross section area;
D_m — mass flow rate (kg/s);
v_{Ri} — rate of reaction i (kmol/m^{3}s);
k_{0i}, E_i, k_i — preexponential factor, activation energy and rate constant;
C_j, p_j — concentration and partial pressure of j-th component;
λ_f — friction factor;
r_c — radius of the bends;
α — angle described by the bend (180°C);
d_t — tube diameter;

F_e — factor used in pressure drop equation;
Re — Reynolds number;
r — number of chemical reactions in the kinetic model;
R — ideal gas constant;
β — positive constant (in this study $\beta = 0.15$);
ρ_{am} — reaction mixture density (kg/m^3);
w — flow rate of reaction mixture;
η_{am} — reaction mixture viscosity (kg/m.s);
I — performance index;
v_{RC} — global coking rate ($kmol/m^3s$);
x_i — state variable "i";
X — state vector;
λ_i — costate (adjoint) variables;
η_j — outlet yield (kg j/kg naphtha).

REFERENCES

[1] R. W. J. Robertson, and D. Hanesian, *Ind. Eng. Chem., Process Des. Dev.*, **14**, 216 (1975).
[2] J. T. Wilson and P. R. Belanger, IEE Trans. on Automatic Control, AC-17, **6**, 756 (1972).
[3] R. Mihail and O. Muntean, "Reactoare chimice", Ed. Didactică și Pedagogică, Bucharest, 1983.
[4] M. Hirato and S. Yoshioka, *Int. Chem. Engineernig*, **13**, 347 (1973).
[5] G. F. Froment and K. B. Bischoff, "Chemical Reactor Analysis and Design", John Wiley, N. Y., 1976.
[6] G. Bozga, J. Towfighi and O. Floarea, *Rev. Roumaine Chim.*, **33**, 87 (1988).
[7] W. H. Ray and J. Szekely, "Process Optimization", Wiley Interscience Publ., 1973.
[8] C. M. Schilmoller, "Hydrocarbon Processing", Sept., 1985, p. 101.

Revue Roumaine de Chimie, **34**, *5*, 1149–1154 (1989)

HYDROGENATION OF AROMATIC NITRO COMPOUNDS IN THE PRESENCE OF DYE-CONTAINING CATALYSTS

A. V. BULATOV
USSR Academy of Sciences, Institute of Chemical Physics,
Chernogolovka, 142432 USSR

Received October 3, 1988

The paper describes a new method of producing highly efficient heterogenized metal complex catalysts based on Pt metals with dyes by successive interaction of the carrier surface with the ligand (oxyanthraquinone), Pt metal complex salt and the modifier. Their catalytic properties and the mechanism of their action in nitroaromatic hydrogenation were studied. Hydrogenation is shown to proceed via radical intermediate formation : catalytically active paramagnetic complexes and anion-radicals of corresponding nitro compounds.

INTRODUCTION

Aromatic amines, halide-containing anilines in particular, are valuable products of fine organic synthesis : they are used for the production of medicines, dyes, antioxidants, etc. They are mainly obtained in the liquid phase catalytic hydrogenation of the corresponding nitro compounds. However, the heterogeneous catalysts known so far cannot often meet modern requirements in selectivity and in activity. Therefore the discovery of new catalysts of nitroaromatics hydrogenation is an urgent task. We have presented the general principles for the choice of such catalysts in our previous works.[1,2]

METHODS

When 50 g of aluminum oxide powder were introduced into an alcoholic solution of purpurine (1, 2, 4-trioxyanthraquinone) (0.175g in 150 ml EtOH), fast binding of the dye was observed. The powder was subsequently filtered, acetone- and ester-washed and dried. An aqueous solution of K_2PdCl_4 (0.446 g in 100 ml H_2O) was poured to the dry powder and stirred at 50–60°C till Pd was completely consumed (~ 10 min). The powder was filtered off again, acetone- and ester-washed and dried. Then there was 'Pd_2purp/Al_2O_3' catalyst, 1 g containing 2.76×10^{-5} mol Pd. Modification of the catalyst was performed in the following way : the solution of the modifier is poured to a certain amount of the catalyst (Pd : L = = 1 :1 for a bidentate ligand and 1 : 2 for a monodentate one).

Hydrogenation was carried out in a thermostated reactor under intense stirring. The reaction rate was determined by the hydrogen consumption. The reaction products were identified by their melting points, elemental analysis, and NMR- and mass-spectra.

RESULTS AND DISCUSSION

We have shown earlier[3,4] that the Pt and Pd complexes with alizarine (aliz) and alizarine red C (ARC) are highly efficient homogeneous catalysts of nitrobenzene hydrogenation. To simplify the separation between the products and catalysts the complexes have been heterogenized on the surface of different carriers. It turned out that the catalytic activity of heterogenized complexes was not lower than that of their homogeneous analogs.[5]

We used the method of surface synthesis shown below:

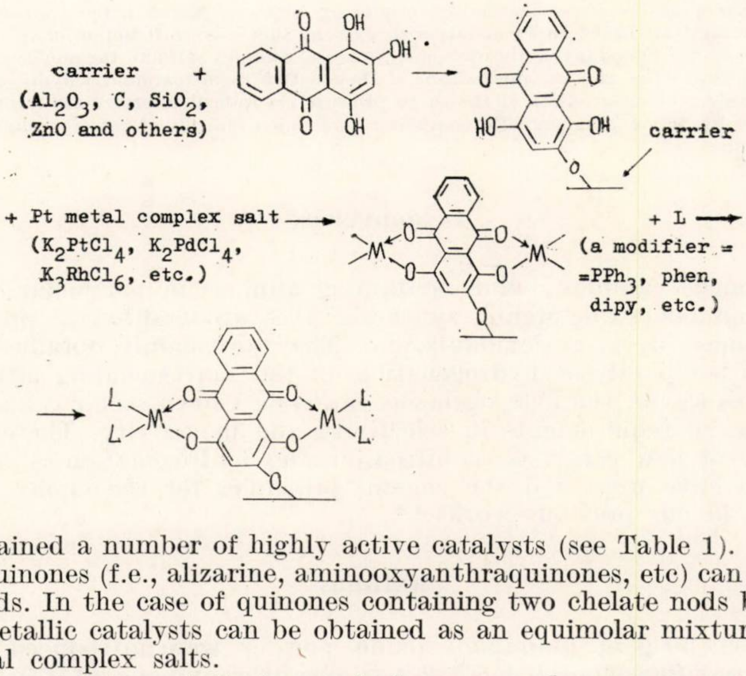

carrier +
(Al2O3, C, SiO2, ZnO and others)
O
OH
OH
O
OH
O
O
HO
OH
O
carrier
+ Pt metal complex salt
(K2PtCl4, K2PdCl4, K3RhCl6, etc.)
M
O
O
O
O
M
O
+ L
(a modifier = PPh3, phen, dipy, etc.)
L
L
M
O
O
O
O
M
L
L
O

and obtained a number of highly active catalysts (see Table 1). Other quinones (f.e., alizarine, aminooxyanthraquinones, etc) can be used as ligands. In the case of quinones containing two chelate nods binuclear heterometallic catalysts can be obtained as an equimolar mixture of two Pt metal complex salts.

The catalytic activity is seen to increase or decrease upon the introduction of a modifying agent, which can cause the required selectivity, in particular, in hydrogenation of halide-containing nitro compounds. We have developed another way of production of heterogenized complexes based on the method proposed by A. Ya. Yuffa and coworkers [6] and the scheme below

$$>SiOLi + (Bu_4N)_2PdCl_4 \xrightarrow[40°C]{} >Si-O-PdCl_3(Bu_4N)_2 + aliz \longrightarrow >Si-O-Pd-Cl\ aliz\ (Bu_4N)$$

The Pd content in this case is 1%.

Table 1

Catalytic activity of Pt- and Pd complexes heterogenized on alumina in nitrobenzene hydrogenation into corresponding amines

Complex	Modifier L	Substrate	Solvent	°C	$W = \frac{\text{mol } H_2}{\text{mol min}}$
Pdaliz	—	NB	i-C_3H_7OH	45	51
,,	—	,,	,,	75	56
,,		,,	octane	75	44
,,	8—Ox	,,	,,	45	63
,,	Phen *	,,	EtOH	45	13
,,	$P(PhCH_3)_3$	,,	,,	45	66
,,	pyrrolidon	m-ClNB	,,	45	46
Pd_2purp	—	NB	octane	65	62
,,	8—Ox	,,	,,	65	60
,,	PhAN	,,	EtOH	45	84
,,	,,	m-ClNB	,,	45	55
,,	$SnCl_2$	NB	,,	50	35
Pt^{II} aliz	—	,,	,,	50	56
,,	$SnCl_2$	,,	,,	50	31
,,	PhAN	,,	,,	50	89
Pt^{IV} aliz	—	o-NBA	CH_3COOH (30%)	45	63
,,	PPh_3	,,	,,	45	83

* Catalytic properties are shown after $NaBH_4$ treatment; 8—Ox — 8-oxyquinoline, PhAN — Phenylazonaphthol; NB — nitrobenzene, m-ClNB — m-chloronitrobenzene, o-NBA — o-nitrobenzoic acid.

This complex appeared to be highly efficient in nitrobenzene hydrogenation.

Thus, the conclusion is that dye-based catalysts of Pt metals heterogenized in different ways are highly efficient catalysts which can be used in the production of compounds containing amino groups.

If heterogenized Pt complexes are subjected to thermal treatment on alumina at 350°C, the metallic catalysts formed differ from their analogs obtained through traditional saturation method, Pt content being the same (0.2% Pt) in both cases. The catalytic properties were compared in the reaction of cyclohexane dehydrogenation (Fig. 1):

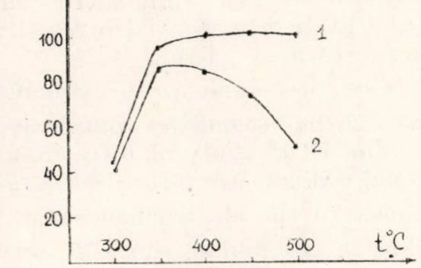

Fig. 1. — 1—0.2% Pt on Al_2O_3, obtained in Pt-purpurine complex pyrolysis; 2—0.2% Pt on Al_2O_3, obtained by H_2PtCl_6 saturation.

The catalyst obtained by pyrolysis of the Pt-dye complex is seen to be more active and selective, an undesirable process of cyclohexane hydrogenolysis being observed for the saturated catalyst.

A great attention was paid to the nature of the catalysts obtained and to the mechanism of their action. The formation of the surface complexes was detected by the diffuse reflectance spectroscopy. A new absorption band with $\lambda_{max} = 500$ nm appeared in the spectrum of purpurine supported on Al_2O_3, whereas a new one with $\lambda_{max} = 595$ nm appeared after the treatment with K_2PdCl_4. X-ray photoelectron spectroscopy showed that there was no complex decomposition and metal reduction to zero-valent state under catalysis, though the change in the bond energy (Table 2) and the satellite appearance in the Pd spectrum ($E_b = 345$ eV) evidenced for the change in the metal oxidation state from $+2$ to $+1$.

Table 2

Bond energies (E_b) of the metal internal shells

Compound	$3d_{5/2}$ Pd	$4f_{7/2}$ Pt
$Pt(ARC)_2/Al_2O_3$	—	72.3
,, $+H_2$	—	71.6
K_2PtCl_4	—	73.1
Pt^0	—	71.3
$Pd(ARC)_2/Al_2O_3$	338.1	—
,, $+H_2$	335.8, 345.0	—
K_2PdCl_4	338.4	—
Pd^0	335.3	—

We showed earlier [2] that the treatment of Pd- and Pt-alizarine complexes with hydrogen resulted in the formation of paramagnetic intermediates, their paramagnetism being caused by the ligand transfer to the semiquinone state.

Heterogenized complexes appeared to become paramagnetic under their treatment with hydrogen or hydrazine : the EPR spectra showed singlet signal with $g = 2.0038 \pm 0.0001$, the signal width (ΔH) depending on the nature of the modifier.

When nitrobenzenes were added to the intermediate paramagnetic complexes, their EPR signals disappeared and the formation of anion-radicals of corresponding nitro compounds was observed instead. Analogous EPR spectra were also registered in the process of catalysis for some radicals formed (Table 3).

Thus we came to the conclusion that the mechanism of homogeneous and heterogenized complexes action is one and the same.

The EPR study of nitro halides revealed anion-radicals (sometimes nitroxyl radicals are formed[2]) containing all the halide atoms, whereas they eliminate in the electrochemical hydrogenation of anion-radicals of nitro halides, in particular, those in ortho-position.[7]

Table 3

The nature and HFS constants of polyhalide nitro compounds

Initial nitro compound	Catalyst	Radical	HFS constants, G				
			a_N	a_{NH}	a_H^o	a_H^p	a_H^m
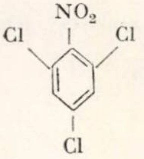	PdQ_2/Al_2O_3	$Cl_3Ar\dot{N}HO$	12.30	15.02	—	—	—
	$Pd(QBu_4N)_2$	$Cl_3ArNO_2^{\bar{\cdot}}$	15.80	—	—	—	0.85
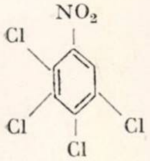	PdQ_2	$Cl_4Ar\dot{N}HO$	8.20	10.90	3.00	—	—
	$Pd(QBu_4N)_2$	$Cl_4ArNO_2^{\bar{\cdot}}$	8.02	—	3.05	—	—
	$Pd(B)/C$	$Cl_4Ar\dot{N}HO$	8.12	10.87	2.90	—	—
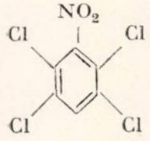	$Pd(QBu_4N)_2$	$Cl_4ArNO_2^{\bar{\cdot}}$	15.50	—	—	1.30	—
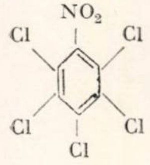	PdQ_2/Al_2O_3	$Cl_5Ar\dot{N}HO$	8.20	10.90	—	—	—
	$Pd(QBu_4N)_2$	$Cl_5ArNO_2^{\bar{\cdot}}$	17.20	—	—	—	—
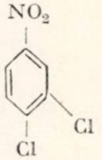	IrClAA	$Cl_2ArNO_2^{\bar{\cdot}}$	9.84	—	3.17	—	1.18
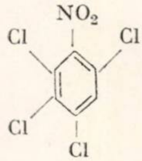	$Pd(B)/C$ *	$Cl_4ArNO_2^{\bar{\cdot}}$	17.16	—	—	—	—
	$Pd(QBu_4N)_2$	$Cl_4ArNO_2^{\bar{\cdot}}$	17.03	—	—	—	—

* Hydrazine hydrate is used as a reductant; Q — alizarine, QBu_4N — alizarine salt with Bu_4N^+, Pd(B)/C — 5% Pd boride catalyst on medicinal charcoal, ClAA — chloroanilic acid.

REFERENCES

[1] A. V. Bulatov, E. G. Chepaikin and M. L. Khidekel, *Proc. XIX ICCC*, 1978, p. 23.

[2] A. V. Bulatov, M. V. Klyuev and M. L. Khidekel, *Kinetika i Kataliz*, **28** (1987) 263.

[3] A. V. Bulatov and M. L. Khidekel, *Trans. Met. Chem.*, **5** (1980) 123.

[4] A. V. Bulatov, E. N. Izakovich, L. N. Karelin and M. L. Khidekel, *Izv. Akad. Nauk SSSR, ser. khim.*, (1981) 2032.

[5] A. V. Bulatov, M. V. Klyuev and M. L. Khidekel in: "Catalysts containing supported complexes", Novosibirsk, Pt. 2, 1980, p. 14.

[6] G. V. Lisichkin and A. Ya. Yuffa, "Heterogeneous Metal Complex Catalysts", Khimiya, Moscow, 1981.

[7] J. G. Lawless and M. D. Hawless, *J. Electroanal. Chem.*, **21** (1969) 365.

Revue Roumaine de Chimie, 34, 5, 1155—1161 (989)

THE EVALUATION AND SIGNIFICANCE OF KINETIC PARAMETERS k_i AND k_t IN THE EMULSION POLYMERIZATION OF VINYL CHLORIDE

V. BUTUCEA, ADRIANA SÂRBU, CECILIA-SPERANȚA GEORGESCU, ADRIANA IONESCU and I. DEACONESCU

ICECHIM — Research Centre for Plastic Materials,
Bucharest 79611, Romania

Received November 28, 1987
Revised March 26, 1988

The present paper proposes an evaluation method of kinetic parameters k_i and k_t based on the kinetic expression of polymerization rate, R_p, and of average degree of polymerization. The significance of the values of these parameters from kinetical point of view and of the possible mechanism of reaction is discussed.

INTRODUCTION

The kinetics of emulsion polymerization process is described by the values of kinetic parameters represented by the rate constants of the initiation, k_i, propagation, k_p, termination, k_t, and desorption of radicals, k_d. Concerning the k_p value, one may admit that a value of $1 \times 10^4 \mathrm{dm}^3\mathrm{mol}^{-1}\mathrm{s}^{-1}$ at 50°C is generally accepted, for vinyl chloride, at least in processes of saturation with monomer.[1] For the values of the other kinetic parameters mentioned, the situation is more complicated. The value k_i depends on the nature and concentration of tenside and cotenside utilized and also on monomer. [2-4] The desorption of radicals, illustrated by the value k_d, is a characteristic process for the monomers which present a strong tendecy of transfer to monomer, vinyl chloride being one of them. The desorption process of radicals from polymer particles refers especially to the radicals resulted from transfer to monomer, radicals formed from one monomer unit. [5-7] The rate of desorption process depends on the diameter of polymer particles. [7] The desorption of radicals will also influence the kinetics of polymerization process, the rate of polymerization, R_p, and the average degree of polymerization, $\bar{P}_n$. The desorption and reabsorption of radicals increase the probability of termination reactions, therefore k_t values, so that the situation may appear in which the average number of radicals per polymer particle, $\bar{n}$, may be $\bar{n} < 0.5$, according to the classical kinetic theory. [8] It comes out that k_t and $\bar{P}$ values will depend also on the diameter of polymer particles. The value of $\bar{n}$ for a given polymerization process is determined by the relative proportion between the rates of initiation, desorption and termination. Therefore any kinetic model concerning $\bar{n}$ or R_p must necessarily include all kinetic parameters mentioned. The check-up of a kinetic model by comparing the calculated values of $\bar{n}$, based on a given model, with those experimentally determined, $\bar{n}_{ex}$, imperiously requires the knowledge of kinetic parameters for a given particular case.

A polymer with a given value of $\bar{P}_n$, results from a polymerization process which occurred with a given kinetic behaviour. As a consequence, the same values of kinetic parameters k_i, k_t and k_d will determine both values of R_p and $\bar{P}_n$. Thus, due to this aspect and considering the kinetic expressions of R_p and $\bar{P}_n$ one may evaluate the kinetic parameters k_i and k_t from a single pair of values R_p and $\bar{P}_n$. The value of k_d is calculated independently of these kinetic expressions. [7]

In this paper is suggested an evaluation method of kinetic parameters k_i and k_t based on kinetic expressions of polymerization rate R_p and of average degree of polymerization $\bar{P}_n$. One discusses the significance of the values of these parameters from the kinetical point of view and of the possible mechanism of reaction.

EXPERIMENTAL PART

The polymerizations were carried out in a 4-liter stainless steel reactor provided with a jacket for temperature control and a stirrer having 1 m/s peripheral speed. For oxygen removal, after charging the water phase, the reactor was purged with N_2 under stirring. The monomer/water ratio was 1/2. The initiator (potassium persulphate) was injected, under pressure, as solution, after reaching 50°C, at which temperature the polymerization was carried out. The amount of vinyl chloride was 1000 g. In runs nos 1, 2 and 3, sodium dodecyl sulphate (SDS) was used as tenside. For runs nos 4 and 5 sodium di-butyl-sulphosuccinate (DBS) was used. In runs nos 6 and 7 for obtaining larger particles, the association complex between high fatty alchools C_{16-18} (FA) and SDS was used in ratio of FA/SDS = 3/1 in run no. 6 and FA/SDS = 6/1 in run no. 7. These complexes were prepared according to paper.[9]

The substances used had the following characteristics :

— technical vinyl chloride of polymerization grade of 99.99 %, purity determined by gas chromatography.

— demineralised water of 2 μS conductivity.

— commercial sodium dibutyl-sulphosuccinate (DBS) was purified by recrystallization from ethyl acetate ; sodium dodecyl sulphate (SDS) LOBA was used as such.

— a technical blend of C_{16-18} alcohols (96 % total alcohol content of which C_{18}= 70 %) was used as such.

— potassium persulphate LOBA p.a. was used without further purification.

The conversion curves were plotted based on hourly measurements of the polymer formed. The rates of polymerization, R_p, were calculated from the conversion curves by graphical derivation at a conversion of 200 g PVC/dm^3.

The diameter of polymer particles was measured by electronic microscopy counting and classifying about 1000 particles. The average surface diameter $\bar{d}_{1,2}$ of the particles was calculated as[10] :

$$\bar{d}_{1,2} = \frac{\sum n_i d_i^3}{\sum n_i d_i^2} \qquad (1)$$

The K values (the Fikentscher constant) were determined by viscometry from 0.5 % cyclohexanone solution at 25°C. The $\bar{P}_v$ values (viscometric average degree of polymerization), corresponding to K values were taken from reference.[11] The $\bar{P}_n$ values which were used in kinetic calculations were obtained considering $\bar{P}_v/\bar{P}_n \simeq 1.8$, from reference.[12]

Data regarding the experiments as well as the characteristics of the polymers are given in table 1.

RESULTS AND DISCUSSION

The experiments conceived had in view two objectives, necessary to elaborate this paper:

— To obtain PVC latexes with polymer particles of widely different average diameters enabling thus to find out if the size of particles influences the kinetic parameters and polymer characteristics.

— To find out, using various tensides, to what extent their nature affects the k_i values.

Table 1

Experimental data

No.	Initiator conc. mol · dm^{-3} × 10^3	Tenside	Tenside conc. g·dm^{-3}	K	$\overline{P}_v$	$\overline{P}_n$	$R_p \times 10^4$ mol · · dm^{-3}s^{-1}	$N_p \times 10^{-16}$ dm^{-3}	$\bar{d}_{1,2}$ dm ×10^6	$S \times 10^{-5}$ dm^2·dm^{-3}
1	1.48	SDS	0.492	65.6	990	550	2.66	64.000	0.752	11.30
2	4.44	SDS	2.600	62.0	850	472	6.80	590.000	0.358	23.80
3	1.48	SDS	3.930	62.5	870	483	3.80	780.000	0.327	26.20
4	2.96	DBS	2.000	69.7	1180	655.5	3.30	4.700	1.790	4.73
5	5.92	DBS	2.000	69.0	1140	633	4.44	4.300	1.850	4.62
6	4.44	FA :SDS 3 :1	2.600	71.1	1265	703	3.30	0.597	4.090	3.13
7	4.44	FA :SDS 6 :1	2.600	71.7	1310	728	2.48	0.293	5.180	2.47

Examination of the results given in tabele 1 shows the following:

— The average degree of polymerization $\overline{P}_n$, obviously depends on the size of particles i.e. these increase with increasing the average diameter $d_{1,2}$ of polymer particles. In this respect the results may be grouped as follows: — exp. 1, 2 and 3 in which SDS was used the smallest average diameters, $\bar{d}_{1,2}$, resulted, of 10^{-7} dm order and $\overline{P}_n$ values below 600; in exp. 4 and 5 where DBS was used as tenside, the $\bar{d}_{1,2}$ values are greater, having about 1.8×10^{-6} dm and $\overline{P}_n$ values 655 and 633; — in exp. 6 and 7 the largest particles were obtained having $\bar{d}_{1,2}$ about 4×10^{-6} and 5×10^{-6} dm and $\overline{P}_n$ values above 700. The same grouping of results is noticed concerning the number of particles N_p and the total surface area, S.

As one may notice the three groups of experiments differ one from another by the nature of tenside. The remarkable differences between these groups, regarding the values of $\overline{P}_n$, $\bar{d}_{1,2}$, N_p and S show that the polymerization process occurred with relatively different proportions between the rates of initiation desorption of radicals and termination. Comparison of experiments regarding the kinetic and possible mechanism of reaction, is obviously necessary to know the values of kinetic parameters.

The desorption of radicals, illustrated by the k_a value, was calculated from the expression [7]:

$$k_a = \frac{12D_w \cdot \delta z}{md^2} C_M \tag{2}$$

where k_d = rate constant of desorption, s^{-1}; D_w= diffusion coefficient of radicals in water, $dm^2 \cdot s^{-1}$; δ = ratio between mass transfer resistance in film and total resistance; z = coefficient which depends on the ratio between the total number of active particles and those which contain a certain number of radicals; m = partition coefficient of radicals between particle and water phase; d = diameter of polymer particle, dm; C_M = = transfer coefficient to monomer which represents $C_M = k_{trm}/k_p$ (where k_{trm} = rate constant of transfer to monomer, $dm^3mol^{-1}s^{-1}$ and k_p = rate constant of propagation, $dm^3mol^{-1}s^{-1}$).

According to indications in the paper[7] for vinyl chloride, the following values were used: $D_w = 2.5 \times 10^{-7} dm^2s^{-1}$; $\delta = 1$; $z = 1$; $m = 35$; $C_M = 1.2 \times 10^{-3}$. The values calculated from expression (2) are given in table 2.

Table 2

Calculated kinetic parameters k_i and k_t based on a single pair of R_p and $\bar{P}_n$ values according to the method proposed

No.	$\bar{n}_{ex.} \times 10^3$	$[R\cdot] \times 10^9$ $mol \cdot dm^{-3}$	$R_p/S \times 10^9$	k_d s^{-1}	$k_i \times 10^{-6}$ s^{-1}	$k_t \times 10^{-9}$ $dm^3 \cdot mol^{-1}s^{-1}$	$R_i/S \times 10^{13}$
1	5.560	5.91	0.235	181.8	8.07	64.70	0.0634
2	1.540	15.10	0.285	802.5	8.42	45.60	0.0940
3	0.652	8.44	0.145	961.9	7.15	144.00	0.0241
4	93.900	7.33	0.697	32.1	14.70	4.90	0.5440
5	138.000	9.86	0.961	30.0	13.60	3.60	1.0200
6	739.000	7.33	1.050	6.1	14.20	1.58	1.0200
7	1132.000	5.51	1.000	3.8	9.96	1.37	0.7740

To calculate the values of kinetic parameters it was taken into account that the kinetic of polymerization process is in correlation with the molecular characteristics of the polymer resulted and thus k_i and k_t values determine both the kinetic expression of R_p and $\bar{P}_n$. In this respect, for R_p we have considered the best the kinetic expression of Ugelstad et al. [6]:

$$R_p = \frac{k_p[M]_p}{N_A} (k_i[I])^{0.5} \left[\frac{V_p}{2k_t} + \frac{N_p}{2k_d}\right]^{0.5} \tag{3}$$

where: R_p = polymerization rate at a given conversion, $mol \cdot dm^{-3}s^{-1}$, $[M]_p$= conc. of monomer in polymer particles, $mol \cdot dm^{-3}$; $[I]$ = conc. of initiator, $mol \cdot dm^{-3}$; V_p = volume of polymer at a given conversion, $dm^3 \cdot dm^{-3}$; N_p = total number of polymer particles, dm^{-3}; k_d = rate constant of radicals desorption, s^{-1}; k_t = rate constant of termination, $dm^3 \cdot mol^{-1} \cdot s^{-1}$; N_A = Avogadro's number; k_i = rate constant of effective initiation, s^{-1}, which represents $k_i = 2fk_s$, where k_s = rate constant of initiator decomposition generating primary ion radicals, s^{-1} and f = = efficiency of initiation. In this expression the value $[M]_p$ is considered to be the same in all experiments because these were carried out in saturation conditions. The value, calculated acording to reference[12], is $[M]_p$ = $= 4.5\ mol \cdot dm^{-3}$.

The epression taken into account for P_n is that well known :

$$\frac{1}{\bar{P}_n} = \frac{k_t^{0.5}(k_i[I])^{0.5}}{k_p[M]_p} + C_M \tag{4}$$

Considering the experimental data R_p, $[\mathrm{M}]_p$, V_p, N_p and $\bar{P}_n$, the values of k_p and C_M adopted as well those calculated for k_d from expression (2), and based on expressions (3) and (4) one may calculate the values of kinetic parameters k_i and k_t. Therefore k_i and k_t can be separated from expression (3) :

$$C = \frac{k_i}{k_t} A + k_i B \tag{5}$$

$$C = R_p^2\,;\ A = \frac{k_p^2[\mathrm{M}]_p^2[\mathrm{I}]V_p}{2N_A}\ ;\quad B = \frac{k_p^2[\mathrm{M}]_p^2[\mathrm{I}]N_p}{2k_d N_A}$$

Also from expression (4) one obtains :

$$k_i k_t = \frac{k_p^2[\mathrm{M}]_p^2\left(\dfrac{1}{\bar{P}_n} - C_M\right)^2}{[\mathrm{I}]} = D \tag{6}$$

Taking the value k_i from (6) and replacing it in (5) one obtains :

$$Ck_t^2 - BDk_t - AD = 0 \tag{7}$$

which enables the calculation of k_t. Thus, the values of k_i and k_t from a single pair of values of R_p and $\bar{P}_n$ can be calculated. From these calculations k_i and k_t are obtained in molecular units. The calculated values are given in table 2 in the usual molar units. Table 2 gives also the values of the average number of radicals per polymer particle, $\bar{n}_{\mathrm{ex}}$, calculated on the basis of experimental data as follows :

$$R_p = k_p[\mathrm{M}]_p[R\cdot] = k_p[\mathrm{M}]_p\bar{n}_{\mathrm{ex.}}\frac{N_p}{N_A} \tag{8}$$

where : $[R\cdot]$ = conc. of radicals, mol · dm^{-3}, which is also given in table 2.

Examination of all the data shows the following :

— a dependence of k_t on average diameter, $\bar{d}_{1,2}$, i.e. these are increasing with the decrease of $\bar{d}_{1,2}$ values. Since we take into account that $\bar{P}_n$ values depend also on $\bar{d}_{1\,2}$ it comes out that $\bar{P}_n$ values depend on k_t values namely as the rate of termination reactions decreases the $\bar{P}_n$ values increase ;

— the k_i values depend firstly on the nature and concentration of tenside used. As it was mentioned $k_i = 2fk_s$, therefore k_i refers to the effective process of initiation. Since k_s is known one may find out the efficiency of initiation, f. For example, in case of exp. 3, considering a value [4] of $k_s = 10^{-5}\mathrm{s}^{-1}$, $f = 0.357$ results ;

— the k_d values depend obviously on diameter of particles. One notices that in case of exp. 4—7 the rates of desorption processes are very reduced in comparison with those from exp. 1—3 ;

— the $\bar{n}_{ex.}$ values show that in these experiments the polymerization processes occurred following a kinetics which deviated from the classical theory i.e. these values are $\bar{n}_{ex.} < 0.5$ in case of exp. 1—5 and $\bar{n}_{ex.} > 0.5$ in case of exp. 6 and 7. This behaviour is characteristic for vinyl chloride.

From the experimental data and the values of kinetic parameters given in tables 1 and 2 some conclusions regarding the mechanisms of reaction come out. The process of initiator decomposition illustrated by k_s is the determining factor for radicals generation. Due to some reactions with impurities solved in water or with desorbed alkyl radicals from particles, or as a consequence of transfer reactions not all primary radicals will succeed to initiate effectively. The effective initiation illustrated by k_i will be achieved by the tenside ionradicals [14] which will succeed in reaching the initiation loci i.e. micelles [15], drops, [16] polymer particles or autoprecipitation. [17] On the other hand, the desorbed alkyl radicals may initiate as consequence of reabsorption. Because of desorption of radicals there is no direct dependence between rate of polymerization and rate of initiation. Due to these aspects it is obviously necessary to know both k_i and k_s for a better understanding of initiation process. For example let us consider exp. 2,6 and 7 in which the initiator concentration was the same. One may notice that k_i values of exp. 6 and 7 are greater than those of exp. 2, particularly of exp. 6. These differences can be explained by differences of k_s values but at the same time we may suppose that these differences are due to different efficiencies, f. Considering also the surface area S one observes an about tenfold area of polymer particles from exp. 2 than those from exp. 6 and 7. This aspect enables us to suppose that the great values of k_s are responsible for the greater values of k_i in the main part.

The length of the kinetic chain within the particle will depend on the diameter of particle i.e. it increases with the increase of diameter. This is due to the fact that the probability of meeting with a new entered radical decreases with increase of particle diameter. This aspect is confirmed by k_t values which are greater, the smaller the diameter of particles and consequently the $\bar{P}_n$ values are also affected, namely, they increase with the increase of particle diameter.

One must mention that in many papers referring to polymerization kinetic of vinyl chloride concerning R_p[14, 18] or the models concerning the calculation of $\bar{n}$[6, 7, 19, 20], to cite only few of them, the k_i and k_t values were adopted rather arbitrarily, a fact demonstrated by the lack of any reference to $\bar{P}$ values. Applying the method proposed in this paper the k_i and k_t may be evaluated based on a single pair of R_p and $\bar{P}$ values. The accuracy of these values will depend on the accuracy of determination of R_p, N_p, $\bar{d}_{1.2}$, $\bar{P}_n$ and on the $[M]_p$ value which is disputable.

REFERENCES

[1] G. M. Burnett and W. W. Wright, *Proc. Roy. Soc. (London) Ser.*, **A**, **60**, 121 (1954).

[2] I. M. Koltoff and I. K. Miller, *J. Amer. Chem. Soc.*, **73**, 3055 (1951).

[3] C. E. M. Morris and A. G. Parts, *Makromol. Chem.*, **119**, 212 (1968).

[4] J. Neelsen, W. Jaeger, G. Reinisch and H. J. Schneider, *Acta Polym.*, **38** (1), 1 (1987)

[5] J. Ugelstad, P. C. Mork and J. O. Aasen, *J. Polymer Sci.*, **5**, 2281 (1967).

[6] J. Ugelstad, P. C. Mork, P. Dahl and P. Rangnes, *J. Polymer Sci.*, **27**, 49 (1969).

[7] M. Nomura and M. Harada, *J. Appl. Polymer Sci.*, **26**, 17 (1981).
[8] W. V. Smith and R. H. Ewart, *J. Chem. Phys.*, **16**, 592 (1948).
[9] J. Ugelstad and P. C. Mork, *Brit. Polym. J.*, **2**, 31 (1970).
[10] H. Zecha and H. Schlacken, *Acta Polym.*, **30**, 215 (1979).
[11] G. Matthews, "Vinyl and Allied Polymers", vol. 2, London Iliffe Books, 1972, p. 320.
[12] M. Morton, S. Kaiserman and M. W. Altier, *J. Colloid Sci.*, **9**, 300 (1954).
[13] C. Tanford "Physical Chemistry of Macromolecules", John Wiley, 1961.
[14] B. S. Hawkett, D. H. Napper and R. G. Gilbert, *J. Polymer Sci. Chem. Ed.*, **19**, 3173 (1981).
[15] W. D. Harkins, *J. Amer. Chem. Soc.*, **69**, 1428 (1947).
[16] J.Ugelstad, K.H. Kaggerund, F. K. Hansen and A. Berge, *Makromol. Chem.*, **180**, 737, (1970).
[17] R. M. Fitch and C. H. Tsai, "Polymer Colloids", R. M. Fitch Ed. Plenum Press, New York (1971), p. 73.
[18] N. Friis and A. E. Hamielec, *J. Appl. Polymer Sci.*, **19**, 97 (1975).
[19] H. J. Schneider, N. Jaeger and W. Dietzel, *Acta Polym.*, **34**, 9 (1983).
[20] V. Lukovitzky, *Vysokomol. Soedineniya* (A) XXIII, **9**, 2039 (1981).

Revue Roumaine de Chimie, 34, 5, 1163—1167 (1989)

РОЛЬ ГАЗОВ ЭЛЕКТРОЛИЗА В ЭЛЕКТРОХИМИЧЕСКОЙ СТАБИЛИЗАЦИИ ГИДРОКСИДА АЛЮМИНИЯ

ТАТЬЯНА Я. ДАЦКО и В. И. ЗЕЛЕНЦОВ
Лаборатория электрической флотации веществ ИПФ АН МССР,
Кишинев, СССР

Получена 2 октября 1988 г.

На примере гидроксида алюминия с помощью данных адсорбционного и химического анализов исследован вклад газовой составляющей электрообработки (ЭО) в степень стабилизации геля гидроксида. Показано, что около 40% степени стабилизации гидроксида алюминия обеспечивается за счет газа электролиза — CO_2. Рассматривается вероятный механизм стабилизации.

The contribution of the gaseous component of electric treatment (ET) to the stabilization level of the gel hydroxide has been investigated on aluminium hydroxide and on the data of adsorption-structural and chemical analysis. It has been shown that about 40% of the stabilization level of aluminium hydroxide is provided at the expense of the electrolytic gas CO_2. The probable mechanism of stabilization is treated.

ВВЕДЕНИЕ

Старение гидроксидов металлов — самопроизвольный процесс, направленный на уменьшение свободной поверхностной энергии системы, сопровождающийся сокращением удельной поверхности, кристаллизацией первоначально рентгеноаморфных соединений.[1] Проблема повышения устойчивости, продления жизни дисперсной системы — одна из самых важных и сложных в коллоидной химии.

Значительное число работ посвящено различным способам стабилизации свойств гидроксидов металлов, например, введением поверхностно-активных веществ,[2] применением гидротермальной [3] и термальной обработки,[4] озвучиванием ультразвуком [5] и др.

Нами было установлено явление стабилизации гидроксидов алюминия и железа в результате электрообработки (ЭО) дисперсий гидроксидов в бездиафрагменном электролизере с графитовым анодом и катодом из нержавеющей стали. Подвергнутые ЭО гидроксиды в течение всего времени старения под слоем маточного раствора сохраняют высокое значение удельной поверхности и сорбционного объема пор, равное исходному, также кристаллическую структуру — остаются рентгеноаморфными. Необработанные образцы за это же время подвергаются кристаллизации, удельная поверхность и сорбционный объем пор у них значительно уменьшаются.

Текстурные свойства ксерогелей, являясь отражением их внутренней структуры, связаны со свойствами гидрогелей, из которых они получены. Гидрогели гидроксидов также показывают стабилизацию своих свойств после ЭО и старения под слоем маточного раствора — вязкость, седиментационный объем и размер частиц у обработанных гелей остаются на уровне исходных, у контрольных они существенно меняются.

Установлено, что из всех слагаемых ЭО — материала электродов, состава электролита, контактного заряжения частиц дисперсии гидроксида с электродами, диспергирующего действия газов электролиза, адсорбции поверхностью частиц гидроксида растворимых продуктов электрохимических реакций — только два последних процесса имеют определяющее значение для стабилизации геля гидроксида. Влияние сорбции растворимых продуктов электролиза было подробно исследовано [6] и показано, что только специфическая сорбция карбонатов, образующихся при электрохимическом окислении графитового анода, способствует стабилизации гидроксидов.

Настоящее исследование посвящено выяснению роли газов электролиза в стабилизации гидроксида алюминия при ЭО.

ЭКСПЕРИМЕНТАЛЬНАЯ ЧАСТЬ

Гидроксид алюминия синтезировали путем сливания по каплям 1 М раствора нитрата алюминия и гидроксида натрия. Затем в специально сконструированном бездиафрагменном электролизере обрабатывали как дисперсию гидроксида с содержанием 1,3% по Al_2O_3, так и маточную жидкость (3 М нитрат натрия) при плотности тока 100 мА/см^2 и продолжительности обработки от 15 до 40 минут. После обработки маточную жидкость соединяли с твердой фазой, от которой она была отделена центрифугированием, и ставили так же, как и обработанную дисперсию на старение. По истечение определенного времени брали пробу, отмывали ее пятикратным объемом дистиллированной воды, отжимали на фильтре и высушивали на воздухе. На этих воздушно-сухих образцах проводили адсорбционно-структурные измерения и рентгенофазовый анализ. Удельную поверхность определяли на адсорбционно-вакуумной установке с кварцевыми пружинными весами Мак-Бена-Бакра, рассчитывали по методу БЭТ. Адсорбатом служил метанол, посадочная площадка которого при расчетах принималась равной 0,25 нм^2. Точность определения удельной поверхности составляла 5%. Химический анализ жидкой фазы проводили по известным методикам аналитической химии[7].

В условиях нашего эксперимента (3 М нитрат натрия, pH = 9, графитовый анод) основным газом электролиза (до 94%) является CO_2. Для выявления влияния природы газа электролиза графитовый анод был заменен на платиновый, а вместо растворимых продуктов электрохимического окисления графита (карбонат-ионов) в дисперсию гидроксида вводили эквивалентное количество бикарбоната натрия. Влияние бикарбонатов, полученных химически, на степень стабилизации гидроксида алюминия (СтСтГа)— отношение величины удельной поверхности гидроксида при данном времени старения к ее исходной величине-сравнивали с действием эквивалентного количества электрохимически полученных бикарбонатов (электролизом жидкой фазы дисперсии с использованием графитового анода) и с эффектом от ЭО дисперсии ГА в маточном растворе.

РЕЗУЛЬТАТЫ И ИХ ОБСУЖДЕНИЕ

Представленные в таблице результаты опытов 1—3 — иллюстрация того, что в условиях ЭО необходимым фактором стабилизации свойств ГА является наличие продуктов электрохимического окисления графита, растворенных — HCO_3^- и газообразных—CO_2. Так, при замене графитового анода на платиновый (оп. 3) стабилизации удельной поверхности не происходит, величина СтСтГА такая же, как и у контрольного образца (оп. 1), несмотря на то, что в этом случае присутствуют газы электролиза (смесь H_2 и O_2). Введением эквивалентного количества бикарбоната натрия (остальные условия такие же, как и в оп. 3) удается повысить СтСтГА лишь до 64% (оп. 5), хотя в данном случае формально присутствуют все значимые элементы ЭО — газы электролиза (здесь-смесь H_2 и O_2) и растворимые карбонаты. Добавление же только бикарбоната натрия в дисперсию без ЭО (оп.4) приводит к аналогичному значению СтСтГА — 64%. Обобщая данные опытов 1—5, приходим к выводу:

— один только растворенный бикарбонат не обеспечивает максимальной СтСтГА,

— газы электролиза в виде смеси водорода и кислорода не оказывают заметного влияния на СтСтГА, следовательно, кроме наличия, важна также природа газа электролиза.

Таблица

Степень стабилизации гидроксида алюминия в зависимости от условий обработки

№ п/п	Условия обработки	$C_{HCO_3^-}$ (ммоль/л)	Степень стабилизации, %
1	Гидроксид без обработки (контрольный)	0	34
2	Гидроксид ЭО в маточном растворе (графитовый анод)	27	94
3	Гидроксид ЭО в маточном растворе (платиновый анод)	0	35
4	Гидроксид в маточном растворе + бикарбонат натрия, без ЭО	27	61
5	Гидроксид ЭО в маточном растворе (платиновый анод) + HCO_3^-	27	64
6	ЭО гидроксида в маточном растворе (платиновый анод) + HCO_3^-	40	61
7	...„...„...„...„...„...„...	60	64
8	...„...„...„...„...„...„...	100	65
9	HCO_3^- получен электрохимически (графитовый анод) + $Al(OH)_3$	27	74
10	HCO_3^- получен электрохимически (графитовый анод)+$Al(OH)_3$	40	75
11	HCO_3^- получен электрохимически (графитовый анод)+$Al(OH)_3$	55	92
12	HCO_3^- получен электрохимически (графитовый анод) + удаление газа из раствора+$Al(OH)_3$	40	65
13	...„...„...„...„...„...„...	55	75

Исходная удельная поверхность гидроксида равна (400 ∓ 20) м²/г, отбор проб — через 15 суток старения в растворе

Карбонаты, полученные в эквивалентном количестве электрохимическим путем при электролизе маточного раствора с использованием графитового анода (оп. 9—11) дают гораздо более высокую СтСтГА, чем аналогичная концентрация бикарбоната натрия. Повышая концентрацию электрохимически полученного бикарбоната путем увеличения времени электролиза, можно достичь все более высокого значения СтСтГА (оп. 9—11), в то время, как повышение концентрации химически полученного карбоната практически не влияет на СтСтГА и она остается в пределах 60—65% (оп. 5—8). Подобное явление может быть связано с наличием в растворе большого количества оставшихся мельчайших пузырьков электролитического CO_2 (газового «тумана»), которые при последующем контакте с твердой фазой ГА оказывают активное действие. При удалении остатка углекислого газа барботированием через раствор гелия (оп. 12, 13) растворенные продукты электрохимического окисления графита оказывают приблизительно такое же стабилизирующее влияние, как и химически полученные (оп. 6,7). И лишь ЭО одновременно и жидкой и твердой фазы дисперсии ГА с использованием графитового анода (оп. 2) приводит к эффективной стабилизации (СтСтГА составляет 94%). Только в этих условиях совместно присутствуют факторы, обеспечивающие стабилизацию — растворенные карбонаты и газ электролиза CO_2. При этом вклад электролитических пузырьков CO_2 довольно значителен и составляет около 40%. Данное положение может быть объяснено, наряду с диспергирующим влиянием, также большой проникающей способностью, высокой дисперсностью и насыщенностью всего объема дисперсии пузырьками электролитического CO_2. Указанные условия способствуют максимальной адсорбции карбонатов поверхностью частиц геля гидроксида алюминия с образованием поверхностных гидроксокарбонатов, которые имеют электроповерхностные свойства, отличные от свойств исходного геля. А такие свойства геля, как вязкость, седиментационный объем, устойчивость частиц к коагуляции определяются состоянием поверхности частиц.[8] Из литературных источников известно, что адсорбция анионов поверхностью частиц геля гидроксида алюминия, в частности это касается карбонат-ионов, часто приводит к повышению кинетической стабильности геля.[9] По-видимому, подобный механизм имеет место и при электрохимической стабилизации гидроксидов. Дополнительный эффект вносит присутствие стабилизирующено агента — карбоната — в виде мелкодисперсных пузырьков электролитического газа CO_2. Именно в этом заключается специфика стабилизации гидроксидов при ЭО их дисперсий в бездиафрагменном электролизере с использованием графитового анода.

ЗАКЛЮЧЕНИЕ

Таким образом, исследовав вклад каждого из компонентов ЭО в стабилизацию гидроксидов, можно утверждать, что механизм электрохимической стабилизации гидроксидов основан на комплексном воздействии растворенных и газообразных продуктов электрохимического окисления графитового анода. Причем основной вклад принадлежит растворенным продуктам, а остальное стабилизирующее влияние достигается за счет газа электролиза CO_2.

ЛИТЕРАТУРА

[1] В. П. Чалый, «Гидрооксии металлов», «Наукова думка», Киев 1975.

[2] В. С. Комаров и И. Б. Дубницкая , «Физико-химические основы регулирования пористой структуры адсорбентов и катализаторов», «Наука и техника», Минск, 1981.

[3] В. М. Чертов, В. И. Зеленцов и И. Е. Неймарк, *Коллоидный журнал*, **33,** № 6, 926(1971).

[4] Н. Ф. Ермоленко и М. Д. Зфрос, «Регулирование пористой структуры окисных адсорбентов и катализаторов», «Наука и техника», Минск, 1971.

[5] М. А. Егоров, *Коллоидный журнал*, **23** № 6, 834 (1971).

[6] Т. Я. Дацко и В. И. Зеленцов, *Известия АН МССР, сер. химич. и биологич. наук*, № 5(1988).

[7] Г. Шарло, «Методы аналитической химии Количественный анализ неорганических соединений», «Химия», Москва, 1969.

[8] J. R. Feldcamp, D. M. Chan, S. L. Meyer, J. L. White and S. L. Hem, *J. Pharm. Sci.* **70,** N. 6,638(1981).

[9] C. J. Serna, J. L. White and S. L. Hem, *Soil Sci. Soc. Am.* J., **41,** 1009(1977)

Revue Roumaine de Chimie, 34, 5, 1169–1173 (1989)

HYDROQUINONE ELECTROSYNTHESIS FROM PHENOL

A. DEAKY, T. ŞIMANDAN, N. MIRICĂ, S. DRAGOŞ and M. MEDELEANU
ICECHIM-Institute of Chemical and Biochemical Energetics, Bucharest, Romania
Electrochemical Energetics Department Timişoara, Romania

Received November 5, 1988

The paper presents the results of laboratory works concerning the electrochemical synthesis of hydroquinone in uncompartmented electrolyzers with forced circulation of the electrolyte consisting of an acidified aqueous phenolic solution. Both electrode reactions are of interest and consist in anodic oxidation of phenol to *p*-benzoquinone and in quinone reduction to hydroquinone, respectively. The process occurs with a yield of transformation of $>85\%$ and a current efficiency of $>35\%$.

Electrochemical synthesis of hydroquinone shows many more advantages than the classical chemical methods. The most important advantage is the obtention of a relatively pure primary product practically free of isomers and other by-products. The economical effect induced by the simplicity of separation and purification exceeds the energy consumption increase during the synthesis.[1]

The major part of the known industrial methods use benzene or phenol as raw material.[2] The phenol method uses aqueous electrolyte and is performed in more favorable energetic conditions and with less complicated equipment.[3]

The experimental laboratory work tested the possibility to obtain hydroquinone directly from phenol, using uncompartmented electrolyzers, as well as to determine the proper conditions conducting to a selective process, at the maximum current efficiency.

The useful electrode reactions are :

$$(+)\qquad (C_6H_5){-}OH + H_2O - 4e \rightarrow O{=}(C_6H_4){=}O + 4\,H^+ \qquad (1)$$

$$(-)\qquad O{=}(C_6H_4){=}O + 2\,H^+ + 2e \rightarrow HO{-}(C_2H_4){-}OH \qquad (2)$$

$$(-)\qquad 2H^+ + 2e \rightarrow H_2 \qquad (3)$$

$$(C_6H_5){-}OH + H_2O \rightarrow HO{-}(C_6H_4){-}OH + H_2 \qquad (4)$$

It can be noticed that the total faradayc effort can be distributed over cathodic reactions (2) and (3).

In the absence of secondary reactions, the global reaction (4) provides a practical constant pH. Beside the obtention of isomers and of other by-products, secondary reactions of hydroquinone re-oxidation and oxygen evolution on the anode, respectively additional hydrogen evolution on the cathode are possible.

The experimental set-up used is shown in Fig. 1.

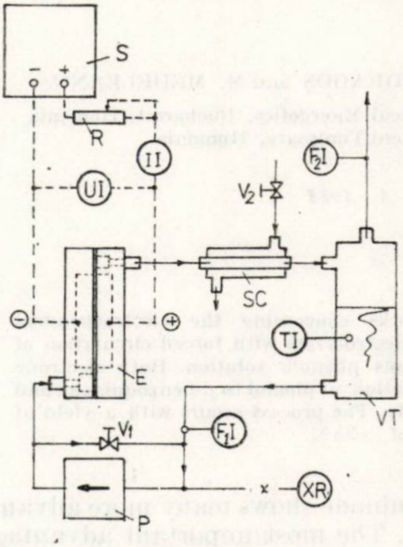

Fig. 1. — Experimental set-up.

The electrolyte pathflow includes: pump P, electrolyzer E, heat exchanger SC and buffer tank VT, acting also as a degasifier.

The electric supply is accomplished by the power supply S through the resistor R. The installation was equipped with measuring instruments for current (II), cell tension (UI), gas- and electrolyte flow (FI-1, FI-2), electrolyte temperature (TI) and organic composition (XR). The electrolyte composition was periodically determined by LLC, using MICROPACK MCH-10 column, methanol-aq. solvent 1 mL/min, UV detection at 254 nm.

The electrolyser is equipped with equal area plane electrodes, at small interelectrodic gap. The anode used was titanium supported lead dioxide and the cathode was stainless steel. The electrolyte having at start 2—4% phenol, 1—3% H_2SO_4, 0.05—0.4% $CuSO_4$, was continuously recirculated through the interelectrodic gap.

The preliminary attempts showed that, for avoiding side reactions and for increasing current efficiency, a suitable correlation between current density, interelectrodic gap and electrolyte flow rate is necessary.

It has been also determined that within this correlation range, the current efficiency can be optimised by suitable modification of electrolyte component concentrations.

In order to find the influence of H_2SO_4 and $CuSO_4$ concentration on reaction yield, series of electrosyntheses at an initial concentration of 3% phenol, 1000 A/m², 300 L/h electrolyte flow rate and an interelectrodic gap less than 1 mm, were performed. All these syntheses were carried out for cca. 30% of the total necessary time, the current efficiency being determined with the help of the phenol LLC peak area.

Fig. 2 shows the shape of a synthesis chromatogram.

The total absence of by-products is noticed, being present only quinone and hydroquinone.

Table 1 shows the *p*-benzoquinone peak area S_Q and the current efficiency η_c at different initial $CuSO_4$ concentrations C_{CuSO_4}, at a H_2SO_4 concentration of 3%.

Concomitantly with the minimum value of quinone concentration, corresponding to $C_{CuSO_4} = 0.2\%$, the current efficiency reaches the maximum.

A new series of experiments was carried out, maintaining the conditions above, using an optimal $CuSO_4$ concentration and varying the H_2SO_4 concentration in the range of 1—3%. The results are shown in table 2.

One remarks that electrolyte acidification determines a continuous growth of the current efficiency η_c concomitantly with the cell tension diminution.

Table 1

Influence of the copper sulphate concentration

C_{CuSO_4}, %	0.05	0.10	0.15	0.20	0.25	0.30	0.35
S_Q, cm^2	0.61	0.49	0.31	0.24	0.28	0.33	0.37
η_c, %	38.2	41.9	45.3	47.6	45.9	43.6	42.1

In the case of hydroquinone separation by extraction, the process performances testing is useful at a higher acidity.

In order to determine the global current efficiency and the specific power consumption, prolonged electrosyntheses were performed, until an advanced exhaustion of the electrolyte phenol.

Table 2

Influence of the sulphuric acid concentration

$C_{H_2SO_4}$, %	1	1.5	2	2.5	3
U, V	3.60	3.48	3.35	3.21	3.10
η_c, %	38.1	40.5	42.2	44.8	47.6

For illustration, Fig. 3 presents the data obtained in several LLC analyses of the organic components during a 4-hour reaction carried out in the conditions above, the initial composition of the electrolyte being: 3% phenol, 2% H_2SO_4 and 0.2% $CuSO_4$.

The process was developed always in conditions of selectivity for hydroquinone. The residual concentration of phenol is 0.39% corresponding to an exhaustion degree of 87%.

Fig. 4 presents the evolution in time of the global current efficiency η_{cg}, the momentary current efficiency η_{ci} and the cell tension U.

One observes a slow decrease of the global current efficiency from 42.1% to 37.5%, in the meantime the momentary current efficiency decreasing much more abruptly to 26.6%, at the end of the process. The cell tension decreased continuously during the process, thus moderating the growth of the specific power consumption.

Fig. 5 presents the evolution in time of the global power consumption E_S, as well as the ΔE_S and $-\Delta \eta_g$ variations expressed in percent of the initial values.

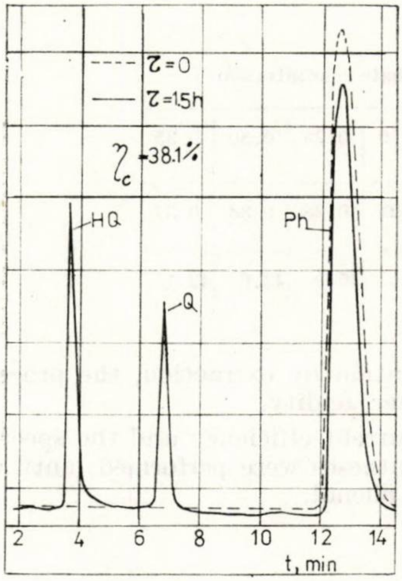

Fig. 2. — Organic components chromatogram at 1.5 h. 1 % H_2SO_4 : 0.2 % $CuSO_4$.

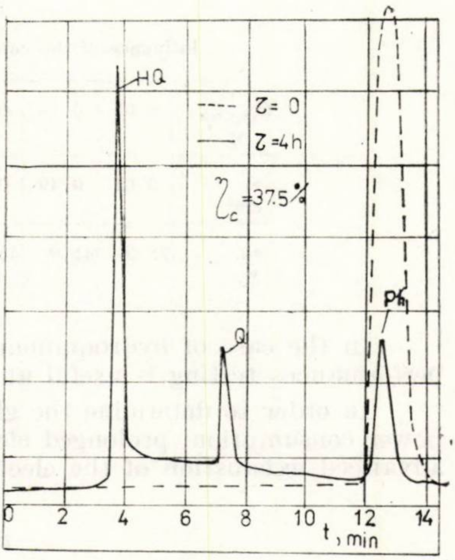

Fig. 3. — The chromatogram of a complete electrosynthesis.

The specific power consumption growth begins at about 180 min after the electrolysis is started, when the global current efficiency is 40.2 % and the phenol exhaustion degree is about 70%.

The optimal residual phenol content depends on the hydroquinone separation method, too. In the case of separation by extraction, the electrosynthesis process can be stopped at a phenol exhaustion degree of 70%.

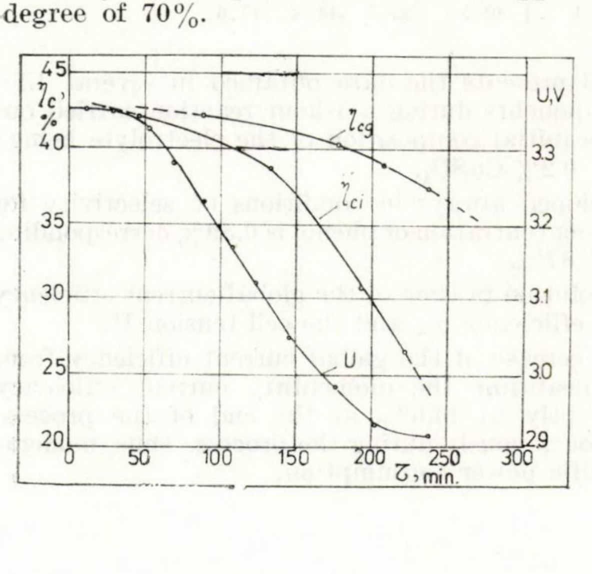

Fig. 4. — Evolution in time of the current efficiency and cell voltage.

The separation by concentration requires a more advanced exhaustion degree, about 80%. In this case the global specific power consumption increases with about 2%, but the possibility of phenol crystallization at the end of concentration is avoided.

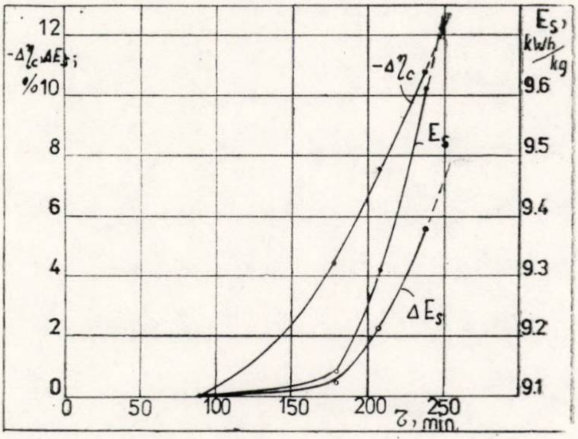

Fig. 5. — Evolution in time of the specific power consumption and ΔE_S, $-\Delta\eta_c$ variations.

The residual content of *p*-benzoquinone is less than 0.1% and requires a minimum reactant consumption for reduction to hydroquinone by chemical methods.

The data presented in the paper demonstrate the industrial applicability of the hydroquinone electrosynthesis from phenol in uncompartmented electrolyzers, with forced circulation of the electrolyte. Further research aims at process operation with higher current densities and a better correlation of the electric, hydraulic and geometrical parameters of the electrolyzer for improving the current efficiency.

REFERENCES

[1] M. Ya. Fioshin and V. A. Smirnov, "Organic Electrosynthesis", Khimiya, Moscow, 1976, 273–275.

[2] * * * "A. I. Ch. E. Symp. Ser.", 1981, 77, No. 204, 264–272.

[3] M. Ya. Fioshin and V. A. Smirnova, "Electrochemical Systems in the Chemical Products Synthesis", Khimiya", Moscow, 1986, 223.

Revue Roumaine de Chimie, **34**, 5, 1175–1182(1989)

MOLECULAR TOPOLOGY. I

VALENCE GROUP ELECTRONEGATIVITY AS A VERTEX DISCRIMINATOR

MIRCEA V. DIUDEA * and IOAN SILAGHI-DUMITRESCU
University of Cluj-Napoca, Faculty of Chemical Technology, Arany Janos Street, 11, 3400 Cluj-Napoca, Romania

Received October 17, 1988

On the basis of the Sanderson group electronegativities (S), a new approach to the heteroatom problem in molecular topology is proposed. Thus, a Randić type topological index (DSI) is derived, which correlates well with physical and biological properties in series of alcohols, amines and halogeno-derivatives.

INTRODUCTION

It is well known [1–4] that a molecular structure may be represented by a molecular graph (G), wherein the vertices are atoms and the edges stand for covalent bonds. Many topological indices (TI's) have been proposed to convert chemical structures into numerical values useful for quantitative structure-property relationship (QSPR) or quantitative structure – activity relationship (QSAR) studies. A synopsis of TI's is available in ref. [3]

Among the TI's, the Randić's connectivity χ index is the simplest one and, in the extended form indicated by Kier and Hall [2] (see below) has found numerous applications to QSAR (local anesthetics[5], hallucinogenic activity of amphetamines[6], mutagenicity of nitrosamines[7], etc.) and QSPR studies (boiling points, heat of atomization and formation, molar refraction, polarizability[2], etc.) (see also [4,8,9]).

THE HETEROATOM QUESTION

Randić [1] calculated χ_R by eq. 1 :

$$\chi_R = \sum_{\text{all edges}} (v_i v_j)^{-1/2} \tag{1}$$

where v_i is the degree (connectivity) of vertex i in the hydrogen depleted graph, and equals the sum of all entries of i-th row in the adjacency matrix

---

* Author to whom all correspondence should be addressed.

A of G. The entries a_{ij} of $\mathbf{A}(G)$ have the value 1 if i, j-atoms are connected (adjacent), otherwise are zero. As examples, two test molecules, isopentane ($G1$ and t-butanol ($G2$), are given below:

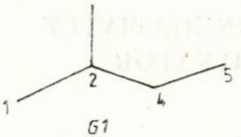

$\underset{\sim}{G1}$

$$\mathbf{A}(G1) = \begin{array}{c|ccccc|c} & 1 & 2 & 3 & 4 & 5 & v_i \\ 1 & 0 & 1 & 0 & 0 & 0 & 1 \\ 2 & 1 & 0 & 1 & 1 & 0 & 3 \\ 3 & 0 & 1 & 0 & 0 & 0 & 1 \\ 4 & 0 & 1 & 0 & 0 & 1 & 2 \\ 5 & 0 & 0 & 0 & 1 & 0 & 1 \end{array}$$

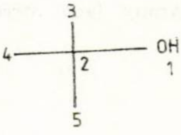

$\underset{\sim}{G2}$

$$\mathbf{A}(G2) = \begin{array}{c|ccccc|cc} & 1 & 2 & 3 & 4 & 5 & v_i & \delta_i^v \\ 1 & 0 & 1 & 0 & 0 & 0 & 1 & 5 \\ 2 & 1 & 0 & 1 & 1 & 1 & 4 & 4 \\ 3 & 0 & 1 & 0 & 0 & 0 & 1 & 1 \\ 4 & 0 & 1 & 0 & 0 & 0 & 1 & 1 \\ 5 & 0 & 1 & 0 & 0 & 0 & 1 & 1 \end{array}$$

In the initial form[1] (eq. 1), χ_R did not account for the chemical nature of atoms. For the graph $G1$, ${}^1\chi_R = 2(1 \times 3)^{-1/2} + (3 \times 2)^{-1/2} + (2 \times 1)^{-1/2} = 2.270$.

Kier and Hall[2] extended the connectivity concept considering the edge as the simplest case of a path length l (edge: $l = 1$) and extending the summation in eq. 1 over all possible paths of length l:

$$ {}^l\chi = \sum_{\text{paths}} (v_i v_j \ldots v_{l+1})^{-1/2} \qquad (2)$$

Indices ${}^l\chi_R$ of order higher than three are expected to bring small contributions to the molecular properties and, therefore, have been used only in particular cases (see ref.[2,8]).

In order to discriminate the chemical nature of atoms (vertices), Kier and Hall[2] have proposed the δ_i^v (valence delta values) instead of v_i values, according to eq. 3:

$$\delta_i^v = Z_i^v - H_i \qquad (3)$$

Z^v and H_i are the number of valence electrons of the i-atom, and respectively the number of hydrogen atoms attached to this atom. In the graph $G2$, $\delta_1^v = 5$ ($Z_1^v = 6$; $H_1 = 1$). For atoms beyond the second row in the Periodic System, the expression leading to δ_i^v is modified as in eq. 4 (see ref.[4,8,9]):

$$\delta_i^v = \frac{Z_i^v - H_i}{Z_i - Z_i^v} \qquad (4)$$

where Z_i is the atomic number of atom i. The new index χ^v is given by eq. 5:

$$ {}^l\chi^v = \sum_{\text{paths}} (\delta_i^v \delta_j^v \ldots \delta_{l+1}^v)^{-1/2} \qquad (5)$$

For $G2$, ${}^1\chi^v = (5 \times 4)^{-1/2} + 3(4 \times 1)^{-1/2} = 1.724$. The Z_i number was also used by Trinajstić et al.[10] For other attempts in this regard see [11].

An important contribution in resolving the heteroatom question was performed very recently by Balaban.[11] The author considered the electronegativities S_i, as recalculated by Sanderson [12] on Pauling's scale, with fluorine having the value 4 and hydrogen 2.592. In order to account for the periodicity of the main properties of heteroatoms, Balaban linearized Sanderson's [12] electronegativities (by using Z_i and G_i = the number of the group in Mendeleev's short form of the periodic chart, as adjusting parameters). Moreover, he divided the linearized S_i values by the calculated value for carbon electronegativity (2.629), thus obtaining non-dimensional relative electronegativities with carbon as a standard. These relative electronegativities (available in ref.[11]) were used to multiply the heteroatom distance sums in the calculation of J index[11]. This approach thus provides a good tool for discriminating the chemical graphs according to the chemical nature of their vertices.

VALENCE GROUP ELECTRONEGATIVITIES

Although Balaban's approach contributes to solving the heteroatom question, the linearized electronegativities do not account for the heteroatoms in the valence state. Moreover, the carbon atoms in different valence states (connections) have not the same value of electronegativity (see [13]).

According to Sanderson's electronegativities equalizing principle[14], we considered here the geometric mean of atomic electronegativities of the atoms belonging to the same vertex, as a vertex (group) electronegativity. This means that the hydrogen atoms should be taken into account in the molecular graph. The consideration of hydrogen atoms in molecular topology has a precedent just in the Kier and Hall's approach [2] for heteroatoms (see eq. 3).

Thus, the group electronegativities may be calculated according to eq. 6 :

$$S_{i,\,\mathrm{group}} = (S_{A,i} \times S_H^{H_i})^{1/(1+H_i)} \tag{6}$$

where $S_{A,i}$ and S_H are Sanderson's [12] electronegativities for the atom A_i and hydrogen, respectively. H_i has the above mentioned significance, and may be calculated by eq. 7 :

$$H_i = (8 - G_{A,i}) - v_i \tag{7}$$

where $G_{A,i}$ is the number of the group in the short form of the periodic chart, and v_i is the degree of vertex i. When $v_i > (8 - G_{A,i})$ then by definition $H_i = 0$. When multiple bonds appear in G, then v_i should be replaced by $\sum^{j} b_{ij}$ = sum of the bond orders on A_i. Subsequently, we will limit ourselves to single bonds in connected graphs.

Taking into account both $S_{i,\,\mathrm{group}}$ and the adjacency of the i-vertex, we may now define the valence (group) electronegativity S_i for the vertex i as in eq. 8 :

$$S_i = (S_{i,\,\mathrm{group}})^{1/(1+v_i)} \tag{8}$$

S_i may be used as a vertex discriminator in a Randić type index, eq. 9

$$ {}^{l}\mathrm{DSI} = \sum_{\mathrm{paths}} (S_i S_j \ldots S_{l+1})^{-1/(l+1)} \qquad (9)$$

Note that both S_i and DSI represent geometric means of the component electronegativities : for S_i we assumed that vertex i is connected to atoms with hypothetical electronegativity equal to unity.

As above mentioned, the most used order for ${}^{l}\mathrm{DSI}$ is $l = 1$, and the expression (9) reduces to :

$$\mathrm{DSI} = \sum_{\mathrm{all\ edges}} (S_i S_j)^{-1/2} \qquad (10)$$

Subsequently, we tested the ability of DSI to correlate with physical and biological properties in a selected group of alcohols. The considered properties were molar polarizability (α), and non-specific local anesthetic activity (as log MBC = log of the minimal nerve blocking concentration). Molecular polarizability is related to the intermolecular London forces (or dispersion interactions) important in drug — receptor interactions, as well as in processes of partition between water and an organic phase. Table 1 lists the experimental and calculated values for the considered properties and ${}^{1}\chi$ and DSI indices, calculated for the alcohols. Statistics of the QSAR — QSPR studies are given in Table 2. Although this is not a severe test for DSI, one can see its usefulness in predicting some of the properties, alone or in correlation with ${}^{1}\chi$. The intercorrelation value between the two indices was here 0.9981.

Table 1

Polarizability and local anesthetic activity of alcohols

No.	Compound	α[a]	log MBC[b]	${}^{1}\chi$	DSI	α calcd. by DSI	log MBC calcd. by		
							${}^{1}\chi$	DSI	${}^{1}\chi$ & DSI
1	Ethanol	12.9	2.75	1.414	1.310	12.875	2.809	2.866	2.785
2	Isopropanol	17.6	2.55	1.732	2.057	17.649	2.489	2.320	2.550
3	n-Propanol	17.5	2.40	1.914	2.034	17.502	2.291	2.337	2.272
4	n-Butanol	22.1	1.78	2.414	2.757	22.123	1.774	1.809	1.760
5	n-Pentanol	26.8	1.20	2.914	3.481	26.750	1.256	1.280	1.247
6	n-Hexanol	31.4	0.56	3.414	4.205	31.377	0.738	0.751	0.735
7	n-Heptanol	36.0	0.20	3.914	4.928	35.998	0.220	0.223	0.222
8	n-Octanol	40.6	−0.16	4.414	5.652	40.625	−0.297	−0.306	−0.290

[a] from ref.[2]; [b] from ref.[15]

Table 2

Statistics of QSPR/QSAR studies on alcohols (N = 8)

Topological index	Property	R	a	b	s	F	T	EV
${}^{1}\chi$[a]	α	0.9982	0.6595	9.0204	0.5772	717.1	37.8	0.9959
DSI	α	0.9999	4.5026	6.3911	0.0321	232530.0	681.9	0.9999
${}^{1}\chi$	logMBC	0.9958	4.2772	−1.0365	0.1030	296296.9	24.4	0.9902
DSI	logMBC	0.9923	3.8229	−0.7305	0.1392	161.5	17.9	0.9822
${}^{1}\chi$ & DSI	logMBC	0.9961	4.46837	−1.4856 0.3182	0.0986	172.8	22.7	0.9892

[a] calculated values for α not given

The next example is a list of 15 halogenoderivatives *vs.* molar refraction, MR (Table 3). Because of the mixed character of list, the correlation is not good but on selecting e.g. bromo-derivatives (entries 4 to 9) the following QSPR was obtained:

$$\mathrm{MR} = 7.0284\ \mathrm{DSI} + 11.1638 \tag{11}$$

$$(N = 6;\ R = 0.9998;\ s = 0.0746;\ F = 10981.4;\ T = 104.7)$$

In a list of 20 amines (Table 4), DSI showed a good correlation *vs.* MR, in a single variable regression. A similar good result was found for a set of 31 alcohols (Table 5).

Table 3

Molar refraction of halogenoderivatives

No.	Compound	DSI	MR obs.	MR calcd.	Statistics
1	1-Chloropropane	2.014	20.847	22.3322	$R = 0.9422$
2	1-Chloro-2-methylpropane	2.764	25.360	28.9366	$s = 2.6760$
3	3-Chloropentane	3.488	30.161	35.3042	$F = 102.7$
4	2-Bromopropane	2.051	23.935	22.8385	$T = 10.1$
5	1-Bromopropane	2.028	23.679	22.6360	$a = 4.7764$
6	2-Bromobutane	2.775	28.651	29.2131	$b = 8.8047$
7	1-Bromo-2-methylpropane	2.777	28.537	29.2246	
8	1-Bromobutane	2.750	28.347	28.9912	
9	3-Bromopentane	3.501	33.068	35.6036	
10	2-Iodobutane	2.800	33.940	29.4297	
11	3-Iodopentane	3.526	38.354	35.8211	
12	2-Iodopentane	3.524	38.314	35.8008	
13	1-Iodopentane	3.498	38.264	35.5710	
14	1-Iodohexane	4.221	42.891	41.9421	
15	1-Iodoheptane	4.945	47.610	48.3132	

Table 4

Molar refraction of amines

No.	Compound	DSI	MR obs. [a]	MR calcd.	Statistics
1	Trimethylamine	2.037	19.595	19.2368	$R = 0.9992$
2	1-Aminopropane	2.050	19.401	19.3201	$s = 0.2912$
3	2-Amino-2-methylpropane	2.829	24.257	24.3906	$F = 11537.3$
4	1-Aminobutane	2.774	24.079	24.0326	$T = 107.4$
5	1-Amino-2,2-dimethylpropane	3.557	28.471	29.1291	$a = 5.9767$
6	1-Amino-3-methylbutane	3.524	28.672	28.9143	$b = 6.5089$
7	3-Aminopentane	3.526	28.617	28.9273	
8	Dipropylamine	4.210	33.515	33.3794	
9	1-Aminopentane	3.498	28.728	28.7451	
10	Diisopropylamine	4.262	33.641	33.7179	
11	Butyldimethylamine	4.209	33.816	33.3729	
12	Trimethylamine	4.211	33.794	33.3860	
13	Butylethylamine	4.210	33.452	33.3794	
14	1-Aminohexane	4.221	33.290	33.4510	
15	Dimethylpentylamine	4.933	38.281	38.0854	
16	2-Aminoheptane	4.971	38.038	38.3328	
17	1-Aminoheptane	4.945	38.003	38.1635	
18	Diisobutylamine	5.713	42.920	43.1624	
19	Dimethylisobutylamine	4.238	33.852	33.5617	
20	Tripropylamine	6.382	47.783	47.5169	

[a] from ref.[2]

Table 5

Molar refraction of alcohols

No.	Compound	DSI	MR		Statistics
			obs.$^{a)}$	calcd.	
1	Isopropanol	2.057	17.705	17.5649	$R = 0.99951$
2	n-Propanol	2.034	17.529	17.4197	$s = 0.24614$
3	2-Methyl-1-propanol	2.784	22.103	22.1522	$F = 29656.7$
4	n-Butanol	2.757	22.067	21.9818	$T = 172.2$
5	2-Methyl-2-butanol	3.539	26.722	26.9161	$a = 4.5854$
6	2-Pentanol	3.506	26.680	26.7079	$b = 6.3099$
7	3-Methyl-1-butanol	3.508	26.904	26.7205	
8	2-Methyl-1-butanol	3.510	26.697	26.7332	
9	n-Pentanol	3.481	26.801	26.5502	
10	3-Pentanol	3.509	26.618	26.7268	
11	2-Methyl-2-pentanol	4.262	31.211	31.4782	
12	3-Methyl-3-pentanol	4.266	31.183	31.5034	
13	4-Methyl-2-pentanol	4.257	31.351	31.4466	
14	4-Methyl-3-pentanol	4.260	31.138	31.4656	
15	4-Methyl-1-pentanol	4.231	31.489	31.2826	
16	2-Methyl-1-pentanol	4.233	31.164	31.2952	
17	2-Ethyl-1-butanol	4.236	31.180	31.3141	
18	n-Hexanol	4.205	31.429	31.1185	
19	2,4-Dimethyl-3-pentanol	5.011	35.675	36.2043	
20	3-Ethyl-3-pentanol	4.993	35.822	36.0907	
21	2-Methyl-1-hexanol	4.957	35.931	35.8636	
22	n-Heptanol	4.928	36.094	35.6806	
23	2-Methyl-2-heptanol	5.710	40.899	40.6149	
24	3-Methyl-3-heptanol	5.713	40.447	40.6338	
25	4-Methyl-4-heptanol	5.713	40.439	40.6338	
26	6-Methyl-1-heptanol	5.678	40.737	40.4130	
27	2-Ethyl-1-hexanol	5.683	40.625	40.4446	
28	n-Octanol	5.652	40.638	40.2489	
29	2,6-Dimethyl-4-heptanol	6.456	45.521	45.3221	
30	2-Methyl-2-octanol	6.433	45.207	45.1770	
31	4-Ethyl-4-heptanol	6.440	44.920	45.2211	

COMPUTER PROGRAM

The above procedure for calculating DSI index was coded into a small superBasic computer program. The adjacency matrix is introduced from the keyboard at line 220, by subroutine AINP. The dialogue with this subroutine must end with a −9, 0, 0 sequence. The same program line directs to the printing of A matrix for a final checking. The next input requires the atomic number of elements. These are needed to access the Sanderson electronegativities file which has been read in at lines 140−180. The degree of vertex i, the number of valence electrons Z_i^v, and H_i are then calculated and finally DSI displayed.

```
100 CLS 2: CLS 0
110 Restore
120 DIM ga(100), sa(100), h(50), d(100)
130 i=0
140 REPeat reading
150 i=i+1:READ ss
```

```
160 if ss=−9 then exit reading
170 sa(i)=ss
180 end repeat reading
190 Input “MOLECULE:”; t$
200 Input ‘ Nr. of atoms”; na
210 dim a(na, na), v(na), s(na)
220 ainp:matip a, t$
230 Print “INPUT at. nr. of elements”
240 for i=1 to na
250 Print i; : Print “ga(“;i;”)=”;: Input ga(i)
260 next i
270 For i=1 to na
280 v(i)=0
290 For j=1 to na
300 if a(i, j) > 0 then v(i)=v(i) + a(i, j)
310 next j
320 ng=ga(i)
330 ng=group(ng)
340 h(i)=8−ng−v(i)
350 if h(i) < 0 then h(i)=0
360 ng=ga(i)
370 s(i)=(sa(ng)*(sa(1))∧ h(i)) ∧ (1/(1+h(i)))
380 d(i)=(s(i))∧(1+v(i)))
390 next i
400 id=0
410 for i=1 to na
420 for j=i to na
430 if a(i, j)<>0 then id=id+(d(i)  *d(j))∧(−0.5)
440 next j
450 next i
460 Print:Under 1
470 print t$: Under 0
480 Print “DS INDEX=”; id
490 Input “Other case? (y/n)”; c$
500 if c$=“y” or c$=“Y” then run
510 stop
540 Define function group(ng)
550 gp=ng−2
560 if gp < 0 then ret ng
570 gg=gp−8
580 if gg < 0 then ret gp
590 end define
600 Define procedure ainp
610 Local i,j, aij
630 Repeat ainput
640 input “i=”;i: input “j”;j: input”a(i,j)=”; aij
640 if i<=na and j<=na and i>0 and j>0 then a(i,j)=aij:
     next ainput
650 if i=−9  then
660 exit ainput
670 else
680 Print “The last element is incorrect”
690 Print “Check it!”
700 end if
710 end repeat ainput
720 end define
730 Define procedure matip(a,t$)
740 under 1
750 Print t$: Under 0: Print
760 for i=1 to na
770 for j=1 to i: print! a(i,j)!
780 print
790 next i
```

```
800 Print
810 Print "Is it correct (y/n)": Input c$
820 if c$="n" or c$="N" then ainp
830 end define
840 data 2.592,0,0,0
850 data 2.275,2.746,3.194,3.654, -9
```

ACKNOWLEDGEMENTS. We are deeply indebted to professor A. T. Balaban (Polytechnic Institute — Bucharest) and to professor Z. Simon (Institute of Medicine — Timişoara) for helpful discussions.

REFERENCES

[1] M. Randić, *J. Amer. Chem. Soc.*, **97**, 6609 (1975).
[2] L. B. Kier and L. H. Hall, "Molecular Connectivity in Chemistry and Drug Research", Acad. Press, New York, 1976.
[3] A. T. Balaban, I. Moţoc, D. Bonchev and O. Mekenyan, "Topological Indices for Structure—Activity Correlations", *Topics in Current Chemistry*, **114**, 21(1983).
[4] A. Sabljić and N. Trinajstić, *Acta Pharm. Jugosl.*, **31**, 189 (1981).
[5] L. B. Kier, L. H. Hall, W. J. Murray and M. Randić, *J. Pharmacol. Sci.*, **64**, 1971 (1975).
[6] L. B. Kier and L. H. Hall, *J. Med. Chem.*, **20**, 1631 (1977).
[7] L. B. Kier, R. J. Simons and L. H. Hall, *J. Pharmacol. Sci.*, **67**, 725 (1978).
[8] A. Sabljić, *J. Chromatogr.*, **314**, 1 (1984).
[9] A. Sabljić and M. Protić, *Chem. Biol. Interact.*, **42**, 301 (1982).
[10] M. Barysz, G. Jashari, R. S. Lall, V. K. Srivastava and N. Trinajstić, in "Chemical Applications of Graph Theory and Topology", R. B. King ed., Elsevier, Amsterdam, 1983, pp. 222.
[11] A. T. Balaban, *Math. Chem.*, **21**, 115 (1986).
[12] **R. T. Sanderson, "Polar Covalence", Academic Press, New York, 1983, p. 41.**
[13] R. T. Sanderson, "Chemical Bonds and Bond Energy", Academic Press, New York, 1971.
[14] R. S. Mulliken, *J. Chem. Phys.*, **46**, 497 (1949).
[15] D. Agin, L. Hersh and D. Holtzman, *Proc. Nat. Acad. Sci.*, **53**, 952 (1965).

Revue Roumaine de Chimie, **34**, *5*, 1183–1193 (1989)

REARRANGEMENT OF 4-ALKYL-3-(*o*-CARBOXYPHENYL)SYDNONES TO 1-ACYL-1,2-DIHYDRO-3*H*-INDAZOL-3-ONES *

FLOREA DUMITRAŞCU and DAN RĂILEANU
Organic Chemistry Center — ICECHIM, 202 B, Spl. Independenței 78100 Bucharest, Romania

Received August 22, 1988

The thermolytic rearrangement of 4-alkyl-3-(*o*-carboxyphenyl)sydnones (**1a**—**c**) to 1-acyl-3-indazolones (**2a**—**c**) in various solvents or neatly is described. The temperature was in the range 100°—160°. In acetic anhydride 3-acetoxy-1-acylindazoles (**5a**—**b**) resulted. The 4-unsubstituted 3-(*o*-carboxyphenyl)sydnone **1d** did not react under these conditions. A more drastic treatment led to 3-indazolone (**4**). The ^1H—NMR spectra of **2a**—**b** and **4** showed them to exist in Py—d_5 under the keto form. The rearrangement mechanism involves a proton transfer from the carboxyl group to the sydnone ring. Acetylenedicarboxylic ester reacted normally with sydnones **1a**, **d** affording in both cases the corresponding pyrazoles **13a**, **d**. However, in refluxing xylene the rearrangement became predominant in the case of **1a**.

To our knowledge no thermal rearrangement of relatively low energy has been observed in the case of sydnones. Nevertheless photochemical rearrangements of excited states of sydnones have been much discussed.[1]

It has been found now that neat 3-(*o*-carboxyphenyl)-4-methyl sydnone (**1a**) by simple heating to its melting point (162°) rearranges to 1-acetyl-3-indazolone (**2a**) in theoretical yield. The reaction took place with CO_2 elimination. In boiling acetic acid, benzonitrile or water, the same transformation occurred although the yields were somewhat lower (Table 1). The 1-acetyl-3-indazolone (**2a**) was identified by its transformation into 1-acetyl-3-methoxyindazole (**3**).[2] In aniline the rearrangement was accompanied by a transacylation reaction with formation of 3-indazolone (**4**).

It has also been found that the sydnone **1a** in refluxing acetic anhydride leads to 3-acetoxy-1-acetylindazole (**5a**). In order to ascertain the intramolecular origin of the N-acetyl group the reaction was also carried out in propionic anhydride when 1-acetyl-3-propionyloxyindazole (**6**) resulted.

The starting material for synthesis of **1a** was the N-(*o*-carboxyphenyl)-N-nitrosoalanine (**7a**). The reaction took place in acetic anhydride at 70°. This was a modification of the method of Eade and Earl[3]-

---

* The abbreviated form "3-indazolone" will be used throughout this work instead of 1,2-dihydro-3*H*-indazol-3-one and 3-indazolinone.

which gave 3-(*o*-carboxyphenyl) sydnone (**1d**) with an yield of 47% improved now to 75% and which attained 70% in the case of sydnone **1a**. In refluxing acetic anhydride both **1a** and **7a** gave **5a**.

Starting from N-(*o*-carboxyphenyl)-2-ethyl-N-nitrosoglycine (**7b**) and its 2-butyl analogue (**7c**) the corresponding 4-ethylsydnone **1b** and 4-butylsydnone **1c** were obtained which could be further transformed into 1-propionyl- and 1-valeryl-3-indazolone (**2b**—**c**). Both **1b** and **7b** in acetic anhydride at reflux gave 1-propionyl-3-acetoxyindazole (**5b**).

CHART I

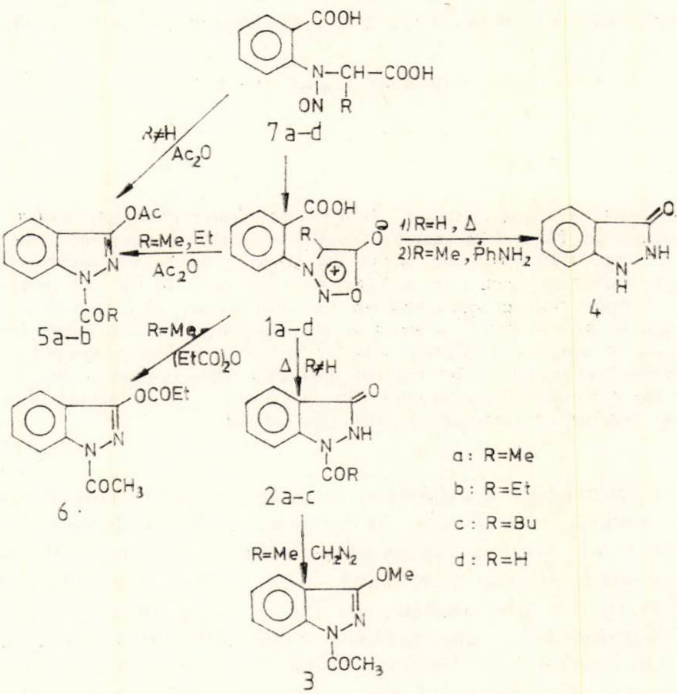
COOH
N—CH—COOH
ON R
7 a–d
R≠H
Ac₂O
OAc
R=Me, Et
Ac₂O
COR
5a–b
COOH
R
1) R=H, Δ
2) R=Me, PhNH₂
O
NH
H
4
1a–d
R=Me
(EtCO)₂O
OCOEt
COCH₃
6
Δ
R≠H
O
NH
COR
2a–c
a : R=Me
b : R=Et
c : R=Bu
d : R=H
R=Me
CH₂N₂
OMe
COCH₃
3

Table 1

Rearrangement of **1a** to **2a** in various media

Medium	Yield %	Conditions
neat	100	vacuum sublimation at the melting point
AcOH	90	reflux 30 min
PhCN	85	short heating near the boiling point
water	55	one hr reflux

The method proved to be of preparative value for the 1-acyl-3-indazolones **2a**—**c**. The known methods[4] of synthesizing these compounds imply the cyclization of *o*-(1-acylhydrazino) benzoic acids which are difficult to obtain while some confusion exists concerning the direct acylation of 3-indazolones. On the other hand the selective hydrolysis of 3-acetoxy-1-acetylindazole (**5a**) is rather difficult to conduct, the given yield starting from 3-indazolone being of 47%.[5]

It is important to point out that the 4-unsubstituted sydnone **1d** did not rearrange in refluxing acetic anhydride, acetic acid or water, **1d** being recovered unchanged. On refluxing for three hours in benzonitrile moderate amounts of impure deformylated 3-indazolone (**4**) were isolated. Better results were obtained when sydnone **1d** was submitted to vacuum sublimation at 200° just under its melting point when yields rose to about 60%. The reaction was accompanied by decarbonylation of the formyl group. The same phenomenon occurred when we tried to obtain 2-formyl-3-indazolone (**9**) by cyclization of the *o*-(2-formylhydrazino)benzoic acid (**8**) at room temperature in Ac_2O—Py. The reaction product was the deformylated indazole **5a**. Evolution of gas could be observed. Similarly when the 1-formyl-3-indazolone (**12**) obtained from 3-indazolone and formic acid was heated above its melting point (170°), the starting material **4** was recovered. Comparatively 3-acetoxy-1-formylindole (**11a**) and 3-acetoxy-1-formyl-2-methylindole (**11b**) could be obtained at reflux of Ac_2O—NaOAc by the cyclization of N-(*o*-carboxyphenyl)-N-formylglycine (**10a**) and of N-(*o*-carboxyphenyl)-N-formylalanine (**10b**) respectively. However the N-formylindoxyl[6] proved to be a quite unstable compound, its synthesis and purification being conducted under rigorous exclusion of oxygen.

CHART II

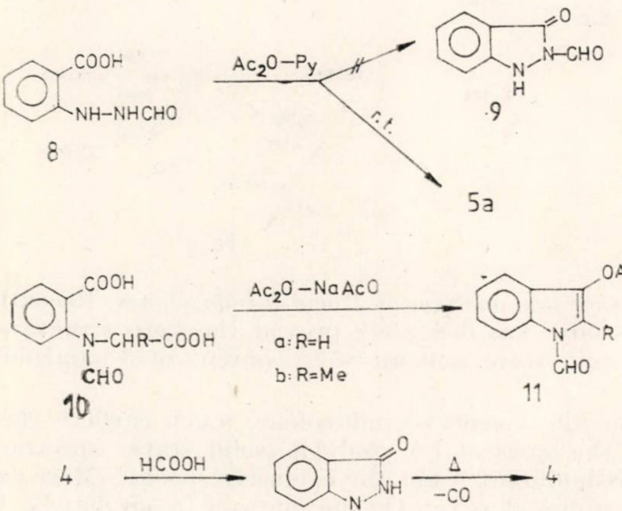

The difference of reactivity between 4-unsubstituted- (**1d**) and the 4-alkylsydnones **1a**—**c** was also ostensible in the case of the 1,3-dipolar cycloaddition of acetylenedicarboxylic ester (DMAD). The 4-methylsydnone **1a** in refluxing benzene led to the expected pyrazole **13a** while in refluxing xylene the rearrangement product, namely the indazolone **2a** was formed. Therefore the free energy of activation is higher in the latter case as well as the rate constant. When the 4-unsubstituted sydnone **1d** was submitted to the same reaction conditions, the corresponding pyrazole **13d** resulted in both cases.

CHART III

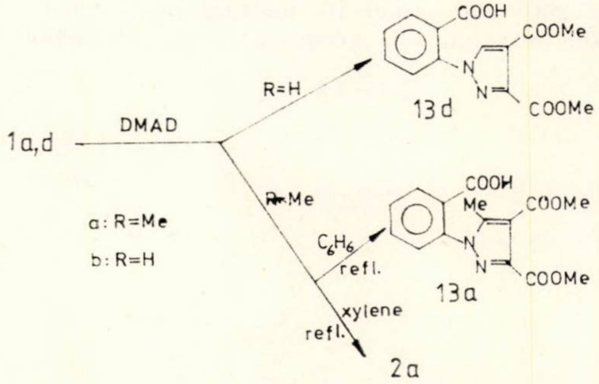

The keto-enol tautomerism of 1-acyl-3-indazolones. Recently an X-ray and ^{1}H-NMR study[7] has definitely proved the keto structure of 3-indazolone in the solid state and an 85% content of 3-indazolol in DMSO solution.

Concerning the 1-acetyl-3-indazolone, much earlier[2] the conclusion was drawn on the basis of UV and IR (solid state) spectra of the enol as being the predominant if not the exclusive species. More recent studies have not been published as yet. On the contrary in our hands the 1-acyl-3-indazolones, namely **2a**—**b** in Py-d_5 solution, on the ^{1}H-NMR scale of magnitude proved themselves to be exclusively in the keto form. Two well-resolved doublets were separated by deshielding from the rest of the aromatic protons (Fig. 1). The strongly deshielded double doublet (δ 8.75 for **2b** and 8.72 for **2a**) was ascribed to the 7-H proton on the basis of the preferred conformation **2A** (Chart 4). It could be observed also in the case of the 1-acyl-3-acyloxyindazoles (**5a**—**b** and **6**) and of the 1-acetyl-3-methoxyindazole (**3**). The second doublet which is less deshielded pertains to the 4-H proton as being adjacent to the 3-CO double bond (δ 8.02 and 8.03 for **2a**—**b** respectively). This implies a planar structure for the five-membered ring. As a matter of fact an envelope conformation can be excluded by the strongly polarized lactam structure as can be inferred from the ^{1}H-NMR peaks of 2-NH at δ 13.10 and 13.68 for **2a**—**b** respectively. As model compounds we can take into account **14**,[8a] **15**[8b] and **16**[9a] which exhibit similar deshieldings for the corresponding protons. Contrary to our expectation, also the parent compound

3-indazolol (**4**) proved itself to exist in d_5-Py solution under its lactamic form. A doublet at δ 8.20 corresponds to the 4-H which is deshielded by the adjacent 3-CO group. No such down-field absorptions are displayed by model compounds containing a C=N bond, part of a ring or not, adjacent to an aromatic proton, for example : isoquinoline, [8c] 2,3,3-trimethylindolenine [9b] and oxime **17**. [8d]

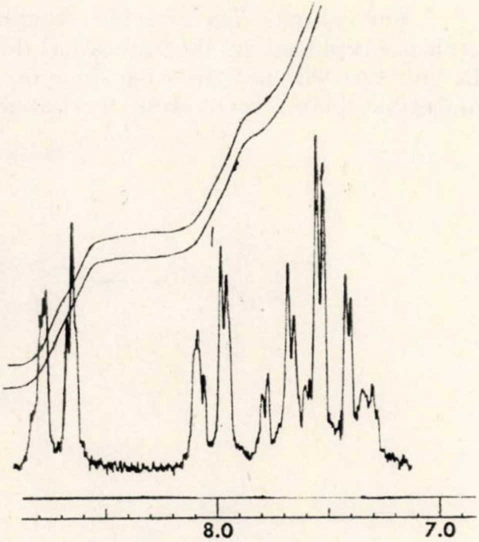

Fig. 1. — ^{1}H-NMR spectrum of 1-acetyl-3-indazolone (**2a**) at 60 MHz.

CHART IV

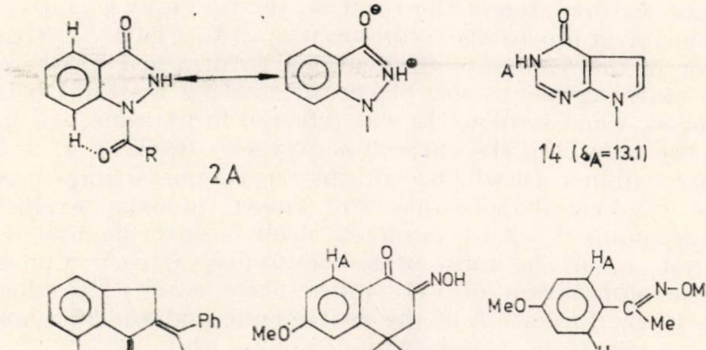
H
O
NH
N
H
O
R
2A
O⊖
NH⊕
N
O
A
HN
N
N
14 (δA=13.1)
Ph
HA
O
HB
15 (δA=7.92)
HA
O
NOH
MeO
Me
Me
16 (δA=8.17)
HA
N–OMe
MeO
C
Me
HA'
17 (δA,A'=7.58)

Reaction mechanism. The presence of a readily transferable carboxylic proton rules out the possibility either of an intramolecular cycloaddition of the carbonyl group to the 1,3-dipolar sydnone or of an electrocyclic reaction with formation of a transient 1*H*-diazirine intermediate.

This would mean a photoinduced-allowed electrocyclic disrotatory ring closure of the sydnone to form a bicyclic diaziridine in accordance with the allowed reaction predicted for the parent hydrocarbon, the bicyclo [2.1.0] pent-2-ene.[10] However it is known that isoelectronic substitution, namely CH replaced by N, O^+, etc., in the molecular framework may favor allowed thermal reactions in some cases in contrast to the parent hydrocarbon. Consequently in that case an electrocyclic reaction which occurs readily by a photoinduced disrotatory path may take place but with some difficulty, *via* a thermal path,[11] for example in our case the heating of **1a** at 160°.

The above mechanisms should operate also when the carboxyl group is replaced by its functional derivatives : ester, amide or hydrazide. In fact this was not the case since no rearrangement occurred, the starting materials being recovered unchanged.

CHART V

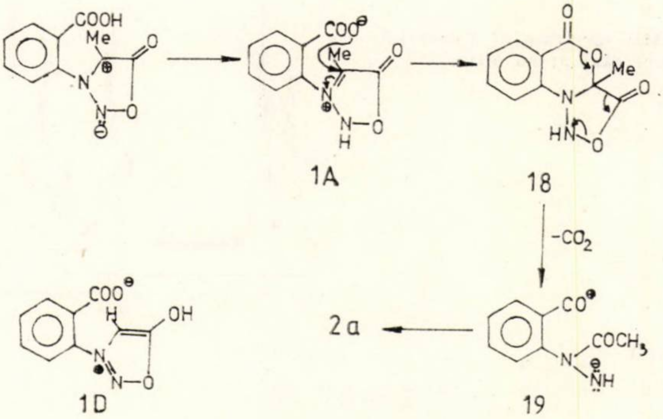

Therefore the first step of the reaction should imply a proton transfer from the carboxyl group to the sydnone ring (**1A**; Chart 5). Strong evidence in favor of this course of the reaction is furnished by the observation that no rearrangement took place, the starting material being recovered unchanged, when sydnone **1a** was refluxed in pyridine, a good proton acceptor. In the next step the carboxylic oxygen attack at 4—C leads to an intermediate adduct **18** which contains an oxazinone ring fused to an oxadiazolone. 1,2,3-Oxadiazol-5-ones are known to exist exclusively as mesoionic compounds.[12] 1,2,3-Oxadiazole itself is unstable and could not be isolated but under the form of its benzo-derivative.[13] Consequently the heterolytic elimination of CO_2 takes place readily by thermolysis which results in the formation of the zwitterionic aminide **19** whose cyclization leads to the final 1-acetyl-3-indazolone (**2a**).

The reaction mechanism by proton transfer can also explain the fact that the 4-unsubstituted sydnone **1d** undergoes the rearrangement only on comparatively drastic conditions and with low yields. It is known that 3-monosubstituted sydnones are protonated at the exocyclic oxygen.[14] Consequently the attack of a carboxylic oxygen at 4—C becomes less probable (**1D**; Chart 5). The presence of the methyl group in the 4-position reverses the charge distribution by stabilizing the positive charge on the adjacent carbon, stability still enhanced by the unshared pair of 3-N (**1A**). Accordingly, protonation takes place at 2—N atom. As a result the attack at 4—C will follow quite readily now.

Literature data express some doubt on the structure of the protonated 3,4-disubstituted sydnones and although protonation at 2-N appears more reasonable no decisive proof has as yet been provided.[14] Anyhow, kinetic measurements have assumed protonation on 2-N of the sydnone ring.[15] This may be considered as a good substantiation for the proposed mechanism which in its turn corroborates the 2-N protonation of 3,4-disubstituted sydnones.

EXPERIMENTAL PART

UV spectra were measured with a Specord Carl Zeiss-Jena instrument and IR spectra with a UR-20 Carl Zeiss-Jena spectrometer. ^{1}H—NMR spectra were recorded on a Varian A 60-A spectrometer with TMS as internal standard, the chemical shifts being expressed in δ values.

N-(o-Carboxyphenyl)alanine. To a solution of 93 g of Na_2CO_3 in 600 mL of water were successively added and dissolved 75 g of anthranilic acid and 90 g of 2-bromopropionic acid. The reaction mixture was refluxed for 3 hrs. After cooling and acidification with HCl 80 g of the title product were obtained with mp 205° (dec.),[16] yield 70%.

N-(o-Carboxyphenyl)-N-nitrosoalanine (7a) and ***3-(o-Carboxyphenyl)-4-methylsydnone (1a).*** To a solution of 5 g of NaOH in 250 mL of water were successively added and dissolved 21 g of N-(*o*-carboxyphenyl)alanine and 7 g of $NaNO_2$. In the cooled solution 30 mL of conc. HCl were dropped under stirring, the temperature being maintained under 5°. A precipitate of **7a** separated which was thoroughly washed with water on the Büchner funnel and dried over P_2O_5 in a vacuum desiccator. The yield of **7a** was 21 g (90%). After recrystallization from benzene-ether mp 117° (dec.).

IR (KBr): 1450 (NO), 1712 and 1740 cm^{-1} (COOH). ^{1}H—NMR (d_6-acetone): 1.30 (d, 3, Me), 5.04 (q, 1, C*H*Me), 6.62 (s, 2, COOH), 7.83 (m, 3, arom. protons), 8.18 (dd, 1, 3—H).

The crude nitroso derivative **7a** was added to 110 mL of acetic anhydride. The reaction mixture was brought to 70°—80° when dissolution occurred. Subsequently the excess anhydride was removed *in vacuo* and the oily residue treated with ice-water when crystals of **1a** separated which were filtered with suction, washed with water and left to dry. The yield was 13.6 g of crude **1a** (70%) with mp 159° (dec.). A small sample was recrystallized for analysis from nitromethane, mp 163° (dec.).

Found: C, 54.75; H, 3.89; N, 12.46. Calc. for $C_{10}H_8N_2O$: C, 54.54; H, 3.64; N, 12.18%. UV: λ_{max}^{EtOH} (log ε) = 309 (3.783), 224 nm (3.891). IR (KBr): 1680 (COOH), 1730 cm^{-1} (sydnone-CO). ^{1}H—NMR (d_6-DMSO): 1.91 (s, 3, Me), 7.88 (m, 5, arom. protons + COOH).

1a, *Methyl ester* .To an ethereal solution of diazomethane obtained from 11 g of nitrosomethylurea, 7 g of sydnone **1a** were added with caution in order to avoid a strong nitrogen evolution. The reaction mixture was stirred for a few minutes and its volume reduced to a third *in vacuo*. After filtration and washing with a small amount of ether 7 g of the methyl ester of **1a** were obtained (94%) A longer reaction time led to formation of appreciable amounts of methyl benzoate as by-product. After recrystallizaton from methanol mp 104°.

Found: C, 56.44; H, 4.52; N, 11.96. Calc. for $C_{11}H_{10}N_2O_4$: C, 56.41; H, 4.27; N, 11.97% UV: λ_{max}^{EtOH} (log ε): 309 nm (3.879). IR (CCl_4): 1743 (COOMe), 1764 cm^{-1} (sh.; sydnone-CO). ^{1}H—NMR (d_6-acetone): 1.97 (s, 3, sydnone-Me), 3.87 (s, 3, COOMe), 8.02 (m, 3, arom. protons), 8.25 (dd, 1, 3′—H).

1a, *Amide*. In 100 mL of 25% ammonia liquor, 8 g of **1a**-ester were added with stirring which was maintained until complete dissolution ocurred. Left overnight the amide of **1a** separated, 5.5 g (75%). After recrystallization from acetonitrile mp 186°.

Found: C, 54.89; H, 4.26; N, 19.31. Calc. for $C_{10}H_9N_3O_3$: C, 54.79; H, 4.11; N, 19.18%, UV: λ_{max}^{EtOH} (log ε) = 310 nm (3.913). IR (HBr): 1628 and 1684 (amide-CO I and II), 1730 (sydnone-CO), 3183 and 3413 ($CONH_2$), 3320 and 3370 cm^{-1} (w, associated NH). ^{1}H—NMR (d_6-DMSO): 1.95 (s, 3, Me), 7.33 (m, 4, arom. protons), 7.58 and 8.17 (singlets, 2, amide NH_2 removable by deuteration).

1a, *Hydrazide*. To 4 mL of hydrazine hydrate in 7 ML of methanol 5 g of **1a**-ester were added. After one hour the hydrazide crystallized from the homogeneous mixture when 4.5 g were obtained, yield 85 %. After recrystallization from methanol mp 170° (dec.).

Found: C, 51.51; H, 4.48; N, 23.75. Calc. for $C_{10}H_{10}N_4O_3$: C, 51.28; H, 4.27; H, 23.93 % UV: λ_{max}^{EtOH}(log ε) = 309 nm (3.825). IR (KBr): 1615 (w), 1635 (m), 1670 (m) and 1710 (s; CO), 3245, 3280 and 3318 cm^{-1} (—$NHNH_2$). ^1H—NMR (d-$_6$DMSO): 2.05 (s, 3, Me), 5.67 (very broadened, 3, —$NHNH_2$), 7.93 (apparent singlet, 4, arom. protons).

***N*-(*o*-Carboxyphenyl)-2-ethylglycine.** To a solution of 102 g of Na_2CO_3 in 600 mL of water, 82.5 g of anthranilic acid and 105 g of 2-bromobutyric acid were added and the homogeneous mixture was refluxed for 4 hours. After cooling and acidification 90 g of the title compound were obtained, yield 67 %. After reprecipitation from a slightly warm ammoniacal solution which had been treated before with active charcoal, mp 209° (dec.).[17]

***N*-(*o*-Carboxyphenyl)-2-ethyl-N-nitrosoglycine (7b)** and **3-(*o*-Carboxyphenyl)-4-ethylsydnone (1b).** The same method was used as in the case of **7a.** From 33 g of N-(*o*-carboxyphenyl)-2-ethylglycine 34 g of **7b** were obtained, mp 120 (dec.), yield 91 %.

IR (KBr): 1438 (NO), 1700 cm^{-1} (COOH).

To 80 mL of acetic anhydride, 25 g of the nitroso acid **7b** were added and the whole was alternatively shaken and heated on a water bath until dissolution occurred. After removing *in vacuo* the volatile, the residue on treatment with water afforded after filtration and drying 19 g of **1b** (81 %). After recrystallization from nitromethane mp 155° (dec.).

Found: C, 56.70; H, 4.47; N, 11.86. Calc. for $C_{11}H_{10}N_2O_4$: C, 56.41; H, 4.27; N, 11.96 %. UV: $^{EtOH}_{max}$(log ε) = 217 (3.995), 307 nm (3.896). IR (KBr): 1693 (COOH), 1730 cm^{-1} (sydnone-CO). ^1H—NMR (d_6-DMSO): 1.00 (t, 3, $CH_2C\mathit{H}_2$), 2.32 (q, 2, $C\mathit{H}_2CH_3$), 6.00 (broad, 1, COOH), 7.88 (m, 3, arom. protons), 8.08 (dd, 1, 3′—H).

1b, *Methyl ester*. Obtained as described above, yield 87 %, mp 101° (from methanol).

Found: C, 58.34; H, 5.12; N, 11.36. Calc. for $C_{12}H_{12}N_2O_4$: C, 58.06; H, 4.84; N, 11.29 %.

1b, *Hydrazide*. Obtained as described before, yield 85 %, mp 169° (dec.) from methanol.

Found: C, 53.04; H, 4.83; N, 22.70. Calc. for $C_{11}H_{22}N_4O_3$: C, 53.22; H, 4.84; N, 22.58 %. IR (KBr): 1610 (w), 1642, 1675 and 1728 (s; CO), 3238, 3290 and 3330 cm^{-1} (—$NHNH_2$).

2-Butyl-N-(*o*-carboxyphenyl)glycine, 2-Butyl-N-(*o*-carboxyphenyl)-N-nitrosoglycine (7c) and **4-Butyl-3-(*o*-carboxyphenyl)sydnone (1c).** In a solution of 30 g of Na_2CO_3 in 200 mL of water 30 g of 2-bromo-hexanoic acid and 20.5 g of anthranilic acid were introduced and refluxed as described before when 30 g of the first title compound were obtained, mp 198° (dec.),[17] yield 75 %. The nitroso acid **7c** was obtained by the method described before. The yield was 72 %, mp 120° (dec.). In acetic anhydride (60 mL) 20 g of the nitroso acid **7c** were added the procedure being the same as for **7a—b.** After working-up 7.5 g of sydnone **1c** were obtained (yield 40 %) with mp 133° (dec.) after recrystallization from nitromethane.

Found: C, 59.70; H, 5.50; N, 10.94. Calc. for $C_{13}H_{14}N_2O_4$: C, 59.54; H, 5.34; N, 10.69 %.

1-Acyl-1,2-dihydro-3Y-indazol-3-ones 2a—c. Thermolysis of 4-alkyl-3 (*o*-carboxyphenyl) sydnones 1a—c. An amount in the range of 0.1—0.5 g of sydnone (**1a—c**) was introduced when decomposition occurred suddenly, which was followed by the sublimation of the corresponding 1-acyl-3-indazolone. Yields were practically theoretical of 1-acetyl-3-indazolone (**2a**: mp 214°; lit.[18] 211°), 1-propionyl-3-indazolone (**2b**: mp 192° from acetonitrile) and 1-valeryl-3-indazolone (**2c**: mp 153° from nitromethane). Vacuum conditions: 40 Torr.

2a: ^1H—NMR (d_5-Py): 2.65 (s, 3, $COCH_3$), 7.28—7.80 (m, 2, 5— and 6—H); 8.02 (dd, 1, 4—H, J = 7 and 2 Hz), 8.72 (d, 1, 7—H, J = 7 Hz), 13.10 (broad, 1, NH).

2b: Found: C, 63.27; H, 5.37; N, 14.62. Calc. for $C_{10}H_{10}N_2O_2$: C, 63.15; H, 5.26; N, 14.75 % IR (KBr): 1710 (CO), 3000 cm^{-1} (v. broad; OH). ^1H—NMR (Py—d_5): 1.32 (t, 3, $CH_2C\mathit{H}_3$), 3.17 (q, 2, $OC\mathit{H}_2CH_3$), 7.24—7.83 (m, 2, 5— and 6—H), 8.03 (dd, 1, 4—H), 8.75 (dd, 1, 7—H), 13.68 (s, 1, NHCO).

2c: Found: C, 65.76; H, 6.42; N, 13.12. Calc. for $C_{12}H_{14}N_2O_2$: C, 66.03; H, 6.46; N, 12.84 %. IR (KBr): 1690 (CO), 3000 cm^{-1} (v. broad; OH).

1-Acetyl-3-methoxyindazole (**3**): from **2a** with diazomethane.[2] ^1H—NMR (d_5—Py): 2.65 (s, 3, $COCH_3$), 4.08 (s, 3, OCH_3), 7.18—7.83 (m, 3, 4— 5— and 6—H), 8.58 (dd, 1, 7—H).

3-(*o*-Carboxyphenyl)sydnone (1d). In 100 mL of acetic anhydride 21 g of **7d**[19] were added and the suspension was evaporated *in vacuo* at 30 Torr with gentle heating when dissolution occurred. The crystalline residue was washed with a small amount of acetone and after filtration 14.5 g of sydnone **1d** were obtained. After recrystallization from acetic acid or ethanol mp 214° (dec.); lit.[3]: 205° (dec.).

1,2-Dihydro-3*H*-indazol-3-one (4). A. Thermolysis of 1d. In a vacuum sublimator 117 mg of sydnone **1d** were introduced and gradually heated near to the melting point at about 200° while the vacuum was maintained at 40 Torr. The sublimed 3-indazolone began to separate but after a while sudden decomposition occurred which caused an impurification of the sublimed product. After resublimation 42 mg of **4** were obtained with mp 244° (yield 55 %).

^{1}H—NMR (d_5—Py): 7.07—7.72 (=, 3, 5—, 6— and 7—H), 8.20 (d, 1, 4—H, J = 7 Hz) 12.07 (s, 2, —NHNH—).

B. From sydnone 1a. To 20 mL of freshly distilled aniline 2 g of sydnone **1a** were added and the resulted solution was refluxed for 5 min. The reaction mixture was left to cool when crystallization occurred. After filtration and washing with ether 1 g of **4** was obtained, mp 243° (yield 83 %).

3-Acetoxy-1-acetylindazole (5a). A. From sydnone 1a. Sydnone **1a** (2.2 g) was refluxed in 20 mL of acetic anhydride for 30 min. After removal *in vacuo* of the solvent the residue was taken up with ethanol and after filtration and drying 1.4 g of **5a** mere obtained (yield 66 %) with mp 110° (lit.[4] 113°).

B. From 7a. In 20 mL of acetic anhydride 5 g of **7a** were dissolved with gentle heating and the solution was refluxed for 45 min. Working-up like above yielded 2 g (42 %) of mp 112°.

C. From *o*-(2-formylhydrazino)benzoic acid (8). To a suspension of 0.5 g of **8**[20] in 2 mL of acetic anhydride, 0.75 mL of pyridine was carefully added with stirring and external cooling with ice-water. Dissolution occurred and the stirring was continued for one hour after which time the separated precipitate was filtered, 0.55 g of **5a** with mp 112° (yield 90 %). A mixed melting point with an authentic sample showed no depression.

3-Acetoxy-1-propionylindazole (5b). A. From sydnone **1b**. The method **A** described for **5a** was followed: 2.34 g of syndone **1b** in 20 mL of acetic anhydride. Yield 1.6 g of **5b** (70 %) with mp 75°.

Found : : C, 61.80 %; H, 5.41; N, 12.20. Calc. for $C_{12}H_{12}N_2O_3$: C. 62.07; H, 5.17; N, 12.07 % ^{1}H—NMR ($CDCl_3$) : 1.30 (t, 3, CH_2CH_3), 2.42 (s, 3, $OCOCH_3$), 3.13 (q, 2, $COCH_2CH_3$), 7.25—7.70 (m, 3, 4-, 5- and 6-H), 8.45 (dd, 1, 7-H).

B. From nitroso acid 7b. The same procedure was followed as for **5a** (method **B**). From 9 g of **7b** in 25 mL of acetic anhydride, 3.4 g of **5b** were obtained, yield 41 %. After recrystallization from ethanol mp 77°.[21]

1-Acetyl-3-propionyloxyindazole (6) : 2.2 g of **1a** were refluxed for 45 min. in 15 mL of propionic anhydride. After removal of the excess anhydride *in vacuo*, treatment of the residue with ethanol and filtration, 1.3 g of **6** (56 %) were obtained with mp 76° (from methanol of ethanol).

Found : C, 62.31; H, 5.28; N, 12.27. Calc. for $C_{12}H_{12}N_2O_3$: C, 62.07; H, 5.17; N, 12.07 % IR (CCl_4) : 1728 (nonmesomeric amide), 1787 cm^{-1} (3-indazolol ester). ^{1}H—NMR (CCl_4) : 1.33 (t, 3, OCH_2CH_3), 2.50 (s, 3, $COCH_3$), 2.53 (q, 2, OCH_2CH_3), 7.07—7.47 (m, 3, 4- 5- and 6-H), 8.22 (dd, 1, 7—H).

N-(*o*-**Carboxyphenyl)**-*N*-**formylglycine (10a)**. Mixed formic-acetic anhydride was prepared from 20 mL of acetic anhydride and 9.6 mL of formic acid (98—100 %)[22] and dropped during an interval of 30 min . at room temperature with stirring in a solution of 20 g of *o*-carboxyphenylglycine and 16.6 g of Na_2CO_3 in 160 mL of water. Stirring was continued for 30 min. after which time the reaction mixture was acidified to pH = 1.5 and extracted with ethyl acetate. After solvent evaporation the residue was formed of 18 g **10a** (80 %) with mp 163°, (dec.) after recrystallization from acetic acid.

Found : C, 54.07 %; H, 4.15; N, 6.38. Calc. for $C_{10}H_9NO_5$: C, 53.81; H, 4.03; N, 6.28 % IR (KBr) : 1650 (N—CHO), 1695 (assoc. *CO*OH), 1742 (*CO*OH), 3200 cm^{-1} (broad; CO*OH*). ^{1}H—NMR (d_6-acetone); 4.43 (s, 2, N—CH_2), 6.38 (s, 2, COOH), 7.60 (m, 3, 4-5- and 6-H), 7.98 (m, 1, 3-H), 8.18 (s, 1, N—CHO); equilibrium conformer of the amide geometric isomerism (11—12 %) : 4.58 (s, 2, N—CH_2), 8.32 (s, 1, N—CHO).

3-Acetoxy-1-formylindole (11a). In 15 mL of acetic anhydride 2g of each **10a** and anhydrous sodium acetate were added and the whole refluxed for 20 min. After removal *in vacuo* of the excess anhydride and on treatment with water, a precipitate was obtained which after drying was chromatographed on a neutral alumina column and eluted with methylene chloride. After recrystallization from ethanol mp 70°. The yield was 1 g (55 %).

Found : C, 65.28; H, 4.73; N, 7.12. Calc. for $C_{11}H_9NO_3$: C, 65.02; H, 4.43; N, 6.90 %, Indigo positive text.

N-(o-Carboxyphenyl)-N-formylalanine (10b). To 15 mL of acetic anhydride 7.5 mL of formic acid were added and the whole was maintained for 15 min. at 50°. Under stirring 5.2 g of *o*-carboxyphenylalanine were added and the stirring continued for 15 min. after which time the excess of acylating agent was removed under vacuum. The residue consisted mainly of the seven-membered anhydride of the acid **10b**, which was identified as such by its IR and ^1H-NMR spectra (mp 134°).

IR (KBr): 1729 (N—CHO), 1808 (anhydride-CO). ^1H-NMR (d_6-acetone): 1.32 (d, 3, $CHCH_3$), 7.70 (m, 3, 4—, 5— and 6—H), 8.00 (m, 1, 3—H), 8.17 (s, 1, CHO).

On treatment with 100 mL of 5% $NaHCO_3$ and after stirring at room temperature for 5—6 hours, acidification, extraction with ethyl acetate and removal of the solvent, 3.5 g of **10b** were obtained (yield 65%). After recrystallization from acetic acid mp 104° (dec.).

Found: C, 55.75; H, 4.95; N, 6.11. Calc. for $C_{11}H_{11}NO_5$: C, 55.70; H, 4.67; N, 5.91%. IR (KBr): 1644 (N—CHO), 1700 (*C*OOH), 3450 and 3532 cm^{-1} (COO*H*). ^1H-NMR (d_6-acetone): 1.32 (d, 3, $CHCH_3$), 4.95 (q, 1, $CHCH_3$), 6.62 (s, 2, COOH), 7.65 (m, 3, 4—, 5— and 6—H), 7.97 (m, 1, 3—H), 8.10 (s, 1, CHO).

3-Acetoxy-1-formyl-2-methylindole (11b): 9 g of the acid **10b** were dissolved in a mixture of 45 mL of acetic anhydride and 8 g of anhydrous sodium acetate. The whole was refluxed for one hour. The excess anhydride was removed *in vacuo* and water was added to the residue when an oil separated which crystallized on staying, 7.5 g (yield 90%). After recrystallization from ethanol mp 103°.

Found: C, 66.47; H, 5.30; N, 6.69. Calc. for $C_{12}H_{11}NO_3$: C, 66.36; H, 5.07; N, 6.45%. IR (KBr): 1720 (N—CHO), 1780 (hetaryl acetate), 2928 cm^{-1} (CH_3). ^1H-NMR (d_6-acetone): 3.37 and 3.43 (singlets, 6, CH_3), 727 (m, 3, 4—, 5— and 6—H), 8.20 (dd, 1, 7—H), 9.27 (s, 1, CHO).

1,2-Dihydro-1-formyl-3H-indazol-3-one (12): 1 g of 3-indazolone was refluxed for 1.5 hr. in 10 mL of formic acid (98—100%). After removal *in vacuo* of the excess formic acid, 1.15 g of **12** were obtained (yield 95%). After recrystallization from formic acid (98—100%) mp 172° (dec.).

Found: C, 59.28; H, 3.89; N, 17.63. Calc. for $C_8H_6N_2O_2$: C, 59.26; H, 3.73; N, 17.28% IR (KBr): 1650 and 1700 (CO), 2550—3200 cm^{-1} (OH, NH). ^1H-NMR (Py-d_5): 7.48—7.67 (m, 2, 5— and 6-H), 8.03 (dd, 1, 4-H), 8.58 (d, 1, 7-H), 9.50 (s, 1, CHO), 13.23 (s, 1, NH).

Thermolysis of 12. An amount of 0.1 g of **12** was heated for about 10 min. around the temperature of 200°. An evolution of gas took place. After cooling the crystallized residue displayed a mp of 242°. The mixed melting point and IR spectrum showed it to be 3-indazolone (**4**).

Dimethyl 1-(o-carboxyphenyl)pyrazole-3,4-dicarboxylate (13 d). To a solution of 1.5 mL of dimethyl acetylenedicarboxylate in 30 mL of xylene, 2.1 g of sydnone **1d** were added and also 2 mL of DMSO for solubilization. The reaction mixture was refluxed for 1.5 hr., the xylene removed *in vacuo* and the residue on treatment with water separated the cycloadduct **13d** which after filtration and drying represented 2.7 g (yield 90%) with mp 102° (from benzene).

Found: C, 53.43; H, 4.32; N, 8.94. Calc. for $C_{14}H_{12}N_2O_6$. :1/2 H_2O: C, 53.57; H, 4.15; N, 8.71% ^1H-NMR (d_6-acetone): 3.83 and 3.88 (singlets, 6, COOMe), 4.15 (s, 1, COOH + + H_2O), 7.72 (m, 3, 4′—, 5′— and 6′-H), 8.02 (m, 1, 3′—H), 8.48 (s, 1, 5-H)

13d, *Trimethyl ester*: with diazomethane.

Found: C, 56.42; H, 4.21; N, 8.58. Calc. for $C_{15}H_{16}N_2O_6$.: C, 56.60; H, 4.40; N, 8.80% ^1H-NMR ($CDCl_3$): 3.75, 3.90 and 3.98 (singlets, 9, COOMe), 7.62 (m, 3, 4′—, 5′— and 6′-H), 7.95 (m, 1, 3′-H), 8.23 (s, 1, 5-H).

Cycloaddition of dimethyl acetylenedicarboxylate to 1a. A. In xylene at reflux. The same procedure was followed as for **1d** but results were quite different:1-acetyl-3-indazolone (**2a**) was obtained with an yield of 40%.

B. In benzene at reflux. Dimethyl 1-(o-carboxyphenyl)-5-methylpyrazole-3,4-dicarboxylate (13a). By replacing xylene as a solvent with benzene the pyrazole **13a** was obtained in 90% yield, mp 149° (from water).

Found: C, 56.77; H, 4.69; N, 8.96. Calc. for $C_{15}H_{14}N_2O_6$: C, 56.60; H, 4.40; N, 8.80% ^1H-NMR ($CDCl_3$): 2.33 (s, 3, 5-Me), 3.90 and 3.93 (singlets, 6, COOMe), 7.42 (m, 1, 6′-H), 7.70 (m, 2, 4′— and 5′-H), 8.18 (m, 1, 3′-H), 8.27 (s, 1, COOH).

REFERENCES

[1] A. Padwa, "Photochemical Rearrangements of Five-Membered Ring Heterocycles", *Rearrangements in Ground and Excited States*, vol. 3, (ed. P. de Mayo), Academic Press, 1980, pp. 488 and 539—540; A. Lablache-Combier, "Photoisomerisation of Five-Membered Heterocyclic Compounds", *Photochemistry of Heterocyclic Compounds*, (ed. O. Buchardt), Wiley-Interscience, 1976, p. 183; R. Kellogg, "Photochemically Induced Fragmentation Reactions of Heterocyclic Compounds", ibid., pp. 425—427.

[2] N. A. Evans, D. J. Whelan and R. B. Johns, *Tetrahedron*, **21**, 3351 (1965).

[3] R. A. Eade and J. C. Earl, *J. Chem. Soc.*, **1948**, 2307.

[4] L. Baiocchi, G. Corsi and G. Palazzo, *Synthesis*, **1978**, 633.

[5] I. J. Jenen and H. P. Eerdekens, U. S. Pat. 2964402 (Gevaert, 1960); *Chem. Abstr.*, **55**, 9129 (1961).

[6] E. Giovannini and Th. Lorenz, *Helv. Chim. Acta*, **41**, 113 (1958).

[7] P. Ballesteros, J. Elguero, R. Claramunt, R. Faure, M. De la Conception Foces-Foces, F. Hernandez Cano and A. Rousseau, *J. Chem. Soc.*, *Perkin Trans.* 2, **1986**, 1677.

[8] N. S. Bhacca, D. P. Hollis, L. F. Johnson and E. A. Pier, "NMR Spectra Catalog", vol. 2, Varian Associates, Palo Alto Cal., 1962, (a) No. 611; (b) No. 649; (c) No. 520; (d) No. 561.

[9] N. S. Bhacca, L. F. Johnson and J. N. Shoolery, *ibid.*, vol. 1, 1962, (a) No. 324; (b) No. 286.

[10] A. M. Trozzolo, T. M. Leslie, A. S. Sarpotdar, R. D. Small, G. J. Ferraudi, T. DoMinh and R. T. Hartless, *Pure Appl. Chem.*, **51**, 261 (1979).

[11] D. R. Kelsey, *J. Comput. Chem.*, **1**, 21 (1980).

[12] H. U. Daeniker and J. Druey, *Helv. Chim. Acta*, **46**, 805 (1963).

[13] Nguyen Minh Tho, A. F. Hogarty and J. Elguero, *Angew. Chem.*, **97**, 704 (1985).

[14] L. Stefaniak, M. Witanowski, B. Kamienski and G. A. Webb, *Org. Magn. Reson.*, **13**, 274 (1980).

[15] S. Aziz, A. F. Cockerill and J. G. Tillet, *J. Chem. Soc. B*, **1970**, 416; S. Aziz, A. J. Buglass and J. G. Tillet, *ibid.*, **1971**, 1912.

[16] J. van Alpen, *Rec. Trav. chim.*, **61**, 888 (1942); E. Tighineanu, F. Chiraleu and D. Răileanu, *Tetrahedron*, **36**, 1385 (1980).

[17] E. Moser, A. Bolleter and C. Wittwer, U. S. Pat. 2781338 (Ciba, 1954/1957); *Chem. Abstr.*, **51**, 13923 (1957).

[18] S. Viebel and H. Lillelund, *Tetrahedron*, **1**, 201 (1957).

[19] A. van Ekenstein and J. Blanksma, *Rec. Trav. chim.*, **24**, 36 (1905).

[20] M. Bianchi, E. Häusermann and I. Rossi, *J. Heterocycl. Chem.*, **16**, 1411 (1979).

[21] R. M. Anderson, *J. Chem. Res.*, *Synop.*, **1985**, 376.

[22] L. Fieser and M. Fieser, "Reagents for Organic Synthesis", vol. 1, Wiley, 1967, p. 4 and literature cited therein.

Revue Roumaine de Chimie, **34**, *5*, 1195–1201 (1989)

KINETIC STUDY OF THE MALTODEXTRINE HYDROLYSIS CATALYZED BY IMMOBILIZED GLUCOAMYLASE

EMIL DUMITRIU, VASILE HULEA, MILENA STOICA[a] and SPIRIDON OPREA
Faculty of Chemical Technology, Splai Bahlui 71, Jassy 6600
[a]Institute of Food Researches, Bucharest

Received January 11, 1988

We studied the kinetics of maltodextrine hydrolysis catalyzed by glucoamylase which was covalently immobilized over an acrylic polymer having primary amino groups in the side chains. The yield of immobilization was equal to 74%, calculated on the basis of enzymatic activity. The content of protein in the catalyst was about 21.48 mg/mL for the wet catalyst and 171 mg/g for the dry catalyst. The kinetic parameters (v_{max}, K_M and E_a) were determined. Also, the influence of certain factors such as temperature, feed concentration, reaction time etc. on the catalytic activity was studied both for the continuous and discontinuous operation of the reactor.

The immobilization of biocatalysts by physical adsorption, ionic and covalent bonding on synthetic supports[1–7] allowed the access on a large scale of these materials in the industrial practice.[8–11] The supports based on poly(2-hydroxypropyl methacrylate) proved to be valuable materials for the chromatography of biopolymers,[12–15] whereas the supports like PONILEX-CC and PONILEX-AS obtained by the alkaline hydrolysis or aminolysis [16] of the ternary copolymers of ethyl acrylate, acrylonitrile and divinylbenzene have a large utilization for the enzyme immobilization.[17–19]

These studies have stated that the glucoamylase can be immobilized at the high yields on the copolymers of the PONILEX-AS type by the covalent or ionic binding. This paper has the aim to study the kinetic of maltodextrine hydrolysis on the covalent immobilized glucoamylase.

EXPERIMENTAL

Materials. As polymeric support for the covalent binding of glucoamylase was used the weakly basic ion exchanger PONILEX-AS having an overall ionic exchange capacity of 0.311 mval/mL and 7.46 mval/g respectively. Soluble glucoamylase (E.C.3.12.13) was provided by the Institute of Food Researches—Bucharest. The maltodextrine (MD) used in this study was prepared by the same institute by the partial hydrolysis of corn starch with an alpha amylase.

o-Toluidine was freshly distilled before use. Glacial acetic acid was reagent grade.

Immobilized enzyme preparation. Firstly, the support was washed with a buffer solution (sodium acetate-acetic acid, pH = 4.5) and then this resin was contacted for 24 h at pH of 4.5 with an aqueous solution of glucoamylase having a known protein concentration and enzymatic activity. Further, the support containing the ionic immobilized enzyme was removed by filtration, washed with buffer solution and the mother liquor was collected.

The amount of retained enzyme was established on the basis of the difference between the enzymatic activity of the initial solution and those of the mother liquor.

The covalent binding was performed upon the ionic immobilized enzyme with the aid of a glutardialdehyde solution of 2.5% (by weight) concentration.

The activity of soluble and immobilized glucoamylase was determined using a solution of 15% maltodextrine buffered with 0.02 m acetate at pH 4.5, at 50°C, using a ratio R of 14.8 (R = mg enzyme/g substrate). The theoretical yield of immobilization ($\alpha\%$) was calculated on the basis of the difference between the initial and residual enzymatic activity of the two solutions. The practical yield of immobilization ($\beta\%$) was calculated from the specific activities of the soluble and immobilized enzyme, respectively. The following results were obtained :

- the content of protein : 21.48 mg/mL wet resin,
  171.02 mg/g dry resin
- specific activity : 1.8 (I.U./mg) for soluble enzyme,
  1.34 (I.U./mg) for immobilized enzyme
- theorethical yield of immobilization $\alpha = 78.4\%$,
- practical yield of immobilization $\beta = 74.0\%$.

The reactions were carried out on two types of reactors : well-stirred reactor and plug-flow reactor. In the second case the catalyst was used in fixed bed, the grain sizes being in the range of 0.5–0.8 mm. All experiments were performed in the buffered solutions (buffer solution sodium citrate-hydrochloride acid) at constant temperature.

The extent of reaction was determined measuring the extinction of the coloured products resulting from glucose and *o*-toluidine. These measurements were performed in the visible range, 620 nm, in acid medium (acetic acid) at 50°C.

RESULTS AND DISCUSSION

In our study two aspects were followed : (i) – the determination of kinetic parameters and (ii) – the measurement of the catalytic properties of immobilized enzyme in relation to various parameters as : pH, temperature, feed concentration, reaction time etc.

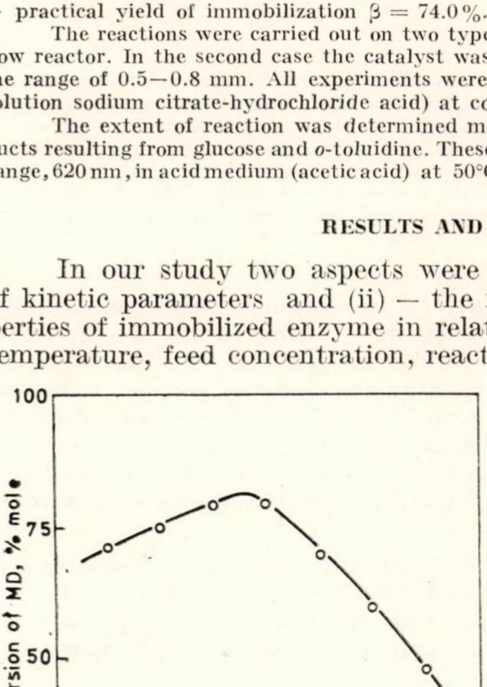

Fig. 1. — The variation of the activity of immobilized enzyme *vs.* pH at 50°C and initial concentration of 2% MD.

As is known, the stability and catalytic activity of enzymes are decisively influenced by the pH values. Therefore, at the beginning, we have studied the relation between the activity of immobilized gluco-amylase and the pH values. The function catalytic activity vs. pH-value is shown in Fig. 1.

As can be seen the maximum activity appears at pH values of 4.0–4.5 and, as a consequence, we have chosen the value of 4.3 for all further experiments.

The kinetic study was performed on the basis of the fundamental scheme of enzymatic reactions proposed by Michaelis and Menten:[20]

$$E + S \underset{k_2}{\overset{k_1}{\rightleftharpoons}} ES \xrightarrow{k_3} E + P \tag{1}$$

Where : E — enzyme;
S — substrate;
P — product
ES — activated complex.
k_1, k_2, k_3 — rate constants

Based on this reaction scheme the following kinetic equation was obtained :

$$v = \frac{v_{\max}}{\dfrac{K_M}{C_S} + 1} \tag{2}$$

where : v — initial rate of the product formation;
$v_{\max}$ — maximum reaction rate;
K_M— the value of initial concentration of the substrate for which the initial rate is half from the $v_{\max}$ value;
C_S — initial concentration of substrate.

This equation allows to determine the values of $v_{\max}$ and K_M on the basis of the variation of initial reaction rate versus the initial substrate concentration.

Equation (2) can be linearized in the following forms :

— equation Eadie-Hofstee [21]

$$v = v_{\max} - \frac{K_M \cdot v}{C_S} \tag{3}$$

— equation Linewever-Burk [22]

$$\frac{1}{v} = \frac{1}{v_{\max}} + \frac{K_M}{v_{\max} \cdot C_S} \tag{4}$$

which are more reliable to be applied for the determination of kinetic parameters than equation (2). The values of initial reaction rate *versus* the initial concentration of substrate (C_S), at various temperatures, are shown in table 1.

These results are processed using the above-presented equations and thus the values of $v_{\max}$ and K_M are obtained (Table 2).

As can be seen from this table both $v_{\max}$ and K_M rise with the temperature and, for the same value of temperature (50°C), there is not an essential difference between the soluble and immobilized enzymes. This fact denotes a remarkable activity for the insolubilized enzyme very close to that of the free enzyme.

Table 1

The values of initial reaction rate (v) *vs* · the initial concentration of MD (C_S); reaction time of 30 min., pH = 4.3

C_S, $\mathrm{mol \cdot L^{-1} \cdot 10^3}$	v, $\mathrm{mol \cdot L^{-1} \cdot s^{-1} \cdot 10^6}$				
	for immobilized enzyme at				for free enzyme
	35°C	40°C	45°C	50°C	50°C
27.7	1.07	1.33	1.37	1.41	1.44
55.5	1.60	2.02	2.42	2.44	2.50
83.3	1.83	2.45	3.02	3.30	3.37
111.1	2.01	2.73	3.46	3.95	4.08
166.6	2.23	3.09	4.04	4.90	5.04
222.2	2.36	3.31	4.41	5.58	5.70
277.7	2.44	3.46	4.66	6.10	6.14
388.8	2.54	3.64	5.02	6.81	6.88

Table 2

The values of v_{max} and K_M parameters for different temperatures

	T, °C	v_{max} $\mathrm{mol \cdot L^{-1} \cdot s^{-1} \cdot 10^2}$	K_M $\mathrm{mol \cdot L^{-1} \cdot 10^3}$
Immobilized enzyme	35	2.84	45.6
	40	4.20	59.4
	45	6.08	84.0
	50	9.60	158.8
Free enzyme	50	9.81	178.0

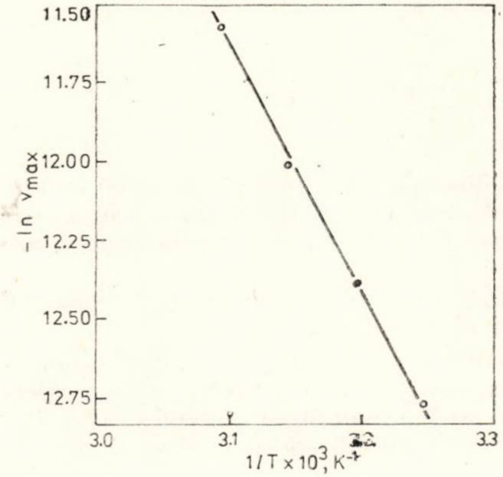

Fig. 2. — The Arrhenius plot for the immobilized glucoamylase on PONILEX-AS.

Taking into account the direct proportionality between v_{max} and the rate constant k_3, at the constant concentration of enzyme, the value of activation energy ($E_a = 61.82$ kj/mol) can be obtained from the Arrhenius plot (see Fig. 2).

The second aspect followed by us was the study of the catalytic performances of this immobilized enzyme, in the process of MD hydrolysis, in relation with some factors (temperature, substrate concentration etc.).

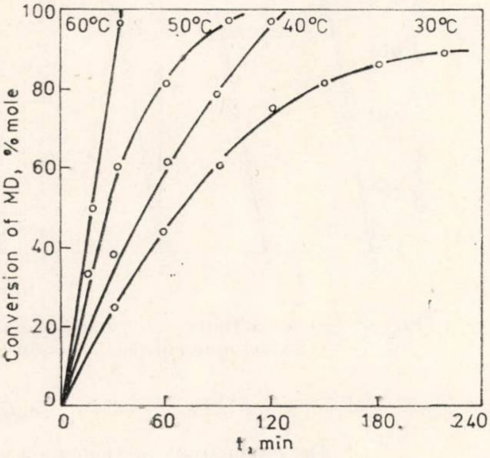

Fig. 3. — The influence of temperature and time of reaction on the conversion of MD; $C_S = 0.055$ mol/L; pH = 4.3.

As can be observed from Fig. 3 the conversion of MD rises as the temperature is risen.

The amount of glucose obtained by hydrolysis also depends on the initial concentration of MD (Fig. 4). The concentration of glucose as reaction product rises up to an initial concentration of MD of about 15% (by weight) but the further increase of MD concentration in feed does not lead to the increase of glucose concentration, the latter remaining approximately constant due to saturation of the catalyst by substrate.

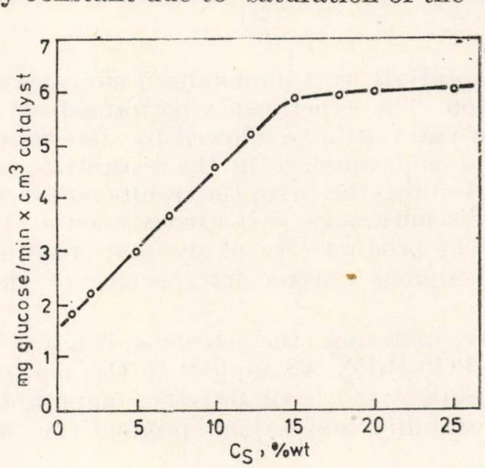

Fig. 4. — The influence of the MD concentration in feed on the amount of resulted glucose; $T = 40°C$, pH = 4,3, reaction time = 120 min.

It would be interesting to state if this type of immobilized enzyme keeps its activity for a prolonged time of operation. Figure 5 shows that the activity remains approximately constant after 75 cycles of operation.

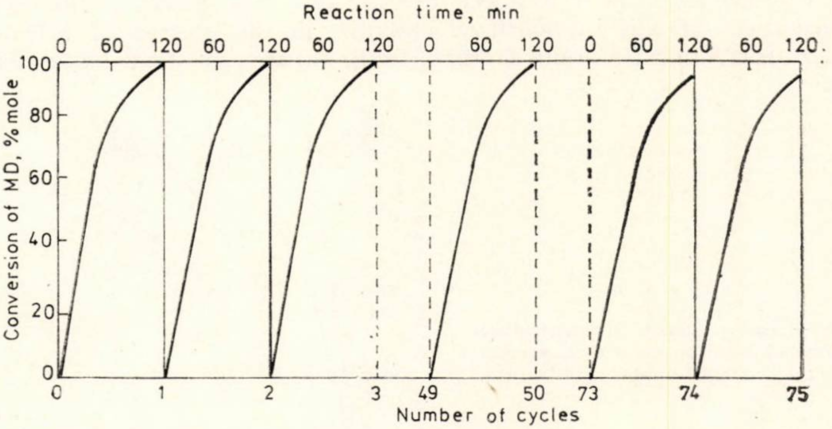

Fig. 5. — The activity of immobilized glucoamylase *vs.* the number of cycles of operation ; $T = 50°C$, $pH = 4.3$, $C_S = 5\%$ (wt).

Table 3

The productivity of the dynamic reactor and those of the discontinuous reactor for different temperatures ; $C_S = 0.11\ mol \cdot L^{-1}$

Temperature, °C	kg glucose/h · m³ catalyst	
	dynamic reactor	discontinuous reactor
40	360	204
50	588	387
60	830	573

A great advantage offered by catalysis with immobilized enzymes is the possibility of dynamic operation. The experiments performed on a dynamic reactor with a fixed bed of catalyst have allowed to determine the performances of the immobilized glucoamylase in the hydrolysis of MD. The results are presented in table 3 together with the results obtained in similar conditions but using a discontinuous well-stirred reactor. It can be noticed from this table that the productivity of dynamic reactor is greater than those of the discontinuous reactor, irrespective of the temperature.

As a conclusion to our study we underline the excelent behaviour of the immobilized glucoamylase on PONILEX-AS support in the maltodextrine hydrolysis. This enzymic catalyst shows an activity comparable with those of the enzyme, a good stability and a high productivity in continuous operation conditions.

REFERENCES

[1] J. Kukara and M. Kminkora, *Czech. C.S.* 209556, Feb. 1982.

[2] Daicel Chem. Ind. Ltd. Jpn. Kokai, Tokkyo Koho, J.P. 58 212 786, Dec. 1983.

[3] I. V. Berezin, N. N. Ugarova and L. Yu. Brovko, U.S.S.R., S.U. 660 378, Dec. 1982.

[4] Matsushita Elect. Works Ltd. Jpn. Kokai Tokkyo Koho, J.P. 58179494, Oct. 1983.

[5] Mitshubishi Chem. Ind. Co. Ltd. Jpn. Kokai Tokkyo Koho, J.P. 57 152 886, Sept. 1982.

[6] Reanal Finomvegyszergyo PCT, Int. Appl. WO, 8300345, Feb. 1983, Eur. Pat. Appl. E.P. 37 667, Oct. 1981.

[7] Sumimoto Chem. Co. Ltd. Eur. Pat. Appl. E.P. 37 667, Oct. 1981.

[8] L. Boroş, I. Iozsef, L. Daroczi and B. Szayam, PCT, Int. Appl. 80/1 782, July 1980.

[9] Nitto Electric Instruments Co. Ltd. Kokai Tokkyo Koho, J.P. 58 152 486, Oct. 1983.

[10] Kokai Tokkyo Koho, J.P. 81 137 882, Oct. 1981.

[11] Kokai Tokkyo Koho, J.P. 58 116 683, July 1983.

[12] O. Mikes, P. Strop and J. Zbrozek, *J. Chromatog.*, **180**, 17(1979).

[13] O. Mikes and P. Strop, *J. Chromatog.*, **192**, 159(1980).

[14] O. Mikes, P. Strop and Z. Hostomska, *J. Chromatog.*, **301**, 93(1984).

[15] O. Mikes, P. Strop and Z. Hostomska, *J. Chromatog.*, **261**, 363(1983).

[16] S. Maxim, A. Flondor, A. Carpov, M. Macoveanu, Al. Tofan, I. Bunia and E. Avădănii, Rom. Pat. 84 729, April 1982.

[17] S. Maxim, A. Flondor, A. Carpov, V. Rugină, D. Cojocaru and N. Topală, *Biotechnol. Bioeng.*, **28**, 294(1986).

[18] Cr. I. Simionescu, V. Popa, S. Maxim, V. Rusan and M. Rusan, *Reactive Polymers*, **5**, 191(1987).

[19] S. Maxim, A. Flondor, A. Carpov, "Ionic Binding of Biologically Active Proteins on Cross-linked Acrylic Macroreticular Supports", *Biotechnol. Bioeng.* (in press).

[20] L. Michaelis, M. L. Menten, *Biochem. Z.*, **49**, 333(1913).

[21] G. S. Eadie, *J. Biol. Chem.*, **85**, 146(1942).

[22] H. Linewever, D. Burk, *J. Amer. Chem. Soc.*, **56**, 658(1934).

Revue Roumaine de Chimie, **34**, *5*, 1203–1207 (1989)

INTERACTIONS BETWEEN THE EMULSIFIERS UTILIZED IN POLYMERIZATION OF VINYL ACETATE

KRISTIANA GOŞA[a], DAN DONESCU[a], NICOLETA CARP[b] and LIANA FUSULAN[a]
[a]Institute of Chemical Research, Research Center for Plastic Materials
[b]Center of Physical Chemistry, Splaiul Independenţei no. 202, Bucharest
77208, Romania

Received March 7, 1988

Hydrophobic interactions were studied which characterize nonionic emulsifiers as hydroxyethyl cellulose (HEC)/nonyl phenol ethoxylate (NPXEO) employed in polymerization of vinyl acetate (VAc). The formation of macromolecular emulsifier-tenside complex alters the initial splitting rate of potassium persulphate (KPS) which initiates polymerization and slows down the splitting of HEC by KPS.

INTRODUCTION

The kinetics of polymerization in emulsion of Vac in the presence of HEC[1,2] is modified by addition of coemulsifier of NPXEO type [3] (X stands for the number of oxyethylene units per molecule). At addition of coemulsifier, the rate of polymerization decreases with the concentration of NPXEO. The rate of polymerization depends on the degree of hydrophobicity of the coemulsifier with a maximum at NP8EO.

These results have suggested two questions :

— whether the two emulsifiers HEC and NPXEO interact to an extent depending on the degree of ethoxylation, i.e. are of hydrophobic nature

— whether splitting of KPS employed as initiator of VAC polymerization is influenced by the presence of macromolecular emulsifier-tenside complex.

Studies of light diffraction [4] have evidenced a preferential absorption of micelles of NPXEO about HEC chains at concentrations of NP20EO lower than 2 g/l and of NP14EO lower than 3 g/l.

This contribution deals with splitting occurring in HEC, NPXEO and KPS aqueous solutions affected by formation of HEC/NPXEO complex, evidenced by other methods than light diffraction.

EXPERIMENTAL

Hercules-Natrosol 250 LR Hec was used; the NPXEO coemulsifiers were commercial products without any additional purification (the ethylene oxide content was determined by NMR).

The viscosity of solutions was measured by Ubbelohde viscometer. UV spectra were recorded with a UV—VIS Carl Zeiss Jena spectrophotometer in 0.1 and 1.0 cm cells. The interfacial tension was measured by the stalagmometric method. The initial splitting rate of KPS and the KPS consumption were determined by titration by the method described in reference.[5]

RESULTS AND DISCUSSION

UV spectra of NPXEO in water exhibit an absorption at 277 nm which correspond to phenyl ring. A plot of absorbance versus the logarithm of concentration points to the existence of three critical concentrations (c.c.).

The first c.c. which decreases with the increasing hydrophobicity was considered micellar c.c.

We may assume that at the second c.c. the aggregation of NPXEO begins and above the third c.c. we obtain aggregates of regular structure

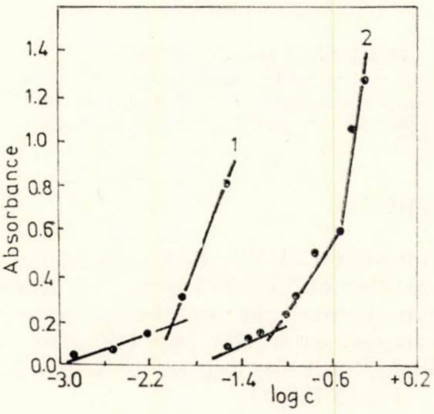

Fig. 1. — Absorbance at 277 nm versus concentration for NP8EO in 1.0 cm (1) and 0.1 cm (2) cells.

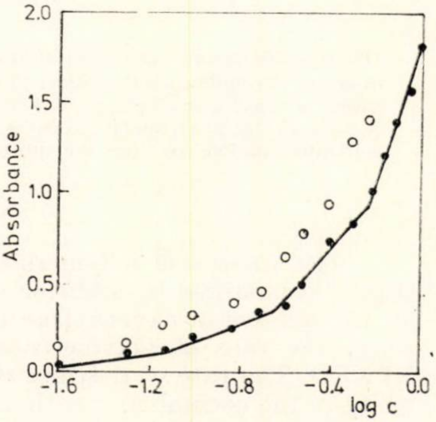

Fig. 2. — Absorbance at 277 nm versus concentration for NP16 EO before (●) and after KPS addition (○).

Addition of the same HEC concentration in all NP 16 EO solutions rises the absorbance at 277 nm pointing to the existence of some interactions between HEC and NP16EO at hydrophobic level. The presence of HEC does not preclude micellization, aggregation and compacting of micellar aggregates but rises the three c.c. 's (Table 1).

Table 1

Type of NPXEO	HEC g/100 cm³	T (°C)	$c \cdot c_1$ (g/100 cm³)	$c \cdot c_2$ (g/100 cm³)	$c \cdot c_3$ (g/100 cm³)
NP8EO	—	25	0.01	0.09	0.30
NP16EO	—	25	0.09	0.23	0.58
NP16EO	—	65	0.09	0.23	0.55
NP16 EO	0.5	25	0.12	0.36	0.81
NP16EO	0.5	65	0.12	0.36	0.76

Because the hydrophobic interactions strengthen as temperature rises, at 65°C the aggregates of ordered structure appear at a lower c.c. than at 25°C.

The adsorption of NPXEO molecules and micelles modifies the HEC chain solubility and consequently the reduced viscosity of HEC is lower in NPXEO solutions than in water (Fig. 3).

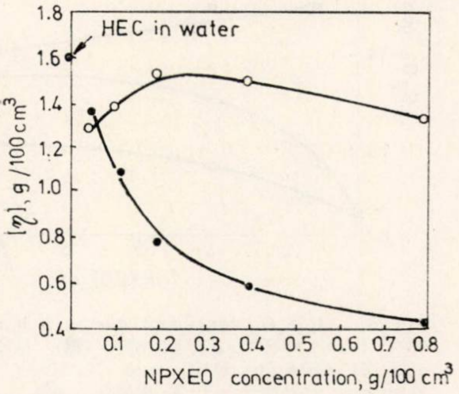

Fig. 3. — Intrinsic viscosity of HEC in NP8EO (●) and in NP16EO (○) solution.

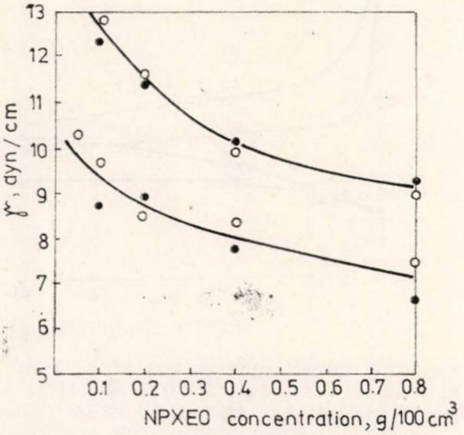

Fig. 4. — Interfacial tension between AcV and NPXEO solution (●) and between AcV and HEC and NPXEO solution (○) ([HEC] = = 0.8 g/100 cm³).

The slight increase of viscosity for NP16EO concentrations ranging between the first and the second c.c. points to the further fixation and to the aggregation of micelles on HEC chains. Packing of HEC/NP16EO aggregate following ordering of NPXEO micelles causes the viscosity to decrease at and over the three c.c. of NPXEO.

The concentration range studied lies above the second c.c. of NP8EO. Therefore, any decrease of viscosity was observed for NP8EO.

The interfacial tension between VAc and aqueous solutions of NPXEO does not change in the presence of HEC (Fig. 4). This is a confirmation of the hypothesis that HEC chains lie inside the HEC/NPXEO complex while at monomer-micellar solution interface there are only tensides.

The initial KPS splitting rate and the KPS consumption in 5 hours at 65°C in HEC and NPXEO solutions are higher in water. It turns out that KPS forms a redox system both with HEC and NPXEO (Figs. 5 and 6).

In NPXEO and HEC solutions the initial splitting rate is higher than in water but decreases with increasing NPXEO concentration. This may be accounted for only in terms of the formation of macromolecular emulsifier-tenside complex which hinders the action of the KPS–HEC redox system, more so as NPXEO concentration increases, i.e. as the largeness of tenside protective layer around the HEC chains increases.

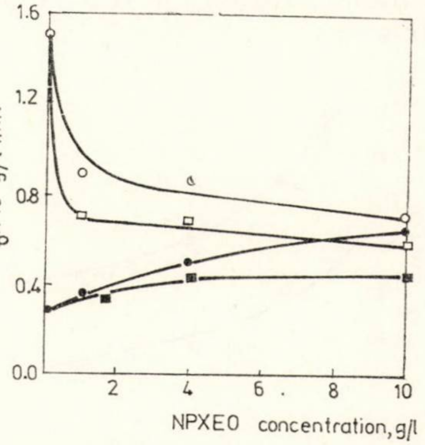

Fig. 5. — Initial splitting rate af KPS at 65 °C in NP16EO (●), NP8EO (■), HEC and NP16EO (○), HEC and NP8EO (□) solutions ([HEC] = 0.5 g/100 cm^3).

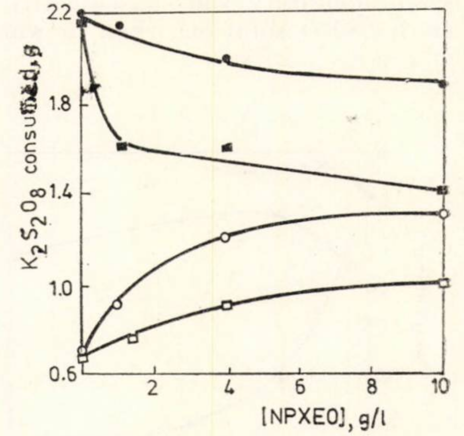

Fig. 6. — $K_2S_2O_8$ consumed during 5 h at 65 °C in NP16EO (●), NP8EO (■), HEC and NP16EO (○), HEC and NP8EO (□) solutions ([HEC] = 0.5 g/100 cm^3).

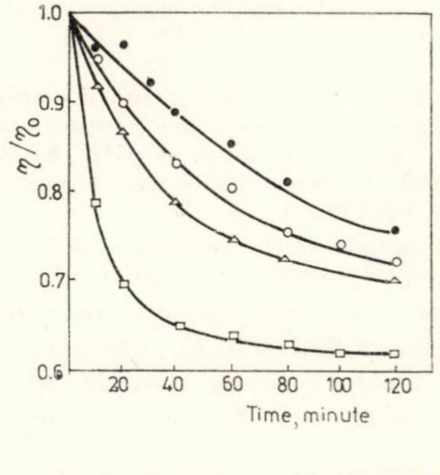

Fig. 7.—Time dependence of ratio of instantaneous over inital viscosity of HEC for various NP16EO concentrations; NP16EO = 0.0 (□); 0.1 (△); 0.7 (○); 1.08 (●) g/100 cm^3 ([HEC] = 0.5 g/100 cm^3).

The UV spectra of NPXEO solutions show an increase of absorption corresponding to the phenyl ring after addition of HEC (Fig. 1). This means that a degradation of NPXEO occurs because the absorption of phenyl is higher at lower ethoxylation degrees. It is known that in presence of KPS and HEC an oxidative degradation occurs [2] evidenced by the decrease of viscosity of aqueous solutions. The viscosity of HEC and NPXEO solutions decreases after addition of KPS made less than the viscosity of HEC solutions (Fig. 7).

In conclusion the splitting of HEC occurs both in the presence and absence of NPXEO but in the latter case this process is slowed down by :

— the decrease of the initial splitting rate of KPS

— the formation of micellar NPXEO aggregates in which HEC is caught inside

— the KPS consumption in the process of NPXEO splitting.

REFERENCES

[1] D. Donescu, K. Goşa, I. Deaconescu, M. Mazăre and N. Carp in "Emulsion Polymerization of Vinyl Acetate", ed. M. El-Aasser and J. W. Vanderhoff, Applied Science Publishers, London and New Jersey, 1981, p. 203.

[2] D. Donescu, I. Deaconescu and K. Goşa, *Rev. Roumaine Chim.*, **29**, 483 (1984).

[3] D. Donescu, I. Deaconescu, K. Goşa, M. Mazăre and I. Gavăt, *Rev. Roumaine Chim.*, **25**, 975 (1980).

[4] Y. Boscher, F. Lafuma and C. Ouivorn, *Polymer Bulletin*, **9**, 533 (1983).

[5] I. M. Kolthoff and E. M. Carr, *Anal. Chem.*, **25**, 298 (1953).

Revue Roumaine de Chimie, 34, 5, 1209–1216 (1989)

THE STUDY OF THE VAPOR-LIQUID EQUILIBRIUM IN THE DIOXANE-WATER SYSTEM

OLGA IULIAN, ORTANSA LANDAUER, DAN GEANĂ and
CORNELIA MATEESCU
Dept. Physical Chemistry/TSCO, Polytechnic Institute, Bucharest, Romania

Received November 3, 1988

Vapor-liquid equilibrum data (T-P-X) for the dioxane-water mixture in the temperature range between 303.15 and 323.15 K are presented. The results of the data correlation by the Wilson model of activity coefficients are also presented.

The study concerning the vapor-liquid equilibrium in the dioxane water system is part of a series of such studies dealing with the binary systems, water-organic component, between which interactions are established and which consequently present deviations from ideality.

The experimental vapor-liquid equilibrium data, in the binary systems can be obtained by: a) static methods, from which isothermal pressure – phase composition data result, that is P–X–Y for T = ct; b) dynamic methods from which isobaric temperature – phase composition data result, that is T–X–Y for P = ct. In the case of the static methods the measurements can be limited only to the composition of the liquid phase (X), the composition of the vapor phase (Y) being computed.

For appreciating the quality of the measured data, the latter are correlated by different G^E models presented in literature,[1–5] which were discussed in detail in the previous papers.[6–7]

The system dioxane-water has been studied with the aim to obtain some further liquid-vapor data in wider ranges of temperatures. A comparison of our data with those of the literature gives the possibility to appreciate their quality. The data were obtained by a static method. The measurements are limited to temperature – pressure – liquid composition (T–P–X) at the temperatures 303.15, 313.15 and 323.15 K. The results of the data correlation by the Wilson model are also presented.

I. EXPERIMENTAL DETERMINATIONS

Static method for the measurement of vapor-liquid equilibrium has become increasingly used in recent years. This is the conclusion of Abott's authorised review of the techniques for measurement of low pressure v-l equilibrium.[8]

The apparatus used in this work is a glass isoteniscope of the Smith and Menzies type[4] with some modifications, which allows the measurement of vapor-liquid equilibrium at pressures between 5 and 760 mm Hg and at temperatures up to 150°C.

The total pressure and the liquid phase compositions were measured at constant temperatures in the range between 303 and 323 K.

The used substances were purified by distillation. The water was tetradistilled und the dioxane was distilled at T = 274.35 K. The purity was verified by IR spectroscopy, by chromatography and by refraction index. The temperature was controlled by a thermostat of the type U 10 (GDR). The temperature was measured with a mercury thermometer with accuracy to 0.1 °C. The pressure was measured with a mercury manometer which is accurate to 0.5 mm Hg.

Liquid phase compositions were measured by means of the refraction index. The calibration curve was obtained at $T = 296$ K. The regression function is :

$$n = 1.3439239 + 0.1955768\ X_1 - 0.1255355\ X_1^2$$

With the variance $\sigma^2 = 3.491 \cdot 10^{-5}$ and the correlation coefficient $\rho = 0.97924 \cdot n$ — represents the refraction index, X_1 the molar fraction of the dioxane. The values for σ^2 and ρ show a very good representation of the data.

II. THE CORRELATION METHOD AND THE COBELV PROGRAM

The experimental vapor-liquid equilibrium data were correlated with a method of the Barker type based on the Wilson model of the activity coefficients.

The used computer program was COBELV (the correlation of the binary vapor-liquid equilibrium) which was described in another work.[6]

The method for correlating the limited P—T—X data in binary systems is based on a model of the activity coefficients having two or more parameters. The values of these parameters were computed, which minimizes the function :

$$\min Q_P = \sum_{k=1}^{N} \frac{(P_k^{\text{exp}} - P_k^{\text{calc}})^2}{\sigma_{Pk}^2}$$

where P_k represent the experimental, respectively, computed total pressures $\sigma_{P_k}^2$ the standard deviation of the measured pressure, N — the number of experimental points.

The given pressure is computed on the basis of thermodynamic equilibrium equations :

$$P^{\text{calc}} = Y_1 P + Y_2 P = \frac{\gamma_1 X_1 f_1^{\circ}}{\varphi_1} + \frac{\gamma_2 X_2 f_2^{\circ}}{\varphi_2}$$

where Y_1, Y_2 are the molar fractions in vapour phase,
X_1, X_2 — the molar fractions in liquid phase,
γ_0, γ_0 — the activity coefficients,
f_1^0, f_2^0 — the standard pure component fugacities,
$\varphi_1^{\circ}, \varphi_2^{\circ}$ — the fugacity coefficients.

In the calculation we considered the ideal behaviour of the vapour phase ($\varphi_i = 1, f_i^{\circ} = P_i^{\circ}$) and the real behaviour of the liquid phase. The calculation of the pressure is a "Bubble-P" type.[1]

The following equations were used for vapour pressure of the pure substances :

— for dioxane, $\ln P = 16.1327 - \frac{2966.88}{T - 62.15}$, mm Hg, $T \in (275\text{-}410\ \text{K})$

— for water, $\ln P = 18.3036 + \frac{3816.44}{T - 46.13}$, mm Hg, $T \in (284\text{-}441\ \text{K})$

The minimization of the Q_P function is a segment of the COBELV program. On the basis of this program and simultaneously with the optimal parameters of the activity coefficients model, we calculate the composition of the vapour phase. The COBELV program contains a series of subroutines for the calculation of the fugacity coefficients, of the standard fugacity etc., in the necessary cases.

The Wilson, NRTL and NRTL/H models were tested as models for the calculation of the activity coefficients. It was noticed that the Wilson model correlated better and it was adopted for the system dioxane-water because of its wide use. The wilson model is given by the expressions :

$$G^E = -X_1 \ln(X_1 + \Delta_{12}X_2) - X_2 \ln(X_2 + \Delta_{21}X_1)$$

$$\ln \gamma_1 = -\ln(X_1 + \Delta_{12}X_2) + X_2\left[\frac{\Delta_{12}}{X_1+\Delta_{12}X_2} - \frac{\Delta_{21}}{\Delta_{21}+X_2}\right]$$

$$\ln \gamma_2 = -\ln(X_2 + \Delta_{21}X_1) - X_1\left[\frac{\Delta_{12}}{X_1+\Delta_{12}X_2} - \frac{\Delta_{21}}{\Delta_{21}+X_2}\right]$$

$$\Delta_{ij} = \frac{V_j^L}{V_i^L}\exp\left[-\frac{\lambda_{ij}-\lambda_{ii}}{RT}\right], \quad i \neq j = 1,2$$

where G^E is the molar excess free enthalpy,

V_j^L — the molar volume of the j component in liquid phase,

$\lambda_{ij}-\lambda_{ii}$ — the parameters of the model, that are energetic terms giving the difference between the interaction energy of the pair $i-j$ and that of the pair $i-i$. For the binary system these parameters are :

$$\lambda_{12} - \lambda_{11} \text{ and } \lambda_{12} - \lambda_{22}.$$

III. RESULTS AND DISCUSSION

The experimental vapor-liquid equilibrium data on pressure-composition of liquid phase at temperatures 303.15 ; 313.15 and 323.15 are shown in tables 1—3.

There are presented the values of the total experimental pressure for different compositions of the liquid phase determined by measuring the refraction index. The tables include the results of the correlations on the basis of the Wilson model : the computed values of the total pressure and of the molar fractions in vapor phase. The values of the deviations of the pressure ΔP are also presented.

The precision of the measurements and of the correlations is evidenced by the value of the criterion function Q_P, of the total variance σ^2 and of the deviations, ΔP. $\sigma_{P_k} = 1$ mm Hg. We can notice the quality of the correlation at all temperatures, especially at 303.15 and 313.15. The values of the deviations, ΔP, having a means of ± 1.5 mm Hg, characterize the data as being satisfactory. The system dioxane-water presents an azeotrope with maximal pressure at all the three temperatures.

Table 1

Vapor-liquid equilibrium data for the system dioxane (1) — water (2) for $T = 303.15$ K. Correlation with the Wilson model; $P_1^{\circ} = 45.65$ mm Hg; $P_2^{\circ} = 31.82$ mm Hg; $V_1^{\circ} = 85.29$ cm^{3}mL^{-1}; $V_2^{\circ} = 18.05$ cm^{3}mol^{-1}

	X_1	p^{exp}, mm Hg	p^{calc}, mm Hg	Y_1	ΔP, mm Hg
1	1	—	45.65	1	—
2	0.9285	56	55.48	0.7763	0.52
3	0.8271	59	60.11	0.6777	−1.11
4	0.6724	61	61.73	0.6236	−0.73
5	0.6436	60.5	61.99	0.6175	−1.29
6	0.6367	64	61.80	0.6161	2.20
7	0.5749	61	61.79	0.6048	−0.79
8	0.4603	60	61.41	0.5857	−1.41
9	0.3629	62	60.64	0.5672	1.36
10	0.2360	60	58.29	0.5289	−1.17
11	0.1524	54	54.71	0.4786	−0.71
12	0.1112	53	51.63	0.4346	1.37
13	0.0628	46	45.92	0.6435	0.08
14	0.0449	41	42.92	0.2877	−1.92
15	0	—	31.82	0	—

$Q_P = 21.975$; $\sigma^2 = 1.997$; $\rho_{12} = -0.871$
$\lambda_{12} - \lambda_{11} = -152.86 \pm 62.97.$
$\lambda_{12} - \lambda_{22} = 1778 \pm 75$

Table 2

Vapor-liquid equilibrium data for the system dioxane (1) — water (2) for $T = 313.15$ K. Correlation with Wilson model; $P_1^{\circ} = 74.62$ mm Hg; $P_2^{\circ} = 55.32$ mm Hg; $V_1^{\circ} = 85.29$ cm^3 mol^{-1}; $V_2^{\circ} = 18.05$ cm^3 mol^{-1}

	X_1	p^{exp}, mm Hg	p^{calc}, mm Hg	Y_1	ΔP, mm Hg
1	1	—	74.62	1	—
2	0.9285	93.5	91.98	0.7647	1.52
3	0.8271	100	100.36	0.6626	−0.36
4	0.6724	104	103.48	0.6072	0.52
5	0.6436	102	103.62	0.6010	−1.62
6	0.6367	103	103.64	0.5996	0.65
7	0.5749	102	103.71	0.5882	1.71
8	0.4603	102	103.22	0.5693	1.22
9	0.3629	103	102.08	0.5512	−0.91
10	0.2360	100	98.49	0.5140	−1.51
11	0.1524	94	92.87	0.4652	−1.12
12	0.1112	89	87.97	0.4225	−1.02
13	0.0628	78.5	78.72	0.3339	0.22
14	0.0449	72	73.79	0.2796	1.79
15	0	—	55.32	0	—

$Q_P = 18.8965$ $\sigma^2 = 1.7178$ $\rho_{12} = -0.8715$
$\lambda_{12} - \lambda_{11} = -135.88 \pm 36.69$
$\lambda_{12} - \lambda_{22} = 1829.94 \pm 42.81$

Table 3

Vapor-liquid equilibrium data for the system dioxane (1) — water (2) for $T = 323.15$. Correlation with the Wilson model. $P_1^{\bullet} = 117.37$ mm Hg; $P_2^{\bullet} = 92.51$ mm Hg; $V_1^{\bullet} = 85.29$ cm^3 mol^{-1}; $V_2^{\bullet} = 18.05$ cm^3 mol^{-1}

	X_1	p^{exp}, mm Hg	p^{calc}, mm Hg	Y_1	ΔP, mm Hg
1	1	—	117.37	1	—
2	0.9285	147	144.64	0.7635	2.36
3	0.8271	159,5	159.52	0.6511	−0.02
4	0.6724	165,5	165.82	0.5874	−0.32
5	0.6436	164	166.18	0.5803	−2.18
6	0.6367	166	166.24	0.5787	−0.24
7	0.5749	165	166.54	0.5661	−1.54
8	0.4603	163	166.04	0.5462	−3.04
9	0.3629	166	164.55	0.5286	1.45
10	0.2360	162	159.72	0.4945	2.28
11	0.1524	152	151.90	0.4504	0.10
12	0.1112	147	144.81	0.4114	2.19
13	0.0628	131	130.83	0.3288	0.17
14	0.0449	129	123.09	0.2773	5.91
15	0	—	92.51	0	—

$Q_P = 38.584 \quad \sigma^2 = 3.507 \quad \rho_{12} = 0.873$

$\lambda_{12} - \lambda_{11} = -60.72 \pm 36.27$

$\lambda_{12} - \lambda_{22} = 1797.2 \pm 36.$

The obtained data were compared with those existing in literature.[9-10] In fig. 1 the relative deviations are represented comparatively, $(\Delta P/P) \cdot 100$, calculated for a set of data from literature and for a set of data obtained by us, at $T = 313.15$ K. For the data in literature, we can notice values of the relative deviation of approximately $\pm 1\%$ and for the data in this work of approximately $\pm 1.5\%$. For the latter there exists a maximal deviation of 2.2% which is to be noticed in the extreme domain of concentration, for which there are no data in literature.

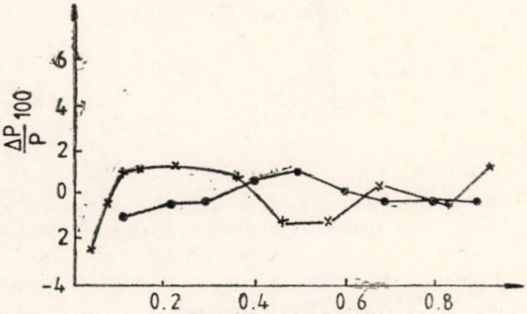

Fig. 1. — The variation of the relative deviation of the pressure with the composition for $T = 303.15$ for the system dioxane-water; × experimental data; ● data in literature.[9]

Using the COBELV program the activity coefficients of the two components γ_1, γ_2 were computed. Fig. 2 presents the dependence of the activity coefficients of the composition, the limiting values at infinite dilution of these coefficients being given. We have also computed and represented the variation of the excess free enthalpy of the system. The values of the activity coefficients between 1 and approx. 8 show that the system dioxane-water presents important deviations from ideality. The excess free enthalpy presents a curve with a maximum and positive deviations from ideality. For the temperatures 313.15 and 323.15 K similar results were obtained, with values of the activity coefficients and of the excess free enthalpy situated between approximately the same limits.

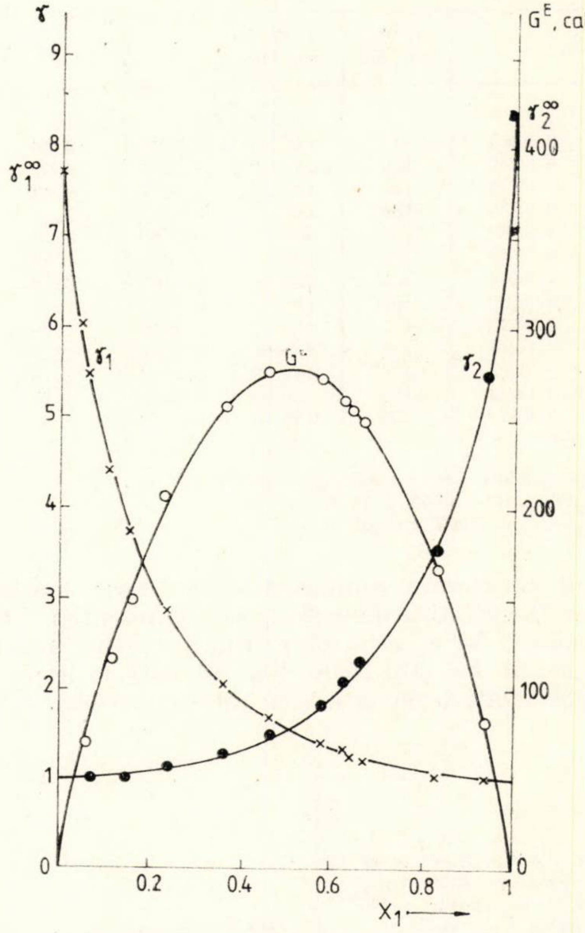

Fig 2. — The variation of the activity coefficients and the free excess molar enthalpy with the composition for the system dioxane-water for $T = 303.15$ K.

We have studied the influence of the temperature on the Wilson model parameters values that were obtained from the experimental data and from the literature. Generally this dependence is neglected or is linearily approximated. In fig. 3 the curves 1—3 represent the variation of the $\lambda_{12}-\lambda_{11}$ parameter for the data in literature,[9-10] and respectively for our experimental data; the curves 1′—3′ represent the variation of the $\lambda_{12}-\lambda_{22}$ parameter for the same data. We can notice that there exists a dependence with the temperature, each parameter varying differently;

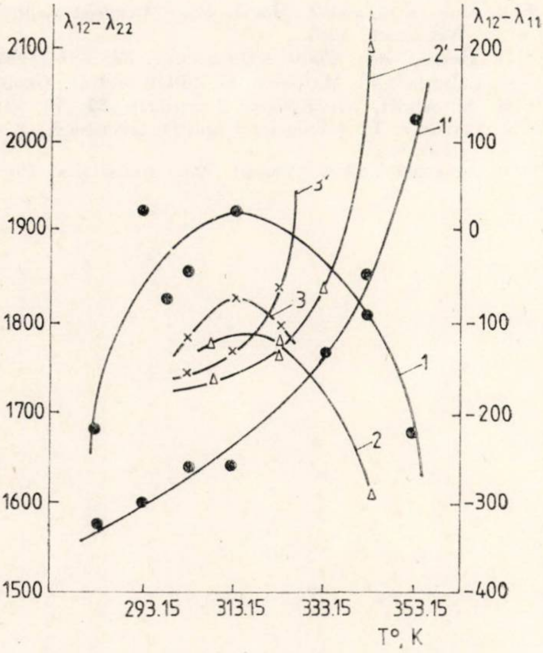

Fig. 3. — The variation of Wilson parameters with the temerature for the system dioxane-water : * — experimental data ; ● data from literature[9]; Δ — data from literature.[10]

for the same parameter the variation is the same, irrespective of the source, but the values of the parameters present differences from one author to another.

It should be noticed that all measurements are compatible, but the quality of the data, the influence of the working method, etc., determine these differences. The results obtained in this work are within the limits of those in literature, this being another confirmation of the quality of our data.

IV. CONCLUSIONS

Vapor liquid equilibrium data in the system dioxane water were experimentally determined. The data were correlated with the Wilson model of the activity coefficients on the basis of the computer program COBELV. The activity coefficients and the excess free enthalpy were computed, the system presenting important positive deviations from ideality. The influence of temperature on the parameters of the model was also studied and compared with the data in literature.

REFERENCES

[1] J, M. Prausnitz, C. A, Eckert, R. V. Orye and J. P. O'Connel, "Computer calculations for Multicomponent Vapor-Liquid Equilibria", Prentice Hall, New York, 1967.

[2] H. Renon, L, Asselineau, G. Cohen and C. Raimbault, "Calcul sur ordinateur des équilibres liquide-vapeur et liquide-liquide", Technip Paris, 1971.

[3] J. A. Barker, *Australian J. Chem.* **6**, 207 (1953).

[4] E. Hálá, J. Pick, W. Fried and O. Vilim, "Vapour-Liquid Equilibrium", Pergamon, Oxford, 1967.

[5] A. Maczynski and Z. Macznsyka, "Verified Vapor-Liquid Equilibrium Data", vol. 5, PWN, Warszawa, 1981.

[6] D. Geană, *Rev. Chim. (Bucureşti)*, **32**, 337 (1981).

[7] O. Landauer, C, Mateescu, O. Iulian and D. Geană, *Rev. Roumaine Chim.*, **33**, 237 (1988).

[8] M. M. Abott, ***Fluid Phase Equilibria*** **29**, 193 (1986).

[9] P. Hovorka, R. A. Schaefer and D. Dreisbach, *J. Amer. Chem. Soc.*, **58**, 2264 (1936) (cited in lit.[5]).

[10] G. Kortüm and V. Valent, *Ber. Bunsenges. Phys. Chem.*, **81**, 752 (1977) (cited in lit.[5]).

Revue Roumaine de Chimie, **34**, *5*, 1217–1223 (1989)

A STUDY OF THE ISOTHERMAL FLOW INSTABILITY OF POLYMERIC FLUIDS

GHEORGHIȚA JINESCU and ALEXANDRU ȘTEFAN
Polytechnic Institute Bucharest, Faculty of Chemical Technology, Department of Chemical Engineering, Splaiul Independenței, 313, Bucharest, Romania

Received October 21, 1988

This paper analyzes the isothermal flow instabilities for melted polymers due to the sliding effect. A complex flow model is developed and new relations are advanced for the design of plastic processing equipment. A more rational low energy consuming technology is presented. A numerical application illustrates its usefulness in research and development activities.

1. PHYSICAL MODEL

Rheological analysis of fluid flow through channels presents industrial interest because it predicts the pressure drop and pumping energy consumption for plastics processing machines.[1,2,3] This paper focuses on incompressible isothermal flow of a power law fluid, taking into account the sliding effect.

Qualitative analysis of polymer flow led us to the following conclusions (Fig. 1):

a) melted hard PVC, polyethylene with high average numerical molecular weight and rubber blend obey the wall adherence hypothesis;

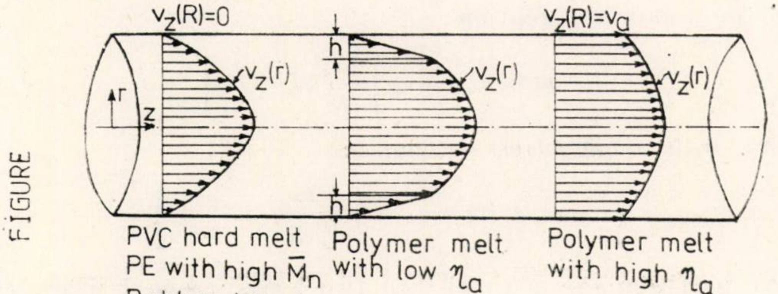

Fig. 1. — Velocity profiles.

b) melted polymers with low apparent viscosity exhibit a linear variation of the flowing velocity in the wall vicinity (length *h*);

c) melted polymers with high apparent viscosity present the sliding effect;

In fully developed steady state flow most of the melted polymers present a velocity profile which is intermediate between the plug flow and the parabolic one.

2. MATHEMATICAL MODEL

Taking into account the hypothesis mentioned above, the moment conservation equation becomes :

$$\frac{\mathrm{d}p}{\mathrm{d}z} = -\frac{1}{r}\frac{\mathrm{d}}{\mathrm{d}r}(r\tau_{rz}) \tag{1}$$

with the following boundary conditions :

$$\begin{aligned} r &= 0\,;\ \tau_{rz} = 0 \\ r &= R\,;\ \tau_{rz} = \tau_R \end{aligned} \tag{2}$$

The solution of this problem reads as follows :

$$\tau_R = \frac{R}{2}\frac{\mathrm{d}p}{\mathrm{d}z} \tag{3}$$

Because under sliding conditions the wall shear stress is not constant and due to the pressure loss along the channel, the following dependence is advanced :

$$\tau_R = -p\mu_a \tag{4}$$

where μ_a stands for the friction wall coefficient.

From eqs (3) and (4) we obtain :

$$\frac{R}{2}\frac{\mathrm{d}p}{\mathrm{d}z} = -p\mu_a \tag{5}$$

having the following solution :

$$p(z) = p_L \exp\left[\frac{2\mu_a}{R}(L - z)\right] \tag{6}$$

The wall shear stress becomes :

$$\tau_R(z) = |-p_L\mu_a| \exp\left[\frac{2\mu_a}{R}(L - z)\right] \tag{7}$$

We partition the channel into two zones : zone I where the fluid adheres to the wall and zone II where we have the sliding effect. Zone I is for $z \in [0, z_1]$ where z_1 is the axial position from which sliding begins. The wall shear stress is constant and the pressure drop is linear as presented in Fig. 2 :

$$p(z) - p_\theta = \frac{p_0 - p_1}{z_1} z \tag{8}$$

The pressure drop along the first zone is :

$$\Delta p = p_0 - p_1 = \frac{2mz_1}{R}\left[\frac{(\varepsilon+3)\,D_v}{\pi R^3}\right]^n \tag{9}$$

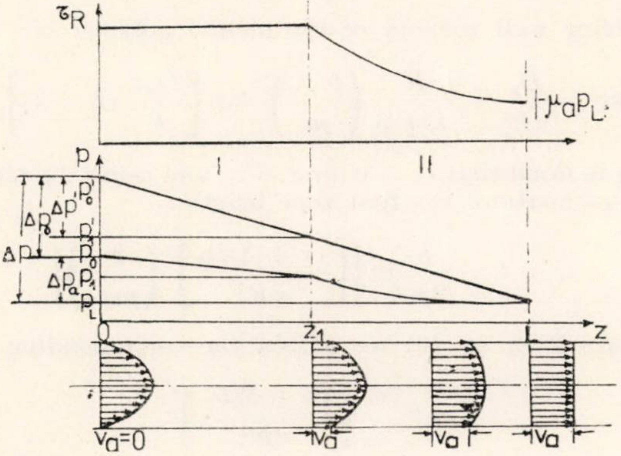

Fig. 2. — Axial profiles of the pressure and shear stress.

and the corresponding entrance pressure is :

$$p_0 = p_1 + \frac{2mz_1}{R}\left[\frac{(\varepsilon+3)D_v}{\pi R^3}\right]^n \tag{10}$$

Zone II is for $z \in (z_1,\ L]$ where L is the channel length and the wall shear stress is given by eq. (7). To estimate the flowing velocity we use the constitutive equation together with the radial distribution of the shear stress :

$$\tau_{rz} = m\left(-\frac{\mathrm{d}v_z}{\mathrm{d}r}\right)^n = \tau_R \frac{r}{R} \tag{11}$$

Taking into account eq. (7) the shear rate deformation is given by

$$-\frac{\mathrm{d}v_z}{\mathrm{d}r} = \left(\frac{\tau_R}{m}\frac{r}{R}\right)^\varepsilon = \left\{\left|-\frac{p_L\mu_a}{m}\right|\exp\left[\frac{2\mu_a}{R}(L-z)\right]\frac{r}{R}\right\}^\varepsilon \tag{12}$$

with the boundary condition at the wall :

$$r = R\,;\ v_z = v_a \tag{13}$$

having the following solution :

$$v_z = v_a + \frac{R}{\varepsilon+1}\left\{\frac{p_L\mu_a}{m}\exp\left[\frac{2\mu_a}{R}(L-z)\right]\right\}^\varepsilon\left[1-\left(\frac{r}{R}\right)^{\varepsilon+1}\right] \tag{14}$$

Using this result, the volumetric flow rate is estimated as :

$$D_v = \int_0^{2\pi}\int_0^R v_z r \mathrm{d}r \mathrm{d}\theta = \pi R^2 v_a + \frac{\pi R^3}{\varepsilon + 3}\left(\frac{p_L \mu_a}{m}\right)^{\varepsilon} \exp\left[\frac{2\mu_a \varepsilon}{R}(L - z)\right)\Bigg] \quad (15)$$

and the resulting wall velocity of the melted polymer is :

$$v_a = \frac{D_v}{\pi R^2} - \frac{R}{\varepsilon + 3}\left(\frac{p_L \mu_a}{m}\right)^{\varepsilon} \exp\left[\frac{2\mu_a \varepsilon}{R}(L - z)\right] \quad (16)$$

Keeping in mind that $v_a = 0$ for $z = z_1$, and using eq. (16) we obtain the following estimate of the first zone length :

$$z_1 = L - \frac{R}{2\mu_a}\ln\left\{\left[\frac{(\varepsilon + 3)D_v}{\pi R^3}\right]^n \left(\frac{m}{p_L \mu_a}\right)\right\} \quad (17)$$

and introducing it in eq. (6) we obtain the corresponding p_1 pressure :

$$p_1 = \frac{m}{\mu_a}\left[\frac{(\varepsilon + 3)D_v}{\pi R^3}\right]^n \quad (18)$$

Using eqs (10) and (15)—(18) we get the corresponding entrance pressure :

$$p_0 = p_1 \exp\left(\frac{2\mu_a z_1}{R}\right) \quad (19)$$

The radial position for which the fluid velocity is equal to the average velocity is given by :

$$r = R\left(\frac{2}{\varepsilon + 3}\right)^{\frac{1}{\varepsilon+1}} \quad (20)$$

3. NUMERICAL APPLICATION

To illustrate the usefullness of the above presented model we give the following numerical application. We consider melted polyethylene with the consistence index $m = 2.277 \cdot 10^4$ Pa · s^n and the power law index $n = 0.4$, flowing through a capillary having 8.2 mm i.d. and 3 cm length. The operating conditions are : the volumetric flow rate is $9 \cdot 10^{-6}$ m^3/s, the exit pressure is $p_L = 10^5$ Pa and the wall friction coefficient $\mu_a = 0.2$. The numerical results are listed in Table 1. The pressure and the wall shear stress axial profiles, together with the radial velocity profile, are presented in Figures 3—4. The radial position for which the fluid velocity is equal to its average velocity is $\frac{r}{R} = 0.75$.

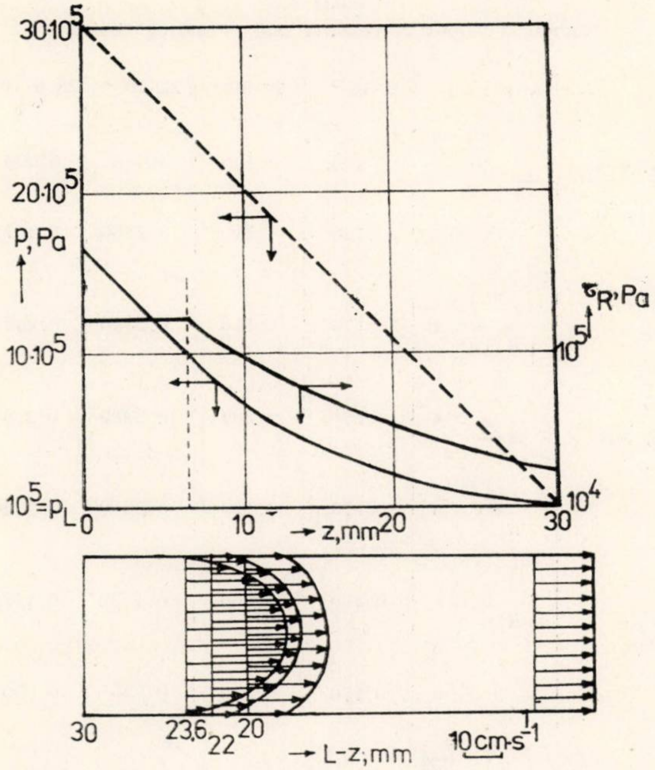

Fig. 3. — Axial profiles of the pressure and wall shear stress and radial profiles of velocity.

We observe that the sliding effect appears at $z_1 = 6.4$ mm from the entrance. The parabolic entrance velocity profile becomes closer and closer to the plug flow one, and is practically flat with 1 mm before the exit.

The total pressure drop under the fluid adherence to the wall is 3 MPa while our model predicts only 1.6 MPa.

4. CONCLUSIONS

The present model seems to allow a more rational design of the plastic processing equipments. Moreover, this model gets a deeper insight of the process, explaining the flow instabilities.

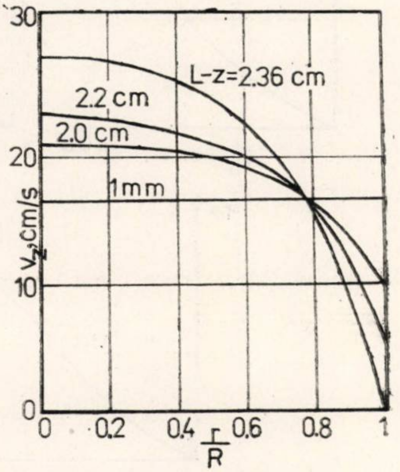

Fig. 4. — Radial profiles of the velocity.

Table 1

Numerical values of velocity and of sliding velocity

$L - z$, m		$1 \cdot 10^{-3}$	$20 \cdot 10^{-3}$	$22 \cdot 10^{-3}$	$23.6 \cdot 10^{-3}$
v_a, m/s		0.170	0.100	0.055	0.000
v_z, m/s	$\frac{r}{R} = 0$	0.170	0.210	0.2360	0.2677
	$\frac{r}{R} = 0.2$	0.170	0.210	0.2356	0.2674
	$\frac{r}{R} = 0.4$	0.170	0.207	0.2289	0.2569
	$\frac{r}{R} = 0.6$	0.170	0.193	0.2059	0.2229
	$\frac{r}{R} = 0.8$	0.170	0.160	0.1532	0.1451
	$\frac{r}{R} = 1.0$	0.170	0.100	0.055	0.000

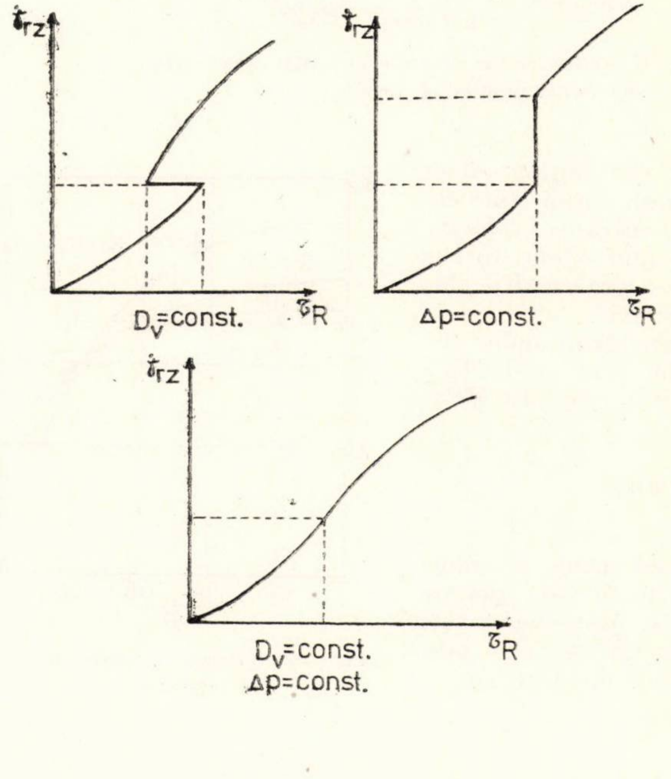
$\dot{\gamma}_{rz}$
τ_R
D_V=const.
$\dot{\gamma}_{rz}$
τ_R
Δp=const.
$\dot{\gamma}_{rz}$
τ_R
D_V=const.
Δp=const.

Fig. 5. — Instable flowing diagrams.

For any volumetric flow rate the shear rate deformation remains constant for a given range of the total pressure drop. On the other hand for any total pressure drop the wall shear stress is constant for a given range of the volumetric flow rate (see Figures 5).

Visualisation of the current lines or measurements of the total pressure drops could give a good validation of the theoretical analysis presented above.

NOTATIONS

D — capillary diameter
D_v — volumetric flow rate
L — capillary length
m — consistency index
n — flow index of a power law fluid
$\bar{M}_n$ — average numerical molecular weight
p — dynamic pressure
r — radial coordinate
R — capillary radius
v_a — slip velocity
v_z — velocity in the z direction
$\bar{v}$ — average velocity
z — axial coordinate
greek letters
Δp — pressure drop
ε $= 1/n$
η_a — apparent viscosity
μ_a — friction coefficient
τ_{rz} — shear stress
τ_R — shear stress at the capillary wall
θ — tangential coordinate
subscripts
o — capillary entrance
1 — axial position delimitating zone I from zone II
L — capillary exit

REFERENCES

[1] A. Ştefan, "Modelarea matematică a proceselor reologice de prelucrare a polimerilor" Ph. D. Thesis, Polytechnic Institute Bucharest, 1986.

[2] R. Mihail, and A. Ştefan, "Reologie aplicată la prelucrarea polimerilor", Polytechnic Institute Bucharest, 1985.

[3] G. Jinescu, "Procese hidrodinamice şi utilaje specifice", Ed. Didactică şi Pedagogică, Bucharest, 1983.

Revue Roumaine de Chimie, **34**, *5*, 1225–**1240** (1989)

ПУТИ СИНТЕЗА О-АНТИГЕННЫХ ПОЛИСАХАРИДОВ*

Н. К. КОЧЕТКОВ
Институт органической химии им. Н. Д. Зелинского Академии наук СССР, Москва

Получена 23 декобря 1988 г.

Биополимеры, локализующиеся на поверхности микробной клетки и несущие функции антигенов, т. е. соединений, вызывающих образование специфических антител в организме хозяина, относятся к различным классам и разнообразны по структуре; состав всей сложной композиции антигенных биополимеров определяется природой микроорганизма и является его важнейшей характеристикой.

Для грамотрицательных бактерий, к которым относятся возбудители многих инфекционных болезней, в том числе и особо опасных инфекций, наиболее характерными биополимерами с антигенными свойствами являются липополисахариды — гликоконъюгаты, содержащие наряду с углеводными и типичные липидные компоненты[1]. Липополисахариды, находясь на поверхности грамотрицательной бактерии и выполняя здесь роль так называемых соматических или О-антигенов, определяют не только специфичность образующихся в организме хозяина антител, но и многие другие существенные свойства поверхности микробной клетки, участвуя в таких важных биологических актах, как взаимное узнавание клеток, фиксация бактериофагов и т. д.

Принципы построения липополисахаридов в настоящее время хорошо известны [2]. Они состоят из трех частей: липофильной части (« липида А»), являющейся матрицей, погруженной в мембрану клетки, короткого олигосахарида («кора») и полисахаридной цепи, прикрепленной через «кор» к липидной части. Именно структура этой полисахаридной цепи, так называемого О-антигенного полисахарида, высоко специфична и определяет всю исключительно высокую биологическую специфичность О-антигена (липополисахарида) в целом.

Общий принцип построения О-антигенных полисахаридов в настоящее время также выяснен и установлены структуры более чем 250 полисахаридов этого типа.

Оказалось, что все они построены по единому плану и являются регулярными блок-полимерами, состоящими из повторяющихся олигосахаридных звеньев, которые могут быть линейными или разветвленными и содержать от двух до десяти моносахаридных единиц самой различной структуры [3], например

---

* Напечатана в *Известия Академии наук СССР, Химическая серия,* Москва, *1* (1984).

$$A-B-C-(A-B-C-)_n A-B-C \text{ или}$$

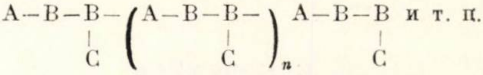

$$A-B-\underset{\overset{|}{C}}{B}-\left(A-B-\underset{\overset{|}{C}}{B}-\right)_n A-B-\underset{\overset{|}{C}}{B} \text{ и т. п.}$$

где A, B, C — остатки моносахаридов. В последние годы в нашей лаборатории [4–7], а далее и во многих других [8–10] успешно осуществлен синтез ряда подобных олигосахаридных повторяющихся единиц О-антигенных полисахаридов из бактерий рода Salmonella, Shigella, Escherichia и др. Более того, необычайно быстрый прогресс современного олигосахаридного синтеза открывает путь к получению большого количества синтетических олигосахаридных звеньев и их близких аналогов; количество работ в этом направлении быстро возрастает.

Вместе с тем следующий шаг к получению О-антигенных полисахаридов — соединение друг с другом повторяющихся олигосахаридных звеньев, приводящее к созданию строго регулярной блок-полимерной структуры, соответствующей природному биополимеру, — до самого последнего времени сделан не был; более того, не существовало и путей для решения подобной задачи. Между тем решение и этой задачи — синтеза самих О-антигенных полисахаридов — становится в настоящее время возможным и имеет огромное значение для дальнейшего изучения биологических свойств и возможностей практического медицинского использования этих важнейших биополимеров.

Сам принцип строения О-антигенных полисахаридов однозначно указывает, что наиболее целесообразный путь их синтеза — сборка биополимера из готовых олигосахаридных единиц. Практическое решение этой задачи может идти несколькими путями, из которых мы рассмотрим три следующих наиболее очевидных (ср. [11]).

1. Последовательное наращивание олигосахаридных повторяющихся звеньев (ступенчатый синтез).
2. Полимеризация олигосахаридов химическими методами.
3. Ферментативная полимеризация олигосахаридов.

Главным требованием к синтетическому О-антигенному полисахариду является его полная регио- и стереоспецифичность. Понятно, что любая, даже одна единственная ошибка в типе связей между звеньями или в стереохимии этой связи сразу вызывает нарушение конформации всей полисахаридной цепи в целом и, как следствие, резкое изменение ее физикохимических характеристик и биологических свойств. По этой причине наиболее серьезная общая проблема при реализации любого из указанных трех подходов к синтезу О-антигенных полисахаридов — это обеспечение регио- и стереоспецифичности реакции при соединении между собой двух соседних повторяющихся звеньев, которые представляют собой сложные полифункциональные соединения.

С другой стороны, осуществление каждого из этих подходов требует решения своих частных синтетических проблем и имеет свои преимущества и слабости. В лаборатории химии углеводов ИОХ АН СССР ведутся работы по всем трем направлениям, они и будут изложены в этой статье.

СТУПЕНЧАТЫЙ СИНТЕЗ

Ступенчатое наращивание повторяющихся олигосахаридных звеньев является наиболее очевидным и в то же время наиболее трудоемким путем, ведущим к получению соответствующего блок-полимера. Практическая реализация этого подхода прежде всего требует должной функционализации олигосахарида. Эта функционализация должна предусмотреть возможность последующей «сшивки» между собой олигосахаридных единиц и, стало быть, создание гликозилирующей группировки X на восстанавливающем моносахаридном звене гликозилирующего олигосахарида A и гликозилируемой группы — свободного или активированного гидроксила YO — в месте возникновения гликозидной связи гликозилируемого олигосахарида B. Остальные функциональные группы должны быть защищены подходящей временной защитой

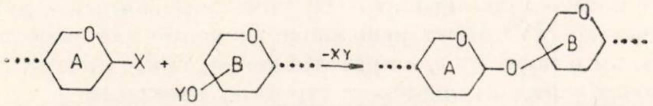
A
X
+
B
YO
-XY
A
O
B

Для стандартной процедуры наращивания олигосахаридного звена, которая может повторяться несколько раз для получения полимера нужного молекулярного веса, эффективный стандартизованный синтез производных A и B из исходного олигосахарида — существенная часть задачи. Наиболее рациональная методика ступенчатого синтеза будет достигнута, когда оба производных легко получаются из одного и того же предшественника.

Наращивание полимерной цепи может проводиться как с восстанавливающего, так и с невосстанавливающего конца цепи, однако первый вариант кажется более удобным. Этот путь к О-специфическим полисахаридам был изучен в нашей лаборатории.

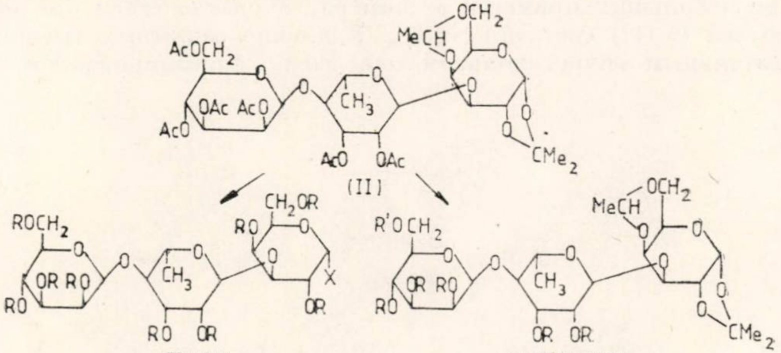
AcOCH2
OAc AcO
AcO
CH3
AcO OAc
MeCH
OCH2
CMe2
(II)
ROCH2
OR RO
RO
CH3
RO OR
CH2OR
RO
X
OR
(III),(IV)
R'OCH2
OR RO
RO
CH3
OR OR
MeCH
OCH2
CMe2
(V),(VI),(VII)
AcOCH2
OAc AcO
AcO
CH3
AcO OAc
AcOCH2
AcO
AcO
CH2
OR RO
RO
CH3
OR OR
MeCH
OCH2
CMe2
(VIII)

R = Ac, X = OAc(III); R = Ac, X = Br(IV); R = R′ = H(V);
R=H, R′=*p*-MeOTr(VI); R = CH$_2$Ph, R′ = H(VII); R = CH$_2$Ph(VIII)

В качестве примера, иллюстрирующего реализацию ступенчатого наращивания цепи, можно привести синтез гекса- и нонасахаридов — «димера» и «тримера» повторяющегося звена полисахарида S. newington[12]. Повторяющееся звено S. newington, как известно, имеет структуру β-*D*-Manp-(1 → 4)-α-*L*-Rhap-(1 → 3)-*D*-Gal (I). Повторяющиеся звенья в полисахариде связаны между собой β-галактозил (1—6)-маннозной связью.

Синтез трисахарида (I) разработан в нашей лаборатории в нескольких вариантах [4,13,14]. Для ступенчатого синтеза наиболее удобно исходить из производного (II), служащего исходным и для гликозилирующего и для гликозилируемого производного. Синтез (II) был специально отработан для этой цели [15]. Для получения гликозилирующего производного (II) превращается в декаацетат (III) и далее обработкой HBr в смеси $CHCl_3$ — AcOH при 0° в гликозилбромид (IV). Разумеется, для получения бромида (IV) можно использовать (I), синтезированный другими методами [4,14]. Качество (IV) имеет решающее значение для успеха последующей конденсации и поэтому его приготовление, как и других галогенидов сложных олигосахаридов, подлежит строгому контролю.

Для получения гликозилируемого производного (II) дезацетилировали действием NEt_3 — MeOH, единственную первичную гидроксильную группу в получившемся (V) замещали метокситритилированием, полученный (VI) бензилировали и после деметокситритилирования 1%-ной трифторуксусной кислотой в дихлорметане был получен гликозилируемый компонент (VII). Он является производным, которое может употребляться для стандартного наращивания цепи блок-полимера.

Конденсация гликозилбромида (IV) и производного (VII) в присутствии $Hg(CN)_2$ в ацетонитриле, употребляя высоковакуумную технику для полного исключения влаги (ср.[16]), дала производное гексасахарида (VIII). Полученный препарат был освобожден посредством хроматографии от небольших примесей α-аномера, образующегося при конденсации; выход (VIII) составил >80%. Удаление защитных группировок последовательным гидрогенолизом над Pd/C, ацетилированием, ацето-

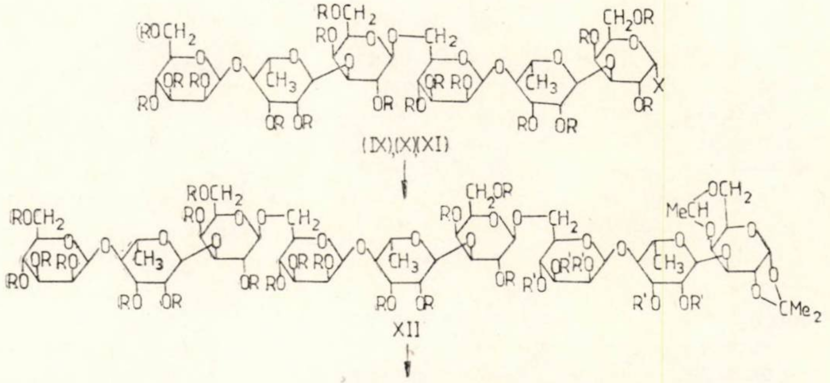

β-*D*-Manp-(1 → 4)-α-*L*-Rhap-(1 → 3)-β-*D*-Galp-(1 → 6)-β-*D*-Manp-(1 → 4)-α-*L*-Rhap-(-1 → 3)-β-*D*-Galp-(1→6)β-*D*-Manp-(1→4)-α-*L*-Rhap-(1→3)-*D*-Gal(XIII)

R = H, X = OH(IX); R = Ac, X = OAc(X); R = Ac, XBr(XI);

R = Ac, R′ = CH_2Ph(XII).

лизом и гидролизом дало свободный гексасахарид (IX) — «димер» повторяющегося звена, который ацетилированием превращался в октадекаацетат (X).

Для осуществления следующего этапа ступенчатого синтеза и получения «тримера» (X) снова превращали стандартным методом в гликозилбромид (XI), который при конденсации с производным (VII) аналогично описанному выше дал производное нонасахарида (XII) (выход 57%), удаление защитных групп дало сам «тример» повторяющегося звена (XIII)

Понятно, что ступенчатое наращивание полимерной цепи может быть продолжено и далее по стандарту: полиацетат олигомера превращается в гликозилбромид и конденсируется со стандартным производным (VII). Нужно только иметь в виду, что получение высших гликозилбромидов требует особенно тщательного контроля, а выходы продуктов конденсации по мере увеличения олигомера будут закономерно падать.

Приведенный пример демонстрирует, что таким путем могут быть получены полисахариды или соответствующие им высшие олигосахариды, состоящие из регулярно повторяющихся олигосахаридных блоков, к которым относятся и наиболее сложные из полисахаридов этого класса — О-антигенные полисахариды грамотрицательных бактерий. Принципиальной слабостью такого подхода является его огромная трудоемкость, особенно для последовательного наращивания значительного числа сложных по структуре олигосахаридных звеньев. При этом следует заметить, что должная функционализация сложного олигосахарида — узловой момент всей схемы — часто может представлять непреодолимые трудности. Нужно также иметь в виду, что очистка полученных олигополимеров от примеси аномеров, образующихся при конденсации, естественно усложняется также с ростом молекулярного веса.

Вместе с тем только ступенчатым методом и только этим путем можно получить олигомеры повторяющихся единиц со строго определенной степенью полимеризации, что необходимо для решения некоторых вопросов иммунохимии.

ХИМИЧЕСКАЯ ПОЛИМЕРИЗАЦИЯ ОЛИГОСАХАРИДОВ

Полимеризация олигосахаридного повторяющегося звена является наиболее естественным и прямым путем к получению блок-полимера, состоящего из регулярно повторяющихся олигосахаридных звеньев.

Ясно, что для получения полисахарида строго регулярной структуры, полностью соответствующего природному, полимеризация должна идти с абсолютной регио- и стереоспецифичностью. Отделение примеси с единичным «ложным» типом связи в случае синтеза макромолекулярных структур хроматографией или другим методом не представляется возможным. Принимая во внимание сложность структуры исходного монополиконденсации с абсолютной регио- и стереоспецифичностью представляла очень серьезные трудности и ставила жесткие требования к реакции гликозилирования, на которой должен основываться процесс поликонденсации. Решение проблемы стало возможным после того, как в нашей лаборатории был разработан принципиально новый метод гликозилирования посредством взаимодействия 1,2-О-цианоэтилиденовых производных сахаров с трифенилметиловыми эфирами под действием трифенилметилий-перхлората [16]. Эта реакция, представляющая собой каталитическую гетеролитическую реакцию, инициируемую ионом трифенилметилия, приводит к образованию 1,2-транс-гликозидной связи с абсолютной регио- и, что особенно существенно, стереоспецифичностью. Столь высокая стереоспецифичность конденсации, уникальная для химии сахаров, скорее всего может быть объяснена синхронным (пуш-пульным механизмом замещения[17].

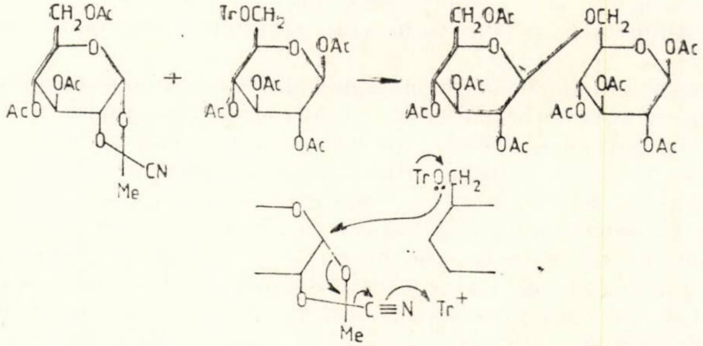

Эта реакция была положена в основу первого достаточно общего по своим возможностям синтеза полисахаридов (см. обзоры [18,19]) посредством поликонденсации моно- или олигосахаридов, содержащих одновременно

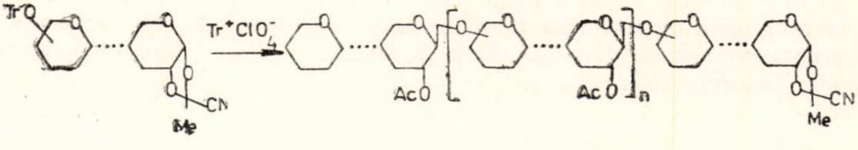

1,2-О-цианоэтилиденовую группу на восстанавливающем конце молекулы и О-тритильную группу у гидроксила, подлежащего гликозилированию. Этот метод впервые открыл возможности получения гомо- и гетерополисахаридов различного типа, в которых мономерные единицы (моно- и олигосахаридные) связаны 1,2-транс-гликозидной связью. Строгая региоспецифичность обеспечена введением в нужное место мономера О-тритильной группы и временной защиты остальных гидроксилов. Однако самое существенное, что обеспечивается абсолютная стереоспецифичность вновь возникающей гликозидной связи, чего не удавалось достигнуть ранее, используя для поликонденсации другие методы гликозилирования — классическую реакцию Кенигса—Кнорра и ортоэфирный синтез (см., например,[20,21]).

Для получения гетерополисахарида, состоящего из регулярно повторяющихся олигосахаридных звеньев, поликонденсации должен быть подвергнут олигосахарид (в нашем случае повторяющееся звено О-антигенного полисахарида), содержащий в нужном месте О-тритильную группу и 1,2-О-цианоэтилиденовую группировку.

В качестве примера можно приевсти синтез О-антигенного полисахарида S. newington, который представляет собой вообще первый химический синтез сложного по структуре биологически специфического гетерополисахарида [17,22] и является важным этапом в развитии синтетической химии углеводов.

Первая и самая трудная задача состоит, как и вообще при синтезе сложных регулярных гетерополисахаридов, в синтезе самого мономера т. е. должным образом функционализированного олигосахаридного повторяющегося звена. Наиболее обычный подход — введение функции в уже готовый олигосахарид

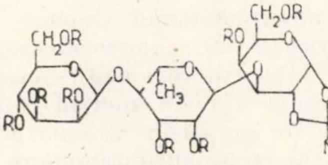

(XIV),(XV)

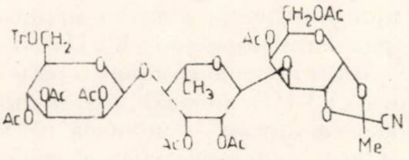

(XVI)

R = Ac(XIV); H(XV).

Для этого трисахарид (I), препаративный синтез которого удобнее всего проводить по, [14] превращался в декаацетат (III) и далее в ацетогалогенид (IV), который взаимодействием с KCN в ацетонитриле [23,24] переводили в 1,2-О-цианоэтилиденовое производное (XIV). Последнее мягкой обработкой разбавленным метилатом натрия превращали в (XV) со свободными гидроксильными группами. Следующая стадия являлась критической, так как нужно было ввести региоспецифически тритильную группу к C^6 маннозного остатка. Как известно, обработка тритилхлоридом в пиридине приводит к замещению преимущественно первичных гидроксильных групп моносахарида, однако в (XV) их две. Действительно, при тритилировании образовалась смесь обоих изомерных моно-О-тритиловых эфиров и ди-О-тритилового эира. К счастью, после ацетилирования нужный О-тритиловый эфир (XVI) удалось выделить хроматографией, хотя и с умеренным выходом.

Мономер (XVI) был введен в реакцию поликонденсации, которая осуществлялась в хорошо отработанных стандартных условиях в растворе CH_2Cl_2 в присутствии 10 мол.% перхлората трифенилметилия и приполном исключении следов влаги, что достигалось удобнее всего использованием высоковакуумной техники. Для больших количеств можно использовать при аккуратной работе и стандартную аппаратуру. Реакция практически заканчивалась через 50—50 ч, после чего она прерывалась добавлением водной CF_3CO_2H, и после нейтрализации и удаления растворителя полученный полимер без очистки подвергали дезацетилированию. Полученный свободный полисахарид (XVII), естественно, представлял смесь полимер-гомологов, из которой гель-фильтрацией выделялась фракция с мол. массой около 5000 (выход 60%). Это соответствовало степени полимеризации трисахаридного звена, равной 11—12, и средней степени полимеризации природного полисахарида. [25] Структура полученного полимера была подвергнута тщательному анализу химическими и физико-химическими методами. Она полностью соответствует структуре природного О-антигенного полисахарида S. newington. Гидролиз (XVII) дал только маннозу, рамнозу и галактозу в соотношении 1: 1: 1. Метилирование с последующим стандартным анализом дало набор частично метилированных полиолов, состоящий из 1, 5, 6-три-О-ацетил-2,3,4-три-О-метилманнита, 1,4,5-три-О-ацетил-2,3-ди-О-метилрамнита и 1,3,5-три-О-ацетил-2,4,6-три-О-метилдульцита, что полностью подтверждает типы связей моносахаридных остатков и свидетельствует о полной региоспецифичности реакции поликонденсации. Специальной тщательной проверке была подвергнута стереоспецифичность реакции поликонденсации. Для этого (XVII) подвергался распаду по Смиту, который привел к окислению остатков маннозы и рамнозы и сохранил нетронутым остаток галактозы с привязанным к нему гликозидной связью остатком глицерина, образовавшимся при окислении остатка маннозы; галактозильная связь в 1-О-галактопиранозилглицерине (XVIII) соответствовала галактозилманнозной связи с синтетическом полисхариде (XVII). Тщательный анализ полученного (XVIII) показал,что он представляет собой чистый β-изомер, т. е. связь галактоза — манноза в (XVII) также имеет только β-конфигурацию, что свидетельствует об абсолютной стереоспецифичности реакции поликонденсации и полной стереорегулярности синтетического полисахарида (XVII).

Полная идентичность структуры (XVII) и природного полисахарида, выделенного известным методом[26] из S. newington, видна также из сравнения спектров ЯМР^{13}С обоих образцов, приведенных в таблице.

Наконец, может быть наибольший интерес представляют биологические испытания синтетического полисахарида. Данные, полученные с помощью реакции ингибирования пассивной гемагглютинации (в системе О-фактор-3 — анти-3-сыворотка), указывают на то, что синтетический образец проявляет высокую иммунологическую активноть, хотя и уступает активности природного полисагарида, очевидно из-за более низкого молекулярного веса. Еще более важны были бы данные о биологической специфичности полученного синтетического антигена. С этой целью нами был получен ближайший аналог природного полисахарида — полисахарид . . . α-*D*-Manp-(1 → 4)-α-L-Rhap-(1 → 3)-β-*D*-Galp-(1 → 6)-α-*D*-Manp-(1 → 4)-α-*L*-Rhap-(1 → 3)-β-*D*-Galp . . . (XIX), который отличался только конфигурацией маннозил-рамнозной связи. Последняя в отли-

Сравнительные данные спектров ЯМР ^{13}С природного и синтетического О-антигенного полисахарида

Остаток сахара	Полисахарид	Химические сдвиги, м.д.					
		C^1	C^2	C^3	C^4	C^5	C^6
Man	Природный	101,75	71.7	74.3	68,1	76,25	70.55
	Синтетический	101,8	71,6	74,3	68,0	76,25	70,25
Rha	Природный	103,3	71,45	71,7	80,7	69,1	18,3
	Синтетический	103,4	71,4	71,6	80,8	69,1	18,5
Gal	Природный	104,4	71,45	81,8	69,75	76,4	62,1
	Синтетический	104,3	71,4	81,8	69,7	76,45	62,1

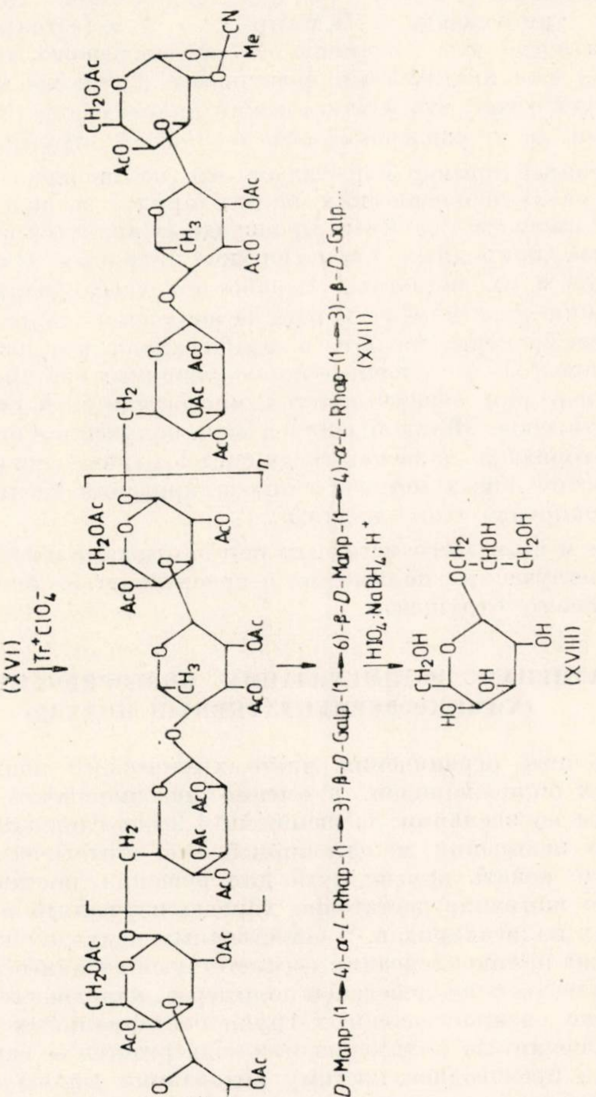
(XVI)
Tr⁺ClO₄⁻
…β-D-Manp-(1→4)-α-L-Rhap-(1→3)-β-D-Galp-(1→6)-β-D-Manp-(1→4)-α-L-Rhap-(1→3)-β-D-Galp…
(XVII)
HIO₄; NaBH₄; H⁺
(XVIII)
CH₂OAc
AcO
OAc
CH₃
CH₂
O
CN
Me
n
CH₂OH
HO
OH
OCH₂
CHOH
CH₂OH

чие от природной β-связи имела α-конфигурацию. Полисахарид (XIX) получен аналогичным путем при поликонденсации соответствующего производного трисахарида α-*D*-Manp-(1 → 4)-α-*L*-Rhap-(1 → 3)-*D*-Gal (XX).[17] Оказалось, что в отличие от синтетического антигена (XVII) аналог (XIX) был практически неактивным в том же тесте. Это ярко свидетельствует о том, что синтетический полисахарид (XVII) не только высокоактивен, но и узкоспецифичен по своей структуре.

Приведенный пример показывает, что поликонденсация повторяющихся звеньев О-специфических полисахаридов в виде О-тритиловых эфиров 1,2-О-цианоэтилиденовых производных является вполне реальным путем синтеза природных биологически активных О-специфических полисахаридов и их аналогов. Разработаны необходимые модификации для расширения приведенного метода на получение полисахридов, включающих также уроновые кислоты и аминосахара, что позволит получать этим путем новые, более сложные полисахаридные системы. В настоящее время в лаборатории осуществляется многостадийный синтез еще двух подобных антигенов. Метод ограничен пока получением полисахаридов, в которых повторяющиеся звенья соединены 1,2-транс-гликозидной связью, однако развитие новых методов гликозилирования вселяет надежды на будущее расширение этого подхода.

Слабым местом этого метода является относительно низкий молекулярный вес получаемых полимеров, и преодоление этой трудности — задача ближайшего будущего.

ФЕРМЕНТАТИВНАЯ ПОЛИМЕРИЗАЦИЯ ПОВТОРЯЮЩИХСЯ ЗВЕНЬЕВ (ХИМИКО-ФЕРМЕНТАТИВНЫЙ ПОДХОД)

Приведенные ограничения чисто химического подхода к синтезу О-антигенных полисахаридов, а именно невозможность пока получать полисахариды со звеньями, связанными 1,2-цис-гликозидной связью, и относительно невысокий молекулярный вес синтетических полимеров, заставили нас искать другие пути для решения поставленной задачи. Принимая во внимание достаточно хорошо изученный путь биосинтеза О-антигенных полисахаридов, [27] естественным подходом к их получению была бы также поликонденсация соответствуюших олигосахаридных повторяющихся звеньев под действием полимераз, являюшихся одной из важных и широко распространенных групп бактериальных ферментов. Однако в ходе биосинтеза полимеризации подвергается не сам олигосахарид, а его сложное производное, поэтому реализация такого подхода требует сначала превращения олигосахаридного повторяющегося звена в это производное — предшественник. Как известно, в ходе, биосинтеза повторяющееся олигосахаридное звено собирается на так называемом липидном переносчике; последний представляет собой пирофосфат сложного полипреноидного спирта, содержащего 55 углеродных атомов. Олигосахарид привязан к фосфатной группе пирофосфата своим восстанавливающим концом и образует соединение типа (XXI), которое и является предшественником биосинтеза. Полипренолпирофосфатолигосахарид типа (XXI) подвергается далее поликонденсации под действием полимеразы соответствующей бактерии.

Полипренолпирофосфатолигосахарид может быть получен как биохимически (последовательный перенос моносахаридных остатков на полипренолпирофосфат с помощью соответствующих гликозилтрансфераз), так и синтезирован чисто химическим путем, после чего подвергнут поликонденсации с помощью полимеразы. В этом случае такой подход можно назвать химико-ферментативным синтезом.

На первый взгляд этот путь синтеза О-антигенных полисахаридов кажется весьма специфичным и крайне трудоемким, требующим для каждого полисахарида выделения своего фермента и своего полипренола из бактериального материала, где тот и другой содержатся в чрезвычайно малых количествах. Однако счастливым образом два обстоятельства позволяют достаточно широко использовать этот подход. Исследования препаратов полимераз, выделенных из нескольких типов Salmonella, показали, что эти ферменты обладают довольно широкой специфичностью [28], т.е. способны вызывать поликонденсацию не только предшественника полисахарида из данного микроорганизма, но и поликонденсацию некоторых предшественников, содержащих другие моносахаридные остатки, хотя процесс и идет с меньшей скоростью. Это важное открытие означает, что, используя синтетические предшественники с иными моносахаридными остатками, можно осуществить синтез других, в том числе и неприродных, аналогов О-антигенных полисахаридов.

С другой стороны, оказалось, что природа полипренола, входящего в состав предшественника — субстрата поликонденсации типа (XXI), также не слишком специфична и в качестве полипренола может быть использован не обязательно полипренол данного микроорганизма. Это существенно облегчает препаративное решение проблемы; дело в том, что бактериальный полипренол содержится в микробной клетке в ничтожных количествах и малодоступен. Однако, как оказалось, он с успехом может быть заменен своим близким аналогом, например одним из доступных растительных полипренолов; мы использовали для этой цели полипренол из шелковицы (Morus alba), названный нами морапренолом, который был выделен и подробно изучен.[29] Интересно отметить, что более низкомолекулярные синтетические полиизопреноидные спирты также способны заменить бактериальный полипренол, хотя они и менее эффективны [30].

Химико-ферментативный подход имеет, естественно, и свои слабости. К их числу относится прежде всего сложность синтеза предшественника — субстрата полипренолфосфоолигосахарида. В настоящее время общий метод синтеза олигосахаридпирофосфатполипренолов типа (XXI) подробно разработан в лаборатории химии углеводов. Хотя этот метод довольно трудоемок, он дает возможность получать достаточно широкий набор таких предшественников.

Сложности связаны также с выделением фермента поликонденсации. Дело в том, что бактериальные полимеразы входят в ферментный ансамбль, обеспечивающий весь биосинтез О-антигенных полисахаридов и прикрепленный к бактериальной мембране. Попытки выделить полимеразы в достаточно очищенном виде пока не увенчались успехом, и по-видимому, солюбилизированный фермент окажется весьма неустойчивым и не подходящим для препаративной работы. По этой причине сегодня реально можно работать лишь с мембранным препаратом, содержащим полимеразу, который, естественно, менее эффективен и не свободен от примесей, осложняющих выделение продуктов поликонденсации.

Хотя химико-ферментативный метод находится ещё в стадии разработки и не применялся пока для получения О-антигенных полисахаридов в препаративных масштабах, уже ясно, что он по своим возможностям очень широк и позволяет получать как природные полисахариды разнообразной структуры, так и многие их аналоги.

В качестве примера рассмотрим синтез О-антигенного полисахарида S. anatum.[31] Он состоит из звеньев трисахарида (I), связанных α-галактозил-(1—6)-маннозной связью в отличие от близкого по структуре полисахарида S. newington, имеющего β-галактозидную связь.

Первым этапом синтеза является получение субстрата ферментативной полимеризации — полипренилпирофосфатгалактозилрамнозилманнозы (XXI). В связи с тем, что при разработке основ химико-ферментативного метода контроль реакции поликонденсации удобнее было осуществлять с использованием изотопных методов, исходный трисахарид (I) предварительно метили введением трития к C^6-остатка галактозы.[32] Меченый трисахарид (XXII) далее превращали в 1-фосфат с α-конфигурацией. Наиболее удобным методом фосфорилирования сложных олигосахаридов оказался метод Мак-Дональда — фосфорилирование безводн. H_3PO_4. Фосфорилирование полного ацетата (XXII) этим методом[33] сопровождается минимальной деструкцией и дает достаточно чистый α-1-фосфат (XXIII). Далее (XXIII) превращали в полипренилпирофосфатолигосахарид (XXI). Как уже упоминалось, при этом исползовался доступный растительный полипренол — морапренол из шелковицы, который,

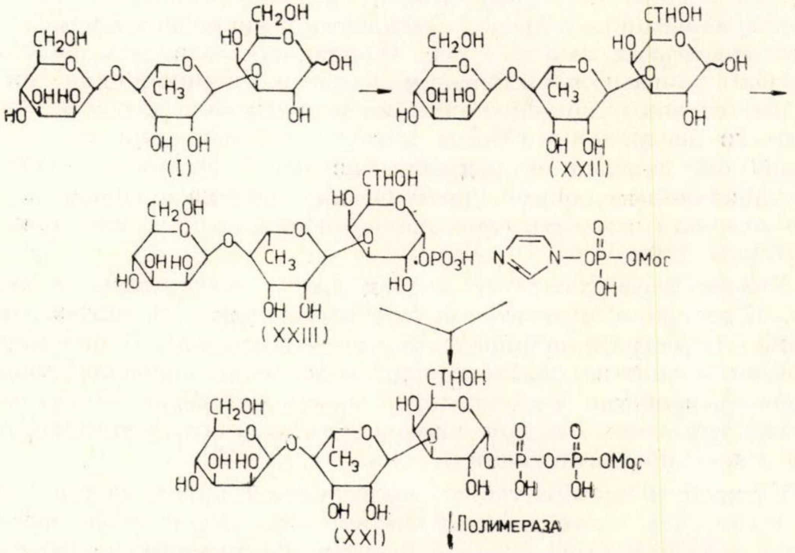

...β-*D*-Manp-(1 → 4)-α-*L*-Rhap-(1 → 3)-α-*D*-Galp-(1 → 6)-β-*D*-Manp-(1 → 4)-α-*L*-Rhap-(1 → 3)-α-*D*-Galp-(1 → 6)... (XXIV)

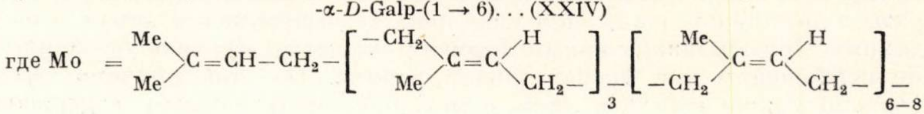

$$\text{где Mo} = \begin{matrix}\text{Me}\\ \text{Me}\end{matrix}\!>\!\text{C}=\text{CH}-\text{CH}_2-\left[\begin{matrix}-\text{CH}_2\\ \text{Me}\end{matrix}\!>\!\text{C}=\text{C}\!<\!\begin{matrix}\text{H}\\ \text{CH}_2-\end{matrix}\right]_3-\left[\begin{matrix}\text{Me}\\ -\text{CH}_2\end{matrix}\!>\!\text{C}=\text{C}\!<\!\begin{matrix}\text{H}\\ \text{CH}_2-\end{matrix}\right]_{6-8}-$$

как было выяснено,[34] может успешно заменить бактериальный полипренол в процессе поликонденсации.

Синтез (XXI) достигался посредством прямой конденсации олигосахарид-1-фосфата (XXIII) с морапренилфосфоимидазолом в смеси ТГФ и ДМСО в мягких условиях.[35] Этот новый метод дает возможность получать полипренолпирофосфатолигосахариды, непосредственно используя фосфаты олигосахаридов с незащищенными гидроксильными группами, и обойти очень серьезные трудности. Дело в том, что единственный известный до сих пор метод основывался на использовании ацетатов олигосахаридов и, следовательно, требовал далее омыления ацетатных групп без затрагивания пирофосфатной связи, что в ряде случаев было невозможно реализовать. Использование в конденсации олигосахаридов с незащищенными гидроксильными группами исключало стадию дезацетилирования и поэтому позволило получать полипренолпирофосфатолигосахариды, включающие моносахаридные остатки с экваториальными гидроксилами у C^2, которые особо чувствительны к разрыву фосфатной связи (галактоза, глюкоза и другие наиболее распространенные моносахариды). Следующая стадия — ферментативная полимеризация несимметричного пирофосфата (XXI) — проводилась под действием препарата, полученного из мембран S. anatum в соответствующем буфере, в присутствии $MgCl_2$. После отделени полипренолпирофосфатного остатка, остающегося на восстанавливающем конце образовавшегося полисахарида, мягким гидролизом и гель-фильтрацией на сефадексе был получен полисахарид (XXIV) с выходом 80%. Исследование его строения методами, подобными указанным в предыдушем разделе, показало, что он представляет собой строго регулярный полисахарид, состоящий из пяти повторяющихся звеньев олигосахарида (I), связанных между собой α-галактозидной связью. Конфигурация этой образовавшейся в ходе ферментативной полимеризации связи была подтверждена гидролизом полисахарида под действием специфического фермента — α-галактозидазы из кофейных зерен, а также получением α-галактозилглицерина при распаде полисахарида по Смиту, подобно описанному выше для β-аналога.

Следует особенно отметить, что практически те же результаты были получены при полимеризации предшественника (XXI) под действием полимераз из других салмонелл, например S.senftenberg. Это демонстрирует достаточно широкую специфичность полимераз, упомянутую выше.

Приведенный пример синтеза О-антигенного полисахарида S. anatum иллюстрирует возможности химико-ферментативного метода. Он важен и интересен, в частности, тем, что этот полисахарид, как и другие полисахариды, в которых повторяющиеся звенья связаны 1,2-цис-гликозидными связями, не может быть получен с помощью химической поликонденсации.

Вероятно, еще более важной в препаративном плане является возможность получать таким путем модифицированные полисахариды благодаря, отсутствию у полимераз узкой специфичности. По имеющимся данным, полученным с использованием меченых субстратов, в реакции поликонденсации могут в тех же условиях использоваться трисахариды типа (I), в которых остаток *D*-галактозы заменен на остаток *D*-фукозы, *D*-глюкозы, *D*-талозы и 4-дезокси-*D*-ксилогексозы, а остаток *D*-маннозы — на остаток *D*-рамнозы, 3-дезокси-*D*-арабиногексозы или остаток

D-глюкозы.[28, 36] При этом успешно получаютсм соответствующие модифицированные полисахариды, хотя их выход при поликонденсации несколько ниже выхода природного полисахарида и в более сильной степени зависит от источника полимеразы. Этим, кстати, демонстрируется, что специфичность полимераз все же имеет вполне определенные границы.

Препаративные аспекты синтеза модифицированных полисахаридов этим методом еще предстоит разработать, но принципиальная возможность широкого использования этого подхода не вызывает сомнений. По видимому, как и в случае химической поликонденсации, наиболее трудоемкой частью синтеза остается получение соответствующего субстрата ферментативной полимеризации. Как можно видеть на приведенном выше примере, химический синтез этих сложных соединений разработан подробно, вместе с тем он остается весьма трудоемким. В этой связи существенно отметить, что для получения небольших количеств полисахаридов можно применить и частичный биохимический синтез полипренолпирофосфатолигосахаридов, используя соответствующие нуклеотиддифосфатсахара и гликозилтрансферазы. Замечательно, что и здесь открыт путь к получению аналогов и неприродных субстратов, так как оказалось, что гликозилтрансферазы, так же как и полимеразы, обладают не слишком узкой специфичностью.[37] Действительно, используя частично химическую, частично биохимическую сборку олигосахаридного остатка на полипренилпирофосфатном остатке и последующую ферментативную полимеризацию, удалось получить несколько полисахаридных систем.[38]

Заканчивая это краткое обсуждение путей получения О-антигенных полисахаридов, следует еще раз подчеркнуть, что три рассмотренных пути различны по своим возможностям и целям.

Первый из них, ступенчатый синтез, очевидно, практически пригоден лишь для получения коротких полисахаридов, содержащих 3—4 повторяющихся звена, но зато дает полисахарид, точнее олигосахарид, со строго определенным числом повторяющихся звеньев, что недоступно двум другим методам.

Метод химической поликонденсации пока разработан лишь для связывания повторяющихся звеньев 1,2-транс-связью, но в этих рамках обладает достаточной широтой как химический метод. Он впервые демонстрирует возможность чисто химического синтеза сложных полисахаридов.

Наконец химико-ферментативный метод, потенциально наиболее широкий по своим возможностям, пока ограничен в отношении синтеза больших количеств полисахарида, а возможность использования его будет определяться широтой специфичности и доступностью соответствующих полимераз.

Можно полагать, что все три подхода найдут свое использование при получении различных О-антигенных полисахаридов и их аналогов, необходимых для решения различных проблем, возникающих при изучении полисахаридов с высокой биологической специфичностью. Использование этих методов открывает возможности для получения сложных полисахаридов со вполне точной структурой, которые послужат важными моделями для изучения взаимосвязи между химической структурой, конформацией полимерной цепи, физико-химическими свойствами и биологической специфичностью этих важных биополимеров.

ЛИТЕРАТУРА

[1] O. Westphal In: International Archives of Allergy and Applied Immunology. Basel, 1974, v. 49, p. 1.

[2] O. Lüderitz, M. A. Freudenberg, C. Galanos, V. Lehmann, E. T. Bietschel, D. H. Shaw, In: « Current topics in membrans and transport » N. Y., 1982, v. 17, p. 79—151.

[3] K. Jann, O. Westphal. In « The Antigens » N. Y., 1975, v. 3, p. 1—125.

[4] N. K. Kochetkov, B. A. Dmitriev, O. S. Chizhov, E. M. Klimov, N. N. Malysheva, A. Ya. Chernyak, N. E. Bayramova, V. I. Torgov, *Carbohyd. Res.*, 1974, **33**, C5.

[5] N. K. Kochetkov, N. N. Malysheva, V. I. Torgov, E. M. Klimov, *Carbohyd. Res.*, 1977, **54**, 269.

[6] N. K. Kochetkov, V. I. Torgov, N. N. Malysheva, A. S. Shashkov, *Tetrahedron*, 1980, **36**, 1099.

[7] N. K. Kochetkov, V. I. Torgov, N. N. Malysheva, A. S. Shashkov, E. M. Klimov, *Tetrahedron*, 1980, **36**, 1227.

[8] H. Paulsen, H. Bünsch, *Tetrahedron Lett.*, **1981**, 47.

[9] H. Paulsen, O. Lockhoff, *Chem. Ber.*, 1981, **114**, 3115; H. Paulsen, H. Bünsch. *Ibid.*, 1981, *114*, 3126; H. Paulsen, W. Kutschker, *Liebigs Ann. Chem.*, **1983**, 557.

[10] S. Josephson, D. R. Bundle. *Can. J. Chem.*, 1979, **57**, 3073.

[11] N. K. Kochetkov, *Pure Appl. Chem.*, 1975, **42**, 327.

[12] B. A. Dmitriev, A. N. Nikolaev, A. S. Shashkov, N. K. Kochetkov, *Carbohyd. Res.*, 1982, **100**, 195.

[13] N. K. Kochetkov, B. A. Dmitriev, N. N. Malysheva, A. Ya. Chernyak, E. M. Klimov, N. E. Bayramova, V. I. Torgov, *Carbohyd. Res.*, 1975, **45**, 283.

[14] V. I. Betaneli, M. V. Ovchinnikov, L. V. Backinowsky, N. K. Kochetkov, *Carbohyd. Res.*, 1980, **84**, 211.

[15] А. В. Николаев, А. С. Шашков, Б. А. Дмитриев, Н. К. Кочетков, *Биорган. химия*, 1981, **7**, 914.

[16] A. F. Bochkov, N. K. Kochetkov, *Carbohyd. Res.*, 1975, **39**, 355.

[17] N. K. Kochetkov, V. I. Betaneli, M. V. Ovchinnikov, L. V. Backinowsky, *Tetrahedron*, 1981, **37**, Supl. 9, 149.

[18] N. K. Kochetkov, Sov. Scientific Reviews. Section B. Chemistry Reviews, 1982, v. **4**, p. 1—69.

[19] Н. К. Кочетков, Изв. АН СССР. Сер. хим., **1982**, 1543.

[20] N. K. Kochetkov,, M. E. Klimov, *Carbohyd. Res.*, 1975, **44**, 138; Н. К. Кочетков, Е. М. Климов, М.В. Овчинников, Изв. АН СССР. Сер. хим., **1977**, 1864.

[21] И. К. Кочетков, А. Ф. Бочков, И. Г. Язловецкий, Изв. АН СССР. Сер. хим., **1968**,. 1818; А. Ф. Бочков, И. В. Обручников, Н. К. Кочетков, Ж. общ. химии, 1974, **44**, 1197.

[22] В. И. Бетанели, М. В. Овчинников, Л. В. Бакиновский, Н. К. Кочетков, *Докл. АН СССР*, **1980**, **251**, 108.

[23] V. I., Betaneli, M. V., Ovchinnikov L. V., Backinowsky N. K. Kochetkov *Carbohyd. Res.*, 1979, **68**, C11.

[24] В. И. Бетанели, М. В. Овчинников, Л. В. Бакиновский, Н. К. Кочетков, *Изв. АН СССР. Сер. хим.*, **1979**, 2751.

[25] J. M. Ryan, H. E. Conrad, *Arch. Biochem. and Biophys.*, 1974, **162**, 530.

[26] O. Westphal, K. Jann, *Methods Carbohydrates Chem.*, 1965, **5**, 83.

[27] В. Н. Шибаев, *Успехи биологической химии*, 1982, **23**, 61.

[28] Н. К. Кочетков, В. Н. Шибаев, Т. Н. Дружинина, Л. М. Гогилашвили, Л. Л. Данилов, В. И. Торгов, С. Д. Мальцев, Н. С. Уткина, *Докл. АН СССР*, 1982, **262**, 139.

[29] Г. И. Вергунова, И. С. Глуходед, Л. Л. Данилов, Г. И. Елисеева, Н. К. Кочетков, М. Ф. Троицкий, А. И. Усов, А. С. Шашков, В. Н. Шибаев, Биорган. химия, 1977, **3**, 1484.

[30] Л. Л. Данилов, Н. А. Калинчук, Т. Н. Дружинина, В. Н. Шибаев, Е. В. Полунин, М. А. Новикова, С. И. Торгова, А. М. Моисеенков, Н. К. Кочетков, *Докл. АН СССР*, 1983, **271**, 358.

[31] В. Н. Шибаев. Т. Н. Дружинина, Н. А. Калинчук, С. Д. Мальцев, Л. Л. Данилов, В. И. Торгов, Н. К. Кочетков, С. Ш. Рожнова, В. А. Килессо, *Биоорган. химия*, 1983, **9**, 564.

[32] В. И. Торгов, В. Н. Чекунчиков, В. Н. Шибаев, Н. К. Кочетков, *Биоорган. химия*, 1981, 7, 401.

[33] L. L. Danilov, M. F. Troitsky, N. S. Utkina, V. N. Shibaev, N. K. Kochetkov, *Carbohyd. Res.*, 1980, **87**, 141.

[34] Ю. Ю. Кусов, Е. В. Киселева, Л.Л. Данилов, В. Н. Шибаев, Н. К. Кочетков, С. Ш. Рожнова, В. А. Килессо, *Биорган, химия*, 1979, **5**, 1863.

[35] L. L. Danilov, S. D. Maltsev, V. N. Shibaev, N. K. Kochetkov, *Carbohyd. Res.*, 1981, **88**, 203.

[36] V. N. Shibaev, L. L. Danilov, T. N. Druzhinina, L. M. Gogilashvili, S. D. Maltsev, N. K. Kochetkov, *FEBS Letters*, 1982, **139**, 177.

[37] V. N. Shibaev, *Pure and Appl. Chem.*, 1978, **50**, 1421.

[38] В. Н. Шибаев, Т. Н. Дружинина, Л. М. Гогилашвили, Н. К. Кочетков, С. Ш. Рожнова, В. А. Килессо, *Докл. АН СССР*, 1983, **270**, 897.

Revue Roumaine de Chimie, **34**, *5*, 1241–1243 (1989)

AN EXTENSION OF THE KOCH-HAAF REACTION. N-ACYL-GLYCINES FROM N-HYDROXYMETHYL-AMIDES AND -IMIDES

CANDIANO LEONTE and EUGENIA CARP
Polytechnic Institute, Department of Organic and Macromolecular Chemistry, Iassy, Romania

Received November 4, 1988

The paper shows that, in the same manner as the simple alkyl carbocations, the carbenium-immonium ions, generated from N-hydroxymethyl-amides and -imides in acid catalysis, react with nucleophilic carbon monoxide, leading to N-acyl-glycines. This "hydroxycarbonyl-de-hydroxylation" is an extension of the Koch-Haaf reaction.

1. THEORETICAL

The Koch-Haaf reaction,[1] in which the alkenes and alcohols react, in acidic medium, with carbon monoxide (often generated *in situ* from formic acid in concentrated sulfuric acid), leads, in a process involving alkyl and acyl cations as reactive intermediates, to carboxylic acids :

$$R^+ \xrightarrow{:\overset{-}{C}\equiv\overset{+}{O}:} R-\overset{+}{C}=\overset{..}{O}: \xrightarrow[-H^+]{HOH} R-COOH$$

The products are always α-branched, since the intermediate carbenium ions (which react with nucleophilic carbon monoxide), resulted directly from the substrates or by subsequent rearrangements, are, in most cases, of tertiary alkyl type.

We have now found that amido- and imido-methyl cations, generated in an SN1 process from N-hydroxymethyl-amides and -imides in acidic media, which are even more stabilized than the simple alkyl cations by a carbenium-immonium resonance type,[2] and which are able to combine with various weak nucleophiles (as aromatic nuclei, amides, nitriles,[2] urethans [3] and others), react with carbon monoxide too, leading, in the conditions of the Koch-Haaf reaction, to N-acyl-glycines :

$$R-CO-NH-CH_2OH \xrightarrow[H-HOH]{H^+} R-CO-\overset{..}{N}H-\overset{+}{C}H_2 \leftrightarrow R-CO-\overset{+}{N}H=CH_2$$

$$\xrightarrow{:\overset{-}{C}\equiv\overset{+}{O}:} R-CO-NH-CH_2-\overset{+}{C}=O \xrightarrow[-H^+]{HOH} R-CO-NH-CH_2-COOH$$

As substrates, the N-methylol derivatives (Ia, b ; Y=OH) of the following aromatic amides and imides were used :benzamide, p-fluoro- and p-chloro-benzamide, and phthalimide.

(p) $X-C_6H_4-CO-NH-CH_2-Y$ (o) $C_6H_4(CO)_2N-CH_2-Y$
Ia(X=H, F, Cl) Ib
Y=OH, COOH Y=OH, COOH

The reaction was carried out by addition of the corresponding N-methylol derivative to a mixture of formic acid (98%) and sulfuric acid (100%). The molar ratio of the reactants was 1 : 9 : 24. The work-up of the reaction mixtures, as described in experimental part, afforded, with moderate yields, the corresponding N-acyl-aminoacetic acids (Ia, b ; Y=COOH). No other organic acids, which, in the conventional acylations of glycine, contaminate the products (e.g. benzoic acid) were found.

It is to note that, by some modifications of the experimental conditions, better yields are likely to be expected, the procedure described here being only prospective. Nevertheless, this type of transformation of N-methylol-amides and -imides ("hydroxycarbonyl-de-hydroxylation") appears to be an attractive alternative to other approaches to N-acyl-glycines and, if it were applied to some similar substrates, it could be of some interest in peptide synthesis.

2. EXPERIMENTAL

As starting materials were used : N-hydroxymethyl-benzamide (Ia, X=H, Y=OH)[4] m.p. 104–106°C (decomp.), from ethanol; N-hydroxymethyl-p-fluorobenzamide (Ia, X=F Y=OH),[5] m.p. 136°C (decomp.), after trituration with ethyl acetate; N-hydroxymethyl-p-chlorobenzamide (Ia, X=Cl, Y=OH),[6] m.p. 145°C (decomp.); N-hydroxymethyl-phthalimide (Ib, Y=OH),[7] m.p. 136–141°C, from ethanol; 98% formic acid; 100% sulfuric acid (if need be, this may be prepared from 20% oleum and ordinary concentrated sulfuric acid).

General Procedure. A mixture of formic and sulfuric acids was previously prepared by dropwise addition, with stirring and cooling (2–3°C), of 80 mmol of 98% formic acid to 480 mmol of 100% sulfuric acid. To this mixture, 20 mmol of finely-powdered N-hydroxymethyl derivative (Ia, b; Y=OH), concomitantly with 100 mmol of 98% formic acid, are gradually added, with stirring and cooling (– 4– 5°C), over a period of 45–60 min., until the solid passes into solution. Stirring is continued at about 15°C for 2 hours.The resultant mixture is allowed to stand overnight at about 0°C and then is poured with stirring onto 60 g of crushed ice. The precipitated product is collected by filtration and washed well with some cold water and, still moist, is dissolved in about 40 mL of 8% sodium hydrogen carbonate solution. The insoluble material is filtered off and the filtrate is acidified with 1 : 1 diluted hydrochloric acid. The N-acyl-glycine separates as colourless precipitate and, after isolation, may be additionally purified by recrystallization.

The following N-acyl-glycines (Ia, b; Y=COOH) were thus obtained : hippuric acid (X=H), 70% yield, m.p. 189–191°C, lit.[8] : 186–187°C (from water); p-fluorohippuric acid (X=F), 51% yield, m.p. 170–171°C (from acetone – chloroform), lit.[9] : 161–161,5°C (from ether) (as metabolization product of p-fluorobenzoic acid); p-chlorohippuric acid (X=Cl), 49% yield, m.p. 147–148°C (from ethyl acetate), lit.[10] : 148°C (from water) ; N,N-phthaloyl-glycine (Ib, Y=COOH), 63.4% yield, m.p. 193–195°C, lit.[11] : 193–195°C (from ethanol). The structures are confirmed by the analytical and IR spectral data. In all instances, except for X=F, authentic samples were used for comparison.

As insoluble in 8% $NaHCO_3$ solution materials, the following by-products, separated from the acidic aqueous medium, were identified : p-chlorobenzamide, m.p. 179°C (from ethanol) N,N'-methylene-bis-benzamide, m.p. 220°C (from ethanol) and N,N'-methylene-bis-phthalimide, m.p. 224–226°C (from acetone), respectively.

REFERENCES

[1] H. Koch, W. Haaf, Ann., **618**, 251 (1958); L. I. Krimen and J. D. Cota, *Org. Reactions*, **17**, 249(1969).
[2] E. H. Zaugg and B. W. Martin, *Org. Reactions*, **14**, 52 (1965).
[3] I. Zugrăvescu, C. Leonte and O. Petrovanu, *Anal. Sti. Univ. "Al. I. Cuza" Iaşi, Sect. I*, T. VI, 1045 (1960).
[4] A. Einhorn, E. Bischkopff and B. Szelinski, *Ann.*, **343**, 223 (1905).
[5] E. Carp, C. Leonte, St. Cilianu and E. R. Bozga, Romanian - Patent 87212/25.I.1985.
[6] C. Leonte, E. Carp, St. Cilianu and E. R. Bozga, Romanian - Patent 94551/1.II. **1988**.
[7] R. S. Buc, *J. Amer. Chem. Soc.*, **69**, 254 (1947).
[8] A. W. Ingersoll and S. H. Babcock, *Org. Synth. Coll.*, **II**, 328 (1961).
[9] M. Coppola, *Gazz. chim. Ital.*, **13**, 523 (1883).
[10] J. Wührer, *Ar. Pth.*, **161**, 719 (1931); G. Z., **1931**, II, 3115.
[11] G. Champetier, M. Guinot, *Compt. rend*, **248**, 1822 (1959); *Chem. Abstr.*, **1960**, 3234g.

Revue Roumaine de Chimie, **34**, *5*, 1245—1250 (1989)

COMPLEX COMPOUNDS OF DIVALENT MANGANESE

D. NEGOIU, MARLENE HANDREA, MARIA NEGOIU and OVIDIU MAIOR
**National Institute of Chemistry, Department of Chemical Technology, Chair of Inorganic Chemistry and Technology, Polizu Street 1,
Bucharest 78126, Romania**

Received May 5, 1988

Six complex compounds of Mn(II) were synthesized : bistriphenylarsonium tetrabromomanganate $[MnBr_4]\cdot[HAs(C_6H_5)_3]_2$, bisoxotritolylphosphine dibromomanganate (II) $MnBr_2\cdot(OPTol_3)_2$, bisphenylphosphonium tetrabromomanganate (II)$[MnBr_4][H_3P(C_6H_5)]_2$, bistrinaphthylphosphonium tetrabromomanganate(II) $[MnBr_4][HP(C_{10}H_7)_3]_2$, bistri(p-N--dimethylethoxyphenylphosphonium) tetrabromanganate(II) $[MnBr_4][HP(C_{10}H_{14}NO)_3]_2$ and bistri-p(p-methoxyphenylphosphonium) tetrabromomanganate(II) $[MnBr_4][HP(C_7H_7O)_3]_2$. The substances were characterized by elemental analysis and UV—VIS spectra. The Racah parameters, the Δ splitting parameter in crystal field and the nephelauxetic parameters were calculated.

INTRODUCTION

Electronic configuration $3d^5$ of bivalent manganese was studied[1,2] using both the weak field[3'4] and the strong field[5] methods. The latter method allows the calculation of the energy of the energetic levels of the $3d^5$ configuration as a function of interelectronic repulsion parameters $B_{\gamma\gamma'}$ and $C_{\gamma\gamma'}$ specialized according to the *e* and t_2 tetrahedral sublevels and also the calculation (on the basis of the experimental spectroscopic data) of the values of the B_{33}, B_{35} and B_{55} parameters and the corresponding $C_{\gamma\gamma'}$ ones. Taking into account all these parameters, the covalence degree of the *e* and t_2 orbitals can be evaluated. The Δ values obtained in this case are determined less exactly because they result only out of corrections due to the second order perturbations.

RESULTS AND DISCUSSION

The complex compounds of divalent manganese were characterized mainly by elemental analysis (Table 1). A good agreement exists between the experimental and theoretical results. The melting points of all the substances obtained were determined and compared with the melting points of the respective phosphines (Table 2).

The absorption spectra in UV-VIS were recorded in chloroform or dimethylformamide (Figs 1—5). These spectra contain 4—5 bands. The assignments given in table 3 were made on the basis of the diagram of

Table 1

Elemental analysis of the divalent manganese compounds

Substance	Mn%		C%		H%	
	theor.	exp.	theor.	exp.	theor.	exp.
$[MnBr_4][HAs(C_6H_5)_3]_2$	5.55	5.06	43.71	42.83	3.25	3.50
$MnBr_2 \cdot (OPTol_3)_2$	5.42	5.13	59.00	61.90	5.00	7.10
$[MnBr_4][H_3PC_6H_5]_2$	5.90	5.23	15.69	17.71	1.75	2.53
$[MnBr_4][HP(C_{10}H_7)_3]_2$	4.57	4.27	59.95	59.21	3.66	3.80
$[MnBr_4][HP(C_{10}H_{14}NO)_3]_2$	3.86	3.25	53.79	52.65	6.42	7.14
$[MnBr_4][HP(C_7H_7O)_3]_2$	5.08	4.93	46.64	45.81	4.72	4.85

Table 2

Melting points of the ligands and of the complex compounds

Complex compound	M.p. (°C)	Ligand	M.p. (°C)
$[MnBr_4][HAs(C_6H_5)_3]_2$	180	$As(C_6H_5)_3$	168
$MnBr_2(OPTol_3)_2$	145	$OPTol_3$	130
$[MnBr_4][H_3PC_6H_5]_2$	290	$H_2PC_6H_5$	liquid
$[MnBr_4][HP(C_{10}H_{14}NO)_3]_2$	286	$P(C_{10}H_{14}NO)_3$	285
$[MnBr_4][HP(C_6H_7O)_3]_2$	150	$P(C_7H_7O)_3$	130−131

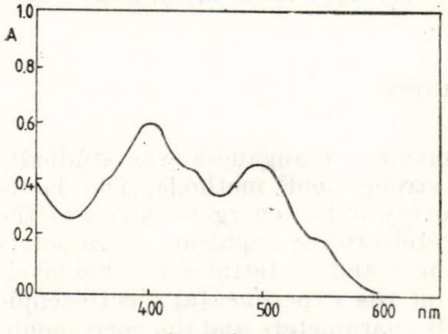

Fig. 1. — Absorption spectra of $[MnBr_4][HAs(C_6H_5)_3]_2$.

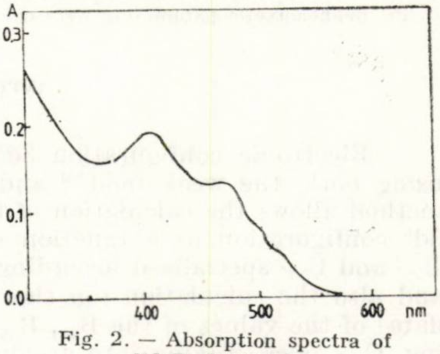

Fig. 2. — Absorption spectra of $[MnBr_2(OPTol_3)_2]$.

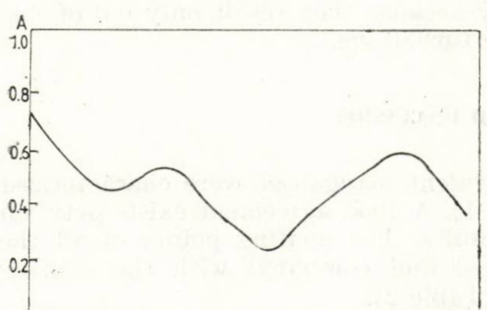

Fig. 3. — Absorption spectra of $[MnBr_4][HP(C_{10}H_7)_3]_2$.

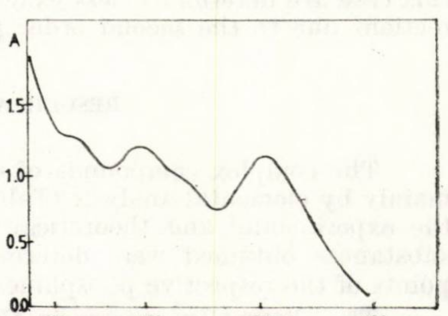

Fig. 4. — Absorption spectra of $[MnBr_4][HP(C_7H_7O)_3]_2$.

the energetic levels calculated in ref.[5] The diagram shows the transitions from $^6A_1$ to the quadruplet group of the $3d^5$ configuration. Otherwise stated, all these transitions are forbidden by the spin rule.

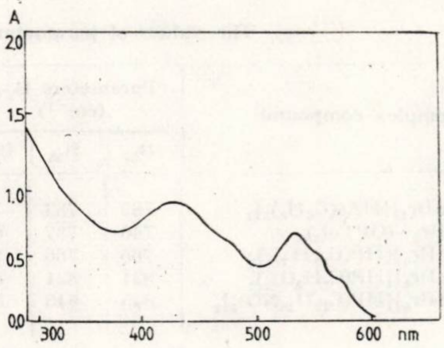

Fig. 5.—Absorption spectra of $[MnBr_4][HPC_{10}H_{14}NO)_3]_2$.

Table 3

UV—VIS Absorption spectra of the Mn(II) complex compounds

Complex compound	Transition from $^6A_1$ to	ν_{max} (cm^{-1})	ε_{mol}
$[MnBr_4][HAs(C_6H_5)_3]_2$	1 $^4T_1(^4G)$	19040	0.01
	2 $^4T_2(^4G)$	21410	0.42
	3 $^4A_1{}^4E(^4G)$	22710	0.36
	4 $^4T_1(^4P)$, $^4T_2(^4D)$	28870	0.40
	5 $^4E(^4D)$	28240	0.30
$MnBr_2 \cdot (OPTol_3)_2$	1 $^4T_1(^4G)$	18180	0.02
	2 $^4T_2(^4G)$	20400	0.15
	3 $^4A_1$, $^4E(^4G)$	28410	0.45
	4 $^4T_1(^4P)$, $^4T_2(^4D)$	23470	0.41
	5 $^4E(^4D)$	25540	0.52
$[MnBr_4][HP(C_{10}H_7)_3]_2$	1 $^4T_1(^4G)$	17069	0.015
	2 $^4T_2(^4G)$	19608	0.10
	3 $^4A_1$, $^4E(^4G)$	22222	0.35
	4 $^4T_1(^4P)$, $^4T_2(^4D)$	25000	0.41
	5 $^4E(^4D)$	29411	0.45
$[MnBr_4][HP(C_7H_7O)_3]_2$	1 $^4T_1(^4G)$	21276	0.02
	2 $^4A_1$, $^4E(^4G)$	23809	0.20
	3 $^4T_1(^4P)$, $^4T_2(^4D)$	26316	0.35
	4 $^4E(^4D)$	29413	0.45
$[MnBr_4][HP(C_{10}H_{14}NO)_3]_2$	1 $^4T_1(^4G)$	16806	0.01
	2 $^4T_2(^4G)$	17241	0.25
	3 $^4A_1$, $^4E(^4G)$	18692	0.32
	4 $^4T_1(^4P)$, $^4T_2(^4D)$	21739	0.36
	5 $^4E(^4D)$	23809	0.42

As a consequence, the intensity of the transitions noticed is weak, in agreement with the theoretical considerations above. This can be also seen in the value of the molal extinction, given in the last column of table 3.

Table 4

The values of parameters $B_{\gamma\gamma'}$, $\beta_{\gamma\gamma'}$ and Δ

Complex compound	Parameters $B_{\gamma\gamma'}$ (cm^{-1})			Parameters $\beta_{\gamma\gamma'}$			Parameter (cm^{-1})
	B_{35}	B_{55}	B_{33}	β_{35}	β_{55}	β_{33}	Δ
$[MnBr_4][HAs(C_6H_5)_3]_2$	783	783	786	0.86	0.86	0.86	5310
$MnBr_2 \cdot (OPTol_3)_2$	740	737	676	0.82	0.82	0.75	4500
$[MnBr_4][HP(C_{10}H_7)_3]_2$	766	766	883	0.85	0.85	0.98	5847
$[MnBr_4][HP(C_7H_7O)_3]_2$	821	821	812	0.91	0.91	0.90	4056
$[MnBr_4][HP(C_{10}H_{14}NO)_3]_2$	645	645	683	0.72	0.72	0.76	3327

The Racah parameters in table 4 may be calculated from the data in table 3 and on account of the energy expression of the sextet and quadruplet terms and of a series of approximations, frequently met in the crystal field theory.

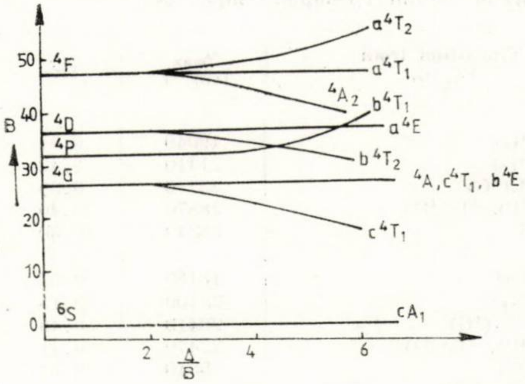

Fig. 6. — Diagram of the energetic levels for the d^5 configuration.

The diagram of the energetic levels[5] is given in Fig. 6. The Racah parameters specialized according to the two subshells e and t_2 are calculated from the experimental data and from the values of the energetic levels as a function of the Racah parameters.[5]

Taking into account the $\overline{B} = B_{35}$ and $C_{\gamma\gamma'} = 3.8B_{\gamma\gamma'}$ approximations from band 3 results :

$$E_1 - E(^4A_1) = 29\ B_{35} = 22710\ \text{cm}^{-1}$$

Therefore $B_{35} = 783$ cm^{-1}.

In the relation above, E_1 = diagonal elements + second order perturbation corrections. This value is obtained for $[MnBr_4] \cdot [HAs(C_6H_5)_3]_2$. The other parameters, B_{55} and B_{33}, are calculated taking into account the value of B_{35}.

The value of parameter Δ may be calculated by the difference $b^4E-c^4T_1$. The Racah parameters values, the Δ parameters and the nephelauxetic parameters are given in table 4. The nephelauxetic parameters are calculated with the value $B = 900\ cm^{-1}$ for the free ion. The values B_{33}, B_{35}, B_{55} are approximately equal, this indicating that the e and t_2 orbitals are approximately equal and slightly involved in covalent bonds. The value of Δ calculated previously may be improved if it is calculated and averaged from other bands.

The IR spectra of the complex compounds obtained were compared with those of the phosphines in the 200—450 cm^{-1} range. For $MnBr_2(OPTol_3)_2$ and the ligand, the respective frequencies are given in table 5.

Table 5

Vibration frequencies in IR of $MnBr_2 \cdot 2OPTol_3$ in comparison with $OPTol_3$

$MnBr_2 \cdot 2OPTol_3$	$\nu \cdot 100\ cm^{-1}$	$OPTol_3$	$\nu \cdot 100\ cm^{-1}$	Assignments
	655		665	Φ(CC)
	700			
	800		815	γ(CH)
	995		1028	β(CH)
	1095			X direction
	1120		1120	
	1160		1193	ν(P = O)
	1270		1310	X (direction)
	1400		1445	ν(CC)
	1440			
	1460			
	1500		1502	ν(CC)
	1600		1603	ν(CC)

Only certain vibration modes are affected by coordination (665, 815, 1028, 1193, 1310 cm^{-1}).

Cotton, Barnes and Bannister[6] studied the complexation effect of the P—O bond on the vibration frequency, and showed that a shift towards frequencies less than maximum 50 cm^{-1} takes place. In the complex mentioned this is 33 cm^{-1}. The P—O bond could have a multiple bond character, as we may suppose that except for the coordinating bond $P^+ \rightarrow O^-$, an inverse bond $P^- \leftarrow 0^+$ may exist, made if the free orbitals dπ, corresponding to phosphorus, overlap the pπ orbitals of the oxygen occupied by electrons. The fact that the P—O bond is somehow double is clearly shown if considering the bond length.

The other complex compounds show that several vibration modes of the phosphines are affected, a proof of formation, of ions HPR_3^+ or HAs, R_3^+.

ESR spectra for some complex compounds prepared were recorded. In the following, the ESR spectrum of $[MnBr_4]\ [H_3PC_6H_5]_2$ will be discussed.

Mn^{2+} presents the spin multiplicity $2I+1 = 6$ that involves the existence of six hyperfine components. For $[MnBr_4] \cdot [H_3PC_6H_5]_2$ an isotropic line, width 330.6 Gauss, centred at 3000 Gauss with the g factor equal to 2.006 is noticed (Fig. 7). The hyperfine splitting due to manganese is not evidenced. The hyperfine structure can be studied on magnetically diluted samples. The enwrapping curve obtained is the result of the dipolar interaction between the M^{2+} ions, with $3d^5$ configuration and the fundamental state $^6A_1$. The ESR spectra of these compounds prepared have similar forms.

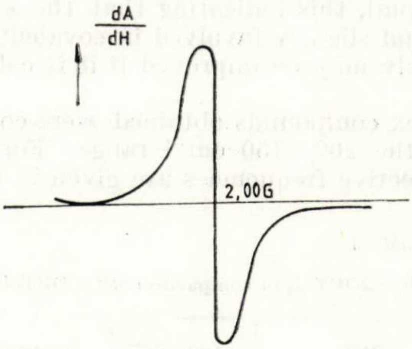

Fig. 7. — ESR spectra of $[MnBr_4][H_3PC_6H_5]$.

EXPERIMENTAL

The IR spectra were recorded with a Zeiss-Jena-Specord 71—IR spectrophotometer, in KBr disk.

The ESR spectra were recorded with a Romanian ART—5 apparatus.

The respective complex compounds were synthesized by using anhydrous $MnBr_2$ to which the respective ligand was added in molar ratio $MnBr_2 : lig = 1 : 1$, in glacial acetic acid. The solution was refluxed for two hours. A yellow colour and a yellow precipitate appeared. The precipitation may be improved by the solution concentration. In the case of the $MnBr_2 \cdot 2OPTol_3$ compound, the synthesis was made in DMF.

The absorption spectra were recorded with a Beckman UV—5260 spectrophotometer in chloroform or DMF as solvents and 1.0 cm cells.

REFERENCES

[1] J. Tanabe and S. Sugano, *J. Phys. Soc. Japan*, **9**, 753 and 766 (1954).
[2] Ch. K. Jörgensen, *Acta Chem. Scand.*, **8**, 1502 (1954).
[3] L. E. Orgel, *J. Chem. Phys.*, **23**, 1004, 1824 (1955).
[4] C. Furlani and A. Furlani, *J. Inorg. Nuclear Chem.*, **19**, 51(1963).
[5] D. Negoiu and C. Furlani, *Lincei-Rend. Sc. fis. mat. e nat.*, **35**, 59(1963).
[6] F. A. Cotton, R. D. Barnes and E. Bannister, *J. Chem. Soc.*, **1960**, 2199.

Revue Roumaine de Chimie, **34**, *5*, 1251–1261 (1989)

MESOIONIC OXAZOLONES. III[1]

PLANAR AND NONPLANAR ACYLATED COMPOUNDS

HORIA PETRIDE and DAN RĂILEANU *
Centre of Organic Chemistry — ICECHIM, Spl. Independenței
202B, 78100 Bucharest 15, Romania

Received December 12, 1987

Mesoionic oxazolones with an oxazolo[3,2-a]pyridinium- or quinolinium-2-olate structure were isolated as mono- and dichloroacetylated derivatives. ^{1}H-NMR spectra showed the acyl group as being coplanar with the mesoionic nucleus in the case of compounds 11 and 12, unlike 13–19 which are sterically hindered. The implications of the planar and nonplanar acylation of the mesoionic oxazolones upon the respective IR and UV absorption spectra are discussed.

Mesoionic oxazolones ("münchnones") with an oxazolo [3,2-a] pyridinium-2-olate structure (**1**) could be isolated only as acylated derivatives **2** or their transformation products.[1–4] From the ^{1}H–NMR spectra of the *in situ* generated compounds **1** it did result that the canonical structure **1B** should have an important contribution to the resonance hybrid.[1] On the other hand, a resonance structure of type **2D** was advocated to prevail in the case of the 3-acylated derivatives **2**.[5,6] As a matter of fact the acyl group, through its negative inductive and electromeric effects, stabilises the molecule but induces an appreciable perturbation of the electronic distribution. This perturbation will be obviously higher for an acyl group which is coplanar to the mesoionic nucleus. If the substituent R^1 displays sufficiently large steric requirements, the acyl group will be deviated from the molecular plane of **2**, the contribution of the canonical structure **2D** being minimized. Consequently, such nonplanar acylated münchnones should behave similarly to their non-acylated precursors **1**, which is not the case for the planar acylated analogs.

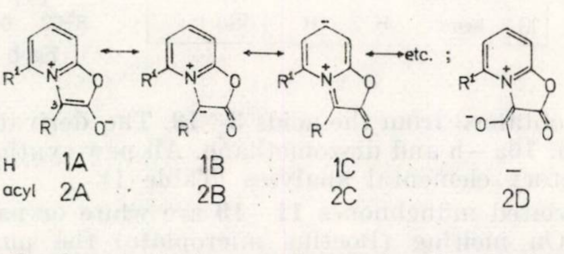

In this paper it is shown on spectral grounds that compounds **2** ($R^1 =$ $=Me$ or fused benzenic ring) are not planar münchnones in contrast with the acylated derivatives **2** ($R^1 = H$). The effect of such in-plane or out-of-plane acylation on the reactivity of these münchnones towards electrophiles (i.e. protonation) and nucleophiles will be discussed in a future paper.[7]

SYNTHESIS

To obtain acylated compounds of type **2** the cyclodehydration of the acids **3**—**10** with an acid anhydride was used. From the preceding paper in this series[1] it was known that acetic anhydride gives the expected reaction products only in the case of the acids **3** and **4**, namely the acetylated derivatives **11c** and **12c**, while the dimeric ketones **20** and **21c** were isolated starting from the acids **5** and **7**, respectively. However, employing a more powerful acylating agent than acetic anhydride, that is its mono- and dichloro-derivatives, the expected acylated compounds **11**—**18** were obtained from the acids **3**—**10**. The derivatives **19a**—**b** were prepared from **16a**—**b** and diazomethane. All new synthesized compounds gave satisfactory elemental analyses (Table 1).

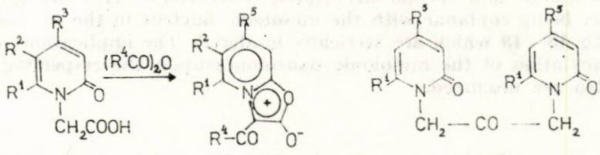

3—10 11—18 20,21c

	R^1	R^2	R^3	R^5	
3	H	H	H	H	11a-b-c
4	H	H	Me	Me	12a-b-c
5	Me	H	H	H	13a-b;20
6	Me	H	OAc	OAc	14a-b
7	Me	H	OH	$OCOR^4$	15a-b;21c
8	Me	H	CO_2H	CO_2H	16a-b
9	Me	CO_2H	H	H	17b
10	benzo		H	H	18a-b

	R^4
a	CH_2Cl
b	$CHCl_2$
c	CH_3

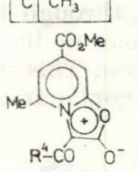

19a-b.

The acylated münchnones **11**—**19** are white or pale-yellow crystalline solids. On melting (Boetius microplate) the purified compounds **13**—**19** do not exhibit sharp melting points, unlike **11** and **12**. On remelting, the former substances gave the melting points of their hydrolysis products.[7] This transformation was confirmed by comparison with the IR and ^1H—NMR spectra of authentic materials. The reason of such different behaviour will be later discussed.[7]

Table 1

Preparation and elemental analyses of compounds **11–19**

Compd. no.	Method (yield, %)	Recryst. solvent	Molecular formula	Elemental analysis, %							
				Calculated				Found			
				C	H	N	Cl	C	H	N	Cl
11a	A(90)[c]	C_6H_6	$C_9H_6NClO_3$	51.08	2.86	6.62	16.76	51.04	3.15	6.68	16.44
11b	A(84)[d]	C_6H_6	$C_9H_5NCl_2O_3$	43.93	2.05	5.69	28.82	43.97	2.25	5.98	29.02
12a	A(50)[e]	CCl_4	$C_{10}H_8NClO_3$	53.23	3.57	6.21	15.71	53.45	3.82	6.43	15.44
12b	A(94)[f]	C_6H_6	$C_{10}H_7NCl_2O_3$	46.18	2.71	5.39	27.27	46.42	2.99	5.64	27.46
13a	A(74)	C_6H_6	$C_{10}H_8NClO_3$	53.23	3.57	6.21	15.71	52.91	3.81	6.20	15.70
13b	A(74)	C_6H_6	$C_{10}H_7NCl_2O_3$	46.18	2.71	5.39	27.27	46.49	2.97	5.59	27.58
14a	A(87)	C_6H_6	$C_{12}H_{10}NClO_5$	50.81	3.55	4.94	12.50	50.71	3.78	4.99	12.75
14b	B(60)	CCl_4	$C_{12}H_9NCl_2O_5$	45.33	2.85	4.40	22.29	45.27	3.06	4.68	22.58
15a	A(86); B(46)	C_6H_6	$C_{12}H_9NCl_2O_5$	45.33	2.85	4.40	22.29	45.47	3.16	4.36	22.37
15b	B(67)	C_6H_6	$C_{12}H_7NCl_4O_5$	37.24	1.82	3.62	36.65	37.03	1.51	3.75	36.97
16a	B(77)	CCl_4	$C_{11}H_8NClO_5$	49.00	2.99	5.19	13.15	48.75	3.05	4.98	13.37
16b	B(83)	CCl_4	$C_{11}H_7NCl_2O_5$	43.45	2.32	4.61	23.32	43.43	2.58	4.59	23.61
17b	B(78)	CCl_4	$C_{11}H_7NCl_2O_5$	43.45	2.32	4.61	23.32	43.60	2.53	4.45	23.65
18a	A(90); B(58)	C_6H_6	$C_{13}H_8NClO_3$	59.65	3.08	5.35	13.54	59.57	3.38	5.59	13.74
18b	A(91)	C_6H_6	$C_{13}H_7NCl_2O_3$	52.72	2.38	4.73	23.94	52.38	2.62	4.60	24.29
19a	C(76)	$CHCl_3$	$C_{12}H_{10}NClO_5$	50.81	3.55	4.94	12.50	51.03	3.68	5.11	12.83
19b	C(62)	$CHCl_3$	$C_{12}H_9NCl_2O_5$	45.33	2.85	4.40	22.29	45.55	3.08	4.56	22.41

[a] see exp. part; [b] anhydrous solvents for **13–19**; $CHCl_3$ free from ethanol; [c] m.p. 196°C; [d] m.p. 163–164°C; [e] m.p. 234–235°C (dec.); [f] m.p. 188–190°C.

^{1}N-NMR spectra

As presented below, from the spectral data of **11–19** (Table 2) two different conformations of the 3-acyl group can be inferred: (3Z)-coplanar for **11** and **12** and noncoplanar for **13–19**.

In aprotic dry solvents the ring protons at the positions 6, 7 and 8 in **11–19** are upfield shifted in comparison with the corresponding protons of the pyridinium cation **22** (in DMSO-d_6),[8] a compound which possesses a "full" positive charge on the aromatic ring. The explanation lies in the fact that the positive charge of the pyridinium cycle in **11–19** is counterbalanced by the negative charge of the oxazole moiety. This comparison is valid particularly for 7-H because of a shielding effect on 6-H and 8-H due to the carbonyloxy-containing ring fused to the pyridinium cycle of **11–19**[1] which is lacking in **22**. On the other hand, the chemical shift of 7-H in **11c** and **13a–b** is quite similar to that of the analogous proton in the ylide **23** (7.8 ppm in $CDCl_3$)[9] or pyridine-N-oxide, both characterized by a back coordination of electrons from the N-ylide or N-oxide group to the pyridine ring.

An interesting example of the influence exerted by conformation on the chemical shift is furnished by the ylides **23** and **24**. The former compound is planar and its α,α'-hydrogens are downfield shifted by the anisotropy of the neighbouring freely-rotating carbonyl group (one interaction hydrogen-oxygen). The latter ylide is no more planar because of the steric hindrance between the α,α'-hydrogens of the pyridine cycle and the carbonyl oxygen atoms (two interactions hydrogen-oxygen).[10] By

Table 2

^{1}H-NMR spectra in aprotic dry solvents[a]

Compd. no.	Solvent	Chemical shifts (δ ppm)[b]				
		R^1	R^2	8-H[c]	R^5	R^4
11c[d]	$CDCl_3$	10.1d	7.2–7.6 m		7.93dd	2.53s
12b	$CDCl_3$	9.75d	7.33d	7.30s	2.63s	7.20s
12c[d]	$CDCl_3$	9.75d	7.1–7.33m		2.58s	2.53s
13a	$CDCl_3$	2.78s	7.29d[e]		7.90dd	4.73s
	CD_3CN	2.70s	7.34d[e]		7.93dd	4.73s
13b	$CDCl_3$	2.80s	7.34d[e]		7.97dd	7.38s
14a	$CDCl_3$	2.78s	7.24d[f]	7.10d[f]	2.40s	4.70s
	CD_3CN	2.65s	7.29d[f]	7.20d[f]	2.32s	4.65s
14b	$CDCl_3$	2.80s	7.30d[f]	7.16d[f]	2.42s	7.35s
15a	CD_3CN	2.68s	7.32d[f]	7.22d[f]	4.50s	4.68s
15b	CD_3CN	2.72s	7.43d[f]	7.33d[f]	6.55s	7.30s
	$CDCl_3$	2.82s	7.2–7.4 m		6.25s	7.33s
16a	$(CD_3)_2CO$	2.78s	7.90m		—	4.73s
16b	$(CD_3)_2CO$	2.80s	7.97m		—	7.43s
18a	CD_3CN	7.6–8.5m		7.55d[g]	8.57d	4.80s
18b	CD_3CN	7.6–8.5m		7.58d[g]	8.60d	7.53s
19a	$(CD_3)_2CO$	2.76s	7.92m		4.02s	4.72s
19b	$(CD_3)_2CO$	2.78s	7.97m		4.03s	7.39s

[a] **11a–b** and **12a** are not soluble in suitable NMR solvents; their spectra in protic solvents wil be discussed in ref.[7]; [b] internal TMS; multiplicity: s-singlet, d – doublet, dd – doublet doublets, m – multiplet; vicinal coupling constants; $J_{5,6} = J_{6,7} = 7$ and $J_{7,8} = 9$ Hz for **11–13** and $J_{4,5} = 9$ Hz for **18a–b**; [c] 4-H for **18a–b**; [d] from ref.[1]; no NMR data for **11c** are given in literature; [e] apparent doublet with J = 8 Hz due to quasi-coincidental chem. shifts; [f] doublet with J = 2 Hz; the assignments for R^2 and 8-H could be inverted; [g] singlet by irradiation of R^5 signal.

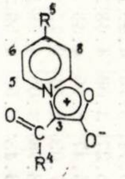
R5
6
8
5
N
O
O
C
3
O⁻
R4

11–12

planar (Z)

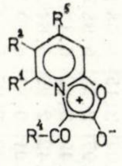
R5
R2
R1
N
O
R4–CO
O⁻

13–19

nonplanar

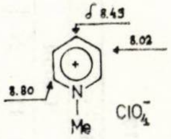
δ 8.49
8.02
8.80
N
Me
ClO4⁻

22

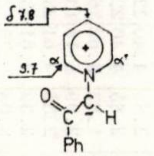
δ 7.8
3.7
α
α'
N
O
C
C
H
Ph

23

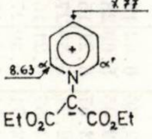
7.77
8.63
α
α'
N
C
EtO2C
CO2Et

24

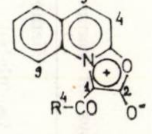
5
4
9
N
O
1
2
R4–CO
O⁻

18a-b

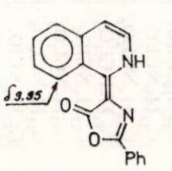
NH
δ 9.95
O
N
O
Ph

25

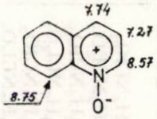
7.74
7.27
8.57
8.75
N
O⁻

26

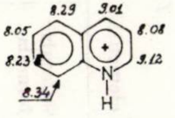
8.29
9.01
8.05
8.08
8.23
9.12
8.34
N
H

27

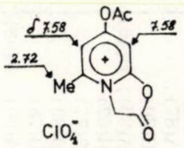
OAc
δ 7.58
7.58
2.72
Me
N
O
O
ClO4⁻

28

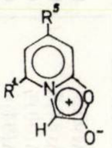

29–32

	R^1	R^5
29	H	H
30	H	Me
31	Me	H
32	Me	OAc

analogy with this case we can adopt the hypothesis that compounds **11** and **12** are also planar molecules, more precisely a (3β Z)-conformation being favoured.

If we take into consideration the quinolinium derivatives **18a—b** a good analogy is offered by the model compound **25** which exhibits δ 9.95 for 9-H, strongly deshielded by the neighbouring carbonyl group.[11] This implies the planarity of the molecule. A similar value may be expected for the chemical shift of 9-H in a (1β Z)-planar conformation of **18a—b**. Actually no signals downfield to 8.6 ppm were observed, the most deshielded proton corresponding to 5-H, *ortho*-coupled with 4-H. Generally speaking all chemical shifts of the quinolinium protons in **18a—b** have intermediate values between those of quinoline-N-oxide **26** (in $CDCl_3$)[12] and those of the quinolinium cation **27** (in TFA),[13] while the chemical shift of 9-H is very close to the corresponding proton in **26**. These observations suggest that the acyl group in **18a—b** is not coplanar with the mesoionic nucleus, as a result of steric hindrance caused by 9-H and observed also on Dreiding molecular models. Alternatively, the absence of downfield shift for 9-H might be due to a planar (1β E)-conformation of the acyl group, but molecular models indicate a larger steric hindrance than in the case of a (1β Z)-arrangement. Therefore this possibility can be ruled out.

The steric requirements in the pyridinium münchnones **13—17** and **19** are somewhat similar to those in the quinolinium derivatives **18a—b**, in the first case the steric hindrance occurring between the acyl and the methyl groups. No deshielding effect is observed for the 5-Me absorption on passing from **28** to **14a**, as required by a planar (3β Z)-conformation. By comparison with the perchlorate **28**,[1] a compound which has a quite analogous skeleton with **14a** but a "full" positive charge on the pyridinium ring, the mesoionic oxazolone **14a** presents upfield shifted signals for 6-H and 8-H, as expected, but for the 5-Me protons a quite similar value (in CD_3CN, 2,65 and 2.72 ppm for **14a** and **28**, respectively).

The influence of the acyl group on the chemical shifts due to the pyridinium protons of the studied münchnones may be rationalized considering the non-acylated precursors **29—32**[1] and their acylated derivatives **11—17** and **19**, more precisely by comparing **31** and **32** with **13** and **14**, respectively. The acylation causes a downfield shift for all the ring protons and especially for 7-H (some 0.3 ppm). This effect could be ascribed for the most part to an increase of the positive charge in the pyridinium ring on acylation. In terms of resonance structures this can be interpreted as different contributions from **1A—C** and **2A—C** to the corresponding resonance hybrids. Canonical structure **1C** which determines a smaller positive charge on the pyridinium carbons than in a "true" pyridinium cation (i.e. **22**) has a greater contribution than **2C** because of the electron-withdrawing inductive effect of the acyl group, its electromeric effect being minimized in **13** and **14**.

IR ABSORPTION SPECTRA

The two carbonyl groups in **11**—**19** present characteristic IR absorptions (Table 3). By analogy with literature data,[2,5,14] in the case of the planar münchnones **11** and **12** the high-frequency band derives from the oxazolone carbonyl bond vibration (ν_{CO}^{oxa}) while the low-frequency band is due to the acyl carbonyl bond (ν_{CO}^{acyl}). A ring vibration may overlap the latter absorption.[5] The low value of ν_{CO}^{acyl} was interpreted as evidence in favour of a greater contribution of the resonance structure **2D**.[14] The presence of chlorine in the acyl group exerts the expected influence[15] upon ν_{CO}^{acyl} band position ; the lowest value pertains to the acetyl group as compared to the mono- and dichloroacetyl carbonyl bonds (**11c** and **12c** versus **11a**—**b** **12a**—**b**, respectively).

Table 3

IR data[a,b] for **11**—**19**

Compd.	ν_{CO}^{oxa}	$\nu_{CO}^{acyl} + \nu_{ring}$	ν_{CO_2H}
11a	1780s	1620m	—
11b	1783s	1631s	—
11c[f]	1750s	1601s	—
12a	1771s	1612s ; 1648w	—
12b	1777s	1629s ; 1648sh	—
12c[f]	1768s	1607s	—
13a	1769s : 1765s[c]	1633s ; 1645sh	—
13b	1772s ; 1755s[c]	1641s ; 1647s	—
14a	1779s ; 1766sh[d]	1641s	—
14b	1783s[d]	1646s	—
15a	1776s[d]	1632sh ; 1642s	—
15b	1781s[d]	1645s	—
16a	1760s ; 1743s[c]	1632m ; 1655m	1700s
16b	1747s ; 1740sh[c]	1610m ; 1640s ; 1659s	1701m
17b	1760sh ; 1738s[c]	1621s ; 1639s	1696s
18a	1767s	1632m ; 1664s	—
18b	1771s	1600m ; 1641s	—
19a	1753s	1635sh ; 1649s	1723s[e]
19b	1766sh ; 1746s[c]	1636s ; 1653s	1731s[e]

[a] absorption bands in cm^{-1} ; relative intensities : s—strong, m — medium, w — weak, sh — shoulder ; [b] spectra in CH_2Cl_2, except **11c**, **16a**—**b**, **17b** and **19a**—**b** (KBr) ; [c] splitting of ν_{CO}^{oxa} band is also observed for other münchnones[14] and sydnones ;[18,19] [d] superimposed with the acyloxy carbonyl bond absorption ; [e] ester carbonyl band ; [f] from ref. [1].

For the nonplanar derivatives **13**—**19** the assignments are less obvious by lack of pertinent data. However, the *gem*-diacetylated olefins

33 and **34**, displaying similar steric requirements to **13**–**19** have for the nonplanar acetyl group absorption a normal value (unconjugated carbonyl bond).[16,17] In our case, owing to the electron-donating effect of the münchnonic ring (see **2B**), a lower value than 1700 cm^{-1} may be expected

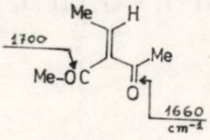

33

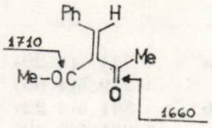

34

for ν_{CO}^{acyl}. Taking into account the resonance structure **2D** which has a significant contribution only for a coplanar acyl group it may be deduced that ν_{CO}^{oxa} and ν_{CO}^{acyl} bands of the nonplanar münchnones should be shifted in opposite directions relative to those of their planar analogs. In fact, on passing from **11a** and **12a** to **13a** or from **11b** and **12b** to **13b** a decrease of 2–18 cm^{-1} for ν_{CO}^{oxa} and an increase of 10–21 cm^{-1} for ν_{CO}^{acyl} can be registered.

The non-acylated mesoionic pyridooxazolones **29**–**32** exhibit lower values of ν_{CO}^{oxa} as compared to **11**–**19**, namely in the range 1700–1750 cm^{-1}.[1] On acylation, ν_{CO}^{oxa} is shifted towards higher frequencies owing to the electron-withdrawing acyl group. The rise in frequency is more pronounced for a coplanar acyl group when both inductive and resonance effects are in action additively.

ELECTRONIC SPECTRA

As it can be seen from Table 4 the studied acylated münchnones exhibit two main absorption bands, the most intense one occurring at a longer wavelength (λ_{max}^{M}) and being more sensitive to solvent effects. A negative solvatochromic shift was observed as well as in the case of the non-acylated precursors **29**–**31**.[1] According to considerations expressed in the preceding paper of this series,[1] the λ_{max}^{M} band could be considered as $\pi \rightarrow \pi^*$ transition associated with an intramolecular charge transfer (from the oxazole to the pyridinium ring). The effect of a carboxyl substituent in the pyridinium ring (**16b**, **17b**) on λ_{max}^{M} is similar to that encountered for N-ylides and 2(1H)pyridinones.[20]

On acylation of **29**–**31**, λ_{max}^{M} is hypsochromically shifted in CH_2Cl_2, but small bathochromic effects could be observed in a more polar solvent ($MeCN-H_2O$; Table 5). Anyhow variations of λ_{max}^{M} are more significant in CH_2Cl_2 solution since strong interactions substrate-protic solvent through hydrogen bonds disturb electronic distribution even in the ground state.[21] As it does result from Table 5 the hypsochromic shifts are about twice as great for a planar acylation (first four entries) with respect to nonplanar acylation (last two entries). This might be interpreted as a relative ground state stabilization for the planar acylated derivatives, due to a greater dispersion of the negative charge. If we accept a major

Table 4

Electronic spectra

Compd. no.	λ_{max} $(\log \varepsilon)^a$		
	CH_2Cl_2	MeCN : EtOH (1 : 1, v/v)	MeCN : H_2O (1 : 1, v/v)
11a	344 (4.20)		
	259.5(4.05)		
11b	341.5(4.22)		
	261.5(4.12)		
12a	339.5(4.17)	335 (4.17)	328 (4.16)
	259.5(4.01)	261.5(4.02)	260 (4.01)
12b	338 (4.19)	336 (4.26)	330.5(4.18)
	264.5(4.07)	263 (4.04)	261 (4.00)
13a	343 (4.13)	336.5 ^{b}	330.5 ^{b}
	265 sh	256 sh	255 sh
13b	343 (4.18)	337 ^{b}	331.5 ^{b}
	263 (4.08)	261.5 ^{b}	261.5 ^{b}
16b			353.5 ^{b}
			265 ^{b}
17b	348 (4.01)		334 ^{b}
	259 (4.07)		256 ^{b}

[a] λ_{max} in nm ; sh — shoulder ;

[b] no reliable log ε values can be given, because of reaction with nucleophiles ; [7] for λ^{M}_{max}, $\log \varepsilon > 4.1$.[1]

Table 5

Variation of λ^{M}_{max} on acylation [a] of **29–31**

Pair of compds.	$\Delta\lambda^{M}_{Max}(nm)^b$		
	CH_2Cl_2	MeCN : EtOH (1 :1, v/v)	MeCN :H_2O (1 : 1, v/v)
(29)–**(11a)**	17.0		
(29)–**(11b)**	19.5		
(30)–**(12a)**	20.5		−2.0
(30)–**(12b)**	22.0		−4.5
(31)–**(13a)**	10.0	5.0	0
(31)–**(13b)**	10.0	4.5	−1.0

[a] the values of λ^{M}_{max} for **29–31** are taken from ref.[1] ;
[b] the sign minus significates a bathochromic shift on acylation.

contribution of **2D** to the ground state of the planar acylated compounds, of **2B** for the nonplanar ones, and of **2C** for the excited states throughout the series, the energy difference between ground and excited states should be greater in the first case. Therefore, as regards UV and IR absorptions the nonplanar acylated compounds are more similar to their non-acylated precursors, according to observations expressed in the introduction of this paper.

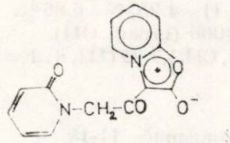

35

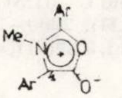

36

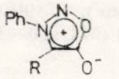

37 R=H
38 R=Ac

Analogous hypsochromic effects were observed by the self-acylation of **29** leading to **35**[5] and also on introduction of an electron-withdrawing *para*-substituent at the 4-aryl group of the monocyclic münchnone **36**.[22] All these UV spectra were registered in CH_2Cl_2 solution. Nevertheless it should be mentioned that the acetylation of sydnone **37** to **38** was accompanied by a 14 nm bathochromic shift of λ_{max}^{M} [23,24] However, in this case the spectra were recordered in ethanol, a protic and quite polar solvent.

CONCLUSIONS

Steric inhibition of resonance is offered as an explanation for the different spectral features shown by the monochloro- and dichloroacetylated oxazolo [3,2-a] pyridinium- and quinolinium-2-olates which are stable derivatives of the corresponding non-isolable mesoionic oxazolones of general type **1**.

EXPERIMENTAL PART

Melting points are uncorrected. IR spectra were recorded with a UR-20 Carl Zeiss Jena spectrometer, UV spectra on a Specord UV—VIS Carl Zeiss Jena double beam spectrophotometer and ^{1}H-NMR spectra with a Varian A-60A apparatus. IR absorption maxima, NMR chemical shifts and coupling constants J are expressed in cm^{-1}, ppm (δ scale, internal TMS) and Hz, respectively.

The acids **3**, **4**, **5**, **7** and **10** were prepared as described in literature.[5,1,25,26,27] Mono- and dichloroacetic anhydrides were obtained from acetic anhydride and the corresponding chlorinated acetic acids in anhydrous toluene.[28]

4-Acetyloxyl-6-methyl-2-oxo-1(2H)pyridineacetic acid (6)

Two grams of perchlorate **28**[1] were triturated with 30 ml water for 10 min. The white solid recovered by filtration and recrystallized from ethanol proved to be **6**. Yield: 78% M.p. 176°C (efferv.). $C_{10}H_{11}NO_5$ requires C-53.33, H-4.92, N-6.22%. Found C-53.60, H-5.10, N-6.22%. IR(KBr): 1645(pyridone), 1721(CO_2H), 1765(OAc).
^{1}H-NMR(DMSO-d_6): 2.30(3H, s, 6-Me or OAc), 2.37(3H, s, OAc or 6-Me), 4.80(2H, s, CH_2), 6.17(2H, m, 3-H and 5-H).

4-Carboxy-6-methyl-2-oxo-1(2H)pyridineacetic acid (8)

The method described by Adams [25] was used, starting from methyl 1,2-dihydro-6-methy 2-oxo-4-pyridinecarboxylate[29] and ethyl bromoacetate. Yield: 35%. M.p. above 360°C (from water). $C_9H_9NO_5$ requires C—51.19, H—4.30, N—6.63%. Found C—51.29, H—4.38, N-6.80%. **IR**(KBr): 1665(pyridone), 1699(shoulder, 4—CO_2H), 1733(CO_2H), 2200—3000 (broad, OH). **^{1}H-NMR**(TFA): 2.78(3H, s, 6—Me), 5.38(2H, s, CH_2), 7.62 and 7.84 (2×1H, 2xs, 3—H and 5—H).

5-Carboxy-6-methyl-2-oxo-1(2H)pyridineacetic acid (9)

The same method as for **8** was employed, starting from ethyl 1,6-dihydro-2-methyl-6-oxo-3-pyridinecarboxylate.[30] Yield : 26%. M.p. above 360°C (from water). $C_9H_9NO_5$ requires C—51.19, H—4.30, N—6.63%. Found C—51.31, H—4.25, N—6.86%.
IR(KBr) : 1648(pyridone), 1739(CO_2H), 2200—3000 (broad, OH).
^1H—NMR (TFA) : 3.03 (3H, s, 6—Me), 5.39(2H, s, CH_2), 7.29 (1H, d, J = 9, 3—H), 8.61(1H, d, J = 9, 4—H).

Synthesis of mesoionic compounds 11-19

Method A (without solvent). In a flask protected from moisture ($CaCl_2$ tube) the appropriate acid anhydride (15 mmoles) was melted at 70—80°C (oil bath). Then 5 mmoles of finely divised acid **3—10** were added, and the mixture was shaken occasionally at 70—80°C for 5—7 min. After the first 2—3 min. the mixture became homogeneous and remained as such, except **12a—b** which precipitated after a time. To the cooled reaction mixture 20—30 mL anh.ether were added and the separation of yellow crystals was hastened by scratching. After filtration and washing with anh. ether the crude material was recrystallized from the solvent indicated in Table 1 (with active charcoal). The purified münchones were kept in a vacuum dessicator.

Method B (with solvent). A solution of 5 mmoles acid **3—10** and 15 mmoles acid anhydride in 30 ml $CHCl_3$ (free from ethanol) was heated under reflux for 0.5—3 hrs. The solvent was removed *in vacuo* at 40°C (bath) and the residue was treated with anh. ether as shown before. The yields were somewhat lower than in method A, but a higher purity of the crude product was found.

Method C (for **19a—b** only). An ethereal solution of CH_2H_2 (cca. 20 mmoles) cooled and dried over KOH pellets was treated with 2 mmoles of **16a—b**. After 2—4 hrs.the deep-coloured solid was separated by filtration and recrystallized from a quite large quantity of $CHCl_3$ with active charcoal.

The ^1H—NMR, IR and UV spectra of **11—19** were presented in Tables 2—4, respectively.

REFERENCES

[1] Part II : H. Petride and D. Răileanu, *Rev. Roumaine Chim.*, **33**, 729(1988).

[2] M. Ohta and H. Kato, "Sydnones and Other Mesoionic Compounds", in "Nonbenzenoid Aromatics", ed. J. P. Snyder, Academic Press, New York, 1969, vol. 1, p. 117 ff.

[3] W. D. Ollis and C. A. Ramsden, "Meso-ionic Compounds", in *Adv. Heterocycl. Chem.*, ed. A. R. Katritzky and A. J. Boulton, Academic Press, New York, 1976, vol. 19, p. 1 ff.

[4] C. A. Ramsden, "Meso-ionic Heterocycles", *Compr. Org. Chem.*, ed. D. Barton, Pergamon Press, Oxford, 1979, vol. 4, p. 1171 ff.

[5] G. V. Boyd and P. H. Wright, *J. Chem. Soc. (C)*, **1970**, 1485.

[6] G. V. Boyd, C. G. Davies, J. D. Donaldson, J. Silver and P. H. Wright, *J. Chem. Soc. Perkin Trans.* 2, **1975**, 1280.

[7] H. Petride and D. Răileanu, in preparation.

[8] A. K. Sheinkman, L. M. Kopman, L. G. Garh, E. V. Titov, S. N. Baranov and A. N. Kost, *Dokl. Akad. Nauk S.S.S.R.*, **193**, 366 (1970).

[10] J. E. Douglas, M. W. Tabor and J. E. Sprandling, *J. Heterocycl. Chem.*, **9**, 53 (1972).

[11] M. Yousif, S. Saeki and M. Hamana, *J. Heterocycl. Chem.*, **17**, 1029 (1980).

[12] K. Tori, M. Ogata and H. Kano, *Chem. Pharm. Bull.*, **11**, 681 (1963).

[13] R. Pastor, J. Musso and A. Cambon, *Bull. Soc. Chim. France*, **1973**, 3009.

[14] G. V. Boyd and P. H. Wright, *J. Chem. Soc. Perkin Trans.* 1, **1972**, 914.

[15] M. Avram and G. D. Mateescu, "Infrared Spectroscopy", Wiley-Interscience, New York, 1972, p. 370 ff.

[16] J. K. O'Loane, C. M. Combs and R. L. Griffith, *J. Org. Chem.*, **29**, 1730 (1964).

[17] L. Birkofer, A. Ritter and H. Vernalek, *Chem. Ber.*, **99**, 2518 (1966).

[18] Y. G. Borodko and Y. K. Sheinker, *Opt. Spectrosc.*, **11**, 482 (1961).

[19] B. E. Zaitzev and Y. K. Sheinker, *Izvest. Akad. Nauk S.S.S.R.*, **1962,** 407.
[20a] A. R. Katritzky, W. K. Yeung, R. C. Patel and K. Burgess, *Heterocycles*, **20**, 623(1983); *Chem. Abstr.*, **99**, 53566 (1983);
[20b] F. Ramirez and A. P. Paul, *J. Org. Chem.*, **19**, 183 (1954).
[21] R. A. Abramovitch and J. B. Davis, *J. Chem. Soc. (B)*, **1966,** 1137.
[22] H. O. Bayer, R. Huisgen, R. Knorr and F. C. Schaefer, *Chem. Ber.*, **103**, 2581 (1970).
[23] D. L. Hammick and D. J. Voaden, *J. Chem. Soc.*, **1961,** 3303.
[24] C. V. Greco, J. Tobias and L. B. Kier, *J. Heterocycl. Chem.*, **4,** 160 (1967).
[25] R. Adams and A. W. Schrecker, *J. Amer. Chem. Soc.*, **71,** 1186 (1949).
[26] S. Garratt and D. Shemin, *J. Org. Chem.*, **28**, 1372 (1963).
[27] M. Mottier, *Helv. Chim. Acta*, **58,** 373 (1975).
[28] J. Hasselmann, Ger. Pat. 1100612, 2 Mar. 1961; *Chem. Abstr.*, **55,** 25760 (1961).
[29] J. Bäumler, E. Sorkin and H. Erlenmeyer, *Helv. Chim. Acta*, **34,** 496 (1951).
[30] N. Anghelide, C. Drăghici and D. Răileanu, *Tetrahedron*, **30,** 623 (1974).

Revue Roumaine de Chimie, **34**, *5*, 1263–1273 (1989)

SOLVOLYSES IN SUBSTITUTED CYCLOPROPYLCARBINYLIC SYSTEMS. 5[1]

BEHAVIOUR OF SPIRO-CYCLOPROPANE-INDANIC ALCOHOLS

ALEXANDRU C. RĂZUŞ[a], MIRCEA D. GHEORGHIU[b] and EMERIC BARTHA[a]
[a] Centre of Organic Chemistry, 202 B, Spl. Independenţei, R – 78100, Bucharest
[b] Department of Organic Chemistry, Polytechnic Institute, Bucharest, Romania

Received October 11, 1988

The solvolysis of several spiro-cyclopropane-indanic alcohols, namely spiro[cyclopropane-1,2′-indan]-1′-ol (**2**), spiro[cyclopropane-1,1′-indan]-2′-ol (**3**) and spiro[cyclopropane-1,1′-indan]-3′-ol (**4**), was undertaken. The solvolysis products were identified and the disappearance rates of the alcohols during solvolysis were compared. Marked differences in solvolytic behaviour of the investigated compounds were observed, depending on the relative positions of the cyclopropanic ring and of the aromatic nucleus to the reaction centre. A reaction mechanism explaining the experimental results was proposed.

The solvolytic behaviour of benzo[b]bicyclo[3.1.0]hex-2-en-4-yl alcohols **1**,[1] in which the bent geometry of the cyclopropylcarbinylic moiety is not favorable for the participation of the cyclopropane ring to the reaction center, suggested the idea of insertion of cyclopropyl rings bisecting the developing carbonium ion center of the indanic framework, as in spiro[cyclopropane-1,2′-indan]-1′-ol **2** and spiro[cyclopropane-1,1′-indan]-2′-ol **3**. In order to obtain a complete picture of the solvolytic behaviour of spiro-cyclopropane-indanyl alcohols, spiro[cyclopropane-1,1′-indan]-3′-ol **4** was taken into account as well, although this alcohol does not generate a cyclopropylcarbinylic cation.

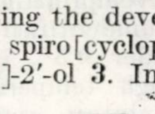

1

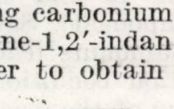

2

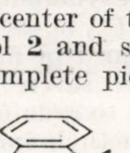

3

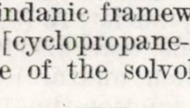

4

Solvolyses of spiranic systems possessing three-membered rings have been reported in the literature.[2] The solvolysis of spiro[2.4]heptan-4-ol **5** gave the cyclobutanic product, bicyclo[3.2.0]heptan-1-ol **6**, as well as the allylcarbinylic product, 3-methylenecyclohexanol **7**.[2a]

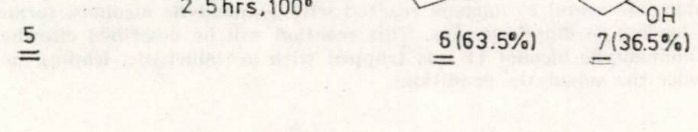

5 **6** (63.5%) **7** (36.5%)

Hydrolysis of spiranic esters **8** in buffered medium leads exclusively to the corresponding alcohols **8**-OH preserving the skeleton.[3]

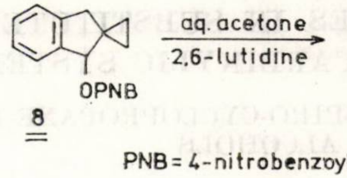

RESULTS AND DISCUSSION

The solvolysis of alcohols **2**, **3** and **4**, whose preparation was reported earlier,[4] was performed in aqueous dioxane * in the presence of perchloric acid. The reaction products were identified and the relative reactivity of these alcohols under solvolytic conditions was determined.

Solvolysis of alcohol **2** gave solely 2-(2-indenyl)-ethanol **9**, the ring-opening product.

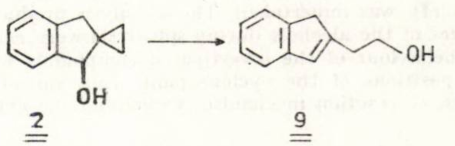

The behaviour of alcohol **3** is quite different; the ring-enlargement product, namely 2a-hydroxy-[1H]-2,2a,7,7a-tetrahydro-cyclobuta[a]indene **10**, was the main reaction product, along with 2-(3-indenyl)-ethanol **11** (less than 2%), 1-methylnaphthalene **12** and spiro[cyclopropane-1,1′-[1H]-indene] **13** (up to 1% in each component). Several unidentified compounds were also obtained in minor amounts (each under 0.5% in the reaction mixture). More severe reaction conditions (high temperature, long reaction time) lead to resinification of the reaction mixture, and only alcohol **11** ** and 1-methylnaphthalene **12** could be identified in the reaction mixture.

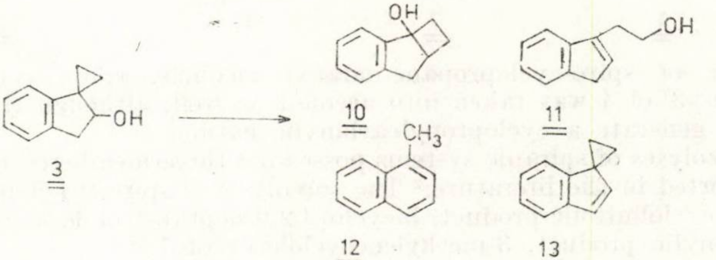

---

* A careful purification [5] of this solvent was necessary; under the solvolytic conditions, traces of acetaldehyde acetal in dioxane reacted with homoallylic alcohols, formed as solvolytic products, leading to dihydropyrans. This reaction will be described elsewhere.

** The homoallylic alcohol **11** was trapped with acetaldehyde, leading to dihydropyrane, stable under the solvolytic conditions.

Under solvolytic conditions, alcohol 4 dehydrated to spiro[cyclopropane-1,1′-[1H]-indene] 13. The formation of dimeric alkene, 2-(spiro-[cyclopropane-1,3′-indane]-1-yl)-spiro[cyclopropane-1,1′-[1H]-indene] 14, along with minor amounts (under 1%) of an unidentified dimer, took place at longer reaction time.

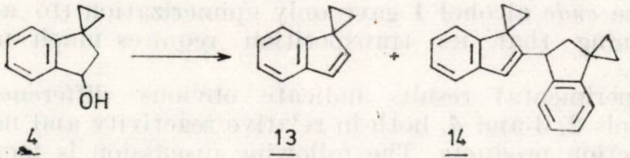

4 13 14

The relative reactivity of alcohols 2, 3 and 4 was qualitatively estimated * comparing the disappearance rates of the respective alcohols (Fig. 1).

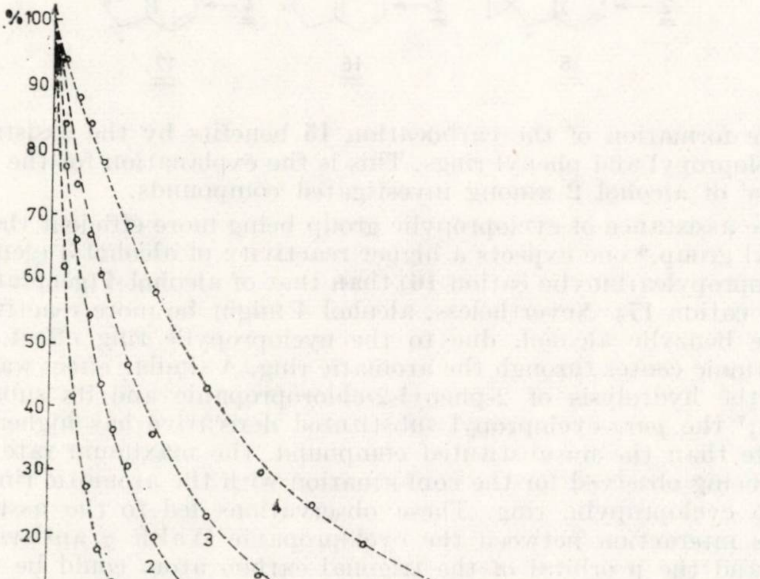

Fig. .—Time-dependent disappearance curves of the alcohols: 1 = alcohol 2, 2 = alcohol 5, 3 = alcohol 4, 4 = alcohol 3.

---

* The solvolysis of the spiro[2,4]heptan-4-ol 5 performed under conditions similar to those described in this paper, as well as kinetic measurements in the solvolysis of the alcohols 2, 3 and 4 are under current investigation; the results will be published in a further paper.

The consumption of alcohol **3** is slower than that of alcohol **4**, in spite of the fact that the former had been solvolysed at higher temperature. The disappearance of alcohol **2** is so fast that kinetic measurements could only be performed at temperatures under 15°C. The reactivity of the non-benzo alcohol **5** is intermediate between the reactivity of alcohol **2** and that of alcohols **3** and **4**.

It is interesting to note that under conditions in which the least reactive among spiranic alcohols, namely alcohol **3**, gave complete rearrangement, the *endo* alcohol **1** gave only epimerization (to approx. 66% extent), meaning that its transposition requires much more drastic conditions.

The experimental results indicate obvious differences between spiranic alcohols **2, 3** and **4**, both in relative reactivity and nature of the solvolytic reaction products. The following discussion is focused on the explanation of these differences.

Ionization of the protonated alcohols gives the carbocations depicted by formulas **15**–**17**.

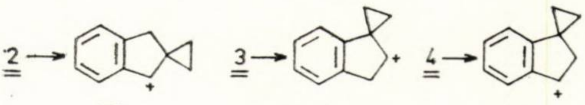

15 16 17

The formation of the carbocation **15** benefits by the assistance of both cyclopropyl and phenyl rings. This is the explanation for the highest reactivity of alcohol **2** among investigated compounds.

The assistance of cyclopropylic group being more efficient than that of phenyl group,[6] one expects a higher reactivity of alcohol **3** (generating the cyclopropylcarbinylic cation **16**) than that of alcohol **4** (generating the benzylic cation **17**). Nevertheless, alcohol **4** might be more reactive than a simple benzylic alcohol, due to the cyclopropylic ring effect at the carbocationic center through the aromatic ring. A similar effect was observed in the hydrolysis of 2-phenyl-2-chloropropanic and its substituted systems;[7] the *para*-cyclopropyl substituted derivative has higher hydrolysis rate than the unsubstituted compound, the maximum rate enhancement being observed for the conformation with the aromatic ring bisecting the cyclopropylic ring. These observations led to the assumption that the interaction between the cyclopropanic Walsh σ antisymmetric orbital and the **p** orbital of the trigonal carbon atom could be through the aromatic electronic π system. A similar effect probably exists in carbocation **17**. The spiranic structure of the system with the cyclopropylic ring bisecting the aromatic nucleus, gives an optimal geometry for the cyclopropylic ring participation to the reaction center through the aromatic ring.

The geometry of the cyclopropylcarbinylic skeleton in alcohol **3** being formally analogous to that of alcohol **5**, the same participation of the cyclopropyl ring to charge development during solvolysis and hence similar rate acceleration is expected for both alcohols. The notable difference observed in the kinetic behaviour of the two alcohols, may be explained only by the annelation of the aromatic ring in alcohol **3**. From the beginning, the inductive effect of the aromatic ring can be easily rejected, since it is known that a phenyl group in α position to the reaction center produces a reactivity enhancement of the cyclopropylcarbinylic system by a factor of approx. 1.3.[8] Steric factors alone cannot explain the solvolysis of alcohol **3** compared to alcohol **5**, since neither the starting materials nor the intermediates are sufficiently different sterically to explain such a different reactivity.

Consequently, the explanation resides in stereoelectronic effects associated with the fixed, bisected position adopted by the aromatic nucleus towards the cyclopropylic ring in alcohol **3** (or in cation **16**). In this alcohol, the geometric restriction is favorable to the conjugation of the aromatic nucleus electrons with the cyclopropanic electronic system (probably through the antisymmetric σ_{cc} Walsh orbital, Fig. 2)[9]. This conjugation produces lowering of ground-state energy in alcohol **3** compared with alcohol **5**. Should the potential energy of the corresponding transition states in the solvolysis of these two alcohols be similar, the activation energy in the solvolysis of alcohol **3** will be higher than that of alcohol **5**, and the corresponding solvolysis rate will be slower. However, the transition states energies are most probably different as well. Presumably, for transition states leading to ionic intermediates in cyclopropylcarbinylic systems, the component of the Walsh orbital at C_3 (or C_4) participates in a certain extent to the charge development at the trigonal carbon atom (C_1). In the solvolysis of alcohol **3**, this participation might be prevented by an interaction between the Walsh orbital component at C_3 and the aromatic electronic system due to favorable position, distance, and "in phase" alignment of this component with the aromatic system. This might lead to an increase in transition state energy and hence a supplemental increase in the activation energy for alcohol **3**.

In general, the solvolysis products of the cyclopropylcarbinyl derivatives are allylcarbinyl- and cyclobutyl derivatives, along with compounds with unchanged carbon atoms skeleton.[10] However, with an electron-donating substituent, such as phenyl, in position 2 of the cyclopropylcarbinylic system (Fig. 2), the reaction product is the benzylic cyclobutanic alcohol.[11] Once formed, such alcohols are converted only with difficulty into homoallylic alcohols. Another extreme case is that in which the major product is the allylcarbinol (sometimes along with small amounts of cyclobutanic derivatives), and this is the case of cyclopropylcarbinylic systems in which the charge-stabilizing substituent is in position 1.[12]

In the carbocation **15**, generated from alcohol **2**, with position 1 of the cyclopropylcarbinylic system being substituted by an aromatic ring, the expected reaction product is a homoallylic alcohol. This is indeed the case : the sole reaction product obtained is the homoallylic alcohol **9**. It is interesting to analyse the reaction path leading from the carbocation **15** to the homoallylic alcohol. The first likely pathway is the attack of the nucleophile at the

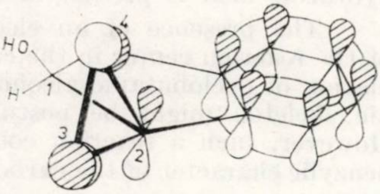

Fig. 2.

carbon atoms in position 3 (or 4) of the cyclopropylcarbinylic system with concerted opening of the ring [13] (Scheme 1).

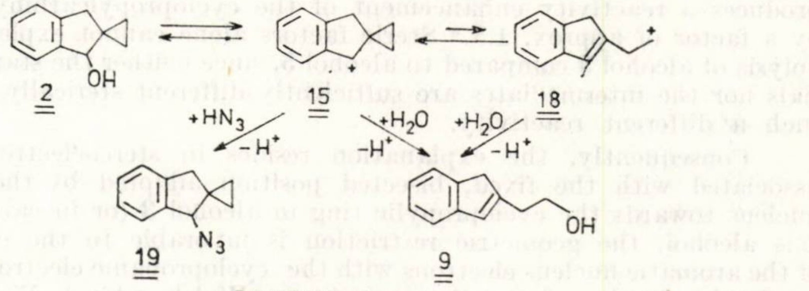

SCHEME 1

However, the trigonal carbon atom has the highest charge density in this cation and consequently is the preferential attack-site for any nucleophile. Should a water molecule be the sole nucleophile in the medium, the product of this attack is the starting material, alcohol **2**, which is going to be reionized till complete consumption by other, less favorable, reaction pathways.

The attack in position 3 (or 4), is less probable due to lower charge density of these sites. Still this pathway leads to the thermodynamically more stable product, namely the alcohol **9**, which consequently slowly accumulates as sole reaction product. An alternative, but energetically less favorable reaction path for ion **15** would involve its conversion into homoallylic ion **18**. Even in small concentration, such a highly reactive ion would lead to the same thermodynamically stable product, the alcohol **9**. In an effort to distinguish between these two reaction paths, a weak nucleophile (hydrazoic acid), leading to non-ionizable products, was added into the solvolysis medium. The highly reactive ion **18** would not select the nucleophiles present in the medium, and a mixture of products with rearranged skeleton, alcohol **9** and the corresponding azide, would be expected. The experimental results indicating the exclusive formation of azide **19**, with unchanged carbon atoms skeleton, the formation of ion **18** is ruled out. The high value of **15** → **2** reaction rate, together with lack of ionization in azide, make azide **19** the sole solvolysis product when hydrazoic acid is present in the medium as well.

The presence of an electron-donating substituent (aromatic ring) at the reaction center in the carbocation **16** would be favorable to the formation of cyclobutanic alcohols. Intermediates with puckered cyclobutanic skeleton might be postulated in these solvolytic transformations. However, such a reaction course is improbable in this case, due to the benzylic character of the carbocationic centre in this intermediate. Indeed, Olah and coworkers had shown [14] that C_1-C_3 interaction into a puckered cyclobutyl-type C_s symmetric intermediate (Fig. 3), suggested by Wiberg,[15], decreases on passing from $R = H$ to $R = CH_3$ and vanishes when $R = C_6H_5$ the carbocation becoming a "classical" one (with charge delocalization in the aromatic nucleus, of course).

It seems reasonable to suppose that the ionic intermediate in the transformation of alcohol **3** is well represented by formula **16**. The feature of this intermediate consists very likely in the possibility of electronic density redistribution (to a more or less extent) from C_3 towards C_1 and simultaneous weakening of the $C_2—C_3$ bond, leading to the cyclobutanic carbocation **20**, tertiary and benzylic as well. Such an intermediate (**16**) might also explain the formation, in small amounts, of homoallylic alcohol **11** and alkene **13** (Scheme 2).

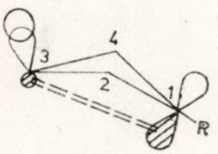

Fig. 3.

The solvolysis of cyclobutanic alcohol **10** under more severe conditions leads exclusively to the homoallylic alcohol **11** and 1-methylnaphthalene **12**. The presence of these compounds as secondary products in the solvolysis of alcohol **13** might also be explained by the formation of **10** as intermediate (or ion **16**).

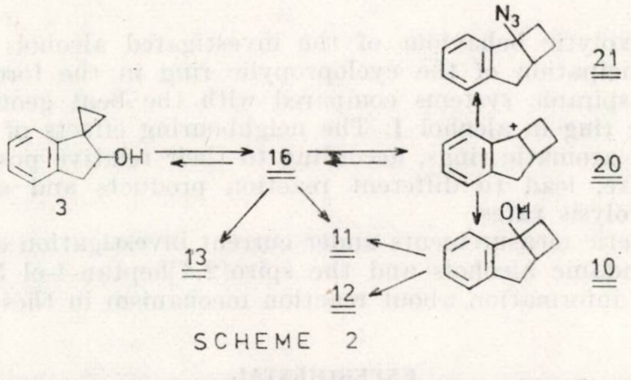

SCHEME 2

The solvolysis of alcohol **3** in the presence of sodium azide gives approx. 10% of azide **21** with rearranged skeleton, along with the same compounds, in the same ratio, as in the solvolysis performed without added azide. This fact might suggest the pronounced tendency of ion **16** to become converted into **20**. Indeed, a long-lived ion **16**, more reactive than ion **15**, would lead solely to an azide with unchanged skeleton, just as in the case of alcohol **2**. The low ionization tendency of alcohol **10**, as well as higher nucleophilicity of water when compared with hydrazoic acid, make the ratio between alcohol **10** and azide **21** in the solvolysis mixture favorable to the former.

Finally, the carbocation **17**, intermediate in the solvolysis of alcohol **4**, is actually not cyclopropylcarbinylic, but benzylic and supplementally stabilized (as pointed out before) by a "through ring" participation of the cyclopropyl ring to the reaction centre. The formation of the reaction products could be explained by the Scheme 3 reaction sequence.

In this case also, introduction of hydrazoic acid in the reaction medium displaces the ionization equilibrium towards the non-ionizable azide **23**. This reaction competing with proton elimination, diminishes the proportion of spiro-cyclopropane-indene **13** and, accordingly, prevents the formation of dimer **14**.

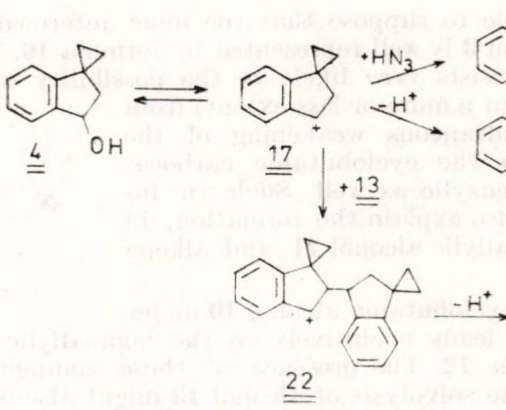

SCHEME 3

The solvolytic behaviour of the investigated alcohols attests the efficient participation of the cyclopropylic ring in the forced bisected geometry of spiranic systems compared with the bent geometry of the cyclopropanic ring in alcohol **1**. The neighbouring effects of both cyclopropanic and aromatic rings, according to their relative position to the reaction centre, lead to different reaction products and substantially different solvolysis rates.

The kinetic measurements under current investigation on the spirocyclopropyl-indanic alcohols and the spiro[2,4]heptan-4-ol **5** are meant to bring new information about reaction mechanism in these solvolyses.

EXPERIMENTAL

The melting and boiling points are both uncorrected. The ^1H-NMR spectra have been recorded on a VARIAN EM 360 L spectrometer, using TMS as internal standard. The $^{13}C-NMR$ spectra have been recorded on a VARIAN FT 80 A spectrometer, using the following parameters: SW = 4000 Hz; pulse width 18 μs, pulse delay 3 s, sensitivity enhancement — 1.3 s. The mass spectra have been recorded on a UR-10 Carl Zeiss-Jena spectrophotometer. The g.l.c. analyses have been performed on a Willy Giede, model 18—3 and a Carlo Erba model Fractovap gas chromatograph, using a flame ionization detector and the following columns: column A: 1 m × 4 mm packed with 7% ethyleneglycol succinate and 4% polyethylene-glycol 20 M on silanized Chromosorb W (60—80 mesh); carrier gas: hydrogen, 60 mL/min, column temperature: 160°C; column B: glass capillary column 30 m × × 0.2 mm coated with SE-54; programmed heating 60—240°C, 10°C/min, H_2 flow of 1 mL/min.

General procedures

Solvolysis of alcohols. The alcohol (2.0 g, 12.5 mmoles) was dissolved under inert atmosphere in 180 mL purified dioxane-water mixture (5:4 volumes) and the solution was stored in a thermostat, at solvolysis temperature. 20 mL of aqueous 5 M perchloric acid solution were thermostated at the same temperature and then, added at once over the alcohol solution, under a positive pressure of inert gas. The mixture was maintained a definite period of time, at desired temperature. The reaction was quenched in 200 mL of saturated aqueous $NaHCO_3$ solution. The aqueous phase was extracted three times with 100 mL ethylic ether, the combined organic layers were washed with water, dried over anhydrous sodium sulphate and the solvent was removed in vacuo.

Solvolysis of alcohols in the presence of sodium azide. The alcohol (0.2 g, 1.25 mmoles) and sodium azide (0.65 g, 10 mmoles) were dissolved in 16 mL purified dioxane-water mixture (5:3 volumes), under inert atmosphere, and the obtained solution was kept at the solvolysis temperature. To this solution, 4 mL aqueous 5 M perchloric acid solution, also thermostated at solvolysis temperature, were suddenly added. The obtained mixture was stored under inert gas a definite period of time, at desired temperature. The reaction mixture was cooled at room temperature and then, the reaction was quenched in 20 mL saturated aqueous $NaHCO_3$ solution. The aqueous phase was extracted three times with 10 mL ethylic ether, the combined ethereal solutions were washed with water, dried over anhydrous sodium sulphate and the solvent was removed in vacuo.

Solvolysis of alcohol 2

Solvolysis of alcohol **2** was performed under the previously described conditions, at 15°C, during 120 min. After working-up as pointed above, an oily product was obtained (yield $> 95\%$), which crystallysis under storage (mp 44–47°C). The g.l.c. analysis of raw product on column B indicated the presence of a main component (97–98%) and of several minor components (each of them, under 0.5%), which have never been separated by preparative g.l.c., nor characterized. The main product is the homoallylic alcohol **9**. After recrystallization from hexane, alcohol **9** (mp 49–50°C) of $> 99.9\%$ chromatographic purity was obtained.

^1H-NMR ($CDCl_3$, δ ppm) 2.3 (s, 1H, OH); 2.65 (t, 2H, $J_1 = 6.8$ Hz, small allylic coupling $CH_2-C=$); 3.27 (bs, 2H, $CH_2-C_6H_5$); 3.78 (t, 2H, $J = 6.8$ Hz, CH_2-OH); 6.5 (bs, 1H, small allylic coupling CH=); 6.9–7.4 (m, 4H, CH-aromatic).

IR (CS_2, CCl_4, cm^{-1}): 720 s, 752 s, 1050 s, 1386 m, 1455 m, 1601 w, 2881 m, 2921 m, 3018 w, 3054 m, 3200–3520 broad band, 3575 w, 3620 m.

Mass spectrum: m/e (rel. int. %): 160 (M, 30.6); 142 (10.5); 129 (100); 128 (34.3); 115 (8.4); 102 (3.0); 89 (1.3); 77 (2.6).

The melting point and the retention time from g.l.c. analysis of homoallylic alcohol **9**, have been compared with those of an authentic sample obtained by selective reduction of the methyl 2-indenyl-acetate with lithium-aluminium hydride.[16]

Solvolysis of alcohol 2 in presence of sodium azide

Working under general conditions, at −10°C, during 6 h, an oily product (azide **19**) was obtained, as sole reaction product:

^1H-NMR ($CDCl_3$, δ ppm): 0.57–1.4 (m, 4H, cyclopropyl); 2.58 (d, 1H, $J = 17$ Hz, CH_2-benzylic); 3.25 (d, 1H, $J = 17$ Hz, CH_2-benzylic); 4.17 (s, 1H, $CH-N_3$); 7.1–7.4 (m, 1H, CH-aromatic).

IR (CCl_4, cm^{-1}): 1240 m, 1311 w, 1323 w, 1431 w, 1456 w, 2098 vs, 2842 w, 2904 m, 2921 m, 2998 m, 3021 w, 3048 w, 3071 w.

Analysis: found: N, 21.68; $C_{11}H_{11}N_3$ requires N, 22.69% (purity 95.11%).

Solvolysis of alcohol 3

Using the general solvolysis conditions, at 65°C, during 90 min, a crystalline product was obtained (yield ∼ 100%), melting between 60 and 78°C. The g.l.c. analysis performed on column A indicated the presence of six components: spiro-cyclopropane-indene **13** (0.2%), 1-methylnaphthalene **12** (0.7%), cyclobutanic alcohol **10** (96.9%), homoallylic alcohol **11** (1.9%) and two other unidentified components in 0.3% and $<0.1\%$, respectively. The above crystalline product was twice recrystallized from hexane and pure alcohol **10** was obtained (mp 78–79°C):

^1H-NMR ($CDCl_3$, δ ppm): 0.65–3.7 (m complex, 8H, CH-aliphatic); 7.1–7.6 (m, 4H, CH-aromatic).

$^{13}C-NMR$ ($CDCl_3$, δ ppm): 18.79 (t); 35.00 (t); 37.15 (t); 75.76 (d); 84.09 (s); 124.23 (d); 125.47 (d); 127.08 (d); 128.47 (d); 143.85 (s); 146.49 (s).

IR (CCl_4, cm^{-1}): 1106 vs, 1348 w, 1467 w, 2852 m, 2940 s, 2986 s, 3017 w, 3064 w, 3607 m.

Mass spectrum: m/e (rel. int. %): 160 (M, 7); 145 (18.0); 133 (10.7); 132 (100); 131 (27); 155 (13.4); 103 (7.6); 91 (6.8); 77 (8.1).

The minor components were identified by comparing the g.l.c. retention times with those of authentic samples (**11**, **12** and **13**).

Homoallylic alcohol **11** was obtained by selective reduction of methyl 1-indenyl acetate **17** with lithium-aluminium hydride, without further purification.

^1H-NMR ($CDCl_3$, δ ppm): 2.8 (t, 2H, J = 6.5 Hz, CH_2 allylic); 3.31 (bs, 2H, small allylic coupling CH_2-indene); 3.83 (t, 2H, J = 6.5 Hz, CH_2-OH); 6.3 (bs, 1H, small allylic coupling CH=); 7.04–7.56 (m, 4H, CH-aromatic).

Solvolysis of alcohol 3 in the presence of sodium azide

Using the general procedure, from alcohol **3** (2 g, 12.5 mmoles), for 24 h at 35°C, 2 g reaction mixture were obtained. The elementary analysis of the mixture indicates 2.22% nitrogen, corresponding to about 10% azide in the reaction product. The mixture was separated by liquid chromathography on a silica gel column (20 cm × 1 cm). The first fraction was eluted with petroleum ether and was identified as azide **21**:

^1H-NMR (CCl_4, δ ppm): 0.85 (m complex, 7H, H-aliphatic); 7.25–7.5 (m, 4H, CH-aromatic).

IR: (CCl_4, cm^{-1}): 1256 s, 1303 m, 1474 w, 2107 vs, 2854 m, 2936 s, 2984 m, 3022 w, 3069 w.

Analysis: found: N, 21.21; $C_{11}H_{11}N_3$ requires N, 22.69% (purity of azide: 93%).

The second fraction eluates with petroleum ether-ethylic ether (4:1). The IR spectrum shows the presence of alcohol signal (intense band at 3600 cm^{-1}) and the absence of the characteristic signal of azide. The g.l.c. analysis (column B) shows that this fraction consists of alcohol **10** (95.4%), alcohol **11** (1.31%) and alcohol **3** (1.23%).

Solvolysis of alcohol 4

Working under the general conditions described above, for 24 h at 25°C, 1.6 g of oily product were obtained. The g.l.c. analysis (column B) indicates the presence of two main components (75% and 18%) and several minor unidentified components (each under 0.5%). The crude reaction mixture was distilled under reduced pressure the fraction with b.p. 100°C/2–3 mm was identified as spiro-cyclopropane-indene **13**, according to ^1H-NMR data.[4] The distillation residue contains 71% of the second main component from the crude reaction product. This was purified by chromatography on silica gel column (25 cm × 1 cm; eluent: petroleum ether b.p. 28–32°C) and, after trituration with petroleum ether, crystalline, gas-chromatographically pure (column B) dimer **14** (m.p. 110°) was obtained.

^1H-NMR ($CDCl_3$, δ ppm): 0.92 (m, 4H, cyclopropyl from indane); 1.6 (bs, 4H, cyclopropyl from indene) 2.07 (dd, 1H, J_{gem} = 12.5 Hz, J_{vic_1} = 7.5 Hz, CH from CH_2-benzylic); 2.3 (dd, 1H, J_{gem} = 12.5 Hz, J_{vic_2} = 7.5 Hz, CH from CH_2-benzylic); 3.78 (t, 1H, J = 7.5 Hz, CH-benzyl allylic); 6.44 (s, 1H, –CH=); 6.6–7.4 (m, 8H, CH-aromatic).

IR: (CCl_4, cm^{-1}): 1456 vs, 1476 m, 1599 w, 2857 m, 2920 m, 2942 m, 2998 m, 3060 m, 3068 m.

Analysis: found: C, 92.63; H, 7.32; $C_{22}H_{16}$ requires C, 92.91; H, 7.09%.

Under general solvolysis conditions (10 h at 45°C), hydrocarbons **13** and **14** are not changed.

Solvolysis of alcohol 4 in the presence of sodium azide

Using the general solvolysis conditions, in the presence of sodium azide, for 24 h at 25°C, 0.22 g oily product was obtained, consisting of azide **25** (87%) and hydrocarbon **13** (13%; according to the ^1H-NMR spectrum of the reaction mixture).

Structure proofs for azide **25** are the following:

^1H-NMR ($CDCl_3$, δ ppm): 0.89 (s, 4H, cyclopropyl); 1.95 (dd, 1H, J_{gem} = 13.5 Hz, J_{vic_1} = 4.5 Hz, CH from CH_2); 2.38 (dd, 1H, J_{gem} = 13.5 Hz, J_{vic_2} = 7.5 Hz, CH from CH_2); 4.7 (dd, 1 H, J_{vic_1} = 4.5 Hz, J_{vic_2} = 7.5 Hz, $CH-N_3$); 6.64 (dd, 1H, J_1 = 8 Hz, J_2 = 5 Hz, CH-aromatic ortho cyclopropyl); 7.0–7.35 (m, 3H, CH-aromatic).

IR (CCl_4, cm^{-1}): 1242 s, 1458 m, 1478 m, 2102 vs, 2854 w, 2921 m, 2960 m, 2998 m, 3020 w, 3053 w, 3070 w.

Analysis: found: N, 18.9 $C_{11}H_{11}N_3$ reaquires N, 22.69% (purity of azide: 83%).

REFERENCES

[1] Part 1, A. C. Răzuş, V. Wertheimer, F. Badea and A. M. Glatz, *Tetrahedron Lett.*, **1975**, 1779; Part 2, V. Wertheimer, A. M. Glatz and A. C. Răzuş, *Rev. Roumaine Chim.*, **22**, 1505 (1977); Part 3, A. C. Răzuş, V. Wertheimer, A. M. Glatz, Zs. Arvay and F. Badea, *ibid.*, **26**, 457 (1981); Part 4, F. Badea, A. M. Glatz and A. C. Răzuş, *ibid.*, **26**, 629 (1981).

[2] (a) W. D. Closson and G. T. Kwiatkowski, *Tetrahedron*, **24**, 2779 (1968); (b) K. B. Wiberg and J. E. Hiatt, *Tetrahedron Lett.*, **1968**, 3009; (c) T. Tsuji, I. Moritani, S. Nishida and G. Tadokoro, *ibid.*, **1967**, 1207.

[3] K. Ohkata, M. Akijama, K. Wanda, S. Sakane, Y. Toda and T. Hanafusa, *J. Org. Chem.*, **49**, 2517 (1984).

[4] E. Bartha, Zs. Arvay and A. C. Răzuş, *Rev. Roumaine Chem.*, **31**, 519 (1986).

[5] L. F. Fieser and M. Fieser, *"Reagents for Organic Synthesis"*, J. Wiley and Sons, New York, 1967, 333.

[6] R. W. Taff, R. H. Martin and F. W. Lampe, *J. Amer. Chem. Soc.*, **87**, 2490 (1965) and G. A. Olah, Ph. W. Westerman and J. Nishimura, *ibid.*, **96**, 3548 (1974).

[7] H. C. Brown and J. D. Cleveland, *J. Amer. Chem. Soc.*, **88**, 2051 (1966).

[8] J. W. Wilt and D. D. Roberts, *J. Org. Chem.*, **27**, 3430 (1962).

[9] A. D. Walsh, *J. Chem. Soc., Trans. Faraday* **45**, 179 (1949); G. L. Closs and H. B. Klinger, *J. Amer. Chem. Soc.*, **87**, 3265 (1965).

[10] H. G. Richey Jr. in *"Carbonium Ions"* vol. III, G. A. Olah and P. v. R. Schleyer, Wiley-Interscience, New York, 1972, chap. 25; K. B. Wiberg, B. A. Hess Jr. and A. J. Ashe, III, ibid. chap. 26.

[11] D. D. Roberts, *J. Org. Chem.*, **30**, 23 (1965).

[12] T. A. Favorskaya, O. V. Sergievskaya and N. P. Ryzhova, *J. Gen. Chem. U.S.S.R.*, **27**, 1018 (1957) and C. G. Richey Jr. and J. M. Richey, *J. Amer. Chem. Soc.*, **88**, 4971 (1966).

[13] N. C. Deno, A. D. Richey Jr., J. S. Liu, D. N. Lincoln and J. O. Turner, *J. Amer. Chem. Soc.*, **87**, 4533 (1965).

[14] G. A. Olah, G. J. Jevall, D. P. Kelly and R. D. Porter, *J. Amer. Chem. Soc.*, **94**, 146 (1972).

[15] K. B. Wiberg, *Tetrahedron*, **24**, 1083 (1968) and K. B. Wiberg and G. Szeimies, *J. Amer. Chem. Soc.*, **90**, 4195 (1968); K. B. Wiberg, *ibid.*, **92**, 571 (1970).

[16] H. Tanida, Y. Hata and H. Jshitobi, *Tetrahedron Lett.*, **1967**, 361; H. Ahmed and N.. Campbell, *J. Chem. Soc.*, **1960**, 4115; E. D. Bergmann and E. Hoffmann, *J. Org. Chem.*, **26**, 3555 (1961).

[17] H. Cristol and F. Plenant, *Bull. Soc. Chem. France*, **1962**, 1325.

Revue Roumaine de Chimie, **34**, 5, 1275–1280 (1989)

COORDINATION COMPOUNDS AS RAW MATERIALS FOR MIXED OXIDES. V *

MIXED COORDINATION COMPOUNDS OF LANTHANIDES AND Co(II), Ni(II) OR Fe(III) WITH GLUCONIC ACID

P. SPACU, LUMINIȚA PATRON, SILVIA PLOȘTINARU, ADRIANA CONȚESCU and N. STĂNICĂ

Center of Physical Chemistry, Bucharest, Romania

Received November 28, 1987

A new class of mixed coordination compounds of Ln (III) and Co (II), Ni (II) or Fe (III) with gluconic acid was synthesized. The complex compounds were characterized by elemental analysis, electronic and IR spectra, magnetic measurements. Thermogravimetric decomposition of these compounds gives mixed $LnCoCO_3$, $LaNiO_3$, Ln_2NiO_4 type oxides.

There is in the literature a great deal of data on gluconic acid — transition metal and gluconic acid — lanthanide systems. It is well known that introduction of hydroxy groups into the molecule of carboxylic acids entails an increase of stability of the resulting complex compounds. The studies of the stability of complexes formed with α-hydroxycarboxylic acids compared to that of compounds of simple monobasic and dibasic acids are very interesting. The higher stability of the former is assigned to the participation of hydroxy groups in the bond which results in the formation of chelate ring.

Most existing studies evidence, on the one hand, the special capacity of gluconic acid chelating towards transition metal ions, and, on the other, the characteristic behaviour of each system with respect to the pH of the medium and the nature of the ion involved. In fact, there are not two gluconic acid-transition metal ion systems which behave identically.

Most studies on this system were carried out in solution by conductometric, polarographic, pH-metric, potentiometric and spectrophotometric methods.[1–4] Only recently the isolation of a large number of gluconates of transition metals and their characterization has become possible.[5,6]

Taking account of the aim of our recent investigation — the obtaining of mixed oxides by nonconventional methods : decomposition of polynuclear coordination compounds — and of the unusual chelating capacity of gluconic acid both with transition metals and lanthanoides, we have initiated a study on Ln(III)-transition metal-gluconic acid.

---

* Part IV is ref. 9.

In this system we have synthesized the following types of mixed complex compounds:

$$[M(II)Ln(III)(Gluc)_4] \cdot nH_2O$$

where $M(II) = Co;\ Ln(III) = La-Tb;\ n = 5$

$$M(II) = Ni;\ Ln(III) = La;\ n = 2$$

$$[Fe(III)Ln(III)(Gluc)_4] \cdot 4H_2O$$

where $Ln(III) = La-Tb.$

The synthesized compounds are all powders: pink for $M(II) = Co$, yellow-green for $M(II) = Ni$ and straw-yellow for $M(III) = Fe$. All are highly soluble in water and hardly insoluble in most of the usual organic solvents. The formulas above were established on the basis of elemental chemical analysis correlated with some physico-chemical studies (spectrophotometric and IR spectrometric, magnetic and thermogravimetric measurements).

To obtain data about the coordination of the ligand with metallic ions, we recorded IR spectra of polynuclear complex compounds in 400–4000 cm^{-1} range and compared the results with the IR spectra of glucono-δ-lactone, of sodium gluconate and transition metal gluconates available in the literature.

The vibration spectra of coordination complexes are generally different from those of free ligands in respect of either the disappearance of some bands characteristic of ligands and the existence of some new bands or the shift or splitting of some bands.

The spectrum of glucono-δ-lactone exihibits one maximum at 1721 cm^{-1} which was assigned to $\nu_{C=O}$ and indicates the presence of free carboxyl groups.[7]

Following complex formation, this band vanishes and two bands appear (one symmetrichl $\nu_{COO^-} = 1390\ cm^{-1} \pm 5$, one asymmetrical $\nu_{COO^-} = 1585 cm^{-1} \pm 5$) which are due to coordinated COO^- group. These bands are typical for the salts of carboxylic acids (Fig. 1).

In case of polyhydroxycarboxylic ligands, the coordination of metallic ions is achieved most often through alcoholic groups. The primary and secondary alcoholic groups yield absorption bands associated with OH distortion and CO frequency in 1000–1400 cm^{-1}.

In sodium gluconate whose interaction between the metallic ion and alcohol groups is assumed minimum, the absorption band at 1090 cm^{-1} was assigned to OH secondary group.[7] The comparison of this spectrum with those of single Co(II) Ni(II) or Fe(III) glucomates as well as those of mixed gluconates points to a shift from 1090 cm^{-1} and 1060 cm^{-1} to lower values which corresponds (in agreement with data in the literature [7]) to coordination of one or more secondary alcohol groups.

The wide bands in the 3000–3400 cm^{-1} range (maximum 3300 cm^{-1}) are assigned to the hydrogen bond in water and/or alcohols. Because each gluconic skeleton contains 5 OH groups and may adsorb water, the salts are hydrated and the IR spectrum confirms this behaviour.

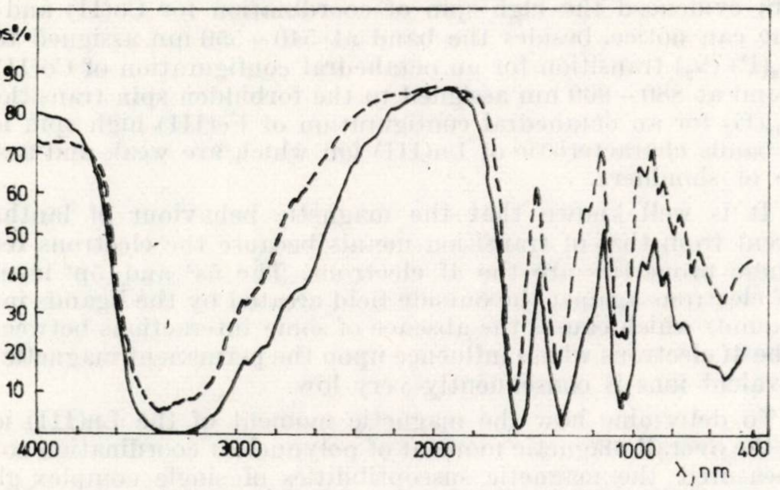

Fig. 1. — IR spectra of Fe(Gluc)·$5H_2O$ — — — — — $FeHo(Gluc)_4·4H_2O$.

The visible spectra for all synthesized mixed compounds of Ln(III) with Co(II), Ni(II) and Fe(III) were recorded and compared with those of respective transition metal gluconates. As one knows, in visible, the lanthanides ions as: Pr(III), Nd(III), Dy(III), Ho(III), Er(III) exhibit a large number of sharp, yet weak, bands due to transitions from background to excited levels of 4*f* configuration (*f*—*f* transitions).

As an example Fig. 2 shows a comparison between the spectra of mixed gluconate $[CoPr(Gluc)_4]·5H_2O$ and $Co(Gluc)_2·2H_2O$ and Fig. 3. $[FeNd(Gluc)_4]·4H_2O$, $[FeHo(Gluc)_4]·4H_2O$ and Fe(Gluc)·$5H_2O$. These

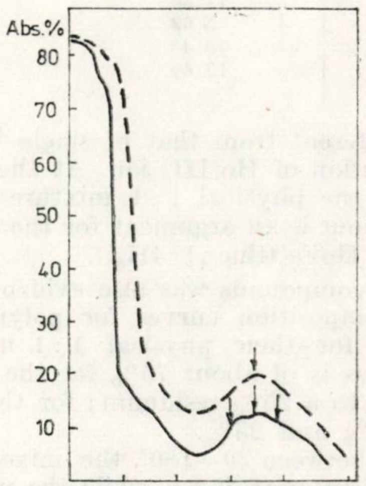

Fig. 2. — Electronic spectra of Co· $Co(Gluc)_2·2H_2O$ — — — $CoPr(Gluc)_4·4H_2O$ ——

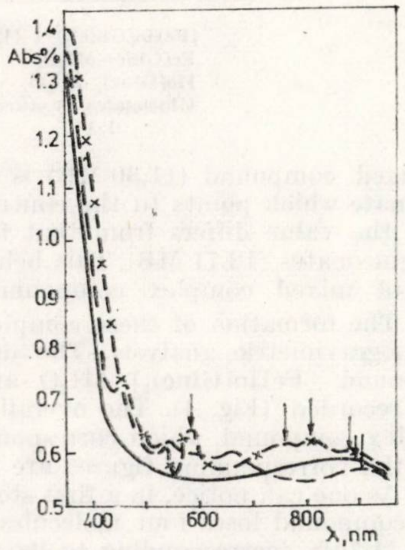

Fig. 3. — Electronic spectra of Fe(Gluc)·$5H_2O$—— $FeHo(Gluc)_4·4H_2O$ — — $FeNd(Gluc)_4·4H_2O$ -x-x-x-

spectra evidenced the high spin of coordination for Co(II) and Fe(III). As one can notice, besides the band at 540–550 nm assigned to $^4T_{1g} \rightarrow {}^4T_{1g}(P)$ (ν_3) transition for an octahedral configuration of Co(II) ion and the band at 880–900 nm assigned to the forbidden spin transition $^6A_{1g} \rightarrow {}^4T_{1g}(G)$ for an octahedral configuration of Fe(III) high spin ion, there exist bands characteristic of Ln(III) ion which are weak and assume the shape of shoulders.

It is well known that the magnetic behaviour of lanthanides is different from that of transition metals because the electrons responsible for these properties are the 4f electrons. The $5s^2$ and $5p^6$ levels screen the 4f electrons against the outside field created by the ligands in complex compounds which causes the absence of some interactions between ligands and the 4f electrons whose influence upon the permanent magnetic moment of trivalent ions is consequently very low.

To determine how the magnetic moment of the Ln(III) ion influences the overall magnetic moment of polynuclear coordination compounds we measured the magnetic susceptibilities of single complex gluconates of Fe(III)and Ho(III) and for the mixed complex gluconate $[HoFe(Gluc)_4] \cdot 4H_2O$. The magnetic susceptibility of a 1 : 1 physical mixture of the two single gluconates has also been recorded for comparison. The susceptibilies are listed in Table 1. It is obvious that the magnetic moment of mixed compound (11,30 MB) is different from that of single Fe(III) gluconate which points to the contribution of Ho(III) ion. At the same time, the value differs from that for the physical 1 : 1 mixture of the two gluconates (12.71 MB). This behaviour is an argument for the formation of mixed complex compound $[HoFe(Gluc)_4] \cdot 4H_2O$.

Table 1

Magnetic moments of complex compounds

COMPOUND	μ_{MB}
$[FeHo(Gluc)_4] \cdot 4H_2O$	11.30
$Fe(Gluc) \cdot 5H_2O$	5.63
$Ho(Gluc)_3 \cdot 2H_2O$	10.46
Gluconates mixture 1:1	12.60

The formation of these complex compounds was also evidenced by thermogravimetric analysis. The decomposition curves for polynuclear compound $[FeHo(Gluc)_4] \cdot 4H_2O$ and for their physical 1 : 1 mixture were recorded (Fig. 4). The overall loss is of about 75% for the mixed complex compound, which corresponds to a 25% residuum; for the mixture the corresponding figures are 77% and 23%.

As one can notice, in a first step, between 20–180°, the mixed complex compound loses four molecules of water (6.35%), while the mixture loses 11.74% (corresponding to its seven molecules of water). It should be emphasized that in this mixture, the decomposition curve indicates the loss of water molecules in two steps which corresponds to the indivi-

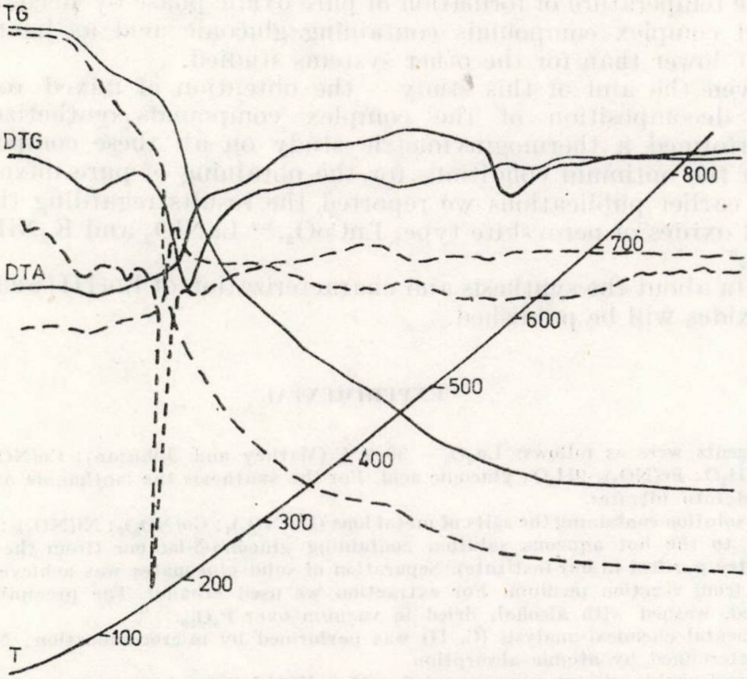

Fig. 4. — Thermal decomposition of $FeHo(Gluc)_4 \cdot 4H_2O$—; physical mixture (1:1) gluconates.

dual loss of water molecules in the two constitutive single gluconates ($5H_2O$ for Fe(III) gluconate and $2H_2O$ for Ho(III) gluconate).

This is not the behaviour encountered in the decomposition of mixed gluconate which is also an argument in favour of the formation of mixed complex compounds.

The second step, between 180° and 700°, corresponds to the decomposition of anhydrous complex compound, i.e. of the mixture of anhidrous gluconates, to elimination of volatile products resulted and the formation of oxidic phases.

The existing data on thermal decomposition of polynuclear complex compound have suggested the following decomposition scheme :

$$[\mathrm{FeHo(Gluc)_4}] \cdot 4\mathrm{H_2O} \xrightarrow[25-180^\circ]{\mathrm{I}} \mathrm{FeHo(Gluc)_4} \overset{\mathrm{II}}{\underset{180-55}{}}$$

$$\rightarrow \mathrm{FeHoO_2(CO_3)} \xrightarrow[550-700^\circ]{\mathrm{III}} \mathrm{HoFeO_3} + \mathrm{CO_2}$$

The X-ray diagrams of the oxidic residues obtained at 700° have indicated the formation of a pure $HoFeO_3$ weakly crystallized oxidic phase, on decomposition of mixed gluconate, and the formation of a mixture of component oxides, on the decomposition of a physical mixture of gluconates.

The temperature of formation of pure oxidic phase by decomposition of mixed complex compounds containing gluconic acid as ligand is at least 100° lower than for the other systems studied.

Given the aim of this study – the obtention of mixed oxides by thermal decomposition of the complex compounds synthetized – we have performed a thermogravimetric study on all these compounds to establish the optimum conditions for the obtaining of pure mixed oxide.

In earlier publications we reported the results regarding the study of mixed oxides of perovskite type, $LnCoO_3$,[8,9] $LaNiO_3$ and K_2NiF_4 type: Ln_2NiO_4.[9]

Data about the synthesis and characterization of Ln(III) and Fe(III) mixed oxides will be published.

EXPERIMENTAL

Reagents were as follows: Ln_2O_3 – 99.9% (Mathey and Johnson); $Co(NO_3)_2 \cdot 6H_2O$; $Ni(NO_3)_2 \cdot 6H_2O$; $Fe(NO_3)_3 \cdot 9H_2O$; gluconic acid. For the synthesis the lanthanide oxides were transformed into nitrates.

The solution containing the salts of metal ions ($Ln(NO_3)_3$; $Co(NO_3)_2$; $Ni(NO_3)_2$; $Fe(NO_3)_3$) was added to the hot aqueous solution containing glucono-δ-lactone (from the wastes of drug industry purified in our institute). Separation of solid gluconates was achieved through extraction from reaction medium. For extraction we used ethanol. The precipitate is left 24h, filtered, washed with alcohol, dried in vacuum over P_4O_{10}.

Elemental chemical analysis (C, H) was performed by microcombustion; Ni, Co and Fe were determined by atomic absorption.

UV and visible spectra were recorded with a VSU-1 Zeiss Jena spectrophotometer, in the 240–980 nm range with MgO as standard;

IR spectra were recorded with a UR-10 Zeiss Jena spectrophotometer, in KBr pellets;

Magnetic measurements on solid samples were performed by the Faraday method, using Mohr salt as standard;

The differential thermal analyses were recorded with an MOM Budapest Paulik-Paulik-Erdey derivatograph.

REFERENCES

[1] S. P. Sinha, "Complexes of the Rare Earth", Pergamon Press, Ltd., 1966, p. 50.

[2] R. L. Pecsok and R. S. Juvet jr., *J. Amer. Chem. Soc.*, **77**, 202 (1955).

[3] R. L. Pecsok and R. S. Juvet jr., *J. Amer. Chem. Soc.*, **77**, 1489 (1955).

[4] N. A. Kostromina, *Zhur. neorg. Khim.*, **11**, 2340 (1966).

[5] G. A. Melson and W. F. Pickering, *Austral. J. Chem.*, **21**, 2889 (1968).

[6] J. F. Ashton and W. F. Pickering, *Austral. J. Chem.*, **23**, 1367 (1970).

[7] G. A. Melson and W. F. Pickering, *Austral. J. Chem.*, **21**, 1205 (1968).

[8] P. Spacu, S. Ploştinaru, L. Patron, A. Conţescu, D. Crişan and N. Stănică, *Rev. Roumaine Chim.*, **32**, 877 (1987).

[9] P. Spacu, L. Patron, S. Ploştinaru, A. Conţescu, D. Crişan and N. Stănică, *Rev. Roumaine Chim.*, **32**, 249 (1987).

Revue Roumaine de Chimie, 34, 5, 1281–1286 (1989)

CONTRIBUTION TO THE CALCULATION OF E—I CURVES, FOR ELECTRODE PROCESSES WITH INSOLUBLE FILMS FORMATION. I

THE INFLUENCE OF THE POTENTIAL SWEEP RATE ON THE Pb/Pb^{2+} ELECTRODE PROCESS, IN SULPHURIC ACID SOLUTIONS

S. STERNBERG[a], V. BRÂNZOI[a] and LILIANA APĂTEANU[b]
[a] Polytechnic Institute of Bucharest, Dept. of Physical Chemistry, Bucharest, Romania
[b] Biochemical and Chemical Energetics Institute, Bucharest, Romania

Received October 5, 1988

Using the cyclic voltammetry method, the influence of the potential sweep rate on the anodic dissolution of lead in concentrated sulphuric acid, with the formation of a passivating, insoluble film of lead sulphate, as well as on the cathodic reduction process of the passivating layer was studied. Determinations were carried out within a relatively wide range of potential sweep rate, that is from 5 to 250 mV/sec. On the basis of the kinetic parameters calculated from the polarization curves, supplementary information concerning the nature and the kinetics of the anodic oxidation and cathodic reduction, in the system under study, were obtained.

INTRODUCTION

In the present sequence of papers several computation methods are tested in order to model the *E—I* curves, at the electrode processes taking place with passivating films formation, according to the reaction :

$$M \underset{k_{-1}}{\overset{k_1}{\rightleftarrows}} M^{z+} + ze \tag{1}$$

where M is a metal. In equation (1) the only anodic reaction which is possible is that of the passivating film formation, a range of active dissolution being non-existent. At the same time one can suppose that the passivating film is not soluble in the electrolyte and it can be removed only by electrochemical reduction. An appropriate example for this purpose is the reaction :

$$Pb \rightleftarrows Pb^{2+} + 2\,e \tag{2}$$

followed by the very fast chemical reaction :

$$Pb^{2+} + HSO_4^- \rightleftarrows PbSO_4 + H^+ \tag{3}$$

In a sequence of previous papers [1-5] we had studied in detail the electrode processes taking place at the $PbSO_4$ formation, by the anodic oxidation of lead in sulphuric acid, as well as at the cathodic reduction of the passivating insoluble film, formed on the metal surface. The studies were carried out in different conditions of concentration, composition and temperature of the electrolyte, using the cyclic voltammetry method.

In the present paper, the influence of the potential sweep rate on the electrode processes in the above-mentioned system was studied, in order to obtain new insight and informations on the nature and kinetics of the anodic oxidation and cathodic reduction process, respectively

EXPERIMENTAL PART

The experimental current-potential curves, in the $Pb|PbSO_4|H_2SO_4$ system, were outlined using the cycle voltammetry method. The potential of the working electrode was scanned within the ($-1200 \div -870$) mV range by means of a PS-3 type potentiostat coupled with an Orion type EMG-1117 pulses generator. The voltammograms were registered by means of an X–Y recorder. As working electrode a lead cylinder having the working surface a circle of 6 mm diameter, was used. A platinum net was used as counterelectrode, and the $Hg|Hg_2SO_4|H_2SO_4$ 1 M electrode was used as reference electrode. The schemes of the electric device and of the cell for electrochemical polarization were described in a sequence of previous papers. [2,3] Determinations were carried out in a sulphuric acid solution of $\rho = 1.28$ g/cm^3 (4.876 M) density, at potential scan rates changing from 5 to 250 mV/sec. Before each run the working electrode surface was mechanically polished with glass paper of different granulation, then it was electropolished in sulphuric acid of $\rho = 1.28$ g/cm^3 density, for 10 minutes, at a potential of -1800 mV, after that is was submitted to cycling with a 5 mV/sec sweep rate, within the above-mentioned potential range, in the working solution, until a number of 20 cycles was performed. Only after that, the working electrode was submitted to cycling at potential sweep rates changing from 10 to 250 mV/sec. At each of this sweep rates a number of 10 cycles was performed. The cycling of the electrode at small sweep rates (5 mV/sec) before each run, had as purpose the obtainment of a reproducible and active porous surface of the electrode. In a sequence of previous papers [2,3,5] it was pointed out that this one is carrying out after about 10–20 charging-discharging cycles. After this preceding processing, reproducible results obtain independently of the order in which the cyclings at different sweep rates are carried out.

The working temperature was maintained constant by means of a UM–210 thermostat, with a ±0.01°C precision.

RESULTS AND DISCUSSIONS

Figure 1 shows the voltammograms obtained on the lead electrode, in a sulphuric acid solution of $\rho = 1.28$ g/cm^3 density at some of the 15 potential sweep rates, on the ($-1200 \div -870$) mV range, and tables 1 and 2 present the kinetic parameters determined from the polarization curves.

The meaning of the peaks on voltammograms, as well as the processes taking place at the electrode are those presented in the introduction (reactions (2) and (3)). Analysis of curves from figure 1 shows that, at the increase of the potential sweep rate, the shape of the voltammograms essentialy does not change. At the same time the potential $E_{p,a}$, corresponding to the anodic current maximum, does not depend on the sweep rate, while the potential $E_{p,c}$, corresponding to the cathodic current maximum, moves with about 30 mV, towards more electronegative values, when

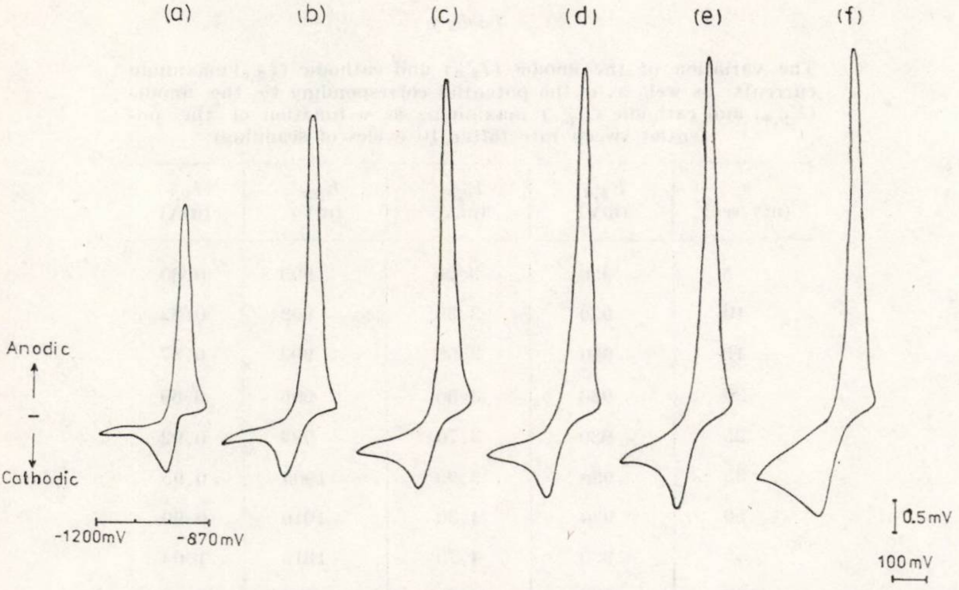

Fig. 1. — Voltammograms of lead electrode, in a sulphuric acid solution, of $\rho = 1.28$ g/cm^3 at several potential sweep rates, within $(-1200 \div -870)$ mV range: a) 10 mV/sec; b) 50 mV/sec; c) 100 mV/sec; d) 150 mV/sec; e) 200 mV/sec; f) 250 mV/sec.

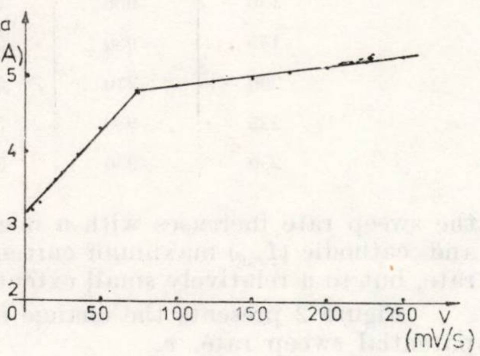

Fig. 2. — The anodic peak current variation as a function of the potential sweep rate.

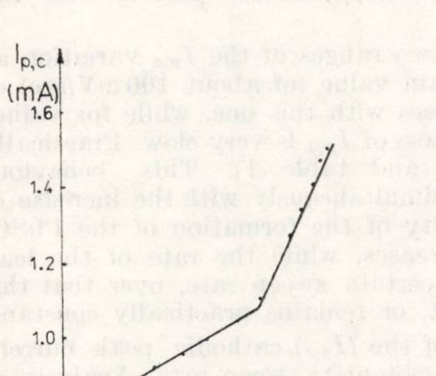

Fig. 3. — The cathodic peak current variation as a function of the logarithm of the potential sweep rate.

Table 1

The variation of the anodic ($I_{p,a}$) and cathodic ($I_{p,c}$) maximum currents as well as of the potential corresponding to the anodic ($E_{p,a}$) and cathodic ($E_{p,c}$) maximum, as a function of the potential sweep rate (after 10 cycles of scanning)

v (mV/sec)	$E_{p,a}$ (mV)	$I_{p,a}$ (mA)	$E_{p,c}$ (mV)	$I_{p,c}$ (mA)
5	−930	3.20	− 990	0.80
10	−930	3.30	− 992	0.82
15	−930	3.50	− 993	0.87
20	−930	3.60	− 996	0.89
25	−930	3.70	− 998	0.92
35	−930	3.95	−1000	0.95
50	−930	4.30	−1010	0.99
75	−930	4.75	−1015	1.04
100	−930	4.86	−1020	1.10
125	−930	4.90	−1022	1.21
150	−930	4.95	−1024	1.27
175	−930	5.05	−1026	1.34
200	−930	5.10	−1028	1.40
225	−930	5.20	−1030	1.47
250	−930	5.25	−1030	1.50

the sweep rate increases with a decade (see table 1). The anodic ($I_{p,a}$) and cathodic ($I_{p,c}$) maximum currents increase with the potential sweep rate, but to a relatively small extent.

Figure 2 presents the change of the ($I_{p,a}$) anodic current with the potential sweep rate, v.

One can observe that there are two ranges of the $I_{p,a}$ variation as a function of v, that is : up to a certain value (of about 100 mV/sec) of the sweep rate, the $I_{p,a}$ rapidly increases with this one, while for values higher than 100 mV/sec of v, the increase of $I_{p,a}$ is very slow. Practically a plateau is obtained (see Fig. 2 and table 1). This behaviour could be explained by the fact that, simultaneously with the increase of the potential sweep rate, the possibility of the formation of the $PbSO_4$ passivating layer by reaction (3) decreases, while the rate of the lead active dissolution increases up to a certain sweep rate, over that this latter increases in a very small extent, or remains practically constant.

Figure 3 presents the variation of the ($I_{p,c}$) cathodic peak current as a function of the logarithm of the potential sweep rate. Analysis of the figure shows that in this case, too, two distinct ranges of the $I_{p,c}$ variation as a function of v obtain. On the first range a slower linear variation is noticed while on the second, a more pronounced variation of $I_{p,c}$ with v appears. In this case, too, this behaviour can be accounted for by the fact that, simultaneously with the increase of the potential sweep rate, an increase of the rate of the electroreduction process takes place too, so much the more as v is higher (see Fig. 3 and table 1).

As pointed out, the anodic and cathodic peak currents are changing to a relatively small extent with the potential sweep rate. Instead of this, a drastic variation of the electricity amounts involved in the anodic (Q_a) and cathodic (Q_c) process, as a function of v is noticed.

Data presented in table 2 show that Q_a as well as Q_c decrease rapidly with the increase of the sweep rate from 5 to 100 mV/sec, and slower and slower at potential sweep rates higher than 100 mV/sec. This behaviour could be explained by the fact that at the increase of the sweep rate, the same potential range is scanned in a smaller and smaller time, hence the thickness (δ) of the active layer from the electrode surface, which participates in the reactions from the interface, is smaller and smaller (see table 2); the electrolyte has no sufficient time to penetrate in depth. Although by the potential slow sweep of the electrode a constant surface of spongeous lead was performed, our results show that the electrode can

Table 2

The variation of the electricity amounts involved in the anodic (O_a) and cathodic (O_c) process as well as of the passivating film thickness formed in the anodic process (δ_{torm}) and dissolved in the cathodic one (δ_{diss}), as a function of the potential sweep rate (after 10 cycles of scanning)

v (mV/sec)	Q_a 10^3 (C/cm^2)	δ_{torm} (μ)	Q_c 10^3 (C/cm^2)	δ_{diss} (μ)
5	61.3	0.155	59.30	0.150
10	43.4	0.110	42.40	0.107
15	33.3	0.084	29.70	0.075
20	25.5	0.065	22.80	0.058
25	21.8	0.055	18.40	0.046
35	16.4	0.041	13.70	0.035
50	12.4	0.031	10.03	0.025
75	9.0	0.023	7.09	0.018
100	7.0	0.018	5.67	0.014
125	5.7	0.014	4.86	0.012
150	4.8	0.012	4.22	0.011
175	4.1	0.010	3.75	0.010
200	3.7	0.009	3.55	0.009
225	3.3	0.008	3.28	0.008
250	3.0	0.0075	3.03	0.0077

be passivated by different amounts of lead sulphate, representing a few monolayers at high sweep rates, until few tens of monolayers, at small sweep rates. The thickness of the passivating film (δ_{form} and δ_{diss}) changes hence, as we already pointed out, as a function of the sweep rate (see table 2). This behaviour is different from that usually indicated in literature,[6-9] in which a constant thickness of the passivating layer is considered, independently of the potential sweep rate.

The various mathematical models from literature,[6-9] which are suggesting $I_p = f(Q)$ relations, refer to constant electricity amounts Q. In our case, such an equation must take into account the existence of a variable Q and will be discussed in the note (II) which follows.

CONCLUSIONS

The study of the influence of the potential sweep rate on the Pb/Pb^{2+} electrode process leads to the following conclusions:

— the shape of the voltammograms does not essentially modify at the increase of the potential sweep rate;

— the potential corresponding to the anodic maximum is independent of the sweep rate, while the potential corresponding to the cathodic maximum moves towards more electronegative values at the increase of the sweep rate (with about 30 mV/dec);

— the electricity amounts involved in the anodic and cathodic process much change with the increase of the potential sweep rate. As a result the thickness of the insoluble film formed on the electrode surface is higher than that of a monolayer, changing itself, from a few tens monolayers (at small sweep rates) to a few monolayers (at high sweep rates);

— for the suggestion of mathematical models for $E-I$ curves computation, a variable Q will be considered instead of a constant one, as appearing in literature.[9-12]

REFERENCES

[1] S. Sternberg, V. Brânzoi, L. Apăteanu and A. Mateescu, *Rev. Roumaine Chim.*, **28**, 583 (1983).

[2] S. Sternberg, V. Brânzoi and L. Apăteanu, *Rev. Roumaine Chim.* **29**, 833 (1984).

[3] S. Sternberg, V. Brânzoi, L. Apăteanu, C. Doboș and E. Comănescu, *Rev. Chimie*, (București), **35**, 427 (1984).

[4] V. Brânzoi, S. Sternberg and L. Apăteanu, *Rev. Roumaine Chim.*, **30**, 199 (1985).

[5] S. Sternberg, V. Brânzoi and L. Apăteanu, *Rev. Roumaine Chim.*, **32**, 121 (1987).

[6] S. Srinivasan and E. Gileadi, *Electrochim. Acta*, **11**, 321 (1966).

[7] N. R. de Tacconi, A. J. Calandra and A. J. Arvia, *Electrochim. Acta*, **18**, 571 (1973).

[8] A. J. Calandra, N. R. de Tacconi, R. Pereiro and A. J. Arvia, *Electrochim. Acta*, **19**, 901 (1974).

[9] D. Devilliers, F. Lantelme and M. Chemla, *Electrochim. Acta*, **31**, 1235 (1986).

Revue Roumaine de Chimie, **34**, 5, 1287–1290 (1989)

COMBINED ION EXCHANGE-SPECTROMETRIC STUDY OF THE Ce(IV)–SULPHANILIC ACID SYSTEM. II[1]

SPECTROMETRIC DETERMINATION OF SULPHANILIC ACID

LUMINIȚA VLĂDESCU and STELUȚA CHIPER
National Institute of Chemistry, Laboratory of Analytical Chemistry,
Splaiul Independenței 202, Bucharest, Romania

Received November 23, 1987

This paper presents the optimum working conditions for the spectrometric determination of sulphanilic acid with Ce(IV) as reagent. By coupling the spectrometric method with a cation exchange system, the pH range may be increased both in the determination of sulphanilic acid with Ce(IV) and of Ce(IV) with sulphanilic acid.

The use of sulphanilic acid for spectrometric determination of Ce(IV) is known in the literature.[2] This method is advantageous but the ways presented by the authors for eliminating interferences require the use of other organic reagents and repeated extraction with organic solvents,[3] electrolysis with platinum electrodes,[4] or operations of precipitation and filtration.[5]

In the previous paper[1] we established the working conditions for using ion exchange resins for eliminating interferences in the spectrometric determination of Ce(IV) with sulphanilic acid.

In the present paper we report the experimental results that prove the redox character of the reaction between Ce(IV) and sulphanilic acid. On this basis a spectrometric method for sulphanilic acid determination was established. The use of a cation exchange resin for extention of the pH range both in determination of Ce(IV) and of sulphanilic acid is proposed.

EXPERIMENTAL

Chemicals and equipment

- Aqueous solutions of known titrum of $Ce(SO_4)_2 \cdot 6\,H_2O$ and $CeCl_3$
- Aqueous solutions of sulphanilic acid 10^{-2}M and 10^{-1}M
- Aqueous solutions of sulphosalicylic acid 10% and 20%
- Aqueous solutions of HCl 4M, NH_3 10% and NH_4Cl 1M.
- Strongly acid cation exchange resin Vionit CS-3
- Strongly basic anion exchange resin Vionit AT-1
- pH buffer solutions (pH 1.5, 2.5, 4.0, 5.5; 8)
- SPEKOL Carl Zeiss Jena spectrophotometer.
- MV 84 pH-meter.

The quantitative determination of Ce(IV) was performed by spectrometry in the presence of sulphanilic acid,[2] or sulphosalicylic acid.[2] Ce(III) was determined spectrometrically by sulphosalicylic acid.[7]

The ion exchange experiences took place in a glass column 15 cm long, 1 cm in diameter, provided with stopcoks at bottom and funnel with ground joint at top.

Known quantities of cation or anion exchange resins were transferred into each column, purified, activated in H^+ or Cl^- form respectively and washed with distilled water up to negative Cl^- test. The NH_4^+ ionic form of the resin was obtained by washing the H^+ cationite with 1M NH_4Cl solution and distilled water.

RESULTS AND DISCUSSION

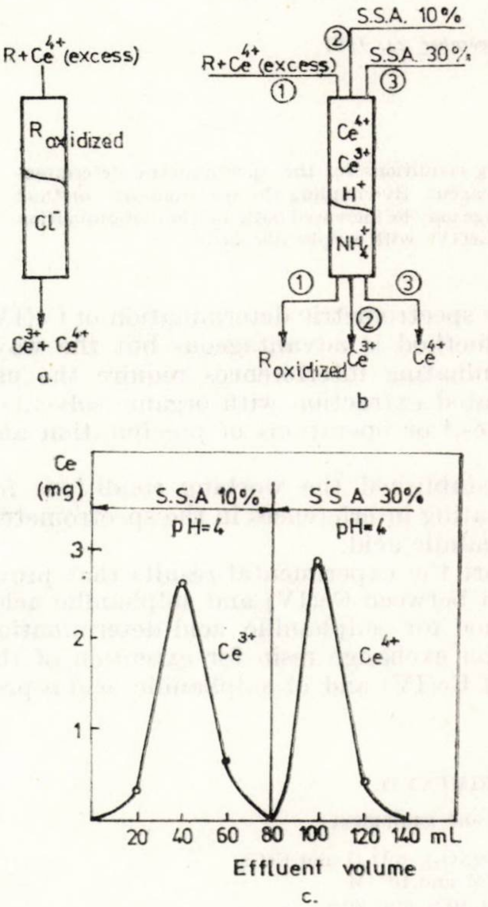

Fig. 1. — Ion exchange behaviour of Ce(IV) in the presence of sulphanilic acid (noted R): a — anion exchange resin (Cl^-); b — cation exchange resin (NH_4^+); c — elution curves of cerium from cationite (NH_4^+).

After passing sulphanilic acid (noted R) and Ce(IV) solution through a column with anion exchange resin in Cl^- ionic form, a red compound was strongly fixed on the upper part of the resin and Ce^{3+} and Ce^{4+} ions were noticed in the effluent (Fig. 1a).

When a solution of sulphanilic acid and Ce(IV) in excess was passed through the column with cationite in NH_4^+ ionic form, the red compound resulted after the reaction between the two reagents was completely collected in the effluent (Fig. 1 b). The absorbance of the effluent solution is proportional to the Ce(IV) amount with which all the sulphanilic acid in the sample reacted, in a 4 :1 Ce : R molar ratio.

The successive passage through the column of several solutions of 10% sulphosalicylic acid (pH = 4) and then 30% sulphosalicylic acid (pH = 4),[7] evidenced, as elution curves (Fig. 1 c), the existence of cerium in the resin, i.e. an amount of Ce(III) corresponding to the amount of sulphanilic acid in the sample and an amount of Ce(IV) corresponding to the excess in this ion versus the sulphanilic acid in the initial solution.

Therefore, the experimental results show (Fig. 1) that an oxido-reduction reaction takes place between Ce(IV) and sulphanilic acid yielding an oxidation product of sulphanilic acid of a red colour and Ce(III) ions. The quantitative determinations showed a 4 : 1 Ce : R molar ratio.

The permanent presence in solution of cerium as Ce(IV) before the reaction and as Ce(III) after the reaction, explains the necessity of the spectrometric determination of Ce(IV) within a limited pH range of 1.6–2.3,[1] because at a higher pH cerium hydrolyzes and at a greater acidity absorbance decreases.

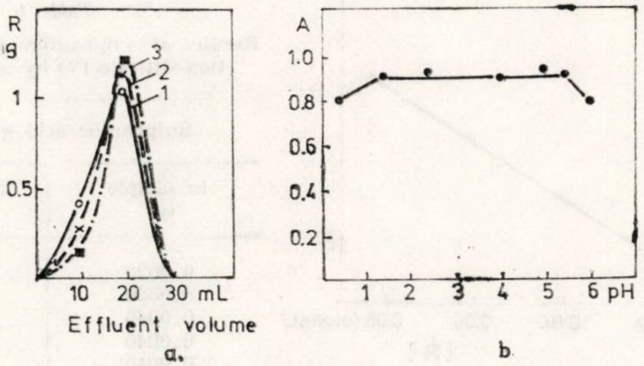

Fig. 2. — Influence of pH on the absorbance of solutions containing the oxidation product of sulphanilic acid after passing through a column with cation exchange resin (NH_4^+) : a — elution curves : 1 — pH = 1.5 ; 2 — pH = 5.5 ; 3 — pH = 8 ; b — dependence of A on pH.

By coupling the spectrometric method with a cation exchange system, Ce(IV) and Ce(III) ions remain fixed in the resin, so that the pH of the effluent solution may be increased, with positive consequences on absorbance (Fig. 2), thus increasing the sensitiveness of the spectrometric method.

The most important consequence of the experimental results obtained is that the redox reaction between sulphanilic acid and Ce(IV) may be at the basis of a spectrometric method for determining sulphanilic acid.

Spectrometric titration of sulphanilic acid with Ce(IV) (Fig. 3) showed a 4 : 1 Ce : R molar ratio.

Dependence between absorbance and sulphanilic acid concentration in the sample is linear within a concentration range of 0.02 — 0.08 mg sulphanilic acid/mL (Fig. 4). Molar absorptivity is ε = 4200 at λ = 495 nm.

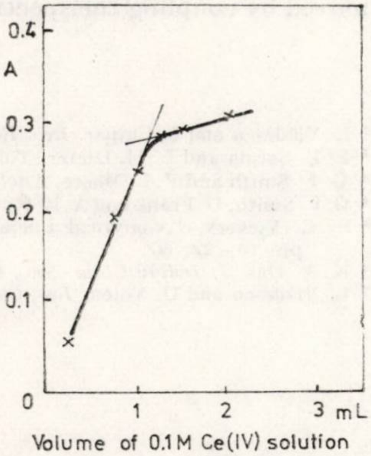

Fig. 3. — Spectrometric titration of sulphanilic acid with Co(IV) : 3 mL of 0.010 M sulphanilic acid solution ; 0.10 M Ce(IV) solution (λ=495nm).

The spectrometric method was checked in determination of sulphanilic acid in synthetic samples. The data given in table 1 show a good agreement between the results obtained by the proposed method and the amounts of sulphanilic acid taken in the sample.

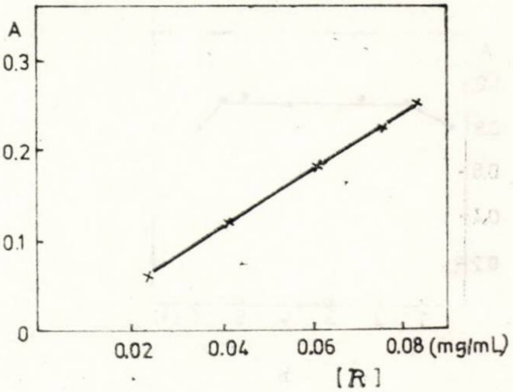

Fig. 4. — Dependence of A on the concentration of sulphanilic acid in solution ($\lambda = 495$ nm).

Table 1

Results of sulphanilic acid determination with Ce(IV) by spectrometry

Sulphanilic acid quantity	
In sample (g)	Determined (g)
0.0020	0.0022
0.0020	0.0019
0.0040	0.0044
0.0040	0.0046
0.0010	0.0014
0.0010	0.0010

CONCLUSIONS

Redox reaction between sulphanilic acid and Ce(IV) may be used as basis of a spectrometric method for the determination of sulphanilic acid. To this end, the absorbance of an aqueous solution containing an unknown amount of sulphanilic acid, and excess of 10^{-1}M Ce(IV) solution in 1M H_2SO_4 is measured at $\lambda = 495$ nm. All ionic interferences may be removed by coupling the spectrometric method with an ion exchange system.

REFERENCES

[1] L. Vlădescu and S. Chiper. *Rev. Roumaine Chim.*, **30**, 1047 (1985).
[2] P. L. Sarma and L. H. Dieter, *Talanta*, **13**, 347 (1966).
[3] G. F. Smith and F. L. Moore, *Analyt. Chem.*, **29**, 448 (1957).
[4] G. F. Smith, G. Frank and A. E. Kott, *Ind. Eng. Chem., Anal. Ed.*, **12**, 268 (1940).
[5] R. C. Vickery, "Analytical Chemistry of Rare Earths", Pergamon Press, Oxford, 1961, pp. 19—22, 60.
[6] K. A. Das, *J. Indian Chem. Soc.*, **10**, 306 (1972).
[7] L. Vlădescu and D. Voicu, *Rev. Chim. (București)*, **30**, 373 (1979).

ORSZÁGOS MŰSZAKI INFORMÁCIÓS KÖZPONT ÉS KÖNYVTÁR 1883

NOTE POUR LES AUTEURS

La **Revue Roumaine de Chimie** publie des articles en anglais, français, russe, allemand ou espagnol. Les auteurs sont priés d'envoyer des articles et des comptes rendus inédits.

Les manuscrits seront dactylographiés à double interligne. La bibliographie, les tableaux et la légende des figures seront placés après le texte.

Si l'article fait partie d'une série numérotée, la partie précédente sera donnée comme première référence.

Chaque article sera précédé d'un résumé comprenant quinze lignes au maximum.

Les références bibliographiques dans le texte seront faites par des exposants sans parenthèses et paraîtront à la fin de l'ouvrage.

Les publications périodiques mentionnées dans la bibliographie seront présentées suivant les prescriptions internationales : le nom de l'auteur précédé de l'initiale du prénom, le titre du périodique abrégé conformément à « Chemical Abstracts » et souligné par une ligne, le numéro du tome indiqué par des chiffres arabes et souligné par deux lignes, suivi de la première page de l'article : à la fin, l'année de la parution sera placée entre parenthèses. Le numéro de la revue ne sera pas indiqué si les pages du volume sont numérotées consécutivement.

Les textes des livres ou traités inclueront : le nom des auteurs, précédés de l'initiale du prénom, le titre du livre entre guillemets et sans être souligné, le numéro du tome précédé par l'abréviation « vol. » (ou « Bd. »), le numéro de l'édition, les éditions (the publisher), la localité de la parution du livre, l'année de la parution et la page de la référence précédée(s) par l'abréviation « p » (ou « S »).

Les brevets seront indiqués comme suit : l'auteur ou la firme, le pays et le numéro du brevet, la date de la revue *(Chem. Abstr.)*. Par ex. : M. Jones (to Union Carbide Co.), Brit. Pat. 610 238, 2 Sept. 1959 : cf. *Chem. Abstr.*, **54**, 12808 (1960).

Si la référence n'a pas été lue en original, on indiquera aussi la revue de références consultée.

Les diagrammes seront tracés à l'encre de Chine sur papier calque. Les tableaux et les figures (en nombre strictement nécessaire), ainsi que les courbes dans les figures seront numérotés par des chiffres arabes. Leur explication sera donnée dans la légende des figures. Prière de ne pas inscrire les mêmes données dans les tableaux et les figures. Chaque tableau aura un titre. On indiquera dans le texte la place approximative des tableaux et des figures. Les formules chimiques seront incluses dans le texte ; en outre, elles seront transcrites sur papier calque, à l'encre de Chine.

Les auteurs sont priés d'indiquer les caractères italiques (en soulignant les lettres au crayon), ainsi que tout autre caractère spécial : les préfixes *ortho*, *méta*, *para*, *cis*, *trans*, etc. seront soulignés pour indiquer leurs caractères italiques et ne seront jamais écrits avec des majuscules.

Aucune correction à la main ne sera admise sur le manuscrit. Les corrections seront frappées à la machine. Les lettres grecques ou d'autres symboles spéciaux seront insérés à la main à l'encre clairement.

Le manuscrit sera signé par l'auteur.

Le titre courant aura 50 lettres au maximum.

L'entière responsabilité du contenu des articles appartient aux auteurs.

Sur demande on peut obtenir une note plus complète.

PRINTED IN ROMANIA

TRAVAUX PARUS AUX ÉDITIONS DE L'ACADÉMIE DE LA RÉPUBLIQUE SOCIALISTE DE ROUMANIE

ELENA CEAUŞESCU, **Răşini de hidrocarburi, vol. 1**, 1988, 344 p.

ELENA CEAUŞESCU, **Progrese în chimia şi tehnologia polimerilor**, 1986, 446 p.

ELENA CEAUŞESCU, **Forschungen im Bereich der Chemie und Technologie der Polymere**, 1986, 444 p.

ELENA CEAUŞESCU, **Cercetări în chimia şi tehnologia polimerilor**, 1983, 520 p.

ELENA CEAUŞESCU, **Noi cercetări în domeniul compuşilor macromoleculari**, 1981, 536 p.

ELENA CEAUŞESCU, **Polimerizarea stereospecifică a izoprenului**, 1979, 307 p.

ELENA CEAUŞESCU, **Research work on synthesis and characterization of macromolecular compounds. Contributions**, 1974, 251 p.

I. G. MURGULESCU, **Introducere în chimia fizică, vol. I. 1. Atomi, molecule, legătură chimică**, 1976, 560 p.

I. G. MURGULESCU, V. EM. SAHINI, **Introducere în chimia fizică, Vol. I, 2. Structura şi proprietăţile moleculelor**, 1979, 604 p.

I. G. MURGULESCU, E. SEGAL, **Introducere în chimia fizică, Vol. II. 1. Teoria molecular-cinetică a materiei**, 1979, 1036 p.

I. G. MURGULESCU, TATIANA ONCESCU, E. SEGAL, **Introducere în chimia fizică, Vol. II. 2. Cinetică chimică şi cataliză**, 1981, 1024 p.

I. G. MURGULESCU, J. PĂUN, **Introducere în chimia fizică, Vol. I, 3. Nucleul atomic, reacţii nucleare, particule elementare**, 1982, 606 p.

I. G. MURGULESCU, RODICA VÎLCU, **Introducere în chimia fizică. Vol. III. Termodinamica chimică**, 1982, 624 p.

I. G. MURGULESCU, O. M. RADOVICI, **Introducere în chimia fizică, Vol. IV. Electrochimia**, 1986, 416 p.

CRISTOFOR I. SIMIONESCU, VALERIA GORDUZA, **Implicaţii bioenergetice ale coloranţilor**, 1988, 208 p.

R. VÎLCU, M. LECA, **Termodinamica polimerilor prin cromatografie de gaze**, 1987, 238 p.

I. ZUGRĂVESCU, M. PETROVANU, **Cicloadiţii 3+2 dipolare**, 1987, 446 p.

RAUL MIHAIL, ION GROZEANU, **Estimarea secvenţială aplicată sistemelor chimice**, 1986, 406 p.

M. BREZEANU, I. PATRON, M. ANDRUH, **Combinaţii complexe polinucleare şi aplicaţiile lor**, 1986, 244 p.

A. T. BALABAN et al., **Labelled Compounds and Radiopharmaceuticals Applied in Nuclear Medicine**, coédition avec John Wiley and Sons, 1986, 742 p.

D. PURDELA, **Nomenclatura chimiei organice — IUPAC**, 1986, 451 p.

PETRU BUDRUGEAC, **Probleme de chimie**, 1986, 280 p.

T. ONCESCU, S. G. IONESCU, **Conversie fotochimică şi stocare de energie**, 1985, 272 p.

V. DRĂGUŢAN, A. T. BALABAN, M. DIMONIE, **Olefin Metathesis and Ring-Opening Polymerization of Cyclo-Olefins**, coédition avec John Wiley and Sons, 1985, 544 p.

C. LITEANU, I. RÎCĂ, **Optimizarea proceselor analitice**, 1985, 360 p.

N. PERESCU, **Chimia extracţiei cu solvenţi şi aplicaţii**, 1985, 212 p.

V. EM. SAHINI, M. HILLEBRAND, **Chimie cuantică în exemple şi aplicaţii**, 1985, 382 p.

GH. MARCU, **Chimia compuşilor coordinativi**, 1984, 415 p.

E. CORDOŞ, C. MANOLIU, **Spectrometria de absorbţie şi fluorescenţa atomică**, 1984, 178 p.

C. BODEA, **Tratat de biochimie vegetală, p. II, t. V**, 1984, 438 p.

N. ASANDEI, A. GRIGORIU, **Chimia şi structura fibrelor**, 1984, 395 p.

N. IONESCU, M. CĂLDĂRARU, **Oxidarea catalitică a olefinelor inferioare**, 1983, 178 p.

C. I. SIMIONESCU, F. DANEŞ, **Originea vieţii**, 1984, 110 p.

C. BODEA, **Tratat de biochimie vegetală, p. II, t. IV**, 1982, 408 p.

CR. SIMIONESCU, VALERIA GORDUZA, **Polimeri biocompatibili şi biologic activi**, 1980, 479 p.

M. FLORESCU, **Metode ştiinţifice în dezvoltarea industriei chimice moderne**, 1979, 495 p.

C. GH. MACAROVICI, **Analiza chimică cantitativă anorganică**, 1979, 457 p.

ISSN 0035—3930

I. P. Informaţia c. 2673

43 426

Lei 40

F 1103

ACADÉMIE DE LA RÉPUBLIQUE SOCIALISTE DE ROUMANIE

REVUE ROUMAINE DE CHIMIE

Hommage à l'académicien
ELENA CEAUŞESCU

TOME 34
Nº 6
Juin 1989

Rev. Roumaine Chim.

RRCHAX, 34, 6, p. 1291 – 1446 (1989), Bucarest

EDITURA ACADEMIEI REPUBLICII SOCIALISTE ROMÂNIA

ACADÉMIE DE LA RÉPUBLIQUE SOCIALISTE DE ROUMANIE

COMITÉ DE RÉDACTION

Rédacteur en chef :

I. G. MURGULESCU, membre de l'Académie de la République Socialiste de Roumanie

Rédacteurs en chef adjoints :

A. T. BALABAN et V. EM. SAHINI, membres correspondants de l'Académie de la République Socialiste de Roumanie

Collège de rédaction :

EM. BRATU, ELENA CEAUȘESCU, ECATERINA CIORĂNESCU-NENITZESCU, CR. SIMIONESCU, membres de l'Académie de la République Socialiste de Roumanie ; P. SPACU, membre correspondant de l'Académie de la République Socialiste de Roumanie ; M. BANCIU, M. D. GHEORGHIU, I. HAIDUC, D. I. MARCHIDAN, G. NIAC et D. SĂNDULESCU

La Revue Roumaine de Chimie paraît 10 fois par an. Toute commande de l'étranger sera adressée à ROMPRESFILATELIA — sectorul Export-Import Presă, P.O. Box 12—201, télex 10376 prsfi r 78104 Bucarest, Calea Griviței nr. 64—66, Roumanie

Les manuscrits, les livres et les revues proposés en échange, ainsi que toute correspondance seront envoyés à la rédaction :

REVUE ROUMAINE DE CHIMIE

125, Calea Victoriei, 79717 Bucarest, Roumanie, téléphone 50 76 80

EDITURA ACADEMIEI REPUBLICII SOCIALISTE ROMÂNIA
125, Calea Victoriei 79717, Bucarest, Roumanie, téléphone 50 76 80

HOMMAGE À L'ACADÉMICIEN
ELENA CEAUȘESCU

ORSZÁGOS MŰSZAKI INFORMÁCIÓS KÖZPONT ÉS KÖNYVTÁR
1883

IN HONOUR OF
ELENA CEAUŞESCU, D. CHEM. ENG., MEMBER OF THE ACADEMY OF THE SOCIALIST REPUBLIC OF ROMANIA

On January 7, this year, we celebrate the birthday and 50 years of revolutionary activity of Academician Elena Ceauşescu. A Doctor of Chemical Engineering, Member of the Executive Political Committee of the Central Committee of the Romanian Communist Party, First Vice-Prime Minister of the Government of the Socialist Republic of Romania, President of the National Council for Science and Education, Dr. Elena Ceauşescu chairs a vast scientific, political and social enterprise meant to bring into effect the country's plans for economic and social development, the important programs geared to a better organization and modernization of production, to increasing work productivity and efficiency, to a comprehensive implementation of the overall policy of the Romanian Communist Party and State, for the benefit of Romanian science, education and culture. The organization and management of the scientific research in this country, most especially in the fields of chemistry, and chemical technology and engineering, largely rely upon the innovative scientific spirit of, and direct guidance by Dr. Elena Ceauşescu.

As a direct outcome, the entire research and development system in chemistry has been given an appropriate coordination and has been integrated, along with the higher education in the field, with the respective industry.

The research work undertaken by Dr. Elena Ceauşescu is focused mainly on the chemistry and technology of macromolecular compounds; she has contributed to elucidating a number of major problems in the area — a most dynamic one in chemistry today, while also providing valuable contributions in all stages of applied research and

engineering, thus fostering the implementation in industry of the results of fundamental research.

Her studies dwell, *inter alia*, upon procedures for monomer and solvent purification; procedures for obtaining polymers via stereospecific polymerization and emulsion polymerization; procedures for obtaining polycondensates; studies on the structural characteristics of polymers and the relationship between structure and properties, as well as methods for the characterization of polymers. A series of studies deal with the use of complex catalysts for polymer synthesis in solution, with special emphasis on catalysts based on transition metals. Other works are concerned with the obtaining of polymers modified by isomerization, degradation and substitution reactions.

The stereospecific polymerization of isoprene holds an important place in the research work developed by Dr. Elena Ceaușescu, owing to the paramount relevance of this problem in today's chemistry of synthetic rubber. Part of the results were gathered in Dr. Ceaușescu's doctoral thesis. A special emphasis was placed on the synthesis of *cis*-1,4-polyisoprenic rubber that displays properties and structures similar to those of natural rubber, and substitutes for the latter in the tyre and technical item industry. Theoretical aspects connected with the reaction mechanism and kinetics, and the properties of the polyisoprene were also dealt with. Research was focused on the optimization of basic parameters, the obtaining of catalytic systems and development of the main steps of the technological flow-chart. The results have led to an industrial process for manufacturing *cis*-1,4-polyisoprenic rubber in Romania.

Dr. Elena Ceaușescu's scientific activity is also reflected in numerous papers published in scientific journals and in six monographs, first put out by Editura Academiei R S. România, Bucharest, namely, "Research Work on Synthesis and Characterization of Macromolecular Compounds" (1974), "Stereospecific Polymerization of Isoprene" (1979), "Recent Research in the Field of Macromolecular Compounds" (1981), "Research in the Chemistry and Technology of Polymers" (1983), "Advances in Polymer Chemistry and Technology" (1986), and "Hydrocarbon Resins" (1988). Many publishing houses worldwide were soon to offer their readers translations of these books.

Dr. Elena Ceaușescu chaired the National Congress of Chemistry in the years 1978, 1981, 1988, and the IUPAC's Macro '83 Symposium. Her opening address at the 1988 National Congress of Chemistry gives important guidelines to the chemical research in Romania, also providing for the strengthening of the international scientific co-operation. Dr. Elena Ceaușescu contributed valuable papers to many scientific congresses and symposia — an outcome of her comprehensive scientific activity in the field of elastomer chemistry.

Dr. Elena Ceaușescu's scientific merits won well-deserved national and worldwide recognition. She is a member of the Academy of the Socialist Republic of Romania. She was also elected member of numerous international chemical societies of high renown and was nominated honorary professor by important higher education institutions abroad. Dr. Ceaușescu is a honorary member of the International Society of Industrial Chemistry, France; active member of the Academy of Sciences, New York; honorary member of the College of Chemists and Chemical Engineers in Costa Rica; honorary member of the University Council and of the Management Council of the Central University in Ecuador; honorary member of the Ecuador Institute of Natural Sciences; honorary member of the School of Information Science of the Central University of Ecuador; honorary professor of the National Engineering University, Peru; honorary member of the American Institute of Chemists (A.I.C.); Doctor Honoris Causa of the University of Buenos Aires; Doctor Honoris Causa of the University of South-Bahia Blanca, Argentina; Doctor Honoris Causa of the Feminine University of Manila, the Philippines; honorary member of the Chemical Society of Mexico; Doctor Honoris Causa of the University of Yucatan, Mexico; Extraordinary Professor of the Autonomous National University of Mexico; Doctor Honoris Causa of Sciences, University of Teheran; honorary member of the Society of Polymer Science in Japan; corresponding member of the Academy of Athens; awardee of the Silver Medal of the Science University of Kuweit; honorary member of the Academy of Arts and Sciences in Ghana; honorary member of the Academy of Sciences of the State of Illinois, USA; Fellow of the Royal Institute of Chemistry, UK; Professor Honoris Causa of the Polytechnics of Central London; member of the European Academy of Sciences, Arts

and Humanities, and member of the Honorary Committee of the Academy; Doctor Honoris Causa of the Technical University of the Middle East, Ankara; Doctor Honoris Causa of the University of Malta; Doctor Honoris Causa for Sciences of the Islamabad University, Pakistan; Doctor Honoris Causa for Sciences of the University of Liberia; Doctor Honoris Causa in Chemical Sciences, D.P.R. of Korea.

The high praise enjoyed by Dr. Elena Ceaușescu is also reflected in her being awarded important titles and distinctions of merit. Among these are: the highest Romanian title of honour "Hero of the Socialist Republic of Romania"; the title "Hero of Socialist Labour"; the medal "Star of the Socialist Republic of Romania", as well as other orders and medals, Romanian and foreign. She was also awarded the Gold Medal of the Institute for the Problems of a New International Economic Order, the Gold Medal "Marie Curie" and the Jubilee Gold Medal of the Institute of International Relations in Rome, and the Gold Badge of the European Academy of Sciences, Arts and Humanities. By virtue of these, Academician Elena Ceaușescu is the most prestigious representative of the Romanian contemporary science, education and culture.

Active in the national scientific and political life as well as in the international arena, presiding over the Romanian National Committee "Scientists and Peace", Academician Elena Ceaușescu makes an outstanding contribution to the carrying into effect of Romania's policy of independent domestic development, many-sided international co-operation, and struggle for peace, a policy designed under the guidance of Comrade Nicolae Ceaușescu, Secretary General of the Romanian Communist Party, President of the Socialist Republic of Romania, Honorary President of the Academy of the Socialist Republic of Romania.

The National Council for Science and Education, the Ministry of the Chemical and Petrochemical Industry, the Academy of the Socialist Republic of Romania and the Central Institute for Chemistry join whole-heartedly in the feelings of highest esteem and praise the Romanian people has for Academician Elena Ceaușescu, and express deepest appreciation for her exceptional contribution

to the building of modern Romania, to the development of scientific research and education in this country, particularly in the field of chemistry, chemical technology and engineering. We wish the most distinguished Romanian scholar many happy returns and a long and fruitful activity in order that science, education and culture in the Socialist Republic of Romania be raised onto ever higher levels of performance, for the benefit of our society, of world progress and peace.

THE NATIONAL COUNCIL
FOR SCIENCE AND EDUCATION

THE MINISTRY
OF THE CHEMICAL
AND PETROCHEMICAL
INDUSTRY

THE ACADEMY
OF THE SOCIALIST
REPUBLIC OF ROMANIA

THE CENTRAL INSTITUTE
FOR CHEMISTRY

REVUE ROUMAINE DE CHIMIE

Tome 34, N° 6 **Juin, 1989**

IN HONOUR OF
ELENA CEAUŞESCU, D. CHEM. ENG.
MEMBER OF THE ACADEMY OF THE
SOCIALIST REPUBLIC OF ROMANIA

ELENA CEAUŞESCU, M. DIMONIE, ANNELIESE CORNILESCU, V. DRĂGUŢAN, ELENA NICOLESCU, S. COCA, MIHAELA CUZMICI, VIORICA APOSTOL, R. MUNTEANU, R. GROSESCU, ALICE VASILESCU and M. TEODORESCU, **Influence of activator in the catalytic systems of ring-opening polymerization of cyclopentene** **1293–1299**

PETRU BALTĂ and MARCEL BIALE, **Redox behaviour of 3d ions in oxide glasses** **1301–1306**

IOAN BERDAN and OLGUŢA COSTINOAIA, **Study of Ni(II) – hydroxylamine reaction system (in French)** **1307–1312**

M. BRUMĂ, I. SAVA, C. HAMCIUC, E. HAMCIUC, C. I. SIMIONESCU, N. M. BELOMOINA, S. A. BABICH, E. S. KRONGAUZ and V. V. KORSHAK, **Synthesis of new polymers containing phenylquinoxaline units** **1313–1320**

C. CRISTESCU and ST. TOMAS, **AS-triazine derivatives with potential therapeutic action. XXIII. Synthesis of 4-thioxo-5(chlorobenzyl)thio-6-azauracil derivatives and their nucleosides** **1321–1327**

VIOREL FEROIU and DAN GEANĂ, **Prediction of vapour-liquid equilibria at low pressure by a general equation of state** **1329–1339**

MIRCEA D. GHEORGHIU, CONSTANTIN DRĂGHICI, LUMINITZA PÂRVULESCU and MIHAI ELIAN, **Nuclear magnetic resonance investigations of small rings. 6. The stereochemistry of cycloaddition of *t*-butylcyanoketene to norbornene derivatives. A multicenter approach for establishing the configuration with the aid of Europium shift reagent of some polycyclic α-*t*-butyl-α-cyanocyclobutanones** **1341–1350**

G. IVAN and MARIA GIURGINCA, **The effect of several hindered amine light stabilizers (HALS) in oxidative degradation of rubber compounds** . . . **1351–1360**

OVIDIU IVANCIUC, **Design on topological indices. 1. Definition of a vertex topological index in the case of 4-trees** **1361–1368**

Rev. Roumaine Chim. **34, *6*, 1291–1446 (1989), Bucarest**

N. JUMATE and I. CHICINAŞ, High voltage plasma applied to determine boron and silicon in superallied metallic powders 1369–1372

Z. KNOR and J. ŠOTOLA, New application of field emission techniques (FEM and FIM) to the study of catalytic systems 1373–1376

GHEORGHE MARIA, CRISTIAN TSAKIRIS, CRISTINA MARIA, ALEXANDRU ISOPESCU and GRIGORE BOZGA, An adapted model to predict operating conditions for a radiant furnace – thermal cracking reactor 1377–1387

STELIANA MAXIM and AURELIA FLONDOR, New crosslinked functionalized acrylic copolymers for biotechnological applications 1389–1395

ALEXANDRU C. RĂZUŞ, MIRCEA D. GHEORGHIU, ZSOLT G. ARVAY, ADRIAN I. IANCU and EMERIC BARTHA, Solvolyses in substituted cyclopropylcarbinylic systems. 6. Solvolysis of spiro[acenaphthene-1,1′-cyclopropan]-2-ol 1397–1403

IOAN SÂRGHIE and CATINCA SIMION, Kinetics of the back-extraction of iron β-diketonates 1405–1411

MIHAELA SPIRATOS, A. AIRINEI, N. STĂNICĂ, N. VOICULESCU and G. I. RUSU, Coordination polymers. VIII. Chelate polymers of 2,4-dihydroxyacetophenone. 1413–1417

J. TARASZEWSKA, Complexation of isomeric chloronitrobenzenes by β-cyclodextrin in the presence of ethanol 1419–1423

CORNELIA UNCUŢA, TEODOR-SILVIU BALABAN, AURICA PETRIDE, FILIP CHIRALEU and ALEXANDRU T. BALABAN, Reaction of pyrylium salts with nucleophiles. XXII. Regioselectivity (formation of aniline derivatives from primary amines and non-symmetrically substituted pyrylium salts) and chemoselectivity (pyridinium vs. aniline formation) 1425–1437

ŞTEFANIA ZUCA and MARIELA CONSTANTINESCU, On the complex ions in molten TlCl – $CdCl_2$ system 1439–1446

Revue Roumaine de Chimie, 34, 6, 1293–1299 (1989)

INFLUENCE OF ACTIVATOR IN THE CATALYTIC SYSTEMS OF RING-OPENING POLYMERIZATION OF CYCLOPENTENE

ELENA CEAUȘESCU[a], M. DIMONIE[b], ANNELIESE CORNILESCU[a],
V. DRĂGUȚAN[c], ELENA NICOLESCU[a], S. COCA[a], MIHAELA CUZMICI[a],
VIORICA APOSTOL[a], R. MUNTEANU[a], R. GROSESCU[d], ALICE VASILESCU[d]
and M. TEODORESCU[b]

[a] Chemical Research Institute, Spl. Independenței 202, Bucharest, Romania
[b] National Institute for Chemistry, Bucharest, Romania
[c] Centre of Organic Chemistry, Bucharest, Romania
[d] Institute of Physics and Nuclear Engineering, Bucharest, Romania

Received November 25, 1988

The paper describes the ways the activators used in the catalytic systems based on WCl_6 and organometallic compounds affect the reaction parameters in cyclopentene ring-opening polymerization. The obtained data allow to systematize the main types of activators employed in respect with the catalytic system sand their mode of action. Conclusions concerning the reaction mechanism and stereochemistry are drawn pointing out the different role of electron-donor and acceptor ligands.

INTRODUCTION

The catalytic systems of WCl_6 employed for ring-opening polymerization of cyclopentene contain along with the organometallic component electron-donor or acceptor compounds named activators.[1] These compounds have various structures and in most cases contain heteroatoms such as oxygen, nitrogen, halogen, etc. Due to their electron-donor or acceptor properties these compounds play a significant part in the polymerization process by increasing the catalytic activity and stability, the system reproducibility and improving the polymer yield.

Although up to now a large number of donors and acceptors have been used as activators,[2] the mechanism of their action upon the intimate stages of the polymerization reaction is not fully understood. The present work highlights some relevant aspects concerning the mode of action of several activators used in cyclopentene polymerization induced by WCl_6-based catalytic systems. As activators various types of compounds containing oxygen, nitrogen, halogen as heteroatom are employed. The work focuses on the mode by which these activators modify the main parameters of reaction and affect the mechanism and stereochemistry of the process.

RESULTS AND DISCUSSION

The polymerization reaction of cyclopentene was carried out in the presence of ternary and quaternary catalytic systems based on WCl_6 and organometallic compounds; one or two compounds of the following series were used as activators: epichlorohydrin, ethyl alcohol, chloranil, 3,3′,5,5′-tetramethyl dibenzoquinone, cyanuric acid, cyanuric chloride and isocyanuric chloride.[3-6] Additionally, maleic anhydride, ethylcelosolv, salicyl aldehyde, phenylisocyanate and s-triazine derivatives have been employed. The main results are presented in Tables 1—3.

Table 1

Effect of epichlorohydrin on the cyclopentene conversion and polypentenamer microstructure

Epichlorohydrin / WCl_6 molar	Cocatalyst	Cocatalyst / WCl_6 molar	Temp. °C	Time min.	Conv. %	η_{inh} dl/g	Microstructure PPM cis %	trans %
2 : 1	Et_3Al	2 : 1	0	45	36	2.59	27.5	72.4
1 : 1	Et_3Al	2 : 1	0	45	38	2.67	22.7	77.3
3 : 1	Et_3Al	2 : 1	0	45	23	2.28	18.4	81.5
1 : 1	$Et_3Al_2Cl_3$	2 : 1	0	45	10	1.62	18.0	82.0
1 : 1	$Et_3Al_2Cl_3$	2 : 1	0	45	5	1.62	16.0	85.0
2 : 1	Et_2AlCl	2 : 1	0	45	19	2.28	14.2	85.5

Table 2

Effect of chloranil on the cyclopentene conversion and polypentenamer microstructure

Chloranil / WCl_6 molar	Cocatalyst	Cocatalyst / WCl_6 molar	Temp. °C	Time min.	Conv. %	η_{inh} dl/g	Microstructure PPM cis %	trans %
1 : 1	Et_3Al	2 : 1	0	45	74	1.81	16.5	83.5
1 : 1	$Et_3Al_2Cl_3$	2 : 1	0	45	55	4.10	15.1	84.8
1 : 1	iBuAl	2 : 1	0	30	48	5.58	10.0	78.9
1 : 1	iBuAl	5 : 1	0	30	72	8.74	28.7	71.3
1 : 1	iBuAl	10 : 1	0	30	70	6.4	—	—
1 : 1	iBuAl	2 : 1	0	90	70	7.54	18.2	81.8
1 : 1	iBuAl	2 : 1	0	90	65	3.03	—	—

Table 3

Effect of various activators on cyclopentene conversion and polypentenamer microstructure

Activator	Temp. °C	Conv. %	η_{inh} dl/g	Microstructure PIM cis %	trans %
Dibenzoquinone	−15	55	4.1	17.0	83.0
Maleic anhydride	0	22	3.0	28.0	72.0
Salicyl aldehyde	0	32	—	19.6	80.4
Ethylcelosolve	0	25	5.10	29.0	71.0
Cyanuric acid	0	37	7.05	25.8	74.2
Cyanuric chloride	0	15	5.12	27.0	73.0
Phenylisocyanate	0	15	3.51	32.0	68.0
2-Hydroxy-4,6-diamino-s-triazine	0	20	5.60	25.0	75.0

As can readily be seen from Table 1, epichlorohydrin displays a moderate effect upon the catalytic activity leading to cyclopentene conversion of 40%. Under these conditions polypentenamer with *trans* configuration between 80 and 85% is obtained. It is noteworthy that the molar ratio epichlorohydrin : tungsten hexachloride plays a decisive role in the catalytic activity and stability. Thus, on varying the molar ratio epichlorohydrin : tungsten chloride from 1 : 1 to 3 : 1 the catalyst activity and stability is constant while over the molar ratio of 3 : 1 the activity strongly diminished and cyclopentene polymerizability vanished.

In contrast to epichlorohydrin, chloranil easily leads to cyclopentene conversions of 60—80% and *trans* configuration of polypentenamer of 80% (see Table 2). The activity of chloranil was very high at short reaction time (Fig. 1).

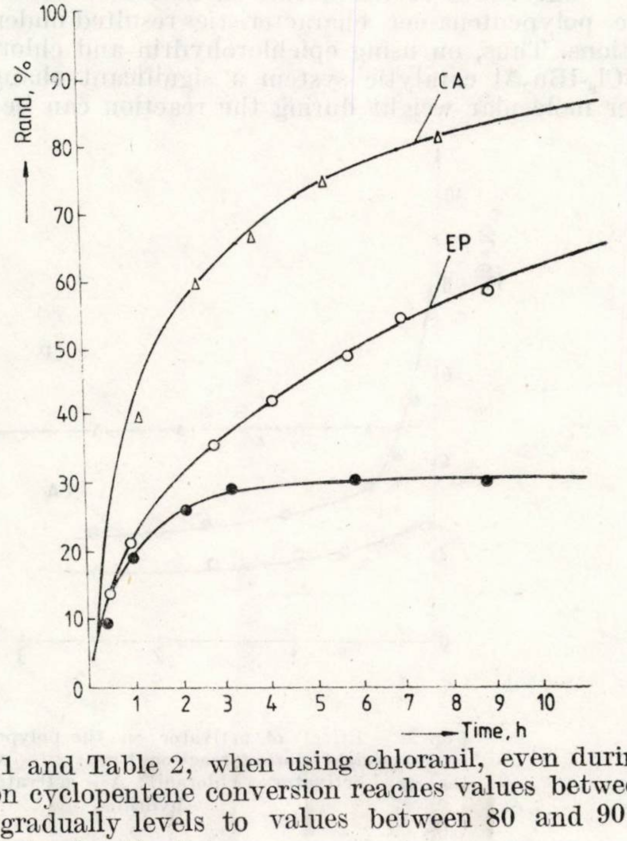

Fig. 1. — Effect of activator on the cyclopentene polymerization in the presence of WCl_6-iBu_3Al : ● — without activator; ○ — activator = epichlorohydrin ; Δ — activator = = chloranil.

As shown in Fig. 1 and Table 2, when using chloranil, even during the first hour of reaction cyclopentene conversion reaches values between 70 and 80% and then gradually levels to values between 80 and 90% while the system seems to deactivate.

Interesting results have also been recorded using a wide range of activators with the WCl_6-iBu_3Al system (Table 3). Of these compounds 3,3′,5,5′-tetramethyldibenzoquinone, salicyl aldehyde and cyanuric acid proved to be quite active and stereoselective. Thus conversions of cyclopentene from 32 to 55% and polymer with *trans* configuration of 75 to 83% have readily been obtained.

Analysis of the results presented in Tables 1–3 and Fig. 1 reveals several kinetic particularities of the catalytic system as follows:

(i) the reaction rate in the presence of the WCl_6-iBu_3Al catalytic system significantly decreases in the course of the process and

(ii) the reaction rate substantially changes when using the ternary catalytic system WCl_6-iBu_3Al-activator. In the case of epichlorohydrin the initial increase of the reaction rate is accompanied by a pronounced deactivation leading to a decrease of the overall process rate. At the same time, on using chloranil as activator in the WCl_6-iBu_3Al catalytic systems, results in a dramatic increase of reaction rate during the first moments of contacting then the activity levels to a maximum value. In contrast to these two activators, the other compounds gave moderate yields in polymer as a function of their chemical structure.

The effect of the nature of activator could be evidenced also by the polypentenamer characteristics resulted under various reaction conditions. Thus, on using epichlorohydrin and chloranil as activator in the WCl_6-iBu_3Al catalytic system a significant change of the polypentenamer molecular weight during the reaction can be observed (Fig. 2).

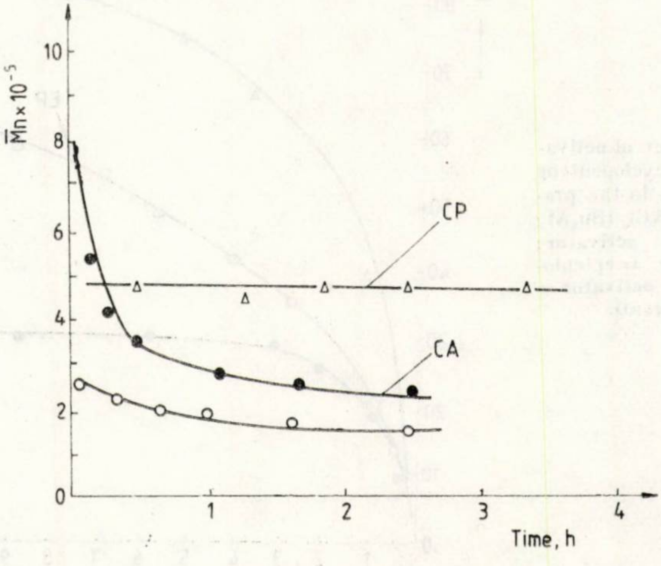

Fig. 2. — Effect of activator on the polypentenamer molecular weight during reaction time: ○ — without activator; ● — activator = chloranil; Δ — activator = epichlorohydrin.

In this case the effect of chloranil is more pronounced though the final molecular weights are relatively higher.

The influence of chloranil and epichlorohydrin on the molecular weight distribution of polypentenamer is of real significance.

As can be seen from Fig. 3, when the ternary catalytic systems consisting of $WCl_6.iBu_3Al$.epichlorohydrin or $WCl_6.iBu_3Al$.chloranil are used a narrow unimodal distribution of the molecular weight is obtained while the quaternary catalytic system $WCl_6 \cdot iBu_3Al \cdot$epichlorohydrin $\cdot$ chloranil leads to a wider molecular weight distribution as a function of the molar ratio of the catalytic components.

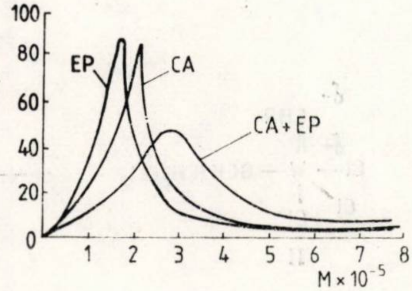

Fig. 3. — Influence of the activator on the polypentenamer molecular weight distribution : EP — activator = epichlorohydrin ; CA — activator = chloranil ; CA + EP — activator = epichlorohydrin + chloranil.

ON THE MECHANISM OF ACTIVATOR ACTION

The specific behaviour of activators incorporated into the ternary and quaternary catalytic systems based on WCl_6 could be explained if we consider that they lead to formation of distinct species by the interaction with the reaction intermediates.[7] Thus the fact that epichlorohydrin readily reacts with WCl_6 to give alkoxytungsten compounds of type I, according to Eq.1, is well known.[8]

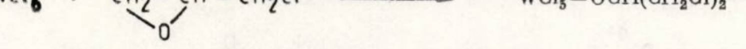

$$WCl_6 + CH_2{-}CH{-}CH_2Cl\ (\text{epoxide}) \longrightarrow WCl_5{-}OCH(CH_2Cl)_2 \qquad (1)$$

Introduction of the $OCH(CH_2Cl)_2$ groups as ligands at the tungsten atom increases the activity of the catalytic system and improves its stability. The effect of epichlorohydrin as activator and stabilizer of the catalytic system can be rationalized by its regulating action on the electron density of the tungsten atom in the metallacarbene species ; this results in a corresponding change of the nucleophilicity of the carbene carbon atom of type II. (Scheme 1).

In addition, introduction of two or three alkoxy groups into the tungsten complex enhances further the stabilizing capacity of the active centres ; however, if more than three epichlorohydrin groups are introduced, the activity of the tungsten complex sharply drops probably due to the strong steric and electronic interaction during cycloolefin coordination or intermediate metallacyclobutane formation.

On the other hand, chloranil acts differently in the catalytic system derived from WCl_6 and organometallic compounds owing to its particular electron-accepting particularity. Thus it was noted that chloranil leads to a high increase of the reaction rate when it is added to the $WCl_6 \cdot$ $\cdot iBu_3Al$ catalyst accompanied by a substantial stability of the active centres. (See Fig. 1). This behaviour can be understood if we admit that chloranil readily forms captodative complexes of types IV and V with the metallacarbene and metallacyclobutane intermediate, respectively.

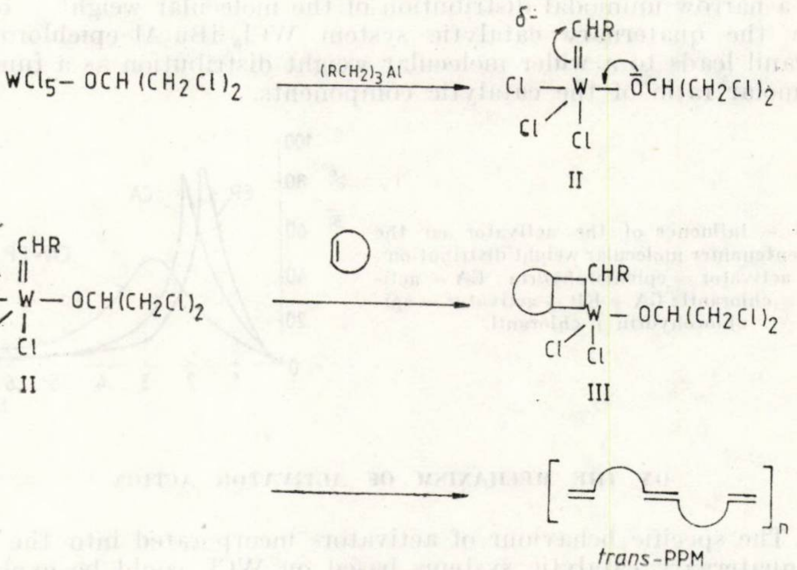

Scheme 1

In the complexes of these types chloranil strongly diminishes the electron density at the tungsten atom and substantially increases the nucleophilicity of the carbene carbon. The synergism of these effects may explain the considerable increase of the activity of the catalytic system in the presence of chloranil. (Scheme 2).

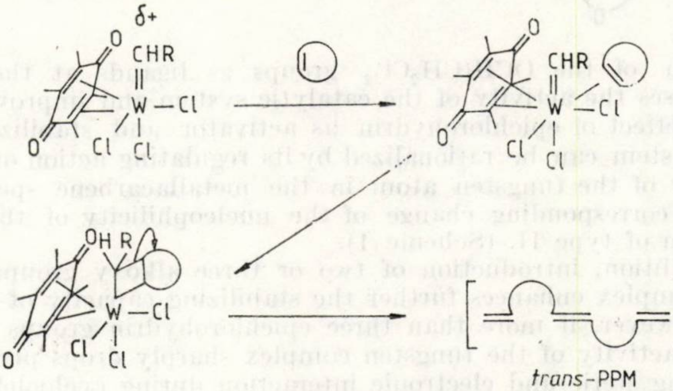

Scheme 2

Analogously, the effect of other activators incorporated into the ternary and quaternary catalytic systems derived from WCl_6 could be rationalized. Due to their electron acceptor and donor particularity, these activators complex at the metallacarbene substantially modifying the electron density of the tungsten atom and the reactivity of the metallacarbene species. In addition, the particular steric restrictions imposed by the bulky ligands formed at the tungsten atom results in a variable content of *cis* and *trans* units in the polypentenamer as shown in Table 3

CONCLUSIONS

As the above results pointed out, the electron donor and acceptor compounds such as epichlorohydrin and chloranil used in the catalytic systems based on WCl_6 and organometallic compounds exert a pronounced action on the activity and stability of the system. The activity of the catalytic system increases distinctly as a function of the electron-donating or accepting particularity of the compound employed as well as of its structure.

The influence of these activators on the catalytic behaviour was explained by considering their complexation at the metallacarbene species and metallacarbene intermediate which results in a change of the electron density in the coordination sphere of the tungsten atom. This change will lead to an increase of the reactivity of metallacarbene species and of the stability of the metallacyclobutane intermediate. In addition, as a function of the volume of the ligand introduced at the tungsten atom by the activator steric interactions arise which modify the stereocourse of the process.

REFERENCES

[1] Elena Ceaușescu, "Recent Research in the Field of Macromolecular Compounds", Ed. Academiei, Bucharest, 1981, p. 100.
[2] V. Drăguțan, A. T. Balaban, M. Dimonie, *Olefin Metathesis and Ring-Opening Polymerization of Cycloolefins*, J. Wiley, Chichester, 1985.
[3] Elena Ceaușescu et al., RO 85121 (1984).
[4] Elena Ceaușescu et al., RO 85378 (1984)
[5] Elena Ceaușescu et al., RO 90752 (1986).
[6] Elena Ceaușescu et al., RO 94191 (1986).
[7] Elena Ceaușescu et al. J. Mol. Catalysis, **28**, 337 (1985).
[8] P. Günther et al., Angew. Makromol. Chem., **14**, 87 (1970).

Revue Roumaine de Chimie, **34**, *6*, 1301–1306 (1989)

REDOX BEHAVIOUR OF 3d IONS IN OXIDE GLASSES

PETRU BALTĂ and MARCEL BIALE
Polytechnic Institute of Bucharest,
Splaiul Independenţei 313, 76206 Bucharest, Romania

Received September 26, 1988

The authors' own data concerning the UV absorption of 3d ions in oxide glasses allowed their arrangement, on the basis of the energy required for the charge transfer, in the order of increasing oxidizing power. The charge transfer energy difference is a measure of the ease of reduction of the higher oxide to the lower one. The position of some ions is altered by the change of glass basicity, the probable causes being discussed. The evidenced correlation between charge transfer energy of 3d ions and the basicity of respective oxides allows the estimation of redox properties by means of the latter, with the advantage that the oxide basicity may be obtained by calculation. As a rule, the electron leaves the more basic oxide for a less basic one.

INTRODUCTION

The transitional metal ions from the first row are used on a large scale for colouring the industrial glasses. The obtained colours and nuances depend essentially on the redox processes between the ions in glass involving the surrounding atmosphere too. From the scientific point of view the redox interaction mechanism is of interest, especially between ions of different transitional atoms.

Various methods were used for data accumulation in this field. Important results have been obtained by means of visible spectroscopy, completed with RES and Mössbauer spectra and chemical analyses. From numerous published works there are cited for illustration only[1-8]. Valuable information is furnished also by the electrochemical methods applied to oxide melts.[9,10] In some cases, the obtained results allowed the ordering of oxides and ions taking into account the relative oxidation potentials,[7] the reduction power[9] or the ease of reduction to the lower oxide.[10] Such an ordering of redox couples is considered[10] in a certain measure independent relative to numerous parameters influencing the redox processes in glasses, e.g.: the melting and cooling conditions, the oxygen fugacity, the glass basicity, the nature and concentration of the transitional ion.

Investigating the charge transfer absorption of 3d ions in oxide glasses, the authors realized the possibility of using the obtained information for the redox behaviour estimation. In the following some of the results are presented.

EXPERIMENTAL

Sodium-borate glasses with the amount of basicity (pB, in percents) of 50 % (containing 10 wt. % Na_2O) and 60 % (27.2 wt. % Na_2O) and a potassium-silicate glass with pB = 70 % (49 wt. % K_2O) were used. The basicity of many industrial glasses is near 60 %. In spite of the fact that the coordination number of atoms in glass (CN), involved in pB calculation,[1,12] is only approximately known, it may be appreciated that the pB values, above mentioned, differ from the actual ones by no more than ±1.5 %.

The melting of glasses has been made in the normal atmosphere, in a platinum crucible, using an electric furnace, during 3 hours at 980 °C in the case of sodium-borate glasses and at 1300 °C for the potassium-silicate ones. The disk shaped samples, about 1 mm thick, were obtained by pressing the melt between two steel plates. The samples were annealed in normal atmosphere, 10 minutes at T_g and then cooled with the furnace.

The transitional ion concentration, introduced as oxide, was 0.1 wt. % of atoms.

In this manner the majority of parameters influencing the redox processes and also the charge transfer absorption, previously identified,[13] have been maintained constant, the results reflecting only the influence of 3d ion nature and of glass basicity.

The electronic spectra were recorded in the range 50,000—20,000 cm^{-1} by means of a double beam spectrophotometer, Specord UV—VIS (GDR), having in the comparison beam an identical sample but without the transitional ion.

In these working conditions the peak position on the spectra obtained on parallel samples does not differ by more than 300 cm^{-1}.

ELECTRON ACCEPTOR POWER OF 3d IONS

In the charge transfer absorption process, taking place in oxide glasses the electron leaves a molecular orbital belonging preponderantly to the oxygen ligand for a d free orbital belonging preponderantly to the transitional ion. Depending on the 3d ion nature, if CN = 6, the free orbital may be of the lower energy group t_{2g}, or of the higher energy group e_g. In the latter case the required charge transfer energy is greater by 10 Dq, respectively by the energy difference between the two groups of d orbitals. For these reasons the ions with a lower oxidation state (OS) absorb, as a rule, in the far UV. On the other hand, the first Laporte permitted transition is determined by the ion with greater OS, having the maximum electron acceptor power.

In order to illustrate the above ideas, in figures 1 and 2 the spectra of Cr, Fe and Cu are presented in two glasses with different basicities.

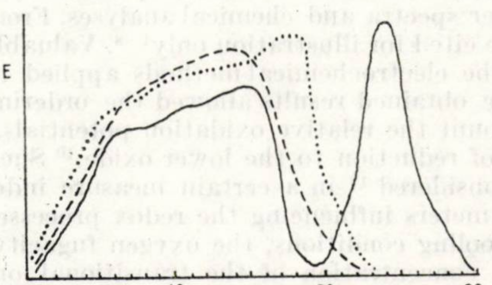

Fig. 1. — The spectra of Cr, Cu and Fe in a glass with pB = 60 %: ——— Cr; ---------- Cu; . . . . Fe

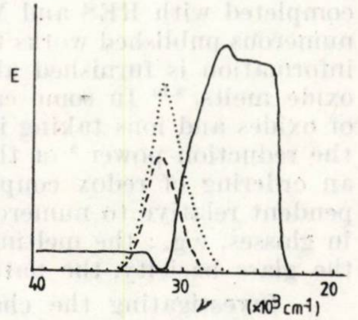

Fig. 2. — The spectra of Cr, Cu and F in a glass with pB = 70 %: ——— Cr; ---------- Cu; . . . . Fe

On all spectra the minimum energy transition, corresponding to the ion with high OS, may be easily localized. As concerns the charge transfer absorption peaks of the ions with lower OS, the localization is more difficult. The energetic structure of molecular orbitals being more complex than the simplified scheme presented above, in the case of Fe^{2+}, for example, four charge transfer transitions are possible,[13] two visible in figure 1 too, throughout the broad envelope. A similar complexity is encountered also in the case of Cr. However, it was possible to identify in the high energy group of maxima the transitions of Cr^{3+} in the two usual coordinations.[13] Accepting some approximation, for the charge transfer energy of the lower OS ions the inflexions in the far UV were considered.

In figure 2, in the glass with pB = 70%, the very simple spectra are assigned to the ions with high OS only.

Taking over this information from the transitional elements spectra in the three mentioned glasses, the diagram in figure 3 was drawn up. The apparently general trend of charge transfer energy diminution by the glass pB increase may be noticed, stressed at pB = 70% by the disappearance of the peaks of the ions with lower OS. But there are also ions which do not alter the transition energy, at least by passing from pB = 50% to pB = 60%, while in the case of Fe^{3+} not even at pB = 70%. The complex reasons of the different behaviour of 3d ions relative to glass basicity include the CN, OS and Dq dependence on the ligand field intensity, variable with pB and the intervention, in some ions, of the Jahn-Teller effect. A tentative of systematization of these causes will be presented in another paper, now in preparation.

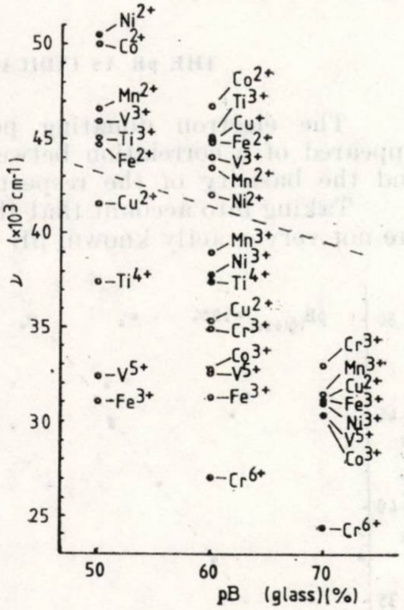

Fig. 3. — The ordering of some 3d ions after the charge transfer energy in glasses with different pB's.

A possible explanation of the absence of lower OS ions in glasses with pB = 70% was discussed in[13] related to the easiness of atmospheric oxygen diffusion in such glasses. One can also remark that the charge transfer energies of six of the ions in figure 3 are distributed over about 2,000 cm^{-1} only, at the boundary of the visible. The only exception are the chromium ions.

Figure 3 evidences the ordering of 3d ions after the electron donating (or accepting) power. From top to bottom, i.e. with the decrease of energy required for charge transfer, diminishes the electron donating power, therefore the ions become less reducing and more oxidizing. By the glass basicity variation the position of some ions alters, a fact remarked also in[7]. The ordering after the charge transfer energy has the advantage of evidencing the proportion of the difference between the redox properties of ions too. It may be observed that in certain cases the differences are within the limits of wave number experimental errors.

Information concerning the ease of reduction or oxidation of the ions of the same element may be obtained considering the energy difference between the respective ions. On this basis an oxide ordering may be done, e.g. after the ease of reduction of the higher oxide.

The results obtained in both ways are comparable, but not identical to those presented in other works,[7, 8, 10] which differ between themselves too. Such differences in the ordering of ions and oxides are probably not avoidable because of the little difference between the redox properties of some ions and their dependence upon numerous parameters, as shown above.

The method of establishing the redox properties of 3d ions in glasses by measuring the charge transfer transition energy has the advantage of a more rigorous control possibility of influencing parameters and of a relative simplicity.

THE pB AS INDICATOR OF REDOX BEHAVIOUR

The electron donating power being measured by pB, the idea appeared of a correlation between the charge transfer transition energy and the basicity of the respective oxide.

Taking into account that the CN's of the transitional ions in glasses are not very exactly known, pB was calculated using the two usual NC's : 4 and 6. These data were represented in figure 4 with the charge transfer energies in the glass with pB = 50 %. It may be seen that for every ion, one of the two points is very near to the straight line, evidencing the correlation sought for. The same correlation is found in the glass with pB = 60%, although the points are more scattered. In the glass with pB = 70% the vicinity of points or even the superposition of the energy values makes the observation of this correlation difficult. The rising in glass pB has a complex and specific influence upon the energy of central ion and ligand molecular orbitals, phenomenon which can not be entirely taken into account by calculating the pB value of the transitional

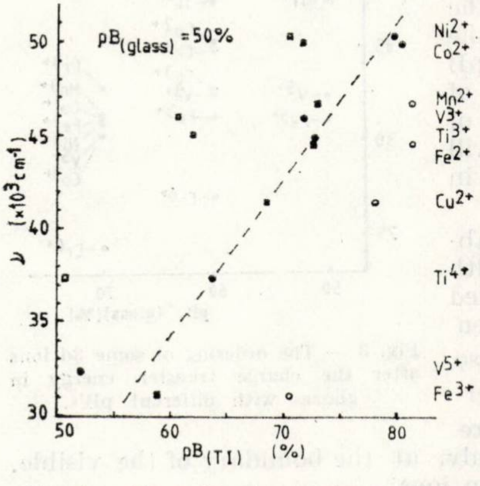

Fig. 4. — The evidencing of the correlation between the charge transfer energy of some 3d ions in a glass with pB = 50 % and the respective oxide basicity. The circles indicate the pB values for CN = 6 and the squares for CN = 4. The full circles and squares are the selected ones.

ion oxide. For a glass pB value of 50% the transitional ion complex is exposed to the lowest ligand field influence and as a result, the correlation is most evident.

Considering the low basicity value of the glass in figure 4 (50%), the majority of CN's indicated by the straight line are plausible. But CN = 4 for Cu^{2+} contradicts the general knowledge and that is why it must be interpreted as an evidence of the fact that, in this case, the charge transfer energy is preponderantly determined by the four ligands drawn nearer as a result of the Jahn-Teller octahedron elongation.

It may be deduced that, in the absence of more precise data about CN's of 3d ions in glasses, the evidenced correlation offers a source of information in this sense. The position of the two points in the case of Co^{2+} and Mn^{2+}, for example, may be interpreted as indicating the presence of both coordinations, for Co^{2+} prevailing CN = 6, but for Mn^{2+} CN = 4. In the case of V^{5+} the CN seems to be greater than 6.

Independently of such possible interpretations, pB may serve as redox properties indicator of 3d ions instead of charge transfer energy, having the great advantage of being accessible by calculation. If the CN of 3d ion has been selected correspondingly the obtained information is of the same value.

So it appears that, in a first approximation, the redox interactions are governed by a simple rule : the electron moves from the higher basicity transitional ion oxide to the lower basicity one.

CONCLUSIONS

Selecting in a reasonable manner the working conditions, the multiple influences upon the charge transfer absorption energy of 3d ions were avoided, evidencing only the influence of the ion nature and of glass basicity.

Using the authors' own data together with some published information the charge transfer absorption energies of 3d ions were established.

On the basis of the charge transfer energies the 3d ions were ordered in the sense of oxidizing power increase. Their ordering after the ease of reduction to the lower OS is also possible. The position of certain ions alters when the glass basicity changes. The ordering after the charge transfer energy benefits by data determined accurately and relatively easily

A linear correlation between charge transfer energy and transitional metal oxide basicity has been evidenced. In this way the redox properties of transitional ions may be appreciated by means of their basicity obtained by calculation.

REFERENCES

[1] W. A. Weyl, "Coloured Glasses", Dawson's of Pall Mall, London, 1959.

[2] C. R. Bamford, "Colour Generation and Control in Glass", Elsevier Sc. publ. Co., Amsterdam, 1977.

[3] A. Paul and R. W. Douglas, *Phys. and Chem. Glasses*, **1**, 1 (1966).

[4] D. Becherescu, V. Cristea et al., *Rev. Materiale de Construcţii*, **16**, 2, 128 (1986).

[5] V. Cristea et al., *Rev. Materiale de Construcţii*, **17**, 192 (1987).

[6] V. Cristea et al., *Rev. Materiale de Construcţii*, **18**, 141 (1988).

[7] J. H. Lee and R. Brückner, *Glastechn. Ber.*, **59**, 233 (1986).

[8] T. Popescu-Negreanu, Thesis, Polytechnic Institute of Bucharest, 1987.

[9] K. Takahashi and Y. Miura, *J. Non-Cryst. Solids*, **38** & **39**, 527 (1980).

[10] H. D. Schreiber et al., *J. Amer. Ceram. Soc.*, (1984) C—106.

[11] P. Baltă, C. Spurcaciu, D. Radu and O. Dumitrescu, *J. Non-Cryst. Solids*, **71**, 69 (1985).

[12] P. Baltă and C. Spurcaciu, *Rev. Materiale de Construcţii*, **15**, 27 (1985).

[13] P. Baltă and M. Biale, Paper presented at 5-CONSILOX, Timişoara, September 1988, in press at *Rev. Materiale de Construcţii*.

Revue Roumaine de Chimie, **34**, *6*, 1307–1312 (1989)

ÉTUDE DU SYSTÈME DE RÉACTION Ni(II) — HYDROXYLAMINE

IOAN BERDAN et OLGUŢA COSTINOAIA
Institut Polytechnique « Gh. Asachi » Iassy
Faculté de Technologie Chimique, Iassy, Roumanie

Reçu le 28 décembre 1987

Dans ce travail on présente les résultats obtenus concernant l'étude du système de réaction Ni(II)-hydroxylamine. Le comportement de l'ion Ni(II) comme acide Lewis (M) vis-à-vis du ligand N-donneur, l'hydroxylamine (L), a été mis en évidence par formation de combinaisons complexes mononucléaires de type ML_n ou $n=1\ldots6$. La formation, la stabilité et la structure des complexes ont été étudiées par des méthodes pH-métriques et spectrophotométriques. Les spectres d'absorption électroniques de type champ cristallin du complexe de rapport molaire $M/L = 1/6$ ont été interprétés à base du diagramme de niveaux énergétiques propres au cas $d^8(Ni^{2+})$ de la symétrie O_h.

The paper reports the characterisation of some Ni(II) complexes with hydroxylamine (L). The complexes correspond to the general type $NiL_n (n = 1\ldots6)$. The formation, stability and structure of the complexes were investigated by pH-metric and spectrophotometric methods. The crystal-field spectra of the NiL_6 complex are characterised by splitting parameter, $Dq = 1{,}000\ cm^{-1}$ and nephelauxetic parameter $\beta_{35} = 0.74$.

1. INTRODUCTION

Dans la série des complexes de l'ion Ni^{2+} on remarque une bonne corrélation structure — propriétés. Ainsi, quant aux propriétés optiques, on constate que la plupart des complexes octaédriques (O_h) sont bleuâtres, ceux de symétrie T_d ont la couleur bleue-intense alors que pour la symétrie plan-carrée, les complexes sont rouge-oranges.

La structure plan-carrée se réalise surtout dans les systèmes de réaction Ni(II) — ligands bidentés tels que : la diméthyl-glioxime,[1] l'éthylènediamine[2] etc. Certains complexes tétraédriques du Ni(II), moins importants, apparaissent dans les systèmes de réaction avec les ligands suivants : X^-(ions halogénures), arsine et phosphine.

La symétrie octaédrique caractérise la plupart des complexes du Ni(II) avec les ligands azote- et oxygène-donneurs. Les complexes pentacoordonnés, qui apparaissent plus rarement, caractérisent les systèmes de réaction de l'ion Ni(II) avec les ligands organiques polydentés.[3]

Dans une série de travaux antérieurs,[4–5] nous avons étudié les systèmes de réaction du Ni(II) avec les ligands de type des oximes. En poursuivant ces études, dans cette note on présente les résultats obtenus sur le système Ni(II)-hydroxylamine. Le choix de ce ligand repose sur la nécessité de connaître la nature des processus chimiques pouvant intervenir lors de l'utilisation du nickel comme catalyseur dans la préparation de l'hydroxylamine à partir du monoxyde d'azote.[6]

2. PARTIE EXPÉRIMENTALE

Comme source de Ni(II), M, nous avons utilisé $Ni(NO_3)_2 \cdot 6H_2O$ en solution aqueuse, de différentes concentrations et de l'hydroxylamine, L, sous forme de chlorhydrate, $NH_2OH \cdot HCl$ (produits p.a.).

Les propriétés acido-basiques de l'hydroxylamine ainsi que le processus de formation des complexes dans le système mentionné ont été étudiées par voies pH-métrique et spectrophotométrique.

Les déterminations de pH ont été effectuées à l'aide du pH-mètre de type MV-85 (R.D.A.).

La formation des complexes a été suivie en faisant réagir la solution aqueuse de Ni(II) avec des quantités appropriées de $NH_2OH \cdot HCl$, à la température ordinaire. Au cours de la réaction, le mélange prend la couleur bleue qui s'enfonce au fur et à mesure qu'on ajoute l'excès de ligand. En solution aqueuse, les espèces complexes formées sont assez stables ; la couleur bleue reste inchangée pendant 24 heures.

La formation, la stabilité et la structure des complexes ayant la formule générale NiL_n, où $n = 1 \ldots 6$, ont été étudiées par pH-métrie et spectroscopie d'absorption électronique (dans le visible et l'ultraviolet). Les spectres électroniques ont été obtenus en utilisant les spectrophotométres suivants : Spekord UV–VIS (200–800 n(m), Spekol (350–800 nm) et VSU-2P (750...1200 nm).

3. RÉSULTATS ET DISCUSSIONS

3.1. Les propriétés acido-basiques de l'hydroxylamine (L) et des mélanges Ni(II)-L

L'hydroxylamine est un ampholite ; sa faible basicité est comparable à celle de $Zn(OH)_2$. Les valeurs des pK_a et pK_b ont été déterminées par le titrage d'une solution aqueuse de $NH_2OH \cdot HCl$ 0,05 m avec une solution de NaOH 0,5 m. Sur le graphe de la figure 1, on constate que l'addition de 1,5 cm³ solution NaOH correspond à la neutralisation du HCl (zone I) :

$$NH_2OH \cdot HCl + NaOH = NH_2OH + NaCl + H_2O$$

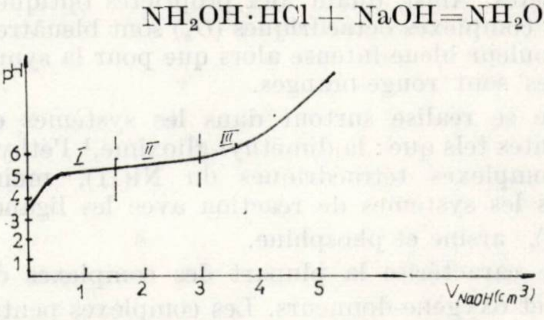

Fig. — Le titrage de l'hydroxylamine (0,05 m) par de la soude (0,5 m) ; volume initial de $NH_2OH \cdot HCl$: 15 cm³.

L'addition d'un volume total de 3 cm³ de NaOH produit une faible augmentation du pH par suite de la neutralisation de NH_2OH (acide faible) :

$$NH_2OH + NaOH = NH_2O^- + Na^+ + H_2O \quad \text{(zone II)}$$

Evidemment, l'addition d'un grand excès de base est accompagnée d'un accroissement du pH (zone III). En sachant que l'addition d'un volume de soude $V = V_E/2$ (ou V_E = volume équivalent) correspond à la formation d'un mélange tampon, il en résulte que $pK_a = pH$; les valeurs expérimentales sont : $pK_a = 5{,}3$ et $pK_b = 8{,}7$.

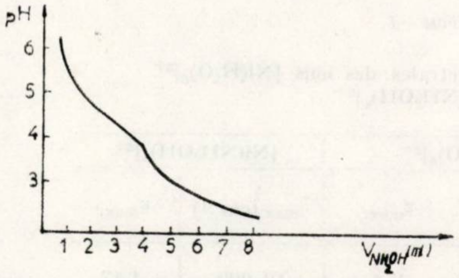

Fig. 2. — Le titrage de la solution de $Ni(NO_3)_2 \cdot 6H_2O$ (0,5 m) par de l'hydroxylamine (0,5 m).

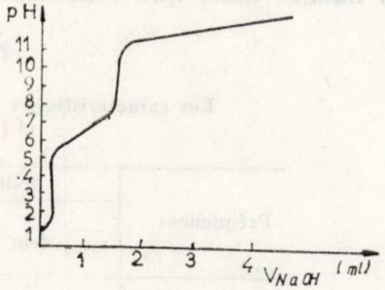

Fig. 3. — Le titrage du mélange : $1Ni^{2+}$(0,5 m) — 6 $NH_2OH \cdot HCl$ (0,5m) par de la soude (5 m) ; volume du mélange : 15 cm³.

L'évolution du système de réaction a été suivie sur des mélanges Ni^{2+}–L de différents rapports molaires et concentrations. Ainsi, dans la figure 2, lors du titrage de la solution de Ni(II) par l'hydroxylamine on observe que l'addition d'une faible quantité de $NH_2OH \cdot HCl$ produit une légère décroissance du pH ; l'addition d'un excès de L ne produit qu'une petite variation du pH. Dans ces conditions, la fonction basique de l'atome d'azote de la molécule du ligand est bloquée, $NH_3OH^+Cl^-$. La fonction donneuse de l'hydroxylamine est mise en évidence à des valeurs de pH plus élevées. En effet, sur le graphe de la figure 3, l'addition d'une faible quantité de NaOH dans le mélange Ni(II)—L produit un saut de pH dont le maximum correspond au volume équivalent de soude qui a neutralisé le HCl. L'addition de soude en excès favorise la formation des complexes de couleur bleue dont l'intensité croit avec le pH à condition qu'il ne dépasse une valeur critique à laquelle précipite le $Ni(OH)_2$. Pratiquement, la formation des complexes a lieu dans l'intervalle de pH : 4,8 . . .10,5, selon l'équilibre :

$$Ni^{2+} + nNH_2OH \rightleftharpoons [Ni(NH_2OH)_n]^{2+}$$

3.2. La composition et la stabilité des complexes

Le processus de formation, la stabilité ainsi qu'une série de caractéristiques des complexes du système Ni(II)—L ont été suivies par voie spectrophotométrique. On a enrégistré les spectres dans l'ultraviolet et visible des réactants et des mélanges Ni(II)—L—NaOH de différents rapports molaires et différentes concentrations. Les caractéristiques spectrales de ceux-ci sont présentées dans le tableau 1. Le spectre électronique de l'ion $[Ni(H_2O)_6]^{2+}$ présente trois bandes d'absorption de type champ cristallin : ν_1 (8.000 cm^{-1}), ν_2 (14.000 cm^{-1}) et ν_3 (25.300 cm^{-1}). Pour l'ion complexe $[Ni(NH_2OH)_6]^{2+}$, les trois bandes d'absorption, qui correspondent à la symétrie octaédrique sont situées à : 10.000 cm^{-1} respectivement 16.950 cm^{-1} (ν_2) et 25.750 cm^{-1} (ν_3). Le déplacement des bandes ainsi que l'intensification de l'absorption observés dans les spectres des mélanges Ni(II)—L, par rapport à l'ion de Ni^{2+} hydraté, sont dûs à l'interaction acido-basique de type Lewis avec formation de complexes.

Tableau 1

Les caractéristiques spectrales des ions $[Ni(H_2O)_6]^{2+}$ et $[Ni(NH_2OH)_6]^{2+}$

Fréquences	$[Ni(H_2O)_6]^{2+}$		$[Ni(NH_2OH)_6]^{2+}$	
	$\bar{\nu}_{max.}$ (cm^{-1})	$\varepsilon_{max.}$	$\bar{\nu}_{max.}$ (cm^{-1})	$\varepsilon_{max.}$
1	8.000	1,1	10.000	4,47
2	14.000	2,5	16.950	5,38
3	25.300	5,5	25.750	9,5

La composition des complexes a été déterminée par la méthode des rapports molaires [7] ; figure 4. Sur le graphe de la variation de l'absorbance (mesurée à 16.949 cm^{-1}) en fonction du rapport molaire L/Ni(II), à pH = 9,5, on observe la formation successive de complexes de différents nombres de coordination : $[Ni(NH_2OH)_n]^{2+}$, où $n = 2 \ldots 6$.

La stabilité des complexes a été déterminée par la méthode Edmonds-Birnbaum [8] qui repose sur la mesure de l'absorbance de deux séries de solution (mélanges) Ni(II)—L, 1 et 2, dont la concentration $[Ni^{2+}]$ est maintenue constante et celle du ligand [L], en excès, mais variable.

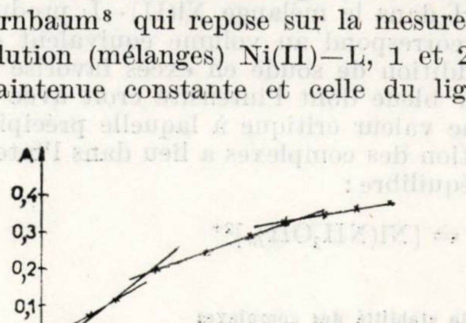

Fig. 4. — Données concernant la détermination de la composition des complexes par la méthode de rapports molaires ; cuve : 1 cm.

Les constantes globales de stabilité des complexes 1 : 4 et 1 : 6 ont les valeurs suivantes : $\beta_4 = 4{,}86 \cdot 10^3$ $L^4 \cdot mol^{-4}$ et $\beta_6 = 4{,}34 \cdot 10^5$ $L^6 \cdot mol^{-6}$; tableau 2.

Tableau 2

Données concernant la détermination de la stabilité des complexes du système Ni(II) — NH_2OH par la méthode Edmonds-Birnbaum ; $\bar{\nu}_{max.} = 16.950\ cm^{-1}$; cuve : 1 cm^2

Paire de solutions	$C_{Ni^{2+}}$	C_L	A	K_n	
				$n = 4$	$n = 6$
1	$7{,}9 \cdot 10^{-3}$	0,111	0,015	$1{,}69 \cdot 10^{-4}$	$1{,}48 \cdot 10^{-6}$
2		0,158	0,025		
1	$7{,}7 \cdot 10^{-3}$	0,111	0,015	$2{,}004 \cdot 10^{-4}$	$2{,}205 \cdot 10^{-6}$
3		0,238	0,033		
2	$7{,}7 \cdot 10^{-3}$	0,158	0,025	$2{,}65 \cdot 10^{-4}$	$5{,}59 \cdot 10^{-6}$
3		0,238	0,033		

3.3. Spectres champ cristallin du complexe $[Ni(NH_2OH)_6]^{2+}$

Les spectres d'absorption de type champ cristallin de l'ion complexe $[Ni(NH_2OH)_6]^{2+}$ ont été interprétés à base de diagramme de niveaux énergétiques propres au cas $d^8(Ni^{2+})$ de la symétrie O_h. Les trois transitions électroniques permises qui produisent les trois bandes d'absorption, ν_1, ν_2 et ν_3, caractéristiques aux complexes du Ni(II) de symétrie octaédrique, sont représentées dans la figure 5.

Dans l'hypothèse d'un champ de ligands faible crée par l'hydroxylamine, les trois bandes d'absorption du complexe 1 : 6 correspondent aux transitions suivantes :

$$\nu_1 : {}^3T_{2g} \rightarrow {}^3A_{2g} ;\ E_1 = 10\,\mathrm{Dq} ;\ 10.000\ \mathrm{cm}^{-1} ;$$

$$\nu_2 : {}^3T_{1g} \rightarrow {}^3A_{2g} ;\ E_2 = 18\,\mathrm{Dq} ;\ 16.950\ \mathrm{cm}^{-1} ;$$

$$\nu_3 : {}^3T_{1g}(\mathrm{P}) \rightarrow {}^3A_{2g} ;\ E_3 = 12\,\mathrm{Dq} + 15\,\mathrm{B} ;\ 25.750\ \mathrm{cm}^{-1}$$

On a calculé aussi les caractéristiques principales des spectres champ cristallin : le paramètre de scission (10 Dq), le paramètre Racah (B) et le terme nephélauxétique (β).

Le paramètre de scission : $\nu_1 = 10\,\mathrm{Dq}$ et donc $\mathrm{Dq} = 1000\ \mathrm{cm}^{-1}$.

Fig. 5. — Le diagramme de niveaux énergétiques propres au cas d^8 et les transitions possibles dans la symétrie octaédrique.

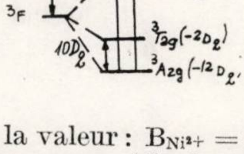

Le paramètre B pour l'ion libre, Ni^{2+}, a la valeur : $B_{Ni^{2+}} = 1041\ cm^{-1}$ mais la valeur $B_{complexe}$ a été déterminée par une méthode graphique [9] à base de représentations de type : $\nu_m/\nu_n = f(\mathrm{Dq}/\mathrm{B})$. En utilisant le rapport ν_3/ν_1, on obtient : $\mathrm{Dq}/B_{complexe} = 1{,}35$ et, par suite, $B_{complexe} = 770{,}7\ cm^{-1}$. Donc $\beta = B_{complexe} / B_{ion\ libre} = 0{,}74$; $\beta < 1$. Il s'ensuit que les valeurs des paramètres Dq = 1000 cm^{-1} et $\beta = 0,74$ sont en accord avec la symétrie octaédrique de l'ion complexe $[Ni(NH_2OH)_6]^{2+}$ dans lequel la liaison Ni—N présente un caractère covalent assez élevé.

4. CONCLUSIONS

Dans le système de réaction Ni(II) – hydroxylamine, en solution aqueuse de pH allant de 4,5 à 10,5, se forme successivement des combinaisons complexes cationiques de formule générale $[Ni(NH_2OH)_n]^{2+}$ ($n = 1 \ldots 6$). En présence d'un grand excès de ligand, il y a formation du complexe à nombre de coordination $n = 6$ avec la constante globale de formation $\beta_6 = 4,34 \cdot 10^5$ $L^6 \cdot mol^{-6}$. Le spectre électronique de l'ion complexe $[Ni(NH_2OH)_6]^{2+}$ interprété à base de la théorie du champ cristallin indique la formation du complexe de symétrie octaédrique dans lequel la liaison Ni—N présente un caractère covalent prépondérant.

BIBLIOGRAPHIE

[1] S. Schibata, *Bull. Chem. Soc. Japan*, **30**, 3755(1957).
[2] S. C. Nyburg and J. S. Wood, *Inorg. Chem.*, **3**, 468(1964).
[3] A. Terzis, K. N. Raymond and T. G. Spiro, *Inorg. Chem.*, **9**, 2415 (1957).
[4] N. Calu, I. Berdan, *Anal. Şti. Univ. "Al. I. Cuza", Iaşi*, tom. XX, f. 1, 101(1974).
[5] N. Calu, I. Berdan, *Anal. Şti. Univ. "Al. I. Cuza", Iaşi*, tom XX, f. 2, 159(1974).
[6] F. Mikula, *Rev. Chemicky Prumysl.*, **9**, 400(1969).
[7] J. H. Joe and A. L. Jones, *Ind. Eng. Chem. Anal.*, **16**, 111(1944).
[8] S. Edmonds and H. Birnbaum, *J. Amer. Chem. Soc.*, **63**, 1471(1941).
[9] A. B. P. Lever, "Inorganic Electronic Spectroscopy", Elsevier—Amsterdam—Londres—New York, 1968.

Revue Roumaine de Chimie, **34**, *6*, 1313–1320 (1989)

SYNTHESIS OF NEW POLYMERS CONTAINING PHENYLQUINOXALINE UNITS

M. BRUMĂ[a], I. SAVA[a], C. HAMCIUC[a], E. HAMCIUC[a], C. I. SIMIONESCU[a],
N. M. BELOMOINA[b], S. A. BABICH[b], E. S. KRONGAUZ[b] and V. V. KORSHAK[b]
[b] Institute of Macromolecular Chemistry, Iași, Romania
[b] Institute of Element-Organic Compounds, Moscow, USSR

Received September 17, 1987

New thermostable polymers containing phenyl substituted quinoxaline and both imide and amide units have been synthesized by low temperature solution polycondensation of diaminophenylquinoxalines with diacid chlorides containing preformed imide rings. Also, certain copolymers have been obtained in which a mixture of diaminophenylquinoxaline and diaminooxadiazole was used in the reaction with the same diacid chlorides. The thermal stability as well as electrical properties of these products are discussed.

INTRODUCTION

Among thermostable heterocyclic polymers widely studied in the last two decades, a special attention has been paid to polyquinoxalines which showed an excellent potential for high temperature applications along with a very good storageability at ambient temperature. Moreover, phenyl substituted quinoxaline polymers have a remarkable solubility in organic solvents which facilitates their detailed study and processing into useful materials.[1]

On the other hand polyimides, very well known for their outstanding resistance at high temperature, have a limited solubility which creates great processing difficulties.[2] Therefore it was expected that a combination into one macromolecule of phenylquinoxaline and imide units would provide high performance physical and thermal characteristics as well as readily processable polymers. At the same time, flexible groups such as amide ones introduced between aromatic and heteroaromatic rings are meant to improve the solubility even more and to generate better mechanical properties of the final materials.

Thus, polyphenylquinoxaline-amide-imide polymers have been synthesized earlier from monomers containing both phenylquinoxaline and imide units already formed.[3] It is the purpose of the present paper to report new polymers containing oxadiazole or/and phenylquinoxaline and imide and amide groups which have been synthesized by polycondensation of heterocyclic diamines incorporating oxadiazole or/and phenylquinoxaline rings with diacid chlorides possessing imide groups.

RESULTS AND DISCUSSION

Diaminophenylquinoxalines I used in the polycondensation reaction have been obtained from 3,4,4′-triaminodiphenylether and bis (α-diketones),[4] according to scheme 1 :

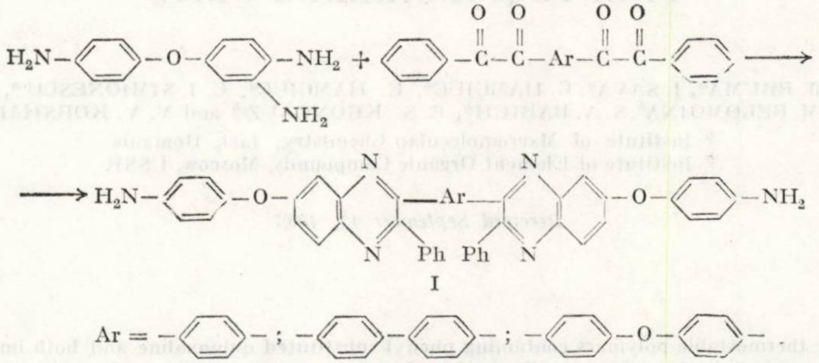
H₂N
O
NH₂
O O
Ar
NH₂
N
Ph Ph
Ar =

I

Scheme 1

The other heterocyclic diamine, 2,5-bis(*p*-aminophenyl)-1,3,4-oxadiazole, has been synthesized from *p*-aminobenzoic acid and hydrazine, according to scheme 2 :

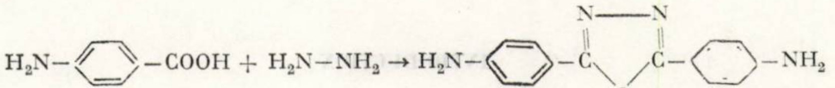
H₂N
COOH + H₂N–NH₂ →
N–N
O
NH₂

I′

Scheme 2

Diacid chlorides II used for polycondensation with the above-mentioned diamines have been prepared by treating with thionyl chloride the corresponding dicarboxylic acids which had been obtained from *p*- or *m*-aminobenzoic acid and trimellitic anhydride,[6] according to scheme 3 :

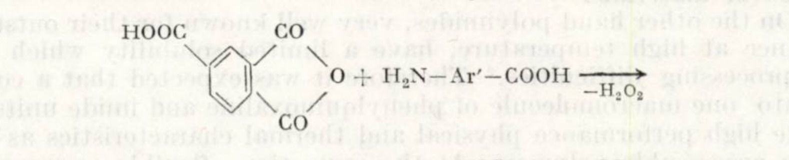
HOOC
CO
O + H₂N–Ar′–COOH
–H₂O
N–Ar′–COOH
SOCl₂
–HCl
–SO₂
ClOC
N Ar′–COCl

II

$Ar' = p\text{-}C_6H_4\ ;\ m\text{-}C_6H_4$

Scheme 3

Low temperature solution polycondensation of 1 mol diaminophenylquinoxaline I and 1 mol diacid chloride II in N-methylpyrrolidone

(NMP) at a concentration of 11–15% using pyridine as acid acceptor gave polyphenylquinoxaline-imide-amides III, according to scheme 4:

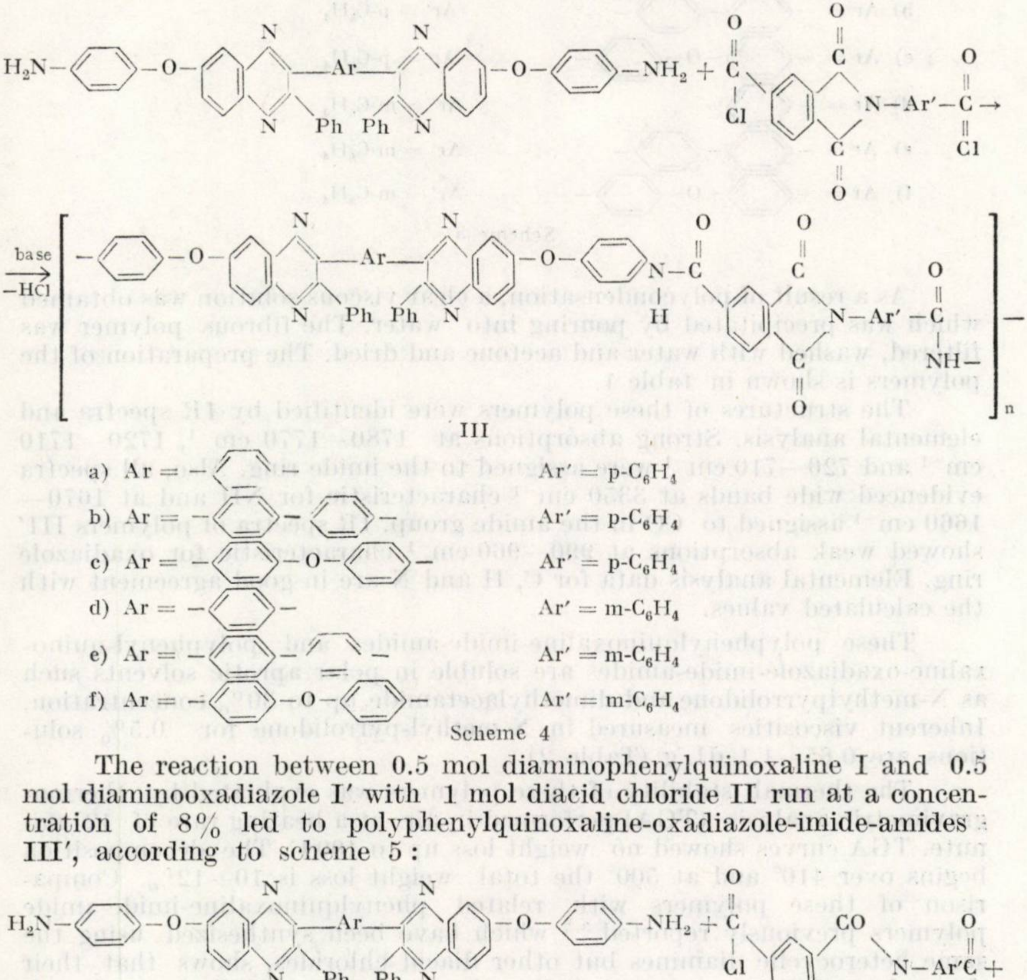
base
–HCl
III
a) Ar =
Ar' = p-C6H4
b) Ar =
Ar' = p-C6H4
c) Ar =
Ar' = p-C6H4
d) Ar =
Ar' = m-C6H4
e) Ar =
Ar' = m-C6H4
f) Ar =
Ar' = m-C6H4

Scheme 4

The reaction between 0.5 mol diaminophenylquinoxaline I and 0.5 mol diaminooxadiazole I' with 1 mol diacid chloride II run at a concentration of 8% led to polyphenylquinoxaline-oxadiazole-imide-amides III', according to scheme 5:

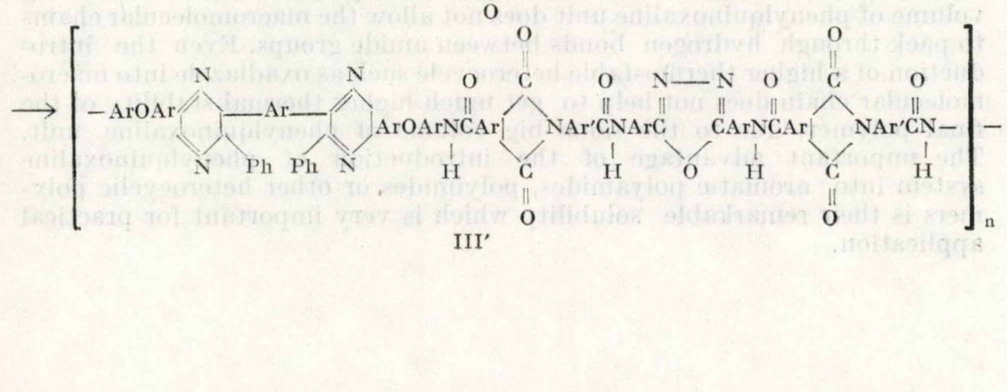

III'

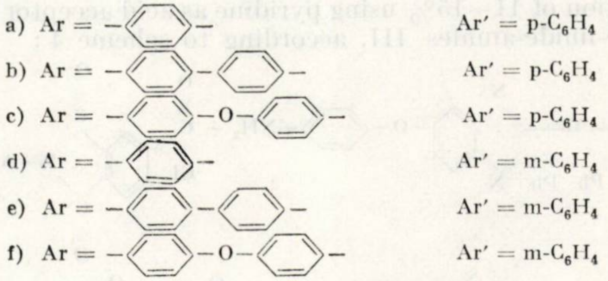

Scheme 5

As a result of polycondensation, a clear viscous solution was obtained which was precipitated by pouring into water. The fibrous polymer was filtered, washed with water and acetone and dried. The preparation of the polymers is shown in table 1.

The structures of these polymers were identified by IR spectra and elemental analysis. Strong absorptions at 1780–1770 cm^{-1}, 1720–1710 cm^{-1} and 720–710 cm^{-1} were assigned to the imide ring. Also, all spectra evidenced wide bands at 3350 cm^{-1} characteristic for NH and at 1670–1660 cm^{-1} assigned to CO in the amide group. IR spectra of polymers III′ showed weak absorptions at 990–960 cm^{-1} characteristic for oxadiazole ring. Elemental analysis data for C, H and N are in good agreement with the calculated values.

These polyphenylquinoxaline-imide-amides and polyphenyl-quinoxaline-oxadiazole-imide-amides are soluble in polar aprotic solvents such as N-methylpyrrolidone and dimethylacetamide up to 30% concentration. Inherent viscosities measured in N-methyl-pyrrolidone for 0.5% solutions are 0.65–1.1 dL/g (Table 2).

The thermal stability of these polymers was evaluated by thermogravimetric analysis (TGA) performed in air at a heating rate of 12°/minute. TGA curves showed no weight loss up to 400°C. The decomposition begins over 410° and at 500° the total weight loss is 10–12%. Comparison of these polymers with related phenylquinoxaline-imide-amide polymers previously reported,[3,7] which have been synthesized using the same heterocyclic diamines but other diacid chlorides, shows that their thermal stabilities are very similar. It means that in all these phenylquinoxaline-imide-amide polymers and copolymers the decomposition begins with the destruction of amide groups. The structure of aromatic diacid chlorides used in the polycondensation process does not influence significantly the thermal stability of the final polymers, because the big volume of phenylquinoxaline unit does not allow the macromolecular chains to pack through hydrogen bonds between amide groups. Even the introduction of a higher thermostable heterocycle such as oxadiazole into macromolecular chain does not help to get much higher thermal stability of the final polymer, due to the same big volume of phenylquinoxaline unit. The important advantage of the introduction of phenylquinoxaline system into aromatic polyamides, polyimides or other heterocyclic polymers is their remarkable solubility which is very important for practical application.

Table 1

Preparation of the polymers

Polymer	Amount of amine (g)		Amount of diacid chloride II. (g)		NMP (mL)	Conc. of the solution (%)
	Diaminophenylquinoxaline I. 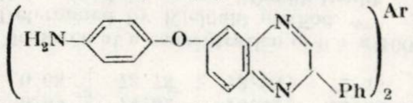	Diaminophenyloxadiazole I′: 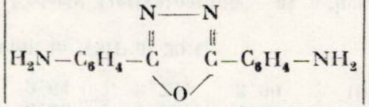	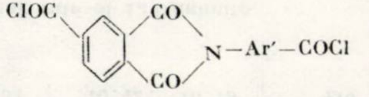			
IIIa	Ar = 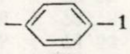 –1.7519	—	Ar′ $=p-_6H_4$	0.87	15	14.88
IIIb.	Ar = 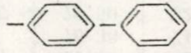 –1.9420	—	"	0.87	22	11.33
IIIc	Ar = 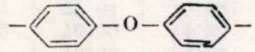 –1.9821	—	"	0.87	24	10.62
IIId	Ar = 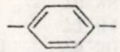 –1.7519	—	Ar′ $=m-C_6H_4$	0.87	22	10.65
IIIe	Ar = 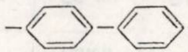 –1.9420	—	"	0.87	22	11.33
IIIf	Ar = 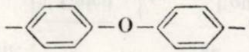 –1.9821	—	"	0.87	22	11.48
III′a.	Ar = 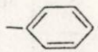 –0.8759	0.327	Ar′ $=p-C_6CH_4$	0.87	25	7.65
III′b.	Ar = 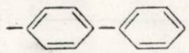 –0.9710	0.327	"	0.87	25	7.98
III′c.	Ar = 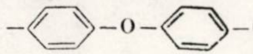 –0.9911	0.327	"	0.87	25	8.05
III′d.	Ar = 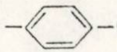 –0.8759	0.327	Ar′ $=m-C_6H_4$	0.87	25	7.65
III′e.	Ar = 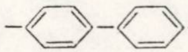 –0.9710	0.327	"	0.87	25	7.98
III′f.	Ar = 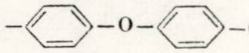 –0.9911	0.327	"	0.87	25	8.05

Table 2

Properties of the polymers

Polymer	* η inh.	Elemental analysis						TGA***	
		C%		H%		N%**		Initial decomp. temp. °C	Weight loss at 500°C
		Calcd	Found	Calcd	Found	Calcd	Found		
IIIa	0.81	76.30	74.72; 75.02	3.80	4.0; 4.18	10.05	10.04; 9.65	410	11
IIIb	1.1	77.64	76.41; 76.02	3.90	4.15; 4.31	9.30	9.41; 9.09	420	10
IIIc	1.1	76.38	74.82; 74.44	3.84	3.92; 3.79	9.18	9.17; 9.08	415	10
IIId.	0.83	76.30	74.92; 74.58	3.80	3.83; 4.0	10.05	9.76; 10.20	410	11
IIIe.	0.97	77.64	75.85; 75.31	3.90	4.18; 4.64	9.30	9.30; 9.52	415	11
IIIf.	1.0	76.38	74.77; 74.56	3.84	3.74; 3.94	9.18	9.23; 9.69	415	11
III′a.	0.77	73.50	72.32; 71.97	3.60	3.82; 4.0	11.18	10.69; 10.85	410	12
III′b.	0.85	74.52	73.05; 72.98	3.68	3.75; 4.0	10.65	10.4 ; 10.12	415	11
III′c.	0.86	73.78	72.90; 72.51	3.64	3.80; 3.92	10.54	10.14; 9.90	410	11
IIId.	0.65	73.50	72.35; 72.18	3.60	3.88; 3.92	11.18	10.81; 10.65	410	12
III′e.	0.69	74.52	73.32; 72.98	3.68	3.90; 4.12	10.65	10.31; 10.08	410	12
III′f.	0.68	73.78	72.80; 72.45	3.64	3.78; 3.90	10.54	10.42; 10.15	410	12

*) Measured at a concentration of 0.5 g/100 mL in NMP at 20°C.

**) Determined by Kjeldahl method.

***) Determined in air on "Paulik-Paulik — Erderly Derivatograph" at a heating rate of 12°C/minute.

Electrical insulating properties of the polymers reported in this paper have been studied on polymer films of 30 microns thickness at room temperature, frequency 800 Hz, using a differential bridge for dielectric constant and dielectric loss tangent of the type TR-9701 (Hungary). The values of dielectric loss tangent, dielectric constant and volume resistivity indicated good electrical insulating properties comparable to those of polyimide film obtained from pyromellitic dianhydride and 4,4′-diaminodiphenylether (film H) (Table 3).

Table 3

Insulating properties of the polymers *)

Polymer	Dielectric loss tangent	Dielectric constant	Volume resistivity ($\Omega \cdot cm$)
IIIa	3×10^{-3}	2.96	3.5×10^{15}
IIIb	3.1×10^{-3}	3.02	4.5×10^{15}
IIIc	4×10^{-3}	3.6	1.2×10^{16}
IIId	5×10^{-3}	3.24	6.6×10^{15}
IIIe	4×10^{-3}	3.7	8.4×10^{16}
IIIf	4.5×10^{-3}	2.98	1.5×10^{16}
III′a	4.2×10^{-3}	3.47	3.8×10^{15}
III′b	2.9×10^{-3}	2.85	7.2×10^{15}
III′c	3.4×10^{-3}	3.1	2.8×10^{15}
Film H	3×10^{-3}	3.5	9×10^{16}

*) All data were obtained on films of 30 – 40 microns

EXPERIMENTAL

Synthesis of the monomers

Diaminophenylquinoxalines I were synthesized by condensation of 3,4,4′-triaminodiphenyl ether (2 mol) with bis(α-diketones) such as 1,4-bis(phenylglyoxalyl) benzene, 4,4′-bis-(phenylglyoxalyl)diphenyl or 4,4′-bis(phenylglyoxalyl)diphenylether (1 mol) in ethanol at reflux temperature, according to a method previously described.[4]

2,5-bis(p-aminophenyl)-1,3,4-oxadiazole I′ was prepared by the reaction of p-aminobenzoic acid (2 mol) with hydrazine hydrate (1 mol) in polyphosphoric acid at 120 – 130°, following a procedure indicated in the literature.[5]

Diacid chlorides II were obtained by treating with excess thionyl chloride at reflux temperature the corresponding dicarboxylic acids resulted from the condensation of trimetillitic anhydride with *p*- or *m*-aminobenzoic acid.[6]

N-methylpyrrolidone (NMP) was dried on NaOH pellets and distilled over phosphorous pentoxide under reduced pressure.

Synthesis of the polymers

Polycondensation was run with equimolecular quantities of diamines and diacid chlorides using N-methylpyrrolidone as solvent, according to the following general procedure.

In a three-necked flask fitted with mechanical stirrer and N_2-inlet and outlet, 0.0025 mol diaminophenylquinoxaline I and 22 mL N-methylpyrrolidone were placed and stirred until complete dissolution. In the case of polyphenylquinoxaline-oxadiazole copolymers the flask was charged with 0.00125 mol diaminophenylquinoxaline I and 0.00125 mol diaminophenlyoxadiazole I′ plus the solvent and it was stirred to dissolve. Then the flask was cooled below – 5°C and 0.0025 mol finely powdered diacid chloride II was added under rapid stirring.

The mixture was kept at − 5°C for 20 minutes, then slowly raised to room temperature within other 20 minutes and kept at room temperature for 2−3 h. The yellow viscous solution was neutralized with a few drops of pyridine. Half part of this solution was used to prepare a film by casting on a glass plate (size 200 × 200 mm) and evaporating the solvent at 100° for 30 minutes, 150° for 1 h and at 200° for other 30 minutes. Film was used to measure the electrical insulating properties. The other part of polymer solution was diluted with 10 ml NMP and was poured into water under rapid stirring. The precipitated yellow polymer was filtered, washed thoroughly with water, then with acetone and dried in vacuum oven. The resulted solid polymer was used to register the IR spectra and to perform the elemental analysis and thermogravimetric analysis. The preparation of he polymers is shown in table 1.

CONCLUSIONS

New polyhenylquinoxaline-imide-amides have been prepared by low temperature solution polycondensation of certain diaminophenylquinoxalines with diacid chlorides containing preformed imide rings. Also, new polyphenylquinoxaline-oxadiazole-imide-amides have been synthesized by using the same monomers and a diamine incorporating the oxadiazole ring. All these polymers are highly thermostable, their decomposition beginning over 410°. They have a remarkable solubility in polar aprotic solvents and their solutions can be cast into transparent, flexible films with good electrical insulating properties comparable to those of polyimide film H.

REFERENCES

[1] E. S. Krongauz, *Vysokomol. Soedineniya, Ser. A*, **26**, 227(1984).

[2] C. E. Sroog, *J. Polymer Sci., Macromol. Reviews*, **11**, 161(1976).

[3] V. V. Korshak, E. S. Krongauz, N. M. Belomoina, M. Brumă, I. Diaconu and C. I. Simionescu, *Angew. Makromol. Chem.*, **144**, 129 (1986).

[4] V. V. Korshak, E. S. Krongauz, N. M. Belomoina, H. Raubach and D. Hein, *Acta Polymerica*, **34**, 213 (1983).

[5] M. Brumă, Doctoral Thesis, "P. Poni" Institute Iaşi (1971).

[6] M. Brumă and G. Neamţu, *Rev. Roumaine Chim.*, **26**, 87 (1981).

[7] V. V. Korshak, E. S. Krongauz, N. M. Belomoina, M. Brumă, I. Sava and C.I. Simionescu, *Rev. Roumaine Chim.*, **32**, 393(1987).

Revue Roumaine de Chimie, 34, 6, 1321–1327 (1989)

AS-TRIAZINE DERIVATIVES WITH POTENTIAL THERAPEUTIC ACTION. XXIII *

SYNTHESIS OF 4-THIOXO-5(CHLOROBENZYL)THIO-6-AZAURACIL DERIVATIVES AND THEIR NUCLEOSIDES

C. CRISTESCU and ST. TOMAS
Chemical and Pharmaceutical Research Institute
112, Şos. Vitan, 74351 Bucharest, Romania

Received June 25, 1988

Thionation with P_2S_5 in pyridine of 5(chlorobenzyl)thio-6-azauracils at a molar ratio substance: P_2S_5 of 2:1 occurs selectively in position 4, yielding 4-thioxo-5(chlorobenzyl) thio-6-azauracils (II). These compounds can be alkylated at S4 atom. 4-Thioxo-5(chlorobenzyl)thio-6-azauridines (VI) were prepared via the silyl modification of the Hilbert-Johnson reaction.

In connection with the investigation on the biological activity of 4-methylthio-5-benzylthio-6-azauracil, we prepared the new 4-methylthio-5(substituted-benzyl)thio-derivatives. The research on 4-methylthio-5(chlorobenzyl)thio-6-azauracils and their nucleosides was undertaken in an attempt to find substances with improved pharmacological and therapeutic properties as compared to 4-methylthio-5-benzylthio-6-azauracil. The study was stimulated by the assumption that the presence of a stronger electron-withdrawing substituent, such as the chloro atom, on the benzylthio-group, increases the binding affinity of the benzyl-group towards the biological receptor.

The selective thionation of 5-benzylthio-6-azauracil with phosphorous pentasulphide was investigated in a previous work.[1] Studies concerned with the thionation of 6-azauracil have demonstrated that the C4-position is the initial site of the reaction.[2–6] Larger amounts of P_2S_5 decreased the quantity of C4-monothiated derivative and favours the formation of the C2, C4-dithiated products. We examined the conditions required for the C4-monothiation of 5-substituted-6-azauracils using phosphorus pentasulphide/pyridine and have found that the best results were obtained at a 5-substituted-6-azauracil/P_2S_5 molar ratio of 2 : 1 using a pyridine with a water content of about 0.1–0.3%.

At the 5(chlorobenzyl)thio-6-azauracil [7] (I)/P_2S_5 2 : 1 molar ratio under similar conditions the 4-thioxo-5(chlorobenzyl)thio-6-azauracil (II) is formed in 50–60% yield. Since II was a critical intermediate for all compounds we devised an alternate method to increase the yield of this substance. Addition of elemental sulphur [8] into the reaction medium and reversal of the I : P_2S_5 molar ratio, increases the yield of the thiolated II with about 20—25% when pyridine with 0.3% water was used.

---

* Part XXII, C. Cristescu and C. Supuran, *Rev. Roumaine Chim.*, **32**, 329 (1987).

Alkylation of monothioxo-derivatives with methyl iodide leads to the corresponding methylthio-derivatives. Thus, 4-thioxo-5(chlorobenzyl)thio-6-azauracils(II a—f) in aqueous alcoholic medium and in presence of sodium hydroxide solution (1 Ec.) lead to 4-methylthio-5(chlorobenzyl)thio-6-azauracils (III a—f). All these reactions take place at room temperature in about 80—85% yield.

The lability of the C4-methylmercapto-group of derivative III, facilitates the replacement of the mercapto-group by the oxo-group. The treatment of III with hydrochloric acid in aqueous alcoholic media gives the starting compounds (I a—f).

Infrared spectra of the compounds II showed an intense absorption band at 1730 ± 30 cm^{-1}$\bar{\nu}$(C=O), indicating the oxostructure of these derivatives.[9–10] The $\bar{\nu}$(C=S) vibration was found near 1140 cm^{-1}.

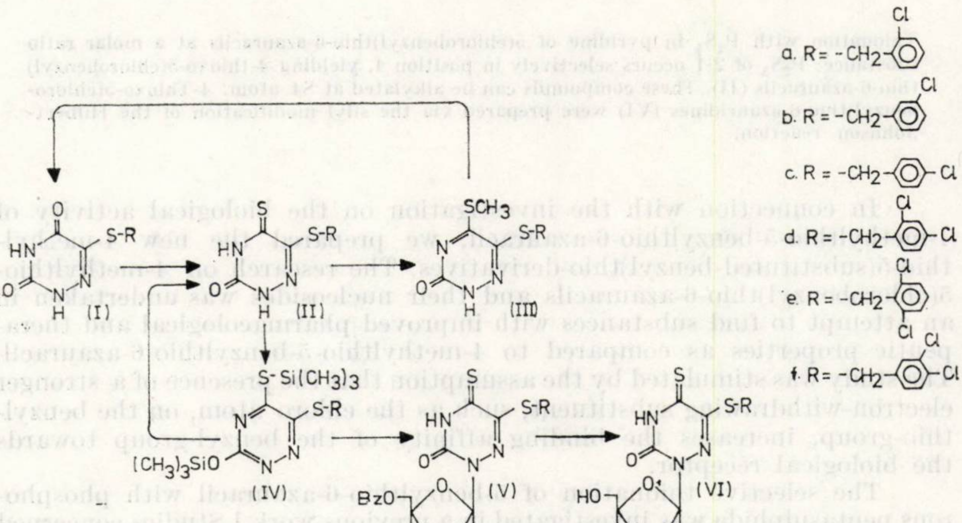

The UV spectra of II either in acidic, neutral and alkaline media show the characteristic absorption peak at the 4-thioxo-derivatives at the 318 nm (acidic and neutral media) and 352 nm (alkaline medium).[12] Alkylation of the C4-thioxo-grup produces a hypsochromic shift in acidic and neutral media and a bathochromic shift in alkaline medium.[2]

Treatment of II with hexamethyldisilazane in the presence of traces of chlorotrimethylsilane, under reflux, gave 2(trimethylsilyloxy)-4(trimethylsilylthio)-5(chlorobenzyl)thio-6-azauracils (IV). The condensation of IV with 1-0-acetyl-2,3,5-tri-0-benzoyl-D-ribofuranoze in dry 1,2-dichloro-

Table 1

Chemical and physical characterization data of the products II-III

No.	mp °C	Recryst[a]. solv.	Yeld %	T.L.C[b]		Paper chrom.[c]		UV Spectra λ max(log ε)			IR Spectra(KBr) cm^{-1}				Formula[d]
				A	B	C	D	Et OH	0.1N HCl	0.1N NaOH	$\tilde{\nu}$ (CO)	$\tilde{\nu}$ (CS)	$\tilde{\nu}$(SCH$_3$)	$\tilde{\nu}$ (C=C)	
II–a	268–269	A	81	0.59	–	0.88	0.75	318(3.87)	318(3.89)	352(3.67)	1730	1140	—	1593,1493	$C_{10}H_8N_3OS_2Cl$
II–b	281–283	A	70	0.59	–	0.88	0.76	318(3.86)	318(3.88)	352(3.72)	1753	1146	—	1600,1480	$C_{10}H_8N_3OS_2Cl$
II–c	263–266	A	75	0.58	–	0.89	0.72	318(3.87)	318(3.86)	352(3.80)	1747	1153	—	1606,1480	$C_{10}H_8N_3OS_2Cl$
II–d	258–259	A	71	0.59	–	0.91	0.77	318(3.86)	318(3.87)	352(3.84)	1740	1140	—	1593,1500	$C_{10}H_7N_3OS_2Cl_2$
II–e	230–232	A	69	0.60	–	0.90	0.76	318(3.88)	318(3.89)	352(3.72)	1700	1140	—	1586,1500	$C_{10}H_7N_3OS_2Cl_2$
II–f	254–255	A	68	0.60	–	0.90	0.75	318(3.87)	318(3.88)	352(3.73)	1727	1140	—	1600,1500	$C_{10}H_7N_3OS_2Cl_2$
III–a	183–185	A	85	0.65	0.11	0.89	0.77	293(3.78)	293(3.79)	335(3.73)	1666	—	2983	1593,1494	$C_{11}H_{10}N_3OS_2Cl$
III–b	193–195	A	86	0.65	0.13	0.89	0.77	293(3.73)	293(3.79)	335(3.73)	1666	—	2990	1600,1500	$C_{11}H_{10}N_3OS_2Cl$
III–c	191–193	A	83	0.65	0.12	0.87	0.77	293(3.79)	293(3.80)	335(3.78)	1666	—	2988	1594,1497	$C_{11}H_{10}N_3OS_2Cl$
III–d	185–187	A	84	0.65	0.12	0.90	0.78	293(3.79)	293(3.80)	335(3.69)	1656	—	2983	1580,1500	$C_{11}H_9N_3OS_2Cl_2$
III–e	215–217	B	81	0.65	0.17	0.90	0.78	293(3.81)	293(3.82)	335(3.80)	1668	—	2986	1580,1500	$C_{11}H_9N_3OS_2Cl_2$
III–f	193–195	A	83	0.64	0.15	0.89	0.79	293(3.86)	293(3.85)	335(3.79)	1646	—	2983	1580,1493	$C_{11}H_9N_3OS_2Cl_2$

a. (A) ethanol; (B) ethanol-water (2:1);

b. spots detected by UV absorption (254 nm); solvent systems: (A) chloroform-methanol (8:2), (B) benzene-ethyl acetate (6:4);

c. spots detected by UV absorption (254 nm); solvent systems; (C) 1-butanol-acetic acid-water (4:1:1); (D) 2-propanol-conc. ammonia-water (7:1:2);

d. analytical results were within ±0.4 % of the theoretical values for C, H, N, S.

Table

Chemical and physical characterization

No.	mp °C	Recryst. solv.[a]	Yield %	T.L.C.[b]		Paper chrom.[c]		$(\alpha)_D^{25}$	UV Spectra λ max(log ε)		
				A	B	C	D		EtOH	0.1 N HCl	0.1NNaOH
V−a	136−138	A	81	—	0.51	0.95	0.86	−123.0[d]	330(3.96)	—	338(4.03)
V−b	145−147	A	83	—	0.50	0.95	0.86	−155.8[d]	330(4.00)	—	338(4.06)
V−c	123−125	A	80	—	0.50	0.95	0.86	−195.2[d]	330(4.01)	—	338(4.05)
V−d	115−117	A	81	—	0.51	0.95	0.86	−145.0[d]	330(3.96)	—	338(4.01)
V−e	133−135	A	85	—	0.51	0.95	0.86	−161.0[d]	330(3.96)	—	338(4.04)
V−f	141−143	B	82	—	0.51	0.95	0.86	−175.0[d]	330(3.99)	—	338(4.05)
VI−a	128−130	A	82	0.35	—	0.79	0.64	− 92.5[e]	326(3.90)	326(4.00)	334(4.15)
VI−b	148−150	C	84	0.34	—	0.79	0.70	−128.0[e]	326(4.22)	326(4.00)	334(4.22)
VI−c	114−116	A	80	0.35	—	0.80	0.69	− 98.0[e]	326(3.86)	326(3.88)	334(4.19)
VI−d	183−185	A	82	0.36	—	0.84	0.71	−178.0[e]	326(4.18)	326(3.69)	334(4.16)
VI−e	155−157	A	84	0.37	—	0.84	0.71	− 91.2[e]	326(3.89)	326(3.90)	334(4.04)
VI−f	189−190	A	83	0.35	—	0.84	0.72	−107.5[e]	326(3.94)	326(3.94)	334(4.09)

a. (A) ethanol; (B) 2-propanol; (C) ethyl acetate; b. spots detected by UV absorption (254 nm) detected by UV absorption (254 nm) after spraying with 0.005 % fluoresceine (in ethanol); (7:1:2); d. C = 1 % in chloroform; e. C = 1 % in ethanol; f. IR Spectra in $CHCl_3$; g. IR $CDCl_3$/TMS; j. ^1H−NMR Spectra in DMSO−d_6/TMS; k. analytical results were within

ethane, at room temperature, in presence of anhydrous stannic chloride, affords only the N-glycosides (V a—f) in 80—82% yield. The second procedure involved the thionation of 1(2′,3′,5′-tri-0-benzoyl-β-D-ribofuranosyl)-5(chlorobenzyl)thio-6-azauracils [7] with phosphorous pentasulphide in pyridine (0.3% water) at a 2 : 1 molar ratio (compound : P_2S_5). The usual work-up afforded a 70—75% yield of V a—f, identical in all respects (TLC, UV, IR) with the above described compounds.

In the infrared spectra of compounds V, the intense absorption of the acyl groups overlaps a considerable number of bands of the heterocyclic and the sugar parts of the molecule. The carbonyl groups absorb in the 1705 ± 5 cm^{-1} region. The absorption bands of the acyl groups, linked to the ribose residue, are 1180, 1126 cm^{-1} $\bar{\nu}(CO \cdot O)$ and 1316, 1290 cm^{-1} $\bar{\nu}(C \cdot CO)$.

Removal of the blocking groups of V with sodium methoxyde in methanol gave 80—84% yield of the 4-thioxo-5 (chlorobenzyl) thio-6-azauridine (VI a—f).

The UV spectra of VI in either acidic, neutra and alkaline media shows the characteristic absorption peak of 4-thioxo-6-azauridine at 326 nm (acidic and neutral media) and 334 nm (alkaline medium).

2

data of the products V–VI

IR Spectra cm^{-1}					^{1}H-NMR Spectra[h] H1′(J1′, 2′)	Formula[k]
$\tilde{\nu}$(CO)	$\tilde{\nu}$(CS)	$\tilde{\nu}$(CO·O)	$\tilde{\nu}$(C·CO)	$\tilde{\nu}$(C=C)		
1700[f]	1146	1183, 1116	1313, 1290	1573, 1500	6.51(d, 3.00)[i]	$C_{36}H_{28}N_3O_8S_2Cl$
1706[f]	1153	1180, 1126	1320, 1293	1580, 1500	6.55(d, 2.50)[i]	$C_{36}H_{28}N_3O_8S_2Cl$
1700[f]	1140	1180, 1126	1316, 1285	1600, 1500	6.48(d, 2.75)[i]	$C_{36}H_{28}N_3O_8S_2Cl$
1710[f]	1153	1180, 1126	1320, 1296	1580, 1500	6.49(d, 2.80)[i]	$C_{36}H_{27}N_3O_8S_2Cl_2$
1710[f]	1153	1180, 1126	1320, 1293	1580, 1500	6.50(d, 2.70)[i]	$C_{36}H_{27}N_3O_8S_2Cl_2$
1700[f]	1146	1186, 1116	1316, 1286	1573, 1500	6.52(d, 2.50)[i]	$C_{36}H_{27}N_3O_8S_2Cl_2$
1700[g]	1140	—	—	1600, 1510	5.97(d, 3.25)[j]	$C_{15}H_{16}N_3O_5S_2Cl$
1700[g]	1140	—	—	1605, 1529	5.95(d, 3.00)[j]	$C_{15}H_{16}N_3O_5S_2Cl$
1700[g]	1150	—	—	1600, 1490	5.93(d, 3.50)[j]	$C_{15}H_{16}N_3O_5S_2Cl$
1693[g]	1142	—	—	1586, 1466	5.98(d, 3.25)[j]	$C_{15}H_{15}N_3O_5S_2Cl_2$
1693[g]	1150	—	—	1586, 1486	5.92(d, 3.50)[j]	$C_{15}H_{15}N_3O_5S_2Cl_2$
1693[g]	1143	—	—	1600, 1486	5.94(d, 3.75)[j]	$C_{15}H_{15}N_3O_5S_2Cl_2$

solvent systems: (A) chloroform-methanol (8:2); (B) benzene-ethyl acetate (6:4); c. spots
solvent systems; (C) 1-butanol-acetic acid-water (4:1:1); (D) 2-propanol-conc. ammonia-water
Spectra in KBr; h. chemical shifts in ppm and I values in Hz; i. ^{1}H–NMR Spectra in
±0.4 % of the theoretical values for C, H, N, S.

The anomeric proton of the nucleosides V and VI appear in ^{1}H–NMR spectra as a doublet at δ 6.50 ppm for V and 5.95 ppm for VI with a coupling constant 2.5–3.5 Hz. The position of the signal suggests that the nucleosides may be the β-anomers (by comparing the ^{1}H–NMR spectra of other nucleosides of this type[11–13]).

EXPERIMENTAL

The melting points were determined on a heating-plate microscope and are not corrected. Thin-layer chromatography was performed on precoated silicagel plates 60 F_{254} (Merck). Paper chromatography was performed by ascending technique on Schleicher & Schüll 2043 b mgl paper. The preparative column chromatography was performed on silicagel 60 (70–230 mesh ASTM) (Merck), a flow-rate of 100 mL per hour being maintained. The fractions were collected at 6-minute intervals. The ultraviolet absorbing substances were determined in eluates by running registration of UV absorption (Uvicord LKB 254 nm). The optical rotation was measured on a Hilger & Watts automatic polarimeter. The ultraviolet spectra were recorded on a Pye Unicam SP 1800 spectrophotometer. The infrared spectra were recorded on a Zeiss-Jena UR-20 spectrophotometer. The ^{1}H–NMR spectra were recorded at 60 MHz on a Varian EM 360 spectrophotometer.

General procedure for the preparation of 4-thioxo-5(chlorobenzyl)thio-6-azauracils (II a—f)

Method A: To a solution of 5(chlorobenzyl)thio-6-azauracils (I a—f; 10 mmoles) in 90 mL dry pyridine (0.1 % water), P_2S_5 (5 mmoles), was added and the mixture was stirred and heated at reflux for 5 hours. The clear orange-red solution was decanted after cooling at room temperature (over night) and concentrated at 40° under reduced pressure. The dry residue was dissolved in 1 N sodium hydroxide solution (50 mL), treated with active charchoal, filtered and adjusted to pH 3 with 10 % hydrochloric acid. After cooling at 4° over night, the product was filtered. Compounds II a—f were recrystallized from the solvent as indicated in table 1.

Method B: A mixture of I a—f (10 mmoles), flowers of sulfur (S_8) 2.5 mmoles and P_2S_5 (20 mmoles) in 90 mL pyridine (0.3 % water) was heated at reflux for 5 hours. The solvent was removed under reduced pressure and the residual solid was covered with water (50 mL) and boiled for 10 minutes. After cooling to room temperature, the solid was filtered, washed with water and dissolved in 1 N ammonium hydroxide (50 mL). The mixture was treated with active charchoal and filtered through a Celite layer and adjusted to pH 3 with 10 % hydrochloric acid. After cooling at 4° (over night) the product was filtered and recrystallized from the solvent as indicated in table 1 to provide II a—f in 68—81 % yield, identical in all respects with II a—f prepared by method A.

General procedure for the preparation of 4-methylthio-5(chlorobenzyl)thio-6-azauracils (III a—f)

4-Thioxo-5(chlorobenzyl)thio-6-azauracils (II a—f; 5 mmoles) was dissolved at 40° in ethanol (25 mL) and 1 N sodium hydroxide (5 mmoles). The stirred solution was cooled to room temperature and methyl iodide (5.5 mmoles) was added in one portion. The reaction was monitored by TLC, and when complete, the solvent was removed under reduced pressure and the residue recrystallized from the solvent as indicated in table 1.

Hydrolysis of 4-methylthio-5(chlorobenzyl)thio-6-azauracils

0.200 g of III a—f was boiled with 10 mL ethanol and 1 mL hydrochloric acid (10 %) for 30 minutes. The solution was evaporated under reduced pressure and the residue was recrystallized from ethanol to furnish 5(chloro-benzyl)thio-6-azauracils (I a—f) identical in all respects (m.p., TLC, UV and IR) with authentical samples.

General procedure for the preparation of 1(2′,3′,5′-tri-O-benzoyl-β-D-ribofuranosyl)-4-thioxo-5(chlorobenzyl)thio-6-azauracils (V a—f)

Method A: A mixture of 4-thioxo-5(chlorobenzyl)thio-6-azauracils (II a—f; 5.5 mmoles), hexamethyldisilazane (10 mL) and chlorotrimethylsilane (0.5 mL) was heated under reflux for 2 hours, until a clear solution was obtained. The excess of hexamethyldisilazane was removed under reduced pressure and the viscous 2(trimethylsilyloxy)-4(trimethylsilylthio)-5(chlorobenzyl)thio-6-azauracil (IV a—f; 5 mmoles) was dissolved in dry 1,2-dichloroethane (20 mL) and added to 1-0-acetyl-2,3,5-tri-O-benzoyl-D-ribofuranose 64.5 mmoles) previously dissolved in dry 1,2-dichloroethane (150 mL). The mixture was stirred for 12 hours at room temperature in the presence of anhydrous stannic chloride (3.5 mmoles). The solution was treated with a saturated aqueous sodium hydrogen carbonate solution (2 × 50 mL) and the organic phase was filtered over Celite 535, dried on anhydrous sodium sulphate and evaporated. The residue was chromatographed on a silicagel column (60 g) with chloroform. The combined collected fractions were evaporated under reduced pressure to give the pure corresponding blocked nucleosides (V a—f) shown in table 2.

Method B: 1(2′,3′,5′-tri-O-benzoyl-β-D-ribofuranosyl)-5(chlorobenzyl)thio-6-azauracil [7] (2 mmoles) was dissolved in pyridine (0.1 % water; 20 mL) and P_2S_5 (1 mmole) was added at 50°. The mixture was heated under reflux and stirring for 3 hours. The clear, reddish-orange solution was decanted after standing at room temperature for 16 hours and concentrated at 40° under reduced pressure. The dry residue was dissolved in chloroform (100 mL) and washed with water and 0.2 N sodium hydrogen carbonate solution, dried (sodium sulphate) and evaporated. The residue was chromatographed on a silicagel column (40 g) with chloroform. The fractions containing the product were pooled and evaporated under reduced pressure to give the pure corresponding blocked nucleosides (V a—f) identical in all respects (TLC, UV, IR, and ^1H-NMR) with V a—f prepared by method A.

General procedure for the preparation of 4-thioxo-5(chlorobenzyl)thio-6-azauridines (VI a—f)

A mixture of the blocked nucleoside VI (2 mmoles), 1 N sodium methoxide (2 mL) and dry methanol (50 mL) was stirred for 6 hours at room temperature. The solvent was evaporated under reduced pressure and the resulting oil was dissolved in water (20 mL) and extracted with ethyl acetate — ether (2:1 v/v; 2 × 10 mL). The aqueous layer was treated with DOWEX 50 × 8 (H^+) at pH 4, filtered and evaporated under reduced pressure. The residue was recrystallized from the solvent as indicated in table 2.

ACKNOWLEDGEMENT. Thanks are due to Veronica Vişan and Ileana Sârbu of the Analytical Department of our Institute for recording the IR and UV spectra, to Cornelia Ioan for the elemental analyses and to D. Ionescu for NMR spectra. The authors express their gratitude to Anca Sava for her invaluable help.

REFERENCES

[1] C. Cristescu and V. Badea, *Rev. Roumaine Chim.*, **14**, 135 (1969).
[2] J. Gut, M. Prystas and J. Jonas, *Coll. Czech. Chem. Comm.*, **26**, 986 (1961).
[3] K. Y. Zee-Cheng and C. C. Cheng, *J. Org. Chem.*, **27**, 976 (1962).
[4] Y. Mizuno, M. Ikehara and K. A. Watanabe, *Chem. Pharm. Bull.*, **10**, 647 (1962).
[5] C. Cristescu and S. Sitaru, *Rev. Roumaine Chim.*, **16**, 135 (1971).
[6] C. Cristescu, *Rev. Roumaine Chim.*, **16**, 311 (1971).
[7] C. Cristescu, *Rev. Roumaine Chim.*, **30**, 117 (1985).
[8] U. Schmidt, A. Luttringhaus and H. Trefzgel, *Liebigs Ann. Chem.*, **631**, 129 (1960).
[9] M. Horak and J. Gut, *Coll. Czech. Chem. Comm.*, **26**, 1680 (1961).
[10] M. Horak and J. Gut, *Coll. Czech. Chem. Comm.*, **28**, 3392 (1963).
[11] M. P. Sweizer, E. B. Banta, J. T. Witkowsky and R. K. Robins, *J. Amer. Chem. Soc.*, **95**, 3770 (1973).
[12] J. D. Stewens and H. G. Fletcher, *J. Org. Chem.*, **33**, 1799 (1968).
[13] F. E. Hruska, A. A. Grey and I. C. Smith, *J. Amer. Chem. Soc.*, **92**, 4088 (1970).

Revue Roumaine de Chimie, **34**, *6*, 1329–1339 (1989)

PREDICTION OF VAPOUR-LIQUID EQUILIBRIA AT LOW PRESSURE BY A GENERAL EQUATION OF STATE

VIOREL FEROIU and DAN GEANĂ

Dept. Physical Chemistry/TSCO, Polytechnic Institute, Bucharest, Spl. Independenţei 313, Romania

Received June 9, 1988

The possibilities of a general equation of state in vapour-liquid equilibria predictions, at low pressures, are studied. An EOS expression for the activity coefficients has been developed. The interaction parameters of the mixing rules have been calculated from the activity coefficients at infinite dilution. It is shown that the general cubic EOS predicts reliable results as compared with those obtained by G^E models.

Phase equilibria are described by practical models which can be divided into two types: equations of state (EOS) and activity-coefficients models.

Generally, the equations of state have been used successfully for PVT and vapour-liquid equilibrium computations of pure and multicomponent fluids, at high pressures. On the other hand, the activity-coefficients approach has been used at low (or moderate) pressures, where the liquid phase is relatively incompressible. The use of EOS has been extended, recently, for vapour-liquid equilibria predictions, at low pressures.[1-3] The phase equilibria calculations based on EOS and on activity models may be done comparatively at low pressures.[4]

A difficult problem of the EOS method is the high sensitivity of computations to the interaction parameters of the mixing rules.

In this paper, we have investigated the possibilities of a general cubic equation of state[5] in vapour-liquid equilibria predictions, at low pressures. An EOS expression for the activity coefficient has been developed, based on the relationship between the fugacity coefficient of a component in the mixture and the fugacity coefficient of the same pure component. The binary interaction parameters of the mixing rules have been estimated from the activity coefficients at infinite dilution, calculated by G^E models. A comparison with the results obtained by using the activity coefficient models is thus possible.

THE GENERAL CUBIC EQUATION OF STATE

The general cubic equation of state presented in the previous works,[5] for fluids mixtures has the following form :

$$P = \frac{RT}{V - b} - \frac{a(T)}{(V - d)^2 + c} \qquad (1)$$

The constants a, b, c, d for a pure component are expressed by :[5]

$$a = \frac{R^2T_c^2}{P_c}\cdot\Omega_a\cdot\beta(T_r)\,;\quad b = \frac{RT_c}{P_c}\Omega_b$$

$$(2)$$

$$c = \frac{R^2T_c^2}{P_c^2}\Omega_c\,;\quad d = \frac{RT_c}{P}\Omega_d$$

where $\beta(T_r)$ is a function of reduced temperature :

$$\beta(T_r) = T_r^{-m} \qquad (3)$$

and Ω_a, Ω_b, Ω_c, Ω_d are functions of α_c (Riedel's criterion), m and Z_c :

$$\Omega_a = \frac{(\alpha_c - 1)^3}{\alpha_c + m}\,;\quad \Omega_b = Z_c - \frac{1 + m}{\alpha_c + m}$$

$$(4)$$

$$\Omega_c = \frac{(\alpha_c - 1)^2(3m + 4 - \alpha_c)}{4(\alpha_c + m)^3}\,;\quad \Omega_d = Z_c - \frac{\alpha - 1}{2(\alpha_c + m)}$$

$$\alpha_c = 0{,}9076[1 + T_f(T_c - T_f)^{-1}\cdot\ln P_c] \qquad (5)$$

The parameters α_c and m can be estimated in different ways, presented in the previous papers.[5] The parameter m can be also fitted at any temperature so that the equation of state (1) gives exactly the saturation pressure of pure component.

The computations at high pressure,[6-8] based on equation (1), have used with good results the classic mixing rules (with a single binary interaction parameter) :

$$a = \sum_i \sum_j X_iX_ja_{ij} \qquad (6a)$$

$$b = \sum_i X_ib_i \qquad (6b)$$

$$c = \sum_i \sum_j X_iX_jc_{ij} \qquad (6c)$$

$$d = \sum_i X_id_i \qquad (6d)$$

with :

$$a_{ij} = (a_i\cdot a_j)^{1/2}(1 - k_{ij}^a) \qquad (7)$$

$$c_{ij} = \pm\,(|c_i|\cdot|c_j|)^{1/2}(\text{“}+\text{” for } c_i, c_j > 0,\ \text{“}-\text{” for } c_i \text{ or } c_j < 0) \qquad (8)$$

These mixing rules do not present a sufficient flexibility, at low pressure, for any systems.

In this paper, mixing rules of the Stryjek-Vera type [9] have been used with the same form for a, b, c, d coefficients as that of equations (6), but with a_{ij} in the form:

$$a_{ij} = (a_i \cdot a_j)^{1/2}(1 - X_i k_{ij} - X_j k_{ji}) \tag{9}$$

where

$$a_{ij} = a_{ji} \text{ but } \quad k_{ij} \neq k_{ji}$$

Other mixing rules with two interaction parameters can be also used. A quadratic form for b coefficient can be used:

$$b = \sum_i \sum_j b_{ij} X_i X_j \tag{10}$$

with

$$b_{ij} = \frac{b_i + b_j}{2}(1 - k^b_{ij}) \tag{10a}$$

and a from equations (6a) and (7).

PREDICTION OF THE BINARY PARAMETERS

A computation method of the activity coefficients from equations of state has been recently presented.[4] It uses the relationship between the activity and fugacity models in expressing the properties of the same phase (e.g. liquid). This relationship is expressed by:[10]

$$\gamma_i(T, P, X) = \frac{\varphi_i(T, P, X)}{\varphi_i^0(T, P)} \tag{11}$$

where γ_i is the activity coefficient of component i in a mixture in the symmetric convention, φ_i is the fugacity coefficient of component i in a mixture and φ_i^0 is the fugacity coefficient of pure component i, all of them being considered at the same temperature and pressure.

The fugacity coefficient φ_i in a mixture has been calculated using the relationship:

$$\ln \varphi_i = \frac{1}{RT}\int_V^\infty \left[\left(\frac{\partial P}{\partial n_i}\right)_{T,V,n_j} - \frac{RT}{V}\right] \mathrm{d}V - \ln Z \tag{12}$$

which becomes for the equation of state (1):

$$\ln \varphi_i = \ln \frac{V}{V-b} + \frac{b + n\dfrac{\partial b}{\partial n_i}}{V-b} - \left(2a + n\frac{\partial a}{\partial n_i}\right)\frac{E}{RT} - \frac{a\left(d + n\dfrac{\partial d}{\partial n_i}\right)}{RT[(V-d)^2 + c]} - \frac{a\left(2c + n\dfrac{\partial c}{\partial n_i}\right)}{2R.T.c}\left[\frac{V-d}{(V-d)^2 + c} - E\right] - \ln Z \tag{13}$$

The partial derivatives in equation (13) are expressed by the relationships :

$$
\begin{aligned}
n\frac{\partial a}{\partial n_i} &= 2\Big(\sum_i X_j a_{ij} - a\Big) - 2\, X_i X_j (k_{ij} - k_{ji}) \\
n\frac{\partial b}{\partial n_i} &= b_i - b \\
n\frac{\partial c}{\partial n_i} &= 2\Big(\sum_j X_j c_{ij} - c\Big) \\
n\frac{\partial d}{\partial n_i} &= d_i - d
\end{aligned}
\tag{14}
$$

and E has the following form :

$$
\begin{aligned}
E &= \frac{1}{2\sqrt{-c}} \ln \frac{V - d + \sqrt{-c}}{V - d - \sqrt{-c}} && \text{for } c < 0 \\
E &= \frac{1}{\sqrt{c}} \operatorname{arctg} \frac{\sqrt{c}}{V - d} && \text{for } c > 0 \\
E &= \frac{1}{V - d} && \text{for } c = 0
\end{aligned}
\tag{15}
$$

The fugacity coefficient of pure component i is expressed by :

$$
\ln \varphi_i^0 = \int_{V_i^0}^{\infty} \left(\frac{P}{RT} - \frac{1}{V_i^0} \right) dV_i^0 + Z^0 - 1 - \ln Z^0 \tag{16}
$$

which for equation of state (1) becomes :

$$
\ln \varphi_i^0 = \ln \frac{V_i^0}{V_i^0 - b_i} + Z^0 - 1 - \ln Z^0 - \frac{a_i \cdot E_i^0}{RT} \tag{17}
$$

where the upper index 0 represents the pure component. One finally obtains an equation for γ_i. The activity coefficient γ_i is a function of volumes V and V_i^0 which are also implicit functions of pressure and must be calculated by solving the equation of state. However, the activity coefficients are almost pressure-independent, and the excess Gibbs energy (G^E) models generally calculate them at an arbitrary reference pressure, which is often taken to be zero. The final expression of γ_i has the following form :

$$
\begin{aligned}
\ln \gamma_i(P = 0) = {} & \ln \frac{V_i^0 - b_i}{V - b} + \frac{b + n\dfrac{\partial b}{\partial n_i}}{V - b} - \left(2a + n\frac{\partial a}{\partial n_i} \right) \frac{E}{RT} - \\
& - \frac{a\left(d + n\dfrac{\partial d}{\partial n_i} \right)}{RT[(V - d)^2 + c]} - \frac{a\left(2c + n\dfrac{\partial c}{\partial n_i} \right)}{2RT \cdot c} \left[\frac{V - d}{(V - d)^2 + c} \right] + 1 + \frac{a_i E_i^0}{RT}
\end{aligned}
\tag{18}
$$

The equation of state (1) is also simplified to a second-order equation in V (since $P \to 0$):

$$V^2 + \left(2d + \frac{a}{RT}\right)V + \left(d^2 + c + \frac{ab}{RT}\right) = 0$$

The equation will have the same form for the pure component i, its expression containing V_i^0 and a_i, b_i, c_i, d_i.

Finally, the activity coefficients at infinite dilution (γ_1^∞ and γ_2^∞ for a binary system) have the following symmetric expressions:

$$\ln \gamma_1^\infty = \ln \frac{V_1 - b_1}{V_2 - b_2} + \frac{b_1}{V_2 - b_2} - 2(a_1 \cdot a_2)^{1/2} \frac{E_2}{RT}(1 - k_{21}) - \\ - \frac{a_2 d_1}{RT[(V_2 - d_2) + c_2]} - \frac{a_2 c_{12}}{TR \cdot c_2} \cdot \left[\frac{V_2 - d_2}{(V_2 - d_2)^2 + c_2} - E_2\right] + \\ + 1 + \frac{a_1 E_1}{RT} \tag{20}$$

$$\ln \gamma_2^\infty = \ln \frac{V_2 - b_2}{V_1 - b_1} + \frac{b_2}{V_1 - b_1} - 2(a_1 a_2)^{1/2} \frac{E_1}{RT}(1 - k_{12}) - \\ - \frac{a_1 d_2}{RT[(V_1 - d_1)^2 + c_1]} - \frac{a_1 c_{12}}{RT\, c_1}\left[\frac{V_1 - d_1}{(V_1 - d_1)^2 + c_1} - E_1\right] + 1 + \frac{a_2 E_2}{RT} \tag{21}$$

It can be observed that, in these conditions, the interaction parameters k_{12} and k_{21} result as solutions of equations (21) and (22). They can be evaluated from the experimental values for γ_1^∞ and γ_2^∞ (when these are available) or from the activity coefficient models, on condition that the parameters of the model have been calculated for the respective system. Of course, this restriction disappears by using a UNIFAC type model,[13] which makes possible the prediction of the activity coefficients only by group-contributions.

RESULTS

Based on the above outlined procedure, two binary systems have been studied: water + methanol and ethanol + n-hexane. These systems are representative for testing the EOS model in liquid-vapour calculations at low pressures. The computations were of bubble-P type, the method being described in detail in a previous work.[8]

The critical parameters of the substances are given in table 1.

The results obtained for water-methanol system at three different temperatures: $T_1 = 308.15$ K, $T_2 = 323.15$ IK and $T_3 = 338{,}15$ K are presented in tables 2—4.

The m and α_c parameters of equation of state (1) were estimated for each substance from saturation pressure and experimental liquid density at normal boiling temperature. The estimation was done by minimisation of the following expression :[5]

$$S(\alpha_c, m) = \left[\left(\frac{P^{\text{ex}} - P^{\text{calc}}}{\sigma_P}\right)^2 + \left(\frac{\rho_L^{\text{ex}} - \rho_L^{\text{calc}}}{\sigma_{\rho_L}}\right)^2\right]_{T=T_f} \tag{22}$$

Table 1

Critical data of pure substances[12]

Substance	T_c(K)	P_c(atm)	V_c(1/mol)	Z_c
Water	647.3	217.6	0.056	0.229
Methanol	512.6	79.9	0.118	0.224
Ethanol	516.2	63	0.166	0.248
n-Hexane	607.4	29.3	0.370	0.260

Table 2

EOS calculations of VLE in water-methanol system at $T = 308.15$ K. Experimental data.[11]

X_1^{ex}	Y_1^{ex}	$P^{\text{ex}}_{(\text{KPa})}$	$k_{12} = 0$; $k_{21} = 0$				$k_{12} = -0.095$; $k_{21} = -0.082$			
			Y_1^{calc}	$P^{\text{calc}}_{(\text{KPa})}$	$\varepsilon_Y(\%)$	$\varepsilon_P(\%)$	Y_1^{calc}	$P^{\text{calc}}_{(\text{KPa})}$	$\varepsilon_Y(\%)$	$\varepsilon_P(\%)$
0.0000	0.0000	28.01	0.0000	27.80	—	—	0.000	27.80	—	—
0.0594	0.0185	26.80	0.0564	27.05	−204.8	−0.93	0.0186	25.85	−0.54	3.54
0.0995	0.0317	25.86	0.0894	27.00	−182.0	−4.4	0.0312	25.02	1.57	3.25
0.1120	0.0364	25.76	0.0986	26.95	−170.9	−4.6	0.0352	24.84	3.29	3.57
0.2049	0.0684	23.98	0.1581	26.14	−131.1	−9.0	0.0647	23.50	5.41	2.00
0.2761	0.0929	22.68	0.1921	26.10	−106.8	−15.1	0.0884	22.29	4.84	1.71
0.3988	0.1389	20.58	0.2298	25.33	−65.4	−23.1	0.1352	19.45	2.66	5.49
0.5306	0.1916	18.35	0.2410	25.22	−25.8	−37.4	0.1889	17.63	1.41	3.92
0.6397	0.2441	16.40	0.2266	25.83	7.2	−57.5	0.2481	15.30	−1.64	6.70
0.7512	0.3262	14.01	0.1959	28.06	39.9	−100.3	0.3221	13.17	1.26	5.99
0.8613	0.4726	10.87	0.1575	33.53	66.7	−208.5	0.4520	10.21	4.36	6.07
0.9592	0.7510	7.33	0.1739	30.29	76.8	−313.2	0.7400	7.05	1.46	3.82
1.0000	1.0000	5.62	1.000	5.20	—	—	1.000	5.20	—	—
Average relative errors			—	—	97.9	70.4	—	—	2.6	4.2

using Rosenbrok's method. The standard deviations were chosen as $\sigma_P = 10^{-3} \cdot P^{\text{ex}}$ and $\sigma_{\rho_L} = 10^{-3} \cdot \rho_L^{\text{ex}}$. The obtained parameter values for the pure substances are presented in table 5.

We have also tried computations using α_c values evaluated from equation (5) and m values obtained by fitting the equation of state (1) to the saturation pressure of pure components at a given temperature. The liquid-vapour equilibrium results, obtained in this way for the water-methanol system, were identical with those presented in tables 2—4.

The experimental values[11] for pressure and vapour phase composition are also presented in tables 2—4. The computations have been done for two different situations, by using the mixing rules of the Stryjek-Vera type :

a) the interaction parameters, $k_{ij} = 0$;

Table 3

EOS calculations of VLE in Water-methanol system at $T = 323.15\,\text{K}$. Experimental data.[11]

X^{ex}	Y^{ex}	$P^{ex}_{(KPa)}$	$k_{12} = 0;\ k_{21} = 0$				$k_{12} = -0.093;\ k_{21} = -0.079$			
			Y^{calc}	$P^{calc}_{KPa)}$	$\varepsilon_Y(\%)$	$\varepsilon_p(\%)$	Y^{calc}	$P^{calc}_{(KPa)}$	$\varepsilon_Y(\%)$	$\varepsilon_F(\%)$
0.0000	0.0000	55.65	0.000	54.81	—	—	0	54.81	—	—
0.0486	0.0283	53.77	0.0465	54.80	−64.3	−1.9	0.0172	53.17	39.2	1.1
0.1475	0.0545	50.19	0.1242	54.31	−127.8	−8.2	0.0522	49.65	4.2	1.1
0.2402	0.0910	46.96	0.1789	53.39	−96.6	−13.7	0.0856	46.40	5.9	1.2
0.3834	0.1480	42.21	0.2334	51.73	−57.7	−22.6	0.1402	41.39	5.3	1.9
0.4589	0.1788	39.79	0.2487	50.86	−39.1	−27.8	0.1717	39.00	3.9	2.0
0.5823	0.2316	35.60	0.2530	50.73	− 9.2	−42.5	0.2318	34.55	−0.08	3.0
0.6863	0.2913	31.99	0.2387	52.28	18.1	−63.4	0.2919	30.70	−0.20	4.0
0.8146	0.4102	25.95	0.2024	58.56	50.7	−125.7	0.4109	24.62	−0.17	5.1
0.8613	0.4773	23.23	0.1897	61.60	60.3	−165.2	0.4777	22.03	−0.08	5.2
0.9137	0.5943	19.56	0.1851	62.92	68.9	−221.7	0.5750	19.66	3.2	−0.51
0.9547	0.7339	16.36	0.2116	55.72	71.2	−240.6	0.7156	16.01	2.5	2.1
1.0000	1.0000	12.33	1.000	11.25	—	—	1.000	11.25	—	—
Average relative errors			—	—	60.4	85.6	—	—	5.9	2.4

Table 4

EOS calculations of VLE in water-methanol system at $T = 338.15\,\text{K}$. Experimental data.[11]

X^{ex}	Y^{ex}	P^{ex}_{KPa}	$k_{12} = 0;\ k_{21} = 0$				$k_{12} = -0.089;\ k_{21} = -0.076$			
			Y^{calc}	$P^{calc}_{(KPa)}$	$\varepsilon_Y(\%)$	$\varepsilon_P(\%)$	Y^{calc}	$P^{calc}_{(KPa)}$	$\varepsilon_Y(\%)$	$\varepsilon_P(\%)$
0.0000	0.0000	103.32	0.000	102.72	—	—	0.000	102.72	—	—
0.0970	0.0395	96.96	0.0874	102.29	−121.2	−5.5	0.0383	96.55	3.0	0.42
0.1972	0.0820	90.71	0.1575	100.82	−92.0	−11.1	0.0776	90.48	5.4	0.25
0.2972	0.1253	84.62	0.2097	98.63	−61.9	−16.6	0.1179	84.40	5.9	0.26
0.4185	0.1758	77.84	0.2513	95.75	−42.9	−23.0	0.1694	77.04	3.6	1.0
0.5080	0.2158	72.64	0.2672	94.25	−23.8	−29.7	0.2114	71.33	2.0	1.8
0.7414	0.3488	57.28	0.2513	97.87	27.9	−70.9	0.3557	55.42	−2.0	3.2
0.8184	0.4282	50.30	0.2324	103.65	45.7	−106.0	0.4337	48.33	−1.3	3.9
0.8672	0.5037	44.96	0.2225	107.19	55.8	−138.4	0.5013	43.66	0.47	2.9
0.9126	0.5982	39.20	0.2234	106.89	62.7	−172.7	0.5882	39.11	1.7	0.23
0.9146	0.6074	39.03	0.2244	106.38	63.0	−172.5	0.5959	38.40	1.9	1.6
1.0000	1.0000	25.00	1.000	24.75	—	—	1.000	24.75	—	—
Average relative errors			—	—	59.7	74.6	—	—	2.7	1.6

Table 5

α_c and m Parameters

Substance	m	α_c	Estimations
Water	0.35	8.15	at $P = 1$ atm; $T_f = 373.15$ K; $\rho_L = = 957.492\ \text{kg/m}^3$
Methanol	0.48	9.50	at $P = 1$ atm; $T_f = 337.8$ K; $\rho_L = = 750.0\ \text{kg/m}^3$
Ethanol	0.705	8.933	α_c eq. (5); m at $T = 323.15$ K
n-Hexane	0.47	7.24	α_c eq. (5); m at $T = 323.15$ K

b) the interaction parameters evaluated from the activity coefficient at infinite dilution, γ_i^∞ (equations (20—21)), calculated by the Wilson model. Wilson's parameters and γ_i^∞ values for each temperature are presented in table 6.

Table 6

Wilson's parameters and γ_1^∞ (Wilson) for water-methanol system

T (K)	$\lambda_{12}-\lambda_{11}$ (cal/mol)	$\lambda_{21}-\lambda_{22}$ (cal/mol)	γ_1^∞	γ_2^∞
308.15	414.35	21.53	1.5530	2.0204
323.15	448.36	36.76	1.6040	2.1228
338.15	453.13	106.68	1.6292	2.2803

The relative errors of calculated pressure and of vapour compositon as well as the average errors at each temperature for (a) and (b) cases, are presented.

A significant improvement of the calculated pressure and vapour phase composition values was obtained when the interaction parametres are estimated from γ_i^∞ (Wilson). The average errors of the calculated results are reduced from 60—100% values to 1—4% values.

For the water-methanol system, the other mixing rules with two interaction parameters (equations (6a, 6c, 10, 6d)) lead to almost identical results.

Table 7 presents the activity coefficient values at $T = 338.15$ K calculated by the equation of state (1) in two situations: a) at $P = 0$ aed b) at $P = P_{\text{equilibrium}}$ (calculated bubble-pressure). For calculations, we have used values of k_{ij} estimated from γ_i^∞ (Wilson), in both cases. As can be seen, from the data presented in table 7, the pressure has a negligible influence on the values of activity coefficients. The last columns

Table 7

The activity coefficients values at $T = 338.15$ K calculated by: a) equation of state (1) at $P = P^{\text{calc}}_{(\text{equil.})}$ b) equation of state (1) at $P = 0$; c) Wilson's model

X	$P^{\text{calc}}_{(\text{KPa})}$	Eq. of state (1)		Eq. of state (1)		Wilson model	
		$\gamma_1(P = P^{\text{calc}})$	$\gamma_2(P = P^{\text{calc}})$	$\gamma_1(P = 0)$	$\gamma_2(P = 0)$	γ_1	γ_2
0.0000	102.72	1.6292	1.000	1.6292	1.0000	1.6292	1.0000
0.0970	96.55	1.5442	1.0034	1.5433	1.0034	1.5355	1.0030
0.1972	90.48	1.4447	1.0147	1.4463	1.0147	1.4445	1.0137
0.2972	84.40	1.3619	1.0350	1.3598	1.0356	1.3598	1.0342
0.4185	77.04	1.2684	1.0769	1.2670	1.0774	1.2657	1.0767
0.5080	71.33	1.2064	1.1219	1.2059	1.1245	1.2027	1.1254
0.7414	55.42	1.0747	1.3633	1.0746	1.3721	1.0690	1.3779
0.8184	48.33	1.0459	1.5443	1.0514	1.5343	1.0372	1.5348
0.8672	43.66	1.0316	1.6868	1.0242	1.6793	1.0211	1.6688
0.9126	39.11	1.0181	1.8649	1.0115	1.8593	1.0097	1.8279
0.9146	38.40	1.0116	1.8848	1.0109	1.8685	1.0093	1.8359
1.0000	24.75	1.000	2.2803	1.000	2.2803	1.0000	2.2803

fo the table give activity coefficients γ_1 and γ_2, calculated by Wilson's model. The values predicted by the EOS method are very close to those obtained with Wilson's model.

The estimated method of the interaction parameters from the activity coefficients at infinite dilution was also tested for the second system: ethanol + n-hexane (azeotropic system). In this case, the results were not very satisfactory, in comparison with the computation results based on zero values of interaction parameters. The average errors in pressure for different temperatures remained high, in the range of 20–25%. The results can be improved using an estimation of the interaction parameters from the azeotropic point. In this case, the average errors in pressure were in the range of 3–7%. The discussion and the results obtained by this method for ethanol + n-hexane system will be presented in another paper.[14]

An explanation for the failure of the first method (the estimation of k_{ij} from γ_i^∞) for this system (and also for other systems, probably) can be given by Figs 1 and 2. In these figures, the dependence of the activity coefficients, γ_1 and γ_2, of the composition, at $T = 323.15$ K was represented. The activity coefficients were calculated by:

(o) the G^E model of Knox-van Ness-Hollinger (KNH).[15] The results obtained with this model were very close to the experimental values $\bar{\varepsilon}_p = 0.3\%$);

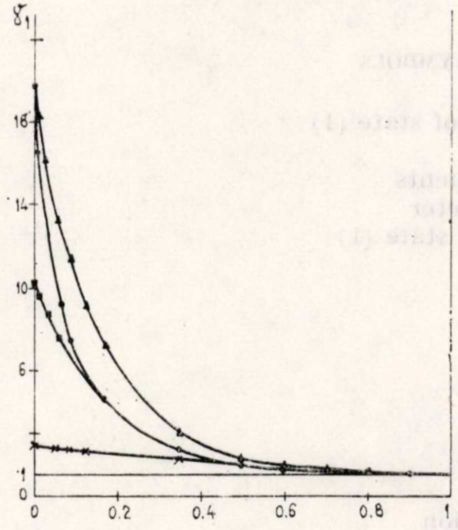

Fig. 1. — Dependence γ_1 *versus* X_1, for ethanol + n-hexane system at 323.15 K.

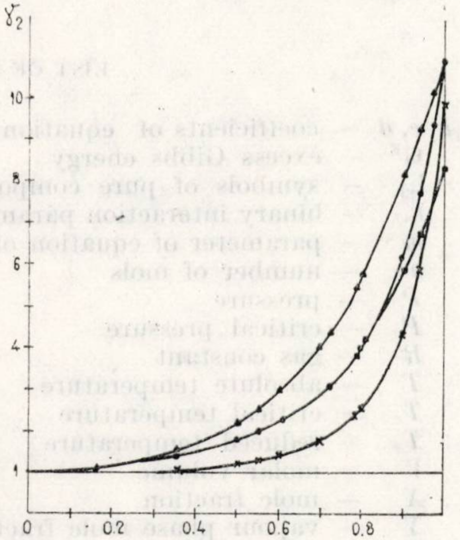

Fig. 2. — Dependence γ_2 *versus* X_1, for ethanol + n-hexane system at 323.15 K.

(x) the equation of state with $k_{ij} = 0$;

(△) the equation of state with $k_{12} = 0.004$ and $k_{21} = 0.192$, estimated values from γ_i^∞(KNH);

(□) the equation of state with $k_{12} = -0.0074$ and $k_{21} = 0.131$, estimated values from azeotropic point.

It is observed that a good prediction of γ_1 and γ_2 values, close to that obtained by the first method, is possible with the equation of state for the case when k_{12} and k_{21} are evaluated from azeotropic point.

The γ_1 and γ_2 values predicted by the equation of state with k_{12}, k_{21} estimated from γ_i^∞(KNH) are different from those obtained with the first method, although the starting points are the same: γ_1^∞(KNH) and γ_2^∞ (KNH).

The γ_1 and γ_2 values computed by the equation of state with k_{12}, $k_{21} = 0$ are completely different from all the other calculations types (γ_1 especially).

The testing of the general cubic equation of state in VLE computation at low pressures gives promising results. The estimation of the interaction parameters from values γ_i^∞(experimental or evaluated from the activity models) ensures for some systems results in good agreement with the experimental ones. At the same time, the behaviour of other-systems (with high nonideality) is unsatisfactorily predicted in comparison with the activity models.

This situation is also mentioned by other authors [4] with different EOS.

The improvement of the mixing rules will ensure in future better results in the computation of vapour-liquid equilibria with EOS, at low pressures.

LIST OF SYMBOLS

a*, *b*, *c*, *d — coefficients of equation of state (1)
G^E — excess Gibbs energy
i,j — symbols of pure components
k_{ij} — binary interaction parameter
m — parameter of equation of state (1)
n — number of mols
P — pressure
P_c — critical pressure
R — gas constant
T — absolute temperature
T_c — critical temperature
T_r — reduced temperature
V — molar volume
X — mole fraction
Y — vapour phase mole fraction
Z_c — critical compressibility factor
α_c — Riedel's criterion
γ — activity coefficient
γ^∞ — activity coefficient at infinite dilution
ε — relative error
$\bar{\varepsilon}$ — average relative error
σ — standard deviation
ρ_L — liquid density
λ — Wilson parameter

REFERENCES

[1] M. J. Huron and J. Vidal, *Fluid Phase Equil.*, **3**, 255(1979).
[2] P. M. Mathias and T. W. Copeman, *Fluid Phase Equil.*, **13**, 91 (1983).
[3] M. Goral, A. Maczynski, G. Schmidt and H. Wenzel, *Ind. Eng. Chem. Fundam.*, **20**, 267 (1981).
[4] J. Schwartzentruber, L. Ponce-Ramirez and H. Renon, *Ind. Eng. Chem. Process Des. Dev.*, **25**, 804(1986).
[5] D. Geană, *Rev. Chim. (Bucureşti)*, **37**, 303 (1986); **37**, 951(1986); **38**, 975(1987).
[6] D. Geană, V. Feroiu and O. Landauer, *Rev. Roumaine Chim.*, **32**, 863 (1987).
[7] D. Geană, V. Feroiu and O. Landauer, *Rev. Chim. (Bucureşti)*, **38**, 887 (1987).
[8] V. Feroiu, D. Geană and O. Landauer, *Rev. Chim. (Bucureşti)*, in print.
[9] R. Stryjek and J. H. Vera, *Fluid Phase Equil.*, **25**, 279 (1986).
[10] H. C. van Ness, "Classical Thermodynamics of Nonelectrolyte Solutions", Pergamon, New York, 1969.
[11] M. L. Mc Glashan and A. G. Williamson, *J. Chem. Eng. Data*, **21**(2), 196(1976).
[12] R. C. Reid, J. M. Prausnitz and T. K. Sherwood, "The Properties of Gases and Liquids", 3rd Edition, McGraw-Hill, New York, 1977.
[13] A. Fredenslund, J. Gmehling and P. Rasmussen, "Vapor-Liquid Equilibria using UNIFAC", Elsevier, Amsterdam, 1977.
[14] V. Feroiu, D. Geană and O. Landauer, *Rev. Chim. (Bucureşti)*, in print.
[15] D. E. Knox, H. C. van Ness and H. B. Hollinger, *Fluid Phase Equilibria*, **15**, 267(1984).

Revue Roumaine de Chimie, **34**, *6*, 1341–1350 (1989)

NUCLEAR MAGNETIC RESONANCE INVESTIGATIONS OF SMALL RINGS. 6

THE STEREOCHEMISTRY OF CYCLOADDITION OF *t*-BUTYLCYANOKETENE TO NORBORNENE DERIVATIVES. A MULTICENTER APPROACH FOR ESTABLISHING THE CONFIGURATION WITH THE AID OF EUROPIUM SHIFT REAGENT OF SOME POLYCYCLIC α-*t*-BUTYL-α-CYANOCYCLOBUTANONES[1]

MIRCEA D. GHEORGHIU, CONSTANTIN DRĂGHICI, LUMINITZA PÂRVULESCU
and MIHAI ELIAN[+]
Department of Organic Chemistry, Polytechnic Institute, *76206* Bucharest–16, Romania

Received November 23, 1988

The stereochemistry of cyclobutanones obtained from the norbornene derivatives 1–6 with t-butylcyanoketene has resulted from the McConnell-Robertson pseudocontact model for the lanthanide induced chemical shift, as having the cyclobutanone ring in *exo*-configuration and the t-butyl group pointing toward the methylene bridge. The *exo*-configuration of cyclobutanone and α-configuration * of t-Bu group gave the best Hamilton factor, while the other models having the cyclobutanone ring and the t-Bu in *exo*-β, *endo*-α and *endo*-β configurations were rejected for the lack of concordance with experimental values. The *exo*-α configurations for the cyclobutanones 8–13 have resulted from co-ordination models of europium with the two lone pairs of oxygen (total population 63 %) and the lone pair of nitrogen (37 % population).

INTRODUCTION

We believe that the norbornene system is a powerful substrate for the study of the reaction mechanism of ketene cycloadditions. However, the set of stereochemical variables are enlarged if the ketene is asymmetric. Unfortunately cycloadditions of norbornene derivatives with asymmetric ketenes as stereochemical gauges for reaction mechanism are virtually unexplored.[2]

Conclusions regarding the reaction mode of norbornene derivatives with an asymmetric ketene could be obtained if several factors are con-

---

[+] decesead September 1988.

* *exo*- refers to the configuration of the cyclobutanone ring with respect to the norbornane skeleton.

α- (as suggested by Chem. Abstr. conventions) is the configuration of t-B ugroup point ing toward the methylene bridge.

sidered when experimental facts are analyzed. Thus is the reaction is concerted occurring according to ${}_{2}\pi_{s} + {}_{2}\pi_{a}$ mode, an *exo*-cyclobutanone, with α-configuration for the largest ketene substituent should be observed as the sole reaction product. A nonconcerted path would lead to any of the products containing either cyclobutanones with *exo*-β, *endo*-α, *endo*-β configurations or/and the transposed products T.

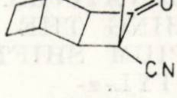

exo-α

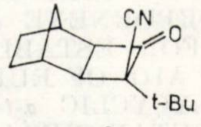

exo-β

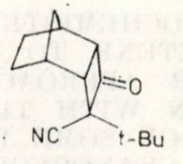

endo-α

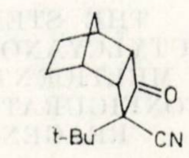

endo-β

The latter compounds would result from the zwitterionic intermediate I, if the addition of ketene to norbornene were a stepwise reaction.

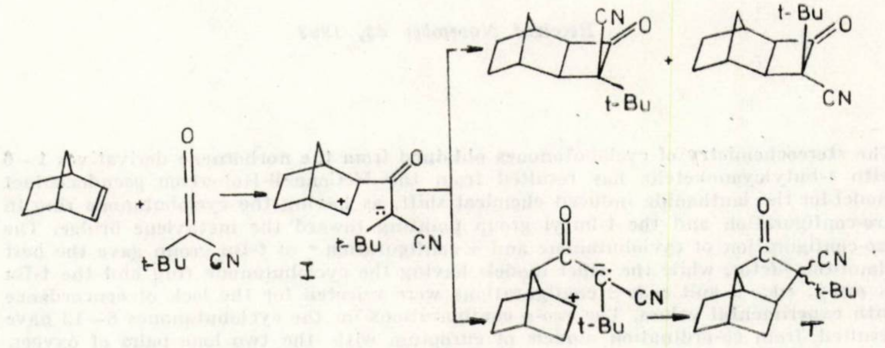

The reported reaction of t-butylcyanoketene (TBCK) with norbornadiene by Brook and our studies [2b,2c,2d] carried out with norbornene **1**–**6** have revealed the formation of cyclobutanones adducts with *exo*-configuration. In the only case of norbornadiene, two reaction products were isolated. In this particular case, the cyclobutanone **9** was accompanied by the 2+2+2 reaction product **7**. Both 2+2 and 2+2+2 cycloaddition products should be regarded as normal outcomes due to the well known ambient reactivity of norbornadiene.[3]

In this report we would like to present our results regarding $Eu(fod)_3 \cdot {}^2H_{27}$ dopped ^{1}H-NMR spectra of cyclobutanones obtained from norbornane derivatives **1**–**6** and TBCK. The stereochemistry of 2+2 adducts has resulted from the comparison of europium induced shifts of the norbornane skeleton protons from compounds **8**–**13**, with those calculated from McConnell-Robertson relationship.[4] As will be shown below, the best fit with experimental result was obtained only if the stereochemistry of cyclobutanones are *exo*- and the t-Bu group has α-configuration. The best model for co-ordination is multicenter, e.g. a time-averaged lanthanide-induced shifts resulted from three discrete rapidly interconverting complexes. The complexation of the shift reagent was supposed to occur unequally on the two pairs of sp^2 hybridized oxygen and on the the lone pair of the nitrogen from the cyano group. The one

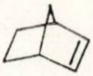
1

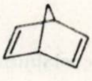
2

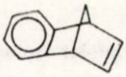
3

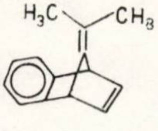

4

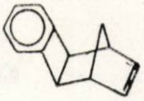
5

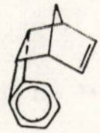
6

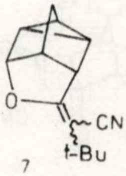

7

site complexation model, assuming a single complex, only at oxygen gave a less satisfactory fit of the calculated versus experimental values for the europium induced shifts.

RESULTS AND DISCUSSION

A. The NMR spectra of cyclobutanones 8—13 in presence of shift reagent

The ^1H-NMR spectra of cyclobutanones **8—13** were recorded in carbon tetrachloride by adding incrementally the shift reagent $Eu(fod)_3 \cdot {}^2H_{27}$. The highest molar ratio substrate/shift reagent (S/SR) was 0.4. In each case good correlation ($R^2 = 0.99$) between the induced chemical shift and the molar ratio S/SR was obtained. The molar induced shift (MIS) and the Hamilton factor as fit criteria [5a] were chosen by us as parameters for characterization of coordination. We have manipulated normalized values of MIS in order to level-off any of the biases originated in fortuitous change in the anhydrous conditions during experimental determination.[5b] All reported values are normalized to the MIS of H_2 and are collected in Table 1. Since the relative MIS (hereafter abbreviated RMIS) are virtually identical for the cyclobutanones **8—13** we are entitled to predict a similar configuration for the cyclobutanone ring and that of t-butyl group in all the compounds. We have chosen for simulation the experimental results associated with compound **9** presented in Table 1.

B. The geometrical model for the cyclobutanones 8—13

According to the methodology, the theoretical calculated MIS require the coordinates of the hydrogen atoms. To our best knowledge there are no literature data regarding the geometry of the annulated cyclobutanones **8—13** or of related compounds. Therefore the geometrical data for our model is a composite resulted from informations based on electron diffraction,[6] X-ray[7], microwave[8], force-field calculations[9] for norbornane skeleton and by microwave [10] and NMR studies in liquid crystals [11] for the cyclobutanone fragment. The resulted hybrid geometry is presented in fig. 1. The C-C bonds from norbornane fragment were taken equal with 1.55 Å, the same distances, but in the planar cyclobutanone fragment are present also in fig. 1a. The carbon-nitrogen triple bond distance was taken

Table 1

Relative molar induced shifts for cyclobutanones

Compound	H_1	H_2	H_3	H_4	H_{7s}	H_{7a}	t-Bu
8 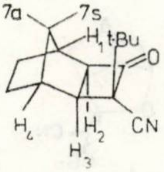 7a 7s H_1 t-Bu O H_4 H_2 CN H_3	0.29	0.47	1	0.82	0.50	-	0.65
9 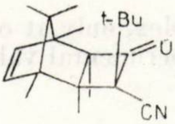	0.28	0.41	1	0.80	0.52	0.27	0.66
10 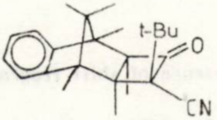	0.31	0.43	1	0.84	0.55	0.30	0.71
11 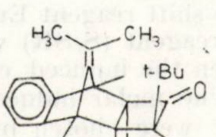	0.27	0.41	1	0.76	-	-	0.70
12 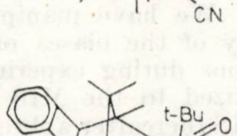	0.27	0.42	1	0.77	0.49	0.27	0.61
13 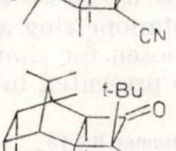	0.30	0.42	1	0.83	0.49	0.26	0.52

equal with 1.162.[12] All carbon-hydrogen bond lengths were considered 1.09 Å. The bridgehead hydrogens H_1 and H_4 were considered coplanar with $C_1-C_7-C_4$ bridge skeleton. The hydrogens H_{7a} and H_{7s} were placed in an orthogonal plane to the $C_1-C_7-C_4$. The hydrogens H_2 and H_3 are in the plane bisecting the dihedral angle γ. The plane containing the cyano group is bisecting the adjacent cyclobutanone angle.

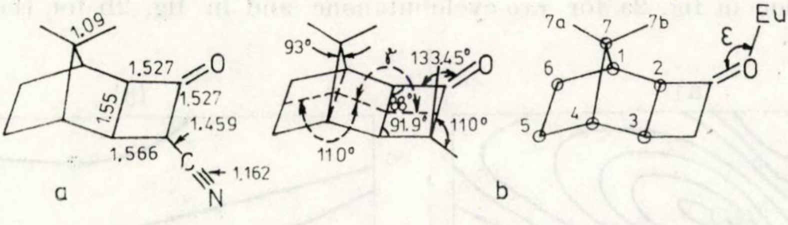

Fig. 1. — The geometry for the model of compounds 9 (a) some bond distances (b) relevant bond and dihedral angles.

C. The Eu-cyanocyclobutanone complex

We have analyzed two models for Eu-substrate complex. The simplest model was based on the assumption that only the carbonyl group is the site of co-ordination. Indeed literature precedences are suggesting that the carbonyl group is a stronger Lewis base than the cyano group,[13] the competing group contained in the structures **8**—**13**. This assumption has been proved to be unsatisfactory. It gave a very soft agreement factor surface, with high values for the agreement factor. For the *exo*-configuration of the cyclobutanone ring, the agreement factor has its lowest value at 12%, and is only slightly better than that obtained for the *endo*-configuration, when the agreement factor is 15.8%.

Encouraged by the good results obtained when the carbonyl group was treated as a two coordinating site[14] and considering the cyano group competitive with the carbonyl group, we have designed a better model for the Eu-substrate complex. With these assumptions, both the configuration of the cyclobutanone ring and that of the cyano group were within reach. Moreover it was very gratifying that the best agreement factor has resulted from a good minimum on the agreement factor surface. Before proceeding to discuss the numerical results, let us look very briefly at preliminary experimental results regarding the $>C=O$ versus $-C\equiv N$ competition in coordinating the europium complex. Experimental determination performed on acetonitrile-acetone and benzocyclobutanone-acetonitrile mixture have revealed that $Eu(fod)_3$, coordinates significantly (15—30%) at the nitrogen atom.[15] Therefore, we believe that the cyano group although a weaker Lewis base than a carbonyl group, cannot be discarded, even in a very rough framework of approximation as it was previously suggested.[13]

The numerical experiments, presented in detail in the experimental part, were carried out in two distinctive steps, having as aim the calculation of the d_1 (O — — —Eu) distance, the bond angle ε defined by the atom $>C=O$— — —Eu, and the dihedral angle γ between the norbornane skeleton and the cyclobutanone ring.

The first step was devoted to search the best ε and γ for all the four configurations *exo*-α, *endo*-α, *exo*-β, *endo*-β. During this search d_1

was allowed to be 2.5Å and then 3Å, while d_2 was kept at 2Å. These figures are popular for >C=O———Eu and —CN———Eu distances[16] respectively. The results of calculations are featured as graphical representation in fig. 2a for *exo*-cyclobutanone and in fig. 2b for the *endo*-isomer.

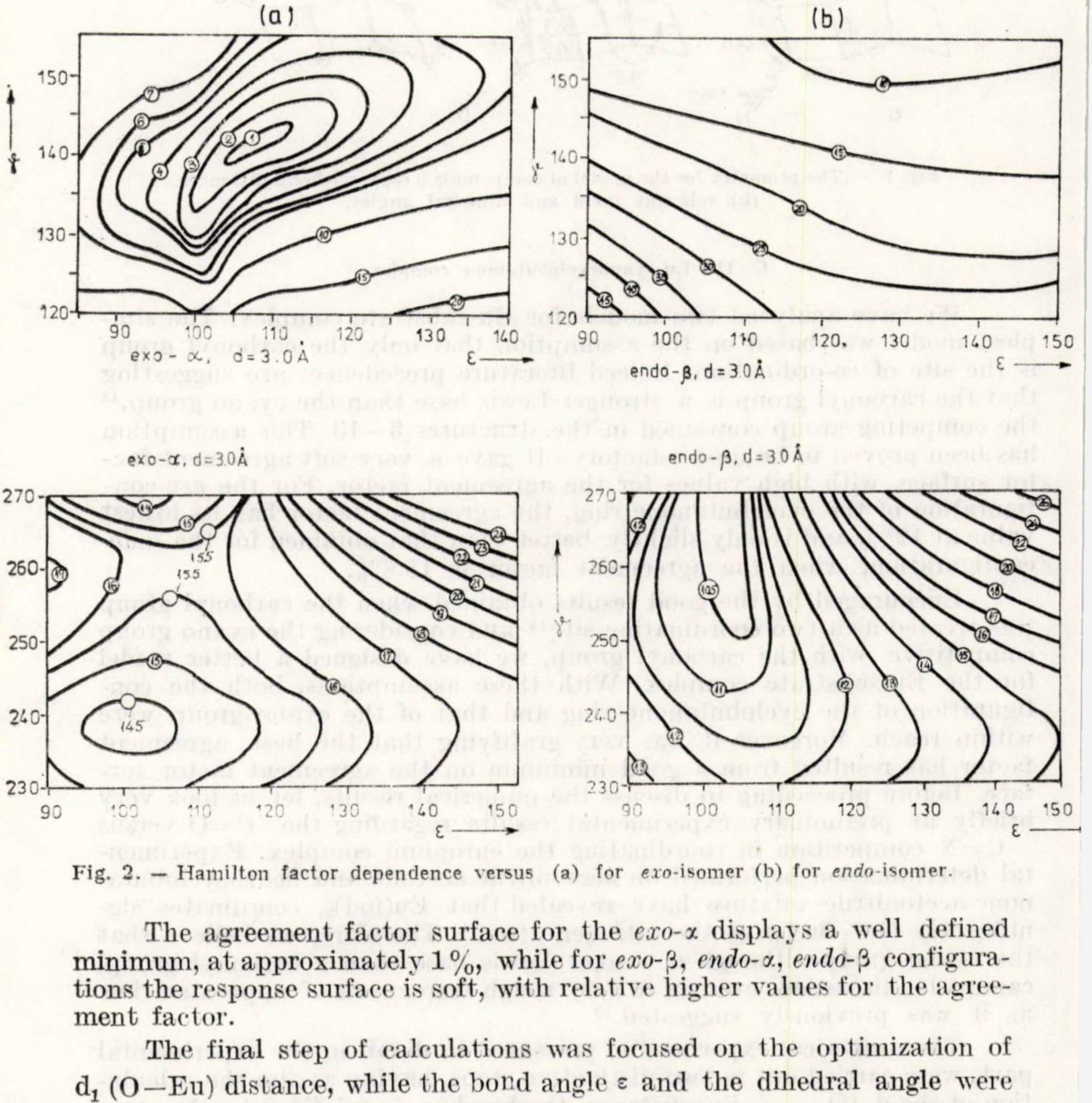

Fig. 2. — Hamilton factor dependence versus (a) for *exo*-isomer (b) for *endo*-isomer.

The agreement factor surface for the *exo-α* displays a well defined minimum, at approximately 1%, while for *exo*-β, *endo*-α, *endo*-β configurations the response surface is soft, with relative higher values for the agreement factor.

The final step of calculations was focused on the optimization of d_1 (O—Eu) distance, while the bond angle ε and the dihedral angle were kept at their best values obtained in the previous stage of calculations. The d_1 parameter was varied within the 2.0—4.0 Å range. The results obtained are presented for both configurations in Fig. 3. In Table 2 are collected the final values for the geometrical parameters d_1, ε and

γ for all the configurations of cyclobutanone fragment and that of cyano groups.

The *exo*-α configuration of cyclobutanone and that of t-butyl group gave the most satisfactory agreement with the experimental results (see Table 3). All the other configurations have either higher values or unacceptable values for the agreement factor. Note also the reasonable bond

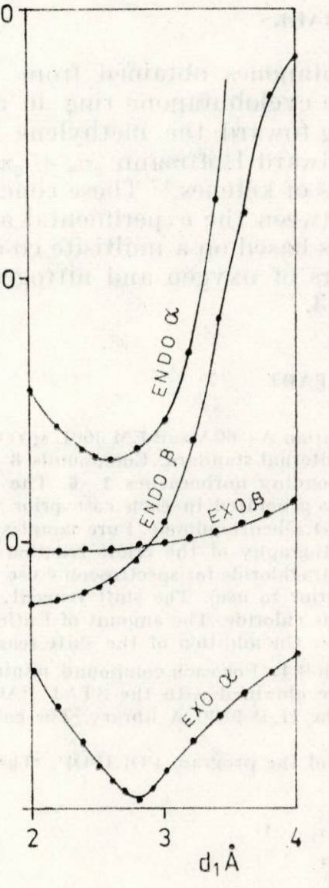

Fig. 3. — The dependence of agreement factor (AF) versus Eu-O distance for *exo*- and *endo*-oriented cyclobutanone.

Table 2

The best values of the agreement factor for configurations *exo*-α, *exo*-β, *endo*-α and *endo*-β.

	H	d_1(Å)	γ	ε
exo-α	0.26	2.8	140	110
exo-β	9.64	2.2	155	140
endo-α	13.20	2.5	270	110
endo-β	7.70	2	270	105

Table 3

Experimental and calculated MIS values for the α-t-butyl-*exo* oriented cyclobutanone (g).

	MIS		RMIS	
	exp.	calc	exp	calc
H_1	1.43	1.44	0.28	0.28
H_2	2.12	2.12	0.41	0.41
H_3	5.13	5.13	1.00	0.99
H_4	4.12	4.11	0.80	0.80
H	2.68	2.69	0.52	0.52
H	1.40	1.41	0.27	0.27

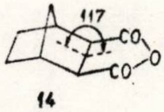

14

angle >C=O — — —Eu of 110°, excepted if the coordination of the lanthanide occurs with the pairs of nonbonded electrons located in an sp^2 orbital. The dihedral angle γ, (140°) apparently is too large, if compared with the same angle (117°) found in the anhydride 14, by X-ray diffraction.[7] We believe that this outcome is originated in the steric repulsion among the $-CH_2-$ bridge and the α-oriented t-Bu group, although $\gamma = 140°$, is somewhat exaggerated.

The total population at the oxygen atom is 0.63, while the nitrogen has 0.37. Our calculations therefore are supporting the view mentioned in the literature concerning that C=O is a stronger Lewis base than the C≡N. However, we would like to point out that the latter group is a good competitor with the former, when europium shift reagent is added to a compound containing both functions.

CONCLUDING REMARKS

The stereochemistry of the cyclobutanones obtained from TBCK and norbornene derivatives **1**—**6** have the cyclobutanone ring in an *exo*-configuration and the t-Bu group pointing toward the methylene bridge. This outcome is in accord with the Woodward-Hoffmann $_{2}\pi_{s} + {}_{2}\pi_{a}$ reaction mode for the concerted cycloadditions of ketenes.[17] These conclusions have resulted from the remarkable fit between the experimental and the calculated MIS. The theoretical model was based on a multisite co-ordination of $Eu(fod)_3 \cdot {}^2H_{27}$ with the lone pairs of oxygen and nitrogen from the α-t-butyl-α-cyanocyclobutanones **8**—**13**.

EXPERIMENTAL PART

The ^1H—NMR spectra were recorded with a Varian A—60A and EM 360L spectrometers in carbon tetrachloride using tetramethylsilane as internal standard. Compounds **8**—**13** were obtained by cycloaddition of TBCK to the corresponding norbornenes **1**—**6**. The cyloadditions were carried out in refluxing benzene. TBCK was generated in each case prior to alkene addition, by thermolysis of 2,5-diazido-3,6-di-t-butyl-1,4-benzoquinone. Pure samples of cyclobutanones **8**—**13** were obtained by column chromatography of the crude reaction products on silicagel, using benzene as eluent.[2d] The carbon tetrachloride for spectroscopic use was kept on anhydrous sodium carbonate (minimum 48 hrs prior to use). The shift reagent, $Eu(fod)_3$ $^2H_{27}$ (Merck) was freshly recrystallized from methylene chloride. The amount of $Eu(fod)_3 \cdot {}^2H_{27}$ resulted from weighting the NMR tube prior and after the addition of the shift reagent. The maximum molar ratio substrate/shift reagent was $0.3\overline{m}\ 0.4$. For each compound minimum five determinations were recorded. The MIS values were obtained with the STAT PAC VOL 1 (linear regression program Hewlett-Packard) from the H P 9830 A library. The calculations were done with a HP—9830A calculator.

The MIS values were calculated with the aid of the program POLIPOP. The program makes use of the McConnell-Robertson equation.

$$M_i = k \frac{3 \cos^2 \alpha_i - 1}{r_i^3} \qquad (1)$$

$$H = 100 \sqrt{\frac{\sum_i (MIS_{exp} - MIS_{calc})_i^2}{\sum_i (MIS_{exp})_i}} \qquad (2)$$

where r_i is distance between hydrogen atom H_i and the Eu atom, and α_i define the angle H_i...hereto atom (O or N)...Eu. The fitness criteria have resulted from Hamilton factor calculated with equation (2) by using experimental (exp) and calculated (calc) MIS values.

For the multicenter complexation equation (1) becomes

$$M_i = k \sum_{j=1}^{m} P_j S_{ij} = \sum_{j=1}^{m} k_j S_{ij} \qquad (3)$$

$$k_j = k \cdot p_j \qquad (4)$$

where j represents the complexation site (j = 1 ... m) and i the hydrogen atoms (i = 1 ... n); p_j — the population on each complexation site :

$$\sum_{j=1}^{m} p_j = 1 \qquad S_{ij} = \frac{3\cos^2\alpha_{ij} - 1}{r_{ij}^2} \tag{5}$$

S_{ij} is resulting from (5);
all other variables having the same meaning as above.

With the condition

$$\sum_{i=1}^{n}\left(M_i - \sum_{j=1}^{m} k_j S_{ij}\right)^2 = \text{minimum} \tag{6}$$

after a simple algebra one obtains :

$$\begin{vmatrix} k_1 \\ \vdots \\ k_m \end{vmatrix} = \text{INV} \begin{vmatrix} \sum S_{i1}^2 & \dots \sum S_{i1}S_{i2} & \dots \sum S_{i1}S_{im} \\ \vdots & \vdots & \\ \sum S_{im}S_{i1} & \dots \sum S_{im}S_{i2} & \dots \sum S_{im}^2 \end{vmatrix} \times \begin{vmatrix} \sum S_{i1}M_i \\ \vdots \\ \sum S_{im}M^i \end{vmatrix} \tag{7}$$

INV meaning the inverse matrix.

Having the k_j from (7) one can obtain population p_j from (9) and the calculated MIS rom (10) :

$$k = \sum_{j=1}^{m} k_j \tag{8}$$

$$P_i = \frac{k_i}{k} \tag{9}$$

$$m_i = \sum_{j=1}^{m} k_j S_{ij} \tag{10}$$

Therefore Hamilton factor becomes :

$$H = 100 \times \sqrt{\frac{\sum_{i=1}^{n} (M_i - m_i)^2}{\sum_{i=1}^{n} M_i^2}}$$

REFERENCES

[1] a) Taken in part from the Ph. D. Thesis of C. D. (Center of Organic Chemistry, Bucharest 1980);

b) For the previous paper: M. D. Gheorghiu, M. Mihai, L. Pârvulescu, A. Vaios and M. Elian, *Rev. Roum. Chim.*, **32**, 1181 (1987).

[2] a) R. C. DeSelms and F. Delay, *J. Org. Chem.*, **37**, 2908 (1972), and the literature cited therein. For the reaction of TBCK with 1 :b) M. D. Gheorghiu, P. Filip, C. Draghici and L. Pârvulescu, *J. Chem. Soc. Chem. Commun.*, 635 (1975); c) with 3—6 : M. D. Gheorghiu, C. Drăghici and L. Pârvulescu, *Tetrahedron*, **33**, 3295 (1977); d) with 2 : P. R. Brook and K. Hunt, *J. Chem. Soc. Chem. Commun.*, **1974**, 989; L. Pârvulescu, Ph. D. Thesis (Polytechnic Institute, Bucharest, 1980).

[3] *See inter alia* : cycloaddition of propynoic ester activated by Lewis acids ; H. Fienemann and H. M. R. Hoffman, *J. Org. Chem.*, **44**, 2802 (1979); cycloaddition of carbene : G. W. Klumpp and P. M. Kwantes, *Tetrahedron Lett.*, **22**, 831 (1981); K. N. Houk,

N. G. Rondon, M. N. Paddon-Row, C. W. Jefford, P. T. Huy, P. D. Burrow and K. D. Jordan, *J. Amer. Chem. Soc.*, **105**, 5563 (1983); for reaction with triazolinediones: W. Adam, L. A. Arias and O. de Lucchi, *ibid.*, **23**, 399 (1982). For the cycloaddition of benzyne see: H. Simmons, *J. Amer. Chem. Soc.*, **83**, 1657 (1961); M. N. Paddon-Row and R. Hartcher, *ibid.* **102**, 662 (1980).

[4] H. M. McConnell and R. E. Robertson, *J. Chem. Phys.*, **29**, 1361 (1958).

[5] a) M. R. Willcott III, R. E. Lenkinski and R. E. Davies, *J. Amer. Chem. Soc.*, **94**, 1742 (1972); R. E. Davies and M. R. Willcott III, *ibid.*, **94**, 1744 (1972); b) for a similar view: J. Epsztajn, A. Bienieck, J. Z. Brzezinski and H.-O. Kalinowski, *Tetrahedron*, **42**, 3459 (1986).

[6] J. F. Chaing, C. F. Wilcox Jr., S. H. Bauer, J. *Amer. Chem. Soc.*, **90**, 3149 (1968); A. Yokozeti and K. Kuchitsu, *Bull. Chem. Soc. Jpn.*, **44**, 2356 (1971).

[7] R. Destro, G. Filipini, C. M. Gramaccioli and M. Simmonetta, *Tetrahedron Lett.*, **1969**, 3223, **1968**, 5955.

[8] R. J. Boyd, J-C. G. Bünzliand and J. P. Snyder, *J. Amer. Chem. Soc.*, **98**, 2398 (1976).

[9] E. M. Engler, J. D. Andose and P. von R. Schleyer, *J. Amer. Chem. Soc.*, **95**, 8005 (1973); N. L. Allinger in "Advances in Physical Organic Chemistry", vol. 13 (V. Gold and D. Bethele, eds.), Academic Press, New York, 1976.

[10] L.-R. H. Scharpen and L. W. Laurie, *J. Chem. Phys.*, **49**, 221 (1968).

[11] K. C. Cole and D. F. R. Gilson, *Can. J. Chem.*, **54**, 657 (1976).

[12] M. Haerl and F. L. Harschfeld, *Acta Cryst.*, **B(31)**, 162 (1975).

[13] A. F. Cockerill, G. L. Davies, R. C. Hardon and D. M. Rackham, *Chem. Rev.*, **73**, 553 (1973); R. von Ammon and R. D. Fischer, *Angew. Chem.*, **84**, 725 (1972); J. K. M. Sanders and D. H. Williams, *J. Amer. Chem. Soc.*, **93**, 641 (1971).

[14] R. F. Newman, *Tetrahedron*, **30**, 969 (1974); R. E. Lenkinski and J. Reuben, *J. Amer. Chem. Soc.*, **98**, 4065 (1976): G. Montaudo, S. Caccamese, V. Librando and P. Maravigna, *Tetrahedron*, **29**, 3915 (1973); P. Pinocchiaro, A. Recca, P. Maravigna and G. Montaudo. *ibid.*, **30**, 4159 (1974); S. Caccamese, G. Montaudo and A. Recca, *ibid.*, **30**, 4129 (1974); R. J. Abraham, D. J. Chadwick, L. Griffths and F. Sancassan, *Tetrahedron Lett.*, **1979**, 4691; R. J. Abraham and D. J. Chadwick, *Tetrahedron*, **37**, 1081 (1981); for a critical view on this topic see: D. J. Raber, J. A. Peters and M. S. Nieuwenhnizen, *J. Chem. Soc. Perkin Trans.* II, 853 (1986), and ref 16a.

[15] C. Draghici, M. Elian, M. D. Gheorghiu, unpublished results, see also ref. 1a.

[16] a) for C = O... Eu distance see: D. J. Raber, C. M. Jauks and J. A. Peters, *Tetrahedron*, **42**, 4347 (1986) and references cited therein; b) for CN...Eu distance see: M. D. Johnston, D. J. Raber, N. K. De Gennaro and J. W. Perry, *J. Amer. Chem. Soc.*, **98**, 6042 (1976).

[17] R. B. Woodward and R. Hoffmann, "The Conservation of Orbital Symmetry", Academic Press, New York, 1970, p. 163.

Revue Roumaine de Chimie, **34**, *6*, 1351–1360 (1989)

THE EFFECT OF SEVERAL HINDERED AMINE LIGHT STABILIZERS (HALS) IN OXIDATIVE DEGRADATION OF RUBBER COMPOUNDS *

G. IVAN and MARIA GIURGINCA
Research Institute for Rubber and Plastics Processing, R-79628 Bucharest, Romania

Received February 8, 1988

In various stages of compounding, processing and utilization, rubber compounds are the subject of thermo-oxidative degradation. The improvement of the properties and the enhancement of the durability request an appropriate protection, and a concern exists in this respect for technical as well as economicals reasons. The present work deals with the effect of several HALS additives, as individual protecting agents as well as in association with phenolic and aminic antioxidants. The efficiency of the antidegradants was followed by spectral methods and by evaluation of physical properties of the samples subjected to accelerated ageing. The results, examined from a kinetic point of view, are used to suggest a possible reaction mechanism in achieving the antidegradant protection.

The destruction of rubbers, rubber compounds and vulcanizates during storage of raw rubbers, processing of rubber compounds, and usage of rubber products is a result of the influence of the medium (mechanical forces acting simultaneously with thermal energy and various chemical substances), frequently including the action of light.

Use of antioxidants associated with photostabilizers in protection of elastomers is a rather new concept [1,2] aiming to limit the destructive process by combining the specific effects of both classes : hindered phenols or secondary aromatic amines used as antioxidants react with free radicals and/or nonradical species resulting from hydroperoxides while photostabilizers act as ultraviolet absorbers, desactivating the excited states, and at the same time, as free radical acceptors. For a mixed protection system it is a primordial request to find the optimal ratio of the protecting agents. The present work was conducted in an attempt to investigate the influence of the ratio of HALS and phenolic or aminic antidegradants on the protecting effect in oxidative or ozonant degradation of elastomers.

EXPERIMENTAL

Natural rubber used as elastomer matrix was purified by precipitation from benzene solution. A benzene solution of 1% purified natural rubber containing the antidegradant or a set of antidegradants was used to cast thin films dried in vacuum at room temperature. The infrared spectra of the films with or without antidegradant in the initial stage or after ageing for a given time were recorded in the domain 4000–200 cm^{-1} using a Perkin-Elmer 577 spectrometer. Ageing of the films was realized for periods till 300 hours at temperatures in the range 80–120°C. The protecting agents used in the present work are listed in Table 1.

---

* Based on a paper presented at the conference "Chemicals for Polymers", 28–30 October 1986, Piestany, Czechoslovakia.

Table 1

Antidegradants used in the study

Symbol	Chemical name	Commercial name (Supplier)
Inh-1	N-isopropyl-N′-phenyl-*p*-phenylenediamine	Santoflex IP (Monsanto Chemical Co.)
Inh-2	N-1,3-dimethylbutyl-N′-phenyl-*p*-phenylenediamine	Santoflex 13 (Monsanto Chemical Co.)
Inh-3	2,6-di-*tert*-butyl-4-methyl-phenol	Topanol OC (Imperial Chemical Industries Ltd.)
Inh-4	2,2′-methylene-*bis*-(4-methyl-6-*tert*-butylphenol)	Sumilizer MPD (Sumitomo Chemical Co.)
Inh-5	2,2,6,6,-tetramethyl-4-pyperidinyl-stearate + + 2,2,6,6,-tetramethyl-4-pyperidinyl-palmitate	Dastib 845 (Czechoslovakia)
Inh-6	*Bis*(2,2,6,6-tetramethyl-4-pyperidinyl) sebacate	Tinuvin 770 (Ciba Geigy Co.)

RESULTS AND DISCUSSION

1. Kinetic approach based on spectroscopic data

The individual antidegradants or couples of antidegradants following the experiments presented in Table 2 were used in amounts of up to 2 parts per 100 parts of elastomer, covering a large domain of the ratio antioxidant : photostabilizer.

The 1720 cm^{-1} band assigned for carbonyl/carboxyl groups was followed. The kinetic curves carbonyl/carboxyl absorption *vs.* time supplied the data concerning the induction periods (t_x). Such a parameter offers a valuable information concerning the protecting ability of the studied system. The collected data were used to evaluate the relative activity of the protecting agents (or systems) relatively to the elastomer protected by 2,6-di-*tert*-butyl-4-methylphenol (Inh—3) used as standard. The relative activity was computed using the relation[3,4]:

$$A_r = (t_x - t_0)/(t_s - t_0) \qquad (1)$$

where t_0 is the induction period for the unprotected elastomer; t_s is the induction period for the elastomer protected by standard antidegradant; t_x is the induction period for the elastomer protected by a given antidegradant (or set of antidegradants). The results are listed in Table 3 and the most relevant kinetic curves are presented in Figure 1.

The data presented in Table 3 reveal the following interesting aspects: (i) the diamine antidegradants exhibit long induction periods, clearly superior to phenolic antidegradants; use of Inh—5 (a photostabilizer) as antioxidant reveals that the efficiency is strongly dependent on concentration and it is able to confer a protection comparable with that of diaminic antioxidants at a temperature around 100°C; the protecting ability of the Inh—6 photostabilizer is similar and independent of concentration; (ii) the binary systems with amine antidegradants (the systems 9—12, 17, 18) exhibit induction periods comparable with Inh—5 and superior

Table 2

Experiments for antidegradant testing

System	Components	Composition, parts per 100 parts of natural rubber
0	Purified natural polyisoprene	Nil (reference)
1	Inh-1	2
2	Inh-2	2
3	Inh-3	2
4	Inh-4	2
5	Inh-5	.5
6	Inh-6	.5
7	Inh-5	.2
8	Inh-6	.2
9	Inh-1 + Inh-5	1.5 + .5
10	Inh-1 + Inh-5	1.5 + .2
11	Inh-2 + Inh-5	1.5 + .5
12	Inh-2 + Inh-5	1.5 + .2
13	Inh-3 + Inh-5	1.5 + .5
14	Inh-3 + Inh-5	1.5 + .2
15	Inh-4 + Inh-5	1.5 + .5
16	Inh-4 + Inh-5	1.5 + .2
17	Inh-1 + Inh-6	1.5 + .5
18	Inh-2 + Inh-6	1.5 + .5
19	Inh-3 + Inh-6	1.5 + .5
20	Inh-4 + Inh-6	1.5 + .5
21	Inh-1 + Inh-3 + Inh-5	1 + .5 + .5
22	Inh-2 + Inh-3 + Inh-5	1 + .5 + .5
23	Inh-2 + Inh-4 + Inh-5	1 + .5 + .5
24	Inh-2 + Inh-4 + Inh-6	1 + .5 + .5

Table 3

Kinetic data for the thermo-oxidative degradation of natural rubber protected by various systems

Protection system	Induction period t_i(h) at temperatures		Relative activity A_r at temperatures		Relative stability S_r at temperatures	
	100°C	120°C	100°C	120°C	100°C	120°C
0 (Nil)	17	8	—	—	—	—
1	110	40	6.2	8.0	.72	.15
2	130	50	7.5	4.1	.68	.11
3	32	15	1.0	1.0	.86	.71
4	80	25	4.2	2.4	.70	.40
5	125	25	7.2	2.4	.34	.50
6	120	20	6.9	1.7	.21	.12
7	50	20	4.1	1.7	.49	.50
8	120	20	6.9	1.7	.17	.12
9	130	50	8.7	6.0	.12	.16
10	100	40	5.5	4.6	.38	.22
11	147	75	8.7	9.6	.11	.14
12	120	35	6.9	3.9	.34	.22
13	116	27	6.7	2.7	.46	.63
14	60	13	2.9	.7	.43	.71
15	115	45	6.5	1.9	.40	.60
16	65	25	3.2	2.4	.42	.65
17	180	90	10.9	11.7	.15	.16
18	240	150	14.9	20.3	.12	.04
19	100	45	5.5	5.3	.41	.70
20	75	25	4.5	2.4	.28	.20
21	75	30	3.9	3.1	.73	.32
22	85	27	4.5	2.7	.74	.22
23	100	45	5.5	5.3	.70	.25
24	250	90	15.5	11.3	.24	.20

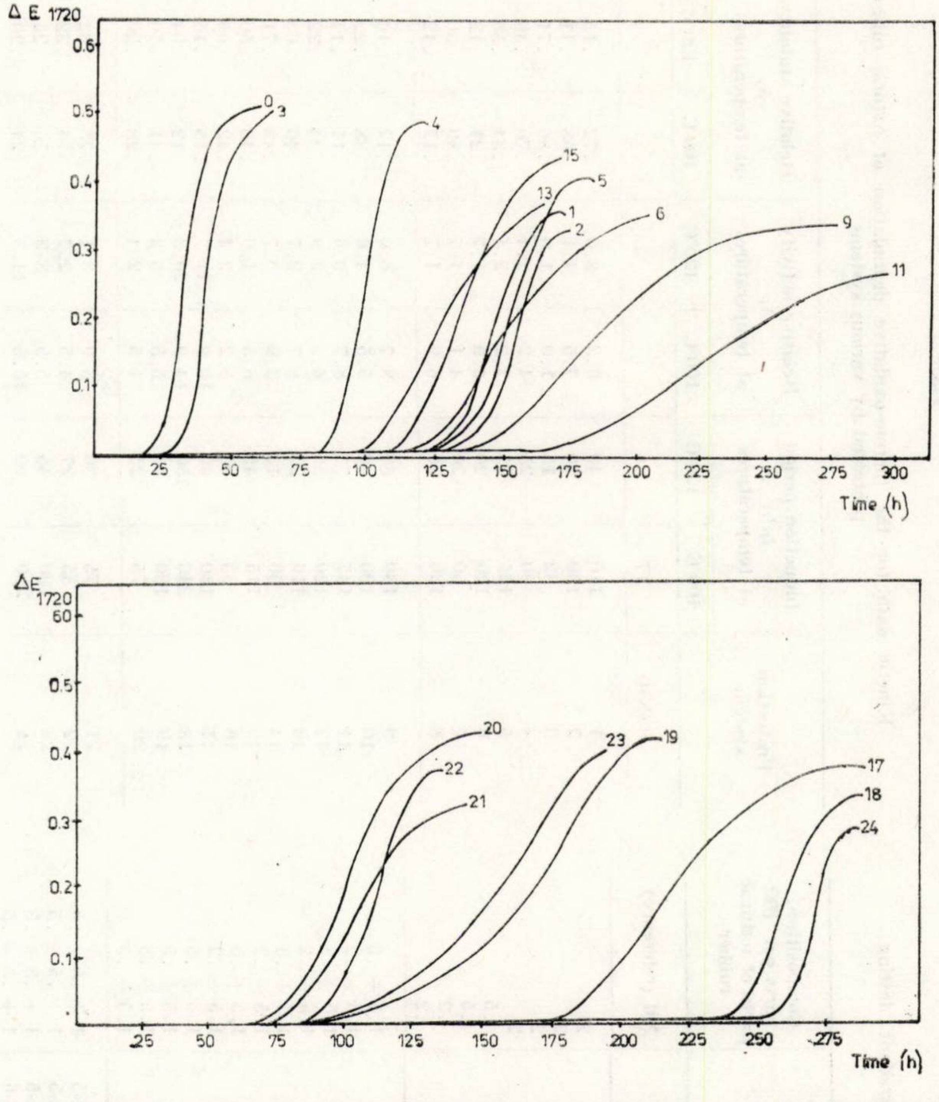

Fig. 1. — Variation of the content of carbonyl/carboxyl groups in unprotected natural rubber and in natural rubber protected by individual antidegradants and by binary and ternary systems of antidegradants (ageing in oven at 100°C). Numbers on the curves are explained in Table 2.

to Inh—6 ; (iii) the binary systems with phenolic antioxidants (the systems 13—16, 19, 20) reveal induction periods superior to individual phenolic antioxidants, about the level recorded for unassociated photostabilizers ; (iv) for the ternary systems 21—23 the induction periods are shorter in comparison with the binary systems containing high concentration of photostabilizer ; the ternary system 24 exhibits a rather surprising behaviour for which a long induction period was recorded suggesting a synergistic effect for this association of antidegradants.

In comparison with the standard system 3, all other systems (individual, binary, and ternary) exhibit an increased capability of protection at low and high temperature; the system 14 is an exception presenting a decreased activity at 120°C. Bearing in mind that, after an induction period, some antioxidants are able to participate in reactions of the propagation stage of the free radical chain process of the oxidation,[5] the relative stability (S_r) was evaluated as a ratio by determining the propagation periods from the kinetic curves:[6]

$$S_r = S_p/S_{unp} \tag{2}$$

where S_p is the oxidation rate of the protected elastomer and S_{unp} is the oxidation rate of the unprotected elastomer, both evaluated after completion of the induction period.

The data presented in Table 3 show that the relative stability ensured by amine antioxidants is higher in comparison with phenolic antioxidants, particularly at high temperature (120°C). The photostabilizer Inh—5 presents for low and high temperature S_r values comparable with the value determined for the *bis*-phenolic antioxidant Inh—4 at 120°C. As a rule, all photostabilizers present a relative stability level at 100°C which is superior in comparison with amine and phenolic antioxidants. The photostabilizer Inh—6 ensures a relative stability which is superior to all other individual antidegradants.

The binary systems amine antioxidant + photostabilizer (systems 9, 11, 17, 18) with high levels of photostabilizer ensure a better stability than systems containing low concentration of photostabilizer (systems 10 and 12).

The relative stability ensured by the systems phenolic antioxidant + photostabilizer (systems 13, 16, 19, 20) is at the same level for high and low temperatures; the systems containing Inh—6 are more efficient in propagation step in comparison with the same systems containing Inh—5.

The ternary protective systems confer a superior relative stability at 120°C in comparison with the stability at 100°C which may be explained by the fact that transformation products from amine antioxidants or photostabilizers are more efficient in breaking the propagation step of the degradation process; the systems containing Inh—6 associated with other antidegradants exhibit a superior protecting capability.

The co-operative (additive, synergistic or antagonistic) activity of protecting systems is evaluated quantitatively by parameter θ calculated by relationship[7]:

$$\theta = t_{1,2}/(t_1 + t_2) \tag{3}$$

where t_1 is the induction (or propagation) period in the presence of the antidegradant 1 at concentration c_1; t_2 is the induction (or propagation) period in the presence of the antidegradant 2 at concentration c_2; $t_{1,2}$ is the induction (or propagation) period in the presence of the system antidegradant 1 + antidegradant 2 at concentration $c_1 + c_2$.

The values for parameter θ computed for induction and for propagation periods are presented in Table 4. The data for induction period at 100°C show that all systems have an antagonistic effect with the exception of the system 18 which presents an additive effect. At higher temperature (120°C), the system 11 presents an additive effect while the systems 17–19 reveal synergistic effects, most enhanced for the system 18.

Table 4

Values of the interaction parameter θ for the thermo-oxidative degradation of natural rubber protected by various systems

Protection system	Values of the interaction parameter θ			
	For induction period at temperature		For propagation period at temperature	
	100°C	120°C	100°C	120°C
9	.5	.8	1.6	.8
10	.6	.7	1.0	.6
11	.6	1.0	2.0	1.0
12	.7	.5	.8	.4
13	.7	.7	.7	.5
14	.7	.4	.9	.4
15	.6	.7	1.0	.6
16	.5	.4	.8	.5
17	.8	1.5	.9	.6
18	1.0	2.1	1.0	1.3
19	.7	1.3	.8	.3
20	.4	.6	.5	.3

For the propagation period, the data presented in Table 4 show that at 100°C the systems 10, 15 and 18 work additively and the systems 9 and 11 exhibit a clear-cut synergistic effect; for the other systems, the values of the parameter θ are about the level corresponding to an additive behaviour. At the temperature 120°C, only the system 18 has a synergistic behaviour and the system 11 presents an additive effect; in all other systems, the antidegradants of the couple work in an antagonistic manner.

The presented data suggest that the amine antidegradants cooperate with photostabilizers more efficiently in the propagation stage of the free radical chain oxidation process sometimes resulting in a synergistic behaviour. Of particular interest seem to be the couples of the diaminic antidegradant Inh-2 with the photostabilizers Inh-5 and Inh-6.

2. Influence of the ageing on physical characteristics

The efficiency of various antidegradant systems containing antioxidants and photostabilizers was evaluated in a simplified recipe based on natural rubber. Cure characteristics and tensile data at room temperature seem to be unaffected by presence of antioxidants, photostabilizers or associations of antioxidants and photostabilizers. The data concerning the behaviour of various recipes (which differ only by contained antidegradant or antidegradant association) in thermooxidative ageing, ozone ageing and resistance to atmospheric factors are presented in Table 5. The presented data reveal that after ageing at 70 and 90°C, the losses of the main tensile characteristics appear more important for the recipes

Table 5

Influence of various ageing circumstances on physical characteristics of the vulcanizates containing various protecting systems

Protection system	Loss (%) of tensile characteristics after oven ageing 72 h at 70°C		Loss (%) of tensile characteristics after oven ageing 72 h at 90°C		Ozone cracking time (h) in static conditions* at		Ozone cracking time (h) in dynamic conditions ** at		Quality retention index after 60 days outdoor exposure ***
	Tensile strength	Ultimate elongation	Tensile strength	Ultimate elongation	25°C	50°C	25°C	50°C	
1	2	12	10	15	25	40	35	49	90
2	3	10	5	12	30	50	39	52	95
3	9	12	18	25	5	4	4	2	20
4	7	14	12	20	5	3	4	2	20
5	3	14	6	15	20	20	16	20	50
6	8	12	11	20	18	15	14	12	50
9	8	18	10	25	49	31	39	30	95
11	5	10	5	14	50	39	40	41	95
13	8	10	18	40	4	4	4	4	25
15	12	12	15	38	4	4	4	4	25
17	6	16	20	30	30	25	25	20	85
19	8	14	11	16	4	5	4	4	90
21	2	10	12	12	32	25	27	19	85
23	2	8	4	12	20	20	17	14	100
24	2	6	4	9	35	25	40	22	100

* Testing in ozone chamber following ISO 1431–72, ozone concentration 50 pphm, 20% elongation.

** Ozone concentration 50 pphm.

*** ASTM D 1171–68.

containing photostabilizers, particularly with the bifunctional one (Inh-6). In ozone ageing, the protecting efficiency of HALS alone is superior in comparison with phenolic antioxidants and inferior in comparison with amine antidegradants; antiozonant effect of the couples HALS + antioxidant is situated at a level comparable with the protection level ensured by the antioxidant alone.

In atmospheric tests, binary systems of amine antioxidant+photostabilizer as well as ternary systems of antidegradants ensured a superior protection. These experimental facts lead to the conclusion that, in the given ageing circumstances, the antagonistic effects are not of practical importance.

The set of physical tests supports the assertions that HALS do not interfere in cure and that initial tensile characteristics are unaffected. In spite of the fact that a significant protecting effect is not revealed in rapid ageing tests, HALS compounds seem to be able to contribute to the maintenance of the level of physical characteristics in atmospheric ageing.

3. Interaction of the antioxidants with HALS

In circumstances of thermal oxidation, the phenolic antioxidant is transformed into a phenoxy radical[5,8,14]; when the system contains a HALS compound (mono- or bifunctional) there exist possible reactions with oxygen or with phenoxy radical:

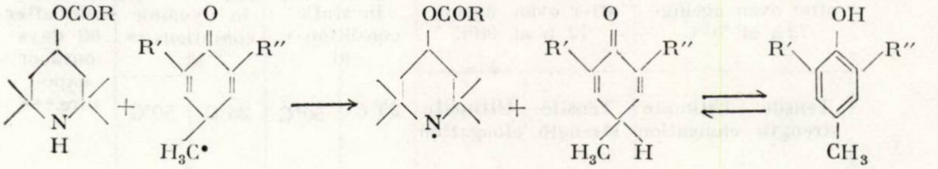

I IIa III IVa IVb (4)

The radical (III) is able to react with oxygen and with the rubber leading to a piperidine-N-oxyl radical (V)

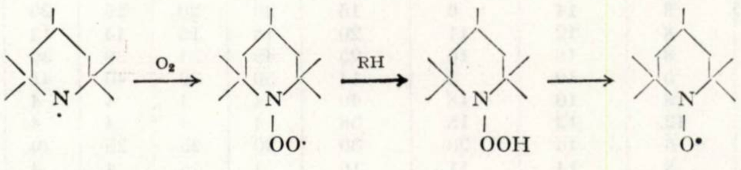

III V (5)

and also to the propagation of the polymer oxidation. The radical (V) is able to react with the phenoxy radical (II) giving a new product (VI) with antidegradant capability:

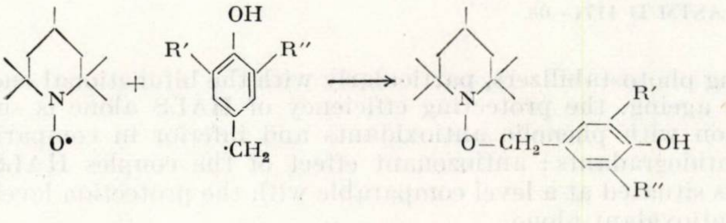

V IIb VI (6)

The examination of the above-presented possible reactions between piperidine radical, phenolic radical and radicals resulting in oxidation of the polymer chain allows to observe that some reactions favour while other reactions hinder the chain breaking process. In these circumstances the couples of phenolic antioxidants + photostabilizer exhibit antagonistic or additive behaviour.

For the diaminic antidegradants, the reaction leading to formation of quinonediimine and semiquinone[15-19] seems to be less affected by the presence of the radicals (III) and (V). This dissimilar behaviour makes possible the exhibition of additive interactions and, possibly, a synergistic cooperation favoured by reaction of the photostabilizer with hydroperoxides to give nonradicalic species. Also, the radical (V) can react, during the propagation step, with radicalic forms of the aminic antidegradant (Inh$^{\bullet}$) preventing the formation of the quinonediimine and, possibly, regenerating the diamine from (VII), giving an antagonistic effect for the global process :

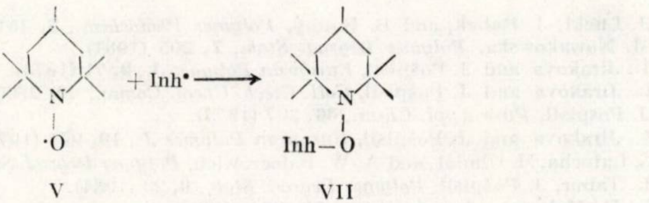

(7)

Similar effects may appear by extraction of a proton from the elastomer macromolecule with the formation of a macroradical (R$^{\cdot}$) able to propagate the chain reaction of oxidation.

Also the radical (III) is able to react with the radical form of the aminic antidegradant (Inh$^{\cdot}$) giving the product (VIII) from which the regeneration of the aminic antioxidant is not possible :

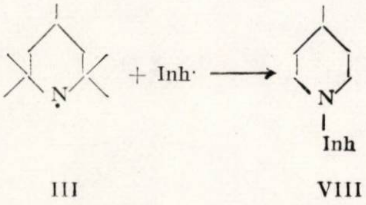

(8)

In addition, the HALS compounds are able to give nitroxyl and hydroxylamine intermediates hindering the propagation of the destruction process by a regenerative mechanism. As a consequence of the parallel development of various processes, it is reasonable to accept that synergistic or additive effects are developed by systems consisting from aminic antioxidant + HALS. The antagonistic behaviour observed for some cases may be explained by the consumption of the species with protection capability in reactions of the type (7) and/or (8).

CONCLUSIONS

In circumstances of thermo-oxidative degradation at temperatures in the domain 80—120°C, in protection of natural rubber by associations antioxidant + HALS compounds, the cooperation of the antidegradants leads to aditive, synergistic or antagonistic behaviour as revealed by kinetic data deduced from spectroscopic measurements. The physical tests support the assertion that HALS compounds do not influence cure behaviour nor the tensile properties of vulcanizates at room temperature.

A significant improvement in protection effect is not revealed by accelerated ageing tests, while outdoor tests revealed that binary systems of amine antioxidant + photostabilizer as well as ternary systems ensured a superior protection of the natural rubber vulcanizates.

REFERENCES

[1] J. Lucki, J. Rabek, and B. Ranby, *Polymer Pholochem.*, **5**, 351 (1984).
[2] M. Nowakowska, *Polymer Degrad. Stab.*, **7**, 205 (1984).
[3] L. Jirakova and J. Pošpisil, *European Polymer J.*, **9**, 71 (1973).
[4] L. Jirakova and J. Pošpisil, *Coll. Czech. Chem. Comm.*, **40**, 2800 (1975).
[5] J. Pospisil, *Pure Appl. Chem.*, **36**, 207 (1973).
[6] L. Jirakova and J. Pošpisil, *European Polymer J.*, **10**, 975 (1974).
[7] C. Latocha, M. Ulmiat, and A. W. Baloerowich, *Polymer Degrad. Stab.*, **7**, 189 (1984).
[8] L. Taimr, J. Pošpisil, *Polymer Degrad. Stab.*, **8**, 23 (1984).
[9] L. R. Mahoney, *Angew Chem.*, **81**, 855 (1969).
[10] J. C. Westfall, C. J. Carman, and R. W. Layer, *Rubber Chem. Technol.*, **45**, 402 (1972).
[11] K. U. Ingold, *Canad. J. Chem.*, **41**, 2816 (1963).
[12] I. Buben and J. Pospišil, *Coll. Czech. Chem. Comm.*, **40**, (1975).
[13] E. C. Horswill and K. U. Ingold, *Canad. J. Chem.*, **44**, 263 (1966).
[14] L. Taimr, H. Pivkova, J. and Pošpisil, *Coll. Czech. Chem. Comm.*, **37**, 1912 (1972).
[15] M. E. Cain and J. R. Gelling, G. T. Knight, P. H. Lewis, *Rubber Ind.*, **9**, 216 (1975).
[16] J. Tsurugi, S. Murakami and K. Goda, *Rubber Chem. Technol.*, **44**, 857 (1971).
[17] F. M. Albert, M. Giurginca, A. Meghea and G. Ivan, *Rev. Chim. (București)*, **31**, 1048 (1980).
[18] F. M. Albert and M. Giurginca, *Industria ușoară*, **27**, 341 (1980).
[19] G. Scott, *Pure Appl. Chem.*, **52**, 365 (1980).

Revue Roumaine de Chimie, **34**, *6*, 1361–1368 (1989)

DESIGN ON TOPOLOGICAL INDICES. 1

DEFINITION OF A VERTEX TOPOLOGICAL INDEX IN THE CASE OF 4-TREES

OVIDIU IVANCIUC
Polytechnic Institute "Traian Vuia", Faculty of Chemical
Technology, Timişoara *

Received July 25, 1988

Distance matrix of a 4-tree was used in defining eighteen vertex topological indices. The best definition was chosen, which ensures a low degeneracy and a large interval of values.

1. INTRODUCTION

Molecular topology determines a large number of molecular properties ranging from physicochemical and thermodynamic properties to chemical reactivity and biological activity. Organic molecules are represented by hydrogen-depleted graphs depicting the covalent bonds between non-hydrogen atoms. In graph theory, alkanes are represented as 4-trees. A 4-tree is a connected graph without cycles and with no vertex with the degree greater than 4. The topology of a chemical structure can be coded in matrix form by the use of the adjacency matrix and the distance matrix.[1]

The adjacency matrix [2] of a graph G with N vertices, A(G) = A, is the square N × N symmetric matrix which contains information about the connectivity of vertices in G. Its entries are defined as :

$$a_{ij} = \begin{cases} 1, & \text{for vertices i, j adjacent} \\ 0, & \text{otherwise} \end{cases}$$

The distance matrix of a graph G with N vertices, D(G)=D, is a square N × N symmetric matrix, whose entries, d_{ij}, are equal to the number of edges connecting vertices i and j on the shortest path between them. The two types of matrices are interrelated and the distance matrix can be computed from the adjacency matrix using a simple algorithm based on the adjacency matrices of higher orders.[3]

From the practical point of view, an efficient way of coding the topology of a chemical structure is represented by the topological indices.[4,5] A topological index (TI) is a numerical quantity which characterizes the bonding topology of a molecule.

The problem of chemical species classification is a difficult task.

---

* Correspondence address : strada N. Grigorescu, 18/2 2750 Hunedoara, Romania

For example, the number of alkane constitutional isomers increases very rapidly with the number of carbon atoms, being equal with [6] 75 for $C_{10}H_{22}$, 366,319 for $C_{20}H_{42}$, 4, 111, 846, 763 for $C_{30}H_{62}$, 62, 481, 801, 147, 341 for $C_{40}H_{82}$ and 1, 117, 743, 651, 746, 953, 270 for $C_{50}H_{102}$. In order to classify such a great number of structures, topological indices with high discriminating power are strongly needed.

An almost general deficiency of topological indices is that they do not characterize uniquely the topology of a molecular graph, but are more or less degenerate, i.e. two or more nonisomorphic structures may lead to the same numerical value for a certain topological index. There are two possible exceptions : the smallest binary notation (SBN) of a graph, introduced by Randić[7–10] and according to Hosoya's conjecture,[11] the distance polynomial and the distance polynomial index Z'.

By definition, the vertex topological index (VII) is a numerical quantity associated with a certain vertex of the chemical graph, which expresses the local topology of the chemical structure.

In the present paper, a design of a VII for 4-trees is presented. The definition obtained ensures a minimum degeneracy and a good distribution of the values. A number of informational TI's are computed, based on the defined VTI's. The rules of branching[12] at constant number of vertices are tested for the computed TI's.

2. THE DEFINITION OF THE VERTEX TOPOLOGICAL INDEX

The molecular topology will be defined by the aid of the distance matrix, because it contains a larger quantity of information concerning the molecular structure. In equations (1)—(18), eighteen types of VTI's are defined. The valence (degree) v_i of the vertex i is equal to the number of neighbours of the vertex i.

$$\mathrm{VTI\text{-}1}_i = \sum_{j=1}^{N} d_{ij} \tag{1}$$

$$\mathrm{VTI\text{-}2}_i = \sum_{j=1}^{N} d_{ij} v_i \tag{2}$$

$$\mathrm{VTI\text{-}3}_i = \sum_{j=1}^{N} d_{ij} v_i^{-1} \tag{3}$$

$$\mathrm{VTI\text{-}4}_i = \sum_{j=1}^{N} d_{ij} v_j \tag{4}$$

$$\mathrm{VTI\text{-}5}_i = \sum_{j=1}^{N} d_{ij} v_j^{-1} \tag{5}$$

$$\mathrm{VTI\text{-}6}_i = \sum_{j=1}^{N} d_{ij} v_i v_j \tag{6}$$

$$\text{VTI-7}_i = \sum_{j=1}^{N} d_{ij} v_i v_j^{-1} \tag{7}$$

$$\text{VTI-8}_i = \sum_{j=1}^{N} d_{ij} v_i^{-1} v_j \tag{8}$$

$$\text{VTI-9}_i = \sum_{j=1}^{N} d_{ij} v_i^{-1} v_j^{-1} \tag{9}$$

$$\text{VTI-10}_i = \sum_{j=1}^{N} d_{ij}^{-1} \tag{10}$$

$$\text{VTI-11}_i = \sum_{j=1}^{N} d_{ij}^{-1} v_i \tag{11}$$

$$\text{VTI-12}_i = \sum_{j=1}^{N} d_{ij}^{-1} d v_i^{-1} \tag{12}$$

$$\text{VTI-13}_i = \sum_{j=1}^{N} d_{ij}^{-1} v_j \tag{13}$$

$$\text{VTI-14}_i = \sum_{j=1}^{N} d_{ij}^{-1} v_j^{-1} \tag{14}$$

$$\text{VTI-15}_i = \sum_{j=1}^{N} d_{ij}^{-1} v_i v_j \tag{15}$$

$$\text{VTI-16}_i = \sum_{j=1}^{N} d_{ij}^{-1} v_i v_j^{-1} \tag{16}$$

$$\text{VTI-17}_i = \sum_{j=1}^{N} d_{ij}^{-1} v_i^{-1} v_j \tag{17}$$

$$\text{VTI-18}_i = \sum_{j=1}^{N} d_{ij}^{-1} v_i^{-1} v_j^{-1} \tag{18}$$

We have to note that VTII has the same definition as the distance sum index.[13]

3. THE SELECTION OF THE BEST VERTEX TOPOLOGICAL INDEX

Computations of the VTI's were done for all 147 4-trees with N = 4 to 10 vertices. For the case of 4-trees with ten vertices, table 1 presents the minimum value, the maximum value, the average value, the standard deviation and the dispersion of the respective VTI. The dispersion of the values of a VTI is defined as :

$$D = \frac{\text{VTImax} - \text{VTImin}}{\text{VTIav}} \tag{19}$$

Table 1

The minimum value, the maximum value, the average value, the standard deviation and the dispersion of the VTI's in the case of 4-trees with ten vertices

No.	VTI	Minimum value	Maximum value	Average value	Standard deviation	Dispersion
1.	VTI-1	14.	45.	25.90	35.24	1.197
2.	VTI-2	22.	96.	42.81	228.77	1.729
3.	VTI-3	3.5	45.	19.26	119.56	2.155
4.	VTI-4	19.0	81.0	42.81	140.95	1.448
5.	VTI-5	11.83	30.0	19.26	12.55	0.943
6.	VTI-6	35.0	156.0	69.42	550.64	1.743
7.	VTI-7	17.25	69.33	32.26	139.28	1.615
8.	VTI-8	4.75	81.0	32.26	374.53	2.364
9.	VTI-9	2.96	30.0	14.19	58.89	1.906
10.	VTI-10	2.83	6.5	4.26	0.729	0.863
11.	VTI-11	2.83	26.0	8.37	35.21	2.767
12.	VTI-12	1.36	4.17	2.74	0.667	1.025
13.	VTI-13	5.55	12.0	8.37	1.76	0.771
14.	VTI-14	1.47	5.08	2.74	0.629	1.321
15.	VTI-15	5.55	46.0	15.74	92.64	2.571
16.	VTI-16	1.47	20.33	5.61	20.59	3.365
17.	VTI-17	1.93	9.67	5.61	4.60	1.380
18.	VTI-18	1.02	2.71	1.70	0.180	0.995

It is not practical to choose a VTI with a small interval of values, or with a small standard deviation, or with a small dispersion, like VTI-10, VTI-12, VTI-13, VTI-14 or VTI-18.

Another comparison considers the distribution of numerical values of the VTI's, exemplified for the 75 decane isomers in table 2. Some of the definitions used give a very uneven distribution of the VTI's: VTI-2, VTI-3, VTI-6, VTI-7, VTI-11, VTI-15, VTI-16 in the lower range; VTI-9, VTI-12 a distribution with gaps T; and VT-14, VTI-5 with a central distribution. More evenly distributed are VTI-1, VTI-8, VTI-10 and VTI-18.

Table 3 presents the number of degenerations of the VTI's for all the 4-trees with N = 4 to 10 vertices. It may be seen that VTI-1, VTI-4, VTI-6, VTI-2, VTI-3 and VTI-8 have a high degeneracy and low selectivity. On the other hand, VTI-15, VTI-17, VTI-19, VTI-7 and VTI-13 have a fairly low degeneracy and high selectivity. VTI-15 and VTI-17 present degeneracy for the same two alkanes: 4-Et-octane and 4-Et-2,3-di-Me-hexane. VTI-9 presents degeneracy for the 4-trees representing 3-Me-nonane, 2,6-di-Me-octane and 3-Et-4-Me-heptane.

At this level of information it is hard to choose between VTI-15, VTI-17 and VTI-9. It is interesting to see if they carry the same type of information on molecular topology. Table 4 presents the intercorrelation matrix of the VTI's. The intercorrelation between VTI's varies from insignificant (for example, between VTI-1 and VTI-7, VTI-2 and VTI-4,

Table 2

Histogram presenting the distribution of the VTI's in the case of 4-trees with ten vertices

	INTERVAL									
	1	2	3	4	5	6	7	8	9	10
VTI-1	52	98	129	139	138	88	56	33	11	6
VTI-2	186	138	122	92	90	66	27	19	7	3
VTI-3	135	148	100	13	33	117	108	60	26	10
VTI-4	52	98	129	139	138	88	56	33	11	6
VTI-5	36	84	123	130	136	109	78	35	14	5
VTI-6	150	163	134	113	85	51	26	16	7	5
VTI-7	222	124	75	101	86	61	38	24	13	6
VTI-8	141	161	84	14	58	124	91	53	18	6
VTI-9	129	104	148	15	0	51	145	106	43	9
VTI-10	58	116	156	95	83	98	47	52	26	19
VTI-11	354	2	206	29	10	76	28	0	17	28
VTI-12	61	99	86	130	20	26	79	86	109	54
VTI-13	34	70	98	125	129	137	81	48	20	8
VTI-14	65	162	134	127	91	55	50	27	26	13
VTI-15	350	18	113	106	32	45	40	18	17	11
VTI-16	354	34	202	1	43	69	2	1	25	19
VTI-17	51	104	100	112	39	51	84	89	68	52
VTI-18	68	145	128	70	68	75	75	71	28	22

Table 3

Number of degenerations of the VTI's and of the informational TI's E, and $\bar{I}$, defined on the respective VTI's, in the case of 4-trees with $N = 4$ to 10 vertices. There are no degeneracies for $\bar{I}$

No	VTI	Number of degenerations of VTI	Number of degenerations of E	Number of degenerations of I
1	VTI-1	115	5	1
2	VTI-2	39	1	0
3	VTI-3	32	2	1
4	VTI-4	115	5	0
5	VTI-5	16	3	0
6	VTI-6	48	1	0
7	VTI-7	5	0	0
8	VTI-8	32	4	0
9	VTI-9	3	1	0
10	VTI-10	13	0	0
11	VTI-11	7	0	0
12	VTI-12	7	2	0
13	VTI-13	6	2	1
14	VTI-14	18	0	0
15	VTI-15	2	0	0
16	VTI-16	18	0	0
17	VTI-17	2	1	0
18	VTI-18	18	2	0

Table

The matrix displaying the intercorrelation coefficients

	VTI-1	VTI-2	VTI-3	VTI-4	VTI-5	VTI-6	VTI-7	VTI-8	VTI-9
VTI-1	1.000	0.112	0.834	0.998	0.977	0.245	−0.008	0.846	0.803
VTI-2		1.000	−0.418	0.073	0.117	0.987	0.982	−0.395	−0.455
VTI-3			1.000	0.852	0.814	−0.302	−0.507	0.999	0.992
VTI-4				1.000	0.968	0.210	−0.051	0.865	0.819
VTI-5					1.000	0.241	0.025	0.822	0.806
VTI-6						1.000	0.945	−0.278	−0.343
VTI-7							1.000	−0.486	−0.530
VTI-8								1.000	0.988
VTI-9									1.000
VTI-10									
VTI-11									
VTI-12									
VTI-13									
VTI-14									
VTI-15									
VTI-16									
VTI-17									
VTI-18									

VTI-13 and VTI-17, VTI-13 and VTI-18), through weak (between VTI-2 and VTI-15, VTI-13 and VTI-17), to high (between VTI-1 and VTI-4, VTI-11 and VTI-16, VTI-12 and VTI-17). The intercorrelation coefficients indicate that VTI-9 and VTI-7 express approximately the same type of information, different from the information contained in VTI-15. Thus, the use of VTI-9 and VTI-17 in developing a TI is almost equivalent and we will prefer VTI-17 for its lower degeneracy.

It is well known that informational TI's are suited for characterizing molecular branching.[12] In order to test the branching rules at constant number of vertices, three types of informational TI's, based on the eighteen types of VTI'-s defined, were computed: the informational energy content [14]

$$E = \sum p_i^2 \tag{20}$$

the total information content [15]

$$I = \sum VTI_i \log_2 \sum VTI_i - \sum VTI_i \log_2 VTI_i \tag{21}$$

the mean information content[16]

$$\bar{I} = - \sum p_i \log_2 p_i \tag{22}$$

where $p_i = \dfrac{VTI_i}{\sum VTI_i}$

Table 3 shows the number of degenerations of the informational TI's computed. The informational energy content has a rather high number of degenerations, in contrast with the total information content index which

4

between the eighteen types of VTI's defined

VTI-10	VTI-11	VTI-12	VTI-13	VTI-14	VTI-15	VTI-16	VTI-17	VTI-18
−0.372	−0.469	0.515	−0.216	−0.460	−0.471	−0.475	0.458	0.417
0.715	0.746	−0.651	0.377	0.714	0.726	0.724	−0.667	−0.614
−0.685	−0.756	0.827	−0.393	−0.748	−0.763	−0.740	0.783	0.724
−0.427	−0.507	0.523	−0.277	−0.505	−0.515	−0.510	0.465	0.420
−0.304	−0.437	0.548	−0.115	−0.388	−0.429	−0.440	0.495	0.489
0.606	0.630	−0.575	0.290	0.600	0.607	0.608	−0.599	−0.554
0.801	0.829	−0.687	0.462	0.814	0.815	0.813	−0.695	−0.621
−0.683	−0.743	0.802	−0.408	−0.742	−0.753	−0.727	0.756	0.696
−0.679	−0.769	0.866	−0.359	−0.739	−0.771	−0.750	0.826	0.785
1.000	0.916	−0.585	0.830	0.952	0.956	0.882	−0.554	−0.484
	1.000	−0.780	0.558	0.954	0.985	0.991	−0.762	−0.693
		1 000	−0.105	−0.683	−0.743	−0.772	0.996	0.963
			1.000	0.675	0.669	0.500	−0.057	−0.015
				1.000	0.957	0.955	−0.655	−0.538
					1.000	0.961	−0.718	−0.657
						1.000	−0.755	−0.669
							1.000	0.968
								1.000

has no degenerate value for all VTI's. We have to note that VTI-15 has no degenerated value, unlike VTI-17 which has a degeneracy in the case of the informational energy index. This fact is an argument in the favour of VTI-15. The analysis based on the order induced by the total information content index, shows that both VTI-15 and VTI-17 closely follow the rules for branching at constant number of vertices. Their value increases when branching increases.

Based on the VTI-1 (the distance sum index) it was defined a very discriminating TI, J.[7,18] By calculations it was determined that there are no J-equivalent nonisomorphic pairs of 4-trees with 11 or less vertices. In the case of 4-trees with 12 vertices, there are six pairs of J-equivalent nonisomorphic graphs.[19] Taking into account that the first degeneracy for VTI-1 appears for a 4-tree with six vertices, representing 2-Me-pentane, we can conclude that a TI defined using VTI-15, whose first degeneracy appears for 4-trees with ten vertices, will be a more discriminating index. Work is in progress in this direction.

REFERENCES

[1] D. H. Rouvray, in "Chemical Applications of Graph Theory", Ed. A. T. Balaban, Academic, New York, 1976, p. 175.

[2] J. J. Sylvester, *Am. J. Math.*, **1**, 64 (1874).

[3] M. Barysz, D. Plavšić and N. Trinajstić, *Match*, **19**, 89 (1986).

[4] A. T. Balaban, I. Motoc, D. Bonchev and O. Mekenyan, *Top. Curr. Chem.*, **114**, 21 (1983), Eds. M. Charton and I. Motoc, Springer, Berlin.

[5] D. H. Rouvray, *Stud. Phys. Theor. Chem.*, **28**, 159 (1983), Ed. R. B. King, Elsevier, Amsterdam.

[6] J. V. Knop, W. R. Muller, K. Szymanski and N. Trinajstić, "Computer Generation of Certain Classes of Molecules", SKTH, Zagreb, 1985, p. 38.
[7] M. Randić, *J. Chem. Phys.*, **60**, 3920 (1974).
[8] M. Randić, *J. Chem. Phys.*, **62**, 309 (1975).
[9] M. Randić, *J. Chem. Inf. Comp. Sci.*, **15**, 105 (1975).
[10] M. Randić, *Chem. Phys. Lett.*, **42**, 27 (1976).
[11] H. Hosoya, M. Murakami and M. Gotoh, *Nat. Sci. Rept. Ochanomizu Univ.*, **24**, 27 (1973).
[12] D. Bonchev and N. Trinajstić, *J. Chem. Phys.*, **67**, 4517 (1977).
[13] D. Bonchev, A. T. Balaban and O. Mekenyan, *J. Chem. Inf. Comp. Sci.*, **20**, 106 (1980).
[14] O. Onicescu, *C.R. Acad. Sci. Paris*, Serie A, **263**, 841 (1966).
[15] L. Brillouin, "Science and Information Theory", Academic, New York, 1956.
[16] C. Shannon and W. Weaver, "Mathematical Theory of Communication", University of Illinois, Urbana, 1949.
[17] A. T. Balaban, *Chem. Phys. Lett.*, **89**, 399 (1982).
[18] A. T. Balaban, *Pure Appl. Chem.*, **55**, 199 (1983).
[19] A. T. Balaban and L. V. Quintas, *Match*, **14**, 213 (1983).

Revue Roumaine de Chimie, 34, 6, 1369–1372 (1989)

HIGH VOLTAGE PLASMA APPLIED TO DETERMINE BORON AND SILICON IN SUPERALLIED METALLIC POWDERS

N. JUMATE and I. CHICINAȘ
Polytechnic Institute, Cluj-Napoca, Romania

Received December 12, 1987

This paper presents a method to determine boron and silicon in superallied metallic powders, using high voltage plasma as a source to excite elements. Samples and standards under the form of solution were used. High voltage plasma was obtained between two electrodes of pure spectral graphite, specially built for this purpose. The sensitivity of the method is under 1 ppm and the accuracy 1 to 4 per cent.

1. INTRODUCTION

The determination of the elemental composition of superallied metallic powders by spectroscopic methods raises several problems from the point of view of using some adequate standards.

Standards ready for delivery are generally made of a compact homogeneous material and they are not suited to superallied metallic powder analysis, because these have different granulosities and they generally consist of 3–4 major components. That is why the analysis under the form of aqueous solution is preferred for these metallic materials.

Silicon and boron, as minor components in these alloys, may be also determined by atomic absorption spectrophotometry, but both elements are hardly excitable. They form stable oxides and can not be excited in acetylene flame, needing nitrogen protoxide flame as an excitation source.

2. EXPERIMENTAL

In order to excite boron and silicon, we have used high voltage plasma obtained from argon as a plasmagen agent and a voltage of 12 kV with a frequency of 300 Hz as an excitation source starting from the idea of inductively-coupled-plasma method. 1,2,3,7.

With the help of a liquid atomizer, the metallic sample, after having been passed into water solution through disintegration with acids, is brought into excitation plasma by means of argon (which plays a double role : spraying gas, and of plasmagen gas).

Plasma is obtained between two electrodes made of pure spectral graphite or tungsten (temperature of about 10,000 K) specially built with that end in view. The upper electrode has a cylindrical shape of 2.5 mm diameter, and the lower one has a central channel of 3 mm diameter, through which aerosols in the sample to be analysed enter the plasma (Fig. 1).

A single-channel spectrophotometer analyzes the radiation emitted by the sample into the plasma.

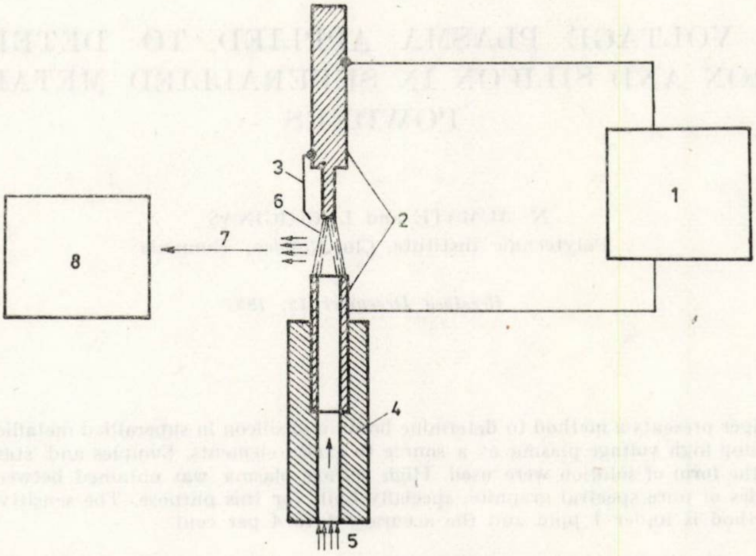

Fig. 1. — Experimental set-up : 1 — HV generator ; 2 — electrodes ; 3 — ionizer ; 4 — PTF sleeve ; 5 — aerosols made of the sample + plasmagen gas ; 6 — HV plasma ; 7 — emitted radiation ; 8 — spectrophotometer.

Optimum analytical conditions :

a) For the high voltage source :	
— Excitation voltage	12 kV
— Capacity	6 μF
— Inductance	1.6 mH
— Resistance	2 Ohms
— Frequency	300 Hz
— Spark gap interval	2 mm
b) For the spectrophotometer :	
— Analytical interval	4–8 mm
— Entrance slit	2 × 25 μm
— Preslit	8 mm
— Argon discharge	400 l/h

3. RESULTS

In the case of boron analysis, we have worked on the line λ = = 2089.6Å (5.94 eV), and of silicon analysis on the line λ = 2516.1 Å (4.95 eV). For these spectral lines, we have checked that no spectral superpositions with the major elements in the sample exist (superpositions caused by the small linear dispersion of the spectrophotometer ($d = = 15$Å/mm)).[4,5]

The signal obtained on the spectrophotometer is relatively noisy, but stable as an average value, being suited to static analyses on the computer.

In order to plot the calibration curves, standard solutions with the matrix having the elemental composition close to the average composition of the samples to be analysed (obtained from pure elements and salts, by a preparation methodology identical with sample-solution preparation) have been used.[5,6] Signal-concentration dependence is linear, having the regression coefficient close to 1 (Fig. 2).

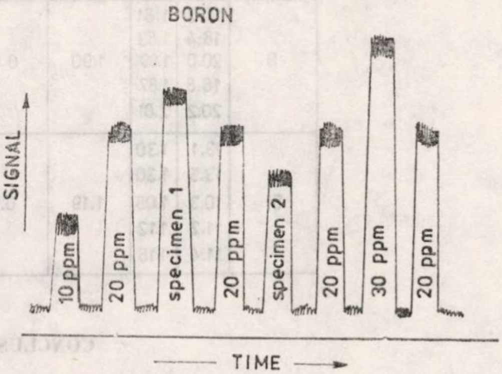

Fig. 2. — Analytical diagram for boron dosage.

Due to the high temperature of the plasma, interferences in plasma are minimum, the method having certain similarity with the solution-analysis method in plasma inductively coupled (ICP).

The dosage was made according to the three-standard method (for plotting the calibration curve) supplemented by the outer-standard method in order to diminish the analytical system instability.

Solutions were fed into plasma according to the diagram in Fig. 2, the second standard being fed after each sample or standard playing a double part in this way : of an outer standard and of a standard for the calibration curve, the intensity of the signal from the sample and the standards having reference to the intensity of the outer standard signal (Fig. 3).

The results of this analysis for a powder of 80—125 μm grain size and the composition : 66% wt Fe, 17% wt Cr, 12% wt Ni, 2% wt Mo are given in table 1.

The relative error of the method is of 2 per cent in the case of boron and 3.5 per cent in the case of silicon.

Using this method, detection limits are placed between those of the atomical-absorption analysis (AAS) and of the inductively-coupled-plasma (ICP) analysis.[2,3,6]

Detection limits of the method proposed are under 1 ppm for boron and silicon. The calibration curve is linear and above 200 ppm.

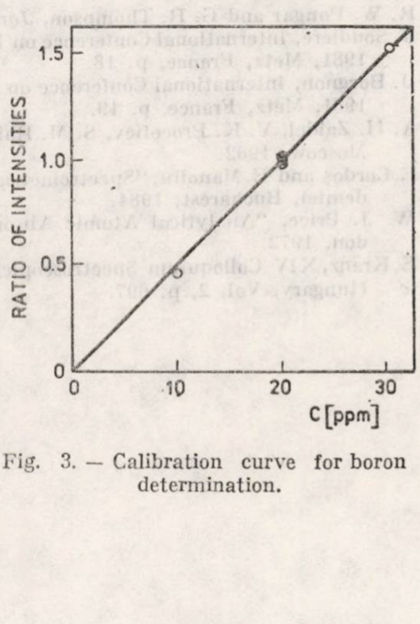

Fig. 3. — Calibration curve for boron determination.

Table 1

Experimental results when determining boron and silicon in superallied metallic powders

Element	Concentration		Average	Std. deviation	Real concentration	Relative error
	ppm	%	%	σ	%	%
B	18.2	1.81	1.90	0.09	1.94	2.0
	18.4	1.83				
	20.0	1.99				
	18.8	1.87				
	20.2	2.01				
Si	13.1	1.30	1.19	0.11	1.15	3.5
	13.5	1.30				
	10.3	1.05				
	11.2	1.12				
	11.4	1.16				

CONCLUSIONS

The results presented in the paper prove that, in high voltage plasma, boron and silicon excitation from aqueous solutions alloys permit determination by spectral emission with a high accuracy and repeatibility of the presence of the two elements as minor components in superallied metallic powders.

The use of high voltage plasma eliminates the problems generated by the excitation of the elements difficult to excite in a flame, and the analysis of samples under the form of solutions solves the problem of the standards for superallied metallic powders.

REFERENCES

[1] R. W. Pongar and G. R. Thompson, *Jarrell — Ash Plasma Newsletter*, 1, (No. 2), 5 (1978).

[2] J. Soudiere, International Conference on Industrial Inorganic Elemental Analysis, 1—5 June 1981, Metz, France, p. 18.

[3] J. Borgnon, International Conference on Industrial Inorganic Elemental Analysis, 1—5 June 1981, Metz, France, p. 19.

[4] A. H. Zaidel, V. K. Procofiev, S. M. Raiski and E. I. Sreider, "Tablitsy spektralnyh linii", Moscow, 1962.

[5] E. Cordoş and E. Manoliu, "Spectrometria de absorbţie şi fluorescenţă atomică", Ed. Academiei, Bucharest, 1984.

[6] W. J. Price, "Analytical Atomic Absorption Spectrometry", Heyden & Son, Ltd., London, 1972.

[7] E. Kranz, XIV Colloquium Spectroscopicum Internationale, 7—12 August 1967, Debrecen, Hungary, Vol. 2, p. 697.

Revue Roumaine de Chimie, 34, 6, 1373 – 1376 (1989)

NEW APPLICATION OF FIELD EMISSION TECHNIQUES (FEM AND FIM) TO THE STUDY OF CATALYTIC SYSTEMS

Z. KNOR * and J. ŠOTOLA
J. Heyrovský Institute of Physical Chemistry and Electrochemistry, Czechoslovak Academy of Sciences, 3, Dolejškova, 182 23 Prague 8, Czechoslovakia

Received October 1, 1988

Field emission techniques have been applied to the study of metal-oxide-metal systems. High temperature treatment of palladium and molybdenum layers deposited under ultra-high vacuum (UHV) conditions onto an oxidized tungsten tip, and nitrogen spillover from Mo to Pd surfaces have been examined in FEM. The atomic structure and crystallographic orientation of sintered palladium clusters has been estimated by FIM.

I. INTRODUCTION

One of the basic problems in practical catalysis is rational choice of a new catalyst for a given chemical reaction. However, in the field of heterogeneous catalysis by individual metals the number of possibilities is rather limited. Therefore, the way towards a new catalyst (a catalyst, having higher selectivity, lower price and/or a longer life-time) has to be looked for in modification of individual metal surfaces and/or in multicomponent systems. Of course, rational construction of a new multicomponent catalytic surface has to be made on the basis of a sufficient knowledge of the role of individual components in such a system.

Commercial metalic catalysts are usually in the form of highly dispersed metals on oxide carriers [1] so that most of the metal atoms are exposed into the gas phase and thereby the mass of the metal is effectively exploited in the catalytic process. Consequently, when looking for the solution of the mentioned basic problem a microscopic approach should be used with the resolution going down to the atomic level (0.1 – 1 nm). The field emission microscopes meet these requirements. There exist examples that the small size of visible area of the sample surface under study in field emission microscopes (5 – 50 nm) has been considered to be a good model of metallic particles in a supported metal catalyst.[2] However, in this case the metallic cluster under investigation is in direct electrical contact with the bulk of a FEM or FIM metal tip. The process occurring on such surfaces – particularly those where electrical charges are transferred – may therefore considerably differ from those occurring on metallic clusters of the same size which, however, reside on an oxide layer. Since it is not possible to work with insulator tips in field emission microscopes, we decided to use as a carrier tungsten oxide, prepared "in situ" on the surface of an ordinary tungsten tip. The active metals can then be deposited onto the tip surface from different directions so that the position of individual catalyst components is exactly known. The role of particular components in a given process can thus be studied with the resolution of FEM or FIM, respectively.

We have chosen a Pd/Mo combination as a model bimetallic catalyst for ammonia synthesis. Molybdenum is able to trap dissociatively nitrogen molecules. However, nitrogen atoms are so strongly held to the molybdenum surface that they are not able to react with hydrogen at room temperature.[3] On the other hand, if nitrogen atoms are deposited onto the surface of platinum group metals (which do not interact with nitrogen molecules at room temperature [4]) either directly from the gas phase [4,5] or by spillover from another metal (e.g.W,[6] Mo [7]) they can be readily hydrogenated [4,5,8].

II. EXPERIMENTAL

An all glass system has been used throughout this study, in which pressures $p \leqslant 8 \times 10^{-8}$ Pa have been routinely attained. The details of the FEM and FIM cells were published elsewhere.[7] Purity of gases has been checked in the FEM and FIM apparatuses by a glass quadrupole partial pressure gauge (AIG CENTRONIC, England) and by an omegatron mass spectrometer (ZD PIE, Poland), respectively.

The oxide layers have been prepared in FEM by exposing the tungsten tip to oxygen atmosphere $p_{O_2} \sim 10^{-4}$Pa for 210 s at 300 K and subsequently raising the tip temperature to about 1100 K for another 30 s. Tungsten oxidation in FIM has been performed in a similar way, viz. the tip has been exposed to oxygen ($p_{O_2} \sim 10^{-3}$Pa) for 220 s at 300 K and then its temperature has been raised to about 1100 K for another 20 s (shorter heating time, needed for preserving the extreme sharpness of the FIM tip, was "compensated" by a higher oxygen pressure).

III. RESULTS AND DISCUSSION

Visibility of metallic clusters on an oxide layer

Visibility of metallic Pd and Mo clusters deposited in FEM or FIM onto the WO_x layer was a crucial question which had to be answered prior to thinking of the application of field emission microscopies to the study of metal-oxide-metal systems.

Oxidation of metal tip considerably increases its work function and thus decreases substantially the emission current in FEM (Fig. 1 a and b). Furthermore, oxidation results in a random atomic structure of the surface similarly as does the low temperature deposition of additional metallic layers. This makes the interpretation of FIM images of such systems difficult (Fig. 2b and c).

FEM images shown in Fig. 1c and 1d represent a positive answer to the mentioned basic question. Namely clusters of palladium and molybdenum deposited onto an oxidized surface of a tungsten tip are visible in FEM as bright regions. This probably results from the resonance-enhanced tunneling in the metal-oxide-metal region.

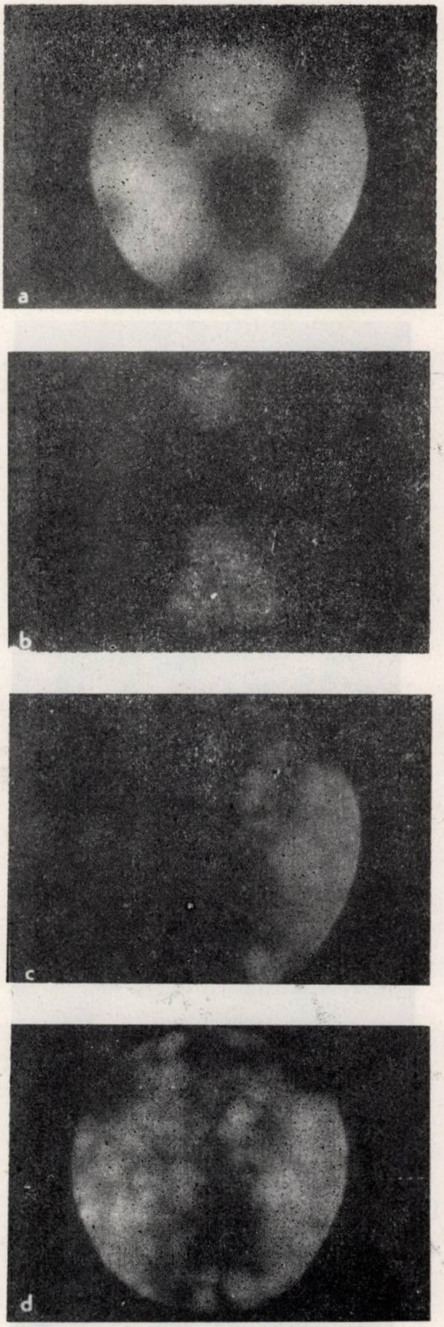

Fig. 1. — FEM images ($T = 78$ K) : a) clean tungsten (imaging voltage $V = 3$ kV), b) oxidized tungsten surface ($V = 4.1$ kV), c) palladium deposited from the right side at 78 K ($V = 4.1$ kV), d) molybdenum evaporated on c) from the left side ($V = 4.1$ kV).

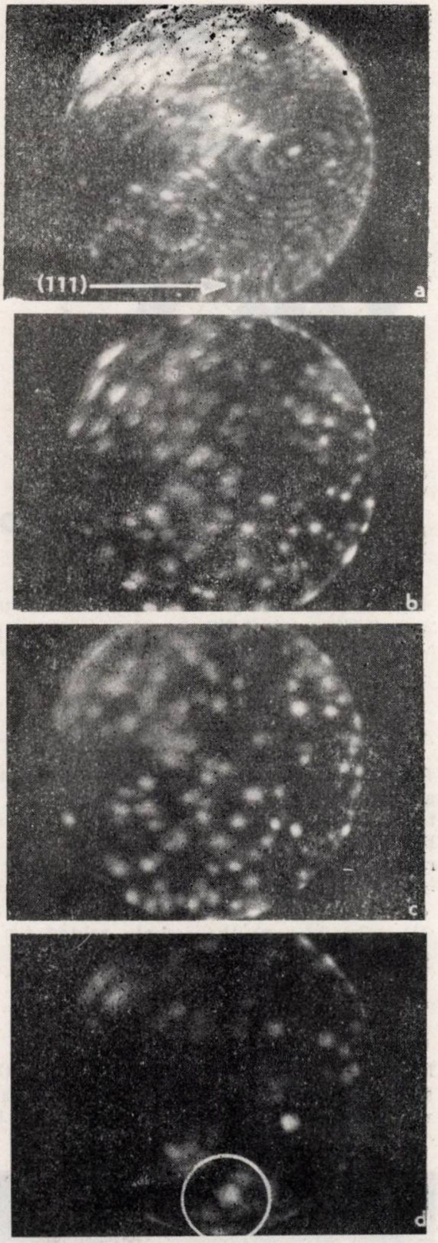

Fig. 2. — FIM images : a) clean tungsten (helium image, best image voltage BIV $= 3.9$ kV, $T = 78$ K, field evaporation voltage FEV $= 4.3$ kV), b) oxidized tungsten surface (neon image, BIV $=$ FEV $= 2.5$ kV), c) palladium layer, deposited at 78 K and subsequently heated for 5 s to about 1100 K in absence of the electric field (neon image BIV $=$ FEV $= 2.5$ kV), d) preceding surface after field evaporation at FEV $= 4.1$ kV (neon image, BIV $= 2.5$ kV

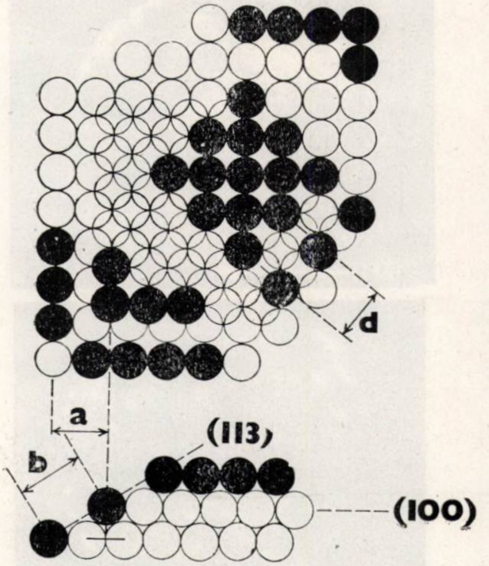

Fig. 3. — Schem of the atomic structure of a palladium crystallite in the region of (111) plane of the original tungsten surface.

→

Fig. 4. — FEM study of the preparation of a Pd/WO$_x$/W sample: a) clean tungsten surface (imaging voltage always at 78 K, V = 6 kV), b) palladium deposited during 15 s from the right side onto the oxidized tungsten tip (V = = 8 kV), c) palladium deposition time 60 s (V = 8 kV), d) total deposition time 150 s (V = 7.5 kV), e) the sample heated for 1 s to about 1200 K in absence of the electric field (V = 7.5 kV).

Fig. 5. — FEM image of Mo, Pd/WO$_x$/W system, showing the lines A and B, along which the photodensity of the image has been measured.

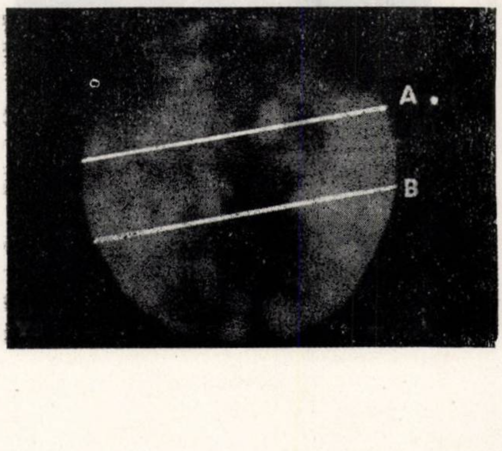

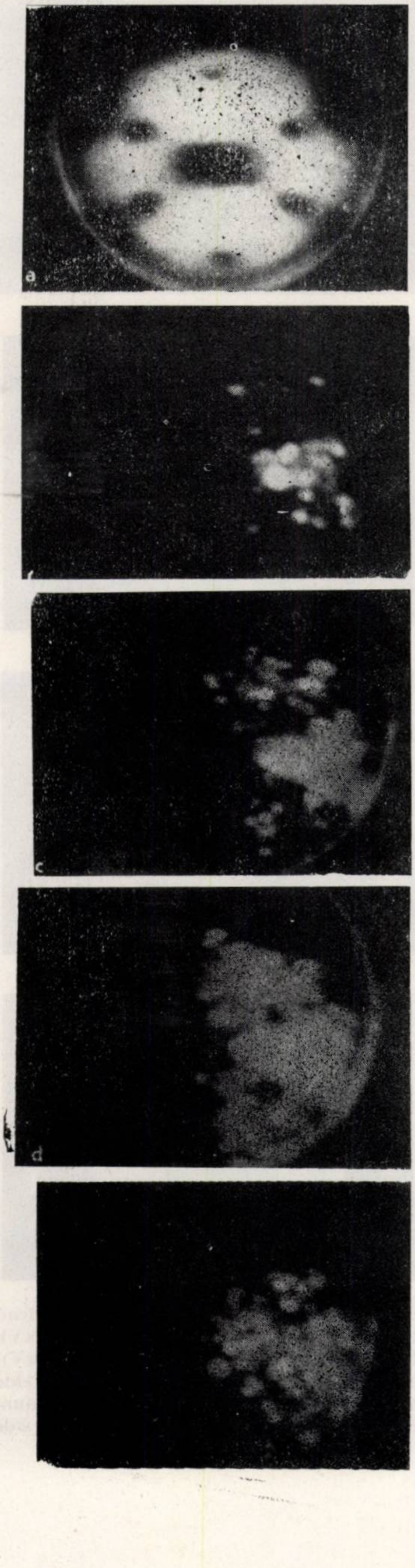

For the study of the atomic structure of sintered palladium crystallites, it is necessary to field evaporate at liquid nitrogen temperature random surface layers, formed by rapid cooling down the sample after the heat treatment. Fig. 2d shows the result of such a procedure. In the lower part of the image (within the white circle) corresponding to the (111) region of the original tungsten surface (exhibiting hexagonal symmetry — c.f. Fig. 2a) a crystallite of tetragonal symmetry can be seen (compare with the scheme on Fig. 3) which represents the image of a palladium cluster on the WO_x surface. From the known magnification [7] one can estimate the real distances, specified in Fig. 3. They are in good agreement with the published data for bulk palladium.[9]

Interaction of metallic clusters with the oxide carrier

Fig. 4 shows the sequence of FEM images (b—d), corresponding to the increasing coverage of palladium on a WO_x layer. When the thick palladium layer is heated for 1 s to about 1200 K in absence of electric field, a coalescence of palladium crystallites can be observed. This could be expected because of the weak interaction of palladium with the underlaying WO_x layer. On the other hand, if molybdenum crystallites are subjected to high temperature treatment (1200 K) the FEM image resembles the appearance of the original image of the oxidized tungsten surface. In this case strong interaction of molybdenum with oxygen on the surface can be expected. "Disappearance of the molybdenum layer" might be a consequence either of MoO_3 sublimation or of a formation of MoO_x continuation of the original WO_x lattice.

Nitrogen spillover from molybdenum to palladium surfaces

Rational construction of a composite catalyst implies a sufficient knowledge of the role of individual components in the overall catalytic process in question, and of the mechanism by which the possible reaction intermediates are transferred between the particular components of the catalyst surface. For example, in our system the reaction intermediates, i.e. the nitrogen atoms, must be able to migrate from molybdenum clusters (where they were formed from trapped nitrogen molecules) towards the palladium surface. In our experiment the bimetallic layer was exposed to nitrogen gas at room temperature. The coverage of the palladium surface by nitrogen, spilled over from molybdenum, has been judged from the photodensity of photographic images of individual stages of the surface. These measurements were performed along the lines crossing the images at different places (see Fig. 5 : line A crosses molybdenum and palladium islands separated by a gap $d \sim 1.5$ nm ; line B crosses the islands, separated by a gap $d > 10$ nm). The obtained data suggest that the nitrogen spillover can take place only across the narrow gap $d \leqslant 1$ nm^{+}.

IV. CONCLUSIONS

The presented results show that the metal-oxide-metal systems can be successfully used for modelling supported metallic and particularly bimetallic catalysts in field emission microscopes. In the paper : (a) the visibility of individual components of a bimetallic system has been demonstrated; (b) the decisive role of the strength of the metal-carrier interaction in the high temperature aging has been observed; (c) it has been proved that within the experimental errors of FIM the structure of sintered palladium crystallites does not differ from the bulk palladium; (d) spillover of nitrogen atoms from molybdenum to palladium surfaces has been observed, provided that the gap between these two surfaces has not exceeded roughly 1 nm.

REFERENCES

[1] C. N. Satterfield, "Heterogeneous Catalysis in Practice", McGraw-Hill, New-York, 1980.

[2] M. Drechsler, *Surface Sci.*, **162**, 755 (1985).

[3] G.E. Moore and F.C. Unterwald, *J. Chem. Phys.*, **48**, 5409 (1968).

[4] K. Kunimori, T. Kawai, T. Kondow, T. Onishi and K. Tamaru, *Surface Sci.*, **54**, 525 (1976); 59, 302 (1976).

[5] Z. Knor and K. Kuchynka, *Coll. Czechoslov. Chem. Commun.*, **50**, 2509 (1985).

[6] Z. Knor, Ch. Edelmann, J. Rudny and J. Stachurski, *Appl. Surface Sci.*, **25**, 107 (1986).

[7] Z. Knor and J. Šotola, *Coll. Czechoslov. Chem. Commun.*, (1988) (in press).

[8] V. V. Gorodetskii and V. A. Sobyanin in "Proc. 7th Internatl. Congr. on Catalysis, Tokyo, 1980", Kodansha, Tokyo, 1981, p. 566.

[9] Ch. S. Barrett and T. B. Massalski, "Structure of Metals", McGraw-Hill, New York, 1966.

Revue Roumaine de Chimie, 34, 6, 1377–1387 (1989)

AN ADAPTED MODEL TO PREDICT OPERATING CONDITIONS FOR A RADIANT FURNACE — THERMAL CRACKING REACTOR

GHEORGHE MARIA[a*], CRISTIAN TSAKIRISI[a], CRISTINA MARIA[b],
ALEXANDRU ISOPESCU[c] and GRIGORE BOZGA[b]
[a] Chemical and Biochemical Energetics Institute, Spl. Independenţei 202, Bucharest 79611, Romania
[b] Department of Chemical Engineering, Polytechnic Institute, Bucharest
[c] Computer Center of Chemical Industry, Bucharest

Received October 26, 1988

A rough way to simulate the coking process for a hydrocarbon cracking reactor in a radiant furnace, without concomitant radiant box model solution, is to pre-establish the radiative heat flux profiles. As a valuable alternative, the flexible rectangular-parallelepipedic space subdivision using the geometric and operating features of the each firebox, and an adequate strategy to solve the coupled radiant section — thermal cracking tubular reactor model allow a very rapid process simulation. This adaptation may be indicated instead of other rigorously coupled models, in order to repeatedly simulate and predict the trends in fuel consumption and in temperatures for economically balancing the coil coking process.

INTRODUCTION

Mathematical models for the hydrocarbon cracking process are extensively discussed in the literature, due to the major importance of the accurate furnace performance predictions. The exact range of the predicted data allows a more reliable and economical design and operating conditions for a thermal cracker furnace. The modelling effort was conducted both for : i) hydrocarbon cracking kinetic schema, coke deposit formation, tubular reactor simulation, and for ii) thermal cracker heater (particularly radiant section) modelling. The furnace accurate simulation involves the coupled reactor-firebox models (as an example see Petryschuk, Johnson ;[1] Eckert et al. ;[2] Filla, Maresca ;[3] Vercammen, Froment ;[4] Goossens et al.[5] Rao et al.,[35] a.o.).

A special attention is paid in the literature to the fired heater simulation, i.e. the ability to predict the heat flux variation throughout the radiant enclosure. These flux profiles depend on the combustion product radiative properties, the characteristics and location of the burners and flames, the furnace geometry and the cracking coil layout. Accuracy and detail in prediction of yields, furnace performance and coking rate are essential both in design and operation. Many firebox models with different orders of complexity and generality were proposed : semi-empirical models, ideally stirred gas models, and zone models (see for instance reviews and discussions of Hottel, Sarofim;[6] Siegel, Howell;[7] Filla, Chiappetta;[8] Nicoară, Suciu;[9] Nogay, Prasad[10]; Kim, Smith[11], a.o.).

---

* Author to whom correspondence should be addressed.

The accurate computation of flux profiles is usually performed using two radiant enclosure simulation methods : the flux method, based on the differential form of the radiative transport equation, and the zone method of Hottel based on the integrated transport equation between each pair of zones. Filla and Chiappetta[8] report that flux methods are faster and require lesser storage than zone method, being more valuable for the coupled radiant furnace – reactor solution.

As resulted, an important problem is to find the best compromise between solution refinement and computation time, particularly for a great nonuniformity of the tridimensional temperature box field (high furnace, some particular burner disposition and flame geometry cases). The computational effort for these cases increases with the number of isothermal zones, in which the volume and surface walls are subdivided, nearly with a power law. These problems are decisive in selecting the adequate simulation method. For instance, Filla and Chiappetta[8] solved it by exploring the sensitivity of results to the number of zones and the radiative properties considered for gas and walls, concluding that : i) zoning of the refractory walls can be substantially coarser than that of the volume and coil walls ; ii) the adequate volume zoning has to take into account the axial and radial temperature gradients due to the flame characteristics, burner disposition and gas recirculation ; iii) the one-gray-gas model is satisfactory for the radiative properties of the combustion products. Another recent paper (Nogay, Prasad[10]) solves the same problem using zone method, attacking with priority the ii) point. Because variations in the burner-to-tube spacing and flame lengths can dramatically affect heater performances, this effect is simulated by subdividing the furnace in a great number of zones, i.e. 50 gas (square or rectangular) and 30 surface isothermal zones (referred to the furnace cross-section). For such a number of zones the computational effort and the required data storage are important, but justified particularly in a design stage, and for obtaining accurate and reliable enough data to make economic considerations.

The aim of this paper is to follow this trend and to test the adaption of a flexible rectangular-parallelepipedic firebox division for obtaining a minimum number of zones. This adaptation together with an adequate strategy to apply the coupled zone method – thermal cracking tubular reactor calculations, allows an approximate but very rapid evaluation of the radiant transfer efficiency and the heat flux nonuniformities for a tested thermal cracking furnace. The resulted procedure could be fast and repeatedly used to predict trends in fuel consumption and in temperatures, for instance to balance the coke deposit formation in our application.

2. FIREBOX SUBDIVISION AND MODEL CONSIDERATIONS

Hottel's zone method to simulate the radiant section of the furnace (Hottel, Cohen;[12] Hottel, Sarofim[6]) requires the subdivision of the entire volume and surfaces of the combustion chamber into a number of zones, each small enough to be considered isothermal. An increasing refined zoning leads, after simulations, to a more accurate tridimensional temperature field, but requiring a considerably increased computer time and storage. In order to obtain rapidly the thermal flux predictions, a realistic compromise is possible using the particularities of each simulated enclosure.

In our application, the radiant box of the furnace (see Fig. 1 and sizes in Table 1) is divided by the two coil screens into one central and two lateral sections which were separately simulated. The spatial arrangement of coils and burners and the parallelepipedic symmetry of sections allow to obtain a minimum necessary number of zones if a rectangular-parallelepipedic subdivision is performed. The central combustion section length, with single-center-burners arrangement of special construction and small burner-to-tube space, was subdivided into five equal zones. Because of experimental information and computative considerations in respect to the flame lengths (Lobo[13]), the box height was subdivided into two unequal parts (with an approximative ratio 1 :3). Thus 10 volume and 34 surface zones are obtained. The lateral combustion sections are similarly subdivided. This flexible way to divide into unequal zones could predict various operating conditions, because zone dimensions can be varied according to the experimental information concerning the temperature gradients and burner working, without introducing new zones.

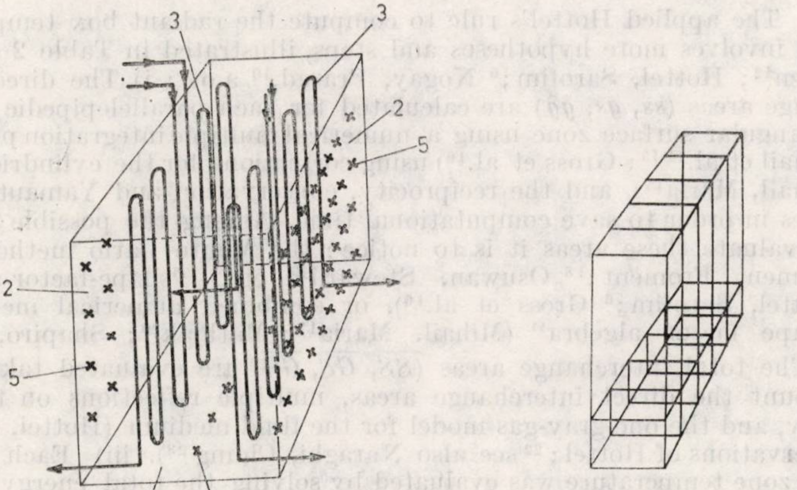

Fig. 1. — Radiant box subdivision (1 — central section, 2 — lateral sections, 3 — coils, 4 — central inferior burners, 5 — lateral burners).

Table 1

Furnace sizes and basic operating conditions

Feed gas properties for the cracking reactor (clean coil):

Feed flow rate: 1450 Kg C_3H_8/hr.; Dilution: 0.4 kg steam/kg C_3H_8; Inlet temperature in radiant section: 600°C; Inlet pressure: 3 atm. abs.; Resulted propane conversion: 90% (experimental); Outlet product temperature: 840°C (experimental)

Reactor coil and refractory walls:

External coil diameter: 0.114 m; Internal coil diameter: 0.095 m; Pitch: 0.286 m; Distance between coil planes: 1.6 m; Total coil length: 88 m; Refractory wall thickness: 290 mm; Internal refractory wall temperature (containing surface diffused flame): approx. 1300°C (experimental) and 1250°C (simulated)

Fuel gas and air:

Inlet composition (%mol): 79.39 CH_4; 14.82 H_2; 5.79 C_2-C_3; Feed rate: 1334 Kg/h (fuel gas); Air excess: 6%vol; Outlet gas temperature from radiant box: 1000°C (experimental) and 1160°C (simulated); Number of central inferior burners: 6 (approx. 59% of fuel gas); Number of lateral burners: 64

Emissivities (mean values) of:

walls: 0.7; coil: $0.35+0.00025\ T$; gas.: $(0.8352-1.942 \times 10^{-4}T)\ (1\text{-}\exp(-\ 0.642\ r))$

Furnace sizes (approximately):

	central section	lateral section
Length:	8.0 m	8.0 m
Width:	1.6 m	0.8 m
Height:	7.2 m	7.2 m

The applied Hottel's rule to compute the radiant box temperature field involves more hypotheses and steps, illustrated in Table 2 (Hottel, Cohen[12]; Hottel, Sarofim;[6] Nogay, Prasad,[10] a.o.): i) The direct interchange areas ($\overline{ss}$, $\overline{gs}$, $\overline{gg}$) are calculated for each parallelepipedic gas and rectangular surface zone using a numerical multiple integration procedure (Mihail et al.[14,15]; Gross et al.[16]) using corrections for the cylindrical tubes (Mihail, Maria[17]), and the reciprocity, conservation and Yamauti's principles in order to save computational time. Among the possible methods to evaluate these areas it is to notice: the Monte Carlo method (Vercammen, Froment;[18] Osuwan, Steward[19] etc.), "shape-factor-algebra" (Hottel, Sarofim;[6] Gross et al.[16]), or combined numerical methods — "shape factor algebra" (Mihail, Maria[17]; Mathiak[20]; Shapiro,[21] a.o.). ii) The total interchange areas ($\overline{SS}$, $\overline{GS}$, $\overline{GG}$) are evaluated taking into account the direct interchange areas, multiple reflections on the gray body, and the one-gray-gas model for the fluid medium (Hottel, Cohen,[12] observations of Hottel;[22] see also Naraghi, Chung[23]). iii) Each isothermal zone temperature was evaluated by solving the total energy balance nonlinear set, using a numerical iterative method (Mihail et al.[15]). The nonlinear equations include radiative and nonradiative terms (i.e. enthalpy and convective flux). The heat transfer coefficients gas-refractory walls for surface zones containing burners with surface diffused flame

Table 2

Hottel's zone method steps for radiant section calculations *

Direct exchange areas ($\overline{ss}$, $\overline{sg}$, $\overline{gs}$, $\overline{gg}$)

$\overline{z_i z_j} = \int\limits_{Z_i}\int\limits_{Z_j} \tau f_i f_j/(\pi r^2)\, \mathrm{d}Z_i \mathrm{d}Z_j$, where $\tau = \exp(-kr)$, and : $z = s$, $Z = A$, $f = \cos\hat{\theta}$, if i, j index a surface zone, $z = g$, $Z = V$, $f = k$, if i, j index a volume zone

Total exchange areas ($\overline{SS}$, $\overline{SG}$, $\overline{GS}$, $\overline{GG}$)

i) $\overline{S_i S_j} = a(T_{s_i})\, [\overline{S_i S_j}]_k + (1 - a(T_{s_i}))\, [\overline{S_i S_j}]_{k=0}$, where $[\overline{S_i S_j}]_k = ({}_{s_i}R_{s_j}) A_{s_j} \varepsilon_{s_j}/(1 - \varepsilon_{s_j})$, and fluxes ${}_{s_i}R_{s_j}$ result from the set : $\sum\limits_j \overline{s_i s_j}({}_{s_m}R_{s_j}) - A_{s_i}({}_{s_i}R_{s_i})/(1 - \varepsilon_{s_i}) = -\varepsilon_{s_m} \overline{s_i s_m}$, $m=1,\ldots$ …, no. of surface zones

ii) $\overline{G_i S_j} = a(T_{g_i})[\overline{G_i S_j}]_k$, where $[G_i S_j]_k = ({}_{g_i}R_{s_j}) A_{s_j} \varepsilon_{s_j}/(1 - \varepsilon_{s_j})$, and fluxes ${}_{g_i}R_{s_j}$ result from the set : $\sum\limits_m \overline{s_j s_m}({}_{g_i}R_{s_m}) - A_{s_i}({}_{g_i}R_{s_j})/(1 - \varepsilon_{s_j}) = -\overline{g_i s_j}$, $i = 1, \ldots$, no. of volume zones

iii) $\overline{G_i G_j} = a(T_{g_i})[\overline{G_i G_j}]_k$, where $[\overline{G_i G_j}]_k = \overline{g_i g_j} + \sum\limits_m ({}_{g_i}R_{s_m})\overline{s_m g_j}$; $\varepsilon = a(T)(1 - \exp(-kpr))$

Energy balances for each zone :

surface zone i : $E_{s_i}(\overline{S_i S_i} - \varepsilon_{s_i} A_{s_i}) + \sum\limits_{j \neq i} E_{s_j} \overline{S_j S_i} + \sum\limits_j E_{g_j} \overline{G_j S_i} - \sum\limits_j h_{s_j} A_{s_i g_j}(T_{s_i} - T_{g_j}) - h_{s_i} A_{s_i}(T_{s_i} - T_{\mathrm{out}_i}) = C_{s_i} \mathrm{d}T_{s_i}/\mathrm{d}t$

gas zone m : $E_{g_m}(\overline{G_m G_m} - 4ka(T_{g_m})V_{g_m}) + \sum\limits_{j \neq m} E_{g_j} \overline{G_j G_m} + \sum\limits_j E_{s_j} \overline{G_m S_j} + \sum\limits_j G_j(H_s + H_c)_j - \sum\limits_j h_{s_j} A_{s_j g_m}(T_{s_j} - T_{g_m}) = C_{g_m} \mathrm{d}T_{g_m}/\mathrm{d}t$

---

* Used notations : A — surface zone area ; $A_{s_j g_m}$ — convective heat transfer area between surface j and gas m ; C — average heat capacity ; $E = \sigma T^4$ — radiation emission rate ; G — molal gas flow rate entering or leaving a gas zone ; h, h_s — heat transfer convective coefficient between a surface and a neighbouring gas volume, ambient or reaction medium ; $H_{c,s}$ — molal chemical or sensible enthalphy ; k — gas absorption coefficient ; p — partial gas pressure ; r — linear distance between two elements ; s or g — surface or gas zone ; t — time ; T — temperature ; V — volume of a gas zone ; ε — emissivity ; $\hat{\theta}$ — angle between r and the normal on surface ; σ — Stefan-Boltzmann's constant ; τ — gas transmissivity.

(i.e. for lateral sections, Fig. 1) was approximated using experimental temperature data. iv) Based on the temperature field, the heat fluxes and the total energy balance of the whole combustion chamber are evaluated.

3. TUBULAR REACTOR MODEL AND COKE FORMATION

The simulated process in this paper is the propane thermal cracking, for which many previous studies were reported. Although well established that thermal cracking proceeds essentially through radical reactions, the prevailing trend is to adopt molecular models. Among the proposed kinetic models, the Sundaram, Froment[24] schema, illustrated in Table 3 was adopted. To obtain the product distribution, reac-

Table 3

The propane cracking kinetic model (Sundaram, Froment[24])

No.	Reaction	Frequency factor (s^{-1} or $l.mole^{-1}.s^{-1}$)	Activation energy (kcal/mole)
1.	$C_3H_8 \rightarrow C_2H_4 + CH_4$	4.692×10^{10}	50.60
2.	$C_3H_8 \rightleftharpoons C_3H_6 + H_2$	5.888×10^{10}	51.29
3.	$C_3H_8 + C_2H_4 \rightarrow C_2H_6 + C_3H_6$	2.536×10^{13}*)	59.06
4.	$2C_3H_6 \rightarrow 3C_2H_4$	1.514×10^{11}	55.80
5.	$2C_3H_6 \rightarrow 0.5C_6 + 3CH_4$	1.423×10^{9}	45.50
6.	$C_3H_6 \rightleftharpoons C_2H_2 + CH_4$	3.794×10^{11}	59.39
7.	$C_3H_6 + C_2H_6 \rightarrow C_4H_8 + CH_4$	5.553×10^{14}*)	60.01
8.	$C_2H_6 \rightleftharpoons C_2H_4 + H_2$	4.652×10^{13}	65.20
9.	$C_2H_4 + C_2H_2 \rightarrow C_4H_6$	1.026×10^{12}*)	41.26
10.	$C_4H_8 \rightarrow C_6$	6.960×10^{7}	34.32
Coke model :			
	$C_3H_6 \rightarrow$ coke	5.820×10^{14}	73.58

*) second order reaction

Table 4

Tubular reactor model *

$$\frac{d\xi_i}{dz} = r_i/\dot{G};\ \xi_i(z = 0) = 0,\ i = 1,2,\ldots,\ \text{index of reaction}$$

$$\frac{pT}{dz} = (\Sigma_i r_i(-\Delta H_i) + 4h(T_{out} - T)/d_t)/(\dot{G}c_g);\quad T(z = 0) = T_0$$

$$\frac{dp}{dz} = \frac{\frac{d}{dz}\left(\frac{1}{M_m}\right) + \frac{1}{M_m}\left(\frac{1}{T}\frac{dT}{dz} + Fr\right)}{\frac{1}{M_m p} - \frac{p}{G^2RT}}$$

where :

$$Nu = h_{in}d_t/\lambda = 0.023\ Re^{0.8}Pr^{0.4} + 429.2\left(\frac{4z}{Re.Pr.d_t}\right)^{-0.0706}$$

$$-\ 544.3(x_{C_3H_8})^{-0.0437}$$ (Sundaram, Froment [34])

$Fr = 0.092\ Re^{-0.2}/d_t$ (straight tube)

$Fr = 0.092\ Re^{-0.2}/d_t + \xi'/\pi R_b$ (bends, see Sundaram, Froment [24])

* Used notations : c_g — gas specific heat ; d_t — reactor tube diameter ; Fr — friction factor ; $\dot{G}$ — flow rate per unit area of reactor cross-section ; h — heat transfer coefficient between gas and external tube skin (index "in" notes the inner coefficient) ; ΔH — heat of reaction ; M_m — mean molecular weight ; Nu — Nusselt number ; p — total gas pressure ; Pr — Prandtl number ; r — reaction rate ; R_b — radius of bend ; Re — Reynolds number ; T — temperature ; x — conversion ; z — reactor length ; λ — thermal conductivity ; ξ_i — molal transformation in the i-th reaction (kmole/kg) ; ξ' — friction factor in the bends.

tion temperature, and pressure profiles along the cracking coil, a set of mass, enthalpy balance and pressure drop equations, was integrated with a constant reactor step length. This reactor model (Table 4) which uses the widely accepted assumptions of one-dimensional plug-flow, presents the advantage of a rapid process simulation.

Under pyrolysis conditions, the main reactions occur in gas phase and are free radical in nature. The formation of carbonaceous material is a side reaction, that is of major importance on overall furnace economics, leading to process inefficiencies. As the coke layer on inner reactor surface increases, it inhibits heat transfer from the tube wall to process gas and consequently increases the wall temperature. This coke layer also increases the coil pressure drop having a negative influence on the ethylene yield, by increasing the hydrocarbon partial pressure. During a typical on stream cycle, the average rate of increase in the tube skin temperature is 1.75 to 2.3°C per day for industrial operations, depending on feedstock (Sundaram, Froment[24]). This results in a 1 – 2 % decrease in firebox efficiency with an increase in fuel consumption of about 5 % (Goossens et al.[5]). When the tube wall temperature or the input pressure reach their maximum allowable values, shutdown of the furnace is necessary for decoking.

Due to the complexity of coking mechanism, it is difficult to obtain an appropriate kinetic expression of coke formation and deposition in the pyrolysis industrial reactors. However, there are a series of studies published on coking mechanisms and kinetics, for the pyrolysis of various feedstocks such as ethane (Petryschuk, Johnson[1]; Li, Johnson[25]; Sundaram, van Damme, Froment[26]), propane (Lichtenstein [27]; Sundaram, Froment [24]), butane (Mihail et al.[28]), n-hexane (Prammik, Kunzru[29]; Mandall, Kunzru[30]), n-octane (Shah et al.[31]), naphtha (Newsome, Leftin[32]; Kumar, Kunzru [33]). Coke formation in industrial cracking coils depends on several factors such as the reaction temperature, hydrocarbon partial pressure and chemical nature of the feedstock. For a given feedstock composition, the coking rate increases as the efluent temperature (i.e. the severity of operation) increases and steam dilution decreases. Other factors which influence the coke formation are related to radiant enclosure construction and operation (i.e. the burners type and disposition around the reactor coil and the fuel feeding of burners).

For the pyrolysis of propane, the most complete study of coking is that published by Sundaram, Froment.[24] Coke formation mechanism and kinetics were studied using a detailed experimental technique. The coking reaction scheme, of consecutive type, is presented in Table 3. The increase in coke thickness $\Delta\delta_c$ in the time interval Δt for the reactor element of length Δz is :

$$\Delta\delta_c = A \exp(-E/R\bar{T})\bar{C}\Delta t/\rho_c,$$

where $\bar{C}$ is the average concentration of propylene, $\bar{T}$ is the average coke surface temperature between z and $z + \Delta z$, A and E are the kinetic coking rate parameters (Table 3), and ρ_c is the density of the coke.

4. OPERATING CONDITION PREDICTIONS TO BALANCE COKING EFFECTS ON REACTOR PERFORMANCES

Adapted coupled model. The coupled radiant sections – reactor simulation starts from some uniform proposed temperature and heat transfer coefficient profiles inside the reactor coils, and a uniform temperature radiant box field (starting solution). After the evaluation of the central and lateral section temperature fields, using Hottel's computational steps (Table 2) the heat fluxes absorbed by coil are obtained (note that since the tube half cross-sections are included in different radiant sections – central or lateral – Fig. 1, the average heat fluxes are performed for each reactor step length). Using these fluxes the reactor simulation allows to obtain the new temperature, coke thickness and heat transfer coefficient profiles, and to predict the product distribution. The reactor simulation is repeatedly applied using a convenient time increment Δt (i.e. 40 h in our application), obtaining the reactor performance and coke thickness time evolutions. The computational procedure is restarted in a new iteration loop, ten iterations being usually sufficient to attain the problem solution. To obtain a rapid procedure, the rule modification proposed by Vercammen, Froment[4] was adopted (step ii) of Hottel's rule is kept out of the inner loops).

In order to save computational time, after the adaptive firebox subdivision, the main alteration from the common computation rule is to keep out of the iteration loops the direct interchange area evaluations. In this strategy, the direct exchange matrices ($\overline{ss}$, $\overline{gs}$, $\overline{gg}$, computed with $\tau = 1$ and $k = 1$, see Table 2), can be stored and further used for simulations under new, but not radically different, operating conditions, or for other process simulations with the same firebox geometry. So, the furnace simulation begins with the adaption of direct exchange areas for the considered case: they are all multiplied by the computed τ_{avg} using the k_{avg} according to Hottel, Cohen[12], and with the k_i if a volume zone i is considered. This rapid way to adapt the direct exchange areas are rougher but simpler than that of Vercammen, Froment,[18] which adapts only the $\overline{ss}$ areas with a complex elaborated formula for τ_{avg} (recommended for the used Monte Carlo integration method), and afterwards computing the $\overline{gs}$, $\overline{gg}$ areas not by direct integration, but computing supplementary $\overline{ss}$ areas in respect to additional fictitious surfaces delimiting the gas volumes. The rapid resulted way for complete furnace simulation (including the coking process, as an example for 240 h of operation) requires in our application (Table 1) at the most 30 min. using a medium size FELIX C512 computer.

Determination of the new burner work levels. The propane thermal cracking furnace, with the data from Table 1, was first simulated under clean reactor surface conditions. The predicted performances (i.e. the outlet propane conversion – 90.2%, and product distribution and temperature – 846°C), the outlet gas temperature from radiant box and some refractory wall temperatures are in fair agreement with the considered experimental data (the basic operating policy of Table 1, and curves 1 from Fig. 2). The only adjustable model parameter (except the number of considered isothermal zones) is the mean temperature of gas entering

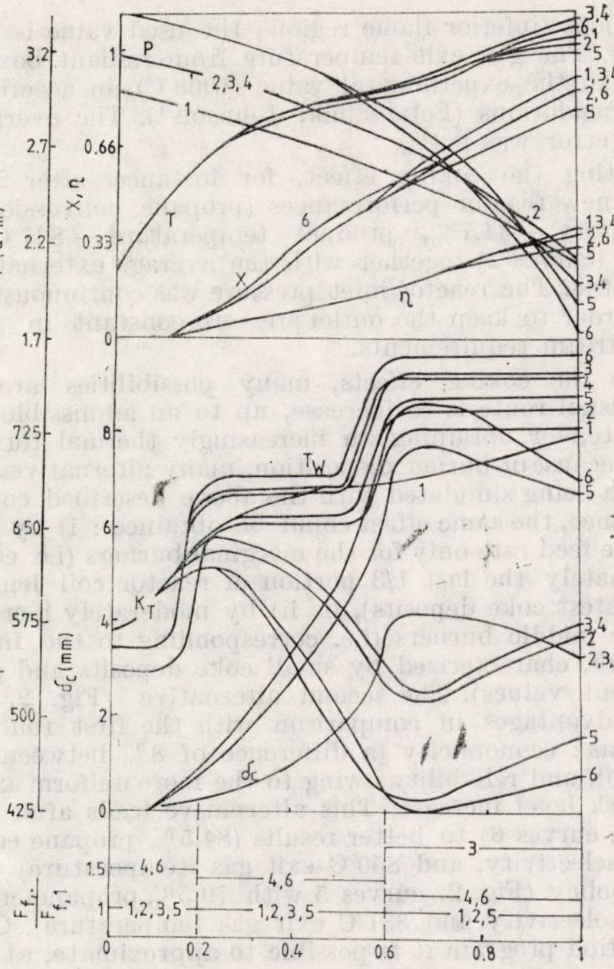

Fig. 2. — Simulated reactor performances under different furnace operating conditions. Curves no. 1 are obtained under basic operating conditions ($F_{f,1}$), i.e. 0 h. of operation, clean coils. Curves no. 2 are obtained after 240 h. operation, including the coking process. Curves nos 3,4 are obtained after 240 h. operation by applying the new fuel gas flow rates policy ($F_{f,3}$ and $F_{f,4}$). Curves no. 5 are obtained after 480 h. operation under the basic operating conditions ($F_{f,1}$) including the coking process. Curves no.6 are obtained after 480 h. operation by applying after 240 h. the $F_{f,4}$ burner working levels.) Used notations: $F_{f,i}$ — burner fuel gas flow rates for different furnace length zones (index $i = 1,\ldots,6$ corresponds with that of curve index); K_T — overall heat transfer coefficient (between coil axis and external tube skin, W/m²K); p — total gas pressure in the cracking coil (atm. abs.); T — gas temperature in the cracking coil (K); T_w — external tube skin temperature (mean values among isothermal coil zones, K); x — propane conversion; δ_c — coke thickness (mm); η — selectivity for ethylene (mole/mole propane feed).

the radiant sections (inferior flame region; the used value is 1680 K in our application). The gas exit temperature from radiant box was with 160°C higher than the experimental value (1000°C), in accordance with Hottel's recommendations (Petryschuk, Johnson[1]). The overall furnace energy balance error was 0.4%.

By simulating the coking effect, for instance after 240 hrs. of operation, the new reactor performances (propane conversion – 84.9%, ethylene selectivity – 34.7%, product temperature – 837°C) are presented in Fig. 2 (curves 2) together with the average external tube skin temperature profile. The reactor inlet pressure was continuously increased in time, in order to keep the outlet pressure constant in accordance with the downstream requirements.

To balance the coking effects, many possibilities are indicated (Section 3). A usual route is to increase, up to an admissible level, the feed fuel gas rate, for obtaining an increasingly thermal flux on each reaction coil. Because of burner disposition, many alternatives are possible, each of them being simulated with the above described coupled procedure. For instance, the same effect could be obtained: i) by cosiderably increasing the feed rate only for the marginal burners (i.e. corresponding to approximately the last 1/3 portion of reactor coil length which contains the greatest coke deposits), or ii) by moderately increasing the feed rate for the middle burners (i.e. corresponding to the first 2/3 of reactor coil length, characterized by small coke deposits and good heat transfer coefficient values). The second alternative (Fig. 2, curves 4) presents some advantages in comparison with the first route (Fig. 2, curves 3), such as: economicity (a difference of 8% between the used fuel gas flow rate), and reliability owing to the more uniform and reasonable burner work level increase. This alternative leads after 480 h. of operation (Fig. 2, curves 6) to better results (84.5% propane conversion, 34.6% ethylene selectivity, and 850°C exit gas temperature) than the basic operating policy (Fig. 2, curves 5 with 79.5% propane conversion, 31.7% ethylene selectivity and 831°C exit gas temperature). Certainly, using the simulation program it is possible to approximate, at any moment, the obtained increased production in connection with the overall used fuel gas quantity and the decrease in furnace run time due to the accelerated coking process. It is to notice that other possible strategies (see for instance Petryschuk, Johnson[1]) could be tested and indicated.

5. DISCUSSION

A rapid and complex simulation of an industrial furnace may be a worthy support to take favourable decisions concerning the operating conditions, even on an hourly basis. An adapted elaborated coupled firebox – reactor model could give fear compromise between the computational time and solution refinement. If a more accurate solution is required, the firebox subdivision could be refined according to the information given by the rapid simulation procedure. From this point of view, the advanced furnace simulation methods could become accessible and rapid instruments to simulate and control the cracking reactions and other similar processes.

REFERENCES

[1] W. F. Petryschuk and A. I. Johnson, *Canad. J. Chem. Engng.*, **46**, 172 (1968).

[2] E. Eckert, V. Hlavacek, M. Marek and J. Mikulas, Scientific papers of the Institute of Chem. Tech. (Prague), **K3**, 71 (1969).

[3] M. Filla and G. Maresca, *Ing. Chim. Ital.*, **12**, 143 (1976).

[4] H. A. J. Vercammen and G. F. Froment, *A. C. S. Symp. Series* **65**, 271 (1978).

[5] A. G. Goossens, M. Dente and E. Ranzi, *Hydroc. Proc.*, **57**, 227 (1978).

[6] H. C. Hottel and A. F. Sarofim, "*Radiative transfer*", McGraw-Hill, New York (1967).

[7] R. Siegel and J. R. Howell, "*Thermal radiation heat transfer*", McGraw-Hill, New York, (1972).

[8] M. Filla and M. Chiappetta, *Comp. Chem. Engng.*, **9**, 527 (1979).

[9] A. Nicoară and G. C. Suciu, *Rev. Chim. (Bucureşti)*, **35**, 519 (1984).

[10] R. Nogay and A. Prasad, *Hydroc. Process.*, **64**, 91 (1985).

[11] T. K. Kim and T. F. Smith, *Int. J. Heat Mass Transfer*, **28**, 2269 (1985).

[12] H. C. Hottel and E. S. Cohen, *A.I.Ch.E.J.*, **4**, 3 (1958).

[13] W. E. Lobo, *Chem. Engng. Progress*, **70**, 65(1974).

[14] R. Mihail, G. Maria and A. Isopescu, *Rev. Chim. (Bucureşti)*, **32**, 988 (1981).

[15] R. Mihail, G. Maria and A. Isopescu, *Rev. Chim. (Bucureşti)*, **33**, 157 (1982).

[16] U. Gross, K. Spindler and E. Hahne, *Lett. Heat Mass Transfer*, **8**, 219 (1981).

[17] R. Mihail and G. Maria, *Int. J. Heat Mass Transfer*, **26**, 1783 (1983).

[18] H.A.J. Vercammen and G. F. Froment, *Int. J. Heat Mass Transfer*, **23**, 329 (1980).

[19] S. Osuwan and F. Steward, *Canad. J. Chem. Engng.*, **50**, 450 (1972).

[20] F. U. Mathiak, *Wärme u.-Stoffübertr.*, **19**, 273 (1985).

[21] A. B. Shapiro, *J. Heat Transfer*, **107**, 730 (1985).

[22] H. C. Hottel, *Ind. Engng. Chem. Fundls.*, **22**, 153 (1983).

[23] M. H. N. Naraghi and B. T.F. Chung, *Int. J. Heat Mass Transfer*, **28**, 245 (1985).

[24] K. M. Sundaram and G. F. Froment, *Chem. Engng. Sci.*, **34**, 635 (1979).

[25] M. C. Li and A. I. Johnson, *Canad. J. Chem. Engng.*, **50**, 786 (1972).

[26] K. M. Sundaram, P. S. van Damme and G. F. Froment, *A. I. Ch. E. J.*, **27**, 946 (1981).

[27] E. Lichtenstein, *Chem. Engng. Progress*, **60**, 64 (1964).

[28] R. Mihail, G. Bozga, A. Isopescu and M. Georgescu, *Rev. Chim. (Bucureşti)*, **34**, 517 (1983).

[29] M. Pramanik and D. Kunzru, *Ind. Engng. Chem. Process Des. Dev.*, **24**, 1275 (1985).

[30] T. K. Mandal and D. Kunzru, *Ind. Engng. Chem. Process Des. Dev.*, **25**, 794 (1986).

[31] Y. T. Shah, E. Stuart and K. Seth, *Ind. Engng. Chem. Process Des. Dev.*, **15**, 518 (1976).

[32] D. S. Newsome and H. P. Leftin, paper presented at the 72nd Annual A.I.Ch.E. Meeting, San Francisco, Nov. 1979.

[33] P. Kumar and D. Kunzru, *Canad. J. Chem. Engng.*, **63**, 598 (1985).

[34] K. M. Sundaram and G. F. Froment, *Chem. Engng. Sci.*, **35**, 364 (1980).

[35] M. Rao, P. M. Plehiers and G. F. Froment, *Chem. Engng. Sci.*, **43**, 1223 (1988).

Revue Roumaine de Chimie, **34**, *6*, 1389–1395 (1989)

NEW CROSSLINKED FUNCTIONALIZED ACRYLIC COPOLYMERS FOR BIOTECHNOLOGICAL APPLICATIONS

STELIANA MAXIM and AURELIA FLONDOR
"Petru Poni" Institute of Macromolecular Chemistry, Aleea Gr.
Ghica Vodă 41 A, 6600 Jassy, Romania

Received September 21, 1987

The paper deals with the physico-chemical characterization of ion exchangers obtained by alkaline hydrolysis or aminolysis with ethylenediamine, diethylenetriamine, 1,6-diaminohexane, N,N-dimethylaminopropylamine and p,p′-diaminodiphenylmethane of the crosslinked acrylic copolymers. The enzymic preparations obtained on acrylic supports have the protein content ranged between 1.7 and 25.1 mg/mL wet support and 7.6 and 290.3 mg/g dry support. Immobilization yield values calculated from enzymic activity ranged between 66.8 and 93.2%.

INTRODUCTION

The stabilization of biocatalysts through physical adsorption and ionic or covalent binding $^{1-3}$ on synthetic supports $^{4-7}$ has made possible their large scale biotechnological application. $^{8-11}$

The low hydrophily and porosity of ion exchangers based on crosslinked poly(acrylic-divinylbenzene) or poly(styrene-divinylbenzene) matrices limit their applications in protein processing.

The ion exchangers based on macroreticular 2-hydroxypropylmethacrylate matrix having high hydrophily proved to be suitable for the chromatography of biopolymers. $^{12-15}$

Acrylic ion exchangers obtained in our laboratory ^{16} by alkaline hydrolysis or aminolysis of the ternary poly-(acrylate-acrylonitrile-divinylbenzene) copolymers proved to be good supports for the enzyme immobilization process. $^{17-19}$

The paper presents some physico-chemical characteristics of high hydrophilic acrylic ion exchangers emphasizing the possibility of their application to ionic immobilization of some enzymes.

EXPERIMENTAL

The following materials were used: ion exchangers of PONILEX–CC^R and PONILEX–AS^R types, respectively, obtained by alkaline hydrolysis or aminolysis with ethylenediamine (EDA), diethylenetriamine (DETA), 1,6-diaminohexane (DAH), N,N-dimethylaminopropylamine (DMAPA) and *p, p′*-diaminodiphenylmethane (DAMPhM) of ternary poly (acrylate-acrylonitrile-divinylbenzene) copolymers; catalase (E.C.1.11.1.6) provided from

FLUKA (F) and Institute of Chemical and Biochemical Energy Bucharest (ICBE), α-amylase (E.C. 3.2.11) provided from Institute of Food Research (I.F.R.) Bucharest, glucoamylase (E.C. 3.2.1.3.) from Merck (M), Novo (N) and I.F.R., glucose oxidase (E.C.1.1.34) from Merck (M), and Böehringer Companies, trypsin (E.C.34.21.4) provided from the Institute of Chemical and Pharmaceutical Research (I Ch Ph R), Bucharest and invertase (E.C.3.2.1.26) provided from SERVA (S).

Maltodextrin (MD) and saccharose (SH) were used as substrates respectively for glucoamylase and invertase.

As buffering substances, 0.02 M disodium phosphate-monosodium phosphate ($pH = 7.0$) and 0.02 M sodium acetate — acid acetic ($pH = 4.5$) were used.

Acrylic ion exchangers were characterized by Romanian Standard Methods determining the total weight exchange capacity (EC_{wt}, expressed as meq/g dry sample), total volume exchange capacity (EC_v, expressed as meq/ml wet sample), volume weight (V_{wt}, expressed as g dry sample/ml wet sample) percent swelling coefficient (SW %, representing the volume variation of an ion exchanger following the transformation from the reference form to hydrochloride form for an anion exchanger and to sodium form for a cation exchanger).

The crosslinking (R %) of ion exchangers was taken as equal to that of the crosslinked acrylic copolymers used for the chemical transformations.

The enzyme uptake coefficient (β %) was expressed as per cent ratio of adsorbed protein and the total amount of the protein taken in the experiment.

Ionic immobilization tests were caried out on 10 ml samples of ion exchangers in the reference form in 20×1.5 cm columns at 20°. Anion exchangers were directly buffered with the buffer solution specific for the particular enzyme. Cation exchangers were transformed into sodium salt, washed first with distilled water and then with the buffer solution specific for the enzyme.

The concentration of the enzyme solutions was 0.2 % (wt/v). The percolation rate of enzyme solutions was 0.3 to 0.4 ml/minute. The amount of the retained protein was determined from percolated solution volume and the difference of the concentration between influent and effluent. The concentrations of enzyme solutions were determined from standard curves obtained representing the variation of U.V. absorption band (275—280 μm) against the concentrations of standard enzyme solutions. Absorption spectra were registered on an UNICAM SP-800 spectrophotometer.

Catalase activity of soluble and immobilized enzyme was determined by iodometry calculating the amount of hydrogen peroxide decomposed per minute. Catalytic activity of soluble and immobilized α-amylase was determined by the Nöelting and Benfeld method, [20] calculating the free maltose formed from starch.

The hydrolytic activity of soluble and immobilized trypsin was determined by the Kunitz method. [21]

The soluble and immobilized glucoamylase activity was determined by iodometry, calculating the amount of glucose obtained from maltodextrin solution (20% wt/v) at 50°. The catalytic activity of soluble and immobilized invertase was determined also by iodometry accounting the amount of invert sugar obtained from a 20 % (wt/v) saccharose solution, at 50°.

RESULTS AND DISCUSSION

Tables 1 and 2 give the physico-chemical characteristics of ion exchangers respectively obtained by aminolysis or alkaline hydrolysis of crosslinked acrylic copolymers. From Tables 1 and 2 data one can see that all types of ion exchangers have high values of the total weight exchange capacity.

Nevertheless, the values of the total volume exchange capacity are quite small owing to the high values of the swelling coefficient.

Figures 1 and 2, respectively, show the dependence of the physicochemical characteristics of anion exchangers obtained by aminolysis with DETA and of cation exchangers obtained by alkaline hydrolysis of crosslinked acrylic copolymers, versus their crosslinking (R %). By comparing the theoretical weight exchange capacity values (curves 1 in both figures) with the experimental values of weight exchange capacity (curves 2 in

Table 1

Physico-chemical characteristics of acrylic anion exchangers obtained by aminolysis with polyalkylene-polyamines or polyarylenepolyamines (PONILEX-AS^R)

No.	Sample	Crosslinking %	Total exchange capacity		Swelling coefficient %	Volume weight g/mL	Amine
			meq/mL	meq/g			
1.	AS–18	2	0.690	4.800	54.0	0.1244	DAH
2.	AS–55	2	0.520	4.700	161.0	0.1104	EDA
3.	AS–56	2	0.560	6.500	154.0	0.0856	EDA
4.	AS–12	3	0.300	4.500	120.0	0.0774	EDA
5.	AS–13	3	0.430	4.200	46.0	0.0787	DAH
6.	AS–31	3	0.640	10.700	118.0	0.0609	EDA
7.	AS–44	3	1.190	10.400	62.0	0.1144	DETA
8.	AS–77	3	1.052	10.120	63.0	0.1250	DETA
9.	AS–88	3	0.946	9.956	65.0	0.0950	DETA
10.	AS–47	3.5	1.610	10.400	55.0	0.1548	DETA
11.	AS–10	4	0.490	4.800	42.0	0.1035	DAH
12.	AS–36	4	1.610	10.300	40.0	0.1563	DETA
13.	AS–53	4	0.300	1.575	49.0	0.1905	DADPhM
14.	AS–16	6	0.760	5.500	27.0	0.1369	EDA
15.	AS–20	6	0.340	2.900	26.0	0.1160	DMPA
16.	AS–21	6	0.370	1.360	15.0	0.2708	DADPhM
17.	AS–23	6	1.570	10.300	35.0	0.1520	DETA
18.	AS–75	6	0.610	3.885	25.0	0.1570	EDA
19.	AS–80	6	0.711	6.164	20.0	0.1153	DAH

Table 2

Physico-chemical characteristics of cation exchangers of PONILEX–CC^R type

No.	Sample	Crosslinking %	Total exchange capacity		Swelling coefficient %	Volume weight g/mL
			meq/g	meq/mL		
1.	CC–11	3	10.10	0.96	966	0.095
2.	CC–21	3	10.28	1.79	953	0.1741
3.	CC–10	4	9.20	2.66	560	0.2891
4.	CC– 4	4	8.60	2.86	547	0.3312
5.	CC– 1	6	7.83	2.68	320	0.3421
6.	CC–18	6	10.90	3.89	340	0.3555

both figures) one can see that experimental weight exchange capacity represents 71–89% from the theoretical values for the anion exchangers, and 72–79%, for the cation exchangers, from the theoretical values. Data from figures 1 and 2 prove that acrylic ion exchangers, with the crosslinking ranged between 2 and 4 %, have expanded elastic and high hydrophylic three dimensional networks.

Figure 3 represents the dependence of the swelling coefficient values on the crosslinking and the chemical nature of functional groups of acrylic anion exchangers. From the figure 3 data, one can conclude that the swelling coefficient values decrease with the increase of the crosslinking value and hydrophobicity of functional groups of anion exchangers.

It is very well known that the swelling coefficient values and the chemical nature of the functional groups of supports have a major importance in the enzyme immobilization process.

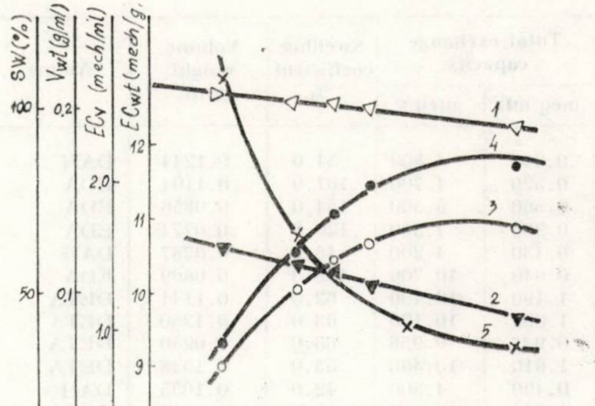

Fig. 1. — Dependence of physico-chemical characteristics of anion exchangers obtained by DETA aminolysis on crosslinking (R%). 1 — theoretical weight exchange capacity; 2 — EC_{wt}; 3 — EC_v; 4 — V_{wt}; 5 — SW (%).

The preferential affinity of proteins for a certain ionic form of acrylic ion exchangers [17] proved the main ionic nature of the enzyme immobilization process on such matrices.

The data presented in figure 4 give the dependence of uptake coefficient values (β %) of catalase (curves 1 and 2), glucose oxidase (curve 3)

Fig. 2. — Dependence of physico-chemical characteristics of cation exchangers on crosslinking (R%). 1 — theoretical weight exchange capacity; 2 — EC_{wt}; 3 — EC_v; 4 — V_{wt}; 5 — SW (%).

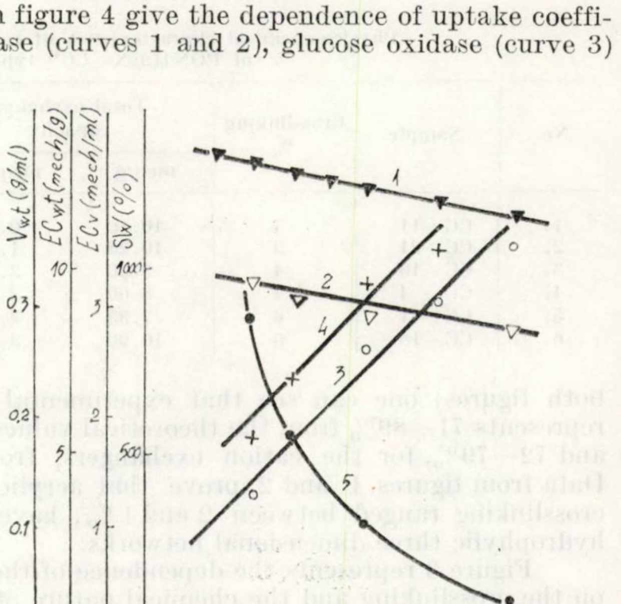

and glucoamylase (curve 4) versus the crosslinking and the chemical nature of functional groups of the anion exchangers obtained by DETA (curve 1) and EDA (curves 2—4) aminolysis. The enzyme uptake coefficient values decrease with the increase of crosslinking of the support. Catalase is better retained on supports possessing amidoethyleneaminic functional groups (curve 2) than on supports with amidodiethylenediaminic functional groups, proving the influence of the chemical nature of functional groups on the enzyme immobilization process. Also, for the same crosslinking and functional groups (curves 2—4), the uptake coefficient values decrease with the increase of enzyme molecular weight.

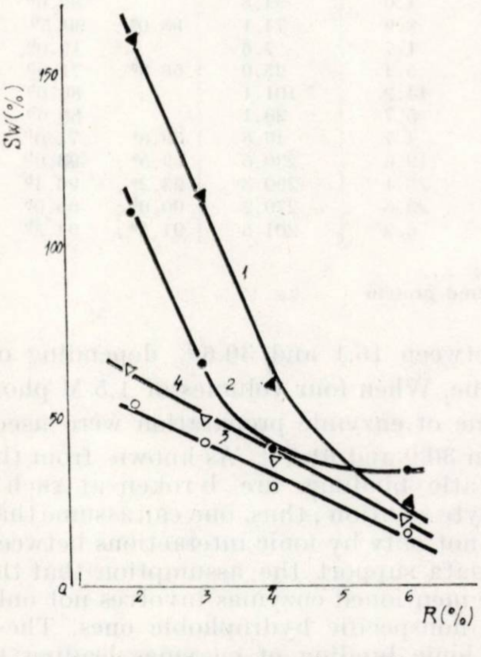

Fig. 3.— Dependence of swelling coefficients on crosslinking and chemical nature of anion exchangers functional groups.
1 — $(-CH_2-CH_2-NH_2)$;
2 — $(-CH_2-CH_2NHCH_2-CH_2-NH_2)$;
3 — $(-(CH_2)_6-NH_2)$.

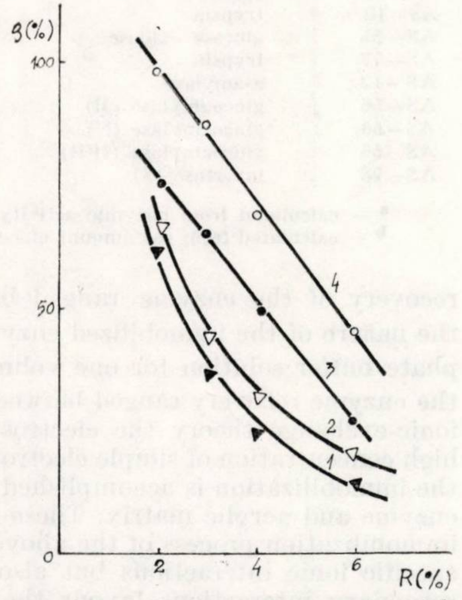

Fig. 4. — Dependence of percent uptake coefficient (β) on crosslinking and chemical nature of support and molecular weight of enzymes. 1 and 2 — catalase; 3 — glucose oxidase; 4 — glucoamylase; 1 — PONILEX-AS (DETA); 2—4—PONILEX-AS (EDA).

Table 3 presents the physico-chemical characteristics of enzymic preparations obtained on acrylic ion exchangers.

To establish the chemical nature of the immobilization process, the enzymic preparations obtained on acrylic supports were undergone to an elution with buffer solutions of 0.2 and 1.5 mol/L concentrations.

Table 4 shows the dependence of desorption function (D%) versus the amount and the concentration of buffer solutions used as desorption agents. The data from Table 4 indicate that using four volumes of 0.2 M phosphate buffer solution for one volume of enzymic preparation, the

Table 3

Physico-chemical characteristics of the enzymic preparations obtained by ionic immobilization of the biologically active proteins on acrylic supports of PONILEX type

Support	Protein	Amount of binding protein		Immobilization yield (γ %)
		mg/mL support	mg/g support	
AS–12	catalase	3.5	30.5	79.8[a]
AS–12	catalase	4.0	34.8	82.0[b]
AS–44	catalase	8.9	74.1	88.0[a]; 90.5[b]
CC–21	catalase	1.7	7.6	15.0[b]
AS–12	trypsin	5.4	25.0	66.8[a]; 71.0[b]
AS–55	glucose oxidase	14.9	101.1	86.0[b]
AS–77	trypsin	5.7	20.1	80.6[b]
AS–12	α-amylase	4.7	40.8	69.8[a]; 71.0[b]
AS–56	glucoamylase (M)	19.6	230.5	89.5[a]; 93.0[b]
AS–56	glucoamylase (N)	25.1	290.3	93.2[a]; 96.4[b]
AS–56	glucoamylase (IFR)	23.5	270.2	90.0[a]; 95.0[b]
AS–98	invertase (S)	6.9	201.5	91.5[a]; 94.5[b]

[a] — calculated from enzymic activity;
[b] — calculated from the amount of bound protein

recovery of the enzyme ranged between 16.1 and 30.6% depending on the nature of the immobilized enzyme. When four volumes of 1.5 M phosphate buffer solution for one volume of enzymic preparation were used, the enzyme recovery ranged between 30.9 and 61.7%. As known from the ionic-exchange theory the electrostatic bindings are broken at such a high concentration of simple electrolyte solution ; thus, one can assume that the immobilization is accomplished not only by ionic interactions between enzyme and acrylic matrix. These data support the assumption that the immobilization process of the above mentioned enzymes involves not only specific ionic interactions but also nonspecific hydrophobic ones. These secondary interactions favour the ionic binding of enzymes leading to their stabilization in the three-dimensional network of the acrylic matrices

CONCLUSIONS

1. The physico-chemical characteristics of acrylic ion exchangers of PONILEX-CC^R and PONILEX-AS^R types confirm that they have elastic, hydrophilic and expanded three-dimensional networks.

2. The immobilization process of catalase, glucoamylase and glucose oxidase is influenced by the crosslinking and chemical nature of the functional groups of the acrylic anion exchangers as well as by the molecular weight of enzyme.

3. The values of immobilization yield (γ) calculated from the catalytic activity of the enzymic preparations proved the possibility of using acryilic supports for the biotechnological applications.

Table 4

Recovery (*D* %) of the biologically active proteins from enzymatic preparations as a function of the amount and concentration of disodiumphosphate solution

Protein	Enzymatic preparation content of protein mg/mL support	Enzymatic preparation content of protein mg/g support	Phosphate 0.2 m/L volumes/volume preparation	*D* %	Phosphate 1.5 mol/L volumes/volume preparation[a)]	*D* %
Catalase	initial		1	7.8	1	42.5
	13.6	112.0	2	15.8	2	52.5
	after elution					
	5.2	42.9	4	30.0	4	61.7
α-Amylase	initial		1	10.2	1	33.6
	10.5	68.3	2	20.4	2	40.8
	after elution					
	5.0	35.2	4	30.6	4	48.0
Glucose oxidase	initial		1	4.4	1	19.3
	14.9	101.2	2	9.1	2	25.1
	after elution					
	10.3	69.9	4	16.1	4	30.9

[a] the elution with 1.5 mol/L phosphate buffer is accomplished on the preparations before subjecting to elution with 0.2 mol/L phosphate buffer

REFERENCES

[1] J. Kukara, M. Kminkova, *Czech. Pat. C.S.*, 209 556 (cl. C12N11/06), Feb. 1982.
[2] Daicel Chem. Ind. Ltd. Jpn. Kokai Tokyo Koho, J.P. 58 212786 (83 212786) (cl. C12N11/12), Dec. 1983.
[3] I. V. Berezin, N. N. Ugarova, L. Yu. Brovko, USSR, S.U. 660 378 (cl. C12N11/02), Dec. 1982.
[4] Matsushita Elec. Works Ltd. Jpn. Kokai Tokyo Koho, J. P., 58 179 494 (83 179 494) (cl. C12N11/02), Oct. 1983.
[5] Mitsubishi Chem. Ind. Co. Ltd. Jpn. Kokai Tokyo Koho, J. P. 57 152 886 (82 152 886) (cl. C12N11/08), Sept. 1982.
[6] Reanal Finomvegyszergyar PCT, Int. Appl. WO, 83 00345 (cl. C12N9/16), Feb. 1983, H.U. Appl. 81/2 088, July 1981.
[7] Sumimoto Chem. Co. Ltd. Eur. Pat. Appl. E.P. 37 667 (cl. C12N11/08), Oct. 1981.
[8] L. Boroș, I. Iozsef, L. Daroczi, B. Szayam, P.C.T.Int. Appl. 80/1 782, July, 1980.
[9] Nitto Electric Instruments Co. Ltd. Kokai Tokyo Koho, J. P., 58 152 486 (83 152 486) (cl. C12 P1/00), 1983.
[10] Kokai Tokyo Koho, J. P. 81 137 882 (cl. C12N11/08), Oct. 1981.
[11] Kokai Tokyo Koho, J. P. 58 116 683 (83 116 683) (cl. C12N11/04) July 1983.
[12] O. Mikes, P. Strop and J. Zbrozek, *J. Chromatog.*, **180,** 17 (1979).
[13] O. Mikes, P. Strop, *J. Chromatogr.*, **192,** 159 (1980).
[14] O. Mikes, P. Strop, Z. Hostomska, *J. Chromatog.*, **301,** 93 (1984).
[15] O. Mikes, P. Strop, Z. Hostomska, *J. Chromatog.*, **261,** 363 (1983).
[16] S. Maxim, A. Flondor, A. Carpov, M. Macoveanu, Al. Tofan, I. Bunia, E. Avădănii, Rom. Pat. 84729, April, 1982.
[17] S. Maxim, A. Flondor, A. Carpov, V. Rugină, D. Cojocaru, I. Bontaș, N. Topală, *Biotechnol. Bioeng.*, **28,** 294 (1986).
[18] Cr. I. Simionescu, V. Popa, S. Maxim, V. Rusan, M. Rusan, *Reactive Polymers*, **5,** 191 (1987).
[19] S. Maxim, A. Flondor, A. Carpov, "Ionic binding of biologically active proteins on crosslinked acrylic macromolecular supports", *Biotechnol. Bioeng.* (in press).
[20] G. P. Noelting, P. Bernfeld, *Helv. Chim. Acta*, **31,** 286 (1948).
[21] M. Kunitz, *J. Gen. Physiol.*, **30,** 291 (1947).

Revue Roumaine de Chimie, 34, 6, 1397–1403 (1989)

SOLVOLYSES IN SUBSTITUTED CYCLOPROPYLCARBINYLIC SYSTEMS. 6[1]

SOLVOLYSIS OF SPIRO[ACENAPHTHENE-1,1′-cyclopropan]-2-OL

[a]ALEXANDRU C. RĂZUȘ,[a] MIRCEA D. GHEORGHIU,[b] ZSOLT G. ARVAY,[a]
ADRIAN I. IANCU[a] and EMERIC BARTHA[a]

[a] Centre of Organic Chemistry, 202 B, Spl. Independenței, R–78100, Bucharest
[b] Department of Organic Chemistry, Polytechnic Institute, Bucharest, Romania

Received October 11, 1988

The solvolysis of spiro[acenaphthene-1,1′-cyclopropan]-2-ol **1** in aqueous dioxane, in the presence of perchloric acid, is described. Cyclopropylic ring-enlargement and cyclopropylic ring-opening products, along with a dimeric alcohol, were obtained. The solvolysis rate of alcohol **1** was compared with that of other spiranic alcohols. A reaction mechanism accounting for the experimental data is proposed.

We have recently reported[1] the solvolytic behaviour of spiro-cyclopropane-indanic alcohols **2**, **3** and **4**, presenting marked differences in both the reaction rates and the nature of the solvolytic products, depending on the benzylic and/or cyclopropylcarbinylic position of the reaction center in the molecule. The solvolysis of spiro[acenaphthene-1,1′-cyclopropan]-2-ol **1** seemed also of interest along the same line.

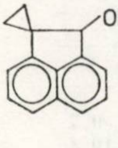

1

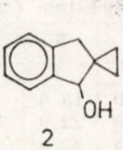

2

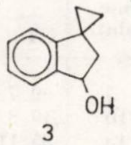

3

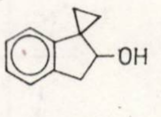

4

The position of the reaction center in alcohol **1** is similar to that in alcohol **2**, enabling the assistance of the aromatic ring as well as the assistance of the cyclopropanic ring. At the same time due to the similar relative position and possibility of interaction between aromatic and cyclopropylic rings, the solvolytic behaviour of alcohol **1** might resemble that of alcohol **4**.

RESULTS AND DISCUSSION

The solvolysis of alcohol **1** was performed in aqueous dioxane, in the presence of perchloric acid. The composition of the reaction mixture was determined by gas-chromatography. The structure assignment for the alcohols obtained as reaction products was based on analytical determinations. Whenever the separation of the alcohols failed, the corresponding acetates or ethers were prepared and separated instead.

The following compounds were identified in the solvolytic reaction mixture: 2-(acenaphthylen-l-yl)-ethanol **5**, the ring-opening product; 6b,7,8,8a-tetrahydro-cyclobut[a]acenaphthylen-8b-ol **6**, the ring-enlargement product; 2-(2-(spiro[acenaphthene-2,1′-cyclopropan]-1-yl)-acenaphthylen-1-yl)-ethanol **7**, a "dimeric" product, and 9,10-dihydro-8H--acenaphtho[1,2-b]pyrane **8**, a product lacking the alcoholic function. Several other unidentified compounds were obtained as well, each component under 0.5% in the reaction mixture.

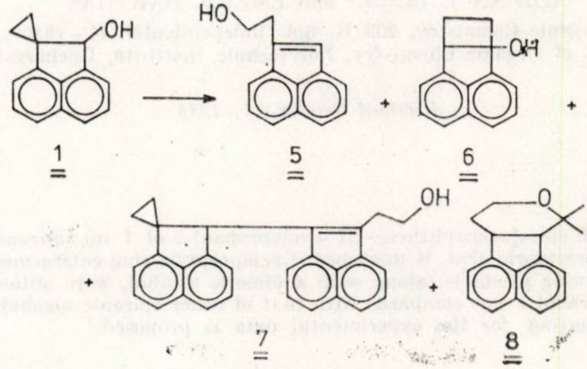

The time-dependent composition of the reaction mixture in a solvolysis carried out at 45°C is displayed in Table 1.

Table 1

Time-dependence of the reaction mixture composition at 45°C

N°	Time (min)	Composition (%) *				
		1	**6**	**5**	**8**	**7**
1	5	69.7	3.0	15.6	0.2	9.7
2	10	49.8	4.9	22.9	0.6	19.4
3	15	35.11	6.4	27.0	0.8	26.7
4	20	24.6	7.4	31.3	1.4	30.6
5	25	21.3	10.1	36.6	1.8	27.8
6	30	11.7	8.5	33.6	2.1	38.9
7	40	5.3	9.2	34.7	2.7	40.4
8	50	2.8	10.0	34.0	3.5	44.1
9	60	1.4	10.0	31.9	4.1	46.0
10	90	0.6	9.0	30.4	6.2	48.8

* up to 100%, unidentified products.

The transformation rate of alcohol **1** during solvolysis is represented by curve A in Figure 1 (for comparison, the correponding curves for the solvolyses of alcohols **2** and **4** performed under comparable conditions of concentration and acidity are displayed).

The first observation to be explained is the appearance of dihydropyran **8**. We have previously[1] noticed the formation, in small amounts, of dihydropyranic compounds during solvolysis of other spiranic compounds. These amounts decrease (and may reach even undetectable concentrations) on careful purification of the dioxane used as solvent. Assuming that acetaldehyde or a hydrolysable acetaldehyde acetal exists as impurity in dioxane, supplemental acetaldehyde was added in the reaction medium. An increase in dihydropyran **8** along with a decrease in homoallylic alcohol **5** was observed. This fact proves that dihydropyran **8** stems from the reaction between the homoallylic alcohol and a carbonyl derivative, a general reaction for the preparation of dihydropyrans [2]. The study of several examples of this reaction is in progress and will be published soon.

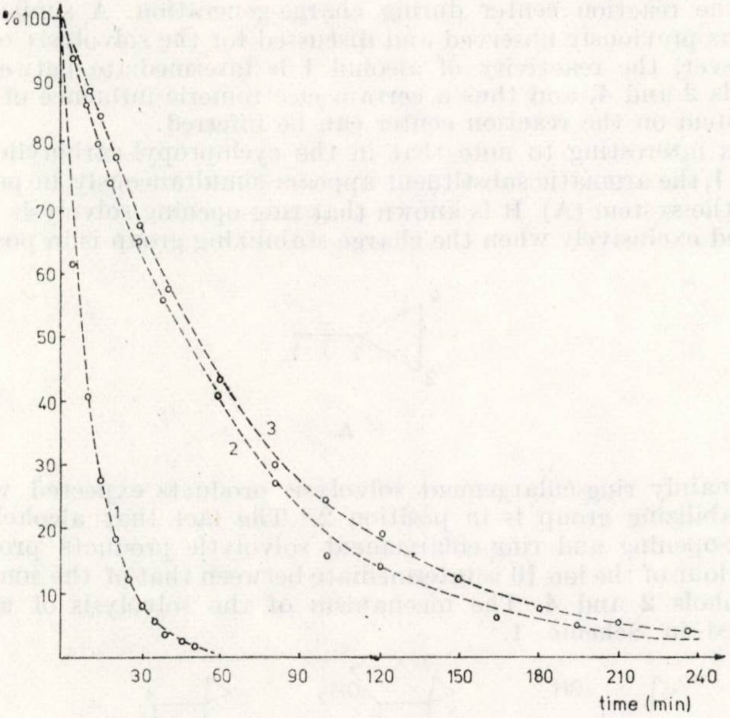

Fig. 1. — Time-dependent disappearance curves of the alcohols: 1 = alcohol **2**; 2 = alcohol **1**; 3 = alcohol **4**.

The experimental data indicate a different solvolytic behaviour of alcohols **1** and **2**. Indeed, while the consumption rate of alcohol **2** is high even at low temperatures, the consumption rate of alcohol **1** is much slower and comparable sooner with that of alcohol **4**.

There is still another important difference between alcohols **1** and **2**. The sole solvolysis product of alcohol **2** is the ring-opening product. In the solvolysis of alcohol **1**, besides homoallylic alcohol **5**, the ring-enlargement product (cyclobutanic alcohol **6**) as well as "dimeric" alcohol **7** were obtained (as discussed above, dihydropyran **8** originates from alcohol **5**).

The slower solvolysis rate of alcohol **1** compared with that of alcohol **2** could be explained by a diminished participation of the cyclopropanic ring to the reaction center during charge-generation. A similar inactivation was previously observed and discussed for the solvolysis of alcohol **4**.[1] However, the reactivity of alcohol **1** is intermediate between those of alcohols **2** and **4**, and thus a certain electromeric influence of the aromatic system on the reaction center can be inferred.

It is interesting to note that in the cyclopropyl-carbinylic system of alcohol **1**, the aromatic substituent appears simultaneously in positions 1 and 2 of the system (A). It is known that ring-opening solvolysis products are formed exclusively when the charge-stabilizing group is in position 1,[3]

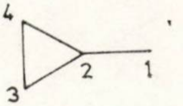

A

whereas mainly ring-enlargement solvolysis products expected when the charge-stabilizing group is in position 2.[4] The fact that alcohol **1** gave both ring-opening and ring-enlargement solvolytic products proves that the behaviour of the ion **10** is intermediate between that of the ions formed from alcohols **2** and **4**. The mechanism of the solvolysis of alcohol **1** is depicted in Scheme 1.

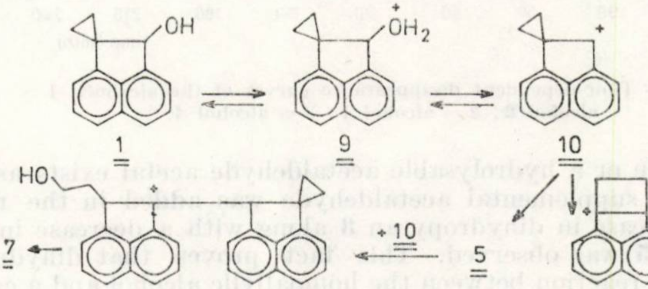

SCHEME 1

The reason for the formation of dimer **7** in the solvolysis of alcohol **1** but not in the solvolysis of alcohol **2** is still to be explained (Scheme 2). In the latter case, formation of the dimer assumes the electrophilic attack of carbocation **13** at the double bond in the homoallylic alcohol **14**. Due to its low electrophilicity, carbocation **13** reacts mainly with the stronger nucleophile in the medium, namely water molecules, regenerating the starting alcohol **2**. The formation of the alcohol **14** takes place through the displacement of the equilibrium towards the thermodynamically most stable product. Should the double bond in alcohol **14** be attacked, it would be with generation of the benzylic carbocation **15**.

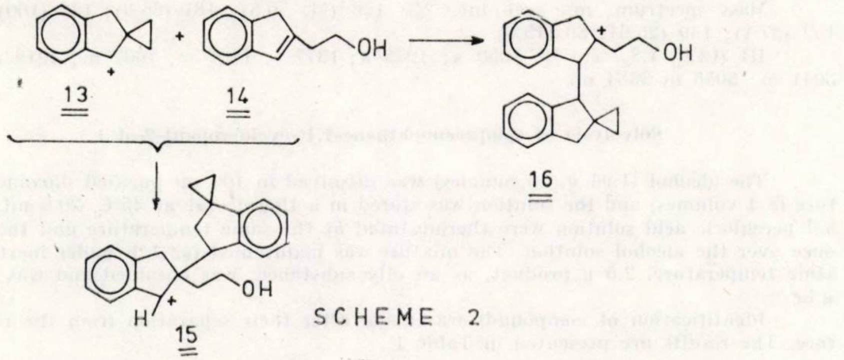

SCHEME 2

In this cation, proton elimination with formation of a double bond is not possible. The formation of ion **16** (in which proton-elimination may occur) is improbable, due to its relatively low stability in comparison with that of ion **13**.

The present results are in good agreement with those previously reported for spiro-cyclopropanindanic series.[1] If in position 2 of the cyclopropylcarbinylic system there is an aromatic substituent which is forced to adopt a position bisecting the cyclopropanic ring, this diminishes the cyclopropyl participation to the reaction center, probably due to stereoelectronic effects. Also, the presence of an aromatic nucleus in position 1 and/or 2 of the system plays a decisive role in the distribution of the solvolytic products.

EXPERIMENTAL

The melting and boiling points are both uncorrected. The IR spectra have been recorded on a Carl Zeiss Jena spectrophotometer. The $^{1}H-NMR$ spectra have been recorded on a VARIAN A 60-A spectrometer, using TMS as internal standard. The $^{13}C-NMR$ spectra have been recorded on a VARIAN FT 80-A spectrometer. The g.l.c. analyses have been performed on a Carlo Erba model Fractovap 230 gas chromatograph, using FID detector and a capillary column made from fused silica, 10 m × 0.2 mm, coated with SE 54; H_2 flow of 1 mL/min; programmed heating 130°C 2 minutes isothermal then 20°C/min 130—230°C.

Synthesis of starting materials

Spiro[acenaphthene-1,1′-cyclopropan]-2-one was prepared by the described method,[5] mp 108°C (methanol; lit.[5] 108°C; the $^{1}H-NMR$ and IR spectra are identical to those described).

Spiro[acenaphthene-1,1′-cyclopropan]-2-ol **1**, was obtained by reduction of spiro[acenaphthene-1,1′-cyclopropan]-2-one in the presence of sodium borohydride, in aqueous methanol, mp 108—110°C (benzene).

$^{1}H-NMR$ ($CDCl_3$, δ, ppm): 0.63—1.83 (m, 4H, cyclopropyl); 2.33 (d, J = 10 Hz, 1H, OH, change with D_2O); 4.92 (d, J = 10 Hz, 1H, C*H*—OH); 6.62 (dd, J_{ortho} = 7.5 Hz,

$J_{meta} = 2$ Hz, 1H, CH-aromatic *ortho* in raport with cyclopropyl); 7.07–7.77 (m, 5H, CH-aromatic).

^{13}C–NMR ($CDCl_3$, δ, ppm): 12.89 (t); 18.21 (t); 33.20 (s); 79.01 (d); 113.04 (d); 120.69 (d); 121.95 (d); 124.75 (d); 127.97 (d); 128.25 (d); 130.56 (s); 136.62 (s); 144.22 (s); 147.56 (s).

Mass spectrum: m/e (rel. int. %): 196 (M, 70.5); 181 (66.9); 168 (100); 165 (65); 152 (37.1); 139 (25.6); 89 (15.6).

IR (CCl_4, CS_2, cm^{-1}): 1050 s; 1079 s; 1377 s; 1491 w; 1602 m; 2919 m; 2997 m; 3041 m; 3056 m 3584 m.

Solvolysis of spio[acenaphthene-1,1′-cyclopropan]-2-ol 1

The alcohol (1.96 g, 10 mmoles) was dissolved in 100 ml purified dioxane-water mixture (5:4 volumes) and the solution was stored in a thermostat at 45°C. 20.0 mL of aqueous 5M perchloric acid solution were thermostated at the same temperature and then, added at once over the alcohol solution. The mixture was maintained for 1 h under inert gas, at the same temperature. 2.0 g product, as an oily substance, was obtained and was analysed by g.l.c.

Identification of compounds was made after their separation from the reaction mixture. The results are presented in Table 1.

Separation and characterization of solvolysis products of alcohol 1

The separation of approx. 2 g raw mixture resulted from solvolysis was performed on a 40 cm × 20 mm column packed with silica gel (Merk, 70/325 mesh). Fraction I: eluent, petroleum ether (bp 28–32°C); under 2% from the mixture to be separed. Content: a mixture of non-identified substances (yellow colored). Fraction II: eluent, petroleum ether: ethylic ether (4:1 volumes); approx. 5% from the mixture. Content: 95–97% dihydropyran **8** and a non-identified compound. This fraction was triturated with a mixture of petroleum ether: ethylic ether (1:1) and dihydropyran **8** was obtained chromatographically pure, as yellow crystals, mp 73–75°C. The characteristic OH bands are absent in the IR spectrum of this fraction. The structure of dihydropyran **8** will be analysed in a following paper. Fraction III: eluent, petroleum ether: ethylic ether (1:1): approx. 10% from the mixture. Content: almost pure cyclobutanic alcohol **6**, m.p. 138–150°C; crystallised from benzene; m.p. 149–150°C.

^1H–NMR ($CDCl_3$, δ, ppm): 1.1–1.5 (m, 1H); 2.1–2.9 (m, 4H); 3.82 (dd, $J = 7_1$Hz, $J_2 = 9.5$ Hz, 1H, CH-benzylic); 7.0–7.8 (m, 6H, CH-aromatic).

^{13}C–NMR ($CDCl_3$, δ, ppm): 22.52 (t); 34.62 (t); 52.40 (t); 84.10 (s); 118.8 (d); 118.85 (d); 122.73 (d); 125.01 (d); 128.24 (d); 131.61 (s); 138.16 (s); 146.37 (s); 147.75 (s).

Mass spectrum: m/e (rel. int. %): 196 (M, 17.2); 181 (20.2); 168 (100); 165 (26.2); 152 (15.4); 139 (19.5); 97 (5.3); 89 (3.3).

IR (CCl_4, CS_2, cm^{-1}): 1086 s; 1359 m; 1488 w; 1601 w; 2857 w; 2946 m; 2984 m; 3051 m; 3250–3550 w; 3589 m.

Fraction IV: eluent, petroleum ether: ethylic ether (1:1); approx. 80% from the mixture. Content: approx. 60% homoallylic alcohol **5** and 40% dimeric alcohol **7**. From this mixture, partially crystallizes the dimeric alcohol. For separation and characterization alcohols **5** and **7** have been transformed into corresponding acetates. Fraction V: eluent, ethylic ether; approx. 5% from the mixture. Contains a mixture of several non-characterized heavy products.

Separation of alcohols 5 and 7

Fraction IV (0.5 g, approx. 1.86 mmoles) was acylated and 0.5 g oily mixture of acetates was obtained. This mixture was chromatographed on a 40 cm × 20 mm column packed with neutral alumina. Fraction 1: eluent, petroleum ether: ethylic ether (4:1 volumes). Content: acetate of alcohol **5** (**5**–OAc), oil, bp 178–180°C/2–3 mm.

^1H–NMR (CCl_4, δ, ppm): 1.91 (s, 3H, CH_3–CO); 2.95 (bt, $J = 7.5$ Hz, $J_{allylic}$ small, 2H, CH_2 allylic); 4.3 (t, $J = 7.5$ Hz, 2H, CH_2–OH); 6.6 (b, $J_{allylic}$ small, 1H, CH=); 7.22–7.7 (m, 6H, CH aromatic).

IR (CCl_4, cm^{-1}): 1052 s; 1242 vs; 1365 m; 1492 m; 1456 w; 1476 w; 1736 vs; 2860 w; 2961 w; 3066 w.

Fraction 2: eluent, petroleum ether:ethylic ether (1:1) Content: acetate of the alcohol **7** (**7**–OAc), mp 179–180°C (acetic acid).

^{1}H–NMR ($CDCl_3$, δ, ppm): 0.72–1.93 (m, 4H, cyclopropyl); 2.04 (s, 3H, CH_3–CO); 3.37 (t, 2H, CH-allylic); 4.41 (t, 2H, CH_2–OH); 5.04 (bs, 1H, CH-benzylic allyl); 6.32 (dd, J_{ortho} = 6 Hz, J_{meta} = 1 Hz, CH-aromatic ortho in relation with cyclopropyl); 6.7–7.85 (m, 11H, CH-aromatic).

IR (CCl_4, cm^{-1}): 1041 s; 1240 vs; 1363 m; 1475 m; 1734 vs; 2860 w; 2954 m; 3049 m; 3064 m.

Alcohol **5** was obtained by hydrolysis of fraction 1, yellow crystals, mp 44–45°C (not stable at storage).

^{1}H–NMR ($CDCl_3$, δ, ppm): 2.65 (bs, 1H, OH, change with D_2O); 2.89 (bt, J = 7.5 Hz, $J_{allylic}$ small, 2H, CH_2 allylic); 3.82 (t, J = 7.5 Hz, 2H, CH_2–OH); 6.68 (bs, $J_{allylic}$ small, 1H, CH=); 7.23–7.88 (m, 6H, CH-aromatic).

IR (CCl_4, cm^{-1}): 1048 vs; 1379 w; 1428 m; 1460 w; 1475 w; 1552 w; 2880 m; 2945 m; 3065 m; 3200–3570 w; 3625 w.

Mass spectrum: m/e (rel. int. %): 196 (M, 19.8); 178 (5.0); 166 (21.3) 165 (100); 152 (2.9); 139 (2.9); 115 (1.1); 88 (1.2); 82 (5.5).

Alcohol **7** was obtained by hydrolysis of fraction 2, yellow crystals, mp 163–165°C (benzene-hexane).

^{1}H–NMR (C_6D_6, δ, ppm) 0.54–1.68 (m, 4H, cyclopropyl); 2.85 t, J = 7.5 Hz, 2H, CH_2 allylic); 3.67 (t, J = 7.5 Hz, 2H, CH_2–OH); 4.98 (bs, 1H, CH-benzylic allyl); 6.63 (dd, J_0 = 6.5 Hz, J_m = 2 Hz, 1H, CH-aromatic *ortho* in relation with cyclopropyl); 6.97–7.87 (m, 11H, CH-aromatic).

IR (CCl_4, cm^{-1}): 1059 s; 1370 m; 1481 m; 1600 m; 2881 m; 2947 m; 3039 m; 3065 m; 3601 m.

Mass spectrum: m/e (rel. int. %): 374 (M, 32.4); 356 (3.5); 343 (18.4) 341 (17); 339 (12); 330 (26); 329 (100); 328 (68.3); 327 (89); 326 (98.1); 325 (30.9); 324 (27.3); 323 (10.5); 316 (19.6); 315 (63.1); 314 (53.8); 313 (65.5); 312 (17.3); 311 (11.6); 303 (10.9); 302 (15.7); 210 (10.1); 209 (64.1); 179 (55.7); 178 (38.3); 170 (17.5); 169 (10.3); 166 (12.6); 165 (59.4); 164 (34.7); 163 (53.3); 157 (28.6).

Separation of methylic ethers of alcohols 5 and 7

The mixture of the alcohols **5** and **7** (0.5 g, 1.86 mmoles), was methylated with methyl iodide in DMSO in the presence of NaOH. The methylation take s place almost quantitatively and gives the methylic ethers **5**-OCH_3 and **7**-OCH_3, which are separated on a 40 cm × 20 mm column packed with neutral alumina. The first fraction, a yellow oil, is eluted with petroleum ether (bp 28–32°C) and is the **5**-OCH_3 ether.

^{1}H–NMR ($CDCl_3$, δ, ppm): 3.01 (bt, J = 7 Hz, $J_{allylic}$ small, 2H, CH_2 allylic); 3.33 (s, 3H, O–CH_3); 3.67 (t, J = 7 Hz, 2H, CH_2–O); 6.68 (bs, $J_{allylic}$ small, 1H, HC=); 7.18–7.62 (m, 6H, CH-aromatic).

The second fraction is eluted with petroleum ether: ethylic ether (9:1) and is the **7**-OCH_3 ether, yellow crystals, mp 119–120°C (petroleum ether).

^{1}H–NMR ($CDCl_3$, δ, ppm): 0.78–1.63 (m, 4H, cyclopropyl); 3.13 (bt, J = 7 Hz, $J_{allylic}$ small, 2H, CH_2 allylic); 3.37 (s, 3H, O–CH_3); 3.7 (t, J = 7 Hz, 2H, CH_2O); 5.08 (bs, 1H, CH-benzylic allyl); 6.31 (d, J = 6.5 Hz, CH aromatic *ortho* in relation with cyclopropyl); 6.7–7.83 (m, 11H, CH-aromatic).

^{13}C–NMR ($CDCl_3$, δ, ppm): 17.28 (t); 18.83 (t); 31.86 (s); 48.76 (d); 58.67 (q); 73.20 (t); 113.03 (d); 120.39 (d); 121.99 (d); 122.98 (d); 123.35 (d); 125.87 (d); 126.73 (d); 127.19 (d); 127.56 (d); 127.85 (d); 127.99 (d); 128.11 (d); 128.26 (d); 128.87 (s); 131.12 (s); 136.06 (s); 138.29 (s); 139.06 (s); 139.20 (s); 140.10 (s); 147.52 (s); 150.62 (s).

IR (CCl_4, cm^{-1}): 1119 s; 1368 m; 1428 m; 2823 m; 2868 m; 2920 m; 2984 m; 3059 m.

REFERENCES

[1] Part 5 ,A. C. Răzuș, M. D. Gheorghiu and E. Bartha, *Rev. Roumaine Chim.*, **34**, 000 (1989)
[2] P. H. Williams, G. G. Ecke and S. A. Ballard, *J. Amer. Chem. Soc.*, **72**, 5738 (1959).
[3] T. A. Favorskaya, O. V. Sergievskaya and N. P. Ryzhova, *J. Gen. Chem. USSR*, **27**, 1018 (1957); C. G. Ricey Jr., and J. M. Ricey, *J. Amer. Chem. Soc.*, **88**, 4971 (1966).
[4] D. D. Roberts, *J. Org. Chem.*, **30**, 23 (1965).
[5] A. Jonczyle, B. Serafim and E. Skulimovska, *Rocz. Chem.*, **45**, 1259 (1971).

Revue Roumaine de Chimie, **34**, *6*, 1405–1411 (1989)

KINETICS OF THE BACK-EXTRACTION OF IRON β-DIKETONATES

IOAN SÂRGHIE and CATINCA SIMION
Faculty of Chemical Technology, Polytechnic Institute Iaşi, Splai Bahlui 71, Iaşi, Romania

Received October 25, 1988

The study of the back-extraction kinetics of the benzoylacetonate, dibenzoylmethanate and iron thenoyltrifluoroacetonate from carbon tetrachloride in strong acid solutions is reported. The partial reaction order with respect to iron and the activation parameters of the back-extraction process have been determined.

INTRODUCTION

In certain cases, in order to determine quantitatively or to separate the elements contained in the organic phase, resulted from an extraction with solvents, these elements must be transferred in another medium (preferably aqueous). The reverse extraction process, that of the metallic ion passage from the organic phase into the aqueous phase was called back-extraction. In order to recuperate the extracted element, the method of evaporating the organic solvent will be used, followed by the complex destruction. When the element extracted in the organic phase as a complex cannot be concentrated by solvent evaporation or the complex in organic phase easily evaporates, the method of back-extraction can be applied using aqueous solutions containing certain reagents able to facilitate the pass of extracted element in aqueous phase. Although the back-extraction is often used, few systematic studies in this field were reported.[1-3]

The kinetics of iron extraction with benzoylacetone,[4] dibenzoylmethane[5] and thenoyltrifluoroacetone[6] in carbon tetrachloride proves that the extraction proceeds slowly, according to a first reaction order with respect to iron.

EXPERIMENTAL

For the back-extraction solutions of iron benzoylacetonate containing 54 μg Fe^{3+}/mL iron dibenzoylmethanate containing 45 μg Fe^{3+}/mL or iron thenoyltrifluoroacetonate containing 68 μg Fe^{3+}/mL in carbon tetrachloride, were used. As back-extraction reagent solutions of hydrochloric or perchloric acid of various concentrations were used. All the experiments were carried out using a thermostated rotating device.[6] It was found experimentally that the process did not depend on the stirring rate within the range of 40–80 r.p.m. and therefore all the experiments were carried out at 60 r.p.m. The iron was determined spectrophotometrically using 1,10-phenanthroline.[7]

RESULTS AND DISCUSSION

Back-extraction of the Iron Benzoylacetonate (Ba – Fe)

The experiment proves that back-extraction of iron in the organic phase containing iron benzoylacetonate with solutions of hydrochloric or perchloric acid with a concentration higher than 1 M takes place rapidly (less than 5 minutes). If the acid concentration is less than 1 M, the process of iron back-extraction from the organic phase in the aqueous phase takes place slowly. The back-extraction percentage ($E\%$) depends both on the strong acid concentration and the temperature at which the equilibrium is attained. The temperature rise increases the back-extraction rate (Fig. 1).

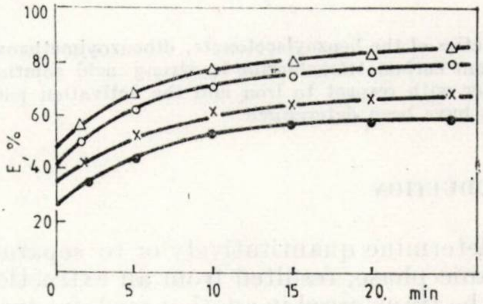

Fig. 1. – Kinetics of the back-extraction of iron benzoylacetonate.
--●--, $t = 8°C$; --x--, $t = 15°C$
--○--, $t = 25°C$; --Δ--, $t = 35°C$.

By plotting $\lg ([Fe]_{(0),\, t=0}/[Fe]_{(0),\, t}) = \lg \alpha$ versus the duration of phase agitation, straight lines are obtained indicating the iron back-extraction from the organic phase containing the iron benzoylacetonate dissolved in carbon tetrachloride with perchloric acid to correspond to a first order kinetics with respect to iron (Fig. 2).

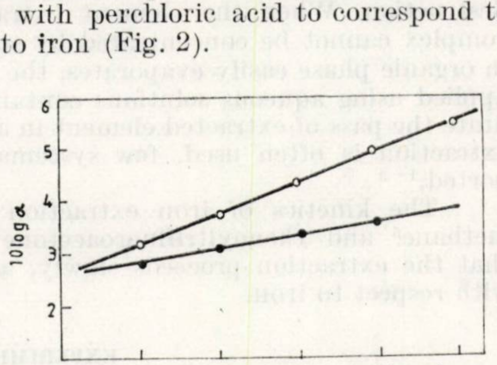

Fig. 2. – Plots lg α versus time for the back-extraction of iron benzoylacetonate with 0.069 M solutions of perchloric acid.
--●--, $t = 8°C$; --○--, $t = 15°C$.

Back-extration of the Iron Dibenzoylmethanate (DBM – Fe)

The stirring rate being kept constant in this case, too, (60 r.p.m.) the back-extraction rate of the iron dibenzoylmethanate depends on both the acid concentration and temperature. By increasing the concentration of perchloric acid and the equilibrium temperature higher back-extraction rates are obtained (Figs 3 and 4). By plotting lg α versus time, straight lines have been obtained which shows a first order kinetics for the back-extraction reaction (Figs 5 and 6).

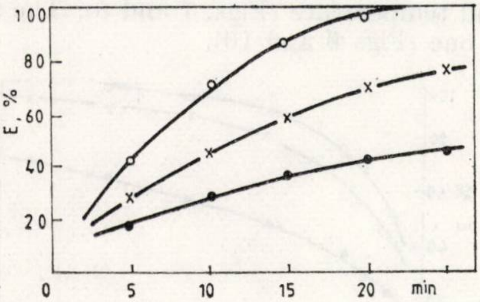

Fig. 3. — Kinetics of the back-extraction of iron dibenzoylmethanate with 1.02 M solutions of perchloric acid.
-- ● --, $t = 15$ °C ; -- x --, $t = 25$°C
-- o --, $t = 35$°C.

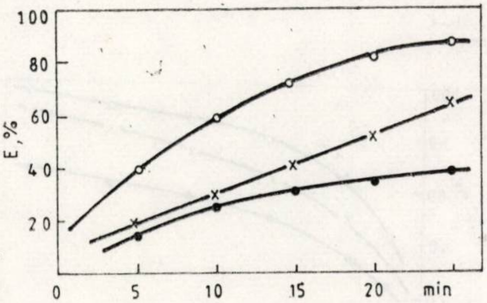

Fig. 4. — Kinetics of the back-extraction of iron dibenzoylmethanate with 0.72 M solutions of perchloric acid.
-- ● --, $t = 15$°C ; -- x --, $t = 25$°C
-- o --, $t = 35$°C.

Fig. 5. — Lgα versus time plots for the back-extraction of iron dibenzoylmethanate with 1.02 M solutions of perchloric acid.
-- ● --, $t = 15$°C ; -- x --, $t = 25$°C
-- o --, $t = 35$°C.

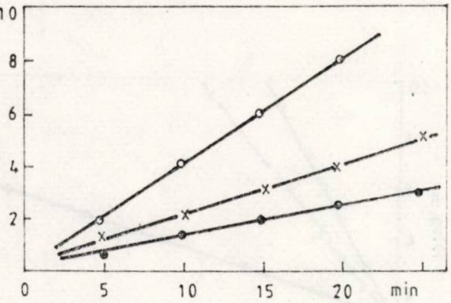

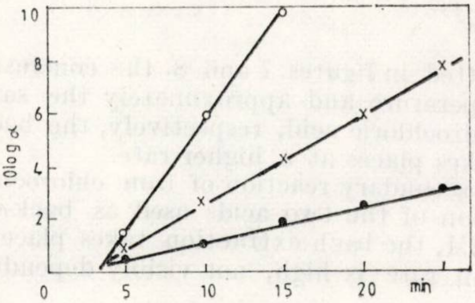

Fig. 6. — Lgα versus time plots for the back-extraction of iron dibenzoylmethanate with 0.72 M solutions of perchloric acid.
-- ● --, $t = 15$°C ; -- x --, $t = 25$°C
-- o --, $t = 35$°C.

Back-extraction of the Iron Thenoyltrifluoroacetonate (TTA – Fe)

As back-extraction reagents 1.46 M perchloric acid and 1.48 M hydrochloric acid have been used. Under constant stirring rate (60 r.p.m.) the back-extraction rate was found to depend on the acid concentration and temperature (Figs. 7 and 8). The reaction order with respect to iron is one (Figs 9 and 10).

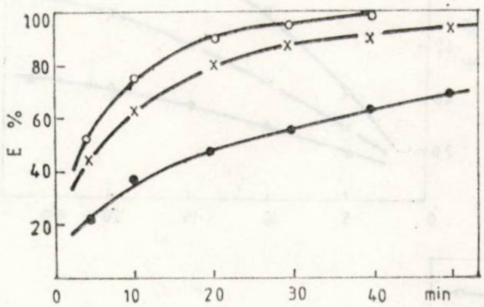

Fig. 7. – Kinetics of the back-extraction of iron thenoyltrifluoroacetonate 1.46 M solutions of perchloric acid.
--●--, $t = 15°C$; --x--, $t = 25°C$; --o--, $t = 35°C$.

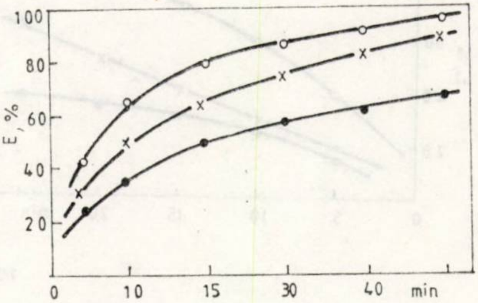

Fig. 8. – Kinetics of the back-extraction of iron thenoyltrifluoroacetonate 1.48 M solutions of hydrochloric acid.
--●--, $t = 15°C$; --x--, $t = 25°C$
--o--, $t = 35°C$.

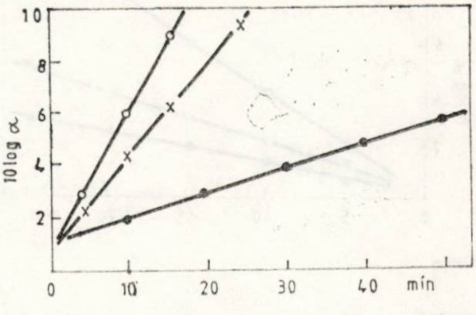

Fig. 9. – Lgα versus time plots for the back-extraction of iron thenoyltrifluoroacetonate with 1.46 M solutions of perchloric acid.
--●--, $t = 15°C$; --x--, $t = 25°C$
--o--, $t = 35°C$

By comparing the results plotted in figures 7 and 8 the conclusion can be drawn that at the same temperature and approximately the same molarity of perchloric acid and hydrochloric acid, respectively, the back-extraction with perchloric acid takes places at a higher rate.

This can be explained by the secondary reaction of iron chlorocomplex formation. If the concentration of the two acids used as back-extraction reagents is higher than 2M, the bach-extraction takes place in a few minutes, the back-extraction rate is high, not visibly depending on the acid type.

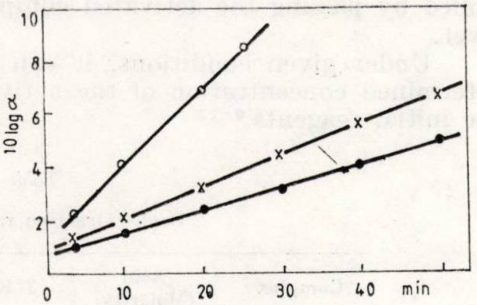

Fig. 10. — Lgα versus time plots for the back-extraction of iron thenoyltrifluoroacetonate with 1.48 M solutions of hydrochloric acid.
--●--, t = 15 °C; --x--, t = 25°C
--o--, t = 35 °C.

Mechanism of the Back-extraction

The analysis of the kinetic data obtained in the slow back-extraction of iron β-diketonates with strong acids shows the back-extraction of the iron benzoylacetonate to take place with diluted acids, while the back-extraction of the dibenzoylmethanate and iron thenoyltrifluoroacetonate can be achieved with more concentrated acids. In case of the iron benzoylacetonate the mechanism of the process can be considered as being given by the repartition of the chelate compound between the two phases, while the back-extraction of iron from the organic solutions containing dibenzoylmethane and thenoyltrifluoroacetone is determined by the chelate decomposition due to the high acidity of the aqueous phase.

The mechanism of the back-extraction is given by the equilibrium :

$$FeR_{3(0)} \rightleftarrows FeR_3$$

$$FeR_3 + 3H^+ \rightleftarrows Fe^{3+} + 3\ HR$$

where HR is the β-diketone and the index (0) refers to the organic phase.

The order of reaction in case of the back-extraction of the iron β-diketonates is equal to one, which corresponds to the proposed mechanism. The concentration of the acid being much higher than the concentration of the β-diketonates, it may be considered that during the whole process of back-extraction, $[H^+]$ is constant and the back-extraction rate is proportional to the concentration of β-diketonate.

Since $t_{1/2}$ can easily be determined graphically, then the back-extraction rate constant (Table 1) for a first-order reaction is

$$k = \frac{0.693}{t_{1/2}}$$

where $t_{1/2}$ is the half life.

Activating Parameters

The activation energy may be calculated using the equations of statistic thermodynamics.[8] Assuming that the reactants are at a given time under the form of activated complex, then the reaction rate is controlled by passing the activated complex through the maximum energy level.

Under given conditions, it can also be admitted that there is a determined concentration of the activated complex in equilibrium with the initial reagents.[9-12]

Table 1

Back-extraction rate constants

Complex	Acid (Molarity)	T°K	$t_{1/2}$ (min)	k (min^{-1})
BA–Fe	$HClO_4$ (0.069 M)	281	5.00	0.1386
		288	4.06	0.1733
		298	3.00	0.2310
		308	2.10	0.3466
DBM–Fe	$HClO_4$ (1.02 M)	288	27.50	0.0252
		298	11.50	0.0603
		308	6.00	0.1155
	$HClO_4$ (0.72 M)	288	39.00	0.0178
		298	17.00	0.0408
		308	7.20	0.0962
TTA–Fe	$HClO_4$ (1.46 M)	288	19.50	0.0355
		298	5.00	0.1384
		308	4.00	0.1733
	HCl (1.48 M)	288	18.60	0.0373
		298	10.50	0.0661
		308	5.30	0.1322

Taking into account the above assumption, the expression of the back-extraction rate constant can be written:

$$k = \frac{KT}{h} \exp\left(\frac{\Delta S^{\neq}}{R}\right) \exp\left(-\frac{\Delta E^{\neq}}{RT}\right) \qquad (1)$$

where K is Boltzmann's constant, R is gas constant, $\Delta E^{\neq}$ is the energy surplus of the activated complex in comparison with the energy of reactants and $\Delta S^{\neq}$ is the entropy of the activated complex.

An approach between equation (1) and Arrhenius' equation:

$$k = A \exp\left(\frac{\Delta E^{\neq}}{RT}\right) \qquad (2)$$

within the considered temperature range can be established if there is a correspondence between them. Using relations (1) and (2), the activation energy and activation entropy of the back-extraction process were calculated, their values being given in Table 2.

In conclusion, assuming that the reactants are at a certain time under the form of activated complex, the activation parameters of the back-extraction process have been calculated.

Table 2

Activation energy and entropy of the back-extraction process

Complex	Acid (molarity)	Dependence of activation entropy of the reaction rate constant on temperature	$\Delta E^{\neq}$ $\frac{\text{kcal}}{\text{mol}}$	$\Delta S^{\neq}$ (20°C) $\frac{\text{U.e}}{\text{mol}}$
BA–Fe	$HClO_4$ (0.069 M)	$\lg k = 0.976 - 0.499 \cdot 10^3\ T^{-1}$ $\Delta S^{\neq} = -42.738 - 4.575\ \lg T$	2.283	−52.651
DBM–Fe	$HClO_4$ (1.02M)	$\lg k = 8.676 - 2.955 \cdot 10^3\ T^{-1}$ $\Delta S^{\neq} = -7.515 - 4.575\ \lg T$	13.518	−17.427
	$HClO_4$ (0.72M)	$\lg k = 9.724 - 3.306 \cdot 10^3\ T^{-1}$ $\Delta S^{\neq} = -2.721 - 4.575\ \lg T$	15.124	−12.634
TTA–Fe	$HClO_4$ (1.46M)	$\lg k = 9.469 - 3.123 \cdot 10^3\ T^{-1}$ $\Delta S^{\neq} = -3.887 - 4.575\ \lg T$	14.285	−13.800
	HCl (1.48M)	$\lg k = 7.137 - 2.470 \cdot 10^3\ T^{-1}$ $\Delta S^{\neq} = -14.556 - 4.575\ \lg T$	11.299	−24.469

REFERENCES

[1] T. Kato, *Bull. Chem. Soc. Japan*, **37**, 1453 (1964).

[2] N. Suzuki and T. Omori, *Bull. Chem. Soc. Japan*, **35**, 595 (1962).

[3] N. Suzuki and T. Kato, *J. Chem. Soc. Japan*, **80**, 132 (1959).

[4] I. Sârghie and S. Fişel, *An. St. Univ. Iaşi* (Romania), **19**, 133 (1973).

[5] I. Sârghie and S. Fişel, The Proceedings of the third National Conference of Analytical Chemistry, Timişoara (Romania), vol. IV, 245 (1971).

[6] I. Sârghie and S. Fişel, *Chimia analitică*, Bucharest, **2**, 113 (1972).

[7] O. G. Koch and G. A. Koch-Dedic, "Handbuch der Spuranalyse", Springer Verlag, Berlin, 544, 1964.

[8] V. N. Kondratiev, *Kinetica Khimicheskikh Gazovykh Reaczij*, Isdatelstvo Akademii Nauk S.S.S.R, Moskva, 162 (1958).

[9] D. Cismaru, *Studii Cercet. Chim. Acad. R.P.R.*, **5**, 119 (1957).

[10] I. Sârghie and A. Bold, *Rev. Chim. (Bucureşti)*, **29**, 1075 (1978).

[11] I. Sârghie and S. Fişel, *Rev. Roumaine Chim.*, **24**, 619 (1979).

[12] I. Sârghie, E. Sârghie and V. Sunel, *Rev. Chim. (Bucureşti)*, **32**, 57 (1981).

Revue Roumaine de Chimie, 34, *6*, 1413 – 1417 (1989)

COORDINATION POLYMERS. VIII[1]

CHELATE POLYMERS OF 2,4-DIHYDROXYACETOPHENONE

MIHAELA SPIRATOS, A. AIRINEI, N. STĂNICĂ *, N. VOICULESCU
and G. I. RUSU
Institute of Macromolecular Chemistry "P. Poni",
R-6600, Iași, Romania
* Center of Physical Chemistry, Bucharest, Romania

Received September 12, 1988

Polychelates derived from 2,4-dihydroxyacetophenone with some divalent ions as iron, cobalt, nickel, copper, zinc and organic acid chlorides were synthesized and characterized in terms of spectral, magnetic, thermal and electrical properties.

In continuation of our studies on the coordination polymers,[1–5] we report here the synthesis and characterization of new polychelates derived from bis(2,4-dihydroxyacetophenone) M^{2+} and bis(2,4-dihydroxyacetophenone)ethylenediimine M^{2+} with organic acid chlorides.

The polychelates have the following general formulae :

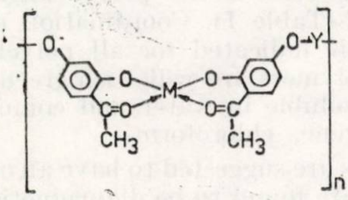

where : M = Fe^{2+} (I) ; Co^{2+} (II) ; Ni^{2+} (III) ; Zn^{2+} (IV) for chelates, and :

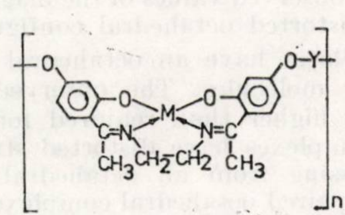

where : M=Fe^{2+}(V) ; Co^{2+} (VI) ; Zn^{2+} (VII) for chelates, and : I_a – VII_a : Y=p – COC_6H_4CO – ; I_b – VII_b : Y=m – COC_6H_4CO – for polychelates.

EXPERIMENTAL

The method described in literature [6] for the synthesis of bis(2,4-dihydroxyacetophenone) Cu^{2+} was employed to prepare the metal chelates with Fe^{2+} (I), Co^{2+} (II) and Ni^{2+} (III).

Bis(2,4-dihydroxyacetophenone) Zn^{2+} (IV) was prepared as described bellow. A solution of 2,4-dihydroxyacetophenone (0.2 mol) in 50 mL of methanol was added to a solution of sodium hydroxide (4 g) in 200 mL water, at room temperature, with good stirring. When the temperature of reaction mixture was 63—65°C, a solution of $ZnCl_2$ (0.1 mol) in 100 mL of water was added under stirring. Then, the reaction mixture was maintained at 65°C for 30 min. The separated product was filtered, washed with ethanol and dried in vacuo.

Bis(2,4-dihydroxyacetophenone)ethylenediimine was obtained in this way: A hot solution of 80% ethylenediimine (0.01 mol) was added to a solution of 2,4-dihydroxyacetophenone (0.2 mol) in 100 mL of ethanol, with good stirring. The reaction mixture was heated on a water bath for two hours, under stirring. The solid was filtered, washed with ethanol (100 mL) and dried in vacuo.

A suspension of bis(2,4-dihydroxyacetophenone) ethylenediimine (0.1 mol) in ethanol (250 mL) was added to a solution of iron chloride, cobalt and zinc acetate, respectively (0.1 mol) in 50 mL of water, under stirring. The reaction mixture was refluxed on a water bath for two hours. The solid products were filtered, washed with hot etanol and dried in vacuo.

The chelate polymers were synthesized from the complexes (I—VII) and organic acid chlorides (terephthaloyl and isophthaloyl chlorides) by interfacial polycondensation.[7,8] The polychelates were purified by repeated extractions with methanol and ethanol.

The polychelates derived from bis(2,4-dihydroxyacetophenone) Cu^{2+} and bis(2,4-dihydroxyacetophenone)ethylenediimine Ni^{2+}, Cu^{2+} were prepared and characterized previously.[2,3]

The infrared and electronic absorption spectra, thermogravimetrical, magnetic and electrical measurements were made as described in earlier communications.[4,5]

X-ray diffraction spectra were performed on a Dron-2 diffractometer using Mo K_α radiation.

RESULTS AND DISCUSSION

The elemental analyses of the polychelates show that the metal to ligand ratio is 1 : 2 (Table 1). Coordination of two water molecules per central metal ion is indicated for all polychelates, excepting Zn^{2+} polychelates. All the polymers are yellowish green to darkish red powders and practically, are insoluble in water and common organic solvents as ethanol, acetone, benzene, chloroform.

These polychelates are suggested to have an octahedral configuration. The Zn^{2+} polychelates are found to be diamagnetic from its expected $3d^{10}$ configuration. The electronic reflexion spectra of the Fe^{2+} polychelates show absorption bands at about 500 nm and 750 nm (shoulder). This band pattern and the smaller observed values of the magnetic moments (Table 1) suggested a strongly distorted octahedral configuration.[9,10]

The Co^{2+} polychelates have an octahedral configuration by coordination of two water molecules. The observed magnetic moment of 2.2 BM is found to be higher than required for a low-spin octahedral structure. The Co^{2+} complexes have distorted structures because of the Jahn-Teller effect, passing from an octahedral geometry into square planar one.[10,11] In spin-paired octahedral complexes of Co^{2+}, the magnetic moment is expected to be 1.8 BM and the higher the magnetic moment, the stronger the distortion.[10,11] The electronic reflexion spectra show the presence of both configurations.

Table 1

Analytical data and physical properties of polychelates

Sample	MW of repeating unit* (g/mol)	C (%)		H (%)		N (%)		M (%)		μ_{eff} (BM)	T_i (°C)
		calcd.	found	calcd.	found	calcd.	found	calcd.	found		
I	393.84	48.74	47.65	4.57	4.21			14.17	13.50		
I_a	523.84	54.97	55.44	3.87	3.83			10.66	9.87	3.26	225
I_b	523.84	54.97	56.09	3.87	3.77			10.66	9.45	3.26	220
II	396.93	48.37	47.96	4.53	3.95			14.84	12.25		
II_a	526.93	54.65	52.86	3.79	4.01			11.18	10.16	2.35	240
II_b	526.93	54.65	53.01	3.79	3.95			11.18	10.23	2.35	235
III	396.71	48.39	47.35	4.53	3.87			14.19	15.97		
III_a	526.71	54.67	54.62	3.79	4.00			11.14	10.20	2.99	210
III_b	526.71	54.67	54.66	3.79	3.95			11.14	9.98	2.99	200
IV	403.37	47.59	48.75	4.46	4.15			16.20	14.50	diamag.	
IV_a	533.37	53.99	53.13	3.74	3.87			12.25	10.75	diamag.	260
IV_b	533.37	53.99	52.50	3.74	3.56			12.25	11.05	diamag.	245
V	417.84	51.69	48.87	5.26	5.75	6.70	7.73	13.36	12.95	paramag.	225
V_a	547.84	56.95	55.01	4.38	4.95	5.11	4.87	10.19	9.23	paramag.	240
V_b	547.84	56.95	55.75	4.38	4.28	5.11	5.01	10.19	8.75	paramag.	220
VI	420.93	51.31	50.48	5.52	5.63	6.65	7.53	14.00	12.91		
VI_a	550.93	56.63	55.20	4.35	4.33	5.08	5.17	10.69	9.05	2.21	
VI_b	550.93	56.63	55.05	4.35	4.12	5.08	6.01	10.69	8.95	2.21	200
VII	427.37	50.54	49.37	5.14	5.37	6.55	6.56	15.29	14.30	diamag.	
VII_a	557.37	55.97	54.78	4.30	4.67	5.02	6.10	11.72	9.50	diamag.	235
VII_b	557.37	55.97	54.94	4.30	4.76	5.02	6.05	11.72	9.77	diamag.	240

* Molecular weights of repeating unit estimated from elemental analysis.

The absorption bands in the electronic spectra of Ni^{2+} polychelates at 380, 500 and 750 nm, as well as the lower observed magnetic moments indicate a distorted octahedral configuration due to the Jahn-Teller effect.[12,13]

The infrared absorption spectra of the polychelates resemble each other in general shape and relative intensity of absorption bands. The chelate polymers show a medium broad band in the 3300–3420 cm^{-1} region, which may be due to the stretching vibrations of phenolic hydroxyl groups as well as of the hydroxyl group of the water molecules associated with the ligand. The broad band of the ligand assigned to OH stretching vibrations disappears to complexation. The bis(azo-oxo) ligand shows C=N stretching vibration at about 1610 cm^{-1}, which shift towards lower frequencies in chelates, indicating involvement of azomethine nitrogen in coordination.[14,15] Also, the infrared absorption spectra of polychelates exhibit a strong absorption band at approximately 1730 cm^{-1}, attributed to carbonyl stretching frequencies as a result of polycondensation reaction between bisphenolic complex and diacid chloride.

The thermal analysis also confirms the presence of water molecules in all polychelates excluding Zn^{2+} polymers. The experimental loss due to water in polychelates approaches the theoretical amounts for dihydrates. The residues from TG curves do not correspond always with the calculated amount of metal oxide, indicating that the polychelates do not decompose completely even at 900°C in the most cases.

The order of thermal stability is : Zn > Ni > Fe > Cu > Co for the bis(azo-oxo) polychelates (Table 1), comparable to the order observed by Goodwin and Bilar.[16] The decomposition of Cu^{2+} and Fe^{2+} polychelates occurred at a lower temperature, probably due to the polymer oxidation by catalytic activity of the metal ions.[17] The higher thermal stability of Zn^{2+} polychelates may be explained taking into account the structure of d-electronic level and the periodical characteristics of zinc atom. The decomposition of the polychelates implies at first the breaking of the metal-ligand bond. The infrared absorption spectra of the residue at 300°C evidenced characteristic absorption bands of the organic ester.

The conductivity measurements were made over a wide range of temperatures (Table 2). The logarithm of the electrical conductivity is a linear function of the temperature reciprocal. The activation energy (E_a) and specific conductivity (σ_0) of the polychelates were evaluated using the relation : $\sigma = \sigma_0 \cdot \exp(-E_a/2kT)$, where σ is the conductivity at T K, k is the Boltzmann constant. E_a, σ_0 and room temperature electrical conductivity are given in Table 2. The activation energy decreases in the following order : Co > Fe > Cu > Ni > Zn, which is in partial agreement with reported results.[18] The bis(azo-oxo) polychelates have smaller values of the activation energy than the bis(dioxo) ones because the central metal ion takes part in formation of more chelate rings.

Table 2

Electrical data of polychelates

Sample	ΔT (K)	E_a (eV)	$\sigma_{298\,K}$ ($\Omega^{-1}cm^{-1}$)	σ_0 ($\Omega^{-1}cm^{-1}$)
I	300–500	1.75	$8.75 \cdot 10^{-9}$	
I_a	300–500	1.50	$8.22 \cdot 10^{-9}$	$2.76 \cdot 10^{4}$
I_b	300–500	1.60	$1.85 \cdot 10^{-9}$	$1.15 \cdot 10^{4}$
II_a	300–500	1.60	$4.65 \cdot 10^{-8}$	$1.06 \cdot 10^{6}$
II_b	300–510	1.70	$6.52 \cdot 10^{-8}$	$1.26 \cdot 10^{7}$
III	300–475	1.75	$3.66 \cdot 10^{-7}$	
III_a	310–490	1.85	$1.12 \cdot 10^{-8}$	$3.11 \cdot 10^{7}$
III_b	320–475	1.80	$2.25 \cdot 10^{-8}$	$2.36 \cdot 10^{7}$
IV_a	300–475	1.25	$6.50 \cdot 10^{-8}$	$1.79 \cdot 10^{3}$
V_a	310–475	1.70	$1.56 \cdot 10^{-8}$	$2.37 \cdot 10^{6}$
V_b	310–510	1.65	$2.52 \cdot 10^{-8}$	$1.51 \cdot 10^{6}$
VI_b	300–475	1.60	$4.82 \cdot 10^{-8}$	$5.18 \cdot 10^{7}$
VII_a	320–480	1.40	$7.58 \cdot 10^{-8}$	$3.74 \cdot 10^{4}$
VII_b	315–470	1.30	$6.50 \cdot 10^{-8}$	$4.68 \cdot 10^{3}$

The diffractograms of the polychelates show a characteristic structure differing by the number and position of the diffraction peaks relating to the initial compounds (Figure 1).

The diffraction patterns of the polychelates indicate the absence of a perfectly ordered crystalline structure. The change of the perfectly ordered structure of the chelates in an amorphous one with some crystallinity degree also supports the polymeric nature of the polychelates

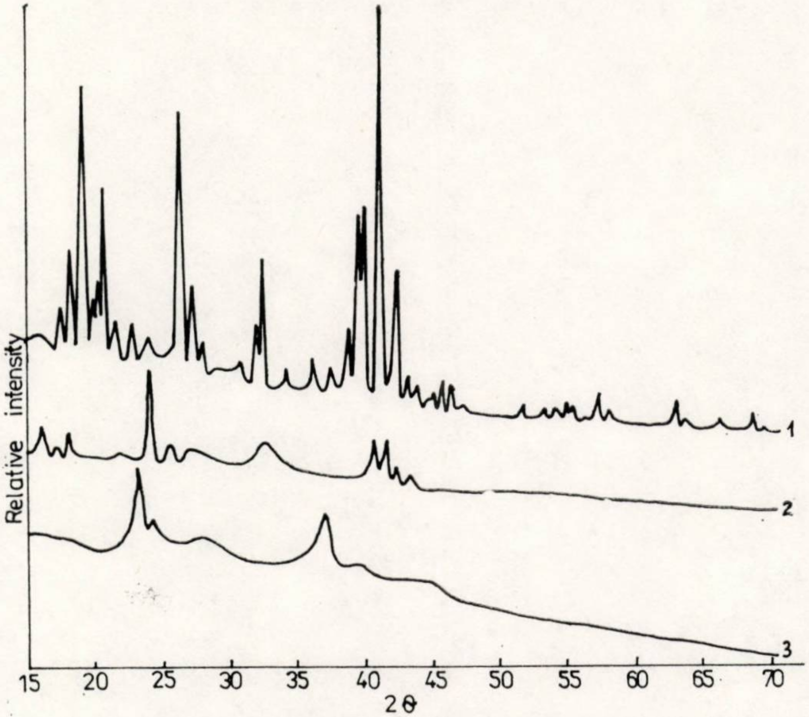

Fig. 1. — X-ray diffractograms of Ni^{2+}-bis(dioxo) complexes. 1 — III; 2 — III_b; 3 — III_a.

REFERENCES

[1] M. Spiratos, A. Airinei and N. Voiculescu, *Angew. Makromol. Chem.*, **138**, 159 (1986).
[2] M. Spiratos, A. Airinei and M. Bostan, *Mater. Plast.*, **16**, 137 (1979).
[3] M. Spiratos, A. Airinei and A. Ciobanu, *Rev. Roumaine Chim.*, **25**, 1083 (1980).
[4] M. Spiratos, G. I. Rusu, A. Airinei and A. Ciobanu, *Angew. Makromol. Chem.*, **107**, 33 (1982).
[5] M. Spiratos, A. Airinei, G. I. Rusu and A. Ciobanu, *Polym. Bull.*, **6**, 243 (1982).
[6] S. V. Vinogradova, V. A. Vasnev and V. V. Korshak, *Vysokomol. Soedin.*, *B*, **13**, 805 (1971).
[7] W. M. Eareckson, *J. Polym. Sci.*, **40**, 399 (1959).
[8] L. V. Interrante and J. C. Bailar, Jr., *Inorg. Chem.*, **3**, 1339 (1964).
[9] J. K. L. F. de Vries, J. M. Trooster and E. de Boer, *J. Chem. Soc., Dalton Trans.*, **1974**, 1771.
[10] A. Earnshow, E. A. King and L. F. Larkworthy, *J. Chem. Soc. A*, **1968**, 1048.
[11] B. N. Figgis and R. S. Nyholm, *J. Chem. Soc.*, **1959**, 338.
[12] R. S. Drago, "Physical Methods in Chemistry", Izd. Mir, Moskva, 1981.
[13] A. D. Harris, H. B. Jonassen and R. D. Archer, *Inorg. Chem.*, **4**, 147 (1965).
[14] J. E. Kovacic, *Spectrochim. Acta*, **23 A**, 183 (1967).
[15] K. Nakamoto, "Infrared Spectra of Inorganic and Coordination Compounds", Izd. Mir, Moscow, 1966.
[16] H. A. Goodwin and J. C. Bailar, Jr., *J. Amer. Chem. Soc.*, **83**, 2467 (1961).
[17] E. C. Winslow and A. A. Manning, *J. Polym. Sci.*, **A 2**, 4903 (1964).
[18] M. M. Patel and R. Manalavan, *J. Macromol. Sci. Chem.*, **A 19**, 951 (1983).

Revue Roumaine de Chimie, **34**, *6*, 1419–1423 (1989)

COMPLEXATION OF ISOMERIC CHLORONITROBENZENES BY β-CYCLODEXTRIN IN THE PRESENCE OF ETHANOL

J. TARASZEWSKA

Institute of Physical Chemistry, Polish Academy of Sciences, 01–224 Warsaw, Poland

Received November 28, 1988

The polarographic method has been used to the determination of the stability constants of isomeric chloronitrobenzenes with β-cyclodextrin in H_2O + ethanol mixtures. Stability constant of ethanol with β-cyclodextrin has been determined as well.

INTRODUCTION

The cycloamyloses (cyclodextrins) are well known to form inclusion complexes with a variety of organic and inorganic compounds.[1] Inclusion processes are often studied in the presence of an organic solvent. One of the common solvents used is ethanol (EtOH) which is often added in order to dissolve guest species slightly soluble in water. The presence of EtOH increases also the solubility of β-cyclodextrin (CD).[2] The maximum of solubility is observed in a mixture containing 20–30% vol. EtOH. In mixtures containing more than 70 vol.% β-CD is insoluble. Molecules of alcohols can also be incorporated into the CD cavity as it has been shown by Matsui and Mochida.[3] Complexation of alcohol can influence the complexation of other guest molecules.

The aim of the presented paper was to study the complexation of isomeric chloronitrobenzenes (ClNB) by β-CD in the presence of EtOH. Complexation of isomeric ClNB by α and β-CD in pure aqueous solutions was studied by us previously [4] using the polarographic method.

EXPERIMENTAL

The reduction of *o*-, *m*-, and *p*-ClNB at the Hg electrode from H_2O + EtOH mixture containing 0.1 M phosphate buffer in the absence and in the presence of increasing concentrations of β-CD was studied polarographically in a three-electrode system at 25±0.5°C The counter electrode was a Pt cylinder. A 1M NaCl NaCl aqueous calomel electrode (NCE) was used as the reference electrode. It was connected to the electrolytic cell via an intermediate vessel filled with the solution under investigation.

Solutions were deaerated by flushing with pure and dried argon presaturated with the solution under investigation; during measurements the gas was passed over the solution.

The polarographic curves were recorded using a measuring system constructed from an EP-20A potentiostat, an EG-20 function generator (both produced by ELPAN – Poland) and a XY/t-102 recorder (ZDEMP – Poland).

β-CD (Chinoin, Hungary) was used as received. Thermogravimetric analysis showed that it contained 11 wt. % of H_2O. *o*-, *m*-, and *p*-ClNB as well as NaH_2PO_4 and KH_2PO_4 used for the preparation of phosphate buffer were p.a. grade reagents (POCh – Poland). EtOH, 99.8% p.a. grade reagent (POCh – Poland) was used without further purification. Triply distilled H_2O was used for preparation of the solutions.

RESULTS AND DISCUSSION

Polarographic reduction of *o*-, *m*-, and *p*-ClNB in H_2O + EtOH mixtures containing 5, 11, 20 and 30 vol. %EtOH is similar to that in pure aqueous solutions and gives a single, well-defined irreversible wave at half wave potential $E_{1/2}$ about -0.4 V vs. NCE which corresponds to a four-electron process as has been found by Ratan et al.[5] The presence of β-CD does not change this picture essentially, however, it causes a decrease in the limiting diffusion currents and a shift of the half-wave potentials towards more negative values. Both these effects are due to the complexation of ClNB by β-CD.

The concentration of ClNB in all experiments was 1.25×10^{-4} M and the concentration of β-CD changed from 3 mM to more than 12 mM. A large excess of CD concentration is required because then the complexation reaction remains at equilibrium everywhere in the diffusion layer.

The diffusion coefficients, D_f, of free ClNB and the observed diffusion coefficients, D_{obs}, in the presence of β-CD were calculated from the polarographic limiting instantaneous currents using the Ilkovic equation corrected for spherical diffusion by Koutecky.[6] The changes in D_{obs} for three isomeric ClNB in the studied H_2O+EtOH mixtures vs. β-CD concentration are shown in Fig. 1.

The method of calculating the stability constants K_s of inclusion complexes based on the knowledge of the diffusion coefficients D_f of the free guest molecules and the observed diffusion coefficients D_{obs} of the guest molecule determined as a function of CD concentration was described by Osa et al.[7] and by us.[4] When a complex of 1 : 1 stoichiometry is formed, as it has been assumed for the complex of ClNB with β-CD, the values of K_s and the diffusion coefficients of the complex, D_c, can be calculated by linear regression analysis using eq. (1)

$$D_{\mathrm{obs}} = \frac{(D_f - D_{\mathrm{obs}})}{K_s \times C_{CD}} + D_c \tag{1}$$

where C_{CD} is the concentration of free CD equal to its analytical concentration.

The values of K_s, D_c and D_f can be also calculated by non-linear iterative minimization of the sum of squares of the deviation from the true line

$$\sum_{i=1}^{N} (D_i^{\mathrm{obs}} - D_i^{\mathrm{calc}})^2 \tag{2}$$

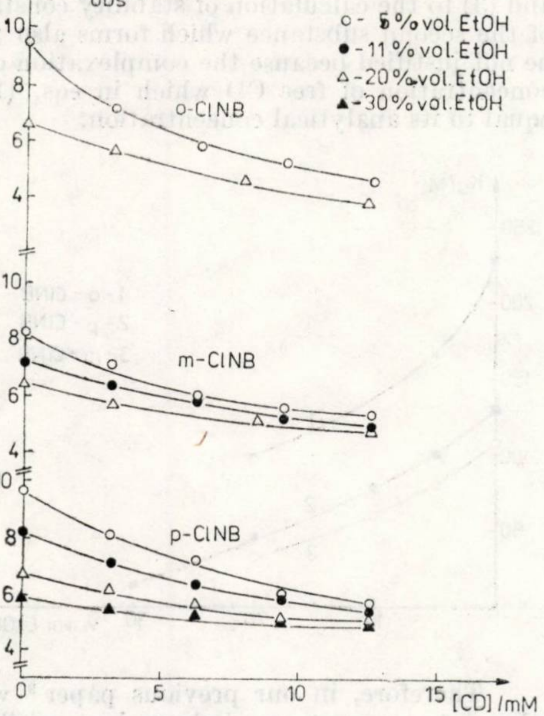

Fig. 1. — Changes in the observed diffusion coefficients D_{obs} of isomeric ClNB in $H_2O + EtOH$ mixtures of 0.1 M phosphate buffer vs. β-CD concentration

where N is the number of points in one set of data and

$$D_i^{calc} = \frac{D_f^* + D_c^* K_s^* C_{CD}}{1 + K_s^* C_{CD}} \tag{3}$$

where K_s^*, D_c^* and D_f^* are the assumed values.

The stability constants K_s of isomeric ClNB with β-CD in $H_2O +$ $+ EtOH$ mixtures containing 0.1M phosphate buffer were calculated using eqs (1) and (3). The numerical values of K_s and D_c did not depend on the method of calculation. The changes in K_s for three isomeric ClNB vs. EtOH content in the mixture are shown in Fig. 2. The results presented show that with increase in the concentration of EtOH in the mixture the complexation of ClNB by β-CD is weaker. The calculated values of D_c are in the limits $2-2.5 \times 10^{-6}$ cm^{2}s^{-1}.

The values of K_s for isomeric ClNB with β-CD determined by us in H_2O + 20 vol. % EtOH are in satisfactory agreement with the data of Zukowski et al. [8] obtained in this mixture by reversed-phase high-performance liquid chromatography.

A decrease of stability constants with increasing concentration of the organic solvent in the mixture has been also reported by other authors

However, as we have shown previously [9] the application of eqs. (1) and (3) to the calculation of stability constant of one guest in the presence of the second substance which forms also inclusion complex with CD can be not justified because the complexation of the second guest changes the concentration of free CD which in eqs. (1) and (3) was assumed to be equal to its analytical concentration.

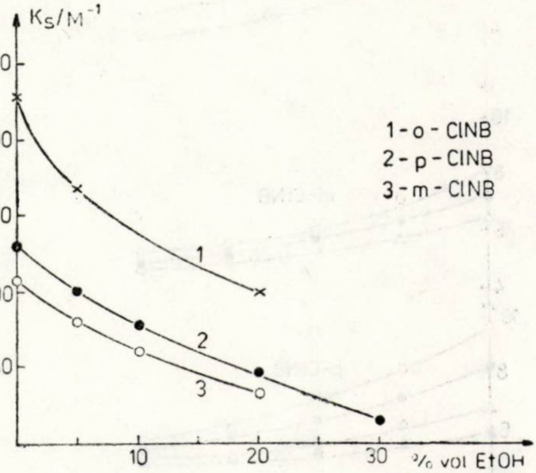

Fig. 2. — Changes in the stability constants K_s of isomeric ClNB vs. EtOH content in the mixture.

Therefore, in our previous paper [9] we derived an equation which takes into account two independent equilibria due to the complexation of guest (1) and guest (2) and which allows to calculate both stability constants. This equation has the following form :

$$D_{\text{obs}} = \frac{K_s^{(1)}\{(D_c + D_f)[1 + K_s^{(2)}(C_2 - C_{CD})] - 2D_c K_s^{(1)} C_{CD} + (D_f - D_c) \times \times \sqrt{(1 + C_{CD} + K_s^{(2)})^2 + C_2 K_s^{(2)}[2 + K_s^{(2)}(C_2 - 2C_{CD})]\}} - 2D_f K_s^{(2)}}{2[(C_{CD}K_s^{(1)} + 1)(K_s^{(1)} - K_s^{(2)}) + K_s^{(1)}K_s^{(2)}C_2]} \tag{4}$$

where C_1, C_2, C_{CD} — analytical concentrations of guest 1, guest 2, and CD respectively.

D_f and D_c — diffusion coefficients of free guest 1 and complex of guest 1 with CD, respectively.

Using eq. (4) we calculated independently the stability constants $K_s^{(1)}$ of isomeric ClNB with β-CD and the stability constant $K_s^{(2)}$ of EtOH with β-CD. We found that the presence of EtOH up to 20 vol. % in the mixture does not cause the decrease of the stability constants of isomeric ClNB with β-CD. The decrease of K_s presented in Fig. 2 was due to the fact that the change in the concentration of free CD with increase of EtOH content was not taken into account .

The complex of EtOH with β-CD is weak. The value of $K_s^{(2)}$ calculated using eq. (4) is equal to $0.5 \pm 0.2M^{-1}$. This value is lower than that reported by Matsui and Mochida. [3]

REFERENCES

[1] J. Szejtli, "Cyclodextrins and Their Inclusion Complexes", Akademiai Kiado, Budapest 1982.

[2] W. Schlenk and D. M. Sand, *J. Am. Chem. Soc.*, **83**, 2312 (1961).

[3] Y. Matsui and K. Mochida, *Bull. Chem. Soc. Japan*, **52**, 2808 (1979).

[4] J. Taraszewska and A. K. Piasecki, *J. Electroanal. Chem.*, **226**, 137 (1987).

[5] R. Ratan, R. Rani and M. Singh, *Indian J. Chem.*, **22**A, 664 (1983).

[6] J. Koutecky, *Czech. J. Phys.*, **2**, 50 (1953).

[7] T. Osa, T. Matsue and T. Fujihira, *Heterocycles*, **6**, 1833 (1977).

[8] J. Żukowski, D. Sybilska and J. Jurczak, *Anal. Chem.*, **57**, 2215 (1985).

[9] J. Taraszewska and A. K. Piasecki, Proc. 4th Intern. Symp. Cyclodextrin, (in press).

Revue Roumaine de Chimie, **34**, *6*, 1425–1437 (1989)

REACTION OF PYRYLIUM SALTS WITH NUCLEOPHILES. XXII[1]

REGIOSELECTIVITY (FORMATION OF ANILINE DERIVATIVES FROM PRIMARY AMINES AND NON-SYMMETRICALLY SUBSTITUTED PYRYLIUM SALTS) AND CHEMOSELECTIVITY (PYRIDINIUM VS. ANILINE FORMATION)

CORNELIA UNCUŢA,[a] TEODOR-SILVIU BALABAN,[a] AURICA PETRIDE,[a]
FILIP CHIRALEU [a] and ALEXANDRU T. BALABAN [b]
[a] Centre of Organic Chemistry, Spl. Independenţei 202 B, 78100 Bucharest, Romania
[b] Polytechnical Institute, Chair of Organic Chemistry, Spl. Independenţei 313, 77206 Bucharest, Romania

Received November 1, 1988

The reaction of pyrylium salts with primary alkylamines RNH_2 presents chemoselectivity (competition between the formation of pyridinium salts and N-alkylanilines) depending both on the nature of the carbon atom in R linked to the amino group, and on the substitution pattern in the pyrylium cation. The nucleophilic attack of the amine RNH_2 to α-methyl versus α-methylene groups in non-symmetrically 2,6-disubstituted pyrylium salts presents high regioselectivity in the benzene-ring closure reaction leading to anilines. Another series of experiments involving non-symmetrically substituted pyrylium salts having two α-methyl groups, one of which is buttressed by a β-substituent (Me, iPr, Ph), also led to significant regioselectivity in the formation of N-alkylanilines. Stereoelectronic effects accounting for these chemo- and regioselectivities are discussed.

INTRODUCTION

The reactions of pyrylium salts with ammonia and primary or secondary amines afford a large diversity of products and continue to provide surprising results such as the formation of non-aromatic 6,6-dimethyl-2,4-cyclohexadienylidene-1-imines from 2,6-diisopropylpyrylium salts and isopropylamine or ethylamine.[1,2]

It is known that secondary amines convert pyrylium salts **1** having 2-methyl or 2-methylene groups into N,N-disubstituted aniline derivatives;[3,4] most textbooks indicate that pyridines and pyridinium salts are the reaction products of pyrylium salts with ammonia and primary amines, respectively. However, the last statement is not always true and the purpose of the present paper is to demonstrate this fact and to report on the regioselectivity of the reaction between non-symmetrically substituted pyrylium salts and primary aliphatic amines.

When pyrylium salts **2** react with ammonia or primary amines, the initially formed product is a doubly vinylogous amide **3** or a tautomer thereof (iminoenol), which may be isolated when R=H and R′=Ph,[5] or when R=*t*-Bu and R′ is an Ar or Alk group.[6]

Otherwise, the compound **3** normally ring-closes (ANRORC reaction [7]), with aromatization as driving force, leading to a pyridine

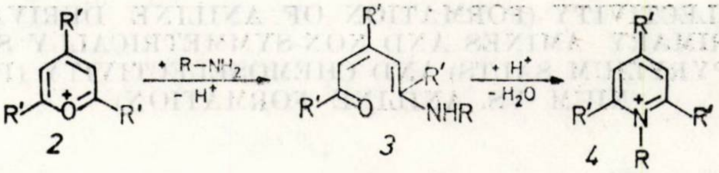

(R=H) or pyridinium salt **4** (R=Ar or Alk). However, pyrylium salts **1** have an alternative pathway for aromatization: competing with the formation of the heterocyclic ring **6**, intramolecular condensation between the carbonyl group and the α-methyl(ene) side-chain leads to the closure of a benzenoid ring and to the formation of an aniline derivative **7** (as in the case of secondary amines which cannot give rise to pyridinic rings).

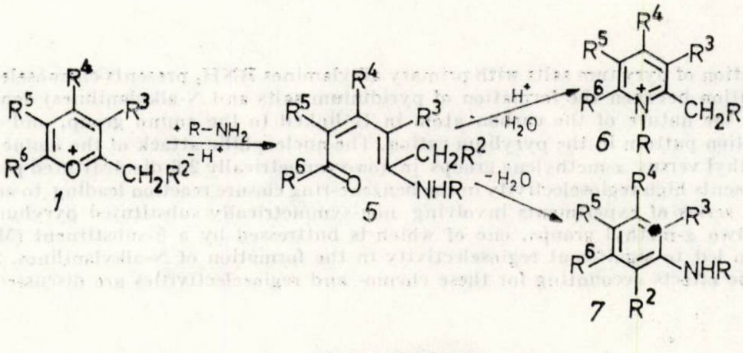

RESULTS

Competition between pyridinium and N-alkylaniline formation

We studied the reaction between one and the same symmetrically substituted pyrylium salt: 2,4,6-trimethylpyrylium perchlorate (**1**, $R^2 = R^3 = R^5 = H$, $R^4 = R^6 = Me$) and a series of primary aliphatic amines: $H_2N-CH_xMe_{3-x}$ ($x = 0, 1, 2, 3$).

The distribution and characterization of the reaction products are presented in Table 1 (all yields in tables 1–5 refer to crude products).

In the context of the present paper, pyridinium **6** *vs.* aniline **7** competition will be denoted as chemoselectivity of the reaction between the pyrylium cation and the primary amine.

A correlation was observed between the reaction chemoselectivity and the nature of the alkyl radical in the amine. Formation of the pyridinium salt **6** prevails when the amino group is linked to a primary carbon atom, while aniline **7** is the main or sole reaction product when the amino group is linked to a secondary or tertiary carbon atom, as indicated in Table 1.

Table 1

Product distribution in the reaction between 2,4,6-trimethylpyrylium perchlorate and primary amines

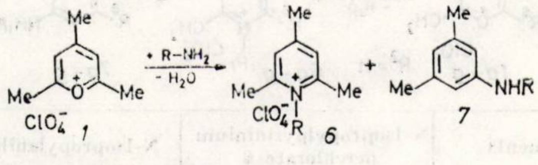

1, $R^2=R^3=R^5=H$; $R^4=R^6=Me$

Prod.	Alkyl	N-Alkyl-2,4,6-trimethyl pyridinium perchlorate **6**		N-Alkyl-3.5-xylidine **7**			Chemo-selectivity (%)	
6; **7**	R	Yield (%)	m.p. (°C)	Yield (%)	Glc purity (%)	b.p. (°C/3 Torr)	**6**	**7**
A	Me	86.6	203–204	13.3	95	95–96	87	13
B	Et	70.9	78–80	28.1	96	103	72	28
C	iPr	14.5	174–175	84.0	96	101–102	15	85
D	tBu	—	—	83.6	63	104	0	100

This result may be explained by invoking steric factors. The increase in steric strain brought about in the pyridinium salt **6** with three adjacent alkyls by the size increase of the median R group tends to favour the formation of a benzenoid ring **7** with no such overcrowding, culminating in the complete exclusion of the former reaction path when R is as bulky as *t*-butyl.

A second series of experiments involved the reaction between one and the same primary amine whose NH_2 group is bonded to a secondary carbon atom, namely isopropylamine, and a series of pyrylium salts possessing alkyl as well as aryl substituents; the pyrylium salt was either (i) symmetrically substituted (**a**–**c**), or (ii) was substituted in position 2 by a methyl group and in position 6 by an isopropyl, a *t*-butyl or a phenyl group(**d**–**g**). In the former case (i), either of the two α-methyl groups gives rise to one and the same aniline by intramolecular ring closure; in the latter case (ii), only the α-methyl group undergoes intramolecular ring closure, so that in all cases the product competition involves one pyridinium salt and one N-alkylaniline. The results are presented in Table 2.

All pyrylium salts in Table 2 show the general trend of favoring aniline **7** formation in the reaction with isopropylamine. However, the substitution pattern in the pyrylium ring is also important for chemoselec-

Table 2

Product distribution in the reaction between isopropylamine and pyrylium salts 1 with alkyl as well as aryl substituents; all pyrylium salts have one (or two symmetrical) α-standing methyl group(s) active in the benzenoid ring closure, therefore only one possibility of ring closure

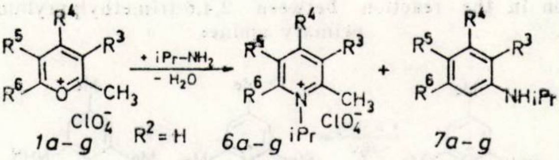

Prod. 6 ; 7	Substituents				N-Isopropylpyridinium perchlorate **6**		N-Isopropylaniline **7**		Chemoselectivity (%)	
	R^3	R^4	R^5	R^6	Yield (%)	m.p. (°C)	Yield (%)	b.p. (°C/1 Torr)	**6**	**7**
a	Me	H	Me	Me	37.0	170–171	55.5	110	40	60
b	Me	Me	Me	Me	39.0	95	56.0	109–112	41	59
c	H	Ph	H	Me	24.6	218	73.3	140	25	75
d	H	Me	H	iPr	12.5	210–211	78.5	107–108	14	86
e	Me	Me	H	iPr	7.5	110–115	90.3	—	8	92
f	H	Me	H	tBu	—	—	93.2	120	0	100
g	H	Ph	H	Ph	6.9	185 (decomp.)	85.9	—	7	93

tivity. An increase in the size of the substituent in position 6 from Me to iPr leads to a decrease in pyridinium yield, while a t-Bu in position 6 entirely prevents formation of pyridinium salt. Substitution of β-positions by methyl groups leads to a decrease in reaction chemoselectivity. Indeed, for pyrylium salts **1a** and **1b** (cf. Table 2), aniline formation prevails only slightly over pyridinium formation. Most probably, the steric hindrance becomes significant in both pyridinium and aniline rings and their formation tendencies appear almost comparable.

Regioselectivity in N-alkylaniline formation from primary amines and non-symmetrically substituted pyrylium salts

Pyrylium salts may be substituted non-symmetrically and lead to regioselective nucleophilic attack by primary amines in two cases: either (a) the nature of the α-alkyl groups is different, leading to two modes of ring closure; or (b), the α-substituents are identical but have different neighbouring groups in β-positions.

Case (a): Ring closure on an α-methyl versus an α-ethyl group

Again we studied the reaction of various primary alkylamines $H_2N-CH_xMe_{3-x}$ ($x = 0, 1, 2, 3$), but using now 2-ethyl-4,6-dimethylpyrylium perchlorate **8**. Results are presented in Table 3.

Besides pyridinium *vs.* benzene ring closure competition (chemoselectivity) discussed so far, a second competition is involved in this case:

Table 3

Product distribution in the reaction between 2-ethyl-4,6-dimethylpyrylium perchlorate 8 and primary alkylamines

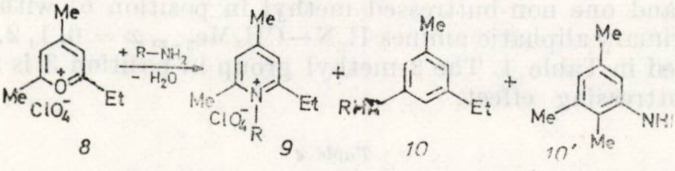

Prod. **9** **10** **10′**	Alkyl	N-Alkyl-2-ethyl 4,6-dimethylpyridinium perchlorate **9**		N-Alkylanilines **10** and **10′**				Chemoselectivity (%)		Regioselectivity Me *vs.* Et (%)	
	R	Yield (%)	m.p. (°C)	Overall yield (%)	Glc composition of crude aniline			**9**	**10** + **10′**	**10**	**10′**
					10 (%)	**10′** (%)	Side products (%)				
A	Me	74.1	153–155	18.5	86.5	8.7	4.8	80	20	91	9
B	Et	63.1	oil	33.9	73.3	21.3	5.4	65	35	77	23
C	iPr	10.1	141–143	83.6	85.3	7.2	7.5	11	89	92	8
D	tBu	—	—	82.6	71.1	4.0	24.9	0	100	95	5

regarding two isomeric anilines resulting from nucleophilic attack of the amine to non-equivalent α-positions (α *vs.* α' regioselectivity).

The yields in pyridinium salts **9** and the overall yields in N-alkylanilines **10** and **10′** are indicative for pyridinium *vs.* benzene ring closure competition. The same trend is observed as in Table 1 : methylamine and ethylamine yield predominantly pyridinium salts, while N-alkylanilines are obtained from isopropylamine (predominantly) and *t*-butylamine (exclusively).

The composition of the crude aniline fraction determined by glc analysis is presented in Table 3. N-Alkylanilines **10** and **10′** are accompanied by variable amounts of unidentified side-products (between cca. 5% and 25%, with individual components not exceeding 3%). To enable an easier comparison of the data, this composition was recalculated for N-alkylaniline only. The recalculated data, presented in Table 3 as well, are a direct measure of the regioselectivity in the benzene-ring closure reaction. The results demonstrate that the methyl group ring-closes intramolecularly appreciably more readily than the ethyl group, i.e. either that the nucleophilic attack occurs close to the methyl rather than to the ethyl group, or that the primary carbanion derived from the methyl group is more stable than the secondary carbanion derived from the ethyl group (or both these effects have comparable contributions).

The α-Me attack is favoured over α-Et attack by a factor of approx. 10 for methyl-, isopropyl- and *t*-butylamine. Surprisingly, the regioselectivity decreases to approx. 3.3 for ethylamine.

Case (b): Ring closure on buttressed versus non-buttressed methyl groups

The next experiments involved the reaction between 2,3,4,6-tetramethylpyrylium perchlorate **11** (which has one buttressed methyl in position 2 and one non-buttressed methyl in position 6) with the same series of primary aliphatic amines $H_2N-CH_xMe_{3-x}$, $x = 0, 1, 2, 3$. Results are presented in Table 4. The β-methyl group in position 3 is responsible for the buttressing effect.

Table 4

Product distribution in the reaction between 2,3,4,6-tetramethylpyrylium perchlorate 11 and primary alkylamines

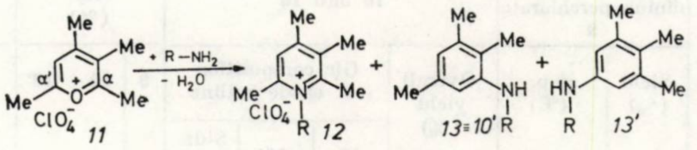

Prod. 12 13≡10' 13'	Alkyl R	N-Alkyl-2,3,4,6-tetramethylpyridinium perchlorate **12**		N-Alkylanilines **13** and **13'**				Chemoselectivity (%)		Regioselectivity (%) Me_α *vs.* $Me_{\alpha'}$	
		Yield (%)	m.p. (°C)	Overall yield (%)	Glc composition of crude aniline			**12**	**13+13'**	**13**	**13'**
					13 (%)	**13'** (%)	Side products (%)				
A	Me	86.5	140–141	13.0	75.4	9.9	14.7	87	13	88	12
B	Et	70.2	97–98	27.5	85.5	9.3	5.2	82	18	90	10
C	iPr	10.3	148	87.2	83.4	8.0	8.6	11	89	91	9
D	tBu	—	—	82.5	44.9	5.9	49.2	0	100	88	12

Again the same trend as in Table 1 is observed for the competition pyridinium *vs.* N-alkylaniline.

The regioselectivity is in favour of the nucleophilic attack at the C-2 atom bearing the buttressed methyl group, and leading to N-alkyl-2,3,5-trimethylanilines (the converse attack in position 6, affording N-alkyl-3,4,5-anilines, occurs about ten times less frequently). It seems probable that this reaction is under kinetic control and that the lower electron density of the 2-position than of the 6-position is responsible for the regioselective nucleophilic attack. We know from experimental data based on specifically deuterated compounds [8] that the ^1H-NMR chemical shifts of pyrylium salt **11** in trifluoroacetic acid are 2.87 ppm for the 6-position and 2.92 ppm for the 2-position, demonstrating the more pronounced electron deficit (deshielding effect) in position 2.

The last series of experiments (Table 5) involved two pyrylium salts (related to the preceding one, **11**, with four methyl groups) having three methyl groups in positions 2, 4 and 6, and a 3-substituent which is either isopropyl or phenyl; in both cases, reaction with isopropylamine affords a low amount of pyridinium salt and large amounts of N-isopropylanilines. For the first compound in Table 5, **14 h**, with a 3-phenyl group, the regioselectivity of the reaction is due to the nucleophilic attack occurring predominantly in position 2, as in the preceding cases; the quantitative results are comparable to those obtained with 2,3,4,6-tetramethylpyrylium. However, the last compound in Table 5, **14j**, with a 3-isopropyl group, presents a low and reverted regioselectivity, with a 2 : 1 probability of nucleophilic attack in position 6 *vs.* 2. This fact is probably due to a combination of steric and electronic factors.

Table 5

Product distribution in the reaction between non-symmetrically substituted pyrylium salts 14 and isopropylamine

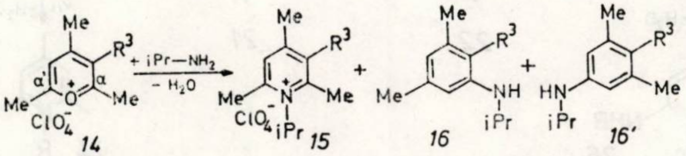

Prod. **15** **16** **16′**	R³	N-Isopropyl-2,4,6-trimethyl-3-R³ pyridinium perchlorates **15**		N-Isopropylanilines **16** and **16′**				Chemoselectivity (%)		Regioselectivity (%) Me$_\alpha$ *vs.* Me$_{\alpha'}$	
				Overall yield (%)	Glc composition of crude aniline						
		Yield (%)	m.p. (°C)		**16** (%)	**16′** (%)	side-products (%)	**15**	**16**+**16′**	**16**	**16′**
h	Ph	7.4	163–164	88.0	91.4	4.7	3.9	8	92	95	5
j	iPr	13.0	97–98	77.4	35.0	64.2	0.8	14	86	35	65

DISCUSSION OF THE RESULTS

The mechanism of the reaction between pyrylium salts and primary amines will be taken into account for explaining the experimental data presented above. Following nucleophilic attack (i) of the amine to the electron-deficient α-position in pyrylium cation **17**, and (ii) base-catalysed formation of the cyclic 2-H pyran derivative **19**, the thermally-allowed electrocyclic ring-opening reaction (iii) leads to the ketodienaminic intermediate **20** and its tautomers **21**, **22** through protolytic equilibria (iv), (v); formation of the latter involves the hydrogen atom from a benzylic position in pyrylium cation. The open-chain enol-iminic intermediate **21** may cyclize (vi) in acid catalysis to dihydropyridinium intermediate **23** which dehydrates (vii) with aromatization as driving force to pyridinium cation **24**.

The competing reaction in the chemoselective dichotomy involves either : (a) electrocyclization (viii) of the enol-enaminic tautomer **22** to the cyclohexadienic intermediate **25** which dehydrates (ix), again with

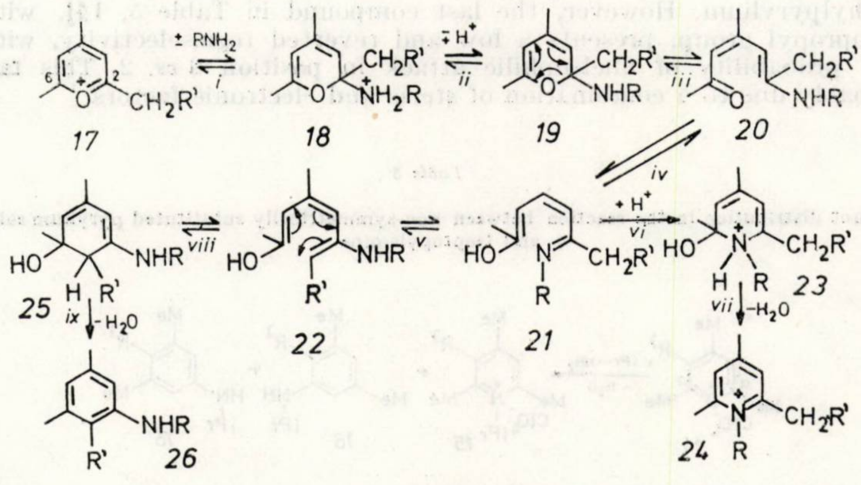

Scheme 1

aromatization as driving force, to the aniline derivative **26**, or (b) the intramolecular nucleophilic attack of the anion formed by deprotonation from the benzylic position of **20** on the carbonyl group ; the same delocalized anion results from the enol **22**.

A rationalization of the experimental data concerning the chemoselectivity of this reaction (i.e. pyridinium *vs.* aniline competition) may be achieved by considering the protolytic equilibria between open-chain intermediates. Indeed, steric strain due to increasing size of alkyl group R in pyridinium salts **24** may be, at least partly, relieved in aniline derivatives **26** in which the bulky group R is in a remote position. Under the experimental conditions used in this work, an R group as bulky as *t*-Bu cannot be accommodated with two other contiguous alkyl groups on the planar framework of the pyridinium ring.

The experimental data concerning regioselectivity of the benzenoid ring closure plead for a kinetic control in reaction step (i), namely preferential nucleophilic attack to the more positively-charged α-position (for the non-symmetrical tetramethylpyrylium cation **11** by a factor of about 10, regardless of amine). However, electronic factors are no longer decisive when steric factors become important. Indeed, in the pyrylium salt possessing in position 3 an isopropyl group instead of methyl or phenyl, the approach of the nucleophile is directed to the less crowded 6-position, leading to a reversed and lower regioselectivity.

Literature data indicate that unlike the reaction between non-symmetrically substituted pyrylium salts and alkali hydroxides which affords phenols in good yield but with variable * regioselectivity,[9] the same pyrylium salts react with secondary amines with high regioselectivity affording N,N-dialkylanilines ; this difference may be explained by assuming thermodynamic control in the former reaction and kinetic control in the latter reaction, as in the formation of N-monosubstituted anilines from similar pyrylium salts and primary amines as discussed in the present paper.

Finally, the synthetic merits of the reaction between pyrylium salts and primary amines will be discussed. So far, the ring-transformation reaction leading from pyrylium to N-alkyl/aryl-substituted pyridinium salts has made a successful synthetic career. On the other hand, with alkylamines such as isopropyl- or *t*-butylamine, this reaction becomes of preparative interest for N-isopropyl and N-*t*-butylanilines. The examples presented in this paper illustrate the potential of this method of preparation. Indeed, taking into account the variety of substitution patterns in the starting pyrylium salts (see Table 2) as well as the regioselectivity of this reaction (see Tables 3—5), one may achieve substitution patterns in the benzenoid ring of N-alkylanilines which are difficult to obtain by other methods such as benzenic-ring substitution (e.g. nitration, followed by reduction and N-alkylation) or methods through benzyne intermediates.

EXPERIMENTAL PART

^{1}H-NMR Spectra were recorded on a Varian A-60A instrument ; glc analyses were performed on a Caro Erba FRACTOVAP-2450 instrument using a capillary glass column (20 m × 0.2 mm ; stationary phase methylsilicone SE 30), hydrogen as carrier gas, flame-ionization detector, in the temperature-range 110—220° (10°/min heating rate). Melting points were determined in open capillary tubes.

The reaction of pyrylium salts with primary amines was performed according to the following general procedure : a mixture of pyrylium perchlorate and excess amine (1 : 3 molar ratio) in absolute ethanol or isopropanol as solvent was heated for two to three hrs. at gentle reflux The solvent was distilled off under reduced pressure ; the oily residue was treated with dilute aqueous ammonia then extracted with ethyl ether for the substituted aniline.

The pyridinium perchlorate was extracted in methylene chloride from the aqueous layer. After evaporation of the solvents, the crude substituted aniline and the pyridinium perchlorate were purified by high vacuum distillation and recrystallization from isopropanol (unless otherwise stated), respectively. All yields reported refer to crude products. All new compounds gave satisfactory elemental (% nitrogen) analysis. ^{1}H-NMR Chemical shifts are given as δ (ppm) values from TMS internal standard in tables 6 and 7. The assignment of signals is either straightforward, or based on consistency of the data within the series ; for the latter case, the chemical shift values are marked by asterisks.

The reaction of 2,4,6-trimethylpyrylium perchlorate with methylamine afforded 1,2,4,6-tetramethylpyridinium perchlorate **6A** (lit.[6] m.p. 202—204°) and N, 3,5-trimethylaniline **7A**.

The reaction of 2,4,6-trimethylpyrylium perchlorate with ethylamine afforded 1-ethyl-2,4,6-trimethylpyridinium perchlorate **6B** (lit.[6] m.p. 72—74°) and N-ethyl-3,5-dimethylaniline **7B**.

The reaction of 2,4,6-trimethylpyrylium perchlorate with isopropylamine afforded 1-isopropyl-2,4,6-trimethylpyridinium perchlorate **6C** (lit.[11] m.p. 171—172°) and N-isopropyl-3,5-dimethylaniline **7C**.

---

* For 2-ethyl-4,6-dimethylpyrylium, both phenols are obtained in almost equal amounts, but for 2,3,4,6-tetramethylpyrylium the reaction has a regioselectivity of 70% in 2,3,5-trimethylphenol.

Table 6

^{1}H-NMR Chemical shifts (δ, ppm, from TMS internal standard) of N-alkylpyridinium perchlorates **6**; 60 MHz; solvent $CDCl_3$, unless otherwise stated; room temperature. An asterisk indicates assignments based on consistency within the series

Comp.	R	R^2	R^3	R^4	R^5	R^6	R	CH_2R^2	R^3	R^4	R^5	R^6
6A[a]	Me	H	H	Me	H	Me	4.05	2.77	7.49	2.53	7.49	2.77
6B	Et	H	H	Me	H	Me	1.53; 4.60	2.88	7.65	2.55	7.65	2.88
6C	iPr	H	H	Me	H	Me	1.78; 5.52	2.95 (bs)	7.65	2.54	7.65	2.95 (bs)
6a[b]	iPr	H	Me	H	Me	Me	1.83; 5.59	2.84	2.47	7.96	2.47	2.84
6b	iPr	H	Me	Me	Me	Me	1.78; 5.50	2.83	2.40	2.45	2.40	2.83
6e[b]	iPr	H	H	Ph	H	Me	1.88; 5.57	3.05	7.92	7.53–7.78	7.92	3.05
6d[b]	iPr	H	H	Me	H	iPr	1.87; 5.55 (bm)	2.91 (bs)	7.53 *	2.61	7.67 *	1.53; 3.92 (bm)
6e[b]	iPr	H	Me	Me	H	iPr	1.88; 5.63	2.92 (bs)	2.47	2.61	7.65	1.53; 3.82 (bm)
6g[b]	iPr	H	H	Ph	H	Ph	1.72; 5.42	3.18	Multiplet in the range 7.62–8.08			
9A	Me	Me	H	Me	H	Me	4.11	1.38; 3.08	7.58	2.54	7.58	2.78
9B	Et	Me	H	Me	H	Me	1.53; 4.58	1.43; 3.16	7.70	2.59	7.70	2.87
9C	iPr	Me	H	Me	H	Me	1.78; 5.51	1.44; 3.26	7.63	2.57	7.63	2.98 (bs)
12A	Me	H	Me	Me	H	Me	4.09	2.73	2.38	2.48	7.59	2.73
12B	Et	H	Me	Me	H	Me	1.53; 4.63	2.82	2.39	2.50	7.59	2.82
12C[b]	iPr	H	Me	Me	H	Me	1.84; 5.52	2.91 (bs)	2.43	2.54	7.49	2.91 (bs)
15h[b]	iPr	H	Ph	Me	H	Me	1.86 : 5.63	2.67	7.25–7.67	2.26	7.25–7.67	3.02
15j[b]	iPr	H	iPr	Me	H	Me	1.84; 5.55	2.98 *	1.48; 3.68	2.66	7.48	2.91 *

[a] In $CDCl_3$ + TFA; [b] In trifluoroacetic acid (TFA). The notation bs indicates a broad singlet, and bm a broad multiplet.

Table 7

^{1}H-NMR Chemical shifts (δ, ppm, from TMS internal standard) of N-alkylanilines **7**; 60 MHz; solvent $CDCl_3$, unless otherwise stated; room temperature. An asterisk indicates assigment based on consistency within the series

Comp.	R	R²	R³	R⁴	R⁵	R⁶	N–R	R³	R⁴	R⁵	R⁶	R²	NH
7A[a]	Me	H	H	Me	H	Me	2.62	6.05	2.21	6.27	2.21	6.05	3.27
7B[a]	Et	H	H	Me	H	Me	1.10; 2.98	6.07	2.19	6.25	2.19	6.07	3.15
7C[a]	iPr	H	H	Me	H	Me	1.08; 3.51	6.07	2.18	6.23	2.18	6.07	3.03
7D[a]	tBu	H	H	Me	H	Me	1.28	6.28	2.18	6.28	2.18	6.28	3.12
7a	iPr	H	Me	H	Me	Me	1.18; 3.58	2.00 *	6.76 *	2.12 *	2.18 *	6.43 *	3.09
7b	iPr	H	Me	Me	Me	Me	1.22; 3.65	2.00 *	2.27	2.13 *	2.27	6.41	3.15
7c	iPr	H	H	Me	H	Ph	1.04; 3.53	6.27 *	2.23	6.68 *	7.17–7.53	6.53 *	3.28
7d	iPr	H	H	iPr	H	Me	1.15; 3.60	6.24	1.21; 2.77	6.38	2.24	6.24	3.30
7e	iPr	H	Me	Me	H	iPr	1.22; 3.65	1.97 *	2.24 *	6.43	1.25; 2.79	6.43	3.25
7f	iPr	H	H	tBu	H	Me	1.16; 3.60	6.42 *	1.27	6.53 *	2.25	6.23 *	3.30
7g	iPr	H	H	Ph	H	Ph	1.23; 3.74	6.78	Multiplet in the range		7.13–7.72	6.78	3.52
10A	Me	H	H	Et	H	Me	2.77	6.29	1.19; 2.53	6.43	2.26	6.29	3.48
10B	Et	H	H	Et	H	Me	1.19; 3.13	6.28	1.19; 2.53	6.40	2.25	6.28	3.42
10C	iPr	H	H	Et	H	Me	1.14; 3.58	6.26	1.19; 2.50	6.38	2.23	6.26	3.22
10D	tBu	H	H	Et	H	Me	1.32	6.46	1.20; 2.54	6.46	2.25	6.46	3.13
13A≡10′A	Me	H	Me	Me	H	Me	2.83	1.97 *	2.24 *	6.43 *	2.27 *	6.35 *	3.36
13B≡10′B	Et	H	Me	Me	H	Me	1.22; 3.12	1.94 *	2.22 *	6.40 *	2.26 *	6.34 *	3.20
13C≡10′C	iPr	H	Me	Me	H	Me	1.18; 3.61	1.94 *	2.20 *	6.37	2.25 *	6.37	3.22
13D≡10′D	tBu	H	Me	Me	H	Me	1.38	2.02 *	2.24 *	6.70 *	2.27 *	6.48 *	3.43
16h	iPr	H	Ph	Me	H	Me	1.06; 3.62	7.38	1.94 *	6.47	2.33 *	6.47	3.12
16j[a]	iPr	H	H	Me	iPr	Me	1.17; 3.49	6.17	2.31	1.30; 3.32	2.31	6.17	3.12

[a] In CCl_4

The reaction of 2,4,6-trimethylpyrylium perchlorate with *t*-butylamine afforded N-*t*-butyl-3,5-dimethylaniline **7D**.

The reaction of 2,3,5,6-tetramethylpyrylium perchlorate **1a** with isopropylamine afforded 1-isopropyl-2,3,5,6-tetramethylpyridinium perchlorate **6a** (lit.[11] m.p. 168°) and N-isopropyl-2,4,5-trimethylaniline **7a**.

The reaction of 2,3,4,5,6-pentamethylpyrylium perchlorate **1b** with isopropylamine afforded 1-isopropyl-2,3,4,5,6-pentamethylpyridinium perchlorate **6b** (lit.[11] m.p. 157°; the present sample is impurified with 4-ethyl-1-isopropyl-2,3,6-trimethylpyridinium perchlorate originating from 4-ethyl-2,3,6-trimethylpyrylium perchlorate present as by-product in **1b**) and N-isopropyl-2,3,4,5-tetramethylaniline **7b**.

The reaction of 2,6-dimethyl-4-phenylpyrylium perchlorate **1c** with isopropylamine afforded 1-isopropyl-2,6-dimethyl-4-phenylpyridinium perchlorate **6c** and N-isopropyl-3-methyl-5-phenylaniline **7c**.

The reaction of 2-isopropyl-4,6-dimethylpyrylium perchlorate **1d** with isopropylamine afforded 1,2-diisopropyl-4,6-dimethylpyridinium perchlorate **6d** and N,3-diisopropyl-5-methylaniline **7d**.

The reaction of 6-isopropyl-2,3,4-trimethylpyrylium perchlorate **1e** with isopropylamine afforded 1,6-diisopropyl-2,3,4-trimethylpyridinium perchlorate **6e** and N,5-diisopropyl-2,3-dimethylaniline **7e**.

The reaction of 2-*t*-butyl-4,6-dimethylpyrylium perchlorate **1f** with isopropylamine afforded 3-*t*-butyl-N-isopropyl-5-methylaniline **7f**.

The reaction of 2-methyl-4,6-diphenylpyrylium perchlorate **1g** with isopropylamine afforded 1-isopropyl-2-methyl-4,6-diphenylpyridinium perchlorate **6g** (recrystallized from ethanol/ethyl ether) and N-isopropyl-3,5-diphenylaniline **7g**.

The reaction of 2-ethyl-4,6-dimethylpyrylium perchlorate **8** with methylamine afforded 2-thyl-1,4,6-trimethylpyridinium perchlorate **9A** and an aniline fraction containing 3-ethyl-N,5-dimethylaniline **10A** and N,2,3,5-tetramethylaniline **10′A** (≡ **13A**).

The reaction of 2-ethyl-4,6-dimethylpyrylium perchlorate **8** with ethylamine afforded 1,2-diethyl-4,6-dimethylpyridinium perchlorate **9B** and an aniline fraction containing N,3-diethyl-5-methylaniline **10B** and N-ethyl-2,3,5-trimethylaniline **10′B** (≡ **13B**).

The reaction of 2-ethyl-4,6-dimethylpyrylium perchlorate **8** with isopropylamine afforded 2-ethyl-1-isopropyl-4,6-dimethylpyridinium perchlorate **9C** and an aniline fraction containing 3-ethyl-N-isopropyl-5-methylaniline **10C** and N-isopropyl-2,3,5-trimethylaniline **10′C** (≡ **13C**

The reaction of 2-ethyl-4,6-dimethylpyrylium perchlorate **8** with *t*-butylamine afforded an aniline fraction containing N-*t*-butyl-3-ethyl-5-methylaniline **10D** and N-t-butyl-2,3,5-trimethylaniline **10′D** (≡ **13D**).

The reaction of 2,3,4,6-tetramethylpyrylium perchlorate **11** with methylamine afforded 1,2,3,4,6-pentamethylpyridinium perchlorate **12A** and an aniline fraction containing N,2,5,3,. tetramethylaniline **13A** (≡ **10′A**) and N,3,4,5-tetramethylaniline **13′A**.

The reaction of 2,3,4,6-tetramethylpyrylium perchlorate **11** with ethylamine afforded 1-ethyl-2,3,4,6-tetramethylpyridinium perchlorate **12B** and an aniline fraction containing N-ethyl-2,3,5-trimethylaniline **13B** (≡ **10′B**) and N-ethyl-3,4,5-trimethylaniline **13′B**.

The reaction of 2,3,4,6-tetramethylpyrylium perchlorate **11** with isopropylamine afforded 1-isopropyl-2,3,4,6-tetramethylpyridinium perchlorate **12C** (recrystallized from ethanol) and an aniline fraction containing N-isopropyl-2,3,5-trimethylaniline **13C** (≡ **10′C**) and N-isopropyl-3,4,5-trimethylaniline **13′C**.

The reaction of 2,3,4,6-tetramethylpyrylium perchlorate **11** with *t*-butylamine afforded an aniline fraction containing N-*t*-butyl-2,3,5-trimethylaniline **13D** (≡ **10′D**) and N-*t*-butyl-3,4,5-trimethylaniline **13′D**.

The reaction of 2,4,6-trimethyl-3-phenylpyrylium perchlorate **14h** with isopropylamine afforded 1-isopropyl-2,4,6-trimethyl-3-phenylpyridinium perchlorate **15h** (recrystallized from ethanol/ethyl ether) and an aniline fraction containing N-isopropyl-3,5-dimethyl-2-phenyl aniline **16h** and N-isopropyl-3,5-dimethyl-4-phenylaniline **16′h**.

The reaction of 3-isopropyl-2,4,6-trimethylpyrylium perchlorate **14j** with isopropylamine afforded 1,3-diisopropyl-2,4,6-trimethylpyridinium perchlorate **15j** (recrystallized from ethanol/ethyl ether) and an aniline fraction containing N,2-diisopropyl-3,5-dimethylaniline **16j** and N,4-diisopropyl-3,5-dimethylaniline **16′j**.

REFERENCES

[1] Preceding part; C. Uncuţa, M. D. Gheorghiu, F. Chiraleu, M. Plăveţi, M. Elian and A. T. Balaban, *Rev. Roumaine Chim.*, **33**, 719 (1988).

[2] C. Uncuţa, M. D. Gheorghiu and A. T. Balaban, *Tetrahedron. Lett.*, **28**, 3143 (1987).

[3] O. Diels and K. Alder, *Ber. dtsch. chem. Ges.*, **60**, 716 (1927).

[4] Review: A. T. Balaban, A. Dinculescu, G. N. Dorofeenko, G. W. Fischer, A. V. Koblik, V. V. Mezheritskii and W. Schroth, "Pyrylium Salts. Syntheses, Reactions, and Physical Properties", Adv. Heterocyclic Chem., Suppl. Vol. 2, Academic Press, New York, 1982.

[5] A. T. Balaban and C. Toma, *Tetrahedron*, Suppl. **7**, 1 (1966).

[6] C. Toma and A. T. Balaban, *Tetrahedron*, Suppl. **7**, 9 (1966).

[7] H. C. Van der Plas, *Acc. Chem. Res.*, **11**, 462 (1978).

[8] A. T. Balaban, C. Uncuţa and F. Chiraleu, *J. Labelled Comp. Radiopharm.*, **19**, 783 (1982).

[9] H. G. Rajoharison, H. Soltani, M. Arnaud, C. Roussel and J. Metzger, *Synth. Commun*, **10**, 195 (1980).

[10] P. Vernaudon, H. G. Rajoharison and C. Roussel, *Bull. Soc. Chim. France*, 205 (1987).

[11] C. Roussel, A. T. Balaban, U. Berg., M. Chanon, R. Gallo, G. Klatte, J. A. Memiaghe, J. Metzger, D. Oniciu and J. Pierrot-Sanders, *Tetrahedron*, **39**, 4209 (1983).

Revue Roumaine de Chimie, **34**, *6*, 1439—1446 (1989)

ON THE COMPLEX IONS IN MOLTEN $TlCl-CdCl_2$ SYSTEM

ŞTEFANIA ZUCA * and MARIELA CONSTANTINESCU
Institute of Physical Chemistry — ICECHIM, Splaiul Independenţei 202, Bucharest, Romania

Received October 28, 1988

The cationic self-diffusion coefficients in the molten $TlCl-CdCl_2$ system were measured as a function of temperature and concentration by the "diffusion into the capillary" technique. The results are explained taking into account the possible structural changes occurring on mixing as destruction of double octahedron type entities and tetrachloro complex ion ($CdCl_4^{2-}$) formation. The concentration of both ionic species is quantitatively established in terms of the diffusion coefficients, at all temperatures and compositions considered.

Complex ions in molten salts are generally defined as structural groups whose central ion is strongly bonded to a certain number of oppositely charged ions for a time longer than 10^{-13} s. However, it is difficult to establish the existence of such groups because all methods of investigation are marred by certain limitations. The diffusion coefficients of ionic constituents of the melt supply information regarding the motion of existing species and together with other information either spectral or thermodynamic, may, contribute to the elucidation of the structure of molten salts.

In order to provide more information on the ionic interaction in the molten $TlCl-CdCl_2$ system, whose phase diagram[1] points to the existence of the compound $CdCl_2 \cdot TlCl$, we have investigated the self-diffusion coefficients of both cationic constituents as depending on temperature and composition.

EXPERIMENTAL

The "diffusion into the capillary method" was used as previously described. Because TlCl and its mixtures with $CdCl_2$ are slightly soluble in water, the radioactivity of each capillary at the end of the diffusion run was measured on samples solidified directly into the capillary. In order to reproduce the counting geometry, the radioactivity of the bath was measured on similar samples. The error of analysis was thus within $\pm 3\%$, i.e. higher than in the measurements in solution. Taking into account all error sources an overall error of the method of $\pm 5\%$ was estimated.

Reagent grade TlCl and $CdCl_2$ were used. Special precautions were taken in preparing and melting them. Thus, argon gas saturated with CCl_4 was bubbled through the melts in order to remove traces of water and decomposition products. ^{204}Tl and ^{115m}Cd radioactive isotopes were employed as tracers. The self-diffusion coefficients $D_{Cd^{2+}}$ and $D_{Tl^{+}}$ were measured as a function of temperature for the whole concentration range from pure $CdCl_2$ to pure TlCl. Because of the thermal instability of the melts the temperatures ranged only to ≈ 50 K above melting point.

RESULTS AND DISCUSSIONS

Our results are listed in Table 1; each entry represents the average of the values obtained simultaneously in the four capillaries employed in the run. The corresponding standard deviations are also listed.

Because the diffusion coefficients for the studied mixtures have not been measured so far, a comparison with literature data was possible for

Table 1

Self-diffusion coefficients $D_{Cd^{2+}}$ and $D_{Tl^{+}}$ in molten $CdCl_2$–TlCl system

x_{CdCl_2}	t, K	$D_{Cd^{2+}} \cdot 10^5$ $cm^2 \cdot s^{-1}$	t, K	$D_{Tl^{2+}} \cdot 10^5$ $cm^2 \cdot s^{-1}$
1	865	2.24±0.06		
	876	2.29±0.01		
	900	2.59±0.04		
	908	2.72±0.04		
0.80	781	1.57±0.05		
	789	1.70±0.04		
	799	1.82±0.03		
	815	1.97±0.02		
0.70	783	1.67±0.02	778	1.77±0.04
	795	1.85±0.04	792	1.95±0.05
	809	2.07±0.05	807	2.19±0.04
	833	2.45±0.06	822	2.56±0.06
0.60	757	1.90±0.05		
	770	2.11±0.01		
	787	2.43±0		
	797	2.59±0.04		
0.50	763	2.33±0.08	757	2.25±0.02
	781	2.66±0.09	767	2.32±0.03
	788	2.88±0.08	799	2.56±0.03
	797	2.96±0.10	787	2.64±0.02
0.25	746	2.85±0.06	759	3.14±0.09
	761	2.92±0.06	769	3.38±0.04
	769	2.95±0.04	782	3.60±0.08
	778	3.10±0.03	790	3.92±0.12
0			759	4.03±0.03
			782	4.57±0.10
			788	4.74±0.08
			794	4.90±0.06

single salts only. As shown in Fig. 1, the present $D_{Cd^{2+}}$ data are in good agreement with more recent data obtained by the diffusion out of the capillary method,[3] but differences of 6—15% are found for older data.[4,5]

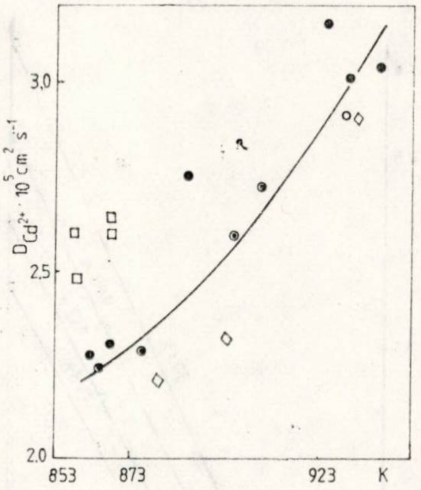

Fig. 1. — Self-diffusion coefficient of Cd^{2+} in molten $CdCl_2$. ○ our data ● Koster;[3] □ Argell and Tomlinson[4]; ◇ Richards.[5]

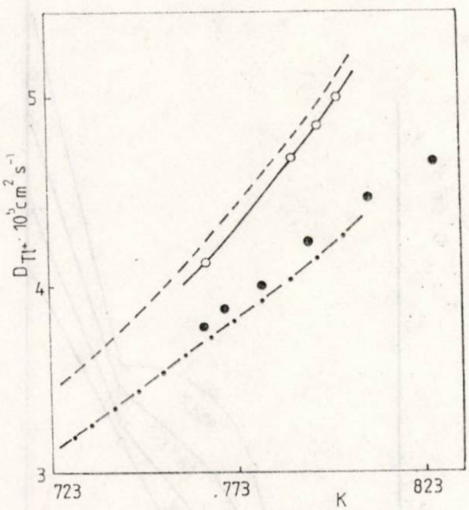

Fig. 2. — Self-diffusion coefficient of Tl in molten TlCl ○ our data ——— Sjoblom and Andersson;[6] ● Berne and Klemm;[7] ○—○—○ Angell and Tomlinson.[8]

Regarding D_{Tl^+}, Fig. 2 indicates a very close agreement (within 2%) of the present data with those obtained by the porous frit method with short diffusion times,[6] while the data obtained by the classical capillary method [7,8] agree within 12%.

The composition dependence of self-diffusion coefficients $D_{Cd^{2+}}$ and D_{Tl^+} in molten $CdCl_2$—TlCl mixtures is shown in Figs. 3 and 4.

As seen in Fig. 3, there is a steep increase of $D_{Cd^{2+}}$ within the range $0.8 \geqslant x_{CdCl_2} \geqslant 0.5$ and then, as $x_{CdCl_2} \to 0$, the increase is slower, and moreover at $x_{CdCl_2} = 0.25$ an inflection is evident. As temperature decreases, this inflection becomes weaker so that, at 748 K, D_{Cd^+} varies linearly with the melt composition.

As far as the D_{Tl^+} isotherms are concerned, they exhibit (Fig. 4) a linear dependence which suggests that the Tl^+ ion moves freely over the entire temperature and concentration ranges studied. Obviously any interpretation of $D_{Cd^{2+}}$ isotherms should be correlated to the special structure of single $CdCl_2$ melt[9] and to the tendency of forming complexes when TlCl is added to $CdCl_2$, as indicated by different physico-chemical data.[10-13] In addition, according to spectral data [14] solid $CdCl_2$ is characterised by a layer structure (probably octahedral chains $(CdCl_3)_n^{n-}$ with $n = 4$, held together by chlorine bridges), which persists to a certain degree in the liquid state.[9] As stated,[15] the degree of association in $CdCl_2$ melt is considerable and the calculated values[5] have come to 0.3—0.8 for the 873—973K temperature range.

On the other hand, given the d^{10}s^2 structure of Tl$^+$ ion, melted TlCl is expected to exhibit a pronounced covalency. Consequently, mixing of these two components should be accompanied by important structura changes: either distortion of the remanent CdCl$_2$ lattice up to total destruction or changes in anion-cation bond energy. According to Bredig [16] on addition of a monovalent chloride, the hexahedral coordination of Cd^{2+} ions in single CdCl$_2$ changes toward tetrahedral coordination also involving an asymmetric polarization of the common anion; Illyasov and Berman [17] have identified an octahedral complex in CdCl$_2$−TlCl mixtures too.

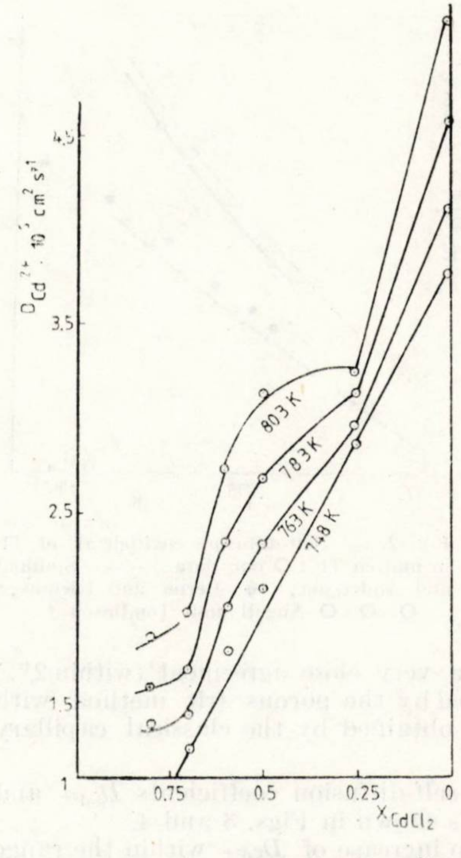

Fig. 3. — $D_{Cd^{2+}}$ vs. composition in molten CdCl$_2$−TlCl system.

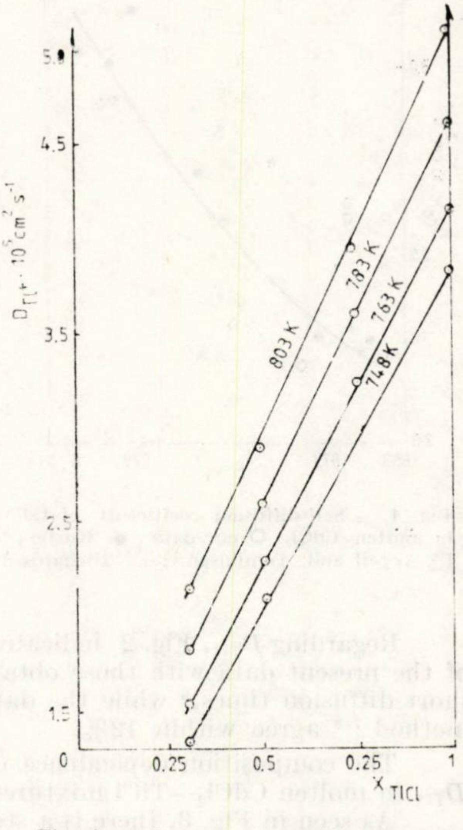

Fig. 4. — D_{Tl^+} vs. composition in molten CdCl$_2$−TlCl system.

Recent spectral data [18] have indicated too strong interactions at $x_{TlCl} = 0.82$.

According to Pelton's complex ion model [19] assuming a complete complexing at $x_{CdCl_2} \leqslant 1/3$, we have obtained the picture of ionic species existing over the whole concentration range as given in Table 2.

The calculated energy of formation of one mole of complex at $x_{CdCl_2} \leqslant 1/3$, based on the measured enthalpies of mixing by Meschel

Table 2

Pelton complex ion model applied in molten CdCl$_2$ – TlCl system

Ionic species	$x_{CdCl_2} \leqslant 0.4$	$x_{CdCl_2} \geqslant 0.4$
Cd^{2+}	0	$x_{CdCl_2} - \frac{(2x_{C\ C} + x_{TlCl})}{4}$
Tl$^+$	x_{TlCl}	x_{TlCl}
CdCl$_4$]$^{2-}$	x_{CdCl_2}	$\frac{(2x_{CdCl_2} + x_{TlCl})}{4}$
Cl$^-$	$x_{TlCl} - 2x_{CdCl_2}$	0

and Kleppa,[12] is of −65.34 kJ/mole, that is sufficient to justify the existence of a stable compound (CdCl$_4$)Tl$_2$.

Because the diffusion coefficients characterize the motion of each constituent ionic species of the medium, they are expected to provide additional structural information, which could not come from the other physico-chemical data, as the enthalpy of mixing,[10] the molar volume,[11] the electrical conductivity[12,13] which characterize the melt in the bulk.

If the temperature dependence is considered, then as evidenced by the data in Fig. 5 there is a linear dependence of log $D_{Cd^{2+}}$ vs. 1/T excepting the $x_{CdCl_2} = 0.25$ mixture, which exhibits a non-Arrhenius behaviour.

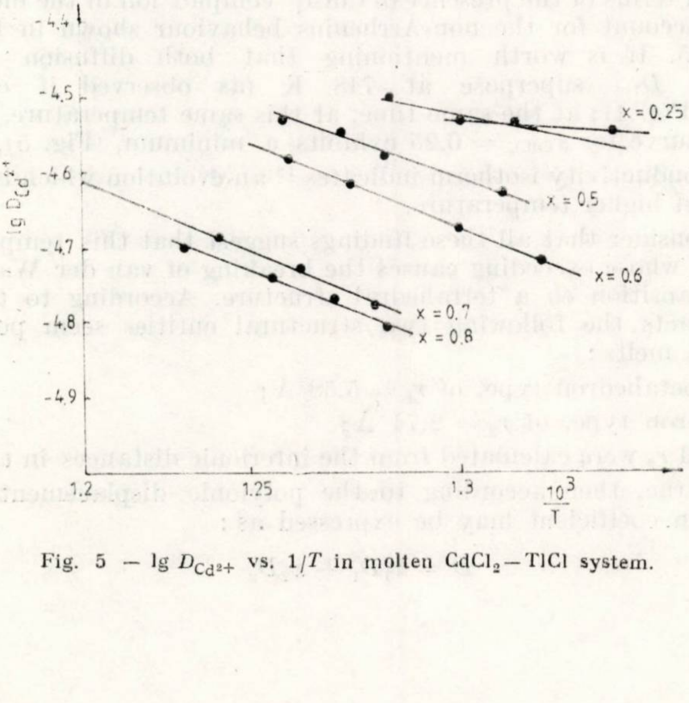

Fig. 5 – lg $D_{Cd^{2+}}$ vs. $1/T$ in molten CdCl$_2$ – TlCl system.

The activation energies, E_{D_+}, calculated from the slope of log D vs. $1/T$ lines for both cations are listed in Table 3. The corresponding standard deviations are also listed.

Table 3

Activation energies $E_D^{Tl^+}$ and $E_D^{Cd^{2+}}$ at different compositions in molten $TlCl-CdCl_2$ system

x_{CdCl_2}	$E_D^{Tl^+}$ kJ/mol	$E_D^{Cd^{2+}}$ kJ/mol	Temperature range, K
1	—	30.19 ± 4.67	863–913
0.80	—	34.91 ± 4.93	773–823
0.70	44.05 ± 4.54	41.23 ± 1.36	773–833
0.60	—	39.34 ± 1.46	753–798
0.50	28.01 ± 5.16	37.04 ± 5.44	753–798
0.25	33.99 ± 5.61	—	743–793
0	27.99 ± 0.96	—	753–798

Examination of data in Table 3 shows that both $E_{D_{Cd^{2+}}}$ and $E_{D_{Tl^+}}$ have a maximum at $x_{CdCl_2} = 0.7$ which points to a certain hindrance of the diffusion of the two cations in this region. Most probably the first addition of TlCl to $CdCl_2$ leads to a distortion of the remanent lattice of $CdCl_2$ melt accompanied by a more compact structure if the mixture. The process reaches the maximum extent at $x_{CdCl_2} = 0.7$ and then, upon further addition of TlCl as suggested by E_{D^+} values in Table 3, the motion of ions is made easier, most probably as a result of systematical destruction of the existing lattice. Indeed, all above specified data [10-13] were discussed in terms of the presence of $CdCl_4^{2-}$ complex ion in the melt, which may also account for the non-Arrhenius behaviour shown in Fig. 5, at $x_{CdCl_2} = 0.25$. It is worth mentioning that both diffusion isotherms $D_{Cd^{2+}}$ and D_{Tl^+} superpose at 748 K (as observed if comparing Fig. 3 and Fig. 4); at the same time, at this same temperature, the non-Arrhenius curve for $x_{CdCl_2} = 0.25$ exhibits a minimum, (Fig. 5), and the electrical conductivity isotherm indicates [13] an evolution which is different from that at higher temperature.

We consider that all these findings suggest that this temperature is a threshold whose exceeding causes the breaking of van der Waals bonds and the transition to a tetrahedral structure. According to the above discussed facts the following two structural entities seem possible in $TlCl-CdCl_2$ melts:

— double octahedron type, of $r_1 = 5.58$ Å;

— tetrahedron type, of $r_2 = 2.74$ Å;

where r_1 and r_2 were calculated from the interionic distances in the solid.[20] If this is true, then according to the polyionic displacement model,[21] the diffusion coefficient may be expressed as:

$$D = x_1 D_1 + x_2 D_2 \tag{1}$$

where x_1, x_2, D_1 and D_2 refer to the mole fraction and the diffusion coefficients of the two structural forms. As $x_1 + x_2 = 1$, it follows from eq. (1) that:

$$x_1 = \frac{D - D_2}{D_1 - D_2} \tag{2}$$

which allows one to estimate the concentration of ionic species existing in the melt at any given temperature from the experimental D value provided that D_1 and D_2 values are available. As already proved [22] at constant temperature $D \cdot r = \text{ct.}$ and accordingly eq. (1) can be written as:

$$x_1 D_1 r_1 + x_2 D_2 r_2 = \text{ct.} \tag{3}$$

which yields:

$$\text{for } x_1 = 0 \qquad D_2 = \text{ct.}/r_2 \tag{4}$$

$$\text{for } x_2 = 0 \qquad D_1 = \text{ct.}/r_1 \tag{5}$$

If Pelton's complex ion model for molten halides [11] is accepted, then in the concentration range $x_{\text{CdCl}_2} \leqslant 1/3$ there are only CdCl_3^{2-} ions in the melt and, consequently, the experimentally measured $D_{\text{Cd}^{2+}}$ stands just for D_2. Then from eqs. (4) and (5) one obtains D_1 and finally eq. (2) can be used as mentioned above.

Table 4 illustrates the results obtained for 783 K. Examination of Table 4 shows that $x_{\text{CdCl}_2} = 0.7$ is the onset of structural changes caused by mixing, which is also suggested by the experimental results in Fig. 3 and Table 3. Besides, it is obvious that the transition toward tetrahedral coordination increases with increasing TlCl concentration, as already assumed.[16] Unfortunately one cannot conclude that these polyionic associations are thermodynamically stable complex ions.

Table 4

Concentration of associated ionic species at 783 K in CdCl$_2$—TlCl system

x_{CdCl_2}	$D_{\text{Cd}^{2+}} \cdot 10^5$ $\text{cm}^2 \cdot \text{s}^{-1}$	$x_{1[\text{CdCl}_6]^{4-}}$	$x_{2[\text{CdCl}_4]^{2-}}$
1	—	1	0
0.80	1.57	1	0
0.70	1.57	0.91	0.09
0.60	2.43	0.50	0.50
0.50	2.66	0.30	0.70
0.25	3.14	0	1

REFERENCES

[1] A. P. Polkin and I. P. Palyura, *Zhur. neorg. Khim.*, **4**, 253 (1959).
[2] S. Zuca and M. Constantinescu, *Rev. Roumaine Chim.*, **17**, 385 (1972).
[3] J. Koster, Ph. D. Thesis, Amsterdam, 1971.
[4] C. A. Angell and J. W. Tomlinson, *Discus. Faraday Soc.*, **32**, 237 (1961).
[5] S. Richards, Ph. D. Thesis, Univ. of Penns.. 1967.
[6] C. A. Sjöblom and J. Andersson, *Z. Naturf.*, **23a**, 197 (1968).
[7] E. Berne and A. Klemm, *Z. Naturf.*, **8a**, 400 (1953).
[8] C. A. Angell and J. W. Tomlinson, *Trans. Faraday Soc.*, **61**, 2312 (1965).
[9] W. Bues, *Z. Anorg. allgem. Chem.*, **104** 279 (1955).
[10] S. V. Meschel and O. J. Kleppa, *J. Chem. Phys.*, **46**, 1853 (1967).
[11] H. Bloom, P. W. D. Boyd, J. L. Laver and J. Wrong, *Australian J. Chem.*, **19**, 1591 (1966).
[12] H. Bloom, *Pure and Appl. Chem.*, **7**, 398 (1963).
[13] P. I. Protsenko, *Izv. Vyssh. Ucheb. Zaved. Khim. i Khim. Technol.*, **4**, 345 (1961).
[14] M. Tanaka, K. Balasubramanyan and J. O'M. Bockris, *Electrochim. Acta*, **8**, 621 (1963).
[15] G. Bertozzi and G. Soldani, *J. Phys. Chem.*, **72**, 353 (1968).
[16] M. A. Bredig, "Molten Salts", ed. G. Mamantov, M. D. Dekker, New York, 1969, p. 55.
[17] I. I. Illyasov and A. G. Berman, *Zhur. neorg. Khim.*, **7**, 181 (1962).
[18] V. D. Prisyazhnaji, B. M. Voronin, I. V. Obolonchik and V. N. Mirnyi, *Koord. Khim.*, **7**, 997 (1981).
[19] A. D. Pelton, *Canad. J. Chem.*, **49**, 3919 (1971).
[20] D'ANS. LAX, "Taschenbuch für Chemiker and Physiker", Springer Verlag, Heidelberg, (1970), pp. 3–429, 3–454.
[21] F. Lantelme, Ph. D. Thesis, Paris, 1965.
[22] Mc Laughlin, *Trans. Faraday Soc.*, **55**, 29 (1959).

ORSZÁGOS MŰSZAKI INFORMÁCIÓS KÖZPONT ÉS KÖNYVTÁR 1883

NOTE POUR LES AUTEURS

La **Revue Roumaine de Chimie** publie des articles en anglais, français, russe, allemand ou espagnol. Les auteurs sont priés d'envoyer des articles et des comptes rendus inédits.

Les manuscrits seront dactylographiés à double interligne. La bibliographie, les tableaux et la légende des figures seront placés après le texte.

Si l'article fait partie d'une série numérotée, la partie précédente sera donnée comme première référence.

Chaque article sera précédé d'un résumé comprenant quinze lignes au maximum.

Les références bibliographiques dans le texte seront faites par des exposants sans parenthèses et paraîtront à la fin de l'ouvrage.

Les publications périodiques mentionnées dans la bibliographie seront présentées suivant les prescriptions internationales : le nom de l'auteur précédé de l'initiale du prénom, le titre du périodique abrégé conformément à « Chemical Abstracts » et souligné par une ligne, le numéro du tome indiqué par des chiffres arabes et souligné par deux lignes, suivi de la première page de l'article : à la fin, l'année de la parution sera placée entre parenthèses. Le numéro de la revue ne sera pas indiqué si les pages du volume sont numérotées consécutivement.

Les textes des livres ou traités inclueront : le nom des auteurs, précédés de l'initiale du prénom, le titre du livre entre guillemets et sans être souligné, le numéro du tome précédé par l'abréviation « vol. » (ou « Bd. »), le numéro de l'édition, les éditions (the publisher), la localité de la parution du livre, l'année de la parution et la page de la référence précédée(s) par l'abréviation « p » (ou « S »).

Les brevets seront indiqués comme suit : l'auteur ou la firme, le pays et le numéro du brevet, la date de la revue *(Chem. Abstr.)*. Par ex. : M. Jones (to Union Carbide Co.), Brit. Pat. 610 238, 2 Sept. 1959 : cf. *Chem. Abstr.*, **54**, 12808 (1960).

Si la référence n'a pas été lue en original, on indiquera aussi la revue de références consultée.

Les diagrammes seront tracés à l'encre de Chine sur papier calque. Les tableaux et les figures (en nombre strictement nécessaire), ainsi que les courbes dans les figures seront numérotés par des chiffres arabes. Leur explication sera donnée dans la légende des figures. Prière de ne pas inscrire les mêmes données dans les tableaux et les figures. Chaque tableau aura un titre. On indiquera dans le texte la place approximative des tableaux et des figures. Les formules chimiques seront incluses dans le texte ; en outre, elles seront transcrites sur papier calque, à l'encre de Chine.

Les auteurs sont priés d'indiquer les caractères italiques (en soulignant les lettres au crayon), ainsi que tout autre caractère spécial : les préfixes *ortho, méta, para, cis, trans,* etc. seront soulignés pour indiquer leurs caractères italiques et ne seront jamais écrits avec des majuscules.

Aucune correction à la main ne sera admise sur le manuscrit. Les corrections seront frappées à la machine. Les lettres grecques ou d'autres symboles spéciaux seront insérés à la main à l'encre clairement.

Le manuscrit sera signé par l'auteur.

Le titre courant aura 50 lettres au maximum.

L'entière responsabilité du contenu des articles appartient aux auteurs.

Sur demande on peut obtenir une note plus complète.

PRINTED IN ROMANIA

66

TRAVAUX PARUS AUX ÉDITIONS DE L'ACADÉMIE DE LA RÉPUBLIQUE SOCIALISTE DE ROUMANIE

ELENA CEAUŞESCU, **Răşini de hidrocarburi, vol. 1,** 1988, 344 p.
ELENA CEAUŞESCU, **Progrese în chimia şi tehnologia polimerilor,** 1986, 446 p.
ELENA CEAUŞESCU, **Forschungen im Bereich der Chemie und Technologie der Polymere,** 1986, 444 p.
ELENA CEAUŞESCU, **Cercetări în chimia şi tehnologia polimerilor,** 1983, 520 p.
ELENA CEAUŞESCU, **Noi cercetări în domeniul compuşilor macromoleculari,** 1981, 536 p.
ELENA CEAUŞESCU, **Polimerizarea stereospecifică a izoprenului,** 1979, 307 p.
ELENA CEAUŞESCU, **Research work on synthesis and characterization of macromolecular compounds. Contributions,** 1974, 251 p.
I. G. MURGULESCU, **Introducere în chimia fizică, vol. I. 1. Atomi, molecule, legătură chimică,** 1976, 560 p.
I. G. MURGULESCU, V. EM. SAHINI, **Introducere în chimia fizică, Vol. I, 2. Structura şi proprietăţile moleculelor,** 1979, 604 p.
I. G. MURGULESCU, E. SEGAL, **Introducere în chimia fizică, Vol. II. 1. Teoria molecular-cinetică a materiei,** 1979, 1036 p.
I. G. MURGULESCU, TATIANA ONCESCU, E. SEGAL, **Introducere în chimia fizică, Vol. II. 2. Cinetică chimică şi cataliză,** 1981, 1024 p.
I. G. MURGULESCU, J. PĂUN, **Introducere în chimia fizică, Vol. I, 3. Nucleul atomic, reacţii nucleare, particule elementare,** 1982, 606 p.
I. G. MURGULESCU, RODICA VÎLCU, **Introducere în chimia fizică. Vol. III. Termodinamica chimică,** 1982, 624 p.
I. G. MURGULESCU, O. M. RADOVICI, **Introducere în chimia fizică, Vol. IV. Electrochimia,** 1986, 416 p.
CRISTOFOR I. SIMIONESCU, VALERIA GORDUZA, **Implicaţii bioenergetice ale coloranţilor,** 1988, 208 p.
R. VÎLCU, M. LECA, **Termodinamica polimerilor prin cromatografie de gaze,** 1987, 238 p.
I. ZUGRĂVESCU, M. PETROVANU, **Cicloadiţii 3+2 dipolare,** 1987, 446 p.
RAUL MIHAIL, ION GROZEANU, **Estimarea secvenţială aplicată sistemelor chimice,** 1986, 406 p.
M. BREZEANU, I. PATRON, M. ANDRUH, **Combinaţii complexe polinucleare şi aplicaţiile lor,** 1986, 244 p.
A. T. BALABAN et al., **Labelled Compounds and Radiopharmaceuticals Applied in Nuclear Medicine,** coédition avec John Wiley and Sons, 1986, 742 p.
D. PURDELA, **Nomenclatura chimiei organice — IUPAC,** 1986, 451 p.
PETRU BUDRUGEAC, **Probleme de chimie,** 1986, 280 p.
T. ONCESCU, S. G. IONESCU, **Conversie fotochimică şi stocare de energie,** 1985, 272 p.
V. DRĂGUŢAN, A. T. BALABAN, M. DIMONIE, **Olefin Metathesis and Ring-Opening Polymerization of Cyclo-Olefins,** coédition avec John Wiley and Sons, 1985, 544 p.
C. LITEANU, I. RÎCĂ, **Optimizarea proceselor analitice,** 1985, 360 p.
N. PERESCU, **Chimia extracţiei cu solvenţi şi aplicaţii,** 1985, 212 p.
V. EM. SAHINI, M. HILLEBRAND, **Chimie cuantică în exemple şi aplicaţii,** 1985, 382 p.
GH. MARCU, **Chimia compuşilor coordinativi,** 1984, 415 p.
E. CORDOŞ, C. MANOLIU, **Spectrometria de absorbţie şi fluorescenţa atomică,** 1984, 178 p.
C. BODEA, **Tratat de biochimie vegetală, p. II, t. V,** 1984, 438 p.
N. ASANDEI, A. GRIGORIU, **Chimia şi structura fibrelor,** 1984, 395 p.
N. IONESCU, M. CĂLDĂRARU, **Oxidarea catalitică a olefinelor inferioare,** 1983, 178 p.
C. I. SIMIONESCU, F. DANEŞ, **Originea vieţii,** 1984, 110 p.
C. BODEA, **Tratat de biochimie vegetală, p. II, t. IV,** 1982, 408 p.
CR. SIMIONESCU, VALERIA GORDUZA, **Polimeri biocompatibili şi biologic activi,** 1980, 479 p.
M. FLORESCU, **Metode ştiinţifice în dezvoltarea industriei chimice moderne,** 1979, 495 p.
C. GH. MACAROVICI, **Analiza chimică cantitativă anorganică,** 1979, 457 p.

ISSN 0035–3930

I. P. Informaţia c. 2873

43 426

Lei 40

F 1103

ACADÉMIE DE LA RÉPUBLIQUE SOCIALISTE DE ROUMANIE

REVUE ROUMAINE DE CHIMIE

TOME 34
N° 8
Août 1989

Rev. Roumaine Chim.

RRCHAX, 34, *8*, p. 1625–1816 (1989), Bucarest

EDITURA ACADEMIEI REPUBLICII SOCIALISTE ROMÂNIA

ACADÉMIE DE LA RÉPUBLIQUE SOCIALISTE DE ROUMANIE

COMITÉ DE RÉDACTION

Rédacteur en chef :

I. G. MURGULESCU, membre de l'Académie de la République Socialiste de Roumanie

Rédacteurs en chef adjoints :

A. T. BALABAN et V. EM. SAHINI, membres correspondants de l'Académie de la République Socialiste de Roumanie

Collège de rédaction :

EM. BRATU, ELENA CEAUŞESCU, ECATERINA CIORĂNESCU-NENITZESCU, CR. SIMIONESCU, membres de l'Académie de la République Socialiste de Roumanie; P. SPACU, membre correspondant de l'Académie de la République Socialiste de Roumanie: M. BANCIU, M. D. GHEORGHIU, I. HAIDUC, D. I. MARCHIDAN, G. NIAC et D. SĂNDULESCU

La Revue Roumaine de Chimie paraît 10 fois par an. Toute commande de l'étranger sera adressée à ROMPRESFILATELIA – sectorul Export-Import Presă, P.O. Box 12–201, télex 10376 prsfi r 78 104 Bucarest, Calea Griviţei nr. 64–66, Bucureşti, Roumanie

Les manuscrits, les livres et les revues proposés en échange, ainsi que toute correspondance seront envoyés à la rédaction :

REVUE ROUMAINE DE CHIMIE

125, Calea Victoriei, 79717 Bucarest, Roumanie, téléphone 50 76 80

EDITURA ACADEMIEI REPUBLICII SOCIALISTE ROMÂNIA
125, Calea Victoriei, 79717 Bucarest, Roumanie, téléphone 50 76 80

REVUE ROUMAINE DE CHIMIE

Tome 34, N° 8 **Août, 1989**

S. STERNBERG, N. BONCIOCAT, ADINA COTÂRȚĂ and T. VIȘAN, Electrode processes with interfacial generation of the electrochemical active species. II. The case of some charge transfer- or diffusion-limited processes . . . 1627—1636

HERNANDEZ E. J. ALONSO, QUERO J. L. VILCHEZ and CARRILLO T. GUARDIA, Study of pyrazinhydroxamic acid reduction on a mercury electrode 1637—1644

R. E. CACHAU, E. OTTAVIANELLI and E. A. CASTRO, Improved two parameter omega technique. IX. On the use of the ITPOT/RF on the study of excited states (in Spanish) . . . . 1645—1650

NISTOR PERESCU and RENATO CHIARIZIA, Extraction of europium(III) from nitric and perchloric media by neutral bifunctional carbamoylmethylenephosphonates . . . . 1651—1660

P. M. SHIUNDU and S. B. JONNALAGADDA, A novel spectrophotometric method for determination of peroxydisulphate ion using *o*-dianisidine-S_2O^{2-}—Cu(II) reaction . . . . 1661—1666

M. ALCOLEA PALAFOX, Torsional and inversion potential function of amino group (in Spanish) . . . . 1667—1675

ÜNEL KÖKLÜ and TÜLAY ORKUN, Lead, chromium and barium in Turkish printing inks and colored newspapers . . . . 1677—1679

VASILE COCHECI, GHEORGHE PETCA and EUGEN GLÜCK, Studies concerning calcium carbonate scales formation and its prevention. I. Kinetics of calcium carbonate precipitation from hyperthermal water. . . . . . . 1681—1689

H. SINGH and S.P.S. TOMAR, Micellar behaviour of calcium and magnesium soaps of higher fatty acids in dilute aqueous solutions at different temperatures 1691—1698

ANIȘOARA BOLD, AURELIA VASILE, ANGELICA POPA, M. CRUCEANU, EVELINE POPOVICI and MARIA ALEXANDROAEI, Ion-exchange with transition metals on highly silicious zeolites of ZSM-5 type. I. Behaviour of Ag(I) and Cu(II) . . . . 1699—1704

RANJANA DIXIT and BHAGWAN S. GARG, Stabilities of bivalent metal complexes with ω-benzoyl-2-hydroxy-4-methoxy-3-methyl acetophenone (BHMMA) . . . . 1705—1710

A. C. BANCIU, SILVIA PLOȘTINARU, MARIUS ANDRUH, LUMINIȚA PATRON and ADRIANA CONȚESCU, Oxidation of cumene with molecular oxygen in presence of Co(II) acetylacetonate complexes heterogenized on silane modified silica . . . . 1711—1720

MAHER M. GIRGIS and ZARIF H. KHALIL, Charge-transfer complexes of hydroxy styryl cyanine dyes and their analogues with nicotine. Structure-activity relationship studies . . . . 1721—1731

ORSZÁGOS MŰSZAKI INFORMÁCIÓS KÖZPONT ÉS KÖNYVTÁR

Rev. Roumaine Chim. **34,** *8,* 1625—1816 (1989), Bucarest

R. JAOUHARI, General study of the benzylation of functionalized aromatic hydrocarbons catalyzed by ruthenium complexes (in French) . . . 1733—1743
ALEXANDRU T. BALABAN, Chemical graphs. Part 51. Valence isomers of bis-homoannulenes . . . . 1745—1752
E.F.SAAD and E. A. HAMED, Addition compounds of isolated, fused and isolated-fused aromatic systems with 2,4,6-trinitrophenol. A spectroscopic study 1753—1759
V. MUREȘAN, I. FENEȘAN and L. PASKUCZ, 2-Arylthio-5-methyl-2-thiono-1,3,2-dioxaphospholanes . . . . 1761—1767
G. L. AGRAWAL and Ku. SHAMI JHA, Oxidation of ethylene glycol with pyridinium chlorochromate. A kinetic approach . . . . 1769—1773
AMAL SABET YANNI, ALI ALI ABDEL-HAFEZ and AHMED MOHAMED MOHARRAM, Synthesis of some new 7-substituted aminomethyl-8-hydroxy-quinoline-5-substituted sulphonamides of biological interest . . . 1775—1778
MIRCEA D. GHEORGHIU and ANGELA POPESCU, Nuclear magnetic resonance of small rings. 8. ^{13}C-NMR spectra of 8-substituted 5,9-methano-5H-benzo[3,4]cyclobuta [1,2] cycloheptenes . . . . 1779—1785
A. GĂLUȘARU, Why life can be only a carbon based chemistry . . . . . . 1787—1798
STELIAN PETRESCU, Study of the solid dissolution kinetics using the sedimentation technique (in French) . . . . 1799—1808

BOOK REVIEWS . . . . 1809—1816

Revue Roumaine de Chimie, **34**, *8*, 1627 – 1636 (1989)

ELECTRODE PROCESSES WITH INTERFACIAL GENERATION OF THE ELECTROCHEMICAL ACTIVE SPECIES. II[1]

THE CASE OF SOME CHARGE TRANSFER- OR DIFFUSION-LIMITED PROCESSES

S. STERNBERG, N. BONCIOCAT*, ADINA COTÂRŢĂ* and T. VIŞAN
Laboratory of Applied Physical Chemistry, Faculty of Chemical Technology, Polytechnic Institute, Bucharest, Romania
*. Institute of Chemical and Biochemical Energetics, ICECHIM, Bucharest, Romania

Received December 20, 1988

On the basis of a kinetic model for the electrode processes with interfacial generation of the electrochemical active species, the polarization curves for two limiting situations were discussed: the cases with charge transfer control and with diffusion limitation. An equation for this last situation was verified experimentally for cathodic polarization of molten lead electrode in the $LiCl-KCl+PbCl_2$ (low concentration) systems.

THE KINETIC MODEL

In an earlier work[1] some equations were proposed for the density of current in the case of electrode processes with interfacial chemical reaction, based on a model illustrated in Figure 1. This model represents the particular case of the liquid lead electrode, which works in contact with the molten electrolyte LiCl–KCl eutectic + $PbCl_2$ (low concentration), at 500°C. In another work,[2] the hypothesis was advanced that the working of this electrode could be interpreted on the basis of

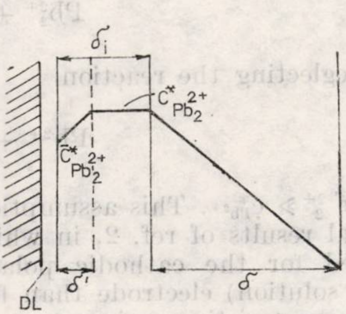

Fig. 1. — The "reaction box" of the kinetic model; δ_i — the thickness of the reaction box; δ' — the thickness of inner diffusive layer of the reaction box; δ — the thickness of outer diffusive layer towards the melt bulk; DL — the double layer of the electrode.

the formation of a metal — molten salt solution, according to the equation

$$\mathrm{Pb} + \mathrm{Pb}^{2+} \rightarrow \mathrm{Pb}_2^{2+} \tag{1}$$

or to the equation

$$\mathrm{Pb} + \mathrm{Pb}^{2+} \rightarrow 2\ \mathrm{Pb}^{+} \tag{1'}$$

It should be noticed that the literature does not offer adequate data to make a choice between mechanisms (1) and (1′). In the discussion that follows we will accept the mechanism (1), which seems to be more plausible; [2,3] this will not affect but the numerical values of the final parameters β and λ in the equations proposed by us.

Under the given experimental conditions ($t = 500$°C), molten lead dissolves in the molten halogenides electrolyte, which contains Pb^{2+} ions, so that reaction (1) does not proceed only on the surface of the metallic lead electrode, but in a "reaction box" of thickness δ_i (Fig. 1). By using a chronoamperometric technique described in ref. 2, one can detect a transition state in which

$$\overset{*}{c}_{\mathrm{Pb}_2^{2+}} \gg c^*_{\mathrm{Pb}^{2+}} \tag{2}$$

The asterisk refers to the concentration of the ions in the "reaction box". The remaining notations on Figure 1 have the following meaning: δ' is the thickness of the diffusion layer of the Pb_2^{2+} ions from the interior of the reaction box to the surface of the liquid lead electrode; δ is the thickness of the diffusion layer to the bulk of the melt, which is considered to be much larger than δ'. $c^s_{\mathrm{Pb}_2^{2+}}$ is the concentration of Pb_2^{2+} ions on the surface of the lead electrode and $c^*_{\mathrm{Pb}^{2+}}$ is the concentration of Pb^{2+} ions in the reaction box.

The discussion is based on the assumption that the cathodic process is

$$\mathrm{Pb}_2^{2+} + 2\ \mathrm{e} \rightarrow 2\ \mathrm{Pb} \tag{3}$$

thus neglecting the reaction

$$\mathrm{Pb}^{2+} + 2\ \mathrm{e} \rightarrow \mathrm{Pb} \tag{4}$$

since $c^*_{\mathrm{P}}{}_2^{2+} \gg c^*_{\mathrm{Pb}^{2+}}$. This assumption was made on the basis of the experimental results of ref. 2, in which much larger cathodic currents were obtained for the cathodic polarization curves of the Pb(liquid)/Pb^{2+} (dilute solution) electrode than for the inert graphite electrode, as well as a characteristic maximum.

In order to form a reaction box of constant thickness δ_i irrespective of the applied polarization, in which the inequality (2) would be observed, it is necessary that every potential pulse have a constant and relatively short duration. Indeed, under such conditions the species Pb_2^{2+} generated on the electrode surface by reaction (1) will spread into a reaction box of thickness proportional to $\sqrt{t}$. In our experiments a time $t = 30$ s was used.[2] Hence, under certain experimental conditions one can form the reaction box required by our model,[1] based on a stationary state assumption.

It results from the above data that we can regard the cathodic polarization curves obtained by us as an electrode process with interfacial chemical generation, for which we have proposed the following equation[1] :

$$i(P) = \frac{i_0 \left[\frac{v(P)}{v_0} \exp\left(-\frac{\alpha z F P}{RT}\right) - \exp\left(\frac{(1-\alpha) z F P}{RT}\right)\right]}{1 + \frac{v(-\infty)}{v_0} \frac{i_0}{i(-\infty)} \exp\left(-\frac{\alpha z F P}{RT}\right)} \tag{5}$$

where $i(P)$ is the current density for a polarization P, i_0 — the exchange current density, and $v(P)$ and v_0 — the chemical reaction rates for the polarizations P and $P = 0$, respectively. The latter situation is the reference state, in which the current $i(P = 0) = 0$ and the concentration in the reaction box is c_0^*. Since the reference state is not an equilibrium state but rather a stationary state, we have used everywhere the polarization P instead of the overvoltage η. The current $i(-\infty)$ is the limiting current, for which the concentration in the reaction box is $c^*(-\infty)$ and the reaction rate is $v(-\infty)$. By noting $f = F/RT$, eq. (5) may be written as

$$i(P) = \frac{i_0 \left[\frac{v(P)}{v_0} \exp(-\alpha z f P) - \exp((1-\alpha) z f P)\right]}{1 + \frac{v(-\infty)}{v_0} \frac{i_0}{i(-\infty)} \exp(-\alpha z f P)} \tag{6}$$

Starting from the basic equation of our model,[1]

$$v(P) = \frac{i(P)}{zF} + \frac{D c^*(P)}{\delta} \tag{7}$$

one gets the expression of the reaction rate for the state of zero current :

$$v_0 = \frac{D c_0^*}{\delta} \tag{8}$$

and the expression of the limiting current :

$$i(-\infty) = zF\, v(-\infty) = \frac{D z F c^*(-\infty)}{\delta} \tag{9}$$

1. Variation of Reaction Rate as a Function of Overvoltage

In order to apply eq. (6), we adopted the following relation for the dependence of the reaction rate on the cathodic polarization P:

$$\frac{v(P)}{v(-\infty)} = r_v = 1 + \beta \exp \ (\lambda z f P) \tag{10}$$

In equation (10) one can suppose that $v(-\infty) \leqslant v(\eta = 0)$, in other words this equation only refers to a reaction rate which decreases when the cathodic polarization increases; r_v is the "overall rate factor" which expresses the fact that the reaction rate decreases r_v times when the polarization varies from P to $-\infty$. At the same time, r_v depends on P and on the parameters β and λ.

The dependence of the ratio r_v as a function of λ is illustrated in Figure 2. The values $\alpha = 0.5$ and $z = 2$, which correspond to the example discussed herein (see Eq. (3)), were taken. Also, we have put $\beta = 2.74$, this value being justified in Section 3. When $\lambda \to 0$, the rate $v(P)$ decreases very slowly as a function of P and does not reach $v(-\infty)$ in experimentally accesible polarization ranges; the larger is λ, the quicker r_v goes to the limiting value ($r_v = 1$).

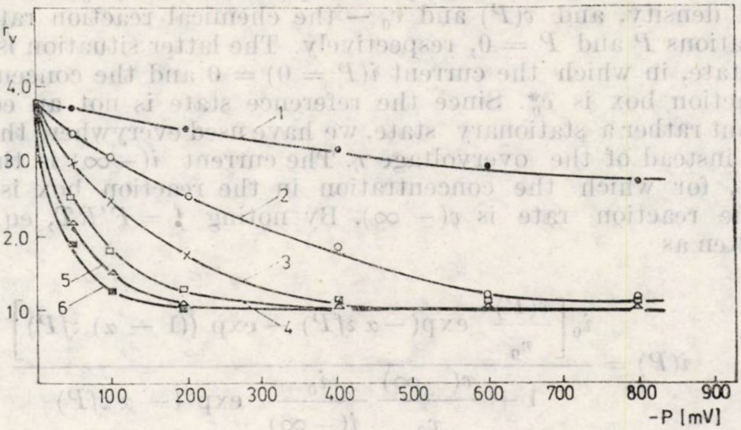

Fig. 2. — Variation of r_v ratio as a function of parameter λ: $\beta = 2.74$; $1 - \lambda = 0.02$; $2 - \lambda = 0.1$; $3 - \lambda = 0.22$; $4 - \lambda = 0.4$; $5 - \lambda = 0.6$; $6 - \lambda = 0.8$.

Equation (10) satisfies the following limiting conditions:

$$r_v(P = 0) = 1 + \beta \quad \text{and} \qquad r_v(P = -\infty) = 1 \tag{11}$$

When $\beta = 0$ the reaction rate is independent of the potential, i.e. $v(P) = v_0$. It is useful to introduce also the ratio r'_v, which can be easily derived from eq. (10):

$$\frac{v(P)}{v_0} = r'_v = \frac{1}{1+\beta}\,[1 + \beta \cdot \exp\,(\lambda z f P)] \tag{12}$$

and which satisfies the limiting conditions

$$r'_v(P = 0) = 1 \text{ and } r'_v(P = -\infty) = \frac{1}{1+\beta} \tag{13}$$

2. Charge Transfer-Limited Electrode Processes

Let us discuss first the general equation (6) in case that the cathodic process is controlled by charge transfer, i.e. that $i_0 \ll i(-\infty)$. In this case, eq. (6) becomes

$$i(P) = i_0 \left[\frac{v(P)}{v_0} \exp(-\alpha\, zfP) - \exp((1-\alpha)\, zfP) \right] \tag{14}$$

which is the equation of an electrode process with charge transfer and interfacial chemical reaction. When the reaction rate is independent of P, i.e. $v(P) = v_0 = \text{constant}$, eq. (14) becomes a classical equation for a charge transfer-limited process, in which, however, i_0 refers to reaction (3) and is expressed as a function of c_0^*. By inserting r'_v into eq. (14), the relation

$$i(P) = i_0 \left[\frac{1}{1+\beta} \exp(-\alpha\, zfP) + \frac{\beta}{1+\beta} \exp(-(\alpha-\lambda)\, zfP) - \exp((1-\alpha) zfP) \right] \tag{15}$$

is obtained. If $P = 0$, $i(P) = 0$, and if $P = -\infty$, $i \to \infty$, as it may be easily seen, irrespective of the sign of the difference $(\alpha - \lambda)$. Hence, relation (15) predicts a polarization curve without saturation. Under these conditions, since the diffusion is much more rapid than the charge transfer, the diffusion "antechamber" to the reaction box disappears (i.e. $\delta' \to 0$).

It should be mentioned that this case has also been treated under the hypothesis that the reaction rate varies as a function of the potential, according to eq. (10). Some polarization curves $i(P)$, corresponding to several values of λ, are given in Figure 3.

In what follows, we will treat in more detail the case in which $i_0 \gg i(-\infty)$ in eq. (6).

3. Diffusion-Limited Electrode Processes with Interfacial Chemical Generation

When the exchange current fulfills the condition $i_0 \gg i(-\infty)$, eq. (6) becomes

$$i(P) = i(-\infty) \left[\frac{v(P)}{v(-\infty)} - \frac{v_0}{v(-\infty)} \exp(zfP) \right] \tag{16}$$

which is the equation of an electrode process with interfacial chemical reaction and diffusion controlled. In the particular case in which the reaction rate is constant, i.e. $v(P) = v_0 = v(-\infty)$ (that is $\beta = 0$ in eq. (10)), relation (16) becomes

$$i(P) = i(-\infty)\,[1 - \exp(zfP)] \tag{17}$$

which is a typical equation with saturation. In this case, from (9) it results that one can write the relation

$$i(-\infty) = zFv_0 - \frac{DzFc^*(-\infty)}{\delta} \tag{18}$$

Likewise, from (7) it results that for $v(P)$=constant, too, the concentration $c^*(P)$ decreases when the cathodic polarization increases. When $v(P)$ is not constant, the relation

$$i(P) = i(-\infty)\,\{[1 - \exp(zfP)] + \beta[\exp(\lambda zfP) - \exp(zfP)]\} \tag{19}$$

obtained by introducing relation (10) in (16), is valid. Equation (19) represents a curve with a limiting current and with a maximum, as we will show in what follows.

Let us derive $i/i(-\infty)$ with respect to P; the expression

$$\frac{\mathrm{d}(i/i(-\infty))}{\mathrm{d}P} = -zf\exp(zfP_{\max}) + \beta\cdot\lambda\cdot zf\exp(\lambda zfP_{\max}) - \beta zf\exp(zfP_{\max}) \tag{20}$$

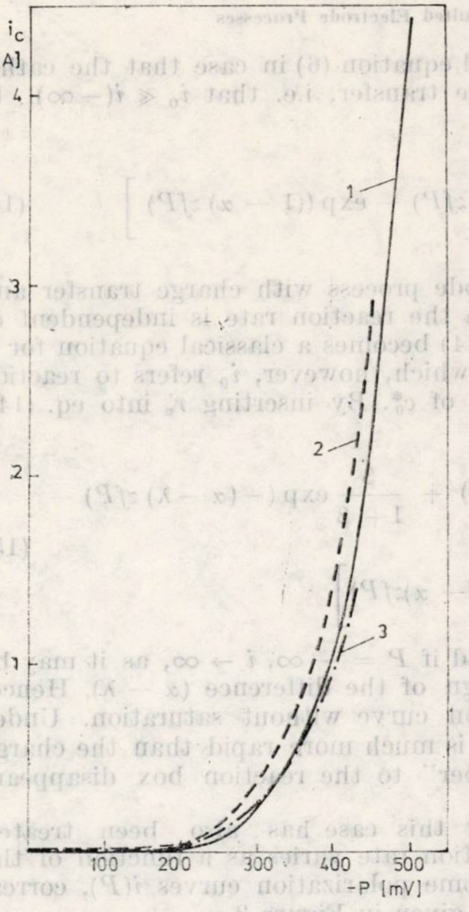

Fig. 3. — The dependence $i_c = f(P)$ for the different values of parameter λ; 1 — $\lambda = 0.5$; 2 — $\lambda = 0.22$; 3 — $\lambda = 0.8$.

results. By noting by X the expression

$$\exp(zfP_{\max}) = \mathrm{X} \qquad (21$$

one obtains

$$\mathrm{X}^{\lambda-1} = \frac{\beta+1}{\beta\cdot\lambda} \quad \text{or} \quad (\lambda-1)\ln \mathrm{X} = \ln\frac{\beta+1}{\beta\cdot\lambda} \tag{22}$$

But $\ln X = zfP_{\max}$, which leads to the value

$$P_{\max} = \frac{\ln \frac{\beta + 1}{\beta \cdot \lambda}}{zf(\lambda - 1)} \tag{23}$$

Figure 4 shows the dependence $P_{\max} = f(\lambda)$, estimated according to eq. (23), whereas Figure 5 gives the dependence $i_{c\max} = f(\lambda)$, obtained by replacing $P_{\max}$ in eq. (19). One can notice that there exists an interval within which $i_{c\max}$ has values with physical meaning, the "validity domain" of eq. (10) contained between $0 < \lambda < 1$. For $\lambda > 1$, negative values are obtained for $i_{c\max}$; they lack physical significance in the framework of the hypothesis accepted in this work.

Figure 6 gives the variation of the $i_{\max}/i(-\infty)$ ratio as a function of P, for the different values of β. One sees that both the $i(P)/i(-\infty)$ ratio and the value of $i_{\max}/i(-\infty)$ ratio increase when β increases.

Figure 7 shows several polarization curves obtained using different λ values for β = constant. One sees that for small values of λ, i does not reach its limiting value, not even for very large polarization. Also, the increase of λ leads to the decrease of the currents $i(P)$ and $i_{\max}$. In Figure 7 is also given the experimental curve obtained by us, which is compared with the curve computed on the basis of eq. (19). The following parameters had been chosen : $\beta = 2.74$ and $\lambda = 0.22$, values which were obtained by means of a computer optimization program. A good agreement can be seen between the experimental results and those obtained based on eq. (19).

The decrease of the reaction rate with increase of P can be accounted for as follows : the rate of reaction (1), $Pb + Pb^{2+} \rightarrow Pb_2^{2+}$, is given by the expression

$$v_r = k' \cdot [Pb] \cdot [Pb^{2+}] \tag{24}$$

Since the concentration of metallic lead Pb is considered to be constant, the reaction rate becomes

$$v_r = k\ [Pb^{2+}] \tag{25}$$

In the expression (25) the concentration $[Pb^{2+}]$, which refers to the reaction box, is not invariable, but it depends of polarization P. At small P values, $[Pb^{2+}]$ concentration is close to the concentration of the Pb^{2+} ions in the bulk of the melt, so that the reaction (whose reaction rate is given by relation (25)) is kinetically controlled. When P and, consequently, $i(P)$ increase, a diffusive zone of the Pb^{2+} ions is created, their concentration decreases and, implicitly, the reaction rate will decrease.

CONCLUSIONS

The general equation proposed by us in ref. 1 for electrode processes with interfacial generation of the electrochemical active species, was applied to the case of an interfacial generation of a chemical nature, in two limiting situations : kinetical control of the charge transfer and diffusion control.

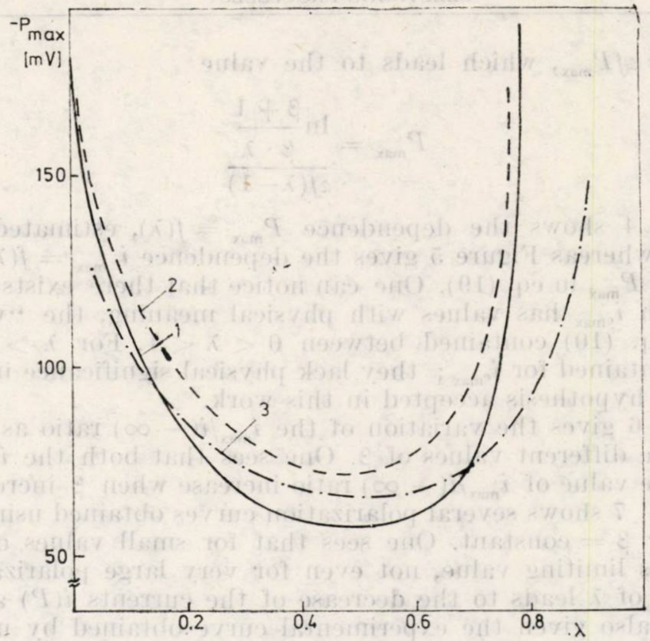

Fig. 4. — The dependence $P_{\max} = f(\lambda)$ for different values of parameter β ; $1 - \beta = 5.5$; $2 - \beta = 2$; $3 - \beta = 2.74$; (optimal value).

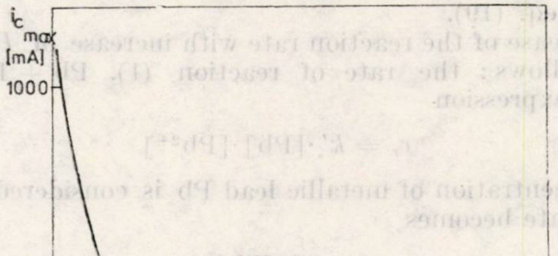

Fig. 5. — The dependence $i_{c\max} = f(\lambda)$ for different values of parameter β ; $1 - \beta = 5.5$; $2 - \beta = 2$; $3 - \beta = 2.74$ (optimal value).

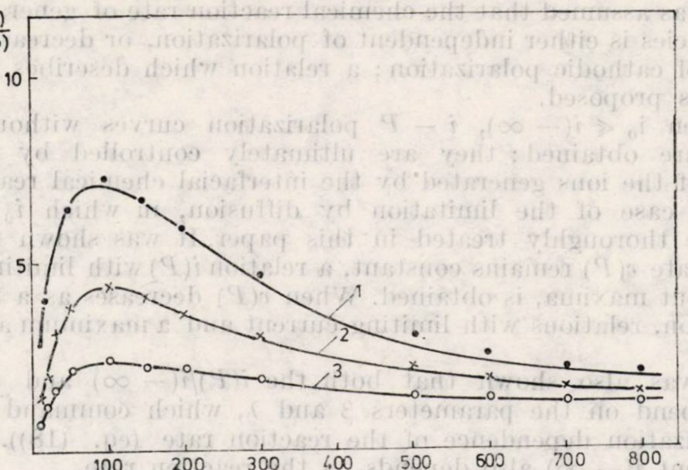

Fig. 6. — Variation of $\frac{i(P)}{i(-\infty)}$ ratio as a function of polarization P, at a constant value of parameter $\lambda(\lambda = 0.22)$; $1 - \beta = 9$; $2 - \beta = 5$; $3 - \beta = 2$.

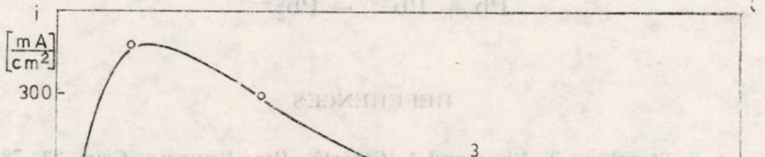

Fig. 7. — The polarization curves in the case of interfacial chemical generation ; 1 — the experimental curve in LiCl — KCl + 0.05 M $PbCl_2$ electrolyte ($t = 500°C$) using a liquid lead electrode ; 2 — optimized curve, with $\beta = 2.74$ and $\lambda = 0.22$; 3 — calculated curve, with $\beta = 2.74$ and $\lambda = 0.04$; 4 — calculated curve with $\beta = 2.74$ and $\lambda = 0.5$; 5 — calculated curve with $\beta = 2.74$ and $\lambda = 0.6$; 6 — calculated curve with $\beta = 2.74$ and $\lambda = 0.8$.

It was assumed that the chemical reaction rate of generation of the active species is either independent of polarization, or decreases with the increase of cathodic polarization; a relation which describes this dependence was proposed.

When $i_0 \ll i(-\infty)$, $i - P$ polarization curves without limiting current are obtained; they are ultimately controlled by the charge transfer of the ions generated by the interfacial chemical reaction.

The case of the limitation by diffusion, in which $i_0 \gg i(-\infty)$, was more thoroughly treated in this paper. It was shown that if the reaction rate $v(P)$ remains constant, a relation $i(P)$ with limiting current, but without maxima, is obtained. When $v(P)$ decreases as a function of polarization, relations with limiting current and a maximum are deduced (eq. (19)).

It was also shown that both the $i(P)/i(-\infty)$ and $i_{\max}/i(-\infty)$ ratios depend on the parameters β and λ, which command ultimately the polarization dependence of the reaction rate (eq. (18)). The limiting current $i(-\infty)$ also depends on the reaction rate.

Finally, eq. (19) was verified by comparing its predictions with the $i = f(P)$ curves observed experimentally for the cathodic polarization of a molten lead electrode in the $LiCl-KCl + PbCl_2$ (low concentration) melts at 500°C, in which the interfacial chemical generation is carried out by the reaction

$$Pb + Pb^{2+} \rightarrow Pb_2^{2+} \qquad (26)$$

REFERENCES

[1] N. Bonciocat, S. Sternberg, T. Vișan and A. Cotârță, *Rev. Roumaine Chim*, **33**, 781 (1988).

[2] S. Sternberg, T. Vișan, N. Bonciocat and A. Cotârță, *Rev. Roumaine Chim.*, **32**, 883 (1987).

[3] S. V. Volkov, V. S. Naumov and A. A. Omelchuk, *Ukr. khim. Zhur.*, **50**, 154 (1984).

Revue Roumaine de Chimie, 34, 8, 1637–1644 (1989)

STUDY OF PYRAZINHYDROXAMIC ACID REDUCTION ON A MERCURY ELECTRODE

HERNANDEZ E. J. ALONSO, QUERO J. L. VILCHEZ
and CARRILLO T. GUARDIA
Department of Analytical Chemistry, Faculty of Science, University of Grenade,
18071 — Grenade, Spain

Received May 23, 1987

The reduction of pyrazinhydroxamic acid at the dropping mercury electrode has been investigated. The reagent captures two electrons and one or two hydrogen ions depending on the pH of solution. The reaction orders together with Tafel's slopes have been calcuculated. From i—E curves the irreversibility of the systems was deduced.

INTRODUCTION

Hydroxamic acid has been used for many years in analytical chemistry as colorimetric and gravimetric reagent.[1-5] Previously we showed that pyrazinhydroxamic acid (PHA) reacts with several metallic cations Cu(II), Ni(II), Pd(II), Mn(II), giving in each case a coloured solid and with Fe(III), Ti(IV), Mo(VI) and V(V), giving coloured complexes on solutions, the colour depending on the pH.

Some of these compounds formed by pyrazinhydroxamic acid with the metallic ions in solution can be extracted with organic solvents, leading to more sensitive determination methods than in an aqueous media.[3] Also the PHA-Fe(III) system can be used as a complexometric indicator.[4] Pyrazinhydroxamic acid has been also used as a catalyzer in the hydrolysis of organic fluorophosphates and fluorophosphonates.[6]

Here we complete the study of electrochemical reduction of pyrazinhydroxamic acid by conventional polarography, voltametric and coulometric techniques.

We have studied the influence of the height of the Hg column, temperature, concentration of the reagent and pH on the height of the polarographic wave. We note as a result of this research that our PHA as well as pyrazin acid studied by other authors [7-10] can be interpreted through a reduction of the pyrazinic ring.

EXPERIMENTAL

Chemical

— The pyrazinhydroxamic acid is obtained by the method of Forks and Sawlewicz,[11] purified by recrystallization in water and identified by elemental analysis, melting point, IR and NMR spectroscopy.

— AcOH—AcONa and $(CH_3)_4NBr$ are used as supporting electrolyte buffer.

— All the measurements were done under pure dry nitrogen atmosphere at 25 ± 0.1°C.

Apparatus

Current-voltage curves were recorded on an AMEL 471 multipurpose unit (with the damping circuit completely supressed) equipped with a combination of dropping mercury electrode, platinum electrode and saturated calomel electrode.

The capillary characteristic in AcOH—AcONa buffer, was $m = 4.7$ mgs^{-1}, $t = 2.06$ s and in $(CH_3)_4NBr$, $m = 2.6$ mgs^{-1}, $t = 2.63$ s, at a mercury height of 41 cm (corrected for back pressure). All measurements were made on a CRISON 501 pH-meter. The cyclic voltametric curves were obtained using an E410 Metrohm mercury hanging drop electrode. The coulometric method using a mercury pool cathode was used for determining the values of n, the number of the electrons involved in the reduction process.

RESULTS AND DISCUSSION

DC Polarography

The PHA reduced at the dropping mercury electrode showed one, two or three polarographic waves depending on the concentrations, temperatures, pH values and supporting electrolyte used.

Figure 1 shows representative polarograms at AcOH—AcONa and $(CH_3)_4NBr$ electrolytes. One can observe the existence of only one wave ($E_{1/2} = -0.67$ V at pH = 4.6) in the first electrolyte and three waves ($(E_{1/2})_1 = -0.92$ V, $(E_{1/2})_2 = -1.39$ V and $(E_{1/2})_3 = -2.16$ V at pH = 5.9) in the second electrolyte respectively.

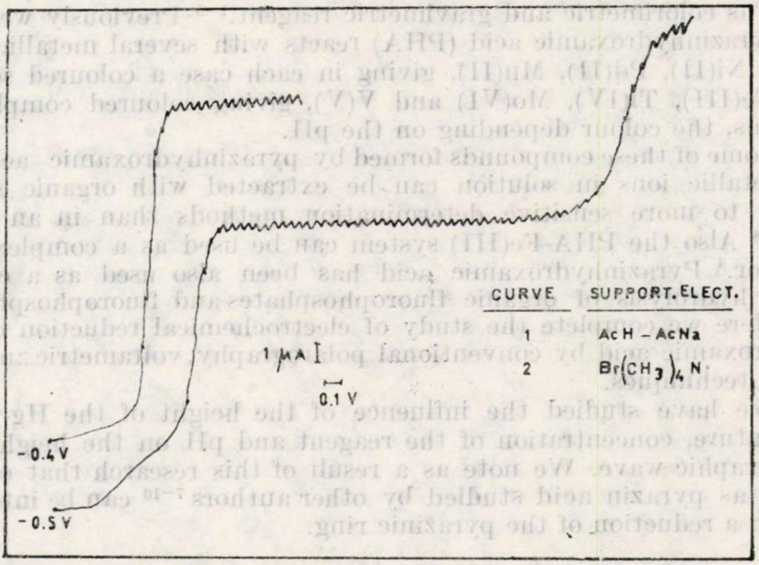

Fig. 1. — Polarograms at AcOH — AcONa and $(CH_3)_4NBr$ supporting electrolyte.

The observation of the electrocapillary curves obtained for 10^{-3} M PHA and supporting electrolyte solutions, shows a great depression of the drop time at the reduction potentials. Based on this fact we can deduce that the product drug is surface-active and is strongly absorbed on the drop mercury electrode surface.

The effect of pH on the current-potential curves was also determined. Thus in AcOH—AcONa buffer the half-wave potential shifts towards more negative values with an increase in electrolyte pH value indicating that hydrogen ions are consumed in the electrode reaction. There is a linear relationship between both magnitudes according to the equation: $E_{1/2} = -0.32 - 0.07$ pH. The limit intensity remains constant.

In $(CH_3)_4NBr$ three well defined polarographic waves appear at pH values under 6.7. The height of the first wave decreases before disappearing at pH = 8. The potential of half wave is independent of the pH for the three observed waves.

The limit intensity of the first and second waves varies with the pH, being independent of the third wave.

Influence of the height of the Hg column

The study carried out on a solution of PHA 10^{-3} M in supporting electrolyte AcOH—AcONa (pH = 4.6) shows that the intensity of the wave varies linearly with the square root of the h_{corr} of the mercury column, showing its diffusive character. Likewise, if the electrolyte is $(CH_3)_4NBr$ (pH = 5.9) the limit intensity of the 1st and 3rd polarographic waves is independent of h_{corr}, while the limit intensity of the second wave varies linearly with $(h_{\text{corr}})^{1/2}$. These facts show that the second wave has a diffusive nature and the first and third have a light kinetic or adsorptive nature.

Influence of the temperature

This study, carried out in solution of reagent 10^{-3} M and using the ground electrolyte mentioned above on identical operative conditions, in a temperature range going from 20°C to 55°C and a height of the mercury column of 41 cm, shows that the limit intensity varies with the temperature of the solution for all the waves observed.

Table 1

Lg i_1 vs T

Supporting electrolyte	$\frac{\delta \lg i}{\delta T}$
AcOH—AcONa	0.0075
$(CH_3)_4NBr$ 1st wave	—
2nd	0.008
3rd	0.0015

The values of the slope of log i_1 vs T appear in table 1.

Table 1 confirms the diffusive nature of the observed wave in AcOH—AcONa. Since the first wave in $(CH_3)_4NBr$ disappears on heating, its nature is adsorptive. The influence of the temperature on the second wave in the same medium confirms its diffusive character, while the third wave presents the characteristic dependence on the temperature of a kinetic wave.

Influence of the concentration of the reagent

Polarograms of several solutions with increasing concentrations of PHA between $2.3\ 10^{-3}$ M — $1.2\ 10^{-4}$ M at AcOH—AcONa and $1.1\ 10^{-3}$ M — $1.1\ 10^{-4}$ M at $(CH_3)_4NBr$ indicate a linear dependence, the limit intensity and the concentration of the reagent for the wave which appears at AcOH—AcONa pH=4.6 and for the second and third wave appearing in $(CH_3)_4NBr$. The first wave observed in the latter case shows the typical dependence of an adsorptive wave.

With the data given by the graphic representation of the limit intensity versus the concentration we were able to calculate the value of the rate diffusive current in AcOH—AcONa, with $I = 3.55$, were I is the diffusion current constant and $D = 2.3\ 10^{-5}\ cm^2s^{-1}$ (pH = 4.6).

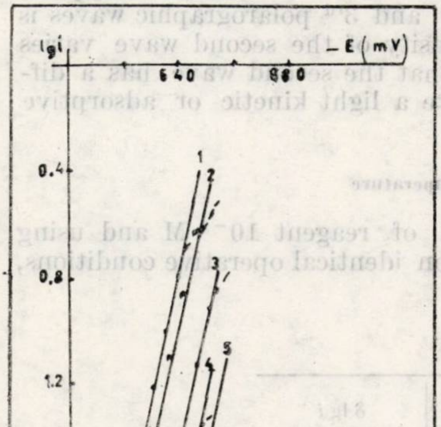

Fig. 2. — Tafel's slope.

The transfer coefficient determined from Tafel's slope is 0.6 (Fig. 2) and the order of the reaction with respect to the (PHA) concentration is one in AcOH—AcONa.

The data found are in the line of other derivatives of the pyrazine to be found in the scientific literature. [3,7,8,9,12]

We note that the number of waves observed depends on the supporting electrolyte used and on the solution. Further, we bear in mind that there are two reducible functional groups in the molecule: the pyrazinic ring and the hydroxamic group to set up the sequence of the reduction of the PHA.

In order to elucidate which of the fundational groups is responsible for this reduction we have made the polarographic study of the pyrazine-2-carboxylic acid in both supporting electrolytes in the same experimental conditions; whereas in the AcOH—AcONa there is only one wave in $(CH_3)_4NBr$ there are two. The behaviour of this acid in both supporting electrolytes and with the same pH, bears a strong resemblance to the experiment with PHA. There, one more wave is observed in the case of $(CH_3)_4NBr$ than with pyrazine-2-carboxylic acid for the more negative potentials with $E_{1/2} = -2.14$ V. We attribute this wave to the reduction of the hydroxamic group.

Coulometry

We carried out controlled potential coulometry to determine the number of electrons which the PHA takes in its reduction process. For this experiment we have used a pool of mercury as cathode, a reference electrode of saturated calomel and a platinum wire as an auxiliary electrode. The working conditions and the values of n found, mean of three determinations, are 2.03 in AcOH—AcONa(pH=4.6) and 1.8 in $(CH_3)_4NBr$ (pH = 5.9). Therefore the reagent captures two electrons in its process of reduction.

Reversibility of the system

For this study we have applied Meites[13] criterion

$$E_{3/4} - E_{1/4} = \frac{0.0564}{n\alpha}$$

Here $n\alpha$ in AcOH—AcONa is 1.97, while in $(CH_3)_4NBr$ for the 2nd waves it is of 0.8 for pH = 6.9.

Having in mind that in both cases we are dealing with bielectronic waves, as established by coulometry, we can deduce that the process is reversible for the AcOH—AcONa supporting electrolyte while in $(CH_3)_4NBr$ it is irreversible.

Cyclic voltametry

The cyclic voltametry curves were recorded at different scan rates (Figs 3 and 4). They always show a single cathodic wave, and another anodic peak in AcOH—AcONa between —0.40 V and —0.90 V while in $(CH_3)_4NBr$ they present two cathodic peaks and one anodic peak between —0.50 V and —1.7 V.

The plot of log i_p value versus the log scan rates is 0.48 in AcOH—AcONa (pH = 4.6) and 0.40 in $(CH_3)_4NBr$ (pH = 7.9).

The difference of the potentials $E_p - E_{1/2}$ is 0.035 V in the first electrolyte and 0.090 V in the second.

These values agree with those found in the literature for compounds similar to PHA.[12,14]

From the voltamograms carried out of the PHA at a concentration range of 10^{-3} M to 10^{-4} M and at different scan rates we can obtain the value of the current function. This is accomplished plotting the current function ($i_p/v^{1/2}$) vs. the scan rate (Fig. 5) in both supporting electrolytes. The process is controlled mainly by the diffusion in the first of the electrolytes used, while in $(CH_3)_4NBr$ it has kinetic character.

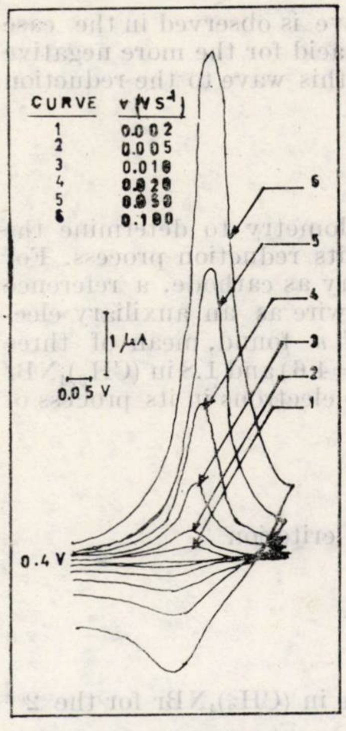

Fig. 3. – Cyclic voltametry curves in AcOH – AcONa.

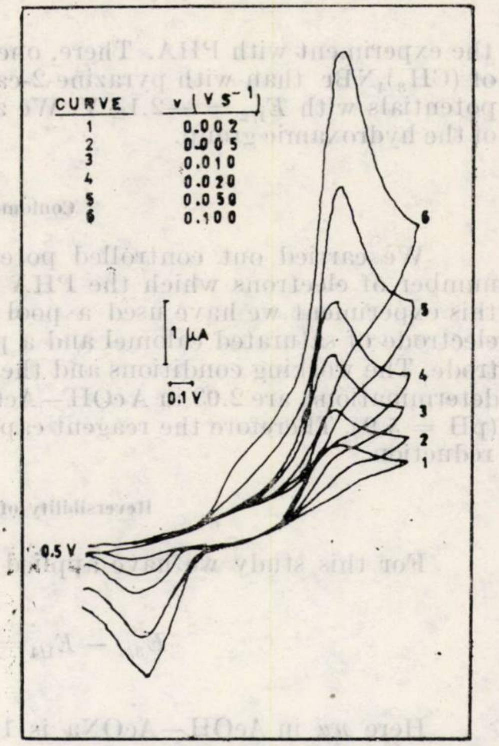

Fig. 4. – Cyclic voltametry curves in $(CH_3)_4NBr$.

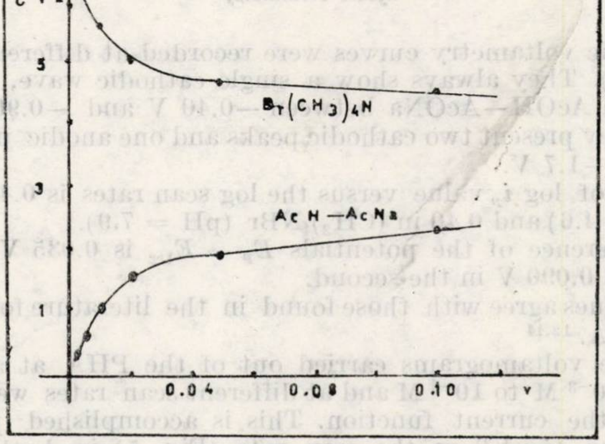

Fig. 5. – The current function $(i_p/v^{1/2})$ vs the scan rate.

Identification of the reduction product

For identification purposes, we obtained the product through electrolysis in the same working conditions as for coulometry (the concentrations of PHA and the buffer solution of 10^{-1} M). The electrolysis was carried out for 10 hours, so that reduction could be completed. We could observe that after two hours of reduction a violaceus-yellow solid appeared. Once we had finished the electrolysis the solvent was eliminated by vacuum-pumping and we extracted the product of reduction in methyl alcohol. The crude obtained is purified by recrystallization and identified by the following methods :

A) Elemental analysis

		%C	%H	%N
$C_5H_7N_3O_2$	calculated	42.55	4.96	28.78
	found	43.70	5.22	30.97

B) NMR

The NMR spectrum of the reduced product shows a multiplet at 9.11, 8.77 and 8.52 MHz, whose integrals correspond with the there protons of the ring, without any other peaks.

C) IR spectroscopy

The IR spectrum was made with a supporting pellet. The main fact observed is the appearance of characteristic secondary amine bands at 625, 655 and 750 cm^{-1}. The typical aromatic and tertiary amine bands (1180, 1550 cm^{-1}), were not observed however in the PHA IR spectrum.

CONCLUSION

The experiment here described shows that the pyrazinhydroxamic acid in a mercury electrode is reduced in two well defined steps, corresponding to the reduction of the pyrazinic ring and the hydroxamic group, respectively.

It has been proved that in the first processes the reduction of the reagent captures two electrons and two protons, according to the following scheme :

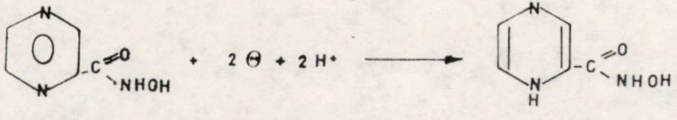

Evidence of adsorption of the PHA on the electrode surface is supported by the observation of electrocapillary curves, the study of the current function variation against the scan rate of potential by D.C. polarography, and cyclic voltametry analysis as a function of the electroactive substance concentration.

REFERENCES

[1] R. Nery, *Analyst*, **91**, 388, 1966.

[2] V. C. Boss and J. H. Yoe, *Talanta*, **13**, 735 (1966).

[3] E. J. Alonso H. and T. Cuardia C., XX Bienal Sociedad Española de Química, Castellón (Spain), **8**, 124 (1984).

[4] E. J. Alonso H. and T. Guardia C., 8° Encontro da Sociedade Portuguesa de Química. Braga (Portugal), C—130, 1985.

[5] E. J. Alonso H., T. Guardia C. and A. M. Camara A., *Quim. Anal.*

[6] B. E. Hackley, R. Plapinger, M. Stolberg, and T. Wagner-Jauregg *J. Am. Chem. Soc.*, **77**, 3651 (1955).

[7] L. F. Wiggins and W. S. Wise, *J. Am. Chem. Soc.*, **78**, 4780 (1956).

[8] K. B. Wiberg, and T. P. Lewis, *J. Am. Chem. Soc.*, **92**, 7154 (1970).

[9] W. Allen, R. L. Pasternak and W. Seaman, *J. Am. Chem. Soc.*, **74**, 3264 (1952).

[10] E. J. Alonso H. and T. Guardia C., XX Bienal Sociedad Española de Química. Castellón (Spain) **8**, 123 (1984).

[11] H. Fork and J. Sawlewicz, *Acta Polo. Pharm*, **21**, 432 (1969).

[12] J. Swatz and F. C. Anson, *J. Electroanalyt. Chem.*, **114**, 117 (1980).

[13] P. Zuman, "The Elucidation of Organic Electrode Processes", Academic Press, New York, 1969.

[14] P. Cinquantini, P. Zanello and G. A. Manzzocchim, *J. Electroanalyt. Chem.*, **80**, 387 (1977).

Revue Roumaine de Chimie, **34**, *8*, 1645–1650 (1989)

UNA TÉCNICA OMEGA BIPARAMÉTRICA MEJORADA. IX

APLICACIÒN DEL ITPOT/RF A ESTADOS EXCITADOS. ESTUDIO DE INDICADORES DE CONSTANTE DIELÉCTRICA

R. E. CACHAU, E. OTTAVIANELLI y E. A. CASTRO

INIFTA, División Química Teórica, Suc. 4, C. C. 16 (1900) La Plata, Argentina

Recibido: el 21 de agosto de 1987

Se utiliza por primera vez la técnica ITPOT/RF (Improved Two Parameter Omega Technique) para el estudio de estados exitados, sobre indicadores de constante dieléctrica. Los cálculos con electrones promovidos a estados excitados preservan la simplicidad del método, y corrigen algunos de sus desvíos. Se analiza la mejora obtenida en términos del modelo de campo de reacción (RF).

It is shown that the consideration of the excited states by the same iterative procedure used for the calculation of the ground state, improves strongly the description of the excited states. The case of dye indicators is analyzed and the improvements explained in terms of the developments of the reaction field technique.

INTRODUCCIÓN

Las técnicas Omega y otras relacionadas se han utilizado en gran cantidad de estudios, en especial dada su simplicidad en el estudio de sistemas conjugados de gran extensión.[1] Por otro lado, en trabajos anteriores de esta serie, se ha puesto de manifiesto la ductilidad y confiabilidad del método ITPOT/RF en diversos tipos de cálculo que involucran generalmente parámetros de carga o enlace, tales como densidad pi total (móvil) sobre un átomo, orden de enlace pi, y otros como el orden de enlace de Coulson, etc., así como evaluaciones del grado de aromaticidad de un hidrocarburo pi-conjugado por medio de estudios sobre su energía total, en relación con el número de enlaces conjugados, usando diversos critérios para ello.[2]

En todos los casos mencionados, y aún en aquellos en que se estudia reactividad de moléculas (generalmente analizando relaciones entre las energías HOMO/LUMO)[3] estos se analizan calculando solamente su estado fundamental. Al comparar la información estructural que nos aporta el ITPOT con la que se puede obtener de la técnica PPP, estas tienen un gran parecido, según se ha mostrado en trabajos de esta misma serie.[4] De modo que, conociendo que la técnica PPP se ha usado exitosamente en el estudio de transiciones $\pi - \pi^{*5}$, podría esperarse que ese mismo tipo de estudio pudiera realizarse con la técnica ITPOT/RF. Las ventajas de emplear la ITPOT/RF residen en el hecho de que este método es más sencillo y directo que el pocedimiento PPP, lo cual obviamente redunda en la mayor economía de cálculo. Este aspecto es particularmente importante cuando se plantea el cálculo de moléculas o agregados moleculares de gran tamaño.

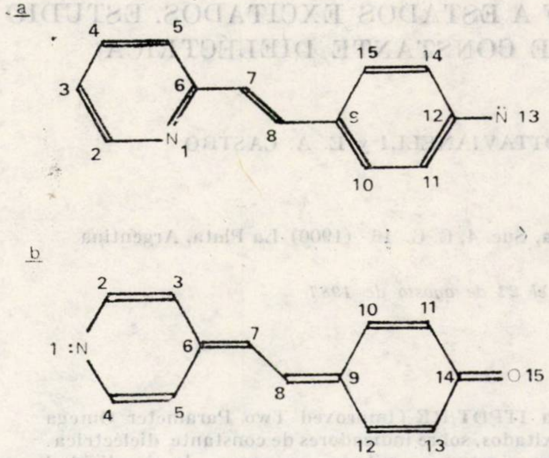

Fig. 1. — a — Numeración de los átomos de la Stirilcianina b — Numeración de los átomos de la Merocianina

En el presente trabajo compararemos los resultados obtenidos en el estudio de dos compuestos, la Merocianina, y la Stirilcianina (Fig. 1), típicos indicadores de constante dieléctrica. Se calcula la energía de transición del modo habitual, por la diferencia de energía HOMO/LUMO sobre los OM obtenidos en el estado fundamental, y por la diferencia de energía entre el estado singlete y el primer triplete, obtenidos ambos por cálculo directo.

En un trabajo anterior de esta serie[6] describimos la posibilidad de incorporar el campo de reacción a la técnica ITPOT, con lo cual las ecuaciones fundamentales para este cálculo resultan, para la integral monocéntrica :

$$\alpha_\mu = \alpha^* + (N_\mu - q_\mu)\,\omega\beta\,(1 - f(e)) - \sum_{\nu \neq \mu} (2 + f(e))(N_\nu - q_\nu)\,\omega'\beta \tag{1}$$

y para los terminos no diagonales :

$$H_{\mu\nu} = H^0_{\mu\nu} \exp(0.55\, p_{\mu\nu} - 0.366) \tag{2}$$

donde $f(e) = (1 - e^{-1/2})$, y e representa la constante dieléctrica del medio, N_μ la carga del core, q_μ la carga gruesa (pi), $p_{\mu\nu}$ el orden de enlace pi, β la integral de resonancia de Hueckel y ω y ω' los parámetros Omega que caracterizan esta técnica.

En nuestros calculos, para describir el primer estado excitado solo modificamos el cálculo de las poblaciones y ordenes de enlace :

$$q_\mu = \sum_i NO(i)\,|C_{i\mu}|^2 \ (3); \qquad P_{\mu\upsilon} = \sum NO(i)(C^*_{i\mu}C_{i\upsilon} + C^*_{i\upsilon}C_{i\mu})/2 \qquad (4)$$

donde ahora NO(i) es el número de ocupación del i-ésimo OM y $C_{i\mu}$ es el coeficiente del OM i-ésimo para el átomo μ.

Se ha mostrado con anterioridad [7] que en los límites de constantes dieléctricas altas las ecuaciones del campo de reacción para el método CNDO coinciden con las del ITPOT, en tanto el campo de reacción separa los orbitales profundos de los de frontera.

Sin embargo, dado que el campo de reacción se calcula a partir de las cargas atómicas calculadas a su vez a partir de los OM ocupados,[8] no es garantía suficiente de que el ITPOT de resultados similares a los del CNDO para estados excitados, si estos se calculan a partir de la promoción de un electrón sobre los OM calculados para el estado fundamental. Es por ello que proponemos aquí realizar este cálculo a partir de los resultados obtenidos por el cálculo de capa cerrada para el estado fundamental y aquellos que resultan de promover un electrón y obtener, (iterativamente, del modo habitual) los OM para obtener el estado triplete.

RESULTADOS

En la tabla 1 se expresa la energía de la transición HOMO/LUMO (em eV), para la Stirilcianina. En ella puede observarse claramente que tanto el modo tradicional de evaluar esta transferencia como el que proponemos en este trabajo manifiestan un fuerte desvio en la serie *a*, en tanto que en la serie *b* ambos tiene un comportamiento cualitativamente correcto. Esto pone de manifiesto una limitación a-priori del método que estamos usando y es la imposibilidad de describir interacciones específicas entre el soluto y el solvente. Para todos los solventes de la serie *a* se postula la existencia de fuertes interacciones entre el N13 (fig. 1a), al tiempo que esta interacción altera, por efecto estérico la forma plana del compuesto, rompiendo de este modo la conjugación. Este inconveniente, y otros propios de la técnica ITPOT deberán ser tenidos encuenta entonces para poder analizar las posibles ventajas el modo de cálculo propuesto.

La tabla 1b, así como la tabla 2 muestran que el cálculo de la transición es mejor descripta cualitativa y cuantitativamente por el modo propuesto.

El mismo análisis podemos realizar sobre la Merocianina (tabla 3), encontrando en este caso que la aproximaciòn ususal no es suficiente para describir, al menos cualitativemente, el comportamiento de la transición HOMO/LUMO en este compuesto, en tanto que si puede conseguirse al menos ese nivel de aproximación con la técnica que hemos propuesto.

Mucho menos satisfactorio resulta el análisis de los cambios en la distribución de carga y ordenes de enlace del compuesto (que se ha ejemplificado para la Stirilcianina en la tabla 4) debido fundamental-

Tabla 1

Diferencia de energía HOMO/LUMO (expresadas en eV) calculada en la forma usual (ITPOT), y del modo propuesto (ITPOT*), comparada con el valor experimental[11] para dos series de soluciones con stirilcianina: a — Con grupos OH y b— Sin grupos OH. *e* constante dieléctrica del medio.

Solv.	e	ITPOT	ITPOT*	Exper.
a —				
Agua	78.5	0.479	0.811	2.863
MeOH	32.6	0.497	0.870	2.695
EtOH	24.3	0.498	0.873	2.672
i-PrOH	18.3	0.499	0.876	2.649
t-BuOH	10.9	0.502	0.884	2.627
b—				
DMSO	46.4	0.497	0.868	2.695
DMF	36.7	0.497	0.869	2.725
Acetona	20.7	0.499	0.874	2.725
Acetato de Etilo	6.2	0.506	0.897	2.749
Dioxano	2.2	0.521	0.945	2.805

Tabla 2

Diferencia de energía HOMO/LUMO para la stirilcianina (ref. tabla 1) en mezclas Dioxano-agua

% Dioxano	e	ITPOT	ITPOT*	Experim.
100	2.21	0.521	0.945	2.805
90	9.50	0.517	0.932	2.731
80	12.01	0.516	0.928	2.701
70	19.07	0.512	0.915	2.684
60	27.21	0.507	0.901	2.695
50	35.85	0.502	0.886	2.701
40	44.54	0.498	0.871	2.707
30	53.28	0.493	0.856	2.719
20	61.86	0.488	0.841	2.743
0	78.48	0.479	0.812	2.863

Tabla 3

Diferencia de energía HOMO/LUMO para la Merocianina (ref. tabla 1) con diversas constantes dieléctricas.
CNDO—RF[12]

e	ITPOT	ITPOT*	Experim.
1	0.602	0.781	2.94
4	0.535	0.838	2.98
50	0.514	0.843	3.88
100	0.512	0.844	4.26

mente a que el método ITPOT en la descripción del estado fundamental tiene varios enlaces y cargas mal descriptos. Sin embargo, si tomamos esto a favor de la técnica propuesta al pasar al análisis de capa abierta, resulta nuevamente que ésta se manifiesta más estable en cuanto a los cambios que propone (en los ordenes de enlace y cargas) al pasar del estado fundamental al primero excitado, y cualitativamente más correcta en comparación con el procedimiento ususal. De todos modos, este análisis fue mucho menos concluyente que aquel que se obtiene para los valores de ΔE HOMO/LUMO para cualquiera de los dos compuestos analizados.

DISCUSIÓN

Del análisis de los resultados encontrados podemos concluir la validez del tipo de cálculo propuesto, al tiempo que señalar que este modo de cálculo mejora en general la descripción cualitativa y tiende a los resultados cuantitativos correctos, tanto en su comparación con técnicas más sofisticadas como el CNDO como en la comparación con resultados experimentales. Sin embargo, también es evidente que si bien este modo de cálculo muestra una tendencia favorable hacia los resultados cuantitativos, esta aún lejos de alcanzar los mismos. Esto podemos entenderlo desde dos puntos de vista : el primero consiste en comprender que las parametrizaciones usuales[9] pueden resultar inconvenientes para describir estados de capa abierta, por lo que se deberá intentar reparametrizar los ω y seguramente los valores de k y h (parámetros del metodo de Hueckel) para este tipo de cálculo. Y, por otro lado, en un trabajo reciente[10] hemos mostrado la inconveniencia del modo de ajuste de los parámetros Omega que se han utilizado hasta el presente. De modo que gran parte del error en la descripción, especielmente de las distribuciones de carga del compuesto, deben tener su origen en este hecho, tál como se mostro en la tabla 4 al señalar que aún en el estudio del estado fundamental la distribución de cargas obtenidas tiene importantes errores.

Tabla 4

Distributiones de carga y ordenes de enlace en la Stirilcianina (ref. tabla 1) en el estado fundamental (π) y en el "LUMO" (π^*)

At.	π		π^*			Enl.	π		π^*		
	ITPOT	CNDO	ITPOT	ITPOT*	CNDO		ITPOT	CNDO	ITPOT	ITPOT*	CNDO
1	1.671	1.502	1.486	1.455	1.737	1−2	0.593	0.474	0.567	0.569	0.429
2	0.912	0.817	0.941	0.913	0.835	2−3	0.747	0.757	0.739	0.715	0.738
3	1.069	1.073	1.031	0.970	1.035	3−4	0.547	0.573	0.537	0.538	0.579
4	0.948	0.782	1.018	1.018	0.908	4−5	0.764	0.703	0.727	0.726	0.671
5	1.054	1.091	0.993	0.941	0.978	5−6	0.508	0.587	0.558	0.539	0.560
6	0.912	0.790	1.019	1.000	1.014	1−6	0.489	0.454	0.433	0.419	0.310
7	1.167	1.212	1.000	0.907	0.978	6−7	0.590	0.501	0.540	0.564	0.546
8	0.974	0.720	1.094	0.973	0.922	7−8	0.636	0.752	0.647	0.584	0.590
9	1.146	1.151	0.983	0.979	1.006	8−9	0.670	0.446	0.589	0.600	0.527
10	0.977	0.892	1.072	0.927	0.910	9−10	0.567	0.575	0.624	0.612	0.498
11	1.132	1.087	1.025	0.974	1.052	10−11	0.739	0.708	0.629	0.579	0.738
12	0.970	0.846	1.025	0.967	0.814	11−12	0.466	0.602	0.527	0.558	0.554
13	1.250	1.889	1.262	1.020	1.856	12−13	0.797	0.352	0.688	0.617	0.384
14	1.001	1.084	1.016	0.991	1.047	12−14	0.321	0.605	0.360	0.382	0.557
15	0.988	0.891	1.038	0.914	0.966	14−15	0.945	0.705	0.916	0.891	0.734
						9−15	0.545	0.557	0.514	0.520	0.500

De este modo puede concluirse que el estudio de estados de capa abierta es factible con este tipo de técnicas, y se deberá contemplar este hecho al redefinir los parámetros necesarios para realizar este tipo de cálculos.

Varios estudios sobre estos aspectos se estan llevando a cabo actualmente en nuestros laboratorios y los resultados serán presentados oportunamente en las publicaciones peródicas pertinentes.

BIBLIOGRAFÍA

[1] M. J. S. Dewar, "The Molecular Orbital Theory of Organic Chemistry", Mc Graw Hill, N. Y. (1969).
[2] H. O. Villar, E. A. Castro and F. M. Fernandez, *Chem. Scripta*, **22**, 49 (1983).
[3] A. Streitwieser, "Molecular Orbital Theory for Organic Chemists", J. Wiley, N. Y. (1961).
[4] F. M. Fernandez and E. A. Castro *Z. Naturforsch.*, **34a**, 1365 (1979).
[5] M. S.A. Abd El Mottaleb, *Z. Phys. Chemie*, **264**, 957 (1983).
[6] H. O. Villar, R. E. Cachau y E. A. Castro, *Acta sud Am. Quim.*, **3** , 67(1983).
[7] R. Constanciel, *Theoret. Chim. Acta*, **54**, 123(1980).
[8] R. Constanciel and O. Tapia, *Theoret. Chim. Acta*, **48**, 75(1978).
[9] S. C. Mathur, D. C. Singh, B. Kumar and S. Mitra *Int. J. Quant. Chem.*, **11**, 759 (1977).
[10] R. E. Cachau, G. Estiu y E. A. Castro (enviado).

Revue Roumaine de Chimie, **34**, *8*, 1651–1660 (1989)

EXTRACTION OF EUROPIUM(III) FROM NITRIC AND PERCHLORIC MEDIA BY NEUTRAL BIFUNCTIONAL CARBAMOYLMETHYLENEPHOSPHONATES*

NISTOR PERESCU[a] and RENATO CHIARIZIA[b]

[a] Institute of Nuclear Power Reactors, P. O. Box 78, 0300 Pitești, Romania
[b] ENEA – Casaccia, TIB–GHI, Via Anguillarese 301, 00060, Rome, Italy

Received August 30, 1987

The distribution of Eu(III) between acidic solutions of nitrates and perchlorates and organic phases containing di-n-hexyl-N,N-diethylcarbamoylmethylenephosphonate (DHDECMP) and di-(2-ethylhexyl)-N,N-di-ethylcarbamoylmethylenephosphonate (DEHDECMP) in n-heptane and mesithylene has been investigated. To purify the crude extractants several procedures were tried and the purity of the products was tested by elemental analysis, gas-chromatography and Am(III) distribution. Some information regarding the stoichiometry of the extracted species and the influence of different parameters (diluent, acidity, temperature) on the distribution ratios is also presented.

INTRODUCTION

The first information on the extractive properties of some diphosphine oxides ($(R_2PO(CH_2)_nPOR_2)$) was published in 1952.[1] Later, other bifunctional organophosphorus compounds such as di-phosphonates ($((RO)_2PO(CH_2)_nPO(OR)_2)$) and carbamoylmethylenephosphonates ($((RO)_2PO(CH_2)_nCONR_2$, with $n \geqslant 1$) were synthetized, physico-chemically characterized and studied for their potential use as extractants.[2–17] A review of these compounds was published in 1966[18] and some more papers appeared in the following years[19–24]. Recently, the interest on some compounds of the carbamoylalkylene-phosphonate, -phosphinate and -phosphine oxide class has sharply increased. Using known synthesis methods,[25, 26] large quantities of some derivatives such as di-n-hexyl-N,N-di-ethylcarbamoylmethylene-phosphonate (DHDECMP), di-(2-ethylhexyl)-N,N-di-ethylcarbamoylmethylenephosphonate (DEHDECMP) and, very recently, n-octyl (phenyl)-N,N-diisobutylcarbamoylmethylenephosphine oxide (O0D(iB)CMPO), have become commercially available. Efforts have been devoted to identify the impurities in crude products[27, 28] and to purify them,[27–36, 50] as well as to investigate their extractive properties towards several chemical species, especially actinides and lanthanides.[27–50] An exhaustive review of the existing data until 1978 has been published by Schulz et al.[50]

---

* Work performed under the auspices of UNPD – IAEA, Vienna, Contract ROM/8254

The increased interest for this class of bifunctional (called sometimes bidentate) extractants is primarily due to the high distribution ratios (D) found when extracting trivalent lanthanides and tri-, tetra- and hexavalent actinides from aqueous solutions of moderate to high nitric acid concentrations. The importance of these extractants in the last steps of the nuclear fuel cycle, especially for partitioning actinides from fission products or for the removal of actinides from high level acidic nuclear wastes [54–59] appears remarkable since trivalent actinides and lanthanides are poorly extracted by most monofunctional extractants from acidic solutions.

The extraction mechanism of inorganic (acids and salts) species by some of these bifunctional extractants is not completely understood. In many fundamental studies carried out measuring Am(III) distribution, [37, 44–46, 50] it has generally been found that D values are dependent on the inorganic acid concentration. For DHDECMP, a plot of log D vs log $[HNO_3]$ shows a fractional slope of 1.44.[37] This might be due to a number of factors such as : a) different reactions take place simultaneously ; b) hydrogen and nitrate ion concentrations have specific influences on the D values (a slope of 2 is obtained from log D vs log$[NO_3^-]$ plots at constant $[H^+]$, and no dependency or even a negative slope is obtained from log D vs log $[H^+]$ plots at $[NO_3^-]$ = constant). Also, log D vs log [DHDECMP] gives a slope of 3,[37] the same value being found for Ce(III) extraction from nitric acid by DHDECMP.[13] This seems to suggest that Am(III) is extracted as a dinitrato-species with three molecules of extractant : $(Am(NO_3)_2\,(DHDECMP)_2)^+(DHDECMP)^-$. This formulation involves an acidic character of the protons between the phosphoryl and carbonyl groups[52] like in beta-diketons. Other studies found more reasonably the same slope value of 3, both for log D vs log $[NO_3^-]$ and log D vs log [DHDECMP] plots without any observed chelation effect when extracting Am(III) and Eu(III) from low acid solutions of $LiNO_3$.[44] At higher (1–5 *M*) concentrations of nitric acid, an internal buffer capacity of the amide group, that protects the phosphoryl-metal bond from the attack by H^+, was observed.[44]

The fractional values of the slopes : 3.2 from log D vs log [DHDECMP], 1.5 from log D vs log $[HNO_3]$ and 2.5 from log D vs log [DEHDECMP] plots (all in the case of Am(III) extraction from nitric acid solutions), as well as the change of dependency as a function of the diluent nature,[42] clearly indicate the complexity of the involved processes. Several other works [23, 29, 30, 34] report an actinide (III) (or lanthanide (III)) to extractant ratio equal to 3 (i.e. a trisolvate formation), but it is not unambiguously stated if the extractants behave as mono- or polydentate compounds, the stoichiometry being readily changed by small modifications of the extraction conditions.

Much more characterized and understood seems to be the reaction between trivalent actinides and O0D(iB)CMPO, thoroughly investigated in a number of recent publications by Horwitz et al.[60] In this case it has been determined that the extracted complex has the composition metal : nitrate : extractant = 1 : 3 : 3. Also in this case, however, no definite conclusion has been reached yet on whether chelation is a factor of any importance.

The carbamoylmethylenephosphonates and related compounds, having a phosphoryl group and a carbonyl group in beta position to each other, should in theory be characterized by an asymmetric donor power and by an enolic tautomerism capable of giving them some acidic character. Also, the respective positions of the two oxygen atoms of the donor groups make the molecule a potential chelating agent. The extractive properties of a particular compound depend on the inductive effects and on the steric hindrance of the substituents. Therefore, depending on the nature and size of the substituents and on other extraction parameters of the aqueous phase, these compounds can act as solvating (generally through P—O) ligands and as chelating agents. The difficulty to exactly define the extraction mechanism can then be ascribed to the possibility for all these potential properties to be met for a given reagent in some given conditions.

In the present work a distribution study of Eu(III) between nitrate and perchlorate aqueous solutions and organic solutions containing DHDECMP is given. Aim of the work was :

i) to try and compare different purification procedures for two bifunctional phosphonates characterized by different substituents on the phosphoryl group ;

ii) to compare the extraction behavior of the two compounds in different diluents and from different aqueous media, namely nitric and perchloric, in controlled conditions of ionic strength ;

iii) to obtain information on the acidic character of the hydrogen atoms of the methylene bridge.

EXPERIMENTAL

Chemicals

Crude DHDECMP and DEHDECMP were obtained from Wateree Chemical Co., Lugoff, S. Carolina, USA, as technical grade (about 49% purity) products. To purify them various routes have been tested.

$^{152\text{-}154}$Eu, as Eu(III) nitrate, from Amersham (U.K.), was used in the distribution experiments. All other chemicals were of A. R. grade.

Purification procedures

1. DHDECMP.

From the original stock of crude DHDECMP, three types of materials have been obtained by means of the following purification procedures :

1a. A method already reported for the purification of other extractants, including carbamoylmethylenephosphonates [44], has been tried. A volume of 20 % (v/v) DHDECMP in n-heptane was equilibrated for 5 minutes with 0.5 volumes of 8 *M* HNO_3. Three liquid phases (one aqueous and two organic) were formed. After phase separation, the heavy organic layer was collected and washed with 0.25 volumes of NaOH 1 *M* to remove HNO_3 and other acidic impurities, and with water up to neutrality. From the resulting organic phase, the n-heptane was then removed in a rotating evaporator.

1b. The same procedure as before has been followed using 70% H_3PO_4 instead of 8 *M* HNO_3 as initial aqueous phase. The choice of concentrated phosphoric acid was based on its higher specificity toward formation of an insoluble adduct (in paraffinic hydrocarbons) with neutral organophosporous compounds [53] thus improving the product purity.

1c. Purification by mercury (II) precipitation has been performed [36].

2. DEHDECMP.

From the original stock of crude DEHDECMP two types of materials have been obtained as follows:

2a. The same procedure as in 1b has been carried out. The procedure indicated in 1a was not successful since no second organic layer was formed by contacting the crude product with 8 M HNO_3.

2b. A volume of 30 % (v/v) crude DEHDECMP was equilibrated for 5 minutes with 0.5 volumes of 70 % H_3PO_4. Three phases were formed. The heavy organic layer was washed many times with water to remove the extracted H_3PO_4. In this way a preliminary separation of the valuable component from the impurities was expected. To the heavy organic phase more hexane (up to an extractant concentration of 20 %) was added and the 1b procedure performed.

Original and purified samples have been tested by elemental analysis, Am(III) distribution and, partially, by gas-chromatography. The results are presented in Tables 1 and 2 and in Figure 1, respectively. From the Tables it can be seen that the purification routes

Table 1

Elemental analysis of crude and purified products

Element	Theoretical	Crude	Purification procedure		
			1a	1b	1c
DHDECMP					
C	59.48	57.28	58.73	57.18	58.65
H	10.54	10.16	10.38	10.28	10.35
N	3.85	3.37	2.99	2.67	3.87
P	8.52	—	—	—	8.22

Element	Theoretical	Crude	Purification procedure	
			2a	2b
DEHDECMP				
C	62.98	62.11	62.86	62.49
H	11.05	10.75	10.73	10.99
N	3.34	2.76	2.63	2.57
P	7.38	—	—	6.40

Table 2

Americium (III) distribution test*
Organic phase: 30 % (v/v) extractant in diethylbenzene
Aqueous phase: 0.1 M HNO_3 + ^{241}Am tracer
Phase ratio = 1, temperature = 22 ± 1 °C

Extractant	D_{Am}
DHDECMP, crude	2.9
,, 1a	2.9×10^{-1}
,, 1b	2.0
,, 1c	1.7×10^{-2}
DEHDECMP, crude	2.1
,, 2a	9.0×10^{-1}
,, 2b	1.5

*The americium stock used in this test was purified from plutonium by extraction with 20 % tri-caprylaine in xylene. Its purity was checked by alpha-spectrometry.

perchloric aqueous media (both of 1 *M* ionic strength) is the same, the different slope values could be due to the different behavior of HNO_3 and $HClO_4$ when extracted by DHDECMP. The presence of $HClO_4$ in organic phase may modify the chemical state of the extracted metallic species and the general properties of the organic phase, significantly increasing the europium (III) distribution ratio. To determine the stoichiometry and structure of the extracted species from perchloric solutions more experimental work is necessary.

Diluent dependency

The nature of the diluent can strongly influence the thermodynamic activity of an extracting agent and its availability for extraction of inorganic chemical species. Large differences in the distribution behavior of a solute and sometimes third phase formation can occur by changing the diluent. Both effects have been met in the present investigation. As it can be seen in Fig. 2, the distribution ratios of Eu(III) are higher by more than a factor 5 when n-heptane instead of mesithylene is used as a diluent of DHDECMP, under comparable extraction conditions. This behavior is due to the chemical inertness of the paraffinic hydrocarbons (n-heptane) as compared to the aromatic ones (mesithylene). The former interact less with the extractant, leaving DHDECMP more available for extraction of inorganic species from the aqueous phase. The extraction of Eu(III), even at tracer level, from perchloric medium (0.1 *M* $HClO_4$ + + 0.9 *M* $LiClO_4$) by DHDECMP in n-heptane, cannot be performed because of the formation of a second organic layer. This is an evidence that $HClO_4$ is very easily extracted by DHDECMP and the diluent (n-heptane) is not able to dissolve the extracted species (probably a solvate). Such a behavior might be useful to purify crude DHDECMP by third phase formation using an aqueous solution of $HClO_4$ at low concentration instead of concentrated HNO_3 or H_3PO_4.

Acid, Eu(III) concentration and temperature dependencies

Distribution ratios were measured for the extraction of Eu(III) from nitrate media having the same ionic strength (1 *M*) but variable

Table 3

Eu(III) (tracer) distribution as a function of HNO_3 concentration

Aqueous phase	D	
	0.25 *M* DHDECMP in n-heptane	0.40 *M* DHDECMP in mesithylene
0.10 *M* HNO_3 + 0.90 *M* $LiNO_3$	0.50	0.33
0.05 *M* ,, + 0.95 *M* ,,	0.50	0.34
0.03 *M* ,, + 0.97 *M* ,,	0.49	0.34
0.02 *M* ,, + 0.98 *M* ,,	0.49	0.34

HNO_3 concentrations into DHDECMP solutions in n-heptane and mesithylene. The results, reported in Table 3, show no variation of the D values over the investigated range of HNO_3 concentration in both cases.

This is an indication that the hydrogen atoms of the methylene bridge connecting the phosphoryl and carbonyl groups are not involved in the extraction reaction.

The distribution of Eu(III) between 0.05 M HNO_3 + 0.95 M $LiNO_3$ and 0.25 M DHDECMP in n-heptane or 0.4 M DHDECMP in mesithylene, as well as between 0.05 M $HClO_4$ + 0.95 M $LiClO_4$ and 0.17 M DHDECMP in mesithylene, was measured as a function of europium concentration in the range 1×10^{-4} M — 1×10^{-3} M. No significant variation (within the limits of experimental errors) of the D values was observed indicating that the formation of polynuclear species can be excluded.

By measuring the extraction of Eu(III) as a function of temperature in the range 18—40 °C, a lowering of the distribution ratios with increasing temperature was observed. This exothermal effect was found for the extraction of Eu(III) from nitrate media into DHDECMP in n-heptane and mesithylene as well as from perchloric solutions into DHDECMP in mesithylene. The obtained experimental data, however, are not sufficient to permit a meaningful thermodynamic treatment.

Using the organic phases prepared with DEHDECMP (sample 2b) in n-heptane and mesithylene, some Eu(III) extraction experiments were carried out from nitrate and perchlorate media. Unfortunately, the mass balance was not respected. This is likely due to the presence of acidic impurities in the product. A high purity product should be prepared in order to investigate its extraction properties.

SUMMARY AND CONCLUSION

Attempts to purify DHDECMP and DEHDECMP by taking advantage of third phase formation during the contact of the organic phase with concentrated nitric or phosphoric acid have led to only modest results. In the case of DHDECMP, however, the very simple procedure followed provided a product showing much better extraction characteristics than the starting material. A similar procedure, properly optimized by using, for example, $HClO_4$ at low concentration as an aqueous phase, could be considered as a preliminary treatment prior to the use of other more complex methods such as the Hg(II) salt precipitation. The importance of using high purity products in obtaining information on the basic chemistry of these bifunctional extractants has been stressed out. With DEHDECMP, for example, no meaningful Eu(III) distribution data were obtained, due to the lack of purity of the extractant.

A large diluent effect has been experimentally evidenced when passing from an aliphatic to an aromatic hydrocarbon. With aliphatic diluents more favorable distribution ratios are obtained, but the risk of forming third phases is higher, as shown in the case of the DHDECMP-heptane-perchlorate system. The use of a phase modifier as suggested previously [58,59] when using n-paraffinic diluents seems then necessary in order to develop useful flowsheets for extraction processes.

Another important parameter to be considered for applications of these extractants regarding actual radioactive solutions is the temperature. Radioactive decay heat causes, for example, high level liquid wastes to be at a temperature somewhat higher than 25°C. The decline of distribution ratios at higher temperatures has to be properly taken into account for process applications.

Eu(III) distribution experiments have allowed us to exclude the formation of polynuclear complexes. The reported stoichiometry [44-60] of metal : anion : extractant = 1 : 3 : 3 has been confirmed at least with a nitric aqueous medium. While no new information has been obtained on the possible chelate formation between extractant and metal ions, the experiments performed at fixed anion concentration with different acidities seem to exclude any contribution of acidic hydration atoms to the overall extraction reaction.

REFERENCES

[1] C. A. Blake, J. G. Moore and W. M. Whatley, ORNL-1480 (1952).

[2] J. E. Mrochek, J. W. O'Laughlin, H. Sakurai and C. V. Banks, *J. Inorg. Nucl. Chem.*, **25**, 955 (1963).

[3] J. J. Richard, K. F. Burke, J. W. O'Laughlin and C. V. Banks, *J. Amer. Chem. Soc.*, **83**, 1722 (1961).

[4] J. R. Parker and C. V. Banks, *J. Inorg. Nucl. Chem.*, **27**, 583 (1965).

[5] J. E. Mrochek and C. V. Banks, *J. Inorg. Nucl. Chem.*, **27**, 589 (1965).

[6] J. E. Mrochek, J. E. O'Laughlin and C. V. Banks, *J. Inorg. Nucl. Chem.*, **27**, 603 (1965).

[7] J. E. Mrochek, J. J. Richard and C. V. Banks, *J. Inorg. Nucl. chem.*, **27**, 625 (1965).

[8] J. R. Parker and C. V. Banks, *J. Inorg. Nucl. Chem.*, **27**, 631 (1965).

[9] T. H. Siddal, III, and C. A. Prohaska, *Nature* (London), **202**, 1088 (1964).

[10] T. H. Siddal, III, and C. A. Prohaska, *Inorg. Chem.*, **4**, 783 (1965). T. H. Siddal, III, U. S. Patent 3, 243, 254 (1966).

[11] W. E. Stewart and T. H. Siddall, III, *J. Inorg. Nucl. Chem.*, **30**, 3281 (1968).

[12] T. H. Siddal, III, *J. Inorg. Nucl. Chem.*, **25**, 883 (1963).

[13] T. H. Siddal, III, *J. Inorg. Nucl. Chem.*, **26**, 1991 (1964).

[14] H. Saisho, *Bull. Chem. Soc. Japan*, **34**, 859 (1961).

[15] H. Saisho, *Bull. Chem. Soc. Japan*, **34**, 1254 (1961).

[16] J. Goffart and G. Duyckaerts, *Anal. Chim. Acta*, **39**, 57 (1967).

[17] J. Goffart and G. Duyckaerts, *Anal. Chim. Acta*, **48**, 99 (1969).

[18] J. W. O'Laughlin, "Some Neutral Bifunctional Organophosphorus Compounds as Solvent Extractants", in Progress in Nuclear Energy, Series IX. Analytical Chemistry, Vol. 6, D. C. Stewart and H. A. Ehon, Eds, Pergamon Press, New York, 1966, p. 97.

[19] D. F. Peppard, "Liquid-Liquid Extraction of Metal Ions", in "Advance in Inorganic Chemistry and Radiochemistry", vol. 9, H. J. Emeleus and A. G. Sharpe, Eds, Academic Press, New York, 1966, p. 33.

[20] D. C. Perricos, A. K. Tsolis and E. P. Belkas, *Talanta*, **17**, 551 (1970).

[21] A. K. Tsolis, E. P. Belkas and D. C. Perricos, *Radiochim. Acta*, **11**, 117 (1969).

[22] H. F. Aly and M. A. El-Haggan, *Radiochem. Radioanal. Lett.*, **3**, 249 (1970).

[23] H. F. Aly and R. M. Latimer, *J. Inorg. Nucl. Chem.*, **32**, 3081 (1970).

[24] H. F. Aly, A. H. T. Kandil and M. Raieh, *Z. Anal. Chem.*, **258**, 281 (1972).

[25] K. Moedritzer and R. R. Irani, *J. Inorg. Nucl. Chem.*, **22**, 297 (1961).

[26] J. A. Cade, *J. Chem. Soc.*, 2266 (1959).

[27] C. T. Bahner, R. R. Shoun and W. J. McDowell, ORNL-TM-5878 (1977).

[28] J. D. Navratil, "Secondary Americium and Plutonium Recovery at Rocky Flats", Conf. on Actinides Recovery from Acidic Wastes, Rocky Flats Plant, Colorado, May 4—5, 1976.

[29] W. W. Schulz and L. D. Mc Isaac, "Removal of Actinides from Nuclear Fuel Reprocessing Waste Solutions with Bidentate Organophosphorus Extractants", in "Transplutonium 1975", W. Müller and R. Lindner, Eds, North-Holland, 1976, p. 433.

[30] W. W. Schulz and L. D. McIsaac, Report ARH-SA-263 (1977).

[31] W. W. Schulz, U. S. Patent 4, 051, 203 (1977).

[32] L. D. McIsaac, J. D. Baker, J. F. Krupa and N. Schroeder, ORNL-TM-6174 (1978).

[33] R. K. Owen, Report ARH-CD-953 (1977).

[34] W. W. Schulz, Report ARH-SA-203 (1974).

[35] N. C. Schroeder, L. D. McIsaac, D. H. Meikrantz, J. F. Krupa and J. D. Baker, *J. Inorg. Nucl. Chem.*, **42**, 1029 (1980).

[36] N. C. Schroeder, L. D. McIsaac and J. F. Krupa, Report ENICO-1026 (1980)

[37] L. D. McIsaac, J. D. Baker, J. F. Krupa, R. E. La Pointe, D. H. Meikrantz and N. C. Schroeder, ICP-1180 (1979).

[38] L. D. McIsaac, J. D. Baker and J. W. Tkachyk, ICP-1080 (1975).

[39] L. D. McIsaac, J. D. Baker and D. H. Meikrantz, ICP-1106 (1976).

[40] L. D. McIsaac, J. D. Baker, J. F. Krupa, D. H. Meikrantz and N. C. Schroeder, ICP-1141 (1978).

[41] L. D. McIsaac, J. D. Baker, J. F. Krupa and N. C. Schroeder, ICP-1132 (1977).

[42] R. R. Shoun, W. J. McDowell and B. Weaver, Proc. Intern. Solv. Extr. Conf. ISEC'77, Toronto, 1977, p. 101.

[43] E. P. Horwitz, D. G. Kalina and A. C. Muscatello, *Sep. Sci. Technol.*, **16**, 403 (1981).

[44] E. P. Horwitz, A. C. Muscatello, D. G. Kalina and L. Kaplan, *Sep. Sci. Technol.*, **16**, 41 (1981).

[45] D. G. Kalina, E. P. Horwitz, L. Kaplan and A. C. Muscatello, *Sep. Sci. Technol.*, **16**, 1127 (1981).

[46] D. G. Kalina, G. W. Mason and E. P. Horwitz, *J. Inorg. Nucl. Chem.*, **43**, 579 (1981).

[47] M. K. Chutova, N. E. Kochetkova and B. F. Myasoedov, *J. Inorg. Nucl. Chem.*, **42**, 897 (1980).

[48] H. Petrzilova, J. Binka and L. Kuca, *J. Radioanal. Chem.*, **51**, 107 (1979).

[49] E. A. Filippov, V. V. Yakshin, V. A. Belov, G. G. Arkhipova, M. I. Tymoniuk and B. N. Laskorin, *Radiokhimiya*, **22**, 162 (1980).

[50] W. W. Schulz and J. D. Navratil, Recent Develop. in Separ. Sci., vol. VII, chap. 2, N.N. Li Ed., C.R.C. Press, Inc., Boca Raton, Florida, 1982, p. 32; W. W. Schulz and L. D. McIsaac, Proc. Intern. Solv. Extr. Conf. ISEC '77, Toronto, 1977, p. 619.

[51] ORNL-TM-4783 (1975).

[52] F. A. Cotton and R. A. Schunn, *J. Amer. Chem. Soc.*, **85**, 2394 (1963).

[53] L. Humblet and J. Van Geel, Report ETR-312 (1981).

[54] E. P. Horwitz, H. Diamond and D. G. Kalina, "Carbamoylmethylphosphoryl Derivatives as Actinide Extractants" in "Plutonium Chemistry", chap. 27, ACS Symposium Series 216, W. T. Carnall and G. R. Choppin, Eds., American Chemical Society, 1983.

[55] E. P. Horwitz, H. Diamond, D. G. Kalina, L. Kaplan and G. W. Mason, "Octyl(phenyl)-N,N-Diisobutylcarbamoylmethylphosphine Oxide as an Extractant for Actinides from Nitric Acid Wastes", Proc. Internat. Solv. Extr. Conf. ISEC'83, Denver, Colorado, 1983, p. 451.

[56] G. F. Vandegrift, R. A. Leonard, M. J. Steindler, E. P. Horwitz, L. J. Basile, H. Diamond, D. G. Kalina and L. Kaplan, "Transuranic Decontamination of Nitric Acid Solutions by the TRUEX Solvent Extraction Process-Preliminary Development Studies", Report ANL-84-45 (1984).

[57] E. P. Horwitz, D. G. Kalina, H. Diamond, G. F. Vandegrift and W. W. Schulz, *Solvent Extr. Ion Exch.*, **3**, 175 (1985).

[58] E. P. Horwitz, D. G. Kalina, H. Diamond, L. Kaplan, G. F. Vandegrift, R. A. Leonard, M. J. Steindler and W. W. Schulz, "TRU Decontamination of High-Level PUREX Waste by Solvent Extraction Utilizing a Mixed Octyl(phenyl)-N,N-diisobutylcarbamoylmethylphosphine Oxide/TBP/NPH (TRUEX) Solvent, in Actinide/Lanthanide Separations, G. R. Choppin, J. D. Navratil and W. W. Schulz, Eds., World Scientific Publication, Co., LTD, Republic of Singapore, 1985, p. 43.

[59] E. P. Horwitz and W. W. Schulz, "Solvent Extraction and Recovery of the Transuranic Elements from Waste Solutions Using the TRUEX Process", Proc. Internat. Meeting on Solv. Extract. and Ion Exch. in the Nuclear Fuel Cycle, AERE Harwell, U. K., Sept. 3—6, 1985, Ellis Harwood Ltd, Market Cross House, W. Sussex, England, 1985, p. 137.

[60] E. P. Horwitz and D. G. Kalina, *Solv. Extr. Ion Exch.*, **2**, 179 (1984).

Revue Roumaine de Chimie, **34**, *8*, 1661–1666 (1989)

A NOVEL SPECTROPHOTOMETRIC METHOD FOR DETERMINATION OF PEROXYDISULPHATE ION USING *o*-DIANISIDINE—$S_2O_8^{2-}$—Cu(II) REACTION

P. M. SHIUNDU[a] and S. B. JONNALAGADDA[b]

[a] Department of Chemistry, University of Nairobi, P. O. Box 30197, Nairobi, Kenya
[b] Department of Chemistry, University of Zimbabwe, Box MP 167, Harare, Zimbabwe

Received August 15, 1987

A simple and sensitive method for determination of peroxydisulphate ion is proposed. Peroxydisulphate ion catalysed by Cu(II) oxidises *o*-dianisidine to diimine, a red compound with absorption peak at 450 nm. By use of the described method as low as 10^{-6}M peroxydisulphate concentration can be determined fast and easily.

INTRODUCTION

Peroxydisulphate ion is one of the strongest oxidising agents known in aqueous solution ($S_2O_8^{2-}/2SO_4^{2-}$ — 2.01 V). In the majority of its reactions peroxydisulphate undergoes either a one electron reduction with formation of one sulphate radical ion or a fiddion of the weak oxygen-oxygen bond with formation of two sulphate radical ions. The importance of peroxydisulphate ion is evident from the ability of ion to oxidise various organic and inorganic substrates in acidic, basic and neutral media.[1] Literature survey shows that although peroxydisulphate ion has been used as an oxidising species in a number of reactions, very few methods are known for its analysis. Classical iodometric method involves the reaction of peroxydisulphate with potassium iodide and the titration of liberated I_2 with standard thiosulphate solution.[2,3] This titrometric method is not accurate in the concentration range of $10^{-4} - 10^{-5}$ M and is less sensitive. The polarographic[4] and polarographic amplification[5] methods afford low detection limits with precision, but the sample need to be free from interfering cations. Peroxydisulphate ion oxidises *o*-dianisidine (oda) to diimine, a red compound with absorption peak at 450 nm.[6] The reaction is found to be a suitable indicator reaction for fast determination of peroxydisulphate concentration. This short communication describes the studies on optimum conditions for analysis of low concentrations of $S_2O_8^{2-}$ ion in aqueous solutions and the recommended procedure using Cu(II) as the catalyst. The effect of ionic strength and pH on the method are discussed.

EXPERIMENTAL

All the reagents used were of Analar grade or high purity chemicals and all the solutions were prepared in deionised distilled water.

Procedure

Maintaining pseudo excess concentrations of reactants compared to peroxydisulphate ion, requisite volumes of the reagents were added to oda solution and then the reaction mixture was adjusted to desired pH, either with dilute sulphuric acid or dilute sodium hydroxide. Reaction was started with the addition of peroxydisulphate ion. Final volume of the reaction mixture was made to 10 mL. The progress of the reaction was followed by measuring the absorbance at different time intervals till a steady value was reached.

RESULTS AND DISCUSSION

The detailed kinetics and mechanism of the reaction will be reported in a separate communication.[6] The red coloured oxidation product which has an absorption peak at 450 nm is a diimine (1,1′-biphenyl-3,3′-dimethoxy-4,4′-diimine).[7]

Effect of pH and buffers

Preliminary experiments carried out at neutral and at different acidic and alkaline pHs with oda 6.0×10^{-4}M and peroxydisulphate 1.0×10^{-4}M showed that reaction is highly pH dependent. At neutral pH, absorbance values reach a maximum in 14 minutes, while on either side, at acidic or alkaline pH conditions reaction slowed down, consuming longer time to attain the same maximum value. Effect of buffers, acetic acid-sodium acetate buffer (1.0×10^{-4}M to 0.1 M) and $H_3PO_4 - K_2HPO_4$ buffer (0.02 M) (after adjusting the pH to 7) were studied and it is observed that both the buffers retard the reaction. Hence all the further studies were conducted at neutral pH without buffers.

Effect of cations

To reduce the reaction time, the effect of different cations on the oxidation reaction is investigated. Fe(II), Al(III), Ce(IV) etc. up to $1.0 \times \times 10^{-4}$ M have showed negligible influence on the reaction, while Ag(I), Cu(II), Mn(II) and Mo(VI) have exerted appreciable catalytic effect even at low concentrations. Figure 1 illustrates the positive effect of different cations on the oda$-S_2O_8^{-2}$ reaction. The curves indicate that Ag(I) has higher catalytic efficiency than other cations. Since Ag(I) precipitates in the presence of halide ions, Cu(II) is chosen as the catalyst for the reaction. Studying the reaction progress with different initial concentrations of Cu(II), 5.0×10^{-4}M is found to be optimum concentration to hasten the reaction rate satisfactorily.

Effect of neutral salts

It is observed that the presence of KCl up to 2.0×10^{-3}M and K_2SO_4 up to 1.0×10^{-3}M had no appreciable effect on the reaction rate, while higher concentrations slowed down the reaction. But the presence of low concentrations of nitrate ion, 10^{-4}M interfered in the reaction, decreasing both the reaction rate and maximum absorbance value.

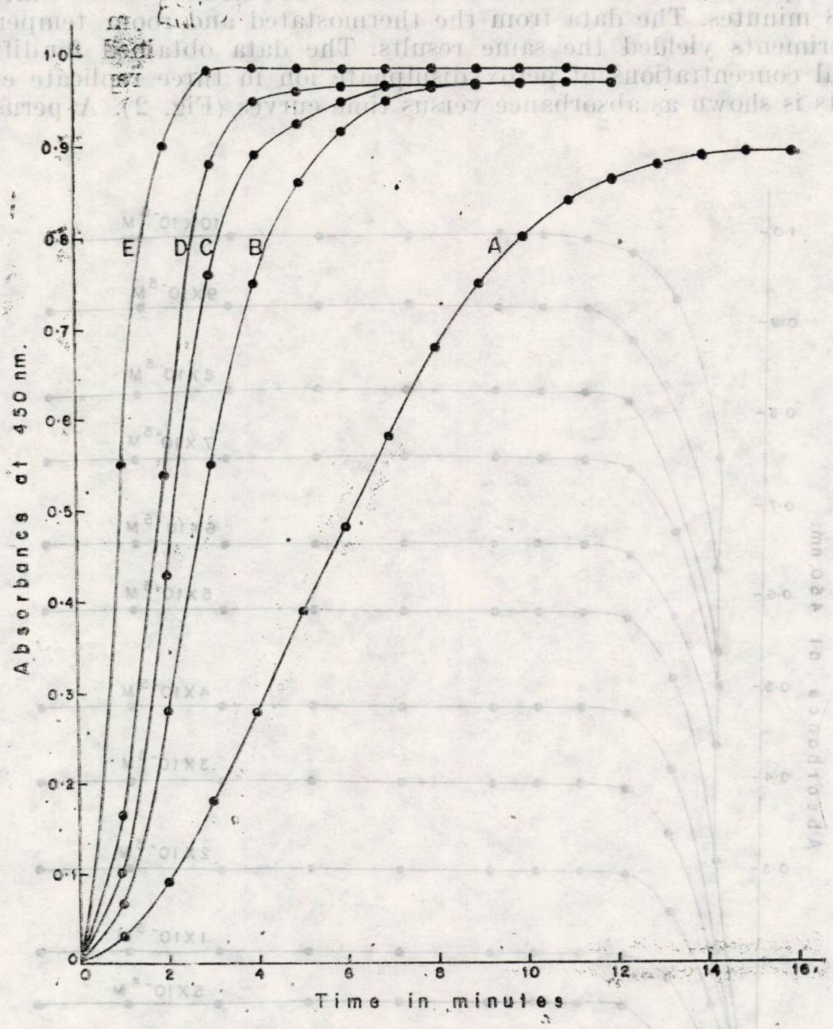

Fig. 1. — Absorbance versus time curves (at 450 nm).
Effect of cations on *o*-dianisidine-peroxydisulphate reaction : [oda] 6.0×10^{-4}M, $[S_2O_8^{2-}]$ 1.0×10^{-4} M.
A — Uncatalysed reaction, B — [Mn(II)] 10^{-5}M,
C — [Mo(VI)] 10^{-5} M, D — [Cu(II)] 10^{-5} M and E — [Ag(I)] 7.0×10^{-7} M.

Analytical method

For the standardization of the method a number of runs of indicator reaction were studied both in a thermostat (20°C ± 0.1°) and at room temperature (20°C ± 2°) employing 8 mL of 7.5×10^{-4}M oda (6.0×10^{-4}M), 0.5 mL of 0.01 M Cu(II)SO_4 (5.0×10^{-4}M) and requisite volumes of water to make up the final volume to 10 mL and different initial concentrations of peroxydisulphate ion (5.0×10^{-6}M $- 1.0 \times 10^{-4}$M). For each experiment the absorbances were measured at 30s or 60 s intervals for 8 minutes. The data from the thermostated and room temperature experiments yielded the same results. The data obtained for different initial concentrations of peroxydisulphate ion in three replicate experiments is shown as absorbance versus time curves (Fig. 2). A perusal of

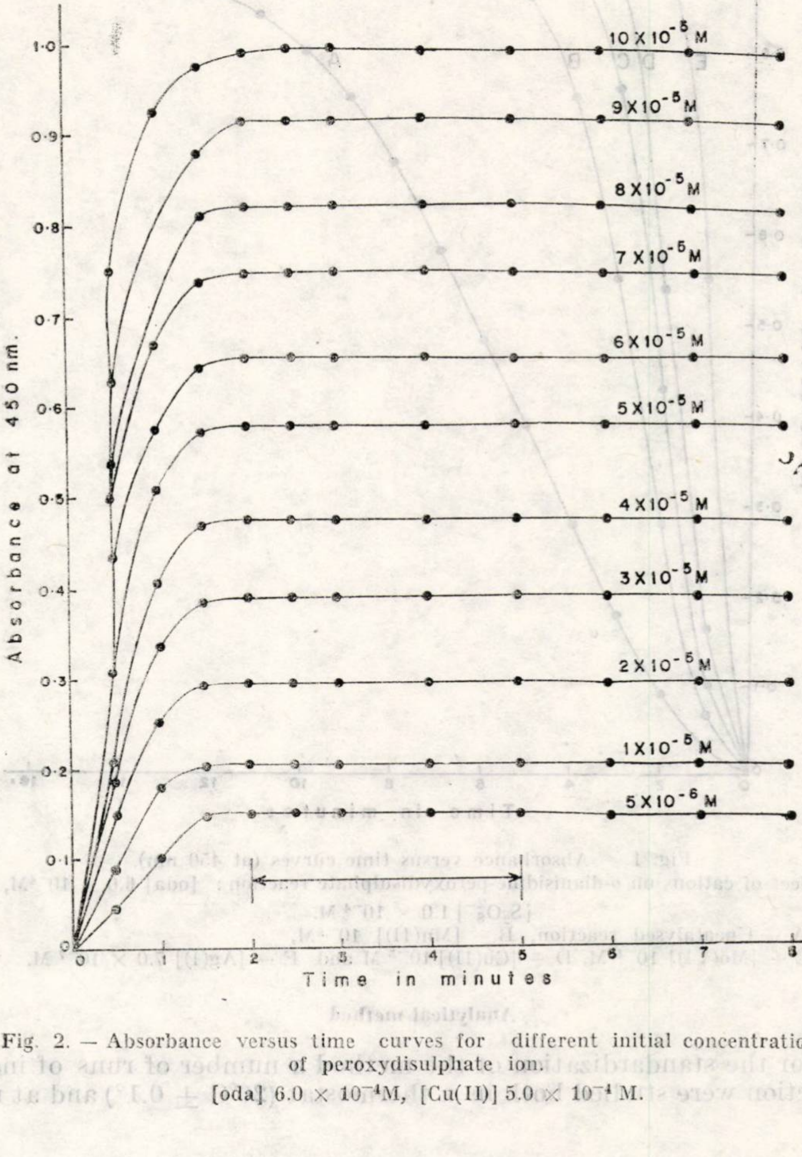

Fig. 2. — Absorbance versus time curves for different initial concentrations of peroxydisulphate ion.
[oda] 6.0×10^{-4}M, [Cu(II)] 5.0×10^{-4}M.

Fig. 2 shows that in all the curves the maximum absorbance value is attained within 60 s and the value remains the same up to 300 s, although a slight decrease is observed after 300 s in some curves. Using the data presented in Fig. 2, the absorbance values (between 60—300 s) were plotted against peroxydisulphate ion concentration. A fairly straight line with gradient 8.8×10^3 (corr. 0.96) was obtained, if absorbance values below 0.16 are excluded, which could be used as a calibration curve for determination of peroxydisulphate ion concentration from the corresponding absorbance values.

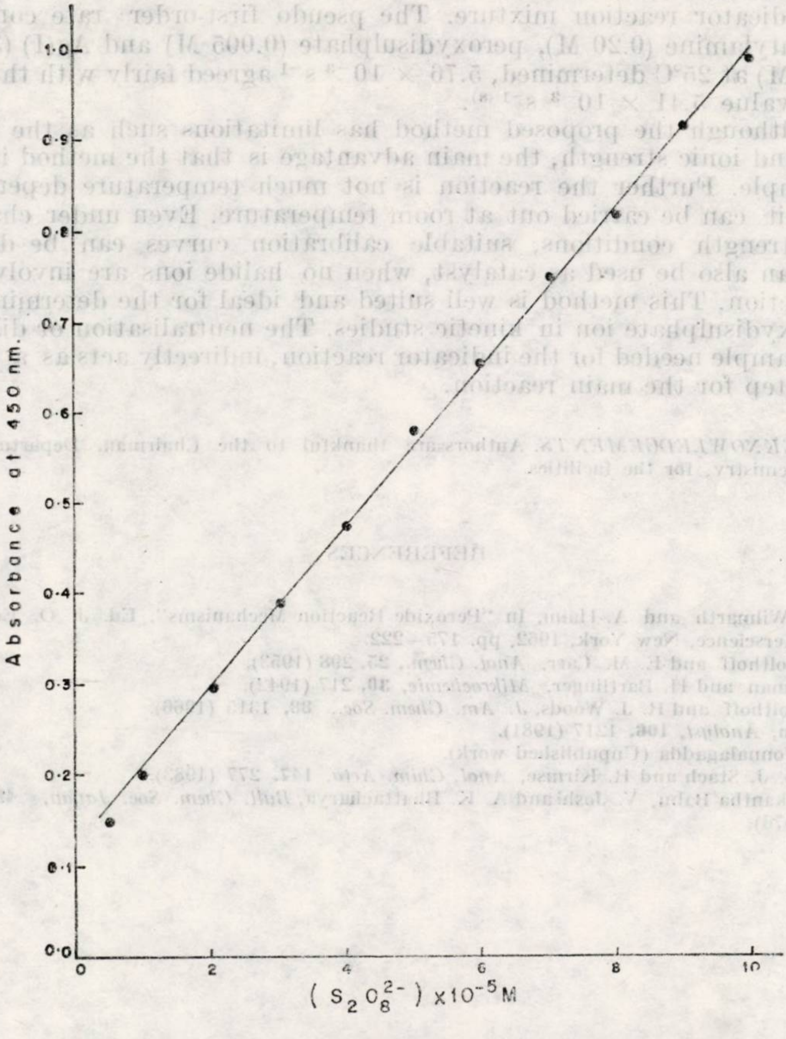

Fig. 3. — Calibration curve : Absorbance versus peroxydisulphate ion concentration. The same conditions as in Fig. 2.
Entries are from three replicate experiments and values had 4% average deviation.

The validity of oda-$S_2O_8^{2-}$ — Cu(II) reaction as the indicator reaction was tested by using it to monitor the kinetics of Ag(I) catalysed reaction between n-butylamine and potassium peroxydisulphate at 25°C. The peroxydisulphate ion concentration at fixed intervals was determined by neutralising the aliquots of reaction mixture and reading the corresponding absorbances at 450 nm after incubation for about three minutes with indicator reaction mixture. The pseudo first-order rate constant for n-butylamine (0.20 M), peroxydisulphate (0.005 M) and Ag(I) ($3.0 \times \times 10^{-4}$M) at 25°C determined, 5.76×10^{-3} s^{-1} agreed fairly with the literature value 5.41×10^{-3} s^{-1} (8).

Although the proposed method has limitations such as the effect of pH and ionic strength, the main advantage is that the method is fast and simple. Further the reaction is not much temperature dependent. Hence, it can be carried out at room temperature. Even under changed ionic strength conditions, suitable calibration curves can be drawn. Ag(I) can also be used as catalyst, when no halide ions are involved in the reaction. This method is well suited and ideal for the determination of peroxydisulphate ion in kinetic studies. The neutralisation or dilution of the sample needed for the indicator reaction, indirectly acts as a quenching step for the main reaction.

ACKNOWLEDGEMENTS. Authors are thankful to the Chairman, Department of Chemistry, for the facilities.

REFERENCES

[1] W. K. Wilmarth and A. Haim, In "Peroxide Reaction Mechanisms", Ed. J. O. Edwards, Interscience, New York, 1962, pp. 175—222.

[2] I. M. Kolthoff and E. M. Carr, *Anal. Chem.*, **25,** 298 (1953).

[3] W. Gelman and H. Bartlinger, *Mikrochemie*, **30**, 217 (1942).

[4] I. M. Kolthoff and R. J. Woods, *J. Am. Chem. Soc.*, **88,** 1315 (1966).

[5] D. Amin, *Analyst*, **106,** 1217 (1981).

[6] S. B. Jonnalagadda (Unpublished work).

[7] M. Otto, J. Stach and R. Kirmse, *Anal. Chim. Acta*, **147,** 277 (1983).

[8] J. Sreekantha Babu, V. Joshi and A. K. Bhattacharya, *Bull. Chem. Soc. Japan*, **49**, 1820 (1976).

Revue Roumaine de Chimie, **34**, *8*, 1667–1675 (1989)

FUNCIÓN POTENCIAL DE TORSIÓN E INVERSIÓN DEL GRUPO AMINO

M. ALCOLEA PALAFOX

Departamento de Química Física I (Espectroscopia), Facultad de Ciencias Químicas. Universidad Complutense de Madrid. Madrid 28040

Recibido: el 16 de agosto de 1987

A partir del método CNDO/2 se han calculado las funciones potenciales de torsión e inversión del grupo p-amino en los anestésicos locales benzocaína y procaína. Se ha optimizado tambien por este método la geometría de dicho grupo, existiendo un ángulo de inclinatión en el enlace C—N.

CNDO/2 calculations have been made to obtain the torsional and inversion potential functions of p-amine group in the local anesthetics benzocaine and procaine. The geometry of this group has been optimized, there being a tilt in the C—N bond.

INTRODUCCIÓN

Los anestésicos locales elegidos, benzocaína y procaína, responden al esquema estructural común de los anestésicos locales, estando formados por un radical lipofílico (anillo aromático), una cadena intermedia (que contiene tres miembros en la benzocaína y ocho en la procaína) y un grupo hidrofílico terminal ($-NH_2$).

Experimentalmente por métodos espectroscópicos [1] se ha observado que este grupo $-NH_2$ sufre con diferencia un mayor intercambio isotópico H → D en el proceso de deuteración con respecto a los otros grupos funcionales presentes en las moléculas. Diversos trabajos ademas con estos anestésicos locales [2-6] parecen indicar que en la formación de un complejo por enlaces de hidrógeno entre la droga y un grupo aceptor en la membrana, solamente el grupo amino en posición *para* y no el grupo carbonilo participa en dichos enlaces. No obstante y dada la complejidad del problema,[7] en el caso concreto de la procaína ha sido postulado [8] que puede haber otro sitio adicional de enlace a los grupos aceptores de la membrana, siendo ésta realizada a traves del grupo amino terciario terminal.

Centrando por tanto el estudio en el análisis de este grupo $-NH_2$, se ha elegido como punto de partida la molécula de anilina. Los procesos de torsión e inversión de los grupos NH_2, NHD y ND_2 en la anilina han sido repetidamente analizados por diversos autores. [9-17] Así es bien conocido que el grupo $C-NH_2$ en la misma tiene una estructura piramidal con un ángulo fuera del plano (ángulo de inversión) aproximadamente de 37.5°.

RESULTADOS Y DISCUSION

Geometría utilizada. Optimización del parametro ε

Usando el método CNDO/2 con parametrización standard[18] se han optimizado los parámetros geométricos, angulos y longitudes de enlace, del grupo $-NH_2$ (tabla 1). Sieiro y col.[19] demostraron que este método es aplicable siempre que se realice sobre un enlace no conjugado. Siendo bien conocido que la deslocalización electrónica del enlace N—H es pequeña (su orden de enlace es proximo a la unidad), indica que puede ser analizado este grupo con razonable confianza.

Tabla 1

Longitudes y ángulos de enlace del grupo amino calculados por el método CNDO/2.

	Longitud de enlace (A°)	Ángulo de enlace (°)
C—N	1.39	
N—H	1.07	
$\widehat{HNH}$		107
$\widehat{HNC}$		111.5
CN-plano del anillo bencenico (ε)		3.60
H_2N-plano del anillo bencenico (ω)		51.8

Para el resto de la molécula se ha usado la geometría descrita en las referencias,[1, 20, 21], asi como valores standard.[22]

Dadas las pequeñas diferencias encontradas entre ambas moléculas, benzocaina y procaína, los valores dados en la tabla 1 pueden considerarse validos para ambas.

Es de particular interés señalar la presencia en esta tabla del parametro ε, el cual se refiere al angulo de inclinación (traducción de la palabra inglesa ,,tilt'') que forma el enlace C—N con el plano que contiene al anillo bencénico y el resto de la molécula (fig. 1). La existencia de este ángulo de inclinación ε es totalmente coherente con los resultados espectroscópicos obtenidos.[1] Este angulo parece más bien el resultado de dos efectos combinados, uno inercial del propio grupo NH_2 y otro elec-

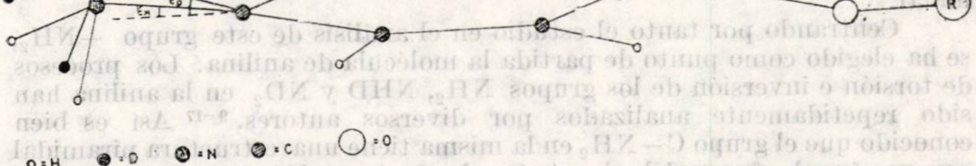

Fig. 1. — Ubicación del ángulo de inclinación ε en las moléculas en estudio.(NH_2 y tambien ND_2)

trónico que se puede estimar por los datos suministrados del método CNDO/2.

Así con el fin de confirmar la influencia de efectos electrónicos en el valor de este angulo, relacionados con las propriedades estáticas del grupo amino respecto al resto de la molécula, se ha realizado su cálculo mediante el citado método CNDO/2, obteniendo su valor óptimo el cual se representa en la fig. 2. El mínimo de la curva para ambas moléculas es de 3.60°, tanto cuando el átomo de nitrógeno esta situado en dirección opuesta a los átomos de hidrógeno del grupo amino, como cuando estan en la misma dirección. No obstante, en el primer caso se alcanza un mínimo más pronunciado en concordancia con una conformación más estable.

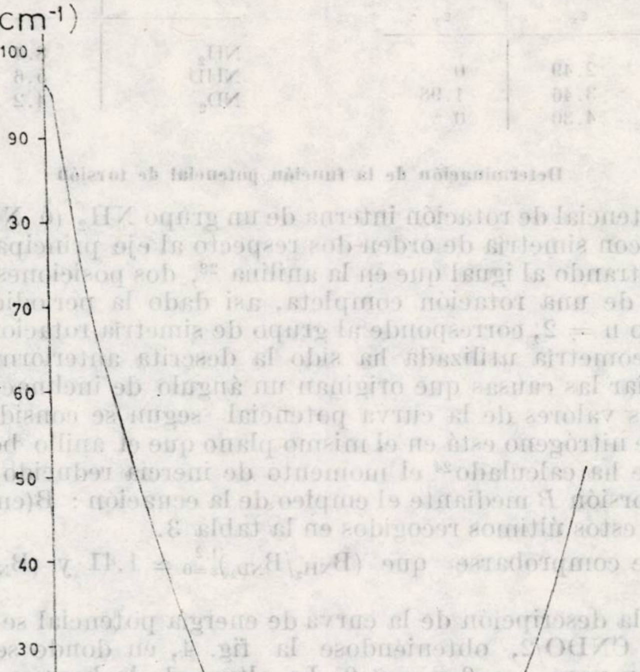

Fig. 2. — Optimización del angulo ε.

Por otro lado, el cálculo del ángulo de inclinación a partir de consideraciones dinámicas se efectua con las ecuaciones señaladas en la fig. 3, obteniéndose los valores dados en la tabla 2.

Tabla 2

Valores óptimos del ángulo de inclinación obtenidos a partir de consideraciones dinámicas

Grupo	$\varepsilon(°)$	
	ε_x	ε_y
NH_2	2.49	0
NHD	3.46	1.98
ND_2	4.30	0

Tabla 3

Valores de la constante de torsión en cm^{-1}

Grupo amino	$\varepsilon = 0$	$\varepsilon \neq 0$
NH_2	8.4	8.8
NHD	5.6	6.0
ND_2	4.2	4.5

Determinación de la función potencial de torsión

El potencial de rotación interna de un grupo NH_2 (ó ND_2) se puede considerar con simetría de orden dos respecto al eje principal de la molécula, encontrando al igual que en la anilina [23], dos posiciones equivalentes a lo largo de una rotación completa, asi dado la periodicidad de este movimiento n = 2, corresponde al grupo de simetría rotacional C_2.

La geometría utilizada ha sido la descrita anteriormente, si bien para estudiar las causas que originan un ángulo de inclinación ε, se han recogido los valores de la curva potencial segun se considere o no que el átomo de nitrógeno está en el mismo plano que el anillo bencénico.

Asi se ha calculado[24] el momento de inercia reducido *Ir* y la constante de torsión *B* mediante el empleo de la ecuación : $B(cm^{-1}) = h/8\pi^2c\ Ir$, estando estos últimos recogidos en la tabla 3.

Puede comprobarse que $(B_{NH_2}/B_{ND_2})^{1/2}_{\varepsilon=0} \simeq 1.41$ y $(B_{NH_2}/B_{ND_2})^{1/2}_{\varepsilon\neq 0} \simeq$ $\simeq 1.39$.

Para la descripción de la curva de energía potencial se ha empleado el método CNDO/2, obteniéndose la fig. 4, en donde se realiza una comparación para $\varepsilon = 0$ y $\varepsilon \neq 0$. La altura de la barrera hallada esta recogida en la tabla 4.

Tabla 4

Altura de la barrera en cm^{-1}

Función potencial	$\varepsilon = 0$	$\varepsilon \neq 0$
Torsión $(\hat{V}_t)$	1842	1795
Inversión $(\hat{V}_i)$	2861	3051

De la carencia de una diferencia en las barreras torsionales de ambos compuestos puede deducirse razonablemente que la rotación del grupo NH_2 tiene el mismo grado de impedimento para ambos compuestos y que dicha rotación no es sensible al cambio en la estructura química

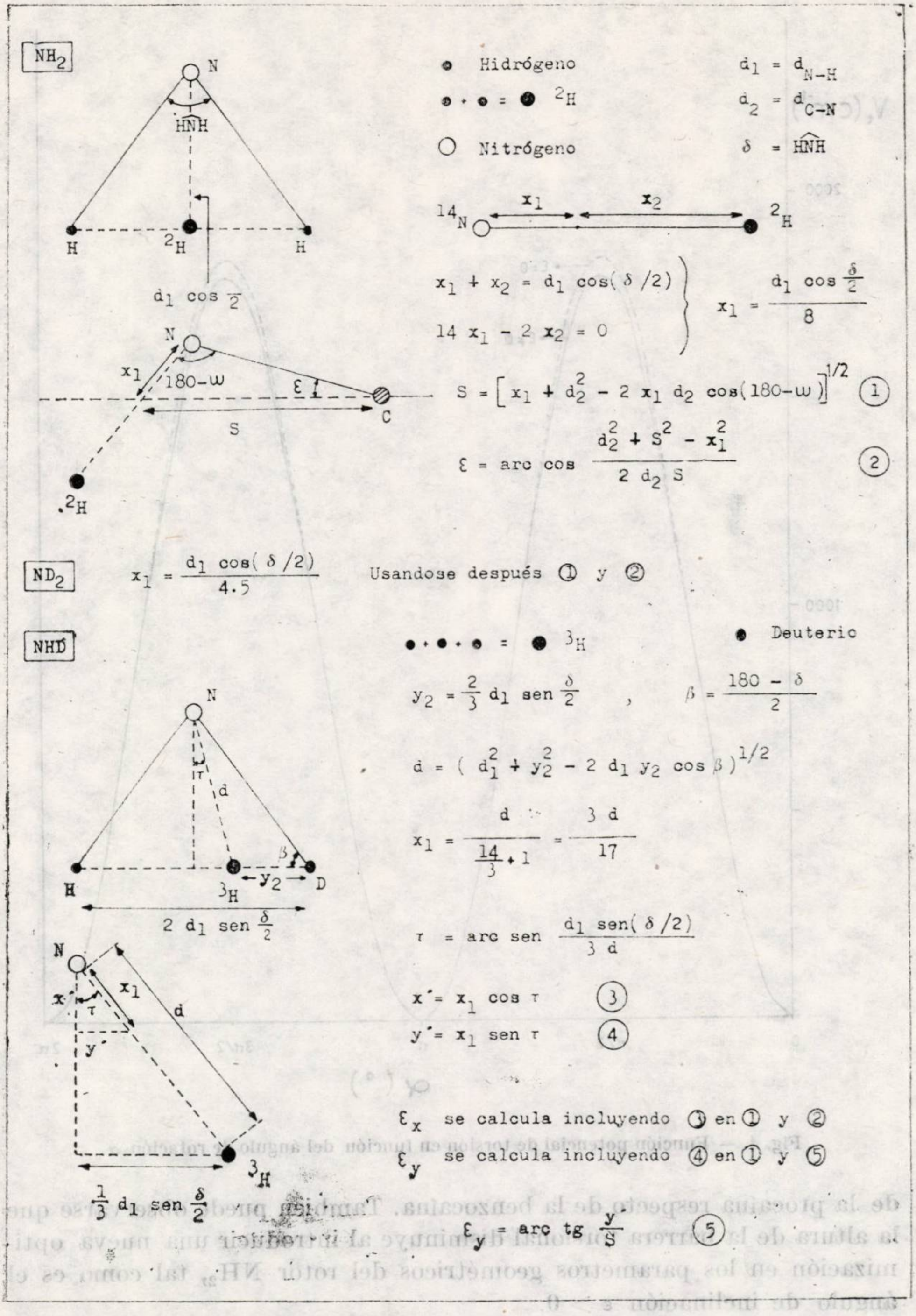
NH₂
N
HNH
H
²H
H
d₁ cos δ/2
● Hidrógeno
● + ● = ● ²H
○ Nitrógeno
d₁ = d_N-H
d₂ = d_C-N
δ = HNH
¹⁴N
x₁
x₂
²H
x₁ + x₂ = d₁ cos(δ/2)
14 x₁ − 2 x₂ = 0
x₁ = d₁ cos δ/2 / 8
N
x₁
180-ω
ε
C
S
²H
S = [x₁ + d₂² − 2 x₁ d₂ cos(180−ω)]^1/2 ①
ε = arc cos (d₂² + S² − x₁²) / (2 d₂ S) ②
ND₂
x₁ = d₁ cos(δ/2) / 4.5
Usandose después ① y ②
NHD
● + ● + ● = ● ³H
● Deuterio
y₂ = 2/3 d₁ sen δ/2 , β = (180 − δ)/2
d = (d₁² + y₂² − 2 d₁ y₂ cos β)^1/2
x₁ = d / (14/3 + 1) = 3 d / 17
τ = arc sen d₁ sen(δ/2) / 3 d
x′ = x₁ cos τ ③
y′ = x₁ sen τ ④
N
τ
d
β
H
³H
y₂
D
2 d₁ sen δ/2
N
x′
τ
x₁
d
y′
³H
1/3 d₁ sen δ/2
ε_x se calcula incluyendo ③ en ① y ②
ε_y se calcula incluyendo ④ en ① y ⑤
ε_y = arc tg y′/S ⑤

Fig. 3. — Fórmulas para el cálculo de ε a partir de consideraciones dinámicas.

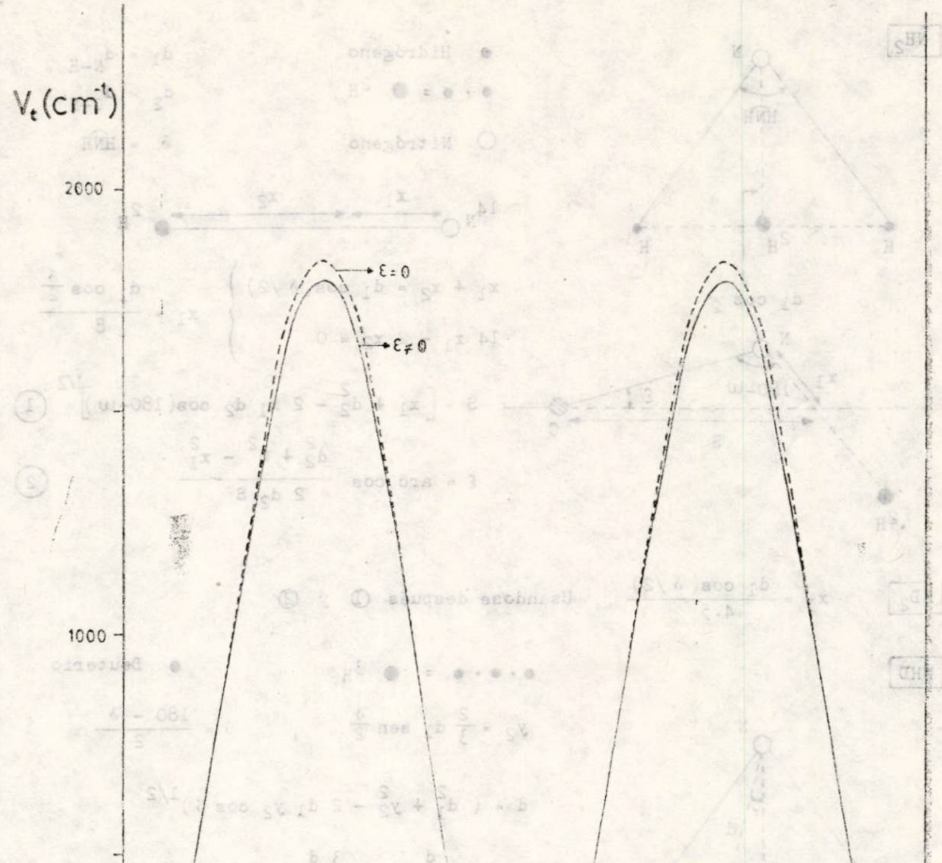

Fig. 4. — Función potencial de torsión en función del ángulo de rotación α.

de la procaína respecto de la benzocaína. Tambien puede observarse que la altura de la barrera torsional disminuye al introducir una nueva optimización en los parametros geométricos del rotor NH_2, tal como es el ángulo de inclinación $\varepsilon > 0$.

Determinación de la función potencial de inversión

El movimiento de inversión de los grupos NH_2, NHD y ND_2 es el que conduce de una molécula con los dos hidrógenos del grupo amino situados por debajo del plano que contiene la molécula, a una conformación donde los dos hidrógenos mencionados están situados por encima de dicho plano. La vibración de inversión (análoga a la vibración de „paraguas'' del amoniaco) envuelve asi el movimiento de los dos hidrógenos a través de este plano, con simultanea inversión del par solitario de electrones del átomo de nitrógeno.

Para llevar a cabo este movimiento, la molécula debe vencer una determinada barrera pontencial, cuya altura máxima corresponde a una geometría en la que el grupo NH_2 esta en el mismo plano del anillo bencénico. Al igual que el movimiento de rotación, cada una de estas vibraciones cuando son excitadas con suficiente amplitud, pueden superar completamente las bajas barreras potenciales y producir inversión en un caso y una rotación interna en el otro.

Para determinar la función potencial de inversión impedida del grupo amino en estas moléculas se ha empleado al igual que en la torsión el método CNDO/2, a partir de la geometría descrita en la tabla 1. Esta función potencial se ha determinado para la consideración de existencia o no del ángulo de inclinación ε, quedando reflejada esta diferencia en la fig. 5.

En ambos casos y tanto para la benzocaína como para la procaína se ha obtenido un único valor óptimo del ángulo de inversión ω de 51.8°, siendo coincidente con el determinado en la molécula de anilina[23,25,26] empleando en este caso métodos „ab initio'', y todos ellos excesivamente elevados si se tiene en cuenta el ángulo experimentalmente determinado [27] por microondas para la misma cuyo valor es $37.5 \pm 2°$. Una posible explicación a este hecho ya fue dado por Niu y col. [25,26]

Por otra parte, el mayor valor determinado para la altura de la barrera (tabla 4) cuando $\varepsilon \neq 0$, a diferencia de lo obtenido para el movimiento de rotación, se interpreta [1] en terminos de la mayor estabilidad que presenta para $\omega = 0$ la conformación totalmente plana con $\varepsilon = 0$, pues prima en este caso la deslocalización [27] de electrones del mismo dentro del sistema π del anillo. Cuando el $\omega = 51.8°$ prima en este caso la localización de electrones en el par solitario del átomo de nitrógeno, siendo así la conformación más estable para $\varepsilon \neq 0$. De esta forma se produce un mayor altura de la barrera para $\varepsilon \neq 0$ que para $\varepsilon = 0$ ($\Delta\hat{V}_i \simeq 190$ cm^{-1}), siendo justo el doble de la existente para el ω entre las conformaciones $\varepsilon = 0$ y $\varepsilon \neq 0$ ($\Delta\hat{V}_i \simeq 96$ cm^{-1}). En el caso de la rotación, al producirse ésta para un ω ya determinado de inversión, solo prima la localización de electrones en el átomo de nitrógeno, de aquí la menor altura de la barrera para $\varepsilon \neq 0$.

Por último se dirá con respecto a los movimientos de rotación e inversión, que se producen en los mismos cambios totalmente marcados en la estructura del grupo amino con alteraciones en las longitudes del enlace N—H y angulos CNH y HNH. Así los cambios en los ángulos son tan amplios como los correspondientes a una hibridación sp^2 pura en el caso completamente planar, y practicamente sp^3 en la conformación piramidal girada o invertida. De esta forma, los valores asignados a las diferencias energeticas entre las conformaciones correspondientes a una

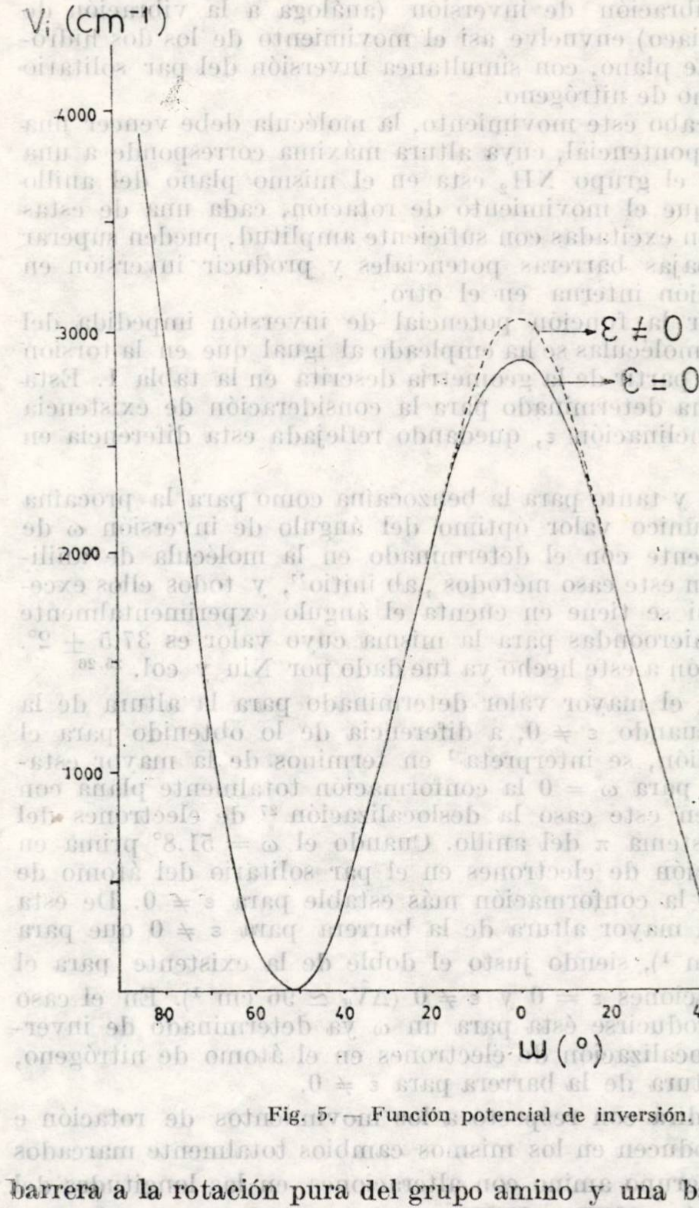

Fig. 5.—Función potencial de inversión.

barrera a la rotación pura del grupo amino y una barrera a la inversión pura del mismo, llevaran consigo una cierta imprecisión a causa de la incertidumbre en la geometría del equilibrio.

REFERENCIAS

[1] M. Alcolea, Tesis Doctoral. Univ. Compl. Madrid (1987).
[2] M. Remko, y P. T. Van Duijnen, *J. Mol. Struct*. **104**, 451 (1983).
[3] R. Beall, J. Herdklotz, y R. L. Sass, *Biochem. Biophys. Res. Commun.*, **39**, 329 (1970).
[4] M. Sax, J. Pletcher, y R. Gustaffson, *Acta Cryst.*, **B 26**, 114 (1970).
[5] J. Pletcher, M. Sax, y C. S. Yoo, *Acta Cryst.*, **B 28**, 378 (1972).
[6] P. O. Dideberg, J. Lamotte, y L. Dupont, *Acta Cryst.*, **B 36**, 1500 (1980).
[7] Y. Boulanger, S. Schreier, L. C. Leitch, I. C. P. Smith, *Can. J. Biochem.*, **58**, 986 (1980).
[8] G. R. Freeman, y C. E. Bugg, *Acta Cryst.*, **B 31**, 96 (1975).
[9] C. Berlorgeot, P. Quintard, P. Delmorme, y V. Lorenzelli, *Can. J. Spectry*, **21**, 119 (1976).
[10] C. Berlorgeot, P. Quintard, y J. Gerbier, *C. R. Acad. Sci. Paris*, **269 B**, 1105 (1970).
[11] J. C. D. Brand, D. R. Williams, y T. J. Cook, *J. Mol. Spectry.*, **43**, 87 (1972), ; **20**, 359 (1966).
[12] M. Quack, y M. Stockburger, *J. Mol. Spectry*, **43**, 87 (1972).
[13] R. A. Kydd, y P. J. Krueger, *Chem. Phys. Letters*, **69**, 2, 827 (1978) ; **72**, 1, 280 (1980).
[14] A. Nonat, A. Bouchy, y G. Roussy, *J. Mol. Spectry.*, **99**, 407 (1983) ; *J. Mol. Struct.*, **116**, 227 (1984).
[15] W. J. Hehre, L. Radom, y J. A. Pople, *Chem. Comm.*, **1972**, 669.
[16] R. A. Kydd, y A. R. C. Dunham, *J. Mol. Struct.*, **98**, 39 (1983).
[17] J. Waite, y M. G. Papadopoulos, *J. Chem. Phys.*, **82**, 3, 1427 (1985).
[18] J. A. Pople, y D. L. Beveridge, "Approximate Molecular Orbital Theory", McGraw-Hill, New York, 1970, p. 75.
[19] C. Sieiro, P. Gonzales-Diaz, yY. G Smeyers, *J. Mol. Struct.*, **24**, 345 (1975).
[20] T. F. Lai, yR. E. Marsh, *Acta Cryst.*, **22**, 885 (1967).
[21] S. Kashino, M. Ikeda, y M. Haisa, *Acta Cryst.*, **B 38**, 1868 (1982).
[22] "International Tables for X-ray Crystallography", Birmigham, Kynoch Press 1962, 111, p. 202.
[23] C. C. Strametz, y H. H. Schmidtke, *Theoret. Chim. Acta*, **42**, 13 (1976).
[24] K. S. Pitzer, *J. Chem. Phys.*, **14**, 239 (1946).
[25] Z. Niu, K. M. Dunn, J. E. Boggs, *Mol. Physics*, **55**, 2, 421 (1985).
[26] Z. Niu, y J. E. Boggs, *J. Mol. Struct. Theochem.*, **109**, 381 (1984).
[27] D. G. Lister, J. K. Tyler, J. H. Hog, y N. W. Larsen, *J. Mol. Struct.*, **23**, 253 (1974).

Revue Roumaine de Chimie, 34, *8*, 1677–1679 (1989)

LEAD, CHROMIUM AND BARIUM IN TURKISH PRINTING INKS AND COLORED NEWSPAPERS

ÜNEL KÖKLÜ and TÜLAY ORKUN
Faculty of Science and Letters, Technical University of Istanbul,
Maslak — Istanbul, Turkey

Received January 7, 1988

In the present study, the heavy metals such as lead, chromium and barium were determined in Turkish printing inks and colored newspapers by A. A. S. techniques with respect to the health hazards.

INTRODUCTION

In the last years organic printing inks and paints have been produced granting attention to environment and health problems, however some of the newest contain inorganic elements in their organic structures. Besides, many organic pigments are deposited on an inorganic core. Therefore, severe rules should not be given since there are exceptions in every case. On the other hand, health hazards arising from the environmental problems have reached such a point that each country should take her precaution strictly according to the local parameters. Universal interest of trace amounts of the health hazardous elements and their distribution in human organs have stimulated many scientists to investigate the normal values, illnesses, occupational diseases and the toxic effect. [1,2,3]

In this study, taking into consideration the above given points, Turkish printing inks and colored newspapers of different publishers were analysed for completion of the previous study [4] and for the last years' revision of the materials with regard to health hazards was suggested.

EXPERIMENTAL

Chemicals and Standard Solutions

The chemicals used were reagent grade quality and the primary standard solutions of A. A. Spectrometry were commercially available.

Instrument

A computerized Perkin Elmer 2380 A. A. Spectrophotometer equipped with graphite furnace was employed. Air-acetylene flame was used for lead, chromium and nitrous oxide and acetylene flame for barium.

Table 1

Analytical data of colored Turkish newspapers of different publishers

Newspapers of different publishers	$10^{-2} \cdot \overline{X}$ values (ppm)		
	Pb	Ba	Cr
A_1	0.49	36.92	<0.25
A_2	0.15	12.01	0
A_3	0	0	0
A_4	0.58	43.56	0
B_1	0.98	72.33	0
B_2	0	0	<0.24
B_3	0.33	22.03	0
B_4	0.30	22.45	0
C_1	0	0	0
C_2	0.87	65.23	0
C_3	0.27	21.84	<0.27
C_4	0.27	21.90	0.54
D_1	0	0	0
D_2	0.47	35.49	<0.23
D_3	0.49	36.85	0
D_4	0.25	20.27	<0.25
E_1	0	0	0
E_2	0.48	38.97	2.43
E_3	0	0	<0.23
E_4	0	0	0
F_1	0	0	0
F_2	0	0	<0.36
F_3	0.23	17.49	0
F_4	0.27	21.95	0.55
G_1	0.49	36.12	0.90
G_2	0	0	0.59
G_3	0.48	32.38	0
G_4	0.39	28.75	0
H_1	0.47	35.22	0
H_2	0.89	64.62	0.28
H_3	0.55	39.66	0.39
H_4	0.23	18.54	0

The subscripts of the capital letters refer to the colors:
1 – blue 2 – green 3 – yellow 4 – red.

$\overline{X}$: Average value of concentration

Table 2

Analytical data of printing inks

Manufacturers	Type of color	$10^{-2} \cdot \overline{X}$ values (ppm)		
		Pb	Ba	Cr
A	Blue	0.12	8.71	0.32
	Yellow	0.17	12.84	0.55
	Red	0.092	6.90	0.48
	Black	0.068	5.44	0.071
B	Blue	0.11	7.75	0.403
	Yellow	0.19	14.21	0.49
	Red	0.085	5.82	0.52
	Black	0.073	7.02	0.069
C	Blue	0.14	9.08	0.39
	Yellow	0.15	11.79	0.61
	Red	0.083	6.57	0.46
	Black	0.063	5.98	0.075

Method and Procedure

In this study, for the colored neswpapers the same procedure was carried out as in the previous papers.[4] It was concerned in extractable amounts of the elements rather than their total values in the samples. Accordingly an extraction test simulating the conditions of human stomach was devised.

The colored newspapers of eight different printers were ground in a mill. 4 grams of each sample were placed in a 250 mL stoppered flask and 125 mL of 0.1 M HCI were added and the flasks were kept in a thermostat at 37.5°C and shaken gently at 30 min intervals over a total period of 4 hr. At the end of this period, samples were filtred through Whatman no. I papers and the filtrates were diluted to 250 mL in a volumetric flask. Finally all solutions were measured by A. A. S. technique.

The samples of printing inks were weighed as 1 gram and placed in a 250 mL beaker. The organic matter was destroyed by a nitric acid — perchloric acid digestion and was evaporated to dryness carefully. The residue was dissolved with a mixture of 2.5 mL of HCI and 125 mL of distilled water. The content of the beaker were decanted to a 250 mL volumetric flask and diluted to 250 mL with distilled water for measurement, by the A.A.S. technique.

The setting of the A. A spectrophotometer was adjusted as specified in the instrument manual. Any interference was compensated automatically. After the adjustment of the specific wavelength of the element measured the result was read as an average value on the digital scale. Air-acetylene flame was used for Pb and Cr and nitrous oxide-acetylene flame for Ba.

The moisture content of the sample was determined in a separate sample at 110°C and the results were given as moisture free samples.

RESULTS AND DISCUSSION

Analytical data (on a moisture-free basis) of Pb, Cr and Ba in samples are listed in Tables 1 and 2.

The heavy metals such as Pb, Cr and Ba constitute a real health damage to children, who might chew and swallow paper.

The extractable amounts of lead, chromium determined in both samples, printing inks and newspapers were found very low which might not give any health risk. The results showed that the printing inks did not contain the lead-chromate pigments which are commonly used in printing by the rotary letterpress method.

The extractable amount of barium is considered as relatively high. The accumulation and absorption of barium might paralyze the central nervous system of the children. Also the dust of materials which contain barium compounds can be collected in lungs and give serious damage in health.

It is also possible that some of the lead, chromium and barium come from other sources than the pigment of the printing ink. These sources might be the filling materials such as talc, calcite, china clay and kaolinite.

REFERENCES

[1] H. A. Roels, J. P. Buchet, A. Bernard, L. A. Lanwerys and J. M. Guerit, *Arch. Belg. Med. Soc. Hyg. Med. Trav. Med. Leg.*, **37**, 589 (1979).

[2] Shoji Kitamura, *Soda to Enso*, **31** (**360**), 3 (1980).

[3] P. Minkkinen, Eripainos Kemia-Kemi, **3**, 282 (1976).

[4] Tülay Orkun and Ünel Köklü, "Studies on Turkish Children's Colored Magazins, Paintings Dyes and Colored Chalks", *Chimica Acta Turcica* (in press).

Revue Roumaine de Chimie, **34**, *8*, 1681–1689 (1989)

STUDIES CONCERNING CALCIUM CARBONATE SCALES FORMATION AND ITS PREVENTION. I

KINETICS OF CALCIUM CARBONATE PRECIPITATION FROM HYPERTHERMAL WATER

VASILE COCHECI, GHEORGHE PETCA and EUGEN GLÜCK

Faculty of Chemical Technology, Polytechnic Institute "Traian Vuia"
Timișoara, Bd. 30 Decembrie No. 2, Romania

Received December 18, 1988

In the present paper the kinetics of calcium carbonate precipitation under the conditions of hyperthermal water exploitation was studied, at temperatures ranging between 65–80°C and supersaturation degrees ranging from 4.44 to 28.28. Under these conditions calcium carbonate precipitation follows a second order equation with respect to calcium ion supersaturation for supersaturation degrees lower than 10, and a first order equation with respect to calcium ion supersaturation for higher supersaturation degrees than 10.

INTRODUCTION

Owing to the high content of bicarbonates, elevated temperatures and the presence of the gaseous phase in contact with water, in the exploitation of hyperthermal waters and oil deposits, an unwanted but frequently encountered phenomenon is the formation of calcium carbonate scales. [1–4] They form in large quantities in well pipes of water or water-oil mixture, in pumps, degassing equipment, a.s.o., leading to productivity diminution and finally to equipment shut-down.

Scales formation is determined by the equilibria change in the $CaO-CO_2-H_2O$ system and by calcium carbonate crystals formation kinetics. Scales formation can be prevented, either acting on the equilibria from the system, or on calcium carbonate precipitation kinetics.

Understanding of calcium carbonate precipitation kinetics under the specific conditions of hyperthermal water is of paramount importance in the knowledge of scales formation mechanism and the methods of their prevention.

Both the kinetics of homogenous precipitation and the kinetics of heterogenous precipitation were studied by a great number of workers, who stated kinetic expressions, empirical, semiempirical or based on the mechanism of calcium carbonate crystals formation.[5–17] The majority of the expressions were established for crystal growth, respectively under the conditions of seeding the reaction environment with calcium carbonate crystals, closer conditions to the actual conditions of calcium carbonate scales formation.[9–14,16–17]

Among the stated kinetic expressions, the expressions proposed by Reddy,[11] Reddy and Nancollas,[9] Davies-Jones,[17] Nielsen, House[15] represent better the experimental data obtained at the precipitation of calcium carbonate. All these authors studied the kinetics of calcium carbonate precipitation by the addition of calcium carbonate crystals to a supersaturated solution of calcium bicarbonate, obtained by mixing a calcium chloride solution with a sodium bicarbonate solution or sodium carbonate-bicarbonate mixture solution, at temperatures ranging between 20 – 40°C and concentrations of calcium ion between 0.25 – 3.29 mmole/dm³.

In order to state a relationship for the calculation of inhibitor dosage as a function of water characteristics[2] and exploitation conditions,[3] we proposed ourselves to establish the kinetic equation which follows better calcium carbonate precipitation under hyperthermal water exploitation conditions.

MECHANISM OF HYPERTHERMAL WATER DESTABILIZATION

Formation of calcium carbonate scales is frequently encountered in plants where water is used as heat bearer. In the majority of these cases, the process occurring under isobar conditions, scales formation is due to equilibria modification in the system $CaO-CO_2-H_2O$, as a consequence of temperature increase. In case of hyperthermal water, the conditions of scale formation are completely different. Water destabilization and calcium carbonate precipitation occur under practically isothermal conditions but with a great pressure variation. In well pipes, water can be considered as an isolated system. In an isolated system, the components can be found in three aggregations, gaseous, liquid and solid. Consequently the following equilibria can be considered :

$$
\begin{array}{c}
CO_{2(g)} \rightleftarrows CO_{2(l)} \\
\hline
CO_{2(l)} + H_2O \rightleftarrows H_2CO_3 \\
H_2CO_3 + H_2O \rightleftharpoons H_3O^+ + HCO_3^- \\
HCO_3 + H_2O \rightleftarrows H_3O^+ + CO_3^{2-} \\
\hline
Ca^{2+} + CO_3^{2-} \rightleftarrows CaCO_{3(s)} \\
CaCO_{3(aragonite)} \rightleftarrows CaCO_{3(calcite)}
\end{array}
$$

In hyperthermal water well pipes can exist two or all the three phases. As water mounts in the pipe and pressure lowers, the gaseous phase separates, resulting a heterogenous water-gas system. As a consequence of the formation of the gaseous phase, carbon dioxide desorbs as pressure lowers, and the equilibria in the liquid phase change to carbonate formation which once precipitates calcium carbonate.[18] Consequently calcium carbonate precipitation is determined by the desorption of carbon dioxide from water, respectively by a certain partial pressure of carbon dioxide in the gaseous phase. This pressure can be calculated on the basis of water characteristics.[19]

EXPERIMENTAL

Application of some efficient methods for prevention of calcium carbonate deposition, supposes the use of some experimental methods, which reproduce accurately hyperthermal water exploitation plants conditions. Starting from hyperthermal water destabilization mechanism, for the study of calcium carbonate scales formation the apparatus presented in figure 1 was used. The apparatus allows the realization of different temperatures and supersaturation degrees of calcium carbonates throughout hyperthermal water route. Water temperature from the reaction vessel 8 is maintained constant by the thermostat 12. The desired partial pressure of carbon bioxide in the gaseous phase is achieved by the modification of the air-carbon dioxide mixture content, which is bubbled into the studied sample from the vessel 8, through the porous plate G_1. Air and carbon dioxide flow is measured by the rotameter 2 and the pneumatic resistance 7, respectively. Air-carbon dioxide mixture, with a flow of 60 dm^3/h at 20°C and 110 kPa, is preheated in the preheater 3 and moistened in the moistening vessel 4. Water vapours trained by the gas are condensed in 11 and condensed water goes back into the vessel 8. Sodium carbonate solution of desired concentration was introduced in the thermostated vessel 8, which has a capacity of 2.5 dm^3. By bubbling the air-carbon dioxide mixture, the change of carbonate into bicarbonate was achieved, the degree of transformation being determined by the air/carbon bioxide ratio. After the attainment of the desired temperature and the equilibrium between the gaseous phase and solution, which was monitored by measuring the pH, calcium carbonate crystals were added. For this purpose calcium carbonate A. R. MERCK was used. By X-ray analysis it was found that crystals consisted in calcite. After the suspension homogenization a 0.01 N calcium chloride solution was added under continuous stirring. Calcium carbonate crystals determined the heterogenous precipitation of calcium carbonate. Water samples were withdrawn at intervals and after rapid cooling were filtered. Calcium ion concentration was determined by atomic absorption spectroscopy. The variation of pH against time was also monitored, which although decreased at the beginning of the experiment, after a relatively short while returned to its initial value. pH lowering was due to carbon dioxide formation, as a consequence of calcium carbonate precipitation reaction, but which is desorbed by the air-carbon dioxide mixture. Under these conditions, owing to the high bicarbonate content, relatively low calcium ion content and bubbling of air-carbon dioxide mixture, it can be considered that calcium carbonate precipitation occurred throughout the experiment under constant bicarbonate ion concentration conditions.

Plots of calcium ion concentration versus time were obtained, of the type presented in figure 2.

RESULTS AND DISCUSSION

Starting from the kinetic expressions stated by Reddy and Reddy and Nancollas, we tried to establish which of these relationships represent better the kinetics of calcium carbonate precipitation under the conditions of hyperthermal water, characterised by elevated concentrations of bicarbonate ion and low of calcium ion.

Data obtained under various experimental conditions were processed in order to establish the kinetic expression, using initially Reddy's equation [11]:

$$-\frac{dC}{dt} = kGf_D^2([Ca^{2+}]_t - [Ca^{2+}]_e)^2 \qquad (1)$$

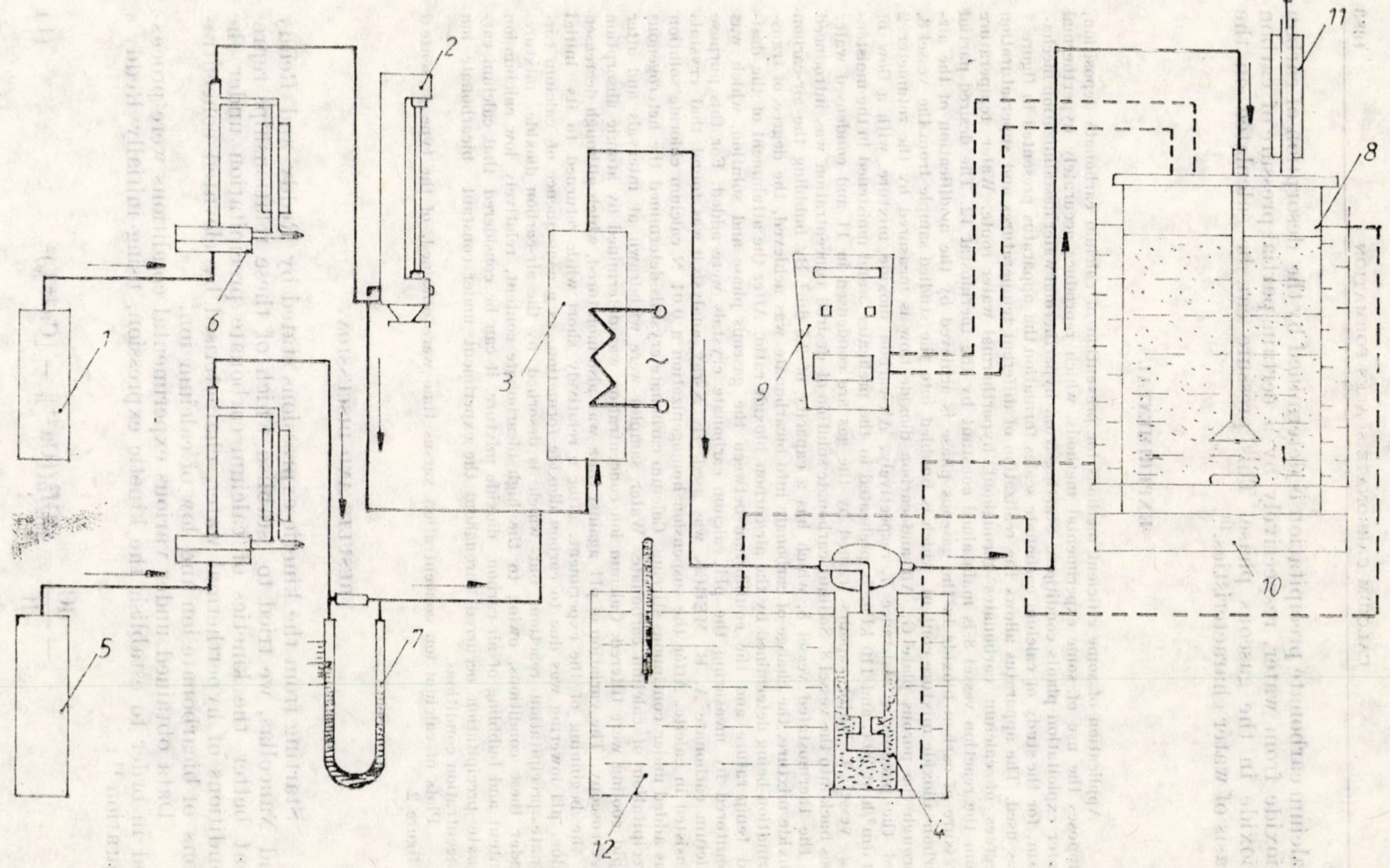

Fig. 1. — Apparatus for the study of the kinetics of calcium carbonate precipitation. 1 — Air supply; 2 — Rotameter; 3 — Electrical resistance for heating; 4 — Moistening vessel; 5 — Carbon dioxide supply; 6 — Pin valve; 7 — Differential manometer; 8 — Thermostated vessel with gas bubbler; 9 — pH-meter; 10 — Magnetic stirrer; 11 — Condenser; 12 — Thermostat.

where $[Ca^{2+}]_t$ and $[Ca^{2+}]_e$ represent calcium ion concentration at time t and at equilibrium, respectively (mole/dm^3); G — amount of seed crystals (g/dm^3); k — rate constant (dm^6/mole.s.g.); f_D — activity coefficient for divalent ion, calculated from the modified Debye-Hückel equation proposed by Davies [20]:

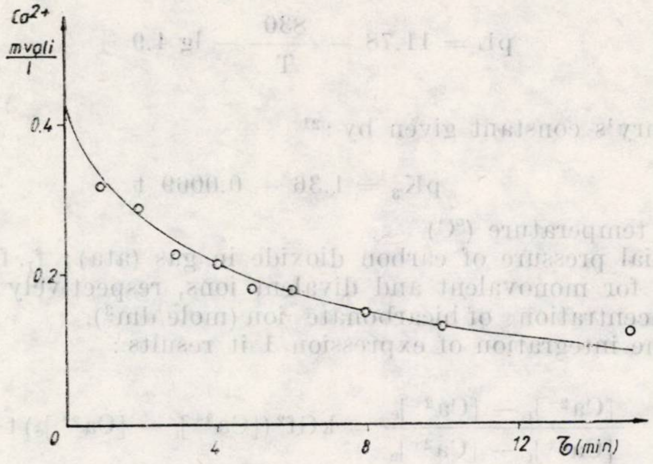

Fig. 2. — Calcium ion concentration variation versus time: Exp. 2

$$\lg f_D = -Az^2\left(\frac{\sqrt{\mu}}{1+\sqrt{\mu}} - 0.3\,\mu\right)$$

where μ is the ionic strength, z — ion valency and A — a constant.

The concentration of calcium ion at equilibrium was calculated on the basis of $CaO-CO_2-H_2O$ system equilibria, using the expression:

$$\lg [Ca^{2+}]_e = D_1 - 2\lg [HCO_3^-] + \lg p_{CO_2}$$

where:

$$D_1 = pK_2 - pL - pK_1 - 2\lg f_1 - \lg f_2 - \lg K_3 + \lg\frac{1000}{18} -$$

$$- 2\lg[HCO_3^-] + \lg p_{CO_2}$$

pK_1, pK_2, pL are carbonic acid dissociation constants and calcium carbonate solubility product, respectively, parameters determined by the expressions [12]:

$$pK_1 = \frac{17052}{T} + 215.21\lg T - 0.12675\,T - 545.56$$

$$pK_2 = \frac{2092 \cdot 39}{T} - 6.498 + 0.02379\ T$$

$$pL = 11.78 - \frac{830}{T} - \lg 4.9$$

pK_3 is Henry's constant given by :[21]

$$pK_3 = 1.36 + 0.0069\ t$$

where t is temperature (°C)
p_{CO_2} = partial pressure of carbon dioxide in gas (ata); f_1, f_2 = activity coefficients for monovalent and divalent ions, respectively; $[HCO_3^-]$ = molar concentration of bicarbonate ion (mole/dm³).

By the integration of expression 1 it results :

$$\frac{[Ca^{2+}]_i - [Ca^{2+}]_e}{[Ca^{2+}]_t - [Ca^{2+}]_e} = kGf^2([Ca^{2+}]_i - [Ca^{2+}]_e)\,t \qquad (2)$$

expression which allows the determination of the rate constant.

Table 1

Rate constants as a function of experimental conditions

Exp.	t °C	p_{CO_2} ata	C_{Ca_i} $\frac{meq}{dm^3}$	C_{Ca_e} $\frac{meq}{dm^3}$	$\frac{C_{Ca_i} - C_{Ca_e}}{C_{Ca_e}}$	G $\frac{g}{dm^3}$	$C_{HCO_3^-}$ $\frac{meq}{dm^3}$	Kk_2 $\frac{dm^6}{mole.\ s.g.}$	k_1 $\frac{dm^6}{mole.\ s.g.}$
1	80	0.0827	0.468	0.064	6.31	0.1	23	426.25	—
2	80	0.0827	0.468	0.064	6.31	0.4	23	320.4	—
3	80	0.0827	0.468	0.064	6.31	0.2	23	440	—
4	70	0.108	0.468	0.086	4.44	0.4	27.5	181.77	—
5	70	0.108	0.937	0.086	9.89	0.4	27.5	166.45	—
6	70	0.108	0.468	0.086	4.44	0.2	27.5	203.58	—
7	65	0.117	0.937	0.132	6.09	0.4	27.5	72.45	—
8	65	0.117	0.937	0.132	6.09	0.4	27.5	108.66	—
9	80	0.0827	1.875	0.064	28.29	0.4	23	—	305.51
10	80	0.0827	0.937	0.064	13.64	0.4	23	—	236
11	80	0.0827	0.937	0.032	28.28	0.4	34.5	—	188.8

The rate constants were determined under the conditions presented in table 1. A satisfactory linear correlation of data according to expression 2 was found only for experiments 1—8, as it results from figure 3. In case of experiments 9 — 11 the obtained results did not follow a second order kinetic equation with respect to calcium ion concentration, as it is seen from figure 4. Using halving times method it was found that in these cases the reaction is of first order with respect to calcium ion concentration; for this reason, an attempt was made to correlate the

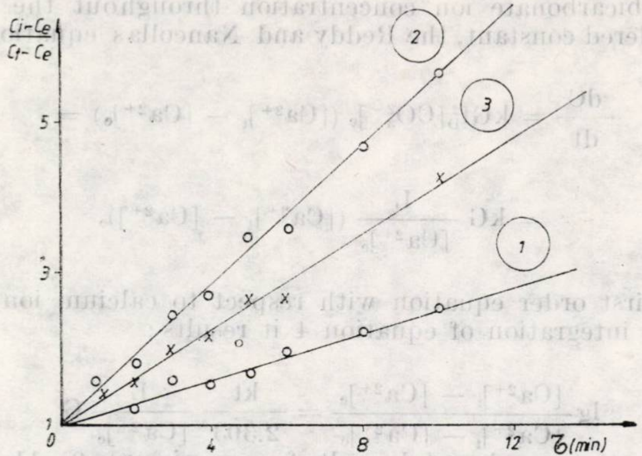

Fig. 3. — Dependence of parameter $\frac{[Ca^{2+}]_i - [Ca^{2+}]_e}{[Ca^{2+}]_t - [Ca^{2+}]_e}$ versus time : 1—Exp. 1, 2—Exp. 2, 3—Exp. 3

data in these cases, using the Reddy and Nancollas equation[9] :

$$-\frac{dC}{dt} = kGf_D^2([Ca^{2+}]_t\,[CO_3^{2-}]_t - [Ca^{2+}]_e\,[CO_3^{2-}]_e) \tag{3}$$

Under the experimental conditions, where owing to high concentration of bicarbonate ion and a good contact between the gaseous and liquid

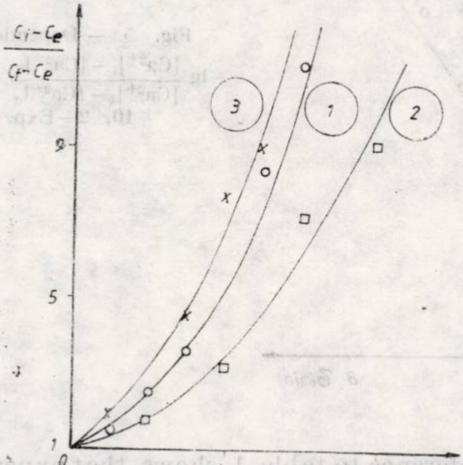

Fig. 4. — Dependence of parameter $\frac{[Ca^{2+}]_i - [Ca^{2+}]_e}{[Ca^{2+}]_t - [Ca^{2+}]_e}$ versus time : 1—Exp. 9, 2—Exp. 10, 3—Exp. 11

phases, the bicarbonate ion concentration throughout the experiment can be considered constant, the Reddy and Nancollas equation becomes :

$$\frac{dC}{dt} = kGf_D^2[CO_3^{2-}]_e\,([Ca^{2+}]_t - [Ca^{2+}]_e) =$$

$$= kG\,\frac{L}{[Ca^{2+}]_e}\,([Ca^{2+}]_t - [Ca^{2+}])_e \qquad (4)$$

resulting a first order equation with respect to calcium ion concentration. By the integration of equation 4 it results :

$$\lg\frac{[Ca^{2+}]_i - [Ca^{2+}]_e}{[Ca^{2+}]_t - [Ca^{2+}]_e} = \frac{kt}{2.303}\,\frac{L}{[Ca^{2+}]_e}\,G \qquad (5)$$

Plotting the experimental results for experiments 9–11, in figure 5 a good correlation of experimental data was obtained, according to expression 5. The experimental conditions and rate constant values are presented in table 1. Reference to table 1 shows that experimental data can be correlated with the Reddy equation only in case of supersaturation degrees of solutions with calcium carbonate lower than 10. At high degrees of supersaturation experimental data follow the Reddy and Nancollas equation.

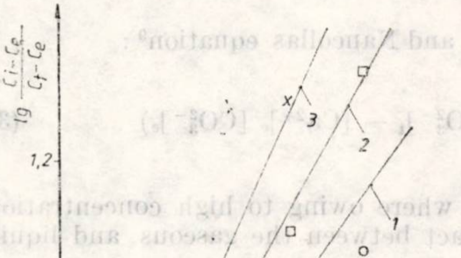

Fig. 5. — Dependence of parameter $\lg\frac{[Ca^{2+}]_i - [Ca^{2+}]_e}{[Ca^{2+}]_t - [Ca^{2+}]_e}$ versus time : 1—Exp. 10, 2—Exp. 9, 3—Exp. 11

CONCLUSIONS

The kinetics of calcium carbonate precipitation was studied under the conditions of hyperthermal water exploitation. For relative supersaturation degrees of calcium carbonate lower than 10, the kinetics is described by a second order expression with respect to calcium ion superconcentration. At higher supersaturation degrees than 10, the kinetics is described by a first order kinetic equation with respect to calcium ion superconcentration.

REFERENCES

[1] V. Cocheci and Gh. Petca, "Simpozion — Probleme actuale ale protecției, tratării și epurării apelor în Republica Socialistă România", vol. II, Timișoara, 1984, p. 233.

[2] V. Cocheci, Gh. Petca and V. Dalea, *Bul. St. și Teh. Inst. Pol. Traian Vuia, Timișoara, Seria Chimie*, **27**.

[3] V. Cocheci and Gh. Petca, "Simpozion — Utilizarea apelor geotermale", Timișoara, 1982, p. 22.

[4] L. Iosifescu, G. Chitanu and A. Carpov, *Hidrotehnica*, **93**, 143 (1984).

[5] R. Stumper and F. Classen, *Compt. rend.*, **228**, 83 (1949).

[6] J. L. Bischoff and W. S. Fyfe, *Am. J. Sci.*, **226**, 65 (1968).

[7] J. L. Bischoff, *Am. J. Sci.*, **226**, 80 (1968).

[8] H. Roques and A. Girou, *Wat. res.*, **8**, 907 (1974).

[9] G. H. Nancollas and M. M. Reddy, *J. Colloid Interface Sci*, **37**, 824 (1971).

[10] M. M. Reddy and G. H. Nancollas, *J. Colloid Interface Sci.*, **36**, 166 (1971).

[11] M. M. Reddy and G. H. Nancollas, *Desalination*, **12**, 61 (1973).

[12] H. N. S. Wiechers, P. Sturrock and G.v. R. Marais, *Wat. res.*, **9**, 835 (1975).

[13] T. F. Kazmierczak, M. B. Tomson and G. H. Nancollas, *J. Phys. Chem.*, **86**, 103 (1982).

[14] E. K. Giannimaras and P. G. Koutsoukos, *J. Colloid, Interface Sci.*, **116**, 423 (1987).

[15] W. A. House, *J. Chem. Soc., Faraday Trans. I.*, **77**, 341 (1981).

[16] G. E. Cassford, W. A. House and A. D. Pethybridge, *J. Chem. Soc., Faraday Trans I*, **79**, 1617 (1983).

[17] C. W. Davies and A. L. Jones, *Trans Faraday Soc.*, **51**, 812 (1955).

[18] V. Cocheci and Gh. Petca, "Simpozion — Probleme actuale ale protecției, tratării și epurării apelor în Republica Socialistă România", vol. II, Timișoara, 1984, p. 237.

[19] V. Cocheci and Gh. Petca, "Simpozion — Probleme actuale ale protecției, tratării și epurării apelor în Republica Socialistă România", vol. II, Timișoara, 1984, p. 241.

[20] C. W. Davies, "Ion Association", Butterworths, Washington, 1962, pp. 34—54.

[21] R. E. Loewenthal and G. v. R. Marais, "Carbonate Chemistry of Aquatic Systems : Theory and Application", vol. I. Ann Arbor Sci. Publ. Inc., 1982.

Revue Roumaine de Chimie, 34, 8, 1691–1698 (1989)

MICELLAR BEHAVIOUR OF CALCIUM AND MAGNESIUM SOAPS OF HIGHER FATTY ACIDS IN DILUTE AQUEOUS SOLUTIONS AT DIFFERENT TEMPERATURES

H. SINGH and S.P.S. TOMAR

Department of Chemistry, J. V. College, Baraut — 250611 (Meerut), India

Received April 6, 1987

The critical micelle concentration (CMC) of aqueous solutions of calcium and magnesium soaps of higher fatty acids has been determined at (35 – 50°C) by means of surface-tensiometric and viscosity measurements. The CMC are found to be independent of temperature but decrease with increasing chain length of fatty acids in calcium soaps. Experimental data have been discussed in the light of B. Szyszkowski's equation. The viscosity of soap solutions may be calculated using the Vand and Moulik equations in the concentration range in which these equations hold good. The Vand and Moulik equations are applicable above CMC of soaps. The effect of temperature on viscosity of soap solutions has been evaluated in terms of Arrhenius and Eyring's equations and the activation parameters for fluidity of aqueous soap solutions ΔH^*, ΔS^* and ΔG^* have been calculated.

INTRODUCTION

A number of studies have been made on viscosity of solutions of surfactants [1–7] to evaluate critical micelle concentration. Surface tension of manganese soap solutions of higher fatty acids was measured in organic solvents [8] and in multicomponent system[9] at 40°C. Critical micelle concentration of magnesium soaps of lower fatty acids in water and alcohols has been determined by Varma et al.[10] In the present investigation the physical properties i.e. surface tension and viscosity of magnesium and calcium soaps of higher fatty acids in water have been studied to determine whether or not the micelle aggregates are formed in these soap solutions. The work is initiated for these soaps in aqueous solutions to determine CMC and the nature of micelles formed under different conditions.

EXPERIMENTAL

Merck or B.D.H. reagent grade magnesium chloride, calcium hydroxide, capric and lauric acids were used. The purity of reagents was confirmed by their melting and boiling point measurements. Deionized distilled water was used for the preparation of all the solutions. The magnesium and calcium soaps were prepared by direct metathesis of sodium soaps with the required amount of magnesium chloride and calcium hydroxide respectively at 50 – 55°C. The precipitated soap was washed with distilled water and then with ethanol. The free precipitant and acid were removed. After initial drying in an air oven at 100 – 105°C, it was again dried under reduced pressure. The procedure for the measurement of surface tension was the same as reported earlier.[11] An Ostwald viscometer was used to determine the viscosity of soap solutions. The densities were measured with an accuracy of ± 0.0001 g with a dilatometer. The accuracy of the results was checked by measuring these physical properties of known solutions.

RESULTS AND DISCUSSION

The typical experimental results are best presented graphically. The plots (Fig. 1) of surface tension, ν versus concentration of soap solutions, *c*, show a sharp change in surface deficiency of the soap at definite concentration indicating the micelle formation. The CMC of these soaps is independent of temperature but decreases as chain length of fatty acids in calcium soaps increases. The plots (Fig. 2) of ν vs. log *c* are found to be linear at 35 – 50°C, showing that the results are in good agreement with Szyszkowski's empirical equation[12]

$$\frac{\nu}{\nu_0} = 1 - X \ln(c/Y)$$

where X and Y are constants. The surface area A (i.e. reciprocal of adsorption excess ν) covered by the soap micelles formed per 1 g mol of soap has been calculated from Gibbs' adsorption equation.

$$A = 1/\tau = RT/X\,\nu_0$$

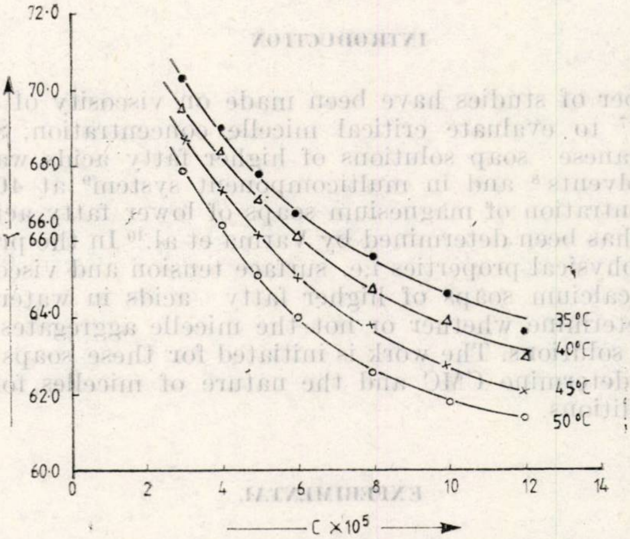

Fig. 1. — Plot of surface tension, γ (dynes cm^{-1}) vs concentration, c (g mole dm^{-3}) of magnesium caprate in water at 35 – 50°C.

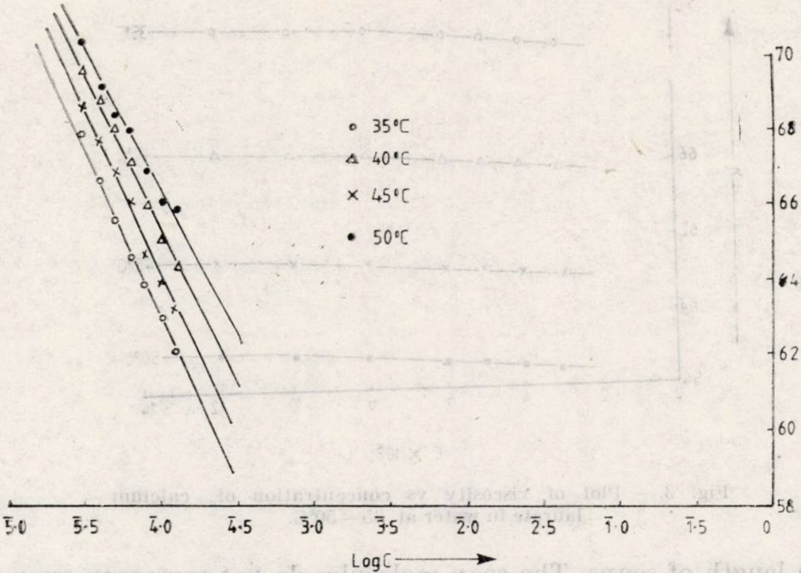

Fig. 2. — Plot of surface tension, γ (dynes cm^{-1}) vs log c of calcium caprate in water at 35—50°C.

The values of constants X and Y (Table 1) were calculated from the slopes $(-2.303X\,\nu_0)$ and intercepts $[=\nu_0[1+X\ln Y)]$ of linear plots of ν vs. log c. Constant X increases as temperature increases but is independent of soap chain. The values of constant X are fairly higher for magnesium caprate than for calcium caprate. The values of constant Y are found to decrease with increasing temperature and soap chain. These are lower for caprate of magnesium than calcium.

The surface area A (Table 1) decreases with increasing temperature and soap chain. The values of A are lower for magnesium caprate than that of calcium caprate.

VISCOSITY

The viscosity, η of soap solutions increases with increasing temperature and soap concentration. The plots (Fig. 3) of viscosity vs. soap concentration, c are characterised by an intersection of two straight lines at a definite concentration (CMC), at all temperatures (i.e. 8×10^{-5}, 9×10^{-5} and 8×10^{-5} for magnesium caprate calcium caprate and calcium laurate respectively). The CMC of calcium soaps decreases with increasing chain length of fatty acids in them but is independent of temperature. It appears that longer molecules impart greater viscosity at equal concentrations but the extrapolated values of viscosity for zero soap concentration are in good agreement with the corresponding experimental values (Table 4) at different temperatures and are independent

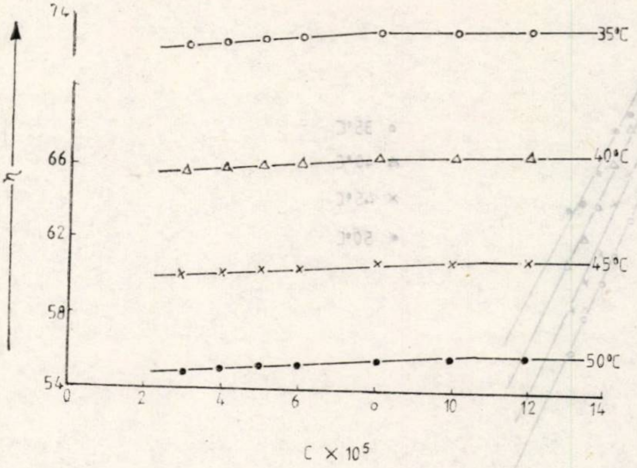

Fig. 3. — Plot of viscosity vs concentration of calcium laurate in water at 35—50°C.

of chain length of soaps. The soap molecules do not aggregate appreciably below critical micelle concentration.

The viscosity of soap solution has been satisfactorily represented by the Vand[13] and Moulik [14] equations. The Vand parameter Q i.e. inter-

Table 1

Surface tension parameters for aqueous calcium and magnesium soap solution at 35° — 50°C

Temperature in °C.	X	$Y \times 10^5$	$A \times 10^{-7}$
Magnesium caprate			
35	0.064	3.015	569.047
40	0.067	2.981	558.430
45	0.070	2.634	549.657
50	0.073	2.284	542.509
Calcium caprate			
35	0.047	3.077	774.143
40	0.050	3.020	748.212
45	0.053	2.656	725.695
50	0.056	2.312	706.151
Calcium laurate			
35	0.048	2.752	758.011
40	0.050	2.600	733.554
45	0.054	2.374	712.264
50	0.056	2.194	693.764

Table 2

Viscosity parameters for aqueous calcium and magnesium soap solutions at 35–50°C

Temperature in °C	Tested conc. limit (Moles/litre) $C \times 10^5$	Valid zones Moles/litre $C \times 10^5$	$\overline{V} \times 10^3$	$Q \times 10^{-2}$	M	$K' \times 10^{-4}$
Magnesium caprate						
35	3–12	8–12	13.262	11.461	1.0170	95
40	3–12	8–12	10.407	12.491	1.0225	130
45	3–12	8–12	9.947	13.069	1.0235	160
50	3–12	8–12	6.815	14.673	1.0410	165
Calcium caprate						
35	3–12	9–12	15.473	29.729	1.0135	75
40	3–12	9–12	13.262	31.668	1.0162	85
45	3–12	9–12	11.052	32.573	1.0200	95
50	3–12	9–12	9.947	36.192	1.0220	102
Calcium laurate						
35	3–12	8–12	9.210	76.003	1.0175	95
40	3–12	8–12	7.184	97.441	1.0210	100
45	3–12	8–12	6.079	115.158	1.0230	105
50	3–12	8–12	5.710	122.587	1.0250	110

action coefficient (Table 2) increases with increasing temperature and chain length of soap while the molar volume $\overline{V}$ (Table 2) decreases with increasing temperature and chain length of soap. However values of Q for magnesium caprate are exceptionally lower than caprate of calcium. The values of the Moulik constant M and K' (Table 2) increase with increasing temperature and chain length of the soap. However the values of K′ are exceptionally higher for caprate of magnesium than calcium. Table 2 reveals that the Vand and Moulik equations are valid in the concentration range above CMC. Further it may be mentioned that the Vand parameter $\overline{V}$ is well defined and Q is only approximately obtained.[15] Most probably Q is a specific property of a solute and not a general one.[16] The Moulik parameters M and K' are not yet defined. Several empirical and theoretically derived relationships connecting viscosity and temperature have been proposed from time to time. The equation of Arrhenius[17]

$$\frac{1}{\eta} = A \exp(- E_{\varphi}/RT)$$

Table 3

Activation parameters for fluidity of aqueous calcium and magnesium soap solutions

Conc. of soap in moles litre^{-1} $C \times 10^5$	ΔH^* Kcals · mole^{-1}	$-\Delta S^*$ cals. deg^{-1} mole^{-1}	ΔG^* at 35°C k cals. mole^{-1}
Magnesium caprate			
3	3.569	40.944	16.180
4	3.615	40.953	16.228
5	3.661	40.962	16.277
6	3.706	40.972	16.325
8	3.757	40.981	16.378
10	3.780	40.990	16.404
12	3.798	40.999	16.425
Calcium caprate			
3	3.478	40.908	16.077
4	3.533	40.917	16.135
5	3.565	40.926	16.169
6	3.569	40.940	16.179
8	3.606	40.953	16.219
10	3.670	40.962	16.286
12	3.716	40.972	16.335
Calcium laurate			
3	3.523	40.917	16.126
4	3.573	40.926	16.179
5	3.620	40.935	16.227
6	3.665	40.944	16.276
8	3.706	40.958	16.322
10	3.752	40.967	16.370
12	3.775	40.981	16.397

Table 4

Extrapolated and experimental values of viscosity in poise of magesium and calcium soap solutions for zero soap concentration at 35 – 50°C in water

Tempera ture in °C	Extrapolated values ($\eta \times 10^4$)			Experimental values ($\eta \times 10^4$)
	Magnesium caprate	Calcium caprate	Calcium laurate	
35	72.00	72.20	71.80	72·24
40	65.60	65.35	65.20	65.58
45	59.84	59.88	59.70	59.90
50	55.00	54.84	54.70	54.96

has been found to hold good for the soap solutions. The term E_φ, is defined as the activation energy of viscous flow, A is a constant. According to Ward, this energy is associated with the configurational changes produced by shearing and depends upon interatomic and intermolecular forces etc. This activation energy of viscous flow $E_\varphi = (= \Delta H^*)$ (Table 3) has been calculated from the slopes of the linear plots of log η vs. $1/T$ (Fig. 4). The interpretation of viscous flow according to the theory of absolute reaction rates has also been presented by Eyring and coworkers.[18] The variation of fluidity, $\frac{1}{\eta}$ with temperature has been evaluated in terms of Eyring's equation.

$$\frac{1}{\eta} = \left(\frac{V}{hN}\right) \exp.(-\Delta G^*/RT)$$

$$= \left(\frac{V}{hN}\right) \exp.\ (-\Delta H^*/RT)$$

$$\exp.\ (\Delta S^*/R)$$

The entropy of activation ΔS^* has been calculated by equating Arrhenius' coefficient, A with $\left(\frac{V}{hN}\right)$, exp. $(\Delta S^*/R)$. h and N are Planck's constant and Avogadro's number respectively, V is the molecular volume of the solvent. The free energy of activation, ΔG^* is then calculated at 35°C from Gibbs' equation.

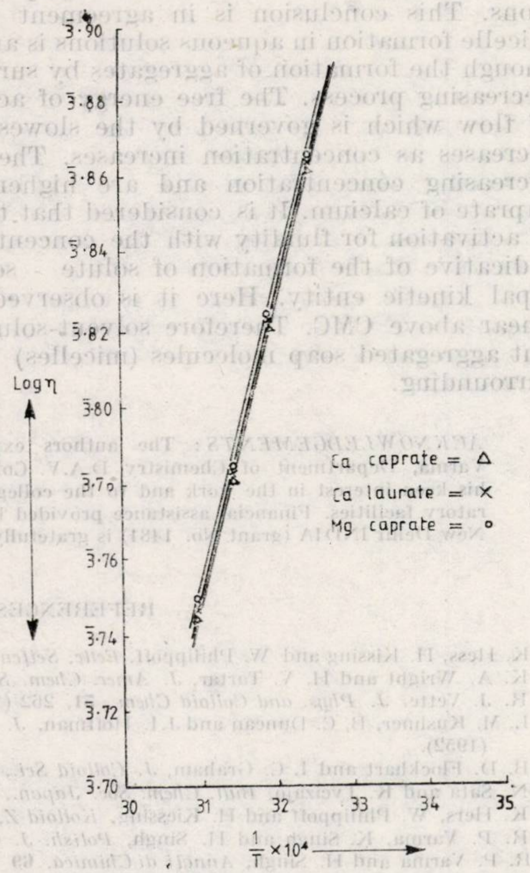

Fig. 4. — Plot of log η vs $\frac{1}{T}$ of magnesium and calcium soaps in water at concentration (8×10^{-5} g mole dm^{-3}).

The activation energy of viscous flow, ΔH^* increases as concentration increases. However values of ΔH^* for magnesium caprate are higher than calcium caprate. It measures the energy barrier to fluid motion and increases in ΔH^* with concentration, and the chain length of the soaps indicates less fluidity and thus confirms structured solvent and micellar aggregation. The entropy of activation ΔS^* also shows a little change with change in concentration and it decreases as concentration increases.

The values of ΔS^* for magnesium caprate are lower than calcium caprate. This implies that negative free energy of micellization is mainly the result of the entropy term in the water-soap system at very low concentrations. This conclusion is in agreement with the general concept that micelle formation in aqueous solutions is an entropy directed process even though the formation of aggregates by surfactant molecules is an entropy decreasing process. The free energy of activation ΔG^* controls the rate of flow which is governed by the slowest step in the fluid process. It increases as concentration increases. The values of ΔG^* increase with increasing concentration and are higher for magnesium caprate than caprate of calcium. It is considered that the non-linearity of free energy of activation for fluidity with the concentration of added solute becomes indicative of the formation of solute - solvent aggregate,[19] as the principal kinetic entity. Here it is observed that plots of $\Delta G^* - C$ are linear above CMC. Therefore solvent-solute aggregation does not occur but aggregated soap molecules (micelles) remain in an overall ordered surrounding.

ACKNOWLEDGEMENTS : The authors express their thanks to Dr. R. P. Varma, Department of Chemistry D.A.V. College, Muzaffarnagar INDIA for his keen interest in the work and to the college authorities for providing laboratory facilities. Financial assistance provided by University grants Commission New Delhi INDIA (grant No. 1481) is gratefully acknowledged.

REFERENCES

[1] K. Hess, H. Kissing and W. Philippoff, *Felle, Seifen*, **48**, 377 (1941).
[2] K. A. Wright and H. V. Tartar, *J. Amer. Chem. Soc.*, **61**, 544, (1936).
[3] R. J. Vetter *J. Phys. and Colloid Chem.*, **51**, 262 (1947).
[4] L. M. Kushner, B. C. Duncan and J.I. Hoffman, *J. Research Mall. Bur. Standards*, **49**, 85 (1952).
[5] B. D. Flockhart and I. C. Graham, *J. Colloid Sci.*, **8**, 105, (1953).
[6] N. Sata and K. Tycizajo, *Bull. Chem. Soc. Japan.*, **26**, 177 (1953).
[7] K. Hers, W. Philippoff and H. Kiessing, *Kolloid Z*, **88**, 40 (1939).
[8] R. P. Varma, K. Singh and H. Singh, *Polish. J. Chem.*, **55**, 1115 (1981).
[9] R. P. Varma and H. Singh, *Annali di Chimica*, **69** 1 (1979).
[10] R. P. Varma and K. Kumar, **Rev. Roumaine Chim**, **24**, 757 (1979).
[11] K. N. Mehrotra and S. C. Bhargava, *Bull. Chem. Soc. Japan*, **40**, 1255 (1967).
[12] B. Szyszkowski, *Z. Phys. Chem*, **64**, 385 (1908).
[13] V. Vand *J. Phys. Colloid Chem.*, **52**, 277 (1948).
[14] S. P. Moulik, *J. Phys. Chem.*, **72**, 4682 (1968).
[15] Intl, Encylo, *Phys. Chem and Chem. Phys.*, Pergamon Press, 1965, Topic 16, Vol. 3 P_4 f.
[16] S. P. Moulik, *J. Indian Chem. Soc.*, **49**, 483 (1972).
[17] S. Arrhnius, Meddel Nobeliest, Vetenskapsakad, **3**, 20 (1916).
[18] S. Glasstone, K. J. Laidler and H. Eyring, "Theory of Rate Process" Mcgraw Hill, New York, N. Y., 19 1941 Chapter 9, pp. 477—516.
[19] J. C. Mac Donald, J. Ser Phillips and J. C. Guerera, *J. Phys. Chem.*, **77**, 370 (1973)

Revue Roumaine de Chimie, **34**, *8*, 1699–1704 (1989)

ION-EXCHANGE WITH TRANSITION METALS ON HIGHLY SILICIOUS ZEOLITES OF ZSM-5 TYPE. I

BEHAVIOUR OF Ag(I) and Cu(II)

ANIŞOARA BOLD, AURELIA VASILE, ANGELICA POPA, M. CRUCEANU,
EVELINE POPOVICI and MARIA ALEXANDROAEI

Department of Chemical Technology, Polytechnic Institute, Splai Bahlui 71, Iaşi, Romania

Received April 30, 1988

The present paper reports the results obtained in studying the kinetics and thermodynamics of the ion-exchange $Ag^+ \rightleftharpoons Na^+$ and $Cu^{2+} \rightleftharpoons 2Na^+$ on ZSM-5 zeolites crystallized in similar conditions but in the presence of various organic compounds. It was shown that though both organic templates used in the synthesis favour the formation of the same ZSM-5 zeolite structure they distinguish themselves by the different peculiarities in the ion-exchange imparted to the zeolite product.

INTRODUCTION

The highly silicious ZSM-5 zeolite reported by Argauer and Landolt [1] in 1972 can be considered as a catalyst useful in a wide range of catalytic reactions in petrochemistry.

After its discovery the researches have been directed towards the obtaining of various morphological and compositional forms, with catalytic properties of immediate use in the industry. Later on, the studies have been directed towards elucidating some theoretical features of the synthesis and properties of this zeolite type.

Though the study on the ion-exchange leads to the obtaining of significant information on the structure of ZSM-5 zeolite network and represents at the same time the theoretical basis for obtaining some stable and selective catalysts, it was rather scarcely approached and only partially.[2–4] Thus the exchange kinetics and equilibrium have been investigated for a small number of cations,[4,5] the relationship between the kinetical and thermodynamical amounts and the conditions of ZSM-5 zeolite synthesis being unknown.

In the present paper are reported the results obtained in studying the kinetics and thermodynamics of the ion-exchange $Ag^+ \rightleftharpoons Na^+$ and $Cu^{2+} \rightleftharpoons 2\,Na^+$ on ZSM-5 zeolites crystallized in similar conditions but in the presence of various organic compounds. The influence exerted by the organic template on the behaviour during the ion-exchange of the obtained ZSM-5 structure has been followed.

EXPERIMENTAL

The silicious zeolite products of ZSM-5 type were obtained according to an original procedure,[6] N-methylpyrrolidone and ethylic alcohol being used as templates.

Since during the synthesis the organic template remained ocluded in the zeolite network pores the access of ions into and out of the structure was not allowed. The ion-exchange was facilitated by the removal of the organic compound by thermal or chemical treatment.[7]

Consequently, the Na–ZSM-5 form used in studying the ion-exchange was obtained by calcinating in air, at 550°C, for 4 hours, the products resulted from the synthesis, followed by an exchange step with 0.1 n NaCl solution.

The occurrence of additional influences, caused by the significant differences in grain size, was avoided by choosing fractions of the same size. The size of zeolite particles was determined by means of a microscope provided with reticle and represented the mean value of 3–4 series of about 150–200 measurements each.

The activation of Na-ZSM-5 samples for the ion-exchange was accomplished at 450°C for 4 hours.

The ion-exchange was carried out under static conditions at 15, 25 and 50°C and the exchange kinetics and equilibrium for the Ag^+ and Cu^{2+} ions was studied on two Na–ZSM-5 zeolite products whose main characteristics are given in Table 1. For the exchange $4 \cdot 10^{-3}$ n $AgNO_3$ and $4 \cdot 10^{-3}$ n $Cu(NO_3)_2$ solutions were used.

Table 1

Characteristics of the Na-ZSM-5 zeolite products

Zeolite product	Organic template	Composition, mole ratio		Crystallinity %	Mean radius μ	Maxium exchange capacity, m equiv./g anhydrous zeolite
		$\frac{SiO_2}{Al_2O_3}$	$\frac{Na_2O}{Al_2O_3}$			
Z–1	Ethanol	48.70	0.990	97	2.65	0.8
Z–2	N M P*	54.40	0.901	97	1.81	0.6

* – N-methylpyrrolidone

The maximum ion-exchange capacity determined for the Na-ZSM-5 products, expressed as m equiv./g anhydrous zeolite exhibits the highest values in agreement with literature data.[2]

RESULTS AND DISCUSSION

Kinetics of the ion-exchange

The kinetics curves obtained for the investigated ions at 15, 25 and 50°C are depicted in Figs 1 and 2. As can be seen, unlike the exchange $NH_4^+ \rightleftharpoons Na^+$,[5] the temperature increase favours the process with both types of the investigated cations.

Assuming that the diffusion of interchangeable ions in the chanel system characteristic of the ZSM-5 structure will evidence the peculiarities of the investigated zeolite products, the apparent diffusion coefficients have been calculated for both cations.

The Boyd-Adamson equation has been used :

$$U(t) = 1 - \frac{6}{\pi^2} \sum_{n=1}^{\infty} \frac{1}{n^2} \exp\,(-\,nBt) \qquad (1)$$

where $U(t)$ is the degree of equilibrium attainment;

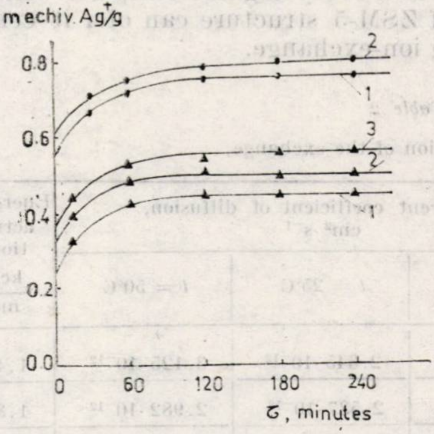

Fig. 1. — Kinetics of the $Ag^+ \rightleftharpoons Na^+$ exchange on Na−ZSM-5 silicious zeolites.
1. ● — product Z−1 ; $t = 25°C$;
2. ● — ,, Z−1 ; $t = 50°C$;
1. ▲ — ,, Z−2 ; $t = 15°C$;
2. ▲ — ,, Z−2 ; $t = 25°C$;
3. ▲ — ,, Z−2 ; $t = 50°C$;

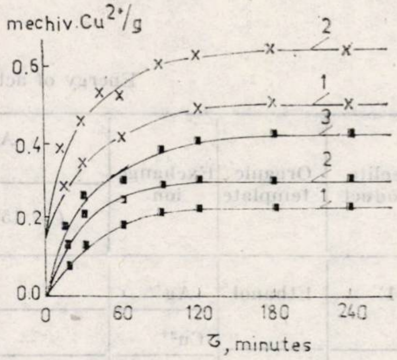

Fig. 2. — Kinetics of the $Cu^{2+} \rightleftharpoons 2Na^+$ exchange on Na−ZSM-5 silicious zeolites.
1. × — product Z−1 ; $t = 25°C$;
2. × — ,, Z−1 ; $t = 50°C$;
1. ■ — ,, Z−2 ; $t = 15°C$;
2. ■ — ,, Z−2 ; $t = 25°C$;
3. ■ — ,, Z−2 ; $t = 50°C$.

t — time of exchange ;
n — whole number (particle number) ;
$B = \frac{\pi^2 \cdot D_1}{r^2}$ — coefficient (the characteristic frequency) ;
D_1 — apparent coefficient of diffusion, $cm^2 \cdot s^{-1}$
r — radius of zeolite particle, cm.

From the experimental data the values $U(t)$ have been calculated and by means of Reichenberg tables[8] the values of the function Bt have been found. The B coefficient has been evaluated by plotting Bt versus t and on this basis the apparent coefficients of diffusion have been calculated.

The energy of activation of the exchange, E_a, has been calculated by plotting the Arrhenius equation in $\log D_1$ versus $10^3 \cdot \frac{1}{T}$ coordinates.

$$D_1 = D_0 \exp(-E_a/RT) \tag{2}$$

The values obtained for the apparent coefficients of diffusion and the energy of activation of the exchange are given in Table 2.

The differences which occur in both ion diffusivity and in the activation energy of the exchange on the two zeolite products are due to the different nature of the organic template found in the medium the investigated zeolite products have been recrystallyzed from. The ethanol favours the formation of some ZSM-5 zeolite networks more suitable for the ion-exchange than those obtained with N-methylpyrrolidone. This fact leads to the conclusion that the role and the action mode of the two organic templates are different and every organic template which is able to favour the crystallization of ZSM-5 structure can ofer it certain peculiarities of the behaviour during ion-exchange.

Table 2

Energy of activation of the exchange

Zeolite product	Organic template	Exchange ion	Apparent coefficient of diffusion, $cm^2 \cdot s^{-1}$			Energy of activation, $\frac{kcal}{mol}$
			$t = 15°C$	$t = 25°C$	$t = 50°C$	
Z—1	Ethanol	Ag^+	—	$2.645 \cdot 10^{-12}$	$3.125 \cdot 10^{-12}$	1.487
		Cu^{2+}	—	$2.537 \cdot 10^{-12}$	$2.982 \cdot 10^{-12}$	1.353
Z—2	NMP*	Ag^+	$1.347 \cdot 10^{-12}$	$1.617 \cdot 10^{-12}$	$2.259 \cdot 10^{-12}$	2.426
		Cu^{2+}	$0.752 \cdot 10^{-12}$	$0.887 \cdot 10^{-12}$	$1.234 \cdot 10^{-12}$	2.166

* — N-methylpyrrolidone

Both investigated samples of ZSM-5 zeolite distinguish themselves by small values of the energy of activation of the exchange with the investigated cations which indicates the process improvement on this zeolite type. The small differences found between the energies of activation characteristic to mono- and divalent cations lead to the conclusion that in case of ZSM-5 silicious zeolites the exchange does not mainly depend on the cation charge.

Exchange equilibrium

The results obtained in studying the exchange equilibrium are given in Figs. 3 and 4.

The affinity of ZSM-5 zeolite structure for the studied ions has been evidenced by calculating the separation factor α_B^A by means of the relationship (3):

$$\alpha_{\mathrm{B}}^{\mathrm{A}} = \frac{\mathrm{A_z}/\mathrm{A_s}}{\mathrm{B_z}/\mathrm{B_s}} = \frac{\mathrm{A_z} \cdot \mathrm{B_s}}{\mathrm{A_s} \cdot \mathrm{B_z}} \tag{3}$$

where A — denotes the Ag^+ or Cu^{2+} ions;

B — Na^+ ion;

z,s — are indices referring to the zeolite and exchange solution, respectively.

The free enthalpy of exchange (Gibbs energy) $\Delta G°$ has been calculated by means of equation (4):

$$\Delta G° = -\frac{\mathrm{RT}}{\mathrm{Z_A Z_B}} \ln K_a \tag{4}$$

where K_a is the thermodynamic equilibrium constant;

Z_A, Z_B are the charges of interchangeable cations.

The thermodynamic equilibrium constant K_a has been calculated by means of the equation :

$$\ln K_a = (Z_B - Z_A) + \int_0^1 \ln K_c \, d A_z \tag{5}$$

where K_c is the corrected coefficient of selectivity.

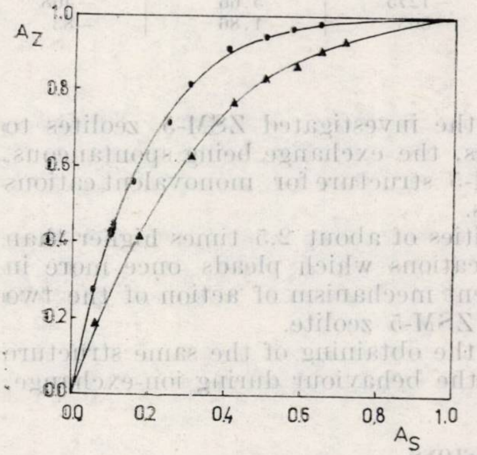

Fig. 3. — Exchange isotherm on the Z—1 zeolite.
● — exchange isotherm for Ag^+ ;
▲ — exchange isotherm for Cu^{2+}.

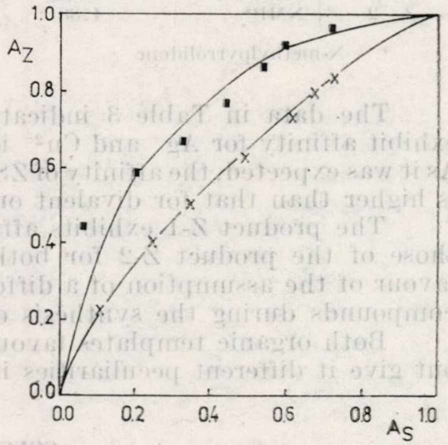

Fig. 4. — Exchange isotherm on the Z—2 zeolite.
■ — exchange isotherm for Ag^+ ;
× — exchange isotherm for Cu^{2+}.

The value of the integral in equation (5) has been determined graphically by plotting in $\log K_c - A_z$ coordinates.

In case of $Ag^+ \rightleftharpoons Na^+$ exchange since the ratio of the activity coefficients $AgNO_3$ and $NaNO_3$ is about 1 for diluted solutions, it was assumed that $\alpha_B^A = K_c$.

For the $Cu^{2+} \rightleftharpoons 2Na^+$ exchange the coefficients of activity of the salts in the solution at equilibrium have been calculated by means of relationship (6) where μ is the ionic strength of the corresponding salt, z_+, z_- the charges of the ions formed by the respective salt :

$$\log \gamma_\pm = -0.505 \cdot z_+ \cdot z_- \cdot \sqrt{\mu} \tag{6}$$

The corrected coefficient of selectivity has been calculated by means of the relationship :

$$K_c = \frac{A_z \cdot B_s^2}{B_z^2 \cdot A_s} \cdot \frac{\gamma^4_{\pm BY}}{\gamma^3_{\pm AY_2}} \tag{7}$$

where AY_2 and BY are $Cu(NO_3)_2$ and $NaNO_3$ respectively. The obtained results are listed in Table 3.

Table 3

Separation factors and calculated free enthalpy

Zeolite product	Organic template	Ag^+		Cu^{2+}	
		Separation factor $Ag_s^+ = Na_s^+ = 0.5$	$\Delta G°$, $\frac{cal}{mol \cdot grad}$	Separation factor $Cu_s^{2+} = Na_s^+ = 0.5$	$\Delta G°$, $\frac{cal}{mol \cdot grd}$
Z–1	Ethanol	15.66	–1275	5.66	–468
Z–2	NMP*	4.88	–803	1.86	–83

* – N-methylpyrrolidene

The data in Table 3 indicate the investigated ZSM-5 zeolites to exhibit affinity for Ag^+ and Cu^{2+} ions, the exchange being spontaneous. As it was expected, the affinity of ZSM-5 structure for monovalent cations is higher than that for divalent ones.

The product Z-1 exhibits affinities of about 2.5 times higher than those of the product Z-2 for both cations which pleads once more in favour of the assumption of a different mechanism of action of the two compounds during the synthesis of ZSM-5 zeolite.

Both organic templates favour the obtaining of the same structure but give it different peculiarities in the behaviour during ion-exchange.

CONCLUSIONS

The study on the kinetics and thermodynamics of the ion-exchange on ZSM-5 silicious zeolites reported in the present paper brings additional information concerning both the values of the amounts characteristic to the ion-exchange process and the relationship between the nature of organic template and the behaviour during ion-exchange of the obtained zeolite products.

It was shown that though both organic templates used in the syntheses favour the formation of the same ZSM-5 zeolite structure they distinguish themselves by the different peculiarities in the ion-exchange imparted to the zeolite product.

REFERENCES

[1] R. J. Argauer and G. R. Landolt, U. S. Patent 3.702.886 (1972).

[2] P. Chu and F. G. Dwyer, ACS Symposium Series 218, Intrazeolite Chemistry, p. 59, Copyright 1983 by the American Chemical Society.

[3] E. F. Vansant, Uytterhoeven, *Adv. Chemistry Series*, **101**, p. 426.

[4] D. P. Matthews and L. C. V. Rees, *Adv. Catal.*, **1985**, 495.

[5] Aurelia Vasile, Doctoral Thesis Iași, (1987).

[6] Aurelia Vasile, M. Cruceanu and V. Ababi, RSR Patent, 86.668 (1984).

[7] P. Chu and N. J. Woodbury, U. S. Patent 3.766.093, (1973).

[8] D. Reichenberg, *J. Am. Chem. Soc.*, **75**, p. 589, (1953).

Revue Roumaine de Chimie, **34**, *8*, 1705–1710 (1989)

STABILITIES OF BIVALENT METAL COMPLEXES WITH ω-BENZOYL-2-HYDROXY-4-METHOXY-3-METHYL ACETOPHENONE (BHMMA)

RANJANA DIXIT and BHAGWAN S. GARG*

Department of Chemistry, University of Delhi, Delhi — 110007, India

Received May 23, 1987

The stability constants of chelate species formed by the interaction of ω-benzoyl-2-hydroxy-4-methoxy-3-methyl acetophenone (BHMMA) with transition metal ions were determined potentiometrically at different ionic strengths (0.02, 0.05, 0.1 and 0.15 M $NaClO_4$) and at different temperatures (20, 30, 40 and 50°C) in 75% (v/v) ethanol $-H_2O$. The parameters $\bar{n}$, the average number of ligand molecule bound per metal ion and pL, the free ligand exponent, were determined by the expressions described by Irving and Rossotti[1] in order to evaluate pKa of the ligand and the stability constants of complexes. The stability constants were computed on an IBM 360 FORTRAN IV computer using a weighted least squares method patterned after that of Sullivan et al.[2] to give β_n values. The S_{min} values were also calculated. The thermodynamic stability constants have been obtained by extrapolating the log K_1 vs $\sqrt{\mu}$ plot to zero ionic strength. Other thermodynamic functions have also been calculated from the stability constants obtained at different temperatures and at constant ionic strength.

INTRODUCTION

2-Hydroxyacetophenone and its derivatives are the most important precursors for the laboratory and biogentic synthesis of naturally occurring polyphenols. Metal chelates of substituted hydroxyacetophenone find wide applications and are important analytical reagents. These ketones have great affinity for various biologically active metal ions. ω-Benzoyl-2-hydroxy-4-methoxy-3-methyl acetophenone is well known for its antifungal and antibacterial properties. Literature survey reveals that no work has been done on the bivalent complexes of ω-benzoyl-2-hydroxy-4-methoxy-3-methyl acetophenone. So the present study was undertaken to determine the stability constants of transition metal complexes with BHMMA.

EXPERIMENTAL

A digital pH meter (ECIL model) pH-5652 in conjuction with a glass electrode was used for pH measurements. The pH meter was standardised with potassium hydrogen phthalate and phosphate buffers before performing the titration.

---

* Author to whom all correspondence should be directed.

A solution of the 2-benzoyloxy-4-methoxy-3-methyl acetophenone (2 g) in dry pyridine (15 mL) was treated with powdered potassium hydroxide (1 g) and the resulting mixture was throughly stirred at 45°C. In about 45 minutes the solution became semi-solid due to the formation of potassium salt of β-diketone. The mixture was cooled and then treated with ice and dilute HCl which gave the final product ω-benzoyl-2-hydroxy-4-methoxy-3-methyl acetophenone, which was recrystallised from ethanol and its purity was checked by IR., elemental analysis and T.L.C. The ligand solution was prepared in 75% ethanol $-H_2O$ media. To ensure constant ionic strength during titration an inert electrolyte, $NaClO_4$ (Riedel) was added in a concentration greater than that of the complexing constituents. $HClO_4$ was standardised with sodium carbonate. Me_4NOH(TMAH) (0.04M) was used as titrant. Its solution was standardised with oxalic acid. All metal ions were prepared from A. R. (B DH) samples of the corresponding nitrates or sulphates and were standardised by conventional methods. Ethanol was purified by the method given by Vogel.[3]

Experimental procedure involved the potentiometric titration of the following solutions against 0.04 M TMAH in 75% ethanol-water medium: (i) 3 mL $HClO_4$ (0.02M) + 1 mL $NaClO_4$ (2M) + 0.5 mL K_2SO_4 (0.02M) + 0.5 mL H_2O + 10 mL ligand (0.01M) + 5 mL ethanol, (ii) 3 mL $HClO_4$ (0.02M) + 1 mL $NaClO_4$ (2M) + 0.5 mL K_2SO_4 (0.02M) + 0.5 mL H_2O + 10 mL $NaClO_4$ (2M) + 0.5 mL metal solution (0.02M) + 0.5 mL H_2O + 10 mL ligand solution (0.02M) + 5mL ethanol.

These titrations were repeated for ionic strengths ($\mu = 0.02$, 0.05 and 0.15 M $NaClO_4$) and for various temperatures (20, 30, 40 and 50°C). The titrations were carried out under a continuous stream of nitrogen with stirring, the titrant being added in small portions. The volume corection[4] factor was applied for ethanol$-H_2O$ mixture and the pH values in aquo-organic mixtures were corrected using the method of Van Uitert and Haas[5].

Table 1

Stability constants of bivalent metal complexes with BHMMA at 30 ± 0.1°C at different ionic strengths

System	Stability constants	Ionic strength (M $NaClO_4$)			
		0.15	0.1	0.05	0.02
BHMMA	log K_1^H	9.14	9.38	9.54	9.84
Mg^{II} – BHMMA	log K_1	3.97	4.66	4.74	5.45
	log K_2	3.28	3.89	4.39	4.33
	S_{min}	0.0012	0.0152	0.0268	0.0045
Mn^{II} – BHMMA	log K_1	4.29	4.98	5.19	5.99
	log K_2	3.60	4.03	4.52	4.64
	S_{min}	0.0010	0.0022	0.0108	0.0278
Cd^{II}-BHMMA	log K_1	4.71	5.06	5.64	6.18
	log K_2	3.75	4.32	4.94	4.90
	S_{min}	0.0024	0.0024	0.0278	0.0032
Pb^{II}-BHMMA	log K_1	5.34	5.50	5.85	6.39
	log K_2	4.60	4.47	5.42	5.16
	S_{min}	0.0084	0.0062	0.0148	0.0153
Zn^{II}-BHMMA	log K_1	5.75	5.92	6.11	6.42
	log K_2	5.07	4.96	5.76	5.45
	S_{min}	0.0124	0.2493	0.0106	0.0007
Co^{II}-BHMMA	log K_1	5.89	6.30	6.42	6.62
	log K_2	5.16	5.08	6.12	5.75
	S_{min}	0.0226	0.0299	0.1228	0.0042
Ni^{II}-BHMMA	log K_1	5.91	6.49	6.63	7.03
	log K_2	5.37	5.44	6.33	6.01
	S_{min}	0.0858	0.0030	0.0433	0.0729

Table 2

Stability constants of bivalent metal complexes with BHMMA at $M = 0.1$ MNaClO$_4$ at different temperatures and their thermodynamic parameters at $M = 0.1$ M NaClO$_4$ at 30 ± 0.1°C.

System	Stability constants	Temperature (°C)			$-\Delta G$ KJ mol^{-1}	$-\Delta H$ KJ mol^{-1}	ΔS KJ mol^{-1} deg^{-1}
		20	40	50			
BHMMA	$\log K_1^H$	9.53	9.26	9.10	—	—	—
Mg^{II}-BHMMA	$\log K_1$	4.69	4.53	3.98	36.98	1.14	0.0514
	$\log K_2$	3.38	3.37	3.41	—	—	—
	S_{min}	0.0025	0.0054	0.0035	—	—	—
Mn^{II}-NHMMA	$\log K_1$	4.99	4.72	4.20	38.87	1.91	0.0322
	$\log K_2$	3.57	3.65	3.66	—	—	—
	S_{min}	0.0013	0.0070	0.0013	—	—	—
Cd^{II}-BHMMA	$\log K_1$	5.08	5.02	4.70	29.33	3.82	0.0840
	$\log K_2$	4.01	3.89	3.78	—	—	—
	S_{min}	0.0154	0.0063	0.0023	—	—	—
Pb^{II}-BHMMA	$\log K_1$	5.55	5.44	5.33	31.88	7.61	0.0803
	$\log K_2$	4.19	4.01	3.98	—	—	—
	S_{min}	0.0018	0.0354	0.083	—	—	—
Zn^{II}-BHMMA	$\log K_1$	6.12	5.87	5.78	34.30	8.57	0.0849
	$\log K_2$	5.40	4.43	4.72	—	—	—
	S_{min}	0.0601	0.0127	0.0088	—	—	—
Co^{II}-BHMMA	$\log K_1$	6.33	6.10	5.90	36.52	19.12	0.0573
	$\log K_2$	5.16	4.90	4.82	—	—	—
	S_{min}	0.0086	0.0008	0.0025	—	—	—
Ni^{II}-BHMMA	$\log K_1$	6.52	6.43	5.97	37.61	7.61	0.0991
	$\log K_2$	5.42	5.16	5.40	—	—	—
	S_{min}	0.0078	0.0054	0.0159	—	—	—

The log β_n values were calculated by weighted least squares method. This treatment determines that set of β_n values which make the function (1) nearest to zero, by minimizing the function (2) as β_n varies.

$$\sum_{n=0}^{N} (y - x - nz)\, \beta_n x^n \tag{1}$$

$$\sum_{i=1}^{I} U^2 (x_i y_i z_i) \tag{2}$$

The function (2) minimized, designated S_{min}, has the same statistical distribution as χ^2 with K degrees of freedom and with weight defined in accordance with Rydberg and Sullivan[6]. It can be equated to χ^2.

RESULTS AND DISCUSSION

The protonation constant and stability constants were calculated at four different ionic strengths and temperatures. The values are recorded in Tables 1 and 2.

Effect of ionic strength

In the present study, the value of dissociation constant of ligand (pKa) (Fig. 1) and stability constants of complexes were found to decrease with increasing ionic strength of the medium, in agreement with the Debye-Hückel equation.[7] The thermodynamic stability constants are obtained by extrapolating the straight line plot of log K_1 vs $\sqrt{\mu}$ to zero ionic strength.

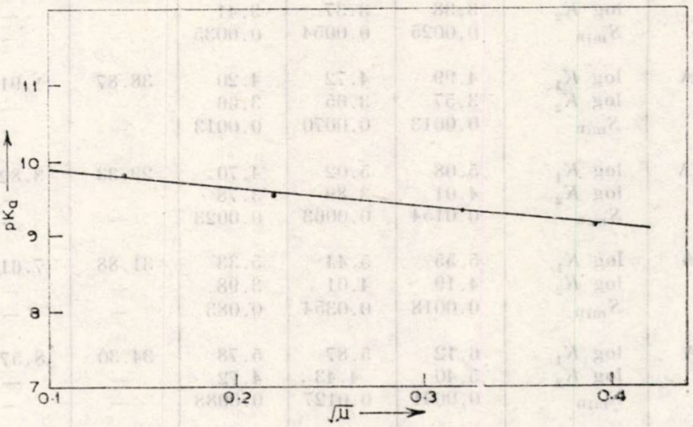

Fig. 1. — Plot of pK_a of BHMMA vs $\sqrt{\mu}$ (ionic strength).

Table 3

Er(Mn—Zn) and δH value for chelation of BHMMA

Parameters	Metal ions			
	Mn^{2+}	Co^{2+}	Ni^{2+}	Zn^{2+}
log K_1^0	6.24	6.76	7.20	6.42
ΔF^a (kcal/mol)	8.65	9.37	9.98	8.90
ΔF_R^b (relative to value for Mn^{2+})	—	0.72	1.33	0.25
ΔH_H^c (relative to value for Mn^{+})	—	43.00	62.00	49.60
ΔH_L^d (relative to value for Mn^{2+})	—	43.72	63.33	49.85
$[(n-5)/5]Er^e$	—	19.94	29.91	—
δH	—	23.78	33.42	—

a) ΔF = Free energy change = 2.303 RT log K_1^0; where R, T and K_1^0 have the usual significance and temp. = 303°K; b) ΔF_R = = Change in heat content for the formation of the complex in solution; c) ΔH_H = Heat of hydration of metal ion; d) ΔH_H = Heat of complexation referred to the metal ion in gaseous state and the ligand in solution; n = number of electrons in the 3d orbital; e) $[(n-5)/5]Er$ = Lattice energy difference for Mn^{2+} to Zn^{2+} complexes; f) δH = Thermodynamic stabilization energy; log K_1 = Values employed for the above calculations, have been obtained by extrapolating log K_1 vs μ (straight line) to zero ionic strength.

Effect of temperature

The overall free energy, enthalpy and entropy changes were calculated by standard method[8]. The results indicate that ΔH and ΔG are negative, which show that complex formation reactions take place spontaneously with the liberation of energy. The positive ΔS shows that the system is entropy stabilized. The ligand field stabilization energy, 'δH' and Er(Mn—Zn) values have been calculated according to the method of George and McClure[9] and are listed in Table 3. The order of ligand field stabilization energy, 'δH' is Co $<$ Ni and the order of enthalpies (ΔH_L) and free energies (ΔF) for chelate formation for BHMMA is : Mn^{2+} $<$ $<$ Co^{2+} $<$ Ni^{2+} $<$ Zn^{2+}. The plots of ΔH_L and ΔH_H of BHMMA complexes as a function of the number of d-electrons in the metal ion are shown in Fig. 2.

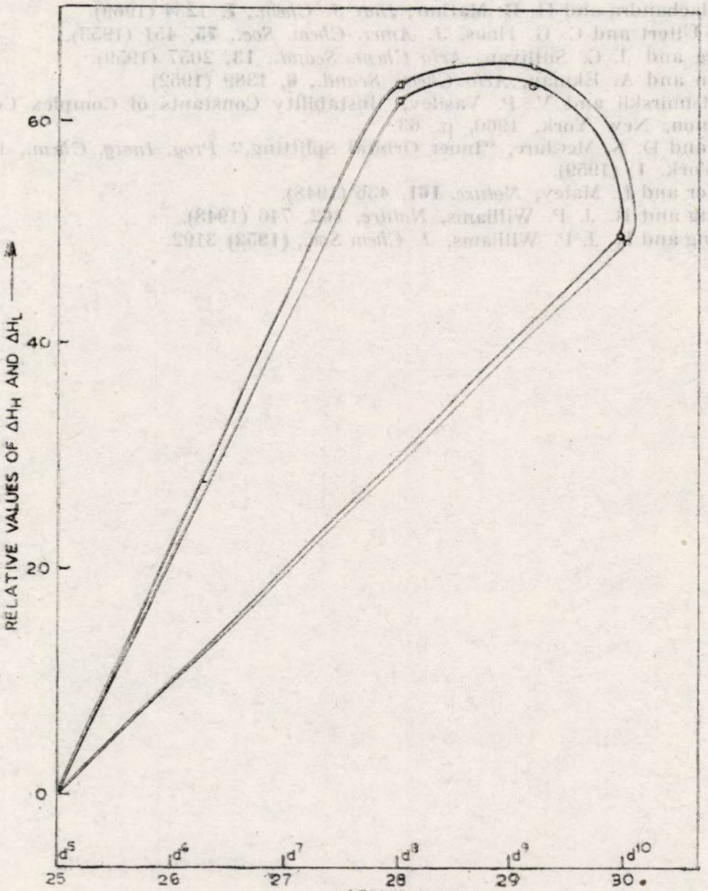

Fig. 2. — Plots of relative values of ΔH_L and ΔH_M against the number of 3d electrons for BHMMA complexes.

Order of stability constant

It is evident from Tables 1 and 2 that the stability constants of the complexes follow the order as found by Mellor and Maley[10] and Irving and Williams[11,12] : $\mathrm{Mg}^{2+} < \mathrm{Mn}^{2+} < \mathrm{Cd}^{2+} < \mathrm{Pb}^{2+} < \mathrm{Zn}^{2+} < \mathrm{Co}^{2+} <$ $< \mathrm{Ni}^{2+}$.

ACKNOWLEDGEMENT. One of the authors (RD) thanks the U.G.C., New Delhi for providing financial assistance.

REFERENCES

[1] H. M. Irving and H. S. Rossotti, *J. Chem. Soc.*, **(1954)** 2904.
[2] J. C. Sullivan, J. Rydberg and W. F. Miller, *Acta Chem. Scand.*, **13**, 2023 (1959).
[3] A. I. Vogel, "A Textbook of Practical Organic Chemistry" Longmans, New York, 1956 p. 166.
[4] U. Rao Balachandra and H. B. Mathur, *Ind. J. Chem.*, **7**, 1234 (1969).
[5] L. G. Van Uitert and C. G. Haas, *J. Amer. Chem. Soc.*, **75**, 451 (1953).
[6] J. Rydberg and J. C. Sullivan, *Acta Chem. Scand.*, **13**, 2057 (1959).
[7] R. Nasanen and A. Ekman, *Acta Chem. Scand.*, **6**, 1389 (1952).
[8] K. B. Yatsimirskii and V. P. Vasilev, "Instability Constants of Complex Compounds", Pergamon, New York, 1960, p. 63.
[9] P. George and D. S. McClure, "Inner Orbital Splitting," *Prog. Inorg. Chem.*, Interscience, New York, **1**, (1959).
[10] D. P. Mellor and L. Maley, *Nature*, **161**, 436 (1948).
[11] H M. Irving and R. J. P. Williams, *Nature*, **162**, 746 (1948).
[12] H. M. Irving and R. J. P. Williams, *J. Chem Soc.*, **(1953)** 3192.

Revue Roumaine de Chimie, **34**, *8*, 1711–1720 (1989)

OXIDATION OF CUMENE WITH MOLECULAR OXYGEN IN PRESENCE OF Co(II) ACETYLACETONATE COMPLEXES HETEROGENIZED ON SILANE MODIFIED SILICA

A. C. BANCIU, ŞILVIA PLOŞTINARU, MARIUS ANDRUH, LUMINIŢA PATRON
and ADRIANA CONŢESCU
ICECHIM – Center of Physical Chemistry, 79611 – Bucharest, Spl. Independenţei 202, Romania

Received February 13, 1988

By using as support a sample of chromatographic grade silica with the specific surface of 195 m^2/g and the pore diameters comprised between 200...600 Å a heterogenized complex of Co(II) acetylacetonate was synthesized. This complex has a high cobalt content, of 5.6% (*i.e.* a concentration of 2.93 Co(II) ions on 1 nm^2 of silica surface) and consists of a mixture of tetrahedral and octaherdral Co(II) complexes. It has been used for the cumene oxidation, in liquid phase, with molecular oxygen, in a concentration of 3×10^{-3} moles complex/mole of hydrocarbon. The heterogenized complex allows an advanced oxidation of cumene under the conditions of attainment of a high cumyl hydroperoxide concentration (up to 29 %) in the reaction liquid. A radicalic heterogeneous – homogeneous reaction mechanism has been proposed for the cumene oxidation with molecular oxygen in the presence of heterogenized Co(II) acetylacetonate complexes.

INTRODUCTION

It is well-known that the transition metal ions (Co(II), Mn(II), Fe(II)) catalyze the oxidation of hydrocarbons in liquid phase with molecular oxygen.[1–3]

The action of the transition metal ions is based, surely, on the decomposition, initiated by a one-electron transfer of the hydrocarbon hydroperoxides, ROOH (the initial oxidation products), after which the RO· and ROO· radicals are formed. These radicals produce chain-branching in the radicalic hydrocarbon oxidation.[1–3]

There are, however, only relatively few data regarding the catalysis of the oxidation reactions of hydrocarbons with molecular oxygen via the heterogenized transition metal complexes. Recent papers in this field are due to A. Ia. Yuffa, V. V. Berentsveig and their coworkers. Thus, the synthesis of some Co(II) acetyl-acetonate complexes heterogenized on silica as well as their catalytic action on tetraline oxidation in liquid phase are described.[4] The same oxidation reaction has been studied in the presence of other heterogenized Co(II) complexes, synthesized with EDTA, α,α′-dipyridyl, trimethylenediamine, 1,10-phenanthroline and other ligands.[5] The catalytic action of Cu(II) chloride heterogenized on silica in the oxidation reaction of cumene in liquid phase has been also reported[6]. Based on the data earlier obtained [5] and on further researches [7,8] and using a mathematical modelling the mentioned authors have proposed a reaction mechanism for the oxidation with molecular oxygen of the hydrocarbons at which a secondary carbon atom is oxidized (tetraline, cyclohexene) in presence of heterogenized Co(II) complexes.[9]

The structural (concentration, coordination geometry) and the catalytic properties of the heterogenized complexes strongly depend on the nature of the used support. The present paper describes the synthesis of a Co(II) acetylacetonate complex heterogenized on a silica which differs from that elsewhere used [4–6] as well as its electronic spectrum and its catalytic action in the oxidation reaction of cumene, in liquid phase, with molecular oxygen.

EXPERIMENTAL PART

The support used was a silica for chromatography, prepared at the Chemical Institute of Cluj-Napoca, having a specific surface $A = 195$ m^2/s and the most part of the pore diameters comprised within 200 – 600 Å. Before use the silica was anhydrized, in vacuum, at 190 – 200°C for 5 hours.

The synthesis of the heterogenizad Co(II) complex was made using, in general lines, a method earlier reported,[4] to which some changes were made. It consisted of the following steps:

1. *The 1st modification of silica.* 30.0 g of anhydrized silica were introduced in a flask with ground stopper, fixed with steel springs, into a mixture of 8.6 mL γ – chloropropyl – trimetoxysilane ("Merck", 97%) and 60 mL absolute toluene. The heterogeneous reaction mixture was shaken for 15 min. at room temperature and then kept for 11.5 hours at 100°C in a cabinet dryer. The liquid phase was then separated and the modified silica washed for three times with a small amount of absolute toluene. By this treatment the silanolic groups on the silica surface were substituted by $-O-Si(OCH_3)_2(CH_2)_3Cl$ groups.

2. *The 2nd modification of silica.* The silica treated as before was covered with 150 mL dimethyldichlorosilane ("Merck", 98 %, b.p. 69°) (in [4] this modification was made with trimethylchlorosilane) and kept at boiling by refluxing on a water bath for 6.5 hours. The liquid was then removed and the modified silica washed for three times with small amounts of absolute benzene and then dried in a cabinet dryer at 100° for 5 hours. By this treatment the silanolic groups still remained on the silica surface were substituted by $-O-Si(CH_3)_2Cl$ groups.

3. *The treatment of the silane-modified silica with sodium acetyl-acetonate.* 10.8 g pure metallic sodium cut off in small pieces was left to react, in a reaction flask provided with two Dimroth reflux condensers, assembled one over another, with 47 mL (stoichiometric amount) of acetylacetone ("Merck", p.a.). The reaction product, impurified with byproducts, still contained unreacted small sodium balls. The reaction mass was taken with 250 mL absolute ethanol, then warmed on a water bath up to complete solvation and then into the ethanolic solution (of brown colour) was introduced the silica, modified as above. The heterogeneous reaction mixture was boiled by refluxing on a water bath, for 4 hours. The still warm liquid was separated and the silica extracted for three times, for 30 min. with 70 – 80 mL absolute ethanol in a Soxhlet equipment. (The first ethanolic extraction solution had pH $\sim$ 8 – 9, the second one $\sim$ 7 – 8 and the last one 7). After the last extraction, the silica was further washed for four times with small amounts of hot absolute ethanol. Then, it was dried in a cabinet dryer, at 100° for 3 hours. As a consequence of this treatment, the alkyl chloride[10] (linked on the silica surface by the previous treatments) underwent a S_N2 attack from the median carbon atom of the acetylacetone anion (which still contained one enolizable hydrogen atom), a new C–C bond being thus formed. In this way acetylacetone chelate rings occurred on the silica surface, being linked on the surface by a propylenic chain followed

by a Si–O bond, **(I)**:

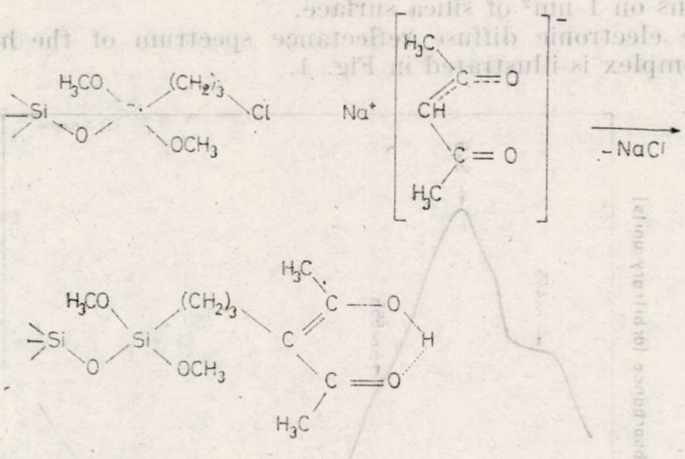

I

After all these treatments the mass of modified silica, isolated, washed and dried, weighted 32.0 g.

4. *The formation of the Co(II) acetylacetonate complex on the silica surface.* 10.0 g $CoCl_2 \cdot 6H_2O$ ("Reactivul", Bucharest, p.a.) were finely powdered in a mortar and then (for a partial drying) warmed in a cabinet dryer, at 115°, for 30 min. The partially anhydrized salt, of dark-blue colour, was cooled at the room temperature in a desiccator, and then quickly powdered and solved into 140 mL of warm (~ 50°) absolute ethanol. An amount of 16.0 g of modified silica was introduced into the concentrated dark-blue solution obtained. The heterogeneous reaction mixture was strongly and continuously shaken for 80 min., at 50–60°. The still warm solution was separated and the silica with the Co(II) acetylacetonate complex heterogenized on its surface was washed for three times with small amounts of hot absolute ethanol. To remove as much as possible the physically adsorbed Co(II) ions from the silica pores it was made an extraction, in absolute ethanol, for 20 hours, in a Soxhlet equipment. The complex heterogenized on silica was finally dried in a cabinet dryer, for 3 hours, at 110°. The sample was of violet-blue colour, of mean intensity.

The metal content of the sample was determined by atomic absorption spectroscopy.

The electronic diffuse reflectance spectrum of the heterogenized Co(II) complex was recorded within the 380 – 1100 nm range by means of a VSU-2 Carl Zeiss (Jena) spectrophotometer, using chromatographic grade silica as a standard.

The tests of cumene oxidation in liquid phase were made discontinuously, using ~100 mL cumene in a thermostated reaction flask of 175 mL provided with a KPG stirrer, a Dimroth reflux condenser and a bubbling tube. The oxygen was bubbled though the strongly stirred cumene with a flow rate of 2–3 bubbles/second.

The cumene used was previously purified according to [3].

During the oxidation *the content of the cumyl hydroperoxide* achieved in the reaction liquid was determined by iodometric titration.

The gaschromatographic analysis of the cumene conversion was made by means of Fractovap 2400 equipment ("Carlo Erba") using a SE 30 column filling, deposited on Chromosorb WHP (100–120 mesh).

RESULTS AND DISCUSSION

The obtained heterogenized Co(II) acetylacetonate complex is characterized by a high metal content, of 5.6 % Co, corresponding to a concentration of 2.93 Co(II) ions on 1 nm^2 of silica surface. Using a "Silohrom S-120" silica, with $A = 140$ m^2/g and working in a similar way the heterogenized Co(II) acetylacetonate complex synthesized in[4] contained 0.3 % Co, which would correspond to a concentration of 0.21 Co(II) ions on 1 nm^2 of silica surface.

The electronic diffuse reflectance spectrum of the heterogenized Co(II) complex is illustrated in Fig. 1.

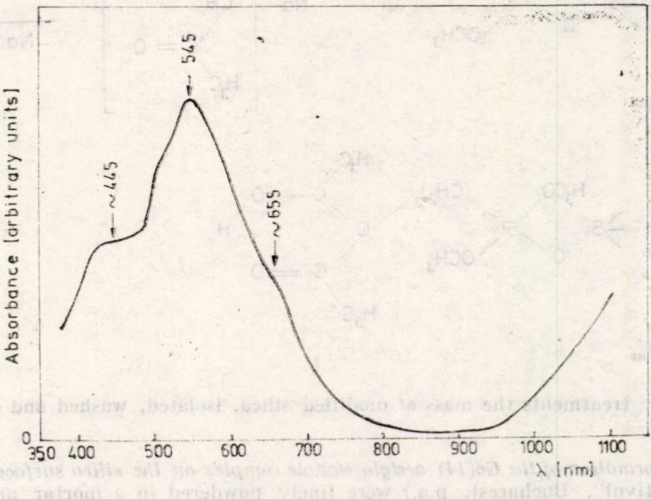

Fig. 1. — The electronic diffuse reflectance spectrum of the heterogenized Co(II) acetylacetonate complex.

One observes that it obviously differs from the corresponding spectrum of the heterogenized Co(II) complex reported in.[4]

The "most intense" absorption band at 545 nm (see below) represents, certainly, the ${}^4T_{1g} \rightarrow {}^4T_{1g}$ (P) transition for the octahedral Co(II) complexes.[11] It occurs in the spectrum in admixture with other bands, due to the spin forbidden transitions to the doublet states resulted from ${}^2G$ and ${}^2H$ terms of the free Co(II) ion.[11] This absorption band is responsible for the violet colour of the heterogenized Co(II) complex. The band occurring as a shoulder, at ~ 655 nm represents, surely, the transition ${}^4A_2 \rightarrow {}^4T_1(P)$ of the tetrahedral Co(II) complexes.[11] This transition is always more intense than the first one mentioned.[11] In the electronic spectrum of our Co(II) complex the band at 655 nm is less intense than the band at 545 nm, an explanation being on the one side the fact that the tetrahedral species are in minority against the octahedral ones and, on the other hand, that the electronic reflectance spectra (unlike the absorption spectra) cannot correctly illustrate the band intensities[12] (except the case when the Kubelka — Munk[13] method is used). From these reasons the band due, most likely, to a charge transfer occurs also less intense in the reflectance spectrum, outlined only as a shoulder, at ~ 445 nm. The broad band which begins at 950 nm having the maximum at over 1100 nm (outside the investigated range) represents, most probably, a mixture of the tetrahedral ${}^4A_2 \rightarrow {}^4T_1(F)$ and the octahedral ${}^4T_{1g} \rightarrow {}^4T_{2g}$ transitions, both occurring even in this range.[11] The heterogenized Co(II) complex is therefore constituted from a mixture of octahedral and tetrahedral species. Because the chelate acetylacetonate ring allows only the dicordination of the Co(II) ion, the other metal chemical bonds to satisfy the tetra- and hexacoordination respectively, are made with the chloride ions (existent in the reaction medium and which neutralize an electric charge of the Co(II) ion) and with neutral molecules, containing donor atoms, as ethanol (the solvent used in the synthesis) or water molecules (also existent in the reaction medium of the synthesis). The heterogenized complex is therefore represented especially by the tetrahedral, (**II**),

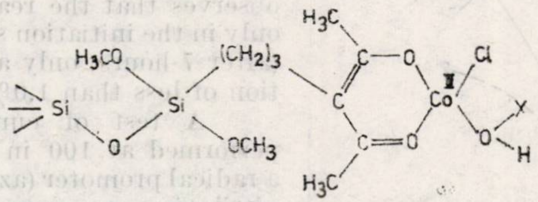

II.

and octahedral, (**III**),

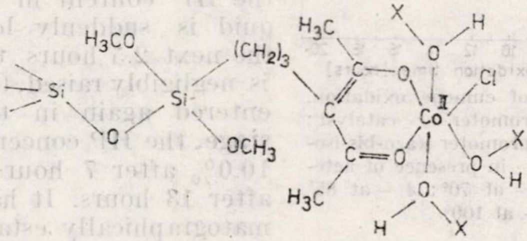

III

species. In these formulas XOH represents C_2H_5OH or H_2O. It is also possible that some Co(II) ions are linked to the silica surface not only via the chelate acetylacetonate rings, but also via chlorine bridges. (The chlorine atoms are covalently bonded to the silica surface as a consequence of the 2nd silica modification, made with dimethyldichlorosilane; see the experimental part).

Finally, due to the high transition metal content of the heterogenized Co(II) ions, it should be also possible that not all the Co(II) ions be covalently linked to the silica surface, a part of them be only physically adsorbed on the suport surface. In this case the adsorption must be particularly strong, because for the Co(II) complex maintained in hot cumene (in the oxidation tests) the metal content remains practically unchanged.

One knows that the oxidation of cumene in liquid phase, with molecular oxygen, is technically made (the Hock procedure), with high yields and without radical promoter or catalysts. [14,15] This is, however, possible only by using a series of reactors, for long times of cumene retention in the reactors, by recycling the unoxidized cumene, and under the conditions of removing any traces of acidity from the reaction mass. The same oxidation, discontinuously performed, in laboratory conditions, takes place more difficultly and requires the use of radical promoters. This is the only way to get a 20% concentration of cumyl hydroperoxide (HP) in the reaction liquid.[3,16]

Indeed, a blind test of cumene oxidation, without promoters or catalysts, made at 100° took place as shown by line 1 in Fig. 2. One observes that the reaction remained only in the initiation stage and finally (after 7 hours) only a HP concentration of less than 1.0% was reached.

A test of cumene oxidation performed at 100° in the presence of a radical promoter (azo-bis-isobutyronitrile) in a concentration of 3×10^{-3} moles/mole of cumene is shown by curve 2 (Fig. 2). After initiation, the radicalic reaction is quenched and the HP content in the reaction liquid is suddenly lowered. During the next 2.5 hours this HP content is negligibly raised, then the reaction entered again in the propagation stage, the HP concentration being of 10.0% after 7 hours and of 15.3% after 13 hours. It has been gaschromatographically established that in this last stage (after 13 hours) the reaction liquid contained 66.5 % unconverted cumene, 15.3% HP and 18.2% a lot of other five reaction products, among them three are significant and one is predominant. The cumene conversion to HP was therefore approximately equal to the cumene conversion to other oxidation products.

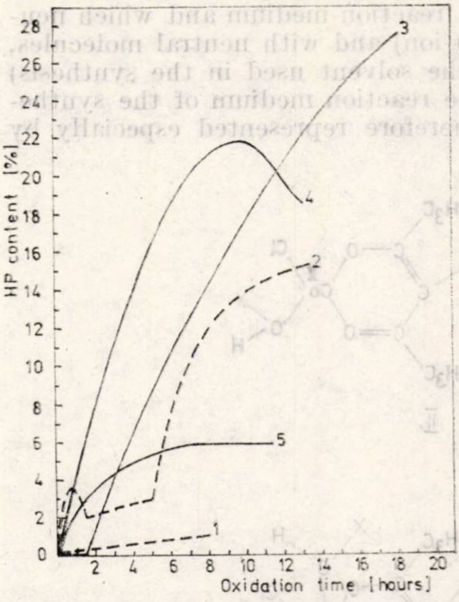

Fig. 2. — The tests of cumene oxidation. *1.* — in absence of promoter or catalyst; *2.* — in presence of promoter (azo-bis-isobutyronitrile); *3.* — *5* — in presence of heterogenized complex: *3* — at 70°; *4* — at 85° and *5* — at 100°.

Fig. 2 shows, too, the tests of cumene oxidation performed at different temperatures in the presence of the Co(II) complex heterogenized on silica. In all these tests the complex was used in a concentration of 3×10^{-3} g-atoms Co/mole of cumene. This concentration of the catalyst is recommended as optimal in a series of papers concerning the homogeneous catalysis,[7–20] as well as to the use of promoters in the radicalic oxidations.[3,16]

In the test performed at 70° (curve 3 in Fig. 2) the reaction remained for 1.5 hours in the inhibition stage, thereafter the radicalic oxidation took suddenly place and did not undergo any interruption for other 16.5 hours. One observes that at this oxidation test at longer reaction times the highest HP concentrations were reached. It has been gaschromatographically established that at the reaction end (after 18 hours) the reaction liquid contained only 39.3 % unreacted cumene, but 27.6 %

HP and 33.1 % other five oxidation products (among them one product is predominant and other two are significant).

In the test performed at 85° (curve 4 in Fig. 2) the initiation stage was practically absent. The HP content in the reaction liquid suddenly raised at the beginning and after that a more obvious diminution of its raise is observed, a maximum (of 21.85 % HP) being present after 10 hours of oxidation. It has been gaschromatographically established that after 7 hours of oxidation (during the raising of the HP content) the reaction liquid contained only 36.1 % unreacted cumene, but 20.1 % HP and 43.8 % a lot of five oxidation products, among them one being most significant. Finally, after 13 jours of oxidation (during the lowering of the HP content) the reaction liquid contained only 22.9 % unreacted cumene, but 18.7 % HP and 58.4 % other five oxidation products. During the last 5 hours of oxidation the HP content in the reaction liquid was insignificantly changed, but an obvious increase in the content of the other five oxidation products (from 43.8 % to 58.4 %) was observed.

The test performed at 100° (curve 5 in Fig. 2) is quite different. The radicalic reaction began without the induction step and presented during the first 7 hours a smooth increase of the HP content (compared with the other tests); after that the HP content (of 5.9 %) remained rigorously constant. In other words, at 100°, in this reaction stage, the HP formation rate was exactly equal to the rate of its decomposition to other subsequent oxidation products.

It must be mentioned that the oxidation of tetraline, performed in a very similar way, led to a lower content of tetralyl hydroperoxide and to a mixture of four oxidation products, among them two being significant. These last products are, surely, the α-tetralol and the α-tetralone (see below).

In the case of cumene oxidation in the presence of the heterogenized Co(II) complex the oxidation takes place differently: from the five oxidation products subsequent to HP only one is predominant (see above). This is due to the fact that in the cumene oxidation one oxidizes a tertiary carbon atom from the molecule (and not a secondary one, as in the case of tetraline or cyclohexene).

For the cumene oxidation in the presence of the heterogenized Co(II) complex we propose the following reaction mechanism:

$$\mathrm{RH} + \mathrm{O_2} \rightarrow \mathrm{HOO\cdot} + \mathrm{R\cdot} \qquad \text{0.a.}$$

$$\mathrm{RH} + \mathrm{O_2} + \mathrm{RH} \rightarrow \mathrm{H_2O_2} + 2\mathrm{R\cdot} \qquad \text{0.b.}$$

$$[\mathrm{Co(II)}]_s + \mathrm{O_2} + \mathrm{RH} \rightarrow [\mathrm{Co(II)}]_s + \mathrm{HOO\cdot} + \mathrm{R\cdot} \qquad \text{1.}$$

$$\mathrm{R\cdot} + \mathrm{O_2} \rightarrow \mathrm{ROO\cdot} \qquad \text{2.}$$

$$\mathrm{ROO\cdot} + \mathrm{RH} \rightarrow \mathrm{ROOH} + \mathrm{R\cdot} \qquad \text{3.}$$

$$[\mathrm{Co(II)}]_s + \mathrm{ROOH} \rightleftharpoons [\mathrm{Co(II)\ ROOH}]_s \qquad \text{4.}$$

$$[Co(II)\ ROOH]_s + ROOH \rightarrow [Co(II)_s] + ROO\cdot + RO\cdot + H_2O \tag{5.}$$

$$[Co(II)\ ROOH]_s \rightarrow [Co(III)\ (OH)]_s + RO\cdot \tag{5.a.}$$

$$[Co(III)\ (OH)]_s + ROOH \rightarrow [Co(II)]_s + ROO\cdot + H_2O \tag{5.b.}$$

$$[Co(III)\ (OR'')]_s + ROOH \rightarrow [Co(II)]_s + ROO\cdot + R''OH \tag{6.}$$

$$RO\cdot + RH \rightarrow ROH + R\cdot \tag{7.}$$

$$HOO\cdot + RH \rightarrow H_2O_2 + R\cdot \tag{8.}$$

$$ROO\cdot + ROO\cdot \rightarrow R'{=}O + ROR'' + O_2 \tag{9.a.}$$

$$[Co(II)]_s + ROO\cdot \rightarrow [Co(III)\ (R''O)]_s + R'{=}O \tag{10.a}$$

Here the square brackets having the indices "s" mean the different Co(II) and Co(III) surface complexes, R is the $C_6H_5-C(CH_3)_2$ (cumyl) group, R′ the $C_6H_5-\overset{\|}{C}(CH_3)$ group and R″ the $-CH_3$ group. For instance, $[Co(III)\ (R''O)]_s$ means a surface Co(III) acetylacetonate complex similar to those above represented by the formulas (**II**) and (**III**), but where one ligand is the methoxide anion, CH_3O^-, instead of one of the neutral molecules XOH (in **II** or **III**).

The reactions 0.a. and 0.b. are, surely, the starting reactions of the uncatalyzed hydrocarbon oxidation in the gaseous and liquid phases, respectively.[21] They are not properly involved in the mechanism of the catalyzed oxidation, but they are mentioned to show the similarity between them and reaction 1.

Reaction 1 represents the catalyzed starting reaction, reactions 2 and 3 represent the unbranched propagation reactions of the radicalic chain, reactions 4—8 the chain-branching reactions and reactions 9 and 10 the most important chain-breaking reactions.

Reactions 5.a. and 5.b. represent in detail the overall decomposition reaction 5, initiated by an one-electron transfer ($HO\cdot + e^- \rightarrow HO^-$), of ROOH, into the RO· and ROO· radicals.

The radicalic heterogeneous-homogeneous reaction mechanism is very similar to that proposed by Yuffa and Berentsveig, for the tetraline and/or cycloxene oxidation.[9] It differs from [9] in what the reactions 6, 9.a. and 10.a. are concerned. Thus, reaction 6 takes place in the cumene oxidation and cannot be involved in the oxidation of a secondary carbon atom (tetraline, cyclohexene). Reactions 9.a. and 10.a. take place differently in the reaction mechanism earlier reported.[9] In this mechanism reaction 9.a. is substituted by 9.b.:

$$ROO\cdot + ROO\cdot \rightarrow R'{=}O + ROH + O_2 \tag{9.b.}$$

(this reaction leads to the alcohol ROH, instead of the ether, ROR″), and reaction 10.a. is substituted by 10.b.:

$$[CoII)]_s + ROO\cdot \rightarrow [Co(III)\ (OH)]_s + R'{=}O \tag{10.b.}$$

(this reaction leads to the same surface complex of the Co(III) ion as reaction 5.a.).

In rest, all the reactions of the reaction mechanism proposed by us (for cumene oxidation) are identical with those proposed [9] for tetraline and cyclohexene oxidation.[9] Obviously, in the case of the tetraline oxidation $R = C_{10}H_{11}$ and $R' = C_{10}H_{10}$, and in the case of cyclohexene oxidation $R = C_6H_9$ and $R' = C_6H_8$. In the particular case of cyclohexene oxidation besides reactions 1—8, 9.b. and 10.b., reaction 11 takes also place :

$$ROO\cdot + RH \rightarrow R > O + RO\cdot \qquad 11.$$

where $R > 0$ means the 1,2-epoxy-cyclohexane. (This reaction has not its equivalent in the oxidation of tetraline).

One may observe that in both reaction mechanisms under discussion the surface complexes of the Co(II) ion react in a triple way : *1.* with the molecular oxygen, which makes it active (reaction 1); *2.* with the initially formed hydroperoxides which are decomposed, to form RO. and ROO· radicals (reactions 4 and 5); and *3.* with the peroxy radicals, ROO·, which undergo decomposition (reactions 10.a. and 10.b., respectivelly).

According to the reaction mechanism proposed by us seven reaction products are to be expected : H_2O, H_2O_2, CH_3OH, $C_9H_{11}OOH$ (cumyl hydroperoxide), $C_6H_5C(CH_3)_2(OH)$ (dimethylphenylcarbinol), $C_6H_5COCH_3$ (acetophenone) and $C_6H_5C(CH_3)_2(OCH_3)$ (methyl-(α-phenyl-isopropyl)-ether). Among them, under the working conditions of the gas-chromatograph, H_2O_2 easily decomposes to H_2O. The remained six reaction products were experimentally detected in the reaction liquid (HP and other five products, among them one being the most predominant). The predominant product is, most likely, the acetophenone, $R' = 0$, which results from reactions 9.a. and 10.a., the main chain-breaking reactions. The other two compounds also important are, most likely, the methyl-(α-phenyl-isopropyl)ether, ROR″ (as results from reaction 9.a.) and the dimethyl-phenyl-carbinol, ROH, (as results from reaction 7). The carbinol and acetophenone also occur as secondary products in the industrial devices of cumene oxidation, in the absence of promoters or catalysts.[15] It must be mentioned that the two important products of the tetraline oxidation are, surely, the α-tetralone, $R' = O$, and the α-tetralol, ROH (which result especially from reaction 9.b., the most important chain-breaking reaction).

CONCLUSIONS

1. The silica used as a support and the adopted synthesis allow the obtention of a heterogenized Co(II) acetylacetonate complex having a high content of transition metal (5.6 % Co).

2. The heterogenized Co(II) acetylacetonate complex is actually formed from a mixture of tetrahedral and octahedral Co(II) species.

3. Used as catalyst in the cumene oxidation with molecular oxygen, in liquid phase, in optimal concentration (3×10^{-3} g-atoms Co/mol hydrocarbon), this heterogenized Co(II) complex allows an advanced cumene oxidation, under the conditions of attainment of a high concen-

tration (up to 29 %) of cumyl hydroperoxide in the reaction liquid. The heterogenized Co(II) complex is more efficient for the cumene oxidation than the azo-bis-isobutyronitrile, one of the best known and most used organic radical promoters.

4. The radicalic heterogeneous-homogeneous reaction mechanism proposed for the cumene oxidation in the presence of the heterogenized Co(II) complex explains fairly good the reaction process and the differences existing between this oxidation (of cumene, where a tertiary carbon is oxidized) and the oxidations of tetraline or cyclohexene (where a secondary carbon atom is oxidized).

REFERENCES

[1] C. D. Nenițescu, "Chimie organică", vol. 1. ed. VIII, Ed. Didactică și Pedagogică, Bucharest, 1980, p. 521.

[2] I. G. Murgulescu, Tatiana Oncescu and E. Segal, "Introducere în chimia fizică", vol. II, 2, Ed. Academiei, Bucharest, 1981, p. 600.

[3] * * * "Organicum", Ed. Științifică și Enciclopedică, Bucharest, 1982, p. 188.

[4] A. Ia. Yuffa, *et al.*, *Kietika i Kataliz*, **22**, 1469 (1981).

[5] V. V. Berentsveig *et al.*, *Neftehimia*, **21**, 254 (1981).

[6] A. Ia. Yuffa, *et al.*, *Kinetika i Kataliz*, **27**, 174 (1986).

[7] A. Ia. Yuffa *et al.*, Proc. 5th International Symposium "Relations Between Homogeneous and Heterogeneous Catalysis", vol. 2, part 2, Novosibirsk, 1986, p. 147.

[8] A. Ia. Yuffa *et al.*, 5th International Symposium "Relations Between Homogeneous and Heterogeneous Catalysis", Abstracts of Poster Communications, Novosibirsk, 1986, p. 279.

[9] V. V. Berentsveig *et al.*, 5th International Symposium "Relations Between Homogeneous and Heterogeneous Catalysis", Abstracts of Poster Communications, Novosibirsk, 1986, p. 31.

[10] Margareta Avram, "Chimie organică", vol. 2, Ed. Academiei Bucharest, 1983, p. 301.

[11] A. B. P. Lever, "Inorganic Electronic Spectroscopy", Elsevier, Amsterdam, 1968, p. 317.

[12] H. L. Schläfer and G. Glieman, "Einführung in die Ligandenfeldtheorie", Akademische Verlagsgesellschaft, Leipzig, 1967, p. 15.

[13] P. Kubelka and F. Munk, *J. Opt. Soc. Amer.*, **38**, 448 (1948).

[14] "Ullmanns Encyklopädie der technischen Chemie", vol. 18, 4. Auflage, Verlag Chemie, Weinheim, 1979, p. 182.

[15] Kirk-Othmer, "Encyclopedia of Chemical Technology", vol. 17, 3rd Edition, John Wiley, New York, 1982, p. 374.

[16] * * * "Reaktionsverhalten und Syntheseprinzipien", Arbeitsbuch, vol. 7, VEB Deutscher Verlag für Grundstoffindustrie, Leipzig, 1976, p. 50.

[17] M. Zawadzki and J. J. Ziolkowski, *React. Kinet. Catal. Lett.*, **10**, 119 (1979).

[18] M. Naki *et al.*, *Chubu Kogyo Daigaku Kyo*, **5**, 151 (1969).

[19] M. A. Bennett *et al.*, *J. Chem. Soc.*, *Chem. Commun.*, **1978**, 582.

[20] G. Henrici-Olive and S. Olive, *Angew. Chem.*, **86**, 561 (1974).

[21] "Ullmanns Encyklopädie der technischen Chemie", vol. 17, 4. Auflage, Verlag Chemie, Weinheim, 1979, p. 490.

Revue Roumaine de Chimie, 34, *8*, 1721–1731 (1989)

CHARGE-TRANSFER COMPLEXES OF HYDROXY STYRYL CYANINE DYES AND THEIR ANALOGUES WITH NICOTINE. STRUCTURE-ACTIVITY RELATIONSHIP STUDIES

MAHER M. GIRGIS and ZARIF H. KHALIL
Chemistry Department, Faculty of Science, Assiut University
Assiut, Egypt

Received August 15, 1987

UV-visible spectrophotometric studies on the possibility of charge-transfer interaction of nicotine with hydroxy styryl cyanine dyes and their analogues [dyes (I–IX)] in 10% (v/v) aqueous ethanol mixture at 29°C demonstrate the formation of charge-transfer complexes of dyes (I, III–VI)only with nicotine. Addition of increasing amounts of nicotine to a solution containing fixed [dye] causes a decrease in the dye absorptivity with a gradual development of a new band at considerably longer wavelength characteristic of the complex formed. The spectra show a clear unique isosbestic point. The stability constants and the molar absorptivities of the complexes formed were calculated by assuming 1 :1 complexes. The experimental results were interpreted in terms of the molecular structure of the interacting molecules.

INTRODUCTION

Nicotine finds growing interest not only for tobacco industry but also for its biochemical[1] and pharmacological[2, 3] effects. The synthesis of nicotine analogues is important in the development of radioimmunoassay for tobacco alkaloids[4] and gives better understanding to nicotine pharmacology.[5] Exposure to nicotine enhances the behavioral response and increases binding of [^{3}H] acetylcholine to nicotinic receptors of the cerebral cortex.[6,7] Nicotine metabolites are organ-specific and local carcinogens.[8] N-Methylnornicotinium ion, a nicotine metabolite product,[9] is the precursor of N′-nitrosonornicotine which disrupts the hydrogen bond between guanine-cytosine base pair and forms new H-bonds with guanine[10] causing a local carcinogen. This assumption is based on frontier MO, HOMO and LUMO calculation of electron densities, electron configurations and energy levels of nicotine, its intermediates and nucleotides bases and base pairs. [10]

An interest has been focused on the biochemical effect of cyanine dyes beside their uses in photographic industry[11] and other purposes.[12] The biological activity of cyanine dyes may be due to the interference of the adsorbed dye molecule on active sites of the living cell.[13] Structure-

-activity relationship has been conducted among styryl and aza cyanine dye analogues to study their effect on breaking period of dormancy in Garlic,[14] essential oil production in sweet marjoram (*Origanum majorana*, L)[15] and chromosomal behaviour in *Vicia faba* seeds.[16] To shed some light on the cause of bioeffect of aza cyanine dyes, CT-complex studies with one of the nucleic acid bases (adenine) were done,[17] and the results obtained are in agreement with their biological activity when applied as bioregulator for *Vicia faba* seeds in the field. Recently, cyanine dyes have been used as growth promotors for cultured fish[18] and in controlling bacterial and fungal diseases in aquatic animals.[18] The use of cyanine dyes as plant growth hormones[19] and anticancer[20] agents was studied.

The interactions between nicotine and drugs have been of much concern and the subject of many investigations.[3,21] The interactions between nicotine and cyanine dyes were not mentioned before. In this work we aimed to study the charge-transfer interaction of nicotine with hydroxy styryl cyanine dyes and their analogues and the effect of distance geometry[22] on the complexation to select the proper structure for the development of radioimmunosasay for tobacco alkaloids.[4], *

EXPERIMENTAL

Nicotine was obtained commercially (BDH) and used without further purification. Styryl cyanine dyes (I–IX) (scheme I) were prepared in a way similar to the method described before.[23] The solid products obtained were recrystallized from ethanol. Analytical data of these dyes are in accordance with their structure. The electronic absorption spectra of dyes I, III, IV and VI are represented in Fig. 1.

All experiments were carried out in 10% (v/v) aqueous ethanol mixture. The calculated volumes of nicotine (0.05 M), dye (0.001 M) and ethanol were transferred to a 10 ml dark flask and the volume was completed to the mark with doubly distilled water. The solutions were freshly prepared each day, and their absorbances were measured within 5 hours. Most operations were performed in an air-conditioned room (– 22°C) with subdued light to avoid photochemical transformations.

Spectrophotometric measurements were recorded on a Shimadzu UV-200 S double beam spectrophotometer, using a rectangular 1 cm path length cell. The baselines were recorded before running the spectrum of a given set of solutions, using 10% (v/v) aqueous ethanol mixture in the cells of the sample and reference compartments. The absorbance was measured at fixed wavelengths to minimize errors arising from the steepness of absorption spectra. The absorption band of the complex formed between nicotine and dye was detected at wavelengths longer than those of the individual pure substances having identical concentrations to those in the mixture. The mixture was measured within ~ 10 min. after mixing the solutions and placing the cell in a thermostated cell holder for equilibrium. The accuracy of the measurements was ± 0.01 absorbance unit.

RESULTS

For some dye-nicotine combinations, the visible absorption band of the dye diminishes gradually with increasing nicotine content in the mixture accompanied by a gradual appearance of a new band at longer wavelength. The spectra of these combinations show a clear unique isosbestic point, c.f. Figs. 2 and 3. This behaviour was noticed only for nico-

---

* Further studies are conducted now on the use of some cyanine dyes as analytical reagents for estimation of nicotine and the results will be published later.

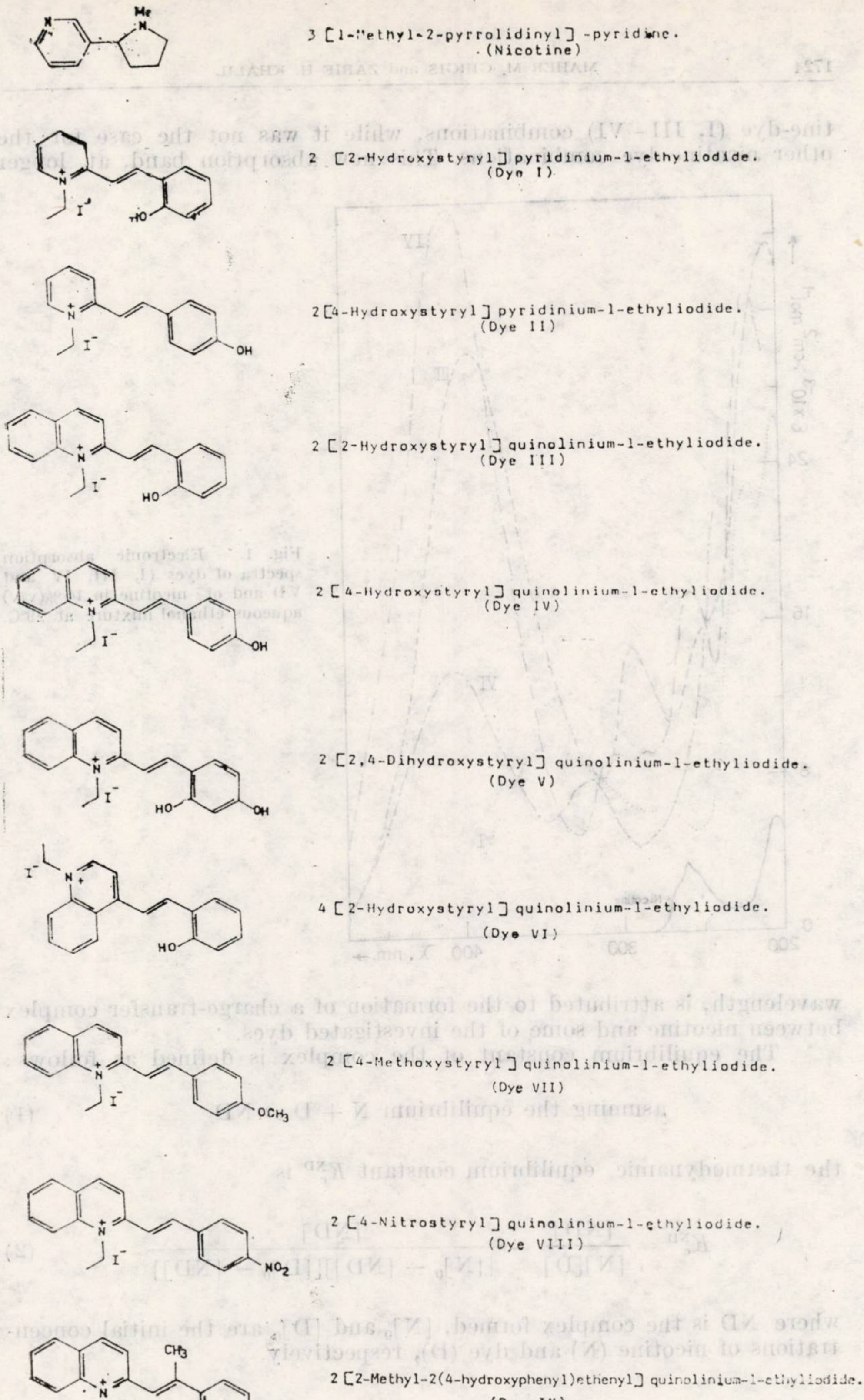
Me
3 [1-Methyl-2-pyrrolidinyl] -pyridine.
(Nicotine)
2 [2-Hydroxystyryl] pyridinium-1-ethyliodide.
(Dye I)
2 [4-Hydroxystyryl] pyridinium-1-ethyliodide.
(Dye II)
2 [2-Hydroxystyryl] quinolinium-1-ethyliodide.
(Dye III)
2 [4-Hydroxystyryl] quinolinium-1-ethyliodide.
(Dye IV)
2 [2,4-Dihydroxystyryl] quinolinium-1-ethyliodide.
(Dye V)
4 [2-Hydroxystyryl] quinolinium-1-ethyliodide.
(Dye VI)
2 [4-Methoxystyryl] quinolinium-1-ethyliodide.
(Dye VII)
2 [4-Nitrostyryl] quinolinium-1-ethyliodide.
(Dye VIII)
2 [2-Methyl-2(4-hydroxyphenyl)ethenyl] quinolinium-1-ethyliodide.
(Dye IX)
HO
OH
OCH3
NO2
CH3
I⁻

Scheme I

tine-dye (I, III—VI) combinations, while it was not the case for the other nicotine-dye combinations. This new absorption band, at longer wavelength, is attributed to the formation of a charge-transfer complex between nicotine and some of the investigated dyes.

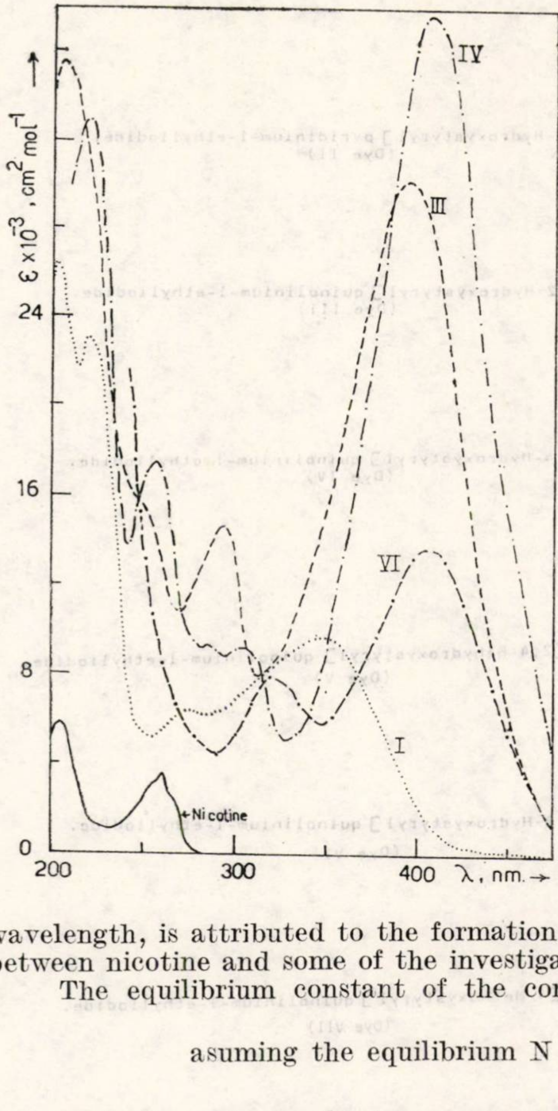

Fig. 1. — Electronic absorption spectra of dyes (I, III, IV and VI) and of nicotine in 10%(v/v) aqueous ethanol mixture at 29°C.

The equilibrium constant of the complex is defined as follows:

$$\text{asuming the equilibrium } \mathrm{N} + \mathrm{D} \rightleftharpoons \mathrm{ND} \tag{1}$$

the thermodynamic equilibrium constant K_c^{ND} is

$$K_c^{\mathrm{ND}} = \frac{[\mathrm{ND}]}{[\mathrm{N}][\mathrm{D}]} = \frac{[\mathrm{ND}]}{[[\mathrm{N}]_0 - [\mathrm{ND}]][[\mathrm{D}]_0 - [\mathrm{ND}]]} \tag{2}$$

where ND is the complex formed, $[\mathrm{N}]_0$ and $[\mathrm{D}]_0$ are the initial concentrations of nicotine (N) and dye (D), respectively.

Eq. (2) may be rearranged :

$$\frac{[\mathrm{D}]_0}{[\mathrm{ND}]} = \frac{1}{K_c^{\mathrm{ND}}} \cdot \frac{1}{[\mathrm{N}]_0} + \frac{[\mathrm{D}]_0}{[\mathrm{N}]_0} + 1 - \frac{[\mathrm{ND}]}{[\mathrm{N}]_0} \tag{3}$$

Since the absorbance in the region of the new band is due to the complex ND, c.f. Figs. (1—3), and the solution is of 1 cm path length,

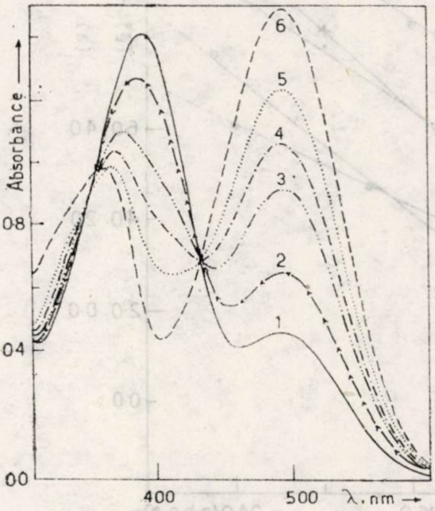

Fig. 2. — Absorption spectra of 5.56 × × 10^{-5} M dye (III) in 10 % (v/v) aqueous ethanol mixture at 29°C to which the following amounts of nicotine (M × 10^4) were added : (1) 0.50 ; (2) 0.86 ; (3) 1.72 ; (4) 2.50 ; (5) 5.00, (6) 50.00.

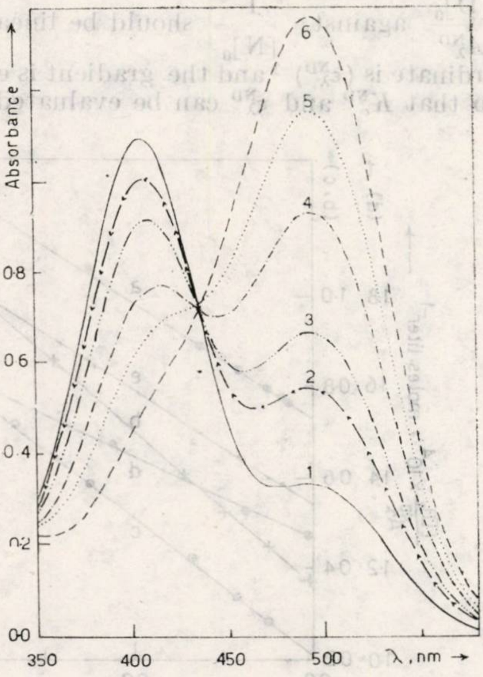

Fig. 3. — Absorption spectra of 3.87 × 10^{-2} dye (IV) in 10 %(v/v) aqueous ethanol mixture at 29°C to which the following amounts of nicotine (M × 10^4) were added : (1) 0.4 ; (2) 0.75, (3) 1.00 ; (4) 1.85 ; (5) 2.94 ; (6) 5.00.

for two molecules complexing according to Eq. (1), the molar absorptivity of the complex at wavelength λ is given by

$$\varepsilon_\lambda^{\mathrm{ND}} = \frac{A_\lambda^{\mathrm{ND}}}{[\mathrm{ND}]} \tag{4}$$

where A_λ^{ND} is the absorbance of the complex at the wavelength λ.

From Eqs. (3) and (4) :

$$\frac{[\mathrm{D}]_0}{A_\lambda^{\mathrm{ND}}} = \frac{1}{K_c^{\mathrm{ND}} \cdot \varepsilon_\lambda^{\mathrm{ND}}} \cdot \frac{1}{[\mathrm{N}]_0} + \frac{[\mathrm{D}]_0}{[\mathrm{N}]_0\, \varepsilon_\lambda^{\mathrm{ND}}} + \frac{1}{\varepsilon_\lambda^{\mathrm{ND}}} - \frac{[\mathrm{ND}]}{[\mathrm{N}]_0 \varepsilon_\lambda^{\mathrm{ND}}} \tag{5}$$

Since $[N]_0 \gg [ND]$ it is possible to neglect the final term in Eq. (5)[24(a)], so that:

$$\frac{[D]_0}{A_b^{ND}} = \frac{1}{[N_0]}\left(\frac{1}{K_c^{ND}\cdot\varepsilon_\lambda^{ND}} + \frac{[D]_0}{\varepsilon_\lambda^{ND}}\right) + \frac{1}{\varepsilon_\lambda^{ND}} \qquad (6)$$

For a series of solutions of constant $[D]_0$ and varying $[N]_0$ a plot of $\frac{[D]_0}{A_\lambda^{ND}}$ against $\frac{1}{[N]_0}$ should be linear. The intercept of the line with ordinate is $(\varepsilon_\lambda^{ND})^{-1}$ and the gradient is equal to $[(K_c^{ND}\cdot\varepsilon_\lambda^{ND})^{-1} + [D]_0(\varepsilon_\lambda^{ND})^{-1}]$ so that K_c^{ND} and ε_λ^{ND} can be evaluated. Plots of Eq. (6) for nicotine-dye (I, III—VI) combinations at 29°C are represented in Fig. 4 while K_c^{ND} and ε_λ^{ND} values are given in Table 1.

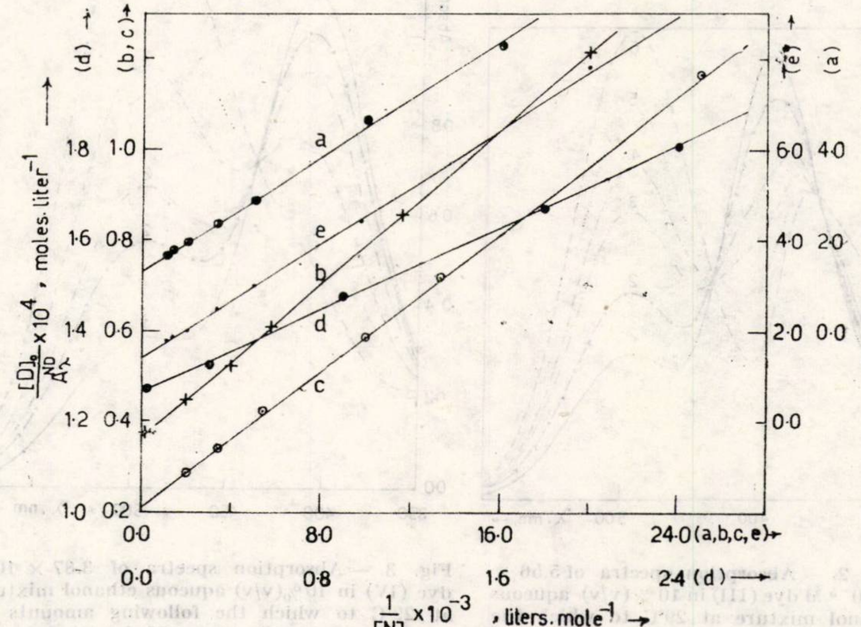

Fig. 4. — Plots of $[D]_0/A_\lambda^{ND}$ versus $1/[N]_0$ for 10% (v/v) aqueous ethanol mixtures containing fixed [dye] and different [nicotine] at 29°C. The combinations are:
(a) nicotine-dye(I) ([dye I] = 7.40×10^{-5} M);
(b) nicotine-dye (III) ([dye III] = 5.58×10^{-5} M);
(c) nicotine-dye (IV) ([dye IV] = 3.87×10^{-5} M);
(d) nicotine-dye (V) ([dye V] = 9.27×10^{-5} M);
(e) nictoine-dye (VI) ([dye VI] = 9.30×10^{-5} M).

DISCUSSION

Various pyridinium salts are utilized as coenzyme models. Pyridine and its derivatives, e.g. nicotinic acid, act as electron donors on mixing with electron acceptor sites such as riboflavin[25] and iodine[26] forming charge-transfer complexes. Kosower and his co-workers[27] show that pyridinium ion acts as an electron-acceptor on forming intermolecular charge-transfer complexes with iodide ion as the electron-donor species. Such complexes are essentially ion-pairs in the ground state.[24(b)] Absorption of energy within the CT-band causes excitation to a covalent excited state. The coloured nature of the quinolinium iodides[28] compared with the lake of visible absorption by most of their other salts was explained in terms of charge-transfer interaction between the two ions. Bis-pyridinium cation derivatives form 1 :1 charge-transfer complexes with neutral donor species[29]. The formation of CT-complexes between neutral donors and aromatic cations has also been reported.[30]

Table 1

The $\lambda_{max}(\varepsilon_{max})$ values of the CT-bands of styryl cyanine dyes (I—IX) and nicotine-dye combinations, isosbestic points position and equilibrium constants associated with the interactions of dye (I, III—VI) with nicotine.

	CT-band			Isosbestic	
Dye	$\lambda_{max}^{D}(\varepsilon_{max}^{D} \cdot 10^{-3})$	Combination	$\lambda_{max}^{ND}(\varepsilon_{max}^{ND} \cdot 10^{-3})$	point position (nm)	$K_c^{ND} \cdot 10^{-3}$ (M^{-1})
I	348(9.7)	Nicotine-dye(I)	424(7.7)	375	5.99
II	330*sh*(8.3)	Nicotine-dye(II)	—	—	—
III	394(30.2)	Nicotine-dye(III)	506(27.4)	434	16.40
IV	406(37.7)	Nicotine-dye(IV)	496(47.6)	436	7.08
V	511(4.0)	Nicotine-dye(V)	549(7.9)	473	11.66
VI	404(13.7)	Nicotine-dye(VI)	505(7.1)	444	7.61
VII	400(29.0)	Nicotine-dye(VII)	—	—	—
VIII	364(29.5)	Nicotine-dye(VIII)	—	—	—
IX	585(6.3)	Nicotine-dye(IX)	—	—	—

i) λ_{max} in nm ; ε_{max} in cm^2 mole^{-1}.
ii) All measurements were carried out in 10%(v/v) aqueous ethanol mixture at 29°C.
iii) Nicotine has a characteristic band : $\lambda_{max} = 261$ nm ($\varepsilon_{max} = 3.5 \times 10^3$ cm^2 mole^{-1}).

Experimental results showed that nicotine absorption spectra is not changed by the addition of iodide ions, indicating that there is no charge-transfer interaction between nicotine and iodide ions.

Addition of various amounts of nicotine to a solution containing fixed concentration of dyes (I, III—VI) causes a decrease in the dye absorptivity with a gradual development of a new band at considerably longer wavelength, characteristic for the complex formed (c.f. Figs. 2 and 3). The spectra show isosbestic point which may be taken as an evidence for 1 :1 complex formation.[31] Application of Eq.(6) gives linear slopes supporting this suggestion (c.f. Fig. 4). The results show wavelength independence of the equilibrium constant indicating the formation of one type of complex.[32]

Exact complex geometry cannot be determined from the present absorption measurements, but parallel stucking interactions between nicotine and dye can be invoked as they have been for similar systems.[33]

In the present investigation, it was found that the ability of nicotine to form charge-transfer complexes with styryl cyanine dyes depends mainly on their molecular structure. Thus, 2[2-hydroxystyryl] pyridinium-1-ethyl iodide (dye I) forms charge-transfer complex on mixing with nicotine. This CT-complex is assumed as 1 :1 parallel stucking interaction between nicotine as an electron donor and dye (I) as an electron acceptor species. The acceptor character of the dye results from the two partially positive centres located at the quaternary nitrogen and the oxygen atom of the hydroxystyryl moiety (c.f. Scheme II-A). The hydrogen atom of the hydroxyl group may act as a bridge between the 0-phenyl of dye(I) and the unshared electron pair located at the N-pyridine of nicotine molecule. The two partially positive centres of dye (I) are located at a distance adopted for that of the two N-atoms of pyridine and pyrrolidinyl moieties of nicotine, since the distance geometry [22] is approximately the same. The suggested 1 :1 parallel stucking interaction is represented by Scheme II-B.[34] Supporting this suggestion, 2[4-hydroxystyryl] pyridinium-1-ethyl iodide (dye II) does not form CT-complex with nicotine as the two positive centres of dye (II) do not fit the distance geometry [22] and the ring-ring [35] size formation with nicotine.

On the other hand 2[2-hydroxystyryl] quinolinium-1-ethyl iodide (dye III) form CT-complex with nicotine similar to that of dye (I); 2[4-hydroxystyryl] quinolinium 1-ethyl iodide (dye IV) gives a CT-complex in contrast to dye (II). This may be attributed to the more delocalization of the positive charge at the N-quaternary atom of quinolinium moiety, due to the extra fused benzene ring which enables the formation of a stable CT-complex with nicotine. The stability constant K_c^{ND} of nicotine-dye (IV) complex (7.08×10^3 M^{-1}) is much less than that of nicotine- dye(III) complex (16.40×10^3 M^{-1}). The use of 2[2,4-dihydroxystyryl] quinolinium-1-ethyl iodide (dye V) gives a CT-complex with $K = 11.66 \times 10^3$ M^{-1}. This value is one half the sum of the stability constants of dyes (III and IV) (c.f. Table 1). This may be interpreted by the fact that dye(V) has two resonance hybrid structures giving two types of complexes (c.f. Scheme II—C). 4[2-Hydroxystyryl] quinolium-1-1-ethyl iodide (dye VI) gives a CT-complex with nicotine of $K_c^{ND} = 7.61 \times \times 10^3$ M^{-1}. This value is much less than that of nicotine-dye (III) complex. The stability constant is approximately the same as that for nicotine-dye(IV) complex (7.08×10^3 M^{-1}); as dyes (IV) and (VI) have approximately the same distance geometry [22] between the two partially positive centres.

Substitution of the hydroxyl group in 4-hydroxystyryl moiety by a methoxyl group (electron releasing) as in dye(VII), or a nitro group (electron withdrawing) as in dye(VIII), abolishes the formation of CT-complexes. This adds new evidence to the rule of the H-bridge formed between the hydrosxystyryl and the N-pyridine moieties, since this hydrogen bridge is cancelled in dyes (VII) and (VIII); consequently no CT-complex will be formed.

Substitution at the ethenyl moiety (—CH = CH—) of the 4-hydroxy styryl group (dye IX) abolishes, also, the formation of CT-complex with nicotine. This may be due to steric congestion between the interacting molecules and the inability to adopt ring-ring conformations needed.[35]

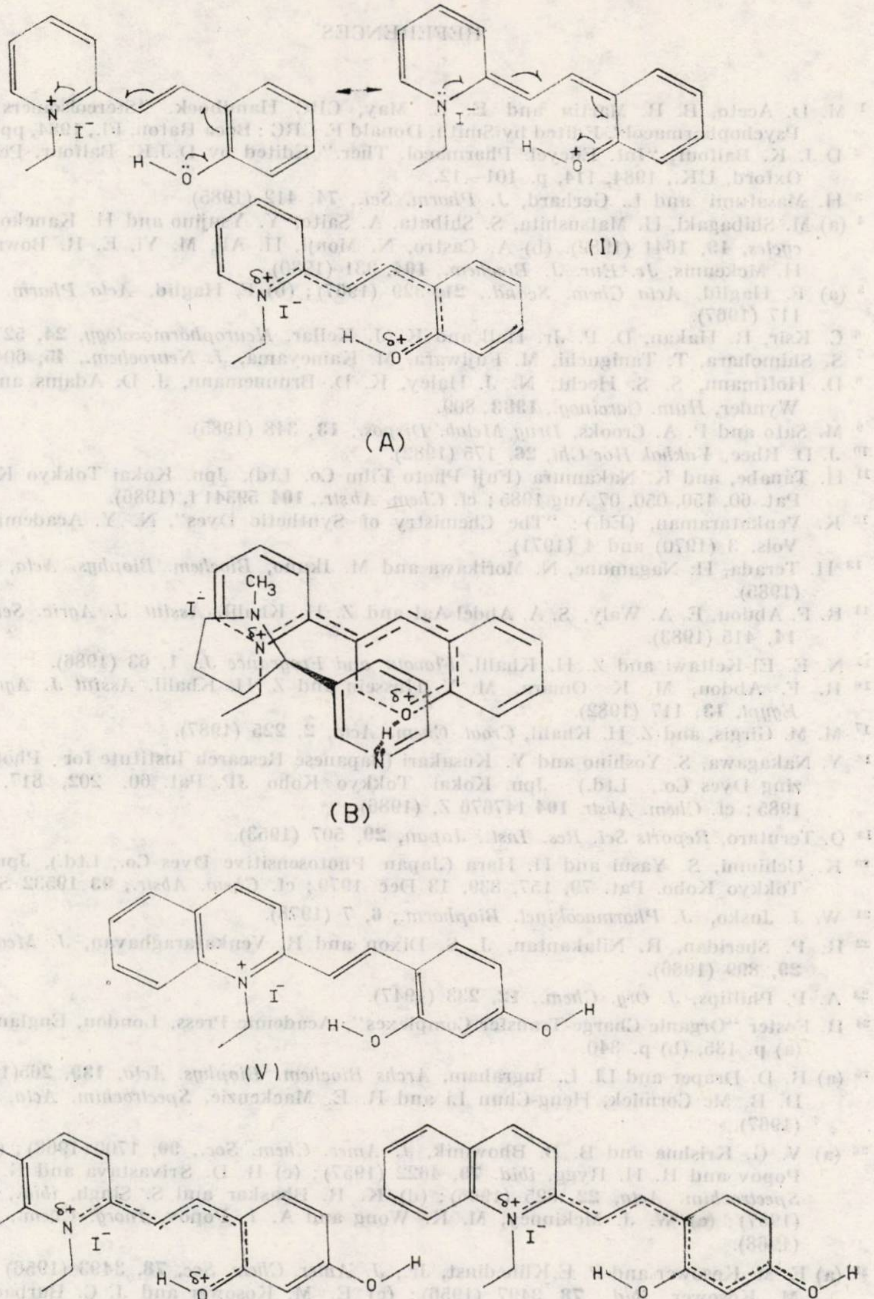
N+
I−
H
O
(I)
δ+
CH3
(A)
(B)
(V)
(C)

Scheme II

REFERENCES

[1] M. D. Aceto, B. R. Martin and E. L. May, CRC Handbook. "Stereoisomers : Drugs Psychopharmacol". Edited by Smith, Donald F. CRC : Boca Raton, Fl., 1984, pp. 67–78.

[2] D.J. K. Balfour, "Int. Encycl. Pharmacol. Ther." Edited by D.J.K. Balfour, Pergamon ; Oxford, UK., 1984, 114, p. 101–12.

[3] H. Masafumi and L. Gerhard, *J. Pharm. Sci.*, **74**, 412 (1985).

[4] (a) M. Shibagaki, H. Matsushita, S. Shibata, A. Saito, Y. Ysujino and H. Kaneko, *Heterocycles*, **19**, 1641 (1982). (b) A. Castro, N. Monji, H. Ali, M. Yi, E. R. Bowman and H. Mckennis, *Jr. Eur. J. Biochem.*, **104**, 331 (1980).

[5] (a) F. Haglid, *Acta Chem. Scand.*, **21**, 329 (1967) ; (b) F. Haglid, *Acta Pharm. Suec.* **4**, 117 (1967).

[6] C. Ksir, R. Hakan, D. P. Jr. Hall and K. J. Kellar, *Neuropharmacology*, **24**, 527 (1985).

[7] S. Shimohara, T. Taniguchi, M. Fujiwara, M. Kameyama, *J. Neurochem.*, **45**, 604 (1985).

[8] D. Hoffmann, S. S. Hecht, N. J. Haley, K. D. Brunnemann, J. D. Adams and E. L. Wynder, *Hum. Carcinog.*, **1983**, 809.

[9] M. Sato and P. A. Crooks, *Drug Metab. Dispos.*, **13**, 348 (1985).

[10] J. D. Rhee, *Yakhak Hoe Chi*, **26**, 175 (1982).

[11] H. Tanabe, and K. Nakamura (Fuji Photo Film Co. Ltd), Jpn. Kokai Tokkyo Koho JP. Pat. 60, 150, 050, 07 Aug 1985 ; cf. *Chem. Abstr.*, **104** 59341 f, (1986).

[12] K. Venkataraman, (Ed.) : "The Chemistry of Synthetic Dyes", N. Y. Academic Press, Vols. 3 (1970) and 4 (1971).

[13] H. Terada, H. Nagamune, N. Morikawa and M. Ikuno, *Biochem. Biophys. Acta*, **807**, 168 (1985).

[14] R. F. Abdou, E. A. Waly, S. A. Abdel Aal and Z. H. Khalil, *Assiut J. Agric. Sci., Egypt* **14**, 415 (1983).

[15] N. E. El-Keltawi and Z. H. Khalil, *Flavour and Fragrance J.*, **1**, 63 (1986).

[16] R. F. Abdou, M. K. Omara, M. Y. Hussein and Z. H. Khalil, *Assiut J. Agric. Sci., Egypt*, **13**, 117 (1982).

[17] M. M. Girgis, and Z. H. Khalil, *Croat. Chem. Acta*, **2**, 225 (1987).

[18] Y. Nakagawa, S. Yoshino and Y. Kusakari (Japanese Research Institute for Photosensitizing Dyes Co., Ltd.) Jpn. Kokai Tokkyo Koho JP. Pat. 60, 202, 817, 14 Oct 1985 ; cf. *Chem. Abstr.* **104** 147676 Z, (1986).

[19] O. Terutaro, *Reports Sci. Res. Inst., Japan*, **29**, 507 (1953).

[20] K. Uchiumi, S. Yasui and H. Hara (Japan Photosensitive Dyes Co., Ltd.), Jpn. Kokai Tokkyo Koho. Pat. 79, 157, 839, 13 Dec 1979 ; cf. *Chem. Abstr.*, **93** 19532 S, (1980).

[21] W. J. Jusko, *J. Pharmacokinet. Biopharm.*, **6**, 7 (1978).

[22] R. P. Sheridan, R. Nilakantan, J. S. Dixon and R. Venkataraghavan, *J. Med. Chem.*, **29**, 899 (1986).

[23] A. P. Phillips, *J. Org. Chem.*, **12**, 233 (1947).

[24] R. Foster "Organic Charge-Transfer Complexes", Academic Press, London, England, 1969, (a) p. 135, (b) p. 340.

[25] (a) R. D. Draper and Ll. L. Ingraham, *Archs Biochem. Biophys. Acta*, **139**, 265(1970) ; (b) D. B. Mc Cormick, Heng-Chun Li and R. E. Mackenzie, *Spectrochim. Acta*, **23**, 2353 (1967).

[26] (a) V. G. Krishna and B. B. Bhowmik, *J. Amer. Chem. Soc.*, **90**, 1700 (1968) ; (b) A. I. Popov and R. H. Rygg, *ibid.* **79**, 4622 (1957) ; (c) R. D. Srivastava and G. Prasad, *Spectrochim. Acta*, **22**, 825 (1966) ; (d) K. R. Bhaskar and S. Singh, *ibid.*, **23**, 1155 (1967) ; (e) W. J. Mckinney, M. K. Wong and A. I. Popov, *Inorg. Chem.*, **7**, 1001 (1968).

[27] (a) E. M. Kosower and P. E.Klinedinst, Jr., *J. Amer. Chem. Soc*, **78**, 3493 (1956) ; (b) E. M. Kosower, *ibid.*, **78**, 3497 (1956) ; (c) E. M. Kosower and J. C. Burbach, *ibid.*, **78**, 5838 (1956) ; (d) E. M. Kosower, *ibid.*, **80**, 3253 (1958) ; (e) E. M. Kosower, J. A. Skorez, W. M. Schwarz, Jr. and J. W. Patton, *ibid*·, **82**, 2188 (1960) ; (f) E. M. Kosower and J. A. Skorez, *ibid.*, **82**, 2195 (1960) ; (g) E. M. Kosower, "Molecular Biochemistry", McGraw-Hill, New York (1962), p. 180.

[28] (a) S. F. Mason, *J. Chem. Soc.* **1960** 2437 ; (b) G. Briegleb, W. Jung and W. Herre, *Z. phys. Chem. Frankf. Ausg.*, **38**, 253 (1963).

[29] (a) A. Nakahara and J. H. Wang, *J. phys. Chem., Ithaca*, **67**, 496 (1963). (b) A Ledwith, and D. H. Iles, *Chem. in Britain*, **4**, 266 (1968).

[30] (a) M. Feldman and S. Winstein, *J. Amer. chem. Soc.*, **83**, 3338 (1961); (b) G. Briegleb, W. Rüttiger and W. Jung, *Angew Chem.*, **75**, 671 (1963).

[31] M. Gouterman and P. E. Stevenson, *J. Chem. Phys.*, **37**, 2266 (1965).

[32] G. D. Johnson and R. E. Bower, *J. Amer. chem. Soc.*, **87**, 1655 (1965).

[33] (a) J. L. Dimicoli and C. Helene, *J. Amer. chem. Soc.*, **95**, 1036 (1973); (b) J. L. Dimicoli, *Bichem. Biophys. Acta*, **254**, 349 (1971).

[34] J. C. M. Tsibris, D. B. Mc Cormick and L. D. Wright, *Biochemistry*, **4**, 504 (1965).

[35] I. S. Jaffrey, V. S. Henry, H. Homer and G. Roseanne, *J. Amer. chem. Soc.*, **102**, 7741 (1980).

Revue Roumaine de Chimie, **34**, 8, 1733–1743 (1989)

ÉTUDE GÉNÉRALE DE LA RÉACTION DE BENZYLATION DES HYDROCARBURES AROMATIQUES FONCTIONNELS, CATALYSÉE PAR DES COMPLEXES DE RUTHÉNIUM

R. JAOUHARI
Laboratoire de Chimie de Coordination (CNRS UA415)
Université de Rennes, Campus Beaulieu 35042 Rennes Cedex France

Reçu le 21 novembre, 1987

On décrit une nouvelle réaction de benzylation des composés aromatiques fonctionnalisés. On a étudié les paramètres réactionnels. La benzylation peut être réalisée sans solvant et on peut recycler les complexes catalytiques du ruthénium.

A new ruthenium catalysed reaction of the benzylation of functional aromatic compounds is described. An examination of reactional parameters is studied. The benzylation reaction may be carried out without the use if any solvent, and the recycle of complexes is possible.

L'alkylation des substrats aromatiques, soit à partir d'halogénures d'aryle ou d'alkyle, soit à partir de benzylalcools, représente toujours un potentiel synthétique important en chimie organique.[1] Le centre d'intérêt de cette réaction a été accru ces dernières années, si on se réfère aux nombres des publications et brevets d'invention déposés, concernant la nature des produits synthétisés et les applications industrielles qui en dérivent.

L'alkylation d'un substrat aromatique comme le phénol ou l'un des dérivés, par un radical benzyle, permet d'accéder à des produits ayant un intérêt comme des agents antioxydants pour un nombre variable des matériaux organiques,[2] ou possédant des propriétés anti-bactérielles.[3]

Récemment, un brevet américain a décrit l'alkylation du phénol par le benzylalcool en phase hétérogène, en présence d'alumine Al_2O_3 comme catalyseur et à des températures élevés : 220° — 450°C. Le rendement du produit benzylé « benzyle-2 phenol » atteint dans les meilleurs conditions 20% et dépend fortement du rapport $PhCH_2OH/PhOH$[2]. Le même produit a été breveté par Mitsubishi Chemical Industries Co. Ltd.,[4] en phase homogène et avec l'utilisation d'alumine comme catalyseur, le rendement étant 49,9 %. La benzylation de chloro-4 phénol en position *ortho* de la fonction OH, possédant les propriétés microbiologiques, a été breveté avec un rendement de 20%, le catalyseur ayant un copolymère divinylbenzène-styrène sulfonique.[5]

D'autre part, l'alkylation des hydrocarbures aromatiques e.g. le benzène, les alkylbenzènes, le naphtalène, par le radical benzyle, conduit à des intermédiaires synthétiques permettant de modifier les propriétés chimiques de certains types d'huiles, ces produits possédant des viscosités variables, sont thérmiquement stables au dessus de 200° – 300°C. De cette façon, la benzylation de p-xylène et t-butyl-4-toluène par le chlorure de benzyle a été brevetée,[6] en utilisant comme catalyseurs le stéarate de zinc et de fer, des salycylates de fer ou d'acétylacétonate de fer, la zone de température employée étant entre 110° – 140°C.

Le BASF, pour sa part, a breveté la benzylation du toluène en présence de silicate d'aluminium et d'alumine [7] ou en présence des acides minéraux ou acides de Lewis.[8]

Dans la course d'élaborer la réaction de benzylation et de rechercher des nouvelles espèces catalytiques nous décrirons dans cet article un nouveau accès synthétique à la benzylation des divers types des substrats aromatiques, catalysée par des complexes de ruthénium.

La benzylation des composés aromatiques par des complexes de ruthénium n'a jamais été citée en littérature, de même, la mise en évidence du comportement spécifique de ces complexes, en tant qu'initiateur d'alkylation dans une réaction type « Friedel-Crafts ».

Les substrats aromatiques étudiés ont été regroupés en trois catégories :

I — Hydrocarbures aromatiques possédant des groupements fonctionnels donneurs par effet de mésomérie (Effet + M) : phénol, triméthyle-2,4,6 phénol, chloro-4 phénol méthyle-4 phénol et anisole.

II — Hydrocarbures fonctionnels possédant des groupements fonctionnels donneurs par effet électronique (Effet + I) : éthylbenzène, benzène, naphtalène et p-xylène.

III — Hydrocarbures aromatiques possédant deux groupements fonctionnels ayant des effets électroniques opposés (Effets +I et – I) : bromo-4-éthylbenzène, bromo-2-éthylbenzène et chloro-4-toluène.

I. HYDROCARBURES AROMATIQUES POSSÉDANT DES GROUPEMENTS FONCTIONNELS DONNEURS PAR EFFET DE MÉSOMÉRIE

I.1. Phénol

La benzylation du phénol a conduit dans les divers essais réalisés à deux isomères : benzyle-2 et benzyle-4-phénol sont facilement séparables par chromatographie sur silice, tout en tenant compte de la différence de polarité entre les deux produits. La formation de deux produits benzylés est accompagnée par celle de bibenzyle en quantités très faibles (5%).

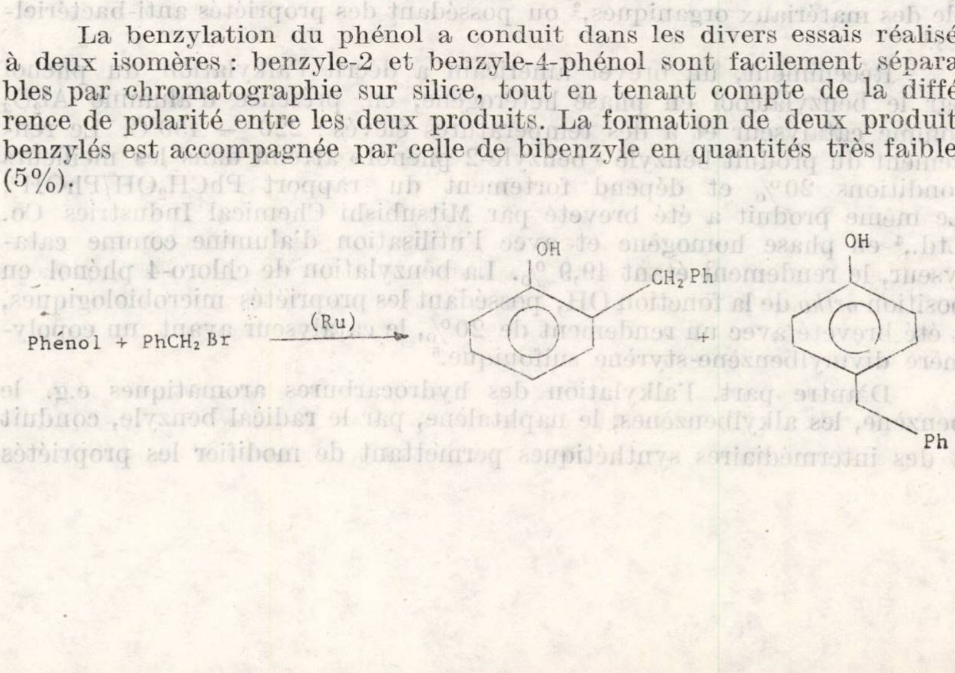

Afin de déterminer les meilleures conditions opératoires pour rendre la réaction plus sélective, nous avons examiné les divers paramètres de la réaction. L'examen a pris en considération : les proportions relatives entre les réactifs, la nature du complexe de ruthénium, l'effet de la température et celui du solvant. Cet examen nous a conduits par la suite à constater que la sélectivité est ameliorée considérablement en l'absence du solvant. La récupération du complexe est possible. En effet, le complexe « recyclé » catalyse la réaction, mais le rendement observé ne représente que la moitié de celui obtenu avec le complexe de départ.

En présence d'un solvant comme le THF, le taux de conversion du phénol en produits benzylés est d'env. 40%. En présence du pentane le rendement atteint 52% et en l'absence du solvant le rendement est 60% (tableau 1) ; celui-ci est de l'ordre de 28% si la réaction est réalisée avec un complexe « recyclé » (tableau 1).

En l'absence du solvant, un dégagement d'acide bromohydrique HBr est sensiblement observé. Par contre, en présence d'un solvant comme le THF, l'acide HBr réagit avec le solvant, d'où l'absence d'un dégagement gazeux en fin de la réaction.

Tableau 1

Effet du solvant sur la benzylation du phénol

Solvant	Conversion [a]	% ortho	% para
THF	38,5	49	51
CH_2Cl_2	18,5	47,5	52,5
CH_3CN	26,5	44,3	55,7
C_5H_{12}	50,3	50,1	49,9
non solvant	58,5	33,6	66,4

[a] déterminée par chromatographie en phase vapeur (méthode de l'étalon interne)

La nature du complexe contribue également à la sélectivité de la réaction de benzylation, dans le sens décroissant suivant : $RuCl_3, xH_2O > RuCl_3, xH_2O + PBu_3 > PcyRuCl_2PMe_3 > (Ru(CO)_2\ (OAc)\ (PPh_3))_2 > (PcyRuCl_2)_2 > Ru_3(CO)_2$

Comparativement à un acide de Lewis e.g. $ZnCl_2$, $SnCl_2$, les complexes de ruthénium sont largement éfficaces pour catalyser la réaction, dans les conditions opératoires appliquées (tableau 2).

Tableau 2

Effet du catalyseur sur la benzylation du phénol[a]

Catalyseur	Conversion	% ortho	% para
$RuCl_3$, xH_2O	38,5	49	51
$PcyRuCl_2PMe_3$[b]	34,9	43,3	56,7
$(PcyRuCl_2)_2$	24,9	47,15	52,85
$[Ru(CO)_2(OAc)(P(C_6H_5)_3)]_2$	26,5	56,5	43,5
$RuCl_3$, $xH_2O + PBu_3$	20,2	59,8	40,2
$Ru_3(CO)_{12}$	11,7	30,25	69,75
$ZnCl_2$	20,5	59,8	40,2
$SnCl_2$	18,5	62,5	47,5

[a] solvant de la réaction : THF.

[b] Pcy = para-cymène

D'autre part, la réaction de benzylation dépend du rapport (PhOH)/(Ru). Pour un rapport égal à 107, la formation des produits benzylés est favorisée. Une augmentation excessive de la concentration en bromure de benzyle par rapport au substrat favorise la formation du bibenzyle et, par conséquent, une diminution du rendement de la réaction (tableau 3).

Tableau 3

Effets des rapports $(PhCH_2Br)/(Ru)$ et $(PhCH_2Br)/(phénol)$ sur la benzylation du phénol

$(PhCH_2Br)/(Ru)^a$	$(PhCH_2Br)/(phénol)$	Conversion	%	
			ortho	para
27,5	1,1	22,5	41	59
53,2	1,1	34,6	37	63
107	1,1	38,5	49	51
107	2,2	17,2	47	53

[a] $(Ru) = (RuCl_3, xH_2O)$

L'effet de la température est important. Pour retrouver le meilleur taux de la conversion du phénol en produits réactionnels, il faut atteindre le seuil de 155°C (tableau 4).

Tableau 4

Effet de la température sur la benzylation du phénol

Température/Temps		Conversion	%	
0°C	h		ortho	para
25	24	0		
75	24	9,1	34,1	65,9
155	24	38,5	49	51

I.2. Phénols substitués

Triméthyle-2,-4,-6-phénol, méthyle-4-phénol et chloro-4-phénol en solution dans le bromure de benzyle et en la présence catalytique de $RuCl_3$, xH_2O sont benzylés avec des rendements 60, 51 et 46% respectivement (tableau 5).

Tableau 5

Benzylation des phénols substitués

Substrat	Conversion	Produits benzylés
Triméthyle-2, -4, -6 phénol	60	Triméthyle-2, -4, -6 benzyle-2-phénol
Méthyle-4-phénol	51^a	Méthyle-4-benzyle-2-phénol *I* Méthyle-4-benzyle-2-phénol *II*
Chloro-4-phénol	46	Chloro-4-benzyle-2-phénol

a) rapport des isomères *I*/*II* = 83/17

I.3. Anisole

L'anisole, en solution dans le THF, est benzylé en deux positions : *ortho* et *para*. Le rendement de la réaction dépend fortement du rapport $(PhOCH_3)/(Ru)$. Pour un rapport égal à 53, le rendement est de 20%. Celui-ci atteint 50% pour un rapport de 107.

Les complexes de ruthénium ne semblent pas avoir d'efficacités catalytiques différentes.

$$RuCl_3, xH_2O \sim PcyRuCl_2PMe_3 \sim (PcyRuCl_2)_2$$

La formation de l'isomère *para* est un peu plus favorisée dans le cas de l'anisole que dans celui du phénol, ceci étant dû probablement à l'effet stérique provoqué par le groupe méthoxy.

En l'absence du solvant, ou en présence du pentane, la réaction de benzylation conduit à la formation de benzyle-2 et -4-phénol (80%) (tableau 6).

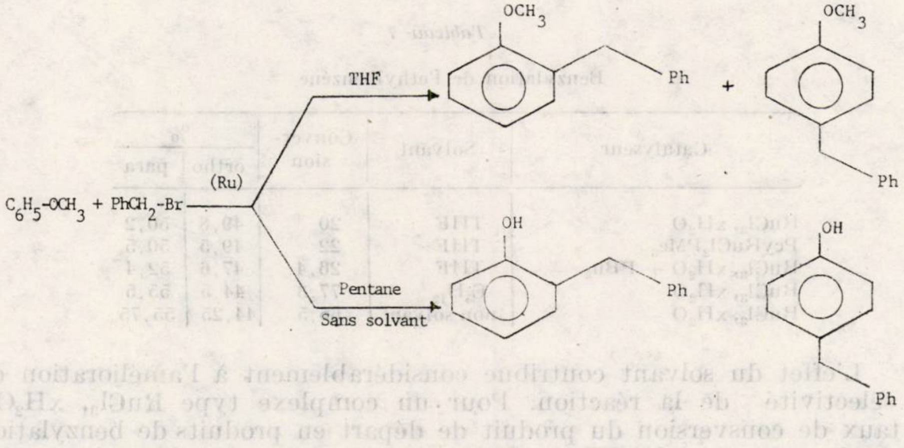

Tableau 6

Benzylation de l'anisole

Catalyseur	$(PhOCH_3)/(Ru)$	$(PhCH_2Br)/(PhOCH_3)$	Solvant	Conversion	% ortho	% para
$RuCl_3, xH_2O$	53,2	1,1	THF	20,1	39,9	60,1
$RuCl_3, xH_2O$	107	1,1	THF	51,4	38,8	61,2
$RuCl_3, xH_2O$	107	1,1	THF	48,7	34,7	65,3
$PcyRuCl_2PMe_3$	107	1,1	THF	49,8	32,8	67,2
$(PcyRuCl_2)_2$	107	1,1	THF	50,6	38,9	61,1
$RuCl_3, xH_2O$	107	1,1	non solvant	79[a]	25,7	74,3

[a] Rdt du benzyle-2 et -4-phénol

En effet, l'acide bromohydrique formé au cours de la réaction, provoque l'hydrolyse de l'éther benzylé ; par contre, en présence de THF, l'acide dégagé, en réagissant de préférence avec le THF, ne provoque pas l'hydrolyse de la fonction éther.

II. Hydrocarbures aromatiques possédant des groupements fonctionnels donneurs par effet électronique

II.1. Ethylbenzène

En présence d'un complexe de ruthenium, l'éthylbenzène est alkylé par le radical benzyle en positions *ortho* et *para*, dont les proportions relatives ne subissent pas une modification notable, en raison de la variation des conditions opératoires (tableau 7).

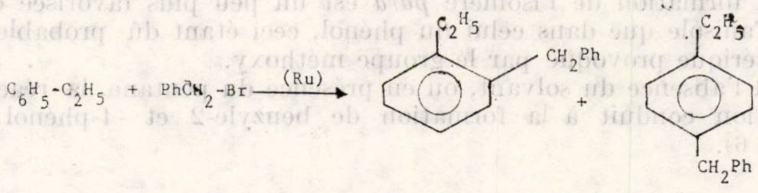

Tableau 7

Benzylation de l'ethylbenzéne

Catalyseur	Solvant	Conversion	% ortho	% para
$RuCl_3, xH_2O$	THF	20	49,8	50,2
$PcyRuCl_2PMe_3$	THF	22	49,5	50,5
$RuCl_3, xH_2O + PBu_3$	THF	26,4	47,6	52,4
$RuCl_3, xH_2O$	C_5H_{12}	77,3	44,5	55,5
$RuCl_3, xH_2O$	non solvant	65,5	44,25	55,75

L'effet du solvant contribue considérablement à l'amélioration de la sélectivité de la réaction. Pour un complexe type $RuCl_3$, xH_2O^2, le taux de consversion du produit de départ en produits de benzylation passe de 24% dans le THF à 78% dans le pentane. L'extraction des produits est plus aisée dans la pentane, dû à la solubilité des produits benzylés dans le pentane, alors que le complexe « recyclé » n'est pas soluble. Ce dernier, soluble dans le THF, est analysé en C.P.V.; l'analyse permet de détecter de très faibles quantités réstantes de produits benzylés, inférieures à 8%. Dans le THF, la formation de bibenzyle ne représente que 5%.

II.2. Benzène, naphtalène et p-Xylène

Le taux de conversion de benzène en diphénylméthane est 16%, si la réaction est réalisée en l'absence du solvant. Par couplage C.P.V. — spectrométrie de masse, on détecte des produits lourds correspondant à une disubstitution et trisubstitution du benzène et du diphénylméthane.

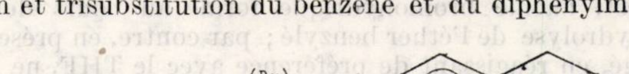

Le naphtalène, possédant une réactivité plus grande que celle du benzène en matière de substitution électrophile pourrait se convertir en produits benzylés avec un rendement de 27% dans le THF et en présence d'un catalyseur type : $PcyRuCl_2PMe_3$. Les deux isomères possibles ont été formés : benzyle-1-naphtalène (*1*) et benzyle-2-naphtalène(*2*), dont les proportions relatives reflètent réellement la réactivité des deux sites alkylés par le radical benzyle (*1/2* = 70/30) (tableau 8).

Tableau 8

Benzylation du benzène, naphtalène et p-xylène

Substrat	Catalyseur	Solvant	Conversion	Rapport des isomères *1/2*
Benzène	$RuCl_3$, xH_2O	THF	10,3	
	$PcyRuCl_2PMe_3$	THF	8,2	
	$(PcyRuCl_2)_2$	THF	8,1	
	$RuCl_3$, xH_2O	non solvant	16,2	
Naphtalène	$RuCl_3$, xH_2O	THF	23,9	78,7/21,3
	$PcyRuCl_2PMe_3$	C_5H_{12}	27,4	70,5/29,5
	$RuCl_3$, xH_2O	non solvant	35,5	25,5/74,5
p-Xylène	$RuCl_3$, xH_2O	non solvant	38	

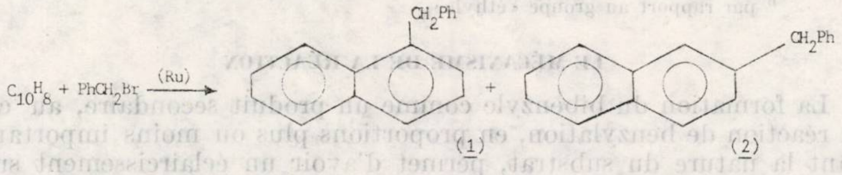

Un inversement des réactivités est observé, si la réaction est réalisée sans solvant, les proportions étant : *1/2* = 25/75 et le rendement de la réaction est 36%.

Le p-xylène conduit au cours de la réaction de benzylation catalysée par $RuCl_3$, xH_2O à un seul produit : benzyle-2-méthyle-4-toluène avec 38% de conversion du produit de départ.

III. Hydrocarbures aromatiques possédant deux groupements fonctionnels ayant des effets électroniques opposés

L'alkylation d'un hydrocarbure aromatique possédant un groupe électrono-attracteur comme le brome, le chlore, l'éthoxycarbonyl ou l'acétyl, par le radical benzyle, n'a pas eu lieu au cours de la réaction avec le bromure de benzyle catalysée par des complexes de ruthenium. En effet, le bromobenzène reste inactif vis-à-vis de la réaction de benzylation ; l'addition d'un groupe « ethyle » sur le bromobenzène en position 2 ou 4 donne lieu a des faibles quantités des produits benzylés.

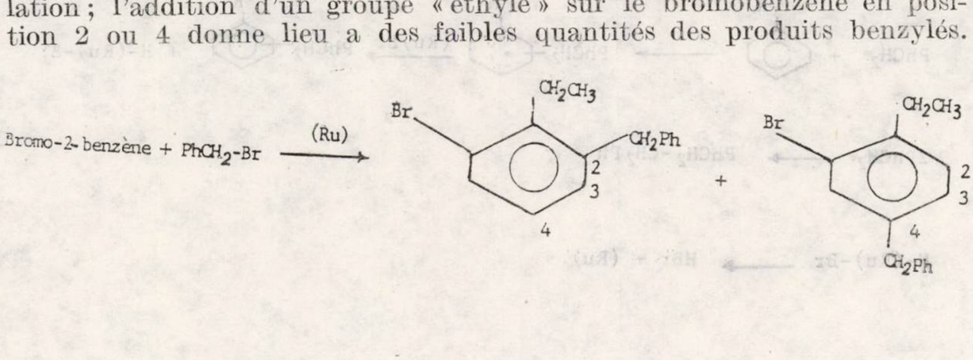

L'alkylation de ces substrats exige une concentration du catalyseur par rapport au substrat, plus importante que celle employée dans la benzylation de l'éthylbenzène. Le taux de conversion du bromo-4-éthylbenzène en produits de réaction passe de l'ordre des traces, pour un rapport (substrat)/(Ru) = 20, jusqu'à 7%, pour un rapport égal à 7. Le même phénomène a été constaté dans le cas de bromo-2- éthylbenzène et chloro-4 toluène (tableau 9).

Tableau 9

Benzylation des divers hydrocarbures aromatiques fonctionnels[a]

Substrat	Catalyseur	Conversion	Substitution[b]		
			2	3	4
Bromo-2-éthylbenzène	$RuCl_3$, xH_2O	7,5	47		53
Bromo-4-éthylbenzène	$RuCl_3$, xH_2O	7	100		
Chloro-4-éthylbenzène	$(PcyRuCl_2)_2$	8	100		

[a] (Ru) = 1 mmol, (substrat) = 7 mmol, ($PhCH_2Br$) = 12 mmol, 160°C/30h.

[b] par rapport au groupe « éthyle ».

LE MÉCANISME DE LA RÉACTION

La formation du bibenzyle comme un produit secondaire, au cours de la réaction de benzylation, en proportions plus ou moins importantes, suivant la nature du substrat, permet d'avoir un éclaircissement sur le mécanisme de la formation du produit benzylé.

En effet, il a été constaté que plus le taux de conversion du substrat en produit benzylé est élevé, plus la formation du bibenzyle est défavorisée, et vice-versa. Par ailleurs, il est bien connu que les complexes de ruthénium peuvent se comporter comme des initiateurs radicalaires,[10] en abstractant un halogène, tout en dépendant des conditions opératoires utilisées. Il est très probable dans nos conditions que le radical benzyle soit formé à la suite d'un déplacement homolytique du brome dans le bromure de benzyle provoqué par le complexe de ruthénium, ce qui permet de penser que la formation du bibenzyle est due au couplage de deux radicaux benzyle ; toute autre possibilité est écartée, en raison de la difficulté imposée par l'assimilation d'un complexe de ruthénium à un acide de Lewis.

$$(Ru) + PhCH_2Br \longrightarrow (Ru)\text{-}Br + PhCH_2^{\bullet}$$

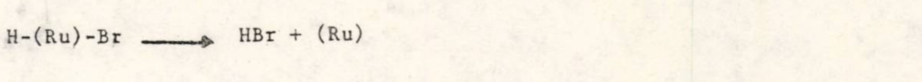

$$2PhCH_2^{\bullet} \longrightarrow PhCH_2\text{-}CH_2Ph$$

$$H\text{-}(Ru)\text{-}Br \longrightarrow HBr + (Ru)$$

Le mécanisme suggéré tient compte du fait que : (1) le complexe résiduel à la fin de la réaction n'est que le complexe de départ, en raison de la possibilité du recyclage du complexe dans un nouveau processus catalytique ; (2) l'acide bromohydrique est présent à la fin de la réaction, si celle-ci est effectuée sans solvant ou en présence d'un solvant aprotique.

CONCLUSION

Parallèlement aux procédures industrielles qui sont généralement limitées à une seule catégorie des produits, la réaction de benzylation en présence des complexes de ruthénium est applicable à diverses catégories d'hydrocarbures aromatiques fonctionnels ou non. D'autre part, le recyclage du complexe est possible. La réaction de benzylation est réalisable sans la nécessité d'un solvant, de même, l'extraction des produits benzylés est facilitée par l'absence ou les très faibles quantités des produits secondaires. Enfin, les deux isomères obtenus dans la plupart des cas étudiés sont facilement séparables sur chromatographie liquide-solide ou sur H.P.L.C..

SECTION EXPÉRIMENTALE

Les substrats aromatiques, et le bromure de benzyle sont commercialisés et utilisés sans aucune purification préalable.

Benzyle-2 et -4-anisole sont préparés par réaction de l'iodure de méthyle sur le sel de sodium du phénol correspondant. Les produits benzylés authentiques de tous les autres substrats étudiés sont synthétisés par réaction de l'organomagnesium du dérivé bromé correspondant, soit sur le bromure de benzyle, soit sur le chlorure de benzoyle suivie par la réduction de Clemenson [9].

Les analyses quantitatives par C.P.V. sont réalisées sur Intersmat IGC 1200 DFL, avec détecteur à ionisation flamme. Les spectre d'I.R. ont été enregistrés à partir de l'appareil Perkin-Elmer 457, les échantillons ont été préparés dans une suspension de Nujol. Les spectres de masses à 70 ev ont été déterminés avec un appareil Varian Mat 311, les spectres RMN ^{1}H et ^{13}C sont enregistrés sur le spectromètre Bruker 300 WB à 300MHz pour ^{1}H et 75.47 MHz pour ^{13}C.

PROCÉDURES GÉNÉRALES DE BENZYLATION DES SUBSTRATS AROMATIQUES FONCTIONNELS

* Benzylation du phénol

Dans un tube de Schlenk de 250 ml, muni d'un barreau aimanté et purgé à l'argon, on introduit successivement : 0,062 g (0,25 mmol) du complexe de $RuCl_3, xH_2O$, 2,5 g (26,6 mmol) du phénol et 3,5 ml (29,43 mmol) du bromure de benzyle. On agite et on chauffe le mélange dans un bain d'huile thermostaté à 155°C pendant 24h, puis on le ramène à la température ambiante. On additionne 10 ml (5/5) de deux solvants THF/pentane, en laissant agiter le mélange pendant 15 minutes. Le mélange est filtré, le filtrat est analysé par Chromatographie en Phase Vapeur (C.P.V.) (Chromosorb W 80/100 mesh, FFAP à 10%, détecteur F.I.D., $T_{four} = 220°$ C, $T_{inj} = T_{det} = 280°$C, $P_{N_2} = 2{,}4$ bar). Le taux de conversion du phénol en hydroxy-2 et hydroxy-4-diphénylméthane est de 58,5% (méthode de l'étalon interne : triphénylméthane) (proportions relatives : 33,6/66,4).

Le filtrat est évaporé et repris par 5 ml d'éther, on purifie le résidu sur une colonne d'alumine (20 × 2 cm), 50 g Al_2O_3). L'élution avec des mélanges benzène / éther conduit à l'obtention de l'hydroxy-2 et 4-diphénylméthane avec un rendement global de 48%. Les deux produits ont été identifiés en C.P. par comparaison avec des échantillons authentiques.

Benzylation de l'éthylbenzène

Dans un autoclave en acier, muni d'un barreau aimanté et purgé à l'argon, on place successivement : 0,132 g (0,5 mmol) de $RuCl_3$, xH_2O, 2,5 ml (20,4 mmol), 3,5 ml (29,4 mmol) de bromure de benzyle et 10 ml de pentane.

On agite et on chauffe le mélange dans un bain d'huile thermostaté à 160°C, pendant 24h. Apres un traitement similaire à celui utilisé dans la benzylation du phénol, les produits benzylés sont extraits par distillation. Les deux isomères éthyle-2 et 4-diphénylméthane ont été obtenus (proportions relatives 44,5/55,5), ils ont été identifiés en C.P.V. par comparaison avec des échantillons authentiques préparés. Le rendement de la distillation est 61,5% (en C.P.V., le taux de conversion est 77,3 (étalon interne : diphénylméthane, FFAP « décrit précédement », programmation de température : 6°C/1 min. entre 100° – 220°C à partir de 1 bar/N_2).

Les deux isomères ont été séparés sur alumine en utilisant comme éluant le benzène. Chaque isomère a été obtenu souillé par 20–25% de l'autre isomère.

EFFET DE L'AGENT DE BENZYLATION

Selon les mêmes procédures expérimentales, nous avons étudié, parallèlement au bromure de benzyle, d'autres halogénures de benzyle : chlorure de benzyle, iodure de benzyle, bromo-2 et 4-bromure de benzyle et méthyle-2 et 4-bromure de benzyle. Quoi qu'il en soit, la nature de l'agent de benzylation n'affecte pas la réaction de l'alkylation catalysée par des complexes de ruthénium.

REMERCIEMENT. L'auteur remercie la S.N.P.E. pour l'aide financier apporté à la réalisation de ce travail. Le professeur P. H. Dixneuf est gracieusement remercié pour ces suggestions fructueuses, ainsi que le Dr C. Ruppin, pour sa participation à la préparation des complexes de ruthénium.

REFERENCES

[1] N. Mine, Y. Fujiwara et H. Taniguchi, *Chemistry Letters*, 357 (1986), et références citées. K. Laali, *J. Org. Chem.*, **50**, 3638 (1985).

[2] A. H. Filbey, H. G. Jr. Braxton et B. K. Melsmer U. S., 4,514,577 30 avr. 1985, Appl. 334, 827, 15 oct. 1982.

[3] I.R.C.B.A., Fr. Demande 2,144,578, 23 Mar 1973, Appl. 7 124, 694, 06 juil. 1973.

[4] Mitsubishi Chemical Industries Co. Ltd. Jpn. 84,186,937, 23 oct. 1984, Appl. 83,60, 539, 06 avr. 1983.

[5] Z. Vodak, F. Krsnak et L. Bechtold Czech, 170,972, 15 jan. 1978, Appl 74/392 22 jan. 1974.

[6] V. V. Borodovitsyn, R. P. Savayah, Yu. V. Pozdnyakovich et S. M. Shein USSR, SU, 1, 020, 418, 04 mai 1983, Appl. 3, 339, 703 07 sept. 1981.

[7] F. Nestler, K. G. Baur, M. Patsch et T. Jacobsen Ger. Offen., 2,547,030, 05 mai 1977, Appl. 21 oct. 1975.

[8] H. Elingsfeld, M. Patsch, K. G. Baur et W. Ruehenbeck Ger. Offen., 2,456,747, 10 juin 1976, Appl. 30 Nov. 1974.

[9] A. Ramasubbu, R. H. Scott et P. Stevenson, *J. Chem. Soc., Perkin Trans.*, 1515 (1987).

[10] K. Von Auwers et T. Markovits, *Chem. Ber.*, 2332 (1908).

Revue Roumaine de Chimie, **34,** *8*, 1745–1752 (1989)

CHEMICAL GRAPHS. PART 51.[1]

VALENCE ISOMERS OF BIS-HOMOANNULENES

ALEXANDRU T. BALABAN
Polytechnic Institute, Organic Chemistry Department, Splaiul Independenţei 313,
77206 Bucharest, Romania

Received April 2, 1989

Constitutional graphs of bis-homoannulenes $(CH)_{2k}(CH_2)_2$ with $p = 2k + 2 = 4$, 6, and 8 carbon atoms are displayed. The same constitutional formulas are valid for the corresponding diones. Known interconversions among some of the valence isomers are discussed in the introduction section and possible new interconversions in the concluding section.

INTRODUCTION

Valence isomers of bis-homoannulenes are hydrocarbons with general formula $(CH)_{2k}(CH_2)_2$, where $k = 1, 2, \ldots$. From such hydrocarbons, mono- or diketones may be obtained theoretically by replacing one or two methylene groups by carbonyl groups; whereas the numbers of diketonic formulas are equal to those of the hydrocarbons, the monoketones will be more numerous because some of the $(CH_2)_2$ groups are chemically nonequivalent.

Historically, several interesting isomerizations were reported in this series which is fairly easily accessible because it consists in dihydroderivatives of annulene valence isomers. Attention should be paid, however, to distinguish *valence isomers* from *isomers*:[2] while the two tetrahydronaphthalenes **1** and **2** correspond to compounds forming the object of the present paper (their molecular graphs have 8 vertices of degree three and 2 vertices of degree two), tetralin **3** does not because it has vertices of degree four; tetralin is *isomeric* with the *valence isomers* **1** and **2**.

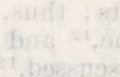
1

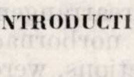
2

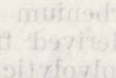
3

Furstoss and Lehn[4] reported almost simultaneously with Masamune[5] and Dauben's groups[6] the synthesis of basketene $(CH)_{10}$; however, the spectra of products differed though the mp's were the same. What had happened was that the first authors had obtained snoutene, another $(CH)_{10}$ isomer, by a rearrangement catalyzed by silver(I) ions.

The correct structure elucidation triggered the rapid development of metal ion catalyzed rearrangements. Practically equivalent rearrangements occur with dihydrobasketene (1,8-bis-homocubane derivatives) **4** which in the presence of silver(I) or palladium(II) complexes or salts yield dihydrosnoutenes **5**, but in the presence of Rh(I) or Ni(0) complexes afford stereoisometric dihydro-Nenitzescu hydrocarbon derivatives **6a**, **6b**.[7–10] Such valence-isomerizations provided much experimental background material for the rationalization by Woodward and Hoffmann[11] of thermally-forbidden reactions which become allowed in the presence of transition metal ions such as Ag(I), Rh(I), Pd(II), Ni(0), etc.

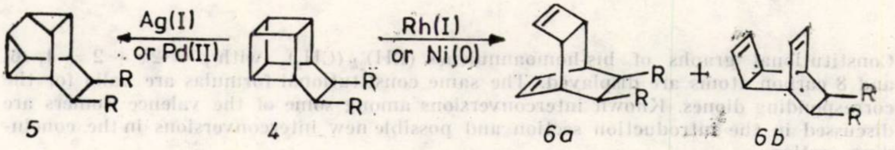

Another aspect involving bis-homoannulene valence isomers is connected with carbenium ion rearrangements; thus, bis-homocyclobutenium dications derived from norbornadiene,[12] and 1,3-bishomocubyl derivatives **7**, **8** in solvolytic reactions, were discussed.[13]

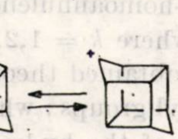

The $AlCl_3$-catalyzed dimerization of hexachlorocyclopentadiene **9** leads to Dechloran, **10**, $(CCl)_8(CCl_2)_2$ which owing to its symmetry has an elevated melting point (485°); this compound is an insecticide, and can also be formed under the catalytic action of $AlCl_3$ or $SbCl_5$ from the dimer **12** of perchlorocyclopentadiene formed via **11**, by reductive dechlorination followed by photochemical chlorination;[14,15] **10** results also from the corresponding ketone (chlordecone **13**) and PCl_5; this ketone is also an insecticide.[16] For both **10** and **13** the initial structure assignment had been in error, and structures **14** and **12** had been discussed and patented.[17–19] The correct structures were determined by McBee.[14,15] Apparently, the structures **10** or **13** are potential energy minima for valence isomers $(CH)_{2k}\,(CH_2)_2$ despite the presence of 4-membered rings, just as adamantane is the most stable valence isomer among saturated tricyclic hydrocarbons with formula $(CH)_4(CH_2)_6$; in the former case (**12** → **10**), a double bond counts as a cycle, and indeed Coulson's model of bent double bonds equates a double bond with a two-membered ring.

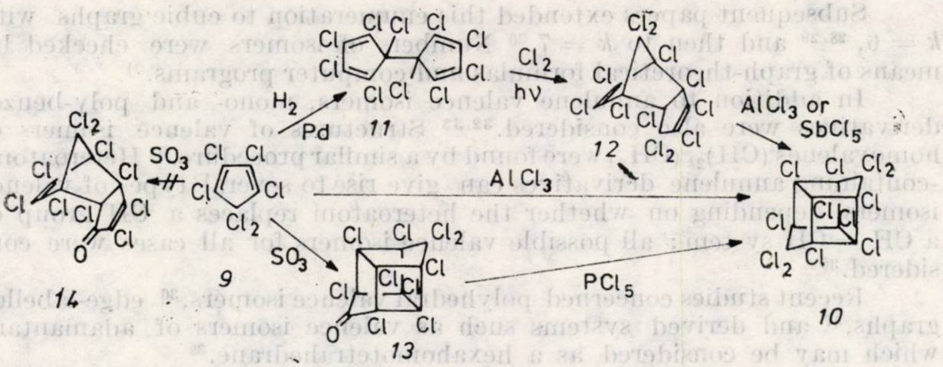

Photochemical valence isomerizations of different bis-homocubane derivatives are also known (Dilling's review[20] may be consulted). The Diels-Alder *endo* dimer of cyclopentadiene **15** undergoes photochemical rearrangement in the presence of acetone as sensitizer affording 1,3-bis-homocubane **16**;[21] on UV irradiation through pyrex, the ketonic derivative **17** yields similarly the monoketo-1,3-bis-homocubane **18**;[22] similar conversions occur with the corresponding tetrachloro- and octachloro-monoketones:[23] UV irradiation of the octachloro-diketone **19** through quartz leads to the perchloro-bis-homocubanedione **20**.[24]

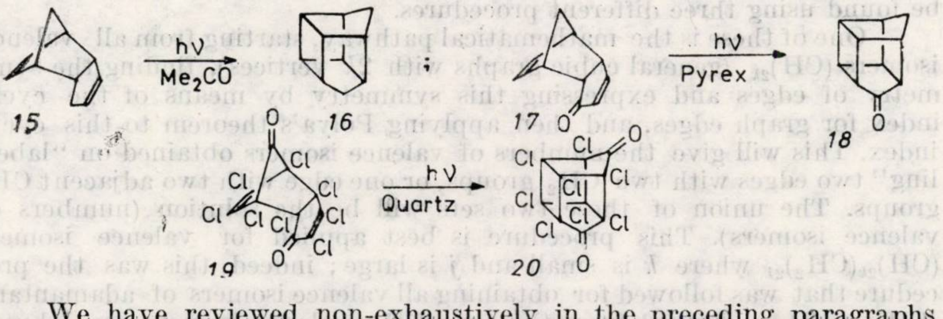

We have reviewed non-exhaustively in the preceding paragraphs a few valence isomerizations of bis-homoannulene valence isomers insisting especially on systems with ten carbon atoms. Many more examples are to be found in a recently published book.[25]

ENUMERATION OF VALENCE ISOMERS

In earlier papers of this series, valence isomers of annulenes $(CH)_{2k}$ with up to ten CH groups ($k = 2$ to 5) were modelled by cubic graphs, in which each vertex symbolizes a CH group and is connected by three edges to other vertices.[2,26] Valence isomers were defined as graphs with the same partition of vertex degrees. Cubic graphs $(CH)_{2k}$ with $k = 1$ to 5 were enumerated and their structures were displayed by means of general cubic multigraphs, in which a vertex may be doubly connected with another vertex and may be also connected with itself by a loop.[27]

Subsequent papers extended this enumeration to cubic graphs with $k = 6$,[28,29] and then to $k = 7$.[30] Numbers of isomers were checked by means of graph-theoretical formulas and computer programs.[31]

In addition to annulene valence isomers, mono- and poly-benzoderivatives were also considered.[32,33] Structures of valence isomers of homovalenes $(CH)_{2k}(CH_2)$ were found by a similar procedure.[34] Heteroatom-containing annulene derivatives can give rise to several types of valence isomers, depending on whether the heteroatom replaces a CH group or a $CH = CH$ system; all possible valence isomers for all cases were considered.[35]

Recent studies concerned polyhedral valence isomers,[36] edge-labelled graphs,[37] and derived systems such as valence isomers of adamantane which may be considered as a hexahomotetrahedrane.[38]

Reviews on these enumerations were published, bringing up-to-date chemically relevant information.[26,29,33] A 3-volume book summarizes the possible numbers of valence isomers for annulenes, benzo-, hetero- and homo-derivatives, as well as the known compounds.[25] Only a minor fraction is known from the large set of such annulene valence isomers and related systems.

VALENCE ISOMERS OF BIS-HOMOANNULENES $(CH)_{2k}(CH_2)_2$

Structural formulas for valence isomers of bis-homoannulenes can be found using three different procedures.

One of these is the mathematical pathway, starting from all valence isomers $(CH)_{2k}$ (general cubic graphs with $2k$ vertices), finding the symmetry of edges and expressing this symmetry by means of the cycle index for graph edges, and then applying Pólya's theorem to this cycle index. This will give the numbers of valence isomers obtained on "labelling" two edges with two CH_2 groups, or one edge with two adjacent CH_2 groups. The union of these two sets will be the solution (numbers of valence isomers). This procedure is best applied for valence isomers $(CH)_{2k}(CH_2)_{2j}$ where k is small and j is large; indeed, this was the procedure that was followed for obtaining all valence isomers of adamantane $(CH)_{2\times 2}(CH_2)_6$, derived from the two $(CH)_4$ valence isomers (cyclobutadiene and tetrahedrane) and from the connected general cubic graphs with four vertices and at most six loops.

In the present case with lower k and larger j values, a more economical procedure may be adopted, taking also into account the fact that homoannulene formulas $(CH)_{2k}(CH_2)_1$ are already available. The procedure consists in inserting on every nonequivalent edge of homoannulene a new CH_2 group.

We shall adopt the simplest, third procedure based upon the already published tables of general cubic graphs.[27] From these tables we select the graphs with two non-geminal loops; these correspond to valence isomers of bis-homoannulenes if the loop and the point adjacent to it are assimilated with a CH_2 group. As a checkout, for lower $p = 2k + 2$ numbers, from the tables of graphs with degrees 4 or less,[39] we select the graphs $(CH)_{2k}(CH_2)_2$.

There exists also a fourth approach, by using sophisticated computer programs which yield all isomers with given formulas, such as those developed at Stanford by Lederberg et al. (heuristic DENDRAL)[40] or at Novosibirsk by Piottykh-Peletskii et al.[41]

We disregard stereoisoimerism, and consider only constitutional isomers.

Table 1 presents the constitutional formulas of valence isomers of bis-homoannulenes $(CH)_{2k}(CH_2)_2$ with $p = 2k + 2$ carbon atoms, for $p = 4$, 6, and 8. The CH_2 or CO groups are shown as black dots. The

Table 1

Bio-homoannulenes $(CH)_{p-2}(CH_2)_2$ with β double bonds (black dots symbolize CH_2 groups, or CO groups in the corresponding diones)

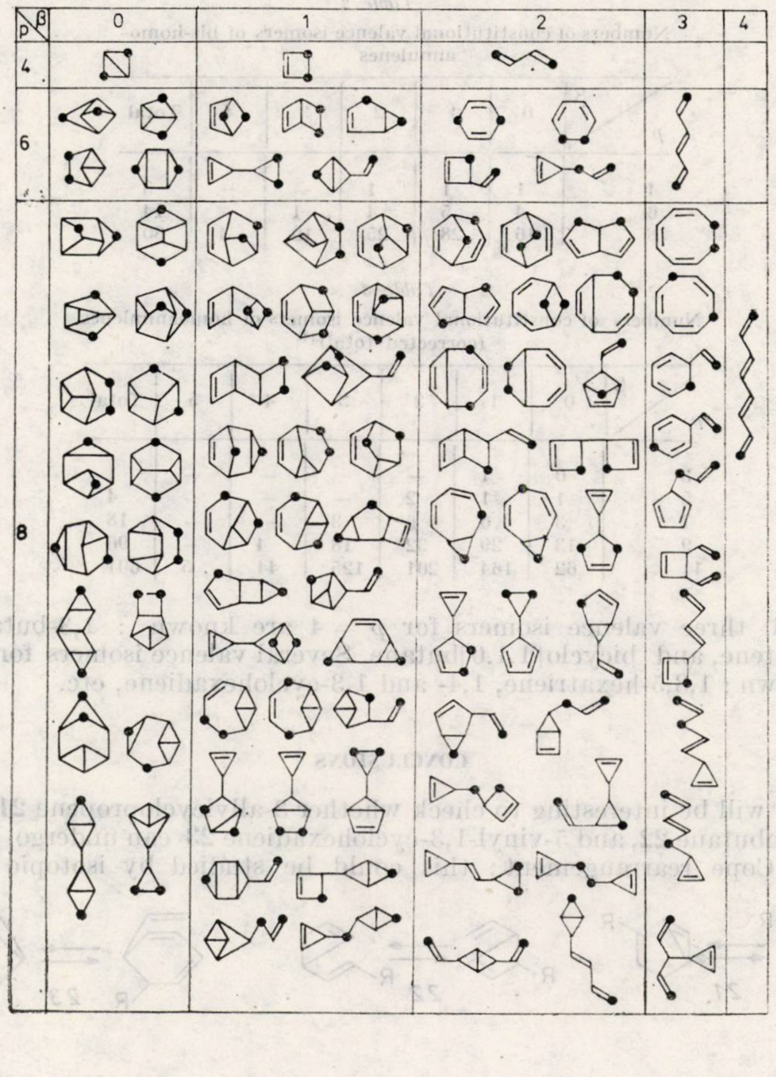

structures are displayed according to the numbers p of carbon atoms and β of double bonds, in the order of increasing numbers of 3- and 4-membered rings; thus, the first structures will have the smallest numbers of 3-membered rings, and their numbers of 4-membered rings will increase gradually; then the number of 3-membered rings will be augmented by one, and again the number of 4-membered rings will increase gradually. When there are no 3- or 4-membered rings, the rings will start from the larger to smaller rings.

The resulting numbers of valence isomers are shown in Table 2, again broken down according to p and β. As for homoannulenes, whose numbers are shown in Table 3, the numbers of valence isomers increase fast with increasing p. The figures from Table 3 for a given $p + 1$ and Table 2 for the corresponding p value bear an approximate parallelism.

Table 2

Numbers of constitutional valence isomers of bis-homoannulenes

p \ β	0	1	2	3	4	Total
4	1	1	1	—	—	3
6	4	5	4	1	—	14
8	16	28	25	10	1	80

Table 3

Numbers of constitutional valence isomers of homoannulenes (corrected total)[34]

p \ β	0	1	2	3	4	5	Total
3	0	1	—	—	—	—	1
5	1	1	2	—	—	—	4
7	3	6	6	3	—	—	18
9	13	29	32	18	4	—	96
11	62	164	201	125	44	5	601

All three valence isomers for $p = 4$ are known : 1,3-butadiene, cyclobutene, and bicyclo[1.1.0]butane. Several valence isomers for $p = 6$ are known : 1,3,5-hexatriene, 1,4- and 1,3-cyclohexadiene, etc.

CONCLUSIONS

It will be interesting to check whether 3-allylcyclopropene **21**, 3-vinylcyclobutane **22**, and 5-vinyl-1,3-cyclohexadiene **23** can undergo a degenerate Cope rearrangement; this could be studied by isotopic or by

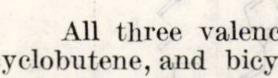
21

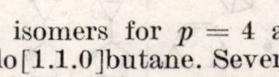
22

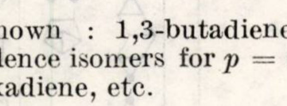
23

chemical labelling (e.g. with R = Alk, the thermodynamically stable isomer would have the more substituted double bond).

It is interesting to speculate also if mild yet powerful isomerization catalysts such as those employed[42,43] for converting [1.1.1.1]pagodane into dodecahedrane (Rh/C) might bring about isomerizations of unsaturated compounds into polycyclic ones, analogously to the reaction **12** → **10** but with hydrogen instead of chlorine atoms; unsaturated hydrocarbons may be polymerized by Lewis acid catalysts, such as $AlCl_3$, which convert the hydrogenated cyclopentadiene dimer (**15** + $2H_2$) into adamantane. Among the strongest catalysts one can mention the molten mixture $AlCl_3$+NaCl which automerizes [^{13}C]–phenanthrene,[44] and Olah's "magic acids", e.g. $SbF_5 + FSO_3H$;[45] these superacids can protonate C–H bonds via dielectronic tricentric bonds.

Thus, thermal, photochemical or electrochemical activation of bonds, as well as catalysts (Lewis or Brönsted catalysts or transition metal ions) have a chance of causing interesting interconversions of valence isomers reported here.

For obtaining structures of higher valence isomers, namely with $p = 10, 12, \ldots$ carbon atoms, one should extend the present approach.

REFERENCES

[1] This paper is preceded by Part 41, A. T. Balaban and I. Tomescu, *Math. Chem.*, **17**, 91 (1985), Part 42, A. T. Balaban, D. Biermann and W. Schmidt, *Nouv. J. Chim.*, **9**, 443 (1985); Parts 43 and 47 are refs. 31 and 30, respectively, in the present paper; parts 44–46 are A. T. Balaban, *Rev. Roum. Chim.*, **31**, 679, 695, 795 (1986); Part 48, A. T. Balaban, *Math. Chem.*, **21**, 115 (1986); Part 49, A. T. Balaban and I. Tomescu, *Discrete Appl. Math.*, **19**, 6 (1988) reprinted in "Application of Graphs in Chemistry and Physics", edited by J. W. Kennedy and L. V. Quintas, North Holland, Amsterdam, 1988, p. 6; Part 50, A. T. Balaban, *Math. Chem.*, **24**, 29 (1989).

[2] A. T. Balaban, *Rev. Roum. Chim.*, **11**, 1097 (1966).

[3] A. T. Balaban, in "Chemical Applications of Graph Theory" (ed. A. T. Balaban), chapter 5, p. 63, Academic Press, London, 1976.

[4] R. Furstoss and J. M. Lehn, *Bull. Soc. Chim. Fr.*, 2497 (1966).

[5] S. Masamune, H. Cuts and M. G. Hogben, *Tetrah. Lett.*, 1017 (1966).

[6] W. G. Dauben and D. L. Whalen, *ibid.*, 3743 (1966); *J. Amer. Chem. Soc.*, **93**, 7244 (1971); W. G. Dauben, C. H. Schallhorn and D. L. Whalen, *J. Amer. Chem. Soc*, **93**, 1446 (1971).

[7] W. G. Dauben and A. J. Kielbania Jr., *J. Amer. Chem. Soc.*, **93**, 7345 (1971).

[8] J. M. Lehn and G. Wipf, *Chem. Commun.*, 747 (1973).

[9] L. A. Paquette, *Acc. Chem. Res.*, **4**, 282 (1971); L. A. Paquette and R. S. Beckley, *J. Amer. Chem. Soc.*, **97**, 1084 (1975); L. A. Paquette, R. S. Beckley and W. B. Farnham, *ibid.*, 1089; L. A. Paquette, R. A. Boggs, W. B. Farnham and R. S. Beckley, *ibid.*, 1112.

[10] R. Noyori, M. Yamakawa and H. Takaya, *J. Amer. Chem. Soc.*, **98**, 1471 (1976).

[11] R. B. Woodward and R. Hoffmann, "The Conservation of Orbital Symmetry", Verlag Chemie, Weinheim, 1970; *Angew. Chem Internat. Ed. Engl.*, **8**, 781 (1969).

[12] J. B. Lambert and A. G. Holcomb, *J. Amer. Chem. Soc.*, **91**, 1572 (1969).

[13] W. L. Dilling and J. A. Alford, *J. Amer. Chem. Soc.*, **96**, 3615 (1974).

[14] E. T. McBee, J. D. Idol and C. W. Roberts, *J. Amer. Chem. Soc.*, **77**, 4375 (1955).

[15] E. T. McBee, C. W. Roberts, J. D. Idol and R. H. Earle, *J. Amer. Chem. Soc.*, **78**, 1511 (1956).

[16] H. E. Ungnade and E. T. McBee, *Chem. Rev.*, **58**, 283 (1958).

[17] E. E. Gilbert and S. L. Giolito, to Allied Chem. Co., U.S. Pat. 2616825 (1951).

[18] H. J. Prins, *Rec. Trav. Chim.*, **65**, 455 (1946).

[19] J. S. Newcomer and E. T. McBee, *J. Amer. Chem. Soc.*, **71**, 952 (1949).

[20] W. L. Dilling, *Chem. Rev.*, **66**, 373 (1966).

[21] G. O. Schenck and R. Steinmetz, *Chem. Ber.*, **96**, 520 (1963).

[22] R. C. Cookson, R. R. Hill and J. Hudec, *J. Chem. Soc.*, 3043 (1964).

[23] P. Yates and P. Eaton, *Tetrahedron*, **12**, 13 (1961).

[24] G. W. Griffin and A. K. Price, *J. Org. Chem.*, **29**, 3192 (1964).

[25] A. T. Balaban, M. Banciu and V. Ciorba, "Annulenes, Benzo-, Hetero-, Homo-Derivatives and their Valence Isomers", CRC Press, Boca Raton, 1987, vol. 3, p. 81, chapter 9 ; vol. 2, p. 47.

[26] A T. Balaban and M. Banciu, *J. Chem. Educ.*, **61**, 766 (1984).

[27] A. T. Balaban, *Rev. Roum. Chim.*, **15**, 463 (1970).

[28] A. T. Balaban, *Rev. Roum. Chim* , **17**, 865 (1972).

[29] M. Banciu, C. Popa and A. T. Balaban, *Chem. Scripta*, **24**, 28 (1989).

[30] A. T. Balaban and C. Deleanu, *Rev. Roum. Chim.*, **32**, 271 (1987).

[31] A. T. Balaban, R. Vancea, I. Moţoc and S. Holban, *J. Chem. Inf. Comput. Sci.*, **26**, 72 (1986).

[32] A. T. Balaban, *Rev. Roum. Chim.*, **19**, 1185 (1974).

[33] M. Banciu and A. T. Balaban, *Chem. Scripta*, **22**, 188 (1983).

[34] A. T. Balaban, *Rev. Roum. Chim.*, **19**, 1611 (1979) ; erratum, *ibid.*, **23**, 311 (1978).

[35] A. T. Balaban, *Rev. Roum. Chim.*, **19**, 1323 (1974).

[36] A. T. Balaban, *Rev. Roum. Chim.*, **31**, 679 (1986).

[37] A. T. Balaban, *Rev. Rum. Chim.*, **31**, 695 (1986).

[38] A. T. Balaban, *Rev. Roum. Chim.*, **31**, 795 (1986).

[39] A. T. Balaban, *Rev. Roum. Chim.*, **18**, 635 (1973) ; erratum, *ibid.*, **19**, 338 (1974).

[40] J. Lederberg, G. L. Sutherland, B. G. Buchanan, E. A. Feigenbaum, A. V. Robertson, A. M. Duffield and C. Djerassi, *J. Amer. Chem. Soc.*, **91**, 2973 (1969).

[41] S. G. Molodtsov and V. N. Piottyhk-Peletskii, in "Algoritmy analiza strukturnoi informatsii", *Vychlislitelnye systemy*, **103**, 51 (1984) ; Inst. Matem. Sibirsk. Otdel. Akad. Nauk SSSR, Novosibirsk.

[42] W. D. Fessner, A. R. Bulusu, C. Murty and H. Prinzbach, *Angew. Chem.*, **99**, 482 (1987)

[43] W. D. Fessner, B.A.R. Murty, J. Worth, D. Hunkler, H. Fritz, H. Prinzbach, W. D. Roth, P.V.R. Schelyer, A. B. McEwen and W. F. Maier, *Angew. Chem. Internat. Ed, Engl.*, **26**, 452 (1987).

[44] A. T. Balaban, M. D. Gheorghiu, A. Schiketanz and A. Necula, *J. Amer. Chem. Soc.*, **111**. 734 (1989).

[45] G. A. Olah, *Chem. Scripta* **18**, 97 (1981) ; *Top. Curr. Chem.*, **80**, 19 (1979) ; G. A. Olah, G. K. Surya Prakash and J. Sommer, "Superacids", Wiley, New York, 1985.

Revue Roumaine de Chimie, **34**, *8*, 1753 – 1759 (1989)

ADDITION COMPOUNDS OF ISOLATED, FUSED AND ISOLATED-FUSED AROMATIC SYSTEMS WITH 2,4,6-TRINITROPHENOL. A SPECTROSCOPIC STUDY

E. F. SAAD* and E. A. HAMED
Chemistry Department, Faculty of Science, Alexandria University,
Moharem Bay, Alexandria, Egypt

Received May 30, 1987

Addition compounds of some biphenyls, fused aromatics and 1,1′-bis(2-naphthol) with 2,4,6-trinitrophenol were studied and investigated by IR and ¹H-NMR spectroscopy. Types of interaction were determined, the effect of the OH group on the types of interaction is discussed, spectral shifts were correlated and a comparative study is reported for the systems in question.

INTRODUCTION

Over the years, evidence has accumulated and much has been published concerning addition compounds, many papers describing the formation of these addition compounds by UV, IR and ¹H-NMR spectroscopy.[1–9]

Biphenyls were the subject of many industrial uses, especially the chlorinated ones, as plasticizers and plastic liners. Being pollutants, scientists are undertaking researches to remove their harmful effect. The importance of this class of compounds has led us to study their ability to form addition compounds with 2,4,6-trinitrophenol, and in turn draw our attention to study 1,1′-bis(2-naphthol) as a donor comprising an isolated-fused aromatic system.

Addition compounds of fused aromatics containing or not functional groups with 2,4,6-trinitrophenol (XI) has been studied,[3,9] and it was concluded that binding takes place through an overlap of π-orbitals of the 2,4,6-trinitrophenol (XI) and the aromatic ring, (termed $\pi - \pi^*$ interaction), as well as hydrogen bonding, yet the study was confined to IR spectral investigation, and limited to the use of naphthalene, anthracene, 1-naphthol and 2-naphthol as examples.

The present article provides further examples, and includes the results of IR and ¹H-NMR spectroscopic investigations of the addition compounds prepared by the interaction of biphenyl (I), biphenyl 4,4′-diol (II), 4,4′-diamino biphenyl (III), (class A), naphthalene* (IV), anthracene* (V), phenanthrene (VI), 1-naphthol* (VII), 2-naphthol* (VIII), naphthalene 1,5-diol (IX) (class B), and 1,1′-bis(2-naphthol) (X) (class C) with 2, 4, 6-trinitrophenol (XI).

---

* ¹H-NMR study

EXPERIMENTAL

The chemicals used in the present investigation were of pure (Koch-light) grade. The addition compounds were prepared by the usual method[5]; as they are known to be susceptible to decomposition by hydroxylic solvents, they were not easily crystallised, and were washed with little ether, then dried on a porous tile. Their purity was checked by TLC. The IR spectra were recorded in the solid state applying the KBr disc technique, on a Pye-Unicam SP 2000 instrument. The ^{1}H-NMR spectra were recorded in the central laboratory of the Faculty of Science, Alexandria University on a Varian EM 390-90 MHz spectrometer using d_6-acetone as a solvent.

RESULTS AND DISCUSSION

IR Spectra

The spectra of the addition compounds, generally, were compared with the 2,4,6-trinitrophenol (XI), and with the donor molecules I—X. Shifts in the different stretching frequencies were taken as an indication of the addition compounds formation.

1. *Class A* (Table 1, Figs 1 and 2)

Table 1

Colours, melting points and IR spectra (cm^{-1}) of the addition compounds of class A with 2,4,6-trinitrophenol

Biphenyl compound	Colour	M.P. °C	ν_{OH}	ν_{NO_2} asym.	ν_{NO_2} sym.	ν_{C-C}	ν_{NH_2}
I	Pale yellow	88	3109	1547	1350	1177 1163*	—
II	Almond green	207	3101 3410 3389*	1545	1350	1187 1180*	—
III	Dark brown	118	—	1554	1347	1165 1182*	3400 3221*
XI	Yellow	122	3112	1555	1348	—	—

* Value of the free donor.

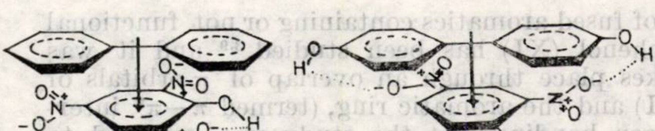

Fig. 1

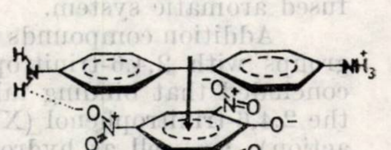

Fig. 2

Biphenyls form two types of addition compounds involving a $\pi-\pi^*$ interaction (I, II), and proton transfer besides $\pi-\pi^*$ interaction III. The addition compounds display change in their spectra compared to those of their components.

---

* ^{1}H—NMR study

i. The ν_{OH} band of the acceptor molecule, 2,4,6-trinitrophenol (XI) is shifted to lower wavenumbers in case of I and II. This shift indicates a stronger intramolecular H-bonding in the addition compound in comparison to the free acceptor molecule, which favours a possible increase in the charge density on the acceptor molecule and a decrease in the charge density on the aromatic (biphenyl) ring of the donor molecule. The ν_{OH} band of the donor molecule II is shifted to higher wavenumber; this denotes a stronger intermolecular H-bonding in the addition compound.

ii. Addition product II is not capable of contributing in $n-\pi^*$ interaction, as this type depends on the relative positions of the $-OH$ donor, NO_2 groups; if the $-OH$ group faces one NO_2 group, the interaction would take place between the polarised $-OH$ donor and $-NO_2$ groups, as the $-OH$ donor group is located between the two $-NO_2$ groups, the $n-\pi^*$ interaction is not favoured and only the intermolecular hydrogen bonds prevail besides the $\pi-\pi^*$ interaction.

iii. The ν_{OH}, ν_{NH_2} bands are no more observed in the addition compound III, and a new band appears within the range 3000–2400 cm^{-1} characteristic for the $-NH_3^+$ structure.[3] Hence III involves the transfer of a proton from the $-OH$ group of the acceptor molecule to the $-NH_2$ group of the biphenyl derivative. The blocking of the lone pair on the nitrogen atom of the donor by the proton of the acceptor prevents $n-\pi^*$ interaction. The second ν_{NH_2} band is shifted to a higher wavenumber indicating intermolecular hydrogen bonding between the $-NH_2$ and $-NO_2$ groups.

iv. The shift of the ν_{NO_2} bands to lower values in I, II and III is in accordance with the increased charge density on the ring of the acceptor molecule XI.

v. The ν_{C-C} bands of the addition compounds I, II are shifted to higher values whereas that of III displays an opposite shift; this indicates a decrease of charge density on the donor molecules I and II. One would assume a possible decrease in the double bond character of this $C-C$ in case of I and II, whereby resonance is inhibited. The opposite is liable to happen in the addition compound III, where resonance is established by the proton transfer from the acceptor to the donor, a situation where $-NH_3^+$ structure, $-NH_2$ group exist. This leads to an increase in the double bond character in III.

Class B (Table 2, Figs 3 and 4)

i. The ν_{OH} band of the acceptor molecule in the addition compound V acquired a shift to a lower value; this indicates a stronger H-bonding which supports the higher charge density at the $-NO_2$ groups.[3,9] The magnitude of the shift in VI is higher than IV and V; this is due to its enrichment in electron density. The addition compound IX displays the shift of ν_{OH} to lower values similarly to IV, V and VI.[3,9]

The ν_{OH} bands of the donor IX denote a shift to a higher value; an intermolecular H-bonding plays a role in this addition compound. This was also facilitated by the position of the hydroxyl group in the donor molecule. This case is reminiscent of the addition compound II.

Table 2

Colours, melting points and IR spectra (cm^{-1}) of the addition compounds of class B with 2,4,6-trinitrophenol

Compound	Colour	M.P. °C	ν_{OH}	ν_{NO_2}	
				asym.	sym.
IV[a]	Bright yellow	150	3096	1561	1354
V[b]	Red	138	3091	1560	1352
VI	Golden yellow	148	3088	1563	1350
VII[a]	Pale red	189	3091, 3451 3280[c]	1546	1344
VIII	Orange	159	3072, 3512 3290[c]	1550	1346
IX	Brick red	203	3095, 24400 3259[c]	1535	1346
XI	Yellow	122	3112	1555	1348

[a, b] ref. [3,9] here revised
[c] value of the free donor.

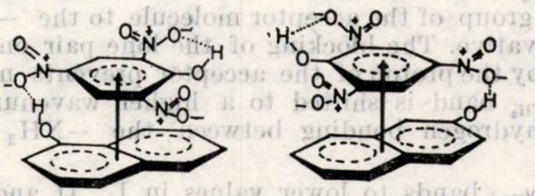

Fig. 3

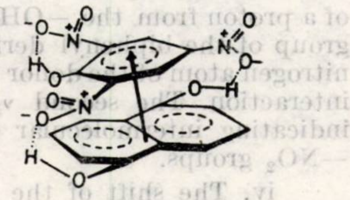

Fig. 4

ii. The ν_{NO_2} bands of XI in the addition compound VI retained its resolved appearance and was shifted to higher values denoting a stronger H-bonding.[3,9] The opposite is displayed in the addition compound IX where ν_{NO_2} acquired a shift to lower value. This addition compound exhibited a stronger intermolecular H-bonding besides the conventional $\pi-\pi^*$ interaction.

Class C (Table 3, Fig. 5)

Table 3

Colours, melting points and IR spectra (cm^{-1}) of the addition compounds of class C with 2, 4, 6-trinitrophenol

Compound	Colour	M.P. °C	ν_{O-H}	ν_{NO_2}		ν_{C-C}
				asym.	sym.	
X	Light green	125	3418 3096, 3500 3488* 3800*	1534	1347	1178 1178*
XI	Yellow	122	3112	1555	1348	—

* Value of the free donor.

i. The ν_{OH}, ν_{NO_2} bands of the acceptor molecule in the addition compound X exhibit similar behaviour to that of I and VIII, i.e., they are shifted to lower values in accordance with the explanation mentioned in classes A and B.

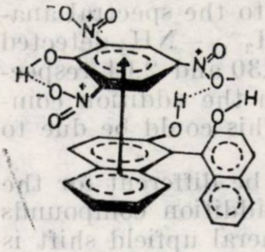

Fig. 5

ii. In contrast to the behaviour of the ν_{OH} band of the donor VIII, the ν_{OH} bands of the donor X exhibited no change in the addition compound; one would assume an intramolecular H-bonding within itself (the two hydroxyls).

The donor molecule X, being racemic (±), the two hydroxy naphthyl rings are non planar, and inclined to each other due to the steric and replusive effects. A case, whereby restricted rotation is exhibited and entirely attributed to spatial effect. Based on these facts, the ν_{C-C} band of the donor X showed no change in the formed addition compound, different to the behaviour of the ν_{C-C} of the donors I and II.

^{1}H-NMR Spectra

The ^{1}H-NMR spectra of the addition compounds and their components were correlated with their structures. The data are consistent with the formation of simple 1 :1 addition compound. The position of the hydroxyl proton in the addition compound was taken as a reference signal which had been assumed to be constant.

Class A (Table 4)

Table 4

^{1}H-NMR Chemical shifts (dppm) of addition compounds of class A

Compound	δOH	δNH_2	δAromatic protons
I	5.93[a]	— (2,2′,6,6′,)	7.53[d] ; 3,3′, 5,5′ 7.40[d] — 9.07[g]
II	8.00[a,b]	— (2,2′, 6,6′)	6.86[e] ; 3,3′, 5,5′ 7.33[e] — 9.03[g]
III	—	1.37 (3H) ; 1.53[c] (2H) (2H)(2,6) (2′, 6′)	6.97[f] ; 3.5 7.20[f] — 8.67[g] 7.50[f] ; 3′, 5′ 7.70[f]

[a] δOH XI 8.69
[b] δOH II 8.20
[c] δNH_2 III 3.57
[d] δaromatic protons I 7.60, 7.47
[e] δaromatic protons II 6.86, 7.40
[f] δaromatic protons III 6.37, 7.30
[g] δaromatic protons XI 9.40

The chemical shifts of the hydroxyl protons, amino protons as well as those of the biphenyl protons were affected in the addition process.

On evaluating the resonance of the hydroxyl protons, biphenyl protons of the addition compounds I and II, one notices a difference in their chemical shifts, in respect to both components. These shifts are generally upfield, and could be attributed to the decrease in diamagnetic current of the biphenyl nucleus caused by induction of the hydroxyl group(s).[10] The formation of the addition compounds I and II indicates the great interaction between both components as well as mutual shielding, which occurred proved by the appearance of a maximum upfield shift.

On the other hand, the interaction between the components leading to the formation of the addition compound III caused the disappearance of the hydroxyl proton signal; in support to the spectral analysis, two singlets appear and were assigned to $-NH_3^+$, $-NH_2$ detected at $\delta = 1.27, 1.53$, yielding an upfield shift of $\delta\Delta = 2.30$ and 2.04 respectively. Deshielding effect of the biphenyl protons in the addition compound III was also observed ($\delta\Delta = 0.40 - 0.24$). This could be due to the presence of the $-NH_3^+$ structure.

There is no reason to expect the situation to be different for the signals of the two protons of the acceptor in the addition compounds I, II and III from the biphenyl protons, i.e., a general upfield shift is observed.

Class B (Table 5)

Table 5

^{1}H-NMR Chemical shifts (δppm) of addition compounds of class B

Compound	δOH	δAromatic protons	
IV	6.54[a]	(1,4,5,8) 7.83[e]; (2,3,6,7) 7.45	−9.03
V	6.73[a]	(1,4,5,8) 8.07[f]; (2,3,6,7) 7.47[f]; 9,10 8.43[f]	−9.03
VI	5.27[a]	(1,8) 7.86[g]; (2,7) 7.57[g]; 3,6 7.62[g]; 4,5 8.70[g]; 9,10 7.73[g]	−9.03
VII	7.33[a,b]	(2) 6.83[h]; (4) 7.23[h]; 3,6,7 7.47[h]; 5 7.80[h]; 8 8.17[h]	−9.03
VIII	6.17[a,c]	(4,5,8) 6.80[i]; (1,3,6,7) 7.63[i]	−0.03
IX	5.67[a,d]	(2,6) 6.83[j]; (3,7) 7.23[j]; 4,8 7.70	−9.07

[a] δOH XI 8.69
[b] δOH VII 8.89
[c] δOH VIII 8.56
[d] δOH IX 8.72
[e] δaromatic protons IV 7.85, 7.40
[f] δaromatic protons V 7.96, 7.30
[g] δaromatic protons VI 7.93, 7.30, 8.37
[h] δaromatic protons VII 6.70, 7.17, 7.38, 7.38, 7.73, 8.13
[i] δaromatic protons VIII 7.20, 7.67
[j] δaromatic protons IX 6.33, 6.92, 7.63

The hydroxyl proton, the two protons of the acceptor ($\delta\Delta = 0.37 - 0.33$) and hydroxyl protons of the donors VII, VIII and IX ($\delta\Delta = 3.42 - 1.96$) are shifted upfield when complexed to form the addition compounds IV — IX. This positive shielding may be due to the ring current of the donors as well as through the conventional $\pi - \pi^*$ bonding.

This type of interaction which manifests a positive shielding was also reflected in the donor aromatic protons in their addition compounds ^{1}H-NMR spectra with the notable exceptions (addition compounds of V, VII and IX) where deshielding has occurred; this is probably due to the geometry of the addition compound itself. X-ray structural determination may be needed to elucidate it.

Class C (Table 6)

A general upfield shift, though insignificant, was observed in the addition compounds X, i.e., those of the hydroxyl protons, aromatic protons of both components, probably reflecting that the amount of interaction between the naphthyl rings and the phenyl ring of XI is weak; this may be due to the stereochemistry of X.

Table 6

^{1}H-NMR chemical shifts (δppm) of addition compound of class C

Compound	δOH	δAromatic protons
X	7.40^{a,b}	(3,3′) 7.07^{d} ; (4,4′) 7.17^{d} ; (5,5′) 7.23^{d} ; (6,6′, 7,7) ′7.33^{d} ; (8,8′) 7.83^{d}–9.10^{e}

[a] δ OH XI 8.69 [c] δ aromatic protons XI 9.40
[b] δ OH X 7.93 [d] δ aromatic protons X 7.07, 7.17, 7.23, 7.33, 7.83.

REFERENCES

[1] R. S. Mullikan and W. B. Person, in "Molecular Complexes : A Lecture and Reprint Volume", Wiley, New York, 1964.

[2] R. Foster in "Charge-Transfer Complexes", Academic Press, New York, 1969.

[3] R. M. Issa and M. M. El-Essawey, *Z. Physik* (Leipzig), **253**, 96 (1973).

[4] S. D. Ross and M. M. Labes, *J. Amer. Chem. Soc.*, **77**, 4916 (1955).

[5] A. M. Hindawey, A. M. G. Nassar and M. Issa., *Indian J. Chem.*, **19A,** 615 (1980).

[6] M. M. Asadi, M. R. Arshadi, *Indian J. Chem.*, **15A**, 453 (1977).

[7] A. M. Hindawey, A.M.G. Nassar and R. M. Issa, *Acta Chimica Acad. Sci. Hungarica*, **88**, 341 (1976).

[8] A. M. Hindawey, A. M. G Nassar and R. M. Issa, *Acta Chimica Acad. Sci. Hungarica*, **92**, 263 (1977).

[9] A. M. Hindawey, Y. M. Issa, Y. A. Marghalani, and R. M. Issa, *Monatsh. Chemie*, **111**, 1143 (1980).

[10] L. M. Jackman and S. Sternhell, "Applications of Nuclear Magnetic Resonance Spectroscopy in Organic Chemistry", 2nd ed ; Chapt. 3–6, Pergamon Press, Oxford, 1972.

Revue Roumaine de Chimie, **34**, *8*, 1761–1767 (1989)

2-ARYLTHIO-5-METHYL-2-THIONO-1,3,2-DIOXAPHOSPHOLANES

V. MUREȘAN, I. FENEȘAN and L. PASKUCZ
Institute of Chemistry, str. Fîntînele 30, 3400 Cluj-Napoca, Romania

Received December 25, 1987

The synthesis, structure and properties of 2-arylthio-5-methyl-2-thiono-1,3,2-dioxaphospholanes (I) are described. According to their ^{31}P-, ^{1}H- and ^{13}C-NMR spectra, compounds I consist of two racemic mixtures, *Z* and *E* respectively, diastereomeric to each other, the *Z* diastereomer being energetically favoured. Basic hydrolysis of compounds I takes place *via* rupture of the P—S bond. Compared to acyclic analogues, compounds I have less marked insecticidal properties.

INTRODUCTION

Earlier investigations on several 5-methyl-2-thiono-1,3,2-dioxaphospholanes and 5,5-dimethyl-2-thiono-1,3,2-dioxaphosphorinanes carried out in our laboratory[1,2,3] dealt with 2-arylsulphonyl-amido derivatives, thus containing an S=P—N substructure. This work has been now extended upon compounds I.

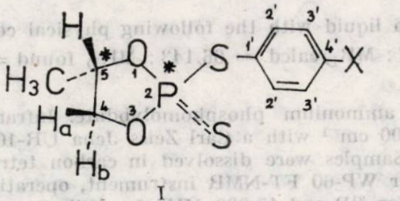

I

I1 : X = OCH_3 ; I2; X=CH_3 ; I3 : X=H ; I4 : X=F ; I5 : X=Cl ; I6 : X=Br

It seemed of interest to study the influence of the S=P—S substructure contained in compounds I upon the configuration, chemical and biological behaviour of the 5-methyl-2-thiono-1,3,2-dioxaphospholanes.

EXPERIMENTAL

Synthesis of 2-arylthio-5-methyl-2-thiono-1,3,2-dioxaphospholanes. I (general method): Equimolar amounts (0.2 moles) of 2-chloro-5-methyl-2-thiono-1,3,2-dioxaphospholane (II) (prepared as described in ref.[4]) and the appropriated sodium thiophenolate (III) were dissolved in 50 mL benzene and refluxed for 8 hours. After cooling, the reaction mixture was washed with water in order to remove both unreacted sodium thiophenolate and the sodium chloride formed in the reaction. The organic layer was dried over magnesium sulphate for 12 hours. The solvent was evaporated *in vacuo* and the solid residue was recrystallized from benzene-hexane (1 :1).

Alkaline hydrolysis of compound I5 : 1 g of I5 was suspended in 10 mL of 20% aqueous sodium hydroxide and stirred at 50° for 30 min. After cooling, the reaction mixture was neutralized with diluted hydrochloric acid, the residue (0.3 g) filtered off and dried *in vacuo*. This solid was identified as *p*-chloro-thiophenol, by its m.p. (53–4°) and mixed m.p. with an authentic specimen.

Analyses and spectra : Physical constants and analytical figures for compounds I are given in Table 1. Carbon, hydrogen and sulphur contents were determined by standard combustion, phosphorous as ammonium phosphomolybdate. Infrared absorption spectra were recorded between 350–3600 cm^{-1} with a Carl Zeiss Jena UR-10 double-beam spectrophotometer using salt optics. Samples were dissolved in carbon tetrachloride. All NMR spectra were recorded on a Bruker WP-60 FT-NMR instrument, operating at a field of 14.1 kG (60 MHz for ^{1}H, 24.28 MHz for ^{31}P and 15.086 MHz for ^{13}C). Samples were dissolved in $CDCl_3$ ($CHCl_3$ for ^{31}P-measurements). ^{1}H-and ^{13}C-chemical shifts were related to internal TMS, ^{31}P-shifts to external D_3PO_4.

Table 1

Melting points, yields and analytical figures for compounds I

Compound	m.p. °C	Yield %	Analysis :		calcd./found	
			%C	%H	%P	%S
I1	59–61	45	43.46 43.57	4.74 4.50	11.21 11.29	23.21 23.29
I2	90–92	42	46.13 46.04	5.03 5.30	11.89 11.93	24.63 24.48
I3	98–99.5	39	43.88 43.75	4.50 5.01	12.57 12.66	26.03 25.95
I4	a	40	40.90 40.86	3.81 3.82	11.72 11.66	24.27 24.37
I5	102–104	40	38.50 38.80	3.59 3.54	11.03 11.28	22.84 22.47
I6	114–116	50	33.24 33.32	3.10 3.09	9.52 9.76	19.72 19.77

[a] Compound I4 is a liquid with the following physical constants : [b] p . 156°/0.7 torr, $d_4^{20} = 1.342$; $n_D^{20} = 1.587$; MR_D calcd. = 66.143 ; MR_D found = 66.156.

RESULTS AND DISCUSSION

Compounds I were obtained by the general reaction :

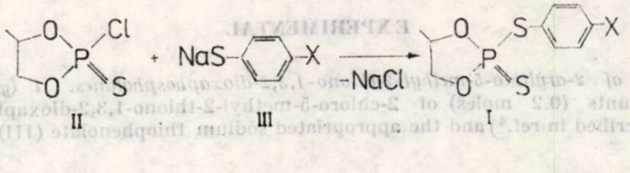

All compounds I are white crystalline solids, except I4, which was obtained as a yellow liquid. All compounds I exhibit intense IR absorption bands at $640-660\ \mathrm{cm}^{-1}$, characteristic for the S=P—S substructure, as well as at 890, 910 and at 932, $1032\ \mathrm{cm}^{-1}$, attributed[5] to the C—C and respectively to the C—O bonds in the phospholane ring.

Having two chiral centers (marked with asterisks in the formulae below), compounds I are expected to form two racemic mixtures, IA—IB and IC—ID respectively, diastereomeric to each other.

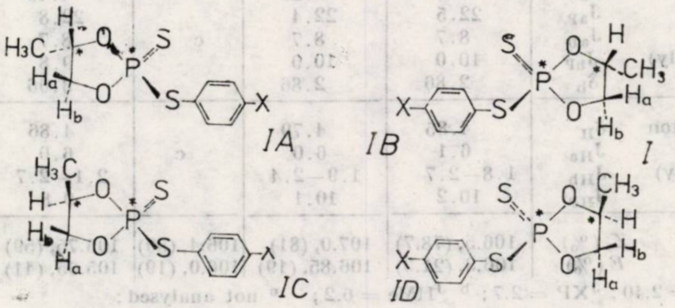

According to the priority rules, IA—IB should be termed as the *Z*-racemic (CH_3 and S= on the same side of the phospholane ring), IC—ID being the *E*-racemic. According to the literature data [6-8] and as expected theoretically, the diastereomer with the bulkiest substituents on opposite sides of the phospholane ring will be energetically favoured and therefore should be preferentially formed in the synthesis. This means that compounds I should consist mostly of the *Z*-racemic IA—IB. An analogous situation was found in the case of 2-arylsulphonylamido-5-methyl-2-thiono-1,3,2-dioxaphospholanes studied by us in earlier works.[1,2]

NMR-spectroscopy proved to be a very valuable tool in the investigation of this kind of isomerism; the two diastereomers being magnetically non-equivalent, their corresponding nuclei exhibit different chemical shifts. For compounds I this doubling of signals could be unambiguously attested in the ^1H-spectra (Table 2) for the $5-CH_3$ substituent, in the ^{31}P-NMR spectra (Table 2), as well as in the ^{13}C-NMR spectra (Table 3) for most of the carbon nuclei. The isomeric ratios included in tables 2 and 3 were calculated from the integrated peak intensities; as it may be seen, for most compounds, the three separate measurements (^1H, ^{31}P and ^{13}C) afforded roughly concordant isomeric compositions. We can thus conclude that with the exception of I4, the *Z*-racemic is preferentially formed for compounds I, too. For the 2-arylsulphonylamido-2-thiono-1,3,2-dioxaphospholanes studied previously[1,2] we were able to obtain in several cases practically pure *Z*-diastereomers by successive recrystallizations of the crude reaction products. The interpretation of the NMR data was thus based on the spectra recorded for these pure stereoisomers. Unfortunately, for compounds I all attempts

Table 2

H- and ^{31}P-NMR spectra of compounds I ; chemical shifts in ppm (δ values ; ^{1}H-standard internal TMS, ^{31}P-standard external D_3PO_4) ; coupling constants J, in Hz

Compound		I2	I3	I4	I5	I6
X		CH_3^a	H	F	Cl	Br
5-CH_3 protons[b]	Z, (%)	1.02, (81.4)	1.01, (88.5)	1.10, (36)	1.12, (65)	1.12, (87.5)
	E, (%)	1.38, (18.6)	1.38, (11.5)	1.42, (64)	1.43, (35)	1.43, (12.5)
methylene	δ_a	4.35	4.29		4.40	4.31
protons[b]	J_{aP}	22.5	22.4		22.8	22.8
(4)	J_{ab}	8.7	8.7	c	8.7	8.8
(*Z*-isomer only)	J_{bP}	10.0	10.0		9.8	10.1
	δ_b	2.86	2.86		3.06	3.06
methine proton	δ_H	4.85	4.79		4.86	4.76
(5)	J_{Ha}	6.1	6.0	c	6.0	6.0
(*Z*-isomer only)	J_{Hb}	1.8–2.7	1.9–2.4		2.1–2.7	2.1–2.7
	J_{HP}	10.2	10.1		9.8	9.6
phosphorus	Z, (%)	106.5, (78.7)	107.0, (81)	106.4, (50)	105.75, (59)	105.0, (80)
	E (%)	106.3, (21.3)	106.85, (19)	106.0, (19)	105.65, (41)	104.88, (20)

[a] $\delta_X = 2.40$; $^{J}XP = 2.7$; [b] $^{J}HMe = 6.2$; [c] not analysed ;

Table 3

^{13}C-NMR spectra of compounds, I ; chemical shifts in ppm (δ values, internal TMS) standard coupling constants J, in Hz.

Compound		I2	I3	I4		I5		I6
X		CH_3^a	H	F		Cl		Br
diastereomers[b]		Z	Z	Z(40 %)	E, (60 %)	Z, (64 %)	E, (36 %)	Z
C–5	δ	75.56	75.53	75.87	77.47	75.58	77.32	75.77
	J_{CP}	1.7	1.6	1.7	2.8	1.5	3.4	1.4
5–CH_3	δ	17.41	17.38	15.58	19.56	17.63	19.51	17.63
	J_{CP}	9.4	9.0	9.0	6.2	9.0	6.0	9.0
C–4	δ	73.88	73.82	73.86	73.01	73.74	72.91	73.74
	J_{CP}	3.5	3.2	3.5	2.8	3.4	2.6	2.8
C–1′	δ	c	c	131.74[d]	131.25[d]	c	c	c
	J_{CP}			7.9	7.9			
C–2′	δ	136.19	136.41	138.44[e]	137.87[e]	137.44	137.12	137.65
	J_{CP}	4.5	4.6	4.8	4.8	4.8	4.8	4.2
C–3′	δ	130.27	129.50	116.81[f]	116.81[f]	129.70	129.70	132.68
	J_{CP}	3.5	3.2	3.2	3.2	2.8	2.8	2.8
C–4′	δ	140.77	130.27	163.85[g]	163.85[g]	c	c	125.05
	J_{CP}	4.1	3.5	4.5	4.5			4.5

[a] $\delta_X = 21.33$, $J_{XP} = 1.4$; [b] for compounds I2, I3 and I6 the signals of the *E*-racemic are not strong enough to be analysed ; [c] signal not found ; [d] J_{CX}0.5 ; [e] $J_{CX} = 4.5$; [f] $J_{CX} = 21.8$; [g] $J_{CX} = 252.1$.

to separate the diastereomers IA—IB from IC—ID failed; the assignments of the observed NMR signals are based on theoretical considerations and analogy with the previous data.[1,2,6–8]

A more detailed consideration of the NMR data in Tables 2 and 3 and their comparison with previous data on related compounds[1,2,6–8] enabled the following statements to be pointed out:

a. *^{1}H-Resonance*: *5-Methyl-protons*: These protons are more deshielded in the *E*-diastereomer IC—ID than those of its *Z*-counterpart, IA—IB. This deshielding is most probably due to the anisotropic effect of the aromatic substituent bound to the phosphorus. The anisotropic effect of the aromatic ring upon the 5—CH_3 substituent should be more powerful in IC—ID, where the two substructures are on the same side of the phospholane ring, that is closer to each other than in IA—IB. This explanation is further supported by the fact that this chemical shift difference between the signals assigned to the two diastereomers *Z* and *E* is much more important in compounds I (0.30 — 0.38 ppm) than in the corresponding sulphonylamido phospholanes (0.04 ppm[2]); the two interacting substructures (CH_3 and the aromatic ring) are much closer to each other in compounds I than in the corresponding sulphonylamido phospholanes. *5-Methine protons*: From the very complex pattern afforded by this single proton, only the lines due to the more abundant *Z* isomer could be identified and analysed as shown in Table 2. *4-Methylene protons*: Again, only the signals of the more abundant *Z*-isomer could be analysed. The two protons H_a and H_b show a very pronounced diastereotopic magnetic nonequivalence, as expected from the asymmetric structure of compounds I. The chemical shift difference between the protons designed H_a and H_b is again much more important (1.25 — 1.50 ppm) in compounds I than in the corresponding sulphonylamido phospholanes (0.65 ppm). Consequently it seems logical to ascribe this shift difference to the different anisotropic contributions of the aromatic ring. According to previous work,[2] we advance the tentative hypothesis, that in the *Z*-diastereomer IA—IB, H_b is the proton on the same side of the phospholane ring as the 5—CH_3 group, as shown in formulae IA—IB. Further, the interpretation of the observed coupling constants ($J_{aP} \gg J_{bP}$) in terms of dihedral angles indicates [2,6–8] a preferred conformation for IA—IB according to formula IV, that is with the 5—CH_3 group in equatorial position. However, the purely speculative nature of these geometrical presumptions should be underlined again.

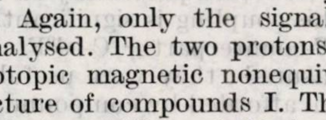

IV

b. *^{31}P-Resonance*: The ^{31}P-nucleus in compounds I appears substantially (with 32 — 33 ppm) more deshielded than in the corresponding arylsulphonylamido phospholanes. This additional deshielding is doubtlessly due to the P—S bonds in compounds I. It is generally known that thiophosphonic compounds have their ^{31}P-nuclei resonating at substantially lower fields than in the analogous molecules containing P—O or P—N bonds. This effect is generally well known,[9] and appeared invariably in several classes of organophosphoric derivatives studied recently in our laboratory.[2,10]

c. ^{13}*C-Resonance*: The signals of only one geometrical isomer (most probably *Z*) could be observed for compounds I2, I3 and I6, samples which, according to ^{1}H and ^{31}P-measurements contain less than 20% of the *E*-diastereomer. Both isomers were however observed for compounds I4 and I5, in which the ratio of the *E*-diastereomer is more substantial. Carbon 5 of the phospholane ring and that of its 5—CH_3 substituent appear more deshielded in the *E*-isomer than in its *Z*-counterpart, in accordance with the above-mentioned observation upon 5—CH_3 ^{1}H-chemical shifts. On the other hand, C—4 is slightly more shielded in the *E*-diastereomer. Only partial characterization of the aromatic ring carbons was obtained, as some presumably weak absorption peaks due to the quaternary carbons C—1′ and/or C—4 were not always found. There is some qualitative evidence that the C—1′ signals for compounds I2, I3, I5, and I6 are covered by the strong C—2′ resonance signals. All carbons in compounds I show detectable coupling to the ^{31}P-nucleus. The strong "beta-coupling" of the 5—CH_3 carbon to the phosphorus is to be mentioned; as it was observed previously for the analogous sulphonylamido-phospholanes,[2] this coupling is significantly larger in the *Z*-diastereomers than in their *E*-counterpart. ^{13}C—^{19}F coupling constants in compound I4 could be measured; they were useful in the interpretation of the aromatic subspectrum afforded by compounds I.

The alkaline hydrolysis of compound I5 proceeds *via* a nucleophilic attack on the phosphorus, breaking the P—S bond and thus yielding p-chloro-thiophenol. After p-chloro-thiophenol was filtered off, aliquots

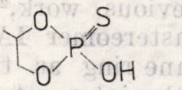

V

of the remaining solution were treated with Pb^{2+} or Ni^{2+} to form insoluble complexes of the thiophosphonic acid V; no such complexes were obtained, which makes us believe that the alkaline hydrolysis of compound I5 implies breaking of the phospholane ring too.

Earlier papers from our laboratory[11] showed that compounds containing the S=P—S substructure, as O,O-dialkyl S-aryl phosphorodithioates exhibit pronounced insecticidal properties. Consequently it seemed of interest to test the influence of the phospholane ring structure appearing in compounds I on this insecticidal activity. It is generally known, that the phosphorylating properties and thus cholinesterase inhibiting activity of the organophosphoric compounds increases with the increasing electrophilic character of the phosphorus atom. In this respect it must be emphasized that electrophilic character of the phosphorus is greater in the phospholane ring than in the acyclic analogs. Nevertheless, the cholinesterase inhibiting activity of the organophosphoric compounds depends very much upon sterical factors too. As it resulted from biological tests effected under comparable conditions, compounds I exhibit a lower insecticidal activity than the above-mentioned acyclic analogues. This fact proves that in the case of compounds I steric hindrance prevails over electronic effects in determinating their biological activity.

REFERENCES

[1] Part. LIII. : L. Almasi, V. Mureșan and A. Barabás, *Z. anorg. allg. Chem.*, **458**, 62 (1979).

[2] A. Barabás, V. Mureșan and L. Almasi, *Org. Magn. Resonance*, **12**, 313 (1979).

[3] I. Feneșan, V. Mureșan, A. Barabás and M. Bogdan, *Rev. Roumaine* Chim., **29**, 76 (1984).

[4] A. B. Arbuzov, K. B. Nikonorov and Z. G. Shishova, *Izvest. Akad. Nauk SSSR*, **1954**, 823.

[5] R. R. Shagidulin, I. H. Shakirov, A. H. Plyanovati, L. I. Gurani and E. I. Mukmenew, *Zhur. obschei Khim.*, **76**, 1021 (1976).

[6] R. H. Cox and M. G. Newton, *J. Amer. Chem. Soc.*, **94**, 4212 (1972).

[7] J. Devillers, M. Cornus, J. Roussel, J. Navech and R. Burgada, *Org. Magn. Resonance*, **6**, 205, 211 (1974).

[8] W. G. Bentrude and H. W. Tan. *J. Amer. Chem. Soc.*, **98**, 1850 (1976).

[9] J. R. Van Wazer, *J. Amer. Chem. Soc.*, **78**, 5709 (1956).

[10] A. Barabás, R. Popescu, V. Mureșan and L. Almași, *Org. Magn. Resonance*, **10**, 35 (1977).

[11] L. Almași and A. Hantz, *Studii și cercetări Chim. Fil. Cluj*, **11**, 135 (1960) ; **12**, 129 (1961).

Revue Roumaine de Chimie, **34**, *8*, 1769–1773 (1989)

OXIDATION OF ETHYLENE GLYCOL WITH PYRIDINIUM CHLOROCHROMATE. A KINETIC APPROACH

G. L. AGRAWAL and Ku. SHAMI JHA
Department of Chemistry, Gour University, Sagar (M.P.), 470003, India

Received December 7, 1987

The kinetics of the oxidation of ethylene glycol with pyridinium chlorochromate, $C_5H_5N^+HClCrO_3$ (PCC) has been studied in dichloromethane-nitrobenzene mixture. The reaction under pseudo-first order condition, is first order both in [Oxidant] and [Ethylene glycol]. The reaction is catalysed by an acid, the acid catalysed reaction being very fast which precluded the determination of its order in the acidic medium. The reaction does not induce polymerisation of acrylonitrile. Increasing percentage of nitrobenzene in the medium decreases the rate constant. Activation energy and the thermodynamic parameters have been determined. A probable mechanism consistent with the experimental observation is suggested.

INTRODUCTION

Though several oxidants have been employed for the oxidation of glycols, the mechanism of glycol fission has been the subject of much controversial discussion in which the relative merits of homolytic bond fission and heterolytic decomposition of the intermediate cyclic complexes have been argued.[1–5] A survey of literature shows that the oxidation of diols by the recently discovered oxidant, pyridinium chlorochromate (PCC), has not been investigated so far. We have therefore studied kinetically the oxidation of ethylene glycol by pyridinium chlorochromate in nitrobenzene-dichloromethane mixture as a first attempt to throw light on the exact mechanism of the reaction.

EXPERIMENTAL

All the inorganic and organic materials were commercial reagent grade unless otherwise stated and were obtained from British Drug Houses, Koch Light Ltd. and Sarabhai Merck Ltd. The purity of organic substrates was checked by measuring the physical constants. Pyridinium chlorochromate (PCC) was prepared by the method described in literature.[6]

All kinetic runs were carried out in a thermostated bath at the desired temperature. The reactions were carried out under pseudo-first order conditions i.e. the concentration of substrate being a large excess over PCC. The reaction was started by adding the required quantity of the PCC to a thermally equilibrated solution of the ethylene glycol in dichloromethane-nitrobenzene mixture. Portions (2 mL) of the reaction mixture were withdrawn at suitable time interval, and cooled to room temperature. The reactions were followed by moni toring the disappearance of Cr(VI) iodometrically. In the solvent composition used, the reaction mixture was homogeneous throughout the course of the reaction.

The pseudo-first order rate constant, k_{obs} were determined from the plot of $\log_{10}$ [oxidant] against time.

RESULTS AND DISCUSSION

The main kinetic features of the oxidation have been identified with ethylene glycol as substrate by monitoring the disappearance of Cr(VI) iodometrically.

Dependence of rate of oxidation

(a) *Concentration of pyridinium chlorochromate*

Kinetic runs have been carried out in the presence of ethylene glycol at different concentrations of PCC. $\log_{10}$ [PCC] *vs* time gave a good first order plot. The order of reaction with respect to PCC is that shown in table 1.

(b) *Concentration of ethylene glycol*

To ascertain the rate constant dependence and the order of reaction in substrate concentration, oxidations were carried out at different concentrations of ethylene glycol. Pseudo-first order rate constants (k_{obs}) were determined from the gradients of the first order plots (Table 2).

The order of reaction was determined from the gradient of the plot of $\log k_{obs}$ against $\log_{10}$ [initial substrate]. The overall bimolecular rate constants k_{obs}/[ethylene glycol] show constant values confirming first order dependence in substrate concentration.

Table 1

Variation of rate constant with [PCC] in dichloromethane-nitrobenzene mixture: [ethylene glycol] = 0.05 *M*, solvent composition = 90 :10 (V/V), temp. = 35°C

10^3[PCC]/M	10.0	8.0	6.6	4.0	2.0
$10^3 k_{obs}/s^{-1}$	1.863	1.909	2.132	1.914	1.892

Table 2

Variation of rate constant with [substrate] in dichloromethane-nitrobenzene mixture: [PCC] = 0.004 *M*, solvent composition = 90 :10 (V/V), temp. = 35°C

[ethylene glycol]/M	0.025	0.050	0.075	0.100	0.125
$10^3 k_{obs}/s^{-1}$	1.045	1.915	3.126	4.232	5.052
k_{obs}/[ethylene glycol] $= 10^2 k_1$	4.18	3.830	4.17	4.23	4.045

(c) *Acid concentration*

Attempts to study the acid catalysed reaction involving *p*-toluenesulphonic acid were unsuccessful as the addition of *p*-toluenesulphonic acid renders the system heterogeneous. However the addition of dichloroacetic acid catalyses the reaction but the reaction is too fast to measure the rate.

Table 3

Variation of rate constant on solvent composition : [PCC] = 0.004 M [Ethylene glycol] = 0.05 M, temp. = 35°C

Nitrobenzene : Dichloromethane (V/V)	$k_{\text{obs}} \times 10^3$ (s^{-1})
100 :00	1.089
95 :05	1.745
90 :10	1.909
85 :15	2.645

(d) *Ionic strength*

The effect of ionic strength on the rate constant could not be studied as the addition of sodium perchlorate makes the system heterogeneous. However it has been reported that the rate constants were unaffected by changes in ionic strength of the medium for the chromic acid oxidation of diols.[7]

(e) *Solvent composition*

The oxidation of ethylene glycol was studied by varying the proportions of nitrobenzene and dichloromethane at 35°C. Increasing percentages of nitrobenzene in the medium were found to decrease the rate constant suggesting that the more polar solvent may require longer reaction time. This is in agreement with the observation of Corey and Suggs.[6]

(f) *Radical scavenger*

The rate constants are not observably affected by acrylonitrile. In the presence of acrylonitrile no polymer precipitation was observed. This rules out the possibility of the formation of free radicals under the reaction conditions used.

(g) *Effect of temperature*

Experiments have been carried out at 25, 30, 35 and 40°C under identical condition of reagents in nitrobenzene-dichloromethane medium.

Activation energy (E_a) was calculated from the Arrhenius plot and using this E_a, related thermodynamic parameters were evaluated.

The data are recorded in table 4.

Table 4

Thermodynamic parameters

[PCC] = 0.004 *M* [ethylene glycol] = 0.10 *M*. Solvent composition = 90 :10 (V/V)

Temp °K	$10^3\ k_{obs}$ (s^{-1})	E_a (kJ mol^{-1})	$-\Delta S^{\neq}$ ($JK^{-1}\ mol^{-1}$)	$\Delta H^{\neq}$ (kJ mol^{-1})	$\Delta G^{\neq}$ (kJmol^{-1})
298	2.146		123.18	11.72	85.76
303	2.576	51.97 (298−303° K)	124.62	11.72	86.77
308	4.230	51.53 (303−313 °K)	123.40	11.70	86.98
313	4.926		124.72	11.693	87.97

DISCUSSION

The experimentally observed kinetic laws for this reaction are expressed by equation (1)

$$-\frac{d[PCC]}{dt} = [PCC]\ [\text{Ethylene glycol}] \qquad (1)$$

indicating that the velocity at any instant is largely proportional to the concentration of oxidant and substrate.

The reaction is supposed to follow direct hydride ion transfer as shown below :

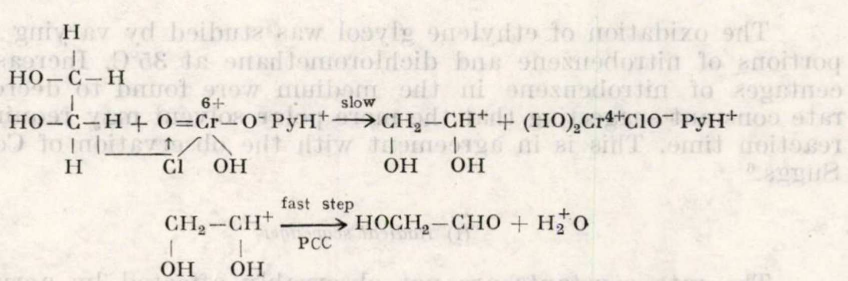

$$\text{HO-CH}_2\text{-CH}_2\text{-OH} + \text{O}=\overset{6+}{\text{Cr}}(\text{Cl})(\text{OH})-\text{O}^-\text{PyH}^+ \xrightarrow{\text{slow}} \underset{\text{OH}}{\text{CH}_2}-\underset{\text{OH}}{\text{CH}^+} + (\text{HO})_2\text{Cr}^{4+}\text{ClO}^-\text{PyH}^+$$

$$\underset{\text{OH}}{\text{CH}_2}-\underset{\text{OH}}{\text{CH}^+} \xrightarrow[\text{PCC}]{\text{fast step}} \text{HOCH}_2-\text{CHO} + \text{H}_2\overset{+}{\text{O}}$$

The oxidation product is the hydroxy aldehyde which has been identified by characteristic spot test.[8] No complex formation is observed spectroscopically between PCC and ethylene glycol. The hydride ion transfer is similar to the oxidation of alcohols [9,10].

Further confirmation of the hydride ion transfer comes from the dependence of the observed solvent effect which involves C—H bond rupture.

The data of large increase in the rate constant with acidity favour a reaction involving protonated Cr^{6+} species in the rate determining step.

Involvement of such species is very well known in the chromic acid oxidation[11]. Thus one can conclude that the primary reaction is essentially a C—H bond fission under these condition, leading to hydroxy aldehyde.

The entropy of activation for oxidation of ethylene glycol by PCC has been found to be negative. This is due to the compactness of the transition state, as compared to the ground state, causing a restriction on the translational and rotational freedom, thus reducing the entropy of activation.

ACKNOWLEDGEMENT. The authors thank Prof. S. P. Banerjee, Head, Chemistry Department, for providing the research facility.

REFERENCES

[1] W. A. Waters, *Trans. Faraday Soc.*, **42**, 184, (1946).
[2] A. A. Forist and F. R. Duke, *J. Amer. Chem. Soc.*, **71**, 2790 (1949).
[3] V. J. Shinerjen and C. A. Bunton, *J. Chem. Soc.*, **1960**, 1593.
[4] R. N. Mehrotra, *J. Chem. Soc.*, **B**, **1968**, 1123.
[5] C. S. Reddy and E. V. Sundram, *Int. J. Chem. Kinet.*, **15**, 307, (1983).
[6] E. J. Corey and J. W. Suggs, *Tetrahedron Letters*, **1975**, 2647.
[7] P. S. Radhakrishnamurthy and P. C. Behera, *Ind. J. Chem.*, **19**, 41, (1971).
[8] F. Fiegel, "Spot Tests in Organic Analysis", Elsevier, Amsterdam, 1975, p. 325.
[9] K. K. Banerjee, *J. Chem. Soc. Perkin II*, **1978**, 639.
[10] K. K. Banerjee, *Bull. Chem. Soc. Japan*, **51**, 2732, (1978).
[11] K. B. Wiberg, "Oxidation in Organic Chemistry", Academic Press, New York, 1965, Part IV, p. 71.

Revue Roumaine de Chimie, 34, 8, 1775—1778 (1989)

SYNTHESIS OF SOME NEW 7-SUBSTITUTED AMINOMETHYL-8-HYDROXY-QUINOLINE-5-SUBSTITUTED SULPHONAMIDES OF BIOLOGICAL INTEREST

AMAL SABET YANNI, ALI ALI ABDEL-HAFEZ and AHMED MOHAMED MOHARRAM*

Chemistry Department, Faculty of Science, Assiut University,
Assiut, Egypt

Received September 15, 1987

7-Aryl (or alkyl) aminomethyl-8-hydroxyquinoline 5-sulphonamide derivatives II—V have been prepared by the Mannich reaction on 8-hydroxyquinoline-5-sulphonylchloride with primary and secondary amines. The compounds obtained were verified by elemental and spectral data and biologically screened.

The chemistry of quinoline and *p*-toluene sulphonamide has attracted special attention because of their therapeutic properties.[1–2] Some of the sulphonamides were used as drugs for diseases like cancer,[3] tuberculosis,[4] diabetes,[5] malaria,[6] leprosy,[7] and convulsion.[8] Substituted 8-hydroxyquinolines were reported as potential amoebicides.[9–12] The Mannich derivatives of 5-benzyl and 5-(*p*-chlorobenzoyl)-8-hydroxyquinolines were also reported as potential ameobicides.[11] Moreover, 7-substituted aminomethyl-8-hydroxyquinoline-5-sulphonic acids[13] have been found to exhibit a remarkable antibacterial activity. Therefore we have endeavoured the synthesis of a new series of 7-substituted aminomethyl-8-hydroxyquinoline-5-sulphonamide derivatives II—V to evaluate their biological activity.

Interaction of 8-hydroxyquinoline with chlorosulphonic acid afforded 5-sulphonylchloride derivative (I). The title compounds were prepared through Mannich reaction according to the usual procedure [11,12] and identified by elemental analysis and spectral (IR, UV) data. The UV spectra in methanol displayed $\pi-\pi$ transition bands due to phenyl and heterocyclic rings around 210(S), 245(S), 263 (shoulder), and 310 nm (broad). IR spectra showed absorptions at 3280—3350 cm^{-1} (ν NH) 1310—1320 cm^{-1}, 1130 — 1150 cm^{-1} (ν SO_2).

The bactericidal activities of selected compounds were determined by the usual disc assay method against *Staph. aureus*, *Bacillus cereus*, *Micrococcus luteus*, *Proteus vulgaris*, *Pseudomonas aeruginosa*, *E. Coli*, *Serratia sp*.

---

* Botany Department.

Most of them showed remarkable bactericidal activity against ***Pseudomonas aeruginosa*** and a promotion effect towards ***Micrococcus luteus***. Some of them have a promotion effect towards ***Staph aureus***. It was also noticed that replacement of the sulphonamide group by a heterocyclic nucleus or an alkyl group enhances the activity as in case of compounds III b, IV b, V a. From our previous studies, it is also worthy to note that replacement of 5-sulphonamide group by 5-sulphonic group[13] induced differences in the bactericidal activity, depending on type of substituent and bacterial species used.

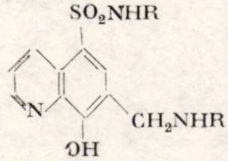

II

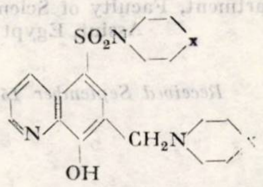

III

II a, R = C_6H_5
b, = p-$NO_2-C_6H_4$ -
c, = $p-COOH-C_6H_4-$
d, = $p-OCH_3-C_6H_4-$
e, = $1-C_{10}H_7-$
f, = $2-C_5H_5N-$
g, = CH_3-
h, = C_4H_9-
k, = $COOH-CH_2-$

III a, x = CH_2
b, x = O

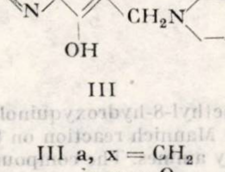

IV

IV a, R = CH_3-
b, = C_2H_5-

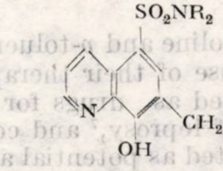

V a, R = CH_3-
b, = C_7H_7-
c, = C_4H_9-

EXPERIMENTAL

Melting points are uncorrected. IR spectra in KBr were recorded on a Unicam SP 200 G spectrophotometer using 1 cm matched silica cells. UV-visible absorption spectra were recorded on a Pye Unicam SP 8000 ultraviolet recording spectrophotometer using 1 cm matched silica cells.

8-Hydroxyquinoline-5-sulphonylchloride (I)[14]

It was prepared by the action of chlorosulphonic acid on 8-hydroxyquinoline at a temperature not exceeding 15°C and was left for one hour, then poured on crushed ice with continuous stirring, when I was separated immediately.[14]

7-Aryl (or alkyl) aminomethyl-8-hydroxyquinoline-5-sulphonamides II, III, IV

A mixture of 8-hydroxyquinoline-5-sulphonamide (0.004 mol), paraformaldehyde (0.004 mol) and the primary or secondary aromatic or aliphatic amine (0.008 mol) was kept for 30—40 hr during which time most of the starting material appeared to have dissolved before precipitation of the product. The separated products II—IV were filtered and crystallised from acetic acid, yield 60—70%. These compounds were insoluble in chloroform, carbon tetrachloride, dioxan, ether and acetone, moderately soluble in gl-acetic acid, methanol, ethanol and soluble in hot diluted HCl. Their characterisation data are given in table 1.

Table 1

Characterisation data of 7-substituted aminomethyl-8-hydroxyquinoline-5-sulphonamides II—V

Compound	Colour	m.p. (°c)	Yield (%)	Molecular formula	Found (%)		Calc. (%)	
					N	S	N	S
II_a	greenish yellow	325 dec.	60	$C_{22}H_{19}O_3N_3S$	10.22	7.78	10.37	7.90
II_b	brownish yellow	275	55	$C_{22}H_{17}O_7N_5S$	13.92	6.24	14.14	6.46
II_c	greenish yellow	334	50	$C_{24}H_{19}O_7N_3S$	8.25	6.30	8.52	6.49
II_d	reddish brown	285	60	$C_{24}H_{23}O_5N_3S$	8.70	6.53	8.84	6.73
II_e	greenish	295	65	$C_{30}H_{23}O_3N_3S$	8.18	6.16	8.32	6.34
II_f	,, ,,	268	50	$C_{20}H_{19}O_3N_5S$	16.98	7.69	17.11	7.82
II_g	grey	295	60	$C_{12}H_{15}O_3N_3S$	14.80	11.18	14.95	11.39
II_h	buff	253	50	$C_{18}H_{27}O_3N_3S$	11.38	8.57	11.51	8.77
II_k	yellow	235	70	$C_{14}H_{15}O_7N_3S$	11.18	8.43	11.38	8.67
III_a	buff	280	70	$C_{20}H_{27}O_3N_3S$	10.58	8.04	10.79	8.22
III_b	pink-buff	291	50	$C_{18}H_{23}O_5N_3S$	10.40	7.95	10.69	8.14
IV_a	white	320	60	$C_{14}H_{19}O_3N_3S$	13.38	10.43	13.59	10.35
IV_b	pink-buff	271	60	$C_{18}H_{27}O_3N_3S$	11.39	8.58	11.51	8.77
V_a	,, ,,	305	60	$C_{16}H_{21}O_3N_3S$	12.36	9.40	12.54	9.55
V_b	buff-grey	258	60	$C_{22}H_{25}O_3N_3S$	9.99	7,56	10.22	7.78
V_c	white	265	60	$C_{19}H_{27}O_3N_3S$	10.96	8.27	11.14	8.49

8-Hydroxyquinoline-5-piperidylsulphonamide

8-Hydroxyquinoline-5-sulphonylchloride (0.004 mol) and piperidine (0.008 mol) were refluxed in ethanol for 2 hr. The separated pale yellow product was filtered off and crystallised from water into greenish pale yellow crystals m.p. 324°. Anal. calcd. for $C_{14}H_{16}O_3N_2S$: C, 57.53 ; H, 5.48 ; N, 9.59 ; S, 10.96. Found C, 57.75 ; H, 5.64 ; N, 9.45 ; S, 10.80 %.

7-Substituted aminomethyl-8-hydroxyquinoline-5-N-piperidyl-sulphonamide V

A mixture of 8-hydroxyquinoline-5-piperidyl sulphonamide (0.004 mol) and the amine (0.004 mol) was refluxed in ethanol (50 mL) for 30 hr. The separated products were filtered off and crystallised from water into buff crystals of V. Characterisation data are given in table 1.

Antibacterial activity of compounds II – V

The antibacterial activity of compounds II a – d, g – k, IIIa,b, IVb, Va) was determined by the usual disc assay method against *Staph. aureus*, *Bacillus cereus*, *Micrococcus Luteus*, *Proteus vulgaris*, *Pseudomonas aeruginosa*, *E. Coli*, *Serratia sp.* at concentrations (5 microgram per disc). The culture medium used was of normal nutrient agar containing one gram yeast/litre. The bacterial suspensions was prepared by adding one mL of sterile distilled water to a 24-hour-old culture of the test organism grown on nutrient agar slant.

REFERENCES

[1] Proffit Elmar and G. Buchman, *Arzneim. Forsch.* **10**, 181 (1960); *Chem. Abs.* 53, 2229 i.
[2] Hisako Nishihara, *J. Biol. Chem.*, Japan, **40**, 579 (1953).
[3] Hoffmann La Roche & Co. Swiss Patent, 416648 (1967).
[4] J. A. Vaichulis, U. S. Patent, 3272352 (1966).
[5] H. Dietrich, Swiss Patent, 454874 (1968).
[6] L. H. Schmidt, *Ann. Rev. Microbiol.*, **23**, 427, (1969).
[7] G. Tarbini, Int. Cong. Chemotherapy, Proc. 5th (2), 909 (1967).
[8] S. Aktiesel, and F. Kabet, Dan. Patent, 108626 (1968).
[9] R. Gopalchari, S. P. Popli, Nitya Nand & Dahr M. L., *J. Scient. ind. Res.* **13B**, 15 (1954).
[10] R. Gopalchari and M. L. Dahr, *J. Sci. Ind. Res.*, **19c**, 233 (1960).
[11] Gopalchari R., *J. Sci. Ind. Res.*, **16c**, 143 (1957); **19c**, 296 (1960); **21B**, 266 (1961).
[12] Th. H. Porter, F. S. Skelton and K. Folkers, *J. Med. Chem.*, **15**, 34 (1972).
[13] A. S. Yanni and A. A. Timawy, *Indian J. Chem.*, **21 B**, 705 (1982).
[14] G. D. Tiwari and M. N. Mishra, *J. Indian Chem.*, **LIX**, 362 (1982).

Revue Roumaine de Chimie, **34**, *8*, 1779—1785 (1989)

NUCLEAR MAGNETIC RESONANCE OF SMALL RINGS. 8

^{13}C-NMR SPECTRA OF 8-SUBSTITUTED 5,9-METHANO-5H-BENZO[3,4]CYCLOBUTA[1,2]CYCLOHEPTENES [1]

MIRCEA D. GHEORGHIU* and ANGELA POPESCU
Department of Organic Chemistry, Polytechnic Institute-TCH,
76206 Bucharest — 16, Romania

Received March 15, 1989

The ^{13}C-NMR spectra of ten benzocyclobutanobicyclo[3.2.1]oct-2-ene derivatives are reported. By annelation with an *exo* benzocyclobutano ring on the five-membered side of bicyclo[3.2.1]oct-2-ene,the C-8-methano-bridge signal is shifted upfield by *ca.* −5 ppm, while the benzocyclobutano fragment in *endo* configuration is deshielding C−8 with *ca.* +5 ppm. The allylic hydroxy group has a shielding effect when it is *exo*, and a deshielding effect when it is in *endo* configuration upon the same methano bridge carbon atom C−8. The signals of sp^2 hybridized carbon atoms C−2 and C−3 were assignned with the aid of Eu(fod)$_3$·d$_{27}$ in a reverse order than quoted in the literature for the related bicyclo[3.2.1]oct-2-ene allylic alcohols.

INTRODUCTION

The chemistry of bicyclo[3.2.1]oct-2-enes subsituted at C—4 is richly illustrated by many reactions, among which the reaction occurring *via* allylic ions are best documented.[2] Nevertheless the spectral characterizations of bicyclo[3.2.1] oct-2-ene derivatives, although better referenced in the literature [1b, 2a, 3] in the case of ^{1}H-NMR, is less ilustrated for ^{13}-C-NMR. In fact the only contributions for ^{13}C-NMR are originated from the Stothers' group[4] and are devoted to bicyclo[3.2.1]oct-2-ene and some derivatives.

As a rule of thumb, the allylic C—4 carbon atom in the parent system is more deshielded than the methano bridge carbon atom C—8; bridgehead C—1 is more deshielded than the bridgehead C—5, the alkenic C—2 is more deshielded than the alkenic C—3, and C—7 is more deshielded than C—6. To summarize in the bicyclo[3.2.1]oct-2-ene system the C—7—C—1—C—2 flank is more deshielded than their counterparts C—6—C—5—C—3. Stothers' assignment of the carbon atoms from the compound **3a** parallels the relative charges calculated at the *ab-initio* STO—3G level,[2g] except for $-CH_2-CH_2-$, where C—6 has a slight excess of negative charge compared with C−7. However, there are convincing evidences that C−6 is more deshielded than C−7 in the parent hydrocarbon **3a**.[4] A hydroxy group in an allylic position (at C−4)[+] is shielding the atom C−6, irrespective of the *endo-* or *exo*-stereochemistry of this group. If the configuration of hydroxy group at C−4 is *exo*, C−8 is experiencing a γ-shielding effect of *ca.* − 5 ppm.

---

* correspondence author

In our report, we would like to support the above findings and also to reveal the effect of benzocyclobutano fragment upon the chemical shift of the bridge methano carbon atom C−8. If the configuration of

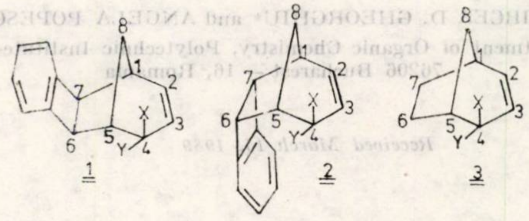

1 2 3

	a	b	c	d	e	f
X	H	OH	H	OAc	H	−O−(C$_4$=O)
Y	H	H	OH	H	OAc	

the benzocyclobutano fragment is *exo*, the signal of C−8 is shifted upfield and when the configuration of benzocyclobutano fragment is *endo* then the same signal is shifted downfield. A similar effect was observed by us in the case of norbornanes annelated on one side with cyclopropane in *exo*-configuration and on other side of norbornane skeleton with *exo-* and *endo*-benzocyclobutane group.[5] Moreover, the α, β, γ and δ effect of the C−4 substituents will be discussed, revealing, as expected, similar effects in the case of benzocyclobutano annelated bicyclo [3.2.1] octenes as they were unveiled by Stothers in the case of the bicyclo[3.2.1] octenes.[4]

DISCUSSION OF THE RESULTS

Tables 1 and 2 are presents the ^{13}C-NMR spectra of *exo-* (**1**) and *endo*-benzocyclobutanobicyclo[3.2.1]octene (**2**) and their derivatives at C−4 (see the footnote at Table 1). In Table 3, ^{13}C chemical shifts are presented for the nonannelated compounds **3** and are quoted from the contributions of Stothers.[4]

A. The assignment of ^{13}C-NMR signals to carbon atoms

a. The CH$_2$ groups from hydrocarbons 1a and 2a

The assignment of the carbons C−4 and C−8, having the same multiplicity in off-resonance experiments, was done by comparison of

---

[+] The numbering of carbon atoms for the alcohols and ketones is unconventional, having as aim to preserve the same labelling for all systems discussed here and thus to facilitate the comparisons among the various related compounds. The *Chemical Abstracts* nomenclature is presented in the title of our paper. For convenience, we shall use throught out this paper the nomenclature mentioned above.

the ^{13}C-NMR spectra of **1a** and **2a** with the 3-chloroderivatives **4** and **5**, respectively.[6]
The substitution with chlorine at C−3 is expected to alter substantially the chemical shift of the vicinal C−4, while the more remote C−8 should have a chemical shift very close to the chemical shift of C−8 in the unsubstituted derivatives **1a** and **2a**, respectively. Indeed, the chemical shift of C−8 in **1a** is at 30.33 ppm, while in the 3-chloroderivative **4** is 29.99 ppm; the *endo*-benzocyclobutano isomer **2a** displays for C−8 a signal at 40.26 ppm, while in the corresponding 3-chloroderivative **5**, it appears at 39.75 ppm. Therefore we have assigned for C−8 the chemical shift presented in Table 1 for alkene **1a** and in Table 2 for alkene **2a**.

Table 1

Chemical shifts of carbon atoms belonging to the bicyclo [3.2.1]octene derivatives annelated with *exo*- benzocyclobutano fragment **1** (δ, ppm, internal TMS, $CDCl_3$)

Compound	X	Y	C_1	C_2	C_3	C_4	C_5	C_6	C_7	C_8
1a	H	H	36.15	133.26	124.57	34.41	35.29	54.60	57.60	30.33
1b	OH	H	36.51	126.48	137.06	69.84	42.90	49.23	53.89	26.19
1c	H	OH	36.14	127.98	135.26	71.44	43.10	45.95	54.51	32.51
1d	OAc	H	36.23	122.81	138.82	71.40	40.01	48.90	53.92	26.83
1f	=O		37.99	155.42	128.10*	201.27	48.00	51.72	52.67	34.92

* for the sake of convenience, carbon atoms, irrespective of the priority of substituent at C-4, are numbered alike for all compounds.

Table 2

Chemical shifts of carbon atoms from the bicyclo [3.2.1]octene derivatives annelated with *endo*- benzocyclobutano fragment **2** (δ, ppm, internal TMS, $CDCl_3$)*

Compound	X	Y	C_1	C_2	C_3	C_4	C_5	C_6	C_7	C_8
2a	H	H	33.99	132.23	126.26	32.37	32.25	53.40	56.89	40.26
2b	OH	H	34.53	128.06	134.81	67.90	39.07	48.53	52.29	35.92
2c	H	OH	35.25	127.54	132.95	74.24	43.25	49.91	55.14	41.28
2d	OAc	H	33.93	123.05	136.64	69.83	36.26	47.95	51.91	36.26
2f	=O		36.05	153.34	129.86	200.48	47.49	50.03	51.13	46.07

* See footnote at Table 1

b. The bridgehead carbon atoms C−1 and C−5

In the parent system **I** the chemical shift of the allylic bridgehead C−5 was assigned to the higher field signal than that of the homoallylic bridgehead C−1.[4] We believe that by annelation with the benzocyclobutano fragment the relative chemical shifts of C−1 and C−5 in the case of hydrocarbons **1a** and **2a** are similar with those from the bicyclo[3.2.1]octene **3a**. Therefore in Table 1 and Table 2, δ_{C-1} is greater than δ_{C-5} for the hydrocarbons **1a** and **2a**. For C−4 substituted compounds **1b**, **1c**, **1d**, **1f**, **2b**, **2c**, **2d** and **2f**, due to the β-deshielding effect of the substituent, obviously the homoallylic bridgehead carbon atom is relatively shifted downfield, and thus $\delta_{C-5} > \delta_{C-1}$. Note that the signals of C−1, relatively remote from C−4, are occurring at *ca.* 35 ppm, differing only slightly in respect with the actual substituent at C−4, and thus are positioned very close to the chemical shift observed for the parent hydrocarbons **1a** and **2a** (see also Table 4).

Table 3

Chemical shifts of the carbon atoms belonging to bicyclo [3.2.1] octene derivatives* **3**

Compound	X	Y	C_1	C_2	C_3	C_4	C_5	C_6	C_7	C_8	lit.
3a	H	H	35.6	134.7	123.8	37.5	33.6	30.6	35.5	35.5	5a
3b	OH	H	35.6	137.9^x	125.2^x	72.1	40.5	24.8	[31.0]	[30.8]	5b
3c	H	OH	35.2	135.9^x	127.1^x	73.7	41.8	21.3	32.5	37.5	5b
3f	=O		37.4	156.5	127.2	203.2	50.6	24.5	29.4	40.2	5a

* See footnote at Table 1. Square bracket suggests ambigous assignment

^{x} These signals were reversed for the corresponding entries from Table 4.

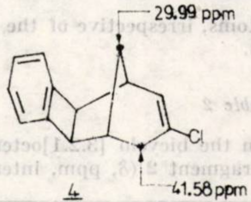

4

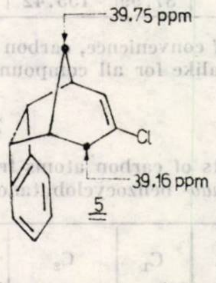

5

c. The benzylic carbon atoms C−6 and C−7

Although the assignments of C−6 and C−7 were attributed by analogy with the parent hydrocarbons presented in Table 3, we have convincing experimental evidence that indeed C−6 is shielded relative to C−7; albeit evidenced here for only one compound we believe it could be safely extrapolated to all compounds presented in Tables 1 and 2. Thus recording the spectra of alcohol **1b** dopped with the shift reagent $Eu(fod)_3 \cdot d_{27}$, the more shielded signal (49.23 ppm) has a greater gradient for the induced shift than the relatively deshielded signal (53.89 ppm). Accordingly the latter signal was assigned to C−7 as being the more remote atom from the complexation center. This assignment is identical with that proposed by Stothers[4b] for the alcohols **3b** and **3c**.

d. The alkenic C−2 and C−3 atoms

By selective proton decoupling, Stothers had assigned in the parent hydrocarbon **3a** for C−2 the lower field signal (132.23 ppm) leaving for C−3 the upper field signal (126.56 ppm).[4a] By annelation with *exo*- or *endo*-benzocyclobutano fragment, there are no reasons whatsoever to reverse the assignments for alkenic carbons in **1a** or **2a**. Therefore by analogy with Stothers' work we have assigned the lower field signal for C−2 for both alkenes **1a** and **2a**.

On the contrary, when C−4 was substituted with −OH and −OAc we have reversed the assignments of Stothers. The lower field signal was attributed to the vicinal C−3, in both *exo*- and *endo*-benzocyclobutano annelated bicyclo[3.2.1]octenes. The assignment was based upon results obtained from ^{13}C-NMR spectra of *exo*-benzocyclobutano substituted alcohol **1b** in the presence of shift reagent Eu(fod)$_3 \cdot d_{27}$. The induced shift for C−3 is roughly twice the induced shift for C−2. Therefore we have reversed the assignment of Stothers also for the unannelated alcohol **3b** and **3c** (see Table 3)[7].

c. The carbinyl C−4

This signal is readily assigned from its deshielded position within the range of 67−72 ppm.

B. Substituent effects

a. Hydroxy group

The changes in shielding produced by hydroxy group are of particular interest as probes for stereochemical analysis and for some assignments of the ^{13}C shieldings. Therefore we have collected in Table 4 the differences $\delta_C^{ROH} - \delta_C^{RH}$.

Table 4

Effect of *exo*- and *endo* hydroxyl group on the skeletal shieldings in the bicyclo [3.2.1] octenol non- and annelated with benzocyclobutano fragment (see footenote Table 1)*. Entries are calculated by substrating the chemical shifts of the carbon atom belonging to the monosubstituted skeleton from the corresponding substituted derivative ($\delta_{ROH} - \delta_{RH}$)

Compound	X	Y	C_1	C_2	C_3	C_4	C_5	C_6	C_7	C_8
3b	OH	H	0	−9.5	14.1	34.6	6.9	−5.8	−4.5	−4.7
3c	H	OH	−0.4	−7.6	12.1	36.2	8.2	−9.3	−3.0	2.0
1b	OH	H	0.36	−6.78	12.49	35.43	7.61	−5.37	−3.71	−4.14
1c	H	OH	0	−5.28	10.69	37.03	7.81	−8.65	−3.09	2.18
2b	OH	H	0.54	−4.17	8.25	35.53	6.82	−4.87	−4.60	−4.34
2c	H	OH	1.26	−4.69	6.39	41.87	11.0	−3.49	−1.75	1.02

* The increments of the −OH substituent at C−4 in bicyclo[3.2.1] octanols were calculated using the data from reference 4b. In the case of C−2 and C−3, the assignments were reversed by us (see text).

For comparison, the corresponding alcohols of bicyclo [3.2.1] octene **3** are also included in Table 4. For the carbon atoms belonging to the alkenic fragment as mentioned already, we have reversed the original assignment of Stothers.[4]

The hydroxy group in *exo*-configuration exerts a shielding effect of *ca.* − 4 ppm upon the methylene bridge carbon atom C−8. A hydroxy group in *endo*-configuration has an opposite effect, deshielding slightly C—8(with *ca.* 1—2 ppm). Therefore a negative magnitude of the γ-effect is a good probe for defining the *exo* stereochemistry of hydroxy group at C—4.

The α-effect of hydroxy group is generally within the range of 35—37 ppm; a larger deshielding effect namely 41.87 ppm was noted in the particular case of the alcohol **2c**.

The β-effect upon the vicinal bridgehead C—5 is deshielding. An *endo*-OH is more strongly deshielding than an *exo*-oriented —OH. The β-effect upon the C—3 sp² carbon atom is larger when the OH is *exo* oriented. In an *exo*-alcohol when acetylated, the most pronounced effect is at C—2, which is shifted upfield (with *ca.* — 4 ppm) relative to the corresponding alcohols. The β-effect upon the bridgehead carbon atom C—5 is of *ca.* — 2.5 ppm. The effect of *exo*-OAc upon the bridge methylene group is less significant than expected as a result of increased steric repulsions; it amounts to *ca.* — 0.4 ppm.

b. Benzocyclobutano fragment

We have noticed that the configuration of the benzocyclobutano fragment annelated on the bicycloheptane skeleton has a γ shielding effect (— 6.7 ppm) when it is in *exo* configuration, and a γ deshielding effect (+ 5.9 ppm) when it is in *endo* configuration.[5] In compounds **1** and **2** the benzocyclobutano fragment is annelated to the five-membered as in our previous examples. Thus, *a priori*, it is reasonable to expect a very similar effect of the benzocyclobutano fragment upon C—8. Indeed, in *exo*-configuration, the benzocyclobutano fragment is responsible for the upfield shift of C—8 with — 5.17 ppm in hydrocarbon **1a**, — 4.61 ppm in the *exo*-alcohol **1b** and — 5.28 ppm in the ketone **1f.** The *endo*-benzocyclobutano fragment deshields the methano bridge C—8 with + 4.76 ppm in the alkene **2a**, with + 5.12 ppm for the *exo*-alcohol **2b** and + 5.87 ppm in the case of the ketone **2f.** Thus the relative shift of C—8 is a powerful probe for defining the configuration of benzocyclobutano fragment paralleling the similar effect of the allylic OH group.

CONCLUSIONS

The stereochemistry of the bicyclo[3.2.1]oct-2-ene system substituted at C—4 with a hydroxy group and annelated on C—6—C—7 with benzocyclobutano fragment is defined the relative chemical shift of the methano bridge C—8 atom. The *exo*-configuration of the hydroxy group and of the benzocyclobutano fragment has shielding effect upon C—8. The magnitude is of approximatively — 4 ppm in the case of *exo*—OH group and of — 5 ppm for benzocyclobutano fragment. In *endo*-configuration, both OH and benzocyclobutano fragment deshield C—8; OH with *ca.* 1—2 ppm and the benzocyclobutano group with a mean value of 5 ppm. The assignment of ^{13}C signals for the parent hydrocarbon and the C—4 derivatives was done i) by analogy with the results of Stothers,[4] ii) supported also by $Eu(fod)_3 \cdot d_{27}$ experiments and iii) is consistent with the substituent induced shifts accounting for α, β and γ effects. We believe that the alkenic carbon atoms in alcohols **1b,1c, 2b** and **2c** have δ—C—3 layer than δ—C—2, contrary to the assignment of Stothers.[4b]

We are now examining the ^{13}C-NMR spectra of benzocyclobutano-derivatives of 3-chlorobicyclo [3.2.1.]octenes with the aim of recognizing the effect of the chloro substituent and for obtaining other experimental facts for a better design of the increments of benzocyclobutano fragment in the *exo*- and *endo*-configuration.

EXPERIMENTAL PART

The ^{13}C-NMR spectra were recorded with FT-80A instrument. The parameters were for : spectral windows 4000 and 5000 Hz, pulse width 15µs, pulse delay 3.5 s and aquisition time 2.047 s or 1.637 s. All spectra were run in $CDCl_3$ with internal standard tetramethylsilane.

The hydrocarbons **1a** and **2a** were synthetized by the method described in reference 8. Details regarding the synthesis of the compounds **1b** — **1f** and **2b**—**2f** will be published in a forthcoming paper.

ACKNOWLEDGEMENTS. We are grateful to Dr. E. Georgescu (Chemical Research Center Rimnicu-Vilcea) for material support.

REFERENCES

[1] a) Taken in part from Ph. D. Theis of A. P. b) For the preceding paper see : M. D. Gheorghiu, A. Popescu and Gh. Surpăţeanu, *Rev. Roumaine Chim.*, **34**, 481 (1989).

[2] a) S. Winstein, M. Ogliaruso, M. Sakai and J. M. Nicholson, *J. Amer. Chem. Soc.*, **89**, 3656 (1967) ; b) J. M. Brown and J. L. Occolovitz, *J. Chem. Soc. B*, **1968**, 411 ; c) A. F. Diaz, M. Sakai and S. Winstein, *J. Amer. Chem. Soc.*, **92**, 7477 (1970) ; d) W. Kirmse and Th. Olbricht, *Chem. Ber.*, **108**, 2616 (1975) ; e) G. B. Trimitsis and A. Tuncay, *J. Amer. Chem. Soc.*, **97**, 7193 (1975) *ibid.*, **98**, 1997 (1976) ; f) J. B. Grutzner and W. L. Jorgensen, *J. Amer. Chem. Soc.*, **103**, 1372 (1981) ; g) E. Kaufman, H. Mayr, J. Chandraseckhar and P.v.R. Schleyer, *J. Amer. Chem. Soc.*, **103**, 1375 (1981) ; h) M. Christl, H. Leininger and D. Brückner, *J. Amer. Chem. Soc.*, **105**, 4843 (1983) ; i) W. N. Washburn, *J. Org. Chem.*, **48**, 23, 4287 (1983) ; j) G. B. Trimitsis and P. Zimmerman, *J. Chem. Soc., Chem. Commun.*, 1984, 1506 ; k) M. Christl and D. Brückner, *Chem. Ber.*, **119**, 2025 (1986) ; l) R. E. Lee and R. R. Squires, *J. Amer. Chem. Soc.*, **108**, 5078 (1986).

[3] W. R. Moore, W. R. Moser and J. E. La Prade, *J. Org. Chem.*, **28**, 2200 (1963) ; R. C. De Selms and C. M. Combs, *ibid.*, 28, 2206 (1963) ; C. W. Jefford and K. C. Ramey, *Tetrahedron*, 24, 2927 (1968) ; M. Battiste, J. M. Coxon and R. Edelman, *Tetrahedron Letters*, **1972**, 4577 ; M. A. Battiste, J. M. Coxon, A. J. Jones, R W. King, G. W. Simpson and P. J. Steel, *Tetrahedron Letters*, **1983**, 307 ; M. A. Battiste, J. M. Coxon, G. W. Simpson and P. J. Steel, *Tetrahedron*, **40**, 3137 (1984).

[4] a) J. B. Stothers, J. R. Swenson and C. T. Tan, *Can. J. Chem.*, **53**, 581 (1975) ; b) J. B. Stothers and C. T. Tan, *ibid.*, **55**, 841 (1977). The corresponding saturated derivatives of **1** were discussed by : E. Lipmaa, T. Pehk, N. A. Belikova, A. A. Bobyleva, A. N. Kalinichenko, M. D. Ordubaki and A. F. Platé. *Org. Mag. Reson.*, **8**, 74 (1976) and A. N. Kalinichenko, A. A. Bobyleva, N. A. Belikova, A. F. Platé, T. Pehk and E. Lipmaa, *Zh. Org. Khim.*, **10**, 1449 (1974).

[5] M. D. Gheorghiu and E. Olteanu, *J. Org. Chem.*, **52**, 5158 (1987).

[6] M. D. Gheorghiu and A. Popescu, manuscript in preparation.

[7] The generally accepted assignment for the alkene carbons of allylic alcohol or ethers is in accordance with our propsal : R. C. Levy, R. L. Licter and G. L. Nelson, "Carbon-13 Nucear Magnetic Resonance Spectroscopy", 2nd Edition, Wiley, New York, 1980, pp 83 and 84.

[8] A. Popescu, L. Pârvulescu, L. Stănescu and M. D. Gheorghiu, *Rev. Roumaine Chim.*, **31**, 1025 (1986) ; in fig. 2 the assignments of C—1 and C—4 from compounds **2** should be reversed.

Revue Roumaine de Chimie, 34, 8, 1787–1798 (1989)

WHY LIFE CAN BE ONLY A CARBON BASED CHEMISTRY

A. CĂLUȘARU
Institute of Chemical Research, 77208 Bucharest, Romania

Received August 20, 1988

A considerable amount of information on the living matter forming capacity of the carbon atom can be obtained within the rigorous conception about the five component vectors of valence states (VVS) of the chemical elements. When the relationship between each VVS component and the atomic number is considered, one gets quantitative data about the combinatorial ability of the carbon atom : it has a considerable number of valence states (35 from 139 possible ones), can form the highest number of radicalic species as reaction transients and has the ability to form VVS containing a high or the highest number of simple, double and triple bonds.

When chemistry based on one element is studied as a possible structural form of the living matter, two main aspects proved to have an outstanding significance : (a) energetics of both formation and breaking of the chemical bonds and (b) chemical combinatorial ability of the involved element. As reference frame, serves obviously the empirical fact that the carbon based chemistry is a possible form of the living matter and the only one known.

The first point includes two different problems of equal weight. One of them refers to the very important property of an element to have close energies of binding with other elements. The carbon atom has this interesting property since there are almost equal energies of formation for C—C (81.6 kcal), C—H (98.8 kcal), C—O (81.5 kcal), C—Cl (78.0 kcal)[1] and also for other chemical bonds with a series of elements. Silicium, the nearest congener of carbon in the periodic table, has not this favourable property since the energy of Si—Si (42.5 kcal) bonds is lower than that of Si—H (75.1 kcal), Si—O (89.3 kcal) and Si—Cl (85.8 kcal).[1] Owing to the much lower stability of the Si—Si bonds, the long chains molecules cannot be formed in this case. However the long C chains are not always the most important ones in the structure of the living matter for which the building blocs are the amino acids. The proteins are constituted by arrangements of amino acids attached by peptide links, therefore not through C—C, but through C—N bonds. Also the most important bases of nucleic acids such as purines and pyrimidines are heterocyclic compounds containing alternate C and N atoms.

The second problem belonging also to the energetics aspects, concerns the activation energy of bond breaking, therefore the stability of a chemical bond, already formed. As an element of the first row in the periodic table, the carbon atom has no extra-orbitals and consequently many carbon compounds are stable in conditions of metastability or thermodynamic instability [1,2]; the saturated carbon compounds especially have a slow reactivity, ensuring the above specified chemical stability. This is why in living organisms a compound can subsist a long time until a specific transformation is produced by the action of enzymes.

These energetics aspects, known for a long time,[1,2] although of particular importance, are too scarce to allow the explanation of the huge number of structures constituting the living matter and the organic chemistry in general.

One can expect more promising possibilities if one takes into account the combinatorial ability of chemical elements. But within the too simplified old conception on the valence states of elements, only very scarce data can be available. However a considerable amount of information can be got in quantitative form, if the new procedure of vectorial encoding of the combinatorial state of an atomic species is used. One of the most salient aspects of the mathematical symbolization of the chemical transformations and structures takes into account the new interpretation and definition of valence state (VS) as the configuration of outer shell electrons of an atomic species in the molecule. In this way any structural form of atom in the frame of a molecular structure can be encoded as a multicomponent vector of valence state (VVS). Yet in the literature a four component vector was proposed and used in expert systems for chemistry in the form (*nsdt*) [3]: *n* is the number of nonparticipating electrons, *s* of single bonds, *d* of double and *t* of the triple ones. But for a more comprehensive interpretation, we found necessary, as we will show below, to use a five component vector, since the nonparticipating electrons can be found in the form of both unpaired (*u*) or paired (*p*) electrons. Therefore we use the following VVS: (*upsdt*).

According to this rigorous interpretation, the number of VS is considerably higher than the one of valence forms in the old conception. Taking into account the known combinations of the chemical elements it has been found that for atoms in general 139 different VS are possible.[4,5] Obviously only a part of these can be encountered in the case of a definite species. Considering the definite VS of individual elements we have found that these forms can be correlated with the atomic number, showing in this way salient aspects about both amounts of structures for the chemistry in general and especially for life chemistry.

1. NUMBER OF VALENCE STATES *vs* ATOMIC NUMBER

Of particular interest is to take into account the number of VS of the chemical elements. The plot in Fig. 1 shows the correlation between the number of VS and the atomic number (AN) for the first *cca* 36 elements and also for iodine (53) and xenon (54). At higher AN a rather monotonic variation around 10 VS can be expected for the majority of the corresponding elements.

It is interesting to specify the obvious periodicity of the VS number as a function of AN. Three peaks can be visibly noticed on this figure each of them located between two successive argonides and having a definite element at the top. But it is also worth noting the region before helium, where a singular species can be found, amounting to hydrogen atom. As shown below, the hydrogen behaves as a top element of a virtual peak. It can either donate its single electron, or share this electron with other atoms to complete the K shell. This ambivalent behaviour gives to hydrogen a unique symmetry among the chemical elements. An important consequence of this symmetrical ambivalence to form both typical ionic and covalent bonds is the possibility to form in addition hydrogen bonds, a unique property, indispensable to the life processes. It is also important to notice that the stable and strong covalent C—H bonds are the main source of non-polar side groups in biological molecules, conferring the hydrophobic effect in interaction with the quasi-crystalline structure of water. This effect results in a solvation cage, whose outstanding role in biochemical processes consists in modelling the shape of enzymes and nucleic acids, conferring in this way the high selectivity of biological reactions in the living tissues.

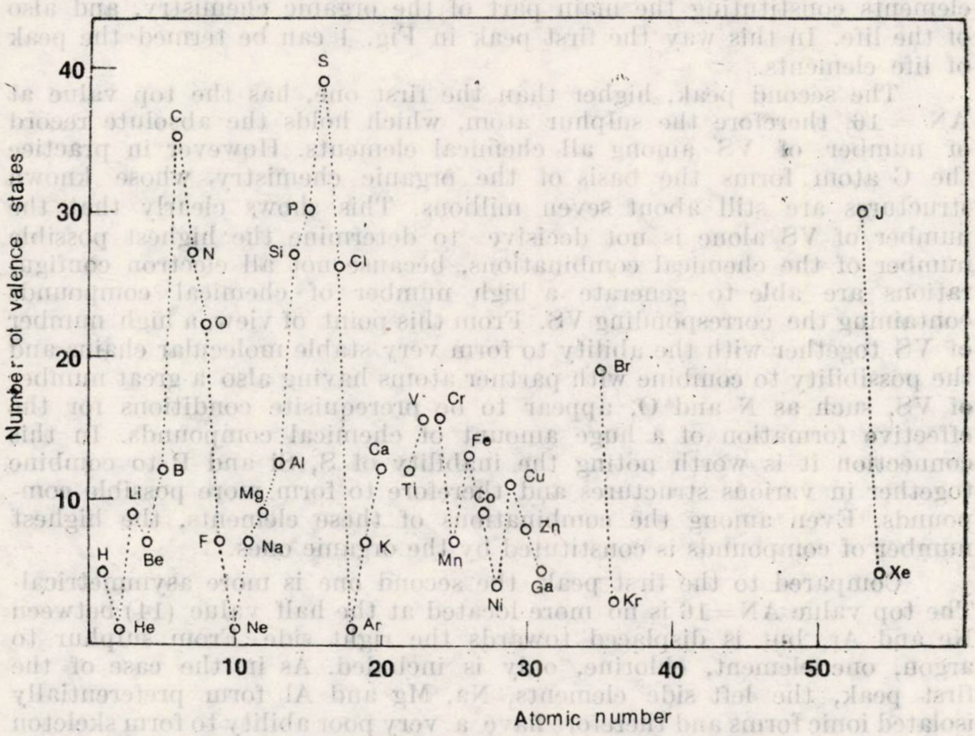

Fig. 1. — Number of valence states *vs* atomic number.

The first proper peak starts with the atoms Li, Be and B, which form especially ionic forms or oxide compounds rather than skeleton structures and therefore the number of VS is not high. At the top of the first peak is the carbon atom with 35 VS, followed by nitrogen with 28 VS and oxygen with 22 VS. The fluorine atom follows with few VS, in contrast with the other halogens having a multitude of possible electron configurations. The top of the peak is located at the half value (6) between He and Ne, corresponding to AN of carbon. For the chemistry it is interesting to note that the three elements with values of VS, over 20, therefore C, N and O, together with H, label the elements constituting the main part of the organic chemistry, and also of the life. In this way the first peak in Fig. 1 can be termed the peak of life elements.

The second peak, higher than the first one, has the top value at AN = 16, therefore the sulphur atom, which holds the absolute record of number of VS among all chemical elements. However in practice the C atom forms the basis of the organic chemistry, whose known structures are still about seven millions. This shows clearly that the number of VS alone is not decisive to determine the highest possible number of the chemical combinations, because not all electron configurations are able to generate a high number of chemical compounds containing the corresponding VS. From this point of view, a high number of VS together with the ability to form very stable molecular chains and the possibility to combine with partner atoms having also a great number of VS, such as N and O, appear to be prerequisite conditions for the effective formation of a huge amount of chemical compounds. In this connection it is worth noting the inability of S, Si and P to combine together in various structures and therefore to form more possible compounds. Even among the combinations of these elements, the highest number of compounds is constituted by the organic ones.

Compared to the first peak, the second one is more asymmetrical· The top value AN=16 is no more located at the half value (14) between Ne and Ar, but is displaced towards the right side. From sulphur to argon, one element, chlorine, only is included. As in the case of the first peak, the left side elements, Na, Mg and Al form preferentially isolated ionic forms and therefore have a very poor ability to form skeleton structures by peptide-like bonds. The chance of the elements of the second peak to form a chemistry similar to the organic one was therefore missed. No other element can be able to substitute the carbon atom to form any type of life. But the second peak lends to the first one its own atoms for a series of structures and functions indispensable to living tissues. The most important are obviously the phosphorous and sulphur atoms, congeners of nitrogen and oxygen respectively, in the second row of the periodic table. Like the atoms of the first row, these ones tend also to form an octet of electrons, but the formation of an octet does not saturate the third outermost shell. In the third shell, the second row atoms still possess the five *3d* orbitals, able to maintain five pairs of electrons. But just this additional bond-forming capacity of P and S confers the essential role they play in biological systems.

The situation changes over AN=18, where the period is no more closed after 8 AN-units, but after 18 ones, since the fourth noble gas, krypton, has AN=36. The previous regularities cannot be found in this case since all elements between Ar and Kr, excepting Br, have a predominant metallic character. This is why all these elements behave like the left side ones of the two previous peaks, forming preferentially isolated ionic species rather than covalent bonds. However one can clearly observe the tendency of V atom to be located on the top of an enlarged peak having a sharp increase with bromine at the right limit of the period.

Over AN=36 the number of VS varies in a similar fashion with the third peak. Here the sharp increase for iodine (N=53) is even higher.

2. NON-PARTICIPATING UNPAIRED ELECTRONS IN VVS *vs* AN

As it has been already emphasized, non-participating electrons can be found as both unpaired or paired ones. An atom having one unpaired electron, therefore a radical, is in general an unstable chemical species, arising the most often as a transient in chemical transformations. The transition of an atom from one to another VS, or even between the forms of the same one, can occur thereby either by one elementary step of electron regrouping, or by several such steps. This type of reactions shows clearly that the occurrence of radicalic species considerably enlarges the number of both possible structures and reaction paths.

In this context it is easy to understand that the greater is the ability to form radicalic species, all the more probable is the amount of both structures and chemical transformations. Information of particular significance for chemistry can be obtained if the ability of chemical elements to form radicalic species, and therefore colhom * reactions [6] as a function of AN is known. The relationship between these two parameters is shown in Fig. 2, where two sharp peaks occur, excepting the H-atom, which always behaves as a top atom of a presumable peak. The first proper peak on Fig. 2 has at the top the C atom with 12, followed by the N atom with 11 and the O atom with 7 possible radicaalic forms of the structures containing these atomic species. Again the F atom with 3 units only on the ordinate axis behaves unlike all the other halogens.

These figures show that the C atom holds in this case the absolute record of the number of radicalic forms among the chemical elements. The radicalic species are unstable, but very reactive, allowing the propagation of a multi-step reaction once started. With the highest number of radicalic VS the carbon has an outstanding importance in the evolution process and also for the emergency of life, which can occur spontaneously only if a wide variety of highly reactant species is available; for the make-up of the first living being this variety of many different reactive forms appears as a particularly necessary property. In the same way one can now understand why a wide variety of carbon structures which are known to be precursors of biological molecules of higher complexity were found in laboratory experiments to be spontaneously formed under conditions similar to those presumed to have taken place during the initial phases of Earth formation.[7] Although this interpretation has been not proved experimentally, since no nucleotides are formed in these conditions, one can think that even if the reaction pathway, allowing the spontaneous formation of the building-blocks of nucleic acids, is in practice much longer than that shown above, the prerequisite condition for the occurrence

---

* By analogy with the term *redox* the term *colhom* (*col*-igation, *hom*-olysis) was proposed since both *redox* and *colhom* reactions are the most elementary processes, constituting any other chemical transformation.

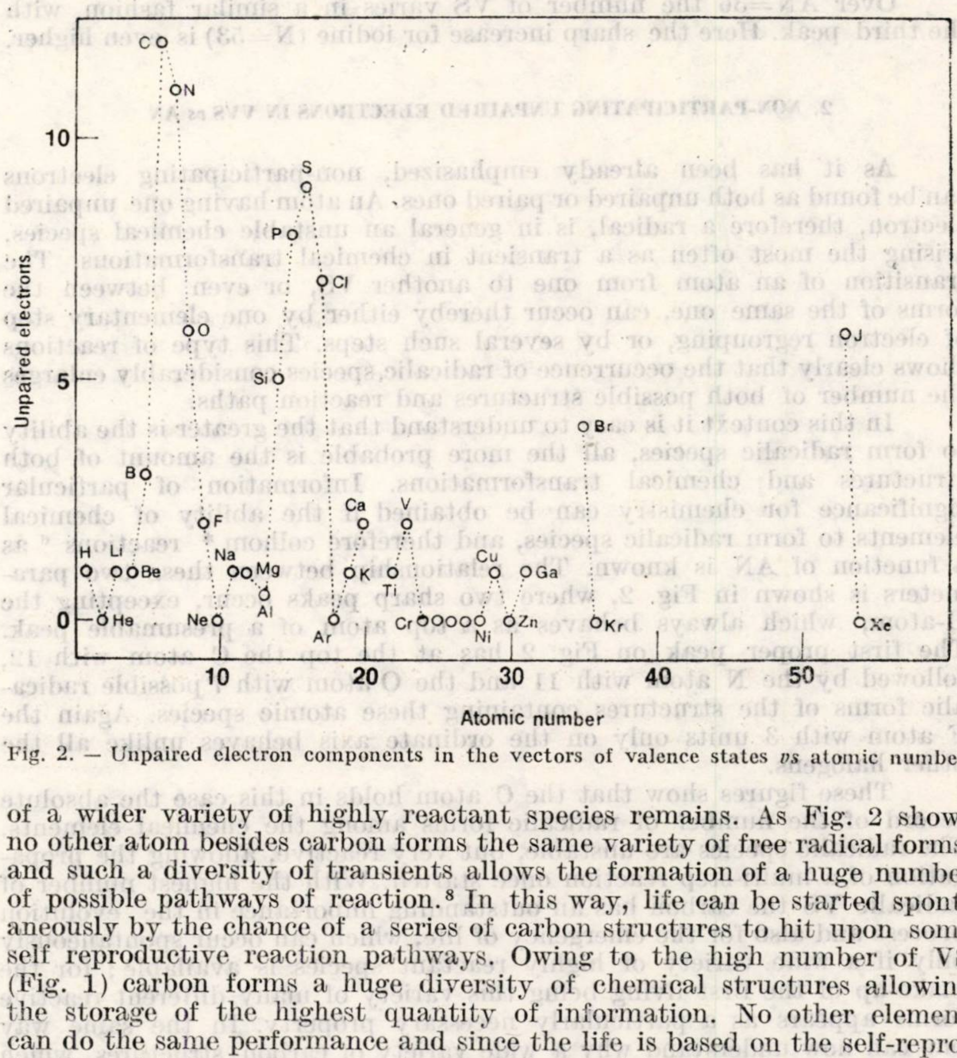

Fig. 2. — Unpaired electron components in the vectors of valence states *vs* atomic number.

of a wider variety of highly reactant species remains. As Fig. 2 shows no other atom besides carbon forms the same variety of free radical forms, and such a diversity of transients allows the formation of a huge number of possible pathways of reaction.[8] In this way, life can be started spontaneously by the chance of a series of carbon structures to hit upon some self reproductive reaction pathways. Owing to the high number of VS (Fig. 1) carbon forms a huge diversity of chemical structures allowing the storage of the highest quantity of information. No other element can do the same performance and since the life is based on the self-reproduction of information, a carbon based chemistry is uniquely suited to serve as basis. The further analysis of the VVS components *vs* AN will add similar arguments.

With an equivalent weight to that of C in forming radicalic species is the N atom. Besides carbon, nitrogen also plays an essential role in the chemistry of life. It is an indispensable element of the amino acids, purines, pyrimidines and forms with carbon peptide type bonds.

Nitrogen is followed by oxygen with 7 radicalic forms only. On this basis one can expect that the atomic vector formed by the doublet (C, N) as a center of reaction will produce the highest number of both radicalic products and intermediates and therefore the largest number of reaction paths, where radicals form one or more transient steps. Of particular importance in organic chemistry are also the atomic vectors forming the group (C, O). Thus for the stepwise transformations in living matter the following three atomic vectors are of essential importance: (C, C), (C, N) and (C, O).

The second peak is formed by the Si, P, S and Cl atoms with S atom at the top (9 forms of radicalic VS). A strong brake to form radicalic species or intermediates is the inability of these elements to form atomic vectors where the elementary steps, therefore *redox*, *colhom* and *heterolytic* processes can occur according to as much as possible different reaction paths. But the high number of radicalic forms of VS in the case of S atom suggest the potential interest for the study of the (C, S) and (N, S) atomic vectors, by the methods of expert systems based on molecular modelling or graphics.

Singular high values were found for Br and I atoms. But in the case of Cl, Br and I, the amount of compounds is strongly limited by the peculiarity of the halogens to be bound preferentially as side atoms, with single bonds or as oxygenated compounds.

3. NON-PARTICIPATING PAIRED ELECTRONS IN VVS *vs* AN

The second type of non-participating electrons is constituted by the single or multiple pairs belonging to a definite atomic species. The pair group is more stable than the unpaired electron. In Fig. 3 the plot of Σp_i *vs* AN is drawn up. It is particularly interesting to notice the analogy of this figure with figure 2, although no correlation may be established between the unpaired and paired electrons in VVS. Here are also two peaks only, located in the same propositions; yet the top atoms are different, with O on the first peak and Cl on the second one. The F and Cl atoms are located on higher positions on these peaks owing to the seven outer shell electrons of the halogens, allowing different forms of regrouping, where at least a pair remains unoccupied. The same situation holds for Br and I atoms. But, in spite of these high positions, the halogens remain in molecules mainly as side atoms, owing to the already mentioned inability to be included in skeleton structures.

It is interesting to notice that the oxygen as the top element of the first peak of life elements, in molecular form, has unpaired electrons with unopposed spin. This is why the molecular oxygen readily shows the more active form with two unpaired electrons. This tendency to an easy dissociation adds in the reactivity of oxygen. One can interpret in this way the strong property of the oxygen atom to share an electron with the other atoms in order to form these strong covalent bonds. With hydrogen the oxygen reacts to form water in one of the most energetic chemical reactions, by which the living organisms are supplied with energy.

From the point of view of a possible reaction path, the most interesting property of the one unoccupied electron pair is to constitute a site of a potential chemical binding, where a positive charged or electron deficient species can be attached to form either a covalent or a coordinative bond. The electron pairs enhance in this way the possibility to bind a chemical species, according to the VS of this component. But this path of reaction is not the most reactive one and the peak elements in Fig. 3 and especially the halogens are not the elements reacting mainly in this way. By comparing the figures 2 and 3 one can see clearly that for the ability to form a large number of compounds the VS containing unpaired electrons are considerably more important than those containing paired electrons. However Fig. 3 shows very accurately the elements constituting the components of chemical group having the highest ability to form coordinative compounds; halogens only are excepted.

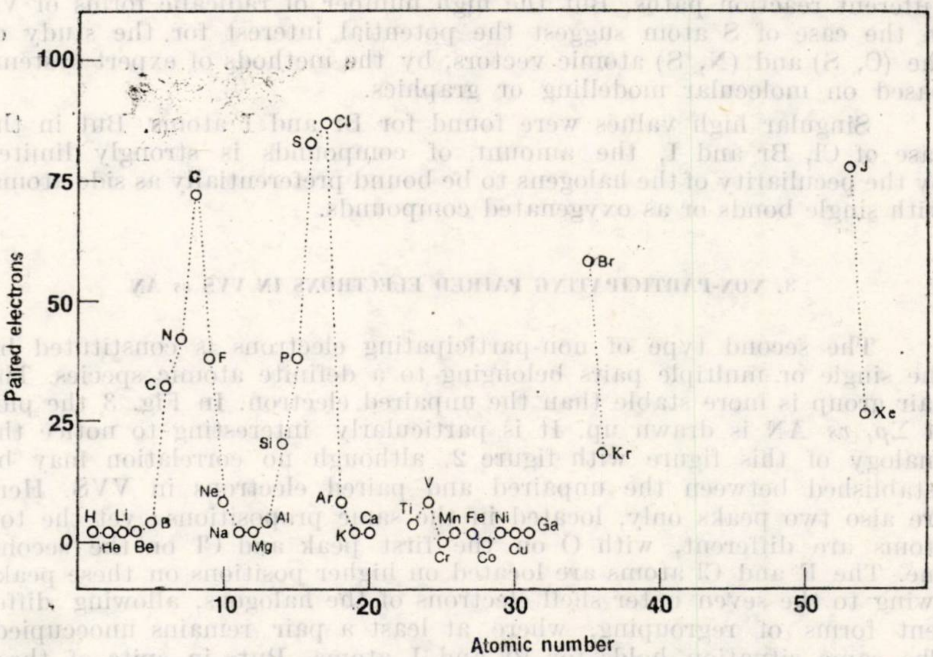

Fig. 3. — Paired electron components in vectors of valence states *vs* atomic number.

4. COMPONENTS OF SINGLE BONDS *vs* AN

Fig. 1 was drawn up independently of the components of VVS. But when the total number of the vectorial components corresponding to single bonds, therefore Σs_i, is plotted *vs* AN, a graph similar with the one in Fig. 1 is obtained. This close analogy between these two graphs shows that the number of valence states of the chemical elements is mainly determined by the occurrence of the single bonds, therefore the third component of the five-member VVS. The specifications in the paragraph 1 for the total number of VS hold also in general for the single bonds. However one can note that the three peaks having at the top C, S and V atoms are of comparable height. One can also see that for the three triads (V, Cr, Mn), (Fe, Co, Ni) and (Cu, Zn, Ga) the first atoms have a high ordinate value and the last ones a much lower one. The vectorial number corresponding to the single bonds is perhaps of particular significance for the characterization of chemical properties of an element among the components of VVS.

5. COMPONENTS OF DOUBLE BONDS *vs* AN

The sum of the components corresponding to the double bonds in VVS *vs* AN is given in Fig. 4. The three main peaks can also be found in this case, although no relation seems to exist between the occurrence of the simple and double bonds. However the peaks are now formed starting from and ending to zero values. For instance the first peak of the life elements rises suddenly from Be to B with 5 ordinate units and further at the top value of C having 13 units. The descending part of this peak is slower, passing over three atomic species N, O, F at zero value, with Al having 3 and then Si with 13 units, equating thus the highest value of the sum of vectorial components related to the double bonds. It is interesting to note that for the life chemistry the large number

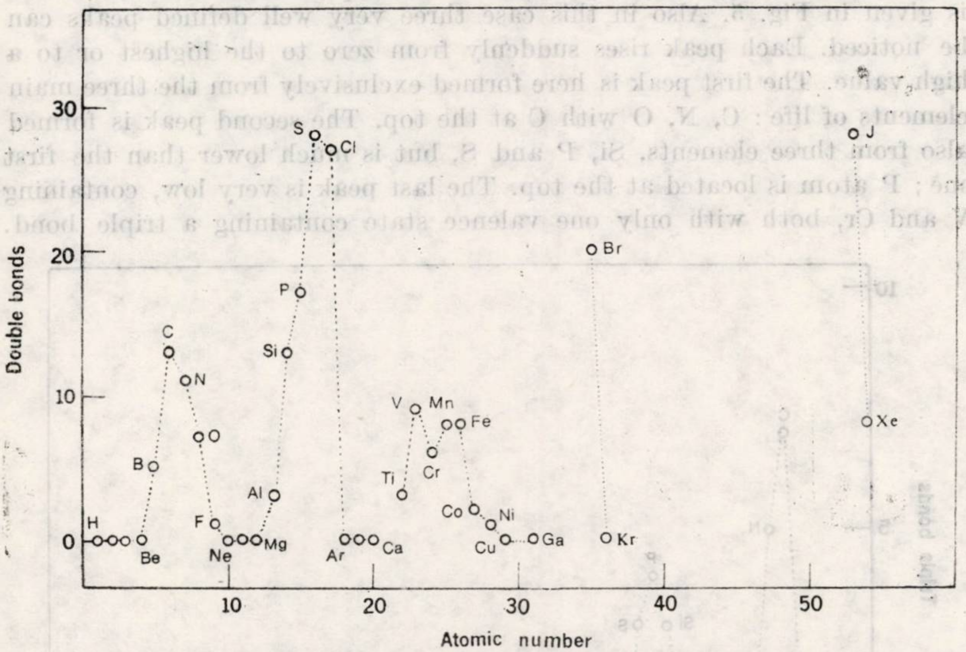

Fig. 4. — Double bond components in vectors of valence states *vs* atomic number.

of vectors containing double bonds is not the most significant parameter. The first peak shows that the value of 13 units for C atom is the optimal one, while the exceeding value of 28 units for S atom is excessive and cannot contribute to increase the number of possible combinations. This conclusion holds still better for Cl and further for Br and I, where the variety of forms containing double bonds is not accompanied by the possibility to form a large variety of compounds with these VS. The second peak descends abruptly to Ar.

The third peak is lower having V, Mn and Fe as top elements. Also in this case the major part of VVS with double bonds is formed by oxygenated compounds.

6. COMPONENTS OF TRIPLE BONDS *vs* AN

The last component of VVS corresponds to the triple bonds. Obviously these last ones are the less frequent in the frame of the chemical structures. The sum of components of the triple bonds in VVS *vs* AN is given in Fig. 5. Also in this case three very well defined peaks can be noticed. Each peak rises suddenly from zero to the highest or to a high value. The first peak is here formed exclusively from the three main elements of life : C, N, O with C at the top. The second peak is formed also from three elements, Si, P and S, but is much lower than the first one ; P atom is located at the top. The last peak is very low, containing V and Cr, both with only one valence state containing a triple bond.

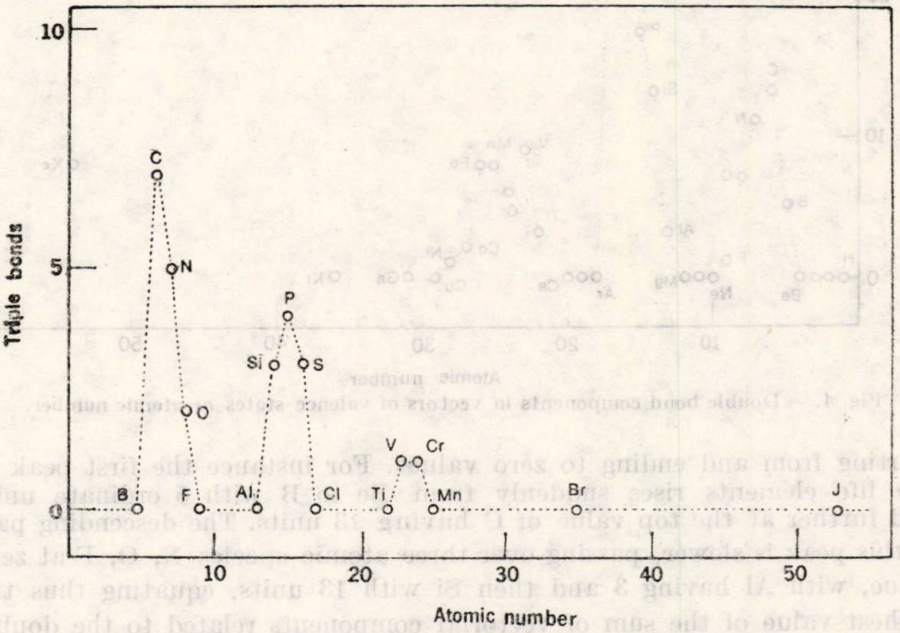

Fig. 5. — Triple bond components in vectors of valence states *vs* atomic number.

7. DISCUSSION

The relationship between the atomic number and the components belonging to the VVS in the above shown definition allows a quantitative evaluation of the most peculiar chemical properties of elements to form stable structures or reaction transients. The higher is this ability, the greater is the number of chemical compounds that can be formed. The total VVS counts the variety of chemical forms belonging to each element and is determined mainly by the frequency of the single bonds, which is the third component of the five-member VVS. Among the VS a specified form may be found in one or a few structures, while other forms can be constituents of a larger number of compounds. It is possible in this way to explain that the S atom which has the highest number of VS does not form the largest variety of structures, while the C atom can do this owing to the favourable VS forms.

One can get much more quantity of useful and specific information when each component of the VVS is studied individually. Any VVS with its components expresses a possible structural shape that proved to be significant in the explanation of some properties which can be important also for the living matter. With the too scarce old conception on the valence state, the chemistry had yet not an effective tool to prove if another element, except for carbon, should be able to form a chemistry, providing a possible alternative form of life.

A quantitative evaluation, able to give a rigorous answer to th problem of the unicity of carbon atom for chemistry of the living matter is based on the above shown relationship between the components of VVS *vs* AN. The problem can be simply formulated as follows : has one or several elements similar properties with carbon atom from the point of view of structural shape, combinatorial capacity and bond energetics? The answer is that no other element has such similar properties. As in the case of the VS number, for each vectorial component it matters not only the amount of forms, but also some special characteristics such as the occurrence and nature of electrical charges and the ability of structures to allow various or even unlimited chemical alternatives to be contained in the specified structure as intrinsic component. The electrical charge is of special importance also in the case of radicalic species, where the reactivity of the unpaired electron adds to the direction and selectivity of a reaction path among several possible ones. But in conferring the above shown properties to an atomic species two factors play the important role : (1) the symmetry of the electronic structure, which is the highest in the case of hydrogen (one electron from two possible) and carbon (four valence electrons from eight possible); (2) the absence of extra-orbitals able to destroy the above shown symmetry, a condition fulfilled only by K and L electron shells. The properties of outstanding importance for life in the case of the binding abilities of hydrogen were already shown. In a similar context the symmetry of the occupied and free electron orbitals of carbon confers to this atom the favourable coincidence of shape, charge and reactivity within a defined VS, factors indispensable to this peculiar chemical geometry enabling the formation of the huge quantity of structures belonging to the organic chemistry and indispensable to the living matter. This is the source of generation of the high number of valence states of the most favourable configuration and the most suited arrangements of the vectorial components, therefore of non-participating electrons and simple, double and triple bonds. These circumstances contribute to the best equilibration of some opposite, but inseparable existential principles, necessary for a living being to occur. There is no other equivalent place, excepting hydrogen, in the periodic table of elements with so high general symmetry and therefore no other element enables a chemistry of life.

The above presented discussion, based mainly on structural shapes and, to some extent, on the combinatory ability, is based on the five-member VVS of the chemical elements, having the peculiarity to refer to the simplest chemical state: the element itself. This procedure is the only one which enables to present quantitatively significant aspects related to the general chemical ability of chemical elements to form both structures and reaction paths in a very simple, easily comprehensive and synoptic form. A similar analysis based on the next complexity level, corresponding to atomic vectors with two chemical species, should lead to an enormous complexity which cannot allow a simple basic interpretation, providing a huge amount of possible variants that are beyond the normal possibility of men, and feasible only by high capacity computers.

REFERENCES

[1] J. T. Edsoll and J. Wyman, "Biophysical Chemistry", Vol. I, Academic Press, N. Y., 1958.

[2] W. V. Sidgwick, "The Chemical Elements and Their Compounds", Vols I and II, Oxford University Press, Oxford, 1950.

[3] I. Ugi, J. Brandt, J. Friedrich, J. Gasteiger, C. Iochum and W. Schubert, *Angew. Chem.* (Int. Ed. Engl.), **18**, 111(1979).

[4] M. Kratochvil, J. Koča and V. Kvasnička, *Chem. Listy*, **79**, 807(1983).

[5] A. Călușaru, "Representation of Chemical Structures by Matrices and Computer Algorithms" Chap. 32 in: "Heat and Mass Transfer", Vol. 3 (N. P. Cheremisinoff, Editor), Gulf Publishers, New Jersey, 1989, p. 1197; A. Călușaru, *Rev. Chim. (Bucureşti)*, **38** 965(1987).

[6] A. Călușaru, *Rev. Chim. (București)*, **38**, 869(1987); A. Călușaru and M. Apostol, *Rev. Roumaine Chim.*, **33**, 25(1988); A. Călușaru, *Rev. Roumaine Chim.*, **33**, 921 (1988).

[7] S. W. Fox and K. Dose, "Molecular Evolution and Origin of Life", 2nd edn., Marcel Dekker, N.Y., 1977.

[8] A. E. Nedham, "The Uniqness of Biologic Materials" Pergamon Press, N.Y., 1965.

Revue Roumaine de Chimie, 34, 8, 1799–1808 (1989)

ÉTUDE CINÉTIQUE DE LA DISSOLUTION DES SOLIDES UTILISANT LA TECHNIQUE DE SÉDIMENTATION

STELIAN PETRESCU
Institut Polytechnique de Iassy, Splai Bahlui 71, Roumanie

Reçu le 12 septembre 1988

On présente une nouvelle méthode d'étude pour la cinétique des processus de dissolution des solides par la détermination de la vitesse de dissolution et du coefficient individuel de transfert de masse en différentes étapes de la sédimentation. La méthode est utilisée pour l'étude de l'influence des paramètres cinétiques de la vitesse de dissolution des granules sphériques d'urée en solution aqueuse d'urée de différentes concentrations.

This paper presents a new method for the study of the solid dissolution kinetics process based on the determination of the dissolution rate and of the individual mass transfer coefficient at different moments of the sedimentation. The method is used in order to study the influence of the kinetics parameters on the dissolution rate of the urea spherical particles in aqueous solution of urea of different concentrations.

1. INTRODUCTION

La littérature en la matière comprend de nombreux travaux sur la cinétique de la dissolution des solides utilisant à cet effet a technique des vaisseaux avec agitateur[1–6] ou la technique du disque rotatif[7–14]. Peu de travaux[7, 15, 16] traitent de la cinétique de la dissolution des solides par la technique de sédimentation, quoique celle-ci permette l'obtention rapide d'informations quantitatives sur la dissolution des solides.

Utilisant la technique de sédimentation, dans ce travail est présentée une méthode d'étude de la cinétique de la dissolution des solides, qui présuppose la détermination expérimentale de la vitesse de dissolution et du coefficient individuel de transfert de masse lors de la dissolution des granules sphériques de solides pendant les différentes étapes de la sédimentation. En s'étayant sur les valeurs de la vitesse de dissolution, on a étudié l'influence de la concentration initiale de la solution ainsi que celle de la vitesse de sédimentation sur la vitesse du processus global de dissolution.

Pour les expérimentations ont été utilisés les granules d'urée et, en tant que solvant, une solution aqueuse d'urée de différentes concentrations. Les données nécessaires aux calculs, respectivement les propriétés physiques générales et d'équilibre, ont été extraites de la littérature[17,18].

2. ÉTABLISSEMENT DES ÉQUATIONS POUR LE CALCUL DE LA VITESSE DE DISSOLUTION ET DU COEFFICIENT INDIVIDUEL DE TRANSFERT DE MASSE

La vitesse de dissolution d'un composant quelconque (A) d'un granule peut être définie par la relation ci-après :

$$V_D = \frac{dm_A}{Sdt} \qquad (1)$$

où : m_A est la masse du composant A du granule ;
S — l'aire de la surface extérieure du granule ;
t — la durée du processus.

La masse du composant A qui passe en phase liquide dans l'intervalle de temps infinitésimal (dt) est :

$$dm_A = \rho_p \cdot X_{Ap} \cdot dV_p \qquad (2)$$

La variation du volume du granule dans le temps dt, ainsi que l'aire de la surface du granule au moment t résultent de la figure 1.

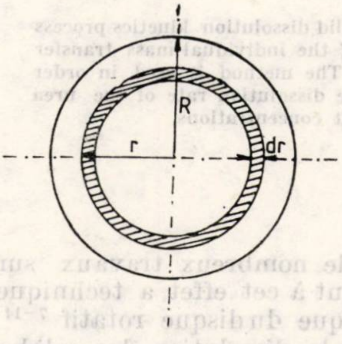

Fig. 1. — Le modèle du granule sphérique.

$$dV_p = 4\pi\, r^2 dr \qquad (3)$$

et

$$S = 4\pi r^2 \qquad (4)$$

En substituant les équations (3) et (4) par (1), il résulte :

$$V_D = \rho_p \cdot \overline{X}_{Ap} \frac{dr}{dt} \qquad (5)$$

Cette équation permet de calculer la vitesse de dissolution des granules sphériques conformément à la variation des dimensions des granules dans le temps. L'équation (5) peut acquérir aussi la forme suivante :

$$v_D = \frac{\rho_p \cdot \overline{X}_{Ap}}{2} \cdot \frac{dd_p}{dt} \qquad (6)$$

Si le granule est formé d'une seul composant, $\overline{X}_{Ap} = 1$ et l'équation (6) devient :

$$v_D = \frac{\rho_p}{2} \cdot \frac{dd_p}{dt} \qquad (7)$$

La variation du diamètre de la particule dans le temps peut être obtenue selon la variation de la vitesse de sédimentation dans le temps

À ce que l'on sait, la vitesse de sédimentation d'une particule sphérique de solide est donnée par la relation[19,20] :

$$v_0 = \left[\frac{4}{3} \frac{g}{\zeta} \cdot \frac{(\rho_p - \rho)}{\rho} \cdot d_p \right]^{1/2} \tag{8}$$

où : g est l'accélération gravitationnelle ;

ρ, ρ_p — la densité de la phase, respectivement la densité de la particule ;

ζ — le coefficient de résistance.

Le coefficient de résistance dépend du numéro Re et de la forme de la particule et peut être exprimé par une relation générale de la forme suivante :

$$\zeta = a \cdot \mathrm{Re}^{-n} \tag{9}$$

En mettant la vitesse au carré et en remplaçant la relation (9) par (8), il résulte :

$$v_0^2 = \frac{4}{3} \cdot g(\rho_p - \rho) \cdot a^{-1} \cdot \rho^{n-1} \cdot \eta^{-n} \cdot d_p^{n+1} \cdot v_0^n \tag{10}$$

De l'équation (10) on obtient le diamètre de la particule qui sédimente en fonction de la vitesse de sédimentation et des propriétés pysiques de la particule et du milieu de sédimentation :

$$d_p = \left(\frac{3}{4}\right)^{\frac{1}{n+1}} [g(\rho_p - \rho)]^{-\frac{1}{n+1}} \cdot a^{\frac{1}{n+1}} \cdot \rho^{\frac{1-n}{n+1}} \cdot \eta^{\frac{n}{n+1}} \cdot v_0^{\frac{2-n}{n+1}} \tag{11}$$

Conformément aux équations (6) et (11) et en passant aux différences finies, on peut écrire l'équation suivante pour calculer la vitesse de dissolution d'un granule sphérique :

$$v_D = \frac{\rho_p}{2} \cdot \overline{X}_{Ap} \left(\frac{3}{4}\right)^{\frac{1}{n+1}} [g(\rho_p - \rho)]^{-\frac{1}{n+1}} \cdot a^{\frac{1}{n+1}} \rho^{\frac{1-n}{n+1}} \cdot \eta^{\frac{n}{n+1}} \cdot \Delta v_0^{\frac{2-n}{n+1}} \cdot \Delta t^{-1} \tag{12}$$

Dans le cas où le déterminant de vitesse est le processus élémentaire de transfert du composant A par la phase liquide, la vitesse de dissolution peut s'exprimer comme suit :

$$v_D = K_l(C^e - C) \tag{13}$$

et considérant l'équation (12) on obtient pour le coefficient individuel de transfert de masse l'équation :

$$K_l = \left(\frac{3}{4}\right)^{\frac{1}{n+1}} \frac{\rho_p}{2} \cdot \overline{X}_{Ap} [g(\rho_p - \rho)]^{-\frac{1}{n+1}} \cdot a^{\frac{1}{n+1}} \cdot \rho^{\frac{1-n}{n+1}} \cdot \eta^{\frac{n}{n+1}} \cdot (C^e - C)^{-1} \cdot \Delta v_0^{\frac{2-n}{n+1}} \cdot \Delta t^{-1} \tag{14}$$

La vitesse moyenne de sédimentation est déterminée éxpérimentalement en utilisant la relation :

$$v_0 = \frac{\Delta H_0}{\Delta t_0} \tag{15}$$

où : ΔH_0 est la distance parcourue par la particule entre deux repères fixes de la colonne de sédimentation,

Δt_0 — la durée du déplacement entre les deux repères.

Les équations (12) et (14) démontrent que dans le cas des particules sphériques qui sédimentent, on peut calculer la vitesse de dissolution et respectivement le coefficient individuel de transfert de masse uniquement par la détermination expérimentale de la vitesse de sédimentation de la particule, les propriétés physiques du milieu de sédimentation se retrouvent dans la plupart des cas dans la littérature.

En fonction du domaine de sédimentation, les équations (12) et (14) acquierent les formes suivantes :

a) pour le domaine Stokes :

$$v_D = 2{,}1213 \cdot \rho_p \cdot \overline{X}_{Ap}[g(\rho_p - \rho)]^{-0{,}5} \cdot \eta^{0{,}5} \cdot \Delta v_0^{0{,}5} \cdot \Delta t^{-1} \tag{16}$$

$$K_1 = 2{,}1213 \cdot \rho_p \cdot \overline{X}_{Ap}[g(\rho_p - \rho)]^{-0{,}5} \cdot \eta^{0{,}5} \cdot (C^e - C)^{-1} \cdot \Delta v_0^{0{,}5} \cdot \Delta t^{-1} \tag{17}$$

b) pour le domaine Allen :

$$v_D = 2{,}5874 \cdot \rho_p \cdot \overline{X}_{Ap}[g(\rho_p - \rho)]^{-0{,}625} \cdot \rho^{0{,}25} \cdot \eta^{0{,}375} \cdot \Delta v_0^{0{,}875} \cdot \Delta t^{-1} \tag{18}$$

$$K_1 = 2{,}5874 \cdot \rho_p \cdot \overline{X}_{Ap}[g(\rho_p - \rho)]^{-0{,}625} \cdot \rho^{0{,}25} \cdot \eta^{0{,}375} \cdot (C^e - C)^{-1} \cdot \Delta v_0^{0{,}875} \cdot \Delta t^{-1} \tag{19}$$

c) pour le domaine Newton :

$$v_D = 0{,}165 \cdot \rho_p \cdot \overline{X}_{Ap}[g(\rho_p - \rho)]^{-1} \cdot \rho \cdot \Delta v_0^2 \cdot \Delta t^{-1} \tag{20}$$

$$K_1 = 0{,}165 \cdot \rho_p \cdot \overline{X}_{Ap}[g(\rho_p - \rho)]^{-1} \cdot \rho \cdot (C^e - C)^{-1} \cdot \Delta v_0^2 \cdot \Delta t^{-1} \tag{21}$$

La détermination expérimentale de la vitesse de dissolution et du coefficient individuel de transfert de masse lors de la dissolution des solides pendant les différentes étapes de la sédimentation exige la détermination au préalable de la variation en temps de la vitesse de sédimentation des granules.

3. TECHNIQUE EXPÉRIMENTALE

Afin d'établir les valeurs expérimentales de la vitesse de sédimentation des granules d'urée en solution aqueuse d'urée, on a utilisé une installation constituée d'une colonne de verre longue de 1,5 m et d'un diamètre de 0,045 m, fermée à une extrémité avec un bouchon de caoutchouc et pourvue de cinq divisions : A, B, C, D et E. Cette colonne est fixée à l'aide d'une pince sur un support métallique. A l'extrémité libre de la colonne se trouve un entonnoir de verre servant à introduire les granules.

Les recherches expérimentales ont été effectuées sous la pression atmosphérique et à la température de 20 °C. En tant que milieu de sédimentation a été utilisée une solution aqueuse d'urée à 10% et 20% masse. Les granules d'urée ont été sélectionnés selon la grandeur à l'aide d'un micromètre. Pendant les recherches ont été utilisées trois granulosités différentes : dp = 1,55 m ; dp = 1,82 mm et dp = 2,07 mm. Pour chaque expérience ont été utilisées 5—6 granules, pratiquement du même diamètre, prenant en considération dans les calculs ultérieurs le granule qui a sédimenté sans rouler et sans atteindre les parois de la colonne.

La solution à la température de 20 °C a été introduite dans la colonne. Environ 5 minutes après on a commencé à introduire les granules et le chronométrage de leur déplacement entre les divisions A—B, A—C, C—D et C—E. À cette fin ont été utilisés deux chronomètres, l'un pour les intervalles A—B, A—C et l'autre pour les intervalles C—D, C—E. Pour chaque granule on a procédé de la même manière. Pendant les expériences, la température a été vérifiée en permanence et maintenue constante a la valeur fixée.

4. RÉSULTATS ET DISCUSSIONS

Les données expérimentales obtenues sur les durées de déplacement des particules entre les divisions A—B, B—C, C—D et C—E sont presentées au tableau 1. Ces données ont été interprétées dans les coordonnées suivantes : H—t, figures 2, 3, qui mettent en évidence la variation de la hauteur de sédimentation dans le temps pendant le déplacement des granules d'urée, en solution aqueuse d'urée de concentration de 10% et de 20% masse.

Tableau 1

Durée du déplacement des granules d'urée dans les intervalles A—B, A—C, C—D etC—E

C° (% masse)	dp [mm]	A—B	A—C	C—D	C—E
10	1,55	4,4	11,6	8,5	15,3
	1,82	4,2	11,0	7,6	13,7
	2,07	4,0	10,0	6,1	12,1
20	1,55	4,9	12,9	9,2	16,7
	1,82	4,7	12,2	8,1	14,6
	2,07	4,35	10,75	6,2	11,3

On constate que les dépendances H—t sont approximativement linéaires sur la distance A—C, mais les durées de sédimentation sont plus grandes pour ce qui est des granules plus petits, indifféremment de la concentration de la solution d'urée.

Si la concentration initiale de la solution d'urée augmente la durée de sédimentation des granules augmente aussi. Les courbes de sédimentation des fig. 2 et 3 ont permis de calculer la vitesse de sédimentation des granules aux différentes hauteurs de sédimentation.

Le tableaux 2 et 3 donnent les valeurs de la vitesse de sédimentation.

Conformément aux tableaux 2 et 3, on constate que la vitesse de sédimentation diminue en fonction de la réduction de la hauteur de sédimentation et qu'elle croît en fonction de l'augmentation du diamètre des

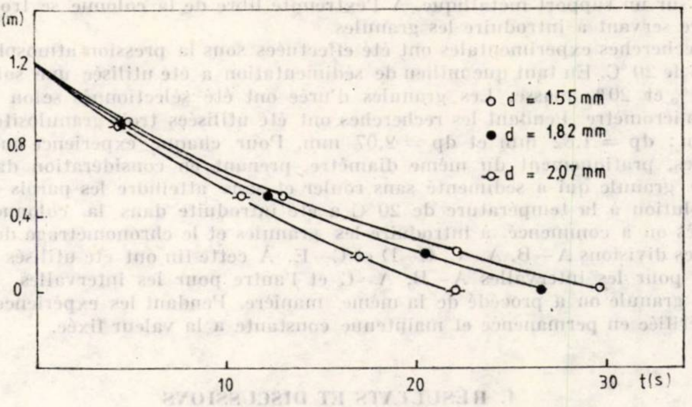

Fig. 2. — La variation de la hauteur de sédimentation dans le temps, C° = 10% masse.

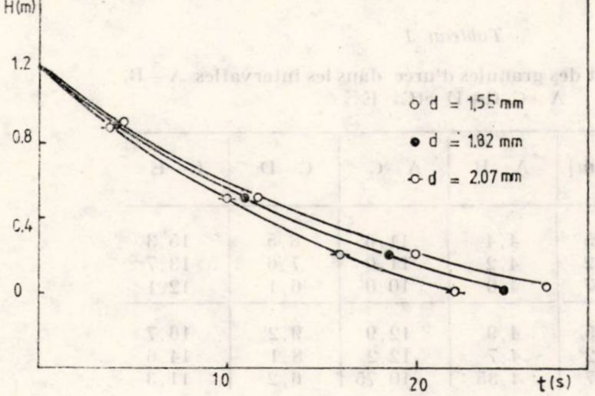

Fig. 3. — La variation de la hauteur de sédimentation dans le temps, C° = 20% masse.

particules et de la diminution de la concentration initiale de la solution d'urée.

Ensuite on a calculé la vitesse de dissolution et le coefficient individuel de transfert de masse lors de la sédimentation des granules sphériques d'urée. Parce que, expérimentalement, on a constaté que les granules d'urée de 1,5—2,1 mm de dimension sédimentent dans le domaine d'Allen, pour les calculs on a utilisé les équations (18) et (19), dans lesquelles on a considéré $X_{AP} = 1$, les granules d'urée utilisés ayant une concentration de plus de 99% masse. Les résultats obtenus sont présentés au tableau 4 et dans les figures 4 et 5.

Les données du tableau 4 montrent que la vitesse de dissolution des granules d'urée en solution aqueuse d'urée de n'importe quelle concentration baisse tandis que la durée de sédimentation croît. Quant aux petite durées, jusqu' à 14 s, l'influence de la concentration initiale de la solu-

Tableau 2

Variation de la vitesse de sédimentation des granules d'urée en fonction de H et dp, C° = 10 % masse.

dp [mm]		H [m]					
		1,1	0,9	0,7	0,5	0,3	0,1
1,55	ΔH [m]	0,2	0,2	0,2	0,2	0,2	0,2
	t [s]	2,90	3,10	3,70	4,40	5,40	6,90
	v_0[m/s]	0,06896	0,06451	0,05405	0,04545	0,03703	0,02898
1,82	ΔH [m]	0,2	0,2	0,2	0,2	0,2	0,2
	t [s]	2,70	2,90	3,40	4,20	5,00	5,90
	v_0[m/s]	0,07407	0,06896	0,05882	0,04761	0,0400	0,03389
2,07	ΔH[m]	0,2	0,2	0,2	0,2	0,2	0,2
	t [s]	2,45	2,65	3,10	3,70	4,20	4,80
	v_0[m/s]	0,08163	0,07547	0,06451	0,05405	0,04761	0,04166

Tableau 3

Variation de la vitesse de sédimentation des granules d'urée en fonction de H et dp, C° = 20 % masse

d_p [mm]		H[m]					
		1,1	0,9	0,7	0,5	0,3	0,1
1,55	ΔH [m]	0,2	0,2	0,2	0,2	0,2	0,2
	t [s]	3,24	3,60	4,20	4,90	6,00	7,40
	v_0[m/s]	0,06172	0,05552	0,04761	0,04081	0,0330	0,02702
1,82	ΔH [m]	0,2	0,2	0,2	0,2	0,2	0,2
	t [s]	3,00	3,27	3,75	4,30	5,00	6,00
	v_0[m/s]	0,06666	0,06100	0,05321	0,04651	0,04000	0,03333
2,07	ΔH [m]	0,2	0,2	0,2	0,2	0,2	0,2
	t [s]	2,73	2,87	3,20	3,60	4,10	4,80
	v_0[m/s]	0,07326	0,06968	0,06250	0,05555	0,04878	0,04166

Tableau 4

Variation de la vitesse de dissolution et du coefficient K_l par rapport à la concentration de la solution initiale d'urée et par rapport à la durée du déplacement des granules d'urée

C° (% masse)	d_p = 1,55 mm			d_p = 1,82 mm			d_p = 2,07 mm		
	t [s]	V_D [kg/m^2·s]	$10^5 \cdot K_l$ [m/s]	t [s]	V_D [kg/m^2·s]	$10^5 \cdot K_l$ [m/s]	t [s]	V_D [kg/m^2·s]	$10^5 \cdot K_l$ [m/s]
10	6,30	0,03873	7,9773	5,85	0,04015	8,2698	5,32	0,04702	9,6848
	10,05	0,02733	5,6292	9,40	0,03765	7,7548	8,50	0,03873	7,9773
	14,60	0,02264	4,6632	13,60	0,02163	4,4551	12,15	0,02092	4,3089
	20,25	0,01773	3,6519	18,65	0,01497	3,0834	16,40	0,01724	3,5509
20	7,14	0,02966	7,8631	6,56	0,03114	8,2555	5,76	0,03250	8,6161
	11,39	0,02159	5,7237	10,39	0,02369	6,2804	9,00	0,02848	7,5503
	16,49	0,02118	5,6150	14,77	0,02028	5,3764	12,65	0,02488	6,5959
	22,64	0,01353	3,5869	19,92	0,01794	4,7560	16,85	0,02305	6,1108

tion d'urée est peu significative, mais pour ce qui est des durées plus grandes, l'influence de la concentration devient insignifiante. La croissance de la concentration de la solution initiale conduit à la réduction de la valeur de la vitesse de dissolution.

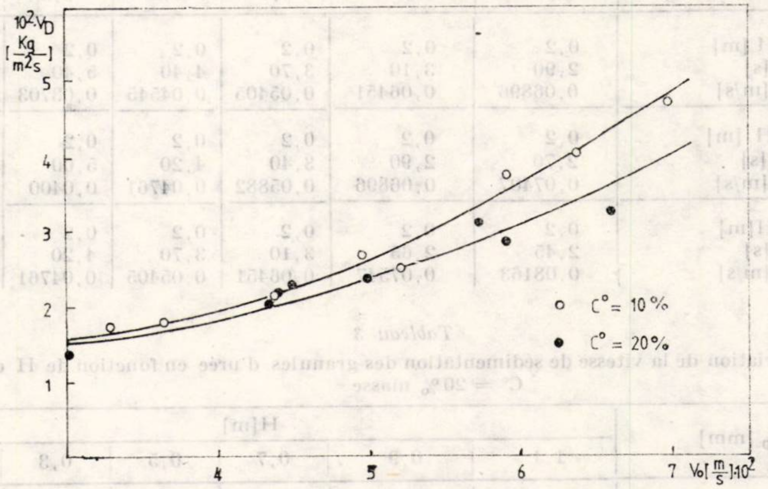

Fig. 4. — La variation de la vitesse de dissolution avec la vitesse de sédimentation et la concentration, C°.

En ce qui concerne la variation de la vitesse de dissolution par rapport à la vitesse de sédimentation (fig. 4), on peut préciser que cette dernière influence positivement la vitesse de dissolution. Aux petites vitesses de sédimentation jusqu'à 0,0475 m/s, la vitesse de dissolution est peu influencée par la concéntration, mais aux grandes vitesses de sédimentation, l'influence de la concentration est plus significative.

Le tableau 4 présente la variation du coefficient individuel de transfert de masse dans le temps, tandis que la figure 5 présente la variation du même coefficient en fonction de la vitesse de sédimentation de la particule aux concentrations de 10% et 20% masse. On constate que les dépendances K_1—t et K_1-vo sont semblables à celles du tableau 4 et de la fig. 4, à la seule différence que, au cas des dépendances K_1 — t, pour les durées petites du processus, respectivement dans l'intervalle $0-8_s$, l'influence de la concentration initiale de la solution sur la valeur du coefficient K_1 est insignifiante et, de même, aux vitesses grandes de sédimentation, respectivement $v_0 > 0{,}055$ m/s, la concentration initiale n'influence pas de manière significative la valeur du coefficient individuel de transfert de masse.

De ce qui a été présenté jusqu'ici, il résulte que, à mesure que la particule d'urée se déplace dans la solution, la vitesse de sédimentation diminue, conséquemment à la réduction de la dimension de cette même particule pendant la dissolution et que la vitesse de dissolution diminue de manière similaire.

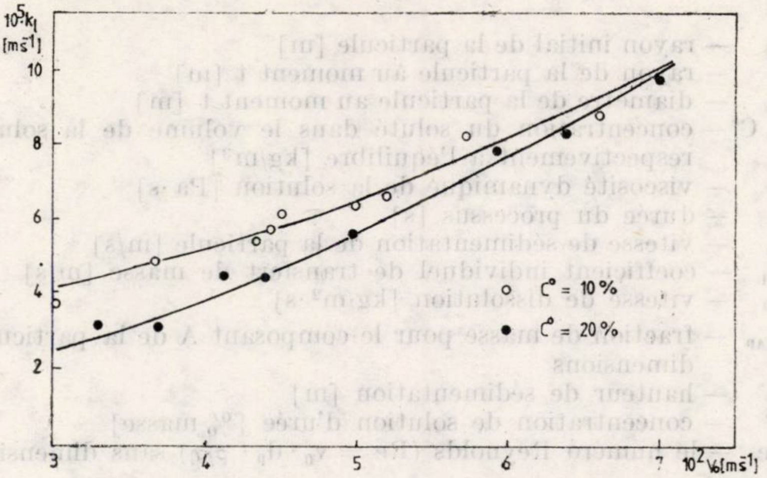

Fig. 5. — La variation du coefficient individuel de transfert de masse avec la vitesse de sédimentation et la concentration, C°.

Les dépendances $V_D - V_0$ et $K_l - v_0$ mettent en évidence le fait que la vitesse de dissolution et le coefficient individuel de transfert de masse sont influencés positivement par la vitesse de sédimentation et, par conséquent, dans le processus global de dissolution des granules sphériques d'urée en solution aqueuse d'urée, le déterminant de vitesse est le processus élémentaire de transfert de l'urée par la phase liquide.

5. CONCLUSIONS

À la suite de ces expériences, on a mis au point une nouvelle méthode de recherche de la dissolution des solides par la détermination de la vitesse de dissolution et du coefficient individuel de transfert de masse des particules sphériques de solides qui sédimentent, au cours des diverses étapes de sédimentation.

Selon la relation entre la définition de la vitesse de dissolution et l'équation de la vitesse de sédimentation, ont été établies les équations du calcul de la vitesse de dissolution et du coefficient individuel de transfert de masse pour les trois domaines de sédimentation.

Expérimentalement a été déterminée la variation de la vitesse de sédimentation dans le temps pour ce qui est des granules sphériques d'urée sédimentont en solution aqueuse d'urée à $T = 20°C$ et ont été calculés v_D et K_l.

Les données expérimentales mettent en évidence l'influence de la concentration initiale de la solution d'urée et de la vitesse de sédimentation sur la vitesse de dissolution et sur le coefficient individuel de transfert de masse de l'urée en solution d'urée. De même, on a mis en évidence le processus élémentaire déterminant de la vitesse.

NOTATIONS

R — rayon initial de la particule [m]
r — rayon de la particule au moment t [m]
d_p — diamétre de la particule au moment t [m]
C, C^e — concentration du soluté dans le volume de la solution et respectivement à l'équilibre [kg/m^3]
η — viscosité dynamique de la solution [$Pa \cdot s$]
t — durée du processus [s]
v_0 — vitesse de sédimentation de la particule [m/s]
K_1 — coefficient individuel de transfert de masse [m/s]
v_D — vitesse de dissolution [$kg/m^2 \cdot s$]
$\overline{X}_{AP}$ — fraction de masse pour le composant A de la particule sans dimensions
H — hauteur de sédimentation [m]
C° — concentration de solution d'urée [% masse]
Re — le numéró Reynolds ($Re = v_0 \cdot d_p \cdot \rho/\eta$) sans dimensions.

BIBLIOGRAPHIE

[1] W. J. Horwarth, *Chem. Eng. Sci.*, **16**, 909 (1962).
[2] W. J. Horwarth, *Chem. Eng. Sci.*, **18**, 47 (1963).
[3] H. Blasinski et K. W. Pyc, *Int. Chem. Eng.*, **15**, 409 (1975).
[4] G. Baldi, A. Conti et A. Gianetto, *A. I. Ch. E. J.*, **27**, 1017 (1981).
[5] S. Boon-Long, C. Languerie et I. P. Coudere, *Chem. Eng. Sci.*, **33**, 813 (1978).
[6] C. Leonte, Al. Szep et S. Petrescu, *Rev. Chim.* **36**, 233 (1985).
[7] V. G. Levici, « Fiziko-himicheskaja ghidrodinamica, Gosudarstvenoe Izdatelistvo fiziko-matematicheskoj literatury », Moskva, 1959.
[8] Z. P. Şulman, M. A. Pokrivailo, V. I. Kordonskii, V. P. Liaşkevici et A. K. Nesterov, *Int. Chem. Eng.*, **13**, 10 (1973).
[9] F. D. Pakanjpe, D. L. Oehlbeck et F. F. Erian, *Lett. Heat Mass. Trans.*, **4**, 393 (1977).
[10] D. E. White, M. Litt et G. J. Heymach, *Ind. Chem. Fundam.*, **13**, 143 (1974).
[11] T. Dabras et Z. Adamczyk, *Chem. Eng. Sci.*, **34**, 1041 (1979).
[12] A. Jguchi, K. Komoni et R. Jzumi, *Int. J. Heat Mass Trans.*, **22**, 1319 (1979).
[13] A. Inoue et T. Tsujino, *Ind. Eng. Chem. Proc. Dev. Des.*, **23**, 122 (1984).
[14] A. F. M. Barton et H. M. Wilde, *Trans. Farad. Soc. I.*, **67**, 3590 (1971).
[15] R. G. Rice et P. J. Jones, *Chem. Eng. Sci.*, **34**, 847 (1979).
[16] S. Petrescu, Doctoral Thesis I. P. Iaşi, 1987.
[17] * * * — Spravochinik azotchika, tom 2, Izd. Khimia, Leningrad, 1969.
[18] C. Calistru, C. Leonte, I. Siminiceanu, et C. Hagiu, « Tehnologia îngrăşămintelor minerale », vol. I, E. T., Bucureşti, 1984.
[19] R. Z. Tudose, I. Ibănescu, M. Vasiliu, A. Stancu, G. Cristian et M. Lungu, « Procese, operaţii, utilaje în industria chimică » Edit. Didactică şi Pedagogică, Bucureşti, 1977.
[20] G. Jinescu, « Procese hidrodinamice şi utilaje specifice în industria chimică », Edit. Didactică şi Pedagogică, Bucureşti, 1983.

Revue Roumaine de Chimie, 34, 8, 1809–1816 (1989)

COMPTES RENDUS

"Spin Labels and Probes in Biology and Medicine. Book 1: Spin Labeling Method. Problems and Perspectives" (edited by M. N. Emanuel and R. I. Zhdanov), 268 pp., 1986, 3.25 Rbl. Book 2: Nitroxyl Radicals. Synthesis, Chemistry and Applications (edited by E. G. Rozantsev and R. I. Zhdanov), 267 pp., 1987, 4.10 Rbl. Book 3: Biomacromolecules in Spin Labeling (edited by G. I. Likhtenshtein and R. I. Zhdanov), 263 pp., 4.10 Rbl. Nauka, Moscow (in Russian).

The series edited by well-known scientists contains so far 14 + 11 + 12 = 37 chapters written by Soviet specialists in the chemical, physical and biomedical aspects involving spin-labelling with nitroxyls (aminoxyls, nitroxides). Actually, the beginning of nitroxyl chemistry 20 years ago is associated with the names of E. G. Rozanstev in USSR and, later, A. Rassat in France. Dr. Zhdanov, who is one of the editors for each of the three volumes, is a close coworker of Dr. Rozantsev.

The high sensitivity of the ESR technique allows the easy detection, in minute concentrations, of paramagnetic species (spin-labelled analogues). Moreover, ESR spectra give information on molecular orientations, an invaluable asset for studies of biological membranes, synthetic polymers or biopolymers.

The first volume starts with a foreword and a chapter written by the late Acad. Prof. N. M. Emanuel who headed the Department of Chemical and Biological Kinetics of the Moscow Institute of Chemical Physics of the USSR Academy of Sciences.

The first chapter of vol. I presents the use of nitroxyls in tumor chemotherapy: N. M. Emanuel and I. P. Konovalova show that the introduction of one tetramethylpiperidine-N-oxyl group into chemotherapeutic agents such as thio-triethylenephosphoramide (thio-TEPA) or triethylene-melamine (TEM) leads to products which are ten times less toxic, yet more active, than the initial compounds.

Subsequent chapters deal with: the interaction of spin-labelled biologically active compounds with DNA; the use of relaxation processes of nitroxyls in molecular biology, especially for evaluating distances between paramagnetic centers (G. I. Likhtenshtein et al.); the uses of nitroxide biradicals in biomedical investigations; investigations of conformational mobility and association of membrane proteins such as rhodopsin or Ca-ATPase by means of spin labels (V. A. Livshits); spin-labelled peptidic (snake) neurotoxins and their interaction with acetylcholine receptors (by the late Yu. A. Ovchinnikov and V. I. Tsetlin); synthesis, properties and applications of spin-labelled phospholipids having mono- or diradicalic character, and possessing differently structured polar parts (by R. I. Zhdanov et al.); ESR studies of Ca-ATPase of sarcoplasmatic reticulum (topography of functional groups, modifications during the functioning, protein-lipid interactions); structural-functional interactions between physiologically active compounds and biomembranes: testing biological activity of chemical compounds by means of spin labels; spin probes for studies of thermoinduced structural changes in cell organelles and biomembranes of normal and cancerous cells; E. K. Ruuge and E. N. Gerasimova as well as O. A. Azizova et al. use hydrophobic, spin labelling for investigating the interaction between spin probes and blood plasma lipoproteins or cell membranes for diagnosing dislipoproteidic and ischemic disorders; this confirms the membrane hypothesis of atherogenesis and artherosclerosis; the final chapter by E. G. Rozantsev and R. I. Zhdanov is a general review of biologically active organic paramagnetic compounds, in particular nitroxyls with similar shape or functional groups which exhibit neuro- or psychotropic, antitumoral, or other pharmacological properties. In his concluding remarks, R. I. Zhdanov presents in detail the unique advantages of the ESR cum spin label techniques.

The second volume is the most chemical of the series. The foreword is written by E. G. Rozantsev and R. I. Zhdanov. In the first chapter, E.G. Rozantsev, E.Sh. Kagan and V.D. Sholle describe triacetoneamine 4-oxo-(2,2,6,6-tetramethylpiperidine) and its leading role in the chemistry of nitroxyl radicals; the reactions of nitroxyls discovered by Rozantsev in 1961, which proceed without destruction of the radicalic center, allow a large variety of conversions. The concluding part of this review indicates possible strategies for synthesizing new nitroxyls. Recipes are appended throughout this chapter. Subsequent chapters are on: electrochemical synthesis of nitroxyls, catalysis of redox processes in aqueouses solutions by nitroxyls, involving either ion-radical, or ion-molecular mechanisms; organo-phosphorus nitroxyls (by R. I. Zhdanov, M. I. Kabachnik et al.); spin-labelled steroids (it should be mentioned that spin-immunological methods allow the detection of steroid hormones or addictive drugs in urine or saliva); QSAR methods for biologically active nitroxyls (R. I. Zhdanov et al.); spin trapping in chemistry and biology (by V. E. Zubarev), stressing solvent effects; Ya. S. Lebedev et al. describe the possibilities offered for studying molecular motions by using 2 mm radiations, instead of the usual 3—30 cm wavelengths; another technically-oriented chapter presents the method of continuous saturation of ESR spectra, which is useful for determining relaxation times with a more sensitive technique, applied to biomolecules; a computer algorithm is presented for simulating ESR spectra in the absence of rapid rotations; S. N. Dobryakov describes a system of differential equations for the dynamics of spin exchange in biradicals.

The third volume has a preface by G. I. Likhtenshtein and R. I. Zhdanov. Three chapters are written by Zhdanov and coworkers: investigations of cholinesterases by means of spin labeling; active centres of ATPases and the spin-labelled analog of ATP; participation of first and second fatty acyl residues in lipid-protein interactions evidenced by spin labelling. A series of chapters present results obtained by spin labels for Ca-ATPase, Na-, K-ATPase, nitrogenase (A. A. Boldyrev et al.). V. A. Livshits, et al. discuss the spatial structure of rhodopsin in solution elucidated by ESR spectroscopy of spin labelled products (so-called short and long spin labels) under illumination and in the dark, including conformational changes brought about by photoirradiation. A. I. Kyäväränen reviews the large-scale dynamics of immunoglobulins studied by relaxation times of spin-labeled proteins. Spin-labeled glycoproteins and polynucleotides are discussed in separate chapters. The last chapter reviews briefly computer programs for obtaining parameters from ESR spectra by means of personal computers.

The high quality of the chapters and the up-to-date literature survey make this series an invaluable instrument for all those who prepare or use spin traps and spin labels; instead of searching isolated chemical, physical or biomedical abstract journals, this series offers a critical and systematic evaluation of recent literature in the expanding field of nitroxyls.

A. T. Balaban
Polytechnical Institute Bucharest

S. J. CYVIN and I. GUTMAN, "Kekulé Structures in Benzenoid Hydrocarbons", Lecture Notes in Chemistry No. 46, Springer-Verlag, Berlin, 1988, 346 pp., soft cover, ISBN 3-540-18801-0

The authors: S. J. Cyvin, from the University of Trondheim, the Norwegian Institute of Technology, and I. Gutman, from the Faculty of Science, University of Kragujevac, developed a fertile research in the field of Kekulé structures of benzenoid hydrocarbons. Their collaboration resulted in many papers published in all important mathematical chemistry journals. This book presents the majority of the important results obtained in this field.

The first 58 pages are a presentation of basic facts. In a short introduction there are described benzenoid hydrocarbons, their history and the importance of Kekulé structures. The next chapter presents some definitions and describes mathematical modelling of the structure of benzenoid hydrocarbons using graphs. Also, some classifications and enumerations of benzenoids are presented. In the third and fourth chapters the authors present some general results about Kekulé's structures and their enumeration and some basic theorems for the calculation of K{G}, the number of Kekulé structures of the hydrocarbon represented by graph G. These results are based on the decomposition of graph G or its adjacency matrix, or monotonic paths matrix. In this chapter are given also lower and upper bounds of K, depending on h, the number of hexagonal rings from the hydrocarbon structure.

There are described the general methods for Kekulé structures enumeration: empirical methods, algorithms, recurrence relationships, summation formulas, combinatorial formulas and others. Chapter five is a short presentation of a very interesting problem: the characterization of non-Kekuléan benzenoid systems. A more detailed description and some new results on this topic can be found in the recent papers of the same authors.

In short, these first pages of the book help the reader to understand the subject and to get accustomed with basic results.

The next 110 pages present some types of benzenoids and describe algorithms and formulas for the calculation of Kekulé structures. Authors present first catacondensed annelated benzenoids. After these, using a geometric classification based on the arrangement of benzenoid rings, peri-condensed structures are classified into : hexagons, chevrons, ribbons, parallelograms, rectangles, pentagons, triangles, multiple zigzag-chains and regular three-, four- five- and six-tier strips. In chapters 14 and 15 one can find some determinant formulas derived from the John-Sachs theorem and a general algorithm to determine the K number for a class of Kekuléan systems as "constructable".

In the next pages there are presented some formulas for K of all-benzenoids, related systems and for special types of benzenoids with repeated units.

The last chapter contains some statistical aspects and the "sieve method" to determine the number of normal benzenoids with a given K.

The work contains an important amount of scientific information and also a remarkable graphic presentation. The large number of examples and figures make it user-friendly.

The book has also some parts of interest only for mathematical chemists who work in the field. For readers who are not mathematical chemists and want to use the results as combinatorial formulas for K for classes of benzenoids and numerical K values, the authors introduced an arrangement of CHARTS within half of the chapters. The CHARTS contain : some definitions for classes of benzenoids using figures, collections of K formulas and full references to the original sources. Thus these CHARTS represent a quick guide which increases the usefulness of the book. The authors avoided complicated mathematical demonstrations so that organic chemists should be able to use it without difficulties.

In conclusion this book is a comprehensive overwiew of the field of Kekulé structures in benzenoid hydrocarbons. For complicated mathematical demonstrations and other detailed data one can use the numerous references.

Cristian Artemi
Faculty of Mathematics, Bucharest

"Transactions of Thirteenth Annual Meeting of the Society for Biomaterials in conjunction with the Nineteenth International Biomaterials Symposium" ; June 3–7, 1987 ; New York, N. Y. USA (editor J. B. Koeneman), vol X, Birmingham Alabama Society for Biomaterials 1987, XU + 299.

This paperbound volume of large format includes the program of the Symposium, the preprints of 283 lectures, communications and posters presented in different sessions, author and subject indexes and the list of Membership Roster of Society of Biomaterials.

The subjects of the sessions reflect the actual stage and the trends in the science of biomaterials, they include the following topics : Bone Implant Interface, Nerve Regeneration, Polyurethane Degradation, Analysis of Retrieved Implants : Orthopaedics and Cardiovascular, Dental Implants. Polymers Materials and Applications, Ion Release Systemic Effects, Soft Tissue Joining, Protein Adsorption, Drug Delivery Systems, Biology of Cartillage, Bone Substitute : Maxillofacial, Charged and Heparinized Surfaces, Orthopaedic Biomaterials Compatibility, Biodegradable Materials, Platelet-Surface Interaction, Properties of Bone, Polymers for Dental Restorations, Cell Polymer Interactions, PMMA Interface, Tissue Regeneration, Valve Calcification, Ligaments and Tendons, Vascular Grafts, In Vitro Corrosion, Bone and Cartillage Repair, Oral and Maxillofacial Materials, Blood Surface Interactions, Orthopaedic Composites, Bioadhesion & Biointeraction, Two Special Symposiums : Wound Healling and Calcification Cardiovascular Implants and four Poster Sessions related to the topics discussed in the communication sessions.

Unfortunately some of the preprints do not include bibliographic references or they are too short.

This volume provides a very useful information source on the world-wide new achievements and developments in the science and engineering of biomaterials.

Adrian Carpov

A. D. WILSON, H. J. PROSER (editors), "Development in Ionic Polymers" — 2, London — Elsevier Applied Science Publishers — 1986 XII + 356 p., ISBN 0-85334-419-1.

The second volume in this series presents the latest progress in the new and important field of ionic polymers, one of the main domains of functional polymers.

This multi-authors volume includes seven chapters and a six page index.

Chapter 1 points out the principal achievements in the synthesis of anionic and cationic polymers (P. A. M. Thompson).

In the following chapter a neglected topic till now — the hybrid silicate organic structures as ionic macromolecules is presented (G. Lagalay).

In chapter 3 is presented an updated review on carboxylated rubbers (M. Pineri).

Another quasi-neglected topic in the past years was the field of ionomers. By his comprehensive contribution T. Tsutsui reviews the main aspects of the synthesis, characterization and application of these special ionic polymers (chapter 4).

The fast developing field of polymeric complexes is outlined in a comprehensive and well documentated contribution (chapter 5) of E. Tsuchida and K. Abe.

Among the many applications of ionic polymers one of great practical interest is the presentation and uses of ionic membranes which is covered in chapter 6 (P. J. Brookman and J. W. Nicholson).

The polymeric complexes are largely used as biomaterials, supports for controlled release drugs, of formulation aids, etc. These applications are presented in chapter 7 (F. G. Hutchinson).

In chapter 8 which ends this volume a short review on the use of ionic polymers in the electrophoretic coating polymers (F. Beck) is presented.

The second volume is complementary to the first one and the classic work of Hollyday "Ionic Polymers".

The editors of this volume are well known scientists with fundamental contributions in ionic polymers and they have selected an outstanding team of specialists from different countries in order to do a very nice piece of work.

Adrian Carpov

"Solubility Data Series, Volume 31; Alkali Metal Orthophosphates", Pergamon Press Oxford, 1988, 347 p., Ed. Eysseltova and P. Dirkse, ISBN 0-08-035937-X.

This volume, which is the of 31st IUPAC Solubility Data Series, presents and evaluates solubility data for orthophosphates of lithium, sodium, potassium, rubidium and caesium. Like the entire Solubility Data Project, this volume is concerned with preparing a comprehensive critical compilation of data on solubility of the above mentioned chemical substances, useful for fundamental understanding of processes relevant to agronomy, biology, chemistry, geology, metallurgy and materials science.

The compilation deals with literature on alkali metal orthophosphates, over the period 1920 — 1984. The main source in locating the papers in this subject area was *Chemical Abstracts*, as well as Gmelin's Handbuch der Anorganischen Chemie, references cited in articles that have been reviewed, and Weddrow and Kobe's review article in *Chem. Rev.*, **54**, 89 (1954), for data published prior to 1920.

The various systems are treated in the order in which the alkali metals are listed in Group 1 of Periodic Table. There are 12 chapters followed by System Index, Registry Number Index and Author Index. Every chapter deals with detalied evaluation of the system, binary, ternary and multicomponent aqueous system containing alkali orthophosphates. Additionally, some chapters give data on mixed solvents — alkali orthophosphates systems.

Using the new IUPAC approach to numerical data presentation, the treatment of any given solute-solvent system consists in two essential parts.

a) Critical Evaluation and Recommended Values.

b) Compiled data sheets.

The critical evaluation part gives the following information:

— an evaluation text concerning the quality of data after consideration of purity of materials, experimental methods employed, reproducibility of the data, etc.;

— a fitting of the data to mathematical functions using suitable statistical texts;

— a set of recommended data with smoothing equations endorsed by the evaluator;

— a graphical plot of recommended data.

To fulfill this task, the evaluator covered all the relevant literature. Every effort was made to detect the best quality and to disqualify the poor or wrong data. Both accepted and unaccepted data are presented alongside. Thus the user can have confidence in the evaluator's brief comment, alerting him to areas that need more work.

The typical data sheet carries the following information:

— compound (names, formulas and *Chemical Abstracts* registry number);
— reference to primary source;
— experimental variables;
— identification of compiler;
— experimental values in the primary source.

Under the general heading every sheet summarizes essential experimental details:

— experimental method;
— type of apparatus;
— source and purity of material;
— estimation error;
— references.

In this view the data compilation ranks high above any other handbook or tabulated compilation which, as a rule, is uncritical.

Ana Zaharia
The Polytechnic Institute, Bucharest

"The Interface Structure and Electrochemical Processes at the boundary Between Two Immiscible Liquids", Edited by Vladimir E. Kazarinov, Springer-Verlag, Berlin, Heidelberg, New York, London, Paris, Tokio, 1987, ISBN 3-540-17519-9, ISBN 0-387-17519-9 Hard cover, 246 p.

The monograph edited by Vladimir Kazarinov is devoted to a subject with wide technological applications and essential implications in the natural phenomena observed in biological systems — the electrochemical processes proceeding at the interface between two immiscible liquids. The book is intended to gain insight into the structure of the interface between immiscible liquids, as well as into the main features of the complex electrochemical reactions occurring at this interface.

The subject is not a very new one: the first studies in this area date back to the beginning of this century; however, the last decades have marked an important development in both the theory and practice of this field; a large number of research works demonstrated a spectacular increase of interest in the fundamental and applicative aspects of the problem. In view of this progress, a monograph devoted to the electrochemistry of the boundary between immiscible liquids should be welcomed.

The book contains nine exhaustive reviews concerning some of the most interesting subjects in the investigated area, written by scientists who are active workers in this field.

The opening article is written by professor J. Koryta, a pioneer of the electrochemistry at the boundary between immiscible solutions. The review presents in a concise (perhaps too concise) form the basic theory and experimental procedures and applications of the electrolysis at the interface between two immiscible electrolyte solutions.

The subsequent chapter, written by A. M. Kuznetsov and Yu. I. Kharkats is devoted to the quantum theory of charge transfer reactions at the interface between two immiscible liquids. The quantum mechanical theory of the electron transfer reactions is mainly considered, whereas the transfer of ions is only briefly discussed.

Chapter 3, written by V. S. Krylov, is concerned with the hydrodynamics and mass exchange at the phase boundaries with regular dissipative structures.

Chapter 4 contains a comprehensive coverage of the state-of-art and achievments in the area of the electrochemistry of liquid interfaces at equilibrium. Basic concepts, data and knowledge on the Galvani and Volta potentials at the interface of immiscible electrolyte solutions are thoroughly reviewed by Z. Koczorowski. The bibliography of this chapter, covering the literature between 1909 and 1984, is exhaustive.

The next two chapters are devoted to the investigation of the electrical double layer structure at oil/water interfaces by electrocapillary curves (prof. M. Senda and coworkers) and by impedance measurements (Z. Samec and V. Marecek).

The last three chapters deal with biologically important cases of electrochemical processes at interfaces between immiscible liquids. Thus, chapter 7, written by L. I. Boguslavsky and A. G. Volkov, deals with the redox and photochemical reactions in membrane/electrolyte systems. The interest of the research in this field is provided by the extraordinary importance of such processes in bioenergetics — for instance, the energy storage in photosynthesis.

Chapter 8, written by A. N. Popov, deals with counterions and adsorption of ion-exchange extractants at the water/oil interface. The review is concerned with the relation between the extractant surface activity and the extraction characteristics of the system.

The last review, written by M. G. Kuzmin and N. K. Zaitsev, is devoted to the kinetics of the photochemical charge separation in micellar solutions. The investigated problem is of a great practical importance for modern biochemical applications, such as the use of biological processes in the storage of solar energy and in molecular electronics.

In conclusion, the monograph contains consistent information on the fundamental studies and practical applications of the electrochemical processes proceeding at the boundary between two immiscible liquids. The subject is very modern and covers a large area of interest. The book is intended for experienced electrochemists, but shall be found useful also for unexperienced researchers, to be used in the planning and execution of new electrochemical experiments. The monograph contains a large number of references, covering the literature up to 1985, which makes it very useful as a source book and literature guide.

Mariana Ciureanu
Electrochemistry Department, Faculty of Chemical Technology
Polytechnic Institute of Bucharest
Bucharest, Romania

KLARA KISS, "Problem Solving With Microbeam Analysis", Akadémiai Kiadó, Budapest, 1988, 410 pp.

Some of the analysis techniques which are known today as "microbeam" analysis techniques are in fact centuries old – e.g. optical microscopy (abbreviated OM); other are somewhat younger, e.g. transmission electron microscopy (TEM), whereas still others have only emerged during the last few decades or even few years. The latter are the most numerous and, at the same time, have turned out to be the most useful in various branches of modern science and technology. We might particularly cite among these the techniques of analysing surfaces or electronic microcircuits (scanning electron microscopy – SEM, Auger and photoelectronic spectroscopies – AES and ESCA, the ion beam techniques – ISS or SIMS, the laser microprobes – LIMA or LRM, etc. During the last few years, several variants and combinations of these techniques have emerged – and the number of acronyms assigned to them has increased accordingly, so that international agreement turns out now to have become necessary.

In this way, a great variety of techniques of this kind, mostly automated or computer-controlled, have become available to specialists; they have reduced the analysis time to minutes instead of hours or days. In other cases, these techniques have permitted to get results in problems which have been considered as insoluble until then. Use of microbeam devices (which still remain costly) has evidenced the close correlation existing between the microstructure of a solid material and its macroscopic properties (such as mechanical resistance, resistance to corrosion, conductivity, adhesion, catalytic activity, etc.). The characterisation of microstructure is now regarded as an essential condition for the understanding and control of materials' properties.

The book reviewed here wishes – and to a great extent even succeeds – to be a survey of all existing microbeam analysis techniques. Part I of the book is devoted to a discussion of the theory, techniques and instrumentation for some of the microbeam methods. Since the avowed purpose of the book is to offer the industrial analyst "whose field of expertise is other than microbeam analysis" a guide as practical as possible on the capabilities of these methods, the author emphasises, even in this "theoretical" section of her work, the aspects of principle of the methods, without dwelling too much into details, the construction of the instruments, and the main advantages and shortcomings of each technique when estimating their usefulness (and cost) for solving specific problems. The main purpose – the industrial applications – is consistently pursued throughout the book. For this reason, Part II, which is devoted to specific case histories and applications in various branches of technology, fills as much as half of the space. In this part, the applications are described by topics: synthetic polymers, microelectronics, metallurgy, corrosion, glass and ceramics, catalysts, fibers, food and cosmetic products, environmental problems, etc. Numerous examples of problems deftly solved by microbeam techniques are given – e.g. the identification of "fisheyes" in polystyrene/polybutadiene copolymers by laser Raman microprobe (LRM), the problems of polymer/metal adherence or of pigment dispersion in plastics investigated by ESCA, the characterisation of epitaxial layers by TEM and selected-area electron diffraction (SAED) or of composites and polymer blends by OM, TEM and SEM, of polymer or fiber surfaces by ESCA, of fluoropolymer surface chemistry by ESCA, of polymer laminates by LRM, etc. – to quote only a few examples among the many encountered in the synthesis and processing of polymers. In microelectronics, the microbeam techniques turned out to be most useful for the final quality control of integrated circuits, for identifying the causes of inter-layer diffusion, deposit formation or contaminations, for pin-pointing defects on large-area integrated circuits, etc.

The clear and concise way in which the principle and application of various microbeam techniques are described, at the level just needed by industrial analysts, the well-researched exposition (over 800 references cited) of the problems occurring in various fields and their solution, and the coherent treatment of wide and apparently disparate fields of application make the book extremely useful to specialists in today's front-line technologies, who are faced today with multiple problems and have to choose the most appropriate and cost-effective way of solving them.

A. Bulucelea

I. BÁN, "Biomathematics and its Applications in Plant Cultivation", Akadémiai Kiadó, Budapest, 1988, 204 p., ISBN-963-05-4519-5 (joint edition with Elsevier Science Publishers).

The book is the English version of the text published in 1977 and written by the head of the Computer and Development of the Hungarian Ministry for agriculture and food, forest management service. Almost half of the text is a general introduction into probability and statistics applied to biomathematical problems. Because of the wide problems discussed concisely, the book is useful also for chemists, biochemists, pharmacologists, physicians, biologists, and ecologists.

The treatment is eclectic : for some aspects an in-depth coverage is given, while other problems are not discussed. Examples of topics which are likely to interest a wider range of readers are the probit transformation based upon logit values, the Moor-Roxer procedure (a variational method for the determination of the regression function, exposed in E. Roxer's books published in Hungarian language, Sopron, 1964, 1970), and the multivariable examination method with relative coordinates.

The second part of the book consists of detailed examples from the area of plant protection such as : optimum sampling rates, optimization of plant protection costs versus benefits, effects of insecticides using modulation according to the control list, distribution of leaf dimensions in uninfected and virus-infected plants.

For its clear presentation the book is recommended to people who are already familiar with basic statistics.

A. T. Balaban
Polytechnic Institute Bucharest

GY. MATOLCSY, M. NÁDASY and V. ANDRISKA, "Pesticide Chemistry", Akadémiai Kiadó, Budapest, 1988 (joint publication with Elsevier Science Publishers as vol. 32 in the series ,,Studies in Environmental Science") 808 pp., ISBN 963-05-4573 X

This excellent and comprehensive book, with many references (mostly pre-1980) and with clearly written formulas, allows a global view of one of the most important sectors of chemical. industry. Pesticides help in preventing disease, loss of agricultural products, and soil erosion.

The book is organized into six unequal parts, along traditional lines : anti-insect agents (240 pp), acaricides (15 pp), nematocides (6 pp), rodenticides (10 pp), fungicides (213 pp), and herbicides (298 pp). In turn, the three major parts are further subdivided according to the chemical nature of compounds, and to the mode of their action (thus, chemosterilants and pheromones for insects are discussed in separate sections).

Detailed information is provided, wherever possible, on the mode of action and on quantitative structure-activity relationships.

Although the three authors have written separately the three major parts of the book, the style and the treatment are consistent throughout the book.

Though pesticides are often cited by trade names, the book uses generally their common names, and trade names are given only for compounds of outstanding importance or of historical interest.

The book has a well-organized systematic table of contents, and a comprehensive subject index.

The book is highly recommended to all those who wish to become acquainted with this field, and is especially useful for students, teaching staff and research scientists interested in pesticides and their development.

A. T. Balaban
Polytechnic Institute Bucharest

E. GARFIELD, "Essays of an Information Scientist", volumes 1—9. ISI Press, Philadelphia. ISBN 0-89495-081-9. Hard covers (the numbers of pages per volume ranges from 450 for vol. 9 to 890 for vol. 3, averaging 660 pages). Indexes are appended.

The inventor of the *Science Citation Index*, *Chemistry Citation Index*, *Current Abstracts of Chemistry and Index Chemicus*, *Index Chemicus Online*, of *Current Contents* (various sections, including Life Sciences; Physical, Chemical and Earth Sciences; and eight other sections), *ISI Atlas of Science*, etc. who is President of the Institute for Scientific Information (ISI) in Philadelphia, is also a distinguished historian of science, with a degree of bachelor of science in chemistry and Ph. D. in structural linguistics awarded in 1961 by the University of Pennsylvania. Actually he prefers to describe himself, as in the title of the books under discussion, as an information scientist. The books collect his essays published in *Current Contents* (now they appear weekly). Coverage is as follows: vol. 1, 1962—1973; vol. 2, 1974—1976; vol. 3, 1977—1978; vol. 4, 1970—1980; vol. 5, 1981—1982; vol. 6 onwards, one-year periods starting with 1983.

Beginning with volume 7, each book in the series has its own title; vol. 7: *The Awards of Science and Other Essays*; vol. 8: *Ghostwriting and Other Essays*; vol. 9: *Towards Scientography*. Each volume in the series has a foreword by a well-known personality such as the Nobel Prize winner Joshua Lederberg for volumes 1 and 2, D. J. de Solla Price for vol. 3, Harriet Zuckerman for vol. 4, R. K. Merton for vol. 5, V. V. Nalimov for vol. 6, G. Holton for vol. 7, Estelle Broadman for vol. 8, and A. Thackray for vol. 9.

Although most scientists will already know Dr. Eugene Garfield's essays from the *Current Contents* column, the collection allows an easy grasp of the tremendous variety of topics discussed in these essays. First and foremost are the topics directly relevant to information dissemination, such as the most cited papers or authors in various fields, the development and use of citation indexes, analysis of Nobel Prizes, citation clustering, co-citation, research front mapping, etc. Dr. Garfield's reminiscences on how he founded ISI, on people he met, or on personal events ("To remember my mother" is one example) are written in a direct, frank and very readable style. Many topics are of general interest to any reader, for instance on medical applications, on ecological, moral and social problems, on humanitarian aspects, etc.

Some topics gave rise to polemical debates; thus the essay "Is French science too provincial?" reprinted from "*La Recherche*" caused a heated debate in French scientific circles, and even the former Prime Minister of France, Michel Debré, jointed the debate deploring the demise of French as international scientific language, and questioning some of Dr. Garfield's proposals and conclusions (such as the conclusion that the true international scientific language is English and that France should join other countries and publish English editions of its scientific journals). Other controversial issues are on animal experimentation, etc.

The volumes contain in addition to the *Current Contents* columns, occasional reprints of Dr. Garfield's publications in periodicals; Volume 7 contains the reprint of the his Ph. D. thesis entitled "An algorithm for translating chemical names to molecular formulas".

It is necessary to dwell on the essays which gave the names of the last three volumes. The awards of science are numerous, though less publicized than the Nobel prizes. Ghostwriters are people who, acknowledged or otherwise, write texts published under other names. Scientography is a term coined by G. Vlăduţ, who is now ISI's manager of basic research, and denotes the graphical mapping of science by successive iterations of citation clustering pioneered by E. Garfield and H. Small.

One has to recall that in 1984 the first Derek de Solla Price Memorial Medal instituted by the journal *Scientometrics* (managing editor: T. Braun, Budapest) was presented to Dr. E. Garfield for his distinguished contributions to Scientometrics, the present-day term for the "science of science".

In the Silver Jubilee issue of the *Journal of Chemical Information* and *Computer Science*, Dr. Garfield published a paper entitled "History of citation indexes for chemistry: a brief review", reprinted in the ninth volume of Essays; he quotes one of his 1987 papers entitled "Breaking the subject index barrier: a citation indexing for chemical patents" (unfortunately, proposals for a Patent Citation Index were ignored).

Dr. Garfield has made a great service to the scientific community by inventing, managing and making available *Science Citation Index* and all the other publications, magnetic tapes, and services of the ISI. His witty and well-documented essays prove that he is a truly interdisciplinary scientist. All volumes provide entertaining and instructive reading.

A. T. Balaban
Polytechnic Institute Bucharest

THE PLASTICS PROCESSING ENTERPRISE—BUZĂU—

The Plastics Processing Enterprise in Buzău, 132, Transilvaniei Street, telephone 13425, Telex 56227, manufactures a large variety of products, that may be classified into four main groups, according to the manufacturing technology:

A. semi-finished and finished plastic products;
B. filters and filtering component parts;
C. protection devices for the breathing passages;
D. active carbon.

A. Semi-finished and Finished Plastic Products

The Plastics Processing Enterprise in Buzău manufactures products from: HDPE, LDPE, PVC in suspension, impact modified PP and PS, by different technologies such as: extrusion, extrusion-blowing, extrusion granulating, sintering, injection, thermoforming.

A.1. Polyethylene Products

1. The Plastics Processing Enterprise in Buzău manufactures and delivers HDPE and LDPE sheets for a wide range of applications in agriculture, industry and other fields of activity.
   The PE foils may be clear or opaque, uncoloured or pigmented.

a. According to the application, there are manufactured four types of LDPE foils with width (in pipe-form) ranging from 150 to 6,500 mm:

- for packaging applications;
- for general purposes;
- for industrial bags;
- covers for agriculture use;

The following values of thickness are given for each type of foil: 0.025—0.045 mm; 0.045—0.25 mm; 0.25—0.32 mm; 0.100—0.160 mm.

b. The HDPE foils have values of thickness ranging from 0.020 to 0.060 mm and width from 150 to 1.100 mm.

The PE sheets are delivered rolled on PVC cores; the maximum weight of a roll is of 50 kg.

Our enterprise is also manufacturing:

- LDPE and HDPE sheets with flaps, for agriculture use (covers for crops of vegetables);
- LDPE sheets for insulating irrigation canals; their width ranges from 750 to 3 000 mm and their thickness from 0.5 to 1 mm.

c. Coextruded LDPE and HDPE foils.

2. PE sheets with the following applications:

- packagings (bags, carrier bags, thin sacks, hoods) for different products (chemical products, food, clothes) or protection covers for pallets (containing construction materials, equipments etc.).

They may be unprinted or printed in one to six colours.

- thick sacks for chemical fertilizers or for other types of powders or granules: maximum load for each sack is of 50 kilos. They may be unprinted or printed in one or two colours.

3. The Plastics Processing Enterprise in Buzău also produces high load packagings (for capacities ranging from 20 to 1,000 litres) by means of technological process used only in this enterprise in Romania, namely rotational or static moulding (sintering) of LDPE powders.

These packagings may have different shapes and colours, their application including boats and objects for sanitary use, tanks and silos, cans and containers that are to be palletized. The material used for these applications — LDPE — is characterized by thermal stability between — 5 and + 60°C, good impact strength, stiffness, chemical resistance to almost all chemical substances and it is also a good electrical insulator; in a word, it shows a unique combination of qualities.

It may be applied in food industry as it meets the requirements for food contact use, approved by the Ministry of Public Health.

On Buyer's request, the range of the existing types and dimensions of products can be extended, either by manufacturing new products or by adjusting connecting pieces, valves and corks to the already existing products.

4. The Plastics Processing Enterprise in Buzău also manufactures and delivers HDPE rifled or punched pipes for draining water in agriculture, with a nominal diameter of 50, 65 or 80 mm.
5. Our enterprise manufactures and delivers LDPE slings, reinforced with thread of viscose cord, used to fasten the pallets containing bags or boxes, with a maximum weight of one ton.

A.2. Semi-finished and Finished Products Made from PVC in Suspension

Our enterprise manufactures and delivers granules, pipes and insulating tubes made from PVC.

Major applications of PVC granules include:

- primary or secondary electrical insulations for pipes or electric cables;
- footwear and different component parts for footwear, such as soles, heel pieces, straps, welts;
- construction materials, namely pressure pipes, fittings, handrails:
- records.

Applications of PVC pipes include technological and sanitary-engineering installations, used as conveyers for drinking water, waste water or liquids that do not attack PVC, for irrigations or as channels for cables.

The Plastics Processing Enterprise in Buzău also manufactures pipes with an outer diameter determined by the values of pressure of the conveyed fluid: simple pipes Type 1 (light) for 2.5 atm., Type 3 (medium) for 6 atm. and Type 4 (heavy) for 10 atm., the values of diameters range from 32 to 110, 16 to 160 and, respectively, from 16 to 110 mm; and coupling pipes with ring, for pressure of 10 atm., with a diameter of 125 to 315.

The coupling pipes are provided with a rubber gasket to ensure a proper sealing. The gaskets are delivered together with the coupling pipes. The insulating pipes made from PVC are used for protective applications of the pipe-lines of electric wirings with voltages up to 1,000 V or used to replace the metallic pipes of the Bergman or Pantzer type.

Our enterprise is manufacturing insulating tubes with an outer diameter of 16—50 mm.

A.3. The Plastics Processing Enterprise in Buzău manufactures packagings from impact-modified polystyrene sheets by thermoforming

These packagings are of different shapes and dimensions, according to the Buyer's requirements and they include: baskets, casseroles, cells, glasses, cases, stands and are used as containers for fruit, frozen food, dairy products, candies, drugs, spare parts for industry etc.

The material used for packaging in the food industry meets the requirements for food-contact use, approved by the Ministry of Public Health.

Thermal stability of the packagings made from impact-modified PS ranges from —10 to +50°C.

A.4. Products Made from Polypropylene

1. Our enterprise manufactures and delivers PP tapes, with a width of 13 mm and a thickness of 0.5 mm, used for fastening different packagings (packs, boxes).
2. We also manufacture and deliver PP woven sacks, with the following dimensions: 550 × 1,000 mm, 650 × 1,150 mm, used as packagings for different chemical products, both for internal consumption and for export.
3. Our enterprise manufactures strings and ropes from flat PP threads used for fastening, attaching or binding different products.
   Twisting technology is used for manufacturing strings with a diameter of 1.5—3.5 mm and ropes with a diameter of 6—14 m, that show a very good resistance.

B. Filters and Filtering Parts

The Plastics Processing Enterprise in Buzău is the largest manufacturer of filters and filtering parts in Romania.

The filters and the filtering parts are used as component parts of the equipments and engines made in Romania or imported, such as greasing and hydraulic

THE PLASTICS PROCESSING ENTERPRISE—BUZĂU—

The Plastics Processing Enterprise in Buzău, 132, Transilvaniei Street, telephone 13425, Telex 56227, manufactures a large variety of products, that may be classified into four main groups, according to the manufacturing technology:

A. semi-finished and finished plastic products;
B. filters and filtering component parts;
C. protection devices for the breathing passages;
D. active carbon.

A. Semi-finished and Finished Plastic Products

The Plastics Processing Enterprise in Buzău manufactures products from: HDPE, LDPE, PVC in suspension, impact modified PP and PS, by different technologies such as: extrusion, extrusion-blowing, extrusion granulating, sintering, injection, thermoforming.

A.1. Polyethylene Products

1. The Plastics Processing Enterprise in Buzău manufactures and delivers HDPE and LDPE sheets for a wide range of applications in agriculture, industry and other fields of activity.

   The PE foils may be clear or opaque, uncoloured or pigmented.

a. According to the application, there are manufactured four types of LDPE foils with width (in pipe-form) ranging from 150 to 6,500 mm:

- for packaging applications;
- for general purposes;
- for industrial bags;
- covers for agriculture use;

The following values of thickness are given for each type of foil: 0.025–0.045 mm; 0.045–0.25 mm; 0.25–0.32 mm; 0.100–0.160 mm.

b. The HDPE foils have values of thickness ranging from 0.020 to 0.060 mm and width from 150 to 1.100 mm.

The PE sheets are delivered rolled on PVC cores; the maximum weight of a roll is of 50 kg.

Our enterprise is also manufacturing:

- LDPE and HDPE sheets with flaps, for agriculture use (covers for crops of vegetables);
- LDPE sheets for insulating irrigation canals; their width ranges from 750 to 3 000 mm and their thickness from 0.5 to 1 mm.

c. Coextruded LDPE and HDPE foils.

2. PE sheets with the following applications:

- packagings (bags, carrier bags, thin sacks, hoods) for different products (chemical products, food, clothes) or protection covers for pallets (containing construction materials, equipments etc.).

They may be unprinted or printed in one to six colours.

- thick sacks for chemical fertilizers or for other types of powders or granules: maximum load for each sack is of 50 kilos. They may be unprinted or printed in one or two colours.

3. The Plastics Processing Enterprise in Buzău also produces high load packagings (for capacities ranging from 20 to 1,000 litres) by means of technological process used only in this enterprise in Romania, namely rotational or static moulding (sintering) of LDPE powders.

These packagings may have different shapes and colours, their application including boats and objects for sanitary use, tanks and silos, cans and containers that are to be palletized. The material used for these applications – LDPE – is characterized by thermal stability between – 5 and + 60°C, good impact strength, stiffness, chemical resistance to almost all chemical substances and it is also a good electrical insulator ; in a word, it shows a unique combination of qualities.

It may be applied in food industry as it meets the requirements for food contact use, approved by the Ministry of Public Health.

On Buyer's request, the range of the existing types and dimensions of products can be extended, either by manufacturing new products or by adjusting connecting pieces, valves and corks to the already existing products.

4. The Plastics Processing Enterprise in Buzău also manufactures and delivers HDPE rifled or punched pipes for draining water in agriculture, with a nominal diameter of 50, 65 or 80 mm.
5. Our enterprise manufactures and delivers LDPE slings, reinforced with thread of viscose cord, used to fasten the pallets containing bags or boxes, with a maximum weight of one ton.

A.2. Semi-finished and Finished Products Made from PVC in Suspension

Our enterprise manufactures and delivers granules, pipes and insulating tubes made from PVC.

Major applications of PVC granules include :

● primary or secondary electrical insulations for pipes or electric cables ;

● footwear and different component parts for footwear, such as soles, heel pieces, straps, welts ;

● construction materials, namely pressure pipes, fittings, handrails :

● records.

Applications of PVC pipes include technological and sanitary-engineering installations, used as conveyers for drinking water, waste water or liquids that do not attack PVC, for irrigations or as channels for cables.

The Plastics Processing Enterprise in Buzău also manufactures pipes with an outer diameter determined by the values of pressure of the conveyed fluid : simple pipes Type 1 (light) for 2.5 atm., Type 3 (medium) for 6 atm. and Type 4 (heavy) for 10 atm., the values of diameters range from 32 to 110, 16 to 160 and, respectively, from 16 to 110 mm ; and coupling pipes with ring, for pressure of 10 atm., with a diameter of 125 to 315.

The coupling pipes are provided with a rubber gasket to ensure a proper sealing. The gaskets are delivered together with the coupling pipes. The insulating pipes made from PVC are used for protective applications of the pipe-lines of electric wirings with voltages up to 1,000 V or used to replace the metallic pipes of the Bergman or Pantzer type.

Our enterprise is manufacturing insulating tubes with an outer diameter of 16—50 mm.

A.3. The Plastics Processing Enterprise in Buzău manufactures packagings from impact-modified polystyrene sheets by thermoforming

These packagings are of different shapes and dimensions, according to the Buyer's requirements and they include : baskets, casseroles, cells, glasses, cases, stands and are used as containers for fruit, frozen food, dairy products, candies, drugs, spare parts for industry etc.

The material used for packaging in the food industry meets the requirements for food-contact use, approved by the Ministry of Public Health.

Thermal stability of the packagings made from impact-modified PS ranges from −10 to + 50°C.

A.4. Products Made from Polypropylene

1. Our enterprise manufactures and delivers PP tapes, with a width of 13 mm and a thickness of 0.5 mm, used for fastening different packagings (packs, boxes).
2. We also manufacture and deliver PP woven sacks, with the following dimensions : 550 × 1,000 mm, 650 × 1,150 mm, used as packagings for different chemical products, both for internal consumption and for export.
3. Our enterprise manufactures strings and ropes from flat PP threads used for fastening, attaching or binding different products.

   Twisting technology is used for manufacturing strings with a diameter of 1.5—3.5 mm and ropes with a diameter of 6—14 m, that show a very good resistance.

B. Filters and Filtering Parts

The Plastics Processing Enterprise in Buzău is the largest manufacturer of filters and filtering parts in Romania.

The filters and the filtering parts are used as component parts of the equipments and engines made in Romania or imported, such as greasing and hydraulic devices of the industrial equipments or filtering devices for air and liquid fuels (gasoline, gas oil). They are also used as component parts of different automotive products: cars of DACIA, OLTCIT, SKODA, LADA, MOSKVICI type, trucks of DAC, ROMAN, ARO and FIAT type, motor tractors and excavators.

The performances of the filtering elements are given both by the dimensions of the smallest particle that will not pass through the device and by the flow of the fluid that is filtered.

These devices include: air-filtering elements, with a filtering accuracy of 20–25 microns, for a maximum flow of 250 m^2/hr, oil-filtering parts, with a filtering accuracy of 5–8, 9–12, 10–15, 20–25 microns for flows ranging from 9 up to 1,000 liters/min. and filtering parts for liquid fuels with an accuracy of 5–8 and 8–11 microns, for flows of 0.15 up to 6.25 liters/min.

C. **Protection Devices for the Breathing Passages**

- protection masks with free aspiration of fresh air for environments with toxic gases (chlorine, ammonia, phosgene, cyanic compounds, organic solvents, aerosols, sulphur dioxide, carbon oxide, hydrogen sulphide etc.):
- dust-masks;
- rescue apparatus for mines;
- masks used in painting industry.

D. **Active Carbon**

The Plastics Processing Enterprise in Buzău manufactures active carbon in granular form (used as degasolination agent for oil-well gases, as purifying agent for industrial waters, as retainer of the traces of oil from the compressed air), in coalbrick form (used as catalyst for cyanuril chloride synthesis), in powder form (used as decolourizing agent for glucose, lactose and molasses in solution, syrups and other types of solutions) and as purifying, decolourizing and deodorizing agent for chemical and pharmaceutical oils and greases, animal and vegetable fats).

The Plastics Processing Enterprise in Buzău can offer, on your request, the technical assistance of its specialist in order to satisfy as well as possible, the demands of your enterprises.

devices of the industrial equipments or filtering devices for air and liquid fuels (gasoline, gas oil). They are also used as component parts of different automotive products: cars of DACIA, OLTCIT, SKODA, LADA, MOSKVICI type, trucks of DAC, ROMAN, ARO and FIAT type, motor tractors and excavators.

The performances of the filtering elements are given both by the dimensions of the smallest particle that will not pass through the device and by the flow of the fluid that is filtered.

These devices include: air-filtering elements, with a filtering accuracy of 20–25 microns, for a maximum flow of 250 m^2/hr, oil-filtering parts, with a filtering accuracy of 5–8, 9–12, 10–15, 20–25 microns for flows ranging from 9 up to 1,000 liters/min. and filtering parts for liquid fuels with an accuracy of 5–8 and 8–11 microns, for flows of 0.15 up to 6.25 liters/min.

C. Protection Devices for the Breathing Passages

- protection masks with free aspiration of fresh air for environments with toxic gases (chlorine, ammonia, phosgene, cyanic compounds, organic solvents, aerosols, sulphur dioxide, carbon oxide, hydrogen sulphide etc.):
- dust-masks;
- rescue apparatus for mines;
- masks used in painting industry.

D. Active Carbon

The Plastics Processing Enterprise in Buzău manufactures active carbon in granular form (used as degasolination agent for oil-well gases, as purifying agent for industrial waters, as retainer of the traces of oil from the compressed air), in coalbrick form (used as catalyst for cyanuril chloride synthesis), in powder form (used as decolourizing agent for glucose, lactose and molasses in solution, syrups and other types of solutions) and as purifying, decolourizing and deodorizing agent for chemical and pharmaceutical oils and greases, animal and vegetable fats).

The Plastics Processing Enterprise in Buzău can offer, on your request, the technical assistance of its specialist in order to satisfy as well as possible, the demands of your enterprises.

ORSZÁGOS MŰSZAKI INFORMÁCIÓS KÖZPONT ÉS KÖNYVTÁR 1983

NOTE POUR LES AUTEURS

La Revue Roumaine de Chimie publie des articles en anglais, français, russe, allemand ou espagnol. Les auteurs sont priés d'envoyer des articles et des comptes rendus inédits.

Les manuscrits seront dactylographiés à double interligne. La bibliographie, les tableaux et la légende des figures seront placés après le texte.

Si l'article fait partie d'une série numérotée, la partie précédente sera donnée comme première référence.

Chaque article sera précédé d'un résumé comprenant quinze lignes au maximum.

Les références bibliographiques dans le texte seront faites par des exposants sans parenthèses et paraîtront à la fin de l'ouvrage.

Les publications périodiques mentionnées dans la bibliographie seront présentées suivant les prescriptions internationales : le nom de l'auteur précédé de l'initiale du prénom, le titre du périodique abrégé conformément à « Chemical Abstracts » et souligné par une ligne, le numéro du tome indiqué par des chiffres arabes et souligné par deux lignes, suivi de la première page de l'article : à la fin, l'année de la parution sera placée entre parenthèses. Le numéro de la revue ne sera pas indiqué si les pages du volume sont numérotées consécutivement.

Les textes des livres ou traités incluront : le nom des auteurs, précédé de l'initiale du prénom, le titre du livre entre guillemets et sans être souligné, le numéro du tome précédé par l'abréviation « vol. » (ou « Bd. »), le numéro de l'édition, les éditions (the publisher), la localité de la parution du livre, l'année de la parution et la page de la référence précédée(s) par l'abréviation « p » (ou « S »).

Les brevets seront indiqués comme suit : l'auteur ou la firme, le pays et le numéro du brevet, la date de la revue *(Chem. Abstr.)*. Par ex. : M. Jones (to Union Carbide Co.), Brit. Pat. 610 238, 2 Sept. 1959 : cf. *Chem. Abstr.*, **54**, 12808 (1960).

Si la référence n'a pas été lue en original, on indiquera aussi la revue de références consultée.

Les diagrammes seront tracés à l'encre de Chine sur papier calque. Les tableaux et les figures (en nombre strictement nécessaire), ainsi que les courbes dans les figures seront numérotés par des chiffres arabes. Leur explication sera donnée dans la légende des figures. Prière de ne pas inscrire les mêmes données dans les tableaux et les figures. Chaque tableau aura un titre. On indiquera dans le texte la place approximative des tableaux et des figures. Les formules chimiques seront incluses dans le texte ; en outre, elles seront transcrites sur papier calque à l'encre de Chine.

Les auteurs sont priés d'indiquer les caractères italiques (en soulignant les lettres au crayon), ainsi que tout autre caractère spécial : les préfixes, *ortho*, *meta*, *para*, *cis*, *trans*, etc. seront soulignés pour indiquer leurs caractères italiques, et ne seront jamais écrits avec des majuscules.

Aucune correction à la main ne sera admise sur le manuscrit. Les corrections seront frappées à la machine. Les lettres grecques ou d'autres symboles spéciaux seront insérés à la main à l'encre clairement.

Le manuscrit sera signé par l'auteur.

Le titre courant aura 50 lettres au maximum.

L'entière responsabilité du contenu des articles appartient aux auteurs.

Sur demande on peut obtenir une note plus complète.

PRINTED IN ROMANIA

TRAVAUX PARUS AUX ÉDITIONS DE L'ACADÉMIE DE LA RÉPUBLIQUE SOCIALISTE DE ROUMANIE

ELENA CEAUŞESCU, **Răşini de hidrocarburi, vol. 1, 1988, 344 p.**
ELENA CEAUŞESCU, **Progrese în chimia şi tehnologia polimerilor, 1986, 446 p.**
ELENA CEAUŞESCU, **Forschungen im Bereich der Chemie und Technologie der Polymere,** 1986, 444 p.
ELENA CEAUŞESCU, **Cercetări în chimia şi tehnologia polimerilor, 1983, 520 p.**
ELENA CEAUŞESCU, **Noi cercetări în domeniul compuşilor macromoleculari, 1981, 536 p.**
ELENA CEAUŞESCU, **Polimerizarea stereospecifică a izoprenului, 1979, 307 p.**
ELENA CEAUŞESCU, **Research work on synthesis and characterization of macromolecular compounds. Contributions,** 1974, 251 p.
I. G. MURGULESCU, **Introducere în chimia fizică. Vol. I. 1. Atomi, molecule, legătură chimică,** 1976, 560 p.
I. G. MURGULESCU, V. EM. SAHINI, **Introducere în chimia fizică, Vol. I. 2. Structura şi proprietăţile moleculelor,** 1979, 604 p.
I. G. MURGULESCU, E. SEGAL, **Introducere în chimia fizică. Vol. II. 1. Teoria molecular-cinetică a materiei,** 1979, 1036 p.
I. G. MURGULESCU, TATIANA ONCESCU, E. SEGAL, **Introducere în chimia fizică. Vol. II. 2. Cinetică chimică şi cataliză,** 1981, 1024 p.
I. G. MURGULESCU, J. PĂUN, **Introducere în chimia fizică. Vol. I. 3. Nucleul atomic, reacţii nucleare, particule elementare,** 1982, 606 p.
I. G. MURGULESCU, RODICA VÎLCU, **Introducere în chimia fizică. Vol. III. Termodinamica chimică,** 1982, 624 p.
I. G. MURGULESCU, O. M. RADOVICI, **Introducere în chimia fizică. Vol. IV. Electrochimia,** 1986, 410 p.
R. VÎLCU, M. LECA, **Termodinamica polimerilor prin cromatografie de gaze, 1987, 238 p.**
I. ZUGRĂVESCU, M. PETROVANU, **Cicloadiţii 3+2 dipolare, 1987, 446 p.**
RAUL MIHAIL, ION GROZEANU, **Estimarea secvenţială aplicată sistemelor chimice, 1986,** 406 p.
M. BREZEANU, I. PATRON, M. ANDRUH, **Combinaţii complexe polinucleare şi aplicaţiile lor,** 1986, 244 p.
A. T. BALABAN et al., **Labelled Compounds and Radiopharmaceuticals Applied in Nuclear Medicine,** coédition avec John Wiley and Sons, 1986, 742 p.
D. PURDELA, **Nomenclatura chimiei organice — IUPAC,** 1986, 451 p.
PETRU BUDRUGEAC, **Probleme de chimie,** 1986, 280 p.
T. ONCESCU, S. G. IONESCU, **Conversie fotochimică şi stocare de energie, 1985, 272 p.**
V. DRĂGUŢAN, A. T. BALABAN, M. DIMONIE, **Olefin Metathesis and Ring-Opening Polymerization of Cyclo-Olefins,** coédition avec John Wiley and Sons, 1985, 544 p.
C. LITEANU, I. RÎCĂ, **Optimizarea proceselor analitice,** 1985, 360 p.
N. PERESCU, **Chimia extracţiei cu solvenţi şi aplicaţii,** 1985, 212 p.
V. E. SAHINI, M. HILLEBRAND, **Chimia cuantică în exemple şi aplicaţii, 1984, 378 p.**
GH. MARCU, **Chimia compuşilor coordinativi,** 1984, 415 p.
E. CORDOŞ, C. MANOLIU, **Spectrometria de absorbţie şi fluorescenţă atomică, 1984, 178 p.**
C. BODEA, **Tratat de biochimie vegetală, p. II, t. V,** 1984, 438 p.
N. ASANDEI, A. GRIGORIU, **Chimia şi structura fibrelor,** 1983, 395 p.
N. IONESCU, M. CĂLDĂRARU, **Oxidarea catalitică a olefinelor inferioare, 1983, 178 p.**
C. I. SIMIONESCU, F. DANEŞ, **Originea vieţii,** 1983, 110 p.
C. BODEA, **Tratat de biochimie vegetală, p. II, t. IV,** 1982, 408 p.
CR. SIMIONESCU, VALERIA GORDUZA, **Polimeri biocompatibili şi biologic activi, 1980,** 479 p.
M. FLORESCU, **Metode ştiinţifice în dezvoltarea industriei chimice moderne, 1979, 495 p.**
C. GH. MACAROVICI, **Analiza chimică cantitativă anorganică, 1979, 457 p.**

ISSN 0035 - 3930

1990 IAN 09

/

I. P. INFORMAŢIA c. 1327

43 426

Lei 40

F 1103

ACADÉMIE DE LA RÉPUBLIQUE SOCIALISTE DE ROUMANIE

REVUE ROUMAINE DE CHIMIE

TOME 34

N°s 9—10

Septembre — Octobre 1989

Rev. Roumaine Chim.

RRCHAX, 34, *9—10*, p. 1817—2010 (1989), Bucarest

EDITURA ACADEMIEI REPUBLICII SOCIALISTE ROMÂNIA

ACADÉMIE DE LA RÉPUBLIQUE SOCIALISTE DE ROUMANIE

COMITÉ DE RÉDACTION

Rédacteur en chef:

I. G. MURGULESCU, membre de l'Académie de la République Socialiste de Roumanie

Rédacteurs en chef adjoints:

A. T. BALABAN et V. EM. SAHINI, membres correspondants de l'Académie de la République Socialiste de Roumanie

Collège de rédaction:

EM. BRATU, ELENA CEAUȘESCU, ECATERINA CIORĂNESCU-NENITZESCU, CR. SIMIONESCU, membres de l'Académie de la République Socialiste de Roumanie; P. SPACU, membre correspondant de l'Académie de la République Socialiste de Roumanie; M. BANCIU, M. D. GHEORGHIU, I. HAIDUC, D. I. MARCHIDAN, G. NIAC et D. SĂNDULESCU.

La Revue Roumaine de Chimie paraît 10 fois par an. Toute commande de l'étranger sera adressée à ROMPRESFILATELIA — sectorul Export-Import Presă, P.O. Box 12—201, télex 10376 prsfi r 78104 Bucarest, Calea Griviței nr. 64—66, Bucarest, Roumanie

Les manuscrits, les livres et les revues proposés en échange, ainsi que toute correspondance seront envoyés à la rédaction :

REVUE ROUMAINE DE CHIMIE

125, Calea Victoriei, 79717 Bucarest, Roumanie, téléphone 50 76 80

EDITURA ACADEMIEI REPUBLICII SOCIALISTE ROMÂNIA
125, Calea Victoriei 79717 Bucarest, Roumanie, téléphone 50 76 80

REVUE ROUMAINE DE CHIMIE

ORSZÁGOS MŰSZAKI INFORMÁCIÓS KÖZPONT ÉS KÖNYVTÁR 78933

Tome 34, N°s 9–10 **Septembre–Octobre 1989**

MARILENA VASILESCU, Quenching of fluoranthene fluorescence by amines 1819–1827

IONEL CIUCANU and CONSTANTIN LUCA, Permethylated dextran as stationary phase in gas chromatography 1829–1833

J. EPPERLEIN, B. BLAU and U. SCHIERIG, UV-VIS-spectral behaviour of arylazo compounds. III. Solvent effects on the visible absorption band of 4-amino-substituted azobenzenes 1835–1842

ANTONINA GUȚU and M. VASS, Work function and electron impact desorption studies on CO/W adsorption states 1843–1847

CONSTANTIN LUCA, ANDREI DĂNEȚ and CORNEL RADU, Mercury determination in water and atmosphere at concentrations lower than parts per billion 1849–1856

A. C. BANCIU, Electronic transitions in the square-planar $Rh(PPh_3)_3SnCl_3$ complex (PPh_3 = triphenylphosphine) 1857–1865

S. NEAGOE, D. NEGOIU, V. NEAGOE, M. NEGOIU, E. BADAU and G. BREBEANU, Pd(II) complex compounds with thioethers. II. Pd(II) compounds of bis(benzylthio-*p*-phenyl)ethers 1867–1875

S. K. MISHRA, A. P. MISHRA and K. L. YADAVA, Study of mixed ligand complexes of Hg(II), Be(II) and Cu(II) by paper electrophoresis (M-Nitrilotriacetate-adenine systems) 1877–1885

A. SYAMAL, Studies on biguanide derivatives: copper(II) complexes with ethylenedibiguanide, trimethylenedibiguanide, *meta*-phenylenedibiguanide, piperazinedibiguanide and phenylbiguanide 1887–1893

GABRIELA STĂNCIUC, MIRON-TEODOR CĂPROIU, HORIA CĂLDĂRARU, AGNETA CARAGHEORGHEOPOL, TITUS CONSTANTINESCU and ALEXANDRU T. BALABAN, Factors affecting stability and equilibria of free radicals. XVI. Preparation and EPR spectra of capto-dative N-alkoxy-dinitrophenyl-aminyls 1895–1905

MIRCEA D. BANCIU, CĂTĂLINA HADA, DANA ALBAIU and CONSTANTIN DRĂGHICI, The physico-chemical characterization of Z-4b, 10b-dihydrochrysene 1907–1919

MIRCEA D. BANCIU, MICHAELA DINA STĂNESCU and FILIP CHIRALEU, Heterocycles with annelated dibenzocycloalkane skeletons. III. Pyrazoles with dibenzobarrelene- and dibenzohomobarrelene skeletons 1921–1930

MIRCEA D. GHEORGHIU, EMILIA OLTEANU, LIGIA STĂNESCU, MARGARETA AVRAM and GHEORGHE SURPĂȚEANU, The syntheses of benzonorbornane, *exo*-benzocyclobutano- and *endo*-benzocyclo-

Rev. Roumaine Chim. **34**, *9–10*, 1817–2010 (1989), Bucarest

butanonorbornanes annelated with *exo*-cyclobutene ring *via* Shechter reaction 1931–1944

I. COCÎRLĂ, LUCIA TĂTARU, M. VÂŢĂ, I. MAZILU, LUMINIŢA WAGNER, D. SCUTARU and CAMELIA PETRESCU, Study on the reactivity of some *AS* naphthols possessing benzimidazolonic rest 1945–1948

O. M. O. HABIB, A. H. ABD EL-RAHMAN and D. S. BADAWY, Synthesis and reactions of some new benzofurano[3,2-c]pyrazol-3-one and benzofurano[3,2-c]isoxazol-3-one derivatives of expected biological activity 1949–1955

MOHAMED F. ABDEL MEGEED and MOHAMED A.H.SALEH,Synthesis and reactions of D-glucosyl derivatives of 2-aryl-4(3H)-quinazolinones and their thione derivatives 1957–1962

MONEER A. I. SALEM, A. M. EL-GENDY and S. I. EL-NAGDY, Behaviour of 4-(4′-bromo-3′-methyl)phenyl-1(2H)-phthalazinone towards some nucleophiles and electrophiles 1963–1971

M. R. MAHMOUD, S. EL-NAGDY and F. A. EL-BASSIOUNY, The condensation of some aromatic aldehydes and ketones with dimethyl homophthalate 1973–1978

S. EL-NAGDY, F. A. EL-BASSIOUNY, I. ATTIA and M. R. MAHMOUD, Studies on the condensation of 1,3-diaryl-propen-1-one with ethyl cyanoacetate 1979–1985

ABDEL-BADIH A. G. GHATTAS, MAHMOUD ABDEL-RAHMAN, MOHAMED T. EL-WASSIMY and GAMAL A. EL-SARAF, Benzofurans. Part III. Synthesis and antifungal activity of some new Mannich bases and sulphides derived from (1,3,4-thiadiazolyl)- and (1,2,4-triazolyl)-benzofurans 1987–1993

N. MOGA, OCTAVIA CUCU, ALINA PĂNESCU and MARIANA POPESCU, Considerations on the synthesis and properties of usual surfactant-free acrylic dispersions 1995–2006

BOOK REVIEWS 2007–2009

Revue Roumaine de Chimie, **34**, *9–10*, 1819–1827 (1989)

QUENCHING OF FLUORANTHENE FLUORESCENCE BY AMINES

MARILENA VASILESCU
ICECHIM — Center of Physical Chemistry
Splaiul Independenţei 202, Bucharest — Romania

Received February 21, 1988

The quenching of fluoranthene fluorescence by various secondary and tertiary, aromatic and aliphatic amines was studied by fluorescence spectroscopy and nanosecond fluorometry; the formation of exciplexes between fluoranthene and amines was evidenced. The fluorescence of exciplexes was characterized from fluorimetric and kinetic viewpoint and the influence the solvent nature and temperature exert upon it was studied.

1. INTRODUCTION

Quenching of aromatic hydrocarbon fluorescence is generally accompanied by formation of exciplex — a molecular complex which is stable in excited state and unstable in ground state. The formation of exciplexes was first mentioned by Leonhardt and Weller[1] in perylene — aromatic amines system in non-polar solvent; since then it has been evidenced in many aromatic hydrocarbons in presence of amines (the reviews[2–5]).

The formation of exciplexes implies an electric charge transfer from electron donor to acceptor molecules. The molecule in excited state is more reactive; it is characterized by a lower ionization potential (IP) and a higher electron affinity (EA) than in the ground state.

$$IP^* = IP - \Delta E_{0,0}$$

$$EA^* = EA + \Delta E_{0,0}$$

where $\Delta E_{0,0}$ is the electron transition energy. The electron transfer in fluorofor-quencher system is determined by the inequation:

$$(IP + EA)_A > (IP + EA)_D$$

The aromatic hydrocarbon molecule is electron acceptor in excited state in presence of some electron donors. Perylene, pyrene and other condensed polynuclear aromatic hydrocarbons form AD complexes with aniline, dimethyl-aniline and other amines which are generally electron donor molecules.[6-10] Fluoranthene or benzo(j, k)fluorene is a condensed aromatic hydrocarbon with cyclopentadiene ring.

This contribution proves that the fluorescence of this aromatic hydrocarbon (fluoranthene) is quenched by amines according to the mechanism established for polynuclear condensed aromatic hydrocarbons.

2. EXPERIMENTAL

The fluorescence excitation and emission spectra of fluoranthene solutions were recorded with 204 Perkin Elmer and Aminco-Bowman SPF 500 spectrofluorimeters. The decay of fluoranthene fluorescence in ns range was studied by means of LIF 200 fluorometer (G.D.R.) with laser pulses. The fluoranthene fluorescence was excited by 337 nm radiation of N_2 laser whose pulse had a half-width of 1 ns, an energy of 20 μJ and a power of 40 kW. The pulse repetition frequency was 84 Hz.

To lower the oxygen concentration, which is by itself a fluorescence quencher, two methods were employed :

— 5—10 min. bubbling of solution with dry purified nitrogen ;

— 5—6 cycles of freezing — defreezing of the solution in the cell attached to a vacuum line (10^{-5} torr) followed by torch cell sealing

The fluoranthene was p.a. grade (Fluka). The amines were freshly distilled.

3. RESULTS AND DISCUSSION

Fluoranthene has some spectrophotometric particularities : the $^1A \rightarrow {}^1L_b(S_1)$ absorption band is very weak, being masked by the $^1A \rightarrow {}^1L_a(S_2)$ band which is intense, with well defined vibrational structure (Fig. 1). The same phenomenon may be noted in the fluorescence excitation spectrum of fluoranthene (Fig. 2) where the $^1A \rightarrow {}^1L_a(S_2)$ band may also be observed.

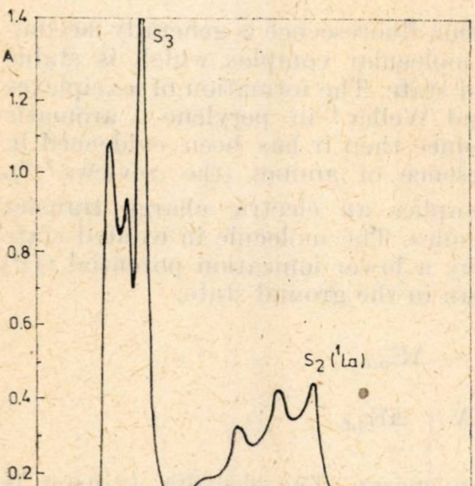

Fig. 1. — The UV absorption spectrum of fluoranthene solution in cyclohexane ($5 \cdot 10^{-5}$ M).

The fluorescence spectrum of the solution of fluoranthene in cyclohexane shows a wide band in the 400—600 nm range with well defined vibrational structure compared to vibrational structure of fluorescence band of fluoranthene acetonitrile solution (Fig. 3).

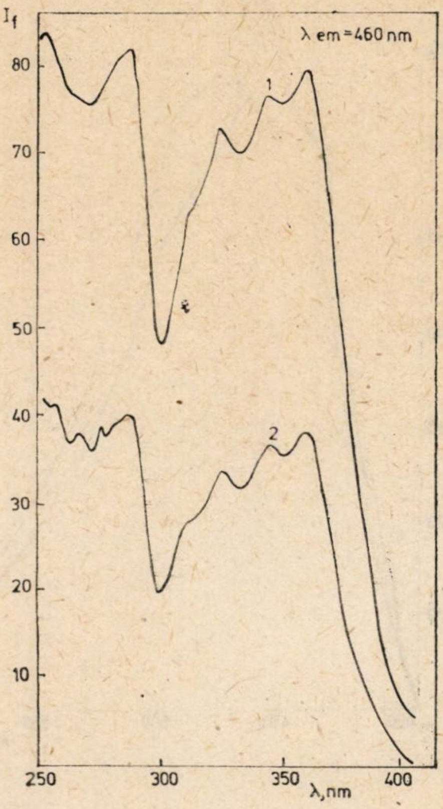

Fig. 2. — The fluorescence excitation spectrum (quantically corrected) of fluoranthene solution in cyclohexane (10^{-4}M) degased (curve 1) and undegased (curve 2); frontal illumination; $\lambda_{em} = 460$ nm; I_f = fluorescence intensity.

The fluorescence intensity values, at different times, taken from fluorescence decay curves, recorded on an x · y chart were processed by computer with a linear regression program to determine the value of fluorescence lifetime τ. The τ value is affected by the presence of oxygen and depends on the spectral range of measurements.

τ values were employed in calculation of rate constant of fluorescence quenching.

The following amines were employed as quenchers: diethylamine (DEA,, di-n butylamine (DBA), triethyltetraamine (TETA), triethylamine (TEA) and dimethylaniline (DMA).

The fluorescence intensity ratio I_0/I (I_0 and I standing for the intensity of fluorescence of fluoranthene solutions in cyclohexane without and with quencher, respectively) is proportional to molar concentration of quencher [Q]: $I_0/I = 1 + K_{SV}[Q]$; the slope of the plot is the Stern-Volmer constant, K_{SV}. Fig. 4 shows the linear Stern-Volmer dependence in the systems under study.

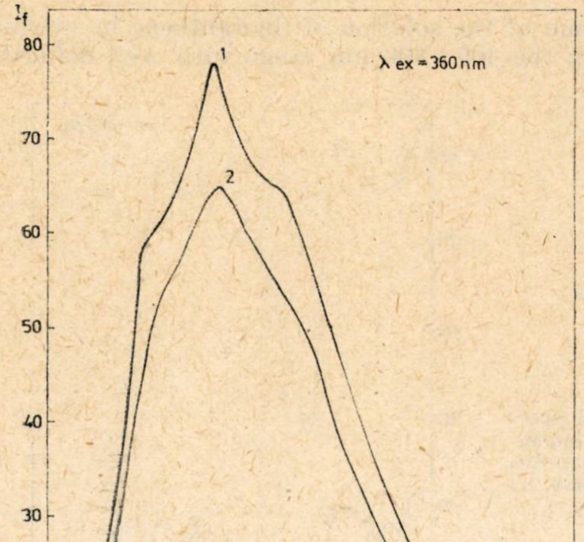

Fig. 3. — The corrected fluorescence spectra for a fluoranthene solution (10^{-4} M) in cyclohexane (curve 1) and acetonitrile (curve 2); λ_{exc} = 360 nm.

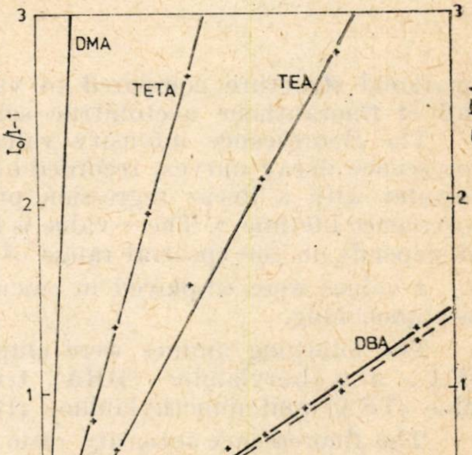

Fig. 4. — The Stern-Volmer linear dependence of fluorescence quenching in fluoranthene — cyclohexane solutions at amine addition.

The fluoranthene fluorescence quenching was studied in solutions degased by N_2 bubbling ($\tau_0 = 44$ ns) as well as in undegased solutions ($\tau_0 = 38$ ns); the k_q values ($= K_{SV}/\tau_0$) calculated for degased and undegased solutions are in a very good agreement. Table 1 lists the values of various parameters of fluorescence quenching.

Table 1

The parameters of fluoranthene — cyclohexane solution (10^{-4}M) fluorescence quenching with various quenchers

Quencher	IP (eV)	$K_{SV}(M^{-1})$	$k_q(M^{-1}s^{-1})$	γ	α
DEA	8.01	4.45 3.90[a]	$0.11 \cdot 10^9$ $0.10 . 10^9$	0.009	—
DBA	7.69	12.60 14.40[b] 9.60	$0.33 \cdot 10^9$ $0.33 \cdot 10^9$ $0.25 \cdot 10^9$	0.026	—
TETA	—	64.60	$1.70 \cdot 10^9$	0.137	—
TEA	7.50	35.80	$0.94 \cdot 10^9$	0.075	0.082
DMW	7.30	245.10	$6.44 \cdot 10^9$	0.519	1.080

[a] resulted from the τ_0/τ dependence on quencher concentration;

[b] resulted from solution degased by bubbling nitrogen.

Addition of DEA, DBA or TETA secondary amines to fluoranthene solutions in cyclohexane diminishes the intensity of fluorescence without any other alteration of the spectrum.

The aromatic tertiary amine DMA forms exciplexes with excited fluoranthene molecules. The fluorescence emitted by the exciplex is intense (green) even in solutions which were not degased (Fig. 5).

The intensity of fluoranthene fluorescence is diminished, a phenomenon accompanied by an increase of exciplex fluorescence intensity with quencher concentration up to about $1.5 \cdot 10^{-1}$M; then, at higher concentration it decreases and the exciplex fluorescence wavelength shifts towards higher values.

Triethylamine (TEA) which is a tertiary aliphatic amine is a much weaker quencher of fluoranthene fluorescence and therefore its exciplex forming probability is much lower; its solution in cyclohexane has evidenced no exciplex fluorescence.

Calculation of fluorescence lifetime in absence (τ_0) and presence of quencher (τ) from the decay curves and plotting $\tau_0/\tau - 1$ versus quencher molar concentration has yielded straight lines which afford graphical evaluation of quenching the Stern-Volmer, K_{SV}, constant. Table 2 lists, for comparison, the values of constant K_{SV} in fluoranthene—cyclohexane—DBA and fluoranthene — acetonitrile — DBA solutions as determined

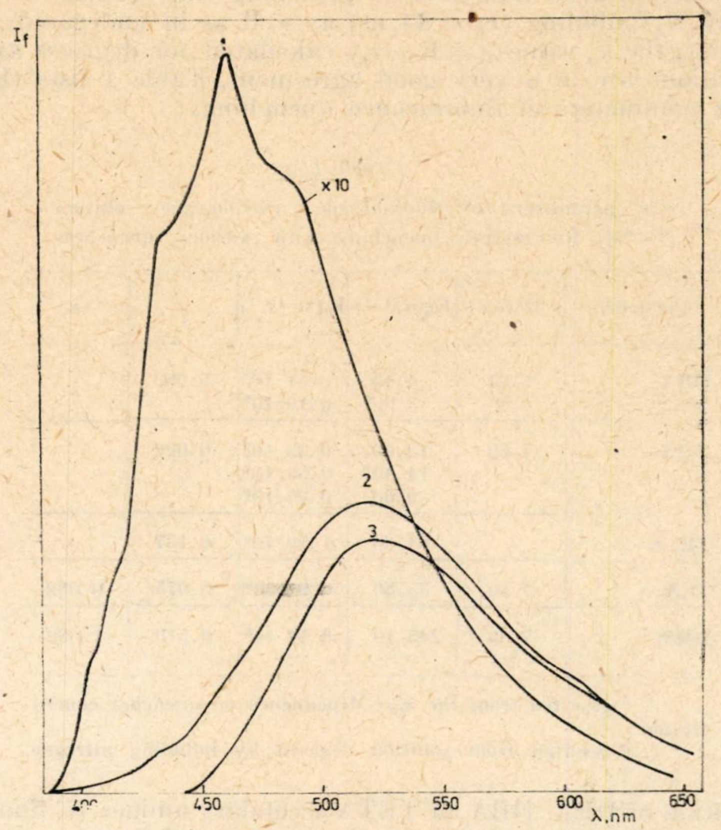

Fig. 5 — The fluorescence spectra of fluoranthene (10^{-4}M) in cyclohexane (curve 1) and fluoranthene in cyclohexane DMA (curve 2, $[Q] = 5 \cdot 10^{-2}$M) and the fluorescence spectrum of the exciplex (curve 3).

Table 2

The values of the Stern-Volmer constant determined from the dependence on quencher concentration of fluorescence intensity $(K_{SV})_S$ and of fluorescence lifetime $(K_{SV})_d$; quencher = DBA

Solvent	$(K_{SV})_S(M^{-1})$	$(K_{SV})_d(M^{-1})$	
	20°C	20°C	40°C
acetonitrile	114.2	106.8	115.4
cyclohexane	12.6	9.6	10.8

from fluorescence intensity measurements (stationary state) and from lifetime measurements at two temperatures : 20° and 40°C. The quenching coefficient is positive ; the K_{SV} value tends to increase with increasing temperature, which may be accounted for the dynamic character of quenching.

As to solutions of fluoranthene in cyclohexane with DMA addition, decay of fluorescence is no longer exponential. To study the decrease of fluoranthene fluorescence lifetime with DMA concentration and, at the same time, determine the lifetime of exciplex fluorescence the two emission bands were separated as accurately as possible into two emission bands, i.e. of the monomer and of the exciplex by employing BG 25 (Schott Jena) optical filtres and the 550 nm cut-off filter. It was found out that the lifetime of fluoranthene fluorescence (monomer) decreases with the increase of DMA concentration up to about $5 \cdot 10^{-2}$, then, at higher concentrations, τ remains practically unchanged. The τ value of excimer fluorescence lifetime obtained at $5 \cdot 10^{-2}$ M DMA is 25 ns.

To study the influence of solvent nature upon fluoranthene fluorescence quenching by DMA the following solvents were tested; n-pentane, cyclohexane, ethylic ether, ethanol, methanol and acetonitrile, whose dielectric constant ranges within 1.84 and 37.5. The K_{SV} values are large in solvents with higher dielectric constant, but no exciplex emission may be noted; this latter was observed in n-pentane, cyclohexane and ethylic ether.

Table 3 lists spectral characteristics of fluoranthene exciplex with DMA in the three solvents. The fluorescence band of the exciplex was obtained by subtracting the normalized spectra at a wavelength which is not emitted by the exciplex. Table 3 also gives the value of wave number of emission band maximum $\tilde{\nu}_{max}$ and the shift $\Delta\tilde{\nu}$ of exciplex emission maximum with respect to the emission maximum of fluoranthene.

The intensity of exciplex fluorescence corresponding to emission maximum, I_E, and the intensity of fluoranthene fluorescence at 460 nm, I_F, were measured, then I_E/I_F was calculated and its value for cyclohexane was taken as unit.

Table 3

Spectrofluorimetric characteristics of fluoranthene-DMA exciplex

Solvent	ε	I_E/I_F	$\tilde{\nu}$ max (cm^{-1})	$\Delta\tilde{\nu}$ (cm^{-}
n-pentane	1.84	1.4	19600	1950
cyclohexane	2.22	1	19230	2320
ethylic ether	4.30	0.9	18340	3210

One can notice in table 3 that the value of this ratio depends on the dielectric constant of the solvent. The stability of the complex decreases with increasing ε even within a narrow range.

The intensity of fluoranthene fluorescence in cyclohexane was measured in the range 20°—60°C to evidence the influence of temperature upon quenching. It was found out that the intensity of fluorescence decreases with temperature; the intensity of exciplex fluorescence also decreases with increasing temperature, between 50° and 60° C the decrease is slower and the fluorescence maximum shifts towards smaller wavelengths. At higher temperatures the exciplex dissociates and the fluoranthene molecules may be reactivated on the singlet excited state

4. CONCLUSIONS

The Stern-Volmer quenching constant, K_{SV}, and the rate constants of quenching, k_q, were calculated from the Stern-Volmer liniar dependence. The values of these constants depend on the ionization potential of the quencher (Table 1).

Amine-quenching of fluoranthene fluorescence is a dynamic process. The k_q values are lower than the rate constants of the diffusion-controlled collision process ($k_0 = 1.24 \cdot 10^{10} M^{-1} s^{-1}$). The quenching efficiency γ was calculated from the equation :

$$k_q = \gamma k_0$$

The values obtained are listed in Table 1.

Addition of tertiary amines to the solution entails formation of a new emission band assigned to the exciplex. The fluoranthene — DMA exciplex fluorescence band was noted in low dielectric constant solvents : n-pentane, cyclohexane, ethylic ether. In ethanol, methanol and acetonitrile no fluorescence of the exciplex was noted.

As in polar solvents dealt with in literature, in this case one may consider that the encounter complex, initially formed by the excited molecule and quencher, dissociates to form a pair of solvated ions, which do not emit fluorescence. If solvation is weak or the ion pair is not stable, as in inert solvents there is no ionization and fluoranthene fluorescence quenching is followed by exciplex formation accompanied by the appearance of new fluorescence bands.

The formation and dissociation of the exciplex occurs according to the scheme :

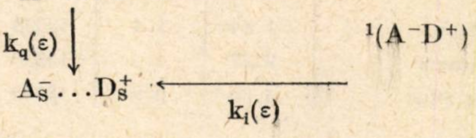

where $^1A^*$ is a fluorofor in excited singlet state, D — a quencher, k_i the rate constant of exciplex ionic dissociation (dependent on ε), k_c the rate constant of exciplex formation from the $^1A^* \ldots D$ encounter complex, k_q the rate constant of fluorescence quenching by solvated ion (dependent on ε).

The probability of exciplex formation, α, depends on ε; α decreases with increasing ε :

$$\alpha = \frac{k_c}{k_c + k_q}$$

k_e does not depend on ε, k_q increases with increasing ε. The exciplex energy $h\tilde{\nu}_{em}$ depends on ε; the exciplex fluorescence maximum shifts towards red with increasing ε, which supports the hypothesis regarding the CT character of the exciplex.

The exciplex fluorescence decreases with increasing temperature, possibly due to exciplex dissociation at higher temperatures: at higher temperature, reactivation of fluoranthene molecules on the singlet excited state becomes possible.

REFERENCES

[1] H. Leonharht, A. Weller, *Ber. Bunsenges. Phys. Chem.*, **61**, 791 (1963).

[2] J. B. Birks, "Photophysics of Aromatic Molecules", John Willey and Sons, New York, 1970, chapter IX.

[3] P. Froehlich, E. L. Wehry, "Modern Fluorescence Spectroscopy", vol. 2, ed. E. L. Wehry—Heyden, 1976, p. 319.

[4] B. Stevens, *Advan. Photochem.*, **8**, 161 (1971).

[5] A. Lablache-Combier, *Bull. de la Societé Chimique de France*, **12**, 4791 (1972).

[6] N. Orbach, R. Potashnik, M. Ottolenghi, *J. Phys. Chem.*, **76**, 1133 (1972).

[7] N. Mataga, K. Ezumi, *Bull. Chem. Soc. Japan*, **40**, 1355 (1967).

[8] H. Beens, H. Knibbe, A. Weller, *J. Chem. Phys.*, **47**, 1183 (1967).

[9] A. Weller, *Pure and Applied Chemistry*, **54** (10), 1885 (1982).

[10] A. S. Cherkasov, V. I. Shirokov, *Opt. i spectr.*, **47** (4), 689 (1979).

Revue Roumaine de Chimie, **34**, *9–10*, 1829–1833 (1989)

PERMETHYLATED DEXTRAN AS STATIONARY PHASE IN GAS CHROMATOGRAPHY

IONEL CIUCANU[a] and CONSTANTIN LUCA[b]

[a] Centre of Chemistry, Blvd. Mihai Viteazul 24, 1900 Timişoara, Romania

[b] Centre of Physical Chemistry—ICECHIM, Splaiul Independenţei 202, 77208 Bucharest, Romania

Received November 28, 1988

The testing of permethylated dextran as stationary phase for gas chromatography is described. The phase has a very good thermostability, gives a stable baseline and a high efficiency for thermolabile compounds.

INTRODUCTION

Gas chromatography uses a large variety of stationary phases such as polysiloxane, polyethers, polyesters, polyamides, polyphenylethers, etc.

Carbohydrates and their derivatives are a special class of stationary phases used in gel permeation chromatography, high resolution liquid chromatography and gas chromatography. Carbohydrates, as such, are not used as stationary phases in gas chromatography since they have a low thermostability. The esters and ethers of carbohydrates such as sucrose acetate and isobutyrate, cyclodextrines(CD)-peracetate, -perpropionate, or -perbutyrate and permethylated CD were used very much as stationary phases in gas chromatography.[1–6] Permethylated β-CD led to separation of a wide variety of structural, positional and optical isomers.[5,6] However, these stationary phases have a low thermostability. Increases in temperature can result in losses of the phase by evaporation or/and in chemical decomposition of the phase by pyrolysis. The first of these disadvantages can be eliminated by immobilization of the stationary phase on a solid support *via* several different spacer arms.[4]

This paper presents a new stationary phase for gas chromatography obtained by the permethylation of dextran. The permethylation was performed according to our methylation procedure.[8] The performance of this stationary phase was compared with that of a methyl phenyl silicone polymer (OV–17).

EXPERIMENTAL

Materials

Dextran with a molecular weight of 40.000 was obtained from Fluka (Switzerland). Dimethyl sulphoxide, methyl iodide, methyl palmitate and rhamnose were obtained from Merck (FRG).

Apparatus

The testing of stationary phase was carried out on a gas chromatograph model GCHF 18.3(DRG) modified for on-column injection and equipped with a flame ionization detector. The stationary phase was coated on Gas Chrom Q (80—100 mesh). Columns were made of Pyrex borosilicate glass tubes (0.7 m × 3.2 mm) leached with 20% HCl at 120°C for 10 hours. The carrier gas was nitrogen.

Methylation

To 50 mg dextran dissolved in 10 mL dimethyl sulphoxide was added 250 mg freshly powdered sodium hydroxide and 1 mL methyl iodide. The mixture was stirred for 10 min at 25—30°C. The permethylated dextran was isolated by addition of chloroform (8 mL) and water (20 mL) for extraction. The chloroform layer was washed with water (3 × 50 mL) and then the solvent was evaporated with a nitrogen stream.

The melting point of permethylated dextran was 260—263°C.

Immobilization of stationary phase

The stationary phase and free radical generator were dissolved in chloroform and were applied by the evaporation method on Gas Chrom Q. The free radical initiator was dicumyl peroxide in proportion of 40% from the amount of stationary phase. The immobilization was accomplished by flushing the column with a slight nitrogen stream at 140°C for 3 hours. In these conditions, we achieved a yield of 93% phase immobilization. The column was purged before use, for 2 hours at 300°C with nitrogen in order to eliminate the degradation products.

RESULTS AND DISCUSSION

The dextran is a (1 → 6)-linked α-D-glucan with about 5% of branch linkages attached to the 3-positions of the backbone.

The degree of methylation of dextran was established by acid hydrolysis, reduction and acetylation of permethylated dextran, followed by gas chromatography analysis of the products. We obtained only 2,3,4-tri-O-methyl, 1,5,6-tri-O-acetyl sorbose which indicated a full methylation of hydroxyl groups.

The thermal stability of permethylated dextran (DX-M) was evaluated by thermoanalysis and by the shape of the baseline of chromatogram in bleed rate experiments. The thermoanalysis of DX—M in an inert atmosphere shows that decomposition begins at 350°C. Deterioration of the OV—17 phase at elevated temperature results from the loss of phase by evaporation and by chemical decomposition by pyrolysis. The shape of baseline for DX—M phase (Fig. 1) shows that deterioration results primarily from chemical decomposition, because this phase has a very low viscosity. The immobilized DX—M phase gave the same baseline shape as the DX—M phase.

The polarity of DX—M phase was expressed using the Rohrschneider constants (ΔI) and was compared with that of immobilized DX—M phase (Table 1). The immobilization with dicumyl peroxide shows the least deleterious effect on the polarity of cross-linked DX—M.

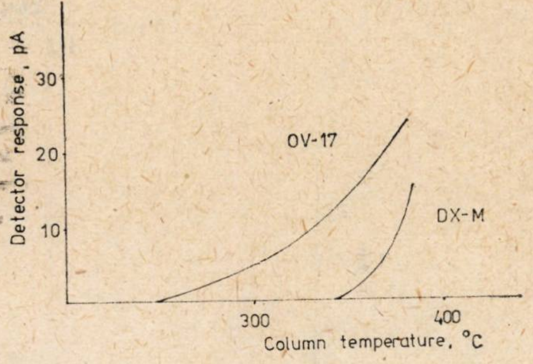

Fig. 1. — The baseline stability of chromatogram in bleed rate experiments for DX-M and OV-17 phases. Glass column (0.7m × 3 mm) with 1% stationary phase on Gas Chrom Q (80—100 mesh); temperature: to 380°C with 5°C/min; carrier gas: nitrogen at 20 mL /min (250°C).

The performances of columns with DX—M as stationary phase were evaluated by a series of van Deemter curves for methyl palmitate at 115°C and 130°C and were compared with a similar column with OV—17 as stationary phase. The van Deemter curves are a graphic representation of equation (1)

Table 1

Rohrschneider constants at 100°C for DX-M and immobilized DX-M

Solute	Rohrschneider constants (ΔI)	
	DX-M	Immobilized DX-M
Benzene	123	125
Ethanol	186	187
2-Pentanone	190	190
Nitropropane	256	258
Pyridine	210	212
$\Sigma\Delta I$	965	972

$$h = A + B/\bar{u} + (C_g + C_1)\cdot\bar{u} \qquad (1)$$

where h is the equivalent height of the theoretical plate, $\bar{u}$ is the average liniar gas velocity, and A, B, C_g and C_1 are constants.

Figure 2 shows that at lower column temperature the efficiency of separation is increased and the mobile phase optimun average velocity ($\bar{u}_{opt}$) is shifted to higher values. The curves are liniar at higher values than $\bar{u}_{opt}$ and their slopes are represented by $C_g + C_1$ constants from eq. (1). The slopes of curves I and II for DX—M phase are higher than the slope of curve III for OV$-$17 phase. Since the value of the C_g constant is the same for DX$-$M and OV$-$17 phases, these differences can only be attributed to an increase of the C_1 constant, which is defined as:

$$C_1 = \frac{2kd_f^2}{3(1+k)^2 D_1} \tag{2}$$

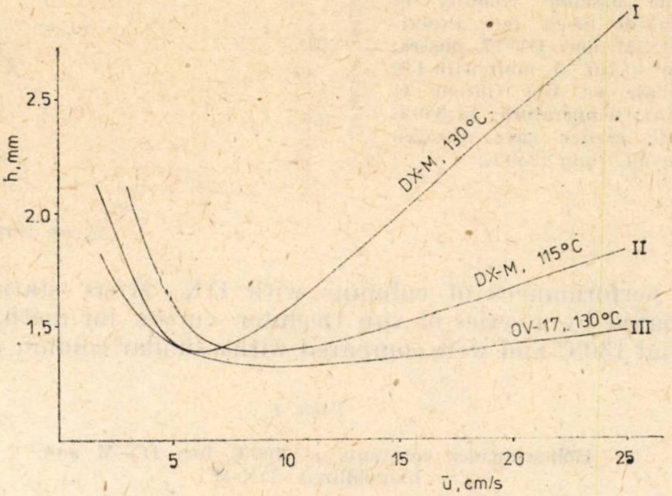

Fig. 2. — Van Deemter curves of DX-M and OV$-$17 phases at different temperatures. Curves: (I) — 130°C, DX-M (II) — 115°C, DX-M; (III) — 130°C, OV-17; glass columns (0.7 m × 3 mm) with 1% stationary phase on Gas Chrom Q (80$-$100 mesh); carrier gas: nitrogen; sample: methyl palmitate.

where k is the capacity factor, d_f is the thickness of stationary phase film and D_1 is the diffusion coefficient of solute in stationary phase. The higher value of the C_1 constant for DX$-$M phase than for OV$-$17 phase is primarily the result of decrease of D_1 term by increasing the viscosity of stationary phase in accordance with Stokes-Einstein's law. In the range of tested temperature, the DX$-$M phase is solid and its D_1 term is unmodified by temperature. For this reason, the decrease of the curve slope for DX$-$M phase at lower column temperature can only be caused by changing the capacity factor and diffusion coefficient of solute in mobile phase.

Figure 3 shows the separation of α and β isomers of permethylated rhamnose on DX$-$M and OV$-$17 phases. The isomers of permethylated rhamnose exhibit a very good peak shape and an excellent resolution on DX$-$M phase. At the same degree of separation of isomers, the retention time and separation temperature are lower on DX$-$M phase than on OV−17 phase. For these reasons, the DX−M phase is indicated for analysis of thermolabile substances.

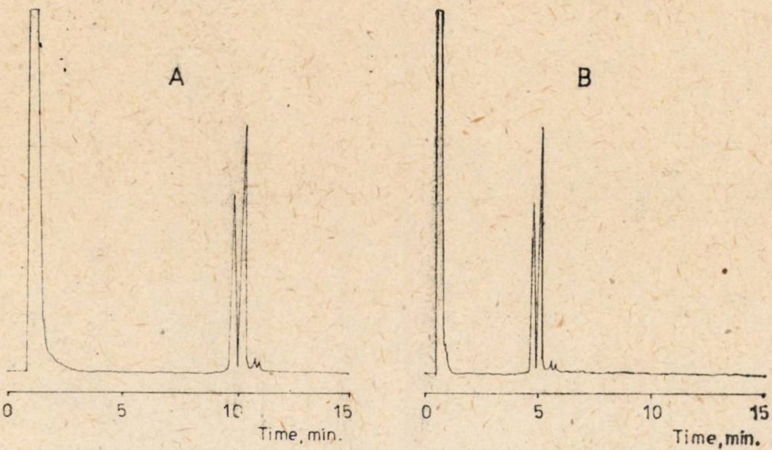

Fig. 3. — Separation of isomers of permethylated rhamnose on OV-17 (A) and DX-M (B) phases. Glass columns (0.7 m × 3 mm) with 1% stationary phase on Gas Chrom Q (80−100 mesh); carrier gas: nitrogen; column temperature: isotherm (A) — 120°C, (B) — 90°C.

REFERENCES

[1] D. M. Sand and H. Schlenk, *Anal. Chem.*, **33**, 1624 (1961).
[2] H. Schlenk, J. L. Gellerman and D. M. Sand, *Anal. Chem.*, **34**, 1529 (1962).
[3] B. Casu, M. Reggiani and C. R. Sanderson, *Carbohydr. Res.*, **76**, 59 (1979).
[4] M. Tanaka, S. Kawano and T. Shono, *Fresenius Z. Anal. Chem.*, **316**, 54 (1983).
[5] Z. Juvacz, G. Alexander and J. Szejtli, *J. High Resolut. Chromatogr. Chromatogr. Commun.*, **10**, 105 (1987).
[6] G. Alexander, Z. Juvancz and J. Szejtli, *J. High Resolut. Chromatogr. Chromatogr. Commun.*, **11**, 110 (1988).
[7] Y. Mizobuchi, M. Tanaka and T. Shono, *J. Chromatogr.*, **194**, 153 (1980).
[8] I. Ciucanu and F. Kerek, *Carbohydr. Res.*, **131**, 209 (1984).

Revue Roumaine de Chimie, **34**, *9–10*, 1835–1842 (1989)

UV-VIS-SPECTRAL BEHAVIOUR OF ARYLAZO COMPOUNDS. III*

SOLVENT EFFECTS ON THE VISIBLE ABSORPTION BAND OF 4-AMINO-SUBSTITUTED AZOBENZENES

J. EPPERLEIN, B. BLAU and U. SCHIERIG
Chemistry and Materials Science Department,
Technical University Karl-Marx-Stadt, Karl-Marx-Stadt, DDR – 9010

Received January 22, 1989

Solvent effects on $\tilde{\nu}_{max}$ values of 4-amino-substituted azobenzenes are studied and correlated with solvent polarity parameters. Impracticable correlations are found between $\tilde{\nu}_{max}$ values with functions of dielectric constant or refraction index of solvents. A comparison of spectral data with E_T scale shows a poor correlation, too. The correlations with the E_T values are significantly better if the protic solvents are excluded. Introduction of specific interaction parameters (γ values) results in good correlations of $\tilde{\nu}_{max}$ with E_T values for protic solvents. The best relationship resulted with the empirical solvent parameters π^*.

INTRODUCTION

The position of absorption maxima from azobenzenes depends on their substituents as well as on the solvent. The influence of different solvents on the absorption shift of solute organic dyes is called solvatochromism. Negative solvatochromism exists, if λ_{max} of dyes decreases with increasing solvent polarity. In case of increasing the λ_{max} of dyes with increasing solvent polarity we can speak of positive solvatochromism. The values of the absorption shifts can be very different from dye to dye. Substances with large absorption shifts depending on the solvent are used as sensors. Azo dyes show positive solvatochromism, as has already been investigated.[1–5] The solvatochromism of the following azo dyes with the present new substituents has never been published before. A quantitative description and prediction of solvent effects on these azo dyes is possible by means of correlation with various parameters of solvent polarity.

UV-VIS-spectra of 20 azobenzenes in 16 different solvents have been recorded.

---

* Part II, J. Epperlein and B. Blau, *Rev. Roumaine Chim.*, **33**, 685 (1988).

Table 1

Azo dyes, which are investigated*

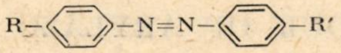

Number	R	R′
1	H	NHBz
2	Cl	NHBz
3	NO_2	NHBz
4	CH_3	NHBz
5	H	NBz_2
6	Cl	$NBzz_2$
7	NO_2	NBz_2
8	CH_3	NBz_2
9	H	NMeBz
10	Cl	NMeBz
11	NO_2	NMeBz
12	CH_3	NMeBz
13	H	NHPh
14	Cl	NHPh
15	NO_2	NHPh
16	CH_3	NHPh
17	H	NPh_2
18	Cl	NPh_2
19	NO_2	NPh_2
20	CH_3	NPh_2

UV-VIS-SPECTRA OF 4-AMINO-SUBSTITUTED AZOBENZENES IN DIFFERENT SOLVENTS

The azobenzenes listed in table 1* are measured in the solvents listed in table 2.

Unsymmetric azobenzenes in table 1 are arranged in the direction of increasing donor strength of the amino-substituents. Table 3 shows the $\tilde{\nu}_{max}$ values of the dyes from table 1 in different solvents.

The solvents are ordered in direction of increasing dielectric constant.

CORRELATION OF $\tilde{\nu}_{max}$ VALUES WITH DIELECTRIC CONSTANT, REFRACTION INDEX, DIPOLE MOMENT AND FUNCTIONS OF THESE CONSTANTS

Sheppard, Nesome and Brode [6] showed that in no case linear relations exist between solvatochromic in-

Table 2

E_T —, π^*_T —, γ-values of solvents, which are used

Number	Solvent	E_T	π^*	γ
1	n-Hexane	30.9	−0.081	0
2	Carbon tetrachloride	32.5	0.294	0
3	1,4-Dioxane	36.0	0.553	9.7
4	Toluene	33.9	0.535	4.5
5	Diethyl ether	34.6	0.273	13.0
6	Chloroform	39.1	0.760	1.5
7	Chlorobenzene	37.5	0.709	1.5
8	Acetic acid	51.2	0.664	—
9	Dichloromethane	41.1	0.802	1.5
10	Cyclohexanone	40.8	0.755	11.7
11	Ethyl-methyl-ketone	41.3	0.674	7.7
12	Ethanol	51.9	0.540	18.7
13	Methanol	55.5	0.580	18.7
14	N,N-Dimethylformamide	43.8	0.875	11.7
15	Acetonitrile	46.0	0.713	—
16	Dimethylsulphoxide	45.0	1.000	11.7

*** Note that in Table 1 Bz means benzyl and not benzoyl; the same non-standard abbreviation was used in Part I of this series, *Rev. Roumaine Chim.*, 33, 473 (1988).**

Table 3

$\tilde{\nu}$ values of azo dyes 1 — 20 in 16 solvents (10^{-3} cm^{-1})

azo dyes / solvent	1	2	3	4	5	6	7
n-hexane	26.25	25.35	22.60	26.10	25.00	24.50	21.75
carbon tetrachloride	25.75	25.20	22.10	25.35	24.70	24.20	21.55
1,4-dioxane	25.10	24.55	21.70	24.90	24.50	24.00	21.20
toluene	25.25	25.00	21.90	25.30	24.60	24.00	21.40
diethyl ether	25.25	25.00	22.00	25.25	24.70	24.20	21.50
chloroform	25.00	24.85	21.60	25.15	24.40	24.00	20.90
chlorobenzene	25.10	24.75	21.60	25.05	24.40	23.90	21.05
acetic acid	25.10	24.80	21.60	25.00	24.50	24.00	21.15
dichloromethane	24.90	24.80	21.50	25.00	24.40	23.90	20.90
cyclohexanone	24.80	24.30	21.20	24.70	24.30	23.80	20.95
MEK	24.80	24.40	21.00	24.85	24.30	23.90	21.00
ethanol	24.95	24.45	21.70	24.90	24.70	24.10	21.30
methanol	24.80	24.55	21.80	24.95	24.50	24.00	21.20
DMF	24.40	23.70	20.60	24.20	24.00	23.50	20.80
acetonitrile	24.70	24.55	21.50	24.80	24.50	23.80	21.00
DMSO	24.25	23.40	20.40	24.15	23.90	23.40	20.75

azo dyes	8	9	10	11	12	13	14
n-hexane	24.90	24.85	24.50	22.45	24.75	25.00	24.70
carbon tetrachloride	24.70	24.65	24.00	21.75	24.60	24.70	24.60
1,4-dioxane	24.70	24.35	23.75	21.40	24.25	24.40	24.40
toluene	24.65	24.40	23.80	21.45	24.30	24.65	24.65
diethyl ether	24.75	24.70	23.95	21.65	24.70	24.60	24.60
chloroform	24.30	24.10	23.50	20.70	24.30	24.25	24.25
chlorobenzene	24.40	24.20	23.65	20.85	24.10	24.45	24.45
acetic acid	24.60	24.55	23.80	21.15	24.30	24.40	24.40
dichloromethane	24.25	24.25	23.30	20.65	24.15	24.15	24.40
cyclohexanone	24.35	24.15	23.60	20.55	23.90	24.20	23.70
MEK	24.45	24.25	23.50	20.75	24.10	24.20	23.80
ethanol	24.65	24.60	23.85	21.10	24.30	24.25	23.80
methanol	24.60	24.40	23.75	21.00	24.30	24.35	23.80
DMF	24.10	24.85	23.20	20.30	23.70	23.90	23.10
acetonitrile	24.40	24.25	23.70	20.70	24.05	24.40	24.10
DMSO	24.00	24.05	23.00	20.05	23.55	23.80	22.80

azo dyes / solvent	15	16	17	18	19	20
n-hexane	23.00	24.80	24.95	24.25	21.50	24.35
carbon tetrachloride	22.50	25.00	24.55	24.05	20.90	24.30
1,4-dioxane	21.80	24.40	24.25	23.90	20.90	24.10
toluene	22.10	24.90	24.30	23.90	21.00	24.20
diethyl ether	21.70	24.80	24.50	23.95	21.10	24.30
chloroform	22.00	24.90	24.15	23.40	20.40	24.00
chlorobenzene	21.80	24.70	24.10	23.65	20.60	24.05
acetic acid	21.70	24.60	24.20	23.75	20.80	24.15
dichloromethane	21.90	24.60	24.10	23.30	20.30	24.00
cyclohexanone	20.90	24.10	24.10	23.45	20.40	24.00
MEK	21.30	24.40	24.15	23.60	20.30	24.00
ethanol	20.90	24.10	24.20	23.85	20.85	23.90
methanol	21.20	24.10	24.15	23.80	20.80	23.85
DMF	20.50	23.70	24.05	23.25	20.20	23.90
acetonitrile	21.70	24.50	24.10	23.60	20.60	24.10
DMSO	20.30	23.10	23.75	22.95	20.00	23.55

fluence on the colour-giving band and refraction index or dipole moment of the solvent.

The dielectric constant also does not correlate with the shift of the absorption maxima.[7] Functions or combinations of these physical constants also do not prove better results.

CORRELATION OF $\tilde{\nu}_{\max}$ VALUES WITH E_T VALUES OF REICHHARDT AND DIMROTH [11]

Between the empirical parameter E_T[12] and the $\tilde{\nu}_{\max}$ values exist correlations in form of equation 1 :

$$\tilde{\nu}(E_T) = \tilde{\nu}_0 + rE_T \tag{1}$$

The slope of E_T values is proportional to the sensitivity of the dye in comparison with the solvent polarity. $\tilde{\nu}_0$ is equivalent to the absorption maximum of the azo dye for $E_T = 0$. The results of this correlation are given in Table 4. The correlation coefficient amounts to 0.90 on average. Figure 1 demonstrates that four protic solvents must be neglected in this correlation. Introduction of specific interaction parameters for protic solvents are necessary. The best correlations are obtained with equation 2 :

Table 4

Results of correlation between $\tilde{\nu}_{\max}$ values and E_T values in form of equation (1) for 12 solvents

Dye number	$\tilde{\nu}_0 \cdot 10^3$ cm^{-1}	r	R
1	28752	−0.096	0.816
2	28967	−0.115	0.888
3	26614	−0.134	0.959
4	28948	−0.104	0.901
5	26 863	−0.064	0.956
6	26228	−0.060	0.917
7	23924	−0.073	0.955
8	26517	−0.054	0.902
9	25606	−0.033	0.688
10	26114	−0.065	0.939
11	25978	−0.131	0.960
12	26771	−0.067	0.848
13	27206	−0.075	0.982
14	28025	−0.105	0.826
15	27533	−0.155	0.890
16	28741	−0.109	0.837
17	25765	−0.040	0.864
18	26714	−0.081	0.973
19	24213	−0.094	0.960
20	25425	−0.035	0.955

$$\tilde{\nu}_{\max}(E_T) = \tilde{\nu}_0 + r' \cdot E_T + t\gamma \tag{2}$$

where γ is a specific interaction parameter.[13] Table 5 shows the results of this correlation. The correlation coefficient R amounts to 0.93 on average. Acetonitrile and acetic acid are excluded, because γ values are not available.

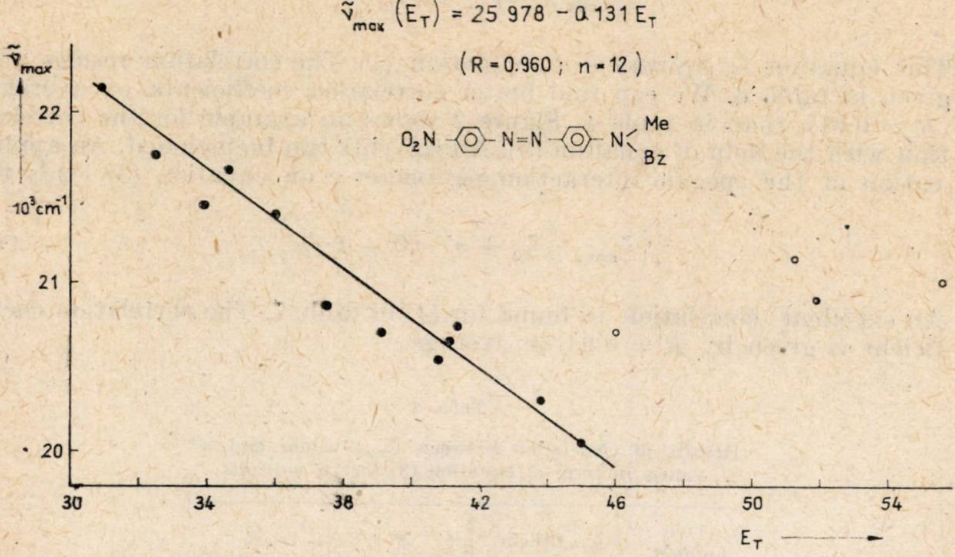

Fig. 1. — Plot of correlation of $\tilde{\nu}_{max}$ values with E_T — values of Reichhardt and Dimroth for azodye number 11.

Table 5

Results of correlation between $\tilde{\nu}_{max}$ values and E_T values in form of equation (2) for 14 solvents

Dye number	$\tilde{\nu}_0 \cdot 10^3$ cm^{-1}	r'	t	R
1	28583	−0.084	−0.047	0.942
2	28645	−0.120	−0.029	0.916
3	26439	−0.127	−0.016	0.966
4	28641	−0.091	−0.028	0.932
5	26831	−0.063	−0.003	0.957
6	26172	−0.058	−0.005	0.920
7	24137	−0.081	0.009	0.970
8	26619	−0.059	0.014	0.949
9	26213	−0.052	0.011	0.832
10	26197	−0.065	0.011	0,961
11	26077	−0.136	0.016	0.963
12	26760	−0.067	−0.002	0.848
13	27172	−0.073	−0.003	0.983
14	27543	−0.086	−0.044	0.893
15	26813	−0.126	−0.065	0.965
16	28168	−0.087	−0.044	0.923
17	25816	−0.043	0.007	0.884
18	26865	−0.087	0.012	0.987
19	24393	−0.101	0.016	0.974
20	25476	−0.037	0.004	0.963

CORRELATION OF $\tilde{\nu}$ VALUES WITH π^* VALUES OF KAMLET[4]

The relation between $\tilde{\nu}_{\max}$ values and π^* values results in the formula

$$\tilde{\nu}_{\max} = \tilde{\nu}_0 + s \cdot \pi^* \tag{3}$$

This equation is equivalent to equation (1). The correlation results are given in table 6. We can find better correlation coefficients, on average ($R = 0.91$), than in table 4. Figure 2 shows an example for the correlation with the help of equation (3). All solvents can be included. An application of the specific interaction parameter γ on equation (3) leads to

$$\tilde{\nu}_{\max} = \tilde{\nu}_0 + s' \cdot \pi^* + t \cdot \gamma \tag{4}$$

An excellent correlation is found for (4) in table 7. The correlation coefficient is given by $R = 0.94$ on average.

Table 6

Results of correlation between $\tilde{\nu}_{man}$ values and π^* values in form of equation (3) for 16 solvents

Dye number	$\tilde{\nu}_0 \cdot 10^3\ \mathrm{cm}^{-1}$	S	R
1	26070	−1.813	0.925
2	25530	−1.678	0.852
3	22692	−1.953	0.898
4	25920	−1.656	0.936
5	25010	−0.933	0.926
6	24498	−0.909	0.915
7	21789	−0.063	0.959
8	25127	−1.011	0.885
9	25006	−1.122	0.985
10	24381	−1.143	0.876
11	22406	−2.278	0.923
12	25109	−1.494	0.962
13	24985	−1.033	0.917
14	24851	−1.547	0.814
15	22853	−2.281	0.841
16	25546	−1.748	0.890
17	24726	−0.809	0.941
18	24351	−1.043	0.911
19	21494	−1.369	0.923
20	24391	−0.482	0.922

CONCLUSIONS

All correlation between $\tilde{\nu}_{max}$ values and E_T- or π^*-values provide the same conclusions: donor-acceptor-substituted azobenzenes have the greatest solvent sensitivity especially the azo dyes with NO_2-groups.

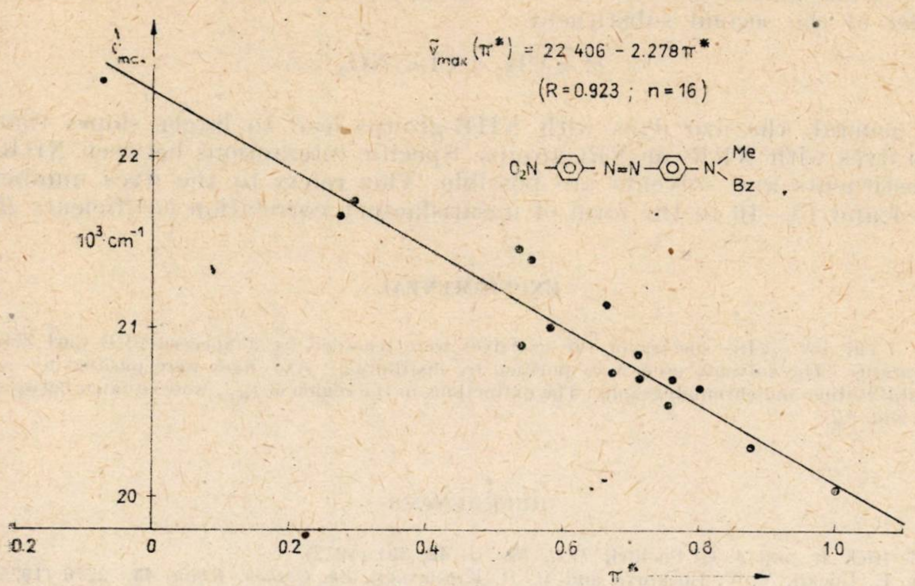

Fig. 2. — Graphical representation of the linear regression equation (3) for azo dye number 11.

Table I

Results of correlation between $\tilde{\nu}_{max}$ values and π^* values in form of equation (4) for 16 solvents

Dye number	$\tilde{\nu}_0 \cdot 10^3$ cm^{-1}	s'	t	R
1	26160	−1.355	−0.035	0.938
2	25602	−1,640	−0.016	0.903
3	22669	−2.041	−0.004	0.911
4	26036	−1.637	−0.017	0.955
5	25014	−0.935	−0.002	0.933
6	24507	−0.901	−0.002	0.922
7	21775	−1.077	0.003	0.962
8	25065	−1.008	0.006	0.922
9	24976	−1.134	0.004	0.995
10	24362	−1.192	0.003	0.924
11	22553	−2.344	−0.015	0.960
12	25096	−1.537	0,002	0.984
13	25025	−1.027	−0.008	0.946
14	24931	−1.521	−0.018	0.887
15	23088	−2.042	−0.050	0.956
16	25650	−1.473	−0.030	0.949
17	24757	−0.823	−0.003	0.974
18	24287	−1.090	0.005	0.927
19	21443	−1.425	0.008	0.945
20	24391	−0.503	0.000	0.945

For some amino-substituents the sensitivity increases in the following order of the second substituent:

$$H < CH_3 < Cl < NO_2$$

In general, the azo dyes with NHR-groups lead to larger slopes than azo dyes with NRR′ or NR_2 groups. Specific interactions between NHR-substituents and solvents are possible. This refers to the dyes number 1—4 and 13—16 in the form of unsatisfactory correlation coefficients *R*.

EXPERIMENTAL

The UV—VIS—spectra of the azo dyes were recorded by a Specord-VEB Carl Zeiss apparatus. The solvents used were purified by distillation. Azo dyes were purified by recrystallisation and chromatography. The extinctions in the region of λ_{max} were situated between 0.8 and 1.2.

REFERENCES

[1] G. Irick Jr. and J. G. Pacifici, *Text, Res. J.* **42**, 391 (1972).
[2] A. E. Luckij, V. V. Bocarova and M. R. Kreslavskij, *Zh. Obshch. Khim.* **45**, 2276 (1975).
[3] H. Mustroph and J. Epperlein, *J. prakt. Chem.* **322**, 305 (1980).
[4] C. Reichhardt, "Solvents and Solvent Effects in Organic Chemistry", Verlagsgesellschaft, Weinheim 1988.
[5] S. Hünig and K. Requardt, *Liebigs Ann. Chem.*, **592**, 180 (1955).
[6] S. E. Sheppard and P. T. Nersome, *J. Am. Chem. Soc.*, **64** 2937 (1943).
[7] W. R. Brode, H. J. Gould and G. H. Wymann, *J. Am. Chem. Soc.*, **75**, 1856 (1953).
[8] E. G. McRae, *J. Phys. Chem.* **61**, 562 (1957).
[9] N. Mataga, Y. Torihashi and K. Ezumi, *Theor. Chim. Acta* **2**, 158 (1964).
[10] F. W. Fowler, A. R. Katritzky and R. J. D. Rutherford, *J. Chem. Soc., B* 460 (1971).
[11] K. Dimroth, C. Reichhardt, T. Siepmann and F. Bohlmann, *Liebigs Ann. Chem.* **661** 1 (1963).
[12] C. Reichhardt and K. Dimroth, *Fortschr. Chem. Forsch.* **11**, 1 (1968).
[13] G. J. Breatley and M. Kasma, *J. Am. Chem. Soc.*, **77**, 4462 (1955).

Revue Roumaine de Chimie, 34, *9–10*, 1843–1847 (1989)

WORK FUNCTION AND ELECTRON IMPACT DESORPTION STUDIES ON CO/W ADSORPTION STATES

ANTONINA GUŢU and M. VASS
ICECHIM — Centre of Physical Chemistry, Spl. Independenţei 202, Bucharest 79611, Romania

Received September 19, 1988

Electron impact desorption and work function change measurements were used to study the adsorption of carbon monoxide on tungsten. Appearance of a "mixed α-CO state", characterized by the simultaneous formation of α-CO state and a high temperature β-CO state is discussed. The formation of the "mixed α-CO state" is accompanied by a negative work function variation and accordingly, by the appearance of electropositive layers on the tungsten surface. A lying down binding state is proposed for the high temperature β-CO state.

INTRODUCTION

The great number of studies concerning the CO/W system, using different methods, [1–12] is a sign of the interest shown to this system, not for catalytic reasons, tungsten not being a catalyst for CO reactions, but for modelling real cases.

The carbon monoxide molecule offers the possibility of different binding states on the tungsten surface depending on the adsorption temperature.

We present in this paper the results obtained in the work function and electron impact desorption studies on the interaction between CO and tungsten.

EXPERIMENTAL

The electron impact desorption (EID) and work function (WF) measurements were performed at room temperature, in a cell of Redhead type [13] connected to a conventional ultra-high vacuum system.

The polycrystalline tungsten ribbon was cleaned in a usual way, by heating under low residual pressure ($10^{-8}-10^{-9}$ torr). Temperatures up to 2473 K were measured indirectly by monitoring the electrical resistance of the tungsten ribbon and by using a conversion curve $\rho - T$ reported in literature [14].

RESULTS AND DISCUSSION

(a) Work function variations

The work function variations induced by successive introductions of gas doses were monitored by the diode method.

The work function change values were calculated both from the current — voltage curves displacements in their linear region ($\Delta\Phi_1$) and from the semilogarithmic, $\ln I = f(V)$, displacements in the retarding field range ($\Delta\Phi_2$).

The results obtained by these two modes of estimating the work function changes with the adsorption dose led to similar values, as seen in Table 1.

Table 1

Work function changes in CO/W system as a function of exposure time

Partial adsorption dose (L)	120	60	60	60	60	60	180	180	180
Total adsorption dose (L)	120	180	240	300	360	420	600	780	960
$\Delta\Phi_1(V)$	-0.16	-0.26	-0.425	-0.56	-0.63	-0.66	-0.70	-0.76	-0.85
$\Delta\Phi_2(V)$	-0.15	-0.26	-0.40	-0.56	-0.64	-0.685	-0.69	-0.75	

The maximum value of the work function change was -0.85 V. The negative value of $\Delta\Phi$ indicates the formation of an electropositive layer. It is well known[15–18] that this type of variation characterizes the formation of the $\alpha-$CO state.

Plotting the work function change as a function of CO adsorption dose, a fast linear increase is observed until -0.63 V, followed by a slow increase reaching a limiting value. This behaviour suggests the appearance of two binding states of CO adsorbed on the tungsten surface.

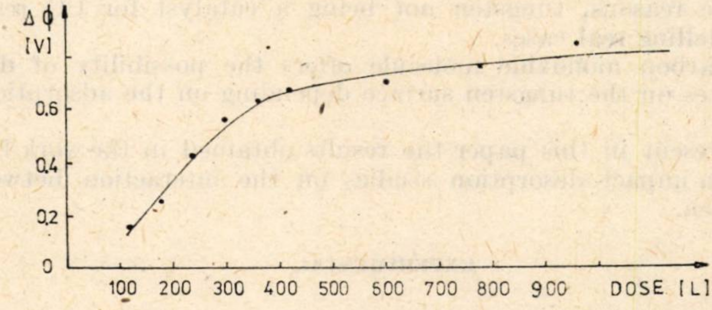

Fig. 1. — Tungsten surface work function variation on CO adsorption at room temperature.

It has also been observed that the formation of the electropositive layers takes place only when a CO adsorption occurs on a surface heated at 1073 K. When the surface heating exceeds 1473 K, CO adsorption on tungsten leads to the formation of an adsorbed electronegative layer, involving a work function change of $+0.74$ V.

(b) The Evaluation of Electron Impact Desorption Parameters

Further information regarding the number and the nature of the binding states formed upon CO adsorption on tungsten surfaces heated at 1073 K were obtained by the EID technique.

In order to identify the CO binding states, a study of the desorbed ion energy distribution was performed. Two peaks were observed (Fig. 2) at retarding potentials of 2 V and 6.25 V, respectively.

Fig. 2. — Ion energy distribution for species desorbed from CO/W system (i_a = 20 μA, a_x = 2.5 V/cm, a_y = 0.25 V/cm).

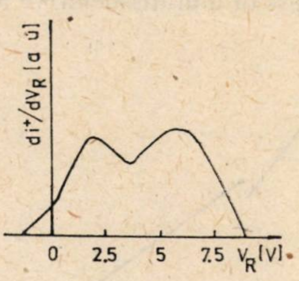

These results are in good agreement with data existing in the literature concerning the formation of two CO absorption species on the tungsten surface: a weak bound one (α—CO) and a strong bound one (β—CO).

The electron bombardment of a tungsten surface precovered with adsorbed CO leads to an increase of the peak height observed at 6.5 V, coupled with a decrease of the peak appearing at 2 V. This suggests, in our opinion, that the desorption process of the weak bound state, α—CO, is accompanied by its partial conversion to the tight bound state, β—CO (Fig. 3). The electron impact study gave qualitatively similar results on the polycrystalline and single crystal (110) [18] substrates examined so far.

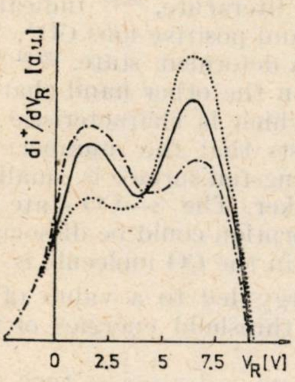

Fig. 3. — Ion energy distribution for species desorbed from CO/W system: — · — after an exposure of 90 L CO; ——— after an electron bombardment at i_a = 70 μA for 14 s. ooo after an electron bombardment at i_a = 70 μA for 28 s. showing the conversion of α-CO form in β-CO form.

Following the variation in time of the concentration of the adsorbed species at constant electron bombardment current, the ionisation cross-sections can be evaluated by the equation:

$$Q_j = \frac{\ln i^+}{t} \cdot \frac{A \cdot \varepsilon}{i_a}$$

The time dependence of the ion current for the desorbed species ($\ln i^+ = f(t)_{i_a = ct}$) in the system CO/W, shown in Fig. 4, leads to two cross-sections, evaluated as $Q_1 = 6.2 \times 10^{-18}$ cm² and $Q_2 = 2.78 \times 10^{-18}$ cm², meaning that the state corresponding to Q_2 is stronger bound than the state characterized by Q_1.

The binding state α—CO present on surface until 400 K, corresponds to a process of non-dissociative adsorption of CO. This has been proved by

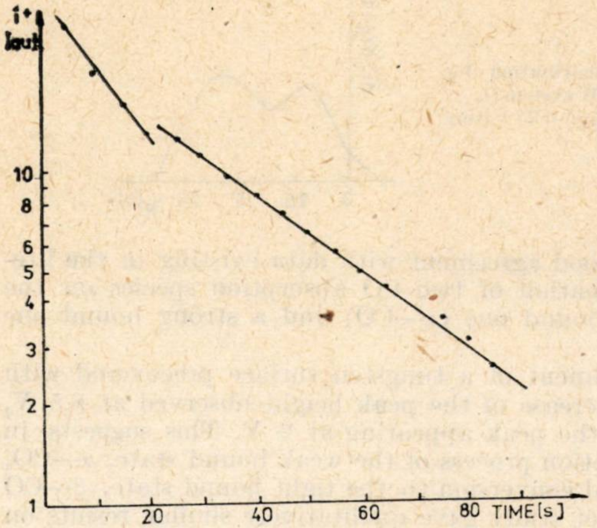

Fig. 4. — The plot of time dependence of the desorbed ion current $\ln i^+ = f(t)_{i_a = \mathrm{ct}}$ for the system CO/W.

the isotope mixing experiments reported in literature, [16,19] indicating the formation of both neutral molecules of CO and positive ions CO^+. The CO molecule adsorbed in this case is not in a deformed state. [20,21] The IR studies reported by Yates at al. [9,10] show on the other hand that α—CO state has a frequency band in a region which is characteristic for the triple bond of CO. The triple bond suggests that the number of electrons shared by the CO molecule and the tungsten surface is smaller and, consequently, the gas — metal bond is weaker. The β—CO state releases instead only O^+ ions, meaning that the adsorption could be dissociative or in a bridge position, when the C — O bond in the CO molecule is weaker.

Measurements of the threshold energy led to a value of 16 eV, which is an average value of the known threshold energies of two CO adsorption states on tungsten.

Since the CO adsorption on tungsten-ribbon heated at 1073 K leads always to negative work function changes and the EID parameters have underlined the formation of two distinct binding states we propose the term "mixed α—CO". This is a mixture of α—CO and β—CO states obtained by a readsorption process at 300 K on a surface heated previously at 1073 K.

For the β—CO state we suggest that the formation of lying down bound CO molecule on tungsten is likely. This model is supported by the observation that a surface blockage with carbon takes place in time on repeated cycles of adsorption-desorption steps.

CONCLUSIONS

The results obtained by electron impact desorption and work function studies on CO/W system could be summarized as follows :

— CO adsorption on tungsten surface, heated at 1073 K, yields to a state labelled "mixed — α—CO" ;

— this state is characterized by the formation of electropositive layers ;

— the "mixed—α—CO" state represents a mixture of α—CO and β — CO states.

REFERENCES

[1] G. Ehrlich, *J. Chem. Phys.*, **34**, 39 (1961).
[2] P. A. Redhead, *Trans. Faraday Soc.*, **57**, 641 (1961).
[3] B. J. Hopkins and S. Usami, *Suppl. Nuovo Cimento*, **5**, 483 (1967).
[4] R. A. Armstrong, *Canad. J. Phys.*, **46**, 949 (1968).
[5] J. W. May and L. H. Germer, *J. Chem. Phys.*, **44**, 2995 (1966).
[6] J. M. Baker and D. E. Eastman, *J. Vac. Sci. Technol.*, **10**, 223 (1973).
[7] P. L. Young and R. Gomer, *Phys. Rev. Letters*, **30**, 955 (1972).
[8] J. W. Gadzuk and E. W. Plummer, *Rev. Mod. Phys.*, **45**, 487 (1973).
[9] J. T. Yates and D. A. King, *Surface Sci.*, **30**, 601 (1972).
[10] J. T. Yates, R. G. Groenler, I. Ratajczykova and D. A. King, *Surface Sci.*, **36**, 739 (1973) .
[11] P. A. Redhead, *Appl. Phys. Letters*, **4**, 166 (1964).
[12] D. Menzel and R. Gomer, *J. Chem. Phys.*, **41**, 3311 (1964).
[13] P. A. Redhead, *Suppl. Nuovo Cimento*, **5**, 586 (1967).
[14] Landolt — Börnstein, Springer Verlag, vol. 2, (1964).
[15] D. Menzel, *Ber. Bunsenges. Physick Chem.*, **72**, 591 (1968).
[16] T. Engel and R. Gomer, *J. Chem. Phys.*, **50**, 2428 (1969).
[17] R. Gomer, *Japan. J. Appl. Phys. Suppl.* 2, Pt. 2, (1974).
[18] C. Leung, M. Vass, and R. Gomer, *Surface Sci.*, **63**, 67 (1977).
[19] I. G. Newsham, J. V. Hogue and D. R. Sandstrom, *J. Vac. Sci. Tehnol.*, **9**, 596 (1972).
[20] A. E. Bell and R. Gomer, *J. Chem. Phys.*, **44**, 1065 (1966).
[21] C. Kort and R. Gomer, *Surface Sci.*, **40**, 71 (1973).

Revue Roumaine de Chimie, **34**, *9–10*, 1849–1856 (1989)

MERCURY DETERMINATION IN WATER AND ATMOSPHERE AT CONCENTRATIONS LOWER THAN PARTS PER BILLION

CONSTANTIN LUCA, ANDREI DĂNEȚ and CORNEL RADU
Department of Analytical Chemistry, Faculty of Technological Chemistry,
Polytechnic Institute, Bucharest, Splaiul Independenței 313, 77206

Received March 31, 1989

The working parameters have been established for two methods of concentrating the mercury from water with a mercury content of the order of 10^{-11} g Hg/mL. The mercury concentration was carried out by reduction on copper powder and electrodeposition on a copper wire. After being concentrated, mercury was thermally desorbed and then determined by atomic absorption by means of an experimental apparatus described in a previous paper. The same apparatus was also employed for concentration and direct determinations of mercury at concentrations of ng/m^3 in air. The proposed methods for concentrating mercury in water are quite simple as they need only a minimum of equipment because concentration can be done immediately after sampling, even on the spot, thus avoiding both contamination and also mercury losses from samples.

There is a natural background concentration of mercury in surface water, atmosphere and soil (generally in the environment) which has increased steadily in the last decades due to the human activities, such as mercury utilization in industry, agriculture and medicine, as well as due to the increase of fuel consumption.[1]

The presence of mercury in water and air is very damaging even at low concentrations because this element can be accumulated by a series of trophic chains in living beings and has also the property to be transformed through biochemical processes into methylmercury which is utterly toxic.[2,3] For all these reasons, very sensitive analytical methods are necessary for mercury determination at concentrations close to the natural background concentration.

Among the proposed methods, the flameless atomic absorption spectrophotometry is the most suitable for the trace determination of mercury as it has been established in many other studies.[4–16]

The above-mentioned method is sensitive as it allows for measuring concentrations of the order of ng/ml. To analyse samples with a lower mercury content, a prior increase of concentration is necessary.

An important factor which leads to errors in mercury determination at very low concentrations is sampling and sample storage, due to important losses in mercury by volatilization, adsorption through the vessel walls and on suspension, etc.[17,18] Therefore, it is appropriate either to anlyse the sample immediately or to concentrate the mercury by a suitable method as soon as possible after sampling.

A series of methods are presented in literature on the subject of mercury concentration in water by using active charcoal,[19] ion-exchanging resins[20] or by reduction on metals.[21,22] The mercury in the air is concentrated mainly by amalgamation with gold and silver.[23,24]

In the present work we present a study concerning the mercury concentration and determination from water and air at the very limit of parts per billion.

The mercury from water was concentrated by reduction on copper powder as well as electrodeposition on a copper wire. The mercury thus concentrated was then determined by means of a set up previously described in an invention patent.[25]

The mercury from the air was concentrated by using an adsorbent included in the mercury determination set up.

EXPERIMENTAL PART

Reagents and apparatus

100 μg/ml titre mercury chloride solution.

99.99% copper powder (Serva) and 0.3 mm diameter copper wire.

P.a. reagent grade nitric, sulphuric (Merck) and perchloric (U.C.B.) acids.

All solutions and synthetic samples were prepared with tri-distilled water.

The copper powder for mercury retention was introduced in glass tubes of 3 mm inner diameter and 40 mm length. In order to remove any trace of mercury left behind, the tubes were heated for two hours at $\sim$350°C. The copper layer was located at the middle of the tube between two silica wool plugs. The tube was again heated for two hours at 350°C.

The mercury electrodeposition was studied by using a d.c. source of 3V and 1A. The analysis after mercury concentration on copper was carried out by means of the apparatus built at the Department of Analytical Chemistry, Faculty of Chemical Technology, Polytechnic Institute Bucharest and Center of Physical Chemistry, Institute of Chemical Research,[25] coupled to an AAS-1N, Carl Zeiss atomic absorption spectrophotometer. The mercury determination was based on sample calcination in air current and selective retention of the resulted mercury vapor, the latter being then desorbed and analyzed by atomic absorption.

The block-scheme of the apparatus is shown in Fig. 1.

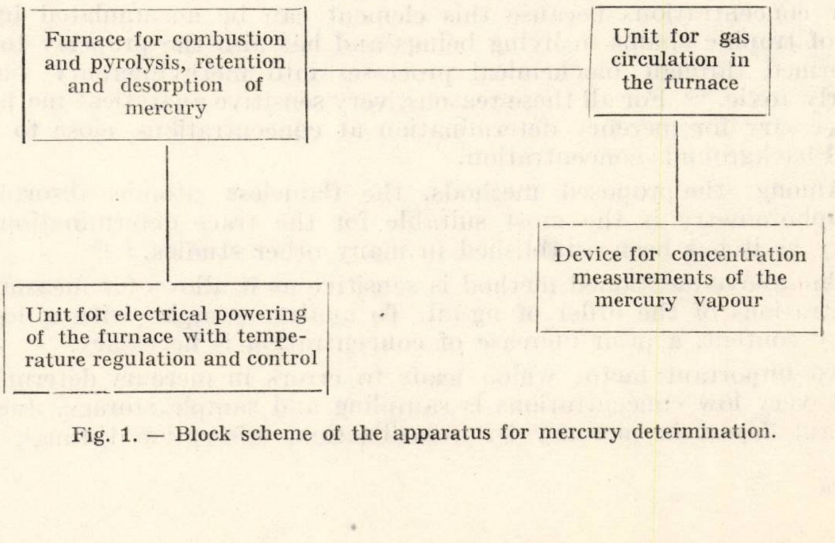
Furnace for combustion and pyrolysis, retention and desorption of mercury
Unit for gas circulation in the furnace
Device for concentration measurements of the mercury vapour
Unit for electrical powering of the furnace with temperature regulation and control

Fig. 1. — Block scheme of the apparatus for mercury determination.

In Fig. 2, a calibration curve for mercury determination is presented.

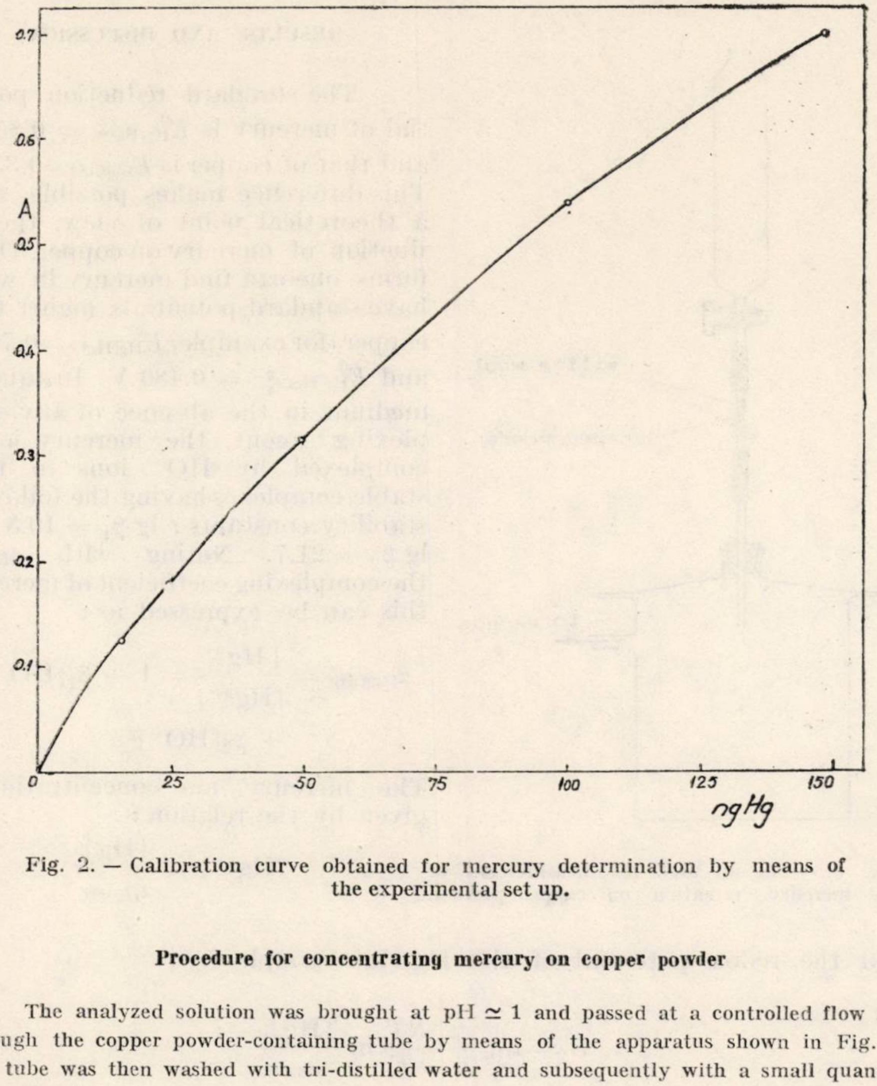

Fig. 2. — Calibration curve obtained for mercury determination by means of the experimental set up.

Procedure for concentrating mercury on copper powder

The analyzed solution was brought at pH $\simeq 1$ and passed at a controlled flow rate through the copper powder-containing tube by means of the apparatus shown in Fig. 3. The tube was then washed with tri-distilled water and subsequently with a small quantity of methanol.

The copper powder was removed from the tube with a glass stick and introduced directly into the cuvette employed for mercury determination.

Procedure for concentrating mercury by electrodeposition on copper

The mercury electrodeposition was performed on a cathode made of a bundle of 0.30 mm diameter copper wire with a total surface area of approximately 1000 mm^2, using an anode made of platinum wire of 0.5 mm diameter and 2 cm length. The mercury electrodeposition was studied under continuous stirring of the solution. The anylyzed sample was acidulated in order to ensure the solution conductivity. After mercury electrodeposition, the copper wire bundle was washed with tri-distilled water and then introduced into the measurement cuvette.

RESULTS AND DISCUSSION

The standard reduction potential of mercury is $E^0_{Hg/Hg^{2+}} = 0.854$ V and that of copper is $E^0_{Cu/Cu^{2+}} = 0.337$V. This difference makes possible, from a theoretical point of view, the reduction of mercury on copper. Other forms one can find mercury in water have standard potentials higher than copper (for example, $E^0_{Hg/Hg^{2+}} = 0.793$ V and $E^0_{Hg/HgCl_4^{2-}} = 0.480$ V). In aqueous medium, in the absence of any complexing agent, the mercury ion is complexed by HO^- ions to form stable complexes having the following stability constants : lg $\beta_1 = 10.3$ and lg $\beta_2 = 21.7$. Noting with $\alpha_{Hg(OH)}$ the complexing coefficient of mercury, this can be expressed as :

$$\alpha_{Hg(OH)} = \frac{[Hg]_t}{[Hg^{2+}]} = 1 + \beta_1[HO^-] + \beta_2[HO^-]^2$$

The mercury ion concentration is given by the relation :

$$[Hg^{2+}] = \frac{[Hg]_t}{\alpha_{Hg(OH)}}$$

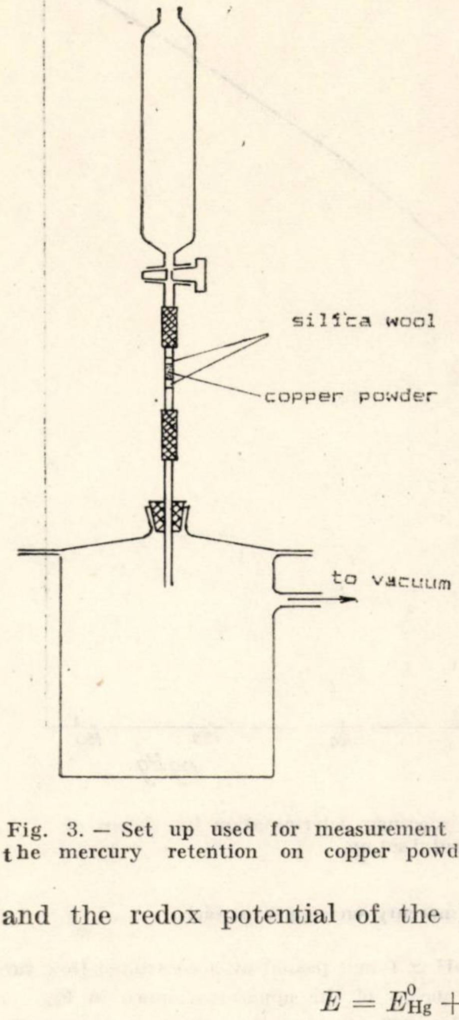

Fig. 3. — Set up used for measurement of the mercury retention on copper powder.

and the redox potential of the Hg/Hg^{2+} couple by :

$$E = E^0_{Hg} + \frac{RT}{nF} \ln \frac{[Hg]_t}{\alpha_{Hg(OH)}}$$

Taking into account the standard potentials of the two systems as well as the $\alpha_{Hg(OH)}$ coefficient, it results that theoretically, mercury can be quantitatively reduced on copper to a concentration of $10^{-10.3}$ M at pH =1 and only to $10^{-9.8}$ M at pH = 7.

The above finding determined us to undertake studies concerning mercury retention by reduction on copper powder in acid medium, when the formation of the mercury hydroxocomplexes is regressed.

The flow rate of the liquid passing through the column with cooper powder varied between 0.5 and 8 ml/min.

When we worked with a copper layer height of 5 mm and synthetic samples of 100 ml at pH = 1 containing 100 pg Hg/ml, mercury was retained quantitatively for all these values. Subsequent measurements were carried out at a flow rate value of 5 ml/min. The height of the copper layer was varied between 2 and 20 mm (0.04–0.4 g copper powder). While working with a synthetic sample of 100 ml at pH = 1 which contains 100 pg Hg/ml and at a liquid flow rate of 5 ml/min, we observed that the mercury is practically quantitatively retained for the minimum value of the copper layer height as well as for the maximum one. Subsequent measurements were made for a copper layer height of 5 mm. Our results are in good agreement with some data reported in literature on mercury reduction with copper powder. [21]

The experimental results obtained for mercury determination after its concentration by reduction on copper powder are listed in Table 1. A series of synthetic samples as well as a surface water have been analyzed.

Table 1

Experimental results for mercury determination after its concentration by reduction on copper

No.	Sample	pH	Determined mercury concentration	Observations
1	100 ml tridistilled water + 1 ml 20% $HClO_4$.	2	430 ng/ml 450 ng/ml 420 ng/ml	Mercury concentration determined in 20% $HClO_4$
2	100 ml tridistilled water + 0.3 ml 98% H_2SO_4.	1	30 ng/ml 25 ng/ml 31 ng/ml	Mercury concentration determined in 98% H_2SO_4
3	100 ml tridistilled water + 0.3 ml 98% H_2SO_4 + 100 ng Hg.	1	1.04 ng/ml 0.98 ng/ml 1.06 ng/ml	Values determined after deducing the amount of mercury introduced with H_2SO_4
4	300 ml surface water + 50 ng Hg + 0.9 ml 98% H_2SO_4	1	226 pg/ml 214 pg/ml 229 pg/ml	Values determined after deducing the amount of mercury introduced with H_2SO_4 After deducing 50 ng Hg initially introduced, the following mercury concentrations were determined in the surface water : – 60 pg/ml – 48 pg/ml – 63 pg/ml.
5	300 ml surface water + 0.9 ml 98% H_2SO_4.	1	75 pg/ml 62 pg/ml 60 pg/ml	Values determined after deducing the amount of mercury introduced with H_2SO_4.

The yield variation of the mercury electrodeposition is presented in Fig. 4 as a function of the electrolysis time. A quantity of 50 ng Hg contained in 100 ml volume of 1.25 M nitric acid solution was employed. A practically quantitative mercury deposition was noticed over a time interval of 90 min. The solution acidity does not influence the mercury electrodeposition within the 0.1–0.5 M HNO_3 range.

Table 2 presents the experimental results obtained for mercury determination in synthetic samples with known amounts of mercury and in surface water. In all cases, the mercury electrodeposition was carried out for two hours.

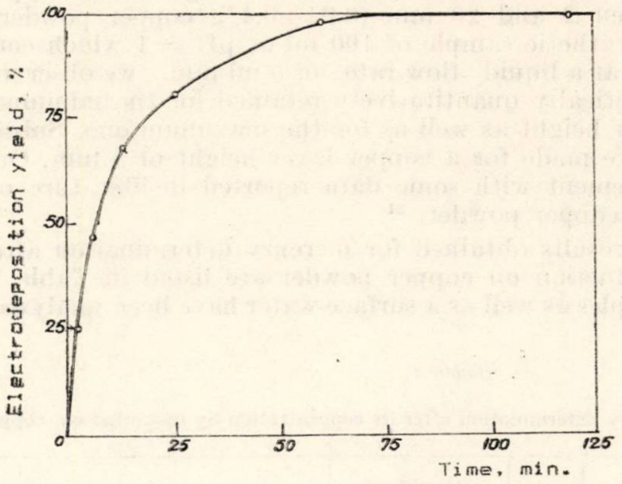

Fig. 4. – Variation of the mercury electrodeposition yield as a function of the electrolysis time.

In order to determine the mercury in air, a known volume of air (which was not previously purified) was passed over the adsorbent which specifically retains mercury and which is contained in the experimental

Table 2

Experimental results for mercury determination after its concentration by electrodeposition on copper

No.	Sample	Mercury concentration	Observation
1	100 ml tridistilled water + 1.5 ml 67% (0.24 M) HNO_3	16 pg/ml 18 pg/ml 16 pg/ml	Mercury concentration determined in 67% HNO_3.
2	100 ml surface water + 25 ng Hg + 1.5 ml 67% HNO_3.	0.31 ng/ml 0.33 ng/ml 0.32 ng/ml	Values determined after deducing the amount of mercury introduced with HNO_3. After deducing 25 ng Hg initially introduced in the surface water, the following mercury concentrations were determined : — 60 pg/ml — 80 pg/ml — 70 pg/ml.
3	100 ml surface water + 1.5 ml 67% HNO_3.	75 pg/ml 85 pg/ml	Values determined after deducing the amount of mercury introduced with HNO_3.

set up for mercury determination. The mercury was then desorbed thermally and determined by flameless atomic absorption. The experimental results obtained for mercury determination in air are listed in Table 3.

Table 3

Experimental results for mercury determination in air

A	μg Hg/m
0.155	5.25
0.175	6.00
0.165	5.51
0.146	4.55
0.152	5.00
0.156	5.25
0.170	5.75
0.165	5.50
0.150	4.75
0.175	6.00
Mean value	5.35
σ	0.502

CONCLUSIONS

The studied methods employed in mercury concentration allow for determination of this element in water at concentrations of about 10^{-11} g/ml, which are of the same order of magnitude as the natural background in some surface waters. Mercury is concentrated by some very simple means available even under the condition of the minimum of equipment. Mercury is concentrated immedialely after sampling thus eliminating the occurrence of mercury losses taking place on storage, losses which for very low mercury concentrations can reach tens of percents. The deposition on copper of other elements beside mercury or of some solid suspensions (even organic in nature) does not hinder the subsequent mercury analysis, the experimental apparatus allowing for its determination even from complex samples with important organic load.

The mercury can be determined in air at concentration of ng/m^3 without interferences, the specific absorbent for mercury (silica wool on which a gold layer was deposited) contained in the apparatus ensuring its selective concentration.

REFERENCES

[1] P. A. D'Itri and F. M. D'Itri, "Mercury Contamination — A Human Tragedy", John Wiley and Sons, 1977, p. 169.

[2] P. H. Abelson, *Science*, **169**, 237 (1970).

[3] S. Jensen and A. Jernelov, *Nature*, **223**, 753 (1969).

[4] S. Chilov, *Talanta*, **22**, 205 (1975).

[5] N. S. Poluektov. R. A. Vikun and Y. V. Zelyukova, *Zh. Anal. Khim.*, **18**, 33(1963).

[6] J. Komarek, V. Otruba and M. Cernikova, *Chem. Listy*, **80** (2), 206 (1986).

[7] W. R. Hatch, and W. L. Ott, *Anal. Chem.*, **40**, 2085 (1968).

[8] G. Cumont, *Chim. Anal.*, **53**, 634 (1971).

[9] H. Pinstock and F. Umland, *Fresenius Z. Anal. Chem.*, **320**, 237 (1985).

[10] Soo-Long Tong and Wooi-Kwee Lieow, *Anal. Chem.*, **52**, 581 (1980).

[11] J. Olafsson, *Analyt. Chim. Acta*, **68**, 207 (1974).

[12] E. Harsonyi, L. Polos and E. Pungor, *Analyt. Chim. Acta*, **67**, 229 (1973).

[13] J. R. Baltisberger and C. L. Knudson, *Analyt. Chim. Acta*, **73**, 265 (1974).

[14] L. H. J. Lajunen, A. Kinnuenn and E, Yrjanheikki, *At. Spectrosc.*, **6**, 49 (1985).
[15] C. Luca, A. F. Dăneţ and C. Radu, *Rev. Chimie (Bucharest)*, **36**, 856 (1985).
[16] Z. Wittmann, *Talanta*, **28**, 271 (1981).
[17] C. Feldman, *Anal. Chem.*, **46**, 99 (1974).
[18] J. L. Bricker, *Anal. Chem.*, **52**, 492 (1980).
[19] A. H. Sloot and H. H. Sas, *Analyt. Chim. Acta.* **73**, 225 (1974).
[20] A. F. Dăneţ, M. Popescu and O. Maior, *Rev. Chim. (Bucharest)*, **30**, 583 (1979).
[21] S. Dogan and W. Haerdi, *Analyt. Chim. Acta*, **76**, 345 (1975).
[22] J. J. Kim and J. Hoste, *Analyt. Chim. Acta*, **35**, 61 (1966).
[23] W. F. Fitzgerald and G. A. Gill, *Anal. Chem.*, **51**, 1714 (1979).
[24] P. E. Trujillo and E. E. , Campbell, *Anal. Chem.*, **47**, 1629 (1975).
[25] A. F. Dăneţ, M. Tarabic, C. Luca, V. Magearu, E. Dascalescu, V. Diaconescu and V. Sarachie, Romanian Patent 79 405/1982.

Revue Roumaine de Chimie, **34**, *9—10*, 1857—1865 (1989)

ELECTRONIC TRANSITIONS IN THE SQUARE-PLANAR $Rh(PPh_3)_3SnCl_3$ COMPLEX
(PPh_3=TRIPHENYLPHOSPHINE)

A. C. BANCIU
ICECHIM — Centre of Physical Chemistry
79611 Bucharest, Spl. Independenţei 202, Sector 6, Romania

Received February 8, 1989

In the 277—740 nm range the electronic absorption spectrum of the square-planar $Rh(PPh_3)_3SnCl_3$ complex shows a CT band (at 290 nm) and three bands (at ~377, ~450, and ~625 nm) which may be ascribed to some *d—d* transitions. These bands are interpreted in the frame of the ligand field theory.

I. INTRODUCTION

The Rh(I) ($4d^8$) ion forms quite numerous complexes, but almost exclusively they involve π-bonding ligands. The majority are square-planar but there are also some five-coordinate complexes. [1]

Some of the square-planar Rh(I) complexes have a wellknown activity in the homogeneous catalysis, such as $Rh(PPh_3)_3Cl$ (the so-called Wilkinson complex — in the hydrogenation reactions of olefins and acetylenes — and $Rh(PPh_3)_2ClCO$ — in the hydroformylation reactions.[1]

Structure and catalytic properties similar to the wellknown Wilkinson complex shows the $Rh(PPh_3)_3SnCl_3$ complex, discovered in 1964 by Young, Gillard and Wilkinson. [2] Heterogenized on silica, chemically modified with buthyl-lithium, this complex catalyses the hydrogenation reaction of cyclohexene as well the hydrogenation and isomerization reaction of n-hexane. [3,4]

The electronic spectra of the square-planar Rh(I) complexes are still less investigated and interpreted than those of other square-planar complexes, i.e. of Ni(II), Pd(II), Pt(II) and Au(III). This is so because in these spectra almost always the *d—d* transition are overlapped by strong CT (charge transfer) transitions. Therefore in the spectra only a single *d—d* band is most frequently outlined. Thus, an electronic spectrum such as that of RhCl(BT)(COD) (BT = benzothiazole; COD = 1,5 cyclooctadiene) consisting from a band with ε = 7250 at 280 nm and another with ε = 1150 at 385 nm is considered as "typical for tetracoordinate Rh(I)". [5]

The present paper deals with the electronic spectrum of the $Rh(PPh_3)_3SnCl_3$ complex in which three bands which may be reasonably ascribed to some $d-d$ transitions are outlined.

II. EXPERIMENTAL

The $Rh(PPh_3)_3SnCl_3$ complex was synthesized, in general lines, after the method described in[2]. The complex was purified by recrystallization from benzene. The elemental chemical analysis agrees with the formula of the comlpex.

The electronic absorption spectrum of the complex was recorded with a Specord UV-VIS spectrophotometer (G.D.R.) on benzene solutions of 1×10^{-4} M concentration (in the 277—357nm range) and of 1×10^{-3} M concentration (in the 333—740 nm range).

III. RESULTS AND DISCUSSIONS

The $Rh(PPh_3)_3SnCl_3$ complex is formed exclusively by π-acceptor ligands. Indeed, both PPh_3 and the anionic ligand $SnCl_3^-$ belong to the class of π-acceptor ligands, more exactly to that of the ligands which form $d_\pi - d_\pi$ back-bonds with the central metal ion.[6] Both ligands have tetrahedral structure, with the donor atom (P and respectively Sn) in sp^3 hybridization.[7]

The complex is diamagnetic, square-planar, of deep red-brown colour. The benzene solution (1×10^{-3} M) of the complex is orange.

The electronic spectrum of the complex is shown in Fig. 1. One observes that in the investigated range (277—740 nm) it contains four bands, different each from other in intensity: at 290 nm ($\varepsilon_{max} = 2.75 \times 10^4$) with f = 1.15, at ~ 377 nm ($\varepsilon_{max} \sim 2.0 \times 10^3$) with f ~ 3.80×10^{-2}, at ~ 450 nm ($\varepsilon_{max} = 8.6 \times 10^2$) with f ~ 1.50×10^{-2} and at ~ 625 nm ($\varepsilon_{max} \sim 1.4 \times 10^1$) with f ~ 1.92×10^{-4}.

From these the very intense band placed at 290 nm represents surely an allowed CT transition (the involved ligands absorb much weaker at this wavelength).

The band at ~377 nm appears intensified (f ~ 3.80×10^{-2}) since it is mostly overlapped by the very intense band centered at 290 nm. In reality it represents a less intense transition, *absolutely comparable* with that placed at ~450 nm (f ~ 1.50×10^{-2}). Undoubtedly the last mentioned band represents a spin-allowed $d-d$ transition whereas the weak band (f ~ 1.92×10^{-4}) at ~625 nm represents a spin-forbidden $d-d$ transition (The $d-d$ bands of the complexes of 4*d* ions are more intense thanthose. of the 3*d* ions). For the $d-d$ nature of the band at ~ 377 nm plead other considerations, too. Thus, at the RhCl(BT)(COD) complex (see above) at which the CT band (from 280 nm) is less intense the band placed at 385 nm has $\varepsilon = 1150$, a value comparable with $\varepsilon \sim 860$ which is the value of the $d-d$ band situated at ~450 nm of the complex under discussion. Finally, if the band from ~377 nm were of CT type, it would signify that the energy difference between the two CT bands (at 290 and ~377 nm) is of 7960 cm^{-1}. This value is too high to be plausible. It is known that at the square-planar complexes of ions with d^8 configuration, formed with π-acceptor ligands (such as the CN^- ions) the energy distance between the CT transition is always much smaller, from under 4000 cm^{-1}. [8,9]

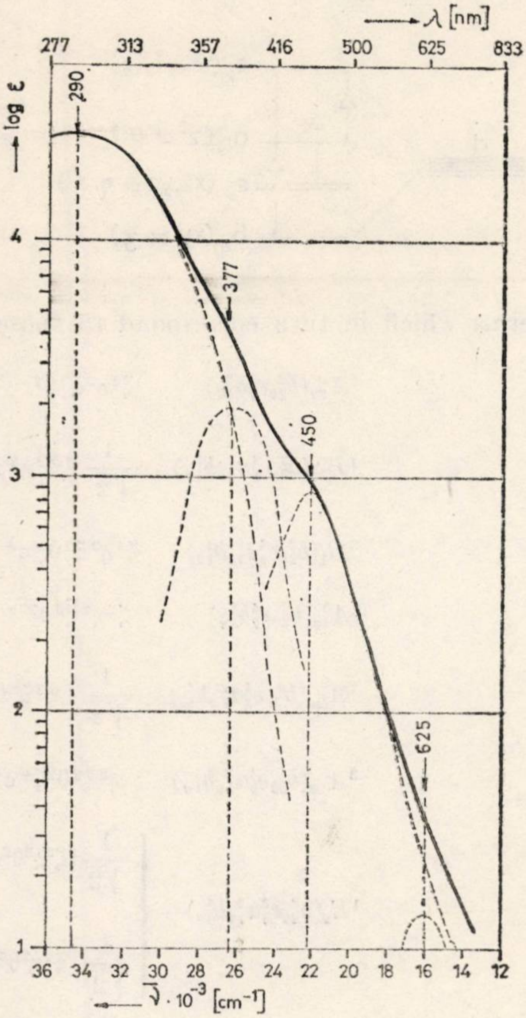

Fig. 1. — Absorption spectrum of the $Rh(PPh_3)_3\ SnCl_3$ complex.

It results, from all these, that the intense bands (for $d-d$ transitions) from ~377 and ~450 nm may be very resonably ascribed to some spin-allowed transitions, whereas the weak band from ~ 625 nm to a spin-forbidden $d-d$ transition.

Therefore, the following attempt to explain theoretically these bands in the frame of the ligand field theory is made.

The energies of the spectral terms between which $d-d$ transitions may occur were calculated using the strong field coupling scheme [10] for the sequence of the antibonding orbitals arisen from the interactions of the 4*d* orbitals of the Rh(I) ion with the ligand orbitals. The scheme is shown in Fig. 2.

The electronic strong field configurations, corresponding to the d^8 configuration of the free Rh(I) ion, the eigen functions and the spectral terms which in turn correspond to those are:

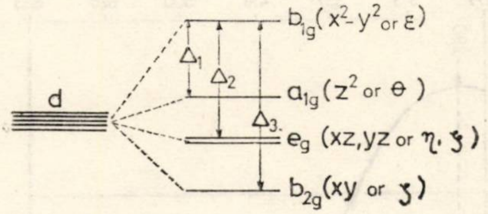
$b_{1g}(x^2-y^2$ or $\varepsilon)$
Δ_1
Δ_2
Δ_3
d
$a_{1g}(z^2$ or $\theta)$
e_g (xz, yz or η, ξ)
b_{2g}(xy or ζ)

Fig. 2. — Antibonding "*d*" molecular levels for a square-planar complex, ML_4, of D_{4h} symmetry.

$$^1A^a_{1g}(b^2_{2g}e^4_g a^2_{1g}) \qquad \zeta^2\eta^2\xi^2\theta^2$$

$$^1B_{1g}(b^2_{2g}e^4_g a^1_{1g}b^1_{1g}) \qquad \frac{1}{\sqrt{2}}\,[\zeta^2\eta^2\xi^2\theta^+\varepsilon^- - \zeta^2\eta^2\xi^2\theta^-\varepsilon^+]$$

$$^3B_1(b^2_{2g}e^4_g a^1_{1g}b^1_{1g}) \qquad \zeta^2\eta^2\xi^2\theta^+\varepsilon^+$$

$$^1A^b_{1g}(b^2_{2g}e^4_g b^2_{1g}) \qquad \zeta^2\eta^2\xi^2\varepsilon^2$$

$$^1A_{2g}(b^1_{2g}e^4_g a^2_{1g}b^1_{1g}) \qquad \frac{1}{\sqrt{2}}\,[\eta^2\xi^2\theta^2\zeta^+\varepsilon^- - \eta^2\xi^2\theta^2\zeta^-\varepsilon^+]$$

$$^3A_{2g}(b^1_{2g}e^4_g a^2_{1g}b^1_{1g}) \qquad \eta^2\xi^2\theta^2\zeta^+\varepsilon^+$$

$$^1E_g(b^2_{2g}e^3_g a^2_{1g}b^1_{1g}) \quad \begin{cases} \dfrac{1}{\sqrt{2}}\,[\zeta^2\xi^2\theta^2\eta^+\varepsilon^- - \zeta^2\xi^2\theta^2\eta^-\varepsilon^+] \\[2ex] \dfrac{1}{\sqrt{2}}\,[\zeta^2\eta^2\theta^2\xi^{2+}\varepsilon^- - \zeta^2\eta^2\theta^2\xi^-\varepsilon^+] \end{cases}$$

$$^3E_g(b^2_{2g}e^3_g a^2_{1g}b^1_{1g}) \quad \begin{cases} \zeta^2\xi^2\theta^2\eta^+\varepsilon^+ \\ \zeta^2\eta^2\theta^2\xi^+\varepsilon^+ \end{cases}$$

By neglecting the relativistic effects (the spin-orbit coupling) the following energy expressions for the spectral terms are obtained:

$$\begin{array}{c|cc|} ^1A^a_{1g} & W + 2E(\zeta) + 4\,E(\eta,\xi) + 2E(\theta) - E & 4B + C \\ ^1A^b_{1g} & 4B + C & W + 2E(\zeta) + 4E(\eta,\xi) + 2E(\varepsilon) - E \end{array} = 0$$

$$E(^1B_{1g}) = W + 2E(\zeta) + 4E(\eta, \xi) + E(\theta) + E(\varepsilon) - (4B + C)$$

$$E(^3B_{1g}) = W + 2E(\zeta) + 4E(\eta, \xi) + E(\theta) + E(\varepsilon) - 3(4B + C)$$

$$E(^1A_{2g}) = W + 4(E(\eta, \xi) + 2E(\theta) + E(\zeta) + E(\varepsilon) - C$$

$$E(^3A_{2g}) = W + 4\,E(\eta, \xi) + 2E(\theta) + E(\zeta) + E(\varepsilon) - 3C$$

$$E(^1E_g) = W + 2E(\zeta) + 2E(\theta) + 3E(\eta, \xi) + E(\varepsilon) - (3B + C)$$

$$E(^3E_g) = W + 2E(\zeta) + 2E(\theta) + 3E(\eta, \xi) + E(\varepsilon) - 3(3B + C)$$

where $W = E^{\mathrm{core}} + 28\,A - 38B + 24\,C$, E^{core} is the energy of the molecular core (which also includes the bonding molecular levels), A, B and C are the Racah parameters for the electronic repulsion radial integrals and $E(\zeta)$, $E(\eta)$ ... are the energies of the levels from Fig. 2.

Between these spectral terms the following transitions are theoretically provided :

$$\nu[^1A^a_{1g} \rightarrow {}^3B_{1g}] = \sqrt{\Delta_1^2 + (4B + C)^2} - 3(4B + C)$$

$$\nu[^1A^a_{1g} \rightarrow {}^1B_{1g}] = \sqrt{\Delta_1^2 + (4B + C)^2} - (4B + C)$$

$$\nu[^1A^a_{1g} \rightarrow {}^3A_{2g}] = \Delta_3 - \Delta_1 + \sqrt{\Delta_1^2 + (4B + C)^2} - 3C$$

$$\nu[^1A^a_{1g} \rightarrow {}^1A_{2g}] = \Delta_3 - \Delta_1 + \sqrt{\Delta_1^2 + (4B + C)^2} - C$$

$$\nu[^1A^a_{1g} \rightarrow {}^3E_g] = \Delta_2 - \Delta_1 + \sqrt{\Delta_1^2 + (4B + C)^2} - 3(3B + C)$$

$$\nu[^1A^a_{1g} \rightarrow {}^1E_g] = \Delta_2 - \Delta_1 + \sqrt{\Delta_1^2 + (4B + C)^2} - (3B + C)$$

$$\nu[^1A^a_{1g} \rightarrow {}^1A^b_{1g}] = \sqrt{\Delta_1^2 + (4B + C)^2}$$

where the parameters Δ_1, Δ_2 and Δ_3 are the energy distances between the levels shown in Fig. 2.

The most plausible assignment for the absorption maxima from the spectrum of the $\mathrm{Rh(PPh_3)_3SnCl_3}$ complex appear to be $^1A^a_{1g} \rightarrow {}^1B_{1g}$ for the maximum placed at ~ 450 nm (~ 22220 cm^{-1}) and $^1A^a_{1g} \rightarrow {}^1E_g$ for the maximum located at ~377 nm (~ 26520 cm^{-1}). On the basis of this assignment and taking into account the most plausible values for the B and C parameters for the Rh(I) ion found in a ligand field of D_{4h} symmetry, those of $B = 350$ cm^{-1} and $C = 2450$ cm^{-1}, [8,11] with the above formulae, the following values for the spectral parameters were obtained :

$$\Delta_1 = 25780 \text{ cm}^{-1} \text{ and}$$

$$\Delta_2 = 28680 \text{ cm}^{-1}.$$

The third spin-allowed transition, ${}^1A^a_{1g} \rightarrow {}^1A_{2g}$, must appear in spectrum at > 32000 cm^{-1} (< 313 nm). In contrary case it would be outlined in spectrum, as a shoulder of the intense CT band. From the energy expression of the transition it results :

$$\Delta_3 > 35200 \text{ cm}^{-1}.$$

The last spin-allowed transition, ${}^1A^a_{1g} \rightarrow {}^1A^b_{1g}$, appears in the spectrum in the far UV range, at 52140 cm^{-1} (192 nm).

By means of these values of the spectral parameters and with the above formulae there were calculated the wavenumbers of the three spin-forbidden transitions. They are :

$${}^1A^a_{1g} \rightarrow {}^3B_{1g} = 14520 \text{ cm}^{-1} \text{ (688 nm)},$$

$${}^1A^a_{1g} \rightarrow {}^3E_g = 21620 \text{ cm}^{-1} \text{ (463 nm) and}$$

$${}^1A^a_{1g} \rightarrow {}^3A_{2g} > 24990 \text{ cm}^{-1} \text{ (< 400 nm)}.$$

The last two of them are obscured in spectrum by much stronger transitions. In exchange, the first computed transition shows a difference of only ~ 1480 cm^{-1} (~ 60 nm) from the weak band experimentally found in spectrum, at ~ 625 nm (~ 16000 cm^{-1}).

The above accounts were affected by the following main error sources : 1. the determiation errors of the maxima of the bands located at ~ 377, ~ 450 and ~ 625 nm, which appear all outlined only as shoulders in spectrum ; 2. the neglection of the spin-orbit coupling, which is greater for the Rh(I) ($4d^8$) ion that for the ions from the first transitionow (for the free Rh(I) ion $\zeta = 1212$ cm^{-1}, comparatively with $\zeta = 535$ cm^{-1}, $\zeta = 649$ cm^{-1} and $\zeta = 829$ cm^{-1} for the free Co(II), Ni(II) and Cu(II) ions, [12] respectively) and 3. the estimation errors of the B and C Racah parameters for the metal ion found in a D_{4h} *ligand field*. (For the *free* Rh(I) ion $B = 667$ cm^{-1} and $C = 2313$ cm^{-1}. [12] One observes that the value $C = 2450$ cm^{-1} taken after [8,11] into account is almost equal to the free ion value, whereas the B value used into calculations (of 350 cm^{-1}) is much less).

Taking into account all the mentioned determination errors, one may conclude that the concordance between calculation and experiment for the transition ${}^1A^a_{1g} \rightarrow {}^3B_{1g}$ may be considered as good.

From the above accounts result the followng splittings (Fig. 3.a.) between the antibonding orbitals arisen from the "d" orbitals of the free Rh(I) ion.

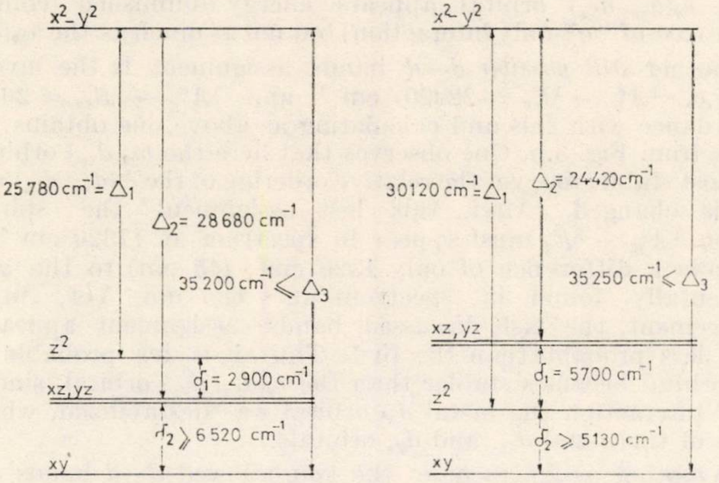
x^2-y^2
$25780\ cm^{-1} = \Delta_1$
$\Delta_2 = 28680\ cm^{-1}$
$35200\ cm^{-1} \leqslant \Delta_3$
z^2
$\delta_1 = 2900\ cm^{-1}$
xz, yz
$\delta_2 \geqslant 6520\ cm^{-1}$
xy
x^2-y^2
$\Delta_2 = 24420\ cm^{-1}$
$30120\ cm^{-1} = \Delta_1$
$35250\ cm^{-1} \leqslant \Delta_3$
xz, yz
$\delta_1 = 5700\ cm^{-1}$
z^2
$\delta_2 \geqslant 5130\ cm^{-1}$
xy

Fig. 3. — Calculated splittings between the antibonding molecular orbitals arisen from the "d" orbitals of the free (Rh(I) ion : a. for the assignment ${}^1A^a_{1g} \to {}^1B_{1g} = 22220$ cm^{-1} and ${}^1A^a_{1g} \to {}^1E_g = 26520$ cm^{-1};

b. for the assignment ${}^1A^a_{1g} \to {}^1E_g = 22220$ cm^{-1} and ${}^1A^a_{1g} \to {}^1B_{1g} = 26520$ cm^{-1}.

One observes : 1. a very high energy separation ($\Delta_1 = 25780$ cm^{-1}) between the $b_{1g}(d_{x^2-y^2})$ and the immediately next orbital, $a_{1g}(d_{z^2})$; 2. much less energy differences (of 2900 cm^{-1} and of $\geqslant 6520$ cm^{-1}) between the other orbitals, and 3. the fact that the $b_{2g}(d_{xy})$ orbital is the most stable.

This energy order of the "d" antibonding orbitals is the most plausible, being in concordance with the chemical intuition with regard to the formation of the chemical bonds in the complexes with $d_\pi - d_\pi$ back bonds. Accordingly, the $b_{1g}(d_{x^2-y^2})$ orbital is high in energy, since the metal $d_{x^2-y^2}$ orbital interacts strongly, "σ", with the sp^3 hybrid orbitals of the ligand donor atoms (P and Sn). The antibonding $a_{1g}(d_{z^2})$ orbital is much smaller in energy, since the metal d_{z^2} orbital interact "σ" weaker, only by means of its toroid part, with the ligand sp^3 hybrid orbitals. Besides, the metal d_{z^2} orbital may "π" interact too, with the four empty ligand d_{z^2} orbitals. Through the last mentioned interaction the energy of the $a_{1g}(d_{z^2})$ orbital appears decreased, comparatively with the case of "σ"-ony interaction.

In the "π" interaction are involved especially the d_{xy}, d_{xz} and d_{yz} metal orbitals. Each of them interacts strongly with the ligand orbitals of the same symmetry and spatial orientation (d_{xy} metal with d_{xy} ligand, etc.). The strongest interacts "π" the metal d_{xy} orbital. It has great overlaps with *all the four empty* d_{xy} ligand orbitals. As a results of this "π"

interaction the antibonding $b_{2g}(d_{xy})$ orbital appears as the most stable, from all the "d" antibonding orbitals. Each of the metal d_{xz} and d_{yz} orbitals may "π" interact *only with two empty* d orbitals (d_{xz} and d_{yz} respectively) of the ligands placed in *trans*. As a result of this interaction the antibonding $e_g(d_{xz}, d_{yz})$ orbital appears energy-diminished (comparatively with the case of "σ"-only interaction) but not as much as the $b_{2g}(d_{xy})$orbital.

Another *still possible* $d-d$ bands assignment is the inverse of the above i.e. ${}^1A_{1g}^a \to {}^1E_g = 22220$ cm^{-1} and ${}^1A_{1g}^a \to {}^1B_{1g} = 26520$ cm^{-1}. In accordance with this and calculating as above one obtains the orbital sequence from Fig. 3.b. One observes that here the $b_{2g}(d_{xy})$ orbital appears as the most stable, too, yet the relative ordering of the $e_g(d_{xz}, d_{yz})$ and $a_{1g}(d_{z^2})$ orbitas is changed. After this last assignment the spin-forbidden transition ${}^1A_{1g}^a \to {}^3E_g$ must appear in spectrum at 17320 cm^{-1} (580 nm). This shows a difference of only 1320 cm^{-1} (45 nm) to the weak band experimentally found in spectrum at $\sim$ 625 nm. Yet, in spite of this agreement, the last discussed bands assignment appears as somewhat less probable than the first. Thus, it is les probable that the $a_{1g}(d_{z^2})$ orbital becomes stabler than the $e_g(d_{xz}, d_{yz})$ orbital, since through the "σ" interaction the metal d_{x^2} orbital was destabilized, what was not the case of the metal d_{xz} and d_{yz} orbitals.

Any other assignement of the spin-allowed $d-d$ bands out of the above discussed leads to unplausible results (as, for example, orbital sequences with the $a_{1g}(d_{z^2})$ orbital as the most stable, or with the $b_{2g}(d_{xy})$ orbital as the most unstable, after the $b_{1g}(d_{x^2-y^2})$ orbital a.s.o.).

From all these considerations the bands assignments made and the orbital sequences from Fig. 3 appear to be the most plausible.

It is possible that at other square-planar Rh(I) complexes too (especially those formed with substituted phosphines, arsines and stibines) which are of orange, red or brown colour, the $d-d$ transitions will occur exactly in the same range like at the complex under discussion. (At the Rh(I) complexes of yellow colour, which are quite numerous, these transitions would be hypsochromically shifted, comparatively with the case of the above discussed complex).

IV. CONCLUSIONS

1. The electronic absorption spectrum of the square-planar $Rh(PPh_3)_3SnCl_3$ complex shows, in the 277–740 nm range, four bands, different from each other in intensity (at 290, $\sim$377, $\sim$450 and $\sim$625 nm).

2. The most intense band, located at 290 nm, represents an allowed CT transition, of metal → ligand type.

3. The bands situated at $\sim$377 and $\sim$450 nm may be most plausible ascribed each to one of the $d-d$ transitions ${}^1A_{1g}^a \to {}^1E_g$ and ${}^1A_{1g}^a \to {}^1B_{1g}$, of the square-planar complexes of d^8 ions.

4. The weak band placed at ~625 nm represents one of the spin-forbidden transitions $^1A^a_{1g} \rightarrow {}^3B_{1g}$ or $^1A^a_{1g} \rightarrow {}^3E_g$.

5. On the basis of the above mentioned assignments of the bands located at ~377 nm and ~450 nm the energy sequences from Fig. 3. result as possible. There, in both cases, the $b_{1g}(d_{x^2-y^2})$ orbital is the highest in energy, the $b_{2g}(d_{xy})$ orbital is the most stable, whereas the $e_g(d_{xz}, d_{yz})$ and $a_{1g}(d_{z^2})$ orbitals are of intermediate energies.

REFERENCES

[1] S. E. Livingstone, "Complexes of Rhodium (I)" in " Comprehensive Inorganic Chemistry", vol. 3, Pergamon Press, Oxford, 1973, p. 1237.

[2] F. J. Young, R. D. Gillard and J. Wilkinson, *J. Chem. Soc.*, **1964**, 5176.

[3] S. A. Panichev, G. V. Kudryavtsev and G. V. Lisichkin, *Vestnik Moskow Univ. Ser. Khim.*, **19**, 730 (1978).

[4] S. A. Panichev, G. V. Kudryavtsev and G. V. Lisichkin, *Koord. Khim.*, **5**, 1141 (1979).

[5] M. Aresta, *Inorg. Chim. Acta Lett.*, **44**, L3 (1980).

[6] * * * "Reaktionsverhalten und Syntheseprinzipien", Lehrbuch 7, 2nd Edition, VEB Deutscher Verlag für Grundstoffindustrie, Leipzig, 1975, p. 333.

[7] F. A. Cotton and G. Wilkinson, "Advanced Inorganic Chemistry", Interscience, London, 1966, p. 461.

[8] H. B. Gray and C. J. Balhausen, *J. Amer. Chem. Soc.*, **85**, 260 (1963).

[9] H. B. Gray, "Electronic Structures of Square-Planar Metal Complexes" in "Transition Metal Chemistry", vol. 1, M. Dekkert, New York, 1965, p. 239.

[10] J. S. Griffith, "The Theory of Transition-Metal Ions", Univ. Press, Cambridge, 1961, p. 226.

[11] R. F. Fenske, D. S. Martin Jr. and K. Ruedenberg, *Inorg. Chem.*, **1**, 441 (1962).

[12] J. S. Griffith, Op. cit., p. 438.

1. The weak band found at ~4050 cm represents one of the spin-forbidden transitions [illegible]

2. [illegible] assignments of the bands located at ~[illegible] nm and ~430 nm the energy [illegible] from Fig. 3 would be [illegible]. Thus, in both cases, the [illegible] orbital is the highest in energy, the [illegible] orbital is the most stable, whereas the [illegible] and [illegible] [illegible].

REFERENCES

[illegible]

Revue Roumaine de Chimie, **34**, *9–10*, 1867–1875 (1989)

Pd(II) COMPLEX COMPOUNDS WITH THIOETHERS. II[1]

Pd(II) COMPOUNDS OF BIS(BENZYLTHIO-*p*-PHENYL) ETHERS

S. NEAGOE,[a] D. NEGOIU,[b] V. NEAGOE,[c] M. NEGOIU,[b] E. BADAU[d] and G. BREBEANU[a]
[a] Petroleum and Gas Institute, Ploiești, Blvd București-Ploiești no. 3–5, Romania
[b] Polytechnic Institute, Bucharest, Department of Chemical Technology, Polizu Street no. 1, Bucharest, Romania
[c] School no. 50, Sector 2, Bucharest, Romania
[d] Institute of Medicine and Pharmacy, Bucharest, Romania

Received March 26, 1989

The paper reports the synthesis and study of several compounds of Pd(II) with ether-bisthioether compounds from the bis(benzylthio-*p*-phenyl)ether series. The compounds obtained are of the $PdLCl_2$ type. The proposed structure was based on the elemental chemical analysis, molecular weight determinations, thermal analysis, electric conductivity determinations, and analyses of the IR, UV–VIS and NMR spectra.

INTRODUCTION

The compounds formed by thioethers as ligands with metals having d^8 electronic structure have been much investigated.[1–3] Schmidt[4] showed that thioethers form, with Pt(II) or Pd(II), chelates with stable rings of six atoms. The coordination at the central metallic ion is achieved by the thioetheric sulphur atoms, the ligands being bidentate.

The present paper reports on the results of a study on some Pd(II) compounds with ether-bisthioether compounds in the bis(benzylthio-*p*-phenyl)ether series, known in the literature:[5,6]

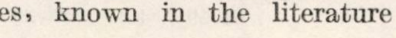

in which Ar is:

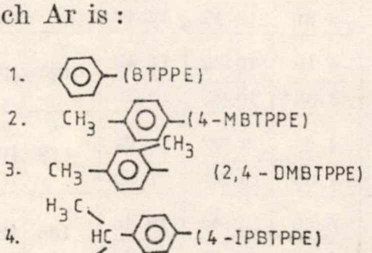

bis(benzylthio-*p*-phenyl)-ether
(4-methyl bis(benzylthio-*p*-phenyl)ether
(2,4-dimethyl bis(benzyl-thio-*p*-phenyl)-ether
(4-isopropyl bis(benzyl-thio-*p*-phenyl)-ether
4-chlorine bis(benzylthio-*p*-phenyl)-ether

RESULTS AND DISCUSSION

Pd(II) complex compounds with ether-bisthioethers in the bis(benzylthio-*p*-phenyl)ether series are microcrystalline powders having yellow, orange or red colours, as a function of the ligand used. The melting points are generally higher than those of the noncomplexed ligands. The compounds are easily soluble in dimethyl-sulphoxide (DMSO), dimethylformamide (DMF), dichlormethane (CH_2Cl_2) and nitromethane.

These compounds are generally obtained by adding the thioether (dissolved in acetone) to a solution of palladium (II) chloride slightly acidulated with HCl, followed either by stirring for 1/4—3 hours at room temperature or by reflux for 1—3 hours on a water bath.

The elemental chemical analyses of the obtained compounds are presented in Table 1.

Table 1

Elemental chemical anaylsis of bis(benzylthio-*p*-phenyl) ethers and oftheir complex compounds with Pd(II)

No.	Compound/System	Element analyzed, Theor./Exp. (%)					M.p. °C	Formula suggested
		Pd	C	H	S	Cl		
1	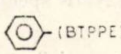	—	75.32 75.02	5.34 5.54	15.46 15.20	—	129	—
2	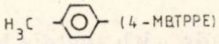	—	75.97 76.10	5.92 5.78	14.48 14.30	—	147	—
3	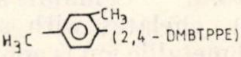	—	76.55 76,06	6.42 6.70	13.70 13.08	—	145	—
4	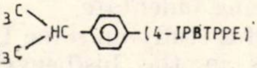	—	77.28 77.68	6.87 7.02	12.85 12.45	—	89	—
5	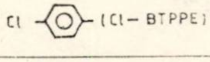	—	64.59 64.88	4.17 4.29	13.26 13.44	—	135	—
6	Pd(II)—(BTPPE)	17.98 17.75	52.71 53.10	3.72 3.81	10.81 10.17	11.98 12.42	134	$[PdLCl_2]$
7	Pd(II)—(4-MBTPPE)	17.16 17.00	54.20 54.00	4.19 3.82	10.32 10.65	11.43 10.76	125	$[PdLCl_2]$
8	Pd(II)—(2,4-DMBTPPE)	16.42 16.70	55.55 56.20	4.63 4.80	9.88 9.58	10.94 11.20	119	$[PdLCl_2]$
9	Pd(II)—(4-IPBTPPE)	15.74 15.86	56.80 57.20	5.03 5.00	9.46 10.00	10.48 10.83	166	$[PdLCl_2]$
10	Pd(II)—(*p*-ClBTPPE)	16.11 16.32	47.26 47.60	3.03 3.00	9.69 10.19	21.47 21.38	215	$[PdLCl_2]$

The correlation of these results permits the assignment of the following general formulation for the synthesized compounds : $[PdLCl_2]$, where L = the ligands 1–5 (Table 1).

This formulation is supported and confirmed by molecular weight determinations, and also by the measurements of electrical conductivity. The experimental results are given in table 2.

Table 2

Molar weights and molar conductivities of the Pd(II) complex compounds with ether-bisthioethers in the bis(benzylthio-*p*-phenyl) ether series

No.	Compound	Molecular weight		Concentration $X \cdot 10^{-4}$ M	Molar conductivity $(\Omega^{-1} \cdot cm^2 \cdot mol^{-1})$
		Theoretical	Experimental		
1	$[Pd(BTPPE)Cl_2]$	591.85	569.80	3.04	3.44
2	$[Pd(4\text{-}MBTPPE)Cl_2]$	619.90	589.04	1.13	2.80
3	$[Pd(2,4\text{-}DMBTPPE)Cl_2]$	647.96	624.39	1.54	1.44
4	$[Pd(4\text{-}IPBTPPE)Cl_2]$	676.01	656.48	1.66	1.73
5	$[Pd(p\text{-}ClBTPPE)Cl_2]$	660.20	640.00	5.37	2.43

Molecular weights of the synthesized complex compounds were determined by Rast's method :[7] the solvent used was camphor.

The values obtained experimentally are in agreement with the theoretical ones calculated according to the above general formulation.

The electrical conductivities were determined in DMSO.[8] The results obtained show that these compounds are nonelectrolytes. Thus, the general formulation $PdLCl_2$, suggested for the compounds is correct.

Thermal analysis

The thermal analysis of the Pd(II) complex compounds indicates their thermal stability and permits the calculation of the metal-ligand combination ratio.

Analysis of the ATD, TGD and TG diagrams of some of the compounds studied (Table 1) led to the data in table 3.

At 200°C the decomposition of the $[Pd(BTPPE)Cl_2]$ and $[Pd(2,4\text{-}DMBTPPE)Cl_2]$ begins, and at 180°C that of the $[Pd(p\text{-}ClBTPPE)Cl_2]$.

The complete oxidation of the organic remainder reaches sometimes 900–1000°C and that is why the thermal effect corresponding to the PdO decomposition is more difficulty noticed in the thermal curves.

From the data of the TG diagram, the combination ratio ligand : metal = 1 : 1 was calculated (Table 1).

Table 3

Results of the thermal analysis of some Pd(II) complex compounds with ether-bisthioethers

Compound	Molecular weight	Residue %: Form of the resulted residue	Residue %: Theor. / Exp.	Temperature of some thermal effects: Decomp. begin.	Temperature of some thermal effects: Ist thermal effect	Temperature of some thermal effects: Final oxid temp.	Residue thermal trarsf. °C
[Pd(BTPPE)Cl_2]	591.85	Pd	17.98 / 18.75	200	220	650	875
[Pd(2,4-DMBTPPE)Cl_2]	647.92	Pd	16.42 / 17.06	200	220	920	masked effect
[Pd(*p*-ClBTPPE)Cl_2]	660.20	Pd	16.12 / 19.21	180	255	1000	masked effect

Spectral analysis

IR spectra of thioethers and the corresponding complex compounds obtained with them are systematized and presented in table 4.

Within the 600—3200 cm^{-1} spectral range, the characteristic frequencies of the valence vibrations ν_{CH}, $\nu_{CH_3 asym}$, $\nu_{CH_3 sym}$, $\nu_{CH_2 asym}$, $\nu_{CH_2 sym}$, ν_{C-C}, $\nu_{C-O asym}$, $\nu_{C-O sym}$, ν_{C-S} and of the thioetheric groups[5,6,9] and also deformation vibrations ν_{CH} appear.

Within the 3000—2800 cm^{-1} spectral range, the bands corresponding to the valence vibrations $\nu_{CH_3 asym}$, $\nu_{CH_2 asym}$ and $\nu_{CH_2 sym}$ appear.

Within the spectra of the complex compounds with Pd(II). these bands appear either shifted or with modified intensities.

The shifts of the bands in the spectra of the Pd(II) complex compounds, in comparison with the spectra of the noncomplexed ligands, and also the change in their intensity due to the $-CH_2-$ groups in the vicinity of the sulphur thioetheric atom, $-S-$, leads to the conclusion that the thioetheric sulphur atoms are involved in the coordination with the central metallic atom.

The 1600—1400 cm^{-1} spectral range includes the frequencies due to the valence vibrations ν_{C-C} in the benzenic nuclei. Unlike the ligand spectrum, the spectrum of the complex compounds, with Pd(II) shows these bands either at the same frequency, with lower intensity, or shifted towards lower frequencies with maximum 10 cm^{-1}. It has thus been proved that the complexation leads to the perturbation of p-π conjugation in the noncomplexed ligands, because the sulphur donor atoms are linked directly to the benzenic nuclei in the ligand.

The 1300—1000 cm^{-1} range includes the frequencies corresponding to the asymmetrical and symmetrical ν_{C-O-C} valence vibrations. In the bis(benzylthio-*p*-phenyl)ether series, the ether bond with the aromatic nuclei is represented by the band corresponding to the antisymmetric ν_{C-O-C} valence vibration splitted in two intense bands ; one of them appe-

Table 4

Characteristic frequencies in the IR spectra of ether-bisthio-ethers in the bis(benzyl-*p*-phenyl) ether series and of their complex compounds with Pd(II) (cm^{-1})*

Compound	3100–3000	3000–2800			1600–1400	1300–1000		900–700	700–600
	ν_{CH}	ν_{CH_3} asym	ν_{CH_2} asym	ν_{CH_2} sym	$\nu_{C \cdots C}$	ν_{C-O} asym	ν_{C-O} sym	ν_{CH}	ν_{C-S}
BTPPE	3085w 3050w 3020i	—	2925w	2845m	1590i 1490i	1240i 1275w	1160m	700i 770m 810w	680i
4-MBTPPE	3090w 3060w 3020i	2960w	2925w	2865w	1590i 1490i	1255i 1275m	1165m	820i	680m
2,4-DMBTPPE	3090w 3060w 3020i	2965w	2925m	2855i	1590i 1490i	1250i 1275w	1165m	870i 820i	680m
4-IPBTPPE	3090m 3060w 3020i	2960i	2925m	2855i	1590i 1490i	1255i 1275m	1185m	820i	680m
p-ClBTPPE	3090w 3050w 3030w	—	2925m	2855m	1590i 1490i	1255i 1275m	1165m	820m	680m
[Pd(BTPPE)Cl$_2$]	3095sh 3065sh 3030sh	—	2915sh	2835sh	1580w	1235i	1160m	705i 775m 815sh	685sh
[Pd(4-MBTPPE)Cl$_2$]	3090sh 3050w	2960sh	2925w	2860w	1580m 1490i	1255i 1275w	1165m	830m	680sh
[Pd(2,4-DMBTPPE)Cl$_2$]	3090sh 3020w	2960w	2925w	2860sh	1590m 1490m	1245i 1275w	1165m	875m 825l	675w
[Pd(4-IPBTPPE)Cl$_2$]	3095sh 3060w 3020sh	2970m	2940sh	2880w	1580m 1490i	1255l 1275w	1185m	835m	665sh
[Pd(p-ClBTPPE)Cl$_2$]	3090sh 3050w 3020sh	—	2925sh	2860w	1590m 1490m	1255i 1275m	1165m	820sh	680sh

* i = intense ; sh = shoulder ; m = medium ; w = weak ; l = large.

ars at 1240—1255 cm^{-1} and the other at 1275 cm^{-1}. The $\nu_{C-O-C_{sym}}$ valence vibration is represented by the less intense band at 1160—1185 cm^{-1}.

In the spectra of the corresponding complex compounds formed with Pd(II), these bands are not changed versus the ligands.

It follows that the ether-aromatic oxygen atom does not take part in complexation.

Within the 900—700 cm^{-1} range the bands due to the γ_{CH} deformation vibration of the hydrogen atoms bonded to the benzenic nuclei appear. These nuclei are different in number and position because the ligands used have a different number of substituents.

In the spectra of the complex compounds with Pd(II), these bands appear changed, generally less intense and sometimes shifted towards higher frequencies. It has been thus proved that the electronic configuration of the noncomplexed ligands is perturbed by complexation because the benzenic nuclei are in the vicinity of the thioether sulphur atoms directly involved in coordination.

Within the 700—600 cm^{-1} range, the bands corresponding to the ν_{C-S} valence vibration of thioetheric bond appear. These bands are usually weak and appear at variable frequencies as a function of the nature of the thioether and of the substituents on the aromatic nuclei.

The change of the band at 680 cm^{-1}, in the spectra of complex compounds in comparison with that of the noncomplexed ligands proves that the sulphur atom is involved in coordination.

UV—VIS spectra. The electronic reflectance spectra in the UV—VIS range, after pelletization in magnesium oxide, were recorded both for the noncomplexed ligands and for the corresponding complex compounds obtained with Pd(II).

Assignment of the bands was made on the basis of the data offered by Gray and Ballhausen.[10] Comparison of the bands observed in the electronic spectra of the complex compounds with those of $[PdCl_4]^{2-}$ and $[PdBr_4]^{2-}$ enabled the following assignments:

a) the band at 600 nm (16670 cm^{-1}) was assigned to the $b_{2g}(\pi^*) \rightarrow \rightarrow b_{1g}(\sigma^*)$; $^1A_{1g} \rightarrow {}^1A_{2g}$;

b) the shoulder at 440 nm (22773 cm^{-1}) was assigned to the $a_{1g}(\sigma^*) \rightarrow \rightarrow b_{1g}(\sigma^*)$, $^1A_{1g} \rightarrow {}^1B_{1g}$;

c) the band at 400 nm (25000 cm^{-1}) was assigned to the $e_g(\pi^*) \rightarrow \rightarrow b_{1g}(\sigma^*)$, $^1A_{1g} \rightarrow {}^1E_{1g}$.

These transitions are of the *d—d* type, spin-permitted and forbidden by parity.

Study of these spectra leads to the conclusion that the complex compounds formed with Pd(II) in the bis(benzyl-*p*-phenyl)ether series have a square-planar disposition belonging to the D_{4h} symmetry group.

^1H—NMR spectra. The ^1H—NMR spectra of the ligands and their complex compounds with Pd(II) were obtained in deuterated DMSO. They include the signals corresponding to the species of protons in the proposed formulas.

Table 5 gives the values of the chemical shifts of the protons in the 2,4-DMBTPPE and BTPPE ligands in comparison with those corresponding to their complex compounds with Pd(II).

Table 5

Values of the ^1H-NMR chemical shifts of the protons in the Pd(II) complex compounds of bis(benzyl thio-*p*-phenyl) ether series in comparison with the noncomplexed thioethers

Assignments	Ligand		Complex coumpound	
	δ(ppm)	Multiplicity	δ(ppm)	Multiplicity
	2,4-DMBTPPE		$[Pd(2,4\text{-}DMBTPPE)_2]$	
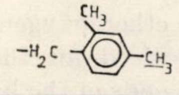	2.22	s	2.22	s
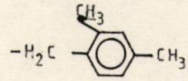	2.30	s	2.30	s
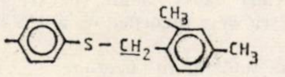	4.10	s	4.11	s
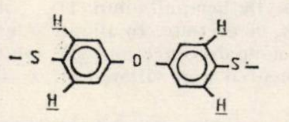	7.37	d	6.86	d
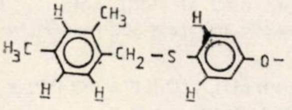	6.78–7.15	s	7.00	s
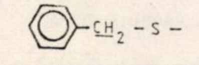	BTPPE		$[Pd(BTPPE)Cl_2]$	
	4.16	s	4.17	s
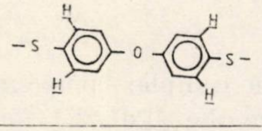	7.35	d	6.87	d
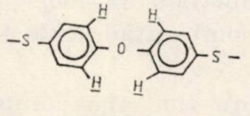	7.36	d	7.36	d
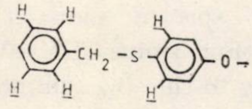	6.82–7.12	s	7.27	s

s = singlet ; d = doublet.

A sensible change of the aromatic zone is noticed. The spectrum shows a slight deshielding of the aromatic protons of the benzenic nucleus linked by the thioether sulphur atom.

A slight shift of the protons in the methylene group linked to the thioether sulphur atom is noticed allowing the conclusion that the thioether sulphur atom is involved in coordination.

The aromatic protons in the close vicinity of the ether oxygen atom are not influenced by coordination. This is also noticed for the protons of the methyl group on the aromatic nuclei at the ends of the ligands.

EXPERIMENTAL

Apparatus : IR spectra were recorded on a UR–20 Carl Zeiss Jena spectrophtometer using anhydrous KBr pellets. The reflectance UV-VIS spectra were recorded on a UV-VIS type Carl-Zeiss Jena spectrophotometer in MgO pellet.
Reagents : $PdCl_2$, solution 0.02 M in HCl ; thioethers : solution 0.02 M in acetone.

The complex compounds : dichloro-bis(benzylthio-*p*-phenyl)-ether-palladium(II), $[Pd(BTPPE)Cl_2]$, and dichlorobis(4-methyl-benzylthio-*p*-phenyl)ether-palladium(II), $[Pd(4\text{-}MBPPE)Cl_2]$ were prepared by adding 10 mL thioether solution, in acetone, to 10 mL solution 0.02M $PdCl_2$. Acetone was then added till the disappearance of opalescence and the solution was magnetically stirred for 3 hours. The yellow crystals sedimented were filtered off, washed and vacuum-dried.

Dichloro-bis (2,4-dimethyl-benzylthio-*p*-phenyl)ether-palladium(II), $[Pd(2,4\text{-}DMBTPPE)Cl_2]$, and dichloro-bis(*p*-chlorine-benzylthio-*p*-phenyl)ether-palladium(II), $[Pd(\text{-}p\text{-}ClBTPPE)Cl_2]$ were prepared by adding 10 mL thioether solution to 10 mL 0.02 M $PdCl_2$ solution, followed by refluxation on a water bath for an hour. The red-orange crystals sedimented were filtered off, washed and vacuum dried.

Dichloro-bis(4-isopropyl-benzylthio-*p*-phenyl)ether-palladium(II), $[Pd(4^{-}IPBTPPE)Cl_2]$ was obtained by adding 10 mL thioether solution in 10 mL 0.02 M PdC_2 solution, in acetone. The solution was treated on water bath for 5 minutes, followed by stirring with a magnetic stirrer. The red-orange crystals obtained were filtered off, washed and vacuum dried.

CONCLUSIONS

The present study led to the conclusion that the complex compounds of Pd(II) with bis(benzylthio-*p*-phenyl) ethers have the $[PdLCl_2]$ form.

The elemental chemical analysis, the determination of molecular weight and thermogravimetrical analysis show a combination ratio Pd : ligand = 1 : 1.

The electrical conductivity determinations show that the complex compounds studied are nonelectrolytes. This suggests a donor-acceptor type bond. Analysis of the IR and ^1H–NMR spectra shows that the coordination is performed by the thioether sulphur atoms. UV–VIS spectra show a square-planar arrangement belonging to the D_{4h} symmetry group.

REFERENCES

[1] D. Negoiu, S. Neagoe, M. Negoiu, E. Bădău and E. Gherman, *Rev. Roumaine Chim.*, **32**, (1987).

[2] M. Schmidt and G. G. Hoffmann, *Phosphorus and Sulfur*, **4**, 239 (1978).

[3] M. Schmidt and G. G. Hoffmann, *Phosphorus and Sulfur*, **4**, 249 (1978).

[4] M. Schmidt and G. G. Hoffmann, *Z. Anorg. allg. Chem.*, **445**, 167 (1978).

[5] E Bădău, Doctoral Thesis — 1981, Polytechnic Institute, Bucharest.

[6] M. Iovu and A. Angelescu, *Rev. Roumaine Chim.*, **18**, 263 (1973).

[7] I. Tănăsescu and M. Ionescu, "Lucrări practice de chimie anorganică", vol. 2, Ed. Tehnică, Bucharest, p. 143, 1975.

[8] W. J. Geary, *Cood. Chem. Rev.*, **7**, 81 (1971).

[9] D. Negoiu, S. Neagoe, M. Negoiu, E. Bădău and E. Gherman, *Rev. Roumaine Chim.*, **32**, 91 (1987).

[10] H. B. Gray and C. J. Ballhausen, *J. Amer. Chem. Soc.*, **85**, 260 (1963).

Revue Roumaine de Chimie, 34, *9–10*, 1877–1885 (1989)

STUDY OF MIXED LIGAND COMPLEXES OF Hg(II), Be(II) AND Cu(II) BY PAPER ELECTROPHORESIS

(M-NITRILOTRIACETATE-ADENINE SYSTEMS)

S. K. MISHRA,* A. P. MISHRA and K. L. YADAVA
Electrochemical Laboratories, Department of Chemistry,
University of Allahabad, Allahabad — 211002, India

Received May 16, 1987

A new method, involving the use of paper electrophoresis is described for the study of the equilibria in mixed-ligand complex systems in solution. The technique is based on the movement migration of a spot of metal ion under an electric field with the complexants added in the background electrolyte at a fixed pH 8.5. The concentration of primary ligand (NTA) was kept constant while that of secondary ligand (adenine) was varied. The plots of − log [adenine] against mobility were used to obtain information of the mixed complex and to calculate its stability constants. The binary equilibria M(II)—adenine and M (II)-NTA have also been studied since it is prerequisite for the study of mixed complexes. log *K* values have been found 5.95, 5.65 and 4.60 for mixed complexes of Hg(II), Be(II), Cu(II) respectively at $\mu = 0.1$ and temp. 35° ± 0.1°C.

INTRODUCTION

Paper electrophoresis (PE) was applied to the study of metal complexes in solution ; attempts were made to determine the stability constants of the complex species. [1,2] In the recent work of these laboratories a new method has been developed for the study of the stepwise complex formation. [3-5] Although the use of paper electrophoresis for the study of metal complex systems with single ligand seems to be well established, there is no systematic study for mixed complexes. However Czakis-Sulikowska [8] made some qualitative observations on the formation of mixed ligand complexes of Hg(II), and which do not throw light either on the nature of the species or on their stabilities. Publications [9,10] from our laboratories described a new method for the study of mixed complexes. The electrophoretic technique usually suffers from a number of defects. [6,7] Temperature during electrophoresis, capillary flow on the paper, electro-osmosis, adsorption and molecular sieving affect the mobility of the charged moieties. The technique described here is almost free from these vitiating factors. In the present investigation Hg(II), Be(II) and Cu(II) complexes of adenine and mixed ligand complexes of NTA with adenine as secondary ligand have been studied.

---

* Present address for correspondence : Dr. S. K. Mishra, Lecturer in Inorganic Chemistry, Department of Chemistry, Agra College, Agra — 282002, India.

EXPERIMENTAL

Apparatus

Electrophoresis equipment (Systronics model, 604 India) built in power supply A.C.—D.C. which is directly fed to a paper electrophoresis tank was used.

In most of electrophoresis instruments no attention is paid to the control of temperature. The electric current running through paper strips generated heat which caused evaporation of background electrolyte leading to serious error. In order to eliminate it, two hollow metallic plates coated outwardly with thin paper plastics were used for sandwiching paper strips and thermostated water (35°) was circulated through them.

pH measurements were made with Elico Model L_{1-10} pH meter using glass electrode.

Chemicals

Hg(II), Be(II) and Cu(II) perchlorates were prepared by precipitating the corresponding carbonates with sodium carbonate from solutions of nitrates, washing the precipitate thoroughly with boiling water treated with a suitable amount of 1% perchloric acid. The resulting mixtures were heated to boiling on a water bath and then filtered. The metal contents of filtrates were determined as usual and the final concentration was kept at 5.0×10^{-3} M.

Hydrogen sulphide water was used for detecting Hg(II) ions while 1-(2-pyridylazo)-2-naphthol (PAN), 0.1% (w/v) in ethanol was used for detecting Cu(II) ions. Aluminium-ammonium acetate 0.1 (w/v) solution in water was used for detecting Be(II). Glucose spot, electroosmotic indicator was detected by spraying aqueous silver nitrate in acetone and 2% ethanolic caustic soda : a black spot was observed.

Background Electrolyte

Stock solution of 9.0 M perchloric acid, 2.0 M sodium hydroxide and 0.5 M adenine were prepared from AnalaR samples (BDH, Poole, Great Britain); 0.01 M nitrilotriacetic acid was prepared from a sample obtained from E-Merck (Darmstadt F.R.G.). Each solution was standardized as usual. The background electrolyte in study of binary complexes consisted of 0.1M perchloric acid and 1.0×10^{-2} M adenine, 1.0×10^{-3} NTA, while in study of ternary complexes, it consisted of 0.1 M sodium perchlorate, 1.0×10^{-3} M NTA and varying amount of 1.0×10^{-2} M adenine, which was maintained at pH 8.5 by addition of sodium hydroxide.

Procedure

(i) *For binary complexes*

Paper strips Whatman No. 1 (30 × 1 cm) in triplicate were spotted in middle with metal ions. An extra strip was marked with glucose. The strips were sandwiched between two insulated hollow metal plates. The plates were then mounted in electrophoresis equipment with end of paper strips dipping in two tanks of the instrument. Each tank was filled with 150 mL of background electrolyte.An hour was allowed for strips to get wet by diffusion with background electrolyte solution. Subsequently electrophoresis was carried out for 60 minutes under the influence of 200 volts potential difference between the two tanks solutions. The strips were then removed from tank dried and migrated spots were detected with specific reagents. The distances travelled by spots were measured from the previously marked point. Triplicate strips always recorded less than ± 3% variation in travelled distances. Mean of the three was taken for calculation of mobility. Movement of glucose was used as correction factor for electroosmosis. The electrophoretic migration of metal spot on paper was observed at different pH's of the background electrolyte. Distances travelled towards anode were assumed to be negative and those towards cathode to be positive. The length of unimmersed strips above the tank containing background electrolyte is 26.5 cm ; so potential gradient applied in each experiment is 7.5 v/cm. Dividing movement by potential gradient yield the mobilities plotted in figs 1 and 2.

(ii) *For ternary complexes*

Strips are marked with metal ions in triplicate alongwith additional one marked with glucose. After drenching the strips with the background electrolyte the electrophoresis was

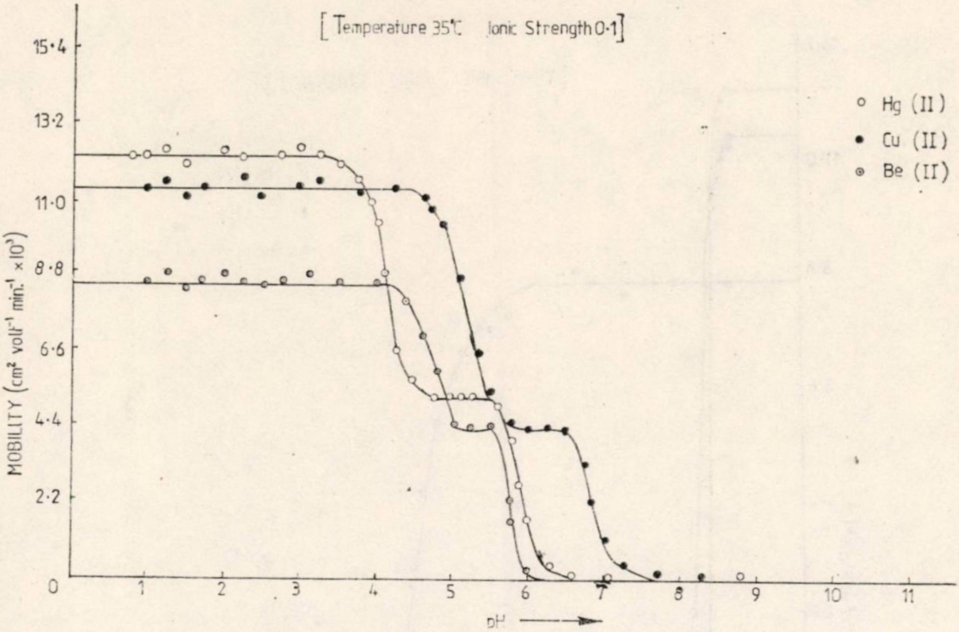

Fig. 1. — Mobility curve M(II) adenine system.

carried for one hour at the same potential difference as in case of binary complexes. For r subsequent observations, the adenine solution maintained at pH 8.5 was added progressively and ionophoretic mobility was recorded. A plot of mobility against log adenine was made, as shown in fig. 3.

RESULTS AND DISCUSSION

1. Metal-adenine binary systems

The plot of overall electrophoretic mobility of metal spot against pH gives a curve with a number of plateaus shown in fig. 1. A plateau is obviously indication of a pH range where speed is practically constant. This is possible only when a particular complex is overwhelmingly formed. Thus every plateau indicates the formation of a certain complex species. The first one in beginning corresponds to a region in which metal ions are uncomplexed. It lies in low pH region where the concentration of protonated species of adenine (H_2L^+) is obviously maximum, hence it is concluded that this protonated species of adenine is non-complexing. Beyond this range, metal ion spot has progressively decreasing velocity and hence complexation of metal ion should be taking place with other ionic species of adenine whose concentration increases progressively with increase of pH. The figure reveals that a second plateau in each case with positive mobility indicates the formation of 1 : 1 complex of cationic nature. Further increase in pH gives rise to a third plateau with zero mobility in each case which indicates formation of electrically neutral metal complex. This is possible only when two anionic species of adenine (L^-)

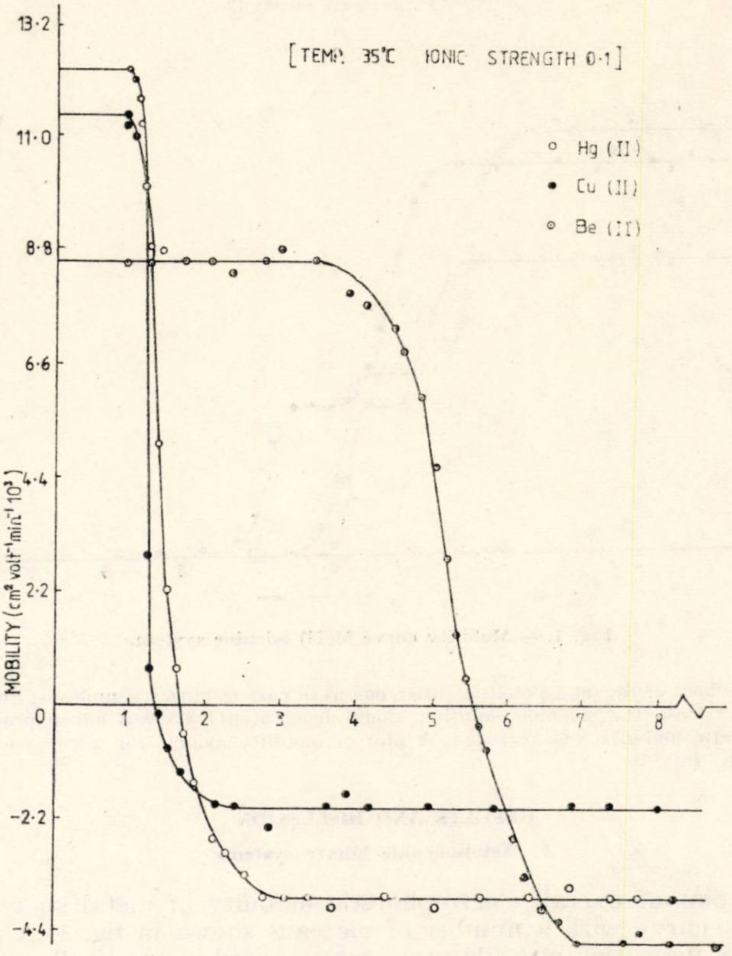

Fig. 2. — Mobility curve M(II) — NTA system.

combines with one bivalent metal ion. Chemical literature also assigns prominent liganding property to unprotonated anionic species of adenine ruling out any such property to the zwitter ion [12,13,14]. Further increase of pH has no effect on the mobility of metal ions.

In view of the above observation the complexation of metal ion with adenine anion (L^-) may be represented as:

$$M^{2+} + L^- \xrightleftharpoons{K_1} ML^+$$

$$ML^+ + L^- \xrightleftharpoons{K_2} ML_2$$

The metal spot on the paper is thus a conglomeration of uncomplexed metal ions, 1 : 1 complex and 1 : 2 complex. The spot moving under the

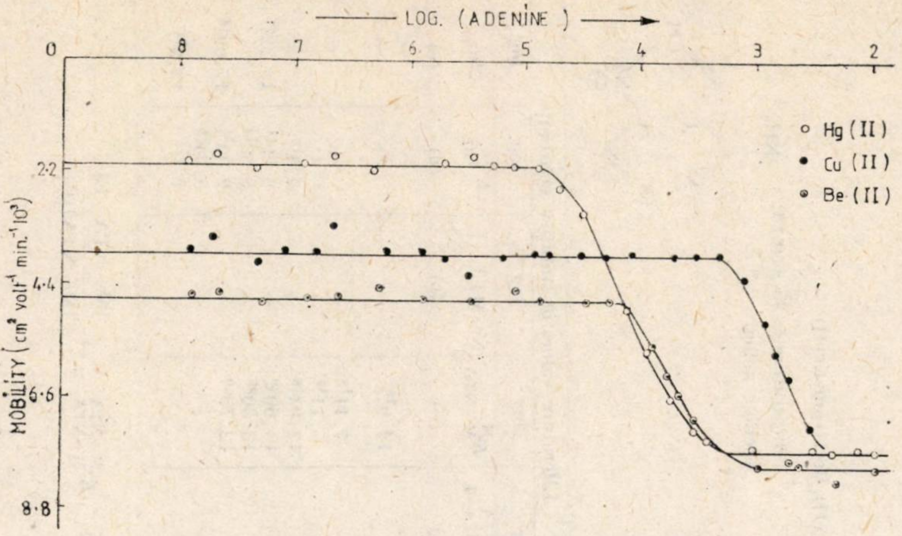

Fig. 3. — Mobility curve M(II) — NTA — adenine system.

influence of electric field, the overall mobility is given by equation:[1]

$$u = \Sigma\, u_n f_n$$

where u_n and f_n are mobility and mole fraction of a particular complex species. This equation is trasformed into the following form on taking into consideration different equilibria :

$$u = \frac{u_0 + u_1 K_1 [L^-] + u_2 K_1 K_2 [L^-]^2}{1 + K_1 [L^-] + K_1 K_2 [L^-]^2}$$

where u_0, u_1 and u_2 are mobilities of uncomplexed metal ion, 1 : 1 metal complex and 1 : 2 metal complex respectively. This equation has been used for calculating stability constants of the complexes of metal ions with adenine anion. For calculating the first stability constant K_1, the region between first and second plateau is pertinent. The overall mobility U will be equal to the arithmetic mean of mobility of uncomplexed metal ion, u_0 and that of the first complex u_1 at a pH where $K_1 = \frac{1}{L^-}$. With the help of dissociation constants of adenine (electrophoretically obtained our values $K_1 = 10^{4.41}$, $K_2 = 10^{9.90}$) the concentration of adenine anion L^- is determined for the pH, from which K_1 can be calculated. The stability constants K_2 of the second complex can be calculated by taking into consideration the region between the second and third plateau of the mobility curve. These calculated values are given in Table 1.

2. Metal-NTA binary systems

The observations on overall mobility of metal spots in the presence of NTA at different pH values are represented in fig. 2. As is evident from the figure that with all the three metal ions two plateaus are obtained,

Table 1

Stability constants for binary and ternary complexes of Hg(II), Be(II) and Cu(II)

Ionic strength 0.1

NTA Anion = $N-(CH_2COO)_3^{3-}$

Temperature = 35 ± 0.1°C

Adenine anion = L^- =

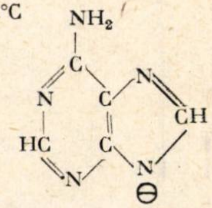

Metal ion	Calculated values of stability constants					Literature values of stability constants				
	log $K'^{M-NTA}_{M-NTA-L}$ (a)	log K^{M}_{M-NTA} (b)	log M−NTA−L (c)	log $K^{M}_{1_{ML}}$ (d)	log 2_{ML_2} (e)	log $K^{M-NTA}_{N-NTA-L}$ (a)	log K^{M}_{M-NTA} (b)	log N−MTA−L (c)	log $K^{M}_{1_{ML}}$ (d)	log $^{2}ML_2$ (e)
Hg(II)	5.95	13.30	19.25	7.81	13.92	—	14.6^{18}	—	—	—
	±0.05	±0.07	±0.12	±0.06	±0.11					
Be(II)	5.65	7.10	12.75	7.20	13.40	—	7.11^{18}	—	—	—
	±0.06	±0.06	±0.12	±0.05	±0.10		7.11^{19}			
Cu(II)	4.60	12.71	17.31	6.73	11.80	—	12.94^{18}	—	7.4^{13}	—
	±0.04	±0.06	±0.10	±0.04	±0.09	—	13.60^{20}	—	6.99^{21}	13.32^{21}
						—	13.30^{20}	—	8.53^{12}	—
						—	12.75^{20}	—	9.00^{14}	17.00^{14}
						—	—	—	8.94^{22}	—
						—	—	—	7.1^{14}	13.5^{14}

$$\text{where } K^{M}_{1_{ML}} = \frac{[ML]}{[M][L]}\ ;\ K^{M}_{2_{ML_2}} = \frac{[ML_2]}{[ML][L]}\ ;\ K^{M}_{M-NTA} = \frac{[M-NTA]}{[M-][NTA]} \quad \text{and} \quad K'^{M-NTA}_{M-NTA-L} = \frac{[M-NTA-L]}{[M-NTA][L]}$$

the mobility of last plateaus lies in the negative region, showing negatively charged nature of the complexes. Hence only one NTA anion is assumed to be combined with one bivalent metal ion to give 1 : 1 M—NTA—complex which is in agreement with the findings of others. [15–17] The stability constants of complexes with NTA are calculated in a manner described in the preceding paragraph (by using electrophoretically obtained dissociation constants values $K_1 = 10^{1.80}$, $K_2 = {}^{2.45}$, $K_3 = 10^{3.65}$). The calculated values are given in Table 1.

3. Metal-NTA-adenine ternary systems

The study of this system has been done at pH 8.5. It is observed from the mobility curves of M-adenine and M-NTA binary systems that binary complexes, M-adenine and M-nitrilotriacetate are formed at a pH lower than 8.5. Thus it would be proper to study the transformation of M—NTA complex into M-NTA-adenine complex at pH 8.5 in order to avoid any side interaction.

The plot of mobility against logarithm of concentration of added adenine gives a curve (Fig. 3) containing two plateaus, one in the beginning and the other in the end. The mobility in the range of first plateau corresponds to the mobilities of 1 : 1 M—NTA complexes. The mobility in this range is also in agreement with mobility of 1 : 1 M—NTA complex as evinced in the study of binary M—NTA system. The mobility of the last plateau is more negative than that of the first plateau. So it indicates the formation of more negatively charged complex. Further since the mobility in the last plateau does not tally with the mobility of 1 : 1 and 1 : 2 metal adenine complex (observed in our study of binary M-adenine system), it is inferred that the moiety in the last plateau is due to coordination of adenine anion to 1 : 1 M—NTA moiety resulting in the formation of 1 : 1 mixed complex (M—NTA-adenine) as:

$$[\mathrm{M}-\mathrm{NTA}^-] + L^- \overset{K'}{\rightleftharpoons} [\mathrm{M}-\mathrm{NTA}-\mathrm{L}]^{2-}$$

In the present electrophoretic study the transformation of a simple complex into mixed complex takes place, hence the overall mobility is given by:

$$u = U_0 f_{\mathrm{M-NTA}} + U_{f_{\mathrm{M-NTA-L}}}$$

where u_0, u_1 and $f_{\mathrm{M-NTA}}$; $f_{\mathrm{M-NTA-L}}$ are mobilities and the mole-fraction of M—NTA, and M—NTA—L^{2-} complexes respectively. Substituting the values of mole fractions, the overall mobility is given by the equation

$$U = \frac{u_0 + u_1 K'[L^-]}{1 + K'[L^-]}$$

u_0 and u_1 are the mobilities in the regions of the two plateaus of the curve. From the figure, the concentration of adenine at which the overall mobility is the mean of the mobilities of two plateaus is determined. Concentration of adenine anion at pH 8.5 for this adenine concentration is calculated. K' is obviously equal to $1/[L^-]$. All these calculated values of K' are given in Table 1.

A perusal of Table 1 reveals that the order of stability constants viz Hg(II), Be(II) and Cu(II) is the same for M(II)-adenine and M(II)—NTA-adenine complexes while in M(II)—NTA binary complexes, the order is Hg(II)> Cu(II)> Be(II). It might be by virtue of different dentacity and nature of adenine ligands. Column (a) of the table gives an idea about the formation of mixed complexes through coordination of an adenine anion to 1 : 1 M—NTA complex. It also visualizes the complexing tendency of the adenine anion to form a mixed complex. It is meaningful to compare column (a) with (d) which gives an idea of the affinity of anionic adenine for metal ion. It is seen here that though the gradation in the tendencies of the adenine anion is the same, it is smaller when is combines with the binary complex (M—NTA) in comparison to that of uncomplexed metal ion. The comparison of log $K^{M}_{M-(Ade.)}$ and log $K^{M(Ade)}_{M(Ade)_2}$ also elucidates the same view.

The conclusion that the combining capacity of a ligand is reduced when it acts as a secondary ligand instead of primary ligand, [23,24] can be further substantiated by considering the role of NTA as a secondary ligand. The values of log ($K^{M-L}_{M-L-NTA}$ (11.44, 5.55, 10.58 for M(II)-adenine-NTA terary complex of Hg(II), Be(II) and Cu (II) respectively) can be computed from the expression :

$$\log K^{M-L}_{M-L-NTA} + \log \beta_{M-NTA-L} - \log K^{M}_{ML}$$

that gives a measure of the tendency of NTA coordinating with binary 1 : 1 complex of the metal ion with adenine (ML). Comparison of log K^{M}_{M-NTA} with log $K^{ML}_{M-L-NTA}$ substantiates the same view while log K^{M}_{M-NTA} and log $K^{M}_{M-Ade.}$ represent better coordinating capacity of NTA over adenine.

Adenine anion forms chelate with metal ions coordinating through $ON_{(3)}$ and $N_{(9)}$. [25,26] Our observations obtained electrophoretically definitely reveal that negatively charged species (L^-) of the adenine is the coordinating species which is in agreement with the finding of others, [11,12,14-25,26,27] while a few workers [28,29] consider neutral species to be the sole coordinating species.

Our electrophoretically determined values resemble the available literature values ; the slight difference may be due to change in temperature, ionic strength and experimental conditions.

REFERENCES

[1] V. J. Jokl, *Chromatography*, **14**, 71 (1964).

[2] J. Biernat, *Rocz. Chem. Ann. Soc. Chim. Polonorum*, **38**, 343 (1964).

[3] R. K. P. Singh, J. K. Sircar, J. R. Yadava, P. C. Yadava and K. L. Yadava, *Electrochim. Acta*, **26**, 395 (1980).

[4] R. K. P. Singh, J. K. Sircar, R. Khelawan and K. L. Yadava, *Chromatographia*, **13**, 709 (1980).

[5] R. K. P. Singh, J. R. Yadava, P. C. Yadava and K. L. Yadava, *Z. phys. Chem.*, Leipzig, **264**, 3 (1983).

[6] H. J. McDonald, "Ionography, Electrophoresis in Stabilized Media", Year Book Publication, Chicago (1955).

[7] D. J. Shaw, "Electrophoresis", Academic, London and New York, pp. 99—103 (1969).

[8] M. Czakis-Sulikowska, *Zesz. nauk. Politech. Ldz. Chem.*, **6**, 2039 (1967).

[9] J. R. Yadava, J. K. Şirkar, K. L. Yadava, *Electrochem. Acta*, **26**, 391 (1981).

[10] R. K. P. Singh, J. R. Yadava and K. L. Yadava, *J. Electrochem. Soc.*, **30**, 250 (1981).
[11] A. Albert, and E. P. Serjeant, *Biochem. J.*, **76**, 62 (1960).
[12] M. M. Taqui Khan and C. R. Krishnamoorthy, *J. Inorg. Nuclear Chem.*, **33**, 1417 (1971).
[13] E. E. Kriss and K. B. Yatssmirskii, *Zhur. neorg. Khim.*, **13**, 2370 (1968).
[14] T. R. Harkins and H. Freiser, *J. Amer. Chem. Soc.*, **80**, 1132 (1958).
[15] N. G. Elenkova and R. A. Tsoneva, *J. Inorg. Nuclear Chem.*, **35**, 84 (1973).
[16] D. L. Rabenstien and G. Blankey, *Inorg. Chem.*, **12**, 128 (1973).
[17] V. V. Ramanujam, M. Rajlakshmi and M. Shivashankar, *Ind. J. Chem.*, **20A**, 531 (1981).
[18] A. E. Martell and R. M. Smith, "Critical Stability constants", Vol. 1 (Amino acids) Planum Press, New York and London, p. 139.
[19] L. G. Sillen and A. E. Martell, "Stability Constants of Metal in Complexes", Special Publication No. 17, Chemical Society, London (1964), pp. 452—455.
[20] D. D. Perrin, "Stability Constants of Metal Ion Complex, Part B (Organic Ligand)", Pergamon Press, Oxford, I.U.P.A.C.
[21] H. Reinert and R. Wein, *Hopp-seylor's Z. Physiol. Chem.*, **350**, 1310 (1969).
[22] G. E. Chency, H. Freiser, and Q. Fernands, *J. Amer. Chem. Soc.*, **81**, 2611, (1959).
[23] D. Hopgood and J. R. Angelici, *J. Amer. Chem. Soc.*, **90**, 2508 (1968).
[24] J. D. Joshi, *Ind. J. Chem.*, **21A**, 531 (1981).
[25] A. N. Speca, C. M. Mukulski, F. J. Iaconianni, L.L. Pytleswski and N. M. Karayannis, *J. Inorg. Nuclear Chem.*, **43**, 2771 (1981).
[26] B. T. Khan, S. Vijayakumari and G. Narsagoud, *Ind. J. Chem.*, **21A**, 264 (1982).
[27] R. Ghose, M. C. Chattopadhyaya and A. K. Dey, *Ind. J. Chem.*, **19A**, 783 (1980).
[28] M. M. Taqui Khan and M. S. Jyoti, *Ind. J. Chem.*, **15A**, 1002 (1977).
[29] G. K. R. Makar and D. R. Williams, *J. Inorg. Nuclear Chem.*, **36**, 1675 (1974).

Revue Roumaine de Chimie, **34**, *9–10*, 1887–1893 (1989)

STUDIES ON BIGUANIDE DERIVATIVES: COPPER(II) COMPLEXES WITH ETHYLENEDIBIGUANIDE, TRIMETHYLENEDIBIGUANIDE, *meta*-PHENYLENEDIBIGUANIDE, PIPERAZINEDIBIGUANIDE AND PHENYLBIGUANIDE*

A. SYAMAL

Department of Chemistry, Regional Engineering College,
Kurukshetra 132119, Haryana, India

Received August 15, 1987

Copper(II) complexes of quadridentate ligands ethylene-dibiguanide, trimethylendibiguanide, *meta*-phenylenedibiguanide, piperazinedibiguanide and bidentate ligand phenylbiguanide have been studied by electron paramagnetic resonance in polycrystalline form and in the corresponding nickel(II) complex matrix. EPR spectra of the complexes in the corresponding nickel(II) complex matrix exhibit nine nitrogen superhyperfine lines on the high field 3/2↔3/2 cooper hyperfine splitting components indicating the presence of four equivalent nitrogen atoms around the copper(II) ion. The evaluation of the covalency parameters from the EPR data indicates that the unpaired electron of copper(II) spends about 31–36% of its time in the nitrogen donor sites of the ligands. The EPR spectra of the complexes suggest the presence of CuN_4 coordination sphere in the complexes. A comparison of the bonding parameters of the copper(II) dibiguanide complexes with those of the copper(II) complexes of biguanide and phenylbiguanide indicates that the bridging group in quadridentate dibiguanides has negligible effect on the EPR spectra and bonding parameters. A comparison of the bonding parameters of the present complexes with those of the copper(II) complexes of tetrapenylporphine and phthalocyanine indicates that biguanides and dibiguanides rank among strong field ligands.

INTRODUCTION

Biguanides (I) and their metal complexes exhibit medical properties [1] and are used as hypoglycaemic and antimalarial agents. Biguanides and dibiguanides (II–V) are considered to be strong field ligands. Biguanides have stabilized a large number of unusual oxidation states of transition metal ions (Co^{1+}, Ni^{3+}, Ni^{4+}, Mn^{4+}, Ag^{3+}, Au^{3+}, Mo^{3+} etc.) and have produced metal complexes of very high formation constant values.[2] Metal complexes of biguanides exhibit aromatic character.[3] The introduction of a bridging group connecting two biguanide molecules e.g.

---

* Presented at the 22nd Annual Convention of Chemists held at Ravinshankar University, Raipur, India in November, 1985.

in ethylenedibiguanide(II) is expected to influence the stability and bonding parameters in dibiguanide complexes. We report here the EPR spectra of copper(II) doped in diamagnetic nickel(II) complexes of ethylenedibiguanide(II), trimethylenedibiguanide(II), *meta*-phenylenedibiguanide(IV), piperazinedibiguanide(V) and phenylbiguanide(VI) with the view of noticing the effect of bridging groups in the ESR spectra and bonding parameters of the copper (II) complexes of biguanide and dibiguanides. EPR spectrum of copper(II) complex of biguanide has been reported earlier.[4]

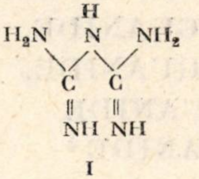

I

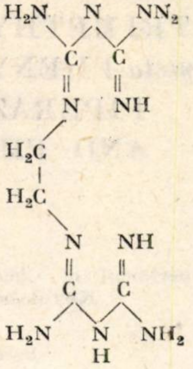

II

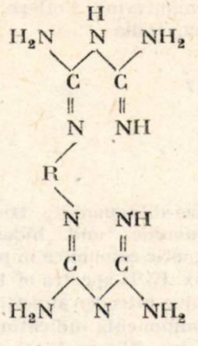

III, IV, V

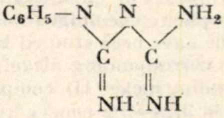

IV

III. $R = -CH_2-CH_2-CH_2-$

IV. $R = m-C_6H_4$

V. 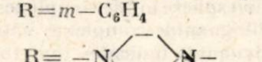

EXPERIMENTAL

Materials — Nickel(II) sulphate hexahydrate and copper(II) sulphate pentahydrate were the analar products of Glaxo Laboratories. Dicyandiamide was purchased from SD's Lab. Chem. Industries. Phenylbiguanide was obtained from Aldrich Chemical Co. (U.S.A.). Ethylenedibiguanide sulphate, trimethylenedibiguanide sulphate, *meta*-phenylenedibiguanide sulphate and piperazinedibiguanide sulphate and their copper(II) complexes were prepared according to the published procedures. [2] Bis(phenylbiguanide)nickel(II) dichloride and bis(phenylbiguanide) copper(II) dichloride were prepared according to the method of Ray and Chakravarty.

Method for the preparation of Cu(ethylenedibiguanide)-doped sample of Ni(ethylenedibiguanide) — Nickel(II) sulphate hexahydrate (95% of 0.005 mol) and copper(II) sulphate pentahydrate (5% of 0.005 mol) were dissolved in 40 mL of water. Ethylenedibiguanide sulphate (0.006 mol) was dissolved in a minimum amount of $4N$ solution of sodium hydroxide, and to this the above solution containing the metal ions was added slowly while strirring magnetically. The pH of the mixture was adjusted to 10 with $4N$ sodium hydroxide solution. The separated precipitates were filtered under reduced pressure, washed thoroughly with water and then with ethyl alcohol, and was dried *in vacuo* at room temperature.

In case of other dibiguanides the copper(II)-doped complexes in the corresponding nickel(II) complex matrix were prepared by following a similar procedure as described above.

$[Ni(phenylbiguanide)_2]Cl_2 \cdot 2H_2O$ was doped by recrystallising a mixture of the copper(II) and nickel (II) chloride complexes (5%; 95% respectively) of the ligand from water.

Spectral measurements — Electronic spectra were recorded in nujol mull with the help of a Cary Model 14 recording spectrophotometer. EPR spectra were obtained on a Varian V45 02—12 X-band spectrometer with 100 kHz modulation. A cylindrical quartz sample tube was used for the spectra of powdered samples. A minutely powdered sample of diphenylpicrylhydrazil free radical was used as a g-marker in a dual channel cavity and the frequency was monitored with the help of a frequency meter.

RESULTS AND DISCUSSION

The copper(II) complexes of the nitrogen donor ligands ethylenedibiguanide, trimethylenedibiguanide, *meta*-phenylenedibiguanide, piperazinedibiguanide, and phenylbiguanide were doped into the corresponding diamagnetic, square planar nickel(II) complexes in order to obtain the magnetic dilution. EPR spectra of the polycrystalline samples of Cu(ethylenedibiguanide), Cu(trimethylenedibiguanide), Cu(*meta*-phenylenedibiguanide), Cu(piperazinedibiguanide), and $[Cu(phenylbiguanide)_2]Cl_2$ exhibit a single exchange-narrowed line at $g = \sim 2.08$ with a peak to peak separation of about 110 gauss. But the magnetic dilution to the correspondig square planar and diamagnetic nickel(II) complex matrix results in the resolution of the copper(II) nuclear hyperfine splittings and nitrogen superhyperfine splittings. The EPR spectra of the complex are comparable to the EPR spectrum of the copper(II) complex of biguanide.[4] The EPR spectra appear to be axial and the spin-Hamiltonian constants obtained from the spectra are given in Table 1. EPR data indicated that $g_{||} > g_{\perp}$, $A^{Cu}_{||} > A^{Cu}_{\perp}$ and $A^{N}_{\perp} > A^{N}_{||}$ and are according to the expectations. Kivelsion and Neiman[6] have indicated that $g_{||}$ is a moderately sensitive parameter for predicting covalency. For covalent environments, $g_{||}$ is less than 2.3 and for ionic environments $g_{||}$ is usually $\geqslant 2.3$. Thus, the ESR data (Table 1) indicate that the metal-ligand bonding in the copper(II) complexes of ethylenedibiguanide, trimethylenedibiguanide, *meta*-phenylenedibiguanide, piperazinedibiguanide, and phenylbiguanide are covalent.[6] The evaluation of the EPR covalency parameters (discussed later) also supports this. The parameters $g_{\perp}$, $g_{||}$, $A^{Cu}_{\perp}$, $A^{Cu}_{||}$, $A^{N}_{\perp}$ and $A^{N}_{||}$ where measured from the anisotropic spectra of the magnetically dilute polycrystalline solids. The observations of nine nitrogen superhyperfine lines on the high field $3/2 \Leftrightarrow 3/2$ copper hyperfine splitting components indicates the presence of four equivalent nitrogen atoms around copper(II) ion with CuN_4 chromophore which is consistent with the single crystal X-ray studies.[7] The EPR spectra of the complexes are quite comparable with the EPR spectra of $Cu(biguanide)_2$ and Cu(O-methyl-1-amidinourea)$_2$ which contain CuN_4 chromophore.[4,8] There

Table 1

Spin — Hamiltonian constants of [Cu(dibiguanide)], [Cu(phenylbiguanide)$_2$/Cl$_2$ and related complexes

Compound	Medium	$G = \frac{(g_{\parallel} - 2)}{(g_{\perp} - 2)}$	g_{av}^{a}	$g_{\parallel}$	$g_{\perp}$	$A_{\perp}^{Cu}$ $\times 10^4 cm^{-1}$	$A_{\parallel}^{Cu}$	$A_{\parallel}^{N}$ $\times 10^4 cm^{-1}$	$A_{\perp}^{N}$ $\times 10^4$
[Cu(ethylenedibiguanide)]	Powder	3.91	2.08						
[Cu(trimethylenedibiguanide)]	Ni(II) complex	3.91	2.10	2.19	2.05	208	32	11	14
	Ni(II) complex	3.50	2.09	2.17	2.05	220	33	12	15
[Cu(piperazinedibiguanide)]	Ni(II) complex	3.71	2.09	2.18	2.05	132	36	10	17
[Cu(*m*-phenylenedibiguanide)]	Ni(II) complex	3.29	2.09	2.16	2.05	169	35	12	16
[Cu(phenylbiguanide)$_2$/Cl$_2$	Ni(II) complex	3.29	2.09	2.16	2.05	188	35	15	17
[Cu(biguanide)$_2$]	Ni(II) complex^b	2.78	2.098	2.169	2.062	208	24	16^e	
[Cu(phthalocyanine)]	Free ligand^c	3.69	2.098	2.179	2.050	202	19	16.7	
[Cu(tetraphenylporphine)]	Chloroform, free ligand^d	2.77	2.112	2.193	2.071	202	29	15.9	

[a] $g_{av} = 1/3(g_{\parallel} + 2g_{\perp})$; $A_{av} = 1/3\,(A_{\parallel} + 2A\perp)$.

[b] Reference 4. [c] Reference 16. [d] Reference 15.

[e] A_{O}^{N}.

was no indication of more than two g-values in the EPR spectra of the copper(II) complexes of the present ligands. This information and the occurrence of an electronic spectral band at around 19600 cm^{-1} in these copper(II) complexes indicate also the presence of square planar CuN_4 coordination sphere and D_{4h} symmetry for these complexes.[7-8]

The EPR spectra of the copper(II) complex in tetragonal crystal field is described by the following spin-Hamilltonian :

$$H = g_{\|}\beta H_z S_z + g_{\perp}\beta(H_x S_x + H_y S_y) + A_{\|}^{Cu} I_z S_z + A_{\perp}^{Cu}(I_x S_x + I_y S_y) + S \cdot \Sigma A_n \cdot I_n$$

where H is the applied magnetic field, β is the Bohr magneton, S is the total spin operator, I_n is the ligand atom nuclear spin, and A_n is superhyperfine structure tensor for the n ligand atoms.

The ground state wave functions in LCAO—MO model in D_{4h} symmetry copper(II) complexes are given[9] by :

$$\psi_{B_{1g}} = \alpha d_{x^2-y^2} - \frac{1}{2}\,\alpha'(-\sigma_x(1) + \sigma_y(2) + \sigma_x(3) - \sigma_y(4))$$

$$\psi_{B_{2g}} = \beta_1 d_{xy} - \frac{1}{2}\,\beta_1'(p_y(1) + p_x(2) - p_y(3) - p_y(4))$$

$$\psi_{A_{1g}} = \alpha_1 d_z 2 - \frac{1}{2}\,\alpha_1'(\sigma_x(1) + \sigma_y(2) - \sigma_x(3) - \sigma_y(4))$$

$$\psi_{E_{1g}} = \begin{cases} \beta d_{xz} - \beta'/\sqrt{2}(p_z(1) - p_z(3)) \\ \beta d_{yz} - \beta'/\sqrt{2}(p_z(2) - p_z(4)) \end{cases}$$

The A_{1g} and B_{1g} states represent the σ bonding, and the E_{1g} and B_{2g} states account for the out-of-plane and in-plane π bonding, respectively. The larger the value of the square of the σ bonding coefficients (α', α_1') the more covalent is the bonding. The ligand orbitals involved in the in-plane σ bonding are taken as sp^2 hybridised orbitals.[10] α is related[11] to S, the overlap integral between the $d_{x^2-y^2}$ orbital and the normalised nitrogen orbitals, as follows :

$$\alpha^2 - 2\,\alpha\alpha' S + \alpha'^2 = 1 \tag{1}$$

Eq. (1) is obtained by the normalisation of B_{1g} orbital. S has the value[11] of 0.093. The value of α'^2 which is equal to $(1 - \alpha_{Cu}^2)^{1/2} - \alpha S$ (where α_{Cu} represents σ bond metal-ligand parameter) was calculated from A_{av}^{N} value and was used to calculate the value of α^2. The $\alpha_N'^2$ value (0.31—0.36) of the present complexes represents approximately the percent of electron delocalisation and thus the copper(II) unpaired electron ($3d^9$) spends about 31—36% of its time in the nitrogen donor sites of the biguanide ligands. Thus, the EPR evidence indicates that the unpaired

d electron of the metal ion is delocalized on to the ligands. A comparison of $\alpha_N'^2$ values of the present copper(II) complexes with those of copper(II) complexes with the acknowledged strong field ligands such as tetraphenylporphine ($\alpha_N'^2 = 0.36$) and phthalocyanine ($\alpha_N'^2 = 0.35$) indicates that biguanide and dibiguanides rank among the strong field ligands. The work of MacDonald has indicated that the position of ethylenedibiguanide in spectrochemical series is slightly below the strong field ligand cyanide ion.[12] α_N^2 values of the complexes were found in the range 0.73—0.77.

The in-plane σ covalency parameter, α_{Cu}^2 was calculated using the expression given by Kivelson and Neiman :[11]

$$\alpha_{Cu}^2 = -\left(\frac{A_{||}}{0.036}\right) + (g_{||} - 2.002) + \frac{3}{7}(g_\perp - 2.002) + 0.04 \qquad (2)$$

and was compared with the $\alpha_N'^2$ and $\alpha_N^2 \alpha_{Cu}^2$ value accounts for the fraction of the unpaired electron density situated on the copper(II) ion and is 0.71 -0.84 for the present complexes. The α_N^2 values calculated from the nitrogen superhyperfine splittings are in general low in comparison to the analogous α_{Cu}^2 values and thus $\alpha_N^2 \neq \alpha_{Cu}^2$. This discrepancy has been explained in terms of variation of copper 4s electron density which has been assumed to be constant in equation (2).[12] A comparison of these α_{Cu}^2 values with the α_{Cu}^2 values of copper(II) tetraphenylporphine ($\alpha_{Cu}^2 = 0.82$)[15] and copper (II) phthalocyanine ($\alpha_{Cu}^2 = 0.80$)[16] indicates the similarity of the present biguanide complexes with the copper(II) complexes of strong field ligands phthalocyanine and tetraphenylporphine, all having CuN_4 chromophore.

In D_{4h} symmetry copper(II) complexes with a $^2B_{1g}$ ground state g values are given[13] by

$$g_{||} = 2.002 - 8\, k_{||}^2 \lambda_0 / \Delta E_{xy}$$

and

$$g_\perp = 2.002 - 2k_\perp^2 \lambda_0 / \Delta E_{xz}$$

where $k's$ are the orbital reduction factors. The combination of the above two expressions leads to

$$G = \frac{(g_{||} - 2.002)}{(g_\perp - 2.002)} = \frac{4k_{||}^2 \Delta E_{xz}}{k_\perp^2 \Delta E_{xy}}$$

If the G value is less than 4.0, the ligands forming the copper II complexes are regarded as strong field ligands.[14] The G values for the presents complexes are in the range 3.29—3.91 and indicate the strong field nature of the ligands biguanides and dibiguanides. G values of the present complexes are comparable to those of copper(II) complexes of strong field ligands tetraphenylporphine ($G = 2.77$)[15] and phthalocyanine ($G = 3.69$).[16]

A comparison of the spin-Hamiltonian parameters and bonding parameters (α_N^2, $\alpha_N'^2$, σ_{Cu}^2) of the present copper(II) dibiguanide complexes containing the bridging group with those of the copper(II) complexes of biguanide and phenylbiguanide in which no bidging group is present, indicates that the nature of the bridging groups in dibiguanides has little effect on the EPR spectra and bonding parameters. Similar observations were also noticed in case of oxovanadium(IV) complexes of biguanide and dibiguanides.[17] The bridging groups like $-CH_2-CH_2-$, $-CH_2-CH_2-CH_2-$, $-C_6H_4-$ etc. bridge two biguanide molecules in one side (see II—V) leaving the other side unbridged. The bridging in both the sides would produce a macrocylic ligand in which case a pronounced effect of the bridging groups is expected to be noticed. Thus, the one sided bridging and the absence of a macrocyclic system do not effect appreciably the delocalisation of electrons in comparison to the non-bridging system (see I and VI) as is evident from the bonding parameters.

ACKNOWLEDGEMENT. The author is indebted to the Council of Scientific and Industrial Research, New Delhi 110001 for the financial support of the work.

REFERENCES

[1] G. D. Cambel, "Oral Hypoglycemic Agents", Academic Press, New York, 1969.
[2] P. Ray, *Chem. Rev.*, **61**, 313 (1961).
[3] A. Syamal, *J. Scient. Indust. Res.*, **37** (1978) 661.
[4] John R. Wasson and Zacharopaules P., *J. Inorg. Nucl. Chem.*, **31**, 3881 (1969).
[5] P. Ray and K. Chakravarty, *J. Indian Chem. Soc.*, **18**, 609, 620 (1941).
[6] D. Kivelson and R. Neiman, *J. Chem. Phys.*, **35**, 149 (1961).
[7] M. Mathew and N. R. Kuncber, *Acta Crystallogr.*, **26B** 2054 (1970).
[8] John R. Wasson and Charles Trapp, *J. phys. Chem.*, **73**, 3763 (1969).
[9] A. H. Maki and McGarvey B. R., *J. Chem. Phys.*, **29**, 31 (1958).
[10] A. H. Maki and B. R. McGarvey, *J. Chem. Phys.*, **29**, 357 (1958).
[11] D. Kivelson and R. Neiman, *J. Chem. Phys.*, **35**, 149 (1961).
[12] D. J. MacDonald, *Inorg. Chem.*, **6**, 2269 (1967).
[13] C. J. Balhausen, *Introduction to Ligand Field Theory*, McGraw-Hill Bucb Co., New York, 1962; I. M. Proctor, B. J. Hathaway and P. Nicholls, *J. Chem. Soc.*, **A.**, **1968**, 1678.
[14] J. M. Assour, J. Goldmacher and S. E. Harrison, *J. Chem. Phys.*, **43**, 159 (1965).
[15] J. M. Assour, *J. Chem. Phys.*, **43**, 2477 (1965).
[16] S. E. Harrison and J. M. Assour, *J. Chem. Phys.*, **40**, 365 (1964).
[17] A. Syamal, *Indian J. Pure Appl. Physics*, **21**, 130 (1983).

Revue Roumaine de Chimie, 34, *9–10*, 1895–1905 (1989)

FACTORS AFFECTING STABILITY AND EQUILIBRIA OF FREE RADICALS. XVI[1]

PREPARATION AND EPR SPECTRA OF CAPTO-DATIVE N-ALKOXY-DINITROPHENYL-AMINYLS

GABRIELA STĂNCIUC,[a] MIRON-TEODOR CĂPROIU,[a] HORIA CĂLDĂRARU,[b] AGNETA CARAGHEORGHEOPOL,[b] TITUS CONSTANTINESCU[b]
and ALEXANDRU T. BALABAN *[c]
[a] Center of Organic Chemistry, Bucharest
[b] Center of Physical Chemistry, Bucharest
[c] Polytechnic Institute, Organic Chemistry Chair, Splaiul Independenţei 313, 77206 Bucharest, Romania

Received May 18, 1989

The oxidation of N-alkoxy-2,6- and -2,4-dinitroanilines (alkoxy = methoxy, ethoxy, isopropoxy and benzyloxy) and of N-alkoxy-4-alkyl-2,6-dinitroanilines (where alkoxy = methoxy, ethoxy and isopropoxy; alkyl = methyl and t-butyl) afforded the corresponding aminyls, whose EPR spectra were completely interpreted (by simulation) and assigned. According to their hyperfine splitting constants (hfc's) pattern, these aminyls as well as their previously investigated picryl analogs can be classified as π-radicals.

INTRODUCTION

Capto-dative (push-pull) free radicals were first discussed in the case of nitrogen-centered systems (diarylaminyls and N,N-disubstituted hydrazyls); [2] subsequently, Katritzky [3] and Viehe [4] with their coworkers advocated the idea that carbon-centered free radicals may also possess enhanced persistence due to the capto-dative effect[4] (a term introduced by Viehe) or to merostabilization [3] (an equivalent term coined by Katritzky).

Theoretical and experimental investigations on the magnitude of the capto-dative effect have not yielded conclusive evidence because some authors argue for substantial capto-dative stabilization,[5] whereas other authors find a low or negligible effect for carbon-centered free radicals.[6,7]

Experimental evidence starting with Goldschmidt's discovery of hydrazyls such as 1,1-diphenyl-2-picrylhydrazyl (DPPH)[8] followed by results of our laboratory on capto-dative diarylaminyls,[9] alkoxyaminlys[40] and various other hydrazyls[11] indicates that some of the most persistent known radicals, e.g. DPPH, belong to this group. Linnett's rationalization [12] which is close to Pauling's "three electron bond" accounts for the stability of hydrazyls and for the enhanced intramolecular rotation barrier observed by us in hydrazyls,[13] owing to the increased bond order of the N—N bond in hydrazyls relative to the parent hydrazines.

In addition, one may perceive an analogy between capto-dative hydrazyls such as DPPH and nitroxides which are also persistent free radicals; in DPPH the picryl group enhances the electronegativity of the aminyl nitrogen making it comparable to that of the oxygen atom in nitroxides.

The present paper continues the preceding investigations on N-alkoxy-N-arylaminyls wherein the aryl group is now a phenyl made a strong electron-acceptor by substitution with 2,4- or 2,6-dinitro groups. Previous work had concentrated on 2,4,6-trinitrophenyl (picryl) analogs.[14]

RESULTS AND DISCUSSION

All N-alkoxy-2,6-dinitrobenzeneamines, and N-methoxy-2,4-dinitrobenzeneamine, were prepared from the corresponding chlorodinitrobenzenes and alkoxyamine hydrochlorides in the presence of potassium hydroxide.

$$\mathrm{Ar{-}Cl} + \mathrm{RO\overset{+}{N}H_3\overset{-}{Cl}} + \mathrm{2KOH} \xrightarrow[-\mathrm{H_2O}]{-\mathrm{2KCl}} \mathrm{Ar{-}NH{-}OR}$$

They are yellow crystalline compounds which have been characterized by elemental analysis, IR and ^1H—NMR spectra.

On oxidation with various oxidizing agents (Ag_2O, lead dioxide or tetraacetate, NO_2) these N-alkoxy-dinitroanilines afforded solutions whose EPR spectra showed an unexpected transient behaviour. Unlike their picryl analogues which on oxidation yielded the N-alkoxy-picrylaminyls as a single paramagnetic species, in the present cases depending upon the oxidation conditions, three types of radicals could be detected under static conditions, at room temperature:

(a) a short-lived nitroxide radical, with unknown structure, because it could not be obtained as a single paramagnetic species in solution;

(b) the expected N-alkoxy-dinitrophenylaminyl which could be obtained under certain conditions;

(c) the corresponding N-alkoxy-picrylaminyl, whose mechanism of formation will be discussed in a forthcoming paper (Part XVII).[1] The latter radical is the most stable and on longer standing at room temperature in solution, it remains as the only paramagnetic species.

N-Alkoxy-dinitrophenylaminyls

With Ag_2O as oxidant, conditions were attained when only the expected N-alkoxy-dinitrophenylaminyl radicals were observed.

The EPR spectra of these radicals were analyzed and simulated for obtaining the hyperfine coupling constants. Line half-widths are 0.1–0.25 Gauss. Figures 1–4 present experimental and simulated EPR spectra; in some cases, the simulation is extended over the whole EPR spectrum; when however, the large a_N hfc can be measured directly from the spectrum

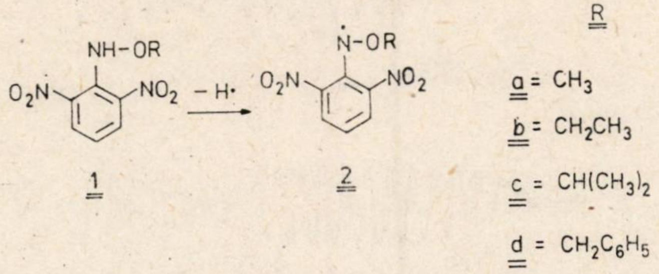

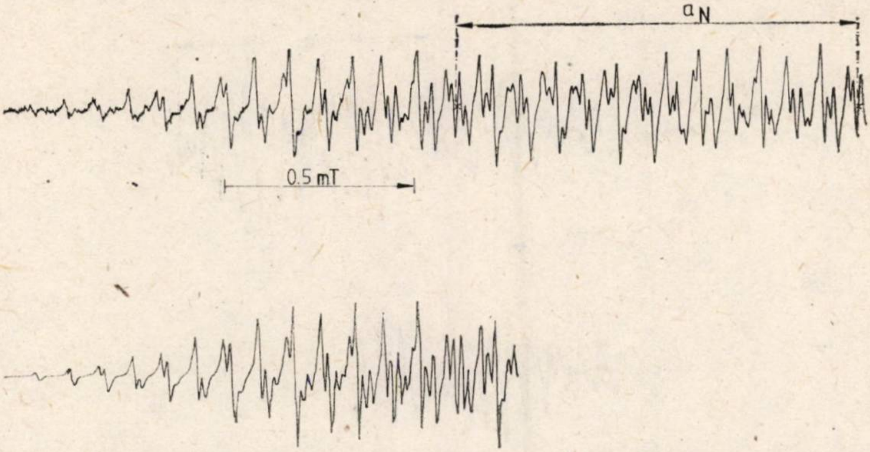

Fig. 1. — Experimental (upper) and simulated (lower) EPR spectrum of the methoxy-aminyl **2a**. Only half of the experimental spectrum is shown, up to the central line.

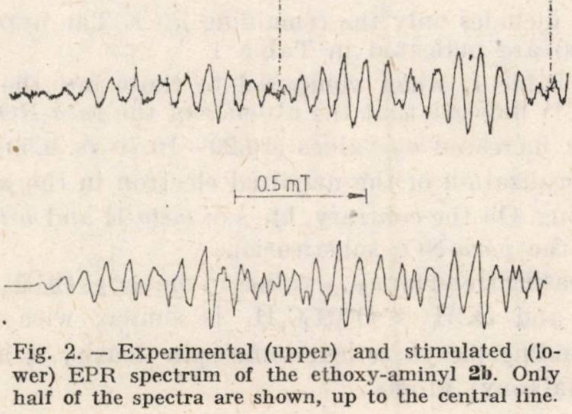

Fig. 2. — Experimental (upper) and stimulated (lower) EPR spectrum of the ethoxy-aminyl **2b**. Only half of the spectra are shown, up to the central line.

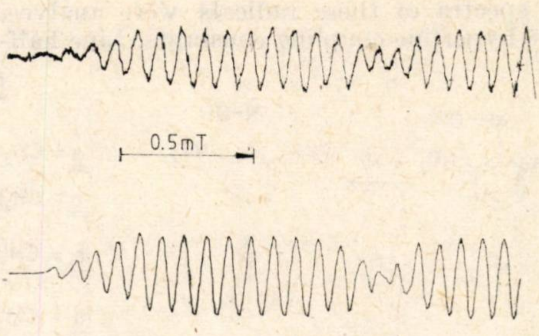

Fig. 3. — Experimental (upper) and simulated (lower) EPR spectrum of the isopropoxy-aminyl **2c**. Only half of the spectra are shown, up to the central line.

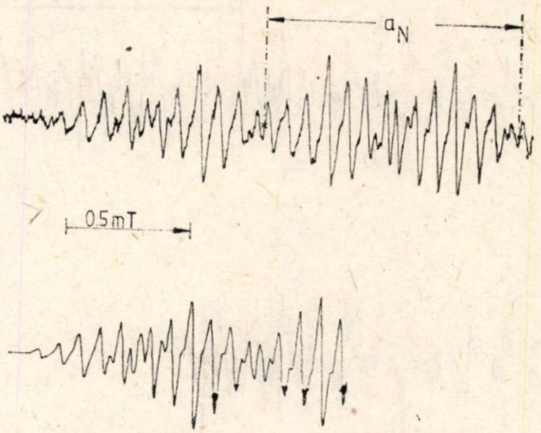

Fig. 4. — Experimental (upper) and simulated (lower) EPR spectrum of the benzyloxy-aminyl **2d**. Only half of the experimental spectrum is shown.

the simulation includes only the remaining hfc's. The hyperfine coupling constans (hfc's) are indicated in Table 1.

Data in Table 1, when compared to those for the corresponding picryl analogs, [14] indicate that the absence of the *para*-NO_2 group results in significantly increased a_N values (10.20—10.70 vs. 9.50—9.85 G) indicating the delocalization of the unpaired electron in the *para* position of the aromatic ring. On the contrary, hfc's of *meta*-H and *ortho*-NO_2 are not influenced by the *para*-NO_2 substitution.

The decreasing trend for $a_{\beta-H}$ values in the series $OCH_3 > OCH_2CH_3 > OCH(CH_3)_2$ and $OCH_3 > OCH_2C_6H_5$ is similar with that observed in the corresponding picryl series; some spin density is also delocalized on the γ-OR (alkoxy) atoms.

Table 1

Hfc's (Gauss) * of free radicals **2a-d** obtained in toluene by oxidation of **1a–d** with Ag_2O. In brackets are presented the numbers of equivalent nuclei (H or N)

Comp.	R	a_N	a_{NO_2}	a_{m-H}	a_{p-H}	$a_{\beta-H}$	Fig.
2a	CH_3	10.70	0.91 (2)	1.66 (2)	5.36 (1)	3.32 (3)	1
2b	CH_2CH_3	10.25	0.88 (2)	1.57 (2)	5.06 (1)	2.85 (2)	2
2c	$CH(CH_3)_2$	10.25	0.84 (2)	1.50 (2)	6.00 (1)	2.50 (1)	3
2d	$CH_2C_6H_5$	10.19	0.85 (2)	1.59 (2)	5.10 (1)	2.82 (2)	4

* For conversion into the SI unit, 10^4 Gauss = 1 Tesla

N-Alkoxy-4-alkyl-2,6-dinitrophenylaminyls

The oxidation of N-alkoxy-4-alkyl-2,6-dinitroanilines **3a–c** and **5a–c** with Ag_2O proceeded normally and afforded the corresponding persistent N-alkoxy-arylaminyls **4a–c** and **6a–c**, respectively, where the 4-alkyl group is methyl for **3** and **4**, and t-butyl for **5** and **6.**

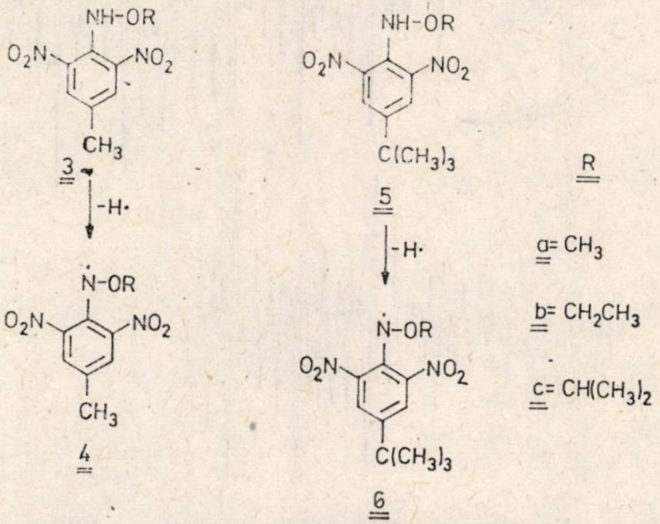

The values of hfc's are indicated in Tables 2 and 3, respectively, and the experimental and simulated EPR spectra are presented in Figures 5–10.

In agreement with earlier observations, the hfc for a_{p-H} is about the same for the unsubstituted position in **2a–d** and for the three methyl protons of **4a–c**.

Table 2

Hfc's (Gauss*) of free radicals **4a-c** obtained in toluene by oxidation of **3a-c** with Ag_2O. In brackets are shown the numbers of equivalent nuclei (H or N)

Comp.	R¹	a_N	a_{NO_2}	a_{m-H}	a_{p-H}	$a_{\beta-H}$	Fig.
4a	CH_3	10.10	0.87 (2)	1.53 (2)	5.72 (3)	2.92 (3)	5
4b	CH_2CH_3	10.25	0.88 (2)	1.65 (2)	5.70 (3)	2.57 (2)	6
4c	$CH(CH_3)_2$	11.25	0.84 (2)	1.50 (2)	4.80 (3)	2.30 (1)	7

* For conversion into the SI unit, 10 Gauss = 1 mT.

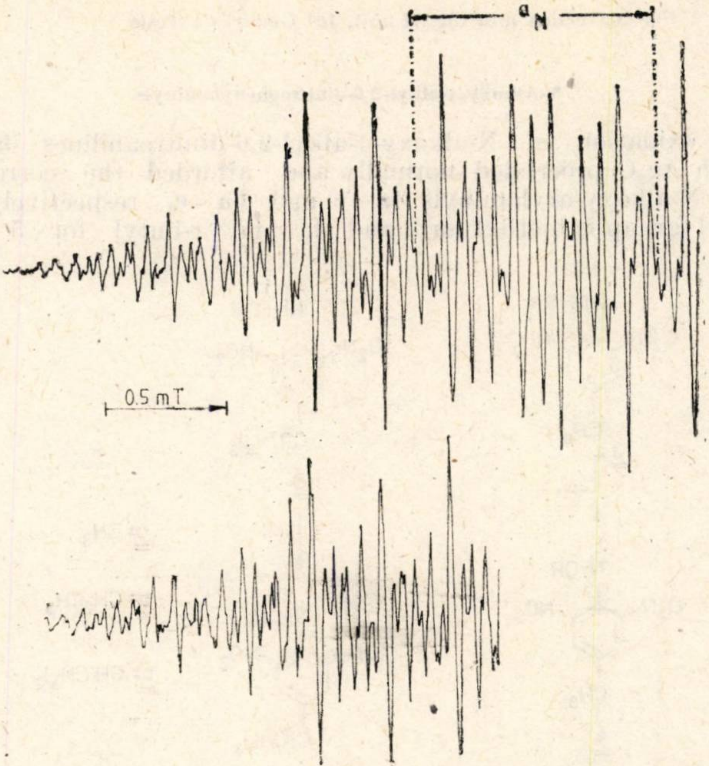

Fig. 5. – Experimental (upper) and simulated (lower) EPR spectrum of the methoxy-derivative **4a**. Only half of the experimental spectrum is shown.

The data in Tables 2 and 3 compared to those of picryl analogs [14] indicate that the replacement of *para*-NO_2 group by methyl or *tert*-butyl group brings a significant increase in a_N values, while the hfc's of *meta*-H and *ortho*-NO_2 are not influenced.

Table 3

Hfc's (Gauss *) of free radicals **6a-e** obtained in toluene from **5a-e** by oxidation with Ag_2O or with $Pb(OAc)_4$. In brackets are shown the numbers of equivalent nuclei (H ori N).

Comp.	R	a_N	a_{NO_2}	a_{m-H}	a_{p-H}	$a_{\beta-H}$	$a_{\gamma-H}$	Fig.
6a	CH_3	10.09	0.88 (2)	1.56 (2)	0.19 (9)	3.16 (3)	—	8
6b	CH_2CH_3	9.90	0.87 (2)	1.67 (2)	0.16 (9)	2.55 (2)	0.16 (3)	9
6e	$CH(CH_3)_2$	9.98	0.82 (2)	1.43 (2)	0.16 (9)	2.19 (1)	0.16 (6)	10

* For conversion into the SI unit, 10 Gauss = 1 mT.

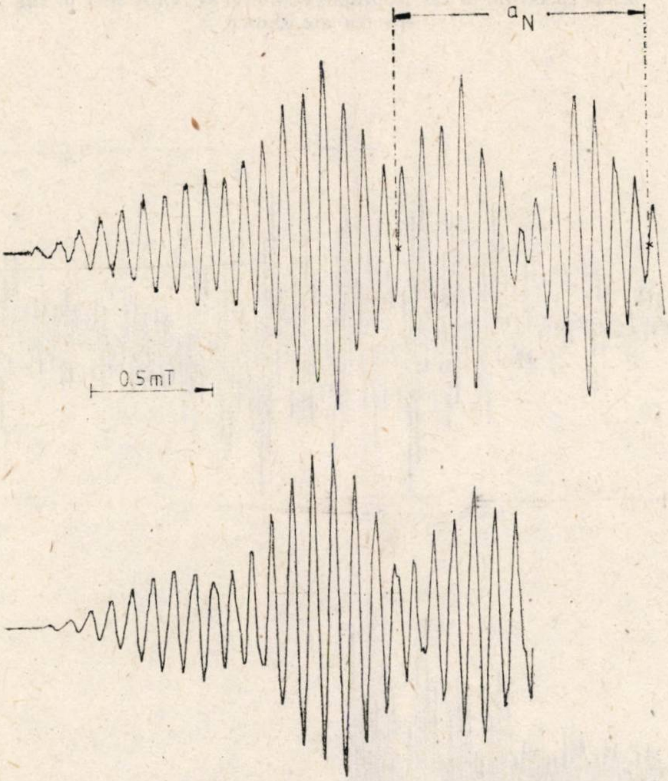

Fig. 6. — Experimental (upper) and simulated (lower) EPR spectrum of the ethoxy-aminyl **4b**. Only half of the spectrum is shown.

The decreasing trend of $a_{\beta-H}$ in the series $OCH_3 > OCH_2CH_3 > OCH(CH_3)_2$ observed for the picryl analogs [14] and the dinitroaminyls **2a–d** (Table 1) is maintained also for the aminyls **4a–e** and **6a–e.**

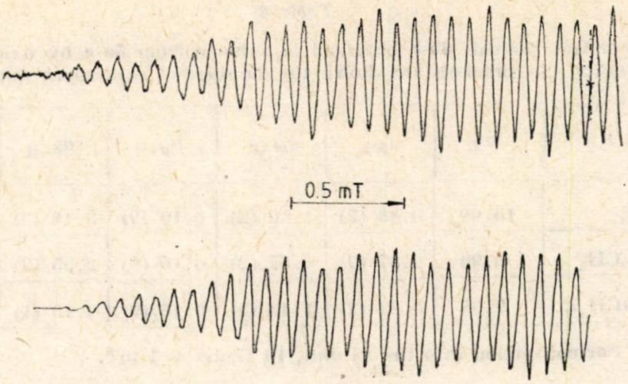

Fig. 7. — Experimental (upper) and simulated (lower) EPR spectrum of the isopropoxy-aminyl **4c**. Only half of the spectra are shown.

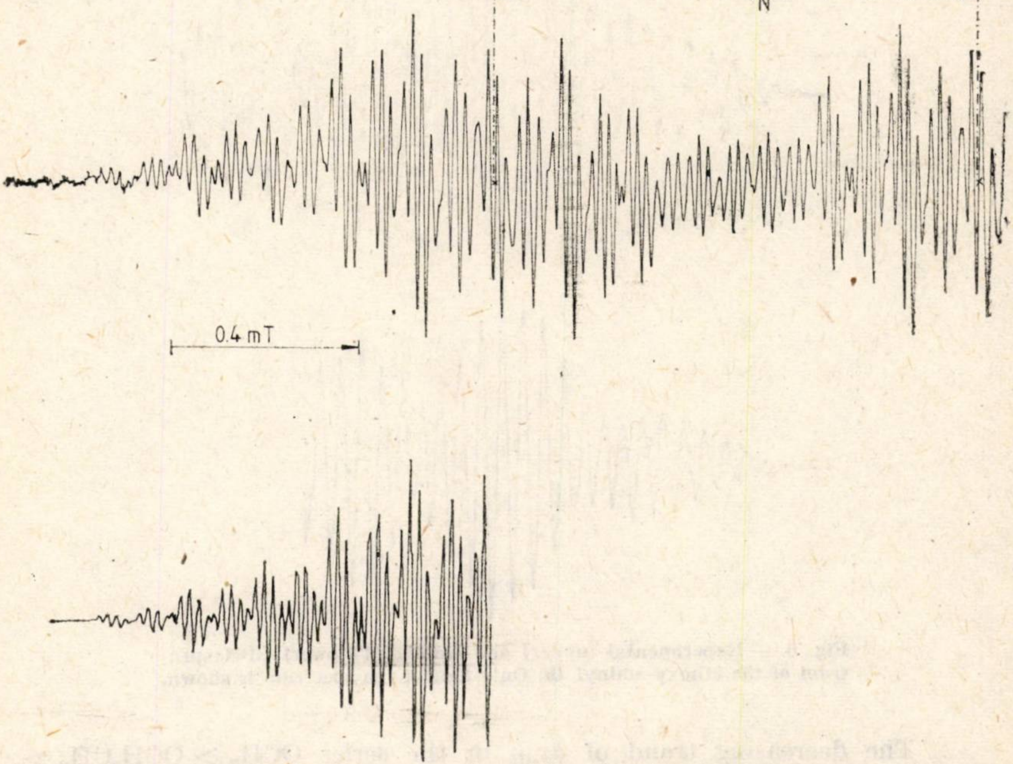

Fig. 8. — Experimental (upper) and simulated (lower) EPR spectrum of the methoxy-aminyl **6a**. Only half of the experimental spectrum is shown.

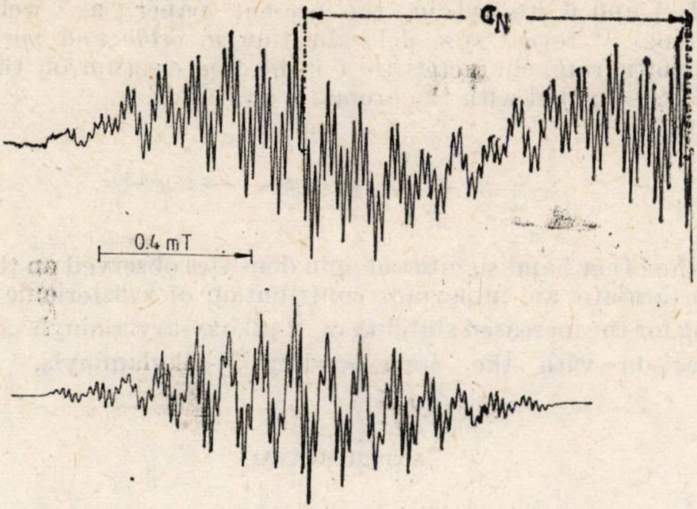

Fig. 9. — Experimental (upper) and simulated (lower) EPR spectrum of the ethoxy-aminyl **6b**. Only half of the experimental spectrum is shown.

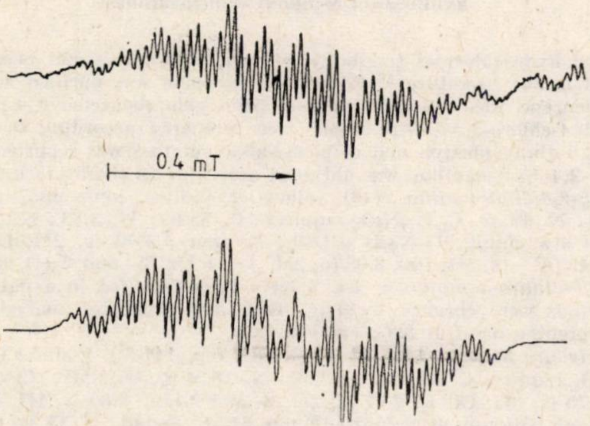

Fig. 10. — Experimental (upper) and simulated (lower) EPR spectrum of the isopropoxy-aminyl **6c**. Only half of the spectra are shown.

CONCLUSION

Aminyl radicals can adopt a π or σ electron configuration; the last one is expected only when the energy gain due to the delocalization energy of two electrons versus one electron is greater than the promotional energy of one electron from a nonbonding σ hybrid orbital into the spin-bearing p_π orbital. Danen and Neugebauer [15] have suggested that such a situation could occur in picrylaminyls. However, the hfc's of the N-alkoxy-dinitroaminyls **2**, **4** and **6** studied in the present paper, as well as their picryl analogs,[14] reveal spin delocalization in *ortho* and *para* positions of the aromatic ring, characteristic for the free electron on the nitrogen p_π orbital, conjugated with the aromatic π orbitals.

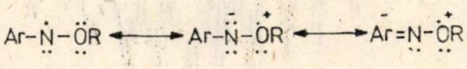

$$\mathrm{Ar}-\underset{\cdot\cdot}{\dot{\mathrm{N}}}-\underset{\cdot\cdot}{\ddot{\mathrm{O}}}\mathrm{R} \longleftrightarrow \mathrm{Ar}-\underset{\cdot\cdot}{\overset{-}{\ddot{\mathrm{N}}}}-\underset{\cdot\cdot}{\overset{+}{\dot{\mathrm{O}}}}\mathrm{R} \longleftrightarrow \overset{-}{\mathrm{Ar}}=\underset{\cdot\cdot}{\mathrm{N}}-\underset{\cdot\cdot}{\overset{+}{\dot{\mathrm{O}}}}\mathrm{R}$$

On the other hand significant spin densities observed on the OR-fragment substantiate an important contribution of zwitterionic structures, accounting for the increased stability of N-alkoxy-arylaminyls $\mathrm{Ar}-\underset{\cdot\cdot}{\dot{\mathrm{N}}}-\mathrm{OR}$ in comparison with the corresponding N-alkylaminyls, $\mathrm{Ar}-\underset{\cdot\cdot}{\dot{\mathrm{N}}}-\mathrm{R}$.

EXPERIMENTAL

All melting points are uncorrected. IR spectra were recorded with a Jena UR-20 instrument. ^{1}H-NMR spectra were obtained at 60 MHz with a Varian EM-360 instrument.

Synthesis of N-alkoxy-dinitroanilines

Alkoxyamine hydrochlorides (methoxy, ethoxy, isopropoxy and benzyloxy) were prepared as indicated in the literature.[16] Commercial dioxane was purified according to ref.[17]. Chloro-2,6-dinitrobenzene was obtained starting from chlorobenzene.[18] 4-t-Butyl-2,6-dinitrochlorobenzene and 4-chloro-3,5-dinitrotoluene were prepared according to literature data[19]. The synthesis of 2,6-dinitrophenyl- and of picryl-alkoxyamines was reported in an earlier paper[10a] N-Methoxy-2,4-dinitroaniline was obtained according to the literature.[10b]

N-Benzyloxy-2,6-dinitroaniline (**1d**) yellow crystalline compound, mp. 76°; Found: C, 53.47; H, 3.90; N, 14.39. $C_{13}H_{11}N_3O_5$ requires: C, 53.89; H, 3.83; N, 14.53%. IR (CCl_4) 3300 cm^{-1} for NH stretching. ^{1}H-NMR ($CDCl_3$, δ, ppm): 4.90 (s, 2H, CH_2), 7.02 (t, 1H, J = 8 Hz, 4-H), 7.43 (Ψ — s, 5H, Ph), 8.08 (d, 2H, J = 8 Hz, 3- and 5-H), 8.08 (s, 1H, NH).

N-Alkoxy-2,6-dinitro-4-toluidines **3a**, **b** have been reported in a patent[19]. Our yellow crystalline compounds were checked by TLC, GLC and elemental analysis; all compounds exhibit an NH stretching band at 3300 cm^{-1} in CCl_4.

Methoxy-derivative **3a**, mp. 145—6° (reported[20] mp. 141-3°). Found: C, 42.49; H, 3.89; N, 18,41. $C_8H_9N_3O_5$ requires C, 42.30; H, 3.99; N, 18.50%. ^{1}H-NMR ($CDCl_3$, δ, ppm): 2.44 (s, 3H, 4-CH_3); 3.75 (s, 3H, OCH_3) 7.97 (s, 2H, 3- and 5-H); 9.80 (s, 1H, NH).

Ethoxy-derivative **3b**, mp. 65° (reported[20] mp. 64-5°. Found: N, 17.31. $C_9H_{11}N_3O_5$ requires N, 17.42%. ^{1}H-NMR ($CDCl_3$, δ, ppm,; 1.20 (t, 3H, J = 7 Hz, Et-CH_3); 2.43 (s, 3H, 4-CH_3); 3.95 (q, 2H, J = 7 Hz, CH_2); 7.91 (s, 2H, 3- and 5-H); 9.72 (s, 1H, NH).

Isopropoxy-derivative **3c**, mp. 98°. Found: N, 15.29. $C_{10}H_{13}N_3O_5$ requires N, 16.4 %, ^{1}H-NMR($CDCl_3$, δ, ppm); 1.21 (d, 6H, J = 7 Hz, iPr—CH_3); 2.41 (s, 3H, CH_3); 4.08 (septet, 1H, J = 7Hz, iPr—CH); 7.80 (s, 2H, 3- and 5-H); 8.04 (s, 1H, NH).

4-t-Butyl-2,6-dinitro-N-alkoxyanilines **5a-c**. All compounds are new, yellow, crystalline substances which exhibit an NH stretching band at 3300 cm^{-1} in CCl_4.

Methoxy-derivative **5a**, mp. 105°. Found: N, 15.43. $C_{11}H_{15}N_3O_5$ requires N, 15.62%. ^{1}H-NMR ($CDCl_3$, δ, ppm): 1.41 (s, 9H, tBu); 3.75 (s, 3H, OCH_3); 8.80 (s, 2H, 3- and 5-H); 9.78 (s, 1H, NH).

Ethoxy-derivative **5b**, mp. 42°. Found: N, 14.62. $C_{12}H_{17}N_3O_5$ requires N, 14.83%. ^{1}H-NMR (CCl_4, δ, ppm); 1.20 (t, 3H, J = 7 Hz, Et—CH_3); 1.40 (s, 9H, tBu); 3.90 (q, 2H-J = 7 Hz, Et—CH_2); 8.00 (s, 2H, arom); 9.45 (s, 1H, NH).

Isopropoxy-derivative **5c**, mp. 30—2°. Found: N, 14.07. $C_{13}H_{19}N_3O_5$ requires N, 14.13 %. ^{1}H-NMR (CCl_4, δ, ppm): 1.25 (d, 6H, J = 7 Hz, iPr—CH_3); 1.43 (s, 9H, tBu); 4.15 (septet, 1H, J = 7 Hz, iPr—CH); 8.01 (s, 2H, arom.); 9.83 (s, 1H, NH).

Preparation of the radicals

The radicals were generated in a vial by mixing the oxidizing agent, Ag_2O, with deoxygenated solutions of N-alkoxy-arylamines, in toluene.

EPR spectra

All EPR spectra were recorded on a JES—3B (JEOL) spectrometer with 100 kHz field modulation using X-band frequency. The hfc constants and g factors were measured by comparison with potassium peroxylamine disulphonate ($a_N = 13.09G \pm 0.04G$ and $g = = 2.00550 \pm 0.0005$[21]).

The spectra were computed with a Lorentzian line shape.

REFERENCES

[1] Part XV, U. Bologa, A. T. Balaban, N. Grecu, N. Negoiţă, M. T. Căproiu and R. I. Walter, *J. Org. Chem.*, **52**, 4176 (1987); Part XVII, G. Stănciuc, M. T. Căproiu, H. Căldăraru, A. Caragheorgheopol, T. Constantinescu and A. T. Balaban, *Z.Naturforsch.*(in press). A. T. Balaban, N. Negoiţă, S. M. Shein and A. D. Khmelinskaya, *Rev. Roum. Chim.*, **32**, 501 (1987) is part XVIII in the series.

[2] A. T. Balaban, *Rev. Roum. Chim.*, **16**, 725 (1971).

[3] A. R. Katritzky and F. Soti, *Heterocycles*, **1**, 67 (1973); *J. Chem. Soc. Perkin Trans.*, I, 1427 (1974); R. W. Baldock, P. Hudson, A. R. Katrizky and F. Soti, *ibid.*, 1422 (1974).

[4] H. G. Viehe, R. Merenyi, L. Stella and Z. Janousek, *Angew. Chem. Int. Ed. Engl.*, **18**, 917 (1979); Z. Janousek, F. Huys, L. René, M. Masquetier, L. Stella, R. Merenyi and H. G. Viehe, *ibid.*, **18**, 616 (1979); "Substituent Effects in Radical Chemistry", editors H. Viehe, Z. Janousek and R. Merenyi, D. Reidel Rublisbing Co. (1986) .

[5] D. Crans, T. Clarke and P. von R. Schleyer, *Tetrahedron Lett.*, **21**, 3681 (1980).

[6] C. Rüchardt and H. D. Beckhaus, *Top. Curr. Chem.*, **130**, 1 (1985); G. Leroy, *Int. J. Quntum Chem.*, **23**, 271 (1983); G. Leroy, D. Peeters, M. Sava and G. Willante, "Substituent Effects in Radical Chemistry", eds. H. Viehe, Z. Janousek and R. Merenyi, D. Reidel Publishing Co., pag. 1 (1986).

[7] D. J. Pasto, R. Krasnansky and C. Zercher, *J. Org. Chem.*, **52**, 3062 (1987).

[8] S. Goldshmidt and K. Renn, *Ber. dtsch. chem. Ges.*, **55**, 628 (1929).

[9] A. T. Balaban, P. T. Frangopol, M. Frangopol and N. Negoiţă, *Tetrahedron*, **23**, 4661 (1967); M. T. Căproiu, N. Negoiţă and A. T . Balaban, *Tetrahedron*, **39**, 3943 (1983).

[10] a) G. Stănciuc and A. T. Balaban, *Org. Prep. Proced. Int.*, **16**, 401 (1984).
b) G. Biggi and F. Pietra, *J. Chem. Soc.* (B), 44 (1971).

[11] A. T. Balaban, M. T. Căproiu and R. Baican, *Tetrahedron*, **33**, 2249 (1977).

[12] J. W. Linnett, "The Electronic Structure of Molecules", Methuen, London, 2nd Ed., 1974; *J. Amer. Chem. Soc.*, **83**, 2643 (1961).

[13] M. T. Căproiu, M. Elian, N. Grecu, N. Negoiţă and A. T. Balaban, *J. Chem. Soc. Perkin Trans. II.* 591 (1983).

[14] G. Stănciuc, M. T. Căproiu, A. Caragheorgheopol, H. Căldăraru, A. T. Balaban and R. I. Walter, *J. Magn. Reson.*, **75**, 63 (1987).

[15] W. C. Danen and F. A. Neugebauer, *Angew. Chem. Int. Ed. Engl.*, **14**, 783 (1975).

[16] A. Chimiek and T. Kolasa, *Bull. Acad. Pol. Sci., Ser. Chim.*, **22**, 195 (1974).

[17] R. L. Augustine and J. A. Caputo, Org. Synth. Coll. Vol. **5**, 869.

[18] H. Schultz, Org. Synth. Coll. Vol. **4**, 365; F. D. Gunstone and S. H. Tucker, Org. Synth. Coll. Vol. **4**, 160.

[19] E. V. P. Tao and C. F. Christie, *Org. Prep. Proc. Int.*, **4**, 73 (1972); E. V. P Tao (to Eli Lilly Co.), U. S. Pat. 3,665,042, May 23, 1972.

[20] J. C. Williams (to Elli Lilly Co.), U. S. Pat. 4,143,073, March 6, 1979.

[21] R. J. Faber and G. K. Fraenkel, *J. Chem. Phys.*, **47**, 2462 (1967).

[illegible]

Preparation of the radicals

[illegible]

EPR spectra

[illegible]

[illegible]

[illegible]

Revue Roumaine de Chimie, **34**, *9—10*, 1907—1919 (1989)

THE PHYSICO-CHEMICAL CHARACTERIZATION OF Z-4b,10b-DIHYDROCHRYSENE

MIRCEA D. BANCIU,[a] CĂTĂLINA HADA,[a] DANA ALBAIU[b]
and CONSTANTIN DRĂGHICI[b]

[a] Laboratory of Organic Chemistry, Polytechnic Institute, TCH, Spl. Independenţei 313, 76206 Bucharest, Romania
[b] Centre of Organic Chemistry — ICECHIM, Spl. Independenţei 202B, 78100 Bucharest, Romania

Received April 25, 1989

The title dibenzo$(CH)_{10}$ hydrocarbon (**1**) was characterized physico-chemically. The charge transfer complex of **1** with tetracyanoethene proved an electronic distribution of **1** similar to that corresponding to two adjacent styrene moieties. An unrearranged $PdCl_2$-complex of the type 1 : 1 was obtained. UV-irradiation of **1** proceeds with aromatization to chrysene (**3**). No reaction was observed on treatment with bromine in acetic acid whereas reaction with N-bromosuccinimide afforded **3**. Photochemical reaction with bromine produced 6,12-dibromochrysene (**13**) *via* the addition product **14**. Dibromoderivative **13** was obtained also on photochemical bromination of chrysene. Attempted photochemical or metal ion-catalyzed valence isomerization of dibenzo [*c,i*]tetracyclo-[$4.4.0.0.^{2,8}\,0^{5,7}$]deca-3,9-diene (**2**) (the thermal precursor of **1**) failed.

INTRODUCTION

The domain of valence isomers of annulenes and of their benzoannelated derivatives presents a continuous and increasing interest in recent years. [1]

In spite of the impressive development of the chemistry of $(CH)_{10}$ valence isomers as well as of their monobenzoannelated derivatives,[1] the "dibenzo$(CH)_{10}$ hydrocarbons" were only scarcely investigated. All 102 possible dibenzoderivatives of valence isomers of [10]annulenes — from which 79 are not *o*-quinonoid — were tabulated, [2] but only nine from these were obtained (until 1986) as stable compounds. [1,2] Three other dibenzo $(CH)_{10}$ valence isomers were suggested by us as reactive intermediate in the pyrolyses of stable isomers. [1,3]

In 1986 we [4] described the isolation of Z-4b,10b-dihydrochrysene (**1**), one of the three pyrolytic dibenzo$(CH)_{10}$ intermediates suggested earlier. [3b] The hydrocarbon **1** was obtained[4] in high yield on flow-vacuum pyrolysis of dibenzo[*c, i*]tetracyclo-[$4.4.0.0^{2,8}.0^{5,7}$]deca-3,9-diene(**2**) at 500°. In turn, hydrocarbon **2**, another dibenzo$(CH)_{10}$ valence isomer, could be easily obtained — according to Stiles [5a] and Friedman [5b] — from benzobarrelene and benzyne.

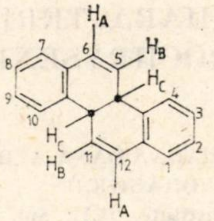

1

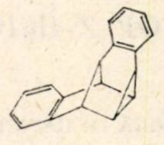

2

In this paper we present a physico-chemical characterization of Z-4b, 10b-dihydrochrysene (**1**) as well as attempted new valence isomerizations of **2**.

RÉSULTS AND DISCUSSION

As presented in our preliminary paper, [4] Z-4b,10b-dihydrochrysene (**1**) is a white solid, m.p. 95–97°, with characteristic UV- and ^{1}H-NMR spectra. Flow-pyrolysis of **1** or treatment with 2,3-dichloro-5,6-dicyano-*p*-benzoquinone (DDQ) at room temperature affords chrysene (**3**) whereas catalytic hydrogenation produces Z-4b,5,6,10b,11,12-hexahydrochrysene (**4**). [4]

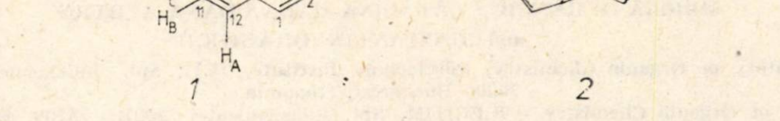

3 1 4

Charge transfer complex of 1 with tetracyanoethene

It is well-known [6] that charge-transfer (CT) complexes between aromatic compounds as electron donors and tetracyanoethene or other electron acceptors may reveal new data on electronic distribution and reactivity of the starting aromatic compounds or could even lead to new interesting properties such as enhanced electric conductivity ("organic metal ")[7].

Addition of tetracyanoethene (TCNE) to a solution of dihydrochrysene **1** in dichloromethane at room temperature was immediately followed by the development of a deep blue colour. In the electronic spectrum two absorption bands appear in the visible range at 422 nm and 555.5 nm. Since these bands are due neither to dihydrochrysene nor to TCNE, they must be attributed to a charge-transfer complex. The above absorptions remain unchanged on storing the solution for three days at room temperature.

Using the Benesi-Hildebrand equation,[8] modified by Scott[9] (eq. 1), the stability constant, K and $\varepsilon_{\max}$ values for the charge-transfer complex could be determined.

$$\frac{C_A \cdot C_B \cdot l}{E} = \frac{1}{K \cdot \varepsilon_{\max}} + \frac{1}{\varepsilon_{\max}} \cdot C_A \qquad \text{(eq. 1)}$$

In eq. 1 C_A, C_B are the molarities of reactants (A stands for TCNE and B for **1**) with $C_A > C_B$, E is the absorbance of the complex and l (cm) is the cell length.

A good linear correlation was obtained in the graphical representation of $\dfrac{C_A \cdot C_B \cdot l}{E}$ versus C_A (Fig. 1).

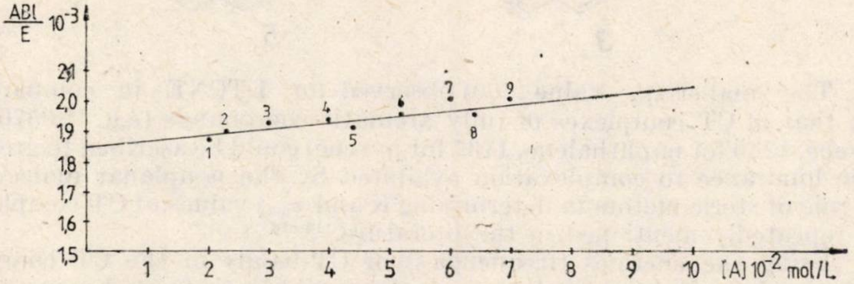

Fig. 1. — Variation of $C_A \cdot C_B \cdot l/E$ *versus* C_A for highest wave-length absorption of CTC between **1** and TCNE.

From values of the slope (2×10^{-3}) and intercept (1.85×10^{-3}) in the Fig. 1 the values of $\varepsilon_{\max} = 500$ L · mole^{-1} · cm^{-1} and K = 1.08 L. · mole^{-1} were calculated. According to the good linear correlation in the Scott relationship the stoechiometry of 1 : 1 for CT-complex could be assumed :

$$\mathbf{1} + \text{TCNE} \overset{K=1.08}{\rightleftarrows} \mathbf{1}\text{-TCNE}$$

The appearance of two (new) distinct maxima in the electronic spectrum of the CT complex of aromatic donors was repeatedly mentioned in the literature.[6,10] The occurrence of these two bands was attributed to two rotational isomers of the CT complex.[11] More recently, experimental[12] and theoretical[13] evidence has been provided for the existence of two geometries responsible for the observed CT-bands. In the case of **1**-TCNE these isomers could be (**1**—TCNE) and (**1**—TCNE)$_b$.

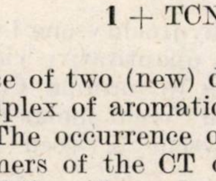

(1-TCNE)$_a$

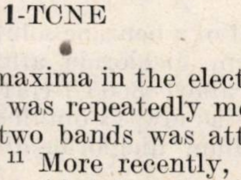

(1-TCNE)$_b$

The calculated K value of 1.08 for **1** is smaller than that of benzene ($K = 2.0$ [14]), but comparable with that of chlorobenzene ($K = 0.770$ [14]) or even bromobenzene ($K = 0.611$ [14]). These data suggest that in **1** the aromatic rings are to some extent deprived in electrons; thus the electronic structure of dihydrochrysene **1** is very close to that of two adjacent styrene moieties.

It may be added that the addition of TCNE to chrysene (**3**) solutions in CH_2Cl_2 produces CT-bands at 543 and 641 nm whereas similar treatment of **5** (isomeric with **1**) affords maxima at 490 and 659 nm, thus appreciably shifted bathochromically (in comparison with **1**) due to the extended aromatic framework.

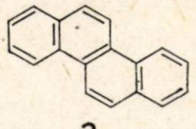

3

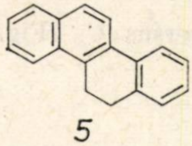

5

The smaller ε_{max} value (500) observed for **1**-TCNE in comparison with that of CT complexes of fully aromatic compounds (e.g. [14] 3570 for benzene, 1240 for naphthalene, 1137 for pyrene) could be ascribed to greater steric hindrance to complexation exhibited by the nonplanar molecule[1]. The role of steric factors in determining K and ε_{max} values of CT complexes was repeatedly mentioned in the literature. [14–16]

Using the energies (frequencies) of CT-bands in the CT complex the ionization potential of electron donors could be estimated using semiempirical equations, [6a] like eq. 2 used for TCNE (as acceptor) and polynuclear aromatic hydrocarbons (as donors). [15]

$$I_p(\text{eV}) = 5.21 + 165\times10^{-4}\cdot\tilde{\nu}_{CT}\ (\text{cm}^{-1}) \qquad \text{(eq. 2)}$$

Thus, for dihydrochrysene **1** a value of 8.18eV may be estimated, in good agreement with known (experimental) I_p-values of related compounds. [13]

Palladium chloride complex of 1

Treatment of a benzene solution of dihydrochrysene **1** with bis(benzonitrile)-palladium dichloride afforded, in quantitative yield, a dark-red complex (m.p. above 360°C) corresponding to formula $C_{18}H_{14}PdCl_2$. The same complex was always obtained using different molar ratios: bis(benzonitrile)-palladium dichloride/dihydrochrysene between 1.2/1 and 3/1.

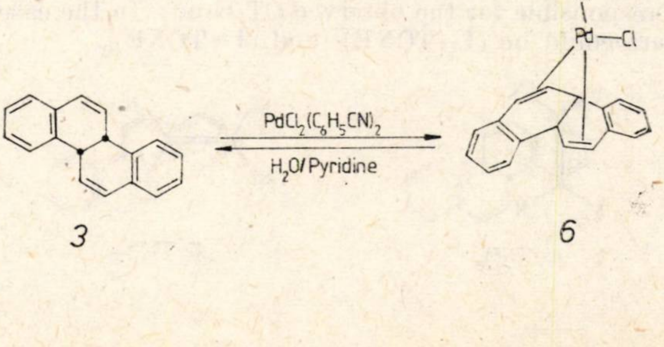

3

6

Decomposition of the complex with pyridine/water at room temperature regenerates **1** in quantitative yield.

In agreement with the above data, the structure **6** can be proposed for the complex.

UV-irradiation of 1

Irradiation of dihydrochrysene **1** at room temperature in acetone or hexane solution with UV light in a thoroughly oxygen-free apparatus conducted to extensive aromatization. After 6 hrs of irradiation about 33% chrysene was formed; along with this aromatic hydrocarbon and starting material **1**, only minor components of the reaction mixture and polymeric material were identified. This behaviour contrasts with that of Z-4b,8a-dihydrophenanthrene (the monobenzo$(CH)_{10}$ hydrocarbon analogous to **1**) whose UV-irradiation[17] proceeds with rearrangement to 2,3-benzobicyclo[4.2.2]deca-2,4,7,9-tetraene.

It seems that the aromatization tendency of **1** is far greater than that of 4b,8a-dihydrophenanthrene. Indeed, following sections of this paper will bring new data for the very easy aromatization of **1**.

Bromination of 1

No reaction was observed to occur between dihydrochrysene **1** and bromine in acetic acid either at room temperature, at 60°C or at reflux; it follows that **1** does not react with bromine in polar medium.

Attempted bromination of **1** with N-bromosuccinimide (NBS) failed. Treatment of **1** in CCl_4 solution with NBS in presence of benzoyl peroxide at reflux afforded only chrysene (**3**). It seems that the primarily formed radicalic intermediate **7** (Scheme 1) reacts further with another bromine atom affording chrysene *via* **8** instead of reacting with molecular bromine (formed from NBS and HBr present in the reaction medium) to give bromoderivative **9** (which should be sterically hindered).

Scheme 1

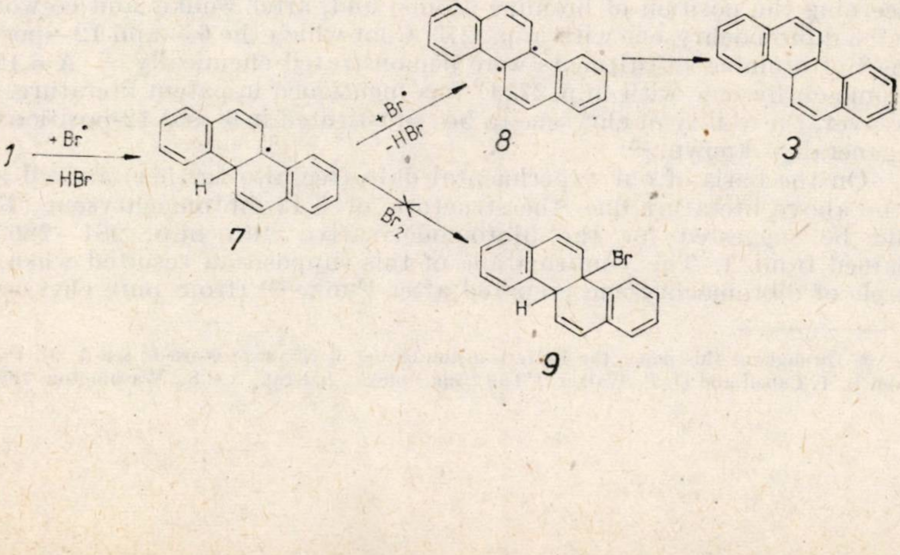

The oxidative (dehydrogenative) action of NBS is well-known. Recently, McOmie *et al.*[18] observed also the easy loss of two benzylic hydrogens during the reaction of **10** with NBS.

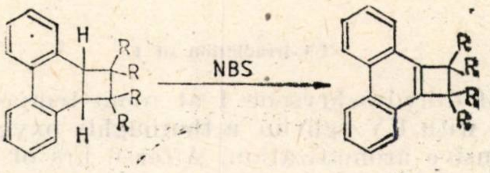

10 **11**

Treatment of dihydrochrysene **1** at room temperature with excess elemental bromine in CCl_4 solution in the presence of UV-light was accompanied by a vigorous evolution of gaseous hydrogen bromide and precipitation of a solid (m.p. 284—286°) which corresponds to the formula $C_{18}H_{10}Br_2$, thus to a dibromochrysene. Due to its insolubility in all usual solvents, no satisfactory ^{1}H-NMR spectrum could be obtained. The UV-spectrum (see Experimental) differs from that reported[19] for 2,8-dibromochrysene * (**12**), one of the two dibromoderivatives of chrysene described in the literature. It should be added that **12** was syntesized by aromatization of a dihydroderivative or by modification of other functional groups and not by bromination.

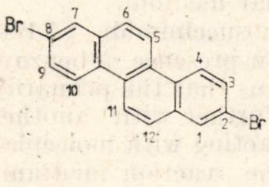

12

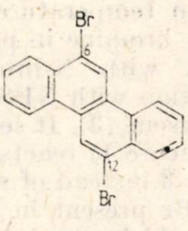

13

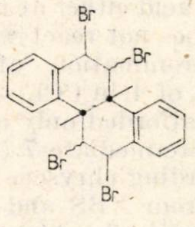

14

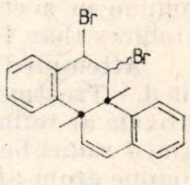

15

On the other hand, the scarcely investigated bromination of chrysene affords, after Schmidt[20] a dibromochrysene with m.p. 273°C (no mention concerning the position of bromine atoms) and, after Funke and co-workers[21] a dibromochrysene with m.p., 270° C for which the 6— and 12—positions * of bromine substituents were demonstrated chemically.[21] A 6,12-dibromo-chrhysene with m.p. 272°C was mentioned in patent literature.[22] Moreover, the ability of chrysene to be substituted in 6- and 12-positions* is generally known.[23]

On the basis of our experimental data (see also further) as well as of the above literature ones the structure of 6,12-dibromochrysene (**13**) could be suggested for the dibromoderivative with m.p. 284—286°C obtained from **1**. The confirmation of this supposition resulted when a sample of dibromochrysene prepared after Funke[21a] (from pure chrysene and showing a m.p. 285—286°C) proved to be identical (m.p., UV- and IR-spectra) with the compound **13** obtained from **1**.

---

* Throughout this paper the Patterson numbering of chrysene is used ; see A. M. Patterson, L. T. Capell and D. F. Walker, "The Ring Index", 2nd Ed., A.C.S., Washington, 1960.

In order to gain further information concerning the bromination of **1**, its reaction with elemental bromine (two equivalents) in CCl_4 was stopped after 5 minutes of UV-irradiation (the colour of bromine disappeared). The usual work-up afforded a thick oily product which crystallized on standing. Its ^1H-NMR spectrum suggested the presence of two addition products : the tetrabromide **14** and the dibromide **15**. Attempted purification by column — or thin layer chromatography failed due to extensive aromatisation.

UV-Irradiation of the crude addition product (**14**+**15**) with an excess of bromine in CCl_4 solution conducted to the same dibromoderivative **13** which was obtained from **1**. Thus, it seems very probable that **13** is formed (Scheme 2) from **1** *via* **15** and **14**. The conversion of **14** to **13** could be explained by a radicalic mechanism similar to that involved in the reaction of **1** with NBS *(vide supra)*.

Scheme 2

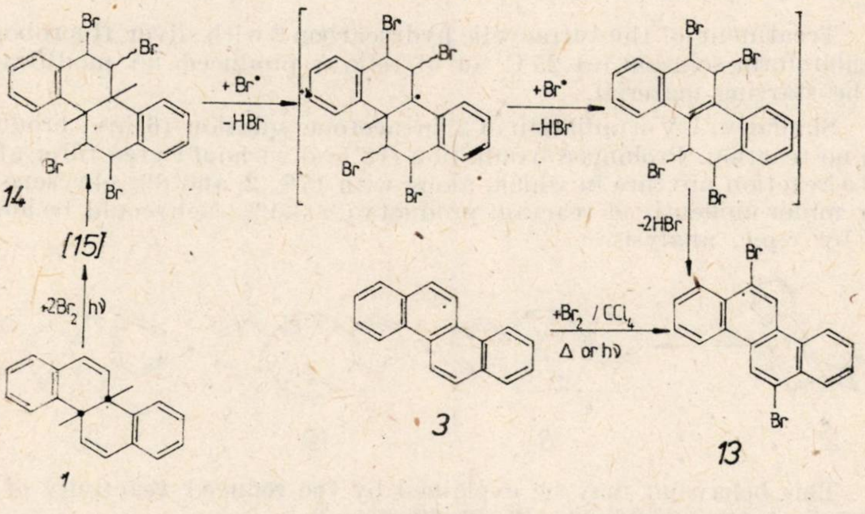

The easy loss of 4b- and 10b-hydrogen atoms from **1** finds an analogy in the E-4b,10b-dihydrochrysene derivatives investigated by Dann [19] and Paquette. [24]

Interestingly, treatment of pure chrysene (**3**) (as a suspension in CCl_4) with excess molecular bromine in the presence of UV-light at room temperature afforded the same dibromoderivative **13**. This procedure seems to be a new alternative for bromination of chrysene.

Other reactions of 1

Hydroboration of **1** followed by H_2O_2/HO^- treatment afforded a crude hydroxylic reaction product, containing probably the diol **16**. Attempts to purify the reaction product conducted invariably to chrysene

(**3**). A similar dehydration/dehydrogenation was mentioned[19] in the E-4b,10b-dihydrochrysene series.

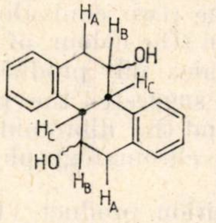

16

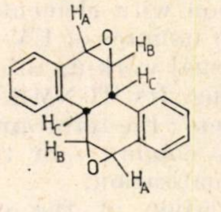

17

Epoxidation of **1** with *m*-chloroperbenzoic acid conducted to a crude epoxidic material, containing mainly **17**. All attempts of purification failed.

Both above reactions were not further investigated.

Attempted valence isomerizations of dibenzo[c, i] tetracyclo [4.4.0.0^{2,8}0^{5,7}] deca-3,9 diene (2)

Treatment of the tetracyclic hydrocarbon **2** with silver fluoroborate in chloroform solution (at 25°C or at reflux) produced no modification of the starting material.

Similarly, UV-irradiation of **2** in acetone solution (6 hrs) produced also no reaction. Prolonged irradiation (13 hrs) without Pyrex filter afforded a reaction mixture in which, along with 17% **2** and 8% chrysene (**3**), only minor unidentified reaction products ($< 3.5\%$ each) could be identified by v.p.c. analysis.

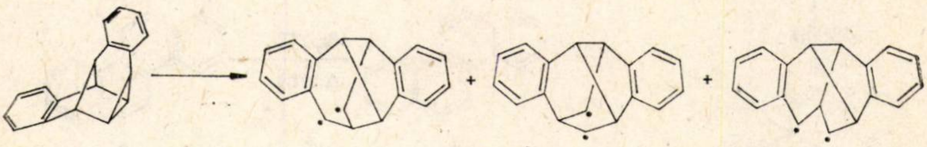

2 *18* *19* *20*

This behaviour may be explained by the reduced reactivity of the primarily formed diradicals (**18**, **19**, **20**) from **2**.

Thus, the unique valence isomerization of **2** seems to be its thermal conversion to **1**.[4]

CONCLUSIONS

Dihydrochrysene **1** could be obtained pyrolytically from hydrocarbon **2** which affords no other valence isomerization (photochemically or by metal catalysis).

Dihydrochrysene **1**, which could also not be further valence isomerized, presents an electronic structure close to that of two adjacent styrene moieties. Chemically, **1** affords easy chrysene (**3**) by aromatization. The aromatization tendency seems to be greater than in $(CH)_{10}$- or benzo$(CH)_{10}$ series. It has been also shown that radicalic bromination of **1** affords 6,12-dibromochrysene (**13**) *via* the addition product **14** and the same dibromoderivative **13** could be obtained by photochemical bromination of chrysene.

EXPERIMENTAL

Melting points are uncorrected. The IR spectra were recorded with an UR—20 C. Zeiss-Jena double-beam spectrophotometer, the electronic spectra with a SPECORD UV—VIS C. Zeiss-Jena double beam spectrophotometer and ^{1}H-NMR spectra with a VARIAN A60—A spectrometer using TMS as internal standard.

Dibenzo[c, i]*tetracyclo*$[4.4.0.0^{2,8}.0^{5,7}]$*deca-3,9-diene* (**2**) was obtained after Friedman from benzobarrelene and benzyne (generated from diazoanthranilic acid with propene oxide) in 1,2-dichloroethane (3hrs at reflux). Purification by column chromatography on neutral alumina afforded pure **2** with m.p. 154—155°C (lit. [5b] m.p. 154—155°C.)

4b,10b-Dihydrochrysene (**1**) was obtained as described in a previous paper [4] by flow-vacuum pyrolysis of **2** at 500°C. After recrystallisation from ethanol a pure hydrocarbon **1**, m.p. 95—97°C was obtained.

IR spectrum (KBr, cm^{-1}) : 748m, 752m, 770m, 782m, 1445w, 1479w, 2851w, 3016w, 3031w and 3042w.

UV spectrum (methanol) λ max, nm (ε max) : 218.5 (35300) ; 225(34500) ; 256(15900) ; 266.5 (sh ; 13400) ; and 298.5 nm (1700).

^{1}*H— NMR spectrum* ($CDCl_3$; δ ppm, : 3.83 ($2H^C$, singlet) ; 5.63 ($2H^B$; doublet) ; 6.47($2H^A$; doublet) and 6.9—7.3 (8H arom.).

Charge transfer complex of 1 with tetracyanoethene

Tetracyanoethene (TCNE) was recrystallized twice from chlorobenzene prior use ; m.p. 198.5—200°C. Dichloromethane was refluxed over P_2O_5 then distilled. Different solutions of **1** in dichloromethane were prepared as noted in Table 1 (no absorption over 400 nm was observed). Addition of TCNE in determined excess (Table 1) over the above solutions —at 20°C— was accompanied by the appearance of a deep blue colour.

Table 1

Charge transfer complex of **1** with TCNE (t ≐ 20°C, l = 0,996 cm ; volume of samples 5 mL)

No.	**1** (B)		TCNE (A)		E_1 cor. (λ = 555.5nm)	E_2^{cor}, (λ = =422 nm)	$\frac{C_A \cdot C_B \cdot l}{E_1} \cdot 10^2$	$\frac{C_A \cdot C_B \cdot l}{E_2} \cdot 10^2$
	mg/5 mL	mol/L	mg/5 mL	mol/L				
1	11.5	0.010	12.8	0.020	0.105	0.12	0.189	0.166
2	14.4	0.0125	14.8	0.023	0.150	0.16	0.1909	0.1909
3	17.4	0.0151	19.7	0.0308	0.240	0.260	0.193	0.1781
4	23.0	0.020	25.6	0.040	0.410	0.41	0.194	0.194
5	26.5	0.023	28.1	0.044	0.526	0.530	0.191	0.1901
6	30.4	0.026	33.9	0.052	0.688	0.684	0.195	0.196
7	34.5	0.030	38.4	0.060	0.860	0.84	0.208	0.213
8	36.8	0.032	40.9	0.064	1.040	1.04	0.196	0.196
9	40.0	0.0348	44.5	0.0695	1.180	1.14	0.204	0.211

The extinctions of the two absorption maxima observed in the visible region are noted in Table 1. Application of Scott's equation conducted to a linear correlation $C_A \cdot C_B \cdot l/E$ *vs.* C_A (Fig. 1) from which K and ε max values were deduced (see text).

Palladium chloride complex (6) of 1

A freshly prepared and filtered solution of bis(benzonitrile)palladium dichloride (90 mg; 0.23 mmoles) in 5mL anhydrous benzene was poured at room temperature over a solution of dihydrochrysene **1** (35 mg; 0.15 mmoles) in 3 mL benzene. After one hour the dark-red precipitate formed was filtered and washed with pentane (20 mL). The obtained solid **6** (60 mg; 97 %) does not melt until 360°C.

Found: C 53.34; H, 3.78; Pd, 26.63; Cl, 17.30. Calcd. for $C_{18}H_{14}PdCl_2$: C. 53.00; H, 3.44; Pd, 26.14; Cl, 17.42 %.

IR spectrum (KBr; cm^{-1}); 493m, 509s, 536m, 749s, 768m, 806m, 949s, 1223s, 1439, m, 1485m, 1500s and 1595s.

The same complex (IR spectrum, elemental analysis) was obtained using molar ratios between 1.2/1 and 3/1 bis(benzonitrile) palladium dichloride/dihydrochrysene(**1**).

Decomposition of the above complex with 7 mL pyridine/water (2/1) solution at room temperature afforded — after ether extraction, neutralization, drying and evaporation of the solvent — pure dihydrochrysene (**1**) in practically quantitative yield.

UV-irradiation of 1

A solution of **1** (50 mg) in 10 mL freshly distilled anhydrous acetone was deoxygenated by bubbling during 1 hr a stream of purified argon (passed over a freshly activated deoxygenating catalyst) followed by short intermittent connections to a vacuum source. The solution was then irradiated with an imersion Hg—UV lamp (medium pressure; 150 watt, Rasotherm filter) for 6 hrs during which time the bubbling of argon was continued. After filtration of a yellow polymeric material the solution was evaporated *in vacuo* under argon and the solid residue was v.p.c.-analyzed. About 33% chrysene along with 50% starting material **1** and numerous minor unidentified components were observed in gas-chromatogram.

The similar irradiation of **1** in pentane solution afforded, after 4 hrs, 63% starting material along with 5% chrysene, minor components ($< 2.5\%$) and a polymeric material.

Prolonged irradiations conducted to greater amounts of chrysene.

Bromination of 1

a) *Attempted bromination with bromine in acetic acid*

Treatment of acetic acid solutions of **1** with excess bromine at room temperature, at 60°C or at 118°C produced no reaction; only starting material **1** was identified after usual work-up of the reaction mixture.

b) *Reaction of* **1** *with N-bromosuccinimide*

A mixture of dihydrochrysene **1** (0.1 g; 0.4 mmoles), N-bromosuccinimide (0.077 g; 0.4 mmoles or 0.155 g; 0.8 mmoles), benzoyl peroxide (0.02 g; 0.08 mmoles) in 6 mL anhydrous CCl_4 was refluxed for 10 minutes then filtered warm. The solid obtained (m.p. 120—3°C) was identical with an authentic sample of succinimide. The organic filtrate, diluted with 5 mL CCl_4, was washed with water until pH 7, dried and evaporated *in vacuo*. The residual solid (85 mg, 86%) was recrystallized from 2 mL ethanol affording chrysene (**3**) m.p. 255—6°C, identical by UV- and ^1H-NMR spectra with a pure sample.

c) *Photochemical bromination of* **1**

c_1) Over a solution of dihydrochrysene **1** (0.55 g, 2.38 mmoles) in 20 mL anhydrous CCl_4, a solution of bromine (0.6 mL; 1.9 g; 11.8 mmoles) in CCl_4 (6 mL) was poured. The mixture was irradiated in a quartz flask with a medium pressure Hg—UV lamp (150 watt; Rasotherm filter) for 5 hrs. During the irradiation a vigorous evolution of gaseous HBr was observed simultaneously with precipitation of a yellowish solid. The reaction mixture was filtered, the filtrate concentrated to 1/4 of the initial volume and filtered again. The combined solid products (600 mg; 65%) were recrystallized from benzene affording pure **13** with m.p. 284—286°C.

Found: C, 55.73; H, 2.98; Br, 40.91; Calcd. for $C_{18}H_{10}Br_2$: C, 55.96; H, 2.59; Br, 41.45%.

IR spectrum (KBr, cm^{-1}): 430m, 550w, 580w, 700w, 760s, 770s, 872s, 921m, 1410w, 1530w and 1590w.

UV spectrum (cyclohexane) λ max, nm (ε max); 248.5 (33000); 257.5 (67000); 262 (83500); 267.5 (120000); 271.5 (145500); 277 (196000); 296.5 (17500); 309.5 (24000); 323.5 (38000); 338.5 (38000); 352.5 (5000) and 372.5 (3000).

c_2) A solution of dihydrochrysene **1** (0.360 g; 1.56 mmoles) in 10 mL anhydrous CCl_4 was treated with two molar equivalents of bromine (0.5 g; 0.158 mL; 3.12 mmoles) dissolved in 1.5 mL anhydrous CCl_4. The mixture was irradiated with the above mentioned Hg—UV lamp (Rasotherm filter) for five minutes (the bromine colour disappeared). The solution was filtered from traces of insoluble material then evaporated *in vacuo* at room temperature. The thick oily residue (0.80 g) crystallized overnight affording an oily pale-red solid containing a mixture of the addition products **14** and **15**.

IR spectrum (CCl_4; cm^{-1}): 1108 m, 1157m, 1185m, 1449w, 1485w, 2858w, 2920w, 3030w and 3068w.

^1H—NMR spectrum ($CDCl_3$; δ ppm): (i) singnals of tetrabromide **14**: 4.2—4.5 (m; H^B and H^C): 5.15 (m; H^A); 7.2—7.9 (m; H arom);

(ii) signals of dibromide **15**: 3.9—4.3 (m; H^B and H^C); 5.15 (m; H^A); 5.8—6.7 (m; H vinyl); 7.1—7.8 (m; H arom).

Attempted separation and purification of the addition products by column — or thin-layer chromatography on SiO_2 conducted to extensive aromatization (UV— and ^1H—NMR spectra).

UV—Irradiation of the addition products (as a mixture) for about 2 hrs in presence of excess bromine in CCl_4 (using the above mentioned UV lamp) afforded the dibromochrysene **13** identical (m.p., UV— and IR—spectra) with that obtained directly from **1** (see c_1).

Bromination of chrysene (3)

a) *Thermal bromination*

The procedure of Funke, Müller and Vadasz[21a] was used. A suspension of pure chrysene (**3**) (1.5 g; 6.5 mmoles) in 60 mL anhydrous CCl_4 was treated with elemental bromine (3.14 g; 1 mL; 19.6 mmoles) then the mixture was refluxed for 5 hrs. (evolution of gaseous HBr). Filtration of the deposited solid, 2.2. g (87%) and recrystallization from benzene afforded the 6,12-dibromoderivative **13** as white crystals, m.p. 285—6°C; UV — and IR—spectra were identical with those of the product obtained from **1** (*vide supra*) or from **3** by photochemical bromination (*vide infra*).

b) *Photochemical bromination*

A suspension of chrysene(**3**) (1 g; 4.33 mmoles) in 50 mL anhydrous CCl_4 was treated with bromine (2 g; 0.64 mL; 12.5 mmoles) in a quartz vessel which was then UV—irradiated (using the above mentioned UV — lamp: Rasotherm filter) for 10 hrs at room temperature (evolution of gaseous HBr). After elimination of a few crystals on unreacted **3** lying on the surface of CCl_4 the remaining reaction product was filtered *in vacuo* affording a pale yellowish solid (1 g; 59%). Recrystallization from benzene afforded 6,12—dibromochrysene (**13**) m.p. 284—5°, with IR— and UV—spectra identical to those of the products obtained on thermal bromination of **3** (see a) or on photochemical bromination of dihydrochrysene (**1**) (*vide supra*).

Hydroboration/oxidation of 1

Diborane was generated by dropping during 1.5 hrs a solution of $NaBH_4$ (0.114 g: 3 mmoles) in 6 mL freshly distilled diglyme over a solution of $BF_3 \cdot (C_2H_5)_2O$ (0.852 g; 6 mmoles) in 3 mL diglyme. The obtained B_2H_6 was bubbled in a solution of dihydrochrysene (**1**) (0.2 g; 0.87 mmoles) in 5 mL diglyme maintained at 0°C. The reaction mixture was maintained 2 hrs at room temperature, decomposed with 0.5 mL cooled water then treated with a solution of H_2O_2 (30%) (1 mL) and 3N NaOH (0.5 mL). After 2 hrs the reaction mixture was decomposed with water (10 mL), ether extracted (4 × 25 mL) and the ethereal extracts were washed with water (4 × 40 mL), dried and evaporated *in vacuo*. The oily residue (0.2 g; 86%) indicated spectral data in agreement with structure **16**.

IR spectrum ($CHCl_3$; cm^{-1}); 1048m, 1389m, 1468m, 1620w, 2858m, 2930s, 3017m, 3300—3500 large and 3591w.

^1H—NMR spectrum ($CDCl_3$; δppm): 2.6—3.2 (m; 10 H alif.) and 7.1—7.4 (m; 8H arom).

Attempted purification by recrystallization or liquid chromatography conducted to large amounts of chrysene.

Epoxidation of 1

A mixture of dihydrochrysene (**1**) (0.2 g; 0.87 mmoles) in anhydrous CH_2Cl_2 (10mL) and 70% *m*-chloroperbenzoic acid (0.45 g; 1.82 mmoles was stirred under inert atmosphere during 10 hrs at room temperature. The reaction mixture was washed with 10% NaOH solution, then with water and the organic layer was dried and evaporated *in vacuo*. The oily residue (0.19g ; 83.7 %) presented ^{1}H-NMR- and IR-spectral data in agreement with structure **17**.

IR spectrum ($CHCl_3$; cm^{-1}) 965m, 1228vs, 1451m, 1505w, 1520w, 3005s and 3030 shoulder.

^{1}H-NMR spectrum ($CDCl_3$; δppm) : 3.88(m ; 2H ; H^C) ; 4.02 (d ; J = 3.5 Hz ; 2H ; H^A) ; 4.30 (m ; 2H ; H^B) and 7.1—7.4 (m ; 8H ; Harom).

The crude product **17** could not be purified by column chromatography on SiO_2 or by recrystallization due to extensive aromatization.

Attempted valence isomerisations of 2

a) *Treatment with silver fluoroborate*

A solution of **2** (100 mg ; 0.43 mmoles) in purified chloroform (100 mL) was treated with catalytic amounts of silver fluoroborate. No reaction occurred either at room temperature during 72 hrs or at 70°C during 7 hrs.

b) *UV irradiation of* 2

Solutions of **2** (100 mg ; 0.43 mmoles in purified acetone (150 mL) were irradiated with medium presure Hg—UV lamp (150 watt) either directly or through a Rasotherm filter. After 2—6 hrs of irradiation the starting material remained unchanged. After 13 hrs of irradiation (without filter) numerous minor components, including 8 % chrysene were observed on v.p.c. - analysis.

ACKNOWLEDGMENT : The authors express their thanks to Drs. Ligia Stănescu and Aurica Petride for v.p.c.-analyses.

REFERENCES

[1] A. T. Balaban, M. Banciu and V. Ciorba, "Annulenes, Benzo-, Hetero-, Homo-derivatives and Their Valence Isomers", CRC Press, Boca Raton, Fla., 1987.

[2] A. T. Balaban, *Rev. Roumaine Chim.*, **19**, 1185 (1974) ; review : M. Banciu and A. T. Balaban, *Chem. Scr.*, **22**, 188 (1983).

[3] a) M. Elian, M. Banciu, L. Stănescu and E. Ciorănescu. *Rev. Roumaine Chim.*, **21**, 89,(1976) ; b) M. Banciu, M. Elian, Phan Le Thuy, C. Drăghici and E. Ciorănescu, *Rev. Roumaine Chim.*, **27**, 19 (1982).

[4] M. Banciu, D. Elian, M. Elian, L. Stănescu and E. Ciorănescu, *Rev. Roumaine Chim.*, **31**, 503 (1986).

[5] a) M. Stiles, U. Burckhardt and G. Freund, *J. Org. Chem.*, **32**, 3718 (1967) ; b) L. Friedman, *J. Amer. Chem. Soc.*, **89**, 3071 (1967).

[6] a) R. Foster, "Organic Charge Transfer Complexes", Academic Press, London, 1969 ; b) R. S. Mulliken and W. B. Person "Molecular Complexes", Wiley, New York, 1969 ; c) R. E. Merrifield and W. D. Philips, *J. Amer. Chem. Soc.*, **80**, 2778 (1958).

[7] a) H. J. Keller (ed.) "Chemistry and Physics of One Dimensional Metals", Plenum Press, New York, 1977 ; b) L. Alcácer (ed.), "The Physics and Chemistry of Low-Dimensional Solids", Reidel, Dordrecht, Holland, 1980.

[8] H. A. Benessi and J. H. Hildebrand, *J. Amer. Chem. Soc.*, **71**, 2703 (1949).

[9] R. L. Scott, *Req. Trav. Chim.*, **75**, 787 1956).

[10] a) Z. Yoshida and T. Kobayashi, *Tetrahedron*, **26**, 267 (1970) ;
b) E.-M. Vasilescu and D. Săndulescu, *Rev. Roumaine Chim.*, **31**, 605 (1986).

[11] J. L. Lippert, H. W. Hanna and P. J. Trotter, *J. Amer. Chem. Soc.*, **91**, 4035 (1969).

[12] K. H. Michaelian, R. E. Rieckhoff and E. V. Voigt, *Proc. Natn. Acad. Sci. USA*, **72**, 4196 (1975).

[13] J. Cioslowski, *Tetrahedron*, **42**, 735 (1986).

[14] E. E. Merrifield and W. D. Phillips, *J. Amer. Chem. Soc.*, **80**, 2778, (1958).

[15] G. C. Aloisi and S. Pignataro, *J. Chem. Soc. Faraday I*, **1973**, 534.

[16] J. E. Frey and E. C. Kitchen, *J. Amer. Chem. Soc.*, **105**, 2175 (1983).

[17] L. A. Paquette, M. J. Kukla and J. C. Stowell, *J. Amer. Chem. Soc.*, **94**, 4920 (1972).

[18] N. P. Hacker and J. F. W. Mc Omie, *Tetrahedron*, **40**, 5249 (1984).

[19] O. Dann, G. Volz, E. Demant, W. Pfeifer, G. Bergen, H. Fick and E. Walkenhors, *Liebigs Annal. Chem.*, **1973**, 1112.

[20] E. Schmidt, *J. prakt. Chem.*, **9**, 241 (1874).

[21] a) K. Funke, E. Müller and L. Vadasz, *J. prakt. Chem.*, **144**, 265 (1936); cf. *Chem. Zentr.*, **1936**, I, 4157; b) K. Funke and J. Ristic, *J. prakt. Chem.*, **145**, 309 (1936) cf. *Chem. Zentr.*, **1936**, II, 2361.

[22] a) I. G. Farbenindustrie, *F. P.* 793893 (1935): cf. *Chem. Zentr.*, **1936**, I, 4075; see also: b) *Swiss pat.*, 222468 (1942); cf. *Chem. Abstr.*, **43**, 7711 (1949).

[23] a) M. S. Newmann and J. A. Catchcart, *J. Org. Chem.*, **5**, 618 (1940); b) E. H. Rodd (ed.), "Chemistry of Carbon Compounds", Elsevier, Amsterdam, 1956, p. 1480; c) E. Clar, "Aromatische Kohlenwasserstoffe", Springer, Berlin, 1941, p. 108; d) S. E. Hunt and A. S. Lindsey, *J. Chem. Soc.*, **1958**, 2227.

[24] L. A. Paquette, M. R. Short and J. F. Kelly, *J. Amer. Chem. Soc.*, **93**, 7179 (1971).

Revue Roumaine de Chimie, **34**, *9–10*, 1921–1930 (1989)

HETEROCYCLES WITH ANNELATED DIBENZOCYCLOALKANE SKELETONS. III *

PYRAZOLES WITH DIBENZOBARRELENE- AND DIBENZOHOMOBARRELENE SKELETONS

MIRCEA D. BANCIU, [a] MICHAELA DINA STĂNESCU [a] and FILIP CHIRALEU [b]

[a] Organic Chemistry Department, Polytechnic Institute, TCH, Splaiul Independenței 313, 76206 Bucharest, Romania

[b] Centre of Organic Chemistry – ICECHIM, Splaiul Independenței 202B, 78100 Bucharest, Romania

Received May 3, 1989

Formyl derivatives **5** and **7** of dibenzobicyclic ketones **4** and **6**, respectively, afforded on treatment with hydrazyine, phenylhydrazine and 2,4-dinitrophenylhydrazine – the corresponding pyrazoles **8a-c** and **9a-c** with annelated dibenzobarrelene- and dibenzohomobarrelene skeletons, respectively. The IR-, UV- and ^{1}H-NMR spectral data along with chemical evidence support the structures **8** and **9** as well as the mechanism of reaction.

INTRODUCTION

In connection with the continuing interest exhibited by polycyclic heteroaromatic compounds we described in previous papers [1-3] the synthesis of pyrylium salts and pyridines with triptycene (**1**) and homotriptycene skeletons (**2** and **3**).

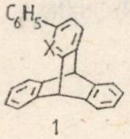

1

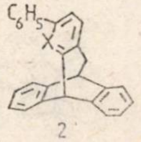

2

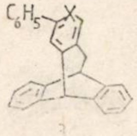

3

$a: X=\overset{+}{O};\ ClO_4^-$ $\quad b: X=N$

In this note we present the synthesis of new pyrazoles with annelated dibenzobarrelene and dibenzohomobarrelene skeletons.

---

* Notes I and II in this series should be considered references 1 and 2 respectively.

RESULTS AND DISCUSSION

Syntheses

The starting materials in the syntheses of pyrazoles were the known ketones **4**[4] and **6**[5] which were converted, as described in our previous papers, into the formyl derivatives **5**[2] and **7**,[6] respectively, existing mainly in their hydroxymethylenic tautomeric forms **5b**[2] and **7b**[6], respectively.

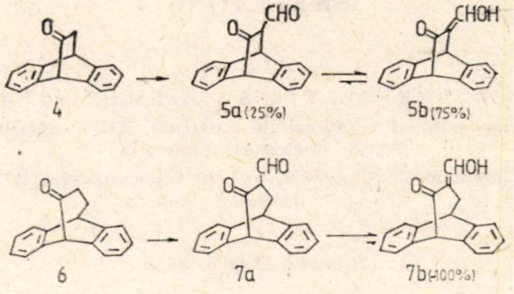
CHO
CHOH
4
5a (25%)
5b (75%)
CHO
CHOH
6
7a
7b (100%)

Refluxing of **5** and **7** with hydrazine hydrate, phenylhydrazine or 2,4-dinitrophenylhydrazine in toluene in the presence of catalytic amounts of *p*-toluenesulphonic acid led to pyrazoles with annelated corresponding bicyclic skeleton. The solid products were recrystallized and their structures were established on the basis of their IR-, UV- and ^{1}H-NMR data.

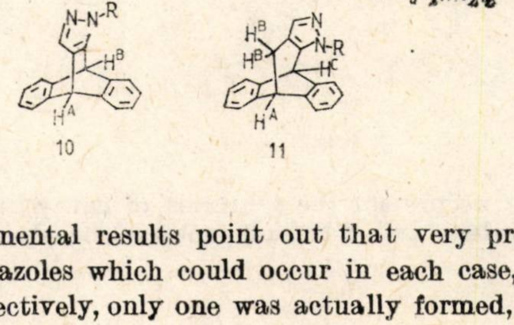
R
H^B
H^A
8
R
H^B
H^B
H^C
H^A
9
a: R=H
b: R=C_6H_5
c: R=$C_6H_3(NO_2)_2$
N-N-R
H^B
H^A
10
H^B
H^B
N-R
H^C
H^A
11

The experimental results point out that very probably from the two isomeric pyrazoles which could occur in each case, namely **8** or **10** and **9** or **11** respectively, only one was actually formed, namely **8** and **9** (see later).

IR spectra

The IR spectra of pyrazoles (see Experimental) are in agreement with the proposed structures (**8a**—**c** and **9a**—**c**). Some characteristic absorptions of the above pyrazoles are collected in Table 1. All compounds exhibit the characteristic $\nu_{C=N}$ absorption of pyrazole rings between 1579 and 1609 cm^{-1}. Only the N-unsubstituted pyrazoles **8a** and **9a** present an absorption between 3200—3440 and 3100—3450 cm^{-1} respectively, characteristic for associated NH bonds. Pyrazoles with an N-phenyl substituent **8b** and **9b** show the characteristic γ_{CH} band of monosubstituted benzenes at 695 and 692 cm^{-1} respectively, whereas pyrazoles with a dinitrophenyl substituent present specific ν_{NO_2} bands: along with the $\nu_{NO_2}^{sym}$ band at 1350 cm^{-1} both compounds **8c** and **9c** indicate two absorptions for $\nu_{NO_2}^{asym}$ at 1530 and 1540 cm^{-1}.

Beside the above-mentioned bands characteristic of pyrazole ring and R-substituent, the IR spectra also show characteristic absorptions for the annelated dibenzobarrelene-(**8a**—**c**) or dibenzohomobarrelene (**9a**—**c**)-skeletons (see Table 1 and Experimental). In this respect pyrazoles **9a**—**c** differentiate from their lower homologs **8a**—**c** by the presence of characteristic $\nu_{CH_2}^{asym}$ and $\nu_{CH_2}^{sym}$ bands at 2916—2920 and 2846—2848 cm^{-1} respectively, which are missing in compounds **8a**—**c**.

Electronic absorption spectra

The electronic spectra of pyrazoles **8a**—**c** and **9a**—**c** in methanol solution are presented in the Experimental part. A comparison of the UV-spectra of the N-unsubstituted pyrazoles **8a** and of triptycene (**12**)[7,8] (Table 2) reveals a striking resemblance in position (λ_{max}) and intensity ($\lg\varepsilon_{max}$) of the characteristic absorption maxima. It seems that the electronic systems of **8a** and **12** are very similar. Literature data[7] showed that the UV-spectrum of triptycene (**12**) is essentially that of an *ortho*-disubstituted benzene, and consequently this resemblence may be also applied to **8a**. However, the somewhat lower lg ε values observed for **8a** as compared to **12** suggest that the electronic transitions are less favoured in the compound **8a** with two *ortho*-substituted benzenic rings and an *ortho*-disubstituted pyrazolic one in comparison with tripycene (**12**) containing three *ortho*-disubstituted benzenic rings. Very probably, important through-space interactions among the π-electron systems like those proved by PE spectral data in the triptycene **12**[9] are also operant within the pyrazole **8a**.

Another interesting comparison could be made between UV spectra of pyrazoles **8a** and **9a** (Fig. 1). As may be seen in fig. 1, all absorption bands of **9a** are hypsochromically and hypochromically shifted in comparison with the corresponding absorptions of **8a**. It follows that the extent of conjugation is higher in the rigid and strained molecule **8a** in comparison with the less rigid molecule **9a**.

Table 1

Characteristic IR absorptions of pyrazoles **8a-c** and **9a-c**

Compound / Vibration	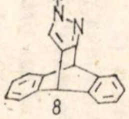 8			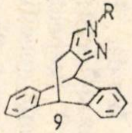 9		
	a ; R=H*	**b** ; R=Ph **	**c** ; R=$C_6H_3(NO_2)_2$*	**a** ; R=H*	**b** ; R=Ph**	**c** ; R=$C_6H_3(NO_2)_2$*
A. Vibrations of pyrazole ring and its substituent R						
νC=N	1585	1603	1603	1579	1602	1609
νNH (assoc.)	3200–3440	—	—	3100–3450	—	—
γCH (monosubstit. benzene)	—	695	—	—	692	—
γCH (trisubstituted benzene)	—	—	835 ; 850	—	—	840 ; 855
γNO_2(sym.)	—	—	1350	—	—	1350
γNO_2 (asym.)	—	—	1530 ; 1540	—	—	1530 ; 1540
B. Vibrations of annelated dibenzocycloalkane skeleton						
νCH_2 (sym.)	—	—	—	2846	2846	2848
νCH_2 (asym.)	—	—	—	2920	2916	2920
γCH (*o*-disubstit. benzene)	741	739 ; 759	748	736 ; 751 ; 765	742 ; 751	732 ; 746
νCH (aryl)	3045	3022 ; 3047	3018 ; 3060	3015	3022 ; 3050	3010 ; 3040

* KBr disc ; ** CS_2 and CCl_4 solution.

Table 2

UV-spectral data of pyrazole **8a** and triptycene (**12**) [7,8]

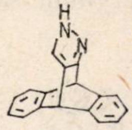

8a

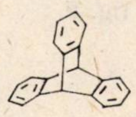

12

λ_{max} nm	lg ε_{max}	λ_{max} nm	lg ε_{max}
235 (shoulder)	3.99		
256	3.15		
263	3.28	264 (shoulder)	3.30
271	3.30	271	3.55
278.5	3.45	279	3.67

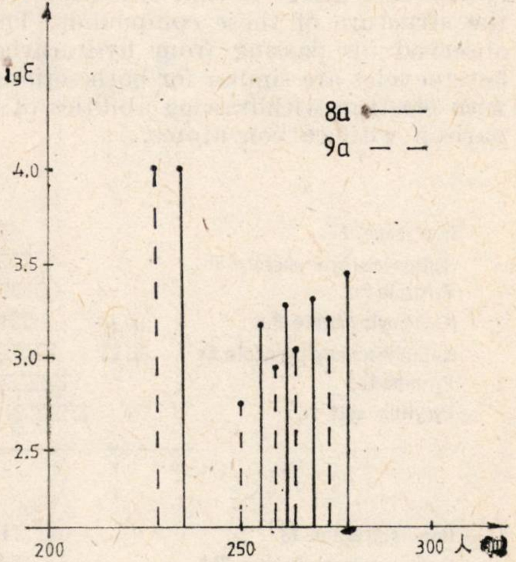

Fig. 1. — Comparison of the UV-absorption maxima of pyrazoles **8a** and **9a**.

In the pyrazoles with N-phenyl and N-dinitrophenyl substitutents, the above parallelism of the spectral data for systems **8** and **9** is less visible probably due to the complication of the chromophoric system. Dinitrophenylpyrazoles **8c** and **9c** present end-absorptions in the visible range, appearing thus yellow-coloured.

^{1}H-NMR spectra

The ^{1}H-NMR spectra (see Experimental) are also in agreement with the proposed structures **8a**—**c** and **9a**—**c** for the synthesized pyrazoles. A graphical representation of characteristic signals of **8a**—**c** along with those of tryptycene (**12**),[10] hydroxymethyleneketone **5b**,[2] pyridine **1b**[2] and pyrylium salt **1a**[2] on one hand and of the signals for pyrazoles **9a**—**c** along with those of homotriptycene (**13**)[11], hydroxymethyleneketone **7b**[6], pyridine **2b**[1] and pyrylium salt **2a**[19] on the other hand, is given in fig. 2.

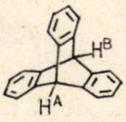

12

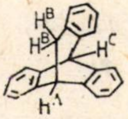

13

A good correlation is observable between signals of similar protons from all compounds with annelated dibenzobarrelene skeleton on one hand, and the compounds with annelated dibenzohomobarrelene skeleton on the other hand. Whereas the bridgehead protons H^A, H^B in triptycene derivatives appear as singlets, the pattern of H^A, H^C, (and H^B) in homotriptycene derivatives is that of a triplet/singlet/(doublet), in agreement with the structure of these compounds. The deshieldings of aliphatic protons observed on passing from hydrocarbons **12** and **13** to corresponding heterocycles are similar for both series of derivatives and are in agreement with electron withdrawing abilities of neighbouring heteroatoms in comparison with carbon atoms.

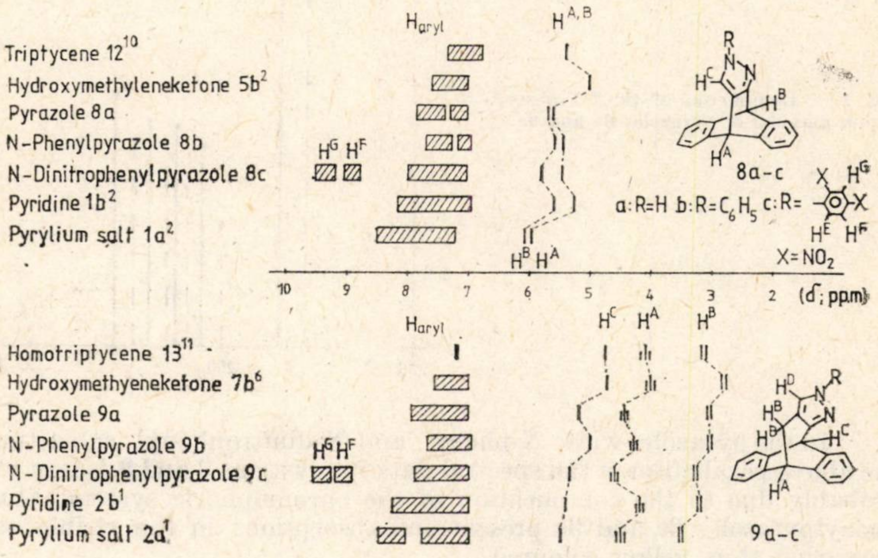

Fig. 2. — Correlation of ^{1}H-NMR data for pyrazoles 8a-c, 9a-c and related compounds.

It should be mentioned that the NH-proton from unsubstituted pyrazoles **8a** and **9a** could not be individually evicenced in the ^{1}H-NMR spectra: in solvents which contain traces of water (d_6-acetone or d_6-DMSO) this proton was included in the HO-signal whereas in anhydrous solvents (CCl_4 : $CDCl_3$; C_6D_6 ; $AsCl_3$; hexachlorobutadiene) the compounds **8a** and **9a** are practically insoluble.

An interesting and useful information (though an indirect one) concerning the structures of the new pyrazoles results from ^{1}H-NMR spectra. Examination of Dreiding stereomodels of **10** and **11** reveals that a pronounced shielding of H^B and H^C protons respectively by the N-phenyl substituent would be expected for structures **10b,c** and **11b,c** due to the position of these protons lying under the benzenic ring. An approximate shielding of 0.75 ppm and 1 ppm for **10** and respectively **11** was evaluated from Johnson-Bovey diagrams [12] whereas from Haigh-Mallion data [13] the same shieldings would be 0.35 ppm and 0.5 ppm.

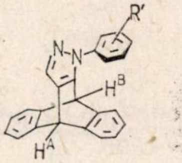

10b, c

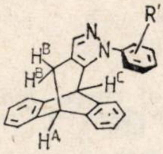

11b, c

Due to the fact that no such shielding of H^B or H^C (in comparison with H^A) was observed in the ^{1}H–NMR spectra of the synthesized pyrazoles, it follows that *the correct structure of these pyrazoles is* **8** *and* **9** *respectively*. Dreiding stereomodels indicate that in compounds **8** or **9** the shielding of H^B and H^C by the very remote phenyl ring would be inoperant.

The reaction mechanism

As in other cases, [14] formation of pyrazoles from 1,3-dicarbonyl derivatives seems to proceed stepwise *via* the hydrazones which undergo further cyclization.

The tautomeric dicarbonylic compounds **5** and **7** could afford two types of hydrazones, namely **14** and **15** (Scheme 1).

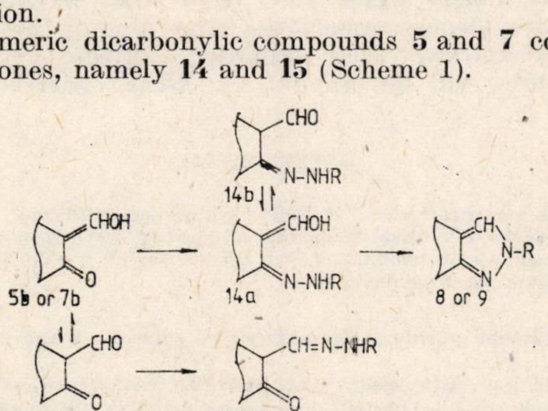

Scheme 1

Elimination of water from **14** should afford **8** or **9** whereas elimination of water from enolic tautomers of hydrazones **15** should lead to pyrazoles **10** or **11**. The present results suggest the formation of pyrazoles **8** or **9** via **14**. A proof of this mechanism was brought by isolation of the intermediate monohydrazones **14** when the reaction of **5** and **7** with 1,4-dinitrophenylhydrazine was stopped at a short reaction time.

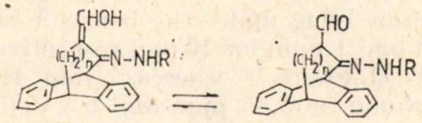

14a 14b

A: n=0 B: n=1 $R=C_6H_3(NO_2)_2$

The IR spectra of these hydrazones (KBr pellets) are in agreement with the structures **14a-A** ($\nu_{C=N} = 1590\ cm^{-1}$; $\nu_{C=O}^{aldeh.} = 1720\ cm^{-1}$) and **14a-B** ($\nu_{C=N} = 1610\ cm^{-1}$; $\nu_{OH}^{assoc.} = 3200 - 3400\ cm^{-1}$). Both compounds **14** afforded a positive reaction of aldehydic group with the Fehling reagent. If the intermediate hydrazones had been **15**, they would not have indicated positive aldehyde tests. Moreover, an enolic tautomeric form **15b** of hydrazones **15** seems improbable keeping in mind the fact that neither **5** or **7** present a tautomeric form **5c** or **7c** similar to **15b** (probably due to additional strain in the bicyclic system).

In conclusion, this work presented the synthesis of six new pyrazoles with annelated dibenzocycloalkane skeletons: three of them, **8a—c**, possess a dibenzobarrelene skeleton and the other three, **9a—c**, a dibenzohomobarrelene moiety. The IR-, UV- and ^1H-NMR spectra as well as chemical evidence support the structures of these pyrazoles and the stepwise mechanism of their formation. Further confirmation of the proposed structures will be brought by X-ray analysis in the future.

EXPERIMENTAL

Melting points are uncorrected. ^1H-NMR spectra were performed on a VARIAN A 60—A spectrometer (TMS as internal standard). IR spectra were registered on a UR—20 C. Zeiss Jena double beam spectrophotometer and UV spectra on a SPECORD UV — VIS. C. Zeiss Jena double beam spectrophotometer.

General procedure for synthesis of pyrazoles 8 and 9

A mixture of hydroxymethyleneketone **5**[2] or **7**[6] (2.0 mmoles), hydrazine derivative (85 % hydrazine hydrate, freshly distilled phenylhydrazine or 2,4-dinitrophenylhydrazine) (2.4 mmoles), catalytic amounts of *p*-toluenesulphonic acid (0.1 mmoles) in 25 mL toluene was refluxed for 12 hrs separating small quantities of water with an ASTM device. (After 1—2 hrs of reflux formation of an abundant solid was visible in the reactions with 2,4-dinitrophenylhydrazine; *vide infra*).

The obtained solutions were washed with water until pH=7, dried and evaporated *in vacuo*. The thick residual products crystallized on scratching with petroleum ether. Recrystallization from proper solvents afforded the pure pyrazoles (**8** -**c**) or (**9** -**c**).

1′,2′-Pyrazolo[b]*dibenzo*[e, *h*]*bicyclo*[2.2.2]*octa-2,5,7-triene* (**8**); yield 61 %; m.p. 300—303°C (from ethanol).

IR spectrum (KBr ; cm^{-1}) : 500m, 530m, 630m, 662m, 741s, 757m, 810m, 891w, 910w, 956m, 1020m, 1120m, 1155m, 1190w, 1296w, 1413m, 1458s, 1585m, 2970w, 3045w and 3200—3440 large.

UV spectrum (methanol ; λ_{max}^{nm} ; lg ε_{max}) : 235 shoulder (3.99) ; 256 (3.15) ; 263 (3.28) ; 271 (3.30) and 278.5 (3.45).

^1H—NMR spectrum (d$_6$-acetone ; δ ppm) : 5.59s (1H ; H^A) ; 5.62s (1H ; H^B) ; 7.0—7.3m (4H ; H$_{benzo}$) ; 7.31—7.8 (m ; 5H ; 4H$_{benzo}$ + H^C).

1′,2′-Pyrazolo[b]*dibenzo*[f,i]*bicyclo*[3.2.2]*nona-2,6,8-triene* (**9a**) : yield 71 % ; m.p. 265—267°C (from ethanol).

IR spectrum (KBr, cm^{-1}) : 497m, 585m, 615m, 670m, 697w, 736s, 751m, 765m, 822m, 960m, 1045m, 1100w, 1175w, 1210w, 1340w, 1385w, 1450m, 1470m, 1579m, 2846w, 2920m, 3015w and 3100 — 3450 large.

UV spectrum (methanol ; λ_{max}^{nm} ; lg ε_{max}) : 227 shoulaer (3.99) ; 252 (2.74) ; 259 (2.93) ; 266 (3.09) and 273.5 (3.20).

^1H—NMR spectrum (d$_6$-acetone ; δ ppm) : 3.05 d (2H ; H^B ; J = 4Hz) ; 4.45 t (1H ; H^A ; J = 4Hz) ; 5.2s (1H ; H^C) ; 7—7.9m (9H ; 8H$_{benzo}$ + H^D).

1′-Phenyl-1′,2′-pyrazolo[b]*dibenzo*[e, h]*bicyclo*[2.2.2]*octa-2,5,7-triene* (**8b**) ; yield 85 % ; m.p. 186—9°C (from ethanol).

IR spectrum (CS$_2$; CCl$_4$; cm^{-1}) 640m, 695m, 739s, 759s, 853w, 948w, 988w, 1382m, 1415w, 1458m, 1515m, 1603m, 1680w, 2975w, 3022w, 3047w and 3072w.

UV spectrum (methanol ; λ_{max}^{nm} ; lg ε_{max}) : 237.5 shoulder (4.22) ; 272.5 (3.87) and 281 (3.83).

^1H—NMR spectrum (CDCl$_3$; δ ppm) : 5.4s (1H ; H^A) 5.6s (1H ; H^B) ; 6.9—7.15m (4H ; H$_{benzo}$) ; 7.2—7.7m (10H ; 9H$_{benzo}$ + H^C).

1′-Phenyl-1′,2′-pyrazolo[b]*dibenzo*[f,i]*bicyclo*[3.2.2.]*nona-2,6,8-triene* (**9b**) ; yield 62 % ; m.p. 186—7°C (from ethanol).

IR spectrum (CS$_2$; CCl$_4$; cm^{-1}) : 692w, 742s, 751m, 955m, 1048w, 1327w, 1382s, 1455w, 1472w, 1500m, 1602m, 2846w, 2916m, 3022w, 3050w and 3072w.

UV spectrum (methanol ; λ_{max}^{nm} ; lg ε_{max}) : 269 shoulder (4.33) and 275 (4.37).

^1H—NMR spectrum (CDCl$_3$; δ ppm) : 3.1d (2H : H^B ; J = 4Hz) ; 4.3t (1H ; H^A ; J = 4Hz) ; 5.1s (1H ; H^C) ; 6.9—7.65m (14H ; 13H$_{benzo}$ + H^D).

1′(2,4-dinitrophenyl)-1′,2′,pyrazolo[b]*dibenzo*[e, h]*bicyclo*[2.2.2]*octa-2,5,7-triene* (**8c**) ; yield 73 % ; m.p. 268—270°C (from acetic acid).

IR spectrum (KBr ; cm^{-1}) : 494m, 633m, 748 s, 795w, 835m, 850m, 875w, 918m, 985m, 1035w, 1080m, 1142m, 1350s, 1389m, 1460m, 1530s, 1540s, 1603s, 3018w, 3060m, and 3120w.

UV spetrum (methanol ; λ_{max}^{nm} ; lg ε_{max}) : 239 shoulder (4.12) ; 265.5 (3.94) ; 271.5 (3.94) ; 281 (3.98) and 300 large (3.94).

^1H—NMR spectrum (F$_3$C—COOH) ; δ ppm) : 5.45s (1H ; H^A) ; 5.8s (1H ; H^B) ; 7.0—7.9m (10H ; 8H$_{benzo}$ + H^C + H^E) ; 8.75—9.1m (1H ; H^F) ; 9.25—9.5m (1H ; H^G).

1′(2,4-dinitrophenyl)-1′,2′-pyrazolo[b]*dibenzo*[f, i]*bicyclo-*[3.2.2]*nona-2,6,8-triene* (**9c**) ; yield 87 % ; m.p. 249—251°C (from acetic acid).

IR spectrum (KBr ; cm^{-1}) : 590w, 615w, 630w, 715m, 732s, 746s, 775m, 840m, 855m, 915m, 970w, 1087m, 1350s, 1530s, 1540s, 1609s, 2840w, 2848w, 2920w, 3010w, 3040w and 3080w.

UV spectrum (methanol : λ_{max}^{nm} ; lg ε_{max}) : 250 shoulder (4.03) ; 265 (3.85) : 274 (3.84) and 321 large (3.82).

^1H—NMR spectrum (F$_3$C—COOH : δppm) : 3.25d (2H ; H^B) ; 4.65t (1H ; H^A) : 5.35s (1H ; H^C) ; 7.0—7.9m (10H ; 8H$_{benzo}$ + H^D + H^E) 8.9—9.25m (1H ; H^F) ; 9.3—9.6m (1H ; H^G).

Dinitrophenylhydrazone (**14b-A** *of* **5** ; yellow crystals, m.p. 230—3°C.

IR spectrum (KBr ; cm^{-1}) : 780w, 850w, 1080m, 1150m, 1325s, (ν_{NO_2}) ; 1420 m ; 1500s (ν_{NO_2}) ; 1590s ($\nu_{C=N}$) ; 1720s (ν_{CHO}).

Dinitrophenylhydrazone **14a-B** of **7** ; pale yellow crystals ; m.p. 212—5°C ;

IR spectrum (KBr ; cm^{-1}) : 720w, 780w, 850w, 1140m, 1180s, 1240m, 1350s (ν_{NO_2}) ; 1380s, 1520m (ν_{NO_2}) ; 1610 ($\nu_{C=N}$) ; 3200—3400 large (ν_{OH} assoc.).

ACKNOWLEDGMENT : ^{1}H—NMR spectra of **8b** and **9b** were registered by Eng. Ana Schiketanz to whom our thanks are due.

REFERENCES

[1] M. Banciu, A. T. Balaban, C. Drăghici and R. Vlad, *Rev. Roumaine Chim.*, **27**, 1037 (1982).

[2] M. Stănescu, M. Banciu and A. T. Balaban, *Rev. Roumaine Chim.*, **34**, 617 (1989).

[3] M. Banciu, M. Stănescu, C. Florea, A. T. Balaban and E. Ciorănescu, *Rev. Roumaine Chim.*, **32**, 1161 (1987).

[4] P. F. Huldrik, A. M. Huldrik and Chung Non Wan, *J. Org. Chem.*, **40**, 1116 (1975).

[5] E. Ciorănescu, M. Banciu, R. Jelescu, M. Elian and C. D. Nenitzescu, *Tetrahedron Letters*, **1969**, 1871 ; *Rev. Romaine Chim.*, **14**, 911 (1969).

[6] M. Banciu, *Rev. Roumaine Chim.*, **27**, 769 (1982).

[7] C. F. Wilcox and A. C. Craig, *J. Org. Chem.*, **26**, 2491 (1961) ; C. F. Wilcox, *J. Chem. Phys.*, **37.** 1874 (1960).

[8] W. Theilacker, K. Albrecht and H. Uffmann, *Chem. Ber.*, **98**, 428 (1965).

[9] T. Kobayashi, T. Kubota and K. Ezumi, *J. Amer. Chem. Soc.*, **105**, 2172 (1983).

[10] K. G. Kidd, G. Kotonycz and T. Schaefer, *Canad. J. Chem.*, **45**, 2155 (1967) ; K. Bowden, J. G. Irvig and A. M. J. Price, *ibid.*, **46**, 3903 (1968).

[11] S. J. Cristol and D. K. Pennelle, *J. Org. Chem.*, **35**, 2357 (1970).

[12] C. E. Johnson Jr. and F. A. Bovey, *J. Chem. Phys.*, **29**, 1012 (1958).

[13] C. W. Haigh and R. B. Mallion, *Org. Magn. Reson.*, **4**, 203 (1972).

[14] T. L. Jacobs, "Pyrazoles and Related Compounds", in "Heterocyclic Compounds", (R. C. Elderfield, ed.) J. Wiley, New York, 1957. vol. 5, p. 46 ; L. A. Paquette, "Principles of Modern Heterocyclic Chemistry", Benjamin Inc., New York, 1968; G.R. Newkome and W.W. Paudler, "Contemporary Heterocyclic Chemistry", J. Wiley, New York, 1982

Revue Roumaine de Chimie, 34, *9–10*, 1931–1944 (1989)

THE SYNTHESES OF BENZONORBORNANE, *exo*-BENZOCYCLOBUTANO- AND *endo*-BENZOCYCLOBUTANO-NORBORNANES ANNELATED WITH *exo*-CYCLOBUTENE RING *via* SHECHTER REACTION[1]

MIRCEA D. GHEORGHIU, [a,*] EMILIA OLTEANU, [a] LIGIA STĂNESCU, [a]
MARGARETA AVRAM + and GHEORGHE SURPĂŢEANU [b]

[a] Department of Organic Chemistry, Polytechnic Institute – TCH, 76206 Bucharest 16
Romania

[b] Department of Organic Chemistry, Polytechnic Institute, Jassy, Romania

Received May 18, 1989

The synthesis and spectral characterization of three cyclobutenes **1**, **2** and **3** are reported. All cyclobutenes were obtained by Shechter reaction, *e.g.* thermal decomposition of the corresponding cyclopropyl aldehyde tosylhydrazone in presence of sodium methoxide. Together with the cyclobutene, representing the ring enlargement product resulted from the intermediate cyclopropylcarbene, cycloreversion product was also isolated. The molar ratio insertion product/cycloreversion product was *ca.* 2 : 1. Molecular mechanics calculation predict that cyclobutene **2** is more stable than the isomeric cyclobutene **3**. The relative stability is originating from the lower torsional interactions along C_3-C_{3a} and $C_{7b}-C_8$ bonds in the *exo* annelated benzocyclobutano derivative **2**.

INTRODUCTION

In 1966, five different groups [3–7] reported syntheses in the series of cyclobutenes annelated in *exo* or *endo* configuration to norbornane skeleton. The *exo*-cyclobutenonorbornane **4** resulted in 0.8% overall yield by photochemical cycloaddition of dimethylmaleic ester to norbornene, followed by conversion to dibromoderivative and halogen elimination. [3] By trapping cyclobutadiene with cyclopentadiene, the *endo*- cyclobutenonorbornane **7** was obtained.[4] The same compound was obtained in an alternative way from the Diels-Alder adduct of cyclopentadiene with *cis*-1,2-dichlorocyclobutene.[5] A mixture of *exo*- and *endo*-cyclobutenenorbornenes **6** and **7** respectively (13 : 20) resulted from the electrocyclic ring closure of bicyclo(4.2.1)nona-2,4,7-triene promoted by ultraviolet irradiation.[6] The *exo*-cyclobutenonorbornane **6** was also noticed as reaction product in the thermal decomposition of the norbornadiene dimer.[6,7]

After the 1966 outburst of contributions, the next twenty years hardly doubled the number of references concerning cyclobutenonorbornanes. Thus in 1968, Sauers designed a better procedure for the synthesis

---

+ deceased 1983

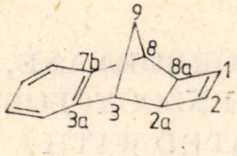

1

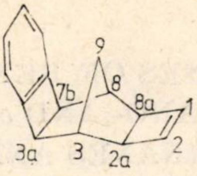

2

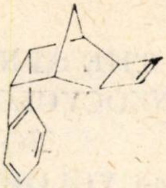

3

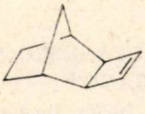

4

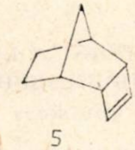

5

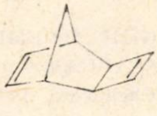

6

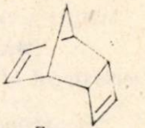

7

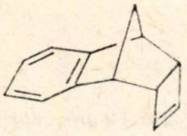

8

of compound 4. When the lithium salt of cyclopropylaldehyde tosylhydrazone **9** was subjected to thermolysis, the cyclopropylcarbene **10** gave, *via* insertion, the cyclobutene 4, together with the cycloreversion product **11**.[8]

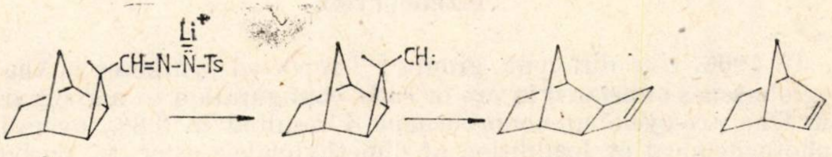

This is the first example of a Shechter reaction[2] applied to a norbornanecyclopropylcarbene. Irradiation of bicyclo(4.2.1)nona-2,4-diene gave a 1 : 2 mixture of *exo* (4) and *endo*-cyclobutenenorbornane (5).[9] Compounds 4–7 were also synthesized from the corresponding cyclobutanone tosylhydrazone[10] by a Bamford-Stevens reaction.[11]

In the present contribution we present data regarding the synthesis and spectral characterization of cyclobutenes **1**, **2** and **3**. The benzonorbornanecyclobutene **1** was briefly mentioned in a short communication in 1975.[12] Since then, no synthetical or structural details were disclosed to our best knowledge. A summary presentation from this laboratory was dedicated to *endo*-benzocyclobutanonorbornanecyclobutene **3**.[13] Also it should be noted that compounds **1**, **2** and **3** structurally related to the carbomethoxycyclobutenes **12**[14] and cyclobutanones **13**,[15a] were obtained previously in our laboratory.

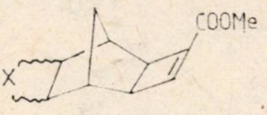

12

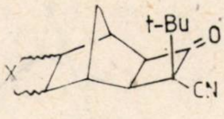

13

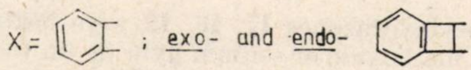

In this paper we present results regarding the synthesis of norbornanocyclobutenes annelated with benzo-, *exo*-benzocyclobutano- and *endo*-benzocyclobutano — fragment by means of Shechter reaction. The precursors of cyclopropylcarbene are easily available from the reaction of norbornenes **14**, **15** and **16**, by cyclopropanation with ethyldiazoacetate, in the presence of Pd catalysts.[15b]

A. SYNTHESIS

For the syntheses of benzonorbornanocyclobutene **1** and of the *exo*- (**2**) and *endo*-benzocyclobutanonorbornanocyclobutene **3**, we employ the Shechter reaction.[2] Under normal structural circumstances, cyclopropylcarbene reacts *via* two reaction modes. The insertion of carbene into the cyclopropane C—C bond has as result a cyclobutene, while the concurrent cycloreversion (or cheletropic reaction) converts the cyclopropylcarbene into an alkene and acetylene. The ratio of insertion *versus* cycloreversion products is generally rated at *cà*. 2 : 1 molar ratio.

At present, there is no firm grasp of the factors governing the magnitude of the insertion/cycloreversion ratio.[16] When the cyclobutene is the aim of the synthesis, one should accept that at best the yields will be medium (equal or less than 60%). So far there are only few examples presenting a sole reaction mode, either cyclobutene formation or cycloreversion. Thus from 1-phenylcyclopropylcarboxaldehyde tosylhydrazone resulted only cyclobutene,

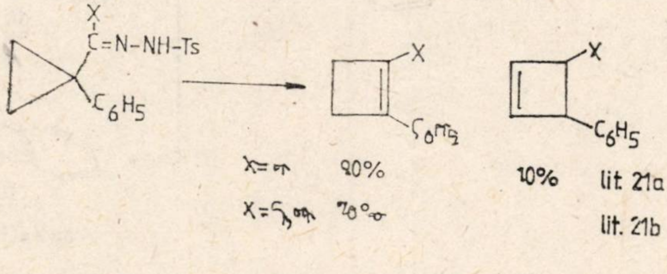

namely a mixture of isomeric phenylcyclobutenes. [21a] A similar rezult, *e.g.* the formation only of a cyclobutene derivative, was obtained using as cyclopropylcarbene precursor the tosylhydrazone of cyclopropylphenyl ketone. [21b] On the other hand, tricyclo(2.2.1.0^{2,6})-3-heptylidene gave only 4-ethynylcyclopentene, as cycloreversion product. [22]

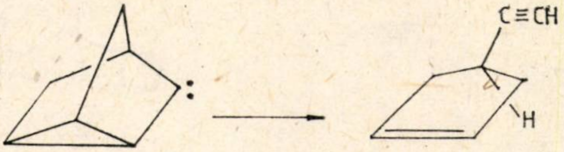

When the tosylhydrazones **17**, **18**, **19** were heated under argon at 130°C with sodium methoxide or sodium hybride (in the case of compound **17**) in diethyleneglycol dimethyl ether (DME) a mixture of cyclobutenes **1**, **2**, **3**, norbornene derivatives **14**, **15**, **16** and a small amount of cyclopropane derivatives **20a**, **21**, **22** resulted. The reaction mixture analyzed by GC and GC—MS revealed that the molar ratio of products is only slightly dependent on the molar ratio of tosylhydrazone : base (sodium methoxide or sodium hydride).

a) Synthesis of 2aα, 3α, 8α, 8aα-tetrahydro-3,8-methanocyclobuta(b)naphthalene (1)

A mixture (1 : 2 molar ratio) of tosylhydrazone **17** and freshly prepared sodium methoxide (from anhydrous methanol and sodium) was heated at 130°C, under argon, for one hour, under stirring. GC analysis of the crude reaction mixture revealed the composition : cyclobutene **1** : norbornene **14** : cyclopropane **20a** as 46 : 16 : 3.7. Pure samples of the cyclobutene **1** were obtained by column chromatography on Al_2O_3, using petroleum ether (b.p. 36°C) as eluent. An alternative way consisted in a careful bromination of the reaction mixture, when the norbornene 14

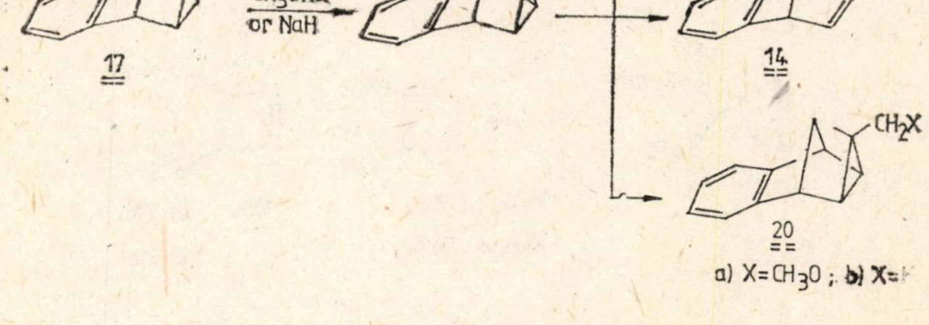

reacted more rapidly than the cyclobutene **1**. By column chromatography, the less polar cyclobutene **1** was easily separated from the more polar dibromoderivative of norbornene **14** [23] and the cyclopropylmethylether **20a**. The methyl ether **20a** [24] results either by trapping the intermediate cyclopropylcarbene by the methoxy anion or by reaction with the residual methanol. The amount of the methyl ether **20a** is relatively reduced, therefore, we do not rule out the possibility that in trapping were involved also traces of methanol, despite our special precaution to remove carefully the excess of methanol. The methyl ether was obtained independently by alkylation of the cyclopropylmethanol **20c**[5c] with methyl iodide in the presence of sodium hydroxide, using dimethylsulfoxide as solvent. By using sodium hydride to generate the sodium salt of tosylhydrazone **17**, which was subsequently thermally decomposed, the methylsubstituted cyclopropane **20b** was identified by GC only in slight amounts (2.5%). The independent synthesis of the methylcyclopropane **20b**, was carried out from the tosylate of the alcohol **20c** subjected to reduction with lithium aluminium hydride.

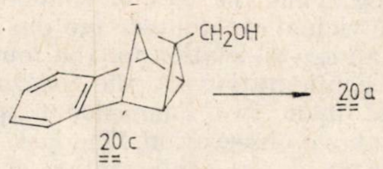

b) Synthesis of 2aα, 3α, 3aα, 7bα, 8α, 8aα-hexahydro-3,8-methanocyclobuta(b)biphenylene (2) and 2aα, 3α, 3aα, 7bα, 8α,8aα-hexahydro-3,8-methanocyclobuta(b)biphenylene(3)

The *exo*-annelated isomeric cyclobutenes **2** and **3**, resulted in *ca*. 50% yield by thermal decomposition of the sodium salt of the tosylhydrazones **18** (*exo*-benzocyclobuta isomer) and **19** (the *endo*-benzocyclobuta isomer) respectively. As byproducts were isolated the alkenes **15** and **16** (approximately 30%) and the methylethers **21** and **22**. The latter

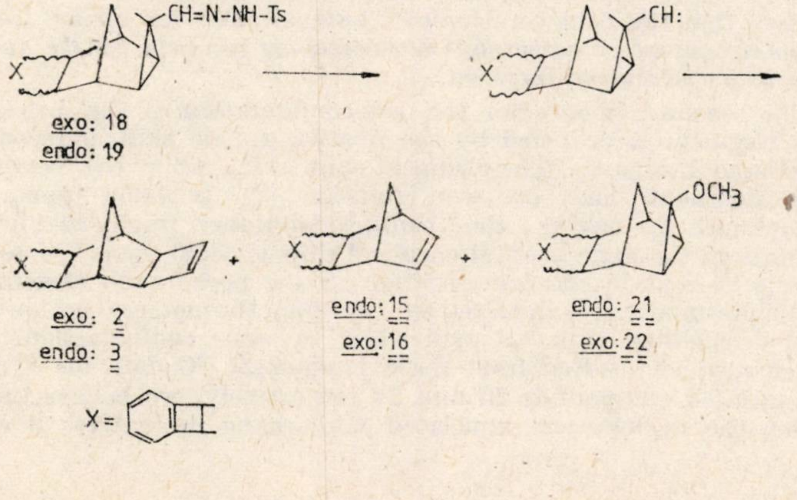

compounds resulted when the sodium salt of the tosylhydrazones **18** and **19** were generated with sodium methoxide. The ethers **21** and **22** were obtained by independent route, analogously with that employed for the preparation of ether **20a**.

B. SPECTRAL DATA

a. ^{1}H-NMR and ^{13}C-NMR results

The NMR spectral data are consonant with the *exo*-configuration of the cyclobutene ring. Thus the lack of coupling between the bridgeheads $H_3(H_8)$ with the vicinal cyclobutene protons $H_{2a}(H_{8a})$ is convincing for the assignment of an *exo*-annelation for the four-membered ring.[5,6a,25] The *exo*- and *endo*- configuration of the benzocyclobutano fragment was established based upon two independent spectral characteristics. One is similar to the above observation. The lack of bridgehead-benzylic proton coupling indicates an *exo*-configuration of the benzocyclobutano ring. The *endo* configuration of the benzocyclobutano ring is shown by the *ca.* 4Hz coupling constant among the bridgehead proton $H_3(H_8)$ and the benzylic $H_{3a}(H_{7b})$ protons.[25] Molecular mechanics calculations (MM2)[26] carried out for the cyclobutene **2** and **3**, have accrued information regarding the dihedral angles $H_{3a}-C_{3a}-C_3-H_3$ and $H_3-C_3-C_{2a}-H_{2a}$. In the *exo*--benzocyclobutano derivative **2**, the calculated dihedral angle between the vicinal benzylic H_{3a} and the bridgehead proton H_3 is 72°, whereas in the *endo*-benzocyclobutano derivative **3**, the same dihedral angle is 37°. In both isomers **2** and **3**, the cyclobutene when in *exo*-configuration, the dihedral angles between the bridgehead proton H_3 and the vicinal proton belonging to the four-membered ring H_{2a}, is *ca.* 72°. From the Karplus equation,[27] the calculated coupling constant corresponding to the $H_{endo}-H_{bridgehead}$ is 5.05 Hz, while that for the $H_{exo}-H_{bridgehead}$ is equal to 0.3 Hz. Indeed, these figures are very close to coupling constants observed experimentally. We believe that we provide for the first time the most reliable dihedral angles between the bridgehead proton and the both vicinal ones. The figures quoted previously[25c] originate from dihedral angles measured on standard models.[25c] Therefore, we believe that the Schleyer-Laszlo[25a] seminal rules for *vicinal coupling constants recognized for norbornane derivatives are valid also for the annelated systems with cyclobutene fragment.*

The second evidence for the *exo*-configuration of the benzocyclobutano fragment is provided by the relative upfield shift induced upon the methano bridge C_8. The chemical shift of C_8, when the benzocyclobutano fragment has *exo* configuration (**2**) is 24.53 ppm, while in compound **3**, having the benzocyclobutano fragment in *endo* configuration, the experimental chemical shift is 36.36 ppm. We reported previously[15c] that in *exo* configuration on the norbornane skeleton, the benzocyclobutano ring is shielding by -6.7 ppm the methano bridge carbon C_8, and deshielding with 5.9 ppm when in *endo* configuration. These increments, which resulted from the experimental ^{13}C data for cyclopropane annelated compounds **23** and **24** respectively, we believe are still valid for the cyclobutene annelated norbornane derivatives **2** and **3**.

Assuming as reference compounds the mono annelated, *exo*-**25** and *endo*-**26**, by *exo*-annelation with cyclobutene as in **2** and **3** respectively, C_8 is shielded with -7.41 ppm and -7.34 ppm, respectively. The mean value -7.37 ppm, considered as increment for an *exo*-cyclobutene ring and using our previous increments for the *exo*- and *endo*- benzocyclobutane fragment, one could

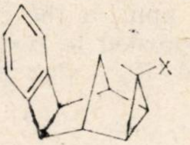

23

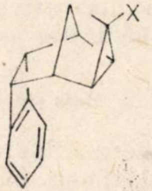

24

a: X=H
b: X=COOCH$_3$
c: X=CH$_2$OH
d: X=CHO

estimate, starting with the known chemical shift of C_8 from norbornane, [28] the chemical shift of the same atom from the cyclobutane **2** and **3**, respectively.

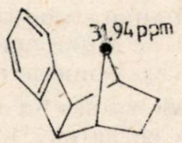

25

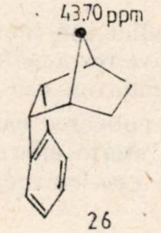

26

Indeed, as presented in the scheme, the calculated values are in excellent agreement with the experimental results. The $^{13}C-NMR$ spectrum of the cyclobutanonorbornane **28**, is to our best knowledge unknown,

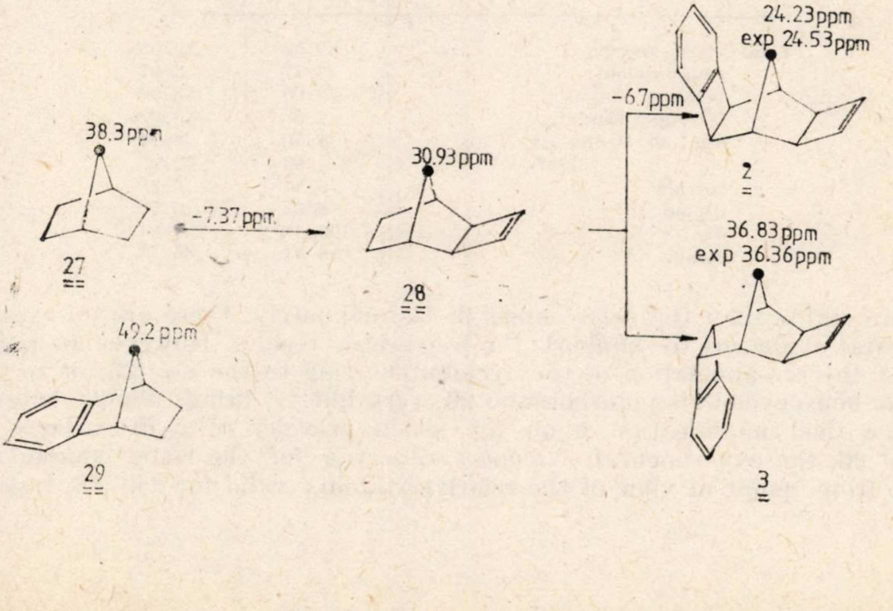
38.3 ppm
27
-7.37 ppm
30.93 ppm
28
-6.7 ppm
24.23 ppm
exp 24.53 ppm
2
36.83 ppm
exp 36.36 ppm
3
49.2 ppm
29

therefore the $\delta = 30.93$ ppm for C_8, represents our prediction,[27] for the ^{13}C chemical shift of this carbon atom.

The configuration of the cyclobutene ring is also *exo* in the benzonorbornane derivative **1**. The lack of coupling between the bridgehead proton and the vicinal methine proton supports, as it was discussed above, the *exo* configuration of the four-membered ring. The *exo*-cyclobutene ring is also shielding the C_8, but with -8.73 ppm, if the chemical shift of C_8 from the cyclobutene derivative **1** is regarded in respect with the benzonorbornane **29**. In the latter compound $\delta C_8 = 49.2$ ppm.[30]

b. Mass spectral data

The MS spectra of the configurational isomers cyclobutenes **2** and **3** are practically identical. Their molecular peaks have a diminished intensity (5%) and display the base peak at $m/z = 129$. On the contrary, for the cyclobutene **1**, the molecular peak has a remarkable intensity, while the base peak is at the $M-1$ mass number.

c. Molecular mechanics calculations (MM2)

In order to predict the thermodynamic stabilities and to understand which interractions are responsible for the difference in stability, we have carried out MM2 calculations for the two isomeric cyclobutenes **2** and **3**.

In Table 1 are collected calculated values for the total and for the components of the steric energy, the enthalpies of formation and the strain energies. The *exo*-benzocyclobuta isomer **2** is with *ca.* 2 kcal/mol more stable than the *endo* isomer **3**. Unfortunately, there are no experimental evidences to support the numerical results. However assuming that the *exo*-annelation of the cyclobutene ring to the *exo*-(**25**) or to the *endo*-benzocyclobutanonorbornane **26**, very likely, brings about identical force field modification upon the strain energies of hydrocarbons **25** and **26**, the experimental evidences observed for the latter compounds are from point of view of the relative stability valid for **2** and **3**. Indeed

Tabele 1

Molecular mechanics (MM2) results (in kcal/mole)

	compound 2	compound 3
Total steric energy	87.52	89.35
compression	3.77	3.97
bending	73.06	73.54
streching-bending	−2.88	−3.02
van der Waals 1,4	8.50	8.74
others	−1.88	−2.25
torsion	6.31	7.80
dipole	0.65	0.58
H_f	203.49	205.31
strain	83.91	85.74

there are a wealth of experimental facts originating from works of Avram[31c] and Baker[31a] indicating, for example if ionic reaction conditions are met, than *endo*-benzocyclobutanobicyclo (2.2.1) heptenes are converted into the more stable thermodynamically *exo*-benzocyclobutanobicyclo (2.2.1)heptenes.

Why the *endo* annelation of the benzocyclobutano fragment renders less stability relative to the *exo* annelation? The examination of the data presented in Table 1, reveals that the most notable differences in the steric energy of the isomeric cyclobutene **2** and **3** are provided by the torsional energy. Among the torsional interactions, those responsible for the relative stability are located on the C_3-C_{2a} and C_8-C_{8a} bonds. In Table 2 are presented the torsional energy values associated to the nine atoms sequence in the *exo*- and *endo*-benzocyclobutano isomers. The most important torsional interractions, responsible for the relative thermodynamic stability of the *exo*-benzocyclobutano isomer **2** are the more stable *anti*

Table 2

Torsional interactions along the $C_{3a}-C_3$ bond (in kcal/mol). Identical values were obtained around the symmetrical $C_{7b}-C_8$ bond

No.	Atom sequence	*exo* (**2**)	*endo* (**3**)
1	$C_{3b}-C_{3a}-C_3-C_{2a}$	0.043	0.266
2	$C_{3b}-C_{3a}-C_3-H_3$	0.037	0.459
3	$C_{3b}-C_{3a}-H_3-C_9$	0.316	0.289
4	$C_{7b}-C_{3a}-C_3-C_9$	0.306	0.308
5	$C_{7b}-C_{3a}-C_3-C_{2a}$	0.200	0.383
6	$C_{7b}-C_{3a}-C_3-H_3$	0.061	0.046
7	$H_{3a}-C_{3a}-C_3-C_9$	0.056	0.103
8	$H_{3a}-C_{3a}-H_3-C_{2a}$	0.007	0.036
9	$H_{3a}-C_{3a}-C_3-C_9$	0.025	0.074

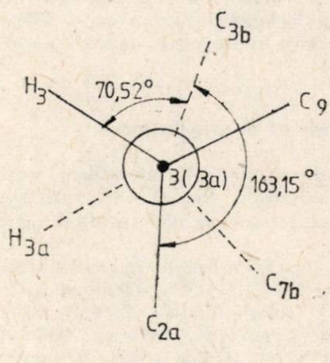

exo-2

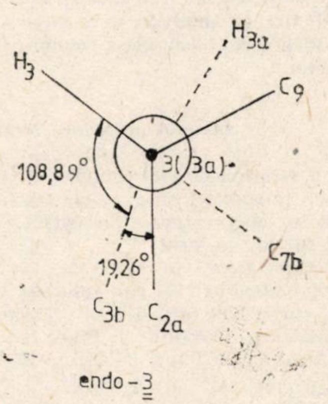

endo-3

like (163.15°) configurations of C_{3b} in respect with C_{2a} from the sequence $C_{3b} - C_{3a} - C_3 - C_{2a}$ than the gauche-like(13.26°) in the *endo* isomer **3.** Additionally the H_3-C_{3b} interactions are less favorable when the H_3-C_3- $-C_{3a}-C_{3b}$ dihedral angle is 108.89°, as in the *endo* isomer **3**, while the same angle being 70.52°, in the *exo* isomer **2**, the torsional energy is relatively lowered (see Table 2). Therefore we believe that these two interactions are ultimately responsible for the relative stability of the *exo*-benzocyclobutano isomer **2** versus the *endo*-isomer **3**.

CONCLUSIONS

The syntheses of the benzonorbornane, *exo*- and *endo*-benzocyclobutanorbornane annelated with an *exo* cyclobutene ring are presented. The three cyclobutene derivatives were obtained by Shechter reaction from the corresponding cyclopropylcarbene. The insertion reaction (formation of cyclobutene) and the cycloreversion reaction (formation of alkene and acetylene) of the cyclopropylcarbene are the two major reaction paths to give the reaction products cyclobutene : alkene in a 2 : 1 molar ratio.

The configurations of cyclobutene on one side of the norbornane skeleton, and that of the benzocyclobutano fragment on the other side of the skeleton are resulting from the analysis of the $^1H-$ and $^{13}C-NMR$ spectra. MM2 calculations are suggesting that the *exo*-benzocyclobutano isomer is more stable than the *endo*-benzocyclobutano isomer, due to some favorable torsional interactions along the C_3-C_{3a} and $C_{7b}-C_8$ bonds.

EXPERIMENTAL

The following instruments were used for spectra : IR with Carl Zeiss Jena UR-10, ^1H-NMR with Varian EM 360 L, $^{13}C-NMR$ with Varian FT 80A and mass spectra with Dupont DP 102. GC analyses were carried out with a Carlo Erba Fractovap — 2450 instrument, equipped with a capillary glass column (20 × 0.2 mm), hydrogen as carrier gas, flame ionization detector.

General procedure for the synthesis of tosylhydrazones

To a solution of 11.4 mmoles of tosylhydrazine in 200 mL chloroform, was added 11.4 mmoles of cyclopropylcarboxyaldehyde and 5 g anhydrous Na_2SO_4. The mixture was kept three days in refrigerator. After filtration and solvent removal, the resulted tosylhydrazones were used further as such.

Tosylhydrazone of 1aα, 2α, 7α, 7aα-tetrahydro-1β-carboxyaldehyde-2,7-methano-1-H-cyclopropa(b)naphthaline (**17**) is a colorless solid, mp = 164°C (MeOH), obtained with 90% yield. IR (KBr, cm^{-1}) 550 (m), 675 (s), 620(w), (675(s) ; 710(w), 775(m), 810(m), 850(w) ; 900(w) 910(w), 1015(m), 1100(m), 1170(s), 1235(w), 1260(w), 1295(w), 1320(m), 1350(m), 1430(w), 1450(w), 1600(w) 2970(m), 3050(m), 3235(m). ^1H-NMR ($DMSO-d_6$, δ, ppm) : 1.21 (1H, H_8^{syn}) ; 1.25 (1H, H_8^{anti}), 2.38(3H, s, $-CH_3$) ; 2.53 ($1H_3H-1$), 3.3 (2H, H-2 ; H-7) ; 6.6-7.85 (4H, m, Arom). Anal. Calcd for $C_{20}H_{20}N_2SO_2$: C, 68.15 ; H, 5.72 ; N ; 7.95 ; S, 9.10. Found : C, 68.07 ; H, 5.60 ; N, 7.50 ; S, 8.80.

Tosylhydrazone of 1aα, 2α, 6bα, 7α, 7aα-hexahydro-1β-carboxaldehyde-2,7-methano-1H-cyclopropa(b)biphenylene (**18**) is a colorless (EtOH) solid, mp 182°C (EtOH), obtained with 85% yield. IR (KBr, cm^{-1}) : 550(m), 595(s), 675(s), 690(s), 715(w), 745(s), 775(w), 800(w), 810(m), 840(w), 850(w), 900(w), 910(m), 960(w), 1045(m), 1100(m), 1172(s), 1195(m), 1315(s), 1345(m), 1430(w), 1460(w), 1495(w), 1600(w), 1620(w), 2945(m), 2970(m), 2995(m), 3030(m), 3221(m).

^{1}H$-$NMR (DMSO$-$d$_6$, δ, ppm) : 0.35(1H, m) ; 0.65 (1H, m) ; 1.2 (2H, m) ; 1.8 (1H, m) ; 2.5 (3H, s) ; 2.63 (2H, s) ; 3.45 (2H, s), 7.25$-$8 (5H, m, arom). Anal. Calcd. for $C_{22}H_{22}N_2SO_2$: C, 69.81 ; H, 5.85 ; N, 7.4 ; S, 8.47. Found C, 69.67 ; H, 5.70 ; N, 7.2 ; S, 8.47.

Tosylhydrazone of 1aα, 2α,2aβ, 6bβ, 7α, 7aα-hexahydro-1β-carboxaldehyde-2,7-methano--1H-cyclopropa(b)biphenylene (19), obtained with 90% yields is a colorless solid, with mp = = 177°C (MeOH). IR(KBr, cm^{-1}) : 505(w) ; 540(m) ; 570(m) ; 595(s) ; 615(w) ; 685(s) ; 705(m) ; 740(m) ; 760(m) ; 810(m) ; 900(m) ; 930(m) ; 1040(m) ; 1060(m) ; 1100(w) ; 1171(s) ; 1195(m) ; 1340(m) ; 1372(m) ; 1480(m) ; 1605(w) ; 1638(w) ; 2980(s) ; 3040 (m) ; 3060(m) ; 3183(s).

^{1}H$-$NMR (acetone$-$d$_6$, δ, ppm) : 0.55 (2H, d, J = 2Hz) ; 1.09 (1H, d, J = 11.5 Hz) ; 1.36 (1H, d, J = 11.51 Hz) ; 1.6 (1H, m) ; 2.4 (3H, s), 2.5 (2H, m) ; 3.57 (2H, m) ; 6.63 (1H, m) ; 6.93 (5H, m, arom) ; 7.47 (4H, m, arom).
Anal. Calcd. for $C_{22}H_{22}N_2SO_2$: C, 69.81 ; H, 5.85 ; N, 7.4 ; S, 8.47 ; Found, C. 69.67 : H, 5.77 ; N, 7.1 ; S, 8, 31.

General procedure for the synthesis of exo-cyclobutenonorbornanes 1, 2 and 3

a) In a suspension of 10 mmoles of sodium methoxide (freshly prepared) in 40 mL diethylenglycoldimethylether (Diglyime) and argon atmosphere, at 130°C, was added 5 mmoles of tosylhydrazones **17**, **18** or **19**. The mixture was stirred an hour at this temperature. After cooling at room temperature, 10 mL of water was added. The mixture was extracted with CCl_4 (3 × 30 mL). The organic layer was washed with water until the pH became neutral and then dried over $MgSO_4$. The solvent was removed under vacuum. The crude reaction mixture was subjected to column chromatography over Al_2O_3, using petroleum ether (bp 36°C) as eluent.

b) In the second approach we employed sodium hydride, instead of sodium methoxide. All reaction conditions are similar with those described above.

2aα, 3α, 8α, 8aα-Tetrahydro-3,8-methanocyclobuta(b)naphthalene (**1**). From the crude reaction mixture, cyclobutene **5** was isolated in 50$-$60% yield. An alternative way, for isolation of cyclobutene **5** was by careful bromination of the reaction mixture. The benzonorbornadiene **14** reacted faster than the cyclobutene **5** with a solution of bromine in carbon tetrachloride. By elution chromatography on Al_5O_3, cyclobutene **5** (with more than 90% purity by glpc) was isolated in lower yields than above, due probably to the losses occurring in the reaction bromine.

GC$-$MS (SE$-$30 cappillary column, 25 m, 140$-$240°C/40 minutes, source 220°, 70 eV) and GC (SE$-$30, 100$-$270°C/22 minutes, injection temperature 225°C) analysis of the crude reaction mixture evidenced the cyclobutene **5**, the benzonorbornadiene **14** and the methyl ether **20a** in a molar ratio 12 : 5 : 1. When the thermal decomposition of tosylhydrazone was carried out in presence of sodium hybride, GC analysis had revealed a molar ratio 20 : 8 : 1 (cyclobutene **5** : benzonorbornadiene **14** : hydrocarbon **20b**.

IR (CS_5, CCl_4, cm^{-1}) : 525 (w) ; 590 (w) ; 695 (s), 749 (s) ; 755 (s) ; 855 (w) ; 950 (m) ; 1265 (m) ; 1290 (w) ; 1455 (m) ; 2200 (w) ; 2310 (s) ; 2800 (w) ; 2940 (s) ; 2960 (s) ; 3010 (w) ; 3040 (m) ; 3070 (w).

^{1}H$-$NMR (δppm, CCl_4) : 1.65 (1N, d, J = 9Hz, H_9^a) ; 2.57 (2H, s, H_{2a}, H_{8a}) ; 2.87 (2H, bs, H_3, H_8) ; 6.18 (2H, s, H_2) ; 7.02 (4H, m, Harom).

^{13}C$-$NMR (δ, ppm, $CDCl_3$) : 40.47 (t, C_9) ; 40.67 (d, C_{2a}, C_{8a}) ; 48.33 (d, C_3, C_8) ; 121.43 (d, Carom) ; 125.34 (d, Carom) ; 137.79 (d, C_1, C_2) ; 147.82 (s, Carom).

MS (70 eV, source temperature, % intensity) : 168 (80) ; 167 (100) ; 166 (25) ; 165 (40) ; 153 (50) ; 152 (40) ; 141 (20) ; 115 (40) ; 83 (10) ; 52 (20).

Calcd. for $C_{13}H_{12}$: C, 92.81 ; H, 7.18 ; Found ; C, 92.77 ; H, 7.13.

2aα, 3α, 3aα, 7bα, 8α, 8aα, Hexahydro-3,8-methanocyclobutene[b]biphenylene (**2**). After carbon tetrachloride evaporation, from 4 g (10.6 mmoles) of tosylhydrazone **18**, have resulted 2 g of crude reaction mixture. GC analysis of crude reaction mixture evidenced cyclobutene (**2**) : norbornene (**16**) ; methyl ether **22** in 16 : 46 : 3.7 ratio. Elution on neutral Al_2O_3 with petroleum ether (b.p. 36°C) gave the title compound (yield 60$-$65%), of 93% purity assesed by GC (SE$-$30, 100$-$270°C/22 minutes; injection temperature 225°C). Pure samples, as a liquid, were obtained by careful bromine addition, to either the crude reaction mixture or to the previously resulted sample, in order to remove the faster reacting *exo*-benzocyclobutanorbornene **16**, followed by chromatography on neutral Al_2O_3 with petroleum ether as eluent.

IR (CCl_4, cm^{-1}) : 1100 (m) ; 1150 (m) ; 1275 (w) ; 1010 (w) ; 1460 (m) ; 2860 (s), 2935 (s) ; 3040 (w) ; 3070 (w).

^{1}H$-$NMR (δ, ppm, CCl_4) : 0.82 (1H, d, J = 11 Hz) ; H_9^a) ; 1.42 (1H, d, J = 11, H_9^s) ; 2.0 (2H ; s, H_{2a}, H_{8a}) ; 2.52 (2H, s, H_3, H_8) ; 3.03 (2H, s, H_{3a}, H_{76}) ; 5.83 (2H, s, H_1, H_2) ; 6.95 (4H, m, Harom).

^{13}C$-$NMR (δ, ppm, $CDCl_3$); 24.53 (t, C_9); 34.42 (d, C_3, C_8); 49.26 (d, C_{2a}, C_{8a}); 49.44 (d, C_{3a}, C_{76}); 121. 82 (d, C_4, C_7); 127.19 (d, C_5, C_6); 147.1 (s, C_{3b}, C_{7a}).

MS (70 eV, source temperature 220°C, % intensity): 194 (5); 193 (11.2); 180 (6.2); 179 (40); 178 (30.6); 166 (7.3); 165 (19.7); 153 (7.2); 152 (10.1); 141 (15.6); 130 (11.8); 129 (100); 128 (38.4); 127 (7.3); 116 (8.1); 115 (21.7).

Anal. Cald for $C_{15}H_{14}$: C, 92.73; H, 7.26. Found; C, 92.67; H, 7.17.

2α, 3α, 3aα, 7bβ, 8α, 8aα-Hexahydro-3,8-methanocyclobuta[b]biphenylene **(3)**. The crude reaction mixture, after removal of carbonatetrachloride was 1.8 g. GC analysis (condition as above) evidenced a 16.7 : 39.2 : 3.4 ratio among the *endo*-benzocyclobutanorbornene **15**, cyclobutene **3** and the methyl ether **21**.

Pure samples have resulted proceeding as in the case of the *exo*- isomer, described previously. Yield are in the range of 55$-$65 %.

IR (CS_2, CCl_4, cm^{-1}): 600 (w); 630 (m), 690 (m), 740 (s), 765 (s), 930 (w), 1100 (m), 1185 (w); 1270 (w), 1290 (w); 1340 (w), 1450 (w), 3875 (w); 29.50 (s), 3030 (m); 3070 (w), 3110 (w).

^{1}H$-$NMR (δ, ppm, CCl_4): 1.39 (1H, H_{9}^{s},); 1.97 (1H, H_{9}^{s}); 2.12 (2H, m, H_3, H_8); 2.38 (2H, s, H_{2a}, H_{8a}); 3.63 (2H, n, H_{3a}, H_{76}); 5.67 (2H, s, H_1, H_2); 6.93 (4H, m, Harom).

^{13}C$-$NMR (δ, ppm, $CDCl_3$): 34.41 (t, C_9); 36.36 (d, C_3, C_8); 47.96 (d, C_{2a}, C_{8a}); 49.43 (d, C_{3a}, C_{76}); 123.84 (d, C_4, C_7); 126.60 (d, C_5, C_6); 135.71 (d, C_1, C_2); 146.48 (s, C_3b, C_{7a}).

MS (70 eV, source temperature 250°C; % intensity): 194 (5); 193 (9.6); 179 (34.6); 178 (29.1); 165 (16.6); 153 (6.3); 152 (9); 141 (10.4); 130 (11); 129 (100); 128 (34.6); 116 (6.9); 115 (15.1); 102 (14.8); 89 (8.2).

Anal. Calcd for $C_{15}H_{14}$: C, 92.73; H; 7.26; Found: C, 92.69; H, 7.15.

General procedure for the synthesis of methyl ethers 20a, 21 and 22

A mixture of carbinol (3 mmoles) **21, 23c** or **24c**) and methyl iodide (6 mmoles) was added to a suspension of finely ground sodium hydroxide in dimethylsulfoxide. After stiring 8 hours at room temperature, the reaction mixture was kept over night. Then 15 mL of water was added and extracted with carbon tetrachloride (3 × 10 mL). The organic layer was washed with 2 × 10 mL water, dried, and evaporated.

The methyl ether of 1aα, 2α, 7α, 7aα-tetrahydro-1β-(hydroximethyl)-2,7-methano-1H-cyclopropa[b]naphthalene (**20a**). Colorless oil, yield 90 %. IR(CS_2, CCl_4, cm^{-1}): 560 (w); 630 (m); 730 (m); 750 (s), 1100 (s); 1135 (s); 1190 (m); 2050 (w); 2080 (w); 1370 (w); 1405 (w); 1450 (m); 1470 (m); 2810 (m); 2850 (s); 2915 (s); 2975 (s); 3020 (m).

^{1}H$-$NMR ($CDCl_3$, δ ppm): 0.99 (d, $J = 3$ Hz), 2H, H_{1a}, H_{7a}); 1.22 (dd, $J = 10.8$ Hz, 1H, H_{8}^{s}); 1.54 (dd, $J = 10$ Hz, 1H, H_{8}^{a}); 2.05 (m, 1H, H_1), 3.12 (d, $J = 7$ Hz, 2H, CH_2); 3.25 (d, 2H, H_2, H_7); 3.27 (s, 3H, CH_3); 6.8$-$7.2 (m, 4H, Harom).

Calcd. for $C_{14}H_{16}O$: C, 83.96; H, 8.05. Found: C, 83.8; H, 8.20.

The methyl ether of 1aα, 2α, 2aβ, 6bβ, 7α, 7aα-hexahydro-1β-(hydroxymethyl)-2,7-methano-1H-cyclopropa[b]biphenylene (**2.1**).

Colorless solid, mp. 39°C, yield 85 %.

IR (CCl_4, cm^{-1}): 930 (w); 1000 (w); 1100 (s); 1140 (s); 1180 (m); 1260 (w); 1370 (w); 1450 (m); 2810 (w); 2850 (m); 2925 (s); 2950 (s); 3020 (m); 3060 (m).

^{1}H$-$NMR ($CDCl_1$, δppm): 0.28 (d, $J = 2.5$ Hz, 2H, H_{1a}, H_{7a}); 0.8$-$1.6 (m, 3H, H_1, $2H_8$); 2.56 (s, 2H, H_2, H_7); 2.87 (d, $J = 6.5$ Hz, 2H, $-CH_2O$); 3.17 (s, 3H, $-CH_3$); 3.60 (d, $J = 3.8$ H_2, H_{2a}, H_{66}); 6.9$-$7.2 (m, 4H, Harom).

Calcd. for $C_{16}H_{18}O$: C, 84.96; H, 8.05. Found: C, 84.70; H, 7.90.

The methyl ether of 1aα, 2α, 2aα, 6bα, 7α, 7aα-hexahydro-1β-(hydroxymethyl)-2,7-methano-1H-cyclopropa[b]biphenylene (**22**).

Colorless oil, yield 88 %.

IR (CCl_4, cm^{-1}): 930 (w); 970 (w); 1005 (w); 1040 (w); 1105 (s); 1150 (s); 1180 (m); 1190 (m); 1265 (w); 1295 (w); 1370 (w); 1450 (m); 1470 (w); 2815 (m); 2860 (m); 2950 (s); 2970 (s); 3020 (m); 3065 (m).

^{1}H$-$RMN ($CDCl_3$, δ, ppm): 0.43 (d, $J = 11$ Hz, 1H, H_{8}^{s}); 0.71 (d, $J = 11$Hz, 1H, H_{8}^{s}); 0.72 (d, $J = 3.5$Hz, 2H, H_{1a}, H_{7a}); 1.23 (m, 1H, H_1); 2.32 (s, 2H, H_2, H_7); 3.07 (d, $J = 7.5$Hz, 2H, $-CH_2O$); 3.26 (s, 5H, $-CH_2^{-0-}$, H_{2a}, H_{6b}), 6.8$-$7.2 (m, 4H, Harom).

Calcd. for $C_{16}H_{18}O$: C, 84.91; H, 8.01. Found: C, 84.60; H, 7.85.

REFERENCES

[1] Taken in part from the Ph. D. Thesis of E. O. We have coined as Shechter reaction the cyclopropylcarbene rearrangement to cyclobutene ring. [2]

[2] L. Friedman and H. Shechter, *J. Amer. Chem.* Soc., **82**, 1002 (1960).

[3] M. Hara, J. Odiara and S. Tsutsumi, *Tetrahedron*, **22**, 95 (1966).

[4] L. Watts, J. D. Fitzpatrick and R. Pettit, *J. Amer. Chem. Soc.*, **88**, 623 (1966).

[5] M. Avram, I. G. Dinulescu, G. D. Mateescu and C. D. Nenitzescu, *Liebigs Ann. Chem.*, **69**, 6919 (1966).

[6] L. G. Cannell, Tetrahedron Letters, **1966**, 5967.

[7] N. V. Maatschappij (Shell International Research) Neth. Appl. 6,504,000 *(Chem. Abstr.* **64**, 80576 (1966)); *ibid.*, 6,503,999 *(Chem. Abstr.* **64**, 11163 h (1966)).

[8] R. R. Sauers, S. B. Schlosberg and P. E. Pfeffer, *J. Org. Chem.*, 33, 2175 (1968).

[9] H. M. Frey, J. Metcalfe and J. M. Brown, *J. Chem. Soc.*, *(B)*, **1970**, 1586.

[10] R. D. Miller and D. L. Dolce, *Tetrahedron Letters*, **1973**, 4403.

[11] W. R. Bamford and T. S. Stevens, *J. Chem. Soc.*, 1952, 4735; R. H. Shapiro, *Organic Reactions*, **24**, 405 (1976).

[12] R. Hahn, R. P. Johnson, *J. Amer. Chem. Soc.*, **97**, 212 (1975).

[13] I. G. Dinulescu, A. Ghenciulescu, L. Enescu, E. Olteanu and M. Avram, *Bul. Instit. Politehnic București, Ser. Chim.—Metalurgie*, **43**, 92 (1981).

[14] L. Enescu, M. D. Gheorghiu, A. Ghenciulescu, I. G. Dinulescu and M. Avram, *Rev. Roumaine Chim.*, **28**, 1001 (1983).

[15] a) M. D. Gheorghiu, P. Filip, C. Drăghici and L. Pârvulescu, *J. Chem. Soc. Chem. Commun.*, **1975**, 635; M. D. Gheorghiu, C. Drăghici and L. Pârvulescu, *Tetrahedron*, **33**, 3295 (1977); M. D. Gheorghiu, L. Pârvulescu and C. Drăghici, *Rev. Roumaine Chim.*, **24**, 1005 (1979); M. D Gheorghiu, C. Drăghici, L. Pârvulescu and M. Elian, *Rev. Roumaine Chim.*, **34**, 1341 (1989).
b) A. Ghenciulescu, L Enescu, H. L. Prasad, F. Chiralea, I. G. Dinulescu and M. Avram, *Rev. Roumaine Chim.*, **23**, 1441 (1978).
c) M. D. Gheorghiu and E. Olteanu *J. Org. Chem.*, **52**, 5158 (1987).

[16] Cyclobutene versus cycloreversion products ratio is unaffected by the relative stereochemistry of the substituents on the cyclopropyl fragment, and the ring size to which the three-membered ring is annelated. [17] The relative stereochemistry of the substituents on the cyclopropyl ring is retained in both the cyclobutene [18] reaction products and in the cycloreversion alkene. [18b] The spin state of cyclopropylcarbene, generated photochemically from the corresponding diazocompounds is triplet. [19] The ring expansion of the cyclopropylcarbenes can certainly be associated to the singlet state, [20] which is reached by intersystem crossing with the triplet state.

[17] W. Kirmse and K.-H. Pook, *Chem. Ber.*, **98**, 4022 (1965).

[18] (a) J. A. Berson, W. Bauer and M. M. Campbell, *J. Amer. Chem. Soc.*, **92**, 7515 (1970); (b) R. R. Galluci and M. Jones, Jr., *ibid.*, **98**, 7704 (1976).

[19] R. A. Moss and W. P. Wetter, Tetrahedron Lett, **22**, 997 (1981).

[20] S. S. Olin and R. M. Vemable, *J. Chem. Soc., Chem. Commun.*, 1974, 273; W.W. Schoeller, *J. Org. Chem.*, 45, 2161 (1980); B. Wang and C. Dong, *Tetrahedron*, 44, 7355 (1988).

[21] (a) M. A. Battiste and M. E. Burns, *Tetrahedron Lett.*, **1966**, 523;
(b) J. W. Wilt, J. M. Kosturile and R. C. Orlowsky, *J. Org. Chem.*, **30**, 1052 (1965).

[22] S. J. Cristol and J. K. Harrington, *J. Org. Chem.*, **28**, 1413 (1963).

[23] G. Wittig and E. Knaus, *Chem. Ber.*, **91**, 895 (1958).

[24] A literature scrutinity of Shechter reaction promoted by sodium methoxide or other nucleophiles revealed only scarce mentioning of the cyclopropylcarbinylmethyl ether or related trapping compounds derivatives. Accordingly, we believe that either the authors have paid little attention to this by product or it was actually not observed. For a general survey see: R. H. Shapiro, *Org. Reactions*, **24**, 405, (1976).

[25] (a) P. Laszlo and P. R. von Schleyer, *J. Am. Chem. Soc.*, **86** 1171 (1964).
(b) D. I. Schuster and C. W. Kim, *ibid.*, **96**, 7437 (1974).
(c) T. A. Antkowiak, D. C. Sanders, G. B. Trimitsis, J. B. Press and H. Shechter, *ibid.*, **94**, 5366 (1872).

[26] N. L. Allinger, *J. Amer. Chem. Soc.*, **99**, 8127 (1977). For an up to date status of MM2 programs see footnotes included in the paper; J. P. Bowen, V. V. Reddy, D. G. Patterson, Jr. and N. L. Allinger, *J. Org. Chem.*, **53**, 5471 (1988).

[27] M. Karplus, *J. Amer. Chem. Soc.*, **85**, 2870 (1963).

[28] J. B. Stothers, C. T. Tan and K. C. Tes, *Can. J. Chem.*, **51**, 2893 (1973).

[29] Work is in progress in our laboratory for the synthesis and the recording of the ^{13}C-NMR spectra of the cyclobutenonorbornene **28**.

[30] K. To, M. Uemaya, T. Tsiji, H. Matsanuva, H. Tanida, H. Iwamura, K. Kushida, T. Nishida, and S. Satoh, *Tetrahedron Letters*, 1974, 327.

[31] (a) A. Ghenciulescu, I. G. Dinulescu, H. L. Prasad, L. Enescu and M. Avram, *Rev. Roumaine Chim.*, **24**, 1159 (1979);

(b) M. Avram, I. Pagany, I. G. Dinulescu, F. Chiraleu and C. D. Nenitzescu, *ibid.*, **15**, 1207 (1970);

(c) M. Avram, I. Pogany, F. Badea, I. G. Dinulescu and C. D. Nenitzescu, *Tetrahedron Letters*, **1969**, 3851.;

(d) R. Baker and I. Hudec, *Chem. Commun.*, 1967, 929; R. Baker and I. C. Saltar, *J. Chem. Soc., Perkins Trans 2*, **1973**, 150; R. Baker and T. J. Mason, *ibid.*, **1972**, 18; R. Baker and T. J. Mason, *J. Chem. Soc.* (B), 1971, 1144.

Revue Roumaine de Chimie, 34, *9—10*, 1945—1948 (1989)

STUDY ON THE REACTIVITY OF SOME *AS* NAPHTHOLS POSSESSING BENZIMIDAZOLONIC REST

I. COCÎRLĂ,[a] LUCIA TĂTARU,[a] M. VÂŢĂ,[a] I. MAZILU,[a] LUMINIŢA WAGNER,[b] D. SCUTARU[a] and CAMELIA PETRESCU[a]

[a] Polytechnic Institute of Jassy, Spl. Bahlui, 71, 6600 Jassy, Romania

[b] ICECHIM, Research Center for Dyestuffs, Spl. Independenţei 202, Bucharest 77208, Romania

Two AS naphthols having bezimidazolonic ring in the molecule have been characterized by the semi-empirical HMO method. Calculations led to comparable results with the experimental data observed from electronic transitions and thermal behaviour of the compounds.

INTRODUCTION

In a previous paper, [1] we have discussed the reactivity and electronic spectra of some AS naphthols derivatives, i.e. anylide and (*o*-, *p*-) toluidides of 2-hydroxy-3-naphthoic acid.

The present investigation extends the study to two related compounds: 5-(2-hydroxy-3-napthoyl)-aminobenzimidazolone-2 (I) and 5-(1-formyl-2-hydroxy-3-naphthoyl)-aminobenzimidazolone-2 (II).

The introduction of the benzimidazolonic rest in the molecule is meant at increasing the stability of such substances, used in azopigments synthesis as coupling compounds.

EXPERIMENTAL

The synthesis of compound I was performed through a non-conventional technique, [2] which, as compared to the classical method, [3,4] has the advantages of a small reaction duration, an increased yield, and a product of high purity, without evidencing special problems of corrosion. [5]

Compound II was obtained through formulating product I with *para*-formaldehyde and hexamethylentetramine.[6]

The products were characterized through UV spectra and thermogravimetric analysis. Experimental data were compared with the results obtained from the calculation of Hückel molecular orbitals. [7] Electronic spectra were registered with a Specord spectrophotometer — Carl Zeiss Jena, at $2 \cdot 10^{-5}$ M methanolic solutions while derivatogrammes were plotted with a Q-derivatograph-MOM Budapest.

RESULTS AND DISCUSSION

In order to estimate the reactivity of compounds I and II in the coupling reaction the method of molecular orbitals in Hückel approximation has been applied, using for heteroatoms the following parameters[8,9]:

$$h_{\dot{O}} = 0.7 \; ; \; h_{\ddot{O}} = 2 \; ; \; h_{\ddot{N}} = 1.4 \; ; \; k_{C-\ddot{N}} = 0.8 \; ; \; k_{C-\dot{O}} = 1.1 \; ; \; k_{C-\ddot{O}} = 0.6$$

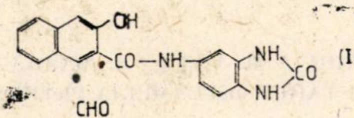
(I)

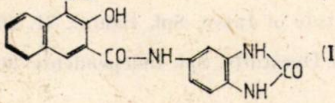
(II)

Standard parameters have been used for all other atoms.

Analyzing molecular diagrams (Fig. 1) and data listed in Table 1, the same electronic distribution is to be found on the bezimidazolonic skeleton of the two compounds; only in the case of the naphtalenic ring the distribution is different.

Table 1

Results yielded by Hückel OM calculations

Molecule	$E_{\pi(\beta)}$	E_{HOMO}	E_{LUMO}	$DE_{(\beta)}$*	DE/n_{π}*	f_r^{E}*
I	42.4063	0.5204	0.4943	18.806	0.671	0.0018 (17) 0.0015 (19) 0.0004 (21)
II	45.8794	0.5205	0.3729	21.579	0.719	0.001 (17) 0.0009 (19) 0.0002 (21)

f_E^r — electron density at atom r for the HOMO (electrophilic attack)
DE — delocalization energy
n_{π} — number of π — electrons.

Consequently, the introduction of the formyl group influences only the reactivity of the naphthalenic nucleus. The coupling position **17** is more reactive in compound II, to the electrophilic attack of the diazoic compound, due to the increased electronic density and higher value of the f_r^E index.

This situation assumes the substitution of the formyl rest in the coupling reaction, through the electrophilic reactant. Similar cases are to be met with some AS naphthols, which have in this position a methyloyl or carboxyl group, which is replaced in the coupling reaction.[10] In our case, the introduction of the formyl group induces the increase of naphtharilide II stability, as well as a higher reactivity of the coupling position. According to the derivatogrammes, in the 285—400 °C range, product I loses 20% of its weight, compared to 12%—for the formylated product (II).

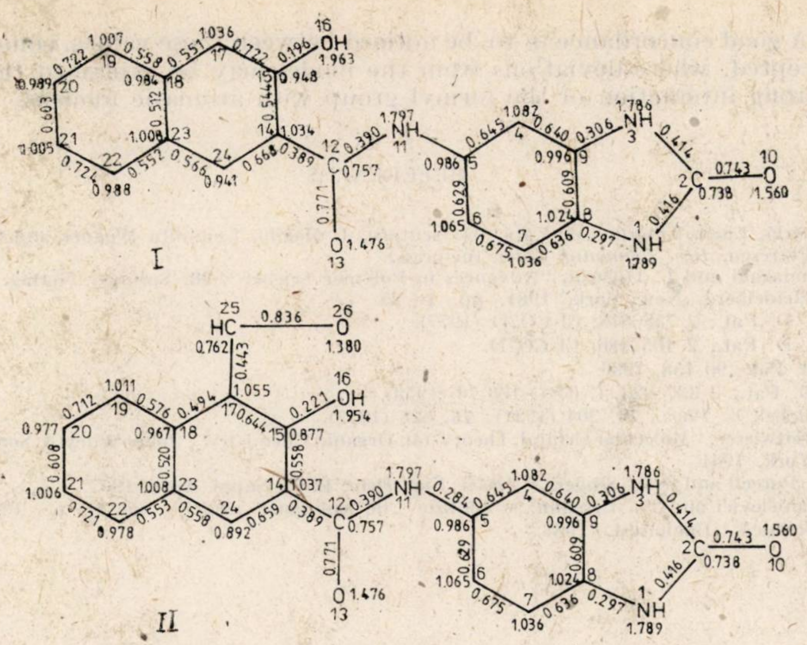

Fig. 1. — Molecular diagrams of the investigated compounds.

Electronic spectra show absorptions located at 209–211 nm, 237–239 nm and 310–317 nm, respectively. The bands may be attributed to some $\pi-\pi^*$ transitions, on which $n-\pi^*$ type transitions and charge transfer transitions are superposed. The correlation of the HMO calculations with the experimental results has to consider the configurational interaction, according to the model discussed in a previous paper, using the same values for the β_α, β_p and β_β parameters[1]:

$\beta_\alpha = 3.15$ eV, $\beta_p = 4.78$ eV and $\beta_\beta = 4.66$eV as compounds I and II belong to the same type of AS naphthols. Data obtained from these calculations, as well as some experimental ones, are listed in Table 2.

Table 2

Calculated and experimental values of transition energies

Investigated molecule	Electronic band	Δn	ΔE eV		$\Delta(\Delta E)$ $\Delta Exp-\Delta E$ Theory
			Exp.	Theory	
I	α	1.2072	4.00	3.80	0.20
	p	1.0147	4.90	4.85	0.05
	β	1.2072	5.93	5.62	0.31
II	α	1.0933	3.91	3.44	0.47
	p	0.8934	4.79	4.27	0.52
	β	1.0933	5.88	5.08	0.79

A good concordance is to be noticed between these values, compound II excepted, where deviations from the model may be explained through the strong interaction of the formyl group with aromatic nucleus.

REFERENCES

[1] I. Cocîrlă, Lucia Tătaru, M. Vâţă, D. Scutaru, I. Mazilu, Luminiţa Wagner and Camelia Petrescu, *Rev. Roumaine Chim.* (in press).
[2] N. Yamazaki and F. Higashi, "Advances in Polymer Science", **38**, Springer Verlag, Berlin, Heidelberg, New York, 1981, pp. 1—25.
[3] B. R. D. Pat., 2 758 818, Cl CO7D (1977).
[4] B. R. D. Pat., 2 405 986, Cl CO7D.
[5] R.S.R. Pat., 90 158, 1986.
[6] B.R.D. Pat., 2 337 023, C 07 C 103/76 (1979).
[7] E. Hückel, *Z. Phys.*, **70**, 204 (1931); **76**, 628 (1932).
[8] A. Streitwieser, "Molecular Orbital Theory for Organic Chemistry", John Wiley & Sons, New York, 1961.
[9] W. P. Purcell and J. A. Singer, *J. Chem. Eng. Data*, **12** (2) Suppl. April, 1967.
[10] H. Sanielevici and F. Urseanu, "Sinteze de coloranţi azoici" vol. 1, p. 157, Ed. Tehnică, Bucharest, 1987.

Revue Roumaine de Chimie, 34, *9—10*, 1949—1955 (1989)

SYNTHESIS AND REACTIONS OF SOME NEW BENZOFURANO [3,2-c]PYRAZOL-3-ONE AND BENZOFURANO[3,2-c] ISOXAZOL-3-ONE DERIVATIVES OF EXPECTED BIOLOGICAL ACTIVITY

O. M. O. HABIB, A. H. ABD EL-RAHMAN and D. S. BADAWY
Chemistry Department, Faculty of Science, Mansoura University
Egypt

Received June 8, 1987

Methyl salicylate was condensed with α-chloroacetanilide and its *p*-chloro-derivative to give the benzofurano-β-ketoanilides Ia-c. Treatment of I with hydrazine hydrate, phenylhydrazine, hydroxylamine hydrochloride, polyphosphoric acid and Mannich bases was studied. Reaction of the pyrazolone derivative II with chloroacetyl chloride, benzenediazonium chloride and Mannich bases was also investigated.

It has been reported in literature that pyrazole, isoxazole, pyridine and benzofuran derivatives show marked biological activity. [1-5] This fact has encouraged the authors to synthesize some new products containing these moieties from benzofuran-β-ketoanilide derivatives Ia—c.

In the present work, benzofuran-β-ketoanilides Ia—c were prepared by the condensation of methyl salicylate with α-chloroacetanilide and its *p*-chloro-derivative. The IR spectra of Ic showed absorption frequencies at 3400—3300, 1660 and 1630 cm^{-1} characteristic for the NH, CO and CONH groups, respectively[1]. H—NMR spectra of Ic gave signals at δ3.8 ppm (s. 3H, OCH_3), δ8.2—8.4 ppm (broad, 1H, CONH) and δ7.1—7.4 ppm (m, 8H, aromatic).

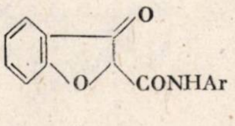

I

a, Ar = C_6H_5
b, = C_6H_4Cl-*p*
c, = $C_6H_4OCH_3$-*p*

In the previous studies we have prepared some pyrazolone derivatives *via* the reaction of hydrazine hydrate with β-ketoanilides. [6-8] In the present investigation, Ia—c reacted with hydrazine hydrate either in ethanol or in acetic acid and gave benzofurano[3,2-c]pyrazol-3-one II. The IR spectrum of II revealed absorption bands at 3300, 1660 and 1620 cm^{-1}

assignable to the NH, CO and C=N groups, respectively. ^{1}H—NMR spectrum of II gave signals at δ10.4 ppm (broad, 1H, NH) and δ7.6 ppm (m, 4H, aromatic).

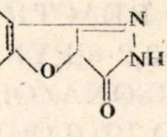

II

On the other hand, when compounds Ia, b were treated with phenylhydrazine in acetic acid, the corresponding N-phenylpyrazolone III was obtained. On carrying out the reaction in ethanol, the products were the corresponding N-phenylhydrazone derivatives IVa, b. Cyclisation of IVa, b into the corresponding N-phenylpyrazol-3-one III was achieved by refluxing in acetic acid.

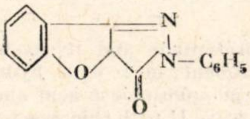

III

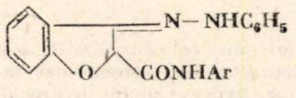

IV

a, Ar = C_6H_5
b, = C_6H_4Cl-*p*

The structure of the N-phenylpyrazol-3-one III was proved by elemental analysis and IR spectra which showed bands at 1690 and 1635 cm^{-1} attributable to the CO and C=N groups, respectively. The IR spectrum of IVa revealed bands at 3400—3350, 1680 and 1640 cm^{-1} characteristic for the NH, CO and C=N groups, respectively. ^{1}H—NMR spectrum of IVa indicated signals at δ4.6 ppm (s, 1H, NNH); δ8.3 ppm (broad, 1H, CONH) and δ7—7.3 ppm (m, 14H, aromatic).

Treatment of Ia—c with hydroxylamine hydrochloride afforded the benzofurano-[3,2-c] isoxazol-3-one V.

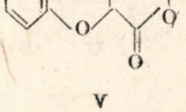

V

The structure of V was deduced from correct elemental analysis and IR spectrum which revealed absorption bands at 1680 and 1625 cm^{-1} characteristic for the CO and C=N groups, respectively. ^{1}H—NMR spectrum gave a signal at δ7.1—7.4 ppm (m, 4H, aromatic).

It has been reported in literature that when acetoacetanilides were treated with dehydrating agents they were converted into the corresponding 2-quinoline derivatives. [9,10] Therefore it is of interest to study the effect of dehydrating agents on β-ketoanilides. Thus, treatment of compounds Ia—c with polyphosphoric acid gave the corresponding benzofurano-[3,2-c] naphthridine-6(5H)-one derivatives VIa—c. The structure of VIa—c was substantiated from analytical data and IR spectra which showed bands at 3400—3300 and 1690 cm^{-1} assignable to the NH and CO groups, respectively. ^{1}H—NMR spectrum of VIa gave signals at δ11.2 ppm (broad, 1H, CONH) and 7.2—7.6 ppm (m, 4H, aromatic).

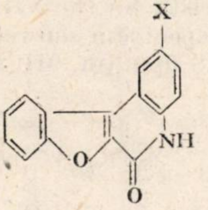

VI

a, X = H
b, = Cl
c, = OCH$_3$

The behaviour of compound Ia towards aminomethylation was also studied. Thus, treatment of Ia with piperidine and formaldehyde in methanol and in the presence of few drops of hydrochloric acid afforded the Mannich base as the hydrochloride salt VII. The structure of VII was inferred from elemental analysis and IR spectrum which showed bands at 3400—3350, 1680 and 1650 cm^{-1} attributable to the NH and the two CO groups, respectively.

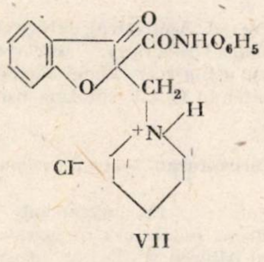

VII

On the other hand, the reaction of the pyrazolone derivative II with different reagents was studied. Thus, compound II was treated with chloroacetyl chloride and gave the N-chloroacetyl derivative VIII, which revealed bands at 1710, 1660 and 1620 cm^{-1} characteristic for the two CO and C=N groups, respectively. The ^{1}H—NMR spectrum of VIII showed signals at δ3.2 ppm (s, 2H, CH$_2$) and 7.6—7.8 ppm (m, 4H, aromatic).

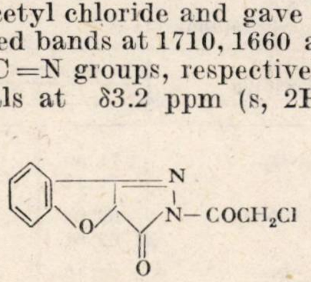

VIII

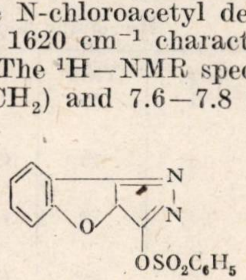

IX

Treatment of compound II with benzenesulphonyl chloride in pyridine afforded the corresponding O-benzenesulphonyl derivative IX. The structure of IX was inferred from elemental analysis and IR spectrum which showed the absence of the carbonyl absorption band.

Reaction of the pyrazolone II with benzenediazonium chloride gave the corresponding benzofurano[3,2-c]phenylazo-pyrazol-3-one X. The IR spectrum of X showed absorption bands at 3400—3300, 1665, 1624 and 1600 cm^{-1} characteristic for the NH, CO, C =N and N = N groups, respectively. The ^1H—NMR spectrum showed signals at δ 10.2—10.4 ppm (broad, 1H, NH) and 7.6—7.8 ppm (m, 9H, aromatic).

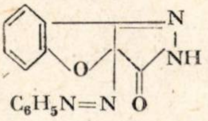

X

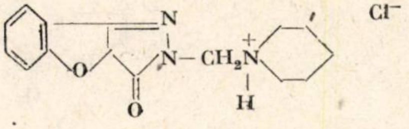

XI

The presence of the cyclic —CONH— linkage in compound II prompted us to investigate its behaviour towards aminomethylation. Thus, when compound II was treated with piperidine and formaldehyde in methanol and in the presence of few drops of hydrochloric acid, it gave the correspondig benzofurano[3,2-c]-2-piperidinomethyl-pyrazol-3-one XI as a hydrochloride salt. The structure of XI was deduced from elemental analysis and IR spectrum which showed bands at 1660 and 1620 cm^{-1} assignable to the CO and C =N groups, respectively.

EXPERIMENTAL

All melting points are uncorrected. Analytical data were determined by the Microanalytical Unit, Faculty of Science, Mansoura University. Infrared spectra were recorded on a Pye-Unicam SP—1100 Spectrophotometer using KBr Wafer technique. The ^1H—NMR spectra were run on a Varian 60 MHz Spectrometer in $CDCl_3$ solution using TMS as an internal standard. Chemical shift in δ, ppm.

Synthesis of benzofuran-3-oxo-2-carboxanilides Ia-c

To methyl salicylate (0.01 mole) and the appropriate α-chloroacetanilide (0.01 mole) in dimethylformamide (10 mL), anhydrous potassium carbonate (1.0 g) was added. The reaction mixture was refluxed for four hours, filtered while hot into water (200 mL) and then acidified with hydrochloric acid. Recrystallisation of the obtained solid products from ethanol gave compounds Ia—c (cf. Table 1).

Table 1

Benzofuran-3-oxo-2-carboxanilides Ia-c

Compound No.	M.p. °C	Yield %	Formula	Analyses % C	Analyses % H	Found Calcd.
Ia	194	70	$C_{15}H_{11}NO_3$	71.50 71.14	4.20 4.34	
Ib	207	70	$C_{15}H_{10}ClNO_3$	63.00 62.61	3.20 3.47	
Ic	184	40	$C_{16}H_{13}NO_4$	68.10 67.84	4.40 4.59	

Reaction of Ia-c with hydrazine hydrate. Formation of benzofurano-[3,2-c]-pyrazol-3-one II

A mixture of each of Ia-c (0.01 mole) and hydrazine hydrate (0.01 mole) in either ethanol or acetic acid (50 mL) was refluxed for four hours. The reaction product was cooled and the obtained solid was filtered off and recrystallised from ethanol to give compound II m.p. 169°C, 60%.
Analysis : Found : %C 62.20 ; %H 3.40. Calcd. for : $C_9H_6N_2O_2$: %C 62.07 ; %H 3.45.

Reaction of Ia, b with phenylhydrazine

A. *In ethanol. Formation of benzofuran-2-carboxanilide-3-phenyl-hydrazones IVa, b*

These compounds were prepared according to the procedure described above. Crystallisation of the resulting solids from ethanol gave the products IVa, b (cf. Table 2).

Table 2

Benzofurano-2-carboxanilide-3-phenyldrazones IVa, b

Compound No.	M.p. °C	Yield %	Formula	Analyses % C	Analyses % H	Found Calcd.
IVa	175	65	$C_{21}H_{17}N_3O_2$	73.50	5.10	
				73.47	4.95	
IVb	234	65	$C_{21}H_{16}ClN_3O_2$	66.80	4.20	
				66.75	4.24	

B. *In acetic acid. Formation of benzofurano-[3,2-c]-2-phenylpyrazol-3-one III*

The same procedure described for the reaction of Ia—c with hydrazine hydrate was used. Crystallisation of the obtained solid product from acetic acid gave compound III, m.p. 185°C, yield 60%.

Analysis : Found %C 71.80 ; %H 3.70. Calcd for $C_{15}H_{10}N_2O_2$: %C 72.00 ; %H 4.00

Conversion of benzofuran-2-carboxanilide-3-phenylhydrazones IVa, b into N-phenylpyrazol-3-one derivative III

Compounds IVa, b (1.0 g in each case) were refluxed with acetic acid (20 mL) and sodium acetate (0.5 g) for one hour. A rapid change in colour was immediately observed and the resulting solid product was proved to be identical with the N-phenylpyrazolone derivative III (melting point and mixed melting points).

Reaction of Ia-c with hydroxylamine hydrochloride. Formation of benzofurano 3,2-c isoxazol-3-one V

A mixture of each of Ia—c (0.01 mole) and hydroxylamine hydrochloride (0.01 mole) in ethanol (30 mL) and pyridine (0.5 mL) was refluxed for three hours. Crystallization of the obtained solid from ethanol gave compound V, m.p. 154°C, yield 40%.

Analysis. Found : %C 62.00 ; %H 2.60. Calcd. for : $C_9H_5NO_3$: %C 61.71 ; %H 2.85

Condensation of Ia-c with polyphosphoric acid. Formation of benzo-furano-3,2-c-naphthridine-6(5H)-ones VIa-c

Compounds Ia—c (1.0 g in each case) were heated with polyphosphoric acid (20 mL) for two hours at 130—140°C, then the reaction mixture was cooled and poured onto ice-cold water. Recrystallisation of the obtained solids from ethanol gave compounds VIa—c (cf. Table 3).

Table 3

Benzofurano [3,2-c]-naphthridine-6(5H)-ones VIa-c

Compound No.	M.p. °C	Yield %	Formula	Analyses % C	H	Found Calcd.
VIa	120	70	$C_{15}H_9NO_2$	76.10 76.59	3.64 3.82	
VIb	145	70	$C_{15}H_8ClNO_2$	66.90 66.79	3.27 2.96	
VIc.	158	75	$C_{16}H_{11}NO_3$	73.00 72.45	4:48 4.15	

Mannich reaction with Ia. Formation of benzofurano-3-oxo-2-piperidinomethyl-2-carboxanilide VII

To a mixture of Ia (0.01 mole) and piperidine (0.01 mole) in methanol (50 mL), aqueous formaldehyde (35 %, 2.5 mL) and hydrochloric acid (0.5 mL) were added. The reaction mixture was refluxed on a steam bath for eight hours, kept overnight at room temperature and diluted with water. The formed solid was filtered off and crystallised from ethanol to give compound VII as a hydrochloride salt, m.p. 75°C, yield 40 %.

Analysis Found : %C 65.40 ; %H 5.80. Calcd for : $C_{21}H_{23}ClN_2O_3$: %C 65.20 ; %H 5.95

Reaction of benzofurano-[3,2-c]pyrazol-3-one II with chloroacetyl chloride. Formation of the N-chloroacetyl derivative VIII

To a mixture of II (0.01 mole) and chloroacetyl chloride (20 mL), few drops of pyridine were added. The reaction mixture was refluxed on a steam bath for two hours and left to stand overnight at room temperature. Crystallisation of the precipitated solid from ethanol gave N-chloroacetyl derivative VIII, m.p. 250°C, yield 60 %

Analysis Found : %C 52.80 ; %H 3.00. Calcd. for : $C_{11}H_7ClN_2O_3$: %C 52.69 ; %H 2.79

Reaction of II with benzenesulphonyl chloride. Formation of the O-benzenesulphonyl derivative IX

To a solution of II (0.01 mole) in pyridine (15 mL) benzensulphonyl chloride (0.01 mole) was added. The reaction mixture was refluxed for fourty minutes on a steam bath, cooled and then poured onto ice-cold water. The brown solid so formed was crystallised from ethanol to give the O-benzensulphonyl derivative IX, m.p. 125°C, yield 50 %.

Analysis Found : %C 56.90 ; %H 3.10. Calcd. for : $C_{15}H_{10}N_2O_4S$: %C 57.32 ; %H 3.18.

Reaction of II with benzenediazonium chloride. Formation of benzofurano-[3,2-c]phenylazo-pyrazol-3-one X

To a cold solution of II (0.01 mole) in ethanolic sodium hydroxide (10 %, 40 mL), benzene-diazonium chloride (0.01 mole) was added. Crystallisation of the obtained solid from ethanol afforded the phenylazo derivative X.

Analysis Found : %C 64.30 ; %H 3.40. Calcd for : $C_{15}H_{10}N_4O_2$ %C 64.74 ; %H 3.59

Mannich reaction of II. Formation of benzofurano-2-piperidinomethyl pyrazol-3-one XI

To a mixture of II (0.01 mole) and piperidine (0.02 mole), in methanol (40 mL), aqueous formaldehyde (35 %, 2.5 mL) was added. The reaction mixture was refluxed for ten hours, left to stand in refrigerator for two days and the resulting solid product was filtered off and crystallised from methanol to give the N-Mannich base XI as hydrochloride salt, m.p. 150°C, yield 40 %.

Analysis Found : %C 58.10 ; %H 5.70. Calcd for $C_{15}H_{18}ClN_3O_2$: %C 58.53 ; %H 5.85

REFERENCES

[1] W. Treb and F. Reisses, German Patent, 1,934,459 (1970); *Chem. Abstr.* **72**, 90307 (1970).

[2] O. H. Hishmat, A. H. Abd el Rahman, E. M. Kandeel and E. Ismail, *Arzneim-Forsch.*, **27**, 2035 (1977).

[3] A. H. Abd el Rahman and E. M. Ismail, *Arzneim-Forsch.*, **26**, 756 (1976).

[4] G. Raynaud, B. Pourrias, J. Thomas and Thomas, *Chim. Ther.*, **8**, 479 (1973).

[5] G. Raynaud, B. Pourrias, J. Thomas and M. Thomas, *Chim. Ther.*, **9**, 85 (1974).

[6] O. M. O. Habib, I. I. Abd El-Gawad, E. M. Khalil and H. A. Etman, *Polish J. Chem.*, in press.

[7] O. M. O. Habib, I. I. Abd El-Gawad, E. M. Kandeel and D. S. Badawy, *Rev. Roumaine Chim.*, under publication.

[8] O. M. O. Habib, I. I. Abd El-Gawad and D. S. Badawy, *Rev. Roumaine Chim.*, under publication.

[9] G. E. Kaslow and R. A. Reck, J. *Amer. Chem. Soc.*, **69**, 864 (1947).

[10] R. Huisgen, *Liebigs Ann. Chem.*, **559**, 101 (1948).

Revue Roumaine de Chimie, **34**, *9–10*, 1957–1962 (1989)

SYNTHESIS AND REACTIONS OF D-GLUCOSYL DERIVATIVES OF 2-ARYL-4(3H)-QUINAZOLINONES AND THEIR THIONE DERIVATIVES

MOHAMED F. ABDEL MEGEED and MOHAMED A. H. SALEH
Chemistry Department, Faculty of Science, Tanta University, Tanta, Egypt

Received May 16, 1987

2-Aryl-4(3H)-quinazoline (**1a-e**) and their corresponding thiones (**2a-e**) reacted with tetra-O-acetyl-α-D-glucopyranosyl bromide in the presence of potassium hydroxide to yield mainly the N-glucoside derivatives (**3a-e**) and (**4a-e**), respectively in a good yield, and O-glucosides (**5a-e**) or S-glucosides (**6a-e**) in a poor yield. Oxidation of the N-glucoside thiones (**4a-e**) with potassium permanganate yielded the corresponding 4-oxo derivatives (**3a-e**), whereas, S-gycosyl derivatives (**6a-e**) yielded the corresponding sulphones (**7a-e**). The obtained products were characterized by UV-, IR- and H-NMR-spectroscopy.

INTRODUCTION

4(3H)-quinazolinones are considered to be important precursors for synthesis of heterocyclic compounds of potential physiological activity[1–10] or as thermostable polymers [11–14]. Since glucosyl derivative of 4(3H)-quinazolinones as well as their corresponding thiones have not previously been described; and in view of biological importance of glucosides in which the aglycone moiety is a pyrimidine derivative, [15–17] we now report the preparation and some reaction of D-glucosyl derivative of 6-substituted-2-aryl-4(3H)-quinazolinones (**1a**–**e**) and their corresponding 6-substituted-2-aryl-4(3H)-quinazolinones (**2a**–**e**). 6-Substituted-2-aryl-4(3H)-

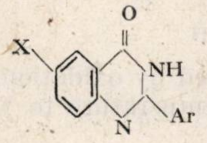

1

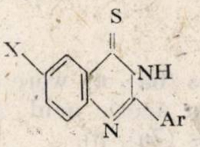

2

	Ar	X
a ;	C_6H_5	H
b ;	C_6H_5	Br
c ;	C_6H_5 - Cl-p	Br
d ;	C_6H_5 - CH_3-p	Br
e ;	C_6H_5 - NO_2-p	H

-quinazolinones (**1a**—**e**) were prepared by the reaction of 5-substituted anthranilic acid with the appropriate aroyl chloride in pyridine as a reaction medium. [18] The resulting 6-substituted-2-aryl-3,1-4H-benzoazinones were treated with formamide according to the method described by Patel and Patel [19] to obtain the desired quinazolinones. The corresponding thiones (**2a**—**e**) were prepared by the action of phosphorous pentachloride in triethyl amine [20] with the appropriate quinazolinones. Tetra-O-acetyl--α-D-glucopyranosyl bromide [21] was prepared by the reaction of hydrobromic acid in acetic anhydride.

The quinazolinones (**1a**—**e**) and their corresponding thiones (**2a**—**e**) reacted readily with 2,3,4,6-tetra-O-acetyl-α-D-glucopyranosyl bromide in the presence of potassium hydroxide, presumably via Walden inversion [22,23] to produce mainly the N-glucosyl derivatives, 6-substituted-2-aryl-3--(2,3,4,6-tetra-O-acetyl-β-D-glucopyranosyl)-4(3H)-quinozolinones (**3a**—**e**) and 6-substitued-2-aryl-3-(3, 3, 6,-tetra-O-acetyl-β-D-glucopyranosyl -4(3H)-quinazolinthiones (**4a**—**e**) in a fairly good yield together with the O-glucosides, 6-substituted-2-aryl-4-(2,3,4,6-tetra-O-acetyl-β-D-glucopyranosyloxo)-1,3-quinazoline (**5a**—**e**) and the S-glucosides, 6-substituted-2-aryl-4-(2,3,4,6-tetra-O-acetyl-β-D-glucopyranosylthio)-1,3-quinazoline (**6a**—**e**), respectively in a poor yield.

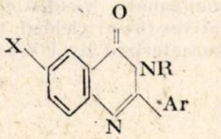

3

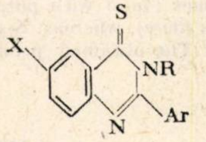

4

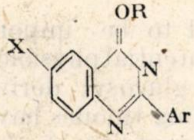

5

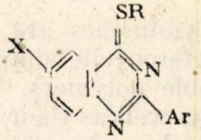

6

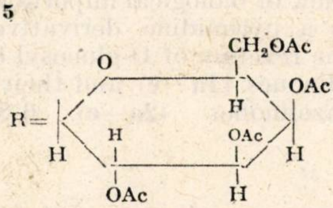

The S-glucosides (**6a**—**e**) were characterised by oxidation with potassium permanganate in acetic acid at room temperature to yield the corresponding sulfones (**7a**—**e**).

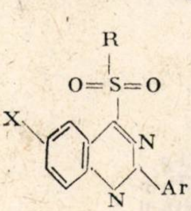

7

Oxidation of the N-glucosides (**4a**—**e**) under the same conditions gave the corresponding N-glucosides of 4-oxoderivatives (**3a**—**e**). The tautomerism in 4(3H)-quinazolinone derivatives (**1a**—**e**) and their corresponding thiones (**2a**—**e**) was confirmed by methylation with dimethyl sulphate to obtain both N-methyl together with $O-CH_3$ or $S-CH_3$ derivatives, respectively. The structures of N-glycosides (**3a**—**e**) and (**4a**—**e**) and O-glucosides (**5a**—**e**) or S-glucosides (**6a**—**e**) were confirmed by comparing their main electronic absorption bands with those reported in the literature. The electronic absorption spectra of the quinazoline structure i.e. the O-glucosides (**5a**—**e**) or S-glucosides (**6a**—**e**) comprise two main absorption bands. The first one located at 220—225 nm ($\log \varepsilon = 4.30-4.42$) assigned as $1L_a \leftarrow 1_A$ transition in the phenyl ring. The second band appears within 300—310 nm region ($\log \varepsilon = 4.10-4.22$) and corresponds to $\pi-\pi^*$ transition in the pyrimidine moiety. The N-glucosides (**3a**—**e**) and (**4a**—**e**) exhibit three main absorption bands. The first band appears within 220—225 nm region ($\log \varepsilon = 4.37-4.48$) due to $^1L_a \leftarrow 1$ transition of the phenyl group. The second band is located at 275—280 nm ($\log \varepsilon = 3.62-3.68$) assigned as $\pi-\pi^*$ transition of carbonyl or thiocarbonyl groups. The third band appears within 325—335 nm region ($\log \varepsilon = 3.26-3.36$) assigned as C.T. within the whole molecule. This band shows bathochromic shift in the case of N-glucosides of the quinazolinthione derivatives (**4a**—**e**).

The IR-spectra of the N-glucosides (**3a**—**e**) and (**4a**—**e**) and O-glucosides (**5a**—**e**), S-glucosides (**6a**—**e**) and the sulphono-glucosides (**7a**—**e**) are characterised by the absence of νNH and/or νOH and the presence of ν$C=O$ of the acetate carbonyl within 1780—1755 cm^{-1}. The carbonyl group of the quinazolone ring in compounds (**3a**—**e**) appears in 1960—1680 cm^{-1} region, whereas the $N-C=S$ group [28] in compounds (**4a**—**e**) appears at 1380—1370 cm^{-1}. The symmetric and asymmetric stretching vibrations of the O-glucoside linkage ($C-O-C$) [29] in compounds (**5a**—**e**) appear with 1050—1030 cm^{-1} and 1260—1250 cm^{-1}, respectively. The S-glucoside (**6a**—**e**) are characterized by a very strong absorption band with 695—690 cm^{-1} attributed to ($C-S-C$) [29] stretching vibrations. Compounds (**7a**—**e**) exhibit their symmetrical and asymmetrical stretching vibrations of the sulphone group at 1180—1155 cm^{-1} and 1370—1360 cm^{-1}, respectively. The ^1H-NMR spectra of the glucosides under investigation are characterised by the absence NH, OH and/or SH signal of the original quinazolinones (**1a**—**e**) or quinazolinthiones (**2a**—**e**). The ^1H-NMR — spectra are also characterised by the presence of a doublet at $\delta = 6.45-6.72$ ppm corresponding to the anomeric proton of the sugar moiety. Another doublet appears at $\delta = 4.22-4.31$ ppm assigned as CH_2 proton of the sugar part. The four protons of the glucopyranosyl ring resonate as multiplet at $\delta = 5.10-5.81$ ppm. The remaining four acetyl groups appear as four singlets at $\delta = 1.66-2.16$ ppm. The aromatic protons exhibit a multiplet at 8.3—7.2 ppm. Generally the S-glucopyranosyl protons resonate at a lower magnetic field than those corresponding to O-glucopyranosyl protons. This suggests that the electron density on the S-glucopyranosyl system might be lower due to the electronegativity of the sulphur atom.

Attempts to deacetylate the glucosides are tried using methylamine,[24] ammonia,[25] hydrochloric acid[26] or sodium hydroxide in some cases[27] to prepare the corresponding deacetylated derivatives. In all cases the starting aglycone quinazolinones (**1a—e**) or quinazolinthiones **2**(**a—e**) are generated through the cleavage of either N-sugar or O-sugar and S-sugar bonds. This cleavage can be explained by the splitting that may occur on either the glucoside linkage depending on the nature of the aglycone or on sugar-oxygen and sugar-sulphur bonds, when the sugar residue is able to take electrons from the aglycone.

EXPERIMENTAL

Melting points are uncorrected. UV—spectra were determined for solution in ethanol with a UNICAM SP—8000 Spectrophotometer, and IR—spectra for potassium bromide discs with a UNICAM 1200 spectrometer. The ^{1}H—NMR — spectra were measured for solution DMSO—d$_6$ with VARIAN—A—60 spectrometer using tetramethylsilane as internal reference.

Reaction of 2,3,4,6-tetra-O-acetyl-α-glucopyranosyl bromide with (**1a—e**) *-and* (**2a—e**) : A solution of the glucosyl bromide (4.1 g, 0.01 mol) in acetone (50 mL) was added to solutions of the appropriate quinazolinone (**1a — e**) or quinazolinthione (**2a—e**) (0.01 mol) in water (6 mL) containing potassium hydroxide (0.6 g, 0.01 mol). The reaction mixture was shaken for 5 hrs at room temperature and then concentrated under reduced pressure at room temperature. The residue was washed with water to remove the potassium bromide and then continuously extracted with cyclohexane. The solid which precipitated from the extract was collected and recrystallised from cyclohexane to give colourless needles of the N-glucosides (**3a—e**) and (**4a—e**), respectively (Table 1). The remaining solid in the extraction thimble was crystallised from ethanol to yield colourless crystals of the O-glucosides (**5a—e**) or S-glucosides (**6a—e**) in poor yield (Table 1).

Oxidation of N-glucosides (**4a—e**) *and S-glucosides* (**6a—e**) *with potassium permanganate* : To a solution of substrate (2 m mol) in glacial acetic acid (25 mL) a solution of potassium permanganate (0.06, 4 m mol) in water (10 mL) was added gradually with stirring during 30 min. Stirring was continued for 5 hrs at room temperature and the mixture was then poured into crushed ice. The solid precipitated was collected and a solution in ethanol was filtered to remove manganese salts, and then concentrated and recrystallised. Compounds (**4a— e**) yielded the corresponding 4-oxo-derivatives (**3a—e**), identified by comparing m.p. and mixed m.p. compounds (**6a—e**) yielding the corresponding sulphones (**7a—e**) was crystallised from cyclohexane (see Table 1).

Action of ammonia on (**3a—e**), (**4a—e**), (**5a—e**), (**6a—e**) *and* (**7a—e**) : To a suspension of the appropriate tetraacetate glucoside derivative (2 m mole) in methanol (25 mL), methanol (25 mL) saturated with ammonia was added. The reaction mixture was kept at v −10°C for 2 days, then filtered and concentrated under reduced pressure at room temperature. The residue was triturated for several times with chloroform and dissolved in the minimal amount of ethanol and the solution was filtered and concentrated. Recrystallisation of the residue from ethanol gave the starting aglycon products.

The same deacetylating procedure was carried out using methylamine, hydrochloric acid or sodium hydroxide. The isolated products were characterised as the starting aglycons, identified by comparison of m.ps and mixed m.ps.

REFERENCES

[1] J. C. Sircar, T. Capiris, J. S. Kesten and J. D. Herzing, *J. Med. Chem.*, **24**, 735 (1981).

[2] M. P. Pandey, *Acta Cienc. Indica* [*Ser*] *Chem.*, **10**, 778 (1985).

[3] V. D. Rao, R. V. Rao and P. Raghunada, *Ind. J. Chem.*, *Sect. B*, **24B**, 988 (1985).

[4] S. Buyuktimkin, *Pharmazie*, **40**, 393 (1985).

[5] N. Sighal, I. S. Gupta and P.C. Bansal, *J. Ind. Chem. Soc.*, **61**, 690 (1984).

[6] R. S. Varma, S. Bahadur and A. K. Agniboti, *Ind. J. Chem.*, *Sect. B*, **18B**, 275 (1979).

[7] M. J. Kornet, T. Varia and W. Beaven, *J. Heterocycl. Chem.*, **20**, 1553 (1983).

Table 1

Analytical and other data for compounds (**2a-e**), (**3a-e**), (**4a-e**) (**5a-e**), (**6a-e**) and (**7a-e**)

Compound (yield %)	m.p. °C	Formula	$[\alpha]^{25(CHCl_3)}_{degrees}$	Found/Calc			
				C%	H%	N%	S%
3a	207–8	$C_{28}H_{28}N_2O_{10}$	+24	60.60	5.10	5.00	
(65)				60.86	4.11	5.07	
3b	211–12	$C_{28}H_{27}BrN_2I_{10}$	+88	53.10	4.30	4.30	
(73)				53.36	4.31	4.44	
3c	221–22	$C_{28}H_{26}BrClN_2O_{10}$	+39	50.40	3.82	4.00	
(68)				50.50	3.94	4.21	
3d	212–13	$C_{29}H_{29}BrN_2O_{10}$	+51	53.80	4.42	4.30	
(70)				53.96	4.53	4.34	
3e	198–99	$C_{28}H_{27}N_3O_{12}$	+67	56.10	4.40	7.00	
(72)				56.28	4.56	7.03	
4a	163–64	$C_{28}H_{28}N_2O_9S$	+87	59.20	4.80	4.80	5.50
(63)				59.14	4.96	4.93	5.64
4b	188–89	$C_{28}H_{27}NBrN_2O_9S$	+74	51.80	4.00	4.20	4.90
(60)				51.94	4.02	4.33	4.95
4c	223–24	$C_{28}H_{26}BrClN_2O_9S$	+36	49.20	3.80	4.00	4.60
(67)				49.31	3.84	4.11	4.70
4d	176–77	$C_{29}H_{29}BrN_2O_9S$	+48	52.60	4.30	4.10	4.70
(56)				52.65	4.42	4.24	4.85
4e	212–13	$C_{28}H_{27}N_3O_{11}S$	+23	54.80	4.30	6.70	5.10
(63)				54.81	4.44	6.85	5.23
5a	163–63	$C_{28}H_{28}N_2O_{10}$	+29	60.70	5.10	5.00	
(12)				60.86	5.11	5.07	
5b	158–59	$C_{28}H_{27}BrN_2O_{10}$	+59	53.30	4.30	4.40	
(13)				53.26	4.31	4.44	
5c	147–48	$C_{28}H_{26}BrClN_2O_{10}$	+45	50.20	3.80	4.20	
(15)				50.50	3.94	4.21	
5d	166–76	$C_{29}H_{29}BrN_2O_{10}$	+74	53.80	4.50	4.20	
(15)				53.96	4.53	4.34	
5e	137–39	$C_{28}H_{27}N_3O_{12}$	+86	56.30	4.62	7.20	
(16)				56.28	4.56	7.03	
6a	142–43	$C_{28}H_{28}N_2O_9S$	+36	59.20	4.90	4.82	5.50
(10)				59.14	4.96	4.93	5.64
6b	191–92	$C_{28}H_{27}BtrN_2O_9S$	+82	51.80	4.00	4.20	4.80
(12)				51.94	4.02	4.33	4.95
6c	178–79	$C_{28}H_{26}BrClN_2O_9S$	+75	49.40	3.80	4.00	4.70
(16)				49.31	3.84	4.11	4.70
6d	182–84	$C_{28}H_{29}BrN_2O_9S$	+46	52.66	4.40	4.10	4.80
(18)				52.65	4.42	4.24	4.85
6e	173–74	$C_{28}H_{27}N_3O_{11}S$	+35	54.80	4.30	6.80	5.30
(10)				54.81	4.44	6.85	5.23
7a	152–53	$C_{29}H_{28}N_2O_{11}S$	+28	55.70	4.60	4.60	5.40
(85)				55.99	4.70	4.67	5.34
7b	148–49	$C_{28}H_{27}BrN_2O_{11}S$	+64	49.60	4.11	4.00	4.80
(88)				49.49	4.01	4.12	4.72
7c	196–97	$C_{28}H_{27}BrClN_2O_{11}S$	+77	47.00	3.80	3.80	4.60
(82)				47.04	3.81	3.92	4.48
7d	180–81	$C_{29}H_{29}BrN_2O_{11}S$	+84	50.30	4.20	4.00	4.50
(75)				50.22	4.21	4.04	4.62
7e	188–89	$(C_{28}H_{27}N_3O_{11}S)$	+56	52.10	4.20	6.50	5.00
(78)				52.09	4.22	6.51	4.97

[8] S. Bahadur and M. Saxena, *Arch. Pharm.* (Weinheim. Ger.). **316**, 964 (1983).

[9] P. Kumar, C. Nath, K. P. Bhargava and K. Shanker, *Pharmazie*, **37**, 802 (1982).

[10] M. N. Aboul-Enein and I. A. Eid, *Pharm. Acta Helv.*, **56**, 239 (1891).

[11] S. S. Tiwari, R. K. Satsange and S. Misra, *Ind. J. Pharm. Sci.*, **40**, 40 (1978).

[12] J. Tani, Y. Yamada, T. Oine, T. Ochiai, R. Ishide and I. Inoue, *J. Med. Chem.*, **22**, 95 (1979).

[13] A. Fukami and S. Nishizaki, *Mitsubichi Denki Lab. Rep.*, **12**, 37 (1971).

[14] R. Salle, B. Sillion and G. DeGaudamaris, *Fr. FR.* 1603/28, 30 Apr. 1971 (1971).

[15] T. Nishimura and I. Iwai, *Chem. Pharm. Bull.*, **12**, 257 (1964).

[16] G. T. Rogers, R. S. Sodbolt and T. L. V. Ulbricht, *J. Chem. Soc.*, **C** (2), 203 (1969).

[17] G. T. Rogers, R. S. Sodbolt and T. L. V. Ulbricht, *J. Chem. Soc.*, **C** (2), 209 (1969).

[18] D. I. Bain and R. K. Smally, *J. Chem. Soc.*, **13**, 1593 (1968).

[19] V. S. Patel and S. R. Patel, *J. Ind. Chem. Soc.*, **42** 53 (1965).

[20] B. Dash, K. E. Dora and C.S. Panda, *Heterocycles*, **19**, 2093 (1982).

[21] E. Fischer, *Ber. dtsch. chem. Ges.*, **44**, 1901 (1911).

[22] H. B. Wood and H. G. Fletcher; *J. Am. Chem. Soc.*, **78**, 207 (1956).

[23] W. A. Bonner, *J. Am. Chem. Soc.*, **81**, 1448 (1959).

[24] M. L. Wolform and A. Thomson, *J. Am. Chem. Soc.*, **56**, 80 (1934).

[25] H. M. A. Abdel-Bary, F. M. E. Abdel-Magied, Z. El-Hewehi and M. A. F. El-Kaschef; *J. Prakt. Chem.*, **314**, 461 (1872).

[26] W. A. Bonner and W. L. Koehler, *J. Am. Chem. Soc.*, **70**, 314 (1948).

[27] G. Wagner and H. Pischel, *Pharmazie*, **19**, 197 (1964).

[28] A. Hetzheim and K. Moekel. *Adv. Heterocycl. Chem.*, **7**, 218—224 (1966).

[29] N. B. Colthup, I. H. Daly and S. E. Eilder, "Introduction to Infrared and Raman Spectroscopy", Academic Press, New York, 1964.

Revue Roumaine de Chimie, 34, 9–10, 1963–1971 (1989)

BEHAVIOUR OF 4-(4′-BROMO-3′-METHYL)-PHENYL-1(2H)-PHTHALAZINONE TOWARDS SOME NUCLEOPHILES AND ELECTROPHILES

MONEER A. I. SALEM,[a] A. M. EL-GENDY[b] and S. I. EL-NAGDY[a]
[a] Chemistry Department, Faculty of Science, Ain Shams University, Abbassia, Cairo, Egypt
[b] Faculty of Science, El-Zagazig University, El-Zagazig, Egypt

Received October 31, 1987

The phthalazinones (IIa-c) have been synthesized by treatment of acid (I) with hydrazines and semicarbazide hydrochloride. Acid (I) reacts with hydroxylamine hydrochloride and gives the desired oxazinone (III). Compound IIa reacts with $PCl_5/POCl_3$ to yield 1-chlorophthalazine (IVa) which reacts with sodamide, benzylamine and hydrazine hydrate to give IVb-d. Anthranilic acid reacts with IIa to give V. Behaviour of phthalazinone (IIa) towards methyl iodide, acid anhydride and acid chlorides has been investigated. Condensation of aromatic aldehydes with VIb was carried out to give the Claisen products VII. 4-Aryl-1(2H)-phthalazinone (IIa) undergoes cyanoethylation to yield 2-cyanoethyl-1(2H)-phthalazinone (VIIIa) which on hydrolysis gives the corresponding carboxylic acid (VIIIb).

It was previously reported that the reaction of hydrazines with acid I leads to the formation of 1(2H)-phthalazinones II,[1] which are useful as remedies for artheriosclerosis and thrombosis and also useful developable light-sensitive material.[2,3]

A recent publication by El-Hashash et al.[4] prompted us to study the chemical reactivity of compounds which exhibit lactam-lactim equilibrium. We report here on the behaviour of 4-(4′-bromo-3′-methyl)phenyl-1-(2H)-phthalazinone(II) towards some nucleophilic and electrophilic reagents with a view to synthesize phthalazine derivatives and to throw more precise information on the concept of lactam-lactim dynamic equilibrium as well. Thus *o*-(4-bromo-3-methylbenzoyl)-benzoic acid (I) reacts with hydrazine hydrate or phenylhydrazine in boiling ethanol to give 4-(4′-bromo-3′-methyl)phenyl-1(2H)-phthalazinone (IIa) or 2-phenyl-4-(4′-bromo-3′-methyl)phenyl-1(2H)-phthalazinone (IIb), respectively, and reacts with semicarbazide hydrochloride in pyridine yielding IIc.

Phthalazinone IIa reacts with hydroxylamine hydrochloride in pyridine to give 4-(4′-bromo, 3′-methyl)phenyloxazinone (III).

The action of $PCl_5/POCl_3$ mixture on IIa gives the desired 1-chlorophthalazine (IVa).

Nitrogen nucleophiles, namely sodamide, benzylamine and hydrazine hydrate react with 1-chlorophthalazine derivative (IVa) to give 1-(N-substituted)-phthalazine derivatives (IVb–d) respectively. On the other hand, IVa reacts with anthranilic acid by fusion at 150–160°C to give V.[5] From the foregoing reactions the authors concluded that compound IIa really exists in the lactam-lactim dynamic equilibrium. The question as to whether the compound IIa exists predominantly in either the hydroxy form of the amide form cannot be determined from their chemical behaviour because reaction of the minor tautomer will shift the equilibrium. In order to favour the lactam tautomer we investigate the behaviour of 4-(4′-bromo-3′-methyl)phenyl-1(2H)-phthalazinones (IIa) towards alkyl halides, acid anhydride and acid chlorides, the reaction being carried out without solvent. The result indicated that the oxo-form is predominant and gave the desired products VIa—e respectively.

Condensation of aromatic aldehydes with 2-acetyl-4-aryl-phthalazinone (VIb) in the presence of sodium ethoxide[6] as catalyst gave the corresponding 2-cinnamoyl-4-aryl-1 (2H)-phthalazinones (VIIa—d).

Phthalazinone derivative (IIa) reacts with acrylonitrile[7] affording 2-cyanoethylated phthalazinone (VIIIa). The hydrolysis of VIIIa with alkali (10% KOH) gave the corresponding carboxylic acid (VIIIb).

All the structures were confirmed by microanalysis and where possible — IR and ^1H-NMR spectral data.[8,9] Results are listed on tables 1 and 2.

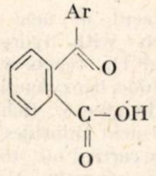

(I)

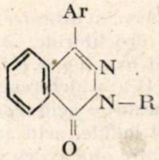

(II)

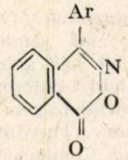

(III)

a) $-R=H$
b) $-R=C_6H_5$
c) $-R=CO-NH_2$

$Ar = C_6H_3-CH_3,\ Br-3,4$

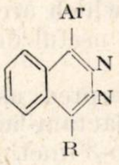

(IV)

a) $-R=Cl$
b) $-R=NH_2$
c) $-R=NH.CH_2.C_6H_5$
d) $-R=NH.NH_5$

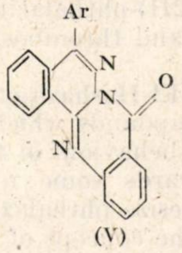

(V)

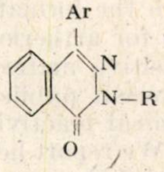

(VI)

a) $-R=CH_3$
b) $-R=-CO-CH_3$
c) $-R=-CO-CH_2-Cl$
d) $-R=-CO-C_6H_5$
e) $-R=-CO-C_6H_4-Cl-p$

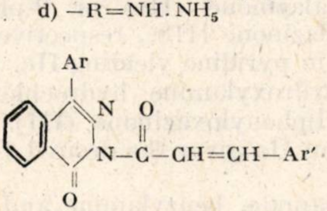

(VII)

a) $Ar'=C_6H_5$
b) $Ar'=C_6H_4-OCH_3-p$
c) $Ar'=C_6H_4-Cl-o$
d) $Ar'=C_6H_4-Br-m$

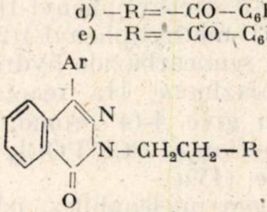

(VIII)

a) $-R=C\equiv N$
b) $-R=COOH$

$Ar = C_6H_3-CH_3,\ \ Br-3,4$

Table 1

Physical data of prepared compounds

Compd.	M.p. °C (colour)	Solv. of cryst. * Yield %	M.F.	Analysis Calcd/Found		
				C %	H %	N %
IIa	> 250 (yellowish-white)	E + A (57)	$C_{15}H_{11}ON_2Br$	57.14 57.55	3.49 3.62	8.89 8.58
IIb	176–77 (colourless)	M (55)	$C_{21}H_{15}ON_2Br$	64.45 64.27	3.84 3.92	7.16 7.34
IIc	> 250 (pale-yellow)	E (61)	$C_{16}H_{12}O_2N_3Br$	53.63 53.96	3.35 3.18	11.73 11.91
III	146–47 (yellowish-brown)	B + L.P (55)	$C_{15}H_{10}NO_2Br$	56.96 57.22	3.16 3.09	4.43 4.64
IVa	> 250 (brown)	Bu (47)	$C_{15}H_{10}N_2ClBr$	53.97 54.32	3.00 3.13	8.36 8.48
IVb	> 250 (pale-brown)	M (54)	$C_{15}H_{12}N_3Br$	57.32 57.58	3.82 4.04	13.38 13.10
IVc	228–29 (colourless)	B (66)	$C_{22}H_{18}N_3Br$	65.35 65.66	4.46 4.70	10.40 10.16
IVd	194–95 (yellow)	B (72)	$C_{15}H_{13}N_4Br$	53.41 53.76	3.86 4.00	18.99 19.21
V	250–51 (pale-yellow)	E (53)	$C_{22}H_{14}N_3OBr$	63.46 63.16	3.36 3.55	10.10 10.19
VIa	145–46 (pale-yellow)	E (59)	$C_{16}H_{13}N_2OBr$	58.36 58.44	3.95 4.18	8.51 8.32
VIb	151–52 (faint-yellow)	B (62)	$C_{17}H_{13}N_2O_2Br$	57.14 57.31	3.64 3.82	7.84 8.00
VIc	>250 (pale-yellow)	B (57)	$C_{17}H_{12}N_2O_2ClBr$	52.11 52.00	3.07 3.10	7.15 7.32
VId	162–63 (colourless)	M (56)	$C_{22}H_{15}N_2O_2Br$	63.01 62.96	3.58 3.51	6.68 6.80
VIe	175–76 (colourless)	B (64)	$C_{22}H_{14}N_2O_2ClBr$	58.21 58.52	3.09 3.10	6.17 6.22
VIIa	159–60 (pale-brown)	B (67)	$C_{24}H_{17}O_2N_2Br$	64.72 65.09	3.82 4.11	6.29 6.18
VIIb	185–86 (yellow)	B (58)	$C_{25}H_{19}O_3NBr$	52.17 52.60	3.30 3.09	4.87 4.96
VIIc	188–89 (colourless)	B (64)	$C_{24}H_{16}O_2N_2ClBr$	60.06 60.42	3.34 3.28	5.84 5.68
VIId	181–82 (pale-yellow)	B (59)	$C_{24}H_{16}O_2N_2Br_2$	54.96 55.34	3.05 3.21	5.34 5.10
VIIIa	167–68 (colourless)	E (47)	$C_{18}H_{14}ON_3Br$	58.70 58.29	3.80 3.53	11.41 11.40
VIIIb	213–14 (colourless)	E (53)	$C_{18}H_{15}O_3N_2Br$	56.69 57.04	3.94 3.81	7.35 7.54

* E = Ethanol, A = Acetic acid, M = Methanol, B = Benzene, Bu = *n*-Butanol and L.P. = Light petrol (b.p. 60– 80°C).

Table 2

IR and ^{1}H-NMR data of prepared compounds

Compd		IR	^{1}H-NMR, δ values
IIa	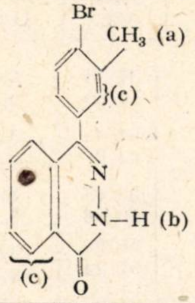 Br CH$_3$ (a) (c) N N—H (b) (c) O	ν—C=N at 1640 cm^{-1}, νC=O at 1680, 1690 cm^{-1}, νCH at 2960 cm^{-1}, νNH at 3350 cm^{-1} and νOH at 3420 cm^{-1}	a) *s*, *3H*, 2. 82 b) *b*, *1H*, 7.18 c) *m*, *7H*, 7.34—7.6.8
IIc	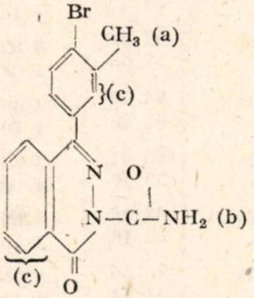 Br CH$_3$ (a) (c) N O N—C—NH$_2$ (b) (c) O	ν—C=N at 1640 cm^{-1} νC=O at 1690, 1680 cm^{-1} νCH a 2980 cm^{-1} and νNH at 3450 cm^{-1}	a) *s*, *3H*, 2.85 b) *b*, *2H*, 6.22 c) *m*, *7H*, 7.30—7.70
III	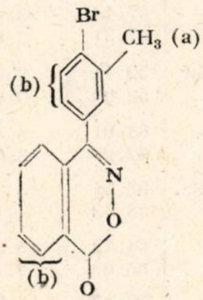 Br CH$_3$ (a) (b) N O (b) O	νC=N at 1635 cm^{-1}, νC=O at 1700 cm^{-} and νC—H at 2950 cm^{-1}	a) *s*, *3H*, 2.84 b) *m*, *7H*, 7.28—7.65
IVa	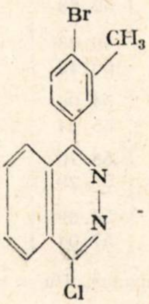	νC=N at 1640 cm^{-1} and νC—H at 2970 cm^{-1}	—.—.—.—.—.—

Table 2 (continued)

compd		IR	^{1}H-NMR, δ values
IVb	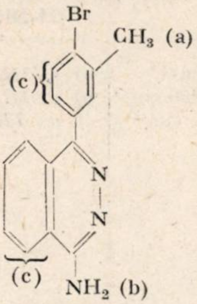 Br CH$_3$ (a) (c) N N (c) NH$_2$ (b)	νC=N at 1645 cm^{-1}, νCH at 2940 cm^{-1} and νNH at 3420	a) *s*, *3H*, 2.85 b) *b*, *2H*, 5.66 c) *m*, *17H*, 7.32—7.61
IVc	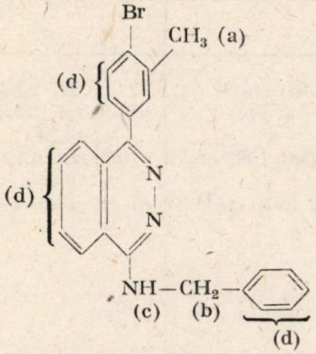 Br CH$_3$ (a) (d) (d) N N NH—CH$_2$— (c) (b) (d)	νC=N at 1625 cm^{-1}, νCH at 2970 cm^{-1} and νNH at 3370 cm^{-1}	a) *s*, *3H*, 2.80 b) *d*, *2H*, 4.18 c *b*, *1H* 5.94 d) *m*, *12H*, 74.0—7.72
V	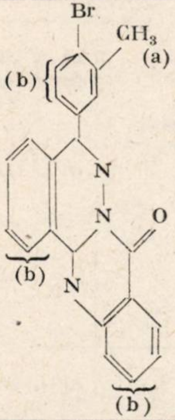 Br CH$_3$ (a) (b) N N O (b) N (b)	νC=N at 1630 cm^{-1}, νC=O at 1680 cm^{-1} and νCH at 2970 cm^{-1}	a) *s*, *3H*, 2.80 b) *b*, *11H*, 7.34—8.12
VIa	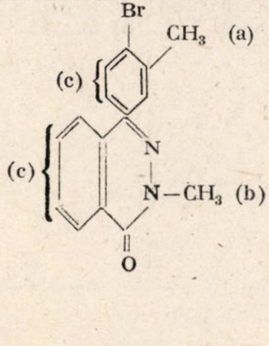 Br CH$_3$ (a) (c) (c) N N—CH$_3$ (b) O	νC=N at 1640 cm^{-1}, νC=O at 1675 cm^{-1} and νCH at 2950 cm^{-1}	a) , *s*, *3H*, 2.82 b) *b*, *3H*, 3.17 c) *m*, *7H*, 7.38—7.78

Table 2 (continued)

Cdmpd		IR	^{1}H-NRM. δ values
VIb	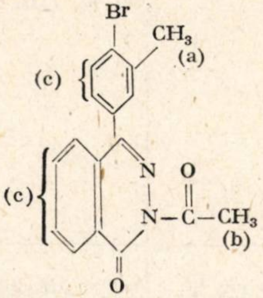 Br CH$_3$ (a) (c) (c) N O N—C—CH$_3$ (b) O	νC=N at 1640 cm^{-1}, νC=O at 1660, 1690 cm^{-1} and νCH at 2980 cm^{-1}	a) *s*, *3H*, 2.05 b) *s*, *3H*, 2.84 c) *m*, *7H*, 7.41—7.86
VIIa	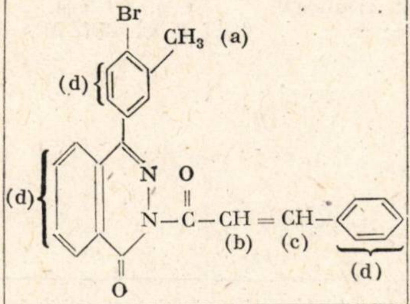 Br CH$_3$ (a) (d) (d) N O N—C—CH = CH— (b) (c) (d) O	νC=C at 1610 cm^{-1}, νC=N at 1640 cm^{-1}, νC=O at 1660, 1685 cm^{-1} and νCH at 2970 cm^{-1}	a) *s*, *3H*, 2.84 b) *d*, *1H*, 5.58 (J_t = = 16.2) c) *d*, *1H*, 6.12 (J_t = = 16.2) d) *m*, *12H*, 7.15—7.68
VIIc	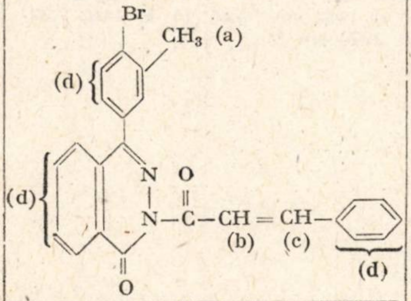 Br CH$_3$ (a) (d) (d) N O N—C—CH = CH— (b) (c) (d) O	νC=C at 1610 cm^{-1}, νC=N at 1630 cm^{-1}, νC=O at 1670,1690 cm^{-1} and ν CH at 2940 ct^{-1}	a) *s*, *3H*, 2.78 b) *d*, *1H*, 5.49 (J_t = = 14.6 c) *d*, *1H*. 5.96 (J_t = = 14.6) d) *m*,*11H*, 7.22—7.74
VIIIa	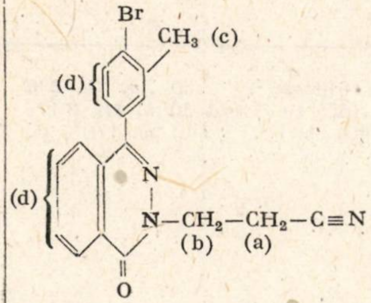 Br CH$_3$ (c) (d) (d) N N—CH$_2$—CH$_2$—C≡N (b) (a) O	νC=N at 1635 cm^{-1}, νC=O at 1680 cm^{-1}, νC≡N at 2220 cm^{-1} and νCH at 2970 cm^{-1}	a) *t*, *2H*, 2.4—2.6 b) *m*, *2H*, 2.7—2.8 c) *s*, *3H*, 2.86 d) *m*, *7H*, 7.34—7.78

Table 2 (continued)

Compd		IR	^{1}H-NMR, δ values
VIIIb	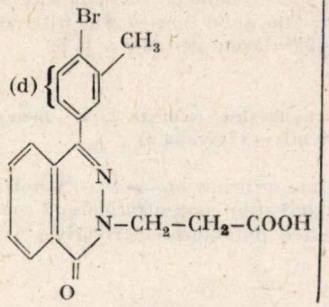	$\nu C=N$ at 1640 cm^{-1} $Cv=O$ at 1670 cm^{-1} $\nu C=O$ (acid) at 1710cm^{-1} and νOH broad at 3440–3480 cm^{-1}	— . — . — . — . — . —

EXPERIMENTAL

All the melting points are uncorrected, the infrared absorption spectra were determined with a Perkin Elmer spectrophotometer Model 577 using KBr pellet technique, while the ^1H-NMR spectra were determined with a Varian VN 1009 (S–60T) instrument, $CDCl_3$ used as a solvent and TMS as internal standard.

Reaction of the acid I with hydrazines; formation of 4-(4′-bromo-3′-methyl)phenyl-1(2H)-phthalazinone derivatives (IIa and b)

A solution of the acid I (0.01 mol) in ethanol (40 mL) was treated with hydrazines, namely hydrazine hydrate or phenylhydrazine (0.012 mol) and the mixture was refluxed for 6 hr. The solid that separated after cooling was crystallized from the proper solvent to give the coresponding phthalazinones IIa and b respectively.

Reaction of the acid I with semicarbazide hydrochloride; formation of phthalazinone derivative (IIc)

A solution of the acid I (0.01 mol) in pyridine (40 mL) was treated with semicarbazide hydrochloride (0.015 mol), the reaction mixture refluxed for 5 hr, cooled, then 100 mL of cold dilute hydrochloric acid was added. The solid that separated was filtered off and crystallized from the suitable solvent to give the phthalazinone derivative IIc.

Reaction of the acid I with hydroxylamine hydrochloride; formation of 4-(4′-bromo-3′-methyl)phenyl-oxazinone (III)

A mixture of the acid I (0.01 mol) in pyridine (20 mL) and hydroxylamine hydrochloride (0.01 mol) with few drops of water was refluxed for 4 hr and the cooled mixture was poured into ice cold dilute hydrochloric acid. The solid separated was crystallized from the proper solvent to give the desired oxazinone III.

Action of PCl_5POCl_3 on phthalazinone IIa; formation of 1-chlorophthalazine derivative (IVa)

A suspension of IIa (1 g), PCl_5 (0.5 g) and $POCl_3$ (10 mL) was heated on a water bath for 6 hr. The reaction mixture was poured gradually into crushed ice and the solid that separated was filtered off and crystallized from the proper solvent to give 1-chlorophthalazine derivative IVa.

Action of sodamide on 1-chlorophthalazine derivative IVa; formation of 1-amino-4-(4′-bromo-3′-methyil)phenylpthalazine (IVb)

A solution of IVa (0.01 mol) in dry xylene (25 mL) was treated portionwise with sodamide (0.01 mol), and the reaction mixture refluxed for 48 hrs; the solid formed was filtered off and crystallized from the suitable solvent to give 1-aminophthalazine derivative IVb.

Reaction of 1-chlorophthalazine derivative IVa with hydrazine hydrate and benzylamine; formation of phthalazine derivatives (IVc and d)

A mixture of IVa (0.01 mol) and hydrazine hydrate or benzylamine (0.012 mol) in ethanol (40 mL) was refluxed for 6 hrs. The solid that separated after concentration and cooling was crystallized from the proper solvent to give 1-substituted phthalazine derivatives IVc and d respectively.

Action of anthranilic acid on 1-chlorophthalazine derivative IVa; formation of 4-(4′-bromo-3′-methyl phenyl)-phthalazino-o-(1,2-b) quinazolin-8(H)-one (V)

A mixture of IVa (0.01 mol) and anthranilic acid (0.02 mol) was heated at 150—160°C for 4 hrs in an oil bath, cooled, then decomposed with hot water (100 mL) and boiled for 1/2 hr. The solid that separated was filtered off and washed for three times with hot water; the solid obtained was crystallized from the suitable solvent to give the desired quinazolinone V.

Reaction of phthalazinone derivative IIa with methyl iodide; formation of 2-methyl-4-(4′-bromo-3′-methyl)phenyl-1(2H)-phtalazinone (VIa)

Method (*A*)

A solution of phythalazinone derivative IIa (0.01 mol) in methanol (10 mL) and methyl iodide (0.04 mol) was added to methanolic sodium methoxide (0.01 mol in 10 mL methanol). The reaction mixture was refluxed for 6 hrs, cooled and concentrated. The solid that separated was filtered off and crystallized from the proper solvent to give the corresponding 2-methylphthalazinone derivative (VIa).

Method (*B*)

A mixture of IIa (0.01 mol), pyridine (10 mL) and methyl iodide (0.04 mol) was heated on a steam bath for 3 hrs. The reaction was acidified by ice/dil HCl; the solid obtained was crystallized from the suitable solvent to give VIa.

Reaction of phthalazinone derivative IIa with acid anhydride and acid chlorides; formation of 2-acetyl and aroyl-4-(4′-bromo-3′-methyl)phenyl-1(2H)-phthalazinone derivatives (VIb-e)

A mixture of phthalazinone derivative (IIa) (0.01 mol), acid anhydride or acid chlorides (0.015 mol) namely acetic anhydride or chloroacetyl chloride or benzoyl chloride or *p* chlorobenzoyl chloride was heated for 2 hr at 130—140°C in an oil bath, cooled and then decomposed with crushed ice. The solid obtained was crystallized from the suitable solvent to give (VIb—e) respectively.

Independent synthesis of 2-substituted 4-(4′-bromo-3′-methyl)-phenyl-1(2H)-phthalazinone derivatives (VIa-b and d)

A solution of the acid I (0.01 mol) in ethanol (50 mL) was refluxed for 5 hrs with methylhydrazine or acid hydrazides, namely acetyl hydrazine and benzoylhydrazine (0.01 mol). The solid that obtained after concentration and cooling was crystallized from the proper solvent and gave products identified as VIa—b and d respectively by m.p. and mix. m.p. determination and comparsion of their IR data.

Condensation of VIb with aromatic aldehydes; formation of 2-cinnamoyl-4-(4′-bromo-3′-methyl)phenyl-1(2H)-phtalazinone derivatives (VIIa-d)

A mixture of VIb (0.01 mol) and aromatic aldehydes, namely benzaldehyde, anisaldehyde, *o*-chlorobenzaldehyde, and *m*-bromobenzaldehyde (0.01 mol) in ethanol (25 mL) was added to ethanolic sodium ethoxide (0.01 mol in 40 mL ethanol) and stirred for 3 hr at room temperature, kept overnight, then the reaction mixture poured into ice-hydrochloric acid (6N). The solid that separated was filtered off and washed several times with water and crystallized from the proper solvent to give VIIa—d respectively.

Cyanoethylation of phthalazinone derivative IIa; formation of 2-cyanoethyl-4-(4′-bromo-3′-methyl)phenil-1(2H)phthalazinones (VIIIa)

Method (*A*)

A solution of phthalazinone derivative IIa (0.01 mol) in pyridine (40 mL) was treated with acrylonitrile (0.015 mol) and the mixture was refluxed for 6 hr, cooled and then poured into ice-hydrochloric acid; the solid that separated was filtered off and crystallized from the suitable solvent to give the desired compound VIIIa.

Method (*B*)

Acrylonitrile (0.015 mol) was added to a solution of IIa (0.01 mol) in dioxane (40 mL), then the reaction mixture was refluxed for 4 hr at 110—120°C in an oil bath, cooled and decomposed with ice-water. The solid that separated was filtered off and crystallized from the proper solvent to give the corresponding 2-cyanoethylated phthalazinone derivative VIIa.

Hydrolysis of 2-cyanoethylated phthalazinone VIIIa; formation of the carboxylic acid VIIIb

A mixture of VIIIa (0.01 mol), KOH (1 g) dissolved in water (10 mL) and ethanol (40 mL) was refluxed for 4 hr. Ethanol was then removed and the residue acidified by 1 N hydrochloric acid. The solid that separated was filtered off and washed several times with water and crystallized from the proper solvent to give the corresponding carboxylic acid VIIIb.

REFERENCES

[1] A. A. Afify, M. A. Sayed, A. El-Farargy and G. H. Tamam, *J. Chem. Soc. Pakistan*, **8** No. 1, (1986).

[2] Inou Michira, Ishikawa Masyuki, Tsuchiya Takashi, Shinamoto, Tokio; *Chem. Abstr.*, **83,** 136899, 179091, 179092 and 179093, (1975).

[3] S. Ikenove, T. Masuda, S. Sakawaki, *Chem. Abstr.*, **94,** 9988 (1981).

[4] M. A. El-Hashash, M. M. Mohamed, M. A. Sayed and O.A. AboBakr; *Pakistan J. Sci. Ind. Res.***28,** 104 (1985).

[5] H. Jahine, A. H. Zaher, Y. Akhnookh and Z. El-Gendy, *Indian J. Chem.*, **16 B,** 689 (1978).

[6] M. El-Deek, M. A. I. Salem, A. A. Hamed and M. Samann, *Rev. Roumaine Chim.*, **26,** 775 (1981).

[7] J. R. Merchant, S. D. Kulkarni and M. S. Venkatash, *Indian J. Chem.*, **19B**, 914 (1980).

[8] R. M. Silverstein, G. C. Bassler and T. C. Morrill, "Spectrometric Identification of Organic Compounds", 4th ed.; Wiley, New York (1981).

[9] L. H. Bellamy, "The Infrared Spectra of Complex Molecules", 2nd ed., Wiley, New York, pp. 132—61. 179, 263, 334 and 350 (1966).

Revue Roumaine de Chimie, **34**, *9–10*, 1973–1978 (1989)

THE CONDENSATION OF SOME AROMATIC ALDEHYDES AND KETONES WITH DIMETHYL HOMOPHTHALATE

M. R. MAHMOUD, S.EL-NAGDY and F. A. EL-BASSIOUNY
Department of Chemistry, Faculty of Science, Ain Shams University,
Cairo, A. R. Egypt

Received October 30, 1987

Fluorenone, N,N-dimethyl-*p*-aminobenzaldehyde and *p*-nitrobenzaldehyde have been condensed with dimethyl homophthalate, in the presence of sodium hydride to give the expected half-ester (1a 2a,b) in excellent yield. The configuration of the half-esters was inferred by cyclisation with sodium acetate in acetic anhydride to the corresponding lactone derivatives (7, 8 a, b). Hydrolysis of the half-esters gives the diacids (1b, 2c, d) which can be converted to the anhydrides (3, 4a, b). Cyclisation and methanolysis of the anhydrides was also described.

The behaviour of dimethyl ester of homophthalic acid in the Stobbe condensation has been studied.[1] Several examples are recorded where derivatives of the acid were condensed with aldehydes and ketones.[2,3,4] In this communication we wish to introduce a synthesis of some arylidene homophthalic anhydride and polycyclic aromatic compounds *via* Stobbe condensation; and this constitutes an extension of Stobbe condensation of aldehydes and ketones with dialkyl homophthalates. Thus when fluorenone, N,N-dimethyl-*p*-aminobenzaldehyde and *p*-nitrobenzaldehyde were condensed with dimethyl homophthalate in the presence of sodium hybride, each of the expected half-esters (1a and 2a, b) were obtained in pure form with very high yield (about 80–85%).

The structure of the half-esters was shown by elemental analysis, and the position of the double bond by oxidation with akaline permanganate to the original ketone and aldehydes. Furthermore, they exhibited $\nu_{C=O}$ at about 1718 cm^{-1} for 2,3-unsaturated ester and about 1685 cm^{-1} for aryl-conjugated carbonyl group.[5]

However, the structure of the half-esters (2a, b) was supported by the ^{1}H–N.M.R spectra which were consistent with their proposed structure. The half-ester (2a) shows the following signals : a singlet at δ 2.9 ppm, a singlet at δ 3.7 ppm, a multiplet at δ ranging from 6.4 to 7.8 ppm; these signals are in the ratio 6 : 3 : 9 and represent the following groups respectively : the two CH_3 – of the $-N(CH_3)_2$ group, CH_3– of the ester group and the aromatic protons involving also the olefinic proton. The half-ester (2b) shows the following signals : a singlet at δ 3.65 ppm, a multiplet at δ ranging from 7.1 to 8.1 ppm, in the ratio 3 : 9 and represents the CH_3- of the ester goup and the aromatic protons involving also the olefinic proton, respectively.

The configurations of the half-esters (1a and 2a) were determined *via* cyclisation of the derived anhydrides (3 and 4a) as follows :

Saponification of the half-esters (1a and 2a, b) gave the corresponding diacids (1b and 2c, d) in pure crystalline state. The position of unsaturation

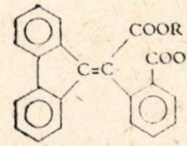

(1)

	R	R'
a,	CH_3	H
b,	H	H
c,	H	CH_3

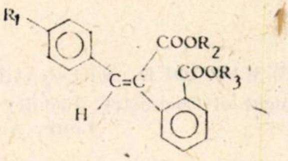

(2)

	R_1	R_2	R_3
a,	$-N(CH_3)_2$	CH_3	H
b,	$-NO_2$	CH_3	H
c,	$-N(CH_3)_2$	H	H
d,	$-NO_2$	H	H
e,	$-N(CH_3)_2$	H	CH_3
f,	$-NO_2$	H	CH_3

in the three dibasic acids was proved both by oxidation of the original ketone and aldehydes, and by their displaying $\nu_{C=O}$ for 2,3-unsaturated and aryl conjugated carbonyl functions [5] at about 1672 cm^{-1} and 1683 cm^{-1} respectively.

The three dibasic acids (1a and 2c,d) were converted by refluxing in acetyl chloride as dehydrating agent to the corresponding anhydrides (3 and 4a, b) which exhibited the expected carbonyl coupling bands [5] at about 1720 cm^{-1} and 1770 cm^{-1}. The hydrolysis of the anhydrides to the original diacids proved the retention of configuration during anhydride formation.

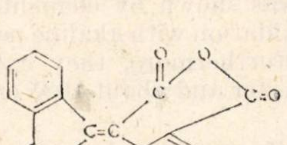

(3)

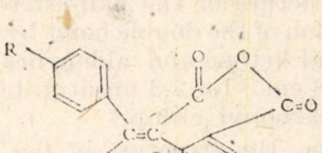

(4)

a, R = $-N(CH_3)_2$

b, = $-NO_2$

Attempted cyclisation of the half-ester (1a and 2a) by zinc chloride in acetic acid — acetic anhydride mixture or phosphorous oxychloride gave the corresponding anhydrides (3 and 4a).

The fluorenylidene, and N,N-dimethyl-*p*-aminobenzylidene homophthalic anhydride (3 and 4a) were cyclised with anhydrous aluminium chloride in presence of dry acetylene tetrachloride to give the corresponding oxoacids (5 and 6) respectively, in very high yield (70–80%).

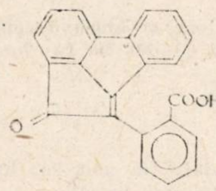

(5)

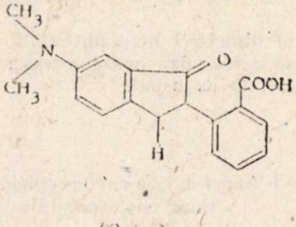

(6)

Similar treatment of the *p*-nitrobenzylidene homophthalic anhydride (4b) gave the corresponding dibasic acid (2d) as the sole acidic product.

The structure of the oxo-indenyl acids (5 and 6) follows from the elemental analysis, solubility in sodium carbonate, yellow and red colour, formation of 2 : 4-dinitrophenylhydrazones and the presence of the $\nu_{C=O}$ for the aryl-conjugated carboxyl and 2,3-unsaturated ring ketonic group[5] (at ca 1685 and 1705 cm^{-1}).

The electronic spectra of the acids (5 and 6) λ_{max} 241–346, ϵ 22,000–35,000, λ_{max} 221–312, ϵ 18,000–42,000) closely resemble those of analogous compounds.[3,6] The longer wavelength bands extend well into the violet region thus reflecting the yellow and red colour of these compounds.

Methanolysis of the anhydrides (3 and 4a, b) by refluxing methanol led to the expected ring cleavage to give the corresponding isomeric half-esters (1c and 2e, f) respectively, in about 80–85% yield. The I.R. spectra of the isomeric half-esters (1c and 2c, f) displayed $\nu_{C=O}$ at ca 1700–1712 cm^{-1}.

The half-esters (1a and 2a, b) refluxed with a mixture of acetic anhydride, acetic acid and sodium acetate yielded the lactonic methyl ester (7 and 8a, b) which may be the postulated intermediate product in the Stobbe condensation, as it was cleaved to the half-esters (1a and 2a, b) by cold alcoholic potassium hydroxide. The structure of the lactonic methyl esters (7 and 9a, b) was determined by microanalysis and the I.R. spectrum which displayed $\nu_{C=O}$ at ca 1742 cm^{-1}.

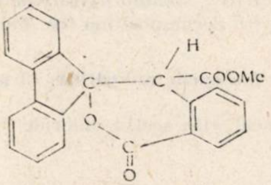

(7)

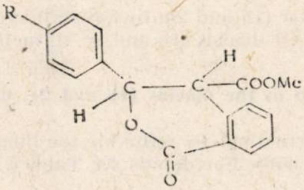

(8)

a, R = $N(CH_3)_2$

b, = NO_2

EXPERIMENTAL

Melting points are not corrected. Infrared (KBr) and ultraviolet spectra were recorded on Unicam SP 1200 (infrared) and Unicam SP 1800 spectrophotometers, respectively.

a) Formation of methyl-β-aryl-α-[2-o-carboxyphenyl]-acrylate by Stobbe condensation

A mixture of dimethyl homophthalate, the ketone or aldehyde and sodium hybride (1.5 : 1 : 1.5 mol) in excess dry benzene was stirred at 60−80° for two hrs, and the reaction mixture was worked up as usual.[3]

Table 1

Methyl-β-aryl-α-[2-*o*-carboxyphenyl]-acrylate (la and 2a, b) and their corresponding diacids (1b and 2c, d)

No.	M.p. (°C) (solvent of crystalization) *	Formula	Analysis % Calcd/Found		
			C	H	N
1a	230−2	$C_{23}H_{16}O_4$	77.5	4.5	
	(Bz−M)		77.2	4.2	
2a	160−1	$C_{19}H_{19}NO_4$	70.15	5.8	4.3
	(Bz−M)		69.9	5.6	3.9
2b	176−8	$C_{17}H_{13}NO_6$	62.4	3.97	4.3
	(Bz−M)		62.4	4.20	3.9
1b	265−6	$C_{22}H_{14}O_4$	77.19	4.09	
	(Bz−L.P.80°)		77.50	4.2	
2c	214−6	$C_{18}H_{17}NO_4$	69.5	5.5	4.5
	(T)		69.9	5.4	3.9
2d	200−1	$C_{16}H_{11}NO_8$	61.3	3.5	4.4
	(A)		61.7	4.0	4.1

* Bz = Benzene, L.P.80 = Light petroleum (b.p. 80−100°), T = Toluene, A = Dil. acetic acid and M = Methanol.

Fluorenone (18 g): (Stirring for two hours) gave a half-ester (1a) (30.1 g 85 % yield) which was filtered off and crystallised from a suitable solvent (cf. Table 1).

N,N-Dimethyl-p-aminobenzaldehyde (14.9 g): (Stirring for one hour) gave a half-ester (2a) (26.1 g, 80 % yield) which was filtered off and crystallised from a suitable solvent (cf. Table 1).

p-Nitrobenzaldehyde (10 g): (Stirring for two hours). The insoluble acidic product (2b) (17.4 g, 81 % yield) was filtered off and crystallized from a proper solvent (cf. Table 1).

b) Saponification of the half-esters

The half-ester (1a and 2a, b) was refluxed with 10 % sodium hydroxide (10 ml per gram ester) for 3 hrs. All diacids (1b and 2c, d) melted with decomposition (cf. Table 1).

c) Conversion of the diacids (1b and 2c, d) to the cyclic anhydrides (3 and 4a, b)

This was carried out by refluxing the dibasic acid with acetyl chloride (10 ml per 1g acid); (80−85 % yield). For details see Table 2.

d) Action of aluminium chloride upon the cyclic anhydrides
Formation of oxoindenyl acids (5 and 6)

Aluminium chloride (1.2 mol.) and a solution of the anhydride (1 mol.) in acetylene tetrachloride (10 ml per g anhydride) were stirred for 12 hrs and left overnight at room tempe-

Table 2

Arylidene homophthalic anhydrides (3 and 4a, b)

No.	M.p. (°C) (solvent of crystallization) *	Formula	Analysis % Calcd/Found C	H	N
3	156—8 (Bz/L.P.80°)	$C_{22}H_{12}O_3$	81.5 81.9	3.7 3.6	
4a	186—8 (T)	$C_{18}H_{15}NO_3$	73.7 73.1	5.1 4.9	4.8 4.9
4b	155—7° (T)	$C_{16}H_9NO_5$	65.08 65.3	3.05 3.4	4.7 4.2

* Bz = Benzene ; T = Toluene.

rature. The acidic reaction product (70—80% yield) was obtained as yellow and red crystals For details see Table 3.

When the anhydride (4b) was subjected to the same procedure, the corresponding. dibasic acid (2b) was recovered in considerably high yield.

Table 3

The oxo-indenyl acids (5 and 6) and their 2 : 4-dinitrophenylhydrazones

No	M.p. °C (Solvent of crystn.) *	Formula	Analysis % C	H	N	M.P. °C (Solvent of crystn). *	2,4-Dinitrophenylhydrazones Formula (Mol. Wt.)	Analysis % Calcd/Found N	N
5	256—8 (alc)	$C_{22}H_{12}O_3$	81.5 81.9	3.7 3.6		243—5 (alc)	$C_{28}H_{16}N_4O_6$ (504)	11.1	11.5
6	222—4 (Bz-alc)	$C_{18}H_{15}NO_3$	73.7 73.4	5.1 4.9	4.8 4.4	258/9 (T/alc)	$C_{24}H_{19}N_5O_6$ (473)	14.7	15.1

* Bz = Benzene, alc = Methanol and T = Toluene.

e) **Conversion of anhydrides (3 and 4a, b) to the isomeric half-esters (1c and 2e, f)**

The anhydride was refluxed for 6 hrs with excess of absolute methanol (30 mL per 1 g anhydride) (75—85% yield). For details, see Table 4.

Table 4

β-Aryl-α-(2-carbomethoxyphenyl) acrylic acid (1c and 2e, f)

No	M.p. (°C) (solvent of crystallization)*	Formula	Analysis % Calcd/Found C	H	N
1c	196—8 (Bz/L.P. 80°)	$C_{23}H_{16}O_4$	77.5 77.9	4.5 4.2	
2e	152—4 (alc)	$C_{19}H_{19}NO_4$	70.2 70.0	5.8 5.4	4.3 4.4
2f	160—2 (T)	$C_{17}H_{13}NO_6$	62.4 62.8	3.97 4.3	4.3 4.2

* Bz = Benzene, L.P. 80° = Light petroleum (b.p. 80—100°),
T = Toluene and alc = Methanol

f) Conversion of the half-esters (1a and 2a, b) to the lactonic methyl esters (7a and 8a, b)

A mixture of the half-ester (1 mol) acetic acid (10 ml), acetic anhydride (10 ml) and a catalytic amount of freshly fused sodium acetate (0.5 g) was refluxed for 6 hrs. The reaction mixture was worked up as usual[3] (60—65% yield). For details, see Table 5.

Table 5

3-Aryl-4-methoxycarbonyl-3,4-dihydroisocoumarin (7 and 8a, b)

No	M.p. (°C) (solvent of crystallization) *	Formula	Analysis % Calcd/Found C	H	N
7	189—191	$C_{23}H_{16}O_4$	775	4.5	
	(Bz.L. P.80°)		77.5	4.4	
8a	204—6	$C_{19}H_{19}NO_4$	70.2	5.8	4.3
	(T)		69.7	5.7	4.7
8b	162—4	$C_{17}H_{13}NO_6$	62.4	3.97	4.3
	(alc)		62.9	3.4	4.3

* Bz = Benzene, L.P. 80° = Light petroleum (b.p. 80—100°), T = Toluene and alc = Methanol

REFERENCES

[1] M. Doub and Johnson, *J. Amer. Chem. Soc.*, **70**, 418 (1948).
[2] H. J. E. Lowenthal and R. Pappo, *J. Chem. Soc.*, **(1952)**, 155, 4799.
[3] M. F. El-Newaihy, W. I. Awad, and H. A. Abdel-Hamid, *Egypt. J. Chem.*, **15**, 297 (1972).
[4] M. F. El-Newaihy, M. R. Salem, E. I. Enayat and H. A. Abdel-Hamid, *J. Ind. Chem.*, **20B**, 564 (1981).
[5] L. J. Bellamy, "The Infrared Spectra of Complex Molecules", Vol. I, 3rd edn., Chapman and Hall, London, 1975.
[6] M. F. El-Newaihy, M. R. Salem, E. I. Enayat and H. A. Abdel-Hamid, *Aust. J. Chem.*, **32**, 1159 (1979).

Revue Roumaine de Chimie, **34**, *9–10*, 1979–1985 (1989)

STUDIES ON THE CONDENSATION OF 1,3-DIARYL-PROPEN-1-ONE WITH ETHYL CYANOACETATE

S. EL-NAGDY,[a] F. A. EL-BASSIOUNY,[a] I. ATTIA[b] and M. R. MAHMOUD[a]

[a] Department of Chemistry, Faculty of Science, Ain Shams University, Cairo, A.R. Egypt

[b] Faculty of Engineering, Ain Shams University, Cairo, A.R. Egypt

Received October 31, 1987

Michael condensation of 1-[*p*-bromophenyl]-3-[*p*-chlorophenyl]-propen-1-one (I) with ethyl cyanoacetate in the presence of ammonium acetate leads to the formation of 6-[*p*-bromophenyl]-2-hydroxy-4-[*p*-clorophenyl] nicotinonitrile, (II) and nicotinamide (III) as a major product. The reaction of (II) with phosphorous oxychloride, Grignard reagents and ethyl bromoacetate gives 2-chloro-(IV), 3-acyl-(X) and 2-alkoxy (VII) pyridine derivatives. Reactions of (IV) with amines, hydrazine hydrate, sodamide and alkoxides were also investigated. Compound (X) reacted with hydrazine hydrate and hydroxylamine hydrochloride to give substituted 1H-pyrazolopyridine (XI) and isoxazolopyridine (XII). Also, reactions of (VI) with hydrazine hydrate and of (I) with urea, thiourea, hydrazine hydrate, phenylhydrazine and oxidation with hydrogen peroxide are described.

The literature [1-4] reports that chalcones react with ethyl cyanoacetate under Michael conditions in the presence of ammonium acetate at high temperature to give the corresponding pyridones.

In the present work, the authors reinvestigated the same procedure using chalcone (1), and it was found that (I) condensed with ethyl cyanoacetate in the presence of ammonium acetate at high temperature affording a mixture of (II) and (III) respectively. The structures of (II) and (III) were confirmed by microanalysis (Table 1), beside their I.R. spectra which displayed $\nu C\equiv N$ at 2225 cm^{-1}, νCO of amides at 1670–1650 cm^{-1} beside broad absorption band in the 3μ region, correlated for νNH, OH and $-CONH_2$ frequency. As a point of interest, the presence of (II) in lactam $\rightleftharpoons$ lactim tautomeric equilibrium has been investigated, since, on its treatment with $POCl_3$, the 2-chloro-4,6-diarylnicotinonitrile [5] (IV) was obtained, whose IR spectrum lacks the carbonyl absorption, while displaying $\nu C\equiv N$ at 2220 cm^{-1} and $\nu C=N$ at 1595 cm^{-1}.

Alkylation [6-8] of 2-chloropyridine derivative (IV) was investigated; thus treatment of (IV) with sodium methoxide and ethoxide yielded 2-alkoxy pyridine derivative (Va, b) whose structure was supported by micro-analysis (Table 1) beside their IR spectra which showed a strong absorption band characteristic of $\nu C\equiv N$ (2230–2220 cm^{-1}), $\nu C=N$ at (1592–1590 cm^{-1}) and absence of –OH, –NH and –CO group.

The well known reactivity[9] of 2-halogen substituents in the pyridine nucleus promoted a study of the replacement of chlorine atom with amines. Therefore 2-chloropyridine derivative (IV) reacted with benzylamine, hydrazine as well as with phenylhydrazine in absolute ethanol producing the 2-benzyl-amino-, 2-hydrazino-, and 2-phenylhydrazino-3-cyano-4,6-diaryl pyridine (VIa–c). The IR spctrum of (VI) showed well defined absorptions for νNH at 3542, 3280 and 3320 cm^{-1}, $\nu C=N$ at 1615, 1610 and 1616 cm^{-1}, $\nu C\equiv N$ at 2228, 2224 and 2228 cm^{-1}.

Furthermore, treatment of (IV) with sodamine in dry xylene produced 2-aminonicotinonitrile (VId), whose IR spectrum showed characteristic bands at 2223 cm^{-1} for $C\equiv N$, at 1618 cm^{-1} for $C=N$ and at 3280 cm^{-1} for NH. Moreover, the 3-cyanopyridone derivative (II) was treated with ethyl bromoacetate affording the *o*-alkylation product (VII). The structure of (VII) was confirmed by its IR spectrum which displayed νCO at 1748 cm^{-1}, characteristic for ester group, and $\nu C\equiv N$ at 2226 cm^{-1}. Reaction of (VII) with hydrazine hydrate in boiling ethanol gave the hydrazine derivative (VIII). The IR spectrum showed bands at 1655, 2224 and (3290–3330) cm^{-1} attributable to νCO, $\nu C\equiv N$ and νNH respectively. Another chemical proof for the existence of (II) in such lactam $\rightleftharpoons$ lactim tautomeric equilibrium is its acid hydrolysis to the corresponding 3-carboxypyridone derivative (IX) which showed νCO of carboxylic group at 1680 cm^{-1}. Alkaline hydrolis is of (III) was found to give the same product (IX).

The behaviour of pyridone (II) was also investigated towards Grignard reagent. Thus, treatment of (II) with methyl magnesium iodide yielded the 3-acetyl-1H-pyrid-2-one (X). The IR spectrum of (X) revealed a strong absorption band at 1680 cm^{-1} characteristic for νCO and absence of $C\equiv N$ group. Compound (X) underwent condensation with hydrazine hydrate in boiling ethanol and with hydroxylamine hydrochloride in boiling pyridine to give the substituted 1H-pyrazolo-, and isoxazolo-pyridine derivatives (XI) and (XII) respectively. The IR spectrum of (XI) showed characteristic bands around 1620, 1505 and 3410 cm^{-1} attributable to $C=N$, and NH respectively, and that of (XII) showed band at 1614 cm^{-1} characteristic for $\nu C=N$. Treatment of chalcone (1) with urea in acidic medium (conc. H_2SO_4) and with thiourea in alkaline medium gave 2-hydroxy-6-[*p*-bromophenyl]-4-[*p*-chlorophenyl]-dihydropyrimidine (XIIIa) and 2-mercapto-6-[*p*-bromophenyl]-4-[*p*-chlorophenyl]-dihydropyrimidine (XIIIb), respectively.

It is known that hydrogen peroxide reacts with α, β-unsaturated carbonyl compounds to give αβ-epoxy ketone.[10] This reaction has now been applied to the chalcone (1) for the synthesis to the α,β-epoxy ketone (XIV). The IR spectrum of XIV showed strong bands characteristic of ν_{CO} at 1680 cm^{-1}, and epoxy linkage at 1250 cm^{-1}.

In general the oxirane ring of 1,2-epoxy ketones is opened by nucleophilic agents.[11,12] Thus the reaction of 1,2-epoxy ketone (XIV) with aqueous sodium hydroxide (as oxygen nucleophile) gave the atrolactic acid derivative (XV), *via* the intermediate α-diketone. The IR

Table 1

Characterized data of compounds prepared

Compd	M.p. (°C)	Recrystal-lization solvent * yield %	Mol. Formula	Analysis, %, Calcd./Found		
				C	H	N
I	160	E, 93	$C_{15}H_{10}ClBrO$	55.98	3.10	—
				55.61	3.31	
II	>280	B, 28	$C_{18}H_{10}ClBrN_2O$	56.03	2.59	7.26
				56.42	2.73	7.42
III	139–40	L.p, 70	$C_{18}H_{12}ClBrN_2O_2$	53.53	2.97	6.93
				53.14	5.15	7.21
IV	225	A, 70	$C_{18}H_9Cl_2BrN_2$	53.46	2.22	6.93
				53.21	2.41	7.23
Va	268	B, 60	$C_{19}H_{12}ClBrN_2O$	57.07	3.00	7.00
				56.83	3.20	7.11
Vb	219–20	B, 55	$C_{20}H_{14}ClBrN_2O$	58.04	3.38	6.77
				57.89	3.25	6.58
VIa	190	B, 71	$C_{24}H_{15}ClBrN_3$	62.54	3.25	9.12
				62.41	3.15	9.31
VIb	216–7	B, 66	$C_{18}H_{12}ClBrN_4$	54.06	3.00	14.02
				54.23	3.14	14.21
VIc	249–50	B, 67	$C_{24}H_{16}ClBrN_4$	60.56	3.36	11.77
				60.23	3.15	11.54
VId	>270	E, 71	$C_{18}H_{11}ClBrN_3$	56.17	2.86	10.92
				56.24	2.67	10.73
VII	153–4	E, 80	$C_{22}H_{16}ClBrN_2O_3$	55.99	3.39	5.93
				55.67	3.26	6.17
VIII	>280	E, 68	$C_{20}H_{14}ClBrN_4O_2$	52.45	3.06	12.24
				52.32	3.32	12.14
IX	158	A, 45	$C_{18}H_{11}ClBrNO_3$	53.39	2.71	3.46
				53.12	2.56	3.21
X	238–9	E, 73	$C_{19}H_{13}ClBrNO_2$	56.64	3.22	3.47
				56.81	3.45	3.61
XI	280	E, 80	$C_{19}H_{13}ClBrN_3$	57.21	3.26	10.54
				57.42	3.14	10.32
XII	247	B, 75	$C_{19}H_{12}ClBrN_2O$	57.70	3.00	7.00
				57.38	3.21	6.82
XIIIa	>280	B, 60	$C_{16}H_{11}ClBrN_2O$	52.96	3.03	7.72
				52.74	3,21	7.59
XIIIb	245	B, 78	$C_{16}H_{11}ClBrN_2S$	50 72	2,90	7,39
				50.43	3.11	7.15
XIV	124	L.p., 65	$C_{15}H_{10}ClBrO_2$	53.33	2.96	—
				53.49	3.11	
XV	247–8	B, 68	$C_{15}H_{12}ClBrO_3$	50.63	3.37	—
				50.91	3.48	
XVIa	62–3	E, 85	$C_{15}H_{12}ClBrN_2$	53.65	3.57	8.34
				53.82	3.74	8.49
XVIb	148–9	E, 82	$C_{21}H_{16}ClBrN_2$	61.24	3.88	6.80
				61.06	3.69	6.58

* E = Ethanol, B = Benzene, L.p. = Light petroleum (b.p. 60–80°C), A = Acetic acid

spectrum of (XV) showed bands at 1685 and 3380 cm^{-1} attributable to νCO and νOH. Moreover, the hitherto unknown chalcone (I) reacted with hydrazine hydrate and phenylhydrazine in boiling ethanol affording the pyrazolines[13] (XV a, b), whose structures were confirmed by microanalysis (Table 1), beside the IR spectra which showed bands at 1600—1610 cm^{-1} for νC=N and 3300—3400 νNH.[14]

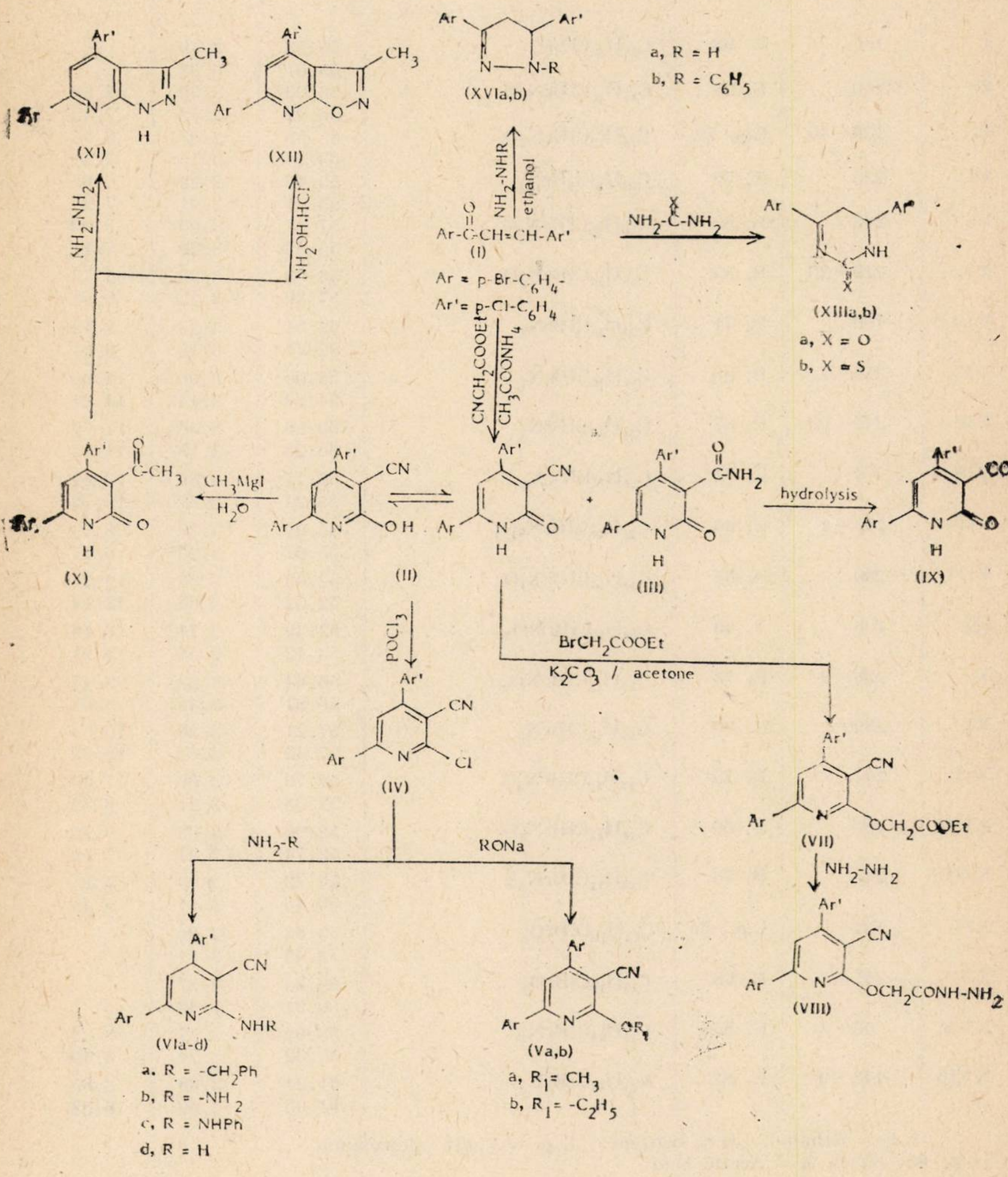
Ar'
CH3
Ar
N
N
H
(XI)
Ar'
CH3
Ar
N
O
N
(XII)
Ar
Ar'
N
N-R
(XVIa,b)
a, R = H
b, R = C6H5
NH2-NHR
ethanol
NH2-NH2
NH2OH.HCl
Ar-C-CH=CH-Ar'
(I)
Ar = p-Br-C6H4-
Ar' = p-Cl-C6H4
NH2-C(X)-NH2
NH
(XIIIa,b)
a, X = O
b, X = S
CNCH2COOEt
CH3COONH4
C-CH3
CH3MgI
H2O
(X)
CN
OH
(II)
C-NH2
(III)
hydrolysis
COOH
(IX)
POCl3
Cl
(IV)
BrCH2COOEt
K2CO3 / acetone
OCH2COOEt
(VII)
NH2-NH2
OCH2CONH-NH2
(VIII)
NH2-R
RONa
NHR
(VIa-d)
a. R = -CH2Ph
b, R = -NH2
c, R = NHPh
d, R = H
OR1
(Va,b)
a, R1 = CH3
b, R1 = -C2H5

EXPERIMENTAL

The infrared spectra were determined with PYE UNICAM and PERKIN ELMER 683 spectrophotometers using KBr wafer technique. Melting points are uncorrected. Characterization data of all compounds prepared are given in Table 1.

Formation of 6-[p-bromophenyl]-2-hydroxy-4-[p-chlorophenyl]-nicotinonitrile (II) and nicotinamide (III)

A mixture of ethyl cyanoacetate (0.03 mol), I(0.03 mol) and ammonium acetate (0.24 mol) was heated at 150—160°C in an oil bath for 4 hr. The reaction mixture was cooled and the yellow oil obtained was washed several times with water, then fractionally crystallized using light petroleum (b.p. 60—80°C) and benzene; compounds II and III were separated.

Action of phosphorous oxychloride on II (Formation of IV)

A suspension of (II) (1 g) and phosphorous oxychloride (5 mL) was heated on a water bath for 2 hrs. The reaction mixture was poured gradually onto crushed ice. The solid which separated was filtered off and crystallized from the suitable solvent to give (IV).

Reaction of 2-chloro-4,6-diaryl nicotinonitrile (IV) with sodium methoxide and ethoxide; formation of Va, b

A solution of (IV) (1 g) in methanol or ethanol (20 mL) was treated with sodium methoxide or ethoxide (prepared by dissolving 0.23 g sodium in 10 mL methanol or ethanol respectively) and refluxed for 5 hrs, then allowed to cool. The solid obtained upon dilution of the reaction mixture with water was filtered off and crystallised from the suitable solvent to give (Va, b).

Formation of 2-benzylamino-4,6-diaryl-pyrid-2-one (VIa)

A suspension of (II) 0.5 g and benzylamine (4 mL) was refluxed for 2 hrs and allowed to cool. The reaction mixture was triturated with cold ethanol and the solid obtained was crystallised from the proper solvent to give (VIa).

Action of hydrazine hydrate on (I, IV, VII, X), and phenylhydrazine on (I, IV); formation of (XVIa, VIb; VIII, XI and XVIb, VIc)

A solution of I, IV, VII and X (0.01 mol) and hydrazine hydrate or phenylhydrazine (0.01 mol) in absolute ethanol (30 mL) was refluxed for 5 hrs. The products obtained after concentration and cooling were crystallized from a suitable solvent to give XVIa, VIb, VIII, XI and XVIb, VIc, respectively.

Formation of 2-amino-3-cyano-3,6-diaryl pyridine VId

A mixture of IV (0.01 mol), sodamide (0.012 mol) and dry xylene was refluxed for 12 hrs. The reaction mixture was diluted with water, then extracted with ether. The solid separated was crystallised from a suitable solvent to give VId.

Reaction of II with ethyl bromoacetate; formation of (VII)

A mixture of II(0.01 mol) ethyl bromoacetate (0.02 mol), 2 g of anhydrous potassium carbonate and dry acetone (30 mL) was refluxed on water, bath for 30 hrs. The excess acetone was evaporated and the reaction mixture was poured on water. The solid separated was filtered off and crystallized from a suitable solvent to give VII.

Hydrolysis of II to the corresponding acid ; formation of (IX)

A mixture of II (0.01 mol) acetic acid (20 mL) and hydrochloric acid (20 mL) was refluxed for 5 hrs, cooled, then poured onto water and filtered. The solid product was crystallised from the proper solvent to give IX.

Action of Grignard reagent on II ; Formation of (X)

A suspension of II (2 g) in dry benzene (50 mL) was added to an ethereal solution of methyl magnesium iodide (prepared from 0.9 g magnesium, 7 g methyl iodide and 40 mL dry ether). The reaction mixture was refluxed (on steam bath) for 10 hrs, set aside at room temperature and then decomposed with a cold solution of hydrochloric acid (10 %). The yellow solid obtained was crystallised from a suitable solvent to give X.

Reaction of X with hydroxylamine hydrochloride ; Formation of (XII)

A mixture of X (0.01 mol) hydroxylamine hydrochloride (0.012 mol), pyridine (20 mL) and a few drops of water was refluxed for 5 hrs. The reaction mixture was poured into ce-cold HCl. The solid separated was crystallised from suitable solvent to give XII.

Action of urea on chalcone I ; formation of (XIIIa)

A mixture of 1 (0.01 mol), urea (0.015 mol), ethanol (20 mL) and conc. sulphuric acid (5 mL) was refluxed for 5 hrs. The mixture was concentrated, cooled, then neutralized by ammonium hydroxide. The solid obtained was filtered off, washed with water, and crystallized from a suitable solvent to give XIIIa.

Action of thiourea on I ; formation of (XIIIb)]

A mixture of 1 (0.01 mol) thiourea (0.01 mol), sodium hydroxide (30 mL 2 % and ethanol (30 mL) was refluxed for 5 hrs. The solid product obtained after concentration and cooling was filtered off and crystallized from a suitable solvent to give XIIIb.

Epoxidation of chalcone I ; Formation of (XIV)

A solution of 1 (0.01 mol) in acetone (50 mL) and methyl alcohol (20 mL) was mixed with 5 % aqueous sodium hydroxide (10 mL) followed by the addition of hydrogen peroxide (30 %, 5 mL). The solution was shaken for one hour, then allowed to stand overnight at room temperature ; water was then added. The solid that separated was crystallized from a suitable solvent to give XIV.

Action of sodium hydroxide on the epoxide XIV ; formation of (XV)

The epoxide XIV (0.01 mol) was refluxed with 10 % aqueous sodium hydroxide (10 mL for each g of epoxide) for 2 hrs. The alkaline solution was treated with charcoal, and extracted with ether. The aqueous layer on acidification by dilute HCl-ice gave the product XV, which was filtered off and crystallized from a suitable solvent.

REFERENCES

[1] A. Sammour, Y. Akhnoukh and H. Jahine, *J. Chem. U.A.R.*, **13,** 421 (1970).

[2] C. Barat, *J. Ind. Chem. Soc.*, **8,** 699 (1931).

[3] H. K. Sen-Gupta, *J. Chem. Soc.*, **1915,** 107, 1347.

[4] I. I .Abdel-Gawad, A. M. Khalil. T. Zimaity and S. Fouda, *J. Ind. Chem., Soc.*, **54,** 626 (1977).

[5] T. Kametani, K. Ogassawara and M. Shio, *Yakugaku Zasski*, **86,** 809 (1966).

[6] B. Gogalimska, *Acta Pol. Pharm.*, **24** 343 (1964).

[7] D. J. Cook, R. E. Bowon, P. Sorter and E. Doniels, *J. Org. Chem.*, **2** , 4949 (1961).

[8] E. Spinner and J. C. B. White, *J. Chem. Soc.*, **10B,** 991 (1966).

[9] D. Nantka — Namirski, *Acta Pol. Pharm.*, **24** 111 (1967).

[10] M. El-Kady, M. M. Mohamed and M. A. El-Hashash, *Rev. Roumaine Chim.*, **24,** 1499 (1979).

[11] A. Sammour and M. El-Kasaby, *J. Chem.*, **13,** 151 (1970).

[12] M. A. El-Hashash and M. El-Kady, *Rev. Roumaine Chim.*, **23,** 1581 (1978).

[13] E. A. Soliman, I. A. Attia and A. M. Guber, *Egypt. J. Chem.*, **27,** 3 (1984).

[14] L. J. Bellamy, "The I.R. Spectra of Complex Molecules" Wiley, IInd edition, New York, 1957.

Revue Roumaine de Chimie, 34, *9–10*, 1987–1993 (1989)

BENZOFURANS. PART III

SYNTHESIS AND ANTIFUNGAL ACTIVITY OF SOME NEW MANNICH BASES AND SULPHIDES DERIVED FROM (1,3,4-THIADIAZOLYL)- AND (1,2,4-TRIAZOLYL)-BENZOFURANS

ABDEL-BADIH A. G. GHATTAS, MAHMOUD ABDEL-RAHMAN,
MOHAMED T. EL-WASSIMY and GAMAL A. EL-SARAF
Chemistry Department, Faculty of Science, Assiut University
Sohag, Egypt

Received October 30, 1987

A series of new Mannich bases (IIIb-q and IVb-g) and sulphides (Va-c and VIa-c) were synthesized from benzofuran derivatives I and II, respectively. The corresponding hydroxymethyl derivatives (IIIa and IVa) were obtained by reacting compounds I and II with formaldehyde alone, respectively. All the new compounds were screened for their antifungal activity.

In recent years 1,3,4-thiadiazoles and 1,2,4-triazoles have received much attention as potential bactericides, [1,2] fungicides,[3,4] insecticides, [5,6] herbicides, [7] and tuberculotherapeutic agents. [8] Similarly, some benzofuran derivatives have been reported to be pharmacologically active [9,10]. Extending our previous work on synthesis of new thiadiazoles [11–13] and benzofurans [14,15] and in view of the above observations it was thought of interest to synthesize a new series of compounds in which a benzofuran nucleus is linked with a thiadiazole or triazole ring. The present work describes the synthesis of new Mannich bases and sulphides derived from 2-(5-mercapto-1,3,4-thiadiazol-2-yl)- and 2-(4-phenyl-3-mercapto-1,2,4-triazol-5-yl)-benzofurans (I and II), respectively. Further, the activities of the synthesized compounds were screened for their antifungal activity.

The parent compound I was not known before and it was prepared from the corresponding hydrazide [16] following the method of Young and Wood [17] in 35% yield; compound II was reported in our previous work. [15] The IR spectra of compound I showed the bands at 3120 (NH), 1620 (C=N), and 1180 (C=S). Its MS showed the molecular ion at m/e (rel. int. %): 234 (100).

Compounds I and II reacted with formaldehyde alone in boiling ethanol to give the corresponding hydroxymethyl derivatives, IIIa and IVa, respectively (cf. Table 1, Scheme 1). The IR of the products showed the absence of the bands corresponding to the NH groups while exhibiting the characteristic absorption bands at 3480–3200 (OH).

Table I

Physical data of compounds III and IV

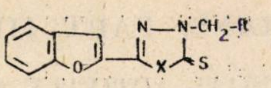

III, X = S

IV, X = N-Ph

Comp. No.	R	M.P. °C	Yield %	Found/Calc. % C	H	N
IIIa	-OH	216-17 (B+P)	60	50.23 50.00	3.10 3.03	10.39 10.61
b	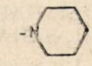	176-77 (B+P)	45	58.26 58.01	4.96 5.14	12.50 12.69
c	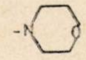	188-89 (P)	50	53.90 54.05	4.40 4.50	12.60 12.61
d	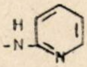	212-13 (B+P)	50	56.60 56.47	3.50 3.53	16.10 16.47
e	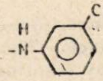	173-74 (P)	65	54.85 54.62	3.10 3.21	11.00 11.24
f	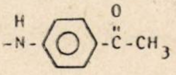	205-207 (B+P)	60	59.93 59.84	4.15 3.94	11.28 11.02
g	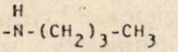 $-\overset{H}{N}-(CH_2)_3-CH_3$	134-35 (P)	45	56.34 56.43	5.24 5.33	13.11 13.17
IVa	-OH	265-66 (B)	70	63.49 63.16	4.21 4.02	13.00 13.00
b	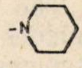	187-88 (B)	55	67.90 67.69	5.54 5.64	14.30 14.36
c	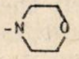	180-81 (B)	60	64.10 64.29	5.24 5.10	14.48 14.29
d	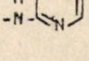	202-203 (M+P)	60	65.90 66.17	4.20 4.26	17.36 17.54
e	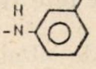	190-91 (B)	55	63.68 63.82	3.86 3.93	13.11 12.95
f	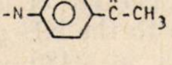	148-50 (B)	60	68.37 68.18	4.45 4.55	12.70 12.73
g	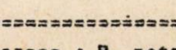 $-\overset{H}{N}-(CH_2)_3-CH_3$	168-69 (B)	65	66.43 66.67	5.90 5.82	14.62 14.61

B, benzene ; P, petroleum ether 60/80; M, methylene chloride.

When compounds I and II were treated with a mixture of formaldehyde and primary or secondary amine in absolute ethanol, a series of Mannich bases IIIb—g and IVb—g (Scheme 1, Table 1) were obtained in good yields. The ^{1}H—NMR spectrum of compound IIIb showed four aromatic and one vinylic protons at 7.82—7.25 and aliphatic protons at 5.20 (s, 2H; N—CH_2—N), 3.00—2.55 (m, 4H, CH_2—N—CH_2), 1.56—1.20 (m, 6H, 3 CH_2—). The MS of compound IVb showed the molecular ion at m/e (rel. int. %) : 390 (32) ; the physical data of compounds III and IV are presented in Table 1 and Experimental part.

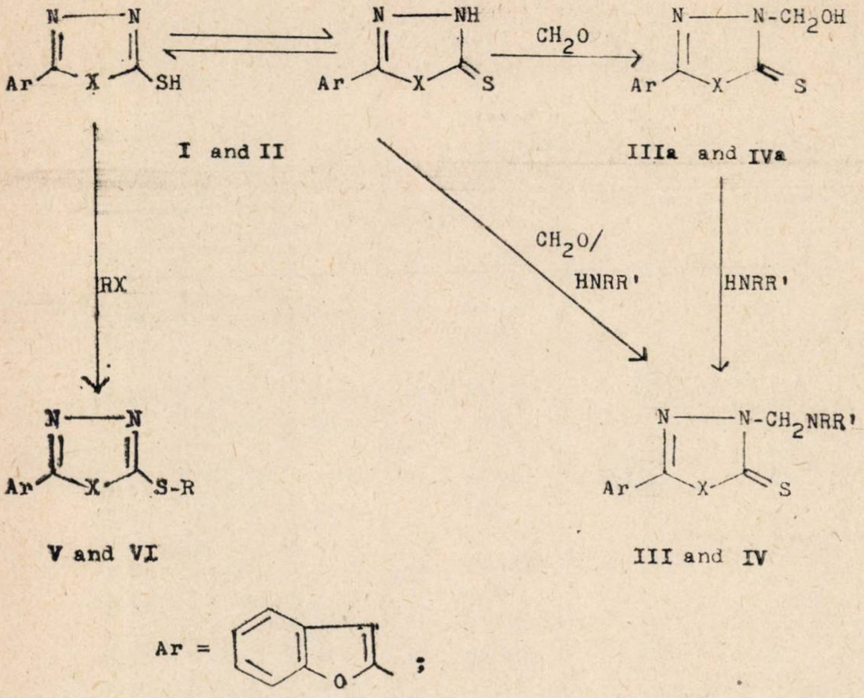

I, III, V, X= S ; II, IV, VI, X= N-phenyl

Scheme 1

Compounds I and II reacted with some halo compounds namely : methyl iodide, benzyl chloride, and 2,4-dinitro-chlorobenzene, in alkaline medium to give the corresponding sulphides (Va—c and VIa—c), respectively (cf. Table 2, Scheme 1). The ^{1}H—NMR spectra of compound Va showed three protons of the CH_3 group at 2.75, whereas MS of compound VIa showed the molecular ion at m/e (rel. int. %) : 307 (100).

The activity of the synthesized compounds was screened for their antifungal activity and most of them showed an inhibitory effect on the growth of pathogenic fungi (cf. Table 3).

EXPERIMENTAL

All melting points are uncorrected. IR spectra (cm^{-1}) were recorded on a Perkin Elmer 137 Spectrophotometer in KBr. ^{1}H–NMR spectra were recorded at 60 MHz on a Varian A–60 Spectrometer. The chemical shifts are expressed in δ values (ppm). DMSO was used as solvent. TMS was used as internal reference standard. The mass spectra were recorded on a CEC 21–104 single focusing mass spectrometer operating at 70 eV using direct inlet. Elemental analyses were done by Microanalytical Laboratory, Cairo University, Giza, Egypt. All compounds were checked for their purity on TLC plates.

Table 2

Physical data of compounds V and VI

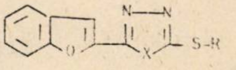

V, X = S

VI, X = N-Ph

Comp. No.	R	M.P. °C	Yield %	Found/Calc. % C	H	N
Va	-CH$_3$	185-86	80	53.45	3.41	11.20
		(E)		53.23	3.23	11.29
b	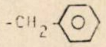	153-54	60	62.74	3.69	8.78
		(E)		62.96	3.70	8.64
c	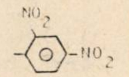	183-85	55	48.23	2.10	13.82
		(M)		48.00	2.00	14.00
VIa	-CH$_3$	178-79	85	66.40	4.43	13.55
		(E)		66.45	4.23	13.68
b	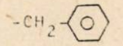	136-37	70	71.98	4.67	12.10
		(E)		72.06	4.44	10.97
c	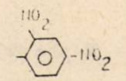	248-49	70	57.30	2.80	14.95
		(B)		57.52	2.83	15.25

E, ethanol; B, benzene ; M, methylene chloride.

2-(5-Mercapto-1,3,4-thiadiazol-2-yl)benzofuran (I)

It was prepared by the method of Young and Wood[17] in 35% yield, m.p. 210°C (ethanol/water). (Found: C, 51.35; H, 2.80; N, 12.10; S. 27.00%, $C_{10}H_6N_2OS_2$ requires: C, 51.28; H, 2.56; N, 11.97; S, 27.36%). MS m/e (rel. int. %): 234 (M$^+$, 100), 161 (14), 160 (15), 158 (70), 143 (49), 138 (7); 115 (23), 114 (7), 103 (23), 89 (14), 88 (9), 64 (30), 45 (15), IR: 3120 (NH), 1620 (C=N), 1590 (C=C), 1180 (C=S), 1025 (C–O–C).

2-(4-Phenyl-3-mercapto-1,2,4-triazol-5-yl)benzofuran (II)

See ref. 15.

Action of formaldehyde on compounds I and II

Formaldehyde (1.5 mL, 40% soln.) was added to the benzofuran derivative I or II (0.005 mole) dissolved in absolute ethanol (60 mL). The reaction mixture was refluxed for 4 hrs, concentrated, and cooled to yield the corresponding hydroxymethyl derivative IIIa or IVa, respectively (cf. Scheme I, Table 1).

Table 3

Antifungal activity of all synthesized compounds

Comp. No.	Pathogenic Fungi								
	1	2	3	4	5	6	7	8	9
I	++	++	++	+	-	-	+	-	++
II	+	++	++	+	+	+	+++	-	-
IIIa	+++	++	++	++	+++	++	++	++	++
b	++	++	++	+	++	++	++	++	++
c	++	++	+++	+	++	+	+	+	+
d	++	++	++	++	++	+	++	+	+++
e	+++	++	+++	++	++	+++	++	++	+
f	++	+++	+++	++	++	+	++	+	++
g	+++	++	++	++	+	++	+++	+++	++
IVa	+	-	-	++	+	-	-	-	-
b	++	-	-	-	-	-	-	-	-
c	++	+	-	+	-	++	-	++	-
d	++	++	-	-	-	++	++	++	-
e	+	++	+++	-	-	++	++	++	++
f	++	-	-	++	++	-	++	-	++
g	-	+	-	++	++	+	++	-	-
Va	-	++	+++	+	+	++	+	-	++
b	++	++	++	+	++	-	+	-	-
c	+++	++	++	++	++	+	++	++	+
VIa	+	-	-	++	++	-	++	-	+
b	+	-	++	+++	++	-	-	+	-
c	++	-	-	+++	-	-	+	-	+

1- Aspergillus flavus , 2- Microsporium canis.
3- Trichophytom rubrum , 4-Candida albicans.
5- Histophasma capsulatum, 6-Microsporium cookei
7- Microsporium gypseum, 8-Trichophyton violaceum
9- Geotrichum cordidum.

inhibition zone (mm):

No effect ; + weak ; ++ moderate ; +++ strong.

Mannich reaction with compounds I and II (general procedure)

Formaldehyde (1.5 mL, 40% soln) was added to the benzofuran derivative I or II (0.005 mole) dissolved in absolute ethanol (60 mL). The reaction mixture was refluxed for 4 hrs.; after cooling at room temperature, the appropriate primary or secondary amine (0.005 mole) was added and the reaction mixture stirred at room temperature for 6 hrs. The precipitate was filtered off and recrystallized from the appropriate solvent to give the Mannich bases IIIb–g and IVb–g (cf. Scheme 1, Table 1).

Compound IIIb: ^1H-NMR: 7.82–7.25 (m, 5H, aromatic and vinylic), 5.20 (s, 2H, $N-CH_2-N$), 3.00–2.55 (m, 4H, CH_2-N-CH_2), 1.56–1.20 (m, 6H, $3\,CH_2$), MS m/e (rel. int. %): 314 (M^+, –17, 30), 280 (13), 236 (40), 2.34 (100), 223 (32), 222 (20), 202 (45), 196 (20), 158 (67), 157 (81), 143 (43), 116 (19), 112 (13), 98 (25), 84 (29), 58 (14), 44 (31), 32 (30), 28 (72), 26 (27).

Compound IIIc: ^1H-NMR: 7.85–7.49 (m, 5H, aromatic and vinylic), 5.20 (s, 2H, $N-CH_2-N$), 3.50 (s, 4H, CH_2-O-CH_2), 2.65 (s, 4H, CH_2-N-CH_2). MS m/e (rel. int. %): 315 (M^+ –18, 8), 312 (58), 238 (27), 235 (42), 221 (18), 181 (8), 157 (14), 114 (11), 100 (100), 99 (17), 85 (9), 70 (10), 56 (26), 43 (8), 42 (10), 28 (34), 17 (15).

Compound IVb: MS m/e (rel. int. %); 390 (M^+, 32), 375 (29); 371 (29), 295 (41), 294 (100), 292 (77), 220 (71), 205 (30), 171 (23), 165 (30), 149 (56), 143 (100), 115 (52), 99 (77), 98 (91), 97 (100), 96 (80), 91 (34), 89 (43), 84 (61), 82 (43), 76 (43), 71 (37), 70 (64), 69 (80), 68 (63), 57 (100), 51 (88), 44 (95), 42 (85), 39 (43.)

Compound IVc: MS m/e (rel. int. %): 392 (M^+, 15), 294 (24), 293 (94), 292 (54), 234 (7), 220 (15), 171 (6), 158 (6), 149 (13), 144 (6), 143 (32), 118 (6), 115 (9), 103 (12), 101 (90), 100 (100), 99 (29), 98 (14), 89 (7), 77 (67), 70 (14), 56 (80), 51 (14), 42 (29), 28 (17).

Action of halo compounds on I and II

Compound I or II (0.005 mole) was dissolved in sodium hydroxide solution (50 mL), 10% and treated with halo compound (methyl iodide, benzyl chloride, or 2,4-dinitrochlorobenzene (0.005 mole), dissolved in ethanol (30 mL); the reaction mixture was refluxed for one hour. After cooling the precipitate was filtered off, washed with water and recrystallized from the appropriate solvent to give the sulphides Va–c and VIa–c, respectively (Scheme 1, Table 2).

Compound Va: ^1H-NMR: 7.88–7.45 (m, 5H, aromatic and vinylic), 2.75 (s, 3H, $S-CH_3$).

Compound Vb: ^1H-NMR: 7.92–7.10 (m, 10H, aromatic and vinylic), 4.52 (s, 2H, $S-CH_2-$phenyl). MS m/e (rel. int. %); 324 (M^+, 4), 241 (35), 239 (31), 220 (6), 179 (11), 160 (14), 148 (100), 132 (15), 131 (16), 99 (6), 92 (7), 91 (100), 90 (100), 64 (29), 63 (15), 45 (37), 39 (11).

Compound VIa: MS m/e rel. int. %); 307 (M^+, 100), 292 (55), 278 (64), 277 (64), 275 (55), 274 (32), 234 (36), 230 (34). 224 (23), 221 (36), 205 (35), 170 (32), 162 (54), 154 (64), 153 (36), 151 (36), 149 (80), 144 (100), 143 (100), 136 (30), 135 (100), 131 (54), 121 (23), 115 (100), 110 (36), 103 (100), 92 (100), 89 (72), 88 (64), 78 (54), 76 (84), 75 (50), 65 (94), 64 (32), 63 (56), 62 (30), 45 (64).

The IR compounds Va–c and VIa–c showed the absence of NH groups and characteristic bands at 680–690 (C–S–C); in the case of compounds Vc and VIc, the characteristic bands of NO_2 groups appeared at 1515–1520 and 1330–1380 cm^{-1}.

Fungicidal Activity

Petri dishes (9 cm), each having 10 mL, of suitable medium (Czapek's agar). Plates were inoculated each with 0.1 mL; suspension of one of tbe test organisms 7 mm. Filter paper discs were saturated with the tested compound (0.1% concentration) and transferred immediately to the surface of each plate. Each plate contained 4 discs. Plates were then incubated for 7 days at 30°C. Antifungal activity was expressed as zones of inhibition which were measured in millimeters.

In general, compounds having thiadiazole ring were found to show higher antifungal activity; on the other hand, compounds containing m-chloroanilinomethyl-group are more effective fungicides (cf. Table 3).

ACKNOWLEDGEMENT. The authors express their sincere thanks to Prof. A. Finch. Chemistry Department, Royal Holloway & Bedford New College, University of London and Dr. A. Senning, Institute of Chemistry, Aarhus University, Denmark for ^1H-NMR and MS. Also, to Dr. El-Sharouny, Botany Department, Faculty of Science, Sohag, Egypt, for fungicidal screening.

REFERENCES

[1] V. Etablissement, FR. DEMANDE 2, 356, 656, 1978 ; *Chem. Abstr.*, **1978,** 168587y.

[2] A. K. Sengupta and A. A. Gupta, *Indian J. Chem.*, **22B,** 263 (1983).

[3] L. Nuesslhin, E. A. Pieroch and K. Roeder, (Sohering A. G.) U.S. Pat. 4 061, 645 ; *Chem. Abstr.*, 1978, 62397k.

[4] J. Wagner, J. Kamecki and S. Leistner, *Pharmazie*, **30,** 804 (1975).

[5] S. S. Tiwari, A. K. Sengupta and J. Kumar, *Indian J. Pharm.*, **32,** 91 (1970).

[6] G. Laurenz and M. Willy, Ger. Offen, 2, 739, 084 (1977) ; V.A., 1978, 190844r.

[7] C. Metzger, L. Eue and R. R. Schmidt, (Bayer A.G.) Ger. Offen., 2, 411, 288, 1975 ; C.A., 1975, 17867g.

[8] J. Lang and H. Tondys, *Pol. Pharmacol. Pharm.*, **27,** 211 (1975) ; *Chem. Abstr.*, **197** , 17236p

[9] K. M. Basavaraja and Y. S. Agasimundin, *Indian J. Chem.*, **22B,** 458 (1983).

[10] J. H. Musser, R. E. Brown, B. Loev, K. Bailey H. Jones, R. Kahen, F.-C. Huang, A. Khandwala, M. Leibowitz, P. Sonnino-Goldman and D. Donigi-Ruzza, *J. Med. Chem.*, **27,** 121 (1984).

[11] F. M. E. Abdel-Megeid, M. A. F. El-Kaschef and A. A. G. Ghattas, *Egypt. J. Chem.*, **20,** 235 (1977).

[12] M. A. Salama, F. M. A. Moti, A. A. G. Ghattas and A. Abdullah, *Egypt. J. Chem.*, **24,** 47 (1981).

[13] A. E. Abdel-Rahman, A. M. Mahmoud, H. A. El-Sherief and A. A. G. Ghattas, *Rev. Roumaine Chim.*, **27,** 781 (1982).

[14] A.-B. A. G. Ghattas, M. T. El-Wassimy, M. Abdel-Rahman, and G. El-Saraf, *Sulfur Lett.*, **XXX** (1987).

[15] A.-B. A. G. Ghattas, M. Abdel-Rahman, M. T. El-Wassimy, and G. El-Saraf, *Sulfur Lett.*, Submitted.

[16] S. Kakimoto, I. Sekikawa, J. Nishie, *Chem. Soc., Japan Pure Chem. Sect.*, **74,** 636 (1953) ; *Chem. Abstr.*, **1954,** 12071.

[17] R. W. Young and K. H. Wood, *J. Am. Chem. Soc.*, **77** 400, (1955).

Revue Roumaine de Chimie, 34, *9–10*, 1995–2006 (1989)

CONSIDERATIONS ON THE SYNTHESIS AND PROPERTIES OF USUAL SURFACTANT-FREE ACRYLIC DISPERSIONS*

N. MOGA, OCTAVIA CUCU, ALINA PĂNESCU and MARIANA POPESCU
Anticorrosive Protections, Paints and Varnishes Research Centre,
Bucharest, Blvd. Chimiştilor 309, Romania

Received February 8, 1988

This paper reports on the synthesis and some properties of an acrylic dispersion which contains copolymerisable active surface agents. The effect of the peculiar monomer ratio, the variation of the chain transfer agent and initiator ratio and the variation of addition time of the copolymerisable active surface agent, on the stability and water resistance of the dispersion, were studied.

INTRODUCTION

The advantages of using aqueous dispersion copolymers for different purposes are already well-known : the half or entire elimination of solvents, the diminution of environment pollution, the elimination of fire risk, etc.

By all means, such aqueous dispersion copolymers exhibit, comparatively with solution copolymers, a few disadvantages too : water sensitivity, which confines the field of application, and a lower time stability.

Lately, numerous research works [1–8] were accomplished in order to obtain surfactant-free dispersions, having various destinations.

In general, the aqueous dispersion copolymerization systems involve one or more emulsifying agents as one of the components. The emulsifying agent, consisting of a long chain molecule having both a hydrophilic and a hydrophobic portion, functions initially to disperse the monomer and to form micelles in which polymerisation will be initiated. Subsequently, once the polymer particle formed, it is protected from coagulation by a layer of adsorbed emulsifying agent on its surface, which forms an electrostatically charged double coat.

In this case, the emulsifying agent takes, chemically speaking, no part in the copolymerization process.

Literature data show that many works were accomplished in order to synthesize various chemical structures bearing chemical bonds capable of copolymerization and chemical groups capable of granting stability to the polymer chain already formed.

---

* Paper presented at Symposium on Chemistry of Colloids and Surface, Cluj-Napoca, Septembre, 8–10, 1986.

Examples of such structures, resulting from literature data, used in aqueous dispersion copolymer synthesis, are :

I.

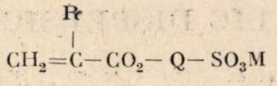

$$\overset{R}{\overset{|}{CH_2=C}}-CO_2-Q-SO_3M$$

where : R = hydrogen, halogen atom, or organic radical ;
Q = bivalent organic radical, the two valences being placed on two different carbon atoms (alkylene, for example) ;
M = hydrogen, ammonium, or metallic atom.

II.

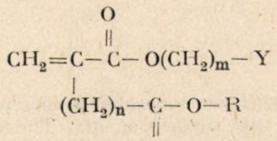

$$CH_2=\underset{\underset{(CH_2)_n-\underset{\underset{O}{\|}}{C}-O-R}{|}}{C}-\overset{\overset{O}{\|}}{C}-O(CH_2)_m-Y$$

where : m = whole number between 2 and 4 ;
n = whole number between 1 and 2 ;
R = alkyl radical containing 1—22 carbon atoms.

III.

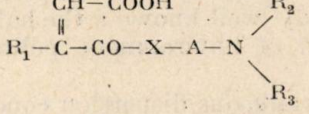

$$R_1-\overset{\overset{CH-COOH}{\|}}{C}-CO-X-A-N\begin{matrix}\diagup R_2\\ \diagdown R_3\end{matrix}$$

IV.

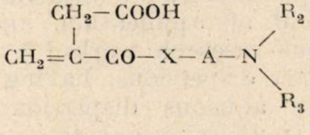

$$CH_2=\overset{\overset{CH_2-COOH}{|}}{C}-CO-X-A-N\begin{matrix}\diagup R_2\\ \diagdown R_3\end{matrix}$$

where : R_1 = hydrogen or methyl ;
X = oxygen or NH ;
A = alkylene group containing 2—12 carbon atoms ;
R_2, R_3 = hydrogen atoms or alkyl groups containing no more than 4 carbon atoms.

V.

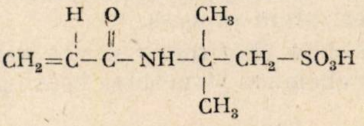

$$CH_2=\overset{\overset{H}{|}}{C}-\overset{\overset{O}{\|}}{C}-NH-\overset{\overset{CH_3}{|}}{\underset{\underset{CH_3}{|}}{C}}-CH_2-SO_3H$$

2-acrylamido-2-methylpropane-1 sulphonic acid.

This structure was accomplished by using the Ritter synthesis:

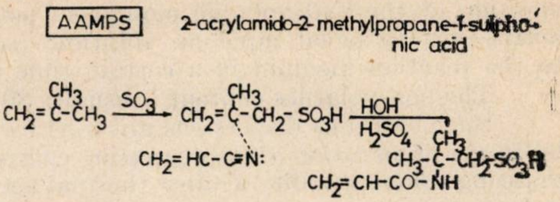

Fig. 1. — Ritter's synthesis of 2-acrylamido-2-methylpropane-1-sulphonic acid.

By using such structures in the aqueous dispersion polymerization process, they do take part in the copolymerization with other monomers.

Stabilization against particles coagulation or deposition is accomplished by means of the hydrophilic groups bound to the polymer chain during the polymerization process.

Hydrophilic groups introduced in the polymer chain may be anionic, cationic or nonionic.

— anionic groups: carboxylate, sulphate, sulphonate, phosphate;

— cationic groups: quaternary ammonium, $-\overset{+}{N}R_3$, phosphonium, $\overset{+}{P}R_3$, etc.

— nonionic groups: hydroxyl $-OH$, amine, $-NR_3$.

Such electrically charged hydrophilic groups, by which stabilization is accomplished, can be introduced into the polymer chain by using other methods too. A similar effect can be accomplished by using a radical initiator ratio greater than that stoichiometrically necessary in the copolymerization process.

Suitable initiating agents release hydratable radicals hydroxyl groups $-OH$ for example, and these attach themselves at the bottom of the polymer chain, stabilizing in this manner the polymer particles.

Another method for introducing hydrophilic groups in the polymer chain is that using monomers containing hydrophilic groups: $-NH_2$, $-COOH$, $-OH$, for example (hydroxypropyl methacrylate dimetyl — aminoethyl methacrylate, acrylic acid, methacrylic acid).

Any initiating agent capable of releasing hydratable on electrically charged stabilizing groups may be used in order to obtain an initiation--stabilizing effects combination.

Ammonium or alkali metal persulphates may release hydratable $-OH$ groups, these themselves being capable of stabilizing the polymer chain.

In combination with initiators, water — soluble reducing agents such as: thiocarbamide, thiosulphates, bisulphites, may be used for the same purpose.

Chain transfer agents like: thioglycolic acid or mercapto-ethanol can also supply bottom hydratable groups on the polymer chain.

Therefore a usual surfactant — free copolymerization system may comprise: hydrophobic monomers, copolymerisable active surface agents, capable of functioning simultaneously as monomers and stabilizing agents, an initiator that initiates the polymerization and supplies hydrophilic groups in order to increase system stability, a chain transfer agent, and the reaction medium, water.

Experimentally, the process for preparing an aqueous dispersion copolymer, by using copolymerisable active surface agents involves the addition of the hydrophobic monomers portion and the copolymerisable active surface agent aqueous solution (separately but simultaneously) to the reaction medium in a certain time and a certain temperature.

The non-volatiles content is usually 30—40 per cent.

Such aqueous dispersions are used for various purposes in the textiles in the preparation of impregnating compositions, in the paper industry, granting colour stability against thermal agents, [3] in paints and varnishes industry [6].

EXPERIMENTAL

The purpose of this work was to synthesize an aqueous dispersion acrylic copolymer by using a copolymerisable active surface agent and to study the variation of the stability and water resistance (as whitening of the film when coming into contact with water) depending on the copolymerisable active surface agent ratio, the intiator and chain transfer agent ratio and the addition time of the copolymerisable active surface agent.

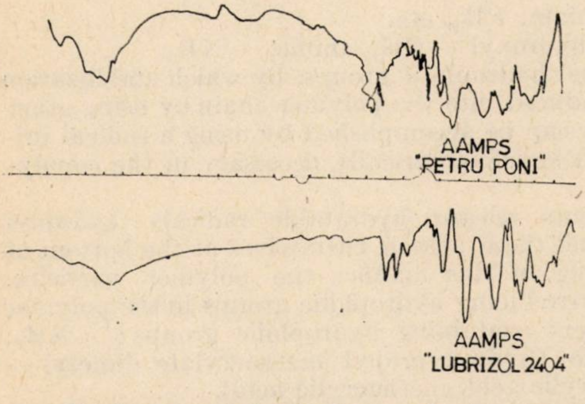

Fig. 2. — I.R. spectra of native and foreign AAMPS.

The 2-acrylamido-2-methylpropane-1-sulphonic acid was used as copolymerisable active surface agent; the reagent was supplied by "Petru Poni" Institute, Iași and "Lubrizol" Company — USA.

Fig. 3. — Copolymer chain possible sequence.

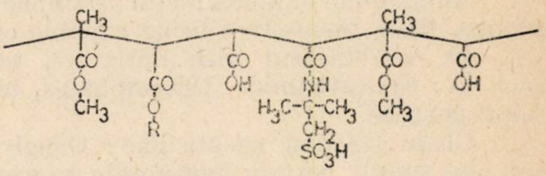

A monomeric mixture consisting of: methyl methacrylate (MMA)., an acrylic acid ester (Ax), acrylic acid (AAc), N-methylolacrylamide (N-methylol AA) and 2-acrylamido-2-methylpropane-1-sulphonic acid (AAMPS) was used, the monomer ratios being varied as follows:

— methyl methacrylate (MMA) between 31 and 40% by weight of the total monomer mixture, and correspondingly the AAMPS ratio was varied between 0 and 9% by weight;

— the acrylic acid ester (Ax) between 50 and 59% by weight of the total monomer mixture, and correspondingly the AAMPS ratio was varied between 0 and 9% by weight;

— the acrylic acid (AAc) and N-methylolacrylamide(N-methylol-AA) remained constant, and the sum of all monomers ratios, including AAMPS, was always 100%.

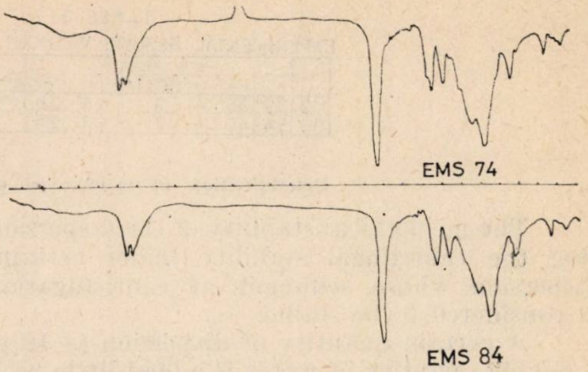

Fig. 4. — I.R. spectra of the copolymer obtained by using native AAMPS (EMS 74) and foreign AAMPS (EMS 84)

The variation of centrifugal stability (a measure for time stability of the aqueous dispersion copolymer), and the variation of whitening of the film when coming into contact with water (a measure for water resistance of the films) were studied depeding on these parameters.

TABLE 1

EXPERIMENTAL RESULTS WITH NATIVE AAMPS

CHARGE	CHARGE COMPOSITION AND AAMPS ADDITION TIME								ANALYSIS		
	AX	MMA	AAc	AAMPS	Methylol AA	DDM	PP	Addition time	APPEARANCE	Sediment	Whitening
67	56	35	4	3	2	-	1	2h	milky-white		15.9
69	50	35	4	9	2	-	1	2h	"		27.1
70	54	37	4	3	2	-	1	2h	"		-
71	54	33	4	7	2	-	1	2h	"	3.1	21.2
72	54	31	4	9	2	-	1	2h	"	3.9	22.3
73	52	35	4	7	2	-	1	2h	white		28
74	54	35	4	5	2	-	1	2h	white-bluish	0.45	7.8
75	54	35	4	5	2	1	1	2h	milky-white	5.45	-
76	54	35	4	5	2	2	1	2h	"	4.25	-
77	54	35	4	5	2	-	0.75	2h	"	0	-
78	54	35	4	5	2	-	1.25	2h	"	1.9	-
79	54	35	4	5	2	-	1	1h	"	0.5	-
80	54	35	4	5	2	-	1	1.5h	white	0	-
81	54	35	4	5	2	-	1	25h	milky-white	6.2	-

AX=acrylic ester; MMA=methyl methacrylate; AAc=acrylic acid; AAMPS=2-acrylamido-2-methylpropane-1-sulphonic acid; Methylol AA=N-methylol-acrylamide; DDM=t-dodecylemercaptane; PP=potassium persulphate

Other parameters that varied considering a standard charge (from the standpoint of monomeric composition) were: the chain transfer agent (t-dodecylmercaptane), the initiator (potassium persulphate), and the addition time of the copolymerisable active surface agent to the reaction mass.

TABLE 2

XPERIMENTAL RESULTS WITH AAMPS LUBRIZOL 2404

CHARGE	CHARGE COMPOSITION AND AAMPS ADDITION TIME								ANALYSIS		
	AX	MMA	AAc	AAMPS	Methylol AA	DDM	PP	Addition time	APPEARANCE	Sediment	Whitening
83	56	35	4	3	2	-	1	2h	milky-white	2	20.6
84	54	35	4	5	2	-	1	2h	white-bluish	0.03	19
85	52	35	4	7	2	-	1	2h	milky-white	9.5	33.4
86	50	35	4	9	2	-	1	2h	"	–	Gel
87	54	37	4	3	2	-	1	2h	"	0.8	44.7
88	54	33	4	7	2	-	1	2h	"	1	29.9
89	54	31	4	9	2	–	1	2h	"	1.3	Gel
90	54	35	4	5	2	1	1	2h	"	1.4	–
91	54	35	4	5	2	2	1	2h	"	3.6	–
92	54	35	4	5	2	–	1.25	2h	"	1	–
93	54	35	4	5	2	-	0.75	2h	"	0.2	–
95	54	35	4	5	2	–	1	15h	"	0.5	–
96	54	35	4	5	2	–	1	1h	"	9.3	–
97	54	35	4	5	2	--	1	2h	"	9.2	–

Further on, the description of the methods used for determination of mechanical stability and the withening of the film when coming into contact with water are given.

TABLE 3

EXPERIMENTAL RESULTS WITHOUT AAMPS

CHARGE	CHARGE COMPOSITION							ANALYSIS	
	AX	MMA	AAc	Methylol AA	DDM	PP	Addition time	APPEARANCE	Sediment
112	59	35	4	2	-	1	2h	milky-white	27.8
113	54	40	4	2	-	1	2h	"	47.2

Determination of mechanical stability

The mechanical stability of the dispersion was determined by measuring the centrifugal stability under certain conditions. Any aqueous dispersion whose sediment at centrifugation does not exceed 10%, is considered to be stable.

A certain quantity of dispersion (~12 g) is weighed in a glass and a double quantity of water is added little by little, with good agitation.

From this diluted and well homogenized dispersion a 15 g quantity is weighed in centrifugation ampoules (always two parallel tests).

The ampoules containing the dispersion are subjected to centrifugation at 3500 rotations/minute, for 30 minutes (the work instructions for the 10 000 rotations/minute centrifuge are observed).

After centrifugation time, the separated liquid is decanted and the surface of the nut is lightly washed with distilled water, thus eliminating the intermediary layer. The ampoule is then dried with a dry rag.

The dried ampoule containing the sediment nut is weighed and A grams are obtained.

After removing the sediment nut, the empty ampoule is weighed and B grams are obtained. The deposited sediment percent is related to the emulsion quantity in the diluted sample subjected to centrifuation (C grams, this quantity being approx. 5 g).

$$\%\ \text{Deposited sediment} = \frac{A-B}{C} \cdot 100$$

The given result is the average between the two parallel tests (the difference must not exceed 0.5 g deposited sediment).

Determination of water resistance (CCPALV method)

This method is based on the total re-emission of the lights radiations transmitted by the acrylic film that whitens when coming into contact with water.

This re-emission is measured by using a galvanometer that records the variations of the electric current of a photoelectric cell. This value percent is related to the corresponding value of the light re-emission of a white porcelain plate considered as standard.

The apparatus used for the determination involves :

— "Multiflex" galvanometer endowed with :

a) light source ;

b) regulation device of the light spot on the scale ;

c) graduated scale;

d) measuring range: sensibility 0.1/100; 1/10; 1/1.

— "Dr. Lange" device for measuring the glitter; its photoelectric cell is set at 45° against the light source in order to record the re-emission, not the reflexion of the light radiations on the film surface;

— galvanometer whose transformer supplies the light source;

— current stabilizer;

— obscure chamber (a 20 × 20 × 40 cm box lined with black paper);

— quartz tank (10 × 5 × 5 mm).

The determination is achieved as follows:

1. The electric contacts of the apparatus are connected by using the corresponding terminals.

2. The "nul" position of the indicator on the sensibility scale is then checked up.

3. The quartz tank is filled with distilled water and the glass plate with the film is placed above; it is very important for the contact between the water surface and the film to be perfect and free from air-bubbles.

The tank is then placed in the obscure chamber and the "Dr. Lange' device is placed on the glass plate. After a certain time period (1 or 2 hours), the value of the light re-emission is read on the scale.

The comutator of the "Multiflex" galvanometer is changed in the desired sensibility range and the alimentation comutator of "Dr. Lange" device's galvanometer is opened. After about 5 minutes, the value may be read on the "Multiflex" galvanometer scale. Immediately, the "Dr Lange" device is placed on the standard plate and the value of the respective light re-emission is registered.

The comutator is then changed on the "nul" position of the sensibility scale and the main supply is interrupted.

4. The same operations sequence is resumed in order to measure the light re-emission of the respective glass plate after film removal, concomitently with the measuring of the standard plate light re-emission value.

5. The electric contacts of the apparatus are disconnected.

The percent whithening of the film when coming into contact with water is expressed in relation with the standard white, as follows:

$$\%\ \text{whitening across the standard white} = \left(\frac{a}{c_a} - \frac{b}{c_b}\right) \cdot 100$$

where:

a = the value of the reading that corresponds to the film

b = the value of the reading that corresponds to the glass plate

c_a = the value of the reading that corresponds to the standard plate

c_b = the same for b value

Effect of AAMPS ratio on the variation of centrifugal stability

The lowest values of the centrifugation sediment for both AAMPS series were achieved for 5% ratio.

These values grow both with the diminution and the increase of this ratio.

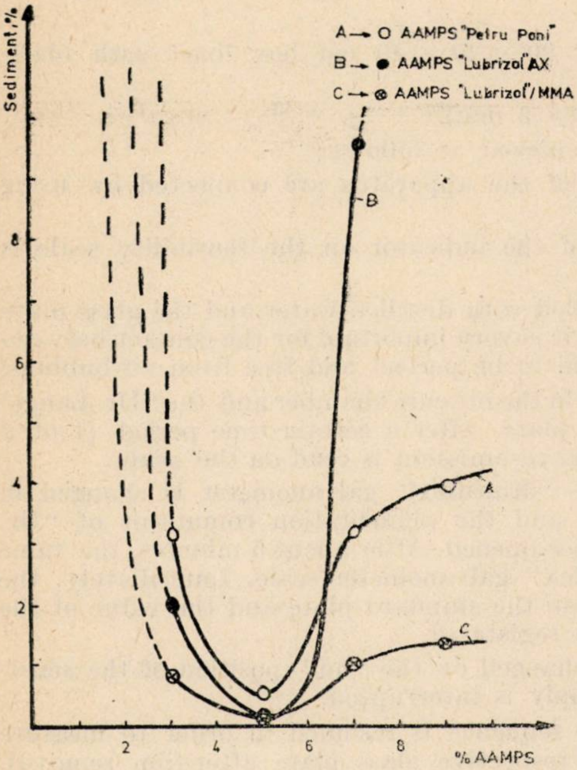

Fig. 5. — Effect of AAMPS ratio upon the centrifugal mechanichal stability of the dispersion.

In the case of the native AAMPS a total instability for a value of less 3% ratio is to be noticed, whereas in the case of the foreign AAMPS, the same instability is to be noticed even at values less than 4% ratios.

When native AAMPS is used, an acceptable stability is to be noticed even at a 9% ratio.

In the case of "Lubrizol" AAMPS, the sediment values grow very much at a 7% ratio against the AX ester ratio; at a 9% ratio against MMA ratio, in spite of the good sediment values achieved, gelatination occurs after a 10 days period.

Effect of AAMPS ratio on whitening when coming into contact with water

The best values for these parameters occur, with no difference between the two AAMPS series, at a 5% ratio. It is to be underlined that the best values were achieved for the native product.

For more than a 3% native AAMPS ratio, the values are better until a 5% ratio.

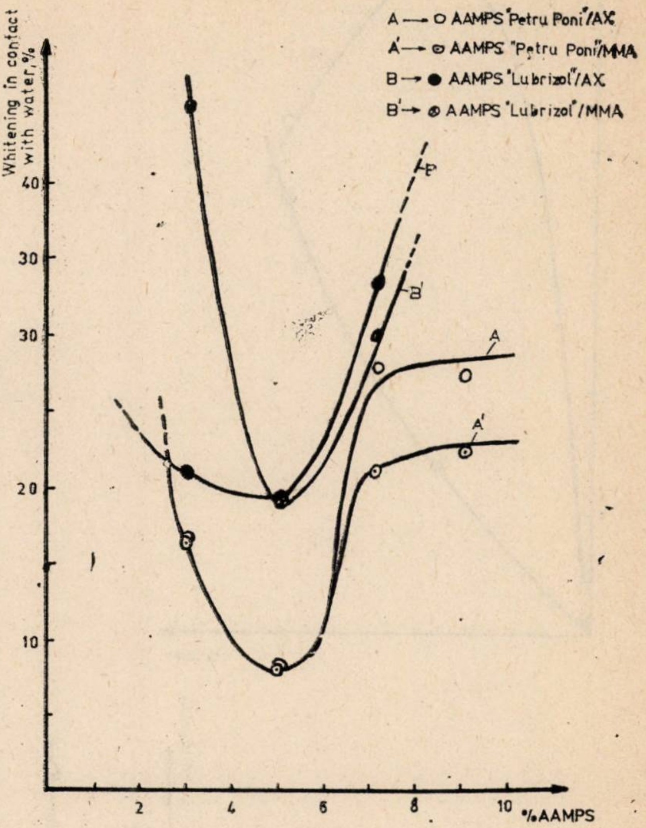

Fig. 6. — Effect of AAMPS ratio upon the whitening of the film in contact with water.

Effect of chain transfer agent ratio on the centrifugal stability

The introduction of a chain transfer agent (*t*-dodecylmercaptane) leads to the worsening of the dispersion stability with no difference for both AAMPS series. Especially for the native product, the instability is higher at a 1% AAMPS ratio.

Effect of initiator ratio on the centrifugal stability

The initiator ratio was varied between 0.75 and 1.25% based on the monomeric blend.

The best stabilities were achieved with an initiator ratio between 0.75 and 1% for both, native and foreign AAMPS series. The instabilities increase very much beginning with a 1.25% initiator ratio based on the monomeric blend, in case of "Lubrizol" AAMPS and with a 1% initiator ratio based on the monomeric blend in case of native AAMPS.

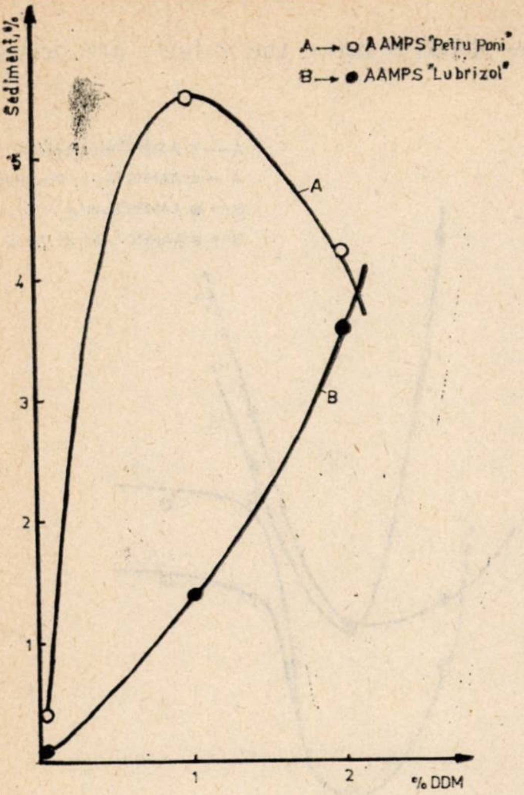

Fig. 7. — Effect of chain transfer agent ratio upon the centrifugal stability of the dispersion.

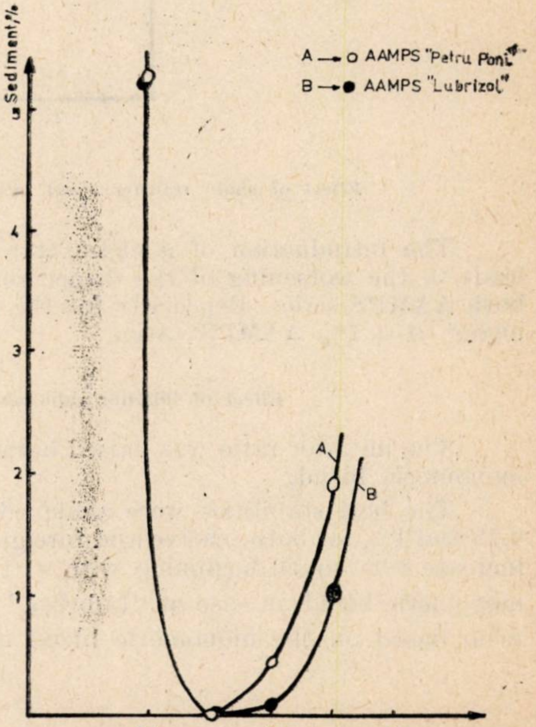

Fig. 8. — Effect of initiator ratio upon the centrifugal mechanical stability of the dispersion.

Effect of the AAMPS alimentation time on the centrifugal stability

The AAMPS addition time varied between 1 and 2.5 hours; the dispersion that exhibited the lowest centrifugation sediment was achieved at an addition time between 1.5 and 2 hours. The instability tendency outside this range is more noticeable in the case of the foreign product.

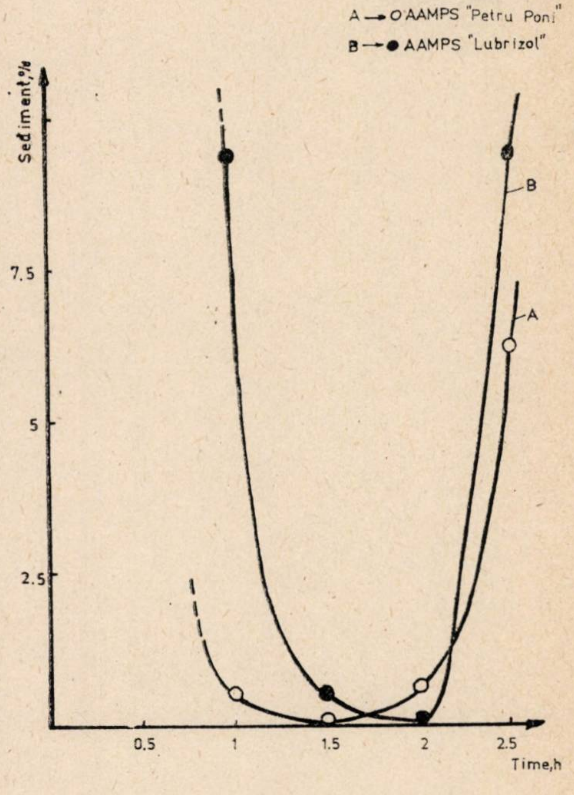

Fig. 9. —Effect of AAMPS addition time upon the centrifugal mechanical stability of the dispersion.

CONCLUSIONS

It appears that hydrophilic groups are uniformly distributed along the polymer chain, in the case of an addition time between 1.5 and 2 hours.

By using a monomeric blend of 54/35/5/4/2/Ax/MMA/AAMPS//AAc/Methylol — AA/, a 0.75 — 1% potassium persulphate, based on the monomeric blend, and an addition time of 1.5—2 hours, a uniform repartition of the hydrophilic groups along the polymer chain, and therefore a better mechanical stability and water resistance, is achieved.

REFERENCES

[1] Fr. Pat. 1.563.269.
[2] US Pat. 3.501.432.
[3] Brit. Pat. 1.470.528.
[4] US Pat. 3.795.648.
[5] US Pat. 3.541.138.
[6] A. Paterkofsky and J. Paul, *Pitture e vernici*, **52**, (8), 289 (1976).
[7] US Pat. 3.308.081.
[8] SRR Pat. 90.605.

Revue Roumaine de Chimie, 34, *9–10*, 2007–2009 (1989)

COMPTES RENDUS

C. Jochum, M. G. Hicks and J. Sunkel (editors), "Physical Property Prediction in Organic Chemistry", Proceedings of the Beilstein Workshop, 16–20 May 1988, Schloss Korb (Italy), Springer-Verlag, Berlin, 1988, 554 pages, hard cover, DM 148. ISBN-3-540-50367-6.

The book is a collection of 33 papers reproduced directly from authors' manuscripts, plus an author index, an introduction, and a review-epilogue.

An international group of scientists met in Northern Italy, close to Bolzano, in a workshop sponsored by the Bundesministerium für Forschung und Technologie (BMFT) and organized by the Beilstein Institute in Frankfurt-am-Main. As outlined by the first contribution (J. M. Czermak from the BMFT), the Chemical Abstracts Service databases concentrate on bibliographic information, while the Federal Republic of Germany specializes in data and factual information. The Beilstein and Gmelin Institutes will soon be computerized and their handbooks will be published in English. The Beilstein ONLINE database will become accessible to the public but it will be fully implemented after 8—10 years.

The next two contributors deploy their activity in the Beilstein Institute : Clemens Jochum who reports on data estimation for the Beilstein Information System ; L. Domokos, whose paper is entitled "Data about data". In both papers it is emphasized that Beilstein owns the world's largest collection of factual data of organic chemistry. Both authors address the dilemma whether to include only the measured data, or also calculated data which are more extensive but apparently less reliable.

S. R. Heller discusses the process of estimating properties of chemicals by means of programs such as PCGEMS or CHEMEST. A. Barth (from the Fachinformationszentrum Karlsruhe which has started the numerical database for heterocyclics on the STN International network) refers to numerical features of the Beilstein database.

— N. Marsh and R. C. Wilhoit from the Thermodynamics Research Center of the Texas A&M University present the five continuing TRC projects for the collection of thermodynamic properties of organic and non-metallic inorganic compounds. The European counterpart is presented in two papers by J. Gmehling who developed the Dortmund Data Bank ; his communications deal with thermodynamic properties of mixtures, and these properties have been analyzed by means of computer programs based upon excess Gibbs energies in therms of group contributions. Other papers using group contribution methods are by authors of Air Products and Chemicals, Inc., USA ; Linde A. G., F. R. Germany ; University of Sussex, England ; and University of Kansas, USA. Mixture properties are also discussed by Czechoslovak authors who developed the Data Bank of the Prague Institute of Chemical Technology.

Biological activities are discussed by G.W.A. Milne and L. Hodes from the National Cancer Institute in Bethesda, Maryland, USA, whereas environmental problems are addressed by R. Brüggemann and B. Münzer (München, F. R. Germany) and A. Sabljić (Zagreb, Yugoslavia) ; the latter author used topological indices for modelling soil sorption, bioconcentration and acute toxicity. For ecological problems, only the vapor pressures at ambient temperatures are significant, therefore empirical equations proposed earlier by Mackay and by Fromherz were tested by the former authors.

J. Gasteiger discusses side-products of the EROS (Elaboration of Reactions for Organic Synthesis) program system for the calculation of energetic and electronic effects. Moleculra orbital and force-field calculations are reviewed by T. Clark.

P. C. Jurs and coworkers make predictions of physico-chemical properties based on structure-property relationships (SPR) using geometric indices called shadow areas for shape analysis. For boiling points of 123 olefins with 2—10 carbon atoms, taken from the TRC Thermodynamic Tables (1986) an 8-parameter equation including molecular-topological parameters gives a correlation factor of 0.999.

P. Jochum discusses numerical interpolation methods by means of various mathematical functions, in particular splines. Fuzzy search methods constitute the topic of the paper by M. Otto and H. Bandemer from GDR. Japanese authors (S. Sasaki, Y. Takahashi and K. Funatsu) present a total system of molecular design based on various computer programs for organic synthesis (AIPHOS), structure elucidation (CHEMICS), and bioactive structure prediction (TUTORS).

P. Willett from the University of Sheffield describes structural similarity used to rank chemical structures in databases.

In his closing remarks, Dr. M. G. Hicks from the Beilstein Institute summarized the conclusions of the meeting which will probably have other follow-up workshops. The enormous task of the Beilstein Institute requires careful consideration of al alternatives, and such workshops do just that.

A. T. Balaban
Polytechnic Institute, Bucharest

B. P. Mundy and M. G. Ellerd, "Name Reactions and Reagents in Organic Synthesis", Wiley, Chichester, 1988. 546 pp., hard cover, £ 27.05.ISBN 0-471-83626-5.

This large-format book belongs to the laboratory shelf, along with *Organic Syntheses*, Fiesers' *Reagents for Organic Synthesis*, and March's *Advanced Organic Chemistry* (note that all these are Wiley books). It provides a quick entry for everyday tasks into the literature (including the above books) and gives many useful hints for the practising organic chemist.

There are two main sections with approximately equal lengths; the first is on Name Reactions, and the second is on Reagents for Organic Synthesis. Both are meant for quick and easy reference in that they consist of two facing pages for each entry. At a glance, for each named reaction (or generically-indicated reaction such as aldol reaction), one can see: the relevant page(s) in March's book (3rd edition, 1984), the general scheme (formulas), the reaction mechanism, with a few notes where necessary, and then in easily followed formulas 4—5 examples with the corresponding references (mostly recent papers, but sometimes also reviews or preparations from *Organic Syntheses*). Thus are listed 117 reactions. They are completed with additional 46 reactions on 11 pages where only the general scheme is provided.

The second section of the book is devoted to most commonly-used reagents (organic and inorganic) in synthetic organic chemistry. Again, two facing pages are reserved for each entry. After the name, follow: the formula with physical constants, the references to the 12 volumes of the Fiesers' book and to March's book, then the major uses (one to six), a few hints on preparation, notes on precaution in handling, and then examples (again expressed by structural formulas with relevant references and notes where necessary). Thus, 145 reagents are indicated.

A major advantage of both parts of the book is its orientation towards modern reactions, such as McMurry olefin synthesis, Ramberg—Backlund reaction, Corey-Sharpless oxidation, etc. (in the named reaction section), as well as (in the reagents section); Wilkinson's catalyst, tosyl azide, phase transfer catalysts, diphenylphosphoryl azide, diphenyl diselenide, dimethylsulfonium methylide, dimethyloxosulfonium methylide, 9-borabicyclo[3.3.1]nonane, 1,5-diazabicyclo[4.3.0]-nonene, 1,4-diazabicyclo[2.2.2]octane, diimide, chlorosulfonyl isocyanate, etc.

The book emerged from students' lecture notes, out of cards prepared for a short random quiz at the end of each lecture; professor Mundy and graduate student Ellerd are to be praised for having produced a very useful book for day-to-day laboratory practice in organic chemical laboratories.

A. T. Balaban
Polytechnic Institute Bucharest

"George de Hevesy (1885—1966) Festschrift", Akadémiai Kiadó, Budapest, 1988, 165 p.

The book contains lectures about the interdisciplinary application of nuclear methods, held in Budapest at the centenary celebration of the birth of George de Hevesy.

Two chapters of the book (by G. Marx and G. Pallo) present some biographical data of George de Hevesy, born in 1885 in Budapest, dead in 1966 in Freiburg: coworker of E. Rutherford, friend of N. Bohr, discoverer in 1922 of the element 72, Hafnium (with D. Coster) using X-ray spectroscopic methods, discoverer in 1913 of the radioactive tracing (with F. Paneth), winner of Nobel Prize in chemistry in 1943 "for his work on isotopes as indicators in studying chemical processes", inventor of neutron activation analysis (with Hilde Levy), distinguished with the Atom for Peace Award, in 1958, for his "discovery and development of tracer technique in chemistry, biology and medicine".

The chapter entitled "The era of cosmochemistry and geochemistry, 1922—1935" (by G. Arrhenius and Hilde Levi) details some scientific research of Hevesy in this domain e.g.: the abundance and distribution of elements (including a detailed history of discovery of hafnium), age of the earth and the solar system, radioactive rare earth elements as tracers of planetary processes.

R.L. Mössbauer presents some interesting "Historical remarks on the gamma resonance method" detailing the story of demonstration of the existence of the recoilless transitions of gamma radiations in crystals.

V. I. Goldanskii's contribution "Advanced Mössbauer spectroscopy, kinetical and dynamical studies", discusses the utility of Mössbauer absorption spectroscopy and of Rayleigh scattering of Mössbauer radiation — methods which make possible remarkable developments of the studies of structural and dynamical properties of biopolymers (e.g. proteins) in wide ranges of temperatures, hydration degrees etc.

In the chapter "Neutral spin echo", F. Mezei discusses the principles, the apparatus and applications of the title method underlining its utility in studies of dynamics of biopolymers, of atomic and molecular diffusion etc.

K. Siegbahn presents a detailed interesting and accessible survey on "Electron spectroscopy for chemical analysis" (ESCA) including modern instrumentation and various applications in inorganic and organic chemistry.

The complete Hevesy bibliography (397 works) ends this interesting book.

Mircea Banciu
Polytehnic Institute, Bucharest

NOTE POUR LES AUTEURS

La Revue Roumaine de Chimie publie des articles en anglais, français, russe, allemand ou espagnol. Les auteurs sont priés d'envoyer des articles et des comptes rendus inédits.

Les manuscrits seront dactylographiés à double interligne. La bibliographie, les tableaux et la légende des figures seront placés après le texte.

Si l'article fait partie d'une série numérotée, la partie précédente sera donnée comme première référence.

Chaque article précédé d'un résumé comprenant quinze lignes au maximum.

Les références bibliographiques dans le texte seront faites par des exposants sans parenthèses et paraîtront à la fin de l'ouvrage.

Les publications périodiques mentionnées dans la bibliographie seront présentées suivant les prescriptions internationales : le nom de l'auteur précédé de l'initiale du prénom, le titre du périodique abrégé conformément à « Chemical Abstracts » et souligné par une ligne, le numéro du tome indiqué par des chiffres arabes et souligné par deux lignes, suivi de la première page de l'article : à la fin, l'année de la parution sera placée entre parenthèses. Le numéro de la revue ne sera pas indiqué si les pages du volume sont numérotées consécutivement.

Les textes des livres ou traités inclueront : le nom des auteurs, précédés de l'initiale du prénom, le titre du livre entre guillemets et sans être souligné, le numéro du tome précédé par l'abréviation « vol. » (ou « Bd. »), le numéro de l'édition, les éditions (the publisher), la localité de la parution du livre, l'année de la parution et la page de la référence précédées(s) par l'abréviation « p » (ou « S »).

Les brevets seront indiqués comme suit : l'auteur ou la firme, le pays et le numéro du brevet, la date de la revue *(Chem.Abstr.)*. Par. ex. : M. Jones (to Union Carbide Co.), Brit. Pat. 610 238, 2 Sept. 1959 : cf. *Chem. Abstr.*, **54**, 12808 (1960).

Si la référence n'a pas été lue en original, on indiquera aussi la revue de références consultée.

Les diagrammes seront tracés à l'encre de Chine sur papier calque. Les tableaux et les figures (en nombre strictement nécessaire), ainsi que les courbes dans les figures seront numérotés par des chiffres arabes. Leur explication sera donnée dans la légende des figures. Prière de ne pas inscrire les mêmes données dans les tableaux et les figures. Chaque tableau aura un titre. On indiquera dans le texte la place approximative des tableaux et des figures. Les formules chimiques seront incluses dans le texte : en outre, elles seront transcrites sur papier calque, à l'encre de Chine.

Les auteurs sont priés d'indiquer les caractères italiques (en soulignant les lettres au crayon), ainsi que tout autre caractère spécial : les préfixes *ortho, méta, para, cis, trans*, etc. seront soulignés pour indiquer leurs caractères italiques, et ne seront jamais écrits avec des majuscules.

Aucune correction à la main ne sera admise sur le manuscrit. Les corrections seront frappées à la machine. Les lettres grecques ou d'autres symboles spéciaux seront insérés à la main à l'encre clairement.

Le manuscrit sera signé par l'auteur.

Le titre courant aura 50 lettres au maximum.

L'entière responsabilité du contenu des articles appartient aux auteurs.

Sur demande on peut obtenir une note plus complète.

PRINTED IN ROMANIA

ORSZÁGOS MŰSZAKI INFORMÁCIÓS KÖZPONT ÉS KÖNYVTÁR 1883

TRAVAUX PARUS AUX ÉDITIONS DE L'ACADÉMIE DE LA RÉPUBLIQUE SOCIALISTE DE ROUMANIE

ELENA CEAUŞESCU, **Răşini de hidrocarburi**, vol. 1, 1987, 344 p.
ELENA CEAUŞESCU, **Progrese în chimia şi tehnologia polimerilor**, 1986, 446 p.
ELENA CEAUŞESCU, **Forschungen im Bereich der Chemie und Technologie de Polymere**, 1986, 444 p.
ELENA CEAUŞESCU, **Cercetări în chimia şi tehnologia polimerilor**, 1983, 520 p.
ELENA CEAUŞESCU, **Noi cercetări în domeniul compuşilor macromoleculari**, 1981, 536 p.
ELENA CEAUŞESCU, **Polimerizarea stereospecifică a izoprenului**, 1979, 307 p.
ELENA CEAUŞESCU, **Research work on synthesis and characterization of macromolecular compounds. Contributions**, 1974, 251 p.
I. G. MURGULESCU, **Introducere în chimia fizică, vol. I. 1. Atomi, molecule, legătură chimică**, 1976, 560 p.
I. G. MURGULESCU, V. EM. SAHINI, **Introducere în chimia fizică, Vol. I. 2. Structura şi proprietăţile moleculelor, 1979**, 604 p.
I. G. MURGULESCU, E. SEGAL, **Introducere în chimia fizică, Vol. II. 1. Teoria molecular-cinetică a materiei**, 1979, 1036 p.
I. G. MURGULESCU, TATIANA ONCESCU, E. SEGAL, **Introducere în chimia fizică, Vol. II.2. Cinetică chimică şi cataliză**, 1981, 1024 p.
I. G. MURGULESCU, J. PĂUN, **Introducere în chimia fizică, Vol. I. 3. Nucleul atomic, reacţii nucleare, particule elementare**, 1982, 606 p.
I. G. MURGULESCU, RODICA VÎLCU, **Introducere în chimia fizică. Vol. III. Termodinamica chimică**, 1982, 624 p.
I. G. MURGULESCU, O. M. RADOVICI, **Introducere în chimia fizică. Vol. VI. Electrochimia**, 1986, 410 p.
CRISTOFOR I. SIMIONESCU, VALERIA GORDUZA, **Implicaţii bioenergetice ale coloranţilor**, 1988, 208 p.
R. VÎLCU, M. LECA, **Termodinamica polimerilor prin cromatografie de gaze**, 1987, 238 p,
I. ZUGRĂVESCU, M. PETROVANU, **Cicloadiţii 3 + 2 dipolare**, 1987, 446 p.
RAUL MIHAIL, ION GROZEANU, **Estimarea secvenţială aplicată sistemelor chimice**, 1986, 406 p.
M. BREZEANU, I. PATRON, M. ANDRUH, **Combinaţii complexe polinucleare şi aplicaţiile lor**, 1986, 244 p.
A. T. BALABAN et al., **Labelled Compounds and Radiopharmaceuticals Applied in Nuclear Medicine**, coédition avec John Wiley and Sons, 1986, 742 p.
D. PURDELA, **Nomenclatura chimiei organice — IUPAC**, 1986, 451 p.
PETRU BUDRUGEAC, **Probleme de chimie**, 1986, 280 p.
T. ONCESCU, S. G. IONESCU, **Conversie fotochimică şi stocare de energie**, 1985, 272 p.
V. DRĂGUŢAN, A. T. BALABAN, M. DIMONIE, **Olefin Metathesis and Ring-Opening Polymerization of Cyclo-Olefins**, coédition avec John Wiley and Sons, 1985, 544 p.
C. LITEANU, I. RÎCĂ, **Optimizarea proceselor analitice**, 1985, 360 p.
N. PERESCU, **Chimia extracţiei cu solvenţi şi aplicaţii**, 1985, 212 p.
V. E. SAHINI, M. HILLEBRAND, **Chimie cuantică în exemple şi aplicaţii**, 1984, 378 p.
GH. MARCU, **Chimia compuşilor coordinativi**, 1984, 415 p.
E. CORDOŞ, C. MANOLIU, **Spectrometria de absorbţie şi fluorescenţă atomică**, 1984, 178 p.
C. BODEA, **Tratat de biochimie vegetală, p. II, t. V**, 1984, 438 p.
N. ASANDEI, A. GRIGORIU, **Chimia şi structura fibrelor**, 1983, 395 p.
N. IONESCU, M. CĂLDĂRARU, **Oxidarea catalitică a olefinelor inferioare**, 1983, 178 p.
C. CAŞCAVAL, **Studiul polimerilor prin piroliză şi cromatografie de gaze**, 1983, 220 p.
C. I. SIMIONESCU, F. DANEŞ, **Originea vieţii**, 1983, 110 p.
C. BODEA, **Tratat de biochimie vegetală, p. II, t. IV**, 1982, 408 p.
I. GĂLĂŢEANU, **Procese şi metode radiochimice în energetica nucleară**, 1981, 234 p.
CR. SIMIONESCU, VALERIA GORDUZA, **Polimeri biocompatibili şi biologic activi**, 1980, 479 p.
M. FLORESCU, **Metode ştiinţifice în dezvoltarea industriei chimice moderne**, 1979, 495 p.
C. GH. MACAROVICI, **Analiza chimică cantitativă anorganică**, 1979, 457 p.

ISSN 0035—3930

1990 JAN 09

I. P. INFORMAŢIA c. 1394

43 426

Lei 40